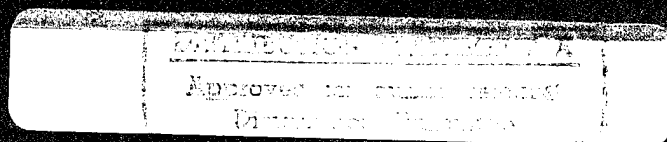


Proceedings of
ION GPS-95

*The 8th International Technical Meeting of
The Satellite Division of The Institute of Navigation*

Part 1 of 2



**September 12-15, 1995
Palm Springs Convention Center
Palm Springs, California**



| | |
|--------------------------------------|---|
| Accession For | |
| NTIS | CRA&I <input checked="" type="checkbox"/> |
| DTIC | TAB <input type="checkbox"/> |
| Unannounced <input type="checkbox"/> | |
| Justification | |
| By | |
| Distribution / | |
| Availability Codes | |
| Dist | Avail and/or Special |
| A-1 | |

Proceedings of

ION GPS-95

*The 8th International Technical Meeting of
The Satellite Division of The Institute of Navigation*

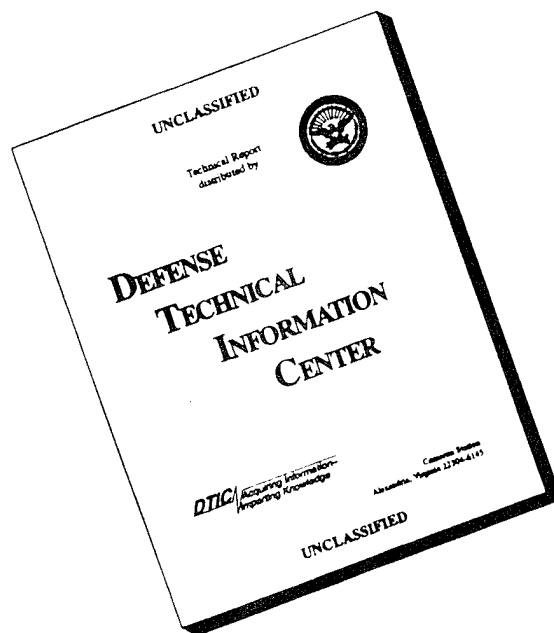
Part 1 of 2

19951219 060

September 12-15, 1995
Palm Springs Convention Center
Palm Springs, California

2025 RELEASE UNDER E.O. 14176

DISCLAIMER NOTICE



THIS DOCUMENT IS BEST QUALITY AVAILABLE. THE COPY FURNISHED TO DTIC CONTAINED A SIGNIFICANT NUMBER OF PAGES WHICH DO NOT REPRODUCE LEGIBLY.

THE INSTITUTE OF NAVIGATION



The Purpose of the ION

The Institute of Navigation is a scientific, non-profit organization, founded in 1945. Its programs are directed toward elevating standards of navigation by coordinating the knowledge and achievement of practicing navigators, scientists and those involved in the development and production of navigation equipment.

DTIC QUALITY INSPECTED 1

ACKNOWLEDGMENTS

The Institute wishes to acknowledge the combined efforts of a dedicated group of individuals whose contributions were invaluable to the success of GPS-95 Meeting. This acknowledgement is in no way all inclusive, but serves as recognition of principal contributors.

ION GPS-94 PROGRAM CHAIRS



Dr. Richard Greenspan
General Chair



Dr. M. Elizabeth Cannon
Program Chair



Mr. Mark Leach
Technical Chair Track A



Mr. Ron Hatch
Technical Chair Track B



Ms. Karen Van Dyke
Technical Chair Track C



Dr. Peter Daly
Technical Chair Track D

MEETING ORGANIZERS

Mr. Phillip Ward: ION Satellite Division Chair
 Mr. Gaylord Green: Satellite Division Vice Chair
 Mr. Ron Hatch: Satellite Division Treasurer
 Dr. Penina Axelrad: Satellite Division Secretary
 Col. Zdzislaw (Stan) Lewantowicz: ION President
 Ms. Carolyn McDonald: ION Meetings Chair
 Mr. Ken Holland: Technical Chair Product Training & Demonstration
 Mr. Loic Camberlein: European Technical Advisor
 Mr. Otto Pietersen: European Technical Advisor
 Dr. Masaaki Murata: Asian Technical Advisor
 WGCdr Keith McPherson: Australian Technical Advisor
 Sqdrn. Ldr. Scott Wallis: Australian Technical Advisor
 Mr. Naser El-Sheimy: Student Session Chair
 Mr. Gaylord Green: Conference Publicity Chair
 Mr. James Thebeau: Press Relations Chair
 Dr. R. Grover Brown: Publications Chair
 Mr. Phillip Arndt: Exhibit Publicity Chair
 Mr. Ron Hatch: Awards Chair

SESSION CHAIRS & CO-CHAIRS

Session A1—Surveying and Geodesy: Chair, Mr. Steve Malys; Co-Chair, Dr. Tom Herring
 Session B1—Product Announcements: Chair, Dr. Jim Sennott; Co-Chair, Ms. Debra Diefes
 Session C1—Space Applications: Chair, Dr. Willy Bertiger
 Session D1—Student Competition Winners: Chair, Mr. Naser El-Sheimy
 Session A2—Military Applications and Requirements: Chair, Dr. Arnold Tucker; Co-Chair, Mr. Ben Roth
 Session B2—DGPS Technology and Applications: Chair, Dr. Alison Brown; Co-Chair, Dr. Trent Skidmore
 Session C2—Space: Orbit and Attitude: Chair, Dr. Bob Schutz; Co-Chair, Mr. Kenn Gold
 Session D2—Wide Area Augmentation Systems: Chair, Dr. Sally Basker; Co-Chair, Mr. Bruce DeCleene
 Session A3—Precision Landing: Chair, Dr. Per Enge; Co-Chair, Ms. Cecelia Feit
 Session B3—Specialized User Equipment Technology: Chair, Capt. Ben Peterson; Co-Chair, Dr. Triveni Upadhyay
 Session C3—Maritime Applications: Chair, Mr. Jim Morgan; Co-Chair, Mr. Fred Forbes
 Session D3—GLONASS: Chair, Mr. Scott Fearheller; Co-Chair, Dr. Jacques Beser
 Session A4—DGPS Algorithms: Chair, Dr. Gerard Lachapelle; Co-Chair, Dr. Paul Cross
 Session B4—Earth Observation and Timing: Chair, Mr. David Allan; Co-Chair, Mr. Greg Bishop
 Session C4—Land Vehicular Applications: Chair, Mr. Robert Denaro; Co-Chair, Mr. Jim Arnold
 Session D4—GNSS Policy and Technology Issues: Chair, Mr. Keith McDonald; Co-Chair, Maj. Gen. Ralph Jacobson, USAF, Ret.
 Session A5—Precise Real-Time Positioning: Chair, Ms. Sally Frodge; Co-Chair, Mr. Richard Barker
 Session B5—GPS User Equipment Technology: Chair, Dr. Sergei Gourevitch; Co-Chair, Dr. Durk Van Willigen
 Session C5—Airborne Applications: Chair, Mr. Warren Hundley; Co-Chair, Ms. Lois Pilley
 Session D5—GPS Reference and Testing: Chair, Mr. Mike Hadfield; Co-Chair, Mr. Stewart Teasley
 Session A6—Attitude Determination: Chair, Dr. Penina Axelrad; Co-Chair, Mr. Ron Brown
 Session B6—Integrated Systems: Chair, Mr. Jeff Geier; Co-Chair, Dr. Manfred Haverland
 Session C6—Emerging Applications: Chair, Mr. Glen Gibbons; Co-Chair, Dr. David Tyler
 Session D6—Integrity: Chair, Dr. John Diesel; Co-Chair, Ms. Marie Lage

ION GPS-95 PROCEEDINGS TABLE OF CONTENTS

Plenary Session

| | |
|---|------|
| GPS – The Ultima Thule of Navigation | |
| James Schlesinger, <i>Keynote Speaker ION GPS-95</i> | 3-6 |
| Panel Discussion: GPS Critical Technology, Policy, and Institutional Issues | |
| Moderator: Keith McDonald, <i>Sat Tech Systems</i> ; Panel Members: Dr. James Schlesinger, Joseph Canny, Gil Klinger, Larry Adams, Charles Trimble, Dr. Scott Pace, and Col. John Caldwell, USAF | 7-14 |

Session A1: Surveying and Geodesy

| | |
|--|---------|
| A Comparison of GPS and Satellite Altimetry for Height Monitoring on an Offshore Production Platform | |
| Moirá Tighe and John Macgregor, <i>Shell U.K. Exploration and Production</i> | 17-23 |
| A GPS Positioning Results Using Precise Satellite Ephemerides, Clock Corrections and Ionospheric Grid Model with Jupiter | |
| Yang Gao, James McLellan, and Mohamed Abousalem, <i>Pulsesearch Navigation Systems, Inc.</i> | 25-34 |
| A Compact Earth Tides Algorithm for WADGPS | |
| James Sinko, <i>SRI International</i> | 35-44 |
| Evaluation of DoD GPS Satellite Orbits Using NASA Laser Ranging Data | |
| James O'Toole and Michael Merrigan, <i>Naval Surface Warfare Center</i> | 45-54 |
| Improved Ambiguity Resolution by Regional Differential Modelling of the Ionosphere | |
| Lambert Wanninger, <i>TU Dresden, Germany</i> | 55-62 |
| An Efficient Algorithm for Batch Estimation of Non-Dynamic Parameters of Double-Differenced GPS Phase Measurement | |
| H. Rim, B. Schutz, and B. Tapley, <i>University of Texas at Austin</i> | 63-71 |
| Determining Earth Orientation by Global Positioning System at the US Naval Observatory | |
| Peter Kammeyer and James Rhode, <i>US Naval Observatory</i> | 73-81 |
| Programme of Research of CEI (Central European Initiative) Countries in Geodesy and Geodynamics | |
| Janusz Sledzinski, <i>Warsaw University of Technology</i> | 83-91 |
| Sakhalin Island GPS Survey: A Case History | |
| Paul Godwin, <i>Mobile Oil Corporation</i> ; Sergey Duginov, <i>Romona Ltd.</i> ; John Brown, <i>Geodetic Technology Company</i> | 93-104 |
| Economics of GPS and CORS | |
| William Young, <i>Riverside</i> ; Yehuda Bock and Shelley Marquez, <i>Scripps Institute of Oceanography</i> | 105-113 |

Session B1: Product Announcements

| | |
|---|---------|
| Open Architecture Design for GPS Applications | |
| Yves Théroux, <i>Canadian Marconi Company</i> | 117-121 |
| Two Piece Chipset for GPS Makes a Four Chip GPS Receiver | |
| Philip Mattos, <i>SGS-Thomson Microelectronics</i> | 123-132 |
| What's New From NovAtel | |
| Simon Newby and Wendy Corcoran, <i>NovAtel Communications Ltd.</i> | 133-140 |
| GPS Tensor™ GPS Receiver for Attitude and Orbit Determination | |
| J. Kurt Brock, <i>Space Systems/LORAL</i> | 141-142 |
| Hitachi HGA-D Fiber Optic Gyroscope for Vehicular Applications | |
| Bob Yoshida, <i>Hitachi Cable America</i> ; Vincent Martinelli, <i>Corning Incorporated</i> | 143-146 |
| Honeywell's DGPS Local Area Augmentation System Ground Station | |
| Steve Serfling, <i>Honeywell</i> | 147-156 |
| Starwatch™: An Off-the-Shelf GPS Asset Location System | |
| John Lavrakas, <i>Advanced Research Corporation</i> | 157-160 |
| The XR5-PC12 – Position and Time/Frequency From a Single Plug-in Module | |
| Tony Haddrell, <i>Navstar Systems Ltd.</i> | 161-166 |
| Ashtech RTZ, Real-Time Kinematic GPS with OTF Initialization | |
| Sergei Gourevitch, Frank van Diggelen, Xinhua Qin, and Mark Kuhl, <i>Ashtech</i> | 167-170 |

Session C1: Space Applications

| | |
|---|---------|
| An Autonomous GNSS-based Orbit Determination System for Low-Earth Observation Satellites | |
| Jorge Potti, Juan Carlos Carmona, and Pelayo Bernedo, <i>GMV S.A.</i> ; Pierluigi Silvestrin, <i>ESA/ESTEC</i> | 173-182 |
| Results of a Automated GPS Tracking System in Support of Topex/Poseidon and GPSMet | |
| Ronald Muellerschoen, Stephen Lichten, Ulf Lindqwister, and Willy Bertiger, <i>Jet Propulsion Laboratory</i> | 183-193 |
| GPS Multipath Modeling and Verification Using Geometrical Theory of Diffraction | |
| Susan Gomez, Robert Panneton, and Penny Saunders, <i>NASA/LBJ Space Center</i> ; Shian and Ba Lu, <i>Lockheed Martin</i> | 195-204 |
| Application of Fuzzy Logic and Multisensor Data Fusion Techniques to On-board GPS-based Spacecraft Navigation | |
| Stefano Giacomini, <i>University of Milano</i> ; Livio Marradi, <i>LABEN S.p.A.</i> | 205-216 |
| GPS Autonomous Relative Navigation and Time Transfer for Orbiting Space Vehicles | |
| Duncan B. Cox, Jr., <i>DBC Communications, Inc.</i> ; John D.W. Brading, <i>Brading Systems and Technology</i> | 217-228 |
| GPS Tracking Experiment of a Dree-Flyer Deployed from Space Shuttle | |
| Bob Schutz, P.A.M. Abusali, Christine Schroeder, and Byron Tapley, <i>University of Texas at Austin</i> ; Michael Exner and Rick McCloskey, <i>University Corporation for Atmospheric Research</i> ; Russell Carpenter, Michael Cooke, and Samantha McDonald, <i>NASA/Johnson Space Center</i> ; Nick Combs, <i>University of Houston</i> ; Courtney Duncan, Charles Dunn, and Tom Meehan, <i>NASA/JPL</i> | 229-235 |
| GPS Receiver Design and Requirement Analysis for the Stanford Gravity Probe B Relativity Mission | |
| Hirohiko Uematsu and Bradford Parkinson, <i>Stanford University</i> ; E. Glenn Lightsey, <i>NASA Goddard Space Flight Center</i> | 237-246 |
| National Satellite Testbed (NSTB) GPS Satellite Clock/Ephemeris Determination Analysis and Results | |
| Scott Pogorelc, Mark Lorenz, Kelly Murdock, Brent Harding, Tim Cashin, and Donna Kraus, <i>Stanford Telecommunications</i> | 247-256 |
| GPS Techniques for Navigation of Geostationary Satellites | |
| Pascale Ferrage, Jean-Luc Issler, Genevieve Campan, and Jean-Claude Durand, <i>French National Space Agency (CNES)</i> | 257-268 |
| Relative GPS Navigation for ATV Rendezvous | |
| Michael Frezet, Herve Marcille, Virginie Pascal, and Jean Michael Pairot, <i>Matra Marconi Space</i> ; Hubert Barré, Massimo Cislighi, and Ulrich Thomas, <i>European Space Agency</i> | 269-278 |

Session D1: Student Competition Winners

| | |
|--|---------|
| Aircraft Tracking Using GPS Position and Velocity Reports | |
| Ran Gazit, <i>Stanford University</i> | 281-290 |
| High Precision Highway Profiles Using Helicopter Borne 'On-The-Fly' GPS | |
| Paul Hansen and Chris Joy, <i>The University of Nottingham</i> | 291-298 |
| A New Concept for GPS Phase Ambiguity Resolution On-The-Fly: The Maximum a Posteriori Ambiguity Search (MAPAS) Method | |
| Christophe Macabiau, <i>Laboratoire de Traitement du Signal et des Télécommunications of the ENAC</i> | 299-308 |
| A New Navigation Algorithm Using Only Information From Measurement | |
| Benlin Xu, <i>University of New Brunswick</i> | 309-318 |
| A Prototype Portable Vehicle Navigation System Utilizing Map Aided GPS | |
| Blake Bullock, <i>The University of Calgary</i> | 319-329 |
| Efficient Ambiguity Search Using Genetic Algorithms | |
| Zuofa Li, <i>The University of Calgary</i> | 331-337 |
| Airborne Gravimetry by GNS/INS A Comparison of Filtering Methods | |
| Youcef Hammada, <i>The University of Calgary</i> | 339-347 |
| Ambiguity Recovery for GPS Long Range Kinematic Positioning | |
| Shaowei Han, <i>The University of New South Wales</i> | 349-360 |

Session A2: Military Applications and Requirements

| | |
|---|---------|
| Use of the GPS Aided Inertial Navigation System in the Navy Standard Missile for the BMDO/Navy LEAP Technology Demonstration Program | |
| Todd Moore, Kevin Rudolph, and Frank Ziolkowski, <i>Hughes Aircraft Co.</i> ; Alfred Luckau, <i>Hughes Missile Systems Co.</i> | 363-371 |
| Integrated GPS/INS/SAR/GMTI Radar Precision Targeting Flight Test Results | |
| R. Guarino and Paul Isben, <i>Westinghouse Norden Systems</i> | 373-379 |

| | |
|---|---------|
| Anti-Jamming Performance of TIDGET in Guided Munitions Applications | |
| Armando Montalvo, Bruce Johnson, and Alison Brown, <i>NAVSYS Corporation</i> | 381-390 |
| Robust Implementation of Relative GPS Guidance | |
| Mark Youhanaie, David Hartman, and Frank Ziokolwski, <i>Hughes Aircraft Co.</i> ; Neeraj Pujara, <i>Wright Laboratory</i> | 391-398 |
| A Global DoD-Optimized DGPS for Precision-Strike | |
| Earl Blackwell, Mark Moeglein, and David Nakayama, <i>SRI International</i> | 399-411 |
| Navigation Performance Analysis for the Edge Program | |
| Donald Kelly and Pamela Harms, <i>Sverdrup/TEAS</i> ; Capt. John Dargen, <i>USAF</i> ; Chuck Eckert, <i>Honeywell</i> | 413-422 |
| Preliminary Results from a GPS-based Portable Impact Location System | |
| Jimmy Saunders and Miguel Cardoza | 423-430 |
| Precise Absolute Navigation: An Evaluation of PPS Position Improvement | |
| Bruce Hermann, <i>Naval Surface Warfare Center</i> ; Stephen Malys, <i>The Defense Mapping Agency</i> | 431-436 |
| GPS Translator for Artillery Projectiles – A Progress Report | |
| George Wiles, <i>US Army Research Laboratory</i> ; Jeff Smuk, <i>Hittite Microwave Corporation</i> | 437-441 |
| The Reduction of Airborne Magnetic Noise Via GPS | |
| L. Bobb, W. Gelatka, D. DePersia, A. Salik, and S. Swyers, <i>Naval Air Warfare Center</i> | 443-447 |
| GPS Operational Control System Modernization: Alternative Architectural Concepts | |
| Jaynarayan Lala and Laura Burkhardt, <i>Draper Laboratory</i> | 449-459 |

Session B2: DGPS Technology and Applications

| | |
|--|---------|
| Design of a GNSS: Coverage, Accuracy and Integrity | |
| V. Ashkenazi, T. Moore, C. J. Hill, W. Y. Ochieng, and Wu Chen, <i>The University of Nottingham</i> | 463-472 |
| Differential GPS Evaluation at UK Airports | |
| Hemant Mistry and Richard Farnworth, <i>UK National Air Traffic Services</i> | 473-479 |
| Floating Differential GPS (FDGPS) | |
| James L. Brown, <i>Aydin Corporation (East)</i> | 481-490 |
| Characterization of Phase and Multipath Errors for an Aircraft GPS Antenna | |
| C. Douglas Hardwick and Jeffrey Liu, <i>National Research Council of Canada</i> | 491-498 |
| Precise Positioning Using GPS/GLONASS Carrier Phase and Code Phase Observables | |
| David Walsh, Stuart Riley, John Cooper, and Peter Daly, <i>The University of Leeds</i> | 499-506 |
| Differential GLONASS, Differential GPS and Integrated Differential GLONASS/GPS – Initial Results | |
| Jacques Beser, Anushia Balendra, Eric Erpelding, and Sonia Kim, <i>3S Navigation</i> | 507-515 |
| Performance Evaluation of a Global IGS-Based Differential GPS System | |
| Don English, Gene Howell, and Wang Tang, <i>ARINC</i> | 517-523 |
| Satisfying Airport Operational Requirements Using Seamless GNSS Techniques, Procedures and Processing | |
| Lois Pilley and Robert Pilley, <i>DSDC</i> | 525-532 |
| Selective Availability via the Levinson Predictor | |
| Timothy Barnes, <i>Zeta Associates, Inc.</i> | 533-542 |

Session G2: Space: Orbit and Attitude

| | |
|--|---------|
| GPS Attitude Determination and Navigation Flight Experiment | |
| J. Kurt Brock, Rich Fuller, Brian Kemper, Dave Mleccko, J. Rodden, and Alfred Tadros, <i>Space Systems/LORAL</i> | 545-554 |
| The GPS Attitude Determination Flyer (GADFLY): A Space-Qualified GPS Attitude Receiver on the SSTI-Lewis Spacecraft | |
| Frank Bauer, E. Glenn Lightsey, Stephen Leake, Jon McCullough, James O'Donnell, Kate Hartman, and Roger Hart, <i>NASA Goddard Space Flight Center</i> | 555-562 |
| Argos Navigation and Attitude Determination System | |
| Jon Petway, <i>Rockwell</i> | 563-572 |
| Experimental Results of Using the GPS for SFU Onboard Navigation | |
| Tsutomu Ichikawa and Keiken Ninomiya, <i>The Institute of Space and Astronautical Science</i> ; Susumu Kumagai and Masaki Mistutake, <i>Hitachi Ltd.</i> | 573-577 |
| A Practical Demonstration of Low Cost Autonomous Orbit Determination Using GPS | |
| Martin Unwin and Martin Sweeting, <i>University of Surrey</i> | 579-587 |

| | |
|--|---------|
| Applicability of GPS-based Orbit Determination Systems to a Wide Range of HEO Missions | |
| Jorge Potti and Pelayo Bernedo, <i>GMV S.A.</i> ; Alessandro Pasetti, <i>ESA/ESTEC</i> | 589-598 |
| Performance Evaluation of the GPS Yaw Bias Implementation | |
| Yoaz Bar-Sever, <i>Jet Propulsion Laboratory</i> | 599-611 |
| Effect of GPS Orbit Accuracy on GPS-determined Topex/Poseidon Orbit | |
| H. J. Rim, B. E. Schutz, P.A.M. Abusali, and B. D. Tapley, <i>University of Texas at Austin</i> | 613-617 |
| Use of GPS for Precise and Operational Orbit Determination at ESOC | |
| Tomás Martín Mur, John Dow, and Nicholas Bondarenko, <i>European Space Agency</i> ; Stefano Casotto, <i>Univeritá Padova</i> ; Joachim Feltens, <i>mbp Informationstechnologie GmbH</i> ; Carlos García Martínez, <i>GMV S.A.</i> | 619-626 |

Session D2: Wide Area Augmentation Systems

| | |
|--|---------|
| A Wide Area Augmentation System (WAAS) Service Volume Model and Its Use in Evaluating WAAS Architectures and Design Sensitivities | |
| Walter Poor, Thomas Albertson, and Pauline Yen, <i>The MITRE Corporation</i> | 629-637 |
| An Algorithm for Inter-frequency Bias Calibration and Application to WAAS Ionosphere Modeling | |
| Yi-chung Chao, Yeou-Jyh Tsai, Todd Walter, Changdon Kee, Per Enge, and Brad Parkinson, <i>Stanford University</i> | 639-646 |
| Incorporation of Orbital Dynamics to Improve Wide-Area Differential GPS | |
| Juan Ceva and Bradford Parkinson, <i>Stanford University</i> ; Willy Bertiger, Ron Muellerschoen, and Thomas Yunck, <i>JPL</i> | 647-659 |
| Validation of the RTCA Message Format for WAAS | |
| Yeou-Jyh Tsai, Per Enge, Yi-Chung Chao, Todd Walter, Changdon Kee, Jennifer Evans, Andrew Barrows, David Powell, and Bradford Parkinson, <i>Stanford University</i> | 661-670 |
| The Ability of a RADGPS to Provide the Accuracy and Integrity Required for En-Route Navigation | |
| Richard Farnworth, <i>UK National Air Traffic Service</i> ; Stuart Jolley, <i>Roke Manor Research</i> ; Andrew Lovett, <i>Racal Avionics</i> | 671-676 |
| Integrating WAAS with LAAS to Avoid Signal Spoofing | |
| Vis Sankaran and Donald Benson, <i>Dynamics Research Corporation</i> | 677-684 |
| Exact Formula for User Range Error in Wide Area Differential GPS | |
| Henry Beisner, <i>Paradeigma, Inc.</i> ; Arthur Dorsey, <i>Loral Federal Systems</i> | 685-693 |
| WAAS Sensor Interference Testing | |
| Trent Skidmore, <i>Ohio University</i> ; Mark Johnson, <i>Rockwell International</i> | 695-703 |
| A Study for Performance Enhancements of the Asian-Australian GPS Augmentation System (AAAS) | |
| Yanming Feng, Kurt Kubik, and Jizhang Sang, <i>Queensland University of Technology</i> ; Jingnan Liu, <i>Wuhan TU</i> | 705-711 |

Session A3: Precision Landing

| | |
|--|---------|
| FAA-Wilcox Electric Category IIIB Feasibility Demonstration Program Flight Test Results | |
| W. Hundley, S. Rowson, and G. Courtney, <i>Wilcox Electric</i> ; V. Wulschleger and R. Velez, <i>FAA Technical Center</i> ; R. Benoist, <i>Litton Aero Products</i> ; P. O'Donnell, <i>MITRE/CAASD</i> | 715-726 |
| FAA/Ohio University/United Parcel Service DGPS Autoland Flight Test Demonstration | |
| Frank van Graas, David Diggle, and Maarten Uijt, <i>Ohio University</i> ; Dave Lamb and Mark Dimeo, <i>Systems Resources Corporation</i> ; Greg Kuehl and Robert Hilb, <i>United Parcel Service</i> | 727-737 |
| FAA/FEDSIM—E-Systems Cat IIIB Feasibility Demonstration Flight Test Preliminary Results | |
| Glyn Romrell, Ron Brown, and Greg Johnson, <i>E-Systems</i> ; Dave Kaufmann, <i>NASA Ames</i> | 739-753 |
| Application of INS/GPS Systems Integration to Increase Performance of Automatic Landing Systems | |
| Jochen Meyer-Hilberg and Harald Harder, <i>Daimler-Benz Aerospace AG</i> | 755-762 |
| A340-DGPS Landing Experiment | |
| Julie de Cevins, <i>Airbus Industrie</i> ; Pascal Ponsot, <i>Aerospatiale</i> | 763-772 |
| FAA's Cat III Feasibility Program: Status and Accomplishments | |
| R. Braff and P. O'Donnell, <i>The MITRE Corporation</i> ; V. Wulschleger, C. Mackin, and R. Velez, <i>FAA Technical Center</i> ; R. Swider and P. Enge, <i>Stanford University</i> ; F. van Graas, <i>Ohio University</i> ; D. Kaufmann, <i>NASA Ames Research Center</i> | 773-780 |
| GNSS Receiver Interference: Susceptibility and Civil Aviation Impact | |
| Mark Johnson and Robert Erlandson, <i>Rockwell</i> | 781-791 |
| Observed GPS Signal Continuity Interruptions | |
| Stewart Cobb, David Lawrence, Jock Christie, Todd Walter, Y.C. Chao, David Powell, and Brad Parkinson, <i>Stanford University</i> ... | 793-795 |

| | |
|---|---------|
| Integrity and Continuity of Service Analysis of LADGPS and WADGPS Architectures with SNAPSIS Simulator | |
| D. Flament and N. Marchel, <i>Thomson-CSF</i> ; B. Christophe, <i>Onera</i> ; J. L. Jonquiere, <i>DGAC/STNA</i> | 797-806 |
| Interoperability and Traditional Nav-aid Considerations for DGPS Standards | |
| Lori Hill and Ken Ganther, <i>Wilcox Electric</i> | 807-814 |

Session B3: Specialized User Equipment Technology

| | |
|---|---------|
| Development and Testing of a Mobile Pseudolite Concept for Precise Positioning | |
| Tom Holden, <i>Stanford Telecom</i> ; John Racquet, Gerard Lachapelle, Weigen Qiu, and C. Pelletier, <i>The University of Calgary</i> ; Anthony Nash, <i>746th Test Squadron</i> ; Patrick Fenton, <i>NovAtel</i> | 817-826 |
| Precision Landing Tests with Improved Integrity Beacon Pseudolites | |
| Stewart Cobb, David Lawrence, Boris Pervan, Clark Cohen, David Powell, and Brad Parkinson, <i>Stanford University</i> | 827-833 |
| A Combined GPS/GLONASS High Precision Receiver for Space Applications | |
| Stuart Riley, Neil Howard, Eric Aardoom, and Peter Daly, <i>University of Leeds</i> ; Pierluigi Silvestrin, <i>ESA ESTEC</i> | 835-844 |
| Integrated GPS/GLONASS Antenna for High Performance Applications | |
| Taymoor Hekmat and Norbert Niklasch, <i>ViCon Engineering GmbH</i> ; Martin Maurer, <i>MAN Technologie AG</i> | 845-851 |
| Tracking Measurements From a Miniature GLONASS Receiver | |
| Oliver Leisten, Geraint Ffoulkes-Jones, Gerald Whitworth, and David Belton, <i>Navstar Systems Ltd.</i> | 853-859 |
| Power Minimization Techniques for GPS Null Steering Antenna | |
| Anton Gecan, <i>E-Systems</i> ; Michael Zoltowski, <i>Purdue University</i> | 861-868 |
| Performance of a Miniature Dielectrically Loaded Volute Antenna | |
| Oliver Leisten and Geraint Ffoulkes-Jones, <i>Navstar Systems Ltd.</i> | 869-877 |
| An Effective GPS Application for Helicopter Operations | |
| William O'Keefe, <i>Newcomb Communication, Inc.</i> | 879-886 |

Session C3: Maritime Applications

| | |
|--|---------|
| Verification of USCG DGPS Broadcast Parameters | |
| Mark Lunday, Joseph Spalding, and Marylouise Dowd | 889-897 |
| DGPS Positioning Accuracy Performance Analysis with RTCM | |
| Message Types 1/9 and 18-21 Using Various Receiver Technologies | |
| G. Lachapelle, M. E. Cannon, H. Lan, and C. Tang, <i>The University of Calgary</i> ; S. Wee and S. Ryan, <i>Canadian Coast Guard</i> | 899-906 |
| Boosting Shipboard RAIM Availability | |
| James LaMance and Alison Brown, <i>NAVSYS Corporation</i> ; Joseph Spalding, <i>US Coast Guard R&D Center</i> | 907-912 |
| The Virtual Anchor | |
| Glen Robertson, <i>Rhodan Marine Equipment</i> ; John Webster, <i>Holst-Webster Enterprises</i> | 913-918 |
| Use of DGPS for an In-Water Acoustic Survey for the PTS SWIMSS | |
| Robert Reid, <i>Naval Undersea Warfare Center</i> | 919-923 |
| Autonomous Underwater Vehicle Navigation | |
| Stewart Cannon, <i>Pelagos Corporation</i> ; Jeff Smith, <i>Applied Remote Technology</i> | 925-933 |
| Performance Analysis of the Interrupted Data Acquisition Receiver Obtained From Operational Missions | |
| Gerald Whitworth, <i>Navstar Systems Ltd.</i> ; David Meldrum, <i>Dunstaffnage Marine Laboratory</i> | 935-940 |
| Results of Testing on a GPS-Based Compass | |
| Joseph Spalding and Mark Lunday, <i>US Coast Guard R&D Center</i> | 941-948 |
| The Use of GPS for Underwater Navigation, Sea Trial Results | |
| M. H. G. Thomas, <i>ACSA</i> | 949-955 |

Session D3: GLONASS

| | |
|---|---------|
| The GLONASS System Status and Prospects for Development | |
| Michael Lebedev and Victor Gorev, <i>CSIC</i> ; Alexander Ganin and Victor Kulnev, <i>CRI of the Russian Space Forces</i> | 959-969 |
| The Place of GLONASS in the Radionavigation Plan of the CIS | |
| Vladimir Denisov, <i>Internavigation Research and Technical Center</i> | 971-984 |

| | |
|--|-----------|
| The GLONASS and GLONASS-M Programs | 985-990 |
| V. Kazantsev, <i>NPOPM</i> | |
| Ways of GLONASS System Advancing | 991-1011 |
| Nicolay Ivanov, Vadim Salischev, and Alexander Vinogradov, <i>RISDE</i> | |
| Marine Radiobeacon DGPS/DGLONASS Service and Regional Centers for Differential GLONASS/Alpha/Chayka Services | |
| Pytor Bogdanov, Valery Chistyakov, Sergey Filatchenkov, Arvid Gevorkyan, and Vladlen Khimulin, <i>Russian Institute of Radionavigation and Time</i> | 1013-1020 |
| GLONASS Approaches Full Operational Capability (FOC) | 1021-1030 |
| Peter Daly, <i>The University of Leeds</i> | |
| Evaluation of GLONASS Performance in Practical Applications: Comparison with GPS-Based Ionospheric TEC Values | 1031-1039 |
| Nestor Zarraoa, Esther Sardon, Dietmar Klähn, and Arne Jungstand, <i>DLR-DFD Neustrelitz</i> | |
| Processing GLONASS Carrier Phase Observations—Theory and First Experience | 1041-1047 |
| Alfred Leick and Jinye Li, <i>University of Maine</i> ; Jacques Beser, <i>3S Navigation</i> ; Gerald Mader, <i>National Geodetic Survey</i> | |
| Differential GLONASS in Russia: The Ways of Development | 1049-1060 |
| Alexander Ganin, <i>GLONASS Coordination Research and Information Center</i> | |
| Kalman Filter Procedures for GPS/GLONASS-Signals | 1061-1068 |
| Norbert Niklasch, <i>ViCon Engineering</i> ; Martin Maurer and Martin Haunschild, <i>MAN Technologie AG</i> ; Walter Richert, <i>LMU</i> | |

Session A4: DGPS Algorithms

| | |
|---|-----------|
| Computation and Quality Control of Differential GPS Corrections | 1071-1079 |
| Xin-Xiang, Hans van der Marel, and Cees de Jong, <i>Delft University of Technology</i> | |
| Effects of the Ionosphere and Cycle-Slips in Long Baseline Dynamic Positioning | 1081-1090 |
| George Dedes and Angela Mallett, <i>The Ohio State University</i> | |
| Using the Ionosphere for DGPS Measurement Error Control | 1091-1100 |
| Gregory Bishop, <i>USAF Phillips Laboratory</i> ; Andrew Mazzella and Elizabeth Holland, <i>NorthWest Research Associates</i> | |
| Fast Ambiguity Resolution Using an Integer Nonlinear Programming Method | 1101-1110 |
| Ming Wei and Klaus-Peter Schwarz, <i>The University of Calgary</i> | |
| Improving the Reliability of OTF Ambiguity Resolution with Dual Frequency GPS Observations | 1111-1116 |
| Gang Lu, M. Elizabeth Cannon, and Gerard Lachapelle, <i>The University of Calgary</i> | |
| Ambiguity Resolution Over Long Baselines for Airborne Differential GPS Positioning | 1117-1126 |
| J. Sonntag and C. Martin, <i>EG&G</i> ; W. Krabill, <i>NASA Goddard Space Flight Center</i> | |
| Adaptive Modeling of Receiver Clock for Meter-Level DGPS Vertical Positioning | 1127-1135 |
| P. Misra, M. Pratt, B. Burke, and R. Ferranti, <i>MIT</i> | |
| Comparison of Different On-The-Fly Ambiguity Resolution Techniques | 1137-1144 |
| Günter Hein and Wolfgang Werner, <i>University FAF Munich</i> | |
| A New Method for Constructing Multi-satellite Ambiguity Combinations for Improved Ambiguity Resolution | 1145-1153 |
| Chris Rizos and Shaowei Han, <i>The University of New South Wales</i> | |
| Long Period Systematic Errors in GPS Measurements | 1155-1163 |
| Shane Nelson, <i>University of Texas</i> | |

Session B4: Earth Observation and Timing

| | |
|--|-----------|
| Sensing the Atmosphere From a Low-Earth Orbiter Tracking GPS: | |
| Early Results and Lessons From the GPS/MET Experiment | 1167-1174 |
| George Hajj, Rob Kursinski, Willy Bertiger, Stephen Leroy, Larry Romans, and Tim Schofield, <i>Jet Propulsion Laboratory</i> | |
| Time Calibration Using the INMARSAT Geostationary Overlay Signal From the AOR-W Satellite | 1175-1181 |
| James LaMance and Alison Brown, <i>NAVSYN Corporation</i> ; Bruce Haines, Willy Bertiger, and Sien Wu, <i>JPL</i> | |
| Real Time Estimation of Ionospheric Delays | 1183-1191 |
| Evelin Engler, Esther Sardón, and Dietmar Klähn, <i>DLR-DFD Neustrelitz</i> | |
| Real-Time TEC Determination for Ionospheric Modeling in WADGPS | 1193-1197 |
| José Fraile-Ordóñez, <i>Kayser-Threde GmbH</i> | |
| An Improved Ionospheric Correction Method for Wide-Area Augmentation Systems | 1199-1208 |
| Anthony Mannucci, Brian Wilson, and Dah-Ning Yuan, <i>Jet Propulsion Laboratory</i> | |

| | |
|--|-----------|
| Application of SCORE Techniques to Improve Ionospheric Observations | |
| Gregory Bishop, <i>USAF Phillips Laboratory</i> ; Andrew Mazzella and Elizabeth Holland, <i>NorthWest Research Associates</i> | 1209-1218 |
| Test Results of Wilcox Electric's Ionospheric Monitoring Network | |
| Craig Stull, <i>Wilcox Electric</i> ; A. J. Van Dierendonck, <i>AJ Systems</i> | 1219-1228 |
| Precise GPS Time Transfer to a Moving Vehicle | |
| Tor Egil Melgård and David Last, <i>University of Wales</i> ; Bernard Thomas, <i>DCN Brest (DGA)</i> | 1229-1236 |
| WADGPS Ionospheric Correction Model Performance Simulation | |
| Tysen Mueller, <i>Seagull Technology, Inc.</i> ; Bob Hamry and Andrew Johnson, <i>Rockwell International</i> | 1237-1246 |
| Development of Real-Time Algorithms to Estimate the Ionospheric Error Bounds for WAAS | |
| Robert Conker, Bakry El-Arini, and Thomas Albertson, <i>The MITRE Corporation</i> ; John Klobuchar, <i>USAF Phillips Laboratory</i> ; Patricia Doherty, <i>Boston College</i> | 1247-1258 |

Session C4: Land Vehicular Applications

| | |
|---|-----------|
| Kinematic GPS for Closed-Loop Control of Farm and Construction Vehicles | |
| Michael O'Connor, Gabriel Elkaim, and Bradford Parkinson, <i>Stanford University</i> | 1261-1268 |
| An Examination of the Relative Merits of Various Sensors for Vehicle Navigation | |
| Eric Abbott and David Powell, <i>Stanford University</i> | 1269-1284 |
| Nonlinear Smoothing of Dead Reckoning Data with GPS Measurements | |
| Ren Da and George Dedes, <i>The Ohio State University</i> | 1285-1294 |
| Next Generation Fiber Optic Gyroscopes for Use with GPS in Vehicle Navigation and Location Systems | |
| Vincent Martinelli, <i>Corning Inc.</i> ; Ray Ikeda, <i>Hitachi Cable America</i> | 1295-1299 |
| Hybrid GPS for Land Vehicle | |
| S. Ishikawa, Y. Suwa, N. Nakahara, T. Ito, T. Yamamoto, Y. Murakami, and T. Yasuda, <i>AISIN SEIKI Co., Ltd.</i> | 1301-1306 |
| VISAT: A Mobile City Survey System of High Accuracy | |
| Naser El-Sheimy, Klaus-Peter Schwarz, and Ming Wei, <i>The University of Calgary</i> ; Martin Lavigne, <i>GEOFIT Inc.</i> | 1307-1315 |
| Field Test Results of an Enhanced GPS Coverage Through Map Aiding in Urban and Canyon Environments | |
| James LaMance and Alison Brown, <i>NAVSYS Corporation</i> | 1317-1322 |
| GPS Receiver Structures for the Urban Canyon | |
| Benjamin Peterson, Richard Hartnett, and Geoffrey Ottman, <i>U.S. Coast Guard Academy</i> | 1323-1332 |
| Autonomous Vehicle Using WADGPS | |
| Daljit Singh, <i>Naval Air Warfare Center</i> ; Harkirat Grewal, <i>American GNC</i> | 1333-1338 |

Session D4: GNSS Policy and Technology Issues

| | |
|--|-----------|
| GPS: A Shared National Asset—A Summary of the National Research Council Report | |
| Laurence Adams, <i>Chair NRC Committee</i> ; Allison Sandlin and Dave Turner, <i>NRC</i> ; Keith McDonald, <i>Sat Tech Systems</i> | 1341-1350 |
| GPS: Charting the Future—A Summary Report by the GPS Panel of the National Academy of Public Administration | |
| Arnold Donahue and Roger Sperry, <i>Co-Directors of the NAPA Study</i> | 1351-1361 |
| GPS Performance Characteristics and Trends | |
| Rob Conley, Mark Fryt, and Sean Scott, <i>Overlook Systems Technologies, Inc.</i> | 1363-1371 |
| Practical Measurements of Radio Frequency Interference to GPS Receivers and an Assessment of Interference Levels by Flight Trials in the European Regions | |
| Paul Nisner, <i>National Air Traffic Services</i> ; John Owen, <i>Defence Research Agency</i> | 1373-1382 |
| The Role of GPS in Automatic Dependent Surveillance (ADS) and a Methodology for the Formulation of Requirements in That Role | |
| Michael Ashbury, <i>Civil Aviation Authority</i> ; Rolf Johannessen, <i>Lambourne Navigation Ltd.</i> | 1383-1391 |
| Aircraft Approach and Landing Studies with the Global Positioning System | |
| Douglas Hardwick and Jeffrey Liu, <i>National Research Council of Canada</i> | 1393-1401 |
| Global Optimization of GPS Augmentation Architectures Using Genetic Algorithms | |
| Samual Pullen, Per Enge, and Bradford Parkinson, <i>Stanford University</i> | 1403-1415 |
| GNSS Combined with Head-Up Display for Precision Landing | |
| Jean-François Jehl and Luc Baron, <i>SEXTANT Avionique</i> | 1417-1424 |
| Implementation of a GPS-Based Oceanic Air Traffic Control System | |
| Joseph Fee, <i>Federal Aviation Administration</i> ; Theodore Simpson, <i>AdsysTech Inc.</i> | 1425-1430 |

Session A5: Precise Real-Time Positioning

| | |
|--|-----------|
| High Precision Real-Time Positioning Using Low Cost OEM Sensors | |
| Adel Tabsh and Hugh Martell, <i>Premier GPS, Inc.</i> ; Darren Cosandier, <i>The University of Calgary</i> | 1433-1441 |
| High-Rate Precise Real-Time Positioning Using Differential Carrier Phase | |
| Dariusz Lapucha, Richard Barker, and Ziwen Liu, <i>John E. Chance & Associates</i> | 1443-1449 |
| Maintaining GPS Positioning in Steep Turns Using Two Antennas | |
| David Lawrence, H. Stewart Cobb, Clark Cohen, Jock Christie, J. David Powell, and Bradford Parkinson, <i>Stanford Univ</i> | 1451-1459 |
| Precise RTK Positioning Using the New RTCM-104 V2.1 Standard | |
| J.P. Thomas Goguen and Timo Allison, <i>Trimble Navigation</i> | 1461-1466 |
| First Results Using the New DGPS Real-Time Deformation Monitoring System "DREAMS" | |
| Günter Hein and Bernhard Riedl, <i>University FAF Munich</i> | 1467-1475 |
| Real-Time Precise Marine Navigation: Description and Results | |
| Hans-Jürgen Euler and Craig Hill, <i>Leica AG</i> ; Urs Müller, <i>terra vermessungen</i> | 1477-1484 |
| Development and Implementation of a Centimeter-Accurate Real-Time-Kinematic Positioning System | |
| Herbert Landau, Christian Pagels, and Ulrich Vollath, <i>terraSat GmbH</i> | 1485-1491 |
| Temporal Characteristics of Multipath Errors | |
| Ahmed El-Rabbany, <i>Alexandria University</i> | 1493-1497 |
| Utilizing a Low Cost GPS Receiver for Centimeter to Sub-meter Accuracy Real-Time and Post-Processed Applications | |
| Geraint Ffoulkes-Jones, <i>Navstar Systems Ltd.</i> ; Darren Cosandier, <i>Premier GPS Inc.</i> | 1499-1508 |

Session B5: GPS User Equipment Technology

| | |
|---|-----------|
| A Comparison of Three Multipath Mitigation Approaches for GPS Receivers | |
| Armando Montalvo and Alison Brown, <i>NAVSYS Corporation</i> | 1511-1520 |
| Achieving Theoretical Accuracy Limits for Pseudorange in the Presence of Multipath | |
| Lawrence Weill, <i>Magellan Systems and California State University at Fullerton</i> | 1521-1530 |
| Comparison of Continuity and Integrity Characteristics for Integrated and Decoupled Demodulation/Navigation Receivers | |
| Jim Sennott and Dave Senffner, <i>Bradley University</i> | 1531-1537 |
| L1 Carrier Phase Multipath Error Reduction Using MEDLL Technology | |
| Bryan Townsend, Patrick Fenton, and Keith Van Dierendonck, <i>NovAtel Communications</i> ; Richard van Nee, <i>Consultant</i> | 1539-1544 |
| Test Results on Mitigation of SATCOM-Induced Interference to GPS Operation | |
| Triveni Upadhyay, George Dimos, and Wassim Ferzali, <i>Mayflower Communications Co.</i> ; Dennis Weed, <i>FAA</i> | 1545-1552 |
| A Modified Frequency-Locked Loop for Improved WAAS Carrier Tracking | |
| Gary McGraw and Bernard Schnafer, <i>Rockwell International</i> | 1553-1562 |
| Monograph on GPS Antispoofing | |
| Phillip Ward, <i>Navward GPS Consulting</i> | 1563-1571 |

Session C5: Airborne Applications

| | |
|---|-----------|
| Flight Test Program to Develop a New Terminal Instrument Procedures TERPS for GPS Approaches | |
| John Fagan, Hazem Hejjo, Travis Fox, and Bill Archer, <i>University of Oklahoma</i> ; Ralph Sexton, <i>Innovative Solutions International</i> ; Gerry McCartor, <i>FAA</i> | 1575-1587 |
| Attitude DGPS/INS Based Real-Time Flight Guidance System for Airborne Sensors | |
| Günter Hein, Bernd Eissfeller, and Jürgen Pielmeier, <i>Institute of Geodesy and Navigation</i> | 1589-1596 |
| Geometric Correction of Airborne Multispectral Scanner Imagery Using GPS Position and Attitude and Digital Elevation Models | |
| Lawrence Fisher, <i>Lockheed Environmental Systems and Technologies</i> | 1597-1606 |
| Interferometric Flight Inspection Systems: Development and Flight Test Results | |
| D. Stratton, <i>Parker Hannifin Corporation</i> | 1607-1614 |
| Flight Tests of a 3-D Perspective-View Glass-Cockpit Display for General Aviation Using GPS | |
| Andrew Barrows, Per Enge, Bradford Parkinson, and J. David Powell, <i>Stanford University</i> | 1615-1622 |
| An Evaluation of Precise Kinematic On-The-Fly GPS Positioning with Respect to a Moving Aircraft | |
| Alan Evans, Bruce Hermann, and Christopher Law, <i>Naval Surface Warfare Center</i> ; Benjamin Remondi, <i>The XYZ's of GPS, Inc.</i> ; Thomas Briggs and Thomas Nelson, <i>Navla Air Warfare Center</i> | 1623-1628 |
| Satellite Based Integrated Navigation and Communication System of the German Air Rescue | |
| Manfred Haverland and Harry Evers, <i>Aerodata</i> ; Dr. Hindemith-Boose and Roland Kirschenlohr, <i>DRF</i> | 1629-1634 |

Session D5: GPS Reference and Testing

Development of High-Rate Differential GPS Reference for Operational Testing

William Mosle and Andy Chasko, *746th Test Squadron, Holloman AFB* 1637-1644

Summary of the Initial GPS Test Standards Document: ION STD-101

Stewart Teasley, *Rockwell Telecommunications*; James Bybee, *Cibola Information Systems* 1645-1653

The 746th Test Squadron: An All-Inclusive GPS Test and Evaluation Facility

Dan Crouch, Chip Mosle, and Michael Novy, *746th Test Squadron, Holloman AFB* 1655-1664

Time to First Fix: A Definition and Recommended Test Method

Leonard Kruczynski, *Trimble Navigation*; Stewart Teasley, *Rockwell Communications* 1665-1672

Carrier Phase GPS Time, Space, Position Information Demonstration (CAPTIDE)

Greg Costable, *Elgin AFB* 1673-1680

The Effect of Tropospheric Propagation Delay Errors in Airborne GPS Precise Positioning

Virgilio Mendes, J. Paul Collins, and Richard Langley, *University of New Brunswick* 1681-1689

Measuring User Equipment Errors from Holloman Flight Test Data

Joseph Clifford and Raymond DiEsposi, *The Aerospace Corp.*; Andrew Chasko, *Amcomp Corporation*;
Kenneth Wernle, *CIGTF*; Gregory Fairbanks, *GPSJPO, AFSMC, LA AFB* 1691-1701

Mobile Inertial Test System: A Dynamic Testbed for the EDGE Flight Tests

Theodore Herrera and Brian Taylor, *Elgin AFB* 1703-1711

HIL Testing of the Navy LEAP GPS/INS Package

George Stupp and David Lehnus, *JHU Applied Physics Laboratory* 1713-1719

Session A6: Attitude Determination

A Single-Baseline Attitude Measurement System Using Low-Cost C/A-Code Receivers

James Gilkey, David Richardson, and Christopher Terndrup, *SRI International* 1723-1732

Accurate Azimuth from a Single PLGR+GLS DoD GPS Receiver Using Time Relative Positioning

Karl Ulmer, Patrick Hwang, Brent Disselkoen, and Mark Wagner, *Rockwell* 1733-1741

Results of DC-10 Tests Using GPS Attitude Determination

Leonard Kruczynski and John Delucchi, *Trimble Navigation*; Timothy Iacobacci, *United Airlines* 1743-1750

Attitude Determination: Exploiting All Information for Optimal Ambiguity Resolution

Hans-Jürgen Euler and Craig Hill, *Leica AG* 1751-1757

Tightly Coupled Attitude Determination Using GPS Carrier Phase Observables

Gene Howell and Wang Tang, *ARINC* 1759-1766

GPS Modeling in the Attitude Determination Error Analysis System: Development and Application to TRACE

Eleanor Ketchum and Joseph Garrick, *NASA Goddard Space Flight Center*; Mohammad Rokni, *Computer Science Corp.* 1767-1774

A GNSS-Based Attitude Determination System for Low-Earth Observation Satellites

Jesús Serrano, Pelayo Bernedo, and Pablo González, *GMV S.A.*; Pierluigi Silvestrin, *ESA/ESTEC* 1775-1784

A Comparison of GPS-Based Attitude Estimation Techniques for Spinning Satellite

Penina Axelrad and Charles Behre, *University of Colorado* 1785-1796

A New Spacecraft Attitude Determination Scheme Based on the Use of GPS Line-Of-Sight Vectors

Jesús Serrano, Jorge Potti, and Pelayo Bernedo, *GMV S.A.*; Pierluigi Silvestrin, *ESA/ESTEC* 1797-1806

Session B6: Integrated Systems

An Artificially Intelligent Vehicle Highway System

Vidal Ashkenazi, Terry Moore, Mark Dumville, David Lowe, and Maria Tsakiri, *The University of Nottingham* 1809-1818

Making the Best with GPS in Car Applications

Ralph Moussa, *Renault* 1819-1823

GPS/Inertial Mapping (GIM) System for Real Time Mapping of Roadways Using WADGPS

Tim Ash, Randy Silva, Alison Brown, and James LaMance, *NAVSYS Corporation* 1825-1830

Twenty-Centimeter Kinematic DGPS Positioning With Digital Barometry

John Schleppe, James McLellan, Jill Battie, and J. Scott McCarron, *Pulsesearch Navigation* 1831-1840

H-764G GPS/INS High Dynamics GPS Tracking Tests Using a Roller Coaster

Al Hasselbring, *Honeywell, Inc.* 1841-1846

| | |
|--|-----------|
| Integration of a Fibre Optical Gyro Attitude and Heading Reference System with Differential GPS | |
| Manfred Bäumker, <i>FH Bochum</i> ; Manfred Hüllenkremer and Axel Lehmann, <i>LITEF GmbH</i> | 1847-1855 |
| A Proposed GPS Block IIF Satellite Design with Civilian Dual Frequency and WAAS Signals | |
| Mohan Ananda, Prem Munjal, and K.T. Woo, <i>The Aerospace Corporation</i> ; | |
| Rich Cole, <i>Innovative Solutions International</i> ; Steve Steiner, <i>U.S. Air Force</i> | 1857-1868 |
| New Approach to Kalman Time Propagation for GPS/INS Integrated Systems | |
| Leonid Schimelevich and Rahel Naor, <i>Israel Aircraft Industries Ltd.</i> | 1869-1873 |

Session C6: Emerging Applications

| | |
|---|-----------|
| Real-Time Landslide Detection System Using Precise Carrier Phase GPS | |
| Hitoshi Kondo, <i>Furuno Electric Co., Ltd.</i> ; M. Elizabeth Cannon, <i>The University of Calgary</i> | 1877-1884 |
| GPS-Based Launched Vehicle Tracking Using a Common Multi-Patch Antenna Configuration | |
| M. Santina, J. Leung, G. Smit, J. Tekawy, and G.T. Seng, <i>The Aerospace Corporation</i> ; | |
| J. McKay and S. Bandel, <i>Hughes Aircraft Co.</i> | 1885-1893 |
| GPS Goes 'Beyond the Gate' | |
| Samuel Shaw, <i>California Maritime Academy</i> ; Jack Hunter, <i>California DOT</i> | 1895-1903 |
| Experimental Demonstration of GPS for Rendezvous Between Two Prototype Space Vehicles | |
| Kurt Zimmerman and Robert Cannon, <i>Stanford University</i> | 1905-1913 |
| Application of GPS Technology to Part 141 Flight Training | |
| James Lyall, <i>Embry-Riddle Aeronautical University</i> | 1915-1921 |
| A GPS Based Nuclear Radiation Detection Device Training System | |
| Edward Groeber, <i>U.S. Army Chemical and Biochemical Defense Command</i> | 1923-1926 |

Session D6: Integrity

| | |
|--|-----------|
| New Techniques Relating Fault Detection and Exclusion Performance to GPS Primary Means Integrity Requirements | |
| Young Lee, <i>The MITRE Corporation</i> | 1929-1939 |
| A General RAIM Algorithm Based on Receiver Clock | |
| P. Misra, M. Pratt, R. Muchnik, and B. Manganis, <i>MIT</i> | 1941-1948 |
| Integrated GPS/Inertial Fault Detection Availability | |
| Mats Brenner, <i>Honeywell CAS-SPO</i> | 1949-1958 |
| GPS/IRS AIME: Calculation of Thresholds and Protection Radius Using Chi-Square Methods | |
| John Diesel and Sherry Luu, <i>Litton Aero Products</i> | 1959-1964 |
| USDRAM: An Innovative Approach to Increasing RAIM Availability | |
| Jonathan Bernick and William Michaelson, <i>Worcester Polytechnic Institute</i> | 1965-1973 |
| GPS Carrier-Phase RAIM | |
| William Michaelson and Hua Hua, <i>Worcester Polytechnic Institute</i> ; Duncan Cox, <i>DBC Communications, Inc.</i> | 1975-1984 |
| An Analysis of Using Carrier Phase to Fulfill Cat III Required Navigation Performance | |
| David Walsh and Peter Daly, <i>The University of Leeds</i> ; Tim Rowe, <i>U.K. National Air Traffic Services</i> | 1985-1993 |
| Weighted RAIM for Precision Approach | |
| Todd Walter and Per Enge, <i>Stanford University</i> | 1995-2004 |
| Solving Integrity Insufficiencies of Sat Nav Systems with Complementary Navigation Information | |
| Stefan Vieweg, <i>Institute of Flight Guidance and Control</i> ; Carsten Butzmuehlen, <i>TU Braunschweig</i> | 2005-2013 |
| Effects of Worst Case Geometries on RAIM Testing | |
| Christine Easton, <i>Rockwell Defense Electronics</i> ; William Michalson, <i>Worcester Polytechnic Institute</i> | 2015-2022 |
| Worst Case GPS Integrity Monitoring | |
| Donald Benson, <i>Dynamics Research Corporation</i> | 2023-2031 |
| Analysis of Risk Affecting Integrity and Continuity | |
| Jizhang Sang, Kurt Kubik, and Yanming Feng, <i>SCSN, Queensland University of Technology</i> | 2033-2040 |
| Authors Index | 2041-2045 |
| Conference Registrants | 2047-2078 |

ION GPS-95 CROSS LISTING OF PAPERS BY SUBJECT

Air Traffic Control

- Aircraft Tracking Using GPS Position and Velocity Reports**
 Ran Gazit, *Stanford University* 281-290
- The Role of GPS in Automatic Dependent Surveillance (ADS) and a Methodology for the Formulation of Requirements in That Role**
 Michael Ashbury, *Civil Aviation Authority*; Rolf Johannessen, *Lambourne Navigation Ltd.* 1383-1391
- Implementation of a GPS-Based Oceanic Air Traffic Control System**
 Joseph Fee, *Federal Aviation Administration*; Theodore Simpson, *AdsysTech Inc.* 1425-1430

Airborne Instrumentation Applications

- Flight Tests of a 3-D Perspective-View Glass-Cockpit Display for General Aviation Using GPS**
 Andrew Barrows, Per Enge, Bradford Parkinson, and J. David Powell, *Stanford University* 1615-1622

Ambiguity Resolution (see Phase Ambiguity Resolution)

Antennas

- Integrated GPS/GLONASS Antenna for High Performance Applications**
 Taymoor Hekmat and Norbert Niklasch, *ViCon Engineering GmbH*; Martin Maurer, *MAN Technologie AG* 845-851
- Power Minimization Techniques for GPS Null Steering Antenna**
 Anton Gecan, *E-Systems*; Michael Zoltowski, *Purdue University* 861-868
- Performance of a Miniature Dielectrically Loaded Volute Antenna**
 Oliver Leisten and Geraint Ffoulkes-Jones, *Navstar Systems Ltd.* 869-877
- An Effective GPS Application for Helicopter Operations**
 William O'Keefe, *Newcomb Communication, Inc.* 879-886

Attitude Determination (also see Spacecraft Orbit and Attitude Determination)

- A Single-Baseline Attitude Measurement System Using Low-Cost C/A-Code Receivers**
 James Gilkey, David Richardson, and Christopher Terndrup, *SRI International* 1723-1732
- Accurate Azimuth from a Single PLGR+GLS DoD GPS Receiver Using Time Relative Positioning**
 Karl Ulmer, Patrick Hwang, Brent Disselkoen, and Mark Wagner, *Rockwell* 1733-1741
- Results of DC-10 Tests Using GPS Attitude Determination**
 Leonard Kruczynski and John Delucchi, *Trimble Navigation*; Timothy Iacobacci, *United Airlines* 1743-1750
- Attitude Determination: Exploiting All Information for Optimal Ambiguity Resolution**
 Hans-Jürgen Euler and Craig Hill, *Leica AG* 1751-1757
- Tightly Coupled Attitude Determination Using GPS Carrier Phase Observables**
 Gene Howell and Wang Tang, *ARINC* 1759-1766
- GPS Modeling in the Attitude Determination Error Analysis System: Development and Application to TRACE**
 Eleanor Ketchum and Joseph Garrick, *NASA Goddard Space Flight Center*; Mohammad Rokni, *Computer Science Corp.* 1767-1774
- A GNSS-Based Attitude Determination System for Low-Earth Observation Satellites**
 Jesús Serrano, Pelayo Bernedo, and Pablo González, *GMV S.A.*; Pierluigi Silvestrin, *ESA/ESTEC* 1775-1784
- A Comparison of GPS-Based Attitude Estimation Techniques for Spinning Satellite**
 Penina Axelrad and Charles Behre, *University of Colorado* 1785-1796
- A New Spacecraft Attitude Determination Scheme Based on the Use of GPS Line-Of-Sight Vectors**
 Jesús Serrano, Jorge Potti, and Pelayo Bernedo, *GMV S.A.*; Pierluigi Silvestrin, *ESA/ESTEC* 1797-1806

| | |
|--|-----------|
| Experimental Demonstration of GPS for Rendezvous Between Two Prototype Space Vehicles | |
| Kurt Zimmerman and Robert Cannon, <i>Stanford University</i> | 1905-1913 |
| Results of Testing on a GPS-Based Compass | |
| Joseph Spalding and Mark Lunday, <i>US Coast Guard R&D Center</i> | 941-948 |
| Geometric Correction of Airborne Multispectral Scanner Imagery Using GPS Position and Attitude and Digital Elevation Models | |
| Lawrence Fisher, <i>Lockheed Environmental Systems and Technologies</i> | 1597-1606 |

Differential GPS (DGPS)

| | |
|--|-----------|
| A Compact Earth Tides Algorithm for WADGPS | |
| James Sinko, <i>SRI International</i> | 35-44 |
| Honeywell's DGPS Local Area Augmentation System Ground Station | |
| Steve Serfling, <i>Honeywell</i> | 147-156 |
| Differential GPS Evaluation at UK Airports | |
| Hemant Mistry and Richard Farnworth, <i>UK National Air Traffic Services</i> | 473-479 |
| Floating Differential GPS (FDGPS) | |
| James L. Brown, <i>Aydin Corporation (East)</i> | 481-490 |
| Differential GLONASS, Differential GPS and Integrated Differential GLONASS/GPS – Initial Results | |
| Jacques Beser, Anushia Balendra, Eric Erpelding, and Sonia Kim, <i>3S Navigation</i> | 507-515 |
| Performance Evaluation of a Global IGS-Based Differential GPS System | |
| Don English, Gene Howell, and Wang Tang, <i>ARINC</i> | 517-523 |
| Satisfying Airport Operational Requirements Using Seamless GNSS Techniques, Procedures and Processing | |
| Lois Pilley and Robert Pilley, <i>DSDC</i> | 525-532 |
| Selective Availability via the Levinson Predictor | |
| Timothy Barnes, <i>Zeta Associates, Inc.</i> | 533-542 |
| A Global DoD-Optimized DGPS for Precision-Strike | |
| Earl Blackwell, Mark Moeglein, and David Nakayama, <i>SRI International</i> | 399-411 |
| Navigation Performance Analysis for the Edge Program | |
| Donald Kelly and Pamela Harms, <i>Sverdrup/TEAS</i> ; Capt. John Dargen, <i>USAF</i> ; Chuck Eckert, <i>Honeywell</i> | 413-422 |
| The GLONASS System Status and Prospects for Development | |
| Michael Lebedev and Victor Gorev, <i>CSIC</i> ; Alexander Ganin and Victor Kulnev, <i>CRI of the Russian Space Forces</i> | 959-969 |
| Ways of GLONASS System Advancing | |
| Nicolay Ivanov, Vadim Salischev, and Alexander Vinogradov, <i>RISDE</i> | 991-1011 |
| Marine Radiobeacon DGPS/DGLONASS Service and Regional Centers for Differential GLONASS/Alpha/Chayka Services | |
| Pytor Bogdanov, Valery Chistyakov, Sergey Filatchenkov, Arvid Gevorkyan, and Vladlen Khimulin, <i>Russian Institute of Radionavigation and Time</i> | 1013-1020 |
| Differential GLONASS in Russia: The Ways of Development | |
| Alexander Ganin, <i>GLONASS Coordination Research and Information Center</i> | 1049-1060 |
| Twenty-Centimeter Kinematic DGPS Positioning With Digital Barometry | |
| John Schleppe, James McLellan, Jill Battie, and J. Scott McCarron, <i>Pulsesearch Navigation</i> | 1831-1840 |
| Integration of a Fibre Optical Gyro Attitude and Heading Reference System with Differential GPS | |
| Manfred Bäumker, <i>FH Bochum</i> ; Manfred Hüllenkremmer and Axel Lehmann, <i>LITEF GmbH</i> | 1847-1855 |
| Experimental Demonstration of GPS for Rendezvous Between Two Prototype Space Vehicles | |
| Kurt Zimmerman and Robert Cannon, <i>Stanford University</i> | 1905-1913 |
| A340–DGPS Landing Experiment | |
| Julie de Cevins, <i>Airbus Industrie</i> ; Pascal Ponsot, <i>Aerospatiale</i> | 763-772 |
| FAA's Cat III Feasibility Program: Status and Accomplishments | |
| R. Braff and P. O'Donnell, <i>The MITRE Corporation</i> ; V. Wullschleger, C. Mackin, and R. Velez, <i>FAA Technical Center</i> ; R. Swider and P. Enge, <i>Stanford University</i> ; F. van Graas, <i>Ohio University</i> ; D. Kaufmann, <i>NASA Ames Research Center</i> | 773-780 |
| Interoperability and Traditional Nav-aid Considerations for DGPS Standards | |
| Lori Hill and Ken Ganther, <i>Wilcox Electric</i> | 807-814 |
| Verification of USCG DGPS Broadcast Parameters | |
| Mark Lunday, Joseph Spalding, and Marylouise Dowd | 889-897 |
| Boosting Shipboard RAIM Availability | |
| James LaMance and Alison Brown, <i>NAVSYS Corporation</i> ; Joseph Spalding, <i>US Coast Guard R&D Center</i> | 907-912 |

| | |
|---|-----------|
| The Virtual Anchor | |
| Glen Robertson, <i>Rhodan Marine Equipment</i> ; John Webster, <i>Holst-Webster Enterprises</i> | 913-918 |
| Use of DGPS for an In-Water Acoustic Survey for the PTS SWIMSS | |
| Robert Reid, <i>Naval Undersea Warfare Center</i> | 919-923 |
| Computation and Quality Control of Differential GPS Corrections | |
| Xin-Xiang, Hans van der Marel, and Cees de Jong, <i>Delft University of Technology</i> | 1071-1079 |
| Effects of the Ionosphere and Cycle-Slips in Long Baseline Dynamic Positioning | |
| George Dedes and Angela Mallett, <i>The Ohio State University</i> | 1081-1090 |
| Using the Ionosphere for DGPS Measurement Error Control | |
| Gregory Bishop, <i>USAF Phillips Laboratory</i> ; Andrew Mazzella and Elizabeth Holland, <i>NorthWest Research Associates</i> | 1091-1100 |
| Adaptive Modeling of Receiver Clock for Meter-Level DGPS Vertical Positioning | |
| P. Misra, M. Pratt, B. Burke, and R. Ferranti, <i>MIT</i> | 1127-1135 |
| Precise RTK Positioning Using the New RTCM-104 V2.1 Standard | |
| J.P. Thomas Goguen and Timo Allison, <i>Trimble Navigation</i> | 1461-1466 |
| First Results Using the New DGPS Real-Time Deformation Monitoring System "DREAMS" | |
| Günter Hein and Bernhard Riedl, <i>University FAF Munich</i> | 1467-1475 |
| Development of High-Rate Differential GPS Reference for Operational Testing | |
| William Mosle and Andy Chasko, <i>746th Test Squadron, Holloman AFB</i> | 1637-1644 |
| Interferometric Flight Inspection Systems: Development and Flight Test Results | |
| D. Stratton, <i>Parker Hannifin Corporation</i> | 1607-1614 |

GLONASS, GPS/GLONASS, and GNSS

| | |
|--|-----------|
| Design of a GNSS: Coverage, Accuracy and Integrity | |
| V. Ashkenazi, T. Moore, C. J. Hill, W. Y. Ochieng, and Wu Chen, <i>The University of Nottingham</i> | 463-472 |
| Precise Positioning Using GPS/GLONASS Carrier Phase and Code Phase Observables | |
| David Walsh, Stuart Riley, John Cooper, and Peter Daly, <i>The University of Leeds</i> | 499-506 |
| Differential GLONASS, Differential GPS and Integrated Differential GLONASS/GPS – Initial Results | |
| Jacques Beser, Anushia Balendra, Eric Erpelding, and Sonia Kim, <i>3S Navigation</i> | 507-515 |
| The GLONASS System Status and Prospects for Development | |
| Michael Lebedev and Victor Gorev, <i>CSIC</i> ; Alexander Ganin and Victor Kulnev, <i>CRI of the Russian Space Forces</i> | 959-969 |
| The Place of GLONASS in the Radionavigation Plan of the CIS | |
| Vladimir Denisov, <i>Internavigation Research and Technical Center</i> | 971-984 |
| The GLONASS and GLONASS-M Programs | |
| V. Kazantsev, <i>NPOPM</i> | 985-990 |
| Ways of GLONASS System Advancing | |
| Nicolay Ivanov, Vadim Salischev, and Alexander Vinogradov, <i>RISDE</i> | 991-1011 |
| Marine Radiobeacon DGPS/DGLONASS Service and Regional Centers for Differential GLONASS/Alpha/Chayka Services | |
| Pytor Bogdanov, Valery Chistyakov, Sergey Filatchenkov, Arvid Gevorkyan, and Vladlen Khimulin, <i>Russian Institute of Radionavigation and Time</i> | 1013-1020 |
| GLONASS Approaches Full Operational Capability (FOC) | |
| Peter Daly, <i>The University of Leeds</i> | 1021-1030 |
| Evaluation of GLONASS Performance in Practical Applications: Comparison with GPS-Based Ionospheric TEC Values | |
| Nestor Zarraoa, Esther Sardon, Dietmar Klähn, and Arne Jungstand, <i>DLR-DFD Neustrelitz</i> | 1031-1039 |
| Processing GLONASS Carrier Phase Observations—Theory and First Experience | |
| Alfred Leick and Jinye Li, <i>University of Maine</i> ; Jacques Beser, <i>3S Navigation</i> ; Gerald Mader, <i>National Geodetic Survey</i> | 1041-1047 |
| Differential GLONASS in Russia: The Ways of Development | |
| Alexander Ganin, <i>GLONASS Coordination Research and Information Center</i> | 1049-1060 |
| Kalman Filter Procedures for GPS/GLONASS-Signals | |
| Norbert Niklasch, <i>ViCon Engineering</i> ; Martin Maurer and Martin Haunschild, <i>MAN Technologie AG</i> ; Walter Richert, <i>LMU</i> | 1061-1068 |
| A Combined GPS/GLONASS High Precision Receiver for Space Applications | |
| Stuart Riley, Neil Howard, Eric Aardoom, and Peter Daly, <i>University of Leeds</i> ; Pierluigi Silvestrin, <i>ESA ESTEC</i> | 835-844 |
| Integrated GPS/GLONASS Antenna for High Performance Applications | |
| Taymoor Hekmat and Norbert Niklasch, <i>ViCon Engineering GmbH</i> ; Martin Maurer, <i>MAN Technologie AG</i> | 845-851 |
| Tracking Measurements From a Miniature GLONASS Receiver | |
| Oliver Leisten, Geraint Ffoulkes-Jones, Gerald Whitworth, and David Belton, <i>Navstar Systems Ltd.</i> | 853-859 |

Gravimetry (see Surveying, Geodesy, and Gravimetry)

Integrated Systems

Use of the GPS Aided Inertial Navigation System in the Navy Standard Missile for the BMDO/Navy LEAP Technology Demonstration Program

Todd Moore, Kevin Rudolph, and Frank Ziolkowski, *Hughes Aircraft Co.*; Alfred Luckau, *Hughes Missile Systems Co.* 363-371

Integrated GPS/INS/SAR/GMTI Radar Precision Targeting Flight Test Results

R. Guarino and Paul Isben, *Westinghouse Norden Systems* 373-379

Navigation Performance Analysis for the Edge Program

Donald Kelly and Pamela Harms, *Sverdrup/TEAS*; Capt. John Dargen, *USAF*; Chuck Eckert, *Honeywell* 413-422

Integrated GPS/Inertial Fault Detection Availability

Mats Brenner, *Honeywell CAS-SPO* 1949-1958

GPS/IRS AIME: Calculation of Thresholds and Protection Radius Using Chi-Square Methods

John Diesel and Sherry Luu, *Litton Aero Products* 1959-1964

Solving Integrity Insufficiencies of Sat Nav Systems with Complementary Navigation Information

Stefan Vieweg, *Institute of Flight Guidance and Control*; Carsten Butzmuehlen, *TU Braunschweig* 2005-2013

Tightly Coupled Attitude Determination Using GPS Carrier Phase Observables

Gene Howell and Wang Tang, *ARINC* 1759-1766

An Artificially Intelligent Vehicle Highway System

Vidal Ashkenazi, Terry Moore, Mark Dumville, David Lowe, and Maria Tsakiri, *The University of Nottingham* 1809-1818

Making the Best with GPS in Car Applications

Ralph Moussa, *Renault* 1819-1823

GPS/Inertial Mapping (GIM) System for Real Time Mapping of Roadways Using WADGPS

Tim Ash, Randy Silva, Alison Brown, and James LaMance, *NAVSYS Corporation* 1825-1830

Twenty-Centimeter Kinematic DGPS Positioning With Digital Barometry

John Schleppe, James McLellan, Jill Battie, and J. Scott McCarron, *Pulsesearch Navigation* 1831-1840

H-764G GPS/INS High Dynamics GPS Tracking Tests Using a Roller Coaster

Al Hasselbring, *Honeywell, Inc.* 1841-1846

Integration of a Fibre Optical Gyro Attitude and Heading Reference System with Differential GPS

Manfred Bäumker, *FH Bochum*; Manfred Hüllenkremer and Axel Lehmann, *LITEF GmbH* 1847-1855

A Proposed GPS Block IIF Satellite Design with Civilian Dual Frequency and WAAS Signals

Mohan Ananda, Prem Munjal, and K.T. Woo, *The Aerospace Corporation*;
Rich Cole, *Innovative Solutions International*; Steve Steiner, *U.S. Air Force* 1857-1868

New Approach to Kalman Time Propagation for GPS/INS Integrated Systems

Leonid Schimelevich and Rahel Naor, *Israel Aircraft Industries Ltd.* 1869-1873

Application of INS/GPS Systems Integration to Increase Performance of Automatic Landing Systems

Jochen Meyer-Hilberg and Harald Harder, *Daimler-Benz Aerospace AG* 755-762

Next Generation Fiber Optic Gyroscopes for Use with GPS in Vehicle Navigation and Location Systems

Vincent Martinelli, *Corning Inc.*; Ray Ikeda, *Hitachi Cable America* 1295-1299

Hybrid GPS for Land Vehicle

S. Ishikawa, Y. Suwa, N. Nakahara, T. Ito, T. Yamamoto, Y. Murakami, and T. Yasuda, *AISIN SEIKI Co., Ltd.* 1301-1306

Field Test Results of an Enhanced GPS Coverage Through Map Aiding in Urban and Canyon Environments

James LaMance and Alison Brown, *NAVSYS Corporation* 1317-1322

Attitude DGPS/INS Based Real-Time Flight Guidance System for Airborne Sensors

Günter Hein, Bernd Eissfeller, and Jürgen Pielmeier, *Institute of Geodesy and Navigation* 1589-1596

Satellite Based Integrated Navigation and Communication System of the German Air Rescue

Manfred Haverland and Harry Evers, *Aerodata*; Dr. Hindemith-Boose and Roland Kirschenlohr, *DRF* 1629-1634

Integrity (also see Wide Area Augmentation System)

| | |
|---|-----------|
| New Techniques Relating Fault Detection and Exclusion Performance to GPS Primary Means Integrity Requirements | |
| Young Lee, <i>The MITRE Corporation</i> | 1929-1939 |
| A General RAIM Algorithm Based on Receiver Clock | |
| P. Misra, M. Pratt, R. Muchnik, and B. Manganis, <i>MIT</i> | 1941-1948 |
| Integrated GPS/Inertial Fault Detection Availability | |
| Mats Brenner, <i>Honeywell CAS-SPO</i> | 1949-1958 |
| GPS/IRS AIME: Calculation of Thresholds and Protection Radius Using Chi-Square Methods | |
| John Diesel and Sherry Lui, <i>Litton Aero Products</i> | 1959-1964 |
| USDRAIM: An Innovative Approach to Increasing RAIM Availability | |
| Jonathan Bernick and William Michaelson, <i>Worcester Polytechnic Institute</i> | 1965-1973 |
| GPS Carrier-Phase RAIM | |
| William Michaelson and Hua Hua, <i>Worcester Polytechnic Institute; Duncan Cox, DBC Communications, Inc.</i> | 1975-1984 |
| An Analysis of Using Carrier Phase to Fulfill Cat III Required Navigation Performance | |
| David Walsh and Peter Daly, <i>The University of Leeds; Tim Rowe, U.K. National Air Traffic Services</i> | 1985-1993 |
| Weighted RAIM for Precision Approach | |
| Todd Walter and Per Enge, <i>Stanford University</i> | 1995-2004 |
| Solving Integrity Insufficiencies of Sat Nav Systems with Complementary Navigation Information | |
| Stefan Vieweg, <i>Institute of Flight Guidance and Control; Carsten Butzmuehlen, TU Braunschweig</i> | 2005-2013 |
| Effects of Worst Case Geometries on RAIM Testing | |
| Christine Easton, <i>Rockwell Defense Electronics; William Michalson, Worcester Polytechnic Institute</i> | 2015-2022 |
| Worst Case GPS Integrity Monitoring | |
| Donald Benson, <i>Dynamics Research Corporation</i> | 2023-2031 |
| Analysis of Risk Affecting Integrity and Continuity | |
| Jizhang Sang, Kurt Kubik, and Yanming Feng, <i>SCSN, Queensland University of Technology</i> | 2033-2040 |
| Boosting Shipboard RAIM Availability | |
| James LaMance and Alison Brown, <i>NAVSYS Corporation; Joseph Spalding, US Coast Guard R&D Center</i> | 907-912 |
| Comparison of Continuity and Integrity Characteristics for | |
| Integrated and Decoupled Demodulation/Navigation Receivers | |
| Jim Sennott and Dave Senffner, <i>Bradley University</i> | 1531-1537 |
| Precision Landing Tests with Improved Integrity Beacon Pseudolites | |
| Stewart Cobb, David Lawrence, Boris Pervan, Clark Cohen, David Powell, and Brad Parkinson, <i>Stanford University</i> | 827-833 |

Interference and Interruptions

| | |
|---|-----------|
| GNSS Receiver Interference: Susceptibility and Civil Aviation Impact | |
| Mark Johnson and Robert Erlandson, <i>Rockwell</i> | 781-791 |
| Observed GPS Signal Continuity Interruptions | |
| Stewart Cobb, David Lawrence, Jock Christie, Todd Walter, Y.C. Chao, David Powell, and Brad Parkinson, <i>Stanford University</i> ... | 793-795 |
| Integrity and Continuity of Service Analysis of LADGPS and WADGPS Architectures with SNAPSIS Simulator | |
| D. Flament and N. Marchel, <i>Thomson-CSF; B. Christophe, Onera; J. L. Jonquiere, DGAC/STNA</i> | 797-806 |
| Performance Analysis of the Interrupted Data Acquisition Receiver Obtained From Operational Missions | |
| Gerald Whitworth, <i>Navstar Systems Ltd.; David Meldrum, Dunstaffnage Marine Laboratory</i> | 935-940 |
| Comparison of Continuity and Integrity Characteristics for | |
| Integrated and Decoupled Demodulation/Navigation Receivers | |
| Jim Sennott and Dave Senffner, <i>Bradley University</i> | 1531-1537 |
| Test Results on Mitigation of SATCOM-Induced Interference to GPS Operation | |
| Triveni Upadhyay, George Dimos, and Wassim Ferzali, <i>Mayflower Communications Co.; Dennis Weed, FAA</i> | 1545-1552 |
| A Modified Frequency-Locked Loop for Improved WAAS Carrier Tracking | |
| Gary McGraw and Bernard Schnaufer, <i>Rockwell International</i> | 1553-1562 |
| Power Minimization Techniques for GPS Null Steering Antenna | |
| Anton Gecan, <i>E-Systems; Michael Zoltowski, Purdue University</i> | 861-868 |
| Practical Measurements of Radio Frequency Interference to GPS Receivers and an | |
| Assessment of Interference Levels by Flight Trials in the European Regions | |
| Paul Nisner, <i>National Air Traffic Services; John Owen, Defence Research Agency</i> | 1373-1382 |

Ionosphere and Earth Observation

| | |
|---|-----------|
| Improved Ambiguity Resolution by Regional Differential Modelling of the Ionosphere | 55-62 |
| Lambert Wanninger, <i>TU Dresden, Germany</i> | |
| An Algorithm for Inter-frequency Bias Calibration and Application to WAAS Ionosphere Modeling | 639-646 |
| Yi-chung Chao, Yeou-Jyh Tsai, Todd Walter, Changdon Kee, Per Enge, and Brad Parkinson, <i>Stanford University</i> | |
| Evaluation of GLONASS Performance in Practical Applications: Comparison with GPS-Based Ionospheric TEC Values | 1031-1039 |
| Nestor Zarraoa, Esther Sardon, Dietmar Klähn, and Arne Jungstand, <i>DLR-DFD Neustrelitz</i> | |
| Effects of the Ionosphere and Cycle-Slips in Long Baseline Dynamic Positioning | 1081-1090 |
| George Dedes and Angela Mallett, <i>The Ohio State University</i> | |
| Using the Ionosphere for DGPS Measurement Error Control | 1091-1100 |
| Gregory Bishop, <i>USAF Phillips Laboratory</i> ; Andrew Mazzella and Elizabeth Holland, <i>NorthWest Research Associates</i> | |
| Sensing the Atmosphere From a Low-Earth Orbiter Tracking GPS: | |
| Early Results and Lessons From the GPS/MET Experiment | 1167-1174 |
| George Hajj, Rob Kursinski, Willy Bertiger, Stephen Leroy, Larry Romans, and Tim Schofield, <i>Jet Propulsion Laboratory</i> | |
| Time Calibration Using the INMARSAT Geostationary Overlay Signal From the AOR-W Satellite | 1175-1181 |
| James LaMance and Alison Brown, <i>NAVSYS Corporation</i> ; Bruce Haines, Willy Bertiger, and Sien Wu, <i>JPL</i> | |
| Real Time Estimation of Ionospheric Delays | 1183-1191 |
| Evelin Engler, Esther Sardón, and Dietmar Klähn, <i>DLR-DFD Neustrelitz</i> | |
| Real-Time TEC Determination for Ionospheric Modeling in WADGPS | 1193-1197 |
| José Fraile-Ordóñez, <i>Kayser-Threde GmbH</i> | |
| An Improved Ionospheric Correction Method for Wide-Area Augmentation Systems | 1199-1208 |
| Anthony Mannucci, Brian Wilson, and Dah-Ning Yuan, <i>Jet Propulsion Laboratory</i> | |
| Application of SCORE Techniques to Improve Ionospheric Observations | 1209-1218 |
| Gregory Bishop, <i>USAF Phillips Laboratory</i> ; Andrew Mazzella and Elizabeth Holland, <i>NorthWest Research Associates</i> | |
| Test Results of Wilcox Electric's Ionospheric Monitoring Network | 1219-1228 |
| Craig Stull, <i>Wilcox Electric</i> ; A. J. Van Dierendonck, <i>AJ Systems</i> | |
| WADGPS Ionospheric Correction Model Performance Simulation | 1237-1246 |
| Tysen Mueller, <i>Seagull Technology, Inc.</i> ; Bob Hamry and Andrew Johnson, <i>Rockwell International</i> | |
| Development of Real-Time Algorithms to Estimate the Ionospheric Error Bounds for WAAS | 1247-1258 |
| Robert Conker, Bakry El-Arini, and Thomas Albertson, <i>The MITRE Corporation</i> ; | |
| John Klobuchar, <i>USAF Phillips Laboratory</i> ; Patricia Doherty, <i>Boston College</i> | |

Land and Intelligent Vehicle Highway Systems (IVHS)

| | |
|---|-----------|
| A Prototype Portable Vehicle Navigation System Utilizing Map Aided GPS | 319-329 |
| Blake Bullock, <i>The University of Calgary</i> | |
| An Artificially Intelligent Vehicle Highway System | 1809-1818 |
| Vidal Ashkenazi, Terry Moore, Mark Dumville, David Lowe, and Maria Tsakiri, <i>The University of Nottingham</i> | |
| Making the Best with GPS in Car Applications | 1819-1823 |
| Ralph Moussa, <i>Renault</i> | |
| GPS/Inertial Mapping (GIM) System for Real Time Mapping of Roadways Using WADGPS | 1825-1830 |
| Tim Ash, Randy Silva, Alison Brown, and James LaMance, <i>NAVSYS Corporation</i> | |
| Kinematic GPS for Closed-Loop Control of Farm and Construction Vehicles | 1261-1268 |
| Michael O'Connor, Gabriel Elkaim, and Bradford Parkinson, <i>Stanford University</i> | |
| An Examination of the Relative Merits of Various Sensors for Vehicle Navigation | 1269-1284 |
| Eric Abbott and David Powell, <i>Stanford University</i> | |
| Nonlinear Smoothing of Dead Reckoning Data with GPS Measurements | 1285-1294 |
| Ren Da and George Dedes, <i>The Ohio State University</i> | |
| Next Generation Fiber Optic Gyroscopes for Use with GPS in Vehicle Navigation and Location Systems | 1295-1299 |
| Vincent Martinelli, <i>Corning Inc.</i> ; Ray Ikeda, <i>Hitachi Cable America</i> | |
| Hybrid GPS for Land Vehicle | 1301-1306 |
| S. Ishikawa, Y. Suwa, N. Nakahara, T. Ito, T. Yamamoto, Y. Murakami, and T. Yasuda, <i>AININ SEIKI Co., Ltd.</i> | |
| VISAT: A Mobile City Survey System of High Accuracy | 1307-1315 |
| Naser El-Sheimy, Klaus-Peter Schwarz, and Ming Wei, <i>The University of Calgary</i> ; Martin Lavigne, <i>GEOFIT Inc.</i> | |

| | |
|---|-----------|
| Field Test Results of an Enhanced GPS Coverage Through Map Aiding in Urban and Canyon Environments | |
| James LaMance and Alison Brown, NAVSYS Corporation | 1317-1322 |
| GPS Receiver Structures for the Urban Canyon | |
| Benjamin Peterson, Richard Hartnett, and Geoffrey Ottman, <i>U.S. Coast Guard Academy</i> | 1323-1332 |
| Autonomous Vehicle Using WADGPS | |
| Daljit Singh, <i>Naval Air Warfare Center</i> ; Harkirat Grewal, <i>American GNC</i> | 1333-1338 |

Maritime Applications

| | |
|--|---------|
| Verification of USCG DGPS Broadcast Parameters | |
| Mark Lunday, Joseph Spalding, and Marylouise Dowd | 889-897 |
| DGPS Positioning Accuracy Performance Analysis with RTCM | |
| Message Types 1/9 and 18-21 Using Various Receiver Technologies | |
| G. Lachapelle, M. E. Cannon, H. Lan, and C. Tang, <i>The University of Calgary</i> ; S. Wee and S. Ryan, <i>Canadian Coast Guard</i> | 899-906 |
| Boosting Shipboard RAIM Availability | |
| James LaMance and Alison Brown, NAVSYS Corporation; Joseph Spalding, <i>US Coast Guard R&D Center</i> | 907-912 |
| The Virtual Anchor | |
| Glen Robertson, <i>Rhodan Marine Equipment</i> ; John Webster, <i>Holst-Webster Enterprises</i> | 913-918 |
| Use of DGPS for an In-Water Acoustic Survey for the PTS SWIMSS | |
| Robert Reid, <i>Naval Undersea Warfare Center</i> | 919-923 |
| Autonomous Underwater Vehicle Navigation | |
| Stewart Cannon, <i>Pelagos Corporation</i> ; Jeff Smith, <i>Applied Remote Technology</i> | 925-933 |
| Performance Analysis of the Interrupted Data Acquisition Receiver Obtained From Operational Missions | |
| Gerald Whitworth, <i>Navstar Systems Ltd.</i> ; David Meldrum, <i>Dunstaffnage Marine Laboratory</i> | 935-940 |
| Results of Testing on a GPS-Based Compass | |
| Joseph Spalding and Mark Lunday, <i>US Coast Guard R&D Center</i> | 941-948 |
| The Use of GPS for Underwater Navigation, Sea Trial Results | |
| M. H. G. Thomas, <i>ACSA</i> | 949-955 |

Military

| | |
|---|---------|
| Use of the GPS Aided Inertial Navigation System in the Navy Standard Missile for the BMDO/Navy LEAP Technology Demonstration Program | |
| Todd Moore, Kevin Rudolph, and Frank Ziolkowski, <i>Hughes Aircraft Co.</i> ; Alfred Luckau, <i>Hughes Missile Systems Co.</i> | 363-371 |
| Integrated GPS/INS/SAR/GMTI Radar Precision Targeting Flight Test Results | |
| R. Guarino and Paul Isben, <i>Westinghouse Norden Systems</i> | 373-379 |
| Anti-Jamming Performance of TIDGET in Guided Munitions Applications | |
| Armando Montalvo, Bruce Johnson, and Alison Brown, NAVSYS Corporation | 381-390 |
| Robust Implementation of Relative GPS Guidance | |
| Mark Youhanaie, David Hartman, and Frank Ziolkowski, <i>Hughes Aircraft Co.</i> ; Neeraj Pujara, <i>Wright Laboratory</i> | 391-398 |
| A Global DoD-Optimized DGPS for Precision-Strike | |
| Earl Blackwell, Mark Moeglein, and David Nakayama, <i>SRI International</i> | 399-411 |
| Navigation Performance Analysis for the Edge Program | |
| Donald Kelly and Pamela Harms, <i>Sverdrup/TEAS</i> ; Capt. John Dargen, <i>USAF</i> ; Chuck Eckert, <i>Honeywell</i> | 413-422 |
| Preliminary Results from a GPS-based Portable Impact Location System | |
| Jimmy Saunders and Miguel Cardoza | 423-430 |
| Precise Absolute Navigation: An Evaluation of PPS Position Improvement | |
| Bruce Hermann, <i>Naval Surface Warfare Center</i> ; Stephen Malys, <i>The Defense Mapping Agency</i> | 431-436 |
| GPS Translator for Artillery Projectiles - A Progress Report | |
| George Wiles, <i>US Army Research Laboratory</i> ; Jeff Smuk, <i>Hittite Microwave Corporation</i> | 437-441 |
| The Reduction of Airborne Magnetic Noise Via GPS | |
| L. Bobb, W. Gelatka, D. DePersia, A. Salik, and S. Swyers, <i>Naval Air Warfare Center</i> | 443-447 |
| GPS Operational Control System Modernization: Alternative Architectural Concepts | |
| Jaynarayan Lala and Laura Burkhardt, <i>Draper Laboratory</i> | 449-459 |

| | |
|---|-----------|
| Accurate Azimuth from a Single PLGR+GLS DoD GPS Receiver Using Time Relative Positioning | |
| Karl Ulmer, Patrick Hwang, Brent Disselkoen, and Mark Wagner, <i>Rockwell</i> | 1733-1741 |
| A Proposed GPS Block IIF Satellite Design with Civilian Dual Frequency and WAAS Signals | |
| Mohan Ananda, Prem Munjal, and K.T. Woo, <i>The Aerospace Corporation</i> ; | |
| Rich Cole, <i>Innovative Solutions International</i> ; Steve Steiner, <i>U.S. Air Force</i> | 1857-1868 |
| GPS-Based Launched Vehicle Tracking Using a Common Multi-Patch Antenna Configuration | |
| M. Santina, J. Leung, G. Smit, J. Tekawy, and G.T. Seng, <i>The Aerospace Corporation</i> ; | |
| J. McKay and S. Bandel, <i>Hughes Aircraft Co.</i> | 1885-1893 |
| A GPS Based Nuclear Radiation Detection Device Training System | |
| Edward Groeber, <i>U.S. Army Chemical and Biochemical Defense Command</i> | 1923-1926 |
| Mobile Inertial Test System: A Dynamic Testbed for the EDGE Flight Tests | |
| Theodore Herrera and Brian Taylor, <i>Elgin AFB</i> | 1703-1711 |
| HIL Testing of the Navy LEAP GPS/INS Package | |
| George Stupp and David Lehnus, <i>JHU Applied Physics Laboratory</i> | 1713-1719 |

Multipath Effects and Reduction

| | |
|---|-----------|
| Characterization of Phase and Multipath Errors for an Aircraft GPS Antenna | |
| C. Douglas Hardwick and Jeffrey Liu, <i>National Research Council of Canada</i> | 491-498 |
| GPS Multipath Modeling and Verification Using Geometrical Theory of Diffraction | |
| Susan Gomez, Robert Panneton, and Penny Saunders, <i>NASA/LBJ Space Center</i> ; Shian and Ba Lu, <i>Lockheed Martin</i> | 195-204 |
| Long Period Systematic Errors in GPS Measurements | |
| Shane Nelson, <i>University of Texas</i> | 1155-1163 |
| Temporal Characteristics of Multipath Errors | |
| Ahmed El-Rabbany, <i>Alexandria University</i> | 1493-1497 |
| A Comparison of Three Multipath Mitigation Approaches for GPS Receivers | |
| Armando Montalvo and Alison Brown, <i>NAVSYS Corporation</i> | 1511-1520 |
| Achieving Theoretical Accuracy Limits for Pseudoranging in the Presence of Multipath | |
| Lawrence Weill, <i>Magellan Systems and California State University at Fullerton</i> | 1521-1530 |
| Comparison of Continuity and Integrity Characteristics for | |
| L1 Carrier Phase Multipath Error Reduction Using MEDLL Technology | |
| Bryan Townsend, Patrick Fenton, and Keith Van Dierendonck, <i>NovAtel Communications</i> ; Richard van Nee, <i>Consultant</i> | 1539-1544 |

New Product Announcements

| | |
|---|---------|
| Open Architecture Design for GPS Applications | |
| Yves Thérout, <i>Canadian Marconi Company</i> | 117-121 |
| Two Piece Chipset for GPS Makes a Four Chip GPS Receiver | |
| Philip Mattos, <i>SGS-Thomson Microelectronics</i> | 123-132 |
| What's New From NovAtel | |
| Simon Newby and Wendy Corcoran, <i>NovAtel Communications Ltd.</i> | 133-140 |
| GPS Tensor™ GPS Receiver for Attitude and Orbit Determination | |
| J. Kurt Brock, <i>Space Systems/LORAL</i> | 141-142 |
| Hitachi HGA-D Fiber Optic Gyroscope for Vehicular Applications | |
| Bob Yoshida, <i>Hitachi Cable America</i> ; Vincent Martinelli, <i>Corning Incorporated</i> | 143-146 |
| Honeywell's DGPS Local Area Augmentation System Ground Station | |
| Steve Serfling, <i>Honeywell</i> | 147-156 |
| Starwatch™: An Off-the-Shelf GPS Asset Location System | |
| John Lavrakas, <i>Advanced Research Corporation</i> | 157-160 |
| The XR5-PC12 – Position and Time/Frequency From a Single Plug-in Module | |
| Tony Haddrell, <i>Navstar Systems Ltd.</i> | 161-166 |
| Ashtech RTZ, Real-Time Kinematic GPS with OTF Initialization | |
| Sergei Gourevitch, Frank van Diggelen, Xinhua Qin, and Mark Kuhl, <i>Ashtech</i> | 167-170 |

Operational Control Segment (OCS)

GPS Operational Control System Modernization: Alternative Architectural Concepts

Jaynarayan Lala and Laura Burkhardt, *Draper Laboratory* 449-459

Phase Ambiguity Resolution

Improved Ambiguity Resolution by Regional Differential Modelling of the Ionosphere

Lambert Wanninger, *TU Dresden, Germany* 55-62

A New Concept for GPS Phase Ambiguity Resolution On-The-Fly:

The Maximum a Posteriori Ambiguity Search (MAPAS) Method

Christophe Macabiau, *Laboratoire de Traitement du Signal et des Télécommunications of the ENAC* 299-308

Efficient Ambiguity Search Using Genetic Algorithms

Zuofa Li, *The University of Calgary* 331-337

Ambiguity Recovery for GPS Long Range Kinematic Positioning

Shaowei Han, *The University of New South Wales* 349-360

A Single-Baseline Attitude Measurement System Using Low-Cost C/A-Code Receivers

James Gilkey, David Richardson, and Christopher Terndrup, *SRI International* 1723-1732

Attitude Determination: Exploiting All Information for Optimal Ambiguity Resolution

Hans-Jürgen Euler and Craig Hill, *Leica AG* 1751-1757

Fast Ambiguity Resolution Using an Integer Nonlinear Programming Method

Ming Wei and Klaus-Peter Schwarz, *The University of Calgary* 1101-1110

Improving the Reliability of OTF Ambiguity Resolution with Dual Frequency GPS Observations

Gang Lu, M. Elizabeth Cannon, and Gerard Lachapelle, *The University of Calgary* 1111-1116

Ambiguity Resolution Over Long Baselines for Airborne Differential GPS Positioning

J. Sonntag and C. Martin, *EG&G*; W. Krabill, *NASA Goddard Space Flight Center* 1117-1126

Comparison of Different On-The-Fly Ambiguity Resolution Techniques

Günter Hein and Wolfgang Werner, *University FAF Munich* 1137-1144

A New Method for Constructing Multi-satellite Ambiguity Combinations for Improved Ambiguity Resolution

Chris Rizos and Shaowei Han, *The University of New South Wales* 1145-1153

Temporal Characteristics of Multipath Errors

Ahmed El-Rabbany, *Alexandria University* 1493-1497

Policy, Status, and Institutional Concerns

GPS – The Ultima Thule of Navigation

James Schlesinger, *Keynote Speaker ION GPS-95* 3-6

Panel Discussion: GPS Critical Technology, Policy, and Institutional Issues

Moderator: Keith McDonald, *Sat Tech Systems*; Panel Members: Dr. James Schlesinger, Joseph Canny,

Gil Klinger, Larry Adams, Charles Trimble, Dr. Scott Pace, and Col. John Caldwell, *USAF* 7-14

GPS: A Shared National Asset—A Summary of the National Research Council Report

Laurence Adams, *Chair NRC Committee*; Allison Sandlin and Dave Turner, *NRC*; Keith McDonald, *Sat Tech Systems* 1341-1350

GPS: Charting the Future—A Summary Report by the GPS Panel of the National Academy of Public Administration

Arnold Donahue and Roger Sperry, *Co-Directors of the NAPA Study* 1351-1361

GPS Performance Characteristics and Trends

Rob Conley, Mark Fryt, and Sean Scott, *Overlook Systems Technologies, Inc.* 1363-1371

Practical Measurements of Radio Frequency Interference to GPS Receivers and an

Assessment of Interference Levels by Flight Trials in the European Regions

Paul Nisner, *National Air Traffic Services*; John Owen, *Defence Research Agency* 1373-1382

The Role of GPS in Automatic Dependent Surveillance (ADS) and a

Methodology for the Formulation of Requirements in That Role

Michael Ashbury, *Civil Aviation Authority*; Rolf Johannessen, *Lambourne Navigation Ltd.* 1383-1391

Aircraft Approach and Landing Studies with the Global Positioning System

Douglas Hardwick and Jeffrey Liu, *National Research Council of Canada* 1393-1401

| | |
|---|-----------|
| Global Optimization of GPS Augmentation Architectures Using Genetic Algorithms | |
| Samual Pullen, Per Enge, and Bradford Parkinson, <i>Stanford University</i> | 1403-1415 |
| GNSS Combined with Head-Up Display for Precision Landing | |
| Jean-François Jehl and Luc Baron, <i>SEXTANT Avionique</i> | 1417-1424 |

Power Reduction in GPS Receivers

Precision Landing

| | |
|--|-----------|
| FAA-Wilcox Electric Category IIIB Feasibility Demonstration Program Flight Test Results | |
| W. Hundley, S. Rowson, and G. Courtney, <i>Wilcox Electric</i> ; V. Wulschleger and R. Velez, <i>FAA Technical Center</i> ; | |
| R. Benoist, <i>Litton Aero Products</i> ; P. O'Donnell, <i>MITRE/CAASD</i> | 715-726 |
| FAA/Ohio University/United Parcel Service DGPS Autoland Flight Test Demonstration | |
| Frank van Graas, David Diggle, and Maarten Uijt, <i>Ohio University</i> ; Dave Lamb and Mark Dimeo, | |
| <i>Systems Resources Corporation</i> ; Greg Kuehl and Robert Hilb, <i>United Parcel Service</i> | 727-737 |
| FAA/FEDSIM—E-Systems Cat IIIB Feasibility Demonstration Flight Test Preliminary Results | |
| Glyn Romrell, Ron Brown, and Greg Johnson, <i>E-Systems</i> ; Dave Kaufmann, <i>NASA Ames</i> | 739-753 |
| Application of INS/GPS Systems Integration to Increase Performance of Automatic Landing Systems | |
| Jochen Meyer-Hilberg and Harald Harder, <i>Daimler-Benz Aerospace AG</i> | 755-762 |
| A340-DGPS Landing Experiment | |
| Julie de Cevins, <i>Airbus Industrie</i> ; Pascal Ponsot, <i>Aerospatiale</i> | 763-772 |
| FAA's Cat III Feasibility Program: Status and Accomplishments | |
| R. Braff and P. O'Donnell, <i>The MITRE Corporation</i> ; V. Wulschleger, C. Mackin, and R. Velez, <i>FAA Technical Center</i> ; | |
| R. Swider and P. Enge, <i>Stanford University</i> ; F. van Graas, <i>Ohio University</i> ; D. Kaufmann, <i>NASA Ames Research Center</i> | 773-780 |
| GNSS Receiver Interference: Susceptibility and Civil Aviation Impact | |
| Mark Johnson and Robert Erlandson, <i>Rockwell</i> | 781-791 |
| Observed GPS Signal Continuity Interruptions | |
| Stewart Cobb, David Lawrence, Jock Christie, Todd Walter, Y.C. Chao, David Powell, and Brad Parkinson, <i>Stanford University</i> ... | 793-795 |
| Integrity and Continuity of Service Analysis of LADGPS and WADGPS Architectures with SNAPSIS Simulator | |
| D. Flament and N. Marchel, <i>Thomson-CSF</i> ; B. Christophe, <i>Onera</i> ; J. L. Jonquiere, <i>DGAC/STNA</i> | 797-806 |
| Interoperability and Traditional Nav-aid Considerations for DGPS Standards | |
| Lori Hill and Ken Ganther, <i>Wilcox Electric</i> | 807-814 |
| An Analysis of Using Carrier Phase to Fulfill Cat III Required Navigation Performance | |
| David Walsh and Peter Daly, <i>The University of Leeds</i> ; Tim Rowe, <i>U.K. National Air Traffic Services</i> | 1985-1993 |
| Weighted RAIM for Precision Approach | |
| Todd Walter and Per Enge, <i>Stanford University</i> | 1995-2004 |
| Analysis of Risk Affecting Integrity and Continuity | |
| Jizhang Sang, Kurt Kubik, and Yanming Feng, <i>SCSN, Queensland University of Technology</i> | 2033-2040 |
| The Effect of Tropospheric Propagation Delay Errors in Airborne GPS Precise Positioning | |
| Virgílio Mendes, J. Paul Collins, and Richard Langley, <i>University of New Brunswick</i> | 1681-1689 |
| Precision Landing Tests with Improved Integrity Beacon Pseudolites | |
| Stewart Cobb, David Lawrence, Boris Pervan, Clark Cohen, David Powell, and Brad Parkinson, <i>Stanford University</i> | 827-833 |
| Aircraft Approach and Landing Studies with the Global Positioning System | |
| Douglas Hardwick and Jeffrey Liu, <i>National Research Council of Canada</i> | 1393-1401 |
| GNSS Combined with Head-Up Display for Precision Landing | |
| Jean-François Jehl and Luc Baron, <i>SEXTANT Avionique</i> | 1417-1424 |

Precise Real-Time Positioning (also see Surveying, Geodesy, and Gravimetry)

| | |
|--|-----------|
| High Precision Real-Time Positioning Using Low Cost OEM Sensors | |
| Adel Tabsh and Hugh Martell, <i>Premier GPS, Inc.</i> ; Darren Cosandier, <i>The University of Calgary</i> | 1433-1441 |
| High-Rate Precise Real-Time Positioning Using Differential Carrier Phase | |
| Dariusz Lapucha, Richard Barker, and Ziwen Liu, <i>John E. Chance & Associates</i> | 1443-1449 |

Maintaining GPS Positioning in Steep Turns Using Two Antennas

David Lawrence, H. Stewart Cobb, Clark Cohen, Jock Christie, J. David Powell, and Bradford Parkinson, *Stanford Univ.* 1451-1459

Precise RTK Positioning Using the New RTCM-104 V2.1 Standard

J.P. Thomas Goguen and Timo Allison, *Trimble Navigation* 1461-1466

First Results Using the New DGPS Real-Time Deformation Monitoring System "DREAMS"

Günter Hein and Bernhard Riedl, *University FAF Munich* 1467-1475

Real-Time Precise Marine Navigation: Description and Results

Hans-Jürgen Euler and Craig Hill, *Leica AG*; Urs Müller, *terra vermessungen* 1477-1484

Development and Implementation of a Centimeter-Accurate Real-Time-Kinematic Positioning System

Herbert Landau, Christian Pagels, and Ulrich Vollath, *terraSat GmbH* 1485-1491

Temporal Characteristics of Multipath Errors

Ahmed El-Rabbany, *Alexandria University* 1493-1497

Utilizing a Low Cost GPS Receiver for Centimeter to Sub-meter Accuracy Real-Time and Post-Processed Applications

Geraint Ffoulkes-Jones, *Navstar Systems Ltd.*; Darren Cosandier, *Premier GPS Inc.* 1499-1508

Interferometric Flight Inspection Systems: Development and Flight Test Results

D. Stratton, *Parker Hannifin Corporation* 1607-1614

An Evaluation of Precise Kinematic On-The-Fly GPS Positioning with Respect to a Moving Aircraft

Alan Evans, Bruce Hermann, and Christopher Law, *Naval Surface Warfare Center*;

Benjamin Remondi, *The XYZ's of GPS, Inc.*; Thomas Briggs and Thomas Nelson, *Navla Air Warfare Center* 1623-1628

Development and Testing of a Mobile Pseudolite Concept for Precise Positioning

Tom Holden, *Stanford Telecom*; John Racquet, Gerard Lachapelle, Weigen Qiu, and C. Pelletier,

The University of Calgary; Anthony Nash, *746th Test Squadron*; Patrick Fenton, *NovAtel* 817-826

Precise Time and Frequency

Time Calibration Using the INMARSAT Geostationary Overlay Signal From the AOR-W Satellite

James LaMance and Alison Brown, *NAVSYS Corporation*; Bruce Haines, Willy Bertiger, and Sien Wu, *JPL* 1175-1181

Precise GPS Time Transfer to a Moving Vehicle

Tor Egil Melgård and David Last, *University of Wales*; Bernard Thomas, *DCN Brest (DGA)* 1229-1236

RAIM (see Integrity)

Selective Availability Estimation

Selective Availability via the Levinson Predictor

Timothy Barnes, *Zeta Associates, Inc.* 533-542

Space Applications

An Autonomous GNSS-based Orbit Determination System for Low-Earth Observation Satellites

Jorge Potti, Juan Carlos Carmona, and Pelayo Bernedo, *GMV S.A.*; Pierluigi Silvestrin, *ESA/ESTEC* 173-182

Results of a Automated GPS Tracking System in Support of Topex/Poseidon and GPSMet

Ronald Muellerschoen, Stephen Lichten, Ulf Lindqwister, and Willy Bertiger, *Jet Propulsion Laboratory* 183-193

GPS Multipath Modeling and Verification Using Geometrical Theory of Diffraction

Susan Gomez, Robert Panneton, and Penny Saunders, *NASA/LBJ Space Center*; Shian and Ba Lu, *Lockheed Martin* 195-204

Application of Fuzzy Logic and Multisensor Data Fusion Techniques to On-board GPS-based Spacecraft Navigation

Stefano Giacomini, *University of Milano*; Livio Marradi, *LABEN S.p.A.* 205-216

GPS Autonomous Relative Navigation and Time Transfer for Orbiting Space Vehicles

Duncan B. Cox, Jr., *DBC Communications, Inc.*; John D.W. Brading, *Brading Systems and Technology* 217-228

| | |
|--|---------|
| GPS Tracking Experiment of a Dree-Flyer Deployed from Space Shuttle | |
| Bob Schutz, P.A.M. Abusali, Christine Schroeder, and Byron Tapley, <i>University of Texas at Austin</i> ; | |
| Michael Exner and Rick McCloskey, <i>University Corporation for Atmospheric Research</i> ; | |
| Russell Carpenter, Michael Cooke, and Samantha McDonald, <i>NASA/Johnson Space Center</i> ; | |
| Nick Combs, <i>University of Houston</i> ; Courtney Duncan, Charles Dunn, and Tom Meehan, <i>NASA/JPL</i> | 229-235 |
| GPS Receiver Design and Requirement Analysis for the Stanford Gravity Probe B Relativity Mission | |
| Hirohiko Uematsu and Bradford Parkinson, <i>Stanford University</i> ; E. Glenn Lightsey, <i>NASA Goddard Space Flight Center</i> | 237-246 |
| National Satellite Testbed (NSTB) GPS Satellite Clock/Ephemeris Determination Analysis and Results | |
| Scott Pogorelc, Mark Lorenz, Kelly Murdock, Brent Harding, Tim Cashin, and Donna Kraus, <i>Stanford Telecommunications</i> | 247-256 |
| GPS Techniques for Navigation of Geostationary Satellites | |
| Pascale Ferrage, Jean-Luc Issler, Genevieve Campan, and Jean-Claude Durand, <i>French National Space Agency (CNES)</i> | 257-268 |
| Relative GPS Navigation for ATV Rendezvous | |
| Michael Frezet, Herve Marcille, Virginie Pascal, and Jean Michael Pairot, <i>Matra Marconi Space</i> ; | |
| Hubert Barré, Massimo Cislighi, and Ulrich Thomas, <i>European Space Agency</i> | 269-278 |
| A Combined GPS/GLONASS High Precision Receiver for Space Applications | |
| Stuart Riley, Neil Howard, Eric Aardoom, and Peter Daly, <i>University of Leeds</i> ; Pierluigi Silvestrin, <i>ESA ESTEC</i> | 835-844 |

Spacecraft Orbit and Attitude Determination (also see Attitude Determination)

| | |
|--|---------|
| Evaluation of DoD GPS Satellite Orbits Using NASA Laser Ranging Data | |
| James O'Toole and Michael Merrigan, <i>Naval Surface Warfare Center</i> | 45-54 |
| GPS Attitude Determination and Navigation Flight Experiment | |
| J. Kurt Brock, Rich Fuller, Brian Kemper, Dave Mleccko, J. Rodden, and Alfred Tadros, <i>Space Systems/LORAL</i> | 545-554 |
| The GPS Attitude Determination Flyer (GADFLY): A Space-Qualified GPS Attitude Receiver on the SSTI-Lewis Spacecraft | |
| Frank Bauer, E. Glenn Lightsey, Stephen Leake, Jon McCullough, James O'Donnell, | |
| Kate Hartman, and Roger Hart, <i>NASA Goddard Space Flight Center</i> | 555-562 |
| Argos Navigation and Attitude Determination System | |
| Jon Petway, <i>Rockwell</i> | 563-572 |
| Experimental Results of Using the GPS for SFU Onboard Navigation | |
| Tsutomu Ichikawa and Keiken Ninomiya, <i>The Institute of Space and Astronautical Science</i> ; | |
| Susumu Kumagai and Masaki Mistutake, <i>Hitachi Ltd.</i> | 573-577 |
| A Practical Demonstration of Low Cost Autonomous Orbit Determination Using GPS | |
| Martin Unwin and Martin Sweeting, <i>University of Surrey</i> | 579-587 |
| Applicability of GPS-based Orbit Determination Systems to a Wide Range of HEO Missions | |
| Jorge Potti and Pelayo Bernedo, <i>GMV S.A.</i> ; Alessandro Pasetti, <i>ESA/ESTEC</i> | 589-598 |
| Performance Evaluation of the GPS Yaw Bias Implementation | |
| Yoaz Bar-Sever, <i>Jet Propulsion Laboratory</i> | 599-611 |
| Effect of GPS Orbit Accuracy on GPS-determined Topex/Poseidon Orbit | |
| H. J. Rim, B. E. Schutz, P.A.M. Abusali, and B. D. Tapley, <i>University of Texas at Austin</i> | 613-617 |
| Use of GPS for Precise and Operational Orbit Determination at ESOC | |
| Tomás Martín Mur, John Dow, and Nicholas Bondarenco, <i>European Space Agency</i> ; Stefano Casotto, <i>Univeritá Padova</i> ; | |
| Joachim Feltens, <i>mbp Informationstechnologie GmbH</i> ; Carlos García Martínez, <i>GMV S.A.</i> | 619-626 |
| An Autonomous GNSS-based Orbit Determination System for Low-Earth Observation Satellites | |
| Jorge Potti, Juan Carlos Carmona, and Pelayo Bernedo, <i>GMV S.A.</i> ; Pierluigi Silvestrin, <i>ESA/ESTEC</i> | 173-182 |
| National Satellite Testbed (NSTB) GPS Satellite Clock/Ephemeris Determination Analysis and Results | |
| Scott Pogorelc, Mark Lorenz, Kelly Murdock, Brent Harding, Tim Cashin, and Donna Kraus, <i>Stanford Telecommunications</i> | 247-256 |

Surveying, Geodesy, and Gravimetry

| | |
|---|-------|
| A Comparison of GPS and Satellite Altimetry for Height Monitoring on an Offshore Production Platform | |
| Moirá Tighe and John Macgregor, <i>Shell U.K. Exploration and Production</i> | 17-23 |
| A GPS Positioning Results Using Precise Satellite Ephemerides, Clock Corrections and Ionospheric Grid Model with Jupiter | |
| Yang Gao, James McLellan, and Mohamed Abousalem, <i>Pulsesearch Navigation Systems, Inc.</i> | 25-34 |
| A Compact Earth Tides Algorithm for WADGPS | |
| James Sinko, <i>SRI International</i> | 35-44 |

| | |
|--|-----------|
| Evaluation of DoD GPS Satellite Orbits Using NASA Laser Ranging Data | |
| James O'Toole and Michael Merrigan, <i>Naval Surface Warfare Center</i> | 45-54 |
| Improved Ambiguity Resolution by Regional Differential Modelling of the Ionosphere | |
| Lambert Wanninger, <i>TU Dresden, Germany</i> | 55-62 |
| An Efficient Algorithm for Batch Estimation of Non-Dynamic Parameters of Double-Differenced GPS Phase Measurement | |
| H. Rim, B. Schutz, and B. Tapley, <i>University of Texas at Austin</i> | 63-71 |
| Determining Earth Orientation by Global Positioning System at the US Naval Observatory | |
| Peter Kammeyer and James Rhode, <i>US Naval Observatory</i> | 73-81 |
| Programme of Research of CEI (Central European Initiative) Countries in Geodesy and Geodynamics | |
| Janusz Sledzinski, <i>Warsaw University of Technology</i> | 83-91 |
| Sakhalin Island GPS Survey: A Case History | |
| Paul Godwin, <i>Mobile Oil Corporation</i> ; Sergey Duginov, <i>Romona Ltd.</i> ; John Brown, <i>Geodetic Technology Company</i> | 93-104 |
| Economics of GPS and CORS | |
| William Young, <i>Riverside</i> ; Yehuda Bock and Shelley Marquez, <i>Scripps Institute of Oceanography</i> | 105-113 |
| High Precision Highway Profiles Using Helicopter Borne 'On-The-Fly' GPS | |
| Paul Hansen and Chris Joy, <i>The University of Nottingham</i> | 291-298 |
| Airborne Gravimetry by GNS/INS A Comparison of Filtering Methods | |
| Youcef Hammada, <i>The University of Calgary</i> | 339-347 |
| Twenty-Centimeter Kinematic DGPS Positioning With Digital Barometry | |
| John Schleppe, James McLellan, Jill Battie, and J. Scott McCarron, <i>Pulsesearch Navigation</i> | 1831-1840 |
| Effects of the Ionosphere and Cycle-Slips in Long Baseline Dynamic Positioning | |
| George Dedes and Angela Mallett, <i>The Ohio State University</i> | 1081-1090 |
| Fast Ambiguity Resolution Using an Integer Nonlinear Programming Method | |
| Ming Wei and Klaus-Peter Schwarz, <i>The University of Calgary</i> | 1101-1110 |
| Improving the Reliability of OTF Ambiguity Resolution with Dual Frequency GPS Observations | |
| Gang Lu, M. Elizabeth Cannon, and Gerard Lachapelle, <i>The University of Calgary</i> | 1111-1116 |
| Ambiguity Resolution Over Long Baselines for Airborne Differential GPS Positioning | |
| J. Sonntag and C. Martin, <i>EG&G</i> ; W. Krabill, <i>NASA Goddard Space Flight Center</i> | 1117-1126 |

Testing

| | |
|---|-----------|
| Development of High-Rate Differential GPS Reference for Operational Testing | |
| William Mosle and Andy Chasko, <i>746th Test Squadron, Holloman AFB</i> | 1637-1644 |
| Summary of the Initial GPS Test Standards Document: ION STD-101 | |
| Stewart Teasley, <i>Rockwell Telecommunications</i> ; James Bybee, <i>Cibola Information Systems</i> | 1645-1653 |
| The 746th Test Squadron: An All-Inclusive GPS Test and Evaluation Facility | |
| Dan Crouch, Chip Mosle, and Michael Novy, <i>746th Test Squadron, Holloman AFB</i> | 1655-1664 |
| Time to First Fix: A Definition and Recommended Test Method | |
| Leonard Kruczynski, <i>Trimble Navigation</i> ; Stewart Teasley, <i>Rockwell Communications</i> | 1665-1672 |
| Carrier Phase GPS Time, Space, Position Information Demonstration (CAPTIDE) | |
| Greg Costable, <i>Elgin AFB</i> | 1673-1680 |
| The Effect of Tropospheric Propagation Delay Errors in Airborne GPS Precise Positioning | |
| Virgilio Mendes, J. Paul Collins, and Richard Langley, <i>University of New Brunswick</i> | 1681-1689 |
| Measuring User Equipment Errors from Holloman Flight Test Data | |
| Joseph Clifford and Raymond DiEsposti, <i>The Aerospace Corp.</i> ; Andrew Chasko, <i>Amcomp Corporation</i> ; Kenneth Wernle, <i>CIGTF</i> ; Gregory Fairbanks, <i>GPSJPO, AFSMC, LA AFB</i> | 1691-1701 |
| Mobile Inertial Test System: A Dynamic Testbed for the EDGE Flight Tests | |
| Theodore Herrera and Brian Taylor, <i>Elgin AFB</i> | 1703-1711 |
| HIL Testing of the Navy LEAP GPS/INS Package | |
| George Stupp and David Lehnus, <i>JHU Applied Physics Laboratory</i> | 1713-1719 |
| Flight Test Program to Develop a New Terminal Instrument Procedures TERPS for GPS Approaches | |
| John Fagan, Hazem Hejjo, Travis Fox, and Bill Archer, <i>University of Oklahoma</i> ; Ralph Sexton, <i>Innovative Solutions International</i> ; Gerry McCartor, <i>FAA</i> | 1575-1587 |

Theoretical and Tutorial Subjects

Monograph on GPS Antispoofing

- Phillip Ward, *Navward GPS Consulting* 1563-1571

Unique and Emerging Applications

A New Navigation Algorithm Using Only Information From Measurement

- Benlin Xu, *University of New Brunswick* 309-318

The Reduction of Airborne Magnetic Noise Via GPS

- L. Bobb, W. Gelatka, D. DePersia, A. Salik, and S. Swyers, *Naval Air Warfare Center* 443-447

Real-Time Landslide Detection System Using Precise Carrier Phase GPS

- Hitoshi Kondo, *Furuno Electric Co., Ltd.*; M. Elizabeth Cannon, *The University of Calgary* 1877-1884

GPS-Based Launched Vehicle Tracking Using a Common Multi-Patch Antenna Configuration

- M. Santina, J. Leung, G. Smit, J. Tekawy, and G.T. Seng, *The Aerospace Corporation*;
J. McKay and S. Bandel, *Hughes Aircraft Co.* 1885-1893

GPS Goes 'Beyond the Gate'

- Samuel Shaw, *California Maritime Academy*; Jack Hunter, *California DOT* 1895-1903

Experimental Demonstration of GPS for Rendezvous Between Two Prototype Space Vehicles

- Kurt Zimmerman and Robert Cannon, *Stanford University* 1905-1913

Application of GPS Technology to Part 141 Flight Training

- James Lyall, *Embry-Riddle Aeronautical University* 1915-1921

A GPS Based Nuclear Radiation Detection Device Training System

- Edward Groeber, *U.S. Army Chemical and Biochemical Defense Command* 1923-1926

Geometric Correction of Airborne Multispectral Scanner Imagery Using

GPS Position and Attitude and Digital Elevation Models

- Lawrence Fisher, *Lockheed Environmental Systems and Technologies* 1597-1606

Wide Area Augmentation System

A Wide Area Augmentation System (WAAS) Service Volume Model and Its Use in

Evaluating WAAS Architectures and Design Sensitivities

- Walter Poor, Thomas Albertson, and Pauline Yen, *The MITRE Corporation* 629-637

An Algorithm for Inter-frequency Bias Calibration and Application to WAAS Ionosphere Modeling

- Yi-chung Chao, Yeou-Jyh Tsai, Todd Walter, Changdon Kee, Per Enge, and Brad Parkinson, *Stanford University* 639-646

Incorporation of Orbital Dynamics to Improve Wide-Area Differential GPS

- Juan Ceva and Bradford Parkinson, *Stanford University*; Willy Bertiger, Ron Muellerschoen, and Thomas Yunck, *JPL* 647-659

Validation of the RTCA Message Format for WAAS

- Yeou-Jyh Tsai, Per Enge, Yi-Chung Chao, Todd Walter, Changdon Kee, Jennifer Evans,
Andrew Barrows, David Powell, and Bradford Parkinson, *Stanford University* 661-670

The Ability of a RADGPS to Provide the Accuracy and Integrity Required for En-Route Navigation

- Richard Farnworth, *UK National Air Traffic Service*; Stuart Jolley, *Roke Manor Research*; Andrew Lovett, *Racal Avionics* 671-676

Integrating WAAS with LAAS to Avoid Signal Spoofing

- Vis Sankaran and Donald Benson, *Dynamics Research Corporation* 677-684

Exact Formula for User Range Error in Wide Area Differential GPS

- Henry Beisner, *Paradeigma, Inc.*; Arthur Dorsey, *Loral Federal Systems* 685-693

WAAS Sensor Interference Testing

- Trent Skidmore, *Ohio University*; Mark Johnson, *Rockwell International* 695-703

A Study for Performance Enhancements of the Asian-Australian GPS Augmentation System (AAAS)

- Yanning Feng, Kurt Kubik, and Jizhang Sang, *Queensland University of Technology*; Jingnan Liu, *Wuhan TU* 705-711

GNSS Integrity Monitoring at High Latitudes

- Gillian Richards, Andrew McGregor, and Reg Harlow, *DRA Bedford*; Andrew Watt and Bernd Tiemeyer, *Eurocontrol* 689-696

A Proposed GPS Block IIF Satellite Design with Civilian Dual Frequency and WAAS Signals

- Mohan Ananda, Prem Munjal, and K.T. Woo, *The Aerospace Corporation*;
Rich Cole, *Innovative Solutions International*; Steve Steiner, *U.S. Air Force* 1857-1868

| | |
|--|-----------|
| National Satellite Testbed (NSTB) GPS Satellite Clock/Ephemeris Determination Analysis and Results | |
| Scott Pogorelc, Mark Lorenz, Kelly Murdock, Brent Harding, Tim Cashin, and Donna Kraus, <i>Stanford Telecommunications</i> | 247-256 |
| Time Calibration Using the INMARSAT Geostationary Overlay Signal From the AOR-W Satellite | |
| James LaMance and Alison Brown, <i>NAVSYS Corporation</i> ; Bruce Haines, Willy Bertiger, and Sien Wu, <i>JPL</i> | 1175-1181 |
| Real-Time TEC Determination for Ionospheric Modeling in WADGPS | |
| José Fraile-Ordóñez, <i>Kayser-Threde GmbH</i> | 1193-1197 |
| An Improved Ionospheric Correction Method for Wide-Area Augmentation Systems | |
| Anthony Mannucci, Brian Wilson, and Dah-Ning Yuan, <i>Jet Propulsion Laboratory</i> | 1199-1208 |
| Test Results of Wilcox Electric's Ionospheric Monitoring Network | |
| Craig Stull, <i>Wilcox Electric</i> ; A. J. Van Dierendonck, <i>AJ Systems</i> | 1219-1228 |
| WADGPS Ionospheric Correction Model Performance Simulation | |
| Tysen Mueller, <i>Seagull Technology, Inc.</i> ; Bob Hamry and Andrew Johnson, <i>Rockwell International</i> | 1237-1246 |
| Development of Real-Time Algorithms to Estimate the Ionospheric Error Bounds for WAAS | |
| Robert Conker, Bakry El-Arini, and Thomas Albertson, <i>The MITRE Corporation</i> ; John Klobuchar, <i>USAF Phillips Laboratory</i> ; Patricia Doherty, <i>Boston College</i> | 1247-1258 |
| Autonomous Vehicle Using WADGPS | |
| Daljit Singh, <i>Naval Air Warfare Center</i> ; Harkirat Grewal, <i>American GNC</i> | 1333-1338 |
| A Modified Frequency-Locked Loop for Improved WAAS Carrier Tracking | |
| Gary McGraw and Bernard Schnauffer, <i>Rockwell International</i> | 1553-1562 |
| Global Optimization of GPS Augmentation Architectures Using Genetic Algorithms | |
| Samual Pullen, Per Enge, and Bradford Parkinson, <i>Stanford University</i> | 1403-1415 |



Plenary Session

General Chair:

Dr. Richard Greenspan
Draper Laboratory

Program Chair:

Dr. M. Elizabeth Cannon
The University of Calgary

GPS – The Ultima Thule of Navigation

James Schlesinger

Keynote Address

The Satellite Division of The Institute of Navigation
8th International Technical Meeting
Palm Springs, California
September 12, 1995

Ladies and Gentlemen:

I am delighted to be here with you this evening. It is my responsibility to launch this symposium on the impact of the Global Positioning System. This stunning technological achievement, created by our Department of Defense, probably (though not certainly) provides the Ultima Thule in navigation. When the ancient Greek explorers ventured beyond the Pillars of Hercules and proceeded north along the coast of western Europe they reached a place, the northernmost part of the inhabited world, where the sun shone continuously and which they called Thule. They also envisaged going even further toward a place they called Ultima Thule—a phrase which in modern times has come to mean the farthest limit possible. With the deployment of the Global Positioning System, mankind is now approaching such a limit for navigation.

Yet even as we approach this long dreamed of goal, we seem to be encountering new problems (though really reinforced old problems). Our attitude towards this monumental achievement appears to be marked by ambivalence. For navigation in the past the fatal risk lay in—inaccuracy. Navigational error regularly entailed catastrophic results. Now new fears are being generated regarding the consequences of—accuracy. Perhaps there is something in human nature that invents challenges; if something is inaccurate, how do I make it accurate? But, paradoxically, if it is accurate, my God, how do I make it inaccurate? If GPS provides the ultimate solution to the problems of navigation, while removing much of its adventure, nonetheless it does generate problems of its own.

Perhaps I should acknowledge my own limited credentials for addressing this professional Society. During World War II many was the flight which, due to errors in navigation, wound up in the wrong country. I, however, once had a boss at RAND who claimed to be the only navigator in the Air Corps who managed to navigate his plane to the wrong continent.

In those days at RAND, since we recognized the need to pursue high missile accuracy for hard-target kill, we were concerned about systematic bias in inertial guidance systems. Therefore when I arrived at the Pentagon, I demanded that the Services do something to develop a hard-target kill capability, which the Soviets were on the verge of introducing into their own forces. In particular I insisted that the Navy acquire accuracy for the Poseidon force. (The Navy at the time was quite disinterested in accuracy, regarding itself as a force oriented towards city-busting.) In my office I would ruminate about RAND-type fixes such as star-trackers or transponders. In the course of this persistent pursuit of missile accuracy, I gave a substantial, if though somewhat unintentional push, to the development of GPS. Some six months after my arrival at the Pentagon, full development of the GPS was authorized. It ultimately led to substantial improvement in most forms of precision-guided weapons—though at the time the main motive may have been simply to soothe the boss.

Though we did not realize it then, development of GPS perhaps represents the culmination of the long and intriguing history of navigation. Those South Sea Islanders who developed techniques of navigation, not yet fully understood by us, thereby acquired a power and status just below the ruling monarch, consequently sought to preserve those techniques as jealously guarded secrets. In the fourth century B.C. in the West, Pytheas of Massilea, whose works are now largely lost to us, ventured out into the Atlantic and reached Thule. In the fifteenth century, Prince Henry the Navigator, established at Cape Vincent a school of navigation. This was followed by the mapping of Africa by Vasco daGama and others and the development of new routes to India and the East. Then came the voyages and (Dare I say it in this era of political correctness?) the discoveries of Columbus. For two and a half millennia, the progress of navigation has been one spectacular adventure.

But there is a problem. Those who develop the techniques of navigation, wish to exploit them, yet deny their

use to other parties for "improper" purposes. One can fully sympathize with this objective. Still, history offers scant encouragement that it can be achieved for a very long period. The rain falls on the just and the unjust. Technology becomes available to both the good and the bad. When the sextant was developed in the eighteenth century, all too soon it became available to pirate raiders. In 1714 the English Government offered a prize of twenty thousand pounds to whoever could solve the problem of accurately measuring longitude. With remarkable diligence John Harrison labored for decades to develop his maritime timekeeper—though it took many additional decades before he received the appropriate recognition and award. It took almost another century before the British Navy equipped its ships with chronometers.

Who would then have imagined that those chronometers would ultimately be used by a German Empire to threaten through unrestricted submarine warfare the very existence of Britain herself? Admiral Jellicoe called the submarine menace "the greatest peril, which ever threatened the population of this country." The British rather huffily asserted that such attacks on commercial shipping "involve a total disregard of the canons of naval warfare." When the Germans declared the waters surrounding Great Britain as closed to shipping, the British (and the Americans) proclaimed that such action was not "legitimate." That did not prevent the British some seventy years later from declaring an exclusion zone around the Falklands during the Argentine war. The belief that one nation can benefit from the techniques of navigation while denying it to their foes is quite simply an illusion. It is, in fact, the illusion of that inspired inventor of rugby football who believed that he alone would be allowed to pick up the ball and run with it. Britain, after all, was destined to rule the waves. Who would imagine that some day German upstarts might abuse the very techniques that the British themselves had painfully developed.

What is the relevance for today? Technologies cannot for long be denied to others. (We cannot successfully emulate those South Sea Islanders who preserved their techniques as hereditary secrets.) The very use of technology will likely accelerate its spread. A balance must be struck between exploitation and protection—and that balance must be thought out with care, recognizing the real forces at play.

Free societies—more precisely, open societies—are by their nature particularly vulnerable to seeing their own technical achievements turned against them by their foes. During much of the Cold War, on the first of the month, when new maps went on sale, a woman from the Soviet Embassy would regularly appear at the Geological Survey to purchase the newly published maps. Her appearance was so reliable that the staff at the Survey had a package of the new maps

ready and waiting for her when she arrived. In brief, we were providing the Soviet Union with information on the location of their targets in our country far better than we then had on target location in the Soviet Union. And, by the nature of our society, we could do little about it. We would be forced to compensate by other means.

All this casts light on the interconnected and perplexing problems that the National Academy of Public Administration (NAPA) and the National Research Council addressed in their joint study for the Congress of the Global Positioning System. If I may be so bold as to suggest, the two parts of the study complemented and reinforced each other very effectively. In my remarks this evening, however, I shall primarily be addressing the NAPA portion of the joint study. The charge given to NAPA by the Congress was to study the national security, governance, commercial, and international aspects of GPS technology. The way the charge was worded seemed to suggest that these issues could be addressed individually. We soon discovered that the synergies among them were so strong that they would all have to be addressed simultaneously. Let me review the evolution in our thinking.

The initial predisposition of our panel was to state that national security was preeminent and that judgments about commercial or international considerations should derive from the primacy of national security. The United States had a major asset in the GPS system managed by the Department of Defense, which had done so noteworthy a job in bringing the system on line. Our predisposition with respect to governance was therefore based on the ancient rule of thumb—"if it ain't broke, don't fix it". With respect to governance, consequently, we saw no need to change the system of Air Force operational management and DoD dominance in policy matters.

Gradually our views were altered by the weight of rapidly changing conditions. To address national security in isolation and to ignore these rapid changes in conditions would, we came to believe, ultimately undermine the American position.

First, we were simply staggered by the unanticipated explosion in the non-military uses of GPS. These included, of course, civilian usage, as in aviation, still substantially determined by government policies. But it also included a veritable explosion of commercial uses wholly separated from government. No one had ever dreamed the use of GPS would expand so rapidly. Moreover, the DoD grossly underestimated the demand at the margin for accuracy in civilian uses—and the consequent spur to differential systems. The pace of growth in commercial activities and its expected continuation meant that these commercial considerations would come to dominate policy. Commercial

activities would soon exceed 90 percent of total demand and military usage would shrink to less than 10 percent. If we attempted to sustain the status quo in perpetuity, we would be swept away.

Second, the explosion appeared to be growing even more rapidly outside of the United States. To a greater or lesser extent other nations expressed some degree of unease regarding a system whose control lay in the hands of the U. S. Department of Defense. The suspicion of and resistance to relying permanently on such arrangements appeared to be increasing.

It was our belief that the satellite system was a "natural monopoly", in the sense that long-run cost curves continued to decline. That meant that the service would most efficiently and at lowest cost be provided by a single supplier. But if foreign unease about the control of the system was not quieted, even though there would be a loss of efficiency, over time other systems were likely to come into play in addition to the DoD's GPS system. There has been at least some preliminary discussions overseas of developing a separate network not subject to DoD control. Some of it was associated with upgrading the Russian GLONASS system to make it into a more effective alternative. Once again, it became clear that any attempt simply to maintain the status quo would over the long run be self-defeating.

Thus, both the commercial and the international aspects meant that our initial predisposition not to change what had not appeared to be broken could not be sustained. This ultimately determined our views regarding governance. We decided that operational management should remain with the Air Force. We concluded that, even with the best will in the world, the DoD would not adequately take into account the growing and somewhat specialized needs of the civilian community. Consequently, we argued that the civilian agencies have a growing role in determining policy. In particular, the Department of Transportation should take the lead on behalf of civilian agencies—but, if and only if, the Department substantially strengthened its capacity to contribute to policy formation. We also believed that, over time, other nations would have to be granted a greater voice in policy councils for the system. This would be necessary to provide sufficient assurance to other nations that their needs would be met, that they would not go off on their own. But that greater voice for other nations would also imply their contribution to the cost of the system.

This brings us back to the fundamental dilemma regarding the conflicting impulses with respect to policy—and the ambivalence that springs from those conflicts to which I referred at the outset. On the one hand, we fear that the GPS signal will in the future be exploited by hostile parties to inflict damage on us either in military operations

or in attacks on civilian targets. Yet, on the other hand, we demand the benefits of high accuracy for many civilian purposes—above and beyond U. S. or Alliance military operations. The compromise, intended to provide some degree of protection against the abuse by others of accuracy, is selective availability—through which the DoD "dithers" the signal intended for civilian users. But we are still uneasy with the compromise; indeed we are downright schizophrenic. After the Exxon Valdez accident, the Congress prescribed that all tankers would be GPS-equipped to help preclude a similar accident. Therefore the Coast Guard will provide for navigational purposes a correction of the dithered signal. In addition, we seek extremely high accuracy for air traffic control, especially in the vicinity of crowded airports. Therefore we are providing local differential systems and the FAA is proceeding to establish a Wide Area Augmentation System. Quite clearly the effect is to undermine the impact of the deliberately dithered signal. Perhaps more significantly, from the standpoint of military operations, other nations are proceeding to correct the signal through their own differential systems. Over time, the dithered signal will be corrected nigh-on universally, and selective availability will lose whatever purpose it serves.

In what is, no doubt, the most controversial recommendation, the two panels recommended that selective availability be turned off now. While all of us understand the original motives for developing selective availability, we believe that in these changed circumstances selective availability has become counterproductive even on national security grounds. In particular, it has accelerated the worldwide spread of differential systems which would counter its potential utility in times of crisis. It has increased awareness in foreign military establishments of the possibilities and the consequences of the dithered signal—and the need for countering the effects. The National Research Council panel concluded that any country sufficiently sophisticated to exploit the GPS signal would be sufficiently sophisticated to include the differential adjustments needed to offset selective availability.

It is to be noted that, although selective availability normally is turned on, it has been turned off on two interesting occasions: during Desert Storm and during the invasion of Haiti. The assumption quite clearly was that our foes were not in a position to exploit the GPS signal at all—certainly not in their weapons systems. But the latter is also true for other relevant nations. This results in the following irony. In the initial period, while other nations have had insufficient time to incorporate the GPS system into their attack capabilities, selective availability remains on. It also spurs the rapid spread of differential systems, which neutralize selective availability. By the time other nations are finally able to exploit a GPS signal in their offensive capabilities, selective availability will have been rendered essentially useless. Not

only does selective availability carry with it the seeds of its own destruction, it accelerates that destruction. In our judgment it would be far better to turn selective availability off now, and turn it on only when it becomes relevant in an actual confrontation.

The DoD reaction has been to fight tooth and nail against the Panel's recommendation. The DoD has stated that "any change in the implementation of SA will be a virtually irrevocable step". Why irrevocable? Is this an example of a perennial Pentagon fear that the final decisionmakers cannot be counted on to do the sensible thing in times of crisis? So why not limit their options? If the final authorities cannot be relied upon, selective availability should be on continuously. Scant consideration is given to the inconvenience and to the substantial and growing costs to the civilian sector or to scientific measurement which result from selective availability being continuously on—ultimately to guard against the untrustworthiness of the highest authorities.

The DoD has also suggested that failure to keep selective availability on continuously—even before foreign foes have introduced use of the signal in their offensive capabilities—endangers our forces in the field. It is noteworthy that no realistic scenario has been put forward to indicate just how our forces are put at risk. I can only infer that, in the absence of selective availability, someone is going to launch a surprise attack on U. S. forces—prior to SA being turned on. I am not sure just who might be planning to launch such an attack. Iran? Iraq?

I find that scenario lacking in credibility, to say the least. There have been very few parties prepared to launch surprise attacks against U. S. forces in past decades. Any such attacks have taken place after U. S. forces are deployed and engaged. Given the immense shift in the balance of power since the end of the Cold War and given the preponderant military position of the United States, such a scenario stretches credulity. Few nations really are seeking to deliberately bring the United States into the field against them.

Nonetheless, it is true that once other countries acquire a GPS capability, absent appropriate U. S. measures, U. S. forces will be in greater danger from precision-guided and other weapons. There are, however, steps the United States can and should take to reduce those dangers. We must take further advantage of electronic warfare. It is always necessary to invest further to maintain military advantage.

The GPS signal poses many serious problems for the military with which we are yet to come to grips. Some are procurement problems. One notes that on December 17 of last year, a U. S. Army helicopter was shot down after straying into North Korea. Though it was moving along one

of the touchiest frontiers in the world, the chopper was not equipped to receive the GPS signal. One also recalls that during the Gulf War civilian receivers were quickly procured—because of the cost, weight and production problems associated with the military version. Incidentally, those receivers were purchased by the Japanese as part of their contribution to the Gulf War. This may have been due to the Japanese not being hampered by cumbersome U. S. procurement procedures.

In addition to such procurement problems, perhaps even more serious is the reality that U. S. military commanders have yet to come to grips with the simple fact that in the future our foes may be taking advantage of the GPS signal. There remains a belief that, like that inspired inventor of rugby football, we alone can pick up the ball and run with it.

Let me repeat. When the system was laid down, given the many, many uncertainties, there was excellent reason to incorporate selective availability. Even now, selective availability would certainly add to the cost and might add to the uncertainty of a hypothetical foe exploiting the signal against us. Nonetheless, with the change in circumstances, selective availability has on balance become either useless or even counterproductive. At best it lies somewhere between a talisman and a smokescreen. It is a capability, for which the original motivation has passed, and for which justification is still sought for its continuous employment. It reflects a frequently-encountered military belief that even when a capability is useless or counterproductive, it should remain in the inventory—until a replacement is found.

Let me close with this observation. It will be recalled that on his first voyage to America, Columbus kept two sets of charts—one to mislead his crew to prevent their worrying too much about their location, the other for himself—a dramatic, if early example of selective availability. (History does not record whether or not Columbus used the term, dithering, in reference to these false charts.) Eventually it turned out that the charts for the crew, which were intended to deceive, were more accurate than the charts Columbus intended for his own use. Ladies and Gentlemen, there just might be a moral there. To be sure, Columbus' deception may have been more likely to succeed in fooling others than our own selective availability. Yet, in such deceptions, the real risk is that we may fool ourselves.

Thank you and have a productive meeting.

GPS Critical Technology, Policy and Institutional Issues

Panel Discussion

The Satellite Division of The Institute of Navigation, 8th International Technical Meeting
Palm Springs, California, September 12, 1995

Edited text from transcript of panel discussion prepared from audio tape of panel.
Text edited by Damon Hart and Keith McDonald

Panel Members:

Moderator - Mr. Keith McDonald

Dr. James Schlesinger, Mr. Joseph Canny, Mr. Gil Klinger, Mr. Larry Adams,
Mr. Charles Trimble, Dr. Scott Pace, and Col. John Caldwell, USAF

Dr. Elizabeth Cannon, ION GPS-95 Program Chairman: "The last part of our program, which I think will be very exciting, is our panel discussion, and that will be chaired by Mr. Keith McDonald. Keith is President of Sat Tech Systems, a satellite technology consulting firm, and is also Chairman and Technical Director of Navtech Seminars. He served as Scientific Director of the DOD navigation satellite program and as Executive Director of the Steering Group which initiated the Navstar GPS system in the 1970s.

Following this, he served in the FAA as Director of the Aeronautical Satellite Division, and later the Systems Analysis Division. Mr. McDonald has been active in the work of RTCA Special Committees. He has been very active within the Institute of Navigation, and served as ION President in 1990-1991. He received the Norman P. Hayes award for his contributions to the advancement of navigation and served as a member of the National Academy of Sciences/ National Research Council Study on the Future of GPS."

Mr. McDonald: "Good evening. We have an interesting program this evening, the subject of which has caused some controversy recently. We have an outstanding group of people to address the recent developments in GPS as well as the controversy.

The format for the panel tonight will dispense with any initial speeches or overview discussions. We will proceed directly to questions. However, I would like to set the stage for a moment. To obtain an interesting set of questions for the session this evening, I asked several of the panel members, among others, to provide questions, and they were very helpful. Actually, one submitted four questions complete with answers. (laughter) It occurred to me that we could provide answers to the panel and see if they could come up with the questions. If I recall, Johnny Carson used to do that with some success. Answers might include: "leave SA alone!", "5-10 meters", and "we don't care". (laughter)

There have been a number of important investigations relating to GPS during the last few years. These investigations include the study by the National Academy of Sciences and the National Research Council, an investigation that spanned about a year and was chaired by Mr. Larry Adams, who is on our panel tonight. Concurrently, the National Academy of Public Administration (NAPA) completed a study, chaired by Dr. James Schlesinger. The White House Office of Science and Technology Policy has also recently completed a study. We have with us Dr. Scott Pace, the chair of that study. There also have been a number of studies which the DOT has sponsored; Mr. Joe Canny of DOT, who was involved in these, is with us tonight.

We have as well, representatives of the DOD management of GPS. Some may criticize certain aspects of GPS, but I think we all agree that the DOD certainly gets high marks for bringing a very capable GPS into operation and for continuing its deployment. This system has changed the course of navigation. We have Mr. Gil Klinger with us from the Office of the Secretary of Defense in the Pentagon, and we have Col. John Caldwell, Deputy Program Manager of the GPS Joint Program Office. I would now like to formally introduce our panel and then we will go directly to the questions.

Mr. Joseph Canny is Deputy Assistant Secretary for Transportation Policy and International Affairs. He majored in physics, science and political science at MIT, attended Rutgers and Yale, worked in city government in New Haven originally, and joined DOT in 1970. He was appointed Deputy Assistant Secretary for Transportation Policy and International Affairs in 1990. Joe Co-Chaired the 1993 DOD/DOT Task Force on GPS and was instrumental in elevating that activity to the Assistant Secretary level, thereby achieving a higher profile for this work in the Department. He also serves on the DOT GPS Executive Board.

Directly to his left is Scott Pace. Dr. Pace is a Public Policy Analyst with the Rand Corporation's Critical Technology Institute, and chairs the White House OSTP Study. He is also Senior Vice President and a member of the Board of Directors of the National Space Society.

Next is someone we have seen frequently over the years—Charlie Trimble, President of Trimble Navigation. He received his bachelor's in Engineering Physics with Honors, and his Master's in Electrical Engineering from Cal Tech. He has four patents, one in GPS, and he runs perhaps the leading company in the world in the manufacture of GPS equipment.

Dr. James Schlesinger has already been introduced. Mr. Larry Adams, to his left, is the retired President and Chief Operating Officer of the Martin Marietta Corporation. He is an Aeronautical Engineer from the University of Minnesota, and was President of the Aerospace Division before becoming Martin Marietta's President. He has served on numerous US Air Force committees and panels, and has chaired several National Research Council committees. Larry is a former President of the American Institute of Aeronautics and Astronautics, and recently chaired the National Research Council study on GPS.

Next is Mr. Gil Klinger. He is with the Office of the Under Secretary of Defense for Acquisition and Technology, and is the Principal Assistant Deputy Under Secretary for Space. Mr. Klinger also was with the Rand Corporation as a Political Science consultant, with the Carnegie Endowment for International Peace, and a number of years ago, worked as an intern and analyst for Senator Proxmire. He did his master's in Public Policy at the John F. Kennedy School at Harvard University.

Finally, we have Colonel John Caldwell, who assumed duties as the Deputy Director of the GPS Joint Program Office earlier this year. Born in Kansas City, Missouri, he received a Bachelor of Science in Electrical Engineering from Arizona State, and was commissioned in 1971. Col. Caldwell also has a Master's in Business Administration. He went through navigator training and combat training with the F4 Phantom at Mather Air Force Base. He also completed a tour as a Staff Development Engineer with the Defense Nuclear Agency. Prior to this session, I mentioned to John that there might be some DOD-bashing tonight, and he said his tour at DNA had given him a thick skin. He served as F16 System Program Manager at Wright Patterson AFB, and was Program Manager for the acquisition of the Block-40 version of the F16's. He went to the JPO in early 1994 as Program Manager of user equipment.

I would now like to start the prepared questions. After three or four of these, we will take a few questions from the audience.

The first question is for Dr. Schlesinger, Mr. Adams, and Mr. Trimble."

QUESTION 1: If SA is removed from the GPS civil signal and some other evolutionary improvements are made to the control segment, it appears that stand-alone civil GPS accuracy at this time would be reduced from the 100 meter level to the 5-10 meter level. Will this have an adverse effect on the differential equipment manufacturers and cause a decrease in the growth of the GPS industry? Also, what is the view of the GPS manufacturers on this?

Mr. Adams: "We, in the course of our study, addressed that issue. We were a little concerned that we may be killing the goose that laid the golden egg, so to speak. So we actually contracted with Booz, Allen and Hamilton, who had done studies and analyses on GPS for several years.

They first gave us a presentation of the work they had done with SA present on the GPS signal. We asked them to analyze the impact of removing SA. The result was that there would be, in a certain segment of the differential GPS market, an impact from the improved accuracy of GPS. However, Booz Allen's analysis indicated that this "loss" would be more than recovered by the provision of differential services in the higher accuracy realm. The removal of selective availability would indeed make systems better in many applications, and more accurate, and also increase their use.

GPS systems, it appeared, would be much more effective and in greater demand, especially for uses needing more and more accuracy. That is where we came down. I believe that the NAPA study independently arrived at similar results."

Dr. Schlesinger: "The question is, with the increase in civil accuracy, that is, achieving 5-10 meters, would that adversely affect the differential equipment manufacturers? The answer is, sure. It obviously will affect them because there may be a lesser quantity of their services. As Larry has underscored, the studies we have done indicate a much larger expansion of the differential area and the equipment may or may not be cheaper, and the aggregate revenues of the industry may or may not be less."

Mr. Trimble: "In terms of looking at SA in the near term, there is very little question that removing SA would affect the augmenting suppliers. However, most of this would be because of the uncertainty - especially in the investment community of what the effect would be.

If you look at the fact that GPS is really an information technology in a mobile environment, you require computation, communication, and position. You are virtually always going to have both communication and positioning and the real opportunities of the augmented service suppliers are in

providing a combination of messaging with differential corrections. So there is a service that is natural and is major.

The other thing to look at is that most commercial demands on differential GPS are not for use at the 2 meter and less demanding accuracy levels. There is a great expansion in the submeter level now. A 7-meter system without selective availability doesn't help when you need good accuracy as well."

Mr. McDonald: "Thank you. The next question is for Mr. Canny of DOT."

QUESTION 2: DOD apparently plans to maintain selective availability for the foreseeable future. The NAPA and NRC studies concluded that SA serves no useful purpose and should be turned to zero immediately and deactivated within three years. As the current joint manager in GPS Policy and Planning with DOD, what is the current DOT position on SA? Do you agree with the current NAPA and NRC recommendations? If not, please explain.

Mr. Canny: "Secretary Schlesinger made a very compelling case with his remarks as to why we need to look beyond the historical basis for survival purposes for putting SA in place. In our relationship with defense, we are not quite that far apart and we are prepared to defer to their judgment on the national security policy for SA. The results of the joint task force study that we did about two years ago concluded that turning off SA would be neither necessary nor sufficient for the users."

Dr. Schlesinger: "The DOD Senate FY96 authorization bill from the Senate Armed Services Committee states that SA should be turned off at a date certain, well before the end of the century."

Mr. McDonald: "Thank you very much. We have a copy of the bill which Dr. Schlesinger cited, the *National Defense Authorization Act for Fiscal '96*, which has the language he referred to. The next question is to Mr. Canny and Mr. Klinger."

QUESTION 3: One of the recent NAPA/NRC study recommendations for enhancing GPS performance for civil and commercial users, is that immediate steps be taken to authorize the use of a second civil L-band frequency for an additional GPS civil signal and that this new signal be added to the Block IIR Satellites at the earliest opportunity. As the civil interface between DOD and the public, is DOT taking the necessary steps to insure that future GPS satellites contain an additional civil L-band frequency, and if so, what is the status of these efforts? Also, how does the DOD view these recommendations?

Mr. Canny: "Let me first say one last thing on the prior question. The FAA is going to need to deploy an augmentation system to meet their requirements, irrespective of any access to SA or the cost associated with these navigational systems.

With respect to the issue of a second L-Band frequency: yes, we have gone forward and it is an excellent example of the cooperation between the DOT, the FAA and the DOD. The RFP for the Block IIF satellites will contain an option for adding a second civil frequency. We are in the process of trying to provide that additional frequency, and if it is positive, we will try and come up with a source of funding. We will be looking at that cooperation."

Mr. McDonald: "Joe, are these comments related to the IIR or the IIF?"

Mr. Canny: "The IIF. The IIR is a different problem. Retrofitting the IIRs may not be cost effective."

Mr. Klinger: "As a matter of policy, we have no objection to an additional civil frequency (on the GPS satellites) with a couple of caveats. One is that we would not place an additional civil frequency on top of current military frequencies. We are vigorously opposed to that for reasons that are probably beyond the need to discuss here. Anyone who is familiar with the GPS issues for discussion can ask Colonel Caldwell, who can speak to the technical issues far better than I. But as a matter of policy, we are supportive of that kind of change.

The second caveat goes to the issue of Block IIR. Dr. Schlesinger, you have described rather colorfully the ineptitude that the Department manifests in major system acquisitions and procurements. All I can do is agree with that. In my experience, that is the way we do business. One thing we don't need to do is to add to that track record. In that regard our feeling is that to make a change to Block IIR right now would bust that procurement wide open. And the guidance that Paul Kaminsky and Bill Perry have given to Bob Davis and myself is that under no conditions are we to take any actions with regard to the GPS constellation that presents even a minimal risk of opening up a hole in that constellation. I think fooling around with a Block IIR procurement at this point would pose just that sort of risk and we are profoundly risk-averse to doing that. Making this kind of change to the Block IIF we will look at with DOT, but we will probably draw a line in the sand."

Mr. McDonald: "Thank you. The next question also relates to this area, and is for Dr. Schlesinger and Mr. Canny:"

QUESTION 4: Currently there appear to be no substantial incentives for the DOD to accommodate civil needs. For

example, there are few mechanisms for civil funding or involvement in DOD satellites. Also, placing civil requirements on DOD satellites typically impact schedule, cost and operational capabilities. In what ways can these concerns be addressed so that GPS can become a system that is effectively managed for both civil and defense purposes?

Dr. Schlesinger: "As I indicated in my opening comments, the DOD, with the best will in the world, is not going to be sufficiently sensitive to civil needs. Therefore, there should be a stronger place for those needs in policy deliberations. To this point, this has been a lopsided arrangement because DOD is frequently much stronger, much abler and much better informed than civilian agencies. We recommended the establishment of an executive board. But the strength and the position on that executive board, particularly of the DOT which is supposed to be the ultimate voice of the civilian community, depends on DOT's strengthening its own capabilities and providing a better voice with regards to these requirements.

However, DOD is not invariably a charitable institution. And, to the extent that there are adjustments in the satellite configuration designed for civilian purposes, it is the civilian agencies that should fund the augmentation costs. That should be understood. DOD ought not to be called upon to make expensive adjustments to this program in order to accommodate civil agencies. Unless there is money there, the civilian agencies are going to be able to talk, but they are not going to be able to effectively help."

Mr. Klinger: "I think it is true by definition, that given the mission of the DOD, we do not focus, strictly speaking, on civilian equities and issues that are of mutual interest to the department, namely, national security matters and matters that spill over, and an increasingly large number of matters do spill over into the civilian sector. Having said that, I would point out that there are three tenets to the policy framework with regards to GPS in the DOD. Two of them deal directly with military matters; namely, that as a matter of policy we are going to develop and maintain a capability to deny to an adversary the use of GPS in any form, whether augmented or the basic system. The second tenet is that while doing that we will maintain an uninhibited and uninterrupted capability for US forces and our allies to make use of GPS in whatever form is necessary.

The third tenet, and in fact it is the first one listed by Paul Kaminsky in any discussion about GPS, is this one: DOD recognizes that even now, its equities with regard to GPS constitute, by number or percentage, only a minority of equities associated with this system. Civil and commercial equities dwarf those of the DOD. Therefore, as the operator of the system, while protecting the military requirements associated with the system, we are obliged to ensure that civilian and commercial uses both now in place and in future

programs are accounted for in everything that we do. That includes the procurement, maintenance and operation of the system.

Having said that, we have in place a formal relationship with the DOT that I would say from my own experience has been improving every day, as DOD and DOT struggle and try to understand the cultural differences between our two missions and roles. We rely upon the DOT to be the voice for a lot of the civilian user community. At the same time, civil and commercial uses are reflected in GPS operational requirement documents and the presence of DOT representatives in Colorado Springs and elsewhere reflects the recognition of the Department of its responsibility to account for civilian users."

Mr. Trimble: "DOD stewardship has clearly helped the civil sector. The playing field has been established for all users of the system. Nationally and internationally, over a billion dollars of civilian user equipment is being purchased this year, with probably 50% of it outside the United States, a great export market for the US. Whether motivation is explicitly there or not, the stewardship is."

Mr. McDonald: "That's an interesting perspective. This next question is for Dr. Pace."

Question 5: The study on GPS which you chaired with the White House Office of Science and Technology Policy was recently completed but has not been released. Would you comment on the following two areas:

- a) the status of the report and in particular the domestic and international concerns; and
- b) from the Office of the President's perspective, what do you see as the need for national policy?

Dr. Pace: "The issues that prompted the study are really very simple; this technology is powerful and is transforming sector after sector. One of the things that happened about two years ago was that many people at the policy level found themselves talking about this strange thing called GPS. Effectively, what they were doing was addressing disaster relief, transportation, aviation; and then we had others addressing GPS for timing, critical to the operation of communications. They were coming together, dealing with the same overlapping technology.

What we have been trying to do in this past year is to scope out these issues. What needs to be decided at the highest level? The agencies should be commended for the amount of progress that has been made in this area. Nevertheless, there remain a series of top level decisions that really can only be made at the highest level. We will soon see, I hope, the first really comprehensive statement on GPS policy since

President Reagan made the system available after the KAL flight disaster. Now this statement will not be revolutionary, but will be a clear concise statement on GPS system policy."

Mr. McDonald: "Thank you. Now questions from the floor."

Question 6, from audience by Mr. Bob French: "I have a 2-part question for Mr. Canny relating to SA."

(1) You explained that the impact of SA on the FAA's augmentation system will be nil. How about the Coast Guard System? Will that be abandoned or will they press for higher accuracies?

(2) What are the implications of turning off SA for the Intelligent Transportation System program, ITS. In particular, for the automated Highway System part of ITS?"

Mr. Canny: "With respect to the Coast Guard system, that system is essentially complete and is about to become operational. With respect to Harbor Access, it is essentially done in the Great Lakes and other areas. I don't think the Coast Guard envisions any significant improvements in that system. That is a relatively inexpensive system, around fifteen million dollars. Regarding intelligent transportation systems, that is probably the area - land transportation use - that has a variety of purposes. Whether it is transportation, risk reduction, truck and transit, you name it, that is probably the area where the greatest expansion and use of GPS will occur. Just to get some sense, your question implied accuracies far better than are obtainable with SA turned off."

Mr. Trimble: "The biggest indicator that SA is involved in ground transportation, comes in the car navigation business. Roughly 600,000 car navigation systems will be sold worldwide this year. That's a 100% annual rate of increase, and this is in spite of SA on the signal."

Dr. Pace: "SA and GPS policy issues come back to the point that there is no issue about international acceptance of GPS. It is accepted! People are buying it every day, paying for it, and using it. The distinction is that governments issue certifications of safety, are responsible for national defense, and have legitimate concerns. But those topics are really not sticking points. The United States has a very important role in helping to shape that dialogue, and the implementation of this technology around the world. So we should keep an eye on those governments that are trying to catch up."

Mr. McDonald: "Thank you, Dr. Pace. Another question from the floor."

Question 7 by unidentified speaker in audience: "My question is to Mr. Trimble or Col. Caldwell, and has to do with whether it is preferable to turn off Anti-Spoofing or SA?"

Mr. Trimble: "The answer is several things. This is not really an issue that violates security or degrades the military system because fundamentally what we're trading off is vulnerability to electronic jamming. There is an impact on cost."

Question 8 from same speaker in audience: "Why can't the C/A code be transmitted on the L2 channel in the Block IIR and IIF satellites?"

Mr. Trimble: "There is equipment available today (to receive the code information on L2). If you had asked a person to sign up for that three years ago, he probably wouldn't have. It is a system approach that uses technology. GPS forms an underpinning that is very useful. If someone paid for a C/A code on L2, we would clearly use it."

Mr. McDonald: "Along that line, I might mention that the Defense Science Board, NAPA, and NRC reports recommended that a C/A code should not be placed on the existing GPS L2 frequency. We have another question from the floor."

Question 9 from the audience by Mr. Tom Stansell: "I would like to make three statements. One is to express a great deal of gratitude to Dr. Schlesinger for the leadership that he has been demonstrating to us in thinking about the future of the system. It is really exciting to take a fresh view, a fresh approach. I really would like to see that kind of proactive leadership show up in the civilian agencies that represent the civil user."

Second, we have talked about the impact of SA being turned off as a simple issue of accuracy improvement. That is true, but what hasn't been discussed, and is equally important, is that turning off SA produces rather significant improvements to differential GPS. Differential GPS achieves higher levels of integrity. Some signals can get lost and fewer signals might get through and you could still have good differential GPS services. Because of that, coverage is vastly improved. The Coast Guard System will have significantly greater coverage, simply because SA is turned off.

Third, without having to change the model, the accuracy of differential services will be improved if SA is turned off. So turning SA off doesn't necessarily invalidate, or eliminate the need for differential services, but it vastly improves the utility of differential. With respect to the integrity issue, one of the things that needs to be really thought through (and I appreciate Dr. Schlesinger's comment in this direction) is that with SA off, RAIM integrity monitoring becomes so much more robust with GPS alone or augmented, I really think there is a question needing to be thoroughly discussed, and that is, do you really need WAAS?"

Mr. McDonald: "Thank you, Tom. I think we will return now to the panel. A question for Mr. Adams and Dr. Schlesinger:"

Question 10: If SA is **not** performing a useful military function, why did the NRC and NAPA include the option for the National Command Authority to reinstate it for three years if it really has no use? Are there any valid reasons that come to mind?

Mr. Adams: "I'll comment on that. It is a fact that if enemy forces are using (civil) GPS, SA will indeed make their unaugmented accuracy poorer - to about 40 meters CEP versus 10 meters without SA. So if you were in a battle situation and it is apparent that enemy forces are using the straight GPS signal and did not have available the differential signal corrections, then indeed, you would want SA to help you with point targets, because of the 40 m. to 10 m. difference.

When you get to the three years, there is another situation that occurs. When L1 is denied, GPS receivers have some difficulties since they use information from the CA code on L1 for P/Y-code acquisition. It was our belief that in three years time, the DoD should be able to develop receivers which could directly acquire the P/Y code. And if there were some lag in that, then one could develop and train people in operational procedures which would allow you to operate in the presence of jamming. We recommended many ways for doing that and I am sure the military could come up with many others. That is the rationale for the three years."

Dr. Schlesinger: "The first point: SA always has a usable military function. The question is whether, on balance, it is useful militarily. It is performing a useful military function in that, to a hypothetical foe out there, it is clearly adding to the cost of his use of the GPS signal, and it may or may not, add to the uncertainty with which he deploys his forces. So there is a military use for it.

Second point: In the transitional period, SA has probably been counterproductive rather than useful, in that it has speeded up the process of providing differential systems around the world and it has speeded up the process in the United States. And one worries about domestic terrorism.

Down the road, not in this initial period, not in the present sense, but in the future, we have the case Larry describes. A hypothetical foe acquires a useful capability utilizing the GPS signal. If that hypothetical foe hasn't also incorporated differential corrections with his weapons systems, then if we turned on selective availability, it would confuse that hypothetical foe. One of the problems with selective availability continuously running is that it speeds the day when that hypothetical foe would incorporate such adjustments (e.g. differential corrections) into his weapon systems."

Mr. McDonald: "Thank you. Now, a comment from Mr. Klinger:"

Mr. Klinger: "I feel somewhat compelled to lay out some sort of response relating to this SA issue which in my experience with GPS is to some degree missing the point. I think Dr. Schlesinger has articulated correctly the question, which is not that SA is useless, the question is exactly, on balance, are we better or worse off with regard to having SA in place.

The economics of the issue is such that, even with SA turned off continuously, there is still a requirement for differential services of the type that are in place. What does happen, however, is that we immediately level the playing field in an adverse manner. All the US receiver equipment manufacturers currently have a leg up on foreign manufacturers of receiver equipment. Now ultimately, we might get that comparative advantage back, but that is not something that I think the taxpayer would be very happy giving up to begin with.

But to go back to this military argument. During the course of the NAPA/NRC studies, we made available, a two-phonebook study, clear evidence that there were over eighty some-odd missions that an adversary could perform with SA turned off, that now, cannot be performed as easily. Your point was that the adversaries, if determined enough, if bloody-minded enough, will go off and do that. With the enemy perspective, I am just not in a hurry to give them those advantages.

And here is one of the ironies about SA. As Charlie Trimble pointed out, our industry is going to make a boatload of money from very precise navigation, which still requires differential services. The irony is that the terrorists in the world are going to be able to come after us in ways that they can't right now, without any differential services, but with SA off.

Added to that, one of the things that this conference is looking at, is the interrelationships between navigation and GPS and other facets of information capabilities that are now available. In that regard, I will point out to you that there is about to be unrestricted availability of one meter or ultimately better, satellite-based, commercially-derived imagery. Imagine what Hamas or his following, or the Iraqis or the Iranis are going to do with Helios I- or Helios II-derived imagery, overlaid with an SA turned-off high-precision navigation system. There are all sorts of point targets that are not available to these people right now for which a capability can be achieved only for a fairly significant investment. I am not in a hurry to make their jobs easier.

To add to this, I think inside the Beltway, reality is - if we turn SA off, it doesn't matter what the contingency is, it is never

coming back on. It is just not going to happen! And for evidence of that, I will disagree once again (with Dr. Schlesinger and the NAPA/NRC studies). I don't view this as a position that reflects a judgement about the skill of Mr. Perry as a decision-maker. I believe it reflects reality in Washington.

I have a point on what Colin Powell and Dick Cheney did in Desert Shield. We did not just take 100,000 - 200,000 troops and their equipment and put them into the area of responsibility that General Schwartzkopf had. We brought a hammer. We brought the biggest movement of men and women and materiel that we have seen since the end of Vietnam. One of the motivations that Cheney and Powell had was the sure knowledge that if they had to go back to the well twice and try and get permission later on to get more support, it was highly uncertain that they would get that permission.

My lesson from that is: If we shut off SA, it is not coming back on. By the way, what better indication to an adversary, that the 82nd Airborne will appear at your door shortly, than if suddenly in an environment in which SA was turned off, we now turned it back on. The fact of the matter is that in the Persian Gulf, precisely because of the shortcomings in our acquisition system, as Dr. Schlesinger pointed out, we didn't have enough military receivers to go around.

In Haiti we had a big advantage. We had, mercifully, an adversary who turned out to be not an adversary at all in the sense we expected. We had an adversary who simply lacked the wherewithal to make any use whatsoever of GPS, and therefore, there was no thought (or concern) of turning off SA. But I will tell you, inside the Pentagon there was great consternation when that decision was made precisely because if somebody had been listening in Haiti, they would have known that something was up, because we shut it off. The point I am making to you is the reverse situation causes just as great concern.

The last point I will make and then I will get off this soapbox, is that both reports contend that one of the things that SA does is incentivize some undefined party to put up their own navigation system. I think that this is a false premise in two major ways. One, is that GPS is a system of technical complexity that is fairly daunting. It is daunting to anyone that is not in the space business. The other point is that space is the last place you would ever want to go to do a job if you could avoid it. I do not believe it is a simple matter that not turning off SA immediately translates either to the willingness or the capability of any other country to be able to simply go and put up a satellite system. I would characterize the GLONASS system (of Russia) as an example of that. They have tremendous difficulty maintaining that system." (applause)

Mr. McDonald: "Dr. Schlesinger, you have a comment?"

Dr. Schlesinger: "I am delighted to see you on your soapbox! In the first place, no-one was raising questions about the way Washington works or who is the ultimate decision-maker.

Secondly, the interesting point that you raise about the advantages to American industry of having selective availability is to say that we pose this as a wonderful trade barrier and not a tariff barrier of the sort that we object to with other nations, such as Japan. No doubt it works; it works for the Japanese, it works for us, but it happens to be against United States policy.

Third, with regard to terrorism, we have differential systems sprinkled all over this country, particularly in the neighborhoods of the crowded urban airports, and near most of the juicy targets such as the Pentagon where you work. It happens to be covered by differential systems."

Mr. Klinger interruption: "Most of my enemies are in the E-ring of the Pentagon." (laughter)

Dr. Schlesinger continues: "When you referred to terrorists, I didn't think you were referring to your colleagues in the Pentagon! (great laughter)

Now, with regard to overseas questions, there are a sprinkling of differential systems that will permit others to go after targets. And, as everybody in the Pentagon knows, over time, the only way to deal with these matters is by using other ways to approach them.

Finally, one should look at other problems with SA on occasion. This adds to the force of the recommendation. It increases the difficulty and inaccuracy of scientific measurements. ...

If Senator Proxmire were still giving Golden Fleece Awards, SA would win one. ..."

[Unfortunately, audio tape was of poor quality throughout and shut off at this point. Convention center technicians did not continue recording the panel for about 15-20 minutes. Panel continues with Mr. Trimble discussing GPS receivers:]

Mr. Trimble: "... If you look at the average selling price of a GPS receiver on the OEM market, it's \$120 and dropping at 30 percent a year. The big deal isn't the application solutions. It's a tracking and information system. We see a factor of ten in terms of growth of user equipment and systems in the next five years, and it's basically going to be in information systems.

We have already discussed L4; if something happens to L2, we need the additional civil frequency."

Mr. McDonald: "I think with that we have given Charlie Trimble the last word tonight. It is time to close the session.

I would like to give my thanks to the members of the panel: Dr. Schlesinger, Larry Adams, Scott Pace, Gil Klinger, Joe Canny, Charlie Trimble and John Caldwell for their participation tonight. Belatedly, I would also like to introduce the new Director of the GPS Joint Program office. Colonel John Clay, USAF is with us this evening. (great applause)

Thanks again to the Panel and I return the program to your Program Chairman, Elizabeth Cannon."

Dr. Cannon: "Thank you very much, Keith. I will close this evening's Plenary Session. I would just like to thank our keynote speaker, Dr. Schlesinger and Colonel Worden, as well as our panel members and Keith for chairing our Panel discussion. It was an exciting program this evening and a great start to our meeting over the next three days. Have a good evening. I will see you all bright and early tomorrow morning." (applause)

Plenary session closed.



Session A1

Surveying and Geodesy

Chair:

Mr. Steve Malys
Defense Mapping Agency

Co-Chair:

Dr. Tom Herring
MIT

A Comparison of GPS and Satellite Altimetry for Height Monitoring on an Offshore Production Platform

Moira Tighe and John Macgregor
Shell U.K. Exploration and Production

BIOGRAPHY

Moira Tighe has a BSc. in Mathematics & Surveying and a Ph.D. in Satellite Geodesy from the University of Newcastle upon Tyne, U.K.

John Macgregor has a BSc. in Topographic Sciences from the University of Glasgow, U.K.

Both joined Shell U.K. in 1992 as project surveyors.

ABSTRACT

In 1993, Shell U.K. Exploration and Production, operator in the U.K. sector of the North Sea for Shell and Esso, carried out a precise GPS campaign for the purpose of providing offshore height benchmarks on several North Sea production platforms. The intention was to reference the platforms to stable land points in order that reliable monitoring of platform height could be carried out in the future.

In 1994, a feasibility study for using Satellite Altimetry in conjunction with a Transponder was carried out on one of the platforms. This paper describes the Transponder trial and provides a comparison between the heights derived from GPS and altimetry.

INTRODUCTION

Shell U.K. Exploration and Production is the operator of many oil and gas production platforms in the U.K. sector of the North Sea. Recent modification work on several of the production platforms has been carried out to extend the field life and ensure that the platforms continue to be a safe working environment. One of the aspects of the work has been to develop and implement a precise measuring scheme, which will be used to help determine information about the nature of long term platform motions.

The Global Positioning System (GPS) provides a method of gaining centimetric positional accuracy over

very long baselines. The relatively new method of using satellite radar altimetry in conjunction with a ground based transponder provides an additional means of determining accurate height. Although it may be beneficial to have the three dimensional information provided by GPS, the main interest offshore is in the height dimension. The altimetry method, therefore, provides an interesting alternative to GPS.

BACKGROUND

Until recently, it was not possible to provide a reliable means of absolute heighting for offshore production platforms. The distances from the coast (and hence from any stable reference points) have ruled out conventional surveying techniques. The hostile offshore working environment has also limited the accurate use of GPS, especially when reduced coverage made multipath and cycle slips a limiting processing problem. It was generally found that integer fixing was not possible over the long baselines between most platforms and the shore, which limited the positional accuracy to decimetre level.

Over recent years, the completion of the GPS constellation, the continuing progress in instrumentation design and the use of enhanced processing techniques have enabled relatively cheap methods of relating widely separated points to each other in a consistent co-ordinate reference frame. These developments provided the opportunity to use GPS to determine accurate positions for offshore production platforms.

GPS BENCHMARKING CAMPAIGN

In 1993, taking account of the increasing emphasis on safety in the North Sea and an improvement in measuring technology, it was decided that a prototype benchmarking scheme would be carried out on several offshore platforms, all located at a distance of some 200kms from the coast line (*ref. 3*). The intention was to aim for an accuracy in the order of a few centimetres and a five day observation campaign was

planned to ensure that sufficient data could be collected to achieve this.

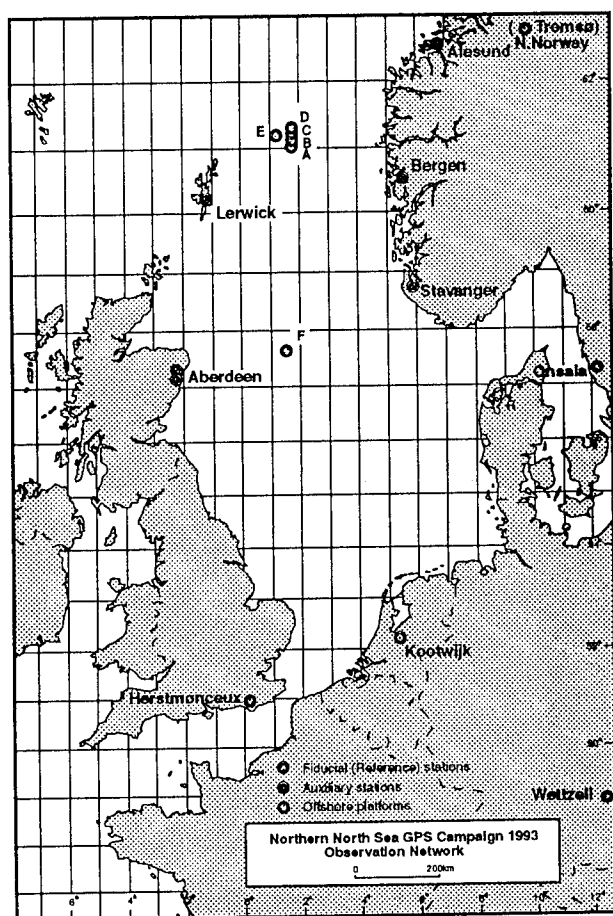


Fig. 1 1993 GPS Network

The network included data from six offshore platforms and six other unknown land based sites (fig. 1). These were included to minimise baseline lengths from the platforms to the coast and thus help with the integer fixing in GPS processing.

By including data from five permanent GPS reference stations (see Table 3) and using precise orbits determined by the International Geodynamics Service (IGS), the unknown sites could be referenced to the International Terrestrial Reference Frame, ITRF92. The epoch used was 1993.740 (knowledge of this enables any future co-ordinates to be corrected for tectonic movement of reference stations by using plate motion models).

Although there was no means of reliably checking the absolute accuracy of the data, the standard deviations were in the order of one centimetre (see Table 1) which was a very acceptable result.

| Platform | $\sigma X, \sigma Y, \sigma Z$ (m) |
|----------|------------------------------------|
| A | 0.008, 0.002, 0.013 |
| B | 0.007, 0.002, 0.011 |
| C | 0.007, 0.002, 0.011 |
| D | 0.006, 0.002, 0.011 |
| E | 0.007, 0.002, 0.013 |
| F | 0.008, 0.002, 0.012 |

Table 1 Standard Deviations from 1993 GPS Survey

The results were archived with the intention of repeating the campaign annually and waiting to see whether any significant movement could be identified. Consultation with academics who had experience in other precise monitoring schemes, however, gave the indication that these discrete measuring campaigns would not be sufficient if future movements were to be reliably detected.

It was, therefore, realised that, if the philosophy of discrete measuring campaigns was followed, it could be a number of years before any apparent platform movement could be reliably identified.

REQUIREMENT FOR CONTINUOUS MONITORING

The advantage of providing continuous data for height monitoring is that a time series can be created to allow outlier detection and determination of trends.

In the environment of operational offshore platforms where structures are subject to drilling/production vibrations, weather/seastate effects and frequent load redistribution there are likely to be many data spikes which could be easily identified on a time series plot.

The recommendation was thus to find a way of removing the effects of these systematic motions by detecting them and then modelling their effect. In order to do this, a means of recording data at a high frequency interval was required.

The method of using Satellite Altimetry in conjunction with a Transponder provides a logistically simple means of collecting height information. It had never previously been tested in an offshore platform environment.

In early 1994, an opportunity arose to carry out a trial using Transponder measurements on an offshore platform. The experiment was to serve the dual purpose of verifying the 1993 GPS benchmark measurements and exploring a means of providing an alternative method for monitoring and predicting platform height changes.

USE OF ERS-1 WITH TRANSPONDERS

The method of Satellite Altimetry utilises a satellite based radar altimeter (frequency 13.6-14.0GHz) to determine a range between the known position of the satellite and a suitable reflective surface. The distance of travel is computed from the time and velocity of the signal and halved to give the range from the satellite to the reflecting surface. ERS-1, a multi-purpose remote sensing satellite, was launched in 1991; its main input to the geodetic community was to provide altimetry over oceans and ice surfaces.

As an extension to the method of ocean heighting, it was found that a Transponder placed close to the satellite ground track (within 7km) (*ref. 5*) could provide a suitable reflecting surface to allow reception and amplification of the signal, which could then be transmitted back to the satellite. The first experiment using such equipment was carried out after the launch of ERS-1 in August 1991 (*ref. 2*). It showed that relative height could be measured over a baseline of 127km with a precision of 3cm.

The satellite radar signal is received by the Transponder, amplified and re-transmitted to the satellite. Vertical ranges can, thus, be computed but limiting factors are :

- atmospheric delay to radar signal,
- satellite orbit uncertainty,
- knowledge of horizontal position of Transponder required (*fig. 4*)

By using a relative measurement technique (*see fig. 2*), height differences can be computed with centimetric accuracy. Meteorological measurements can be used to improve the accuracy of the result and orbit errors can be reduced by utilising laser range observations to ERS-1. The approximate horizontal position can be determined by GPS.

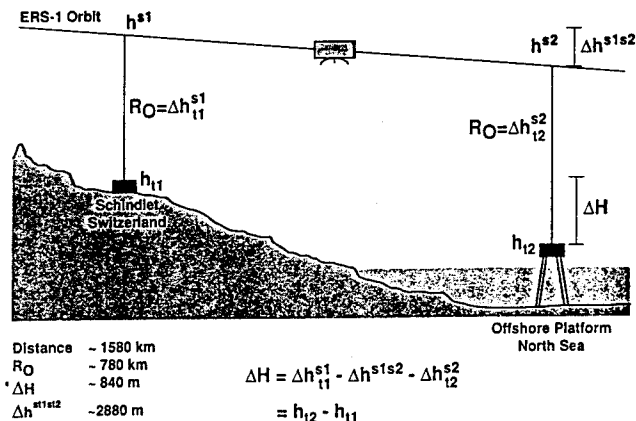


Fig. 2 Relative Height Measurement Using a Reference Station with Known Height

In addition to exploring the feasibility of the Transponder method, a secondary aim of the offshore trial was to determine the requirements for supplementary measurements. This could be done by assessing the extent to which accuracy would be compromised if meteorological measuring equipment was to be minimised.

The main participants of the 1991 experiment were the Rutherford Appleton Laboratory (RAL), a U.K. Research Laboratory, in conjunction with the University of Newcastle upon Tyne, U.K. and the University of Graz in Austria. All provided assistance with the Shell offshore Transponder trial in 1994.

BENEFITS OF THE TRANSPONDER METHOD

The operation of the Transponder itself is very simple. It transmits for a period of only four seconds during each satellite overpass and data is then recorded on board the satellite and downloaded by the European Space Agency (ESA). Minimum operator intervention is, therefore, required once a Transponder has been deployed.

The method provided an attractive alternative to GPS and the following conditions were favourable for designing a height monitoring scheme :

- from early 1995, ERS-1 would change from an experimental phase to a fixed orbit with a 35 day repeat period (which would allow height recording every 35 days),
- ERS-2 would be launched to replace ERS-1 (overlapping in operation),
- ERS-2 would pass over several North Sea oil fields,
- ERS-2 would also cross land at a suitable site, allowing simplified logistics for reference station deployment.

THE OFFSHORE TRANSPONDER TRIAL

The Shell offshore platform chosen as the ideal site for the experiment was Platform A from the 1993 GPS network. It was situated about 3.5km from the satellite ground track (in order to receive the satellite signal, it is necessary for the Transponder to be within 7km of the satellite ground track).

Approval had been given the previous year to operate GPS receivers on the platforms but the physical differences with the equipment to be installed offshore for the Transponder trial were :

- the prototype Transponder to be used was considerably larger than a GPS receiver (1.5 x 0.8 x 0.6m),
- the Transponder emits microwave radiation during retransmission of the amplified satellite signal.

Although the operating time for the Transponder is only about four seconds (time when satellite is directly overhead), it was still necessary to verify that the equipment did not present a safety hazard. This was done in co-operation with platform personnel and the Transponder manufacturer, Ulmo Systems Ltd (U.K.).

A second Transponder (a new, smaller model manufactured for the University of Graz) was deployed at a land site at Schindlet near Zurich in Switzerland. This gave a baseline of about 1580km (*fig. 3*). By determining a height for this using GPS, an absolute height for the offshore site could be determined from the Transponder measurements (*see fig. 2*).

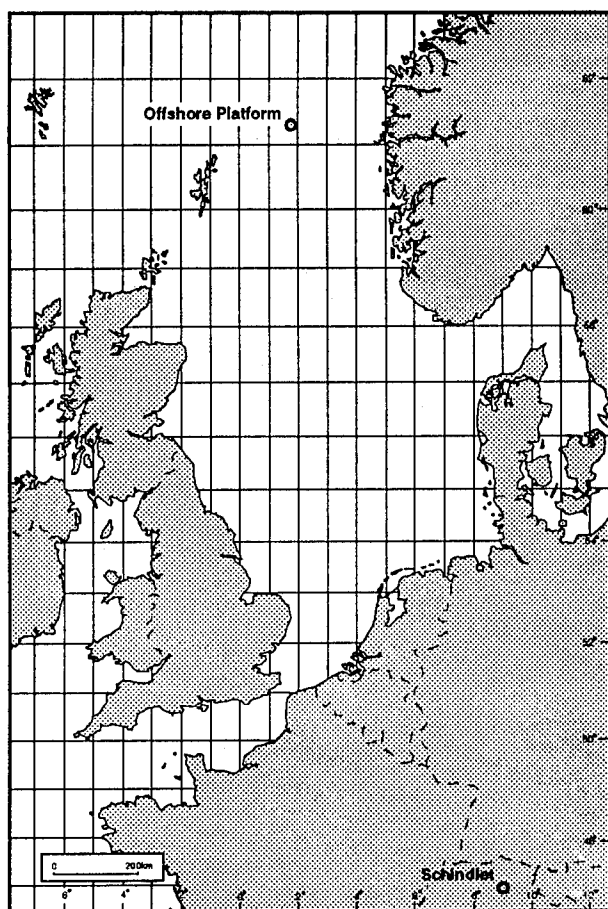


Fig. 3 Transponder Sites

The Swiss site was chosen for logistical reasons, being the closest site on the ERS-1 ground track which was convenient for transport of equipment and personnel from Graz. Additionally, the location facilitated support from the University in Zurich to be provided (specifically with meteorological observations).

FIELDWORK

The prime opportunity to carry out the Transponder measurements was on 10th July, 1994. After

overcoming several logistic problems, both Transponders were successfully deployed and tested in time for the ERS-1 overpass.

The following supplementary measurements were required :

- dual frequency GPS data,
- meteorological data,
- Satellite Laser Ranging (SLR) data.

DUAL FREQUENCY GPS DATA

These were obtained for the following reasons :

- to determine an accurate height for the land site at Schindlet, in order that it could be used as a reference site (*see fig. 2*),
- to compute approximate horizontal positions for both sites so that a vertical range from the satellite could be obtained (*see fig. 4*),
- to compute corrections for the ionospheric delay,
- to tie the results into ITRF so that a comparison for both the ERS-1 derived height and the 1993 GPS benchmark results could be made.

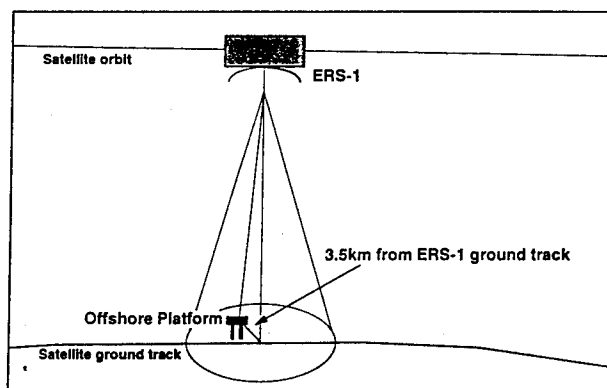


Fig. 4 Horizontal Range Computation

The GPS receivers used at the Transponder sites were Trimble 4000SST (offshore) and SSE (land). The plan was to collect data on the day of the ERS-1 overpass and for one day either side. Due to the problems with fog causing offshore helicopter delays, however, the equipment did not arrive on the platform when expected which meant that the observations only began on the day of the overpass. Only about 40 hours of GPS data was recorded, which degraded the quality of the result but was not a limiting factor (as the results from the 1993 GPS survey could be used for an accurate comparison).

METEOROLOGICAL DATA

This was used to determine tropospheric corrections. In addition to basic meteorological measurements (temperature, humidity and pressure), data from the

ERS-1 Water Vapour Radiometer (WVR), which can only be used over oceans, was used at the offshore site. At the land site, students from the University in Zurich operated meteorological equipment, including a WVR and radio sondes.

SATELLITE LASER RANGING (SLR) DATA

ERS-1 is, theoretically, in a known orbit but, in order to gain centimetric accuracy, a precise orbit arc between Transponder sites must be measured by SLR at the time when observations are taking place. Fortunately, this is routinely done and the required orbits could be purchased from the Royal Greenwich Observatory (RGO) in Herstmonceux, U.K.

ERS-1 DATA PROCESSING

Prior to the computation of final height differences (carried out at the University of Newcastle upon Tyne), the uncorrected ranges from ERS-1 to each Transponder were computed from the raw data at RAL. The data itself was received from ESA.

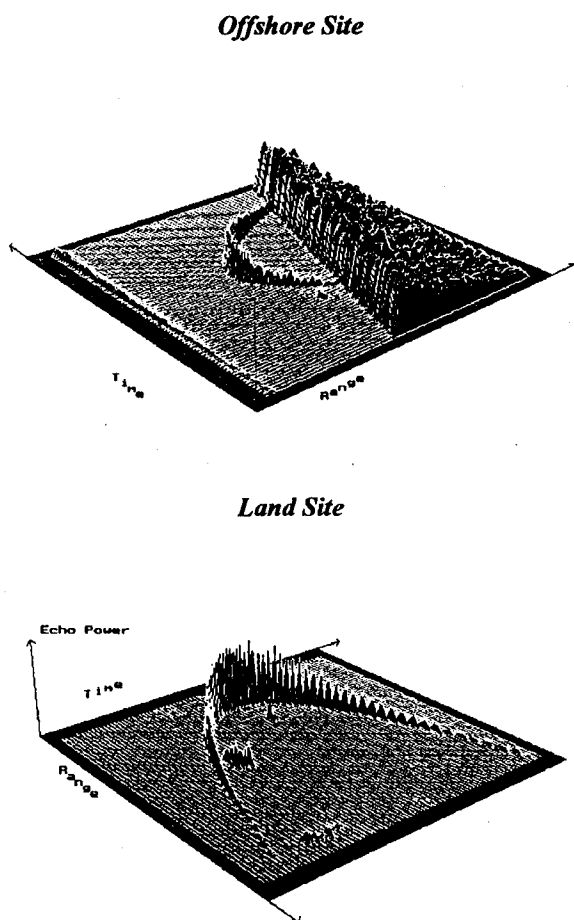


Fig. 5 ERS-1 Radar Altimeter Returns from Transponders

GPS DATA PROCESSING

Echoes from both Transponders were clearly identified and plotted as hyperbolae (fig. 5). A detailed

description of the computation can be found in (ref. 1) and it will suffice to say that a quadratic function is fitted to smooth the waveforms. The minimum points on the hyperbolae represent the exact points where the range is required (fig. 6).

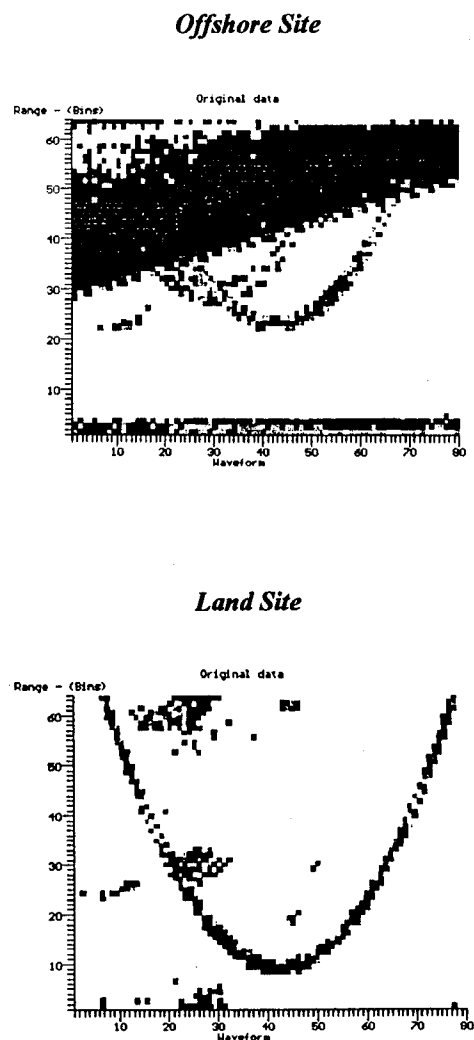


Fig. 6 Ranges Plotted as Hyperbolae

It can be seen (figs. 5,6) that a sea surface reflection can be identified at the offshore site. This can be filtered out. The uncorrected ranges can be found in Table 2.

| | Offshore Site | Land Site |
|--------------------------------|---------------|--------------|
| Predicted UTC of minimum range | 21:21:16.70 | 21:17:20.60 |
| Measured UTC of minimum range | 21:21:16.670 | 21:17:20.578 |
| Uncorrected range | 781430.935m | 777695.052m |

Table 2 Uncorrected Ranges from Transponders to ERS-1 Satellite (and UTC Times).

The GPS processing was carried out in the Surveying Department at the University of Newcastle upon Tyne using the following data :

- a total of 32.5 hours common to the land and offshore sites,
- ten permanent GPS reference stations (*Table 3*) to determine co-ordinates in ITRF (*ref. 3*).

The three dimensional GPS vector between the land and offshore sites was computed with a standard deviation of 1cm.

| | |
|--------------|------------------|
| Tromso | Norway* |
| Onsala | Sweden* |
| Metsahovi | Finland |
| Kootwijk | The Netherlands* |
| Herstmonceux | U.K.* |
| Wetzell | Germany* |
| Graz | Austria |
| Zimmerwald | Switzerland |
| Matera | Italy |
| Madrid | Spain |

Table 3 GPS Reference Stations for 1994 GPS Network (also used in 1993 network)*

IONOSPHERIC CORRECTIONS

Table 4 shows the ionospheric corrections which were computed using the GPS data.

| | Site Data | Ref. Data | Difference |
|---------------|-----------|-----------|------------|
| Offshore Site | -0.022m | -0.014m | 0.008m |
| Land Site | -0.021m | -0.022m | -0.001m |

Table 4 Ionospheric Corrections Computed from GPS Data Collected on Site and also at Permanent Reference Stations.

It can be seen that the ionospheric corrections are in the order of 2cms. Table 4 also shows that it would be possible to compute these corrections without significantly limiting the accuracy by using GPS data from the permanent reference stations. This would avoid the requirement to deploy a GPS receiver at the unknown site (once its horizontal position is known).

TROPOSPHERIC CORRECTIONS

The dry path delay was computed from surface meteorological data and compared with a standard model with a difference of 2cms. It is known that this is a fairly reliable method for computing dry path

delay. It can be seen from Table 5, however, that the wet path delay varies with different data sources.

| | Offshore Site | Land Site | Difference |
|--------------|---------------|-----------|------------|
| Surface Data | -0.131m | -0.116m | -0.015m |
| Radio Sonde | -0.105m* | -0.102m | -0.003m |
| WVR | -0.122m | -0.092m | -0.030m |
| Model | -0.095m | -0.040m | -0.055m |

Table 5 Wet Path Delay Corrections to Ranges

* The offshore radio sonde data was from Lerwick Observatory (in the Shetland Islands off the North East coast of Scotland, about 190km from the offshore site).

If it is assumed that the WVR data is most likely to be correct, then it can be seen that the model does not fit well in an offshore environment. The surface data introduces an error of 1.5cm which is not really significant, especially as it would be practically beneficial to avoid the expense of using WVR data for full time observations.

ORBIT ARC COMPUTATION

Two orbits for ERS-1 were computed from SLR data at the Royal Greenwich Observatory (RGO). One was a global orbit, computed from laser data recorded at 30 global sites over a period of five days (*ref. 4*).

A more precise orbit was computed by the short arc method using data from six European sites which recorded data for five minutes during the Transponder trial. This allowed corrections to the global arc to be computed which resulted in a standard deviation for the ERS-1 orbit between the land and offshore sites in the order of 3cm.

This result could have been bettered if the baseline between the two sites had been shorter (this would preferably be the case if the Transponder method was to be used for long term operation).

FINAL RESULTS

After applying the atmospheric and orbit corrections, a final height for the offshore site was computed. Several results were computed using the two orbit models and the different wet path delay corrections. The mean of these (ignoring obviously poor approximations) was used to make a comparison with the GPS result.

In order that the comparison of methods could be made, it was necessary to measure the height differences between Transponder and GPS receiver locations using calibrated theodolite and EDM measurements (*Table 6*).

| Reference Point | Offshore Site | Land Site |
|-----------------|---------------|-----------|
| GPS Marker | 98.892m | 939.987m |
| ΔH | 0.679m | 0.622m |
| Transponder | 99.571m | 940.609m |

Table 6 Height differences between Transponder Location and GPS marker.

The resulting heights computed for the offshore platform are given in Table 7.

| GPS | Transponder | Difference |
|---------|-------------|------------|
| 99.571m | 99.564m | 0.007m |

Table 7 Difference between Transponder and GPS derived heights for offshore platform.

The heights can also be compared with those derived from the 1993 GPS survey (see Table 8).

| GPS | Transponder | Difference |
|---------|-------------|------------|
| 99.604m | 99.564m | 0.040m |

Table 8. Difference between 1994 Transponder height and 1993 GPS height for offshore platform.

The difference is not thought to be significant, considering the small volume of data which has been analysed (i.e. other effects at the offshore site could have caused a difference of this magnitude).

CONCLUSIONS

- The Transponder method gave results which agreed reasonably with GPS results,
- Deployment on an offshore production platform did not impair the performance of the Transponder,
- Processing of orbit and atmospheric data implied that data collected could be reduced to a minimum, although the wet path delay could limit the accuracy to a couple of centimetres,
- It should be possible to guarantee a relative height accuracy of at least 5cm (using minimum meteorological data), which should enable modelling of any platform height change if a Transponder was deployed permanently,
- This was an experimental situation and consideration of future logistics should be taken into account before further long term operational work,

- Verification that ESA show future commitment to programming the satellite would be necessary (it is believed that they have expressed a great interest in supporting offshore applications),

It can be concluded that the comparison between GPS derived heights (1993 and 1994) verifies the Satellite Altimetry method and that either method (or a combination of both) has potential for use in a future height monitoring scheme for offshore production platforms.

ACKNOWLEDGEMENTS

Many thanks are extended to the following who helped with the Shell offshore trial of Transponder measurements in conjunction with Satellite Altimetry :

Andrew R Birks, Rutherford Appleton Laboratory, U.K. Tel. 44 (0) 1235 821900

Bert Burki, University of Zurich, Switzerland.

Paul A Cross & Paul H Denys, University of Newcastle upon Tyne, U.K. Tel. 44 (0) 191 222 6445

Peter Pesec, University of Graz, Austria.

Redvers J Powell, Ulmo Systems Ltd, U.K. Tel. 44 (0) 1491 872176

REFERENCES

- (1) Birks A R. *Report on the ERS-1 Radar Altimeter Data from the Transponder Deployments on 10th July 1994.* Shell U.K. Report, August 1994.
- (2) Denys P H, Birks A R, Cross P A, Powell R J. *Precise Height Determination using the ERS-1 Radar Altimeter and Active Ground Based Transponders.* ESTEC Contract 93/0804, Final Report, December 1993.
- (3) Denys P H, Cross P A. *The Newcastle Processing and Computational Procedures for the Shell Northern North Sea GPS Campaign September 1993.* Shell U.K. Report, August 1994.
- (4) Denys P H, Birks A R, Cross P A, Powell R J. *The Shell Transponder Altimetry Trial.* Shell U.K. Report, October 1994.
- (5) Powell R J, Birks A R, Bradford W J, Wrench C L, Biddiscombe J. *Using Transponders with the ERS-1 Altimeter to Measure Orbit Altitude to +/- 3cm.* Space Radar Group RAL, 1992.

A GPS Positioning Results Using Precise Satellite Ephemerides, Clock Corrections and Ionospheric Grid Model with Jupiter™

Dr. Yang Gao, James McLellan, and Mohamed Abousalem
Pulsearch Navigation Systems, Inc.

BIOGRAPHY

Yang Gao is a Research Scientist at Pulsearch where his work has been focused on algorithm design and software development for high precision static and kinematic GPS positioning. Prior to joining Pulsearch, he conducted research on Wide Area Differential GPS using the Canadian Active Control System at The Geodetic Survey Division of Geomatics Canada. Mr. Gao holds a Ph.D. in Geomatics Engineering from The University of Calgary, Canada.

James F. McLellan is the Vice President and General Manager of Pulsearch. He has B.Sc. and M.Eng. in Surveying Engineering from University of New Brunswick and The University of Calgary, Canada. Mr. McLellan has geodetic and engineering experience in the design of geodetic software, establishment of geodetic control networks, and design and development of integrated navigation and fleet tracking systems.

Mohamed A. Abousalem is a Geomatics Engineer at Pulsearch with B.Sc. in Civil Engineering from Alexandria University, Egypt, and M.Sc. in Geomatics Engineering from The University of Calgary, Canada. His work includes GPS positioning and navigation system development, wide area differential GPS systems, Kalman filtering techniques, and statistical testing and quality control of navigation systems. Mr. Abousalem is an Honourary Killam Scholar at The University of Calgary where he is currently pursuing his Ph.D. studies.

ABSTRACT

Over the past few years, increased attention has been given to the use of precise GPS satellite ephemerides, satellite clock corrections and ionospheric models as an economical and efficient alternative to conventional DGPS. Precise satellite ephemerides and clock corrections are used to overcome the effects of broadcast ephemerides and clock errors including Selective

Availability. Precise ionospheric models, on the other hand, are essential to single-frequency users for better estimation of ionospheric delays than just using the standard broadcast ionospheric model.

Investigated in this paper is the achievable positioning accuracy using precise satellite ephemerides, satellite clock corrections and ionospheric grid model available from the Canadian Active Control System. A few tests were conducted using datasets collected at Algonquin Park, Ontario, and Calgary, Alberta. Jupiter™, a GPS post-processing software package developed by Pulsearch, was used for all data processing and management. Unsmoothed instantaneous least squares position fixes were computed, and the results were compared to the known coordinates of the stations occupied. Results have indicated that a one-to-three metre positioning accuracy is achievable using precise satellite ephemerides and clock corrections. The use of the precise ionospheric grid model, currently under development at the Geodetic Survey Division of Geomatics Canada, slightly improved the horizontal positioning, yet biases still remained in the height.

INTRODUCTION

Autonomous GPS positioning accuracy is significantly degraded by GPS satellite ephemerides and clock errors, particularly errors due to Selective Availability (SA). For single frequency users, the accuracy is further degraded by ionospheric delays which are only partly accounted for by using the broadcast ionospheric model. Therefore, in order to achieve one-to-three-meter level positioning accuracy, differential GPS (DGPS) has to be employed.

In DGPS, two receivers are used with one serving as a base (reference) station, with precise known coordinates, and the other as the remote for which positioning is required. Due to the use of a base station, the method is effective only for short baselines; over long baselines, spatial decorrelation of error sources degrades the

resulting positioning accuracy. In addition, the positioning solution is relative to the known base position. Also, for real-time applications, a continuous data link is required between the base and remote stations.

Lately, increased attention has been given to the use of precise satellite ephemerides, clock corrections and ionospheric models. The use of such precise data provides an economical and efficient alternative to conventional DGPS. Users can perform precise absolute point positioning without the need for a base station which allows the users to precisely and directly tie into modern spatial reference frames, for example WGS84, NAD83 or ITRF [Kouba and Popelar, 1994].

Precise satellite ephemerides and clock corrections are becoming available from various organizations on a regular basis. To our knowledge, the Geodetic Survey Division (GSD) of Natural Resources Canada (NRCan) is the only organization that produces precise satellite clock corrections at high rate (i.e. 30 seconds) on a regular basis. Accordingly, considerable research has been conducted to date to determine the achievable positioning accuracy using this data [Heroux et al., 1993, Lachapelle et al., 1993 and Gao, 1994]. In this paper results of various tests are presented to demonstrate the achievable positioning accuracy using precise data and to compare the results to DGPS positioning results.

Precise ionospheric models are of a particular interest to single-frequency GPS users, especially for GPS surveys conducted at high latitudes where the GPS broadcast ionospheric model is significantly degraded. These models, however, are only available from a few organizations at a non-regular basis. Therefore, there has not been much research on their use. A few tests have been conducted by Pulsesearch to assess the quality of one of these models as compared to the broadcast ionospheric model.

PRECISE SATELLITE DATA

The precise GPS satellite ephemerides and clock corrections used in the tests presented herein were obtained from the Canadian Active Control System (CACS) developed at GSD of NRCan [Kouba et al., 1993]. The data is available to subscribers on a regular basis via the Canadian Geodetic Bulletin Board Service (CGBBS). The data is available in 24-hour files with the ephemerides in the internationally recognized NGS-SP3 format [Remondi, 1989], and the clock corrections in a proprietary format. Standardization of clock data format will soon become necessary. Details about precise

satellite data generation are given below and further details can be found in Kouba et al. [1993].

Precise Satellite Ephemerides

Since August 1992, the GSD has been generating precise GPS satellite ephemerides from the CACS stations augmented with data from other globally distributed core stations of the International GPS Service for Geodynamics (IGS). Precise ephemerides are computed in the International Terrestrial Reference Frame (ITRF), which is compatible with WGS84 and agrees with NAD83 within a fraction part per million. Typically, within 3 days following the observations, CACS's precise ephemerides are generated, archived and made available to users. Precise ephemerides are available in NGS-SP3 format containing Cartesian coordinates (x, y and z) for all GPS satellites at 15-minute intervals.

According to results reported from GSD, e.g., Kouba et al. [1994], CACS precise ephemerides errors have typical Root Mean Square (RMS) value of 20 cm. The RMS of the broadcast GPS ephemerides errors, however, normally range from a few meters to tens of meters.

Precise Satellite Clock Corrections

In addition to precise satellite ephemerides, precise satellite clock corrections are also computed daily at GSD based on the precise ephemerides and observational data from CACS. These precise satellite clock corrections account for satellite clock errors including the dithering introduced by SA. The corrections are available for GPS satellites visible in Canada at 30 second intervals. Corrections for global GPS satellites are also available. Reports from GSD have shown that the precise satellite clock correction errors have a typical RMS of 1 to 2 ns or 30 to 60 cm [Heroux et al., 1995].

PRECISE IONOSPHERIC DELAY MODEL

The precise ionospheric grid model used in the tests presented herein were also obtained from the GSD of NRCan. At the GSD, a single-layer grid model has been adopted within a geomagnetic coordinate system to simplify the representation of the ionospheric effect and to facilitate the precise ionospheric modeling. The use of a precise ionospheric model allows single-frequency GPS users to achieve positioning accuracy compatible with that obtained by dual frequency users.

A crucial part in precise ionospheric modeling is the precise determination of the instrumental biases in the GPS satellites and tracking receivers. Research conducted at GSD has demonstrated 0.5 to 1 ns accuracy

of the bias estimates. Under Anti-Spoofing (AS), however, some degradation is experienced due to higher measurement noise [Gao et al., 1994]. Test results have indicated that an average of about 30 cm accuracy of ionospheric delay correction has been achieved when satellite elevation angle is higher than 20 degrees [Heroux, 1994]. The precise ionospheric grid model is currently under development, thus unavailable for the CGBBS subscribers. The model is, however, expected to be available in the near future as part of CACS products.

GPS SINGLE-POINT POSITIONING USING PRECISE GPS DATA

GPS pseudorange measurements contain a few biases and errors which would significantly distort the computed position if left unaccounted for. In the following sections, the GPS pseudorange measurement model containing the various measurement errors and biases is presented. The different error mitigation procedures are then discussed with the focus on using precise ephemerides, clock corrections and ionospheric models.

Pseudorange Measurement Model

The measured GPS pseudorange (or carrier-smoothed pseudorange) between a tracking receiver and a GPS satellite j can be modeled by:

$$p^j = \rho^j + e^j \Delta r^j + c (dt^j - dT) + dion^j + dtrop^j + dmult^j + \epsilon^j \dots \quad (1)$$

- p^j is the measured pseudorange between the tracking receiver and satellite j ,
- ρ^j is the true geometric range between the tracking receiver and satellite j ,
- Δr^j is the orbital error vector of satellite j ,
- e^j is the unit vector joining the tracking receiver and satellite j ,
- dT is the tracking receiver clock offset,
- dt^j is the clock offset of satellite j including SA effects,
- $dion^j$ is the ionospheric delay between the tracking receiver and satellite j ,
- $dtrop^j$ is the ionospheric delay between the tracking receiver and satellite j ,
- $dmult^j$ is the multipath error at the tracking receiver,
- ϵ^j is the pseudorange measurement noise, and
- c is the speed of light.

GPS Satellite Error Mitigation

When using precise ephemerides, the satellite position error in Equation (1) can be virtually removed. Also,

when using precise satellite clock corrections, the satellite clock offset (dt^j) can be removed. In this case, Equation (1) reduces to Equation (2) as follows:

$$p^j = \rho^j - c \cdot dT + dion^j + dtrop^j + dmult^j + \epsilon^j \dots \quad (2)$$

Since precise satellite ephemerides are available in NGS-SP3 format, interpolation is required to derive the precise satellite position for a given measurement instant. Regular high-order polynomials provide cm-level interpolation accuracy [Remondi, 1989]. For users who prefer using the standard RINEX navigation message format, conversion procedures will be required.

The same applies to precise satellite clock corrections which are available at 30-second intervals. For high measurement data rates (e.g. 1 Hz), such clock corrections need to be interpolated. Preliminary tests indicate no appreciable degradation in the positioning accuracy due to the interpolation process.

Note that although the precise satellite clock corrections account for both satellite clock errors and SA effects, other time corrections are still needed for precise processing, e.g. relativistic time effects, using simple standard formulas documented in the ICD-GPS-200.

Ionospheric Delay Mitigation

Dual frequency GPS users have the privilege of being able to remove most of the ionospheric effect in the pseudorange measurements by using the ionosphere-free linear combination of pseudoranges measured on the two frequencies [Hofmann-Wellenhof et al., 1994]. Single frequency users, however, can account for the ionospheric effects using the standard GPS ionospheric model parameters transmitted with the GPS navigation message. The standard ionospheric model, however, is unlikely to be more than 75% effective, especially during high ionospheric activity periods [Wells et al., 1986].

The alternative for single-frequency users is to use calibrated ionospheric models in order to achieve the meter-level positioning accuracy. An example of such a model is the CACS model investigated herein which is the single-layer grid model supplied by the GSD. The model parameters are provided in the form of a grid currently with spacings of 3 degrees in the latitude and 1 degree in the longitude.

The procedure involved in using the CACS ionospheric grid model include the following steps:

a) determine the geomagnetic coordinates of the intersection point between the receiver-to-satellite line of sight and the single ionospheric layer.

b) use the determined geomagnetic coordinates to derive the vertical grid ionospheric delay values from the precise ionospheric grid model. Note that the CACS ionospheric grid model contains an RMS value for each grid delay value which can be used for quality assurance.

c) map the vertical grid delay derived from the ionospheric model to the slant path delay based on the zenith angle on the ionospheric layer.

After applying the ionospheric delay corrections derived from the ionospheric grid model, Equation (2) is reduced to the following:

$$p^j = \rho^j - cdT + dtrop^j + dmult^j + \varepsilon^j \dots\dots\dots (3)$$

Tropospheric and Multipath Errors

From Equation (3), the pseudorange measurements still contains tropospheric and multipath errors. The tropospheric delay effect can be estimated precisely (90%) using the standard GPS tropospheric model [Hofmann-Wellenhof et al., 1994], i.e. the Hopfield model, and thus can be removed from Equation (3).

Multipath errors, on the other hand, can be minimized through careful site selection, the use of antenna ground planes and choke rings as well as carrier phase smoothing techniques. GPS receivers from some manufacturers also have the capability to further mitigate multipath effects using the narrow correlator technology [Fenton et al., 1991]. The residual multipath effects can then be neglected. Accordingly, the troposphere and multipath-free pseudorange can be modeled as follows:

$$p^j = \rho^j - cdT + \varepsilon^j \dots\dots\dots (4)$$

Note that the reduced pseudorange measurement modeled by Equation (4) includes, in addition to random errors, the receiver clock offset which can be estimated along with the unknown receiver position parameters. Also note that the random error (ε^j) contains not only the raw measurement noise but also the residual satellite position and clock errors, residual ionospheric and tropospheric delays as well as residual multipath.

Since the accuracy of the precise satellite ephemerides, satellite clock corrections and ionospheric models are all claimed to be better than one metre, the reduced pseudorange measurements can thus be applied for precise metre-level single point positioning.

DATA PROCESSING AND ANALYSIS

This section aims to evaluate the achievable GPS positioning accuracy using precise satellite ephemerides, clock corrections and ionospheric model through data analysis and comparison.

Dataset Description

Two datasets were used in this research. The first dataset was provided by the GSD. It was collected on June 20, 1995 at the CACS tracking station located in Algonquin Park, Ontario, at 30 second intervals using a TurboRogue receiver. Anti-Spoofing (AS) was turned off on that day and thus the pseudoranges were collected on P-code.

The second dataset was collected by Pulsesearch on August 21, 1995 at an Alberta Survey Control Marker in Calgary at 1 second intervals using NovAtel RT-20 receiver. Data was also collected simultaneously at a base station using a NovAtel 2151R receiver for DGPS comparison purposes. Baseline length is approximately 8 km. Note that AS was turned on that day.

Jupiter™, a GPS post-processing software package developed by Pulsesearch, was used for all data processing and management. In the following section, details on the software features and capabilities are presented.

Jupiter™ Software

Jupiter is a Windows®-based multi-purpose GPS post-processing software package. Jupiter uses Kalman filtering and least squares estimation techniques to compute position and velocity parameters in either static or kinematic modes [Abousalem et al., 1994]. The software processes pseudorange and carrier phase rate data in single-point and single-difference (differential) modes. Jupiter also processes the integrated carrier phase measurements in double difference processing mode. The software is capable of processing a variety of receiver data formats including NovAtel, Trimble, Leica, Motorola and CMC Allstar receivers. The standard RINEX format is also supported. It is also capable of processing dual-frequency data, if available, for ionospheric calculations to replace the standard GPS broadcast ionospheric model.

Jupiter contains many data processing and management features like reliability analysis, geodetic computations, point database, file utilities and others; providing the operator with a full stand-alone data processing environment. Coordinates from the point database can be exported into one of the various pre-defined formats including Arc/Info™, GENerate, Geolab™, DXF (for

AutoCAD™), NavTrax™ and SEG-P1. Data can also be exported in a variety of user-defined formats.

To perform the tests described in this paper, Jupiter was adapted to process precise satellite ephemerides in NGS-SP3 format and precise satellite clock corrections in the GSD proprietary format within its single-point processing mode. This has become a processing feature of the software production version 2.00. Use of precise ionospheric models will be included in the near future once they become available on a regular basis.

Data Processing

Jupiter was used to compute unsmoothed instantaneous least squares static position fixes for both datasets. Since the prime objective is to assess the positioning accuracy using precise GPS data, Kalman filtering was not used. This was to avoid any possible filter smoothing effects. Jupiter was also used to export the results into a customized data sheet.

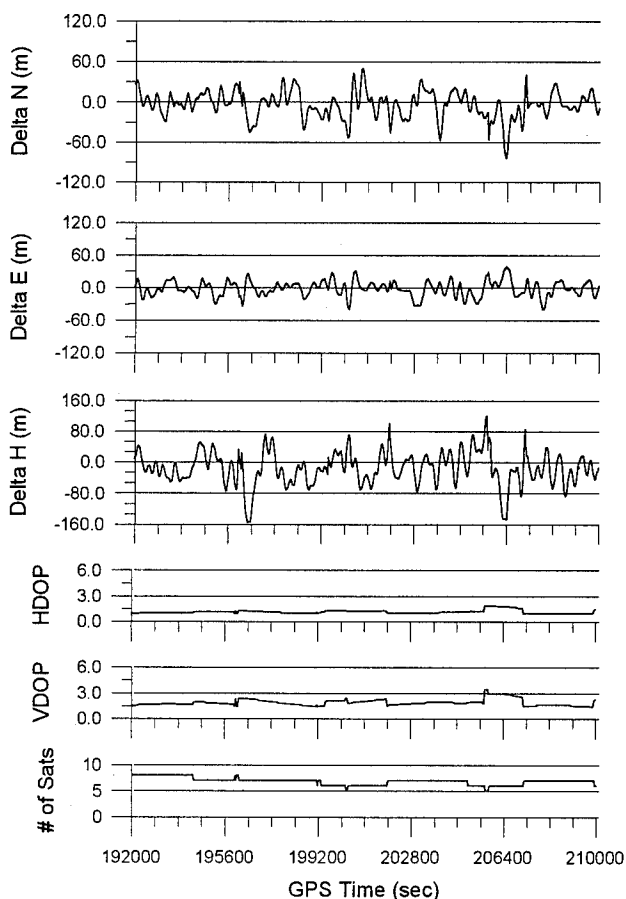


Figure 1 Autonomous Single-Point Positioning Errors Using Broadcast Ephemerides and Ionospheric Model [Algonquin Park, 20 June 1995]

The results were differenced with the true station coordinates known within a few centimetres. The errors in the three position components are presented. HDOP and VDOP values and the number of GPS satellites used in the solution are also presented for analysis purposes. A 10 degree elevation mask was used during processing.

Results and Analysis

Autonomous Single-Point Positioning

Shown in Figures 1 and 2 are the single-point positioning processing results using the broadcast satellite ephemerides, clock parameters and ionospheric model for the two datasets.

It is clear from the two figures that SA was in effect during the data collection periods. Typical SA positioning errors of more than 100 metres in the horizontal and 150 metres in the vertical are demonstrated. It is also noticeable that SA effects on 21 August were more severe.

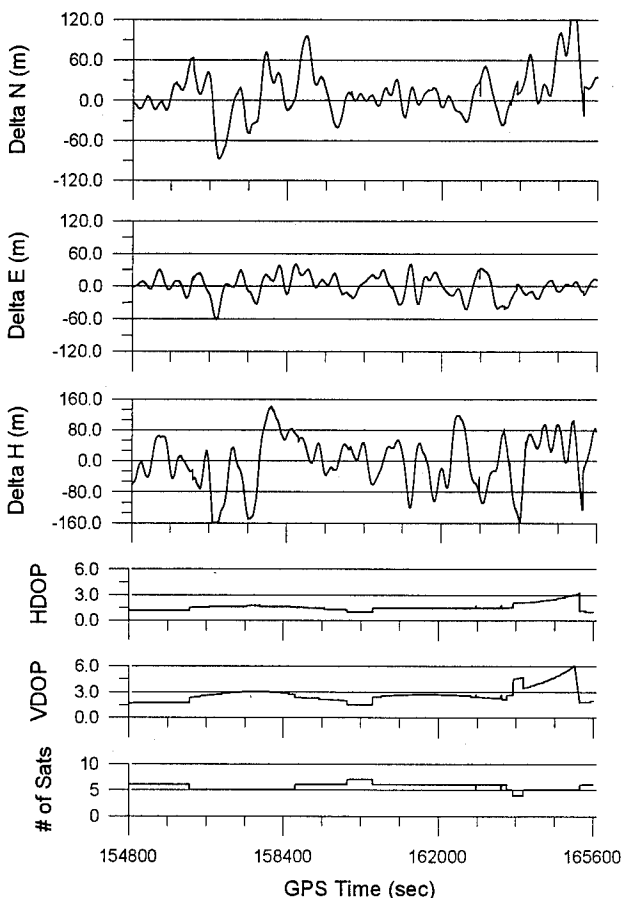


Figure 2 Autonomous Single-Point Positioning Errors Using Broadcast Ephemerides and Ionospheric Model [Calgary, 21 August 1995]

Single-Point Positioning Using Precise Satellite Clock Corrections

Since the major GPS error source is the satellite clock dither caused by SA, positioning accuracy was first investigated using only precise satellite clock corrections. Both Algonquin and Calgary data were processed using broadcast satellite ephemerides and ionospheric model with precise satellite clock corrections obtained from GSD. The results are shown in Figures 3 and 4.

By comparing Figures 3 and 4 to Figures 1 and 2, respectively, the improvement in the positioning accuracy in the two datasets is significant. The achieved level of accuracy, however, is not satisfactory to most GPS users. Therefore, precise ephemerides are necessary to overcome the epsilon component of SA and hence to improve the positioning accuracy.

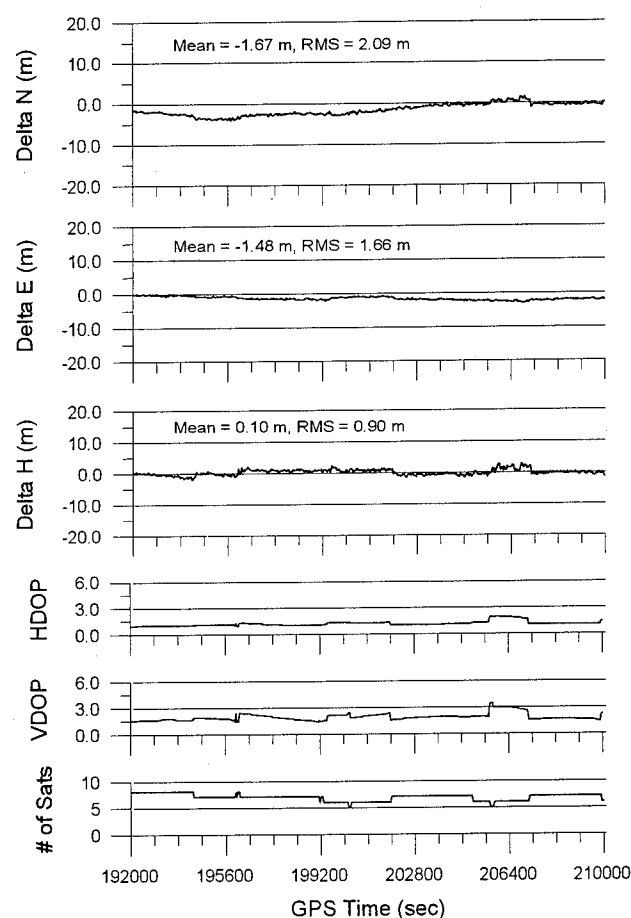


Figure 3 Single-Point Positioning Errors Using Precise Satellite Clock Corrections with the Broadcast Ephemerides and Ionospheric Model [Algonquin Park, 20 June 1995]

Note the higher positioning precision and accuracy in the June 20 results. This is because of the less noisy and more accurate P-code pseudorange measurements tracked on that day. C/A code pseudoranges were tracked on August 21 instead because AS was turned on. Also, note the correlation between the number of satellites used in the solution, the DOP values and the positioning accuracy.

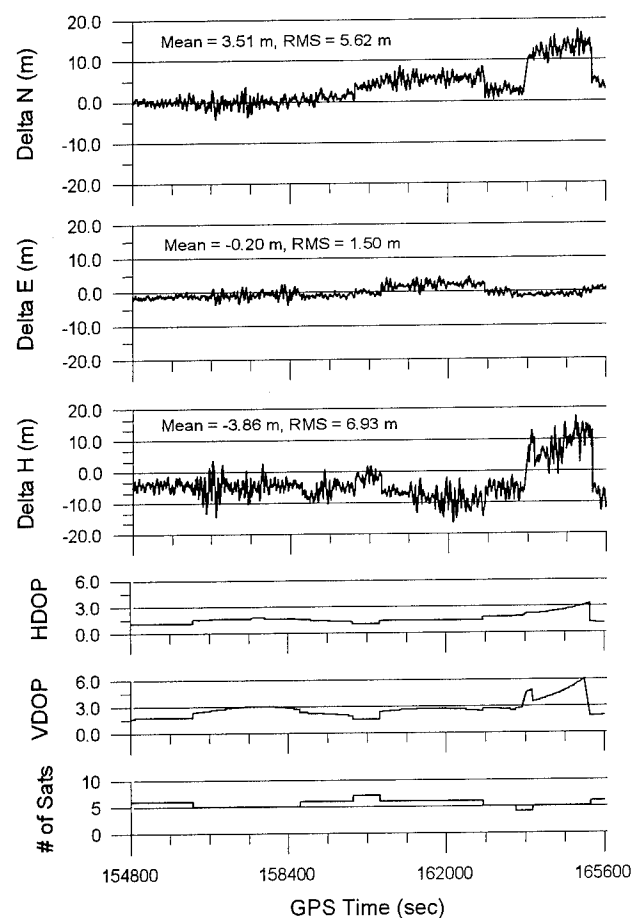


Figure 4 Single-Point Positioning Errors Using Precise Satellite Clock Corrections with the Broadcast Ephemerides and Ionospheric Model [Calgary, 21 August 1995]

Single-Point Positioning Using Precise Satellite Ephemerides and Clock Corrections

Besides precise satellite clock corrections, precise satellite ephemerides were used and the resulting positioning accuracy was investigated. Shown in Figures 5 and 6 are the single-point positioning processing results of the two datasets using precise satellite ephemerides and clock corrections.

By comparing Figures 5 and 6 to Figures 1 and 2 and Figures 3 and 4, respectively, it is clear that the positioning accuracy is further improved by using precise satellite ephemerides with precise clock corrections. In other words, to achieve one-to-three metre level of positioning accuracy, GPS users need to overcome both SA components: satellite clock dither and satellite ephemeris degradation.

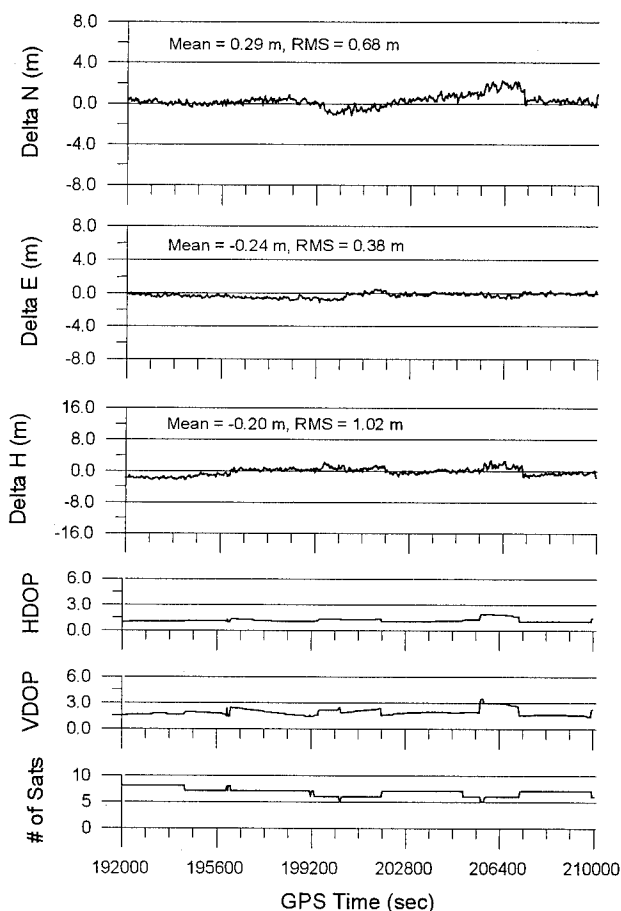


Figure 5 Single-Point Positioning Errors Using Precise Satellite Ephemerides and Clock Corrections with the Broadcast Ionospheric Model
[Algonquin Park, 20 June 1995]

From the mean and Root Mean Square (RMS) values shown, the positioning error RMS of the June 20 P-code dataset is 0.8 m in the horizontal and 1.0 m in the vertical. On the other hand, the RMS values are 3.0 m and 5.3 m, respectively, for the August 21 C/A code data.

In addition, biases are noticeable in both the horizontal and vertical components in Figure 6. This is believed to be mainly due to the residual ionospheric delay effect using the broadcast ionospheric model.

Also, note that the degradation in the positioning accuracy towards the end of the survey period in Figures 5 and 6 correlates to the decrease in the number of used satellites and the consequential increase in the HDOP and VDOP.

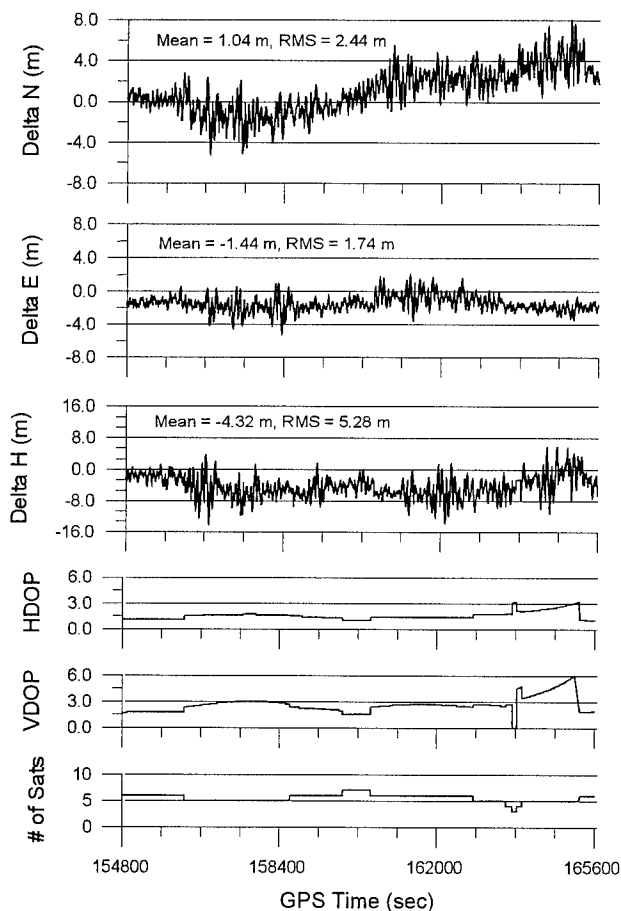


Figure 6 Single-Point Positioning Errors Using Precise Satellite Ephemerides and Clock Corrections with the Broadcast Ionospheric Model
[Calgary, 21 August 1995]

Single-Point Positioning Using Precise Satellite Data and Ionospheric Model

The first datasets was reprocessed using the precise ionospheric model available from GSD together with precise satellite ephemerides and clock corrections. The results are shown in Figure 7. Results indicate that the horizontal positioning accuracy is further improved. A bias, however, is introduced in the height component.

A probable cause for the introduced height bias would be the fact that, during ionospheric modeling, the receiver and satellite inter-frequency biases are estimated with reference to a selected receiver. The reference receiver inter-frequency bias may have not been calibrated and thus the bias would still be contained in the ionospheric grid model.

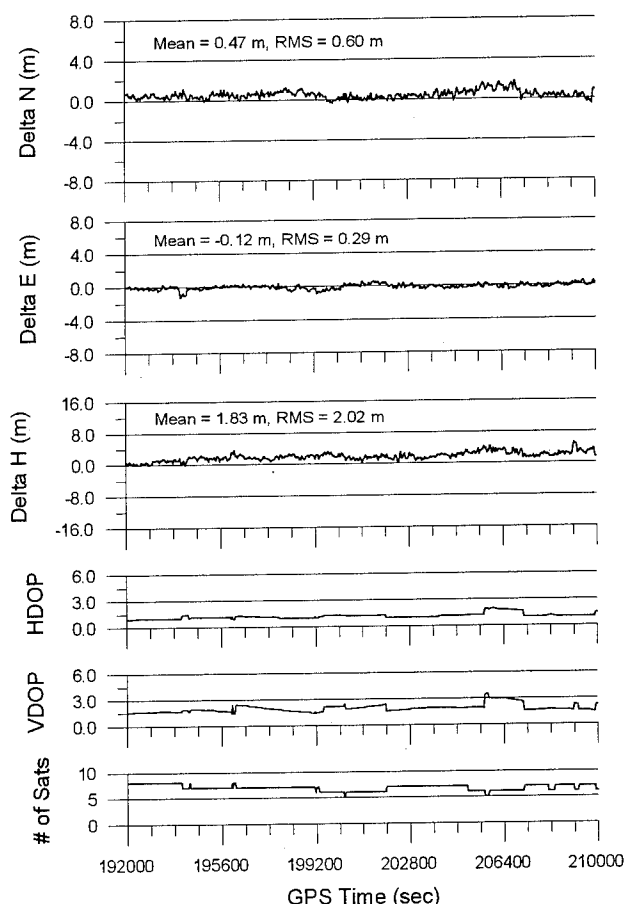


Figure 7 Single-Point Positioning Errors Using Precise Satellite Ephemerides and Clock Corrections with the GSD Ionospheric Grid Model [Algonquin Park, 20 June 1995]

Since the GSD ionospheric grid model is still under development, the height bias will be overlooked for the time being from the accuracy point of view. Accordingly, only the precision of the model will be assessed by computing the RMS of the height error with respect to the mean value. This value is 0.85m which indicates the possible improvement in the height component once the bias issue is resolved.

Due to the current non-availability of precise ionospheric grid model, single-frequency users will have no alternative to using the broadcast ionospheric model while dual frequency users use the standard dual-frequency ionospheric corrections [Hofmann-Wellenhof et al., 1994]. For completeness, the June 20 dataset was processed using the precise satellite data and the standard dual-frequency ionospheric corrections. The resulting positioning errors are shown in Figure 8.

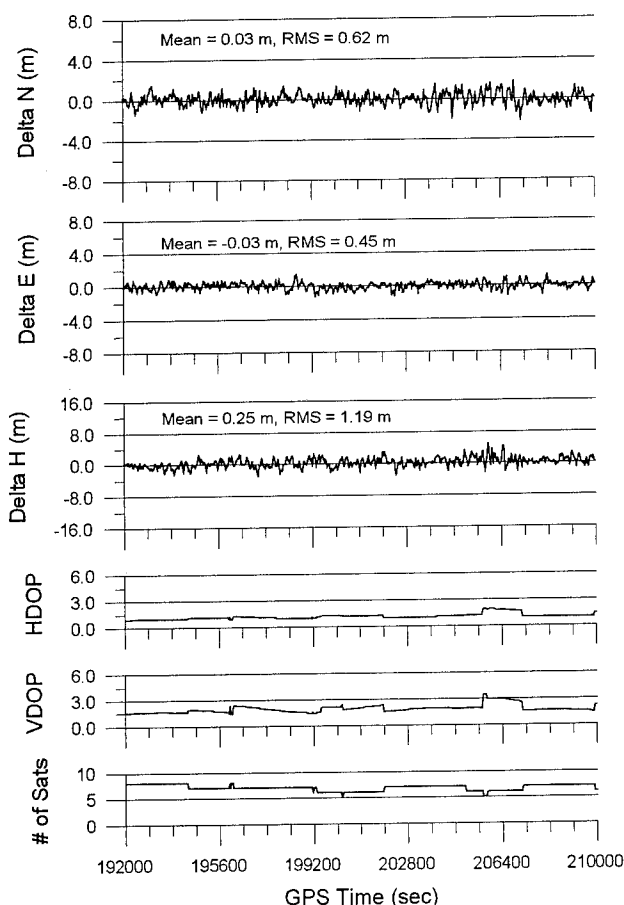


Figure 8 Single-Point Positioning Errors Using Precise Satellite Ephemerides and Clock Corrections with the Dual Frequency Ionospheric Corrections [Algonquin Park, 20 June 1995]

Differential Positioning

To further demonstrate the achievable positioning accuracy using precise satellite data, the results are compared to DGPS. The August 21 data was differentially processed using the data collected simultaneously over an 8 km baseline. The DGPS results are shown in Figure 9. DGPS results yielded RMS of approximately 1.25 m horizontally and 2.9 m vertically.

The resulting larger RMSs are due to the few large spikes caused by the low number of valid differential corrections available from the base station. In Jupiter, a 2D position determination with height fixed is carried out when valid number of differential measurements is not enough for a 3D solution. If these epochs were ignored, sub-metre RMS values would be obtained.

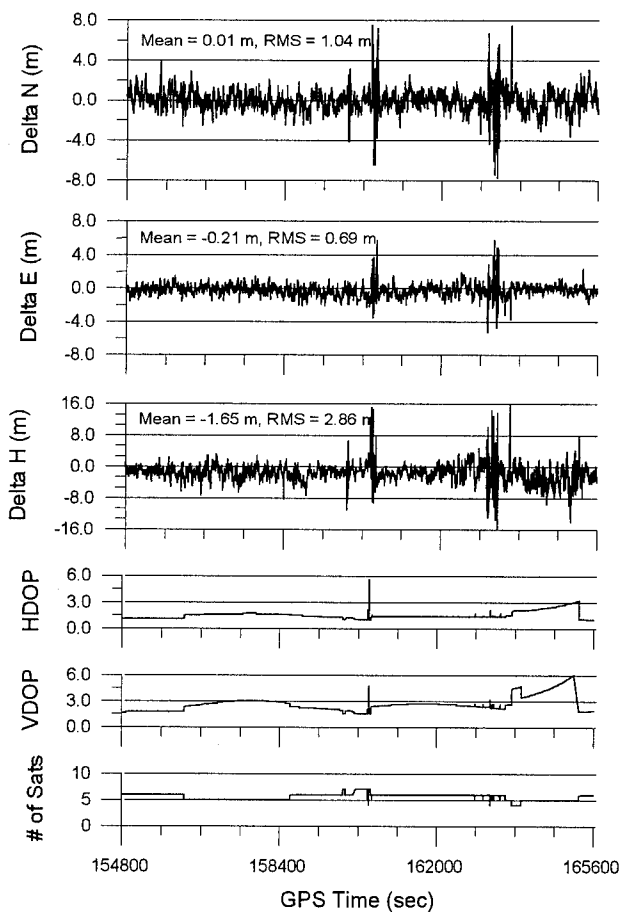


Figure 9 Differential Positioning Errors Using Broadcast Ephemerides and Ionospheric Model [Calgary, 21 August 1995]

Comparing the DGPS solution in Figure 9 to the results from using the precise satellite data shown in Figure 6, the positioning accuracy seems quite comparable if

ionospheric delay effects can be precisely determined by a precise ionospheric model. Single-point processing using precise data, however, has the advantage of baseline length independence.

CONCLUSIONS

Single-point positioning accuracy using precise satellite ephemerides and clock corrections was investigated and analyzed. The use of the ionospheric grid model, currently under development at GSD, was also investigated. The new approach is an economical and effective alternative to the conventional DGPS approach. The results presented in this paper indicate that a positioning accuracy of one to three meters can be achieved using precise satellite ephemerides and clock corrections. The use of a precise ionospheric model has shown only a slight improvement as the model is still under development. Better results are expected from such a model in the future. Positioning accuracy obtained from using precise satellite data is comparable to that obtained from conventional DGPS.

ACKNOWLEDGMENTS

The Geodetic Survey Division of Geomatics Canada is greatly acknowledged for providing the precise satellite data and ionospheric grid model used in the tests presented in this paper. Special thanks go to Mr. Pierre Heroux for his assistance and advice and to Mr. Robert Duval for his comments.

REFERENCES

- Abousalem, M.A., M.A. Forkheim and J.F. McLellan (1994), "Quality GPS Post-Processing Using Jupiter™". Proceedings of the International Symposium on Kinematic Systems in Geodesy, Geomatics and Navigation, KIS'94, Banff, Alberta, Canada, August 1994, pp. 197 - 206.
- Fenton, P., B. Falkenberg, T. Ford, Ng K., A.J. Van Dierendonck (1991), "NovAtel's GPS Receiver - The High Performance OEM Sensor of the Future". Proceedings of The Institute of Navigation International Technical Meeting, ION GPS-91, Albuquerque, NM, Sept. 10-13, pp. 49-58.
- Gao, Y., P. Heroux and J. Kouba (1994), "Estimation of GPS receiver and satellite L1/L2 signal delay biases using data from CACS". Proceedings of the International Symposium on Kinematic Systems in Geodesy, Geomatics and Navigation, KIS'94, Banff, Alberta, Canada, August 1994, pp. 109 - 117.

Gao, Y. (1994), "GPS Positioning Accuracy Using Precise Real-Time Ephemeris and Clock Correction". *Marine Geodesy*, Vol 17, No. 4.

Heroux, P. (1995). Personal Communication.

Heroux, P., M. Caissy and J. Gallace (1993). "Canadian Active Control System Data Acquisition and Validation". *Proceedings of the 1993 IGS Workshop*, Astronomical Institute, University of Bern.

Heroux, P. and J. Kouba (1995), "GPS Precise Point Positioning with a Difference". Presented at Geomatics '95, Ottawa, Ontario, Canada, June 13-15, 1995.

Hoffman-Wellenhof, H. Lichtengger and J. Collins (1994), "GPS Theory and Practice". Springer-Verlag, Third Revised Edition.

Kouba, J., P. Tetreault, R. Ferland, F. Lahaye (1993), "IGS data processing at the EMR master Active Control System Centre". *IGS Workshop*, Berne, Switzerland.

Kouba, J., F. Lahaye and Y. Mireault (1994), "Comparison and Combination of Precise GPS Satellite Ephemerides Produced by the IGS Analysis Centres". *AGU Spring Meeting*, Baltimore, May 1994.

Kouba, J., J. Popelar (1994), "Modern Geodetic Reference Frames for Precise Satellite Positioning and Navigation". *Proceedings of the International Symposium on Kinematic Systems in Geodesy, Geomatics and Navigation, KIS'94*, Banff, Alberta, Canada, August 1994.

Lachapelle, G., R. Klukas, D. Roberts, W. Qiu and C. McMillan (1994). "One-meter Level Kinematic Point Positioning Using Precise Orbits and Satellite Clock Corrections". *Proceedings of ION GPS94*, Salt City, 20-23 September 1994.

Remondi, B.W. (1989), "Extending the National Geodetic Survey Standard GPS Orbit Formats". *The United States National Oceanic and Atmospheric Administration, NOAA Technical Report NOS 133 NGS 46*.

Wells, D., N. Beck, D. Delikaraoglou, A. Kleusberg, E.J. Krakiwsky, G. Lachapelle, R.B. Langley, M. Nakiboglu, K.P. Schwarz, J.M. Tranquilla, P. Vanicek (1986), "Guide to GPS Positioning". Canadian GPS Associates, University of New Brunswick, Fredericton, New Brunswick, Canada.

A Compact Earth Tides Algorithm for WADGPS

James Sinko
SRI International

BIOGRAPHY

James W. (Jim) Sinko is a Principal Engineer with the Systems Development Division of SRI International and received his B.S. (Engineering Science) and MSEE from Stanford University, and his PhD (EE) from the University of Rochester. He has over 27 years of experience in radar, electronic warfare, and aircraft systems.

ABSTRACT

This paper presents an algorithm for calculating the cyclic displacements of geo-features and locations due to solid earth tides. Wide-area differential GPS (WADGPS) systems designed for accuracies of better than 2 m need to account for tidal effects on the solid earth which can result in coordinate displacements of as much as 45 cm in the vertical direction. Differential position changes as large as 30 cm can occur between stations 3000 km apart.

The algorithm presented is about 50 lines long. This short length is obtained by solving the tidal potential directly rather than by using the traditional harmonic analysis. (The harmonic analysis, while useful for tidal measurements, is not needed for predictions). Since no harmonics are left out, the accuracy of the model is better than 2 cm. The model predicts both radial and horizontal displacements (radial displacements are the dominant effect). The algorithm has been incorporated into Exploitation of Differential GPS for Guidance Enhancement (EDGE), a militarized WADGPS system employed during a recent (June 1995) demonstration on DGPS for precision munition delivery at Eglin Air Force Base, FL. This DGPS network is giving submeter accuracies at locations that are more than 1000 km from the nearest reference receiver.

INTRODUCTION

The tidal forces that cause ocean tides also cause a distortion of the solid earth, which can cause vertical changes of 30 cm above the undisturbed earth and 15 cm below. In addition, there can be movements of a few cm in the north/south and east/west directions.

Short-range differential GPS networks need not worry about solid earth tides because of the close proximity of the reference receiver and the roving receiver. However, earth tides can contaminate WADGPS measurements by introducing periodic changes in range measurements to the satellite vehicles (SVs), principally in the earth's radial (altitude) direction. Since the range corrections for EDGE are accurate to within 10 to 20 cm, it is important to account for range differentials due to earth tides. EDGE is a real-time system, so it is also necessary to have a compact, fast-running algorithm that calculates earth tide displacements to within a couple of centimeters.

Although it provides little mathematical formulation, the book by Darwin (1898) is a very readable description of earth tides. Munk and MacDonald (1960) is also quite readable, but only small portions of their book are devoted to earth tides. A readable description that includes usable mathematical formulations is Bartels (1957). Bartels' description is in terms of harmonic tides, which were used (prior to digital computers) for computational convenience and (after digital computers) because harmonics are closely related to experimental measurements. Longman's (1959) method computes tides directly without expanding the tidal forces into harmonics--a convenient method for digital computers. The standard reference book is Melchior (1983). Although not as readable, it is comprehensive in its coverage, especially with regard to experimental measurements, and contains an exhaustive list of references.

The algorithm described in this paper is based primarily on Longman's method of predicting the vertical tide, and also on Pollack's (1973) corrections and expansion of Longman's method for the horizontal components of the earth tide. Units have been changed to the meter-kilogram-second (MKS) system, and more recent values of constants have been used.

The results produced by Longman's model are good for a simple tide prediction model. However, Archinal (1992)--and almost identical discussions in McCarthy (1989) and Melbourne (1983)--outline a more complicated model. They base their results on a model by Wahr (1981) that involves an elastic structural model of the elliptical earth with fluid core resonances. Wahr's conclusions imply that his model is only needed when accuracies better than one percent are required. (The maximum deviation in station height from the Longman model is only about 1.4 cm.) Details on adding the Wahr correction appear in Archinal (1992).

EQUATIONS

All the symbols used below all have two letters: a capital followed by a lower case. This symbology has been adopted to ease the transition from equations to a programming language. While these symbols are as close to conventional notation as possible, the "conventional notation" is not always standard. Where a Greek letter is used in the conventional notation, we have used the first two letters of the English word for the Greek letter. The appendix to this paper contains the list of symbols, their units, and their meanings.

All equations are listed in the sequence in which they are to be calculated. When they are converted to a programming language, the typical modifications are: insertion of multiplication and exponentiation symbols, conversion of degrees to radians in trigonometric functions, and assignment of symbols to certain functions of variables that occur on the left side of equations.

We have changed Longman's convention for longitude. Longitude should be entered as east longitude (e.g., Menlo Park, CA is -122.17°). It should be noted that Longman takes west longitudes as being positive. This is opposite of the normal convention. Angles are mixed--some in radians and some in decimal degrees.

The first 28 equations are primarily from Longman (1959). The equations for mean longitude of the moon reckoned its orbit from the referred equinox (Sm), mean longitude of lunar perigee (Pm), mean longitude of the

sun (Ls), and longitude of the moon's ascending node in its orbit reckoned from the referred equinox (Nm) are

$$Sm = 270.437422 + 481,267.892 Tc + 0.00252 Tc^2 \quad (1)$$

$$Pm = 334.328 + 4069.0322 Tc - 0.0103 Tc^2 \quad (2)$$

$$Ls = 279.6967 + 36000.7689 Tc + 0.0003 Tc^2 \quad (3)$$

$$Nm = 259.1825 - 1934.1424 Tc + 0.0021 Tc^2 \quad (4)$$

For convenience, the modulus of the four above equations is taken with respect to 360°. These angles are in degrees, so from a programming standpoint, it may be easiest to convert them to radians. The time, Tc, is the fraction of a Julian century since noon of December 31, 1899. The value for Tc can be computed from the FORTRAN algorithm given in Press, et. al (1992). The same authors have similar books for the BASIC, C, and Pascal languages. The date routines in Microsoft Excel are an even more convenient way to calculate Tc from a given time and date. Terms involving Tc³ have been ignored because their values are a small fraction of an arc second.

The inclination of the moon's orbit to the equator (Ie) is given by

$$Ie = \arccos[\cos(In) \cos(Im) - \sin(In) \sin(Im) \cos(Nm)] \quad (5)$$

where In = 23.43929° and Im = 5.145396° are the inclinations (to the ecliptic) of the earth's equator and the moon's orbit. Ie is always positive and less than 28°, so no quadrant problems arise from using an arccos function. Likewise, the longitude in the celestial equator of its intersection Am with the moon's orbit (Nu) is in the interval (-15°, +15°), so it can be found from

$$Nu = \arcsin[\sin(Im) \sin(Nm) / \sin(Ie)] \quad (6)$$

Applying the cosine formula to the spherical triangle OmAmVe and denoting the side OmAm by Al gives

$$\cos(\text{Al}) = \cos(\text{Nm}) \cos(\text{Nu}) + \sin(\text{Nm}) \sin(\text{Nu}) \cos(\text{In}) \quad (7)$$

$$\sin(\text{Al}) = \sin(\text{In}) \sin(\text{Nm}) / \sin(\text{Ie}) \quad (8)$$

For programming purposes, functions of variables [e.g., Cos(Al)] appearing on the left side of an equation are assigned a name which is then used later in the right side of succeeding equations. From the values of the sin and cos of Al, we can compute

$$\tan(\text{Al}/2) = \sin(\text{Al}) / [1 + \cos(\text{Al})] \quad (9)$$

Since Al is in the interval (0, 2 π), Al/2 lies in (0, π) and Al is uniquely determined by

$$\text{Al} = 2 \arctan\{\sin(\text{Al}) / [1 + \cos(\text{Al})]\} \quad (10)$$

For programming purposes, Eq. (9) is never computed, as Al is calculated in Eq. (10). Xi--the longitude in the moon's orbit of its ascending intersection with the celestial equator--is given by

$$\text{Xi} = \text{Nm} - \text{Al} \quad (11)$$

Si--the mean longitude of the moon in its orbit reckoned from Am--is given by

$$\text{Si} = \text{Sm} - \text{Xi} \quad (12)$$

The hour angle of the sun (Ha) is given in degrees by

$$\text{Ha} = 15 (\text{To} - 12) + \text{Lo} \quad (13)$$

where To is time (UTC) in hours and Lo is east longitude in degrees. Ra--the right ascension of meridian of place of observation reckoned from Am--is given by

$$\text{Ra} = \text{Ha} + \text{Ls} - \text{Nu} \quad (14)$$

The longitude of the moon in its orbit reckoned from its ascending intersection with the equator (Lm) is given by

$$\begin{aligned} \text{Lm} = & \text{Si} + 2 \text{Em} \sin(\text{Sm} - \text{Pm}) + \\ & 0.8 \text{Em}^2 \sin[2 (\text{Sm} - \text{Pm})] + \\ & 3.75 \text{Rm} \text{Em} \sin(\text{Sm} - 2 \text{Ls} + \text{Pm}) + \\ & 1.375 \text{Rm}^2 \sin[2 (\text{Sm} - \text{Ls})] \end{aligned} \quad (15)$$

Note that the above equation requires that Si (and thus Lm) be in radians. The zenith angle of the moon (Th) is given by

$$\begin{aligned} \cos(\text{Th}) = & \sin(\text{La}) \sin(\text{Ie}) \sin(\text{Lm}) + \\ & \cos(\text{La}) [\cos^2(0.5 \text{Ie}) \cos(\text{Lm} - \text{Ra}) + \\ & \sin^2(0.5 \text{Ie}) \cos(\text{Lm} + \text{Ra})] \end{aligned} \quad (16)$$

To avoid quadrant determination problems, Th will not be evaluated; only cos(Th) will be used. The mean longitude of solar perigee (Ps) is given in degrees by

$$\text{Ps} = 281.2208 + 1.7192 \text{Tc} + 0.00045 \text{Tc}^2 \quad (17)$$

The longitude of the sun in the ecliptic reckoned from its ascending intersection with the equator (Le), and the right ascension of meridian of place of observation reckoned from the vernal equinox (Rv) are given by

$$\text{Le} = \text{Ls} + 2 \text{Ee} \sin(\text{Ls} - \text{Ps}) \quad (18)$$

$$\text{Rv} = \text{Ha} + \text{Ls} \quad (19)$$

where Ee is the eccentricity of the earth's orbit. Le and the first Ls in Eq. (18) are in radians. The zenith angle of the sun (Ph) is given in the expression. Again, to avoid quadrant problems, Ph will not be evaluated explicitly.

$$\begin{aligned} \cos(\text{Ph}) = & \sin(\text{La}) \sin(\text{In}) \sin(\text{Le}) + \\ & \cos(\text{La}) [\cos^2(0.5 \text{In}) \cos(\text{Le} - \text{Rv}) + \\ & \sin^2(0.5 \text{In}) \cos(\text{Le} + \text{Rv})] \end{aligned} \quad (20)$$

The distance between the centers of the earth and moon (Dm) is evaluated below. Cm = 3.844E8 m is the mean distance between the centers of the earth and moon, and Em = 0.0549 is the eccentricity of the moon's orbit.

$$A_p = 1/[C_m (1 - E_m^2)] \quad (21)$$

$$D_m = 1/\{1/C_m + A_p E_m \cos(S_m - P_m) + A_p E_m^2 \cos[2(S_m - P_m)] + 1.875 A_p R_m E_m \cos(S_m - 2 L_s + P_m) + A_p R_m^2 \cos[2(S_m - L_s)]\} \quad (22)$$

The distance between the centers of the earth and sun (Ds) is found from

$$A_o = 1/[C_s (1 - E_e^2)] \quad (23)$$

$$1/D_s = 1/C_s + A_o E_e \cos(L_s - P_s) \quad (24)$$

where Cs = 1.49598E11 m is the mean distance between the centers of the earth and sun, and Ee = 0.016708617 is the eccentricity of the earth's orbit. The earth radius at the point of observation is given by

$$R_p = R_e/[1 + 0.006738 \sin^2(L_a)] \quad (25)$$

where La is the latitude. The vertical (upward) components of the lunar (Gm) and solar (Gs) tidal acceleration at a point Pt on the earth's surface are given by

$$G_m = \frac{\mu M_m R_p}{D_m^3} [3 \cos^2(\theta) - 1] + \frac{1.5 \mu M_m R_p^2}{D_m^4} [5 \cos^3(\theta) - 3 \cos(\theta)] \quad (26)$$

$$G_s = \frac{\mu M_s R_p}{D_s^3} [3 \cos^2(\phi) - 1] \quad (27)$$

$\mu = 6.67259 \times 10^{-11} \text{ m}^3 \text{ kg}^{-1} \text{ s}^{-2}$ is Newton's gravitational constant, $M_m = 7.3483 \times 10^{22} \text{ Kg}$ is the mass of the moon, and $M_s = 1.9891 \times 10^{30} \text{ Kg}$ is the mass of the sun. To convert vertical tidal acceleration to actual earth deflection, the following equation is used:

$$D_v = \frac{(G_m + G_s) R_e L_v}{\{2 [9.7804 + 0.0517 \sin^2(L_a)]\}} \quad (28)$$

where L_v is the vertical Love number and the denominator is twice the value of gravity at the earth's surface (in MKS units). Love numbers convert the equipotential surface (the height that would be taken by an idealized fluid covering a perfectly rigid earth) into actual earth movement. Measurements of the vertical Love number place its value at about 0.61.

From here to Eq. (44), the equations are primarily from Pollack (1973). The magnitudes of the horizontal components of lunar (Hm) and solar (Hs) tidal acceleration are given by

$$\frac{H_m}{\sin(\theta)} = \frac{3 \mu M_m R_p \cos(\theta)}{D_m^3} + \frac{1.5 \mu M_m R_p^2 [5 \cos^2(\theta) - 1]}{D_m^4} \quad (29)$$

$$\frac{H_s}{\sin(\phi)} = \frac{3 \mu M_s R_p \cos(\phi)}{D_s^3} \quad (30)$$

Note that Eq. (30) corrects an error in Longman's Eq. (4). The declination (Md) and hour angles (Tm) of the moon are related by

$$\sin(M_d) = \sin(I_e) \sin(L_m) \quad (31)$$

$$\cos(M_d) \cos(T_m) = \cos(R_a) \cos(L_m) + \sin(R_a) \sin(L_m) \cos(I_e) \quad (32)$$

and for the sun

$$\sin(S_d) = \sin(I_n) \sin(L_e) \quad (33)$$

$$\cos(S_d) \cos(T_s) = \cos(R_v) \cos(L_e) + \sin(R_v) \sin(L_e) \cos(I_n) \quad (34)$$

With additional analysis, one obtains

$$\cos(M_d) \sin(T_m) = [\cos(L_m) - \cos(R_a) \cos(M_d) \cos(T_m)] / \sin(R_a) \quad (35)$$

$$\cos(Sd) \sin(Ts) = [\cos(Le) - \cos(Rv) \cos(Sd) \cos(Ts)] / \sin(Rv) \quad (36)$$

$$\cos(Ma) \sin(Th) = -\cos(La) \sin(Md) + \sin(La) \cos(Md) \cos(Tm) \quad (37)$$

$$\cos(Sa) \sin(Ph) = -\cos(La) \sin(Sd) + \sin(La) \cos(Sd) \cos(Ts) \quad (38)$$

$$\sin(Ma) \sin(Th) = \cos(Md) \sin(Tm) \quad (39)$$

$$\sin(Sa) \sin(Ph) = \cos(Sd) \sin(Ts) \quad (40)$$

The south tidal accelerations due to the moon and sun are found from the expressions below, which can be evaluated by multiplying Eq. (29) by Eq. (37) and Eq. (30) by Eq. (38), respectively,

$$U_m = H_m \cos(Ma) \quad (41)$$

$$U_s = H_s \cos(Sa) \quad (42)$$

The west tidal accelerations due to the moon and sun are found from the expressions below, which can be evaluated by multiplying Eq. (29) by Eq. (39) and Eq. (30) by Eq. (40), respectively,

$$W_m = H_m \sin(Ma) \quad (43)$$

$$W_s = H_s \sin(Sa) \quad (44)$$

The south and west displacements are found from

$$D_o = L_h R_p (U_m + U_s) / [9.7804 + 0.0517 \sin^2(La)] \quad (45)$$

$$D_w = L_h R_p (W_m + W_s) / [9.7804 + 0.0517 \sin^2(La)] \quad (46)$$

where the horizontal Love number (L_h) has a measured value near 0.09.

The equations have been checked by constructing an Excel spreadsheet from the equations listed above and comparing results with the examples listed in Broucke, et al. (1972).

EARTH TIDE EXAMPLES

Figure 1 shows the radial displacement of the surface due to earth tides at Shalimar, FL, and Menlo Park, CA, using the model. The figure shows the tides for four days in 1990 when the sun and the moon were at opposition and could be expected to cause large tides. The delay between Shalimar and Menlo Park can lead to radial differences of up to 30 cm. During times of lower tides, the maximum difference decreases to about 15 cm.

Although the harmonic analysis of the tides is no longer a convenient way of computing earth surface displacements, it is of value for understanding how the earth tides affect various locations. The earth tide looks different at the equator and the pole because of the combined actions of the semidiurnal, diurnal, and long-term tidal forces (see Figure 2). The semidiurnal (sometimes called "sectorial") tides have a period of approximately 12 hours. They bulge the earth out on the parts nearest and furthest from the moon (and/or sun) and pull it in along the meridians that are perpendicular to the moon's direction. Their effect is maximal at the equator and nil at the poles. The diurnal (sometimes called "tesseral") tides are nil along the equator and at the poles, and at a maximum at the mid-latitudes. They bulge out one side of the earth in the northern hemisphere and the opposite side in the southern hemisphere. The long-term (sometimes called "zonal") tides have periods varying from 14 days to a year. These tides cause the earth to be squished at the poles and bulge all around the equator. They are primarily due to the earth's equator being in a different plane than the ecliptic. The recognition of these effects is attributed to LaPlace.

Figure 3 shows the tides at the equator, Menlo Park, and the North Pole, all at the same longitude. At the equator, we see primarily the semidiurnal tides. In Menlo Park, we see that the addition of diurnal tides to the semidiurnal tides causes one maximum to be much higher than the other maximum. At the North Pole, only the long-term tides have any effect (the graph would have to be carried out for weeks to show periodic changes).

Figures 4 and 5 show examples of the south and west displacements at Shalimar and Menlo Park.

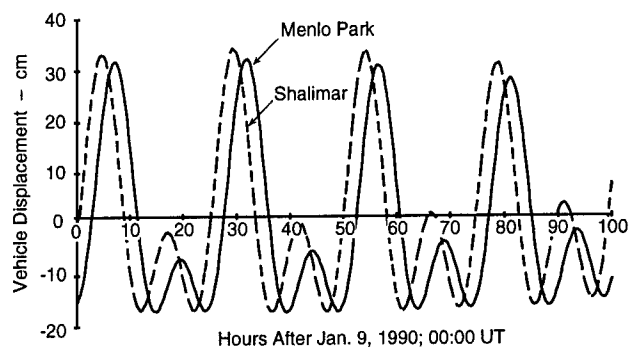


FIGURE 1 EARTH TIDE VARIATIONS FOR TWO LOCATIONS 3300 km APART

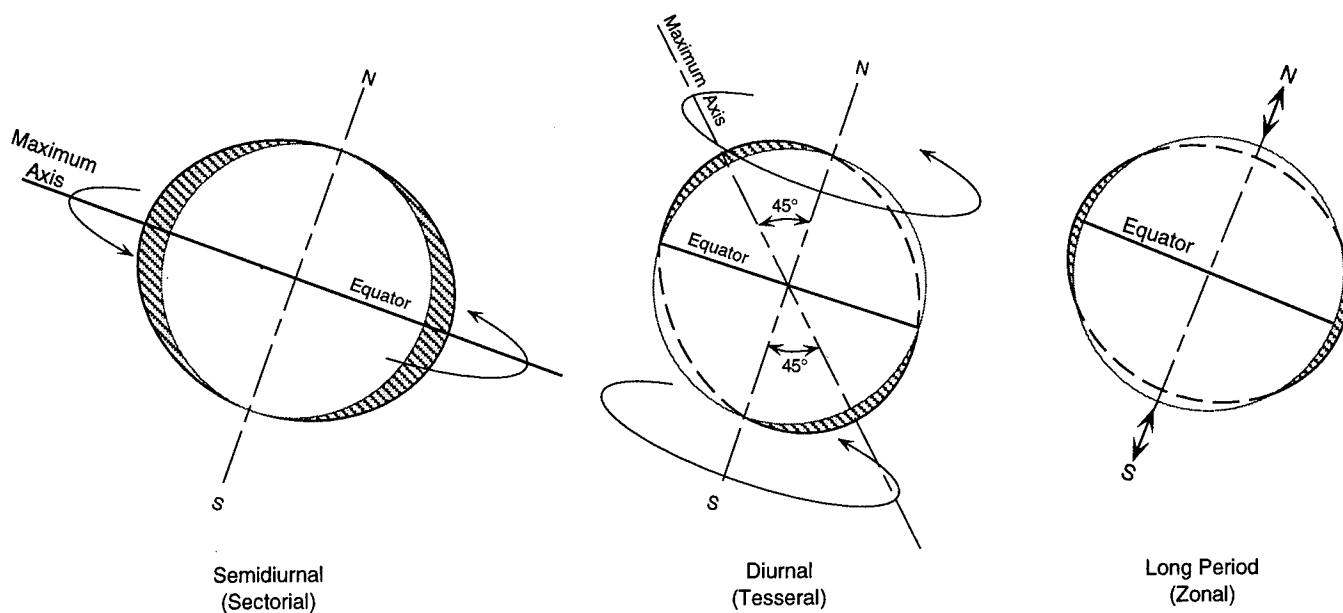


FIGURE 2 THE THREE PRIMARY TYPES OF TIDAL HARMONICS

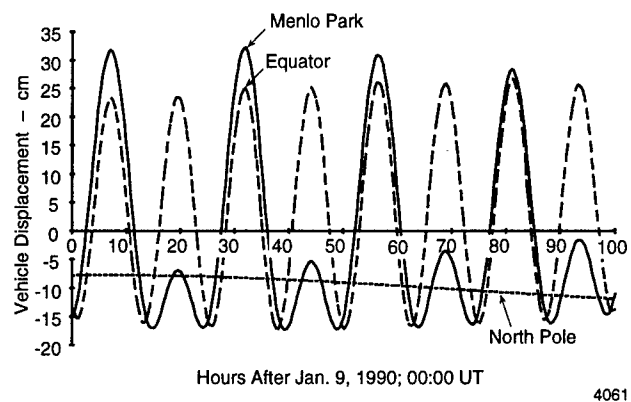


FIGURE 3 EARTH TIDE DISPLACEMENTS AT THE EQUATOR, A MID-LATITUDE POINT, AND THE POLE (the tide at the Pole has a cyclic variation at about 14 days)

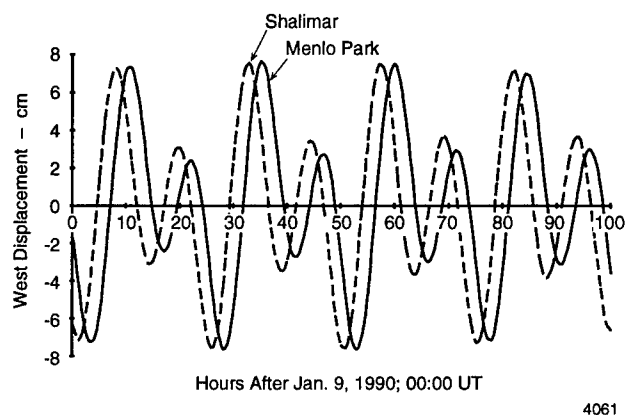


FIGURE 4 EARTH TIDE DISPLACEMENTS IN THE WEST/EAST DIRECTION

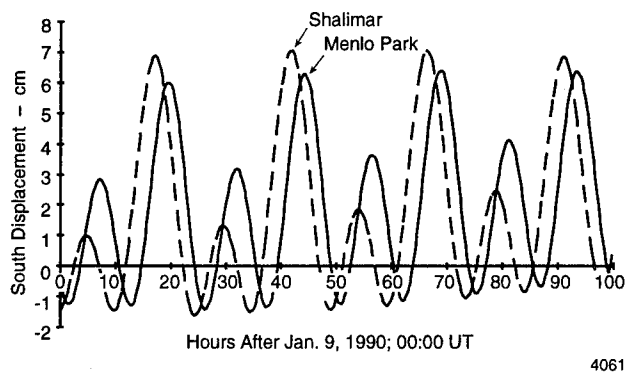


FIGURE 5 EARTH TIDE DISPLACEMENTS IN THE NORTH/SOUTH DIRECTION

OTHER EFFECTS

In addition to the solid earth tide, several tidal and geological effects can affect WADGPS measurements (see Archinal, 1992). Other factors that can affect measures by a few centimeters are described below.

1. *Rotational deformation due to polar motion* can introduce station location radial displacements of up to 2.5 cm and horizontal displacements of up to 0.7 cm. The proximity of Menlo Park and Shalimar should reduce the error to a maximum of 1.5 cm radial and 0.4 cm horizontal (see Archinal, 1992).
2. *Ocean loading due to tides* can cause the land to deflect. Details for computing these defections are outlined in Archinal (1992). A series of tides are multiplied by a phase function and then summed. For San Francisco, the amplitude of the largest component is 1.53 cm. Most East Coast locations have amplitudes of 1 cm or less. It should be noted that some parts of the world can be more seriously affected by ocean loading tides. Schuh (1989) claims up to 20 cm total variation for ocean loading for some isolated locations and shows a measured 12 cm at Kwajalein.
3. *Atmospheric loading* is found from both local barometric pressure and the average pressure in a 2000-km radius circle around the site. If there was a difference of one inch of mercury between the sites and the 2000-km circles around them, an error of about 3 cm would occur. The 3-cm displacement is probably extreme for a one-inch pressure change because the majority (60%) of the effect comes from the average pressure in the 2000-km radius circle, and severe pressure disturbances are usually more localized than a 2000-km circle. However, it should be noted that the lowest recorded pressure was more than four inches below normal.
4. *Relative plate motions* can be as high as 5 cm per year. If the surveyed coordinates are old, there could be noticeable error.

SUMMARY AND CONCLUSIONS

The equations presented in this paper can be easily adapted to common programming languages for a compact earth tides algorithm. For the EDGE project we have used Microsoft Excel for testing and C for the real-time operating code. EDGE attained an RMS position accuracy of 34 cm CEP for a user's stationary receiver that used

corrections data from four remote reference receivers at distances ranging from 1900 to 2400 km.

APPENDIX

This appendix contains an alphabetical list of symbols and their meanings, units, and values (in the case of constants). When "d" is used for a dimension, the quantity is dimensionless. Angles denoted "deg or rad" can be in either form, provided they are compatible with the trigonometric functions in the language (usually radians). When an angle is calculated only in degrees, it will have to be converted to radians if the language requires arguments to be in radians.

| | |
|----|--|
| Al | defined in equations (7) and (8), deg |
| Am | ascending intersection of the moon's orbit with the equator, d |
| Ap | defined in equation (21), m^{-1} |
| Ao | defined in equation (23), m^{-1} |
| Cm | mean distance between the centers of the earth and moon, 3.844E8 m |
| Cs | mean distance between the centers of the earth and sun, 1.49598E11 m |
| Dm | distance between the centers of the earth and moon, m |
| Do | south displacement of the earth at point Pt due to earth tides, m |
| Ds | distance between the centers of the earth and sun, m |
| Dv | vertical displacement of the earth at point Pt due to earth tides, m |
| Dw | west displacement of the earth at point Pt due to earth tides, m |
| Ee | eccentricity of the earth's orbit, 0.016708617, d |
| Em | eccentricity of the moon's orbit, 0.0549, d |
| Er | referred equinox, d |
| Gm | vertical component of tidal acceleration due to the moon, $m s^{-2}$ |
| Go | vertical component of tidal acceleration due to the moon and sun, $m s^{-2}$ |
| Gs | vertical component of tidal acceleration due to the sun, $m s^{-2}$ |
| Ha | hour angle of mean sun measured westward from the place of observations, deg |

| | | | |
|----|---|----|---|
| Hm | horizontal scalar component of tidal acceleration due to the moon, m s^{-2} | Re | equatorial radius of the earth, 6378137 m |
| Ho | horizontal scalar component of tidal acceleration due to the moon and sun, m s^{-2} | Rm | ratio of mean motion of the sun to that of the moon, 0.074804, d |
| Hs | horizontal scalar component of tidal acceleration due to the sun, m s^{-2} | Rp | distance from Pt to the center of the earth, m |
| Ie | inclination of the moon's orbit to the equator, deg or rad | Rv | right ascension of meridian of place of observations reckoned from the vernal equinox, deg |
| Im | inclination of the moon's orbit to the ecliptic, 5.145396° | Sa | azimuth to the sun, reckoned from south to west, at point Pt on the earth's surface, deg or rad |
| In | inclination of the earth's equator to the ecliptic, 23.43929° | Sd | declination of the sun, deg or rad |
| La | terrestrial latitude of point of interest on the earth's surface, deg or rad | Sm | mean longitude of moon in its orbit reckoned from the referred equinox, deg |
| Le | longitude of the sun in the ecliptic reckoned from the vernal equinox, rad | Si | mean longitude of moon in radians in its orbit reckoned from Am, rad |
| Lh | horizontal love number, 0.09, d | Tc | number of Julian centuries from Greenwich mean noon on Dec. 31, 1899 |
| Lm | longitude of the moon in its orbit reckoned from its ascending intersection with the equator, rad | Th | zenith angle of the moon, deg or rad |
| Lo | terrestrial east longitude of point of interest on the earth's surface, deg | Tm | hour angle of moon measured westward from the place of observation, deg or rad |
| Ls | mean longitude of the sun, deg and rad (depending on equation) | To | Greenwich civil time measured in hours |
| Lv | vertical love number, 0.61, d | Ts | hour angle of sun measured westward from the place of observation, deg or rad |
| Ma | azimuth to the moon, reckoned from south to west, at point Pt on the earth's surface, deg or rad | Um | south component of tidal acceleration due to the moon, m s^{-2} |
| Md | declination of the moon, deg or rad | Us | south component of tidal acceleration due to the sun, m s^{-2} |
| Mm | moon mass, $7.3483\text{E}22$ Kg | Ve | vernal equinox, d |
| Ms | sun mass, $1.9891\text{E}30$ Kg | Wm | west component of tidal acceleration due to the moon, m s^{-2} |
| Mu | Newton's gravitational constant, $6.67259\text{E}-11 \text{ m}^3 \text{ kg}^{-1} \text{ s}^{-2}$ | Ws | west component of tidal acceleration due to the sun, m s^{-2} |
| Nm | longitude of the moon's ascending node in its orbit reckoned from the referred equinox, deg | Xi | longitude in the moon's orbit of its ascending intersection with the celestial equator, deg |
| Nu | longitude in the celestial equator of its intersection Am with the moon's orbit, deg | | |
| Om | moon's ascending node, d | | |
| Ph | zenith angle of the sun, deg or rad | | |
| Pm | mean longitude of lunar perigee, deg | | |
| Ps | mean longitude of solar perigee, deg | | |
| Pt | point of interest on the earth's surface, d | | |
| Ra | right ascension of meridian of place of observations reckoned from Am, deg | | |

REFERENCES

- Archinal, B. A. 1992. Explanatory supplement to the *Astronomical Almanac*. pp 199-277, (Ed. P. K. Seidelmann). University Science Books, Mill Valley, CA.
- Bartels, J. 1957. *Tidal Forces*. (abridged translation from German in *Earth Tides*, Ed. by J. C. Harrison, 1985, Van Nostrand Reinhold Co., Inc.)

Broucke, R. A., W. E. Zurn, and L. B. Slichter. 1972. Lunar Tidal Accelerations on a Rigid Earth, in *Flow and Fracture of Rocks*, Geophys. Monogr. Ser., 16, pp 319-24, American Geophysical Union, Washington D. C.

Darwin, G. H. 1898. *The Tides and Kindred Phenomena in the Solar System*. Houghton, Mifflin and Co.

Longman, I. M. 1959. "Formulas for Computing the Tidal Accelerations Due to the Moon and the Sun." *Jn. Geophys. Research*, Vol. 64, pp 2351-55.

McCarthy, D. D., ed. 1989. *IERS Standards 1989*. IERS Technical Note 3. Central Bureau of the International Earth Rotation Service, Observatoire de Paris.

Melbourne, W. and 7 others 1983. Project Merit Standards. U. S. Naval Observatory Circular No. 167.

Melchior, P. J. 1983. *The Tides of the Planet Earth*, 2nd Edition, Pergamon Press, Oxford.

Munk, W. H. and G. J. F. MacDonald 1960. *The Rotation of the Earth: A Geophysical Discussion*. Cambridge Univ. Press.

Pollack, H. N. 1973. "Longman Tidal Formulas: Resolution of Horizontal Components." *Jn. Geophys. Research*, Vol. 78, No. 14, pp 2598-2600.

Press, W. H., S. A. Teukolsky, W. T. Vetterling, and B. P. Flannery. 1992. *Numerical Recipes in FORTRAN*. Cambridge Univ. Press.

Schuh, H. and L. Moehlmann. 1989. "Ocean Loading Station Displacements Observed by VLBI." *Geophysical Research Letters*, Vol 16, pp 1105-8.

Wahr, J. M. 1981. "Body Tides on an Elliptical, Rotating, Elastic and Oceanless Earth." *Royal Astron. Soc. Geophys. Jour.* Vol. 64, pp 677-703.

Evaluation of DoD GPS Satellite Orbits Using NASA Laser Ranging Data

James O'Toole and Michael Merrigan
Naval Surface Warfare Center

BIOGRAPHY

James W. O'Toole received a B.A. degree from Duquesne University in 1959 and a Ph.D. in mathematics from the University of Notre Dame in 1967. Michael J. Merrigan received a B.S. degree from Virginia Polytechnic Institute and State University (VPI) in 1985 and an M.S. degree in Geodetic Engineering from VPI in 1991. Both authors are employed with the Space and Geodesy Branch of the Naval Surface Warfare Center Dahlgren Division.

ABSTRACT

The Global Positioning System (GPS) satellites, designated as PRN5 (SVN35) and PRN6 (SVN36), are equipped with laser retroreflectors. Satellite laser ranging (SLR) observations have been collected by the National Aeronautics and Space Administration (NASA) at a number of their tracking sites since November of 1993. NASA quick look normal points have been processed over selected periods throughout 1993, 1994, and 1995 in order to provide an independent evaluation of two GPS ephemeris products calculated by the Department of Defense (DoD). One product is the real time Kalman filter estimates calculated by the GPS Operational Control System (OCS) and the other is the Defense Mapping Agency (DMA) post fit precise ephemeris. Since the NASA laser ranging data are accurate to a few centimeters, this data type can be used to independently evaluate DoD ephemeris accuracy. While the laser data distribution is sparse, the combined results from several selected analysis periods provide an adequate data sample size for this study. SLR residuals were calculated, using the DoD orbit products, by correcting for tropospheric effects, relativistic effects, the laser retroreflector offset from the satellite's center of mass, station tides, and plate motion. Results are provided in the

form of SLR residuals that vary in value from a few centimeters to a few meters. A statistical summary of these residuals is provided. The results are significant because they have been determined without the use of DMA or OCS processing software or L-Band tracking data.

PROCEDURE

Satellite laser range (SLR) residuals were computed using the Operational Control System (OCS) and the Defense Mapping Agency (DMA) ephemeris for thirty days during 1993-1995. The OCS ephemeris is a real time Kalman filter process, described in Scardera [1], and the DMA ephemeris is a post-fit Kalman filter/smoothing process, described in Swift [2]. The key differences between these two processes are outlined in Table 1. It should be noted that the OCS Kalman filter is 'tuned' to generate predictions of the GPS orbit and clock states while the DMA Kalman filter/smoothing and the IGS process are 'tuned' to generate the best after the fact GPS orbit and clock estimates. One such tuning procedure, as indicated in Table 1, is to adjust the process noise level to prevent clock estimates from following their random component. Although this may improve the prediction, desired by OCS, it would not improve the post-fit results desired by DMA.

Because a recent set of minor revisions to the World Geodetic System 1984 (WGS 84), Malys and Slater [3], have been implemented during the course of this study, special procedures had to be used to account for the implementation of these revisions in the DoD orbit processes. In particular, a revised value for the central term in the WGS 84 Earth gravitational model was implemented at different times in the DMA and OCS orbit processes. This

term, commonly known as 'GM', which represents the product of the universal gravitational constant (G) and the mass of the Earth (M), including the atmosphere, was changed to the internationally recommended value of 398600.4418 km³/s² McCarthy [4]. The original WGS 84 value for this parameter was 398600.5 and the change was shown to cause a 1.29 meter systematic error in the radial positions of the GPS satellites. This radial error, in general did not corrupt navigation user positioning since it was fully compensated for by a corresponding equal and opposite error in the estimated satellite clock offsets. In this way, user navigation solutions did not suffer the effects of this GM error. In the analysis presented here however, this radial error must be carefully accounted for and effectively removed from the DoD orbits which were generated before the improved GM value was implemented.

The DMA orbit process implemented the revised GM value on day 2 of 1994 while the OCS implemented the revised value on days 292 and 305 of 1994 for PRN5 and PRN6 respectively. DMA and OCS orbits generated after these dates did not require adjustment for this WGS 84 GM change.

For the purpose of calibrating results, residuals were also computed using ephemerides obtained from the International GPS Service (IGS). IGS residuals were expected to be much lower due to the size of the IGS tracking network and the fact that some of the SLR tracking sites are colocated with IGS GPS tracking sites. The GM value used by the IGS, during the comparison period, was 398600.4415 and no adjustments were made for this small difference.

NORMAL POINT MEASUREMENTS

A very good discussion on normal points and laser ranging principles in general can be found in Degnan and Pavlis [5]. The NASA quick look normal points used in this study are produced in the field by compressing a number of raw laser ranges into a single value in order to reduce random error. Raw laser ranges are produced by an outgoing laser pulse, containing about 10¹⁷ photons. The pulse is reflected, at the satellite, by a laser retroreflector array, built by the Russian Institute for Space Device Engineering in Moscow under contract to Professor Carroll Alley at the University of Maryland. The pulse is returned to the telescope but only a few of the original photons return. This is partly due to the fact

that most SLR tracking stations are designed for lower orbiting satellites and partly due to the size of the retroreflector array. It is, for example, small by comparison to that on GLONASS which can be tracked easily. The SLR counter has a resolution of 3 millimeters and the departure time of the pulse is recorded to an accuracy of less than a microsecond. The number of raw ranges used to form a quick look normal point can vary from a few to a few hundred, and are compressed over a three minute or five minute interval. The standard error for the normal points can vary from a few millimeters to a few centimeters. The normal points have been corrected for any equipment delay but not for other effects. Laser ranges are not affected by the ionosphere or the wet component of the troposphere. Corrections are made to account for the remaining tropospheric effect by using the Marini & Murray [6] tropospheric model for laser data. This model is accurate to one centimeter above ten degrees and the normal point data used in the study is between twenty and ninety degrees. The typical tropospheric correction is between two and four meters. The GPS laser reflector array is offset from the center of mass and the effect on a range measurement is about negative half a meter. There is a relativistic time delay on laser data which is less than a centimeter. The station position is affected by plate motion and earth tides. The NUVEL NNR-1 plate motion model and the solid earth tide effect on station coordinates are taken from the International Earth Rotation Service (IERS) Standards (1992), McCarthy [4]. These models are used to correct the station position to the current observation time. Residuals in the form of observed minus computed range values are calculated by using the ephemeris provide by the IGS, the DMA, and the OCS. Residuals computed from ephemeris developed with the old GM are adjusted by adding 1.29 meters to their value in order to account for the GM difference. Mean, standard deviation, and peak value statistics are calculated daily and for the entire data set. RMS values are calculated for the entire data set and compared with User Range Error (URE) statistics.

ORBIT EVALUATION RESULTS

Figure 1 indicates the geographical location for each of the NASA SLR tracking sites utilized for collection of the evaluation data. Figures 2, 3, and 4 show the distribution of the GPS tracking networks utilized by the OCS, the DMA and the IGS respectively.

The thirty days of SLR tracking data used in this study were collected between November 1993 and March 1995. Tables 2 and 3 provide a list of the specific days used as well as the daily statistics on the orbit evaluations for all three sets of estimated orbits (IGS, DMA and OCS). Figures 5, 6, 7, and 8 are a graphic representation of the entire set of SLR tracking residuals from the OCS and DMA ephemeris. Because the collection of SLR data used here is spread over seventeen months, the structure of these residuals in an individual day cannot be seen on these particular plots. Separate plots, provided in Figures 9, 10, and 11 show the residuals from all three orbit evaluations over a two day period. The two days selected for this plot were days 11 and 12 of 1995 from PRN5. These results appear to be representative of the overall results which are provided in Tables 4 and 5. Figure 9 indicates that any station related error is less than 20 cm. while Figure 11 shows a 300 cm. variation. Graz, Austria and Herstmonceux, UK see satellite PRN5 at about the same time and have similar IGS residuals but dissimilar DMA and OCS residuals. The variation in the residuals for the OCS and to a lesser extent the DMA, support the belief that the ephemeris error is the dominant component of these residuals.

Since the accuracy of the SLR normal points is expected to be no worse than a few centimeters, the statistics provided in Tables 4 and 5 provide an independent accuracy check of the GPS ephemerides generated by the three organizations. Clearly, the IGS ephemerides are superior to the DMA or OCS estimates while the DMA orbits are superior to the OCS filter states. Recall that the OCS filter states are not derived from any prediction process. In GPS parlance, the Age of Data (AOD) of the OCS filter states is zero. If the broadcast navigation messages, which are based on a prediction process, were evaluated with the laser tracking data described here, the statistics would be considerably larger.

Since the RMS values shown in Table 5 are in essence, a measure of the URE due to ephemeris error, these values can be compared to RMS values of User Range Errors, due to ephemeris error, which have been derived by other investigators using L-Band tracking data. Note however, that the UREs derived from L-Band tracking data are affected by important additional error sources, including those associated with the satellite and receiver clocks.

Note also that it is possible for satellite and receiver clock error to compensate for each other to some degree. Despite these differences, the RMS of laser tracking residuals for the OCS orbits shown in

| DMA | OCS |
|---|---|
| Ten Stations. | Five Stations. |
| Eight day smoother. | Continuous filter. |
| All sats in one partition. | Up to six sats per partition. |
| Rad. & Y-axis modeled as 1st order Gauss-Markov with high noise. No noise on orbit. | Radiation pressure & Y-axis modeled as random walk with low process noise. Process noise on orbit states. |
| High process noise on sat clocks. Q-bumps at clock events. | Low process noise on sat clocks. Q-bumps at clock events. |
| Requires Master Clock. | Requires Composite Clock. |
| Solves for polar motion. | Does not solve for pole. |
| Solves for ut1-utc rate. | Does not solve for ut1-utc rate. |
| Uses ut1-utc predict to move the gradient of potential from ecef to eci. | Does not use ut1-utc predict to move the gradient of potential from ecef to eci. |
| Models zonal tide effects on ut1. | Does not model zonal tide effects on ut1. |
| Models plate tectonic motion. | Does not model plate tectonic motion. |
| Estimates tropospheric parameter per station. | Does not est. tropospheric refraction parameter. |
| Eight day ref. orbit. Five min. step, (other step for force change). | Thirty day reference orbits. Seven and a half min. step, (one min during eclipse). |
| Radiation model uses constant satellite mass. | Radiation model has an option to use a variable mass. |

Table 1 DMA Versus OCS Processing

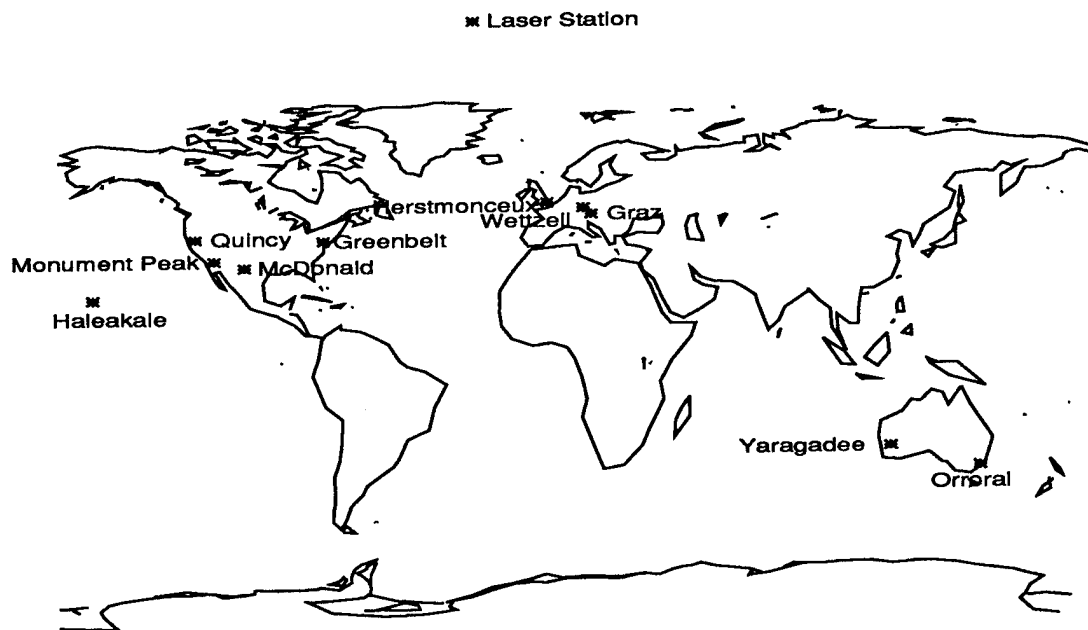


Figure1 NASA SLR GPS Tracking Net

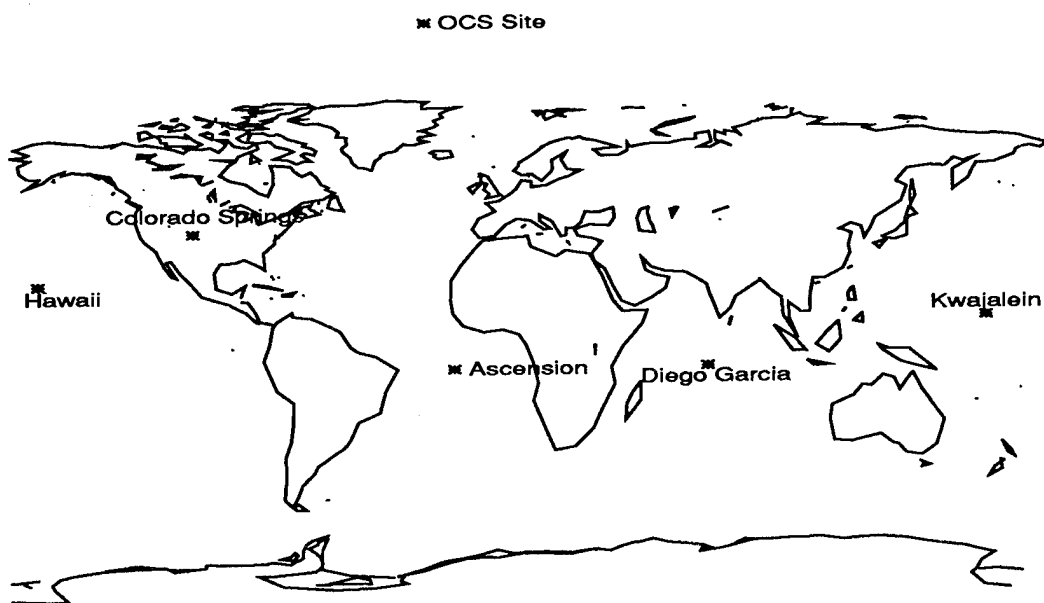


Figure 2 OCS GPS Tracking Network

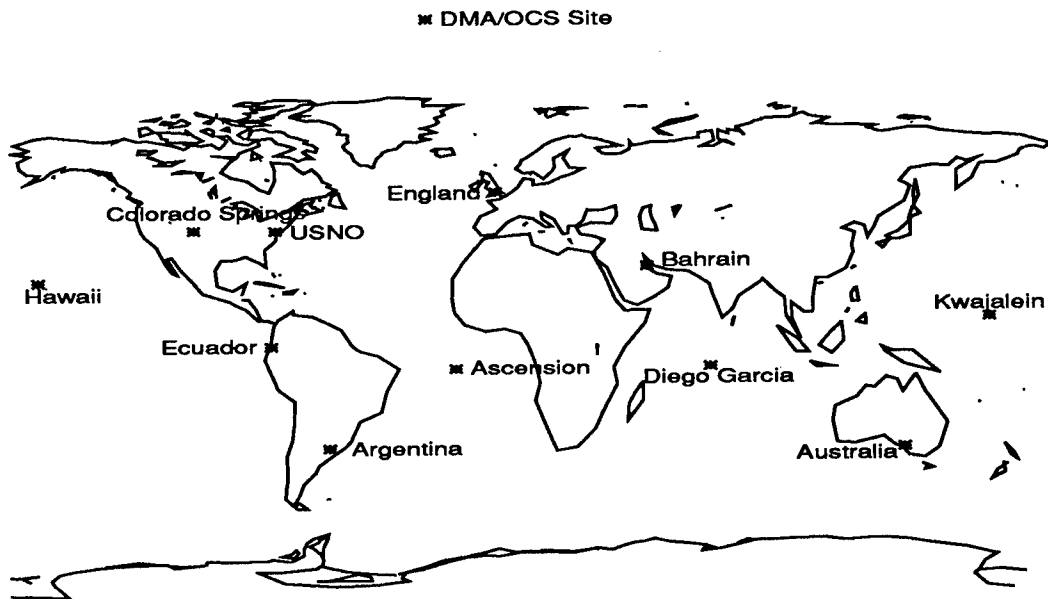


Figure 3 DMA GPS Tracking Network

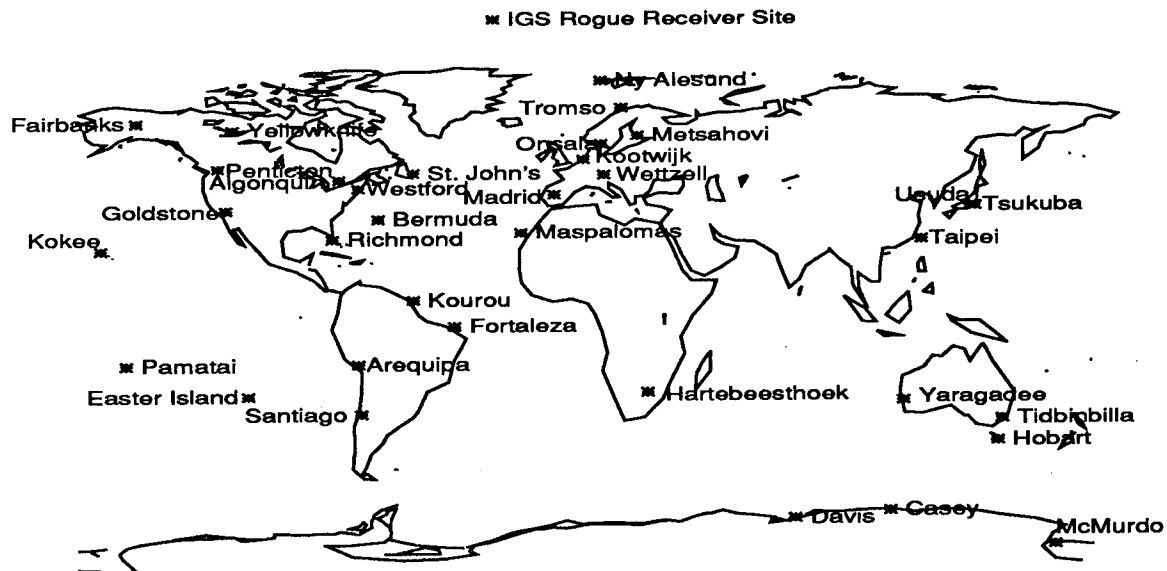


Figure 4 IGS Tracking Network (Global Stations Only*)

*Processed by either 1) two or more IGS Analysis Centers on another continent
or 2) a majority of Analysis Centers.

| PRN5 | | | MEAN (CM.) | | | STD. (CM.) | | | PEAK (CM.) | | |
|------|----|-----|------------|-------|-------|------------|-------|-------|------------|--------|-------|
| Pts. | Yr | Day | IGS | DMA | OCS | IGS | DMA | OCS | IGS | DMA | OCS |
| 27 | 93 | 321 | -8.5 | 9.2 | 59.0 | 1.7 | 6.7 | 19.7 | -10.7 | 24.4 | 109.1 |
| 58 | 93 | 322 | -6.4 | -27.3 | 73.6 | 7.6 | 37.2 | 70.9 | -20.2 | -94.8 | 248.4 |
| 48 | 93 | 323 | -7.5 | -51.8 | 22.9 | 7.2 | 51.4 | 72.2 | -22.5 | -110.4 | 185.7 |
| 11 | 93 | 324 | 1.6 | 15.7 | 104.7 | 3.5 | 23.8 | 26.5 | -5.9 | 45.5 | 135.9 |
| 15 | 94 | 186 | -1.9 | 6.7 | 176.9 | 0.2 | 12.9 | 63.8 | -2.3 | 26.2 | 268.7 |
| 9 | 94 | 214 | 1.7 | -39.6 | 109.4 | 0.2 | 0.5 | 46.5 | 2.1 | -40.0 | 180.0 |
| 11 | 94 | 215 | 11.9 | -71.0 | 166.7 | 1.4 | 7.6 | 17.9 | 13.6 | -81.2 | 187.5 |
| 6 | 94 | 216 | 12.0 | -47.2 | 96.1 | 1.0 | 7.9 | 10.4 | 13.6 | -56.5 | 109.8 |
| 8 | 94 | 217 | 7.1 | -83.9 | 21.2 | 1.1 | 4.9 | 9.5 | 8.3 | -89.9 | 34.2 |
| 9 | 94 | 236 | 6.6 | -30.1 | -10.5 | 4.6 | 9.3 | 36.5 | 14.4 | -38.6 | -48.5 |
| 5 | 94 | 237 | 3.8 | -17.4 | -46.7 | 1.2 | 5.4 | 7.5 | 6.0 | -24.2 | -55.9 |
| 14 | 94 | 292 | 1.4 | 21.7 | 66.1 | 9.7 | 9.0 | 39.2 | 17.7 | 43.6 | 119.8 |
| 4 | 94 | 293 | -2.6 | 8.4 | 41.5 | 0.6 | 0.5 | 3.7 | -3.1 | 8.8 | 46.5 |
| 8 | 94 | 364 | -19.5 | 50.6 | 44.7 | 2.2 | 9.4 | 20.3 | -22.1 | 61.2 | 69.8 |
| 6 | 94 | 365 | -22.1 | 25.5 | -7.4 | 1.2 | 1.6 | 6.1 | -23.4 | 27.9 | -16.5 |
| 7 | 95 | 2 | -9.1 | 33.0 | 52.5 | 1.3 | 4.0 | 8.6 | -11.8 | 37.8 | 64.7 |
| 8 | 95 | 3 | -8.6 | -2.0 | 30.4 | 1.4 | 18.6 | 23.5 | -11.0 | -26.2 | 60.5 |
| 15 | 95 | 4 | 12.4 | -22.7 | 138.8 | 6.3 | 101.8 | 101.7 | 21.5 | -117.5 | 261.3 |
| 11 | 95 | 5 | 14.3 | -44.0 | 104.1 | 1.5 | 21.4 | 19.0 | 16.6 | -75.6 | 133.4 |
| 15 | 95 | 6 | -1.8 | -22.7 | 106.1 | 7.9 | 81.2 | 92.3 | -11.7 | -132.4 | 256.5 |
| 22 | 95 | 11 | -1.9 | -8.1 | 79.5 | 9.7 | 23.3 | 116.3 | -15.2 | -34.1 | 229.5 |
| 14 | 95 | 12 | 14.5 | -24.2 | 93.0 | 5.4 | 27.0 | 129.4 | 21.0 | -57.3 | 276.3 |
| 5 | 95 | 14 | -4.6 | -22.3 | 3.0 | 1.1 | 0.6 | 16.3 | -6.3 | -23.3 | 26.1 |
| 7 | 95 | 16 | 3.4 | 3.7 | 154.6 | 1.5 | 3.6 | 30.4 | 5.2 | 8.5 | 196.1 |
| 6 | 95 | 73 | -3.2 | 15.4 | 85.5 | 1.0 | 4.0 | 45.2 | -4.4 | 19.7 | 139.4 |
| 13 | 95 | 74 | 3.1 | -14.5 | 93.8 | 6.4 | 9.5 | 87.7 | 15.8 | -28.2 | 255.2 |
| 6 | 95 | 75 | 3.8 | 15.7 | 22.7 | 0.6 | 3.6 | 4.1 | 4.6 | 20.7 | 29.1 |
| 10 | 95 | 76 | 3.7 | 15.3 | 35.8 | 3.3 | 8.2 | 46.8 | 7.7 | 26.5 | 173.3 |
| 22 | 95 | 77 | -1.4 | -1.9 | 154.5 | 2.7 | 18.4 | 88.4 | -5.1 | -33.5 | 300.2 |
| 10 | 95 | 78 | 5.3 | 64.6 | 50.2 | 1.0 | 4.3 | 4.8 | 7.0 | 68.8 | 58.4 |
| 11 | 95 | 79 | -4.3 | -5.2 | 206.9 | 0.5 | 0.7 | 23.9 | -5.0 | -6.2 | 242.3 |

Table 2 SLR Residual Statistics By Day (PRN5)

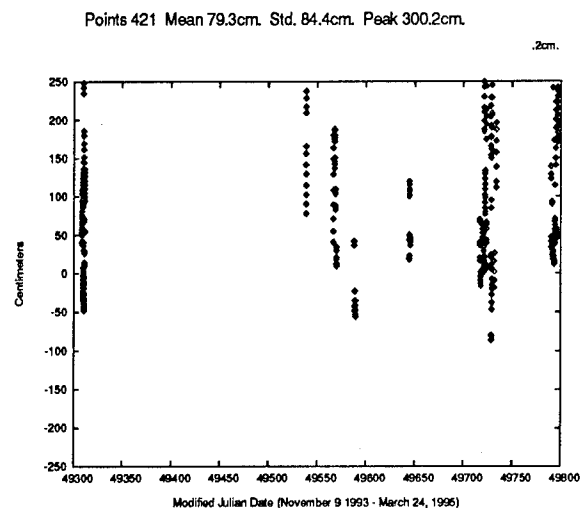


Figure 5 PRN5 OCS SLR Residuals

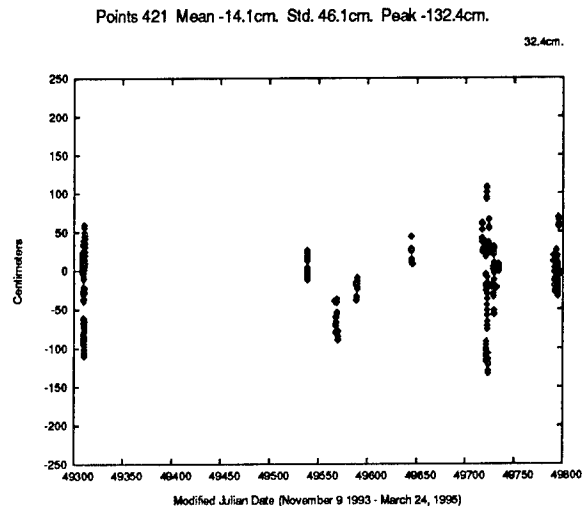


Figure 6 PRN5 DMA SLR Residuals

| PRN6 | | | MEAN (CM.) | | | STD. (CM.) | | | PEAK (CM.) | | |
|------|----|-----|------------|-------|--------|------------|------|-------|------------|-------|--------|
| Pts. | Yr | Day | IGS | DMA | OCS | IGS | DMA | OCS | IGS | DMA | OCS |
| 6 | 94 | 236 | 0.0 | 22.4 | -131.6 | 0.9 | 2.3 | 8.2 | -1.6 | 24.9 | -142.8 |
| 4 | 94 | 237 | 6.2 | 9.2 | -76.2 | 3.2 | 2.9 | 11.1 | 11.5 | 14.1 | -89.6 |
| 3 | 94 | 238 | -1.3 | 4.8 | -98.5 | 0.4 | 0.5 | 5.9 | -1.7 | 5.4 | -105.8 |
| 6 | 94 | 292 | 8.7 | 72.4 | -5.5 | 1.2 | 6.8 | 2.0 | 11.0 | 83.7 | -7.0 |
| 6 | 94 | 295 | 14.1 | 161.2 | -5.3 | 4.0 | 6.7 | 4.4 | 18.2 | 167.7 | -13.1 |
| 16 | 94 | 324 | -1.2 | 20.5 | 7.1 | 3.5 | 14.6 | 9.1 | -8.5 | 41.9 | 27.8 |
| 7 | 94 | 362 | 25.4 | -2.6 | 131.6 | 0.9 | 5.8 | 4.4 | 27.2 | -11.1 | 139.5 |
| 29 | 94 | 364 | 6.7 | 17.6 | 201.9 | 15.5 | 31.3 | 94.6 | 26.1 | 69.1 | 336.4 |
| 7 | 94 | 365 | -12.3 | -19.0 | 91.4 | 0.8 | 3.6 | 5.3 | -13.0 | -24.4 | 98.9 |
| 6 | 95 | 1 | -7.9 | 19.8 | 94.0 | 3.9 | 8.7 | 13.5 | -13.5 | 32.0 | 107.7 |
| 4 | 95 | 2 | -9.9 | 20.6 | 86.6 | 0.8 | 7.1 | 6.3 | -11.0 | 28.0 | 94.1 |
| 7 | 95 | 3 | -3.9 | 0.3 | 122.2 | 1.0 | 3.0 | 7.2 | -5.0 | -4.6 | 131.8 |
| 4 | 95 | 4 | 20.8 | 36.4 | 181.4 | 0.8 | 3.5 | 2.0 | 21.8 | 41.3 | 184.3 |
| 3 | 95 | 5 | 21.5 | -3.4 | 185.6 | 1.0 | 2.1 | 1.3 | 22.6 | -5.3 | 187.4 |
| 4 | 95 | 6 | 21.6 | 10.3 | 156.4 | 1.3 | 5.0 | 1.7 | 23.6 | 18.1 | 159.3 |
| 15 | 95 | 7 | 13.4 | -81.9 | 265.3 | 2.9 | 11.1 | 31.8 | 18.3 | -97.4 | 316.2 |
| 7 | 95 | 10 | -1.3 | 23.2 | 200.8 | 1.3 | 5.0 | 13.2 | -3.6 | 29.2 | 216.9 |
| 11 | 95 | 11 | 5.9 | 27.4 | 79.1 | 16.3 | 20.4 | 11.7 | 22.0 | 47.5 | 92.6 |
| 10 | 95 | 12 | 0.7 | 17.8 | 119.9 | 2.2 | 1.2 | 19.1 | 3.8 | 20.1 | 145.6 |
| 6 | 95 | 13 | 25.7 | 36.4 | 163.0 | 7.9 | 13.4 | 26.8 | 39.6 | 55.7 | 189.1 |
| 11 | 95 | 14 | 1.7 | 13.4 | 247.3 | 8.0 | 26.4 | 125.7 | 18.4 | 68.9 | 380.5 |
| 5 | 95 | 15 | -5.4 | 21.8 | 91.6 | 0.8 | 0.2 | 6.3 | -6.2 | 22.1 | 100.1 |
| 26 | 95 | 74 | 0.3 | -2.9 | 38.4 | 2.7 | 28.8 | 25.4 | -5.7 | -52.0 | 116.3 |
| 5 | 95 | 76 | 21.0 | 9.4 | 147.5 | 1.9 | 4.8 | 2.4 | 23.4 | 17.0 | 149.9 |
| 18 | 95 | 77 | 3.9 | 11.2 | 78.4 | 11.9 | 31.2 | 86.1 | 22.7 | 55.4 | 170.3 |
| 11 | 95 | 78 | -3.6 | 40.9 | 110.8 | 1.8 | 8.9 | 38.8 | -7.5 | 51.5 | 171.5 |
| 7 | 95 | 79 | -7.5 | 84.3 | 127.3 | 1.2 | 1.1 | 29.6 | -9.4 | 85.3 | 171.4 |

Table 3 SLR Residual Statistics By Day (PRN6)

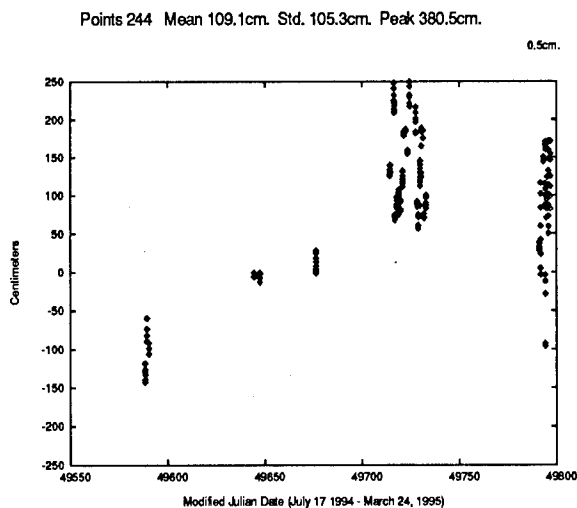


Figure 7 PRN6 OCS SLR Residuals

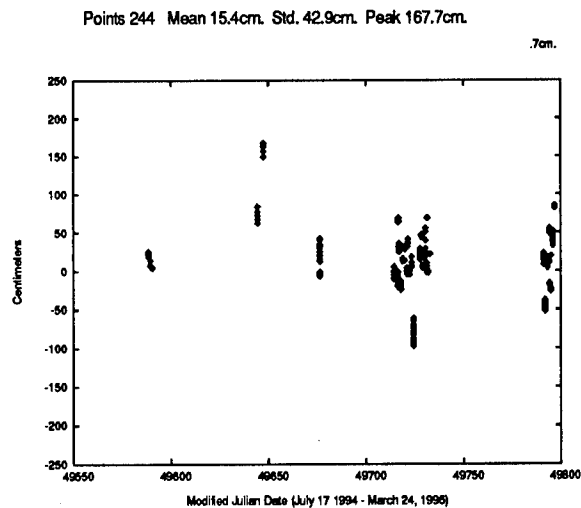


Figure 8 PRN6 DMA SLR Residuals

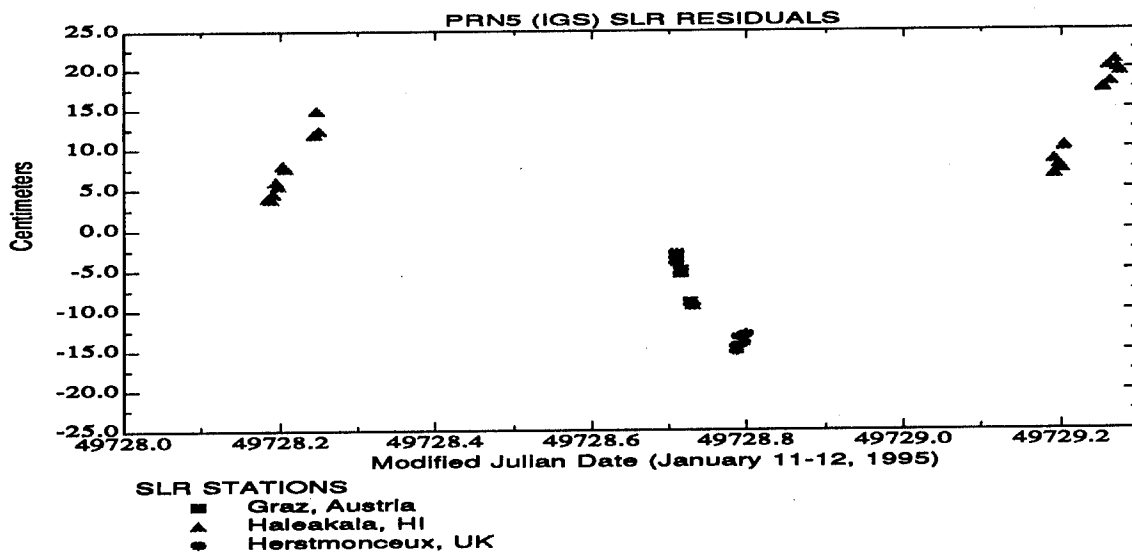


Figure 9 IGS SLR Residuals

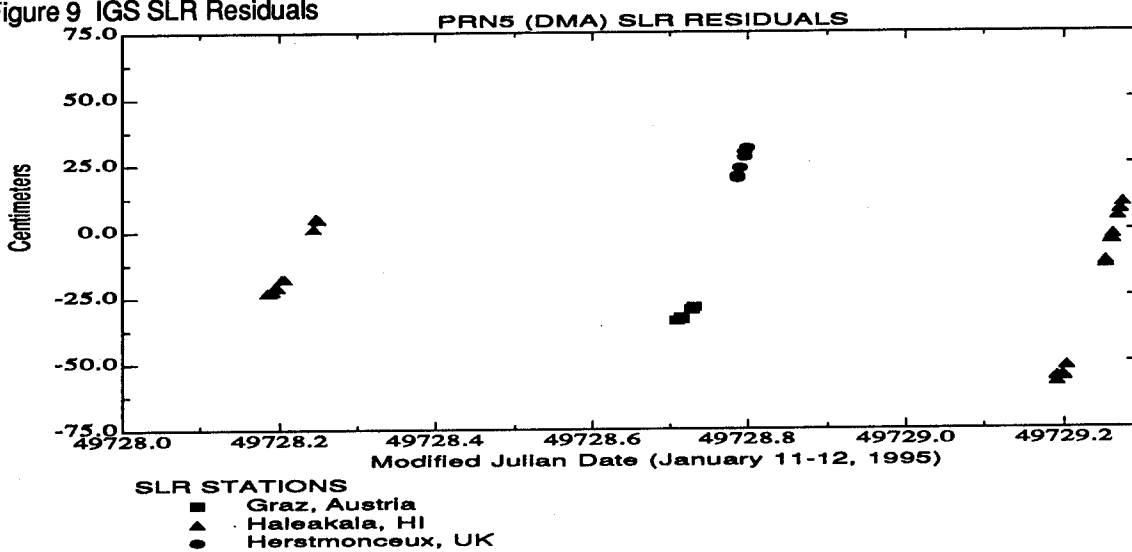


Figure 10 DMA SLR Residuals

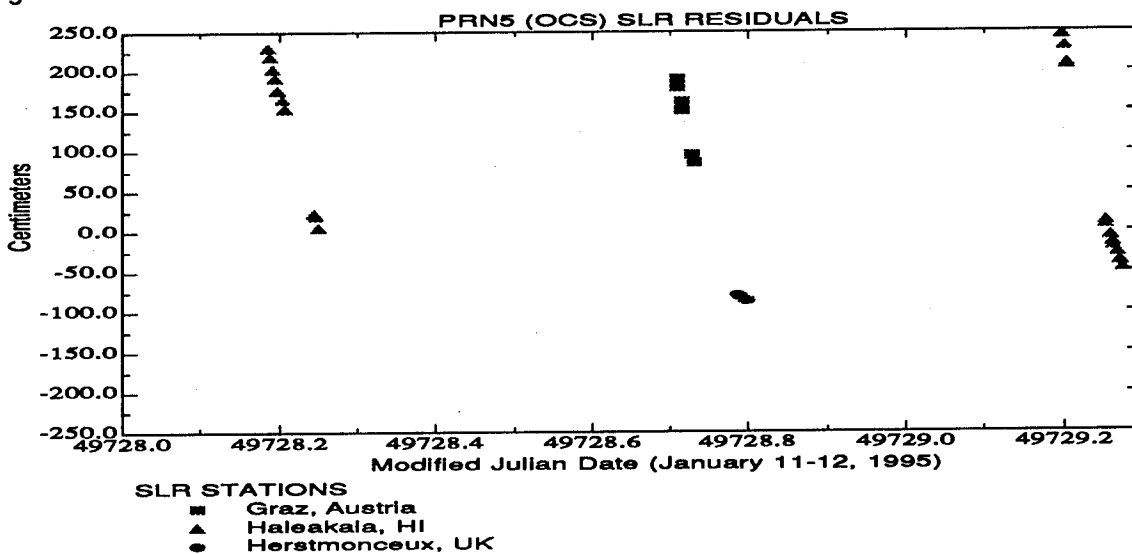


Figure 11 OCS SLR Residuals

| Sat. ID | Pts. | MEAN (CM.) | | | STD. (CM.) | | | PEAK (CM.) | | |
|---------|------|------------|-------|-------|------------|------|-------|------------|--------|-------|
| | | IGS | DMA | OCS | IGS | DMA | OCS | IGS | DMA | OCS |
| PRN5 | 421 | -1.2 | -14.1 | 79.3 | 9.5 | 46.1 | 84.4 | -23.4 | -132.4 | 300.2 |
| PRN6 | 244 | 4.3 | 15.4 | 109.1 | 11.9 | 42.9 | 105.3 | 39.6 | 167.7 | 380.5 |

Table 4 Summary Statistics (SLR Residuals)

| Sat. ID | Pts. | IGS | DMA | OCS |
|---------|------|------|------|-------|
| PRN5 | 421 | 9.6 | 48.2 | 115.8 |
| PRN6 | 244 | 12.7 | 45.6 | 151.6 |

Table 5 RMS Values (CM.) For SLR Residuals From GPS Orbits

Table 5 (116-152 cm.) agree well with the L-Band UREs for the OCS orbits which have been quantified recently. For example, the RMS of 400 days of L-Band Precise Positioning Service UREs, using the entire GPS constellation and the OCS filter states, was 137 cm., Malys [7]. This level of agreement between the laser residuals and the L-Band residuals is quite remarkable and provides an indication that the OCS estimation process, in general, is successfully isolating ephemeris parameters from clock parameters.

The statistics shown for the DMA ephemerides indicate a half meter level of accuracy and are commensurate with the level of a posteriori residuals generated by the DMA ephemeris/clock estimation process.

The statistics shown for the IGS ephemerides show an overall decimeter-level of accuracy and corroborate the results of independent laser data analysis reported by Degnan and Pavlis [7]. Moreover, the decimeter-level ephemeris accuracy claims which appear throughout a large body of IGS literature are supported by the results presented here.

CONCLUSIONS

The paper shows that the OCS continuous Kalman filter product is accurate to about one and a half meters in range and the DMA filter-smoother product is accurate to better than half a meter in range. The

Navigation messages which are broadcast to the real-time user were not evaluated in this study but since they are based on predictions using the OCS filter states as initial conditions, they are known to be less accurate than the filter states themselves. Moreover, the evaluations of all three types of ephemerides (IGS, DMA and OCS) yield results which corroborate the accuracy claims of analysts which have based their conclusions on L-Band tracking data. Because the laser tracking data does not depend at all on the behavior of the satellite clocks, the analysis technique presented here provides a reliable, independent method of ephemeris accuracy evaluation. The results provide an indication that ephemeris parameters and clock parameters are adequately isolated in the estimation processes which are routinely executed at the IGS, DMA and the OCS.

ACKNOWLEDGMENTS

The authors wish to thank Mr. Steve Malys of DMA for suggesting this study and for providing extensive suggestions which greatly improved the quality of this paper. The authors also wish to thank Dr. Erricos Pavlis of NASA for providing data and helpful conversations regarding laser processing and Mr. Ronald Beard, of the Naval Research Laboratory, for coordination activities.

REFERENCES

1. Scardera, M.P., *The NAVSTAR GPS Master Control Station's Kalman Filter Experience*, NASA, Goddard Space Flight Center, Flight Dynamics Symposium, Greenbelt, MD, 1989.
2. Swift, E.R., *Mathematical Description of the GPS Multisatellite Filter/Smoother*, NSWC TR 87-187, Dahlgren, VA, October 1987.
3. Malys, S., and Slater, J.A., *Maintenance and Enhancement of the World Geodetic System 1984*, Institute of Navigation, ION-GPS-94, Salt Lake City, Utah, September 1994.
4. McCarthy, D.D. (ed.), *IERS Technical Note 13, IERS Standards (1992)*, Observatoire de Paris, July 1992.
5. Degnan, J.J., and Pavlis, E.C., *Laser Ranging to GPS Satellites with Centimeter Accuracy*, GPS World, pages 62-70, September, 1994.
6. Marini, J. W. and Murray, Jr., C. W., *Correction of Laser Range Tracking Data for Atmospheric Refraction at Levels Above 10 Degrees*, Goddard Space Flight Center Report X-591-73-351, November 1973.
7. Malys, S., *One Year of OCS Filter Performance Measured by Empirical User Range Errors*, Presentation at the GPS Performance Analysis Working Group (PAWG-95), Colorado Springs, Colorado, August 1995.

Improved Ambiguity Resolution by Regional Differential Modelling of the Ionosphere

Lambert Wanninger
TU Dresden, Germany

Biography

Lambert Wanninger received his Dipl.-Ing. and his Dr.-Ing. in Geodesy in 1988 and 1994 from the Universität Hannover, Germany. He has several years experience in various aspects of precise GPS applications especially in the field of ionospheric effects on GPS and in ionospheric research with GPS. He is currently employed as research associate at the Geodätisches Institut, Technische Universität Dresden, Germany.

Abstract

Fast and on-the-fly ambiguity resolution algorithms are limited to short baselines mainly due to ionospheric refraction. Even under the moderate and mostly undisturbed ionospheric conditions of the mid-latitudes, the differential errors often exceed 1 ppm of the baseline length. Much larger errors are found in the presence of ionospheric disturbances and in the equatorial region.

In order to reduce these differential errors and thus to extend the use of fast and on-the-fly ambiguity resolution from short to medium-length baselines, a differential ionospheric model was developed whose parameters are derived from dual-frequency phase observations of at least three GPS monitor stations. Differential ionospheric corrections are produced epoch-by-epoch and satellite-by-satellite for any other GPS station in the area.

Examples are presented which demonstrate the improvement in ambiguity resolution under undisturbed ionospheric conditions in the mid-latitudes, and also in the presence of ionospheric disturbances (medium-scale Traveling Ionospheric Disturbances). These disturbances are able to prevent fast and on-the-fly ambiguity resolution even on short baselines (≤ 10 km). The differential ionospheric model removes most of these disturbing effects.

Introduction

Resolution of the double difference carrier phase ambiguities is the key to precise (cm accuracy) baseline co-

ordinates from GPS measurements. In recent years, fast ambiguity resolution algorithms and ambiguity resolution on-the-fly were introduced (e.g. Hatch 1990, Frei and Beutler 1990). These algorithms find the correct set of double difference ambiguities after just several seconds or few minutes of observations. They usually produce reliable results if no large observation errors affect the phase and code observations. Thus, code noise needs to be on a low level in order to provide a good initial position estimation from code observations. Multipath effects have to be minimized by antenna design and by careful attention to antenna siting. Moreover, distance-dependent errors have to be kept small by restriction to short baselines. In fact, these distance-dependent errors limit fast ambiguity resolution to baselines with a maximum length of a few kilometers.

Two kinds of distance-dependent errors exist: ionospheric refraction and orbit errors. Even under Selective Availability (SA) broadcast orbit errors have seldom exceeded 10 m. Applying the well known but pessimistic rule-of-thumb that a 20 m orbit error results in 1 ppm baseline error shows that orbit errors contribute to the overall error budget in maximum in the order of 0.5 ppm of the baseline length. The effects of ionospheric errors, however, are often much larger (1 – 2 ppm and more) even under the moderate ionospheric conditions of the mid-latitudes and even at the present minimum of the sunspot cycle. Larger errors occur in the presence of ionospheric disturbances, in the equatorial region, and during years of high sunspot activity. Incidents have been observed where the L_1 ionospheric baseline error exceeded 10 ppm of the baseline length (Wanninger 1993a,b).

In order to illustrate the contributions of orbit errors and ionospheric errors to double difference phase observables, a 24 hour data set of a 44 km baseline has been arbitrarily selected from our database of permanent GPS observations in Germany. After ambiguity fixing, the double difference range residuals have been plotted for L_1 and for the ionosphere-free linear combination L_0 (Fig. 1). Ionospheric refraction affects the L_1 -signal only,

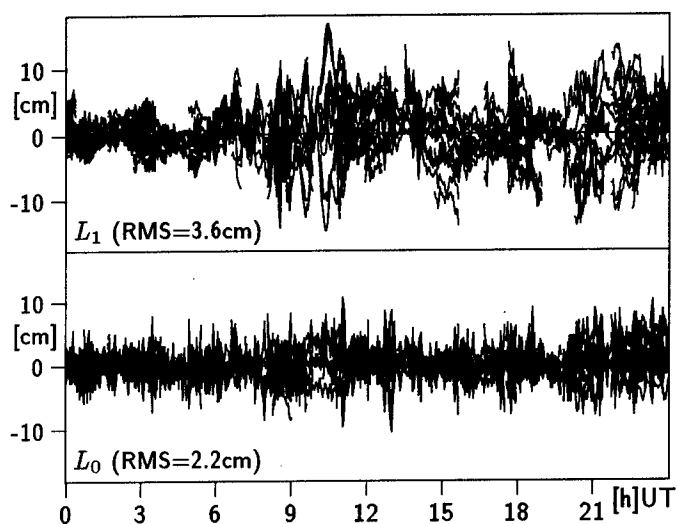


Figure 1: Double difference range residuals in all satellite combinations of a 44 km baseline, for L_1 and the ionosphere-free linear combination L_0 , observed in Germany on September 7, 1994.

whereas both signals contain orbit errors and all other kinds of errors. Hence, the difference between the two plots are mainly due to the ionosphere (some differences can be attributed to the higher observation noise of the L_0 -signal and to multipath). Whereas small differences can be detected between midnight and sunrise (low ionospheric electron content), large differences are found during daylight hours (high electron content). L_2 observations and linear combinations like widelane and narrowlane experience similar ionospheric effects as L_1 . The difference in RMS-values (Fig. 1) illustrates that ionospheric refraction is the main error source in medium-length baselines and that ionospheric refraction causes the main difficulty for ambiguity resolution.

One approach to extend the use of fast ambiguity resolution algorithms to medium-length baselines (10 – 50 km) consists in the reduction of ionospheric errors by application of appropriate ionospheric models. In recent years, various publications dealt with models of the absolute total electron content (TEC) derived from dual-frequency GPS observations of one or several receivers (Fig. 2a). These models were used to reduce single-frequency baseline coordinate errors (Georgiadou and Kleusberg 1988, Wild et al. 1989) and to improve ambiguity resolution on long baselines and for observation sessions of several hours (Mervart et al. 1994). Such a model consists of one set of coefficients for all satellites and an observation session of several hours. Their main limitation lies in the inability to reproduce small-scale or medium-scale structures of the ionospheric electron content.

The idea of differential ionospheric modelling was in-

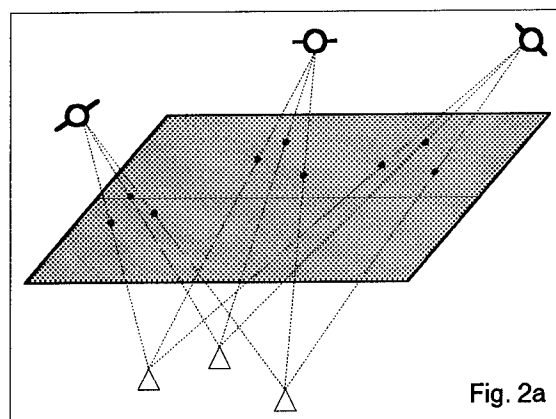


Fig. 2a

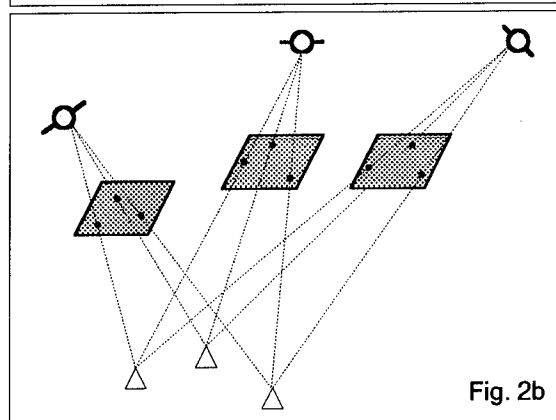


Fig. 2b

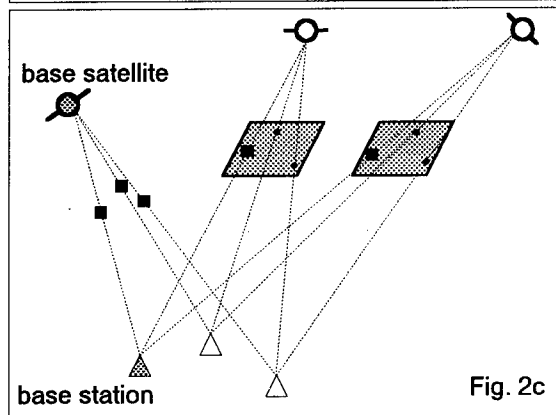


Fig. 2c

Figure 2: Different levels of ionospheric models for differential GPS (simplified concepts). 2a: Modelling of the absolute TEC. 2b: Differential modelling of the ionosphere. 2c: Differential modelling of the ionosphere using double differences.

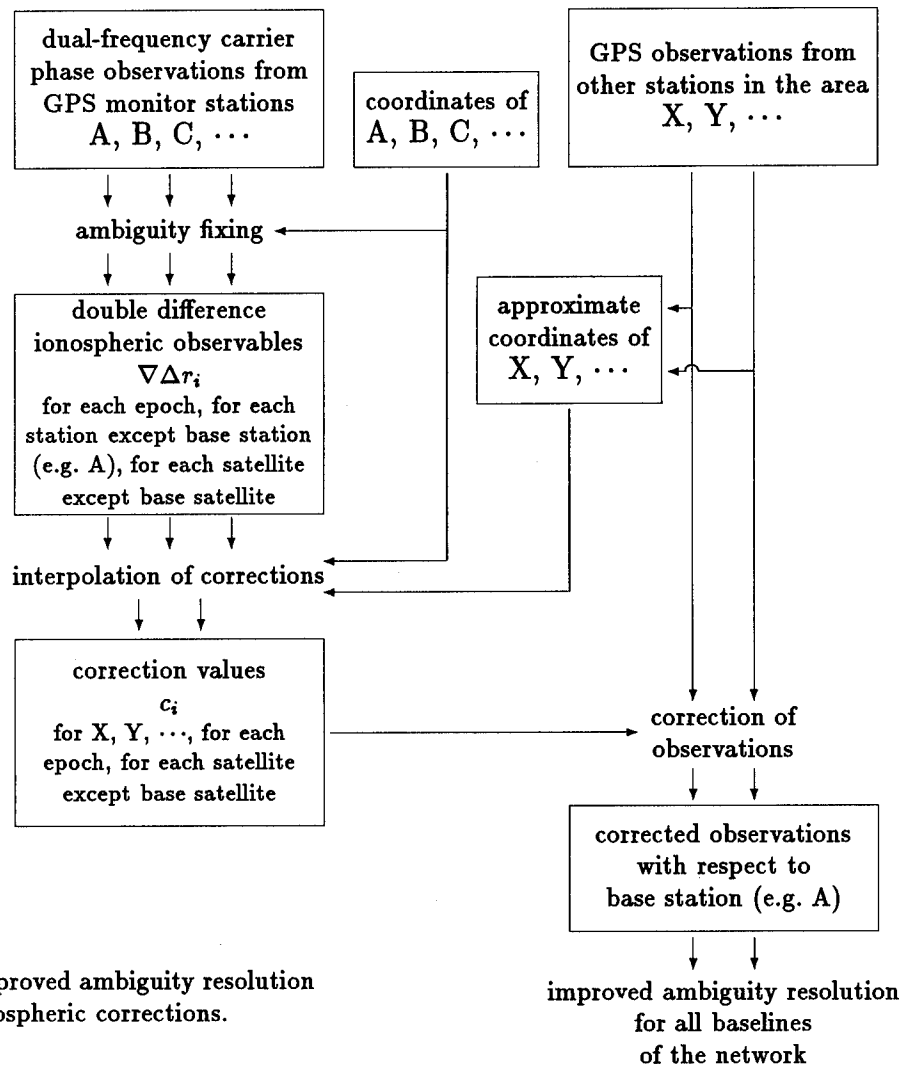


Figure 3:
The concept of improved ambiguity resolution by differential ionospheric corrections.

roduced by Webster and Kleusberg (1992). Their model provides epoch-by-epoch and satellite-by-satellite ionospheric corrections. The ionospheric delays of a station equipped with a single-frequency receiver are estimated from interpolation of ionospheric delay observations of three surrounding monitor stations using the intersection points of the GPS signal paths with an ionospheric single-layer model at a height of 350 km (Fig. 2b). The problem of ambiguities in the ionospheric delays derived from dual-frequency phase data is overcome by assuming that the ambiguity differences between the monitor stations are, on average, equal to zero.

In this research, dual-frequency carrier phase ambiguities are resolved and fixed in the network of monitor stations, thus yielding differential ionospheric delays in the most accurate GPS mode. Correction values are then determined on the level of double differences epoch-by-epoch and satellite-by-satellite from interpolation of

ionospheric delay values of the monitor stations using their coordinates and approximate coordinates of the new station (Fig. 2c). Thus, in contrast to Webster and Kleusberg (1992) our approach requires complete ambiguity fixing between monitor stations. Moreover, the interpolation algorithm has been simplified.

Regional Differential Ionospheric Model

The regional differential ionospheric model is derived from dual-frequency phase data of at least three GPS monitor stations surrounding the area of interest. It is based on the double difference observables of the ionospheric linear combination L_i of the phase observations.

In a first processing step, ambiguity resolution and fixing has to be performed for the network of monitor stations (compare Fig. 3, see also Wanninger 1995). Although their distances may be of the order of 50 km,

ambiguity resolution is simplified because the baseline coordinates are known, dual-frequency receivers are employed and long observation periods can be used. If the modelling is to be accomplished in real-time or almost in real-time, ambiguity resolution in the network of monitor stations must be performed and checked continuously. The reliable fixing of the double difference ambiguities of a newly risen satellite may require several minutes, half an hour, or an even longer period of observation data. As long as the ambiguities of a particular satellite could not be fixed, no ionospheric corrections can be applied to phase observations of this satellite.

After ambiguity fixing, we obtain unambiguous double difference ionospheric observables $\nabla\Delta r_i$ for each epoch. They refer to a base station and a base satellite. In each observation epoch the ionospheric model consists of at least two (number of monitor stations minus one) $\nabla\Delta r_i$ values per visible satellite. Ionospheric corrections c_i for any station in the area can then be computed by interpolation using the known latitude and longitude coordinates of the monitor stations and the approximate latitude and longitude coordinates of the stations to be determined. The correction values are interpolated epoch by epoch, i.e. in every observation epoch an independent set of corrections is produced.

If three monitor stations are available, the interpolation of correction values is performed by a linear interpolation algorithm. If more monitor stations are available, either the best group of three stations (for example the three closest surrounding stations) should be selected or several correction values from sets of three stations can be computed and averaged or a more sophisticated interpolation algorithm could be used. The main advantage of more than three monitor stations lies in the ability to determine correction values even if only some (but at least three) monitor stations including the base station could provide observations.

In a further processing step, the ionospheric correction values are scaled to ionospheric effects on L_1 and L_2 in order to yield corrections for the original phase observations or also for the code observations. Corrections can be applied to the observations of any station in the area including the monitor stations. The observations of the base station and of the base satellite need not to be modified because their correction values are zero.

Since double difference corrections are applied to non-differenced observations, a further baseline processing must only be performed between stations whose observations have been manipulated by correction values based on identical error models. Manipulated data must not be combined with original observations with the exception of the observations of the base station.

These ionospheric corrections have effects on single-frequency and dual-frequency ambiguity resolution and

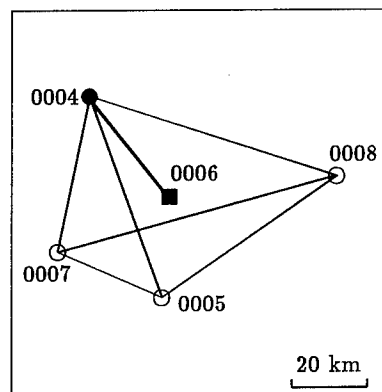


Figure 4: Network of GPS monitor stations and the 34 km baseline 0004-0006.

on single-frequency coordinate results. Ionosphere-free coordinate solutions are not affected. Their results remain unchanged.

In an operational mode, ambiguity resolution in a regional network of several monitor stations surrounding a number of new stations consists of the following processing steps: (a) ambiguity resolution in the network of monitor stations, (b) estimation of ionospheric corrections, (c) modification of the observations of all stations with the exception of the base station, and (d) improved ambiguity resolution for all baselines in the network.

Undisturbed Ionospheric Conditions

Observations were selected arbitrarily from the data sets of the already existing dense network of permanent GPS stations in North Germany (Figure 4). 13 hours of Trimble SST/SSE observations (June 17, 1994) were used to test the described algorithm. The analysis of the ionospheric conditions from dual-frequency phase observations revealed that almost undisturbed and thus average mid-latitude ionospheric conditions were present. The GEONAP software package (Wübbena 1989) was used to perform ambiguity resolution in the network of monitor stations (0004,0005,0007,0008).

Ionospheric corrections were predicted for station 0006 from the dual-frequency phase observations of at least three surrounding permanent tracking stations. When dual-frequency observations of all four surrounding stations existed, the mean of two predicted values (triangle 0004-0007-0008 and triangle 0004-0005-0008) was taken as correction value for the observation of station 0006. In both triangles, station 0004 was used as base station, therefore the observations of 0004 needed not to be corrected in order to perform improved ambiguity resolution for the baseline 0004-0006.

The successful correction of ionospheric effects is shown by comparison of double difference phase residuals of L_1 and the widelane linear combination L_W for

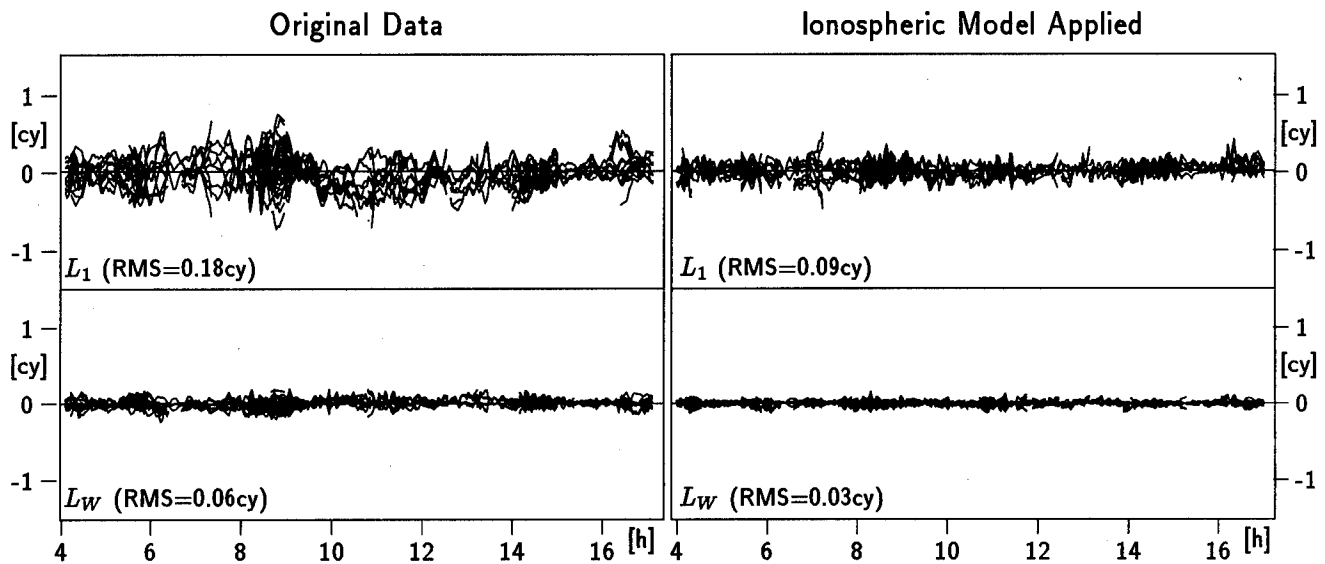


Figure 5: Double difference phase residuals after ambiguity fixing in all satellite combinations, in L_1 and widelane L_W , for the original data and with ionospheric model applied, 34 km baseline of Figure 4, observed under undisturbed ionospheric conditions.

| | original observations | ionospheric model applied |
|-----------------------------|-----------------------|---------------------------|
| correct ambiguities fixed | 45 (87%) | 50 (96%) |
| incorrect ambiguities fixed | 7 (13%) | 2 (4%) |

Table 1: Ambiguity fixing with GPSurvey, 15-min blocks of observations, 34 km baseline of Figure 4, undisturbed ionospheric conditions.

the original data and also for the corrected data (Fig. 5). The RMS of all double difference phase observations improved in L_1 from 0.18 cy to 0.09 cy and in L_W from 0.06 cy to 0.03 cy. Systematic effects of ionospheric refraction which can be identified by constantly large residuals over some period of time were considerably reduced. Whereas 95% of the L_W residuals were smaller than 9.9 cm before ionospheric correction, afterwards 95% of the L_W -residuals were smaller than 6.5 cm. But the corresponding figures for L_1 show no improvement (original data: 95% smaller than 7.0 cm, corrected data: 95% smaller than 7.2 cm). The ionospheric corrections considerably improved the L_1 -RMS value, but nevertheless the number of large residuals could not be reduced. Most probably, they are caused by L_1 -specific but non-ionospheric errors.

In order to verify whether the ionospheric corrections improve ambiguity resolution, 15-min blocks of obser-

vations were processed with a non-scientific manufacturer's software package (Trimble's GPSurvey 2.0). The GPS observations were loaded from RINEX-format, on the one hand the original observations and on the other hand RINEX phase and code observations after ionospheric correction. In 13% of the 15-min blocks, the ambiguity resolution algorithm selected an incorrect set of double difference ambiguities with the original data (the coordinate errors, obtained by comparison of the 15-min baseline solution with the results of the complete data set, considerably exceeded the test limits of 5 cm in the horizontal components or 8 cm in the vertical component). After application of the ionospheric correction this percentage was reduced to 4 (Table 1). The remaining failures are attributed to poor receiver-satellite-geometry causing large coordinate errors in the initial coordinate solution. Hence, with the exception of outages due to poor geometry, the ionospheric model guaranteed correct ambiguity resolution of a 34 km baseline, with 15-min blocks of observations and with a standard software package.

Medium-Size Ionospheric Disturbances

The most common ionospheric disturbances in mid-latitude regions are caused by medium-scale travelling ionospheric disturbances (MSTIDs). They mainly occur during daylight hours in winter months in years of maximum solar activity. They complicate ambiguity resolution even on baselines shorter than 10 km. Single-frequency coordinate errors can exceed 10 ppm of the baseline length (Wanninger 1993a).

An example of strong MSTIDs was found in a 9-hour

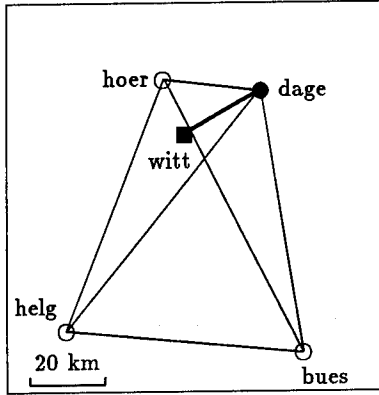


Figure 6:
Network of GPS monitor stations and
the 23 km baseline dage-witt.

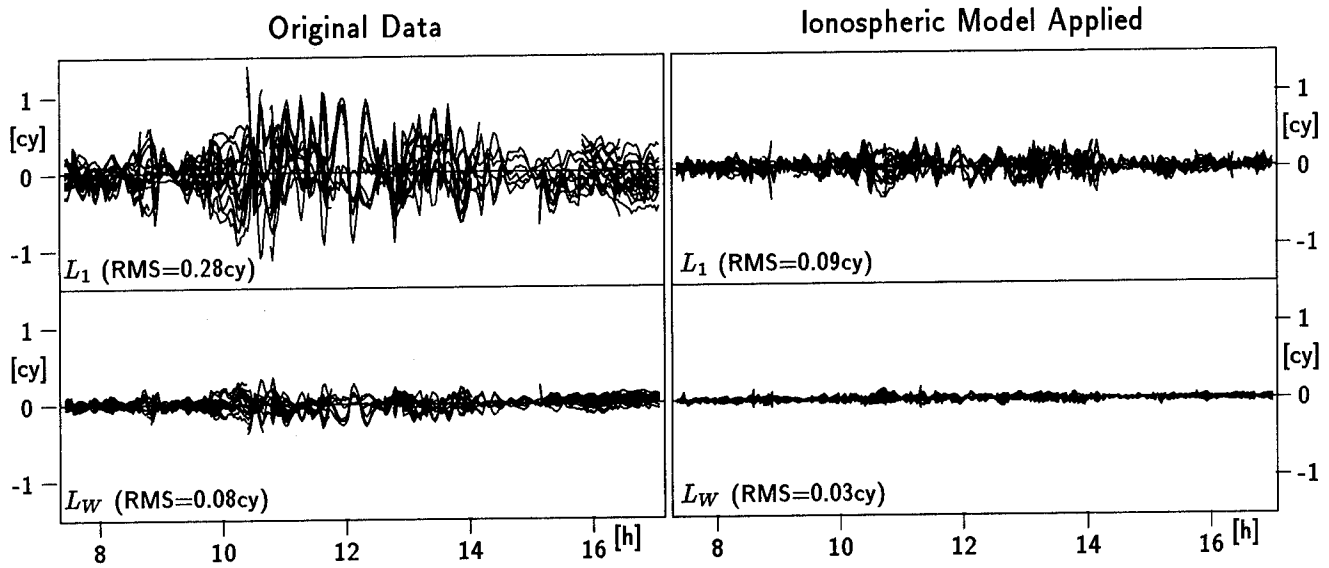


Figure 7: Double difference phase residuals after ambiguity fixing in all satellite combinations, in L_1 and widelane L_W , for the original data and with ionospheric model applied, 23 km baseline of Figure 6, observed during a period of ionospheric disturbances (medium-scale TIDs).

data set observed with Trimble SSE in North Germany on March 16, 1993 (Fig. 6). The analysis of the ionospheric conditions from dual-frequency phase observations revealed large and periodically changing ionospheric effects with typical MSTID-periods of 10 to 20 minutes. These effects can also be observed in the L_1 and L_W double difference phase residuals (Fig. 7). L_1 double difference phase residuals show periodic disturbances with amplitudes up to 1 cycle and periods of 15 to 30 minutes. Here, only epoch-by-epoch and satellite-by-satellite ionospheric modelling can produce accurate corrections.

The comparison of double difference phase residuals in L_1 and in L_W for the original data and for the corrected data demonstrates the successful application of the differential ionospheric model (Fig. 7). The RMS of all double difference phase observations improved in L_1 from 0.28 cy to 0.09 cy and in L_W from 0.08 cy to 0.03 cy. Whe-

reas 95% of the L_1 residuals were smaller than 11,0 cm (L_W : 14,0 cm) before applying ionospheric corrections, afterwards 95% of the L_1 -residuals were smaller than 3.5 cm (L_W : 4.9 cm). Consequently, the disturbing effects of MSTIDs could greatly be reduced.

In order to verify the improvement in ambiguity resolution, GPSurvey was used again to process 15-min blocks of observations of the baseline dage-witt. Whereas ambiguity resolution failed in 24% using the original data, the ambiguities of all 38 15-min blocks could correctly be solved after applying ionospheric corrections (Table 2). Hence, the ionospheric model guaranteed correct ambiguity fixing even under disturbed ionospheric conditions.

Moreover, the 23 km static baseline has been processed in kinematic mode and an ambiguity-fixed widelane solution has been produced, i.e. independent sets of coordinates have been calculated for every epoch using the wide-

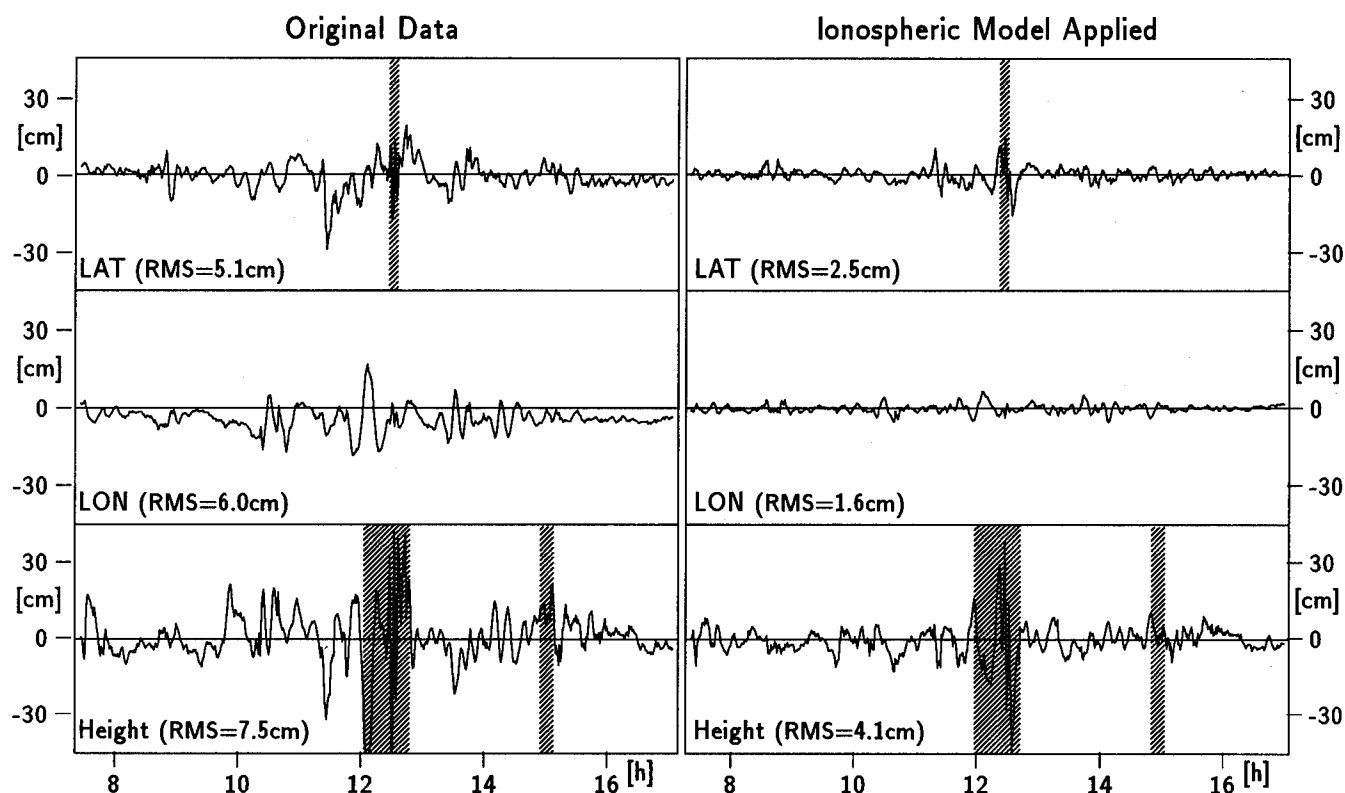


Figure 8: Coordinate errors of a kinematic processing (wideline solution) of the 23 km static baseline of Figure 6, observed during a period of ionospheric disturbances (medium-scale TIDs), shaded areas indicate periods with $DOP \geq 7$.

| | original observations | ionospheric model applied |
|-----------------------------|-----------------------|---------------------------|
| correct ambiguities fixed | 29 (76%) | 38 (100%) |
| incorrect ambiguities fixed | 9 (24%) | 0 (0%) |

Table 2: Ambiguity fixing with GPSurvey, 15-min blocks of observations, 23 km baseline of Figure 6, observed during a period of ionospheric disturbances (medium-scale TIDs).

lane linear combination. Two kinds of ionospheric effects can be distinguished (Fig. 8, original data), medium-scale TIDs causing errors with amplitudes up to 20 cm and with periods of 15 to 30 minutes, and errors constant over several hours due to the absolute ionospheric electron content (see e.g. the fairly constant error of -6 cm in longitude between 1400 and 1700 hours). Ionospheric corrections completely removed the latter effects and considerably reduced the effects of MSTIDs. The RMS of the coordinate errors improved from 5–6 cm to

1.5–2.5 cm in the horizontal components and from 7.5 to about 4 cm in the vertical component.

Conclusion

Regional differential modelling of the ionosphere based on dual-frequency observations of at least three GPS monitor stations can successfully be applied to reduce ionospheric effects on medium-length baselines and thus improve ambiguity resolution. Fast and on-the-fly ambiguity resolution can now be extended from short (≤ 10 km) to medium-length (10 – 50 km) baselines, thus reducing the required minimum observation time.

The requirement of complete dual-frequency ambiguity fixing in the network of monitor stations limits this approach to networks with baseline lengths of less than 50 to 100 km. If the modelling is to be performed in (near-) real-time ambiguity resolution in the network of monitor stations must be performed and checked continuously.

Despite those limitations, these regional ionospheric error models enhance differential GPS in medium-sized networks. Most of the ionospheric effects are removed even under ionospheric disturbed conditions. Ambiguity resolution is improved for all those techniques which rely on small ionospheric effects.

Acknowledgments The GPS observations were made available by the Landesvermessung Hannover, Dezernat Grundlagenvermessung (M. Strerath) and by the Institut für Erdmessung, Universität Hannover (H.-J. Goldan).

References

- Frei, E., Beutler, G. (1990): Rapid static positioning based on the Fast Ambiguity Resolution Approach: theory and first results, *manuscripta geodetica*, 15:325-356
- Georgiadou, Y., Kleusberg, A. (1988): On the effect of ionospheric delay on geodetic relative GPS positioning, *manuscripta geodetica*, 13:1-8
- Hatch, R. (1990): Instantaneous ambiguity resolution, *Proceedings of Kinematic Systems in Geodesy, Surveying, and Remote Sensing (IAG Symposium 107)*, Banff, Canada, September 1990, pp.299-308
- Mervart, L., Beutler, G., Rothacher, M., Wild, U. (1994): Ambiguity resolution strategies using the results of the International GPS Geodynamics Service (IGS), *Bulletin Géodésique*, 68:29-38
- Wanninger, L. (1993a): Der Einfluß ionosphärischer Störungen auf präzise GPS-Messungen in Mitteleuropa, *Zeitschrift für Vermessungswesen*, 118:25-36
- Wanninger, L. (1993b): Effects of the equatorial ionosphere on GPS, *GPS World*, July 1993, pp. 48-54
- Wanninger, L. (1995): Enhancing differential GPS using regional ionospheric error models, *Bulletin Géodésique*, 69:issue 4/95, in press.
- Webster, I., Kleusberg, A. (1992): Regional modelling of the ionosphere for single frequency users of the Global Positioning System, *Proceedings of the Sixth International Geodetic Symposium on Satellite Positioning*, Columbus, March 1992, Vol. I, pp. 230-239
- Wild, U., Beutler, G., Gurtner, W., Rothacher, M. (1989): Estimating the ionosphere using one or more dual frequency GPS receivers, *Proceedings of the Fifth International Geodetic Symposium on Satellite Positioning*, Las Cruces, March 1989, Vol. II, pp. 724-736
- Wübbena, G. (1989): The GPS adjustment software package GEONAP – concepts and models, *Proceedings of the Fifth International Geodetic Symposium on Satellite Positioning*, Las Cruces, March 1989, Vol. I, pp. 452-461

An Efficient Algorithm for Batch Estimation of Non-Dynamic Parameters of Double-Differenced GPS Phase Measurement

H. Rim, B. Schutz, and B. Tapley
Center for Space Research, University of Texas at Austin

BIOGRAPHIES

H. J. Rim received his B.S. and M.S. from Seoul National University, Department of Aeronautical Engineering. He received his Ph.D. from the University of Texas at Austin, Department of Aerospace Engineering and Engineering Mechanics, in 1992. He is currently a research associate at the Center for Space Research, where his efforts include GPS-based precise orbit determination for Topex/Poseidon, EOS ALT/GLAS, and geodetic applications of GPS.

B. E. Schutz is Professor of Aerospace Engineering and Engineering Mechanics at the University of Texas at Austin and holds the Gulf Oil Foundation Centennial Fellowship in Engineering. He is also Associate Director of the Center for Space Research and a member of the Applied Research Laboratory staff.

B. D. Tapley is Professor of Aerospace Engineering and Engineering Mechanics at the University of Texas at Austin and holds the Clare Cockrell Williams Centennial Chair in Engineering. He established the orbit mechanics program in the ASE-EM department in 1961 and the Center for Space Research in 1981, developing both into international centers for study and research. He also serves as the Director of the Texas Space Grant Consortium.

ABSTRACT

The dual frequency GPS phase measurement is commonly used for the high precision GPS geodetic applications. Processing this particular data type involves solving several non-dynamic parameters, such as the ambiguity parameters and the tropospheric parameters. The total number of these measurement parameters to be estimated grows as the number of GPS satellites and ground stations increases, or as the arc length becomes longer, which in turn, requires allocation of large amounts of computer memory. These parameters have special characteristics in their correlation relation with each other. The parameters adjacent in time are highly correlated, while parameters separated in time are not. This special correlation property allows the correlation between time-separated parameters to be ignored, thereby reducing the

parameter set which must be in the memory at any given time. Also, the size of the parameter set which will reside in the memory does not depend on the arc length. Two different types of GPS tracking data have been processed using this approximation to demonstrate significant reduction on computer memory usage and computation time without losing the accuracy level for other geodetic parameters. One is the data set from IGS campaign, the other is the data set from Topex/Poseidon (Topex). The memory requirement reduced by 23% for IGS data and 46% for the Topex data to process one day worth of these data. CPU time also reduced by 26% on Cray J90/16, and by 38% on HP 735/125 workstation for IGS data, while 32% and 64% reduction in CPU time demonstrated for Topex data on Cray J90/16 and HP 735/125, respectively.

INTRODUCTION

For the high precision GPS geodetic applications, the dual frequency GPS phase measurement is commonly used these days. For this particular data type, the phase ambiguity terms should be determined either by the ambiguity resolution techniques or by simply estimating ambiguity parameters. In addition to the ambiguity parameters, the tropospheric parameters should be estimated to account for the media effect for this data type. In the context of the batch estimation, the total number of these measurement parameters to be estimated grows as the number of GPS satellites and ground stations increases, or as the arc length becomes longer.

Figure 1 shows the linear increase of these parameters as the arc length increases. A typical 1-day arc for the International GPS Service (IGS) data from about 30 ground stations requires estimation of more than 1000 non-dynamic parameters. For the Topex data, more than 1600 parameters should be estimated for a 1-day arc from 24 stations. Batch estimation of large number of these parameters requires, in turn, allocation of large amounts of computer memory. Figure 2 compares the memory requirement for processing IGS data and the Topex data for up to 3-day arcs. Figures 3 and 4 demonstrate the CPU time spent on Cray J90 and HP735 for each data type to be processed.

These parameters have special characteristics in their correlation relation with each other. The parameters

adjacent in time are highly correlated, while parameters separated in time are not, as demonstrated in Figure 5. It shows the parameters which have the correlation coefficient greater than 0.7. This special correlation property allows the correlation between time-separated parameters to be ignored, thereby reducing the parameter set which must be in the memory at any particular time. Also, the size of the parameter set which will reside in the memory does not depend on the arc length.

Two different types of GPS tracking data have been processed using this approximation to demonstrate significant reduction on computer memory usage and computation time without losing the accuracy level for other geodetic parameters. One is the data set from IGS campaign, the other is the data set from Topex.

ASSUMPTIONS

This algorithm was developed under certain assumptions. The data type was assumed to be the double-differenced GPS phase measurement. Comparing to the undifferenced phase data, there exists correlations between measurements that must be taken into account to avoid the processing of redundant information (Bierman, 1977). Also, the double-differenced ambiguity parameters were solved in the estimation process. This algorithm was based on a batch-least squares estimation procedure (Tapley, 1973) using square-root free Givens algorithm (Gentlemen, 1973). This algorithm was implemented in the MSODP1 (Multi-Satellite Orbit Determination Program 1), which is a GPS data processing software at CSR (Rim, 1992). Currently, this software runs on Cray J90/16 and HP735/125. And the performance of this algorithm was evaluated on both machines.

DATA SETS

Two types of double-differenced GPS phase observations were processed to evaluate the pass algorithm. One is the double-differenced data between ground stations, such as the IGS data. The other is the double-differenced data between a ground station and Topex/Poseidon satellite. Three days worth of data for both data type were processed from April 23, 1995. 24 GPS satellites from 32 ground stations were used for IGS data, while 24 stations were used for Topex data. For both data sets, 1-day, 2-day, and 3-day arcs were processed. The epoch state, a scale factor of ROCK4, and daily y-bias parameters were adjusted for each GPS, and the ambiguity parameters, 2.5-hour tropospheric zenith delay parameters for all ground stations, and coordinates of selected ground stations were estimated for both data type. The epoch state, daily constant along-track parameter (C_p), and daily once per orbital revolution amplitude and phase coefficients in the along-track and cross-track directions for Topex were adjusted for Topex data.

THE PASS ALGORITHM

The pass algorithm is summarized in Table 1. The observation file is read prior to the data processing to check the pass information for the ambiguity and the tropospheric parameters, which includes the pass number, start and end time for each pass. Assign $mamb+mtrop$ pass parameters in the first part of the estimation vector. After read m observations at any time t , check the latest ambiguity $id-lamb$, and the tropospheric parameter $id-ltrop$. If $lamb$ exceeds $mamb$, save the 1st row of DUZ into a disk space, and rearrange the DUZ such as the 2nd row becomes the 1st row, 3rd row becomes 2nd row, and so on until the $mamb$ -th row becomes $mamb-1$ -th row. Reinitialize the $mamb$ -th row so that this location could be used for the $mamb+1$ -th ambiguity parameter. Repeat the above procedure $lamb-mamb$ times. Same steps are followed for the tropospheric parameters. After process all the observations, the saved DUZ information is used to solve for the ambiguity and the tropospheric parameters using the back-substitution.

PERFORMANCE EVALUATION

To evaluate the pass algorithm, three different cases were compared in terms of the size of the estimation vector, the computer memory usage, and the computation time. Those cases were 1) assigning ambiguity parameters and the tropospheric parameters as the global parameters—**Global** case, 2) treating ambiguity parameters as the pass parameters, while keeping the tropospheric parameters as the global parameters—**Session** case, and 3) treating the ambiguity and tropospheric parameters as the pass parameters—**Pass** case. For each case, 1-day, 2-day, and 3-day arcs were processed for both IGS data and Topex data.

Figure 6 shows the size of the estimation vector for both data sets. For IGS data, the number of ambiguity parameters was reduced to about 250 for Session and Pass cases, and the number of tropospheric parameters was reduced to 150 for Pass case. For Topex data, the number of ambiguity parameters was reduced to 83 for Session and Pass cases, and the number of tropospheric parameters was reduced to 120 for Pass case. Note that these reduced number of parameters does not depend on the arc length. Comparing to the Global case for IGS data, 41%, 53%, and 60% reduction in the estimation vector size was achieved for the Session case in 1-day, 2-day, and 3-day arcs, respectively. For the Pass case, 51%, 71%, and 79% reduction was demonstrated for 1-day, 2-day, and 3-day arcs, respectively. For the Topex data, more reduction in the estimation state vector size was attained, such as 69%, 76%, and 79% for Session case, and 75%, 86%, and 90% for Pass case in 1-day, 2-day, and 3-day arcs, respectively.

Figure 7 shows the computer memory requirement for each case. For IGS data, the required memory was

reduced by 19%, 48%, and 64% for Session case, and by 23%, 57%, and 73% for Pass case for 1-day, 2-day, and 3-day arcs, respectively, comparing to the Global case. For Topex data, the memory usage dropped by 46%, 73%, and 84% for Session case, and by 46%, 76%, and 88% for Pass case in 1-day, 2-day, and 3-day arcs, respectively. Note also that the required memory stayed at the same level even though the arc length increased.

Figure 8 shows the CPU time on Cray J90/16 for each case. For IGS data, the CPU time reduced by 16%, 27%, and 36% for Session case, comparing with Global case, and further reduction of 26%, 45%, and 56% achieved for Pass case for 1-day, 2-day, and 3-day arcs. For Topex data, 28%, 51%, and 65% improvement achieved in CPU time for Session case, and 32%, 55%, and 69% for Pass case in processing 1-day, 2-day, and 3-day arcs.

Figure 9 shows the CPU time on HP735/125 for each case. For IGS data, 25%, 39%, and 47% decrease in CPU time occurred for Session case, and 38%, 61%, and 73% for Pass case. For Topex data, more reduction in CPU time was demonstrated, such as 60%, 74%, and 86% reduction for Session case, and 64%, 79%, and even 90% for Pass case. Note that the quadratic increase of the CPU time with arc length for Global case became a linear trend for Pass case on both machines, since the number of observations linearly increased as the arc length increased, while the required memory stayed about the same level. All of the above comparisons were summarized in Table 2.

SOLUTION EVALUATION

Table 3 compares the Global orbit solutions with the Session and the Pass orbit solutions. The maximum orbit difference in 3-dimensional RSS was less than 1 mm for the Pass solutions, while there was no difference in the orbit solutions for the Session cases. Also, the difference in the estimated station coordinates between the Session case and the Global case was zero, while the maximum difference for the Pass cases was less than sub-mm. These results conform the validity of the approximation of

ignoring the correlation between time-separated non-dynamic parameters.

CONCLUSIONS

Significant reduction in the computer memory usage and the computation time was demonstrated for processing the double-differenced GPS phase measurement using the pass algorithm. It was also demonstrated that the solution accuracy for other parameters was preserved when this algorithm was employed. Since the pass algorithm requires about the same level of memory usage for different arc length, this algorithm definitely paves an efficient way to explore longer arcs than the traditional 1-day arcs in GPS data processing using a batch least-square estimation technique.

ACKNOWLEDGMENTS

This research was sponsored by NASA Contract NAS 5-33021. The data preprocessing effort by Young-Sun Nam was deeply appreciated. Greg Baker made a major contribution for porting MSODP1 on HP735.

REFERENCES

- Bierman, G. J., *Factorization Methods for Discrete Sequential Estimation*, Academic Press, New York, NY, 1977.
- Tapley B. D., "Statistical Orbit Determination Theory", *Advances in Dynamical Astronomy*, pp. 396-425, D. Reidel Pub. Co., Holland, 1973.
- Gentleman, M. W., "Least Squares Computations by Givens Transformations Without Square Roots", *J. Inst. Math. Appl.*, Vol. 12, pp. 329-336, 1973.
- Rim, H. J., *Topex Orbit Determination Using GPS Tracking System*, Ph. D. Dissertation, The University of Texas at Austin, December 1992.

Table 1. Pass Parameter Algorithm

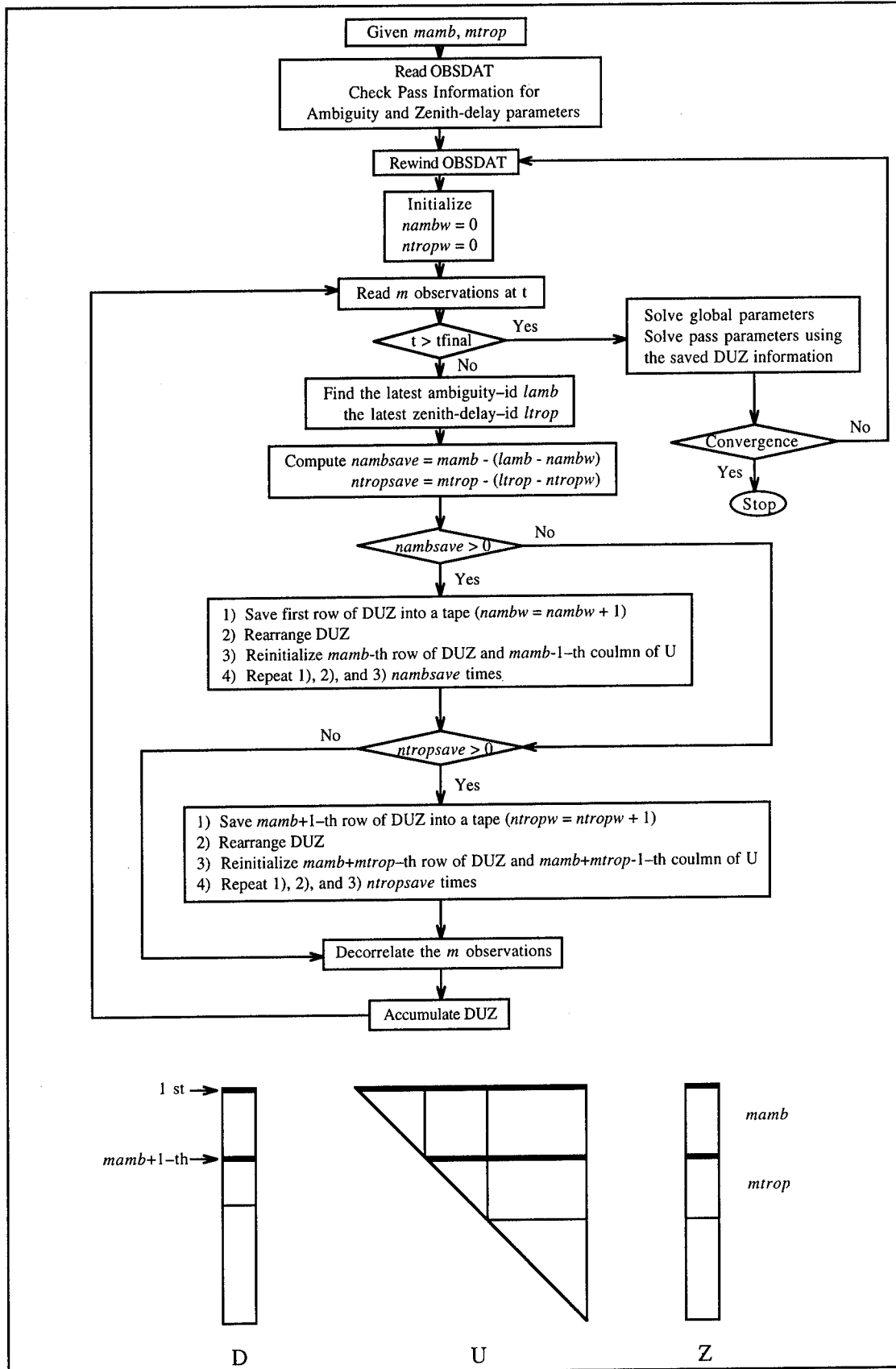


Table 2. Summary of Performance Evaluations

| Case | Arc (days) | Parameter Type | Number of Parameters | Memory (Mw) | CPU (min) | |
|-------|---------------|-------------------|-------------------------|----------------|-----------|-------|
| | | | | | Cray J90 | HP735 |
| IGS | 1 | Global | 1281 | 2.6 | 21.3 | 58.8 |
| | | Session | 757 | 2.1 | 17.8 | 43.9 |
| | | Pass | 633 | 2.0 | 15.7 | 36.2 |
| | 2 | Global | 2352 | 4.6 | 61.2 | 208.0 |
| | | Session | 1094 | 2.4 | 44.4 | 127.8 |
| | | Pass | 687 | 2.0 | 33.8 | 80.6 |
| | 3 | Global | 3454 | 7.8 | 125.2 | 455.5 |
| | | Session | 1389 | 2.8 | 79.8 | 241.0 |
| | | Pass | 712 | 2.1 | 54.9 | 124.8 |
| Topex | 1 | Global | 1874 | 3.5 | 11.1 | 28.2 |
| | | Session | 573 | 1.9 | 8.0 | 11.4 |
| | | Pass | 464 | 1.9 | 7.6 | 10.1 |
| | 2 | Global | 3541 | 7.9 | 36.5 | 111.7 |
| | | Session | 840 | 2.1 | 17.9 | 28.8 |
| | | Pass | 493 | 1.9 | 16.5 | 22.9 |
| | 3 | Global | 5266 | 15.2 | 87.5 | 400.2 |
| | | Session | 1115 | 2.4 | 30.6 | 54.4 |
| | | Pass | 522 | 1.9 | 27.2 | 38.3 |

Table 3. Maximum RSS Orbit Difference with Global Solution [mm]

| Case | Arc | | | | | |
|-------|---------|-------|---------|------|---------|------|
| | 1 day | | 2 day | | 3 day | |
| | Session | Pass | Session | Pass | Session | Pass |
| IGS | 0 | < 0.1 | 0 | < 1 | 0 | < 1 |
| Topex | 0 | 0 | 0 | < 1 | 0 | < 1 |

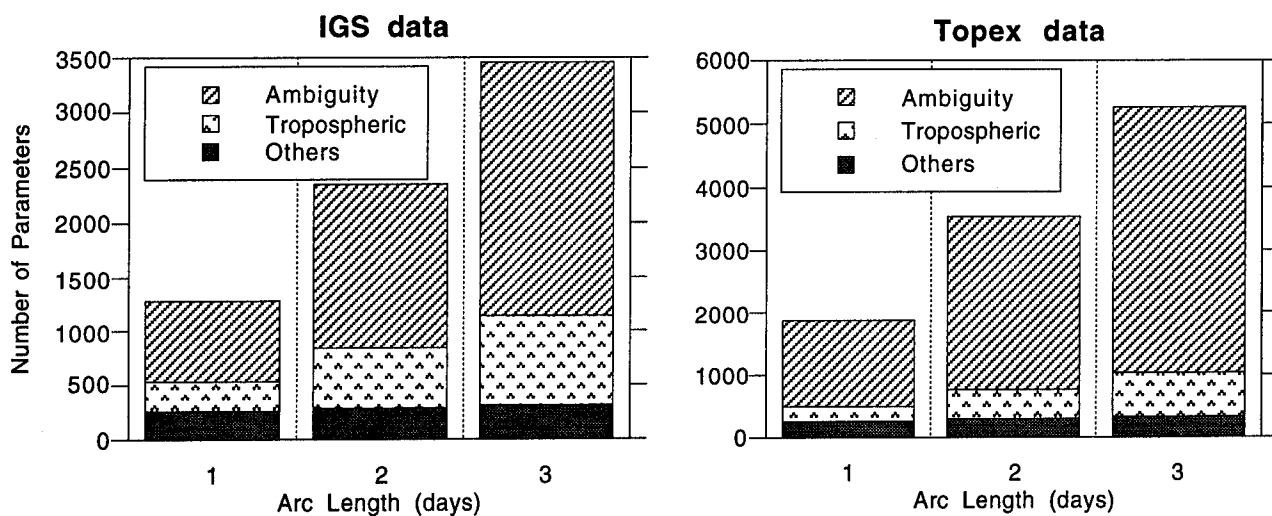


Figure 1. Number of Estimated Parameters

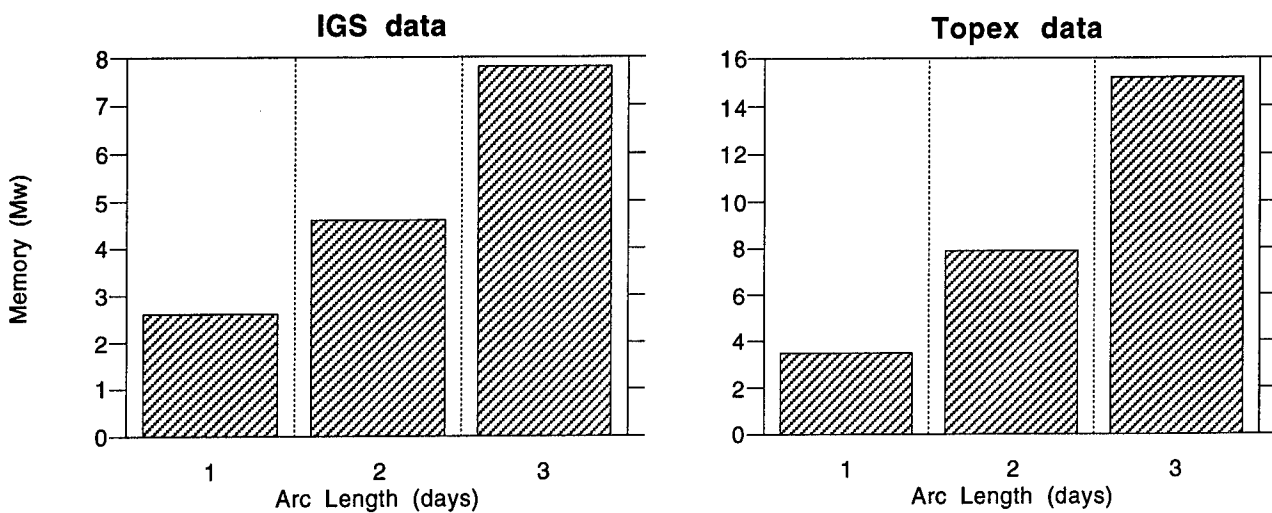


Figure 2. Required Computer Memory [Mw]

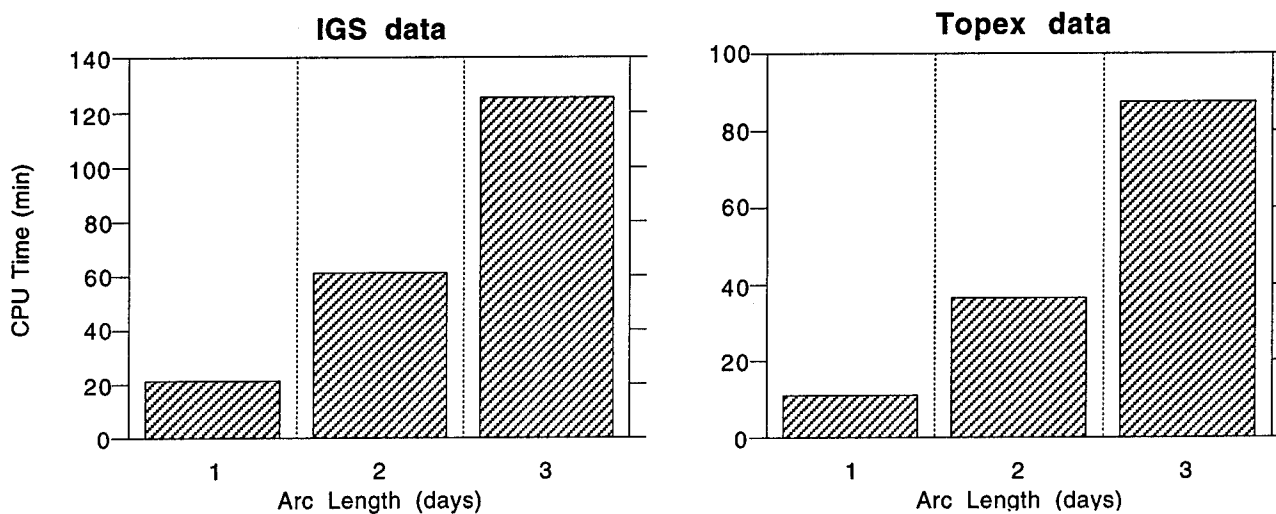


Figure 3 CPU Time on Cray J90 [min]

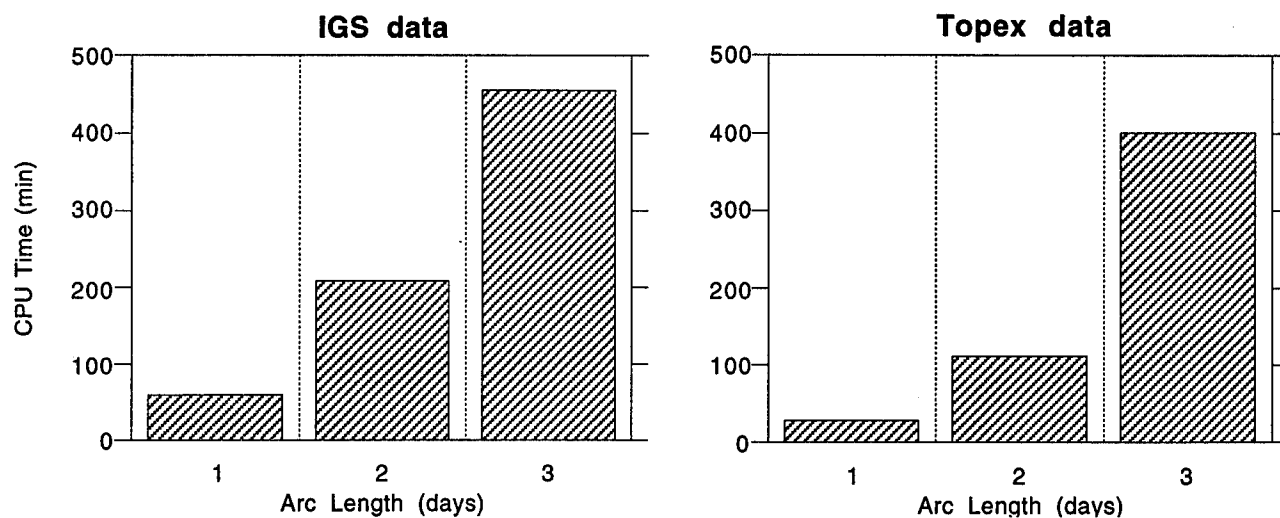


Figure 4. CPU Time on HP735 [min]

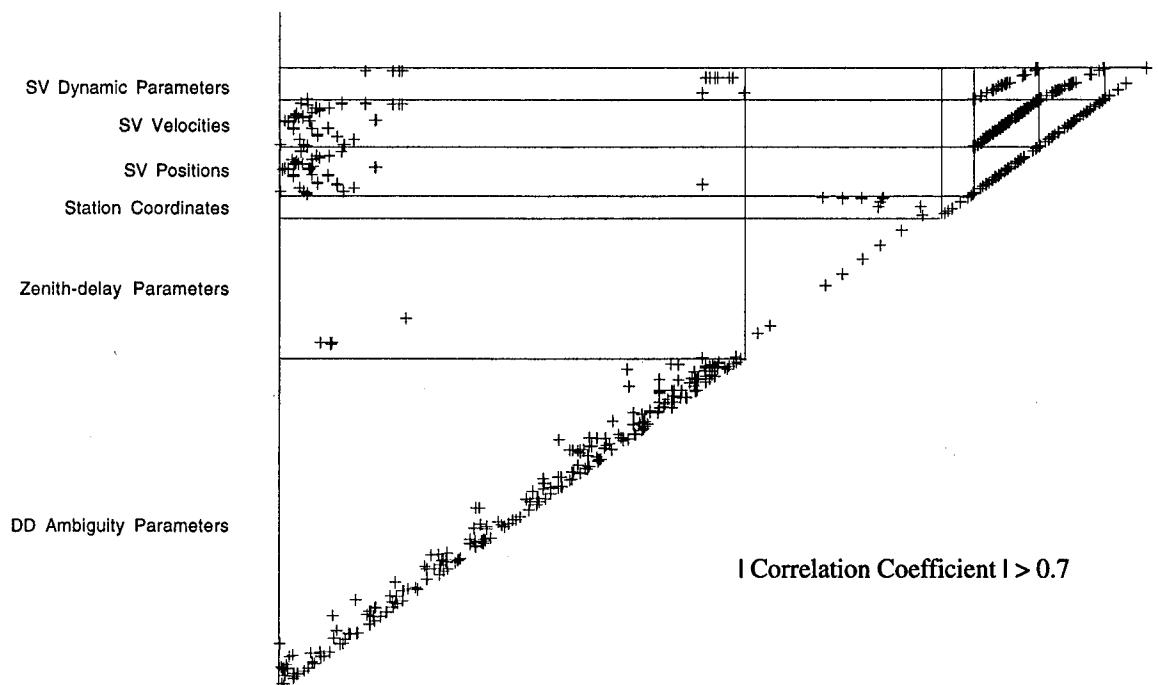


Figure 5. Highly Correlated Parameters

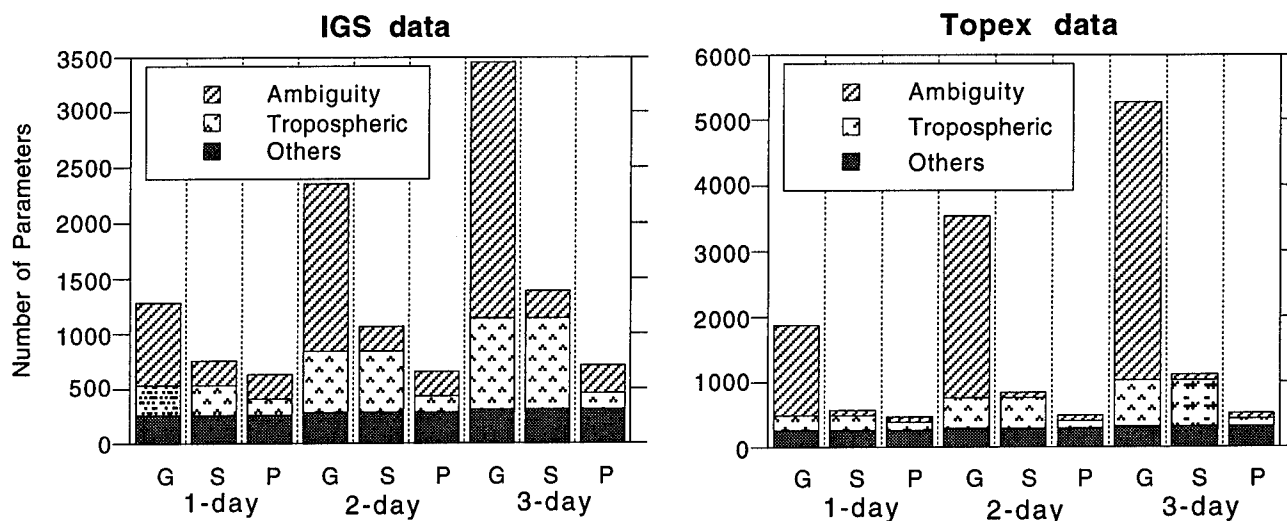


Figure 6. Number of Estimated Parameters (G-Global; S-Session; P-Pass)

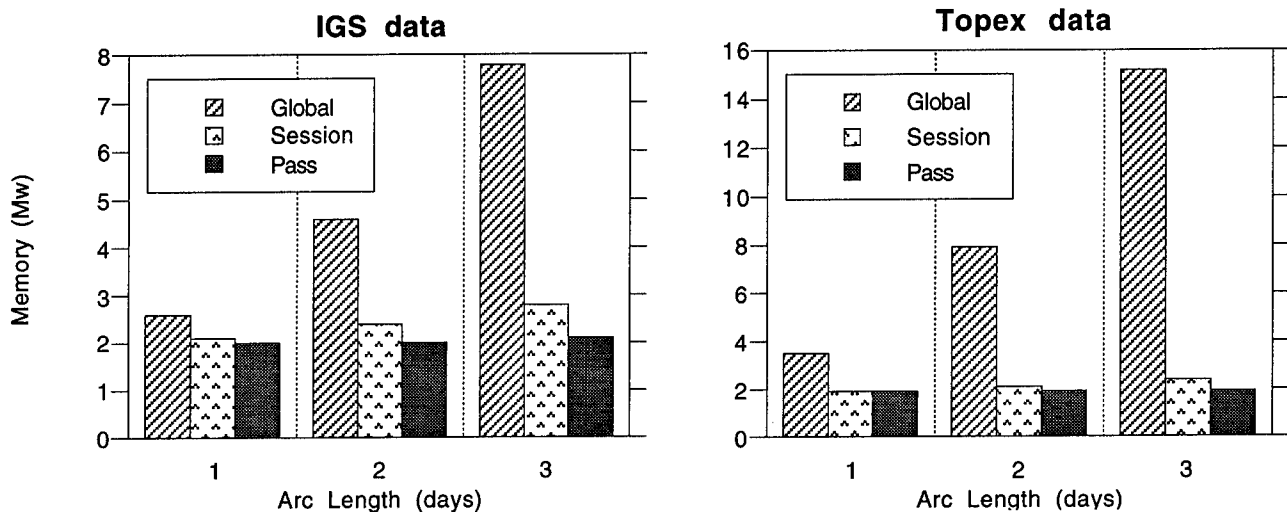


Figure 7. Required Computer Memory [Mw]

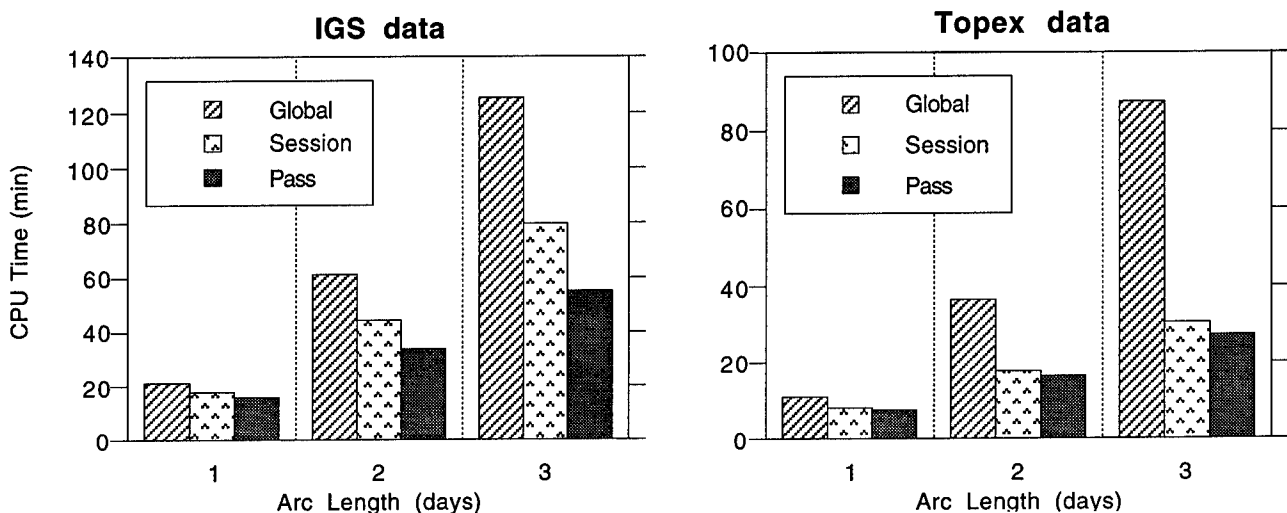


Figure 8. CPU Time on Cray J90 [min]

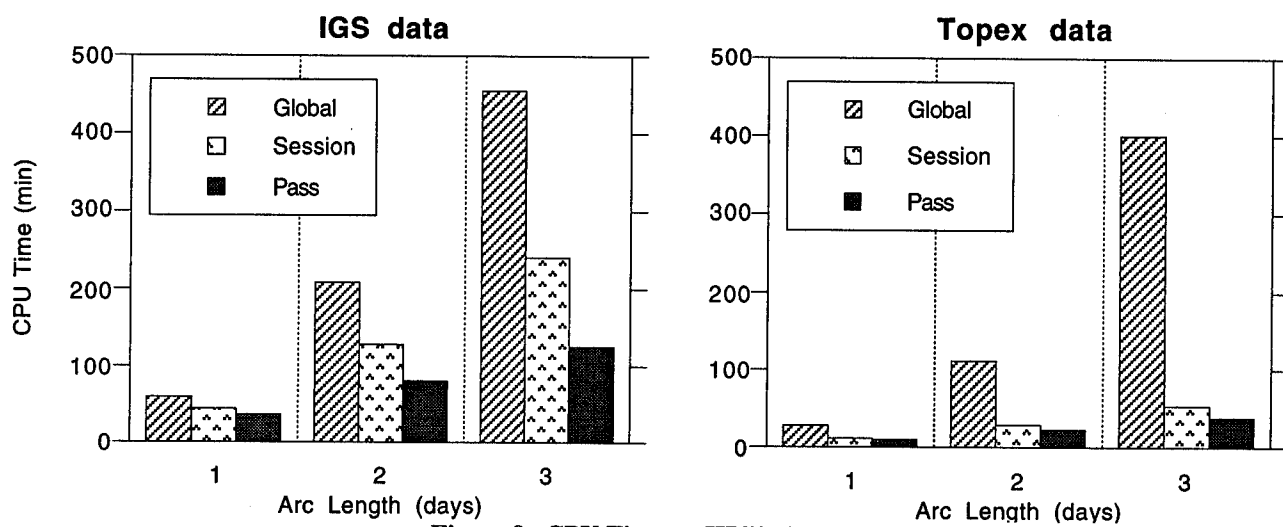


Figure 9. CPU Time on HP735 [min]

Determining Earth Orientation by Global Positioning System at the US Naval Observatory

Peter Kammeyer and James Rhode
US Naval Observatory

BIOGRAPHY

Peter C. Kammeyer received in 1970 a B.S. from the University of Washington and in 1974 a Ph.D. from New York University, both in mathematics; his thesis studied periodic satellite orbits. From 1982 to 1986 he participated in many launches and orbit maneuvers at Communications Satellite Corporation. He came to the Nautical Almanac Office of the U.S. Naval Observatory in 1986 and has worked at the Observatory on ephemeris compression, on optical space tracking, and on other aspects of astrodynamics.

James R. Rohde received a B.Sc. in astrophysics from Indiana University in 1978 and an M.A. in astronomy from the University of Virginia in 1984. At the University of Virginia he studied stellar and solar system astrometry. In 1985, he came to the Nautical Almanac Office of the U.S. Naval Observatory, and he has worked at the Observatory on planetary satellite ephemerides and on propagation of Earth satellite orbits.

In 1994, both authors were transferred to the Earth Orientation Department of the Time Directorate of the U.S. Naval Observatory to begin the Observatory's effort to determine Earth orientation parameters by analysis of GPS orbits.

ABSTRACT

The U.S. Naval Observatory determines the orientation of the Earth from its observations of distant celestial radio sources, also including in this determination other sources of data. Because of the expense of the radio observations, the Observatory would like, if possible, to reduce the required observing time. To maintain accurate knowledge of Earth orientation between observations in a reduced schedule, the Observatory desires to use analysis of observations of GPS satellites.

The Observatory's effort to analyze GPS satellite orbits is directed toward the determination of both polar motion and UT1, the rotation angle of the Earth around its axis. This effort uses a combination of the JPL GIPSY software and additional software developed at the Observatory. Determination of polar motion by analysis of GPS orbits began on a trial basis at the Observatory in late 1994. This paper will report the results obtained for polar motion parameters and give the results of an experiment determining UT1 from length-of-day values found in GPS analysis.

The Observatory's effort to determine UT1 has further led to determination of a mean rate for that part of the motion of the orbit pole, the unit vector normal to the orbit, coming from once-per-revolution terms in radiation pressure acceleration with the effect of varying distance from the sun removed. This additional mean rate depends on the position of the Sun relative to the orbit plane, and that dependence remains nearly the same from year to year. We have thus concluded that it will be possible to obtain UT1, between calibrations by VLBI every two weeks, with an rms error less than 0.2 millisecond.

INTRODUCTION

The U.S. Naval Observatory presently determines Earth orientation from its observations of distant radio sources by very long baseline interferometry (VLBI), also including in this determination other sources of data. In recent years, as reported in the International Earth Rotation Service (IERS) Annual Report, IERS (1993), the Observatory has been able, within a few days, to provide Earth orientation values with rms errors of 1 milliarcsecond for polar motion components and 0.14 millisecond (corresponding to 2.1 milliarcseconds) for UT1. After a few weeks, rms errors have decreased to 0.3 milliarcseconds for polar motion components and 0.03 milliseconds for UT1. The Observatory would

like, if possible, to reduce the required VLBI observing time while maintaining the same level of accuracy.

The Observatory's effort to analyze GPS satellite orbits is directed toward determining polar motion and toward achieving the desired reduction in the VLBI observing time required to determine UT1. This effort has used the GIPSY software developed at JPL (Webb and Zumberge(1993)) and also software developed at the Observatory. Determination of polar motion by analysis of GPS orbits began on a trial basis in late 1994 and has approached the accuracy desired for final values of polar motion components. Our values of polar motion components are now among those from which are calculated the results reported in IERS Bulletin A.

A one-hour-long VLBI observation of distant radio sources by two antennas can be combined with polar motion components determined from analysis of GPS orbits to give a value of UT1R (UT1 with zonal tide terms of period up to 35 days removed) having rms error under 0.03 millisecond. We have recently propagated UT1R, by integrating length-of-day values coming from analysis of GPS orbits, over two weeks with an rms error of a few tenths of a millisecond.

Another way to determine UT1R is to propagate the *orbit pole*--the unit vector in the direction of the angular momentum vector--for each GPS satellite and then obtain UT1R from the comparison between the propagated orbit poles and those determined relative to the body of the Earth by analysis of GPS orbits. We have therefore studied how well one can from past experience predict a GPS orbit pole.

Suppose that the orbit of a spacecraft is circular, that one can ignore the effect of the spacecraft's varying distance from the Sun, that the Earth may be treated as a uniformly reflecting sphere, that the spacecraft's physical properties remain constant, and that the spacecraft's configuration and attitude depend only on the relation between the positions of the Earth and the Sun as observed from it. The spacecraft's radiation pressure acceleration, relative to the orbit pole and the Sun direction, will then depend only on the angle between them and the angle around the orbit to the spacecraft from the projection of the Sun direction. If thruster firings are rare and sufficiently accurate models of other accelerations are used (the gravity model used in our study, JGM-2, is of extremely high quality, as described by Nerem et al. (1995)), the motion of the spacecraft's orbit pole due to radiation pressure acceleration can be determined.

Consider a hypothetical satellite, in a circular orbit in the actual orbit plane, the radius of the hypothetical orbit equal to the actual semimajor axis. The actual radiation pressure, given as a function of angle from ascending node, will cause a motion of the orbit pole for this hypothetical satellite. We will call the mean rate of this motion the *additional mean rate* of orbit pole motion.

Only the component of radiation pressure acceleration which is normal to the orbit plane can affect the orbit pole. The effect, on the motion of the orbit pole of the hypothetical orbit, of each Fourier component of the orbit-normal acceleration can be found from Hill's equations of relative motion, which are discussed by Kaplan (1976) and which are closely related to subjects discussed in Szebehely (1967). Terms with frequencies other than once per revolution can produce only periodic motions of the hypothetical orbit pole. A once-per-revolution term causes, to first order in eccentricity, the same effect on the actual and hypothetical orbit poles.

We call the mean rate of the motion of the pole of the hypothetical orbit the *additional mean rate* because we will break orbit pole motion due to radiation pressure acceleration into that for a perfectly absorbing sphere, which we will treat exactly, and that due to an additional acceleration, which we will treat by approximate methods. The sphere's radiation pressure acceleration, which is constant and thus has no effect on the orbit pole of the hypothetical orbit, will be removed from the part of the orbit pole motion which we will study.

We will determine the additional mean rate by fitting a linear function of time to the angular momentum change, during a one-month fitting interval, arising from the additional acceleration. Fitting a linear function to angular momentum change causes errors to be divided by the fitting interval. The desired part of the angular momentum change will be determined by removing, from the angular momentum change, that part not desired. The part of angular momentum change to be removed is, for each day, that from the beginning to the end of the day for an approximate orbit close to the actual orbit but with once-per-revolution normal accelerations set to zero. From angular momentum values for these approximate orbits are also calculated day-to-day angular momentum changes for the additional acceleration.

In this paper, the fitted angular momentum values are those at a particular time each day. A more accurate approach would fit angular momentum values for the time each day when the satellite and the Sun are in the same half plane bounded by the line containing the angular momentum direction and passing through the center of the Earth. A further

improvement would be to determine angular momentum values from a closer approximation to the reported orbit than the one-day approximation just described.

Determining the additional mean rate is most closely related to the work of Colombo(1989) and Beutler *et al.* (1994). As they did, we paid particular attention to once-per-revolution accelerations and used Hill's equations of relative motion. Like Colombo, we analyzed accelerations into components in the radial and orbit-normal directions together with the direction orthogonal to these: the GIPSY software allows specifying accelerations in these three directions. Like Beutler *et al.*, we found that accelerations become much simpler when analyzed with respect to directions defined using the Sun direction.

Every few days during 1993 and 1994, and for several satellites, we determined the additional mean rate. The largest additional mean rate determined was approximately 2 milliarcseconds per day. This corresponds to an acceleration of approximately 10^{-12} kilometer/second², one per cent of the total radiation pressure and roughly the size of the y-bias included in analyses by other workers, such as Fliegel *et al.* (1992). Our description of orbit-normal accelerations is closer to what is actually observed

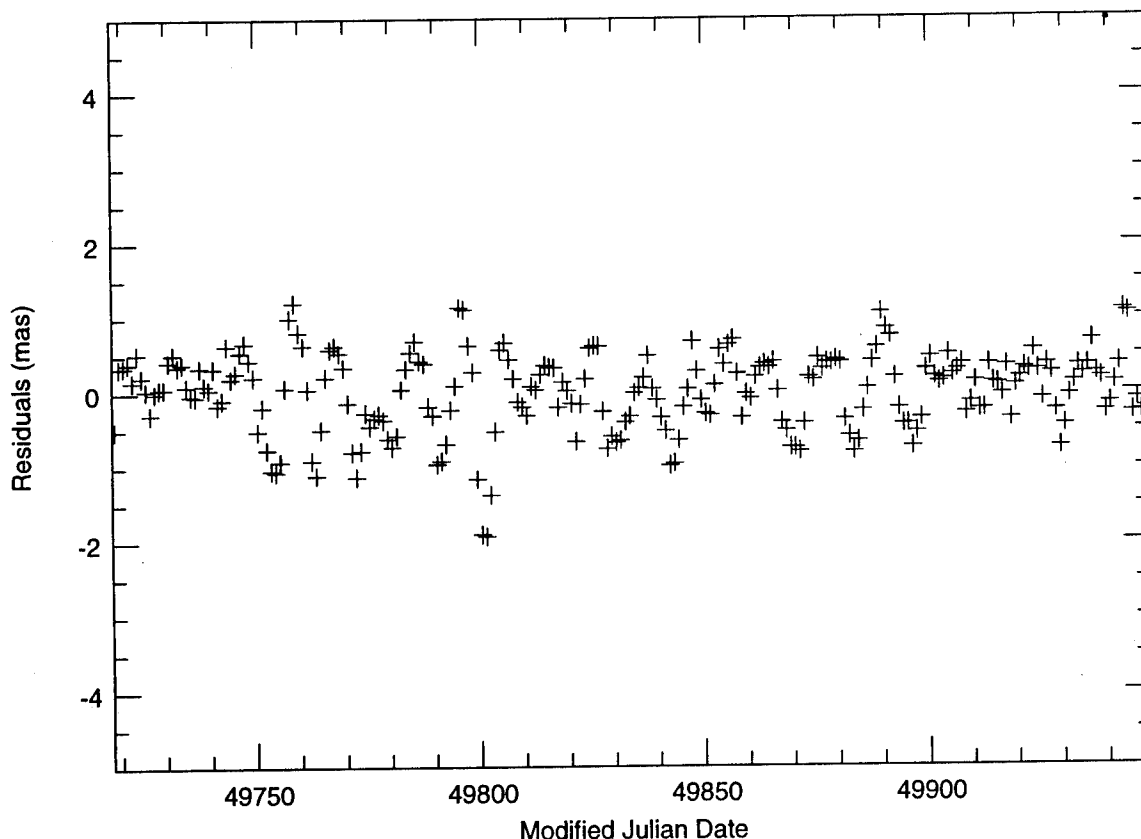
than would be one using y-bias, but an analysis by Slabinski (1995) suggests that a description using y-bias may eventually prove more compact.

The dependence of the determined additional mean rate on the position of the Sun relative to the orbit plane varies little from year to year. For each value of the angle from orbit pole to Sun, determined additional-mean-rate values are similar for different GPS satellites. When determined additional-mean-rate was converted to a once-per-revolution acceleration normal to the orbit plane and equations of motion including that acceleration were solved, the orbit pole was accurately propagated. From our results we have concluded that the use of past experience to predict the additional mean rate will allow determining UT1R with an rms error less than 0.2 millisecond for a two-week period between calibrations with VLBI data.

DAILY GPS ANALYSES

Differences between values for the polar motion component x determined by analysis at U.S. Naval Observatory of GPS orbits in 1995 and corresponding U.S. Naval Observatory final values have a mean of -0.31 milliarcsecond. These differences have an rms difference from their mean of 0.52 milliarcsecond and are shown in Figure 1.

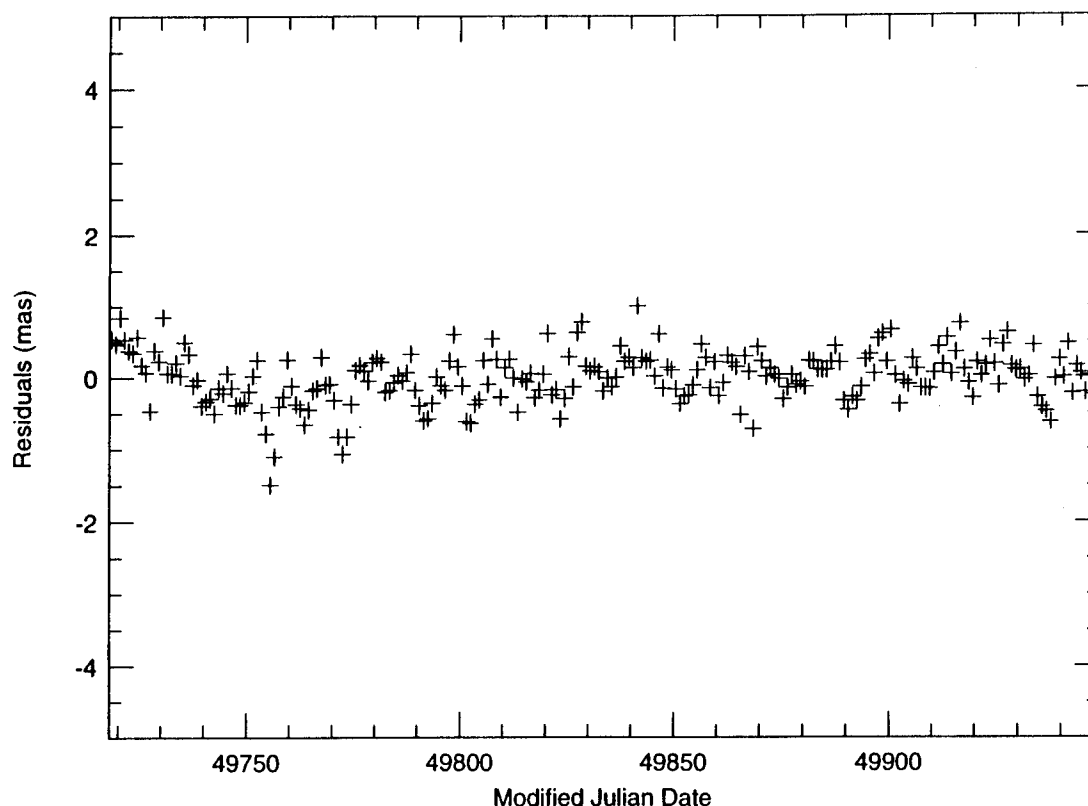
Figure 1. X pole, USNO GPS - USNO final



Differences between values for the polar motion component y, beginning with January 1, 1995, and Naval Observatory final values have a mean of 0.29

milliarcsecond. Deviations of this y residual from the mean have an rms value of 0.36 milliarcsecond and are shown in Figure 2.

Figure 2. Y pole, USNO GPS - USNO final



The Observatory has used GIPSY since 13 November, 1994 to perform daily analyses of GPS observations and, thus, to determine polar motion. At present, a set of 42 globally distributed stations is used. The observations are acquired from the Crustal Dynamics Data Information System (CDDIS) at Goddard Space Flight Center within three days after they are made. When the analysis is done, 35 to 40 stations will typically have reported observations. The number and distribution of the stations has evolved somewhat since the analyses began, as have the methods for dealing with questionable data.

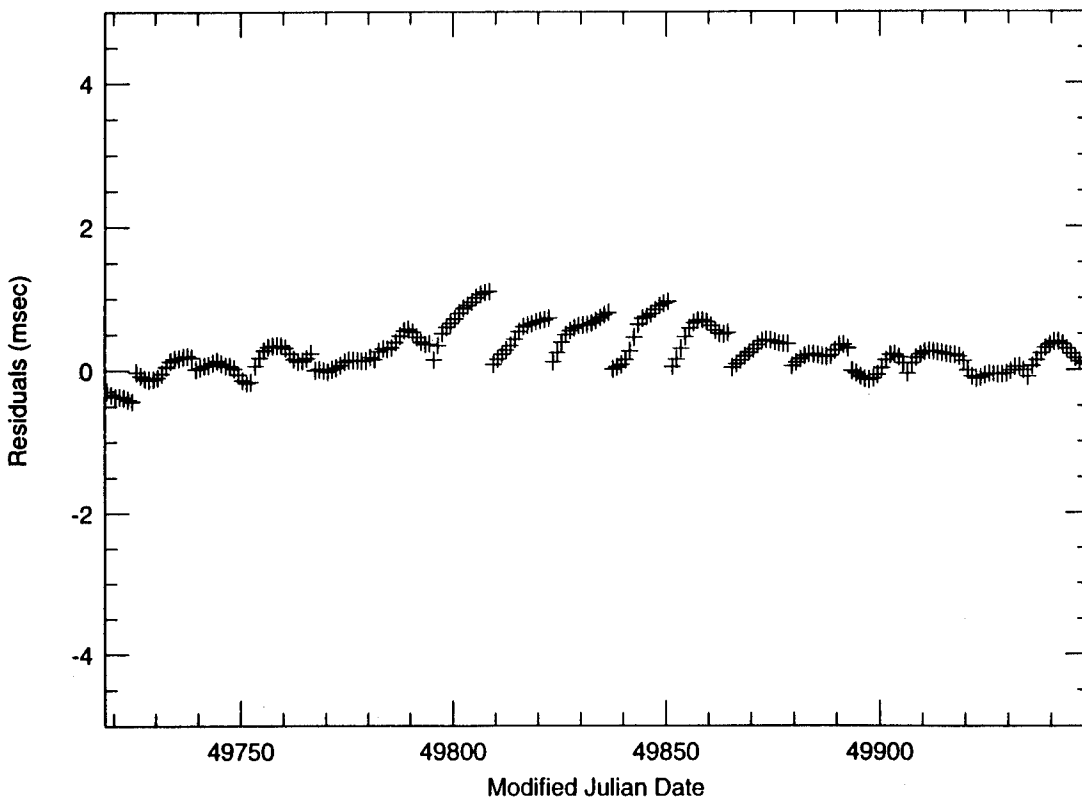
We desired to learn how well length-of-day values found in our daily analysis of GPS orbits could be used to propagate UT1R over two week periods. We chose a contiguous sequence of two-week periods beginning on January 1, 1995. For each period, final Naval Observatory UT1-UTC values for six days centered at the beginning of the period were converted to UT1R-UTC; starting values of UT1R-UTC and length of day were obtained numerically from these UT1R-UTC values. To the starting length-of-day value and to length-of-day values obtained from analysis of GPS orbits during the following two weeks, we fitted a line, all values

having equal weight. Taking length of day from the fitted line, and beginning with the starting value of UT1R-UTC, gave UT1R-UTC during the two weeks. These propagated values of UT1R-UTC have an rms value of 0.40 millisecond and are shown in Figure 3.

VERIFYING THE ADDITIONAL MEAN RATE OF ORBIT POLE MOTION

Recall that the additional mean rate is the mean rate of motion of the orbit pole, the unit vector in the direction of the angular momentum, caused by once-per-revolution terms in the radiation pressure acceleration with the effect of varying distance from the Sun removed. We desired to verify the values of additional mean rate shown in the figures below, and thus compared the orbits reported by JPL for Space Vehicle Number (SVN) 15 during several one-month periods in 1994 to nearby orbits propagated numerically. The position and velocity of SVN15 were reported by JPL in J2000 geocentric coordinates, as are those of every GPS satellite, at fifteen-minute intervals. At those times we calculated the elevation angle which the reported position made with the instantaneous plane of the propagated orbit. From the elevation angle values

Figure 3. UT1R-UTC, USNO GPS integrated LODR - USNO final



a UT1R value has been estimated for each day; the error in the estimated UT1R values suggests the quality of the determined additional mean rate.

Propagated orbits were produced in one-day sections, beginning and ending fifteen minutes after midnight GPS time, by the orbit integrator OI contained within the GIPSY software written at JPL. Position and velocity values at the end of integration over each day, fifteen minutes after midnight GPS time, were used as initial values for integration over the next. The initial position and velocity for the first day of each propagated orbit were obtained by correcting values reported by JPL for error in the Earth orientation parameters provided with them. Since the errors in polar motion components were under one milliarcsecond, only errors in UT1 were corrected. Position values were corrected by rotating them around the celestial pole of date, expressed in J2000 coordinates, and velocity values were corrected the same way. Position and velocity values, reported by JPL, to which such a correction has been applied will be called *corrected JPL values*.

The acceleration model for the propagated orbit included Earth gravity model JGM-2 up to degree and order 12, the gravity of all solar system bodies, the effects of general relativity and of pole, solid-body, and ocean tides, and an empirical radiation pressure. The orbit integrator OI correctly handled

the variation in the intensity of sunlight due to the satellite's varying distance from the Sun. We modelled radiation pressure as the sum of the acceleration for a perfectly absorbing spherical ball and an additional acceleration. The area/mass ratio for the sphere was obtained from experience with the satellite; its value depended on the satellite but not on the day.

The additional acceleration had two components, one in the transverse direction--in the orbit plane, perpendicular to the radius, and pointing forward--and one in the direction normal to the orbit plane. The component in the transverse direction was the sum of a constant term and constant multiples of the cosine and sine of the satellite's angle ϕ from ascending node. The component normal to the orbit plane was the sum of a constant and constant multiples of $\cos\phi$, $\sin\phi$, $\cos 2\phi$, and $\sin 2\phi$. The once-per-revolution terms in this component were obtained by interpolation from a table of additional-mean-rate values, calculated by the process to be described in the next section.

Let the angular momentum of the propagated orbit be \mathbf{h} , propagated radius vector be \mathbf{r} , and the vector in the propagated orbit plane which produces by cross product the small rotation from the propagated to the reported orbit plane be $\boldsymbol{\omega}$. The displacement from the propagated radius vector to the nearest

vector in the reported orbit plane is, to first order, the cross product $\omega \times \mathbf{r}$. The elevation angle is thus, to the same accuracy,
 $(\mathbf{h}/h) \cdot (\omega \times \mathbf{r})/r = \omega \cdot (\mathbf{r} \times \mathbf{h})/rh$.

The vector rotating the orbit plane would be constant if the propagated orbit correctly incorporated the entire acceleration of the satellite and if the reported positions were correct. Although errors in the position of the Earth's axis reported by JPL are negligible, errors in the reported UT1R are not. Suppose errors in the reported UT1R correspond to a rotation by θ , around the celestial pole of date, from the correct J2000 axes to the axes with respect to which positions are reported. Then reported positions are rotated by an angle $-\theta$ in the positive sense around the celestial pole of date. The plane-rotating vector ω thus becomes

$\omega_0 - \theta \mathbf{P}^*$, where ω_0 is the ω value--coming from orbit determination error and orbit propagation error--for a correct UT1R and \mathbf{P}^* is the projection on the orbit plane of the unit vector \mathbf{P} toward the celestial pole of date. The elevation becomes

$(\omega_0 - \theta \mathbf{P}^*) \cdot (\mathbf{r} \times \mathbf{h})/rh$; this may be expressed in terms of the satellite's angle ϕ from ascending node and the unit vectors \mathbf{I} in the node direction and \mathbf{J} in the orbit plane and a quarter revolution away from \mathbf{I} in the direction of satellite motion:

$$\omega_0 \cdot \mathbf{I} \sin \phi - (\omega_0 - \theta \mathbf{P}^*) \cdot \mathbf{J} \cos \phi.$$

For each one-day span starting and ending fifteen minutes after midnight GPS time, we evaluated at fifteen-minute intervals the products of the elevation angle with the sine and the cosine of the satellite's angle ϕ from ascending node and then integrated these products numerically to obtain the Fourier coefficients $\omega_0 \cdot \mathbf{I}$ and $(\omega_0 - \theta \mathbf{P}^*) \cdot \mathbf{J}$. We next estimated UT1R at the middle of the day by ignoring the small rotation vector ω_0 . The estimated UT1R started each one-month period within 0.05 millisecond of the final UT1R obtained by the Naval Observatory and remained within 0.3 millisecond of it, suggesting that errors in the measured additional mean rate are under 0.2 milliarcsecond per day.

DETERMINING THE ADDITIONAL MEAN RATE OF ORBIT POLE MOTION

Seeking, for several GPS satellites, values of the additional mean rate of orbit pole motion during much of 1993 and 1994, we first constructed approximate orbits valid for one-month periods. These orbits were then improved, in an iterative process, to produce one-day approximations. On nearly all days, corrected JPL positions differed less

than one meter in the orbital plane and thirty centimeters normal to that plane from those given by the one-day approximation. A position error of this size can produce an error of at most 0.2 milliarcsecond per day in the mean rate of orbit pole motion over a one-month interval.

Every one-month approximation was constructed with OI. The acceleration model was that used above for orbit propagation, but with radiation pressure restricted to that for a perfectly absorbing sphere plus a transverse acceleration; the transverse acceleration and the area/mass ratio for the sphere remained constant throughout the month. The initial position was a corrected JPL position, and the initial velocity was obtained by multiplying the corresponding corrected JPL velocity value by a constant. The values of this constant, of the area/mass ratio, and of the transverse acceleration were adjusted to make the propagated crossings of the J2000 equator approximate the reported crossings as closely as possible both in time and in radial distance.

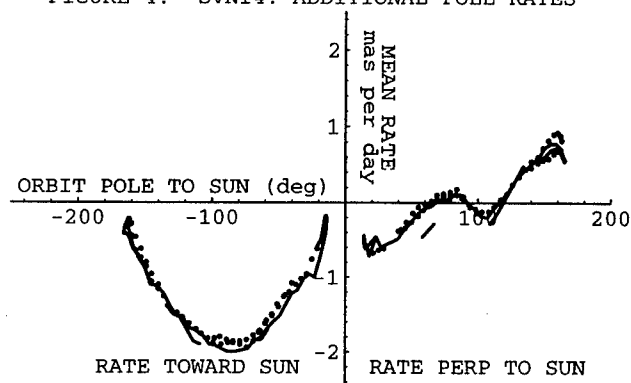
For every one-month approximation, we decomposed the differences between corrected JPL positions and corresponding positions from the approximate orbit into three components. One was in the direction normal to the instantaneous plane of the one-month approximation, one was in the radial outward direction, and one was in the transverse direction. The radial and normal components remained under fifty meters, and the transverse component remained under--usually much under--half a kilometer.

At all stages of the iterative process, each of the components of the deviation between corrected JPL positions and the approximate orbit was represented by a product of the radial distance and a function of the angle ϕ from ascending node. Each of these functions was the sum of a constant and constant multiples of ϕ , ϕ^2 , $\cos \phi$, $\sin \phi$, $\phi \cos \phi$, $\phi \sin \phi$, $\cos 2\phi$, and $\sin 2\phi$. On nearly all days, the error in this representation was at each stage only a few centimeters. This representation and its derivative gave the changes in initial position and velocity required to produce the approximate orbit at the next stage.

The acceleration model used for the final one-day approximation was identical to that used above for the propagated orbit, except that the once-per-revolution terms in the additional normal acceleration were for this approximate orbit set to zero. Setting these terms to zero caused the angular momentum change from beginning to end of day for the actual orbit to differ from that for the one-day approximate orbit; the determined additional mean rate may be viewed as an average of these differences. For the

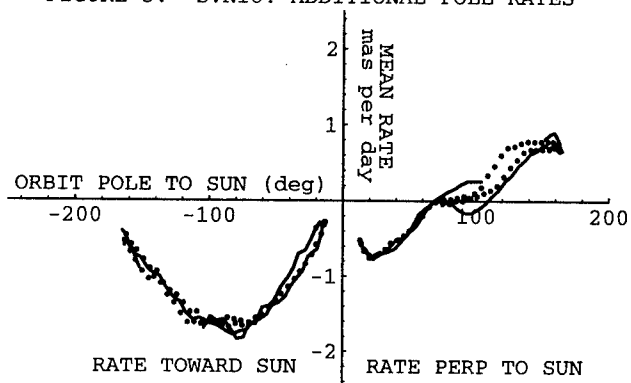
final one-day approximation to the motion of each GPS satellite, the area/mass ratio of the perfectly absorbing sphere was set to the average of the area/mass ratios used for one-month approximations to that satellite's motion in 1994. The constant term in the transverse acceleration, the once-per-revolution terms in the transverse acceleration, and the constant and twice-per-revolution terms in the normal acceleration were obtained by solving Hill's equations to remove corresponding terms in the transverse and normal components of deviations from corrected JPL positions.

FIGURE 4. SVN14: ADDITIONAL POLE RATES



In an operational system to determine UT1R, the terms in the additional acceleration would be obtained from orbit data corrected by an extrapolated UT1R. An error in extrapolated length-of-day would produce errors in the constant and twice-per-revolution terms in the normal acceleration, since GPS orbits are not circular, but these errors would contain as a factor the orbit's eccentricity--less than 0.02. Errors in these terms would in turn produce an error in the long term motion of the orbit pole, containing a further factor of the eccentricity.

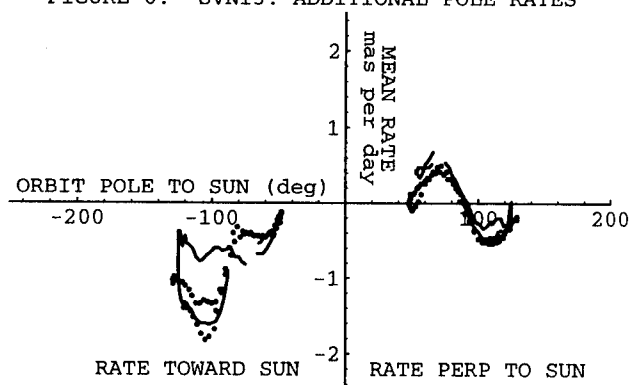
FIGURE 5. SVN18: ADDITIONAL POLE RATES



We were now at last able to obtain values of the additional mean rate. Centered on each time for which we desired the additional mean rate, we defined a one-month interval. At the beginning of each day in this interval, we calculated the difference

between the angular momentum for the final one-day approximation for the day and the angular momentum for a one-month approximation covering the day. We subtracted a running, day-by-day, sum of the change from beginning to end of day in the difference between the angular momenta for the one-day and one-month approximations. We then adjusted the resulting differences for the jump at the transition between one-month approximations. We found the least-squares linear approximation, over the one-month interval, to the adjusted angular momentum differences. Thus was determined the additional mean rate at the middle of the interval.

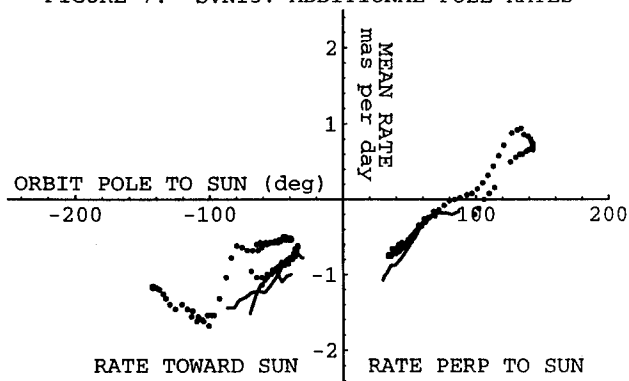
FIGURE 6. SVN13: ADDITIONAL POLE RATES



CURVES OF THE ADDITIONAL MEAN RATE OF ORBIT POLE MOTION

In terms of the position of the Sun, we defined two components of the additional mean rate of orbit pole motion, that along the projection of the Sun direction on the orbit plane for the middle of the fitting interval and that in the perpendicular direction in that orbit plane. The additional mean rate components are plotted, as functions of the angle (expressed in degrees) between the orbit pole and the direction toward the Sun, in Figures 4 to 7.

FIGURE 7. SVN15: ADDITIONAL POLE RATES



Positive and negative angles between the orbit pole and the Sun are physically identical; the component

of the additional mean rate toward the projection of the Sun's direction on the orbit plane is plotted against negative values of the angle. The component a quarter revolution ahead--in the direction of satellite motion--of the projection of the Sun's direction is plotted against positive values of the angle. The vertical axis in each figure gives in milliarcseconds per day the mean rate of the additional motion of the orbit pole; note that one milliarcsecond per day corresponds to an effect in UT1R determination of approximately one millisecond per two weeks.

Solid lines connect additional-mean-rate values in 1993, and dots show additional-mean-rate values observed in 1994 and 1995. We calculated for SVN13, SVN14, SVN15, and SVN18 additional-mean-rate values every five days, except near orbit changes, throughout 1994, and for SVN13 and SVN15 we continued into 1995. For SVN13 we calculated additional mean rate every five days in 1993 except during a gap covering two weeks on either side of a small orbit change on August 30, 1993. For SVN14 we calculated additional mean rate every five days in 1993 except for two gaps; they are centered on an orbit maneuver which occurred in early March, 1993 and some smaller orbit change on April 23, 1993. For SVN15 we calculated additional mean rate every five days during the first six months of 1993; during these months there is one gap, covering the month centered on a small orbit change on April 20, 1993. Finally, for SVN18 we calculated additional mean rate every five days in 1993 except for a gap covering two weeks on either side of an orbit maneuver in early March 1993.

Note that the plots, Figures 4 and 5, for SVN14 and SVN18 are similar, and are symmetrical about an orbit-pole-to-Sun angle of ninety degrees. Symmetrical points have equal separations of the Sun from the orbit plane. For both satellites, the additional-mean-rate values in 1993 and 1994 lie, for any given value of the angle from the orbit pole to the Sun, within a band of width less than 0.5 milliarcsecond per day. In these plots, particularly in that for SVN18, one can further see that many values of the angle from orbit pole to Sun appear not once but twice in 1993. In 1994, although more difficult to see because the plotted points are not connected, this occurs again. The plots for SVN13 and SVN15 are made more complicated by changes in yaw bias, but also show small scatter for the additional mean rate at each value of the angle from orbit pole to Sun.

There appears to have been for SVN13 a rapid transition from one type of behavior to another when the angle from the orbit pole to the Sun was approximately 120 degrees in late May 1993. We suggest that this transition was associated with the one change in yaw bias known to have occurred in

1993. The yaw bias for SVN13 was changed by half a degree in the same direction as was later the case for SVN15 in June, 1994. The solid curve giving 1993 rates after the transition approximates the points giving rates in 1994 and the corresponding points for SVN15 shown in Figure 7.

For SVN15 there was one change in yaw bias: half a degree on June 6, 1994. The calculated additional mean rates, since they were obtained by fitting angular momentum over a one-month interval, should first have been affected about May 20, 1994. The angle from the orbit pole to the Sun was then 60 degrees and was increasing. For orbit-pole-to-Sun angles between 40 and 60 degrees, the additional mean rate was determined in the early parts of 1993, 1994, and 1995. For orbit-pole-to-Sun angles in this range, additional mean rates for 1993 and 1994 can validly be compared; their values are similar to those found for SVN14 and SVN18. For the same range of orbit-pole-to-Sun angles, the component of the additional mean rate along the projection of the Sun direction was significantly higher in 1995. This component approached after May 20, 1994 the values observed in early 1995. The rapid change in this component when the Sun is approximately ninety degrees from the orbit pole appears also in the plot for SVN13, and may be a result of the yaw bias.

IMPLICATIONS FOR DETERMINING UT1

We propose predicting the additional mean rate by the sum of one of its recent values and an estimate of its change from past experience. For the desired reduction in the amount of VLBI observing, the recent value will be three weeks old, two of which are half the four-week interval used to calculate the recent value and one of which is half the two-week interval over which the orbit pole motion is propagated. We note that three weeks corresponds to a change of at most twenty degrees in the angle from the orbit pole to the Sun. Using the additional mean rate in 1993 to predict the change, we find the value of any desired component of the determined additional mean rate can be predicted at nearly any time in 1994 to within 0.2 milliarcseconds per day--equivalent to 0.2 milliseconds in two weeks. This prediction accuracy for the determined additional mean rate suggests, both because errors for different satellites will partly cancel and because rms error includes times before the end of the two weeks, that error in UT1 determination coming from error in additional mean rate will have an rms error under 0.1 millisecond.

While our analysis has not included all errors which would occur in actual, operational, determinations of UT1 from GPS analysis, calibrated once in two weeks

with VLBI observations, it appears unlikely that the rms error in such UT1 determinations would reach 0.2 millisecond.

Jet Propulsion Laboratory, Pasadena, Calif., July, 1993.

ACKNOWLEDGEMENTS

To Dennis McCarthy and Brian Luzum of U.S. Naval Observatory, to Henry Fliegel of Aerospace Corporation, and especially to Victor Slabinski for many useful conversations. To Arvid Myers and Francine Vannicola of U.S. Naval Observatory for assistance in accessing data. To the group responsible for GIPSY at JPL for assistance with software and data. Not to us, but to our world and its Creator, belongs praise for what beauty is in this work.

REFERENCES

Beutler, G., E. Brockmann, W. Gurtner, U. Hugentobler, L. Mervart, M. Rothacher, and A. Verdun, Extended Orbit Modeling Techniques at the CODE Processing Center of the International GPS service for Geodynamics (IGS): Theory and Initial Results, *Manuscripta Geodaetica*, 19, 367-386, 1994.

Colombo, The Dynamics of Global Positioning System Orbits and the Determination of Precise Ephemerides, *J. Geophys. Res.*, 94 (B7)9167-9182, 1989.

Fliegel, H.F., T.E. Gallini, and E.R. Swift, Global Positioning System Radiation Force Model for Geodetic Applications, *J. Geophys. Res.*, 97 (B1)559-568, 1992.

International Earth Rotation Service (IERS), 1993 *IERS Annual Report*, Central Bureau of IERS - Observatoire de Paris, 1994.

Kaplan, M.H., *Modern Spacecraft Dynamics and Control*, John Wiley & Sons, New York, 1976.

Nerem, R.S., C. Jekeli, and W.M.Kaula, Gravity Field Determination and Characteristics: Retrospective and Prospective, *J. Geophys. Res.*, 100 (B8)15053-15074, 1995.

Slabinski, V., private communication, August 19, 1995.

Szebehely, V., *Theory of Orbits--The Restricted Problem of Three Bodies*, Academic Press, New York, 1967.

Webb, F.H. and J.F. Zumberge, eds., *An Introduction to GIPSY / OASIS II*,

Programme of Research of CEI (Central European Initiative) Countries in Geodesy and Geodynamics

Prof. Dr. Janusz Sledzinski
Warsaw University of Technology

BIOGRAPHY

Janusz Śledziński is the University Professor and Director of the Institute of Geodesy and Geodetic Astronomy of the Warsaw University of Technology. He is a member of the American Institute of Navigation, Alexandria, VA, the British Royal Institute of Navigation, London, UK, the American Geophysical Union and the New York Academy of Sciences. Member of the Committee of Geodesy and the Committee of Space Research of the Polish Academy of Sciences. UN Expert on geodesy; 1976-1978 Team Leader and Chief Adviser in UNDP Project in Afghanistan. He is the Chairman and International Coordinator of the CEI (Central European Initiative) Section C "Geodesy" and co-chairman of the CEI Project CERGOP. Wide experience in theoretical and practical aspects of satellite geodesy. Author and co-author of about 250 scientific papers.

ABSTRACT

The broad programme of geodetic projects and geodynamic research initiated by CEI (Central European Initiative) member countries is outlined in the paper. This organisation was originally founded in 1989 as QUADRAGONALE and then developed through PENTAGONALE, HEXAGONALE to the CEI (CENTRAL EUROPEAN INITIATIVE).

Nowadays in the geodetic programme of CEI take part 15 countries (10 member countries and 5 so called associated (consultative) countries). The programme of cooperation of the Section C "Geodesy" includes 3 themes: (a) Interconnection of geodetic control networks in Central Europe, (b) GIS/LIS systems as a data base of the GEOPAR (Geoenvironmental problems of the Circumpannonian and adjacent regions) and (c) Geodynamic investigations of the region. The GPS EUREF campaigns promoted by the CEI Section C with the aim to connect the Central and Eastern European countries to the ITRF geodetic system have been performed in many CEI countries. The list of these actions is given in the paper. The backgrounds of the scientific programme in geodynamics for the region of Central Europe are discussed. Project CEI CERGOP (Central Europe Regional Geodynamics Project) was approved for realisation by the CEI member countries in May 1993. The main objectives of the Project are: to integrate the geodynamic research in the region of Central Europe based on high accuracy space geodetic measurements and an integrated geodynamic network, to provide a precise geodetic frame CEGRN (Central European GPS Reference Network) for studies of geodynamics of Central European area (Pannonia Basin, Teisseyre-Tornquist zone, Carpathian Orogenic Belt, Subalpine and Bohemian Region) and to collect observations for studies and interpretation of geodynamic interactions

in Central Europe. The following countries participate in the Project: Austria, Croatia, the Czech Republic, Germany, Hungary, Italy, Poland, Romania, Slovakia, Slovenia and Ukraine. First GPS zero-epoch observation campaign of the CEGRN'94 was organised from May 2nd to May 6th, 1994. The results of this campaign processed by four CERGOP Processing Centres (Warsaw, Graz, Penc, Pecny) are already available. The second GPS campaign was performed from May 29th to June 3rd, 1995. Project CERGOP is partially financed by EU as a COPERNICUS Project. Other geodynamic projects related to CERGOP (e.g. EXTENDED SAGET) are also outlined in the paper. Four other international campaigns of EXTENDED SAGET Project were performed in 1992, 1993, 1994 and 1995. The work of eleven scientific CERGOP study groups is briefly mentioned. Further plan of action of the CEI Section C is also mentioned in the paper.

1. CENTRAL EUROPEAN INITIATIVE AS THE ORGANISATION OF THE INTERNATIONAL COOPERATION

In November 1989 the Foreign Ministers of Austria, Hungary, Italy and Yugoslavia at the conference in Budapest founded an organisation named QUADRAGONALE. A few months later, in April 1990 (Vienna) former Czechoslovakia joined this organisation forming the PENTAGONALE and in July 1991 at the conference of Prime Ministers in Dubrovnik Poland was admitted creating the HEXAGONALE. In July 1992 the HEXAGONALE was renamed as Central European Initiative. Violent political development in Europe, break-up and civil war in Yugoslavia, disintegration of Czechoslovakia, formation of new countries in the region of Eastern and Southern Europe, all these events caused considerable changes in organisation and international cooperation within the Central European Initiative. In the meantime Yugoslavia's CEI membership was suspended (November 1991), Croatia, Slovenia and Bosnia & Herzegovina (July 1992) and Czech Republic and Slovakia (March 1993), Macedonia (July 1993) were admitted as full members of the CEI. Growing international prestige of the CEI in the last few years is marked by the fact that new countries express their interest and willingness to cooperate in the frame of the CEI working groups. These countries are: Belarus, Bulgaria, Romania, Ukraine (associated countries since March 1994) and Albania (since July 1994). Bavaria and Germany also cooperate closely with CEI.

The current (1.01.1995) status of the CEI membership is the following:

CEI member countries are: Austria, Bosnia & Herzegovina, Croatia, Czech Republic, Hungary, Italy, Macedonia, Poland, Slovakia, Slovenia.

The following countries are members of the Council of Association of the Central European Initiative (associated, consultative countries): Albania, Belarus, Bulgaria, Romania, Ukraine.

The main objectives of the CEI cooperation are to strengthen the stabilisation within the region of Central Europe, to promote all-European integration processes and to help the Central and Eastern European countries in entering the integrated world by adjusting their multi-lateral relations to Western European standards.

The Central European Initiative is a loose grouping of states with no legal status. It was agreed that a Summit (Heads of Governments and Foreign Ministers) would be held once a year in October and a meeting of Foreign Ministers of the member and associated countries would be organised every year in April. Working Groups constitute the basic structural component of the CEI. They plan and approve initiatives, agreements and projects which they promote and complete in cases requiring financing, or which they pass to the National Coordinators or Foreign Ministries for approval and financing. There are sixteen CEI Working Groups at the moment: 1.Environment, 2. Transport, 3. Small and medium size enterprises, 4. Media, 5. Telecommunications, 6. Culture, education, youth exchange, 6. Science and technology, 8. Migration, 9. Energy, 10. Disaster relief, 11. Tourism, 12. Statistics, 13. Agriculture, 14.Civil defense, 15. Minorities, 16. Experts on vocational training, ad-hoc

The Earth sciences and, in particular geodesy, are represented in the Working Group No 7 "Science and Technology." This Working Group was set up in June 1990 with the aim of

- * identifying areas where regional technological cooperation can be developed on a mutual benefit basis,
- * identifying projects of mutual benefit and orienting them towards a Central European perspective,
- * fostering cooperation among universities, research centres and institutions of the Central European region in the field of science, technology and applied research,

- * promoting the training and the mobility of CEI scientists and creating new research opportunities for human resources of Central European region,
- * promoting participation of CEI scientists in international research programmes,
- * encouraging projects which can contribute to the development of innovative technologies and modernisation of small and medium-size enterprises.

The programme of the Working Group on Science and Technology includes presently nine endorsed scientific and technological projects (committees):

1. Centres of Excellence Physics of Matter, 2. Technology Transfer Centre, 3. Earth Science, 4. Experimental Mechanics, 5. Meteorology, 6. Astronomy and Astrophysics, 7. Space, 8. Industrial Technologies and Automation, 9. Parallel Computing.

The work of the Committee for Earth Science is divided into three sections:

- * Section A: "Geology"
- * Section B: "Geophysics"
- * Section C: "Geodesy"

2. GEODETIC RESEARCH PROGRAMME OF THE CEI SECTION C "GEODESY"

The CEI Section C "Geodesy" scientific programme includes three themes:

- Theme No.1: Interconnection of geodetic control networks (horizontal, levelling, gravimetric);
- Theme No.2: Geographic and Land Information Systems. Data quality in geographic information system and cadastre;
- Theme No.3: Geodynamic investigations.

It is worth mentioning that a significant progress and great achievements in the international cooperation of CEI countries are to be pointed out in themes 1 and 3.

In the theme 1. the following main significant achievements can be noted:

- * extension of the EUREF to many CEI member and associated countries. The EUREF GPS campaigns were performed so far in Austria, Italy, Hungary, Czech Republic, Slovakia, Poland, Bulgaria, Romania, Slovenia, Croatia;
- * establishment of national GPS reference networks in the countries of Central and Eastern Europe; such networks were established in Austria, Italy, Poland, Hungary, Czech Republic, Slovakia,

Croatia, Slovenia;

- * Programme of establishment of at least one permanent GPS station in CEI countries. At present 13 permanent stations are operating in CEI countries, other 10 stations are planned in 1995-1996
- * establishment of the absolute gravity networks in some CEI countries (Austria, Italy, Poland)
- * repeated measurements of precise levelling networks and interconnection of gravity and levelling networks of some member countries.

3. GPS EUREF CAMPAIGNS IN CENTRAL AND EASTERN EUROPE

The interconnection of horizontal control networks of CEI countries is recognised in the programme of activities of the Section C "Geodesy" as one of the main tasks. The best way to fulfil this task is the cooperation with the IAG Subcommission EUREF. It is stressed in several Section C resolutions that the national geodetic services of CEI countries should intensify and finish the interconnection of geodetic control networks as soon as possible within the actions of EUREF organised by the Institut für Angewandte Geodäsie, Frankfurt am Main, Germany. This cooperation is gratefully acknowledged by all involved CEI countries. It is also recommended that transformation parameters from the ETRF'89 to the national coordinate systems used in particular countries and vice versa should be available as soon as possible for each CEI country. The EUREF GPS campaigns were performed so far in the following CEI countries: Austria, Italy, Hungary, Czech Republic, Slovakia, Poland, Bulgaria, Romania, Slovenia, Croatia.

4. CEI SCIENTIFIC PROGRAMME IN GEODYNAMICS

4.1. BACKGROUNDS OF THE GEODYNAMIC INVESTIGATIONS IN CENTRAL EUROPE

The area of Central Europe has a particular position from the point of view of geotectonics. This results from the fact that three geological units of various ages contact on the territory of Central Europe: East European Precambrian Platform, Palaeozoic Platform of the Central and Eastern Europe and South European Alpine Orogeny. The Teisseyre-Tornquist's zone separating two above mentioned Platforms is of prime importance for the regional geodynamics of Central Europe.

Another region in Central Europe which should be carefully investigated is the Carpathian Orogeny and its profound geotectonic features. Splendid Carpathian mountains ridge forms gigantic arc, open to the south, about 1500 km long and 200-300 km wide. This relatively young formation was created as a consequence of the collision between the African and the European plates. This process is continuing in present days and is affecting the tectonic regime over areas extending into Austria, Bohemia, Slovakia, Poland, Ukraine and Romania. The Carpathian Basin which includes Hungary tectonically belongs to the Eurasian plate and is considered as relatively quiet, although in the last years several earthquakes were observed also in this region. The dynamic processes in eastern Alps and the Carpathians are accompanied by seismicity which is propagated along the faults which form a deep seated zone characterized by gravity anomalies. Geotectonic activity has a slow, long term character related to tectonic processes but also abrupt episodic changes take place as results of seismic stress release. Detailed geological studies revealed a rather complicated microplate structure and the associated fault system in this area. All this can be genetically related to tectonic processes in the Mediterranean and the Alpine-Adria region. Geology of the region is well studied and also some measurements of the crustal motions were performed. However, so far rather classical terrestrial geodesy was applied, precise levelling first of all. Nowadays, the GPS technique allows us to make completely new approach to the problem of the study of crustal deformation over hundreds and thousands of kilometers.

Considering the key position of the territory of this region for the tectonic of Europe, the geodynamical investigations in this zone are of extra-regional importance. In particular, the geodynamic research in the region of the Teisseyre-Tornquist zone which separates two major European tectonic platforms offers an essential and considerable contribution to all geodynamical projects in this region. Also investigations of the geodynamic interactions in the Carpathian Orogenic Belt, Pannonia Basin and the Bohemian Subalpine Region may contribute to better knowledge of geodynamics of Central Europe.

It can be noted that all these regions, interesting from geological point of view, just coincide generally with the territory of countries of the Central Europe Initiative (former HEXAGONAL group countries). Therefore proposals to join efforts to undertake the investigations and studies, properly organized and

coordinated seem to be of great value for the CEI Section C "Geodesy" and can constitute one of the main items of activities of this Section.

4.2. CONCISE OUTLINE OF THE PROJECT CERGOP. OBJECTIVES OF THE PROJECT

Project CERGOP (CENTRAL EUROPE REGIONAL GEODYNAMICS PROJECT) was initiated in 1993 by the scientists from FÖMI Satellite Geodetic Observatory Penc (Hungary), the Institute of Geodesy and Geodetic Astronomy of the Warsaw University of Technology and the Space Research Centre of the Polish Academy of Sciences. It was approved for realisation by the CEI (Central European Initiative) member countries in May 1993 in Książ Castle, Poland. Eleven countries participate in the CERGOP Project.: Austria, Croatia, Czech Republic, Germany, Hungary, Italy, Poland, Romania, Slovakia, Slovenia, Ukraine.

The main objectives of the Project are the following:

- * to integrate the geodynamic research in the region of Central Europe based on high accuracy space geodetic surveys and an integrated geodynamic network;
- * to foster the international cooperation among research groups of participating countries;
- * to provide a precise geodetic frame - so called Central European GPS Reference Network (CEGRN) - for
 - ** studies on geodynamics of Central European areas of
 - Pannonia Basin,
 - Teisseyre-Tornquist Zone,
 - Carpathian Orogenic Belt,
 - Subalpine and Bohemian Region;
 - ** connection of local geodynamic networks established on the territory of participating countries;
- * to collect satellite observations for studies and interpretation of geodynamic interactions in Central Europe.

The main coordinating body of the Project is the International Project Working Group (IPWG) headed by the Project Chairman Dr. István Fejes (Hungary) and the Project Co-Chairman Prof. Dr. Janusz Śledziński (Poland).

The IPWG is responsible for:

- * scientific progress and scientific level of the Project,
- * administrative management.

Each participating country delegates to the IPWG one representative, the National Investigator (N.I.); the tasks of National Investigators are:

- * organisation and supervision of observation campaigns within their respective countries,
- * supervision of the activities of data and processing centres,
- * contribution to the work of CERGOP study groups,
- * liaison with other overlapping projects,
- * dissemination of information and maintenance of contacts with potentially interested groups or institutions within their particular countries.

It was agreed that the conferences of the International Project Working Group (IPWG) would be organised twice a year to discuss the progress and programmes of scientific research within the Project. The First Working Conference was held on 17-18 February 1994 in Warsaw (Poland) and was followed by the Second Conference organised on 4-5 November 1994 in Penc/Budapest (Hungary). The third Conference was organised on 8 May 1995 in Penc (Hungary). Next Conferences: 6-7 November 1995 in Warsaw (Poland), spring 1996 in Graz (Austria), fall 1996 in Udine (Italy).

Project CERGOP was submitted to the EC Office in Brussels with the request for the financial support within the research programme COPERNICUS'94. As the Project Coordinator serves the Institut für Angewandte Geodäsie Frankfurt, FRG.

4.3 STUDY GROUPS

Eleven study groups were formed by the Second CERGOP Working Conference held in Penc/Budapest on 4-5 November 1994 to carry out research in particular fields. They are:

- CSG 1. Investigation of tropospheric delays. Chairman: P.Pesec (Austria)
- CSG 2. CERGOP site quality monitoring. Chairman: I.Busics (Hungary)
- CSG 3. CERGOP reference frame. Chairman: J.Rogowski (Poland)
- CSG 4. Standardisation of data and processing centres. Chairman: G.Stangl (Austria)
- CSG 5. Permanent and epoch GPS CERGOP stations. Chairman: J.Śledziński (Poland)
- CSG 6. CEGRN and precise levelling. Chairman: J.Šimek (Czech Republic)
- CSG 7. CERGOP gravity network. Chairman: M.Barlik (Poland)
- CSG 8. Geotectonic analysis of the region of Central Europe. Chairman: P.Vyskočil (Czech Rep.)

CSG 9. Geoid in Central Europe. (Chairman will be elected at the next meeting)

CSG10. Monitoring of recent crustal movements in Eastern Alps with GPS. Chairman: Cl. Marchesini (Italy)

CSG11. Threedimensional plate kinematics in Romania. Chairman: D.Ghițău (Romania).

4.4 REALISATION OF THE CENTRAL EUROPEAN GPS REFERENCE NETWORK (CEGRN)

Establishment of a Central European Regional GPS Reference Network (CEGRN) was proposed as the first action within this Project. This Project, however, is not limited itself only to establishment of the geodetic frame necessary for geodynamic studies. Investigation of wide spectrum of geotectonic phenomena will be the core of the Project. The aim of this study is to establish the model of the geodynamic processes of this region, to determine horizontal and vertical motion of the crust, stress and strain fields and to have the possibility to monitor episodic deformation caused by earthquakes.

The CEGRN design concept and the standards for the first zero-epoch GPS observation campaign were developed in 1993 and finally approved by the First CERGOP Working Conference held in Warsaw on 17-18 February 1994. The design required that the sites and monumentations of the CEGRN stations would satisfy optimal conditions for GPS observations as well as identify and fulfil the geodynamical needs. For technical reasons the number of sites of the CEGRN was limited to about 30. It was also decided that Graz Lustbühel Computing Centre (Austria) would serve as the CERGOP Data Centre. There are four CERGOP Processing Centres which will process the observations of the CEGRN campaigns. These centres are: IGS Centre Graz (Austria), IGS Evaluation Centre IG&GA Warsaw (Poland), FÖMI SGO Penc (Hungary) and VUGTK Pecny (Czech Rep.).

The participants of the First Working Conference in Warsaw decided that the first GPS zero-epoch observation campaign of the CEGRN'94 would be organised from May 2nd to May 6th, 1994. The campaign was carried out successfully. Unfortunately four Romanian sites and some other stations were not able to participate in the campaign. First results of processing were presented by the CERGOP Processing Centres. The next CEGRN'95 campaign was organised from 29 May to 3 June 1995. Now the Processing Centres collect the GPS data of this campaign.

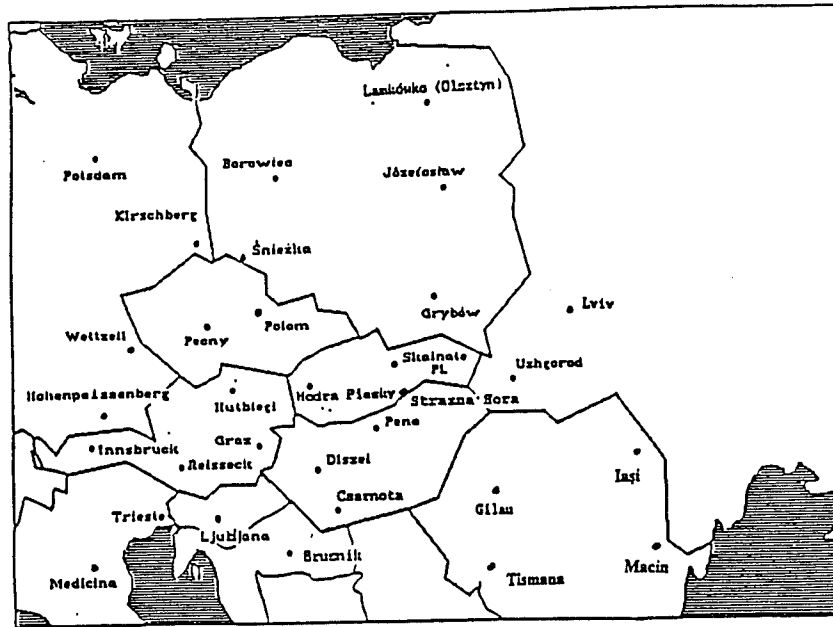


Fig. 1. Stations of the CEGRN

4.5 THE OVERLAP BETWEEN OTHER INTERNATIONAL PROJECTS

There are some geodynamic projects running in Europe that indicate or may indicate some interferences with the CERGOP. These projects are: WEGENER, EXTENDED SAGET, BALTIC SEA LEVEL PROJECT, EUROPROBE, EUREF, IGS.

As an example of the interference of two overlapping projects we can mention the CERGOP and EXTENDED SAGET which was initiated by the Institute of Geodesy and Geodetic Astronomy of the Warsaw University of Technology in 1991 as an extension of the Project SAGET launched at this Institute in 1986.

There is a significant coincidence of scientific aims of both projects. However, there are also some very essential differences. The EXTENDED SAGET network covers much more extended area and an unlimited number of points can be incorporated to this network. This gives an excellent opportunity to all participating institutions to connect new established points to the ITRF coordinate system. The evaluation of these points, their geodetic and geodynamic assessment depending mainly on the type and stability of point monumentation, is the responsibility of involving institution and agencies.

The CERGOP campaigns are envisaged to be organised in the next three years; EXTENDED

SAGET campaigns are thought as long-term action and will be performed at least in the whole of current decade. Table below summarizes all main aspects of both projects under consideration and outlines their similarities and differences.

The following conclusions may be pointed out when comparing both projects::

- The same standards of GPS observations are observed in both CEGRN and EXTENDED SAGET campaigns.,
- EXTENDED SAGET network includes stations of Scandinavia and Mediterranean Region. CEGRN is limited only to CEI countries; only some regions of Ukraine, Rumania and Germany, interesting from tectonic point of view, are included,
- EXTENDED SAGET campaigns give the possibility to connect to ITRF system new points that may be currently needed,
- Both networks (projects) can coexist. Campaigns of both projects may supplement each other.

4.6 ABSOLUTE GRAVITY TRAVERSE FROM BALTIC SEA TO ADRIATIC AND BLACK SEA

There is a concept to launch a new research programme concerning absolute gravity measurements and monitoring of the mean sea level in Central Europe. The main goal of the project is to support the established CEGRN network by a gravimetric network of absolute points located in selected CEGRN stations

Comparison of EXTENDED SAGET and CEGRN

| | EXTENDED SAGET | CEGRN |
|----------------------------------|--|---|
| Area | countries from Scandinavia to Mediterranean Region | CEI countries |
| Number of points | unlimited | limited to about 30 |
| Stations | no any restriction in station distribution; any new station is accepted | only accepted stations |
| Campaigns | 1992, September 7-11 1993, August 2-6 1994, May 2-6 1995, May 29 - June 3 | 1994, May 2-6, zero-epoch 1995, May 29 - June 3 |
| Duration of campaigns | 5 days | 5 days |
| Responsible processing centre(s) | IG&GA WUT | IG&GA WUT (PL) SGO FÖMI PENC (H) GRAZ (A) VUGTK (CZ) |
| Software used | BERNESE | BERNESE |

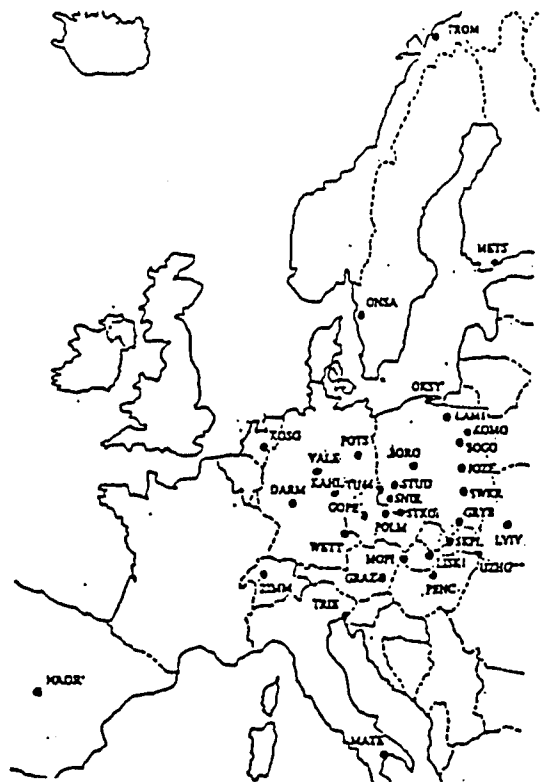


Fig.2. Stations of the EXTENDED SAGET'93



Fig.3. Stations of the EXTENDED SAGET'94/CEGRN'94

and moreover joining also some tide gauges of the Baltic Sea, Adriatic and Black Sea. In this way these points will form a gravimetric absolute traverse between Baltic Sea and Adriatic with the connection to the Black Sea. The scientific background and objective of the proposal is to establish a gravimetric precise frame for (1) interplate vertical monitoring of Central European regions (Alpine Orogeny, Pannonia Basin, Carpathian Belt, Teisseyre-Tornquist Zone, Dinarian Alps), and (2) investigation of global change (GLOSS) and monitoring of the mean sea level change between Baltic Sea, Adriatic and Black Sea.

It is thought that the traverse would be measured at least three times within the next three years. It is assumed that in the campaign will take part 5 absolute gravity meters from the University of Trieste/Italy, Bundesamt fEuV Vienna/Austria, IfAG Frankfurt/Germany, IG&GA WUT Warsaw/Poland and Finnish Geodetic Institute Helsinki/Finland. It is envisaged that for practical reasons the number of points of the gravimetric traverse should be limited to about 16-18. The special Steering Committee of the project has been established. The work will begin next year.

5. REFERENCES

- H.Seeger. EUREF - the new European Reference Datum and its relationship to WGS 84. Paper presented at the GPS 84 Implementation Workshop, 16-18.06.1992, EUROCONTROL INSTITUTE LUXEMBOURG
- M.Barlik, T.Borza, I.Busics, I.Fejes, W.Pachelski, J.Rogowski, J.Śledziński, J.Zieliński. Central Europe Regional Geodynamics Project (CERGOP). Project submitted to the Section C - Geodesy of the Central European Initiative (CEI). Warsaw, 1993.
- I.Fejes, M.Barlik, I.Busics, W.Pachelski, J.Rogowski, J.Śledziński, J.B.Zieliński. The Central Europe Regional Geodynamics Project. Proceedings of the International Seminar "GPS in Central Europe", Penc, Hungary, 27-29 April 1993.
- M.Barlik, T.Borza, I.Fejes, W.Pachelski, J.Rogowski, J.Śledziński, J.B.Zieliński. Central Europe Regional Geodynamics Project (CERGOP). Proceedings of the 2nd Conference of the Section C "Geodesy" of the Central European Initiative, Committee of Earth Sciences, Książ Castle, Poland, 11-14 May 1993.
- M.Barlik, T.Borza, I.Busics, I.Fejes, W.Pachelski, J.Rogowski, J.Śledziński, J.B.Zieliński. Central Europe Regional Geodynamics Project (CERGOP). REPORTS ON GEODESY, IG&GA WUT, No. 2(8), Warsaw, 1993.
- I.Fejes. The GRL Hierarchy of the GPS Reference Frame. Proc. IRIS'93 Workshop, Edit. T.Yoshino, Communication Research Laboratory, Tokyo, Japan.
- E.Erker. CEI Projects and Plans in Connection with EUREF and UELN. Paper presented at the Symposium of the IAG Subcommission EUREF in Budapest, May 17-19, 1993.
- J.Śledziński. Last CERGOP related actions in Poland. Paper presented at the First Working CERGOP Conference, Warsaw, 17-18 February 1994. Proceedings of this Conference: REPORTS ON GEODESY, No. 2(10), Warsaw, 1994.
- J.Śledziński. National Report of Poland. Paper presented at the First Working CERGOP Conference, Warsaw, 17-18 February 1994. Proceedings of this Conference: REPORTS ON GEODESY, IG&GA WUT, No. 2(10), Warsaw, 1994.
- J.Śledziński. Status Report on CERGOP Processing Centre at the IG&GA WUT. Paper presented at the First Working CERGOP Conference, Warsaw, 17-18 February 1994. Proceedings of this Conference: REPORTS ON GEODESY, IG&GA WUT, No. 2(10), Warsaw, 1994.
- J.Śledziński (edit). REPORTS ON GEODESY, Nr. 2 (10), 1994. Special issue on the occasion of the First CEI CERGOP Working Conference, Warsaw, Poland, 17-18 February 1994, Institute of Geodesy and Geodetic Astronomy Warsaw University of Technology.
- J.Śledziński. Geodynamic network of EXTENDED SAGET (Satellite-Geodetic Traverses) in Central Europe. Paper presented at the XIX General Assembly of the European Geophysical Society, Grenoble, France, 25-29 April 1994.
- H.Seeger, P.Franke. EUREF Activities of the IfAG from May 1993 to May 1994. Paper presented at the Symposium of the IAG Subcommission EUREF, Warsaw, June 8-11, 1994.

- H.Seeger, P.Franke. National Report of Germany. Paper presented at the Symposium of the IAG Subcommission EUREF, Warsaw, June 8-11, 1994.
- J.Śledziński, J.Rogowski. Contribution of the permanent IGS GPS station Józefosław to the activities of the International GPS Geodynamics Service (IGS). Symposium of the IAG Subcommission for the EUREF (European Reference Frame), Warsaw, Poland, 8-11 June 1994.
- H.Bednarek, W.Krajewski, W.Graszka, J.Śledziński, J.Rogowski, K.F.Burke, P.Rakowsky. Military first-order geodetic control network in Poland. Joint Polish-American (DMA) Project. Paper presented at the Symposium of the IAG Subcommission for the European Reference Frame (EUREF), Warsaw, Poland, 8-11.06.1994.
- J. Śledziński. Three GPS campaigns of EXTENDED SAGET in Central Europe. Symposium of the IAG Subcommission for the EUREF (European Reference Frame), Warsaw, Poland, 8-11 June 1994.
- I.Fejes, A.Kenyeres. The Central Europe Regional Geodynamic Project. Paper presented at the 1st International Symposium on Deformations in Turkey, Istanbul, 5-9 September 1994
- J.Śledziński. Geodynamic GPS EXTENDED SAGET Network in Central Europe. Paper presented to the 7th International Technical Meeting "GPS Goes Operational: Applications and Technology", ION-GPS'94, Salt Lake City, Utah, USA September 1994.
- J.Śledziński, J.Rogowski. Geodetic and geodynamic projects related to the programme of the CEI (Central European Initiative) Section C "Geodesy". Paper presented at the International Meeting on Cooperation of the Central European Initiative, Section C - Geodesy, Kočovce Mansion, Slovakia, September 20-23, 1994
- J.Śledziński. National Report of Poland. Paper presented at the 2nd CERGOP Working Conference, Penc, Hungary, 4-5 November 1994.
- J.Śledziński. Relations between CEGRN and EXTENDED SAGET networks. Paper presented at the 2nd CERGOP Working Conference, Penc, Hungary, 4-5 November 1994.
- J.Śledziński, J.Rogowski, M.Figurski, L.Kujawa, M.Piraszewski. Results of zero-epoch CEGRN'94 campaign. Paper presented at the 2nd CERGOP Working Conference, Penc, Hungary, 4-5 November 1994.
- J.Śledziński, J.Rogowski, M.Figurski, L.Kujawa, M.Piraszewski. Results of EXTENDED SAGET'94 Campaign. Paper presented at the 2nd CERGOP Working Conference, Penc, Hungary, 4-5 November 1994.
- J.Śledziński. Relations between CEGRN and EXTENDED SAGET networks. Paper presented at the 2nd CERGOP Working Conference, Penc/Budapest, Hungary, 4-5 November 1994
- J.Śledziński (edit). Proceedings of the 2nd CERGOP Working Conference, Penc/Budapest (Hungary), 4-5 November 1994. REPORTS ON GEODESY, IGGA WUT, No. 5 (13), Warsaw, 1994
- J. Śledziński. Concise outline of geodetic and geodynamic projects running at the Institute of Geodesy and Geodetic Astronomy of the Warsaw University of Technology. Contribution to the update of the National Report of Poland. Paper presented at the Third Round Table Session of the Earth Science Committee, Working Group on Science and Technology of the Central European Initiative (CEI), Trieste, Italy, 12-13 December 1994.
- J. Śledziński. CERGOP Project as a multilateral co-operation of CEI countries to set up a GPS monitoring network in Central Europe (invited paper). Paper presented at the Third Round Table Session of the Earth Science Committee, Working Group on Science and Technology of the Central European Initiative (CEI), Trieste, Italy, 12-13 December 1994.
- J. Śledziński. Programme of research in geodynamics of CEI (Central European Initiative) countries. CERGOP and related projects. Paper presented at the XX General Assembly of the European Geophysical Society, Hamburg, Germany. 3-7 April 1995.
- J. Śledziński. Programme of research of CEI countries in geodesy and geodynamics. Paper presented at the Symposium IAG G6 "Geodetic Networks for Addressing Geophysical Issues", Boulder, Colorado, USA, July 1995.

Sakhalin Island GPS Survey: A Case History

Paul Godwin
Mobile Oil Corporation

Sergey Duginov
Romona Ltd.

John Brown
Geodetic Technology Company

Biographies

Paul S. Godwin is a Senior Staff Geophysicist with Mobil Oil Corp. Exploration & Producing Division, New Business Development. He graduated from the University of Surrey, England, in 1968 with BS^C (Electrical Engineering).

Sergey N. Duginov is Manager Asia-Pacific for ROMONA Ltd (Russian Marine Positioning & Survey Company) based in Yuzhno-Sakhalinsk, Russia. He graduated from the Dept. of Satellite Geodesy, Moscow Institute of Geodesy, Air Survey & Cartography in 1989. On completion of formal education he worked as a surveyor for DMIGE Co (Far East Marine Engineering Co) and since the end of 1991 has worked for ROMONA Ltd. Prior to his appointment as Manager Asia-Pacific he was Area Manager for Vietnam based in Vung Tau.

John M. Brown is on educational leave from Chevron Petroleum Technology Company and is currently working on his PhD at The University of Calgary in the area of estimation techniques and reliability measures. He is a part-time consultant with Geodetic Technology Company in Richardson, Texas.

Abstract

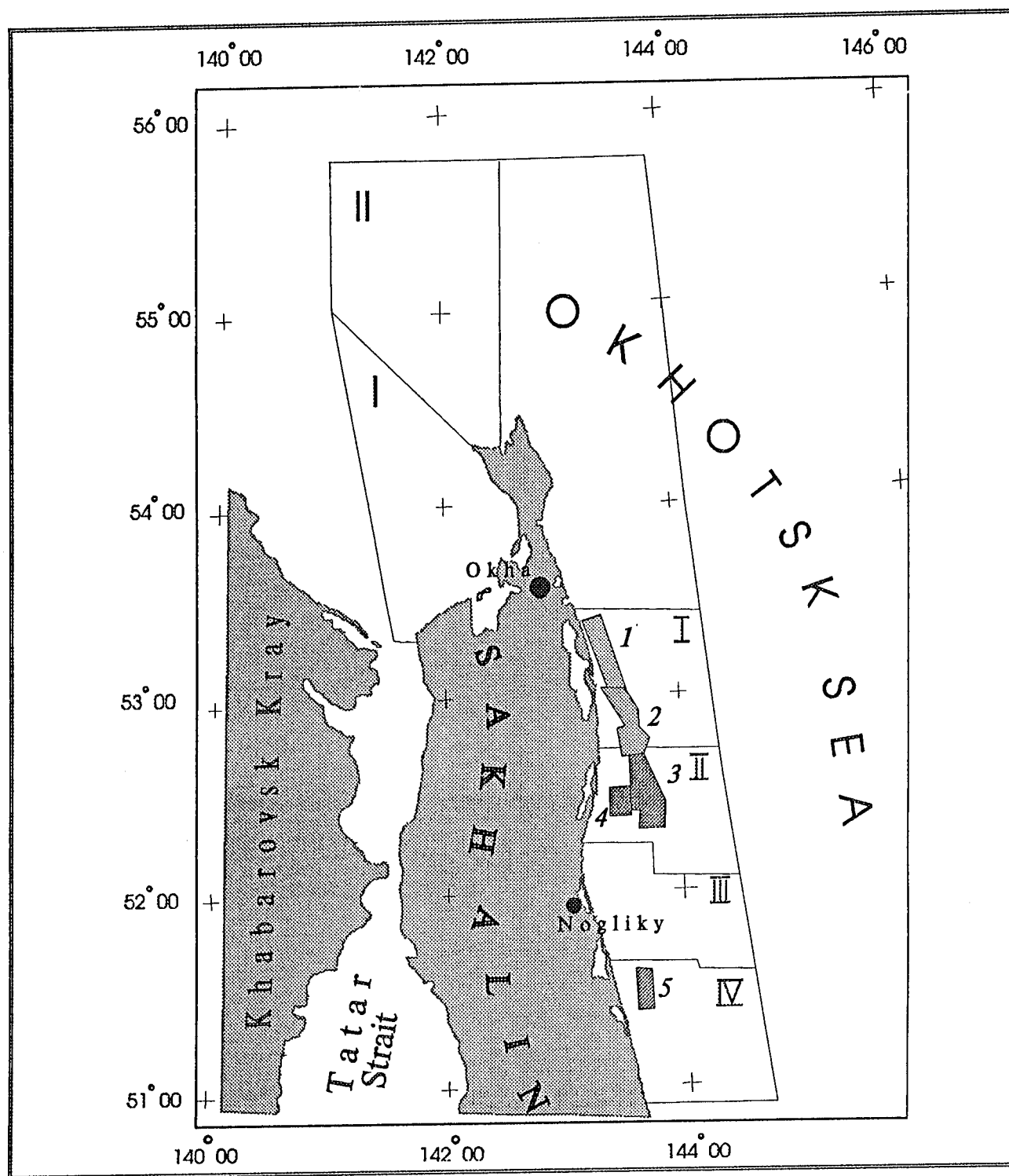
In December 1993 a consortium of Mobil and Texaco was awarded exploration and production rights for the Kirin block, offshore northeast Sakhalin Island in the Russian Far East Territories. Existing seismic data was positioned by various radio navigation systems, whose base station / transponders had been located by TRANSIT receivers operated in the point positioning mode.

A static mode GPS survey was conducted to verify the existing *ad hoc* network, and tie this network to a global system by post-processing with tracking data from the International GPS Service for Geodynamics (IGS). With these confirmations, the consortium believed it would be possible to better estimate the accuracy of the existing seismic data locations and establish absolute control positioning for future work.

The GPS field work, based out of Nogliki, was conducted by ROMONA in July 1994 and the initial in-field processing was also performed there for QC purposes before demobilising. Subsequently, *beta* release Trimble software (GPSurvey v1.98), licenced by Geodetic Technology Company, was loaded on a laptop PC and the long baseline processing, to effect the ties to three IGS stations, was performed in Moscow. The Canadian Energy and Mineral Resources program SPARC (now called GEOPACE) was used to compute absolute point positions to confirm the GPSurvey processing.

Results exceeded expectations. Estimated accuracy between the Sakhalin network and the three IGS stations are +/- 6cm horizontal and +/- 15cm (1 sigma) in the vertical. Differences between IGS ties and SPARC positions were at the sub-metre level. PC based off-the-shelf software capable of taking advantage of IGS data allows GPS surveying to achieve cost effective ties to a global geodetic network at a speed that minimises the impact on overall project cycle time. The power of this new utility requires that client companies select contractors with the proper training and experience and also that software developers recognise the necessity for extensive quality control of both the data and operators' inputs.

Fig. 1 SAKHALIN OFFSHORE (showing lease areas)



LEGEND

- I, II - Exxon Ventures (CIS) Inc., (Project Sakhalin-III)
- IV - Mobil, Texaco, (Project Sakhalin-III)
- 1, 5 - Sakhalin Energy Investment Company Ltd., (Project Sakhalin-II)
- 2, 3, 4 - Exxon Ventures (CIS) Inc., Sodeco, (Project Sakhalin-I)

Introduction

Mobil Russia Ventures Inc., Moscow, Russia and ROMONA Ltd., Yuzhno, Sakhalinsk Region, Russia (hereafter referred to as Mobil and ROMONA) established an eleven point control network on the northeast coastline of Sakhalin Island during the last two weeks of July, 1994. Preliminary absolute WGS 84 position and orientation were obtained through occupation of the control point Nysh (NYSH). In August 1994, ROMONA Ltd. indirectly tied NYSH to a DORIS station located approximately 500km southeast using dual frequency GPS receivers. The DORIS station coordinates used by ROMONA Ltd. were estimated to be within +/- 20cm of their true WGS absolute horizontal position. Mobil requested Geodetic Technology to formally tie the observed network to the International Terrestrial Reference System, 1992 (ITRF 92) using GPS data collected by at least two International Geodynamic System (IGS) stations and precise satellite orbit information. Four IGS stations, located in Usuda, Japan, Tsukuba, Japan, Taipei, Taiwan, and Fairbanks, Alaska respectively, were chosen as the points to which control point NYSH would be tied (See Figure 4). Due to restrictions on exporting classified data from Russia, all processing involving data collected on Sakhalin had to be completed in country. The initial processing and adjustment was performed in Yuzhno-Sakhalinsk and the final long baseline processing was performed in Moscow.

Background & History

Sakhalin Island is located in the Russian Far East Territories and is washed by the Sea of Okhotsk on the north and east and the Tatar & Laperus Straits on the west and south. One of the larger Russian Islands, Sakhalin has a population of only six-hundred thousand and is rich in natural resources such as oil & gas, coal, forest and fish with famous red caviar.

For many years SakhalinMorneftegas (Russian Oil company) has produced oil onshore northern Sakhalin. Formerly, the government of the Soviet Union and subsequently the Russian Government financed the exploration surveys offshore north-east Sakhalin. During this time Russian companies such as Far East Marine Company (FEMCO), Dalmorneftegeofizika (DMNG) and Far East Marine Geological Expedition (DMIGE), carried out 2D seismic, investigation and site surveys and also drilled many wells. The results indicate great potential for hydrocarbon resources offshore

Sakhalin in the Sea of Okhotsk. A challenge is that during winter time the sea around Sakhalin Island is covered with ice which limits exploration activities to the summer period from June to October. Large deposits have been discovered offshore north-east Sakhalin, such as Piltun-Astokhskoye, Kirinskoye, Lunskeye, Chaivo. For future development of these oil & gas fields the Russian Government has invited bids from foreign companies such as Mobil, Exxon, Texaco, Marathon, McDermott, Mitsui, Shell, amongst others.

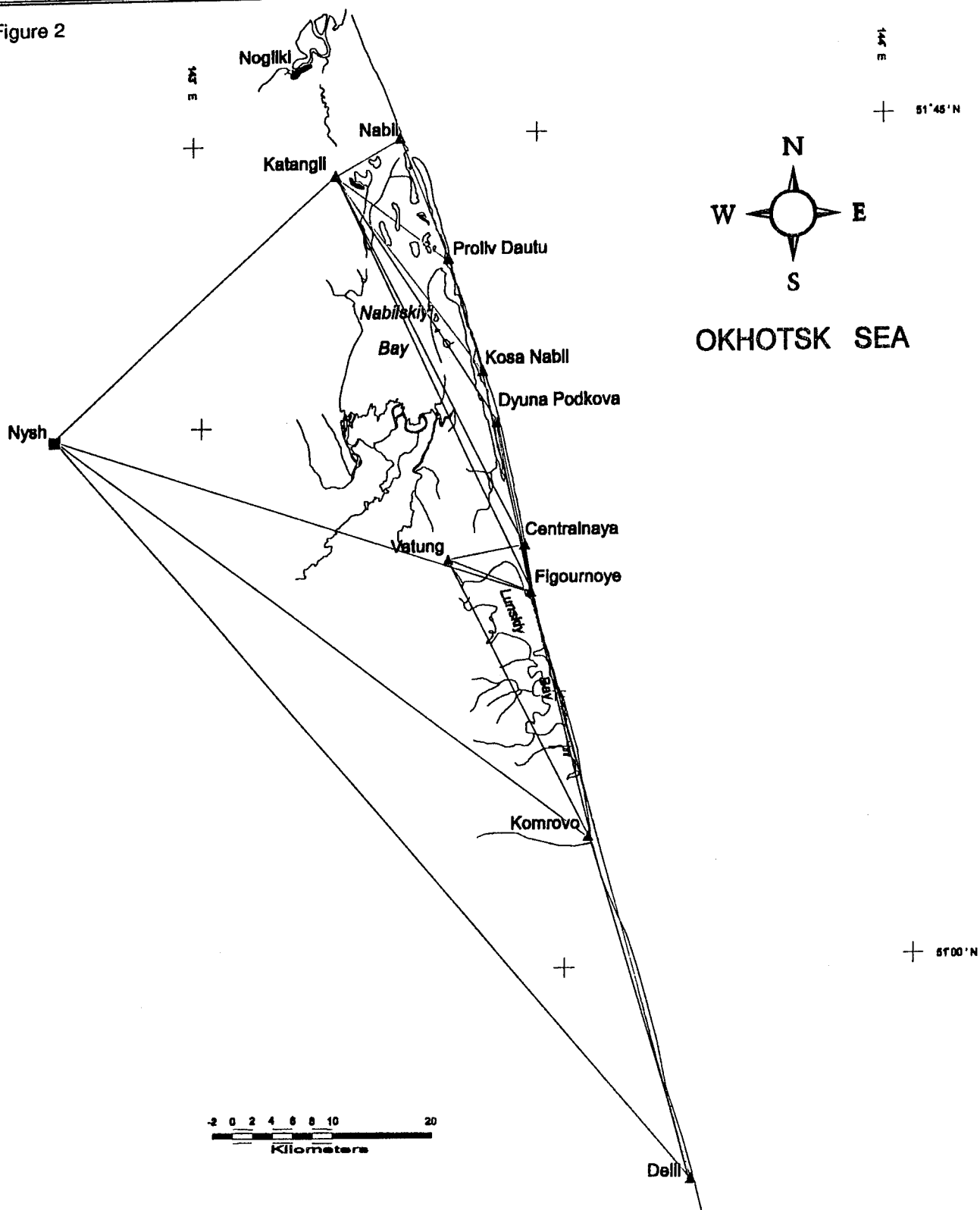
Historically, radio navigation systems were used, e.g. Syledis (French) and Poisk (Russian). Typically the base station coordinates were determined by TRANSIT receivers operated in the point positioning mode, although some were defined using geodetic control points in the Russian State coordinate system (SCS).

GPS technology started to be used in marine surveys in 1990. In 1991 Russian Marine Positioning & Survey Company, Yuzhno-Sakhalinsk, (ROMONA) carried out relative GPS measurements using WM-102 receivers. The pre-existing control point at the ROMONA's office in Yuzhno-Sakhalinsk, named Corpus, was chosen as reference point. Corpus was set using a JMR-4A receiver with not less than 50 TRANSIT satellite passes. Some geodetic control points on the north-east coast were then chosen for future use as base stations for radio navigation systems. Using Magnavox's PoPS software the coordinates for these stations were defined and tied to the local network in World Geodetic System 1984 (WGS-84). The result of this historical activity was that the north-east Sakhalin sites in many cases had multiple coordinate sets, determined over the years since offshore activity started in 1976.

In December 1993 a consortium of Mobil and Texaco was awarded exploration and production rights for the Kirin Block (see Figure.1). The consortium desired to establish or redefine the existing geodetic control points on the north-east coast to remove doubt and confusion before any further exploration activity commenced.

ROMONA was awarded a contract by Mobil to conduct a static mode GPS survey to verify the existing local geodetic network on the north-east coast and to tie this network to a global system. ROMONA supplied the experienced technical personnel and equipment, and their survey team was responsible for the GPS field work and initial in-field and post-processing. Aviation support was provided by a Mi-8-MTV helicopter chartered from the Aerolift Company.

Figure 2



The Field Work

The survey objective was to determine the coordinates of geodetic control points using three dual frequency Trimble 4000SSE GPS receivers.

Originally, it was planned to perform the observations on 13 (thirteen) points.

Checks of the Trimble 4000SSE GPS receivers were performed on short (50 meters) and long (2000-4000 meters) baselines before the beginning of the field work.

A one day helicopter reconnaissance was conducted prior to commencement of any GPS data collection. The purpose of this reconnaissance was to verify and recover the points as well as determine safe access. In fact, two points were not recovered, one had washed away and the other could not be found. Trimble FlightMate handheld GPS receivers were of great assistance. The navigation of the helicopter was aided by a Garmin GPS receiver installed in the cockpit. Due to the absence of the point in the Nysh area, formerly defined by TRANSIT satellite methods, a new site was set there.

The base of operations was Nogliki. Field operations were performed from 15 July to 25 July 1994.

Geodetic Control Point

Dual frequency carrier-phase GPS observations of approximately 50 hours were recorded at Nysh. These data were subsequently processed using precise GPS ephemerides with GPS observation at the International GPS Service for Geodynamics (IGS) stations. (See below). Uninterrupted GPS observations at Nysh were made from 0:57 AM 17 July till 2:19 AM 19 July 1994 (UTC time).

Static GPS Survey

The static GPS survey was conducted using three dual frequency Trimble 4000SSE receivers. GPS observations were performed simultaneously at three geodetic points (triangles) according to Fig. 2. For Nysh-Katangli-Figournoye and Nysh-Figournoye-Komrovo triangles (fundamental control point) sessions were a minimum of four hours each for Komrovo-Figournoye-Delil and Nysh-Komrovo-Delil triangles sessions were of three and a half hours each and on the remaining geodetic points the observation sessions were of at least two hours duration. For control of field measurements GPS observations were performed on the Katangli-Nabil-Proliv Dautu, Figournoye-Vatung-Centralnaya and Nysh-Komrovo-Delil triangles.

For all sessions, an HF/SSB transceiver was installed at each site occupied for efficient

coordination of sessions as well as safety. Adequate camping and survival gear was deployed at each site as weather dictated.

All receivers collected data at 15 second intervals for all sessions. Measurements of temperature, atmospheric pressure and percentage humidity were made at all points and recorded hourly directly into the receiver and the field book. The antenna height measurement was performed both before and after each session and similarly recorded.

The raw data from all three GPS receivers, was downloaded daily to the computer and to floppy disk and checked for quality. Each evening, this data was postprocessed to resolve the relative baseline vector between the GPS points using Trimble's GPSurvey™ v1.01 software. For QC purposes, all such computations were completed before the final demobilisation of the ROMONA team from Nogliki to ROMONA's main base in Yuzhno-Sakhalinsk.

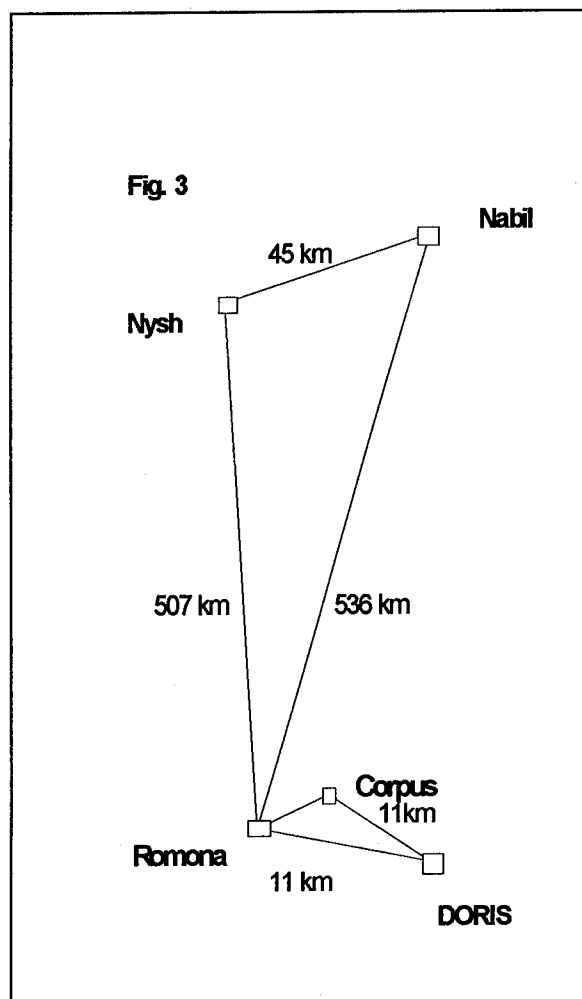
Provisional Network Solution Adjustment

On completion of all the fieldwork, baseline solution and network adjustment were performed in ROMONA's office in Yuzhno-Sakhalinsk. Trimble's GPSurvey™ v1.01 software was used for all calculations of various baselines vectors and network adjustments. Geometric relative positioning accuracy (HOR Prec) of all the measured baselines was better than 1 : 100000, and the HOR Prec. of the baselines between fundamental control points was better than 1:1000000.

GPS Measurements from DORIS Station

For comparison with the future ITRF-92 coordinates, GPS observations were made on 5 and 13 August 1994 incorporating the DORIS reference point located near Yuzhno-Sakhalinsk. The DORIS antenna reference point co-ordinates were defined in 1992 by the Geodetic and Levelling Service of National Geography Institute (IGN/SGN) of France in the Frame of Geodynamic Research International Programme. The DORIS station is located near Yuzhno-Sakhalinsk in the south of Sakhalin Island, approximately 500 km south-east of the existing GPS Network. The scheme of these observations is shown in Figure 3. Session lengths were 1.5 hours for DORIS-ROMONA-Corpus and 5 hours for ROMONA-Nysh-Nabil triangles.

An additional network adjustment was based on the DORIS station as reference point.



Geodetic Survey Division. Data is computed using all available IGS station information and is uploaded approximately 3-7 days post-mission. Accuracies of the 15 minute epoch precise orbital information and precise SV clock corrections are at the 20 cm level and agree with WGS 84 at 0.2 ppm [Kouba et. al.]. The four IGS stations selected to use as ITRF 92 reference points for the project were FAIR, located in Fairbanks, Alaska; USUD, located in Usuda, Japan; TSKB, located in Tsukuba, Japan; and TAIW, located in Taipei, Taiwan (See Figure 4). All IGS stations used in the project are equipped with Allen Osborne Rogue SNR-8000 Receivers using Dorne Margolin R Antennas. The SNR-8000 measures C/A code, P Code, L1 and L2, and obtains the P Code from cross-correlation techniques if A/S is implemented [IGS Documentation, 1994]. Data observation intervals at each IGS station are 30 seconds. GPS observation data in the Receiver Independent Exchange (RINEX) format for the three eastern stations were obtained from Scripps Institute of Oceanography (SIO), and for FAIR from the Jet Propulsion Laboratory (JPL). Both SIO and JPL sources are accessible via anonymous ftp. Current (as of January 10, 1994) ITRF 92 precise Cartesian coordinate estimates were downloaded from SIO's facilities. Unfortunately, Geodetic Technology Company was unable to obtain reliable estimates for the IGS point TSKB. However, since precise Cartesian coordinate values were listed for the three remaining points, it was determined that the missing tie to TSKB would not adversely affect the solution.

Long Baseline Postprocessing

IGS Station Observation and Precise Orbit Data Acquisition

Prior to beginning work in Moscow, Mobil informed Geodetic Technology Company of the data collection periods observed at NYSH during the field survey. Data observation times for NYSH and two additional stations, Figournoye (FIGO) and Komrovo (KOMR) are listed in Table 1.

IGS station GPS measurements and precise orbital information corresponding to these observation periods were obtained through computers accessible through the Internet. Precise GPS satellite (SV) orbits were downloaded from Canadian Energy and Mineral Resources

Table 1 - Data Observation Times for Points in Mobil/ROMONA Network

| Point | Day | Start (UTC) | Stop (UTC) | Total (Hours) |
|-------|------------------|-------------|------------|---------------|
| NYSH | July 17-19, 1994 | 00:57 | 02:19 | 49 h 16 m |
| FIGO | July 17, 1994 | 01:00 | 07:00 | 04 h 00 m |
| FIGO | July 19, 1994 | 03:00 | 07:00 | 04 h 00 m |
| KOMR | July 19, 1994 | 03:00 | 07:00 | 04 h 00 m |
| KOMR | July 21, 1994 | 04:26 | 08:00 | 03 h 34 m |
| NYSH | July 21, 1994 | 04:26 | 08:00 | 03 h 34 m |

ITRF 92 geographic and Cartesian coordinates for the three points used for the project are listed in Table 2.

Table 2 - ITRF 92 Values for Project IGS Control Points

| Name | Latitude/X | Longitude/Y | Ellipsoidal Height/Z |
|------|--------------------------------------|---------------------------------------|-----------------------------|
| USUD | 36° 07'59.2037" N -3741020.511 m | 138° 21' 43.3542" E 3427432.566 m | 1508.696 m 3741020.511 m |
| TAIW | 25° 01' 16.7981" N -3024781.775 m | 121° 32' 11.5388" E 4928936.927 m | 44.007 m 2681234.588 m |
| FAIR | 64° 58' 40.8112" N -2281621.220 | 147° 29' 57.2521" E -1453595.760 m | 318.987 m 5756961.990 m |

Processing Software

Two software packages were used to determine the precise ITRF 92 estimates of the points in the Mobil/ROMONA control point network. The first, Trimble's GPSurvey v1.98, was used as the primary method to determine the baseline lengths between the IGS stations and the selected local network points. At the time of processing, GPSurvey v1.98 was available only to *beta* site companies. The current version, 2.0, with all the features listed below, is now available to the public. The baseline processing package has been modified from version 1.20 by adding the capability to use multiple reference SVs throughout a single observation set and process up to 24 hours of continuous data. The option to use precise SV orbit files in the EF18 binary format is also available and was selected throughout the processing.

The second package providing confirmation of the GPSurvey results was the SPARC single point positioning program developed by Canadian Geodetic Survey Division. SPARC accepts GPS observations files in either RINEX or Rogue format, and SP3 formatted precise SV orbits to compute absolute position estimates at epochs coincident with the precise satellite ephemeris file. These values are then averaged over the data collection interval to estimate a final 3-D position. If precise satellite clock data are used at each estimation epoch, achievable accuracies will approach the sub-meter level, given sufficient data samples, low receiver noise, and minimal multipath effects. Geodetic Survey provides orbit files with precise clock data at 15 minute epochs. Precise SV clock files calculated by Geodetic Survey are only valid for points within Canada and so were not used in the confirmation. L3 pseudorange positions were calculated by SPARC at 15 minute intervals to avoid the effects of selective availability (SA).

Preliminary Processing

Prior to departing for Moscow, data obtained from the IGS stations for July 17 (Day 198) and July 18 (Day 199) were processed by both GPSurveyTM and SPARC. GPSurveyTM baselines results agreed with published IGS values at the 0.05 ppm level and SPARC results were within +/-1.5m (1 σ) in all three components. Geodetic Technology Company performed the pre-processing to help ensure that work in Moscow would proceed smoothly and to verify agreement between the Trimble and Geodetic Survey software.

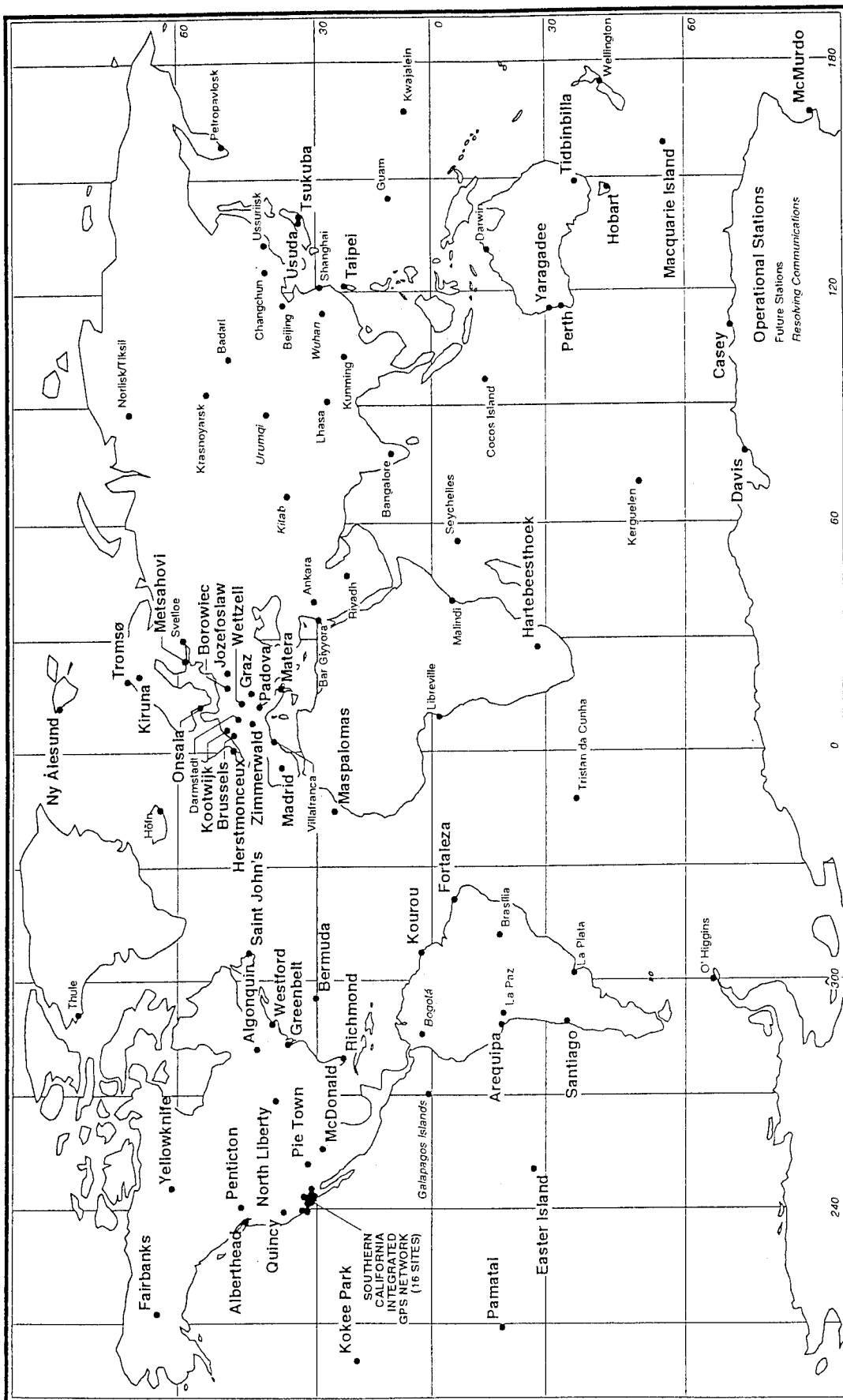
IGS Baseline Ties and Adjustment

NYSH was connected to all three IGS stations on days 198 and 199. Baseline comparisons between days 198 and 199 agreed to within 5 cm horizontal and 15 cm vertical. Points KOMR and FIGO were used as secondary tie points and connected only to stations USUD and TAIW on days 198, 200, and 202 (insufficient data was available to compute the ~5500 km baseline to FAIR). Furthermore, baselines between FIGO, NYSH and KOMR on day 200 were reprocessed using precise ephemeris data to provide strength in the Mobil/ROMONA-IGS network solution. Figure 5 shows the baselines processed. Standard meteorological values (20°C, 1000mb, 50% humidity) were input into the processing software due to the long time span of each session.

Following determination of the baseline measurements, the network was adjusted using TrimNet to estimate final ITRF 92 values for point NYSH, FIGO, and KOMR. The three IGS stations were held fixed and height and centering errors were estimated to be 5mm each. Adjusted baseline accuracies are listed in Table 3.

PPM values between the fixed points are not listed. The baseline accuracies translate to errors between +/- 0.02cm and +/- 0.06cm (1 σ). The highest ppm value, 1.912, is for baseline FIGO-KOMR, expectedly the shortest baseline in the network.

GPS TRACKING NETWORK OF THE INTERNATIONAL GPS SERVICE FOR GEODYNAMICS OPERATIONAL AND PLANNED STATIONS



September 1994

Fig. 4

Standard deviations for the estimated points range from 0.03m to 0.06m in the horizontal components, and from 0.10m to 0.13m in the vertical. Vertical accuracies are larger than horizontal reflecting the poorer SV geometry in determining the vertical component and limitations of the processing software. However, these accuracies are within the +/-0.50m absolute position error required by Mobil and have improved upon the previous WGS 84 estimates. The adjusted ITRF 92 values for point NYSH were compared with the previous coordinate estimates and found to differ 1.99m in horizontal magnitude and 1.58m in height. These previous values were determined by ROMONA using differential GPS (L1/L2) and indirectly measuring to a DORIS station approximately 500km to the southeast.

Confirmation with SPARC v2.1 Processing

To confirm the results of the IGS baseline ties and network adjustment, SPARC was used to determine estimates of points NYSH, FIGO, and KOMR for the four hour sessions collected from 1:00 am to 5:00 am UTC on day 200. Results from this confirmation are presented in Table 4 as well as differences in latitude, longitude and ellipsoidal height from the IGS-tie/ITRF 92 estimates.

Table 4 - SPARC v2.1
Differences between ITRF 92 Positions

| Name | $\delta\phi$ m | $\delta\lambda$ m | δh m |
|------|----------------|-------------------|--------------|
| NYSH | -0.07 | 0.14 | 0.36 |
| FIGO | 0.19 | 0.06 | 0.19 |
| KOMR | -0.65 | -0.09 | 1.63 |

Agreements are at the sub-meter level except for the height component at point KOMR. SPARC will estimate positions only at epochs receiving data from at least 4 satellites both tracked by the receiver and listed in the precise SV orbit/clock correction file. Station KOMR experienced a large number of cycle slips (and therefore loss of measurement data) and only 6 epochs were used to obtain a position. This accounts for the larger differences in the vertical component.

Comparative Results

After the post-processing in Yuzhno-Sakhalinsk the GPS network was defined in WGS-84 based upon the DORIS position. Subsequent to post-processing of the long baseline data in Moscow and the derivation of ITRF-92 coordinates a second network was defined. The differences between ITRF-92 and DORIS co-ordinates for all GPS points are listed in Table 5.

Table 5 - Differences between ITRF-92 & DORIS coordinates.

| Name | $\delta\phi$ sec/m | $\delta\lambda$ sec/m | δh m |
|------|---------------------|-----------------------|--------------|
| CENT | -0.027038 -0.836 | -0.047553 -0.920 | 1.602 |
| DAUT | -0.027757 -0.858 | -0.0472 -0.908 | 1.549 |
| DELI | -0.025360 -0.784 | -0.048786 -0.955 | 1.743 |
| DUNA | -0.027291 -0.843 | -0.047503 -0.916 | 1.583 |
| FIGO | -0.027033 -0.835 | -0.047384 -0.917 | 1.597 |
| KATA | -0.028054 -0.867 | -0.046656 -0.896 | 1.528 |
| KOMR | -0.026347 -0.814 | -0.049291 -0.959 | 1.682 |
| KOSA | -0.027446 -0.848 | -0.047431 -0.914 | 1.573 |
| NABI | -0.028025 -0.866 | -0.046954 -0.901 | 1.524 |
| NYSH | -0.027391 -0.846 | -0.045495 -0.878 | 1.580 |
| VATU | -0.027028 -0.835 | -0.047104 -0.911 | 1.600 |

As previously mentioned the positions of several of the points were determined by different survey methods over the years. The new ITRF-92 co-ordinates were then compared with the existing co-ordinates. The differences between the ITRF-92 and previous co-ordinates for all GPS points are listed in Tables 6 and Table 7.

Sakhalin Island GPS Survey: IGS Ties (Stations KOMR & FIGO omitted for clarity)

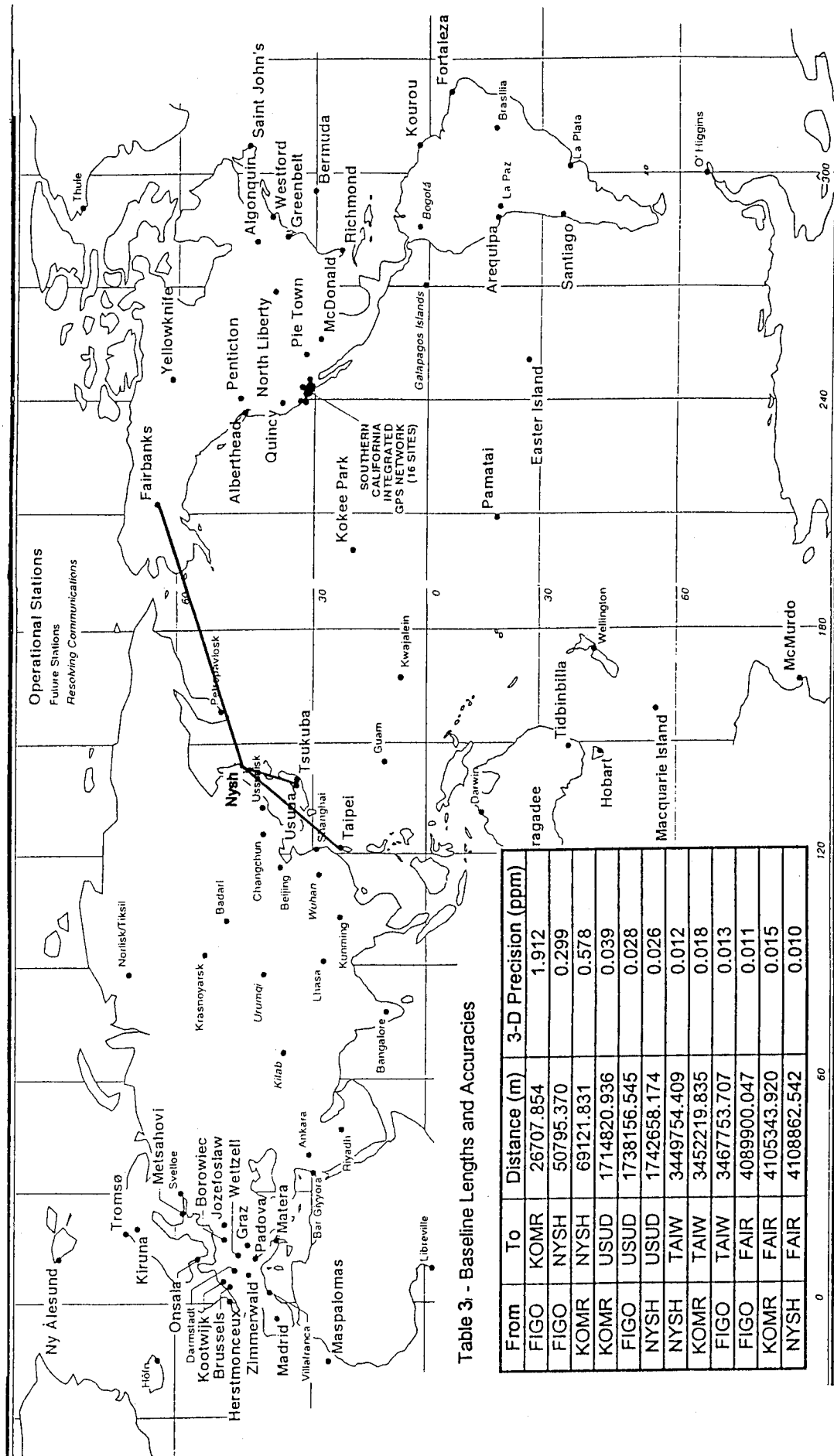


Table 3 - Baseline Lengths and Accuracies

| From | To | Distance (m) | 3-D Precision (ppm) |
|------|------|--------------|---------------------|
| FIGO | KOMR | 26707.854 | 1.912 |
| FIGO | NYSH | 50795.370 | 0.299 |
| KOMR | NYSH | 69121.831 | 0.578 |
| KOMR | USUD | 1714820.936 | 0.039 |
| FIGO | USUD | 1738156.545 | 0.028 |
| NYSH | USUD | 1742658.174 | 0.026 |
| NYSH | TAIW | 3449754.409 | 0.012 |
| KOMR | TAIW | 3452219.835 | 0.018 |
| FIGO | TAIW | 3467753.707 | 0.013 |
| FIGO | FAIR | 4089900.047 | 0.011 |
| KOMR | FAIR | 4105343.920 | 0.015 |
| NYSH | FAIR | 4108862.542 | 0.010 |

Fig. 5

September 1994

Table 6 - Differences between ITRF-92 & TRANSIT coordinates.

| Name | $\delta\phi$ sec/m | $\delta\lambda$ sec/m | δh m |
|------------|--------------------|-----------------------|--------------|
| Katangli | -0.053 -1.65 | -0.185 -3.55 | -6.07 |
| Figournoye | -0.013 -0.40 | -0.01 -0.19 | -3.32 |
| Delil | -0.074 -2.29 | 0.009 0.16 | 2.01 |
| Vatung | 0.079 2.43 | -0.046 -0.90 | -1.56 |

Conclusions and Recommendations

Points NYSH, FIGO and KOMR were successfully tied to ITRF 92 at the sub 50cm level, satisfying the accuracy requirements specified by Mobil. Geodetic Technology Company verified that Trimble's revised GPSurvey v1.98 package reliably computes long baselines (>1000km) to accuracies of +/- 6cm horizontally and +/- 15cm vertically using precise SV ephemeris data. Final ITRF positions were independently confirmed using the EMR software SPARC v2.1, which computes single point position estimates using pseudorange observations corrected with the L3 observable, precise SV positions, and most importantly precise SV clock corrections. These two methods used to determine ITRF 92 positions are different algorithms (differential vs. single point) but are correlated through the use of identical SV orbit files. Nevertheless, agreement between the two strongly indicates that the final ITRF 92 IGS station-referenced positions are both accurate and reliable. Improvements on the position estimates for NYSH, FAIR, and KOMR could be attained by using software that simultaneously computes SV orbit parameters along with the estimates for the new unknown points. Software capable of this is currently available only on UNIX based systems and is impractical for use under the processing location restrictions required by Mobil. All long baseline ties to the IGS stations and single point position estimates were processed at Mobil's office in Moscow on an Intel-based 486DX2 40MHz notebook computer. Additional IGS station ties could be added to increase the precision and accuracies of the three estimated Mobil/ROMONA positions but viable choices for this region are currently limited. However, even without these additional

Table 7 - Differences between ITRF-92 & GPS 1991 coordinates.

| Name | $\delta\phi$ sec/m | $\delta\lambda$ sec/m | δh m |
|--------------|--------------------|-----------------------|--------------|
| Katangli | 0.156 4.82 | -0.083 -1.60 | 1.36 |
| Figournoye | 0.174 5.39 | -0.174 -3.37 | 0.76 |
| Proliv Dautu | 0.165 5.09 | -0.126 -2.43 | 1.07 |
| Duna-Podkova | 0.173 5.32 | -0.125 -2.42 | 0.68 |

improvements, Geodetic Technology Company demonstrated that precise absolute ITRF 92 positions can be generated in-field post-mission at accuracies less than +/- 20cm in all three axes.

Future recommendations include investigating the effects of using measured versus standard meteorological values at stations separated by large distances (and with long data sets), increasing observation times for multiple stations in the observed network (as opposed to one station with 48 hours of data and 2 with 4 hours), and using software capable of computing improved SV orbit parameter estimates. It is expected that these modifications would yield results that would not improve the accuracies of the absolute ITRF 92 estimates at a level significant for applications used in the petroleum exploration industry.

The overall results show that the historic radio navigation station sites were within acceptable tolerances and therefore the existing seismic is similarly acceptable regarding positional accuracy (assuming of course there were no unresolved lane count problems in processing). Future geophysical work positioned with real-time DGPS may be easily tied. The project as a whole amply demonstrates the power and utility of GPS hardware and software available today. However the user bears the ultimate responsibility for all results and therefore the requirement for such work to be performed by those with the proper skill and experience is still evident.

Acknowledgements

The authors wish to acknowledge their colleagues and co-workers for their encouragement and

support. Special thanks to Dr Ruth Neilan and the worldwide staff of IGS.

References

"Comparison of Methods for Obtaining Absolute WGS84 Positions in Remote Locations"; J. Brown, E. Cannon and D. Roberts, The University of Calgary and J. Morgan, Chevron Petroleum Technology Company. ION GPS 94,

" One Meter Level Kinematic Point Positioning Using Precise Orbits and Satellite Clock Corrections " G. Lachapelle, R. Klukas, D. Roberts and W. Qiu, The University of Calgary: C. McMillan, Defence Research Establishment Ottawa. ION GPS 94',

The International GPS Service for Geodynamics
Central Bureau. Tel 818-354-1836 or e-mail
igscb@cobra.jpl.nasa.gov

Economics of GPS and CORS

William Young
Riverside County Flood Control District

Yehuda Bock and Shelley Marquez
Scripps Institute of Oceanography

Biography

Mr. Young is in charge of the Geographic Information System (GIS), Right-of-Way Engineering, Surveying and Photogrammetric Mapping for the Riverside County Flood Control and Water Conservation District. He is licensed with the State of California as a Land Surveyor, Photogrammetrist, and Consulting Engineer. Mr. Young teaches Photogrammetric Engineering at the University of California in Riverside. He is a member of the Southern California Global Positioning System (GPS) Users Group, the California Continuous Operating Reference Stations (CORS) Committee, and the League of California Surveying Organization. His work for the County currently focuses on the fields of GIS, GPS, and softcopy photogrammetry.

Dr. Bock is director of the Scripps Orbit and Permanent Array Center at Institute of Geophysics and Planetary Physics, Scripps Institution of Oceanography, UCSD where he is a research geodesist and senior lecturer. Dr. Bock is a member of the Executive Committee of the Southern California Integrated GPS Network (SCIGN), the California Continuous Operating Reference Stations (CORS) Committee, the Governing Board of the International GPS Service for Geodynamics (IGS), the Executive Committee of the International Association of Geodesy (IGPP), and is an associate editor for *Manuscripta Geodaetica*.

Ms. Marquez is coordinator of the Scripps Orbit and Permanent Array Center and a staff research associate at Scripps. She is responsible for customer service and the maintenance of the SOPAC BBS for Southern California surveyors.

ABSTRACT

Global Positioning System - GPS is convincing many surveyors to change the way they think about the profession. For most of recorded history surveying has used

the same fundamental techniques. Now in a comparative instant of time GPS has introduced a revolution in procedure, a quantum leap in results, and gratifying economies to achieve essentially traditional goals. Continuous Operating Reference Stations (CORS) will continue this trend and will gradually replace the fixed monument reference system used around the world.

Some History - The first true geodetic survey took place in France in the late 1700's. The United States didn't perform its first geodetic survey until 1816-17 under Superintendent Ferdinand Hassler of the Coast Survey. Until the early 1950's surveying was accomplished by measuring angles with a theodolite (transit) and using calibrated rope, rods, chains, or steel tapes to measure distances.



**Measuring Angles
with a THEODOLITE**



**HELIOGRAPH Sighting
distance over 30km**

Over the years instrumentation continued to improve, especially in the accuracy and weight of theodolites. So me of the first geodetic theodolites weighed over 300 pounds and had a horizontal circle 3 feet in diameter. (Mr. Hassler died from a fall while attempting to save his 200-pound theodolite.) The steel tape improved in uniformity and calibration, and with the use of a temperature gauge and spring balance improved distance measuring up to a point.

During the era of steel tape and theodolite, the most any surveyor could hope for in everyday work was an accuracy of about 1:10,000. When doing triangulation over long distances, an accuracy of 1:25,000 to 1:100,000 could be achieved. The U.S. Coast and Geodetic Survey (USC&GS) classified first order work as 1:25,000. However, when checking a triangulation network with a steel tape between points relatively close together, it is difficult to recall any check ever coming out better than 1:10,000. The primary surveying process has not changed from the beginning of recorded history until the early 1950's with the advent of electronic distance measurement (EDM) techniques. It took another twenty years before most self-respecting surveyors were equipped with an EDM instrument.



**Electronic Distance Measuring
EDM**

First Real Changes - Along with EDM came increased accuracies; 1:50,000 became common. This led to the national reference accuracy standards being revised; first order became 1:100,000. In our area there are still hundreds of USC&GS stations with accuracy no better than 1:10,000. Their value is mainly historical. Occasionally we establish new positions for old stations utilizing the North American Datum of 1983 with a new epoch and time tag.

The 1950's also introduced digital computers which, we are all aware, has led to rapid expansion of surveying and engineering technology. Development of survey instrumentation has continued at a rapid pace as computers get smaller and faster with data storage becoming larger and less expensive. All of this has culminated in the Total Station survey instrument which measures angles and distances automatically and has an on-board computer for running programs and storing data. Unless computer technology slows down we are all going to be on a dead run to keep up. With GPS marrying Total Stations procedures, future development of this technology is limited only by our imaginations.

ECONOMICS OF GPS

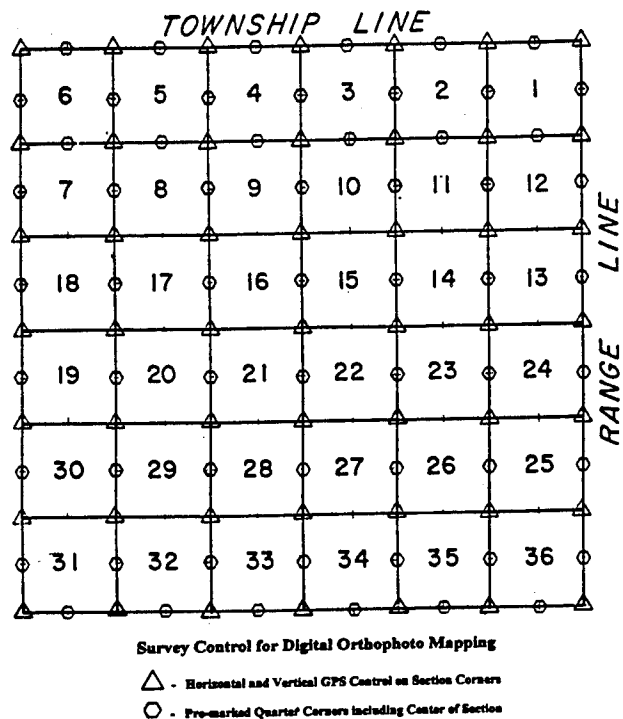
Experiences in Riverside County

The Riverside County Flood Control District has had an on-going program of 1:2400 scale and 4 foot contour mapping. The map sheets are on a square-mile basis. This means establishing positions and elevations on section and quarter corners. Until 1988, internal survey accuracy was

improving in lock step with improvements in survey instrumentation and computer technology. It was routine to achieve 1:50,000 using EDM and a T-3 theodolite. It wasn't until we tied our surveys to the National Geodetic Survey control system that our accuracies fell off drastically. Any good mapping program is based upon the State Plane Coordinate System, and our goal was to produce maps that would meet National Standards. The necessity of

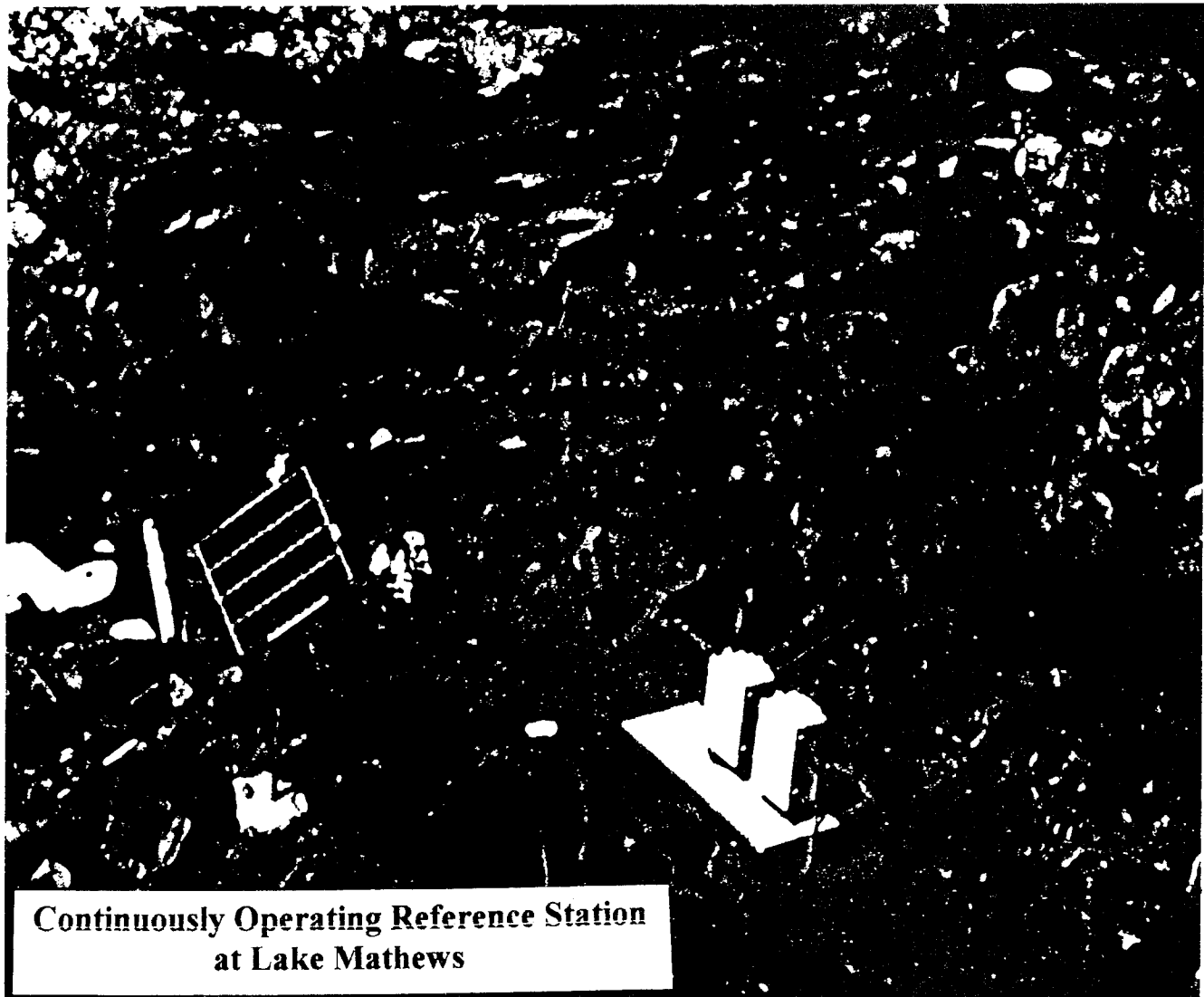
In Riverside County we have two major problems: First the National Reference System (mainly established in the 1930's and 1940's) was not accurate enough to use as a base for modern mapping. Second, crustal motion and earthquakes result in changing ground surfaces. Riverside County covers about 7000 square miles and is bisected by the San Andreas Fault; the western half experiences constant crustal motion. This might seem to be a major burden to any continuing surveying program, as in fact it was until recently.

In 1988 we had our first hands-on experiment with the Global Positioning System. We rented eight receivers and teamed up with the National Geodetic Survey (NGS) to establish a new network of points across Riverside County. Due to rigid observation standards set by NGS, nearly all points observed in the main network were better than 1:1,000,000. In July of 1988, the County's Flood Control District began conversion from conventional ground surveying to utilization of GPS while also developing techniques to account for daily crustal movement and establishing a network of new high precision stations. At that time in 1988 it was costing us approximately \$2,000 per horizontal point and \$110.00 per vertical point to set control to map a township. All of our surveying had to have visual line-of-sight between points, and vertical points were established using differential leveling. We have just completed control for a township in Corona California and the cost was \$223.00 per point for both horizontal and vertical data using GPS. This is only one-tenth our 1988 cost in 1995 dollars. The most important part was that it was more accurate than anything we could produce in the past.



tying to the National Geodetic Survey by juggling stations to best fit our higher-order accuracy surveys was costly and frustrating. This led us to develop our own network of stations across the county based upon the few National Geodetic Survey stations that had an accuracy of 1:100,000. Accuracy improved and adjustments were easier, but line-of-sight geodetic surveying is a costly process.

The Role of Continuously Operating Reference Stations



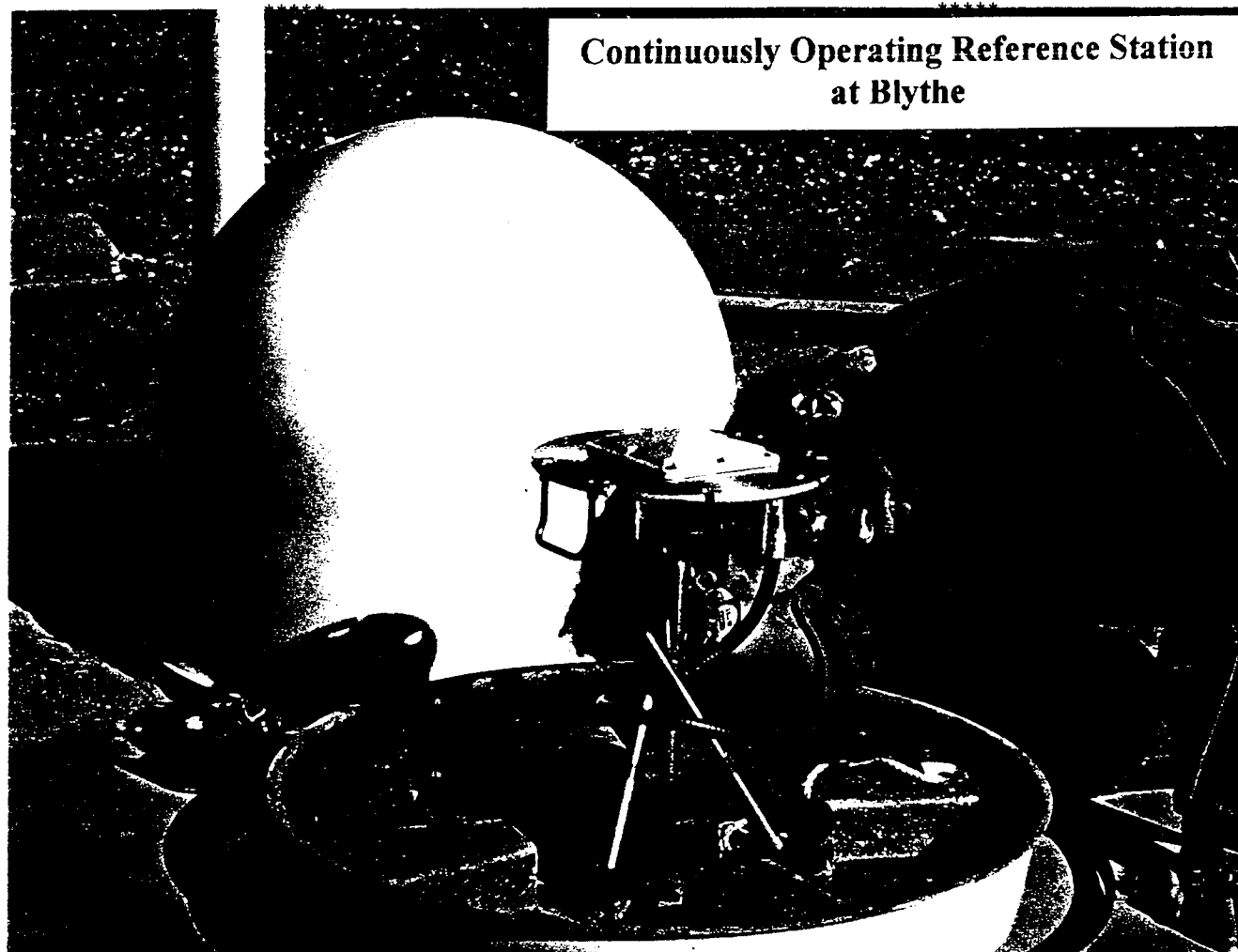
**Continuously Operating Reference Station
at Lake Mathews**

One of the things that helped to reduce the expense of establishing survey control was the introduction in Southern California in 1991 of continuously operating permanent GPS stations, often referred to as Continuously Operating Reference Stations (CORS). Currently, daily horizontal positions for each of the CORS in Southern California are determined with an accuracy of 1-3 mm, with the vertical position accurate to 5-8 mm. The CORS give us the best secular and episodic motion (crustal motion and earthquakes) values available. When needed, we can also utilize the program developed by the National Geodetic Survey to do Horizontal Time Dependent Positioning (HTDP) to bring all components of a survey together. CORS also allows us to monitor movement of the National Special Reference System (NSRS) in Southern California to know when secular and episodic motion have reached the point we must take them into consideration. Currently the District

is using five CORS as the basis for our surveying system. Two of the stations are operated by the County and Flood Control District, the other three by the Southern California Earthquake Center (SCEC). This is equivalent to having five GPS receivers on every job at very little cost. There are twenty-two CORS in Southern California with another six scheduled to come on line. The Southern California sites form the Permanent GPS Geodetic Array (PGGA) operated by the Scripps Orbit and Permanent Array Center (SOPAC) at the University of California, San Diego, Institute of Geophysics and Planetary Physics, Scripps Institution of Oceanography. For more information on how to obtain data see the appendix. In Northern California there are seven CORS sites which form the Bay Area Regional Deformation Array (BARD) operated by University California, Berkeley and the U.S. Geological Survey.

The Scripps Orbit and Permanent Array Center (SOPAC) has been analyzing daily the complete set of PPGA data since August 1991. At its inception, the PPGA consisted of 4 core stations (Goldstone, JPL, Pinyon Flat and Scripps). All sites contain dual frequency, precise P-code GPS receivers. A stable GPS monument has been designed for use in the network and five such monuments have been installed at the Scripps, Pinyon Flat, Vandenberg, Monument Peak and Blythe sites. One form of the monument is: (1) a ground-level base that is anchored to depth, and decoupled from the surface, and (2) an

antenna-mount that can be precisely positioned on this base. Stainless steel rods embedded in stable rock or massive concrete have been used at the other sites. The PPGA provides important infrastructure support for ongoing crustal deformation projects in southern California. It (provides essentially free) data for any survey performed in southern California. Data are recorded at a 30 second interval, 24 hours a day to all visible satellites. With the current network shown in Figure 1, any receiver operating in southern California is within 100 km of a PPGA station.



**Continuously Operating Reference Station
at Blythe**

The following support is available at the SOPAC archive for campaign-type regional surveys in southern California: (a) RINEX files for the PPGA and global tracking stations of the International GPS Service for Geodynamics (IGS) (Zumberge et al., 1995); (b) terrestrial reference frame. The SOPAC archive contains a list of station positions and velocities for the global and PPGA sites tied to the International Terrestrial Reference Frame; (c) daily solution covariance matrices. These files are an invaluable resource for the analysis of regional networks since they contain the complete geodetic content of the global tracking and

regional CORS networks; (d) precise satellite ephemerides; (e) solution summary files. These include PPGA station repeatabilities; (f) interseismic deformation. Since the PPGA sites track continuously they obtain interseismic rates at a fraction of the time required by occasional field campaigns. This is invaluable information when coseismic displacements are desired (especially in the far-field) by surveys that have taken place at a significant amount of time before or after earthquakes. Users have been collecting PPGA and global tracking data from the Scripps archive for more than five years. In the month of April 1994 more than

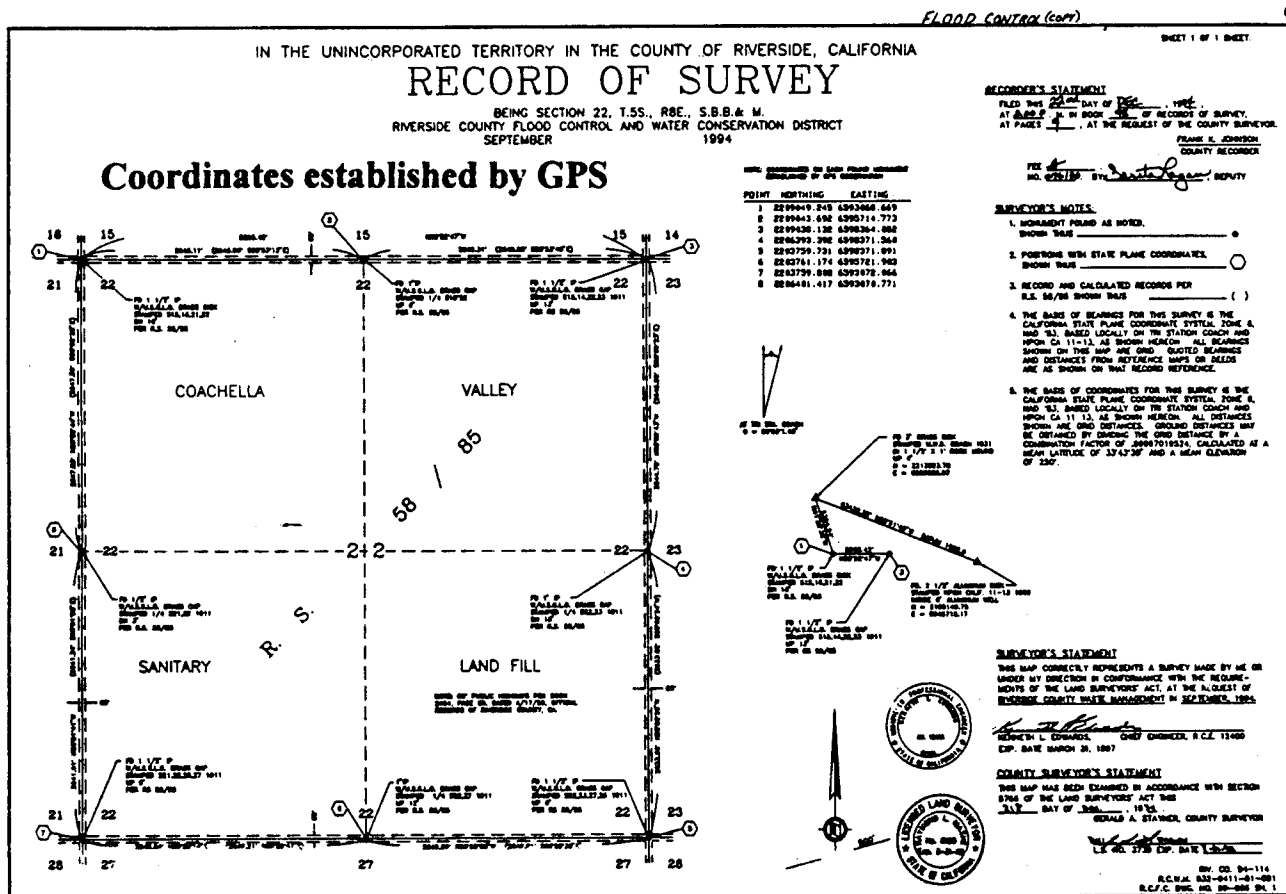
12,000 data files were transferred by external users from the SOPAC archive.

The National Geodetic Survey is in the process of establishing State coordinates for both the Southern and Northern California arrays. These sites will then have legal status and become part of the new National Spatial Reference System (NSRS). Riverside County's site at Blythe will become part of the main National Network of CORS because of its strategic location, solid monumentation, and location on the North American tectonic plate. It will be the primary station for monitoring crustal motion of the other CORS sites in Southern California. The California CORS Committee (CCC) is coordinating both arrays with the National Geodetic Survey through Don D'Onofrio, the State Advisor.

The District uses GPS to establish horizontal and vertical position on every type of survey we do: Photogrammetric

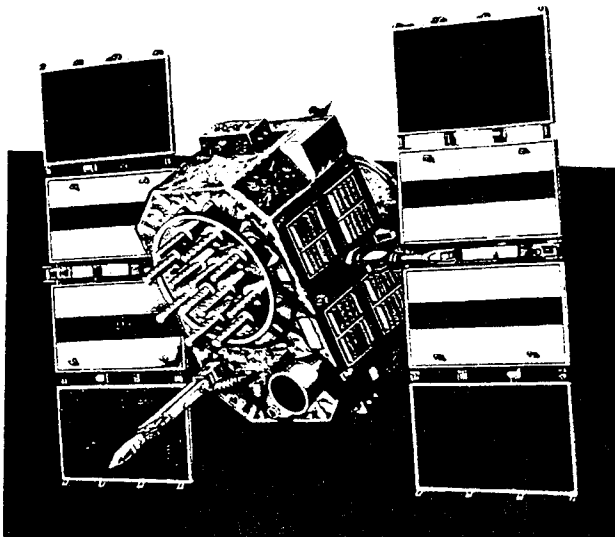
We have a paradox in California. There are more CORS operating here than any place in the nation, resulting in the most accurate surveys ever performed. Though surveying will benefit handsomely in the long run, the primary reason we have so many CORS is crustal motion and earthquakes which complicates surveys and can render the data generated useless after a period of time. As more CORS go in across the nation they will become the backbone of the National Special Reference System. Fixed monuments as we know them today will have diminishing use as CORS become more available and easier to use. In these days of budget slashing it's imperative we use GPS to the fullest. It generates more accurate data, faster, more conveniently, and at less cost. That doesn't happen very often in the real world.

control, Record of Surveys, Property Surveys, Construction staking for dams, channels, bridges, landfills, and roads,



Digital Orthophoto Control Engineering Geographic Information Systems (GIS), Crustal Motion Studies, Densification of the North American Vertical Datum of 1988. In this coming year we plan to put our CORS at Lake Mathews on radio transmission at a five-second sampling rate to our office. Anybody within a 30-mile (18 km) radius, with the proper radio receiver, who is able to use raw Trimble data is welcome to the data. Thirty-second data is also available through SOPAC. We plan to run an experiment in September utilizing four CORS sites sampling at a one-second rate for airborne GPS-controlled aerial photogrammetry.

Our GPS receivers are in use all day every day. When you have cut brush for clearing line-of-sight stations, done night triangulation, performed differential leveling for miles during hot and windy or extremely cold weather, carried car batteries to the top of mountains, or chained with a steel tape for long distances, it's easy to fall in love with GPS. We look forward eagerly to future development of this truly "space-age" technology.



REFERENCES

Yehuda Bock, **Continuous Monitoring of Crustal Deformation**, *GPS World*, Innovation Column, June 1991, 40-47, 859 Willamette St., P.O. Box 10460, Eugene, Oregon, 97440-2460

Yehuda Bock, **Crustal Deformation and Earthquakes**, *Geotimes*, 39, 16-18, 1994, 4220 King St., Alexandria, VA 22302-1507

Yehuda Bock, **Permanent GPS Geodetic Array in Southern California (PGGA)**, Scripps Institution of Oceanography, IGPP-UCSD (0225), 9500 Gilman Drive, La Jolla, CA 92093-0225

Shelley Marquez and Yehuda Bock (1995), **We Have a New Look**, Scripps Institution of Oceanography, IGPP-UCSD (0225), 9500 Gilman Drive, La Jolla, CA 92093-0225

Dean C. Merchant, July, 1991, **GPS-Controlled Aerial Photogrammetry**, Topo Photo Inc., 3894 Chevington Road, Upper Arlington Road, Ohio 43220

Gregory A. Hilmer, PLS, **Four-Dimensional Surveying, The California Spatial Reference System and Deformation Surveys**, The California Surveyor Spring 1995, 1303 Garden Street, 2c, San Louis Obispo, CA, 93401

Joseph F. Dracup, **History of Geodetic Surveying**, ACSM Bulletin, March/April 1995, 5410 Grosvenor Lane, Suite 100, Bethesda, MD 20814-2122; Forum on NOAA's, **National Spatial Reference System**, Committee on Geodesy, National Research Council, 2001 Wisconsin Ave NW Washington, DC 2007; Proceedings, **Airborne Geophysics and Precise Positioning: Scientific Issues and Future Directions**, Committee on Geodesy, National Research Council, 2001 Wisconsin Ave NW Washington, DC 2007

Committee on the Future of the Global Positioning System, **The Global Positioning System, a Shared National Asset**, Committee on Geodesy, National Research Council, 2001 Wisconsin Ave NW Washington, DC 2007

Appendix A: SCRIPPS ORBIT AND PERMANENT ARRAY CENTER - DESCRIPTION OF BBS AND INTERNET SERVICES

Southern California Positioning Service

RINEX and raw (receiver image) data are available from permanent GPS sites in Southern California in 24 hour segments with a one day delay. Sampling is at 30 seconds. These sites, since they operate continuously, serve as base receivers for field surveys. See Figure 1 for location of operational sites. NAD83 coordinates will soon be available for most sites. Data for all sites are available on Internet. Selected important sites are available on a PC-based bulletin board service.

Precise GPS Orbits

We now have precise rapid GPS orbits available within 24 hours of the end of observing day. Regular service GPS orbits are available within 4-5 days of collection. Orbits are available almost continuously from 8/27/91 in NGS SP3 format.

Subscription and Log In Information for BBS

Contact customer service by phone or fax to request a subscriber account and it will be set up within 24 hours. We recommend that you use a modem with a minimum baud-rate of 9600 and communication parameters of 8, N, 1. BBS software is Maximus. Dial-in number is 619/587-2563.

Internet Access Information to SOPAC Data

You may also obtain the data via Internet:

ftp toba.ucsd.edu (132.239.152.80)
name: (toba.ucsd.edu): anonymous
password: your e-mail address
directories: rinex, raw, products
and the World Wide Web: <http://jon.ucsd.edu>

The Scripps archive contains GPS data for selected global sites and for all sites in the Southern California Integrated GPS Network for the entire period that sites have been operating. To access site data, change directory to rinex or raw/95data/day#. To access IGS and rapid orbits, change directory to products/GPSweek#.

SOPAC Acknowledgments

At present there is no charge to access the bulletin board. This public service is made possible by the contributions of the following organizations. We do appreciate acknowledgment of the data usefulness and a copy of any

publications which may result from your research.

Funding provided for SOPAC Bulletin Board Service has been provided by:

Director's Office of SIO
Southern California Earthquake Center (SCEC)
Outreach Program
Riverside County Flood Control and Water
Conservation District
Riverside County Transportation Department
San Diego County Department of Public Works
Orange County Environmental Management Agency
(Survey Division)
State of California Department of Transportation
(Caltrans)

Funding and support for the PGGA has been provided by:

Southern California Earthquake Center (SCEC)
National Aeronautics and Space Administration
(NASA)
U.S. National Science Foundation (NSF)
U.S. Geological Survey (USGS Pasadena)
Jet Propulsion Laboratory (JPL)
Massachusetts Institute of Technology (MIT)
California Institute of Technology (Caltech)
University of Southern California (USC)
University of California, Los Angeles (UCLA)

For more information contact:

SOPAC Customer Service, IGPP 0225,
UC San Diego, 9500 Gilman Drive
La Jolla, CA 92093-0225
Fax: 619/534-9873.
Customer Service: 619/534-8487 or 619/534-7692.
E-mail: pgga@pgga.ucsd.edu.



Session B1

Product Announcements

Chair:

Dr. Jim Sennott
Bradley University

Co-Chair:

Ms. Debra Diefes
DCS Corporation

Open-Architecture Design for GPS Applications

Yves Théroutx
Canadian Marconi Company

BIOGRAPHY

Yves Théroutx, a Project Engineer with Canadian Marconi Company, has eight years of experience in the design, qualification, integration and project engineering of hardware for GPS and Omega navigation and sensor systems.

ABSTRACT

The last few years have seen a new range of GPS products and applications, while the cost of a basic GPS sensor has decreased significantly. The need has emerged for a versatile GPS sensor that can be tailored to any specific application.

This paper describes the architecture of the CMT-1200, a compact and low-cost GPS receiver that permits the incorporation of new software components at different execution levels and rates, thereby providing maximum flexibility without the need of an extra processor or memory. The user can thus easily customize the I/O or navigation filtering, as well as add new data or command processes directly into the core software. This reduces hardware requirements while providing more efficient utilization of software processing power and memory.

The CMT-1200's hardware is also described. The basic design approach includes a high level of circuit integration, and a powerful RISC processor architecture. With two built-in serial ports and many discrete inputs and outputs, the CMT-1200 can be easily expanded to handle additional devices (eg, serial ports, A/D converter, gyroscope, altimeter, etc) with minimum added circuitry.

Finally, examples are provided of specific applications, showing how the software and hardware can be customized with a minimal time to market.

INTRODUCTION

The vast majority of GPS-based applications use the GPS receiver as a peripheral device. For many of these non-critical applications (excluding navigation), the optimal design approach is to integrate the GPS and application electronics in a single processing unit. The CMT-1200's architecture and processing power permits the embedding of a wide range of host applications. The GPS receiver then becomes the heart of the system.

BACKGROUND

The CMT-1200 design effort has been a collaboration between Canadian Marconi Company (CMC) and GEC Plessey Semiconductors (GPSC), combining CMC's strengths in navigation system design with GPSC's know-how in RF analog and digital ASICs. The result is an "open architecture" applied to the following products:

- CMC's CMT-1200 OEM card [1], which can be purchased with a FEPRM that allows the user to develop source code and reprogram it independently
- GPSC's chipset, for very high-volume applications
- CMC's GPS software, to which customized features can be added using GPSC's ARM processor software development kit.

The flexibility of this architecture permits the addition of a GPS-based application directly into the receiver, keeping cost, size and power consumption to a minimum..

HARDWARE ARCHITECTURE

The CMT-1200 GPS receiver is a highly integrated design comprising three chips (see Figure 1):

- RF front end [2]
- digital signal processing (DSP) ASIC [3]
- RISC processor.

The RF chip performs triple IF conversion and analog-to-digital conversion (2 bits), and also includes the PLL and VCO. It also provides the time base for the processor and the DSP chip.

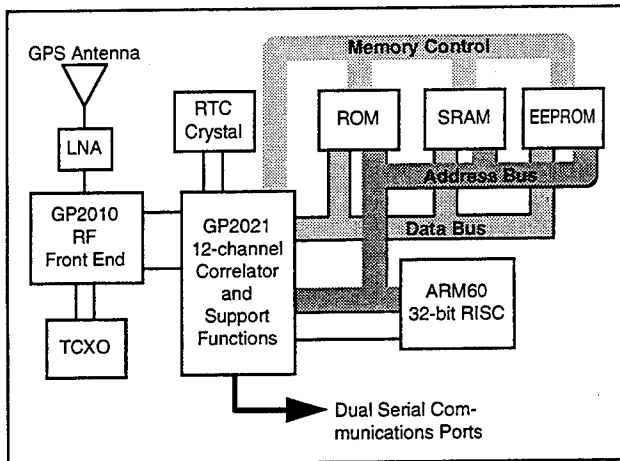


Figure 1 - CMT-1200 Block Diagram

The DSP chip includes 12 GPS tracking channels and the following peripheral circuits:

- two programmable UARTs
- real-time clock
- programmable interrupts
- watchdog and reset circuit
- discrete I/Os.

The processor is the system's critical component. The ARM60 RISC processor was selected because it has:

- the processing power to handle 12 tracking channels
- 30% spare capacity for customized tasks
- low cost and power consumption.

Integration of GPS and customized applications can be achieved either by using the CMT-1200 standard platform, or embedding the GPS chipset onto a custom board with the host application.

The basic CMT-1200 can be enhanced with the following:

- an additional UART
- up to 2 Mbytes ROM/EEPROM
- up to 512 kbytes SRAM
- up to 64 kbytes EEPROM.

The battery back-up input can be used to supply only the real-time clock, or to maintain SRAM as well, in order to accelerate time to first fix (TTFF). The chipset architecture also has the required chip-select to support additional 8/16-bit devices, such as a UART or A/D converter, for full custom applications.

For applications requiring more processing power, such as

a real-time kinematic (RTK) algorithm, the code could be executed totally in SRAM, in order to operate in zero-wait-state memory access. Operational code fetching is then reduced by a factor of three (from two wait-states to zero wait-states). Typically this will improve the CPU power by a factor of two.

SOFTWARE ARCHITECTURE

The CMT-1200's GPS software is broken down into the simplest and most logical modules (Figure 2). Each module is as self-contained as possible to ensure easy development, testing and interfacing. Once the modules were defined, execution rates of 500 μ s, 50 ms, 1 s and background were established, based on previous experience and to provide maximum flexibility for the integration of new tasks.

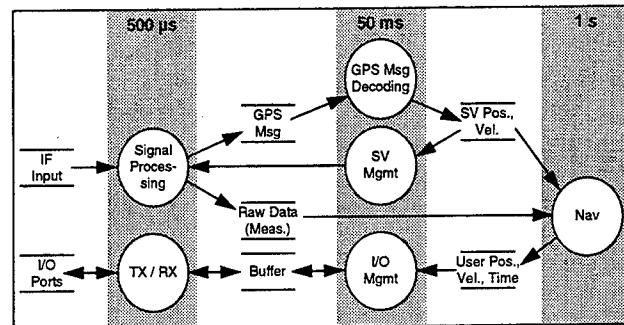


Figure 2 - CMT-1200 Software Data Flowchart

The 500- μ s execution rate is used for the highest priority tasks, signal processing and low-level I/O. The 50-ms execution rate is used for I/O management, GPS data decoding and SV management process. The navigation process is performed every second. Lower-rate processes are executed at the background level. At all execution rates, spare CPU time is available to perform any task. Special built-in checks are incorporated to detect any overloading of the system.

To facilitate the addition of customized features, all important data structures are global, so that a new process can access any of them directly with no waste of CPU time. Special algorithms prevent modification of values at critical times.

Another way to add processes is to execute them just before or after any of the main or underlying modules. This allows for easy modification of the data, eg, to provide an extra filter for pseudo-range measurements prior to navigation processing. A similar filter could be added after the navigator, before the RS-232 output, etc.

This high level of flexibility is made possible primarily by the CMT-1200's memory capacity and CPU power. The software's modularity, on the other hand, permits the addition of processes at almost any level and stage in the generation of the navigation solution. This architecture is ideal for the new GPS market, which calls for many different applications with particular characteristics and requirements.

CUSTOMIZATION

A very wide range of custom software can be embedded in the CMT-1200, for applications including:

- drivers to interface with communications devices
- enhanced navigation units with DR sensors
- RTK positioning
- map matching.

As an example, the implementation of a communications device interface is described herein. Its goal is to provide real-time tracking with differential GPS (DGPS) capabilities, along with two-way driver/base-station messaging, without installing an expensive in-vehicle computer. The proposed solution uses the CMT-1200 as the development platform. A third UART is used to communicate with a modem, resulting in an on-board unit with the following interfaces (Figure 3):

- host on Com 1, ASCII or binary
- DGPS on Com 2, RTCM-104
- communications on Com 3, packet-switched public network modem.

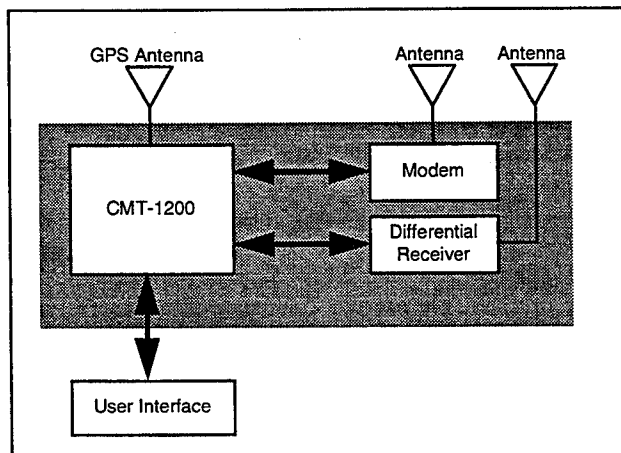


Figure 3 - Communications Unit Block Diagram

The main benefits of this product is that it interfaces to a standard device for vehicle tracking. The host might be a mobile computer, or a simple data-entry keyboard to provide a driver interface. The third UART provides the enhanced functionality to allow the interconnection of a standard differential input and a user interface without having to process differential corrections through a mobile computer, thereby offering significant cost savings. Additional savings result from the use of the packet-switched public network, which provides a data link at a cost much lower than a cellular phone network.

The communications software module can be added to the standard CMT-1200 software in accordance with Figure 4.

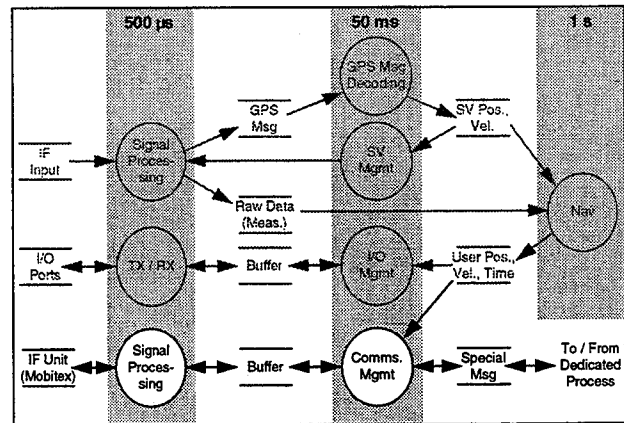


Figure 4 - Data Flowchart with Communications Software

GPS RECEIVER FEATURES AND PERFORMANCE

The GPS receiver has the following features:

- 12 parallel tracking channels, ready for WAAS DGPS
- 24 tracking channels in acquisition mode
- DGPS-ready RTCM-104
- GPS measurements aligned on GPS time (accuracy better than 1 μ s)
- raw measurement rate of 10 Hz.

Related features of the CMT-1200 include:

- time-mark output of 1 Hz, aligned with GPS time
- keep-alive input pin (RAM and/or real-time clock)
- dual UART (third UART optional)
- six input/output discrete control lines
- reprogrammable operational code (FEPROM)
- rechargeable lithium battery (optional).

The CMT-1200 is compatible with both active and passive antennas. When a passive antenna is used, the maximum loss of the cable should not exceed 3 dB, for optimal tracking performance.

From integration work with peripheral circuits, the susceptibility of the CMT-1200 to RF emissions has been proven to be very low.

Performance data for the CMT-1200 are presented in Figures 5 through 7. Typical TTFFs are 60 s with current almanac, position and time, and 30 s with current almanac, position, time and ephemeris. Re-acquisition times are <1 s for obscurations shorter than 5 s, and <3 s for obscurations shorter than 1 hour. TTFFs have been measured when GPS measurements are not aligned with GPS time.

ACKNOWLEDGEMENTS

The author would like to thank Canadian Marconi Company's GPS design team members, especially those who developed the CMA-3012 airborne GPS receiver used by most major airlines. The concept of the CMT-1200 has been derived from this high-end product. Thanks also to GEC Plessey Semiconductors, whose staff has cooperated closely in the design process, thereby achieving the CMT-1200's very high level of integration and quality.

REFERENCES

1. ALLSTAR OEM (CMT-1200) Specification, CMC Document 1826-1127, rev. E, August 1995.
2. GP2010 GPS Receiver RF Front End, GPSC Publication DS4056-2.4, June 1995.
3. GP2021 GPS 12-Channel Correlator with Microprocessor Support Functions, GPSC Publication DS4077-1.6, June 1995.

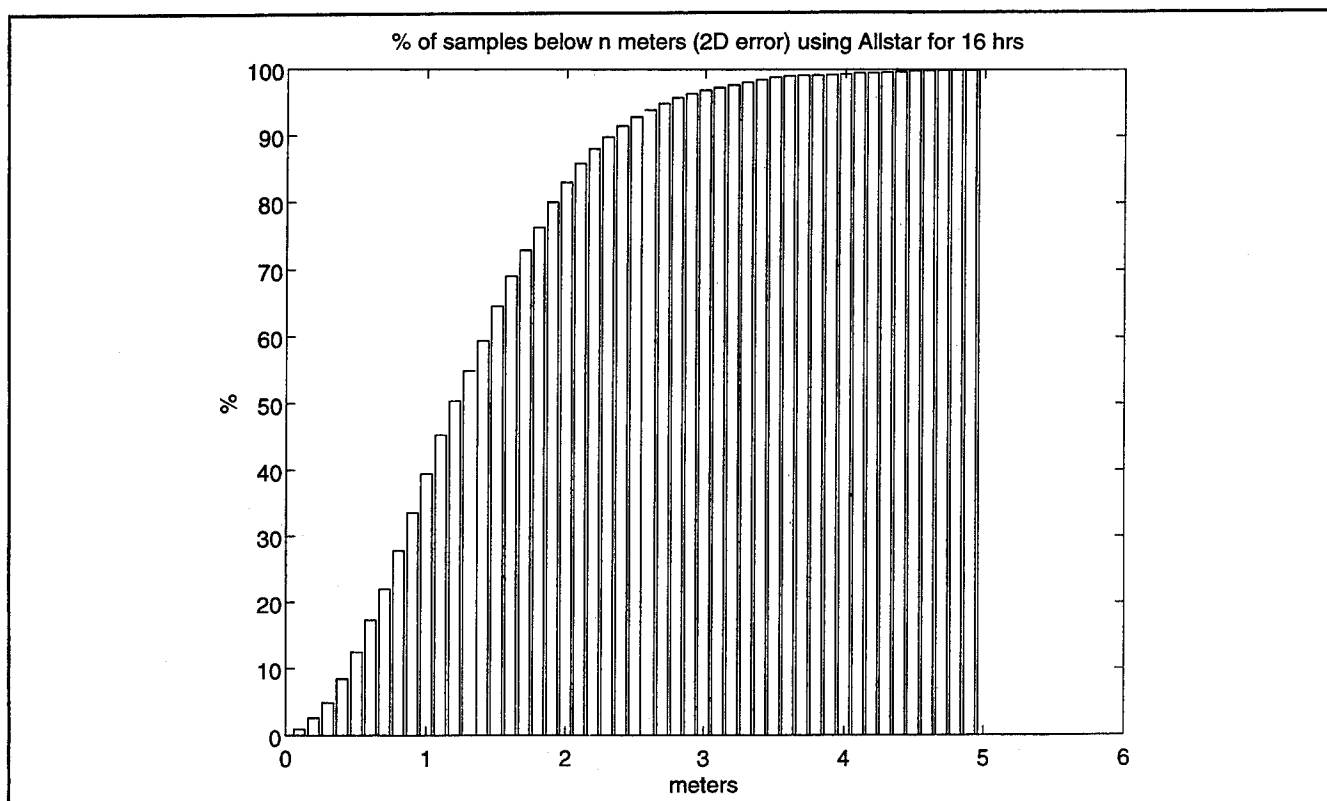


Figure 5 - CMT-1200 GPS Position Accuracy

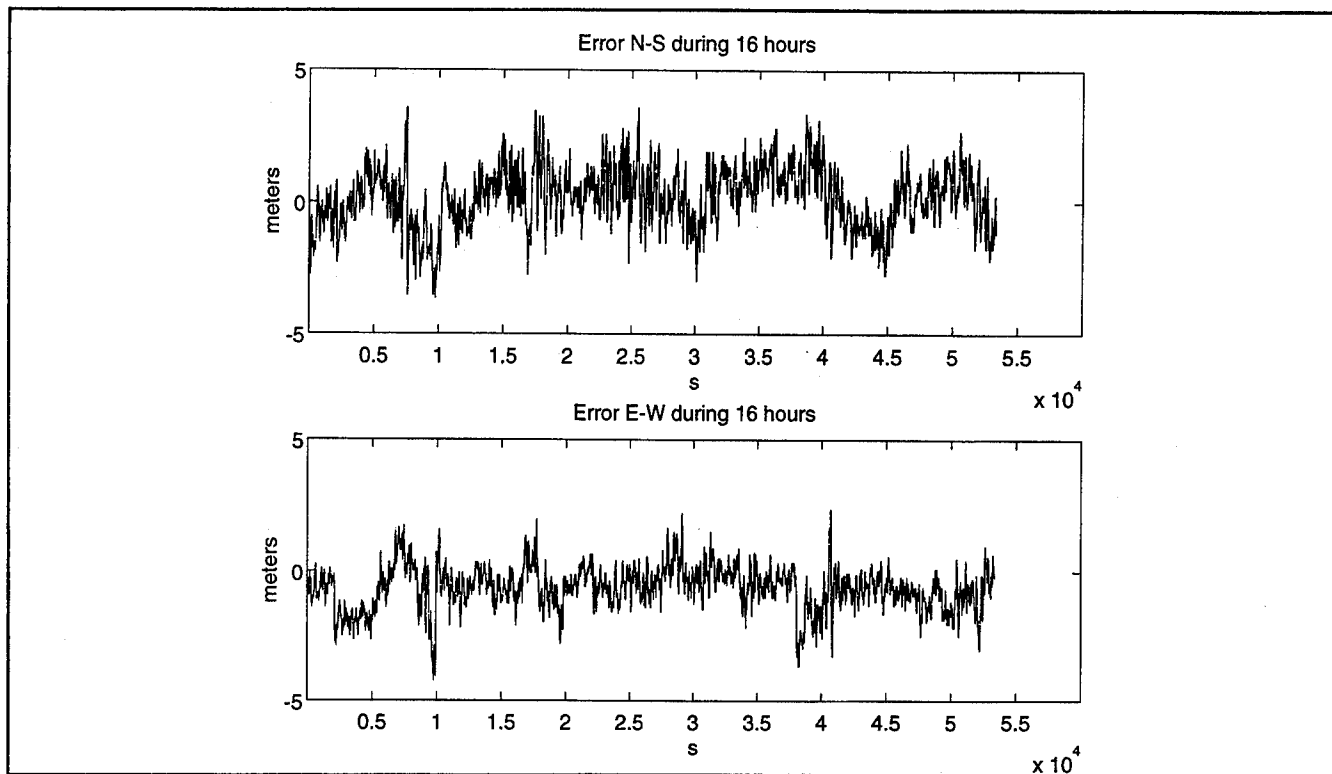


Figure 6 - CMT-1200 N/S and E/S Position Accuracy

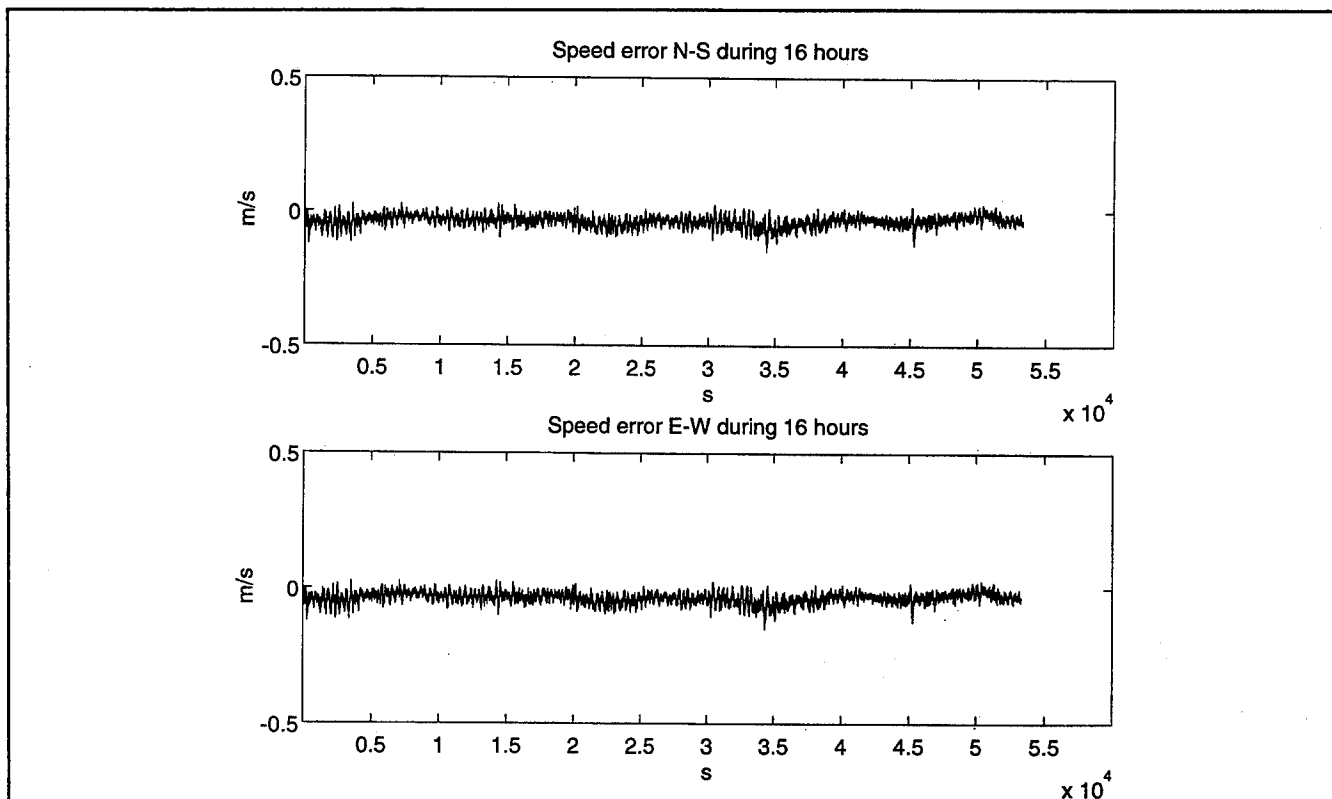


Figure 7 - CMT-1200 N/S and E/S Groundspeed Accuracy

Two Piece Chipset for GPS Makes a Four Chip GPS Receiver

Philip Mattos
SGS-Thomson Microelectronics

BIOGRAPHY

Philip Mattos gained his first degree at Cambridge, followed by MSc 's in Telecomms and Computer Science at Essex, and has just completed his PhD studies at University of Bristol on GPS Receiver innovations.

From 1970 to 1979 he worked for British Telecom Research Centre on Data-comms, radio paging, and microprocessor research. He then joined INMOS(now ST Bristol) at its inception, and after two years in the transputer design team, led the applications teams worldwide, first for memories, then from 1985 for the transputer family of processors.

Working on Navigation systems since 1986, he has specialised in GPS and satellite communications applications since 1989, working with licensees of the technology described here and in earlier papers, and currently as chief architect of the ST20GP1 processor.

ABSTRACT

A 32-bit CPU integrated with both 12 channel dsp hardware and on-chip peripherals (UARTS,parallel I/O, realtime clock) and a matching single chip radio, using a 50ppm crystal rather than expensive TCXO, make the core of the receiver. Add RAM and ROM together with sophisticated software available under licence yields a 4 chip receiver with components parts under \$50 in volume(100k +), but with acquisition times second to none and

only software differences between the oem car model and the centimetre-accurate survey version, and the ability to load user software onto the same CPU makes higher levels of system integration even more cost-effective.

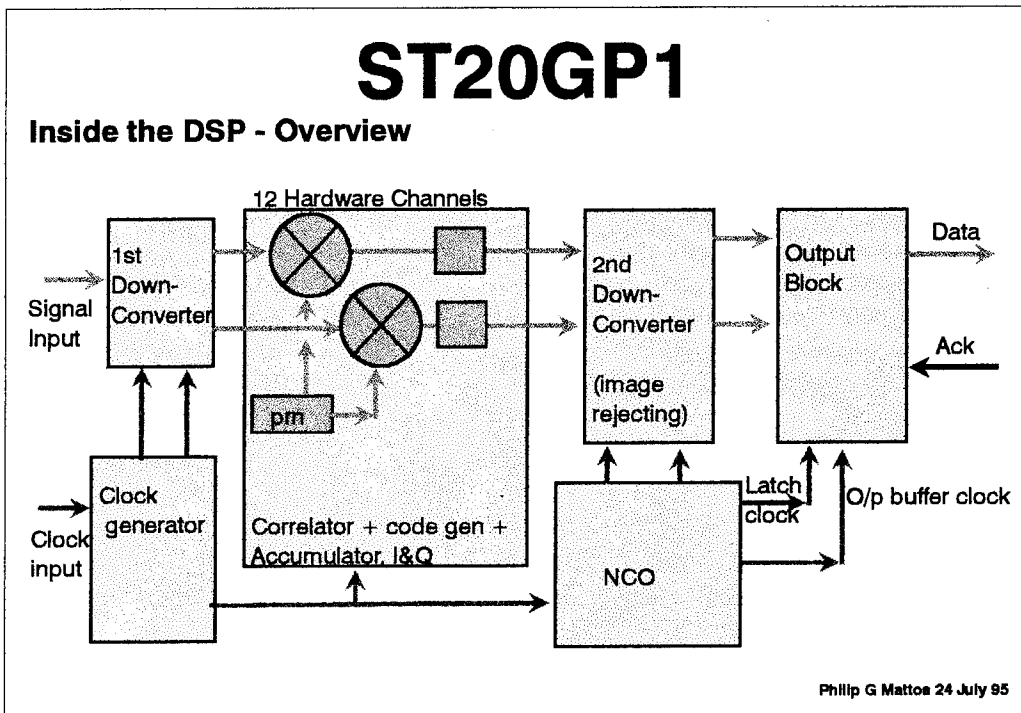
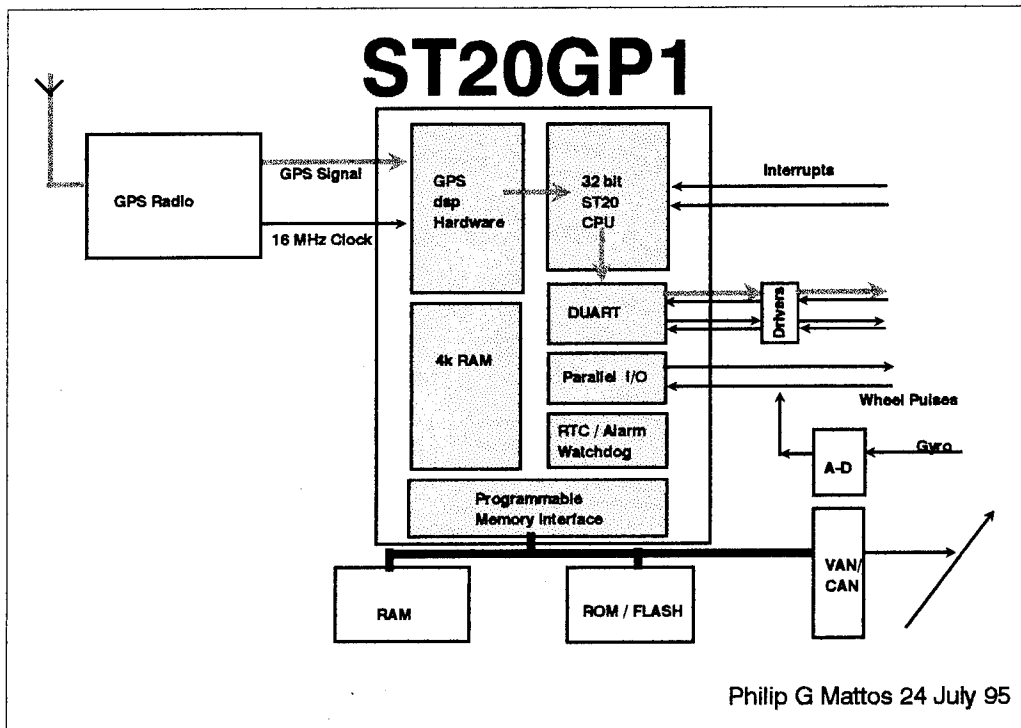
INTRODUCTION

The relentless climb in GPS volumes, and associated fall in prices, especially in the automotive market, mean that the oem card or module is too expensive for the equipment builder to purchase, but gives inadequate profit margin for the supplier.

Led by Japan, where car navigation systems found favour first, and where traffic information systems go live in 1996, the price of oem GPS cards has passed \$200 and promises to reach \$100 next year.

Both the GPS company and the car electronics company need to reduce their costs. In the former case, the solution is a flexible, low component count, low cost chipset. In the case of the car electronics company, the solution is to build from components, rather than the oem card, but this is a little more difficult as they seldom have the required expertise in RF technology and in GPS software.

The chipset described here solves all these problems as a single chip radio, single chip processor that includes 12 channel hardware correlators, ROM and RAM are all that are needed for a complete GPS receiver, and the



radio application information, and GPS software are available under licence to all high volume system builders. It operates from 3.3 volts, making it suitable for low power areas like containers and railway trucks, as well as giving good battery life in portables.

The move to hardware correlators, after 5 years of this author advocating a fully software approach, reflects the volume of the GPS market, now large enough to support a generic silicon vendor, but the major advantages of rapid acquisition time and tolerance of low-cost crystals, rather than expensive TCXO's, have been retained.

Adding the hardware correlators allows the CPU to be downgraded to use narrower, slower memory, saving cost, and allows the CPU to run with a slower clock cycle, saving power. At the same time, peripherals such as real-time clock, watch-dog and UARTs have been added on chip. There is even an alarm for systems that are required to wake up autonomously at intervals to check their position, such as navigation buoys.

Avoiding a TCXO can save \$20 alone, while allowing direct CPU access to the part-processed signal allows the software to take over from the hardware for acquisition, especially of the first satellite, when the frequency ambiguity is greatest.

Two of the twelve channels are configured to support either GPS or INMARSAT WADGPS/FAA WAAS prn codes, allowing the system to support these services as soon as they open.

With the earlier versions of this technology taking a major share of the Japanese GPS market, the new two-chip set promises to move from the 100k units arena into the 1m units/year arena very rapidly.

NEW INTEGRATION

The new levels of integration seen here in Figure 1 are single chip RF, and combining the

DSP ASIC, upgraded to twelve channels, with the 32-bit CPU, together with all the peripherals expected on a microcontroller. No corners have been cut... there is even a wake-up alarm that brings the CPU out of power-down after a software determined period. While this is most relevant for solar powered installations such as navigation buoys and freight containers, it can be used to good effect on cars to guarantee instant start-up. When the car is parked, the system awakes every hour to download ephemeris information.... until after 12 hours, when it relaxes the period to every 4 hours, then after 48 hours it may switch off entirely. This algorithm ensures that the car battery is not discharged when parked for a month's holiday... but that a 10 second or better start-up can be guaranteed in normal use.

Note also that in security applications, for freight or for car alarms, the system may wish to detect if the vehicle has been moved, and radio an alarm .

NEW DSP SECTION

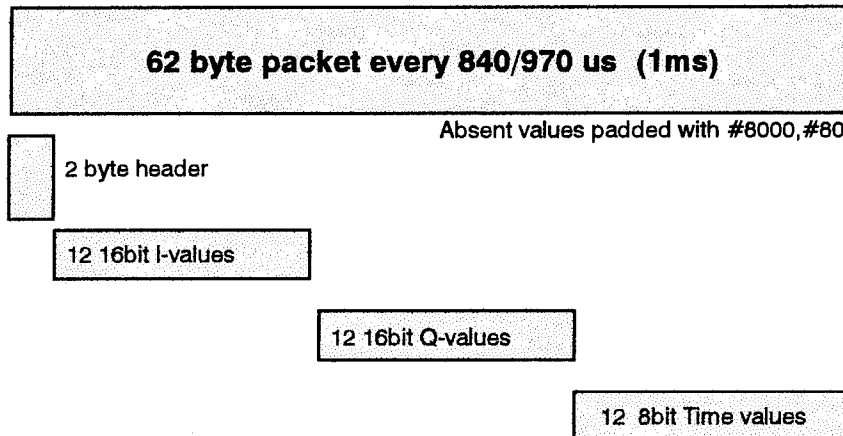
The dsp section handles 12 satellites in parallel, two of which may be using non-GPS codes, such as INMARSAT/FAA RTCA-SC-159 services. The choice of twelve was made to allow permanent all-in-view operation.

The dsp section consists of a downconverter that maps the 4.092MHz signal to nominal baseband in I and Q, followed by 12 IQ correlator/accumulators, then further downconversion using an NCO to remove all residual phase and frequency error. All the processing is performed based on 16MHz sampling of the signal, and 125ns steps in code phase, 1Hz steps in frequency, 3 degree steps in carrier phase.

The output from the DSP section consists of 62 byte packets of data, passed by DMA into the CPU memory. The data consists of 12 16bit words of data for the I channels, 12 for the Q channels, and 12 8 bit time stamps, plus a header. These packets are normally delivered

ST20GP1

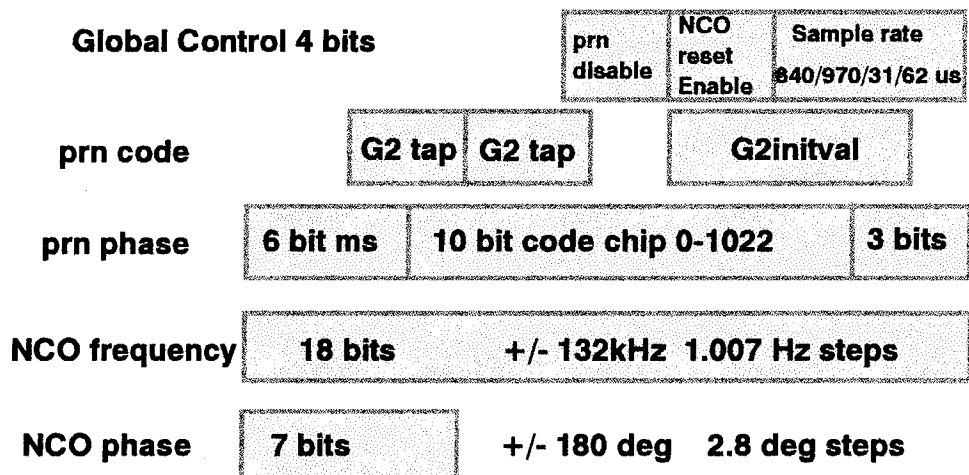
Inside the DSP - Data Format



Philip G Mattos 24 July 95

ST20GP1

Inside the DSP - Control Registers



Philip G Mattos 24 July 95

at a nominal 1 millisecond rate, though provision is made both for doppler and clock error when tracking, and for a much faster sample rate during acquisition.

ACQUISITION....Sensitivity and Speed.

Acquisition performance dominates the availability of the car GPS. While the all-in-view receiver minimises the problem, it is still important. This design continues to use the fast software acquisition algorithm first published in GPS-90 [1], but modified in two directions.

In normal addition of an extra satellite, the dsp hardware only provides samples at a 1 ms rate, rather than the 64us used in the software version.... so the frequency band searched can only be +/-500Hz, rather than +/- 8kHz. This is a benefit when the system is running, because the frequency uncertainty is within this range, so by using 16 sample pairs in an FFT, the acquisition is performed in a 62Hz bandwidth, many dB more sensitive than the 1kHz bandwidth used since 1990.

When starting, however, due to unknown oscillator error, a much wider frequency band must be searched, and due to unknown timing error, the whole millisecond of code phase ambiguity must be searched.... 16 milliseconds at each 500ns phase would take some 32 seconds for a single frequency... clearly not acceptable.

The solution was to give the dsp hardware an "acquisition mode", where it passed the data to the CPU at a much faster rate, ie a much wider filter bandwidth. This has been set at 31 or 62 us rate, and it is the latter which is used here to allow the initial FFT acquisition to cover a 16KHz bandwidth for a single setting of the NCO. The multiple channels of the dsp can be used to search multiple frequency bands in parallel, or multiple code-phases in parallel. This can be done on one satellite (nominally the highest), or on the highest three.

This latter is chosen because the car roof may mask a satellite, as may an adjacent wall. Using four channels per satellite allows the first level

search to take $2046/4$ ie 512ms, the second level $2046*2/4$ ie 1023ms, the third $10 * 16/4$ ms for a total of around 1.6 seconds to acquire the first satellite when oscillator frequency and precise time are unknown. Repeating this for the 16kHz band above and below the most recently known frequency leads to an acquisition time less than 5 seconds, in a very narrow 62Hz bandwidth, with 50KHz variation due to temperature since last use.

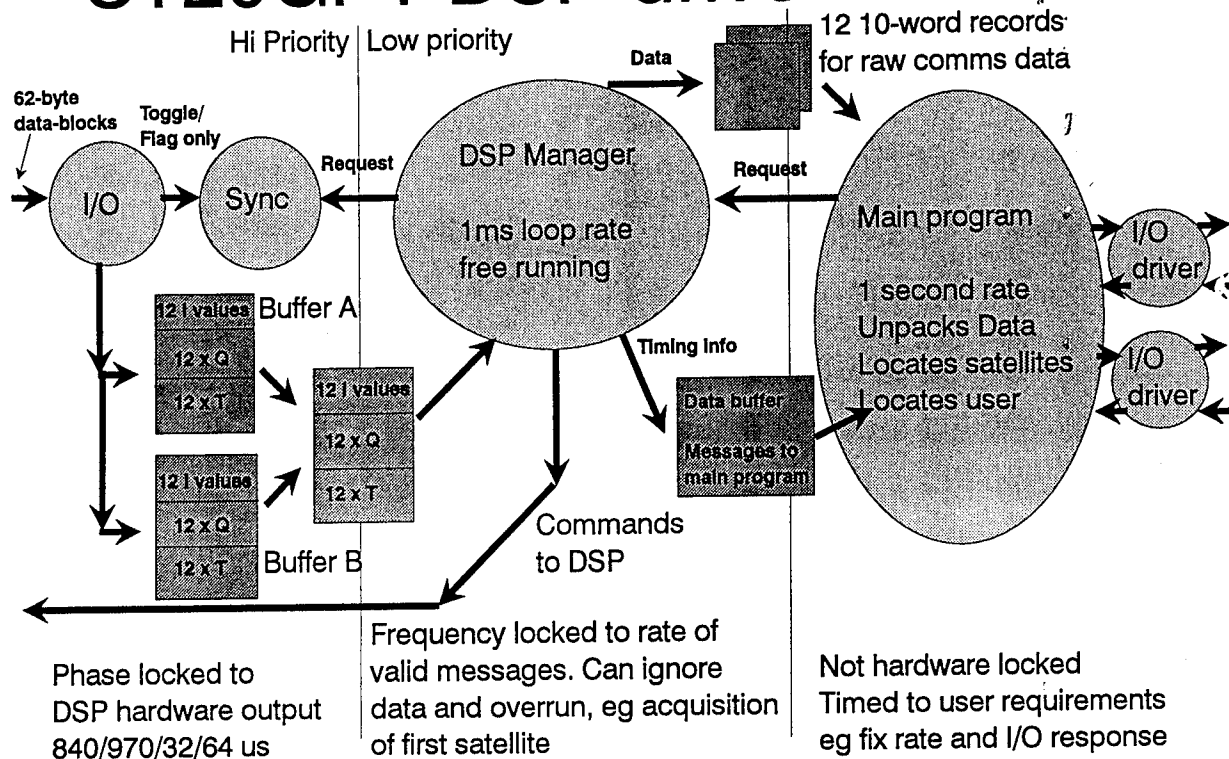
The above algorithm yields the first three satellites in the same time if not obstructed, but is considered successful if even one is found. This one yields a calibration of the receiver oscillator, so in the relatively low velocity situation of the car, the precise frequency of the other satellites can immediately be computed, and also their approximate code phase from the stored position and almanac data. Thus subsequent satellites require around 200 code phases tested at 16ms each, 3.2 seconds if only a single channel is allocated to each.

However 11 channels could be in use at this point, and each phase could need 15 FFTs due to data transitions, so in fact CPU time would be the limit, not the dsp hardware. Thus a multilevel approach is used again, and only 3ms is processed at each code phase, and only if the amplitude is sufficient is the further 13ms loaded. The top 50 candidates then have the full 16ms FFT performed (note 25%, far higher than the $10/2046$ or 0.5 per cent retained in first satellite search.... hence the ability to find satellites down to the horizon under trees in the rain even with a patch antenna) This approach leads to 1.25secs limit on the hardware, and around 2 seconds for the software. As it will be rare that 12 satellites are above the horizon, the software and hardware will match in the general case.

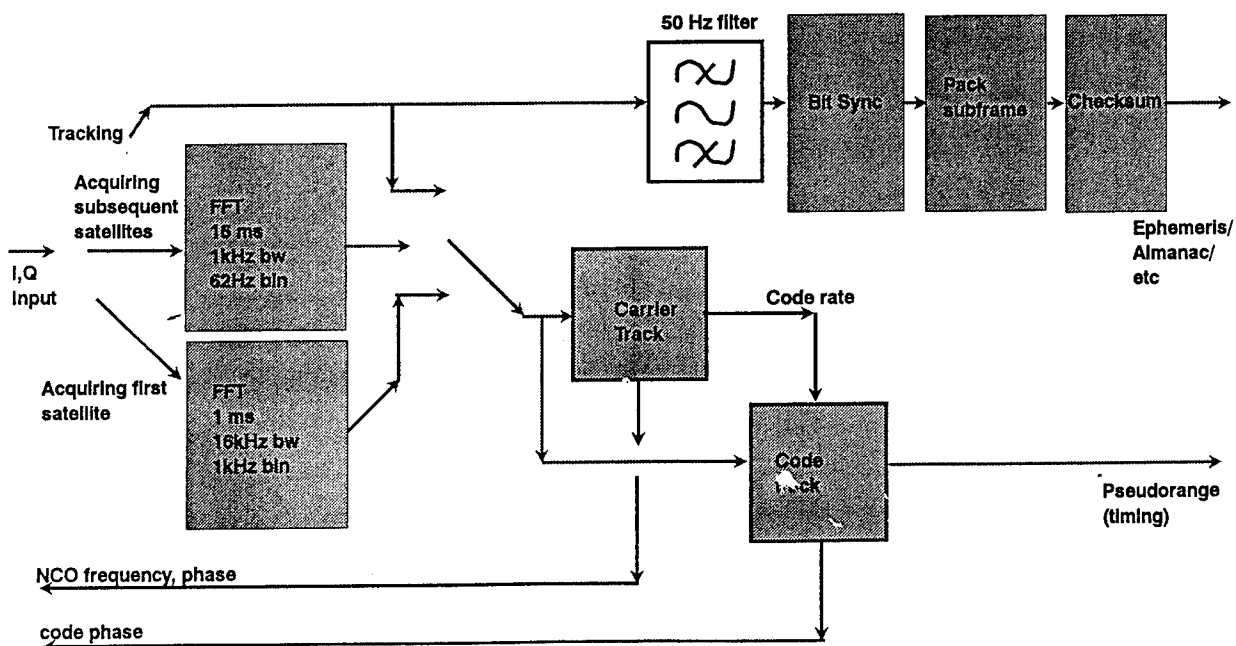
Note that further economies can be made, such as limiting the search to the highest six satellites, of which three will have been found in mode 1. This leaves 9 channels looking for 3 satellites.

By whatever means, once three satellites have

ST20GP1 DSP driver software



GPS DSP Software



been found, a crude, altitude-held position and velocity fix can be generated, even on almanac data. It is the velocity that is needed, for which the old position estimate and very approximate satellite positions are adequate.

Given a crude position and a now-precise frequency pre-knowledge for the remaining satellites, satellites 4-12 can be found without even the FFT work, as the NCO is set up correctly, and only around 20 code-phase possibilities are searched. Retaining the 62Hz bandwidth means $20 * 16\text{ms}$ real time, or 0.3 seconds, all in parallel. We note that the 20 phase search depends on almanacs good to 1500metres range error on the satellites and receiver clock equally good to achieve this. The latter can be managed by waiting until the first channel found has read a downloaded time-of-week, if an extra six seconds delay can be tolerated....no problem for autonomous and cold starts, but difficult for warm starts.

However, by definition, warm starts have downloaded an ephemeris within 4 hours, so using a maximum range rate of 830m/s, a two second error in 4 hours is the maximum tolerable variability ie $2/(3600*4) = 1/7200$ or 140ppm. Note that this is variability.... not error. Static or aging error is calibrated out against GPS time..

RF CHIP

The RF chip is simply an integration of the discrete architecture to minimise assembly complexity and cost, with the added benefits of reduced size and power consumption. The architecture is a single downconversion to 20MHz, aliased down to 4MHz by undersampling at 16MHz.. This has the benefit of an easily filtered image, 40MHz away at RF, and a simple band-shaping filter at 20MHz which needs no set-up, uses 10% components and has to reject images only at 12 and 28 MHz, some 40% away from centre frequency.

The major economy in the radio is the inclusion of the local oscillator chain and reference clock divider. Thus there is no synthesiser or Phase locked oscillator/VCO to provide.

The RF chip was designed using MAXIM's GST2 process, initially on the Quickchip 9/60 in a 28 pin SSOP package, in order to satisfy time-to-market requirements for 1996. As volume builds it will be ported to a full custom chip to reduce costs further, and will be reduced to a 16 or 20 pin package. The initial design is a fully flexible radio, supporting single or dual down conversion with two programmable dividers to generate the second LO and the reference clock. This is justified as there are sufficient transistors on the Quickchip array. The custom chip will supply only the minimal needs of the GPS architecture, ie single conversion and a single, non-programmable divider.

OSCILLATOR

The main oscillator is run at around 80 MHz in the GPS application so that the multiplication ratio to L-band and the division ratio to the processor reference clock are both reasonable, while at the same time the crystal is readily available at minimal cost. The oscillator uses a single transistor, and supplies the 80MHz and the 1.5GHz signals on separate outputs, which minimises the need for further filtering and prevents the digital circuitry from damping the L-band signal. The oscillator transistor is kept separate from the RF chip for two reasons.... access is required to all three terminals of the transistor, so it would increase the pin-count, and also the excellent phase-noise performance achieved by this approach could be compromised by coupling from the digital dividers through the substrate of the RF chip.

FREQUENCY TOLERANCING without a TCXO

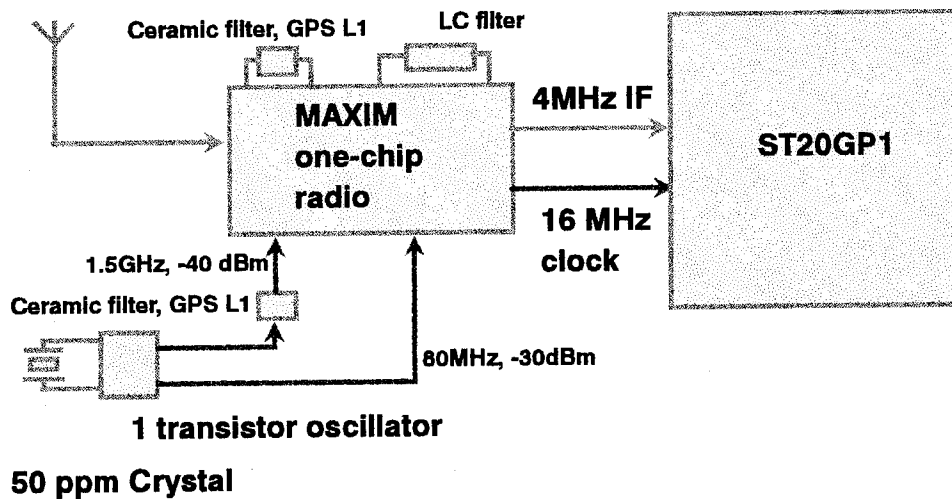
The reason for excluding a TCXO, just as in the software designs from 1989-94, is economic.... it costs as much as the processor. However no performance penalty can be tolerated.

The wider frequency tolerance of an uncompensated crystal brings three problems

- 1) a larger search volume for acquisition of the first satellite

ST20GP1

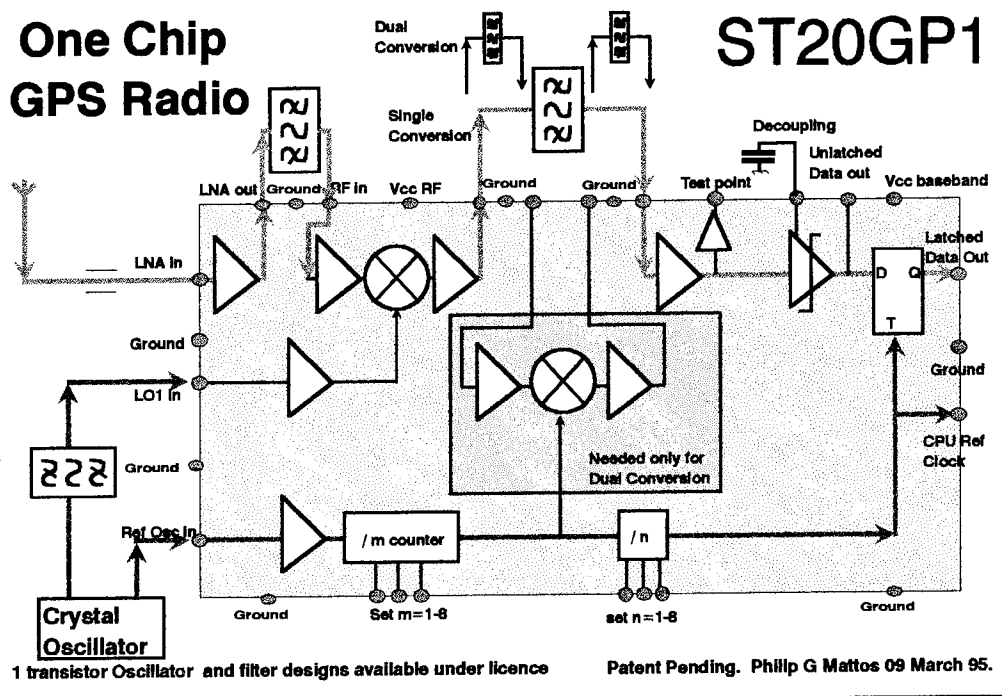
RF architecture



Philip G Mattos 24 July 95

One Chip GPS Radio

ST20GP1



2) The need to handle higher frequency offsets in the dsp work

3) The need to handle more rapid changes in frequency in the tracking algorithm.

The first two of these have been handled above... the hardware supports frequency errors up to 132kHz, and supports a software aided fast acquisition mode that acquires the first satellite(s) in seconds rather than tens thereof.

The third problem, tracking loop dynamics, is not a problem in a non-channelised system. While the 1989-93 software systems had difficulty downloading data during changes between 250Hz channels, the 1994 software system used continuous tuning, and this is repeated in the 1995 hardware dsp with the NCO tuning in continuous 1Hz steps if required. With the carrier phase tracking able to handle 2800 degrees per second, around eight hertz, without even tuning the NCO, and the NCO supporting df/dt rates of up to 1kHz per second, there is ample capability for handling oscillator variation..... in fact the software currently calculates phase/frequency only at databit edges, ie 20ms, in order that minimum noise is introduced to the tracking, and for convenience as integration to the 20ms level is needed for data extraction anyway.

APPLICATIONS INTEGRATION

Building a GPS system from the component level, rather than using an oem GPS board, means that rather than using a second processor to integrate positioning and other sensors, the integration and display, routefinding and user interface algorithms can all be loaded onto the GPS CPU.

This is supported by the availability of around 50% of the CPU time for user applications, after the first 10 seconds used for rapid acquisition. As the gyro has not stabilised, nor the CD-ROM spun up to speed in this time, the entire navigation system, rather than just the GPS work, can run on the ST20GP1.

Additionally, the 6 I/O pins, two interrupt pins, and 8bit stream I/O port allow interfacing to additional hardware. A quarter-VGA screen (320*240) can be directly connected to the stream I/O port, using an EPLD video timing generator, or alternatively the port can be used to stream speech samples to a DAC for verbal route directions..."Turn left in 100 metres".

The 6 I/O are used to interface the gyro serial ADC, and to poll the keyboard, be it a discrete keyboard or soft keys around the screen.

PERFORMANCE

The performance of a stand-alone GPS is no longer measured by accuracy in a benign environment, because all modern receivers are so accurate that it is the signal, by means of SA or ionospheric distortion, that dominates the positional error.

The car GPS is measured by its TTFF under various initialisation conditions, and its percentage availability in city, mountain, forest and highway environments.... all situations that cannot be mathematically defined.

The benign conditions TTFF has been discussed above under fast acquisition.... such that warm starts are now in the 6 second region, and cold starts are dominated by the satellite datarate, which needs 36 seconds worst case after acquisition.

The autonomous start, where the receiver has no position or time estimate, for example on initial delivery of a car from Japan to Europe, also benefits greatly from the fast acquisition mode, and under benign conditions is less than 90 seconds... allowing for limitations such as using default ionospheric models and being unable to report UTC time, as the appropriate almanac packets could take 12.5 minutes to arrive.

In operation, the all-in-view nature of the receiver has two major benefits. It achieves the maximum availability... tracking obscured satellites even in the absence of signal such that

they can take their place in the navigation solution at the smallest window in the obstruction. It also minimises the effects of SA and multipath/reflections by averaging the errors. While a four satellite solution under SA may have a mean error of 50 metres, the 7 satellite solution is more like 20-30 metres.

The ability to track two INMARSAT satellites when available means both an undistorted range measurement to add to the navigation solution, and precise corrections for the GPS satellites, with zero additional hardware cost. The corrections message is received on the GPS frequency, through the GPS radio and decoding mechanism... and the ST20GP1 supports the new prn codes for these satellites. Once this service opens, we can expect a one metres service in our cars !!!.

CONCLUSION

The ST20GP1 offers to the car-electronics manufacturers of the world the opportunity to have the ultimate in GPS performance for the lowest possible system cost, with time to market minimised by available radio designs and licensable, royalty free software. Whilst the car electronics manufacturers need this support, the chip is equally suitable for the oem GPS board manufacturers who have their own radio expertise and software.

As the culmination of 8 years work on GPS that took implementation from traditional hardware through revolutionary software only solutions, and back again to the perfect combination of the two, the ST20GP1 uses integrated hardware for accurate satellite tracking and minimum CPU loading, but allows the 32-bit CPU full access to the signal for the ultimate in fast-acquisition, and with a single chip radio and low cost crystal oscillator makes GPS a commodity product costing tens, not hundreds, of dollars.

What's New From NovAtel

Simon Newby and Wendy Corcoran
NovAtel Communications Ltd.

BIOGRAPHY

Simon Newby received his B.Sc. in Surveying and Mapping Sciences in 1987 from North East London Polytechnic. He received his M.Sc.E. in Surveying Engineering in 1992 from the University of New Brunswick, where his Masters research involved ionospheric modelling with respect to GPS. In 1992 Simon joined Leica Heerbrugg's GPS products group as a customer support engineer. In 1993 he joined NovAtel GPS as a customer support and applications engineer. More recently he has assumed responsibility for support of NovAtel's dealer network.

Wendy Corcoran graduated from the University of New Brunswick in 1986 with a B.Sc. in Surveying Engineering. After graduation she joined Norstar Instruments and worked in GPS software development. In 1989 she joined Ashtech as an applications engineer. In 1991 Topcon and Ashtech signed an OEM agreement and Wendy joined Topcon to establish their GPS division. Wendy has been with NovAtel GPS for the past year as product manager for surveying and mapping products.

ABSTRACT

At ION GPS-94 detailed specifications were presented for an affordable new 20 cm real-time positioning system ... RT-20. One year down the road, with many units in the field, and with many 100's of hours of use, field results are presented which underline the performance, utility and robustness of this exciting new technology.

The new NovAtel MiLLennium dual-frequency receiver is discussed, and plans for new end-user and OEM products are revealed.

INTRODUCTION

This paper summarizes those technologies — recent, new, and forthcoming — which constitute NovAtel's GPS product line. A summary of the real time 20 centimetre RT-20 technology is presented and a brief overview of two multipath mitigation technologies is given. Brief details of the upcoming MiLLennium dual-frequency receiver are presented, and NovAtel's first end-user GPS products are introduced.

RT-20 BACKGROUND

To date, NovAtel's GPS products have been based on Narrow Correlator L1 technology. This technology made real-time C/A-code positioning at the metre level available for the first time in a high performance receiver that was suitable for a wide variety of very challenging applications.

Historically, users of satellite navigation systems have demanded positions of a higher quality than those currently available. Thus, in GPS circles we have seen an ever increasing trend towards real-time phase-based positioning systems.

In line with these market trends and pressures, NovAtel began development of a fixed ambiguity RTK system based on its L1 GPSCard. By September 1993 the first system was completed and successfully demonstrated. However, the fixed ambiguity approach displayed several drawbacks which can be considered inherent limitations with even the best L1 receivers, the most notable of which can be summarized as follows:

- L1 observations cannot successfully model ionospheric delays
- Multipath can affect the quality of pseudoranges and have a huge impact on the size of the initial ambiguity search volume

- Ionosphere and multipath can conspire to make the ambiguity search process lengthy and unreliable

Ultimately, it was decided that these drawbacks compromised the robustness and usability of the system. Thus, further development of the L1 fixed ambiguity approach was deferred until new dual-frequency receiver technology became available.

The fixed ambiguity system relied upon a subset of floating ambiguity algorithms which were used to define the initial limits of the search volume and which ran in parallel with the fixed solution once the ambiguities had been resolved. Testing and development of the fixed ambiguity approach revealed very good agreement between the floating and fixed solutions. This testing also revealed that the float solution was more stable than that of the fixed. Thus, the software engineers concentrated on developing the floating ambiguity solution into a commercial product.

RT-20 Philosophy

In essence, the RT-20 algorithms are a suite of double differencing routines which compute and continuously improve the remote receiver's estimate of each satellite's phase ambiguity. It is important to note that the algorithms never attempt to fix the ambiguities to integer numbers — instead, the estimate of each ambiguity remains unfixed at all times. In practical terms this means it is very unlikely that the system will select incorrect values for the ambiguities. In turn, this means that a solution can always be computed provided that continuous phase data are available from at least 4 satellites.

This scenario has immediate advantages over that of the fixed ambiguity approach where an "all or nothing" approach must be accepted by the user.

As with any differential setup (real-time or post-processed) raw data must be available from both reference and remote locations. The RT-20 remote relies upon reception of raw code and phase data from a reference station. To this end, any NovAtel full data Narrow Correlator receiver can be used to broadcast the necessary RTCM type 3 (reference station coordinates) and type 59 messages (reference station code and phase data). **Table 1** lists the salient characteristics of the type 3 and type 59 messages.

| Message type | Number of bits (maximum) | Update rate (suggested) |
|--------------|--------------------------|-------------------------|
| 3 | 180 | 10 s |
| 59 | 990 * | 2 s |

* Assuming 12 satellites being tracked

Table 1: Main Characteristics of the Reference Station's Data Transmission

Clearly, the demands placed on the radio link are relatively modest, and it is possible to broadcast the necessary reference station messages using a 1200 baud radio link. This is especially true if less than 12 satellites are being tracked.

Typical RT-20 Accuracy

Immediately after power up and reception of the reference station's data the RT-20 remote outputs what essentially amounts to a code differential solution. Narrow Correlator code measurements allows for metre level positioning in this instance. However, a few seconds later the RT-20 floating ambiguity algorithms begin estimating the ambiguities for each satellite, and the solution rapidly starts to improve. After 2 to 3 minutes a nominal horizontal accuracy of 20 cm CEP is typically obtained. With continuous phase lock the accuracy improves further to 2 to 5 cm CEP. This process of a gradually evolving position is most easily likened to that of a gradual transition from a code only differential solution to that of a phase only differential solution — at power up the solution is almost entirely based on code measurements ... after several minutes the solution is based purely on phase data.

Figure 1 illustrates typical static and kinematic convergence times for a short baseline (< 10 km) scenario. It can be seen that kinematic accuracies are comparable to those of the static case, the main difference being convergence times which are nominally three times longer.

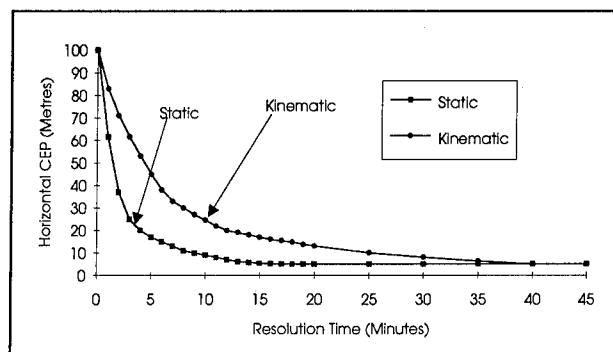


Figure 1: RT-20 Accuracy vs. Convergence Time for Short Baselines

Latency & Safety Issues with RT-20

The RT-20 algorithms utilize a number of novel techniques which are designed to increase the robust nature and usability of the system.

An RT-20 remote can generate its positions at user-selectable rates as high as 5 Hz. In NovAtel receivers a 5 Hz update rate means that raw code and phase data are being measured by the remote receiver five times per second – there is no smoothing or extrapolation involved.

However, the double-differencing RT-20 algorithms require code and phase data from a reference station. Clearly, broadcasting reference station data at rates as high as five times per second would place unreasonable demands on the system's radio link. Fortunately, because the reference station is stationary it is a relatively straightforward task to predict the temporal behaviour of the phase observations. Therefore, the RT-20 reference station need only broadcast its observations once every two seconds. The remote unit then estimates the temporal behaviour of the phase observations using a 3 state extrapolator model. In this manner, accurate 5 Hz reference station data can be constructed using real 0.5 Hz data with no perceptible loss in accuracy. The quadratic 3 state filter has an r.m.s. accuracy of 3% of a wavelength (≈ 6 mm) over 2 seconds, or 30% of a wavelength (≈ 60 mm) over 6 seconds. Clearly, the 2 second update rate for reference station data is preferable.

Extrapolators of this type appear to be gaining popularity and have recently been documented by *Landau & Vollath* (1995) and *Lapucha et al.* (1995).

The extrapolator also helps in greatly reducing data latency times of the RT-20 position updates so that they are typically less than 70 ms. This means that when the user stops moving so does the solution ... almost instantaneously. This scenario often isn't true of other RTK systems.

The extrapolated reference station data are compared with real data at the update rate specified by the data link. If large discrepancies are found then a badly behaving satellite is said to have been detected and its observations will be de-weighted. If large discrepancies are detected for all satellites then a badly behaving reference satellite is said to have been detected and a new one is chosen.

This integrity check offers the distinct advantage that satellite behaviour can be easily monitored, accounted for, and adjusted for.

RT-20 utilizes a default 12.5° elevation cut-off angle. Any satellites below 12.5° are tracked by the receiver and

their ambiguities are determined and maintained, but their observations are severely de-weighted so that they have virtually no impact on the solution. This helps to avoid the use of low elevation satellites and the associated tropospheric and ionospheric problems which can arise.

The RT-20 receiver requires at least 4 satellites in order to deliver 3D positions. If obstructions cause high elevation satellites to be lost such that less than 4 satellites are tracked, then the RT-20 receiver will automatically include the low elevation, low weight observations in its solution. This is accomplished by increasing the weights on the low elevation satellite observations so that they are included in the position solution. This technique endeavours to deliver continuous positions regardless of satellite blockage, and the resultant loss of accuracy is reflected in the standard deviations of the position.

Multipath considerations With RT-20

Because the initial positions are so closely coupled to the code measurements it is imperative to have good quality pseudoranges. Narrow Correlator pseudoranges aid considerably in this respect, but in the presence of poor multipath conditions even the Narrow Correlator's enhanced multipath immunity may not always be as good as one would like. If reference and remote receivers are equipped with choke ring ground planes the effects of multipath can be minimized. However, in many applications this is not always a practical option. For this reason, the RT-20 receiver also runs Multipath Elimination Technology (MET) as a standard feature. MET, which is described in more detail later in this paper, removes some 25% to 50% of the residual code multipath, runs within the receiver firmware, and helps to confine the size of the initial search volume which is used by RT-20's double differencing algorithms.

Ionospheric Considerations with RT-20

The ionosphere and multipath play very important roles in the utility of phase-based L1 positioning systems. Multipath has already been discussed within the sphere of an RT-20 solution, but ionospheric delays are too important to overlook.

During periods of peak ionospheric activity the group delay experienced at GPS frequencies can be as much as 50 m at zenith and three times as much for a satellite at the horizon. The ionosphere is a dispersive medium at radio frequencies ... a property which is fully exploited by dual-frequency receivers by combining observations made on the L1 and L2 frequencies. However, L1

receivers lack the second frequency and must rely on alternative techniques to estimate the ionosphere's effect. Typically, with L1 receivers we either ignore the ionospheric effect altogether or we attempt to model it using one of several empirical models which are available. Empirical ionospheric models are extremely limited in their ability to model the effect and on the average can only remove 50% of the ionospheric delay. Therefore, the residual ionosphere after such modelling is usually a major source of error for which we cannot correct.

Differential processing removes much of the ionospheric effect, but the spatial correlation of the ionospheric delay between reference and remote locations becomes weaker as the baseline length increases, and differential processing becomes less effective in its ability to remove the effect. In a code differential scenario this results in decreasing accuracy as baseline lengths increase.

In L1 phase-based systems the effect is far more severe and can result in a complete inability to resolve ambiguities with any degree of confidence. In fact, in the fixed ambiguity approach the general rule of thumb is that baseline lengths of 15 km to 20 km should not be exceeded if ionospheric problems are to be avoided. RT-20's floating ambiguity approach circumvents these problems by never attempting to fix the ambiguities. Instead, the system accepts the fact that ionospheric decorrelation will impact on the result, and reflects the impact accordingly by showing larger standard deviations. **Figure 2** shows RT-20 accuracy versus baseline length. We see that a solution is always available, albeit of reduced quality as the baseline length increases. Typically, under steady state conditions, RT-20 delivers better than half a metre accuracy CEP, after a period of extended phase lock, over baselines of 50 km.

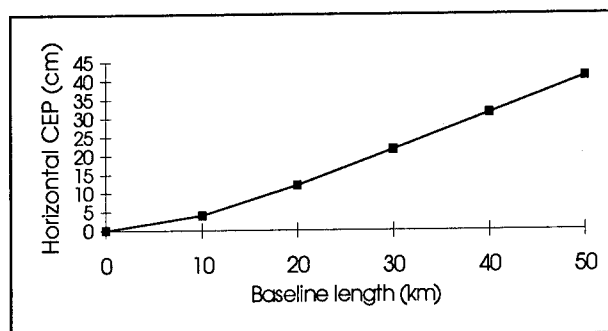


Figure 2: RT-20 Accuracy vs. Baseline Length

To summarize, we can state that the very nature of the RT-20 floating solution overcomes the baseline length

limitations suffered by fixed ambiguity solutions, and offers a seamless transition from short to long baselines.

Current RT-20 Applications

Production versions of RT-20 have been available since January 1995. Since then many units have been delivered to customers and many 100's of hours of field use have been accumulated. The applications for this technology have proven to be many and varied, and include:

- robotics guidance
- precision guidance for agriculture
- precision earth moving
- precision mining
- collision avoidance systems for heavy machinery
- container tracking systems
- truck guidance alarm systems
- seismic surveying
- GIS / surveying
- hydrographic surveying and dredging
- land slide monitoring

In all cases, the RT-20 approach has delivered accurate positions which tie in closely with the system's design specifications. Novel new applications for the technology will undoubtedly continue to emerge.

Summary Float vs. Fixed – Pros & Cons

The previous paragraphs have reviewed some of the major problems which are faced by L1 only phase-based RTK positioning systems. Some the ways in which RT-20's floating solution overcomes or minimizes many of the limitations have also been explained. **Table 2** summarizes the various advantages and disadvantages of the L1 floating solution versus L1 fixed solutions.

Ford & Neumann (1994) presents a thorough overview of the RT-20 technology. The interested reader is directed towards this reference if more details are required.

| L1 FLOATING AMBIGUITY RT-20 | L1 FIXED AMBIGUITY SOLUTION |
|---|---|
| ADVANTAGES | |
| <ul style="list-style-type: none"> • always converges • always gives a position • not CPU or RAM intensive • statistics good indicators of accuracy • foolproof operation • seamless transition from short to long baselines • low cost platform | <ul style="list-style-type: none"> • can give centimetre level accuracy for short baselines |
| DISADVANTAGES | |
| <ul style="list-style-type: none"> • typically decimetre level accuracy | <ul style="list-style-type: none"> • easier to pick the wrong answer • difficult to know if the answer is correct • too long to get a good position • too much CPU and RAM required • doesn't work for long baselines • experience needed to operate • too long to get good position at start up and after loss of lock • operational constraints |

Table 2: Advantages and disadvantages of the RT-20 floating ambiguity solution vs. L1 fixed ambiguity solutions

MULTIPATH MITIGATION TECHNOLOGIES

Multipath signals often cause a bias within the receiver measuring process. Unlike other systematic biases which affect GPS pseudorange and carrier phase observations, multipath effects are not correlated between antenna locations. This means that no form of differential processing, either real-time or post-processed, removes the effect. In real-time applications pseudorange multipath at the reference station will cause errors in the pseudorange corrections. In turn, these errors propagate into position errors at the remote locations.

Traditionally, GPS users have attempted to overcome multipath effects by using choke ring ground planes or by carefully selecting sites for antenna placement. Depending on the intended application both of these methods are either wholly impractical or quite impossible to implement. In a bid to offer more acceptable means for reducing the effects of multipath NovAtel has concentrated on a regime of advanced signal processing techniques which eliminate the requirement for ground plane choke rings and avoid the need for careful site selection.

Multipath Elimination Technology (MET)

Narrow Correlator technology is inherently immune to the effects of multipath. In a standard Narrow Correlator design the power of the early and late correlators is

equalized. However, in the presence of multipath, the correlation function is affected in such a way that is non-symmetric and skewed (Figure 3).

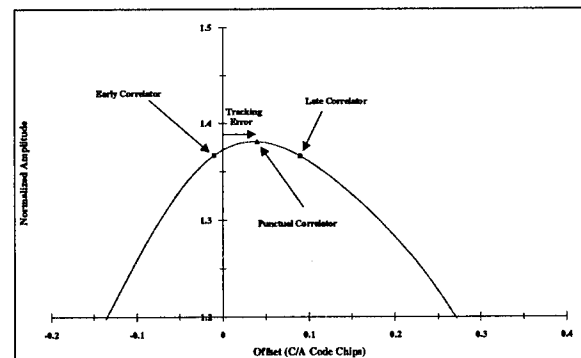


Figure 3: Tracking Error Due to Multipath

Although the power of the early and late correlators has been equalized, it is easy to see that a tracking error still results.

MET differs significantly from the Narrow Correlator method outlined above — it adds two additional correlators (one either side of the correlation function's peak) so that there are two early correlators and two late correlators. Rather than equalizing the power at the correlators, MET positions the correlators either side of the peak of the correlation function (Figure 4).

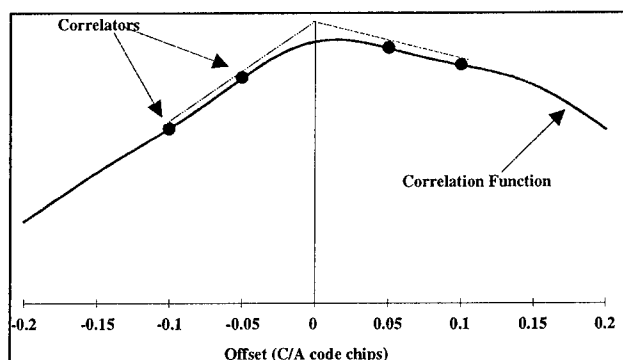


Figure 4: Early Late Slope (ELS) Technique

By positioning the correlators in such a way early slope and the late slope information is determined. The early late slope (ELS) information is then used to correct the receiver's delay lock loop thereby reducing the effects of multipath.

Extensive testing has demonstrated that MET is effective at removing 25% to 50% of residual code multipath. MET is available as a firmware upgrade for any 12 channel NovAtel GPSCard — operation is totally transparent to the user, there is no impact on data latency times or data update rates, and there is always an improvement in pseudorange quality in the presence of multipath.

Multipath Estimating Delay Lock Loop (MEDLL)

Patented MEDLL technology offers a far more rigorous approach to the reduction of multipath effects than that of MET. In essence, MEDLL extends the MET concept further by adding multiple correlators so that the shape of the entire correlation function can be determined (Figure 5).

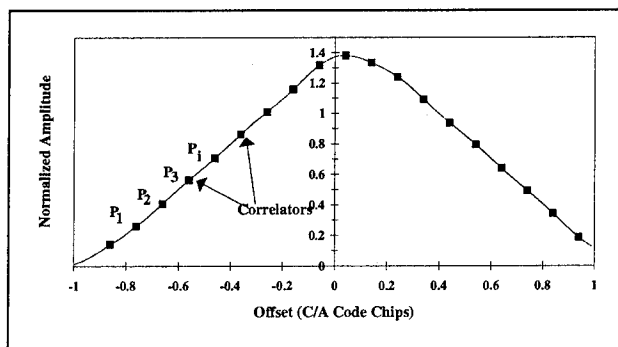


Figure 5: Multiple Correlator Sampling of the Correlation Function

MEDLL decomposes the correlation function into its direct and multipath components — the amplitude, delay, and phase of each multipath component is estimated.

Each estimated multipath correlation is then subtracted from the measured correlation function. The net effect of this process results in an estimate of the direct path correlation function. All that remains is to apply a standard early-late delay-lock-loop to the direct path component, thereby providing an optimal estimate of the code loop tracking error.

First prototypes of the MEDLL concept were successfully tested on a signal channel receiver design over a year ago. Since that time the MEDLL concept has been extended and implemented in a full 12 channel receiver design which necessitates the use of multiple GPSCards. Each GPSCard in the MEDLL receiver is linked to one common RF deck and an OCXO which minimizes inter-channel biases. The MEDLL receiver features exactly the same data interface as a NovAtel GPSCard.

In April 1995 MEDLL receivers were used during 101 successful Category III landings which were performed by Wilcox Electric at the FAA Tech. Center. The same MEDLL technology is incorporated in those receivers which will be delivered to Wilcox Electric for use in the FAA's WAAS program.

Tests have demonstrated that MEDLL receivers successfully account for some 90% of the residual multipath effect.

To date, MEDLL technology has been used to estimate and remove code multipath. The next step in the technology's development concentrates on removal of phase multipath. It is also thought that there may be some scientific interest in producing a version of the MEDLL receiver which can serve as a "multipath meter." The utility of such a receiver will be examined.

For a full insight into MET and MEDLL technologies the interested reader is directed towards *Townsend & Fenton* (1994), *Townsend et al.* (1995a and 1995b), and *van Nee et al.* (1994).

DUAL-FREQUENCY TECHNOLOGY

NovAtel's MiLlennium dual-frequency receiver features two custom designed ASIC 12 channel correlator chips to give a total of 24 configurable tracking channels. In its standard configuration MiLlennium independently tracks Narrow Correlator C/A-code on L1, P-code on L2 (AS on), and provides full wavelength phase observations on L1 and L2.

MiLlennium follows the same philosophy as current NovAtel L1 GPSCards and offers extremely robust tracking loops, high quality low noise observations

available at high update rates (up to 10 Hz), rapid position update rates (up to 5 Hz), and enhanced EMI immunity which is achieved through a combination of 2.5 bit sampling on the receiver's front end and a well designed RF deck.

The receiver is in OEM Eurocard format and features the same electrical interface as current NovAtel GPSCards. The receiver's user interface also remains the same as existing GPSCards. Therefore, the transition from L1 to dual-frequency should be effortless for the vast majority of existing NovAtel GPSCard users.

The receiver accepts position and velocity aiding from INS units, and has hooks to accommodate the GLONASS system. MiLlennium accepts 5 Mhz and 10 Mhz external frequency standards, and a real-time 2 cm option will be offered shortly after production units ship.

MiLlennium uses patent pending P-code Delayed Correlator Technology in order to track the L2 P-code.

END-USER PRODUCTS

NovAtel's innovative Narrow Correlator OEM GPSCard first came to market in late 1992. Since that time the company has established a solid reputation as a manufacturer of high performance OEM receivers. NovAtel is augmenting its line of OEM products by adding end-user products targetted at specific applications. The first of such product offerings are aimed at hydrographic and GIS users. A fully-featured Windows®-based post-processing package will also be offered in 1996.

Hydrographic Surveyor, GPSDredger, and HYPACK™

NovAtel GPS has entered into a distribution agreement with Coastal Oceanographics Inc. to distribute HYPACK™ software with Hydrographic Surveyor and GPSDredger GPS receivers.

The Hydrographic Surveyor is available as a PC card receiver or as an environmentally sealed Narrow Correlator receiver — both units accept RTCM 104 differential corrections and both are compatible with Coast Guard Beacon Receiver corrections. Metre-level positions are available at user-selectable rates as high as 10 Hz, and raw data can be logged for post-processing at rates as high as 20 Hz. A full upgrade path to GPSDredger is also offered.

GPSDredger (also available in PC format or packaged format) offers the same feature set but adds real-time 20 centimetre RT-20 technology. GPSDredger accuracies are available only when using reference stations that transmit RT-20 messages — these could be from local NovAtel reference receivers or from ACCQPOINT's RTK-FM service. Coast Guard Beacon Receivers are not capable of broadcasting the necessary reference station data. In RT-20 mode positions are available at rates as high as 5 Hz.

Both receivers are offered as part of a complete packaged solution that includes Coastal Oceanographic's HYPACK software. HYPACK for Windows® is a complete hydrographic surveying and dredging software package which includes modules for:

- survey design
- data editing and sorting
- digitizing and plotting
- volume computations
- data collection
- DXF import/export
- cross sections

Apart from adding full support for NovAtel receivers, HYPACK also supports multiple hydrographic sensors including echo sounders, side scan sonar, magnetometers, gyro compasses, heave-pitch-roll sensors, and many others.

GISMO (GIS MOBILE)

Following a recent teaming agreement with GIS experts ViaSat Technologies of Montreal, NovAtel now offers its first entry product into the GIS market. The GISMO (GIS MOBILE) is a complete backpack system which includes a ruggedized Narrow Correlator receiver, battery, antenna, controller, and all cabling. The backpack was custom designed by mountaineers to offer day-long comfort and ease-of-use, and features novel routing channels so that cabling is tucked away neatly.

Included in the GISMO package is a Windows® post-processing package that offers interactive or batch pseudorange differential processing for metre-level accuracy. The software offers a host of useful features including:

- overlaying of ortho-rectified vector and raster images
- GPS and vector editing — simple CAD functions, distance and area computations
- user defined data dictionaries
- attribute and position querying
- export to DXF, ASCII, dBase, and others

- support for multiple datums and map projections
- analysis tools for data integrity

In the field, the hand-held controller software gives the user maximum flexibility to control the collection and attribute tagging of GPS data. Audible and visual alarms alert the user to problems such as poor GDOP, too few satellites, loss of radio link etc. etc. Real-time code differential and RT-20 upgrades are available for GISMO, and MET technology is included as a standard feature to help counter the effects of multipath.

GISMO packages are available with or without the controller, and GISMO ships with controller software for DAP 9000, Corvallis, and Husky FS2 units so that reinvestment in costly hand-held data collectors is not always required.

SUMMARY

Plans for new and emerging products from NovAtel have been discussed. In future months, expect to see more technology, more end-user products, and more teaming agreements.

REFERENCES

Ford, T.J., and J. Neumann (1994), *NovAtel's RT20 – A Real Time Floating Ambiguity Positioning System*, Proceedings of ION '94, Salt Lake City, September 20–23, pp.1067–1076.

Landau, H., C. Pagels, and U. Vollath (1995), *Development and Implementation of a Centimeter-Accurate Real-Time-Kinematic Positioning System*, Proceedings of ION '95, Palm Springs, September 12–15, in press.

Lapucha, D., R. Barker, and Z. Liu (1995), *High-Rate Precise Real-Time Positioning Using Differential Carrier Phase*, Proceedings of ION '95, Palm Springs, September 12–15, in press.

Townsend, B.R., and P. Fenton (1994), *A Practical Approach to the Reduction of Pseudorange Multipath Errors in a L1 GPS Receiver*, Proceedings of ION '94, Salt Lake City, September 20–23, pp.143–148.

Townsend, B.R., D.J. Richard van Nee, P.C. Fenton, and K.J. Van Dierendonck (1995a), *Performance Evaluation of the Multipath Estimating Delay Lock Loop*, Proceedings of ION 1995 National Technical Meeting, Anaheim, January 18–20.

Townsend, B.R., P. Fenton, and D.J. Richard van Nee (1995b), *L1 Carrier Phase Multipath Error Reduction Using MEDLL Technology*, Proceedings of ION '95, Palm Springs, September 12–15, in press.

van Nee, D.J.Richard., J. Siereveld, P. Fenton, and B. Townsend (1994), *The Multipath Estimating Delay Lock Loop: Approaching Theoretical Accuracy Limits*, Proceedings of PLANS '94, Las Vegas, April 11–15, pp.246–251.

GPS Tensor™

GPS Receiver for Attitude and Orbit Determination

J. Kurt Brock
Space Systems/LORAL

BIOGRAPHY

Kurt Brock received his M.S. from Stanford University in Aeronautics and Astronautics and his B.S. from the University of California at Berkeley in Mechanical Engineering. In 1992/1993 he served as Chief Systems Engineer on the Globalstar Program and then as the GPS Tensor Program Manager. His current position is Executive Director of Satellite Navigation and Air Traffic Control at Space Systems/LORAL in Palo Alto, California.

ABSTRACT

Space Systems/Loral, a leading manufacturer of meteorological and communications satellites, introduces GPS Tensor™, a space-qualified, solid-state, GPS attitude and orbit determination receiver. This single compact receiver offers 13 output states of navigation and attitude information for guidance and control of space vehicles from launch to orbit. The GPS Tensor™ is an ideal replacement for conventional attitude determination equipment such as earth sensors, sun sensors, and gyros. Accurate trajectory navigation can be accomplished without employment of an extensive worldwide tracking network. GPS Tensor™ delivers roll, pitch and yaw angles, rates, position, velocity, time and filtered orbit determination using a continuously tracking L1, C/A code receiver.

The GPS Tensor™ comprises two major subassemblies: the receiver/processor unit (RPU) with a RS-422 interface, and four patch antennas and preamps. The attitude determination receiver consists of single or redundant circuit cards which makes it ideal for RPU embedded applications. It accepts a wide range of input voltages and consumes less than 12 watts of power.

The GPS Tensor™ is the first space flight qualified GPS attitude and orbit determination receiver and will provide reliable, long life service in radiation environments up to 100 kRad, in addition to withstanding the wide

variety of shock, vibration and temperature extremes encountered in space.

INTRODUCTION

The GPS Tensor™ is planned as a replacement for conventional attitude and ground orbit position determination equipment which when joined with a reaction-momentum wheel and magnetic devices results in a simplified and reliable spacecraft pointing and navigation system. Filtered navigation is generated without ground observation and data processing.

SYSTEM DESCRIPTION

The GPS Tensor™ is a continuous tracking, L1, C/A code receiver. The fully redundant unit is comprised of the dual receiver processor unit (RPU) with a duplex RS-422 interface, and four patch antennas connected through an assembly of four preamplifier each with split outputs. The system works with power voltages between 14 and 40 V dc using about 12 watts per receiver side. The mass of the system, the dual receiver, preamp package and antennas, is under 3.5 kg. The receiver is qualified to operate in space environments up to 100 kRad of radiation.

The system raw position accuracy is 100 meters with Selective Availability. The navigation outputs at 1 Hz are dynamically filtered. Orbit semi-major axis estimates are within 20 meters. A Receiver Autonomous Integrity Monitoring (RAIM) algorithm detects potential failures and eliminates them from being processed while allowing corrective selection of available signals for navigation. An attitude "Dilution of Precision" calculation is also performed. A 1 Hz precision time reference pulse, PPS, is accurate within a microsecond of the GPS time data. The attitude and rate accuracy are 0.1° and 0.1°/s RMS (for a 1.5 meter baseline), respectively, and are output at 10 Hz.

Detailed specifications are included on the next page.

GPS Receiver for Attitude and Orbit Determination

Description and Features

| | |
|---|---|
| Receiver: | Space qualified, continuous, L1, C/A code Attitude and Standard Position Service (SPS), and time reference receiver. For embedded (board set), integrated (sensor unit), or stand-alone applications. |
| Antenna: | Array of 3 or 4 low profile antennas biased and controlled by the receiver. Can be tailored to the satellite platform installation. |
| Attitude determination: | Real-time measurement of roll, pitch, and yaw output up to 10 times per second. |
| Position/velocity determination**: | Three dimensional position determination to 100 m SEP. Velocity determination to 0.1 m/s. Dynamic filtering for orbit determination. |
| Differential GPS position: | RTCM (SC-104) corrections can be supplied for precise differential positioning. |
| Position coordinate systems: | Selectable orbit coordinate systems output in XYZ (ECI), Keplerian. |
| TTFF (position): | 30 minutes cold start, 3.0 min. warm start |
| TTFF (attitude): | Application dependent (<30 sec. nom.) |
| Interface: | Dual, full duplex RS-422 |
| Redundant-RPU weight: | 3.3 kg |
| Redundant-RPU dimensions: | 74 mm x 275 mm x 170 mm |
| Preamplifier dimension: | 51 mm x 138 mm x 76 mm |
| Preamplifier weight: | 0.4 kg |
| Antenna weight: | 0.1 kg each |
| Antenna dimensions: | 73 mm x 73 mm x 5.7 mm (single element) |
| Input voltage: | 14-23 V dc (18 nom.) |
| Input power: | <15 Watts |

Environmental

| | |
|--------------------------------|--|
| Operating temp.: | RPU & Preamplifier: -20°C to +60°C Antenna: -70°C to +60°C |
| Non-Operating: | -40°C to +65°C |
| Shock: | Operating: 40 g for 11 milliseconds Endurance: 0.09 g ² /Hz, 100 to 1,100 Hz |
| Random vibration: | Operating: 0.04 g ² /Hz, 100 to 1,100 Hz Durance: 0.09 g ² /Hz, 100 to 1,100 Hz |
| Vacuum/pressure: | <1 x 10 ⁻⁵ torr |
| Humidity: | 100% condensing |
| EMI/EMC: | MIL-STD-461C, Class A1a |
| Radiation: | 100 kRad SI |
| Reliability (10 years): | Ps = 0.95 single string = 0.99 redundant |

Operational Features:

- Self correcting hardware/firmware to mitigate SEU effect
- Self-surveying antenna installation
- No attitude or position initialization required
- Simultaneous tracking up to 9 satellites through 4 antennas

Accuracy

| | | |
|-------------------|---|--------------------------|
| Attitude*: | Roll: 0.1° (RMS) | Roll Rate: 0.5°/sec |
| | Pitch: 0.1° (RMS) | Pitch Rate: 0.5°/sec |
| | Yaw: 0.1° (RMS) | Yaw Rate: 0.5°/sec |
| Orbit**: | After dynamic filtering (orbit dependent) | |
| | Semi-major axis | <20 m |
| | Eccentricity: | 10 ⁻⁵ |
| | Inclination: | 10 ⁻⁵ radians |
| | RAAN | 10 ⁻⁵ radians |
| | Arg. of perigee | 10 ⁻⁵ radians |
| | Mean anomaly | 10 ⁻⁵ radians |

| | |
|--------------|-------------------------|
| Time: | 1 sec ± 1 µsec GPS time |
|--------------|-------------------------|

*Note: Attitude accuracy is dependent on antenna separation and multipath 0.1° (1σ) at ≈1.5 m baseline.

**Note: All GPS receivers are subject to degradation of position, velocity, and time accuracies under Department of Defense imposed Selective Availability (S/A). Attitude accuracies are not affected by S/A.

For further information contact:

Business Development
Space Systems/Loral
3825 Fabian Way
Palo Alto, CA 94303-4697
(415) 852-6802, FAX (415) 852-4940

Specifications subject to change without notice.

SPACE SYSTEMS/LORAL

Hitachi HGA-D Fiber Optic Gyroscope for Vehicular Applications

Bob Yoshida
Hitachi Cable America

Vincent Martinelli
Corning Incorporated

BIOGRAPHY

Mr. Bob Yoshida is the Marketing Manager for Hitachi Cable America. He has been marketing in the field of fiber-optic gyroscopes for the past 5 years. He has a Bachelor's degree from the School of Commerce (International Marketing) at Waseda University.

Mr. Vincent P. Martinelli is Supervisor of Applications Engineering for Corning Incorporated's Industrial/Government Fiber & Components group. He has been working in the field of optical gyroscopes for past 8 years. He has an S.M. degree in Electronic Materials and a S.B. degree in Materials Science and Engineering, both from the Massachusetts Institute of Technology.

ABSTRACT

The HGA-D fiber-optic gyroscope is the most recent product introduction in Hitachi Cable Ltd.'s line of gyroscopes for land vehicular applications. The HGA-D functions as a complement to the GPS receiver in navigation and location systems. The HGA-D provides dead reckoning information required for route guidance and improves the overall system performance, especially in environments where the GPS receiver may be shielded from satellite signals.

With the HGA-D design, Hitachi has reduced the size and the manufacturing cost compared to previous product generations. These improvements have been achieved without compromising the high performance and reliability of previous FOG designs. Thousands of Hitachi Cable FOGs are currently being used in automotive navigation systems in Japan, where they have operated failure-free for the past three years, as well as in a variety of systems in the US and Europe.

In this paper, we will briefly describe the FOG operating principle, basic design and benefits before focusing on specific performance attributes of the HGA-D. In

particular, we will discuss how the HGA-D is incorporated into vehicular systems that use GPS. We will describe how the FOG has been designed to be highly reliable in vehicular environments. We will also provide an overview of future directions for FOG product improvement.

Introduction

The Hitachi HGA-D fiber-optic gyroscope (FOG) is the latest generation of products designed for use as a dead reckoning sensor in vehicle navigation systems. The HGA-D relies on the proven technology of the all-fiber open loop FOG design - the same basic design that has met the demands of the automotive environment in systems that have been on the road for the past 5 years.

The HGA-D meets all of the technical requirements for vehicle navigation system applications, while featuring reduced size and weight from previous generation FOGs. Investment in improved assembly techniques and automation of component fabrication has simplified the manufacturing process and led to significant reductions in manufacturing costs making the HGA-D attractive for automotive system designers. The HGA-D is currently being produced at rates of tens of thousands annually.

In this product announcement, we will describe the basic operating principle for the FOG and review the HGA-D optical and electronic architecture. We will present the general specification for the HGA-D and discuss environmental test results. We will also describe how failure mode evaluation analysis was used as a tool to design reliability into this product. Finally we will discuss future development efforts to improve FOG products for automotive systems.

Basic FOG Operating Principle

The operating principle of the FOG is based on the Sagnac effect, which describes the relative difference in

pathlength traveled by counter-propagating beams of light in a rotating reference frame. Figure 1 shows counter-propagating light beams launched into a closed path, such as an optical fiber coil, from a beamsplitter, which is at the point BS. When the fiber coil is not rotating, the two beams of light travel exactly the same path before being recombined at BS. In the case where the coil is rotating during the time which it takes for the light to transit the coil, the beamsplitter moves from BS to BS' (for a counter-clockwise rotation). The two beams arrive at the beamsplitter at different times since they have traveled different distances through the coil. The path length difference, ΔL , is given by:

$$\Delta L = \frac{RL}{c} \Omega, \quad (1)$$

where R is the radius of the coil, L is the length of fiber in the coil, c is the speed of light in a vacuum, and Ω is the rotation rate. Note that the pathlength difference is directly proportional to the rotation rate.

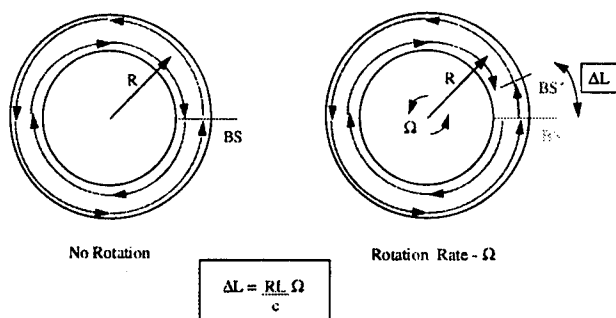


Figure 1. The principle of the Sagnac effect. When viewed from a rotating reference frame, two counter-propagating beams of light travel different distances through a closed path.

In the FOG, an interferometric technique, which detects the change in output intensity for the interference between the two counter-propagating beams, is used to measure the pathlength difference. The rotation rate can be directly determined by this technique.

Open loop all-fiber FOG

Figure 2 is a schematic representation of an open loop all-fiber FOG. The term "all-fiber" refers to the fact that the beamsplitters, polarization control elements and modulator are all built from optical fiber. The beamsplitters in this case are fiber-optic couplers. The polarization control elements include a polarizer, made from elliptical jacket fiber, and a sensing coil made from

elliptical core polarization-maintaining (PM) fiber. Elliptical core fiber meets the technical requirements for the FOG design at a much lower cost than traditional stress-rod type PM fibers. The phase modulator uses a length of fiber wound on a PZT cylinder. Details on these components and on the signal processing scheme used have been published previously.¹

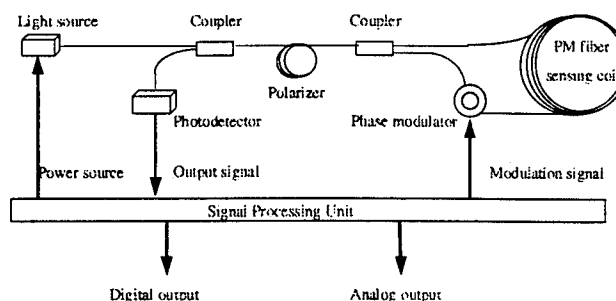


Figure 2. The open loop all-fiber FOG configuration. This type of FOG is in mass production for FOG/GPS vehicle navigation systems.

The open loop all-fiber FOG has been in mass production since 1992. It has met all of the technical requirements for navigation and location systems, including environmental performance.

Benefits of FOG technology

The FOG offers several advantages when compared to other dead reckoning sensor technologies, including:

- high reliability
- superior technical performance
- environmental ruggedness
- consistent unit-to-unit performance
- compact size
- light weight
- quick start-up.

The FOG is inherently reliable due to the absence of moving parts. Its key component technologies, the light source and the optical fiber, have established reliability track records based on use in CD players for consumer electronics and in fiber-optic cable for the telecommunications industry, respectively. Other components have been designed using FMEA tools in order to build reliability into the FOG.

Both consumers and system makers benefit from these FOG attributes. Consumers demand high functionality and 100% system operation - especially in congested urban areas. The FOG offers a performance advantage

and proven reliability making it possible to meet these consumer needs.

System makers count on the FOG's consistent performance to simplify assembly processes, by eliminating the need for expensive calibration and customization steps.

HGA-D design and performance specifications

Figure 3 shows the schematic configuration of the optical and electronic components of the HGA-D. The electronics consist of four lock-in amplifiers, a timer, and a single chip microcomputer containing a 10 bit A/D converter with serial communication interface. The rotation rate is determined by the harmonic ratio method using the proper frequency of 21.7 Hz.

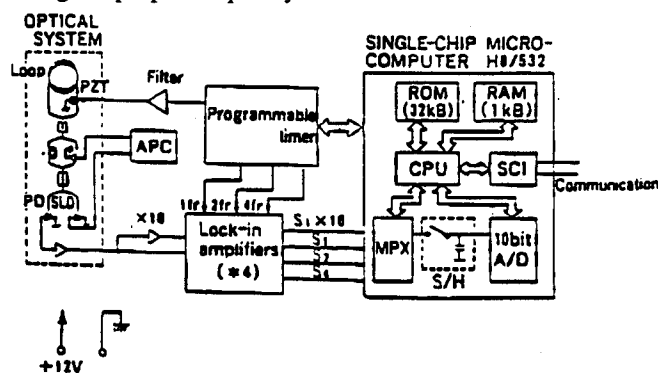


Figure 3. Schematic representation of the main optical and electronic components of the HGA-D.

Table 1 shows the technical specification for the HGA-D. This specification has been developed based on the intended use in vehicle navigation systems where the FOG works in concert with a GPS receiver to provide position information to the onboard navigation computer.

Table 1. Performance specification for the HGA-D FOG.

| | |
|--------------------|---------------------------------------|
| Input rate range | ± 60 deg/s |
| Random walk | 4 deg/ $\sqrt{\text{hr}}$. |
| Initial bias | ± 0.2 deg/s (without zero adjust) |
| Scale factor error | ≤ 1 % |
| Frequency response | 16 Hz |
| Warm up time | 3 s (typical) |
| Output | Serial (TTL) |

| | |
|-----------------------|-------------------|
| Operating temperature | -30 to +75° C |
| Storage temperature | -40 to +85° C |
| Power supply | +12 V DC |
| Dimensions | 120 x 50 x 170 mm |
| Weight | 1 kg |

Table 2 summarizes the environmental requirements for automotive applications along with the results for the HGA-D.

Table 2. Environmental test conditions for HGA-D for navigation and location systems

| Test | Condition | Result |
|----------------------------|---|--------|
| High temperature operation | 75° C, 500 hr. | Pass |
| Low temperature operation | -30° C, 250 hr. | Pass |
| Heat shock | -40 to +85° C, 2 hr./cycle 1500 cycles | Pass |
| Vibration | 8 to 200 Hz, 2.5 G x, y, and z axes, 17 hr. each | Pass |
| Shock | 80 G x, y and z axes, 3 times each | Pass |

Future design improvements

The HGA-D is the latest product in the evolution of FOG technology to reach mass production quantities; however, based on the anticipated demands for continuing improvement in product performance, reducing size and weight, and meeting cost reduction targets, work on the next generation FOG is already begun. The next generation FOG will employ an integrated optical circuit (IOC) to reduce the number of optical components and assembly operations required along with a digital signal processing scheme. The combination of these features will improve the FOG technical performance while reducing size, weight and manufacturing cost. Recent progress on this design has been reported in another paper at this meeting.

Summary

The HGA-D is a mass-produced FOG designed for use in automotive navigation systems. This gyro meets the technical requirements for automotive use and offers all of the benefits of the proven open-loop FOG technology. Efforts are underway to develop the next generation FOG using an IOC. This type of FOG is seen as the successor to the HGA-D model for automotive applications.

ACKNOWLEDGMENTS

The authors are grateful to Dr. H. Kajioka and Dr. T. Yuhara of Hitachi Cable Ltd. and Mr. Ray Ikeda of Hitachi Cable America for their support.

REFERENCES

1. T. Yuhara, T. Kumagai, H. Soekawa and H. Kajioka, "Fiber-optic gyroscopes for automotive applications," *Journal of Circuits, Systems and Computers*, Vol. 5, No. 1, 1995, pp. 17-36.
2. V. Martinelli, R. Ikeda, "Next Generation Fiber Optic Gyroscope for Use with GPS in Vehicle Navigation and Location Systems;" Presented at ION-GPS, Session C4, Sept. 14, 1995.

Honeywell's DGPS Local Area Augmentation System Ground Station

Steve Serfling
Honeywell

BIOGRAPHY

Steve Serfling is Manager of Business Development for GPS Programs, Honeywell Commercial Aviation Systems, Sensor Products Organization. Steve has been with Honeywell for 15 years and has worked on GPS related projects for the past 6 years. He has participated in Honeywell's flight test programs and represented Honeywell on the RTCA SC-159 Committee during development of the SCAT-IMASPS.

ABSTRACT

Honeywell has introduced a Differential GPS (DGPS) Local Area Augmentation System (LAAS) that meets the requirements of RTCA/DO-217 (Minimum Aviation System Performance Standards DGNSS Instrument Approach System: Special Category I). Honeywell provides a total-system approach with both ground-based and airborne equipment. This paper describes Honeywell's Fail Operational DGPS ground based equipment.

Honeywell's SLS-2000 Fail Operational DGPS Ground System is unique in that the architecture allows for continued operation in the presence of faults with less hardware than traditional systems.

Basic system operation consists of multiple differential correction processors (DCP) that are synchronized by a fault tolerant clock resident in each processor function. Each DCP receives serial input data from remote GPS reference receivers to assure that all operations are performed using identical input data. The DCPs then calculate the differential corrections and perform multiple integrity checks on the GPS reference receiver. The output of each processor is compared (bit for bit) using a patented and proven Honeywell technique. Upon successful comparison, the data is output to the RF datalink for transmission.

HONEYWELL MARKET PRESENCE

Honeywell is the world's leading supplier of avionics systems and subsystems for both civil and military aircraft, from small turboprop commuters and corporate business jets to large air transport, cargo and fighter aircraft. With more than 50 years of experience in aircraft avionics and services, Honeywell continues to provide leading edge technology systems to meet the challenges of the ever changing aviation industry. As the industry has matured and air traffic has grown, increased demands have been placed on air traffic management, pilot workload, and airport operations, with added emphasis on reliability, system integrity and operating cost. Honeywell continues to meet these challenges and is today the full cockpit avionics supplier for many aircraft while serving as a major subsystem supplier on most other aircraft.

With this experience and total systems approach, Honeywell is in a unique position to support the aviation industry in lowering cost, increasing traffic capacity and advancing the technology of air traffic management in the future.

HISTORY OF HONEYWELL'S GPS EXPERIENCE

Honeywell has a long history of providing GPS technology to military, air transport and general aviation aircraft. Honeywell has conducted numerous GPS and DGPS flight test demonstrations for aircraft manufacturers, the FAA and other certification authorities world-wide.

Honeywell also has a long history of developing GPS certification requirements and architecture characteristics. Honeywell has charter members of both the SC-159 subcommittee of RTCA and the ARINC 743 subcommittee of AEEC and has

participated in writing numerous sections of the ARINC 743, ARINC 755, DO-208 and DO-217 documents.

Honeywell began development of GPS technology in 1986 with the design of a two-channel, fast sequencing GPS Sensor Unit housed in an Inertial Reference Unit (IRU). This device was successfully flight tested by Boeing on their 767 flight test aircraft. The same design was also successfully tested at Airbus on their A310 flight test aircraft.

Development of our first ARINC 743 compliant, two-channel, all-in-view receiver began in 1988 when the ARINC characteristic started to materialize. This unit was TSO'd in 1990 and is flying on many business aviation aircraft types with over 575 units shipped. Boeing flight tested the device in fall of 1990 during the certification of the 737-500 FMS. This device also received the world's first non-precision approach certification in December 1993.

In the fall of 1990, Honeywell and NASA joined forces to demonstrate the potential of differential GPS to provide guidance for precision approach. During these tests, 34 Category III touchdowns were performed using the Honeywell IRS/DGPS integrated navigation system.

Honeywell teamed with the FAA to determine the feasibility of providing position accuracies sufficient for non-precision and precision approaches using commercially available GPS sensors. Honeywell instrumented their GIV aircraft with a complete GPS/IRS navigation and a data acquisition system. The aircraft was flown at the FAA Tech Center where the approaches were monitored with a laser tracker. The results of these tests were presented at the ION Conference in September 1992.

In 1992, Honeywell teamed with Canadian Marconi Corporation to develop an ARINC 743 12-channel GNSSU for air transport category aircraft. The device was certified for general aviation aircraft in January of 1994 and certified on both Boeing and Airbus aircraft in early 1995. The Honeywell/CMC GNSSU was certified on the first flight of the Boeing 777 in mid-1995. Honeywell has delivered over 800 12-channel certified GPS receivers to date.

Honeywell continues to develop the DGPS technology with our participation in Boeing's Category IIIB flight test evaluation. In late July and early August this year, a NASA owned Boeing 757 successfully completed CAT IIIB automatic landings at NASA's Wallops Island, VA flight test facility. The GPS CAT IIIB flight test program was collaborative effort between NASA, Boeing, and four avionics industry teams: Honeywell, Collins/DASA, Litton/Wilcox, and Interstate Electronics. Each entity had a unique role in the program; NASA supplied the 757 aircraft and flight test facility, Boeing supplied the pilots, ground crew,

maintenance, flight test personnel and performed the aircraft modifications for flight test, and the industry teams supplied the prototype DGPS landing systems.

During the 75 CAT IIIB automatic landings performed during the Honeywell phase of flight testing, the Honeywell DGPS landing system replaced the instrument landing system (ILS) receiver with a DGPS solution that provided equivalent lateral and vertical guidance signals to the airplane's autopilot. The autopilot used the DGPS lateral and vertical guidance signals to control the plane down the glideslope to landing and then used the DGPS lateral guidance signal on the runway after touchdown to keep the airplane on the runway centerline during rollout.

Preliminary performance data from the Honeywell system shows that the predicted system accuracy of approximately 1-2 meters was achieved. Over the coming months, Boeing will process all of the recorded data in a simulation of the entire airplane/GPS environment to determine the accuracy of each system and the behavior of each system under various simulated failure conditions. The simulation results will then be used to help guide the creation of the requirements for future DGPS precision landing systems.

Honeywell has teamed with Canadian Marconi Corporation and Pelorus Navigation Systems Inc. to develop the DGPS Ground Station. CMC will provide the GPS receiver and Pelorus will develop the datalink function and the ground-system chassis.

SCAT I DIFFERENTIAL GPS CONCEPT

GPS has many advantages over existing navigation aids in that it provides highly accurate, world-wide coverage, and can provide navigation for all phases of flight. However, in order to provide precision approach navigation capability, the GPS system must be augmented to provide increased accuracy, integrity, and availability. Implementation of local area DGPS technology significantly increases the accuracy, integrity, continuity of function and availability of the GPS navigation function and has been widely accepted within the navigation community.

To provide for early implementation of DGPS precision approach landing capability, RTCA Special Committee 159 published the Minimum Aviation System Performance Standards (MASPS) DGNSS Instrument Approach System: Special Category I (SCAT-I) (Document no. RTCA/DO-217). THE SCAT-I MASPS provides guidance and design requirements for DGPS instrument approach systems. Figure 1 shows a simplified block diagram of the DO-217 implied ground reference station architecture.

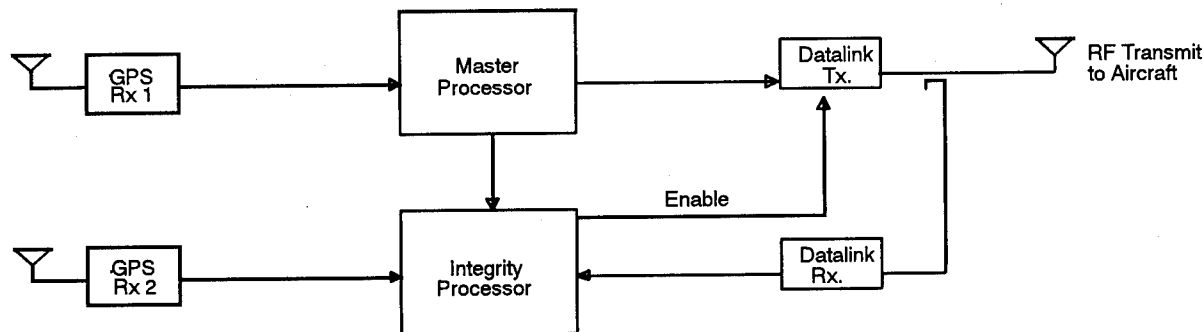


Figure 1. DO-217 Implied Architecture

HONEYWELL DIFFERENTIAL GPS GROUND REFERENCE SYSTEM

Numerous DGPS solutions have been proposed and successfully demonstrated within the GPS community. Honeywell has studied several of these solutions and has chosen to implement a carrier-smoothed code-tracking DGPS approach in our SLS-2000 Differential GPS equipment for SCAT-I precision approach capability. Carrier-smoothed code-tracking DGPS is the most robust SCAT-I compliant solution to implement and has been demonstrated to be very robust. Its accuracy exceeds the needs of all SCAT-I requirements and may be compatible with emerging Category II requirements. In addition, this architecture makes relatively modest demands on the DGPS differential correction datalink.

SYSTEM ARCHITECTURE

Honeywell's SLS-2000 Fail Operational DGPS Ground Station is comprised of equipment to perform two major subfunctions: 1) determine ground-based differential corrections and 2) transmit these corrections to the aircraft using a DO-217 defined datalink. In addition, to complete the system, an aircraft differential GPS receiver and VHF datalink receiver are required onboard a user's aircraft.

The ground-based reference equipment calculates differential corrections for smoothed pseudorange measurements of each Space Vehicle (SV) in view. The primary function of these differential corrections is to remove the Selective Availability (SA) errors that are intentionally induced by the GPS Control Segment and system errors common between the satellite signals received by the airborne and ground components (e.g. tropospheric errors). Removal of these errors significantly increases the accuracy and integrity of the aircraft's GPS navigation solution enabling it to be used for aircraft guidance during Category I approaches. The reference system operates on carrier-smoothed code tracking phase measurements derived from the GPS SVs and WAAS satellite signals.

The datalink equipment provides a means of uplinking the differential corrections, integrity messages, and where required, the desired flight path information from the reference station to the aircraft avionics. The aircraft avionics applies the differential corrections to the GPS smoothed pseudorange measurements prior to calculation of the GPS navigation solution. The aircraft avionics will likewise use the uplinked integrity information to ensure the operational requirements of the navigation solution are met and the flight path information to create the approach path for precision approach.

Honeywell's GPS reference station is a modular design and can be configured in either fail-passive or fail-operational configurations. The fail-passive configuration is designed to meet the DO-217 MASPS minimum requirements and contains less redundant equipment than the fail-operational equipment described in this paper. The fail-operational configuration is designed to exceed the SCAT-I MASPS requirements and provides a deferred maintenance capability.

As shown in Figure 2, the primary physical equipment (fail-operation configuration) consists of: a differential reference station housed in an environmentally controlled shelter, three spatially separated RSMUs, and a VHF transmitting antenna.

Figure 3 shows a simplified block diagram of the Differential Reference Station in a fail-operational configuration. The fail-operational Differential Reference Station is unique in that the architecture allows for continued operation in the presence of faults using less hardware than traditional systems. Fail-operational performance is accomplished by dividing the system into Fault Containment Modules (FCMs) that are I/O buffered using serial data transmissions. The serial data transmission circuitry and multiple power system provide isolation circuitry that prevents one FCM from affecting another. Figure 4 shows the physical layout for the GPS reference station chassis.

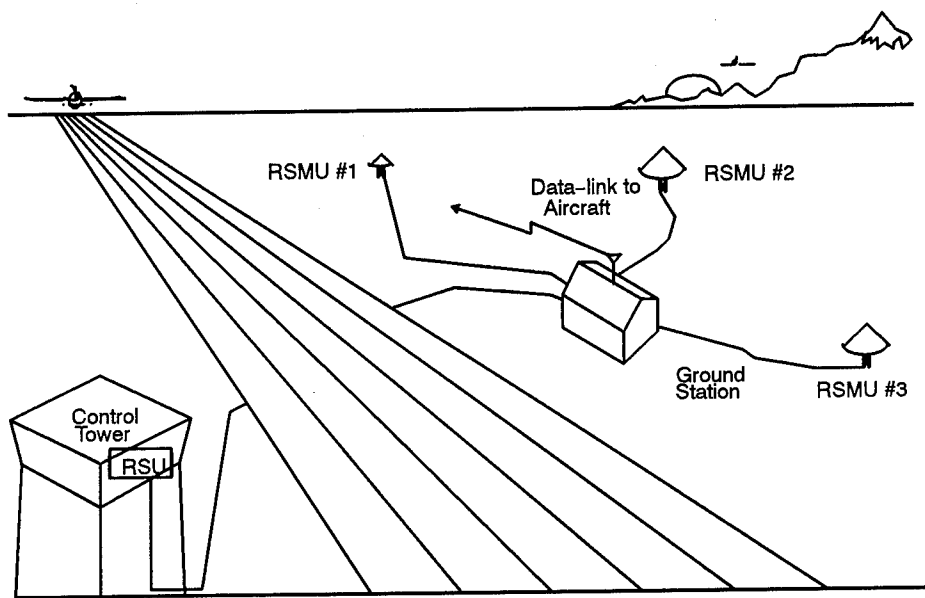


Figure 2. Differential GPS Overview

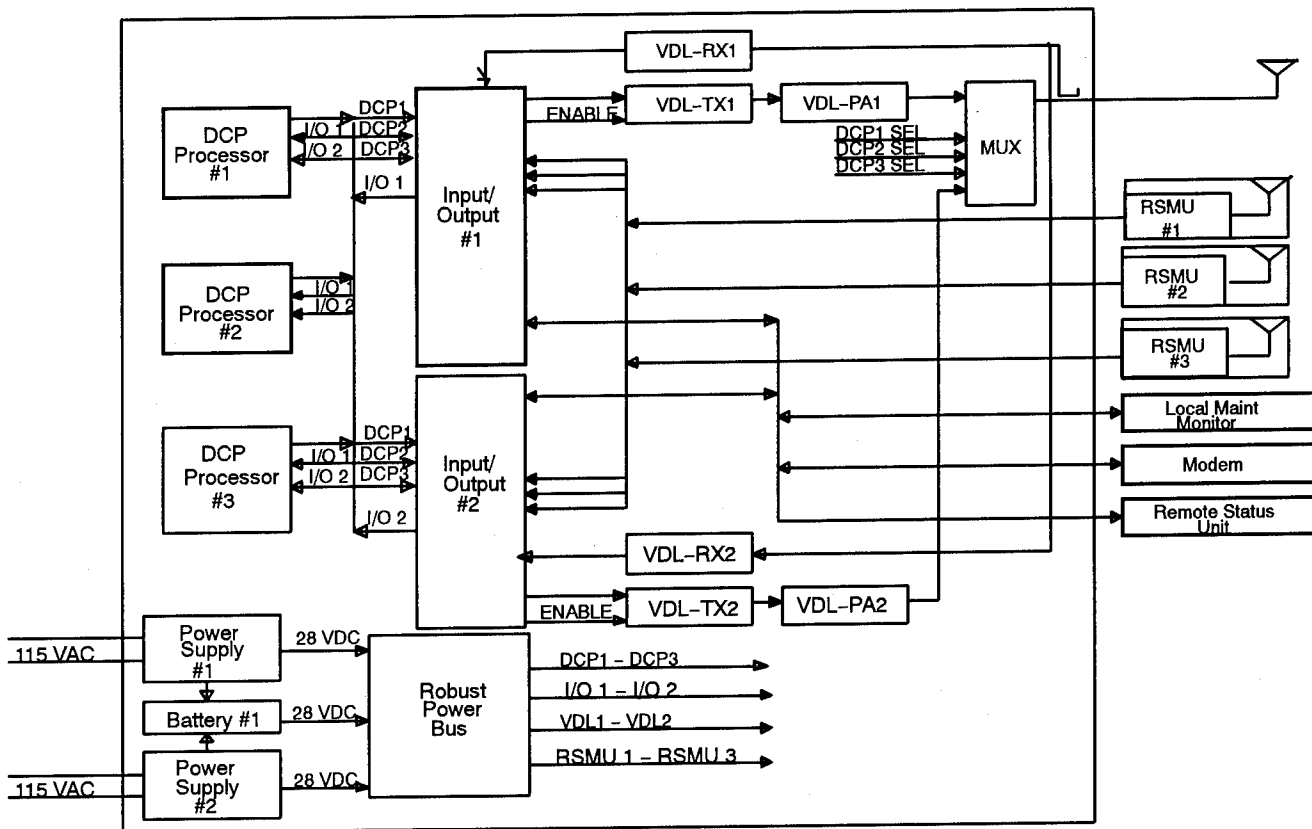


Figure 3. Fail-Operational Differential Reference Component Block Diagram

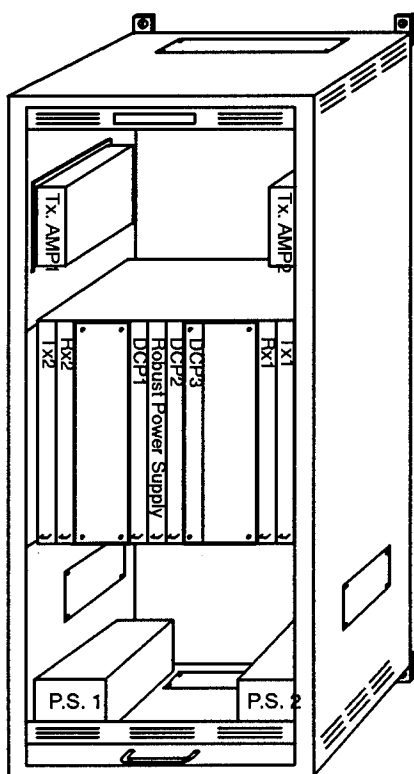


Figure 4. SCAT I Ground Chassis Station

The Differential Reference Station (fail-operational configuration) consists of three identical Differential Correction Processors (DCP), two Datalink Transceivers (RF transmitters and RF wraparound receivers) and two Input/Output functions. The station operates on a fault tolerant power supply system supported by a backup battery which provides an additional one-hour power source in the event of primary power failure.

The three DCPs are synchronized by fault tolerant clocks resident in each processor function. Each processor receives serial input data from: the RSMUs, the datalink wrap-around, and the interface control function each time a request command is generated. This synchronization assures that all processors operate on the same input data. The DCPs calculate the differential corrections and perform RSMU integrity checks using identical RSMU data sets. The differential corrections and other output data (to the datalink) is then compared bit for bit by the fault detection interfaces. Upon a successful comparison, the datalink transmits the message to the user systems. An on-line RF receiver decodes and routes the message back to each DCP to ensure datalink availability.

SYSTEM COMPONENT DESCRIPTION

Differential Correction Processor

The primary function of the Differential Correction Processor (DCP) is to calculate a differential correction message for each tracked Satellite Vehicle (SV) that is considered valid. In the fail-operational configuration, the DCP channels utilize data from three (or more) RSMUs to form independent sets of corrections.

Each of the correction sets is formed, as follows: Within each DCP, pseudoranges are predicted using the surveyed position of the RSMU station antennas and the RSMUs output of SV positions. The predicted pseudoranges are then differenced with the RSMU measured values. The pseudorange differences calculated for each SV contain a common error due to the RSMUs clock error, which can be very large (range equivalent values on the order of 10^6 meters or larger). In order to calculate the pseudorange corrections, an estimate of this clock error is removed from each pseudorange difference by subtracting the average of all valid pseudorange differences from each individual difference. Removal of the clock error and satellite motion from the pseudorange differences reduces the dynamic range of the pseudorange correction messages transmitted across the datalink.

Once the receiver clock error has been removed, a deviation test on the unique correction sets is performed as an added measure of multipath rejection and error detection. This test involves examining the deviation of each SV correction from the mean. If any correction deviates from the mean by a predetermined threshold it will be rejected and the average will be recomputed from the remaining valid corrections. The DCP will then average the remaining sets of differential corrections to further reduce measurement noise including multipath effects. It is this average that will be used as the differential correction transmitted to the aircraft. If particular SV measurements exceed a predetermined threshold, the SV may be declared invalid for a preset time.

The DCPs format data to be transmitted consistent with Type 1, Type 4 and Type 7 messages, as defined by the DO-217 MASPS (Type 1 corresponds to differential corrections, Type 4 corresponds to the precision approach path and Type 7 defines an enhanced integrity message). Growth capability includes all message types. The output data is transmitted at 2 Hz, allowing for reduced data latency and enabling the design to support future Category II and III operations.

Major features of the Differential Correction Processors are:

- Designed with the Intel 80960 32 bit, single chip, RISC processors
- Previously certified, fault tolerant architecture which includes a voted, fault tolerant clock
- Software programmed in "C" and verified per DO-178B Level B
- Differential corrections computed and transmitted at 2 Hz
- Remote programming of software program memory
- Multiple non-volatile memory to provide integrity of site specific data

Datalink

The datalink function is designed to be compliant with SCAT I requirements and transmits in the VHF band from 112 to 117.950 Mhz with 25 Khz channel spacing. The datalink function receives serial formatted correction and waypoint messages from the DCP. The modulator randomizes the data according to RTCA DO-217 Appendix F, providing a Forward Error Correction (FEC) function, and then symbolizes the data for D8PSK modulation at a 10,500 symbol/second rate (31,500 bit/second). The output is then amplified in the Solid State Power Amplifier (SSPA) for transmission from the antenna. Internal monitoring circuitry tests the datalink for modulation accuracy, Time Division Multiple Access (TDMA) burst concurrency, VSWR, power output, and other critical system parameters to ensure that failures in the circuitry are immediately detected and the appropriate alarms issued. The nominal effective range of the datalink is 20 nm with a variable power output from 1 to 20 watts. The DCPs automatically switches transceiver pairs to reduce the probability of latent faults in the ground-based datalink function.

To ensure end-to-end integrity of the differential corrections, Cyclic Redundancy Check (CRC) codes are used on the data transmission. These CRCs are initially created by the DCP critical level software then reconstructed and compared to the received CRC by the airborne equipment critical level software. In addition, the transmitted signal is received and demodulated by the ground station datalink receiver. Demodulated data is fed back to the DCP for verification that data received from the RF link are identical to the original baseband data provided to the datalink function for transmission.

RSMU

Honeywell's current RSMUs use the same advanced technology as aircraft GPS receiver designs to provide standard satellite measurement data sets. The receivers are based on the TSO'ed C129 receivers currently in production for Honeywell. The satellite measurement data set includes satellite position, satellite status, pseudorange, delta range

measurements, measurement time, and equipment status. The RSMUs include a GPS antenna augmented with a choke ring ground plane to reduce multipath effects. In addition, the RSMUs are spatially separated to minimize the effect of multipath errors occurring simultaneously at each GPS receiver. Figure 5 shows the RSMU physical layout and Figure 6 shows a typical RSMU installation. Table 1 defines the RSMU GPS receiver specifications.

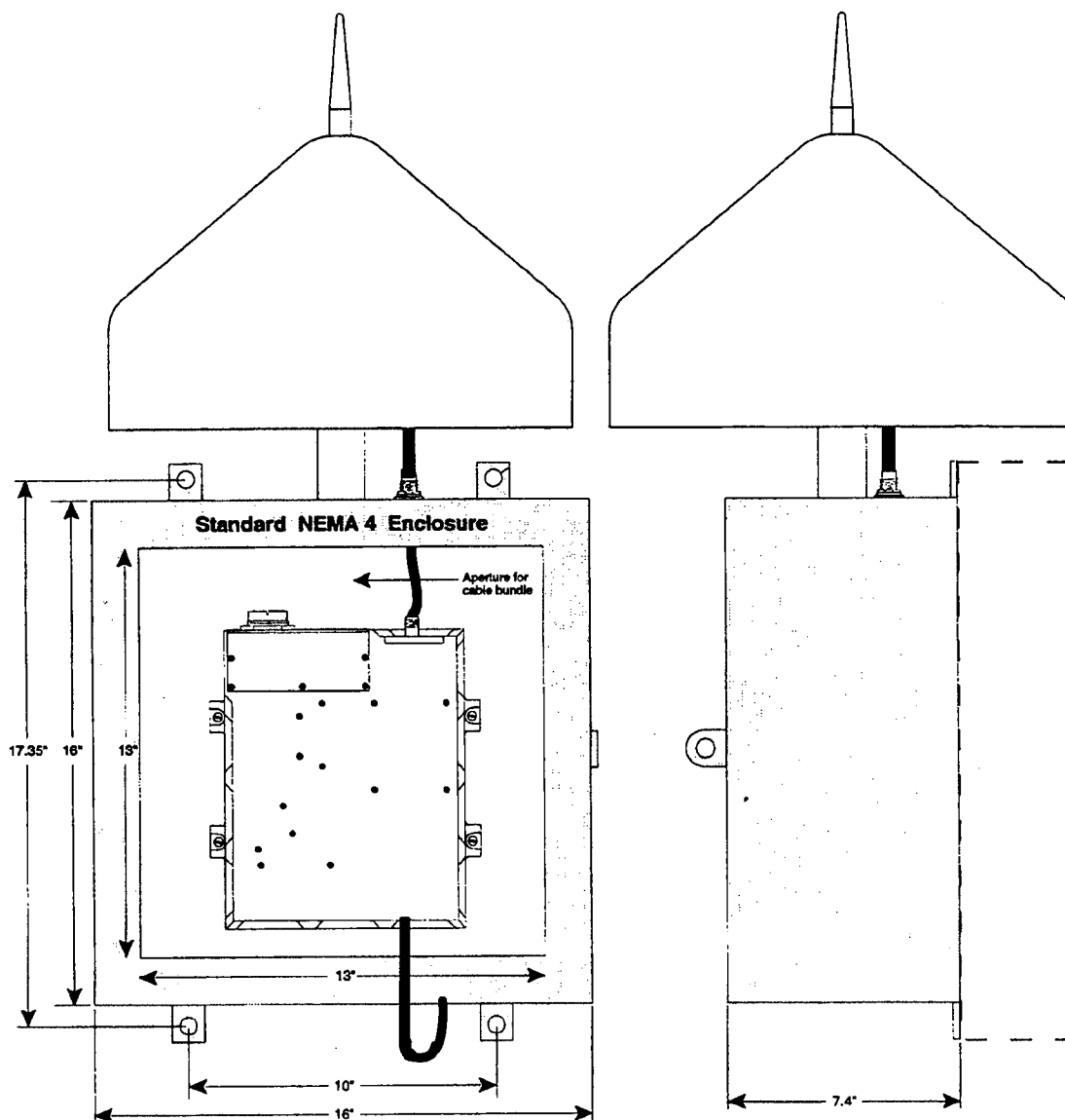


Figure 5. Remote Satellite Measurement Unit (RSMU) Physical Diagram

Table 1. RSMU Specifications

| | |
|-----------------------------|--------------------------------|
| GPS channels | 12 (all in view) |
| Acquisition Time | 75 seconds |
| Signal Interface | Differential digital |
| Power Consumption | 20 Watts |
| MTBF | >40,000 Hrs |
| Mask Angle | Variable |
| Data output rate | 2 Hz |
| Software Updates | Remotely program- mable |
| Operating Temp | -50_C to +70_C |
| Operating Relative Humidity | 0 to 100% |
| Operating Altitude | 0 to 10,000 MSL |
| Rain | 25 millimeters per hour |
| Ice Loading | 1/2 inch radial thick- ness |
| Wind | 0 to 70 MPH |

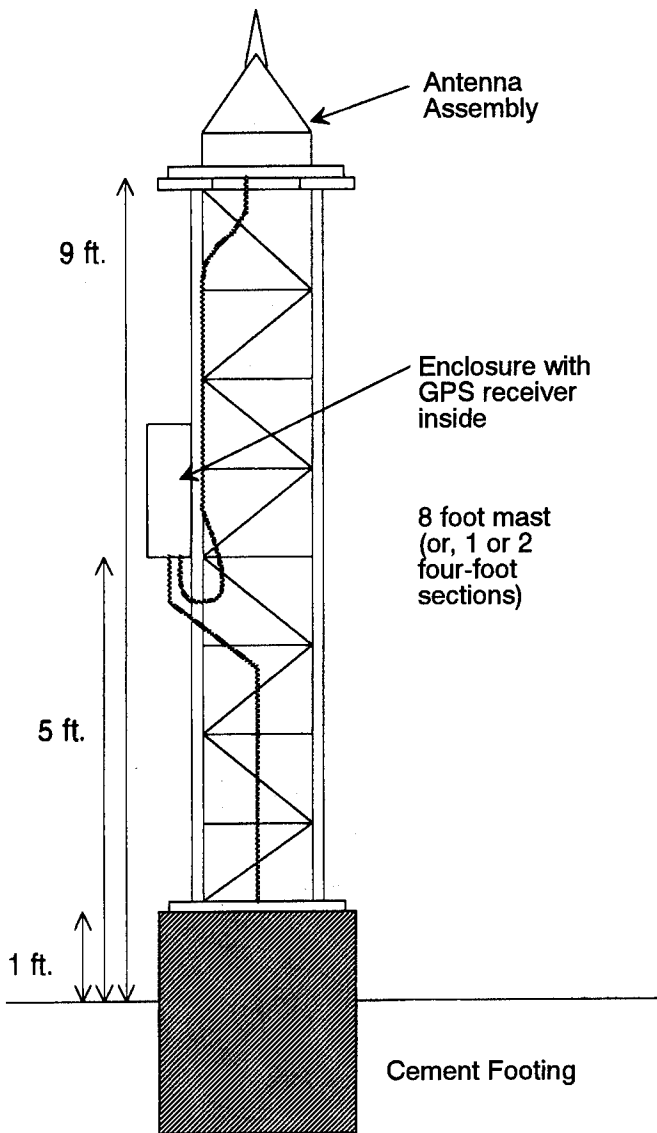


Figure 6. RSMU Installation

SYSTEM PERFORMANCE

Honeywell has performed extensive analysis on the performance of the GPS satellite constellation and the SCAT I equipment under development. Analysis is based on the total SCAT I system design (including the airborne and ground components). The Martinez almanac and the Durand weights are used for satellite failure simulations.

The performance of the SCAT I system is defined through four measures: integrity, availability, accuracy and continuity of function. The Honeywell system identified in this paper is designed to exceed the DO-217 MASPS requirements for each of these measures as identified in Table 2.

While this paper focuses on the DGPS reference station design, the airborne equipment is an integral part of the total system design; therefore, some reference to airborne performance criteria is included.

Table 2. SCAT I Requirements

| REQUIREMENTS | HONEYWELL | RTCA DO-217 |
|-------------------------|--|--|
| Accuracy | RMS pseudorange of <0.9 meters | RMS pseudorange of <1.1 meters |
| Integrity | 1E-8 per approach | 3E-8 per approach |
| Continuity of Function | 1.15E7 per approach | 3.8E-5 per approach |
| Availability | >99% | 98% |
| Integrity Alarm Latency | <1.0 seconds | <3.0 seconds |
| Acquisition Time | 75 seconds | 300 seconds |
| Software Criticality | DO-178B Level B | DO-178B Level B |
| Uplink Rate | 0.5 seconds | 3.0 seconds |
| Datalink Range | 20-40 nmi | 20 nmi (minimum) |
| Datalink Modulation | D8PSK per RTCA/DO-217 Appendix F, Change 1 | D8PSK per RTCA/DO-217 Appendix F, Change 1 |
| Datalink Message | RTCA/DO-217 Appendix A, Types 1, 4 and 7 | RTCA/DO-217 Appendix A, Type 1 |

Integrity

The integrity level provided by the Honeywell SCAT I ground-based system is primarily the result of two major design components:

The first is the use of three RSMUs, fault tolerant architecture, and redundant components to provide a measurement consistency check to identify multipath errors and detect erroneous measurements.

The second is the use of the CRC on the messages transmitted to the aircraft from the ground. The CRC ensures the end-to-end integrity of the differential corrections datalink and eliminates the datalink as a potential system integrity failure point. A separate CRC is also used to ensure the integrity of the uplinked pathpoints.

The integrity level of the Honeywell proposed SCAT I ground-based equipment is 1×10^{-8} /approach.

Availability

The availability of the SCAT I system is a function of the satellite constellation (including failures), the MTBF of the DGPS Ground System equipment, and the integrity requirements (false detection rate, integrity

bound etc.). The constellation related (based on VDOP) availability computed for the Honeywell SCAT I system is 99.7% for the autonomous GPS satellite constellation and 99.9% for the GPS constellation augmented with WAAS satellites. The DGPS Ground Station equipment availability is better than 99.9% for the fail-operational configuration. Analysis has shown that incorporation of a minimum (<24 hour) repair time or added component redundancy will enable the system to meet 99.999% availability.

Accuracy

The accuracy of the SCAT I system is the function of the differential corrections, sensor measurements, and the satellite geometry. The resulting vertical system accuracy of the SCAT I system is 1 - 2m (2σ). Accuracy will continue to be enhanced in future upgrades as requirements for Category II and III are defined.

Continuity of Function

The continuity of function of the SCAT I system is the function of the failure rates of the DGPS Ground Station and the satellite constellation. System outages

(resulting from constellation limitations) which can be predicted by the airborne component do not affect the continuity of function, but do affect availability. The continuity of function computed for the Honeywell SCAT I ground system is 5.5×10^{-7} /approach.

MAINTENANCE

The SCAT I Ground System includes a monitoring system for configuration, control, fault isolation and status. This monitoring function consists of power-up and continuous Built-In-Test, a local maintenance monitor, and provisions for a remote maintenance monitor.

Local Maintenance Monitor

A Local Maintenance Monitor (LMM) system is included with each SCAT I Ground System. The LMM provides system configuration, system control and fault isolation. The LMM is comprised of a Personal Computer configured with software to interface via an RS-232 interface.

The LMM allows the system operating parameters to be initialized and/or changed. This includes field programming of the operating software, thus allowing software updates without disassembling the system. The LMM provides a user friendly menu system that allows the operator to configure the following parameters:

- RSMU Locations
- Datalink Frequency
- Datalink Transmitter Power
- Datalink TDMA slot(s)
- Fail Safe vs. Fail Operational Configuration
- Multipath Information
- Pathpoint Data (multiple inputs)
- Modem Autodial Numbers
- Enable/Disable System

The LMM can request the system status to aid in fault isolation and repair. The Built In Test (BIT) information is transferred from the Ground Systems internal memory to the LMM for easy fault analysis. The BIT information includes a fault identifier, date, time, and detailed snapshot parameters (if available). An optional printer at the Ground System provides a permanent record of the system activities.

Typical Status Parameters include:

- Processor Alarms
- Datalink Transmitter Alarms
- Datalink Power Amplifier Alarms

- Datalink Receiver Alarms
- Power Supply Alarms
- Battery Alarms
- Satellite Failures
- Multipath Alarms
- Shelter Environmental Alarms

Remote Maintenance Monitor

The DGPS reference station is provisioned to allow the system status to be reported via a remote interface. The status can be requested by dialing into the system and logging on with the appropriate passwords. The same Personal Computer/software used for the LMM is used to support this option. The system can also be configured to automatically dial out whenever an alarm condition(s) is detected.

Remote Status Unit

Remote status indications of the Ground System are provided via a dedicated serial line to a Remote Status Unit (RSU). The RSU displays In Service, Maintenance Required and No Service. The system allows for multiple RSUs to be connected to provide status in various locations (i.e. Tower, Maintenance Shop, etc.) if desired.

Certification

Honeywell has extensive experience in developing aircraft equipment and working with the FAA to obtain certification. Honeywell has initiated a project with the FAA to certify the DGPS system for SCAT I precision approach capability during the first quarter of 1996.

The certification process is being accomplished in accordance with the Type Acceptance Test and Evaluation (TATE) plan prepared by the FAA's National Airways Systems Engineering Division (A05-200).

Acknowledgements

The assistance of Rod Stangeland and Randy Hartman in the preparation of this paper was greatly appreciated. Also recognition to the Honeywell GPS design team for their dedication and creative work on the concepts and designs described in this paper.

References

Minimum Aviation System Performance Standards, DGNSS Instrument Approach System: Special Category I RTCA/DO-217; August 1993.

Starwatch™: An Off-the-Shelf GPS Asset Location System

John Lavrakas
Advanced Research Corporation

BIOGRAPHY

John Lavrakas is president of Advanced Research Corporation. He holds a B.S. and M.A. in Mathematics from Harvey Mudd College and Claremont Graduate School, respectively. He has more than fifteen years experience in GPS and time space positioning systems.

ABSTRACT

StarWatch™ is a new GPS Asset Location product of Advanced Research Corporation. It is an off-the-shelf global tracking system, that is low-cost and easy to install. Using the new ORBCOMM communications satellite network and cellular communications, the StarWatch system provides unique solutions for rural and remote tracking and messaging. This paper discusses StarWatch features, including principles of operation, communication means and ORBCOMM features, and how StarWatch benefits users and providers of vehicle and asset tracking systems.

INTRODUCTION

Along with advances in technology come solutions to problems for numerous businesses and individuals. For years many companies have provided systems for vehicle fleet dispatching and management, but the need has grown to track assets in addition to land and marine vehicles. Advanced Research has developed a product that addresses the needs of managers of mobile assets in locating these assets in a timely manner. The product is called StarWatch, and it combines the benefits of Global Positioning System (GPS) positioning technology with digital maps and cellular and satellite communication to provide the ability to manage assets anywhere. Hosted on a personal computer running under Microsoft® Windows™, StarWatch is easy to install and operate. Using point and click operation, StarWatch provides the user a quick and easy view of assets anywhere. StarWatch is specifically designed for small fleet operators and managers of large numbers of assets located anywhere.

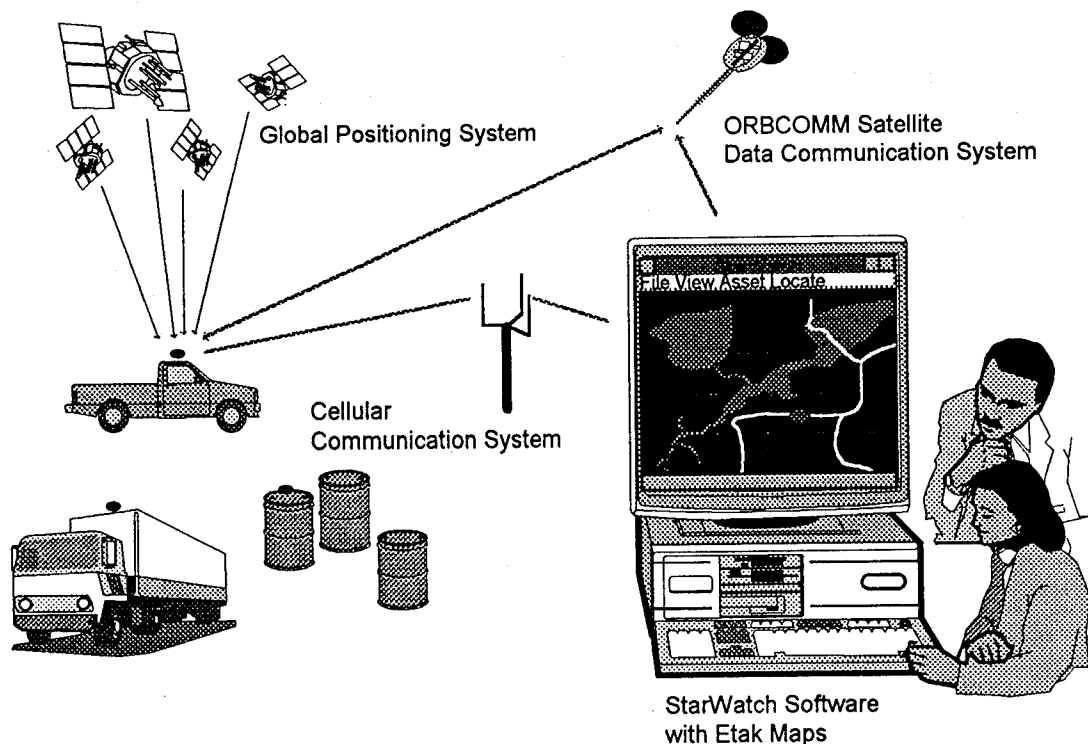


Figure 1. StarWatch Asset Location System

PRODUCT DESCRIPTION

StarWatch is comprised of a PC hosting the system control and map display software, ORBCOMM and cellular communications channels, and positioning sensor and communication units, as illustrated in Figure 1. The proprietary StarWatch software provides access to digital maps provided by Etak, Inc. (Menlo Park, California) using Etak map access software libraries. This permits the user to zoom and pan on the maps and set the level of detail of highways, streets, railroads, lakes, parks, and other features. Assets are identified by means of vehicle icons. The label of each icon is user selectable. StarWatch is able to display multiple maps, which can be arranged by the user in any way they wish using standard Windows controls. See Figure 2 for a sample view of a StarWatch screen.

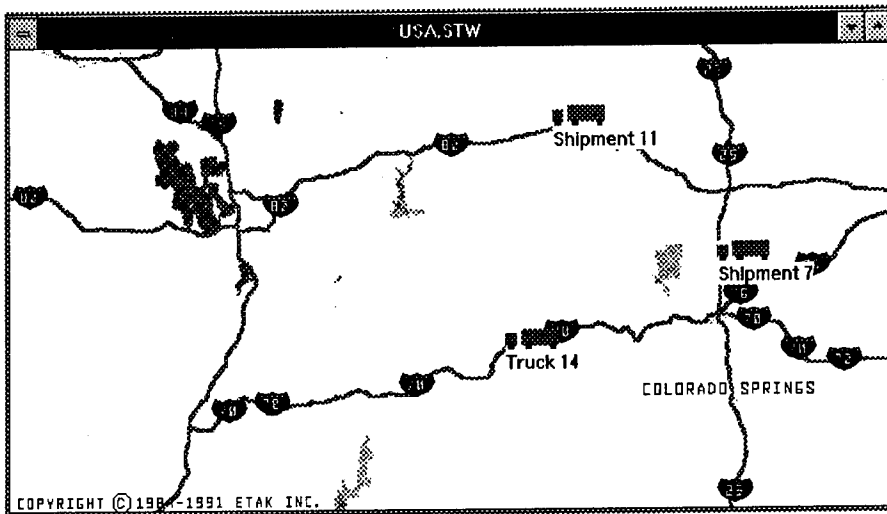


Figure 2. StarWatch Sample Screen

StarWatch provides a data recording capability, in which all data is stored to a user-selected file on disk in ASCII format. This data is then available for later review. StarWatch also provides a messaging capability for tracking units which have a PC attached. This allows the dispatcher to relay messages to the driver of vehicles. All messages can be logged for later reference.

There are two means of communications with StarWatch, both selected for their universality and ease of use. The first is the Advanced Mobile Phone System (AMPS) cellular service, provided in metropolitan areas throughout the United States, as well as a number of other countries. Cellular telephone service is a relatively low cost, high quality, and fully maintained communication network. Costs for cellular service vary by region and are established by individual providers.

Common to them all are a fixed monthly fee (typically under \$50), a per message cost above the monthly allotment (typically about \$0.40) and roaming fees for communications outside the home coverage area.

The other communication channel to be provided by StarWatch is the Orbital Communications Corporation ORBCOMM satellite data messaging service to begin operation by the end of this year. This service will provide worldwide messaging, from any point to any point using low earth orbit satellites and small low power transceivers. ORBCOMM launched two of the eventual thirty-six satellites in April 1995, and are currently going through a satellite and communication check out phase. In October and November ORBCOMM will conduct field (beta) tests of the service with a number of its resellers, including Advanced Research Corporation, and will offer commercial service before year's end.

Costs for ORBCOMM are established by individual ORBCOMM resellers, but include a monthly charge per subscriber communicator (less than \$40) and a per message charge (position messages less than \$1).

For cellular operation, StarWatch uses the Trimble Navigation GPS/Cellular Messenger unit, a commercially available GPS sensor providing high quality communication via cellular telephone. The unit contains a Trimble six-channel GPS sensor that provides time, position, velocity, heading, and status data using the Trimble ASCII Interface Protocol. It

accepts commands for polling and configuration, including notifying the operator when an asset has left an area. The unit physical characteristics are given in Table 1.

Table 1. Trimble Messenger Physical Characteristics

| | |
|-----------|---|
| Power | 11-16 VDC, 3 W receive, 19 W transmit |
| Size | 26 cm x 11.7 cm x 4.8 cm (10.25 " x 4.60" x 1.89") |
| Weight | 1 kg (2.2 lb) |
| GPS | Tracks 8 satellites |
| Interface | Serial RS-232, 9600 baud Comm. Bell 212A (1200 BPS DPSK) |

There are four manufacturers of ORBCOMM subscriber communicators (SC), the transceivers used to communicate with the ORBCOMM satellite system.

Elisra Electronics (Israel)
 Magellan Navigation (San Dimas, California)
 Panasonic Matsushita (Japan)
 Torrey Science (San Diego, California)

Although each of their product offerings is unique, there is a commonality of features. Each will offer GPS positioning. In addition, ORBCOMM provides a coarse positioning capability by means of a Doppler ranging method using their satellites. StarWatch is able to operate with any of these units. ORBCOMM transmits over the frequency range 148.000 to 150.050 MHz and receives over the range 137.000 to 138.000 MHz. The transceivers communicate at 2400 bps uplink and 4800 bps downlink. A presentation of physical characteristics for the individual manufacturers is given in Table 2.

Table 2. ORBCOMM SC Physical Characteristics

| | Torrey Science Trakker 211 | Panasonic KX-G7000 | Elisra EL-2000 |
|-----------|--|---|--|
| Power | 12-24 VDC, 6 W | 12-24 VDC 120-240 mA receive 1.6 A transmit | 12.8 to 36 VDC, 95 mA standby 2.5 A transmit |
| Size | 10.2 x 10.2 x 48.3 cm (4 x 4 x 19") | 15 x 15 x 5.3 cm (5.9 x 5.9 x 2.1") | 20.5 x 12.4 x 6.1 cm (8 x 4.9 x 2.4") |
| Weight | not available | 0.85 kg (30 oz) | 0.96 kg (34 oz) |
| GPS | Yes | Yes | Yes |
| Interface | RS-232 Analog/ digital I/O | RS-232 | RS-232 Analog/ digital I/O |
| Other | Weatherized Battery Intelligent power management | Weatherized Sleep mode | Weatherized Battery Sleep & standby modes |

Note: Information on Magellan unit not available at time of publication

In addition to the subscriber communicators described above, CypherComm (Colorado Springs, Colorado) is offering a secure version of the ORBCOMM. It will offer encrypted data messaging, providing increased security

for locating assets used in law enforcement, military, and high security applications.

StarWatch will be released in two versions: a Cellular version available in October 1995 and an ORBCOMM version in December 1995, coincident with ORBCOMM service. In addition for each major version, StarWatch will be packaged into a low cost demonstration version, called StarWatch Track One, which will have all the features of StarWatch, except that it will only be able to track one asset. It will be bundled with the StarWatch software, EtakMAP USA, and one tracking unit. User's may upgrade to the full StarWatch for an additional fee.

FEATURES AND BENEFITS

StarWatch offers flexibility and convenience in the tracking of assets anywhere. It requires only a PC and a modem, therefore not only can asset location be performed at a dispatch center, but in a manager's office or in a hotel room. Asset location can be performed by a number of people simultaneously. Thus StarWatch offers ultimate flexibility for any organization tracking assets.

With high quality Etak maps, StarWatch provides full continental United States highway coverage with the EtakMAP USA data base and detailed street level coverage with any of its more than 280 Etak coverage area maps. StarWatch's ORBCOMM version release will provide both geo-coded locations ("Show me the location of 123 Main Street") and reverse geo-coded locations ("What is the nearest set of cross streets to my asset?").

StarWatch will offer an object linking and embedding (OLE) interface with its ORBCOMM Version release. This open architecture interface provided by Microsoft Windows, allows disparate programs to communicate with one another easily and in real-time. This feature allows StarWatch to serve as a location engine for other commercial programs for maximum flexibility of operation and use. For example, a user may use the relational data base management program Microsoft Access to define a data base application for tracking shipments, then connect it to StarWatch via OLE to provide positioning information. Information that can be returned from StarWatch include map objects as well as geographic information like city, state, zip code, nearest intersection, and street address range.

StarWatch's ability to transmit text data gives it a powerful capability for data collection. StarWatch can be used as a data collection system.

When integrated with CypherComm's secure communication module, ORBCOMM provides the security of tracking sensitive and high value assets. Position, time, and other message data is encrypted prior to transmission so that only but the intended recipient has access to the information.

LIMITATIONS

Cellular tracking with StarWatch, although offering twenty-four hour access, is restricted to areas of cellular coverage. Assets outside this range cannot be contacted until they move back in the coverage area. The Trimble unit is not weatherized or battery powered for full portability. Advanced Research is pursuing ways of packaging the Messenger so that it will be weatherized, battery powered and portable.

ORBCOMM satellite communications with only two of the eventual thirty-six satellites in operation provides contacts over a six to eight hour period each day. This coverage will continue into mid-1997 until the additional satellites are scheduled to be launched. Although the service is not continuous, it is more than adequate to provide global positioning of assets on a once or twice a day basis which is sufficient for many asset location applications.

APPLICATIONS

Applications of StarWatch include tracking high value property and cargo, tracking stolen vehicles, monitoring shipments, managing high value rental property, and tracking long haul trucking shipments. With its ability to transmit message data, StarWatch serves as an information system as well as asset location system. StarWatch is available for both end users and for systems integrators that focus on various market niches. StarWatch offers an attractive asset location engine to existing niche market transaction software. The OLE interface expedites the integration of StarWatch with other Windows-based applications.

TEST PROGRAM

Advanced Research is scheduled to conduct field tests of StarWatch Cellular in September and October and tests of StarWatch ORBCOMM in October and November. Test applications are identified in Table 3.

Table 3. StarWatch Test Applications

| Test Organization | StarWatch Application |
|--------------------------|--|
| Horse transport company | Dispatching rigs throughout the US |
| Concrete mix company | Tracking trucks into mountainous areas |
| Courier company | Tracking courier vehicles that leave radio coverage area |
| Moving and storage firm | Monitoring trailer shipments |
| Protective services firm | Monitoring high value property against theft |

CONCLUSIONS

StarWatch uses GPS technology, along with advances in communications and PC technology to provide a low-cost, flexible, portable, and easy-to-use asset location system that can be used anywhere. Focusing on low message rate applications by means of cellular and ORBCOMM satellite communication technology, StarWatch user's are assured they can be up and running immediately without the expense and effort of installing a fully customized system.

ACKNOWLEDGMENTS

The author wishes to thank Glenn Marshall for reviewing this paper and providing valuable comments.

REFERENCES

1. Lavrakas, John W. and Marshall, Glenn C., Where Is It and Where Is It Going?: A Comprehensive Look at GPS Asset Location, GPS Solutions, Vol. 1, Num. 1, pp. 13-22.

The XR5-PC12 – Position and Time/Frequency From a Single Plug-in Module

Tony Haddrell
Navstar Systems Ltd.

BIOGRAPHY

Tony Haddrell Bsc ARCs is General Manager of Navstar Systems Ltd, a supplier of radiolocation equipment based in Northampton, UK. He has been associated with GPS Technology and Development for more than 10 years initially with Racal-Decca and latterly Technical Director of Navstar Limited.

ABSTRACT

Navstar's XR5-PC is a new addition to the NavSymm XR5 product family. The module is a plug in PC-AT® expansion card and provides full 12-channel capability in mobile, base station or timing modes.

The module supports rapid data transfer to applications running on the host PC, whilst appearing as a standard IBM comms port to the operating system. This allows the direct use of standard drivers available in Windows®, OS 2® and similar environments.

The paper describes the product and its applications in the field and development environments.

INTRODUCTION

The NavSymm XR5-PC12 is a 12 channel professional quality L1 C/A code GPS receiver on a short length IBM-PC® standard expansion board. The board uses Navstar's proprietary XR5 technology and was developed in response to the ever growing need for faster raw data extraction from the GPS receiver.

The result is a compact module which finds use in a number of applications, especially those involving high integrity and throughput, such as real time cm accuracy work, and differential base stations.

The module also makes use of NavSymm's timing and synchronising expertise, providing accurate Time of Day data, and in later versions, frequency reference output.

OUTLINE

This paper describes the XR5-PC12 in terms of its hardware and software, and highlights some of the advantages and features of using GPS integrated within a PC environment. A short introduction to the XR5 technology stream architecture and performance is also included. Finally, some performance measurements from the XR5-PC12 are presented, of interest to those seeking raw GPS data at high data rates.

XR5 TECHNOLOGY

Navstar's XR5 technology is based upon the company's well proven GPS receiver architecture, and is implemented using a number of in-house designed Integrated Circuits. All development and product design is carried out in the company's Northampton, UK, facility, allowing both rapid response to new requirements, and field support by the design team where necessary.

The quality and accurate reproduction of the designs is assured by manufacture in our own factory, on the same site.

ARCHITECTURE

Figure 1 shows a block diagram of the architecture. In the XR5-PC12 module, the input/output and Power Supply functions are integrated onto the ISA-bus compatible plug in card, and the RF section is carried on a daughter board.

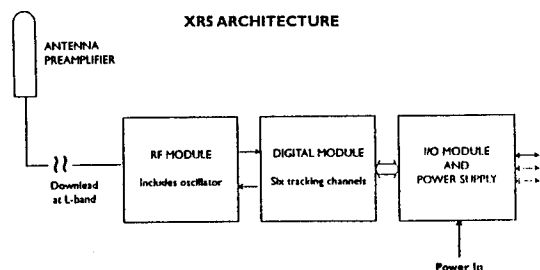


Figure 1

ANTENNA

The architecture provides 12v DC for a L1 active antenna. The current drawn is both limited to protect from fault conditions, and monitored to provide alarm warning if the antenna is disconnected or faulty.

RF CIRCUITS

Figure 2 provides the frequency plan and layout of the RF subsystem. XR5 was designed to provide outstanding rejection of unwanted signals, which is becoming more and more a problem as GPS finds its way into more hostile environments.

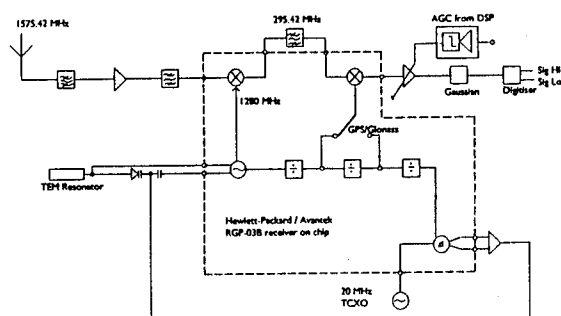


Figure 2

The L-band section of the receiver is realised largely in the ROC (Receiver on Chip) device, fabricated in "Super Silicon", minimising power requirements whilst maintaining maximum anti-jam capabilities.

Filtering at both L-band and IF is used to provide high out of band rejection, the former being an in house designed special component. The IF, AGC and Digitising circuits are implemented in a second chip using mixed CMOS technologies. Interface to the Digital circuits is provided in two level "over sampled" digital form.

The RF module also hosts the reference oscillator, a high performance TCXO, and generates reference frequencies for the digital circuits as well as phase locking all of the local oscillator components.

DIGITAL CIRCUITS

Figure 3 is the block diagram of the Digital part of the receiver. Central to the architecture is the Digital Signal Processing (DSP) ASIC, realised in CMOS and providing 6 channels of code generation, correlation and code and carrier tracking, as well as signal sampling and support for the Motorola 68020 processor and peripheral circuits.

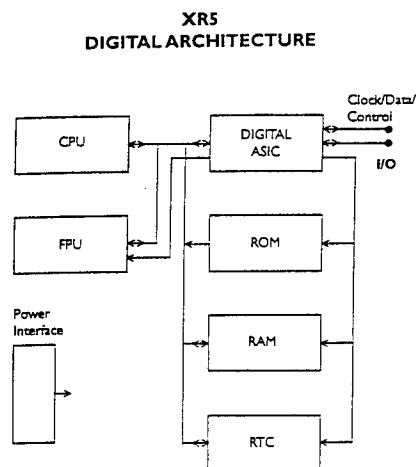


Figure 3

The DSP is configurable to provide various channel architectures and processor support. In the XR5-PC12 two DSPs are used to provide 12 parallel tracking channels and the I/O capability to support the ISA bus circuitry and serial ports. One of these provides memory management and the logic support for the processor and its coprocessor.

The DSP chip also contains circuitry to output an accurate 1pps signal, under processor control.

A Real Time Clock (RTP) is included, as is backed up RAM, to enable the receiver to rapidly provide a first fix, based on stored data from previous sessions, and the time and date.

SOFTWARE

Figure 4 is a representation of the software modularity. The software routines provide acquisition and tracking of the GPS signals, using the DSP hardware, measurements, data demodulation and storage, and satellite prediction calculations.

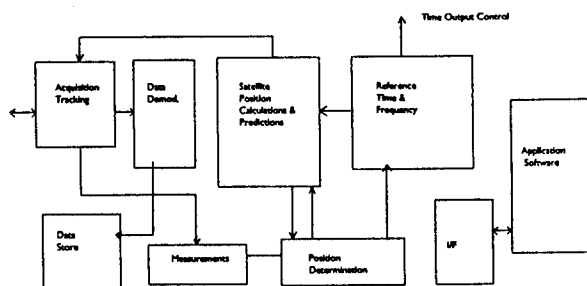


Figure 4

Position and Time determination is carried out using a Kalman filter, with update rates at up to 4 per second.

Serial and Parallel I/O are supported using the DSP chip on board interfaces. Included is Navstar's powerful interface protocol, enabling rapid application development and debugging.

THE XR5-PC12 DESCRIBED

GENERAL

The XR5-PC12 is a plug in module which fits into an IBM-PC compatible PC ISA bus expansion slot. The board does not occupy the full slot length, being only 7.5 inches (190mm) approximately long. It needs two slot widths. This form factor makes the XR5-PC12 compatible with most slimline and full size desktop PCs, and some larger portable machines. Many industrial PCs also provide ISA bus expansion slots.

The module has a standard PC expansion slot rear panel, which houses the connectors for the two serial ports and the GPS antenna. An LED showing status of the module is also provided here.

The ISA bus connection provides power for the XR5-PC12 from the host computer, and data transfer across the bus in a number of modes. Whilst this is the usual port for data transfer, it is

not a requirement for operation, and the module may be used without a host PC if arrangements for provision of power are made.

On the ISA bus, the XR5-PC12 appears as an I/O device and occupies 8 bytes of I/O space. Although a 16 bit card, all data transfers are 8 bit only. Address selection is by DIP switches on the XR5-PC12, offering a choice of 8 locations. The board supports interrupt transfers between itself and the host PC, but can also be configured for streaming data to achieve maximum data rates (over 70k baud!). The interrupt to be used for the former method is selectable on the module.

The module carries a 12 channel GPS receiver, implemented in XR5 technology as described above. A 12 volt DC supply is present at the antenna connector to power the preamplifier in the remote antenna assembly.

The XR5-PC12 is designed around ease of communication to its host devices, and provides a new level of fast data access for applications such as Real Time Positioning. One such improvement is the board's ability to emulate the ISA bus side of a standard PC serial port. This allows data transfer using standard operating system drivers (such as those provided with MS-DOS®, Windows®, OS2® etc.), without being limited by baud rate restrictions (since the serial side of the port is not there). As will be seen below, the data modes provided represent a major improvement in the I/O capability of the GPS receiver.

XR5-PC12 HARDWARE

The PC12 provides a fully featured, high resolution 12 channel L1, C/A code GPS receiver. It utilises FLASH memory for programme retention, and can therefore receive software upgrades via its host computer. Battery backup is provided for critical memory, and the real time clock. For a specification of the receiver, please refer to product literature.

At the heart of the receiver's high data throughput is the Motorola 68020 processor, with a coprocessor to take care of the floating point calculations. Processing in the XR5-PC12 is autonomous, and does not use any of the host computer's resources.

Power supply smoothing is included, to alleviate the effects of the "dirty" power rails often found inside PCs. Similar attention has been paid to the Electro Magnetic Compatibility aspects of being located within a computer.

In addition to the communication ports (RS232, RS422 and ISA bus) the hardware supplies the 1pps signal for timing applications, and a TDMA transmit control function for datalinks. This feature is important if using the XR5-PC12 for Real Time DGPS base station applications.

COMMUNICATIONS

As noted above, the design concept for the XR5-PC12 is for a communications engine. Consequently, the module offers two serial ports and two possible ISA bus ports, together providing maximum flexibility for application development and high performance. The ports are referred to as A, B, C1 and C2, and are described in that order below. All three ports are set-up and operate independently of each other.

PORT A is a partially handshaked serial port conforming to the RS232D standard. It has a male DB9 connector, and can be configured for a number of interface modes and rates (described below).

PORT B is a non handshaked RS422A standard serial port, using a female DB9 connector on the rear panel. It too can also be configured in several ways. This port also provides the 1pps pulse, a 100 microsecond TTL level signal synchronised to UTC. Optionally the output can be double pulsed on the UTC minute marker, or configured to be a 10pps signal.

Both serial ports can be operated at all standard baud rates up to the maximum of 19,200.

The ISA bus port may operate as either C1 or C2. PORT C1 implements the COMM port emulation described above. Depending on the user defined setup, this port can utilise a 512 byte input and output FIFO buffer, resulting in rapid data transfer, under control of the host PC. Navstar's supplied CDU programme uses this mode to communicate with the XR5-PC12 when running on the host PC.

PORT C2 is a data streaming 8 bit parallel port implemented on the ISA bus, and occupying register space not used within the register set of C1. Thus it can operate independently of C1 whilst occupying the same 8 byte I/O block.

The module can be requested to swap the C2 function over to C1 if required. Streaming data achieves the ultimate in data transfer rate, but requires an application on the host PC that is capable of maintaining such a rate. The information to be streamed is requested from the

XR5-PC12, which then outputs as fast as possible using a FIFO structure to isolate the module's processor from the output task.

PROTOCOLS

Various communication protocols are supported by the various ports. These range from simple ASCII status messages to complete question and answer sessions using the data monitor facility. Table 1 shows the availability of these protocols on each port. The port characteristics are set-up from the CDU or application programme, and are remembered in critical memory during power down. A mechanism is provided to enable the user to return to CDU mode if lock up within the embedded application prevents the host from communicating with the GPS.

The CDU interface is available on both the ISA bus and one serial port. This enables the user to run Navsymms CDU software on either the host PC or an external one. The CDU programme implements the Data Monitor debugging and development toolset, so an application programmer can debug the GPS part of his programme from outside of the system if necessary.

| | Port A | Port B | Port C1 | Port C2 |
|-----------------------------|--------|--------|---------|---------|
| CDU Interface | | ✓ | ✓ | ✓ |
| RTCM-104 Interface | ✓ | | | |
| Streaming Data Transfer | | | ✓ | ✓ |
| ASCII Status Output | ✓ | ✓ | | |
| TDMA Modem Control | ✓ | | | |
| Time of Day Message Output | ✓ | ✓ | | |
| One Pulse per Second Output | | ✓ | | |

Table 1 Protocol Availability

PERFORMANCE

The raw measurement and positioning performance of the XR5-PC12 follows closely that of the other members of the XR5 family. The following figures show the results of measurements taken during development of the product, with the host computer being a 486-DX machine running a Data Monitor session to retrieve the wanted data. Data was taken at once a second.

Figure 5 shows the performance in real time differential GPS mode, using a zero baseline and two XR5-PC12s. Similar results were obtained with a variety of mobile receivers, the intent being

to test performance of the XR5-PC12 as a base station.

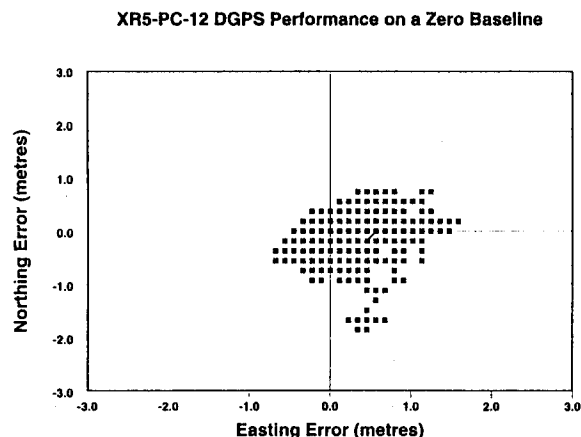


Figure 5

Figures 6 and 7 show the raw measurement performance of code and carrier respectively. The RMS figures for the single difference plots are 15cm for code and around 1 mm for carrier.

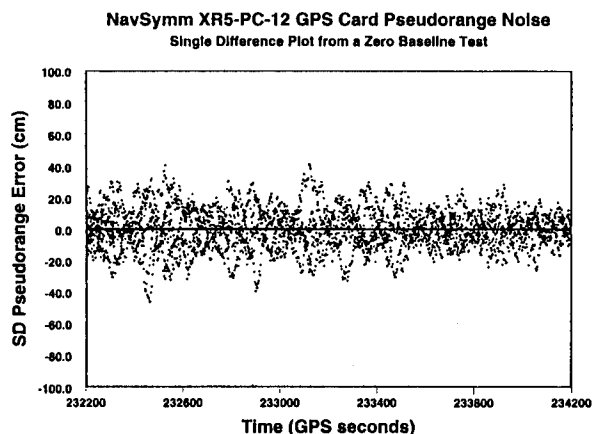


Figure 6

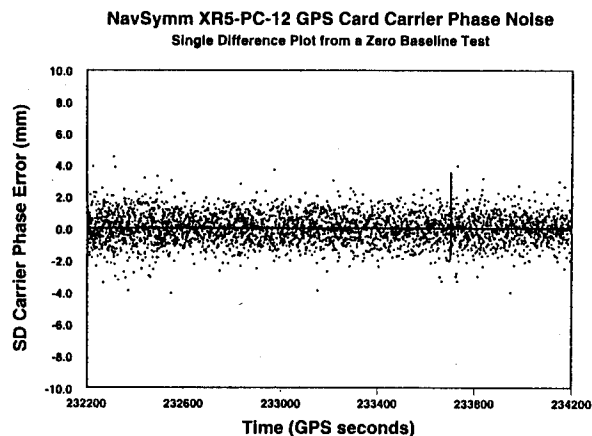


Figure 7

Figure 8 is part of a plot taken from an exercise using the XR5-PC12 in an application environment. In this case, the board was mounted in a small ISA-bus frame along with a single board computer (386 processor) and a power supply unit. The computer was running Real Time Positioning software from Premier GPS. The trial took place on an airfield and consisted of multiple laps of a pre-marked track, at speeds of up to 60mph. The Figure shows the repeatability in height from a number of passes over the same ground, after a rapid static initialisation at the beginning of the trial. The base station was also an XR5-PC12, and the datalink used Navsymm UHF radios. The plot shows repeatability of 1-3 cm in height, some caused by the inability of the driver to follow exactly the same track each time. This demonstrates a potential application of the XR5-PC12, and its accuracy when used in this manner.

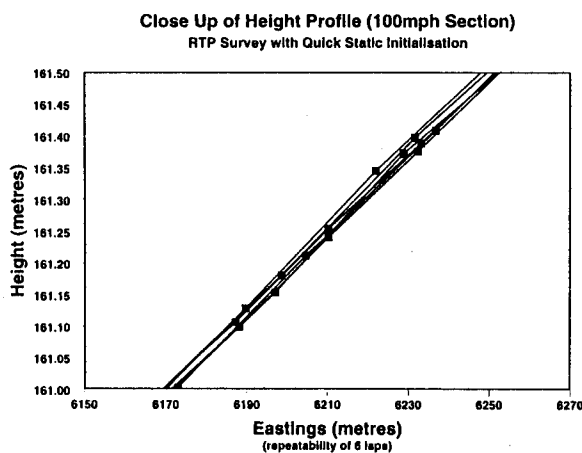


Figure 8

CONCLUSION

This paper has introduced the XR5-PC12 and described some of its features and performance. The product finds use in a wide variety of applications where compatibility with standard PC architecture and software is needed.

ACKNOWLEDGEMENTS

IBM-PC®, OS2® and PC-AT® are trade marks of IBM

MS-DOS® and Windows® are trademarks of the Microsoft Corporation.

REFERENCES

The XR5 Technology Stream
T. Haddrell

Proceedings, ION-GPS-92

Ashtech RTZ, Real-Time Kinematic GPS with OTF Initialization

Sergei Gourevitch, Frank van Diggelen, Xinhua Qin, and Mark Kuhl
Ashtech

BIOGRAPHY

Sergei Gourevitch is a Chief Scientist with Ashtech. Dr. Gourevitch was awarded a Ph.D. in experimental particle physics by Case Western Reserve University. After a term of post-doctoral research at Brandeis University, he joined the radio interferometry group at M.I.T. While at M.I.T. he was part of the group which demonstrated the feasibility of precise, carrier phase GPS geodesy and pioneered the technique. He made important contributions to all areas of GPS geodesy and navigation.

Frank van Diggelen is the Ashtech Marketing Manager for OEM and Navigation products. Dr. van Diggelen received his Ph.D. in Electrical Engineering from Cambridge University. His GPS experience includes the development of RAIM and Fast Ambiguity Resolution techniques for the US Coast Guard and US Air Force respectively. Before GPS he worked in the South African mining industry, and was a navigation officer aboard a South African Navy ship.

Mark Kuhl earned both his B.S.E.E. and M.S.E.E. degrees in 1988 and 1990 from Ohio University. Throughout the last three years of his studies he was employed by Avionics Engineering Center at Ohio University where he worked on projects to augment flight navigation using GPS. Mr. Kuhl has been employed with Ashtech for the past four years as a Design Engineer and is Product Manager.

Dr. Xinhua Qin is a GPS algorithm software group manager and product manager at Ashtech Inc. He received his Ph.D. degree in Aeronautics and Astronautics from Stanford University in 1991. He worked on the Stanford Relativity

Gyroscope Experiment, also known as the Gravity Probe-B program, from 1987 to 1990. Since 1991, Dr. Qin has been with Ashtech and working in the software development of precision GPS and attitude determination systems.

ABSTRACT

Ashtech announces the RTZ real time Kinematic system. This product essentially combines the world leading ASHTECH Z-12 receiver with the leading PNAV post-processing program to provide "in the box" real time solutions that equal the post-processed solutions achievable with Z-12 and PNAV. This system is the heart of an ever growing number of "vertical" applications such as **GPSTopo** (a topographical mapping system), **SEISMARK** (a seismic survey stake out system) and **MINE SURVEYOR** (a survey system optimized for open pit mines. The system is also being used for OEM applications requiring real-time centimeter accuracy.

We wish to make two main points in this paper:

1. Z-12 quality is the key to the success of this product.
2. Time to Fix is not an adequate quality indicator for "On the Fly" integer ambiguity resolving systems. We suggest a better indicator and show its use for the RTZ product.

The Z-12 SNR Advantage Yields:

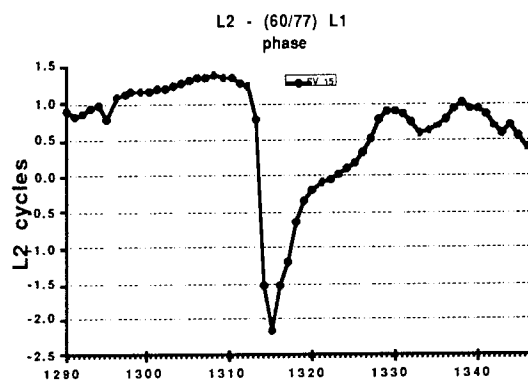
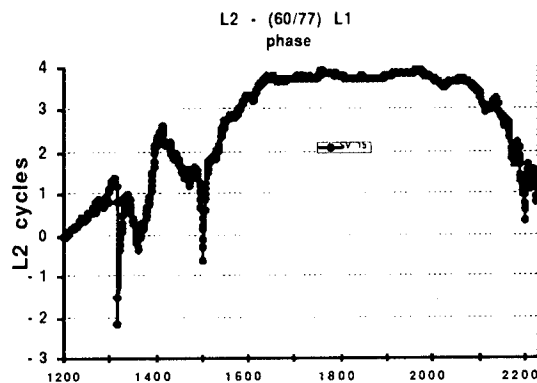
- Lower Noise
- Quicker Acquisition/Settling Time
- Ability to Track Rapidly Changing Ionosphere¹

¹ Yes. The ionosphere is back! (San Jose Mercury News - August 28, 1995). The eleven year sunspot cycle has just passed the point of least activity. Ionospheric interference will increase through the next five years.

All at the Same Time!

At previous IONs we've talked about the Z-12 SNR advantage and showed how quiet the data was; low residuals for the observables. We also talked about the improved settling time. (The amount of time it takes a transient, such as the one experienced on signal acquisition, to die away is proportional to the inverse noise bandwidths of the tracking loops.) In this paper , we would like to mention some of the other Z-12 advantages.

Tracking of Rapidly Varying Ionosphere



The plot on the right is a "blow up" of the largest transient in the full plot shown on the left. The change of 3 L2 cycles in ten seconds in the L2 - (60/77) L1 phase is equivalent to a change in the L1 delay of 6 L1 cycles in ten seconds which is over a meter in 10 seconds. And, the ionospheric delay changed from essentially zero rate to this large rate of change in less than 10 seconds. Cross correlating receivers will not track this much ionospheric variation. The Z-12 "P" variables tracked, with no cycle slips, throughout this period of large transients.

First, the Z-12 unequaled SNR advantage allows it to track rapidly varying ionosphere

We were recently sent some data, which was obtained by a satisfied customer, taken in an area of high ionospheric activity. The following plots demonstrate the ability of the Z-12 to continue tracking the "Y-buster" observables under such conditions.

Another area where the Z-12 is superior is in the area of resistance to jamming. The following table summarizes an independent study² where geodetic receivers from the top four manufacturers (Ashtech, Leica, Allan Osborne and Trimble) were switched on near Rotterdam Harbor Entrance, where users have reported the inability to track GPS satellites. The suspected source of the interference is a radio transmitter which is part of the harbor infrastructure.

% of Visible Satellites Successfully Tracked

| Receiver | Near Rotterdam Harbor Entrance | 1 km from Harbor Entrance | 2 km. from Harbor entrance |
|--------------|--------------------------------|---------------------------|----------------------------|
| Ashtech Z-12 | 100% | 100% | 100% |
| B | 0% | 55% | 67% |
| C | 0% | 63% | 88% |
| D | 0% | 0% | 0% |

² Sluiter, P.G. and Haagmans, M.E.E.; Comparative Test Between Geodetic Y-GPS receivers. Susceptibility to Radio Frequency Interference. GPS Nieuwsbrief, May 1995

Note:

1. The engineers who conducted this test did nothing to purposefully jam the receivers. This performance is the normal performance in the locations tested.
2. Since this test was done, Ashtech Z-12 technology has been improved to give 30 times more jam immunity.

HOW DO WE JUDGE ON THE FLY AMBIGUITY RESOLVERS?

We have seen it suggested that the appropriate specification is TTF (Time to Fix ambiguities.) Indeed we have seen product specifications where TTF is indeed the sole specification.

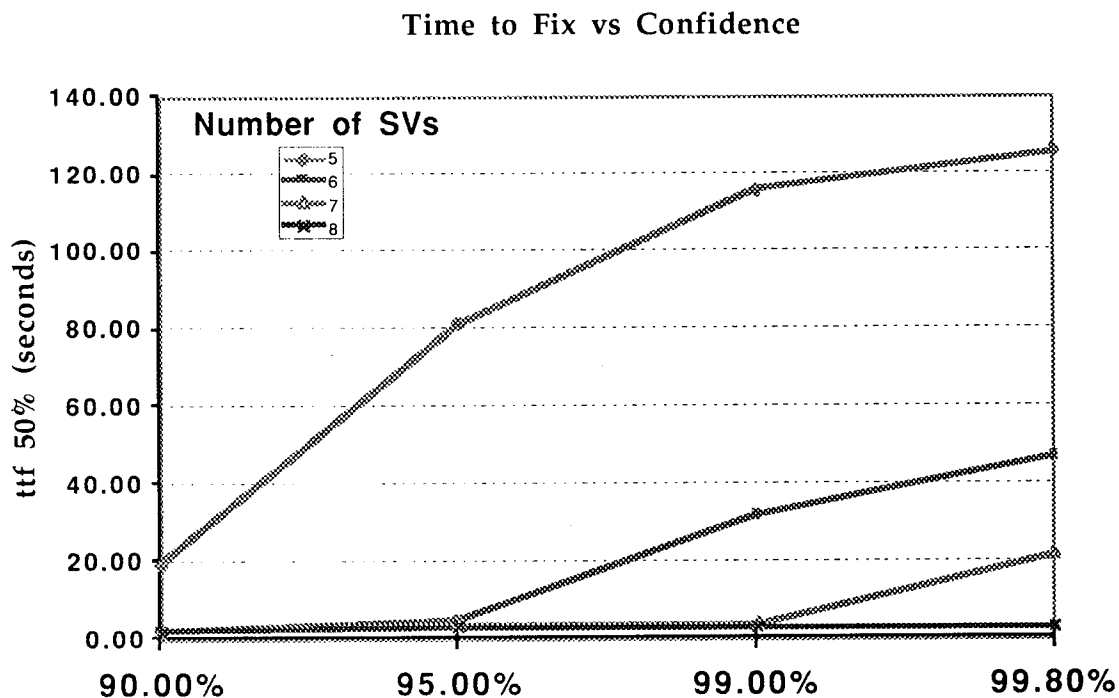
TIME TO FIX IS NOT ENOUGH!

WHAT PERCENTAGE ARE CORRECT?

Suppose manufacturer B's OTF system determined the integer ambiguities 40% faster than manufacturer A's system. However, "B" was correct 70% of the time while "A" was correct 99.8% of the time. "B" would be useless for any kind of surveying work but would win 70% of the head to head "shoot-outs" (where a customer pits one system against another).

Clearly, the TTF is useless without also specifying a confidence level.

Consider the next figure:



We've plotted the curves from our data sheets. Here, one chooses the confidence level (horizontal axis) and the curves tell the user how long it typically takes to determine ambiguities. There are curves for different numbers of observed satellites. These curves are based on actual data under a wide range of conditions.

We see that if there are 8 satellites being tracked, the result is almost instantaneous, as is the case for 7 satellites if 99% confidence is sufficient.

The Z-12 allows the user to select a confidence level, then the system determines integer ambiguities as fast as possible while guaranteeing the confidence level.

The following table summarizes the data which was used to determine the last figure as well as some new data (12,000 test in all) . These are averages over expected satellite number, baseline length, etc.

Average Ambiguity Resolution Speed

| Confidence Level | Average Speed (seconds) |
|------------------|----------------------------|
| 90% | 2 |
| 95% | 5 |
| 99% | 40 |
| 99.8% | 65 |

CONCLUSION

Not only do we believe that our RTZ system is unmatched in centimeter level real time navigation, we also believe that the criteria by which such systems are judged need to reflect the confidence that the obtained solution is correct.

We suggest that the above method, of showing both time to fix ambiguities and actual confidence, provides criteria by which all real-time centimeter systems should be compared.



Session C1

Space Applications

Chair:

Dr. Willy Bertiger

Jet Propulsion Laboratory

An Autonomous GNSS-based Orbit Determination System for Low-Earth Observation Satellites

Jorge Potti, Juan Carlos Carmona, and Pelayo Bernedo
GMV S.A.

Pierluigi Silvestrin
ESA/ESTEC

BIOGRAPHIES:

Jorge Potti (e-mail: jpotti@gmv.es) is Project Manager at GMV (Spain). He received his MS degree in Aeronautical Engineering in 1986 from the Polytechnic University of Madrid (Spain) where he gained the third national award of university studies. Since that time he is working at GMV (Grupo de Mecánica del Vuelo) in the research and development group of the Flight Dynamics and Avionics Division. At present his major areas of research are satellite guidance, navigation and control, including GPS applicability and operational issues.

Juan Carlos Carmona received his MS degree in Physics Science, Control Systems branch, in 1985 from the University of Madrid (Spain). From 1985 to 1990 he worked in the design of real-time digital control systems for chemical plants. In 1990 he joined the Flight Dynamics and Avionics Division in GMV, where he specialized in advanced guidance, navigation and control space systems and signal and data processing.

Pelayo Bernedo received his MS degree in Aeronautical Engineering from the Polytechnical University of Madrid, Spain in 1988. He worked for McDonnell Douglas in the MD-80 twinjet series within the structures group. Since 1991 he works in the Simulation Division in GMV, where he specializes in GPS based navigation for airborne applications and tracking systems for fleets of ground vehicles.

Pierluigi Silvestrin is a Senior Systems Engineer in the Earth Observation Preparatory Programme (EOPP) Division of the European Space Research and Technology Centre (ESTEC) in Noordwijk (The Netherlands). He graduated in Electronic Engineering at the University of Padova (Italy) in 1985, specialising in control systems design. After working for one year at the Joint European Torus (JET) in Abingdon (UK), he joined in 1987 the Attitude and Orbit Control Systems Section of ESTEC. In 1989 he joined the EOPP Division, where he is presently responsible for studies of space systems and supporting technologies for future

Earth observation missions of the European Space Agency.

ABSTRACT:

Earth observation missions which use direct broadcast links for data distribution to local users will benefit from the on-board real-time knowledge of the orbital position, which can be broadcasted for geolocalisation of the observation. The autonomous orbit determination (OD) of the satellite would also reduce the operational costs of the mission through the reduction of the ground stations utilisation.

The European Space Agency (ESA) and GMV (Grupo de Mecánica del Vuelo) are currently investigating a GPS-based OD System for Earth observation missions, using the MetOp mission as a study case. The MetOp system is a European satellite series for operational meteorology and climate monitoring from the polar orbit which will complement the NOAA Polar Orbiting Environmental Satellite System. It is being built for Eumetsat which will operate it after launch in 2001.

This paper reviews and analyses the system requirements leading to orbit, attitude and datation requirements and presents some preliminary analyses on the applicability of GNSS to the autonomous orbit determination (OD) of MetOp including investigations of estimation techniques for attenuating the disturbing effect of selective availability and of the need for an on-board orbits dynamics model and its relevance. A GPS-based OD algorithm is defined in detail. Software implementation in a state-of-the-art simulation system allows to derive detailed performance and sensitivity analysis estimates of the resulting system and the hardware demands of the proposed algorithms.

The proposed GPS-based OD system provides real-time orbit determination to the local users in the order of 15 to 30 m accuracy which is not only far better than what provided by conventional methods but also implies a significant decrease in the operations for the local users.

1. INTRODUCTION

In the frame of the Earth observation satellites carrying high resolution radiometer, and in particular of the MetOp mission, we are primarily interested in solving the problem of pixel localisation, i.e. the knowledge of what point over the surface of the Earth a given instrument is looking at. Analysis have proven that the orbit knowledge is one of the critical contributors to the total pixel localisation error. Initial MetOp design assumes the all-time availability of an orbit knowledge with a precision of order of 900 m (max. values) where this value accounts for both the classical ground-based orbit determination accuracy and the accuracy of the necessary propagations which must be performed by the local users.

With GPS there are obvious potential benefits: no need for ground-based orbit determination, no need for distributing the orbital parameter updates to the local users and no need for the local users to perform orbit propagations. In addition, an autonomous GPS-based OD algorithm would also dramatically increase the real-time orbit determination accuracy. The design of such an autonomous GPS-based OD system must consider the primary objective of solving the problem of pixel localisation error. Current system requirements claim for a pixel localisation error of 1 Km for nadir-looking directions. Taking into account the problem geometry one can deduce that real-time OD errors below 20 to 30 m make the contribution of OD errors to the total pixel localisation error almost negligible. There is an obvious trade-off to be performed between the algorithms complexity (being an on-board application it is particularly important to minimise the hardware demands) and the orbit determination accuracy and efforts have been directed to keep system simplicity while increasing the orbit positioning accuracy to the maximum possible extent.

2. PROBLEM CHARACTERISATION

2.1. MetOp-1 reference orbit

MetOp-1 will operate in the sun synchronous near circular orbit specified in table 1.

| Orbit | |
|--------------------------------|-----------------------|
| • Type | Polar sun synchronous |
| • Repeat cycle | 5 days (71 orbits) |
| • Local solar time (des. node) | 9.00 h |
| • Longitude asc. node | 0.0 deg |
| Mean keplerian elements: | |
| • Semi-major axis | 7,197.939472 Km |
| • Eccentricity | 0.001165 |
| • Inclination | 98.704663 deg |
| • Right ascens. of asc. node | 55.835595 deg |
| • Argument of perigee | 90.000000 deg |
| • Mean anomaly | 270.13359 deg |

Table 1: MetOp-1 reference orbit

2.2. Basic observables

The GPS receiver is the hardware in charge of processing the input GPS signal in order to the pseudorange and integrated Doppler (continuous carrier phase) measurements (for every receiver channel).

2.3. Orbit Determination Concepts and Algorithms

Different tracking concepts might be applied, including GPS based OD, GLONASS based OD, dual GPS/GLONASS based OD, dual GPS/Inmarsat based OD, and combined GPS/GLONASS/Inmarsat based OD.

This paper focuses on the investigations and analyses that have been performed only for the GPS based OD concept. For the particular case of GLONASS the achievable performances will be similar to that provided by GPS improved by switching off some errors sources, namely the selective availability effects.

The GPS based OD will be based on a dynamic approach using a Kalman filter: a MetOp-1 position and velocity evolution prediction model (i.e., an orbit propagation model) will be used. This approach is preferred to the position fix approach because some effects of the errors in the measurements are mitigated in our proposed approach due to the availability of a quite accurate orbit dynamics model, resulting in a significantly better OD accuracy.

2.4. GPS-based OD Performance Drivers

The accuracy of the GPS based OD depends mainly on the following:

- *Ephemeris of the GPS satellites*: the orbital parameters of the GPS satellites broadcasted in the navigation message allow the user to calculate the satellite position with only a certain degree of accuracy. This accuracy is degraded by the US Department of Defence with the so called Selective Availability (SA) up to different levels. Apart from that, both the satellite orbital parameters and the clock correction coefficients are updated approximately once every 4 hours and their validity period extends for 6 hours. Ephemeris data are given for a reference time and so the accuracy degrades as a function of time with respect to the reference time.
- *GPS satellite clock errors*: the Control Segment upload code phase adjustments so as to maintain all GPS satellites times. The fluctuations of the GPS satellite clock are calibrated by the control segment by using a second-order polynomial, the coefficients of which are included in the corresponding GPS navigation message. The GPS receiver will use this polynomial function to correct

the transit time of the GPS signal. The accuracy of this correction is limited and may be degraded with SA.

- **Selective Availability:** SA is an intentional degradation of the broadcast GPS satellites ephemeris (i.e., orbital elements and atomic clock parameters information) and/or a dithering of the oscillator on-board the GPS satellite that results in degraded (single) receiver positioning accuracy. Such degradation is effectively removed using differential techniques, but these are not applicable to our case as they would require continuous communication from ground to satellite. In order to improve the performances of the on-board GPS based OD function, an on-board mitigation of the SA effects is required: due to the identified stochastic characteristics of the SA, an on-board estimation of the SA is required. This issue will be further discussed in section 4.
- **Ionospheric propagation:** its effect is a time delay in the GPS transit time (from GPS satellite to user spacecraft) which will depend on the Sun, spacecraft and GPS satellites position, solar activity, etc. In our case the orbit is at an altitude of 800 Km and it can be shown that the range of ionosphere refraction correction is bounded at values of approximately 2 m. Such an error is much smaller than other disturbing effects (e.g. SA), hence on-board estimation of ionosphere refraction correction is not required.
- **User's clock errors:** a GPS receiver generates a replica of the received C/A code signal. One period of this code lasts 1 ms and consists of 1023 bits of 0.978 microseconds. The edges of this stream of bits have no absolute reference time. By receiving the satellite C/A code and the navigation message, the user's receiver is set to GPS time at a certain initial time. From this moment the user's clock drifts from GPS time due to its frequency drift with time.
- **User's receiver noise:** thermal noise limits the accuracy in the measurement of pseudorange and integrated Doppler to a degree which depends on the design of a particular GPS receiver and the signal power received.

2.5. Assumptions and constraints

The results presented in this paper are based on the assumption of the availability on-board of a multi-channel parallel receiver and an antenna designed and accommodated in such a way to provide 160 deg field of view with the antenna boresight coinciding with the zenith direction, the GPS constellation is assumed as being composed of 24 satellites. Use of differential GPS or of (military) receivers equipped with SA-removal data processing capability is explicitly

excluded. The most significant GPS receiver characterising data is assumed being as follows:

| | |
|---|----------------------------|
| C/A code pseudo-range noise (rms) | 0.5 m |
| Number of GPS receiver channels | 9 |
| Integrated Doppler noise (rms) | 1 mm |
| Initial value of the clock bias | 0.1 msec |
| Initial value of the normalised frequency error | 10^{-9} |
| Normalised frequency error derivative | -10^{-13} s^{-1} |

Table 2: Assumed GPS receiver characterising data

3. OBSERVABILITY ANALYSIS FOR MetOp-1

Figures 1 and 2 show the number of visible satellites for the GPS case and also for some other mixed constellations. As expected, the use of mixed constellations brings advantages in terms of:

- **Accuracy:** the number of observables increases significantly thus, allowing better orbit determination accuracy. The PDOP improves as a result of better constellation geometry.
- **Integrity:** with mixed constellations it is possible to perform receiver autonomous integrity monitoring since in those cases the minimum number of visible satellites exceeds those required to perform failure detection, which requires 5 satellites at least, or failure identification, which requires 6 satellite at least.

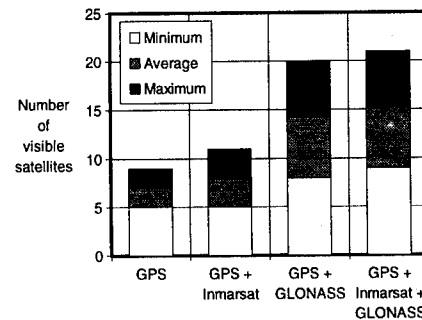


Figure 1: Number of visible satellites for different constellations (antenna coverage of 160 deg).

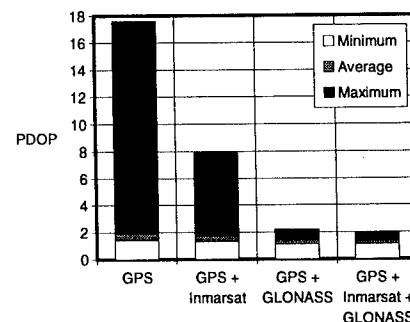


Figure 2: PDOP values for different constellations

4. ESTIMATION TECHNIQUES FOR ATTENUATING THE DISTURBING EFFECT OF SELECTIVE AVAILABILITY

By far the most important source of error which limits the achievable real-time orbit determination accuracy of a GPS-based estimator is SA. Considering the measurement equations for pseudo-range and integrated Doppler it may be seen that they both include correlated noise due to SA. Hence we must augment the system state vector to be able to express the Kalman equations in a form which assumes uncorrelated measurement noise. State vector augmentation implies also to include models for the propagation of the new variables accordingly. The choice of the models and associated parameters becomes a key element for system design. We have considered two lines of search: methods based on system identification, involving the use of a second filter to identify SA model parameters, and a second order Gauss Markov model for SA either with fixed or adapted parameters.

4.1. Methods based on system identification

We have considered the Prony spectral line estimation, the Pisarenko harmonics decomposition and the Rationale transfer function modelling. The Prony spectral line estimation model, as well as the Pisarenko harmonics decomposition model, assumes that the signal to be analysed is composed of a linear combination of several sinusoids, whose amplitude may be damped, embedded in white noise. Whereas Pisarenko's is a spectral decomposition methods, Prony's may be considered as a fitting method, either exact (Hildebrand approach) or approximate with a least squares error minimisation procedure (usually called extended Prony). Although not every discrete-time process (signal) may be represented by a rationale transfer function model (RTF), in most of practical cases it is possible to find some RTF close enough to the actual model, as to allow to extract valuable information characterising the signal. In general, mathematical results based on RTF will suggest, if not produce, acceptable solutions, as far as liner models are applicable.

These methods offer interesting advantages over traditional or classical system identification or spectral determination methods like FFT and others similar. Very few samples are required to match either the frequencies present in the signal (Prony and Pisarenko) or directly the coefficients of an autoregressive (AR) system model (RTF). Typically 64 to 128 samples are enough, or even less in case of reduced orders (two to three frequencies, or up to third order in the AR model). Accurate estimation is performed for frequencies comprised between 0.01 and 0.5 times the sampling frequency. Unfortunately, frequencies below 0.01 times the sampling frequency are difficult to detect, so it is not possible to determine long period components of SA. In

particular, the general statement of the Pisarenko method requires a very accurate estimation of the autocorrelation matrix to avoid the possibility of spurious tones being detected. Moreover, one should think that SA estimates are to be used immediately, hence subsampling to estimate low frequency tones is not useful, also because the number of sub-samples required for a correct estimation would imply times longer than satellite visibility times, thus rendering the low frequency estimate useless.

Besides, the key in the applicability of these methods is the coupling between the on-board EKF and the SA filter. This coupling comes mainly through the covariance matrix components associated with SA model. We have observed a great sensitivity to this coupling to the extent of forcing the EKF to diverge. Correct resetting of covariance is essential whenever a satellite change in a channel is observed. Additionally, the filter computational burden increases with the number of tones being detected, so in practice the number of frequencies to be detected must be fixed and small. As explained, RTF(AR) method requires a limitation in the polynomial order. The case of AR model of order two is equivalent to a Gauss-Markov model of order two, but requires more computations if the AR parameters are to be determined. This fact, among others, suggests that the treatment of a particular 2nd order AR may be directly performed with a single EKF, dispensing with the identification part. Another fact pointing towards the use of a single EKF is that of possible filter instability due to rapid variations in the estimated coefficients, which forces a low pass filtering of these parameters before feeding them back to the first filter.

Hence, Pisarenko, Prony and RTF(AR) methods were discarded, in spite of the fact that in another frame they could be successfully employed.

4.2. Methods based on augmented Kalman filtering

We have considered Gauss-Markov models, including KF with first order, second order and adaptive second order Gauss-Markov models for SA. The first order Gauss-Markov model represents the simplest approach where the state vector being estimated (i.e. user position and velocity, user clock errors and integration Doppler constants) by the KF is extended with a number of ECRV's (once per each receiver channel, usually referred to as range biases) with fixed time constant. Second order Gauss Markov models represent a similar approach but in this case the state vector is further augmented with the range bias derivatives at each receiver channel. Second order Gauss-Markov may be either the damped or the critically damped model. SA model parameters (natural frequency and noise covariance) are constant (i.e. not tuned by the unique KF) and must be set conveniently to avoid filter divergence (natural frequency too high) or lack of

tracking (natural frequency too low). In the case of adaptive second order Gauss-Markov model, two filters are required. The first one is similar to that of the preceding cases, but now, at every step, the second filter adapts the parameters of the second order Gauss-Markov models used by the first filter. This second filter is a simple second order Kalman filter.

In order to preliminary compare first and second order Gauss-Markov models performance, several simulation cases were conducted. Simulations show an average improvement of some six meters if second order Gauss-Markov is used instead of the first order. Such a relatively small improvement does not entirely justify the use of the second order model in our particular application case (we are particularly interested in minimising the software complexity and such an improvement does not imply a significant decrease of our primary concern, the pixel localisation error). Similar analysis were performed with the adaptive version, showing that no significant improvement of the adaptive versus the non-adaptive version is attained, hence second order adaptive Gauss-Markov models were also discarded. Additional analysis of the estimation accuracy with different SA models, also showed that the on-board estimation scheme based on a first order Gauss-Markov model is more robust than the second order version mainly due to the necessity of parameters tuning for every different SA real world model. This re-tuning can be avoided by means of an adaptive filter (robustness should be assessed), but achieved orbit position accuracy obtained with the first order version does not justify the additional burden introduced by an adaptive second order scheme.

5. ORBIT DYNAMICS MODEL

Two kind of on-board dynamics models have been considered, analytic and numerical. Analytic models are in principle less time expensive than numerical models requiring on-board integration. However most

of the available analytic or semi-analytic models lack from the ability of either being self-contained (requiring a set of parameters to be computed on-board and uplinked to the spacecraft, because otherwise after expiration of the validity interval the propagation errors keep growing) or of allowing propagation at short time intervals (of typically 1 sec, the working frequency of our estimation filter). This does not prevent the feasibility of a suitable analytic or semi-analytic on-board dynamics for our purposes of on-board autonomous orbit determination. However, the development of such a model is costly and it was seen not being particularly critical to our application case.

The selected on-board propagator uses as integrator a second order Runge-Kutta method. This ensures minimum computation time while keeping integration accuracy. In the dynamic equations the acceleration model only accounts for the spherical field gravity acceleration plus the J_2 and J_3 terms. This on board dynamic model was compared with reference propagator implementing state of the art orbit dynamics (50x50 Earth gravity field model, accurate third body perturbations due to Sun and Moon, solar radiation pressure and aerodynamic effects computed with the MSIS CIRA-86 atmospheric model). The acceleration model error of our proposed orbit propagator (hereinafter referred to as 2x2 model) is bounded at values of approximately $2 \times 10^{-4} \text{ m/s}^2$.

6. ON-BOARD ORBIT DETERMINATION ALGORITHMS

The on-board software required for performing the autonomous GPS based OD is summarised in figure 3 which represents a particular application case of an extended Kalman filter. Such an algorithm is able to provide real-time estimation, i.e. the time at which the estimate is output coincides with the last measurement point.

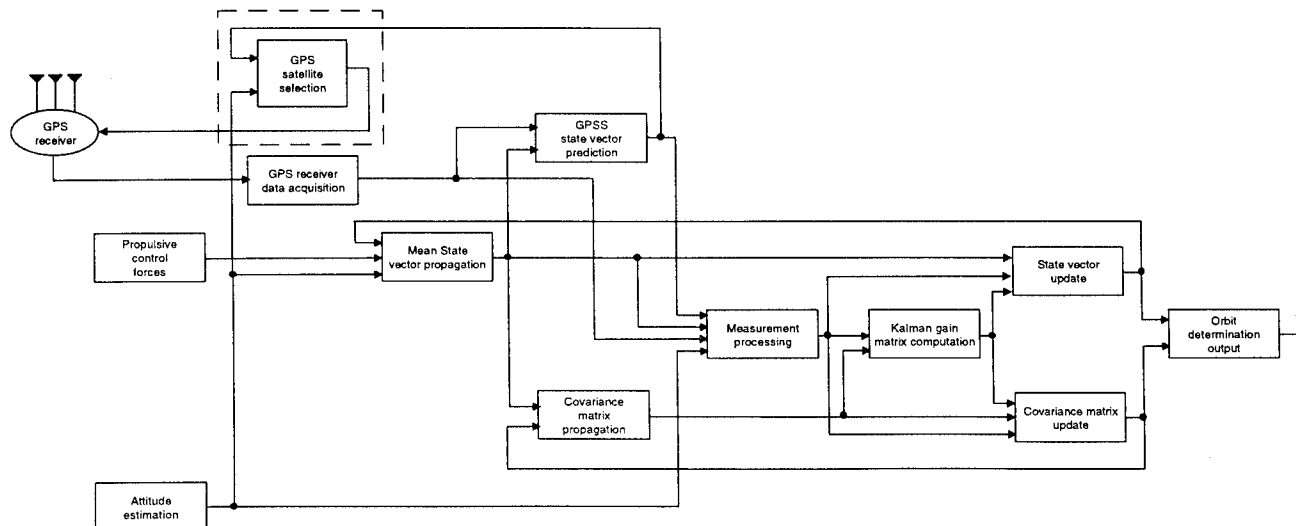


Figure 3: OD function architecture.

It has been assumed that the selection of the GPS satellites to be tracked is performed by the receiver itself. In our case we are assuming having 9 channels which makes that the selection of the GPS satellites to be tracked does not play an important role.

The functions required are here briefly summarised:

- **Acquisition of GPS receiver data:** the GPS receiver will output the following data which feeds our estimation filter: identification of the GPS satellites tracked, the raw GPS measurements (pseudo-range and integrated Doppler) for all the receiver channels and antennas, the time of measurement in the receiver clock, and, the GPS satellite navigation message data, including the ephemeris of the GPS satellites being tracked.
- **Prediction of the GPS satellites state vector:** some GPS satellite data are required for the measurement processing (i.e., GPS satellite position, velocity and acceleration vectors for the observables on-board prediction and for the observation matrix computation, see below). Hence, a GPS satellites state vector prediction is required. Such prediction will be performed from the GPS satellites ephemeris contained in the GPS Navigation Message Data using Keplerian propagation modified to account for second order harmonic perturbations.
- **Initialisation of the state vector and covariance matrix for orbit determination:** the state vector used will consist of $(8+2n_c)$ components as follows (note that n_c stands for the number of GPS receiver channels):

$$\bar{x}_{state} = \left\{ \bar{x}_{C/EQ} \quad \dot{\bar{x}}_{C/EQ} \quad E_{clock} \quad \Delta T_B \quad \bar{b} \quad \bar{I} \right\}^T$$

where $\bar{x}_{C/EQ}$ and $\dot{\bar{x}}_{C/EQ}$ are the spacecraft centre of mass position and velocity vectors expressed in the inertial frame, E_{clock} is the normalised GPS receiver clock frequency error, ΔT_B is the time bias of the GPS receiver clock, \bar{b} is a vector of ranges biases (one per each receiver channel), and \bar{I} is a vector of integration Doppler constants (one per each receiver channel). The initialisation of such vector (mean and covariance) is performed from input parameters.

- **Propagation of the mean state vector:** the state vector is propagated as follows
 - if there is a change of the GPS satellite tracked in a receiver channel, the elements of the state vector corresponding to the associated range bias and integrated Doppler constant are re-initialised,
 - the propagation of the spacecraft position and velocity is performed by integrating numerically the equations of motion in the in-

ertial frame (a second order Runge-Kutta method is used),

- the propagation of other elements of the state vector is performed analytically as follows:

$$\begin{aligned} \hat{E}_{clock} &= e^{-\frac{\Delta t}{\tau_{E_{clock}}}} \hat{E}_{clock}^- + \sigma_{E_{clock}} \sqrt{1 - e^{-\frac{\Delta t}{\tau_{E_{clock}}}}} \eta_{E_{clock}} \\ \Delta \hat{T}_B &= \Delta \hat{T}_B^- + \hat{E}_{clock}^- \Delta t + K_A \sqrt{\Delta t} \eta_A \\ \hat{b}_i &= e^{-\frac{\Delta t}{\tau_b}} \hat{b}_i^- + \sigma_b \sqrt{1 - e^{-\frac{\Delta t}{\tau_b}}} \eta_b \\ \hat{I}_i &= \hat{I}_i^- + c \left(K_I \sqrt{\Delta t} \eta_I + a_{f_i} \Delta t + a_{f_i} \Delta t^2 - \hat{E}_{clock}^- \Delta t \right) \end{aligned}$$

where Δt is the sampling period, $\tau_{E_{clock}}$ and $\sigma_{E_{clock}}$ are the time constant and variance constant for E_{clock} modelling, τ_b and σ_b are the time constant and variance constant for range biases modelling, a_{f_i}, a_{f_j} are constants for modelling the integration Doppler constants, K_A is a state constant for the receiver clock bias modelling, K_I are constant for modelling of the integrated Doppler constants, $\eta_A, \eta_{E_{clock}}, \eta_b, \eta_I$ are white Gaussian noises and c is the velocity of electromagnetic waves in vacuum.

- **Propagation of the state vector error covariance matrix:** the state vector error covariance matrix is propagated as follows

- if there is a change of the GPS satellite tracked in a receiver channel, the elements of the estimated covariance matrix corresponding to the associated range bias and integrated Doppler constant should be initialised,
- the transition matrix of the spacecraft position and velocity vectors is computed analytically by using the formulation of a second order Runge Kutta numerical integrator. The required dynamic matrix is computed analytically from the linearised formulation and using the estimated state vector. The transition matrix of other estimated parameters is constructed analytically from their modelled dynamics.

The overall transition matrix is as follows:

$$\Phi_{TOTAL} = \begin{bmatrix} \Phi(\bar{x}_{C/EQ}, \dot{\bar{x}}_{C/EQ}) & 0 & 0 & 0 & 0 \\ 0 & \Phi(\Delta T_B) & \Phi(\Delta T_B, E_{clock}) & 0 & 0 \\ 0 & 0 & \Phi(E_{clock}) & 0 & 0 \\ 0 & 0 & 0 & \Phi(\bar{b}) & 0 \\ 0 & 0 & \Phi(\bar{I}, E_{clock}) & 0 & \Phi(\bar{I}) \end{bmatrix}$$

where,

$$\Phi(\bar{x}_{C/EQ}, \dot{\bar{x}}_{C/EQ}) = \begin{bmatrix} [I] + \frac{1}{4} \Delta t^2 \left(3 \left[A \left(t + \frac{2}{3} \Delta t \right) \right] - [A(t)] \right) & [I] \Delta t + \frac{1}{6} \Delta t^2 [A(t)] \\ \frac{1}{4} \Delta t \left([A(t)] + 3 \left[A \left(t + \frac{2}{3} \Delta t \right) \right] + \frac{1}{6} \Delta t^2 [A(t)] \left[A \left(t + \frac{2}{3} \Delta t \right) \right] \right) & [I] + \frac{1}{2} \Delta t^2 [A(t)] \end{bmatrix}$$

with Δt is the integration step and $[A(t)]$ is the Jacobian matrix for the acceleration due to the gravitational field, which elements are computed as follows:

$$\begin{aligned} A_{11} &= \frac{\mu_x}{R^3} + 3 \frac{X^2}{R^2} \left\{ \frac{\mu_x}{R^3} + \frac{\mu}{R^3} J_2 \frac{\bar{R}^2}{R^2} \left[2 \left(1 - 5 \frac{Z^2}{R^2} \right) - 1 \right] \right\} \\ A_{12} &= A_{21} = 3 \frac{X Y}{R R} \left\{ \frac{\mu_x}{R^3} + \frac{\mu}{R^3} J_2 \frac{\bar{R}^2}{R^2} \left[2 \left(1 - 5 \frac{Z^2}{R^2} \right) - 1 \right] \right\} \\ A_{13} &= A_{31} = 3 \frac{X Z}{R R} \left\{ \frac{\mu_x}{R^3} + \frac{\mu}{R^3} J_2 \frac{\bar{R}^2}{R^2} \left[2 \left(1 - 5 \frac{Z^2}{R^2} \right) + 4 \right] \right\} \\ A_{22} &= A_{33} = \frac{\mu_x}{R^3} + 3 \frac{Y^2}{R^2} \left\{ \frac{\mu_x}{R^3} + \frac{\mu}{R^3} J_2 \frac{\bar{R}^2}{R^2} \left[2 \left(1 - 5 \frac{Z^2}{R^2} \right) - 1 \right] \right\} \\ A_{23} &= A_{32} = 3 \frac{Y Z}{R R} \left\{ \frac{\mu_x}{R^3} + \frac{\mu}{R^3} J_2 \frac{\bar{R}^2}{R^2} \left[2 \left(1 - 5 \frac{Z^2}{R^2} \right) + 4 \right] \right\} \end{aligned}$$

with

$$\begin{aligned} \mu_x &= \mu \left[1 - \frac{3}{2} J_2 \frac{\bar{R}^2}{R^2} \left(1 - 5 \frac{Z^2}{R^2} \right) \right] \\ (X, Y, Z) &= (X_{C/IEQ}, Y_{C/IEQ}, Z_{C/IEQ}) = \bar{x}_{C/IEQ} \\ R &= \sqrt{X^2 + Y^2 + Z^2} \end{aligned}$$

the submatrices corresponding to the non-dynamic terms of the state vector are,

$$\begin{aligned} \Phi(\Delta T_B) &= 1 \\ \Phi(\Delta T_B, E_{clock}) &= \Delta t \\ \Phi(E_{clock}) &= e^{-\frac{\Delta t}{\tau_{E_{clock}}}} \\ \Phi(\bar{b}) &= e^{-\frac{\Delta t}{\tau_b}} [I]_{NA, NA} \\ \Phi(\bar{I}) &= [I]_{NA, NA} \\ \Phi(\bar{I}, E_{clock}) &= \{-c\Delta t \quad \dots \quad -c\Delta t\}_{1, NA}^T \end{aligned}$$

- the error covariance matrix associated to the state vector is propagated using a discrete formulation. The system noise associated to the spacecraft state vector is computed analytically from the uncertainties in the on-board orbit dynamics model, whereas the system noise covariance matrix associated to the estimated parameters is directly constructed from their on-board modelled dynamics. The covariance matrix propagation is done by using a U-D factorisation in order to reduce the on-board computer workload as well as to improve the numerical stability.

The total system matrix is as follows,

$$Q_{TOTAL} = \begin{bmatrix} Q(\bar{x}_{C/IEQ}, \dot{\bar{x}}_{C/IEQ}) & 0 & 0 & 0 & 0 \\ 0 & Q(\Delta T_B) & Q(\Delta T_B, E_{clock}) & 0 & 0 \\ 0 & Q(\Delta T_B, E_{clock}) & Q(E_{clock}) & 0 & 0 \\ 0 & 0 & 0 & Q(\bar{b}) & 0 \\ 0 & 0 & 0 & 0 & Q(\bar{I}) \end{bmatrix}$$

with,

$$Q(\bar{x}_{C/IEQ}, \dot{\bar{x}}_{C/IEQ}) = \begin{bmatrix} 0 & 0 & 0 & 0 & 0 & 0 \\ 0 & 0 & 0 & 0 & 0 & 0 \\ 0 & 0 & 0 & 0 & 0 & 0 \\ 0 & 0 & 0 & w_a & 0 & 0 \\ 0 & 0 & 0 & 0 & w_a & 0 \\ 0 & 0 & 0 & 0 & 0 & w_a \end{bmatrix} \Delta t^2$$

where w_a represents the acceleration error of the implemented orbit dynamics model.

For practical purposes the system noise covariance matrix is computed as follows,

$$\Gamma_k Q_k \Gamma_k^T = \Phi_{k+1, k} Q(t) \Phi_{k+1, k}^T \Delta t$$

The noise covariance for the non-dynamic terms of the state vector is derived from their propagation models, and thus,

$$Q(E_{clock}) = (\sigma_{E_{clock}})^2 \left[1 - e^{-\frac{2\Delta t}{\tau_{E_{clock}}}} \right]$$

$$Q(\Delta T_B) = K_A^2 \Delta t + Q(E_{clock}) \frac{\Delta t^2}{2}$$

$$Q(\Delta T_B, E_{clock}) = Q(E_{clock}) \frac{\Delta t}{2}$$

$$Q(\bar{b}) = (\sigma_b)^2 \left[1 - e^{-\frac{2\Delta t}{\tau_b}} \right] [I]_{NA, NA}$$

$$Q(\bar{I}) = (K_I)^2 \Delta t [I]_{NA, NA}$$

with the same notation as before.

Finally, the system error covariance matrix is predicted as follows,

$$[\hat{P}] = [\Phi][\hat{P}^-][\Phi]^T + [Q]$$

where $[\Phi]$ is the transition matrix, computed as mentioned previously, $[\hat{P}^-]$ is the system error covariance matrix of the previous step and $[Q]$ is the system noise covariance matrix, computed as per above.

- **Processing of measurements:** the raw measurements provided by the receiver are processed as follows

- the observables selected for the orbit determination (namely, pseudo-range and integrated Doppler) are predicted on-board by using non-linear formulation (an extended Kalman filter is used). The following models are used for pseudorange and integrated Doppler measurements:

$$\begin{aligned} \hat{P}\hat{R}(i) &= \left| \hat{\bar{R}}_{SA/IEQ}(i) - \hat{\bar{R}}_{SA/IEQ}(i) \frac{1}{c} \hat{\bar{R}}_{SA/IEQ} + c\Delta \hat{T}_B + \bar{b}_i \right| \\ \hat{N}(i) &= \frac{f_{GPS}^T}{c} \left(\left| \hat{\bar{R}}_{SA/IEQ}(i) - \hat{\bar{R}}_{SA/IEQ}(i) \frac{1}{c} \hat{\bar{R}}_{SA/IEQ} + c\Delta \hat{T}_B + \hat{\bar{b}}_i + \hat{\bar{I}}_i \right| \right) \end{aligned}$$

with the same notation as above and $\hat{\bar{R}}_{SA/IEQ}(i)$ being the position vector of the antenna of the GPS satellite tracked by the

channel i^{th} w.r.t. the predicted position of the spacecraft antenna, in Inertial Equatorial Frame, and $\hat{\mathbf{R}}_{SA/EQ}(i)$ the velocity of the selected GPS satellite in the same frame.

- the on-board predicted values of the observables are used to compute the corresponding innovations,

$$\hat{\mathbf{I}}_A^{PR}(i) = \mathbf{M}_A^{PR}(i) - \mathbf{P}\hat{\mathbf{R}}(i)$$

$$\hat{\mathbf{I}}_A^N(i) = \mathbf{M}_A^N(i) - \hat{\mathbf{N}}(i)$$

The first processing of the innovations is the sequential filter rejection test, where for each measurement, if

$$|\hat{\mathbf{I}}_A^{PR,N}| > K_\sigma \sqrt{[\mathbf{H}(i)]_{i,N} [\hat{\mathbf{P}}] [\mathbf{H}(i)]_{i,N}^T + [\mathbf{R}]}$$

then, the measurement is rejected. Note that above the term $[\mathbf{H}(i)]$ represents the observation matrix for the measurement provided at channel i at current time, and $[\mathbf{R}]$ is the measurement error covariance matrix.

- the observation matrix to be used for the filtering process is computed as follows: for the pseudorange measurement corresponding to the GPS satellite tracked by the channel i^{th} the line of the observation matrix is:

$$[\mathbf{H}_{GPS}^{PR}(i)] = \begin{bmatrix} -\frac{\hat{\mathbf{R}}_{SA/EQ}(i)}{\|\hat{\mathbf{R}}_{SA/EQ}(i)\|} & 0 & 0 & 0 & c & 0 & \delta_{1,i} & \dots & \delta_{N_A,i} \end{bmatrix}$$

whereas for the integrated Doppler measurements corresponding to the GPS satellite tracked by the channel i^{th} the line of the observation matrix is:

$$[\mathbf{H}_{GPS}^N(i)] = \frac{f_{GPS}}{c} \begin{bmatrix} -\frac{\hat{\mathbf{R}}_{SA/EQ}(i)}{\|\hat{\mathbf{R}}_{SA/EQ}(i)\|} & 0 & 0 & 0 & 0 & 0 & \delta_{1,i} & \dots & \delta_{N_A,i} \end{bmatrix}$$

- a constant (receiver dependent) value of the pseudo-range and integrated Doppler measurements noise is assumed.
- **Update of the state vector and covariance matrix:** for each i^{th} measurement an updating loop process is performed as follows:
 - Check for conditions of updating: the update process is allowed only if the corresponding GPS unit is valid, the corresponding tests declared the measurement as valid, and the measurement is inside the expected range according to the sequential filtering rejection test.
 - Obtain the gain matrix as,

$$[\mathbf{K}(i)]_{N,1} = \frac{[\hat{\mathbf{P}}(i-1)][\mathbf{H}(i)]_{i,N}^T}{1.2[\mathbf{H}(i)]_{i,N} [\hat{\mathbf{P}}(i-1)][\mathbf{H}(i)]_{i,N}^T + [\mathbf{R}]_{i,1}}$$

- State update:

$$\Delta \hat{\mathbf{x}} = \hat{\mathbf{x}}(i-1) + [\mathbf{K}(i)]_{N,1} [\bar{\mathbf{I}}_{A/R}(i) - [\mathbf{H}(i)]_{i,N} \hat{\mathbf{x}}(i-1)]$$

$$\hat{\mathbf{x}}^+ = \hat{\mathbf{x}} + \Delta \hat{\mathbf{x}}$$

- System error covariance matrix update:

$$[\hat{\mathbf{P}}(i)] = [\mathbf{I}] - [\mathbf{K}(i)]_{N,1} [\mathbf{H}(i)]_{i,N} [\hat{\mathbf{P}}(i-1)]$$

which is conveniently performed by using the faster upper diagonal algorithm.

7. PERFORMANCE SIMULATIONS OF THE GPS-BASED OD SYSTEM

7.1. Nominal performances

Simulation results prove that under nominal conditions and the data of tables 2 and 3, the proposed OD algorithm provides an orbit positioning accuracy as shown on figure 4 (all the simulations results presented in this section correspond to a 10 orbits duration).

| | |
|---|----------------------------------|
| Initial user S/C position error | 10 Km |
| Initial user S/C velocity error | 10 m/s |
| On-board acceleration model error | $2 \times 10^{-4} \text{ m/s}^2$ |
| Initial pseudorange bias (\bar{b}) uncert. | 80 m |
| Pseudorange bias (\bar{b}) standard dev. | 30 m/(s) |
| Pseudo-range bias (\bar{b}) time constant | 100 sec |
| Initial uncert. for Doppler constants | 100 |
| Doppler constants K_f | 0.15 |
| Initial uncertainty in E_{clock} | 10^{-6} |
| State noise in E_{clock} | 10^{-7} |
| Initial uncertainty in time bias (ΔT_B) | 1 msec |
| Time bias K_B | 10^{-9} |
| Pseudorange measurements noise | 0.5 m |
| Integrated Doppler measur. noise | 1 mm |

Table 3: GPS-based OD system summary input data

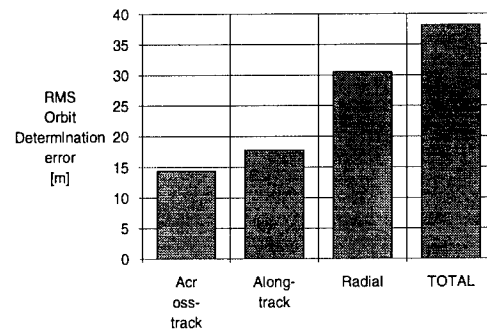


Figure 4: OD system nominal performances for MetOp

7.2. Sensitivity analysis w.r.t. different selective availability models

A set of simulations have been performed to assess the robustness of the proposed OD algorithms with respect to the actual, "real-world" values of SA. A summary of the results is shown in figure 5. The proposed algorithms exhibit a remarkable robustness with respect

to such a variety of selective availability models. Even for the case of the time series selective availability models (i.e. Lear Arima 2x1, Zyla Arima 3x2 and RTCA Gauss Markov SA model, which are regarded as too pessimistic since they provide an output which is too noisy compared to actual SA measurements), the proposed algorithms are still able to maintain the positioning estimation accuracy very close to the nominal case.

| SA MODEL | rms position estimation errors (m) | | | |
|---------------------|------------------------------------|-------------|--------|-------|
| | Along-track | Cross-track | Radial | Total |
| None | 1.5 | 1.2 | 6.2 | 6.5 |
| Lear deterministic | 11.9 | 14.6 | 34.5 | 39.3 |
| Lear random | 8.8 | 9.7 | 21.2 | 24.9 |
| Martínez-Molina | 12.1 | 15.3 | 28.4 | 34.5 |
| Rater Jerk analytic | 14.4 | 17.8 | 30.6 | 38.2 |
| Lear Arima 2x1 | 17.7 | 20.6 | 42.4 | 50.4 |
| Zyla Arima 3x2 | 17.3 | 19.3 | 40.9 | 48.4 |
| RTCA Gauss- Mar. | 16.8 | 25.1 | 46.1 | 55.1 |

Figure 5: OD RMS errors summary results for different SA models

7.3. Sensitivity w.r.t. on-board orbit dynamics models

Previously we discussed the choice of the orbit dynamics model implemented within the proposed OD system. Analysis of the influence of the quality of such a dynamics model in the achievable accuracy of our system was performed. Additional simulations were performed with exactly the same conditions except for the on-board orbit dynamics model (and associated system noise covariance matrix). Three orbit dynamics models were analysed: 2x2, 4x4 and 8x8. The results are shown in table 4. The nominal error level achieved in the 2x2 case is reduced by approximate factors of 0.9 and 0.8 when implementing the 4x4 and 8x8+ models, respectively. Such a relatively small accuracy increase is not worth the additional computational loads and memory demands.

| Orbit Dynamics Model | rms position estimation errors (m) | | | |
|----------------------|------------------------------------|-------------|--------|-------|
| | Along-track | Cross-track | Radial | Total |
| 8x8+ | 12.2 | 15.0 | 24.8 | 31.5 |
| 4x4 | 12.9 | 16.5 | 27.0 | 34.2 |
| 2x2 | 14.4 | 17.8 | 30.5 | 38.2 |

Table 4: OD RMS errors summary results for different orbit dynamics models

7.4. Sensitivity w.r.t. orbit control manoeuvres

There are several ways for the proposed on-board algorithms to cope with the disturbing effect of orbit control manoeuvres:

- The on-board software implements appropriate interfaces to the orbit control system such that it is able to perform propagation of the position and velocity vectors through the commanded manoeuvre and increases the system noise covariance matrix with the "expected" manoeuvre execution errors. This concept requires interfacing the OD software with the on-board software in charge of handling the orbit control thrusters.
- An alternative would be to suppress this interface, and to increase all time the system noise covariance matrix such that it is able to cope with any manoeuvre being executed.
- The simplest solution is to complete ignore the fact that manoeuvres can be performed. In these conditions the filter will diverge during the time of manoeuvres application but the excellent GPS observability conditions will bring back the filter to convergence shortly after the manoeuvre. For MetOp-1 there is no specific requirement for orbit determination accuracy during manoeuvres which makes acceptable a small divergence at that time.

Simulation have been performed under the following conditions:

- The real-world implements realistic manoeuvres corresponding to our MetOp-1 study case.
- The on-board software operates in different modes corresponding to the three candidate methods mentioned earlier.
 1. Nominal case without manoeuvres: the filter tuning was optimised without taking into account the effect of manoeuvres.
 2. The on-board software knows the time and size of manoeuvres being executed (except of manoeuvre execution errors). It also has the ability of propagating the state vector through the commanded manoeuvres.
 3. The on-board software does not know if a manoeuvre is being executed, however, the system noise covariance is increased by an approximate factor of 10 in order to cope with possible manoeuvre being executed at any time.
 4. Ignore absolutely: corresponds exactly to the nominal case (same filter tuning and same on-board propagation model) but the real-world implements the manoeuvres mentioned previously. In this case there is serious mismodelling which causes divergence.

The results are shown in table 5 which reveals that position vector estimation accuracy is only affected by an approximate factor of 1.1 for the worst case of increasing the system noise covariance matrix at any time. The case where we ignore the manoeuvres is par-

ticularly interesting since the performances are identical to that obtained in our nominal case if we exclude from the statistical analysis that portion of time where the manoeuvres are being executed. At those times the filter diverges but it recovers the nominal conditions after some 50 seconds after manoeuvre completion.

Consequently, the estimation algorithms can cope with completely unknown orbit control manoeuvres (both in terms of manoeuvre size and time) and still provide sufficient estimation accuracy.

| Orbit Dynamics Model | rms position estimation errors (m) | | | |
|----------------------|------------------------------------|-------------|--------|-------|
| | Along-track | Cross-track | Radial | Total |
| Case 1 | 14.4 | 17.8 | 30.5 | 38.2 |
| Case 2 | 14.4 | 17.8 | 30.6 | 38.3 |
| Case 3 | 17.3 | 19.7 | 34.9 | 43.7 |
| Case 4 | 17.4 | 18.4 | 32.8 | 41.4 |

Table 5: OD RMS errors summary results for different mechanisms of attenuating the disturbing effects of orbit control manoeuvres

8. HARDWARE REQUIREMENTS OF THE PROPOSED GPS-BASED ORBIT DETERMINATION ALGORITHMS

8.1. General

The previously described GPS-based OD algorithms imply the following hardware demands on-board the host satellite:

- A single antenna located in the anti-Earth face of the spacecraft (i.e. in zenith view) with an antenna beamwidth of 160 deg.
- A C/A code GPS receiver providing pseudorange and integrated Doppler measurements with an accuracy described in table 2 at a 1 Hz frequency:

8.2. Memory and computational loads

Assuming the use of a high level language, the CPU time consumption per step (having assumed a working frequency of 1 Hz, 1 step corresponds to 1 sec of real time) amounts to some 16 msec, running in a Sun-Spark 20 workstation.

Object code size amounts to some 27 Kbytes. Inlining optimiser option has not been used to compute those figures, and no static library calls forced to be included within the objects. Final object code size will depend on particular software design and, among others, on the particular method selected to compile and link the code to produce the on-board executable software. There is always a trade-off between size and execution speed. Inlining, in general, speeds up code execution, but resulting code requires more space to be allocated.

Source code is composed of some 1100 (executable) lines. Memory required by additional static data storage amounts to some 4 Kbytes, whereas dynamic memory requirements (minimum stack size) demands some 15 Kbytes peak. Henceforth, total memory budget is about 40 Kbytes.

9. REFERENCES

- [1] Lear, W.M., "GPS Navigation for Low Earth Orbiting Vehicles", NASA, Mission Support Directorate, Mission Planning and Analysis Division, JSC-32031, 87-FM-2 Rev. 1, March 1989.
- [2] Allan, D.W. and Dewey, W.P.: Time-Domain Spectrum of GPS SA. ION GPS-93. Sixth International Technical Meeting of the Satellite Division of the Institute of Navigation, Salt Lake City, Utah, September 22-24, 1993.
- [3] Bar-Sever, Y.E.; Yunck, T.P. and Wu, S.-C.: GPS-Based Orbit Determination and Point Positioning Under Selective Availability. ION GPS-90. Third International Technical Meeting of the Satellite Division of the Institute of Navigation, Colorado Springs, Colorado, September 19-21, 1990.
- [4] Chou, H.-T.: An Anti-SA Filter for Non-differential GPS Users. ION GPS-90. Third International Technical Meeting of the Satellite Division of the Institute of Navigation, Colorado Springs, Colorado, September 19-21, 1990.
- [5] Raby, P. and Daly, P.: Integrated GPS/GLONASS Navigation: Algorithms and Results. ION GPS-93. Sixth International Technical Meeting of the Satellite Division of the Institute of Navigation, Salt Lake City, Utah, September 22-24, 1993.
- [6] Cadzow, J.A.: Spectral Estimation; An Overdetermined Rational Model Equation Approach, Proceedings of the IEEE, Vol. 70, No. 9, September 1982.
- [7] Thomson, D.J.: Spectrum Estimation and Harmonic Analysis, Proceedings of the IEEE, Vol. 70, No. 9, September 1982.
- [8] Burg, J.P., Luenberger, D.G. and Wenger, D.L.: Estimation of Structured Covariance Matrices, Proceedings of the IEEE, Vol. 70, No. 9, September 1982.
- [9] Marple, S.L. Jr.: A New Autoregressive Spectrum Analysis Algorithm, IEEE Trans. Acoustics, Speech and Signal Processing, Vol. ASSP-28, pp. 441-454, August 1980.

Results of a Automated GPS Tracking System in Support of Topex/Poseidon and GPSMet

Ronald Muellerschoen, Stephen Lichten, Ulf Lindqwister, and Willy Bertiger
Jet Propulsion Laboratory

BIOGRAPHIES

Ronald Muellerschoen received a B.S. degree in physics at Rensselaer Polytechnic Institute and a M.S. degree in applied math at the University of Southern California. He is currently a Member of the Technical Staff in the Earth Orbiter Systems Group at the Jet Propulsion Laboratory (JPL). His work at JPL has concentrated on the development of efficient filtering/smoothing software for processing GPS data and the processing of Topex/Poseidon-GPS data.

Dr. Stephen M. Lichten has worked at the Jet Propulsion Laboratory since 1983, where he presently is the Earth Orbiter Systems Group Supervisor and Radio Metrics manager in NASA's Deep Space Network Advanced Technology Program. He received an A.B. degree from Harvard in 1978 and a Ph.D. in astrophysics from Caltech in 1983. His group specializes in high-precision orbit determination, including automated GPS tracking techniques and software, recently demonstrating 2-cm radial orbit accuracy for Topex/Poseidon. Dr. Lichten was a session co-chair for the ION GPS'93 meeting and a Technical Chairman for the ION GPS'94 meeting.

Dr. Ulf J. Lindqwister received his Ph.D. in physics from Princeton University in 1988. Dr. Lindqwister is supervisor of the GPS Networks and Operations Group at JPL that operates NASA's permanent GPS stations in various global, regional, and local GPS networks (currently approaching 50 stations) and whose group also routinely produces media (ionospheric and tropospheric) calibrations for NASA's deep space and near Earth missions.

Dr. Willy Bertiger received his Ph.D. in Mathematics from the University of California, Berkeley, in 1976, specializing in Partial Differential Equations. Following

his Ph.D., he continued research in maximum principles for systems of partial differential equations while teaching at Texas A&M University. In 1981, he went to work for Chevron Oil Field Research. At Chevron, he worked on numerical models of oil fields and optimization of those models for Super Computers. In 1985, he began work at JPL as a Member of the Technical Staff in the Earth Orbiter Systems Group. His work at JPL has been focused on the use of GPS for high precision orbit determination.

ABSTRACT

A fully automated near real-time GPS tracking system has been developed around JPL's GIPSY/OASIS II software. The system produces < 25 cm (3D rms) GPS orbits and one-half nanosecond (15 cm) clock estimates. The process starts automatically when a favorable global distribution of ground data from the IGS network (International GPS Service for Geodynamics) becomes available. Ionospherically corrected phase and pseudorange data are optimally combined to remove satellite and ground receiver clock errors, including selective availability. After the GPS orbits are determined within the data arc, they are then propagated with empirically determined dynamic force models. Real-time < 2 meter (3D rms) GPS orbits are always available. As a by-product of this process, other calibration estimates such as station clocks, troposphere estimates, and earth orientation parameters are also produced. For 27-hour daily arc fits, the process requires 6-7 hours of CPU time on an HP9000/735 workstation.

Additionally, a second process has been developed that automatically starts when data from the Topex/Poseidon GPS receiver and a favorable distribution of ground stations becomes available. An optimal selection of ground stations is determined and data from these sites are then used to solve for the GPS clocks as well as the Topex/Poseidon orbit. This process makes use of the

previously determined predicted GPS orbits. The Topex/Poseidon orbits determined within the data arc are precise to 5 cm radial (rms) and 18 cm 3D (rms). Real-time predicted orbits are also produced precise to 15 meters 3D (rms). This process has been adopted to also support the precise orbit determination of the GPSMet experiment.

INTRODUCTION

The Topex/Poseidon (T/P) spacecraft was launched into a 1334 km circular orbit in August 1992 and carries a high precision dual frequency GPS receiver. When the GPS Anti-Spoof function is off, the GPS receiver uses P-code to obtain GPS pseudorange and carrier phase observables at L1 and L2 frequencies, providing ionosphere-free pseudorange and phase observables. When the Anti-Spoof function is on, the GPS flight receiver tracks only the L1 C/A signal, which precludes the computation of ionosphere-free observables. Since January 31, 1994 (except for 2 three-week periods in June/July 1995 and April/May 1995), the Anti-Spoof function has been turned on and T/P's GPS receiver has been operating as a single frequency receiver [1].

GPSMet is an experiment on the MicroLab I satellite which was launched into a 790 km circular orbit in April 1995. It carries a modified version of a dual frequency TurboRogue™ GPS receiver [2]. When the Anti-Spoof function is on, the receiver tracks the L1 C/A signal and full wavelength L2 in cross-correlated mode. This provides the generation of ionosphere-free pseudorange and phase observables.

The Topex/Poseidon spacecraft requires near real-time orbit determination for 1.) the production of Interim Geophysical Data Records [3] and 2.) integration with the U.S. Navy's Altimetry Data Fusion Center (ADFC) located at the Stennis Space Center. The ADFC's goal is to combine altimetry data from available sources into oceanographic products and to distribute them to the U.S. Navy in a timely manner. To make use of the Topex/Poseidon altimeter data, an estimate of T/P's radial orbit component to less than 1 meter must be available in less than 24 hours.

The goal of the GPSMet experiment is to make measurements of the Earth's neutral atmosphere such as refractivity index, temperature, and water vapor using radio occultations of GPS signals with the onboard GPS receiver [4]. Precision orbit determination is necessary for proper calibration and processing of the GPS radio occultation data. Although near real-time orbits are not necessary to perform the experiment, being able to demonstrate the capability of providing these

measurements of the Earth's atmosphere in a timely matter is important.

To support the near real-time orbit determination of both these spacecraft, a fully automated GPS tracking system has been developed. The core of this data reduction system is the second generation GPS data processing software system, GIPSY/OASIS II, developed at JPL [5]. This core software set is driven by a highly automated expert data processing system that incorporates various UNIX utilities such as c shell, awk, sed, and perl. When there is a sufficient global distribution of ground data available, the process automatically produces a GPS orbit solution from a 27-hour data arc. The 27-hour data arc includes 3 hours of the previous day and 24 hours of data of the current day. In this way, 3 hours of GPS orbits in the overlapping data segments are used to quickly assess the quality of the GPS orbits. After each daily GPS process completes, predicted GPS orbits are also produced that span 3 additional days past the end of the data arc. It is primarily these precise predicted GPS orbits that are used to support the near real-time orbit determination of Topex/Poseidon and the GPSMet experiment.

After this GPS process has been completed, an e-mail message is automatically compiled and distributed to potential users. The message reports orbit precision, data residuals, data outliers, and potential problems that may have arisen in the processing. All this occurs within 18 hours of UTC midnight (which is the end of the data arc) of the current processing day.

Both the predicted GPS orbits and GPS solutions within the data arc, along with GPS clock and yaw-rate solutions [6], along with earth orientation solutions, are placed on an HP9000/735 workstation. These solutions are available via anonymous FTP from sideshow.jpl.nasa.gov (128.149.70.41) under [pub/gipsy_products/RapidService/orbits](ftp://pub/gipsy_products/RapidService/orbits). A revolving buffer currently allows availability of the two most recent weeks of these RapidService orbits. This occurs on a daily basis and has been in operation since March of 1995.

Besides supporting orbit determination of Topex/Poseidon and the GPSMet experiment, these GPS orbits and clock solutions are also used by JPL's IGS Flinn Analysis [7] to screen all data from the IGS network. Over 100 sites per day are precisely point positioned with these GPS orbits and clock solutions. The technique of precise point positioning refers to processing ground data with fixed GPS orbits and fixed GPS clocks. Only the station's clock, troposphere, station location, and phase biases are estimated. Large postfit residuals of the

phase data are a direct indication that data from a particular station may not be valid.

The paper will cover briefly the automated data acquisition of the IGS data, the determination of a global distribution of ground sites, problem detection and correction within the automated GPS processing, and the results of this processing. The results will indicate orbit precision, both within the data arc and of the predicted GPS orbits, clock precision, expected user position error of using the predicted GPS orbits for WAAS, precision of the Earth orientation estimates, and precise point positioning of global stations. A comparison will be made between the solutions produced by this automated processing and the solutions produced by JPL's IGS Flinn Analysis (JPL Flinn) [7]. The orbits and clock solutions produced by the automated process will be referred to as the JPL quick-look solutions. The nomenclature "quick-look" refers to the fact that these solutions are available within 18 hours of UTC midnight of the solution day, whereas the JPL Flinn solutions are generally not available until two weeks after UTC midnight of the solution day.

The paper will conclude with the production and results of the near real-time Topex/Poseidon orbits and of the MicroLab I satellite.

GROUND DATA ACQUISITION

JPL uploads data via regular telephone lines, Internet, and NASCOM (direct NASA communications lines from the three DSN stations) in 24-hour file segments¹. All routine data uploading and handling operations at the JPL have been automated. The data transfers start immediately after UTC midnight, and under ideal conditions all the data are obtained within 12 hours. In practice, 95+% of the data are collected automatically every day, with the remaining data uploaded the next day by the automated upload system.

The data is uploaded automatically via telephone lines or direct serial connections using Microphone Pro scripts running on Macintosh computers. The networked Macintoshes at JPL use Telebit T2500 Trailblazer modems to dial up 30+ stations with standard telephone connections. Data from 8+ stations are uploaded from the receivers with direct serial connections via Internet. The resulting files are stored on the Macintosh computers until

a DEC 3000/500 Alpha workstation at JPL completes a successful FTP transfer. The Alpha workstation additionally decompresses, inventories, validates, formats, and distributes the data. The process requires about a minute of CPU time on the DEC workstation per station per day.

GPS ground data acquired from agencies besides JPL are additionally obtained via Internet. All data for a particular day are combined and may be accessed via anonymous FTP from bodhi.jpl.nasa.gov (128.149.70.66) under pub/rinex. Approximately 100+ stations per day are eventually acquired, with about 60+ stations available within 12 hours of UTC midnight.

AN OPTIMAL GLOBAL DATA DISTRIBUTION

To obtain the GPS orbits and clock solutions within 6-7 hours of processing time on an HP9000/735 workstation, 18 stations are selected from the available data base and used for the daily processing. An optimal selection of 18 stations is determined by computing the rms value over the Earth of the distance-to-nearest-site function [8]. At an arbitrary point on the Earth (θ, ϕ) the quantity

$$r_n(\theta, \phi) = R_e \cos^{-1} [\sin \theta \sin \theta_n \cos(\phi - \phi_n) + \cos \theta \cos \theta_n] \quad (1)$$

is the great-circle distance from (θ, ϕ) to a ground site n located at (θ_n, ϕ_n). Let

$$r(\theta, \phi) = \min [r_1, r_2, \dots, r_N] \quad (2)$$

be the distance from (θ, ϕ) to the nearest of N ground sites. Define a function "zeta" as the rms value over the Earth:

$$\zeta = (4\pi)^{-1/2} \left[\int d\phi \int d\theta \sin \theta r^2(\theta, \phi) \right]^{1/2} \quad (3)$$

For uniformly distributed stations:

$$\zeta \approx \frac{2}{\sqrt{6}} R_e \sqrt{\pi/N} \quad (4)$$

To achieve a zeta of less than 2000 km, 22 uniformly geographically distributed sites are needed. Given however the non-uniformity of the IGS network, the smallest zeta that can be achieved with 18 stations is 2800 km. In comparison, JPL's IGS Flinn Analysis, which uses 34 stations to compute GPS orbits and clocks, realizes a 2400 km value for zeta.

As ground data are accumulated and the global distribution improves, the value of zeta for a particular

¹ The choice of 24-hour file segments is arbitrary and so far has satisfied the requirements of JPL's sponsors. In principle, data acquisition and processing could be more frequent.

solution day decreases. Table 1 shows the local PDT (Pacific Day-light Savings Time) time that the value of zeta crossed 3400 km in the first two weeks in August of 1995.

| solution day | zeta (km) for 18 stations | local PDT time zeta crosses 3400 km and auto processing starts |
|--------------|---------------------------------|---|
| 95aug01 | 3386 | Aug 02 02:06 |
| 95aug02 | 3096 | Aug 03 04:10 |
| 95aug03 | 3022 | Aug 04 04:13 |
| 95aug04 | 3297 | Aug 05 03:11 |
| 95aug05 | 3158 | Aug 06 04:04 |
| 95aug06 | 3276 | Aug 07 03:13 |
| 95aug07 | 2983 | Aug 08 04:09 |
| 95aug08 | 3028 | Aug 09 04:11 |
| 95aug09 | 2897 | Aug 10 17:11 |
| 95aug10 | 2975 | Aug 11 04:06 |
| 95aug11 | 3000 | Aug 12 04:02 |
| 95aug12 | 2962 | Aug 13 04:06 |
| 95aug13 | 2969 | Aug 14 04:11 |
| 95aug14 | 2994 | Aug 15 04:15 |

Table 1) Local PDT time when an 18 station distribution crosses the 3400 km "zeta" threshold.

When zeta crosses this 3400 km threshold, the automated GPS processing is initiated with the 18 optimally determined ground stations. An acceptable distribution of stations is generally available just after 4:00 AM PDT. This is 11 hours after the end of the processing day's UTC midnight, which is also the end of the processing day's data arc.

PROBLEM DETECTION AND CORRECTION OF THE GPS PROCESSING

Once an optimal distribution of stations is determined, a script is executed that computes the GPS orbits and clocks. This computation requires 6-7 hours of processing on an HP9000/735 workstation for a 27-hour data arc.

One of the first steps in the processing is to perform a fit to the broadcast ephemeris solution. This produces nominal starting conditions of the GPS spacecraft. The 3D rms of this fit is generally a few meters, which is the level of the precision of the broadcast orbits. Should the 3D rms of a GPS satellite exceed 100 meters, the satellite is automatically removed from the processing. In this way, GPS maneuvers are automatically detected. GPS maneuvers were successfully detected to have occurred on 95aug08 for GPS35, 95jul22 for GPS18, 95jul19 for

GPS15, 95jul12 and 95jul14 for GPS23, 95jul01 for GPS21, 95jun23 for GPS10, 95jun22 for GPS34, and 95jun17 for GPS19.

Another step of this GPS processing is to perform linear fits to the ground clock solutions as computed with pseudorange data and the broadcast orbits and clocks. This serves four purposes. First, the prefit (pre-filter) residuals are reduced to at most a few hundred meters. A simple prefit residual test in the filter is then used to remove gross data outliers. Second, clock jumps are detected and recorded. In the filtering process, all clocks are estimated as white noise processes relative to a reference clock. It is therefore undesirable to use a reference clock that has had a clock jump within the data arc. Third, this process aligns all the ground clocks to GPS time. This is particularly important since one of these clocks will serve as the reference clock. A linear fit to a hydrogen maser standard smooths the GPS SA effect to the 1/2 nanosecond level. And fourth, the detection of clock jumps can also aid in the removal of pseudorange outliers.

Even if a station appears to have a good clock based on pseudorange data, the phase data may not be acceptable. To determine this, after the first pass through the filter and smoother, the postfit residuals of the phase data are examined to determine if there are additional cycle-slips. If there are, phase breaks are inserted in the data file and the data is reprocessed through the filter/smoother. If excessive phase breaks need to be inserted, the entire pass is removed from the data file before reprocessing.

To remove outliers from the solution, a simple windowing method is used. If postfit (post-smoother) pseudorange residuals exceed 3 meters or postfit phase residuals exceed 5 cm, the outlying data points are removed with a decentralized SRIF downdating process [9]. When all the residuals are less than their specified window, the GPS orbits are then mapped within the data arc, and the smoothed GPS clocks are tabulated.

RESULTS OF THE GPS PROCESSING

GPS Orbit Precision Within the Data Arc

Orbit overlaps provide a preliminary assessment of the orbit precision. Figure 1 compares the 3-hour orbit overlaps between the JPL Flinn GPS orbits and the JPL quick-look GPS orbits. The average 3D rms overlap for the Flinn orbits is 18 cm; the average 3D rms overlap for the quick-look GPS orbits is 34 cm. Assuming that the daily orbits are relatively uncorrelated, dividing by $\sqrt{2}$ yields an approximate 3D orbit precision of 13 cm for JPL Flinn orbits and 24 cm for JPL quick-look orbits. This is

a pessimistic estimate of the precision since only the tails of the orbits are being used in this statistic. The overall precision of the orbits should be better than this, and especially so in the middle of the data arc.

Figure 2 shows the 3D orbit difference between the JPL Flinn GPS orbits and the JPL quick-look GPS orbits. The average 3D rms orbit difference is 21 cm. Assuming that the Flinn orbits are truth, the 3D precision and accuracy of the quick-look orbits are then 21 cm. This is in close agreement with the 24 cm 3D precision obtained from the orbit overlaps.

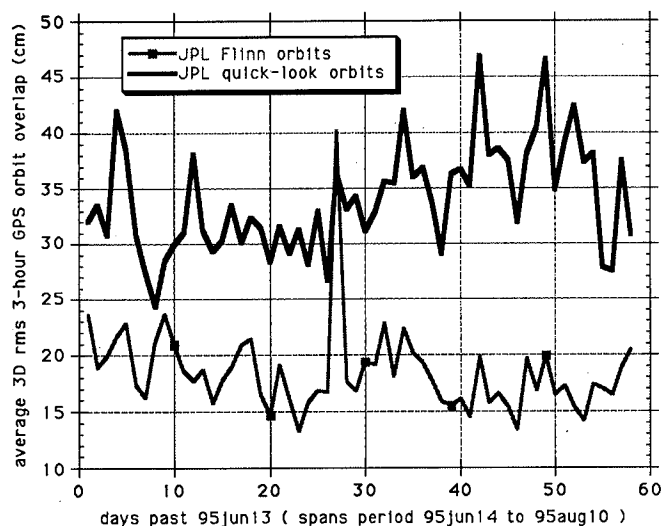


Figure 1) Orbit overlap comparison between JPL Flinn orbits and JPL quick-look orbits. Overlaps indicate a 3D precision of 13 cm for the Flinn orbits and 24 cm for the quick-look orbits.

Orbit Precision of Predicted GPS Orbits

After each GPS process completes, predicted GPS orbits are produced by combining the orbits of the current day with orbits from three previous days. Smoothing is used to remove discontinuities in the overlapping orbit segments. The combined 4-day solution is then fitted to empirically determined force models which include a solar-scale factor, a y-bias parameter, a constant down-track acceleration, and once-per-rev cross and down-track accelerations. Estimating twice-per-rev accelerations or going to longer or shorter than 4-day fits, degrades the precision of the predicted GPS orbits.

This solution is then integrated 3 days past the end of the data arc of the current day. Figure 3 shows the results of averaging 10 days (95jul27-95aug05) of GPS orbit differences between the predicted GPS orbits and the GPS orbits estimated within the data arc. After 24 hours, the 3D precision of the predicted GPS orbits is 1 meter (rms).

After 42 hours, the 3D precision of the GPS orbits is 2 meters (rms). At the 42 hour mark, new GPS orbits from the next day's processing are now available. (In Figure 3, the end of the next day's data arc occurs at 24 hours, the data are accumulated 11 hours after that, and the auto processing requires 6-7 hours to produce the next day's solution.) Therefore, better than 2 meter 3D GPS orbits are available in real-time.

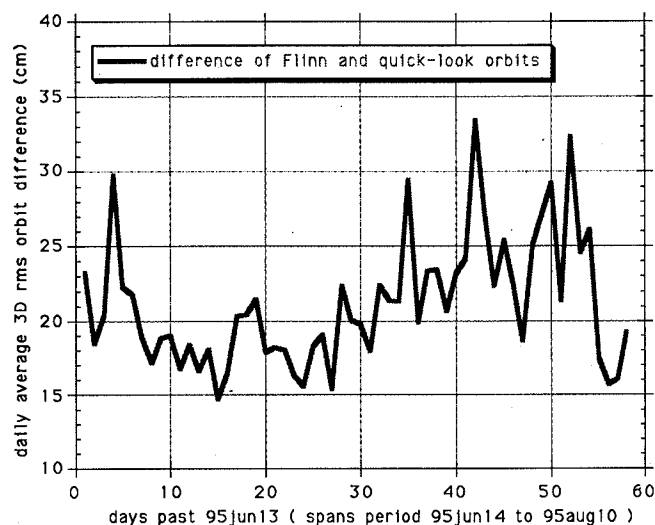


Figure 2) Orbit difference between JPL Flinn orbits and JPL quick-look orbits. The orbit difference shows the quick-look orbits have a 3D accuracy of 21 cm.

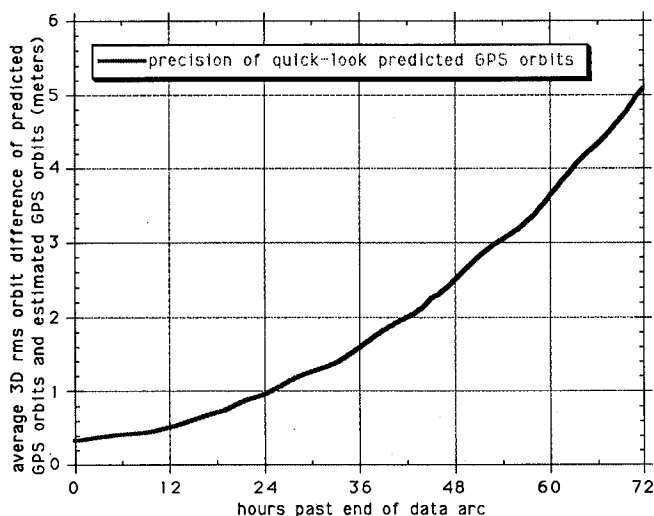


Figure 3) Precision of JPL quick-look predicted orbits. At 42 hour mark, next day's GPS orbits are available.

GPS Clock Precision

GPS clock precision can also be assessed by compiling the differences in the overlapping clock solutions of the daily fits. Table 2 shows the GPS clock overlap

differences for the JPL Flinn and JPL quick-look solutions. Averaging these numbers and assuming the overlapping clock solutions are uncorrelated, the JPL Flinn GPS clock precision is 0.27 nsec and the JPL quick-look GPS clock precision is 0.57 nsec.

| overlap period | rms of quick-look clock overlaps (nsec) | rms of Flinn clock overlaps (nsec) |
|-----------------|---|------------------------------------|
| 95jul23-95jul24 | 0.952 | 0.285 |
| 95jul24-95jul25 | 0.713 | 0.354 |
| 95jul25-95jul26 | 0.783 | 0.318 |
| 95jul26-95jul27 | 0.675 | 0.356 |
| 95jul27-95jul28 | 0.912 | 0.581 |
| 95jul28-95jul29 | 0.703 | 0.436 |
| 95jul29-95jul30 | 0.897 | 0.367 |

Table 2) rms differences of overlapping clock solutions. Overlaps indicate 0.27 nsec precision of the JPL Flinn GPS clocks and 0.57 nsec precision of the JPL quick-look GPS clocks.

Table 3 shows the clock differences between the JPL Flinn clock solutions and the JPL quick-look clock solutions. There are two days in this table with unusually high clock differences. On 95jul11, the reference clock selected by the quick-look processing was the receiver in Arequipa, Peru. This receiver's clock is not linked to a hydrogen maser. Since the Flinn reference clock is always linked to a hydrogen maser, the unusual large clock differences on 95jul11 reflects the instability of Arequipa's clock. On 95jul16, the quick-look process selected the receiver at Algonquin, Canada as a reference clock. Within the 27 hour data arc, the Algonquin receiver had a data outage of 80 minutes. This caused all the clocks in the system to float with a common error, and hence caused the large clock difference with the JPL Flinn solutions. Since this occurrence, additional measures have been built into the automated procedure to detect data outages at receivers and disallow their selection as a reference clock.

| solution day | rms difference of clock solutions (nsec) |
|--------------|--|
| 95jul02 | 0.52 |
| 95jul03 | 0.37 |
| 95jul04 | 0.48 |
| 95jul05 | 0.41 |
| 95jul06 | 0.41 |
| 95jul07 | 0.30 |
| 95jul08 | 0.43 |
| 95jul09 | 0.50 |
| 95jul10 | 0.52 |

| | |
|---------|--------|
| 95jul11 | 114.25 |
| 95jul12 | 0.42 |
| 95jul13 | 0.52 |
| 95jul14 | 0.53 |
| 95jul15 | 0.61 |
| 95jul16 | 249.28 |
| 95jul17 | 0.50 |

Table 3) rms clock differences between JPL quick-look and JPL Flinn clock solutions. The clock differences show that the quick-look clock solutions have an accuracy of 0.46 nsec.

Assuming that the JPL Flinn GPS clocks are truth, and excluding the days 95jul11 and 95jul16, the quick-look GPS clock precision and accuracy is 0.46 nsec. This is in close agreement with the 0.57 nsec precision as obtained from clock overlaps.

Precise Point Positioning

Precise point positioning uses the pre-determined GPS orbits and clocks to compute estimates of a receiver's clock, troposphere, station location, and phase biases. The processing time to point position a single station day on an HP9000/735 workstation is 2-3 minutes. Once the GPS orbits and clocks have been determined, this method can quickly and accurately compute the 100+ station locations of the IGS network.

Table 4 lists the 3D rms station coordinate repeatabilities of 17 globally distributed stations over the 5 week period 95jul02 to 95aug05. Most of the 3D rms repeatability can be attributed to the vertical precision of the station coordinates, while the horizontal precision is in general a few millimeters. The average 3D rms station coordinate repeatability when using the JPL Flinn solution is 16 mm; the average repeatability using the JPL quick-look solutions is 21 mm.

| station | Flinn solutions (mm) | quick-look solutions (mm) |
|------------------------|----------------------|---------------------------|
| Algonquin, Canada | 12.7 | 14.1 |
| Tidbinbilla, Australia | 8.9 | 17.9 |
| Fairbanks, US. | 14.6 | 12.7 |
| Kokee Park, US | 9.7 | 8.5 |
| Kootwijk, Netherlands | 7.5 | 11.1 |
| Madrid, Spain | 9.5 | 9.8 |
| Santiago, Chile | 31.7 | 43.6 |
| Tromso, Norway | 8.7 | 11.6 |
| Arequipa, Peru | 20.7 | 40.7 |
| Bermuda, UK | 16.1 | 18 |
| Kerguelen, France | 17.2 | 25.1 |

| | | |
|------------------------|------|------|
| Kitab, Uzbekistan | 16.2 | 28.3 |
| Maspalomas, Canary Is. | 10.6 | 13.2 |
| Nyalsund, Norway | 11.8 | 15.8 |
| Richmond, US | 30.9 | 41.9 |
| Shanghai, China | 17.4 | 27.5 |
| Usuda, Japan | 27.2 | 24.9 |

Table 4) 3D station coordinate repeatabilities.

Average 3D repeatability is 16 mm (rms) with JPL Flinn and 21 mm (rms) with JPL quick-look solutions.

User Position Error For a WAAS Network

The Wide-Area Augmentation System (WAAS) being developed by the FAA to aid in aircraft navigation is proposed to combine pseudorange data from 20-30 stations in the WAAS network and provide a combined GPS ephemeris and clock correction to the users of the system. Unlike the clock correction which must be computed in real-time, the ephemeris correction is predictable. Table 5 lists the user position errors computed in a WAAS network as a function of the type of GPS ephemeris employed. The method to obtain these user position errors is to simulate users throughout the WAAS network with precise GPS orbits and GPS clocks. This incorporates the error due to the real GPS clocks. The user's position and clock at every data epoch is then estimated using the WAAS GPS ephemeris (the "slow" correction), and estimated GPS clocks (the "fast" correction) as determined by a WAAS network [10]. For this table, the estimated GPS clocks were computed with pseudorange data from 13 stations in the WAAS network.

| type of orbit | vertical rms (meters) | 3D rms (meters) |
|--|-----------------------|-----------------|
| broadcast ephemeris orbit | 1.79 | 2.29 |
| dynamic orbit computed with WAAS network | 0.76 | 0.90 |
| quick-look orbit | 0.43 | 0.49 |
| 1-day predicted | 0.49 | 0.55 |
| 2-day predicted | 0.58 | 0.64 |
| 3-day predicted | 0.60 | 0.68 |

Table 5) User position error as a function of orbit. The "2-day predicted" orbits are real-time GPS orbits.

Although the broadcast ephemeris orbits are accurate to 8 meters (3D rms), the resulting 3D user position error after estimating the GPS clocks is 2.3 meters (rms). This is a result of the clock correction absorbing much of the orbit error. The column labeled "dynamic orbits

computed with the WAAS network" are filtered orbits which use pseudorange data from the WAAS network. The 3D precision of these orbits over the WAAS network is 2.5 meters (rms). The resulting 3D user position error is 0.9 meters (rms). The quick-look and predicted orbits are those generated by the described quick-look GPS processing. The 2-day predicted orbits are essentially real-time GPS orbits. The corresponding 3D user position error is 0.64 meters (rms).

Estimates of Earth Orientation

An important by-product of this GPS process is to provide timely estimates of Earth orientation parameters, pole motion and UT1R-UTC. The two components of polar motion can be directly observed by GPS. However only a time rate of change of UT1R-UTC can be observed since the GPS constellation is insensitive to absolute UT1R-UTC. By integrating this time rate of change, UT1R-UTC can be recovered except for an initial bias. The initial bias must be provided by an external source such as VLBI measurements. The error introduced into the estimate of UT1R-UTC computed in this fashion is expected to resemble a random-walk. Therefore it is not so much the scatter in the estimate of derivative of UT1R-UTC, but the mean of this estimate that will determine how far UT1R-UTC will wander from the truth.

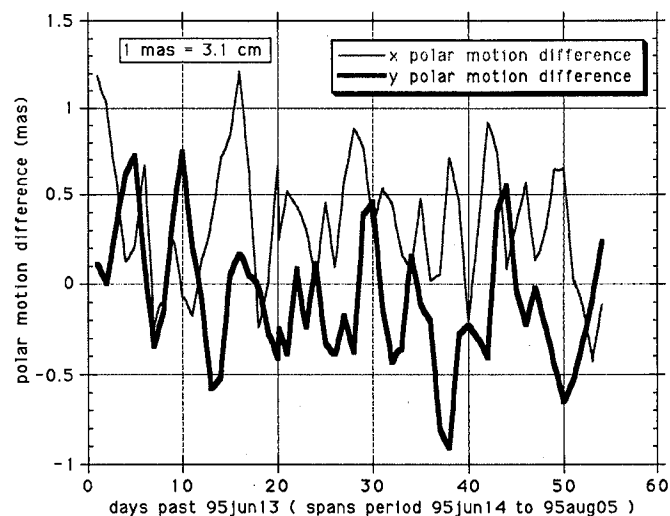


Figure 4) Difference of the JPL quick-look polar motion series and the IERS Bulletin B Final series.

Figure 4 shows the difference between the IERS Bulletin B Final² series [11] and the JPL quick-look polar

² IERS Bulletin B combines estimates of the Earth's orientation from Very Large Baseline Interferometry (VLBI), Lunar and Satellite Laser Ranging (LLR, SLR), and GPS. It is available 1 month after real-time.

motion solutions. 1 mas (milli-arcsecond) is equivalent to 3.1 cm at the Earth's surface. The statistics of these differences are compiled in Table 6. The mean in the statistics represents a known misalignment of the station coordinates, hence the sigma is a more representative number of the precision.

| component | mean (mas) | sigma (mas) | rms (mas) |
|---------------|------------|-------------|-----------|
| x pole motion | 0.34 | 0.33 | 0.48 |
| y pole motion | -0.10 | 0.34 | 0.35 |

Table 6) Difference of the JPL quick-look polar motion series and the IERS Bulletin B Final series. The quick-look solutions yield an equivalent 1-cm precision of the Earth's pole position.

The time derivative of UT1R-UTC is more commonly expressed as a length-of-day (LODR):

$$\text{LODR} \equiv -86400 \frac{\partial}{\partial t} (\text{UT1R-UTC}) \quad (5)$$

Figure 5 shows the LODR for the JPL quick-look solutions and the IERS Bulletin B Final series. The rms difference between these series is 0.042 msec (milliseconds); the mean is 0.0002 msec. The rms difference between the JPL quick-look series and JPL's Kalman Earth Orientation Filter (KEOF) which makes use of VLBI measurements over the period 95jun14 to 95aug28 is 0.034 msec; the mean is 0.001 msec.

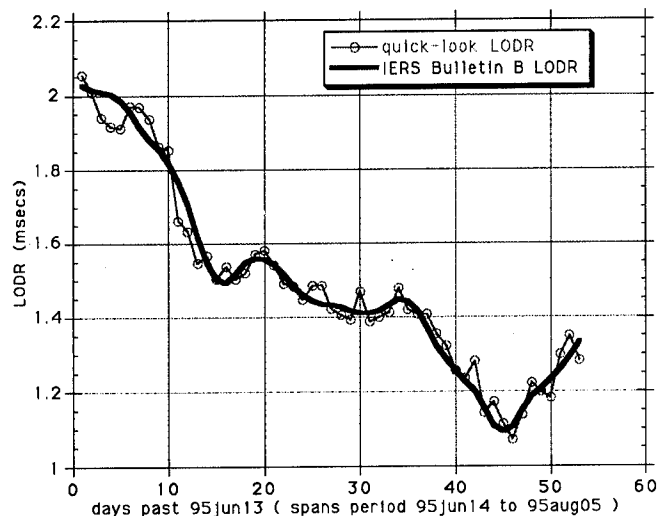


Figure 5) Length-of-day of the JPL quick-look solutions and of the IERS Bulletin B Final series.

Figure 6 shows the difference between the integrated LODR quick-look series and the IERS Bulletin B Final UT1R-UTC series. An initial bias was first removed from the integrated LODR series so that the difference of these series would start at zero. The rms difference is 0.18 msec over the 2 month period. This amount of rotation

corresponds to 8.3 cm on the Earth's equator. The random-walk nature of the integrated error is clearly evident.

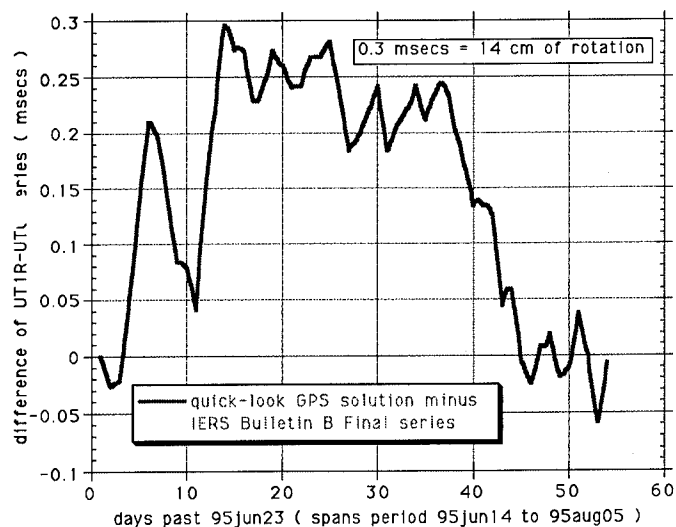


Figure 6) Difference of JPL quick-look integrated LODR solution and IERS Bulletin B Final series for UT1R-UTC.

TOPEX PROCESSING RESULTS

The method to compute the Topex/Poseidon orbit is to make use of the predicted GPS orbits and solve for the GPS clocks. It is sufficient to use a network of 12 stations for this purpose. Table 7 shows the local PDT time that the value of zeta, as computed for an optimal distribution of 12 ground stations, crosses 4000 km for the first two weeks of August 1995.

| solution day | zeta (km) for 12 stations | local PDT time zeta crosses 4000 kms |
|--------------|---------------------------|--------------------------------------|
| 95aug01 | 3807 | Aug 01 22:13 |
| 95aug02 | 3827 | Aug 02 22:03 |
| 95aug03 | 3956 | Aug 03 22:07 |
| 95aug04 | 3873 | Aug 05 02:11 |
| 95aug05 | 3899 | Aug 06 02:06 |
| 95aug06 | 3901 | Aug 07 02:13 |
| 95aug07 | 3930 | Aug 07 22:05 |
| 95aug08 | 3877 | Aug 08 22:04 |
| 95aug09 | 3995 | Aug 10 09:01 |
| 95aug10 | 3827 | Aug 10 22:14 |
| 95aug11 | 3865 | Aug 11 21:10 |
| 95aug12 | 3762 | Aug 13 02:03 |
| 95aug13 | 3807 | Aug 13 22:03 |
| 95aug14 | 3792 | Aug 15 01:11 |

Table 7) Local time when a 12 station distribution crosses the 4000 km "zeta" threshold.

When zeta crosses 4000 km, a secondary process is automatically initiated with the 12 optimally determined ground stations. An acceptable distribution of stations is generally available just after 2:00 AM PDT. This is 9 hours after the end of the processing day's UTC midnight. The process to determine the GPS clocks and T/P orbit requires 2-3 hours on an HP9000/735 workstation. By 5 AM PDT, 12 hours after the end of the data arc, T/P orbits are available. If the radial component of the orbit overlap with the previous day is less than 20 cm, the orbit solution is FTP'd to the sponsor's computer. An e-mail message is compiled reporting the orbit overlaps, residual information, and problems that may have occurred during the processing.

Figure 7 shows the radial and down-track components of the orbit overlaps for the period 95jul26 to 95sep02. The average radial, cross-track, and down-track overlaps for this period are 7.8 cm, 8.8 cm, and 22.1 cm, respectively. If the errors in the overlaps are independent, then this would imply a radial orbit precision of 5.5 cm (rms) and a 3D orbit precision of 18 cm (rms).

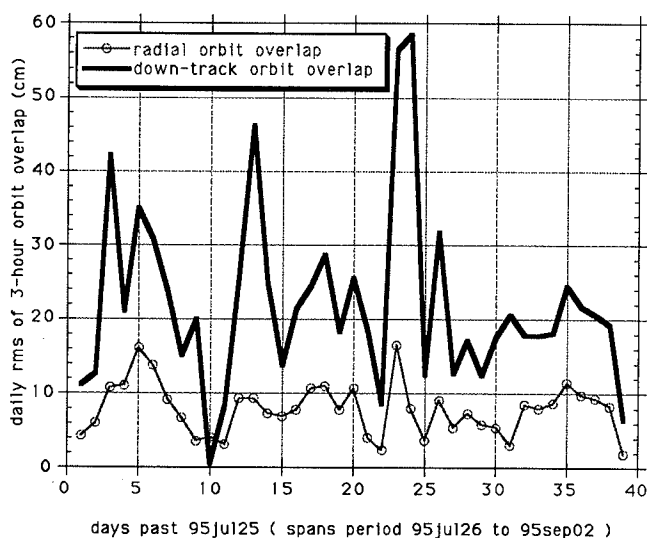


Figure 7) Radial and down-track components of Topex/Poseidon orbit overlaps.

An additional method for assessing the radial orbit accuracy relies on altimeter data collected by the spacecraft. T/P carries a nadir-pointing radar altimeter that can measure the range to the sea surface. These range measurements can be used together with the radial ephemeris to determine the geocentric height of the sea surface. At the points in the ocean where the satellite ground tracks intersect on ascending and descending passes, two such determinations of sea height can be made. In the absence of errors in the orbit and in the media corrections to the altimeter range, the height

difference at the crossing point location is a measure of the true variability of the ocean surface. The difference of the crossover variances with the NASA Precise Orbit Ephemeris, which has a radial precision of < 3.5 cm (rms), indicates that the radial precision of the GPS determined T/P orbits produced by the described processing is 5.0 cm (rms). This is in close agreement with the 5.5 radial precision obtain by computing the orbit overlaps. Note that when AS is off, the T/P receiver operates as a dual-frequency receiver and 2.0 cm (radial) T/P orbits are possible [12].

Figures 8 and 9 show a 10-day average (95jul27-95aug05) of the predicted radial and 3D orbit precision after 48 hours of integration. At the 36 hour mark, a new T/P orbit solution is available from the next day's processing. Hence real-time T/P orbits with a radial precision of 50 cm (rms) and a 3D precision of 15 meters (rms) are available in real-time.

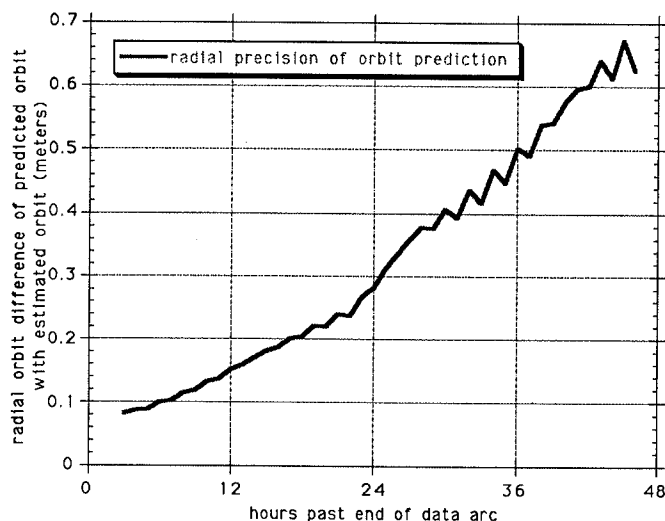


Figure 8) Radial difference of T/P's predicted orbit and the estimated orbit within the data arc.

GPSMET PROCESSING RESULTS

The same technique of using fixed orbits and solving for GPS clocks has also been applied to the GPSMET data to determine the precise orbit ephemeris of the MicroLab II satellite. Precision orbit determination is necessary for proper calibration and processing of the GPS radio occultation data. It is the accuracy of the velocity that is most critical to the experiment. Since the occultation experiment is looking at GPS signals at low elevation angles relative to the spacecraft zenith, the GPS antenna is pointed perpendicular to the spacecraft zenith. This is not an ideal orientation for orbit determination. Although Anti-Spoofing (AS) does not effect orbit determination, it does have a significant effect on the occultation

experiment. Data processing has thus concentrated on the 2 three-week periods in 1995 when AS was off. Here we examine a one week period from June 23, 1995 through June 30, 1995. Currently, orbit determination is not the limiting error source for the occultation experiment and little effort has gone into tuning the dynamic or reduced-dynamic orbits. We believe there is substantial room for improving the orbits which are currently at the decimeter level.

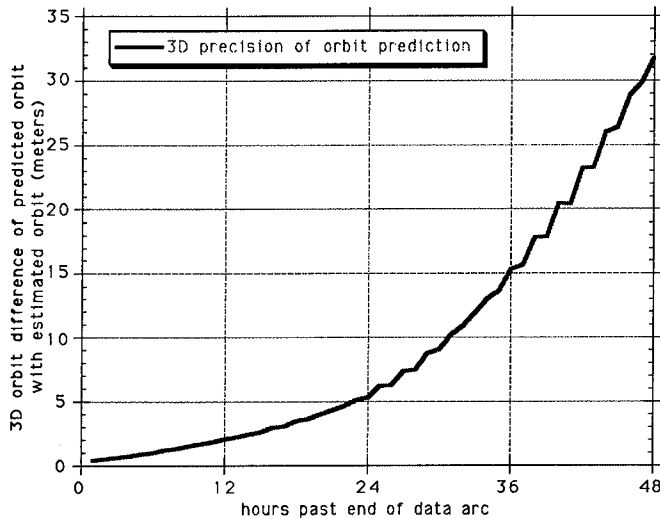


Figure 9) 3D difference of T/P's predicted orbit and the estimated orbit within the data arc.

Reduced-dynamic phase and range residuals are 2.4 cm and 76 cm respectively; the dynamic phase and range residuals are 3.4 cm and 79 cm. There is not continuous tracking data from the GPSMet flight receiver. These data gaps are not due to the receiver operation but other spacecraft and ground systems. Table 8 shows a list of data gaps larger than a one-half hour duration for the period of June 23-30. Note the large gaps in data around midnight June 25/June 26, around midnight June 27/June 28, and on June 24.

| start of gap | end of gap | hours |
|---------------|---------------|-------|
| 95jun23 16:26 | 95jun23 18:04 | 1.6 |
| 95jun24 06:52 | 95jun24 23:54 | 17 |
| 95jun25 06:07 | 95jun25 10:17 | 4.2 |
| 95jun25 16:36 | 95jun26 00:32 | 7.9 |
| 95jun26 07:03 | 95jun26 09:21 | 2.3 |
| 95jun26 15:15 | 95jun26 15:45 | 0.5 |
| 95jun26 15:52 | 95jun26 17:38 | 1.8 |
| 95jun27 15:06 | 95jun28 01:45 | 11 |
| 95jun28 14:21 | 95jun28 16:01 | 1.7 |
| 95jun29 15:17 | 95jun29 15:53 | 0.6 |
| 95jun30 05:47 | 95jun30 09:43 | 3.9 |
| 95jun30 14:32 | 95jun30 16:22 | 1.8 |

Table 8) Data gaps in the GPSMet data, June 23, 1995-June 30, 1995.

Table 9 shows the rms overlaps for this time span. The large data gaps on June 24 and between June 25/26 are responsible for the large orbit overlaps for these days. Excluding these excessive overlaps, the average reduced-dynamic overlaps are 6.8 cm, 4.8 cm, and 11 cm in the radial, cross, and down-track components, respectively

| overlap period | H (cm) | C (cm) | L(cm) |
|-----------------|--------|--------|--------|
| 95jun23/95jun24 | 10.4 | 04.9 | 19.6 |
| 95jun24/95jun25 | 39.7 | 16.3 | 226.7 |
| 95jun25/95jun26 | 67.9 | 43.5 | 1080.3 |
| 95jun26/95jun27 | 6.1 | 1.5 | 9.0 |
| 95jun28/95jun29 | 4.5 | 4.8 | 9.7 |
| 95jun29/95jun30 | 6.3 | 7.9 | 8.3 |

Table 9) Reduced-dynamic overlaps for MicroLab I, June 23, 1995-June 30, 1995.

CONCLUSION

A highly automated GPS data processing system has been developed around JPL's GIPSY/OASIS II software. The process determines when there is a sufficient distribution of ground stations from the IGS network. When such a configuration is achieved, a GPS orbit solution is computed. At completion, the GPS orbit and GPS clock solutions are placed in a data base and an e-mail message is sent out reporting residuals and orbit overlaps with the previous day's solution. The 3D precision of these GPS orbits within the data arc is < 25 cm (rms). In addition, the GPS orbits are predicted such that the 3D precision of these real-time orbits is < 2 meters (rms).

A second automated process makes use of the predicted GPS orbits for orbit determination of the Earth orbiter Topex/Poseidon. When a sufficient distribution of ground stations is available, a T/P orbit solution is computed. At completion, the orbit solution is placed on the sponsor's computer and an e-mail message reports T/P's orbit overlaps, residuals, and data outliers. The 3D precision of these T/P orbits within the data arc is 18 cm (rms). These orbits are generally available within 12 hours after the end of the data arc.

Both these processes are completely automated and require no human intervention. Problems are automatically detected and corrected by the expert system.

ACKNOWLEDGEMENT

The work described in this paper was carried out in part by the Jet Propulsion Laboratory, California Institute of Technology, under contract with the National Aeronautics and Space Administration. A portion of the work was sponsored by the Naval Oceanographic Office, and we thank in particular J. Blaha for his support.

REFERENCES

- [1] Muellerschoen, R. J., Bertiger, W. I., Wu, S. C., Munson, T. N., Zumberge, J. F., Haines, B. J., Accuracy of GPS Determined Topex/Poseidon Orbits During Anti-Spoof Periods, Institute of Navigation Conference, 1994 National Technical Meeting, San Diego, CA, January, 1994.
- [2] Srinivasan, J. M., Meehan, T. K., Young, L. E., Code and Codeless Ionospheric Measurements with NASA's Rogue GPS Receiver, Institute of Navigation Conference, Colorado Springs, Colorado, September 1989.
- [3] Cangahuala, L., Muellerschoen, R. J., Yuan, D., Graat, E., Guinn, J. R., Topex/Poseidon Precise Orbit Determination: Quick-Look Operations with SLR and GPS Data, AAS/AIAA Astrodynamics Conference, Halifax, Nova Scotia, Canada, August 1995.
- [4] Hajj, G., Bertiger, W. I., Kursinski, E., Leroy, S., Romans, L., Schofield, J., Initial Verification of the GPS-LEO Occultation Technique of Mapping the Neutral Atmosphere with the GPSMet Experiment, Institute of Navigation Conference, Palm Springs, CA, September 1995.
- [5] Zumberge, J. F., Webb, F. H., An Introduction to GIPSY/OASIS II, JPL Course Notes, Boulder Colorado, July 1993.
- [6] Bar-Sever, Y. E., A New GPS Yaw Attitude Model - Design and Performance, Institute of Navigation Conference, Palm Springs, CA, September 1995.
- [7] Zumberge, J. F., Jefferson, D. C., Blewitt, G., Heflin, M. B., Webb, F. H., Jet Propulsion Laboratory IGS Analysis Center Report, 1992, *Proceedings of the 1993 IGS Workshop*, edited by G. Beutler and E. Brockmann, pp. 154-163, Astronomical Institute, University of Berne, 1993.
- [8] Zumberge, J. F., Neilan, R. E., Mueller, I. I., Densification of the IGS Global Network, IGS Workshop, Pasadena, CA, December 1994.
- [9] Muellerschoen, R. J., Dowdating a Time-Varying Square-Root Information Filter, Flight Mechanics/Estimation Theory Symposium, Greenbelt, Maryland, May 1990.
- [10] Ceva, J. C., Bertiger, W. I., Muellerschoen, R. J., Parkinson, B., Incorporation of Orbit Dynamics to Improve Wide Area Differential GPS, Institute of Navigation Conference, Palm Springs, CA, September 1995.
- [11] Boucher, C. Z., Altamimi, Duhem, L., ITRF 91 and Its Associated Velocity Field, *IERS Technical Note 12*, Central Bureau of IERS, Observatoire de Paris, October 1992.
- [12] Bertiger, W. I., Yunck, T. P., Gold, K., Guinn, J. R., Reichnert, A., Watkins, M. M., High Precision and Real-Time Tracking of Low Earth Orbiters with GPS: Case Studies with Topex/Poseidon and EUVE, Invited Talk, *Proceedings of the 3rd Workshop on High Precision Navigation*, Stuttgart, Germany, pgs. 97-107, April 1995.

GPS Multipath Modeling and Verification Using Geometrical Theory of Diffraction

Susan Gomez, Robert Panneton, and Penny Saunders
NASA/Lyndon B. Johnson Space Center

Shian Hwu and Ba Lu
Lockheed Martin Engineering & Sciences Company

BIOGRAPHY

Susan F. Gomez is an Aerospace Engineer at NASA-JSC where she has been working on attitude determination for the Space Station since 1993. She received her B.S. from the University of Texas in 1992.

Mr. Robert Panneton received a Bachelor of Electrical Engineering degree from the Catholic University of America in Washington, DC and a MSEE from the University of Illinois in Champaign - Urbana, Illinois as a commissioned officer in the United States Air Force. From 1967 to 1975 he was with TRW Systems Group in Houston, Texas supporting the Johnson Space Center (JSC) in RF communications analysis during the Apollo, Skylab, and Apollo-Soyuz Test Project Programs. He worked for Lockheed Martin Engineering & Sciences Co. in support of the Shuttle Program in the area of communications performance test predictions. He has been employed by NASA/JSC since 1988 working in the area of Space Station antenna system development and performance.

Penny Saunders received a Bachelor of Science degree in Physics from the University of West Florida and a Masters of Science degree in Electro-optics from the University of Houston-Clear Lake. She has been with NASA Johnson Space Center since 1984. She currently serves as manager for the GPS development and test project for the International Space Station Alpha. She has spent the past eight years working on GPS-related projects for the Space Station, Space Shuttle, and other advanced programs.

Dr. Shian Hwu received a diploma from National Taipei Institute of Technology, the M.S. degree from The University of Mississippi, and the Ph.D. degree from University of Houston, all in Electrical Engineering. He was a communication engineer in Taiwan from 1979 to 1982. From 1984 to 1989 he was with the Applied Electromagnetics Lab., University of Houston. He joined Lockheed Martin Engineering and Sciences Co. in 1990 and is now a principal engineer working on antenna development and multipath analysis for communications and tracking systems.

Mr. Ba P. Lu received an Electrical Engineer degree from ESE (Ecole Superieure d'Electricite) in France in 1956 and a MSEE from the University of Pennsylvania in 1971. He has over 35 years of experience in the field of

telecommunications. He has been with Lockheed Martin Engineering and Sciences Co. at the Johnson Space Center for the past fifteen years working on the development, analysis, measurement and evaluation of antenna systems for space programs.

ABSTRACT

In this paper, Uniform Geometrical Theory of Diffraction (GTD) is applied to model and verify the differential carrier phase errors due to multipath for a series of GPS multipath ground tests. The computer simulation technique for predicting GPS signal strength and phase shift is presented. A comparison with experimental measurements was made for two typical International Space Station interference structures: a plate and a cylinder.

Differential carrier phase error results obtained with the GTD model are compared with field test data. Good agreement was noted as well as some discrepancies observed, probably due to the antenna phase center deviation in the low elevations and background noise present in the field test data. Selected measured and predicted differential carrier phase error results are presented and compared. Obtained results indicate that reflections from and diffractions around the multipath producers, located near the GPS antennas, can produce phase shifts of greater than 10 mm. The multipath effects are evident in both the phase shift patterns and in the gain patterns.

INTRODUCTION

The International Space Station (ISS) will use the Global Positioning System (GPS) to provide position, velocity, attitude determination, and time reference. Multipath is a significant error source for GPS attitude determination (Ref 1). The ISS GPS antennas are surrounded by many microwave energy reflecting structures such as various solar panels, thermal radiators, Russian science power platform tower, communications antennas, video cameras and many attached payloads. To characterize the multipath environment for the ISS GPS subsystem, a rigorous computational electromagnetic method, the Uniform Geometrical Theory of Diffraction (GTD), was proposed to calculate the error on the gain and phase of the differential carrier phase measurements due to multipath for the ISS GPS subsystem. In the microwave frequency region, reflection and diffraction become the

dominant mechanisms of interaction between electromagnetic waves and scattering structures. The GTD technique has been used successfully to predict microwave propagation characteristics by taking into account the dominant multipath components due to reflections and diffractions from scattering structures. To evaluate the GTD modeling technique for the ISS GPS multipath model development, a series of GPS multipath field tests that simulated the ISS GPS multipath environment were performed using the NASA/Johnson Space Center GPS and Antenna Laboratory test facilities.

GPS ANTENNA

The antenna is an important element for the GPS receiver system. The GPS antenna receives and translates the GPS satellite signal into amplitude and phase information that is input to the GPS receiver. Therefore, GPS system performance is dependent on the antenna design and resulting antenna patterns.

Two different antennas types, Trimble microstrip patch antennas, shown in Figure 1, and Micropulse choke-ring antennas shown in Figure 2a, were used in this study. The patch antenna is smaller and provides a wider beamwidth, thus better hemispherical coverage. The choke ring antenna consists of several concentric metallic circular fins on a ground plane. The concept is similar to corrugations found on a corrugated horn antenna. The antenna radiating elements are located at the center of the ground plane. The purpose of the choke-ring ground plane is to provide multipath rejection in the low elevation angles and thus better performance for a GPS system operated in a multipath environment. Therefore, the radiation pattern usually exhibits higher boresight and lower broadside gains and better axial ratio. The choke ring antenna is larger and weighs more than the simple microstrip patch antenna.

Since the GPS antenna is right hand circular polarized, it is convenient to represent the antenna patterns in terms of right hand circular polarized (RHCP) and left hand circular polarized (LHCP) field components rather than the commonly used vertical and horizontal linear field components. The definitions of the GPS antenna patterns are shown below.

The electric field at any point in space for the GPS antenna patterns is defined by:

$$\mathbf{E} = \mathbf{r}E_r + \mathbf{l}E_l$$

where the direction unit vectors, \mathbf{r} and \mathbf{l} , for the RHCP and LHCP fields are:

$$\mathbf{r} = \frac{1}{\sqrt{2}}(\bar{\theta} - j\bar{\phi})$$

$$\mathbf{l} = \frac{1}{\sqrt{2}}(\bar{\theta} + j\bar{\phi})$$

and the RHCP and LHCP field components, E_r and E_l are:

$$E_r = \frac{1}{\sqrt{2}}(E_\theta + jE_\phi)$$

$$E_l = \frac{1}{\sqrt{2}}(E_\theta - jE_\phi)$$

where E_θ and E_ϕ are the linear field components in the θ and ϕ directions defined in conventional spherical coordinates.

In this study, the GPS antenna was modeled as a point source with combination of a RHCP pattern and a LHCP pattern that were obtained from the antenna patterns measured in NASA/JSC's anechoic chamber. This simple model provides valid results only for multipath producers located in the far-field range of the GPS antenna. The far-field range R is determined by:

$$R = 2D^2 / \lambda$$

where D is the antenna dimension and λ is the wavelength. For omni type low gain GPS antennas, such as those used in the field tests, D is usually between 0.5λ and 1λ . For the worst case assumption $D=\lambda$, the far-field range $R=2\lambda$ which is about 0.4 meter for GPS L1 frequency. The radiation pattern of this simple equivalent radiation source antenna model exhibits the same polarization sense and similar characteristics as the measured GPS antenna in both gain and phase only in the far field. If multipath producers are located in the near-field distance from the GPS antenna, a more complex antenna model is required to simulate the currents on the antenna to take into account the near field effects.

All GPS antennas are modeled as transmitting sources in this analysis. By reciprocity, the transmitting and the receiving patterns of an antenna are identical.

FIELD TEST DATA COLLECTION

The measured differential carrier phase data was collected on the Building 14 antenna range at NASA - JSC from Julian Day (JD) 045 to JD082 (February 14 - March 23, 1995) using two GPS receivers and two sets of 4 antennas. The test site was selected to be as far away as possible from unintentional multipath producers. For the data collected from JD045 to JD068, both a Trimble Advanced Navigation System (TANS) Vector and TANS Quadrex were used to collect data. For the data collected from JD072 to JD082 only the TANS Quadrex was used. For the test days when both receivers were used, the signal from the antennas was split and sent to both receivers. The only difference between the receivers is that the Vector has the software to compute an attitude, whereas the Quadrex outputs the measurements necessary to compute attitude, but does not compute an attitude internally. The antennas were mounted to an optical table in a 2 foot square planar configuration. The optical table used during this test is flat to within 3 millimeters over its 4 ft. by 8 ft. surface and had been leveled to within 30 arc seconds using a bubble level. The antennas were mounted directly to the table on 3.5 inch tall aluminum mounts that screwed into the optical table. A 12 ft. by

12 ft. ground plane rested on the optical table and was flush with the antennas. The ground plane was constructed out of standard wood 2 by 4's with 3 sheets of aluminum sheeting screwed into the 2 by 4's. Holes were cut into the ground plane to accommodate the antennas. Each receiver had a laptop computer to record the data from that receiver. Figure 1 shows the test setup.

Data was collected in approximately 24 hour periods. Data was collected with no intentional multipath producers and with each of 5 intentional multipath producers introduced individually. For this paper, the data from JD059 and JD074 are presented. For JD059, a 4 ft. by 12 ft. aluminum sheet was placed on the South side of the antennas and at a 45° angle. The Trimble microstrip patch antennas shown in Figure 1 were used for data collection on JD059. For JD074, a 3 ft. diameter, 4 ft. tall cylinder was placed vertically on the ground plane on the south side of the antennas. The Micropulse choke ring antennas shown in Figure 2a were used in combination with the cylinder shown in Figure 2b for data collection on JD074.

Only selected data are presented and discussed in this paper. A complete data package with all configurations investigated in this study can be found in Reference 2.

GEOMETRICAL THEORY OF DIFFRACTION

This section contains a very brief description of the Geometrical Theory of Diffraction (GTD). It outlines a key equation and concept which provide the foundations for this work. The GTD is one of the most widely used Computational Electromagnetics (CEM) techniques. The reasons for this include the increased availability of low cost but powerful computers, increasing interest in electromagnetic interactions with complicated geometry, and the simplicity of the method. The fundamentals of GTD can be understood more easily than other popular CEM techniques.

The GTD technique provides a high frequency approximate solution to the electromagnetic fields including incident, reflected, and diffracted fields and their interactions. They are obtained from an asymptotic solution of Maxwell's equations and are corresponding to the leading terms of the asymptotic expansion for large values of wavenumber or frequency. In the field computation using GTD, the incident, reflected, and diffracted fields are determined by the field incident on the reflection or diffraction point multiplied by a dyadic reflection or diffraction coefficient, a spreading factor, and a phase term. The reflected and diffracted field at a field point r' , $E^{r,d}(r')$, in general have the following form:

$$E^{r,d}(r') = E^i(r) D^{r,d} A^{r,d}(s) e^{-jks}$$

where

$E^i(r)$ is the field incident on the reflection or diffraction point r

$D^{r,d}$ is a dyadic reflection or diffraction coefficient

$A^{r,d}$ is a spreading factor

s is the distance from the reflection or diffraction point r to the field point r'

$D^{r,d}$ and $A^{r,d}$ can be found from the geometry of the structure at the reflection or diffraction point r and the properties of the incident wave at that point.

The application of GTD to a given radiation problem is first to decompose the scattering structure into simple geometrical shapes, and that the reflection and diffraction coefficients for these are known. Next, all field components contributing to the radiation intensity in the field point must be traced, and the individual contributions must be determined. The resultant field is given by summing all the complex contributing components:

$$E^{tot} = E^{inc} + \sum_{n=1}^N E_n^{ref} + \sum_{m=1}^M E_m^{dif}$$

where

E^{tot} is the total field at the observation point

E^{inc} is the direct incident fields from the antennas

E^{ref} is the reflected fields from the plates and cylinders

E^{dif} are the diffracted fields from plates and cylinders

More detailed information about GTD and the specific GTD code used in this study can be found in Reference 3.

DETERMINATION OF DIFFERENTIAL CARRIER PHASE ERRORS ON FIELD TEST DATA

The differential phase error is the measured differential phase subtracted from the ideal differential phase with the line bias compensated for. The measured differential phase is the differential phase measured by the receiver. The ideal differential phase was computed using the measured baselines and the reference or true attitude of the table as shown in the following:

$$\Delta\Phi_{ijideal} = u_j^T M_{Btrue}^{WGS84} b_i^B$$

where:

u_j^T is the transpose of the unit vector from the receiver to satellite j

M_{Btrue}^{WGS84} is the matrix that transforms from the body frame to WGS84 and represents the reference attitude

b_i^B is the baseline vector in the body frame from the master antenna to slave antenna i

The reference attitude was calculated using the following technique. Since the antennas were mounted directly to the optical table using precisely manufactured mounts, the attitude of the table was the same as the attitude of the antennas. Therefore, the roll and pitch of the reference attitude was 0 ± 30 arc seconds since the table had been leveled using a 30 arc second accurate bubble level. The

yaw of the table was determined by sighting the North Star using a theodolite that had been collimated off an optical mirror mounted to the optical table. A more thorough explanation of the method used to determine the reference attitude is given in Reference 4.

The baselines were computed by the TANS Vector receiver during its 'self survey' and were also computed mechanically. The baselines computed mechanically were computed from the center of each antenna using the following technique. Since the optical table contains mounting holes 1 in. \pm 0.001 in. over its entire surface, and the antennas were placed on mounts manufactured to within a tolerance of 0.001 in. so that the center of the antenna was directly over the center of the mounting screw that screwed into the optical table, the locations of the mechanical center of the antennas were determined by measuring the mounting holes on the table. The antennas were mounted in a two foot planar square array. For the results in this paper, the mechanical locations of the center of the antennas are used to determine the baselines.

The Vector receiver output its calculations of the baselines in East, North, UP (ENU) coordinates. The mechanical locations of the baselines were measured in body, or table, coordinates and transformed to ENU coordinates using the reference attitude. The greatest difference between the mechanically measured and 'self survey' baselines was 3.72 mm.

The line bias, β , is defined as the mean difference between the measured differential phase and the ideal differential phase:

$$\beta = \frac{1}{k} \sum_{t=1}^k (\Delta\Phi(t)_{ij_{measured}} - \Delta\Phi(t)_{ij_{ideal}})$$

where t is the measurement number and k is the total number of measurements.

The differential phase error contains errors due to noise and multipath and was computed as follows:

$$\Delta\Phi_{ij_{error}} = \Delta\Phi_{ij_{measured}} - \Delta\Phi_{ij_{ideal}} - \beta_j$$

COMPARISON BETWEEN GTD CALCULATED DIFFERENTIAL CARRIER PHASE ERRORS AND MEASURED DIFFERENTIAL CARRIER PHASE ERRORS

The multipath effects from the multipath producers were measured as differential carrier phase errors in mm which are the differences between the differential carrier phases measured by the GPS receivers in the field and the calculated ideal differential carrier phases with the line bias subtracted out. The GTD calculated differential carrier phase errors are the errors calculated using the computer simulation. The differential carrier phase errors are presented in millimeters of the total GPS carrier wavelength of 190.5 mm as a function of time, given in GPS time of week in hours.

The satellite tracks for two satellites on a day when no intentional multipath producer was added to the test setup are shown in Figure 3. The satellite tracks for satellites selected for comparison on JD059 and JD074 are shown in Figures 4 and 5. Figures 4 and 5 show the reflection region, the diffraction region, and the blockage regions as a function of the satellite azimuth and elevation.

It was noted in the data that on the days when no multipath producer was added to the test setup, there was still noticeable multipath at the lower elevations, usually less than 5 mm and of a low frequency, as shown in Figures 6 and 7. Notice that for satellite 4 in Figure 7, at the higher elevations (98.0 - 100.0 hours), very little background multipath is present, whereas at the lower elevations, as in Figure 6, there appears to be a multipath signature. The appearance of multipath errors at the lower elevations is probably due to the antenna phase center deviations from the average antenna phase center. The background multipath could also be due to the few structures in the area where data was taken. Building 14 and 18 are each located more than 400 m from the test site and a radio tower is located more than 100 m from the test site. Since these structures are so far away, the authors suspect the phase center motion as the probable cause of the multipath signature in the data on the days when no intentional multipath producer was included in the test setup.

Figure 8 shows the comparison between the measured data and the GTD data for satellite 16 on JD059, with the 4 ft. by 12 ft. aluminum plate. Since the direct signal is not present in the blockage region, only weak diffracted signals from around the edges and corners reach the antenna, as noticed in the blockage region (75.0 - 75.7 hours), where significant carrier phase shifts of greater than 10 mm are present. As a result of the interference between the direct signal and strong reflected signal, significant multipath errors on the differential carrier phase of between 5 and 10 mm were observed in the reflection region (75.7 - 78.3 hours). The observed multipath in the diffraction region (78.3 - 79 hours) is significantly lower, usually less than 5 mm. Similar observations are noted for Figure 9, which shows the comparison between the measured and GTD data for satellite 24 on JD059; however, satellite 24 does not move into the blockage region.

Figures 10 and 11 show similar results for JD074 and the 3 ft. diameter cylinder. Notice; however, that the cylinder produces much more significant phase shifts in the blockage region than was noted with the plate. This is due to the cylinder being placed closer to the antennas and vertical, making the blockage region larger. Notice also that satellite 4 on JD074 passes through the blockage region where both antennas are blocked, rather than just one, as was the case for satellite 16 on JD059.

The following summarizes the observations supported by the data presented in this section:

1. Structural blockages cause more than 10 mm (18.9°) phase shift
2. Reflections from and diffractions around the structures cause more than 5 mm (9.45°) phase shift.
3. In the low elevation angle region when no intentional multipath producer is present, two major concerns are antenna phase center deviation and background noise due to unwanted multipath from environment.

CONCLUSIONS

It was demonstrated that the phase errors due to multipath in the precision GPS applications can be modeled and characterized using the GTD technique. The multipath objects introduced more than 10 mm of phase shift in the data. This level of phase shift can produce significant errors in the attitude determination solution. It was also noted from the measured results when no multipath producer was present that there were significant phase errors in the low elevation regions that are probably due to the antenna phase center deviation in that region. This presents a challenging task for GPS antenna design to provide better phase center stability to minimize this error.

ACKNOWLEDGMENTS

The authors would like to acknowledge Jose R. Hernandez and Antha A. Adkins for their valuable contributions.

REFERENCES

1. Cohen, Clark E. and Bradford W. Parkinson, "Mitigating Multipath Error in GPS Based Attitude Determination," 14th Annual Guidance, Navigation and Control Conference, February 1991.
2. Gomez, S. F., R. J. Panneton, P. E. Saunders, S. U. Hwu, and B. P. Lu, "Multipath Field Test Report," not yet completed, contact authors for copy.
3. Marhefka, R. J., and J. W. Silvestro, "Near Zone - Basic Scattering Code User's Manual with Space Station Applications," NASA Contractor Report 181944, ElectroScience Laboratory, Ohio State University, December 1989.
4. Gomez, S., R. Carpenter, and C. Semar, "GPS Attitude Determination Performance Evaluation Using Ground Test Data", ION National Technical Meeting, Jan. 1995.

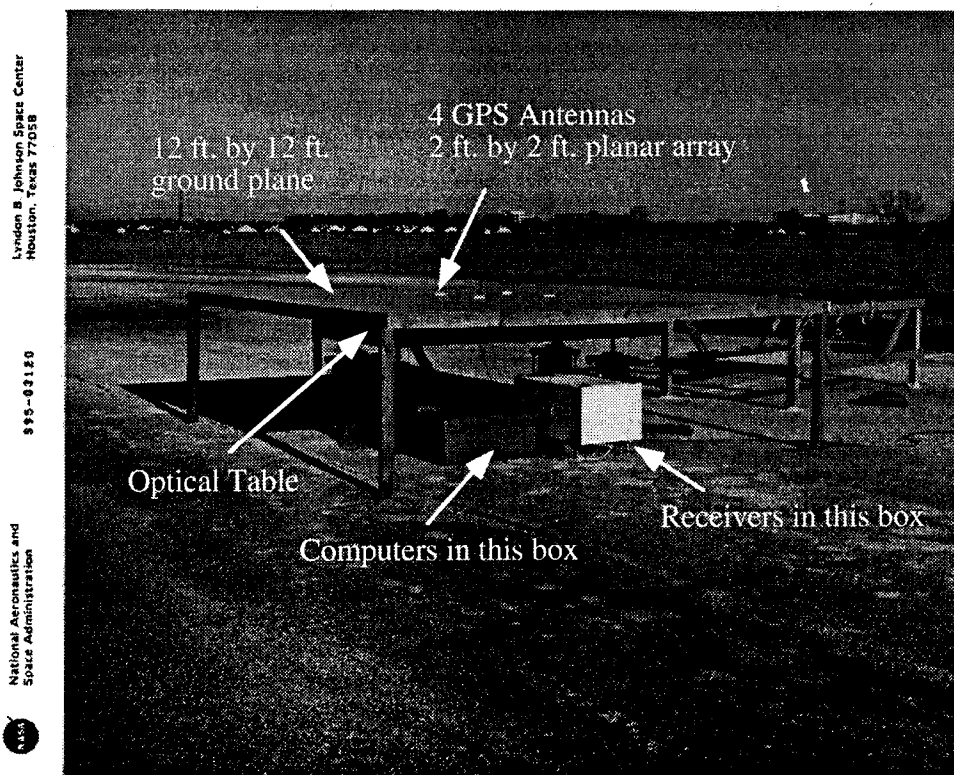


Figure 1 - Test Setup with No Multipath Objects and Patch Antennas

Lyndon B. Johnson Space Center
Houston, Texas 77058

595-04600

National Aeronautics and
Space Administration



Figure 2a - Test Setup with MicroPulse Choke Ring Antennas

Lyndon B. Johnson Space Center
Houston, Texas 77058

595-04233

National Aeronautics and
Space Administration

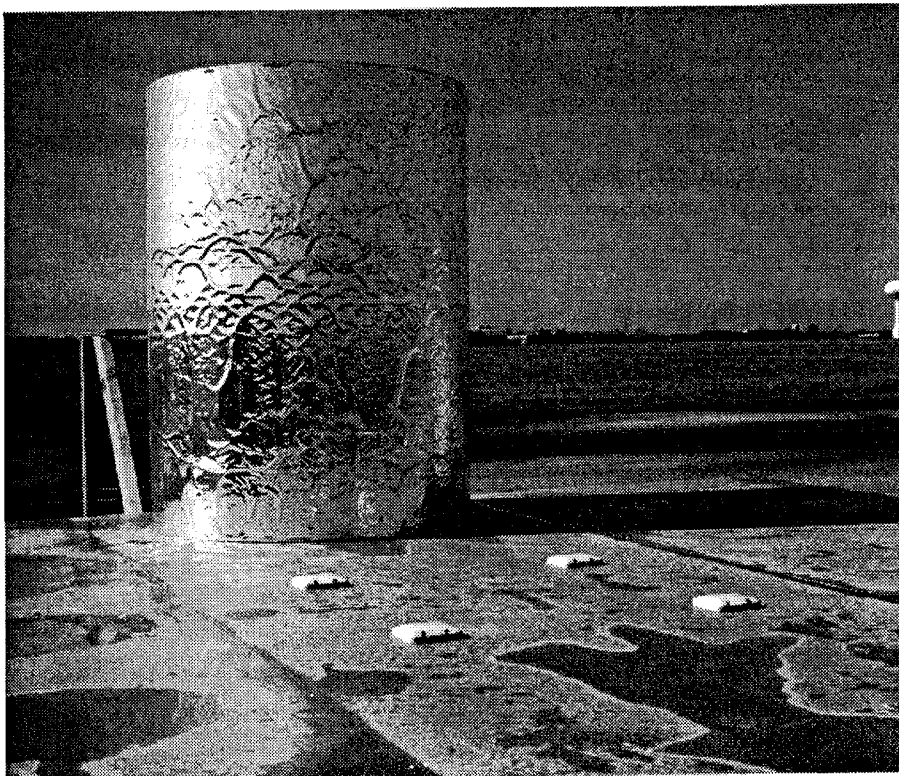


Figure 2b - Test Setup with 3 ft. Diameter Cylinder

Figure 3 - Satellite Tracks for JD046 With No Intentional Multipath Producers and Using Patch Antennas

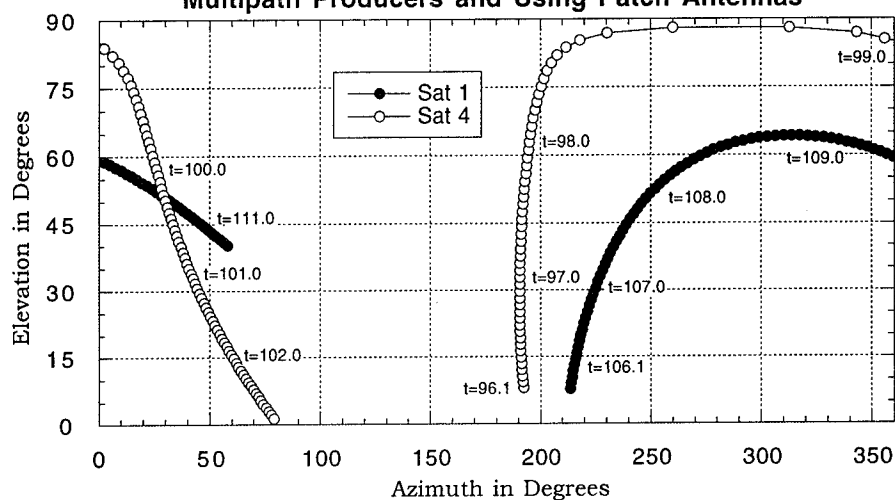


Figure 4 - Satellite Tracks for JD059 with 4 ft. by 12 ft. Aluminum Sheet

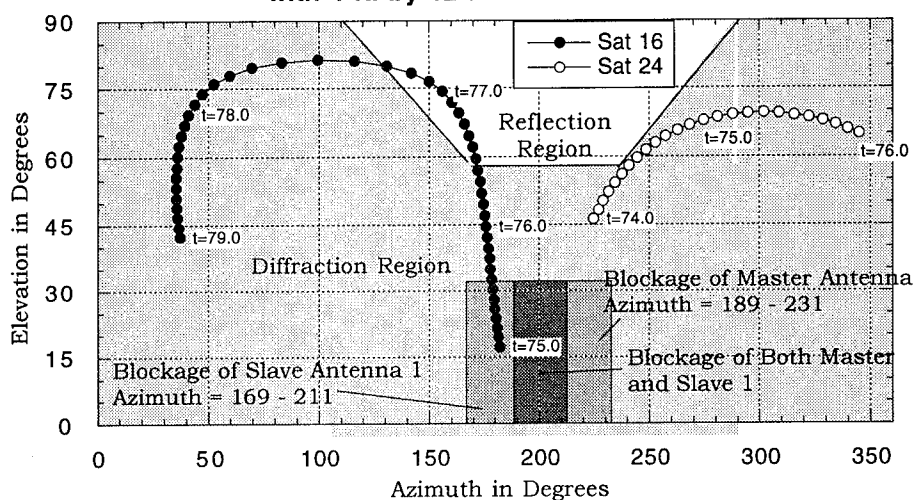


Figure 5 - Satellite Tracks for JD074 with 3 ft. Diameter Cylinder

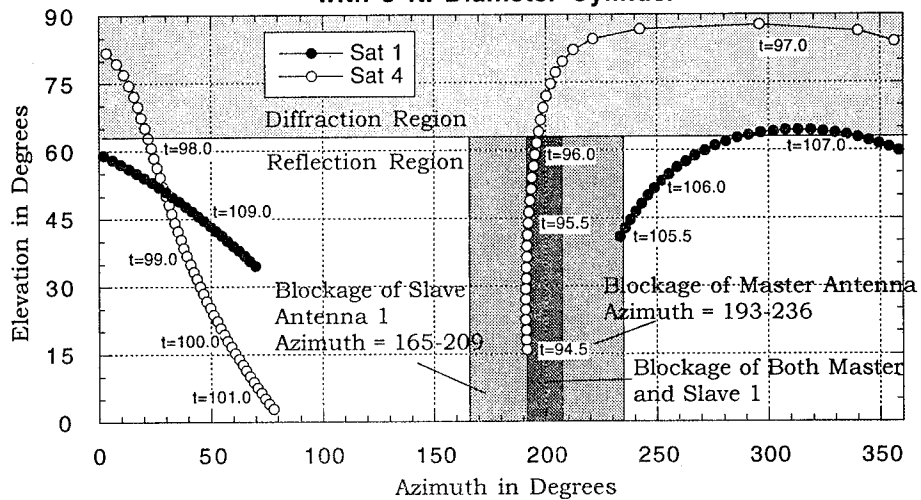


Figure 6 - Measured Differential Carrier Phase Error on JD046 with
No Intentional Multipath Producer - Satellite 1 Antenna 1

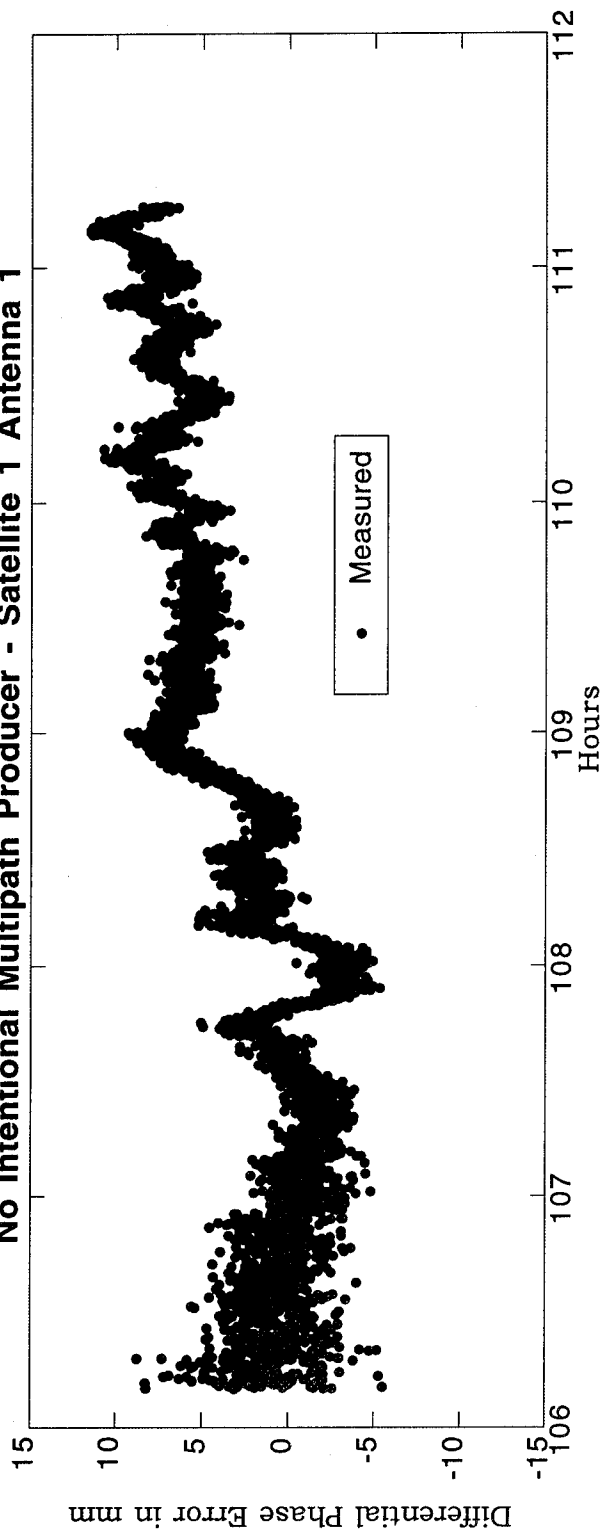


Figure 7 - Measured Differential Carrier Phase Error on JD046 with
No Intentional Multipath Producer - Satellite 4 Antenna 1

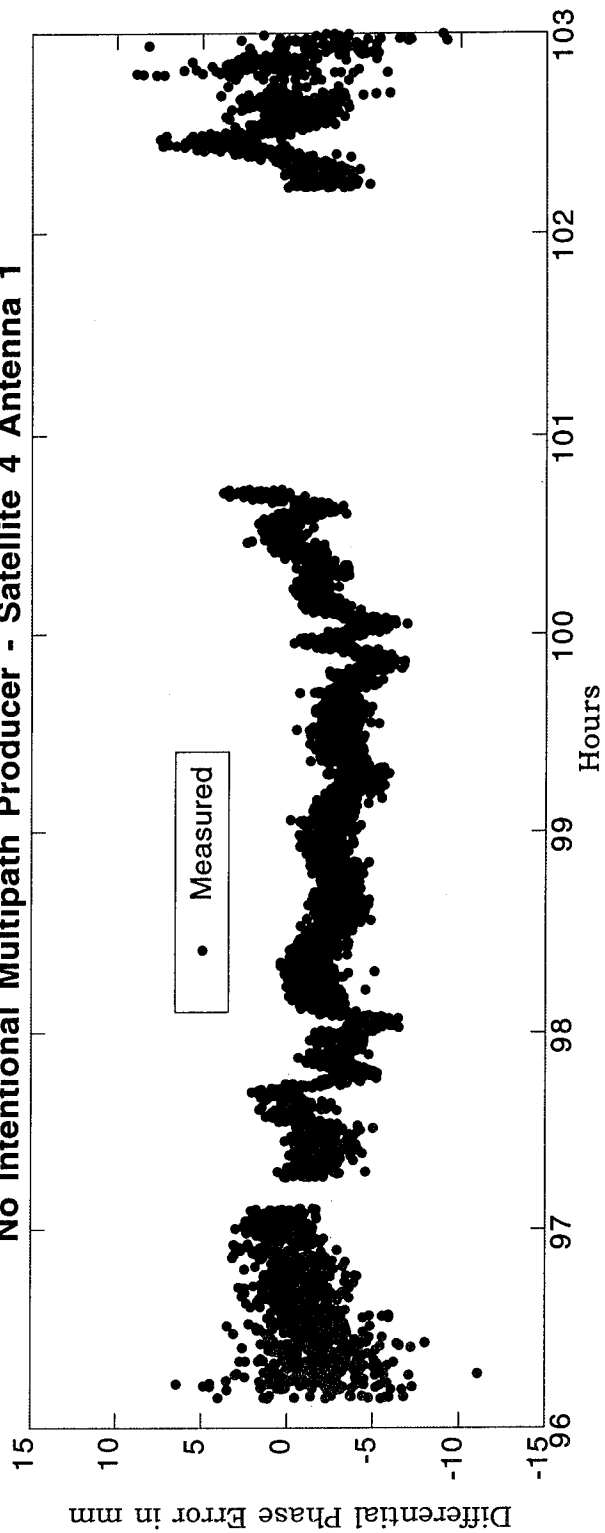


Figure 8 - Comparison of Measured and Predicted Differential Phase Errors on 4 ft. by 12 ft. Aluminum Sheet with Patch Antennas (JD059) - Satellite 16 Antenna 1

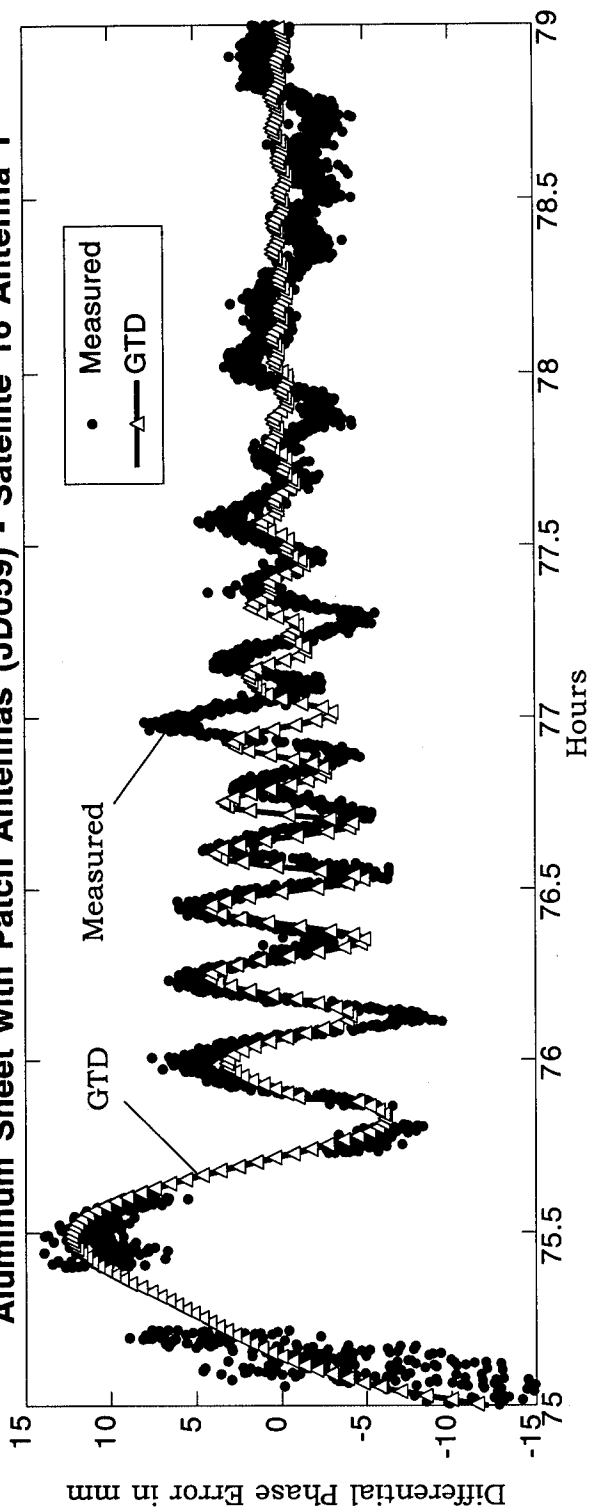


Figure 9 - Comparison of Measured and Predicted Differential Phase Errors on 4 ft. by 12 ft. Aluminum Sheet with Patch Antennas (JD059) - Satellite 24 Antenna 1

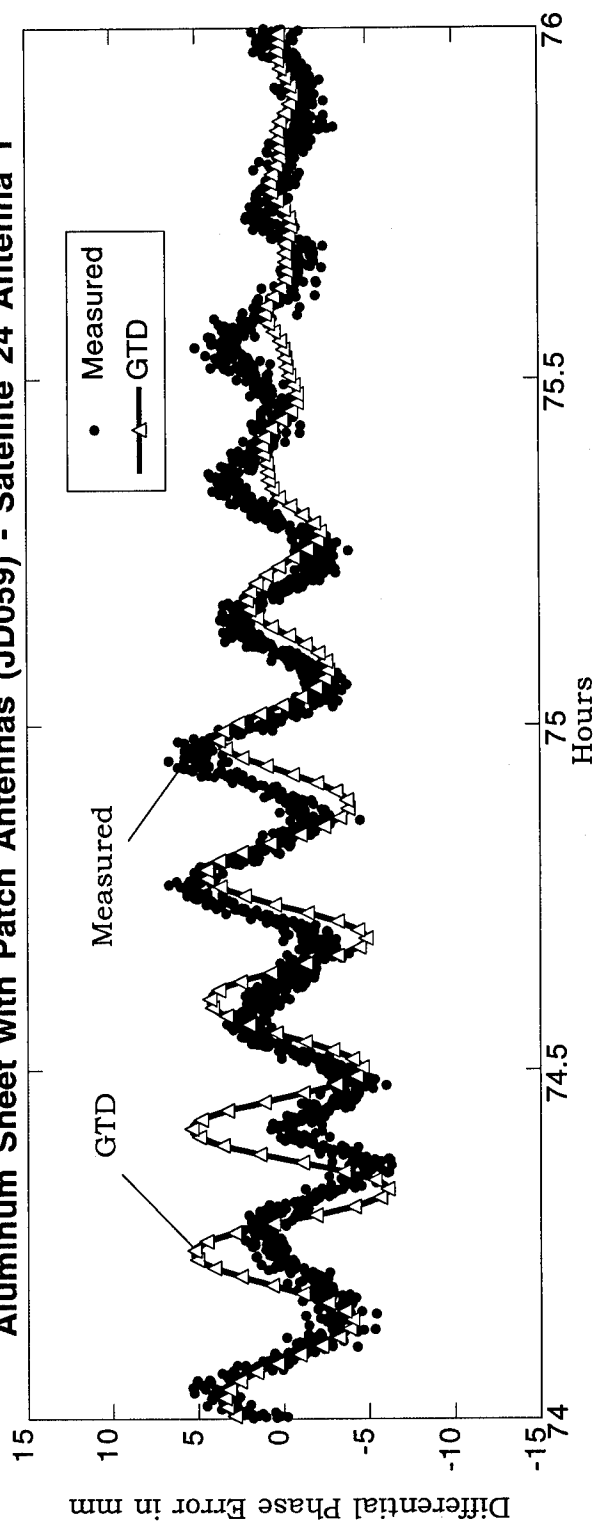


Figure 10 - Comparison of Measured and Predicted Differential Phase Errors on 3 ft. Diameter Cylinder with Choke Ring Antennas (JD074) - Satellite 1 Antenna 1

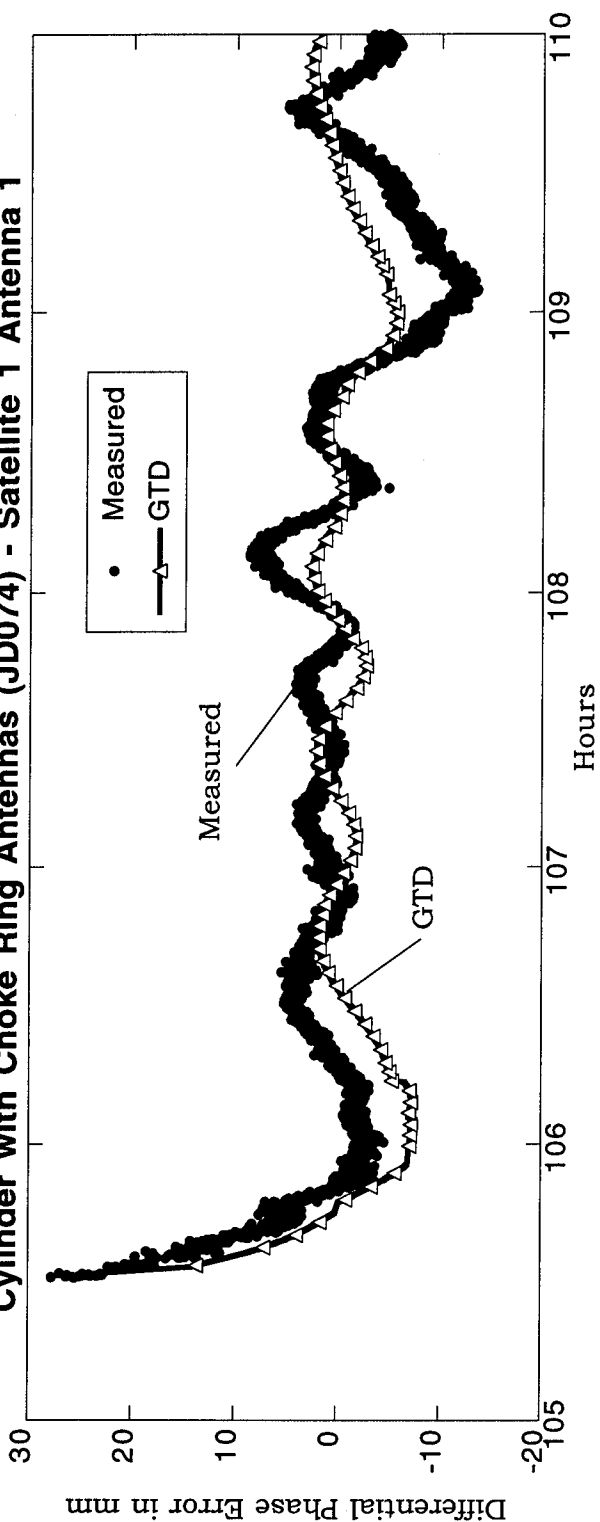
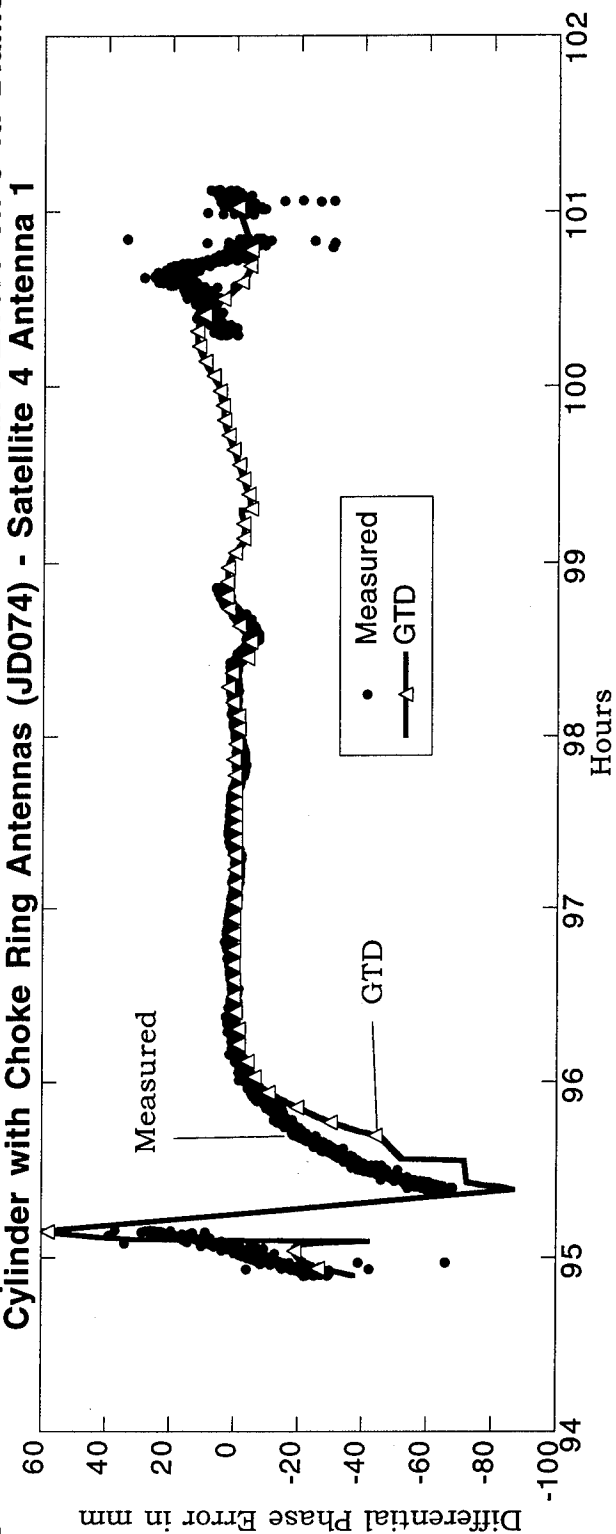


Figure 11 - Comparison of Measured and Predicted Differential Phase Errors on 3 ft. Diameter Cylinder with Choke Ring Antennas (JD074) - Satellite 4 Antenna 1



Application of Fuzzy Logic and Multisensor Data Fusion Techniques to On-board GPS-based Spacecraft Navigation

Stefano Giacomini
University of Milano

Livio Marradi
LABEN S.p.A.

BIOGRAPHY

Stefano Giacomini received a degree in Computer Science from University of Milano in 1995. His research interests lay in fuzzy logic, data fusion algorithms and expert systems.

Livio Marradi received a degree in Physics from University of Bologna in 1985. He was Research Associate in the High Energy Physics Dept. at University College London. He joined Honeywell-Bull Microsystems R&D Dept. from 1987 to 1990. Since then he is at the Research and Strategic Developments Dept. of LABEN. His experience includes design and development of on-board autonomous data handling systems and is currently responsible for the SW developments of the GPS TensorTM receiver.

ABSTRACT

Autonomous on-board spacecraft guidance and navigation can benefit from multisensor data fusion techniques both in terms of achievable accuracies in position and attitude determination, as well as in terms of increased system reliability. In particular, significant benefits can be found in cases where measurement noise conditions may change during the mission and safety-critical spacecraft operations are involved.

Accuracy, reliability and integrity are three of the main requirements which will be involved in autonomous spacecraft navigation and rendez-vous missions. Those requirements may be achieved by integrating, now available, space qualified GPS receivers that provide both position and attitude information with specific mission related instruments and Inertial Navigation Sensors.

LABEN is currently developing a spaceborne GPS receiver for position and attitude determination. In parallel, research activities are currently in progress within the Research and Strategic Developments Dept. of LABEN in the fields of on-board autonomy and multisensor data fusion. A rendez-vous simplified study case has been taken as reference, and involves integration of the GPS receiver data with data from a Laser Range Finder and a three axis Inertial Navigation Sensor.

The core of the data fusion system is based on an Extended Kalman Filter that includes an accurate gravitational dynamic model. Because sensor measurements are all affected by various error sources that are variable in time according to spacecraft-target-GPS relative positions and configurations and due to the presence of GNC rendez-vous manoeuvres, the Kalman filter operation needs to be adapted in real-time to obtain best performance on the basis of the current conditions. This is achieved by acting both on the filter covariance matrices and on the dynamic model itself.

A novel adaptive scheme employs a Fuzzy Logic layer to control the filter performance by analyzing incoming sensors data on the basis of a set of rules. The fuzzy rule set is designed with a twofold objective: achieve better accuracy in position determination and also act as a controller on GNC and sensors operation correctness and consistency.

Preliminary simulation tests of the spacecraft rendez-vous system with the Fuzzy Logic aiding have provided good results and in-sight on the validity of the adopted sensor fusion scheme, compared with the only Kalman filtering of sensors data.

KEYWORDS: Fuzzy Logic, Kalman Filter, GPS, Data Fusion, Autonomy.

1. INTRODUCTION

Space missions will require, in a near future, different levels of on-board autonomy. LABEN is carrying out research projects to consolidate the concepts which are at the basis of future autonomous spacecrafts and to define novel on-board HW and SW architectures capable to provide autonomy features and functionalities [1]. An integrated on-board data handling platform [2] can be easily configured to meet different mission requirements. Four basic guidelines drive these developments:

- integration of all spacecraft functions (classical spacecraft data handling, attitude and orbit control, payloads and experiments control) in a single flexible and modular system;

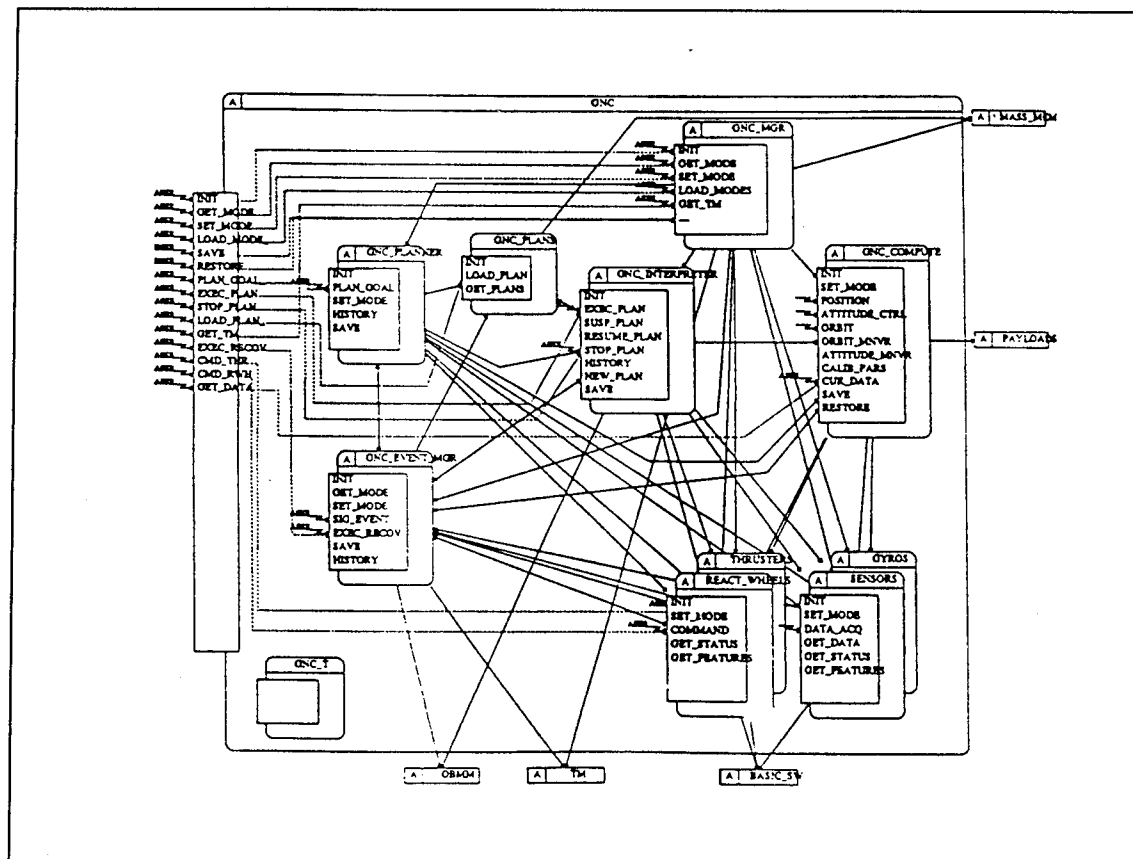


Fig. 1.1-1 - GNC object internal structure

- easy adaptation of system HW interfaces to specific mission equipments (eg. attitude sensors/actuators, specific instruments);
- easy adaptation of system processing capability to mission requirements and mission phases (eg. single/multiple processing nodes);
- abstraction of software architecture from actual physical hardware configuration and reuse of typical subsystem SW objects;

In the frame of this research activity, the present paper provides preliminary results on an on-going work which aims at defining a data processing scheme for fusion of data acquired from attitude and orbit determination sensors [3]. On-board orbit determination and control is a fundamental issue for an autonomous spacecraft. This is particularly true, for example, for such missions that require autonomous rendez-vous with orbiting space stations [4], or in all cases where ground control should be reduced to a minimum.

The initial work has deliberately faced only orbit determination by applying the developed architecture to a simplified spacecraft rendez-vous study case. The preliminary results seem to be quite promising. Development will continue by taking into consideration data fusion from attitude determination sensors as well as from payload sensors, by extending and generalizing the defined architecture.

A GPS receiver developed by LABEN [5] forms the basic instrument on which attitude and orbit determination is based. The receiver data is integrated in a simulation environment with data from a Laser Range Finder and a three axis Accelerometer to provide accurate and reliable information to the Guidance Navigation and Control system (GNC) of the study case.

1.1. On-Board Integrated Spacecraft Control Unit

The Control Unit architecture topology features an integrated and homogeneous system platform, composed of single or multiple symmetric processing *Nodes*, according to the specific mission requirements. The *Nodes* control all spacecraft subsystems through a set of *Segment Busses* to which all the equipments are connected via standard interfaces. The number of *Nodes* and *Segments* and the allocation of subsystems to segments is mission dependent. The processing nodes may be active simultaneously to achieve parallel operations during critical mission phases, or may be set in a cold redundancy configuration during low processing load phases. Architectures with 2 and 4 processing nodes have been prototyped by LABEN [2]. Typical segments would include:

- *GNC* (Attitude & Orbit Sensors, Actuators, GPS);
- *Payloads* (mission dependent experiments and instruments)

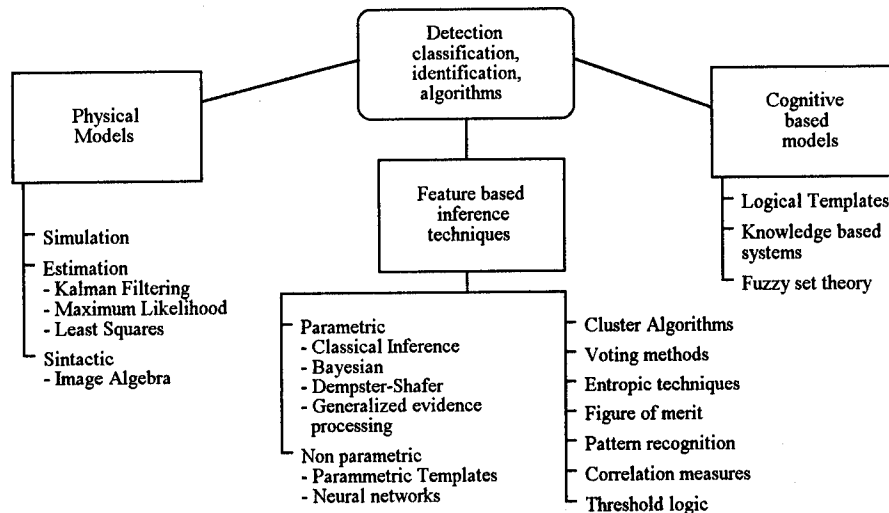


Fig. 1.2-1 - Taxonomy of data fusion techniques

- ♦ *Telecommunications* (Telecommand, Telemetry);
- ♦ *Services* (Power & Thermal controls);

The software architecture follows a hierarchical structure: data handling and S/C operations are as much as possible localized into subsystem and payload SW managers, controlled and coordinated by an On-Board Mission Manager. A Basic SW executive layer provides services to autonomously handle system configuration and communications; in addition it provides SW components for a mission "Goal Oriented" control for autonomous selection and execution of nominal mission plans and for diagnosis of failures and execution of recovery actions. The on-board knowledge base is essentially provided by configurable data tables. The detail which is introduced in the on-board knowledge can provide different levels of autonomy as required by the mission. Software is designed with an object oriented methodology and all subsystem SW objects may be dynamically re-allocated to any of the HW Nodes. Fig. 1.1-1 gives an example of the internal structure of a generic GNC subsystem object.

1.2. Data Fusion Concepts

Data Fusion can be defined as a process which relates data coming from different, and possibly not homogeneous, sources to obtain a piece of information at a higher level with respect to the original data. The main objectives for which sensor data fusion techniques are applied can be found in the wide literature and are summarized as follows:

- ♦ Detection, identification and object/event recognition;
- ♦ Object/event tracing and monitoring;
- ♦ Environment state variation control;
- ♦ Decision making;

Although sensor data fusion objectives may be different, it should be noted that a system designed for a specific task may be easily adapted to achieve additional functionalities.

This feature points out the fact that similar fusion techniques are used for apparently different objectives.

Most of the research in literature makes use of combinations of active and passive sensors. When sensors provide the same type of information (*competitive fusion*), the fusion process is used essentially to obtain better accuracy or increased reliability. On the other hand, when sensors provide complementary data (*complementary fusion*), it is important that they are compatible in terms of field of view, frequency range and sensitivity to external conditions [6]. In this case, a sensors data model relates the data outputs to the final object of the fusion process similarly to an observation matrix that relates measures to the system state vector. In [7] different techniques are reported to correlate "intersecting" sensors data: *averaging*, *deciding* and *guiding*. The averaging technique simply computes a weighted average of the homogeneous sensed data; the deciding technique introduces a priority order of the sensors, while the guiding (or sequential) technique uses information from a primary sensor to guide acquisitions and interrogations to secondary ones. Discrepancies or inconsistencies in the sensors output data may also be used by the fusion process to detect and possibly isolate system failures.

Expressing the sensed environment with a vector $\underline{e} = (e_1, e_2, \dots, e_n)^T$, the relation between sensed object and output of the fusion process (fused data) may be described, in the most general case, by the following equations [8]:

$$s_i(t) = f_i(t, e(t)) \quad i = 1, m$$

$$\phi_j(t) = g_j(t, s(t)) \quad j = 1, p$$

where f represents the sensor transfer function, and g the fusion process. In the simple case where the sensor transfer function and the fusion process can be considered time invariants, the relation reduces to:

$$\phi(t) = g(f(e(t)))$$

which maps an n -state environment vector e to a p -state vector of fused data ϕ , through the sensors transfer functions and the fusion processes.

Many data fusion applications also make use, in addition to the sensor measurements, of other sources of information (knowledge sources) and of knowledge bases to obtain the required fused data. The knowledge sources are activated on the basis of the sensors outputs and according to previously generated hypothesis on a possible solution, which is in this way built up incrementally. In [9] a detailed classification of types of fusion process techniques (fig. 1.2-1) is reported. Three main classes can be identified:

1. *Physical Model* based techniques: the fusion process contains a model of the sensed environment and of the observables; this class includes among others Kalman filtering;
2. *Feature based inference* techniques: the fusion process identifies the sensed environment features by mapping sensors data to internally coded data bases;
3. *Cognitive based* techniques: the fusion process emulates the decision process of the analyst, by making use of internally stored template logical models; fuzzy expert systems lay within this class.

2. THE DATA PROCESSING SCHEME

The selected data fusion scheme for the rendez-vous study case makes use of an extended Kalman filter estimator and predictor, controlled and adapted by a fuzzy rule-set module that pre-processes all the available information and sensor measurements.

The initial objective of the research was to consider simply absolute position/velocity determination of the spacecraft on the rendez-vous trajectory. Main purpose was to verify the possibility of increasing accuracy of the system state vector elements, by integrating data from the three sensors (GPS, Laser and Accelerometer) and by adapting the knowledge of the measurement noise processes as they change in time during the rendez-vous. In addition, take into consideration the frequent manœuvres and thruster forces applied to the spacecraft on the trajectory. A second objective of the fusion process architecture, currently under test, is to provide integrity checks on the information sources and increased reliability on the resulting fused data.

The use of Kalman filters is well known in the field of optimal estimation. This technique is widely adopted, with the increase of microprocessor performances, also in embedded real-time systems. One of the key issues in the design of a Kalman filter is the knowledge of the dynamic process and measurement noise processes, given by the process noise $Q(k)$ and measurement noise $V(k)$ covariance matrices. A significant difficulty in designing an efficient filter is due to the uncertainty in the knowledge of these matrices. With the possibility of real-time tuning, the Kalman filter performance can be enhanced. Different adaptation schemes have already been proposed and applied: *covariance matching* techniques try to keep consistency between the filter residual covariance and its theoretical value while *hill-climbing* methods adopt optimization algorithms to obtain the optimum of the filter performance cost function. Recently expert system techniques based on *fuzzy logic* have been successfully adopted in Kalman filter adaptation schemes [10] and in processing of reliability factors for GPS-based position determinations [11].

Our present research is limited to the adaptation of the measurement noise covariance matrix $V(k)$ by using a-priori knowledge of the time-varying sensors induced environment errors, built into a set of fuzzy logic rules. A block diagram of the overall data fusion scheme for the specific study case is shown in fig. 2-1.

2.1. Information Sources and Pre-Processing

In addition to the three spacecraft sensors, two additional information sources are used in the processing. The GNC subsystem module provides (optional) information on actuators activations. The RF subsystem handles a data link to the target of the rendez-vous, from which it is assumed to obtain highly accurate periodic estimation of its own state vector $xtg(k)$. The Earth Centered Inertial (ECI) coordinate frame is always assumed in the following.

The Accelerometer is modelled as a three axis sensor providing acceleration components in the body frame which are then converted into ECI through instantaneous knowledge of the spacecraft attitude matrix. The spacecraft system is subject to gravitational forces and to GNC applied actuator forces. The accelerometer readings are only triggered by GNC actuator activation signals, $f(k)$, or alternatively may be continuous readings that are pre-processed and passed on to the filter only when raising above a given threshold.

The Laser Range Finder is modelled to provide spacecraft-target range data, $Lr(k)$, in addition to azimuth, $az(k)$, and elevation, $el(k)$, angles in the body frame. Target-miss events are also simulated in the laser model.

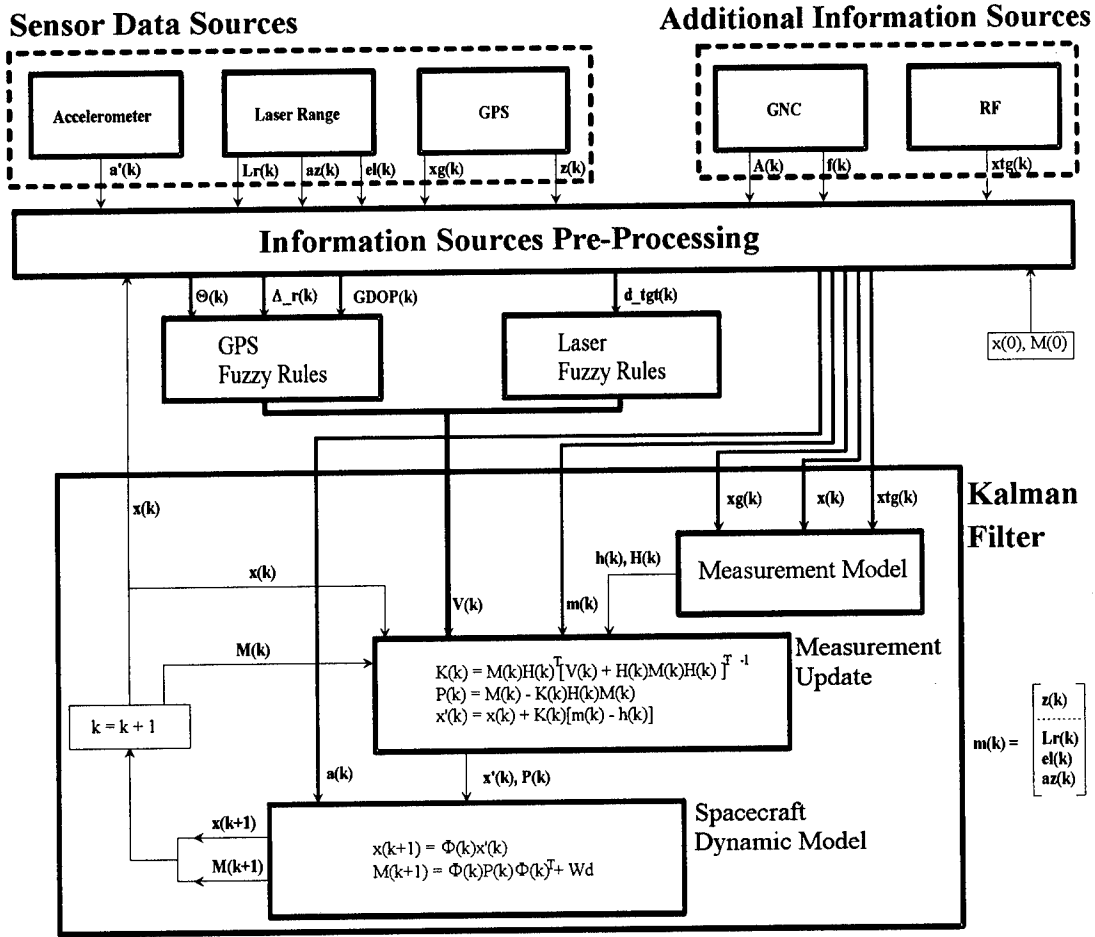


Fig. 2-1 - Overview of Data Fusion Architecture

The GPS receiver is modelled from the LABEN Tensor developments. It features 9 parallel channels that provide up to 9 pseudo-range measurements, $z(k)$, to GPS space vehicles. The pseudo-ranges together with the GPS SV position vectors, $xg(k)$, (simulated over the rendez-vous trajectory), form the principal sensor inputs to the Kalman filter.

2.2. The Kalman Filter

The core of the data fusion architecture is represented by an Extended Kalman Filter. Design of the filter is derived from the GPS Tensor development [12] and modified to include additional measurement sources. The system state is described by an 8-state vector in ECI coordinates, $\underline{x}(k) = (x, y, z, \dot{x}, \dot{y}, \dot{z}, b, \dot{b})^T$, where b ($c\Delta t$) represents the receiver clock bias error. The Kalman filter inputs are the following:

| | |
|----------|------------------------------------|
| $xtg(k)$ | target state vector; |
| $xg(k)$ | GPS SV position vector; |
| $m(k)$ | GPS and Laser measurements vector; |
| $V(k)$ | measurements covariance matrix; |
| $a(k)$ | GNC-induced acceleration vector; |

The form of the equations for the implemented non-linear system are:

$$\begin{cases} x_{k+1} = f_k(x_k) + \Gamma_k \xi_k \\ h_k = g_k(x_k) + \eta_k \end{cases}$$

By linearizing in a Taylor series $f_k(x_k)$ around \hat{x}_k and $g_k(x_k)$ around $\hat{x}_{k|k-1}$ we get:

$$\begin{cases} f_k(x_k) \cong f_k(\hat{x}_k) + \Phi_k(x_k - \hat{x}_k) \\ g_k(x_k) \cong g_k(\hat{x}_{k|k-1}) + H_k(x_k - \hat{x}_{k|k-1}) \end{cases}$$

where:

$$\Phi_k = \left[\frac{\partial f_k}{\partial x_k}(\hat{x}_k) \right] \quad \text{and} \quad H_k = \left[\frac{\partial g_k}{\partial x_k}(\hat{x}_{k|k-1}) \right]$$

The update process of the Kalman matrices is as follows:

$$P_{0,0} = Var[x_0]$$

$$P_{k,k-1} = \Phi_{k-1} P_{k-1,k-1} \Phi_{k-1}^T + \Gamma_{k-1} Q_{k-1} \Gamma_{k-1}^T$$

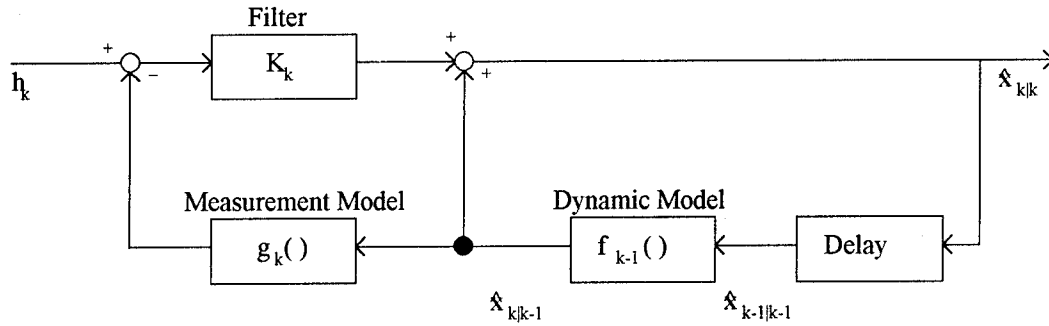


Fig. 2.2-1 - Extended Kalman filter block diagram

$$K_k = P_{k,k-1} H_k^T (H_k P_{k,k-1} H_k^T + V_k)^{-1}$$

$$P_{k,k} = (I - K_k H_k) P_{k,k-1}$$

$$\hat{x}_{0|0} = E[x_0]$$

$$\hat{x}_{k|k-1} = f_{k-1}(\hat{x}_{k-1|k-1})$$

$$\hat{x}_{k|k} = \hat{x}_{k|k-1} + K_k [h_k - g_k(\hat{x}_{k|k-1})]$$

$$k = 1, 2, \dots$$

$$h(k) = \begin{bmatrix} \sqrt{(x-x_1)^2 + (y-y_1)^2 + (z-z_1)^2 + b} \\ \sqrt{(x-x_2)^2 + (y-y_2)^2 + (z-z_2)^2 + b} \\ \vdots \\ \sqrt{(x-x_n)^2 + (y-y_n)^2 + (z-z_n)^2 + b} \\ \hline \sqrt{(x-x_{tg1})^2 + (y-y_{tg1})^2 + (z-z_{tg1})^2} \\ \cos^{-1} \left(\frac{z-z_{tg}}{\sqrt{(x-x_{tg1})^2 + (y-y_{tg1})^2 + (z-z_{tg1})^2}} \right) \\ \tan^{-1} \left(\frac{y-y_{tg}}{x-x_{tg}} \right) \end{bmatrix}$$

A block diagram of the filter is sketched in fig. 2.2-1. The influence of the covariance matrices Q_k and V_k on the filter performance is particularly evident in the equation of the gain K_k .

The filter is designed to output a periodic state vector solution independently of the presence or not of measurements from all sensors. Sensors may have different read-out frequencies. In the absence of measurements, the filter outputs just the state vector prediction from the dynamic model.

It is important that the dynamic model be accurate enough. In particular, a model of the gravitational potential, $U = \frac{\mu}{r} \left[1 - \frac{J_2}{2} \left(\frac{r_e}{r} \right) \cdot (3 \cdot \sin^2(L) - 1) \right]$, is implemented in the filter. The gradient components of U are then added to the pre-processed acceleration components read-out from the accelerometer (only during GNC manoeuvres - accelerometer components are otherwise set to zero) and numerically integrated to obtain the state vector prediction at time $k+1$.

The number of measurements at any time k is variable according to the sampling time of the sensors (GPS and Laser) and to the number of available GPS satellites in view. The measurement model vector

has variable size, $1 \leq n \leq (q+3)$, with $q = 1, \dots, 9$.

Measurements are assumed uncorrelated, therefore only the diagonal of the V_k matrix contains significant values. Those are set-up and updated in real-time by the fuzzy processing layer, as discussed in the following.

2.3. The Fuzzy Logic Layer

The fuzzy adaptation scheme allows to include heuristic knowledge of the environment in which the system operates to tune the Kalman filter covariances. In particular, it allows us to identify a set of system configurations and/or situations that affect the error knowledge of the sensors measurements, in a different way than the default nominal mode. The parameters that are used by the fuzzy processor to identify those situations are made available by the information sources pre-processing module (fig.2-1). In the absence of such external adaptation, the filter performance may considerably degrade during specific situations.

2.3.1. Basic Concepts

The advantage of the fuzzy logic approach with respect to traditional adaptation schemes is related to the possibility of expressing the knowledge in a linguistic form rather than with complex mathematical models. In the specific case, mathematical models (of

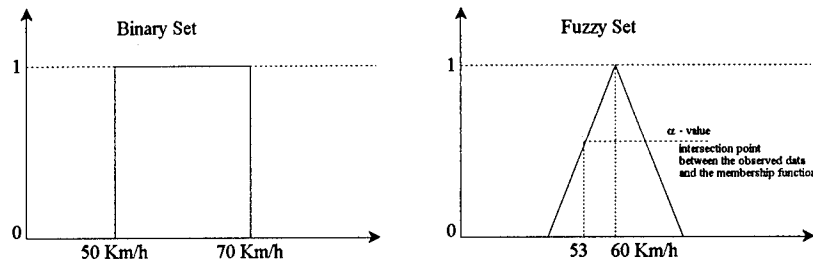


Fig. 2.3.1-1 - Binary and Fuzzy set membership functions

the environment, for example) could be used a-priori to build the heuristic adaptation knowledge base. The adaptation strategy can then be represented in the form of *fuzzy rules*:

IF <antecedent> THEN <consequent>

Both parts of the rule (antecedent and consequent) don't represent definite actions, but rather reference conditions and behaviours. The consequent part of a rule contains a qualitative expression of the action to be performed, while the quantitative expression of the final decision is determined by the combination of all rules. This feature is a great advantage with respect to the use of mathematical models, that are typically tailored to specific and single physical phenomena/effects (eg. the ionospheric model, the S/A model, etc.). The combination of concurrent multiple

fuzzy set is associated with a reference term and is characterized by a collection of objects which are similar to it. The similarity degree is what is denoted as membership degree to the fuzzy set and described by a *membership function*. If, for example, we denote 60 Km/h as a *medium* speed, the closer the speed of the observed parameter is to 60, the higher is its membership degree (fig. 2.3.1-1). By contrast a binary set function is also shown, where a medium speed is denoted as that between 50 and 70 Km/h. It is clear how, with this kind of set, we might obtain a completely different action in going, for example, from 50 Km/h to 49.99.. Km/h.

The fuzzy Reasoning is composed by two computational steps, which permit to infer fuzzy values for the output variables, starting from fuzzy

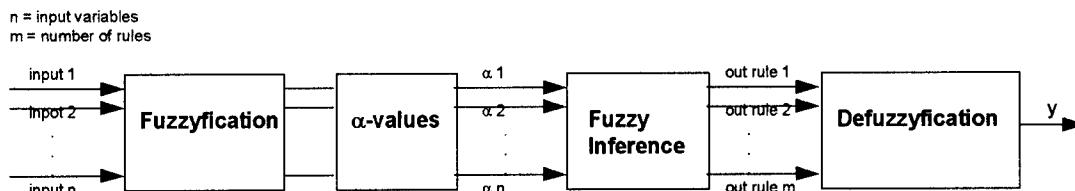


Fig. 2.3.1-2 - Fuzzy computational model

effects could produce very complex mathematical formulations.

In addition, the linguistic approach allows us to deal with uncertain and/or imprecise expressions of the type:

- *Peter is very tall;*
- *Speed is high;*
- *Elevation angle is small;*

in contrast to the classical (0,1) boolean logic for which thresholds should be defined to decide whether elevation angle is big or small. The fuzzy rules then become expressions of the type:

IF the light IS red AND the speed IS high
 THEN the action IS brake;
 IF the light IS green AND the speed IS very low
 AND the crossing IS close
 THEN the action IS accelerate;

To allow the fuzzy processor to take decisions on the basis of the linguistic rules, the observed parameters (information sources) should be evaluated to establish the degree of membership to the reference term. A

values of the input variables. The steps include (fig. 2.3.1-2):

- *Fuzzyfication*: to interface the fuzzy processor to the real system it is necessary to fuzzify the observed data by means of the association with a corresponding function. To speed up and simplify the task, currently the observed data is associated to a crisp value;
- *Alpha-value computation*: computes the membership degree of the input variables to the fuzzy sets by means of membership functions (fig.2.3.1-1). The classical logical operators (OR, AND, NOT) are extended to combine fuzzy sets with a precise mathematical formalism;
- *Fuzzy Inference*: formalizes the fuzzy reasoning by using the fuzzy rules and the α -values to deduce fuzzy outputs. Using the α -values obtained from antecedent parts, the membership functions of the consequent parts are modified and combined from the different rules. The most classical methods are the *max-min* and the *max-dot* methods.

- *Defuzzification*: this last step is used to obtain a precise answer (discrete value of the output variables) for the action to be taken on the system. The most commonly used techniques are the *center-of-gravity* and the *centroid*.

2.3.2. Fuzzy processing and membership functions

The input variables used by the fuzzy processor for the simulated study case are the following:

$\Theta(k)$: elevation angles vector of the GPS satellites at time k , computed from the satellites positions and from the spacecraft position and attitude;

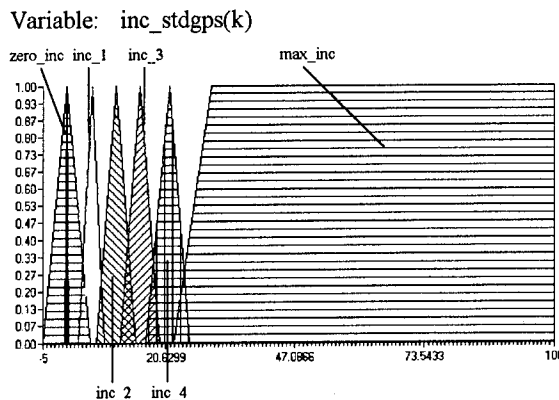
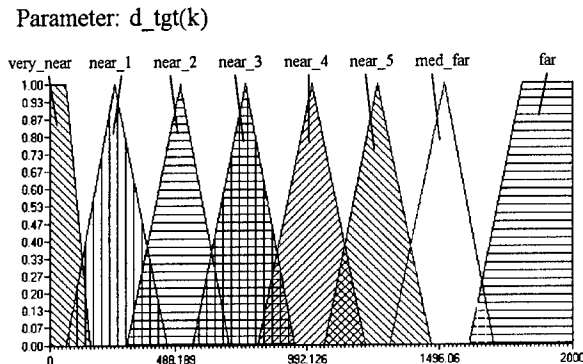
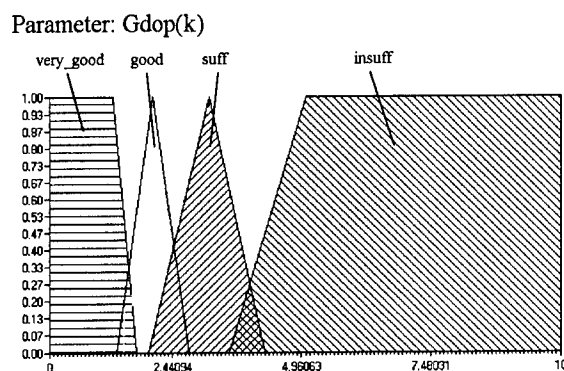
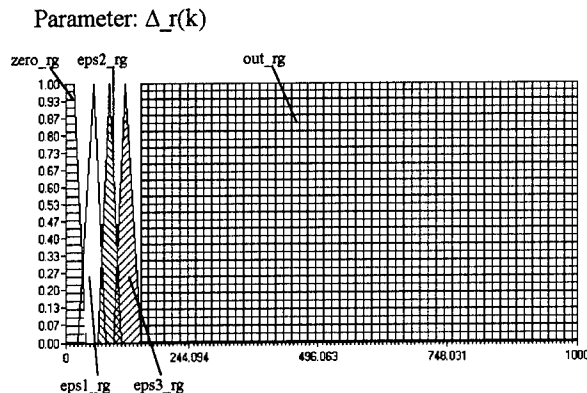
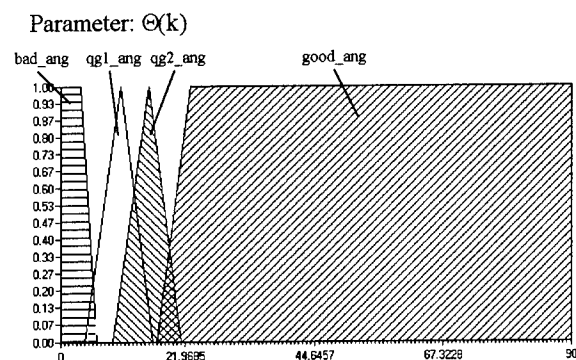
$\Delta_r(k)$: pseudo-range residuals, computed as the difference between the actual measurements and the estimated values;

Gdop(k): geometric dilution of precision parameter computed at time k ;

d_tgt(k): estimated distance between target and spacecraft at time k .

The membership functions for those parameters are shown in fig. 2.3.2-1.

The fuzzy rules are subdivided into two blocks, each associated to a sensor. The outputs, inc_stdgps(k) and diff_stdlr(k), computed by the defuzzification processes of the two blocks, represent corrective values to be applied to the diagonal of the Kalman filter measurement covariance matrix. The membership functions for those variables are shown in fig. 2.3.2-2.



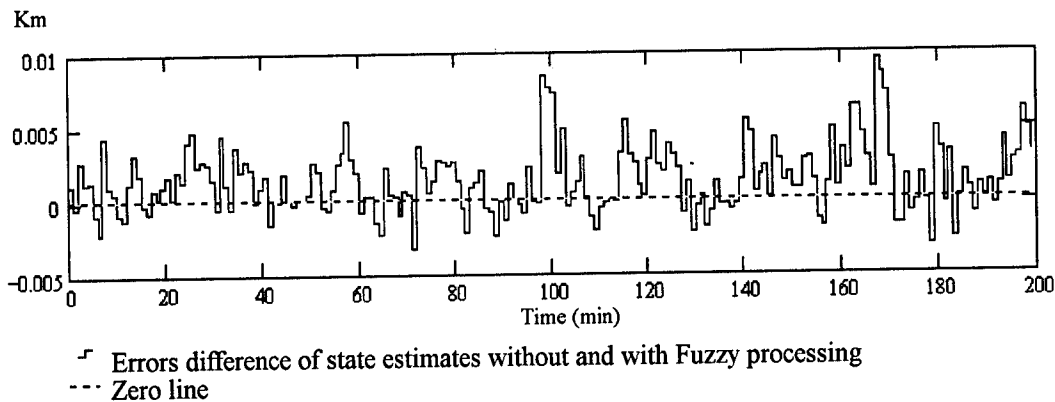
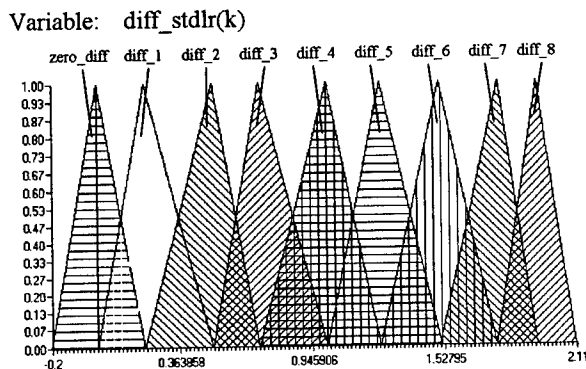


Fig. 3-1 a



The fuzzy rules set uses the input parameters to identify, in the present design, three sources of error and take care of them on the basis of the expert system knowledge:

- Elevation angle of the GPS satellites with respect to the receiver has an effect on the Signal to Noise Ratio, due to antenna gain pattern and to ionospheric distortion;
- "Failure" of a GPS satellite is a second

possible source of error, which may introduce large unwanted bias in the receiver pseudo-range measurement. This source of error is commonly detected by RAIM techniques;

- GDOP provides a kind of quantitative measure of the achievable accuracy given a satellite geometric configuration;
- Distance between target and spacecraft affects the performance of the Laser instrument in a know way.

Those represent just a few of the possible implementation rules. It should be outlined that a promising application of fuzzy processing may be applied to the identification of multipath error sources within GPS receivers for attitude determination.

3. SIMULATION RESULTS

To verify performances of the data fusion architecture, a simulation environment was developed and set-up on a Sun SPARCStation. The target LEO orbit and a complete rendez-vous trajectory for the spacecraft were

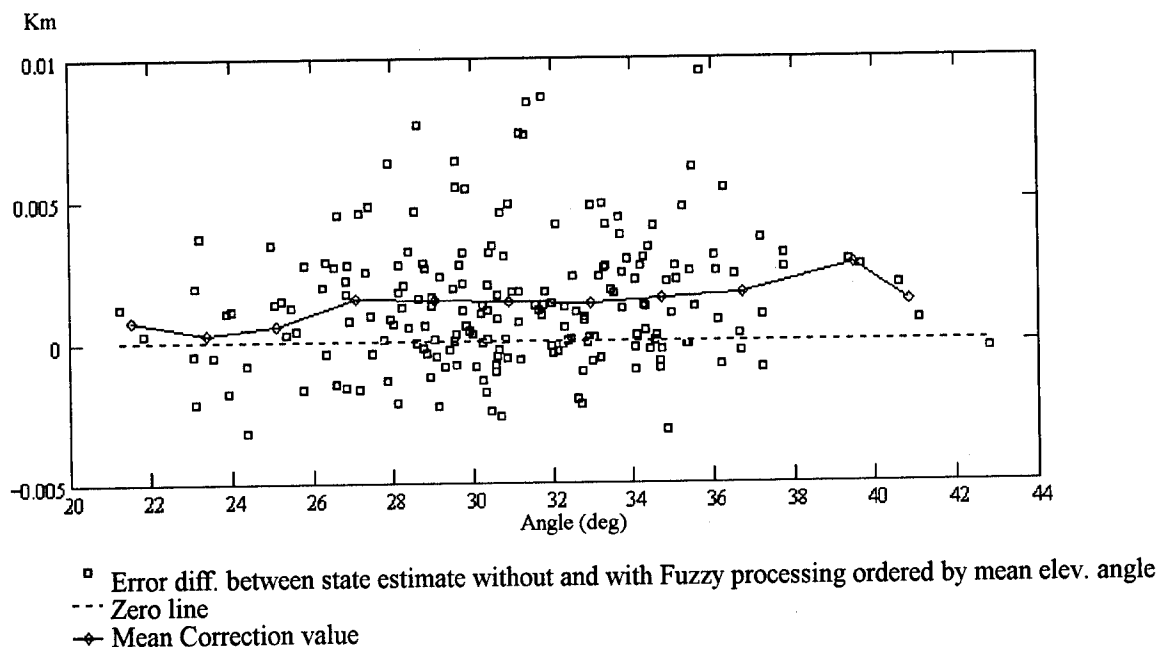


Fig. 3-1 b

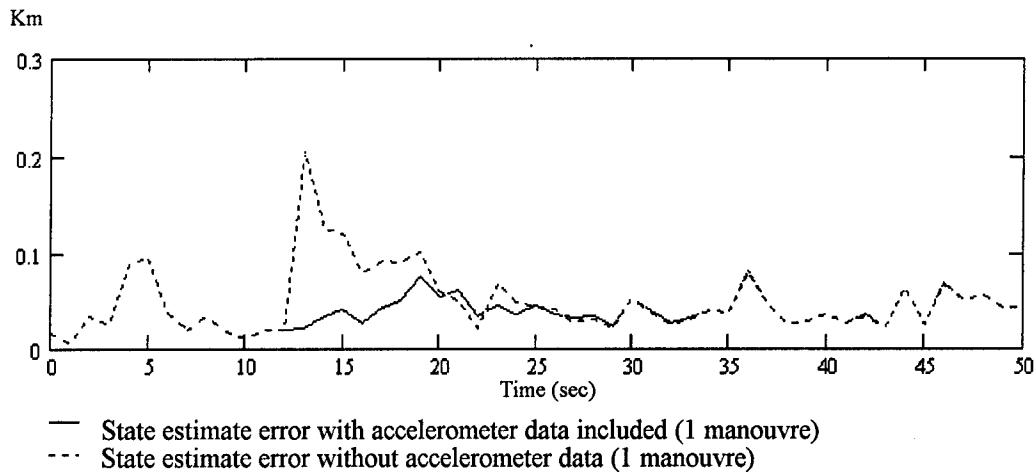


Fig. 3-2

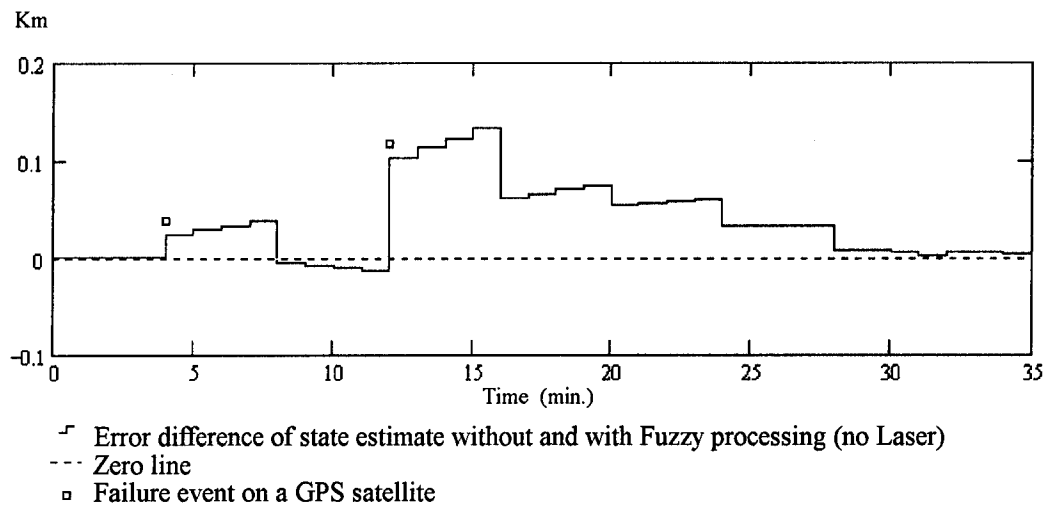


Fig. 3-3

generated, including GNC manoeuvres and actuator forces. Software modules were developed representing sensor instruments simulations, GPS constellation and simplified models of the error sources considered.

Simulations were aimed essentially at verifying the performances of the only Kalman filtering against the combination of fuzzy control and filter, under different operating conditions.

Three main simulation tests provided results on:

1. GPS-only solutions in the absence of manoeuvres;
2. GPS and Accelerometer in the presence of GNC manoeuvres;
3. GPS, Laser and Accelerometer solutions in a global rendez-vous simulation.

The performances evaluation is based on the length of the error vectors \underline{e} formed by the difference of the resulting state vector estimate and the true system generated state vector. In [10] the correlation coefficient R between the estimated and the true state is instead proposed as a figure of merit of the adaptation scheme.

Test 1

No manoeuvres are included in this set of tests, and the only Selective Availability error source is present. Fig. 3-1a plots the difference $(\underline{e}_k - \underline{e}_{fk})$ where \underline{e}_k is the only Kalman filter and \underline{e}_{fk} is the combined Fuzzy+Kalman solution. This plot essentially emphasises the effect of the fuzzy rules on the GPS satellites elevation angles. A positive value indicates an increase in the Fuzzy+kalman approach. Fig. 3-1b plots the same quantity ordered by increasing mean elevation angle.

Test 2

A single thruster (50 sec) manoeuvre is simulated to evaluate the effect of the accelerometer in the Kalman filter. The GPS receiver is operating as in test 1 with the only S/A error. Fuzzy rules are disabled. Fig. 3-2 plots the error vectors with the accelerometer on and off.

Test 3

This test performs a global simulation of the rendez-vous with the three sensors operating in nominal mode. Different kinds of errors are introduced sporadically. Fig. 3-3 plots the result of introducing periodic instantaneous GPS satellite failures to

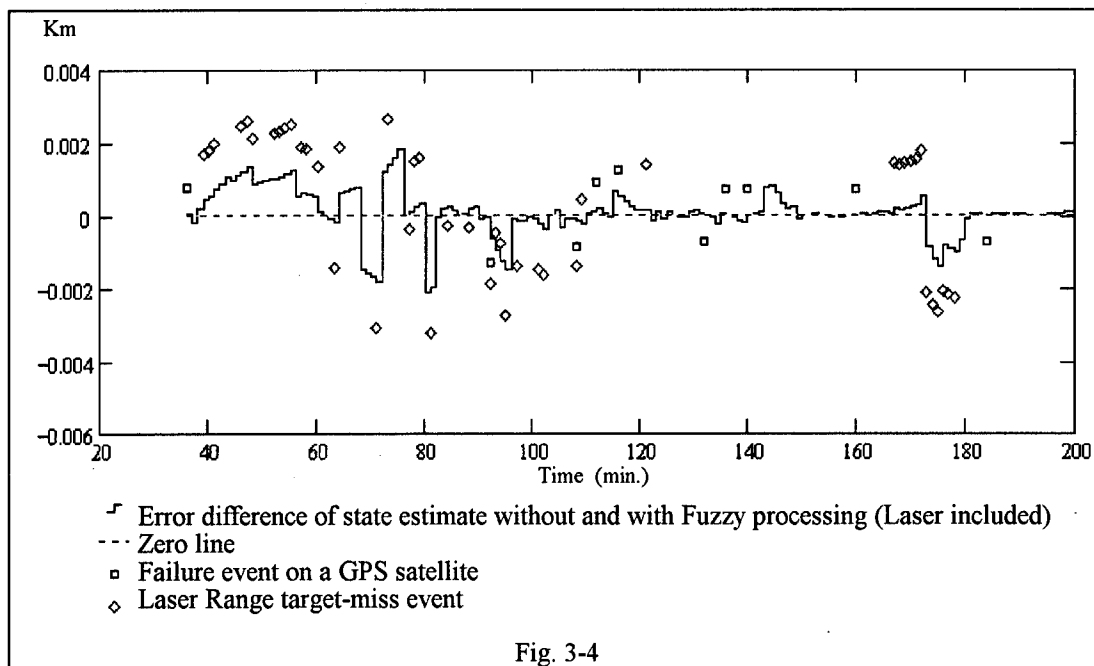


Fig. 3-4

evaluate the effect of fuzzy rules correcting such situations. The convergence time after the failure of the only Kalman filter is quite visible in this plot.

Fig. 3-4 reports the errors after activation of the Laser at close distances from the target. The accuracy of the Laser significantly reduces the error in the state estimate; this is quite evident at the occurrence of laser target-miss events.

The following table summarizes the mean state vector estimation error for the three tests considered above, computed as $\sqrt{\text{tr}(E[(\hat{x} - x)(\hat{x} - x)^T])}$.

| | TEST 1 | | TEST 2 | | TEST 3 |
|----------------------------|--------|----------------------------|--------|----------------------------|--------|
| Fuzzy+Kalman | 24 m | Accelerometer ON | 38 m | Fuzzy+Kalman | 9 m |
| Kalman only | 25 m | Accelerometer OFF | 49 m | Kalman only | 15 m |
| Iterative Least Squares | 59 m | Iterative Least Squares | 74 m | Iterative Least Squares | 61 m |

Processing Time

In view of the application of such a data fusion processing scheme into an embedded real-time spacecraft system, a coarse evaluation of the processing times was performed on a Sun SPARCStation (SPARC processor @ 25 MHz) and are reported in the following table.

| | Mean Processing Time (sec) |
|--|----------------------------|
| Total state estimation for time k (Measurement Pre-Processing+Fuzzy+Kalman) | 0.094 |
| Kalman filter Dynamic Model | 0.001 |
| Measurement Model (Pre-Processing and Kalman filter Measurement Model) | 0.028 |
| Fuzzy Rules processing | 0.037 |

4. CONCLUSIONS AND FUTURE ASPECTS

A data fusion architecture employing a fuzzy expert system based adaptation strategy of Kalman filter covariance matrices has been developed and demonstrated in a simulation environment for a rendez-vous study case. The results demonstrate that the concepts can lead to improvement in system state vector estimate accuracy with respect to a traditional filter approach, in the presence of varying environment and operating conditions. In addition it has been proved that it is possible to integrate, in a

quite flexible architecture, data and measurements from various information sources. In the present work the focus of the data fusion strategy was mainly posed on improvement of accuracy. The second objective of this architecture, currently under study, is the increase of system reliability and data integrity by introducing, when possible, a-priori knowledge in the fuzzy rules of the system evolution.

Although the reference study case is presently based on a rendez-vous application, the aim is to achieve a modular architecture that may be easily adapted and

configured for different applications. In particular, define "standard" interfaces between sensors and the pre-processing layers and for easy inclusion of different fuzzy rule set data bases. Currently available commercial software tools allow to easily define and maintain, through graphical interfaces, the fuzzy set membership functions and rules and to generate data bases, which may be linked to C-language run-time code, and used by the fuzzy inferential engine in a real-time system.

One application, that is already under study and development in LABEN [13], is to tailor this architecture to spacecraft attitude determination by integrating in a common unit a GPS attitude determination receiver with Miniaturized Inertial Measurement Units.

5. REFERENCES

- [1] "Autonomous Spacecraft Data Management System (ASDMS)", LABEN Final Report - ESTEC Ctr.No. 7960/88/PP/NL, Nov. 1994.
- [2] L.Marradi, G.Di Lorenzo, "A prototype on-board data handling platform for autonomous spacecrafts", Proceedings of the Eurospace On-Board Data Management Symposium, Rome, Jan 1994.
- [3] S.Giacomini "Data Fusion and Data Processing in Spaceborne Multisensor Applications", Graduation Thesis, Computer Science Dept. - University of Milano, 1995.
- [4] J.M.Pairot, M.Lellouch, U.Thomas, M.Cislaghi, "ATV Rendez-vous pre-development", CNES, Toulouse, 1995.
- [5] A.Sacchetti, "GPS for orbit and attitude determination: hardware design and qualification plan for a spaceborne receiver", ION-GPS, 1994
- [6] S.A. Shafer, A. Stenz, and C.A. Thorpe, "An Architecture for Sensor Fusion in a Mobile Robot", Proceedings of the 1986 IEEE International Conference on Robotics and Automation, San Francisco, 1986, pp. 2002-11.
- [7] S.Y. Harmon, G.L. Bianchini, and B.E. Pinz, "Sensor Data Fusion Through a Distributed Blackboard", Proceedings of the 1986 IEEE International Conference on Robotics and Automation, San Francisco, 1986 pp. 1449-54.
- [8] R.Tanner, N.K.Loh "A taxonomy of Multi-Sensor Fusion", Journal of Manufacturing Systems, 1992, pp. 314-325.
- [9] L.A. Klein, "Sensor and Data Fusion Concepts and Applications", SPIE-The International Society for Optical Engineering, April 1993
- [10] J.Lalk, "Intelligent adaptation of Kalman filters using fuzzy logic", 1994 IEEE.
- [11] K.Koremura, M.Asakura, C.Matsumoto, "Position accuracy improvement using fuzzy processing on GPS data", ION-GPS, 1994.
- [12] K.Brock, R.Fuller, S.Hur-Diaz, J.Rodden, "GPS attitude and orbit determination for space", ION-GPS, 1994.
- [13] B.Garavelli, L.Marradi, A.Morgan, "Space qualified GPS receiver and MIMU for an autonomous on-board guidance and navigation package", Paris, 1995.

GPS Autonomous Relative Navigation and Time Transfer for Orbiting Space Vehicles

Duncan B. Cox, Jr.
DBC Communications, Inc.

John D. W. Brading
Brading Systems and Technology

BIOGRAPHIES

Dr. Cox is President of DBC Communications, Inc., in Manchester, MA. His technical experience has been primarily in the development of new technology relating to inertial and radio navigation systems, with a strong focus on GPS systems. Currently, he is developing techniques and algorithms employing GPS carrier phase measurements for accurate relative navigation of satellites, for range instrumentation, and for enhancing navigation integrity. He is also developing image processing techniques, algorithms, and software. He was previously a cofounder and chairman of Mayflower Communications Company and a division leader at the C.S. Draper Laboratory. He received a D. Eng. degree from Yale University in 1964.

Mr. Brading has been active in GPS receiver design since 1982. He is currently working with the FAA on the Runway Status Lights program and with DBC Communications on the design of relative GPS navigation algorithms for space applications. Mr. Brading was previously employed by Mayflower Communications working primarily on the Advanced GPS Receiver program and the MLS/GPS/RNAV receiver program. Prior to joining Mayflower, Mr. Brading was employed by Northrop Corporation as chief GPS software engineer. Mr. Brading has a BS in Engineering Mathematics and has authored several articles on GPS receiver development.

ABSTRACT

GPS can be applied advantageously to the problem of autonomous relative navigation and time transfer for two vehicles with communications links between them. This application is significantly different from the navigation of one vehicle with respect to a reference station which has essentially perfect knowledge of position and time.

The focus in this paper is on applications where the two vehicles are orbiting space vehicles. A GPS receiver is placed in each vehicle, and a communications system is used to pass information from one vehicle to the other so that relative navigation and clock-correction estimates can be computed in each vehicle. The vehicles are orbiting near to each other, so that the perturbations in their orbits are significantly correlated and the errors in the GPS measurements to common satellites are significantly correlated. The receivers incorporate SA corrections, and can make pseudorange and accumulated-phase measurements at L1 and L2. Aiding/correction signals are limited to attitude data from on-board sensors and signals sent from one vehicle to another. State-of-the-art accuracies are desired.

This paper addresses the design of the navigation algorithms and the expected performance trends, and illustrates the trends with the results of computer simulations. Several important issues are addressed, particularly, (a) the benefits of utilizing a joint relative-navigation filter, rather than two independent navigation filters, (b) means of incorporating matched (same satellite, same epoch, different vehicle) and unmatched measurements, (c) the benefits of incorporating accumulated-phase measurements, rather than "delta-pseudorange" (delta-phase) measurements, (d) the effects of measurement nonlinearities, (e) modeling the accumulated-phase ambiguity states, (f) the benefits and limitations of using accumulated phase measurements in enhancing the relative accuracy of time transfer, and (g) the dependence of relative navigation accuracy on absolute navigation accuracy and on the distance between the two user vehicles.

BACKGROUND

Many papers have been published on the use of GPS measurements for autonomous absolute navigation of orbiting space vehicles [Munjal, 1992]. The autonomy provided by this system has been shown to result in significant system simplifications and cost reductions in comparison with alternative approaches, and the resulting accuracies have been shown to be sufficient for many space applications. It has been demonstrated that greatly improved accuracies can be achieved by providing corrections to the GPS measurements from one or more reference stations [Davis, 1994, & refs.]. Extensions have been made to incorporate inertial sensors to provide data on measurable specific forces. It has also been shown that six-degree-of-freedom navigation (including attitude determination) can be achieved using GPS accumulated-phase measurements from multiple GPS antennas [Satz, 1991; Ward, 1995]. The use of GPS pseudorange measurements for relative navigation in rendezvous applications has also been described [Hinkel, 1995]. Little, if anything, has been published on the use of GPS accumulated-phase measurements, in addition to GPS pseudorange measurements, for autonomous relative navigation and time transfer for pairs of orbiting space vehicles. The use of accumulated-phase measurements allows unusually great accuracies to be achieved. This paper discusses the approaches that can be used to achieve the best accuracies, and points out some of the pitfalls to be avoided.

ASSUMPTIONS

In this paper we consider the design of filters for autonomous navigation and time transfer for two orbiting space vehicles, which we will call User Vehicle 1 and User Vehicle 2 (UV1 and UV2), as shown conceptually in Figure 1. The filters are to estimate the absolute position, velocity, and clock error for each vehicle, and the relative position, velocity, and clock error of one vehicle with respect to the other. Only local GPS measurements are to be utilized, except that a two-way communications link is available for transmission of measurement data, filter output data, and/or control information from one vehicle to the other.

Simulation results are provided to illustrate the conclusions presented in the text. The simulation truth models utilized for this study are purposely simplified in order to clarify performance trends. The UVs are considered to be point masses with separations ranging from 1000 km to less than 1 km. (Extensions to six-degree-of-freedom representations can follow previously

published approaches.[Satz, 1991]. Lever arms between the navigation centers and the antennas phase centers for each UV are assumed to be known with negligible error, (as determined by other sensors.) The orbits of the UVs are assumed to be almost the same, except for an along-track displacement that is a variable study parameter. The orbit altitudes are generally assumed to be approximately 1000 km, well above the troposphere, and the ionosphere. The GPS satellite ephemeris errors are considered to be random vector biases with component rms magnitudes of 3 m radial, 4 m cross-track, and 5 m along-track. GPS satellite clock errors are assumed to be zero. The UV orbits are assumed to be governed by a gravity field of 7th order and degree (subset of WGS84), and perturbations due to solar pressure and atmospheric drag are assumed to be negligible. The UVs are assumed to be in orbit, without thrusting. (Inertial data can be incorporated in a straight-forward fashion to measure specific force.) The fields of view of the GPS antennas are assumed to be limited to upper hemispheres (with locally level antennas), with the result that the constellation seen by both UVs are almost the same, except when the separation distance between UV1 and UV2 is large. (Further limitations in the fields of view can be introduced in six-degree-of-freedom models.) User clock errors are assumed to be due to random velocity (frequency) and acceleration (frequency drift) noise.

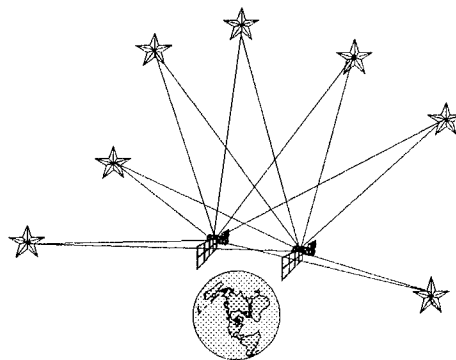


Figure 1. Autonomous navigation and time transfer for two space vehicles

The GPS receivers are assumed to be capable of measuring pseudorange, accumulated phase, and delta accumulated phase, utilizing P/Y codes on L1 and L2 frequencies. Selective availability (SA) errors are assumed to have been compensated in the receiver. Measurements are assumed to be made simultaneously at each measurement epoch. Epochs are assumed to be separated by a period of 10 seconds. Multipath noise is assumed to be random with rms values of about 1.5 m in pseudorange and 1 mm in accumulated phase (2 mm in

double-difference accumulated phase). (Such low values require special attention to antenna design and siting.). Code-loop measurements are assumed to have been aided with carrier-phase-rate data with a time constant of almost 10 seconds. Receiver front-end noise is assumed to result in pseudorange and phase error components that are negligible in comparison with the respective multipath errors.

For low earth orbits, ionospheric errors in pseudorange, and incremental ionospheric errors in accumulated phase, will be important, but can be quite well compensated, on the basis of the differences between measurements at the L1 and L2 frequencies. (L1-L2 inter-channel biases in the receivers should be considered.) Because of the high orbital velocities, ionospheric errors may have significant dynamics. If the measurements and corrections are made independently at each epoch, the correction formula results in an amplification of the rms value of independent front-end and multipath noise by a factor of 3.0. At the high altitude of 1000 km, the baseline for this study, we assume that the ionospheric error is negligible, and we do not apply the correction formula. At lower altitudes using the correction formula would be appropriate, although the random noise levels would be increased accordingly.

GPS ACCUMULATED-PHASE MEASUREMENTS

The GPS receiver in a *User Vehicle* (UV) is assumed to be capable of making measurements of *pseudorange* (PR) and accumulated phase (AP) with respect to any visible GPS Satellite (S). A PR measurement made at UV1 using a signal from S1 can be modeled as

$$PR = |\mathbf{r}_{UV1,S1}| - \tau_{UV1} + \varepsilon_{UV1,S1} \quad (1)$$

where \mathbf{r} is the vector from UV1 to S1, τ is the error of the UV1 clock, and ε is the net measurement error, with all terms being represented in a consistent set of units, e.g., meters. A GPS receiver is also able to measure the phase of the GPS carrier (after removal of the code and data). It is also capable of keeping track of the evolution of whole carrier cycles in the phase measurements, beginning with the initial epoch. If this cycle count is appended to the phase measurement, the result is *accumulated phase* (AP). AP is almost the same functionally as PR, except that there is an initial cycle-count ambiguity N . Hence the accumulated phase measurement can be represented in the form

$$AP = |\mathbf{r}_{UV1,S1}| - \tau_{UV1} - N_{UV1,S1} + \varepsilon_{UV1,S1} \quad (2)$$

This measurement is illustrated in Figure 2.

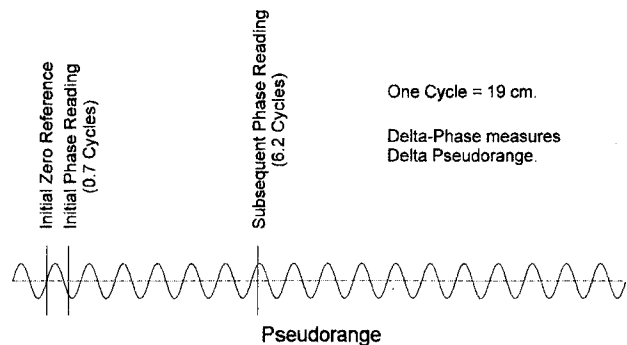


Figure 2. Accumulated phase measurements

The multipath and front-end errors associated with AP are much smaller than the corresponding error components associated with PR. (The propagation errors for AP and PR are essentially the same, except that the ionospheric errors are opposite in sign.) Hence, by fixing the ambiguity constants, the evolution of the trajectory of each user vehicle can be determined with extreme precision.

By taking the differences between AP readings taken at closely spaced sample times, *delta-accumulated-phase* (ΔAP) measurements (known in the classic GPS literature as "delta-pseudorange" measurements) are obtained. An interval of 0.6 seconds is typical. These are useful as estimates of pseudorange derivatives because they are reasonably accurate and can be modeled approximately as instantaneous, rather than average, values. However, using these ΔAP measurements to obtain the evolution of a trajectory results in much greater error than can be obtained with AP measurements, because the former data cannot account for changes in pseudorange outside the short intervals. Generally, utilizing AP measurements, as opposed to ΔAP measurements, involves greater complexity, and requires greater caution, but provides a very significant advantage in performance when the filter is appropriately designed.

ARCHITECTURE ISSUES

We desire an *absolute* navigation estimate for each vehicle, and *relative* navigation estimate showing the spatial vector between the two user vehicles. We also desire estimates of the absolute and relative clock errors. The relative estimates are different from *differential*

estimates, which are obtained when the position and clock error for one of the user vehicles are known essentially perfectly.

The relative estimation problem has some interesting features. Because measurements from two nearby UVs to a common satellite at a given epoch contain highly correlated errors, and because the unknown orbital dynamics perturbations for two nearby UVs are significantly correlated, the absolute estimation errors for the two UVs will be correlated, and the relative estimation errors will be significantly smaller than the absolute estimation errors. Because of this correlation between the absolute estimation errors for UV1 and UV2, a measurement at UV2 can be used to reduce the absolute position error for UV1 as well as for UV2, and vice versa. Furthermore, the relative estimation accuracy will depend upon the absolute estimation accuracy (even when the differential measurement errors magnitudes are held fixed). This dependence is due to the measurement geometry and increases as the separation distance between the UVs increases.

The relative estimation process converges to the differential estimation process when the estimation errors associated with one of the UV's are assumed to be zero.

A desirable output from the estimation filter is the $2n$ -by- $2n$ covariance matrix P for the estimation errors associated with UV1 and UV2. From this matrix the expected mean squared values of differential (as well as direct) measurement residuals can be computed and compared with actual residuals. The results can be used for editing of spurious data and/or for detection of estimator convergence problems. The results can also be used for higher level decision making, e.g., to determine whether relative and absolute errors are deemed to be small enough to be suitable for high-risk operations.

Perhaps the simplest estimator architecture is one with two independent absolute estimation filters, as shown in Figure 3.

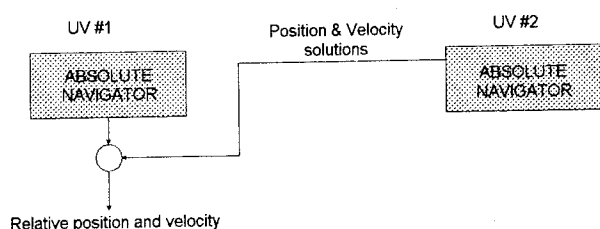


Figure 3. Relative navigation with two absolute navigation filters

With this architecture the estimation results at UV2 are telemetered to UV1, and the absolute estimates are subtracted directly to obtain the relative estimates. However, there are problems with this approach. Achieving good relative-estimation accuracy requires that only pairs of measurements with highly correlated errors be included. If a measurement from one UV with respect to a particular GPS satellite is incorporated in one estimator, a corresponding measurement from the other UV with respect to the same satellite must be incorporated in the other estimator. Since non-common measurements must be excluded, absolute accuracy would be degraded, and there might be a need for separate absolute estimators (incorporating all available measurements), to be utilized exclusively for absolute estimation. With this architecture, measurements made at one UV would not help the absolute estimation at the other UV and, hence, performance would be significantly less than optimal. Furthermore, correlations between UV1 errors and UV2 errors would not be computed and, thus, no projections of the relative estimation errors or of the *a priori* differential residual errors would be available.

An alternative architecture is shown in Figure 4. In this architecture each UV incorporates an integrated estimation filter, which receives raw time-tagged measurements from the other UV, as well as the measurements from its own GPS receiver. This estimator models states from both UV1 and UV2, and provides an integrated covariance matrix of dimension $2n$ -by- $2n$. Although the required computations are more intensive than those for the architecture in Figure 3, the performance is enhanced, the desired covariance results are obtained, and the pooling of measurements facilitates editing of bad measurements. For these reasons we favor using the integrated estimation filter.

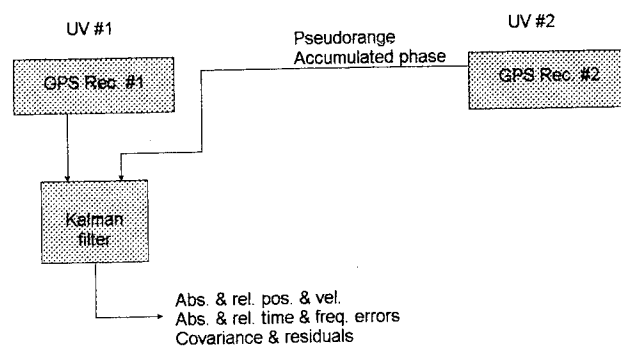


Figure 4. Utilizing an integrated estimation filter.

It may be advantageous in some applications to approximately separate the problem into absolute and relative navigation, thereby providing the desired relative and absolute error covariances with reduced computational burden, and with some reduction in accuracy. These two navigators should be cross-coupled in order to allow the nonlinear measurement and propagation geometry to be taken into account. This is a topic for further study.

GPS MEASUREMENT TRANSFORMATIONS

When the two UVs are close to each other, the errors in the measurements from the two UVs to the same satellite will be significantly correlated. It is essential to reflect these correlations in the noise models used in the integrated estimation filter. However, for computational simplicity it is desirable to use scalar updates with uncorrelated noise. The measurements with correlated errors can be conveniently transformed into average and differential measurements which have uncorrelated noise:

$$PR_{av,S1} = (PR_{UV1,S1} + PR_{UV2,S1})/2 \quad (3)$$

$$PR_{\Delta,S1} = (PR_{UV1,S1} - PR_{UV2,S1})/2 \quad (4)$$

$$AP_{av,S1} = (AP_{UV1,S1} + AP_{UV2,S1})/2 \quad (5)$$

$$AP_{\Delta,S1} = (AP_{UV1,S1} - AP_{UV2,S1})/2 \quad (6)$$

The differential measurements then are modeled as having relatively low rms values of noise in comparison with those of the average measurements. These transformations are used whenever correlated measurements are received; otherwise, unmodified PR and AP measurements are used. Generally, the average measurements are most useful in reducing errors in absolute navigation and time transfer; whereas, the differential measurements are most useful in reducing errors in differential navigation and time transfer. However, there is some cross coupling, as will be described below.

Double-difference accumulated-phase (ddAP) measurements are often used for GPS differential kinematic navigation [Loomis, 1989; Hwang, 1991; Remondi, 1992]. A double-difference measurement is formed by subtracting a single-difference measurement with respect to one GPS satellite from a single-difference measurement with respect to a second satellite. The second differencing operation eliminates user clock errors from the measurement equation and, thus,

provides two useful features: (1) Cycle slips and other mismodeling errors can be detected as being inconsistent with vehicle dynamics (by using a double-difference-measurement-residual test statistic); and (2) the sensitivity of the double-difference measurement to user-clock time error can be set exactly equal to zero, thus eliminating a potential round-off error in the filter update equations.

However, if the GPS satellite-to-satellite differences are always taken, the estimator is prevented from using the measurements to estimate user-clock frequency errors, and thereby is inhibited from achieving the best performance in time transfer and, to a lesser degree, in navigation. If double-difference measurements are employed, the missing information can be supplied as average difference measurements, i.e., the average of two single-difference measurements with respect to the two satellites. The filter-model noise levels associated with the double-difference and average-difference AP measurements would be the same, unless correlations between GPS satellite errors are to be modeled.

Introducing double-difference (and average-difference) AP measurements raises a problem in that these transformed measurements include common source measurements (e.g., with a measurement with respect to one satellite being subtracted from all of the measurements with respect to the other satellites), and are therefore correlated. Taking this correlation into account requires either a vector measurement update or a further transformation of variables to diagonalize the measurement noise matrix. Alternatively, single-difference measurements can be employed as scalar updates, and double differences can be used in a separate residual monitoring operation to detect cycle slips and other mismodeling errors. In general, residual monitoring should employ flexible measurement transformations, adjusted for best sensitivities to likely errors.

GPS MEASUREMENT MODELING

The successful operation of the estimation filter that is used in the navigation and time-transfer process requires an adequately faithful modeling of the measurement processes. These processes are described functionally by Eqs. (1-6). Mismodeling errors can cause the filter to perform poorly or to give completely erroneous results.

The range terms $|r_{UV1,S1}|$ in Eqs (1-2) are nonlinear functions of the coordinates of UV1 and UV2. Errors in

linearization are important considerations. In a batch filtering process, iteration can be used to optimize the solution with full consideration of the nonlinearities. However, the extended Kalman filter depends upon linearized models which are based only on estimates of derivatives at current epochs. This issue is discussed further in the GPS Kinematic Solutions section below.

The measurement error terms $\varepsilon_{UV1,S1}$ in Eqs. (1-2) are transformed by Eqs. (3-6) into average and differential errors. Adequate modeling of these errors is very important.

The errors in average PR measurements are composed of front-end noise, multipath errors, electromagnetic propagation errors, satellite ephemeris errors, and satellite clock errors. Only the first of these is truly independent random (white) noise; the second could be considered as approximately white, although there is significant time correlation. The other errors are slowly varying, and cannot be well modeled as being white. Moreover they may have larger variances than the white error components. In conventional GPS navigation filters, PR measurement errors are modeled as being completely white. This approximation can lead to quite nonsensical behavior. A better choice would be to include Markov processes as average PR measurement error components. As the capabilities of processors improves, the added complexity associated with these models will not be seen as an unreasonable burden.

The average AP measurements contain the same functional error sources as average PR measurements; however, for AP measurements, the front-end-noise and the multipath-error components are very small and the ionospheric phase error is opposite in sign to the group delay. Here it would be completely erroneous to assume that the measurement noise is just a small white component. The large slowly-varying component MUST be modeled separately. These components can be absorbed into the average AP cycle-count-ambiguity models. The simplest procedure is to model these ambiguities as random-walk processes with sufficiently large noise powers to represent the slowly varying measurement errors. First-order Markov processes may offer further significant improvements in performance.

Differential measurement processes have the same error sources as the average measurement processes, except that only a fraction of the GPS satellite and electromagnetic propagation errors appear. The size of the fractional multiplier depends upon the separation distance between the UVs. Hence, if the separation

distances vary widely over the course of the mission, the noise models MUST be made to adapt accordingly. For small separation distances, where only multipath and front-end noise are significant, the measurement errors may be represented by the white-noise term alone. In this case, the AP differential cycle-count ambiguities may be considered to be constants, and the random-walk noise powers can be set equal to zero. Further performance improvements then can be achieved by determining the exact integer values for some or all of the differential cycle-count ambiguities, or of corresponding double-difference cycle-count ambiguities [Greenspan, 1982; Brown, 1983; Remondi, 1984; Loomis, 1989; Hwang, 1991; Satz, 1991; Remondi, 1992].

As new satellites appear and new measurement processes begin, the states and covariances associated with the measurement models must be initialized. The initializations should be established on the basis of the existing states and covariances.

GPS KINEMATIC SOLUTIONS

The UV positions in an arbitrary trajectory can be determined on the basis of AP data alone, as long as cycle-count information is not lost. This is known as the kinematic solution. The kinematic solution yields a much higher accuracy in relative estimation than a solution based on pseudorange measurements and an orbital dynamics model.

The simplest approach to the kinematic navigation solution is to write the double-difference measurement equations for each vehicle and to find the solutions for the UV positions at all epochs such that the sum of the squares of the residuals is minimized. Solutions can be obtained if AP measurements are available from at least 5 GPS satellites. It can be shown, for example, that there is a complete solution if there are seven GPS satellites in a nonsingular geometry and if AP measurements from two epochs are incorporated. [Michalson, 1995]. This solution can be conceptualized by considering AP measurements to four satellites as being used to propagate the UV orbital positions so that the UV can just as well be considered to be stationary, and by considering the AP measurements to the remaining three satellites as being used to determine the location of a stationary UV by observing the change in range from three different perspectives over the observation interval. Over a 10-second interval between epochs, the geometry change is so small that the equations are very poorly conditioned and, equivalently, the PDOP for this method is very high. Accuracies can be improved and time

transfer can be included, by incorporating more data and by making the model more complex; but then the required calculations become extremely complex. We would like to employ a Kalman filter, instead of a batch least-squares formulation, in order to allow large amounts of data and complex models to be utilized.

One approach to using a Kalman filter to obtain a kinematic navigation solution is to use all available ddAP measurements as Kalman updates at each epoch, and to use the changes in all these measurements for state propagation between epochs [van Graas, 1995]. This approach has been shown to produce a useful differential navigation solution when there are at least seven satellites in view. However, the approach is decidedly non-optimum, as can be seen by noting that the process noise is correlated in time and with the measurement noise. Moreover, when there are only four satellites in view, this filter would indicate a falling covariance; whereas, the best that can actually be done under these circumstances is to propagate the trajectory. This problem could be solved by using AP measurements to only four satellites for trajectory propagation, and to use only AP measurements to the remaining satellites for measurement updates. However, there would remain the problem of how to partition the measurements for best results when there are more than 4 satellites.

Another Kalman filter approach, which would seem to be optimum, is to use all the AP measurements as Kalman updates, and to use for propagation a random-walk model with extremely large incremental noise. This model fits the Kalman mold and accurately reflects the assumptions used in obtaining the simple batch-least-squares solution. We have confirmed that this Kalman model does in fact yield the correct deterministic differential navigation solution with AP measurements made to seven satellites at two epochs. However, there is a major impediment to obtaining this solution, namely, the problem of finding the appropriate coefficients for the linear difference equations which are used in the Kalman filter model. Since the solution depends upon past as well as present data, past linearization errors affect present results. Moreover, for short intervals between epochs the equations are extremely poorly conditioned, with the result that minute linearization errors produce large navigation errors. Using a simple extended Kalman filter produces divergent solutions to this problem. We have found that, by iterating the filter backwards and forwards several times, the correct solution can be obtained in the limit. However, this approach is computationally burdensome and convergence is difficult to guarantee under operational conditions.

We have found that there are two keys to solving the problem of linearization errors: (1) initializing the estimation errors at small values, and (2) improving the observability of the states. (Using a second-order estimator is also likely to help [Satz, 1991]). First, utilizing PR measurements, in addition to AP measurements, quickly reduces navigation errors to nominal values and sets the stage for further reductions due to AP measurements. Secondly, incorporating an accurate orbit propagation model (and/or an inertial navigation system propagation model in other applications) significantly increases the observability of the states to the AP measurements. These two augmentations of the Kalman kinematic model reduce the effects of the measurement-model linearization errors to near negligible values. The result is an optimum filter incorporating all the available kinematic information.

Other mismodeling errors also can be important. For example, if the differential-cycle-count ambiguities are modeled as constants, and if differential satellite and electromagnetic propagation errors are not separately modeled, variations in such errors over the course of the trajectory can be completely inconsistent with the model. In such cases the Kalman estimator is unable to avail itself of the information in the AP data and the results are exceedingly poor. A simple solution to this problem is to introduce incremental noise into the state propagation model so that each of the cycle-count ambiguities is modeled as a random-walk processes with a rate of divergence roughly comparable to the rate of change of the satellite and electromagnetic propagation errors seen in the modeled measurement process over the time intervals of interest. The result is that the covariance is reduced more slowly by the AP measurements, but the actual error in estimation is reduced. The actual performance then more closely approximates the performance projected by the covariance.

TIME TRANSFER

Once the navigation solution has been obtained, the time-transfer solution can be obtained by substituting the PR measurement value and the location of the UV into Eq. (1), and by solving for the clock error τ_{UV} . The PR measurements provide solutions for both position and time. On the other hand, AP measurements do not alone provide solutions for time, i.e., user clock error is unobservable if only AP measurements are utilized [Michalson, 1995]. Nonetheless, the AP measurements can be used very effectively to reduce the navigation errors, thereby reducing those components of the error in

estimation of user clock error. For example, if relative navigation error can be reduced to 0.1 m rss (0.3 ft rss), this component of the relative time-transfer error will have been reduced to less than 0.3 ns rms. When navigation errors contribute negligibly to the time-transfer solution, the performance in time transfer will be governed by the PR measurement errors, including the unobservable common-mode biases, and the stochastic model of the user clocks. For high-quality user clocks, the estimation process will then entail long-term averaging of PR measurement noise. This process is well accomplished in an integrated estimation filter. Here we mainly want to point out the value of the AP measurements to the time-transfer process.

EFFECTS OF USER-VEHICLE SEPARATION

As the separation distance between the UVs increases from a small value, the first-difference measurements (both AP and PR) incorporate increasing fractions of line-of-sight satellite ephemeris errors and electromagnetic propagation errors. Hence, the Kalman estimator should adaptively adjust the rms values of differential-cycle-count ambiguity noise and measurement noise in accordance with the estimated separation distance (which can be determined approximately on the basis of PR measurements at a single epoch). If this adjustment is not made, performance can be very poor under some circumstances. If the adjustment is made appropriately, good performance will be achieved, and that performance will depend upon the separation distance. As expected, the best performance will be achieved at small separation distances, where the differential measurement errors are smallest.

It is interesting to note that, even if differential satellite and propagation errors are negligible, there is a dependence of relative navigation accuracy on the separation distance between the UVs. This dependence arises because of the fact that the differential range term in each differential PR and differential AP measurement equation is a function of both absolute and differential errors in position. This can be illustrated algebraically for the example shown in Figure 5.

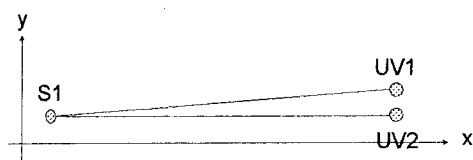


Figure 5. Relative-navigation measurement geometry

For this example, UV1 and UV2 are closely spaced, the vector from the GPS satellite S1 to the UVs lies approximately in the direction of the x axis, and the vector between UV1 and UV2 lies approximately in the direction of the y axis. In this case the ranges r_1 and r_2 from S1 to UV1 and UV2, respectively, are

$$\begin{aligned} r_1 &= |\mathbf{UV}_1 - \mathbf{S}_1| \\ &= [1](x_1) + [|\mathbf{UV}_1 - \mathbf{UV}_2|/r](y_1) \end{aligned} \quad (7)$$

$$\begin{aligned} r_2 &= |\mathbf{UV}_2 - \mathbf{S}_1| \\ &= [1](x_2) + [0]y_2 \end{aligned} \quad (8)$$

Hence, the differential range is

$$\begin{aligned} r_2 - r_1 &= [1](x_2 - x_1) + [|\mathbf{UV}_2 - \mathbf{UV}_1|/2r](y_2 - y_1) \\ &\quad + [|\mathbf{UV}_1 - \mathbf{UV}_2|/2r](y_2 + y_1) \end{aligned} \quad (9)$$

From the last term in Eq. (9), the differential range is seen to be a weak function of the average position of the two user vehicles. Although the amplitude of this term is quite small, it can be important. For example, if the distance between the UVs is 100 km, the amplitude of the term is

$$\begin{aligned} &[|\mathbf{UV}_1 - \mathbf{UV}_2|/2r] \\ &\cong (100\text{km})/(40,000\text{ km}) = 1/400 \end{aligned} \quad (10)$$

If, for example, the average navigation error in the y direction is 10 m rms, this term will contribute an error of 25 mm rms in the differential AP measurement equation. This is an order of magnitude larger than the measurement noise. Hence, it can be important to ensure that absolute errors as well as differential errors are reasonably well estimated, even in cases where differential accuracy is the only ultimate concern.

SIMULATION RESULTS

We provide here some simulation results from an integrated Kalman navigation filter to illustrate some of the conclusions drawn in the discussion above. These results are not meant to indicate the actual performance achievable in a specific application with real hardware and software. However, they illustrate important phenomena which should be taken into account in a design for a specific application.

Figure 5A shows two plots of RSS error in absolute (*average of UV1 and UV2*) position as a function of time for the case where only unmodified PR data are utilized, and where the only significant filter-model errors are white PR measurement noise of amplitude 1.5 m rms, and white acceleration process noise of amplitude 0.02 m/s/(10 sec) rms. GPS satellite ephemeris and clock errors were set at zero. A second-order gravity model (including J2 terms) was used in the filter for orbit and covariance propagation. Estimation errors were computed from the filter covariance. The plots are for UV separations of 1000 and 1 km. Only post-update values are shown. The initial value was 1000 m rss. The behavior is reasonable, given the assumptions. Errors fall abruptly as a result of the first set of measurements, and then fall gradually as the white measurement errors are averaged, until a floor is approached where the increase in error due to orbit propagation balances the decrease due to measurements. The differences between the results for different separation distances are due to differences in constellations seen by the two UVs. Sudden shifts are due to constellation changes. Sample error histories (not shown in the figure) generally fall under the covariance-generated rss values.

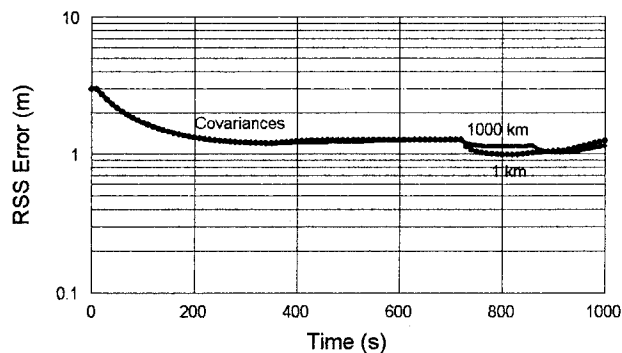


Figure 5A. Absolute navigation error with PR measurements for UV separations of 1000 and 1 km

Figure 5B shows the corresponding RSS errors in relative-navigation (*error in the vector between UV1 and UV2*). Because, the errors of one UV were essentially independent of those of the other UV, the relative-navigation error is about 40% bigger than the absolute navigation error.

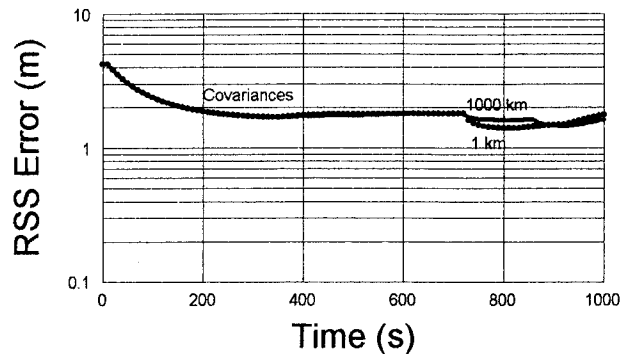


Figure 5B. RSS relative navigation errors with PR measurements with UV separations of 1000 and 1 km

Figure 6A shows the absolute-navigation results when double-difference AP (ddAP) measurements are introduced. The ddAP ambiguities were modeled as random-walk processes with very small velocity noise, 1 $\mu\text{m}/(10 \text{ sec})$ rms. The ddAP measurement noise was modeled as white with rms value 2 mm. Because ddAP measurements are very insensitive to absolute navigation error when UV separations are small, there is essentially no improvement due to the ddAP measurements under these conditions. However, there is a slight improvement at the larger (1000-km) separation, as shown by the lowest curve, because of the last term in Eq. (9).

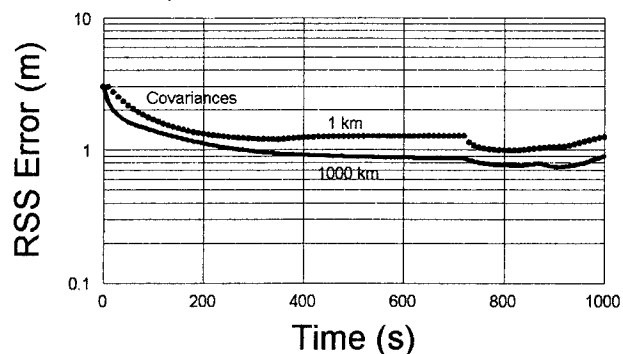


Figure 6A. Absolute navigation errors with PR and ddAP measurements for UV separations of 1000 and 1 km

Figure 6B shows the relative navigation results with the PR and ddAP measurements. Here the benefits of the ddAP measurements are evident. With a UV separation of 10 km or less, as shown by the bottom curves, accuracies of 2 cm are achieved (under our assumption that satellite ephemeris errors have been compensated to negligible values). Note, however, that the errors are

larger at separation distances of 100 and 1000 km, as shown by the upper two curves. This dependence of error on UV separation distance is not due to decreased correlation of measurement errors, because only white measurement noise was present in this experiment. Rather, the dependence of relative navigation error on separation distance is due to the dependence of the ddAP measurement errors on absolute navigation errors in accordance with the last term in Eq. (9). This is a fundamental phenomenon to be considered when designing a system for the ultimate in performance with large separation distances.

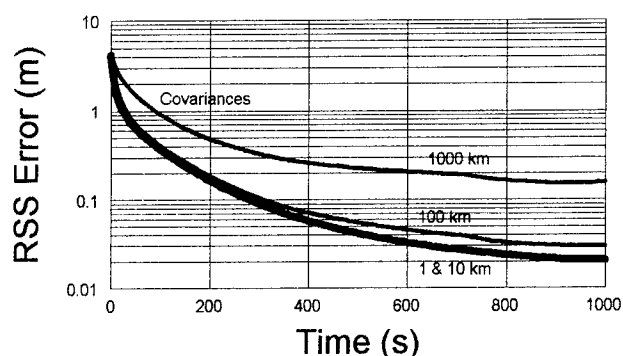


Figure 6B. Relative navigation performance with PR and ddAP measurements for separation distances of 1000, 100, 10, 1 km.

Figure 7A shows what happens to absolute (average UV) navigation error when the truth model is augmented to include satellite ephemeris errors as random constants of rms values 3 m radial, 5 m along-track, and 4 m cross-track. Here the separation distance was set at 1 km. Three sample error histories are shown in addition to the covariance result. The filter white PR noise parameter was increased to 7.2 m rms to account for the increased PR measurement error. But the white-noise model did not represent well the actual PR measurement errors. The filter assumed that averaging would reduce the effects of the measurement errors; but the errors changed very slowly and could not be reduced significantly by averaging. As shown by the sample histories, the actual errors were effectively reduced from the initial value of 1000 m after the first update, but further reductions projected by the covariance could not be produced. This example shows the nonsensical aspect of the white pseudorange noise model that is conventionally used for absolute GPS navigation problems.

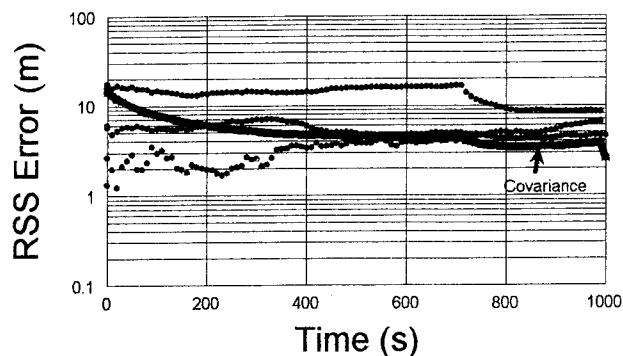


Figure 7A. Absolute navigation errors with 1 km UV separation with GPS satellite ephemeris errors

Figure 7B shows the corresponding relative-navigation errors. Because the separation distance is small, the ddAP measurements contain negligible amounts of the satellite ephemeris errors; hence, the modeling of 2-mm rms measurement noise is essentially correct. The three sample histories show that the covariance projections of 2-cm rss error in 1000 seconds can be met.

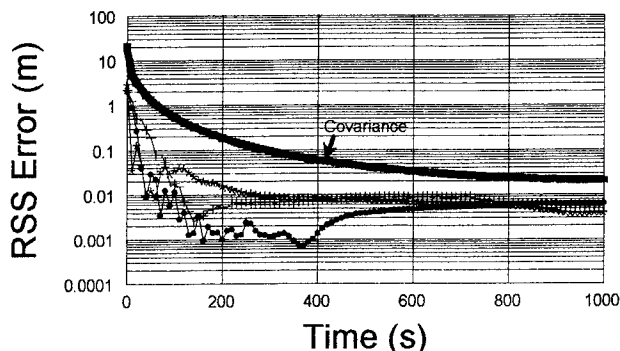


Figure 7B. Relative navigation error with 1-km SV separation and 7-m rss GPS ephemeris error

Figure 8A shows absolute navigation results when the SV separation is increased to 100 km. The covariance results are slightly better than those in Figure 7a for the 1-km separation, because the ddAP measurements at large separations have some sensitivity to absolute navigation errors. However, as before, the sample histories don't reflect the covariance. There is the immediate reduction in error due to incorporation of the first set of pseudorange measurements, but thereafter the gross mismodeling of the measurement errors causes a disagreement between the covariance and sample-history results.

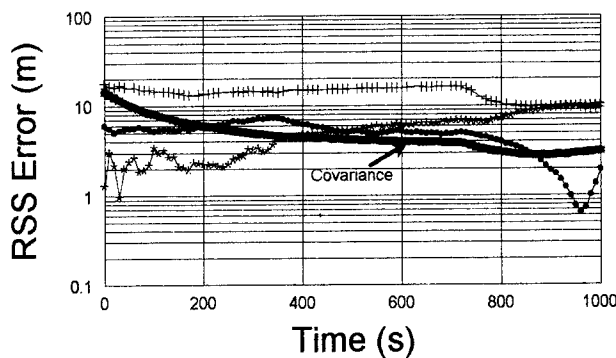


Figure 8A. Absolute navigation errors for a 100-km SV separation with 7-m rss GPS ephemeris errors

Figure 8B shows the corresponding relative-navigation results for the case where the UV separation is 100 km and the GPS ephemeris errors are 7 m rss. Here the covariance projects an rss error of less than 0.1 m after 1000 seconds, somewhat worse than for the 1-km separation case. However, the sample histories suggest an rss error of almost 1 meter. This disappointing result is due to mismodeling, in this case mismodeling of the ddAP measurement error. Because of the large UV separation, an appreciable amount of slowly-varying ephemeris error component corrupts each ddAP measurement, making the 2-mm white noise and the almost-constant cycle-count ambiguities a very poor model.

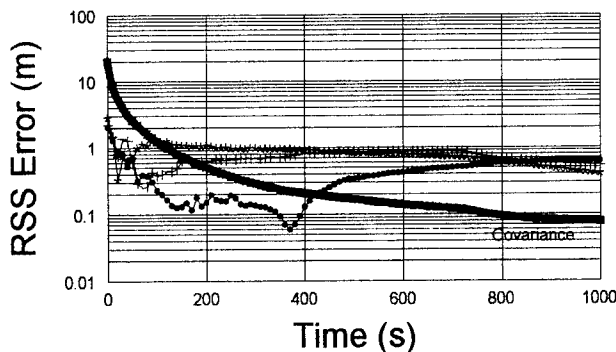


Figure 8B. Relative navigation errors for 100-km SV separation with 7-m rss ephemeris errors and an unmodified ddAP error model

In an effort to remedy the mismodeling relating to Figure 8B, the random-walk noise associated with the ddAP ambiguity constants was increased to 1 mm rms in 10 seconds. As expected, this had only a slight effect on the absolute navigation errors, as shown in Figure 9A, but a

very helpful effect on the relative navigation errors, as shown in Figure 9B.

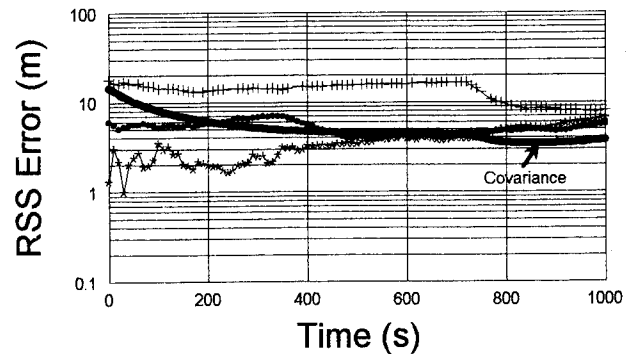


Figure 9A. Absolute navigation errors with 100-km SV separation, 7-m rss GPS ephemeris errors, and increased ambiguity noise

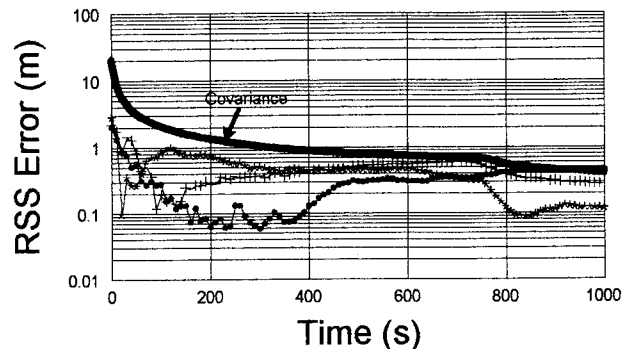


Figure 9B. Relative navigation errors with 100-km SV separation, 7-m rss GPS ephemeris errors, and increased ambiguity noise

As shown in Figure 9B, the relative-navigation error indicated by the covariance falls only to about 0.4 m rss after 1000 seconds, but the sample-history errors are well behaved, stay below the covariance projection, and are much lower than those in Figure 8B.

These results are meant to provide insight into the key modeling issues associated with an integrated Kalman estimator for application to relative navigation for orbiting space vehicles. For a specific application, high-fidelity truth models would be used, all the available data (PR and AP; average, differential, and individual) would be incorporated, and time-transfer (as well as navigation) performance would be considered.

CONCLUSIONS

General guidelines have been presented for designing a system for autonomous navigation and time transfer for pairs of orbiting space vehicles. The system utilizes GPS pseudorange and accumulated-phase data and yields estimates of both absolute (each vehicle alone, or the average) and relative (one vehicle with respect to another) variables. An integrated estimation filter is employed, thereby including consideration of vehicle-to-vehicle correlations. The estimator makes full use of the kinematic information in the accumulated-phase measurements, together with the information in the pseudorange measurements and the orbit propagation model. Achieving good performance requires that special attention be paid to modeling the measurement errors. The error models and the performance depend upon the separation distance between the user vehicles. Absolute navigation errors cause relative navigation errors, except when the separation distance is small. Simulation results have been provided to illustrate the principal design issues.

ACKNOWLEDGMENTS

This work was carried out under Contract N00014-94-C-2170 with the U.S. Naval Research Laboratory (NRL), Washington, DC. The authors wish to express their appreciation to Joseph White, Paul Landis, Ronald Beard, Alan Hope, and Peter Melvin, all of NRL, for their administrative and technical support in carrying out this work.

BIBLIOGRAPHY

- Richard. L. Greenspan, A. Y. Ng, Joseph M. Przyjemski, and James. D. Veale, "Accuracy of Relative Positioning by Interferometry with Reconstructed Carrier GPS: Experimental Results", *3rd International Geodetic Symposium on Satellite Doppler Positioning*, February 1982.
- R. Grover Brown and Patrick Y. C. Hwang, "A Kalman Filter Approach to Precision GPS Geodesy," *Navigation: Journal of The Institute of Navigation*, Vol. 30, No. 4, Winter 1983-84; pp. 338-349.
- Benjamin W. Remondi, *Using the Global Positioning System (GPS) Phase Observable for Relative Geodesy: Modeling, Processing, and Results*, "Ph. D. dissertation, Center for Space Research, The University of Texas at Austin, 1984.
- Peter Loomis, "A Kinematic GPS Double-Differencing Algorithm", *Proceedings of the 5th International Geodetic Symposium on Satellite Positioning*, Physical Science Laboratory, New Mexico State University, March 1989; pp. 611-620.
- Patrick Y. C. Hwang, "Kinematic GPS: Resolving Integer Ambiguities on the Fly", *Navigation: Journal of the Institute of Navigation*, Vol. 38, No. 1; Spring 1991; pp. 205-219.
- Haywood S. Satz, Duncan B. Cox, Jr., Ronald L. Beard, and G. Paul Landis, "GPS Inertial Attitude Estimation via Carrier Accumulated Phase Measurements", *Navigation: Journal of the Institute of Navigation*, Vol. 38, No. 3, Fall, 1991; pp. 273-284.
- Benjamin W. Remondi, "Real-Time Centimeter-Accuracy GPS: Initializing while in Motion (Warm Start vs. Cold Start)", *Proceedings of ION GPS-92*, September 1992; pp. 1053-1061.
- Prem Munjal, William Fees, and Mohan Ananda, "A Review of Spaceborne Applications of GPS", *Proceedings of ION GPS-92*, September 1992; pp. 813-823.
- George Davis, John Ries, Hyung Rim, Bob Schutz, and Byron Tapley, "Orbit Determination Techniques for GPS Tracking of Low-Altitude Satellites", *Proceedings of ION GPS-94*, September 1994; pp. 1221-1231.
- Lisa Ward and Penina Axelrad, "Spacecraft Attitude Estimation using GPS: Methodology and Results for RADCAL", *Proceedings of the ION National Technical Meeting*, January 1995, pp. 813-825.
- Frank van Graas and Shane-Woei Lee, "High-Accuracy Differential Positioning for Satellite-Based Systems Without Using Code-Phase Measurements", *Proceedings of the ION National Technical Meeting*, January 1995, pp. 231-239.
- Heather Hinkel, Young Park, and Wigbert Fehse, "Real-time GPS Relative Navigation Flight Experiment", *Proceedings of the ION National Technical Meeting*, January 1995, pp. 593-601.
- William R. Michalson, Duncan B. Cox, Jr., and Hua Hua, "GPS Carrier-Phase RAIM", *Proceedings of ION GPS-95*, September 1995.

GPS Tracking Experiment of a Free-Flyer Deployed from Space Shuttle

Bob Schutz, P.A.M. Abusali, Christine Schroeder, and Byron Tapley, *University of Texas at Austin*

Michael Exner and Rick McCloskey, *University Corporation for Atmospheric Research*

Russell Carpenter, Michael Cooke, and Samantha McDonald, *NASA/Johnson Space Center*

Nick Combs, *University of Houston*

Courtney Duncan, Charles Dunn, and Tom Meehan, *NASA/Jet Propulsion Laboratory*

BIOGRAPHIES

Bob Schutz is Professor of Aerospace Engineering and Engineering Mechanics at The University of Texas at Austin (UT/Austin) and Associate Director of the Center for Space Research (CSR).

P. A. M. Abusali is Research Scientist with the Center for Space Research at UT/Austin.

Christine Schroeder is Graduate Research Assistant in the CSR at UT/Austin and a graduate student in Aerospace Engineering and Engineering Mechanics.

Byron Tapley is Director of the CSR at UT/Austin, Professor of Aerospace Engineering and Engineering Mechanics and Director of the Texas Space Grant Consortium.

Michael Exner is the Program Manager for the NSF-funded GPS/MET Program, managed by the University Corporation for Atmospheric Research (UCAR).

Rick McCloskey is a System Engineer for the GPS/MET Program, managed by UCAR.

Russell Carpenter is an aerospace engineer at the NASA/Johnson Space Center (JSC) working on the Space Station GPS Project and is pursuing doctoral studies at UT/Austin.

Michael Cooke is an electrical engineer at the NASA/JSC and is the Systems Implementer on the Space Station GPS Project.

Samantha McDonald is an electrical engineer at the NASA/JSC working on the Space Station GPS Project.

Nick Combs is the Wake Shield Facility Experiment Inte-

gration Manager for the Space Vacuum Epitaxy Center at the University of Houston.

Courtney Duncan is a member of the Technical Staff in the GPS Systems Group at the NASA/Jet Propulsion Laboratory (JPL).

Charles Dunn is a member of the Technical Staff in the GPS Systems Group at the NASA/JPL.

Tom Meehan is the GPS flight receiver Group Leader at the NASA/JPL and a co-investigator on GPS/MET.

ABSTRACT

Shuttle mission STS-69 was launched on September 7, 1995, 10:09 CDT, carrying the Wake Shield Facility (WSF-02). The WSF-02 spacecraft included a set of payloads provided by the Texas Space Grant Consortium, known as TexasSat. One of the TexasSat payloads was a GPS TurboRogue receiver loaned by the University Corporation for Atmospheric Research. On September 11, the WSF-02 was unberthed from the Endeavour payload bay using the remote manipulator system. The GPS receiver was powered on prior to release and the WSF-02 remained in free-flight for three days before being retrieved on September 14. All WSF-02 GPS data, which includes dual frequency pseudorange and carrier phase, were stored in an on-board recorder for post-flight analysis, but "snapshots" of data were transmitted for 2-3 minutes at intervals of several hours, when permitted by the telemetry bandwidth. The GPS experiment goals were 1) an evaluation of precision orbit determination in a low altitude environment (400 km) where perturbations due to atmospheric drag and the Earth's gravity field are more pronounced than for

higher altitude satellites with high precision orbit requirements, such as TOPEX/POSEIDON; 2) an assessment of relative positioning using the WSF GPS receiver and the Endeavour Collins receiver; and 3) determination of atmospheric temperature profiles using GPS signals passing through the atmosphere. Analysis of snap-shot telemetry data indicate that 24 hours of continuous data were stored on board, which includes high rate (50 Hz) data for atmosphere temperature profiles. Examination of the limited number of real-time navigation solutions show that at least 7 GPS satellites were tracked simultaneously and the on-board clock corrections were at the microsec level, as expected. Furthermore, a dynamical consistency test provided a further validation of the on-board navigation solutions. Complete analysis will be conducted in post-flight using the data recorded on-board.

INTRODUCTION

The Wake Shield Facility (WSF) is a free-flying spacecraft deployed from the Space Shuttle for the purpose of growing thin semiconductor films for advanced electronics in an ultra-vacuum environment. The ultra-vacuum is created in low Earth orbit by a 4 meter diameter stainless steel disk with a mass of 1979 kg flying with its velocity vector perpendicular to the disk. The vacuum in the disk wake is expected to be 1000-10,000 times better than Earth-based laboratories can achieve. The WSF is a NASA-funded University of Houston experiment, with Space Industries Incorporated (SII) serving as the principal hardware development partner.

Launch of WSF occurred on STS-69, launched from Kennedy Space Center on September 7, 1995, 10:09 CDT. Since this was the second flight of the WSF, it was designated WSF-02. Release of WSF-02 to free-flight was at 06:25 CDT on September 11. The orbit parameters for this flight included an altitude of about 400 km, near zero eccentricity and inclination of 28.5 degrees. The WSF-02 was planned to operate in free-flight for about 48 hours, but operations were extended to 75 hours. The satellite was retrieved at 08:59 CDT on September 14 and Endeavour landed at Kennedy Space Center on September 18 at 06:38 CDT.

The spacecraft design and the orbit parameters make the WSF-02 a suitable platform to conduct other experiments. Several additional payloads were arranged to be WSF-02 Cooperative Experiments, including those provided by the Texas Space Grant Consortium (TSGC). The TSGC payloads were known as TexasSat. As one of the TexasSat components, The University of Texas at Austin proposed to fly a high precision GPS receiver on WSF-02 for the following purposes:

- examine the low altitude space environment and the effect of atmospheric drag and Earth gravity on the motion of the WSF in free-flyer mode,
- evaluate GPS dual-frequency receiver performance in a high precision operation mode that does not require access to the Department of Defense encryption of the GPS signals,
- assess ability to use GPS in a relative satellite positioning mode using the Shuttle GPS receiver and the WSF GPS receiver,
- use the WSF GPS data to obtain atmospheric temperature profiles from the GPS signals that pass through the atmosphere, referred to as "occultations".

Each of the experiment goals will contribute information to other space flight programs. The assessment of low Earth orbit accuracy is important for future satellites that will require high accuracy orbits. Although the 1335 km altitude TOPEX/POSEIDON (T/P) has demonstrated the ability to determine few-centimeter accuracy orbits in three-dimensions [Schutz et al., 1994; Yunck et al., 1994], no demonstration in very low Earth orbit with a high precision GPS receiver has been conducted. In addition, the relative positioning with GPS is potentially important for Space Station applications. The determination of atmospheric profiles will augment and enhance the measurements now being collected by the GPS/MET program [Ware and Exner, 1995].

In the following sections, the GPS receiver characteristics and the operational constraints are described. The operation of the GPS receiver through deployment and retrieval are given in a later section, along with the preliminary results obtained from the in-flight operation. Based on these results, preliminary conclusions are given in the final section.

WSF-02 GPS EXPERIMENT DESCRIPTION

The WSF/GPS experiment developed into a collaboration with the University Corporation for Atmospheric Research (UCAR), which is primarily interested in the GPS goal directed toward determining atmospheric temperature profiles. UCAR has been funded by the National Science Foundation and others to conduct such experiments on the MicroLab 1 satellite, launched in April 1995. UCAR acquired three GPS receivers based on the JPL/Osborne TurboRogue design. These receivers are referred to as the GPS/MET version of the TurboRogue. The availability of the GPS/MET backup receiver for the WSF flight was anticipated well before MicroLab 1 launch, but the availability was complicated by factors introduced by both GPS/MET and Shuttle launch schedule considerations.

The GPS/MET TurboRogue receiver is a flight version of the commercially available geodetic version. This flight version is now marketed by Allan Osborne Associates as the TurboStar. Thermal and vibration tests of the WSF-02 flight unit were conducted at the Ball Aerospace facility in Boulder, CO. This 2.3 kg receiver uses 17 watts during tracking and the dimensions are 25x25x10 cm. The receiver measures pseudorange and carrier phase on both L1 and L2 using a cross-correlation technique when the GPS satellites are transmitting in anti-spoofing mode. The receiver can track up to eight GPS satellites simultaneously. The receiver hardware design, tracking integrated circuits and software were developed at JPL for NASA and flight software enhancements were implemented by JPL under contract to UCAR.

The GPS experiment design was influenced by the bandwidth of the Wake Shield telemetry, especially during operation of the primary WSF experiment of gallium arsenide (GaAs) film growth. During these periods, the full telemetry bandwidth (9600 baud) was dedicated to this experiment. In addition, some GPS experiment objectives required high rate data collection, e.g., a 50 Hz sample rate, which could not be met with the telemetry bandwidth throughout the free-flight operation. With these considerations, it was apparent that all data should be recorded on-board for post-flight analysis. Nevertheless, other requirements for limited real-time data existed, such as health status and to support a NASA Johnson Space Center (JSC) real-time experiment organized by Heather Hinkel and Russell Carpenter, with the participation of Astronaut Jim Newman.

With the considerations for real-time and on-board storage of all data for post-flight analysis, NASA/JSC designed and constructed a solid-state recorder, which was capable of storing 80 mbytes of data. Recorder status information, as well as GPS pseudorange data and navigation solutions, were forwarded to the Shuttle and to the ground operation centers via the WSF telemetry stream. Ground telemetry commands enabled switching the receiver operation (and hence the recorder operation) to reduce the number of occultations recorded, thus slowing the rate of data collection. The atmospheric temperature profile analysis required the high data rate, which was the initial operation mode at receiver power on. Since the recorder had limited capacity, a telemetry command was available to reduce the number of occultations recorded, known as "low data rate".

The GPS antenna placement was a compromise between conflicting requirements. The ideal antenna orientation for atmospheric studies using the signal occultation is to have

the ground plane perpendicular to the velocity vector, but facing in the anti-velocity direction. This orientation was achieved on MicroLab 1. On the other hand, the preferred orientation for precision positioning studies has the antenna facing the zenith direction to enable viewing all satellites with optimum geometry. Since these directions are orthogonal, a compromise was necessary. Additional constraints for the antenna placement were imposed by the Wake Shield.

A side view of the Wake Shield is shown in Fig. 1. While the ideal location for the antenna was the epitaxy housing on the wake side, contamination concerns prevented the placement of the antenna in this area. The compromise location for the antenna ground plane was the outer rim on the zenith side. An additional constraint imposed by WSF-02 required the ground plane to remain outside the epitaxy housing field of view. As a consequence, the ground plane was oriented 26° with respect to the zenith, as shown in Fig. 1. In order to accommodate the change in aerodynamics imposed by the antenna ground plane, similar "trim tabs" were placed elsewhere to provide balancing torques.

The antenna placed on the ground plane is a micro-strip antenna manufactured by Ball Aerospace. This antenna is identical to the antenna used with GPS/MET on MicroLab 1. An 0.5 db noise figure preamplifier was acquired from Miteq.

WSF-02 DEPLOYMENT AND RETRIEVAL

Space Shuttle Endeavour was oriented in a gravity gradient (GG) attitude prior to the WSF-02 deployment operations. The GG orientation was used to eliminate contamination of WSF-02 by Endeavour's attitude thrusters. The Endeavour orientation in GG mode is shown in Fig. 2, which also illustrates the orbiter velocity vector (V).

The WSF-02 was removed from the cross-bay carrier (unberthed) using the Remote Manipulator System (RMS) at 00:51 CDT, September 11, 1995. Mission Specialist Newman maneuvered Wake Shield into the "ram clean mode", an orientation with the wake-side of WSF-02 directed to the incoming wind (opposite the normal orientation of the satellite). The purpose of the ram clean orientation was to use the relative wind to remove contaminants from the wake-side. In this orientation, the GPS antenna was on the Earth side, an undesirable orientation for activation of the GPS receiver. The WSF was held in this mode for about 2.5 hours.

After completion of the ram cleaning, WSF-02 was moved with the RMS under Mission Specialist control to the nor-

mal attitude orientation with the wake-side directed in the anti-velocity vector direction and the ram-side facing the incoming wind. The GPS antenna was on the zenith side as well. While attached to the RMS, the WSF attitude determination and control system (ADACS) underwent checkout. This checkout was conducted for about 45 minutes. Fig. 2 shows WSF-02 in the ADACS checkout mode orientation. The TurboRogue receiver was powered up early in the ADACS checkout mode for the reasons given below at approximately 03:45 CDT.

The WSF-02 was moved with the RMS to the release position after completion of the ADACS checkout. This position is directly above the payload bay. Nominal release of

WSF-02 was within 30 minutes after moving from ADACS checkout to the release orientation. However, communication problems delayed the release by one orbital revolution to about 06:25 CDT on September 11.

After release from the RMS, a nitrogen thruster on the WSF-02 provided a small thrust of 0.25N for approximately 14 minutes to increase the separation between the WSF-02 and the Shuttle. In this period, the Endeavour thrusters continued to be quiet to meet the WSF-02 contamination avoidance requirement. During the thrust period WSF-02 moved past the port side of the Shuttle and then above the Shuttle nose. A second thrust period of WSF-02 was not conducted. Instead, the separation induced by the initial thrust produced a separation of about 12 km, where the Shuttle maneuvering system was activated to further increase the separation to 63 km.

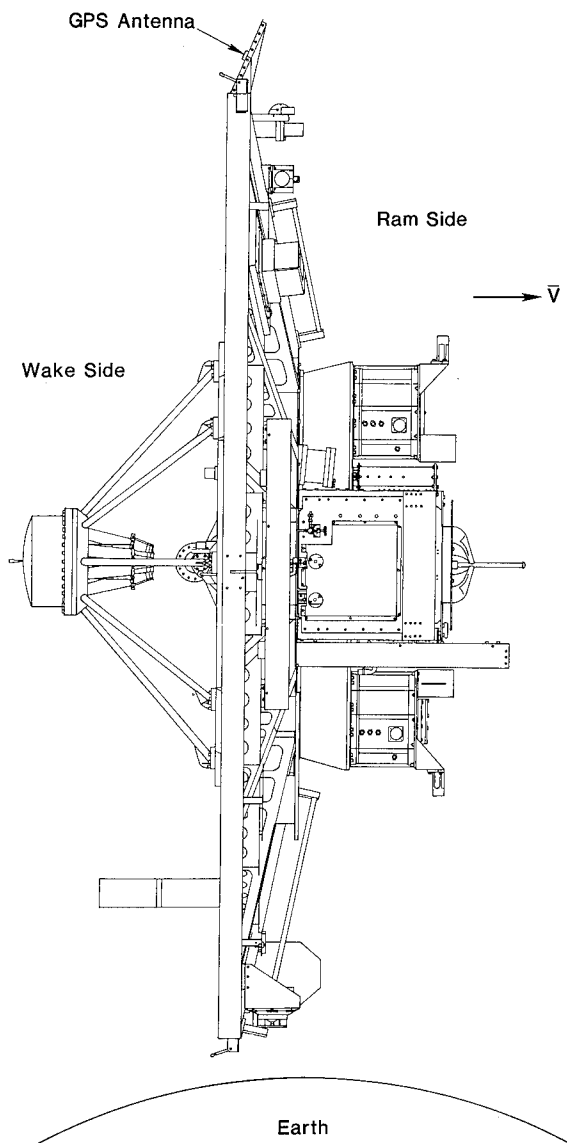


Fig. 1. Side View of Wake Shield Spacecraft

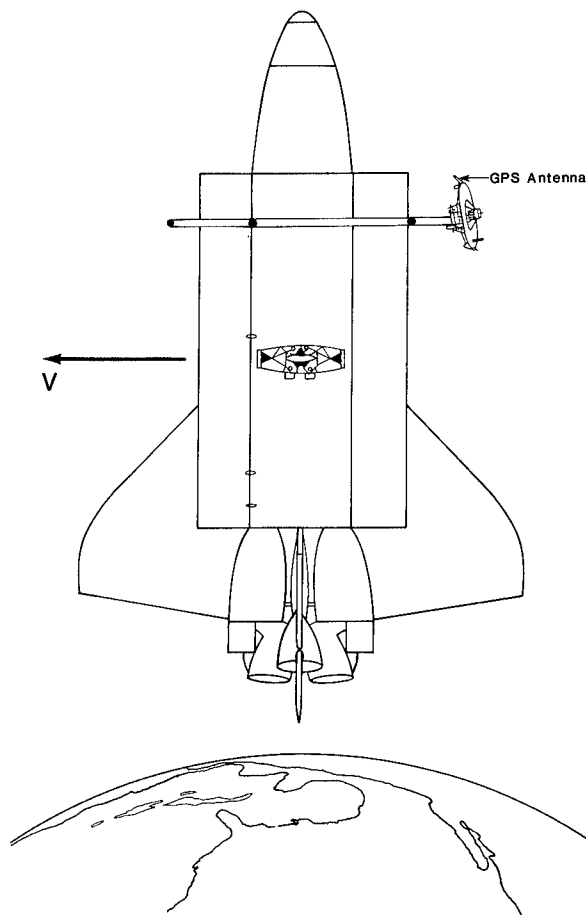


Fig. 2. WSF-02 in ADACS Checkout Orientation

The WSF-02 had been planned to operate in free-flight for about 48 hours; however, ADACS excursions were experienced and steps were taken to correct the system. These steps reduced the time available for the primary epitaxial film growth while in free-flight. As a result, the free-flight was extended to about 75 hours.

After completion of the primary experiment, the Shuttle crew maneuvered Endeavour to the vicinity of the WSF-02. The free-flyer was grappled by the RMS at 08:59 CDT, September 14. WSF-02 remained on the RMS for a few hours before being stowed into the payload bay. Endeavour landed at Kennedy Space Center at 06:38 CDT, Monday September 18.

GPS RECEIVER TESTS AND OPERATION

The solid state recorder, which used flash memory technology, was designed to provide power to the TurboRogue and communicate with the receiver via the receiver's RS-422 interface. In turn, the recorder was attached to the Wake Shield power distribution bus and communicated with the WSF-02 telemetry bus via an RS-485 interface. Because of the telemetry bandwidth considerations, the available telemetry commands were limited to the following:

- Recorder/receiver power on/power off
- Switch receiver data rate to low rate
- Activate/deactivate snap-shot of receiver data
- Reformat disk

As data were output from the receiver to the recorder, it was held in a buffer before writing to the solid state "disk". Under command, the snap-shot data were extracted from the buffer and sent to the WSF-02 telemetry bus. The data contained in the real time snap-shot were:

- Recorder temperatures
- Disk sectors used
- Data rate (high or low)
- Time and pseudo-range from receiver
- Time, receiver position (x,y,z) and clock correction

Various tests were conducted with the receiver and recorder during the year preceding the launch. A test of radio frequency interference (RFI) was conducted at the League City (TX) SII facility in December 1994. No RFI problems were detected while other WSF-02 experiments were activated.

In March, 1995, a test of the WSF-02 TurboRogue was conducted at JSC using a GPS signal simulator which created signals that were consistent with an orbiting receiver.

On April 14, 1995, as part of final testing of the receiver/recorder at JSC, a short baseline (2 m) test was conducted with the WSF-02 TurboRogue and a Collins MAGR, similar to the receiver used on Endeavour. During April 18-20, 1995, the TurboRogue was integrated to WSF-02 at Hangar A/E, Cape Canaveral Air Force Station (FL). A receiver test was conducted using a Dorn-Margolin antenna located outside the clean room containing WSF-02. The coaxial cable with the D-M was attached to a "re-radiating" antenna, which was placed about 0.5 m from the WSF-02 antenna. The test was conducted using the WSF-02 power and telemetry bus. Although difficulties were encountered with the RFI environment in the vicinity of Hangar A/E, proper placement of the D-M antenna outside the hangar to shield it from the RFI sources resulted in a successful preflight test. The receiver was configured for flight at Hangar A/E on May 26 with software that had been tested in orbit on MicroLab 1. Data from the test was left in the recorder, which used 3.97% of the capacity.

The TurboRogue receiver on WSF-02 was activated prior to release from the RMS while in the ADACS checkout mode. The reasons for planned activation during this period were as follows:

- WSF would be in normal attitude or near-normal attitude (e.g., each axis within 30° of nominal attitude),
- WSF would still be attached to the RMS, thus enabling a short baseline calibration with the Shuttle Collins receiver early in the mission,
- WSF/GPS would likely be locked on GPS satellites when released from RMS to provide GPS data during the WSF thrusting period.

Experience with the similar GPS receiver on MicroLab 1 and signal simulations performed at NASA/JSC showed that full GPS lock-on could require up to 30 minutes from power on. Since the last pre-flight receiver test was conducted in May, 1995, under static operation at Kennedy Space Center, the receiver had no meaningful a priori information at the September 11 power on. The almanacs were nearly four months old and a reasonable a priori position was not available to the receiver. At power on, the receiver systematically searched GPS PRN, C/A correlation and doppler space until sufficient tracking data are available to determine the state vector. In summary, the TurboRogue searched for GPS satellites over all expected doppler values until it located C/A signals. These signals were analyzed using discrete Fourier Transforms to enable lock on the C/A code and acquire metric data.

RESULTS

At this writing, only preliminary results are available based on the snap-shot telemetry data. The full analysis

will be conducted with the data recorded on the solid state disk, which will be available in early October.

Fig. 3 shows WSF-02 in free-flight, as seen by the Endeavour crew. The illustrated view shows the ram side and the GPS antenna ground plane is clearly visible as the protrusion on the "top" side, i.e., the side away from the Earth. The GPS receiver/recorder is in the enclosure 90° counter-clockwise from the antenna.

Several snap-shots of data were collected following receiver turn on. These snap-shots were produced under ground command and most had durations of 2-3 min. The snap-shots are summarized in Table 1, which also shows the telemetered solid state disk use. Examination of the first four snap-shots shows that up to seven GPS satellites were tracked simultaneously during the snap-shot periods. The receiver-computed navigation solution, included in the telemetry, shows that the receiver clock was steered to GPS time since the computed clock correction was generally a few microseconds.

As evident from Table 1, the recorder accumulated data from the TurboRogue during several flight regimes. First, about 2.5 hours of data were collected with the WSF-02 attached to Endeavour with the RMS. Second, data was collected during the WSF-02 thrust period. And third, approximately 20 hours, of free-flight data were acquired. In addition, the Collins GPS receiver on Endeavour acquired data throughout the TurboRogue period, so various studies of relative positioning from GPS can be performed. The reason for the apparent premature tracking termination after 24 hours will be determined in the post-flight review of the recorded data and the hardware state.

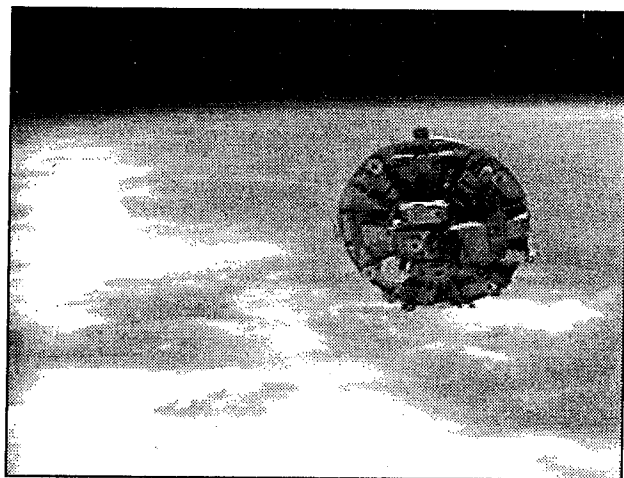


Fig. 3. Endeavour View of WSF-02 Ram Side

TABLE 1. Summary of GPS Snap-Shots and Events

| Time | Event | Disk Use (%) |
|--|-------------------------------|--------------|
| September 11, 1995 | | |
| 03:48 CDT | Receiver/recorder power on * | 3.97 |
| 06:00 CDT | Snap-shot 1 | Not avail. |
| 06:25 CDT | WSF-02 release to free-flight | |
| 06:27 CDT | WSF-02 thrust start | |
| 06:41 CDT | WSF-02 thrust stop | |
| 10:48 CDT | Snap-shot 2 | 12.49 |
| 15:00 CDT | Snap-shot 3 | 24.31 |
| 18:05 CDT | Snap-shot 4 | 25.25 |
| 21:22 CDT | Snap-shot 5 | 26.22 |
| September 12, 1995 | | |
| 03:05 CDT | Snap-shot 6 | 27.58 |
| [All subsequent snap-shots show 27.58% used] | | |

The rate of data accumulation in the solid state recorder through Snap-shot 3 shown in Table 1 is consistent with the expected occultation rate (50 Hz). However, the disk accumulation rate after Snap-shot 3 suggests that fewer occultations were being recorded. The occultation algorithm used in the receiver has been thoroughly tested on MicroLab, but the algorithm does rely on expected spacecraft attitude. No real-time attitude information was provided to the receiver. The reason for the apparent change in occultation scheduling will be investigated further in post-flight analysis.

An initial assessment of the data acquired in the snap-shots was conducted by evaluating the dynamical consistency of the (x,y,z) position solutions. In this test, a sampling of (x,y,z) from the free-flight snap-shots 2, 3 and 4 were used as "observations" for a dynamical orbit determination. In other words, the WSF-02 orbit was modeled with a large gravity field (degree and order 70 JGM-3), atmospheric drag, solar radiation pressure and other small perturbations. In one test, the (x,y,z) "observations" were fit with the University of Texas Orbit Processor (UTOPIA) over the 8 hours of the snap-shots and the WSF-02 initial state was estimated. The observation residuals had a root mean square (rms) of about 60 m. The experiment was repeated, but a drag parameter was estimated also and the resulting fit produced residuals with an rms of 20 m. The level of the residuals is consistent with GPS Selective Availability. This test demonstrated that the navigation solutions, derived from the pseudorange, give a dynamically consistent orbit at the expected level, thereby provid-

ing a strong indication that the GPS data acquired during the WSF-02 flight are valid.

The estimated orbit parameters for WSF-02 from the UTOPIA processing were:

| | |
|---------------------|---------|
| Semimajor axis | 6782 km |
| Eccentricity | 0.0008 |
| Inclination | 28.45° |
| Equatorial altitude | 404 km |

CONCLUSIONS

A TurboRogue GPS receiver was carried on the second flight of the Wake Shield Facility. The receiver successfully operated for approximately 24 hours beginning at 03:48 CDT, September 11, 1995. Based on limited telemetry, high quality measurements were made by the receiver and all objectives of the experiment are expected to be met. Two anomalies were observed: 1) premature termination of tracking, possibly associated with high temperatures, and 2) the receiver appeared to stop scheduling occultations after 12 hours. These anomalies will be resolved with the post-flight return of the flight hardware and recorded data.

The dual frequency pseudorange and carrier phase measurements will be used to compute and study precision orbits for a low altitude (400 km) satellite. The techniques used for the precision orbit determination will be based on methodologies successfully applied to higher altitude satellites, such as TOPEX/POSEIDON. In addition, studies will be performed of relative positioning between the WSF-02 and Endeavour, using the Collins receiver on Shuttle and the TurboRogue on WSF-02.

ACKNOWLEDGEMENTS

This experiment was supported, in part, by the Texas Space Grant Consortium and the NASA Johnson Space Center under grant NAG9-750. The Wake Shield is supported by NASA Grant NAGW-977. Thanks to John Ries for the UTOPIA processing of WSF/GPS data.

REFERENCES

Ware, R., Exner, M. L., et al., GPS sounding of the atmosphere from low Earth orbit: preliminary results, Submitted to *Bulletin of the American Meteorological Society*, 1995.

Schutz, B., B. Tapley, P. Abusali, and H. Rim, Dynamic orbit determination using GPS measurements from

TOPEX/POSEIDON, *Geophys. Res. Letters*, Vol 21, No. 19, 2179-2182, September 15, 1994.

Yunck, T., W. Bertiger, S. Wu, Y. Bar-Sever, E. Christensen, B. Haines, S. Lichten, R. Muellerschoen, Y. Vigue, and P. Willis, First assessment of GPS-based reduced dynamic orbit determination on TOPEX/POSEIDON, *Geophys. Res. Letters*, Vol. 21, No. 7, 541-544, April 1, 1994.

GPS Receiver Design and Requirement Analysis for the Stanford Gravity Probe B Relativity Mission

Dr. Hirohiko Uematsu and Dr. Bradford Parkinson
Stanford University

E. Glenn Lightsey
NASA Goddard Space Flight Center

BIOGRAPHY

Hirohiko Uematsu, Ph.D., is a manager for spaceborne GPS receiver development for the Gravity Probe B Relativity Mission at Stanford University. He received Ph.D. and M.S. degrees from Stanford University and a B.S. degree from University of Tokyo. He has been working on spaceborne receivers since 1990, including Trimble's VECTOR and Loral's TENSOR.

Bradford W. Parkinson, Ph.D., is a tenured professor of Dept. of Aeronautics and Astronautics, Stanford University. He is also a program manager for the Gravity Probe B Relativity Mission. He served for six years as the first program director of the GPS Joint Program Office and has been instrumental in GPS program development.

E. Glenn Lightsey is a Ph.D. candidate at Stanford University working on spaceborne GPS receivers. He is also a full-time employee at the NASA Goddard Space Flight Center, where he works for the Guidance and Control Branch. He has an M.S. degree from The Johns Hopkins University and a B.S.E. degree from Princeton University.

ABSTRACT

The Gravity Probe B (GP-B) program is a relativity

gyroscope experiment primarily designed to test two aspects of Einstein's theory of General Relativity. For space applications, it provides a unique opportunity for GPS to perform not only point-positioning but also time-transfer, attitude determination, and precise orbit determination on a rotating drag-free satellite. This paper describes the mission, requirements and operational conditions imposed on a GPS receiver and design of such a receiver for GP-B based on the TENSOR receiver developed by Space Systems/Loral.

1. INTRODUCTION

The primary objective of GP-B is to measure the relativistic drift of an Earth-orbiting gyroscope as predicted by the General Theory of Relativity [1]. GPS will play one of the key roles providing time tags for the measurements and carrier phase tracking for precise orbit determination. A drag-free satellite in a polar, circular orbit at the altitude of 650 km will carry a GPS receiver and a redundant spare, which will provide real-time navigation solutions, real-time attitude solutions, timing pulses and raw measurements for post-processing. The GPS receiver will be one of the primary navigation sensors not only for the relativity experiment but also for the *clock*, *geodesy* and *aeronomy* coexperiments. It will also provide real-time navigation solutions for *closed-loop orbit trim*.

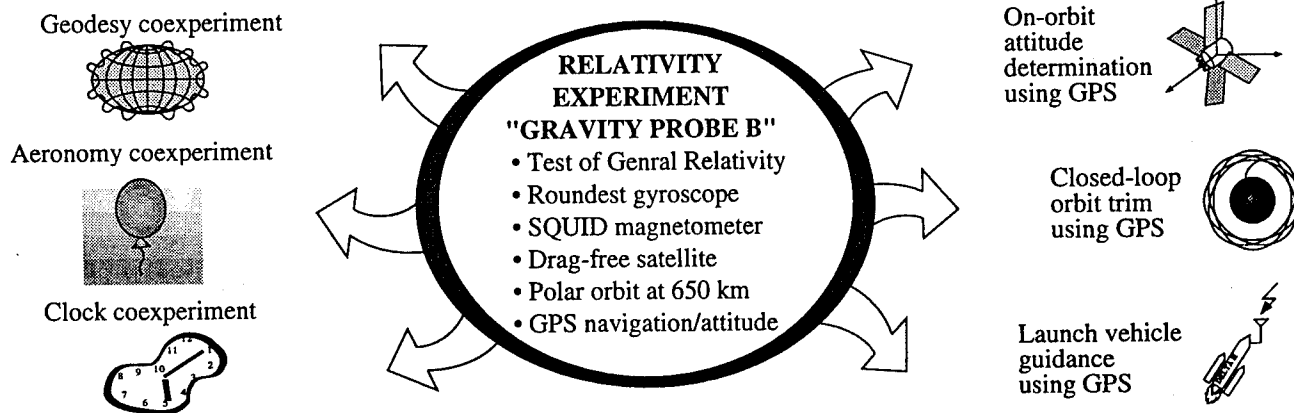


Figure 1 Stanford Gravity Probe B Relativity Experiment, coexperiments and spacecraft operations using GPS

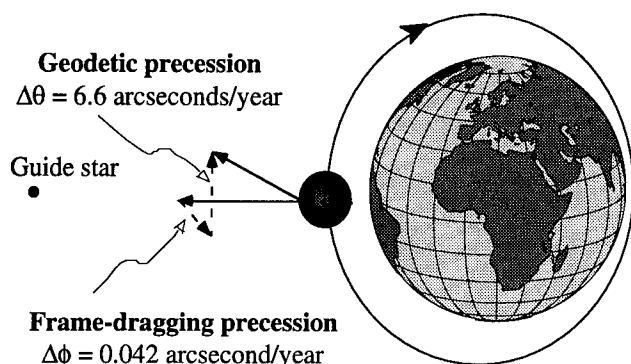


Figure 2 Geodetic and frame-dragging precession rates to be investigated by GP-B

In this paper, we will first describe the mission and requirements imposed on the GPS receiver. We will then discuss the GPS installation to the GP-B spacecraft and operational conditions including antenna coverage and GPS signal reception. We started to design a receiver to comply the GP-B requirements and operational conditions based on the TENSOR receiver developed by Space Systems/Loral and will discuss the design issues in terms of hardware and software development. Finally, other issues such as radiation hardness and handling of single even upsets (SEU) are discussed, and conclusions are presented.

2. MISSION AND GPS REQUIREMENTS

The GP-B program is primarily designed to test the theory of General Relativity, but that is not the only goal of the mission. With state-of-the-art instruments and stringent requirements, it expands the opportunity to perform the geodesy, clock and aeronomy coexperiments, and also to demonstrate the real-time applications of GPS in space such as closed-loop orbit trim and attitude determination on a rotating satellite [Fig. 1]. In the following sections, we will describe the relativity experiment and coexperiments, and discuss the GPS requirements.

RELATIVITY EXPERIMENT

Four gyroscopes carried on a drag-free satellite in a polar, circular orbit will undergo two kinds of relativistic drifts caused by the Earth's gravity: geodetic precession and frame-dragging precession [Fig. 2]. The geodetic precession is caused by the warping of space-time around the Earth by the gravity, and the frame-dragging precession is caused by the spinning of the Earth's body dragging space-time around it. The direction of the gyroscope spin axis is measured with respect to the telescope axis, whose pointing is maintained to within 20 milliarcseconds of a guide star. The guide star as seen from the GP-B spacecraft will serve as a distant inertial reference, which is free from the gravitation effects of the solar system. The drift rate is measured by a superconducting sensor called a *SQUID* (superconducting

| | POS | VEL | TIME | FREQ |
|-------------------------|-------|---------|----------|---------------------------|
| Relativity ¹ | 0.5 m | 0.3 m/s | 0.1 msec | 1e-9 |
| Geodesy ² | 1 cm | — | — | — |
| Clock ³ | — | — | — | 1e-8 (shf) 3e-14 (lmg) |
| Aeronomy ⁴ | 1 km | — | 0.1 sec | — |
| Orbit trim ⁵ | 25 m | 0.5 m/s | 0.1 msec | — |

Table 1 GPS requirements by relativity experiment, coexperiments and orbit trim.

- 1,2,4 10 second time constant with post-processing [2, 3, 4].
- 3 $\tau=1$ sec for short-term and $\tau=1$ year for long-term with post-processing [5].
- 5 1 day time constant with real-time navigation [6].

quantum interference device) magnetometer, which has a $1/f$ noise characteristic. In order to increase the signal-to-noise (S/N) ratio, the satellite body is rotated about the telescope axis at 0.1~1 rpm, which results in the ac modulation of the signal. The GPS receiver will provide navigation solutions for calibrating sensor scale factors and provide time tags for the measurements. The requirements on GPS are summarized in Table 1. The requirements imposed by the relativity experiment are post-processing numbers because the data reduction scheme will process down-linked data on the ground. The velocity requirement is particularly important because the orbital aberration determined by the satellite velocity is used to calibrate the SQUID scale factor [7].

GEODESY COEXPERIMENT

The TENSOR receiver developed by Space Systems/Loral is based on the Trimble VECTOR receiver, which is capable of multiplexing up to four antennas and tracking L1 carrier phase and differential phases among antennas. The measurement noise in the carrier phase is about 2~3 mm over a half second. Combined with this precision and the drag-free requirement ($<10^{-11}g$) on the GP-B spacecraft at 650 km altitude, the GP-B program will provide a unique opportunity to measure the Earth's gravitational equipotential surface. The objective of this coexperiment is to improve the geopotential field determination accuracy by one to two orders of magnitude over degrees 2 to 50, and the requirement on GPS navigation accuracy is better than 1 cm with respect to the ground stations with post-processing [4]. Although the carrier phase measurements of the TENSOR receiver have enough precision, the limiting factors on the accuracy are the temperature dependent bias drift, the SA (selective availability) correction errors and the ionospheric delay. The GP-B spacecraft is scheduled to be launched in 1999, which is close to the next solar maximum and the ionospheric activity is expected to be high during that period. We sought the option to use a dual frequency receiver during the initial tradeoff study, but decided to use a single frequency receiver in order to reduce the scheduling and technical risks for the primary mission. We have accumulated a considerable amount of experience

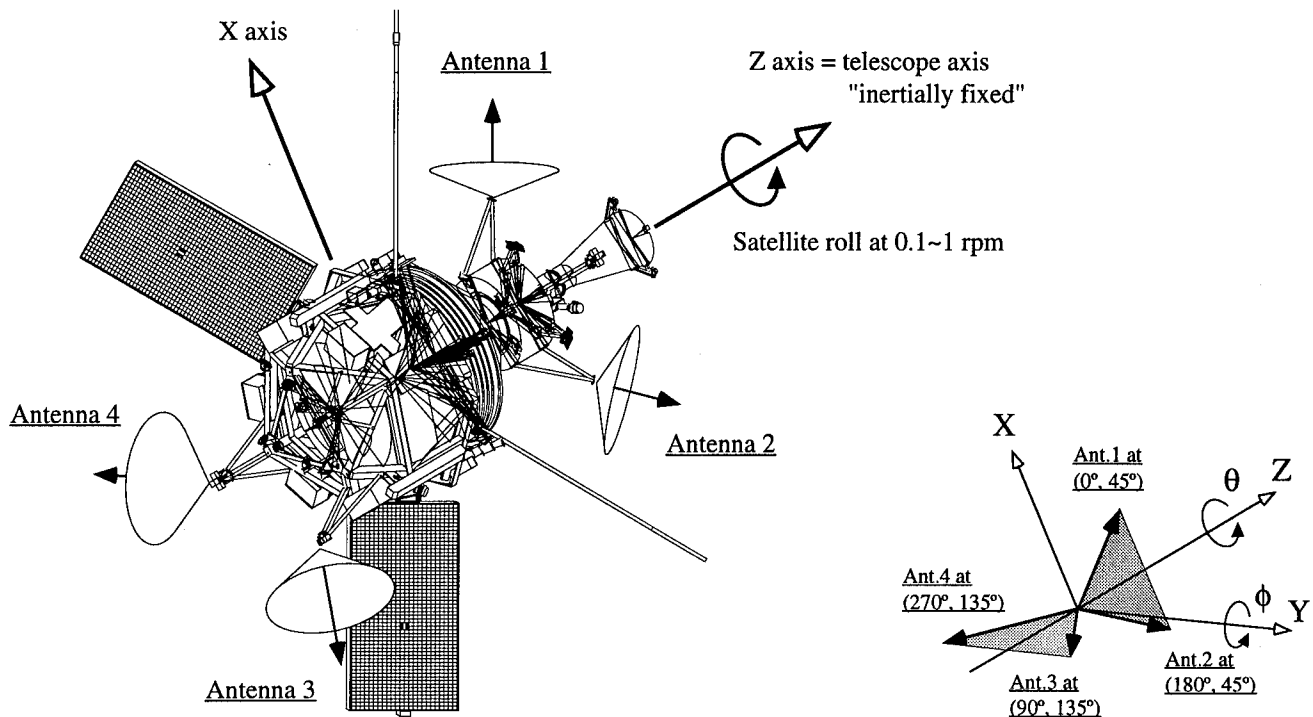


Figure 3 GP-B spacecraft and GPS antenna configuration. GPS antenna directions are defined by 3-2 Euler angles, θ and ϕ , respectively.

with this specific receiver architecture since Cohen [8] started his attitude determination study in 1990, and the multiplexing technology combined with the attitude determination algorithm best suited the mission as described in the later section.

CLOCK COEXPERIMENT

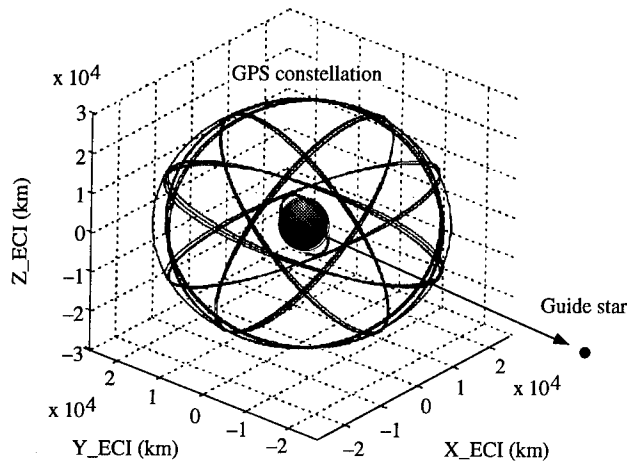
GP-B provides another unique opportunity to test Einstein's equivalence principle regarding the gravitational redshift. As the Earth orbits around the Sun, it moves in and out of the Sun's gravity potential because its orbit is slightly elliptic. A clock kept on or near the Earth will be affected by the Sun's gravity as the frequency shifts by as much as 3×10^{-10} during a year [5]. According to Einstein's equivalence principle, under identical influences, different clocks must keep the same time independently of internal composition, which means that, if we have two clocks of different types, both clocks should be affected in the same way regardless of the type and operating frequency. The GP-B mission provides access to two types of clocks: an atomic clock through GPS and a gyroscope clock whose frequency is measured by the SQUID. These two clocks are expected to generate a null gravitational redshift test to 0.01%.

This coexperiment requires precise timing of measurements for the gyroscope spin speed. The required accuracy is about $1e-8$ over 1 second and $3e-14$ over 1 year. The short-term stability is provided by the temperature compensated crystal oscillator (TCXO) inside

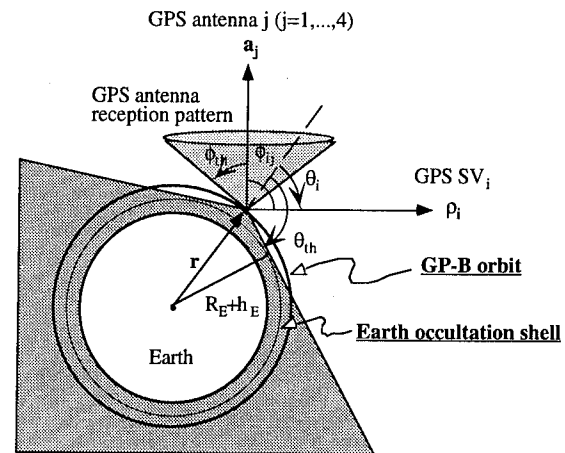
the receiver and the long-term stability is achieved by resolving the TCXO frequency by GPS. In order to accommodate the clock requirements, a hardware modification is being planned for the TENSOR receiver, including a clock signal output directly tied to the TCXO. The TCXO runs at $16f_0$ MHz ($f_0 \equiv 1.023$ MHz) and drives the GPS signal tracking circuits. Both the code phase and the carrier phase measurements are sampled based on this $16f_0$ signal, and the sampling within the payload is driven by the same signal, which is fed through a coax cable from the receiver to the payload. The code and carrier phase measurements are down-linked every second, and the timing of the measurements is resolved within 100 nsec accuracy (post-process) relative to the mission starting time. The limiting factors are the same as those for the geodesy coexperiment.

ORBITAL TRIM AND ATTITUDE DETERMINATION

Another key role of the GPS receiver is to assist the autonomous orbit trim as a navigation sensor. The GPS receiver will provide the spacecraft flight computer with the real-time navigation solutions whose accuracy is limited by SA. The flight computer then filters the solutions over several orbits to achieve the required accuracy listed in Table 1. The TENSOR receiver is also capable of real-time attitude determination although it is not the primary attitude sensor. The TENSOR receiver will be a backup attitude sensor to the star sensor, which is also a backup to the telescope sensor. The accuracy



(a) GP-B orbit and GPS constellation



(b) Geometric diagram for GPS visibility test

Figure 4 (a) GP-B orbit (polar, circular orbit at 650 km altitude) and GPS constellation based on almanac collected on August 16, 1995. (b) Geometric diagram for the GPS satellite visibility test.

requirement is about 0.1° (rms) over 1 second. The attitude determination algorithm becomes complicated because of the configuration of the GPS antennas, which is designed to maximize the signal coverage and to minimize the multipath signals. The following section will describe the antenna installation and the operational conditions of the GPS receiver for GP-B.

3. GPS INSTALLATION AND OPERATIONAL CONDITIONS

We conducted an initial tradeoff study in 1993 and selected Loral's TENSOR receiver as a baseline architecture on which to build the GP-B receiver. We selected this specific receiver mainly because of its radiation hardness and multiplexing capability up to four antennas. The GP-B spacecraft will be built by the spacecraft subcontractor, Lockheed Martin Astronautics, and the GPS receiver will be a customer furnished equipment (CFE) built and supplied by Stanford. One unique aspect of the GP-B spacecraft operation is that it must be failure operational, which means a single point failure must not result in the degradation of operational performance. For this reason, we will have a redundant GPS receiver with A and B sides, each of which is connected to four preamps and four GPS antennas. This means that, if a single point failure occurs in a receiver A, the redundant side B can take over the GPS operation without degrading the GPS performance.

After selecting the GPS receiver, Lockheed designed the GPS antenna configuration [9]. Because of the demanding requirements on the navigation accuracy and continuous operation, the antenna locations were selected in order to maximize the GPS signal coverage and to minimize the multipath signals mainly from the solar panels. Figure 3

shows the proposed antenna configuration for GP-B. Each GPS antenna points outward from the center of the spacecraft so that the entire sky with a solid angle of 4π steradian is covered even with a 10° elevation mask on each antenna. The fore antennas 1 and 2 are perpendicular to one another and out of phase by 180° , and so are the aft antennas 3 and 4. The aft set is out of phase by 90° from the fore set so that the four antennas form a tetrahedron.

This configuration certainly reduces the multipath and maximizes the signal coverage, but at the same time, complicates the GPS receiver operation combined with the fact that the satellite is rotating about the z axis.

GPS VISIBILITY ANALYSIS

We analyzed the GPS satellite visibility from each GPS antenna installed on the GP-B spacecraft in order to plan for the signal search and tracking strategy. Figure 4(a) shows the GP-B orbit and the GPS constellation based on the almanac collected on August 16, 1995. On this date, there were 25 healthy GPS satellites including 24 block II satellites and the last block I satellite, SV12. In this analysis, SV12 was removed from the active satellite list because it may not be operational during the GP-B mission. Figure 4(b) shows the geometric diagram that we used for the visibility test. The visibility is determined by two factors: the antenna elevation mask and Earth occultation. We defined a line of sight vector $\vec{\rho}_i$ to GPS SV_i ($i=1,\dots,32$), a boresight vector \vec{a}_j for antenna j ($j=1,\dots,4$) and a GP-B satellite position vector \vec{r} . We then defined the viewing angles as shown in Figure 4(b).

$$\theta_i = \arccos(\vec{r} \cdot \vec{\rho}_i / |\vec{r}| |\vec{\rho}_i|)$$

$$\phi_{ij} = \arccos(\vec{\rho}_i \cdot \vec{a}_j / |\vec{\rho}_i| |\vec{a}_j|)$$

The threshold angles for the Earth occultation and for the antenna mask are defined by

$$\theta_{th} = 90^\circ + \arccos\left(\frac{R_E + h_E}{|r|}\right) = 106.8^\circ$$

$$\phi_{th} = 90^\circ - \phi_e = 85^\circ$$

where R_E : Earth's radius
 $h_E \equiv 350\text{km}$: occultation height
 $\phi_e \equiv 5^\circ$: antenna elevation mask

A GPS satellite i ($i=1,\dots,32$) is declared visible from an antenna j ($j=1,\dots,4$) if the following condition is satisfied.

$$(\theta_i \leq \theta_{th}) \cap (\phi_{ij} \leq \phi_{th})$$

The occultation height h_E is set to the ionosphere shell altitude [10] in order to minimize the ionospheric delay and the atmospheric refraction. It also satisfies the condition for avoiding the multipath from the Earth's surface [11].

We ran a simulation for a one-day period and the results are shown in Figures 5 and 6. The total number of visible satellites averages to about 12, and the minimum is 10, which is more than the number of channels (9) implemented in the TENSOR receiver. This seems to be an ideal situation with plenty of satellites to track, but Figure 6 reveals a problem. It shows the number of visible satellites from each antenna, which is modulated at two frequencies: the orbital frequency (97 min period shown in Figure 6(a)) and the roll frequency (3 min period shown in Figure 6(b)).

The orbital modulation is caused by the fact that the GP-B spacecraft is inertially pointing at the guide star. The fore antennas 1 and 2 see most of the GPS satellites during half an orbit when the satellite is in front of the Earth, and the aft antennas 3 and 4 are blocked by the Earth's body. The situation reverses when the satellite moves behind the Earth where the aft antennas have most of the visibility. This is why the two plots in Figure 6(a) are out of phase by 180° .

The roll modulation shown in Figure 6(b) is caused by the satellite's rotation about the telescope axis. As discussed in Section 2, the GP-B spacecraft is rotated in order to ac-modulate the SQUID signal, and the number of visible satellites is modulated at the roll frequency as a result. Also, the fore antennas 1 and 2 are out of phase by 180° and so are the aft antennas 3 and 4. The fore set and the aft set are out of phase by 90° because of the antenna configuration shown in Figure 3.

Since the total number of visible satellites is more than that of the receiver channels, we should be able to track as many satellites as 9 even from the inertially pointing, rotating GP-B spacecraft if we plan the tracking strategy right. This task can be accomplished by modifying the software to accommodate the antenna configuration in the

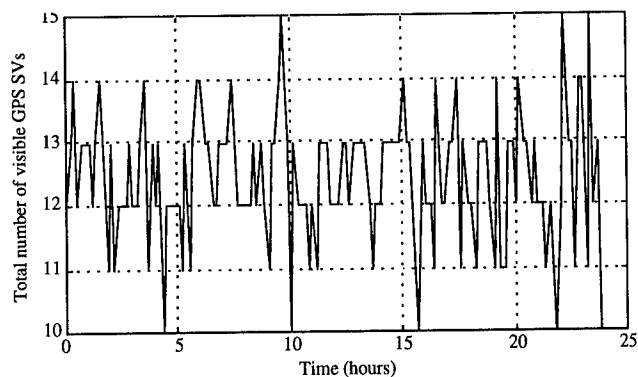
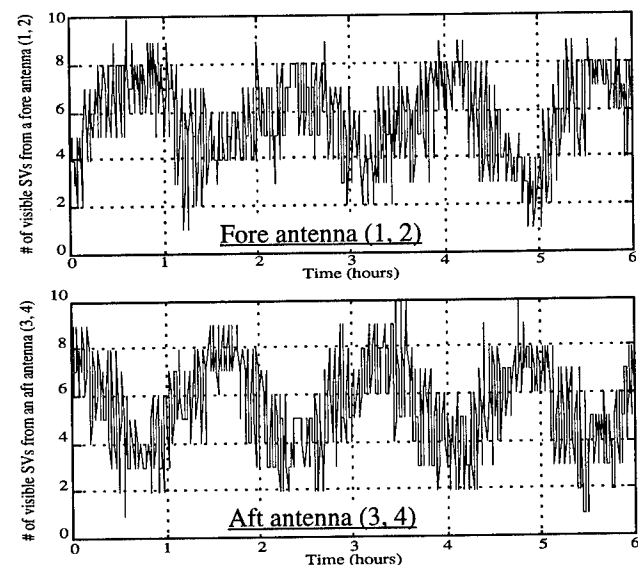
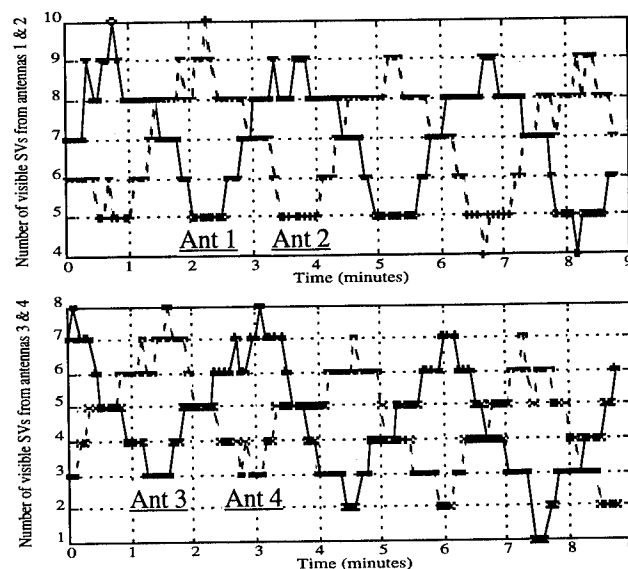


Figure 5 Total number of visible GPS satellites from GP-B spacecraft.



(a) Number of visible GPS satellites from fore and aft antennas over 6 hours.



(b) Number of visible GPS satellites from each antenna over 10 minutes.

Figure 6 Number of GPS satellite visible from each GPS antenna installed on GP-B spacecraft.

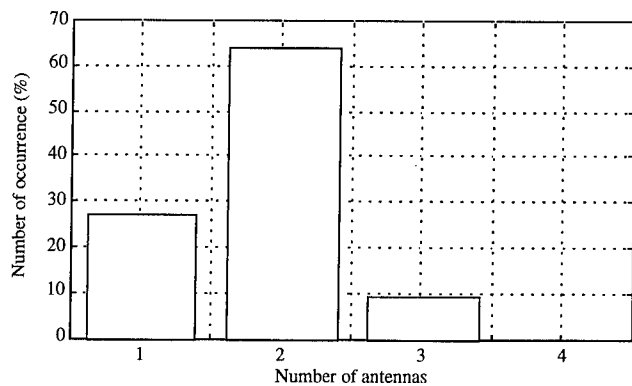
search and tracking algorithm, which we will discuss in Section 4.

GPS ATTITUDE DETERMINATION

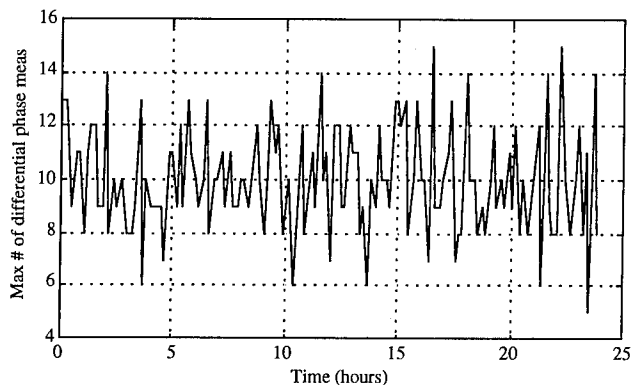
Another interesting question is whether the attitude determination is possible with this antenna configuration. Cohen et al. [12] developed the attitude determination algorithm for four antennas with a common view using the multiplexing technique. The VECTOR software supports attitude determination if 4 antennas have a common view, and the TENSOR software works with 3 or 4 antennas with a common view. For the GP-B case, 3 antennas have a common view for only 10% of the time, and 4 antennas never have a common view as shown in Figure 7(a). Figure 7(b) shows the maximum number of differential phase measurements, which was calculated from the visibility test and not limited by the number of channels or the tracking strategy of the receiver. It averages to about 10 measurements with minimum of 5 and maximum of 15. Our experience with the VECTOR receiver on terrestrial vehicles (model airplanes, land vehicles, etc.) shows that the motion-based integer resolution works well with 12 or more measurements and the attitude algorithm works with 9 or more once the integers are resolved. Figure 7(b) shows a marginal number of measurements compared with our experience, but it is theoretically sufficient (more than 3) and the attitude determination performance can be affected by other factors such as baseline length, vehicle dynamics, observability and line bias calibration.

The baseline length between two fore antennas or two aft antennas is 2.38 m, and that between a fore antenna and an aft antenna is 4.72 m. These baselines are relatively long for spacecraft installation and should improve the accuracy. The vehicle dynamics is also very slow and predictable with 20 marcsec pointing accuracy, which makes Kalman filtering an ideal tool to process sparse data sequentially. Another important factor is the observability. Although the number of measurements is sufficient, they may not span the entire state space. The observability issue can be addressed in terms of *ADOP* (attitude dilution of precision) or eigen vectors of a measurement matrix obtained by *SVD* (singular value decomposition).

The last and possibly the most complicated factor is the line bias, which can be affected by temperature variation, aging, EMI, antenna phase pattern, etc. The line bias can affect the attitude accuracy significantly unless the double differencing technique is employed. The calibration is usually conducted on the ground with flight antennas and cables installed on a truss with the equivalent dimensions, unfortunately, though, the grounding and temperature conditions are quite different in space. The accuracy of pre-flight calibration is limited by how accurately the truss is built, by the temperature dependency and also by the antenna grounding, which affects the phase pattern by as much as 2~4 mm. These factors lead to a suggestion



(a) Histogram: number of antennas with a common view to a GPS satellite.



(b) Maximum number of differential phase measurements available to the GP-B receiver.

Figure 7 Differential phase availability analysis for GPS attitude determination of the GP-B spacecraft.

of in-flight calibration for GP-B. We know the spacecraft attitude to 20 marcsec accuracy from the telescope and the star blipper, and the differential phase measurements are down-linked every second together with the carrier phase measurements. From this flight data, we should be able to estimate the line biases and the antenna phase patterns. We will not investigate the in-flight calibration any further in this paper.

Although required only for the backup mode, the GPS attitude determination of the GP-B spacecraft is possible considering three techniques: attitude filtering, in-flight calibration, and antenna/channel optimization (*ACO*) algorithm, which we will explain in the following section.

4. RECEIVER DESIGN

We selected Loral's TENSOR receiver as the baseline architecture for GP-B for its radiation hardness, antenna multiplexing capability and microprocessor. We plan to modify the TENSOR software and hardware in order to handle the visibility problem and the timing requirements presented in the previous sections. We will describe the baseline architecture first and then discuss the software/hardware modifications.

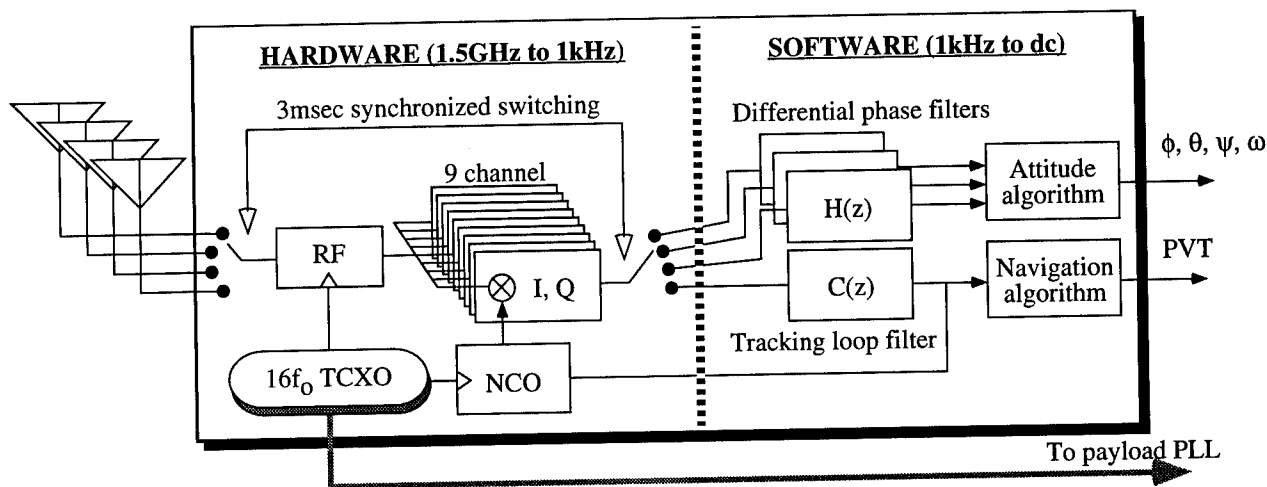


Figure 8 Multiplexing receiver architecture.

BASE ARCHITECTURE

Figure 8 shows the general architecture of the TENSOR/VECTOR receivers. The TENSOR and VECTOR receivers share the same basic architecture with 6 channels for VECTOR and 9 channels for TENSOR. The architecture can be divided into two parts according to the signal frequency being handled: the hardware section handles a signal from 1.5 GHz to 1 kHz and the software section from 1 kHz to dc. Four antennas are multiplexed sharing a single RF path to the correlator channels, whose outputs are then passed to the tracking loop or differential phase filters depending on whether the current antenna is master or slave, respectively. The antenna and filter switching is synchronized by a software trigger. The navigation algorithm then collects master antenna measurements for PVT (position, velocity and time) solutions, and the attitude algorithm uses differential phase measurements from slave antennas for attitude determination. The output directly connected to the TCXO is not supported by the regular TENSOR, but is part of the Stanford modification.

SOFTWARE MODIFICATION

Our motivation for the software modification is to maintain continuous tracking of the GPS signals even on a rotating spacecraft and to optimize the search/tracking algorithm, i.e., to maximize the use of 9 correlator channels minimizing GDOP, PDOP or ADOP, etc. at the same time. The current version of software for VECTOR or TENSOR does not support the GP-B antenna configuration where four antennas are installed on a rotating spacecraft and are pointing perpendicular to each other. We will first describe what is supported by the current software and then describe the modification plan.

The filter selection for each channel and the antenna switching are synchronized by the software trigger. The master antenna is selectable by a user command, and as a

default configuration, all channels share a common master, which means that visible GPS signals are tracked on a single antenna leaving the other three antennas for differential phase measurements. This configuration does not work well for GP-B mainly because the number of visible satellites from each antenna varies from 1 up to 10 satellites according to the orbital motion and the satellite roll as shown in Figure 6. With this configuration, we may have to switch the master antenna every 1.5 minutes (half the roll period) just to maintain 4 or more visible satellites. Another configuration supported by the current software is a roving master antenna configuration, which assigns an antenna with the strongest signal-to-noise ratio as a master to the tracking loop filter. This configuration allows each channel to have a different antenna as a master and works well when each antenna operates under different conditions. A good example is the RADCAL satellite [13] where four antennas were installed pointing 17.5° off the zenith to avoid the multipath signals from a gravity gradient boom. In this case, each antenna can have a different signal level depending on the gain pattern and the line-of-sight (LOS) vector, and it makes a good sense to have the strongest signal as a reference. This configuration may work for GP-B, but the higher level code, which assigns a PRN code to each channel, still assumes that all antennas are pointing in the zenith direction, and this will limit the efficient use of all channels.

In order to utilize all 9 channels in the most efficient way for GP-B, we have introduced the antenna/channel optimization (ACO) algorithm, which incorporates the knowledge of the spacecraft position/attitude, the antenna configuration and the GPS almanac to the selection of a master antenna per channel. Figure 9 shows the general concept of the ACO algorithm. Among four inputs to ACO, the antenna configuration is stored in the receiver ROM, and the other inputs, the spacecraft position/attitude and the GPS almanac, can be fed either from the spacecraft command and telemetry unit (CTU) or from the receiver solutions. The CTU inputs can be

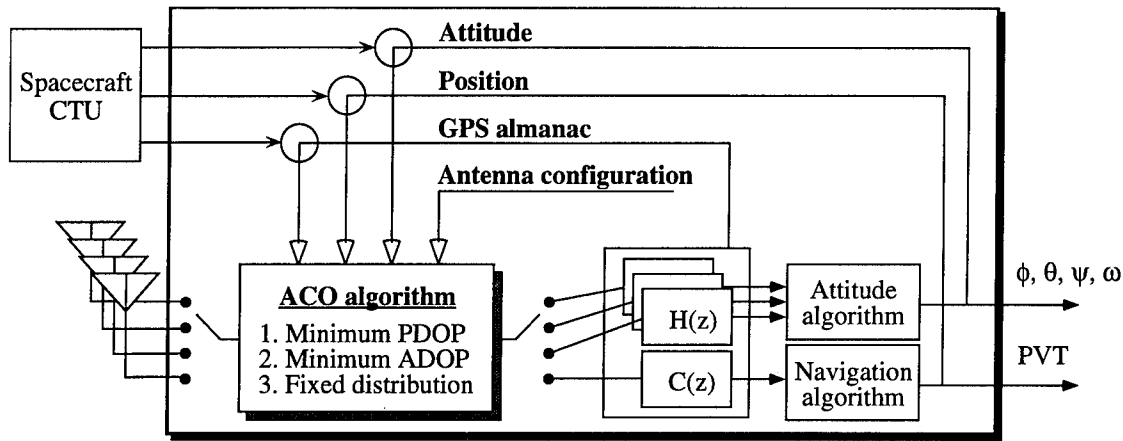
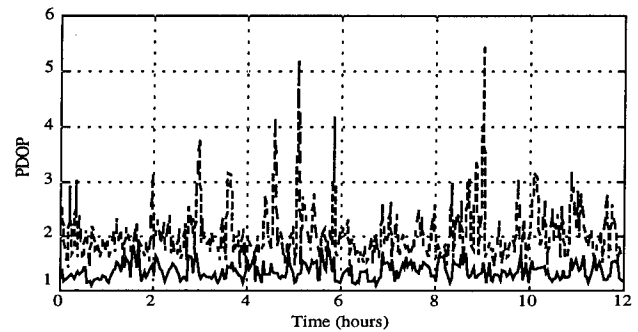


Figure 9 Antenna/channel optimization (ACO) conceptual diagram

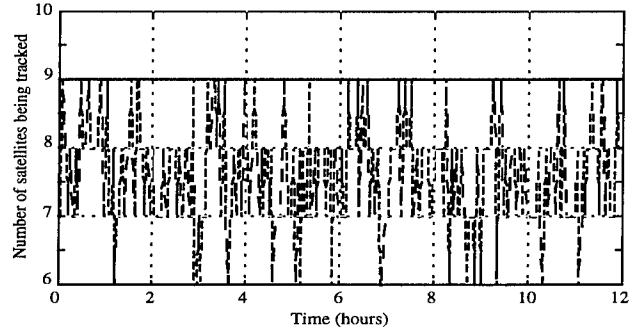
selected during the receiver initialization. Given these inputs, ACO selects a master antenna per channel based on three different criteria: minimum PDOP, minimum ADOP or fixed distribution. The minimum PDOP algorithm is useful for a mission where the navigation accuracy is more important than the attitude accuracy such as the GP-B mission. The minimum ADOP is useful for an opposite situation where the navigation accuracy can be achieved by Kalman filtering sparse range measurements. The last algorithm, the fixed distribution, is the simplest but less generalized because it has to be customized for each mission. In this paper, we will show the results for the fixed distribution algorithm tailored for GP-B.

The fixed distribution algorithm selects GPS satellites and assigns master antennas according to prescribed procedures and is an attractive solution for GP-B because it is simpler to implement, requires less computation and the visibility is very predictable from tight attitude control. The computational load is an important factor because ACO may have to be updated every 30 seconds due to the roll period modulation of the visibility [Figure 6(b)]. As shown in Figure 7(a), we found that 3 antennas share a common view about 10% of the time and 2 antennas about 63% of the time. Assume that N_3 satellites are visible from 3 antennas, N_2 satellites are visible from 2 antennas and N_1 satellites are visible from only one antenna when the ACO algorithm is called ($N_1 < 7$ and $N_3 < 4$ from Monte-Carlo simulations). ACO will then select satellites based on the rules we designed for GP-B as follows:

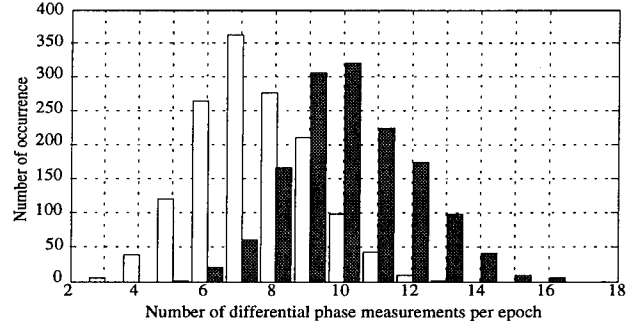
- 1) Select GPS satellites SV_i ($i=1, \dots, N_3$) that are visible from 3 antennas.
- 2) Select an antenna with the highest elevation angle to SV_i as a master and assign it to channel i .
- 3) Select GPS satellites SV_j ($j=N_3+1, \dots, N_1+N_3$) that are visible from only one antenna and assign that antenna to channel j .
- 4) Select GPS satellites SV_k ($k=N_1+N_3+1, \dots, 9$) that are visible from two antennas. Select satellites with higher elevation angles if the total number of visible satellites exceeds 9.



(a) PDOP with (solid) and without (dashed) ACO.



(b) No. of SVs tracked w/ (solid) and w/o (dashed) ACO.



(c) Histogram: number of differential phase measurements per epoch with (gray) and without ACO.

Figure 10 Performance comparison between ACO and the common master configuration.

- 5) Select an antenna with the highest elevation angle to SV_k as a master and assign it to channel k .

We selected the satellites visible from 3 antennas first in order to increase the number of differential phase measurements and to help attitude determination. We then selected those visible from only one antenna because they are most likely to fill the null space left by the other three antennas and should help minimize the PDOP. We filled the remaining channels with satellites visible from 2 antennas. If a satellite chosen is visible from more than one antenna, the antenna with the highest elevation angle to that satellite was selected as a master. By selecting the one with the highest elevation, we could minimize the master reassignment frequency. Figure 10 shows the ACO performance compared with a common master configuration, which is the current default. The common master configuration, where all 9 channels share one antenna as a master, showed PDOP as high as 5.5 and the number of satellites being tracked dropped to as low as 6. The ACO algorithm, meanwhile, kept all 9 channels filled over 12 hours and the PDOP was always below 2.0. In addition, the number of differential phase measurements averaged to about 10 for ACO and about 7 for the common master configuration, which means that the ACO algorithm resulted in the number of measurements close to the maximum according to Figure 7(b).

The ACO algorithm showed superior performance for GP-B maintaining low PDOP and a fair number of differential measurements throughout, and should be useful for any other space missions where the antennas are installed on a rotating or non-nadir pointing spacecraft. This algorithm can also be applied to terrestrial receivers in order to account for banking of an aircraft [14], rolling of a large sea vessel, etc. Remaining issues for the real-time installation of ACO are the update rate, channel assignment, and tracking filter handshakes in the case of antenna switching.

HARDWARE MODIFICATION

As we described in Section 2, the clock coexperiment requires the measurement frequency stability to be $1e-8$ over 1 second and $3e-14$ over 1 year. Although these requirements are achievable by a GPS receiver, the payload electronics and the receiver clock still need to be synchronized for GPS to be able to time tag the science measurements. We and Lockheed Martin designed a phase-locking mechanism between the payload and the GPS receiver by feeding a common clock signal. As shown in Figure 8, a TCXO at $16f_0$ drives not only the RF section but also the correlator channels, which means that all the measurements within the receiver are clocked based on the TCXO signal. As part of the Stanford modifications to the TENSOR receiver, the TCXO signal will be routed to the payload electronics and will be used to phase-lock the sampling sequence within the payload. Figure 11 shows the preliminary timing diagram. Data flows are indicated by solid arrows and electrical signals

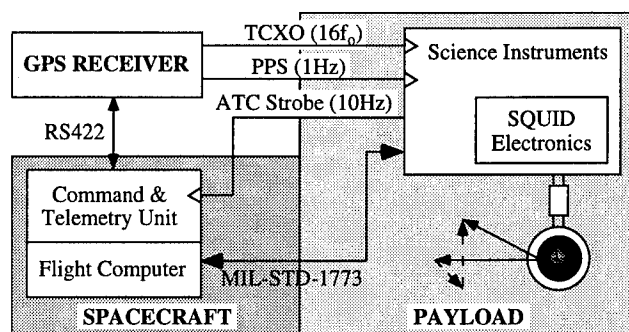


Figure 11 Timing distribution among GPS, spacecraft and payload.

by hollow arrows. The GPS receiver will supply the TCXO signal, from which the sampling triggers are derived. It will also supply the pulse-per-second (PPS) signal in order to synchronize the sampling burst to UTC. The payload will then generate the 10 Hz strobe based on $16f_0$, which will be routed to the spacecraft for synchronizing spacecraft sensor outputs and the payload measurements. We are currently designing the TCXO signal driver.

5. OTHER ISSUES RELATED TO GPS OPERATION IN SPACE

Electronics installation and operation in space becomes challenging because of the harsh space environment such as radiation, temperature, lack of ground command access, etc. The design issues that we did not discuss, but are equally important, include radiation hardening, handling of SEUs, memory-scrubbing algorithm, temperature dependent drift, antenna ground plane design, cold/warm start and cross-strapping.

One of the reasons for selecting the TENSOR receiver is its radiation hardness. It was originally designed for a total dose of 100 kRads(Si) at a 1400 km altitude during a 7 year operation. For our mission, the GP-B spacecraft is expected to receive about 10 kRads(Si) over the 2 year operation. Another strength of TENSOR is its RAD6000 microprocessor. This RISC chip delivers about 20 mips at 20 MHz and more importantly uses an error detection and correction code (EDAC) with four-bit distance, which means that it can correct a one-bit flip and detect two-bit flips. We will not go into these issues any further in this paper.

6. CONCLUSION

Stanford is designing a rad-hard GPS receiver based on the Loral TENSOR receiver for the Gravity Probe B Relativity Mission. The Stanford receiver will be supplied to the spacecraft contractor, Lockheed Martin, as a CFE and will be a primary navigation sensor not only for the relativity mission but also for the geodesy, clock and aeronomy coexperiments and for the closed-loop orbit trim. It will also serve as a backup attitude sensor. We

have described the relativity mission and coexperiments, and presented the GPS requirements derived from each experiment or operation in Table 1.

The GPS antenna configuration for GP-B was designed to minimize the multipath signals from the solar arrays and to maximize the sky coverage. We have conducted the visibility study, which showed that the number of visible satellites from each antenna was modulated at the orbital and roll frequencies. We developed the ACO algorithm to optimize the satellite selection and antenna/channel distribution. It selects satellites and assigns a master antenna to each channel based on the minimum PDOP, the minimum ADOP or the fixed distribution rules. We have demonstrated that the fixed distribution algorithm performed much better for GP-B than the conventional common master configuration maintaining lower PDOP and larger number of differential phase measurements. We have also shown that the attitude determination was feasible considering the ACO algorithm, the attitude Kalman filtering and the in-flight calibration. Lastly, we have presented the timing scheme among GPS, spacecraft and payload, designed for the clock coexperiment. The hardware modification to route the TCXO signal from the GPS receiver to the payload was discussed.

ACKNOWLEDGMENTS

Gratitude is acknowledged to NASA for supporting this research under Contract No. NAS8-39225. Trimble Navigation, Ltd. and Space Systems/Loral are gratefully acknowledged for their support and many contributions. The authors would also like to thank Lockheed Martin for supplying spacecraft and payload materials.

REFERENCES

1. C. W. F. Everitt, "The Stanford Relativity Gyroscope Experiment (A): History and Overview" in *Near Zero: New Frontiers of Physics*, J. D. Fairbank, J. B. S. Deaver, C. W. F. Everitt, P. F. Michelson, Eds. (W. H. Freeman and Company, New York, 1988), pp. 587-639.
2. N. J. Kasdin, B. W. Parkinson, J. Turneaure, C. W. F. Everitt, Stanford University, "Relativity Mission (GP-B) System Design and Performance Requirements," T003, Rev. B (6 October 1994).
3. N. J. Kasdin, B. W. Parkinson, J. Turneaure, C. W. F. Everitt, Stanford University, "Gravity Probe B Twelve Science Requirements," T002, Rev. A (15 April 1993).
4. M. B. Tapley, *A Geodetic Gravitation Gradiometer Coexperiment to Gravity Probe B*, Ph.D. Dissertation, Stanford University, SUDAAR 640 (1993).
5. T. Walter, *A Gyroscope Clock for a Null Gravitational Redshift Experiment*, Ph.D. Dissertation, Stanford University (1993).
6. P. Axelrad, *A Closed Loop GPS Based Orbit Trim System for Gravity Probe B*, Ph.D. Dissertation, Stanford University, SUDAAR 598 (1990).
7. R. Vassar, *Error Analysis for the Stanford Relativity Gyroscope Experiment*, Ph.D. Dissertation, Stanford University, SUDAAR 531 (1982).
8. C. E. Cohen, *Attitude Determination Using GPS*, Ph.D. Dissertation, Dept. of Aeronautics and Astronautics, Stanford University (Dec. 1992).
9. Lockheed Missiles & Space Company, Inc., "Global Positioning System (GPS) Receiver Error Analysis," LMSC/F420300 (10 May 1991).
10. J. A. Klobuchar, "Design and Characteristics of the GPS Ionospheric Time Delay Algorithm for Single Frequency Users," IEEE PLANS (Las Vegas, NV, November 4-7, 1986), pp. 280-286.
11. J. G. Ceva, B. W. Parkinson, "Multipath Interference in Orbiting Receivers Due to Earth Surface Reflections," ION GPS-93 (The Institute of Navigation, Salt Lake City, UT, September 22-24, 1993), vol. 2, pp. 1557-1563.
12. C. E. Cohen, B. W. Parkinson, "Aircraft Applications of GPS-Based Attitude Determination," ION GPS-92 (The Institute of Navigation, Albuquerque, New Mexico, Sep. 16-18, 1992), pp. 775-782.
13. C. E. Cohen, E. G. Lightsey, W. A. Feess, B. W. Parkinson, "Space Flight Tests of Attitude Determination Using GPS," ION GPS-93 (The Institute of Navigation, Salt Lake City, Sep. 22-24, 1993), vol. I, pp. 625-632.
14. D. Lawrence, et al., "Maintaining GPS Positioning in Steep Turns Using Two Antennas," ION GPS-95 (The Institute of Navigation, Palm Springs, CA, September 12-15, 1995).

National Satellite Testbed (NSTB) GPS Satellite Clock/Ephemeris Determination Analysis and Results

Scott Pogorelc, Mark Lorenz, Kelly Murdock, Brent Harding, Tim Cashin, and Donna Kraus
Stanford Telecommunications, Inc.

BIOGRAPHY

All of the authors are currently members of the NSTB systems engineering team at STel's Reston, VA facility.¹

Scott Pogorelc received his AB in Physics from Occidental College and a MS in Aerospace Engineering Sciences from the University of Colorado. Mr. Pogorelc has over 7 years experience with GPS including 4 years working on the NSTB for the FAA. He is task leader for algorithm research and development for the NSTB.

Mark Lorenz received a BS in Engineering Sciences from the U.S. Air Force Academy and a MS in Guidance and Control System Engineering from the Air Force Institute of Technology. He is a task leader for the development of the real-time ephemeris determination capability for the NSTB.

Kelly Murdock received his BS in Aerospace Engineering from Virginia Tech, his MS in Aeronautics and Astronautics from Purdue University, and his MS in Physics from University of Houston at Clear Lake. He is involved in orbit determination and Independent Data Verification and Validation for the NSTB.

Brent Harding received his BS in Aerospace Engineering from the University of Texas and his MS in Physical Sciences from the University of Houston at Clear Lake. He is currently involved with the development of the GPS/GEO orbit estimation software for the NSTB.

Tim Cashin received his BS in Aerospace Engineering from the University of Notre Dame and his MS in Aerospace Engineering from Virginia Tech. He is

currently involved in GPS orbit analysis as well as analysis of NSTB flight data.

Donna Kraus received her BS in Aerospace Engineering from the University of Missouri-Rolla and her MS in Aeronautics from The George Washington University. She is involved in the development and usage of the NSTB Algorithm Simulator environment (ALSIM).

ABSTRACT

The FAA's National Satellite Testbed (NSTB) is a precursor to the Wide Area Augmentation System (WAAS). The testbed is designed to verify the WAAS concept by computing and broadcasting GPS integrity and differential correction information to a user aircraft. In addition to supplying ionospheric and satellite integrity information, one of the testbed's primary functions is to provide separate clock and ephemeris corrections.

To help meet the goal of the testbed and to satisfy the WAAS navigation accuracy requirements, Stanford Telecom (STel) has performed extensive analysis on the problem of separating the clock and ephemeris errors for GPS satellites in near real-time. As a result of this analysis, STel has developed and implemented algorithms which provide the testbed with GPS satellite clock and ephemeris determination capabilities. The algorithms include accurate force models as well as precise earth orientation models to estimate and predict the GPS satellite states. This paper describes the clock/ephemeris algorithms developed for the NSTB, including initial performance analysis and test results. A description of the tests conducted as well as a description of the algorithms is also presented.

**The contents of this paper reflect the views of the authors, who are responsible for the accuracy of the information presented herein, and are not the official views or policies of the FAA.*

1. INTRODUCTION

The FAA is moving rapidly toward the initial implementation of WAAS. The WAAS will enhance the GPS Standard Positioning Service to meet the accuracy, integrity and availability requirements for sole means navigation in the National Airspace System (NAS) for enroute through Category I precision approach phases of flight. In preparation for the development and implementation of the WAAS, the FAA has been supporting the research and development of the NSTB, a prototype of the WAAS. Since 1992, the FAA has been conducting flight tests with the NSTB at the FAA Technical Center (FAATC) in Atlantic City, NJ. Through its continued success, the NSTB has been a primary vehicle of the FAA for verifying the initial WAAS concept, including the verification and validation of meeting Category I accuracy requirements.

In its current configuration, the NSTB consists of an independent network of Testbed Reference Stations (TRS) located in the U.S. and Canada, a Testbed Master Station (TMS), a Ground Earth Station (GES) and a geosynchronous satellite data link to provide a User Platform (UP) with GPS integrity information and wide-area differential corrections. In previous NSTB flight tests, the wide-area differential corrections provided to the UP have consisted of lumped range corrections to mitigate the effects of both satellite fast and slow clock errors as well as satellite ephemeris errors. This simple approach of using a single fast correction to encompass all known satellite errors has proven to be effective [1-3] in a benign environment consisting of the relatively small errors in the broadcast ephemeris and clock parameters [4].

In the future, providing lumped range corrections may no longer be sufficient. The inclusion of TRS sites in Alaska and Hawaii [5] will introduce much longer baselines, and as a result, the spatial decorrelation of ephemeris errors will become more pronounced. In addition, if the broadcast navigation message is degraded (e.g. via a faulty upload or "epsilon" selective availability), the effects of spatial decorrelation could be compounded further. Therefore, to accommodate the expansive WAAS network, possible broadcast message uncertainties, and to meet the accuracy/integrity requirements specified in [5], it will be necessary to provide the capability for the WAAS, and hence the NSTB, to determine GPS satellite clock and ephemeris errors in real-time.

Various approaches have been suggested for GPS ephemeris determination, including the inverse GPS approach [6], kinematic orbit modeling approach [7] and the Precision Orbit Determination (POD) model approach [8]. While all of these methods have merit, there are also

shortcomings. The first approach consists of performing a least-squares solution for the satellite position and clock offset using a set of fixed monitor stations. It is simple and fast, however, it can not be applied when a satellite is viewed by less than 4 monitor stations and it is extremely sensitive to measurement quality. The second method is an enhanced version of the first, this time using a minimum-norm solution to deal with underdetermined cases, and kinematic modeling of the satellite motion to provide smooth estimates. While an improvement over the inverse GPS approach, it still suffers from poor performance in the case of rising satellites. The POD method uses a more standard approach (i.e. including dynamic models) and appears to offer the highest potential orbit determination accuracy. The downside to this approach is that it is based purely on data post-processing and orbit prediction, and this would make the implementation inconsistent with the real-time environment of the NSTB. Instead, STel has decided to implement a Nominal Precision Orbit Determination (NPOD) scheme. This is a slightly modified version of the POD approach in which selected, non-essential dynamic models are omitted and the method is applied in real-time. Though not as precise as the POD approach, this method still delivers high-level performance when solving for the GPS ephemerides and clocks and it is compatible with the NSTB system architecture.

In this paper, a proposed NSTB orbit determination approach is investigated. This includes analysis and results from 4 different test configurations: 1 case involving real GPS data and 3 cases involving simulated GPS measurements. In order to demonstrate the real-time implementation of the algorithms, the processing procedures used during these tests are designed to emulate the operational environment of the testbed. The goal of this paper is to address the following items:

- provide a general description of the algorithms
- provide a description of each test scenario
- present the data analysis and results

The paper concludes with a summary highlighting key test results, and it also describes plans for future enhancements to the NSTB algorithms.

2. EPHEMERIS ALGORITHMS

The NSTB ephemeris determination algorithms consist of approximately 35 program modules (written in C) to implement the dynamic orbit estimation approach. The modules include functions to deal with coordinate and time transformations, satellite dynamic modeling, observation modeling and state estimation. A brief

description for each of these items is provided in the following sections.

2.1 Coordinate Systems

Satellite and station coordinates are initially provided in an Earth-Centered Earth-Fixed (ECEF) coordinate system (e.g. WGS-84). To allow for accurate ephemeris determination, however, the satellite coordinates are transformed to the Earth-Centered space-fixed Earth Mean Equator and Equinox of 2000 (J2000.0) inertial coordinate system. During NSTB orbit processing, all satellite states are maintained in J2000.0 while station coordinates are transformed from ECEF to J2000.0 at each measurement epoch. To compute corrections to the broadcast ephemerides, precise ECEF satellite positions are computed by the NSTB algorithms as needed.

Reconciliation between J2000.0 and the ECEF coordinate system is accomplished using a rigorous coordinate transformation [9,10] between the two systems. Included in the transformation are incremental rotations accounting for lunisolar precession, nutation, polar motion and earth rotation. Accurate representation of the rotation matrices for the latter two effects requires precise values for X and Y polar motion parameters and UT1-UTC. These data are obtained from Bulletin B files published monthly by the International Earth Rotation Service (IERS).

2.2 Time

NSTB network time (the reference time to which all measurements are synchronized) is determined to coincide with GPS time as closely as possible. However, to apply all necessary relativistic effects and to integrate the spacecraft equations of motion, a proper time scale is required [9,10]. The NSTB algorithms use Terrestrial Dynamic Time (TDT) as coordinate time and as the independent variable for the equations of motion.

2.3 Dynamic Modeling

As part of the NPOD strategy, the NSTB algorithms include a set of dynamic models to estimate the GPS satellite ephemerides. In order to minimize the real-time processing requirements in the testbed and yet still maintain a high fidelity dynamic model, a tradeoff study was conducted using JPL's GIPSY II orbit integrator [9]. The goal in developing the NSTB algorithms was to target satellite accelerations responsible for position differences greater than 10 cm when conducting a 24 hour orbit integration comparison between the GIPSY and NSTB orbit models. Based upon this study, the total acceleration model which satisfied the 10 cm constraint was determined to consist of the following components:

- gravitational accelerations due to the geopotential including the central-body and higher order harmonics
- point-mass gravitational accelerations due to the Sun and Moon
- accelerations due to solar radiation pressure and Y-bias

The acceleration components due to the Earth are computed using a spherical harmonic expansion of geopotential [11] with coefficients supplied by the JGM-3 gravity field [12]. Given the nominal altitude of the GPS spacecraft, the gravity field can reasonably be truncated to degree and order 12.

The lunisolar gravitational effects are computed by treating the Sun and Moon as Newtonian point masses. For a given satellite epoch, the NSTB algorithms are able to compute the precise solar and lunar positions in J2000.0 coordinates using the JPL DE200 planetary ephemeris file.

Finally, accelerations resulting from solar radiation pressure and the Y-bias are determined using the ROCK42 GPS solar radiation pressure model which is described by Fliegel and Gallini [13].

2.4 Satellite State Parameters

In addition to the 6 dynamic parameters of the GPS satellite state (position and velocity), the state vector consists of 3 non-satellite dynamic states and 3 satellite clock states. The non-satellite dynamic states are the solar radiation and Y-bias parameters prescribed in the ROCK42 solar radiation model [13]. These states are treated as stochastic parameters whose discrete values are allowed to vary slowly in time by adding small amounts of exponentially correlated process noise. Because pseudorange measurements have already been corrected for the SA clock dither, the satellite clock is modeled as a quadratic polynomial. To account for errors in removing the SA dither and the unknown behavior of the broadcast epsilon, the acceleration parameter is treated stochastically.

2.5 Observation Modeling

Discrete-time pseudorange observables are modeled as a nonlinear function of the observed spacecraft state and TRS location. The observation partial derivatives and pseudorange residuals are computed using the surveyed position of the TRS antenna phase center and the nominal satellite position provided by the reference trajectory. To account for the propagation delay of the GPS signal, a

light-time correction to the satellite dynamic state is performed to determine the position of the GPS antenna phase center at the signal time of transmission. As part of the light-time correction algorithm, corrections for relativity are also included in the modeled range.

2.6 Estimation

Due to the presence of a high-fidelity dynamic model and the real-time operational requirements of the NSTB, a linearized, current-epoch Kalman filter is used in the testbed. The performance of this algorithm was compared to the extended (non-linear) formulation and was preferred for the following reasons:

- reduced transient behavior during start-up
- reduced sensitivity to noisy or randomly biased data

To ensure high accuracy and numerical stability, a U-D mechanization of the Kalman filter algorithm was implemented [14,15]. In addition to its stability, thorough analysis has been conducted to verify the performance of the U-D algorithm and it has been demonstrated to be computationally efficient and well-suited for real-time applications [15].

Formal errors of the satellite state estimates are required in the integrity monitoring function of the NSTB. To support this function, the U-D factors are combined to form the full covariance matrix. In addition, to ensure that the measurement residuals remain within the linear regime, the satellite states are periodically updated with their state error estimates to yield improved reference trajectories.

3. EXPERIMENTAL CONFIGURATIONS

While the NSTB orbit determination algorithms have been tested in a variety of scenarios, this paper focuses on four distinct test cases. The first case consists of a nominal configuration using a complement of TRS sites operating in the U.S. and Canada. Real GPS data were collected from the selected sites in a manner which was consistent with the actual NSTB operational procedures. The second case consists of a data simulation using the same set of stations as the first, while the third case augments the second by adding additional sites in Alaska and Hawaii. The fourth and final case consists of a data simulation where the NSTB network is expanded to include global tracking sites.

3.1 NSTB Real-Time Configuration

The NSTB currently supports nearly a dozen TRS sites in the contiguous U.S. (CONUS) and Canada. For the initial

testing and evaluation of the GPS clock/ephemeris estimation software, 9 of these sites were selected to provide data for the analysis. The site locations are shown in Figure 1. Each of the TRS sites was equipped with the standard suite of hardware items:

- dual-frequency GPS receiver/antenna
- Rubidium oscillator
- 80486 PC
- high-speed modem
- weather station

The TRS sites were remotely configured from the TMS using custom software resident on each TRS PC. Measurements were stored locally at each TRS site for a period of approximately 96 hours. To keep the volume of tracking data manageable, measurements were recorded at 30 second epochs.

Following the collection effort, data from all 9 TRS sites were transferred to the TMS for reduction and analysis. The data types received from each site included observables for the L1-C/A pseudorange and carrier phase, P2-P1 differential group delay and L1-L2 differential carrier phase.

As part of the data pre-processing procedure, pseudorange data were smoothed using the carrier phase data, and then corrected for delays due to the ionosphere and troposphere. TRS clock biases were removed by applying the technique of common-view time transfer, which in turn allowed for the removal of nominal SA fast clock errors. Once the measurements were corrected for atmospheric effects, station clock biases and SA fast clock errors, the pseudorange residuals were computed and screened for outliers.

3.2 CONUS Data Simulations

Using the precise GPS ephemerides computed by the International GPS Service (IGS) as a truth source, 96 hours of GPS observation data were simulated for 2 North American networks: the first consisting of the 9 CONUS stations mentioned in Section 2.1 and the second consisting of the same 9 CONUS stations plus two additional sites in Fairbanks, AK and Kokee Park, HI. For the sake of convenience, orbits were estimated for a satellite subset of the GPS constellation, where 1 satellite was chosen from each of the 6 GPS orbital planes. The simulated observations were augmented with data noise as well as with range errors which modeled the effects of the ionosphere and SA. Random errors were also applied to the measurements to simulate system biases. Nominal satellite slow clock errors were added using values derived from the broadcast ephemerides which were valid

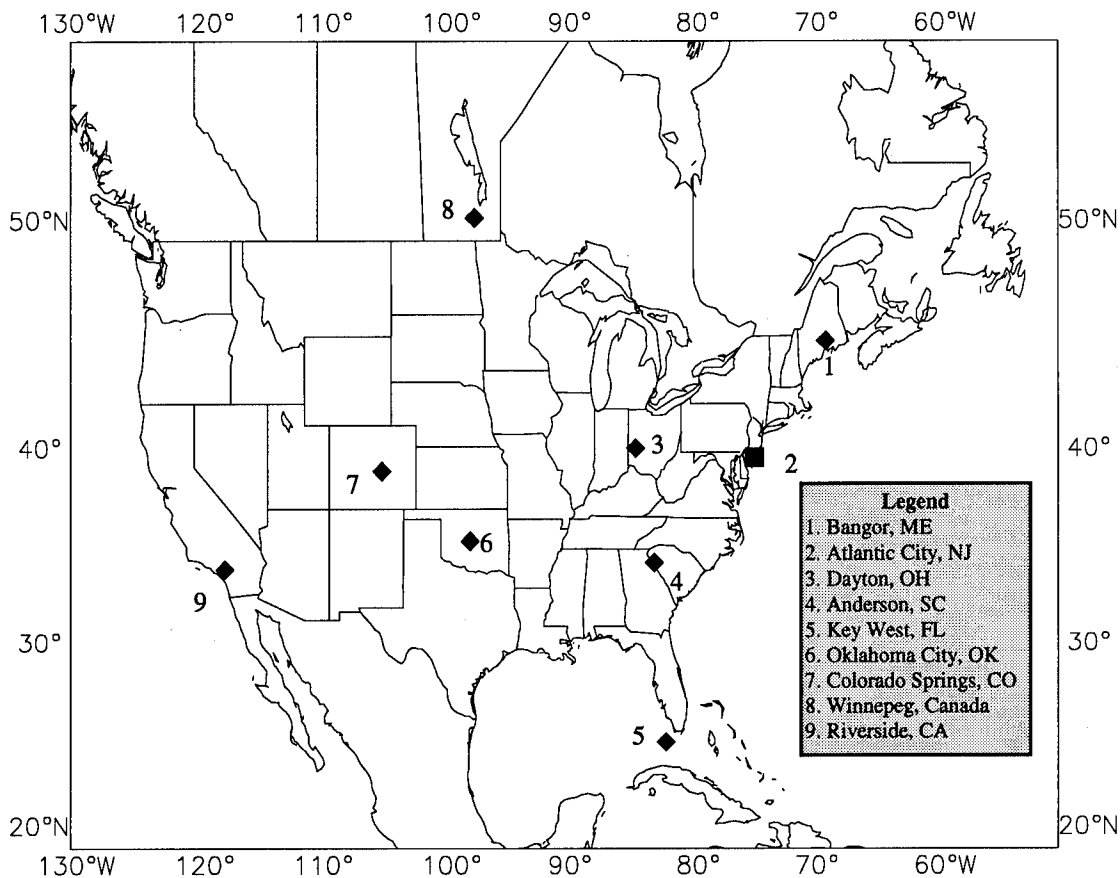


Figure 1: Current NSTB Network

during the simulation interval. With the exception of removing station clock biases and tropospheric delays (which were assumed to be removed perfectly and hence not added), data pre-processing was conducted in the same manner as in the first test case.

3.3 Global Data Simulation

To test the performance of the ephemeris algorithms in the presence of a global WAAS network, measurements were simulated for the same 6-satellite subset (Section 3.2) using an arbitrary choice of 15 IGS tracking sites. The network consisted of the following monitor stations: Pamatei, Tahiti; Kokee Park, HI; Fairbanks, AK; Goldstone, CA; Algonquin Park, Canada; Kourou, French Guyana; Santiago, Chile; Tromso, Norway; Madrid, Spain; Matera, Italy; Hartebeesthoek, South Africa; Tidbinbilla and Yarragadee, Australia; Tapei, Taiwan and Usuda, Japan. Data from these sites were generated and processed using the same criteria described in Sections 3.1 and 3.2.

4. ANALYSIS AND RESULTS

JPL's GIPSY II software package was used as a benchmark to evaluate the dynamic models implemented

in the NSTB. To assess orbit estimation performance with real data, IGS precise ephemerides were used to check the NSTB solution accuracy. For selected cases, the satellite slow clock estimates were compared to the broadcast values. The effect of the resulting GPS orbit errors on navigation accuracy was examined for a static user. To conclude the analysis, the run-time requirements for the ephemeris algorithms were determined to verify that they would function in the real-time environment of the NSTB.

4.1 Verification of the Orbit Integrator

To demonstrate the fidelity of the NSTB's orbit integrator, tests were conducted to compare its performance to that of the GIPSY II orbit integrator over a series of 48 hour arcs. Using identical initial conditions for a given satellite, trajectories were computed for a variety of GPS spacecraft using both orbit integrators. Modeled forces during the tests consisted of those responsible for the accelerations mentioned in Section 3.3. The Height, Cross-Track, Long-Track (HCL) and 3-D RSS position differences for a typical GPS case are shown in Figure 2. Note that since the comparison involved state propagation rather state estimation, the solar radiation parameters were treated as constants over the integration interval.

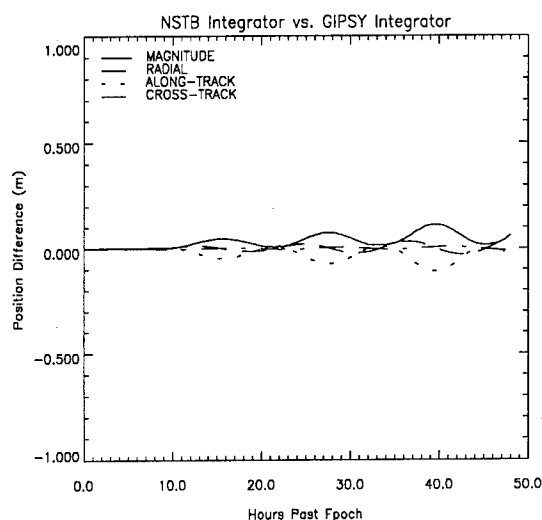


Figure 2: NSTB and GIPSY orbit integrator comparison

4.2 Orbit and Clock Results

During processing and analysis, emphasis was placed on the real data scenario more so than on the simulated test cases. Therefore, the simulated scenarios were constrained to a nominal 6-satellite subset of the GPS constellation in which 1 satellite was chosen from each orbital plane. Plots are provided for the orbit errors computed for PRN19, which was included in each case. Corresponding plots for the PRN19 clock errors are provided for the real data case and for the 9-station data simulation case.

4.2.1 Real Data Results

Using the NSTB TMS and ephemeris algorithms, data for July 30th-August 2nd, 1995 were processed from the network shown in Figure 1. Our analysis indicates that with the given regional NSTB network, each satellite orbit converged after 2-3 complete satellite passes or approximately 48-72 hours. For the final 24 hours (August 2nd), the 3-D RMS orbit error for the entire GPS constellation in the NSTB region was 12.7 meters. While still preliminary, these results indicate that the NSTB algorithms are capable of providing orbit accuracies of the same magnitude as the current "benign" broadcast ephemerides. The error in the estimated position for PRN19 is given in Figure 3 while its corresponding estimated clock error is shown in Figure 4. The sharp transition in the clock error that occurs around the 10 hour mark can be traced to an IODE transition in the broadcast ephemeris.

To put the difficulty of estimating the GPS clocks and ephemerides in perspective, a profile of the Positional Dilution of Precision (PDOP) for PRN19 is given in Figure 5. It should be noted from Figure 5 that careful

consideration must be given to measurement errors and noise when processing pseudorange data. Specifically, due to large PDOP values, orbit accuracy can be severely degraded if data screening and weighting schemes are not applied appropriately, especially in the case of C/A-code pseudorange and cross-correlated group delay data types.

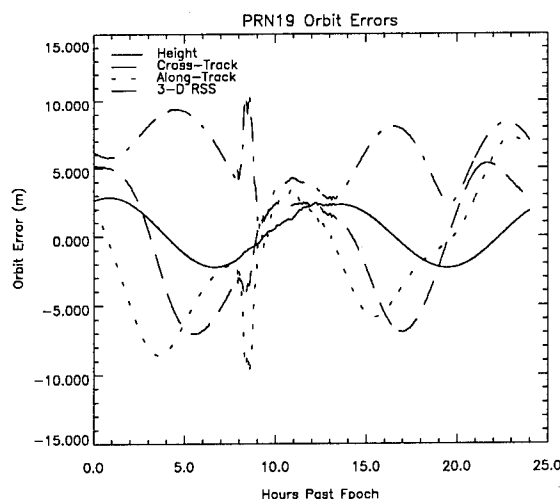


Figure 3: PRN19 Orbit Error from NSTB data

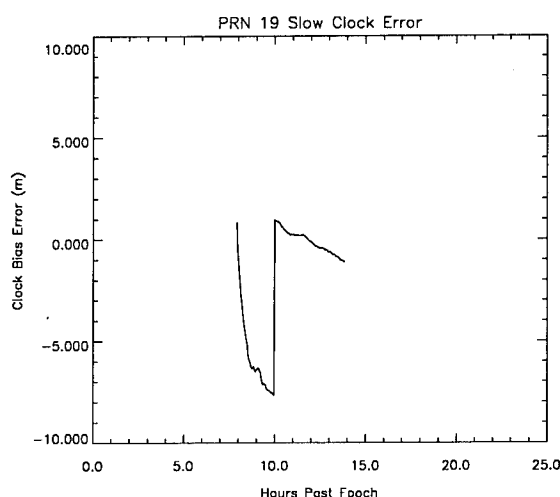


Figure 4: PRN19 Slow Clock Error from NSTB data

4.2.2 Simulated Results with 9-station NSTB Network

The 9-station NSTB network also served as the basis for a 96 hour, 6-satellite simulation. Although meter-level system biases were added to the data, the overall quality of the measurements is believed to be better than that of the real GPS pseudorange data. A comparison of the results from this scenario was performed between the estimated orbit errors for the 6 satellites tested: PRN06, PRN16, PRN17, PRN18, PRN19 and PRN20. The RMS

orbit error over CONUS for this group of spacecraft was 7.9 meters, approximately 4.8 meters better than the 12.7 meter RMS error attained with the real data. This is most likely due to unmodeled systematic errors and the absence of biases (e.g. multipath) in the simulated data.

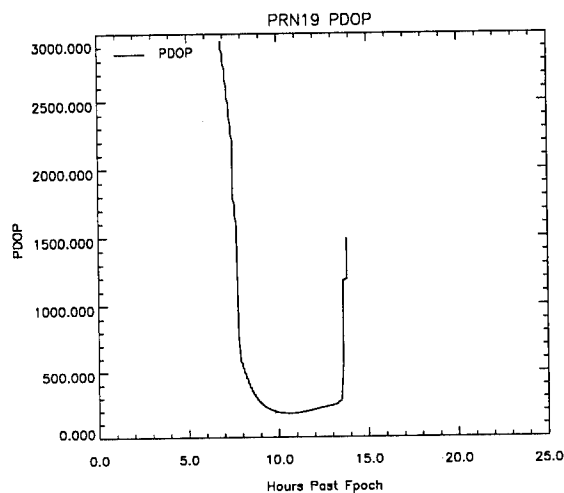


Figure 5: PRN19 PDOP history for NSTB network

Improvements in NSTB measurement pre-processing, including the implementation of a multipath mitigation algorithm should reduce discrepancies between real and simulated data. While the results from the simulation certainly indicate that there is room for improvement with respect to the real data case, the simulation also verifies that the current implementation of the ephemeris algorithms contains no gross errors. To demonstrate the similarity of the results between the real and simulated cases, the corresponding orbit and clock errors for PRN19 are shown in Figures 6 and 7. In the case of the clock error in Figure 7, the near perfect solution is a consequence of the fact that station clocks and the troposphere were perfectly removed (i.e. not added) as was the SA clock dither.

4.2.3 Simulated Results with 11-station NSTB Network

The 9-station NSTB network was expanded to include monitor stations in Alaska and Hawaii. The benefit of including these sites is improved station geometry as well as extended satellite observation intervals. To evaluate the effect of an expanded network on orbit accuracy, the 9-station NSTB network was augmented with specific sites in Fairbanks, AK and Kokee Park, HI and once again a 96 hour simulation was performed. The extended network reduced the RMS orbit error over CONUS 58% (from 7.9 meters to 5.0 meters) for the 6-satellite test case. The orbit errors for PRN19 are given in Figure 8.

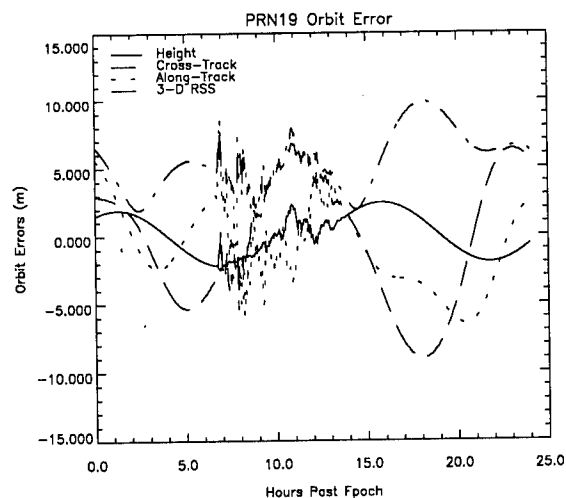


Figure 6: PRN19 Orbit Error (9-station simulation)

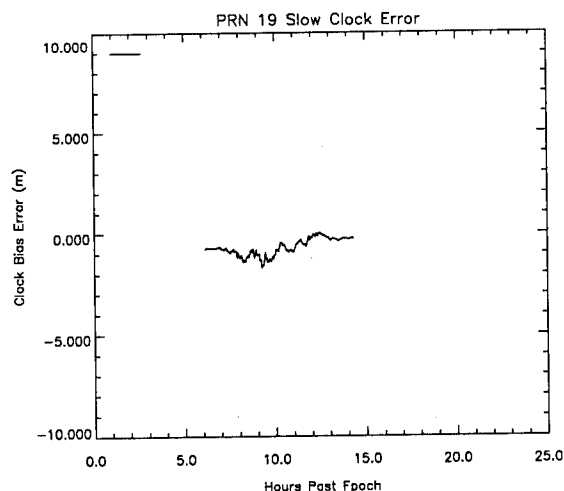


Figure 7: PRN19 Clock Error (9-station simulation)

4.2.4 Simulated Global Network

To evaluate the performance of the NSTB ephemeris algorithms under optimal conditions, a final 96 hour simulation was performed using a global network of 15 IGS sites selected in an effort to provide a set of evenly spaced monitor stations. As a result of the vastly enhanced viewing geometry and data continuity, the orbit accuracy improved dramatically. The global RMS orbit error for this case was 1.8 meters. The stability of the solution as well as the effect of continuous measurement updates can be readily noted in Figure 9.

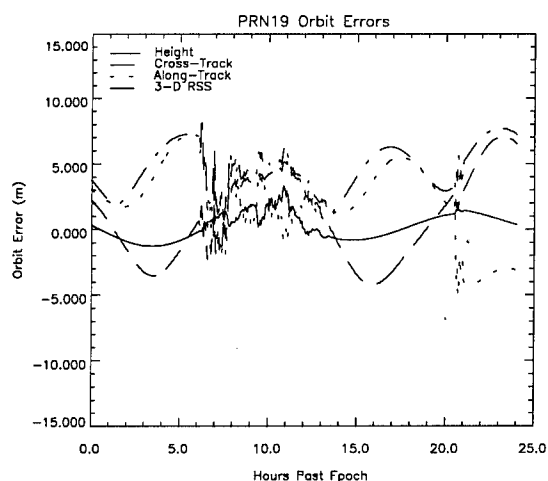


Figure 8: PRN19 Orbit Errors (11-station simulation)

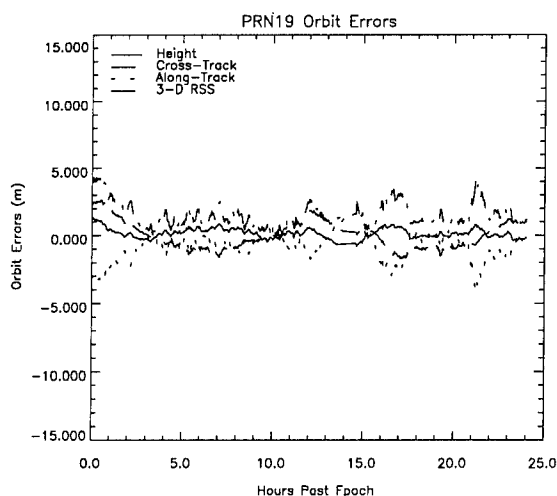


Figure 9: PRN19 Orbit Error (global network simulation)

4.3 Orbit Errors and Spatial Decorrelation

The critical impact of GPS orbit errors on the NSTB is the spatial decorrelation of the user range errors. Within the NSTB network, the user line-of-site vector remains highly correlated with those of the TRS's and therefore only spatially decorrelated range errors will cause a degradation of the user navigation solution. To examine this effect, the spatial decorrelation of the range errors was computed for the entire GPS constellation for August 2, 1995. Considering the 4200 km baseline connecting Bangor, ME and Riverside, CA as the worst case scenario, the RMS differential range error for the 24 hour period was 1.2 meters. A contour plot of the differential range errors over the NSTB region for PRN19 using Bangor as a reference is given in Figure 10.

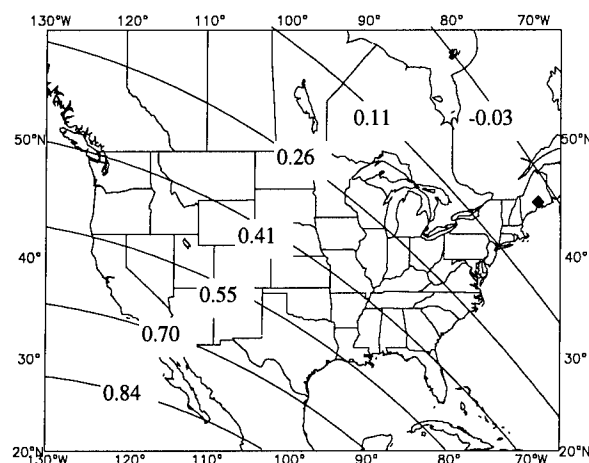


Figure 10: PRN19 Differential Range Error

4.4 Algorithm Hardware Requirements and Timing

The NSTB ephemeris algorithms consist of approximately 4000 lines of C source code and were developed and tested on a multiprocessor Sparc 20 workstation. Timing tests reveal that when running under the operational conditions of the testbed, the ephemeris algorithms were able to execute at a rate which is approximately 1/40th real-time. Thus, preliminary testing confirms that although the NPOD approach is computationally intensive, it can be easily implemented in the real-time environment of the NSTB.

4.5 Implementation and User Accuracy

Incorporation of a real-time GPS ephemeris/clock correction capability into the NSTB is a phased effort. The initial phase (Phase I) has been to re-architect the testbed to separate the TMS processing into foreground and background tasks. Foreground processing consists of computing GPS fast clock corrections, integrity processing and message formatting. The background is responsible for estimating NSTB network time, computing the ionospheric grid for CONUS, and GPS ephemeris/slow clock determination.

Under the Phase I architecture, the ephemeris algorithms produce satellite dynamic and clock states in a manner that is similar to the method that the GPS control segment uses to generate the broadcast ephemerides. That is, the NSTB algorithms provide a set of predicted GPS reference trajectories and clock coefficients. The TMS background process uses this information, to compute satellite ephemeris and clock corrections in real-time.

In the future Phase II architecture real-time estimation of GPS ephemerides and slow clock states will be implemented in place of using predicted GPS reference trajectories and clock coefficients.

As part of the verification procedure for the Phase I architecture, a series of static tests was conducted at STel's Reston facility in late August, 1995. UP navigation solutions were computed using separate ephemeris and clock corrections provided by the TMS. The navigation solutions were referenced to the surveyed location of the user antenna to determine the user position errors. The results for a 33 minute test are summarized in Table 1.

| User Navigation Error | | | |
|------------------------|----------|-----------|---------|
| Component | Mean (m) | Sigma (m) | 95% (m) |
| East | 0.30 | 0.77 | 1.83 |
| North | -0.90 | 1.63 | 4.16 |
| Vertical | 0.32 | 2.56 | 5.44 |
| Number of Points: 2000 | | | |

Table 1: User Navigation Error

It can be noted from this table, that the 95% user vertical error for our test was less than 5.5 meters. These results indicate that when using the proposed GPS ephemeris algorithms, the NSTB accuracy results are consistent with earlier work [1-3] which has demonstrated meeting Category-I RNP performance [5].

5. SUMMARY

The modeling elements and processing approach employed with the GPS ephemeris algorithms developed for the NSTB were presented. Initial results based on real and simulated observations and several TRS configurations are summarized in Table 2.

| Case | Data Source | TRS Sites | RMS Error Performance | | |
|------|-------------|---------------------|-----------------------|----------------|-----------------|
| | | | Orbit (RSS) (m) | Slow Clock (m) | Diff. Range (m) |
| 1 | NSTB (real) | 9 (CONUS) | 12.7 | 7.5 | 1.2 |
| 2 | Sim | 9 (CONUS) | 7.9 | 4.6 | 0.7 |
| 3 | Sim | 11 (CONUS + AK, HI) | 5.0 | 3.9 | 0.4 |
| 4 | Sim | 15 (Global) | 1.8 | 1.5 | 0.2 |

Table 2: NPOD Performance Summary

In case 1 (real data), the mean RSS orbit error exceeds 10 meters for the regional NSTB tracking network of TRSs. However, the RMS differential range error across CONUS was shown not to exceed 1.2 m. The difference between cases 1 and 2 illustrates the sensitivity to observation data quality and preprocessing limitations. Cases 2, 3 and 4 illustrate the sensitivity to the geometric distribution of the tracking network.

Separate clock and ephemeris corrections were applied to the navigation solution of a static user to show consistency with previous results using lumped corrections in a benign environment. The resulting 95% vertical position error was less than 5.5 meters, demonstrating that Category-I accuracy requirements can be met with the NSTB ephemeris algorithms. Because no assumptions were made by the NSTB regarding the quality of the broadcast ephemerides, these results should be indicative of the expected user navigation performance in a non-benign environment as well.

The processing procedures used during the tests emulated those methods used currently by the NSTB. This demonstrated that the ephemeris algorithms are compatible with the NSTB system architecture and can be integrated with nominal effort. Moreover, timing numbers from the tests indicate that the ephemeris algorithms will run in real-time, despite being computationally intensive. Finally, with improved receiver hardware and an expanded NSTB network, it is anticipated that the ephemeris determination capability of the NSTB will be further improved.

6. FUTURE WORK

This paper represents the first generation of GPS ephemeris determination algorithms for the NSTB. Once the GEO ranging capability of the NSTB is firmly established, the algorithms will be optimized to work for the GEO satellite as well. Work is currently under way to improve orbit accuracy by making several enhancements to the algorithms. Improvements based on the following are under consideration:

- improving data pre-processing
- improving reference trajectories of the GPS satellites by curve fitting previous ephemerides
- estimating the wet zenith tropospheric delay
- estimating earth orientation parameters
- processing carrier phase observables and estimating phase biases

7. ACKNOWLEDGMENTS

We wish to thank Joe Murray for his painstaking efforts in collecting the data, and Marie Lage and Bryant Elrod for their valuable comments and suggestion while reviewing this paper. We also would like to thank the FAA Satellite Program Office and the FAA Technical Center for their continued support of the NSTB. This work was supported by the FAA under contract No. DTFAO1-95-C-00026.

8. REFERENCES

1. Lage, M. E., B.D. Elrod, *Flight Testing and Evaluation of Wide Area Differential GPS*, Proceedings of the Institute of Navigation, January 20-22, 1993, pp. 415-423.
2. Haas, F.M. Jr., M.E. Lage, *Analysis of Recent Wide Area Augmentation System (WAAS) Flight Tests*, Proceedings of the Institute of Navigation, January 18-20, 1995, pp. 347-355.
3. Haas, F.M. Jr., "WAAS Cross-Country and Cat-1 Approach Demonstration Results". STel Technical Report #94126 presented to the FAA Technical Center, March 1995.
4. Zumberge, J.F. and W. I. Bertiger, Vol. 1, Chapter 16, *The Global Positioning System - Theory and Application*, (Draft) AIAA, 1995.
5. Wide Area Augmentation System Specification, FAA Document FAA-E-2892, Revision 1, July 1995.
6. Kee, C. and B.W. Parkinson, *High Accuracy GPS Positioning in the Continent: Wide Area Differential GPS*, Navigation, Journal of the Institute of Navigation, Vol. 98, No. 2, Summer, 1991.
7. Tsai, Y., Y. C. Chao, T. Walter, C. Kee, D. Powell, P. Enge and B.W. Parkinson, *Evaluation of Orbit and Clock Models for Real Time WAAS*, Proceedings of the Institute of Navigation, January 18-20, 1995, pp. 539-547.
8. Rim, H.J., B. E. Schutz and B.D. Tapley, *GPS Precise Orbit Determination for Wide Area Differential GPS*, Proceedings of Differential Navigation Satellite Systems (DSNS) '94, Canary Wharf, London, April 18-22, 1994.
9. *An Introduction to GIPSY/OASIS II*, Jet Propulsion Laboratory, 19 July 1993.
10. Seidlemann, K. P., *Explanatory Supplement to the Astronomical Almanac*, University Science Books, 1992.
11. Gottlieb, R.G., *A Fast Recursive Singularity Free Algorithm for Calculating the First and Second Derivatives of the Geopotential*, Johnson Space Center Document JSC-23762, July 6, 1990.
12. Olson, R., Colorado Center for Astrodynamics Research, *Private Communication*.
13. Fliegel, H.F., T.E. Gallini, *Global Positioning System Radiation Force Model for Geodetic Application*, Journal of Geophysical Research, Vol. 97, 10 January 1992.
14. Maybeck, P.S., *Stochastic Models, Estimation, and Control, Vol. 1*, Academic Press, New York, NY, 1979.
15. Bierman, G. J., *Factorization Methods for Discrete Sequential Estimation*, Academic Press, New York, NY, 1977.

GPS Techniques for Navigation of Geostationary Satellites

Pascale Ferrage, Jean-Luc Issler, Geneviève Campan, and Jean-Claude Durand
French National Space Agency (CNES)

BIOGRAPHY

Pascale Ferrage, Jean-Luc Issler, Geneviève Campan and Jean-Claude Durand, of the French National Space Agency (CNES), are involved in work on space radio navigation systems such as the GPS based autonomous navigation for the STENTOR geostationary satellite.

ABSTRACT

Different navigation systems (ground and on board equipment) have been studied in order to design an autonomous navigator for a geostationary satellite. This study focuses on the hardware system description, the mission analysis and the orbit determination accuracy obtained with the presented kinds of localisation measurements.

The presented comparison study considers different navigation techniques based on C/A code characteristics with a dedicated C/A code on board receiver :

a) The use of the C/A codes transmitted by the GPS satellites ;

b) Transmission in Ku, C or S-band of C/A codes by 3 dedicated ground pseudolites, or by feeder-link stations of the host satellite (in Ku-band).

This paper presents the characteristics of each radionavigation system (theoretical background, kind of measurement, frequencies, error models ...) and the method used to estimate the orbit determination accuracy. Then, the results are compared and discussed.

System specification of the on board receiver are given in each case.

The use of the studied system on board geostationary radionavigation satellites is also discussed. Some studies concerning GPS navigation for geostationary transfer orbits are also described.

The GPS application planned for the STENTOR program is also presented.

Introduction

Tracking sessions for geostationary satellites are generally performed by ground stations with classical ranging, Doppler and angular measurements.

In order to minimize the ground segment operations and to develop more and more autonomous orbitography systems (for orbit determination, orbit manoeuvre computation, ...), new GPS techniques are considered, where the measurements are performed and used on board the satellite itself. That constitutes an autonomous navigation system, well matched to spacecraft provided with a ionic propulsion dedicated to North-South station keeping. In such a case, the frequency necessary for the station keeping manoeuvres (typically once a day) induces costly ground operations, if an autonomous navigation system is not used. Autonomous navigation could also be useful for East-West station keeping manoeuvres. The autonomous navigation could also be used to broadcast on-board generated ephemeris (orbital and clock elements), if the associated accuracy is good enough for future GNSS2 payloads.

Two candidate configurations are considered in this paper. First, a general system description of each studied configurations is given :

- hardware description and measurement principle,
- link and error budget,
- system advantages and drawbacks.

Then an orbitography study is detailed with a comparison of the orbit determination accuracy achievable by the differents localisation systems:

- principles about the methods used,
- details of some specific modellings (clock delay, orbit extrapolation error, ...),
- complete description of each simulation (hypotheses, error budget, measurements schedule, results, ...).

The orbit determination accuracy for station keeping of each system is presented.

1. System description

1.1. General description

The studied system is based on the following components :

- A radionavigation receiver placed on board the geostationary spacecraft. This equipment is a multichannel C/A code receiver.

- A network of radionavigation signal transmitters. The clock phase differences of these transmitters are assumed to be known : the system is synchronised. Single way and monofrequency radiolinks are established between these transmitters and the receiver.

- A receiving antenna with its main lobe pointing towards the earth and covering a part of the transmitters network.

- The receiver processes the C/A signals, to produce pseudorange and pseudospeed (Doppler) measurements related to the axis linking the transmitters and the geostationary satellite. The Doppler measurements are performed over an interval T equal to 10 seconds. The pseudorange measurements are performed every 10 seconds.

- The raw measurements are transmitted to an on board processor, performing the autonomous orbitography.

1.2. Raw measurement errors

The first source of short term measurement noise is the thermal noise. These errors are characterized by the following parameters :

σ_{PRth} = Standard deviation of Pseudo Range (m)

σ_{PVth} = Standard deviation of Pseudo Velocity (m/s)

c = Speed of light (m/s)

T = Doppler count interval (s)

f_o = frequency of the carrier processed (Hz)

Rc = Chip rate of the C/A code (chip/s)

Rd = Data rate of the transmitted message (bit/s)

B_{nm} = Noise bandwidth of the D.L.L (Hz)

B_{np} = Noise bandwidth of the Costas Loop (Hz)

Li = Losses between the antenna and the loops.

$\frac{C}{No}$ = Signal to noise density at antenna access (Hz)

$$\sigma_{PDth} \# \frac{c}{Rc} \sqrt{\frac{B_{nm}}{2 \cdot \left(\frac{C}{No} \cdot \frac{1}{Li} \right)}} \left[1 + \frac{2 \cdot Rd}{\left(\frac{C}{No} \cdot \frac{1}{Li} \right)} \right]$$

$$\sigma_{PVth} \# \frac{c}{\pi \cdot f_o \cdot T} \sqrt{\frac{B_{np}}{\left(\frac{C}{No} \cdot \frac{1}{Li} \right)}} \left[1 + \frac{Rd}{2 \cdot \left(\frac{C}{No} \cdot \frac{1}{Li} \right)} \right]$$

The second source of short-term noise is due to the short-term stability of the oscillators used in the system. An estimation of these errors is formulated hereafter :

σ_{PRosc} = Std deviation of Pseudo Range (m)

σ_{PVosc} = Std deviation of Pseudo Velocity (m/s)

ΔFi = frequency difference over the T period (Hz)

Fi = central frequency of the oscillator i (Hz)

The index i is b for the on board oscillator and g for the ground oscillator.

$$\sigma_{PRosc} \# c \cdot T \cdot \sqrt{\left[\frac{\Delta F_b}{F_b} \right]_T^2 + \left[\frac{\Delta F_g}{F_g} \right]_T^2}$$

$$\sigma_{PVosc} \# c \cdot \sqrt{\left[\frac{\Delta F_b}{F_b} \right]_T^2 + \left[\frac{\Delta F_g}{F_g} \right]_T^2}$$

The standard deviations σ_{PD} and σ_{PV} related to the global short term errors are given by :

$$\sigma_{PR} = \sqrt{\sigma_{PRth}^2 + \sigma_{PRosc}^2}$$

$$\sigma_{PV} = \sqrt{\sigma_{PVth}^2 + \sigma_{PVosc}^2}$$

1.3. Study of different location systems

1.3.1. Case a : GPS receiver receiving signal transmitted by the GPS satellites

This case has been well described in previous papers [1], [2], [3], [4]. The transmitters are the GPS Space Vehicles. The frequency used is L1 ($f_0 = 1575.42$ MHz). The RF link analysis is performed with a best case - worst case link budget. The associated geometrical configuration (fig 1.3.1.1) is synthesized by a set of parameters, as follows :

R_{earth} = Radius of the earth

R_{ms} = Radius of an earth centered masking sphere

Θ_{geomax} = GPS SV Aspect angle from a GEO (max)

$\Theta_{geommin}$ = GPS SV Aspect angle from a GEO (min)

Θ_{gpsmax} = GEO Aspect angle from a GPS SV (max)

Θ_{gpsmin} = GEO Aspect angle from a GPS SV (min)

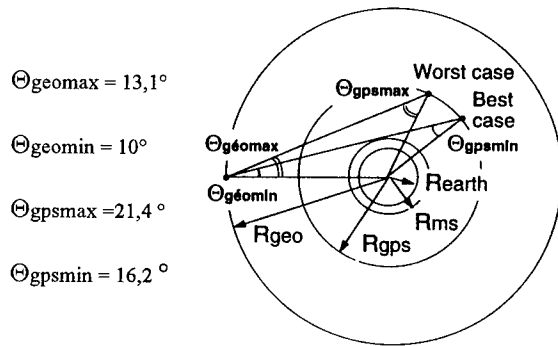


fig 1.3.1.1 : GPS-GEO link budget configuration

The masking sphere allows the receiver or the on board processor to suppress the measurements embeded with strong ionospheric errors. Its altitude has been selected to 1000 km for this study. The ionospheric error on pseudorange measurement has been estimated to 16 m in the worst case, which is the best case of the link budget. The aspect angles in the worst case has been chosen to have a C/No at the antenna port better than to 30 dBHz (with a # 2 dB margin), compatible with the acquisition thresholds of good GPS receivers. The best case aspect angles correspond to the masking sphere. The associated link and error budget is given hereafter (table 1.3.1.2) :

| Case of GPS SV | Best case | Worst case |
|----------------------------|-----------|------------|
| Transmitted power (dBW) | 14 | 14 |
| GPS antenna gain (dB) | 13.4 | 1.4 |
| Free space losses (dB) | 192.9 | 192.8 |
| Other losses (dB) | 3.2 | 4 |
| GEO antenna gain (dB) | 13 | 12 |
| Noise temperature (dBK) | 27.5 | 27.5 |
| Boltzman const (dBW/k/Hz) | -228.6 | -228.6 |
| C/No (dBHz) | 45.4 | 31.8 |
| Internal losses L_i (dB) | 1.5 | 1.5 |
| σ_{PDth} (m) | 1.3 | 6.4 |
| σ_{PVth} (mm/s) | 0.12 | 0.59 |

table 1.3.1.2 : GPS-GEO link budget

Losses due to multipath or ionospheric fadings are more important for the best case of the link budget. Losses due to the degradation of the ellipticity ratio outside the nominal zone of the GPS SV antenna pattern are not well known. An estimation (3 dB) is taken into account in the worst case link budget.

For orbit determination, the choosen standard deviations related to the thermal noise are 10 m and 1 mm/s. They are slightly greater than in the calculated worst case, but still negligible compared to the effects of Selective Availability (table 2.3.1.4). The short term stability of a GPS SV clock is assumed to be majored by 10^{-12} s/s. The short term stability of the receiver clock is choosen to be 10^{-11} s/s. Thus, we obtain :

$$\begin{aligned} \sigma_{PRth} &= 10 \text{ m} & \sigma_{PVth} &= 1 \text{ mm/s} \\ \sigma_{PRosc} &= 0.03 \text{ m} & \sigma_{PVosc} &= 3 \text{ mm/s} \\ \sigma_{PR} &= 10 \text{ m} & \sigma_{PV} &= 3.2 \text{ mm/s} \end{aligned}$$

The maximum pseudorange error ϵ_{PRmult} due to multipath can be estimated with the following elements, considering one single delayed path created by a reflection on the earth itself (fig 1.3.1.3) :

r = reflection coefficient on the earth surface

G_{ed} = GPS SV antenna gain, for the direct path

G_{er} = GPS SV antenna gain, for the reflected path

G_{rd} = GEO antenna gain, for the direct path

G_{rr} = GEO antenna gain, for the reflected path

a = relative amplitude of the reflected signal [5]

$$a = \frac{G_{er} \cdot G_{rr} \cdot r}{G_{ed} \cdot G_{rd}}$$

NB: The multipath errors could be not negligible because $G_{ed} < G_{er}$ and $G_{rd} < G_{rr}$.

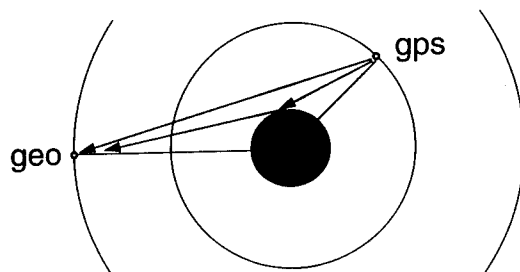


fig 1.3.1.3 : Multipath for a GPS-GEO link.

C_s = chip spacing used in the GPS receiver [5].

$$\epsilon_{PR_{mult}} = \frac{a \cdot c \cdot C_s}{R_c}$$

With a classical chip spacing ($C_s = 1$ chip) and a first estimation of the relative amplitude such as $a \# -14$ dB, we obtain $\epsilon_{PR_{mult}} \# 10$ m. This error can be reduced with a receiver equipped with narrow correlators [5].

1.3.2. Case b - option 1 : GPS Rx receiving GPS-like signals transmitted in Ku band by several host stations

In this case, the transmitters are located on the ground, at feeder-link stations of the host satellite (connection and/or TM/TC stations). The frequency of the uplink signal is assumed to be in the Ku band. One uplink channel could be occupied by a C/A code modulated in baseband by a data message. The main characteristics of this channel are summarized by :

$f_0 \# 14$ GHz ; $R_c = 1.023$ MHz ; $R_b = 50$ bits/s

This concept enables to reuse significant hardware parts pre-existing in the host station (high power amplifier, stable clock, transmitting antenna ...) and in the host spacecraft (receiving antenna ...). The main specific hardware is limited to a monochannel GPS

generator connected to a coherent Ku upconverter (ground parts) and a Ku downconverter connected to a GPS receiver (spacecraft parts). The synchronisation (i.e knowledge of the transmitters clock phase differences) of the system can be performed by external means such as GPS itself. A time GPS receiver is now usually set up in feederlinks stations. The synchronisation could also be performed internally, if the number of stations (or dedicated pseudolites : § 1.3.3) is sufficient. In such a case, autonomous orbitography and system synchronisation are performed simultaneously.

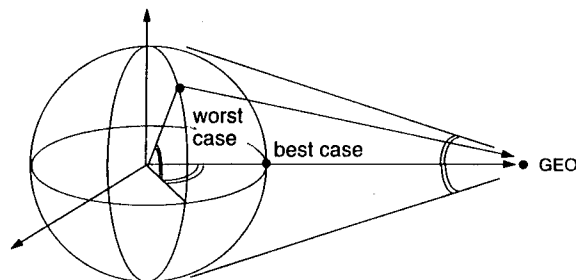


fig 1.3.2.1 : Geometry of the link budget. Case b.

The link budget (table 1.3.2.2) considers a best case with a feeder link station situated on the subsatellite point, and a worst case with station coordinates equal to 45° in latitude and relative longitude (fig 1.3.2.1)

| Feeder link station | Best case | Worst case |
|----------------------------|-----------|------------|
| Transmitted power (dBW) | 7 | 7 |
| station antenna gain (dB) | 45.3 | 45.1 |
| Free space losses (dB) | 206.4 | 207.3 |
| Other losses (dB) | 3.8 | 4.5 |
| GEO antenna gain (dB) | 19 | 18.7 |
| Noise temperature (dBK) | 30.5 | 30.5 |
| Boltzman const (dBW/K/Hz) | -228.6 | -228.6 |
| C/No (dBHz) | 59.1 | 57.1 |
| Internal losses L_i (dB) | 2 | 2 |
| σ_{PDth} (m) | 0.3 | 0.4 |
| σ_{PVth} (mm/s) | 0.05 | 0.07 |

table 1.3.2.2 : feederlink station - GEO link budget

The selected standard deviations related to the thermal noise are finally 0.5 m and 0.1 mm/s. The short term stability of a ground high performance OCXO is assumed to be 5.10^{-13} s/s. The short term stability of the on board clock used for the study is 7.10^{-13} s/s. Thus, we obtain :

$$\begin{aligned}\sigma_{PRth} &= 0.5 \text{ m} & \sigma_{PVth} &= 0.1 \text{ mm/s} \\ \sigma_{PRosc} &= 0.003 \text{ m} & \sigma_{PVosc} &= 0.26 \text{ mm/s} \\ \sigma_{PR} &= 0.5 \text{ m} & \sigma_{PV} &= 0.3 \text{ mm/s}\end{aligned}$$

1.3.3. Case b - option 2 : GPS Rx receiving GPS-like signals transmitted in Ku, C or S band by 3 dedicated ground GPS pseudolites

This case is quite similar to the previous one, except for the ground station concept. It has been presented in [6]. The transmitters are dedicated pseudolites, using Ku, C or S band; i.e. f_0 # 14, 6 or 2 GHz. The link budget configuration is identical to the previous one, as well as the clock stability assumptions.

| Dedicated pseudolites | best case | | | worst case | | |
|------------------------|-----------|--------|--------|------------|--------|--------|
| | Ku | C | S | Ku | C | S |
| Tx power (dBW) | 10 | 11.8 | 10 | 10 | 11.8 | 10 |
| Tx ant gain (dB) | 35.8 | 24.1 | 15.1 | 35.3 | 22.1 | 13.1 |
| F.S Losses (dB) | 206.4 | 199.6 | 189.5 | 207.3 | 200.5 | 190.4 |
| Other losses (dB) | 3.8 | 1.8 | 0.7 | 4.5 | 2.5 | 1.4 |
| Rx ant gain (dB) | 19 | 19 | 19 | 18 | 18 | 18 |
| Noise temp (dBK) | 30.5 | 29 | 28.1 | 30.5 | 29 | 28.1 |
| B cst (dBW/K/Hz) | -228.6 | -228.6 | -228.6 | -228.6 | -228.6 | -228.6 |
| C/No (dBHz) | 52.6 | 52.9 | 54.3 | 49.6 | 48.4 | 49.8 |
| Int losses (dB) | 2 | 2 | 2 | 2 | 2 | 2 |
| σ_{PDth} (m) | 0.6 | 0.6 | 0.5 | 0.9 | 1 | 0.8 |
| σ_{PVth} (mm/s) | 0.06 | 0.11 | 0.09 | 0.08 | 0.18 | 0.16 |

table 1.3.3.1 : Pseudolite-GEO link budget

The global short term noise evaluation table is thus :

| dedicated pseudolites | pseudorange (m) | | | pseudovelocity (mm/s) | | |
|------------------------|-----------------|-------|-------|-----------------------|-------|-------|
| | Ku | C | S | Ku | C | S |
| selected σ_{th} | 1.0 | 1.0 | 1.0 | 0.1 | 0.2 | 0.2 |
| σ_{osc} | 0.003 | 0.003 | 0.003 | 0.260 | 0.260 | 0.260 |
| global σ | 1.0 | 1.0 | 1.0 | 0.3 | 0.3 | 0.3 |

The pseudorange errors are computed with a Total Electron Count (TEC) equal to $7.4.10^{17}$ e/m² in the worst case.

CNES has already tested 3 stations manufactured by IN-SNEC including C-band GPS pseudolites transmitting toward one Inmarsat 2 geostationary payload equipped with a C-L repeater. This experimentation has been performed in the frame of the European GNSS overlay project [7]. The one sigma standard deviation of the pseudorange noise measured with GPS receivers connected to a coherent L-L1 frequency converter was below 2 meters [7]. The orbitography performance obtained with 5 days of measurements leads to an estimation of the radial component better than 4 m (1 σ rms), with 3 pseudolites located in Toulouse (France), Kourou (French Guyana) and Hartebeesthoek (South Africa). The orbit of the geostationary satellite was computed using measurement periods of 1 hour every 6 hours [7].

2. Orbit determination

This second part describes the orbitography analysis performed on these 3 different location systems. This study consists in the estimation of the orbit determination accuracy reached after 3 days of observation.

2.1. Method

The method used is a direct covariance analysis of a least squares orbit determination filter. For each kind of measurement, the covariances of the different kinds of errors are given in input. The results are the covariances of each estimated orbit parameters.

The different types of measurement errors can be simulated by :

- random function,
- bias or serial bias function (systematic error during all the observation period or during shorter periods),
- autoregressive functions (Markov process).

The software used for this study is quite well adapted to classical measurements performed by ground stations: such as ranging, Doppler, elevation or azimuth measurements.

Therefore, to determine the orbit determination accuracy reached with the different solutions, we had to convert their measurements in classical measurements performed by ground stations:

- For the pseudo ranging between GPS satellites and the Geo satellite (case a), we consider a fictive ground station network located at a very high altitude (20132 km) on a circle behind the Earth (§ 2.3.1). Then each GPS signal is converted into a pseudo ranging measurement between the spacecraft and the fictive station, the nearest to the GPS satellite.
- For the cases b (pseudo ranging and Doppler measurements between the spacecraft and ground stations or beacons) no conversion is needed.

Orbit parameters:

The used orbit parameters are adapted to a quasi geostationary orbit:

a: semi major axis

$$\left. \begin{aligned} ex &= e \cos(\omega + \Omega) \\ ey &= e \sin(\omega + \Omega) \end{aligned} \right\} \text{eccentricity vector}$$

$$\left. \begin{aligned} ix &= \sin i \cos(\Omega) \\ iy &= \sin i \sin(\Omega) \end{aligned} \right\} \text{inclination vector}$$

$\ell_m = \omega + \Omega + M - \theta$: mean longitude

where: ω : argument of perigee
 Ω : right ascension of the ascending node

M: mean anomaly
 θ : sidereal time

2.2. Specific errors modelling

2.2.1. Clock delay

The radioelectric measurements considered are one way measurements. So the delay of the clock used to determine the measurement datation must be taken into account as a pseudo range error (a delay of 1 μ s corresponds to a range error of about 300 m).

To take into account this error we have incorporated three new parameters in the resolution system. Two of

them are added to the state vector, in order to be estimated through the least squares filter :

P1 = clock bias ($\sigma_1 = 2.6 \mu$ s)

P2 = clock drift ($\sigma_2 = 3.3 \cdot 10^{-9}$ s/s)

And the third parameter, P3 represents the residual clock drift after estimation ($\sigma_3 = 3.3 \cdot 10^{-9}$ s/s).

This method decreases the observability of the whole state vector but the fact the clock delay can be estimated widely compensates the observability lost.

Different tests have been performed about that. They are detailed on § 2.3.1 (case a).

2.2.2. Error due to the orbit extrapolation model

To represent the error which can be introduced by the orbit extrapolation model of the on-board software (analytical model), we have incorporated an other parameter (uncertain parameter) in the resolution system. This parameter characterizes an unaccuracy on the Earth attraction coefficients μ of $\sigma_\mu = 0.14 \text{ km/s}^2$ which leads to an error of about 5 m on the semi major axis after 3 days of extrapolation. This kind of value is compatible with a CNES analytical model which has been tested and evaluated with respect to an orbit determined by an accurate numerical model with actual measurements [8], but should be adapted with the chosen on board model.

2.3. Study of different location systems

2.3.1. Case a : GPS Rx receiving signal transmitted by the GPS satellites

The measurements are pseudorange between the visible GPS Space Vehicles (SV) and the geostationary satellite. Due to the different antennas geometry (transmitter and receiver), the link budget and the ionospheric effects, the GPS satellites which can be acquired must be located on a crown behind the Earth (fig 1.3.1.1, [1]).

This restriction prevents four GPS satellites from being simultaneously visible (which would allow to know immediately the spacecraft position, and moreover, the on board clock delay). So, the orbit determination must be performed through an estimator (least squares filter for instance).

The following figure shows the distribution of the GPS satellite on the crown behind the Earth after a simulation with the GPS orbits (determined the 4th of august 1994).

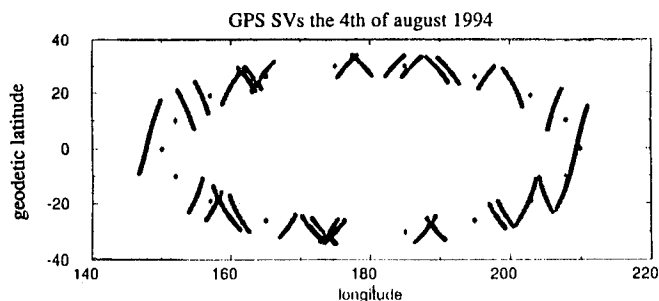


Figure 2.3.1.1

Our analysis software represents the GPS SV visible by the geostationary satellite by 18 fictive ground stations located on this circle. As soon as a GPS SV is acquired by the GEO, the associated pseudorange measurement is simulated, related to the fictive station the nearest of the GPS satellite.

When a GPS satellite is visible, a measurement is performed every 10 s, this frequency leads, on a long observation period, to an effective measurement every 15.1 s (fig 2.3.1.2), taking into account the 24 GPS orbit evolution and the geostationary one's.

Figure 2.3.1.3 shows the distribution of the visible GPS satellites versus time.

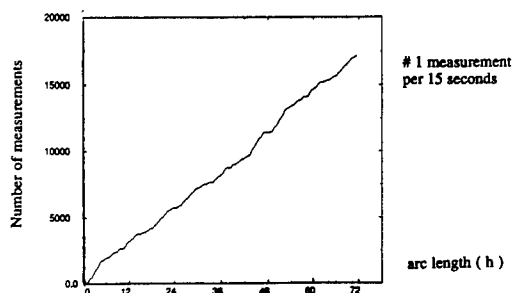


Figure 2.3.1.2 : Cumulated of GPS measurements versus time

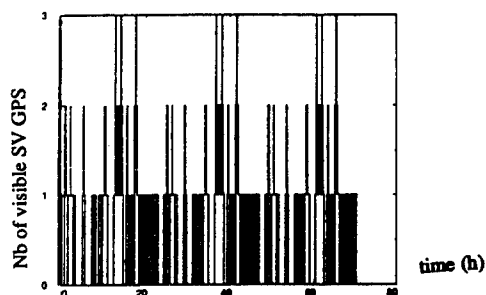


Figure 2.3.1.3 : Number of visible GPS satellites versus time

Measurement plan:

We consider 3 days of orbit observation, with a measurement every 10 s as soon as a GPS satellite is visible.

Measurement errors:

The error budget is given in the following table:

| Error origin | Kind of error | σ (m) |
|--|--|--------------|
| multipath | bias | 10 |
| thermal | random error | 10 |
| ionosphere | bias | 16 |
| short term selective availability (SA) | autoregressive Markov process $\tau = 180$ s | 25 |
| long term SA | autoregressive $\tau = 7200$ s | 30 |

To these errors some others must be added:

- The orbit extrapolation model error due to the attraction coefficient μ error : $\sigma_{\mu} = 0.14 \text{ km}^3/\text{s}^2$, this parameter is estimated (added to the state vector).
- The clock delay is modeled by 2 estimated parameters {clock bias ($\sigma = 2.6 \mu\text{s}$) ; clock drift ($\sigma = 3.3 \cdot 10^{-9} \text{ s/s}$)} and 1 non estimated parameter {residual clock drift (after estimation)}. This error has been simulated as a bias or a random error ($\sigma = 3.3 \cdot 10^{-9} \text{ s/s}$).

Results:

The following table (2.3.1.4) gives the orbit parameter accuracies (after 3 days of orbit observation) and the contribution of each error.

| Model | a (m) | ex | ey | ix (deg) | iy (deg) | l (deg) |
|----------------|-------|---------|---------|----------|----------|---------|
| Short tSA | 1.024 | 3.9e-08 | 4.0e-08 | 1.4e-05 | 1.3e-05 | 1.2e-05 |
| Long tSA | 2.452 | 8.4e-08 | 9.7e-08 | 3.2e-05 | 2.9e-05 | 2.9e-05 |
| Clock-bias | 0.000 | 0.0e+00 | 0.0e+00 | 0.0e+00 | 0.0e+00 | 0.0e+00 |
| Clock drift | 0.000 | 0.0e+00 | 0.0e+00 | 0.0e+00 | 0.0e+00 | 0.0e+00 |
| Residual drift | 0.000 | 0.0e+00 | 0.0e+00 | 0.0e+00 | 0.0e+00 | 0.0e+00 |
| Ionosphere | 0.441 | 5.4e-08 | 5.4e-08 | 1.8e-05 | 1.8e-05 | 4.3e-05 |
| μ | 4.937 | 4.2e-08 | 3.6e-08 | 1.3e-05 | 1.4e-05 | 3.1e-05 |
| Multipath | 0.326 | 4.2e-08 | 3.6e-08 | 1.3e-05 | 1.4e-05 | 3.1e-05 |
| Short-term | 0.075 | 0.0e+00 | 0.0e+00 | 1.3e-06 | 1.4e-06 | 5.7e-07 |
| Troposphere | 0.000 | 0.0e+00 | 0.0e+00 | 0.0e+00 | 0.0e+00 | 0.0e+00 |
| Total | 5.634 | 1.1e-07 | 1.2e-07 | 4.1e-05 | 3.9e-05 | 6.1e-05 |

$\Delta R \approx 5.6 \text{ m}$
 $\Delta T \approx 45 \text{ ns}$
 $\Delta N \approx 31 \text{ m}$

Table 2.3.1.4

This simulation leads to a very good orbit accuracy where the highest error contribution comes from the orbit extrapolation model whereas the SA contributes more slightly to the total error. The very low contribution of the residual clock drift drove us to perform a second simulation where the clock delay (bias and drift) are not estimated. This led to a better

observability but immediately the contribution of the clock error increased (table 2.3.1.5).

For this simulation, the clock delay has been taken into account as a clock drift of 10^{-11} s/s corresponding to a bias of 2.6 μ s after 3 days. The result of this simulation is given in the next table:

| Model | a (m) | ex | ey | ix (deg) | iy (deg) | l (deg) |
|-------------|-------|---------|---------|----------|----------|---------|
| Short t SA | 0.729 | 3.7e-08 | 4.0e-08 | 1.4e-05 | 1.3e-05 | 1.2e-05 |
| Long t SA | 1.729 | 7.9e-08 | 9.4e-08 | 3.2e-05 | 2.9e-05 | 2.8e-05 |
| Clock-bias | 365.9 | 3.1e-06 | 4.0e-07 | 8.5e-05 | 3.7e-05 | 3.1e-04 |
| Clock drift | 1.329 | 1.5e-06 | 9.0e-07 | 2.4e-05 | 1.3e-05 | 7.3e-05 |
| Clock error | 0.000 | 0.0e+00 | 0.0e+00 | 0.0e+00 | 0.0e+00 | 0.0e+00 |
| Ionosphere | 1.994 | 5.2e-08 | 5.0e-08 | 1.8e-05 | 1.8e-05 | 4.2e-05 |
| μ | 3.045 | 4.4e-08 | 3.5e-08 | 1.3e-05 | 1.4e-05 | 3.2e-05 |
| Multipath | 1.473 | 3.9e-08 | 3.5e-08 | 1.3e-05 | 1.4e-05 | 3.1e-05 |
| Short-term | 0.053 | 0.0e+00 | 0.0e+00 | 1.3e-06 | 1.4e-06 | 5.7e-07 |
| Troposphere | 0.000 | 0.0e+00 | 0.0e+00 | 0.0e+00 | 0.0e+00 | 0.0e+00 |
| Total | 366.0 | 3.5e-06 | 9.9e-07 | 9.8e-05 | 5.6e-05 | 3.3e-04 |

$\Delta R \approx 370$ m
 $\Rightarrow \Delta T \approx 240$ m
 $\Delta N \approx 70$ m

Table 2.3.1.5

Several tests have been performed, and led to the same conclusion : the clock delay parameter have to be estimated, so an on board clock with a medium mid term-stability performance could be enough because even if the residual drift is important after a linear estimation ($3.3 \cdot 10^{-9}$ s/s), its influence is minor.

At last, different tests have been performed on shorter periods (36 h, 24 h, 12 h) and have also shown very good results. Table 2.3.1.6 gives the results on the 3 directions (radial R, normal N, and along track T).

| Duration | R deviation | N | T |
|----------|-------------|------|-------|
| 36 h | 10 m | 42 m | 53 m |
| 24 h | 25 m | 50 m | 60 m |
| 12 h | 60 m | 75 m | 155 m |

Table 2.3.1.6

Conclusion of case a :

The orbit determined with those GPS measurements seems to be very accurate even on very short arcs (12 h).

2.3.2. Case b : GPS Rx receiving GPS-like signals emitted in Ku, C or S band by 3 ground beacons.

The measurements are pseudo range (one way) and Doppler between the spacecraft and 3 ground pseudolites.

We consider a 0 deg longitude satellite and 3 ground beacons located in Toulouse, Kourou and Hartebeesthoek. The coordinates choosen for these beacons are given hereafter :

| | Longitude | Latitude | Altitude |
|----------------|-----------|----------|----------|
| Toulouse | 1.5 ° | 43.4 ° | 260 m |
| Kourou | - 52.6 ° | 5 ° | 112 m |
| Hartebeesthoek | 27.7 ° | -25.9 ° | 1151 m |

Measurement plan:

A pseudorange and a Doppler measurement is performed every 10 s during 3 days, for each pseudolites.

Measurement errors:

They are detailed in the following table, for the dedicated pseudolites (case b - option 2).

| Origin of error | σ_{ranging} (m) | | | σ_{doppler} (mm/s) | | | Kind of error |
|---|-------------------------------|---|--------|----------------------------------|-----|-----|---------------|
| | Ku | C | S | Ku | C | S | |
| Short term noise (oscillator + thermal) | 1 | 1 | 1 | 0.3 | 0.3 | 0.3 | random |
| Multipath | 1 | 1 | 1 | 0.1 | 0.1 | 0.1 | bias |
| Ionosphere | 0.4 | 2 | 20 / 6 | 0 | 0 | 0 | bias |
| Troposphere | 3 | 3 | 3 | 0 | 0 | 0 | bias |

The case of feeder link stations (b-option 1) has the same error budget in Ku band, except for the pseudorange short-term noise (0.5 m instead of 1 m). However, it has been verified this difference has no significant influence on the orbitography performance.

The following errors are also taken into account:

- the extrapolation orbit model error: $\sigma_{\mu} = 0.14 \text{ km}^3/\text{s}^2$,
- the clock delay:
 - . clock bias ($\sigma = 2.6 \mu\text{s}$) to be estimated,
 - . clock drift ($\sigma = 3.3 \cdot 10^{-9} \text{ s/s}$) to be estimated,
 - . residual clock drift ($\sigma = 3.3 \cdot 10^{-9} \text{ s/s}$).

Remarks:

1. We consider the ground pseudolites are correctly synchronised.

2. We consider the important ionospheric bias (S band case) could be partially compensated (70 %) through a permanent ground calibration. That's the reason why the study is performed with 2 correction values.

The 4 following tables present the accuracies reached on the orbit parameters and the contribution of each kind of error after three days of measurements, and for the 3 transmission bands (Ku, C and S). For S band, 2 tables are given for each case of ionospheric bias.

| Model | a (m) | ex | ey | ix (deg) | iy (deg) | l (deg) |
|----------------|-------|---------|---------|----------|----------|---------|
| Clock-bias | 0.000 | 0.0e+00 | 0.0e+00 | 0.0e+00 | 0.0e+00 | 0.0e+00 |
| Clock drift | 0.000 | 0.0e+00 | 0.0e+00 | 0.0e+00 | 0.0e+00 | 0.0e+00 |
| Residual drift | 0.000 | 0.0e+00 | 0.0e+00 | 0.0e+00 | 0.0e+00 | 0.0e+00 |
| Ionosphere | 0.000 | 0.0e+00 | 0.0e+00 | 0.0e+00 | 0.0e+00 | 3.7e-06 |
| μ | 4.937 | 0.0e+00 | 0.0e+00 | 0.0e+00 | 0.0e+00 | 9.5e-06 |
| Multipath | 0.000 | 0.0e+00 | 0.0e+00 | 0.0e+00 | 0.0e+00 | 9.5e-06 |
| Short-term | 0.009 | 0.0e+00 | 0.0e+00 | 0.0e+00 | 0.0e+00 | 0.0e+00 |
| Troposphere | 0.000 | 0.0e+00 | 0.0e+00 | 0.0e+00 | 0.0e+00 | 2.8e-05 |
| Total | 4.937 | 0.0e+00 | 0.0e+00 | 0.0e+00 | 0.0e+00 | 3.0e-05 |

$\Delta R \approx 5m$
 $\Delta T \approx 22m$
 $\Delta N \approx 0m$

Table 2.3.2.1 (Ku band)

| Model | a (m) | ex | ey | ix (deg) | iy (deg) | l (deg) |
|----------------|-------|---------|---------|----------|----------|---------|
| Clock-bias | 0.000 | 0.0e+00 | 0.0e+00 | 0.0e+00 | 0.0e+00 | 0.0e+00 |
| Clock drift | 0.000 | 0.0e+00 | 0.0e+00 | 0.0e+00 | 0.0e+00 | 0.0e+00 |
| Residual drift | 0.000 | 0.0e+00 | 0.0e+00 | 0.0e+00 | 0.0e+00 | 0.0e+00 |
| Ionosphere | 0.000 | 0.0e+00 | 0.0e+00 | 0.0e+00 | 0.0e+00 | 1.8e-05 |
| μ | 4.937 | 0.0e+00 | 0.0e+00 | 0.0e+00 | 0.0e+00 | 9.5e-06 |
| Multipath | 0.000 | 0.0e+00 | 0.0e+00 | 0.0e+00 | 0.0e+00 | 9.5e-06 |
| Short-term | 0.009 | 0.0e+00 | 0.0e+00 | 0.0e+00 | 0.0e+00 | 0.0e+00 |
| Troposphere | 0.000 | 0.0e+00 | 0.0e+00 | 0.0e+00 | 0.0e+00 | 2.8e-05 |
| Total | 4.937 | 0.0e+00 | 0.0e+00 | 0.0e+00 | 0.0e+00 | 3.0e-05 |

$\Delta R \approx 5m$
 $\Delta T \approx 22m$
 $\Delta N \approx 0m$

Table 2.3.2.2 (C band)

| Model | a (m) | ex | ey | ix (deg) | iy (deg) | l (deg) |
|----------------|-------|---------|---------|----------|----------|---------|
| Clock-bias | 0.000 | 0.0e+00 | 0.0e+00 | 0.0e+00 | 0.0e+00 | 0.0e+00 |
| Clock drift | 0.000 | 0.0e+00 | 0.0e+00 | 0.0e+00 | 0.0e+00 | 0.0e+00 |
| Residual drift | 0.000 | 0.0e+00 | 0.0e+00 | 0.0e+00 | 0.0e+00 | 0.0e+00 |
| Ionosphere | 0.003 | 0.0e+00 | 0.0e+00 | 8.1e-07 | 8.1e-07 | 1.9e-04 |
| μ | 4.937 | 0.0e+00 | 0.0e+00 | 0.0e+00 | 0.0e+00 | 9.5e-06 |
| Multipath | 0.000 | 0.0e+00 | 0.0e+00 | 0.0e+00 | 0.0e+00 | 9.5e-06 |
| Short-term | 0.009 | 0.0e+00 | 0.0e+00 | 0.0e+00 | 0.0e+00 | 0.0e+00 |
| Troposphere | 0.000 | 0.0e+00 | 0.0e+00 | 0.0e+00 | 0.0e+00 | 2.8e-05 |
| Total | 4.937 | 0.0e+00 | 0.0e+00 | 8.1e-07 | 8.1e-07 | 1.9e-04 |

$\Delta R \approx 5m$
 $\Delta T \approx 140m$
 $\Delta N \approx 1m$

Table 2.3.2.3 (S band, $\sigma_{iono} = 20 m$)

| Model | a (m) | ex | ey | ix (deg) | iy (deg) | l (deg) |
|----------------|-------|---------|---------|----------|----------|---------|
| μ | 4.937 | 3.0e-11 | 2.0e-11 | 1.1e-09 | 1.1e-09 | 1.1e-07 |
| Clock-bias | 0.000 | 0.0e+00 | 0.0e+00 | 0.0e+00 | 0.0e+00 | 0.0e+00 |
| Short-term | 0.009 | 2.2e-10 | 2.1e-10 | 1.5e-07 | 1.5e-07 | 1.0e-07 |
| Clock drift | 0.000 | 1.0e-11 | 1.0e-11 | 2.3e-09 | 1.1e-09 | 0.0e+00 |
| Residual drift | 0.000 | 1.0e-11 | 1.0e-11 | 2.3e-09 | 1.1e-09 | 0.0e+00 |
| Ionosphere | 0.001 | 2.0e-10 | 3.5e-10 | 2.6e-07 | 2.4e-07 | 5.6e-05 |
| Multipath | 0.000 | 3.7e-11 | 5.7e-11 | 4.4e-08 | 4.0e-08 | 9.3e-06 |
| Troposphere | 0.000 | 9.9e-11 | 1.8e-10 | 1.3e-07 | 1.2e-07 | 2.8e-05 |
| Total | 4.937 | 3.2e-10 | 4.5e-10 | 3.3e-07 | 3.1e-07 | 6.3e-05 |

$\Delta R \approx 5m$
 $\Delta T \approx 47m$
 $\Delta N \approx 1m$

Table 2.3.2.4 (S band, $\sigma_{iono} = 6 m$)

Conclusion of case b:

Those results are excellent, the total error is mainly due to the orbit model error and the ionospheric bias in case of S band transmission without ionospheric bias calibration.

Some other tests have been performed on shorter arcs (36 h, 24 h, 12 h) and leads to very good results too, almost with Ku or C transmission. The accuracy stays

very fine until 24 h and is still correct after only 12 h of measurements. It seems to be the most accurate way of on board navigation.

3. main conclusions

The following table summarizes the orbit performances reached with those different location systems. It gives the position accuracy at 1σ :

| System | ΔR (m) | ΔT (m) | ΔN (m) | Remark |
|--|----------------|----------------|----------------|---|
| GPS satellites (case a) | 5 to 6 | 45 | 31 | - possibility to reduce the measurement arc till 12 h without any notable degradation |
| 3 ground beacons (case b) Ku, C band | 5 | 22 | 0 | - Ku, C: very accurate even on short arcs (> 12 h) |
| S band - ionospheric bias not compensated | 5 | 140 | 1 | - S band: - along track deviation due to the ionospheric effect |
| - 70 % of ionospheric bias compensated | 5 | 47 | 1 | - possibility to reduce the measurement arc till 12 h |

A sensitivity study has been performed for ground transmitters related to the pseudovelocity. Its contribution to the global performance is negligible, compared to the influence of the pseudorange. This observation allows to relax the specification of the short term stability of the on board oscillator. All the performance of this oscillator (§ 2.3.1) are thus compatible with a good OCXO (Ovenized Controlled Cristal Oscillator), which could be integrated in the C/A receiver.

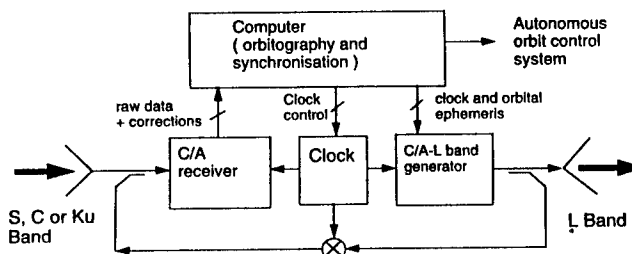


fig 3.1. Autonomous nav & GNSS2 geostationary payload.

The on board receiver could of course take benefit of a clock in the payload, as it could be the case in the

GNSS2 geostationary payloads. If these payload broadcast GNSS-like signals in a band close or equal to L1, a GNSS receiver could not be used on board for electromagnetic compatibility reasons. However, solutions described in case b can be managed for such applications (fig 3.1).

4. GPS navigation in transfer orbit

Progress in the GPS receiver techniques allow to reduce the acquisition and tracking thresholds. An acquisition C/No threshold close to 25 dBHz at the antenna access is now possible. Such performances could allow a navigation during geostationary transfer orbits, using GPS with other measurements or as sole mean.

An operational orbitography performed on ground using both GPS measurements (transmitted during the contacts with the ground) and classical ranging data could reduce the number of used ground stations or/and the cost of the associated ground segment operations before the station keeping.

An orbitography performed on board with GPS measurements could also be possible with good acquisition thresholds (25 dBHz at the antenna port, for instance).

The geostationary satellites are typically sun-pointed during transfer orbits, excepted during some manoeuvres. Studies have shown that number of GPS contacts performed during classical GTO (Geostationary Transfer Orbit) or GDO (Geostationary Drift Orbit) are not numerous enough, if the GPS antenna dedicated to station keeping is used. Two complementary antennas (fig 4.1), mounted on the face pointed toward the sun (-Z) and on the anti-sun face (+Z) of the platform, could be used.

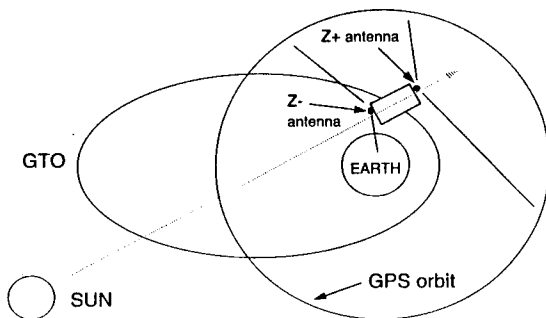


fig 4.1. GPS subsystem for transfer orbits

The pattern of these antennas is assumed to be hemispherical. The associated gain Gr is a function of the aspect angle Θ :

$$Gr(\Theta) = Gr(0) \cdot [\cos(\Theta)]^r \quad \text{if } \Theta < 1.2 \text{ rad}$$

$$Gr(\Theta) = 0 \quad \text{if } 1.2 < \Theta < \pi \text{ rad}$$

The antenna parameters chosen for this study are $r = 1.4$ and $Gr(0) = 2$, i.e $Gr(0)_{dB} = 3 \text{ dB}$. The antenna pattern of the transmitting GPS antenna is modelled as follows (fig 4.2) :

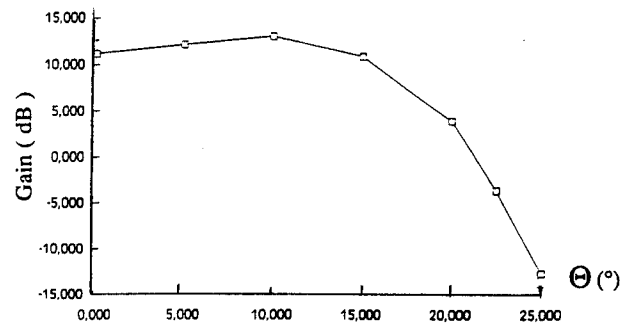


fig 4.2 : Model of the L1 band GPS SV antenna gain.

The dynamic link budget between a GPS SV and the satellite in transfer orbit consider a worst case for non free space losses estimated to 4 dB. The system noise temperature is assumed to be constant (600K) in the study.

The studied transfer orbits are GTO, GDO and SSO (Super Synchronous Orbit). They are described in table 4.3 :

| | GTO | SSO | GDO |
|----------------------|--------|---------|---------|
| Apogee altitude (km) | 36000 | 60000 | 36000 |
| S-major axis (km) | 24580 | 36688 | 41984 |
| Eccentricity | 0.715 | 0.80925 | 0.00675 |
| Inclination (°) | 7 | 7 | 0.06 |
| Argum of perigee (°) | 180 | 180 | 180 |
| Long of asc node (°) | 280.24 | 280.24 | 280.24 |
| Mean anomaly (°) | 0 | 0 | 0 |

table 4.3 : Types of transfer orbit studied.

The following results (fig 4.4, 4.5, 4.6) present the number of GPS satellites visible ($C/No > 25 \text{ dBHz}$) by the 2 hemispherical antennas during the 3 types of orbit presented above.

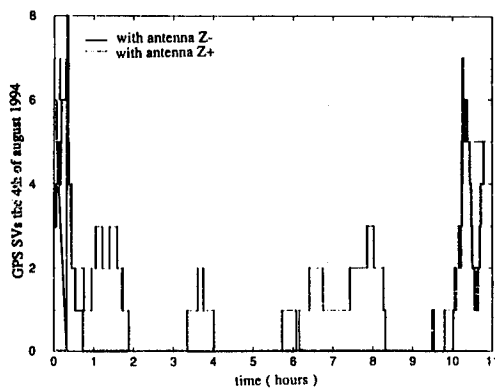


fig 4.4 : Visible GPS satellites for a GTO.

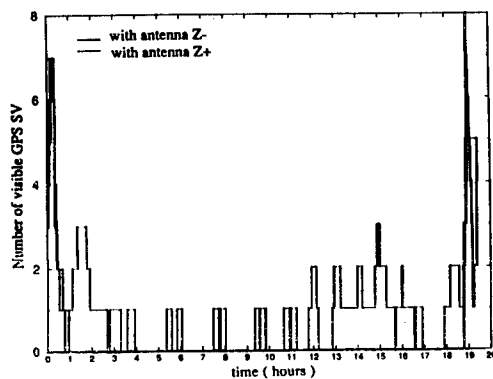


fig 4.5 : Visible GPS satellites for a SSO.

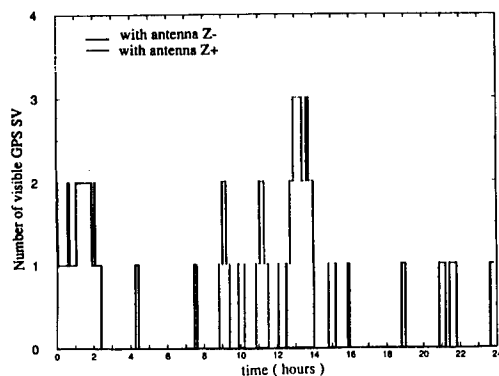


fig 4.6 : Visible GPS satellites for a GDO.

These results encourage to continue further work in this subject. The number of GPS contacts is quite correct. These contacts are well distributed along each orbit. Autonomous orbitography seems to be accessible with modern L1-C/A GPS receivers.

5. Implementation of GPS measurements in STENTOR

The STENTOR project is a french geostationary satellite, dedicated to the experimentation of new space techniques in orbit (STENTOR = Satellite Technologique pour Experimenter des Nouvelles Techniques en ORbite).

The GPS navigation on board geostationary satellite is considered as one of these new techniques. CNES performed several internal works on this subject, such as the one presented in this paper. The first industrial study for CNES concerning the use of different navigation systems using GPS techniques started in 1989. These techniques are now considered as sufficiently mature to be tested in orbit.

An autonomous navigation principle, based on GPS use, will be implemented on-board STENTOR.

The description of this system is very close to the one described in § 1.3.1. It is part of the A.O.C.S subsystem under MMS (Matra Marconi Space) responsibility.

As it is considered as an experiment, it can be superseded by a "standard" (i.e. not GPS-based) procedure.

This experiment will allow to check the actual performances of this solution. A conventional method will be used as a reference.

The use of this system during transfer orbit is still under discussion.

ACKNOWLEDGMENTS

The authors would like to thanks MMS for their excellent work already performed in the frame of the GPS/STENTOR project.

REFERENCES

- [1] Orbit determination of geostationary satellites using the GPS. M.P. Ananda and P.S. Jorgensen. Symposium on Space Dynamics for Geostationary Satellites, CNES, France, aug, 1985.
- [2] Description and performance of the GPS Block I and II L-band Antenna and Link Budget. Francis M. Czopek and Lt. Scott Shollenberg. ION GPS, USA, sept 1993.
- [3] Tracking geostationary satellites with GPS. J.M. Legido Riba, R. Lucas Rodriguez, Paper in ESA-Preparing for the future, Vol .5 N°1, march 1995.
- [4] Considerations for the application of GPS in satellites : GPS system trade study. J. Kronman and Th. McElroy. ION GPS, USA, sept 1994.
- [5] New theories and GPS experiments about effects of multipath and RF jammers. S. Mahooti and R. Landry. ION GPS, USA, sept 1994.
- [6] New applications of GNSS in Orbit and Attitude determination (copy of slides). J-Luc Issler. Symposium on Space Flight Dynamics, Russia, may 1994.
- [7] European complement to GPS : main experimental results. J. Barbier, M. Deleuze, J-L. Issler, ION GPS, USA, sept 94.
- [8] Test of the long-term evolution of a quasi-geostationary orbit using numerical and analytical methods. P. Ferrage, A. Guitart. IAF, Israel, oct 1994.

Relative GPS Navigation for ATV Rendezvous

Michael Frezet, Herve Marcille, Virginie Pascal, and Jean Michael Pairot
Matra Marconi Space

Hubert Barré, Massimo Cislighi, and Ulrich Thomas
European Space Agency

BIOGRAPHY

Michel Frezet received an Engineer Degree from the Ecole Supérieure des Télécommunications (Paris) in 1981. He joined Matra Marconi Space (MMS) in 1982. Since 1989 he is working in Space Mechanics and GNC, covering mostly the Hermes Navigation and Guidance activities. Since 1994, he is responsible of the MMS ATV GNC activities.

Herve Marcille received an Engineer Degree from the Ecole Centrale Paris, France in 1989, and a MSc degree from the Aero&Astro dept of Stanford University in 1990. Since then, he is working as an engineer in the design of Attitude and Orbit Control Systems, at Matra Marconi Space, covering Earth observation satellites (CNES) and scientific missions (ESA). He is now responsible of navigation activities for the ATV Rendezvous Predevelopment (ARP).

Virginie Pascal received an engineer degree from the Ecole Nationale Supérieure de Mécanique et d'Aérotechnique of Poitiers, France in 1990. Since then, she is working as an engineer in the Dynamics and GNC division of Matra Marconi Space. She is currently in charge of the detailed RGPS navigation design within ARP-Kernel.

Jean Michel Pairot received an Engineer Degree from the Ecole Supérieure de l'Aéronautique et de l'Espace (Toulouse, France) in 1980, completed by a DEA in artificial intelligence. In 1983, he joined Matra Marconi Space and worked on spacecraft attitude control, pointing systems and autonomous space rendezvous. Since 1995, he is system engineer responsible for MMS technical activities on the ARP-Kernel project.

Hubert Barré received his Engineer Degree in Energy, Transportation and Propulsion, completed by a DEA in Mechanics and Energetics in 1979, Orleans (France). He worked with Thomson-CSF (France) from 1981 to 1991 on the development of autonomous

controlled and guided weapons, as a system engineer then as a project manager. He joined ESA-ESTEC in 1991 as a system engineer on the ATV and ARC (Automated Rendezvous and Capture) projects. He is currently responsible for the development of a GPS receiver and Rendezvous Sensor within ARP project.

Massimo Cislighi received a Master Degree in Mechanical Engineering at the University of Roma in 1981. He joined ESA/ESTEC in 1988 where he performed System Architecture Analysis (Hermes) and became responsible (1993) for joint ESA/Russian system-level studies in view of possible cooperation. Since 1994, he is delegated by the ESA ATV Project Manager to the management of the ATV Rendezvous Predevelopment (ARP) activities.

Ulrich J. Thomas received his Masters Of Aeronautical Engineering from the technical University of Berlin (TUB) in 1980. He received a PhD from TUB in 1983 for research activities on Life Cycle Costing to Advanced Space Transportation Systems. He joined ESA in 1985, performing successively resources systems engineering then logistics support system for Columbus. In 1990 he joined the Directorate of Space Transportation Systems to be responsible for the ATV phase A activities and now for the technical aspects of the ARP-Kernel project.

ABSTRACT

In 1994, ESA initiated an ATV Rendezvous Predevelopment (ARP) Program in parallel to the ATV phase B. The Automated Transfer Vehicle (ATV) will perform servicing to the International Space Station Alpha (ISSA). The Rendezvous to ISSA is a critical mission phase of the ATV flight involving the safety of both ATV and ISSA vehicles and crews. Therefore, the ARP program primary objective is to demonstrate the maturity of the critical technology involved in the achievement of such rendezvous operations. The baseline relative navigation solution

for the long range proximity operations (12 km to 300 m) is the Relative GPS (RGPS). This paper presents the current results of the ARP activities on the design and development of the so-called RGPS filter.

1. INTRODUCTION

As its major participation to the cost and maintenance of the International Space Station Alpha (ISSA) the European Space Agency (ESA) has decided to develop an ISSA dedicated servicing vehicle, the Automated Transfer Vehicle (ATV). The mission of the ATV will be to perform an orbital rendezvous with the ISSA ending either by a docking along the ISSA velocity axis (Vbar approach) or a berthing until grappling by the ISSA robot arm after a radial approach (Rbar). The relative GPS (RGPS) is baselined as the navigation mean for the long-range part of the proximity operations.

In 1994, the ATV Rendezvous Predevelopment (ARP) program has been initiated by ESA in parallel to the ATV phase B in order to demonstrate Europe capability to master the key technology involved in performing the ATV to ISSA orbital rendezvous (ref [6]), among which the relative GPS navigation. The ARP program includes the following elements and objectives:

- The rendezvous system pre-development (called ARP-Kernel, Matra Marconi Space is prime contractor) which includes:
 - * Design and development of a Rendezvous Control system (RVC) prototype software running in real time in an ATV computer breadboard.
 - * Development and validation of the ground simulation facilities
 - * Verification process for the RVC prototype software
 - * Definition, execution and analysis of flight demonstrations for the Rendezvous Sensor (RVS) and the RGPS.
- The development of a Rendezvous Sensor (RVS) by DASA JENA Optronik (ARP-RVS contractor).
- The procurement of a GPS receiver (ARP-GPS), by Laben (ARP-GPS contractor) based on the Laben/Loral TensorTM, which shall be used during ARP-K activities for verification and demonstration of the relative GPS algorithms (ground tests and flight demonstration).

In the following, we shall focus on the RGPS navigation activities that are currently carried out in the frame of the ARP-Kernel, project including:

- Functional description of the RGPS navigation function

- Description of the implemented RGPS algorithms: choice of the GPS observables, of the state vector and filtering scheme, trade-off performance versus SW complexity.
- RGPS performance prediction based on preliminary simulations.
- Development of a high fidelity functional simulator.
- Test and validation campaign philosophy.

The activities undertaken in the frame of ARP-Kernel for the relative GPS aim at demonstrating in a full scale prototype that the RGPS is a relevant technology element for the automatic Rendezvous foreseen for the ATV.

2. THE RGPS FILTER WITHIN ATV RVC

2.1 Applicable operational conditions

After launcher separation, the ATV mission is composed of two main mission phases. The phasing of the ATV with the ISSA is performed by a succession of Hohmann transfer burns dedicated to approach the altitude of the ISSA while catching up in free drift with ISSA actual on-orbit position. During the phasing, the ATV will rely on absolute GPS navigation and up-linked target ephemeris that will allow to derive coarse relative position/velocity estimates used for active control of the transfer burns. The second mission phase consists in the proximity operations that are triggered by the entry into the ISSA communication range. From this event on, the ATV relative navigation is supposed to work directly in relative mode in order to achieve the necessary performance for a safe approach sequence. This direct, real-time relative navigation is made possible by the established ISSA to ATV UHF link that transmits in real time the necessary ISSA GPS data. The initial position/velocity estimates are available at the transition, derived as previously described (100 m, 0.5 m accuracy).

Both ISSA and ATV are assumed to have a 12 channels C/A code GPS receiver providing raw data at 1 Hz. Thanks to the real-time UHF link the ISSA GPS raw data are made available to the RGPS filter no more than two seconds after they were acquired. The antenna coverage of both receivers are assumed sufficient to provide a nominal common visibility of at least 4 GPS satellites all the time. Considering the small range of proximity operations (< 12 km), and the use of hemispherical antennas with low enough mask angle (< 15°), this feature is easily satisfied with the current 24 GPS satellites constellation.

During all the proximity operations, the ISSA is supposed to be a "co-operative target" in the sense that it does not perform linear control burns.

2.2 RGPS navigation performance requirement

The performance requirements apply to the estimates of the relative position/velocity of the ATV with respect to the ISSA Local Vertical/Local Horizontal (LV/LH) frame, which is used by the guidance function to compute and correct in real time the reference approach trajectory and by the closed loop position/velocity control. Three main drivers apply for the performance specification of the RGPS navigation in the frame of the ATV rendezvous:

- The impact of navigation errors on the relevance of the guidance reference trajectory computation.
- The ability to detect anomalous deviations from the reference trajectory sufficiently early to allow a safe mission reconfiguration (stop-approach or avoidance manoeuvre).
- The acquisition range of the ISSA retroreflector by the optical Rendezvous Sensor (RVS) at the hand-over from RGPS navigation to the final RVS navigation.

These constraints have lead ESA to specify the following performance requirements to the RGPS navigation:

| | |
|----------------|----------------------------|
| position error | < 10 m (3σ) |
| velocity error | < 0.05 m/sec (3σ) |

This specification applies with Selective Availability (SA) active on all GPS satellites.

2.3 RGPS filter functional description

Various filtering scheme for relative navigation with GPS have already been proposed in the literature. The first choice to be performed is whether to derive the relative position/velocity estimates by subtracting the outputs of two independent absolute navigation filters, (one for the chaser and the other for the target), or to use directly both spacecraft GPS data in the same filter. The second option has always been recognised as superior in order to benefit as much as possible from the cancellation of all the external sources of errors in the GPS signal (SA, ionospheric delay, GPS ephemeris errors) that affect similarly the input GPS signal received quasi-simultaneously by both receivers, ref[1][7][8]. This cancellation is obtained by subtracting directly the raw data (pseudo-range, carrier cycle count, range-rate) obtained simultaneously from both GPS receivers. With this simple principle most of the errors inherent to the GPS signal itself vanish directly. The direct processing of differential GPS observables has then been selected for the ATV RGPS filter. Its principle is depicted on figure 2.3/1.

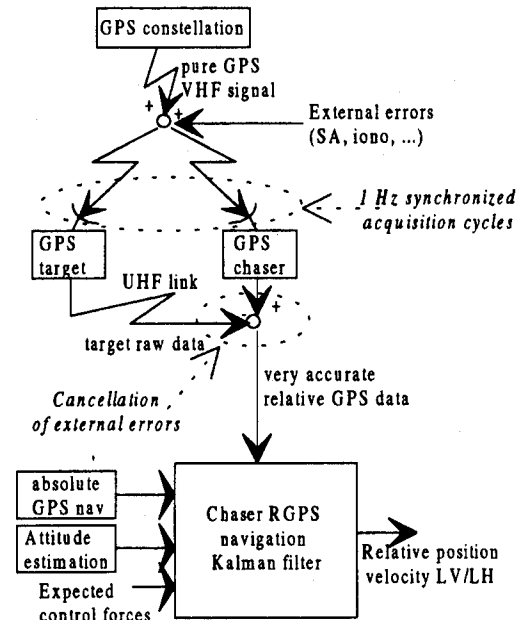


Figure 2.3/1 - Principle of RGPS navigation

However, the derivation of relative navigation from such relative raw data requires also a knowledge of the absolute position/velocity of the target/chaser composite in order to predict the line of sight to the GPS satellites. Ref[4] proposes to include in the same Kalman filter the estimate of both vehicles position/velocity vectors together with range/range-rate biases estimates for each of the GPS satellites commonly tracked by chaser and target. This solution lead to a 27 states filter in ref[4]. In the case of ATV, the absolute navigation of the ATV is already required independently for the phasing mission phase and continues to operate during the rendezvous phase. Absolute navigation data are then readily available for the relative GPS filter. The more economic and modular solution (in terms of size of the state vector) chosen for ATV is then to design an independent RGPS filter, working solely on the relative raw data, and fed by the output of the absolute navigation filter. Despite the fact that the absolute navigation estimates are sensitive to the SA and other external error sources (ionospheric delay, ...), the impact on the accuracy of the RGPS output has been found to be quite acceptable. Note that the method of ref[4] makes use of the relative measurements to improve the absolute navigation solution, while in the ATV case, only the relative navigation benefits from the relative observables.

An other issue of importance in the functional design of the RGPS filter is the introduction of the acceleration model that will feed the dynamics propagation. As already said, the target is "co-operative", thus no input from the target about any control acceleration is needed. On the ATV side, it has been chosen to use the a priori knowledge of the

linear accelerations obtained at the thruster management function level when computing the on-time of the thrusters.

The RGPS filter is also fed with attitude estimates of both the chaser and the target in order to compensate for the lever arm existing between the GPS antenna and the spacecraft's centre of mass to which apply the relative navigation estimates. ISSA attitude data will be received in real time by ATV thanks to the space-to-space UHF link.

3. RGPS filtering algorithm description

3.1 RGPS observables

One essential trade-off to make in designing a GPS-based filter is the choice of GPS observables to process. The three basic observables available from the TensorTM receiver are:

- The pseudo-range measurement (10 m, 1σ)* (issued from code phase measurement) is classically used for instantaneous absolute position fix.
- The carrier cycle count (6mm, 1σ)* (issued from carrier phase measurement)
- The range-rate measurement (5cm/sec, 1σ)* (from the Doppler shift commanded to the carrier tracking loop)

(*) performance figures free from external error sources (from ARP-GPS specification)

Beside these basic raw observables, it is possible to reconstruct a pseudo range-rate observable by back differentiation of carrier cycle count data. This observable will be called the *delta-range observable* in the following. This observable is essentially related to the mean velocity over the integration time step, and therefore can be used instead of the range-rate observable to provide a direct observability of the velocity states.

The past studies performed on RGPS navigation during rendezvous (Hermes, ref[7][8]) have shown that the use of a velocity-related observable to supplement the pseudo-range measurements is highly desirable because it allows a faster estimation dynamics during manoeuvring flight (necessary for feedback control) while providing the necessary improvement to the steady-state accuracy. Regarding the alternative between range-rate and delta-range observables, the carrier phase measurement accuracy provided by the ARP-GPS receiver is greatly in favour of the delta-range option (nearly 10 times more accurate than the range-rate). The size of the state vector is the same in both cases, and the observable processing complexity is quite similar.

Another way to supplement the "coarse" pseudo-range accuracy is to use the carrier cycle count observable as a position measurement by calibrating at first the random Doppler constant representing the actual pseudo-range at GPS satellite acquisition. This *integrated Doppler* method is certainly the most accurate one (ref[1],[2]), both in terms of bandwidth and accuracy. However it requires to augment the state vector by the Doppler constants, i.e. as many as the number of simultaneously tracked satellites (at least 4). This state augmentation, together with the various matrix manipulations that are needed to cope with GPS satellite switching (covariance matrices reinitialisation) make the Kalman filter computations much more burdensome and very sensitive to the number of tracked satellites. For a flight software, this option is then recommended only to cope with very stringent performance specifications.

In the ATV case, the specified performance level allows to choose the **pseudo-range/delta-range** observables option as the best compromise between performance and on-board software complexity. This choice allows to work with a relatively small state vector (8 states) made of:

- 3 relative position estimates*
- 3 relative velocity estimates*
- 1 relative clock bias estimate
- 1 relative normalised frequency error estimate

(*) relative position and velocity are expressed in the target LV/LH frame

3.2 GPS satellites selection algorithm

Only GPS satellites that are available from both chaser and target receivers are used as recommended in ref[3]. It has been chosen to work always with a four GPS satellite configuration (if available) in order to minimise the computation load involved in the measurement update processing. Simulations have shown that only about 10% degradation of the Geometric Dilution Of Precision (GDOP) results from this limitation. However, it is important not to replace the saved workload by a complex GPS satellite selection algorithm. Therefore, a simplified selection algorithm based on the tetrahedral volumic criteria (ref[5], section 6) is preferred to a complete GDOP minimisation algorithm. The average GDOP value of the selected combinations with the simplified algorithm is about 10% higher than the average value obtained with the GDOP minimisation algorithm. This difference does not induce a significant impact on the navigation performances.

3.3 RGPS Filter Characteristics

The RGPS navigation filter is based on a Linearized Kalman Filter (LKF). Unlike an Extended Kalman

Filter which computes a numerical integration to perform state propagation, a LKF uses the same linear transition matrix for the state and covariance propagation. The UD form of the covariance matrix is used in order to preserve naturally the positiveness.

State Propagation

A simple linear transition matrix based on the first order Clohessy Whiltshire equations proves to be adequate for propagation of the relative position/velocity states. It was tested that neither the second order term of the Clohessy Whiltshire equations nor the addition of the differential J2 perturbation bring any significant improvement in the end performance, due to the small relative distance between both spacecraft's (< 12 km). The control thrusts in turn need to be accounted for to feed the propagation dynamics.

State Update

State update is performed at 1 Hz on the basis of the relative raw data obtained by direct difference between chaser and target pseudo-range/delta-range data. The "measurement sharing technique" is used to update sequentially the covariance matrix (directly in UD form) while computing as many gain vectors as there are simultaneous measurements (nominally 8 measurements for a configuration of 4 satellites). A global measurement residuals vector is made by subtracting predicted measurements (based on the propagated state estimate) from current measurements. A global state correction is then computed by applying the correct combination of gain vectors/observation matrices to the measurement residual vector.

Timing and synchronization problems

The bias cancellation property of the RGPS technique relies essentially on the simultaneity of the chaser and target GPS data acquisition that are subtracted to get the relative GPS observables. This is particularly important for cancellation of the selective availability which undergoes relatively short term time variation. For this reason, it is of major importance to insure the best possible synchronization of both receivers, despite the fact that they are physically separated. This can be obtained by insuring that the 1 Hz GPS measurement cycle be synchronous with the true GPS time estimated within each receiver. The remaining desynchronization effect is then the relative clock bias, which is accounted for in the filter. However, the possibility to deal with asynchronous 1 Hz time-tagged data has been implemented within the RGPS filter. This is done by including in the measurement prediction equations a Taylor series development with

respect to the target/chaser desynchronization (obtained from relative time tag). A discussion of synchronization problems encountered experimentally is given in ref[2].

The second major timing issue is the target GPS data ageing due to the UHF link transfer delay (< 2 sec). Chaser data are then bufferized to wait for the corresponding target data. In order to limit the delay on the output estimates of the RGPS filter, the state estimate is interpolated back to the date of the available relative measurement before proceeding to the measurement prediction.

3.4 Specificities of the delta-range processing

The delta-range observable (difference between successive carrier cycle counts), is strictly equivalent to the variation of the pseudo-range over one measurement cycle (1 sec in our case) including the GPS receiver clock stability impact.

As it is stated in ref[5] (p 4-14), the processing of the so-called delta-range observable is not straight forward. The major problem arises from the fact that the actual delta-range is not a direct function of the current state vector, but rather a function of the current and previous step state vectors. Unless the standard state vector is doubled to include the position/velocity components at the beginning and end of each step (better use the integrated Doppler solution in this case), the user is bounded to make some simplifications while preserving the actual accuracy of the overall filtering scheme, by spoiling the intrinsic accuracy of the Doppler count data.

Our experience on the subject lead to adopt the delta-range processing of figure 3.3/1.

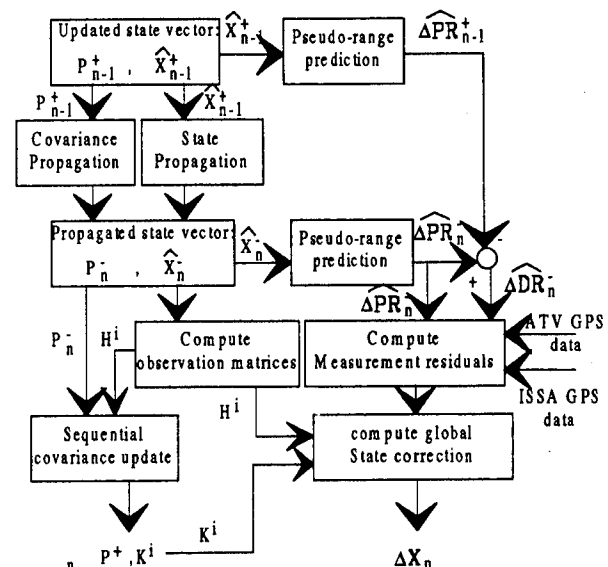


Figure 3.3/1 - Processing of the GPS observables

Where:

\hat{x}_n^+ is the estimated state vector after update at step n
 \hat{x}_n^- is the estimated state vector before update at step n
 P_n^{\pm} are the corresponding covariance matrices (actually in UD form)
 H^i is the i th measurement observation matrix
 $\hat{\Delta PR}$ is the predicted relative pseudo range
 $\hat{\Delta DR}$ is the predicted relative delta range

The major characteristics of this processing are summarised hereafter:

a/ The relative delta-range prediction ($\hat{\Delta DR}_n^-$) is made by back differentiation of the relative pseudo-range prediction $(\hat{\Delta PR}_n^- - \hat{\Delta PR}_{n-1}^+)/\Delta t$. This formulation allows to account exactly for the fact that the delta-range represents exactly a variation of the GPS satellite to GPS receiver range over the integration time step rather than an instantaneous range-rate.

b/ For delta-range prediction, the pseudo-range estimate at the previous step is recomputed based on the updated state vector. Eventually, the pseudo-range prediction is performed twice per simulation step, for each tracked satellite. This feature might appear as a complexification of the measurement prediction computations, however this is balanced by the fact that relative delta-range estimates are straight forwardly derived from pseudo-range estimates. Eventually, only eight complex measurement prediction equations (for 4 GPS satellites) are evaluated at each step to deal with eight independent observables.

c/ The state update is performed globally while the covariance matrix computation is made sequentially. This feature is necessary to insure that the predicted delta-range estimate strictly represents the actual state evolution due to the one-step propagation.

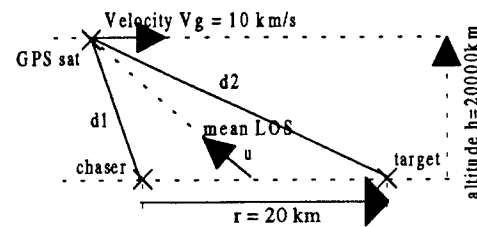
d/ The observation matrices for the delta-range are computed based on a range-rate expression. This approximation allows to avoid a very burdensome expression that would be obtained by true time-derivation of the true relative delta-range expression (i.e. pseudo-range back-difference).

Two problems have been encountered in the design of this delta-range processing and have been solved by using the above implementation. They are detailed hereafter:

Approximating delta-range by range-rate

The easiest approximation would be to treat the delta-range measurement exactly as an instantaneous range-rate data. This solution allows to express the predicted

delta-range directly as a function of the current estimated state vector. However, the authors have found that the resulting accuracy of the measurement prediction is not satisfactory (at the mm/sec level), because it induces two much low frequency errors in the measurement prediction process. This error comes from the approximation of a mean velocity (delta-range) over the integration step by an instantaneous velocity expression (range-rate). Obviously, the first one is delayed by roughly half a step from the second one, leading to an error proportional to the range-rate derivative. The following simple 2D example illustrates the typical error resulting from this approximation:



The relative pseudo-range is:

$$\Delta PR = d_1 - d_2 \approx \vec{r} \cdot \vec{u}$$

The relative range-rate is:

$$\Delta RR = \dot{d}_1 - \dot{d}_2 \approx \dot{\vec{r}} \cdot \vec{u} + \vec{u} \cdot \dot{\vec{r}}$$

The relative delta-range is:

$$\Delta DR_n = \frac{\Delta PR_n - \Delta PR_{n-1}}{\Delta t} \approx \Delta RR_n - \frac{\Delta t}{2} \cdot \Delta \dot{RR}_n$$

Even with a fixed target/chaser configuration, the approximation error amounts to $(\Delta t / 2 \cdot \ddot{u} \cdot \vec{r})$, due to the moving geometry of the GPS satellite versus the target/chaser system. The figure 3.3/1 (from above example) illustrates that a low frequency error up to 2 mm/sec can result:

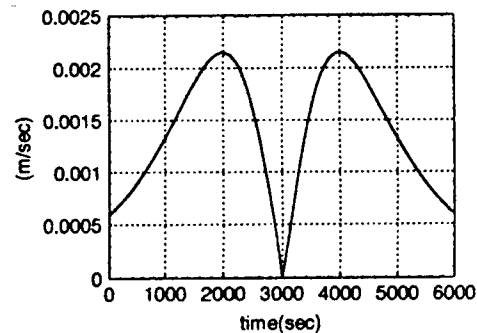


Figure 3.3/1 - Typical prediction error resulting from approximation of delta-range by range rate

Impossibility to update the state vector sequentially

It is mandatory not to adopt a thoroughly sequential algorithm that would consist in updating sequentially the state vector together with the covariance matrix. This implementation problem has been experimented by the authors and is therefore explained here:

One way to implement the measurement sharing technique is to treat all scalar measurements sequentially as if they were separated by a null propagation interval. However, this scheme generates at each step intermediate state estimates that form the basis of the next single measurement state update. In the delta-range case, this approach is not possible because it corrupts the estimated pseudo-range variation with the evolution due to the previous partial updates:

The actual i^{th} delta range is roughly a function (h^i) of the position variation over the step Δt :

$$\Delta DR_n^i = h^i \left(\frac{X_n - X_{n-1}}{\Delta t} \right) = h^i \left(\dot{\bar{X}}_n \right)$$

An i^{th} delta-range prediction based on a partially updated vector \hat{X}_n^{i-1} (with measurements 1 to $i-1$) would lead to the following expression:

$$\Delta \hat{DR}_n^i = \hat{h}^i \left(\frac{\hat{X}_n^{i-1} - \hat{X}_{n-1}^+}{\Delta t} \right) = \hat{h}^i \left(\underbrace{\frac{\hat{X}_n^{i-1} - \hat{X}_n^-}{\Delta t}}_{(1)} + \underbrace{\frac{\hat{X}_n^- - \hat{X}_{n-1}^+}{\Delta t}}_{(2)} \right)$$

The term (2) is homogeneous to the mean velocity ($\dot{\bar{X}}_n$) which is expected to be observed with the delta-range observable. The term (1) represents the range variation due to update 1 to $i-1$. It pollutes the accuracy of the delta-range prediction. Its contribution will falsely be interpreted as an error in the estimated velocity.

Consequently, the sequential processing must be reserved to the update of the covariance matrix and computation of the corresponding Kalman gain vectors. As for the measurement prediction and state update, it must be based solely on the same current "propagated" and previous "updated" state estimates.

3.5 RGPS filter tuning and dynamics

The tuning of the RGPS filter involves the definition of a measurement covariance matrix for the relative pseudo-range and relative delta-range observables, as well as the choice of a propagation model noise covariance matrix. The tuning of the measurement noise covariances is quite natural since, unlike in many applications of Kalman filtering, the relative measurement errors are indeed essentially made of uncorrelated noise, this resulting from the cancellation of most low frequency errors due to the differentiation of target/chaser measurements. This result assumes that the errors generated by the GPS receivers are essentially white noise. This characteristics is even more justified for the relative delta-range observable

which results from two successive differentiations (target from chaser difference + one-step time derivation). According to the noise specifications of the TensorTM receiver, the following tuning is selected:

relative pseudo-range (10m 1σ):

$$R_{pr} = 2 \times 10^2 = 200 \text{ m}^2$$

relative delta-range (6mm, 1σ):

$$R_{dr} = 2 \times 2 \times (6 \cdot 10^{-3})^2 = 1.44 \cdot 10^{-4} \text{ (m/s)}^2$$

Note that a factor of 2 allows to account for target/chaser differentiation, and another for time derivation of Doppler count (delta-range case).

The tuning of the propagation model noise matrix is less straight forward since the actual errors can hardly be directly characterised by uncorrelated random noise (Clohessy Whiltshire errors, control actuation errors ...). It was then preferred to perform this tuning by experimental optimisation (simulation). The model noise covariance matrix is implemented with the following structure for each position/velocity pair[?]:

$$Q_{x,\dot{x}} = K dt \begin{pmatrix} dt^2/4 & dt/2 \\ dt/2 & 1 \end{pmatrix}$$

where dt is the 1 sec sampling period.

A value of $K = 5 \cdot 10^{-7} \text{ m}^2/\text{sec}$ has been found as the best compromise for position/velocity performance. For larger values of K , the delta-range measurement is poorly filtered and the corresponding velocity performance sticks to the delta-range noise at about 1 cm/sec (1σ) (full confidence in the delta-range measurement). For lower values of K , the position performance degenerates into a model drift, as the Kalman filter puts too less weight on the pseudo-range data.

With the above correct tuning, the behaviour of the RGPS filter can be interpreted as the following: The velocity estimate is very accurate thanks to the millimetric relative delta-range measurement. Consequently, most of the filtering of the pseudo-range data is performed according to a prediction relying mostly on velocity integration rather than dynamics model propagation. With respect to the position estimate, the delta-range measurement acts almost as a propagation model, providing both a fast time response of the filter, and a high robustness to model errors such as the thrusters actuation errors. This explains why a quite simple propagation model featured by the first order Clohessy Whiltshire equations is quite sufficient to achieve the desired performance. It also explains why, when increasing K up to $10^{-3} \text{ m}^2/\text{sec}$, the position error does not quite grow up to the pseudo-range measurement error, but instead remains below 2 meters accuracy.

This simple physical interpretation of the pseudo-range + delta-range RGPS filter behaviour allows us to derive approximate dynamics characteristics in steady-state:

The position estimate is mainly formed by a combination of averaged pseudo-range measurements over a time period τ_{pr} , while relying on delta-range integration over the same time period. τ_{pr} can then be determined as the duration over which averaging pseudo-range noise and integrating delta-range noise amount to the same error contribution (according to the tuning of measurement noise covariances), leading to:

$$\tau_{pr} = \sqrt{\frac{R_{pr}}{R_{dr}}} = 1200 \text{ sec}$$

According to the same logic, the time constant of the delta-range measurement filtering is determined by the equivalence of averaged delta-range measurement noise and integrated velocity propagation model noise over the same time period τ_{dr} . this yields:

$$\tau_{dr} = \sqrt{\frac{R_{dr}}{Kdt}} = 17 \text{ sec}$$

These results show that the delta-range measurement is the key feature to this RGPS filter that provides a high bandwidth (< 20sec time constant) that can be accounted for in the control design, while allowing a very extensive filtering of the pseudo-range much less accurate data. Note that the initial convergence of this filter in position is much faster than illustrated by the steady state 1200 sec filtering time constant, thanks to the much higher initial gains obtained through the unstationary feature of the Kalman filter.

4. Preliminary RGPS performance results

At the time being, the high fidelity close loop functional simulator dedicated to the full RVC validation (see § 5), including the relative GPS navigation, is not yet operational. However, the design, tuning and preliminary validation and performance assessment of the above RGPS navigation algorithm has been carried out on a simplified simulator. This simulator features a closed loop rendezvous system with accurate simulation of target and chaser spacecraft dynamics, emulation of GPS raw data based on a realistic 24 satellites GPS constellation with ionospheric errors, commendable desynchronization between chaser/target measurements, typical guidance and control functions and chaser thruster system, allowing the achievement of representative close loop simulations featuring free drift, homing and closing phase using RGPS.

The major simplifications implemented in this simulator are:

- The SA error applied is the same for chaser and target data assuming perfect synchronization.
- The absolute navigation function is emulated as a black box that corrupts the actual ATV position/velocity vector with errors representative of a filtered absolute navigation estimation with C/A code GPS data and SA active.
- The lever arm between GPS antenna and centre of mass is neglected, eliminating the effect of residual attitude motion.
- The data transfer delay between ISSA and ATV is neglected assuming direct availability of both GPS outputs immediately.

The clock errors of both receivers are modelled as a first order gauss-markov process on the normalised frequency error with rms value 10^{-9} and time constant 1 year. Clock biases are initialised at 1 msec error.

Thruster errors are simulated as follows:

| | |
|--------------------|-----------|
| misalignment bias | 1° (3σ) |
| misalignment noise | 0.5° (3σ) |
| scale factor error | 2% (3σ) |

The performance results obtained on a full scale Vbar approach scenario featuring initialisation in free-drift followed by a homing phase and a closing phase are illustrated in figures 4/1,2. Through a preliminary limited statistical simulation campaign (50 runs), the achieved performance can be summarised by:

| | |
|----------------|-----------------|
| position error | < 2.5 m (3σ) |
| velocity error | < 5 mm/sec (3σ) |

These results are very satisfactory with respect to the specification, and yield a comfortable margin to account for the simplifications involved in this preliminary performance evaluation.

Sensitivity to desynchronization

The effect of the target/chaser GPS receivers desynchronization has been evaluated separately as the single error source in otherwise ideal simulations: The results shown in table 4/1 show that despite the open loop compensation, its effect becomes dominant for measurement date offsets greater than 200 msec. Moreover, the effect of differential selective availability would show up through desynchronization. A preliminary analytical evaluation of its impact (table 4/1) based on a second order gauss markov model (range 23 m, range-rate 0.28 m/sec, 1σ, 120sec time constant) allows to expect a significant impact on the velocity performance. Note that for these reasons, it is requested to limit the

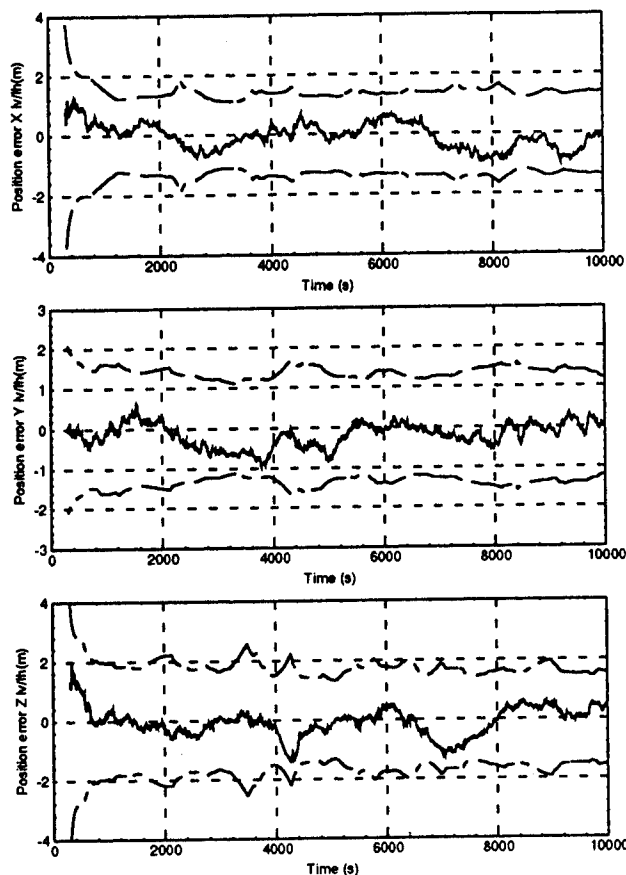


Figure 4/1- RGPS simulation results: position error in X,Y,Z LV/LH and Kalman 3σ envelope (meters)

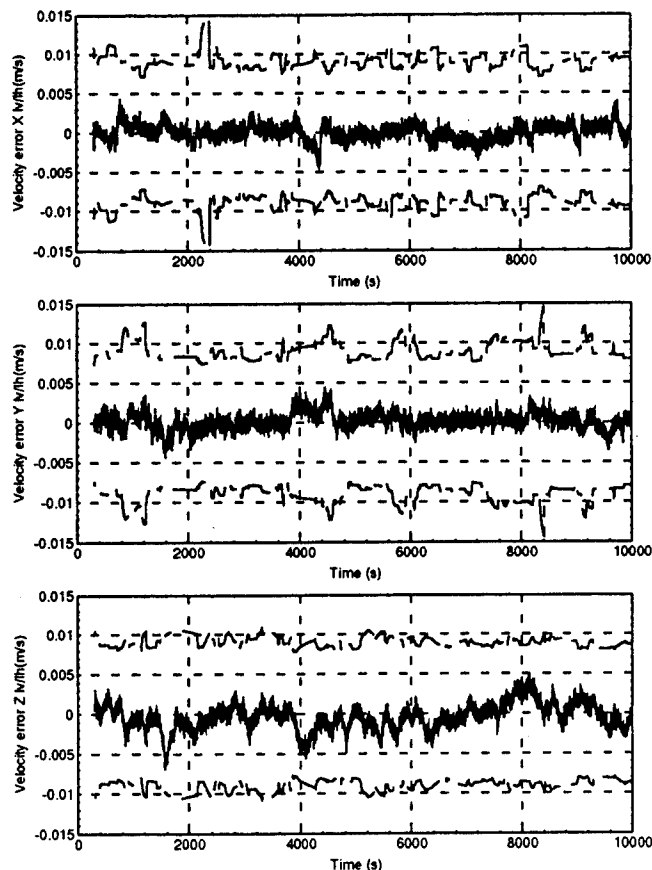


Figure 4/2- RGPS simulation results: velocity error in X,Y,Z LV/LH and Kalman 3σ envelope (m/sec)

desynchronization to less than 10 msec (1 msec would be achieved by using two ARP-GPS receivers).

| | Desynchronization level | | |
|--|-------------------------|----------------|------------------|
| | 0.1 sec | 0.2 sec | 0.3 sec |
| Desynchro. only (simulation results) | 1.2 m 3 mm/s | 3 m 6 mm/s | 5 m 10 mm/s |
| Differential SA only (analytical expectations) | 0.5 m 5 mm/s | 1 m 10 mm/s | 1.5 m 15 mm/s |

Table 4/1 - Impact of desynchronization and differential selective availability on RGPS performances

5. Development of the RVC functional simulator

The complete definitive software implementation of the above RGPS filter is currently being carried out within the global RVC functional simulator. This functional simulator will contain the exact software processing involved in the whole navigation, guidance, control, and mission and vehicle management functions that are developed for the prototype ATV rendezvous system. The resulting RVC simulator will interface with high fidelity environmental models derived from the ESA simulation facility EUROSIM, including chaser and target actual dynamics, all attitude and navigation sensors, a detailed model of the ATV reaction control system and an emulation of the ISSA/ATV UHF link covering transfer delay and synchronisation issues. This closed loop simulator will be used to validate the navigation performance results through an extensive simulation campaign.

For this prototype software, ESA has chosen to apply a new software development approach taking benefit of the design and automatic software generation tools Xmath/SystemBuild by ISI. The basic idea is to obtain from the algorithm designers (specifiers) a complete SystemBuild version of the RVC algorithms that will be used at design and validation level within the high fidelity functional simulator. The same SystemBuild RVC software will then be mapped into an autocoded C-language RVC software that, after interfaces adaptation, shall then be loaded onto the target ATV breadboard for real-time ground simulation/validation.

A detailed mathematical C-coded software model of the GPS receivers is then currently being developed for use within the functional simulator (SystemBuild level) and later on the real-time ground simulation facility. Both target and chaser receiver models will

interface with a high fidelity simulator of the GPS constellation and associated GPS signal errors and navigation data content.

6. Validation process

One step is the verification of the achievable performances by running Monte-Carlo simulations with the high fidelity functional simulator. But this simulator is made of software models that shall be validated by comparison with the real world: this is the objective of the validation campaign to be carried out in the ARPK program (ref [6]).

The first step will be the validation of the GPS receiver software model in the ESTEC GPS laboratory using the ARP GPS receiver. The GPS Lab features a NTC GPS measurement environment simulator that permits to generate RF signals to be plugged in a real GPS receiver. This way, the GPS receiver output and the GPS receiver software model can be compared for various flight conditions.

This validation will be completed in the frame of the RGPS navigation "open loop" tests: the chaser and target GPS raw data are generated with the ARP GPS receiver and/or the GPS receiver software model and the RGPS navigation algorithms are run with the different raw data inputs in order to estimate the relative position and velocity. This test permits to verify that the RGPS navigation performances are achieved and also to complete the validation of the GPS receiver software model.

The final step of the RGPS validation is the execution of flight tests: the flight tests are necessary in order to validate hypotheses that are made for the simulation on ground of the GPS measurements (space environment, delays, multipath, ionospheric effects,...). The basic results of the flight tests will be the recorded GPS raw data of the chaser and target GPS receivers: they will be used for validation of the ground simulator (by comparison with GPS Lab-generated receiver raw data) and for validation of the RGPS navigation performances (by running the RGPS algorithms with recorded raw data and comparison with the real relative trajectory). Two flight tests are currently foreseen in the frame of ARP: one with the Shuttle deploying the scientific DASA satellite ASTROSPAS as the second space vehicle and the other with the Shuttle rendezvousing with Mir.

This proposed incremental scheme allows to verify all the critical elements of the RGPS navigation chain and to demonstrate the applicability of the RGPS technology for the ATV to ISSA rendezvous.

7. Conclusion

The relative GPS navigation filter for ATV to ISSA rendezvous has been presented. A particular effort in on-board software load minimisation has allowed to obtain satisfying performances while keeping the state vector at a reasonable size (8 states). The processing of differentiated carrier cycle count data has been successfully implemented to benefit from the very good accuracy of carrier phase data. Helpful recommendations on the use of this observable have been derived. An ambitious software and hardware validation plan will allow to assess more precisely the performances of this RGPS navigation.

ACKNOWLEDGEMENTS

Thanks go to the ARP-GPS engineering team from Laben, as well as the staff of the ESTEC GPS-lab whose cooperation was helpful for this RGPS activity.

REFERENCES

- [1] J. S. Llorente-Martinez, R. Lucas: *Differential GPS Algorithms Evaluation for Navigation Between Two LEO Spacecraft During Rendezvous*. IEEE NAECON 1991, Dayton, May 1991.
- [2] J.M. Legido, M.A. Martinez, R. Lucas: *Differential and Relative Navigation Results with a GPS Receiver for Space Applications*. Proceedings of ESA International Conference on GNC, Noordwijk, April 1994.
- [3] B.A.C. Ambrosius, E.T. Hesper, K.F. Wakker: *Application of the Global Positioning System for Hermes Rendezvous Navigation*. Journal of Guidance Control and Dynamics Vol.16, N°1, January-February 1993.
- [4] Dr. Lubomyr, V. Zyla, Mr Moises, N. Montez: *Use of two GPS Receivers in Order to Perform Space Vehicle Orbital Rendezvous*. Proceedings of the ION GPS-93 Meeting, Salt Lake City, Utah, Sept. 1993.
- [5] William Lear: *GPS Navigation for Low Earth Orbiting Vehicles*. NASA JSC internal Note, JSC 32031, March 1989
- [6] J.M. Pailot, M. Lellouch, U. Thomas, M. Cislighi: *ATV Rendezvous Pre-development*. Colloque International de Mécanique Spatiale (CNES), Toulouse (France), 19-23 June 1995
- [7] M. Frezet, P. Riant: *Hermes Navigation and Orbital Guidance*. First ESA International Conference on GNC, Noordwijk, June 1991.
- [8] M. Frezet, P. Riant, M. Janvier, M. Caldichoury: *Hermes Rendezvous and Navigation System*. 2nd European in-Orbit Operations Technology Symposium, Toulouse, Sept 1989, ESA-SP-297.



Session D1

Student Competition Winners

Chair:

Mr. Naser El-Sheimy
The University of Calgary

Aircraft Tracking Using GPS Position and Velocity Reports

Ran Gazit
Stanford University

ABSTRACT

A new approach to Air Traffic Control (ATC) calls for every aircraft to periodically broadcast its GPS derived position. The position reports will be received by ATC controllers, and will be used for aircraft tracking and conflict prediction. This technique is expected to increase the quality and extent of ATC surveillance coverage, and to provide a highly accurate Collision Avoidance System.

In this study we identify the required elements of the appropriate tracking algorithms, and estimate the improvement in tracking accuracy that can be obtained by using this technique. A measurement error model that matches the correlation functions of both position and velocity errors is identified. This model is combined with two aircraft models in an adaptive Kalman filter. A switching logic provides the best position and velocity estimates during all phases of flight, and guarantees smooth transition of the estimates during satellite constellation changes.

The filter performance is checked in a Monte Carlo simulation, using real GPS data and simulated aircraft motion. The simulation includes the effect of an imperfect radio data link due to message interference. The tracking accuracy is then compared to the performance of modern ATC radar trackers. The effect of the improved surveillance accuracy on minimum separation standards is demonstrated.

I. INTRODUCTION

Air Traffic Control (ATC) requires timely and accurate information on aircraft position, velocity and heading. This information is obtained today using radar systems that are limited in both accuracy and coverage. A new approach to ATC suggests that every aircraft will periodically broadcast its position and possibly velocity, as measured by an on-board GPS receiver. The reports will be received by ATC ground controllers, and will be used for aircraft tracking and conflict prediction.

This technique, now being evaluated in trials around the world, is known as Automatic Dependent Surveillance (ADS) [1]. It is expected to increase the ATC surveillance accuracy and to allow a decrease in the minimum separation standards. Eventually, it should provide the freedom to select optimum routes and altitudes for time and fuel savings.

A major element in any ATC surveillance system is the tracking filter, which provides smooth estimates of the aircraft position, velocity and heading, based on noisy position measurements. Most of the existing research on aircraft tracking and tracking filter design assume that the aircraft position is measured by radar [2-5]. Using GPS as the position sensor requires a new design of the tracking filter, since the nature of the measurement errors in this case is very different from the nature of the current radar measurement errors.

In addition to the geometric difference between the two systems - radar accuracy depends on the distance from the radar, whereas GPS accuracy is uniform worldwide - we observe a much larger time constant in GPS position errors than the almost white radar measurement errors. An appropriate measurement error model should be identified and incorporated in the new tracking filter design. Other possible error sources should be identified and treated appropriately.

The objective of this work is therefore to design an aircraft tracking filter, which uses measurements provided by airborne GPS receivers. Through the tracking filter design process, we wish to identify and solve the major problems that might occur in GPS-based aircraft tracking. We then study the performance of the new tracking filter and compare its tracking accuracy with the performance of current ATC radar trackers. Finally, we estimate the effect of the improved surveillance accuracy on aircraft separation standards.

We treat the GPS receiver as a standalone sensor, unaided by air data, INS or differential corrections. In that case the position measurement errors are governed

by Selective Availability (SA). Note that these errors are different from pure ranging errors, and the work done on SA model identification [6] is not directly applicable in this case. In section 2 of this paper we identify an appropriate measurement error model by analyzing real GPS data. The data is analyzed with special emphasis on the relationship between the position and velocity errors, since we would like to determine the possible benefits of including velocity information in the aircraft report.

The tracking filter should combine the measurement error model with a dynamic model for the aircraft motion. Section 3 provides a brief description of various aircraft models, and the actual tracking filter design is described in section 4. Section 5 compares the GPS tracking accuracy with the accuracy of ATC radar trackers, and section 6 demonstrates the effect of the increased surveillance accuracy on the minimum separation standards. Section 7 concludes the paper.

II. ERROR MODEL IDENTIFICATION

The first step in tracking filter design is identification of the error model. This was done by analyzing a data base, composed of several five-hour-long recordings of GPS position and velocity errors. The recordings were made at a basic sampling rate of 1Hz, on different days, at different times of the day, using a static Trimble 4000-SSE receiver located at Stanford University.

Data Analysis

The time constants of the position and velocity errors were estimated at the point where the autocorrelation function of the data reaches $1/e$ of its value at zero lag. The average time constant of the position error was 139.7 seconds. This is smaller than the value usually associated with SA, which is 190 seconds [6]. This indicates that SA models are not directly suitable to model the position errors.

The average time constant of the velocity error is significantly large (83.1 sec). The velocity error is therefore not white as sometimes assumed [7], but rather correlated. In order to identify the possible benefits of additional velocity reports, we were interested in a dynamic model that matches the correlation of both position and velocity errors. This requires some analysis of the relationship between the two error components.

We compared between the velocity solution of the receiver and the velocity estimated by first difference of the position solution. The difference between the two values was smaller than 0.05 m/s for about 80% of the time. This is one of the indications that the velocity error can usually be treated as a derivative of the position error.

We have observed sharp transitions between periods of agreement and non-agreement of the two velocity values. The transitions were always associated with a satellite constellation change. Sudden steps in GPS error due to satellite set transitions can be a major error source in aircraft tracking [8], and we must pay special attention to these transitions when designing the tracking filter.

The transfer function between the position and velocity errors was estimated by computing the ratio between their power spectral densities. The results showed that we can consider the velocity error as a derivative of the position error and use one dynamic model for both errors.

The identification of the dynamic error model is based on estimating the sample autocorrelation function of the data and fitting it with autocorrelation functions of known models.

Simple Gauss-Markov Processes

Simple Gauss-Markov processes can be described by the following transfer function:

$$x(s) = \frac{\beta^n}{(s + \beta)^n} w(s) \quad (1)$$

where $w(s)$ describes a zero mean white noise input $w(t)$, with spectral density Q , and n is the process order. For $n = 1$, $x(t)$ is an exponentially correlated signal. The rate of change of an exponentially correlated signal is white, whereas the experimental data clearly shows that the velocity error is correlated. This leads us to higher order models.

We derived the autocorrelation functions of high order ($n = 2, 3, 4$) simple Gauss Markov processes and selected Q and β to match the value of the empirical position autocorrelation at zero lag and at the $1/e$ point. This however does not guarantee that the *velocity* autocorrelation will match the experimental data, as shown in figure 1 for $n=2$. Matching both position and velocity autocorrelations, at both zero lag and $1/e$ points requires four free parameters, where simple Gauss Markov processes have only two. This leads to a general 3rd order process.

A General 3rd Order Gauss-Markov Process

A general 3rd order Gauss-Markov process can be described by the following transfer function:

$$x(s) = \frac{a\omega^2}{(s + a)(s^2 + 2\zeta\omega s + \omega^2)} w(s) \quad (2)$$

In this case we have four free parameters (a, ω, ζ and Q). We can use them to match the correlation functions of

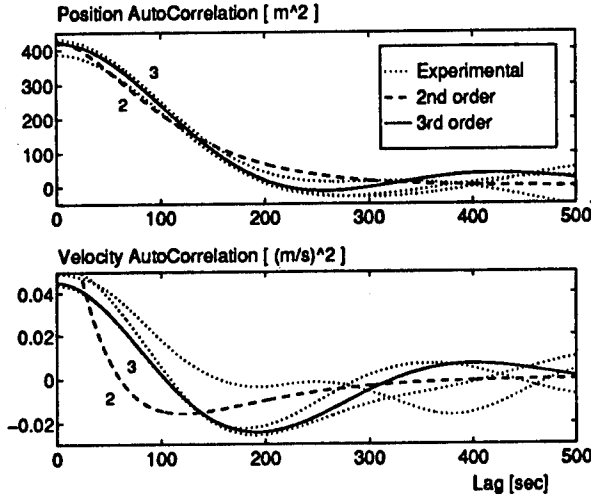


Figure 1: Autocorrelation functions of a simple 2nd order and a general 3rd order GM processes. The dotted lines are autocorrelations of three different five-hour-long recordings of GPS position and velocity errors.

both position and velocity at the required time points. The results, depicted in figure 1 for $a=0.0067\text{sec}^{-1}$, $\omega=0.01634\text{sec}^{-1}$, $\zeta=0.3057$ and $Q=10.6562 \cdot 10^4\text{m}^2\text{sec}$, show good agreement up to 300 seconds lag.

The measurement error model should be combined with a dynamic model for the aircraft motion. The next section proposes several such models.

III. DYNAMIC AIRCRAFT MODELS

Civil aircraft have two basic modes of flight: uniform motion and maneuvering. The uniform motion mode can be described by a 2nd order kinematic (constant velocity) model:

$$\dot{x}(t) = v_x(t) \quad (3)$$

$$\dot{v}_x(t) = w_v(t) \quad (4)$$

where $w_v(t)$ is zero mean white noise with appropriate spectral density, which accounts for the small acceleration disturbances in this stage of flight. The same model applies in the y direction.

In order to account for the aircraft accelerations during maneuvers, the model order can be increased:

$$\dot{x}(t) = v_x(t) \quad (5)$$

$$\dot{v}_x(t) = a_x(t) \quad (6)$$

$$\dot{a}_x(t) = w_a(t) \quad (7)$$

where $w_a(t)$ is zero mean white noise, which accounts for acceleration increments ('jerks') during aircraft maneuvers. The aircraft acceleration is assumed to be nearly constant in this model.

A more accurate description of the kinematic behavior during a turn is given by the coordinated turn model, which assumes a constant turn rate at a constant speed

$$\dot{x}(t) = V \cos \gamma(t) + w_x(t) \quad (8)$$

$$\dot{y}(t) = V \sin \gamma(t) + w_y(t) \quad (9)$$

$$\dot{\gamma}(t) = \omega + w_\gamma(t) \quad (10)$$

where γ is the aircraft heading, and ω is the turn rate. The various disturbances and modeling errors are accounted for by adding the appropriate noise terms [4].

The turn rate ω in this model can be set to a fixed, preselected value, or extracted from the estimated state vector. In that case the discrete time model is nonlinear in ω , and requires an Extended Kalman Filter.

IV. TRACKING FILTER DESIGN

The tracking filter should combine a measurement error model with an aircraft model. The general problem of tracking filter design with correlated measurement noise is discussed first. We then select a simple aircraft model, combine it with several error models and compare the performance of the resulting tracking filters by using a Monte Carlo simulation. Based on this study we decide on a specific error model to be used in the tracking filter, and check its performance with several aircraft models.

Correlated Measurement Noise

The aircraft model and the measurement error model can be described by the following linear systems:

$$x(k+1) = \Phi x(k) + w(k) \quad w \sim N(0, W) \quad (11)$$

$$e(k+1) = \Psi e(k) + v(k) \quad v \sim N(0, V) \quad (12)$$

where x is the aircraft state vector, e is the state vector of the measurement error model, and w and v are independent, zero mean white noise vectors. The measurement vector z is a linear combination of x and e :

$$z(k) = Cx(k) + De(k) \quad (13)$$

The tracking filter should provide an optimal estimate of the aircraft state vector x . In order to use the Kalman Filter formulation, the dynamic model (Eqs. 11-13) should be expressed as a linear system with white process and measurement noise. This is usually achieved by augmenting the aircraft state vector with the error model state vector:

$$x_a = \begin{bmatrix} x \\ e \end{bmatrix}$$

The augmented state space system is:

$$\begin{bmatrix} x(k+1) \\ e(k+1) \end{bmatrix} = \begin{bmatrix} \Phi & 0 \\ 0 & \Psi \end{bmatrix} \begin{bmatrix} x(k) \\ e(k) \end{bmatrix} + \begin{bmatrix} w(k) \\ v(k) \end{bmatrix} \quad (14)$$

and the measurement equation is:

$$z_k = \begin{bmatrix} C & D \end{bmatrix} \begin{bmatrix} x(k) \\ e(k) \end{bmatrix} \quad (15)$$

The augmented system has white plant noise as required, but has no measurement error, since the white noise driving the error model is now part of the augmented process noise. This can lead to a singular covariance matrix in the Kalman filter equations, since linear combinations of the augmented state elements are known perfectly [9].

A possible solution to this problem is to assign some small artificial value to the measurement noise covariance matrix. This value accounts for unmodeled measurement errors, and serves as a design parameter, chosen to match some specific performance requirements.

We have derived a more rigorous solution to the correlated measurement noise problem. It is based on generating a pseudo-measurement, which is a linear combination of two consecutive measurements. This pseudo-measurement is corrupted by white noise, and the Kalman filter equations can now be applied without state augmentation and without introducing artificial parameters. For more details, see [10]. The results obtained are the same when using both approaches.

Filter Initialization

The initial estimate of the augmented state vector $\hat{x}_a(0)$ is obtained after the first two position measurements:

$$\hat{x}_1(0) = z(0) \quad (16)$$

$$\hat{x}_2(0) = [z(0) - z(-1)]/T \quad (17)$$

$$\hat{x}_3(0) = 0 \quad (18)$$

$$\hat{x}_4(0) = 0 \quad (19)$$

where T is the sampling interval, and z is the position measurement. In order to guarantee the consistency of the filter initialization [2], the initial covariance matrix is set to:

$$\hat{P}(0) = \begin{bmatrix} \phi_{xx}(0) & \Delta\phi_{xx} & -\phi_{xx}(0) & -\phi_{xv}(0) \\ \Delta\phi_{xx} & 2\Delta\phi_{xx}/T & -\Delta\phi_{xx} & -\Delta\phi_{xv} \\ -\phi_{xx}(0) & -\Delta\phi_{xx} & \phi_{xx}(0) & \phi_{xv}(0) \\ -\phi_{xv}(0) & -\Delta\phi_{xv} & \phi_{xv}(0) & \phi_{vv}(0) \end{bmatrix} \quad (20)$$

where $\Delta\phi_{xx} \triangleq [\phi_{xx}(0) - \phi_{xx}(T)]/T$ and $\Delta\phi_{xv}$ is defined in a similar way. $\phi_{xx}(\tau)$, $\phi_{xv}(\tau)$ and $\phi_{vv}(\tau)$ are the correlation functions of the specific error model.

We have assumed here one dimensional tracking, using a second order aircraft model, augmented by a second order error model. The extension to other models, and to the case where both position and velocity are measured, can be found in [10].

Error model selection

We now wish to examine the effect of different error models on the tracking accuracy. We form tracking filters that combine the constant velocity aircraft model with an exponential correlation error model, a simple second order error model, and the general third order error model.

The filter performance is checked in a Monte Carlo simulation in the following way: we select at random a 1000-second interval out of a much longer stream of recorded GPS measurements. This is used as the input to the filter. The tracking errors are averaged over 1000 such intervals.

Figure 2 shows the average tracking errors in position and velocity, for an aircraft in uniform motion where only its position is measured. The tracking errors are compared with the average error obtained when not using a tracking filter. In this case the velocity is estimated by a first difference of the position measurement.

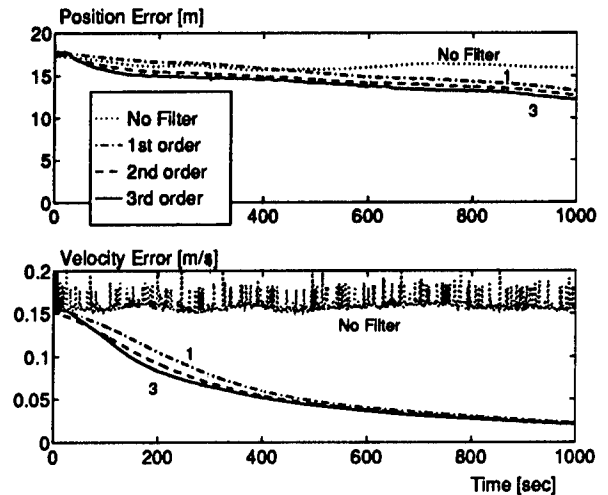


Figure 2: Average tracking errors during uniform motion, using different measurement error models.

The tracking filters were successful in reducing the velocity error, but did not improve the position error. The difference between the various error models is small, and we can see that the time constant of the filter is quite large for any error model.

In order to check our results, we have repeated the same procedure with 'simulated' GPS position errors, using a 2nd order Gauss Markov process which is identical to the model used in the Kalman filter. The average tracking errors in this case were very similar to the case where real GPS measurements were used. This indicates that the poor performance in position is not a result of bad modeling.

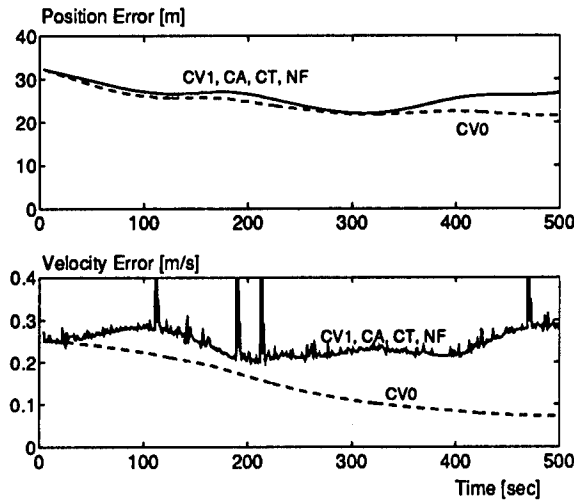


Figure 3: Average tracking errors during uniform motion, using different aircraft models.

Due to the small differences between the error models, we have decided to use the 2nd order error model throughout the rest of this work.

Aircraft model selection

In this section we wish to evaluate the effect of different aircraft models on the tracking accuracy. We combine the 2nd order error model selected in the previous section, with the following aircraft models:

- CV0** Constant Velocity, with zero acceleration
(Eqs. 3-4, $\sigma_v = 0$)
- CV1** Constant Velocity, with random acceleration
(Eqs. 3-4, $\sigma_v = 5\text{m/s}^2$)
- CA** Constant Acceleration, with random increments
(Eqs. 5-7, $\sigma_a = 1\text{m/s}^3$)
- CT** Constant Turn rate, with random disturbances
(Eqs. 8-10, $\sigma_x = \sigma_y = 1\text{m/s}^2$, $\sigma_\gamma = 0.5^\circ/\text{s}$)

The performance of these models is compared with the case where no filter is used. This is denoted in the following discussion as NF.

Figure 3 shows the average tracking accuracy obtained in a 300 knot, straight line motion. All aircraft models, except CV0 cannot do better than the raw measurement accuracy, and provide the same tracking accuracy as NF. The CV0 model cannot improve the position accuracy much, but it does improve the accuracy of the velocity estimate.

Figure 4 shows the average tracking errors that were observed during a $3^\circ/\text{sec}$ turn at the same speed. The turn was initiated at $t = 520$ sec and lasted for 1 minute. As expected, the CT model provides the best steady state accuracy during the turn. However, it has a longer transient phase than the CA model.

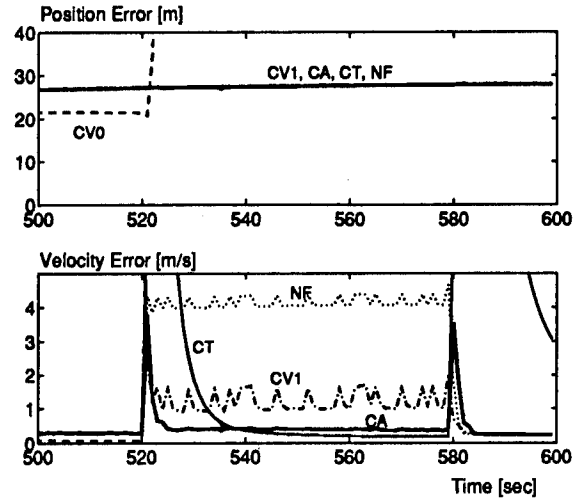


Figure 4: Average tracking errors during a coordinated turn, using different aircraft models.

Data link effect

The input to the filter is provided through a radio data link which is common to all aircraft under ADS. Under most communication protocols we can expect some interference between messages. As a result of this interference, the reports arrive to the filter with some probability, which can be estimated by [11]:

$$P_r = \exp\left(-N \frac{2n_m}{Bt_f}\right) \quad (21)$$

where N is the number of aircraft in the detection range of the receiver, n_m is the report length in bits, B is the bit rate, and t_f is the frame length. It is assumed that aircraft send a report once every t_f seconds, and randomly change the exact transmission time.

We now wish to determine the sensitivity of the tracking filter's performance to missing reports for each aircraft model. In order to provide a suboptimal estimate when a measurement is missing, we set the state estimate equal to the prediction from the time update phase of the Kalman filter in the previous time step.

The simulation study was repeated under the assumption that the position reports are received with a probability of $P_r = 0.7788$. As will be shown below, this specific value represents a future ATC environment, with 1000 aircraft within the detection range of the receiver.

Figure 5 shows the average tracking errors during the aircraft $3^\circ/\text{sec}$ turn, under the imperfect data link assumption. It seems that the CA filter is less sensitive to missing reports than the CT filter. Additional simulation studies proved the CA filter to be more robust to parameter changes, and we conclude that it is more

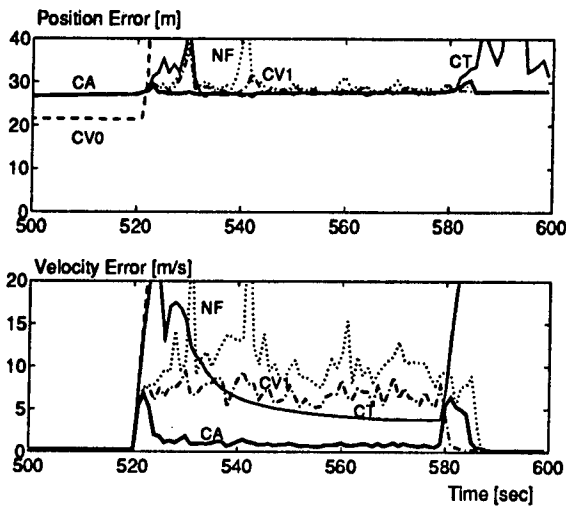


Figure 5: Average tracking errors during a turn, using different aircraft models, under an imperfect data link.

suitable for modeling the aircraft during its maneuver phase.

Multiple-Model Estimation

The results obtained in the previous section show that a tracking filter with the CV0 model is optimal during the uniform motion phase of flight but diverges during turns. A tracking filter with the CA model provides good estimates during turns, however, it does not reduce the velocity error during the uniform motion phase. One of the possible ways to obtain the best estimates during all phases of flight is to use a multiple-model algorithm.

Multiple-model algorithms are composed of a parallel bank of Kalman filters, each based on a different model. The probability for each model being correct is calculated recursively, based on its likelihood function. The state estimate is a weighted average of the model-conditioned estimates, with the model probabilities as weights [2, 9].

A more elaborate scheme of multiple model estimation is the Interacting Multiple Model (IMM) filter, which assumes an underlying Markov chain that governs the probabilities of transition between the different aircraft models. The IMM filter provided excellent position and velocity estimates during all phases of flight, in studies that used many different combinations of different aircraft models [3-5].

We found, however, that any multiple-model algorithm which relies on the filters innovations or likelihood functions fails when tracking GPS reports, due to satellite constellation changes. The discontinuities in position which appear whenever the GPS receiver

changes the set of satellites, trigger any existing maneuver detection algorithm and cause it to switch from a uniform motion mode to a turn mode.

We have decided to design our tracking filter around two Kalman filters that run in parallel: one is based on the CV0 model, and the other uses the CA model. The estimated state is set equal to the output of one of these filters, according to the following tests:

When the current mode of flight is uniform motion, we check the continuity of the position information. This is accomplished by computing the difference between the current position report and the previous one, and comparing it with \bar{v}_o , which is the predicted velocity from the previous time step:

$$\hat{v} = \frac{z - z_{-1}}{t - t_{-1}} \quad (22)$$

$$\delta_v = (\hat{v} - \bar{v}_o)^T (\hat{v} - \bar{v}_o) \quad (23)$$

If δ_v is greater than a specified threshold for more than one time step, we assume that a maneuver is taking place, and the flight mode is switched to the turn mode.

When the flight mode is a turn, we check the statistical significance of the estimated acceleration, in order to determine when the turn is over [2]:

$$\delta_a = \hat{a}^T [\hat{P}_a]^{-1} \hat{a} \quad (24)$$

$$\rho_a = \alpha \rho_a + \delta_a \quad (25)$$

where \hat{a} is the estimated acceleration, and \hat{P}_a is the corresponding block from the covariance matrix of the CA model. ρ_a is a fading memory average of δ_a , and when it drops below a certain threshold, we assume that the turn is completed, and revert to the uniform motion mode.

The state estimate \hat{x} is set equal to the estimate of the filter that matches the current flight mode. This state estimate is used in the time update phases of both filters, so that both filters update the best estimate available.

In the following discussion we will refer to the overall filter described above as the GPS tracking filter. The average tracking accuracy of this filter is compared in figure 6 with the performance of an IMM filter and a single CA filter. The IMM filter we used is based on the same aircraft models as the GPS tracking filter (CV0 and CA). The GPS filter performs better than the other filters, during all phases of flight.

Note that the maneuver detection scheme described above can be avoided if the aircraft will include a 'maneuver flag' in its report. This flag can be used to switch between the appropriate models. However, we still have to detect satellite constellation changes and treat them appropriately.

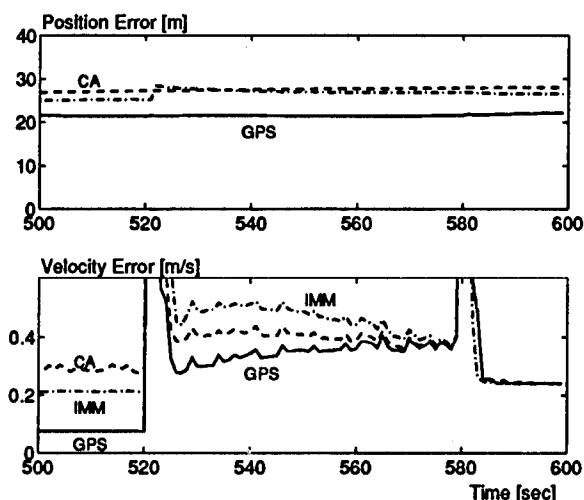


Figure 6: Average tracking errors during a turn, using different tracking filter structures.

This is done by measuring the duration of the discontinuity in the position reports. If δ_v (Eq. 23) is greater than the specified threshold for only one time step, we assume that a constellation change has occurred. The state estimate for the next 5 cycles is computed by propagating the state vector through the time update phase of the current filter, and bypassing its measurement update phase. The CV0 and CA filters, however, continue to operate without any intervention - only the output of the overall filter is affected. After 5 cycles the transient response of the CV0 and CA filters decays, and the state estimate is set equal to the output of one of them.

Figure 7 depicts the position measurement error during a sequence of satellite set transitions, and shows the effect of the discontinuities on the velocity tracking error of the GPS filter described above. For comparison, we show also the tracking error of a simple CA filter.

Velocity reports

The simulation studies so far assumed that only position is measured. We have repeated the same simulation trials when measuring both position and velocity and could not find any significant improvement in the tracking accuracy. Similar observations about the possible benefits of velocity information were made regarding the integration of GPS and INS [7].

As stated earlier, the velocity error is equal most of the time to the derivative of the position error. This reduces the benefits of additional velocity information, since the Kalman filter differentiates the position error anyhow, as part of its estimation process.

Moreover, adding the velocity information to the position report will increase the message length and de-

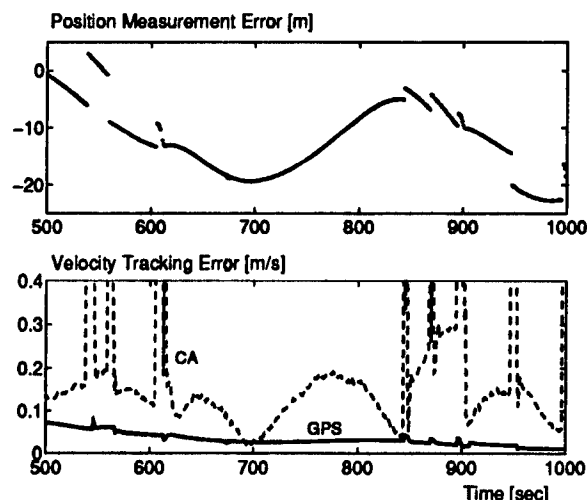


Figure 7: Position measurement error and velocity tracking error during a sequence of satellite set transitions.

crease the probability of clear reception. For example, if the message length increases from 125 bits to 250 bits due to the additional information, the probability of clear reception will decrease from 0.7788 to 0.6065 (based on 1Mbps bit rate, 1sec update rate and 1000 aircraft in the detection range). This caused a severe degradation in the tracking accuracy in simulation studies we made.

Update rate

We have assumed up to this stage that aircraft repeat their reports once in a second. By increasing the interval between messages to 2 seconds, we can increase the probability of clear reception from 0.7788 to 0.8085 when using position measurement only (125 bit long report), or from 0.6065 to 0.7788 when using position and velocity reports (250 bit). This is supposed to increase the filter accuracy.

However, when a report is missing, the estimation error is approximately twice as large for a 2 second interval than a 1 second interval. When averaging the tracking accuracy in a Monte Carlo simulation we have observed that the overall effect of decreasing the update rate is to degrade the filter performance.

The performance study in the next section assumes therefore a 1 second update rate, with position information only.

V. PERFORMANCE STUDY

In order to study the performance of the proposed tracking filter, we define in table 1 three representative aircraft trajectories. Trajectory T1 represents typical

cruise flight maneuver. T2 includes a more rapid turn, and T3 represents a high speed agile target.

| | Speed [knot] | Turn rate [deg/sec] |
|----|--------------|---------------------|
| T1 | 150 | 1 |
| T2 | 300 | 3 |
| T3 | 600 | 6 |

Table 1: Representative trajectories

The average tracking accuracy is calculated over these trajectories, while using real GPS data that was recorded by a fixed receiver. The measurement errors are added to simulated aircraft motion and are sampled according to the probability of clear reception in an ATC environment.

A future ATC environment can be characterized by the following assumptions on the data link: each aircraft broadcasts a 125 bit message once a second, in a 1Mbps bit rate; there are 1000 aircraft within the detection range of the receiver. For comparison, the capacity of a Mode S sensor (a major element in the current surveillance system) is 700 transponder carrying aircraft within 255 nmi [12]. The resulting probability of clear reception is $P_r=0.7788$ (Eq. 21). The effective update rate (which indicates how often a message from a specific aircraft is received, with a probability that is higher than a given reliability level [11]), is 4.58 seconds with 99.9% reliability. This is equivalent (in a probabilistic sense) to the 4 seconds rotation period of current ATC radars.

| | Position [m] | Speed [m/s] | Heading [deg] |
|----|--------------|-------------|---------------|
| T1 | 21.5 | 0.07 | 0.04 |
| T2 | 21.5 | 0.07 | 0.02 |
| T3 | 21.5 | 0.07 | 0.01 |

Table 2: Average tracking errors during uniform motion, on different trajectories, using GPS position measurements.

| | | Position [m] | Speed [m/s] | Heading [deg] |
|----|---------------|--------------|-------------|---------------|
| T1 | max | 21.7 | 1.85 | 1.37 |
| | after 30 sec. | 22.8 | 0.27 | 0.15 |
| T2 | max | 23.8 | 5.7 | 2.6 |
| | after 30 sec. | 22.7 | 0.9 | 0.07 |
| T3 | max | 37.1 | 26.7 | 4.9 |
| | after 30 sec. | 22.5 | 6.5 | 0.24 |

Table 3: Average tracking errors during a turn, on different trajectories, using GPS position measurements.

Table 2 summarizes the average tracking errors during the uniform motion phase of flight, and table 3

shows the tracking errors during the turn phase of the flight.

The average tracking accuracy obtained by using radar measurements is detailed in tables 4 and 5. The relevant radar parameters are: on trajectories T1 and T2 the aircraft is tracked by three monopulse secondary radars, each of which has a range measurement accuracy of 110 meters and a bearing measurement accuracy of 0.07° [3]. On trajectory T3 a single radar is used, which has a bearing accuracy of 0.2° [5]. In all cases the radar rotation period is 4 seconds, and the algorithm used is the Interacting Multiple Model algorithm, which combines the constant velocity aircraft model (CV) with the constant turn rate model (CT) and its associated second order Extended Kalman Filter.

| | Position [m] | Speed [m/s] | Heading [deg] |
|----|--------------|-------------|---------------|
| T1 | 37 | 0.31 | 0.6 |
| T2 | 46 | 0.33 | 0.3 |
| T3 | 150 | 6 | 1.1 |

Table 4: Tracking errors during uniform motion, on different trajectories, using radar measurements.

| | | Position [m] | Speed [m/s] | Heading [deg] |
|----|---------------|--------------|-------------|---------------|
| T1 | max | 204 | 4.11 | 12 |
| | after 30 sec. | 83 | 3.6 | 4 |
| T2 | max | 241 | 6.7 | 20 |
| | after 30 sec. | 74 | 3.6 | 5 |
| T3 | max | 425 | 175 | 32 |
| | after 30 sec. | 215 | 41 | 7.7 |

Table 5: Tracking errors during a turn, on different trajectories, using radar measurements.

The improvement in tracking accuracy is apparent, especially in the velocity and heading estimates. We now wish to study the effect of the improved surveillance accuracy on the minimum separation standards.

VI. RADAR SEPARATION MINIMA

Safe separation between aircraft is maintained today by air traffic controllers, who monitor a minimum separation standard of 3 nmi in the terminal airspace and 5 nmi for enroute traffic. Since the surveillance information that is provided to the controllers is obtained by radar, these standards are usually referred to as radar separation standards and are a function of the radar accuracy.

We wish to estimate the effect of GPS-based surveillance on these standards. Since reduction of in-trail separation is limited by wake-turbulence concerns, we consider here only lateral separation standards. Note

that we do not consider route spacing or track separations, which depend also on the navigation accuracy and control system delay time and are beyond the scope of this work.

The surveillance separation standard affects the collision risk, which can be measured by the probability of close approach. This is defined as the probability that the *true* distance between aircraft is less than the minimum safety distance, when the *measured* distance between the aircraft is equal to the minimum separation standard:

$$P_{ca} \equiv P(\Delta x_t < d \mid \Delta x_m = s)$$

where Δx_t is the true separation between the aircraft, and Δx_m is the measured separation. s is the surveillance separation standard, and d is the minimum safety distance, represented by the horizontal size of a typical aircraft.

Given $f(x)$, the probability distribution function of the surveillance errors, P_{ca} can be computed by the following integral [13]:

$$P_{ca} = \int_{s-d}^{s+d} \left[\int_{-\infty}^{+\infty} f(x) f(x-z) dx \right] dz \quad (26)$$

The probability distribution function of GPS position errors can be modeled by a combination of two normal distributions. One models the 'body' of the measurement errors, and the other models the rare large errors:

$$f(x) = p_1 \frac{\exp[-x^2/(2\sigma_1^2)]}{\sqrt{2\pi}\sigma_1} + p_2 \frac{\exp[-x^2/(2\sigma_2^2)]}{\sqrt{2\pi}\sigma_2} \quad (27)$$

The standard deviations σ_i can be expressed as $\alpha_i \sigma_o$, where σ_o is the standard deviation of the ranging error, and α_i is a multiplier that models the satellite geometry effect on the position error. p_i is equivalent to the probability of having a multiplier α_i .

Figure 8 shows the distribution of more than 50,000 GPS position error samples, that were collected over a period of about 6 months using four Trimble 4000-SSE receivers located at Stanford, San Diego and Arcata, California and Elko, Nevada. A double-Normal distribution (Eq. 27) that fits this data was obtained for $\alpha_1=0.85$, $\alpha_2=3.42$ and $p_1=0.99$. We assumed that the ranging error is described by $\sigma_o=21$ m. This model enables us to estimate the effect of possible SA elimination by reducing σ_o to 5m, while keeping all the other parameters.

Also shown in figure 8 is the effect of using only the first term in Eq. (27). It is clear that the additional term is required to properly model the tail of the experimental distribution function.

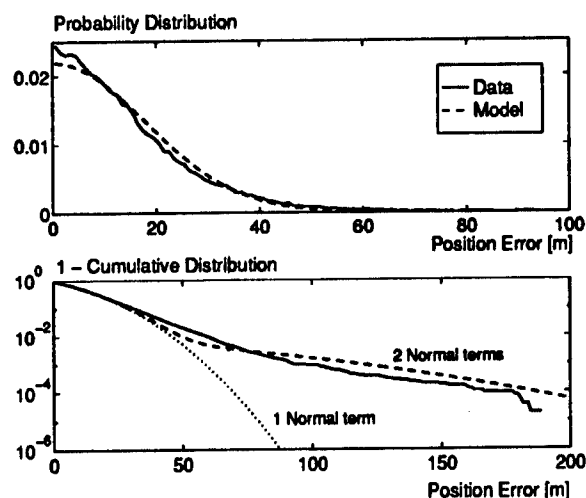


Figure 8: Probability distribution of GPS position errors: experimental data and Normal models.

The probability distribution function of radar azimuth measurement errors can be described by the same double-normal distribution, with $\sigma_1=0.0987^\circ$, $\sigma_2=0.1640^\circ$ and $p_1=0.836$ [13]. These values are multiplied by a range of 200 nmi to model en-route surveillance errors, and by 50 nmi to model terminal traffic surveillance.

The probability of close approach was obtained by analytical and numerical integration of Eq. 26. The results are depicted in figure 9 as a function of the minimum separation standard. We assumed that the minimum safety distance is $d=75$ m.

We see that the en-route separation standard can be reduced to about 0.5 nmi, while keeping the same safety level that is provided today by using radar surveillance and a 5 nmi radar separation standard. The terminal separation standard can be reduced from 3 nmi to about 1 nmi, without increasing the collision risk. In the absence of SA the separation standard can be even further reduced.

VII. CONCLUSION

GPS-based aircraft tracking can yield a significant improvement in the quality and extent of ATC surveillance coverage. This requires a new design of ATC tracking algorithms, since the nature of GPS measurement errors is very different from the nature of the current radar measurement errors. Constellation changes and message interference in the radio data link should be of special concern when designing the tracking filter and evaluating its performance.

The tracking filter designed here combines a 2nd order Gauss Markov process as the measurement error

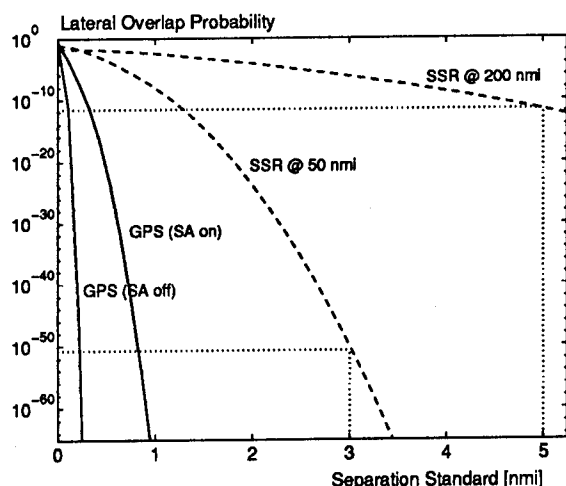


Figure 9: Probability of close approach for Secondary Surveillance Radar (SSR) and GPS-based surveillance.

model, with two dynamic aircraft models, in an adaptive Kalman filter structure. Switching logic identifies aircraft maneuvers and provides smooth transition of the estimates through satellite constellation changes. The average tracking accuracy of the GPS tracking filter was estimated by using real GPS data and simulated aircraft motion, and was compared to the performance of ATC radar trackers. This performance study showed a large improvement in tracking accuracy and a potential for substantial reduction in the minimum separation standards.

The results obtained here are based on data that was collected by fixed, high quality GPS receivers. More research is required to estimate the effect of using dynamic, airborne receivers, and to identify the need for a tracking filter when SA is turned off or when the Wide Area Augmentation System is implemented.

The traditional location of the tracking filter is on the ground, where the current position sensor - the radar - is located. However, when using an airborne sensor, each aircraft can track its own position and broadcast its estimated or predicted state. This will enable each aircraft to use a filter that matches its GPS receiver and flight control characteristics. It will reduce the load of the ATC center and will eliminate the tracking errors caused by the data link. Moreover, other aircraft in the vicinity of the transmitter would be able to receive these reports and predict possible conflicts, without the need to run a tracking filter for each neighboring aircraft. Further research is required to investigate the effects of this technique on aircraft collision avoidance systems.

ACKNOWLEDGMENTS

The author is indebted to Professor J. David Powell for his guidance and support throughout this research. The support of the FAA's Satellite Program Office (AGS-100) is gratefully acknowledged. However, the opinions and views expressed in this paper belong to the author alone, and do not necessarily represent the position of any other organization or person.

REFERENCES

- [1] P. L. Massoglia and R. D. Till, "Automatic dependent surveillance (ADS) pacific engineering trials (PET)," in *IEEE PLANS*, pp. 167-172, 1992.
- [2] Y. Bar-Shalom and T. E. Fortman, *Tracking and Data Association*. Academic Press, 1988.
- [3] P. Vacher, I. Barret, and M. Gauvrit, "Design of a tracking algorithm for an advanced ATC system," in *Multitarget-Multisensor Tracking: Application and Advances* (Y. Bar-Shalom, ed.), vol. 2, Artech House, 1992.
- [4] X. R. Li and Y. Bar-Shalom, "Design of an interacting multiple model algorithm for air traffic control tracking," *IEEE Transactions on Control Systems Technology*, vol. 1, no. 3, pp. 186-194, September 1993.
- [5] W. D. Blair, G. A. Watson, and S. A. Hoffman, "Second order interacting multiple model algorithm for tracking maneuvering targets," in *Signal and Data Processing of Small Targets*, vol. 1954, pp. 518-529, SPIE, 1993.
- [6] H. T. Chou, "An anti-SA filter for non-differential GPS users," in *ION GPS - 90*, pp. 535-542, 1990.
- [7] W. Tang and G. Howell, "Integrated GPS/INS kalman filter implementations issues," in *ION GPS - 93*, pp. 217-224, 1993.
- [8] M. D. Goodwin and J. J. Kusnierek, "Using GPS for airborne formation control," in *ION GPS - 93*, pp. 971-984, 1993.
- [9] P. S. Maybeck, *Stochastic Models, Estimation and Control*, vol. 1. Academic Press, 1979.
- [10] R. Gazit, "Digital tracking filters with high order correlated measurement noise," submitted to *IEEE Transactions on Aerospace and Electronics Systems*, April 1995.
- [11] R. Gazit, "Communication protocols for GPS-based surveillance and TCAS," in *ION GPS - 94*, pp. 923-932, 1994.
- [12] J. L. Baker, V. A. Orlando, W. B. Link, and W. G. Collins, "Mode S system design and architecture," *Proceedings of the IEEE*, vol. 77, no. 11, pp. 1684-1694, November 1989.
- [13] S. Nagaoka, O. Amai, and Y. Watanabe, "Evaluating the feasibility of a radar separation minimum for a long-range SSR," *The Journal of Navigation*, vol. 42, no. 3, pp. 403-416, September 1989.

High Precision Highway Profiles Using Helicopter Borne 'On-The-Fly' GPS

Paul Hansen and Chris Joy
The University of Nottingham

BIOGRAPHIES

Paul Hansen gained a BEng in Civil Engineering from The University of Nottingham in 1992. Since then he has been a PhD student working in the field of kinematic GPS ambiguity resolution on-the-fly in the Institute of Engineering Surveying and Space Geodesy (IESSG) at The University of Nottingham.

Chris Joy gained a BEng in Civil Engineering from The University of Nottingham in 1993. Since then he has been a PhD student working in the field of high precision, GPS assisted helicopter photogrammetry in the IESSG.

ABSTRACT

Kinematic GPS is capable of providing centimetre level positioning for a wide range of applications. This has come about through recent developments in both GPS receiver technology and 'on-the-fly' (OTF) ambiguity resolution techniques.

One application to benefit from this high level of precision is helicopter photogrammetry. The technique uses near vertical photography taken from a helicopter to produce high precision profiles for highway deformation and repair projects. The camera is mounted vertically on the side of the helicopter and integrated with an OTF GPS system to provide exposure coordinates. The aim is the minimisation of ground control, leading to a faster and more cost effective operation.

This paper describes the techniques and software used in the OTF ambiguity resolution process at Nottingham. It then details the present stage of the integration of the GPS and photogrammetric systems. A field trial was performed, and results obtained using a Bell 206B Jet Ranger helicopter equipped with this system. These are compared with the results produced using full conventional ground control. The

performance of the combined system is assessed and future developments to the system are described.

1 INTRODUCTION

An efficient road network is essential for a country's economic activity. Not surprisingly, there is a strong desire to minimise any effects caused by the on-going programs of maintenance and expansion of this network. One such effect, which was identified around 10 years ago by Photarc Surveys Limited (Photarc) of Harrogate, North Yorkshire, was the use of traditional ground survey techniques to provide highway profiles. The necessity to cone off traffic lanes was severely reducing traffic flow and was also hazardous for the surveyors who undertook the work.

A simple non-contact system was conceived and developed to provide the necessary data without disturbing traffic flow (Boardman, 1994). A Zeiss UMK 10/1318 Universal Camera is 'cradled' out of the rear door of a Bell 206B Jet Ranger helicopter to capture stereoscopic images of the highway surface from an altitude of 75m. Photogrammetric techniques can then be utilised to give regular grids of road spot heights to RMSE $\pm 0.005\text{m}$ using control points surveyed at 40m intervals along the hard shoulder of the highway (Smith and Joy, 1995).

The IESSG at The University of Nottingham has extensive research activity in kinematic GPS. It was decided to develop the existing photogrammetric system by investigating the integration of GPS to provide perspective centre coordinates at the centimetre level, and attitude sensors to provide orientation. This was with a view to reducing the number of control points required for the photography by employing exterior orientation parameters in an aerial triangulation computation. Analysis had shown that to achieve the $\pm 0.005\text{m}$ precision level, coordinates would be required at RMSE $X = \pm 0.024\text{m}$, RMSE $Y = \pm 0.028\text{m}$ (plan) and RMSE $Z = \pm 0.007\text{m}$

(height). However, these would be relaxed for the reduced heighting precisions of between $\pm 0.010\text{m}$ to $\pm 0.020\text{m}$, typically required by clients.

The paper begins by detailing the OTF algorithms and software used in support of this project (Section 2). Section 3 then discusses the integration of the GPS and photogrammetric systems. This is followed by details of the initial system evaluation trials and results obtained. The paper is then concluded in Section 5 with the future developments that are planned to the system.

2 OTF ALGORITHMS AND SOFTWARE

In order to achieve centimetre level accuracy using GPS, the carrier phase integer ambiguities must be determined. Conventional kinematic GPS techniques require the user to remain stationary whilst initialising the ambiguities and then maintain lock on at least four satellites during the course of the survey. In the case of helicopter positioning it is unlikely that this will occur. Therefore, a system is required which can initialise the integer ambiguities rapidly whilst the helicopter is moving, i.e. on-the-fly.

One solution to the problem of OTF ambiguity resolution is to employ an ambiguity search technique. Various methods have been proposed, including those of Hatch (1990), Mader (1990) and Euler and Landau (1992). Each employs the same principle, that only the correct integer ambiguity combination will satisfy all of the data and give the best least squares fit. The basic method is also the same for each:

- (i) define a set of possible integer ambiguities
- (ii) search through these to find the best integer ambiguity combination
- (iii) test this to see whether it is significantly better than the next best combination.

An alternative ambiguity resolution technique is to obtain an estimate of the widelane (L1-L2 frequency combination) integer ambiguity directly, by combining dual frequency carrier phase and pseudorange measurements (Melbourne, 1985). The correct integer ambiguities can no longer be obtained instantaneously using this technique, as P code pseudoranges are not available to civilian users under the Anti-Spoofing (A/S) conditions which currently apply and the noise level of C/A code pseudoranges is too high. However, the solution produced is usually within two cycles of the correct widelane integer ambiguity and so is a good starting point for an ambiguity search.

The IESSG's OTF software is a combination of two ambiguity search techniques, together with the option of using direct resolution of the widelane ambiguities.

The method proposed in Euler and Landau (1992) is used to calculate the sum of the squares residual value for a particular integer ambiguity combination, whilst the method used in Ashkenazi *et al* (1993) significantly reduces the number of integer ambiguity combinations that must be considered.

The combined ambiguity search technique recognises that firstly, the integer ambiguities from four satellites will define a unique position and secondly that it is possible to calculate integer ambiguity values to all satellites from a known position. Hence, given four satellites' integer ambiguities, it is possible to calculate the integer ambiguities to any remaining satellites. Therefore, a search loop can be constructed around the integer ambiguities from only four satellites. The values of the integer ambiguities to any remaining satellites are calculated at each integer ambiguity combination or 'node' defined by these four initial integer ambiguities. The integer ambiguity values to each satellite are thus known at each search node, which is necessary for the residual calculation defined in Euler and Landau (1992), yet many fewer combinations need to be considered. For example, with a 7 satellite constellation, the corresponding number of integer ambiguity combinations for a ± 5 cycles search range using single difference ambiguities are:

| | |
|---------------------------|--------------|
| Standard Euler and Landau | |
| = | 19, 487, 171 |
| Combined Search Technique | |
| = | 14, 641 |

The extra computational overhead of calculating the remaining ambiguities at each of the search nodes defined by the four initial satellites is far outweighed by the reduction in the total number of integer ambiguity combinations to be considered. Direct resolution is an option which can be added to further reduce the number of combinations when dual frequency data is available, by decreasing the range over which the ambiguity search has to operate.

The OTF software is based around a simple Kalman filter constructed in a 'UD' factorised manner (Bierman, 1977) to increase the numerical stability of the solution. Single difference pseudorange and carrier phase measurements are used, which eliminates the need for a decorrelation matrix, and a receiver clock offset is solved as an unknown within the Kalman filter's state vector.

At each epoch, the Kalman filter produces an initial, real valued estimate for each of the single difference integer ambiguities and the nearest integer value to each of these is taken as the mid-point of the search along that particular integer ambiguity. The search

range for each ambiguity is determined using either a multiple of its associated standard error, or a pre-set number of cycles. The choice and value of these is decided by the program user. All of the integer ambiguity values within the range are searched and the sum of the squares residual is calculated for each combination as detailed above.

Ambiguity resolution occurs when the best (lowest sum of the squares residual) combination is deemed to be significantly different to the next best combination. This occurs when the ratio of the two combinations' residuals satisfies a statistical test. This is either an F-Test or a fixed ratio test, with the choice of test and F-Test confidence level or fixed ratio value being decided by the program user. The integer ambiguities may then be resolved to the values of the best combination.

The OTF ambiguity resolution software was designed to be flexible, enabling the user to choose the most effective method of processing their kinematic data. The options available include :

- (i) the ability to perform ambiguity searches using single or dual frequency data on up to three frequencies simultaneously
- (ii) direct resolution of the widelane integer ambiguities
- (iii) incorporation of positions determined from other positioning systems
- (iv) the use of up to four reference stations
- (v) the use of any combination of carrier phase and pseudorange data in a processing run.

The OTF software must ensure that an incorrect integer ambiguity combination is not resolved. Two options are present to increase its reliability. These are the direct resolution of the widelane integer ambiguities, used when dual frequency data is available and the use of multiple reference stations, which greatly increases the reliability of the solution (Hansen, 1994). The former also generally has the benefit of decreasing the time required for ambiguity resolution to occur.

The OTF software is currently used in a post processed manner, although this is not an integral part of its design. It is therefore possible to use integer ambiguities obtained in previous processing runs to construct trajectories of the antenna position accurate to the centimetre level. Section 4.2.3 details the data processing performed in the helicopter trials.

3 INTEGRATION OF THE GPS AND PHOTOGRAMMETRIC SYSTEMS

3.1 Introduction

Although the integration of GPS with photogrammetric data acquisition has been investigated with reference to fixed wing aircraft (Ackermann, 1986), the use of low altitude helicopter flight has not been reported. Such an investigation is important because of the unique operational characteristics of this alternative aerial platform. A number of points become apparent :

- (i) Where is the GPS antenna to be mounted ?
- (ii) How can this be related to the perspective centre of the camera ?
- (iii) What quality of positioning data can be acquired, and how can this be processed ?
- (iv) How can GPS positions be attributed to a photographic exposure ?

The IESSG approach from the outset was to develop a system which was as cost effective and versatile as possible. With this in mind, coupled with the need for Photarc to continue commercial operation of the original, purely photogrammetric system during development, a number of alterations were proposed. These are detailed in the following sections.

3.2 Antenna Location and the Perspective Centre-Phase Centre Offset Vector

The GPS antenna should be mounted where it can receive satellite signals with the minimum of obstruction. Prime locations were on the tail, on the roof, and above the rotor housing. These positions are restricted by Civil Aviation Authority (CAA) regulations on airframe modifications, equating to additional costs and delay in implementing a system. The simplest solution was to attach the antenna to the camera mount, thus potentially obscuring half of the satellite signals and probably introducing multipath from the helicopter fuselage.

At this stage, the calculation of the offset vector between the camera's perspective centre and the antenna phase centre became relevant. This is because of the need to obtain the perspective centre coordinates at the instant of exposure. If the camera is to have three degrees of freedom during a sortie, attaching the antenna to the airframe gives a separation vector which varies in both magnitude and direction, as the camera and helicopter are considered as separate platforms. The advantage of the antenna being attached to the camera mount is that the resulting vector is fixed in magnitude and varies only in direction. The three

remaining unknowns are the Euler (rotation) angles about the three principal axes, which could potentially be measured.

As part of the preliminary investigations, it was decided to slightly modify the camera mount so that the antenna could be attached (Figure 1), accepting the degradation of the GPS positioning ability for these trials.

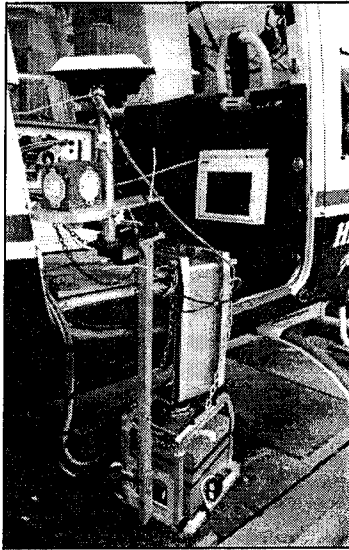


Figure 1 : The integrated system as located on the helicopter

3.3 Exposure Control and Identification

Integration of the camera and the GPS receiver is important to provide both exposure times and positions. Two options were considered :

- (i) use of a timing pulse from the camera to the GPS receiver, to enable interpolation of the perspective centre coordinates between successive epochs; or
- (ii) use of the Pulse Per Second (PPS) output from the receiver to fire the camera on a GPS measurement epoch.

Modern aerial cameras are equipped with a centre of exposure pulse which could be fed to the receiver. It is also possible to add a diode into the image plane of older cameras, and calibrate it to the instant of exposure. However, altering Photarc's UMK 10/1318 Universal Camera was not a viable solution. In addition, the motion of a helicopter is less predictable than that of a fixed wing aircraft, which would make it difficult to interpolate the exposure positions between the GPS coordinate solutions. At a typical flying speed of 15mph (24km/h) and an epoch separation of 1 second, the distance of travel is 6.70 metres.

If the PPS output of the GPS receiver is used to fire the camera, the problem of interpolation is significantly reduced. The only potential adjustment that needs to be made is to allow for the delay between the rising edge of the PPS output and the instant of exposure. With this in mind, control circuitry was designed to allow the PPS output to fire the camera.

3.4 Evaluating the Euler Angles at the Instant of Exposure

As has been discussed, to evaluate the direction of the offset vector the three Euler angles must be measured at the instant of exposure. In the past, the IESSG has made use of a purpose built array of commercially available tilt sensors and it seemed appropriate to test their performance in this new environment. Briefly, these are capacitance based sensors of patented design with a range of ± 60 degrees and a resolution of ± 0.001 degrees. Sampling of the tilt is undertaken by a 486 DX33 personal computer.

3.5 System Integration

Figure 2 shows a schematic of the complete system. The trigger on the camera is pushed at the required instant of exposure, as with previous flights. However, the shutter is unable to fire until the next GPS epoch (at 1 second intervals), as identified and marked by the GPS receiver. At the same time, the PC is instructed to interrogate the tilt sensors and record the tilt of the camera. Time constraints prior to the flight meant that the delay between PPS output and photograph exposure could not be measured and so remained undefined between the range 0-1 seconds. One important function of the electronic control system was to lengthen the PPS pulse from 1 microsecond to the 1 millisecond pulse needed to fire the camera shutter.

4 SYSTEM EVALUATION TRIALS

4.1 The Pontefract Provisional Flight Trial

Field trials were conducted near Pontefract, Yorkshire. The idea was to evaluate the performance of the system in its initial guise, verifying that integration could be achieved. A conventional ground control network was observed along a fictitious highway at the helicopter's home airfield. The trials were performed at the airfield to limit flying time. The system was set up as shown in Figures 1 and 2, with one Trimble 4000 SSE GPS receiver located at the airfield to act as a base station. This resulted in a baseline length which remained under 1km. Due to time constraints on the availability of both the GPS equipment and the helicopter, there was a limited window of opportunity

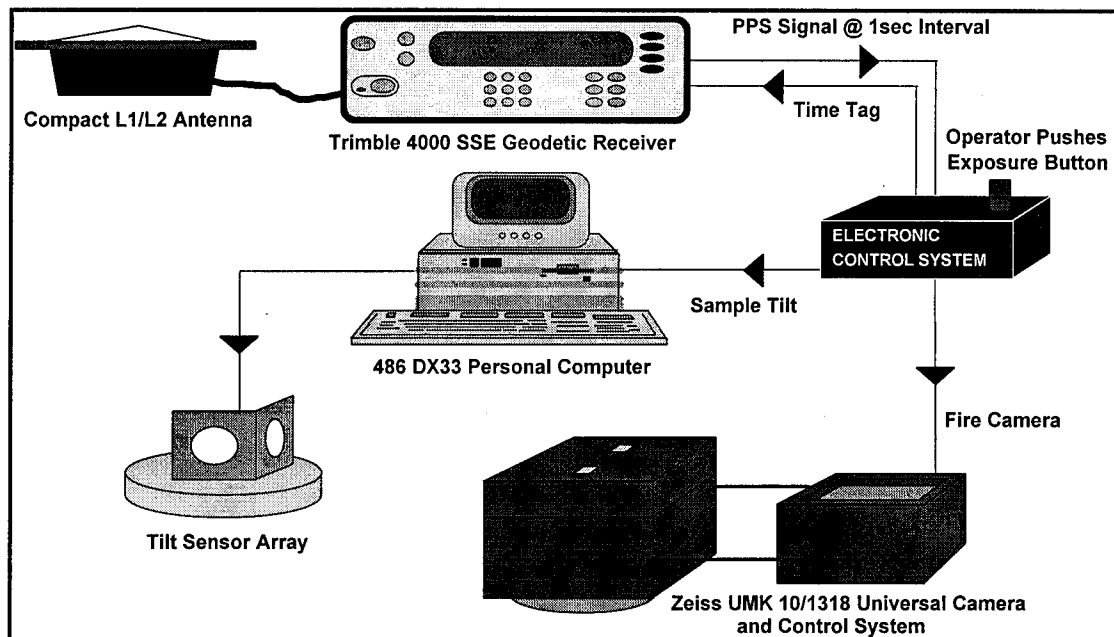


Figure 2 : Schematic diagram of the data capture system design

for the trials, which resulted in them being performed during severe weather conditions.

The helicopter charter company operates a 1968 Bell 206B Jet Ranger helicopter. This is equipped with a CAA approved skymount which is fixed in the rear area so that the camera mount can be attached. The Bell 206 is widely recognised as the most successful civilian helicopter ever manufactured and is operated by most charter companies in the United Kingdom. This factor alleviates the problems of attaching a camera mount to differing helicopters.

In the course of the trials, 5 photographic exposures were taken on each of 3 parallel flight lines along the fictitious highway to ensure a strong geometry for the photogrammetric computations. This was repeated a number of times because of the possibility of weather induced photographic blur. GPS observations were taken at one second intervals throughout the flight, as well as for 10 minutes at the start and end of it, as an aid to ambiguity resolution. Unfortunately, the number and frequency of cycle slips and loss of lock which occurred during the flight itself rendered this initialisation data unusable.

4.2 Processing

4.2.1 Photogrammetric Processing

Conventional photogrammetric techniques were necessary to establish truth coordinates for the perspective centre of the camera and ultimately the GPS antenna phase centre. The procedure can be summarised as follows:

(i) Photogrammetric observation to calculate the coordinates of the four fiducial marks in the ground coordinate system, allowing for the *inter-nodal separation*.¹

(ii) Theodolite Angle Intersection to establish vector magnitude and direction from the four fiducial marks to the antenna phase centre.

(iii) Conversion of the coordinates of the antenna phase centre from the local ground coordinate system to WGS84.

4.2.2 Tilt Sensor Data Processing

The calculation of truth tilt values was necessary for comparison against the tilts recorded by the PC during the flight. The coordinates of all four corners of one of the sensors were calculated for the instant of exposure with the aid of the theodolite intersection data. Simple algebra was then applied to calculate the tilt and compare this against the measured value.

4.2.3 GPS Data Processing

The GPS data obtained during the trial was not ideal for OTF processing, as the techniques require observations to a minimum of five satellites to operate and there were few sections of the data taken on board the helicopter where this was achieved. For the majority of the flight, four and usually only two or three satellites were tracked by the GPS receiver. This was caused by the low antenna position (Section 3.2),

¹ This is defined as the separation between the inner and outer nodes of a camera, which is the distance travelled by a ray as it passes through the lens cone.

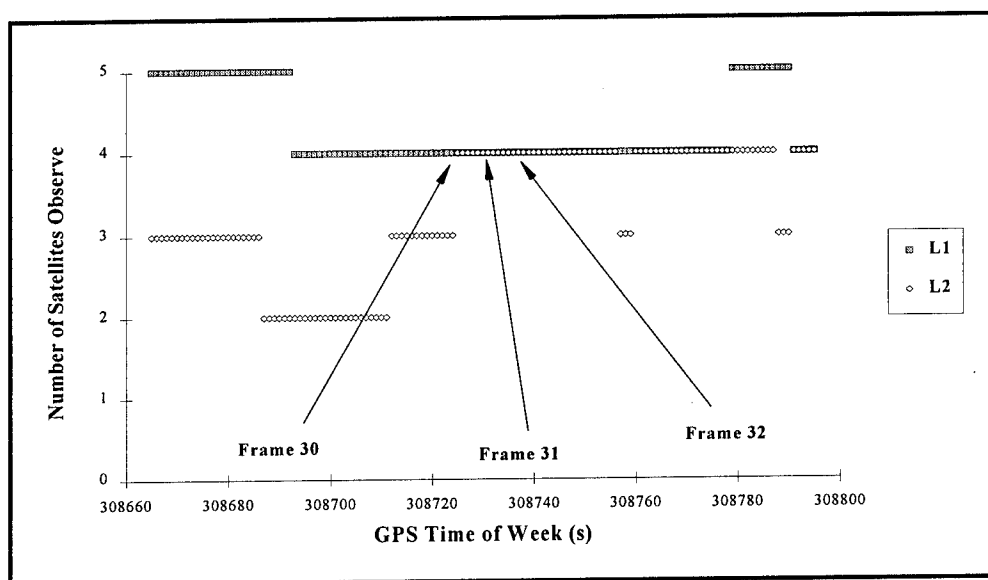


Figure 3 : Number of satellites observed on L1 and L2 frequencies for the time span bracketing Frames 30 - 32

which resulted in masking of half of the sky by the helicopter itself.

It was therefore only possible to process one section of GPS data during which photographs were taken. The number of satellites observed in this period are as shown in Figure 3.

Between GPS time of week 308725 and 308743, the exposure times of Frames 30 and 32 respectively, the GPS receiver mounted in the helicopter tracked four satellites on both L1 and L2. Five satellites were tracked on L1 only for short periods both before and after this section of the data, enabling resolution of the L1 integer ambiguities to be attempted. As Figure 3 shows, L2 is tracked less often than L1. This is because the noise level of the observations was very high throughout the data set and L2 signal-to-noise ratio (SNR) is generally lower than the L1 SNR. Hence, the L2 signal was drowned by the noise level and measurements were not made.

Processing the data with the OTF software was not as straightforward as usual. Rather than being able to use the L1 solution throughout, it was necessary to reinitialise the L1 integer ambiguities in the five satellite section following the exposures and then use knowledge of these L1 integer ambiguities to enable the L2 integer ambiguities to be found. An L2 coordinate solution was thus produced for Frames 30 and 31, whilst an L1 solution was produced for Frames 31 and 32.

4.3 Results

4.3.1 Introduction

The trials showed that it was possible to integrate the GPS and photogrammetry systems successfully to produce a working system. However, the tilt sensors did not prove to be of as much use as had been initially thought and the location of the GPS antenna was a major problem in terms of the OTF positioning capability of the system.

4.3.2 Tilt Sensor Data

| Frame Number | Calculated Tilt (degrees) | Sensor Tilt (degrees) |
|--------------|---------------------------|-----------------------|
| 19 | -2.33 | +2.92 |
| 20 | +0.12 | +0.36 |
| 21 | -2.28 | +3.99 |
| 22 | -2.48 | +2.78 |
| 30 | +0.19 | +0.24 |

Table 1 : Calculated and measured tilts for a sample of the photographic exposures

Table 1 shows the calculated and measured tilts for a selection of the photographic exposures. As can be seen, there is a close correlation for Frames 20 and 30, but a large disagreement for the remaining frames. Their performance was undoubtedly affected by the weather conditions, which would have prohibited a commercial survey. It was speculated that the inherent damping of the sensors was proving excessive.

This was investigated to obtain controlled experimental data to quantify the tilt sensor performance. The principle was to move the sensor between two fixed angles of tilt in an accurately measured time. This could then be superimposed on a plot of the recorded tilt variation as obtained from the datafile. The two important variables derived from the charts that were produced, were the velocity of movement between the two tilts and the corresponding delay between ceasing motion and the sensor reading the correct tilt.

The results showed clearly that the sensors had an inherent delay of 1 second, irrespective of the velocity of movement. In fact, soon after this investigation had been undertaken, it was discovered that the time constant for the sensors was 0.3 seconds, and control theory states that this will always lead to a delay of the order of 0.9 seconds, corroborating the practical test results. It was therefore not possible to use these tilt values for any of the data processing. It is hoped that the tilt sensor array will be of use in a modified role for future work.

4.3.3 OTF GPS Coordinate Solutions

It became clear during processing of the GPS observations that, as expected, the GPS antenna was not mounted in the best place on the helicopter. Masking of the sky and multipath had been expected, but the amount to which these affected the OTF positioning capability of the system had not been anticipated. In most cases, ambiguity resolution could not be attempted due to the limited number of satellites and when it was performed for Frames 30 - 32, an F-test confidence level of 90% had to be used, as resolution did not occur when the preferred level of 99% was employed.

The phase centre coordinates for Frames 30, 31 and 32 were calculated using the perspective centre coordinates and the perspective centre - phase centre offset vector (Section 3.2), and these values compared with the OTF GPS coordinates (Table 2).

These show large vector differences of between 18cm and 31cm between the two positioning systems. The OTF L1 and L2 solutions for Frame 31 do not correspond well in X, but their difference from the perspective centre based truth is similar in Y and Z.

Possible explanations for these differences include the effect of multipath from the helicopter fuselage and the fact that only four satellites were visible during this period. These were in approximately the same plane across the sky, resulting in a PDOP of 12. This could generate a position shift of several centimetres from the truth due to satellite geometry alone.

It was later found that the camera triggering circuit was introducing a delay of 56 milliseconds, corresponding to a movement of 38cm at the flying speed of 15mph. This is a possible cause of some of the offset, but because of the unstable nature of the helicopter flight it was not possible to interpolate the perspective centre coordinates to see how this delay affected the level of agreement with the GPS solution.

5 CONCLUSIONS AND SYSTEM DEVELOPMENTS

5.1 Conclusions

The trial demonstrated the successful integration of the two systems, for exposure control and identification (attributing a time tagged GPS position to each frame). It also showed that the tilt sensor array was not sensitive enough for a high dynamic environment such as this. Their likely use would be as a first approximation to the actual tilt value during photogrammetric processing.

The full potential of the OTF GPS system was not realised in this case because of the lack of data at the instant of exposure. The quality of the GPS data (loss of signal strength) meant that L2 observations were not available for the majority of the data set and so the widelane frequency combination could not be used.

| Frame Number | "Perspective Centre" Solution minus OTF GPS | | | Vector Magnitude Between Solutions (m) |
|--------------|---|--------|--------|--|
| | dX (m) | dY (m) | dZ (m) | |
| 30 (OTF L2) | 0.17 | 0.13 | -0.14 | 0.25 |
| 31 (OTF L1) | 0.14 | -0.10 | -0.05 | 0.18 |
| 31 (OTF L2) | -0.26 | -0.06 | -0.11 | 0.29 |
| 32 (OTF L1) | -0.13 | -0.04 | 0.28 | 0.31 |

Table 2 : Difference between the antenna phase centre coordinates based on the camera perspective centre and those computed using the OTF software

The combined effect of multipath, satellite geometry and delays in the triggering circuitry resulted in an offset between the two methods of coordination of the order of 20 - 30cm.

5.2 Developments to the System

The potential of a combined OTF GPS and photogrammetric system has been demonstrated. However, the preliminary system was limited by the lack of GPS data. The first major development is thus with regards to the location of the GPS antenna.

In order to retain the element of portability in the combined system, the antenna will not be mounted directly on the helicopter. Instead, it will still be attached to the removable camera mount, but will now be mounted on a lightweight pole, long enough to enable satellites on the far side of the helicopter to be visible. A new, smaller dual frequency kinematic antenna will be used to reduce the effect of drag.

As previously stated, the provisional triggering circuitry introduced a delay of around 56 milliseconds from PPS pulse to camera exposure. New triggering circuitry has therefore been designed to alleviate the effect of this delay. In principle, the GPS receiver will be set to produce the PPS output slightly before the measurement epoch such that the camera will fire at exactly the same time as the GPS measurements are made. Improvements to the method of measuring the orientation of the offset vector by tilt sensors are being considered, although it is not anticipated that these will be realised during the immediate lifetime of this project.

Further simulations and another flight trial are envisaged in the coming months. With good quality GPS data and reasonable satellite geometry, the OTF processing software can achieve positional accuracy at the 1-2cm level. It is therefore expected that the new developments being undertaken will produce an integrated system where the perspective centre coordinates are reliably determined to within 5 - 10cm.

ACKNOWLEDGEMENTS

The authors wish to acknowledge the support of their project supervisors, Prof. V. Ashkenazi, Prof. A.H. Dodson and Dr M.J. Smith. The authors would like to thank numerous colleagues from the IESSG, notably Dr D.P. Lowe and Mr G.W. Roberts and also Mr J.C. Boardman of Photarc Surveys Limited. Research into kinematic GPS and its application to helicopter borne photogrammetry in the IESSG is funded by the United Kingdom Engineering and Physical Sciences Research Council and The University of Nottingham.

REFERENCES

- Ackermann F., 1986, The Use Of Camera Orientation Data In Photogrammetry - A Review, *Proceedings ISPRS Symposium 'Progress In Image Sensors'*, Stuttgart 1-5 Sept. 1986.
- Ashkenazi V., Ffoulkes-Jones, G.H., Moore, T. and Walsh, D.M.A., 1993, Real-Time Navigation to Centimetre Level, *Proceedings of the Second International Conference on Differential Satellite Navigation Systems*, Amsterdam, Holland.
- Bierman, G., 1977, Factorization Methods for Discrete Sequential Estimation, *Academic Press*, New-York - San Francisco - London.
- Boardman, J.C., 1994, High Precision Levelling of Motorways by Low Level Helicopter Survey, *Photogrammetric Record*, Vol. 14(84), October 1994, pp 925 - 942.
- Euler H.J. and Landau, H., 1992, Fast Ambiguity Resolution On-The-Fly for Real-Time Applications, *Proceedings of the Sixth International Geodetic Symposium on Satellite Positioning*, Ohio, Vol. 2, pp 650 - 659.
- Hansen, P., 1994, Real-Time GPS Carrier Phase Navigation, *Proceedings of the Third International Conference on Differential Satellite Navigation Systems*, Vol. 2, Paper No. 49, London.
- Hatch, R., 1990, Instantaneous Ambiguity Resolution, *K.I.S. Symposium*, Banff, Canada.
- Mader, G.L., 1990, Ambiguity Function Techniques for GPS Phase Initialisation and Kinematic Solutions, *Proceedings of the Second International Symposium on Precise Positioning with the Global Positioning System*, Ottawa, Canada, pp 1234 - 1247.
- Melbourne, W., 1985, The Case for Ranging in GPS-Based Geodetic Systems, *Proceedings of the First International Symposium on Precise Positioning with GPS*, Rockville, Maryland.
- Smith M.J. and Joy C.I.H., 1995 Investigations into Developments in Using Helicopter Photography for Highway Surveying, *Photogrammetric Record*, Vol. 15(85) April 1995 pp 77 - 84.

A New Concept for GPS Phase Ambiguity Resolution On-The-Fly: The Maximum a Posteriori Ambiguity Search (MAPAS) Method

Christophe Macabiau

Laboratoire de Traitement du Signal et des Télécommunications of the ENAC

BIOGRAPHY

Christophe MACABIAU was born in 1968 in Moissac, France. He graduated in 1992 as an electronics engineer at the Ecole Nationale de l'Aviation Civile (ENAC) in Toulouse, France. He is specialized in signal processing and in radionavigation electronics. After working in 1993 for the MLS Project Office in Ottawa, Canada, he became a Ph.D. candidate at the Laboratoire de Traitement du Signal et des Télécommunications of the ENAC in 1994. He is working on the application of precise GPS positioning techniques to aeronautics.

ABSTRACT

The use of the pseudorange information contained within the GPS carrier phase observables enables to achieve a high level of positioning accuracy, but requires the resolution of the intrinsic cycle ambiguities of the phase measurements. Several methods have been proposed that can solve the ambiguities without static initialization by performing a search of the most coherent values of the double difference ambiguities of four particular satellites. They belong to the class of the multiple hypotheses sequential tests, that check each envisaged hypothesis against a decision criterion. A new method of ambiguity resolution on-the-fly, designed to make an optimal use of all the available measurements, is proposed in this paper. The decision criterion used by this method is the a posteriori probability of each potential solution. The mathematical developments involved in the design of the method are exposed, and the first simulation results obtained are presented, showing the validity of the concept proposed in this paper.

1. INTRODUCTION

The GPS phase measurements delivered by a receiver are related to the geometrical distance between the transmitting satellite and the receiver. These measurements constitute a potential source for a very precise determination of position, as they can be achieved with an accuracy of the order of one centimeter. However, the full access to that accurate geometrical information requires the resolution of the intrinsic integer ambiguities

of the measurements. Since fifteen years, several specialized techniques have been developed to achieve this resolution. Some of them assume the receiver is static during the determination, while the others can be carried out even when the receiver is moving. When the resolution is performed without static initialization, the resolution is said to be made *on-the-fly*. These positioning techniques are very useful tools for static applications, like static baselines surveying, and for mobile positioning in dynamic applications like satellite altimetry, aerial photogrammetry, airborne gravimetry or aircraft landing.

This paper describes a new method for ambiguity resolution on-the-fly of GPS phase measurements, called the *Maximum A Posteriori Ambiguity Search (MAPAS)* method. In section 2, a model of the GPS signal carrier phase measurements is presented and the problem of ambiguity resolution is introduced. Then, the Least Squares Ambiguity Searching Technique is described, followed by a discussion on the statistical aspect of the ambiguity searching techniques. In section 3, the principles of the MAPAS method are exposed, then a presentation of the input data used by the method is made, enabling us to derive the theoretical expressions of the decision criterion, and to build the algorithm. In section 4, the simulated data is described and the results obtained using the MAPAS method are presented and discussed.

2. AMBIGUITY RESOLUTION

The L_1 carrier phase measurements delivered by a suitably equipped civilian GPS receiver are the measurements of the phase of the low frequency signal generated by mixing the received L_1 satellite signal with the output of an oscillator tuned at the nominal carrier frequency. As described by Rocken (Rocken, 1988), a first order model of this beat phase measurement, for satellite i , at epoch k is :

$$\Phi_i(k) = f(\Delta t_R - \Delta t_{S_i}) - \frac{D_i(k)}{\lambda} - N_i + f\tau_{ion} - f\tau_{trop} + b_i(k) + \varepsilon_{mult}(k) \quad (1)$$

where

- f is the L_1 frequency and λ is the corresponding wavelength.
- Δt_R and Δt_S are respectively the receiver and satellite time equivalent phase offset with respect to GPS time.
- $D_i(k)$ is the geometrical distance between the satellite i and the receiver.
- N_i is the initial ambiguity value of the measurement.
- τ_{ion} and τ_{trop} are the ionospheric and tropospheric propagation delays.
- $\varepsilon_{mult}(k)$ is the carrier phase multipath term.
- $b_i(k)$ is the phase measurement noise. In the following, we assume that $b_i(k)$ is a discrete white gaussian noise, having zero mean and variance σ^2 .

As long as the lock on the signal is held, the phase measurement device can keep track of all the detected whole-cycle phase revolutions, and all the phase measurements delivered are biased by the same phase ambiguity N_i . When a *cycle slip* occurs, that is when a loss of lock on the signal is experienced, the phase measurements can not be performed any more. Once the signal is re-acquired, the integer number of whole-cycle revolutions has been lost, and the initial ambiguity has a different value.

The multipath propagation of the signal can be responsible for a loss of phase lock. It may also cause the ambiguities to be resolved to incorrect values. The effect of multipath on the performance of the method presented in this paper will not be investigated here. In consequence, the term $\varepsilon_{mult}(k)$ will be neglected.

Assume now that two receivers, denoted with the subscripts 1 and 2, make the carrier beat phase measurements of the signal transmitted by the satellite i at the same epochs. The receivers are supposed to be close to each other, so that the tropospheric and ionospheric propagation delays affecting their measurements can be considered as identical. This approximation will be valid as long as the distance between them is less than 20 km.

In order to eliminate the satellite clock offset, we can form the single differences of phase

$$\begin{aligned}\Delta\Phi_i(k) &= \Phi_{1i}(k) - \Phi_{2i}(k) \\ &= f\Delta t_{R12} - \frac{\Delta D_i(k)}{\lambda} - \Delta N_i + \Delta b_i(k)\end{aligned}$$

where

- $\Delta t_{R12} = \Delta t_{R1} - \Delta t_{R2}$
- $\Delta D_i(k) = D_{1i}(k) - D_{2i}(k)$
- $\Delta N_i = N_{1i} - N_{2i}$
- $\Delta b_i(k) = b_{1i}(k) - b_{2i}(k)$

Further on, to remove the receiver clock offset, we can form the double differences of phase, as shown in the following. This is achieved by choosing a reference satellite. For demonstration purposes, satellite 1 will be chosen as the reference satellite. If N satellites are being tracked at epoch k , we can form $N - 1$ double differences with the $N - 1$ remaining satellites:

$$\begin{aligned}\nabla\Delta\Phi_{1i}(k) &= \Delta\Phi_1(k) - \Delta\Phi_i(k) \\ &= -\frac{\nabla\Delta D_{1i}(k)}{\lambda} - \nabla\Delta N_{1i} + \nabla\Delta b_{1i}(k)\end{aligned}\quad (2)$$

where

- $\nabla\Delta D_{1i}(k) = \Delta D_1(k) - \Delta D_i(k)$
- $\nabla\Delta N_{1i} = \Delta N_1 - \Delta N_i$
- $\nabla\Delta b_{1i}(k) = \Delta b_1(k) - \Delta b_i(k)$

The model (2) for the double differences depends on the known coordinates of satellite 1 and satellite i , and on the coordinates of the two receivers. Thus, once the double difference ambiguities $\nabla\Delta N_{1i}$ are solved, we may be able to reach the desired positioning information contained within the double differences of phase.

Assume now that the coordinates of one receiver, say receiver 1, are well known. In the case where receiver 2 keeps a constant position during the ambiguity resolution procedure, then the number of unknowns in the system of the double differenced equations at any epoch is $3 + N - 1 = N + 2$, while the number of observations is $N - 1$. Then, the system can be solved using the observations gathered over two epochs if $2(N - 1) \geq N + 2$, that is if $N \geq 4$. The resolution yields an estimate of the double differences ambiguities as well as an estimate of the position of receiver 2.

The double difference model (2) is linearized and solved using an iterative procedure, as described by Remondi (Remondi, 1984), Rocken (Rocken, 1988), Blewitt (Blewitt, 1989), Leick (Leick, 1990) or Hofman et al. (Hofman et al., 1993) for example.

When the position of receiver 2 cannot be modelled as a constant, the system cannot be directly solved, as the number of unknowns increases over time. Performing an active search of the correct solution at each epoch is an adequate strategy for the resolution of the ambiguities. This search is carried out over a physical or a mathematical domain centered around an estimate of the solution. These methods require a great calculation power from the executing processor.

The Ambiguity Function Method, described by Remondi (Remondi, 1984) and by Mader (Mader, 1992) in the dynamic case, searches for the most coherent position in a physical volume, considering the phase measurements. The other searching techniques search for the most coherent combination of the double difference ambiguities in a mathematical set of probable discrete combinations. Numerous methods have been proposed so far. Among them, are the Least Squares Ambiguity Search Technique (LSAST) described by Hatch (Hatch,

1991) or Lachapelle et al. (Lachapelle et al., 1992), the Fast Ambiguity Resolution Approach (FARA) described by Frei and Beutler (Frei and Beutler, 1990), the Fast Ambiguity Search Filter (FASF) described by Chen (Chen, 1993), the optimized Cholesky decomposition method described by Landau and Euler (Landau and Euler, 1992), or the integrated 'on-the-fly' technique described by H. Abidin (Abidin, 1991) which achieves an integration of several techniques.

We will now have a closer look to the methods searching for the ambiguities related to only four particular satellites, like the method described by Hatch (Hatch, 1991) or Lachapelle et al. (Lachapelle et al., 1992). Let us denote N_k as the number of tracked satellites at epoch k . We can split the system of the $N_k - 1$ equations (2) in two parts :

- the system of the 3 double difference equations corresponding to four particular satellites. These satellites are called the *primary* satellites
- the system of the $N_k - 4$ remaining double difference equations corresponding to the other satellites. These satellites are in turn called the *secondary* satellites.

All the quantities related to the primary satellites (resp. the secondary satellites), like the observations, the ambiguities and the phase noise values will be qualified as primary (resp. secondary) quantities.

If the primary ambiguities are known, then the position of the moving receiver can be determined, and the secondary ambiguities can be known. Thus it is not necessary to search for the entire set of the unknown ambiguities, and some computation effort can be saved.

For example, the method described by Lachapelle et al. (Lachapelle et al., 1992) searches for the primary ambiguities that are associated, through the primary system of equations, with a physical position contained within a search cube built around a carrier-phase-smoothed code solution. At each measurement epoch k , for each potential three-integer combination, the difference between the actual secondary phase observations and some computed observations is formed. This secondary *prediction error*, called $z(k)$, together with the secondary observations covariance matrix $\Sigma_{SS}(k)$ can be used to form the *local variance factor*

$$\hat{\sigma}_0^2(k) = \frac{z(k)^T \Sigma_{SS}(k)^{-1} z(k)}{N_k - 4}$$

A *global variance factor* can also be built using all of the local variance factors. A candidate yielding too high a local or global variance factor is rejected from the search set, and thus will not be tested for during the next search epoch. After several rejection epochs, the best combination can be isolated in the set.

Considering the statistical aspect of these methods, we see that the ambiguity searching procedures can be

included in the large group of the *multiple hypotheses sequential tests*. The set of the potential three-integer vectors constitutes the set of the unknown parameters of the probability density function of the primary and secondary observations. Let us call this set \mathcal{N} . Thus, the procedure is built to decide between the hypotheses :

$$H_{abc} = \{[a \ b \ c] : [\nabla\Delta N_{12} \ \nabla\Delta N_{13} \ \nabla\Delta N_{14}] = [a \ b \ c]\}$$

for each three-integer vector $[a \ b \ c] \in \mathcal{N}$. In this discussion, satellites 1,2,3,4 are considered as being the 4 primary satellites.

The decision is taken using the raw data

$$\begin{aligned} \nabla\Delta\Phi_1^n = \\ [\nabla\Delta\Phi_{11}(1) \dots \nabla\Delta\Phi_{1N_1}(1) \dots \\ \nabla\Delta\Phi_{11}(n) \dots \nabla\Delta\Phi_{1N_n}(n)] \end{aligned}$$

The test is a mapping g that associates to the observation data $\nabla\Delta\Phi_1^n$ a particular hypothesis H_{abc} :

$$g(\nabla\Delta\Phi_1^n) = H_{abc}$$

The decision is taken at the epoch n when a preset decision condition is satisfied. Thus the size of the sample $\nabla\Delta\Phi_1^n$ is not known before the test is performed, and a compromise must be struck between the delay in making the decision and the accuracy of that decision by specifying the decision condition. This kind of test is called a *sequential test*. The important sets of parameters used to assess the quality of a sequential test are the set of the *error probabilities* and the set of the *Average Sample Numbers (ASNs)*.

The set of the error probabilities is the set of the conditional probabilities

$$\alpha_{abc} = P[g(\nabla\Delta\Phi_0^n) \neq H_{abc} \mid H_{abc} \text{ true}]$$

We can build the weighted error probability as

$$\bar{\alpha}(g) = \sum_{abc \in \mathcal{N}} P[H_{abc} \text{ true}] \alpha_{abc}$$

The set of the ASNs is the set of the conditional expectations :

$$ASN_{abc} = E[n \mid H_{abc} \text{ true}]$$

A sequential test is usually built by specifying values for the error probabilities. These values are inserted into the theoretical expressions of the decision thresholds to design the test. The ASNs are also determined using their own theoretical expressions.

In the case of the ambiguity searching algorithms, like in the case of most multiple hypotheses sequential tests, these theoretical expressions are hard to derive, and the design is made with empirical threshold values. These values are set so that the measured error probabilities and ASNs are as low as required. The error

probabilities and the ASNs thus become estimated criteria used to assess the performance of the test.

Several decision criteria can be chosen. The LSAST method uses the weighted least squares sum of the prediction errors for each hypothesis. The MAPAS method uses the a posteriori probability of each hypothesis knowing the prediction errors.

3. THE MAPAS METHOD

The Maximum A Posteriori Ambiguity Search (MAPAS) method is based on the same basic principles as the LSAST method described by Hatch (Hatch, 1991). The main difference resides in the decision criterion used by the test: the MAPAS method uses the *a posteriori probability* of each potential solution knowing all the past secondary prediction errors. Thus the criterion is a naturally global parameter, and all the measurements acquired up to the current epoch are considered when a decision is taken.

The principle of this method is inspired from the method described by Brown and Hwang (Brown and Hwang, 1983), where the ambiguities are estimated as unknown parameters of an observation model using a Kalman filter.

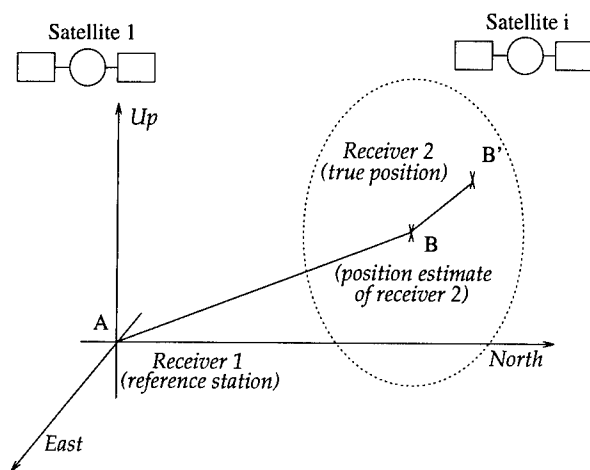


Figure 1: Illustration of the situation of the receivers in a local coordinate system.

The MAPAS method assumes that the measurements made by two receivers, located as described in figure 1, are available at each measurement epoch. Receiver 1 is called the reference station. Its position, denoted A, must be well known, and its code and phase measurements must be known by receiver 2. In the following discussions, we will consider that receiver 2 is located in B'. The ground distance between A and B' should be less than 20 km, and their altitude should not differ by more than 1.5 km. Thus the ionospheric and tropospheric propagation delays will be considered as identical for both receivers. At each measurement epoch, a good estimate of the position of receiver 2, called B, must be

available. This estimation can be made using pseudo-range corrections delivered by the reference station, or using a carrier-phase-smoothed code technique. The standard deviation of the estimate should be less than 1m on either axis in order to restrict the number of ambiguities candidates.

The main steps of the MAPAS method are as follows. The procedure is initialized at epoch 0 by the selection of four particular satellites among the tracked satellites, and by the construction of the set of the candidate primary ambiguities. Then, at each measurement epoch, for each potential solution, a prediction of the secondary phase measurements is made, and subtracted from the actual secondary phase measurements. The a posteriori probability of each potential solution in the set is then computed from the *a priori probability* of each prediction error. That potential solution is rejected from the set if its a posteriori probability is lower than a preset acceptance threshold. If the largest a posteriori probability of the set is higher than a predefined threshold, then the combination related to that best value is elected as the correct solution.

The primary satellites are selected according to their PDOP factor, among the tracked satellites whose elevation is greater than 7.5 deg, in order to ensure their visibility during the whole resolution procedure.

The PDOP of the primary satellites is an important selection criterion, as it seriously affects the performance parameters of the test. If the primary satellites are the satellites meeting the elevation angle requirement with the lowest PDOP factor, then the number of initial potential solutions is at its maximum. Many observation epochs, as well as many computer operations are then required to isolate the correct ambiguities. A minimum PDOP of 5 is usually required. On the other hand, when the PDOP of the primary satellites is too high, the posterior probability of the true solution may be accidentally lowered because of inaccurate intermediate position estimates, as it will be pointed out further. In this case, a reasonable upper bound of 10 is set.

Thus the PDOP of the primary satellites has an opposite influence on the duration of the test and on its error probability, and an ideal mean value has to be selected. In the case of the MAPAS algorithm, the primary satellites are chosen as the satellites of elevation angle greater than 7.5 deg having the PDOP factor which is the closest to the arbitrary value of 7.5.

The double difference model (2) is linearized around the position estimate B. The phase data used by the procedure at each measurement epoch are the double differences of phase that can be formed using the actual phase measurements made by the moving receiver, and the computed phase measurements that could be made by receiver 1 if it was located in point B, corresponding to the position estimate. The computed measurements

are denoted $\Phi_{3i}(k)$. Considering equation (1), we have:

$$\Phi_{1i}(k) - \Phi_{3i}(k) = -\frac{D_{1i}(k) - D_{3i}(k)}{\lambda}$$

$$\Phi_{3i}(k) - \Phi_{2i}(k) = f\Delta t_{R_{12}} - \frac{D_{3i}(k) - D_{2i}(k)}{\lambda} - \Delta N_i + \Delta b_i(k) \quad (3)$$

Therefore, we can use the single differences of phase $\Delta\bar{\Phi}_i(k) = \Phi_{3i}(k) - \Phi_{2i}(k)$, where $\Phi_{3i}(k)$ is generated using ().

$\Delta\bar{\Phi}_i(k)$ has the same ambiguity and noise values as $\Delta\Phi_i(k)$.

As point B is very close to point B', we can linearize the model (3), assuming that the direction cosines ($C_x(k), C_y(k), C_z(k)$) of the satellites are identical for both receivers. This approximation is justified because the distance between B and B' is of the order of a few meters. We have

$$\begin{aligned} D_{3i}(k) - D_{2i}(k) &= C_{xi}(k)(x_B(k) - x_{B'}(k)) \\ &\quad + C_{yi}(k)(y_B(k) - y_{B'}(k)) \\ &\quad + C_{zi}(k)(z_B(k) - z_{B'}(k)) \end{aligned}$$

and if we note

$$\Delta R(k) = [x_B(k) - x_{B'}(k) \quad y_B(k) - y_{B'}(k) \quad z_B(k) - z_{B'}(k)]^T$$

and

$$C_i(k) = \frac{1}{\lambda} [C_{xi}(k) \quad C_{yi}(k) \quad C_{zi}(k)]$$

then we have

$$\begin{aligned} \Delta\bar{\Phi}_i(k) &= f\Delta t_{R_{12}} - C_i(k)\Delta R(k) - \Delta N_i(k) + \Delta b_i(k) \end{aligned}$$

For the N_k tracked satellites, we can form the following linearized models of the double differences of phase :

$$\begin{aligned} \nabla\Delta\bar{\Phi}_{1i}(k) &= -C_{1i}(k)\Delta R(k) - \nabla\Delta N_{1i} + \nabla\Delta b_{1i}(k) \end{aligned} \quad (4)$$

where $C_{1i}(k) = C_1(k) - C_i(k)$.

We can stack the $N_k - 1$ values $\nabla\Delta\bar{\Phi}_{1i}(k)$ obtained in (4) into two separate vectors $\Phi_P(k)$ and $\Phi_S(k)$. $\Phi_P(k)$ contains the 3 values related to the 4 primary satellites, and $\Phi_S(k)$ contains the $N_k - 4$ values related to the secondary satellites. Thus, we get the following primary and secondary systems of equations, using vectors and matrices denoted with the respective subscripts P and S :

$$\Phi_P(k) = -C_P(k)\Delta R(k) - N_P + b_P(k) \quad (5)$$

$$\Phi_S(k) = -C_S(k)\Delta R(k) - N_S + b_S(k) \quad (6)$$

The set of the acceptable three-integer solution vectors can be built using the primary system (5) at the initial epoch 0. The physical search volume can be chosen

as an *ellipsoid* centered on the estimated position B. The semi-axes of the ellipsoid are set to three times the corresponding values of the standard deviations of the position estimate. The first step of the elaboration of the initial set \mathcal{N} can be the calculation of the ambiguities corresponding to the eight corners of the cube englobing the ellipsoid using (5). Then we can build the set of ambiguities delimited by these eight values. Eventually, the set \mathcal{N} is formed by rejecting those ambiguities associated with a position located outside the ellipsoid.

At each epoch k , the position associated with a particular combination $N_{P_{abc}} = [a \ b \ c]$ can be estimated using the primary phase observations. For example, using least squares estimation theory, we get :

$$\Delta\hat{R}_{abc}(k) = -S(k)\Phi_P(k) - S(k)N_{P_{abc}} \quad (7)$$

where $S(k)$ is

$$S(k) = [C_P(k)^T \Sigma_{PP}^{-1}(k) C_P(k)]^{-1} C_P(k)^T \Sigma_{PP}^{-1}(k)$$

and $\Sigma_{PP}(k)$ is the covariance matrix of the primary observations. Using (2) and the assumptions on the phase measurement noise process made in (1), the expression of this matrix can be shown to be

$$\Sigma_{PP}(k) = \sigma^2 \begin{bmatrix} 4 & 2 & 2 \\ 2 & 4 & 2 \\ 2 & 2 & 4 \end{bmatrix} \quad (8)$$

A prediction of the secondary phase measurements at the epoch k can be elaborated if we inspire from the linear measurement model (6). Assume a prediction of the secondary ambiguities $\hat{N}_{S_{abc}}(k)$ is available for each combination $[a \ b \ c]$ in \mathcal{N} .

We can then form the prediction

$$\hat{\Phi}_{S_{abc}}(k) = -C_S(k)\Delta\hat{R}_{abc}(k) - \hat{N}_{S_{abc}}(k) \quad (9)$$

The prediction $\hat{N}_{S_{abc}}(k)$ can be made using all the past secondary observations obtained from the satellites present in $\Phi_S(k)$.

For example, considering the fact that for the true hypothesis the prediction of the secondary ambiguities should be a vector of constant integers, we can choose to use the prediction

$$\begin{aligned} \hat{N}_{S_{abc}}(k) &= [Round(\frac{1}{k - k_i} \sum_{j=k_i}^{k-1} [-C_{1i}(j)\Delta\hat{R}_{abc}(j) \\ &\quad - \nabla\Delta\bar{\Phi}_{1i}(j)])]_{i \in \{5, \dots, N_k\}} \end{aligned} \quad (10)$$

where k_i is the first epoch of lock on the signal transmitted by satellite i . A predicted value of secondary ambiguity concerning satellite i is then computed for the first time at epoch $k_i + 1$.

We need now to introduce the a posteriori probability of each potential value $[a \ b \ c]$, conditionally on the value of the prediction errors. That probability is the

conditional probability for the true value of the primary ambiguities $[p \ q \ r]$ to be equal to $[a \ b \ c]$, given the values of the prediction errors obtained for that hypothesis $[a \ b \ c]$ up to the current epoch.

The actual secondary observations depend on the true primary ambiguities $N_{P_{pqr}} = [p \ q \ r]$. The true position can be expressed as :

$$\Delta R_{pqr}(k) = -S(k)\Phi_{P_{pqr}}(k) - S(k)N_{P_{pqr}} + S(k)b_P(k) \quad (11)$$

so that

$$\Phi_{S_{pqr}}(k) = -C_S(k)\Delta R_{pqr}(k) - N_{S_{pqr}} + b_S(k) \quad (12)$$

Thus, for each candidate $N_{P_{abc}}$, the prediction error can be written as :

$$z_{abc}(k) = \Phi_{S_{pqr}}(k) - \hat{\Phi}_{S_{abc}}(k) \quad (13)$$

Using Bayes' rule, we can write the a posteriori probability of a particular three-integer combination $[a \ b \ c]$ as :

$$P[N_P = [a \ b \ c] | z_{abc_1}^k] = \frac{f(z_{abc_1}^k | N_P = [a \ b \ c]) P[N_P = [a \ b \ c]]}{\sum_{[a \ b \ c] \in \mathcal{N}} f(z_{abc_1}^k | N_P = [a \ b \ c]) P[N_P = [a \ b \ c]]} \quad (14)$$

where $z_{abc_1}^k = [z_{abc}(1) \dots z_{abc}(k)]$ and \mathcal{N} is the set containing all the $[a \ b \ c]$ candidates.

$$f(z_{abc_1}^k | N_P = [a \ b \ c]) \quad (15)$$

is the value of the a priori probability density function of the innovations at the point $z_{abc_1}^k$. We assume that each three-integer combination in \mathcal{N} is equally probable, so that (14) can be reduced to

$$P[N_P = [a \ b \ c] | z_{abc_1}^k] = \frac{f(z_{abc_1}^k | N_P = [a \ b \ c])}{\sum_{[a \ b \ c] \in \mathcal{N}} f(z_{abc_1}^k | N_P = [a \ b \ c])} \quad (16)$$

Thus, at each epoch k , the a posteriori probability of each potential solution in the set can be computed once the current value of (15) is determined for every hypothesis.

The nature of the a priori law of probability of the recorded prediction errors $z_{abc_1}^k$, as well as the value of their conditional mean and covariance matrix has to be determined in order to perform the calculation of (15).

From (13), if we insert (7) into (9), and (11) into (12), we can derive the expression of the conditional prediction error for a candidate solution $[a \ b \ c]$:

$$z_{abc}(k) | N_P = [p \ q \ r] = [a \ b \ c] = \hat{N}_{S_{abc}}(k) - N_{S_{pqr}} - C_S(k)S(k)b_P(k) + b_S(k) \quad (17)$$

Moreover, assuming $N_P = [p \ q \ r] = [a \ b \ c]$, we have

$$\hat{N}_{S_{abc}}(k) = N_{S_{pqr}} \quad (18)$$

If no precaution is taken when using the predictions elaborated with (10), this assumption may not be verified for the true combination $[a \ b \ c]$, especially in the first stages of the procedure, when few measurements have been used to compute the average. A way to counter that is to allow the prediction several averaging epochs to get stabilized to the correct value before using it for statistical selection. However, it is very essential that the algorithm uses all the information available to feed its selection routines within the shortest delay, and the predictions elaborated should be used by the test as early as possible. Moreover, this prediction is not very noise sensitive, and it has proven to be highly accurate during all the trials performed.

Hence, the MAPAS algorithm releases the secondary ambiguity predictions concerning a given satellite only if there exists at least one $[a \ b \ c]$ candidate for which one that prediction has been constant for 2 epochs.

Note that it is important for the validity of assumption (18) that the primary satellites do not have too high a PDOP factor. Indeed, if the estimate (7) is not accurate enough for the true solution, the ambiguity prediction (10) may be biased by a value of one full cycle. In that case, the error prediction will be accidentally large, and the a posteriori probability of the true solution will be abnormally low.

As assumption (18) is made, (17) becomes :

$$z_{abc}(k) | N_P = [a \ b \ c] = -C_S(k)S(k)b_P(k) + b_S(k) \quad (19)$$

Since the additive phase noise measurement assumed in (1) is a white noise process, expression (19) shows that the successive random vectors $z_{abc}(k) | N_P = [a \ b \ c]$ are independent over time. Thus $z_{abc_1}^k$ is composed of k independent vectors. The value of the a priori probability density function (15) can therefore be computed as

$$f(z_{abc_1}^k | N_P = [a \ b \ c]) = \prod_{i=1}^k f(z_{abc}(i) | N_P = [a \ b \ c]) \quad (20)$$

Still using (19), as the phase measurement noise process is assumed to be a white gaussian noise with zero mean, we see that $z_{abc}(k) | N_P = [a \ b \ c]$ is a gaussian vector with zero mean. Its covariance matrix is

$$\begin{aligned} \Sigma(k) &= Cov(z_{abc}(k) | N_P = [a \ b \ c]) \\ &= C_S(k)S(k)\Sigma_{PP}(k)S(k)^T C_S(k)^T \\ &\quad + \Sigma_{SS}(k) - C_S(k)S(k)\Sigma_{PS}(k) \\ &\quad - \Sigma_{PS}(k)^T S(k)^T C_S(k)^T \end{aligned}$$

where

- $\Sigma_{PP}(k)$ is the covariance matrix of the primary observations. Its expression is given in (8).
- $\Sigma_{SS}(k)$ is the covariance matrix of the secondary

observations. Its expression is :

$$\Sigma_{SS}(k) = \sigma^2 \begin{bmatrix} 4 & 2 & \dots & \dots & 2 \\ 2 & 4 & 2 & \dots & \vdots \\ \vdots & 2 & \ddots & 2 & \vdots \\ \vdots & \dots & 2 & 4 & \vdots \\ 2 & \dots & \dots & 2 & 4 \end{bmatrix}$$

- $\Sigma_{PS}(k) = \Sigma_{SP}(k)^T$ is the cross-covariance matrix between the primary observations and the secondary observations. Its expression is :

$$\Sigma_{SP}(k) = \sigma^2 \begin{bmatrix} 2 & 2 & 2 \\ \vdots & \vdots & \vdots \\ 2 & 2 & 2 \end{bmatrix}$$

Thus, $f(z_{abc}^k | N_P = [a b c])$ can be recursively computed by multiplying each of the successive values

$$f(z_{abc}(k) | N_P = [a b c]) \quad (21)$$

$$= \frac{1}{2\pi^{\frac{N_k-4}{2}} \sqrt{\det \Sigma(k)}} \times \exp -\frac{1}{2} z_{abc}(k)^T \Sigma(k)^{-1} z_{abc}(k)$$

The normalization factor $\frac{1}{2\pi^{\frac{N_k-4}{2}} \sqrt{\det \Sigma(k)}}$ does not need to be computed, as the value given in (21) is only used to update (15) through (20), which is in turn used to calculate the a posteriori probability (16), where it cancels.

The algorithm of the procedure is shown in figure 2. The symbol $P(k)$ is used to designate the a posteriori probability of a candidate at epoch k , $f(k)$ designates the corresponding value of the a priori probability density function, and $s(k)$ is the sum of the prior probabilities of all the candidates in the set. P_0 is the upper decision threshold and P_{min} is the rejection threshold.

The algorithm shown in figure 2 evaluates $f(k)$ for the current epoch k , and $P(k-1)$ for the previous epoch $k-1$ using the sum $s(k-1)$. This is done to avoid a second scan of the set to calculate $P(k)$ with the sum of the current $f(k)$ in the big *while* loop. This causes a non-sensitive delay of one epoch in the instant of decision.

If a cycle slip is experienced on the signal received from any primary satellite, the procedure must be restarted.

4. SIMULATION RESULTS

The raw phase data used for the simulations is the double differenced phase data that could have been formed using two receivers in the city of Valence, on October 7th, 1994.

In these simulations, one reference station is considered, and the moving receiver is assumed to be moving along a certain simulated trajectory.

The simulations were run using the satellite constellation visible from 0:00 a.m. till 12:00 a.m. on October

```

selection of primary satellites
read data
construction of  $\mathcal{N}$ 
while best  $P(k) < P_0$ 
  read data
  compute  $\Sigma(k)$ 
  for each  $N_P = [a b c] \in \mathcal{N}(k)$ 
    if  $f(k-1)$  is available then
      compute  $P(k-1)$ 
      reject  $N_P$  if  $P(k-1) < P_{min}$ 
    end if
    if  $N_P \in \mathcal{N}(k)$  then
      update best  $P(k-1)$ 
      compute  $\hat{N}(k)$ 
      compute  $z_{abc}(k)$ 
      compute  $f(k)$ 
      update  $s(k) = \Sigma f(k)$ 
    end if
  end for
end while

```

Figure 2: Main steps of the MAPAS algorithm.

7th, 1994. The procedure ignored the satellites of elevation less than 5 deg. Thus, the number of considered satellites during the various ambiguity resolution trials ranged from 6 to 11.

Phase measurements for these satellites were generated every second. The measurements were considered as affected by the same tropospheric and ionospheric propagation terms, and by a discrete white gaussian noise. The standard deviation of this noise was set to $\sigma = 1 \text{ mm}$.

The ambiguity resolution trials were performed one after the other over the 24 hours. For each trial, the number of measurement epochs and the computation time required for the algorithm to be able to make a decision, as well as the truthfulness of the value of the ambiguities selected were recorded. The size of the search ellipsoid was set with the following values of semi-axes : ($a_x = 2\text{m}, a_y = 2\text{m}, a_z = 2.5\text{m}$).

The design parameters of the procedure are the rejection criterion P_{min} and the upper decision threshold P_0 .

The values assigned to these parameters affect the error probability, the Average Sample Number (ASN), and the computation time of the procedure. The value of the true primary ambiguities does not influence the performance of the procedure, as long it is included in the initial set. Thus only one estimated ASN and one estimated error probability will be given.

A subtle tradeoff must be achieved when specifying the two thresholds P_{min} and P_0 . Both of them must be adjusted so that false solutions are quickly rejected from the set, while the correct combination is kept. Assign-

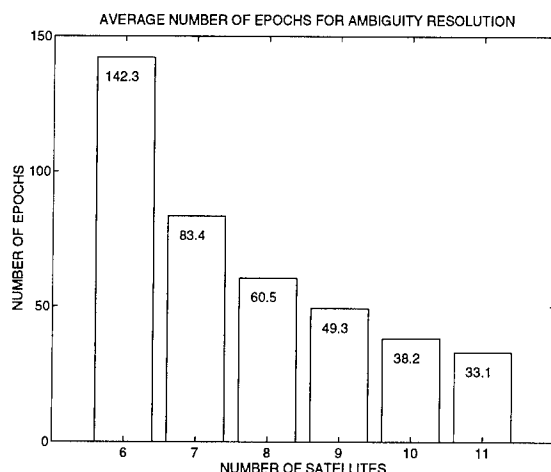


Figure 3: Average duration of the trials in epochs as a function of the number of tracked satellites.

ing a high value to P_{min} will make the algorithm reject quickly the false solutions. However, it will increase the chances for the true combination to be accidentally eliminated as well, and the error probability will be larger. If that value is set too low, then the ASN will be slightly higher, and a prohibitive number of operations will have to be performed by the processor. Similarly, setting P_0 with too low a value may enable a false solution to be elected, and the error probability will increase. On the other hand, setting it with a high value will increase the ASN.

It appears that for reasonable values of P_0 and P_{min} , P_0 has a strong influence on the ASN while P_{min} directly affects the error probability.

The influence of P_{min} is illustrated in table (4). As the abnormal transient values of posterior probability are mostly observed during the first ten epochs, when all the candidates share the unit probability, it happens very often that the a posteriori probability of the true solution reaches a low value. But it is very rare to see a false solution pass the upper acceptance threshold P_0 when the true solution is still in the set.

Thus, if a low error probability is to be reached, it is important that the rejection threshold P_{min} be set to a very low value. However, as the quantity of operations depends strongly on the number of candidates handled by the procedure, specifying too low a value for P_{min} may prevent the use of the algorithm for real time applications.

The adjustment of these different parameters required a lot of simulations, and only the first satisfying results obtained are presented here. The results of 2493 trials are presented in figures 3, 5, 6, 7 and 8. For these trials, the rejection criterion was set to $P_{min} = 10^{-5}$ and the decision threshold was set to $P_0 = 0.9999$. The observed global success rate for all the simulation runs

| P_{min} | Error rate in % | Average computation time in s | ASN |
|-----------|-----------------|-------------------------------|------|
| 10^{-5} | 99.12 | 34.17 | 63.3 |
| 10^{-6} | 99.34 | 36.25 | 63.4 |
| 10^{-8} | 99.56 | 41.51 | 63.5 |

Figure 4: Evolution of the performance parameters when P_{min} decreases, for $P_0 = 0.9999$.

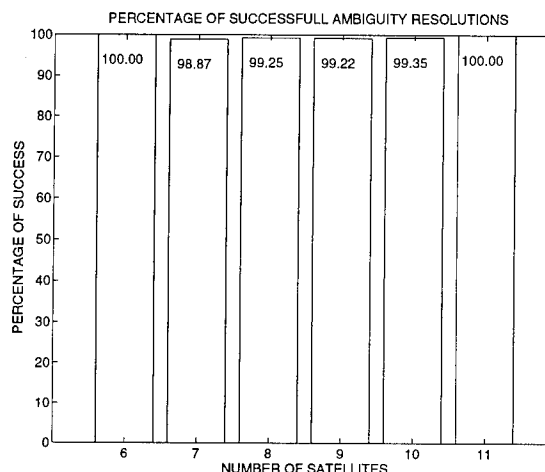


Figure 5: Percentage of successful trials as a function of the number of tracked satellites.

is 0.9912. The ASN is 63.

These performance parameters were estimated for the different numbers of tracked satellites, and are presented in figures 3, 5 and 8.

As the rate of acquisition of the information increases, that is as the number of satellites increases, both the rejection and the selection procedures are more efficient and this results in an improvement of the ASN, as it is shown in figure 3.

As seen in figure 6 and 7, the values selected for the design parameters enable the correct combination to be kept inside the search set despite its erratic initial path, and to be eventually isolated.

The average computation times required to perform the search on an HP 712/80 workstation are shown on figure 8. These durations represent the whole execution time of the entire resolution. The times presented here are to be used as rough indications only, as no particular effort was made to speed up the execution of the procedure so far. The simulation software was only designed to study the validity of the concept of the MAPAS method. However, the trend of the evolution of these figures with the number of satellites can be analysed. As seen in figure 8, the benefit of a larger number of observations per epoch offered by additional satellites is important only when 10 satellites are used. Before that, the gain in the ASN is not big enough to compensate the heavy volume of data processed by the computer.

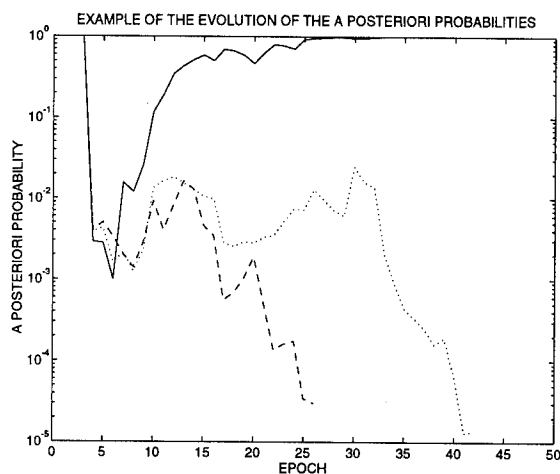


Figure 6: Example of the evolution of the a posteriori probabilities over time. The solid line corresponds to the correct combination. The dashed and the dotted lines correspond to two wrong solutions that are rejected sooner or later.

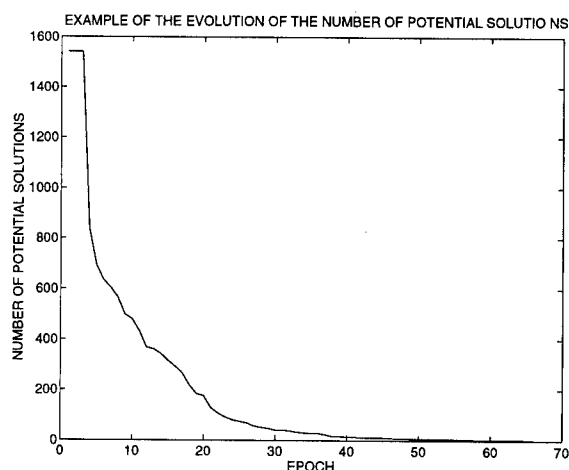


Figure 7: Example of the evolution of the number of potential solutions in the set. The set contains 1541 initial potential solutions.

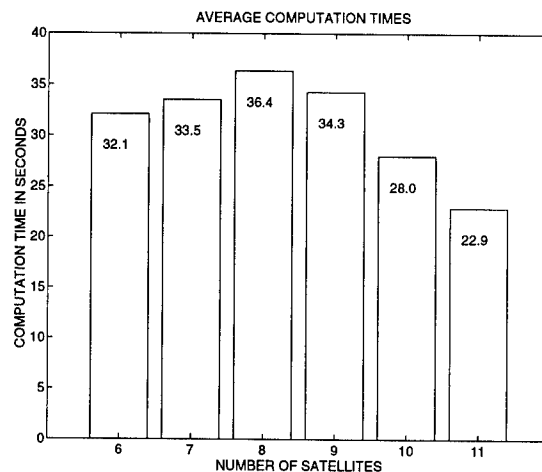


Figure 8: Average execution time of the simulation software as a function of the number of tracked satellites.

5. CONCLUSION

The MAPAS method makes an optimal use of all the current and past code and phase data available to the receiver, as the final decision is taken considering all the acquired data.

This method also provides a means to quantify the confidence that can be made in each potential solution. At each step of the resolution, the a posteriori probability of a particular combination can be delivered by the procedure.

As seen from the first simulation results presented here, over all the possible satellite configurations, the MAPAS method raised the correct ambiguities with a success rate of 99.1 %, and an average number of epochs of 63. This encouraging result demonstrates the validity of the concept of an ambiguity searching procedure based on the a posteriori probability.

Ongoing investigations aim to achieve a better adjustment of the design thresholds as well as an optimization of the algorithm, so that the real time performances of the method can be improved.

ACKNOWLEDGMENTS

The author wishes to thank the company SEXTANT AVIONIQUE for helping him in the development of the MAPAS method. He also wishes to thank the Service Technique de la Navigation Aérienne for enabling him to perform this research by providing funds and precious informations.

REFERENCES

- Abidin H. (1991) "New Strategy for 'On the fly' Ambiguity Resolution", proceedings of ION GPS-91, Albuquerque, September 11-13, The Institute Of Navigation, pages 875-886

- Blewitt G. (1989)** *"Carrier Phase Ambiguity Resolution for the Global Positioning System Applied to Geodetic Baselines up to 2000 Km"*, Journal of Geophysical Research, Volume 94 Number B8, pages 10187-10203
- Brown R.G. and Hwang P.Y.C. (1983)** *"A Kalman Filter Approach to Precision GPS Geodesy"*, Journal of the Institute of Navigation, Volume 30 Number 4, pages 155-166
- Chen D. (1993)** *"Fast Ambiguity Search Filter : A Novel Concept for GPS Ambiguity Resolution"*, proceedings of ION GPS-93, The Institute Of Navigation, Alexandria VA, pages 781-787
- Frei E. and Beutler G. (1990)** *"Rapid Static Positioning based on the Fast Ambiguity Resolution Approach : The Alternative to Kinematic Positioning"*, proceedings of Second International Symposium on Precise Positioning with GPS, Canadian Institute of Geomatics, Ottawa, Canada. September 3-7, pages 1197-1216
- Hatch R. (1991)** *"Instantaneous Ambiguity Resolution"*, proceedings of International Association of Geodesy Symposia 107 on Kinematic Systems in Geodesy, Surveying and Remote Sensing, New York, Springer-Verlag, pages 299-308
- Hofman-Wellenhof B. and Lichtenegger H. and Collins J. (1993)** *"Global Positioning System : Theory and Practice"*, Springer-Verlag
- Lachapelle G. and Cannon M.E. and Lu G. (1992)** *"High-Precision GPS Navigation with Emphasis on Carrier-Phase Ambiguity Resolution"*, Marine Geodesy, Volume 15 Number 4, pages 253-269
- Landau H. and Euler H.J. (1992)** *"On-The-Fly Ambiguity Resolution for Precise Differential Positioning"*, proceedings of ION GPS-92, The Institute of Navigation, Alexandria, September 16-18, Albuquerque, New Mexico, pages 607-613
- Leick A. (1990)** *"GPS Satellite Surveying"*, Wiley-Interscience
- Mader G. (1992)** *"Kinematic GPS Phase Initialization using the Ambiguity Function"*, proceedings of Sixth International Geodetic Symposium on Satellite Positioning, Columbus, Ohio, March 17-20, pages 712-719
- Remondi B.W. (1984)** *"Using the Global Positioning System GPS phase observable for relative geodesy : modeling, processing and results"*, Ph.D. Dissertation, University of Texas at Austin, May 1984
- Rocken C. (1988)** *"The Global Positioning System : A New Tool for Tectonic Studies"*, Ph.D. Dissertation, Universitat zu Koln, Cologne, West Germany.

A New Navigation Algorithm Using Only Information From Measurement

Benlin Xu
University of New Brunswick

Biography

The author has been a Ph.D. candidate in the Dept. of Geodesy and Geomatics Engineering, the University of New Brunswick, Canada since September of 1991. He obtained B.Sc degree from The Jiangxi Institute of Metallurgical Technology, China in 1982, M.Sc degree from Institute of Seismology of State Seismological Bureau of China in 1987, and worked as an engineer at Institute of Seismology, Fuzhou, China during 1987 - 1991. His research activities are mainly on GPS, navigation, digital signal processing, geodesy and earthquake prediction.

Abstract

This is a new self-learning navigation algorithm based on probability space and non-Newtonian dynamics. This new algorithm relies solely on the measurements on a vehicle: positions, velocities and their error statistics. The basic idea behind this new algorithm is two-fold: (1) A cluster of the observed positions contain true kinematic information of the vehicle, (2) A process model associated with the error statistics of the positions is able to squeeze, to a large extent, the information off for use. We base the new algorithm on an analogy. We consider the statistical confidence regions of the position fixes as "sources" tending to "attract" the undetermined trajectory to pass through these regions. With these position fixes and their error statistics, an imaginary real-time potential field is constructed in which an imaginary mass particle is forced to move. To make the new algorithm be flexible to a changing navigation environment, we leave some pa-

rameters unfixed and let the algorithm determine them using a sequence of observations and the criterion of least square errors of the observation. By all the above efforts, the trajectory of the imaginary particle can be a good representative path of the vehicle.

The new navigation algorithm has been tested with both simulated and real navigation data, as an estimator, predictor, smoother and blunder detector. The test results have demonstrated that the new algorithm has some advantages over Kalman filter, but with a slower processing speed.

1 Introduction

When a vehicle is traveling, it is assumed that instantaneous position fixes and the corresponding error statistics can be obtained by one or more navigation services. Our purpose is to estimate the position of the vehicle at present and predict its next position at an interested time instant. Existing navigation services include classical ground-based radio positioning such as Loran, Tacan, Omega; satellite positioning such as GPS and Transit; and self-contained systems such as inertial positioning, gyrocompass and ship's log (used at sea). No matter what navigation services are employed, a navigation algorithm which can suppress random noise in observations is always needed. Even with most advanced GPS service, the detection of blunders or the test of reliability on the coming GPS data may be required, then a navigation algorithm with a blunder detection function may also be desired.

Navigation problems are commonly solved by combining two different kinds of information: observations

of the motion of the vehicle, and a process model derived from some physical laws. Kalman filter is the most often used method. Its application has been very successful in space industry, but not in marine navigation. Dove and Miller [1989] wrote "The lack of recently published papers describing the use of Kalman filters in marine navigation does suggest that perhaps there has not been hoped for progress in this area."

The implementation of Kalman filter is dependent on the filter being tuned with a proper system process model. The difficulty of the application of Kalman filter in marine navigation is usually not related to measurements since nowadays precise observations can be obtained. Instead, the problem arises with the process model. Realistically, in many environments, an *a priori* process model is far from enough to represent the real system process, especially in a marine environment or for a vehicle under heavy maneuvering.

In light of this, we have tried to develop a possible alternative algorithm which relies solely on measurement on a vehicle: positions, velocities and their error statistics.

Section 2 describes the motivation and methodology of the research. A process model to simulate the real process of the vehicle is presented in Section 3. Section 4 talks about the self-learning procedure of the new algorithm. Section 5 is devoted to the computation aspects of the new algorithm. Then, two applications of the new algorithm are presented in Section 6. Numerical result comparisons between a Kalman filter and the new algorithm can also be found in Section 6.

2 Motivation and methodology

This research is motivated by the fact that a cluster of observed position fixes on a vehicle geometrically contain true kinematic information of the vehicle. We desire to abstract the information and use it. Then, how can we get it?

We base our algorithm on an analogy. We consider the statistical confidence regions (geometrical descriptions of error statistics) of the position fixes as "force sources" tending to "attract" the undetermined trajectory to pass through these regions. When the vehicle is traveling, it is assumed that instantaneous position fixes and the corresponding error statistics can

be obtained. Based on these position fixes and error statistics, an imaginary real-time potential field may be constructed in which an imaginary mass particle would be forced to move. The potential field caused by single position fix (we call it position potential field) should reflect the reliability of the position fix, and the produced force on the particle should monotonically decrease with the closeness of the particle to the position fix. When a new fix with its confidence region appears, if the particle is not right in the center of the confidence region, the particle would be attracted with a force of which the magnitude is proportional to the intensity of the potential surrounding the fix and monotonically decreases with the decreasing distance of the particle from the fix. Furthermore, to let the free particle go away from the position fix after the position fix appears, we assume the effect (potential) of the attracting source will be dissipating exponentially with time. By properly choosing position potential function, we believe the trajectory of the imaginary particle could be a representative path of the vehicle.

An attempt to create a new navigation algorithm based on the same motivation was made by Inzinga and Vaníček [1985]. In their research, the force produced by a position potential field on the particle was directly linked with the probability with which the position fix fell into a two-dimensional error ellipse. But the derived equation of the motion of the particle was very difficult, if not impossible, to be analytically treated.

The general strategy used in our new algorithm is described by Fig. 1. Based on the new idea, we must first select a proper potential function for an individual position fix. According to this function we can establish a real-time position potential field for the cluster of the position fixes. Then we can set up an equation of the motion of the particle. We solve it and get the process model of the new algorithm. To be flexible to a changing navigation environment, the potential function contains some parameters. But without known parameters and some initial conditions, it is not known which trajectory is the one currently being generated. We accordingly require some further information in order to enable us to narrow down our choice and to select a trajectory as being the one along which we believe the process to be evolving. We design

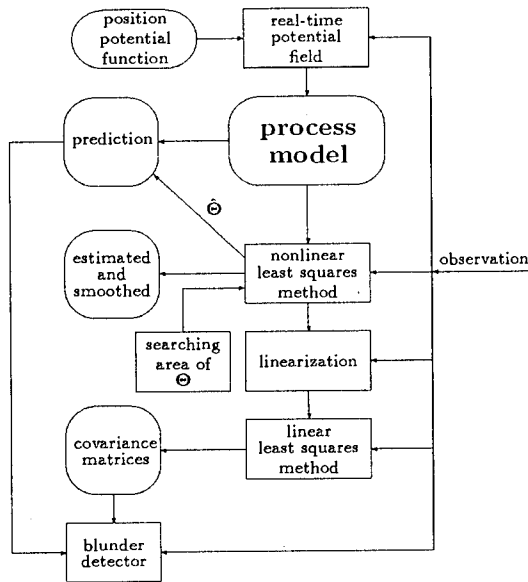


Figure 1: General strategy of the new algorithm

a self-learning procedure for the new algorithm and let it learn the parameters and initial conditions from previous observations. By a so called observation model, the parameters and initial conditions in the process model are related to the previous observations. At this stage the least square errors of observations will be brought in as a criterion for the parameter determination so that the trajectory selection is best in the clearly defined sense. The criterion and the observation model basically form a self-learning component of the new algorithm. Then nonlinear least square method is used to estimate the parameters and the present position as well as the smoothed positions for some previous fixes. The prediction of the position at the interested time instant can be made based on the process model with the estimated parameters and the present position of the vehicle. To get the covariance matrices for the above computed (estimated, predicted and smoothed) positions, we first linearize the observation model using the estimated parameters, and then employ linear least squares method on the linearized model. Blunder detection will be made right upon the arrival of new data according to the compatibility between the prediction and the new data by checking whether the new comer is located within the confidence

region of the predicted position with high confidence level (say, 0.999). If the new comer is not compatible with the prediction, it may be discarded.

3 Movement of a free particle in a non-Newtonian gravitational field

3.1 Position potential field

We assume that the error vector of an observed position is a Gaussian random vector, then the confidence region (error ellipse or ellipsoid) of the position is supposed to completely describe the position accuracy. We select the quadratic form of the confidence region as the major part of the position potential function U_i ,

$$U_i = G(\mathbf{r} - \mathbf{r}_i^0)^T \mathbf{C}_i^{-1} (\mathbf{r} - \mathbf{r}_i^0) e^{-\alpha(t-t_i)},$$

where

$$\mathbf{r} = \begin{pmatrix} x \\ y \end{pmatrix}, \quad \mathbf{r}_i^0 = \begin{pmatrix} x_i^0 \\ y_i^0 \end{pmatrix}$$

are the position vectors of the particle and the i -th position fix respectively, \mathbf{C}_i is the covariance matrix of the i -th position fix reflecting the uncertainty of the position fix, G is a positive parameter which plays a similar role to the gravitation constant (a scale factor), α is a positive dissipating parameter, both G and α are to be determined, t represents time ($t \geq t_i$), and t_i is the time instant when the i -th position fix appeared.

The real-time position potential field U produced by n position fixes is simply the summation of the n individual position potential fields,

$$\begin{aligned} U &= \sum_{i=1}^n U_i \\ &= G e^{-\alpha t} \sum_{i=1}^n (\mathbf{r} - \mathbf{r}_i^0)^T \mathbf{C}_i^{-1} (\mathbf{r} - \mathbf{r}_i^0) e^{\alpha t_i}, \quad (1) \end{aligned}$$

where $t \geq t_n$. It is obvious this potential field is non-Newtonian. Here, we would like to note that in order to make the new algorithm keep pace with the kinematic change of the vehicle as close as possible, as soon as a new position fix appears, the real-time position potential field will be updated to involve the new comer.

3.2 Equation of the motion of the particle

The partial derivative of the real-time position potential function *eqn.*(1) with respect to *r* gives the acceleration of the particle, i.e.,

$$\begin{aligned}\ddot{\mathbf{r}} &= -\frac{\partial U}{\partial \mathbf{r}} \\ &= -e^{-\alpha t}(\mathbf{A}\mathbf{r} - \mathbf{B}), \quad t \geq t_n\end{aligned}$$

where

$$\begin{aligned}\mathbf{A} &= 2G \sum_{i=1}^n e^{\alpha t_i} \mathbf{C}_i^{-1}, \\ \mathbf{B} &= 2G \sum_{i=1}^n e^{\alpha t_i} \mathbf{C}_i^{-1} \mathbf{r}_i^0.\end{aligned}$$

This is the equation of the motion of the particle in the real-time position potential field after the appearances of the *n* position fixes. To avoid possible numerical trouble, we move the origin point of time *t* to the point *t_n*. Now the equation of the motion of the particle can be written as follows:

$$\begin{aligned}\ddot{\mathbf{r}} &= -e^{-\alpha t}(\mathbf{A}\mathbf{r} - \mathbf{B}), \quad t \geq 0 \\ \mathbf{A} &= 2G \sum_{i=1}^n e^{\alpha(t_i - t_n)} \mathbf{C}_i^{-1}, \\ \mathbf{B} &= 2G \sum_{i=1}^n e^{\alpha(t_i - t_n)} \mathbf{C}_i^{-1} \mathbf{r}_i^0.\end{aligned} \quad (2)$$

3.3 Solution for the equation of the motion

In the following, we will confine ourselves to two dimension navigation problems. But this does not mean that the basic idea is not applicable to three dimension problems. Furthermore, for simplicity we assume that the covariance matrices of the position fixes are diagonal. When the covariance matrices are fully populated, a simplification has been validated [Xu, 1995]. We denote the inverses of the diagonal covariance matrices as

$$\mathbf{C}_i^{-1} = \begin{pmatrix} p_{x_i} & 0 \\ 0 & p_{y_i} \end{pmatrix}.$$

Then *eqn.*(2) can be split into two uncoupled ordinary differential equations:

$$\ddot{x} = -(A_x x - B_x)e^{-\alpha t}, \quad t \geq 0 \quad (3)$$

and

$$\ddot{y} = -(A_y y - B_y)e^{-\alpha t}, \quad t \geq 0 \quad (4)$$

where

$$\begin{aligned}A_x &= 2G \sum_{i=1}^n e^{\alpha(t_i - t_n)} p_{x_i}, \\ B_x &= 2G \sum_{i=1}^n e^{\alpha(t_i - t_n)} p_{x_i} x_i^0, \\ A_y &= 2G \sum_{i=1}^n e^{\alpha(t_i - t_n)} p_{y_i}, \\ B_y &= 2G \sum_{i=1}^n e^{\alpha(t_i - t_n)} p_{y_i} y_i^0.\end{aligned}$$

We first derive the solution for *eqn.*(3), then by similarity, we can achieve the solution for *eqn.*(4).

As the first step, let's find the solution for the homogeneous form of *eqn.*(3):

$$\ddot{x} + A_x e^{-\alpha t} x = 0. \quad (5)$$

Let $x(t) = u(s)$ and $s = \frac{2}{\alpha} e^{-\frac{\alpha t}{2}} \sqrt{A_x}$, then,

$$\begin{aligned}\dot{x} &= -e^{-\frac{\alpha t}{2}} \sqrt{A_x} u' \\ \ddot{x} &= e^{-\alpha t} A_x u'' + \frac{\alpha}{2} e^{-\frac{\alpha t}{2}} \sqrt{A_x} u'\end{aligned}$$

where u' and u'' represent du/ds and d^2u/ds^2 respectively, and *eqn.*(5) becomes

$$s^2 u'' + s u' + s^2 u = 0. \quad (6)$$

This is a Bessel equation of order 0. Its solution is a cylindrical function, and the general solution is

$$u = c_1 J_0(s) + c_2 N_0(s), \quad (7)$$

where J_0 and N_0 are Bessel functions of order 0 and of the first, second (Neumann) kind respectively, c_1 and c_2 are constants that will be determined by the initial conditions of the particle. By replacing u and s in *eqn.*(7) with x and $\frac{2}{\alpha} e^{-\frac{\alpha t}{2}} \sqrt{A_x}$ respectively, we get the solution for *eqn.*(5)

$$x = c_1 J_0\left(\frac{2}{\alpha} e^{-\frac{\alpha t}{2}} \sqrt{A_x}\right) + c_2 N_0\left(\frac{2}{\alpha} e^{-\frac{\alpha t}{2}} \sqrt{A_x}\right). \quad (8)$$

The second step is to find a particular solution for *eqn.*(3). By inspection, we find a particular solution for *eqn.*(3): $x = B_x/A_x$. The general solution for a linear ordinary differential equation can be obtained by the summation of the general solution of its homogeneous form and one of its particular solution. So

adding the above particular solution to eqn.(8), we get the general solution for eqn.(3),

$$x = B_x/A_x + c_1 J_0\left(\frac{2}{\alpha} e^{-\frac{\alpha t}{2}} \sqrt{A_x}\right) + c_2 N_0\left(\frac{2}{\alpha} e^{-\frac{\alpha t}{2}} \sqrt{A_x}\right). \quad (9)$$

Because of the similarity between eqn.(3) and eqn.(4), we can obtain the solution for eqn.(4) with little extra effort,

$$y = B_y/A_y + c'_1 J_0\left(\frac{2}{\alpha} e^{-\frac{\alpha t}{2}} \sqrt{A_y}\right) + c'_2 N_0\left(\frac{2}{\alpha} e^{-\frac{\alpha t}{2}} \sqrt{A_y}\right), \quad (10)$$

where c'_1 and c'_2 , like c_1 and c_2 , are undetermined constants. Taking the time derivative of eqn.(9) and eqn.(10) respectively and noting that

$$\begin{aligned} \frac{dJ_0(z)}{dz} &= -J_1(z), \\ \frac{dN_0(z)}{dz} &= -N_1(z), \end{aligned}$$

where, J_1 and N_1 are respectively the first and second (Neumann) kind of Bessel functions of order 1, we get the solutions for velocities,

$$\dot{x} = \sqrt{A_x} e^{-\frac{\alpha t}{2}} \left(c_1 J_1\left(\frac{2}{\alpha} e^{-\frac{\alpha t}{2}} \sqrt{A_x}\right) + c_2 N_1\left(\frac{2}{\alpha} e^{-\frac{\alpha t}{2}} \sqrt{A_x}\right) \right), \quad (11)$$

$$\dot{y} = \sqrt{A_y} e^{-\frac{\alpha t}{2}} \left(c'_1 J_1\left(\frac{2}{\alpha} e^{-\frac{\alpha t}{2}} \sqrt{A_y}\right) + c'_2 N_1\left(\frac{2}{\alpha} e^{-\frac{\alpha t}{2}} \sqrt{A_y}\right) \right). \quad (12)$$

Once parameters G and α are known and the initial conditions of the particle (vehicle), i.e., $(x_n \ y_n)^T$ and $(\dot{x}_n \ \dot{y}_n)^T$, are available, the above four constants c_1 , c_2 , c'_1 and c'_2 can be determined by solving a system of equations obtained from eqns.(9) - (12). Noting that

$$J_1(z)N_0(z) - J_0(z)N_1(z) = \frac{2}{\pi z},$$

we have

$$c_1 = -\frac{\pi}{\alpha} \left[(x_n - B_x/A_x) \sqrt{A_x} N_1\left(\frac{2}{\alpha} \sqrt{A_x}\right) - \dot{x}_n N_0\left(\frac{2}{\alpha} \sqrt{A_x}\right) \right] \quad (13)$$

$$c_2 = \frac{\pi}{\alpha} \left[(x_n - B_x/A_x) \sqrt{A_x} J_1\left(\frac{2}{\alpha} \sqrt{A_x}\right) - \dot{x}_n J_0\left(\frac{2}{\alpha} \sqrt{A_x}\right) \right] \quad (14)$$

$$c'_1 = -\frac{\pi}{\alpha} \left[(y_n - B_y/A_y) \sqrt{A_y} N_1\left(\frac{2}{\alpha} \sqrt{A_y}\right) - \dot{y}_n N_0\left(\frac{2}{\alpha} \sqrt{A_y}\right) \right]$$

$$- \dot{y}_n N_0\left(\frac{2}{\alpha} \sqrt{A_y}\right) \quad (15)$$

$$c'_2 = \frac{\pi}{\alpha} \left[(y_n - B_y/A_y) \sqrt{A_y} J_1\left(\frac{2}{\alpha} \sqrt{A_y}\right) - \dot{y}_n J_0\left(\frac{2}{\alpha} \sqrt{A_y}\right) \right]. \quad (16)$$

Then, the position and velocity at next instant t_{n+1} can be determined by eqns.(9)-(16) with $t = t_{n+1} - t_n$.

3.4 Process model

Having derived the solution for eqn.(2), we can say that S_{n+1} , the state of the particle at t_{n+1} , is the function of parameters G and α and its state at t_n (as initial condition). Let's denote it as

$$S_{n+1} = f_n(\Theta, S_n) \quad (17)$$

where,

$$S_i = \begin{pmatrix} r_i \\ \dot{r}_i \end{pmatrix}, \quad \Theta = \begin{pmatrix} G \\ \alpha \end{pmatrix}$$

with the understanding that the function f_n is specially related to the previously observed position fixes.

This is the process model of the particle. Provided that parameters G and α are known and the initial conditions of the particle are available, the state of the particle can be evolved to the next instant.

4 Self-learning procedure

Assume that observations are being repeatedly taken on the vehicle and are streaming into a computer. They are placed into, what is called "a push-down table". This is a memory storage area in which the most recent data are entered at the top, while all of their predecessors are moved down to make room for them. Each time new data arrive, the procedure is repeated, all previous data being moved down the table and the most recent data again being entered at the top. The push-down table is of fixed length. Upon the next receipt of new data, the bottom-most entry is then simply discarded or forgotten. Let the observation and error vectors at time t_n be, respectively,

$$l_n = \begin{pmatrix} l_{r_n} \\ l_{\dot{r}_n} \end{pmatrix}, \quad v_n = \begin{pmatrix} v_{r_n} \\ v_{\dot{r}_n} \end{pmatrix}$$

where subscripts r_n and \dot{r}_n are used for position and velocity respectively. Using eqn.(17) we have

$$l_n + v_n = f_n(\Theta, l_{n-1} + v_{n-1}). \quad (18)$$

Accordingly we use *eqn.*(18) for each of the instants t_{n-k+1} to t_n (k is the number of the most recent position fixes used), and obtain

$$\mathbf{l} + \mathbf{v} = \mathbf{f}(\boldsymbol{\Theta}, \mathbf{l} + \mathbf{v}) \quad (19)$$

where

$$\mathbf{l} = \begin{pmatrix} \mathbf{l}_n \\ \mathbf{l}_{n-1} \\ \vdots \\ \mathbf{l}_{n-k+2} \\ \mathbf{l}_{n-k+1} \end{pmatrix}, \quad \mathbf{v} = \begin{pmatrix} \mathbf{v}_n \\ \mathbf{v}_{n-1} \\ \vdots \\ \mathbf{v}_{n-k+2} \\ \mathbf{v}_{n-k+1} \end{pmatrix},$$

$$\mathbf{f} = \begin{pmatrix} \mathbf{f}_n \\ \mathbf{f}_{n-1} \\ \vdots \\ \mathbf{f}_{n-k+2} \\ \mathbf{f}_{n-k+1} \end{pmatrix}.$$

By *eqn.*(19) the set of observations made over the extended time span $t_{n-k+1} \leq t \leq t_n$ are related to the parameter vector $\boldsymbol{\Theta}$ and the initial conditions of the vehicle at t_{n-k} . This equation is called the observation equation and will recur over and over again.

As usual, the least square errors of the observations is used as the criterion for parameter determination. That means we will minimize the objective function

$$\Phi = \mathbf{v}^T \mathbf{C}^{-1} \mathbf{v} \quad (20)$$

with respect to parameter $\boldsymbol{\Theta}$. Note that we may regard the initial conditions of the vehicle as pseudo-observations, then we will enlarge the vectors \mathbf{v} and \mathbf{C} to include the corresponding quantities.

5 Computational aspect

We use nonlinear optimization methods [Bard, 1974] to get the solution of *eqn.*(19). Because of the difficulty in the estimation of the covariance matrices of the computed positions with a nonlinear optimization method, after accurate values of these parameters have been obtained, we linearize *eqn.*(19) with respect to the parameters and then use least squares method to get the estimated covariance matrices.

The variable metric method or the conjugate direction method is used to implement the optimization.

Both methods need the gradients of the objective function with respect to the parameters. It has been said that both have the same convergent speed and the former is more stable but needs more memory during processing. To our experience on the problems under investigation, they give the same numerical results.

6 Applications

6.1 Description of data

We applied the new algorithm to two real tracks of our researching boat MARY O. Both had a sampling rate of 10 seconds. C/A-code pseudo-range and carrier phase were observed by using Ashtech GPS receiver. The positions of MARY O during commissions were estimated on-line by PNAV (the Precise Differential GPS Navigation and Surveying software, Ashtech, 1993) with the mode of smoothed C/A-code pseudo-range. Accurate positions were computed by PNAV with mode of pseudo-ranges plus carrier phase and float integer ambiguities and by forward and backward processing after the commissions. According to the post processing results, the internal accuracy of positions was of the level 0.05 m. Fig. 2 depicts the two tracks. It is obvious that the boat was always under maneuvering during the two campaigns.

Comparisons between the PNAV's on-line and post processing outputs revealed the presence of 1-3 meter bias in the on-line position outputs. To show the real merits of the new algorithm, however, in this paper, we demonstrate the applications using simulated data. We add Gaussian noise (with a variance $\sigma = 1$ m) to PNAV's post processing results of positions to get 'observed' positions. We got the velocities by differencing PNAV's post processing results of positions and then added Gaussian noise ($\sigma = 0.05$ m/s) to these velocities to get 'observed' velocities. The errors of the 'observed' position for both tracks are depicted in Fig. 3 and Fig. 5. The position errors of the dead-reckoning technique (i.e., navigation using only the velocity) are depicted in Fig. 4 for the first track and Fig. 6 for the second.

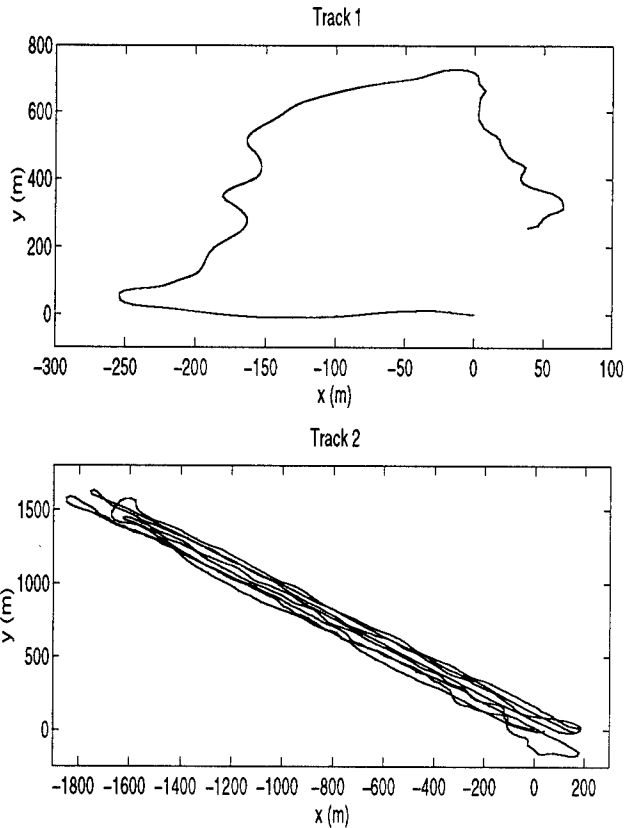


Figure 2: Two Tracks of MARY O

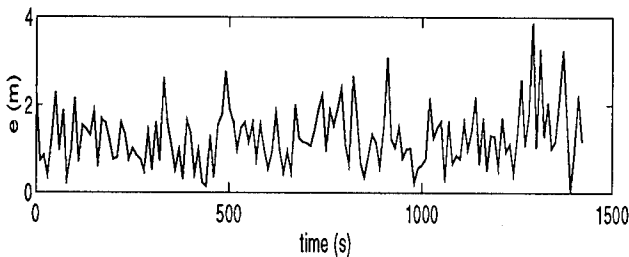


Figure 3: Errors of the 'observed' positions, Track 1

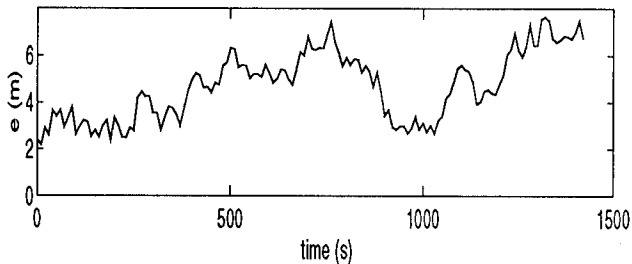


Figure 4: Position errors by dead-reckoning, Track 1

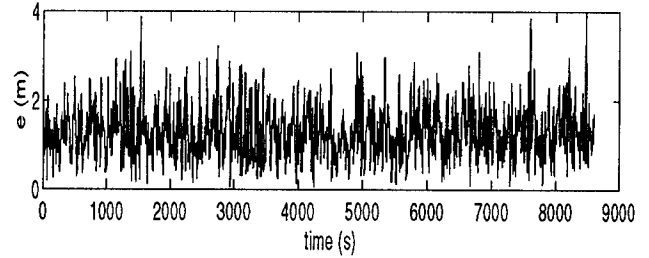


Figure 5: Errors of the 'observed' positions, Track 2

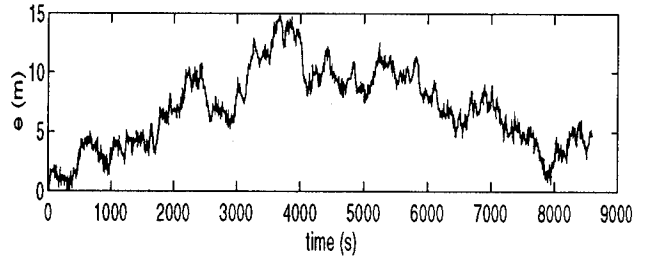


Figure 6: Position errors by dead-reckoning, Track 2

6.2 Results from the new algorithm

Many simulations were done with α and k fixed and a search area for parameters G defined by $0 \leq G \leq 1.0$ in each simulation [Xu, 1995]. The root of the mean square error of the estimated positions (RMS) and the maximum estimated position error (max-e) versus α and k are depicted in Fig. 7 for the first track and Fig. 8 for the second. It is obvious that the maximum estimated position errors by the new algorithm are much lower than the maximum position errors by dead-reckoning. And when α was large enough, the RMS for both tracks were lower than 1 m, and the maximum estimated position errors were lower than the corresponding maximum 'observed' position errors (3.9 m for the first track and 4.1 m for the second) respectively. With $k = 10$ and $\alpha = 25.5$, the errors of the computed positions are drawn in Fig. 9 for the first track Fig. 10 for the second. The errors of the smoothed position was about the position fix 5 fixes backward from the most recent one. Better results could be achieved by some other values of α . We once also supplied the new algorithm with PNAV's on-line output and also got improved position estimations but with unrealistic estimations of their covariance matrices. The new algorithm used 0.11 seconds to process one position fix when $k = 5$, and 0.23 seconds when

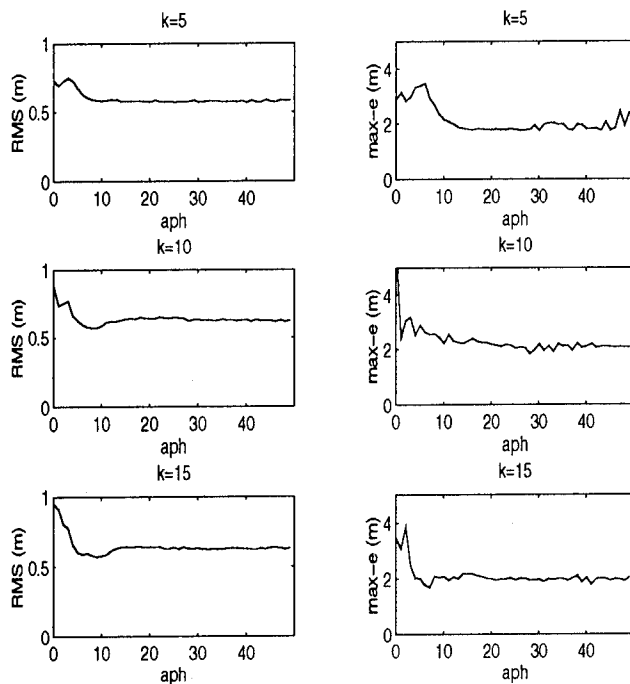


Figure 7: RMS and maximum estimated position error, Track 1

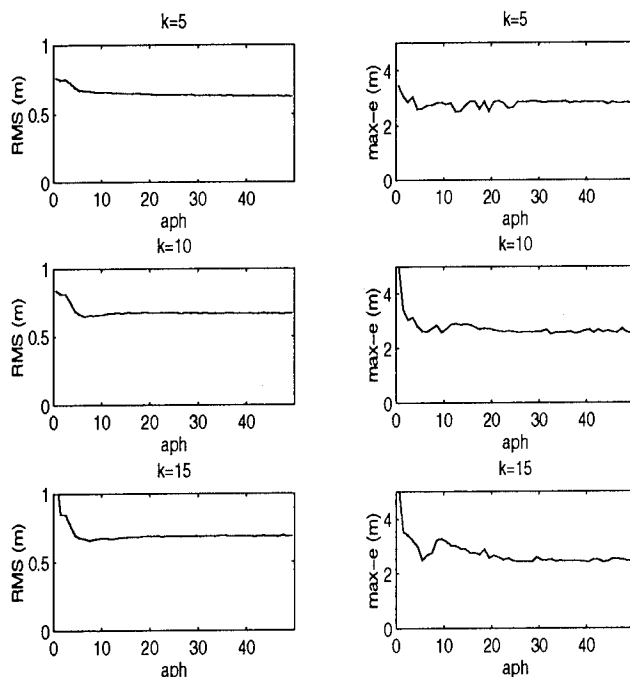


Figure 8: RMS and maximum estimated position error, Track 2

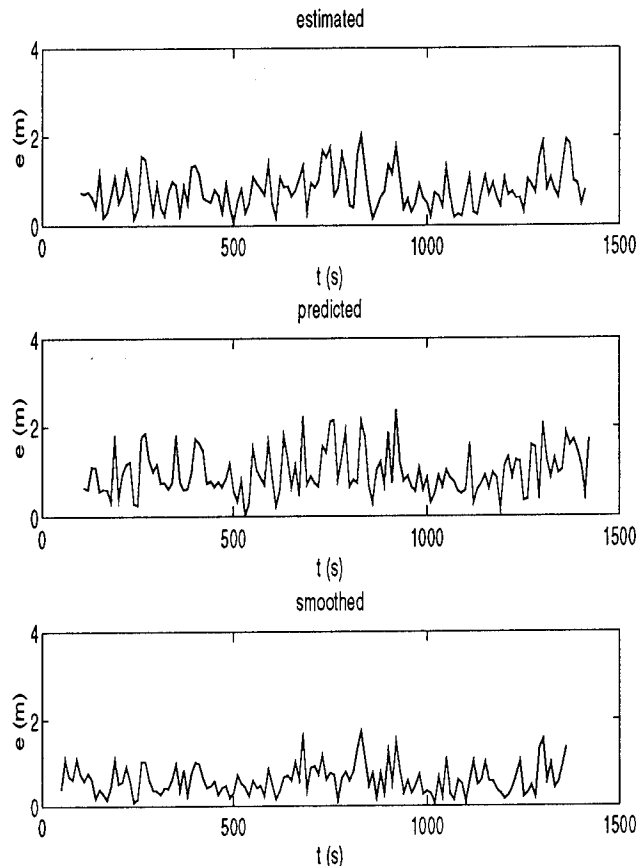


Figure 9: Errors of the computed positions, Track 1

$k = 10$.

Now let's talk about blunder detection. Two blunders were added to the first set of data. The first one was at $t = 400$ seconds with a magnitude of 10 meters in x direction, the second at $t = 800$ seconds with the same magnitude as the first but in y direction. With $k = 10$ and $\alpha = 25.5$, the errors of the estimated positions without or with detection are shown in Fig. 11 and Fig. 12. The confidence level for the confidence regions was 0.999.

6.3 Results from Kalman filter

The system process model used was [Gutman, 1990]

$$\mathbf{x}_n = \Phi \mathbf{x}_{n-1} + \mathbf{A} \mathbf{w}_{n-1}, \quad (21)$$

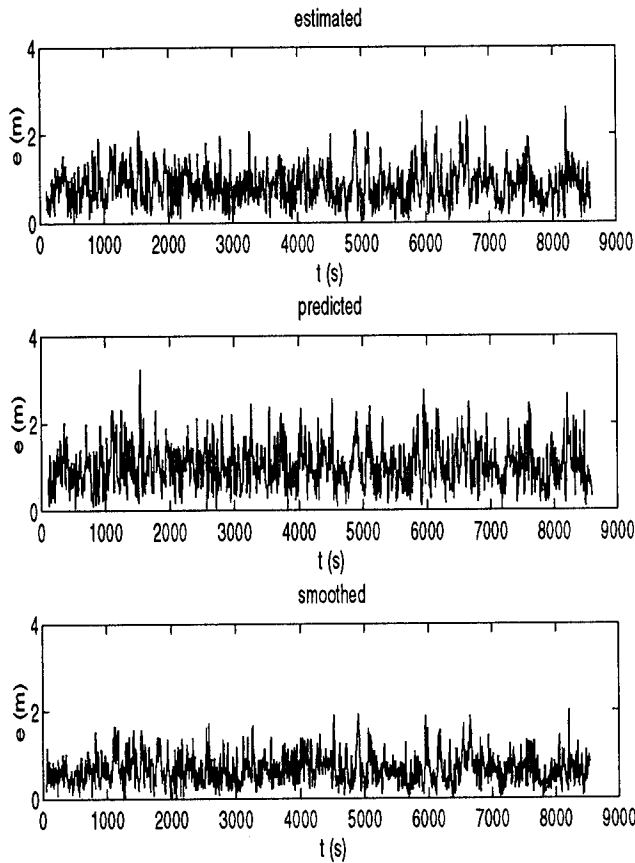


Figure 10: Errors of the computed positions, Track 2

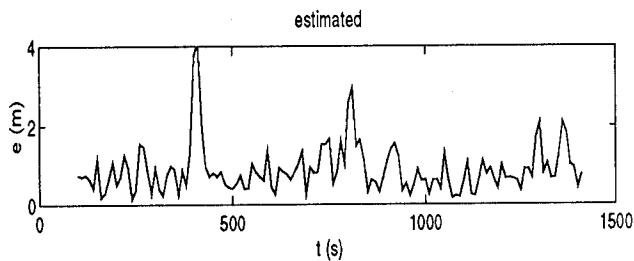


Figure 11: Errors of the estimated positions, without detection

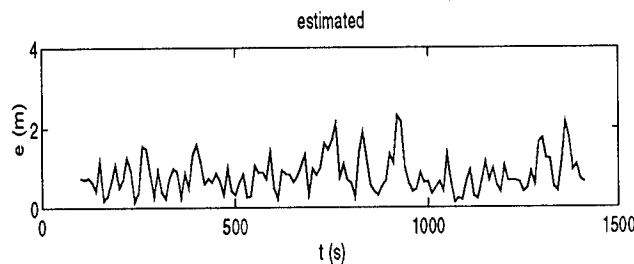


Figure 12: Errors of the estimated positions, with detection

where

$$\mathbf{x} = \begin{pmatrix} x \\ y \\ \dot{x} \\ \dot{y} \\ \ddot{x} \\ \ddot{y} \end{pmatrix} \quad \mathbf{A} = \begin{pmatrix} \frac{1}{6}\Delta t^3 & 0 \\ 0 & \frac{1}{6}\Delta t^3 \\ \frac{1}{2}\Delta t^2 & 0 \\ 0 & \frac{1}{2}\Delta t^2 \\ \Delta t & 0 \\ 0 & \Delta t \end{pmatrix}$$

$$\Phi = \begin{pmatrix} 1 & 0 & \Delta t & 0 & \frac{1}{2}\Delta t^2 & 0 \\ 0 & 1 & 0 & \Delta t & 0 & \frac{1}{2}\Delta t^2 \\ 0 & 0 & 1 & 0 & \Delta t & 0 \\ 0 & 0 & 0 & 1 & 0 & \Delta t \\ 0 & 0 & 0 & 0 & 1 & 0 \\ 0 & 0 & 0 & 0 & 0 & 1 \end{pmatrix},$$

and Δt was the sampling rate, w was assumed to be a zero-mean white noise sequence with covariance matrices

$$q_{ij} = E(w_i w_j) = \begin{cases} q \begin{pmatrix} 1 & 0 \\ 0 & 1 \end{pmatrix} & \text{if } i = j \\ 0 & \text{if } i \neq j \end{cases}$$

The observation model was

$$\mathbf{l}_n = \mathbf{B}_n \mathbf{x}_n + \mathbf{v}_n, \quad (22)$$

where

$$\mathbf{l} = \begin{pmatrix} l_x \\ l_y \\ l_{\dot{x}} \\ l_{\dot{y}} \end{pmatrix}, \quad \mathbf{B} = \begin{pmatrix} 1 & 0 & 0 & 0 & 0 & 0 \\ 0 & 1 & 0 & 0 & 0 & 0 \\ 0 & 0 & 1 & 0 & 0 & 0 \\ 0 & 0 & 0 & 1 & 0 & 0 \\ 0 & 0 & 0 & 0 & 0 & 0 \\ 0 & 0 & 0 & 0 & 0 & 0 \end{pmatrix}$$

and \mathbf{v} was assumed to be a zero-mean white noise vector with a known covariance matrix.

We applied this Kalman filter on the above two sets of data. The best results we could obtain (by testing many values of q) is depicted in Fig. 13 ($q = 10^{-7}$) for the first track and Fig. 14 ($q = 10^{-8}$) for the second. The Kalman filter needed only 0.02 seconds to produce an estimated position.

6.4 Discussion

The reason for the above failures with the Kalman filter was that the eqn.(21) could not keep being valid for a vehicle under maneuvering. Don't blame the Kalman filter. It is user's responsibility to give the filter a correct model. When the vehicle is under maneuvering, q

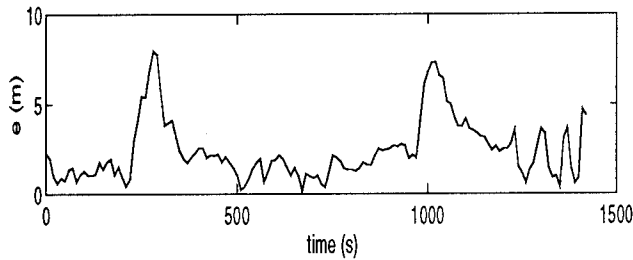


Figure 13: Errors of the estimated positions by Kalman filter, Track 1

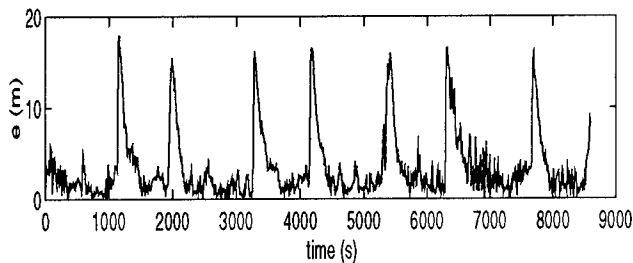


Figure 14: Errors of the estimated positions by Kalman filter, Track 2

may be a function of time. It was because the process model in the new algorithm had been updated from time to time, it could keep pace with the kinematic change of the vehicle and achieve better results.

7 Summary

It is no doubt that a cluster of observed positions contain true kinematic information of the vehicle. The process model associated with the error statistics of the position fixes and based on the analogy is able to squeeze the information off for use. Updating the process model position fix by position fix makes the process model keep pace with the kinematic change of the vehicle to a large extent. The new algorithm can act as an integrator to combine position and velocity observations, and then can supply better navigation than that using either observed positions or velocities (dead-reckoning) alone, and has a good ability for blunder detection. As to the required error statistics of observations, unlike Kalman filter, the new algorithm needs only cofactor matrices (relative size of covariance matrices), and the corresponding variance factor can be estimated. Compared with the Kalman

filter defined by eqn.(21) and eqn.(22), when the vehicle is under maneuvering, the new algorithm is able to achieve better results, but its processing speed is slower.

Acknowledgements

I sincerely thank my supervisor Professor P. Vaníček for his bring me to this topic and also for his guidance, constant support and encouragement throughout this research. Thanks also to Prof. D. E. Wells for his suggestions and criticism on the research. I am truly grateful to Prof. P. Vaníček and the University of New Brunswick for the financial assistance in my study and research in the University, and to Mr. D. W. Dodd for offering me real navigation data.

References

- Bard, Y. (1974). *Nonlinear Parameter Estimation*. Academic Press, New York and London.
- Dove, M. J. and Miller, K. M. (1989). "Kalman filters in navigation systems." *Navigation (UK)*, Vol. 42, No.2.
- Gutman, P-O. and Velger, M. (1990). "Tracking Targets Using Adaptive Kalman Filtering." *IEEE Transactions on Aerospace and Electronic Systems*, Vol. 26, No. 5, pp 691-698.
- Inzinga, T. and Vaníček, P. (1985). "A two-dimensional navigation algorithm using a probabilistic force field.", Presented at Third International Symposium on Inertial Technology for Surveying and Geodesy, Banff, Canada, 1985.
- Schwarz, K. P., Cannon, M. E., and Wong, R. V. C., (1989). "A comparison of GPS kinematic models for the determination of position and velocity along a trajectory." *manuscripta geodaetica*, Vol.14: 345-353.
- Vaníček, P. and Krakiwsky, E. J. (1986). *Geodesy: the concepts*. second edition, Elsevier Science Publishers B. V. 1992.
- Xu, B. (1995). *A New Navigation Algorithm*. Ph.D. dissertation, the Department of Geodesy and Geomatics Engineering, the University of New Brunswick, Fredericton, N.B., Canada E3B 5A3.

A Prototype Portable Vehicle Navigation System Utilizing Map Aided GPS

Blake Bullock
The University of Calgary

BIOGRAPHY

Mr. Bullock received a B.Sc. in Surveying Engineering in 1993 and an M.Sc. in Geomatics Engineering in 1995, both from The University of Calgary. His areas of research include land, air, and marine navigation systems, positioning technologies, and digital road map databases that support land vehicle navigation. He has recently joined Motorola as an Applications Engineer in the Position and Navigation Systems Business.

ABSTRACT

The author has developed a prototype portable vehicle navigation system (PortaNav) based on a notebook computer, a PCMCIA-type GPS receiver, and a digital road map. In order to meet the requirement of portability, the system can not be permanently installed in a vehicle, eliminating the possibility of using dead reckoning sensors. It was necessary to improve the accuracy of GPS positioning in single point mode under the effects of selective availability (SA). Traditionally, this has been done by integrating dead reckoning sensors with the GPS measurements. For this system, a digital road map was used as an auxiliary source of positioning information. A Kalman filter was used to combine the raw GPS measurements with map-derived constraints to improve the positioning coverage, accuracy, and reliability of the navigation system.

Software was developed to log three sets of data for comparison. First, a stand-alone GPS fix is logged to show what unaided GPS provides. Second, the map aided GPS solution is recorded to show the improvement achieved. Finally, a RINEX file is recorded for post-mission precise orbit processing, yielding the most accurate solution. Data was recorded in various urban environments to show the improvements gained.

The paper describes the mathematical basis for the map aiding process. Test results showing GPS alone and map aided GPS in urban canyon, tree canopy, and open road

environments are presented. Conclusions are drawn on the viability of using GPS for vehicle navigation without the use of dead reckoning sensors.

INTRODUCTION

The field of vehicle navigation has advanced significantly over the past five years. This has been due largely to the coming of the Global Positioning System (GPS), and the advancement of computer related technologies. To date, a total of 229 land vehicle navigation systems have been identified in [1]. In the past two years, over twenty portable vehicle navigation systems have emerged. This closely parallels the increased use of personal digital assistants (PDAs), which are described as any portable computing device used for managing personal data. Akin to PDAs are portable navigation assistants (PNAs), defined as any portable navigation system intended for personal use.

A portable vehicle navigation system is described as an autonomous navigator that is not permanently affixed to a vehicle. This includes the hand-held GPS waypoint navigators such as the GARMIN GPS 45 and the Magellan Meridian GPS (Figure 1). These systems provide simple waypoint positioning and navigation, but do not have any mapping (locating) capabilities.

A few of the portable systems are based on notebook computers with an external GPS receiver and a digital road map. Retki, from Liikkuva Systems International, City Streets from Road Scholar Software, and DeLorme MapExpert are three examples of such a system. The author has developed a prototype portable vehicle navigation system (PortaNav) similar to these systems, based on a notebook computer, a low-cost GPS receiver, and a digital road map.

This paper first describes the basic system design, then focuses on the positioning module used in PortaNav. Tests illustrating the system performance are then presented.

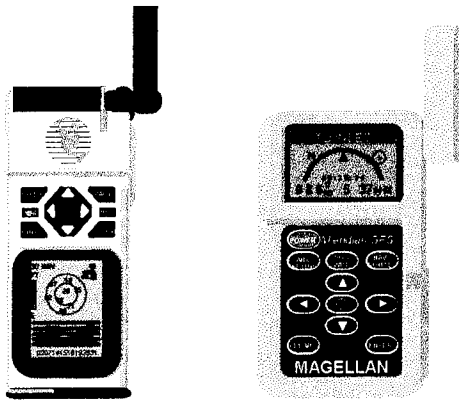


Figure 1. Portable Navigation Assistants (PNAs) - GARMIN GPS 45 (left) and Magellan Meridian GPS

PORTANAV SYSTEM

The objectives behind the design of PortaNav were to keep the cost low, provide nation-wide positioning, provide locating in areas where digital road maps are available, and remain autonomous from the vehicle. End-user products were sought for each of the components. The complete PortaNav system is pictured in Figure 2.

A notebook computer form factor was chosen for the development platform and the end product. An NEC Ultralite Versa 25C with an active matrix colour screen and 486 SLC processor was procured for this purpose. The Versa also has Personal Computer Memory Card International Association (PCMCIA) slots for expansion PC cards. PCMCIA slots provide a standard interface to computing devices that is manufacturer independent [2].

GPS was an obvious choice for the positioning system. No other system can compete at providing absolute nation-wide low-cost positioning. A low-cost C/A code receiver with a simple output interface was sought. Trimble's MobileGPS receiver, which has a PCMCIA interface, was available for under US \$1,000. This six channel receiver tracks up to eight satellites, and the raw measurements can be accessed via a software development kit from Trimble.

The system was developed in Calgary, so a digital road map supplier with coverage in this area was sought to facilitate testing. Etak, of Menlo Park, California was able to provide a beta map of Calgary for this purpose. Etak also has a software development kit for their digital road maps.

POSITIONING MODULE

In autonomous navigation, the primary objective is to show the user the current road of travel. To accomplish this, a position must be computed to an accuracy better than half the average distance between roads (50 m) so that the vehicle can be snapped to the correct road for

display. A solution is sought that provides a relatively smooth trajectory and allows the correct road to be identified as often as possible.

GPS provides a horizontal positioning accuracy of 100m at the 95% confidence level under the effects of selective availability (SA). Many methods of improving single point GPS positioning have been developed over the past decade [3]. Differential GPS, dead reckoning, and map matching have all been used successfully to augment the capabilities of stand-alone GPS [4], [5], and [6].

In order to remain autonomous from the vehicle, the system can not be permanently installed. This eliminates the possibility of using dead reckoning sensors such as odometers, compasses, and rate gyros. The former because they must be attached to the wheels or transmission, and the latter two because they should be mounted on a stable platform, not just a box that is thrown on the front seat.

To keep the cost of the system down, differential GPS (DGPS) could not be used. At the time this project began (two years ago), there were no low-cost DGPS solutions available. Today, an infrastructure exists to provide low-cost corrections via FM sub-carrier waves. Also, the hardware costs for DGPS have reduced dramatically. However, using DGPS still adds cost, bulk, and complexity to the system.

Map matching is the process of correlating the traced path of a vehicle with possible paths in a single line digital road network. Map matching is usually used in conjunction with dead reckoning sensors to augment GPS. Using a digital road map to augment GPS does not increase the hardware cost or the bulk of a navigation system. This is a great advantage in portable navigation.

The positioning module for PortaNav is based on stand-alone GPS and a new approach to using map-derived information to augment GPS. The basic premise is to use the positional information of roads in the digital road map as observations. The map-derived observations are integrated with the raw GPS measurements using a Kalman filter.

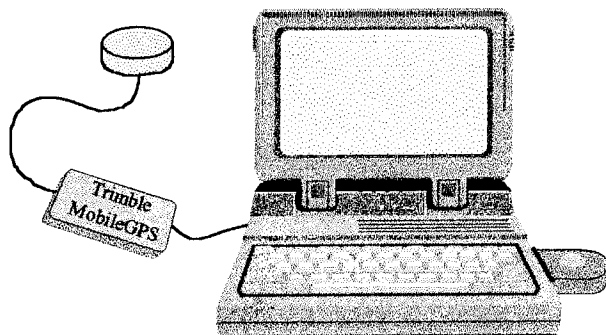


Figure 2. Hardware components of PortaNav

PortaNav uses a centralized Kalman filter to integrate all of the available GPS and map-derived observations. Eight parameters are modelled in the state vector, namely, three geodetic position states (ϕ, λ, h), three velocity states (v_n, v_e, v_h), the receiver clock offset (CdT), and the receiver clock drift rate ($\dot{C}dT$). The C/A code pseudorange and the doppler shift (phase rate) GPS measurements are used to update the filter every epoch. A constant velocity model and a first-order Gauss-Markov noise process are used to model the vehicle dynamics. The effects of SA are not directly modelled; the filter parameters are set loose enough to compensate.

The remainder of this paper focuses on the map aiding approach used in the positioning module of PortaNav. First, map aiding is contrasted with map matching. Then, the coordinate frame and basic observational models for map aiding are presented. The approach taken to identify possible roads of travel is described, and finally, the results of operational tests performed in various urban environments are presented.

MAP MATCHING AND MAP AIDING

The idea of using information from a digital road map in a navigation system is not new. Map matching itself dates back to the sixties. Some map matching techniques involve using road information to correct measurement drift errors, particularly in dead reckoning sensors. Another approach to map matching is to snap the computed solution onto the road network for display purposes only. Several vehicle navigation systems, such as the Etak Navigator [7] use map matching with dead reckoning. Others, such as the Oldsmobile Guidestar [8], use map matching with GPS and dead reckoning.

An approach for using map data to augment GPS without using dead reckoning is given in [9]. The approach is to compute corrections for the GPS data based on a map match. Then an optimum position on the road is selected based on the remaining noise in the measurement data. One other map matching approach worth mentioning is based on correlating the trace of the vehicle track with a path in the road network using fuzzy logic.

The work in this paper differs from other approaches in that map-derived information is treated as an observable and introduced directly into the solution with the other observables. The effect is to influence the filter at the observation level rather than just yank the computed solution to a point on the map. The rationale for this map aiding approach is based on the fact that the digital road maps are not perfect; the absolute coordinates in them have a level of uncertainty, and should be treated as such.

The fundamental assumption behind both map matching and map aiding is that the vehicle is on a road in the road

network. PortaNav uses this assumption in two ways. The first is to introduce a weighted point into the positioning algorithm. The second is to compute a straight line slope-intercept model of the road link and apply this equation as a constraint. In the following sections, each of these two models is described. Before introducing the models, a coordinate frame will be defined.

COORDINATE FRAME FOR MAP AIDING

Throughout the ages of mapping, the world has been represented by using a flat surface. A paper map is based on some map projection that transforms the curvilinear real world to a planar map representation. Digital road maps are constructed in the same way. Knowledge of the transformation algorithm allows one to use the map space coordinates in a curvilinear space. The positioning solution algorithms used in PortaNav are all formed in a geodetic coordinate frame, specifically, using the WGS-84 reference ellipsoid. Etak maps are based on a unique map projection designed to suit the needs of representing a digital road map.

The Etak coordinate system (ECS) is based on the Etak-32 unit, which is an integer value that subtends an angle of $\frac{1}{2^{32}}$ of a great circle. Longitudes have a range of -2^{31} to $+2^{31}$, zero being at the Greenwich meridian and positive being east. Latitudes range from -2^{30} to $+2^{30}$, zero being at the equator, and positive being north. The reason for using this representation is so that coordinate values can be represented by 32-bit integers, thereby reducing the amount of storage space required for the map. The disadvantage to Etak-32 units is the limited resolution. At the equator, the length (d_{ECU}) of an Etak-32 unit is computed as:

$$d_{ECU} = \frac{C_e}{2^{32}} \cong 0.932 \text{ cm}, \quad (1)$$

where $C_e = 40030173$ is the approximate circumference of the Earth (m).

A resolution of one centimetre is more than sufficient for most vehicle navigation requirements.

Due to meridian convergence, the length of an Etak-32 unit varies. In a north-south direction (dy), the Etak-32 unit is constant, and in an east-west direction (dx) it is scaled by the cosine of the latitude. In all other directions the length varies according to the azimuth:

$$dy = lat_2 - lat_1, \quad (2)$$

$$dx = \cos\left(\frac{lat_1 + lat_2}{2}\right) \cdot (lon_2 - lon_1), \text{ and} \quad (3)$$

$$d = \sqrt{dy^2 + dx^2}, \quad (4)$$

where lat_1, lat_2 are the latitudes of points 1 and 2 in ECUs, and
 lon_1, lon_2 are the longitudes of points 1 and 2 in ECUs.

This approximation is valid for short distances relative to the Earth's circumference. For computing long distances accurately, one would need to resort to the spherical distance formula.

The coordinate system used for forming the straight line slope-intercept model is based on a modified local ECS. To form the model, it is best to have a coordinate system where distances are equal in every direction. This is accomplished by multiplying the longitudes by the cosine of latitude. Second, to preserve numerical accuracy, the origin should be shifted nearer to the area of interest. The first computed position is used as the origin for the local ECS. The transformation equations between geodetic coordinates and the local ECS can now be defined:

$$y = \phi \cdot \frac{E_{MAX}}{\pi} - y_{off}, \quad (5)$$

$$x = (\lambda \cdot \frac{E_{MAX}}{\pi} - x_{off}) \cdot \cos(\phi), \quad (6)$$

$$\phi = (y + y_{off}) \cdot \frac{\pi}{E_{MAX}}, \text{ and} \quad (7)$$

$$\lambda = \left(\frac{x}{\cos(\phi)} + x_{off} \right) \cdot \frac{\pi}{E_{MAX}}, \quad (8)$$

where x_{off}, y_{off} are the offsets from the origin (m), and

E_{MAX} is the maximum Etak-32 value $(\frac{1}{2^{31}} - 1)$.

The extents of a road link rarely exceed a few hundred metres, so this coordinate system will serve well to form the straight line slope-intercept model.

It should be noted that the Etak map is based on the NAD-27 datum, which is based on the Clarke 1866 reference ellipsoid. A coordinate transformation must be done between WGS-84 and NAD-27 each time a map-derived position is used in the positioning solution.

Weighted Point Model

Given a computed position, a search is performed in the digital road map database to determine the nearest road. The procedure for the road finding algorithm is outlined later in the paper. The coordinates of the point on the nearest road that are nearest to the computed position are then obtained (Figure 3). These coordinates can be applied to the solution as a weighted point. In least squares, this would be similar to using *a priori* information on the unknown coordinates. The effect is that the coordinates are treated as an observation with some weight. If the weight is of the same order of magnitude as the weights of other observations in the

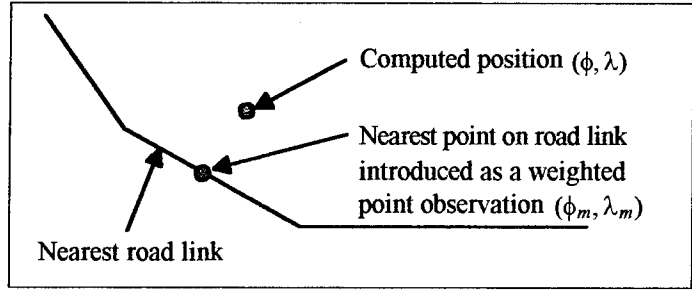


Figure 3. A weighted point observation

adjustment, then the map coordinates will affect the solution significantly.

To evaluate the potential effect of using the weighted point, one must compare the accuracies of the conventional observations with those of the map observations. In PortaNav, the positioning information for the solution is coming primarily from the GPS pseudoranges. As discussed, a horizontal accuracy of about 100 m can be expected for single point GPS solutions. If the coordinates derived from the digital road map have a better accuracy than this, then it may be beneficial to use a weighted point model. Etak claims that their digital road maps are accurate to the fifteen metre level. This claim is not guaranteed by Etak for the beta-release map of Calgary. However, testing did show this claim to be accurate in several areas, and plausibly, the whole map region.

Now that it has been determined that map-derived coordinates will be beneficial, the observation models will be developed. The notation and terminology follows the presentation of the Kalman filtering algorithm in [10]. If the coordinates of the point to be weighted are given in the same geodetic reference frame as the computed GPS solution, the observation equations are:

$$\phi_m = \phi, \sigma_{\phi_m}, \text{ and} \quad (9)$$

$$\lambda_m = \lambda, \sigma_{\lambda_m}, \quad (10)$$

where ϕ_m, λ_m are the map-derived coordinates to be weighted,

ϕ, λ are the unknown geodetic coordinates, and

$\sigma_{\phi_m}, \sigma_{\lambda_m}$ are the standard deviations of the map coordinates.

At any epoch, only one weighted point will be added, so the design matrix will always have two rows. Only the first two columns will be populated:

$$\mathbf{A} = \begin{bmatrix} \frac{\partial \phi_m}{\partial \phi} & \frac{\partial \phi_m}{\partial \lambda} & \frac{\partial \phi_m}{\partial h} & \frac{\partial \phi_m}{\partial v_n} & \frac{\partial \phi_m}{\partial v_e} & \frac{\partial \phi_m}{\partial v_h} & \frac{\partial \phi_m}{\partial C dT} & \frac{\partial \phi_m}{\partial C dT} \\ \frac{\partial \lambda_m}{\partial \phi} & \frac{\partial \lambda_m}{\partial \lambda} & \frac{\partial \lambda_m}{\partial h} & \frac{\partial \lambda_m}{\partial v_n} & \frac{\partial \lambda_m}{\partial v_e} & \frac{\partial \lambda_m}{\partial v_h} & \frac{\partial \lambda_m}{\partial C dT} & \frac{\partial \lambda_m}{\partial C dT} \end{bmatrix} \\ = \begin{bmatrix} 1 & 0 & 0 & 0 & 0 & 0 & 0 & 0 \\ 0 & 1 & 0 & 0 & 0 & 0 & 0 & 0 \end{bmatrix}. \quad (11)$$

Recall that the map coordinates are on the NAD-27 datum while the solution parameters are on the WGS-84 ellipsoid. A coordinate transformation is done on the observations to bring them into the WGS-84 frame. The effect of the transformation on the partial derivatives is negligible, therefore, ignored.

The associated variance-covariance matrix of the observations is simply:

$$C_1 = \begin{bmatrix} \sigma_\phi^2 & \sigma_{\phi\lambda} \\ \sigma_{\lambda\phi} & \sigma_\lambda^2 \end{bmatrix}. \quad (12)$$

And the (2 x 1) misclosure vector is:

$$w = \begin{bmatrix} \phi - \phi_m \\ \lambda - \lambda_m \end{bmatrix}. \quad (13)$$

The weighted point model is formed directly in geodetic space. The observations are map points taken from the digital road map and converted into geodetic coordinates using Equations 7 and 8. The misclosure vector and the variance-covariance matrix of these points are also expressed in geodetic space.

This type of an observation set can be applied in a least squares adjustment or in a Kalman filter. For the least squares adjustment, the extra columns in the design matrix need to be eliminated; for the filter, the misclosure must be negated since the errors are computed rather than the corrections. In PortaNav, when a weighted point update is applied, it is added to the filter after the doppler update in a sequential manner [11].

Slope-Intercept Model

The second type of map aiding model is based on the equation of a straight line. Each road in the digital road map database, whether straight or curved, is broken down into straight line segments. The coordinates of the end points of these line segments can be obtained from the database (Figure 4). With the two sets of coordinates, a straight line equation with a slope and Y-intercept is formed. The equation of the line is then added as an observation to the positioning algorithm. The solution is

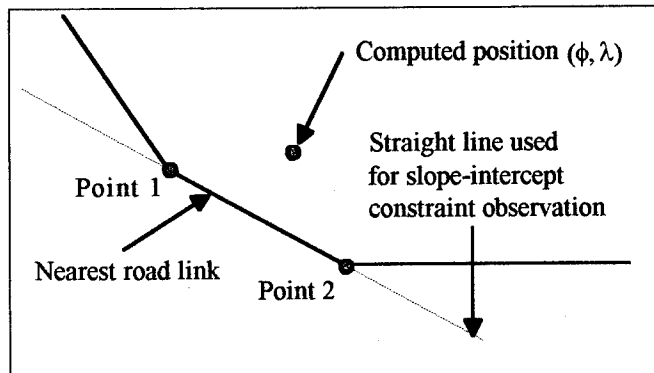


Figure 4. A straight line slope-intercept observation

effectively constrained to a point somewhere on the line rather than to a single point, as was the case in the weighted point observation. Again, decisions on when to use this model are made by the road finding algorithm.

The straight line model is formed in the two dimensional local ECS previously described. Given the two pairs of coordinates (x_1, y_1) , and (x_2, y_2) , the equations for the slope (m) and Y-intercept (b) of the line through them are:

$$m = \frac{y_2 - y_1}{x_2 - x_1}, \text{ and} \quad (14)$$

$$b = y_1 - m \cdot x_1. \quad (15)$$

Assuming the standard deviations of the two points are equal ($\sigma_{x_1} = \sigma_{x_2}$ and $\sigma_{y_1} = \sigma_{y_2}$), the error can be propagated through the model to arrive at:

$$\sigma_m^2 = \frac{2 \cdot k1}{k2}, \quad (16)$$

$$\sigma_b^2 = \frac{(x_1^2 + x_2^2) \cdot k1}{k2}, \text{ and} \quad (17)$$

$$\sigma_{mb} = \sigma_{bm} = \frac{-(x_1 + x_2) \cdot k1}{k2}, \quad (18)$$

where $k1 = \sigma_x^2 \cdot m^2 + \sigma_y^2$, and

$$k2 = 2 \cdot (x_1^2 + x_2^2) - (x_1 + x_2)^2. \quad (19)$$

Now with the slope, intercept, and associated errors of the line, the implicit straight line model can be formed:

$$f(x, l) = m \cdot x + b - y, \quad C_1. \quad (20)$$

In Equation 20, x and y are the unknown coordinates (x) of the vehicle expressed in the two dimensional local ECS, and m and b are the observations (l) as computed in Equations 14 and 15. At any epoch, only one road link will be used as a constraint, so there will only be one equation in this model. The implicit model has two design matrices:

$$A = \begin{bmatrix} \frac{\partial f}{\partial \phi} & \frac{\partial f}{\partial \lambda} & \frac{\partial f}{\partial h} & \frac{\partial f}{\partial v_n} & \frac{\partial f}{\partial v_e} & \frac{\partial f}{\partial v_h} & \frac{\partial f}{\partial c_d T} & \frac{\partial f}{\partial c_a T} \end{bmatrix} \quad (21)$$

$$= \begin{bmatrix} \frac{\partial f}{\partial \phi} & \frac{\partial f}{\partial \lambda} & 0 & 0 & 0 & 0 & 0 & 0 \end{bmatrix}, \text{ and}$$

$$B = \begin{bmatrix} \frac{\partial f}{\partial m} & \frac{\partial f}{\partial b} \end{bmatrix} = \begin{bmatrix} x & 1 \end{bmatrix}. \quad (22)$$

$$\text{where } \frac{\partial f}{\partial \phi} = \frac{\partial f}{\partial x} \cdot \frac{\partial x}{\partial \phi} + \frac{\partial f}{\partial y} \cdot \frac{\partial y}{\partial \phi}, \quad (23)$$

$$\frac{\partial f}{\partial \lambda} = \frac{\partial f}{\partial x} \cdot \frac{\partial x}{\partial \lambda} + \frac{\partial f}{\partial y} \cdot \frac{\partial y}{\partial \lambda}, \quad (24)$$

$$\frac{\partial f}{\partial x} = m, \text{ and} \quad (25)$$

$$\frac{\partial f}{\partial y} = -1. \quad (26)$$

The partial derivatives of the local ECS coordinates with respect to geodetic coordinates are derived by differentiating Equations 5 and 6:

$$\frac{\partial y}{\partial \phi} = \frac{E_{MAX}}{\pi}, \quad (27)$$

$$\frac{\partial y}{\partial \lambda} = 0, \quad (28)$$

$$\frac{\partial x}{\partial \phi} = -\sin(\phi) \cdot \left(\frac{E_{MAX}}{\pi} - x_{off} \right), \text{ and} \quad (29)$$

$$\frac{\partial x}{\partial \lambda} = \cos(\phi) \cdot \frac{E_{MAX}}{\pi}. \quad (30)$$

The elements of the observation variance-covariance matrix are computed in Equations 16 to 18:

$$\mathbf{C}_1 = \begin{bmatrix} \sigma_m^2 & \sigma_{mb} \\ \sigma_{bm} & \sigma_b^2 \end{bmatrix}. \quad (31)$$

And the (1 x 1) misclosure vector is:

$$\mathbf{w} = \left[m \cdot \left(\lambda \cdot \frac{E_{MAX}}{\pi} - x_{off} \right) \cdot \cos(\phi) + b - \left(\phi \cdot \frac{E_{MAX}}{\pi} - y_{off} \right) \right]. \quad (32)$$

Note that the straight line slope-intercept model is formed in the local ECS, so the misclosure and the variance-covariance matrix of the observations (m , b) must be expressed in compatible units. Again, for application in a Kalman filter, the misclosure vector should be negated.

The slope-intercept model and the weighted point model are not both used in the same epoch. If the slope-intercept model is chosen, it is applied after the doppler update in the Kalman filter as was the weighted point model.

ROAD FINDING ALGORITHM

Before either one of the map aiding algorithms can be used, a road must be selected. If an incorrect constraint is introduced into the Kalman filter, the solution may be yanked off course. An algorithm must be designed to find roads and ascertain their validity. If it is not possible to determine which of a number of roads is the correct one at a certain epoch, no map constraints will be applied during that epoch and the filter will rely solely on the GPS measurements available.

Nearest Feature Search

The fundamental task behind selecting a road to use as a constraint is to do a nearest feature search. Given the coordinates of a point, a search is performed on the digital road map database to determine the feature that is closest to that point. The orthogonal distance between a search point and a road link can be found using a vector dot product. The coordinates of the point along the road link that is closest to the search point can then be found using a vector cross product. The procedure for doing this is found in [12].

It is not necessary to search the entire database for the feature nearest to the search point. A search window is defined and used as a mask to limit the search to a small

portion of the digital road map. It is convenient to use the display window as the starting point for the search window. As each road is called up from the database and displayed in graphics space, a record of the road is kept. Only the displayed features are searched, thereby dramatically reducing the computation time required to perform the road finding algorithm. This is crucial in the operation of PortaNav, as multiple searches are performed during each epoch.

Confidence Regions

A confidence region is bounded by a line of constant certainty. If the vehicle is travelling on a road link in the digital road map, then at least one road should fall in the confidence region. The variance-covariance matrix of the estimated parameters computed in the Kalman filter algorithm can be used to determine the semi-major and semi-minor axes and the orientation of a confidence ellipse [13]. The resulting error ellipse is the uncertainty of the position computed in the geodetic coordinate frame. This ellipse does not account for any uncertainty in the positions of the roads in the digital road map.

The uncertainty level in the digital road map is not homogeneous. There is no information stored in the Etak digital road map to quantify the uncertainty, so a global uncertainty level must be chosen. Etak claims a positional accuracy of fifteen metres on average in their production map products. A few areas of the map of Calgary were tested using the precise orbits and clocks. A standard deviation of fifteen metres will in fact be used for the coordinates in the road map.

A good representation of the map uncertainty is a circle of error since the error is not direction dependant. To arrive at a 95% circle of error, the radius is scaled by 2.45. Combining the map error circle with the scaled 95% confidence ellipse of the computed solution yields an ellipse whose axes are extended by the radius of the circle (Figure 5).

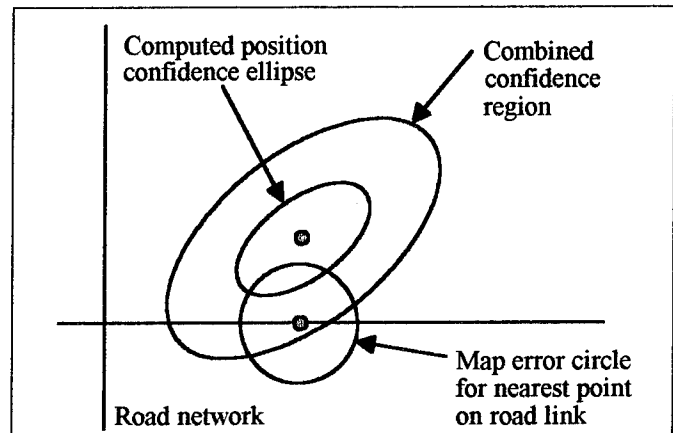


Figure 5. Combination of confidence regions

Now, to find all of the possible roads of travel, a nearest road search should be performed using each of the points of the boundary of the combined confidence ellipse. This is not feasible for a real-time solution, so a simplification is in order. PortaNav uses the centre of the ellipse and the extents of the ellipse as defined by the end points of the semi-major and semi-minor axes. There are five points of interest, so five nearest feature searches are performed. This does not delay the processing significantly, while most of the possible roads will be found. Once the nearest feature search is complete, a list of five possible roads is generated.

Road Selection and Elimination

It is possible that the list of five nearest roads may consist of one to five different roads. If two or more different roads are listed, then further processing is necessary to narrow down the possibilities. A procedure was devised to eliminate unlikely roads based on the azimuths of the road, the direction of travel, and the distance to the nearest point on the identified road.

In order to pass the test of plausibility, a road link must conform to the following two conditions: the azimuth must be near the computed direction of travel, and the road must not be more than a certain distance away from the current point. The first criteria only applies if the vehicle is moving; any road azimuth is valid if the vehicle is stationary. The tolerances chosen for the two conditions were based on the layouts of typical road networks.

The tolerance for the azimuth condition must be large enough to allow for noise in the computed velocities and in the map derived azimuth, while small enough to reject roads that are not in the general direction of travel. A threshold of twenty degrees was chosen for this condition. At most intersections, the intersecting roads are at an angle of 90° . In residential or hilly areas, the

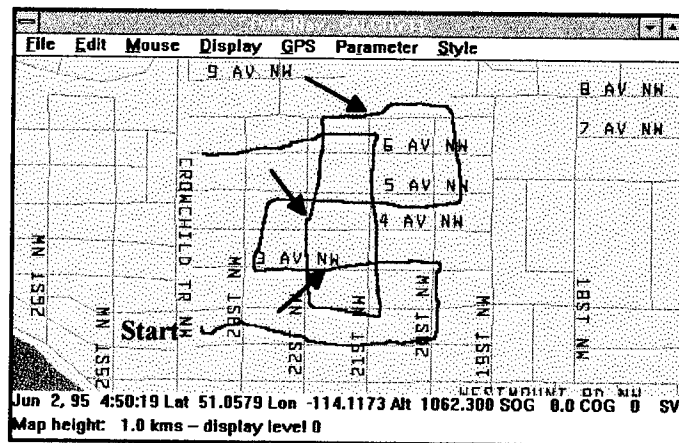


Figure 6. Map aided GPS in open road environment

intersections may be at angles as low as 45° or 50° . The only time where intersections have a smaller angle is in the case of ramps.

The tolerance for distance is required to account for the fact that the vehicle may not be on a road in the database. This is the case when the vehicle is in a parking lot or in an area of the map that is not up to date or complete. Most urban areas have roads spaced at about 100 m. This is the case in most areas of Calgary including both the areas of grid streets and avenues and residential areas. Some of the commercial areas of the city have roads that are spaced further apart.

In order to accept a road, it must be the only found road that has an azimuth that agrees with the direction of travel within twenty degrees either way. Secondly, it must be within 100 m of the computed position of the vehicle. If and only if one road passes both conditions will one of the two map updates be performed.

Map Aided Updates

There is only a small difference in the effect of the two different map-derived updates. The weighted point tends to constrain the solution to that point, while the slope-intercept model tends to constrain the solution to a point somewhere along the road link. Understanding the desired effect is necessary before deciding when one or the other should be applied.

Road vehicles are either stationary or they are moving. If the vehicle is stationary, the solution should be constrained to a point, otherwise, the solution may tend to drift up and down the road link either. If the vehicle is moving, the solution should be allowed the freedom of moving to a different point along the road link. It turns out that a slow moving vehicle should not be allowed the freedom to wander up and down the road link. Therefore a slow vehicle is distinguished from a fast vehicle by some threshold speed. In Calgary, the speed limit for residential areas is 50 km/h. It was decided that the

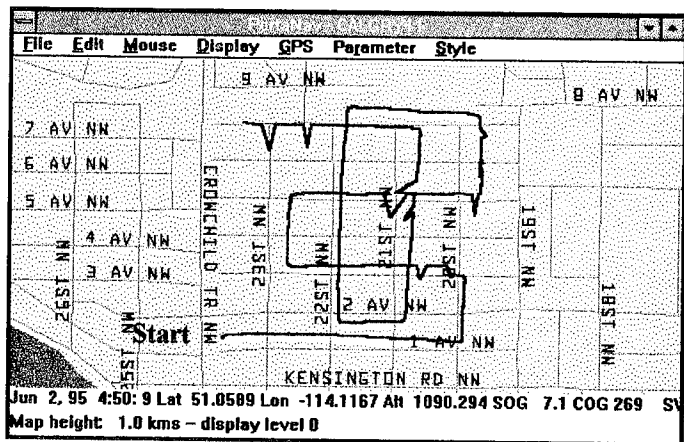


Figure 7. Best DOP fix in open road environment

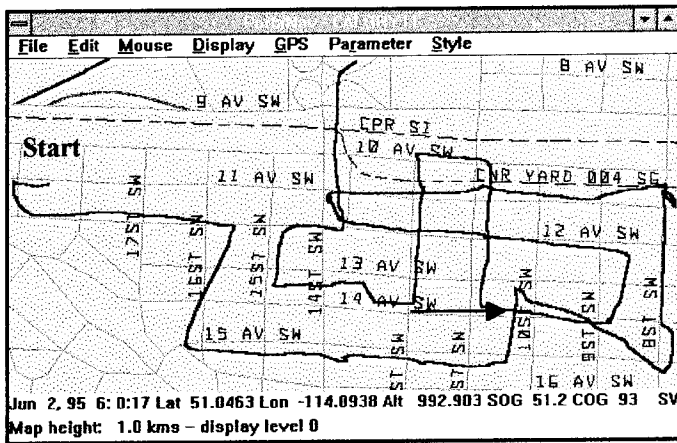


Figure 8. Map aided GPS in tree canopy environment

threshold should be just below this level (45 km/h) so that only vehicles proceeding at slower speeds are constrained using the weighted point algorithm.

SOLUTIONS COMPARED

The first solution using GPS alone is a best DOP unique solution. This solution is arrived at by selecting the four satellites that give the best DOP, and using them in a unique solution to solve for the four unknowns. This solution is computed internally by the Trimble MobileGPS receiver and is logged by PortaNav.

A second GPS stand alone solution uses all of the satellites in view above the cut-off elevation (10°) in a least squares adjustment. Blunder detection and removal is performed if there is redundancy in the adjustment. The results of this solution were even noisier than the best DOP fix because of the increased number of constellation changes. The plots for this solution will not be presented.

The next solution compared is the map aided Kalman filter as outlined in this paper. Again, this algorithm is based on a Kalman filter that uses pseudorange and doppler measurements to filter a state vector with eight

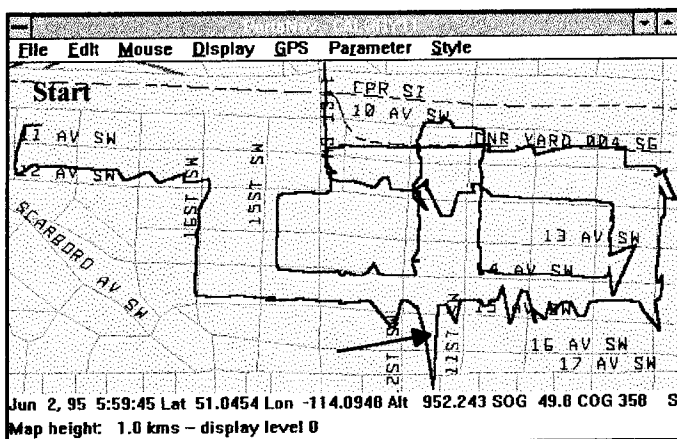


Figure 9. Best DOP fix in tree canopy environment

states. The digital road map is used to find probable roads of travel, and if an acceptable road is found, it is used to update the filter with a spatial constraint.

Finally, the baseline solution against which the above three are compared is arrived at by using precise GPS orbits and clocks to compute a post-mission solution [14]. A static test using the Trimble MobileGPS receiver yielded an RMS of 5.0 m in northing, 4.8 m in easting, and 7.2 m in height. The precise orbits/clocks solution was used to verify the accuracy of the digital road map and confirm the trajectory of the tests. The precise orbits/clocks solutions will not be presented here.

ENVIRONMENTS TESTED

There are three main environments in urban land navigation: open road, tree canopy, and urban canyon. Each of these is described in brief.

Urban canyons are areas where tall buildings line the streets, as is the case in most downtown cores. GPS signals do not penetrate solid matter, so the buildings block the signals, reducing the number of satellites available. Buildings are also highly reflective, so urban canyons tend to be high multipath environments. The maximum multipath error is about 300 m in a pseudorange. Multipath in the order of 150 m is common in urban canyon areas. The effects of multipath are large shifts in the computed positions from epoch to epoch.

Tree canopy refers to areas where the trees are large, have heavy foliage, and possibly even cover the road overhead. GPS signals are affected by the foliage, so the heavier the foliage, the less likely the signal is to reach the receiver. Tree canopy areas tend to not have as bad multipath as the urban canyon areas, however multipath is still apparent. In single point GPS, signal blockage is a large source of noise. This is because each satellite has a different range error due to SA. The result is that when a satellite drops out of or enters the constellation in view, the solution is shifted by up to a few tens of metres. Constellation changes occur frequently in both the tree canopy and the urban canyon environments, causing the solutions to be quite noisy.

The open road is anywhere that does not have obstructions to the satellite signals. Typically these areas are in residential areas with younger trees, major thoroughfares with large right-of-ways, and in areas where the buildings are only one to three stories tall.

KALMAN FILTER PARAMETERS FOR MAP AIDED GPS

There are many parameters that are used to control the behaviour of a Kalman filter. In PortaNav, some

constraints were also introduced to further improve the performance of the filter.

The characteristics of a slow moving vehicle are quite different from those of a fast vehicle. A slow vehicle can change headings quickly, while a fast vehicle can change positions quickly. This knowledge was the basis behind selecting two sets of correlation times and spectral densities. The correlation times, parameter standard deviations, and spectral densities are listed in Table 1. The parameter variances remain the same regardless of the situation. Again, the threshold of 45 km/h was used to distinguish between fast and slow travel. The parameter variances listed were used as the initial variances as well. The relatively high clock variances are due to the fact that the Trimble MobileGPS receiver makes use of a clock that is inexpensive but not very stable.

The standard deviations of the observations appear in Table 2. GPS errors vary largely from situation to situation; the error budget does not always lead to a realistic value. Empirical testing led to the selection of the values listed.

Some of the weaknesses of the Kalman filter can be addressed by adding some constraints to the values of the state vector. Each of the constraints used in PortaNav will be briefly described.

First of all, when the vehicle is stationary, the three velocity components are constrained to zero. This is implemented by observing the velocity as computed independently by the receiver. If the speed over ground (SOG) is less than 2 m/s (7.2 km/h), the vehicle is assumed to be stationary. This assumption is based on the fact that a road vehicle does not normally sustain speeds at this level. Once the static condition has been determined, the velocities are constrained to zero. This is done by setting the velocity states to zero when the states are updated at each epoch. This causes the predicted solution to remain unchanged, while the measurements continue to affect the filtered position.

The second major constraint comes into effect when measurements from only three satellites are available. This happens quite often in areas with tall buildings or trees. If an epoch with only three satellites is used, the height is constrained to the last known value. This allows the filter to remain stable, while making use of the information in the observations to determine the horizontal position and the velocities. This constraint is effectuated in the same manner as the static constraint:

when the state vector is updated, the height parameter is left unchanged.

The final constraint placed on the filter is related to the road that is found. Kalman filters based on a constant velocity dynamics model tend to overshoot the turn when the direction of the vehicle changes. To assist the filter in finding the proper azimuth after changing direction, the azimuth of the first road found is introduced into the state vector. A change in azimuth of more than forty degrees over the span of a few epochs indicates that a significant change in direction has occurred. As soon as an acceptable road is found after a significant change in direction, the azimuth of the road is applied to the

| State parameters | State standard deviation | Spectral density of process noise (m^2/s^3) | | Correlation time of process noise (s) | |
|-----------------------|--------------------------|---|------|---------------------------------------|-------|
| | | slow | fast | slow | fast |
| horizontal positions | 50 m | | | | |
| vertical position | 50 m | | | | |
| horizontal velocities | 10 m/s | 1,000 | 250 | 5 | 20 |
| vertical velocity | 10 m/s | 250 | 125 | 20 | 40 |
| clock offset | 200 m | | | | |
| clock drift | 20 m/s | 80 | 80 | 1,000 | 1,000 |

Table 1. Parameters used in Kalman filter

horizontal velocity components of the filter. Once again, this occurs at the state update phase by projecting the absolute velocity into the easting and northing velocity components using the azimuth of the found road. This constraint causes the predicted position at the next epoch to be along the road, rather than overshooting the road laterally.

Due to the static constraint used, the Kalman filter experiences a lag when the vehicle begins to move again. To help compensate for this, the filter is kick started when the vehicle starts moving after a static period. When the receiver determined SOG rises above the static threshold, the horizontal velocity states in the Kalman filter are set using the receiver determined SOG and course over ground (COG).

TESTS

All of the tests were performed on June 1, 1995. The plots for the map aided solutions show June 2; this is

| Observation | Standard deviation |
|-------------------|--------------------|
| GPS pseudorange | 15 m |
| GPS doppler shift | 0.2 m/s |
| map coordinates | 15 m |

Table 2. Standard deviations of observations

UTC time. The vertical height of each plot is shown on the bottom line of the screen captures. The other parameters are displayed during the run and as the file is played back post-mission. All of the plots are north up.

The plots for the map aided GPS solution are shown in Figures 6, 8, and 10 for the open road, tree canopy and urban canyon environments respectively. The plots of the best DOP fix as computed by the Trimble MobileGPS

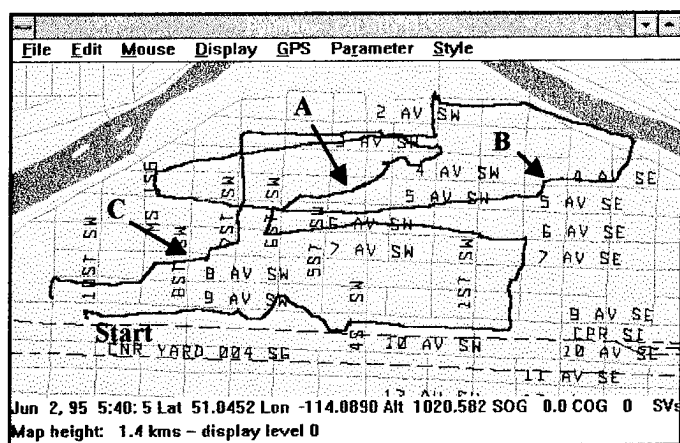


Figure 10. Map aided GPS in urban canyon environment

receiver are shown in Figures 7, 9, and 11. The actual road of travel is easily identified in all of the plots except in the urban canyon plots. Some general comments on each environment follow.

The open road is the most friendly to GPS and that fact is clear in both the map aided and best DOP solutions. The best DOP solution experiences spikes when a satellite is blocked momentarily and the constellation used is changed. From Figure 7, there appears to be a bias to the north and east due to SA. The map aided solution in Figure 6 exhibits a common characteristic of constant velocity Kalman filter models, namely, overshooting the turns. When this happens, the map helps bring the solution into line again. This is evident at the points marked with an arrow in Figure 6.

The primary objective is to identify what street the vehicle is travelling on. The software can do a map match for display purposes, and snap the position onto the road. For the open road case, the snapped solution for each case would be virtually equivalent.

The tree canopy area used has narrow roads, apartment buildings that are two to ten stories high, and large trees that occasionally cover the entire roadway. The effect on the best DOP solution is an increased number of constellation changes, hence several large shifts in the position occur due to SA. The large shift marked with an arrow in Figure 9 is due to multipath. At this point there were two large buildings lining the road.

The trajectory of the map aided solution is much smoother than the best DOP fix, and hence is much more pleasing to the end user. Road identification is still possible at all points in the trajectory except for the area marked with an arrow in Figure 8. The large multipath caused the filter to get lost. The filter was able to avoid the large shift to the south that is apparent in Figure 9, but at the next epoch, an over correction caused the large shift to the north. A blunder this large does not get absorbed by the filter. The filter should be modified to have better blunder detection and removal. The good news is that the filter was able to find the correct position again within two blocks. In Kalman filtering, the solution has the potential to diverge after a large blunder is introduced.

The urban canyon environment is by far the most treacherous for GPS navigation. The signal blockages cause long periods between fixes and frequent instances of high multipath cause large shifts in the positions. The best DOP solution in Figure 11 shows several shifts of up to three hundred metres due to multipath. With the best DOP solution, there are as many fixes near wrong roads as there are fixes near correct roads.

The map aided solution has a smooth trajectory in the urban canyon for the most part. The only time the filter got lost is marked with arrow A. The actual path travelled was north on 6th St. to 3rd Ave., east until 2nd St., south until 4th Ave., then east to 9th St., where the filter finds the correct position. There are two other times where the filter is off course for a block. In the first, marked by arrow B, the vehicle was never on 4th Ave. The problem is caused by an incorrect map update, and was corrected when the vehicle made the next turn. The second instance, marked by arrow C, shows the vehicle traversing blocks diagonally. The actual path of the vehicle was south on 7th St. until 8th Ave., where it turned west. The problem was caused by a long period of blackout. Again, the filter was able to correct itself within two blocks.

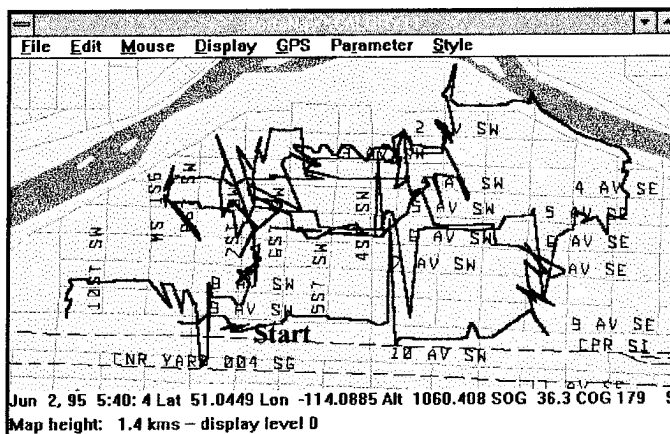


Figure 11. Best DOP fix in urban canyon environment

The performance of the Kalman filter was evaluated with and without each of the state constraints previously described. The static constraint helped the filter remain stable at intersections, and helped to prevent turn overshooting when the vehicle stopped before turning. A disadvantage of the static constraint is when the filter is lost, it takes longer to return to the correct position again. The height constraint only had an effect in the urban canyon. There were a total of 532 epochs over a period of 1,478 seconds in the urban canyon data set. Of these, 273 or 51% were with only three satellites. Over half of the fixes would not have been available without height aiding. The azimuth constraint after a turn helped keep the filter from overshooting the roads laterally. Examples of this occurring are indicated with arrows in Figure 6. The disadvantage to this constraint is that when an incorrect road is found, it takes longer for the true road to be found. The final adjustment to the filter was the kick start applied after static periods, which helped in areas where quick turns were made.

CONCLUSIONS

The map aiding approach taken to augment GPS greatly improves the smoothness of the trajectory in vehicle navigation, particularly in the urban canyon and tree canopy environments. The computed solution enables the vehicle to be displayed on the correct road more often than with GPS alone (with map matching in the display procedure). Map aiding enhances the performance of GPS for autonomous portable vehicle navigation at a low increase in the cost of the system, and with no additional hardware. Map aided GPS provides output that is pleasing to the eye and mind if a user is willing to put up with the filter occasionally becoming lost in the urban canyon environments.

ACKNOWLEDGEMENTS

Partial funding for the research contained herein has been provided by the National Science and Engineering Research Council of Canada (NSERC). Etak of Menlo Park, California, and Trimble Navigation of Sunnyvale, California are acknowledged for their software development support. Precise GPS orbits and satellite clocks for post-mission processing were provided by Geomatics Canada of Natural Resources Canada (NRCAN).

REFERENCES

- [1] Krakiwsky, E.J., M.A. Abousalem, D.J. Szabo, and J.B. Bullock (1995). *IVHS Navigation Systems Database*, Version 4.5. Department of Geomatics Engineering, The University of Calgary, Canada.
- [2] Reimer, J. (1994). "Getting Carded: So, What Are Those PCMCIA Cards All About?" *Pen Computing*, August 1994, Vol. 1, No. 1, pp. 44-48. Pen Computing Inc., Albany, New York.
- [3] Krakiwsky, E.J. and J.F. McLellan (1995). "Making GPS Even Better With Auxiliary Devices." *GPS World*, November 1994, Vol. 6, No. 3, pp. 46-53. Advanstar Communications, Eugene, Oregon.
- [4] Schwarz, K.P., M.E. Cannon, and R.V.C. Wong (1989). "A Comparison of GPS Kinematic Models for the Determination of Position and Velocity Along a Trajectory." *Manuscripta Geodetica*, Vol. 14, No. 5, pp. 345-353.
- [5] Kao, W. (1991). "Integration of GPS and Dead-Reckoning Navigation Systems." *Proceedings of Vehicle Navigation & Information Systems Conference, 1991 (VNIS '91)*, October 20-23, Dearborne, Michigan, pp. 635-643.
- [6] Krakiwsky, E.J., C.B. Harris, and R.V.C. Wong (1988). "A Kalman Filter For Integration of Dead Reckoning, Map Matching, and GPS Positioning." *Proceedings of the IEEE Position, Location, and Navigation Symposium, 1988 (PLANS '88)*, November 29 - December 2, Orlando, Florida.
- [7] Zavoli, W.B. and S.K. Honey (1986). "Map Matching Augmented Dead Reckoning." *Proceedings of Position, Location, and Navigation Symposium, 1986 (PLANS '86)*, Las Vegas, Nevada.
- [8] Tapscott, M. (1994). "On The Road With GPS." *Defense Electronics*, Sept. 1994, Vol. 26, No. 9.
- [9] Scott, C.A. and C.R. Drance (1994). "Increased Accuracy of Motor Vehicle Position Estimation By Utilizing Map Data, Vehicle Dynamics, and Other Information Sources," in *Proceedings of Vehicle Navigation & Information Systems (VNIS '94)*, August 31-September 2, Yokohama, Japan.
- [10] Krakiwsky, E.J. (1992). "The Method Of Least Squares: A Synthesis of Advances." *Department of Geomatics Engineering*, The University of Calgary.
- [11] Brown, R.G. and P.Y.C. Hwang (1992). *Introduction To Random Signals and Applied Kalman Filtering*. Second Edition, John Wiley & Sons Inc., New York.
- [12] Bullock, J.B. (1995). "A Prototype Portable Vehicle Navigation Systems Using Map Aided GPS." M.Sc. Thesis, Department of Geomatics Engineering, The University of Calgary, Canada.
- [13] Mephram, M.P. and B.G. Nickerson (1987). "Preanalysis," *Papers For The CISM Adjustment And Analysis Seminars*. Second Edition, The Canadian Institute of Surveying and Mapping, Ottawa, Canada.
- [14] Geomatics Canada (1994). "GPS Positioning from ACS Clocks and Ephemerides (GPSPACE)." User's guide, Version 2.0. Canadian Active Control System Operations, Geodetic Survey Division, Ottawa, Canada.

Efficient Ambiguity Search Using Genetic Algorithms

Zuofa Li
The University of Calgary

Biography

Mr. Zuofa Li is a Ph.D. candidate in the Department of Geomatics Engineering at the University of Calgary. He received the M.Sc. degree in Surveying Engineering from Wuhan Technical University of Surveying and Mapping in 1987. His current research interests are in the areas of GPS data processing algorithms, airborne gravimetry, multiresolution modeling and estimation in physical geodesy, and applications of fractal geometry and chaos theory in geodesy. He is a student member of ION and an IAG affiliate.

Abstract

In this paper, an efficient search procedure for phase ambiguities is developed using genetic algorithms (GAs). GAs are efficient search techniques based on the mechanism of natural selection, combining a Darwinian survival-of-the-fittest philosophy with a random yet structured information exchange among a population of artificial chromosomes, which correspond to the number of potential ambiguity sets in the ambiguity search procedure. Numerical results show that the correct ambiguities are found after examining only a small portion of the search space using the proposed procedure.

1. Introduction

In GPS positioning, carrier phase is the most precise measurement which makes relative positioning at centimeter level accuracy possible. However since only the fractional part of the phase can be measured, the principal problem in using carrier phase in range mode is the determination of an unknown integer number of wavelengths, known as the phase ambiguity. The phase ambiguities must be resolved correctly to reach centimeter accuracy. The estimation and validation of the phase ambiguities is often referred to as the ambiguity resolution.

During the past few years various approaches have been developed and studied to resolve the phase ambiguities,

e.g. the ambiguity function method (Counselman and Courevitch, 1981; Remondi, 1984; Erickson, 1992), the fast ambiguity resolution approach (Frei and Beutler, 1990; Qiu, 1993), the least squares ambiguity search technique (Hatch, 1991; Lachapelle et al, 1992), Sequential square root information filtering (Landau & Euler, 1992; Euler, 1994), the fast ambiguity search filter (Chen, 1993, 1994), and the ambiguity transform method (Teunissen, 1994; Teunissen and Tiberius, 1994). These ambiguity resolution techniques have a more or less similar strategy for resolving ambiguities. Basically, the procedure starts with an estimation of initial coordinates or initial ambiguities using differential pseudorange solution or float carrier phase solution. Next the potential search space is determined. The search space can be either a physical space (defined in the position domain) or a mathematical space (defined in the ambiguity domain). The ambiguity resolution is then performed by testing many potential coordinates or ambiguity sets inside a predetermined search space. Each potential coordinate set or ambiguity set is tested by applying certain validation and rejection criteria. The search procedure is stopped and ambiguities are fixed when certain assurance criteria are fulfilled.

From the above ambiguity resolution procedure, it is easy to see that the ambiguity search strategies play an important role in the ambiguity resolution. In general, the smaller the search space to be examined, the more efficient an ambiguity resolution procedure will be. The focus of this paper is therefore on developing an efficient search scheme for the ambiguity resolution based on genetic algorithms, which give correct ambiguities after examining only a small portion of the search space.

This paper is organized as follows. The concepts of genetic algorithms are introduced in Section 2, and an efficient search scheme for ambiguity resolution in the ambiguity domain is formulated in Section 3. Numerical examples are given in Section 4 to demonstrate the applicability of the proposed approach.

2. The Concepts of Genetic Algorithms (GAs)

Since Holland's pioneering work (Holland, 1975), there has been a growing number of genetic algorithms for a variety of optimization problems and machine learning tasks because of their robustness and because of their ability to rapidly locate optimal or near-optimal solutions of parameters (e.g. Goldberg and Kuo, 1987; Goldberg, 1989; Grefenstette and Baker, 1989; Siedlecki and Sklansky, 1989; Karr 1991; Karr, et al, 1991; Kumar, 1991).

GAs are search algorithms based on the mechanism of natural genetics. They imitate nature with their Darwinian survival-of-the-fittest approach. This approach allows GAs to speculate on the new points in the search space with expected improved performance by exploiting historical information. GAs use random transition rules, not deterministic transition rules, to guide their search. Although chance is used to define their decision rules, GAs are not random walks through search space. They use the chance efficiently in their exploitation of prior knowledge to rapidly find optimal or near-optimal solutions.

GAs require the natural parameter set of the problem to be coded as a finite string, called a chromosome. In the majority of GA applications, the parameters are coded as binary strings. To understand how this can be done, let us consider the ambiguity resolution problem. If the physical space is chosen, coordinates x , y , and z in the search space have to be coded. Any of these three parameters can be easily represented as a binary string. For example, 6 bits would be interpreted as binary number (e.g. 101010 would be 42). This value would be mapped linearly between x_{\min} and x_{\max} according to the following formula:

$$x = x_{\min} + \frac{\text{bin}}{2^m - 1}(x_{\max} - x_{\min}) \quad (2.1)$$

where bin is the integer value represented by a m -bits string, x_{\min} and x_{\max} are the minimum and maximum of x (or y , or z). The above transformation establishes a one-to-one mapping between m -bits binary strings and real numbers in the interval $[x_{\min} x_{\max}]$ with resolution

$\frac{1}{2^m - 1}(x_{\max} - x_{\min})$. This gives a convenient mean for representing a real number of parameters. Three strings, corresponding to x , y , and z , are then put together to form a string corresponding to the point coordinate (x, y, z) . If the mathematical space is chosen, the ambiguities can be directly coded using the binary representation. Since GAs work with a code of parameters, not parameters themselves, they are difficult to fool because they are not dependent on continuity of the parameter space.

GAs manipulate a set of strings, called population, in the binary space simultaneously. This implicit parallelism gives GAs rapid processing power, which allows simultaneous allocation of search effort to many regions of search space. The population-to-population approach reduces the chance of converging to local maximum in a multimodal search space. Therefore GAs are global search techniques.

A simple GA is composed of three basic operators: 1) reproduction; 2) crossover; 3) mutation. These operators are implemented by performing the basic operations of copying strings, exchanging portion of strings and occasionally altering of a string portion.

Reproduction is an operation by which an old string is copied to a new population according to its fitness value. Here fitness value is defined as non-negative number, which is used to measure the quality of a string. The best string in a search space has maximum fitness value corresponding to an optimal solution of parameters, while the worst has minimum fitness value. In general, the fitness function consists of two functions:

$$f(x)=g(J(x)) \quad (2.2)$$

where J is the objective function, and g transforms the value of the objective function to a non-negative value. The mapping performed by g is always needed when the objective function is to be minimized (since lower objective values must map to higher fitness values) or when the objective function can take on negative values. In this paper, a number of copies is made according to the following distribution:

$$P_i = \frac{f_i}{\sum_{i=1}^n f_i} \quad (2.3)$$

where f_i is the fitness value of a string in the population, n is the number of strings. Reproduction is thus the survival-of-the-fittest step of GAs. The best strings make more copies than the worst.

After reproduction, simple crossover is implemented in two steps. First, the two new strings are selected at random from the strings created by previous selection. Second, a position along the strings is created at random, at which two strings exchange their parts to create two new strings. This is shown as follows. Given two strings [1 0 1 1 0 0] and [0 1 1 0 0 1], crossover at position 4 results in two new strings [1 0 1 0 0 1] and [0 1 1 1 0 0]. Crossover provides a mechanism for strings to mix and match attributes through a random process. When string A loses its desirable qualities to string B, string B is improved and has a better chance to survive in the future generation. However, string A has been weakened, and will die off in future generations.

Crossover in a population is controlled by a crossover rate 'Pcrossover', which is the probability of accepting an eligible pair of chromosomes for crossover. The crossover rate is usually set to a high value to provide sufficient information for processing.

Reproduction and crossover gives GAs the most of their power. The third operation, mutation, increases the variability of the population and prevent premature convergence. The mutation operation introduces occasional random alterations of a string portion. In the binary code, this simply means changing a 1 to a 0 and vice versa. The mutation rate is controlled by the mutation rate 'Pmutation', which is the probability of switching bits in the chromosomes. The mutation rate is typically set to a small value.

After examining the above three operations, an overall processing procedure of a simple GA using the above three operators proceeds in cycles, called generations. First, an initial population of strings (i.e. the first generation) is generated at random. Each string is then decoded yielding the actual parameters. The fitness value for the parameter set corresponding to each string is computed. This fitness value is then used to direct the application of the three operations, which generate a new generation of the population. This simple procedure continues generation by generation until convergence with a population is achieved.

3. An Efficient Ambiguity Search Procedure

In the section, a modified simple GA is applied to develop an efficient procedure for ambiguity search. We will restrict our attention to the efficient search procedure in the mathematical space since searching in the mathematical space is more efficient than in the physical space. However it is also possible to develop an efficient search scheme in the physical space using a similar idea as that described in this section.

The ambiguity search problem in a mathematical space can be formulated as an optimization problem, in which a potential ambiguity set in a predetermined search space is sought such that the estimated ambiguities are equal to the true ones. Since the true ambiguities are always unknown, an objective function is needed to measure the quality of the estimated ambiguities. There are many options available for choosing objective functions. The following objective function is used in this paper:

$$J(\Delta \nabla N) = (\Delta \nabla N - \Delta \nabla \hat{N})^T Q_{\Delta \nabla \hat{N}}^{-1} (\Delta \nabla N - \Delta \nabla \hat{N}) \quad (3.1)$$

where $J(\Delta \nabla N)$ is the objective function for the double difference ambiguity set $\Delta \nabla N$,

$$\Delta \nabla N = \Delta \nabla \Phi - \Delta \nabla \rho,$$

$\Delta \nabla \Phi$ is the observed double difference vector for the true point and $\Delta \nabla \rho$ is the calculated double difference observation, $\Delta \nabla \hat{N}$ is the estimated double difference ambiguity set from the double difference float carrier phase solution, and $Q_{\Delta \nabla \hat{N}}^{-1}$ is the corresponding covariance matrix.

The application of a GA requires some measure for evaluating the quality of the possible solutions represented by individual strings in the population. Since the fitness value must be a non-negative value and the optimal solution should correspond to the maximum of the fitness, the fitness function used here is defined as follows:

$$f(\Delta \nabla N) = b - \log(J(\Delta \nabla N)) \quad (3.2)$$

where b is chosen such that $f(\Delta \nabla N) \geq 0$. The logarithmic mapping is chosen to prevent premature convergence because it exaggerates a small difference when $J(\Delta \nabla N)$ approaches zero.

An ambiguity search procedure based on a modified GA is shown in Figure 1 and can be outlined using the following steps:

Step 1: The real values for the double difference ambiguities are computed using the double difference float carrier phase solution. This can be done by either a sequential adjustment or a Kalman filter.

Step 2: A search cube around the initially estimated double difference ambiguities is defined by a specified set of criteria.

Step 3: An initial population of size n corresponding to a set of double difference ambiguities inside the search cube is selected at random.

Step 4: The strings in the population are decoded and fitness values of these strings are computed according to (3.2). The best string in the population is passed to the next generation.

Step 5: Genetic operations are performed for a given selection criteria, crossover rate and mutation rate.

Step 6: Nominal convergence is checked. If convergence occurs, go to Step 7, otherwise go to Step 4.

Step 7: A new population for the next generation is generated by transferring the best string of the converged population to the new population and then generating the other $n-1$ strings randomly.

Step 8: Go to Step 4 until convergence is achieved.

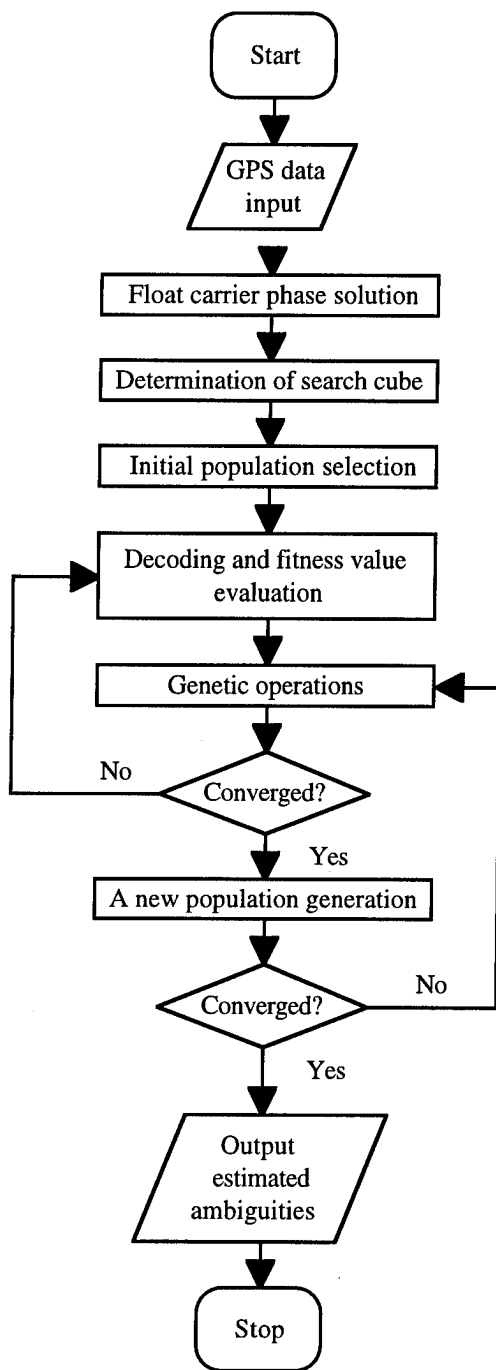


Figure 1. Flow chart for the ambiguity search procedure

The above search procedure is designed for a small population size for reducing the search number of potential ambiguity sets. Because the simple GA described in Section 2 works well when the population size is medium or large (50 ~ 200), it does poorly with a very small population due to insufficient information processing and early convergence to non-optimal results. That is why a modified simple GA is chosen. A flow chart for the proposed search procedure is given in Figure 1. A computer program for such a procedure has been implemented using Matlab-language.

Two important points related to the above ambiguity search procedure need to be addressed:

First, since the application of GAs to the ambiguity search requires only information concerning the quality of the estimated ambiguities, different fitness functions will lead to the same ambiguity search procedure with the exception of the fitness function calculation. Therefore, the above ambiguity search procedure can be generalized.

Second, only three double difference ambiguities corresponding to the four primary satellites are coded in the above search procedures in order to reduce search space. The other double difference ambiguities corresponding to secondary satellites are determined using these ambiguities. Here primary satellites are those satellites necessary to determine a position uniquely, and secondary satellite are the remaining redundant satellites (Hatch, 1991). The advantage of this technique is that only a three-dimensional space needs to be searched regardless of the number of satellites.

4. Numerical Results

To prove the validity of such an ambiguity search procedure, two tests with actual measurements were conducted. The purpose of the first test is to provide validation of the procedure. It is also used to demonstrate the effectiveness of the search procedure. The second test is designed to investigate the performance of the search procedure in static mode, especially in a strong multipath environment.

In the first test, a zero baseline was observed with the NovAtel GPSCard™ receivers on the roof of the Engineering Building of The University of Calgary on May 3, 1995. The zero baseline consisted of two receivers connected to one antenna through an antenna splitter. Since the same observations were received at both receivers, all errors with the exception of receiver noise and a small amount of residual multipath canceled out in double difference mode, given an ideal data set for validation of the proposed procedure. The results to be presented here is based on 5-minute data. The parameter b in the objective function (3.2) is chosen as 10 for both tests. The first test is run with the following two parameter sets:

Case I:

population size=5
string length = 18
Pcrossover = 1.0
Pmutation = 0

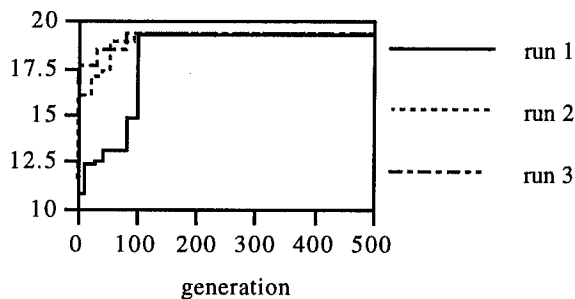
and

Case II:

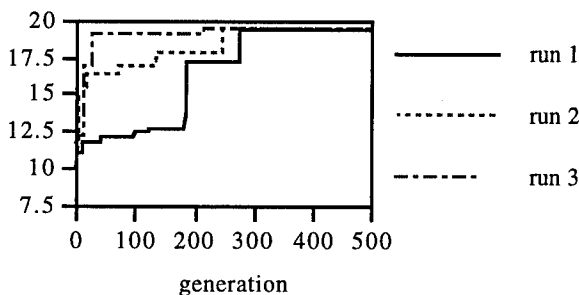
population size=5
string length = 24
Pcrossover = 1.0
Pmutation = 0.

The small population size is chosen to achieve the desired reduction in search number of potential ambiguity sets. The search range for each ambiguity corresponding to the string length 6 is 2^6 , i.e. 64, while the search range for each ambiguity corresponding to Case II is 2^8 , i.e. 256. That means the search cube for both cases consists of 262144 and 16777216 ambiguity sets, respectively. The crossover rate is set to one to facilitate a high order of information processing, while the mutation rate is kept to zero as it is clear that enough diversity will be introduced in the search procedure after Step 7.

Figure 2 shows the fitness value corresponding to the best string in each generation for three independent runs (different initial populations) as it increases with the number of generation. The true and estimated difference ambiguities are given in Table 1.



(a) ambiguity search range: 64 (cycles)



(b) ambiguity search range: 256 (cycles)

Figure 2. Fitness values of test I

| Satellite pairs in differencing | True ΔN (cycles) | Estimated ΔN (cycles) |
|---------------------------------|--------------------------|-------------------------------|
| 4 - 5 | 6301747 | 6301747 |
| 12 - 5 | 110277974 | 110277974 |
| 7 - 5 | 11028053 | 11028053 |
| 9 - 5 | 7877165 | 7877165 |
| 2 - 5 | -52 | -52 |

Table 1: True and estimated double difference ambiguities of Test I

From Figure 2 and Table 1, it is easy to see that the double difference ambiguities have been found correctly for all three runs after no more than 100 generations (i.e. 500 function evaluations or 0.19 % of the search space) in Case I and after no more than 300 generations (i.e. 1500 function evaluations or 0.009% of the search space) in Case II. These results mean that the larger the search range, the more efficient the proposed search procedure will be.

In the second test, two GPS data sets collected in a strong multipath environment are used. The first data set was collected using Magnavox receivers on the roof of the Engineering Building of The University of Calgary on May 12, 1993, and the second one using NovAtel GPSCardTM receivers on the same site on May 27, 1995. Two pillars with known coordinates were chosen for data collection. Therefore the ambiguities can be computed accurately, which will serve as the base for comparisons. The double difference carrier phase residuals of the satellite pair SV 26 - SV 19 for the first data set are shown in Figure 3. The periodic characteristics of the residuals indicates the presence of strong multipath.

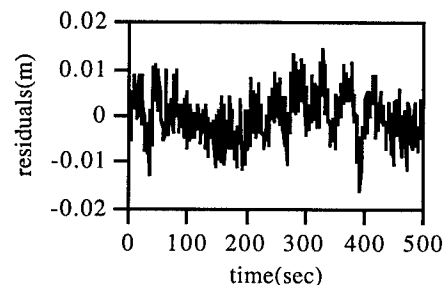
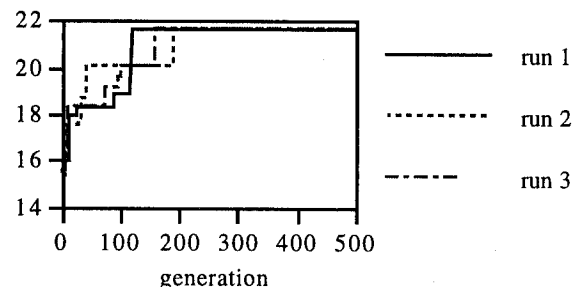
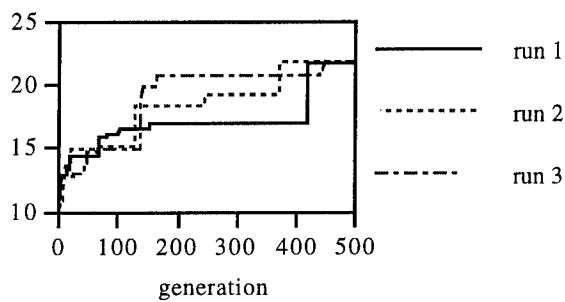


Figure 3. The double difference carrier phase residuals (satellite pair: SV 26 - SV 19)

The second test is also run with the two parameter sets used in the first test. Figures 4 and 5 show the fitness value corresponding to the best string in each generation for three independent runs using two data sets. The true and estimated difference ambiguities for both data sets are given in the Table 2 and 3, respectively.



(a) ambiguity search range: 64 (cycles)

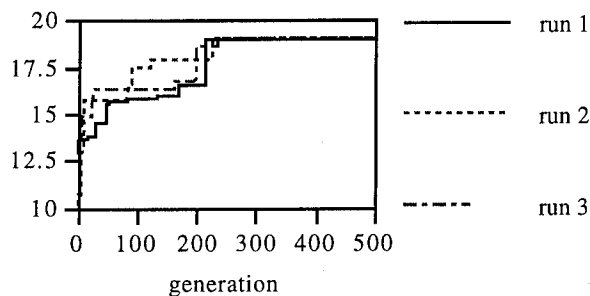


(b) ambiguity search range: 256 (cycles)

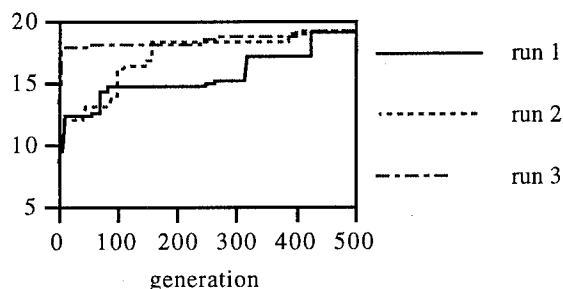
Figure 4. Fitness values for the first data set in Test 2

| Satellite pairs in differencing | True ΔVN (cycles) | Estimated ΔVN (cycles) |
|---------------------------------|---------------------------|--------------------------------|
| 2 - 19 | -20 | -20 |
| 27 - 19 | -40 | -40 |
| 26 - 19 | -58 | -58 |

Table 2: True and estimated double difference ambiguities of the first data in Test 2



(a) ambiguity search range: 64 (cycles)



(b) ambiguity search range: 256 (cycles)

Figure 5. Fitness values for the first data set in Test 2

| Satellite pairs in differencing | True ΔVN (cycles) | Estimated ΔVN (cycles) |
|---------------------------------|---------------------------|--------------------------------|
| 4 - 2 | -3150908 | -3150908 |
| 5 - 2 | -9453253 | -9453253 |
| 14 - 2 | 9452766 | 9452766 |
| 7 - 5 | -15755104 | -15755104 |
| 9 - 2 | 3151081 | 3151081 |
| 24 - 2 | -14186445 | -14186445 |
| 15 - 2 | -14179036 | -14179036 |

Table 3: True and estimated double difference ambiguities of the second data in Test 2

As can be seen from Figures 4 and 5 and Tables 2 and 3, the double difference ambiguities have been found correctly for all three runs after no more than 250 generations (i.e. 1250 function evaluations or 0.48% of the search space) in Case I and 450 generations (i.e. 2250 function evaluations or 0.013% of the search space) in Case II for both data set. Comparing the results from the first test with the second one, one can see that more function evaluations are needed for the second test. That might be due to the multipath effect.

5. Conclusions and Future Work

The above preliminary results are encouraging and show that the ambiguity search procedure based on a GA is an efficient search scheme for ambiguity resolution.

The following work needs to be done to make the algorithm fully operational:

- 1) More tests using a variety of scenarios are needed.
- 2) Comparisons with other ambiguity search methods should be conducted and evaluated.
- 3) A validation method for the proposed search procedure must be developed and tested.

Acknowledgments:

The author would like to thank his supervisor, Dr.K.P.Schwarz, for his guidance and financial support of this research, which was obtained through an NSERC Research grant. W.Qiu, H.Sun, N.El-Sheimy and J.Skaloud are acknowledged for discussions and helpful suggestions during the coding of the ambiguity search procedure. Mrs.J.ML.Lai is also acknowledged for editing the manuscript.

References:

Chen, D.S.(1993): Fast Ambiguity Search Filter (FASF): a Novel Concepts for GPS Ambiguity Resolution, Proceedings of ION GPS-93, Salt Lake City.

- Chen, D.S.(1994): A Comparison of the FASF and Least-Squares Search Algorithms for Ambiguity Resolution On The Fly, Proceedings of KIS94, Banff, Alberta.
- Counselman, C.C and Gourevitch (1981): Miniature Interferometer Terminals for Earth Surveying: Ambiguity and Multipath with Global Positioning System, IEEE transactions on Geoscience, and Remote Sensing, Vol. GE-19, No.4.
- Erikson, C. (1992): Investigation of C/A Code and Carrier Measurements and Techniques for Rapid Static GPS Surveys, Msc Thesis, Publication No. 20044, Department of Geomatics Engineering, The University of Calgary.
- Euler, H.J.(1994): Achieving High-Accuracy Relative Positioning in Real-time: System Design, Performance and Real time Results, Proceedings of IEEE 1994 PLANS, Las Vegas, Nevada, April 11-15, 1994.
- Frei, E. and Beutler (1990): Rapid Static Positioning Based on the Fast Ambiguity Resolution Approach 'FARA': Theory and Their Results, Manuscripta, Geodetica, Vol. 15.
- Goldberg, D.E.(1989):Genetic Algorithms in Search, Optimization and Machine Learning, Addison-Wesley, Reading, MA.
- Goldberg, D.E. and Kuo, C.H.(1987): Genetic Algorithms in Pipeline Optimization, Journal of Computing in Civil Engineering, Vol., No.2, 1987.
- Grefenstette, J.J and Baker, J.E. (1989): How Genetic Algorithms Work: A Critical Look at Implicit Parallelism, Proceedings of the Third International on Genetic Algorithms (Schaffer, T.D.(editor)), Morgan Kaufman Publishes, Inc.
- Hatch, R. (1991): Instantaneous Ambiguity Resolution, Proceedings of IAG Intentional Symposium 107 on Kinematic Systems in Geodesy, Surveying and Remote Sensing, Spring-Verlag.
- Holland (1975): Adaptation in Natural Systems, University of Michigan Press.
- Karr, C.L.(1991): An Introduction of Genetic Algorithms, SPIE Vol. 1515.
- Karr, C.L., Stanley, D.A. and Scheiner, B.J. (1991): Genetic Algorithms Applied to Least Squares Curve Fitting, US Bureau of Mines Report of Investigation, R1 9333, 1991.
- Kumar, K.K(1989): Micro-Genetic Algorithm for Stationary and Non-stationary Function Optimization, SPIE Vol. 1196 Intelligent Control and Adaptive System.
- Lachapelle, Cannon, M.E. and Lu, G.(1992): High-Precision GPS Navigation with Emphasis on Carrier-Phase Ambiguity Resolution, Marine Geodesy, Vol.15.
- Landau, H. and Euler, H.J.(1992): On-the-Fly Ambiguity Resolution for Precise Differential Positioning, Proceedings of the ION GPS-92, Albuquerque, New Mexico, Sept.16-18, 1992.
- Qiu, W. (1993): Analysis of Some Critical Error Sources in Static GPS Surveying, Master Thesis, Publication No. 20054, Department of Geomatics Engineering, The University of Calgary.
- Remondi, B. (1984): Using the Global Positioning System(GPS) Phase Observable for Relative Geodesy: Modeling, Processing and Results, Ph.D. Dissertation, Center for Space Research, The University of Texas at Austin.
- Siedlecki, W. and Sklansky (1989): A Note on Genetic Algorithms for Large-Scale Feature Selection, Pattern Recognition Letter, Vol.10.
- Teunissen, P.J.G (1994): A New Method for Fast Phase Ambiguity Estimation, Proceedings of PLANS94, Las Vegas.
- Teunissen, P.J.G and Tiberius, C.C.J.M(1994): Least-Squares Estimation of the GPS Phase Ambiguities, Proceedings of KIS94, Banff, Alberta.

Airborne Gravimetry by GPS/INS

A Comparison of Filtering Methods

Youcef Hammada
The University of Calgary

Biography

Mr. Youcef Hammada is a M.Sc. student in the Geomatics Engineering Department of the University of Calgary, Canada. His research interests include GPS/INS integration for navigation and positioning, and advanced filtering methods. He holds a bachelor degree in Physics from the University of Algiers, Algeria, and a master's degree in Control Systems from the University of Missouri Rolla, USA.

Abstract

During the last five years, research in airborne gravimetry has been very active due to the fact that aircraft acceleration can now be determined with high accuracy from GPS carrier phase and phase rate measurements. Airborne gravimetry determines the gravity disturbance by differencing a time series of gyro-stabilized accelerometer measurements from an inertial navigation system (INS) and a time series of GPS derived accelerations. The difference is the sum of the gravity disturbance and system noise. The airborne implementation of this principle is so attractive because it allows to measure the gravity signal in large areas in relatively short time.

Both measurements are affected by large noise with different frequency components. Consequently, the gravity disturbance signal is buried in considerable noise and its frequency spectrum resolution will depend on the signal to noise ratio in different frequency bands. The challenge is to derive the most appropriate filtering scheme to recover the useful signal from the noisy measurement. Three approaches are considered and compared in this paper. Finite impulse response low-pass filtering which is basically a frequency domain technique. Kalman filtering with a shaping filter as a stochastic model for the gravity disturbance. Deterministic model filtering that approximates the gravity disturbance by a simple function, such as a constant or a ramp, for a short time interval. The latter approach divides the complete estimation cycle into a series of estimation cycles of short duration, and is therefore quite different from the

other two approaches which consider the whole data span as one function.

The same set of airborne data was used to estimate gravity disturbances by each of the three methods. The gravity disturbance estimates were compared to values obtained through upward continuation of terrain gravity disturbances, used as reference. The deterministic model filtering method showed the expected discontinuities between estimation cycles. After smoothing by an interpolating polynomial, the gravity disturbance estimates reproduced the reference trend. The frequency domain method performance depends on the sensor errors at different frequencies. Again, the gravity disturbance estimates reproduced the reference trend. The Kalman filter method, based on a stochastic model for the gravity disturbance, yielded the best results after a backward optimal Kalman filter smoothing step. The results are preliminary and some possible limitations of the analysis are discussed in the last section.

1 Introduction

The difficulty of extracting the gravity disturbance from the time-synchronized series of GPS and INS measurements is due to the extremely small signal to noise ratio. While the gravity disturbance amplitude would typically be 30 mGal and usually not exceed 100 mGal over distances of about 100 km, the noise level of an airborne gravity system is much higher as Figure 1.1 shows. Although a large part of this is white noise and can be eliminated by low-pass filtering, a considerable part is correlated noise either due to time-dependent system errors or aircraft dynamics. So the problem is to distinguish the gravity disturbance signal from the system measurements which is largely dominated by the system noise, GPS and INS sensors noise.

INS sensor errors due to accelerometer bias, accelerometer scale factor and gyro drift are in the low frequency spectrum range. They affect mainly long wavelength and medium wavelength gravity resolution accuracies. The most predominant GPS error is the aircraft acceleration noise which is amplified by differentiating velocity measurements. It is in the high frequency spectrum range and affects short wavelength gravity resolution accuracy. It

may be useful to emphasize that this is a rather schematic and broad vision. In reality, there exists a region in the error frequency spectrum where both sensor errors are present.

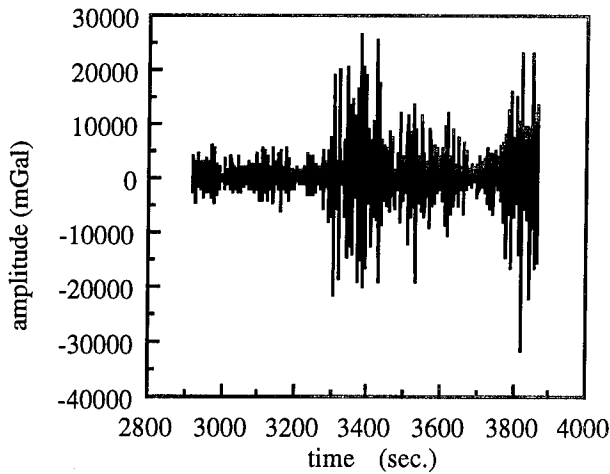


Fig. (1-1) - Gravity system measurements.

The level of "nuisance" of the different error contributors on the gravity disturbance determination accuracy is reviewed. Three different methods to estimate the gravity disturbance are investigated and compared. Only the vertical gravity disturbance estimation, scalar gravimetry, was considered. The theoretical foundations upon which each method is based are quite different. The sensitivities of each method to the error sources affecting the gravity disturbance are also different. Therefore a comparative investigation, based on a numerical test, is insufficient and inappropriate in an absolute sense. However, the opportunity and objective of this paper was to provide the conceptual framework of each method. Consequently, the numerical tests are valuable in a relative sense.

In order to make the comparative study of the three methods meaningful numerically, a common experimental measurement data set was considered. The measurement data were collected during an airborne gravimetry test that took place September 16th, 1994 in Lesser Slave Lake in Alberta, Canada. Furthermore, terrain gravity measurements of the flown area were used to generate an upward continued gravity disturbance grid at flying height. The upward continued gravity disturbances were considered as reference.

2 Concept

The dynamics of the gravity vector, in kinematic mode, are described by Newton's law of motion. When expressed in the local level frame, Newton's second law of motion in the gravitational field of the Earth is of the form (Schwarz and Wei, 1994)

$$\dot{\mathbf{g}}^l = \dot{\mathbf{v}}^l + (2\Omega_{ie}^l + \Omega_{el}^l)\mathbf{v}^l - \mathbf{R}_b^l \mathbf{f}^b, \quad (2-1)$$

where the superscript l denotes that the corresponding vector is expressed in the local level frame, \mathbf{g}^l is the gravity vector, \mathbf{f}^b is the specific force vector expressed in the body aircraft frame, $\mathbf{v}^l, \dot{\mathbf{v}}^l$ is the velocity and acceleration of the aircraft respectively. The parameters Ω_{ie}^l and Ω_{el}^l are the skew-symmetric matrices containing the angular velocities ω_{ie}^l and ω_{el}^l . ω_{ie}^l is the angular velocity of the Earth rotation with respect to the inertial frame and ω_{el}^l is the angular velocity of the local level frame rotation with respect to the Earth fixed frame. The transformation matrix, \mathbf{R}_b^l , represents the orientation of the body frame with respect to the local level frame. The specific force vector in the body frame is sensed by the INS accelerometer triad and the transformation matrix, \mathbf{R}_b^l , can be computed by using body rate measurements ω_{ib}^b sensed by the INS gyro triad. The aircraft position, velocity and latitude are obtained using GPS carrier phase and phase rate measurements. The aircraft acceleration can be obtained by using either GPS position measurements (double differentiation) or GPS velocity measurements (single differentiation). The gravity disturbance is defined as the difference between the actual gravity vector and the normal gravity vector. Therefore, the gravity disturbance dynamic model is given by

$$\delta \mathbf{g}^l = \dot{\mathbf{v}}^l - \mathbf{R}_b^l \mathbf{f}^b + (2\Omega_{ie}^l + \Omega_{el}^l)\mathbf{v}^l - \gamma^l, \quad (2-2)$$

where γ^l is the normal gravity vector which is computed with respect to a specific ellipsoid. In case of scalar gravimetry only the vertical component is of interest (since the north and east gravity vector magnitude components are negligible), the equation (2-2) becomes (Schwarz, Li and Wei, 1994)

$$\delta g_u = \dot{v}_u - f_u + (2\omega_e \cos \varphi + \frac{v_e}{R_N})v_e + \frac{v_n^2}{R_M} - \gamma_u \quad (2-3)$$

where ω_e is the Earth rotation rate, φ is the geodetic latitude, R_N and R_M are the radii of curvature in the ellipsoidal meridian and prime vertical. The subscript u denotes the vertical component.

Clearly, sensor errors directly affect gravity disturbance resolution accuracy. Error sources affecting DGPS carrier phase measurements in kinematic mode, for a short baseline, are essentially receiver noise and multipath. Indeed, the receiver tracking bandwidth has to be sufficiently large to keep track of the satellite signal which makes the receiver noise level higher. Multipath signal has a more random pattern and tends to cancel out. Consequently, GPS in differential mode provides an aircraft velocity with an accuracy of about 1 to 2 cm/s. This value is fully sufficient to make all velocity-dependent corrections in equation (2-3) very accurate. Similarly, normal gravity can be computed with high accuracy using the computed GPS position coordinates,

for details see (Czompo, 1994). On the other hand and despite the highly accurate aircraft position and velocity provided by the differential GPS, the time-differentiation process blows up the error contributed by the aircraft acceleration term, \dot{v}_u , and this error increases rapidly with frequency. This can be seen in the amplitude spectrum of the gravity system measurements of Figure (1-1), given in Figure (2-1). Considering that the amplitudes of the gravity disturbance spectrum are not more than a few mGal in the frequency range 0.1 to 0.5 Hz, the system noise is extremely large. A large part of this noise is due to GPS derived acceleration noise, see for details (Schwarz, Li and Wei, 1994).

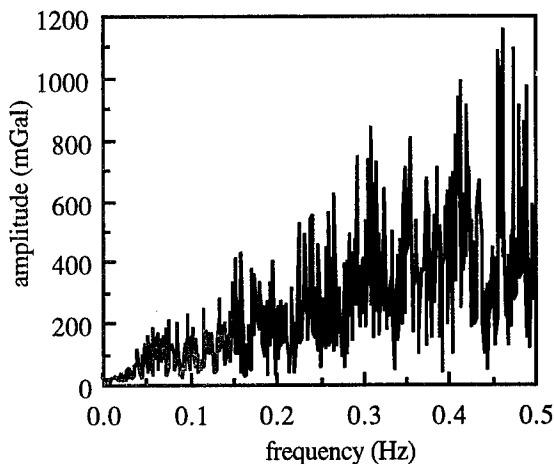


Fig. (2-1) - Measurements frequency spectrum.

The error contributed by the specific force vertical component, f_u , is due to accelerometer measurement noise such as bias and scale factor and to a lesser degree to gyro measurement noise such as gyro drift. However, the so-called accelerometer scale factor contains aircraft vibration effect. These errors are in the same frequency range as the useful signal.

3 Low-pass filtering

Since the gravity disturbance signal being on the low frequency range, it becomes quite natural to consider low-pass filtering methods as a valuable approach. Unfortunately, the large spreading of the sensors noise frequency spectrum lowers the performance expectations of this method.

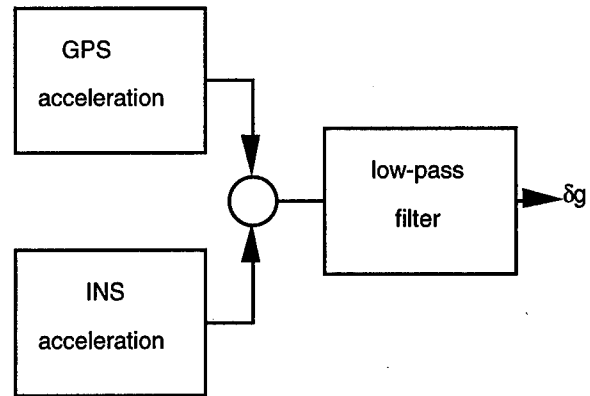


fig. (3-1) - Low-pass filtering diagram.

There are basically two classes of low-pass filters, finite impulse response (FIR) and infinite impulse response (IIR). Finite impulse response low-pass filtering was considered in this paper. Finite impulse response filters are also known as nonrecursive filters, since the current output filter is computed from current and previous inputs. In other words, there is no inherent feedback. The filter has the following mathematical form

$$y(k) = \sum_{n=-N}^N \omega(n)h(n)x(k-n) \quad (3-1)$$

where

- x : filter input
- y : filter output
- h : filter impulse response
- ω : window function.

The finite impulse response low-pass filter is an attractive option because it is inherently stable and does not introduce a phase distortion in the output waveform. The choice of a window function is an important step in the design of a FIR low-pass filter. A window function provides a means of truncating the desired low-pass coefficients, which are generally infinite in extent, in a manner that allows the resulting filter response to be close to the ideal response. Unfortunately, truncation by any window leads to two types of distortion. The first is known as the Gibbs phenomenon, a rippling effect in the filter response due to the window frequency spectrum sidelobes. The second is a broadening of the transition gap between the filter response passband and stopband due to the width of the window's main spectral lobe. A window function is generally chosen (Stearns and Hush, 1990) on the basis of its ability to reduce the Gibbs phenomenon. The sharpness of the transition from passband to stopband may be controlled by the length of the filter, the parameter N in equation (3-1).

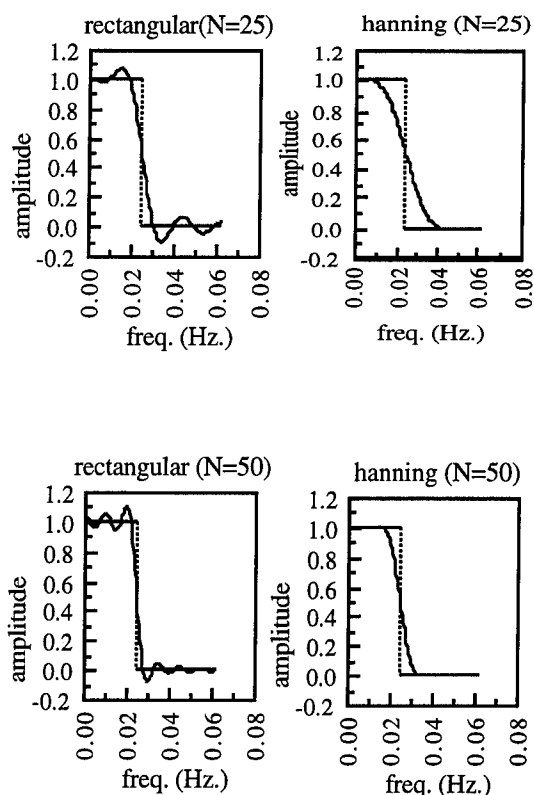


Fig. (3-2) - Ideal versus real low-pass transfer function for two values of N.

3.1 Numerical test

A Hanning window was chosen in this paper because it provides a good trade-off between the main lobe width (passband to stopband transition sharpness) and sidelobe amplitudes (Gibbs phenomenon reduction). A FIR low-pass filter with a cut-off frequency of .007 Hz (150 sec. averaging time corresponding to a 10 km wavelength) was designed to estimate the gravity disturbance.

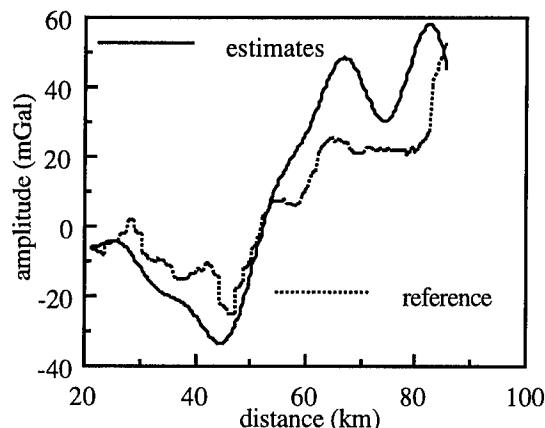


Fig. (3-3) - Low-pass filter estimates versus reference.

The result is relatively good in capturing the trend of the gravity disturbance variation. An accuracy of slightly less than 20 mGal (RMS) is achieved. It shows, however, large biases with respect to the reference solution.

4. Kalman filtering

The gravity disturbance dynamic is described by a shaping filter

$$\delta g_k = F\delta g_{k-1} + G\omega_k, \quad (4-1)$$

for a predetermined gravity disturbance covariance function. Measurements are provided by the differences between INS and GPS accelerations.

$$z_k = H\delta g_k + v_k, \quad (4-2)$$

where ω_k is the white input noise and v_k is the measurement noise. The covariance function describes a statistical model for the local gravity field. It provides the relationship between the gravity field parameters at two different locations. According to previous investigations (E.T. Knickmeyer, 1990, Eissfeller and Spietz, 1989), the gravity statistical model as described in equation (4-1) may be obtained in basically three steps. In the first step, a gravity statistical model described by the covariance function of the anomalous potential is established in the space domain. In the second step, the model is transformed either to the time domain or to the frequency domain. Third step, a shaping filter is derived. Consequently, the starting point in the investigation would be to derive empirically the covariance function from a set of measured terrain gravity disturbances of the flown area. Then a covariance model of the disturbing potential has to be selected from a set of models to fit the empirically determined covariance function. These models are summarized in (E.T. Knickmeyer, 1990). As stated in (Schwarz and Vassiliou, 1987), a good choice for a covariance model is the second order Gauss-Markov model.

4.1 Shaping filter

The shaping filter transfer function, based on the covariance model of the disturbing potential, should produce as output the gravity field states described statistically by the original covariance model when excited by a white noise input. A frequency domain approach, spectral factorization method, is considered for the derivation of the shaping filter. The disturbing potential T is modelled as a second order Gauss-Markov process.

$$C_{TT}(\rho) = \sigma_T^2 (1 + \beta\rho)e^{-\beta\rho}, \quad (4-3)$$

where

- σ_T^2 : variance of T
- ρ : radial horizontal distance
- β : correlation distance

(Schwarz and Vassiliou, 1987).

The state vector may be the disturbing potential and its first derivatives

$$\underline{x} = (T, T_x, T_y, T_z)^T, \quad (4-4)$$

where

$$T_x = \frac{\partial T}{\partial x} = \frac{1}{R \cos \varphi} \frac{\partial T}{\partial \lambda} = -\gamma \eta$$

$$T_y = \frac{\partial T}{\partial y} = \frac{1}{R} \frac{\partial T}{\partial \varphi} = -\gamma \xi$$

$$T_z = \frac{\partial T}{\partial z} = \frac{\partial T}{\partial h} = -\delta g$$

(Moritz 1980).

The parameter γ is the normal gravity, the (x, y, z) coordinates represent the local level frame, ξ meridian deflection component and η the prime vertical deflection component. As stated in (Eissfeller and Spietz, 1989) the spectral matrix is given by

$$S(s) = \frac{2\sigma_T^2 \beta^3}{(\beta^2 - s^2)^2} \begin{bmatrix} 2 & 0 & 2s & 2is \\ 0 & \beta^2 - s^2 & 0 & 0 \\ -2s & 0 & -2s^2 & -2is^2 \\ 2is & 0 & 2is^2 & \beta^2 - 3s^2 \end{bmatrix}$$

which corresponds to

$$S(s) = \begin{bmatrix} S_{TT} & S_{TT_x} & S_{TT_y} & S_{TT_z} \\ S_{T_x T} & S_{T_x T_x} & S_{T_x T_y} & S_{T_x T_z} \\ S_{T_y T} & S_{T_y T_x} & S_{T_y T_y} & S_{T_y T_z} \\ S_{T_z T} & S_{T_z T_x} & S_{T_z T_y} & S_{T_z T_z} \end{bmatrix}$$

To apply spectral factorization, $S(s)$ has to be para-hermitian

$$S(s) = S^T(-s). \quad (4-5)$$

This condition is not met by the off-diagonal elements of the fourth row and column of the spectral matrix. These elements correspond to the cross-correlation between T_z and the other state elements T, T_x, T_y . To alleviate this problem, Eissfeller and Spietz (1989) proposed to neglect these cross-correlation power spectral densities and to split up the problem into the design of a combined potential and deflection shaping filter with the state

$\underline{x}_1 = [T, T_x, T_y]^T$ and a scalar gravity disturbance shaping filter with state $\underline{x}_2 = T_z$, so that

$$S_1(s) = \frac{2\sigma_T^2 \beta^3}{(\beta^2 - s^2)^2} \begin{bmatrix} 2 & 0 & 2s \\ 0 & \beta^2 - s^2 & 0 \\ -2s & 0 & -2s^2 \end{bmatrix}$$

$$S_2(s) = \frac{2\sigma_T^2 \beta^3}{(\beta^2 - s^2)^2} (\beta^2 - 3s^2). \quad (4-6)$$

Only the scalar gravity disturbance shaping filter is considered. The spectral factorization of $S_2(s)$ is such that

$$H(s) = \frac{\sqrt{2}\sigma_T \beta}{(\beta + s)^2} (\beta + \sqrt{3}s). \quad (4-7)$$

Therefore

$$(\beta + s)^2 (-\delta g(s)) = \sqrt{2}\sigma_T \beta (\beta + \sqrt{3}s) \omega(s). \quad (4-8)$$

Using the inverse Laplace transform, the corresponding space domain relation is

$$-\beta^2 \delta g - 2\beta \delta \dot{g} - \delta \ddot{g} = \sqrt{2}\sigma_T \beta^2 \omega + \sqrt{2}\sigma_T \beta \sqrt{3} \dot{\omega}. \quad (4-9)$$

Substituting

$$\delta g_n = \delta g + \sqrt{2}\sigma_T \beta \sqrt{3} \omega. \quad (4-10)$$

Consequently, the gravity disturbance shaping filter is

$$\begin{bmatrix} \delta \dot{g} \\ \delta \dot{g}_n \end{bmatrix} = F \begin{bmatrix} \delta g \\ \delta g_n \end{bmatrix} + G \omega, \quad (4-11)$$

where

$$F = \begin{bmatrix} 0 & 1 \\ -\beta^2 & -2\beta \end{bmatrix}, G = \sqrt{2}\sigma_T \beta \omega \begin{bmatrix} \sqrt{3} \\ -\beta(1 - 2\sqrt{3}) \end{bmatrix}.$$

This spatial domain filter has to be transformed to the time domain which can be accomplished according to the relation

$$\frac{d}{dr} = \frac{d}{dt} \frac{dt}{dr} = \frac{d}{dt} \frac{1}{v}. \quad (4-12)$$

The Kalman filter mechanization is well known, see for instance (Gelb, 1994).

4.2 Numerical test

The estimation required two steps. A forward Kalman filtering and a backward optimal Kalman filter smoothing. The second step was necessary to smooth out the large model uncertainties. Figure (4-1) shows the result after smoothing.

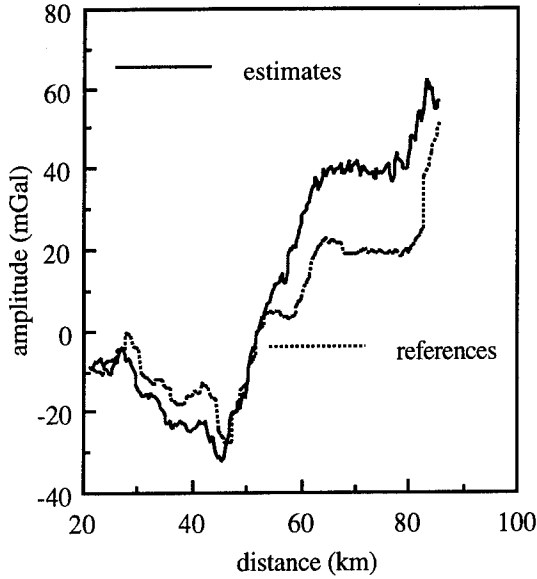


Fig. (4-1) - Kalman filter estimates versus reference.

The trend of the gravity disturbance variation is nicely reproduced although there is still a significant shift between 60 and 80 km. The achieved estimation accuracy is about 10 mGal (RMS).

5 Deterministic model

Based on the fact that the gravity disturbance varies very little over short distances, it may be described by the simple model

$$\dot{x} = 0 \quad \text{or} \quad \delta g_k = \delta g_{k-1} \quad (5-1)$$

The measurement equation remains the same

$$z_k = \delta g_k + v_k \quad (5-2)$$

This approach uses a piecewise continuous function for each estimation cycle. The basic condition that has to be met is that for a short time interval, the gravity disturbance can be considered as a constant or a ramp.

5.1 Constant model

A simple constant model for the gravity disturbance is given in equation (5-1). As stated in (Salychev, 1995), the corresponding Kalman filter is described by

$$\hat{x}_k = \hat{x}_{k-1} + K_k(z_k - \hat{x}_{k-1})$$

$$K_k = \frac{P_o}{kP_o + R}$$

$$P_k = \frac{P_o R}{kP_o + R}$$

where

\hat{x}_k : estimate of δg

K_k : Kalman gain

P_o : initial state error variance
 R : measurement noise variance.

For practical situations, it is realistic to expect the measurement noise variance significantly larger than the initial state error variance. Furthermore there is no a-priori knowledge of the initial state error variance. In order to assess the effect of an overestimation or an underestimation of the initial state error variance on the state estimation, the estimation state error propagation has to be investigated. The estimation state errors may be described by

$$\begin{aligned} \tilde{x}_k &= x_k - \hat{x}_k \\ &= \prod_{i=1}^k (1 - K_{k+1-i}) \tilde{x}_0 \\ &\quad - \sum_{j=0}^{k-1} \left\{ \prod_{i=k+1-i}^j (1 - K_{k+1-i}) \right\} K_{k-j} v_{k-j} \end{aligned} \quad (5-3)$$

where

$$\prod_{i=1}^j (1 - K_{k+1-i}) = 1 \quad \text{for } i > j$$

The corresponding variance can be written as

$$\begin{aligned} P_k &= E[\tilde{x}_k \tilde{x}_k^T] = E[\tilde{x}_k^2] = \\ &= \left[\prod_{i=1}^k (1 - K_{k+1-i}) \right]^2 E[\tilde{x}_0^2] \\ &\quad + \left[\sum_{j=0}^{k-1} \left\{ \prod_{i=k+1-i}^j (1 - K_{k+1-i}) \right\} K_{k-j} \right]^2 E[v_{k-j}^2] \end{aligned} \quad (5-4)$$

where

$$E[\tilde{x}_0^2] = P_o \quad \text{and} \quad E[v_{k-j}^2] = R$$

By expanding both summation terms, a closed form expression for P_k is obtained as

$$P_k = \frac{1}{\left[\frac{kP_o}{R} + 1 \right]^2} P_o + \frac{k^2}{\left[k + \frac{R}{P_o} \right]^2} R \quad (5-5)$$

(Salychev 1995).

The first term in equation (5-5) corresponds to the initial state and the second term corresponds to the measurement noise smoothing. The choice of a large value for P_o will make the first term converge quickly while the second term converges slowly. Therefore the algorithm converges quickly to the initial state, whose value is obtained after a backward estimation run, while the measurement noise is poorly smoothed.

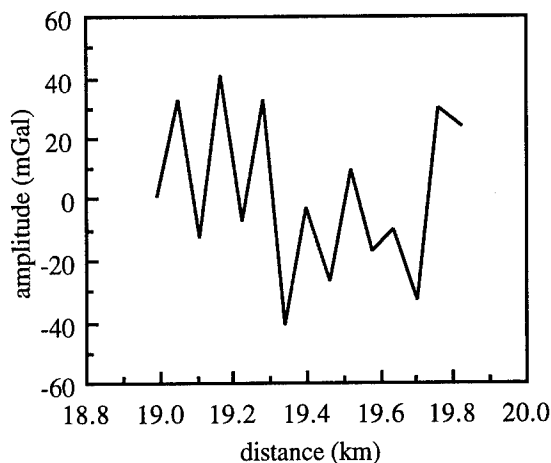


Fig. (5-1) - Estimates for a large P_0 .

Conversely, the choice of a small value for P_0 will make the algorithm strongly smooth the measurement noise while the initial state is poorly estimated.

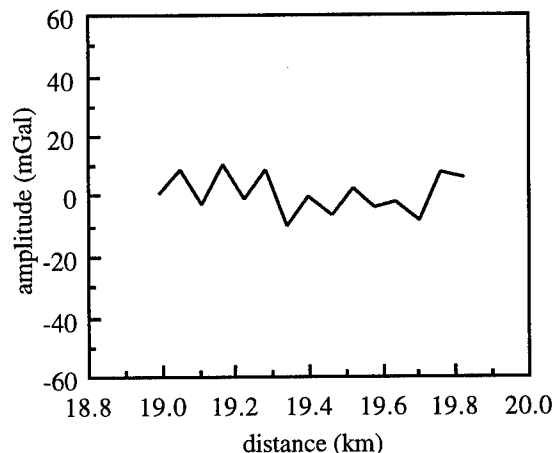


Fig. (5-2) - Estimates for a small P_0 .

One approach to tackle this problem may be to find a trade-off in terms of how accurate the initial state is required and what level of measurement noise smoothing is required. Clearly this approach depends on the length of the estimation interval and the a-priori statistical information. The best trade-off is achievable for a long estimation time interval, which jeopardizes the validity of the constant model for the gravity disturbance. An alternative approach (Salychev 1995) consists of a two step estimation procedure. The first step estimates the initial state vector. The second step smooths the measurement noise by using the gravity disturbance estimates obtained from the first step estimation. Consequently, the measurement noise can no longer be considered as white. The second step estimation may be described by

$$\begin{aligned}\hat{x}_k &= \hat{x}_{k-1} + K_k(z_k - \hat{x}_{k-1}) \\ K_k &= \frac{P_{k-1} - S_{k-1}}{P_{k-1} - 2S_{k-1} + R^*} \\ P_k &= P_{k-1} - K_k(P_{k-1} - S_{k-1}),\end{aligned}\quad (5-6)$$

where

$$R^* = \frac{N^2}{\left[N + \frac{R}{P_0}\right]^2} R$$

$$\begin{aligned}S_{k-1} &= E[\tilde{x}_{k-1} v_k^*] \\ &= \sum_{j=0}^{k-2} \left\{ \prod_{i=1}^j (1 - K_{k-i}) \right\} K_{k-j-1} (N - j - 1)^2 \frac{R}{\left[N + \frac{R}{P_0}\right]^2},\end{aligned}$$

where N is the total number of samples in the interval of estimation. The initial state error variance is provided by the second term of equation (5-5)

$$P = \frac{N^2}{\left[N + \frac{R}{P_0}\right]^2} R$$

(Salychev 1995).

5.1 Numerical test

A basic time interval of 15 second corresponding to a horizontal distance of 900 meters was considered. The next figure shows the particular discontinuity pattern associated with this method.

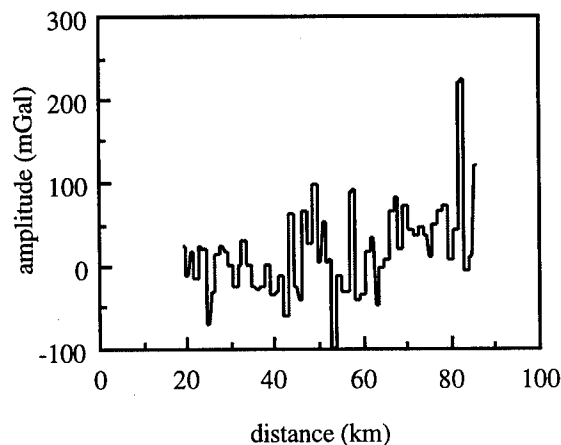


Fig. (5-3) Deterministic model unsmoothed estimates.

A sixth order polynomial was used to interpolate data of the individual pieces of the estimation cycles.

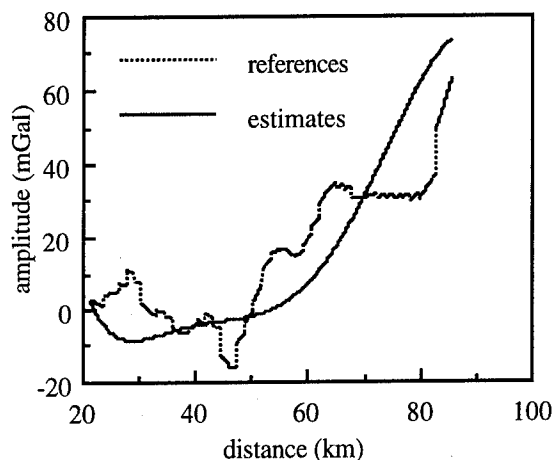


Fig. (5-4) - Deterministic model smoothed estimates versus reference .

A smoothed trend is well reproduced, but all details are lost. The accuracy, in terms of root mean square error, is comparable to the one achieved with the Kalman filter method (about 10 mGal).

6. Discussion and Conclusions

Three methods of gravity disturbance estimation were investigated and numerically tested. Their performances are strongly conditioned by the theoretical assumptions under which they were derived. The conceptual framework of each method was presented. The numerical results can only be assessed in a relative way because the sensitivities of each method to system measurement noise are quite different.

The deterministic model estimates showed, as expected, the discontinuity pattern between consecutive basic estimation cycles. The numerical results showed that interpolating data by using a polynomial was not appropriate. Indeed, despite the smoothing of the discontinuities, signal details were lost. The other factor limiting the estimates accuracy is the effect of accelerometer bias and accelerometer scale factor. Indeed, using the same data set and the same approach, a deterministic model for the gravity disturbance, Salychev (1995) achieved a 1 mGal estimation accuracy. However, a different estimation strategy was used in this case, namely a multi-stage filtering procedure, which consists of four steps. In the first and second step, accelerometer bias and scale factor were removed. Since the accelerometer bias and accelerometer scale factor are the main error source contributors in the low frequency spectrum range, where the useful signal resides, the first two steps revealed to be crucial in achieving a high gravity disturbance resolution accuracy. In the third step, a piecewise gravity disturbance estimation is performed. In the fourth step, a data interpolation using a spline is realized. A spline data

interpolation scheme showed to be more appropriate. Furthermore, using equal length basic interval of estimation for the whole data span may not be optimal, because for some intervals, the deterministic model may not be valid anymore due to the sharp variation of the local gravity field inside these intervals.

The Kalman filter with a shaping filter as a statistical model for the gravity disturbance yielded the best numerical result. Conceptually, the approach is very interesting since the statistical properties inferred in the Kalman filter state model are unique to the local gravity field. Despite the fact that the derivation of the shaping filter requires several approximation stages, the numerical test revealed that a backward optimal Kalman filter will smooth out most of the model uncertainties. In this case, the a-priori removal of the accelerometer bias and the accelerometer scale factor will make the measurements less noisy, and therefore a more conservative choice for the measurement noise covariance matrix is to be considered. On the other hand, the estimation performance should not be affected significantly since the system model reflects only the gravity disturbance statistical properties.

The low-pass filtering method result captured the gravity disturbance variation trend. It missed, however, most of the reference details. In this case, the level of expected accuracy strongly depends on the level of INS sensor noise, accelerometer bias and accelerometer scale factor. Since these errors are in the same frequency range as the useful signal and the low-pass filtering method is frequency content "blind". In addition, accuracy expectation is also conditioned by aircraft vibration effect which is lumped into scale factor effect. Aircraft vibration effect are related to aircraft flight dynamics. As a consequence, its effect varies with frequency, making its detection and removal difficult. The aircraft vibration effect may be reduced by using an aircraft with a smooth flight dynamics. In addition, short wavelength gravimetry is also limited by the low frequency part of the GPS derived acceleration noise. One way to solve or at least to reduce this problem may be simply to avoid it, by increasing the averaging time (decreasing the low pass filter cut-off frequency) using a lower flying velocity aircraft. Another performance limiting factor is the fact that the low-pass filter passband to stopband transition interval cannot be made equal to zero in practice. An a-priori removal of the accelerometer bias and the accelerometer scale factor will obviously improve significantly the performance of this method.

Each method has the potential to achieve a high precision resolution of the gravity disturbance. Provided an a-priori treatment of the sensors noise. A more rigorous derivation of the shaping filter is expected to improve the Kalman filter method.

Acknowledgements

The author would like to thank Dr. K.P. Schwarz for his guidance, support and encouragement. He gratefully acknowledges Dr. O.S. Salychev for providing the INS

field test data and Mr. Argeseanu for preprocessing the GPS data and computing the reference gravity field. He also would like to thank Dr O.S. Salychev for the numerous discussions on airborne gravimetry filtering methods.

References

- [1] **V. Argeseanu (1994)**, "A three-dimensional gravity field model of the Kananaskis area", Msc. thesis, University of Calgary, June 1994.
- [2] **J. Czompo (1994)**, "Airborne scalar gravimetry system errors in the spectral domain", P.h.d thesis, University of Calgary, Canada, May 1994.
- [3] **B. Eissfeller and P. Spietz (1989)**, "Shaping filter design for the anomalous gravity field by means of spectral factorization", manuscripta geodaetica, 14, pp. 183-192.
- [4] **A. Gelb (1974)**, "Applied optimal estimation", MIT Press, Cambridge, Massachusetts, USA.
- [5] **E.T. Knickmeyer (1990)**, "Vector gravimetry by a combination of inertial and GPS satellite measurements", P.h.d thesis, University of Calgary, Canada, September 1990.
- [6] **H. Moritz (1980)**, "Advanced physical geodesy", Herbert Wichmann Verlag Karlsruhe, Abacus Press, Tunbridge, Wells, Kent.
- [7] **K.P. Schwarz, Ye Cai Li, and M. Wei (1994)**, "The spectral window for airborne gravity and geoid determination", KIS94 Banff, Canada, September 1994.
- [8] **K.P. Schwarz and M. Wei (1994)**, "An error analysis of airborne vector gravimetry", KIS94 Banff, Canada, september 1994.
- [9] **K.P. Schwarz and A.A. Vassiliou (1987)**, "Study of the high frequency spectrum of the anomalous gravity potential", University of Calgary, Journal of Geophysical Research, vol. 92, No. B1, pp. 609-617.
- [10] **O.S. Salychev, V.V. Voronov, and K.P. Schwarz (1994)**, "Useful signal in airborne gravimetry application".
- [11] **O.S. Salychev (1995)**, "Airborne gravimetry with high precision resolution", ITS Center Ltd., Moscow, Russia, Report for the University of Calgary, Alberta, April 1995.

Ambiguity Recovery for GPS Long Range Kinematic Positioning

Shaowei Han

The University of New South Wales

BIOGRAPHY

Shaowei Han received a B.Sc. and M.Sc. in Geodesy in 1986 and 1989, respectively, from the Wuhan Technical University of Surveying and Mapping. He then joined the academic staff in the same university and was involved in several projects in GPS rapid static and kinematic positioning, orbit determination and deformation analysis. From 1994, he has been studying at the School of Geomatic Engineering, The University of New South Wales, as a full-time PhD student under the supervision of Dr. Chris Rizos. His research focus is on the use of GPS for precise long range kinematic positioning.

ABSTRACT

Precise long range GPS kinematic positioning to centimetre accuracy requires the carrier phase ambiguities to be resolved. There are many techniques for on-the-fly ambiguity resolution for short baselines (<20km), but none for long range applications (tens to thousands of kilometres). The traditional technique of fixing the integer ambiguity is by initialisation involving a period of static positioning at the beginning of a kinematic session. The weakness of this technique is that it requires a re-initialisation procedure if cycle slips occur during the period the antenna is in motion. Recently, ambiguity resolution procedures have been developed that operate even when the antenna is moving, the so-called "on-the-fly" ambiguity resolution techniques. Ambiguity resolution on-the-fly for long range kinematic mode of positioning, however, is a very difficult task. In this paper, a technique of ambiguity *recovery* is suggested to recover integer ambiguities when cycle slips occur or if the data gap is shorter than a few minutes. This technique comprises three steps. The first step uses the widelane carrier phase observation, together with the combined observation ($-7\phi_1 + 9\phi_2$) and the precise pseudoranges, to detect and remove cycle slips in the one-way carrier phase data. Normally, the cycle slips,

when there are no serious multipath problems, can be detected and removed in this step. The second step uses two combined carrier phase observables ($\phi_1 - \phi_2$ and $-3\phi_1 + 4\phi_2$) and the predicted roving receiver position to detect and remove cycle slips using a Kalman filter algorithm applied to the Ambiguity Function implementation. For the applications when position can be predicted with relatively high precision over a short period, such as the tracking of a railway vehicle, large ship, or aircraft, the second step will be very powerful. The last step involves a validation procedure which determines which integer cycle ambiguity set will be significantly better than other candidate sets. The suggested technique has been successfully tested for various baseline lengths. Results of an aircraft positioning experiment (140km) and a railway tracking experiment (295km) will be presented.

INTRODUCTION

Precise long range GPS kinematic positioning to centimetre accuracy requires the carrier phase ambiguities to be resolved. There are many techniques for on-the-fly ambiguity resolution for short baselines (<20km), but none for long range applications (tens to thousands of kilometres). Colombo et al (1995) suggest a two-step procedure. The first step is an initialisation which can fix the initial integer ambiguity using static data at the beginning of a kinematic session. The second step is to compute the trajectory using a Kalman filter and smoothing algorithm. This technique needs a re-initialisation procedure if cycle slips occur during the period the antenna is in motion. This will involve ambiguity resolution on-the-fly, which is a very difficult task. Based on the analysis of ambiguity resolution techniques such as: search techniques in the *measurement* domain (orbit free techniques); search techniques in the *coordinate* domain (particularly suitable when good approximate initial coordinates are available), and; search techniques in the *estimated*

ambiguity domain using least squares estimation (which makes use of geometric constraints), a technique for ambiguity recovery has been developed which is based on cycle slip detection and repair procedures.

The search technique in the measurement domain used to determine the L1 and L2 whole-cycle ambiguities with the aid of P-code pseudorange data on L1 and L2 was first suggested by Hatch (1986). However it needs a comparatively long time to resolve the ambiguities due to the small wavelengths of the L1 and L2 carrier waves. Subsequently, Wübbena (1989), Dong & Bock (1989), Blewitt (1989), Abidin & Wells (1990) and Goad (1992) proposed the use of P-code pseudorange data on L1 and L2 to determine the integer ambiguities of the widelane observations. The main advantage is that the ambiguities of widelane observations are easily determined and largely independent of the baseline length. But for precise positioning the L1, L2 or ionosphere-free observations are used, not widelane observations, and the integer ambiguities of other independent combined observations should be resolved in order to determine the ambiguities for the L1 and L2 observations. The extra-widelaning technique (Wübbena, 1989) uses widelane, narrowlane and the ionospheric signal phase combinations to determine the integer ambiguity of the widelane and narrowlane observations, aided by P-code pseudoranges on L1 and L2, for static positioning. Abidin & Wells (1990) also use this technique for kinematic positioning. Because the ionospheric effect dramatically increases with increasing baseline length, it is difficult to determine the integer ambiguities of the narrowlane carrier phase observation for long baselines. On the other hand, Dong & Bock (1989), Blewitt (1989) and Goad (1992) use this technique to determine the integer ambiguity of the widelane carrier phase observable using dual-frequency precise pseudorange data for long static baselines first, and then the ionosphere-free combination with L1 ambiguities and the known widelane ambiguity are used to compute the coordinates of the static site and the L1 ambiguities. In this way, the ionosphere-free combination can be processed with free ambiguity parameters and the real-valued ambiguities can be obtained. Because a bias of 10.7cm in the real-valued ambiguities will cause a 1 cycle bias in the L1 ambiguities (eqn (13)), the second step requires a relatively long static observation period to obtain high precision real-valued ambiguity estimates (less than a quarter of 10.7cm). Hence, the L1 ambiguity is not easy to determine for the long range kinematic positioning mode. However, the problem of cycle slip detection and repair does not involve "absolute" ambiguity determination, but rather "relative" ambiguity determination in time. The concern is only with the biases on phase observations

that change with time. It is then possible to carry out cycle slip detection and repair using one-way data within a short period.

The search techniques in the coordinate domain, which are particularly suitable when good approximate initial coordinates are available, mainly use the Ambiguity Function Method (AFM) suggested by Counselman & Gourevitch (1981) and Remondi (1984). Mader (1992) proposed the ionospheric correction technique within the AFM using a trial suite of integers. Han (1993) suggested an integrated technique where the search region for the AFM is defined by the predicted position, and uncertainty, output by the Kalman filter used for kinematic position processing. A highly efficient computation procedure for the AFM using dual carrier phase observations was described by Han & Rizos (1995b). However, the ionospheric effect is the main obstacle for long range kinematic applications, even if the precise ephemeris can be obtained or the orbit biases estimated. If the integer ambiguities at previous epochs are known, the ionospheric delay can be computed and these biases at the current epoch can be predicted with high precision. This means the AFM can then be used to detect and remove cycle slips during a short period, even for long range kinematic applications.

The search technique in the estimated ambiguity domain using integer least squares estimation is the most important technique for short range applications, including kinematic and rapid static positioning (Han, 1995). Many practical searching procedures based on integer least squares estimation have been suggested, such as: Fast Ambiguity Resolution Approach (FARA) (Frei & Beutler, 1990); Cholesky Decomposition method (Landau & Euler, 1992); Spectral Decomposition method (Abidin, 1993); Least Squares Ambiguity Search Technique (Hatch, 1990); Fast Ambiguity Search Filter (FASF) (Chen, 1993), and; Least-squares AMBiguity Decorrelation Adjustment (LAMBDA) (Teunissen, 1994). The main reason these procedures are restricted to short range applications are the orbit bias and ionospheric delay. For long range applications, the ionosphere-free combination observation and the integer ambiguity should be searched if widelane ambiguity is fixed. The short wavelength will result in a large search region and the searching will be difficult for long range applications. If integer ambiguity candidates are available from the cycle slip repair procedure, the searching will become easier and the quadratic form of the residuals can still be used as the criteria for verifying that the selected integer ambiguity set is significantly better than others.

For long range kinematic applications, the preferred option is to resolve cycle slips *and* recover integer

ambiguities instantaneously, and all of the abovementioned general algorithms will make a contribution. In this paper, an ambiguity recovery procedure that integrates the contributions from these three classes of algorithms is proposed.

GPS LONG RANGE KINEMATIC POSITIONING

The observation equations and the ambiguity resolution procedure for high precision long range static positioning were described by Blewitt (1989), Dong & Bock (1989) and Goad (1992), and are based on the following equations:

$$R_1 = \rho + \frac{I}{f_1^2} + \varepsilon_{R_1} \quad (1)$$

$$\varphi_1 \lambda_1 = \rho - \frac{I}{f_1^2} + N_1 \lambda_1 + \varepsilon_{\varphi_1} \quad (2)$$

$$R_2 = \rho + \frac{I}{f_2^2} + \varepsilon_{R_2} \quad (3)$$

$$\varphi_2 \lambda_2 = \rho - \frac{I}{f_2^2} + N_2 \lambda_2 + \varepsilon_{\varphi_2} \quad (4)$$

where R_1 and R_2 are the one-way precise pseudo-ranges; φ_1 and φ_2 are the one-way carrier phase observations in unit of cycles; ρ is the geometric range from station to satellite; I is a function of the Total Electron Content; f_1 , f_2 and λ_1 , λ_2 are the frequencies and wavelengths of the L1 and L2 carrier waves respectively; N_1 and N_2 are the integer cycle ambiguities of the L1 and L2 carrier phase observations; and ε is the observation noise with respect to the observation type indicated by its subscript. The carrier phase combination (i, j) can be represented as (Han & Rizos, 1995a):

$$\varphi_{i,j} = i \cdot \varphi_1 + j \cdot \varphi_2 \quad (5)$$

and its integer ambiguity and wavelength can be represented as:

$$N_{i,j} = i \cdot N_1 + j \cdot N_2 \quad (6)$$

$$\lambda_{i,j} = c / (i \cdot f_1 + j \cdot f_2) \quad (7)$$

where c in eqn (7) is the speed of light in a vacuum. Based on eqns (1-4), the real-valued ambiguity ($N_{i,j}$) estimation formula for a carrier phase combination $\varphi_{i,j}$ can be written as:

$$N_{i,j} = \varphi_{i,j} - \frac{9240(i+j)+289i}{2329 \cdot \lambda_1} \cdot R_1 + \frac{9240(i+j)+289j}{2329 \cdot \lambda_2} \cdot R_2 \quad (8)$$

hence the double-differenced widelane ambiguity can be written as:

$$\Delta \nabla N_{1,-1} = \Delta \nabla \varphi_{1,-1} - \frac{17}{137 \cdot \lambda_1} \cdot \Delta \nabla R_1 - \frac{17}{137 \cdot \lambda_2} \cdot \Delta \nabla R_2 \quad (9)$$

For static data, $\Delta \nabla N_{1,-1}$ can generally be determined using a few tens of minutes of data.

The double-differenced ionosphere-free combination observation can be represented by the formula:

$$\Delta \nabla \varphi_{77,-60} \lambda_{77,-60} = \Delta \nabla \rho + \Delta \nabla N_{77,-60} \lambda_{77,-60} + \varepsilon_{\Delta \nabla \varphi_{77,-60} \lambda_{77,-60}} \quad (10)$$

Because the wavelength of the ionosphere-free combination is very small (0.63cm), $\Delta \nabla N_{77,-60}$ will be very difficult to determine. However, after the widelane ambiguities $\Delta \nabla N_{1,-1}$ are fixed, $\Delta \nabla N_{77,-60}$ can be represented as:

$$\Delta \nabla N_{77,-60} = \frac{60 \cdot i + 77 \cdot j}{i + j} \cdot \Delta \nabla N_{1,-1} + \frac{17}{i + j} \cdot \Delta \nabla N_{i,j} \quad (11)$$

and then substituting in eqn (10), the following form of the observation equation can be obtained:

$$\begin{aligned} \Delta \nabla \varphi_{77,-60} \lambda_{77,-60} &= \Delta \nabla \rho + \Delta \nabla N_{i,j} \left(\frac{17}{i+j} \cdot \lambda_{77,-60} \right) + \\ &+ \Delta \nabla N_{1,-1} \left(\frac{60 \cdot i + 77 \cdot j}{i+j} \cdot \lambda_{77,-60} \right) + \varepsilon_{\Delta \nabla \varphi_{77,-60} \lambda_{77,-60}} \end{aligned} \quad (12)$$

The third term of the right side is therefore a known quantity. The search techniques in the estimated ambiguity domain can be used to resolve $\Delta \nabla N_{i,j}$. The larger the coefficient of $\Delta \nabla N_{i,j}$, the smaller the search region for $\Delta \nabla N_{i,j}$. The maximum value is obtained when $i+j=1$, hence $\Delta \nabla N_{i,j}$ can be represented by $\Delta \nabla N_1$, $\Delta \nabla N_2$ or other combinations which satisfy the condition $i+j=1$, and the same search region will result. In the suggested procedure the least squares ambiguity decorrelation adjustment procedure (LAMBDA) is used, and $\Delta \nabla N_1$ is used. Therefore, eqn (12) can be simply expressed as:

$$\begin{aligned} \Delta \nabla \varphi_{77,-60} \lambda_{77,-60} &= \Delta \nabla \rho + \Delta \nabla N_1 \cdot (17 \lambda_{77,-60}) + \\ &+ \Delta \nabla N_{1,-1} \cdot (60 \lambda_{77,-60}) + \varepsilon_{\Delta \nabla \varphi_{77,-60} \lambda_{77,-60}} \end{aligned} \quad (13)$$

Comparing this equation with the L1 double-differenced phase observation equation, the wavelength of $\Delta \nabla N_1$ in equation (13) is equivalent to 10.7cm ($17 \lambda_{77,-60} = 10.7 \text{cm}$). On the other hand, the orbit bias will affect the ambiguity determination and

though this can be neglected in the short range positioning mode (due to the differential processing), the precise ephemeris is used for long baselines. The effect of the orbit bias on the $\Delta\nabla\rho$ can be approximated as:

$$d\Delta\nabla N_1 = \frac{1}{17\lambda_{77,-60}\bar{\rho}} [\Delta X \cdot (dX^i - dX^j) + \Delta Y \cdot (dY^i - dY^j) + \Delta Z \cdot (dZ^i - dZ^j)] \quad (14)$$

where $(\Delta X, \Delta Y, \Delta Z)$ is the baseline vector; (dX^i, dY^i, dZ^i) and (dX^j, dY^j, dZ^j) are the orbit biases for the three components for satellites i and j ; $\bar{\rho}$ ($\approx 20,000\text{km}$) is the mean value of the distances from receivers to satellites. If we assume the orbit biases at the three components are the same and are random for different satellites, the effect of an orbit bias on $\Delta\nabla N_1$ can be approximated by:

$$m_{\Delta\nabla N_1} = \frac{\sqrt{6}}{51\lambda_{77,-60}\bar{\rho}} \cdot D \cdot m_s \quad (15)$$

where D is the baseline length; m_s is the standard deviation of the satellite orbit information and $m_{\Delta\nabla N_1}$ is the standard deviation of the effect of the orbit bias on the $\Delta\nabla N_1$. If we assume that $m_{\Delta\nabla N_1} < 0.25$ cycle, the maximum length of the baseline for different orbit biases are given in Table 1.

Table 1. Maximum Length of Baseline for Different Orbit Biases

| Orbit Bias (m) | 0.2 | 0.5 | 1.0 | 2.0 | 5.0 | 10.0 |
|---------------------|------|------|-----|-----|-----|------|
| Maximal Length (km) | 3280 | 1312 | 656 | 328 | 131 | 66 |

If the distance from the fixed receiver to the roving receiver is less than 15km, any fast ambiguity resolution technique for static positioning, or ambiguity resolution on-the-fly technique, can be used to obtain the initial integer ambiguities.

After determination of the initial ambiguities $\Delta\nabla N_{77,-60}$ from $\Delta\nabla N_{1,-1}$ and $\Delta\nabla N_1$, double-differenced ionosphere-free combination observations (eqn (10)) can be used for the subsequent GPS long range kinematic positioning within a Kalman filter algorithm. Colombo et al (1995) present decimetre-level accuracies for DGPS kinematic positioning over distances greater than 1000km. The obstacle to practical applications is to *recover* the integer ambiguities if cycle slips do occur while the antenna is in motion. In order to detect and repair a cycle slip in subsequent epochs, the double-differenced ionospheric

delay can be computed using the following relation, if the integer ambiguities are known:

$$\Delta\nabla\left(\frac{I}{f_1^2}\right) = \frac{f_2^2}{f_1^2 - f_2^2} [(\Delta\nabla\varphi_1 - \Delta\nabla N_1)\lambda_1 - (\Delta\nabla\varphi_2 - \Delta\nabla N_2)\lambda_2] \quad (16)$$

CYCLE SLIP DETECTION AND REPAIR FOR ONE-WAY DATA

Cycle slip detection and repair for one-way data was first suggested by Blewitt (1990) for static environment. Han & Rizos (1995a) proposed the widelane and $\varphi_{-7,9}$ combinations for detection and repair of cycle slips for the kinematic positioning mode. After briefly describing the procedure (ibid, 1995a), the validation and rejection criteria are discussed.

1. Real-valued Cycle Slip Estimations

Eqn (8) is suitable for the computation of the real-valued widelane ambiguity at every epoch, but not precise enough to compute the ambiguities for other phase combinations (Han & Rizos, 1995a). Therefore, the ionosphere biased formula is used instead:

$$N_{i,j} = \varphi_{i,j} - \frac{R}{\lambda_{i,j}} + \gamma \frac{I}{f_1^2} \quad (17)$$

where

$$\gamma = \frac{\alpha_{i,j} + \beta}{\lambda_{i,j}} \quad (18)$$

$$\alpha_{i,j} = \frac{4620 \cdot i + 5929 \cdot j}{4620 \cdot i + 3600 \cdot j} \quad (19)$$

$$\beta = \begin{cases} 1 & \text{for } R = R_1 \\ 1.647 & \text{for } R = R_2 \\ 1.323 & \text{for } R = (R_1 + R_2) / 2 \end{cases} \quad (20)$$

R in eqn (17) can be chosen as being either R_1 or R_2 , or the mean value of R_1 and R_2 , which minimise the P-code pseudorange noise (depending on the data available). The larger the wavelength of $\varphi_{i,j}$, the smaller the noise of $N_{i,j}$ if the ionospheric delay can be obtained with high precision. Therefore, widelane and $\varphi_{-7,9}$ combinations are selected for the detection and repair cycle slips.

The biases caused by the ionospheric delay have very strong correlation between epochs and can be

represented as a linear function of time for short periods of up to a few minutes. If some epochs are used to fit a linear function of time and to predict the value at the next epoch, the differences between the predicted value $N_{1,-1}^-(k)$ (or $N_{-7,9}^-(k)$) using previous epochs and the computed value $N_{1,-1}(k)$ (or $N_{-7,9}(k)$), using observations at this epoch in eqns (8) and (17), can be obtained:

$$DN_{1,-1}(k) = N_{1,-1}(k) - N_{1,-1}^-(k) \quad (21)$$

$$DN_{-7,9}(k) = N_{-7,9}(k) - N_{-7,9}^-(k) \quad (22)$$

The standard deviations of $DN_{1,-1}(k)$ and $DN_{-7,9}(k)$ can also be obtained. If no cycle slip or multipath effect is present, the noises of $DN_{1,-1}(k)$ and $DN_{-7,9}(k)$ are dependent on the correlations of the ionospheric delay and the noise of the observations. If the ionospheric delay changes rapidly, the noises will be larger. Figures 4, 5, 6, 8 and 9 illustrate their noise level.

2. Determination of the Integer Cycle Slip Candidates

Based on the cycle slip estimates (eqns (21) and (22)) and their standard deviations, all candidates for integer cycle slips on $\phi_{1,-1}$ and $\phi_{-7,9}$, can be formed using the odd-even relationship.

Based on the definitions of $N_{1,-1}$ and $N_{-7,9}$, the following relation must hold:

$$\begin{aligned} \text{if } N_{1,-1} \text{ is even} &\rightarrow N_{-7,9} \text{ has to be even} \\ \text{if } N_{1,-1} \text{ is odd} &\rightarrow N_{-7,9} \text{ has to be odd} \end{aligned}$$

This odd-even relation implies that when one of these is resolved, the effective wavelength of the other is doubled, and can therefore be resolved more easily. The cycle slips $CS_{1,-1}$ and $CS_{-7,9}$ are subject to the same relations:

$$\begin{aligned} \text{if } CS_{1,-1} \text{ is even} &\rightarrow CS_{-7,9} \text{ has to be even} \\ \text{if } CS_{1,-1} \text{ is odd} &\rightarrow CS_{-7,9} \text{ has to be odd} \end{aligned}$$

Obviously it is easy to determine $CS_{1,-1}$ when $CS_{-7,9}$ is determined and vice versa. The cycle slips on ϕ_1 and ϕ_2 can then be determined using the following relations:

$$CS_1 = \frac{1}{2}(CS_{-7,9} + 9 \cdot CS_{1,-1}) \quad (23)$$

$$CS_2 = \frac{1}{2}(CS_{-7,9} + 7 \cdot CS_{1,-1}) \quad (24)$$

For a static receiver, this step can detect and repair almost all cycle slips due to the low noise. But for a roving receiver, especially where the satellite elevation is relatively low ($< 40^\circ$) or when a few tens of seconds data gap exist, the cycle slip cannot be determined as one unique set. Therefore, many cycle slip candidate sets will be formed. The following tests will be necessary.

3. Validation Criteria for Decision

If the cycle slip in one-way carrier phase cannot be determined as one set using the above procedure, the geometric constraints and Kalman filter prediction information should be used to create validation and rejection criteria in order to resolve the correct set of cycle slips. Using eqns (21) and (22), the real-valued cycle slip estimates and their standard deviations can be computed. The search regions for $DN_{1,-1}$ and $DN_{-7,9}$ can be formed in the one-way case and then to create the search region for the double-differenced observable. The satellite with the highest elevation is selected as the reference satellite. For each double-differenced cycle slips, the following tests should be applied:

Test 1: Tests on the innovation sequences of $\Delta\nabla\phi_{1,-1}$ and $\Delta\nabla\phi_{-7,9}$

The ionospheric delay value for each double-differenced observable can be predicted using the ionospheric delay values computed at the previous epochs (eqn (16)), and the ionosphere-corrected observable of $\Delta\nabla\hat{\phi}_{1,-1}$ and $\Delta\nabla\hat{\phi}_{-7,9}$ can be obtained. The innovation values can be computed using the following equations:

$$\Delta\nabla L_{1,-1} = (\Delta\nabla\hat{\phi}_{1,-1} - \Delta\nabla CS_{1,-1})\lambda_{1,-1} - HX(-) \quad (25)$$

$$\Delta\nabla L_{-7,9} = (\Delta\nabla\hat{\phi}_{-7,9} - \Delta\nabla CS_{-7,9})\lambda_{-7,9} - HX(-) \quad (26)$$

If $\Delta\nabla L_{1,-1} \sim N(0, D_{1,-1} + HP(-)H^T)$ or $\Delta\nabla L_{-7,9} \sim N(0, D_{-7,9} + HP(-)H^T)$, $\Delta\nabla CS_{1,-1}$ or $\Delta\nabla CS_{-7,9}$ will pass the tests, otherwise $\Delta\nabla CS_{1,-1}$ or $\Delta\nabla CS_{-7,9}$ should be rejected. $X(-)$ and $P(-)$ are the Kalman predicted position and its variance matrix; H is the design matrix in the Kalman filter; $D_{1,-1}$ and $D_{-7,9}$ are the variances of $\Delta\nabla\hat{\phi}_{1,-1} \cdot \lambda_{1,-1}$ and $\Delta\nabla\hat{\phi}_{-7,9} \cdot \lambda_{-7,9}$.

Test 2: Test on the quadratic form of the residuals of $\Delta \nabla \hat{\phi}_{1,-1}$

Using the ionosphere-corrected double-differenced widelane observable and the Kalman filter predicted position, the update position and the quadratic form of the residuals $(QF_{1,-1})_i$ with respect to a cycle slip candidate set i can be computed. The following test should then be applied:

$$(QF_{1,-1})_i = V_{1,-1}^T D_{1,-1}^{-1} V_{1,-1} + \delta X_{1,-1}^T P^{-1} (-) \delta X_{1,-1} \quad (27)$$

$$\frac{(QF_{1,-1})_i}{(QF_{1,-1})_{\min}} < \xi_{F_{m,m},1-\alpha} \quad (28)$$

where $V_{1,-1}$ is the residual vector of the widelane observable at this epoch; $\delta X_{1,-1}$ is the correction of $X(-)$ using the widelane observable; $\xi_{F_{m,m},1-\alpha}$ is the Fisher percentile for degrees of freedom m and m and confidence level $1-\alpha$; m is the number of double-differenced observations. If a cycle slip candidate set does not pass the test (eqn(28)), this set should be rejected.

Test 3: Contrast tests on quadratic form of the residuals of $\Delta \nabla \phi_{77,-60}$

Using all cycle slip candidate sets that have passed the previous tests, the cycle slip candidates of the ionosphere-free observable can be formed. Table 2 gives an example in which $\Delta \nabla N_{1,-1}$ and $\Delta \nabla N_{-7,9}$ are $[-2,2]$, and all possible candidate sets are formed for the ionosphere-free observable. The minimum discrepancy among these candidates is 10.7cm. Fixing one set of cycle slips, the current epoch data should be used within the Kalman filter and the quadratic form of the residuals $QF_{77,-60}$ should be computed for each set of cycle slips. If the smallest $(QF_{77,-60})_{\min}$ and $(QF_{77,-60})_i$ with respect to a cycle slip candidate set i are not consistent with the relation:

$$\frac{(QF_{77,-60})_i}{(QF_{77,-60})_{\min}} < \xi_{F_{f,f},1-\alpha} \quad (29)$$

the cycle slip candidate set i should be rejected. $\xi_{F_{f,f},1-\alpha}$ is the Fisher percentile for degrees of freedom f and f and confidence level $1-\alpha$; f is the number of double-differenced observations. If only the current epoch data are used, $f=m$. If all other sets, except the one that has the smallest $(QF_{77,-60})_{\min}$, are rejected, the cycle slip set derived $(QF_{77,-60})_{\min}$ is selected as the correct cycle slip value. Otherwise all cycle slip

sets that have passed the test (eqn (29)) should be treated as candidates for the next epoch.

Table 2. Biases of Different Candidates on Double-Differenced Ranges

| $\Delta \nabla N_{1,-1}$ (cy) | $\Delta \nabla N_{-7,9}$ (cy) | $\Delta \nabla N_1$ (cy) | $\Delta \nabla N_2$ (cy) | $\Delta \nabla N_{77,-60} \cdot \lambda_{77,-60}$ (m) |
|----------------------------------|----------------------------------|-----------------------------|-----------------------------|--|
| -2 | -2 | -10 | -8 | -1.827 |
| | 0 | -9 | -7 | -1.720 |
| | +2 | -8 | -6 | -1.613 |
| -1 | -1 | -5 | -4 | -0.913 |
| | +1 | -4 | -3 | -0.806 |
| 0 | -2 | -1 | -1 | -0.107 |
| | 0 | 0 | 0 | 0 |
| | 2 | +1 | +1 | 0.107 |
| +1 | -1 | +4 | +3 | 0.806 |
| | +1 | +5 | +4 | 0.913 |
| +2 | -2 | +8 | +6 | 1.613 |
| | 0 | +9 | +7 | 1.720 |
| | +2 | +10 | +8 | 1.827 |

CYCLE SLIP DETECTION AND REPAIR USING THE AMBIGUITY FUNCTION METHOD WITH CONSTRAINTS

If there are more than four double-differences for L1 and L2 carrier phase and precise pseudorange, the above procedure will be very powerful. But precise pseudorange data are not always available. Many GPS receivers do not output precise pseudorange data when A/S is on, including the Trimble 4000SSE, Leica System 200, and others. Although some receivers, such as the Ashtech Z12 and the new Leica System 300, output two precise pseudoranges on L1 and L2, the signal-to-noise ratio is relatively low, and the precise pseudoranges are often not available even when L1 and L2 carrier tracking are maintained. If precise pseudorange data are lost for a relatively long period, cycle slip detection and repair using the abovementioned procedure will become difficult. If the carrier phase observable is maintained, but no precise pseudorange data is available, the cycle slip detection and repair step can be performed using a combination of the Ambiguity Function Method (AFM) and Kalman filtering. Details are presented below.

1. Ambiguity Function Method (AFM) for Long Range Kinematic Positioning

The Ambiguity Function Method is insensitive to integer biases such as cycle slips, and hence quite suitable for kinematic positioning applications. The equivalence of AFM and least-squares search methods has been proved (Lachapelle et al, 1992; Han, 1993). The AFM requires good initial positioning in order to

define the search region and a relatively long wavelength carrier phase observation (formed from combinations of dual frequency phase observations), in order to reduce the maxima points and the computation time (Han & Rizos, 1995b). The ionospheric effect is the main obstacle for its application in the long range kinematic case, even when the precise ephemeris is available. If the AFM is not used for positioning, but rather for cycle slip detection and repair, the ionospheric delay can be computed at the previous epochs (eqn (16)) using dual frequency carrier phase observations and the known integer ambiguities. The ionospheric delay at the current epoch can be predicted with high precision if the prediction period is no more than a few minutes.

After integer ambiguities are initialised, Kalman filter processing will be used to determine the position using the double-differenced carrier phase observations. The current version of the software considers the orbit as known. The ionospheric delay can be computed by eqn (16). For the next epoch the ionospheric delay can be predicted and the ionosphere-corrected carrier phase combination observations of $\Delta \nabla \hat{\phi}_{1,-1}$ and $\Delta \nabla \hat{\phi}_{-3,4}$ at the current epoch k can be used to compute the Ambiguity Function value:

$$A(X) = \left| \sum_{s=1}^{m_k} \exp \left[i \cdot \left(2\pi \Delta \nabla \hat{\phi}_{i,j}^s(k) - \frac{2\pi}{\lambda_{i,j}} \Delta \nabla \rho^s(X, k) \right) \right] \right| \quad (30)$$

where X is the trial position within the search region defined by the Kalman predicted position $X(-)$ and its variance $P(-)$; $\Delta \nabla \rho^s(X, k)$ is the computed double-differenced range for the double-differenced observation pair s at epoch k using the trial position X ; m_k is the number of double-differenced observations at epoch k . When $A(X)$ is larger than the 95% of its expectation value, X will be considered to be a maxima point. If only one maxima point is obtained, this point is assumed to be the optimal position.

First, the AFM should be performed using the double-differenced observation $\Delta \nabla \hat{\phi}_{-3,4}$ and the maxima positions obtained. The new search region should be centred at each maxima position and the AFM should be performed using $\Delta \nabla \hat{\phi}_{1,-1}$, and then a set of cycle slip candidates can be obtained for each maxima position. The minimum distance among the maxima points is about twice the observation wavelength ($\lambda_{-3,4} = 1.628\text{m}$) for six visible satellites, and about 1.2 times the observation wavelength in the case of five satellites (Han & Rizos, 1995b).

If only L1 carrier phase is available, the AFM can be performed using the L1 carrier phase observations.

Because the wavelength is only 0.190m, the number of maxima points will be greater than the dual frequency case.

2. AFM with Constraints

Using the AFM, only fractions of the carrier phase observables are used, and hence the data processing is easily implemented. However, there is still other information valuable to positioning, such as the integer ambiguity values, not used. If two or three satellites are still tracking with no cycle slips, or cycle slips that can be repaired using their precise pseudoranges, their integer ambiguities can be used as constraints in the Ambiguity Function Method described above.

Assume the double-differenced observation s has known ambiguities ($\Delta \nabla N_{i,j}^s$) and has been corrected. The constraint can be written as follows:

$$\left| \Delta \nabla \hat{\phi}_{i,j}^s(k+1) - \Delta \nabla N_{i,j}^s - \frac{1}{\lambda_{i,j}} \Delta \nabla \rho^s(X, k+1) \right| \leq \text{EPS} \quad (31)$$

where EPS is a threshold value dependent on the observation accuracies, normally selected as three times the standard deviation of the observation. This constraint will make the search space reduce from three to two dimensions. If three satellites have no cycle slips, two constraints can be constructed and the search space will be reduced to one dimension. Figure 1 shows the search space reduced from two dimensions to one dimension. The maxima points will be reduced from 68 to 4.

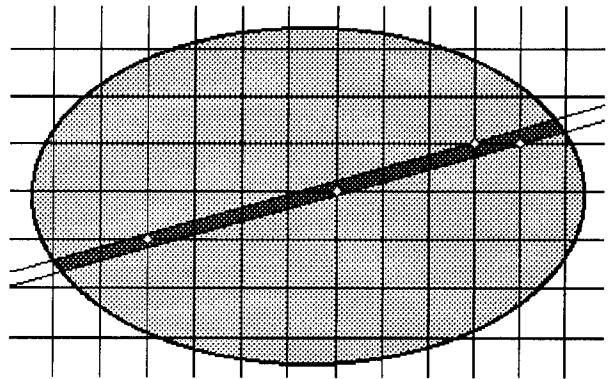


Figure 1. Maxima Points Reduced from Two Dimensions to One Dimension

3. Validation Criteria for AFM in Long Range Applications

Using all cycle slip candidate sets, the ionosphere-free observable can be formed and the current epoch data

used in the Kalman filter. The quadratic form of the residuals $QF_{77,-60}$ should be computed for each set of cycle slips. The same test with eqn (29) should be performed. If all sets except the one that has the smallest $(QF_{77,-60})_{\min}$ are rejected, then the identified cycle slip set is selected as being the correct one. Otherwise all cycle slip sets that passed the test (eqn (29)) should be treated as candidates for the next epoch.

AMBIGUITY RECOVERY PROCEDURES

All data lost at certain epochs will cause gaps. This will occur if all satellite signals are obstructed or a failure in the receiver software occurs. Normally, the best observation environment will be selected for long range kinematic positioning, and hence data gaps seldom occur and are usually only of short duration. The most frequent causes of data loss are due to obstructions of the signal, or a low signal-to-noise ratio caused by bad ionospheric conditions, multipath, high receiver dynamics, or low satellite elevation. Except for the data gap, the data available at an epoch can be divided according to the three cases in Table 3.

Table 3. Cases of Data Loss

| | Data Available |
|----------|---------------------------------------|
| Case I | C/A, ϕ_1, ϕ_2 , P1, or/and P2 |
| Case II | C/A, ϕ_1, ϕ_2 |
| Case III | C/A, ϕ_1 |

Case I: If four or more satellites have Case I data, it is considered that no data loss has occurred because one precise pseudorange is enough to detect and repair cycle slips after a short data gap using the one-way cycle slip detection and repair procedure.

Case II: If less than four satellites have Case I data, but more than four satellites have Case II data, the Kalman filter & AFM procedure for detection and repair of cycle slips can be used. If two or three satellites have precise pseudoranges which can be used to determine any cycle slips, the AFM with constraints procedure can be implemented. $\phi_{1,-1}$ and $\phi_{-3,4}$ will be used in this procedure. If the biases in the observations and the vehicle trajectory can be predicted with high precision, this procedure will be very powerful.

Case III: If four or less satellites have Case II data, but more than four satellites have Case III data, the Kalman filter & AFM with constraints procedure can be used for the single frequency case, but the maxima points will be more numerous than for the dual frequency case due to its short wavelength (0.190m).

Based on the above discussions, the ambiguity recovery procedure can be summarized in Figure 2. After Test 3, if more than one candidate set is left, the current software deletes this epoch and then processes the next epoch. From data processing experience, this normally is caused by multipath and having less than four precise pseudoranges available (Case II or III).

The one-way cycle slip detection and repair procedure can also be used in the ambiguity initialisation step. The cleaned data will then be used in the initialisation procedure.

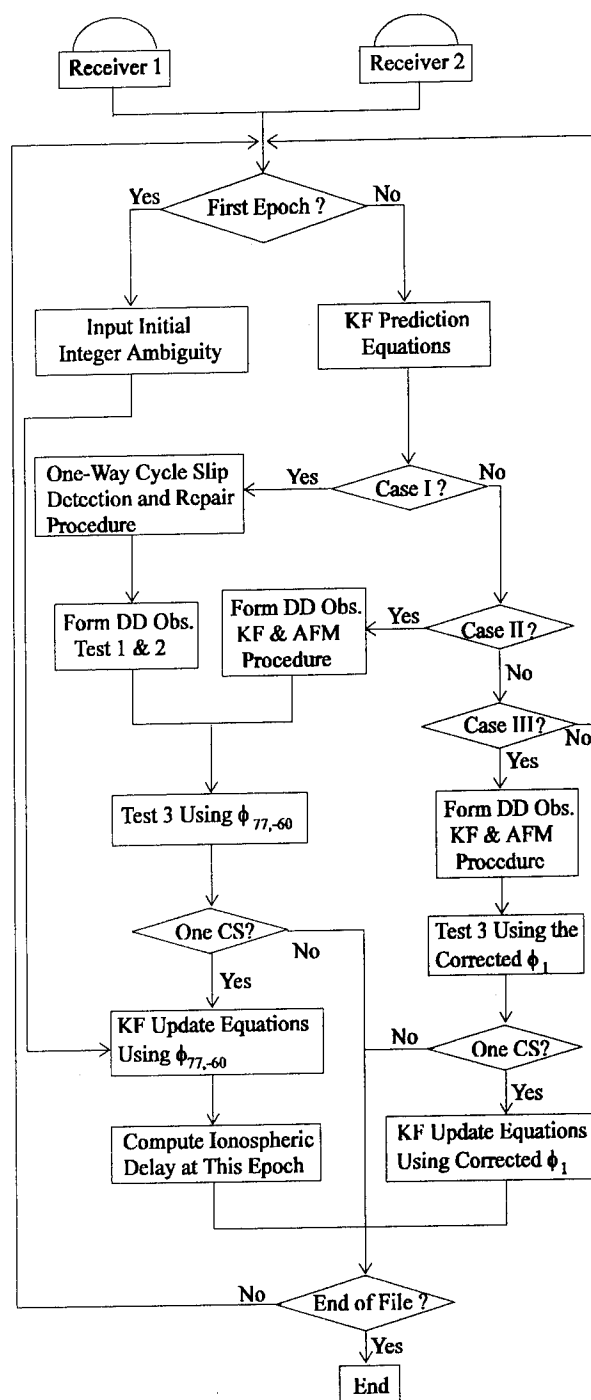


Figure 2. Cycle Slip Detection and Repair Procedure

EXPERIMENTS

1. Aircraft Experiment

This experiment was carried out on June 4, 1992, using Trimble 4000SST GPS receivers capable of measuring a single P-code pseudorange on L2 (R2). The precise ephemeris is available from IGS service. One receiver was mounted on a plane and the other was fixed at a site about 57.5 metres from the initial aircraft location. After 4-5 minutes static tracking the aircraft took off and its trajectory and height are plotted in Figures 3a and 3b. Eqn (17) is used to compute $N_{1,-1}(k)$ and $N_{-7,9}(k)$, and then to predict $N_{1,-1}^-(k)$ and $N_{-7,9}^-(k)$ using the previous several epochs (ten epochs are chosen here). The differences between the predicted value and the computed value using real P-code pseudorange data on L2 and dual frequency carrier phase observations are plotted in Figures 4a and 4b for the aircraft receiver, and Figures 5a and 5b for the stationary receiver. For the roving receiver (Figures 4a & 4b), it can be seen that the noise of $DN_{-7,9}(k)$ is less than 0.25 cycles and $CS_{-7,9}(k)$ normally has one candidate set. If the noise of $DN_{1,-1}(k)$ is larger than 0.5 cycles, $CS_{1,-1}(k)$ normally has more than one candidate set. The odd-even relationship will be very powerful for reducing the cycle slip candidate sets. For the stationary receiver (Figures 5a & 5b), the noise of $DN_{-7,9}(k)$ and $DN_{1,-1}(k)$ is small enough to determine cycle slips. The elevation of this satellite (PRN 23) is plotted in Figure 5a. It can be seen that the lower the elevation, the higher the noise of $DN_{1,-1}(k)$. Based on the cycle slip candidates in the one-way data, the double-differenced cycle slips can be formed and Test 1 and Test 2 then applied using the Kalman filter predicted position and the predicted ionospheric delay value. After Test 3 is applied, only one cycle slip candidate set is left at each epoch for this experiment.

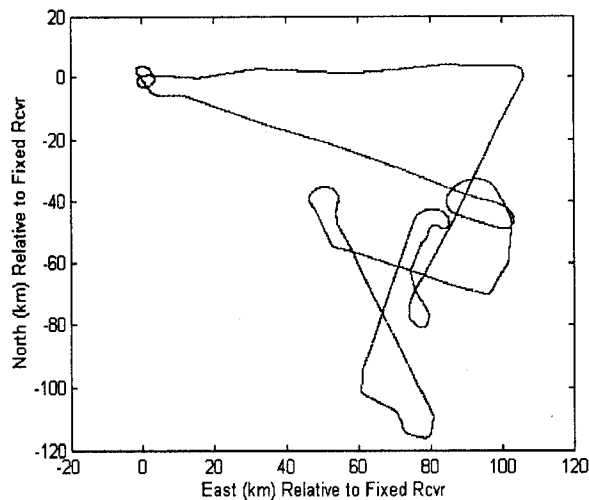


Figure 3a. Aircraft Trajectory Relative to Fixed Rcvr

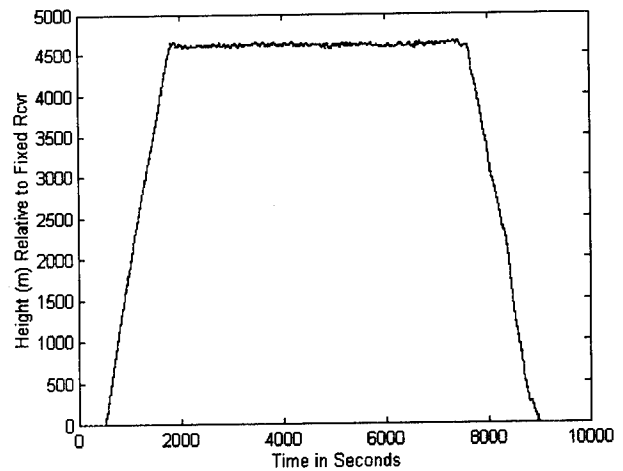


Figure 3b. Aircraft Height Relative to Fixed Rcvr

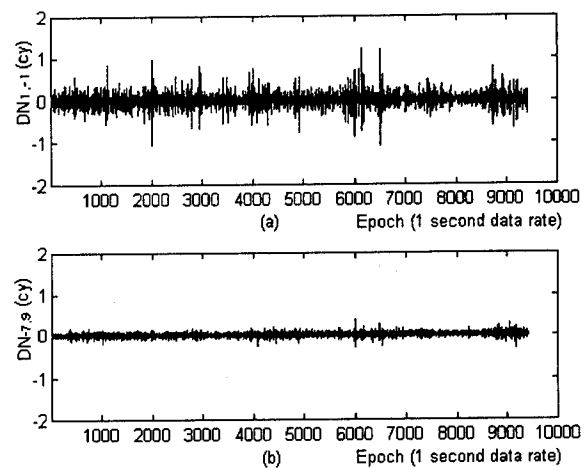


Figure 4. Real-valued Cycle Slip Estimates ($DN_{1,-1}$ (a) and $DN_{-7,9}$ (b)) for Aircraft Receiver

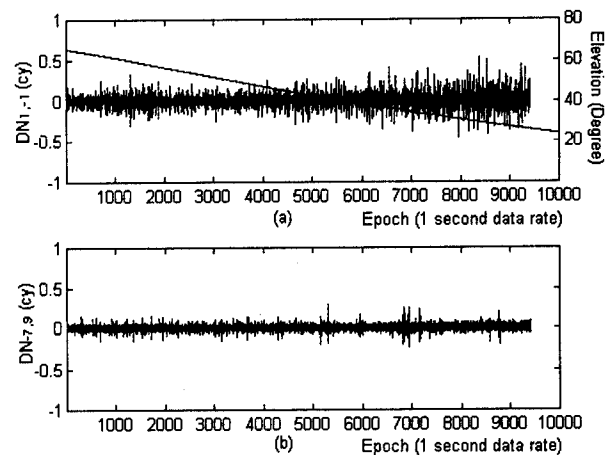


Figure 5. Real-valued Cycle Slip Estimates ($DN_{1,-1}$ (a) and $DN_{-7,9}$ (b)) for Fixed Receiver

In order to test the power of this procedure, a 60 second data gap after epoch k is simulated. The predicted $N_{1,-1}^-(k+60)$ and $N_{-7,9}^-(k+60)$ using 60 epoch data before epoch k can be obtained. The

computed real-valued cycle slips $DN_{1,-1}(k+60)$ and $DN_{-7,9}(k+60)$ at each epoch are plotted in Figures 6a and 6b. It can be seen that the noise of $DN_{1,-1}(k)$ does not change much, but the noise of $DN_{-7,9}(k)$ has increased significantly. The cycle slip detection and repair procedure can successfully determine one cycle slip candidate set. A 5 minute data gap simulation was then selected, but the data processing was not successful.

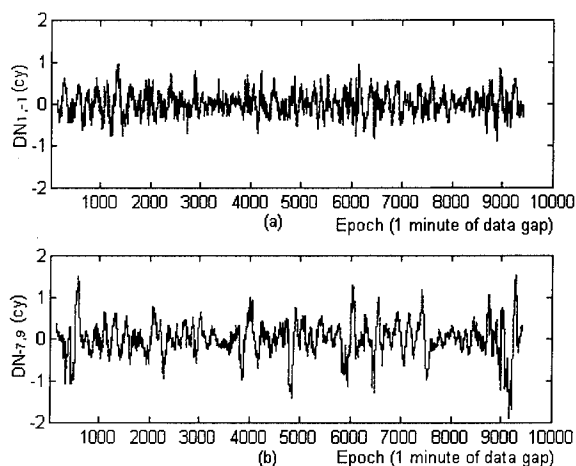


Figure 6. Real-valued Cycle Slip Estimates ($DN_{1,-1}$ (a) and $DN_{-7,9}$ (b)) for Aircraft Receiver Assuming 1 Minute of Data Gap

The KF & AFM procedure neglecting P2 pseudorange is also used to detect and repair cycle slips. For 1-2 second data interval observations, the Kalman predicted position bias is less than 2.5 metres and the cycle slip detection and repair process was successful. For data sample interval greater than 2 seconds, more than one set of cycle slips are left and the process was not successful.

The initialization is carried out using the first and last 5 minutes of static data (baseline length of the order of tens of metres), and the same double-differenced integer ambiguities were obtained, hence furnishing proof that indeed there are no cycle slips left in the data.

2. Train Experiment

This experiment was carried out on October 6, 1994, using the Ashtech Z12 GPS receivers, capable of measuring dual P-code pseudoranges when A/S is on. The precise ephemeris is available from IGS service. Two receivers were set up, separated by about 272 kilometres at the start. One was mounted on a train. After static tracking, the train receiver moved over a period of about 50 minutes. The trajectory and height are plotted in Figures 7a and 7b. Eqns (8) and (17) are

used to compute $N_{1,-1}(k)$ and $N_{-7,9}(k)$ and then to predict $N_{1,-1}^-(k)$ and $N_{-7,9}^-(k)$ using the previous several epochs (ten epochs are chosen here). The differences between the predicted value and the computed value ($DN_{1,-1}(k)$ and $DN_{-7,9}(k)$) are plotted in Figures 8a and 8b for the train receiver. The noise of $DN_{1,-1}(k)$ and $DN_{-7,9}(k)$ is less than about 0.1 cycles. This satellite (PRN 16) has the lowest elevation of the five satellites tracked, and is plotted in Figure 8a. It can be seen that cycle slip detection and repair is very easy for 1 second data rate observations if there is no data gap.

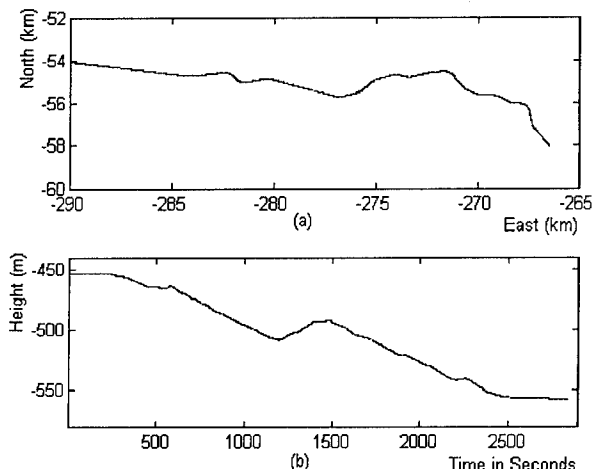


Figure 7. Train Trajectory (a) and Height (b) Relative to Fixed Rcvr

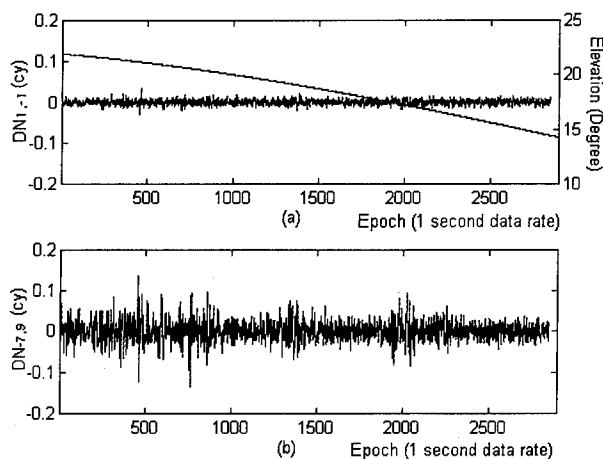


Figure 8. Real-valued Cycle Slip Estimates ($DN_{1,-1}$ (a) and $DN_{-7,9}$ (b)) for Train Receiver

A data gap of 5 minutes is simulated at each epoch, similar to the aircraft experiment, and the real-valued cycle slip estimates are plotted in Figures 9a and 9b. The suggested procedure can successfully determine one set of cycle slip values. The 5 minute cleaned data are used to predict $N_{1,-1}^-$ and $N_{-7,9}^-$ when $DN_{1,-1}$ and $DN_{-7,9}$ are computed.

Multipath effect will cause the real-valued cycle slip estimates to be biased. Figure 10 gives an example of a cycle slip during a short of data gap. The problem is that there are multipath effects before and after the data gap. In this case, the current software will delete all affected data which can be identified by the linear fitting procedure.

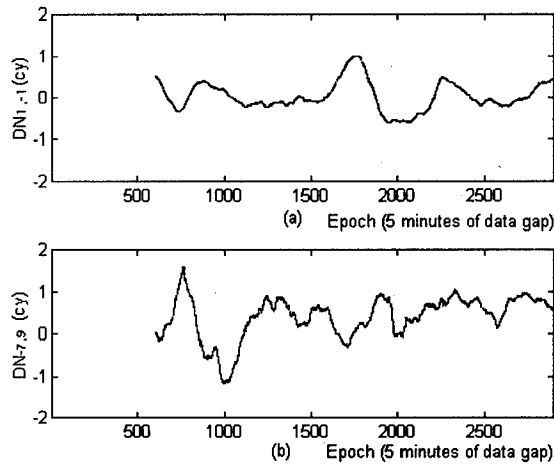


Figure 9. Real-valued Cycle Slip Estimates ($DN_{1,-1}$ (a) and $DN_{-7,9}$ (b)) for Train Receiver Assuming 5 Minutes of Data Gap

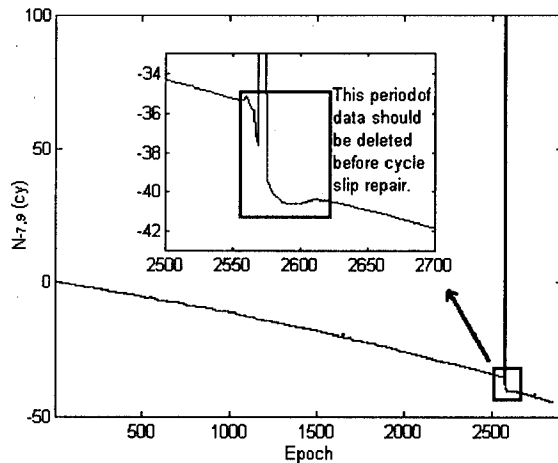


Figure 10. Cycle Slip Occurred in PRN 18 of Train Receiver

The KF & AFM procedure is also used to detect and repair cycle slips. For data with 1-3 second sample rate selected from this data set, the predicted position biases are less than about 2.5 metre, and the cycle slip detection and repair is successful. For the data with larger interval than 3 seconds, more than one set of cycle slip candidates will remain and the result is therefore not successful.

CONCLUSIONS

If precise pseudorange data are available, the combined carrier phase observations $\phi_{1,-1}$ and $\phi_{-7,9}$

are very useful for cycle slip detection and repair in kinematic data. The suggested procedure can repair data gaps up to 1-5 minutes depending on the receiver type and the ionosphere conditions.

If dual frequency, full wavelength carrier phase is available, but no precise pseudorange data, the KF & AFM procedure will be powerful in detecting and repairing cycle slips. The length of data gap can be repaired depends on the dynamics and environment. Normally, if the predicted position bias is less than about 2.5 metres, the cycle slips can be repaired. For GPS receivers outputting precise pseudorange, the KF & AFM procedure can be used together with the first procedure in order to detect and repair cycle slips during any period pseudorange data loss.

The suggested procedure needs ambiguity initialization at the beginning of a session. For short receiver separations at the beginning of a session, the traditional ambiguity resolution method for the static case, or ambiguity resolution 'on-the-fly' for the kinematic case can be used. For long receiver separations at the beginning of a session, static methods are needed to initialize the ambiguities.

Multipath is the main obstacle to the suggested procedure. In the current software, all data seriously affected by multipath will be deleted.

This method can be used for real-time kinematic positioning. After initializing at the start of the session, and if there are no data gaps longer than a few minutes, the integer ambiguities can be resolved instantaneously and the roving receiver position can be determined in real-time.

ACKNOWLEDGEMENTS

The author would like to thank his supervisor, Dr. Chris Rizos, for his guidance and advice during his research. Discussions with Dr. O. Colombo (University of Maryland and NASA Goddard S. F. C.) have been very helpful. The aircraft data was kindly provided by Prof. K. Kubik (Queensland University of Technology) and the train data by Freight Rail, New South Wales. The author is supported by Australian Research Council funding.

REFERENCES

- Abidin, H. A. (1993). Computational and Geometrical Aspects of On-The-Fly Ambiguity Resolution. PhD dissertation, Dept. of Surveying Engineering Tech. Rept. No. 164, University of New Brunswick, Fredericton, New Brunswick, Canada, 314pp.

- Abidin, H. A. and D. E. Wells (1990). Extradilating for 'On The Fly' Ambiguity Resolution: Simulation of Ionospheric Effects. Proc. 2nd Int. Symp. on Precise Positioning with Global Positioning System, Ottawa, Canada, 3-7 September, 1217-1232.
- Blewitt, G. (1989). Carrier Phase Ambiguity Resolution for the Global Positioning System Applied to Geodetic Baselines up to 2000 km. Journal of Geophysical Research. Vol. 94, No. B8, 10187-10203.
- Blewitt, G. (1990). An Automatic Editing Algorithm for GPS Data. Geophysical Research Letters, Vol. 17, No. 3, 199-202.
- Chen, D. S. (1993). Fast Ambiguity Search Filtering (FASF): A Novel Concept for GPS Ambiguity Resolution. Proc. of ION GPS-93 6th Int. Tech. Meeting of the Satellite Division of the Institute of Navigation, Salt Lake City, Utah, 22-24 September, 781-787.
- Colombo, O. L., C. Rizos and B. Hirsch. (1995). Decimetre-level DGPS Navigation Over Distances of More Than 1000km: Results of the Sydney Harbor Experiment. Proc. 4th Int. Conf. on Differential Satellite Navigation Systems, Bergen, Norway, 24-28 April.
- Counselman, C. C. and S. A. Gourevitch. (1981). Miniature Interferometer Terminals for Earth Surveying: Ambiguity and Multipath with the Global Positioning System. IEEE Transactions on Geoscience and Remote Sensing, Vol. GE-19, No. 4, 244-252.
- Dong, D. N. and Y. Bock. (1989). Global Positioning System Network Analysis With Phase Ambiguity Resolution Applied to Crustal Deformation Studies in California. Journal of Geophysical Research, Vol. 94, No. B4, 3949-3966.
- Frei E., J. Yau and D. Sauer (1993). Ambiguity Resolution on the Fly (AROF); Results, Facts, Limitations. Proc. of the ION GPS-93 6th Int. Tech. Meeting of the Satellite Division of the Institute of Navigation, Salt Lake City, Utah, 22-24 September, 1059-1067.
- Goad C. C. (1992). Robust Techniques for Determining GPS Phase Ambiguities. Proc. 6th Int. Geodetic Symp. on Satellite Positioning, Columbus, Ohio, 17-20 March, 245-254.
- Han, S. W. (1993). Improved Ambiguity Function Method and Its Application in Kinematic Positioning. Presented at IAG General Meeting, Beijing, P. R. of China, 9-13 August.
- Han, S. W. (1995). Ambiguity Resolution Techniques Using Integer Least Squares Estimation for Rapid Static or Kinematic Positioning. Proc. of Satellite Navigation Technology 1995 and Beyond, Brisbane, Australia, 26-28 June.
- Han, S. W. and C. Rizos (1995a), A Suggested Procedure for On-The-Fly Ambiguity Resolution for Long Range Kinematic Positioning. Proc. 4th Int. Conf. on Differential Navigation Systems, Bergen, Norway, 24-28 April.
- Han, S. W. and C. Rizos (1995b), Improving the Computational Efficiency of the Ambiguity Function Algorithm. Submitted to Manuscripta Geodaetica.
- Hatch R. R. (1990). Instantaneous Ambiguity Resolution. Proc. of the IAG Int. Symp. No. 107 on Kinematic Systems in Geodesy, Surveying, and Remote Sensing, Springer-Verlag, 299-308.
- Hatch, R. R. (1986). Dynamic Differential GPS at the Centimeter Level. Proc. 4th Int. Geodetic Symp. on Satellite Positioning, Las Cruces, New Mexico, 28 April - 2 May, 1287-1298.
- Lachapelle, G., M.E. Cannon, C. Erickson and W. Falkenberg (1992). High Precision C/A Code Technology for Rapid Static DGPS Surveys. Proc. 6th Int. Geodetic Symp. on Satellite Positioning, Ohio, 17-20 March, 165-173.
- Landau, H. and H. J. Euler (1992). On-The-Fly Ambiguity Resolution for Precision Differential Positioning. Proc. of the ION GPS-92, 5th Int. Tech. Meeting of the Satellite Division of the Institute of Navigation, Albuquerque, New Mexico, 22-24 Sept., 607-613.
- Mader, G. L. (1992). Rapid Static and Kinematic Global Positioning System Solutions Using the Ambiguity Function Technique. Journal of Geophysical Research, Vol. 97, No. B3, 3271-3283.
- Remondi, B. W. (1984). Using the Global Positioning System (GPS) Phase Observable for Relative Geodesy: Modeling, Processing and Results, Doctoral Dissertation, Center for Space Research, University of Texas at Austin, 360pp.
- Teunissen, P. J. G. (1994). A New Method for Fast Carrier Phase Ambiguity Estimation. Proc. IEEE Position Location and Navigation Symp. PLANS94, Las Vegas, 11-15 April, 562-573.
- Wübbena, G. (1989). The GPS Adjustment Software Package - GEONAP - Concepts and Models. Proc. 5th Int. Geodetic Symp. on Satellite Positioning, Las Cruces, New Mexico, 13-17 March, 452-461.



Session A2

Military Applications and Requirements

Chair:

Dr. Arnold Tucker

Applied Research Laboratory

Co-Chair:

Mr. Ben Roth

Defense Mapping Agency

Use of the GPS Aided Inertial Navigation System in the Navy Standard Missile for the BMDO/Navy LEAP Technology Demonstration Program

Todd Moore, Kevin Rudolph, and Frank Ziolkowski
Hughes Aircraft Co.

Alfred Luckau
Hughes Missile Systems Co.

BIOGRAPHY

Todd A. Moore is a Project Engineer for the GPS Navigation Technology Center at Hughes Aircraft Company. He has over 6 years experience with GPS navigation systems and played a key role in the integration and flight test of the prototype GPS Aided Inertial Navigation System (GAINS) in 1990. Since early 1994, Todd has served as Project Manager for GAINS applications. He received his BSEE and MSEE from Loyola Marymount University in 1988 and 1990, respectively.

Kevin E. Rudolph is a Project Manager for the GPS Navigation Technology Center at Hughes Aircraft Company. He has over 10 years experience with advanced GPS navigation system applications. Kevin served as Project Manager for GAINS applications until 1994 and was a key player in the establishment of the Navy LEAP GAINS system. He received his BSEE in 1982 from Purdue University and MS Engineering in 1985 from University of California, Los Angeles.

Frank Ziolkowski is a Scientist/Engineer for the GPS Navigation Technology Center at Hughes Aircraft Company. He has over 10 years experience with GPS navigation systems, specializing in Kalman filter design and integration. Frank was the key designer and integrator of the GAINS Kalman filter. He received his BSEE from University of Illinois in 1985 and MSEE from University of Southern California in 1988.

Alfred M. Luckau is a Senior Engineering Specialist at Hughes Missile Systems Company. He has 15 years experience in configuration design, requirements development, aerodynamics modeling, and performance analysis. Fred was responsible for Navy LEAP Standard Missile mission and system requirements as well as Lead Engineer for the first intercept flight test, FTV-3. He received his BS Aerospace Engineering from Cal Poly, Pomona in 1980.

ABSTRACT

To demonstrate the feasibility of a sea-based theater-wide ballistic missile defense capability, the Navy Program Executive Office Theater Air Defense (PEO TAD), in conjunction with the Ballistic Missile Defense Organization (BMDO), performed two flight tests of a Lightweight Exo-Atmospheric Projectile (LEAP) mounted on a Navy Standard Missile 2 Block III Extended Range Terrier (SM 2 BLK III ER). The SM 2 BLK III ER was augmented with a third stage utilizing an integrated GPS/Inertial Navigation System (INS) allowing increased range, accuracy, and exo-atmospheric control. The SM 2 Flight Test Vehicles (FTV) were fired from the USS Richmond K. Turner (CG-20) located off the coast on the Eastern Test Range, against target vehicles launched from NASA's Wallops Flight Facility on the Virginia coast.

The Navy LEAP mission posed a challenging environment, including high vehicle dynamics, exo-atmospheric operation, and short mission duration. An adapted version of the Hughes Aircraft Company's GPS Aided Inertial Navigation System (GAINS) served as the navigator for the SM 2 third stage. The GAINS unit combines a low cost strapdown Inertial Measurement Unit (IMU) with an embedded GPS receiver module to provide a robust, low cost means of determining position, velocity, attitude, and time. The Navy LEAP Standard Missile flight tests have proven the robustness and reliability of the GAINS unit, successfully achieving the system requirements in the high dynamic and high altitude environment. This paper summarizes the design considerations and flight test results, highlighting the advantages of the low cost, high accuracy GPS aided inertial navigation solution.

INTRODUCTION

In early 1995, the Ballistic Missile Defense Organization (BMDO)/Navy Lightweight Exo-Atmospheric Projectile

(LEAP) Technology Demonstration Program demonstrated the feasibility of deploying a LEAP kinetic kill vehicle (KKV) from a Navy ship to intercept a representative exo-atmospheric Theater Ballistic Missile (TBM) target. The LEAP KKV was carried as a payload on a modified Navy Standard Missile 2 Block III Extended Range Terrier which was surface-launched from the guided missile cruiser USS Richmond K. Turner (CG-20). The Standard Missile was selected as the launch vehicle for these flight tests because of its superior kinematic capabilities and overall compatibility with existing Navy launch systems. The Standard Missile was modified by Hughes Missile Systems Company (HMSC) to include a newly designed third stage for increased range and exo-atmospheric control allowing accurate delivery of the KKV to the desired exo-atmospheric target acquisition point.

Stressing accuracy requirements were placed on the Third Stage Guidance System by the KKV narrow field-of-view (FOV), KKV divert capability, and cooperative engagement scenario. The GPS Aided Inertial Navigation System (GAINS) plays a critical role in meeting these requirements by providing accurate navigation measurements to the Third Stage Guidance System and in the handover of the inertial state vector to the KKV for target acquisition. The GAINS integrates measurements from a strapdown Inertial Measurement Unit (IMU) to maintain the navigational state of the Standard Missile Third Stage, including three axes each of position, velocity, and attitude. The measurements from an embedded GPS receiver are used to correct the navigation state vector to the desired accuracy.

The navigation accuracy provided by the GAINS contributed to the probability of successful TBM intercept. In addition, the GAINS unit provided Universal Time Coordinated (UTC) reference time for guidance calculations involving time tagged target state updates collected by ground tracking stations and uplinked to the Standard Missile by the launch ship. The GAINS IMU also provided measurements of linear acceleration and angular velocity to the Third Stage Attitude Control System (ACS) which maintained stable vehicle orientation.

MISSION OVERVIEW

The BMDO/Navy LEAP Technology Demonstration Program included the launch of four Standard Missile Flight Test Vehicles (FTV). The first Flight Test Vehicle, FTV-1, was flown on 24 September 1992, demonstrating high altitude missile control of a conventional Standard Missile 2 Block III Extended Range

Terrier. The second Flight Test Vehicle, FTV-2, was flown on 27 September 1993, demonstrating the exo-atmospheric performance of the modified Standard Missile, including nosecone separation and KKV ejection. The third and fourth Flight Test Vehicles, FTV-3 and FTV-4, were flown on 4 March 1995 and 28 March 1995, respectively, and demonstrated the feasibility of an exo-atmospheric intercept of a representative TBM target.

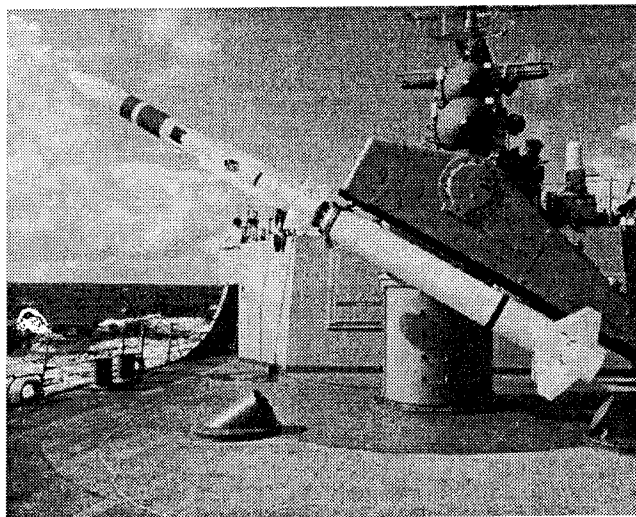


Figure 1. Navy LEAP Modified Standard Missile On USS R.K. Turner Aft Missile Launcher



Figure 2. FTV-4 Launch From USS R.K. Turner

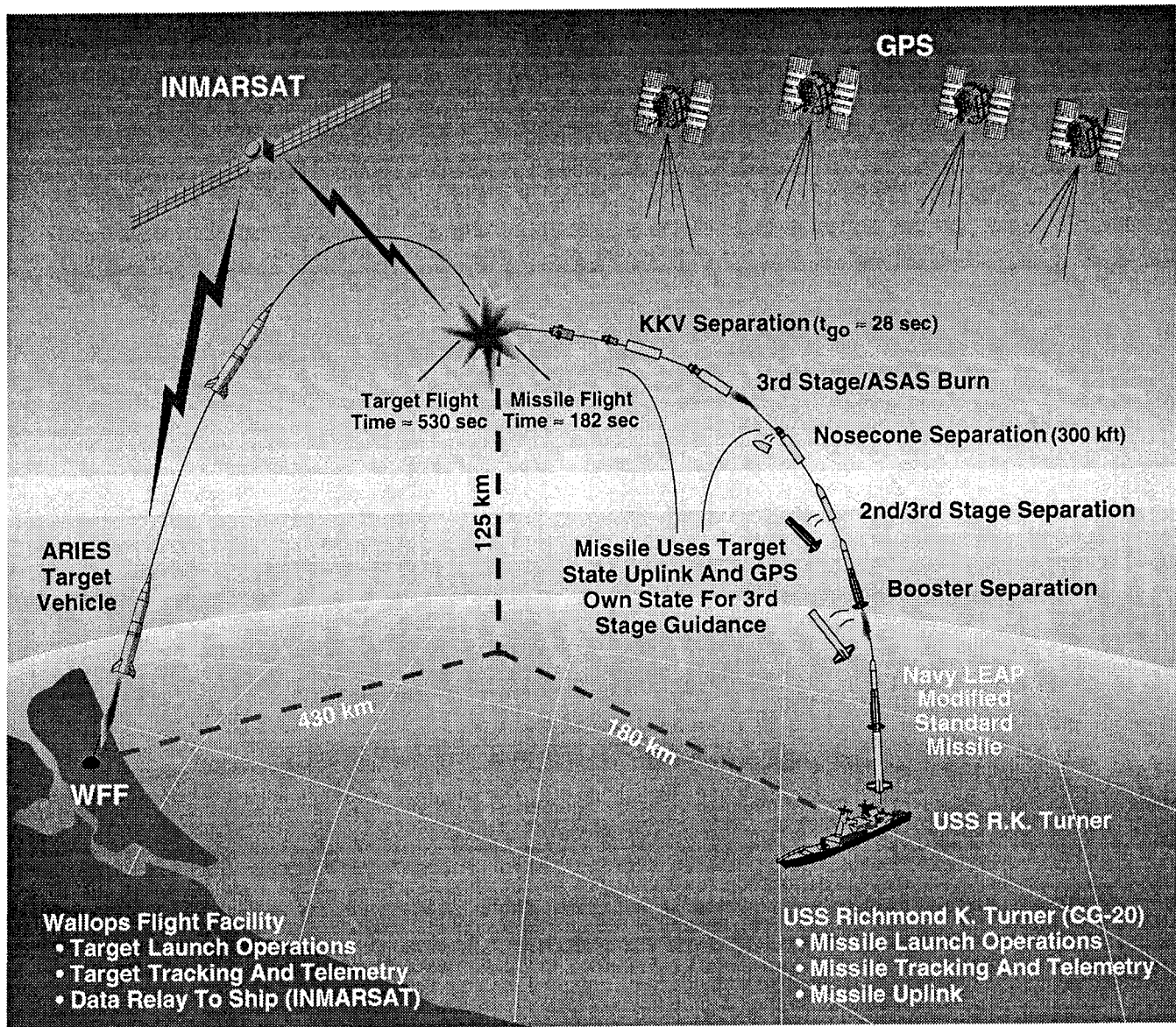


Figure 3. Navy LEAP FTV-3 And FTV-4 Mission Overview

The mission profile for the third and fourth Flight Test Vehicles is shown in Figure 3. The TBM target was launched from NASA's Wallops Flight Facility located on the Virginia coast. After detection of target launch and formation of the fire control solution, the Standard Missile was launched from the USS Richmond K. Turner located off the coast on the Eastern Test Range. The first and second stage operations were similar to the conventional Standard Missile 2 Block III Extended Range Terrier on which it was based. Upon reaching an altitude of approximately 187,500 feet the third stage was separated from the second stage and initiated third stage guidance and control. At an altitude of approximately 300,000 feet, the nosecone was ejected to expose the

KKV. At this time the third stage rocket motor burn initiated and continued for approximately 16 seconds. The third stage guided to the desired exo-atmospheric target acquisition point based on the GAINS navigation solution and target state updates uplinked from the launch ship. At approximately 400,000 feet, the LEAP KKV inertial system was aligned, pointed toward the target, and ejected from the third stage.

The successful operation of the GPS Aided Inertial Navigation System was demonstrated in both the FTV-3 and FTV-4 missions with the performance surpassing expectations. Review of missile telemetry and KKV seeker video data showed that the high accuracy GAINS

navigation solution enabled the third stage to successfully guide to the target acquisition point and point the KKV narrow FOV sensor at the target.

DESIGN OVERVIEW

The GAINS design selected for the Navy LEAP mission was based on a system which had been previously proven in various prior applications by Hughes Aircraft Company. The basic architecture, along with the core of the navigation and Kalman filter algorithms and software, were originally developed under a company research and development program during 1989-1991.

The GAINS prototype design was successfully flight tested in December 1990, during the company funded Advanced Interdiction Weapon System Pre-Prototype Flight Demonstration (AIWS-PPFD) Program. Hundreds of hours of testing were accumulated during the simulation, laboratory, van, and captive flight testing of the prototype system in preparation for the first free-flight test. The AIWS-PPFD design and flight test results were presented at the Institute of Navigation, National Technical Meeting on January 1992 [1].

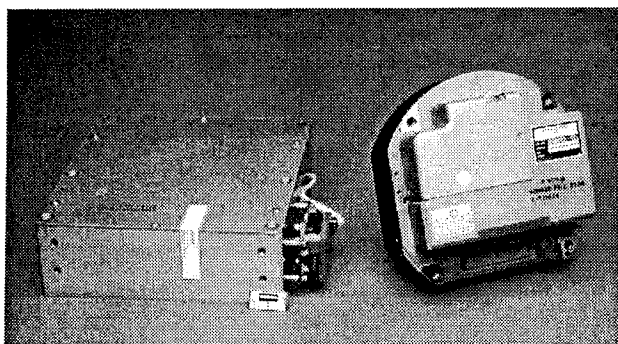


Figure 4. Navy LEAP GPS Aided Inertial Navigation System (GAINS) Receiver Processor Unit (RPU) and Inertial Measurement Unit (IMU)

An upgraded AIWS-PPFD design was the point of departure for the BMDO/Navy LEAP Technology Demonstration Program. The open architecture approach utilized in GAINS development provided increased flexibility, allowing rapid modification to meet the Navy LEAP mission requirements.

The Ada software design utilizes modularity and data structures to de-couple the algorithms from the specific hardware configuration. A major portion of the Ada algorithm software was reused for the Navy LEAP GAINS application with little or no modification.

The GAINS hardware design and packaging were configured to meet the size, weight, power and environmental requirements of the Standard Missile Third Stage. System elements were selected for their conformance with both the physical and mission-derived performance requirements and availability within the aggressive program schedule. GAINS exploited the use of non-developmental items (NDI) where appropriate to reduce cost and risk.

The Navy LEAP GAINS comprised of the Receiver Processor Unit (RPU) and the Inertial Measurement Unit (IMU) as shown in Figure 4. The Receiver Processor Unit integrated a NDI SEM-E form-factor Navigation Processor Board and GPS Receiver Board with the Hughes Interface Board in a single chassis. The IMU was a production Advanced Medium Range Air-to-Air Missile (AMRAAM) form factor IMU.

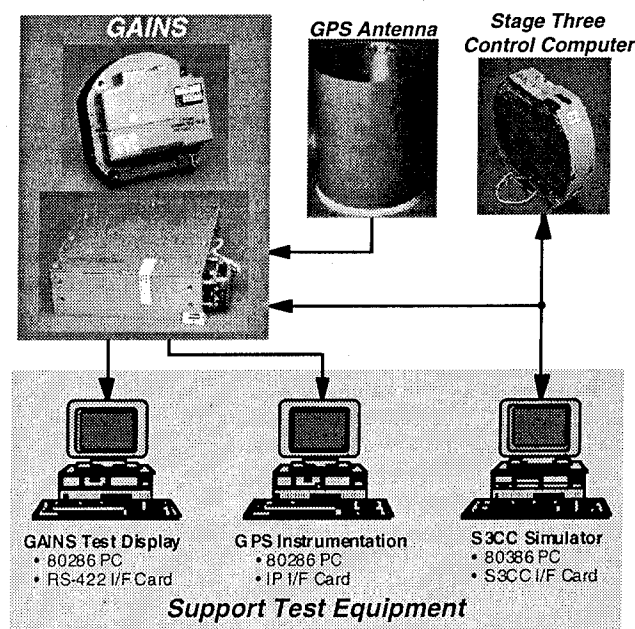


Figure 5. GAINS External Interface Block Diagram

The RPU received inertial measurement information from the strapdown IMU mounted within the third stage and GPS satellite RF signals from the eight element conforal ring antenna surrounding the third stage. GAINS integrated the measurements of the IMU to maintain the third stage position, velocity, and attitude navigation state. The measurements from the embedded GPS receiver were used by the Kalman filter to estimate both the initialization and in run errors and generate corrections to the navigation state. The corrected navigation state was sent by the GAINS to the Stage 3 Control Computer (S3CC) that performed the third stage

guidance and control functions. The GAINS external interface block diagram identifying external interfaces, including the test equipment supporting the development and integration, is shown in Figure 5. The GAINS functional block diagram is shown in Figure 6.

The GAINS corrected navigation state was required only during the third stage phase of flight, but was computed and sent to the Stage 3 Control Computer throughout the entire Standard Missile flyout. GAINS operation during the earlier phases of the flyout sequence provided added error observability and contributed to the overall GAINS performance.

DESIGN CONSIDERATIONS

In the course of adapting the GAINS design for the BMDO/Navy LEAP Technology Demonstration Program, special issues were encountered which required careful consideration during the design, integration, and test phases of the program. The conditions of the Navy LEAP mission were very demanding for an integrated GPS-INS system. Several of the specific issues associated with the operational environment are listed herein.

High Dynamics

The Navy LEAP Standard Missile trajectory includes high levels of jerk and acceleration, some of which exceed the dynamic range of the embedded GPS receiver, causing the receiver to lose code and carrier track of the GPS satellites. The missile acceleration profile measured from the FTV-4 mission is shown in Figure 7. The Earth Centered Earth Fixed X, Y, and Z velocities measured from the FTV-4 mission are shown in Figures 8, 9, and 10, respectively.

As anticipated, in both the FTV-3 and FTV-4 missions the 28 G axial acceleration experienced during the Standard Missile First Stage rocket motor burn exceeded the tracking bandwidth of the GPS receiver, resulting in a temporary GPS signal loss. Inertial aiding was provided to the embedded GPS receiver to enable a rapid post-launch re-acquisition time. In both the FTV-3 and FTV-4 missions, the code and carrier tracking of the GPS satellites was re-established within 17 seconds from loss of lock. In FTV-4, the jerk levels in excess of 580 G/second at the second/third stage separation event resulted in the loss of track on two satellites. The code and carrier track of the two GPS satellites was re-established within 9 seconds from loss of lock.

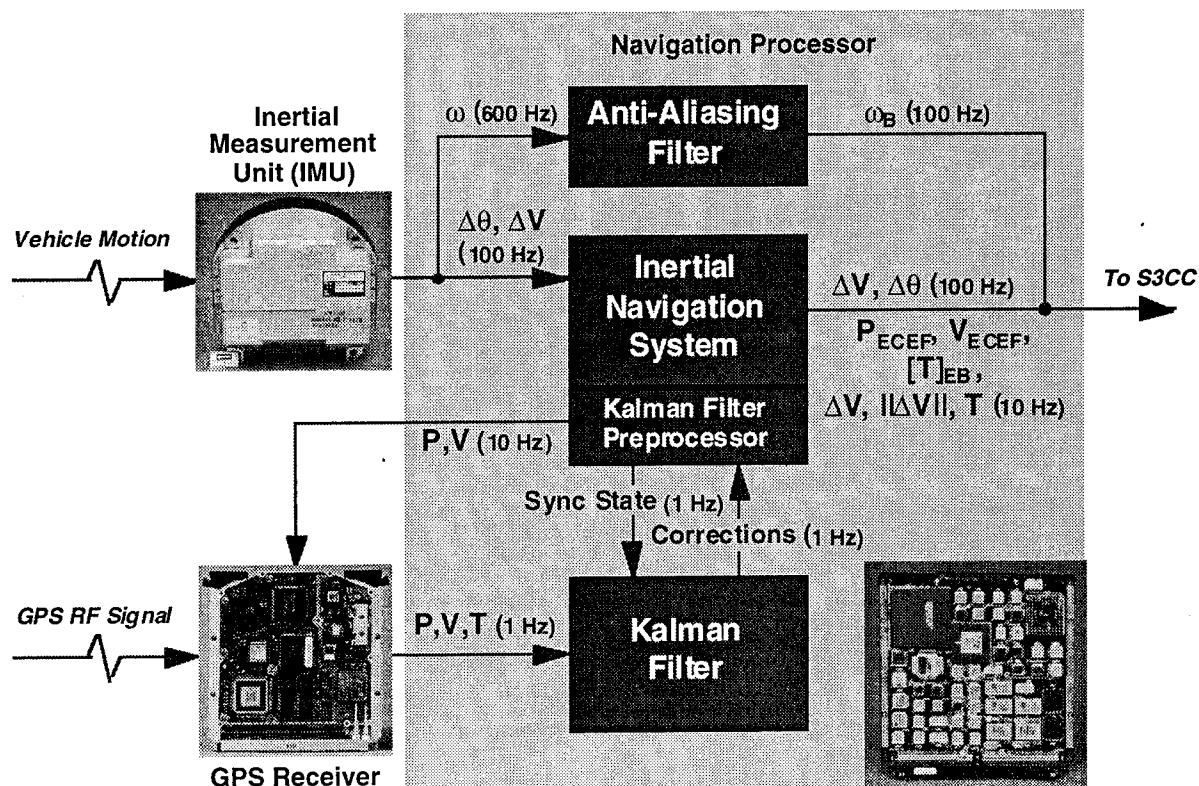


Figure 6. GAINS Functional Block Diagram

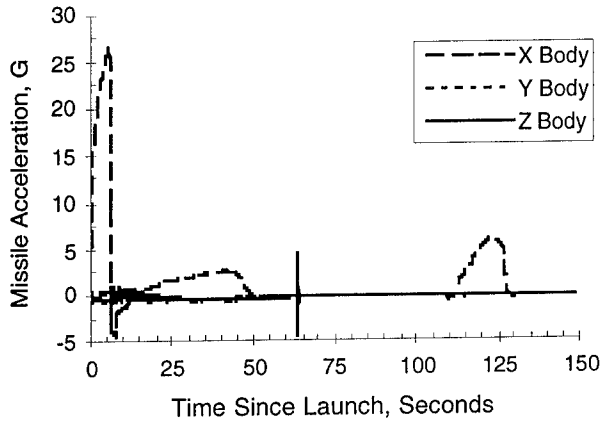


Figure 7. FTV-4 Navy LEAP Standard Missile Body Acceleration History

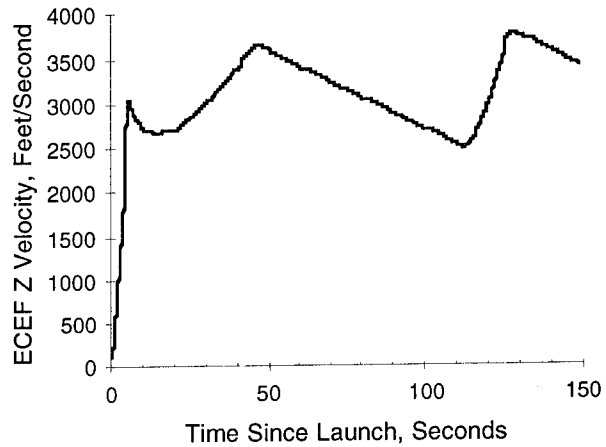


Figure 10. FTV-4 Earth Centered Earth Fixed Z Velocity

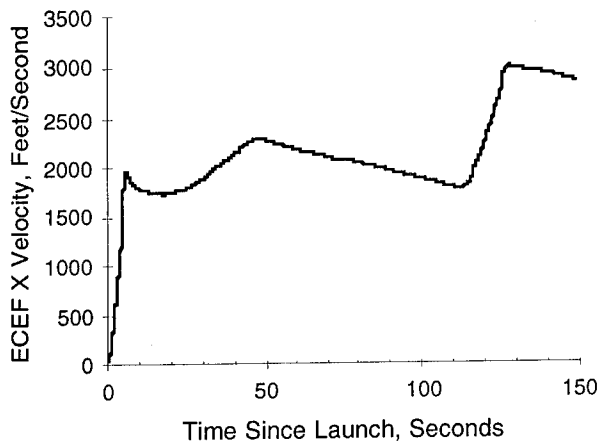


Figure 8. FTV-4 Earth Centered Earth Fixed X Velocity

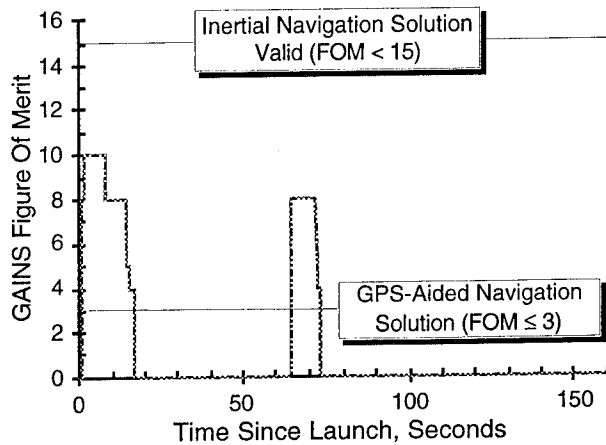


Figure 11. FTV-4 GAINS Figure Of Merit

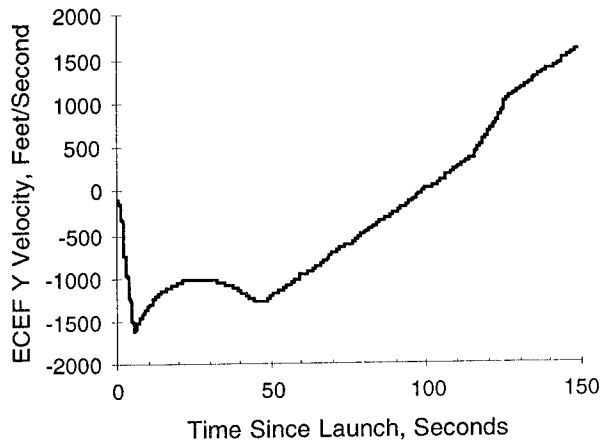


Figure 9. FTV-4 Earth Centered Earth Fixed Y Velocity

A figure of merit (FOM) was computed by GAINS based on the Kalman filter processing mode and GPS tracking state. The navigation solution is valid when the figure of merit is less than fifteen. A zero figure of merit indicates that the navigation solution is fully aided by the GPS measurements. The GAINS Figure of Merit for the FTV-4 mission is shown in Figure 11.

Multipath

The GPS antenna designed for the BMDO/Navy LEAP Technology Demonstration Program is an eight element conformal ring antenna surrounding the third stage rocket motor. The elements are summed to provide a single phase center to the embedded GPS receiver. The measured antenna gain patterns in the pitch and roll planes are shown in Figures 12 and 13, respectively.

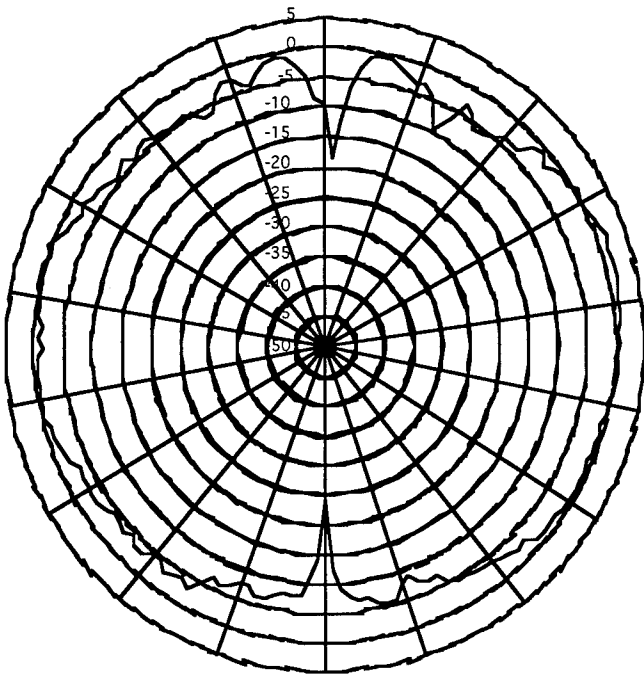


Figure 12. Antenna Gain Pattern In Pitch Plane

The ring antenna design was chosen to maximize the number of visible satellites given the steep launch and flight path angle of the Navy LEAP Standard Missile. The omni-directional design, however, was susceptible to GPS signal multipath from reflected signals off both the launch ship and ocean surfaces. Although the GPS signal multipath was localized to the shipboard environment and diminished significantly subsequent to missile launch, this phenomenon was observed during shipboard testing and in the pre-launch timeline sequence. The critical issue was therefore to evaluate the net effect of the pre-launch multipath on overall system performance. The two main performance considerations were: (i) the quality of the GPS measurements collected in the presence of the multipath induced noise, and (ii) the number of GPS measurements collected during pre-launch to ensure the convergence of the navigation Kalman filter. Extensive shipboard testing was performed to characterize the multipath environment and verify proper convergence of the navigation solution. Post-flight analysis of missile telemetry data confirmed that the FTV-3 and FTV-4 pre-launch and flyout GPS satellite tracking operations were performed as anticipated.

RF Interference

RF interference has always been a concern for GPS receivers due to the low transmitted signal strength from the GPS satellites. GPS receivers are typically equipped with internal bandpass filtering, and the antenna design

itself provides attenuation to out-of-band signals. Even with these safeguards, however, there can be interference from transmitters which operate close enough to the GPS L-band frequencies, or with sufficient power, to jam the GPS satellite signal. As a result, an evaluation was made of all tracking and communication test equipment to be employed in the FTV-3 and FTV-4 flight tests, ensuring compatibility with the GPS receiver operation during both the pre-launch and flyout sequences. In addition, the GPS antenna was characterized for both in-band and out-of-band sensitivity. The potential interference sources were studied both theoretically and empirically. The theoretical study considered all known transmitter frequencies and power levels including both primary frequencies and sub-harmonics. In addition, several empirical tests were conducted with representative flight hardware in the shipboard environment. The exhaustive testing performed did identify several candidates for close scrutiny, but ultimately showed GAINS compatibility with the FTV-3 and FTV-4 flight test participants.

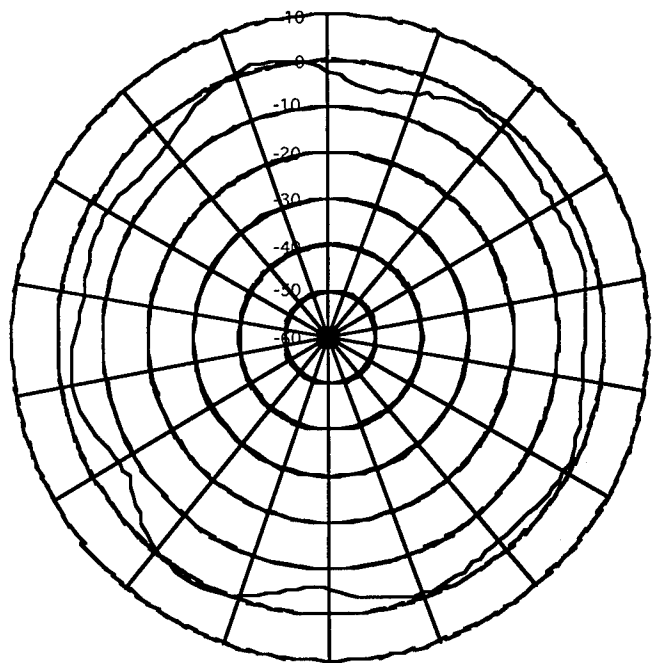


Figure 13. Antenna Gain Pattern In Roll Plane

There were no detectable indications that GPS satellite tracking was affected by RF interference in either the FTV-3 or FTV-4 missions. The carrier-to-noise ratios for the GPS satellite signals tracked in both the FTV-3 and FTV-4 missions were above the minimum desired signal strength. The carrier-to-noise ratios reported by the embedded GPS receiver during the FTV-4 mission are shown in Figure 14.

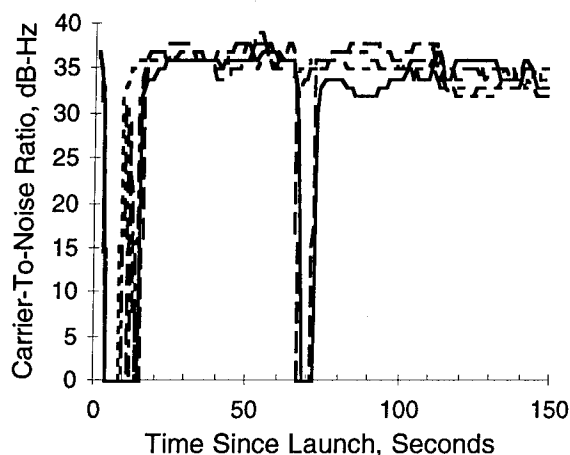


Figure 14. FTV-4 Satellite Carrier-to-Noise Ratio

Satellite Observability

A careful characterization of the GPS antenna gain pattern was performed to determine the observability of GPS satellites for the FTV-3 and FTV-4 missions. A ring antenna, as designed for the BMDO/Navy LEAP Technology Demonstration Program, inherently exhibits nulls in the direction of the nose and tail as shown in Figure 12. Additionally, there are areas where the gain pattern is not uniform as shown in Figure 13. A loss of GPS satellite track due to the antenna gain pattern may result in poor geometry during the mission, potentially degrading the navigation accuracy.

Extensive hardware-in-the-loop testing using a GPS satellite signal simulator test station was performed to evaluate GAINS performance and ensure robustness in Navy LEAP mission [2]. GAINS sensitivity to constellation changes was evaluated by implementing the measured antenna gain pattern in the signal simulator test station and performing missile flyouts with various GPS satellite constellations. Performance predictions for the FTV-3 and FTV-4 missions were achieved by performing flyouts through the anticipated GPS satellite constellation.

Post-flight analysis of missile telemetry data confirmed that there were no observed losses of GPS satellite tracking due to antenna variations in either the FTV-3 or FTV-4 missions.

Satellite Selection

A companion issue to loss of satellite observability due to antenna gain pattern is the rate at which satellite selection is performed by the GPS receiver. A conventional GPS receiver typically updates its satellite selection criteria

over a period of several minutes. This is unacceptable in the high dynamic environment of Navy LEAP mission with its relatively short time of flight. The embedded GPS receiver within the GAINS was modified to reduce the satellite selection period to less than 1 minute, ensuring a minimum of three geometry evaluations within the Standard Missile flyout.

In addition to satellite selection, the time to replace a lost satellite with another available satellite was evaluated. A conventional GPS receiver typically replaces a lost satellite within 30-60 seconds. Given the high dynamic environment of Navy LEAP mission, a replacement period of less than 20 seconds was implemented.

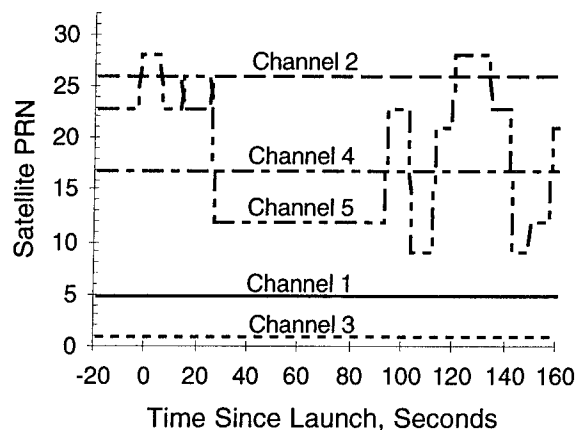


Figure 15. FTV-3 Satellite Tracking

The rapid replacement modification to the embedded GPS receiver was evident in the post-launch re-acquisition of the FTV-3 flight test. The GAINS GPS receiver combined three of the primary four satellites, PRN 1, 5, and 17, with the satellite from the station keeping channel, PRN 23, to form a valid GPS solution within 17 seconds from the launch induced loss of track as shown in Figure 15. After the desired satellite, PRN 26, was re-acquired, it was re-inserted into the GPS solution. This logic provided insurance that a valid GPS solution would be maintained if PRN 26 was not re-acquired.

Navigation Solution Shifts

There are several sources for potential shifts in the navigation solution when using GPS measurements to aid an inertial navigation system. The most common occurs when the GPS receiver chooses a new satellite constellation. This results in a shift in the GPS position measurement bias that may cause transients in the navigation solution. Fortunately, these shifts are observed primarily in the position measurements, which

was not as critical in the FTV-3 and FTV-4 missions as the velocity and attitude solution.

Another potential problem results from the G-sensitivity of the GPS receiver oscillator. The high accelerations experienced during the Navy LEAP Standard Missile trajectory as shown in Figure 7 may cause temporary shifts in the clock frequency. This could result in shifts to the GPS receiver's position and velocity measurements. This effect was carefully studied during hardware-in-the-loop testing using a GPS satellite signal simulator test station and an externally controlled frequency reference to simulate the oscillator G-sensitivity.

The performance observed from the FTV-3 and FTV-4 missions was consistent with the performance predictions generated during hardware-in-the-loop testing.

SUMMARY

The Navy LEAP mission posed a challenging environment for a GPS Aided Inertial Navigation System, including high vehicle dynamics, exo-atmospheric operation, and short mission duration. The Navy LEAP GAINS demonstrated that a NDI-based system, judiciously tailored in both hardware and software, could provide a low cost, high accuracy navigation solution suited to the stressing environment.

A major lesson learned in the Navy LEAP GAINS effort was the value of the simulated dynamic test environment. The ability to perform end-to-end hardware-in-the-loop tests using simulated GPS satellite RF signals with coordinated IMU digital data was critical in ensuring the performance and robustness of the GPS Aided Inertial Navigation System. In addition, the evaluation of the GPS RF link closure in the anticipated environment and

assessment of potential RF interference sources was fundamental in achieving mission success.

The application of the GPS Aided Inertial Navigation System to the BMDO/Navy LEAP Technology Demonstration Program has identified and addressed numerous issues involving the integration of GPS into a surface launched exo-atmospheric missile. All of these issues were successfully resolved through the collective efforts and experience of the Navy LEAP design, integration, and test teams, contributing to the successful flyout of the Navy LEAP FTV-3 and FTV-4 Standard Missiles.

ACKNOWLEDGMENTS

The Hughes Aircraft Company GPS Navigation Technology Center would like to thank the Navy Program Executive Office Theater Air Defense and HMSC Program Offices for the opportunity to participate on the BMDO/Navy LEAP Technology Demonstration Program. In addition, the outstanding engineering efforts provided by the Standard Missile integration/test team and the Johns Hopkins University/Applied Physics Laboratory independent verification team are greatly appreciated.

REFERENCES

- [1] K. Rudolph and M. Youhanaie, "GPS-Inertial Navigation for the Advanced Interdiction Weapon System Flight Demonstration", Institute of Navigation, National Technical Meeting, January 1992.
- [2] G. Stupp and D. Lehnus, "HIL Testing of the Navy LEAP GPS/INS Package", Institute of Navigation, GPS Technical Meeting, September 1995

Integrated GPS/INS/SAR/GMTI Radar Precision Targeting Flight Test Results

R. Guarino and Paul Ibsen
Westinghouse Norden Systems

BIOGRAPHIES

Mr. Guarino joined Norden Systems in 1969. He is presently Manager - Radar Architecture and Analysis, responsible for the design and performance analysis of advanced technology multimode airborne radar and weapon delivery systems. During his career at Norden, he has been responsible for engineering design analysis for the PAVEMOVER radar, the Joint STARS radar, the AN/APQ-173 radar and the Multimode Radar System (AN/APG-76). Mr. Guarino is the holder of two U.S. Patents in radar design. He received his BEE from Manhattan College and his MSEE and Engineer degrees from New York University.

Paul Ibsen is a Senior Systems Engineer at Westinghouse Norden Systems, Norwalk, Connecticut. Mr. Ibsen has worked in Synthetic Aperture Radar (SAR) motion compensation and antenna steering control for 12 years. He is the lead designer of the navigation transfer alignment and antenna control for the AN/APG-76 multimode radar and does planning and performance analysis of SAR precision targeting flight tests. He holds a BSEE/BSCS from the University of Connecticut, 1982. Since 1985, he also has been an instructor at Bridgeport Engineering Institute.

ABSTRACT

This paper summarizes the results of a series of flight tests flown to evaluate the precision targeting performance improvements obtainable with a modern tactical coherent airborne radar when operating with an integrated Global Positioning System/Inertial Navigation System (GPS/INS). The radar used in these experiments was the AN/APG-76 which has both synthetic aperture radar and ground moving target indication (GMTI) modes. Performance was evaluated with two integrated GPS/INS systems, a Honeywell H-764G and a Litton LN-100G both of which are state-of-the-art systems. Each system is implemented in a

tightly coupled GPS/INS configuration with P/Y code GPS receivers. The testbed for these flight tests was a Gulfstream II aircraft that was instrumented to record all radar and GPS/INS data.

Testing was done with both fixed and moving targets. The fixed target tests were performed using an array of surveyed corner reflectors; the moving target tests used a van moving along the edge of a runway. In both cases, the test results show that an order of magnitude improvement in targeting performance is obtained with use of GPS.

INTRODUCTION

The ability to achieve high accuracy weapon delivery from an airborne platform provides significant operational benefits. The accuracy with which targets are located is critical to mission success. To achieve this capability in all weather, the use of radar is required. High resolution SAR provides a means to detect and precisely resolve targets but the ability to measure target location accurately has traditionally been limited by Inertial Navigation System errors. The advent of the Global Positioning System tightly coupled with an INS provides the capability of greatly improved accuracy. Several analytical precision targeting studies [1,2,3] have been published. GPS/SAR experiments with short range test systems are also available [4,5]. This paper summarizes test results of an operational long range tactical GPS/INS/SAR/GMTI system.

Target detections in a SAR image provide targeting information relative to the aircraft. Range and Doppler histories of the target's image along with height above target (HAT) data provide a three dimensional position vector of the target relative to the aircraft. Adding this vector to the radar's GPS derived earth centered position vector provides accurate absolute precision targeting in WGS-84 coordinates.

A GPS/SAR system can provide this absolute targeting with a single image (or frame). The accuracy is limited by height above target errors, velocity/Doppler errors, range, and GPS position errors (listed in descending order of highest error contributors in a typical system). Target elevation is measured using the elevation monopulse aperture in the AN/APG-76 radar to determine the HAT.

A technique to exploit the most accurate (lowest error contributor) measurements can improve the single frame performance. Multiple frames taken from different orientations can minimize HAT errors by using range, Doppler and GPS measurements only. Such multiple frame technique was tested and evaluated. The description and test results are given in a subsequent section.

The preceding techniques apply directly for stationary targets and indirectly for moving targets. For moving targets, the Doppler return seen by the radar is a function of both the spatial location and the velocity of the target. To separate out these effects the target location is measured directly using the azimuth interferometer aperture of the AN/APG-76 radar. This measurement is then correlated with the map data from the surrounding terrain to develop the precise moving target location.

SINGLE FRAME MEASUREMENT TECHNIQUE

The AN/APG-76 has the capability to measure targets in three dimensions relative to the aircraft in a single frame. Ten-foot resolution SAR imagery provides

range and Doppler measurements. Height above target is provided by radar elevation angle measurements. The AN/APG-76 coupled with a GPS aided navigation system provides precise WGS-84 target coordinates. Atmospheric effects on radar range, Doppler and elevation measurements are compensated for in this technique as well as radome effects on elevation.

Target range is measured by round trip propagation time of the radar signal which isolates the detected target to a radius from the aircraft or on a conceptual sphere. The Doppler shift of the fixed target determines the target's angle relative to the radar velocity vector which is a locus that forms a cone. The intersection of these two geometric surfaces forms a circle (Figure 1). The circle represents the ambiguous location of the target as determined by range and Doppler. The location is further isolated to one side of the aircraft by the illumination pattern of the radar antenna. Elevation angle measurements isolate the target to a point on the circle.

SAR Doppler measurements are a function of both target azimuth and elevation. Therefore, target altitude error produces a corresponding cross range error. The altitude error induced cross range error can be eliminated as a factor in weapon delivery performance if the weapon can be commanded to follow the SAR uncertainty circle near the target's estimated position. Figure 2 illustrates this concept. The results section will specify circular error probable (CEP) results both for this optimum weapon delivery case and for the case where the altitude errors are projected

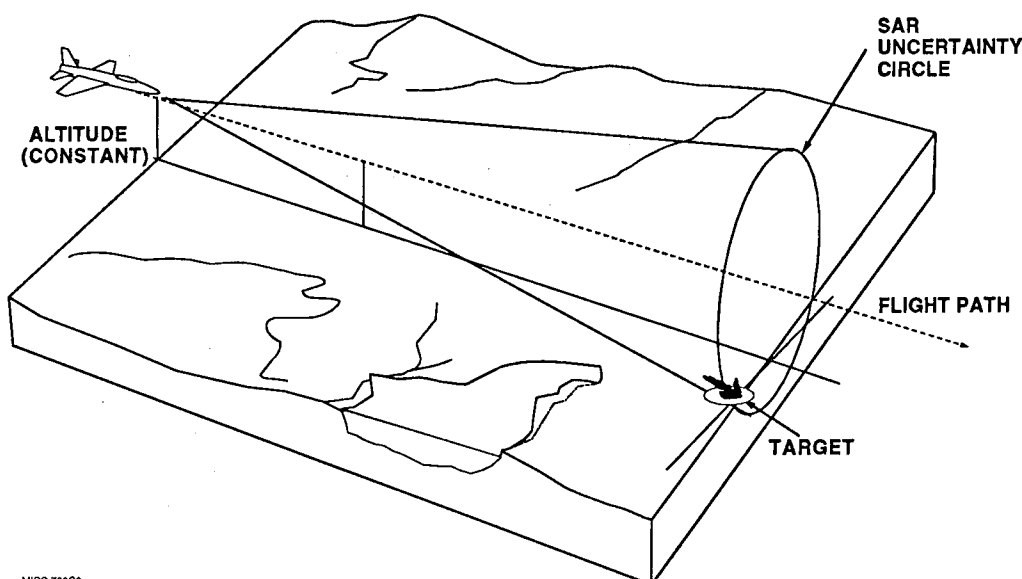


Figure 1. Single SAR Frame Targeting

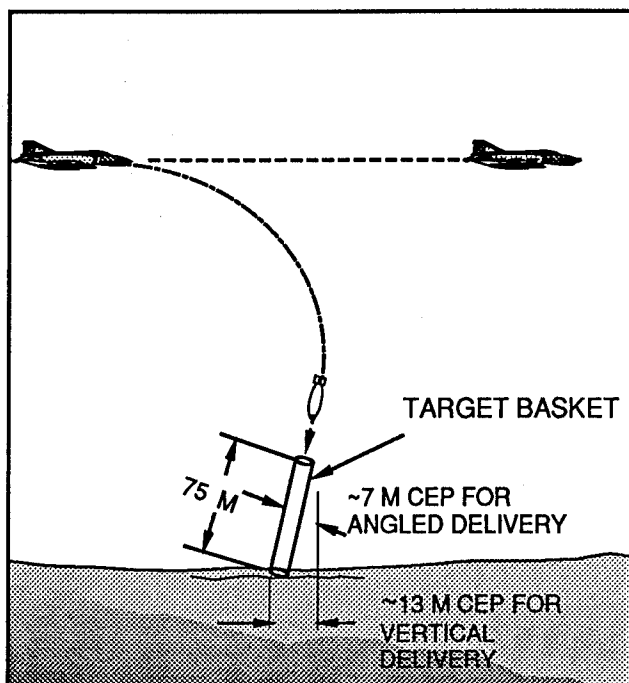


Figure 2. Optimal Weapon Delivery

vertically to the ground. These are the two common ways to project the three-dimensional errors into a two dimensional ground plane CEP error.

MULTIPLE SAR FRAME MEASUREMENT TECHNIQUE

The multiple SAR frame technique (Figure 3) uses two or more SAR images from known GPS positions to

provide improved target location accuracy for fixed targets. Between images the aircraft is flown to change the relative aircraft-to-target geometry, in particular to change the SAR image plane. The objective is to change the relationship of the three components of the location error (range, Doppler and elevation) between measurements. With proper geometry changes, multiple range measurements can be used to minimize Doppler error and multiple Doppler measurements can be used to minimize target altitude error.

The maneuver used for this technique in the flight test experiment exploits the range and Doppler accuracy of the GPS/SAR system to minimize altitude errors (refer to flight profile section for more detail). Range accuracy is exploited by measuring range to the target from two radar positions separated by up to thirty degrees of aspect angle. This geometry allows a triangulation calculation to be employed to solve for azimuth angle to the target, which is normally solved for by Doppler in the single frame technique. The end of the maneuver changes the SAR plane (contains line-of-sight vector and velocity vector) to near orthogonality between two frames. SAR plane changes vary the cross-range shift of the target due to an altitude error. This makes the attitude error observable with Doppler measurements.

The technique requires that the operator designate (with a cursor) the same target (or same point on an extended target) on each of the maps. The accuracy of the redesignation process affects targeting location accuracy. Better SAR resolution improves the ability of the operator to designate the same target point in

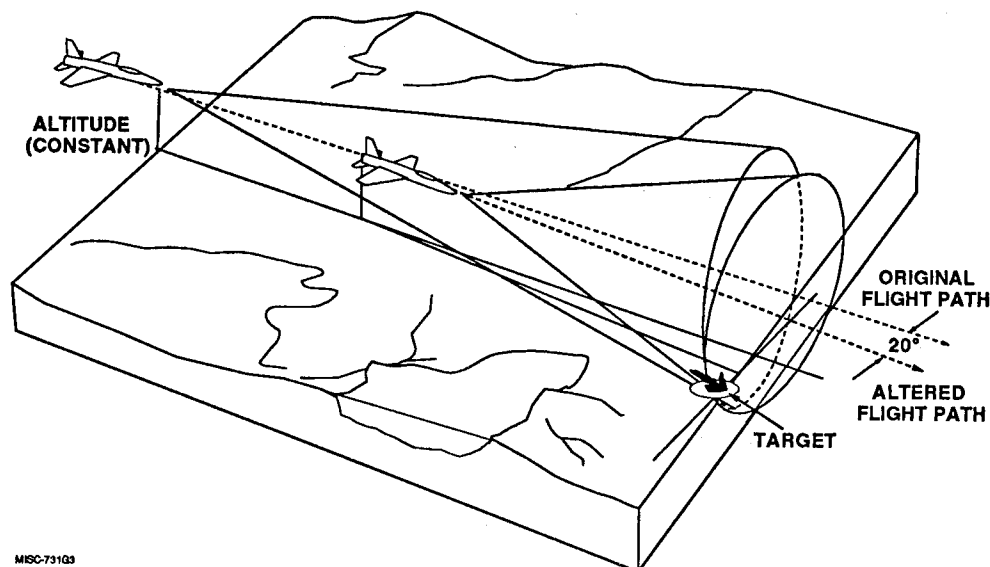


Figure 3. Multiple SAR Frame Targeting

each map. These experiments used ten-foot resolution imagery. Processing for this experiment was done from recorded flight data in a computer laboratory environment and the display was expanded to allow better cursoring.

TEST ASSETS

Testing was conducted using Norden's operational SAR/MTI radar, the AN/APG-76, integrated with each of two tightly coupled GPS/INS navigation systems, a Honeywell H764G and a Litton LN100G. Norden's fully instrumented Gulfstream aircraft was the testbed for the system. The test target was a corner reflector surveyed in WGS-84 coordinates to better than 1 meter accuracy.

AN/APG-76 is a mature, fielded multimode, Ku-band surveillance and fire control radar designed for use in tactical aircraft. It is a long range, high power, coherent system utilizing a mechanically scanned multi-aperture planar array with low sidelobes. Mounted on the array is a strapdown inertial measurement unit (IMU) that provides precise angle and vibration measurements. The system is highly programmable and has the capability to perform a wide spectrum of complex tasks that provide the operator with the modes of operation to accomplish a variety of mission scenarios.

The existing, fielded modes of operation include; real beam ground map, high resolution SAR ground map (with and without GMTI), air-to-ground ranging, and air-to-air search, track, and air combat maneuver. All modes are self-calibrating. The radar also provides an extensive on-board built-in-test (BIT) and fault isolation test capability.

The radar provides a unique simultaneous SAR/GMTI mode in which detected targets are displayed on the SAR map as moving target symbols. The symbols are accurately located at their true azimuth position relative to the map center using the measured azimuth interferometer angle to the target. The map on which the moving target symbol is displayed is collected and processed simultaneously with the GMTI. This illustrated in Figure 4 which shows a simultaneous SAR/GMTI mode image which was recorded in-flight.

FLIGHT TEST PROFILES

Test data for both the single and multiple frame measurement techniques was collected on a series of six flights with repeat passes over an established course around Rentschler Airfield in East Hartford, Connecticut. The surveyed corner reflector was located at Rentschler Airfield. A common radar hardware/soft-

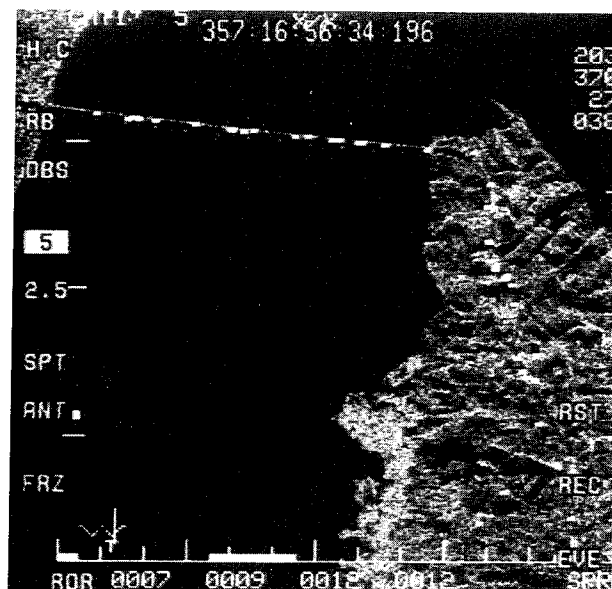


Figure 4. Simultaneous SAR/GMTI Image

ware configuration was maintained for all tests. The aircraft altitude during testing was approximately 25,000 feet and the aircraft ground speed varied between 300 and 350 knots depending on headwinds.

For the single frame measurement technique each test leg began with the surveyed test target located 40 nautical miles (nmi) from the test aircraft and at an angle which was 20° to the right of the aircraft velocity vector. The aircraft flew at a constant heading until the target was 25 nmi from the aircraft and 60° to the right of the aircraft velocity vector. Approximately 75 SAR images were collected on each of nineteen flight legs.

The test profile for the Multiple Frame Measurement technique was selected to induce large changes in both the aspect angle of the target with respect to the aircraft, and, the SAR image plane (the plane defined by the aircraft velocity vector and the line-of-sight vector from the aircraft to the target). The profile began with the surveyed test target located 30 nmi from the test aircraft and at an angle which was 50° to the right of the aircraft velocity vector. The aircraft then flew a 6-degree bank turn until the target was 15 nmi from the aircraft and 20° to the right of the aircraft velocity vector. At this point the aircraft began a 45-degree bank turn which ended with the target 11 nmi from the aircraft and 20° degrees to the left of the aircraft velocity vector. Approximately 50 SAR images were collected on each of three flight legs.

Figure 5 shows a sample SAR image that was generated during the flight testing. The figure shows a scene of Rentschler Airfield with two corner reflector arrays.

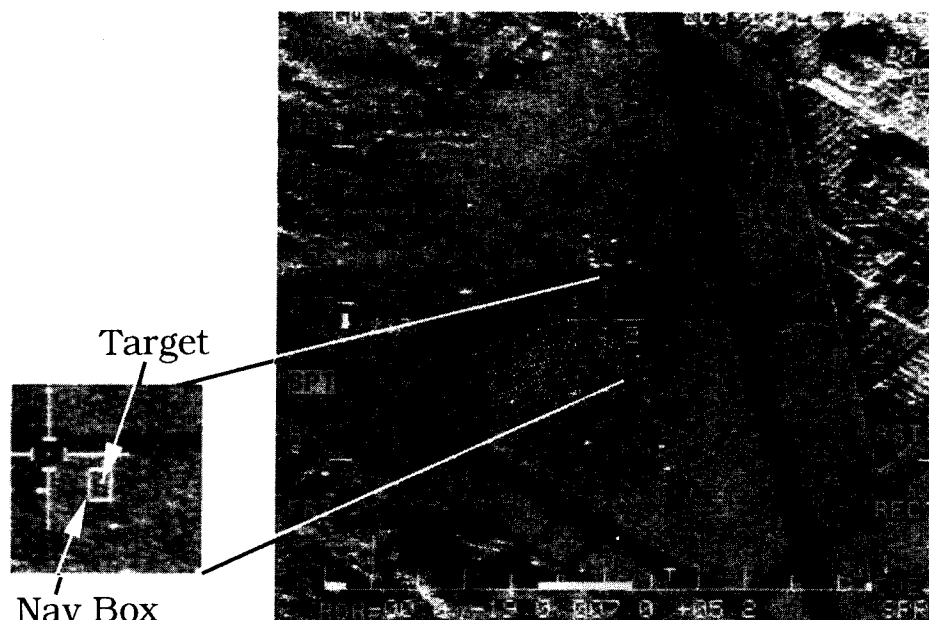


Figure 5. Sample of SAR Image Accuracy

The surveyed corner reflector is the bright spot marked target in the Figure. Also shown in the Figure is a navigation box which is overlaid on the SAR map at the GPS/INS/SAR estimated surveyed reflector location. In this particular frame the target location error is less than 5 meters.

DATA REDUCTION

The target location measurement errors were computed for each SAR image by the following method:

- a. The aircraft position at the mid point of the image collection was obtained from recorded GPS/INS output data.
- b. Each SAR image generated by the radar was digitized and the location of the surveyed corner reflector relative to the image center was measured. Using this data and the surveyed corner reflector location truth data, the true location of the map center was determined.
- c. Using the results of steps a and b and an estimate of the radar signal atmospheric propagation, the true values of range, Doppler and elevation angle at the map center were computed.
- d. The range, Doppler and elevation angle at the map center, as measured by the radar, were then compared to the truth data to determine the measurement errors. These results were then converted into the range, cross range and altitude errors

given in the next section.

Note that computed errors include the GPS/INS position errors of the aircraft. An attempt was made to determine aircraft location to a better accuracy using differential GPS (DGPS) data recorded in flight. These measurements turned out too noisy to be useful.

STATIONARY TARGET TEST RESULTS

The single frame measurement technique was evaluated using data gathered on a total of nineteen test runs taken over an eight month period. A summary the measurement results obtained is presented in the first column of Table 1. As can be seen, the slant plane range measurement is quite accurate and the major errors are in altitude and cross range. The measured altitude error represents approximately a 1-milliradian error in the elevation angle measurement. The second column of the table shows the resulting errors when the altitude error is eliminated. The estimated weapon delivery CEP (neglecting weapon control/steering errors) is shown at the end of the table and demonstrates the accuracy improvements obtainable when the altitude error is reduced.

The estimated performance of the integrated GPS/INS systems used for these tests is summarized in Table 2. As is evident from the table the measured position accuracy is much better than the specification and the measured velocity accuracy is also well within spec.

Table 1. Single Frame Measurement Flight Test Data Summary

| DIMENSION | ACCURACY (M) | |
|--------------------------|----------------------|--------------------|
| | UNCORRECTED ALTITUDE | CORRECTED ALTITUDE |
| RANGE | | |
| SLANT RANGE | 5.5 | 5.5 |
| GROUND RANGE | 9.6 | 5.4 |
| ALTITUDE | 75.4 | — |
| CROSS RANGE | 14.0 | 7.6 |
| CEP | | |
| VERTICAL WEAPON DELIVERY | 13.1 | 7.3 |
| OPTIMUM WEAPON DELIVERY | 7.3 | 7.3 |

Table 2. Estimated Integrated GPS/INS Measurement Errors

| PARAMETER | ACCURACY | |
|---------------------------|---------------|-------------|
| | SPECIFICATION | MEASUREMENT |
| POSITION (m CEP) | 16 | 5.5 |
| HORIZONTAL VELOCITY (m/s) | 0.03 | 0.018 |

Results obtained with the fixed target multiple slant plane technique are shown in Table 3. The results listed in the first column were obtained by taking a sequence of images gathered in each test leg and comparing the first image with each successive image. The second column "N-Point Filter" results were generated by computing a best estimate based on all the images. Overall these results match the single frame measurement technique results with the altitude corrected.

MOVING TARGET TEST RESULTS

Moving target test results are shown in Table 4, which lists the relative location error of the detected moving targets with respect to a SAR map reference. These measurements were taken at ranges between 25 and 40 nmi. The mean error represents an azimuth angle error of approximately 150 microradians. The 1-sigma variation in the results is consistent with the signal-to-noise ratio of the target measurements. The total moving target location error is the root sum square of the relative moving target RMS error and the SAR map location errors and is approximately 20 meters.

Table 3. Multiple Frame Measurement Flight test Data Summary

| DIMENSION | ACCURACY (M) | |
|--------------------------|----------------|----------------|
| | 2-POINT FILTER | N-POINT FILTER |
| SLANT RANGE | 2.1 | 1.1 |
| ALTITUDE | 12.1 | 6.1 |
| CROSS RANGE | 5.4 | 2.1 |
| CEP | | |
| VERTICAL WEAPON DELIVERY | 5.9 | 2.6 |
| OPTIMUM WEAPON DELIVERY | 4.8 | 2.0 |

Table 4. Relative Target Location Error

| TEST LEG | RELATIVE ERROR (M) | | |
|-----------|--------------------|---------|------|
| | MEAN | 1-SIGMA | RMS |
| 053:15:59 | 11.46 | 13.38 | 17.6 |
| 053:16:46 | 16.08 | 9.21 | 18.5 |
| 053:17:33 | 3.18 | 9.78 | 10.3 |
| 074:16:27 | 8.64 | 10.62 | 13.7 |
| 074:17:01 | 9.45 | 13.2 | 16.2 |
| 074:18:13 | 9.27 | 12.33 | 15.4 |
| AVERAGE | 9.68 | 11.42 | 15.3 |

FUTURE WORK

Future precision targeting experiments to be conducted for a Joint Advanced Strike Technology (JAST) Program 95-1 demonstration will include real time operation and improved SAR resolution. Real-time implementation will require the operator to have access to portions of the previous SAR map (showing the cursored target pixel) when he makes the subsequent target designations. Improved resolution will allow the operator to cursor the target more precisely in-flight. Future testing plans also include using carrier phase kinematic DGPS (0.1 meters) as radar truth data to isolate P-Code GPS errors.

ACKNOWLEDGEMENT

The authors wish to thank Dr. James O'Brien and Dr. Lawrence Orwig of Westinghouse Norden Systems for their valuable contributions to this study.

REFERENCES

- [1] Anthony Abbott, Neeraj Pujara, Peter Howe, "GPS Exploitation for Precision Targeting - Observability Using Synthetic Aperture Radar", 49th Annual Meeting Proceedings of the Institute of Navigation, June 1993.
- [2] George R. Beck, et al., "GPS Exploitation For Precision Targeting: Tactical Applications", 49th Annual Meeting Proceedings of the Institute of Navigation, June 1993.
- [3] Dr. George T. Schmidt, Roy H. Setterlund, "Precision Strike Concepts Exploiting Relative GPS Techniques", 49th Annual Meeting Proceedings of the Institute of Navigation, June 1993.
- [4] Scott Burgett, "Target Location in WGS-84 Coordinates Using Synthetic Aperture Radar Images", 49th Annual Meeting Proceedings of the Institute of Navigation, June 1993.
- [5] Richard Gibbs, Matthew Bottkol, Todd Owen, "Flight Test Demonstration of Image Fix-taking with SAR", 49th Annual Meeting Proceedings of the Institute of Navigation, June 1993.

Anti-Jamming Performance of TIDGET in Guided Munitions Applications

Armando Montalvo, Bruce Johnson, and Alison Brown
NAVSYS Corporation

ABSTRACT:

Many guided munitions systems could benefit from the use of GPS position information to augment existing inertial navigation systems. Currently GPS is planned to be used on JDAM, other potential missile systems are, next generation of AMRAAM and Harpoon missiles. These applications however, are characterized by no pre-launch visibility of GPS satellites, short duration, and high launch dynamics, which preclude the use of conventional GPS receivers. Utilizing the TIDGET sensor, NAVSYS developed an innovative approach to GPS/INS data fusion for these demanding applications that optimally combines GPS and INS data from both the launch platform and smart munitions. The advantages of this system include no initialization of GPS sensor pre-launch, rapid signal acquisition even in high dynamic environments (Time To First Fix < 1 sec), and inherent differential operation. But perhaps the most surprising advantage is the improved anti-jamming performance when compared to even an ideal conventional receiver. An ideal conventional GPS receiver will provide a jamming margin of 43 DB for C/A codes and 53 DB for P/Y codes, assuming no quantization and sampling losses. Here we will show that the TIDGET sensor provides jamming margin of up to 70 DB for C/A codes and 68 DB for P/Y codes, for these applications, while still maintaining one meter PR accuracies. Here we present the system's architecture with an analysis of the system performance and J/S margins.

1. INTRODUCTION

1.1 GPS FOR PRECISION WEAPON DELIVERY

Attack aircraft currently carry a suite of precision sensors such as Global Positioning System (GPS), Inertial Navigation System (INS), Forward Looking Infrared (FLIR) systems, and Synthetic Aperture Radar (SAR) that can be used to provide precision air-to-ground or air-to-air targeting. Smart weapons also carry a sensor suite including inexpensive IMUs and sometimes GPS equipment for precision weapon delivery. However, the size, weight, and cost of the missile electronics limit the functions that can be performed on-board. The ability to fuse data from on-board sensors and off-board assets can significantly improve the accuracy of the weapon delivery while reducing the cost of the weapon system.

NAVSYS has designed an innovative tracking system that optimally combines data from the aircraft and missile sensors, including GPS and INS data from both sources. This architecture has the following key advantages over previous GPS/INS missile guidance systems.

- Low cost GPS sensor used in place of a full receiver on the missile.
- No initialization needed of GPS sensor pre-launch.
- Rapid initial signal acquisition even in high dynamic maneuvers (TTFF < 1 sec).
- Sensor fusion of aircraft and missile GPS/INS data performs rapid in-flight alignment of missile INS, reducing time

- Sensor fusion of aircraft and missile GPS/INS data performs rapid in-flight alignment of missile INS, reducing time needed for pre-launch initialization and alignment.
- Enhanced signal processing of GPS data on aircraft increases signal margin and anti-jamming (A/J) performance of missile GPS data.
- "Differential" missile-to-aircraft operation provides improved GPS precision for targeting using aircraft sensors.

The TIDGET/INS Missile (TIM) system concept, is illustrated in Figure 1.

The missile carries on-board an inexpensive, miniaturized GPS sensor, the TIDGET™. The TIDGET is used to periodically collect "snapshots" of the GPS data. This data is formatted into a message that also includes the missile INS position, velocity, and attitude data, which is transmitted back to the aircraft. The aircraft receives the data from the missile and passes it to the TIM tracking system for processing. The TIM tracking system combines the data from the aircraft GPS/INS systems with the TIDGET/INS data received from the missile, and processes this to compute an integrated GPS/INS solution for the relative location and velocity of the missile to the aircraft. This can be combined with FLIR and SAR data to accurately target the weapon system. Several applications can benefit from the use of a TIM tracking system to improve the guidance accuracy. In [1] and [2] the focus was on the use of the technology in an extended range air-to-air missile where a target is acquired by the launch aircraft. The missile is then launched and uses its on-board INS to fly towards an aim point (expected future location of the target) supplied by the launch aircraft. Based on the target motion, the launch aircraft transmits updates of the aim point to the missile during flight. Once the missile reaches the aim point and the target can be acquired by the

missile seeker, the mid-course guidance phase ends and the missile starts using its seeker for terminal guidance to the target. Note that if the missile INS provides inaccurate navigation information, the capability of the missile to reach the aim point will be severely degraded.

Although those papers considered air-to-air applications, the TIM system can be used in any guided missile or bomb that relies on an on-board INS for navigation/guidance.

1.2 TECHNICAL ISSUES

A block diagram of the NAVSYS TIM tracking system is shown in Figure 2. The key technical issues in the design of the TIM system are:

TIDGET/INS Data Fusion

A system that relies on an INS navigation information for guidance is subject to guidance errors due to the fact that the INS (if uncorrected) exhibits errors that grow with time. The magnitude of the INS errors depends on the size of initialization errors, as well as the instrument, i.e. accelerometer and gyro errors. In airborne applications where missiles are launched from wing mounts, a large source of INS error occurs due to incorrect attitude initialization (i.e. incorrect alignment), which results from wing twist etc [1]. Furthermore, if low cost Inertial Measurement Units (IMU's) are used, the accelerometers and gyros will exhibit large errors.

By fusing GPS and INS data, improvements in system accuracy are obtained because of:

- **Improved INS initialization:** by using the appropriate data fusion process, it is possible to significantly reduce the effects of incorrect INS initialization after processing only a few GPS measurements. This means that for example in a hostile jamming environment, only a small number of GPS

measurements are required, whereupon autonomous operation using only the INS is possible.

Improved Navigation information: if the GPS data is used to correct the INS at regular intervals throughout the missile flight, one obtains a system that exhibits the best characteristics of both GPS and inertial navigation systems, viz. the accuracy and stability of GPS, as well as the high bandwidth of an INS.

The key issues regarding TIDGET/INS data fusion are the tradeoffs related to: IMU quality and cost, and number and accuracy of TIDGET/GPS updates required.

Rapid Acquisition of GPS Signal

In many smart munitions applications, a munitions-mounted GPS receiver will not be able to receive GPS signals until launch. Furthermore, launches of smart munitions typically involve high accelerations. Both of these factors are detrimental to conventional GPS receiver operation and result in larger delays for GPS solutions to become available.

Communications Link Bandwidth

The bandwidth of the downlink between the missile and the aircraft will determine the amount of GPS data available for processing. The amount of data available for processing will affect the navigation solution accuracy and availability, especially in jamming scenarios. Given a fixed, effective communications bandwidth, the trade-off is between the TIDGET sampling rate of the GPS signal structure, the quantization level of the TIDGET sampler (number of bits), the length of the TIDGET snapshots, and the frequency of the TIDGET snapshots (i.e. the number of TIDGET snapshots per unit time).

Anti-Jam Capability

The effectiveness of any munitions system is threatened by the use of enemy jammers.

Although GPS signals are spread-spectrum, their low power levels and particular spread spectrum architecture make them susceptible to jamming.

In the remainder of the paper we will describe the TIDGET sensor its operation and its performance in particular its associated J/S margins in a TIM system.

2. TIDGET OPERATION

The proposed TIM system is based on the low cost TIDGET sensor developed by NAVSYS Corporation. The TIDGET sensor architecture is a compromise between a full GPS receiver and a GPS digital translator, which in this application provides the best features of both for missile tracking.

A conventional GPS receiver includes an RF subsystem, frequency synthesizer, digital signal processing (DSP) chip, and a microprocessor. The RF subsystem receives the L1 GPS signals and converts them to a convenient intermediate frequency (IF). The IF signals are filtered and digitized. Typically, a sample rate of at least 2 MHZ is used to digitize the GPS signals which are at 1.023 MHZ for the C/A code. A 20 MHZ sample rate is required to capture the full P/Y code bandwidth. A second down-converter and A/D sampler is used to capture the L2 bandwidth if required.

The digitized GPS signals are then processed in a semi-custom DSP chip to provide code and carrier demodulation. Samples of the demodulated signals are accumulated and processed in the microprocessor to provide pseudo-range (PR) and delta-range (DR) measurements. These measurements are then used to derive the position and velocity of the receiver. In a tracking system implementation, the receiver provides either the raw PR/DR measurements or a position and velocity fix as output from the microprocessor.

This data is transmitted via a telemetry link to a ground station for further processing.

The trade-offs between the receiver-based implementation and the translator include cost, complexity, power, size, bandwidth, and performance. The receiver approach requires that each missile being tracked carry a complete GPS receiver that can process the GPS data for transmission to the ground station. A more efficient approach, which reduces the amount and complexity of the flight hardware, is to perform navigation processing on-board the aircraft, where size and weight constraints are less significant.

A GPS translator implements this idea by retransmitting the raw GPS data from the vehicle to a translator processing system. The front-end of the translator is identical to that of a conventional GPS receiver. The raw (unprocessed) GPS signals are then transmitted via a telemetry link to the ground-based translator processing system.

The advantage of the translator system over a receiver system is in the acquisition and tracking performance. Missile-borne GPS receivers have difficulty in rapidly acquiring and tracking satellite signals due to the high dynamics of the missile. Large swings in the frequency of the receiver's oscillator are introduced by the missile's high dynamics, especially during missile launch. These frequency swings create an extremely difficult acquisition and tracking problem for the receiver, since it has to search over a large Doppler range to find the satellite signals. This problem is compounded by the fact that the receiver may not be able to "see" GPS satellites prior to launch, since the missile is usually located beneath the wing of an aircraft. Even in a static environment, a receiver typically requires several minutes to acquire and track enough satellite signals to provide a navigation solution.

The major disadvantage of translators for this application is the larger telemetry bandwidth required. Existing GPS translator systems developed by the US Navy and by the tri-service Range Applications Joint Program Office (RAJPO) are based on analog translators and therefore require wide bandwidth telemetry systems (>2 MHz) which are not suited for tactical applications.

The NAVSYS design uses a missile sensor that incorporates the size, weight, cost, and performance advantages of a digital translator while requiring only a low bandwidth telemetry link as does a GPS receiver. This system design is based on the patented TIDGET GPS sensor illustrated in Figure 3.

In addition to downconverting and digitizing the GPS signal, the TIDGET also includes a digital data buffer (DDB) to provide the capability to reduce the output data rate. This data rate reduction is achieved by buffering a "snapshot" of the digital GPS data. The selected interval of data is then transmitted to the aircraft with the INS data from the missile. The GPS snapshot and INS data are fused with the aircraft sensor data to derive the missile position, velocity, and attitude solution relative to the aircraft and target. The aircraft uses this information to send fire control data and INS calibration data to the missile across the telemetry link.

3 TIDGET PERFORMANCE

As mentioned before, the TIDGET is a compromise between a full GPS receiver and a GPS digital translator and exhibits performance characteristics, unique to its architecture. We are not only concerned with the TIDGET performance under normal circumstances but also with its performance in the presence of intentional or unintentional jammers. A good way of representing the performance of this sensor is by expressing the maximum jammer-to-signal (J/S) power margin

that can be tolerated by the sensors, while producing reliable data. There are several types of jammers, of which we will only consider the effects and possible counter-measures for the following types: narrowband or continuous wave (CW) jammers, broadband jammers, pulsating jammers and spoofing jammers. The analysis presented here suggest that broadband jammers are expected to be more detrimental to the performance of the TIDGET sensor. Also it is shown that in the presence of a broadband jammer, the J/S margin for the TIDGET sensor is given by:

$$10\log_{10}(J/S) \geq 73.109 - SNR_T + TG_{loss} - PG \quad (dB) \quad (1)$$

where SNR_T is the minimum SNR (in DB-Hz) required to acquire code phase and carrier phase synchronization, for PR measurements, for a given length of data from the TIDGET sensor. TG_{loss} is the SNR degradation (in DB) introduced by the sensor through the translation of the raw GPS signal, and PG is the processing gain (in DB) that can be obtained through proper filtering of the raw GPS signal and processing of the TIDGET sensor data.

3.1 TIDGET SNR DEGRADATIONS

The TIDGET sensor (see Figure 3) includes three main components: (i) the analog front-end where the RF GPS signal is bandpass filtered and downconverted through three stages of mixing; (ii) a presampler filter along with an A/D converter that quantizes the filtered analog signal to 2 bits (sign and magnitude) which then are provided to latches for sampling; (iii) and a component containing the DDB and other control functions required for the proper operation of the interfacing I/Os [1]. Each of these components degrades the receiver SNR by increasing the thermal noise in the received signal, reducing the effective signal strength, or introducing noise to the received signal.

Front End Degradation

The first component, where all the front-end functions are performed, usually reduces the SNR by increasing the effective thermal noise in the received signal. This component of the TIDGET sensor has been carefully designed so that this SNR degradation is no larger than 4 DB [1], which is similar to the majority of receivers and digital translators. Thus the following comparative analysis, ignores this SNR degradation as it is common to all.

Sampling and Quantization Degradations:

The SNR degradations introduced by the presampler/converter component in the TIDGET are usually not encountered in the same fashion on either full receivers or digital translators. These performance degradations are explained below.

- Effect of Sampling Rate: In the presampler/converter, the downconverted GPS signal is filtered, sampled, and quantized by a 1 or 2 bit A/D converter. Aliasing is avoided by bandlimiting the signal through a filter prior to sampling. In a full receiver, the downconverted received signal will be passed through a pair of presampling filters that not only bandlimit the received signal, but also produce a pair of signals that when treated as a complex construct forms an analytical signal. In the TIDGET sensor, the downconverted received signal is only passed through a single presampling filter and then sampled not at the Nyquist frequency but at half the Nyquist frequency. The resulting sampled signal contains only the real or imaginary part of the analytical signal encountered in a full receiver. When correlated with either a P or C/A reference code, this results in an SNR degradation of approximately 3 DB due to the loss of signal power.
- Degradation Due to Quantization In the TIDGET the downconverted received signal, is further quantized by a 1 bit

quantizer. The effects of this quantization in the effective SNR of the TIDGET output data can be seen by considering the output of a typical correlator when this quantized data is used. Assuming coherent detection of the carrier phase and independent noise samples, it can be shown (see [1]) that the performance degradation due to 1 bit quantization for weak signals results in a 1.97 DB loss.

Thus the total SNR loss associated with a typical TIDGET sensor is $TG \text{ loss} = 4.97 \text{ DB}$.

3.2 ACQUISITION PERFORMANCE

The TIDGET sensor data is only used to acquire and track the GPS code and carrier information in order to obtain PR and carrier-range (CR) measurements. The GPS signal structure also carries satellite ephemeris and time information modulated on the spread spectrum signal structure at a 50 bps rate. This data information is not used by the TIDGET, but is gathered at the reference receiver. Because of this, the best acquisition performance can be obtained if the data modulated on the GPS signal is removed before processing the TIDGET data. This process, called data aiding, significantly improves the acquisition and tracking performance of the TIDGET system. Since there no data present the effective coding gain associated with the spread spectrum code is augmented by 16 DB for acquisition and tracking (see [1]).

The GPS signals must be acquired in both time (code phase) and Doppler frequency offsets (carrier phase) before the tracking operation can begin. This implies a search for the single synchronization in both time and frequency. The search problem is greatly simplified, however, if a-priori information about the Doppler frequency is obtained, which allows the use of coherent phase detection. This reduces the two-dimensional

frequency-phase search to only a one-dimensional search over all possible code phases until synchronization is acquired. For the TIM system, the missile inertial information, along with the GPS receiver data, provide a-priori information to permit coherent detection. In order to improve performance even further the TIM system uses a sequential search method, since this allows the use of maximum likelihood detection methods. It can be shown (see e.g. [1], [4]) that the minimum required SNR to guarantee acquisition of the code and carrier synchronization is given by:

$$SNR_T = 10 \log_{10}(-\ln(\beta)) + 10 \log_{10}\left(\frac{1}{PS}\right)$$

where β is the probability of missing detection and PS is the TIDGET snapshot data length. The higher performance obtained results in a more rapid acquisition in a noisy environment (see e.g. [1],[3]).

3.3 TRACKING PERFORMANCE

As indicated earlier, using a-priori information about the carrier phase, obtained through data aiding between sensors, coherent carrier phase demodulation can be obtained and resolved before code phase acquisition and tracking. Once code phase synchronization is obtained, the code phase can be tracked by using a delay lock loop to obtain estimates of the code phase. Typically, receivers track the code phase by using delay lock loops which provide minimum mean square error estimates of the code phase. In order to obtain maximum performance the TIM system uses a Maximum Likelihood Estimator (MLE) instead of a minimum mean square error method. The MLE method results in an improvement in measurement accuracy by at least a factor of 2, depending on the TIDGET snapshot length.

3.4 JAMMING PERFORMANCE

Four types of jammers present a typical threat to the TIM system: spoofing, narrowband or CW jammers, pulsating jammers, and broadband jammers.

Spoofing Jammers

Spoofing jammers are spread spectrum signals that emulate GPS signals by reproducing the GPS signal structure associated with C/A codes. The simplest method to defeat C/A code spoofing jammers, is to process the encrypted P code signals. In this regard, the TIDGET architecture is no different than conventional receivers. If spoofing jammers are a concern, P code signal processing can be used.

Narrowband or CW Jammers

Narrowband or CW jammers are high power signals that occupy narrow or small bandwidths that fall on or close to the GPS carrier frequencies. In an ideal receiver, these signals are spread during the correlation with the reference code. Thus their effects are mitigated by the spreading factor associated with the reference code. However in some cases this reduction in the SNR degradation introduced by the jammer may not be enough in many cases. In the TIDGET, the effects of this type of jammer also include the introduction of spurious responses at the limiter output of the A/D converter, as well as non-linear effects due to stuck faults of the quantization bit in the A/D converter.

The suggested approach to dealing with narrowband jammers is to treat the problem as a cancellation of the narrowband signal (the CW jammer) in the presence of broadband noise (the GPS signal). There are several methods that can be used to reduce the effective power of the narrowband signal before correlation with the reference code is performed (see e.g. [4], [5]). These procedures can be applied equally well to TIDGET and conventional receivers.

Pulsating Jammers

Pulsating jammers are very high power signals of very short duration. These signals have a strong detrimental effect on the data detectors in ideal receivers [7], by acting as a noise source that introduces burst errors on the data stream. The smaller the duration of the jamming pulse, the more power it contains and the more bursty the effective channel behavior is. This type of jammer can be compensated either by introducing error correction capabilities in the transmitted GPS signal or by estimating the jammer state (present or not present) and ignoring the data when the jammer is present.

Fortunately, this problem does not severely affect the performance of the TIDGET sensor if the duration of the pulsating jammer is small compared to the length of the sensor data. Since this is the case for almost all practical cases, it can be presumed that such jammers do not affect significantly the TIDGET performance.

Broadband Jammers

Broadband jammers are signals of moderate power and broad bandwidth centered on or around the GPS carrier frequencies and behave like band-limited white Gaussian noise. The main effect of the this jammer is to degrade the effective SNR by effectively increasing the noise floor.

One defense against broadband jammer signals is to reduce their power by filtering the jammer spectrum in order to reduce its effective bandwidth. This band-limiting operation can be performed by the presampler filter in the TIDGET sensor. Note that band-limiting the received signal spectrum beyond the chip rate of the reference code, either 10.23 MHz for P/Y code signals or 1.023 MHz for C/A code signals, will also reduce the GPS signal power. Since the GPS signal power spectrum has a $\sin(x)/x$ shape, for either P/Y or C/A code signals, intuitively the signal loss will be more gradual than the reduction of noise power, so that an overall

gain can be obtained. It can be shown that any possible SNR gain or losses achieved by band-limiting the received GPS signal an broadband noise can be express as:

$$SNR(f) \equiv PG = 10 \log_{10} \left[\frac{\epsilon(f)}{N_0 BW} \right]$$

where $BW = F_{\max} - F_{\min}$ = bandwidth, N_0 is the effective noise spectral density, and $\epsilon(f)$ is given by:

$$\epsilon(f) = \frac{P}{2\pi^2} \left[\frac{-BW}{f_{\max} f_{\min}} + \frac{\cos(2\pi f_{\max} T)}{f_{\max}} - \frac{\cos(2\pi f_{\min} T)}{f_{\min}} \right] + \frac{PT}{\pi} \int_{-2\pi f_{\min} T}^{2\pi f_{\max} T} \frac{\sin(x)}{x} dx$$

Figures 4 and 5 show this PG as a function of bandwidth for the P/Y code and C/A code respectively. These figures assume a broadband jammer with bandwidth of 20.46 MHz and a relative power of 0 DB. Note that for a 2 MHz bandwidth, the PG is 9.33 DB and 2.98 DB for C/A and P code signals respectively.

By combining these result we can conclude that the performance of the TIDGET is indeed govern by equation (1). Tables and 2 summarize the performance of the TIDGET for this application for various packet sizes, sampling rates. The resulting jamming gains are calculated relative to a broadband jamming signal spread over the full 20.46 MHz of the P/Y code. The last column is the PR accuracy in meters assuming no jamming and 40 DB-Hz signal levels. From these tables we can clearly see that: 1) for the TIDGET-based TIM system, the C/A code signals has slightly larger jamming margins than P/Y code. 2) Undersampling significantly increases the broadband jamming margin for a small cost in PR accuracy. Typically, a factor of five decrease in sampling rate will increase the jamming margins by approximately 10 DB while decreasing the accuracy only by a factor of two. 3) Accuracy and jamming margins increase with increase packet size.

4. CONCLUSIONS

The TIM system, based on the TIDGET GPS architecture and aided with missile-based INS data, provides the capability to obtain accurate navigation information for guided munitions.

By using the unique characteristics of the TIDGET it is possible obtain the benefits of GPS while still meeting the demands for rapid GPS signal acquisition even in high dynamic environments (Time To First Fix < 1 sec), improved Anti-Jamming performance when compared to even an ideal conventional receiver, and inherent differential operation.

REFERENCES:

1. Aircraft Missile Sensor Fusion for Enhanced Weapon Delivery, NAVSYS Technical Report WP-TIM-3414-95-05.
2. J. Coetsee, A. Montalvo, and A. Brown "A TIDGET /Inertial Missile Sensor Fusion System" AAA Guidance, Navigation and Control conference, August 1995.
3. D. Middleton, D. Van Meter, "On Multiple Alternative Detection of Signals in Noise", IEEE Trans. On Info. Theory, 1955.
4. M. Wax, T.J. Shon, T. Kailath, "Covariance Eigenstructure Approach to 2D Harmonic Retrieval", IEEE Conf. On Acoustics, Speech & Signal Proc., Boston 1983.
5. Applied Optimal Estimation, Gelb, MIT Press
6. Cheng, Gupta, "Advanced Midcourse Guidance for Air-to-Air Missiles", AAA Journal on Guidance and Control, March-April 1986.
7. J.G. Proakis, Digital Communications, Mcgraw-Hill, 1989.

Table 1 C/A Code Performance

| Packet Size (ms) | Packet Size (bits) | Sampling Rate (MHZ) | SNR Threshold (DB) | TIDGET Loss (DB) | Jamming Gain (DB) | J/S Margin (DB) | PR Accuracy (40 DB-Hz) (m) |
|------------------|--------------------|---------------------|--------------------|------------------|-------------------|-----------------|----------------------------|
| 4 | 40 k | 10 | 27.57 | 4.96 | 3.11 | 44 | 16.4 |
| 4.7 | " | 8.6 | 26.92 | " | 3.70 | 45 | 15.1 |
| 7 | " | 5.71 | 25.14 | " | 5.40 | 48 | 12.4 |
| 200 | 2 M | 10 | 10.59 | " | 3.11 | 61 | 2.3 |
| 232.6 | " | 8.6 | 9.93 | " | 3.70 | 62 | 2.2 |
| 350.3 | " | 5.71 | 8.16 | " | 5.40 | 65 | 1.8 |
| 1000 | " | 2 | 3.6 | " | 9.33 | 70 | 1.0 |

Table 2 P/Y Code Performance

| Packet Size (ms) | Packet Size (bits) | Sampling Rate (MHZ) | SNR Threshold (DB) | TIDGET Loss (DB) | Jamming Gain (DB) | J/S Margin (DB) | PR Accuracy (40 DB-Hz) (m) |
|------------------|--------------------|---------------------|--------------------|------------------|-------------------|-----------------|----------------------------|
| 4 | 40 k | 10 | 27.57 | 4.96 | 2 | 43 | 5.2 |
| 4.7 | " | 8.6 | 26.92 | " | 2.25 | 44 | 4.8 |
| 7 | " | 5.71 | 25.14 | " | 2.55 | 46 | 3.9 |
| 200 | 2 M | 10 | 10.59 | " | 2 | 60 | 0.7 |
| 232.6 | " | 8.6 | 9.93 | " | 2.25 | 60 | 0.7 |
| 350.3 | " | 5.71 | 8.16 | " | 2.55 | 63 | 0.6 |
| 1000 | " | 2 | 3.6 | " | 2.98 | 68 | 0.3 |

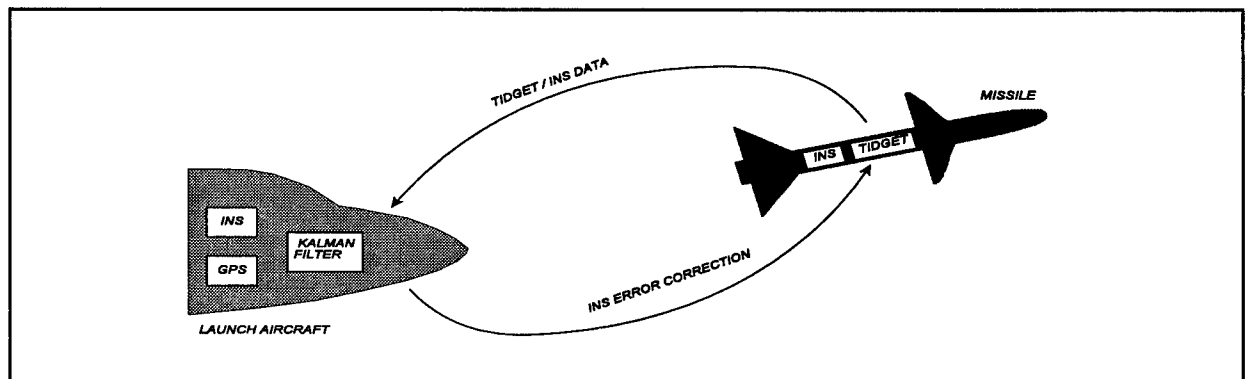


Figure 1: TIM System Concept

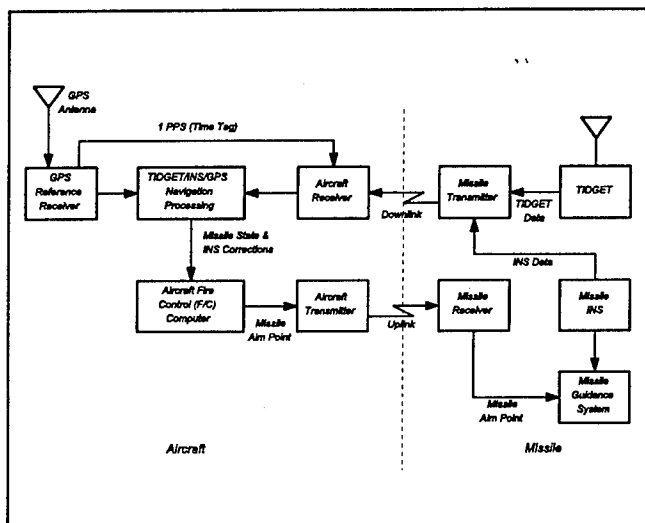


Figure 2: TIDGET/INS Missile (TIM) System Block Diagram

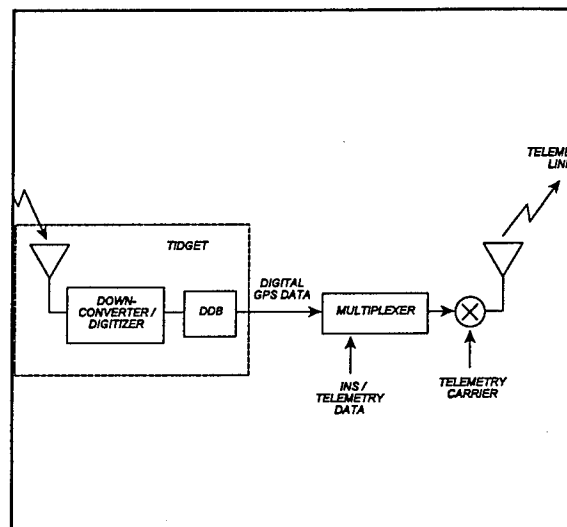


Figure 3: Missile TIDGET Sensor Architecture

10
ION 95

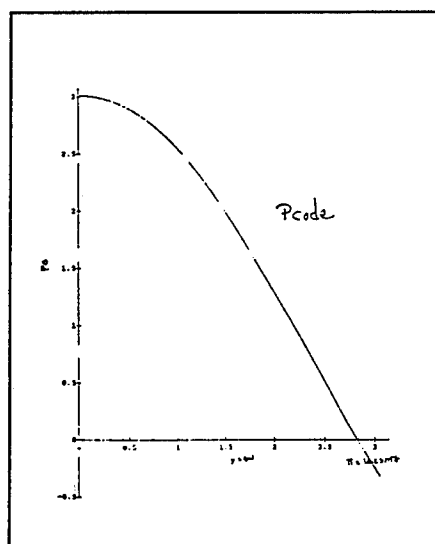


Figure 4 Processing Gain for P Code

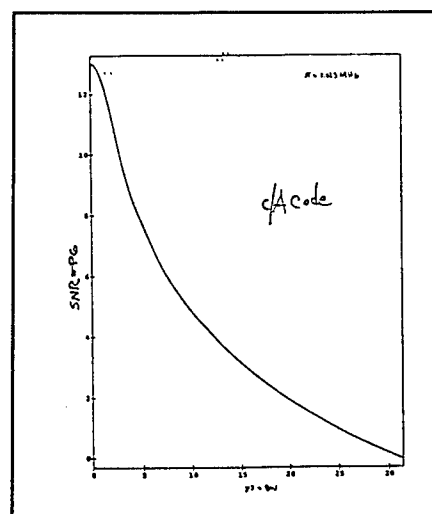


Figure 5 Processing Gain for C/A code

Robust Implementation of Relative GPS Guidance

Dr. Mark Youhanaie, David Hartman, and Frank Ziolkowski
Hughes Aircraft Co.

Neeraj Pujara
Wright Laboratory

BIOGRAPHIES

Dr. Mark Youhanaie is manager of the GPS Navigation Technology Center at Hughes Aircraft Company in El Segundo, California. He has led Hughes' GPS-Inertial systems developments since 1988, prior to which he was manager of the Inertial Navigation Section at Hughes Missile Systems. Dr. Youhanaie holds B.S., M.S., and Ph.D. degrees from the University of Illinois at Champaign-Urbana.

Mr. David Hartman is an engineer in the GPS Navigation Technology Center at Hughes Aircraft Company in El Segundo, California. He has been the lead developer of Hughes' inertial navigation implementations since 1988 and is currently responsible for advanced inertial navigation system analyses. Mr. Hartman holds an M.S. degree from the University of California, Los Angeles.

Mr. Frank Ziolkowski is an engineer in the GPS Navigation Technology Center at Hughes Aircraft Company in El Segundo, California. He has been the lead developer of Hughes' GPS-INS Kalman filter implementations since 1988. Mr. Ziolkowski holds a B.S. degree from the University of Illinois at Champaign-Urbana and an M.S. degree from the University of Southern California.

Mr. Neeraj Pujara is an engineer in the Wright Laboratory Avionics Directorate at Wright-Patterson Air Force Base. He has been engaged in research in the areas of navigation and reference systems integration. He is the Project Engineer for the GPS Electronic Combat Critical Experiment and is the Technical Director for the B-1B Relative Targeting System Demonstration program. Mr. Pujara holds B.S. and M.S. degrees in Electrical Engineering from Wright State University.

ABSTRACT

Much attention has been given recently to the application of Differential GPS (DGPS) phenomenology to improve the accuracy of precision guidance weapons. Specifically, we consider scenarios where a targeting system

provides target coordinates using an on-board GPS for its inertial reference system. By guiding the weapon in a coordinate frame that is correlated to the GPS bias errors inherent in the targeting data, guidance accuracies can be improved to near "precision" level without the use of a terminal guidance seeker. Initial Relative GPS concepts have been proposed to achieve this correlation by slaving the weapon GPS receiver to "track the same four satellites" as the GPS receiver on the targeting aircraft. While this simplistic approach may be effective in some scenarios, it is not sufficiently robust for general implementation. This paper identifies and examines specific issues that must be resolved before Relative GPS guidance can be considered an implementable methodology. Several candidate solutions are presented and evaluated through simulation and analysis. Detailed consideration of these implementation issues was a subject of the USAF GPS Exploitation for Precision Targeting Program with Hughes Aircraft Company.

INTRODUCTION

Recent evaluations of engagement doctrines, subsequent to the experiences of Operation Desert Storm and changing political realities, have motivated the development of new weapon system concepts. Elements common to these emerging concepts include precision strike capability, affordability, and operation in all weather conditions. As a result, Hughes Aircraft Company has developed a weapon system concept that includes a GPS-aided targeting system (GATS) and a synergistic weapon guidance technique called Relative GPS guidance (U.S. Patent Number 5,344,105). Implementation issues of the GATS/Relative GPS weapon system were studied as a part of the USAF GPS Exploitation program under the Precision Strike Initiative.

System concepts that employ GPS-aided targeting, combined with differential or Relative GPS guidance, have been discussed in recent related publications [e.g., 1-3]. This paper presents error budget analyses demonstrating the potential accuracies afforded by Relative GPS guidance and considers issues related to its *implementation in a robust manner*. The simple notion of tracking the same

four SVs as the targeting aircraft, while convenient for feasibility analysis, can result in significant operational limitations. Several candidate solutions are discussed and evaluated through analysis and simulation. An assessment is presented from the standpoint of weapon guidance accuracy and potential consequences for existing aircraft and weapon operations, subsystems, and interfaces.

Overview: Idea and Benefits of Relative GPS

The objective of Relative GPS is to navigate a vehicle from point A to point B where the location of point B is defined by a targeting platform at point C (Figure 1). Assume point B is known very well relative to point C and that the targeting platform has a GPS receiver.

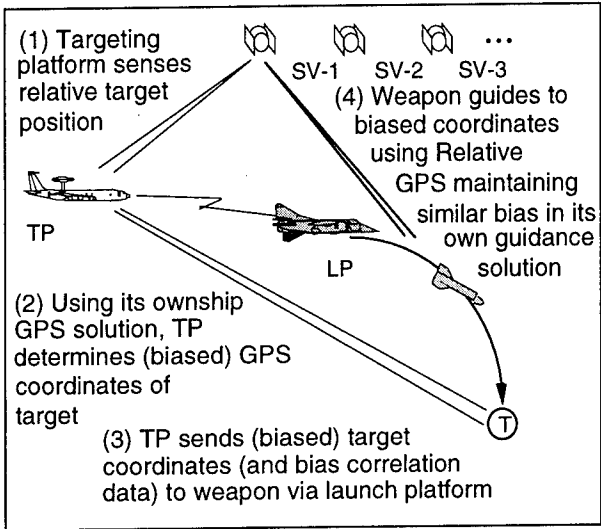


Figure 1. Idea of Relative GPS

If the vehicle also has a GPS receiver, its accuracy in navigating to point B can be better than that of absolute GPS, if it can maintain a high degree of correlation of its absolute GPS position solution errors with those of the targeting platform. In this sense, it navigates relative to the targeting platform in its biased GPS coordinates. Thus, while the vehicle never knows its absolute position better than standard GPS accuracy, it may navigate to point B with a relative accuracy comparable to the absolute accuracies of DGPS.

Relative GPS guidance has the potential of providing near-precision weapon guidance accuracy without requiring a terminal homing seeker, yielding obvious affordability benefits. The global coverage of the GPS results in superior guidance performance compared to pure inertial guidance alternatives. Furthermore, as the GPS utilizes L-band transmission frequencies, its performance is virtually unaffected by weather. Recent trends in GPS receiver developments have made embedded GPS receiver modules even less costly than the inertial sensors required in typical GPS-inertial guidance systems.

Precision Strike Benefits

Error budget analysis at the weapon system level reveals that achievement of precision guidance requires both targeting system and weapon guidance accuracies of better than 3 meters CEP (Figure 2). Three weapon guidance techniques can be considered. The use of a conventional terminally homing (seeker-guided) weapon provides the required accuracy but incurs seeker cost. Use of a conventional GPS for weapon midcourse and terminal guidance does not provide sufficient accuracy because the standard GPS precise positioning service (PPS) accuracy of 16 meters SEP [4] exceeds the precision strike threshold. Relative GPS can provide the required accuracy using standard GPS receiver hardware.

| Error Sources | Values (meters CEP) | | Comments |
|----------------------|---------------------|--------------|------------------------------|
| | Conventional GPS | Relative GPS | |
| GATS targeting error | 3 - 5 | 3 - 5 | GPS-aided SAR |
| Steering error | 1 | 1 | Typical peak transient error |
| Navigation error | 10 | 1 - 2 | Horizontal position |
| Total (RSS) | 10.5 - 11.2 | 3.3 - 5.5 | ≤3 m CEP for "precision" |

Figure 2. Total Weapon Delivery Error Budget

Relative GPS exploits the same phenomena as DGPS to provide comparable accuracies in a mobile environment. DGPS can provide position accuracies on the order of 1 meter by using a stationary "base station" at a surveyed location. Unlike DGPS, Relative GPS does not require a base station and consequently cannot improve absolute accuracies. Instead, it provides a similar degree of *relative* position accuracy between the mobile GPS-equipped targeting platform and the GPS-guided interceptor. The implementation challenge is to maintain, in a robust manner, maximal correlation between the GPS bias errors inherent in the target coordinates and those realized by the guided weapon.

GPS-based guidance provides the benefits of accuracy maintenance, insensitive of flyout range (Figure 3). This feature can be used to relax the accuracy requirements otherwise translated to the weapon's inertial measurement unit (IMU) (although inertial aiding of GPS receivers for antijam improvement typically stresses IMU requirements to the limits of affordability). Analysis of spatial decorrelation affects shows that, for typical tactical scenarios, Relative GPS guidance provides a similar benefit.

Relationship to GATS

The GATS SAR algorithms produce a designated target location in GPS coordinates. Examination of these algorithms reveals that the GPS position solution errors

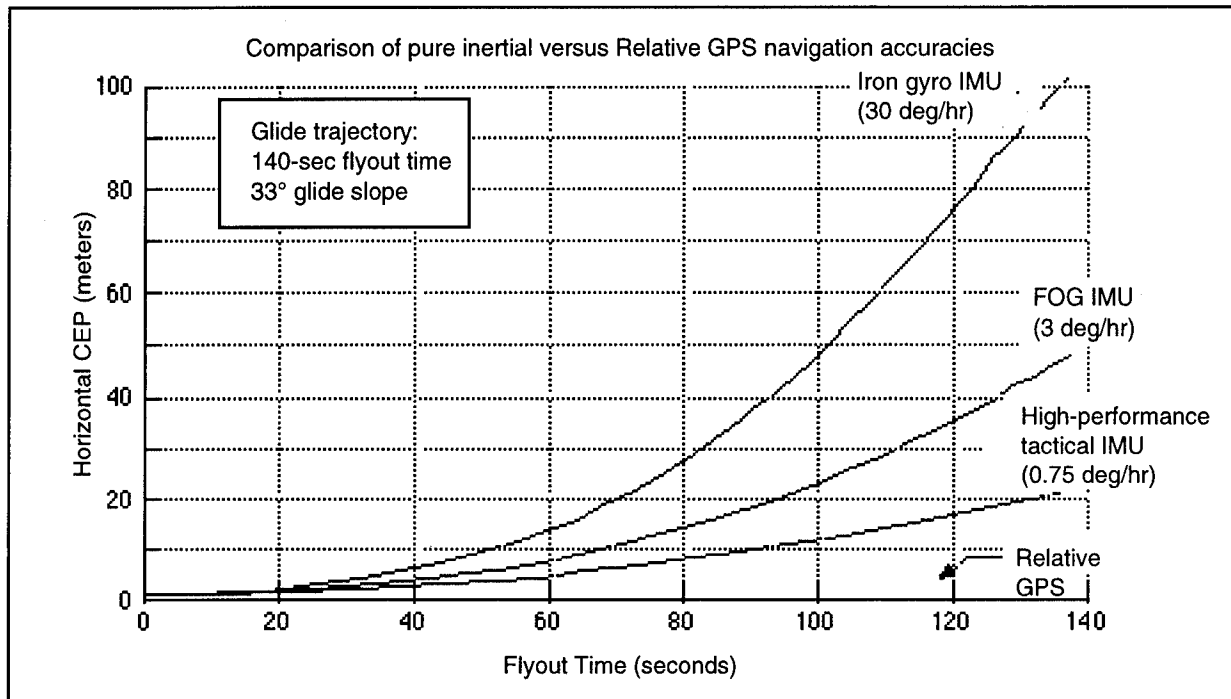


Figure 3. Relative GPS Guidance Accuracy Is Much Less Sensitive to Flyout Range

from the targeting platform's GPS receiver transfer into the target coordinates in an untransformed manner. Therefore, the objective of the Relative GPS mechanization is to maintain maximal correlation of the weapon GPS position solution bias errors to those of the targeting platform. Maintaining this strong bias correlation is the key to Relative GPS guidance accuracy, making Relative GPS implementation a *system* design issue.

THEORETICAL BASIS

DGPS implementations typically employ a GPS receiver at a precisely known location (base station) to observe the bias-like (slowly varying) errors in the pseudorange measurements from each SV. These errors (differential corrections) are then transmitted to all users within the vicinity. The base station is usually an all-in-view receiver that computes and transmits corrections for all visible SVs.

A DGPS remote receiver then performs SV selection, acquisition, and tracking using normal operations, but it applies the received corrections to each pseudorange measurement prior to computing its position solution. In this manner, absolute position accuracies much better than the GPS precise positioning service (PPS) levels are achieved. The value of each observed bias depends on time and the line of sight through the atmosphere. The degree to which to these bias-like errors are eliminated from the position solution depends on their spatial and temporal variations between the base station and the remote receiver.

Review of DGPS Phenomenology

A review of standard GPS error budgets reveals that the total GPS absolute error budget is comprised of bias-like (slowly varying) error sources [5–8]. This is the theoretical basis for DGPS performance. The error budget in Figure 4 is segmented into noise-like and bias-like errors based on assumed operational durations typically less than 5 minutes. User clock error is assumed to be well estimated by both receivers and is therefore not included as a bias-like error. Time transfer error may cause a transient in the second receiver's solution, but the effect on steady-state position solution bias can be expected to be small.

| GPS Noise-like Errors | 1 σ Values |
|--|-------------------|
| Multipath | 1.0 m |
| Quantization | 0.1 |
| Receiver noise | 0.5 |
| Total noise-like error | 1.1 |
| GPS Bias-like Errors | 1 σ Values |
| Satellite ephemeris | 3.0 m |
| Satellite clock | 3.0 |
| Tropospheric residual | 1.0 |
| Ionospheric residual | 1.0 |
| Total bias-like error | 4.5 |
| Total absolute GPS error: RSS $(4.5 + 1.1) \times (\text{DOP} = 1.7) = 8 \text{ m}$ | |

Figure 4. Representative GPS Error Budget

The performance of DGPS or Relative GPS depends then on the ability to achieve bias cancellation over distance and time. A survey of DGPS phenomenology indicates expected temporal and spatial variations in relative errors, as summarized in Figures 5 and 6.

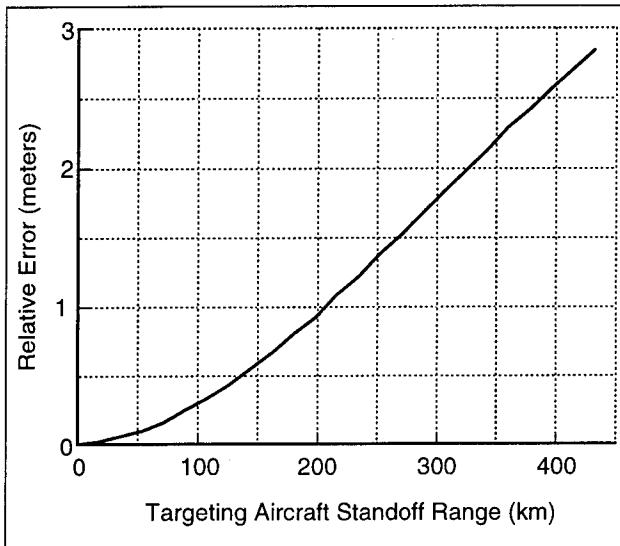


Figure 5. GPS Bias Cancellation Error Over Distance (Spatial Decorrelation)

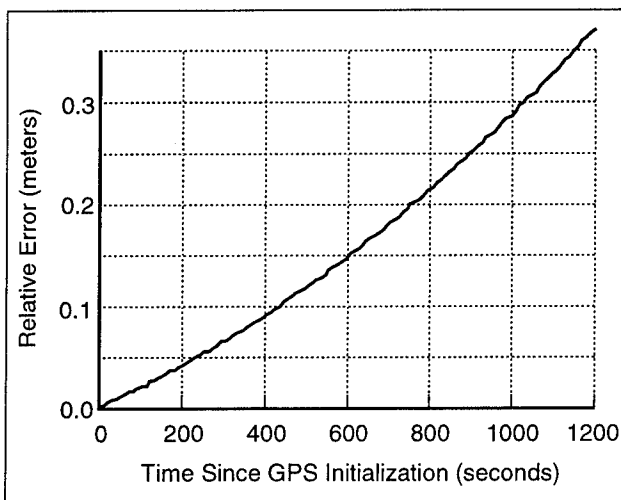


Figure 6. GPS Bias Cancellation Error Over Time (Temporal Decorrelation)

These results show that sufficient bias cancellation can be achieved over times and distances that are small compared to most tactical engagement scenarios.

EVALUATION OF RELATIVE GPS IMPLEMENTATIONS

The implementation problem then becomes one of how to maximize the realized degree of bias cancellation in the presence of real operational events. In addition to the errors in Figure 4, we must allow for an implementation

error to account for deviations from maximal bias correlation.

Tracking the Same Four Satellites

A simplistic idea for maintaining bias cancellation is to have the weapon GPS receiver track the same four satellites as the targeting platform. Unfortunately, this approach lacks robustness due to several operational factors.

First, SV visibility (masking) changes may affect both GPS receivers during the operational timeline, causing constellation changes to occur. Constellation changes just before or during the targeting process may result in a targeting platform bias error that is correlated to more than four SVs. The time constant of the Kalman filter response would determine the "best four" SVs for the weapon receiver to track. A conventional SV selection algorithm could significantly degrade bias cancellation and Relative GPS performance.

Second, Kalman filter gain computations are explicitly dependent on the jamming and atmospheric environments and on vehicle trajectory. At the point in time when target coordinates are computed, the targeting platform position bias errors contain a linear combination of four or more SV-dependent bias errors. The weighting factor on each error is an accumulation of Kalman gain histories that are (GPS receiver) algorithm dependent. Even if the aircraft and weapon receivers tracked identical constellation histories at the same location, they could produce different solution biases. Additionally, the same constellation histories, when subjected to different ECM histories, would produce different gain histories and therefore different solution biases.

A robust implementation approach must consider these deviations. Many improvements are possible, each with a different mixture of benefits and limitations. Four ideas currently under study are discussed below.

Implementation Ideas for Investigation

In this study, four independent mechanization elements have been identified and evaluated. The benefits and implications of each are discussed. The objective of each technique is to maintain maximal correlation between the GPS bias errors inherent in the (GPS-aided) target coordinates and the GPS bias errors in the weapon navigation solution. By maintaining good bias error correlation, accurate Relative GPS guidance accuracy is achieved.

Satellite Correlation Vector

The first approach employs a satellite correlation vector (SCV) algorithm to monitor the operations in the targeting system GPS receiver to identify which SVs the target coordinates are correlated to at all times. The outputs of this algorithm would provide information to the weapon

GPS receiver for use in its satellite selection. The generation of this additional information provides for a more sophisticated version of the "track-the-same-four-satellites" notion. The potential drawbacks of this approach are the need for access to data from the targeting platform GPS not normally provided on a standard GPS interface and the throughput required for the SCV algorithm. An SCV algorithm and corresponding data access requirements are currently in development.

This mechanization can be implemented by deriving information that describes how the biases on the pseudo-range measurements map into biases inherent in the position solution. A sensitivity matrix or satellite correlation vector can be computed from the Kalman filter gain and state transition matrices to approximate this mapping. The matrix would be used to aid satellite selection to minimize of the CEP given a bias shift, if constellation shifts occur during the trajectory.

An error-covariance analysis was performed to evaluate the consequences of replacement satellite selection on Relative GPS navigation accuracy. The horizontal navigation CEP was computed for all four SV constellations possible via replacement of a lost satellite (from the original constellation tracked during the targeting operation). Also computed for comparison were (1) the navigation CEP achieved when the original constellation was tracked throughout the flight (no loss of GPS) and (2) the accuracy achieved when no replacement SV was utilized (use only 3 SVs). Figure 7 summarizes the simulation results. These results show that selection of the replacement satellite can dramatically affect the resultant weapon navigation terminal CEP. As expected, in all cases evaluated here the accuracy is worse than when the original constellation is tracked throughout the trajectory (no loss of GPS).

An interesting finding is that, in some cases, the final accuracy is actually better if no replacement SV is

| Weapon TTF | Fast | Conventional |
|-----------------------|-------------------------------------|-------------------------------------|
| Weapon IMU quality | 1 deg/hr 1 mg 0.075 deg/rt-hr | 1 deg/hr 1 mg 0.075 deg/rt-hr |
| No loss of GPS | 2.10 | 2.11 |
| Use only 3 SVs | 2.21 | 4.67 |
| Satellite combination | Navigation CEP (Horizontal) | |
| 1 | 4.99 | 8.42 |
| 2 | 3.22 | 49.4 |
| 3 | 4.13 | 4.52 |
| 4 | 4.83 | 8.99 |
| 5 | 4.69 | 7.58 |
| 6 | 4.69 | 10.31 |
| 7 | 5.05 | 5.74 |

Figure 7. Simulation Results (50-km Weapon Flyout)
Show Impact of Alternate Satellite Selection on
Relative GPS Performance

selected. This is explained by the fact that, even with a good tactical grade IMU, the navigation CEP growth due to IMU errors is small compared to the bias shift incurred by the best alternate constellation.

The operational implication of these results is that pre-launch (e.g., mission planning) computations can determine whether or not selection of a replacement satellite would provide greater accuracy than simply tracking those remaining from the original constellation. This computation would depend on the time-to-go at the time of satellite loss and the quality of the weapon IMU. In those cases where a replacement SV can provide better performance, an SCV calculation must be employed to correctly identify the best replacement. A suboptimal selection can produce very large navigation errors.

High Elevation Mask

The second approach employs an appropriately large elevation mask angle in the targeting system GPS receiver to ensure that its selected constellation (during targeting) is likely to be visible to the weapons during their engagement timelines. The potential drawbacks of this approach are reduced SV visibility probabilities and degraded GDOP in the absolute accuracies.

The use of a high elevation mask angle to ensure visibility of the same satellites to both the weapon and the targeting aircraft depends on the duration of the total mission timeline, the amount of (line-of-sight) motion of the satellites, and the resulting impact on acquisition and dilution of precision parameters.

For ownship targeting cases, mission duration (start of targeting to weapon impact) depends on the ingress velocity of the targeting aircraft, average velocity of the weapon, and the targeting range. For targeting ranges of 50 to 100 km, mission durations are typically 5 to 10 minutes. Advanced targeting systems with longer range capabilities could extend mission durations to 15 to 20 minutes.

Comparing these numbers with the characteristics of the GPS satellite constellation, we find that mission timelines in the range of 5 to 20 minutes would require a corresponding increase in GPS receiver elevation mask angles by 2.5 to 10°. To avoid large atmospheric errors from satellite signals near the horizon, GPS receivers typically might employ a minimum elevation mask angle of 5 to 10°. The increased mask angle for Relative GPS would be added to this minimum, as summarized in Figure 8.

To determine the effect of increased elevation mask angle on Relative GPS performance, global and time averages were computed using actual GPS satellite orbital parameters.

Figure 9 summarizes the cumulative probability of satellite visibility for total elevation mask angles up to

| Mission Duration (min) | Mask Increase for Relative GPS (deg) | Total Relative GPS Elevation Mask (deg) |
|------------------------|--------------------------------------|---|
| 5 | 2.5 | 12.5 |
| 10 | 5 | 15 |
| 15 | 7.5 | 17.5 |
| 20 | 10 | 20 |

Figure 8. Total Elevation Mask Required

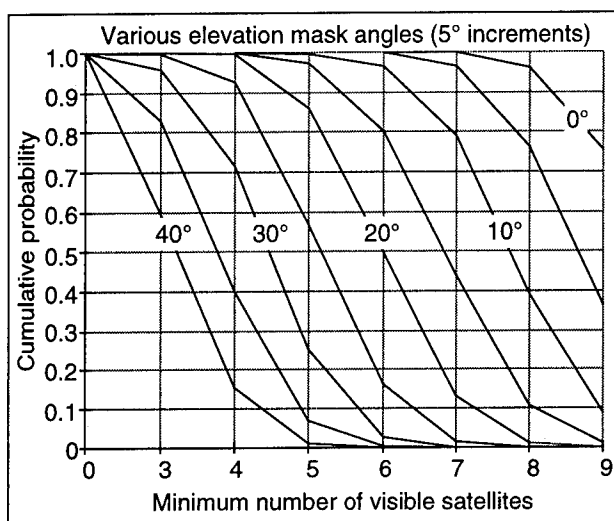


Figure 9. Cumulative Probability of Satellite Visibility With Various Elevation Mask Angles

40°. The satellite lines-of-sight change, relative to a stationary observer, is an approximate rate of 0.5 deg/min. Thus, the 5° increments between the parametric curves shown would correspond approximately to 10-minute intervals in total mission time.

To allow for satellite reliability, we consider five visible satellites with 98 percent visibility to be a minimum acceptable threshold for evaluation of this technique. The analysis results above indicate that mask angles up to 15° can provide threshold capability. Based on typical engagement geometries, this would limit mission timelines to approximately 10 minutes. Next, these results were translated to quantify the effects of elevation mask angle on satellite visibility and dilution of precision. The results are summarized in Figures 10 through 14.

Computations were made using constraints of PDOP <100 and PDOP <6 on selection of points within the analysis program. The PDOP <100 results therefore indicate higher availabilities and higher DOPs, while the PDOP <6 results are more indicative of how an actual GPS receiver would perform. (Although not usually noted, some constraint is usually implicit in published DOP statistics to eliminate near-singular solutions from the statistics.)

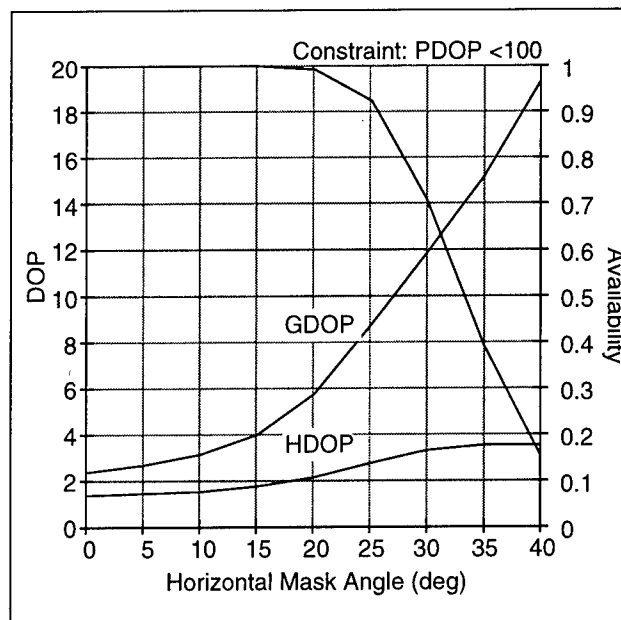


Figure 10. Availability and DOP as Function of Elevation Mask (PDOP <100, i.e., Virtually Unconstrained)

Based on Figure 11, limiting the elevation mask to 15° provides about 96.5 percent availability. Degradation of HDOP and GDOP values (compared to a 10° elevation mask) are 9 and 18 percent, respectively. The suitability of these degraded levels depends on the specifics of a particular system mechanization.

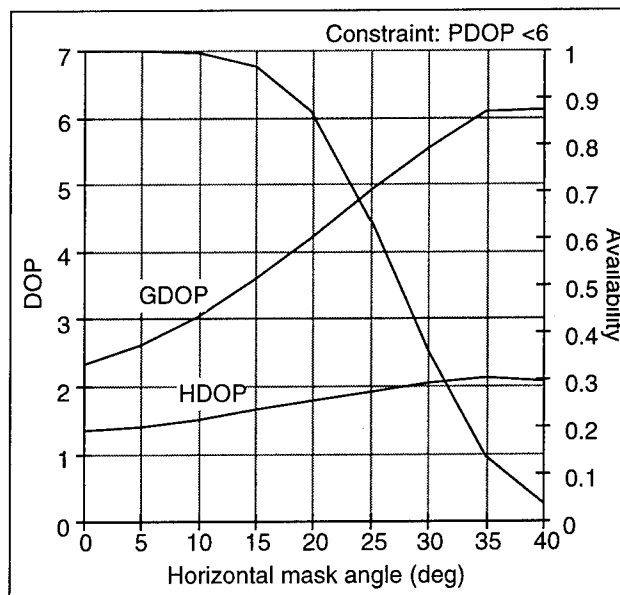


Figure 11. Availability and DOP as Function of Elevation Mask (PDOP <6, i.e., Realistically Constrained)

Fixed-point Smoother

The third approach considered is a fixed-point smoother algorithm designed to estimate shifts in the targeting system GPS position bias. A shift in bias may be observable if the estimator has access to the GPS receiver position outputs and knowledge of constellation change events. The potential drawback of this approach is the indirect nature of the bias cancellation. An undeclared bias shift event may not be detected by the algorithm, resulting in degraded accuracy. Also, additional computational throughput is required for the additional estimator.

The CEP results quoted, based on a weapon trajectory shaped to produce a 90° dive angle into the target, are in the horizontal plane. Different dive angles can produce different CEPs for a given weapon midcourse trajectory.

Figure 12 summarizes the results of an error-covariance study for two trajectories to illustrate the use of the fixed-point smoothing algorithm. The cases explore variations in this Relative GPS implementation. The row labeled "Nominal" has no constellation shift. The row labeled "Constellation shift, no Q bump" shows the degradation in performance that occurs when a constellation shift occurs and nothing is done to compensate in the weapon navigation filter. The row labeled "Constellation shift with Q bump" shows what happens if large process noise is introduced (Q bumping) into the weapon navigation filter. While this filter tuning operation is commonly employed in GPS receivers, it can easily worsen Relative GPS performance. The final row shows the results with the Q bump and the fixed-point smoother. The success in providing Relative GPS performance (approaching that without a constellation shift) indicates that the bias shift is observable and correctable using this approach.

| Parameter | Short Trajectory (meters CEP) | Medium Trajectory (meters CEP) |
|---|----------------------------------|--------------------------------------|
| Nominal | 1.3 | 2.1 |
| Constellation shift, no Q bump | 2.3 | 4.9 |
| Constellation shift with Q bump | 7.8 | 8.5 |
| Constellation shift with Q bump plus fixed-point smoother | 1.5 | 2.5 |

Figure 12. Simulation Results Show That Fixed-point Smoother Can Estimate and Compensate for Bias Shift

Line-of-Sight Dot Product

A fourth approach considered is a line-of-sight (LOS) dot product algorithm, a simple modification to the weapon SV selection algorithm. Here, an attempt is made to track the same four satellites as the targeting system GPS

receiver. When, however, one or more are not visible, a replacement would be selected on the basis of minimal angular difference in the LOS angle relative to the originally desired SV. This approach is based on the assumption that a significant portion of the total bias error is atmospherically dependent and therefore spatially correlated. The degradation of relative accuracy would therefore be minimized by maintaining a constellation as close as possible to the original LOS angles of the one employed by the GPS receiver during the targeting operation. An obvious drawback of this easy-to-implement approach is that only atmospheric bias errors are expected to be spatially correlated, while errors that are SV dependent (e.g., SV clock) are not.

The analysis of this approach was based on a global and time averaging of satellite visibility factors. Beginning with the minimum GDOP constellation, the angular distance to the nearest visible alternate satellite was determined. Statistics were accumulated over time at each position point (Figure 13).

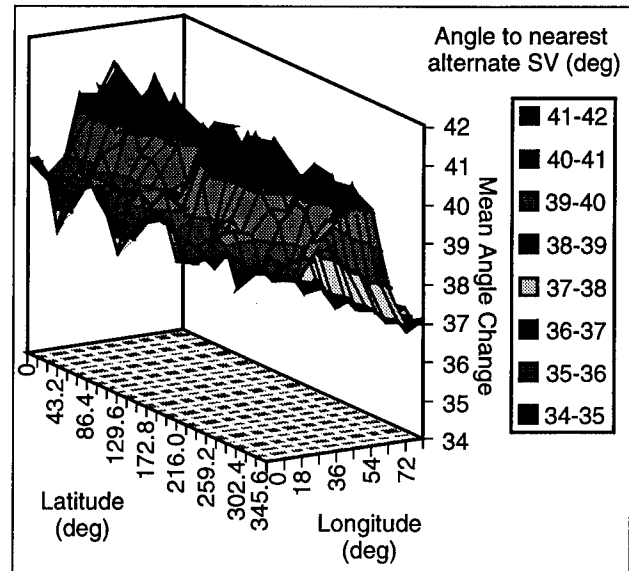


**Figure 13. LOS Dot Product Analysis Results
Mean Distance to Nearest Alternate
SV is 38.8**

The resulting aggregate mean was computed to be 38.8°, with an aggregate standard deviation of 9.6°. These values may be compared to the GPS satellite constellation configuration that consists of four satellites in each of six orbital planes. Although they are not uniformly spaced within these planes, the average distance between satellites would be 90°. The six planes are spaced 30° apart (in right ascension). It is therefore almost certain that the nearest alternate satellite would reside in an orbital plane other than the original.

Figure 13 shows a surface plot from the analysis data generated as described above. An apparent correlation to longitude is confirmed when viewed from the elevation

perspective. The latitude perspective, however, shows no correlation to latitude.

Unfortunately, a mean angular change of 40° would be expected to result in significant variation in atmospheric group delay, particularly when large elevation excursions occur. This result therefore implies that this simple implementation approach would be inferior in Relative GPS performance to alternatives that attempt to avoid a constellation change.

SUMMARY

We have shown that a near-precision strike can be achieved using GPS-aided targeting and a weapon without a seeker, assuming it has sufficiently accurate terminal steering capability. The desires for all-weather operation and affordability are supported by the use of Relative GPS guidance to eliminate the need for a weapon seeker for terminal homing. Differential GPS phenomenology results are used to define theoretical accuracies achievable using Relative GPS.

A number of potential implementation errors exist which may limit the realized accuracy of Relative GPS. The simple notion of tracking the same four satellites as the targeting platform carries significant operational limitations. Four implementation ideas offer the potential to improve robustness and increase the likelihood of approaching theoretical performance, with minimal impact on existing systems.

In summary, each of the four candidate implementations provides some degree of robustness. The findings and implications are summarized in Figure 14.

| Implementation | Utility | Implications |
|------------------------------|---|---|
| High elevation mask | Useful up to mask of 15 to 20° | Requires change to aircraft receiver software |
| Satellite correlation vector | Often best to stay with 3 of original 4 SVs; if alternate is selected, choice is critical | Requires modification to typical weapon satellite selection algorithms |
| Fixed point smoother | Bias shift resulting from alternate SV can be estimated | Most significant impact; requires new aircraft interface and weapon estimation function |
| LOS dot product | Can achieve mean angular change of 39° to minimize atmospheric variation | Requires modification to receiver satellite selection |

ACKNOWLEDGMENTS

The authors wish to thank Kevin Rudolph of Hughes Aircraft Company for his contributions to the development of Relative GPS guidance and its implementation, and also to Bob Jeffers, Michael Brand, and Michael Nowakowski of Hughes Radar Systems for their collaborations on the development of the GPS-aided SAR targeting.

REFERENCES

1. Schmidt, G., and R. Setterlund, "Precision Strike Concepts Exploiting Relative GPS Techniques," Institute of Navigation, Proceedings of the 49th Annual Meeting, June 1993.
2. Beck, G. R., et al, "GPS Exploitation for Precision Targeting: Tactical Applications," Institute of Navigation, Proceedings of the 49th Annual Meeting, June 1993.
3. Abbott, A., N. Pujara, and P. G. Howe, "GPS Exploitation for Precision Targeting - Observability Using Synthetic Aperture Radar," Institute of Navigation, Proceedings of the 49th Annual Meeting, June 1993.
4. "System Specification for the NAVSTAR Global Positioning System," SS-GPS-300, 11 December 1990
5. Martin, E.H., "GPS User Equipment Error Models," *Navigation: Global Positioning System*, Institute of Navigation, Vol. 25, No. 2, Summer 1978
6. Brown, A., "Extended Differential GPS," *Navigation*, Vol. 36, No. 3, Institute of Navigation, Fall 1989.
7. Jorgenson, P., "An Assessment of Ionospheric Effects on the GPS User," *Navigation*, Vol. 36, No. 2, Institute of Navigation, Summer 1989.
8. Youhanaie, M., F.G. Ziolkowski, and N. Pujara, "Issues for Robust Implementation of Relative GPS Guidance for Precision Weapon Delivery," Institute of Navigation, Proceedings of the National Technical Meeting, January 1994.

Figure 14. Implementation Evaluation Results Summary

A Global DoD-Optimized DGPS for Precision-Strike

Earl Blackwell, Mark Moeglein, and David Nakayama
SRI International

BIOGRAPHY

Earl Blackwell graduated from the University of Tennessee in 1957 with a B.S. in engineering physics. He continued graduate work at UCLA and USC and joined SRI International in 1970. Specializing in GPS technology since 1978, he is currently Director of the Advanced GPS Applications Program at SRI.

Mark Moeglein, a Research Engineer at SRI, received a B.S. in engineering from Harvey Mudd College in 1987. He has been involved in the design and development of DGPS systems since joining SRI in 1989.

David Nakayama graduated with distinction from Harvey Mudd College in 1992 with a B.S. in engineering. He is currently a Research Engineer at SRI, where he has been involved in hardware and software systems design and development since 1992.

ABSTRACT

Low-cost, all-weather, precision-strike weapon delivery without the need for expensive seeker-based guidance is of interest to the DoD community. This paper presents concepts based on a militarized version of Differential GPS (DGPS) that offers potential submeter, GPS-based navigation accuracies. Key features of the DoD DGPS concept enable reference receiver/user separations in excess of 1000 nmi and DGPS correction latencies of 30 min or more. This technology could potentially be transferred into the GPS system infrastructure to allow submeter, Precise Positioning Service accuracy.

Results from a concept feasibility demonstration of a long-baseline (2000-nmi) DGPS experiment are presented. Application of this principle to a CONUS-wide DGPS network using four authorized GPS reference receiver sites is also presented, including measurements of network

correction accuracies. The Joint Direct Attack Munition (JDAM) program sponsored development and demonstration of this concept; however, the technology is applicable to virtually every authorized GPS receiver.

INTRODUCTION

Four independent teams conducted nine-month Concept Exploration studies for the JDAM program in response to a 3-m circular error probable (CEP) "precision kit" accuracy requirement. Low cost, all-weather, launch and leave, and in-flight retargeting capability were also fundamental requirements. Although multiple seeker guidance technologies were the principal focus of the study teams, non-seeker solutions were also sought.

On completion of various tradeoff investigations, SRI International's study results strongly supported a non-seeker, differential GPS (DGPS) approach from the standpoints of all-weather, lowest cost, and performance. A strong factor for this conclusion was that JDAM already envisioned using GPS integrated with an Inertial Navigation System (INS) guidance package in its weapon concept. This low-cost, GPS-INS tailkit would be affixed to either an Mk 84 2000-lb bomb or a BLU-109 penetrator. Incorporating DGPS into this unit should be technically straightforward and very low cost.

The JDAM product improvement program further pursued the DGPS option, asking SRI to perform a long-baseline wide-area DGPS (WADGPS) experiment, followed by development of a four-station WADGPS network. SRI developed and supported this network from July 1994 to June 1995 under the Exploitation of DGPS for Guidance Enhancement (EDGE) High Gear program conducted at Eglin AFB, FL.

This paper presents results from this work, showing the feasibility of achieving meter-level Precise

Positioning Service (PPS) navigation accuracy for the weapon guidance unit, leaving a balance of 2.8 m for targeting and guidance errors out of a total 3 m CEP error budget.

BACKGROUND

The DGPS process has been honed by the civilian GPS community to provide very high levels of accuracy for the commercial receiver market. Most civil DGPS architectures compensate for ionospheric delays, satellite clock and ephemeris errors, and selective availability (SA) clock dither. DGPS attempts to remove these error sources, illustrated in Figure 1, by means of pseudorange corrections generated by a surveyed GPS receiver station [Blackwell].


However, effectively applying DGPS to military operational situations required an approach that transcended several basic constraints of civilian DGPS. One constraint to civilian DGPS is the need to maintain relatively close proximity between the user of the DGPS correction and the Reference Receiver (RR) station. Typically, a user receiver is separated from the RR site by a baseline of no more than 300 nmi to preserve commonality of the lines of sight to each satellite. This baseline limitation (necessary to compensate for ionospheric signal delay) is obviously a considerable problem in military battlefield situations. A second constraint is the need for a continuous datalink, sending correction updates at rates up to 1 Hz to offset the effects of SA clock dither.

If one redefines DGPS for only authorized (keyed), dual-frequency GPS receivers, immediate advantages accrue for the military user who is capable of using ionosphere-free L_1/L_2 pseudorange measurements. For example, baseline lengths are no longer constrained to maintaining common ionospheric lines of sight, and are therefore only limited by satellite visibility and (to a lesser extent) satellite orbital error projection differences induced by different satellite-receiver geometry. Also, without SA, correction update rates can be drastically reduced. In effect, a military dual-frequency DGPS correction need only compensate for a satellite's clock and ephemeris drift.

Table 1 summarizes the key principles of this militarized DGPS approach by comparing the correction message content and characteristics between conventional DGPS and the militarized concept.

Table 1: CIVILIAN vs MILITARY DGPS

| Civilian Receivers | DoD Receivers |
|-----------------------------------|---|
| <i>Major Error Sources</i> | |
| Selective Availability | SA Removed by Key |
| Ionospheric Delay | Iono Measurement (L_1/L_2) |
| Satellite Clock | Satellite Clock |
| Satellite Position | Satellite Position |
| Tropospheric Model | Tropospheric Model |
| Multipath | Multipath |
| <i>DGPS Correction Properties</i> | |
| 10-60 updates/min | ~1 update/30 min |
| < 300-400 nmi baselines | Baselines limited only by satellite visibility (global applicability) |

 = Differential Correction Content

MILITARY WADGPS SYSTEM CONCEPT

The strength of the military WADGPS concept is that it can provide DGPS accuracy without the need for RRs and added datalinks in the theater of operations. We recognize that a classical DGPS implementation for military applications can be viewed as essentially a system "band-aid," adding RRs and datalinks where they were not originally intended. But using RR network technology to augment the Operational Control System (OCS) monitoring capability and using the GPS navigation message as the datalink blurs the distinction between DGPS and what is simply a more accurate signal in space (SIS). So, although many of these concepts are demonstrated in a DGPS context, one can envision that their eventual implementation might be in the form of a control segment enhancement.

Enhanced PPS navigation accuracy can be achieved through successful implementation of four principal system elements:

- Reference Receiver Network (RRN)
- Datalink to PPS user
- PPS receiver and measurement environment
- Target location and/or mapping information.

Reference Receiver Network

Due to problems with satellite visibility, as well as to variations in atmospheric delays, a single RR cannot provide accurate DGPS corrections over a wide area (beyond a roughly 300-mi radius) without significant

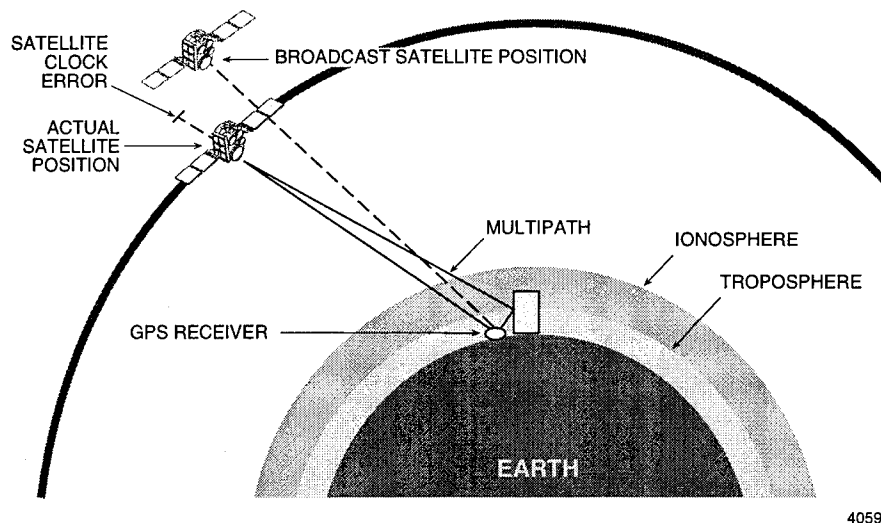


FIGURE 1 GPS MEASUREMENT ENVIRONMENT

accuracy degradation. A network of widely dispersed RRs overcomes this limitation and permits use of significantly larger theaters of operation (RRs can be placed 1000 nmi or more from user receivers).

In general, any RRN (including that of the NAVSTAR OCS) consists of a group of monitor stations, datalinks from the monitor stations to some central site, and a centralized filter. The monitor stations act as sensors, measuring pseudorange and integrated carrier phase to each space vehicle (SV) and sending these measurements along to the centralized filter for processing. The filter combines the raw measurements to generate a set of corrections. The clock bias, atmospheric delay, multipath environment, solid earth tide state, and survey error at each monitor station must be accounted for independently to achieve the sustained accuracy required for submeter PPS navigation.

Correction Datalink

It is difficult to conceive of a datalink more convenient than the navigation message built into the GPS structure, since all users by definition have the datalink receiver and the coverage can be global. Spare pages in Subframe 4 of the navigation message are ideal candidates to carry a list of corrections for all satellites in the constellation, particularly since it is currently difficult to update the ephemerides in Subframes 1-3 of all SVs directly.

In December 1993, in a briefing to the Joint GPS Working Group (JGWG), SRI presented the concept of using the navigation message as the differential correction datalink. In June 1995, Second Space Operations

Squadron (2SOPS) pursued a variant of this idea by embedding expected range deviations (ERDs) for each satellite as a correction list in page 13 of Subframe 4 [Butts and Shank]. These classified ERDs (which are encrypted) do not contain SA clock dither.

In a precision-guided munition (PGM) operational context, the aircraft platform carrying the GPS-guided munition would normally use its embedded GPS avionics receiver to read the navigation messages from all SVs in view and transfer corrected ephemeris data to the weapon prior to its release. Thus, the set of corrections as well as the target's coordinates are transferred to the munition along with the standard GPS initialization. If sufficiently accurate broadcast SV clock and position information is not yet available, alternate datalinks such as the improved data modem (IDM) could be used.

Authorized GPS Receivers

With few (if any) modifications, a PPS receiver would be able to use DGPS corrections to improve its accuracy. However, user receiver-related error sources would likely become the major error contributor once SIS errors are reduced. For highest accuracies, these errors can be reduced using straightforward techniques developed in the civilian community. Multipath can be avoided, measured, calibrated, and/or carrier-smoothed (along with pseudorange measurement noise). Tropospheric models can be refined. Receiver channels can be added to track both frequencies simultaneously and all SVs in view. Satellite-selection algorithms can be improved to account for changes in error sources as well as provide more

flexible user-selectable options. And navigation filters can be tuned with submeter accuracy in mind.

Targeting and Mapping

Accurate target coordinates and/or map information are required for many GPS applications, including a "seekerless" PGM. Although the enhancements we propose can reduce targeting errors, a comprehensive look at the complex issues of targeting and mapping are sensitive and outside the scope of this paper. We should mention, however, that the DGPS RRN could itself be used as an aid to targeting by providing precise SV clock and ephemeris corrections in real time. These corrections could be used in the process of establishing control points within an image. A demonstration of this process is discussed in the results section of this paper.

Notional System Design

Figure 2 depicts one potential military DGPS implementation. Measurements are collected from a small RRN surrounding the theater of operations to ensure correction availability for all SVs in view from the theater. In this example, the list of all corrections are packed into a page in Subframe 4 and uploaded to an SV in the theater. The uploaded corrections from each SV will be broadcast once every 12.5 minutes. (Note that

each SV will have a different list, with varying correction ages.) Each authorized receiver in view of an SV will be able to read and decrypt its associated corrections. Age of uploaded corrections is expected to be on the order of 30 minutes, with update rates of once per hour or longer.

A variant of this wide-area theater network concept was implemented in the EDGE demonstration at Eglin AFB, FL.

CONCEPT VALIDATION

SRI conducted a long-baseline experiment in early 1994 as a precursor for a potential JDAM-like wide-area DGPS (WADGPS) implementation, and to validate some of the assumptions of the system concept.

Experiment Implementation

Three Ashtech Z-12 dual-frequency GPS receivers were placed along an approximately 2300-nmi line of SRI offices, as shown in Figure 3. Each site's antenna location was surveyed by the Defense Mapping Agency (DMA) to serve both as RR location coordinates and user truth at Albuquerque. The purpose of the experiment was to demonstrate that merged SV clock and ephemeris corrections from Florida and California could be used to effectively correct a receiver in New Mexico, given a

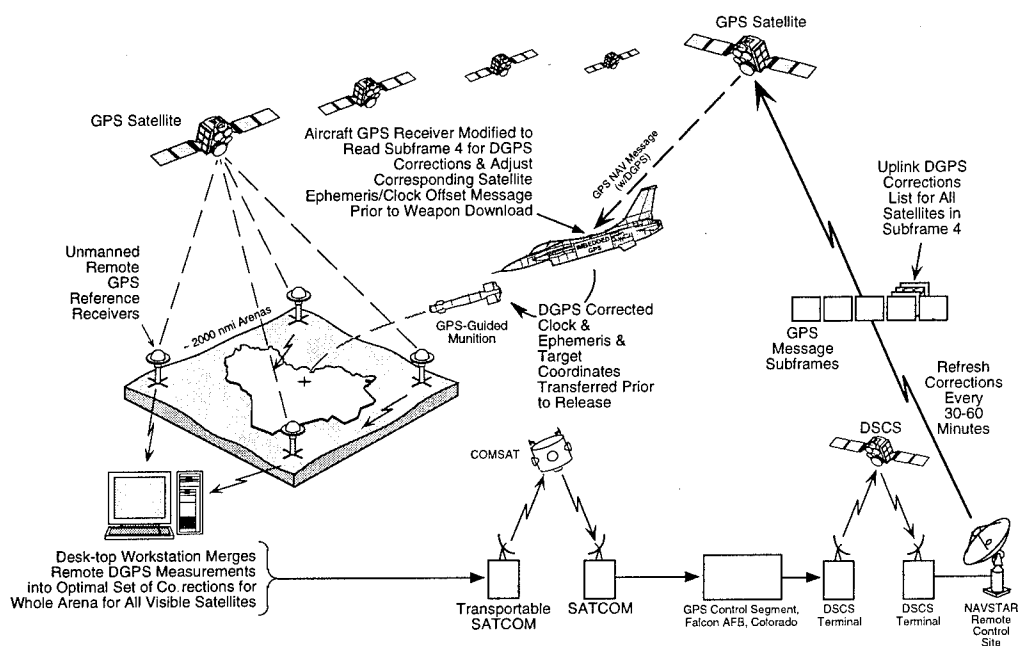


FIGURE 2 DGPS PRECISION-STRIKE WEAPON CONCEPT

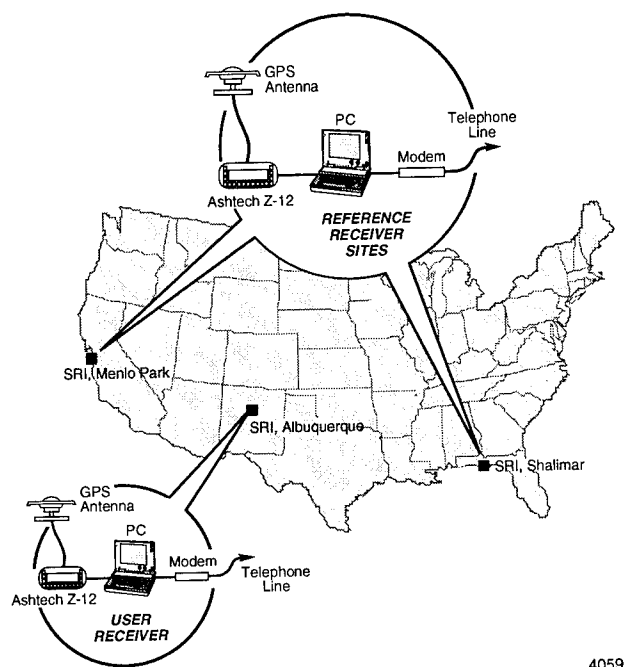


FIGURE 3 LONG-BASELINE EXPERIMENT

dual-frequency receiver. SA values, obtained from 2SOPS, were removed during post-processing of raw data for the purpose of analyzing SV clock and ephemeris drifts.

The experiment procedure was to calculate DGPS corrections for the California and Florida RR sites, then combine them in a weighted fashion to apply to the Albuquerque user receiver's raw measurements to yield the user's corrected position relative to the DMA truth. Data were collected remotely and downloaded for processing in a manner consistent with a real-time implementation. In addition to long-baseline accuracy, the experiment quantified correction accuracy degradation as a function of time and as a function of the user receiver's distance from the place for which the weighted corrections were calculated (i.e., the *virtual* RR).

Experiment Results and Findings

The Albuquerque receiver's corrected position data over a 24-hour period yielded a 50% CEP of 0.97 m. The DGPS corrections used were a linear weighting of the satellite corrections from the California and Florida RR sites optimized for New Mexico. This result demonstrated

the improved position accuracy of DGPS for precision-strike use.

Figure 4 presents the relationship of measured correction error drift with refresh interval. The actual error growth experienced on average for each satellite of the GPS constellation during the 24-hour period is plotted against the update rate. These errors are the sum of clock and ephemeris ranging errors. From these data, one sees an expected RMS drift error of 0.37 m over a 30-min correction update interval.

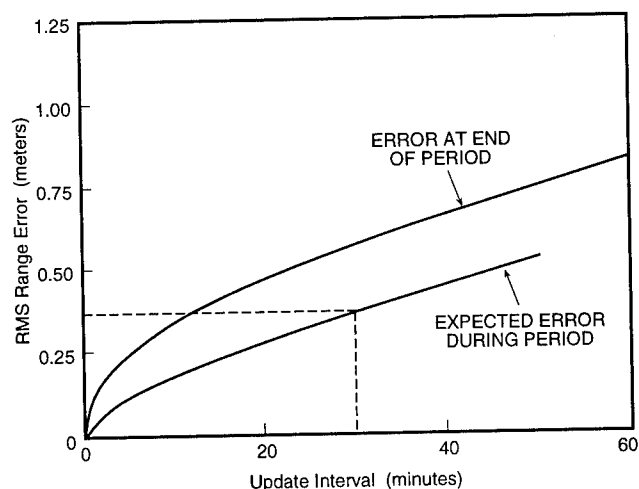


FIGURE 4 MEASURED SV CLOCK AND EPHEMERIS DRIFTS

By moving the virtual RR from the fixed user site in Albuquerque, SRI was able to analyze how DGPS-corrected position accuracy degraded as distance from the virtual RR was increased. The results of this displacement analysis are presented in Figure 5 for the east, north, and up components of corrected positions. One concludes that the DGPS corrections can degrade very slowly with increasing distance from a virtual RR. This low rate of error growth is expected since the difference in range error over a long baseline (due to SV position error) is related to the relatively small difference in viewing angle to the SV.

Lessons learned in this experiment were crucial to successful development of the EDGE RRN a few months later. More accurate surveys were performed for the network, and a more rigorous approach to multipath mitigation was possible using software developed for the experiment. Finally, wet tropospheric delay observability was demonstrated by analyzing the change in integrated

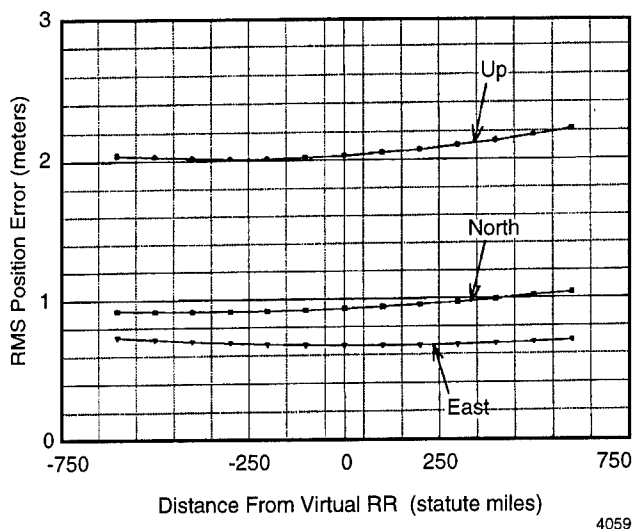


FIGURE 5 WIDE AREA DGPS ACCURACY vs GEOMETRY

carrier phase corrections with changes in each satellite's wet mapping function, a process which reduced residual tropospheric delay (described further in the next section).

This experiment also quantified error sources useful for determining correction error contributions to the overall DGPS error budget, as delineated in Table 2. Thus, following this long-baseline experiment, an RMS correction error of 45 cm was believed achievable with a 30-min correction update rate.

Table 2: DGPS ERROR ESTIMATES (m)

| Errors | Sources | | |
|-------------------------------------|---------|-------|-------|
| | SIS | User* | Total |
| Carrier-smoothed Measurement Error† | 0.15 | 1.0 | 1.01 |
| Residual Tropospheric Delay | 0.2‡ | 0.5 | 0.54 |
| Correction Latency | 0.37§ | | 0.37 |
| Correction Round-off | 0.05 | | 0.05 |
| RMS Range Error Contributions | 0.45 | 1.1 | 1.2 |

*Estimate for a typical militarized, dual-frequency, authorized receiver in a nominal multipath environment.

†Includes residual code noise, multipath, and ionospheric delay.

‡After using carrier phase wet delay measurements.

§Based on 30-min correction update rate.

CONCEPT DEMONSTRATION

At the end of the long-baseline experiment, the EDGE High Gear program was established to demonstrate use of militarized WADGPS technology with a precision-guided munition. Six GBU-15 munitions were retrofitted with a GPS-INS navigation and guidance system that received WADGPS clock and ephemeris corrections from the RRN.

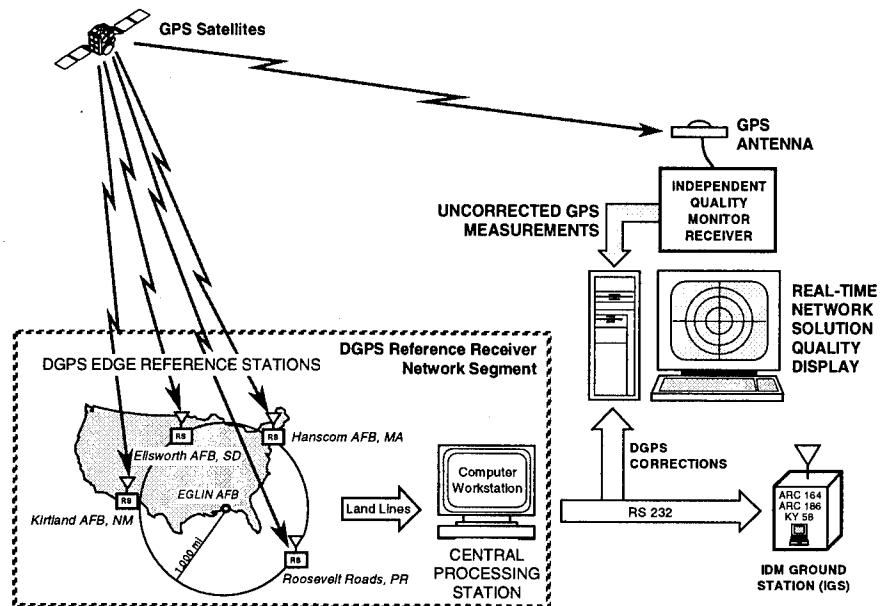
The reference stations (RSs) for the network were placed at least 1,000 nmi from the test range at Eglin AFB, as illustrated in Figure 6. Unclassified receiver measurement data were transmitted to Eglin AFB, where the corrections from each station were generated and merged to form a "network" correction set. These corrections were uplinked (via a secure IDM operational datalink developed by the Naval Research Laboratory [NRL]) to an F-16 carrying the GBU-15. The F-16 then passed the corrections to the munition's integrated flight management unit (IFMU) via the 1553 bus. The IFMU, built by Honeywell, applied the corrections to pseudoranges received from an internal Interstate Electronics Corporation (IEC) GPS receiver before using them in the navigation solution. The weapon navigation and impact results of the EDGE demonstration program are treated in a separate paper [Harms, et al.].

EDGE RRN Implementation

The EDGE RRN consisted of four reference stations, placed at military installations so they would surround the target area, and a central processing station at Eglin AFB. The central processing station consisted of a Data Logger (which communicated with the reference stations via leased line modem), a Network Correction Processor (which computed the network differential corrections), and a Quality Monitor (which served as independent truth to assess correction accuracy).

Reference Stations. Each of the four reference stations consisted of an authorized E-Systems GR-1200 (CU) GPS dual-frequency receiver (formerly Ashtech Z[Y]-12), a simple weather sensor, a desktop computer, and a leased line modem.

Choke ring survey antennas were carefully sited to minimize multipath effects. DMA surveyed the antenna locations into a common grid to within approximately 30 cm and provided these coordinates for use in the Network Correction Processor calculations. A desktop computer collected raw GPS measurements for all



4059

FIGURE 6 EDGE DGPS NETWORK

satellites in view from the GPS receiver as well as pressure and temperature data from the weather sensor. These data were forwarded to the Data Logger in real-time via modem over commercial leased lines.

Data Logger. The Data Logger consisted of four leased line modems and a multiport desktop computer. Data were logged for record and then forwarded to the classified Network Correction Processor for correction generation.

Network Correction Processor. The Network Correction Processor accepted the raw reference station data from the Data Logger. After combining dual-frequency measurements to remove ionospheric delay, performing carrier smoothing on the raw measurements, and applying earth tide and tropospheric models, the Network Correction Processor generated corrections valid for each reference station using an SA-corrected version of the broadcast satellite clock and ephemeris data. Finally, carrier phase data were used to measure and remove wet tropospheric delay.

The corrections (now accounting for broadcast clock and ephemeris errors) were then combined to create a single set of network corrections, valid for the entire theater of operations but optimized for the theater center. These corrections were forwarded to the IDM ground station for uplink to the GPS weapon and to the Quality Monitor for accuracy assessment.

Quality Monitor. The Quality Monitor consisted of a local E-Systems GR-1200 (CU) receiver with choke ring antenna, two relay computers, and a desktop computer. The Quality Monitor processor (in a manner similar to the Network Correction Processor) calculated local DGPS corrections with data from the local receiver.

Network corrections were compared against local corrections to assess accuracy in range space. The Quality Monitor also applied network corrections to local measurements to calculate a corrected position. This corrected position was then compared against the local DMA-surveyed benchmark coordinates to assess position accuracy. Various displays were developed so that real-time assessment of correction quality could take place during operational missions.

Improved Correction Accuracy

Although the RRN was developed and deployed in about six months, we were able to make several significant improvements over the software used in the long-baseline experiment. Of most notable interest are double-differenced weighted carrier averaging of all raw measurements, incorporation of a solid earth tide model, four-station zenith wet tropospheric delay determination, and weighted least-squares network correction determination.

Carrier Averaging. Carrier smoothing or averaging is a process that uses extremely precise integrated carrier phase measurements to aid inherently error-prone code phase pseudorange measurements. This process can dramatically mitigate receiver noise and multipath.

These code-minus-integrated carrier phase offsets were measured from a simultaneous track of PRN 6 at the Kirtland and Ellsworth AFB reference stations (see Figure 7). They are typical of the multipath and code noise observed at these stations for all satellites.

Temperature-dependent effects in the analog GPS receivers introduced errors into this process by causing code and integrated carrier measurements to drift apart as ambient air temperature changed. This effect, common to all channels, was removed from the measurements with an appropriate double-difference smoothing technique that used one channel as a reference.

Solid Earth Tide Models. With more than 2000-nmi distances between reference stations, solid earth tides must be taken into consideration. This effect, caused by deformation of the earth crust due to gravitational forces, can result in relative position differences of significant magnitude when trying to achieve submeter level accuracy. (Relative altitude changes of up to 30 cm were observed between the New Mexico and Massachusetts reference stations.) To compensate for this phenomenon (which primarily affects altitude), we implemented an earth tide model that adjusted the altitude coordinates of each reference station.

In addition, rather than incorporate this model into the munition GPS receiver, the set of corrections optimized for the network center were pre-adjusted to account for solid earth tides before uplink. A further treatment of this topic is presented in another ION '95 paper [Sinko].

Improved Tropospheric Models. Tropospheric model inaccuracy is a major contaminant in WADGPS corrections. A generalized tropospheric model only accounts for "normal" tropospheric delays. Many models are divided into hydrostatic ("dry") and variable ("wet") delays. The unpredictability of wet delay makes most receiver models vulnerable to significant tropospheric errors in hot and humid climates.

The geoscience community's work in measuring plate tectonics with integrated carrier phase suggested that they had a good way of handling variable tropospheric delays over long baselines. Using a variant of these methods [Herring], the EDGE RRN measured the wet delay at each RR site using ionosphere-free GPS integrated carrier

phase. An example of these measurements is provided in Figure 8.

Note that, as would reasonably be expected, the variable "wet" delay at zenith is roughly 0.1 m higher in humid Puerto Rico and Massachusetts than in arid New Mexico and South Dakota. We have collected rawinsonde data to serve as truth data for these measurements and plan to present the results of an accuracy analysis in the near future.

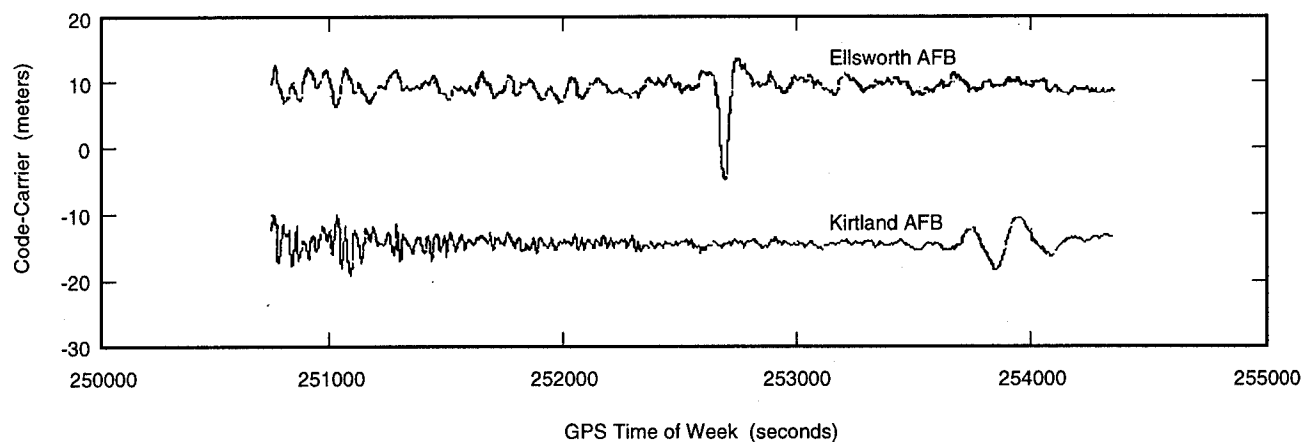
Theater Correction Optimization. The pseudorange corrections from all reference stations were merged to form a single set of corrections, optimized for theater test location. In the first step of an iterative process, all available corrections were averaged to form a network correction. In the second step, the clock bias for each set of station corrections was adjusted to agree with the network corrections. These steps were repeated until their effect became negligible.

Finally, the corrections were combined to form a single set of corrections optimized for theater location. When a satellite was visible to three or fewer stations, an averaged correction was calculated weighted by correction quality. When all four stations tracked a satellite, a geographical weighted average was calculated using weighted least-squares that estimated the rate of change of correction with respect to north and east relative to the virtual RR at Eglin AFB.

Demonstration Results

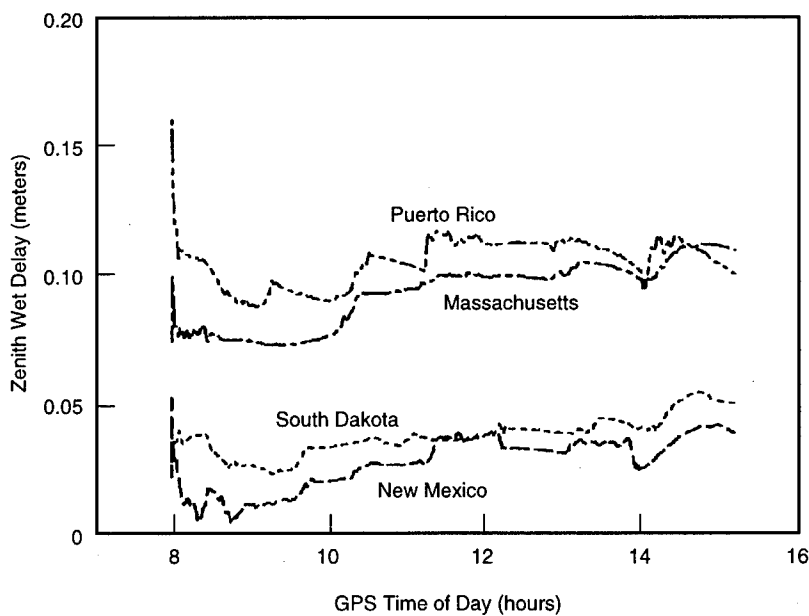
The RRN operated successfully during the course of the EDGE program. It was used to support ground, captive carry, and free-flight drop missions as well as a targeting exercise.

Position Accuracy. Figure 9 shows the EDGE network-corrected position error (relative to a DMA survey) of the local Quality Monitor receiver for the five operational weapon drops--three against horizontal targets and two against vertical targets. For consistency during these missions, the Quality Monitor used the same five satellites as those selected by the munition GPS receiver. (The selection criterion was lowest weighted position dilution of precision [PDOP].) The Quality Monitor position was calculated using weighted least-squares. The error was determined by comparing the RRN-corrected position against the DMA-surveyed benchmark.



4059

FIGURE 7 TYPICAL CODE MULTIPATH AND RECEIVER NOISE (Observed at Kirtland AFB and Ellsworth AFB)



4059

FIGURE 8 WET TROPOSPHERIC DELAY MEASUREMENTS

Table 3: DGPS-CORRECTED QUALITY MONITOR POSITION ERRORS FOR EDGE FLIGHT TESTS

| Drop No. | Position Error (m) | | | | |
|----------|--------------------|-------|-------|-------|--------|
| | East | North | Up | Miss* | Radial |
| 1 | 0.36 | -0.17 | -0.25 | 0.41 | 0.47 |
| 2 | 0.10 | -0.06 | -0.51 | 0.13 | 0.52 |
| 3 | 0.41 | -0.40 | -0.48 | 0.59 | 0.76 |
| 4 | 0.01 | -0.24 | 0.05 | 0.24 | 0.25 |
| 5 | 0.11 | -0.56 | 1.57 | 0.55 | 1.57 |

*Miss is defined as GPS position error in the plane perpendicular to the munition trajectory at impact. Drops 1, 2, and 5 were against horizontal targets, arriving at approach angles of approximately 85 deg. Drops 3 and 4 were against a vertical billboard target, arriving at approximately 20 deg.

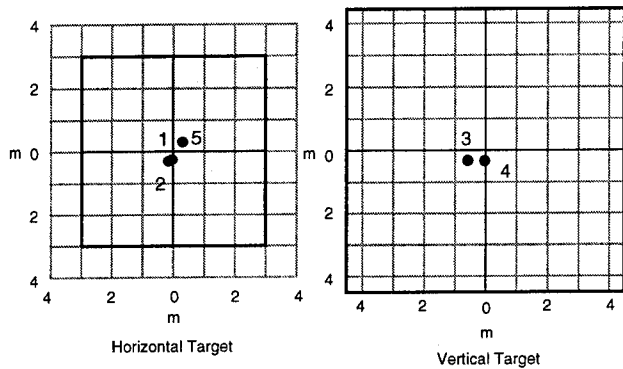


FIGURE 9 DGPS-CORRECTED QUALITY MONITOR POSITION ACCURACY FOR EDGE FLIGHT TESTS

Table 3 provides a comprehensive listing of the corrected position errors. In all five cases, the horizontal corrected position error was well under 1 m, and only once did the vertical error exceed 1 m. During these drops, the actual guidance implementation experienced a nominal 4-m offset miss from the corrected GPS navigation position data in Table 3 [Harms, et al.].

Figure 10 provides another "solution-space" representation of horizontal EDGE RRN accuracies over an extended period of time. The data for this histogram were collected during an extended EDGE captive carry mission lasting 6.5 hours. The 50% CEP for this representative sample against the DMA benchmark is 30 cm.

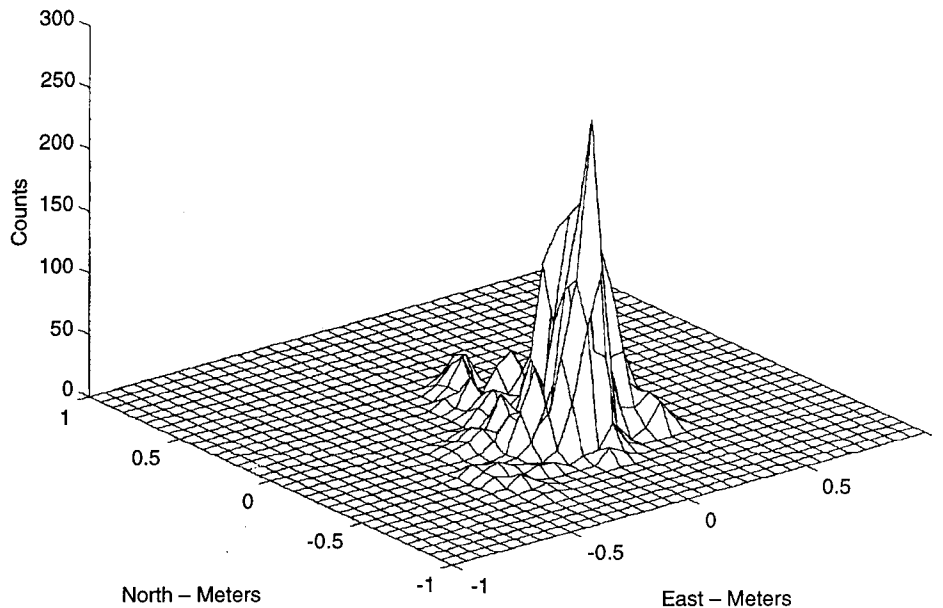


FIGURE 10 MEASURED ERROR IN DGPS CORRECTED 2-D POSITION ~ 6.5 HOURS

Early network testing identified a small but recurring Quality Monitor survey bias, which is demonstrated by the southeast direction of errors for all five drop tests and the corresponding bias in the extended sample in Figure 10. In fact, the 50% CEP for this sample against its mean solution is only 17 cm.

Correction Accuracy. Table 4 demonstrates "zero latency" EDGE RRN performance in range space for the five weapon drop missions. These RRN minus Quality Monitor correction differences are smaller than expected, given test contaminants such as survey error, inadequacy of the standard tropospheric model, and multipath contamination. Even with these contaminants, the correction differences during the five drops measured 40 cm RMS.

Table 4: RRN CORRECTION ACCURACY FOR EDGE FLIGHT TESTS

| Drop No. | RRN minus Quality Monitor Pseudorange Correction Differences (m) | | | | |
|----------|--|-------|-------|-------|-------|
| | ch 1 | ch 2 | ch 3 | ch 4 | ch 5 |
| 1 | 0.21 | 0.38 | 0.16 | -0.05 | 0.11 |
| 2 | 0.27 | 0.03 | -0.35 | 0.27 | 0.09 |
| 3 | -0.40 | 0.85 | 0.01 | -0.19 | 0.09 |
| 4 | -0.04 | -0.51 | 0.19 | -0.01 | -0.03 |
| 5 | -0.81 | 0.14 | 0.60 | 0.00 | 0.38 |

Although the RRN used an advanced version of the wet zenith delay determination demonstrated in the long-baseline experiment, the Quality Monitor was itself limited to a more basic tropospheric model appropriate to use in a PGM. In the often hot and humid Florida weather, we regularly noticed what appeared to be zenith tropospheric delay errors of about 0.1-0.2 m. Also, because the RRN could track satellites well before they were visible at Eglin AFB, the network corrections for all satellites were smoothed before the local Quality Monitor had a chance to track and smooth its own measurements. Thus, almost as a rule, when the Quality Monitor disagreed with the RRN by more than 0.5 m, it was due primarily to Quality Monitor multipath. (Local errors were evidenced by the fact that the network reference stations agreed so well with each other. Quality Monitor multipath in these situations was observed by watching the offsets between raw ionosphere-free pseudorange and integrated carrier phase varying by several meters.)

RRN as Targeting Tool. Defense agencies dedicated to targeting have methods for precisely determining the range and bearing from one point to any other point in a set of aerial photographs and radar imagery. This process is sometimes called "target mensuration." By knowing the coordinates of an identifiable control point in an image, one can obtain precise coordinates for a specified target.

As part of the EDGE program, raw GPS data were collected at three control points visible in a targeting image. Using the RRN as a source of DGPS corrections, surveys were made for these three control points by applying RRN corrections for approximately 30 minutes of collected data. The ability to survey these points to within 0.5 m was demonstrated. By applying targeting vectors to these image control points to obtain the target coordinates, a highly accurate targeting approach was successfully demonstrated.

ENHANCED PPS ACCURACY

Now that the EDGE RRN has demonstrated performance consistent with the SIS accuracy column in Table 2, interest turns to making this technology available to the PPS user. This section discusses some of the available options for improving SIS accuracy, with their associated advantages and disadvantages. It is not intended to recommend any particular approach, but rather to offer suggestions for continued PPS accuracy improvement.

RRN Concepts

The EDGE program successfully demonstrated the functionality of an easily deployable, theater-wide DGPS network in large arenas. Operationally, one might require that consideration be given to providing theater coverage to more than one major region of conflict (MRC) at a time. When two or more regions may be contiguous, the issue arises of correction validity across MRC boundaries, or the necessity to distribute multiple sets of corrections through scarce datalink resources. It is apparent that a more preferable solution would be to simply cover the globe with pre-surveyed, fixed installations and resolve the components of SIS errors, such that a complete set of corrections with global applicability can be distributed to all PPS users for all SVs in the constellation. This solution could more readily support force deployments anywhere in the world without necessarily waiting for network installation and survey.

A preliminary siting analysis suggests that 15 to 20 RR sites could be deployed globally to provide continuous multi-station measurements of each satellite in the complete constellation. Figure 11 illustrates the global network concept. Observe that the 5-deg horizon footprint of a single GPS satellite can always see five to six RRs simultaneously. At a given instant, SV orbital and clock error components can be measured from a small but finite baseline. Although this network has less density than some global RRNs, it represents a dramatic improvement over the current five OCS monitor stations available to PPS users.

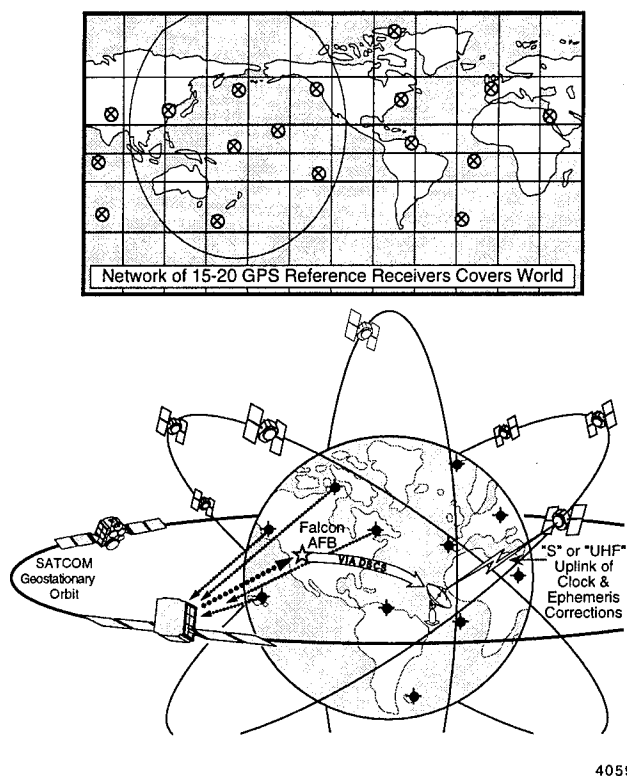


FIGURE 11 GLOBAL DGPS NETWORK

Ideally, this global RRN would be co-located with existing stations wherever possible. The additional stations add redundancy as well as better viewing geometry for all satellites at all times, allowing more accurate and timely uploads. Adding stations farther from the equator improves satellite viewing geometry, allowing more effective discrimination between clock, radial, cross-track, and along-track SV errors.

The addition of this network, initially as an overlay to existing resources, would allow rapid development to support the PPS user community (perhaps through alternative datalinks) while minimally impacting the current control segment. Once proven and refined, the

new RRN could be incorporated into the existing system with no negative impact to satellite operators and PPS users.

Data Distribution to PPS User Receivers

As discussed earlier in this paper, the preferred datalink is clearly the GPS navigation message. But a significant amount of latency is associated with building, uploading, and downlinking the current navigation message. Several methods for reducing these latencies have been suggested in informal discussions with members of the control segment community. Most concepts entail optimizing the current OCS filter or upload process and could potentially reduce latencies dramatically for uploading page 13 correction tables.

One suggested approach appears to be the most far-reaching: using the inter-satellite crosslink of the next-generation Block II-R SVs for communicating rapid navigation message updates. When there is a partial Block II-R constellation, the cross-link could be used to update the page 13 correction tables. As Block II-R SVs gradually replace Block II and II-A vehicles, clock and ephemeris parameter adjustments could replace page 13 differential corrections altogether.

From the point of view of satellite operations, the net effect of this change would likely be a significant reduction in the number of required satellite contacts per day, particularly if the anticipated factor of 2 improvement [Minutes of PAWG] of the Block II-R SV clocks is taken into account. From the point of view of PPS users, improved accuracy would be inherited with the Block II-R SVs without firmware modification to each user receiver.

SUMMARY

A militarized WADGPS can provide the all-weather accuracies needed for PGMs such as JDAM. A long-baseline experiment across CONUS validated the concept's assumptions and quantified error sources. Development of the EDGE High Gear program RRN provided additional insights into DGPS error sources and methods to mitigate them.

The EDGE program demonstrated that accurate pseudorange corrections valid for a network theater with reference stations more than 1000 nmi from the network center could be provided. Submeter, DGPS-corrected position accuracy was also consistently demonstrated over the course of the program.

Approaches for improving accuracy for all authorized users were discussed. RRN options included near-term theater or global overlay networks, as well as an OCS monitor system upgrade. Datalink options range from application-specific systems to near real-time corrections to Subframes 1-3 (removing the DGPS "band-aid"). Finally, if clock and ephemeris errors are reduced, high-accuracy PPS users will have the ability to reduce navigation errors to the submeter level through reductions in receiver-related errors.

ACKNOWLEDGMENTS

The authors would like to acknowledge the work and support of Capt. Chris Shank at the 50th Space Wing and Brian Brottlund of NSR. Special thanks are also due to John Gagliano, LtCol Greg Teman, Capt. John Dargan, and 1Lt Edward (Vince) Jolley at the JDAM SPO, who provided the opportunity to do this work and gave their continued support to make it a reality. Finally, much gratitude goes to numerous colleagues at SRI whose hard work continues to make this program a success.

REFERENCES

- Blackwell, Earl, "Overview of Differential GPS Methods," Global Positioning System--Papers published in *Navigation*, Volume III, ION, 1986.
- Butts, Jim and Shank, Chris, "Navigation Message Correction Tables: A Proposal," *ION Proceedings*, January 1995.
- Harms, P., Kelley, D., and Dargan, J., "Navigation Performance Analysis for the EDGE Program," presented at ION GPS 1995.
- Herring, T.A., "Modeling Atmospheric Delays in the Analysis of Space Geodetic Data," Refraction of Transatmospheric Signals in Geodesy - Proceeding of the Symposium, The Hague, Netherlands, 1992.
- Minutes of the Performance Analysis Working Group (PAWG) meeting held August 23-24, 1995, at Falcon AFB, CO.
- Sinko, James, "A Compact Earth Tides Algorithm for WADGPS," presented at ION GPS 1995.

Navigation Performance Analysis for the Edge Program

Dr. Donald Kelly and Pamela Harms, *Sverdrup/TEAS*

Capt. John Dargan, *USAF*

Chuck Eckert, *Honeywell*

ABSTRACT

The Exploitation of Differential Global Positioning System for Guidance Enhancement (EDGE) High Gear Program substantiates the use of Differential corrections to the Global Positioning System (GPS) for guiding air-to-ground weapons. The EDGE flight vehicle consisted of a 2000 pound GBU-15 glide bomb modified by replacing the seeker head with an Inertial Navigation System / Global Positioning System (INS/GPS). Navigation accuracy enhancement was accomplished using "theater-wide" Differential GPS (DGPS) corrections to the GPS pseudoranges. The DGPS corrections were generated from a reference receiver network of four GPS receiver sites approximately 1,000 nautical miles distant. The DGPS corrections were supplied to an Improved Data Modem (IDM) ground station which transmitted the corrections to the host aircraft.

This paper discusses lessons learned from the EDGE tests in using DGPS to improve the accuracy of the navigation. Static and captive carry tests were conducted, using carrier phase position scoring, to assist in determining the navigation accuracy. This paper also presents GPS lessons learned in satellite selection techniques, dilution of precision (DOP) criteria, GPS constellation maintenance, and satellite masking issues.

1.0 INTRODUCTION

History was made on May 23, 1995 as an Air Force F-16 dropped a modified GBU-15 from an altitude of 25,000 feet and a down range distance of 67,000 feet against a vertical target. The modified GBU-15 became the first seekerless INS/GPS weapon to successfully attack a vertical target, impacting within two meters of the target aimpoint. Figure 1 shows the results of this historic flight which was accomplished in the middle of a successful six-drop test program conducted at Eglin Air Force Base, Florida.

The EDGE program was designated an Air Force Materiel Command High Gear Program, allowing streamlined acquisition and reporting procedures, in response to the Joint Direct Attack Munition (JDAM) plan for adding precision capability to its baseline GPS-guided munition. A precision-capable, seekerless, INS/GPS weapon is a force multiplier in that fewer weapons are needed to strike the target and future host aircraft can be designed to be smaller and more "stealthy" since less weapon carriage is required. As part of the direction establishing EDGE as a

High Gear Program, we were challenged to complete the program in only twelve months. In order to successfully demonstrate this capability in the required time, design analysis was limited to critically essential areas. A streamlined design process was established to identify and prioritize tasking. As a result of this tasking, analysis was limited to assuring the capability to meet primary mission objectives.

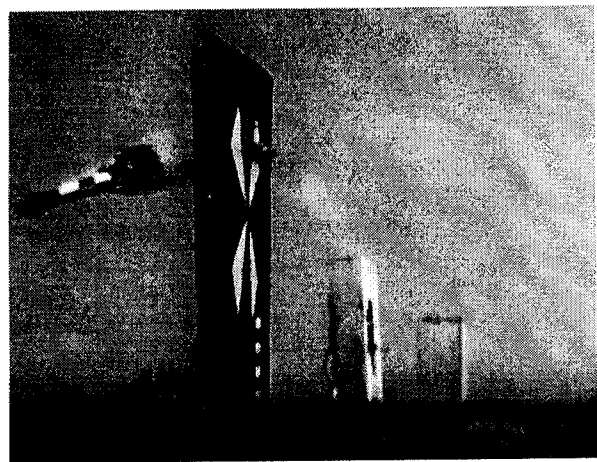


Figure 1. EDGE Flight Against Vertical Target

EDGE met its objective of demonstrating the navigation accuracy improvement potential of differential GPS for guiding air-to-ground munitions through an end-to-end weapon system implementation of DGPS using a DGPS reference receiver network, a modified GBU-15 glide bomb and a Block 50 F-16D launch aircraft. One goal of the EDGE program was to demonstrate the potential of improving current GPS-guided munition accuracy from a thirteen meter circular error probable (CEP) to less than five meters. Table 1 compares the actual radial miss ("hole in the ground") to a calculated non-differential miss using a GPS point solution program. This shows that the differential corrections did improve the solution slightly, and that the EDGE goal of five meter CEP (for drops one through five) was achieved.. Multipath effects can significantly affect navigation performance (refer to section 4.0), as this appears to have contributed to the 9.0 meter miss for drop four. For drop six, the weapon GPS receiver was only able to successfully obtain track on four of the five channels.

Numerous ground, captive carriage, and free flight drop tests were conducted in support of the EDGE program. The demonstration included free flight drops on both

horizontal and vertical targets located on the Eglin Air Force Base test range.

Table 1. Summary of EDGE Test Results

| Drop | Target type | Radial error (m) | w/o DGPS |
|------|-------------|------------------|----------|
| 1 | Horizontal | 4.1 | 5.9 |
| 2 | Horizontal | 4.0 | 3.2 |
| 3 | Vertical | 1.9 | 5.9 |
| 4 | Vertical | 9.0 | 3.2 |
| 5 | Horizontal | 3.9 | 6.6 |
| 6 | Horizontal | 11.4 | n/a |

The EDGE system concept, illustrated in Figure 2, consists of a DGPS reference receiver network, an IDM, a Block 50 F-16D launch aircraft, and the modified GBU-15 glide bomb. This concept allowed an end-to-end test of the weapon system implementation using DGPS.

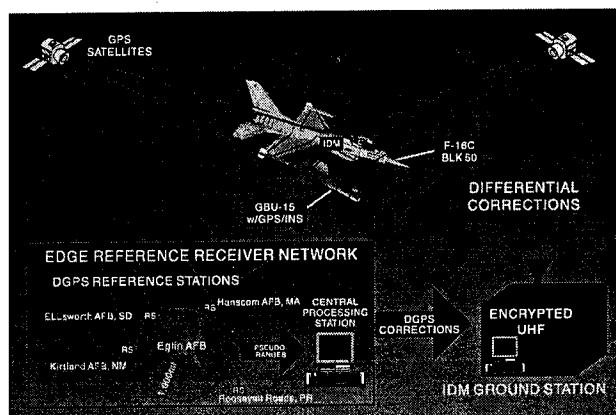


Figure 2. EDGE System Concept

The DGPS reference receiver network consists of four, 12-channel P/Y code reference receivers located at sites approximately 1000 nautical miles distant from the theater of operation at the Eglin AFB test range. The reference receiver network produces "theater-wide" pseudorange corrections that remove most of the GPS space and control segment clock and ephemeris ranging errors. The pseudorange corrections are computed for all GPS satellites in view of the network and are accurate for up to thirty minutes. The reference receiver network provides the corrections to an IDM ground station which transmits them over a UHF data link to the launch aircraft. This single transmission of all the DGPS corrections to the aircraft occurs several minutes prior to weapon launch. The launch aircraft then passes the corrections over a 1553 bus to the GBU-15 Integrated Flight Management Unit (IFMU) where the DGPS corrections are stored for use after weapon launch. The IFMU contains a strapdown INS and embedded five-channel P/Y code fast acquisition GPS receiver. Prior to launch, the IFMU performs a transfer align using the F-16's GPS aided INS as a master reference. During the transfer align, the GPS time is transferred from the F16's GPS receiver to the IFMU over the same 1553 bus as the transfer align data. Once the aircraft launches the GBU-15, the IFMU GPS receiver

enters a fast acquisition mode and acquires five satellites on P/Y code. The GPS receiver pseudoranges, corrected by the DGPS network, are then used in the IFMU's navigation Kalman filter to provide navigation corrections.

2.0 INTEGRATED FLIGHT MANAGEMENT UNIT

The EDGE weapon uses the Honeywell BG1232AG Integrated Flight Management Unit. The IFMU architecture is shown in Figure 3 [1]. The primary components include the inertial measurement module (IMM), Embedded Computer Toolbox and Operating System (ECTOSTM) software, and Interstate Electronics SEM-E five channel GPS receiver.

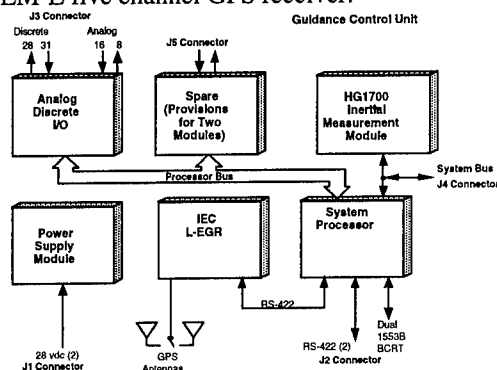


Figure 3. Honeywell BG1232AG IFMU Architecture

The ECTOS embedded software is composed of two parts: 1) the Embedded Computer Operating System (ECOSTM) and 2) the Embedded Computer Toolbox (ECTTM). ECTOS is provided to the user as a packed Ada[®] object library. Control files for compilations and linking are also provided. The relationship between ECTOS, the electronics and the application software is shown in Figure 4. ECTOS provides the interface between the application software and the hardware.

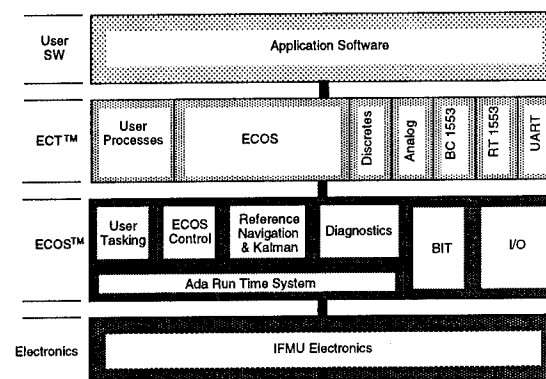


Figure 4. System Hierarchy

3.0 SYSTEM ERROR SOURCES

Table 2 provides a summary of the INS error sources [1]. Navigation error analysis for EDGE was performed using the MatSOFE (Matlab Simulation for Optimal Filter Evaluation) software. MatSOFE is a Monte Carlo analysis simulation used for evaluating Kalman filter designs [2-6]. Table 3 shows the DGPS error budget provided by SRI International at the start of the EDGE program. This budget served as the guide for determining DGPS error states and noise levels for the navigation analysis.

Table 2. Honeywell Sensor Error Model

| Sensor | Error | Model | 1- σ | Correlation |
|---------|---------------|--------------|--------------------------------|-------------|
| RLG | Bias | Gauss-Markov | 1.0 deg/hr | 3 hours |
| | Scale Factor | Gauss-Markov | 50 ppm | 3 hours |
| | Orthogonality | Gauss-Markov | 10 arc-sec | 3 hours |
| | Random Walk | Gauss-Markov | 0.125 deg/hr ^{1/2} | |
| | Quantization | n/a | 2.76 arc/sec | |
| RBA-500 | Bias | Gauss-Markov | 1000 μ g | 3 hours |
| | Scale Factor | Gauss-Markov | 100 ppm | 3 hours |
| | Orthogonality | Gauss-Markov | 10 arc-sec | 3 hours |
| | Misalignment | Gauss-Markov | 20 arc-sec | 3 hours |
| | Nonlinearity | Gauss-Markov | 22 μ g's / g ² | 3 hours |
| | Random | Noise | 0.025 ft/sec/hr ^{1/2} | |

Table 3. EDGE DGPS Error Budget

| ERRORS | SOURCES | | | TOTAL |
|---|---------------------------------|--------------------------------|------------------------------------|--------|
| | DGPS Correction Errors | Correction Distribution Errors | IEC SEME Receiver Predicted Errors | |
| Carrier-smoothed measurement error* | 0.15 m | | 1.0 m | 1.01 m |
| Residual tropo delay | 0.2 m† | | 0.5 m | 0.54 m |
| Latency of corrections | | 0.37 m | | 0.37 m |
| Correction round-off | | 0.05 m | | 0.05 m |
| Displacement from virtual RR | | 0.0 m | | 0.0 m |
| RMS range error contributions | 0.32 m | 0.37 m§ | 1.1 m | 1.2 m |
| | Total Correction Error - 0.49 m | | (UERE) | |
| HORIZONTAL TARGET CEP | 2.1 m | | | |
| ALTITUDE FUZING ERROR (50% PROBABILITY) | 2.0 m | | | |

* Includes code noise, multipath, & residual iono

† Projected tropo error with integrated carrier phase

§ Based on 30-min correction update rate

The major error sources can be divided into guidance (including aerodynamic and autopilot error sources), navigation (both INS and GPS error sources) and target location errors. Errors due to the implementation of the

EDGE guidance algorithm, the autopilot algorithm, and aerodynamic uncertainties are expected to be relatively small as compared to navigation errors. From analysis of data from the 1992 Operation Concept Design (OCD) program [7,8], guidance errors appeared to only contribute approximately 30 cm to the total EDGE CEP error budget. EDGE 6-DOF analysis and data from the EDGE free flights show this to be an accurate assessment.

Target location error, TLE, was a significant error source for the OCD program. For the EDGE program, target locations were surveyed to an approximate 30 centimeter accuracy by the Defense Mapping Agency (DMA). Thus, TLE contributes only a small relative amount (30 cm) of error to the total EDGE CEP.

While Table 3 indicates that a two meter navigation CEP is possible, the EDGE team selected five meters CEP as the EDGE system accuracy goal. Given the 30 centimeter expected contributions to CEP of guidance and TLE, one can solve for the desired contribution of navigation. Table 4 summarizes the EDGE CEP budget goals for INS/GPS and INS/DGPS.

Table 4. EDGE CEP Goals

| | INS/GPS | INS/DGPS |
|------------|---------|----------|
| TLE | 0.3 m | 0.3 m |
| Guidance | 0.3 m | 0.3 m |
| Navigation | ~9.0 m | ~5.0 m |
| CEP | 9.0 m | 5.0 m |

4.0 NAVIGATION PERFORMANCE ANALYSIS

The critical part of achieving the desired navigation performance is properly tuning the flight filter. The objective of the tuning process is to determine optimum filter noise models, filter initialization, and filter parameters such that the filter accurately estimates truth. For navigation analysis and tuning, both the Honeywell covariance analysis software and the MatSOFE Monte Carlo simulation were used. The next few sections provide examples of some of the MatSOFE analysis [9]. In addition to filter tuning, this analysis included evaluating filter performance sensitivity (forming an error budget), analyzing differential GPS (DGPS) versus GPS versus INS-only performance, examining the batch smoothing of measurement residuals between five second filter updates, and examining various GPS measurement turn-off times [9].

Figure 5 shows the CEP for a sample 50-run GPS MatSOFE simulation. MatSOFE simulations shows that for the given GPS error levels, a navigation CEP of seven to eight meters may be expected.

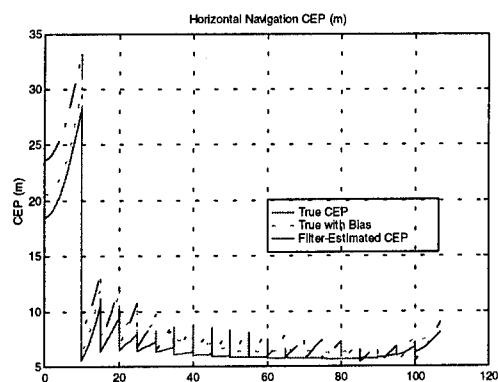


Figure 5. MatSOFE Navigation CEP Estimate for GPS-Only Weapon

Filter analysis was conducted, using MatSOFE, for the DGPS error sources described previously. One of the best approaches for evaluating filter performance is the method described by Mr. Stan Musick, Wright-Patterson AFB, Ohio, in [2,3]. In these references, Musick discusses ten tests, or criteria, for evaluating filter performance. These ten tests consist of five tests for estimation error (state-related) and five residuals (measurement-related) tests. For example, test criteria five, C5, compares the Monte Carlo covariance (standard deviation of 50 Monte Carlo runs) to the filter covariance. Figure 6 provides a sample plot of this test. For this test to be successful, the filter (dotted line) and Monte Carlo (dashed line) covariance results should be approximately equal. In addition to examining expected filter performance prior to free flight, the five residuals tests may be compared to free flight residuals data to ensure actual performance matches simulation.

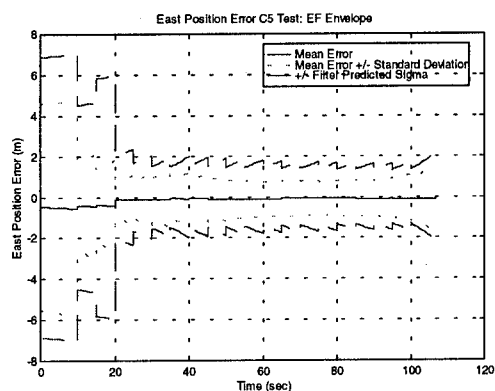


Figure 6. Test for Criteria C5

The navigation CEP goal for the EDGE program was approximately five meters. Again, using the DGPS error levels, the CEP plot of Figure 7 is typical. In this figure, the filter believes the CEP at the end of the flight to be approximately 2.6 meters, whereas the true CEP is approximately 2.0 meters. As will be discussed later, it may be that the assumed DGPS error levels at the

beginning of the EDGE program were somewhat optimistic. This causes the CEP plots, such as Figure 7, to be optimistic as well.

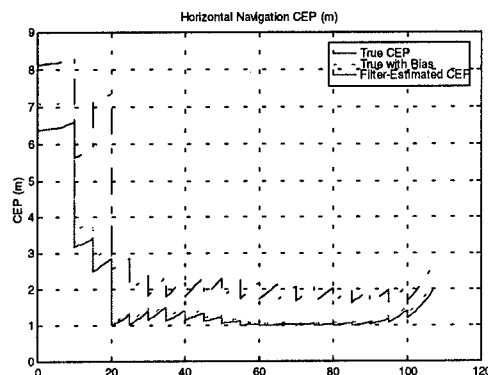


Figure 7. EDGE Navigation CEP Estimate

Additional analysis should be conducted to more accurately determine DGPS errors. For example, Figure 8 provides a navigation CEP plot for the EDGE weapon assuming additional multipath errors [10]. This may be closer to how EDGE really performed, but we cannot be certain without additional analysis and enough free flights to obtain a true statistical sample.

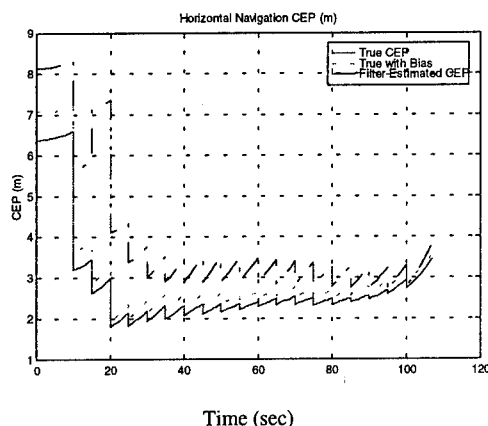


Figure 8. EDGE Navigation CEP Estimate (With Multipath)

Captive Carry Analysis. The Carrier Phase TSPI Demonstration (CAPTIDE) program was initiated in response to a requirement for high accuracy Time Space Position Instrumentation (TSPI) to evaluate precision weapons at Eglin AFB. The 39th Flight Test Squadron (FTS) determined that GPS carrier phase technology was a potential candidate to satisfy this requirement [9,11] and investigated this technology concurrent with the EDGE flight tests.

The EDGE High Gear Program designated one of the captive carry (CC) missions, CC4, to quantify the accuracy associated with a DGPS/INS (EDGE) guidance

system. A secondary objective of CC4 was to compare DGPS/INS system performance with GPS/INS system performance. Two identical modified GBU-15 weapons were used, one using DGPS corrections the other with the DGPS corrections inhibited were mounted on F-16 wing stations three and seven respectively. Twenty-five straight and level passes were flown over Eglin's range B-70 to provide the data for this analysis. Eglin range assets available for CC4 TDOP input included cinetheodites, radars, and aircraft inertial velocity. The average miss distance across all passes was 12.09 (3.69 m) feet compared with CAPTIDE and 12.03 feet (3.67 m) compared with the existing measurement system which uses a Kalman smoother to integrate range assets to form an optimal position and velocity solution (TDOP).

The average horizontal per pass "miss distance" without using DGPS across all passes was 29.53 feet (9.00 m) compared with CAPTIDE and 29.96 feet (9.13 m) compared with TDOP, showing the close agreement between CAPTIDE and the traditional TDOP system. The TDOP average horizontal per pass "miss distance" using DGPS corrections across all passes was 10.92 feet (3.33 m).

Free Flight Test Results. Telemetry data was collected and recorded for all six free flights. This data was used to generate a GPS-only point solution that was compared to the combined INS/GPS solution obtained during the actual flight. When this analysis was performed on the data from the first flight an oscillation in the point solution altitude appears (Figure 9). The guidance did not respond to the altitude oscillation. The oscillation that appears in the point solution is probably affecting the Kalman filter combined INS/GPS solution causing an erroneous slowly varying bias and by increasing the filter residuals. This same oscillation also appears in the pseudorange minus integrated delta range plot for free flight one (Figure 10). Although a final determination on the source of these errors has not been completed, analysis to date indicates that the performance observed is consistent with multipath. It is also interesting to note that when the GPS switched to the rear antenna (all except channel one) at around 61438 seconds, the oscillation seems to disappear and the GPS solution appears to more accurately reflect the true position.

Figure 10 shows a continual oscillation on satellite 19 indicating multipath during the low dynamic part of the flight. It is also interesting to note that satellite two (channel one) never switches antennas, yet slowly diverges from the pack, again leading us to believe that multipath is the source of the error. The big jumps are due to antenna switching from the front antenna to the rear antenna. All channels except channel one switched.

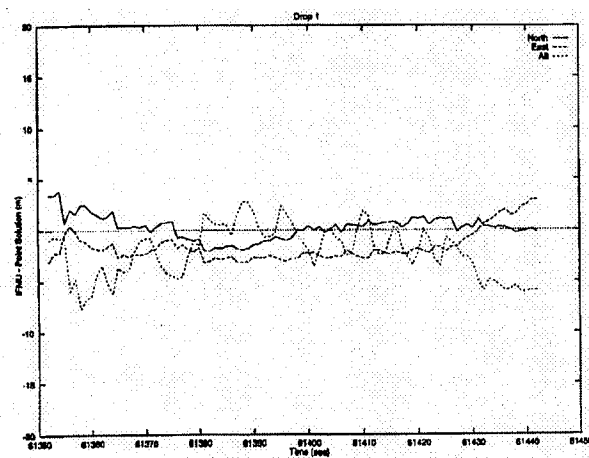


Figure 9. Free Flight 1: INS/GPS Solution - GPS Point Solution

Figure 11 shows the impact points for three of the free flight tests against horizontal targets. The target is located at 0,0 and the diamond symbol indicates where the weapon actually impacted. Analysis of the Telemetry data provided an independent GPS point solution (corrected by DGPS), and the predicted impact point assuming the point solution was used is plotted as the "+" symbol. The "x" symbol is the INS/GPS Kalman filter residual, indicating that the Kalman filter was following the GPS solution. Since the GPS point solution and the IFMU INS/GPS solution agree but appear to be off by approximately three meters, any future improvement in navigation accuracy must be accomplished by improving the GPS accuracy, rather than filter tuning or improvement in INS instruments. The GPS navigation error can be attributed to multipath affecting the GPS receiver. The square symbol indicates the predicted impact point using uncorrected GPS.

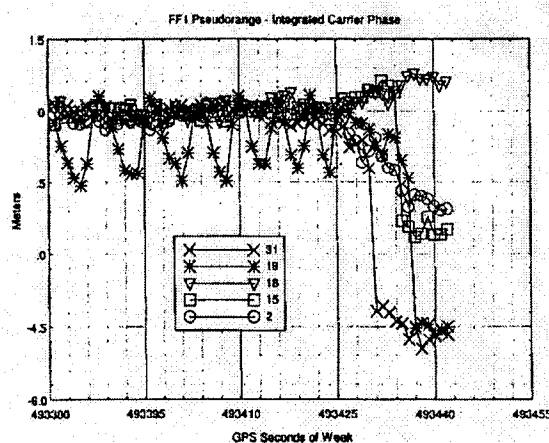


Figure 10. Free Flight 1: Pseudorange - Integrated Deltarange

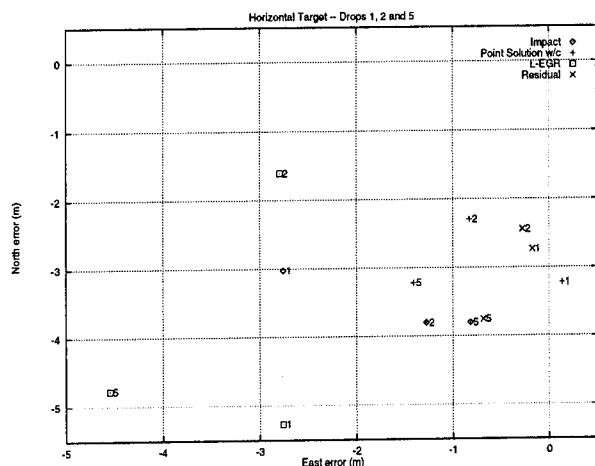


Figure 11. Horizontal Targets: Position Error at Impact

Multipath Effects on EDGE Accuracy. The major navigation error contributor in the EDGE flights was the corruption of the GPS signals by multipath [10]. The test for multipath is to integrate the deltarange minus the pseudorange or “code minus integrated deltarange” plots. The resultant plot of the individual GPS receiver channels should be straight lines with only receiver noise causing some randomness. If the plots show the channels wandering, then either the receiver is seeing multipath or the GPS receiver tracking loops are affected by dynamics. Extensive testing of the GPS receiver using a Northern Telecom simulator showed little effects on the GPS receiver do to dynamics, thus the only conclusion is that the EDGE weapon is significantly effected by multipath.

As an additional check, a point solution using just the GPS receiver supplied data and the differential corrections shows the integrated navigation solution tracking the GPS solution to within a meter, yet the miss distance was consistently around three to four meters, much greater than the less than one meter error predicted by the differential network. The code minus integrated delta range plots for the four free flights against a horizontal target show a significant change when the vehicle pitches over.

As an example, Figure 10 shows a one meter change in channel one (no antenna switch occurred on channel one) during free flight two. The code minus integrated delta range plots for free flight one shows a single channel that is continually effected after launch and before pitch over. This same oscillation shows up in the point solution (Figure 9). The IFMU Kalman filter’s preprocessing smoothes the oscillation by using a least squares fit over five GPS samples, but it is unlikely that the oscillations caused by multipath are random about the true answer. An analysis of the point solution shows that as the vehicle pitches over, the solution starts to move towards the

target, but even the last data point transmitted still is not at the target with the expected accuracy estimated by the differential GPS network. The multipath appears most prevalent when the GPS receiver is using the top mounted antenna, because as the vehicle pitches over and the GPS receiver switches to the rear antenna, the GPS solution (and the integrated INS/GPS solution) start to drive towards the actual target.

The point solution of the GPS data alone (corrected by the differential corrections) shows that the GPS solution is the major error contributor to the miss distance in all flights and most important, the GPS receiver’s solution is corrupted by multipath effects, which are external to the receiver itself. The integrated GPS/INS solution is heavily weighted towards the GPS solution because the differential corrections supplied were assumed to be very accurate. As a result, the integrated GPS/INS solution follows the GPS. Since the GPS solution is in error and misses the target, modifications to the Kalman filter noise parameters alone would not likely improve navigation performance. Correcting the multipath effects of the weapon on the GPS receiver, would result in additional accuracy.

5.0 GPS DISCUSSION

GPSSIM Mission Planning Software. A GPS mission planning software package called GPSSIM was developed by the EDGE team. GPSSIM uses GPS almanac data to compute visible satellites and dilution of precision (DOP) values with respect to a reference location specified by the user. GPSSIM models both a horizon antenna mask angle and a body fixed antenna mask angle. GPSSIM is a Matlab-based tool and its inputs include latitude and longitude information for the reference location (for EDGE, the reference location is Eglin AFB, FL), pitch and heading of the weapon at release (needed in the variable mask angle computation), and GPS almanac data

Upon start-up, the GPSSIM simulation initializes time and date from the computer clock and uses the GPS almanac data to determine what satellites are visible to the reference location. Four windows are displayed by GPSSIM; a DOP table window, a satellite availability window, a GPS receiver masking window, and an input window. These four windows are shown in Figure 12.

This tool proved to be invaluable for examining the DOP for the set of satellites likely to be selected during free flight, ensuring that no masking problems were likely to occur, and in preparing for possible IODE mismatches.

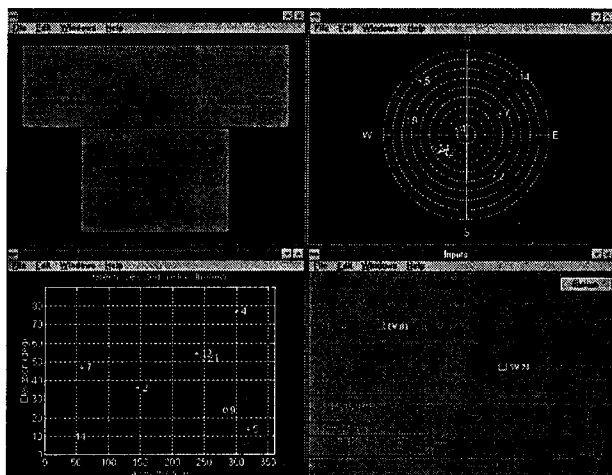


Figure 12. GPSSIM Display (All Four Screens)

EDGE Variable Mask Angle. The weapon GPS receiver configuration for the EDGE Program uses a variable satellite masking angle. The mask angle is used to avoid selecting satellites that are low on the horizon or low with respect to the attitude of the GPS antenna, and thus difficult for the receiver to track. Therefore, the variable mask angle helps ensure fast GPS acquisition and avoids the loss of track on a satellite during flight. The variable mask angle depends on the attitude (heading and pitch angle) of the weapon at release and two additional angles called the horizon mask angle and the body mask angle. The horizon and body mask angles are depicted in Figure 13.

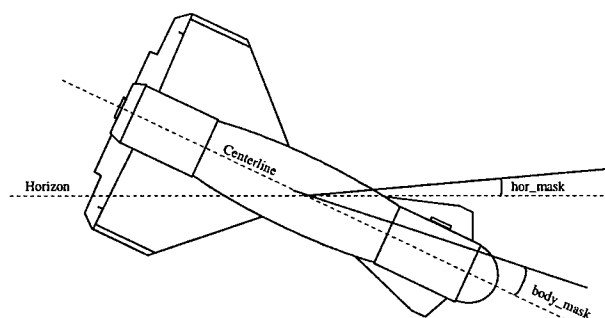


Figure 13. Body and Horizon Mask Angles used in Computation of Variable Mask Angle

The horizon mask angle can be thought of as the minimum value that the variable mask angle can have, as measured from the horizon. The body mask angle is measured relative to the body of the weapon and comes into play when the pitch of the weapon is different from zero. If the weapon attitude is such that the pitch is zero, the EDGE mask angle constant. The EDGE mask angle is variable because it changes as the azimuth angle with respect to the

heading of the weapon changes. The EDGE mask angle is computed according to the following equation:

$$\text{mask_ang}(az) = \max \left(\text{hor_mask}, \text{pitch} \left[1 - \frac{(az - \text{heading})}{90} \right] + \text{body_mask} \right)$$

where az is azimuth angle, $pitch$ is the weapon pitch angle and $heading$ is the weapon heading. Note that all angles are in degrees in the above equation. Thus, the variable mask angle is a function of the azimuth angle and changes as the azimuth angle sweeps from the nose of the weapon to the tail of the weapon. The mask angle directly off the nose of the weapon is the maximum of the horizon mask angle and the sum of the weapon pitch angle and the body mask angle. Directly behind the weapon, the mask angle is the maximum of the horizon mask angle and the body mask angle minus the weapon pitch angle. In the area sweeping from the nose of the weapon to the tail of the weapon, the mask angle varies as a function of the azimuth angle.

Navigation Message Uploads. Ephemeris fit intervals (page changes on-board the GPS satellites) do not significantly affect navigation accuracy. Navigation uploads from 2SOPS to the satellites, however, can cause IODE mismatches between the weapon ephemeris and the ephemeris for which the differential corrections are valid. Software can easily correct this problem, thus this should not be an issue for a fully operational weapon system.

For the EDGE captive carry missions and the first dress rehearsals, no precautions were taken to ensure that navigation uploads did not occur. Data gathered on passes for which IODE mismatches occurred was not useful to some analysis areas. For free flight missions, EDGE engineers worked in close cooperation with 2SOPS operations personnel to ensure that the satellites likely to be used by the weapon GPS receiver did not undergo navigation uploads during the flight test. This practice would have been very helpful on all of the EDGE missions.

GPS Scheduled Maintenance. During periods of scheduled maintenance of the GPS satellites or ground station hardware, the GPS accuracy over certain geographic locations may be degraded. Scheduled maintenance is routinely accomplished for tasks such as orbital maneuvers, attitude adjustments, and battery charging during eclipse periods. In addition, 2SOPS periodically conducts special tests on the GPS constellation. One such test during Phase I of the SRI differential GPS study caused GPS accuracy to be somewhat higher than normal, thus impacting the comparison of baseline GPS accuracy compared to differential accuracy. Mission planning in this area involved checking several bulletin boards (2SOPS and Holloman AFB) for Notice Advisories to Navstar Users (NANUs) which report on scheduled maintenance of the

GPS satellites. Thus, if a satellite is scheduled for maintenance on the mission date, this can be taken into account in the GPSSIM mission planning software by making that satellite unhealthy (a change can be made in the code to force the simulation to consider a satellite not selectable for navigation). There were occasions where mission planning was performed assuming a satellite would be unhealthy (as indicated in a NANU) and the satellite was actually healthy at mission time. There were also occasions where satellites were seen as unhealthy during the mission whereas there had been no NANU reported. In these instances, the GPSSIM mission planning software was run real-time in the Central Control Facility to account for these discrepancies.

GPS Satellite Geometry. Throughout EDGE captive carry and free flight missions, several additional GPS mission planning areas came about as a result of the behavior trends of the IEC receiver. The fast acquisition algorithm in the receiver is dependent on the first channel of the receiver. Thus, if the first satellite was low on the horizon and had a weak signal strength, this often lead to long acquisition times and poor tracking performance. In an attempt to avoid this problem, GPS mission planning involved selecting mission times during which the satellite selected in the first channel of the receiver was not low on the horizon. The cutoff angle for the first satellite was set to ten degrees. The GPSSIM software used a model of the IEC satellite selection algorithm to predict the satellites the receiver would select for navigation. Mission times were selected according to when the first satellite in the list had an elevation angle greater than ten degrees (the IEC receiver sorted the satellites in numerical order based on PRN numbers; therefore, the satellite in the first channel of the receiver was always the selected satellite with the lowest PRN number).

When a satellite is low on the horizon, the ionospheric and tropospheric errors associated with that satellite tend to be larger than those for higher elevation satellites, and the signal strength is generally weaker. The WPDOP satellite selection algorithm, however, has a tendency to select low elevation satellites. For the final EDGE mission, consisting of free flights five and six, an attempt was made to find a mission time during which the receiver selects satellites above fifteen degrees so that these errors would be minimized. Finally, GPS mission planning was used to avoid selecting satellites that were located directly behind the weapon and setting (i.e., low on the horizon) because the receiver had difficulty maintaining track of such satellites.

Weighted PDOP (WPDOP) Satellite Selection Algorithm. The EDGE satellite selection algorithm is based on WPDOP; the set of five visible satellites that are above the variable mask angle with the minimum WPDOP value is the set selected by the receiver for navigation. The weighting in the weighted PDOP algorithm is a

tropospheric weighting, which is shown plotted in Figure 14. In addition, the satellite selection algorithm will only select satellites which it predicts to remain visible and above the variable mask angle for a period of five minutes from the time of selection.

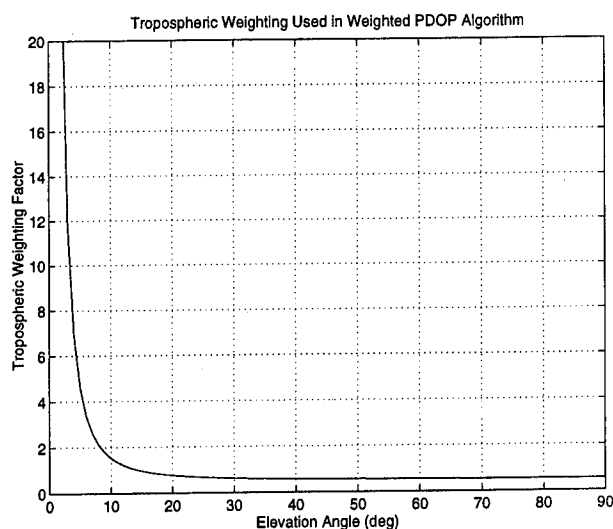


Figure 14. Tropospheric Weighting

6.0 LESSONS LEARNED

Although the EDGE program met all its objectives and achieved phenomenal results of approximately 4 m CEP there were many lessons learned in the area of navigation and GPS during the EDGE program. This section provides suggestions for future programs and identifies some areas for further research that will further enhance precision munitions accuracy.

DGPS Errors. For future programs, additional emphasis should be placed on characterizing the DGPS errors. These errors include the weapon receiver's ability to estimate ionospheric and tropospheric corrections, multipath effects, correction latency errors, errors due to IODE mismatches. Multipath, in particular, may have had a significant influence on the EDGE weapon CEP.

Using Carrier Phase Scoring to Evaluate Navigation Filter Performance. Carrier phase (CAPTIDE) scoring was included as a "piggyback" test under the EDGE test program. Because of the success of the CAPTIDE testing under EDGE, carrier phase offers an excellent method for high accuracy navigation scoring of precision guided munitions (PGMs). To use the fullest capability of carrier phase scoring, CAPTIDE needs to be integrated in the test process at the start of the test program. In addition, the weapon antenna must be placed in such a position as to prevent aircraft masking problems during captive carry (and possible dry passes) missions.

Flight Filter Structure. At the beginning of EDGE, we knew we would have time make only minor modifications

to the flight navigation filter. Several modifications have the potential for further improving navigation accuracy, and these will be pursued in future efforts.

Weapon GPS Receiver. Allowing the receiver to use carrier smoothing may significantly improve the measurement accuracy and/or noise. This is standard in commercial receivers, but we're not aware of its use in military receivers due to increases susceptibility to jamming and dropouts. There might be some way that it could be selectively used by military receivers.

EDGE Satellite Selection Algorithm. Three areas relating to the satellite selection algorithm used in the weapon GPS receiver are important to discuss.

a) The EDGE satellite selection algorithm is based on a weighted position dilution of precision (WPDOP) algorithm, where the weighting factor is based on a tropospheric model. The WPDOP algorithm has a tendency to select low elevation satellites, but the IEC receiver was found to have difficulties acquiring and tracking low elevation satellites. The satellite selection algorithm implemented a variable mask angle based on the attitude of the weapon to help alleviate this problem, although it did not fully overcome the problem. Furthermore, the selection algorithm selects only those satellites that are predicted to remain above the variable mask angle for five minutes past the time of selection. This helped to ensure that the selected satellites would not depart from the field of view for the duration of the mission.

b) There were several "Go/No Go" criteria associated with the set GPS satellites selected by the receiver for navigation. These criteria were checked real-time in the Central Control Facility during missions. Originally, the receiver would reselect satellites every five minutes or whenever it received new ephemeris data. Because there was no control over when the satellite selection algorithm was initiated, there was a risk that selection would occur just prior to weapon release, not allowing enough time to check the GPS "Go/No Go" criteria. This problem was overcome by forcing the satellite selection to occur only when an IDM transmission was made.

c) The IEC receiver ordered the selected satellites by PRN numbers; channel one was designated to track the selected satellite with the lowest PRN number, whereas channel five was designated to track the selected satellite with the highest PRN number. The fast acquisition algorithm in the receiver was dependent on the first channel of the receiver; if the first satellite was low on the horizon and had a weak signal strength, this could lead to a long acquisition

time and poor tracking performance. It may have been preferable to order the satellites from highest to lowest elevation; channel one should track the satellite with the highest elevation angle, i.e., the easiest one to acquire.

Navigation Uploads. Navigation uploads from 2SOPS to the satellites can cause IODE mismatches between the weapon ephemeris and the ephemeris for which the differential corrections are valid. Again, software can easily correct this problem, thus this should not be an issue for a fully operational weapon system.

Location of GPS Antenna for Captive Carry and Dress Rehearsal Missions. The GPS antenna on the EDGE weapon often had difficulty tracking satellites during captive carry missions because the aircraft fuselage blocked its view. Because of this, during many of the captive carry passes the receiver tracked less than five satellites. It may have been helpful to alter the location of the GPS receiver antenna during captive and dress rehearsal missions so that more data could have been collected when the receiver was tracking five satellites, as it was expected to do in free flight.

Secondary Satellite Selection. In the beginning of the EDGE Program, the IEC receiver was setup to select a secondary satellite in any of its five channels should it lose track of an originally selected satellite. This feature was disabled for several reasons. First, GPS mission planning and the EDGE variable mask angle were expected to ensure that the receiver would not select satellites that were likely to depart from the field of view of the receiver. Secondly, if the receiver were to change satellites during the flight, the filter solution would drift and then take approximately twenty seconds to converge, which would degrade the navigation performance of the weapon.

Flight Filter Measurement Residuals. Measurement residuals were somewhat higher than what expected. Even though the simulation verified these levels, it would be worthwhile to investigate this further.

7.0 CONCLUSIONS

The EDGE High Gear program provided an excellent opportunity for developing and testing DGPS in an operational weapon, the GBU-15 2000 pound bomb. The EDGE program successfully met its objectives of improved performance over GPS-only navigation by demonstrating an approximate 4 m CEP. Over the previous twelve months, the EDGE team members have conducted extensive analysis relating to navigation and GPS, and have resolved several issues that directly affecting navigation performance. These areas include examining time to first GPS measurement, satellite selection algorithm, flight filter measurement noise levels,

filter measurement rates, filter measurement types, DGPS error budget, filter shutoff time, and estimating navigation and system CEP.

Many of the lessons learned present opportunities for further research and analysis. There are two that stand out as key lessons. First is the need to better understand DGPS errors, including measurement noise levels and multipath effects. Multipath effects likely had a much greater effect on miss distance (CEP) than originally thought. Secondly, the importance of locating a remote weapon GPS antenna at a location that prevents aircraft masking.

REFERENCES

1. Integrated Flight Management Unit User's Manual, Honeywell Doc. ED7026, Vol I - VI, May 16, 1994.
2. Discussions with Mr. Stan Musick WL/AAAS-3, Wright-Patterson AFB, OH, Oct 1994 - Jun 1995.
3. *Users' Manual for a Multimode Simulation for Optimal Filter Evaluation (MSOFE)*, S.H. Musick and N.A. Carlson, AFWAL-TR-88-1138, Avionics Laboratory, Air Force Wright Aeronautical Laboratories, Air Force Systems Command, Wright-Patterson Air Force Base, Ohio, 45433-6543, April 1990.
4. *Program Design Description for a Multimode Simulation for Optimal Filter Evaluation (MSOFE)*, N.A. Carlson, R.D. Percy, and S.H. Musick, AFWAL-TR-88-1137, Avionics Laboratory, Air Force Wright Aeronautical Laboratories, Air Force Systems Command, Wright-Patterson Air Force Base, Ohio, 45433-6543, February 1989.
5. A test version of MatSOFE was provided by Capt Curtis Evans, Air Force Institute of Technology, Wright-Patterson AFB, Ohio. Capt Evans also provided helpful guidance on how many of the routines functioned.
6. Applications-Oriented Kalman Filtering, Industry Short Course Notes, D.A. Kelly, 1994.
7. "Final Report for the INS/GPS Operational Concept Demonstration (OCD) High Gear," ASC/YHD, Eglin AFB, FL. Document is recorded as Record No. 307, Vitro Technical Services, Inc, Technical Publications Group, Eglin AFB, FL, 12 July 1993.
8. "INS/GPS Operational Concept Demonstration (OCD) High Gear Program," IEEE PLANS, April 1994. Program sponsored by ASC/YHD, Eglin AFB, FL.
9. EDGE Technical Reports, Edited by D.A. Kelly, Contract Number F08635-91-C-0002, 11 August 1995.
10. The discussion on multipath effects (Section 5.9) is provided by Mr. Chuck Eckert of Honeywell, Minneapolis, MN, and is based on analysis conducted by Mr. Eckert and Mr. Mark Moeglein of SRI, Palo Alto, CA.
11. The discussion on CAPTIDE is provided by Mr. Jesse Fowler and Mr. David Reiter. Final CAPTIDE results are to be presented in a final CAPTIDE report to be released soon.

Preliminary Results from a GPS-based Portable Impact Location System

Jimmy Saunders and Miguel Cardoza
Applied Research Laboratories

Biography

CDR Jimmy D. Saunders, USN (Retired), is an Assistant Director and head of the Space and Geophysics Group at Applied Research Laboratories, The University of Texas at Austin (ARL:UT). He holds a B.S. degree in Physics from the University of Mississippi, and a Masters degree in Nuclear Physics from the Naval Postgraduate School, Monterey, California. At ARL:UT, Mr. Saunders manages research and development of systems which employ leading edge technology associated with GPS satellites, and missile and rocket systems.

Michael A. Cardoza received his bachelors degree in Aerospace Engineering from the University of Texas at Austin in 1989. He is currently a Research Engineer Associate with Applied Research Laboratories, The University of Texas (ARL:UT), where he has worked on the design, development, and testing of GPS-based navigation and surveying systems since 1988. His current technical interests are in integrated realtime GPS-based precise positioning and navigation systems.

Abstract

Applied Research Laboratories, The University of Texas at Austin (ARL:UT), has developed a prototype portable impact location system which utilizes air deployed, GPS equipped sonobuoys to localize the acoustic energy released when a projectile impacts the ocean. Meter level impact localization is realized using a low-cost OEM sensor, and DGPS realtime and postprocessing software. This paper reviews the operational concept and development constraints of the portable impact location system, and describes the selection, testing, and integration of a low-cost disposable OEM sensor into an air deployable sonobuoy. In addition, data reduction software developed to optimize DGPS positioning accuracy is discussed, along with

preliminary performance results from open ocean demonstration tests.

Introduction

Current methods for scoring the performance of ballistic weapons, such as naval guns, field artillery, or missiles, rely on extensive test range instrumentation (such as ground based radar tracking systems) and/or field spotters. Many of these test systems require periodic re-surveying and calibration to ensure that accurate scoring is achieved, and provide limited flexibility in testing different operational scenarios (in the case of a fixed testing range, the weapon system must be moved to test a shorter or greater operational range). Perhaps one of the most technically challenging weapons systems to support with accurate test instrumentation is the performance of naval guns. Fixed test ranges typically involve long and costly transit times for ships which must periodically test the performance of their guns or missile systems. Use of GPS technology, combined with traditional acoustic based localization methods, provide a means for accurately scoring such weapons at any time, in any ocean, and with minimal cost.

Applied Research Laboratories, The University of Texas at Austin (ARL:UT), has developed a prototype portable impact location system to score the performance of weapons systems which utilize a ballistic projectile. The system utilizes ship or air deployable GPS equipped sonobuoys to localize the acoustic energy released when the projectile impacts the ocean. Meter level impact localization is obtained through the use of a low-cost, disposable OEM sensor, and DGPS realtime and postprocessing software. The portable impact location system was developed with three key design goals:

- Maintain or improve upon the scoring accuracy provided by current methods,

- The design of the portable impact location system is described graphically in Figure 1. The system utilizes a shipboard reference system, an optional aircraft deployment system, and 10-12 disposable GPS equipped

The diagram illustrates the operational baseline and sonobuoy array configuration. It shows a GPS Equipped Launch Platform (a ship) and a Sonobuoy Deployment and Optional Data Recording Platform (a helicopter) both receiving signals from GPS satellites. The Operational Baseline is indicated as 1-1,000 km. The Sonobuoy Array Diameter is indicated as 1-5 km. The diagram also shows the Impact Point and the location of GPS and Hydrophone Equipped Sonobuys, with VHF Data Telemetry Links connecting the launch platform and the deployment platform to the sonobuoy array.

In operation, the free-floating sonobuoys may be deployed by ship or aircraft in a pattern which encompasses the targeted impact area. During weapons firing, GPS and acoustic data telemetered by the sonobuoys are recorded onto digital tape and onto a personal computer (PC). In addition, the realtime autonomous positions and satellite tracking information from each sonobuoy is displayed to assess the operational performance of the sonobuoys.

data smoothing and differential GPS processing is described in greater detail later in the paper. To obtain impact positions, the relative positions of the sonobuoys are used, in conjunction with the received time of each acoustic signal, to estimate a range from each sonobuoy to the impact point. These ranges are then combined in a least squares solution to determine the position of the impact point(s) relative to the ship.

The portable impact location system is best described as a system comprised of four subsystems; the shipboard reference subsystem, the deployment vehicle recording/display subsystem, the sonobuoy subsystem, and the geolocation subsystem. Each of the subsystems are described in the following sections, with emphasis on issues affecting the use of GPS technology to meet the operational system goals.

Reference Subsystem

The reference subsystem is responsible for tying the DGPS positioning results to a known WGS84 benchmark or to the launch platform (in the case of relative positioning). The system, depicted in Figure 2 below, includes a dual frequency all-in-view GPS receiver, a 486/50 MHz ruggedized PC for data logging, a Davis digital weather station for collection of temperature, pressure and relative humidity data, and an UPS and gasoline powered generator for power. All of these components, with the exception of the generator, are rack mounted in a transportable case. The geodetic quality GPS receiver was selected for use in the reference subsystem due its excellent codeless L2 pseudorange performance (critical for ionospheric correction), its all-in-view tracking capability (important over long baselines), the availability of extensive command and control software, and the option to upgrade to Precise Positioning Service (PPS) capability at a later time. In operation, the PC collects 5 second GPS and 15 minutes weather data continuously throughout the test period. The data is archived to diskette (along with a log file containing benchmark and antenna height information) for geolocation data reduction.

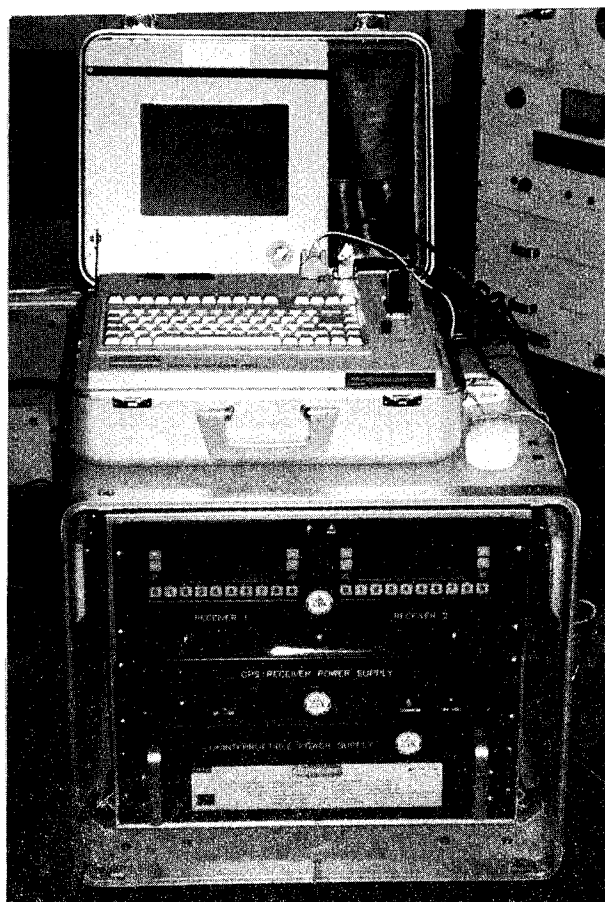


Figure 2. Photograph of the reference subsystem.

Deployment Vehicle Recording/Display Subsystem

The role of the vehicle recording/display subsystem is to provide a "portable" short baseline reference site to the sonobuoy array, and to link the array to the reference subsystem site which may be over a thousand km away. In this capacity, the recording/display subsystem deploys the sonobuoys, records telemetered GPS and acoustic data from the sonobuoys, and records GPS and weather data collected onboard the aircraft. The system hardware, depicted in Figure 3 below, includes 2 dual frequency Ashtech Z-12 all-in-view GPS receivers, 2 Metrum RS512 40 KHz digital tape recorders, an Industrial Computers Pentium 90 MHz PC, and assorted peripherals such as 16 bit A/D converters, multi-port digiboards, time code reader cards, etc. (some of which is located within the PC).

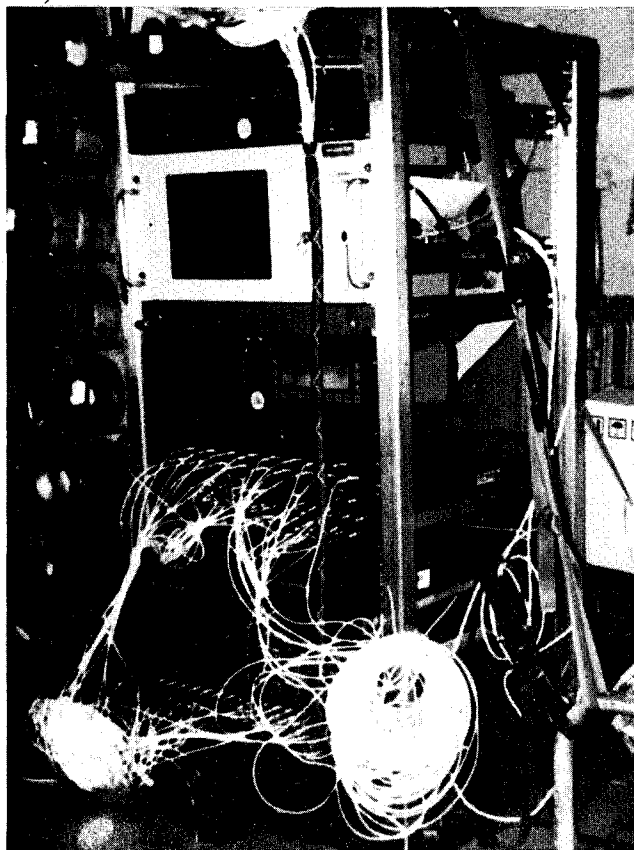


Figure 3. Photograph of the realtime display and recording subsystem.

In operation, the deployment vehicle begins by deploying a sound velocity profile (SVP) buoy to record the sound velocity in the impact area from 10 to 100 meters, and deploys 10 to 12 sonobuoys in an elliptical pattern about the intended impact area. During sonobuoy deployment, realtime display of sonobuoy position and satellite tracking data is used to determine if the pattern provides sufficient geometry to support scoring. If not,

additional buoys are deployed. Throughout the buoy deployment, and for several minutes following the test, GPS data is recorded on the deployment vehicle at a 5 second rate, and weather measurements are logged every 15 minutes. Following the test, post-test engineering diagnostics are generated to provide a quick assessment of system performance, and to ensure that sufficient data are available for postprocessing.

Sonobuoy Subsystem

The portable impact location system sonobuoy, graphically depicted in Figure 4, is designed to transmit, via its 2,400 bps VHF communication link, raw GPS measurement data and acoustic data, at a 1 Hz rate. The cost of recovering the sonobuoys, coupled with the need for a flexible system that could be deployed in severe sea state conditions, led to the design of a disposable sonobuoy. The targeted sonobuoy design goals were:

- Maximum cost <\$1,000.00 per unit
- GPS OEM form factor <4x4 inches
- GPS OEM power draw of <5 watts
- GPS pseudorange measurement noise <1 m (1 σ)
- Survivability rate of 85% (when aircraft dropped)

Design of the portable impact location system sonobuoy was therefore based upon a standard Spartan model AN/QQS-53D sonobuoy, coupled with a low-cost GPS OEM receiver and hydrophone. The primary design issues were an acceptable hydrophone response as a function of range to the impact point, and use of a

calibrated hydrophone to provide some insight into cross-correlation signal processing techniques to improve accuracy.

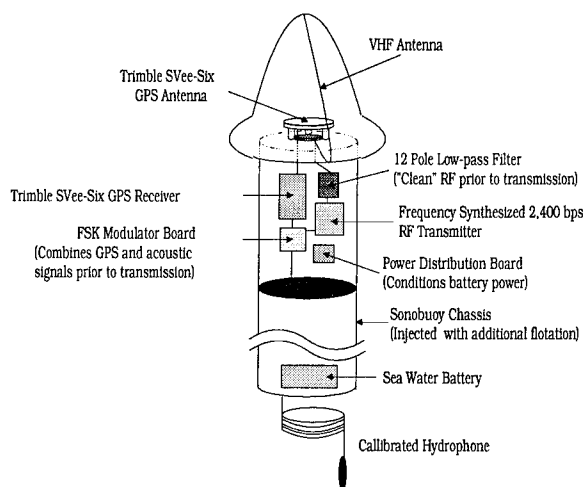


Figure 4. Graphical sketch of the sonobuoy components.

Following a test of several classes of hydrophones in the Gulf of Mexico, a HyTech -168 dB re 1V/mPa hydrophone was chosen for use in the sonobuoy. In selecting the GPS OEM receiver for the buoy, cost became a primary constraint, followed by performance, suitable form factor, and flexible command and control functions. Several OEM receivers were evaluated for use in the portable impact location system sonobuoy. Laboratory test results, displayed in Table 1, were used to identify two primary candidate receivers which were tested in actual aircraft drops in the Gulf of Mexico.

Table 1. Laboratory Test Results GPS OEM Receivers

| Receiver Type | Receiver Cost | Measurement Error 1 Sigma (m) | Size ($<4 \times 4$ in) | Power (<5 watts) | Variable Data Rate | Error Checksums |
|-------------------|---------------|----------------------------------|-----------------------------|------------------------|-----------------------|--------------------|
| Ashtech Sensor II | \$1,200 | 3.5 (22,069 epochs) | Yes | Yes | Yes | Yes |
| NovAtel 2151R | \$6,000 | 0.9 (25,928 epochs) | No | Yes | Yes | Yes |
| Trimble SVee-Six | \$450 | 4.6 (21,322 epochs) | Yes | Yes | No | No |
| Navstar XR5 | \$3,000 | 3.0 (18,569 epochs) | No | Yes | Yes | Yes |

Of the receivers tested, the Trimble SVee-Six GPS OEM receiver was selected for use in the sonobuoy. The SVee-Six receiver did not represent the best available GPS receiver technology with regards to performance. However, given future trends in receiver form factor and capability, the Trimble receiver was identified as the best choice for the current sonobuoy. Use of the SVee-Six OEM receiver did, however, require unplanned development in the postprocessing software to address limitations in receiver command and control and measurement quality.

The OEM command and control interface did not support variable data rates, and therefore the realtime recording system had to be stripped of any processes not critical to data recording in order to keep up with a 1 second data rate. In addition, an error message checksum was not provided on the output messages. This required a modification to the realtime read routines to include a time consuming bit-by-bit read whenever the message was corrupted during transmission. These modifications limited the amount of realtime monitoring and sonobuoy tracking planned, but were mitigated by converting much of the realtime processing software to OS/2 to take

advantage of parallel processing, and by upgrading the PC used in the recording/display subsystem from a 486/50 MHz to a Pentium class 90 MHz PC.

The portable impact location system relies upon meter level relative positioning between sonobuoys to achieve meter level acoustic positioning of the impact points. To achieve this level of positioning, not only must the buoy-to-buoy separation distance be short enough to cancel common mode errors (such as selective availability (SA), satellite orbit, and atmospheric errors), but the measurement quality from the sonobuoys ideally should be at the 1 meter level as well (1 sigma). Statistics from OEM measurement data collected in the laboratory and at sea indicated a 1 sigma pseudorange measurement error of 4.6 to 5.5 meters, as shown in Table 2. Although this was a recognized limitation in the low-cost OEM receiver chosen for the sonobuoy, it was expected that some form of smoothing technique would reduce the random component of the measurement error.

To this end, several measurement enhancement procedures were implemented in the postprocessing software. First, the doppler data reported by the receiver was integrated to form low-noise doppler range. The intent behind this modification was to provide an observable for directly smoothing the pseudorange measurements [Hatch, 1982]. However, doppler integration outside the code tracking loops produced doppler range measurements with repeated cycle discontinuities, which made direct pseudorange smoothing ineffective. However, this observable did provide a reliable model of SA, satellite orbit, and other GPS system trends. Therefore, differencing the pseudorange from the doppler range provided an observable which represented pseudorange measurement noise, signal multipath, and twice the ionospheric drift. A Fast Fourier Transform (FFT) smoothing technique was then applied to this observable to reduce the measurement noise component [Press, W., 1992]. This was performed by using an FFT conversion over a 400 second window of data, and removing the high frequency (10+ KHz) signals which represented measurement noise. The resulting "smoothed" measurements were then re-applied to the doppler range measurement to produce pseudoranges with a 1 sigma measurement error of 1.9 to 2.3 meters; a factor of about 2 improvement over unsmoothed pseudorange measurements. The results of this smoothing approach are summarized in Table 2 below.

Table 2. Results of FFT Smoothing on Trimble SVEE-Six Pseudorange Measurement Data

| Data Type | Laboratory Environment 1 Sigma Error (m) | Ocean Environment 1 Sigma Error (m) |
|--------------|---|--|
| Not Smoothed | 4.6 (21,322 epochs) | 5.5 (111,284 epochs) |
| Smoothed | 1.9 (20,945 epochs) | 2.3 (109,318 epochs) |

Finally, several hardware modifications were required to successfully adapt the low-cost OEM receiver to the AN/QQS-53D sonobuoy. For example, laboratory testing indicated that the 9th and 10th harmonic of the sonobuoy transmitter significantly interfered with the GPS L-band signal. The original transmitter used a crystal frequency multiplier to obtain the transmit frequency, and while this was suitable for its original use, we found it to be unusable even with a 12 pole low pass filter on the transmitter output. Transitioning to a frequency synthesized transmitter and reducing the output power to 0.8 watts (from 1.25-1.50 watts) provided a much cleaner signal and eliminated L-band interference. In addition, it was discovered that the sea water battery induced a power spike into the OEM receiver which erased its pre-loaded command instructions. A power distribution board was therefore added to the system to prevent power spikes from effecting the GPS receiver. Several other electronic and mechanical modifications were required to integrate the GPS receiver into the stock sonobuoy, including development of a Frequency Shift Keying (FSK) modulator board to combine the acoustic and GPS measurement data into a 16 KHz signal for transmission, and injecting additional floatation into the sonobuoy chassis to offset the added weight of the GPS electronics.

Geolocation Subsystem

The geolocation subsystem consists of a Pentium 90 MHz PC with embedded multiport Digiboard, a National Instruments multifunction I/O A/D board, and a Datum PC05XT time code reader board. Sonobuoy GPS and acoustic data recorded to the Metrum digital recorders onboard the aircraft, along with aircraft and reference site GPS and weather data, are all downloaded to the geolocation PC for processing. Several programs written in C and FORTRAN are used to process the GPS and acoustic data. All software is activated through Windows icons, utilizes graphical user interfaces (GUIs), and is designed to run in batch mode. The geolocation postprocessing methodology is described graphically in Figure 5.

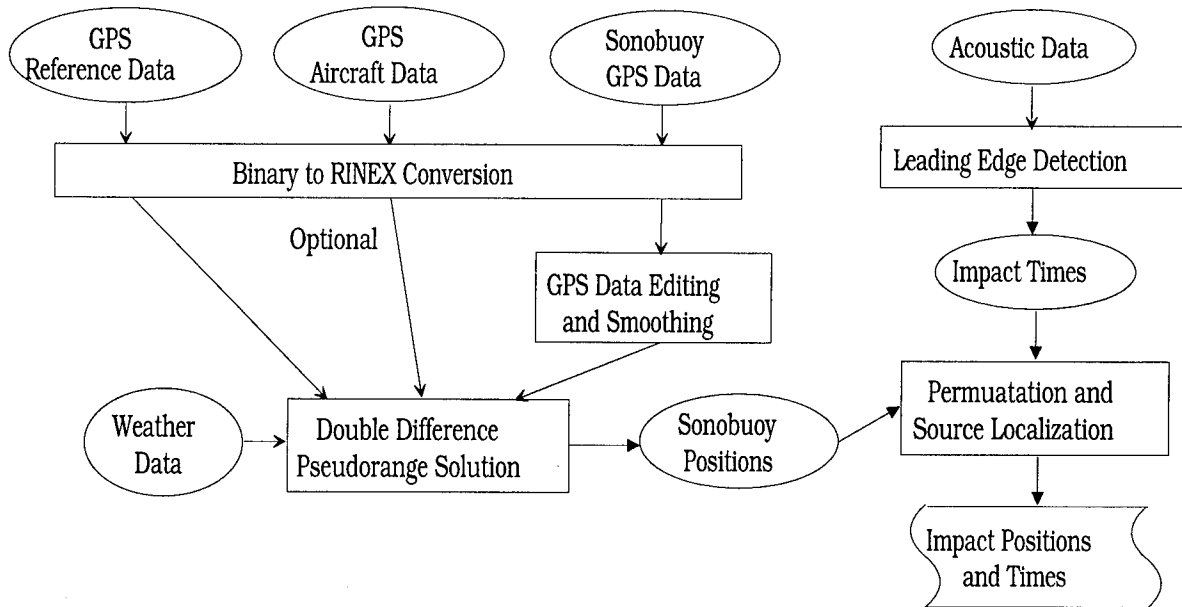


Figure 5. Graphical representation of the geolocation subsystem software.

As shown in Figure 5, the geolocation postprocessing software begins with several batch driven programs for converting the GPS data into RINEX format. Following the conversion process, GPS data from the sonobuoys are edited for spurious pseudorange measurements utilizing the fact that they are constrained to the geoid. In addition, the sonobuoy GPS data is smoothed (discussed earlier), and combined with GPS and weather data from the reference site and aircraft (if used). The weather data is used in a Modified Hopfield model to account for most of the tropospheric error, and dual frequency pseudorange measurements are used to correct for the ionospheric error between the reference site and the aircraft (if necessary). Other errors, such as SA, satellite and receiver clock, satellite orbit, and residual tropospheric errors, effectively cancel in the least squares double difference pseudorange solution algorithm. The relative differential GPS (DGPS) positions for the sonobuoys are then used in the acoustic processing software to determine the positions of the impact points.

Processing of the acoustic data is performed in two steps, 1) the acoustic data is digitized at a 10 KHz rate, and the leading edge of the received signal is time stamped with 1 millisecond timing accuracy, and 2) the impact time tags and corresponding sonobuoy positions are processed through a permutation program to determine a specific impact point which agrees with a set of sonobuoy positions and impact times.

Acoustic data recorded in realtime to tape is played back through a 10 KHz high pass filter, and digitized at a 10 KHz rate. Through the digitization process IRIG-B time code (recorded on one channel of the tape from a

GPS timing receiver) is used to assign a UTC time stamp every 1 millisecond to the digitized samples. Up to 8 sonobuoy channels can be digitized simultaneously using the LabView-based program. In addition, the audio track is monitored during digitization to distinguish actual acoustic events from reverberation, and to limit the amount of data digitized to only the data of interest about the impact period. Once digitized, a high resolution graph of a subset of the captured data is displayed, and the leading edge of the acoustic events for each sonobuoy are tagged. The digitization process concludes with a file of event times for each sonobuoy stored for permutation processing.

The permutation process begins by recording the sound velocity profile of the impact region using a disposable sound velocity buoy. This information, along with precise GPS positions for the sonobuoys and the impact times file created earlier, are used to compute a position for the impact points relative to the sonobuoy positions. This processing is performed using the permutation program GAMARAY [Stotts, 1994], developed at ARL:UT. Source localization begins with a two dimensional grid overlying the entire sonobuoy array. At each grid point a direct path is calculated to each receiver location. A reference receiver (sonobuoy) is chosen arbitrarily to compare the model time structure arrivals with the data. All travel times are then calculated relative to this reference receiver. The horizontal range, R , from grid point (x_i, y_i) to the j^{th} receiver, is given by,

$$R = ((x_i - x_j)^2 + (y_i - y_j)^2)^{1/2} \quad [1]$$

The direct path travel time from grid point (x_i, y_i) , assuming constant sound speed, to the j^{th} receiver is given by

$$T_{ij} = \frac{((x_i - x_j)^2 + (y_i - y_j)^2)^{1/2}}{C_{\text{rec}}} \quad [2]$$

where C_{rec} is the sound speed taken at the receiver depth (10 meters). The relative travel time of the grid point from the reference receiver, r , for the i^{th} receiver is therefore given by

$$T_{ij} = T_{ir} - T_{ij} \quad [3]$$

Based upon these relative travel times, a least squares error term is calculated for each grid point. This error is calculated through the following expression

$$L_i = \sum_{j=1}^N (T_{ij} - T_{dj})^2 \quad [4]$$

where N corresponds to the number of receivers, and the d subscript in the second T term in equation [4] corresponds to the reference receiver data. Next, the minimum value of L_i is found, and the grid location corresponding to this value is saved. This corresponds to

$$E_{\text{min}} = \min(L_i) \quad [5]$$

A new grid is constructed centered about the minimum point, E_{min} , with a smaller grid spacing, i.e., 100 meters. This procedure is repeated for 10 meters and finally 1 meter grid spacing. This final spacing approaches the limit of the GPS buoy location accuracy.

System Performance Results

The prototype portable impact location system has been demonstrated in two sea tests. The first test occurred in mild sea conditions (estimated sea state 2), while the second occurred during fairly rough seas (estimated sea state 4). For both tests the baseline distance between the reference site and the impact region was approximately 2,500 km, and therefore an aircraft deployment/recording platform was used. In both tests the recording/display subsystem performed well, with GPS and acoustic data successfully recorded onto the digital tape recorders, and with realtime displays of the sonobuoy reported PVTs used for deployment of the buoy pattern. Performance of the sonobuoys and the geolocation subsystems are described in greater detail in the following sections.

Sonobuoy Subsystem Performance

Initial aircraft drop tests in a controlled ocean environment were used to assess sonobuoy performance, finalize the baseline sonobuoy configuration, and identify any necessary enhancements prior to the planned at sea tests. Based upon these drop tests, the expected survivability rate for the sonobuoy was approximately 80% (80% of the sonobuoys fully operational following deployment), and the root mean square (RMS) of the smoothed pseudorange measurement error was 2.3 meters (as shown in Table 2).

Sonobuoy performance based upon drop test A, however, was not as successful. Only 4 of the 8 sonobuoys dropped provided realtime PVT information. Further analysis of the recorded data, however, revealed that the aircraft RF receiver control interface introduced errors into the data received from buoys 5, 6, and possibly 7, as shown in Table 3. When taken into account, this indicates a sonobuoy survivability rate of 75% (6 of 8); consistent with the results of the initial drop tests. Another interesting result from test A was the observed GPS measurement noise. The RMS value of the 1 sigma measurement error was approximately 3.1 meters, about 0.75 meters above what was anticipated based upon the initial drop test analysis.

Table 3. Sonobuoy Performance : Drop Test A

| Buoy | GPS Data | No. of Epochs | % >3 SVs | GPS SNR | 1 σ (m) Error |
|------|----------|---------------|----------|---------|----------------------|
| 1 | Yes | 973 | 95.6 | 11.3 | 3.6 |
| 2 | Yes | 652 | 93.6 | 9.0 | 4.8 |
| 3 | Yes | 1047 | 92.4 | 10.7 | 0.9 |
| 4 | Yes | 1036 | 92.7 | 11.8 | 1.3 |
| 5 | Yes | 467 | 54.6 | 12.5 | 34.4 |
| 6 | Yes | 45 | N/A | N/A | N/A |
| 7 | Yes | 38 | N/A | N/A | N/A |
| 8 | No | | | | |

The results of test B were noticeably better; which is particularly promising given the severe sea state condition (sea state 4). Of the 10 sonobuoys deployed, 9 provided GPS and acoustic data suitable for processing; indicating a 90% sonobuoy survivability rate, as shown in Table 4. It is also interesting to note that the RMS value of the 1 sigma measurement error improved to about 2.8 meters. Although this is still about 0.5 meters above the initial estimates, it suggests that the OEM receiver is performing well in this type of ocean environment.

Table 4. Sonobuoy Performance : Drop Test B

| Buoy | GPS Data | No. of Epochs | % >3 SVs | GPS SNR | 1 σ (m) Error |
|------|----------|---------------|----------|---------|----------------------|
| 1 | Yes | 1480 | 86.4 | 9.5 | 4.5 |
| 2 | Yes | 1316 | 86.2 | 14.1 | 1.3 |
| 3 | Yes | 1764 | 77.9 | 13.8 | 0.6 |
| 4 | Yes | 1331 | 86.6 | N/A | 3.1 |
| 5 | Yes | 1472 | 72.2 | 9.5 | 4.6 |
| 6 | Yes | 1426 | 82.5 | 13.3 | 3.7 |
| 7 | Yes | 1608 | 86.1 | 16.1 | 1.6 |
| 8 | Yes | 1451 | 85.9 | 12.5 | 0.8 |
| 9 | Yes | 1662 | 85.7 | N/A | 0.8 |
| 10 | Yes | 46 | N/A | N/A | N/A |

Geolocation Subsystem

The portable impact location system postprocessing time goal is 48 hours from receipt of the raw data, to generation of the final scoring information. During test A, previously discussed aircraft communications problems created several fragmented GPS and acoustic measurement files. Although half of the data were processed in 2-3 hours, a great deal of effort in manual processing and analysis were required to extract any useful information from the remaining sonobuoy data. Test A was therefore not considered a valid estimate of expected geolocation processing time. With the aircraft problem resolved, however, measurement data from the 9 sonobuoys deployed in test B were processed in approximately 6 hours; well within the 48 hour postprocessing goal.

Future System Development Efforts

There are two planned enhancements for the prototype portable impact location system; improvements to the sonobuoy design, and implementation of cross-correlation processing techniques.

Customized MCM GPS Technology

A review of current and future GPS receiver technology developments suggest that a Multi-Chip Module (MCM) GPS receiver design may be well suited for this application. Such a receiver could be customized to improve pseudorange measurement quality, provide a flexibility in customizing measurement data output and output rates to minimize communication bandwidth requirements, and possibly provide phase data to evaluate ambiguity resolution processing between sonobuoys. In addition, use of MCM technology allows for development of a single electronics board assembly, which would reduce the cost of future sonobuoy fabrication.

Cross-Correlation of Acoustic Signals

Presently the portable impact location system utilizes a leading edge detection technique to identify the arrival time of the acoustic signal. If, however, a complete spectrum of data from a calibrated hydrophone were available, a cross-correlation technique could be used to more accurately identify and tag arrival times between sonobuoys, as well as eliminate the need for a permutation program to identify specific impact events. In addition, cross-correlation techniques may provide a means for automated leading edge detection. Currently the process of identifying the impact leading edges is labor intensive, accounting for about 50% (3-4 hours) of the total geolocation postprocessing time.

Summary

ARL:UT has developed and field tested a prototype impact location system. To support this effort, ARL:UT has successfully integrated a low-cost OEM GPS receiver into an air deployable sonobuoy. This disposable sensor provides GPS and acoustic information in realtime, over the existing VHF communication link. Although limited in performance, techniques applied in postprocessing to edit and smooth the sonobuoy GPS data were successful, and allow the portable impact location system to provide scoring of ballistic projectiles with meter level accuracy.

Acknowledgments

The authors would like to thank the Geomatics Systems Division of ARL:UT for their dedication in the development of the portable impact location system.

References

- Hatch, R.on, "The Synergism of GPS Code and Carrier Measurements," Proceedings of the Third International Geodetic Symposium on Satellite Doppler Positioning, Las Cruces, New Mexico, 08-12 February, 1982.
- Press, W., et.al., "Numerical Recipes in C : The Art of Scientific Computing, Second Edition", Cambridge University Press, New York, NY, 1992.
- Stotts, Steve, et.al., "Source Localization Using GPS Technology and Received Arrival Time Structure Analysis," 128th Meeting of the Acoustical Society of America, Austin, Texas, November 1994.

Precise Absolute Navigation: An Evaluation of PPS Position Improvement

Bruce Hermann
Naval Surface Warfare Center

Stephen Malys
The Defense Mapping Agency

BIOGRAPHIES

Bruce R. Hermann received his B.S.E.E. degree from Bradley University in 1965, his M.S. in 1966 from Colorado State University, and his Ph.D. in electrical engineering from the University of Illinois in 1972. Dr. Hermann has been employed at the Naval Surface Warfare Center Dahlgren Division (NSWCDD) in the Space and Geodesy Branch since 1972; and he has been working on various aspects of the Global Positioning System (GPS) since 1978.

Mr. Malys received a Bachelor of Science degree from the Pennsylvania State University and a Master of Science degree in Geodetic Science from The Ohio State University. He is employed as a geodesist at the Defense Mapping Agency Acquisition and Technology Group and has contributed to the agency's geodetic exploitation of satellite systems since 1984.

ABSTRACT

Real time GPS navigation solutions necessarily use the broadcast ephemerides for satellite positions and clock corrections. For civilian applications that use the Standard Positioning Service (SPS), Selective Availability (SA) is the primary source of real time position error, but for military users who employ the Precise Positioning Service (PPS), the limited accuracy of the broadcast ephemerides is the primary source of error. This PPS real time navigation error due to the satellite ephemerides can be reduced if the mission allows the user to save the PPS solutions and reprocess them when the post-fit ephemerides becomes available. Since the SA corrected pseudorange observations that created the PPS solutions are not available to the typical navigation user, these observations cannot be used to improve the position solutions at a later date. Therefore the option to simply reprocess the SA corrected observations with the precise ephemerides and clocks is not available. The precise absolute navigation algorithm described in this paper avoids the need to reprocess the SA corrected observations, but it does require access to the SA corrected broadcast ephemerides for the time of interest, the PPS navigation solutions that are to be corrected, the GPS time of each solution, and a list of the satellites that were used.

The Precise Absolute Navigation (PAN) algorithm is described and its effectiveness tested with equivalent PPS navigation solutions. The precise satellite ephemerides chosen for the navigation improvements are the DMA Precise Ephemerides and clock solutions. The true absolute position at each observation is obtained from On-The-Fly (OTF) kinematic relative position solutions referenced to a known absolute point. The results of several days of testing are discussed.

MOTIVATION

The purpose of the PAN development was to investigate the feasibility of improving, by post-processing, the accuracy of a set of typical PPS navigation solutions. Real time navigation solutions necessarily use the Broadcast Ephemerides as the source of the satellite position and satellite clock estimates, but in certain cases the mission could benefit from more accurate navigation solutions. If the mission is not time critical, it may be acceptable to delay use of the navigation solutions until the post fit Precise Ephemerides are available. In this case, significantly better results may be expected.

With a precise ephemerides, static absolute position solutions can achieve sub-meter repeatability [1], [2]. Meter level navigation solutions have been demonstrated by postprocessing L_1 observations with post-fit precise ephemerides, clock estimates, and an ionospheric model [3]. Applications where precise absolute navigations would be of interest include cases where differential or relative data are not available, or where the track of a moving vehicle or ship is desired at remote locations far from other sites.

In the operational environment, the PPS navigation solutions will be obtained from a user in the field. Presumably these solutions were obtained with a receiver that can correct for the effects of Selective Availability (SA) and AntiSpoofing (AS). AS encrypts and SA corrupts the GPS signals making the precise signal and the full accuracy of the broadcast ephemerides accessible to authorized users only. These receivers can display the navigation solution in real time, but the field-corrected satellite ephemerides and the SA-corrected pseudorange and phase observations are classified

and therefore are not available to the user. The PPS position solutions are unclassified and can be recorded in the field along with the GPS time and the satellites contributing to the solution. Even though the original observations are lost, this information is enough to allow the PPS solutions to be improved at a later time with the post-fit precise ephemerides.

METHOD

It is assumed that the GPS time and the PPS solutions to be improved are given, as is the receiver type and the details of the navigation algorithm it used. The algorithm information is used to establish which satellites, of those in view, produced the particular navigation solution. To compute the difference between the two ephemerides, an independent source of the SA corrected Broadcast ephemerides and the DMA Precise ephemerides and clock estimates are required. Finally, for testing purposes, two frequency SA corrected pseudorange and phase observations from a typical receiver will be needed in addition to the information above.

The form of the observation equations that produced the navigation solution in the field receiver can be reconstructed as in Equation (1). The original observation vector was O_o , the computed ranges were placed in the C_o vector, and the initial guess for the state vector was X_o . Note that none of these vectors used in the field solution was saved.

$$O_o = C_o + \frac{\partial C_o}{\partial X_o} \Delta X_o \quad (1)$$

The solution to (1) is ΔX_o , from which the new state vector X_b (the saved PPS solution) was found: $X_b = X_o + \Delta X_o$. It is clear that if the precise ephemerides were available in the field along with the broadcast ephemerides, the same observation vector O_o would have been used with either set of ephemerides. Thus the common observation vector allows the right hand side of Equation (1) using the broadcast ephemerides (subscript b) to be equated to the equivalent set of equations using the precise ephemerides (subscript p). This is illustrated in Equation (2).

$$C_b + \frac{\partial C_b}{\partial X_b} \Delta X_b = C_p + \frac{\partial C_p}{\partial X_p} \Delta X_p \quad (2)$$

The PPS navigation solution X_b obtained from the field is used in the computation for the vector C on both sides of (2). Assuming operation in the linear region, the solution vector X_b from (1) used along with the original broadcast ephemerides to compute C_b should require no further correction. This makes $\Delta X_b \approx 0$. Therefore (2) can be rearranged into a form similar to that in Equation (1). This result, Equation (3), can be solved in the usual least squares sense to obtain the correction ΔX_p that should be applied to the given X_b to form the precise solution: $X_p = X_b + \Delta X_p$.

$$C_b - C_p = \frac{\partial C_p}{\partial X_p} \Delta X_p \quad (3)$$

The only difference between the computed vectors on the left of Equation (3) is due to the satellite position difference and the satellite antenna offsets. The precise ephemerides are computed for the satellite center of mass, not the antenna phase center. This offset must be subtracted from the range in order to match the observed ranges. The other modeled effects normally included in the computed vector to match the observations, such as tropospheric refraction and relativity [4], are not needed since they would be approximately the same regardless of which ephemeris was used.

STATIC SITE RESULTS

For development and testing purposes, one week of data was collected at the DMA monitor site at the Aerospace Center in St. Louis. The effects of SA were removed from the tracking data and the broadcast ephemerides in the DMA Data Correction Facility (DCF). DMA is an authorized PPS user and has developed this DCF to facilitate post-processing of GPS data collected for the purpose of orbit determination and geodetic survey work. Satellites below 15° elevation were not used in the static solutions; the Geometric Dilution Of Precision (GDOP) for day 072 with this mask angle is plotted in Figure 1. The GDOP for the other days of the week were similar. The figure shows two periods where the GDOP is larger than 6 for a significant interval. In both cases only four satellites were above the 15° elevation mask. During the largest spike, the GDOP exceeded 600 briefly.

The difference between the simulated PPS solutions for day 072 and the given site coordinates are shown in Figure 2. The weighted mean and standard deviation in the east, north and vertical components for all S solutions during the day is

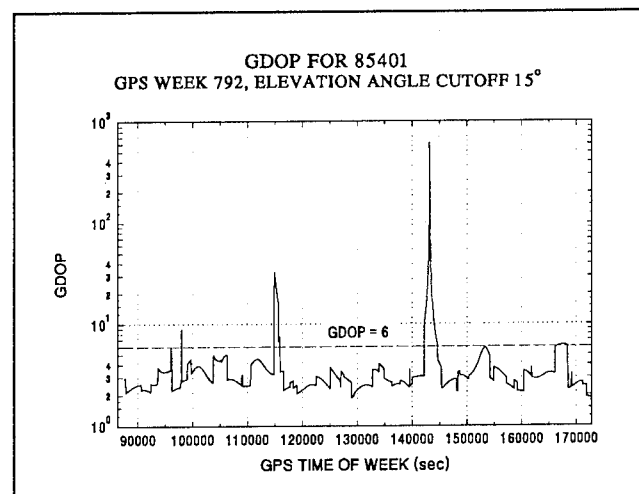


Figure 1. The GDOP For Day 072 With A 15° Elevation Mask Angle

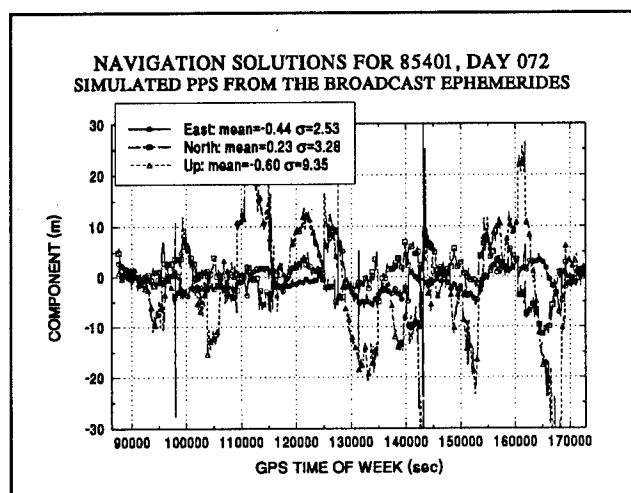


Figure 2. Simulated PPS With Respect to the Surveyed Position

listed along with the results from the other days in Table 1.

In order to minimize the effects of the periods of large GDOP on the statistics, the means and standard deviations were weighted by the function shown in Equation (4). Each component of the navigation solution was multiplied by the weight which is a function of the current GDOP. Solutions determined during large GDOPs were given lower weight (made smaller) so that the means and standard deviations computed over all solutions were not overly influenced by the solutions obtained when GDOP was greater than 6.

$$W_i = \frac{1}{1 + \left(\frac{GDOP_i}{6} \right)^6} \quad (4)$$

Figure 3 shows the PAN solutions for day 072. As was expected, the standard deviations on the position errors are greatly reduced compared to the PPS which uses the broadcast ephemerides. There are several error spikes that appear in both figures. At 97,950s the spike is due to the loss of a satellite for one 30s time step and the consequent

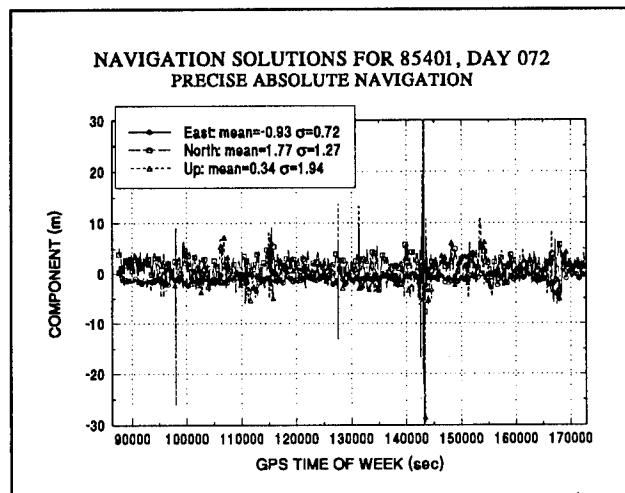


Figure 3. PAN Solutions With Respect to the Surveyed Position

increase in GDOP. At 127,590s a new satellite is acquired. At 131,340s there is no satellite activity and the cause of that spike could not be determined. The multiple jumps between 144,100 and 144,500s are due to the very high GDOP during this period.

The weighted standard deviations obtained by the PAN technique for the entire seven days are presented in Table 2. The PAN consistency from day to day is quite good, though there is an unexplained bias in the north component of about 1.7 to 1.9m. As a check on the accepted position for this site, days 072, 073 and 075 were processed with the DMA GPS Absolute Sequential Positioning software (GASP) [5]. The average differences between the GASP solutions and the given position were -1.03m east, 0.30m north, and -0.44m in height. These results would move the site 30cm north and 103cm west, helping to reduce the apparent PAN solution error in both components.

RESULTS FOR A DYNAMIC SITE

The most interesting application for PAN will be for improving the accuracy of the track traversed by moving vehicles. Though the improved accuracy must wait for the availability of the Precise Ephemerides, for many missions this wait will be acceptable. For example, a military vehicle

| | 071 | | 072 | | 073 | | 074 | | 075 | | 076 | | 077 | |
|---|-------|------|-------|------|-------|------|------|------|-------|------|-------|-------|-------|------|
| | μ | σ | μ | σ | μ | σ | μ | σ | μ | σ | μ | σ | μ | σ |
| E | -0.55 | 2.27 | -0.44 | 2.53 | -0.90 | 2.89 | 1.07 | 1.68 | -0.42 | 2.21 | -1.87 | 8.69 | 1.01 | 1.81 |
| N | -0.28 | 2.99 | 0.23 | 3.28 | 0.52 | 5.12 | 0.80 | 4.29 | 0.56 | 3.12 | 1.45 | 8.07 | -0.52 | 2.75 |
| U | 1.09 | 6.52 | -0.60 | 9.35 | 1.14 | 8.86 | 2.37 | 5.65 | 1.80 | 7.88 | -3.38 | 17.26 | 0.62 | 4.95 |
| S | 2393 | | 2833 | | 2833 | | 1652 | | 2833 | | 2826 | | 719 | |

Table 1. Static PPS Weighted Means (μ meters) and Standard Deviations (σ meters) For Each Day in the East, North, and Vertical Components. Row S Lists the Number of 30s Observations Processed Each Day.

| | 071 | | 072 | | 073 | | 074 | | 075 | | 076 | | 077 | |
|---|-------|----------|-------|----------|-------|----------|-------|----------|-------|----------|-------|----------|-------|----------|
| | μ | σ | μ | σ | μ | σ | μ | σ | μ | σ | μ | σ | μ | σ |
| E | -0.78 | 0.66 | -0.93 | 0.72 | -0.92 | 1.88 | -0.90 | 0.62 | -0.85 | 0.66 | -0.66 | 2.04 | -1.12 | 0.56 |
| N | 1.82 | 1.27 | 1.77 | 1.27 | 1.87 | 1.36 | 1.79 | 1.23 | 1.88 | 1.30 | 1.90 | 4.01 | 1.82 | 1.34 |
| U | 0.09 | 1.88 | 0.34 | 1.94 | 0.17 | 3.21 | 0.70 | 1.80 | 0.19 | 1.85 | -0.41 | 8.29 | 0.42 | 1.75 |

Table 2. Static PAN Weighted Means (μ meters) and Standard Deviations (σ meters) For Each Day in the East, North, and Vertical Components

traveling on a roadway and reporting its PPS position every second (or some other appropriate time interval) can be positioned more accurately with this post-processing technique. The field PPS results, improved by *precise absolute navigation*, can then be used to more accurately establish a *georegistered* Geographic Information System (GIS). This will be especially valuable in areas where no

geodetic control has been established or where the local maps are provided on a non-geocentric datum. Another example is remote absolute positioning of fixed objects by ranging sensors [6]. In this case, the accuracy with which the system can position objects absolutely is based upon knowledge of the sensor location.

To illustrate this capability, PAN results are presented for one of two vehicles traveling around a fixed circuit at the Naval Surface Warfare Center, Dahlgren Virginia. As with the static site data, this dynamic data set was processed by the DCF to remove the effects of SA. Even with SA removed, these data can only approximate the quality of true PPS results. The receiver was not keyed, so the two frequency pseudoranges used for the PPS are C/A quality, not P-code quality.

The truth was obtained from OTF relative positioning between the vehicles in motion and a well known fixed site [7]. The truth tracks for the vehicle labeled 95 are shown in Figure 4. The truth coordinates of this vehicle are shown in the east and north directions, in units of meters, with respect to the fixed site. A small segment of this track (labeled "DETAIL" in Figure 4) was selected for expansion to illustrate the differences between the simulated PPS, the PAN solutions, and truth.

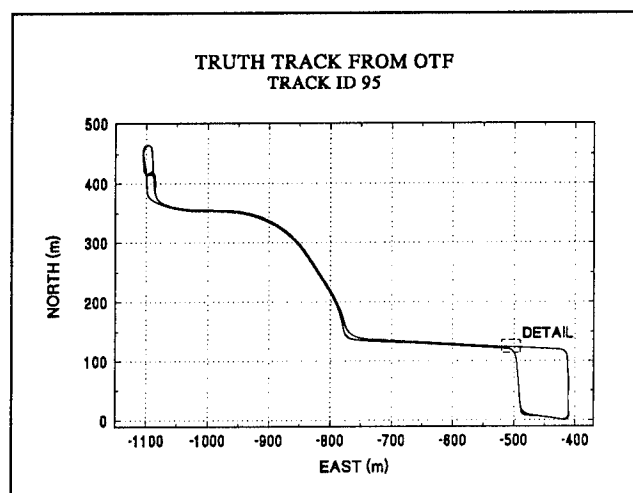


Figure 4. The Circuit Taken by Vehicle 95 Derived From 1s On-The-Fly Solutions

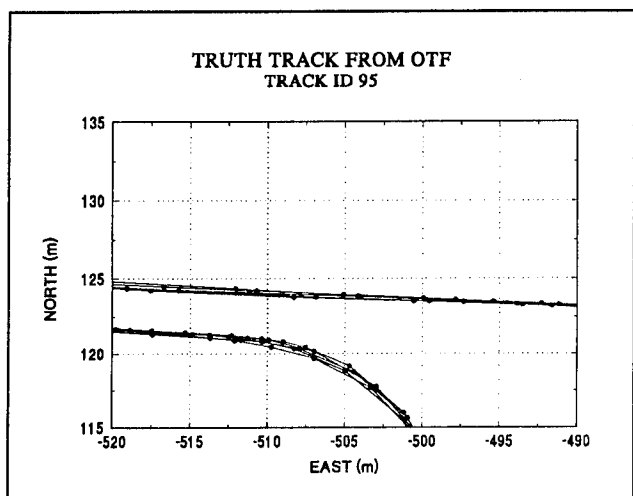


Figure 5. Truth Detail for Vehicle 95 in the East and North Components

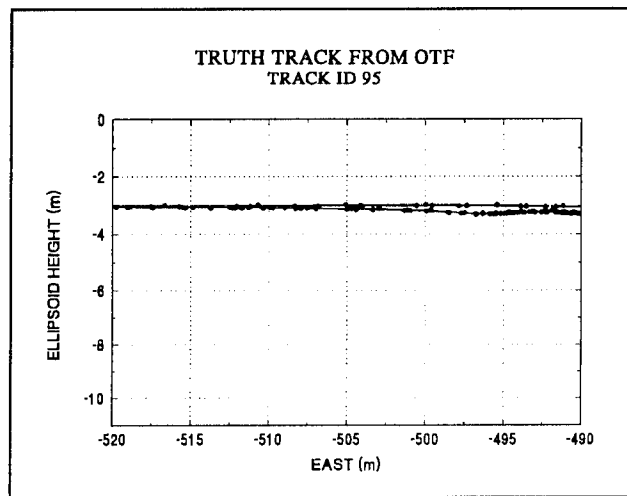


Figure 6. Truth Detail for Vehicle 95 in the East and Vertical Components

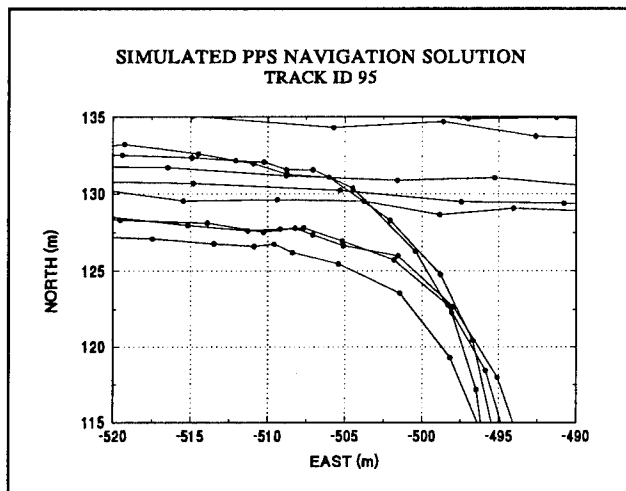


Figure 7. Detail of PPS Results in the East and North Components

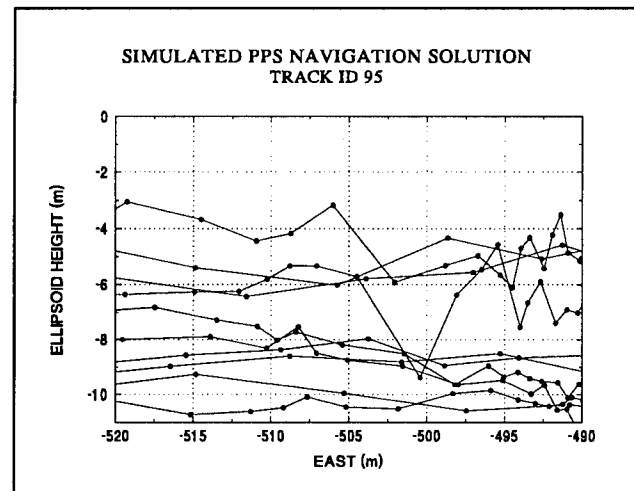


Figure 8. Detail of the PPS Results in the East and Vertical Components

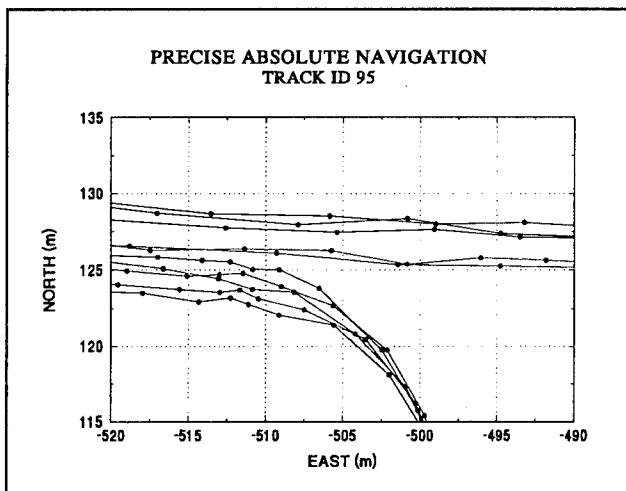


Figure 9. Detail of the PAN Solutions in the East and North Components

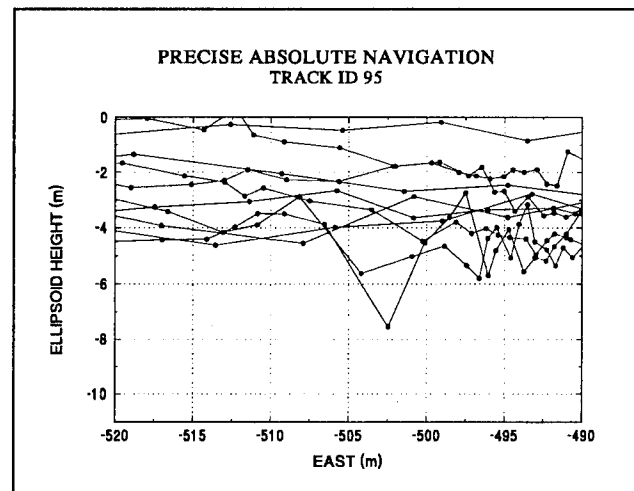


Figure 10. Detail of the PAN Solutions in the East and Vertical Components

The expanded truth track detail is shown in Figures 5 and 6. In Figure 5, the bottom set of tracks show the vehicle traveling east along a two lane road and then turning off toward the south. The top tracks are for the return route when the vehicle was traveling west. There are five overlapping tracks in each direction representing five circuits of the course. The dots represent the 1s On-The-Fly

| Units = meters | PPS - Truth | | PAN - Truth | |
|-------------------|-------------|----------|-------------|----------|
| | μ | σ | μ | σ |
| East | 1.68 | 1.20 | -0.84 | 0.38 |
| North | 8.05 | 2.50 | 3.18 | 1.12 |
| Vertical | -5.61 | 3.31 | -0.89 | 1.92 |

Table 3. PPS and PAN Means (μ) and Standard Deviations (σ) from Vehicle 95 Solutions

solutions at each observation time. The truth ellipsoid heights with respect to the reference site are shown in Figure 6. There is little height variation along this section of the course.

The east-north and east-vertical solutions for the simulated PPS results are shown in Figure 7 and Figure 8 on the same scale as the truth. The corresponding sample of the PAN solutions are shown in Figures 9 and 10. There is a noticeable improvement in the PAN solutions compared to the PPS results. The improvements are quantified in Figures 11 and 12. These two figures show the differences between the solutions and the truth over the entire course as a function of time. Of particular interest is the reduction in the magnitude of jumps that occur in the PPS solutions when the number of satellites being tracked changes. Two examples of this are in Figure 11 at 412,296 and 413,195s. The statistics are summarized in Table 3. The use of the precise ephemerides in the PAN solutions reduces the mean offsets in each component seen in the simulated PPS results

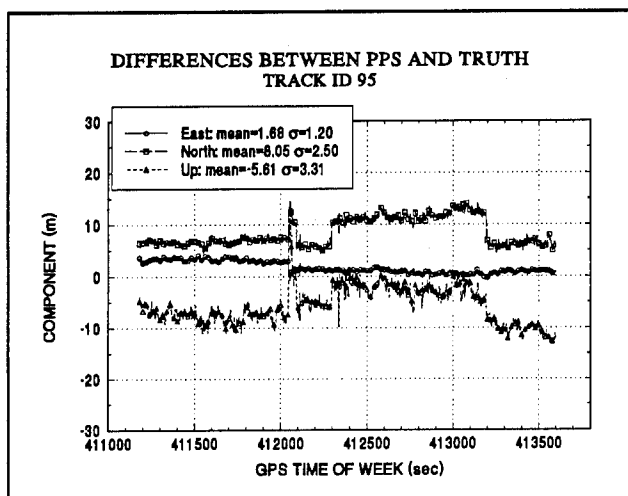


Figure 11. PPS Results Differenced With the Truth for the Entire Vehicle Circuit

and also reduces the standard deviations by about a factor of two. However, the unexplained PAN north component bias, seen in the static site results, remains.

CONCLUSIONS

This paper demonstrates that PPS navigation solutions from field sites can be upgraded to Precise Ephemeris quality without reprocessing the original observations. If files of the unclassified navigation solutions, the time, and the satellites being tracked, are kept and a source of the SA corrected broadcast ephemerides and precise ephemerides are available, then the PPS solutions can be improved at a later date. This capability can make important contributions to military mapping operations where vehicles equipped with PPS receivers can gain access to areas which lack geodetic control points.

ACKNOWLEDGMENTS

The authors wish to thank Dr. Randall Smith of DMA for suggesting this unique investigation. The authors also wish to thank the following individuals: Mr. Brian Tallman, Mr. Kim Kangas, and Mr. Brian Hagan of the Defense Mapping Agency, Aerospace Center for providing the seven days of static test data; Ms. Lisa McCormick, Ms. Mary Carroll, and Mr. David Hanson also of the Defense Mapping Agency, Aerospace Center for correcting the Drive-By data in the DCF; and Dr. Alan G. Evans of the Naval Surface Warfare Center, Dahlgren Division for providing the Drive-By data which was used for the dynamic testing. The operational version of the code was developed by Ms. Bonnie Risinger of the Naval Surface Warfare Center, Dahlgren Division.

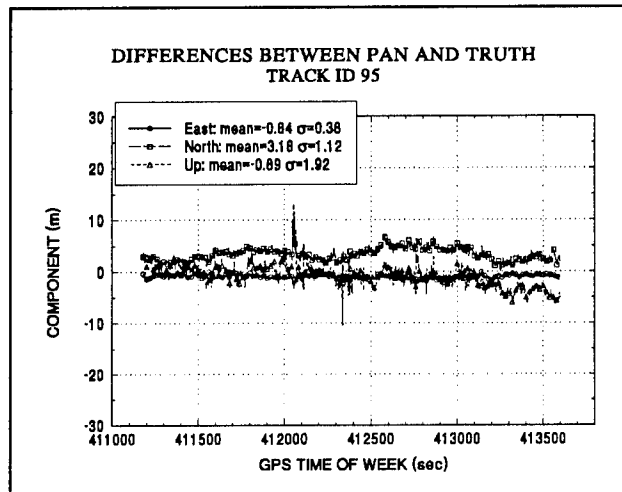


Figure 12. PAN Results Differenced With the Truth for the Entire Vehicle Circuit

REFERENCES

1. Hermann, Bruce, R., *Five Years of Absolute Position at the Naval Surface Warfare Center*, Proceedings of the Sixth International Geodetic Symposium on Satellite Positioning, The Ohio State University, March 1992.
2. Malys, Stephen, Dennis Bredthauer, Bruce Hermann, and James Clynnch, *Geodetic Point Positioning with GPS: A Comparative Evaluation of Methods and Results*, Proceedings of the Sixth International Geodetic Symposium on Satellite Positioning, The Ohio State University, March 1992.
3. Lachapelle, G., R. Klukas, D. Roberts, W. Qiu, and C. McMillan, *One-Meter Level Kinematic Point Positioning Using Precise Orbits and Satellite Clock Corrections*, Proceedings of ION GPS-94, Salt Lake City, Utah, September 1994.
4. Braasch, Michael S., *A Signal Model for GPS*, NAVIGATION, **37**, No. 4, Winter 1990-91.
5. Malys, Stephen and Maria J. Ortiz, *Geodetic Absolute Positioning with Differenced GPS Carrier-Beat-Phase Data*, Proceedings of the 5th International Geodetic Symposium on Satellite Positioning, Las Cruces, NM, March 1989.
6. O'Leary, E. M., A. G. Evans, and T. N. Smith, *An Evaluation of the Use of GPS and Laser Ranging to Position Stationary Objects from a Distance*, The Institute of Navigation, Annual Meeting, Washington D.C., June 1992.
7. Hermann, Bruce R., Alan G. Evans, Christopher S. Law and Benjamin W. Remondi, *Kinematic On-The-Fly GPS Positioning Relative to a Moving Reference*, Proceedings of ION GPS-94, Salt Lake City, Utah, September 1994.

GPS Translator for Artillery Projectiles – A Progress Report

George Wiles
U.S. Army Research Laboratory

Jeff Smuk
Hittite Microwave Corporation

BIOGRAPHY

Mr. Wiles is a senior project engineer and RF system designer with the Acoustics and Special Sensors Branch of the U.S. Army Research Laboratory. He has 12 years of experience in working with artillery-launched electronic systems. He holds a B.S. degree in electrical engineering from Virginia Polytechnic Institute.

Dr. Smuk is a senior microwave design engineer with Hittite Microwave Corporation, where he is currently involved in the design and characterization of multi-function MMIC chips and their integration into miniature subsystems. He holds B. Eng., M. Eng., and Ph.D. degrees in electrical engineering from Carleton University.

SUMMARY

Recent improvements have miniaturized the Global Positioning System (GPS) translator for artillery to fit into a 9-in.³ NATO standard fuze package, including electronics, power supply, and antenna. The device has been successfully tested.

ABSTRACT

The Army has been developing a GPS translator to allow tracking of artillery projectiles as part of the ongoing effort to improve artillery effectiveness. Since the original proof-of-concept test (October 1991), the design has been miniaturized to fit in the 9-in.³ volume of a standard artillery fuze, which can screw onto any of the several million projectiles already in the stockpile. The 9-in.³ package includes translator electronics, a thermal reserve battery, and transmit and receive antennas. The first prototype was successfully tested in December 1994, when an artillery round with translator was tracked 12 km to impact.

This paper details the significant electronic design improvements that miniaturized the translator. An overview of the antenna and power supply system is given, as well as a detailed description of the monolithic microwave integrated circuit (MMIC) translator chip set.

INTRODUCTION

The Army has been conducting research into using the Global Positioning System (GPS) to improve artillery accuracy and effectiveness. A proof-of-concept demonstration had

been conducted, in which two L1 C/A code translators were built and fired [1,2]. The prototype translators were constructed from commercial off-the-shelf electronic components, and configured to fit inside the available volume of an artillery projectile (123 in.³).

Based on the success of that initial effort, a follow-on effort was begun to design a translator to fit in the available 9-in.³ volume of the fuze. To accomplish this, three major efforts took place. The dual-frequency antenna was redesigned to provide more internal volume at the nose; a thermal reserve battery was designed and built to supply primary power for the electronics, and a custom gallium arsenide (GaAs) monolithic microwave integrated circuit (MMIC) chip set was created to replace the off-the-shelf components. The MMIC approach enhances ruggedness and reliability and lowers power consumption. By integrating packaged MMICs together with procured components, a form-fit translator module is realized, which provides over 125 dB of gain with 3 dB noise figure, survives firing shock of over 8000 G, and operates from 0° to 70°C.

SYSTEM ARCHITECTURE

The basic function of the translator is to convert the incoming C/A-coded L1 GPS signals from the NAVSTAR constellation to a higher frequency within the 2200- to 2290-MHz telemetry band and to provide the amplification required to overcome path loss.

The dual-conversion translator architecture, shown in Figure 1, was selected because of the extremely high gain of the module and low isolation between transmit and receive antennas. Active circuit functions are performed within the seven GaAs MMICs shown. Passive L-C and surface acoustic wave (SAW) filters maintain stability and noise figure while limiting output power requirements. The signal path consists of low noise amplification to establish system noise figure, downconversion to an intermediate frequency (IF) within the VHF band, which allows for substantial amplification, and the integration of a high-selectivity SAW filter to limit noise bandwidth, upconversion to the telemetry band, and amplification to the required output power level. The local oscillators are provided by two phase-locked loops using a common reference oscillator to maintain close-in phase coherence. A harmonic of the crystal reference oscillator is coupled into the IF strip to form a pilot signal that

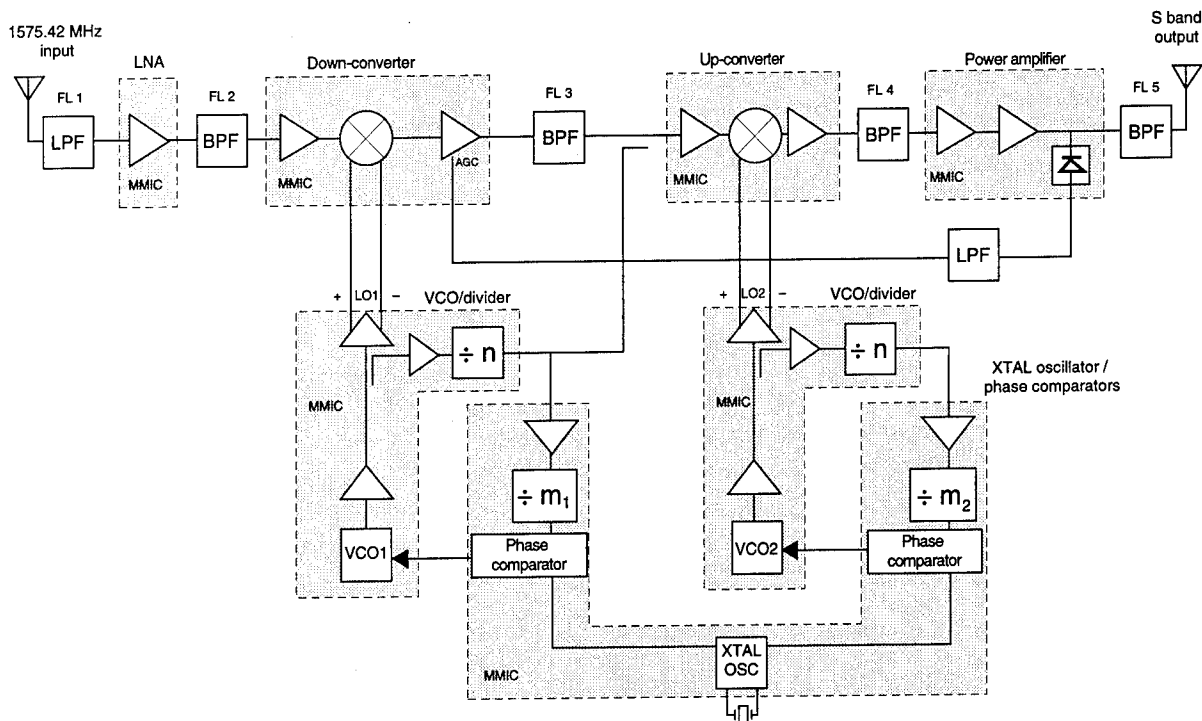


Figure 1. GPS translator block diagram.

allows the translated GPS signals to be acquired by the ground receiver following Doppler-, temperature-, and shock-induced shifts in the output frequency.

The 125-dB overall translator gain includes all the losses associated with the passive components in the signal path, making the total active gain budget for the MMICs higher. The large number of gain stages results in significant gain variation over temperature, which is temperature compensated through an automatic gain control (AGC) leveling loop, consisting of a detector in the output stage of the power amplifier, a low-pass filter, and a variable gain IF amplifier in the down-converter.

PROOF-OF-PRINCIPLE TEST

The miniature translator was created specifically for a proof-of-principle (POP) test of the artillery registration system. Certain operational requirements were relaxed in order to facilitate testing in a cost- and schedule-constrained environment. For example, a C/A code implementation was allowed even though the military requires use of the Y code in battlefield systems. Also, the maximum acceleration level for the POP hardware was 8000 G, or half of the maximum of 16 kG experienced in the longest firings. It is expected that a capability for multiple rounds in the air at one time will be a requirement for a fielded system, which is not implemented in this system.

The design effort focused on the critical areas of antenna, power supply, and electronics to accomplish the necessary size reduction.

SYNTHESIZER

The overall topology of the phase-locked oscillator (PLO) is illustrated in Figure 2, where dotted lines indicate die boundaries. The voltage-controlled oscillator (VCO) output is buffered and passes to a balanced output driver, which feeds the active mixers in the translator. The output also passes through a digital divider chain to an edge-triggered phase/frequency comparator along with the buffered reference oscillator signal. A phase/frequency comparator was selected to suppress reference signal feedthrough while providing reliable locking characteristics over the large range of temperature and power supply voltage required. A charge pump, filtered by a resistor/capacitor network, converts the differential current pulses from the comparator to a voltage level to lock the VCO. External components are limited to a crystal that stabilizes the reference oscillator, an inductor that selects the third crystal overtone, a resistor/capacitor network that establishes the loop bandwidth, and several chip capacitors that bypass the power supply voltage.

To reduce chip size for the L- and S-band LOs, active functions are incorporated on three MMICs, while the VCO tank circuit inductor pairs are contained on two additional MMICs [3]. The reference oscillator, two phase/frequency comparators, two charge pumps, and two digital dividers are combined on a single 2.4 mm × 1.65 mm die, allowing two local oscillators to be phase locked to the same reference. The GaAs crystal oscillator exhibits degraded phase noise compared with a silicon implementation. However, down to less than 1 kHz offset from the carrier, the phase noise performance of the PLOs is dominated by other sources. The VCO

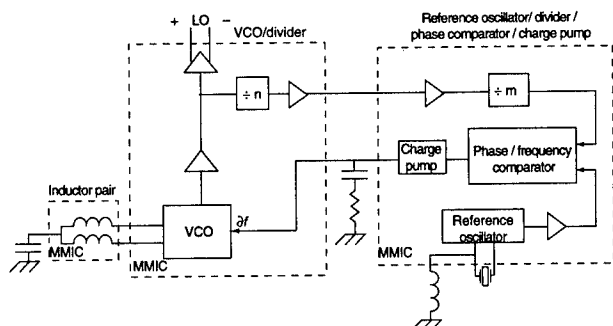


Figure 2. Phase-locked oscillator topology.

and associated high-speed digital divider are integrated on a separate 1.95 mm × 1.2 mm die. Integration of two different tank inductor pairs, on separate die, allowed use of the same VCO/divider MMIC chips in both L and S frequency bands, with more repeatable performance than if discrete single inductors were employed.

Phase lock is maintained over a temperature range from -40° to +80°C. Frequency stability closely follows the inverse parabolic behavior of the SC cut crystal with -75 and -17 ppm deviations at the temperature extremes. Phase lock is also maintained at room temperature over supply voltages ranging from 3.7 to 5.9 V.

SIGNAL PATH MMICs

Table 1 summarizes the performance of the packaged downconverter, upconverter, and power amplifier. A commercial MMIC low-noise amplifier (LNA) (MAAM 12000) provides 1.6 dB noise figure with 25 dB of associated gain.

The downconverter, which provides conversion gain over an extremely wide 37- to 77-dB range, consists of a two-stage RF common-source amplifier with negative feedback, a double-balanced Gilbert cell mixer, and a five-stage variable gain IF amplifier. The IF amplifier consists of a differential input stage, three gain control stages, and an output buffer stage. Chip dimensions are 1.9 mm × 0.8 mm. The upconverter includes a four-stage IF amplifier, a double-balanced Gilbert cell mixer, and a four-stage RF amplifier. Chip dimensions are 1.9 mm × 1.0 mm. The power amplifier consists of a three-stage preamplifier followed by driver and output amplifier stages. The preamplifier stages are based on common-source/source-follower pairs with negative feedback. The output stage is a stacked field-effect transistor (FET) design [4], which distributes the output tank RF voltage swing evenly across two FETs connected in series. The power-leveling AGC control voltage is generated by a diode detector coupled to the output stage. Chip dimensions are 2.3 mm × 1.9 mm.

MMIC FABRICATION AND PACKAGING

The custom downconverter, upconverter, power amplifier VCO, and phase-frequency comparator MMICs are shown in Figure 3. They were fabricated using a standard 1-μm gate-length, enhancement/depletion GaAs MESFET foundry process.

Table 1. MMIC performance summary (at 25°C).

| | |
|---|---------------|
| Downconverter | |
| Conversion gain control range | 37 to 77 dB |
| -1 dB O/P power gain compression | +9 dBm* |
| Noise figure | 13.5 dB* |
| Supply bias | 80 mA at 8 V* |
| Input/output voltage standing wave ratio (VSWR) | <1.6:1* |
| Upconverter | |
| Conversion gain | 36 dB |
| -1 dB O/P power gain compression | +1 dBm |
| Noise figure | 8.8 dB |
| Supply bias | 69 mA at 5 V |
| Input/output VSWR | <1.4:1 |
| Power amplifier | |
| Small-signal gain | 40 dB |
| -1 dB O/P power gain compression | 21.5 dBm |
| -3 dB bandwidth | 32% |
| Noise figure | 5.4 dB |
| Supply bias | 400 mA at 8 V |
| Input/output VSWR | 1.9:1/2.8:1 |

*At 70 dB conversion gain

The power amplifier is soldered into a 7.6 mm × 9.1 mm × 1.4 mm six-lead ceramic package with a high thermal conductivity copper-tungsten base. The other MMICs are epoxied into 6.9 mm × 6.9 mm × 1.8 mm ten-lead glass flatpacks with a kovar base to provide RF grounding. Additional chip capacitors, resistors, and inductors are included within these packages for bias decoupling/filtering and gold bond-wires form interconnections.

TRANSLATOR ELECTRONICS MODULE ASSEMBLY AND EVALUATION

The packaged MMICs, crystal, L-C filters, SAW filter, capacitors, resistors, and inductors are surface-mounted on 10-mil duroid circuit boards, which are attached to copper-tungsten metal matrix disks. Circuitry on each disk is individually tested and de-bugged prior to module assembly.

The translator RF circuitry is contained on three disks, as shown in Figure 4. Miniature coaxial cables are used to carry RF and tuning signals between the lower and middle/upper boards. Coaxial feedthroughs interconnect the middle and upper boards, which are assembled back-to-back. The 7.4-oz, 1.6-in.-diameter by 1.1-in.-high translator fits within a standard artillery fuze, and withstands a firing acceleration of 8000 G, in-flight environments, and a 0° to 70°C temperature range.

ANTENNA

For the original test firings of 1991 and 1992, the GPS antenna was a monopole under a radome at the end of the projectile. A new design was performed by Ball Communications to implement the previously investigated [2] dual-wrap design, which freed considerable internal volume (Figure 5). The pattern remained the same, with a null off of the forward axis, and all of the usable gain directed to the sides and rear.

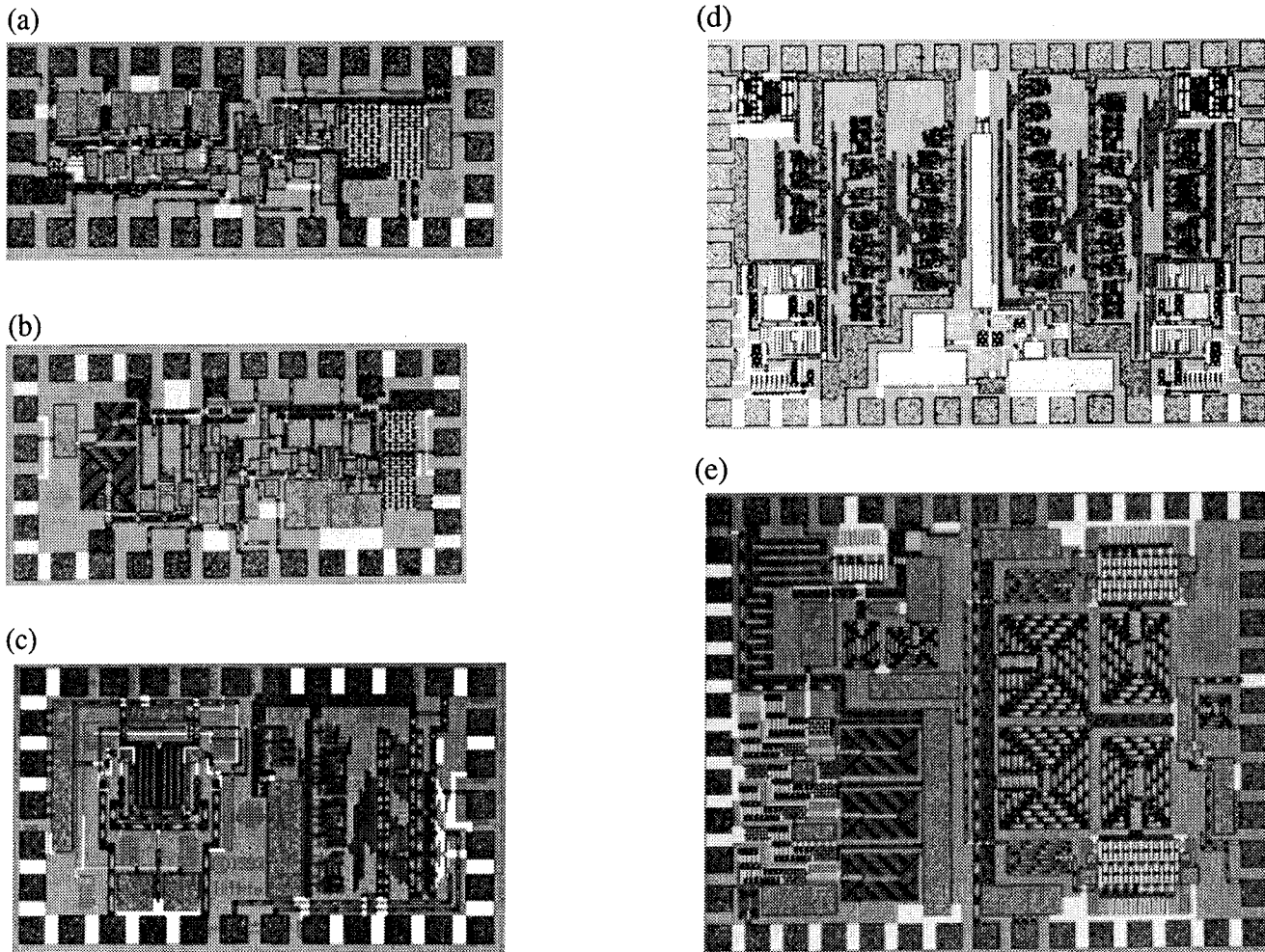


Figure 3. Microphotographs of MMICs: (a) downconverter, (b) upconverter, (c) VCO/divider, (d) phase comparator/divider/oscillator, and (e) power amplifier.

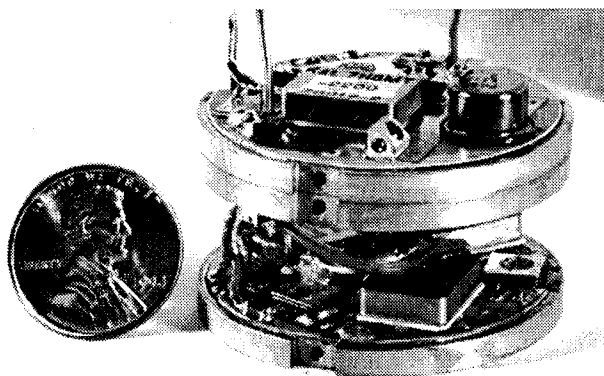


Figure 4. Photograph of a translator electronics module.

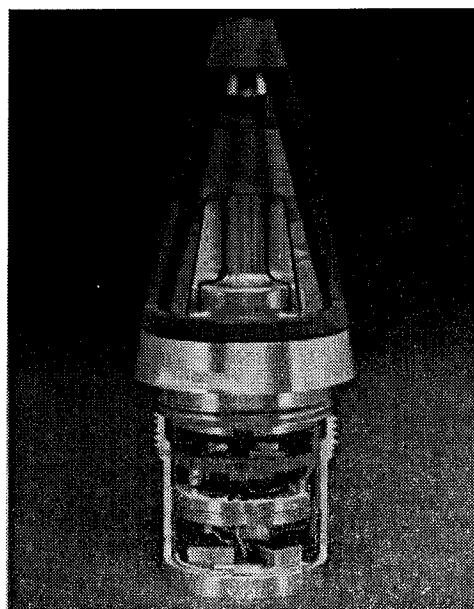


Figure 5. Complete translator, including electronics module, antennas, power conditioner, and battery.

BATTERY

The long shelf life and artillery handling procedures dictate the need for a reserve power supply. A reserve supply is one that can sit inert for years, then upon application of the start-up mechanism, come to life quickly and supply a high-energy density for a short time. A thermal battery was developed by the U.S. Army Research Laboratory (ARL) especially for this application. In the thermal battery, the shock of launch ignites a pyrotechnic train that melts a solid electrolyte. Although thermal batteries have been designed and built before, each new configuration requires careful balancing of pyrotechnic, insulation, and anode and cathode materials (see Fig. 6), to ensure that the internal operating temperature of 400° to 600°C is maintained. Also, the high spin (275 rps maximum) was a new requirement. The operating characteristics achieved for the POP test are 11 to 16 Vdc, 1.2 A, 62-s lifetime [5]. The igniter was mounted on top of the battery in a stacked cylinder configuration, instead of internal to the cell stack, to take advantage of the internal volume at the apex of the conical antenna housing (Figure 5).

POWER CONDITIONER

The power requirements of the translator electronics module are 380 mA at 5 V and 460 mA at 8 V, for a total consumption of 5.6 W at room temperature. A simple circuit consisting of two 3-terminal regulators provides the regulated 8- and 5-V sources for the electronics module. The regulators themselves consume 3.3 W at the minimum battery voltage of 11 V.

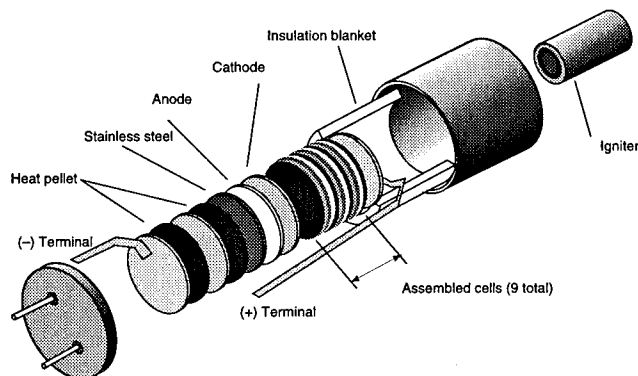


Figure 6. Battery—exploded view.

DISCUSSION AND CONCLUSION

Five different MMIC circuits were designed, fabricated, and evaluated. These were used in the fabrication of a miniature translator module, together with a MMIC LNA, custom filters, crystal, circuit boards, and other nondevelopmental item (NDI) hardware and components. The 9-in.³ prototype translator is the first reported to fit within the envelope of a standard artillery fuze, survive firing shock, and meet all required electrical specifications over a 0° to 70°C operating temperature range.

POP translators mounted on 155-mm artillery projectiles were test fired by ARL personnel. Data from all NAVSTAR satellites above the horizon were successfully translated during the two 45-s flights.

Efforts are ongoing to further reduce the size of the electronics module, and to provide P(Y), multiround, and extended range capability. The artillery translator has been adopted as the first of three artillery improvement devices being developed under the auspices of the U.S. Army Armament Research, Development, and Engineering Center/Army Research Laboratory Low-Cost Competent Munitions (LCCM) program.

REFERENCES

1. G. Wiles, "Tracking Projectiles: The GPS Registration Fuze Program," *GPS World*, September 1992, pp. 50–54.
2. G. Wiles, B. Mays, A. Ladas, and J. Eicke, "Projectile Tracking Device Using GPS," *ION National Technical Meeting Proceedings*, January 1992, Session 2.
3. J. Smuk and P. Katzin, "MMIC Phase Locked L-S Band Oscillators," 1994 GaAs IC Symposium Digest, pp. 27–29.
4. M. Shifrin, Y. Ayasli, and P. Katzin, "A New Power Amplifier Topology with Series Biasing and Power Combining of Transistors," 1992 IEEE Monolithic Circuits Symposium, Albuquerque, NM, 1–3 June 1992, pp. 39–41.
5. F. Kreiger, "Thermal Optimization of Li(Al)FeS₂ Thermal Batteries," *Proceedings of the 36th Power Sources Conference*, pp. 399–403.

The Reduction of Airborne Magnetic Noise Via GPS

L. Bobb, W. Gelatka, D. DePersia, A. Salik, and S. Swyers
Naval Air Warfare Center

BIOGRAPHIES

The authors are employees of the Electro-Optics Development Division of the Naval Air Warfare Center at Warminster, Pennsylvania. The primary studies of this group are related to improving the effectiveness of sensor systems used in anti-submarine warfare.

ABSTRACT

The objective of this study was to demonstrate that magnetic noises which are position related can be removed from an airborne total field magnetometer system. The system contains a helium-4 magnetometer sensor with a sensitivity of 0.003 nanoteslas (nT) in the magnetic anomaly detection (MAD) band of 0.05 to 0.5 Hz. This sensor is housed in the tip of the tailboom of a U. S. Navy P-3 Orion aircraft; this 20 foot separation of the sensor from the main fuselage helps to remove some of the platform noise which arises from the permanent, induced and eddy current moments of the platform. The GPS receiving antenna is also located on this tailboom. The antenna is connected to a single frequency all-in-view narrow correlator spacing C/A code L1 receiver. The data for this study was acquired at altitudes from 500 feet to 20,000 feet off the coast of North Carolina in the Oak Bravo test area near the latitude and longitude of 35°N and 71°W. The magnetic noises which are position (or track) related come from the magnetic geology, the magnetic field of the earth, and the gradients in these fields. The platform magnetic noise is reduced by using the total magnetic field value and the direction cosines in a platform noise model. These parameters may be determined by the GPS and the inertial navigation system (INS). The magnetic gradient noise arises in several ways. The horizontal gradient is approximately 0.003 nT/m and the vertical gradient is approximately 0.030 nT/m. These values are higher in high magnetic geology. The horizontal gradient noise arises from aircraft track changes from a straight line and from horizontal buffeting. The vertical gradient noise comes from vertical buffeting in the vertical gradient field. Small buffets (~0.1m) give rise to magnetic noise

comparable to the sensor sensitivity. The magnetic geology noise was reduced by utilizing a GEODAS map of the geologic field and the GPS to provide position on the map. The frequency of the geology noise was in general below the MAD band; however, the principle of MAD band geologic noise reduction by utilizing a map and the GPS was demonstrated.

INTRODUCTION

One of the non-acoustic approaches used by the U. S. Navy for detecting and localizing submarines is to sense the disturbance of the magnetic field of the earth due to the presence of a submarine. This approach is called magnetic anomaly detection. It requires that a very sensitive magnetometer be operated within the airborne platform, which in this case is a P-3. The sensitivity of the magnetometer is 0.003 nanoteslas in the MAD detection band of 0.05 to 0.5 Hz. To put this number into perspective, the earth's magnetic field is about 50,000 nanoteslas. The total field magnetometer is housed within a fiberglass boom which extends from the rear of the aircraft by about twenty feet. Locating the magnetometer away from the main fuselage of the aircraft helps to remove some of the platform magnetic noise. However, it needs to be kept in mind that the magnetometer is maneuvering through an ambient field which is more than ten million times larger than the magnetometer sensitivity. Small variations in this field create noise in the MAD detection band when the magnetometer is translated. The sources of this noise are the platform, the geology field, the geomagnetic background, ocean waves, and the magnetic gradient fields of the earth. The noises which depend on the spatially varying fields are the geology noise and the gradient noise. Both of these can be mitigated by knowing position vs. time accurately. The platform noise terms arise from the induced and permanent magnetization of the platform as well as from the eddy currents. These noises depend on changes in the orientation of the platform in the field of the earth. In this paper, the reduction of the spatially related magnetic

noises by using a C/A code GPS receiver will be described.

FLIGHT TESTS AND DATA ACQUISITION

A series of flights was conducted with a highly instrumented P-3 in the Oak Bravo test area which is approximately 150 miles off the northern coast of North Carolina. In addition to the total field magnetometer there were current sensors, fluxgate magnetometers, accelerometers, and two GPS antennas. One of the antennas was on the tail boom near the magnetometer and the other was in the middle of the fuselage. The antennas were connected to 10-channel single-frequency C/A code narrow correlator spacing receivers. The ground speed of the P-3 during the tests averaged about 300 knots. Data was collected under all flight conditions, that is, during rolls, pitches, yaws, standard rate and double standard rate turns, and at altitudes from 500 feet to 20,000 feet. Thirty-four channels of information were collected in addition to the GPS data. The data were time synchronized to GPS time. For some of the flights there were two platforms in the air, each with two GPS antennas flying at predetermined separations. These formation flights enabled the reduction of geomagnetic noise which is coherent between the two platforms. The simultaneous use of the four single frequency narrow correlator spacing receivers yields a relative accuracy better than 1 meter SEP for aircraft-to-aircraft positioning using a robust carrier smoothing of the code approach (Lachapelle et al 1994). Additionally, it was shown that the separation between the two antennas on the one platform could be determined at the few millimeter level which is useful for assessing the flexing of the platform in flight. The problems in the GPS data were associated with multipath, satellite drop-outs during maneuvers, constellation changes which yield sudden apparent position changes, and transmitted code errors which were common to all receivers.

ANALYSIS AND RESULTS

One of the most significant sources of magnetic noise is related to the platform itself. The 130,000 pound platform is largely metal, with some components having high permeability and high remnant magnetization. Therefore, as this platform changes its orientation in the magnetic field of the earth, eddy currents are induced in the skin, the induced magnetization changes, and the component of the permanent magnetization along the field of the earth changes. The approach for reducing the platform noise is to use a platform noise model

which takes into account the magnitude and direction of the earth's magnetic field at the platform location, the orientation of the platform and the change in orientation, that is, roll, pitch, and yaw. In this study, two methods were used to acquire the above parameters. The first method was to use the onboard three-axis vector magnetometers (sensitivity of about 1 nT) to measure the magnetic field components of the earth along the longitudinal (L), transverse (T), and vertical (V) axes of the platform. By using these magnetic field values and the derived direction cosines, the platform noise correction terms are calculated. The second approach is to use the GPS position and the International Geophysical Reference Field (IGRF) Model, which gives the core magnetic field of the earth as a function of location, to get the earth's magnetic field value at the platform location. This information when combined with the INS data on roll, pitch, yaw, and heading may also be used to calculate the platform noise correction terms. A comparison between these two approaches for generating the fields along the three principal axes of the aircraft during maneuvers is shown in Figure 1.

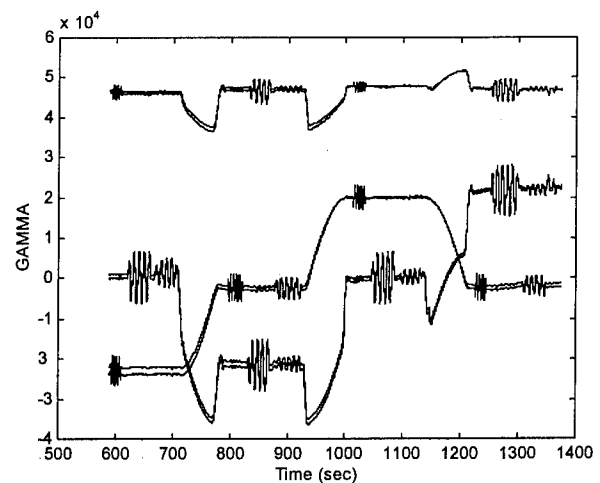


Figure 1: The Comparison between the Modeled Vector Fields and the Measured Fields is Shown. The Upper Trace is the Vertical (V) Component, the Middle Trace on the Right Hand Side of the Figure is the Transverse (T) Component, and the Bottom Trace is the Longitudinal (L) Component.

In this figure, the component values (L, T, and V) for the four cardinal headings are shown for dedicated maneuvers (pure rolls, pitches, and yaws). These six traces show the excellent agreement between the two different approaches. When these magnetic field values along with the direction cosines are used to calculate the platform noise correction terms, the result shown in Figure 2 is obtained. This is a power spectral density (PSD) curve in gamma^2/Hz vs. frequency (where 1 $\text{gamma} = 1 \text{ nT}$). The upper trace is the uncompensated

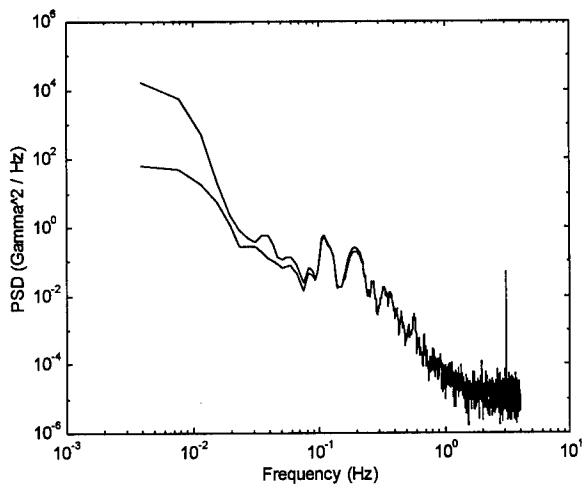


Figure 2: The PSD of the Uncompensated Total Field (TFU, upper trace) is Compared with the PSD of the Platform Noise Correction Field (XX).

total field (TFU) directly from the magnetometer and the lower trace is the platform noise correction term (XX) calculated from above. As can be observed, the match between these two curves is very good from 0.1 Hz to higher frequencies which is where most of the platform noise occurs. The result of subtracting the correction terms from the uncompensated field is shown in Figure 3. These two curves show that as much as 20 dB of noise reduction is obtained by removing the platform noise. The sensor level is at 1×10^{-5} gamma²/Hz. Therefore, substantial (30 to 40 dB) noise remains. The result of reducing the gradient noise and the geology noise will be shown next.

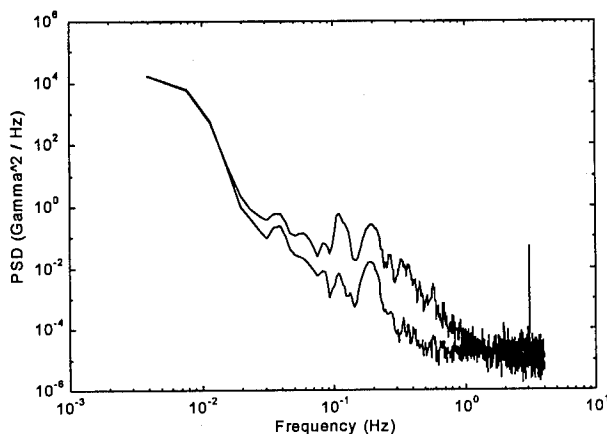


Figure 3: The PSD of the Uncompensated Total Field (TFU, upper trace) and the PSD of the Compensated Total Field (TFU-XX) are Compared.

From the IGRF Model, the earth's core magnetic field and the gradients of this field are known for each location. The IGRF Model does not include the geology field. The platform does not fly along a perfect line, there are heading changes, buffeting, and maneuvering. And, because these occur in a gradient field, the total field will vary with time due to these motions. For example, the vertical gradient is approximately 0.03 nT/m. This means that a 1 m buffet produces a 0.03 nT signal; this is equal to ten times the magnetometer noise level. Thus, small variations from straight line flight can produce measurable magnetic noise. The GPS is used to yield the absolute and the relative position versus time. The variations about the track are determined to about 10 cm (Roberts 1994). This position information combined with the gradient field (which also depends on position) produces the magnetic gradient noise. This noise is the lower trace (TFM) in the PSD shown in Figure 4. It can be seen that this model field matches the corrected (compensated) total field quite well at low frequencies and around 0.1 Hz. In Figure 5 is shown the result of subtracting the model field (TFM) from the compensated total field (TFU-XX). This result is compared with the original starting noise value (TFU). The approach of using the GPS combined with the models of the magnetic fields, the platform, and the motion in the gradient fields produces about 35 dB of noise reduction. From the two platform tests it can be shown that some of the residue near 0.03 Hz is geomagnetic noise. In Figure 6, the magnetic field versus time is displayed for the uncompensated total field (lower trace) and the total field with the above noises subtracted. The power of this noise reduction approach is exemplified in this figure. In addition to using direct subtraction of the noises, both coherent subtraction and adaptive noise cancellation have been employed in the noise reduction studies (Salik 1995).

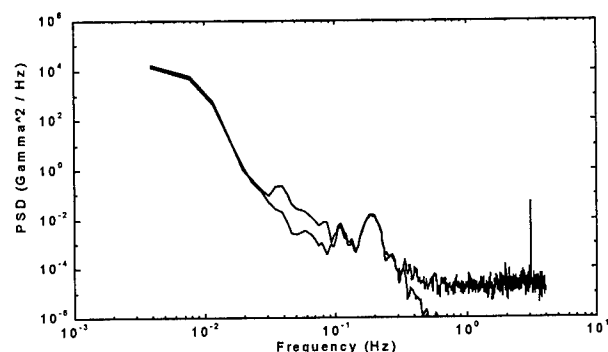


Figure 4: The PSD of the Compensated Total Field (TFU-XX, upper trace) is Compared with the PSD of the Model Field.

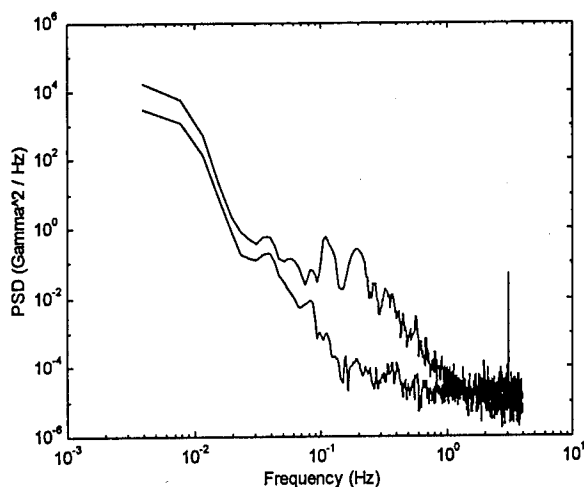


Figure 5: The PSD of the Uncompensated Total Field (TFU, upper trace) is Compared with the PSD of the Model Corrected Compensated Total Field (TFU-XX-TFM).

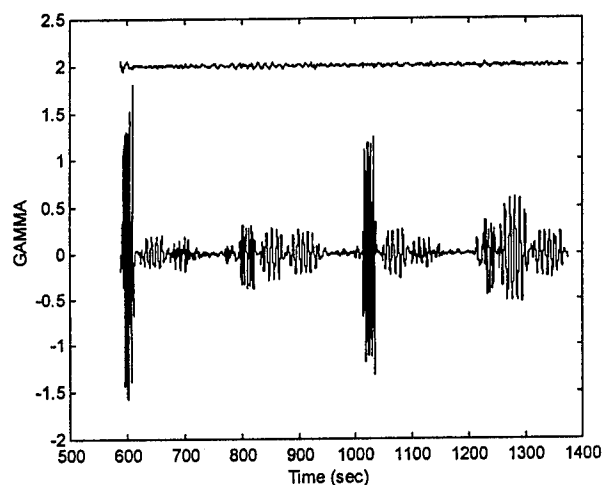


Figure 6: The Uncompensated Total Field (TFU, lower trace) is Compared with the Model Corrected Compensated Total Field (TFU-XX-TFM). An offset of 2 Gammas was Used for Display Purposes.

The magnetic geology noise in this region occurs at low frequency and is not significant above 0.04 Hz. This noise arises from magnetic rock that resides below the sea floor. It can be modeled as a dipole array at the depth of the geology. The periodicity depends on the

depth and the structure. The farther away it is, the lower the frequency. Many measurements of the geology field are compiled in the GEODAS empirical data base from the National Geophysical Data Center. This data base was used to provide sea level magnetic field values as a function of location within the test area. These values are used to calculate the geology field as a function of location at the altitude of the test. Using this modeled field and the GPS information from the flight test, the magnetic geology contribution at each data point is determined and removed. The result of this is shown in Figure 7. In this figure, the total field is shown for a flight without very much maneuvering and buffeting, so the residual noise is low. The geology noise reduction is mostly below 0.02 Hz; however, this does demonstrate the principle of MAD band geology noise removal. Higher resolution measurements to produce a more accurate map will provide significantly higher levels of noise reduction.

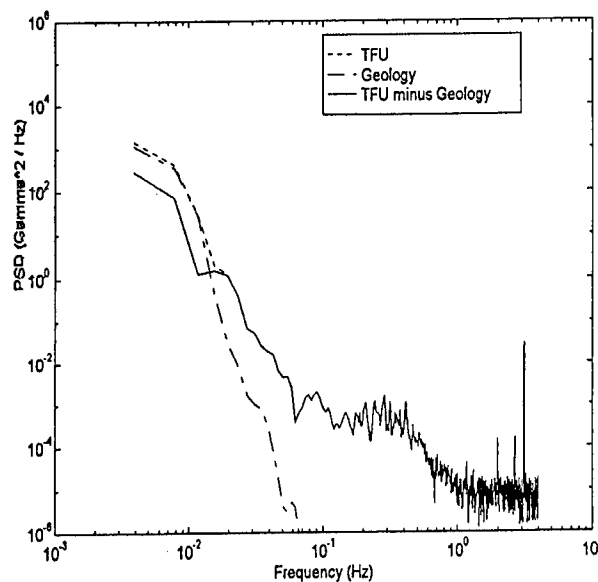


Figure 7: The PSD of the Geology Field is Shown along with the PSD of the Uncompensated Total Field Minus the Geology Field.

CONCLUSIONS

The efficacy of using the GPS to assist in reducing the magnetic noise in an airborne magnetometer has been demonstrated. Within the MAD detection band, 35 to 40 dB of noise reduction has been achieved; and, the utility of using the GPS as a model input for reducing magnetic geology noise was demonstrated.

REFERENCES

LACHAPELLE, G., H. SUN, M.E. CANNON, and G. LU (1994) Precise Aircraft-to-Aircraft Positioning Using a Multiple Receiver Configuration. Proceedings of the National Technical Meeting, Institute of Navigation, San Diego, 24-26 January 1994.

ROBERTS, D. (1994) Determination of Precise Aircraft Trajectory Under Buffeting Conditions Using Both Single Point Positioning and Differential GPS. University of Calgary Progress Report to the Naval Air Warfare Center, 15 June 1994.

SALIK, A. (1995) Electromagnetic Noise Characterization and Reduction. AMPAC Report 95-930-1 to the Naval Air Warfare Center, 1995.

GPS Operational Control System Modernization: Alternative Architectural Concepts

Jaynarayan Lala and Laura Burkhardt
Draper Laboratory

BIOGRAPHIES

Jaynarayan H. Lala is a Principal Member of Technical Staff at the Charles Stark Draper Laboratory in Cambridge, MA. His research interests include design, evaluation, and validation of fault tolerant architectures for high integrity systems. For the past several years he has been the task leader for GPS OCS modernization programs at Draper. He received the Ph.D. in Instrumentation and the M.S. in Aeronautics and Astronautics from the Massachusetts Institute of Technology in 1976 and 1973, respectively. He received the B.S. degree in Aeronautical Engineering from the Indian Institute of Technology, Bombay, India in 1971. Dr. Lala is a Fellow of the IEEE and an Associate Fellow of AIAA.

Laura F. Burkhardt is a software engineer at Draper Laboratory. She has been a principal investigator in several recent government-sponsored efforts to re-engineer the GPS control segment, including a redesign of the MCS hardware and software, specification of the Ground Antenna application software, and the OCS architecture study described in this paper. She received a B.A. in Psychology from Gettysburg College in 1966.

ABSTRACT

This paper discusses options for modernizing the ground control facilities of the Global Positioning System (GPS). Specifically, it discusses the S-band command and status functions that are performed by the Ground Antennas (GAs). In addition to describing hardware upgrades for the GAs, it compares centralized and distributed processing options and describes a transition strategy for migrating from the existing legacy system to a new, modernized system.

1. INTRODUCTION

The satellite constellation of the Global Positioning System (GPS) is operated and controlled by ground-based facilities, collectively known as the Operational

Control System (OCS). The OCS includes a central Master Control Station (MCS) and a number of geographically dispersed Ground Antennas (GAs) and Monitor Stations (MSs), also referred to as remote sites. The OCS was designed and built almost fifteen years ago using 1970's technology. By now, the OCS computer hardware as well as most of the non-computer hardware is obsolete, in some cases not supported by the vendors, and difficult to maintain. The software suffers from typical legacy software problems such as a lack of documented requirements, "brittle" code, and limited modifiability and upgradability. The underlying system architecture is monolithic, proprietary and cannot be easily upgraded to provide the needed higher throughput and memory. Furthermore, the architecture does not take advantage of the recent advancements which have the potential for making the OCS significantly more reliable and available.

Draper Laboratory was a member of the OCS Architecture Task Force that was convened by the GPS Joint Program Office (JPO) in 1994 to produce a set of engineering options for modernizing the OCS. The goal of the study was to produce a variety of well-conceived ideas and alternatives, which would then enable the government to develop a comprehensive evolution strategy. Each industry member of the Task Force concentrated on a subset of the OCS functions assigned to it by the government team. In addition to producing engineering alternatives for the current OCS functionality, a transition plan for integrating any change was required that was incremental and evolutionary, rather than massive and revolutionary.

Draper Laboratory concentrated on the subset of OCS functions relating to S-band command and status communication with the Space Vehicles (SVs). Several options for this S-Band Command and Telemetry (C&T) Subsystem were considered, including bent pipe, store-and-forward and federated architectures. The paper discusses each of these options and illustrates the transition

strategy, using the federated architecture as an example.

2. SYSTEM REQUIREMENTS

2.1 Requirements Identification

At the beginning of the study, the government team identified a set of OCS requirements and refined them with input from the study team members into a final document called the OCS Architecture Plan [1]. Requirements were grouped into major functional areas and represented graphically as bubbles.

Figure 1 shows a hierarchical organization of the OCS functions. The functions are grouped into four layers which represent a progression from the actual problem, i.e., the primary purpose of the OCS, to the solution. Each layer represents a group of functions that is required in support of the functions of all the higher layers, as described below.

Primary Purpose of the OCS. The primary objective of the OCS is to support the GPS satellite missions, particularly the navigation mission. This purpose can be sub-divided into three parts:

1. Ensure correct and sufficient operation of the Space Segment,
2. Support the Navigation Mission,
3. Support the Nudet Detection System (NDS) Mission.

In addition, there are satellite communication functions that enable all three of these sub-purposes to be fulfilled.

Secondary Purpose of the OCS. The secondary purpose of the OCS is to operate the control segment; this is required in order to carry out the primary function. This purpose can be sub-divided into four parts:

1. Manage the MSs,
2. Manage the overall OCS,
3. Manage communications,
4. Manage the GAs.

Operator Monitoring and Control. This layer includes functions that are required in order to accomplish all the functions of Layers 1 and 2. Included here are the Human/Computer Interface, through which the operator controls and monitors the OCS, and Data Analysis.

Software Implementation Functions. This layer includes system-wide functions that are required for computer support. Included here are the System Services and Data Management bubbles.

2.2 Starting Assumptions

At the kick-off meeting for the OCS Architecture Study, there were several lengthy discussions about how the OCS requirements should be viewed by the Task Force. One viewpoint was that the functions as stated in the OCS Architecture Plan, along with formal requirements documents such as the OCS Prime Item Functional Specification [2], should be considered as a set of pure requirements without any regard to the present OCS implementation. At the other extreme was the viewpoint that the present implementation as well as all planned upgrades should be considered as constraints when suggesting new implementation options. In the end, it was concluded that the OCS should be viewed as a geographically distributed set of facilities as shown in Figure 2 and described in the Architecture Plan.

The OCS is thus defined as consisting of a Master Control Station (the MCS); multiple, globally distributed L-band monitoring stations (the MSs); and multiple, globally distributed S-band uplink/downlink stations (the GAs). These facilities are linked by a communications network.

The MCS at a minimum consists of the main computer system for the OCS and the Satellite Operators, who control and monitor various functions within the OCS. At a minimum, the GAs perform a subset of the S-band Uplink/Downlink function, specifically, the subset relating to conversion of binary signals to modulated tones for transmission to the SV. The MSs perform at a minimum the subset of the L-band Reception function relating to receiving L-band signals from the SV, demodulating them and performing a phase-lock loop search on the PRN codes. The MSs also formulate Pseudo Range and Accumulated Delta Range measurements.

All other functions, however, could be reallocated between the MCS, GAs, and MSs. Thus the final OCS architecture could be highly centralized (i.e., no data processing at the remote stations), highly distributed (i.e., most data processing functions at the remote stations) or any point on a continuum between the two extremes.

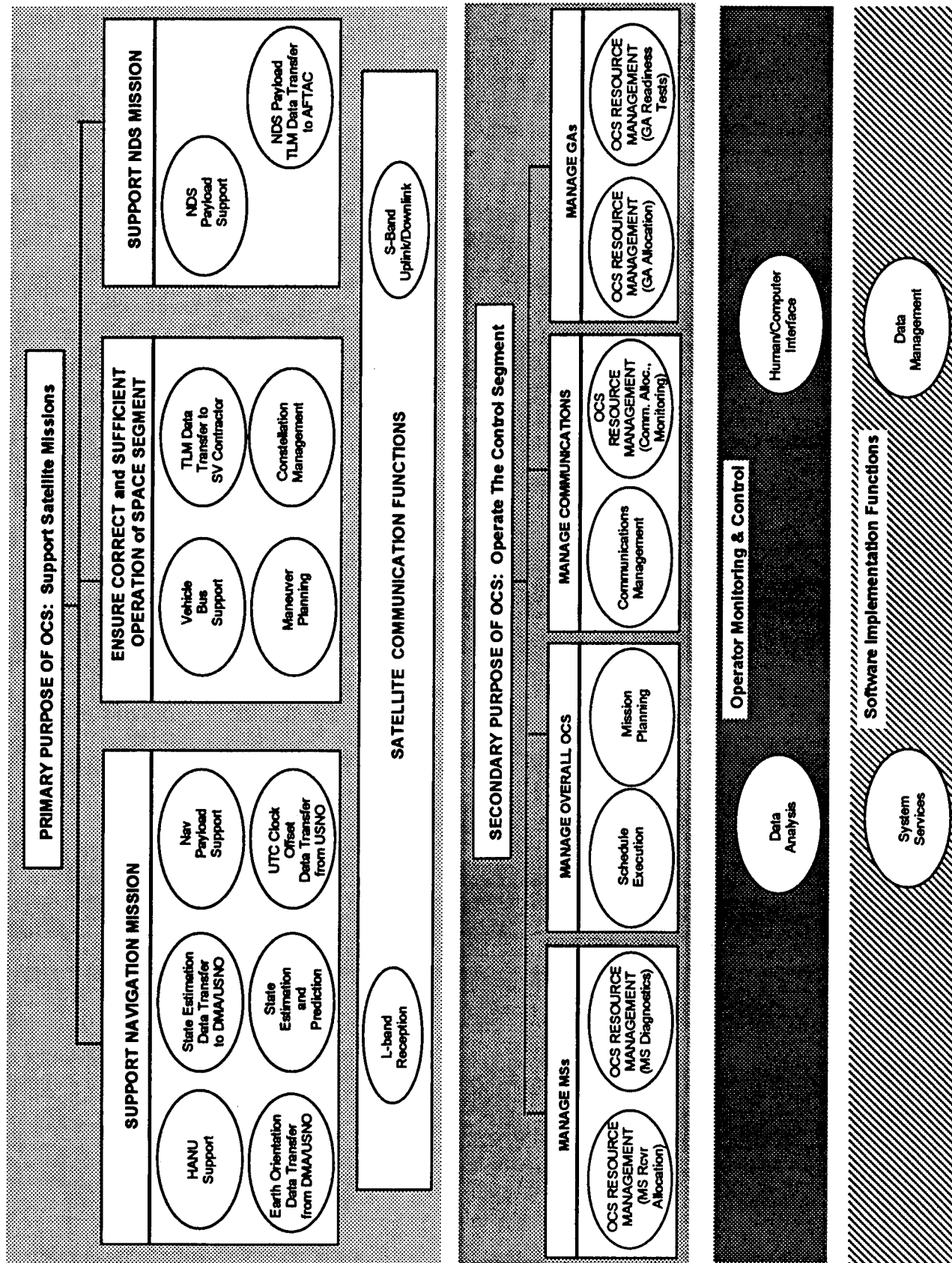


Figure 1. Hierarchy of OCS Functions.

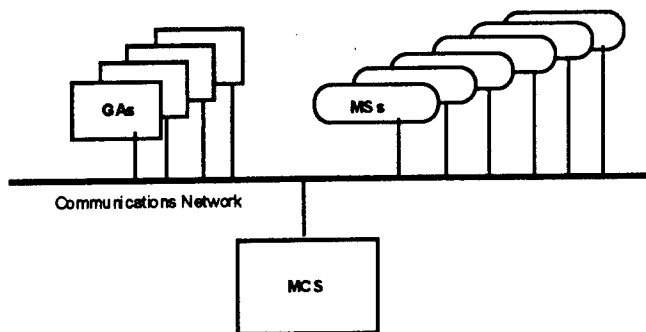


Figure 2. OCS Facilities

In addition, the functionality represented by any particular bubble could be allocated to one or more OCS components (i.e., GA, MCS, MS). Thus a bubble could represent completely self-contained functions or it could represent functions requiring collaboration between two components. In the current OCS, for example, the Maneuver Planning bubble represents functions performed solely by the MCS, while the Vehicle Bus Support bubble is carried out by the MCS in cooperation with the GAs.

3. COMMAND & TELEMETRY SUBSYSTEM: DESIGN OPTIONS

3.1 Overview

The functional areas that make up the Command & Telemetry (C&T) Subsystem are listed below. A brief summary of the requirements of each area is also given.

Vehicle Bus Support. Detect vehicle bus anomalies by monitoring telemetry; determine bus state of health; perform functional verification of uplinked commands; generate commands; generate spacecraft processor program and data loads and commands; transmit commands.

Navigation Payload Support. Detect navigation payload anomalies; generate uploads; determine nav payload state of health; transmit uploads.

NDS Payload Support. Detect NDS payload anomalies; perform functional verification of NDS commands; generate NDS payload commands; transmit and verify NDS payload commands; check NDS payload state of health; generate IONDS telemetry data for transmission to AFTAC.

Part of OCS Resource Management relating to GAs. Perform readiness tests; monitor GA status data to detect anomalies.

S-band Uplink/Downlink. Track the downlink carrier; format, encrypt and convert command data to modulated signals for transmission to the SV; uplink a carrier signal to the SV containing command and

navigation data; acquire, demodulate, decrypt, decommutate, and format S-band telemetry data.

Part of External Data Transfer relating to SV Contractor and AFTAC. Provide NDS Payload Support Data to AFTAC. Provide SV telemetry data to the SV contractor.

In this study several options were considered for the implementation of the Command & Telemetry Subsystem. The principal difference between these options is the allocation of functions between a central facility (the MCS) and the remote site GAs. As discussed in Section 2.2, a continuum of choices exists for this distribution. This is illustrated in Figure 3.

The top row in the figure shows the functions under consideration. The remaining rows illustrate three options for allocating these functions between the MCS and the GAs. The centralized approach and the federated approach represent the two extremes. In the centralized architecture, most of the C&T processing is performed by the MCS, while the GAs only provide the RF uplink to and downlink from the SVs. This is also known as the bent-pipe GA design. The federated design, on the other hand, makes maximum use of the computing resources available at the remote sites. In this design most of the Vehicle Bus Support, Navigation Payload Support and NDS Payload Support functions, in addition to RF uplink and downlink, are performed at the GAs; the MCS only performs those C&T functions that are most efficiently implemented centrally such as command and upload generation. The hybrid approach distributes more processing to the GAs than does the centralized approach, but not as much as the federated approach. The current implementation is such an approach and is called the store-and-forward GA design.

For the centralized and hybrid designs, the Command & Telemetry processing at the MCS could itself be implemented in a centralized or distributed manner. These are referred to as the centralized-at-MCS and distributed-at-MCS suboptions, respectively. In the centralized implementation, one copy of the software would serve multiple users simultaneously, i.e., multiple System Satellite Operators (SSOs) monitoring contacts at different GAs. In the distributed implementation separate copies of the software, each executing on its own workstation, would exist to serve each GA. This implementation more readily allows for an increase in the number of simultaneous contacts and growth in the functionality provided during a contact, while preventing problems with one contact from affecting other concurrent contacts. In the federated design, however, the processing at the MCS is too simple to benefit from a distributed architecture.

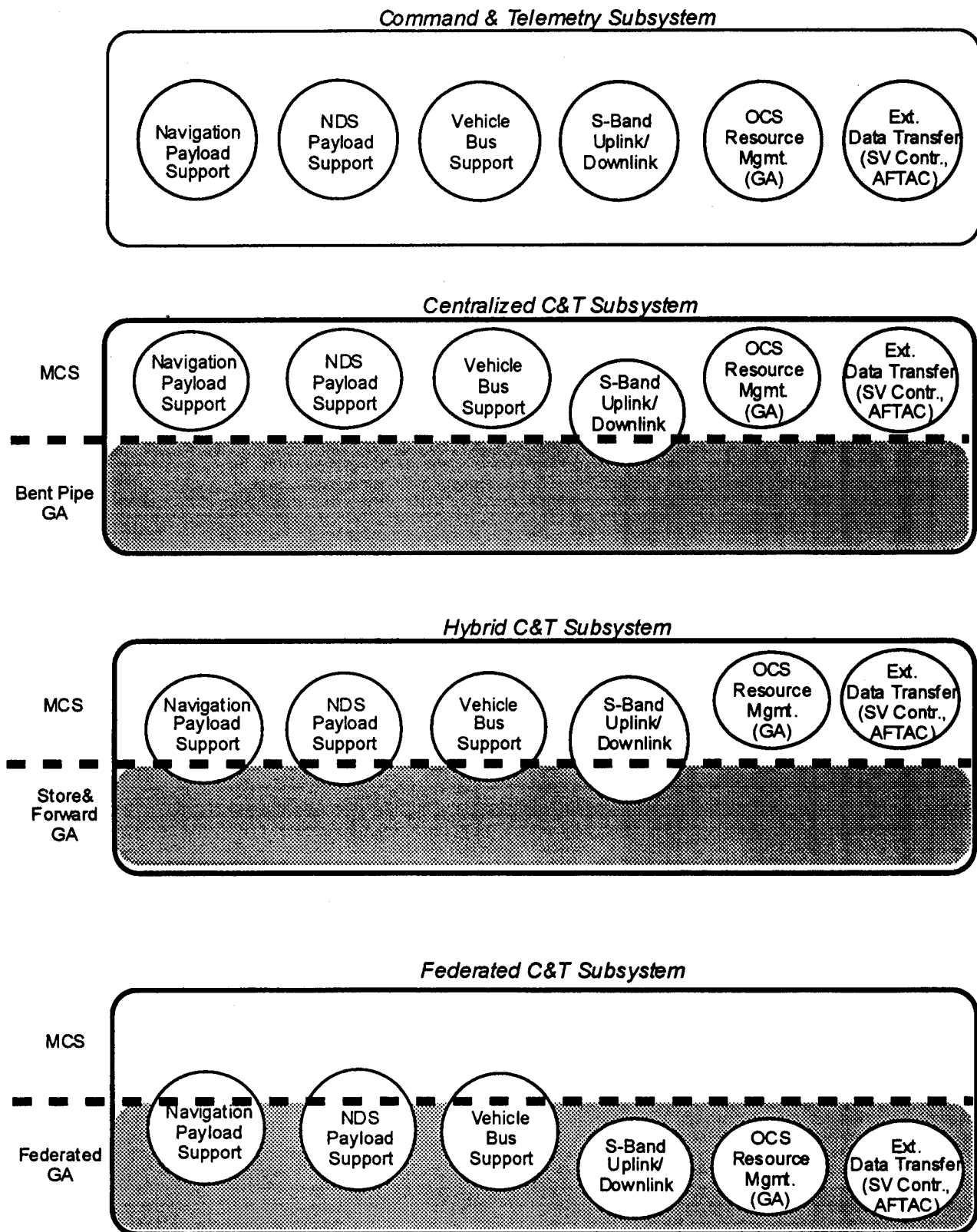


Figure 3. Implementation Options for Command & Telemetry Subsystem.

The following sections describe the three design options in more detail and summarize their advantages and disadvantages.

3.2 Centralized C&T Subsystem

In this design most of the Command & Telemetry functions are performed by the MCS. The purpose of the GAs is solely to provide the RF uplink and downlink to the SVs. The following two subsections describe the implementation of the functions at the MCS and the GAs, respectively, for this option.

3.2.1 MCS

In a centralized architecture, the MCS would perform the following functions in addition to its current functions:

- Command encryption. Commands must be encrypted before being sent to the GA.
- Telemetry decryption and decommutation. Live encrypted telemetry is decrypted at the MCS, decommutated and time-stamped for each frame. Playback telemetry must also be decrypted, decommutated and time-stamped.
- Uplink retry. Retry of commands or upload segments that failed must be done under direct control of the MCS.

However, some processing is also removed from the MCS because there is no longer any need to maintain duplicate copies of command and upload messages at the MCS and the GAs and to ensure that they are synchronized.

3.2.2 Bent Pipe GA

The bent-pipe GA is similar in concept to the Automated Remote Tracking Station (ARTS) of the U.S. Air Force Satellite Control Network (AFSCN). A bent-pipe GA remote site performs the following functions.

- a. Receives SV commands and nav uploads from MCS.
- b. Converts commands/uploads to RF energy and transmits them to the SV. Performs echo check on transmitted data.
- c. Receives, converts from RF to digital, and time stamps beginning of telemetry. (Individual frames are not time-stamped because the decryption and decommutation functions are not performed at the bent-pipe GA.)
- d. Sends raw telemetry to MCS in real time.
- e. Sends GA equipment status to MCS.

To implement the bent-pipe GA, the IBM Series/1 computers in the present GAs would be replaced with dependable, open architecture control computers. The encryption devices, KIT-123s,

would be moved to the MCS, since SV commands would now be encrypted at the MCS. The decryption devices, KGR-28s, would also be moved to the MCS, as downlink telemetry would be decrypted and decommutated at the MCS. The functionality of the control computer will be reduced significantly compared to the Series/1 functionality in the existing GAs. The software to implement this functionality would be custom designed using an object-oriented approach and implemented in Ada, and a COTS POSIX-compliant, real-time operating system would be used.

The principal advantage of the bent-pipe GA design is that it provides commonality with the AFSCN ARTS. It also requires a simpler software design at the remote sites compared to the existing GAs, and it does not require commands and uploads to be stored at the remote sites.

This option has many disadvantages. These include increased processing requirements at the MCS, increased hardware and software complexity at the MCS, and increased dependence of GAs on the MCS to perform their function. It does not take advantage of the distributed processing resources available at the GAs.

3.3 Hybrid C&T Subsystem

The hybrid approach distributes Command & Telemetry processing between the MCS and the GAs. The following two subsections describe the MCS and the GA implementations, respectively, for this option.

3.3.1 MCS

In the hybrid approach, commands and nav uploads are generated at the MCS and sent to the GA for storage and later transmission to the satellite. The MCS maintains duplicate copies of command and upload messages and ensure that they match what is currently at a particular GA. Failed commands and uploads are retired by the GA, following initial direction given by the MCS.

The MCS receives decrypted telemetry frames from the GA and processes the individual status parameters, i.e., performs conversion to engineering units and limit checking. Raw telemetry data is forwarded to the SV Contractor and AFTAC sites. Equipment status sent by the GA is also processed at the MCS; this processing includes computation of derived status, limit checking, and evaluation of overall station status.

3.3.2 Store-and-Forward GA

The store-and-forward GA is identical to the current GA in functionality and performs the following functions.

- a. Receives and stores SV commands and nav uploads from MCS.
- b. Upon separate order from MCS, converts commands/uploads to RF energy and transmits to SV. Performs echo check on transmitted data.
- c. Receives, converts from RF to digital, decrypts, decommutates, time stamps and stores SV telemetry.
- d. Analyzes telemetry to verify SV acceptance of uplink data.
- e. Retries uplinks that failed, as directed by MCS.
- f. Transmits telemetry to MCS in real time. Provides playback telemetry after contact as requested by MCS.
- g. Sends GA equipment status to MCS.

To implement this option the two Series/1 computers at each GA would be replaced by redundant open architecture control computers. The functionality of the Two Channel Switch, Red Black Terminal Interface, Bit Synchronizer, Decommulator and the Time Code Translator would be absorbed in the control computers. The redundant control computers would be integrated with the encryption/decryption hardware in the red shelter and with the RF and baseband hardware in the black shelter over fiber optic links. The echo circuit and the downlink test circuit would be replicated, thereby making the uplink and the downlink subsystems completely dual redundant and eliminating all single point failures in those subsystems.

The existing applications software for the Series/1 computer would be replaced with custom software developed using an object-oriented design approach and implemented in Ada. The current executive would be replaced with a COTS POSIX-compliant real-time operating system.

A principal advantage of the store-and-forward GA design option is that the current functionality of the GA is implemented in a state-of-the-art, dependable, open system architecture. The new GA control and status design would also provide better error detection/retry capability during uplink of large nav messages. The maintainability of the new GA would be much improved compared to the existing GA. Finally, this design takes some advantage of the computing resources available at the GAs.

The principal disadvantage of this design is that it lacks commonality with the ARTS of the AFSCN. This design does not fully leverage distributed computing resources and technology to reduce

MCS complexity. It does not reduce dependence of remote sites on the MCS appreciably. Finally, there is the added complexity of distributed data, i.e., commands and uploads are duplicated at the MCS and the GAs.

3.4 Federated C&T Subsystem

In the federated approach the Command & Telemetry processing is concentrated at the Ground Antennas. The following two subsections describe the MCS and the GA implementations, respectively, for this option.

3.4.1 MCS

Commands and nav uploads are generated at the MCS and sent to the GA for storage and later transmission to the satellite. However, duplicate copies of the messages are not maintained at the MCS. All telemetry processing is performed at the GA. The MCS does receive telemetry parameters for display but only when a change is detected. Telemetry required by AFTAC and the SV Contractor is sent directly from the GA, rather than being routed through the MCS. Failed commands and uploads are retried by the GA, following initial direction given by the MCS.

3.4.2 Federated GA

The federated GA is a concept not yet implemented at the ground antennas for any satellite system. Each federated GA remote site would perform the following functions.

- a. Receive and store SV commands and nav uploads from MCS.
- b. Upon separate order from MCS, convert commands/uploads to RF energy and transmit to SV. Perform echo check on transmitted data.
- c. Receive, convert from RF to digital, decrypt, decommutate, time stamp and store SV telemetry.
- d. Perform all telemetry processing formerly done at MCS, including limit checks, maximum change checks, computation of derived measurements, functional verification of uplinked commands, etc., as well as verifying SV acceptance of uplinked data or commands.
- e. Send telemetry parameters to MCS when a change is detected.
- f. Retry uplinks that failed, as directed by MCS.
- g. Provide playback telemetry after contact as requested by MCS.
- h. Send raw telemetry to SV Contractor and AFTAC.
- i. Process GA equipment status, including computation of derived status, limit checking and evaluation of overall station status.

The implementation of this option would involve the same steps as described for the hybrid approach, i.e., replacing the Series/1 computers at the GA with modern computers, combining and simplifying other equipment in the C/S subsystem, re-implementing the existing EDL application software, etc. At this point, it would be necessary to remove functionality from the MCS and implement it at the GA. This is described in detail in Section 4.

With a federated architecture, as with the hybrid approach, the current functionality of the GA would be implemented in a state-of-the-art, dependable, open system architecture. In its final implementation, however, it would take full advantage of distributed computing resources and technology to reduce MCS complexity. It eliminates duplicate command, upload and tracking messages by storing messages only at the GA. Its principal disadvantage is that it lacks commonality with ARTS, although designs for getting around this limitation have been proposed [4].

4. COMMAND & TELEMETRY SUBSYSTEM: TRANSITION STRATEGY

The design and implementation of the hardware and software required for the federated C&T Subsystem is a challenging engineering task. But an even larger challenge is posed by the transition task: how to migrate from the existing legacy system to a new target system containing open architecture hardware and easily understandable, maintainable, and portable software. The OCS is a large system (several million lines of code). The Architecture Task Force was required to produce a transition plan that was incremental and evolutionary rather than calling for a one-time "flip the switch" cutover. While this constraint was initially inspired by government budget limitations, it also reflects sound engineering practice.

The strategy of rewriting a legacy system from scratch to produce the target system and planning for a one-time total replacement has been called the "Cold Turkey" approach to conversion of legacy systems [3]. This strategy carries substantial risk of failure for a number of reasons, including the constantly changing conditions of the system (the "moving target"), poorly documented specifications, undocumented dependencies, the requirement for almost 100% system up time, and the difficulty of managing large projects. An alternative approach proposed in [3] is the "Chicken Little" approach, which involves migrating the legacy system in place by small incremental steps until the desired long term objective is reached. Each step requires a relatively small resource allocation (e.g., a few person years), takes a short time, and produces a specific, small result toward the desired goal. If one step of this

approach fails, only the failed step must be repeated rather than the entire project. In addition, failures in individual steps may indicate large or previously unforeseen problems. Due to the incremental nature of this approach, such problems can be addressed incrementally. The Chicken Little approach in the long run will probably cost more than the Cold Turkey approach, because it requires the creation of "gateways," software modules introduced between operational software components to mediate between them and to insulate some components from changes being made to others. After the system has been entirely replaced, these gateways will be discarded. But the higher cost of Chicken Little must be balanced against its significantly higher probability of success.

Draper attempted to apply the principles described in [3] to the transition plan developed for migrating from the current OCS architecture to one including a Federated C&T Subsystem. This transition has four main steps:

- (1) replace the computer hardware and software at each Ground Antenna, providing only the current functionality;
- (2) replace the Nav Payload/NDS Payload/Vehicle Bus Support and relevant OCS Resource Allocation functions at the MCS;
- (3) update Ground Antenna RF and baseband equipment, such as the High Power Amplifiers and Bit Synchronizers; also replicate the single-string equipment;
- (4) migrate selected MCS functions to each Ground Antenna.

4.1 Step 1: Replacement of GA Control & Status Subsystem

The purpose of this step is to install an open-architecture computer with a modern operating system and programming language that can serve as the basis for further improvements. The Control & Status Subsystem should be updated in one Ground Antenna at a time. The Control & Subsystem includes the control computers (Series/1) and other digital control equipment such as the Digital Acquisition Control Unit (DACU) and Decommutators. Electrical connections can be replaced with fiber optics. The selected operating system should be installed on the main control computers, system files converted to the target data base, and the object-oriented, Ada version of the GA application program activated. The new GA application program is estimated to be about 60K source lines of code. For replacement of this application, a Cold Turkey approach was proposed for two reasons. One reason was the difficulty of finding COTS communications software written for the Series/1 computer. The other reason was that

there are five GAs world-wide to meet GPS needs. Taking down one of them for a short time does not totally disrupt GPS operations. In addition, several options exist for providing a substitute while a particular GA is being upgraded [4,5].

This step does not have a backout plan. It is assumed that before beginning the conversion, replacement hardware and software have been thoroughly tested using a testbed, the test environment at Cape Canaveral or other means. If problems are encountered during the upgrade, all efforts will be concentrated on solving those problems; re-installing the Series/1 is not an option. The decision to proceed with the upgrade signals a commitment to making the new system work.

This step will result in several new and changed messages being sent to the MCS from the GA. These messages report equipment status and also serious error conditions that result in operator alarms at the MCS. Software must be in place at the MCS to accept these new and changed messages and to generate appropriate operator displays.

4.2 Step 2: Replacement of Relevant MCS Functions

In this step the Nav Payload/NDS Payload/Vehicle Bus Support and relevant OCS Resource Allocation functions are replaced at the MCS. The goal of this step is to provide the same functionality as the current system but to disentangle these functions from the current hardware and software, modularize them and provide clean interfaces between the modules so that future modifications can be more easily accommodated. Since the MCS currently runs on an ES9000 mainframe, communication with other computers or workstations should not be a problem and the Chicken Little approach should be followed for migrating these functions.

Replacements for these functions, either rewritten modules or COTS products, will have previously been obtained. In this step, the existing CPCs from the SV Command/Status Computer Program Configuration Item (CPCI) and Network Control CPCI will be replaced, one Computer Program Component (CPC) at a time, by a replacement function running on an open-architecture workstation. The workstation will also be running a commercially available real-time operating system, an Object Request Broker for inter-process communication and the selected Database Management System (DBMS). The system as it exists before any functions have been migrated is shown in Figure 4.

(It should be noted that an Object Request Broker is simply a specific instantiation of an Inter-Process Communication (IPC) service. An ORB provides a higher-level interface than many IPC products and,

despite its name, does not require that the communicating processes be implemented using object-oriented methods. While ORB has been used in the following discussion to illustrate the transition strategy, any IPC would work.)

The ES9000 containing the current MCS software is shown in the upper half of Figure 4. For simplicity, we have shown only the CPCs from SV Command/Status and Network Control CPCIs. These are represented by rounded rectangles. Each of the disks at the top of the figure represents a single file in the existing system. Access to each file is through a single routine; these routines are grouped together in a CPC called "Common Access Routines." Thus it can be seen that access to each file is controlled through a single point and that once a particular file has been migrated to the target data base, this single control point can be modified to access the desired data from the target system. The ES9000 is connected to the target workstation by a communications link.

In order to replace the existing CPCs one at a time, two types of transition software must be designed and implemented. First, gateways that mediate between the legacy system and the target functions must be designed and implemented. On the ES9000 these gateways will translate legacy messages (i.e., Work Requests) or legacy file accesses into messages the object in the target system understands. On the target system these gateways (or "stubs") will translate messages from objects in the target system into messages (i.e., Work Requests) the legacy system understands or into accesses to legacy files.

In addition, an ES9000-ORB interface must be designed and implemented. This interface is needed because the gateways on the ES9000 must be able to send and receive ORB messages but most ORB products are not implemented for the ES9000. The ES9000-ORB interface will accept low-level packets from the gateways on the ES9000 and translate them into an ORB-type request; it will also accept ORB messages from processes on the workstation and translate them into low-level packets for the ES9000. The gateways and ES9000-ORB interface are illustrated in Figure 5.

One issue not yet addressed is how to deal with data obtained from Compools, e.g., the SV Current Value Table (SV CVT). One possible solution is to first modify the existing software so that all reads and writes of each compool go through a common access routine, similar to the file access routines. This access routine could then be replaced with a gateway that obtains data from the target system as required.

MCS

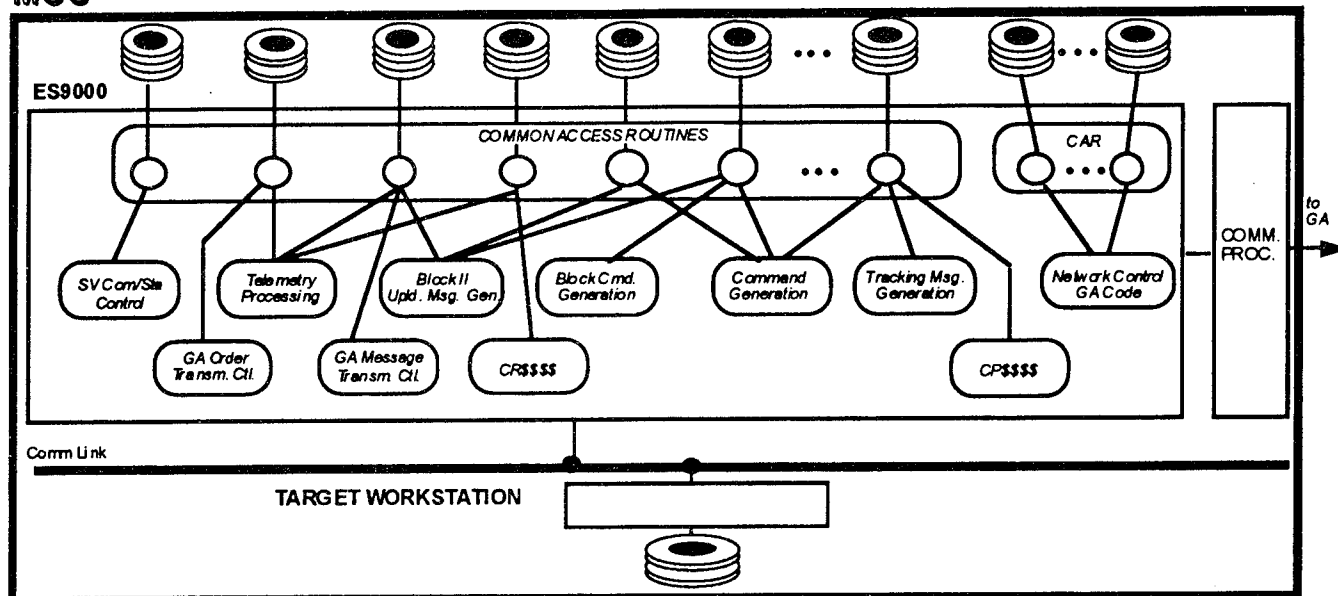


Figure 4. Step 2 Transition at MCS (Before).

MCS

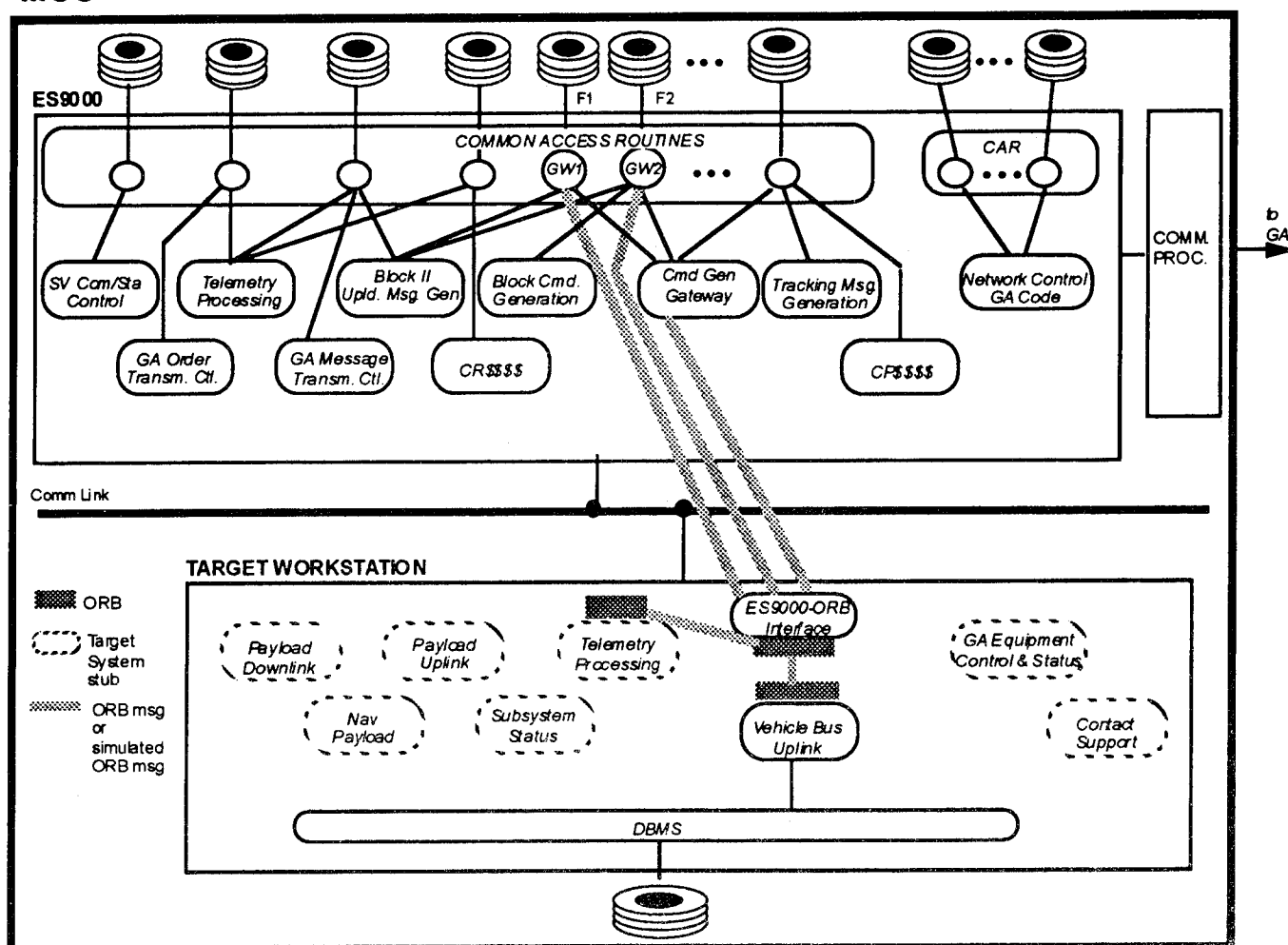


Figure 5. Step 2 Transition at MCS (During).

More details and examples of the transition process are provided in [6]. Two important considerations must be mentioned here. (1) The order in which CPCs are transitioned has performance implications. The CPCs should be cut over in an order such that once a function is being executed on the target workstation it does not cause accesses back to the legacy files, if at all possible. (2) Communication back and forth between legacy and target systems will, nonetheless, impact performance. The challenge will be to keep this impact to the absolute minimum.

Note that the software development effort for Transition Steps 1 and 2 can be proceeding in parallel. Also, the actual execution order of Steps 1 and 2 could be reversed.

4.3. Step 3: Update of GA RF and Baseband Equipment

In this step the Ground Antenna RF and Baseband equipment is updated. This includes replacing existing items such as the High Power Amplifiers and Bit Synchronizers, as well as replicating the echo check circuit and downlink test circuit, which are currently single string. This should require only minor software changes, for example, if replacements for existing equipment require different control parameters or supply different status information.

As in Transition Step 1, the equipment should be replaced in one Ground Antenna at a time and a substitute ground antenna provided while the replacement is occurring.

4.4. Step 4: Migrate Selected MCS Functions to Ground Antennas

In this step the functions identified in Section 4.2 (Figure 4) as residing at the Ground Antenna should be moved from the MCS to the Ground Antennas. This software migration will be incremental in that it will be done in one Ground Antenna at a time, but for that particular Ground Antenna, all designated functions will be moved from the MCS to the GA.

This step requires a strategy similar to that explained for Step 2. Gateways will be required at the MCS but not at the Ground Antenna.

When all Ground Antennas have become federated, the amount of programs and data residing at the MCS will be considerably reduced. The amount of programs and data at the Ground Antennas, on the other hand, will be considerably increased.

5. SUMMARY AND CONCLUSIONS

Several options for rearchitecting a subset of OCS functions collectively known as the Command & Telemetry Subsystem have been described in this paper. These options span the spectrum from a highly centralized architecture to a federated architecture. In addition, a transition plan has been described for migrating from the existing OCS legacy system to a federated Ground Antenna architecture. This transition plan assumes an incremental, evolutionary approach which, while obviously very complex, has a substantially higher probability of success than the traditional one-time, flip-the-switch approach.

6. REFERENCES

1. OCS Architecture Plan, prepared by Brian Finney, Martin-Marietta Corporation, Valley Forge, PA, 10 June 1994.
2. System Segment Specification for the Operational Control System Segment of the Navstar Global Positioning System, SS-CS-300A, 6 January 1989.
3. M. Brodie and M. Stonebraker, "DARWIN: On the Incremental Migration of Legacy Information Systems," University of California, Berkeley, March 1993.
4. GPS Ground Antenna/Colorado Tracking Station Compatibility Study, Draper Laboratory, Cambridge, MA, 30 June 1995.
5. GPS Ground Antenna Phased Implementation Plan, Draper Laboratory, Cambridge, MA, 31 July 1995.
6. L. Burkhardt et. al., GPS OCS Architecture Study Report, Draper Laboratory, Cambridge, MA, August 1994.



Session B2

DGPS Technology and Applications

Chair:

Dr. Alison Brown
NAVSYS Corporation

Co-Chair:

Dr. Trent Skidmore
Ohio University

Design of a GNSS: Coverage, Accuracy and Integrity

Prof. V. Ashkenazi, Dr. T. Moore, Dr. C. J. Hill, Dr. W. Y. Ochieng, and Dr. Wu Chen
The University of Nottingham

BIOGRAPHIES

Professor V Ashkenazi is the Director of the Institute of Engineering Surveying and Space Geodesy (IESSG), the University of Nottingham. Dr T Moore is a Lecturer with the IESSG, Dr C J Hill is a University Research Fellow and Drs W Y Ochieng and Wu Chen are Senior Post-Doctoral Research Assistants with the IESSG.

ABSTRACT

The concept of a civil owned Global Navigation Satellite System (GNSS) has evolved due to the concerns of the civilian navigation community over the current satellite positioning systems, GPS and GLONASS. Neither of these two systems provide continuous satellite availability and integrity, and both of them have been developed as military systems owned by single nations, with no absolute guarantee of continuity of service. In the case of GPS, the implementation of Selective Availability (SA) to degrade navigation accuracy means that full GPS navigation accuracy is inaccessible to the civilian community.

Various options have been proposed, and some implemented, to address these concerns. These range from joint (US) military (DoD) and civilian (DoT) control of GPS, augmentation by using other satellite systems (eg. geostationary communications satellites), to the eventual deployment of a new GNSS wholly owned by the civilian community.

It has also been suggested that the task of finding a successor to GPS should follow an evolutionary process, culminating in the deployment of the new GNSS. The approach is therefore a gradual one, starting with the current GPS constellation and enhancing its potential, in stages, through

augmentation with existing satellites, such as communication satellites in Geostationary Orbits (GEO), GLONASS, and with planned satellite constellations in Low Earth Orbit (LEO) and Medium Earth Orbit (MEO). Suggestions have also been made, involving satellites in Highly Elliptical Orbits (HEO).

The paper addresses the theoretical and practical aspects of candidate configurations and assesses satellite coverage (and hence navigational potential) and the provision of system integrity. The analysis includes an investigation into the design of satellite orbits advocated for use within a GNSS environment such as Geostationary Orbits (GEO), Low Earth Orbits (LEO), Medium Earth Orbits (MEO) and Highly Elliptical Orbits (HEO).

1 INTRODUCTION

The process of GNSS constellation design can be divided into two parts. Firstly, it is possible to design a new configuration of satellites, given specific criteria which it must satisfy. Secondly, it is possible to analyse a given constellation, either resulting from the design process, or based on current satellites, to assess the degree to which it meets the specified requirements. A thorough description of the basic theoretical principles of the design of optimal satellite orbits, in terms of satellite availability, coverage, accuracy, integrity and cost, as implemented in the IESSG design software, is given in this paper. As a demonstration of the analysis principles, a number of GNSS constellations have been tested.

- The full GPS constellation
- GPS plus 4 geostationary (GEO) satellites (the planned geostationary satellites of Inmarsat)
- GPS plus GLONASS

- 30 MEO (Medium Earth Orbits, altitude of approximately 10500 km) satellites augmented with 6 geostationary satellites.

GNSS1 is therefore represented by the two scenarios of GPS plus augmentations. The use of 30 MEO plus 6 GEO satellites offers a typical example of GNSS2.

2 COVERAGE AND ACCURACY

2.1 Design Criteria

The criteria for the design of a satellite constellation can be broadly classified into four major categories namely, purpose, integrity, complexity and cost. The purpose defines the use of the satellite system, examples being navigation and communications. System integrity defines the ability of the system to self-check so that erroneous satellites and receivers can be isolated, whereas complexity involves the nature of technology required to acquire the desired constellation. Once the purpose has been identified, the required constellation has to be designed. This involves the determination of the total number of satellites required to provide adequate coverage of the globe, together with their corresponding orbital parameters. The constellation is then costed and analysed for its navigation or communications potential, satellite availability and system integrity. If the constellation is optimal in terms of the aforementioned criteria, then it is adopted otherwise an iterative procedure is invoked until an acceptable constellation is achieved. This is illustrated by the flow diagram in Figure 2.1.

2.2 Satellite Coverage

A satellite will be visible on earth at any point within a circle whose centre is directly beneath the satellite. The circle diameter increases with satellite altitude, and as one approaches its perimeter, a greater amount of the earth's atmosphere must be traversed to reach the satellite, leading to increased atmospheric errors. Hence, for satisfactory communication and positioning, elevation angles higher than 7.5 degrees are normally used. Clearly, coverage for a system of communication satellites differs from coverage for a constellation of navigation satellites. In the first case, we need to see a minimum of one satellite from any point on Earth. In the case of navigation, we need a minimum of 4 satellites, offering a sufficiently strong geometry for a good navigation fix. The coverage of constellation can therefore be defined as *a measure of the extent to which it can provide the design function over the surface of the earth.*

2.3 Cost Analysis

The overall cost of a satellite system can be broken down into three major components namely, the Research and Development Cost, the Initial Establishment Cost and the Operation and Maintenance Cost. The costing process can be further broken down to involve two of the segments of the system namely, the ground and space segments. The ground segment includes all the tracking, processing, transmission and launching facilities required. The costs of the ground segment will depend on the complexity of these facilities. The launch costs vary depending on whether small rockets are used to place satellites into low earth orbits or whether large boosters are needed to place satellites into higher orbits. Another variable in the determination of launch costs involves the launch procedure where either single or multiple satellite launching can be performed. The space segment cost is proportional to the complexity of the satellites themselves. The small low powered satellite in low orbit will be less expensive than the more complicated high powered, higher orbit satellites. The other major system costing variables include, the number of ground (tracking) stations, the mean satellite life, the number of satellites in the constellation, the projected lifetime of the constellation, the probability of launch success, the annual cost of maintaining a ground station, the annual interest on invested capital and annual insurance associated with the project.

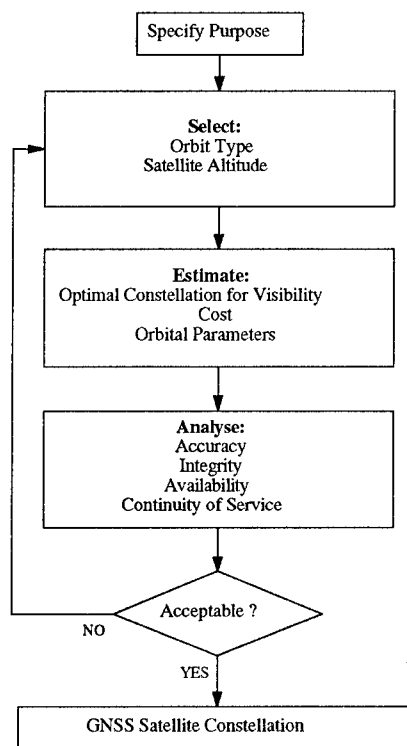


Figure 2.1 - GNSS Constellation Design

2.4 Coverage and Accuracy Analysis

The navigation potential of any satellite constellation is analysed based on the computation of an indicator of positional accuracy, referred to as Position Dilution of Precision (PDOP). The 'maximum PDOP' approach is used where the entire globe is divided into as many grid cells as is practical and PDOP values are computed at every point at regular intervals for a period of 24 hours. In the following analyses, a time interval of 10 minutes is used. This is a compromise between the accuracy of the results, and the time required to compute the results. It is possible that spikes in the PDOP values will be missed by a time interval of 10 minutes. The maximum PDOP value at every point is then recorded to represent the worst case scenario. This technique is superior to the so called 'snapshot' approach as it takes care of both temporal and spatial characteristics of the system. This approach enables a direct comparison of the navigation potential of any two candidate satellite navigation systems for the entire globe over 24 hours.

The following analysis is divided into three parts namely, the current GPS constellation, the GPS augmentation representing GNSS1 and the replacement of GPS representing GNSS2. Analysis has shown that there are 4 or more satellites visible anywhere on the globe for 100% of the time, for the constellations investigated. However, this does not mean that the constellation is 'available' for navigation purposes for 100% of the time. To be available for navigation, the constellation must provide sufficient precision (DOP values) and sufficient integrity (capability to perform RAIM). The following figures illustrate the global coverage of the tested

constellations, based purely on the criterion of PDOP. They are all based on the same colour scale for easy visual comparison.

Figure 2.2 shows the maximum PDOP value contour plot of the entire globe taken over 24 hours for the 24 GPS satellite constellation. It is evident from the plot that the high latitude regions suffer more than the equatorial and mid-latitude areas. Figures 2.3 and 2.4 represent the results of the GPS constellation augmented with 4 geostationary communications satellites and with 24 GLONASS satellites respectively. The result of augmenting GPS with 4 geostationary communications satellites is the provision of most regions with acceptable PDOP values (6 and below). The augmentation of GPS with GLONASS represents the best possible scenario offering PDOP values of 4 and below, anywhere in the world at any time.

The replacement of GPS by a civilian GNSS (GNSS2) may rely on the use of satellites in medium orbits (12000 km in altitude) as a compromise between higher and lower orbits, augmented with geostationary communications satellites. Such a constellation will probably perform the dual task of providing positioning and communications services. Figure 2.5 shows the results of the adoption of 30 Medium Earth Orbit (MEO) satellites augmented with 6 geostationary communications satellites. It can be seen that most of the globe will experience PDOP values of 6 and below with an occasional rise of up to 10 and no worse, making it a viable option for GNSS2 with a little improvement.

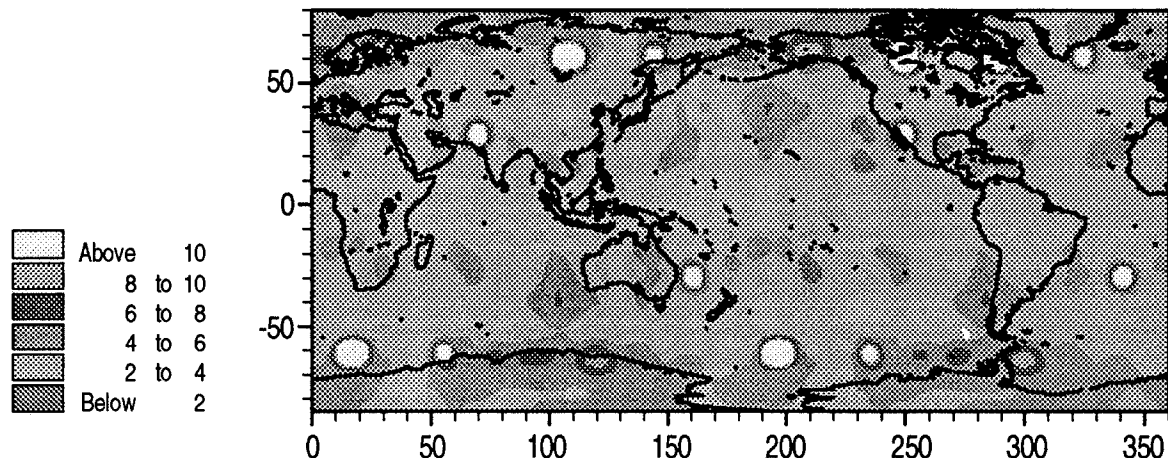


Figure 2.2 - Maximum PDOP Analysis for 24 GPS Satellites

2.5 System Integrity

System integrity is defined by the FRP (Federal Radionavigation Plan) as the ability of a system to provide timely warnings when the system should not be used for navigation. GPS or GLONASS on their own would provide highly accurate and reliable navigation services. However, in some situations such as aircraft navigation, the integrity of the systems is insufficient to ensure safety. Two methods have been proposed for integrity monitoring namely GPS or GLONASS Integrity Channel (GIC) and Receiver Autonomous Integrity Monitoring (RAIM). The GIC integrity monitoring method uses a communication link to transmit real-time integrity messages to the users. The FAA has experimented with GIC. With

this system a network of monitoring stations is used to observe errors in the range measurements. RAIM is a method of checking the validity of the navigation solution in the receiver by taking advantage of redundant information. A detailed discussion on system integrity is given in the next section.

3 INTEGRITY

Integrity is defined by the FRP (Federal Radionavigation Plan) as the ability of a system to provide timely warnings to users when the system should not be used for navigation [DOD/DOT, 1992]. The development of the Global Positioning System (GPS) has clearly demonstrated the advantages of a

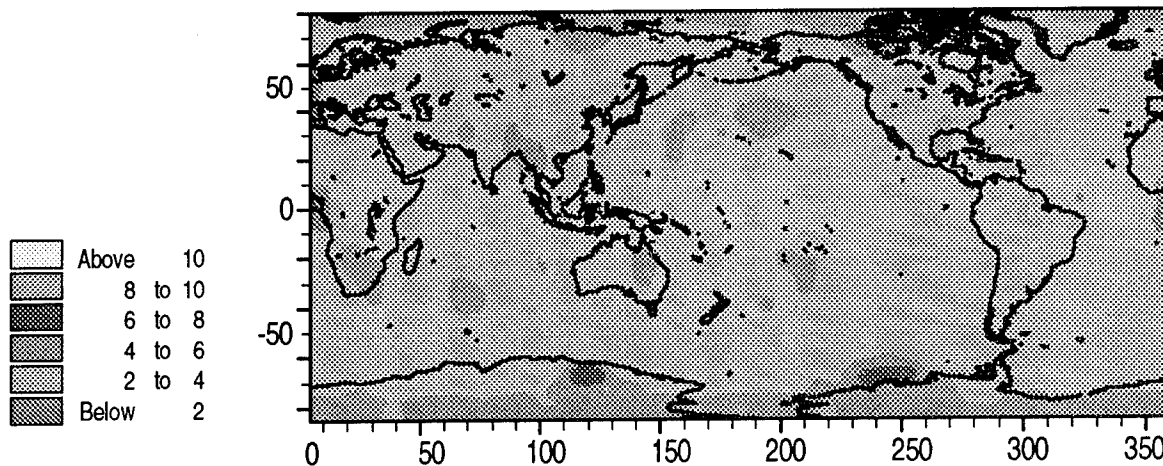


Figure 2.3 - Maximum PDOP Analysis for 24 GPS + 4 GEO Satellites

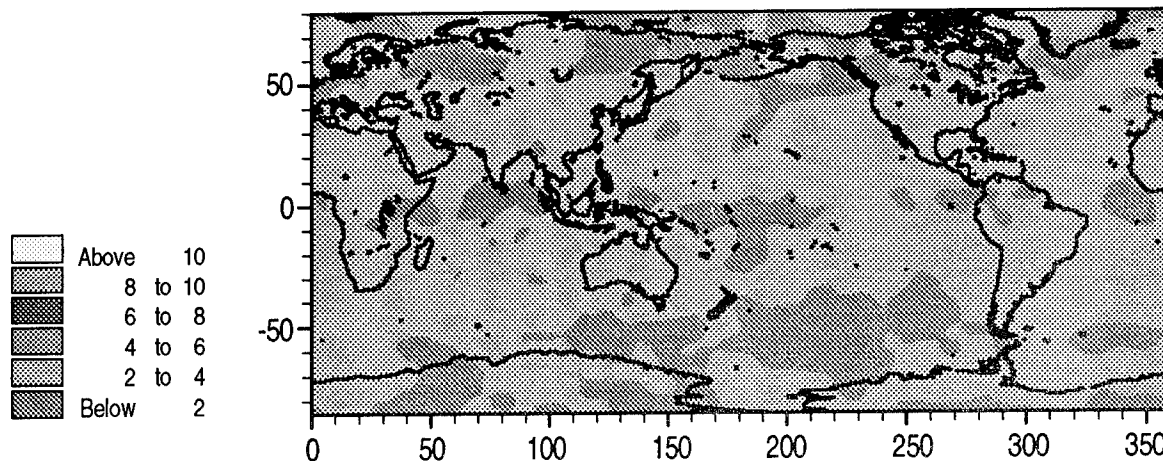


Figure 2.4 - Maximum PDOP Analysis for 24 GPS + 24 GLONASS Satellites

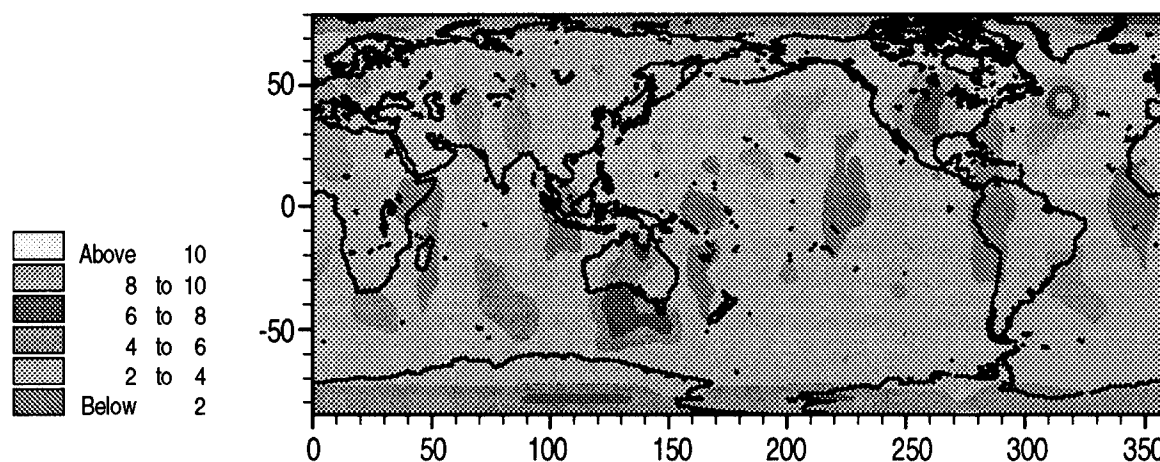


Figure 2.5 - Maximum PDOP Analysis for 30 MEO + 6 GEO Satellites

Global Navigation Satellite System (GNSS). It has global coverage, 24 hour all weather availability, provides a high level of positioning accuracy, and has proven to be cost effective for a variety of applications, from navigation to high precision surveying. However, the civil air navigation community has very demanding requirements for the 'integrity' of any systems used in safety-critical operations. A navigation system can be said to have integrity if it never gives a position which is significantly in error, or if it has the ability to inform the user when the position error is out of tolerance. The RTCA, through its Special Committee 159, has defined the integrity requirements which GPS must meet, in terms of 4 distinct parameters, as follows:

1. **Alarm Limit** : the size of a 'significant' position error, which the user must be informed of. This depends on the proximity of hazards, such as other aircraft (or the ground !), and therefore on the phase of flight
2. **Time to Alarm** : the (maximum) time between the cause of the error, and a warning message reaching the user. Again this depends on the phase of flight.
3. **Maximum False Alarm Rate** : the highest rate at which system errors are flagged, without there being a real problem. This is essentially a 'pilot confidence' factor, since a system which consistently gives false warnings will not be trusted.
4. **Minimum Detection Probability** : the probability that a real error will be detected. This factor is the key to integrity, since safety-critical navigation cannot tolerate system errors which go undetected.

GPS is a complex system, based on data messages transmitted from a constellation of satellites. There is potential for the system to fail at any one of a number of stages, from the production of the data messages and their upload to the GPS satellites, to their transmission, reception and processing within the users' equipment. To counter these possibilities, GPS has a number of built-in checking systems. However, even with all of these self-checks, GPS cannot meet the integrity requirements set out by the RTCA.

3.1 Definition and Requirements for Integrity

Any positioning system uses measurements, such as range, Doppler count, or angle, to compute the position of the users. In addition to the user's coordinates, information about their precision and reliability is also crucial for the users. The precision of a position fix represents the position quality, as affected by the random measurement noises through the geometry of the system. In GPS, this geometric factor of the system is described by the Position Dilution of Precision (PDOP). However, if there are systematic errors or outliers in the measurements, the position error could be very large, but not reflected by the PDOP. For a Global Navigation Satellite System (GNSS), a user may experience large position errors due to various reasons. These include:

- 1 The navigation satellite may transmit incorrect information about its ephemeris and clock.
- 2 Some user related errors (eg errors introduced during signal propagation or by the user's receiver), which cannot be monitored by the system itself, may produce large positioning errors

- 3 When GPS is used as a part of GNSS, the SA error may produce very significant positioning errors on rare occasions.
- 4 Due to the limitation of the GNSS satellite constellation (dependent on the design of the system), the navigation service could be unavailable for users within view of too few satellites in normal operational status. More frequently, the navigation service could be significantly degraded when the satellites have a poor geometric configuration.

Thus, one of the key issues for the GNSS applications is how to monitor the system and position solution, and inform the user when the derived position accuracy does not satisfy the user's requirements. This is the integrity problem. A system can be said to have 'integrity' if

With given probability P , either the position error does not exceed a prespecified threshold R , or an alarm is raised within a time-to-alarm interval duration T , when the position error exceeds the prespecified threshold R .

For any 'yes-no' type decision making, there exist two types of errors. The first type of error occurs when the system *can* be used, but the decision criterion indicates that there is a fault. This is a False Alarm (Type I error). The second type of error occurs when the system *cannot* be used, but the decision criterion does not indicate a problem. This is a Miss Detection (Type II error).

The requirements of integrity are different for various applications. They are usually specified by four quantities: the alarm limit, the time-to-alarm, the maximum false alarm rate, and the minimum detection probability [RTCA SC-159, 1991].

3.2 Integrity Monitoring Methods

Various methods for monitoring the integrity of GNSS have been proposed. Each method aims either to check whether an individual measurement error exceeds a specified threshold, or whether the resulting position error exceeds a specified threshold. The latter approach is more relevant to air navigation, since it is the output of the positioning system, ie the aircraft coordinates, which must be checked against the navigation accuracy requirements during the various phases of flight.

External monitoring of GNSS relies on one or more ground based systems, positioned at known locations.

Individual satellites are then monitored by comparing the measured pseudoranges with those computed from the satellite and monitor station coordinates. If a measurement error exceeds a certain threshold, indicating that a satellite has failed, a warning is relayed to users that the satellite should not be used. This is a powerful approach to integrity monitoring, since the method directly isolates the particular satellite which has failed. If sufficient healthy satellites are still visible to the user, it is still possible to use the system for navigation. However, this approach is not able to identify problems with the user's equipment, which may produce faulty measurements, or which may yield a poor position solution due to masking of one or more satellites. To counter these possibilities, it is necessary to use a monitoring method which relies on the actual measurements used in the positioning solution.

Receiver Autonomous Integrity Monitoring (RAIM) is a method applied by the user to check the consistency of the measurements made from different satellites, to estimate the quality of the resulting position. A number of different algorithms for RAIM have been developed, including position comparison, range comparison, residual analysis, and parity checking methods. With proper selection of the thresholds, it can be shown that all these algorithms are basically equivalent.

The main drawback of RAIM is that it relies on redundancy in the position solution to detect and isolate bad measurements, ie it requires more than the navigation minimum of four satellites. As a result, it is not always possible to carry out a RAIM computation if, for instance, the user is at a weak point in the coverage of the GNSS constellation, or if satellites are masked or lost during aircraft manoeuvres. The power of the RAIM technique can be improved by adding in measurements from other instruments on board the aircraft. The technique is then no longer 'Receiver Autonomous', but 'Aircraft Autonomous'. AAIM can be applied either by comparing the position solution from GNSS with that obtained by other navigation sensors, such as a barometer, or an inertial navigation system, or by integrating the raw measurements from each system into a single solution (with appropriate weighting of the various measurements).

3.3 Capability of GNSS to Provide RAIM

Civil air navigation demands a very high level of integrity of GNSS. To meet these requirements, there must be a method to detect, and preferably isolate, any measurement errors which will cause significant errors in the computed position. Receiver Autonomous Integrity Monitoring (RAIM), is a method designed to

be sensitive not only to errors occurring in the GNSS system, but also to those caused the user's own equipment and environment. The basic input to a RAIM algorithm is the same raw measurements used to compute the user's position.

The ability of a receiver to perform a RAIM calculation depends on the number and geometry of the satellites in view. Thus, using only the receiver's coordinates and the predicted positions of the GNSS satellites, it is possible to determine whether or not a RAIM calculation can be performed, ie whether RAIM is 'available' to the user, as an integrity monitoring technique.

As part of the suite of GNSS design and analysis software, a program to analyse the RAIM availability for any satellite constellation has been developed at the IESSG. This section gives a description of the RAIM availability method and an overview of the structure of the analysis program. For a given satellite constellation, the RAIM availability is calculated within a certain period, for either a given location (eg an airport) or a specified flight route. The RAIM availability is calculated with respect to the integrity requirements of a specified flight phase (the alarm limit, false alarm and minimum detection probabilities), and an assumed measurement noise level.

In the following studies, a number of scenarios have been investigated, based on the requirements of an aircraft using GPS. Since the magnitude of a 'significant' positioning error varies according to the required positioning accuracy, a given constellation may provide RAIM for one level of accuracy, while not providing it for a higher accuracy level. The following studies have therefore investigated the different phases of flight when using GNSS. The studies have also considered differing numbers of inoperative GPS satellites out of the full constellation. In addition, the augmentation of the GPS solution with additional sources of measurements has also been investigated.

The RAIM availability for the different satellite constellations discussed in §2.4 has been investigated on a global grid ($5^{\circ} \times 5^{\circ}$). The satellite constellations considered here are GPS only and GPS with 4 Inmarsat geostationary satellites, GPS plus GLONASS and 30 MEO with 6 geostationary satellites.

3.3.1 RAIM Availability Analysis of GNSS

Due to the inadequacy of coverage and integrity of GPS, different systems have been proposed to augment

or replace GPS to form a new GNSS system and the coverage for various systems has been analysed in §2.4. In this section, the RAIM availability of these systems is analysed and compared. The satellite constellations considered in this analysis include GPS, GPS and 4 Inmarsat-3 satellites, GPS and GLONASS, and 30 medium earth orbit (MEO) satellites plus 6 geostationary satellites. Again, this investigation concentrates on the three flight phases of en-route, terminal, and non-precision approach phases.

The RAIM availabilities are calculated based on a global coverage, with a $5^{\circ} \times 5^{\circ}$ grid cell. The elevation cut-off angle of 7.5° is adopted for all the constellations. A test period of 24 hours and a sample rate of 5 min have again been adopted in the analysis.

Figure 3.1 shows the geographic distributions of the RAIM availability for all three flight phases with the 24 GPS satellite constellation. A GPS pseudorange error of 33 m has been adopted in the tests. It can be seen that for the en-route phase (figure 3.1a) the RAIM availability is over 99% for most areas. At the poles and in low latitude regions (close to the equator), RAIM is available 100% of the time (which is shown in the figure for above 99.8%, because with a 5 min sample rate the resolution is 0.3%), while in the mid-latitude areas RAIM availability is slightly worse and in some small regions RAIM availability is between 98 and 99%. RAIM availability for the terminal phase (figure 3.1b) is generally worse than that of the en-route phase, but is still above 99% in most areas. In some small regions in mid-latitudes, RAIM availability is reduced to just above 95%. The RAIM availability for the non-precision approach phase is much worse (figure 3.1c). It is below 95% for most mid-latitude areas.

The maximum RAIM outage interval of the GPS constellation for the non-precision approach phase results in most regions where RAIM can be continuously unavailable for 10 to 30 min. There are two bands in mid-latitude where RAIM can be continuously unavailable for 30 to 60 min (or even over 1 hour in some small regions).

Figure 3.2 shows the RAIM availability of the non-precision approach phase for the constellation of GPS and 4 Inmarsat satellites. In this test, a pseudorange measurement error of 5 m is adopted for both GPS and Inmarsat satellites, which requires that the differential corrections are transmitted to the user as well. It can be seen that apart from a few small regions (where RAIM is still available more than 99%), RAIM is available 100% in the most areas of the world.

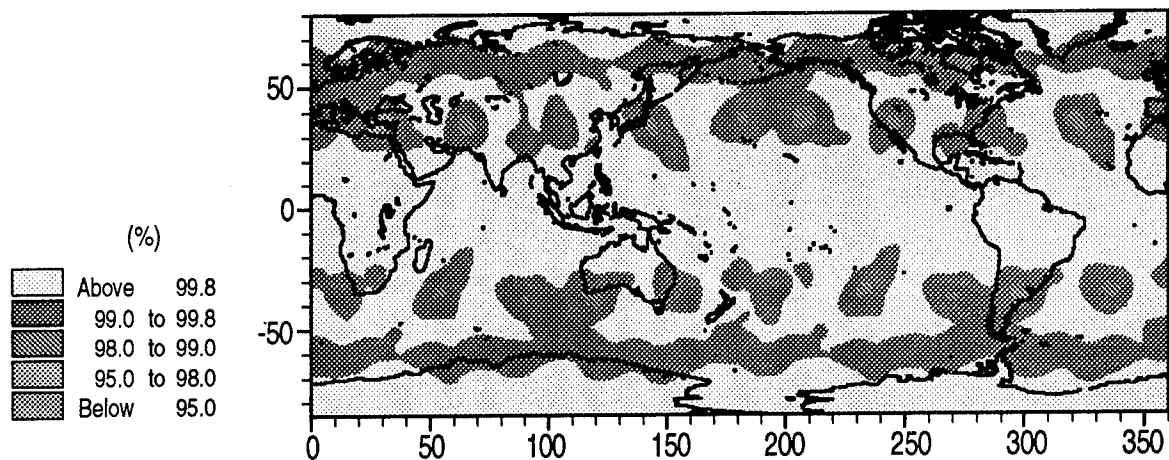


Figure 3.1a - RAIM availability for GPS Only (en-route)

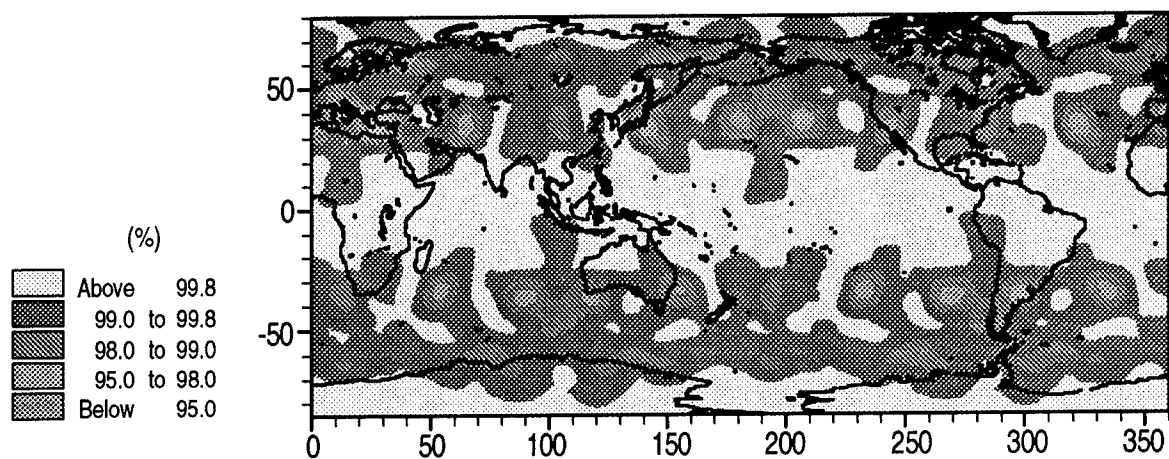


Figure 3.1b - RAIM availability for GPS Only (terminal)

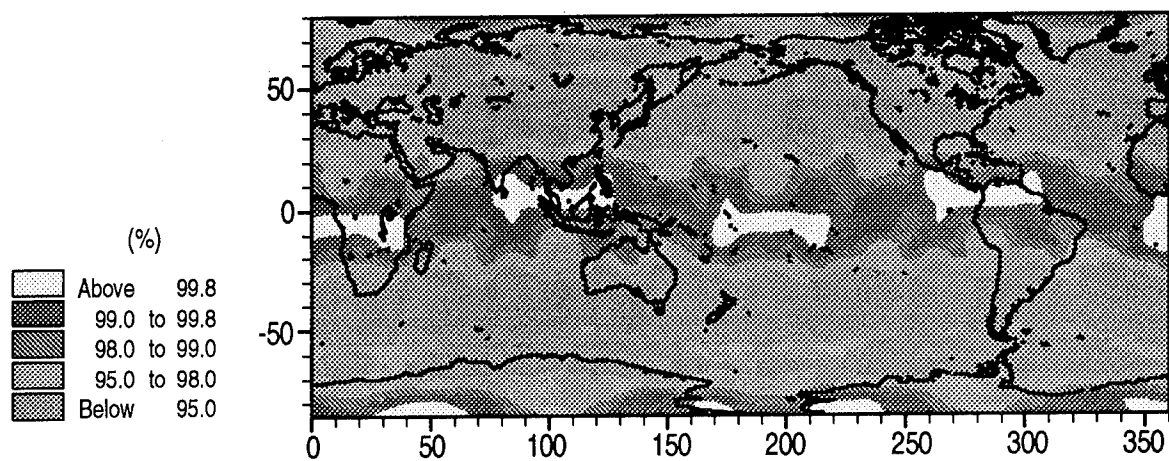


Figure 3.1c - RAIM availability for GPS Only (non-precision Approach)

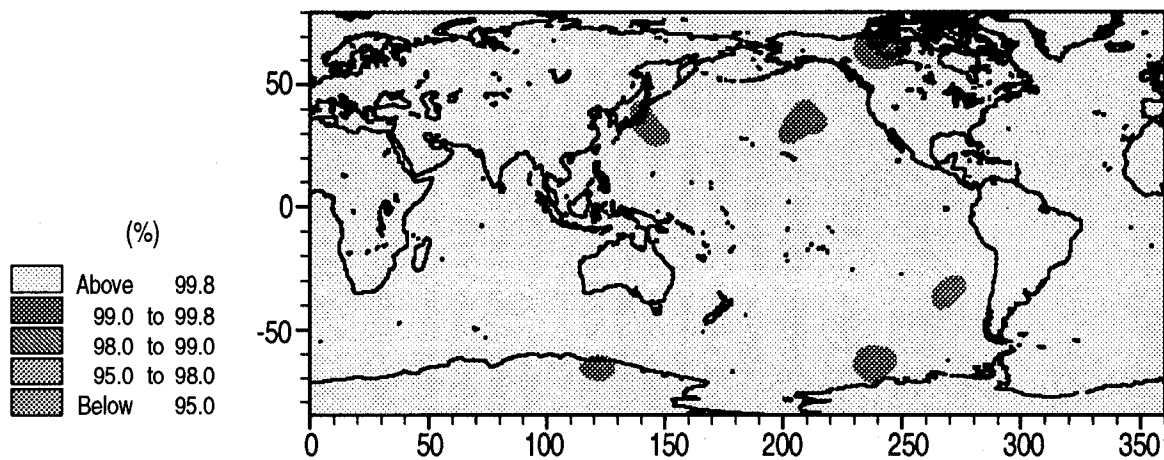


Figure - 3.2
RAIM availability for GPS + 4 Inmarsat (non-precision Approach)

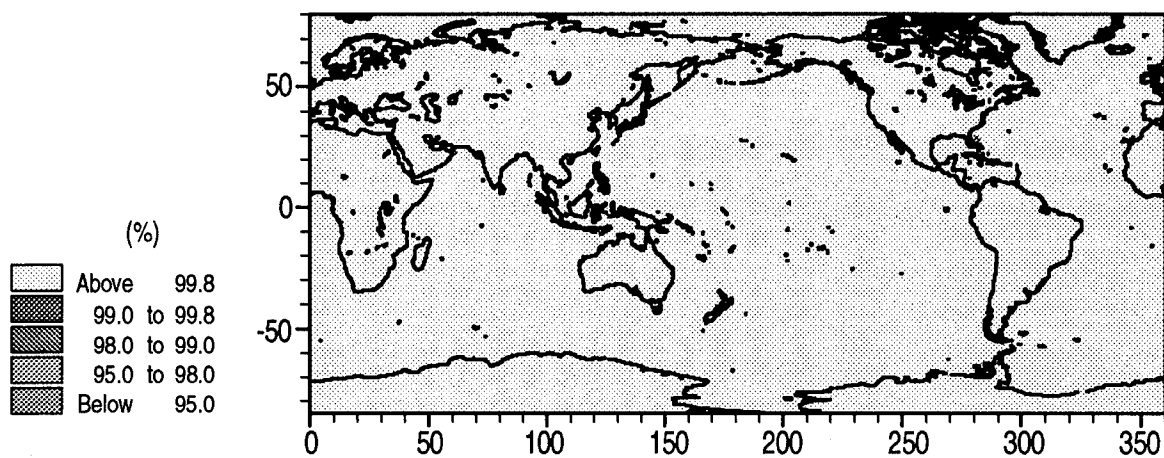


Figure - 3.3
RAIM availability for GPS + GLONASS (non-precision Approach)

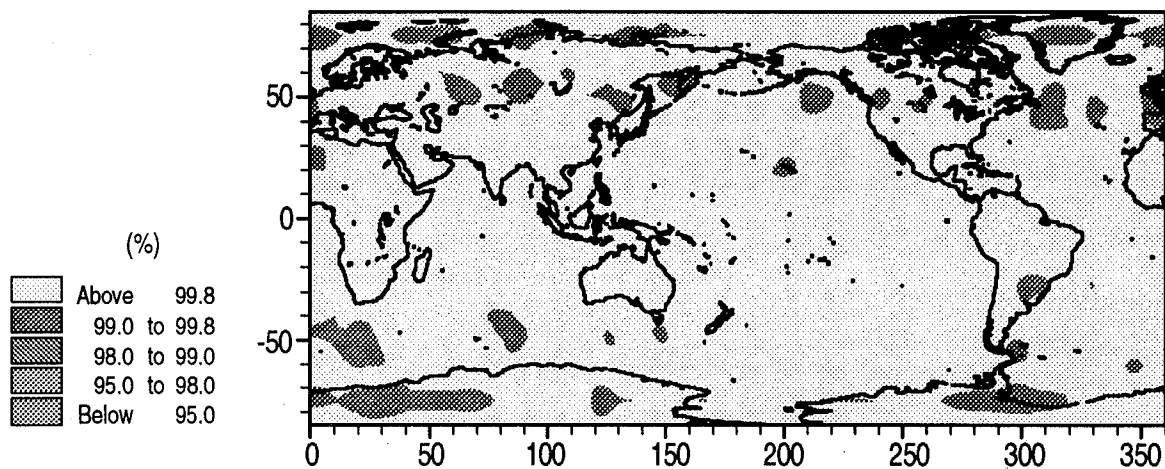


Figure - 3.5 - RAIM availability for 30 MEO + 6 GEO (non-precision Approach)

Combining GPS and GLONASS, the RAIM availability can be further improved (as shown in figure 3.3). In this test, the GPS and GLONASS

measurement errors have been set to 33m and 5 m respectively, due to the fact that GLONASS measurements have no SA errors in them. Apart from two spots, RAIM is available 100% of the time even

for the non-precision approach phase. Figure 3.5 gives the RAIM availability distributions of the non-precision approach phase for the constellation of 30 medium earth orbit (MEO) satellites and 6 geostationary satellites. In this test, a measurement

error of 5 m is assumed for all the measurements. It can be seen that RAIM is still available 100% of the time in most areas. The integrity of this constellation is slightly worse than GPS + Inmarsat (figure 3.2), but significantly better than GPS only (figure 3.1c).

4 CONCLUSIONS

This paper has addressed the three major areas of GNSS constellation design namely, satellite availability, coverage, system integrity and cost. It has been shown that GPS on its own does not satisfy the requirements for sole means navigation. The two main techniques for integrity monitoring namely RAIM and GIC together with their derivatives have also been discussed. It is argued that for robust integrity provision the two techniques should be used in parallel.

The problems of the lack of satellite availability can be overcome to some extent by augmentation with other satellite systems such as Inmarsat geostationary communication satellites. The best situation however, is obtained when GPS is augmented with GLONASS. In the case of total replacement of the current positioning systems, it has also been shown that the solution may lie on satellites in medium earth orbits augmented appropriately with geostationary satellites.

5 REFERENCES

Ashkenazi, V. et al (1993) 'Wide-Area Differential GPS: A Performance Study', *Navigation: Journal of the Institute of Navigation*, Vol 40, No. 3

Brown, A and C. Fosha, (1988) 'Algorithms for a GPS Integrity Channel', *ION GPS-88*

Brown, R.G. and P.W. McBurney (1988) 'Self-Contained GPS Integrity Check Using Maximum Solution Separation', *Navigation: Journal of the Institute of Navigation* Vol. 35, No. 1

Brown, R.G. et al (1991) 'Update on GPS Integrity Requirements of the RTCA MOPS', *Proc. of ION GPS-91*

Chen, W. (1992) 'Integration of GPS/INS for Surveying Applications', PhD thesis University of Newcastle Upon Tyne

DOT/DOD (1992) Federal Radionavigation Plan 1992, DOT-VNTSC-RSPA-92-2/DOD-4650.5

Enge, P. et al (1992) 'A Signal Design for the GIC which Includes Capacity for WADGPS Data', *Proc. of ION GPS-92*

Ochieng, W. (1993) 'Wide Area DGPS and Fiducial Network Design', Ph.D thesis, University of Nottingham

Parkinson, B.W. and Axelrad, P.A (1988) 'Autonomous GPS Integrity Monitoring Using Pseudorange Residual', *Navigation: Journal of the Institute of Navigation* Vol. 35 No. 2

RTCA (1991) 'Minimum Operational Performance Standards for Airborne Supplemental Navigation Equipment Using Global Positioning System (GPS)', RTCA Document DO-208

RTCA (1993) 'Minimum Aviation System Performance Standard DGNSS Instrument Approach System Special Category I - Proposed Final Draft Document', RTCA 272-93/SC159-443

RTCA (1994) 'Wide Area Augmentation System Signal Specification', RTCA Paper No. 114-94/SC-159-508

Shank, C.M. and J. Lavrakas (1993) 'GPS Integrity: An MCS Perspective', *Proc. of ION GPS-93*

Van Dyke, K. (1992) 'RAIM Availability for Supplement GPS Navigation', 48 Annual Meeting of ION, Washington, D.C.

Differential GPS Evaluation at UK Airports

Hemant Mistry and Dr. Richard Farnworth
UK National Air Traffic Services

BIOGRAPHIES

Mr. Hemant Mistry is an engineer employed by the United Kingdom's National Air Traffic Services. He has been extensively involved in the development of the Microwave Landing System and is currently working on R&D projects related to precision approach and landing guidance.

Dr. Richard Farnworth is a research engineer employed by the United Kingdom's National Air Traffic Services which is part of the Civil Aviation Authority (CAA). His responsibilities include the management of R&D projects relating to the application of satellite navigation systems in civil aviation.

ABSTRACT

Many experiments have been undertaken and are currently underway to assess the feasibility of using the Global Positioning System (GPS) to provide precision approach and landing services. Most of these trials have been limited to theoretical analysis and tests carried out under experimental conditions. Although such evaluations can demonstrate system capabilities under specific conditions, they provide no guarantee of a systems performance in a continuous real time operational environment. The assessment of the use of GPS for precision approach services requires a constructive step by step approach under revenue service operational conditions. Project Heathrow has been specifically implemented to satisfy this requirement. The project is a co-operative venture between the National Air Traffic services (NATS) and British Airways and has been designed to provide a direct revenue service comparison between the Instrument Landing System (ILS), Microwave Landing System (MLS) and Differential GPS systems installed at London's Heathrow Airport.

BACKGROUND

The ILS has successfully served the aviation community for over fifty years. Today, the system is capable of providing precision guidance down to Category IIIB minima, that is zero decision height and 75 metres (see to taxi) runway visual range. In Europe the low cloud bases and adverse weather conditions dictate a business requirement for these high levels of ILS operations. In fact of all Category II and III operations world-wide, over 85 percent are carried out within the European Region. However, this operational performance of the ILS can no longer be guaranteed for the foreseeable future because of a number of factors which are inherent in the system design. These include the systems susceptibility to multipath interference from airport buildings and aircraft movements within the beam coverage, the limitation of operational channels and finally the increasing threat from FM broadcast interference which has already forced some airports to reduce their operating limits.

In view of these shortcomings, ICAO developed and adopted the MLS to replace ILS by the turn of the century. Until now progress on the ILS/MLS transition plan has been relatively slow. Member states are reluctant to install MLS in view of advances in satellite technology and the possibility of achieving a precision approach guidance capability using the United States GPS and/or the Russian GLONASS. Most of the assessment work on the use of satellites for precision guidance has been concentrated on the use of GPS because GLONASS receivers have been unavailable. In order to further assess the use the GPS during the final approach and landing segments of flight, more comprehensive studies are required which takes the operational requirements and limitations into account.

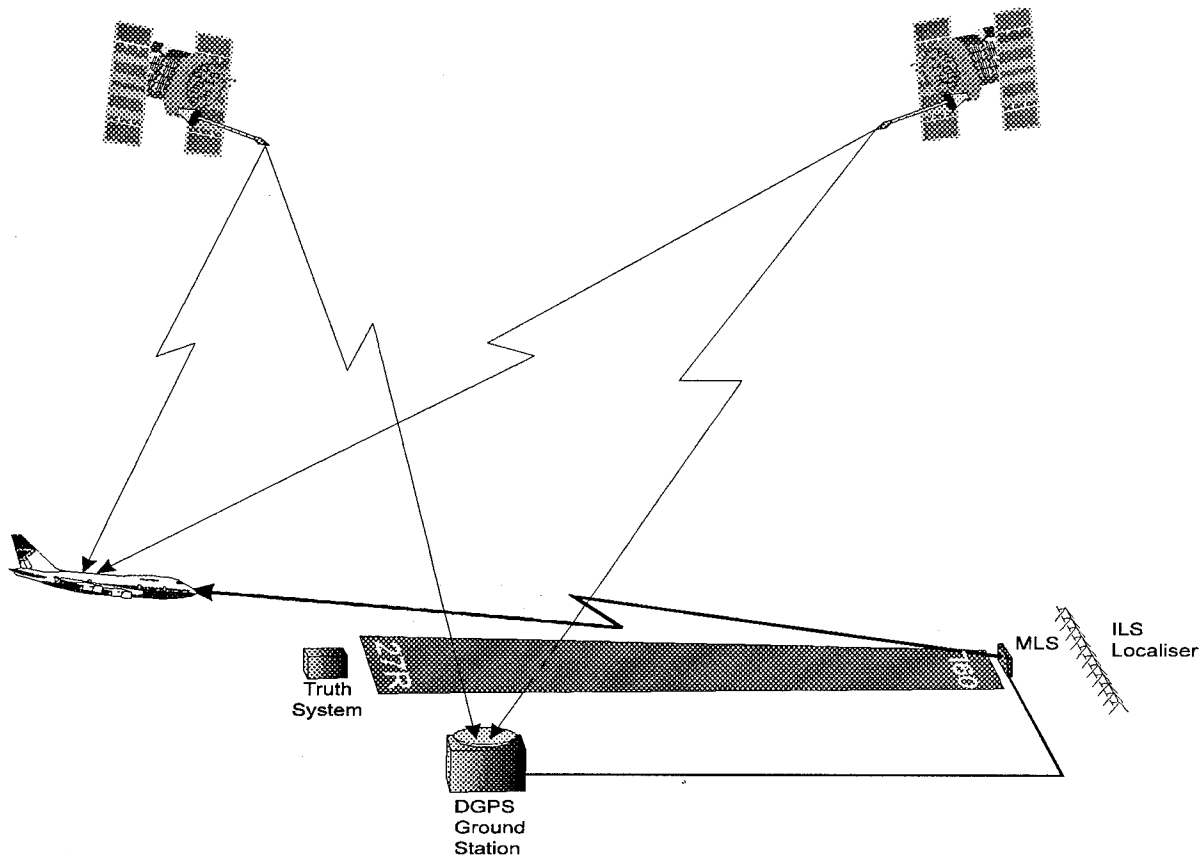


Figure 1. Project Heathrow - DGPS Evaluation

PROJECT SET-UP

The Project Heathrow evaluation is primarily a data collection exercise, the initial results of which were presented to the ICAO world-wide divisional meeting in March this year. The DGPS set-up currently being used for Project Heathrow is based on a 12 channel GPS receiver. The unit is built to ARINC 743A standards and represents equipment specified and currently available for commercial aviation. The aircraft being used in the evaluation is a British Airways Boeing 767 fitted with a dual DGPS and MLS test installation in addition to the existing dual Category IIIB ILS configuration. All relevant parameters output from each of the test units are recorded for detailed analysis along with data from the operational ILS and other navigation systems onboard the aircraft. A specially modified Optical Quick access recorder is used to store the large amounts of data collected during each approach. Figure 2 illustrates the configuration of the airborne installation.

The ground element of the project consists of a Category III ILS, an evaluation MLS and the DGPS

ground station on runway 27R at Heathrow. The satellite differential corrections are transmitted via the MLS auxiliary data channel to the aircraft. Various studies including recent technical analysis by the ICAO All Weather Operations Panel (AWOP) have suggested the C-band datalink to be the most suitable for the transmission of DGPS data in the final approach environment. The MLS C-band datalink provides an ICAO standardised high integrity protocol for the transmission of digital information and its potential to provide an uplink for satellite corrections is being assessed during the project.

An independent automatic photographic truth system, remotely triggered by the aircraft, is being used to provide position information to an order of accuracy better than that of the ILS. Information from this system is used during the data analysis to provide a truth reference for all three of the systems being evaluated. Figure 1 shows an overview for the DGPS evaluation system at Heathrow.

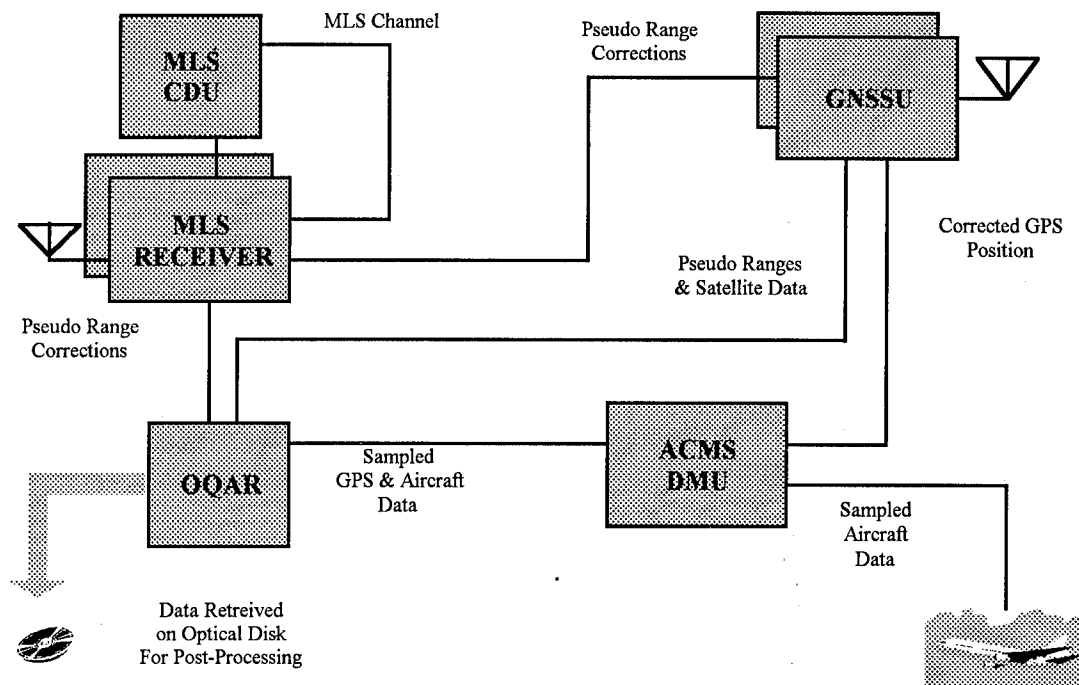


Figure 2. Airborne Architecture

INITIAL RESULTS

Analysis of the results is currently undertaken in three stages for every approach to runway 27R by the aircraft.

- The first stage, undertaken by British Airways, provides an overall assessment of the operational performance of all three systems.
- The second stage is performed by UK NATS and converts the output of the GPS to a ILS look-alike signal. This allows for direct comparison between the recorded MLS (which already has an ILS look-alike output), ILS and DGPS. Data from the independent truth system is additionally used at this stage to provide an assessment of the accuracy achievable using GPS in revenue service applications. Work undertaken here will determine processing requirements for the raw GPS output and will hence aid in the development of the Multi-Mode Receiver (MMR).
- The final stage of analysis is performed by the UK Defence Research Agency (DRA). Here, in-depth analysis is carried out to assess the performance of

the DGPS system during each approach. The performance of the complex algorithms used is checked against data available from the satellites at the time to provide a detailed account of the achievable performance of a DGPS system in an operational environment.

By the very nature of the evaluation, changes to the equipment configuration (airborne, and ground) are dictated by the results obtained. Changes made to the overall set-up provide an iterative account on the performance of DGPS.

Figure 3 shows ILS, MLS and DGPS angular deviations for one of the approaches into Heathrow. To obtain such deviations from a DGPS position, the latitude, longitude and altitude of the aircraft and ground reference point were first converted to Earth Centred, Earth Fixed Cartesian co-ordinates using the WGS-84 Earth spherical model. The position of the aircraft in these co-ordinates was then transferred to a East-North-Up system centred on the reference point. A rotation was then added to align the x-axis of this right-handed system along the reciprocal of the runway heading.

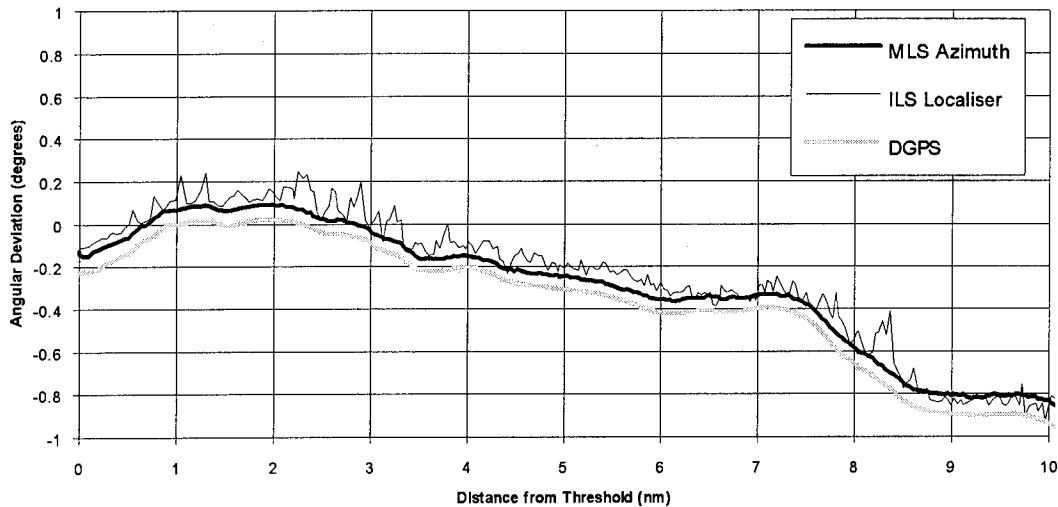


Figure 3. ILS, MLS and DGPS localiser deviation comparisons

FURTHER DEVELOPMENTS

The requirements of integrity, accuracy, continuity of service and availability for all weather operations are very stringent. It is appreciated that the current technology available for commercial aviation would require the resolution of many technical issues before it could be considered for use as an alternative to ILS. It is however recognised that the technology available for GPS is moving forward all the time. The equipment set-up used in this evaluation will thus be upgraded as such improved technology becomes available.

Apart from the assessment of DGPS performance, Project Heathrow is actively involved with the development of concepts to aid the implementation and use of a future GNSS. Two areas that are currently being investigated are (1) Choice of Local Area Datalinks and (2) Extension to the En-route Environment.

THE CHOICE OF DATALINK

An underlying issue for implementation and use of a GNSS during the approach and landing phases of flight is the choice of datalink used to uplink satellite differential correction and integrity messages to the aircraft. Numerous RF modulation schemes have been proposed and assessed for this application including VHF, L-band, C-band and TDMA based datalinks.

The implementation of a GNSS should facilitate maximum interoperability. Not only should this be applicable to the different categories of approach but

also to the use of different technologies within the global augmentation. With respect to the issue of datalink interoperability, the key is a common datalink message format. This would then allow the use of datalink technologies which are most suited for the region and the particular operation.

The choice of datalink for future GNSS applications will be dependent on various factors including spectrum availability, interference resistance and user implementation costs. Table 1 below summarises the desirable characteristics of a GNSS datalink and indicates whether or not the proposed datalink formats possess the characteristics.

Use of a VHF frequency to uplink corrections for future GNSS application shows promise. However, there are several important factors which need resolution before the application can be implemented. The VHF datalink may use the 108-118 MHz frequency band by utilising any unused ILS and VOR frequencies, or the 118-137 MHz communications band. The VHF spectrum, particularly towards the lower frequency end is susceptible to interference from FM radio broadcasting. The potential effect of such interference on a DPSK data message requires further evaluation. Other factors which need to be addressed include VHF spectrum congestion, which is of particular concern in the European region, and transmission capabilities for safety critical and time critical data.

Mode S was designed for secondary surveillance radar operations and includes a 1090 MHz downlink and a 1030 MHz ground station uplink to the aircraft. In a Mode-S/GNSS configuration, the differential and

supporting operational data would be time multiplexed with the other data already existing on the datalink. The Mode-S does not currently possess the requirements for a safety critical datalink and would not be able to do so without a major system upgrade. Its use as a source for a GNSS datalink would also

violate the desired partitioning between navigation, communications and surveillance during flight operations in the terminal environment.

| Desirable Characteristics | Mode-S | L-Band | Pseudolite | VHF | C-Band |
|---|--------|--------|------------|-------|---------------|
| Technical Feasibility | | | | | |
| Sufficient Number of Channels | No | Maybe | Maybe | No | Yes |
| Bandwidth/Data Rate | No | Maybe | Maybe | Maybe | Yes |
| Interference Resistance | Maybe | No | No | No | Yes |
| Available Frequency Spectrum | Yes | No | Maybe | Maybe | Yes |
| Interoperable for all categories of approach services | No | Maybe | Yes | Maybe | Yes |
| Fast track ICAO SARPS for approach services | No | No | No | No | Yes |
| On-Airport siting | Yes | Yes | Yes | Yes | Yes |
| Designed for safety critical applications | | | | | |
| DO-178B/ED-12B | No | No | No | No | Yes |
| DO-160C/ED-14C | No | No | No | No | Yes |
| Meets Integrity, Continuity and Availability | No | No | No | No | ICAO protocol |
| Standard Aircraft Polling (Duplex/Triplex) | No | No | No | No | Yes |
| Designed for 360° aircraft coverage | Yes | Yes | Yes | Yes | Yes |
| Maintains CNS functional partitions | No | Maybe | Maybe | Yes | Yes |
| Easily included in MMR architecture | No | Yes | Yes | Yes | Yes |
| Low costs for operators and users | No | Maybe | No | Yes | Yes |

Table 1. Desirable characteristics for a GNSS datalink

An L-band datalink concept would also require significant development if it is to be considered for a safety critical application. Needless to say, any L-band datalink must not interfere with the GNSS L-band transmissions and care must be taken that the datalink is not susceptible to other potential interference sources in the band such as JTIDS, DME and TACAN. An attraction of this architecture would be its near uniform L-band front end which would simplify future receiver designs.

Currently only the C-band datalink can meet all the requirements for a GNSS datalink. This characteristic is achieved because the C-band datalink protocol was developed as part of the MLS function and therefore provides an ICAO standardised datalink function for all categories of operation. The concept now needs to be further demonstrated as a stand alone GNSS datalink function.

Future developments may lead to a combination of RF modulation schemes adopted for GNSS datalink applications. VHF GNSS datalinks may be further

developed by regions which do not envisage a shortage of VHF channels and corresponding interference problems. On the other hand, regions which do expect problems with VHF channel congestion may adopt the C-band datalink which is proven technology and provides an ICAO approved protocol for early implementation

In order to maintain interoperability onboard the aircraft, the method by which an RF receiver translates the serial data from the data link transmission medium into ARINC words for translation by the GNSS receiver should be independent of the RF modulation scheme or the system used to uplink the message from the ground to the aircraft. Appendix A of Draft 5 of Supplement to ARINC characteristic 743A (MOPS for GNSS Sensor) proposes a suitable physical layer interface for this requirement, summarised as follows:

The ARINC 429 broadcast protocol is independent of the data link used to uplink the differential message and utilises two ARINC 429 labels to

send a message block. The message block transfer begins with a label 045 followed by the transmission of repeating label 046 until the end of the data block. Label 045 designates the start of a broadcast message and contains the length of the application data which follows in terms of the number of ARINC (16 bits) which follow.

It is likely that this methodology will be accepted by the AEEC for the ARINC 743A MOPS and also for the ARINC 755 (Multi-Mode Receiver) MOPS.

In view of the above, there is a requirement to have a common datalink message format which could be

uplinked to the aircraft irrespective of the RF modulation scheme employed by the datalink. Currently the only message format for differential applications is defined in the Minimum Aviation Performance Standards for the Special Category I (SCAT-1) Instrument Approach System (RTCA/D0-217). This format now needs to be extended or redefined so it is applicable and interoperable with other categories of operations. Once a standard GNSS differential message format is agreed, it could be used irrespective of the datalink employed for the particular application. Figure 4 provides an overview of the requirements.

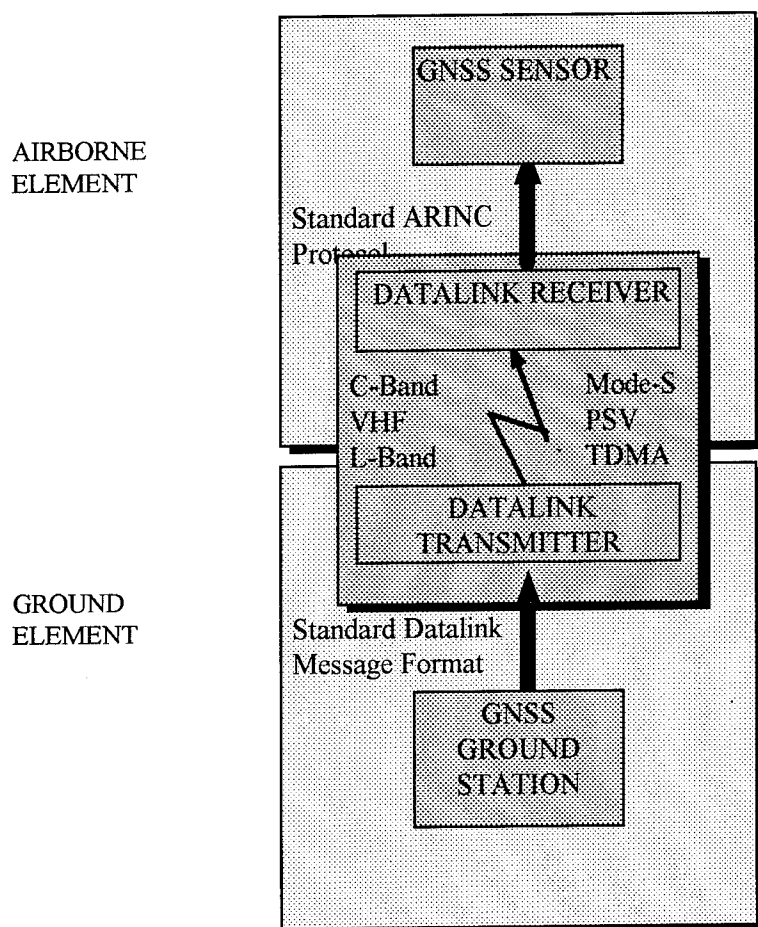


Figure 4. GNSS Datalink Interoperability.

Project Heathrow is currently being extended to include a revenue service DGPS data collection exercise between Heathrow and Munich. The evaluation will use both the C-band and VHF datalinks to uplink the differential corrections and work is currently being undertaken to devise a common message format for the datalinks.

EXTENSION TO THE EN-ROUTE PHASE

An extension to Project Heathrow aims to investigate the application of satellite navigation systems in the en-route environment where it has the potential to give valuable benefits to users and civil authorities. The extension is being carried out in collaboration with Siemens Plessey Systems, Racal Electronics and Roke

Manor Research and the existing Project Heathrow participants. This extension involves the use of a regional area GPS monitoring network and is the subject of another paper to be presented at this conference.

PROJECT ABERDEEN

The technology available for DGPS ground systems and airborne receivers is moving forward. It has been identified that the static receiver is highly susceptible to multi-path interference which might prove to be a problem for differential ground stations. The narrow correlator receiver has been shown to reduce multi-path errors and further multi-path eliminating techniques using advanced software are being developed. Project Aberdeen was carried out by NATS to complement Project Heathrow by investigating the advantages to be gained by using new receiver technologies and careful antenna site selection to reduce multi-path errors at the differential ground station.

At Aberdeen airport an MLS transmitter was installed and modified to transmit differential GPS corrections using the C-Band data link as is done at Heathrow. The DGPS ground station is based around the latest receivers using narrow correlator technology. The antenna has been placed on the ground in a clear site to avoid multi-path interference. The antenna site was carefully selected after performing a multi-path survey of the area.

The airborne equipment consisted of an MLS receiver designed to ARINC 727 standards that is capable of decoding the differential corrections and output them as ARINC 429 labels for the GPS receiver to use. The airborne GPS system also uses the narrow correlator receiver.

Results

A series of flight tests were carried out in December 94 with the main objective of evaluating the performance of the high integrity data-link which looks very promising for the transmission of differential GPS corrections. Carrier phase data was recorded on the aircraft and at the ground station to allow for post processing to give a truth reference with centimetre level accuracy. During most of the approaches sub-meter position accuracies were achieved on the aircraft but there were a small number of anomalies noticed during aircraft dynamics. During dynamic manoeuvres excursions exceeding $\pm 1\text{m}$ from the true position were apparent. This was later identified as a receiver software problem in the implementation of carrier aiding of the code tracking loop. The receiver manufacturer assures us that this

problem has been resolved and does not exist in the new version of their receiver.

These high accuracies were achieved, in part, by careful selection of the ground antenna site. The antenna was placed flat on the ground away from buildings and other obstructions and a 1 sigma multipath error of approximately 10cm was obtained. At a poor site multi-path errors of many meters could theoretically be introduced into individual pseudorange measurements resulting in a significant error in computed position. For a receiver with a standard correlator the errors could be many times more than this. Multi-path errors cannot be removed by the use of differential techniques. It has been found that the location of the ground station antenna is critical to the entire system performance and must be very carefully surveyed for multi-path. The area around the antenna must be protected from future developments. Antennas mounted on poles or buildings are vulnerable from ground reflections which may cause significant multi-path interference.

Initial indications show the levels of accuracy achieved using such a system can meet Cat 1 precision approach accuracy requirements. However, there is still the question of meeting the other RNP parameters such as availability, integrity and continuity of service.

Further trials with this DGPS system are scheduled to be carried out later this year at Boscombe Down Airfield.

CONCLUSIONS

This paper has described projects currently underway at UK airports. The type of step by step qualitative assessment of the performance of DGPS as being done at Heathrow is what is now required to continue to assess the application of GPS in precision approach services. To date, all evaluations undertaken to assess the feasibility of the concept have been conducted under experimental conditions. Attempts have been made to perform more comprehensive studies, however, many problems have been encountered during these projects, the problems caused being indicative of the equipment being immature. Unlike those projects, this evaluation is intended to run over a long period of time, allowing the full range of operational conditions to be examined and subsequent development implemented where necessary. The results will enable performance statistics on the use of GPS under operational conditions to be determined and also be used in the development of standards for the Multi-Mode receiver (MMR), which is seen to provide optimum flexibility and minimise retrofit effort during the transition from ILS.

Floating Differential GPS (FDGPS)

James L. Brown
Aydin Corporation (East)

BIOGRAPHY

James L. Brown is a Senior Systems Engineer at Aydin Corporation (East) in the Business Development unit. He has a BSEE from Michigan State University and an MSEE from Wichita State University. He has over 30 years experience in the design, development, modeling, real time simulation (DIS), and implementation of Navigation and Weapon Delivery Systems, Trainers, All Weather Flight Control Systems, Remote Piloted Vehicles, and associated GPS technologies. The GPS technology started with the analysis and simulation of an automatic fail-operational landing system using the Air Forces 621B Satellite Positioning System, now designated as GPS.

ABSTRACT

The subject of this paper is the control and tracking of vehicles that are Over The Horizon (OTH) and maintain positional accuracies of less than 8 meters by using a floating differential GPS "All-in-view" Reference Receivers. Various existing methods that are in different stages of development/implementation that can solve part of the problem are the Extended Differential GPS, Coast Guard Harbor control, Wide Area Differential GPS (WDGPS) and Radio Data System (RDS). They all use networks of differential and/or monitor stations and FM radio station subcarriers to augment the differential solutions and require monitor and/or ground network stations to function properly. The situation that will be discussed in this paper involves remotely controlled vehicles all OTH with no terrestrial base station Line of Site (LOS). The vehicles can be air, ground, sea vehicles or combinations of each. The remote vehicles of course must be controlled and tracked from a Master Ground Station (MGS) and the Vehicle Control Commands and Time Space Position Information (TSPI) must be passed (datalinked) to and from the vehicles under control. It is defined, for this paper, that all OTH vehicles fall into the category of there is no LOS between the OTH vehicle and the MGS. This could be a vehicle hundreds of nautical miles from the MGS at some altitude or it could be a vehicle in

close proximity of the MGS, but because of the terrain no LOS is possible. In both situations, the OTH vehicle will need a relay to transmit and receive the appropriate differential and trajectory control information. This is illustrated in Figure 1.

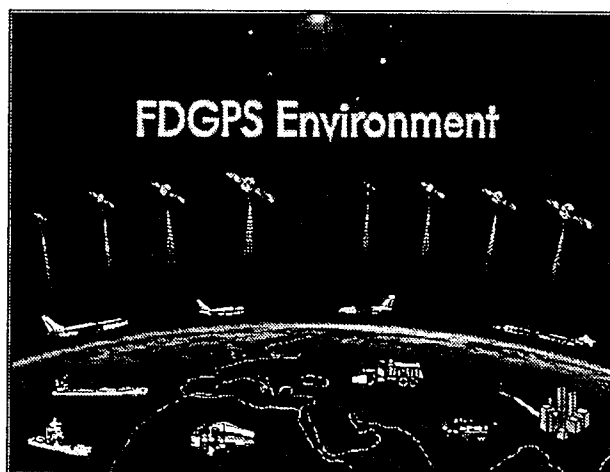


Figure 1. *FDGPS Environment*

DEFINITION

The floating Differential GPS (FDGPS) proposed, is defined that each vehicle contains an "all-in-view" differential GPS and can be utilized as a Reference Receiver.

PRINCIPLE OF OPERATION

The following description will provide the functionality of a floating DGPS. At the MGS, the reference receiver, a DGPS (5 - 12 'all-in-view' channel receiver), is surveyed, and the differential processing is carried out. The appropriate pseudorange, pseudorange rate, and ephemeris data is transmitted via datalink to the LOS vehicles. These LOS vehicles will then use this information to calculate its corrected position. The differential calculations accomplished on the LOS vehicle will now allow it to become a Reference Receiver for other OTH vehicles, which are in LOS of the "reference" vehicle. This

"reference" vehicle will now become a relay. The "reference" vehicle will now transmit the same correction information that the MGS Reference Receiver did, along with any additional pseudorange corrections acquired, but to a new OTH audience. The major item is that the same four Satellite Vehicles (SVs) must be used in the calculation of the differential data. However if the OTH vehicle can use the information from any of the 'all-in-view' Satellite Vehicles (SVs) that the MGS was viewing, the OTH vehicle will calculate its differential information using both the MGS Reference Receiver data and the "reference" vehicle data. The OTH vehicle will then calculate its differential position and will become a "reference" vehicle for other OTH vehicles. The LOS vehicle and all of the OTH vehicles must datalink the appropriate position and velocity information back to the MGS for its processing of control functions and tracking of the vehicles. There can be a series of OTH vehicles which can expand the differential processing over many relays, and in turn many miles.

The remainder of this paper will depict the analysis, development, and generation of error equations used to illustrate the propagation of position errors as a function of the number of relays, GDOP, pseudorange, and other related errors.

Basic Pseudorange Equations

The first item is to identify the standard pseudorange and pseudorange rate equations. The basic equations, References 9 (pg 9) and reference 8 (pgs 305-310) for the navigation equations and Pseudorange (ρ_R) equations.

The basic pseudorange equation is given by:

$$\rho_R = [(x_u - x_s)^2 + (y_u - y_s)^2 + (z_u - z_s)^2]^{\frac{1}{2}} - \epsilon_R$$

where

$$[(x_u - x_s)^2 + (y_u - y_s)^2 + (z_u - z_s)^2]^{\frac{1}{2}}$$

is the true range ρ_{R_T}

x_u, y_u, z_u = user coordinates

x_s, y_s, z_s = Satellite Vehicle (SV) coordinates

ϵ_R = all errors

The error term ϵ_R can be separated into two elements, the error due to time and all other errors.

The time error is defined in ICD-GPS-200 (pg 72) and is expressed as $c\Delta t$, where c is the speed of light and Δt is the time error. The remaining element (σ_{ϵ_p}), which represents the remaining errors is given as:

$$\delta \epsilon_p = [(\epsilon_x^u - \epsilon_x^{s_i})^2 + (\epsilon_y^u - \epsilon_y^{s_i})^2 + (\epsilon_z^u - \epsilon_z^{s_i})^2]^{\frac{1}{2}}$$

Where:

$\epsilon_{x,y,z}^u$ = the position, measurement, Quantization, etc. error associated with the coordinate system for the user.

$\epsilon_{x,y,z}^{s_i}$ = the position, measurement, Quantization, etc. error associated with the coordinate system for the satellite vehicle. The subscribe (i) represents the number of satellites being tracked/measured.

Then it follows that the pseudorange equation for each tracked/measured Satellite is given by:

$$\rho_{R_i} = \rho_{R_T} - c\Delta t - \delta \epsilon_p$$

The Pseudorange Rate equation becomes more involved with the error function having three different element plus the time error function ($c\Delta t$).

The three elements are:

$\rho_{\dot{R}_p}$ position error contribution

$\rho_{\dot{R}_v}$ velocity error contribution

$\rho_{\dot{R}_{pv}}$ second order error contribution

The true pseudorange rate with the time error included is given as:

$$\frac{\rho_{\dot{R}} + c\Delta t}{\rho_{R_T}} = \frac{(x_u - x_s)(\dot{x}_u - \dot{x}_s) + (y_u - y_s)(\dot{y}_u - \dot{y}_s) + (z_u - z_s)(\dot{z}_u - \dot{z}_s)}{\rho_{R_T}}$$

The error contributed as a function of position is given by:

$$\rho_{\dot{R}_p} = \frac{(\epsilon_x^u - \epsilon_x^{s_i})(\dot{x}_u - \dot{x}_s) + (\epsilon_y^u - \epsilon_y^{s_i})(\dot{y}_u - \dot{y}_s) + (\epsilon_z^u - \epsilon_z^{s_i})(\dot{z}_u - \dot{z}_s)}{\rho_{R_T} + \epsilon_R}$$

The error contributed as a function of velocity is given by:

$$\rho_{R_v} = \frac{(x_u - x_{s_i})(\dot{x}_u - \dot{x}_{s_i}) + (y_u - y_{s_i})(\dot{y}_u - \dot{y}_{s_i}) + (z_u - z_{s_i})(\dot{z}_u - \dot{z}_{s_i})}{\rho_{R_r}}$$

The error contributed by second order terms is given by:

$$\rho_{R_p} = \frac{(e_x^u - e_x^{s_i})(\dot{e}_x^u - \dot{e}_x^{s_i}) + (e_y^u - e_y^{s_i})(\dot{e}_y^u - \dot{e}_y^{s_i}) + (e_z^u - e_z^{s_i})(\dot{e}_z^u - \dot{e}_z^{s_i})}{\rho_{R_r}}$$

These equations can be presented as the following and are calculated for each tracked/measured SV.

$$\rho_{R_i} = \rho_{R_r} + \rho_{R_p} + \rho_{R_v} + \rho_{R_{vp}}$$

Pseudorange Measurement and Calculations:

The method of measurement can be illustrated by the following (Reference 8, pg 310);

$$\rho_{m_i} = c(t_{Rx} - t_{Tx})$$

where

c = speed of light

t_{Rx} = time signal received

t_{Tx} = time signal transmitted

When the Pseudorange is known and the position of the satellite(s) are established, the solution for the position and time can be calculated using the simultaneous equations as previously discussed. The method, as is well known and will be used in detail later, is that by knowing the measured Pseudorange and knowing the surveyed position of the reference receiver (DGPS) a pseudo range can be calculated and then the difference between the measured and the calculated will provide a correction factor for the pseudorange for each SV. The correction factor that will be transmitted, is defined as $\Delta \rho_i$ (reference 4, method 1).

The users that are on a Line-Of-Sight (LOS) with the Surveyed Receiver (MGS Reference Receiver) will be defined as LOS_{k_i} , where $k=1$ is the user that is in the LOS of the MGS Reference Receiver (MGSRR), $k=2$ is the user that is in the LOS of the user, as defined, but is not in the LOS of the MGSRR, and $k=3,4$, etc are the ongoing levels of LOS users. For simplicity of discussion, only one user at each level will be addressed in the following analysis results.

With these ground rules set and the first level user will be receiving the pseudorange corrections, the method of establishing the first level user as a Reference Receiver is described in the following manner.

First Level User:

The measurement of pseudorange as defined above is $\rho_{m_i} = c(t_{Rx} - t_{Tx})$ and the corrected pseudorange is given as:

$$\rho_{c_i} = \rho_{m_i} - \Delta \rho_i$$

Now the solution for the user position can be carried out utilizing the equations defined earlier. The solution will result in a x, y, and z position. As was accomplished earlier, the true position is viewed separate from the error element and is viewed as

$$\rho_i = [(x^u - x^{s_i})^2 + (y^u - y^{s_i})^2 + (z^u - z^{s_i})^2]^{\frac{1}{2}} - c \Delta t + [(e_x^u - e_x^{s_i})^2 + (e_y^u - e_y^{s_i})^2 + (e_z^u - e_z^{s_i})^2]^{\frac{1}{2}}$$

Where the error portion of this equation can be written as

$$[(e_x^u - e_x^{s_i})^2 + (e_y^u - e_y^{s_i})^2 + (e_z^u - e_z^{s_i})^2]^{\frac{1}{2}} = [(\delta e_x)^2 + (\delta e_y)^2 + (\delta e_z)^2]^{\frac{1}{2}} = \delta e_p$$

Which when viewed in terms of pseudorange calculations is

$$\delta \rho_i = \rho_{c_i} - \rho_{m_i} + \delta e_p$$

and the error term δe_p is, in effect, $PDOP_{LOS_{k_i}} \cdot e_{LOS_{k_i}} + \delta \sigma_i$, where Geometric Dilution of Precision (GDOP) and the 3D position (PDOP) Dilution of Precision are defined in Reference 1, pgs 10-14. The $e_{LOS_{k_i}}$ is the sum of individual errors (Ephemeris, Ionospheric, etc.) and are defined in Reference 5, Table 1 page 90, and Reference 6, Table 4.1 page 141. The term $\delta \sigma_i$ is the correction factor generated by the differential manipulation. It is the ratio of the Differential GPS error and the GPS error.

From this, the correction that is transmitted to the next LOS user is viewed as

$$\delta \rho_I = \Delta \rho_I + \delta \epsilon_p$$

It has to be noted that if there is a SV in view of the LOSV, and is not part of the MGSRR all-in-view configuration. The procedure to calculate its pseudorange correction must be carried out in the same manner as was accomplished for the MGSRR. The difference is that the "surveyed position" is now the corrected or differential calculated position of the user. It is also deemed necessary to forward the pseudorange correction accomplished by the MGSRR to the next level user. This could alleviate using a corrected pseudorange value versus a more accurate MGSRR pseudorange correction.

Second To n Level Users:

The second level user follows the same procedure as the first level user accomplished. The difference at the second level and remaining levels is the error changes. For example, the second level error term is given by

$$\delta_{\epsilon_p}(2) = PDOP_{LOS_{V_2}} * (\epsilon_{LOS_{V_2}} + PDOP_{LOS_{V_1}} * \epsilon_{LOS_{V_1}} * \delta_{CF_1}) * \delta_{CF_2}$$

The error function at the third level results in error function as described in the following expression.

$$\delta_{\epsilon_p}(3) = PDOP_{LOS_{V_3}} * [\epsilon_{LOS_{V_3}} + \delta_{\epsilon_p}(2)] * \delta_{CF_3}$$

and the fourth level is given by:

$$\delta_{\epsilon_p}(4) = PDOP_{LOS_{V_4}} * [\epsilon_{LOS_{V_4}} + \delta_{\epsilon_p}(3)] * \delta_{CF_4}$$

and continues to propagate to the nth level, and is given by:

$$\delta_{\epsilon_p}(n) = PDOP_{LOS_{V_n}} * [\epsilon_{LOS_{V_n}} + \delta_{\epsilon_p}(n-1)] * \delta_{CF_n}$$

Numeric Calculations:

In the above equation for $\delta_{\epsilon_p}(n)$, each variable has a range of values. Table 1, RANGE ERROR BUDGET, depicts the error budgets that were defined in references 1 through reference 6. The individual elements (ephemeris, ionospheric, etc) errors are defined as $\epsilon_{LOS_{V_n}}$. This includes errors for the GPS and Differential GPSs C/A and P codes. The resultant

of these errors range from 4 meters to greater than 30 meters. PDOP is described in Figure 4 of Reference 1 and has values 2.43 or less for the median and 3.28 or less for the 90 th percentile. The correction factor, δ_{CF_n} , is generated by looking at what the GPS error is with and without differential corrections and using that ratio as the correction factor. For example, P code GPS is 16m or less on given systems. The same GPS system if used with a differential is in the order of 4 meters or less. A different correction factor value for C/A type code would be in the order of 75-100m and with differential would be 10 m or less. This all leads to a set of variables that have to be varied over several ranges. This is illustrated by:

$$\epsilon_{LOS_{V_n}} = 4, 10, 20, 30 \text{ meters}$$

$$PDOP_n = 2.43, 2.75, 3.0, 3.28$$

$$\delta_{CF_n} = 0.1, 0.25, 0.5$$

$$\text{Number of relays} = 8$$

When calculating the $\delta_{\epsilon_p}(n)$ equations for the number of relays ($n = 1, 8$), the results are shown in Table 2. To illustrate the function of these errors, 3 additional 3D graphs are generated. The first graph is shown in Figure 2, which illustrates the resultant error as a function of PDOP and the error magnitude ($\epsilon_{LOS_{V_n}}$) at a given correction factor of 0.25 (4/16).

Figures 3 and 4 are for error magnitudes of 4 and 30 meters respectively and a correction factor of 0.25. For an error magnitude of 4 (Figure 3), the comparison between PDOP and the number of relays and the resultant errors (meters) is depicted. The results in Figure 3 illustrates the nonlinearity in the error as PDOP increases and the number of relays increase. This rise in error is larger in Figure 4, which is depicting the error magnitude of 30 meters and PDOP of 3.28.

It was expected that, as the number of relays increased, the error will increase. The data shows that the error increased for each relay as was expected. There will be another layer of error added onto the new reference receiver number. The magnitude of increase will of course be a function of the initial error magnitude, PDOP, and the correction factor. It should be noted that the correction factor was held constant over the eight relays, while in the real world, the correction factor will be larger as the number of relays increase (0.25 → 0.5). The two extremes of resultant error are also as expected, the

low end as shown in Table (GPS>DAT) for $\epsilon_{LOS_V_n}=4$, $\delta_{CF_n}=0.1$, PDOP=2.43 and eight relays has a resultant error of 1.284 meters. While on the other end of the spectrum, the condition of $\epsilon_{LOS_V_n}=30$, $\delta_{CF_n}=0.5$, PDOP=3.28 and eight relays has a resultant error of 3946 meters.

Conclusions:

The initial numeric results indicate that this method is feasible for conditions where Over-The-Horizon (OTH) or Non-Line Of Sight receiver are required. This method could also complement the WADGPS and other differential GPS ranging methods. For example, one of the methods would be used up to the allowable range past the CONUS coastline. This method would then extend the coastline accuracy over a range for many hundreds of miles. Whereby, maybe a ship could be one of the relays to aide in the range extension.

Acknowledgments:

The author wishes to acknowledge the efforts of Mr. Gary Boswell, Past President of Aydin Computer and Monitor Division and Mr. James Dougherty, Vice-President of Commercial Software of Aydin Computer and Monitor Division. The extra efforts of reviewing the development and final conclusions by both Gary and James are greatly appreciated.

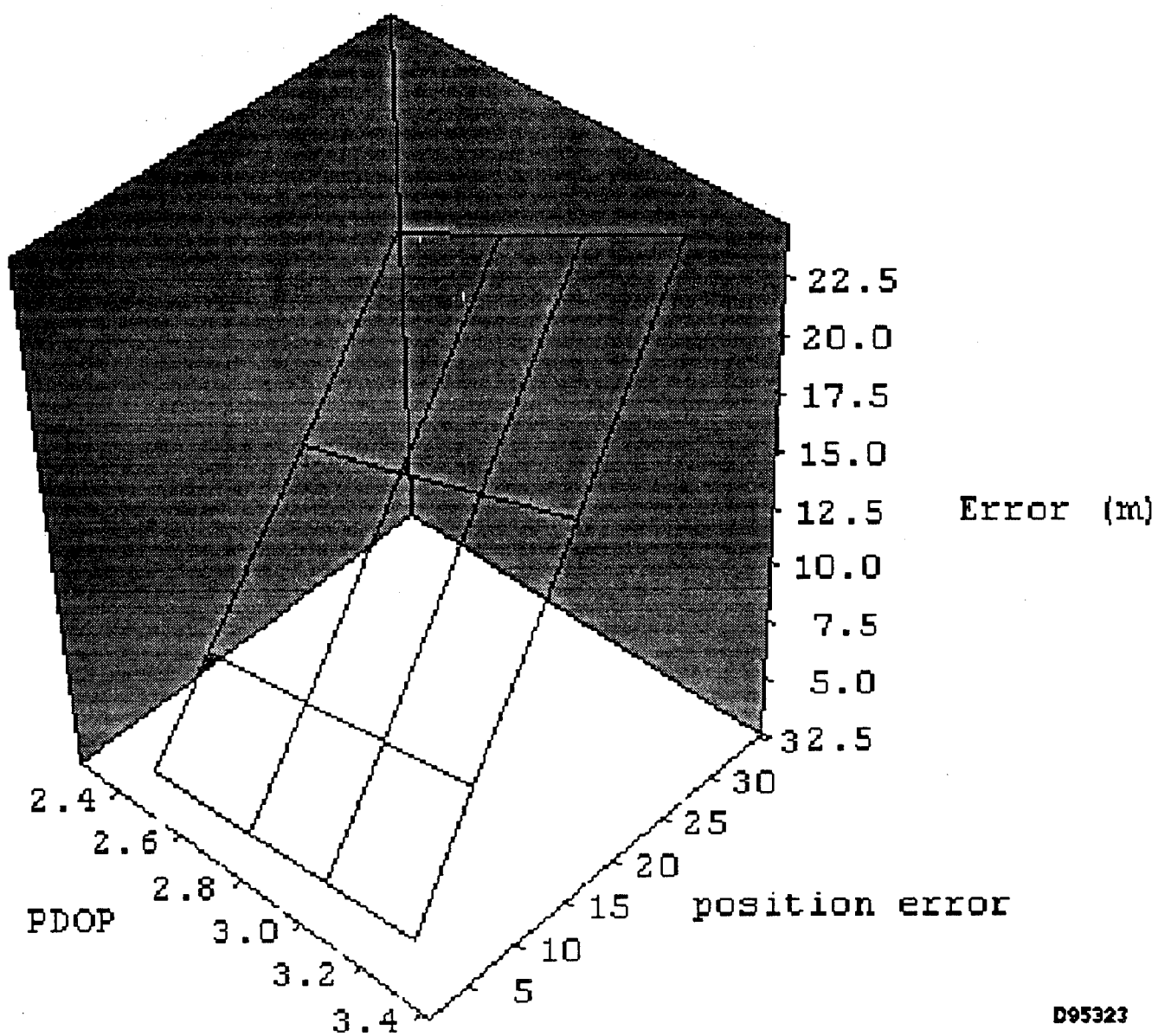
REFERENCES

- 1) NAVSTAR OPERATION
VOL I, ION pg 9
R. J. Milliken & C. J. Zoller
- 2) GPS Pseudolite Locations
Parkinson, et al VOL IV, ION pg 66, 67,
Tables 1, 2, and 3
- 3) GPS Pseudolite Locations
Parkinson, et al VOL IV, ION pg 83, 84,
Tables 8, 9
- 4) Differential GPS Methods
Blackwell
VOL III, ION Pg 93, Table 2
- 5) Differential GPS Methods
Blackwell
VOL III, ION Pg 90, Table 1
- 6) Differential GPS
Besar and Parkinson
VOL II, ION pg 177-183
- 7) Modern Navigation, Guidance, and Control
Processing VOL II, Section 7.5 pg 447-453,
Ching-Fang Lin
- 8) Aerospace Avionics Systems
Section 6.2, pg 305-310
Siouris
- 9) NAVSTAR/Global Positioning System
18 Satellite Constellation
ION VOL II pg 9-11
P. S. Jorgensen
- 10) Extended Differential GPS
Alison Brown
The NAVSYS Corporation
Monument, CO 80132
- 11) ICD-GPS-200

Table 1. Range Error Budget

RANGE ERROR BUDGET
Table 1

| ERROR ELEMENT | Reference 1 | Reference 1 | Reference 2 | Reference 2 | Reference 3 | Reference 4 | Reference 4 | Reference 5 | Reference 5 | Reference 6 | Reference 5 |
|--|--------------------|--------------------|--------------------|--------------------|-------------|--------------|----------------|-------------|-------------|-------------|-------------|
| | Low (meter) | High (meter) | C/A (m) | C/A : SA | DGPS (m) | P (m) (DGPS) | C/A (m) (DGPS) | P (m) | C/A (m) | Absol (m) | Diff (m) |
| SV clock error ¹ & | 1.5 ^{***} | 1.5 ^{***} | 3.5 | 20 | 0.7 | 0 | 0 | 10 | 10 | 2.7 | 2.7 |
| Nav subsystems stability ² | | | | | | | | | | | |
| Ephemeris error | | | 1.7 | 1.7 | 0 | 0 | 0 | 8.6 | 8.6 | 2.5 | 0 |
| Atmospheric Delays | 2.4 | 5.2 | 4 | 4 | 0 | 0.5 | 0.5 | 1.3 | 21 | 2.3 | 0 |
| Ionospheric | | | 0.5 | 0.5 | 0.5 | | | 1.3 | 1.3 | 2 | 2 |
| Tropospheric | | | | | | | | | | | |
| Group Delay (SV eqp) | 1 | 1 | | | | | | | | | |
| Multipath | 12 | 2.7 | 1 | 1 | 1 | 4 | 10 | 4 | 10 | 1.2 | 1.2 |
| Rx noise & Resolution | 1.5 | 1.5 | 3.5 | 3.5 | 3.5 | 0.5 | 2 | 0.8 | 8 | 1.5 | 1.5 |
| Vehicle Dynamics | | | | | | 0.8 | 8 | 0.5 | 2 | | |
| Calibrated Site Resid | | | | | 1.9 | | | | | | |
| Predictability of SV | | | | | | | | | | 1 | 1 |
| Perturbations | | | | | | | | | | | |
| Other | | | | | | | | | | 0.866 | 0.866 |
| RSS | 3.6 | 6.3 | 6.7 | 20.8 | 4.2 | 4.2 | 13 | 13.9 | 27.9 | 5.3 | 3.97 |
| RMS | | | | | | | | | | | |
| 1 Sigma | | | Est ^{***} | Est ^{***} | | | | | | 3 | 3 |
| PDOP | 2.43 | 3.28 | 3 | 3 | | 1.5 | 1.5 | 1.5 | 1.5 | | |
| HDOP | | | | | | | | | | | |
| VDOP | | | | | | | | | | | |
| Totals | | | 20.1 | 62.4 | | 6.3 | 19.5 | 21 | 42 | 16 | 12 |
| ^{***} SV clock & | | | | | | | | | | | |
| Ephemeris error | | | | | | | | | | | |
| ^{***} Estimated value of PDOP | | | | | | | | | | | |



D95323

Figure 2. Resultant Error PDOP/Error Magnitude

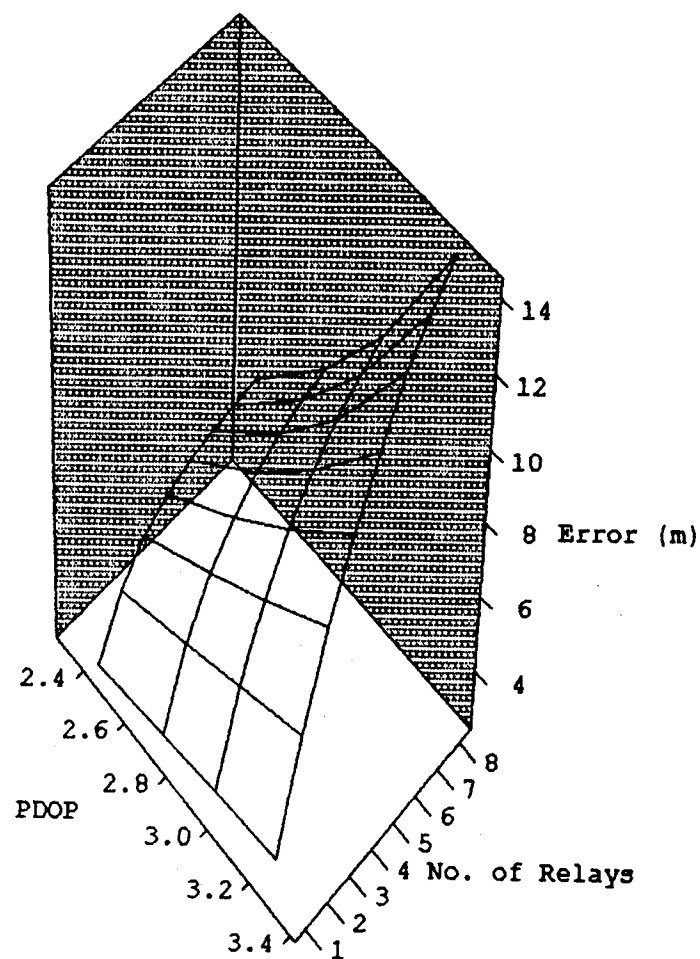


Figure 3. Resultant Error for E4-D25 PDOP vs. Number of Relays

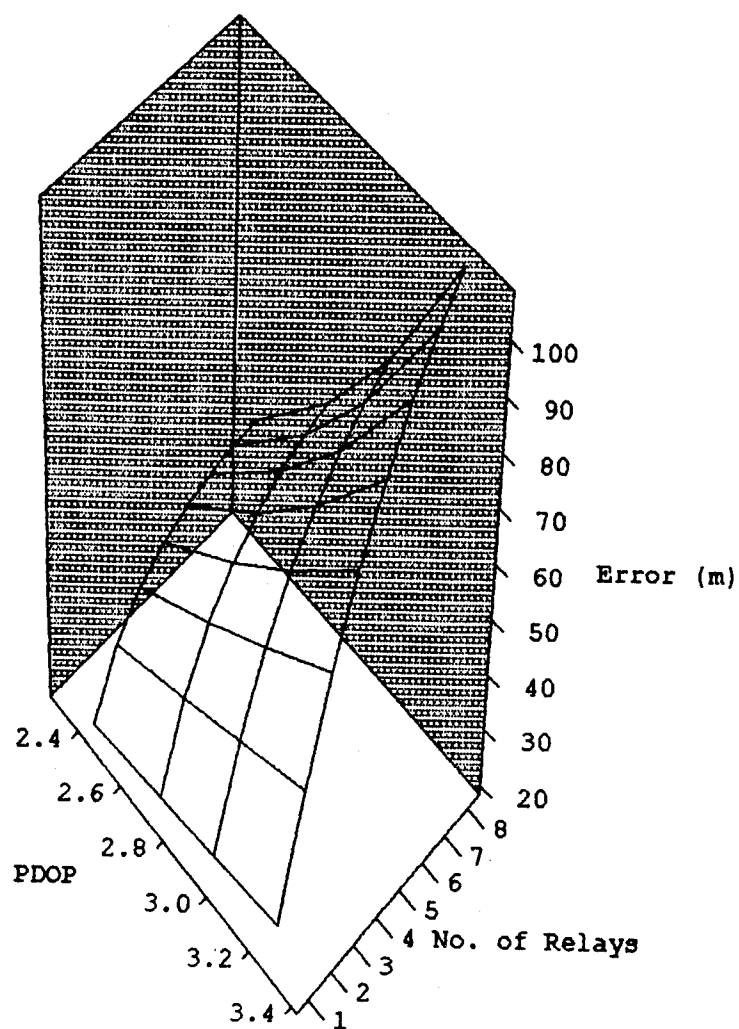


Figure 4. Resultant Error E30_D25 PDOP vs. Number of Relays

Table 2. Pseudorange Error Summary

| ERR | dc1 | PDOP | err1 | err2 | err3 | err4 | err5 | err6 | err7 | err8 |
|-----|------|------|-------|--------|--------|--------|--------|--------|--------|--------|
| 4 | 0.5 | 2.43 | 4.86 | 10.76 | 17.94 | 26.66 | 37.25 | 50.12 | 65.75 | 84.75 |
| | | 2.75 | 5.5 | 13.06 | 23.46 | 37.76 | 57.42 | 84.45 | 121.62 | 172.73 |
| | | 3 | 6 | 15 | 28.5 | 48.75 | 79.13 | 124.69 | 193.03 | 295.55 |
| | | 3.28 | 6.56 | 17.32 | 34.96 | 63.9 | 111.35 | 189.18 | 316.81 | 526.13 |
| 4 | 0.25 | 2.43 | 2.43 | 3.91 | 4.8 | 5.35 | 5.68 | 5.88 | 6 | 6.08 |
| | | 2.75 | 2.75 | 4.64 | 5.94 | 6.83 | 7.45 | 7.87 | 8.16 | 8.36 |
| | | 3 | 3 | 5.25 | 6.94 | 8.2 | 9.15 | 9.86 | 10.4 | 10.8 |
| | | 3.28 | 3.28 | 5.97 | 8.18 | 9.98 | 11.47 | 12.68 | 13.68 | 14.5 |
| 4 | 0.1 | 2.43 | 0.97 | 1.21 | 1.27 | 1.279 | 1.283 | 1.284 | 1.284 | 1.284 |
| | | 2.75 | 1.1 | 1.4 | 1.49 | 1.51 | 1.51 | 1.52 | 1.52 | 1.52 |
| | | 3 | 1.2 | 1.56 | 1.67 | 1.7 | 1.71 | 1.713 | 1.713 | 1.714 |
| | | 3.28 | 1.31 | 1.74 | 1.88 | 1.93 | 1.94 | 1.95 | 1.951 | 1.952 |
| 10 | 0.5 | 2.43 | 12.15 | 26.91 | 44.85 | 66.64 | 93.12 | 125.29 | 164.38 | 211.87 |
| | | 2.75 | 13.75 | 32.66 | 58.65 | 94.4 | 143.55 | 211.13 | 304.05 | 431.82 |
| | | 3 | 15 | 37.5 | 71.25 | 121.88 | 197.81 | 311.72 | 482.58 | 738.87 |
| | | 3.28 | 16.4 | 43.3 | 87.41 | 159.75 | 278.38 | 472.95 | 792.03 | 1315.3 |
| 10 | 0.25 | 2.43 | 6.08 | 9.77 | 12.01 | 13.37 | 14.2 | 14.7 | 15.01 | 15.19 |
| | | 2.75 | 6.88 | 11.6 | 14.85 | 17.09 | 18.62 | 19.68 | 20.4 | 20.9 |
| | | 3 | 7.5 | 13.13 | 17.34 | 20.51 | 22.88 | 24.66 | 26 | 27 |
| | | 3.28 | 8.2 | 14.92 | 20.44 | 24.96 | 28.67 | 31.71 | 34.2 | 36.24 |
| 10 | 0.1 | 2.43 | 2.43 | 3.02 | 3.16 | 3.2 | 3.21 | 3.21 | 3.21 | 3.21 |
| | | 2.75 | 2.75 | 3.51 | 3.71 | 3.77 | 3.79 | 3.79 | 3.79 | 3.79 |
| | | 3 | 3 | 3.9 | 4.17 | 4.25 | 4.28 | 4.28 | 4.28 | 4.28 |
| | | 3.28 | 3.28 | 4.36 | 4.71 | 4.82 | 4.86 | 4.87 | 4.88 | 4.86 |
| 20 | 0.5 | 2.43 | 24.3 | 53.82 | 89.7 | 133.28 | 186.24 | 250.58 | 328.75 | 423.73 |
| | | 2.75 | 27.5 | 65.31 | 117.31 | 188.79 | 287.09 | 422.25 | 608.1 | 863.63 |
| | | 3 | 30 | 75 | 142.5 | 243.75 | 395.63 | 623.44 | 965.16 | 1477.7 |
| | | 3.28 | 32.8 | 86.6 | 174.81 | 319.49 | 556.76 | 945.89 | 1584.1 | 2630.7 |
| 20 | 0.25 | 2.43 | 12.15 | 19.53 | 24.02 | 26.74 | 28.39 | 29.4 | 30.01 | 30.38 |
| | | 2.75 | 13.75 | 23.2 | 29.7 | 34.17 | 37.24 | 39.35 | 40.81 | 41.8 |
| | | 3 | 15 | 26.25 | 34.69 | 41.02 | 45.76 | 49.32 | 51.99 | 53.99 |
| | | 3.28 | 16.4 | 29.85 | 40.88 | 49.92 | 57.33 | 63.41 | 68.4 | 72.49 |
| 20 | 0.1 | 2.43 | 4.86 | 6.04 | 6.33 | 6.4 | 6.41 | 6.42 | 6.42 | 6.42 |
| | | 2.75 | 5.5 | 7.01 | 7.43 | 7.54 | 7.57 | 7.58 | 7.585 | 7.586 |
| | | 3 | 6 | 7.8 | 8.34 | 8.5 | 8.55 | 8.57 | 8.57 | 8.57 |
| | | 3.28 | 6.56 | 8.71 | 9.42 | 9.65 | 9.72 | 9.75 | 9.76 | 9.76 |
| 30 | 0.5 | 2.43 | 36.45 | 80.74 | 134.55 | 199.92 | 279.36 | 376.87 | 493.13 | 635.6 |
| | | 2.75 | 41.25 | 97.97 | 175.96 | 283.19 | 430.64 | 633.38 | 912.14 | 1295.5 |
| | | 3 | 45 | 112.5 | 213.75 | 365.63 | 593.44 | 935.16 | 1447.7 | 2216.6 |
| | | 3.28 | 49.2 | 129.89 | 262.22 | 479.24 | 835.15 | 1418.8 | 2376.1 | 3946 |
| 30 | 0.25 | 2.43 | 18.23 | 29.3 | 36.02 | 40.11 | 42.59 | 44.1 | 45.02 | 45.57 |
| | | 2.75 | 20.63 | 34.81 | 44.55 | 51.26 | 55.86 | 59.03 | 61.21 | 62.71 |
| | | 3 | 22.5 | 39.38 | 52.03 | 61.52 | 68.64 | 73.98 | 77.99 | 80.99 |
| | | 3.28 | 24.6 | 44.77 | 61.31 | 74.88 | 86 | 95.12 | 102.6 | 108.73 |
| 30 | 0.1 | 2.43 | 7.29 | 9.06 | 9.49 | 9.6 | 9.62 | 9.628 | 9.629 | 9.63 |
| | | 2.75 | 8.25 | 10.52 | 11.14 | 11.31 | 11.36 | 11.37 | 11.38 | 11.38 |
| | | 3 | 9 | 11.7 | 12.51 | 12.75 | 12.83 | 12.85 | 12.85 | 12.86 |
| | | 3.28 | 9.84 | 13.07 | 14.13 | 14.47 | 14.59 | 14.62 | 14.64 | 14.64 |

Characterization of Phase and Multipath Errors for an Aircraft GPS Antenna

C. Douglas Hardwick and Jeffrey Liu
National Research Council of Canada

BIOGRAPHY

Douglas Hardwick is Manager of Resource Geoscience at the Flight Research Laboratory, Institute for Aerospace Research, of the National Research Council of Canada. His projects in navigation include the development of one of the first fully automatic VLF Communication Station processors and the integration of VLF, Loran-C and GPS with an inertial navigation system. Current projects include the development of precise differential GPS for airborne gravity.

Mr. Hardwick graduated from the Royal Military College of Canada in 1955 as a navy pilot and obtained a BSc in Electrical Engineering from the University of Toronto. He worked on the design of advanced flight control systems in Canada, the US and Germany before joining the National Research Council in 1971.

Jeffrey Liu received his M.Sc. in Geomatics Engineering from the University of Calgary in 1993. He also holds a B.Sc and M.Sc. in Geodesy from Tongji University, Shanghai, China. He is currently doing research in the areas of GPS development for airborne gravity and precise GPS landing studies at National Research Council of Canada.

ABSTRACT

In the application of GPS to airborne gravity, the centimetre-level phase errors of an aircraft-mounted antenna can influence the results. Furthermore, the aircraft structure can give rise to multipath errors that are even more significant. This paper describes a project to characterize the errors of an aircraft-mounted antenna by carrying out short-baseline measurements over several days to build an error map as a function of satellite direction relative to the aircraft body frame. The calibration model is developed based on a set of carrier phase residuals. The effectiveness of the model is

demonstrated by using an independent set of test data. This antenna calibration should improve the estimation of vertical acceleration of the aircraft.

INTRODUCTION

This study is one component of a joint project between Sander Geophysics Ltd, the National Research Council of Canada, the Geological Survey of Canada and two oil companies, to develop a new generation of airborne gravity measuring system. It is the objective of the project to achieve better than 1 milligal accuracy with as little as 30 seconds of low pass filtering.

It has been well established that, within a GPS antenna, the effective phase centre is not a fixed, known point; it varies with satellite elevation (θ) and azimuth (ϕ) in the antenna coordinate system, as well as varying between the L1 and L2 signals [Schupler et al., 1991; Tranquilla et al., 1988]. In many GPS applications, these small uncertainties are insignificant; but in airborne gravimetry, where DGPS vertical position is double differentiated to produce vehicle acceleration to the accuracy specified above, the antenna errors become significant. In addition to the errors caused by phase centre uncertainty, multipath signal distortion caused by reflective surfaces on the host aircraft can be even more of a problem.

It has been argued that with the inevitable low pass filtering in a final airborne gravity system, no matter how short the time constant, the above errors will be filtered out. However, it should be remembered that there are long-period attitude changes in a helicopter or a fixed wing aircraft that approach the period of the gravity anomalies of interest. An example is the phugoid mode, an under-damped sinusoidal pitching motion with typical periods of 15 to 30 seconds. Furthermore, autopilot outer control loops that are coupled to navigation error signals can cause small roll attitude changes with periods of up to several minutes.

It is the objective of this project to model these errors and to minimize them, thus producing a cleaner, less noisy DGPS-measured vertical acceleration, leading to a decrease in the final low pass time constant.

METHODOLOGY

A helicopter was chosen as the test vehicle for this project because, in the early phases of system development, a slow surveying speed offers less of a challenge in terms of separating vehicle acceleration from gravity anomalies. The helicopter in this case is a Bell 206 Jet Ranger, owned by the National Research Council. The GPS receivers used are the dual frequency TurboRogueTM SNR 8000. The antenna to be characterized is an aircraft model supplied for this receiver, mounted on the helicopter as shown in Figure 1.

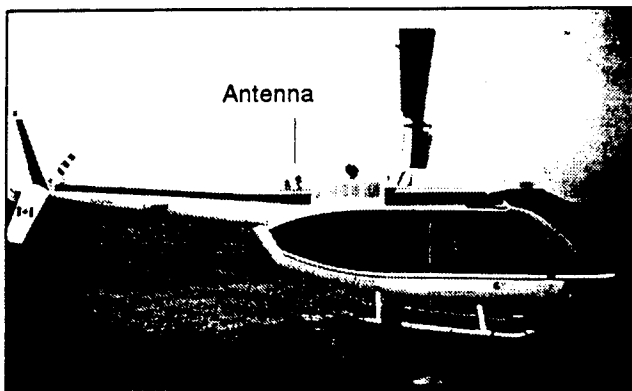


Figure 1. The configuration of an aircraft antenna mounted on the helicopter

The basic approach has been to collect error data with the antenna mounted on the helicopter, rather than trying to characterize the phase centre with the antenna by itself in an anechoic Radio Frequency (RF) chamber, as is sometimes done [Schupler et al., 1994; Tranquilla et al., 1994]. By making the error measurements *in situ*, the multipath errors, which should be a function of aircraft geometry, are included in the data. Measurements are made over a short baseline between the aircraft antenna and a reference antenna, the latter equipped with choke rings to minimize multipath from ground reflections. Using standard carrier phase techniques, the phase residual for each satellite in view is calculated, along with its azimuth and elevation. Double-differencing eliminates clock error between the two receivers, with the highest elevation satellite of satellites in view being used as the reference or "base" satellite. This choice is based on the fact that the higher the elevation, the greater is the freedom from phase-centre errors and multipath; thus, the residual error of the double-difference pair will essentially be that of the lower satellite. Double

differencing also significantly reduces the orbital and atmospheric errors.

There was some uncertainty with respect to the double-differencing approach, because the model has to be single-satellite specific. On the other hand, it would be difficult to map all possible pairs of satellite positions for a model. Single differencing, although difficult because of the differences between the receiver clocks, was done for purposes of comparison with double differencing, and as will be shown in the next section, there is little or no loss of accuracy when the model is based on double differencing as described above.

It is necessary to receive a satellite signal trajectory at virtually every point on the hemisphere of the aircraft antenna. Once this has been achieved, an error model can be created, the arguments for which are satellite elevation (θ) and azimuth (ϕ) in the antenna coordinate system. Once the coefficients for this model have been calculated, they can then be applied to reduce the overall position error residual, which, it is hoped, will lead to improved signal-to-noise in the computed vertical acceleration.

One problem with this approach is that of phase-centre and multipath errors in the reference antenna. This is illustrated in Figure 2, where for two TurboRogue reference antennas with choke rings on a short baseline, residuals are plotted as a function of satellite elevation. Clearly, there are errors associated with reference antennas. If the error model is constructed with the errors of the reference antenna included, the question arises as to what happens when the aircraft and the reference antenna are in a different geometrical relationship from when the model data were taken. For example, characterization data are taken with both antennas level, but when the aircraft changes attitude, the relationship will be different, as illustrated in Figure 3. It can be seen that the errors in the reference antenna should be excluded from the model.

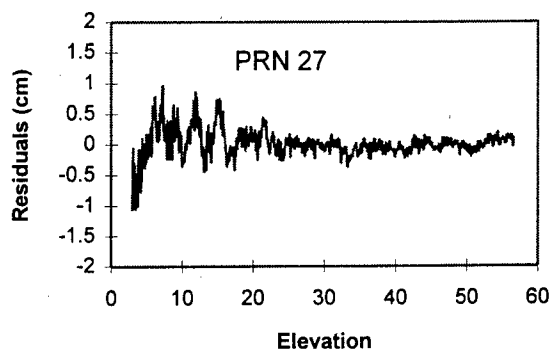


Figure 2. The residuals of one satellite for two TurboRogue reference antennas

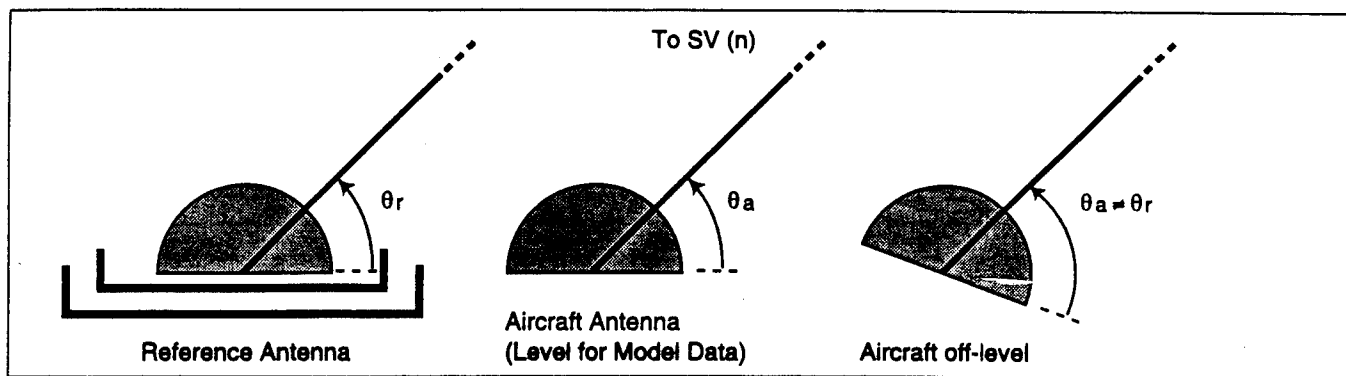


Figure 3. Relationships between reference and aircraft antennas

To accomplish this, an antenna chosen to be the reference was measured in an anechoic chamber and a reasonable representation of its errors as a function of elevation and azimuth was obtained, as shown in Figure 4, which presents the best-fit phase residuals for the reference antenna at L1 frequency. Since the major sensitivity is to elevation and because sensitivity to azimuth variations is small, the latter were neglected and an error model for the reference antenna was based on elevation only. Figure 5 shows the azimuthally averaged phase pattern for the reference antenna.

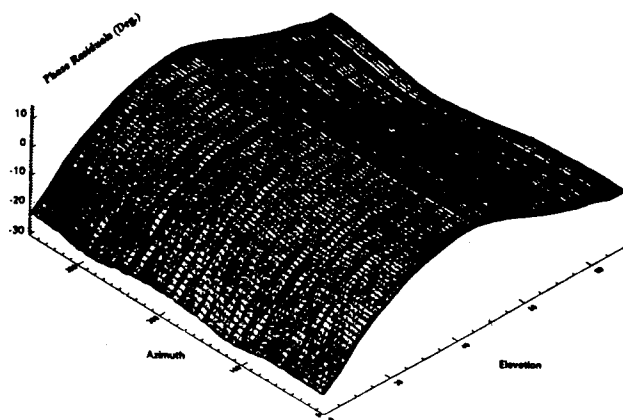


Figure 4. Phase residuals for the reference antenna at L1

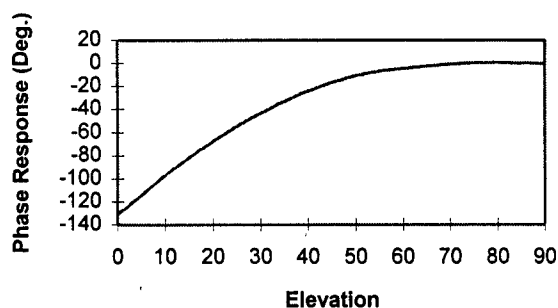


Figure 5. L1 phase pattern for the reference antenna

Thus, the model for the two antennas has the form

$$\text{Residual} = f\{\epsilon_R(\theta, \phi), \epsilon_R'(\theta), \epsilon_A(\theta, \phi)\} \quad (1)$$

where ϵ_R is the error in the reference antenna,
 ϵ_R' is the error characteristic of Figure 4 and
 ϵ_A is the error in the aircraft antenna.

An important consideration in collecting data for the model is to have the satellites more or less uniformly distributed over the hemisphere of the antenna. Otherwise, too much weight will be given to sections with heavy concentrations of satellites, while other sections with sparse concentrations or total voids will lead to a poorly conditioned solution for the model. Figure 6a shows a typical sky coverage at Ottawa over one day of data collection. To obtain uniform coverage, it was necessary to change the heading of the helicopter without in any way altering the antenna baseline. Figure 6b shows the sky distribution for three sessions, each on a different heading.

The modelling results achieved with static testing are shown in the next section.

It is the intention of the project to verify the results in the vertical acceleration domain by flying the antenna on the helicopter over a known elevation profile, during which time the fidelity of height measurement would be verified using a laser altimeter. Because of a shortage of serviceable TurboRogue receivers, which are shared between other partners on the project and with the Geodetic Survey of Canada, the helicopter testing has been delayed. In the interim, as partial verification of the model under conditions of varying antenna attitude, NovAtel single frequency receivers were used for a test in which an aircraft antenna was mounted on a tripod, as shown in Figure 7. The attitude of the antenna mounting plate could be changed and measured dynamically, to simulate aircraft pitch and roll. Results of this experiment are shown in the next section.

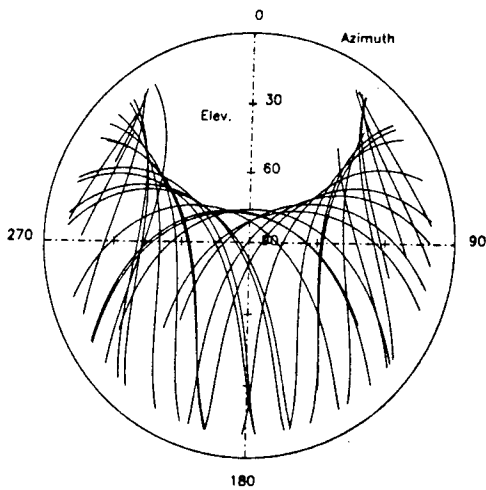


Figure 6a. Satellite sky map at Ottawa over one day

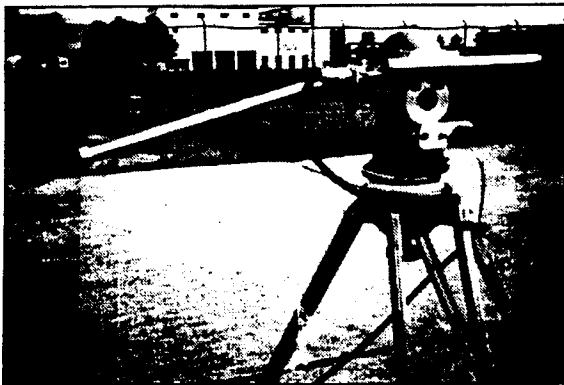


Figure 7. The aircraft antenna mounted for the attitude test

Two methods of modelling residual errors as a function of satellite elevation and azimuth were investigated, spherical harmonics and least-squares fit.

Spherical harmonic model:

$$f(\theta, \phi) = \sum_{l=1}^n \left(J_{l0} P_{l0}(\cos\theta) + \sum_{m=1}^l (P_{lm}(\cos\theta)(C_{lm} \cos m\phi + S_{lm} \sin m\phi)) \right) \quad (2)$$

where J_{l0} , C_{lm} , S_{lm} : spherical harmonics calibration coefficients

$P_{lm}(\cdot)$: Legendre polynomial

Least-squares model:

$$f(\theta, \phi) = \sum_{l=0}^n \sum_{i=0}^l a_{i(l-i)} \theta^i \phi^{(l-i)} \quad (3)$$

A spherical harmonic model with the 8th order gave essentially the same results as a least-squares model with the 10th order, and the spherical harmonic model was chosen as the calibration function for the next section. This model was also chosen in [Cohen et al., 1991].

RESULTS

Pre-testing of Model Parameters

The error model chosen assumes that the residual errors,

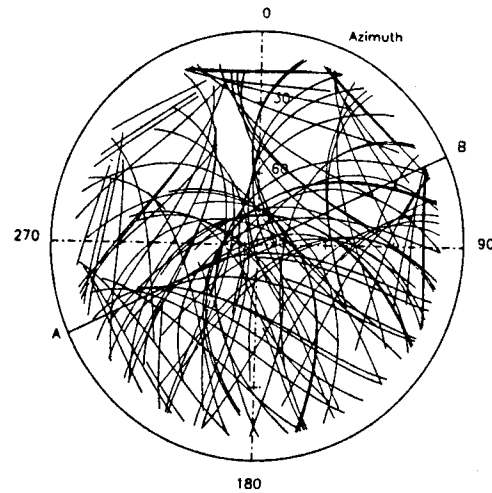


Figure 6b. Satellite sky map for three sessions

on a satellite-by-satellite basis, can be reasonably well represented as a function of only two variables, elevation and azimuth. Dependence on another variable, such as signal-to-noise ratio, would greatly complicate the model. To validate this assumption, multi-day data were taken with the aircraft antenna on a T-33 aircraft in a short baseline test. The objective was to show that different satellites, at similar elevation and azimuth angles, produced similar residuals. Figure 8 shows residuals of PRN 2 and PRN 21, where these two satellites had similar trajectories at different times of the day. Note that the residuals of PRN 21 have been offset by 2 cm for clarity. It is seen that the residuals of PRN 2 and PRN 21 are strongly correlated, and this indicates that multipath has the expected geometrical dependence.

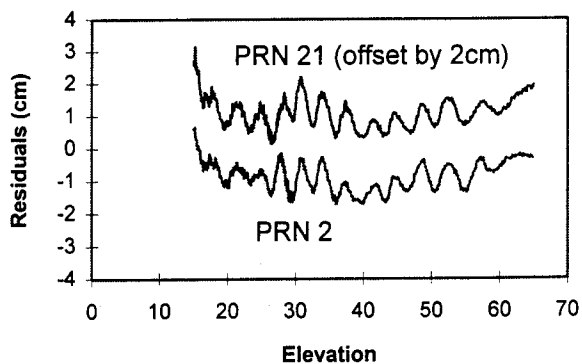


Figure 8. Similarity of residuals for satellites with similar trajectories

In order to further verify the multipath's geometry dependence, some satellite crossing points were selected from the sky map for the run. The results of this test are shown in Table 1. At satellite crossing points, the residuals of different satellites are almost the same and the agreement is better than 2 mm. Similar results were also documented in [Kee et al., 1994].

Table 1. Residual comparisons at cross-points among different satellite sky tracks

| No. | Satellites (PRN) | Elev. (deg.) | Az. (deg.) | Residuals (cm) | | Diff. (cm) |
|-----|------------------|--------------|------------|----------------|-------|------------|
| 1 | SV 20, SV 2 | 30.2 | 290.1 | 1.35 | 1.22 | 0.13 |
| 2 | SV 20, SV 19 | 29.3 | 298.1 | 0.05 | -0.12 | 0.17 |
| 3 | SV 20, SV 23 | 24.9 | 265.7 | -0.24 | -0.25 | 0.01 |
| 4 | SV 20, SV 27 | 26.2 | 307.1 | -0.18 | -0.24 | 0.06 |
| 5 | SV 7, SV 9 | 57.7 | 101.4 | -0.45 | -0.50 | 0.05 |
| 6 | SV 14, SV 16 | 36.5 | 69.3 | -0.96 | -0.80 | -0.16 |
| 7 | SV 14, SV 25 | 35.7 | 89.1 | -1.09 | -1.23 | 0.14 |
| 8 | SV 14, SV 4 | 36.9 | 79.9 | -0.69 | -0.58 | -0.11 |
| 9 | SV 1, SV 6 | 56.5 | 280.8 | -0.11 | -0.01 | -0.10 |
| 10 | SV 1, SV 9 | 57.7 | 100.5 | -0.45 | -0.51 | 0.06 |

Static Testing with the Helicopter

This test was carried out on a flat, obstruction-free, grassy area of the Ottawa International airport. In order to investigate the question of double difference versus single difference, it was decided to use a common clock for two receivers so that both single and double difference data could be generated.

Initial set-up tests were done with the aircraft antenna on a tripod with the same baseline as was to be used with the helicopter, and with a rubidium frequency standard as a common clock for both TurboRogue receivers. It was found that even with the common clock, there were apparent "clock" errors in the receivers of up to 2-3 cm in the single difference mode. These errors were found to be due to temperature changes in the receivers. It was therefore decided to do the data collection for the modelling with an Ashtech 3DF receiver, the type used for attitude measurement, where signals from two or more antennas are processed with a common clock. With this receiver, good single-difference data were obtained and

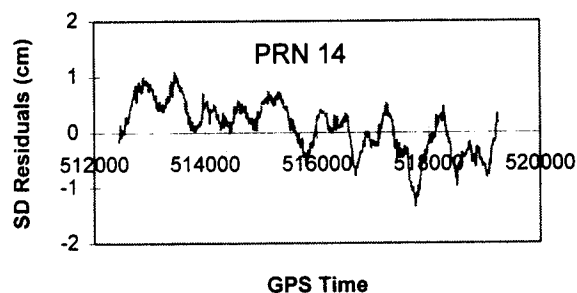


Figure 9. Single difference residuals for satellite PRN 14

we were able to show, as in Figure 9, that there was little to choose between the two methods.

Although early tests had shown that the helicopter blades rotating over the normal operating speed range, had no effect whatsoever on the GPS solution, there was concern that for static testing, the blade angle with respect to the fuselage could change the residuals. Short baseline tests showed that unless a blade was directly above the antenna, the blade angle had no effect. For consistency, the blades were set at 45 degrees to the centreline of the fuselage for all tests.

For the characterization data gathering, the helicopter skids were shimmed to give a level attitude and the position of its GPS antenna was fixed by two transit bearings. The angle between the centre-line of the helicopter and the baseline was also measured by transit bearings. The coordinates of the reference station were determined by a single point solution with precise emperides and satellite clock corrections from the Canadian Active Control System (CACS). The direction of the baseline was obtained from the double difference solution. The heading of the helicopter with respect to true north was then determined.

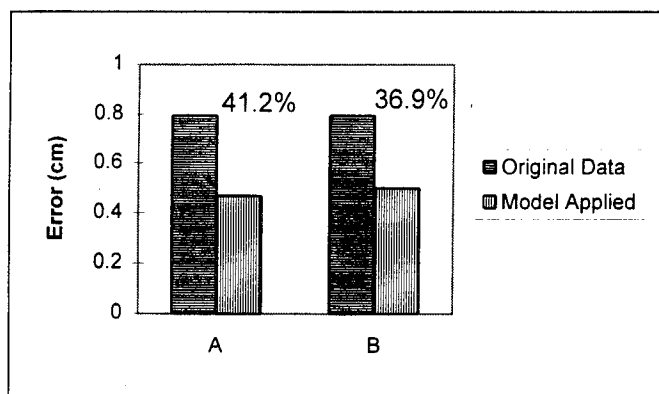
The testing was broken into three sessions, denoted S1 to S3, each on a different heading. The headings were:

S1 --- 329.6° (True)
S2 --- 59.0°
S3 --- 14.6°

Between each session, the helicopter was moved by hand to keep the antenna, as seen by the transits, at the same point above the ground, and the helicopter was re-levelled.

Application of the computed model coefficients to the data from which they were computed, as would be expected, produced a reduction of the residuals. However, we wished to demonstrate robustness of the model and to do so, coefficients from combinations of two sessions were applied to a third session. These subsets of coefficients did display robustness, but with a qualification: Figure 6b is divided approximately into a northern and a southern hemisphere by diagonal AB. In the southern hemisphere, it can be seen that there is a good mix of the satellite tracks for all three sessions, whereas in the northern hemisphere, the tracks for each session are clumped, with much less intersection and intermingling. It is only with data from the southern hemisphere that true robustness could be shown: including data from the other hemisphere in the model

caused deteriorated robustness. In effect, we were asking the model to predict in areas for which it had no data. The results that follow are for the southern hemisphere only. Figure 10 shows the improvement obtained using the model. The robustness is illustrated in case "B", where coefficients from S1 and S2 are applied to the data of S3. Figure 11 shows a surface plot of the model using data from all three sessions.



A Coefficients from S1, S2 and S3, applied to S3
B Coefficients from S1 and S2, applied to S3

Figure 10. Improvement in residuals using the error model in helicopter static test

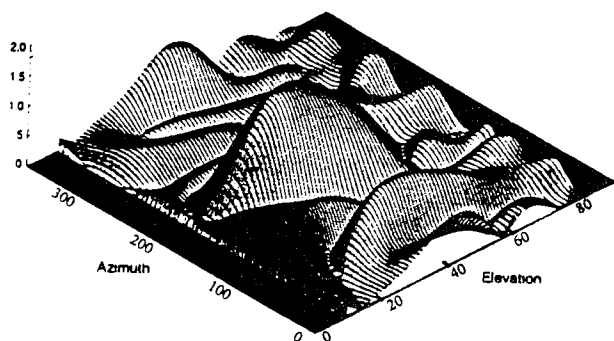


Figure 11. Error model for S1, S2 and S3 in helicopter static test

Simulated Aircraft Attitude Dynamic Test

In this test, the aircraft antenna was mounted on a special tripod whose head could be moved to simulate aircraft attitude changes. A potentiometer was calibrated to measure the antenna attitude and its signal was merged with the receiver data. Due to a temporary shortage of TurboRogue receivers, two NovAtel GPScard receivers were used, and in order to obtain more consistent coverage over the antenna hemisphere than was the case

for the helicopter static test, four sessions totalling about 96 hours were recorded, with the direction of the aircraft antenna being changed 90 degrees for each session. A fifth session of five hours was done simply to confirm robustness. After the model coefficients were calculated from the first four sessions using the 8th-order harmonic model, a simulated aircraft attitude testing of one hour was conducted. Attitude changes of up to ± 30 degrees, at frequencies from 0.1 to 0.3 Hz, were simulated. For this portion of the testing, the sample rate was 5 Hz, as opposed to 0.1 Hz for the static data collection.

Figure 12 shows the sky distribution for the four sessions, each on a heading change of 90 degrees. Note that the areas of the sky map which remain uncovered are much smaller than for the previous helicopter test. Residuals were calculated using double differencing, since, for the reasons outlined previously, this is the preferred method. An error model was calculated using the 8th order spherical harmonics. The error model for all four sessions is shown in Figure 13. In this new model, the elevation limit is about 65 degrees (rather than 80 degrees in the previous helicopter model). The reason is that with double differencing, the highest elevation satellite in view is used as the reference or base satellite and the next highest satellite was seldom higher than 65 degrees.

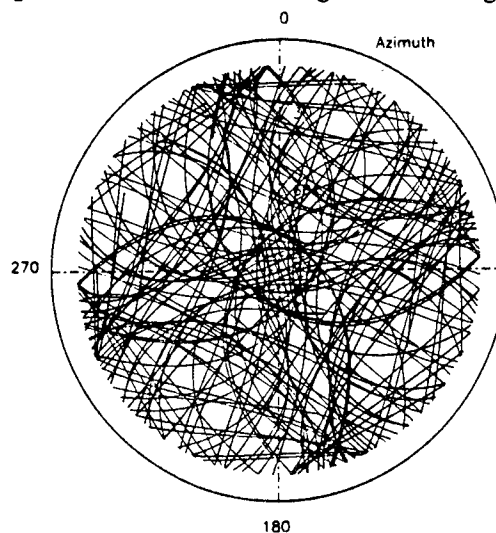


Figure 12. Satellite sky map for four sessions

In evaluating the results of this test, it should be noted that with the aircraft antenna mounted on a tripod rather than on the helicopter, the multipath errors would be greatly reduced and the geometry-associated errors were not much above the uncorrelated receiver noise. Nevertheless, the model did produce a significant reduction in the residuals. As shown in Figure 14, application of the model to the fifth (independent) session produced a reduction of 23.5%, thus confirming robustness.

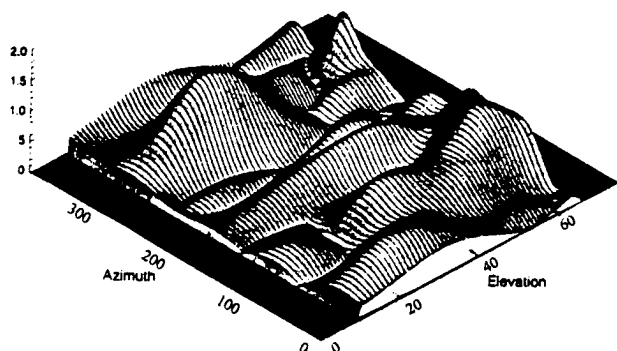


Figure 13. Error model for four sessions

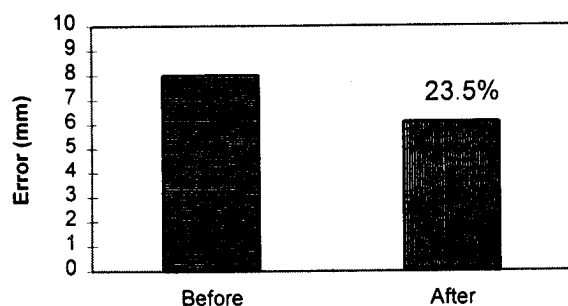


Figure 14. Improvement in residuals using error model for an independent session

For the attitude testing, the height solution had a noise envelope of approximately 7 mm peak-to-peak and it was difficult to see the effect of the error model against this noise background on a stand-alone plot of height. However, as shown in Figure 15, which is a typical section of the attitude test, the height difference with and without the model, is reasonably well correlated with the attitude signal. This shows that the model is generating a height correction signal. It would therefore be safe to conclude that the error model will be effective in the higher multipath environment of the helicopter.

CONCLUSION

It has been shown that phase-centre and multipath errors of an aircraft-mounted GPS antenna, can be characterized by elevation and azimuths of satellites with respect to the antenna hemisphere. An error model based on satellite residuals with elevation and azimuth as independent variables, can be constructed from static data and the model can be implemented as a least squares either by a least-squares surface or by spherical harmonics. An eighth-order spherical model was found to be convenient for this study. The model was not robust unless there was very complete coverage of the antenna hemisphere. This

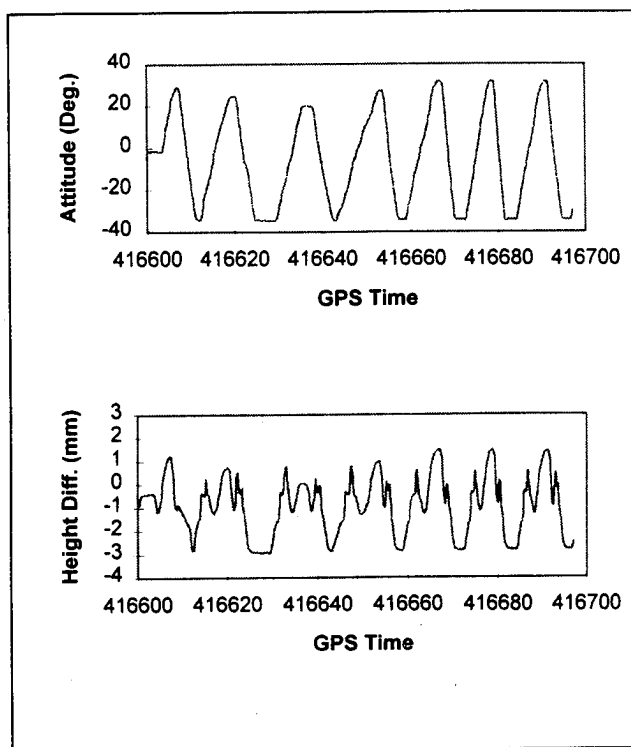


Figure 15. Height solution difference with and without the model

was achieved by collecting data in 24-hour sessions on at least four different azimuths.

For airborne gravity work, double-difference solutions for height are required. It was found that the model could be based on double differences provided that an *a priori* error model of the reference antenna was used in order to isolate its errors from those of the aircraft antenna.

Logistics problems with respect to two-frequency receivers have held up flight testing, but a simulated attitude test of an antenna on a tripod showed the error model to be capable of reducing attitude-related noise in the height solution. This test was carried out with multipath errors just barely above the receiver noise and it is expected that in the higher multipath environment of the helicopter, the height errors will be proportionately reduced, with corresponding reduction in attitude-dependent vertical acceleration noise, which is the objective of the project.

ACKNOWLEDGEMENTS

Funding for this work has been provided by the Industrial Research Assistance Program at National Research Council of Canada, as one component of a joint project between Sander Geophysics Ltd. and Geological Survey of Canada. Their contributions are appreciated.

ACKNOWLEDGEMENTS

Funding for this work has been provided by Sander Geophysics Ltd., the National Research Council of Canada, Mobil Exploration and another oil company. It comprises one component of a joint airborne gravity project involving these funders plus the Geological Survey of Canada. The testing on which this study is based was carried out with the participation of Sander Geophysics, Ltd..

REFERENCES

- Axelrad, P., C.J. Comp, and P.F. MacDoran (1994), Use of Signal-to-Noise Ratio For Multipath Error Correction in GPS Differential Phase Measurements: Methodology and Experimental Results, Proceedings of GPS-94, The Institute of Navigation, Alexandria, VA, pp. 655-666.
- Cohen, C., and B. Parkinson (1991), Mitigating Multipath Error in GPS Based Attitude Determination, Guidance and Control, Vol. 74, Advances in the Astronautical Science, pp. 53-68.
- Kee, C., and B. Parkinson (1994), Calibration of Multipath Errors on GPS Pseudorange Measurements, Proceedings of GPS-94, The Institute of Navigation, Alexandria, VA, pp. 353-362.
- Schupler, B.R., and T.A. Clark (1991), How Different Antennas Affect the GPS Observable, GPS World, Vol. 2, pp. 32-36.
- Schupler, B.R., R.L. Allshouse, and T.A. Clark (1994), Signal Characteristics of GPS User Antennas, Navigation, Vol. 41, No. 3, pp. 277-295.
- Tranquilla, J.M., and B.G. Colpitts (1988), GPS Antenna Design Characteristics for High Precision Applications, in Proc. ASCE Specialty Conference GPS-88 Engineering Applications of GPS Satellite Surveying Technology Specialty Conference, Nashville, TN, pp. 2-14.
- Tranquilla, J.M., J.P. Carr, and H.M. Al-Rizzo (1994), Analysis of a Choke Ring Groundplane for Multipath Control in Global Positioning System (GPS) Applications, IEEE Transactions on Antennas and Propagation, Vol. 42, No. 7, pp. 905-911.

Precise Positioning Using GPS/GLONASS Carrier Phase and Code Phase Observables

Dr. David Walsh, Dr. Stuart Riley, John Cooper, and Prof. Peter Daly
*CAA Institute of Satellite Navigation,
Department of Electronic and Electrical Engineering
The University of Leeds*

BIOGRAPHIES

Dr. Walsh is a Senior Research and Development Engineer at the Civil Aviation Authority (CAA) Institute of Satellite Navigation (ISN) at the University of Leeds. He obtained a PhD from the University of Nottingham in 1994. He has previously worked as a Research Assistant at the Federal Armed Forces University, Munich and at the Centre for Nuclear Research (CERN) in Geneva.

Dr. Riley graduated from the ISN, University of Leeds in 1994 with a PhD in Electronic Engineering. Since 1990 he has been active in integrated GPS/GLONASS receiver design and observable processing. He is currently developing a LEO space platform GNSS receiver for the European Space Agency.

Mr. Cooper is a PhD student at the CAA ISN working in the area of satellite navigation. He is concerned particularly with interference issues for GPS and GLONASS.

Prof. Daly is Director of the CAA Institute of Satellite Navigation at the University of Leeds and has been involved with GPS/GLONASS satellite navigation issues since 1982.

ABSTRACT

The aim of the work described in this paper is to examine the performance of differential positioning using both the GPS and GLONASS satellite systems. Two aspects of performance have been concentrated on, (i) satellite availability, and (ii) positioning accuracy. These aspects are analyzed in some demanding applications.

The increased satellite availability when using both satellite systems is analyzed. The paper then describes precise differential positioning results which have been

obtained using code and carrier phase observables from the 20 channel GPS/GLONASS receiver developed at the University of Leeds. Differential performance on a static baseline using both GLONASS and GPS, GPS alone and GLONASS alone, is described.

Differential GPS/GLONASS tests have also been performed using a land vehicle in urban and semi-urban areas. The results demonstrate the advantages of using both GPS and GLONASS systems for this application. The consequent increase in the number of visible satellites significantly increases the positioning capability in built up areas. The results also show the potential for using a 20 channel GPS/GLONASS receiver to take full advantage of the increased number of satellites.

The paper also describes a flight test where en-route differential GPS/GLONASS positioning was performed for a flight to the North Pole. The results show the satellite availability at very high latitudes and the positioning accuracy over very long distances.

INTRODUCTION

Differential GPS is successfully used worldwide to provide positioning accuracy at the metre level. However, there are a number of applications which would benefit from a greater satellite availability. This may be because a very high level of system integrity is required, eg for Category III precision approach and landing of aircraft, or because positioning is required in areas where there are many obstructions which block satellite signals, eg vehicle positioning in urban areas.

The most obvious choice to improve the satellite availability is to increase the number of satellites by combining the GPS and GLONASS systems. After recent GLONASS satellite launches there are now 22 operating satellites in orbit. This is only 3 below the

number of operating GPS satellites, making a total of 47 satellites available when using both systems. There has been a lot of interest recently in the possibility of combining both systems and the resulting positioning performance.

The Institute of Satellite Navigation has developed a 20 channel GPS/GLONASS receiver capable of obtaining carrier phase and code phase observables from any combination of 20 GPS or GLONASS satellites [1,2]. Each channel can track either GPS or GLONASS satellites. The data is recorded at a 1 Hz rate and a differential position solution can be determined using GPS and GLONASS satellites, just GPS, or just GLONASS. The ability to track over 10 satellites is very important to be able to take full advantage of using both systems. Recent vehicle positioning tests using a 10 channel version of the Leeds receiver have shown that there are not enough channels to take full advantage of combining both systems even in areas where there is a lot of satellite masking [3].

The aim of the work described in this paper is to analyze the performance of GPS/GLONASS positioning with especial regard to satellite availability and positioning accuracy. Comparisons are made between the GPS/GLONASS performance and the performance of both separate systems. The satellite availability is analyzed using software written to determine the average, maximum and minimum number of satellites available in a 24 hour period.

Three tests have also been carried out using actual data. Firstly, a static baseline has been measured to determine the accuracy of the pseudorange and phase smoothed pseudorange position solutions. A position 'truth' source from commercial carrier phase positioning software has been used to give centimetre level positioning accuracy. Secondly, a vehicle positioning test has been carried out in urban and semi-urban areas to look at the satellite availability in a demanding application. Thirdly, a flight test was undertaken to the North Pole to study the receiver performance in a flight environment, to look at positioning accuracy over long distances and to study the satellite availability in the polar region.

GNSS SATELLITE AVAILABILITY

To demonstrate the satellite availability GPS/GLONASS, GPS, and GLONASS simulations have been carried out using the present constellations of 22 GLONASS satellites and 25 GPS satellites (including the one remaining Block I GPS satellite). An elevation mask of 10° was used to reflect the fact that low elevation satellites are more likely to be significantly affected by unmodelled errors. Therefore, some applications may require that only satellites above 10° may be used. The average, maximum and minimum number of satellites in a 24 hour period are

determined for an area of the earth's surface between 40° and -30° degrees longitude and 0° and 80° degrees latitude (roughly approximating to Europe and Northern Africa). The number of satellites is calculated using a $2^\circ \times 2^\circ$ grid spacing and a 600 second time step.

The average number of satellites available for GPS/GLONASS, GPS, and GLONASS are shown in figures 1, 2 and 3.

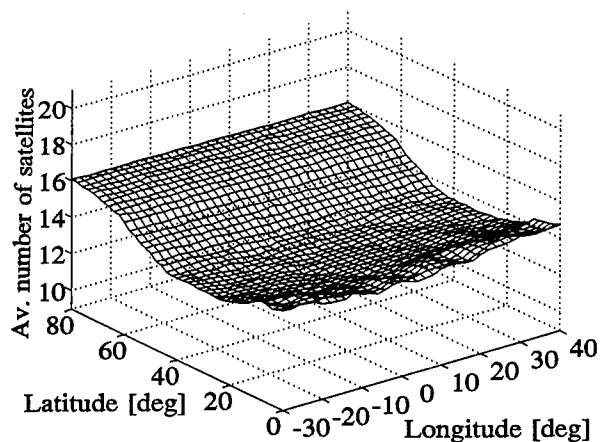


Figure 1 Average number of GPS/GLONASS satellites available with 10° elevation mask

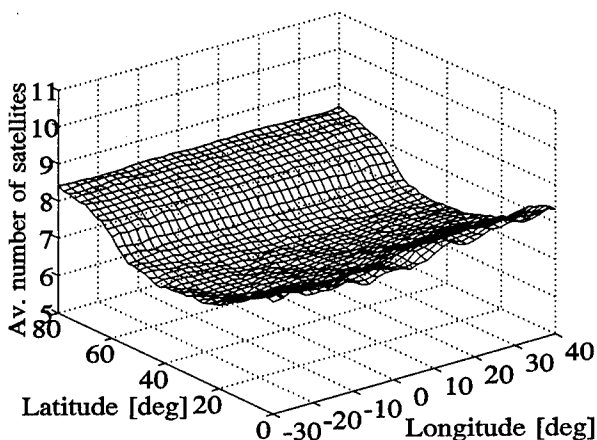


Figure 2 Average number of GPS satellites available with 10° elevation mask

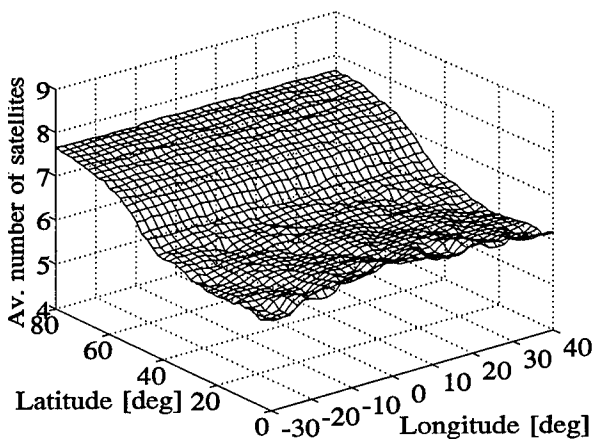


Figure 3 Average number of GLONASS satellites available with 10° elevation mask

Clearly, there is a significant increase when both systems are used. There are at least 13 GPS/GLONASS satellites available on average, rising to 16 at high latitudes. With GPS only the lowest average value is about 7 in mid-latitudes, whereas the lowest average value is 6 with GLONASS only near the equator.

However, it is also important to note the minimum number of satellites available in the 24 hour period. This is because if rigorous applications require a certain minimum number of satellite they will not be available during periods when there are less than this number available. Examples of such applications are the integrity requirements for Cat III precision approach and landing of aircraft, and very fast ambiguity resolution on-the-fly which may well require at least 7 satellites in some cases.

The minimum number of satellites available for GPS/GLONASS is shown in figure 4. The lowest minimum number of satellites is 8, in the mid-latitudes. The minimum number of GPS satellites is shown in Figure 5. The lowest minimum is 4, with 5 being the usual minimum. These figures (with a 10° elevation mask) suggests that using GPS and GLONASS together will provide greater availability and integrity, particularly for rigorous applications.

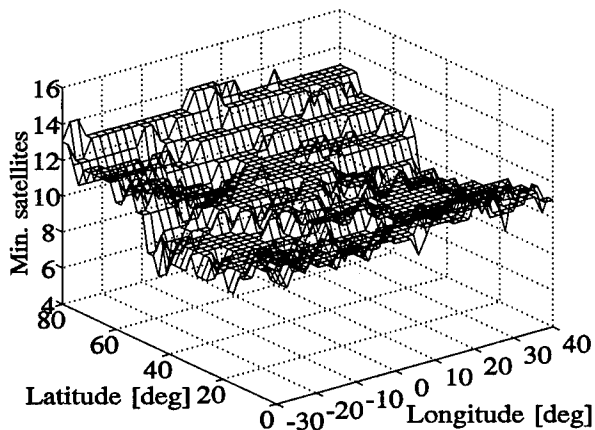


Figure 4 Minimum number of GPS/GLONASS satellites available with 10° elevation mask

The maximum number of GPS/GLONASS satellites is shown in figure 6. At high latitudes it is theoretically possible to obtain 18 to 19 satellites. Although in field conditions the number of visible satellites is often lower due to obstructions.

DIFFERENTIAL GNSS ACCURACY ON A STATIC BASELINE

The aims of this test were to (i) compare the accuracy of the GPS/GLONASS, GPS, and GLONASS differential pseudorange solutions, and (ii) to compare the differential pseudorange and phase smoothed [4] differential pseudorange accuracies, particularly for GLONASS. The smoothing was performed using a

1000 second time average and two parallel filters.

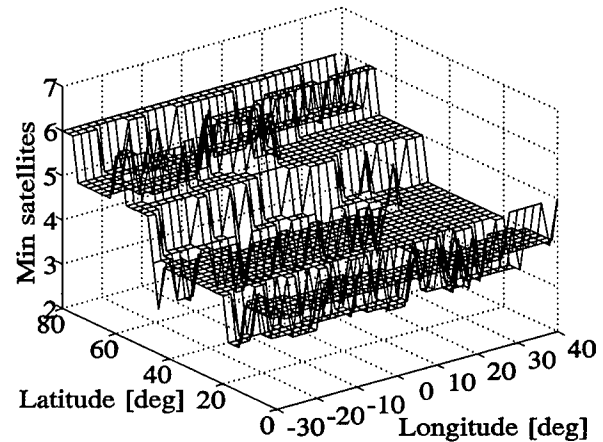


Figure 5 Minimum number of GPS satellites available with a 10° elevation mask

The baseline was just over 10 km and a 0° elevation mask was used. Two 20 channel Leeds GPS/GLONASS receivers were used which measure L1 carrier phase and C/A code phase from all satellites in view. Both antennas were placed in areas where high multipath might be expected due to local obstructions. Trimble broadband kinematic antennas were used to obtain both the GPS and GLONASS frequencies.

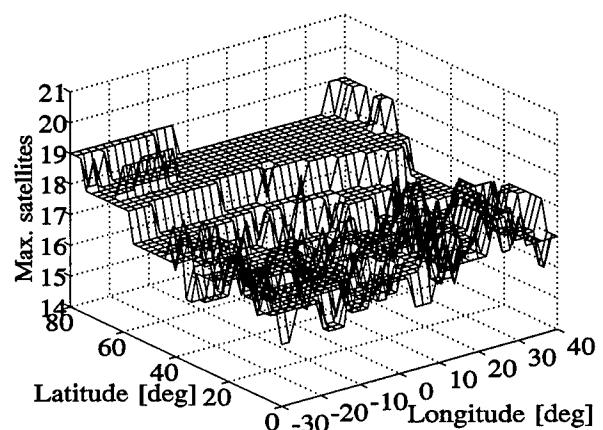


Figure 6 Maximum number of GPS/GLONASS satellites available with 10° elevation mask

The truth in this test was provided using two Trimble SSEs. At each end of the baseline a single antenna was used and the signal was split between a Trimble SSE and a Leeds receiver. Therefore, the Trimble SSE measurements were used to determine the vector between the phase centres of the two antennas. The baseline vector was calculated using the Trimble WAVE software. Only L1 phase measurements and C/A code phase were used for the Trimble solution because the antenna was not specifically designed to receive observables at the L2 frequency and the quality of the L2 observables could not be guaranteed. Approximately 20 minutes of data was taken which was easily sufficient to obtain an L1 ambiguity fixed

solution from the WAVE software with a coordinate precision of approximately 1cm.

A previous test on a static baseline has been carried out at Leeds [3]. The baseline was approximately 278 km and a 10 channel receiver was used. Apparent average coordinate accuracies of about a metre were observed with a differential GPS/GLONASS solution. However, the supplied coordinate truth could not be verified.

The data from the Leeds receivers was processed six times using GPS/GLONASS, GPS, and GLONASS data with and without phase smoothing. The average offsets (in WGS84 X,Y and Z) between the derived epoch by epoch differential positions and the Trimble carrier phase solution are shown in Table 1. The offsets of the smoothed and unsmoothed solutions are approximately the same. The GPS offsets in X, Y and Z are all within 0.5 metres and compare very well with the Trimble GPS pseudorange solution. The GPS/GLONASS offsets are greater in X and Z. This is due to the contribution of the GLONASS satellites as can be seen from the differential GLONASS offsets in X and Z.

The GLONASS offsets may be due to a number of reasons, most likely differing receiver delays between the different GLONASS frequencies, or multipath which has a greater effect on GLONASS code phase because of the lower chipping rate. Because the GLONASS frequencies are different the signals have different signal delays within the analogue sections of the receiver. These can be calibrated but they will vary due to structural changes in the filters and with temperature. The receivers used in this test have not been calibrated recently and were at widely varying temperatures with the reference receiver being in the laboratory and the other receiver being housed in a vehicle on a very hot day. The next generation of receivers at Leeds have been designed to minimise the differential delay problem.

There might also be an error contribution from the different GPS and GLONASS coordinate systems. No attempt has been made to account for the difference in these tests. The difference between the offsets in Y for the phase smoothed GPS/GLONASS, GPS, and GLONASS solutions is shown in figure 7.

The standard deviations in X, Y and Z are shown in Table 2. Clearly the standard deviations of the smoothed solutions are much better than the non-smoothed solutions. The difference between the GLONASS solution and the phase smoothed solution in Y are shown in Figure 8. The phase smoothed solution has been offset by exactly 10 metres to aid presentation. After the usual initial transient before the filter takes effect the improvement in the noise is obvious. Additionally, the effect of multipath can be seen. The GLONASS phase noise is greater than GPS

because the code-phase measurement is inherently less precise because of the lower chipping rate of the GLONASS C/A code phase. As stated before, the GLONASS code phase is therefore more susceptible to multipath.

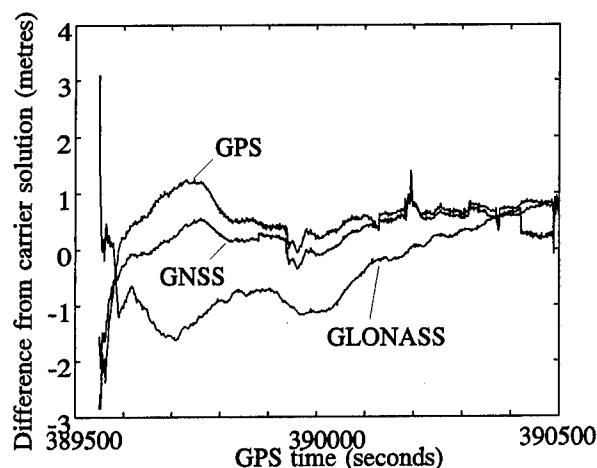


Figure 7 Difference in Y between the GPS/GLONASS, GPS and GLONASS solutions and the L1 carrier phase solution

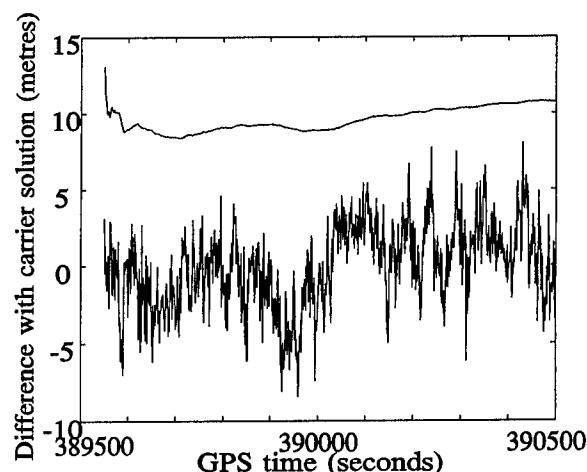


Figure 8 Difference in Y of GLONASS smoothed and unsmoothed solutions and L1 carrier phase solution (smoothed solution is offset by exactly 10 m for presentation)

GPS/GLONASS VEHICLE POSITIONING TEST

The aims of the GPS/GLONASS vehicle positioning test were:

- (1) to determine the advantage of combining GPS and GLONASS in an application where satellite availability is a problem,
- (2) to determine the suitability of equipment and software developed at Leeds for differential vehicle positioning,
- (3) to examine the performance of the system in two different environments, urban and semi-urban.

In urban areas satellite masking by nearby buildings, trees and other vehicles is a great problem. Often only satellites with high elevations can be observed. When there are fewer than 4 satellites, for GPS only, 3D

| | Average X offset (m) | Average Y offset (m) | Average Z offset (m) |
|--------------|----------------------|----------------------|----------------------|
| GNSS (sm) | 1.63 | 0.31 | 3.90 |
| GNSS | 1.65 | 0.58 | 3.93 |
| GPS (sm) | -0.01 | 0.49 | -0.29 |
| GPS | 0.24 | 0.68 | 0.57 |
| GLONASS (sm) | 4.37 | -0.41 | 6.69 |
| GLONASS | 4.16 | -0.04 | 6.75 |

Table 1 Average offset in X, Y and Z between GPS/GLONASS, GPS and GLONASS solutions and L1 carrier phase solution (sm = phase smoothed)

| | Std. in X (m) | Std. in Y (m) | Std. in Z (m) |
|--------------|---------------|---------------|---------------|
| GNSS (sm) | 0.52 | 0.45 | 0.81 |
| GNSS | 1.64 | 1.35 | 3.15 |
| GPS (sm) | 0.58 | 0.52 | 0.81 |
| GPS | 2.24 | 1.55 | 4.03 |
| GLONASS (sm) | 0.28 | 0.72 | 0.88 |
| GLONASS | 2.49 | 2.70 | 3.99 |

Table 2 Standard deviation in X, Y and Z of the difference between the GPS/GLONASS, GPS and GLONASS solutions and the L1 carrier phase solution (sm = phase smoothed)

| | Urban coverage (%) | Semi-urban coverage (%) | Overall (%) |
|---------------|--------------------|-------------------------|-------------|
| GPS & GLONASS | 75 | 88 | 81 |
| GPS | 51 | 67 | 58 |

Table 3 Percentage 3D position coverage of vehicle journey time in urban and semi-urban areas

positioning is not possible without using other sensors or fixing the height. It should be noted that the purpose of the tests was not to produce a usable in-car navigation system, which would obviously require integration with other systems. The purpose is to compare the percentage of time that 3D differential positioning is possible with, and without, combining GPS and GLONASS. This would determine the potential of GPS/GLONASS positioning as a component of an in-car navigation system.

An initial test had been carried out [3] using a 10 channel Leeds receiver mounted in the vehicle. Although there was an improvement when GLONASS was used as well it was limited because only 3 channels were used for GLONASS satellites. Additionally, only 16 GLONASS satellites were available at the time.

As well as increased satellite availability the increase in the number of satellites with GLONASS should

improve the PDOP of the solution compared to GPS. As so much of the sky is masked in urban areas it is likely that if fewer satellites are visible they will not have a very good geometry. It should be noted that with GPS/GLONASS positioning there is an extra unknown in the solution, the GLONASS clock term, which will also affect the DOP values.

Test Description

The test was performed on 3.8.95 when 19 GLONASS satellites were available. A 20 channel receiver was used at the reference point and another 20 channel receiver was used on the vehicle. Both receivers recorded single frequency C/A code and L1 carrier phase observables. Two Trimble SSEs were also connected to the same antennas in the same way as described for the static test to provide a position truth. A Trimble broadband kinematic antenna was mounted on the vehicle in order to receive signals at both the GPS and GLONASS frequencies. The reference receiver had a Trimble L1/L2 antenna with a ground plane. The vehicle used was a van with the kinematic antenna mounted on top. The 20 channel receiver was placed in a rack in the van and powered by a 12v car battery via an inverter. The receiver was connected to a 486-laptop. The 20 channel reference receiver was connected to an antenna placed on the roof of the Electronic and Electrical Engineering Department.

The satellites were selected automatically on both 20 channel receivers as there were enough channels to record data from all satellites in view. Data was recorded at a rate of one per second from all satellites tracked.

The vehicle was driven around Headingley, Leeds for approximately 22 minutes to record some data in an urban environment. Then the vehicle was driven along the Leeds ring road for a further 16 minutes to record some data in a semi-urban environment. The route of the test is shown in Figure 9. This is a plot of the differential GPS/GLONASS position of the vehicle in eastings and northings. The gaps in the data are where less than 5 satellites were observed.

Data Processing and Results

A C/A code differential solution was performed with no carrier smoothing for each of the GPS/GLONASS, GPS and GLONASS solutions. A 0° elevation mask was used to obtain as many satellite as possible. The percentage of the total time that a 3D position solution was determined for GPS/GLONASS and for GPS in urban and semi-urban areas, and overall, is shown in Table 3. The improved results with GPS/GLONASS are clear and significant. The improved percentage in urban areas is approximately 1.5 times as great with GPS/GLONASS compared to just GPS. In semi-urban areas the increase is smaller but still significant at 21%

of the total time. Overall, an increase from 58% to 81% would be significant when using GPS/GLONASS positioning as part of an in-car navigation system.

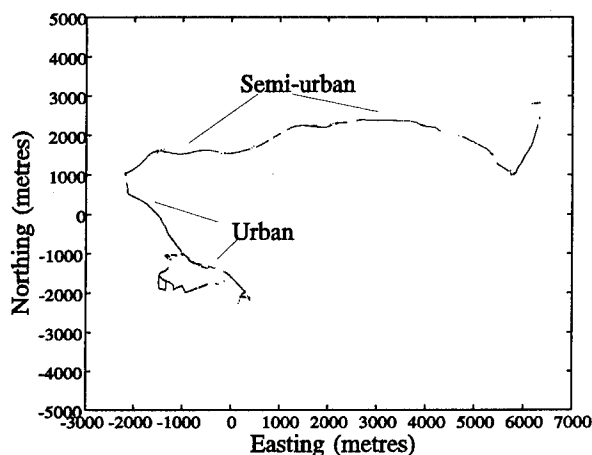


Figure 9 Plot in eastings and northings of vehicle path in urban and semi-urban areas

The Leeds receivers were not originally designed for this application and so some modifications have to be made which will improve the results. In particular, it is possible to speed up the acquisition of satellites after losing lock which will further increase the coverage percentage.

The overall number of satellites available during the test are shown in Figure 10. The number of satellites is only plotted when there are greater than 5 satellites. The periods with less than 5 are shown by diagonal lines on the plot. The average number of GPS/GLONASS satellites is 8 with a maximum of 13. With GPS alone the average is about 4 with a maximum of 7. The average number of GLONASS satellites is between 3 and 4 reflecting the lower number of satellites at that time. The GPS/GLONASS PDOP during the test is shown in Figure 11.

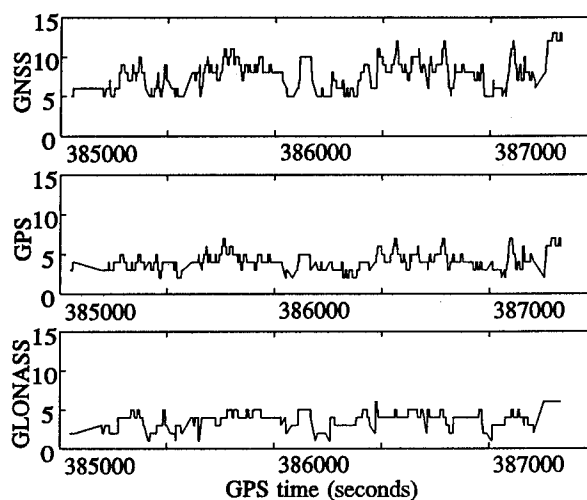


Figure 10 Number of visible GPS/GLONASS, GPS and GLONASS satellites during vehicle journey

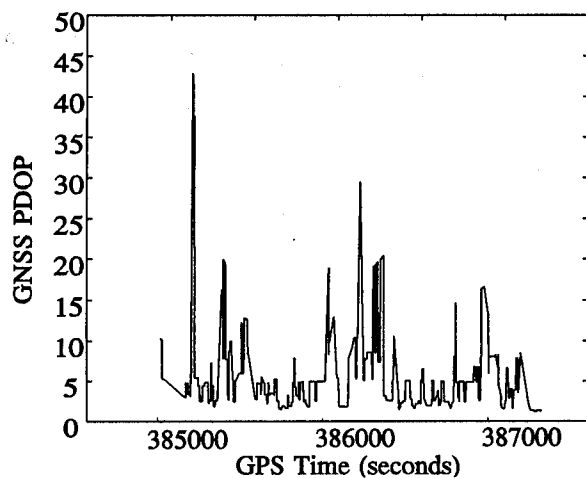


Figure 11 PDOP values for GPS/GLONASS throughout vehicle journey

The accuracy of the epoch by epoch position solution during the test was determined from an L1 carrier phase solution processed using the On-The-Fly ambiguity resolution option from the Trimble WAVE software. However, because there are many short periods of data to be processed it was not always possible to resolve the ambiguities which produces a less precise solution.

A comparison of the height component determined from the GPS/GLONASS solution and the Trimble carrier phase solution is shown on Figure 12. The plot is of the offset between the two solutions. It can be seen that the offset can be quite large due to (i) the large VDOPs experienced when satellite masking was bad, and (ii) the fact that satellite measurements were used down to 0° elevation to maximise the number of satellites seen. This means that pseudoranges with large multipath errors could be obtained. The mean offset is 1.05m and the standard error is 6.01m.

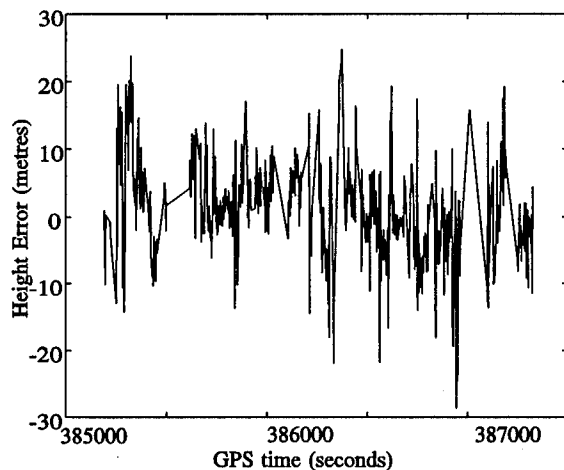


Figure 12 Difference in height between GPS/GLONASS solution and L1 carrier phase solution

POLAR FLIGHT TEST

Differential positioning using two 20 channel receivers was also tested in a flight environment in June of this

year. The aims of the test were:

- (1) to analyze the performance of the receiver in flight dynamics,
- (2) to look at the satellite availability in the polar region,
- (3) to look at the differential positioning accuracy of a moving vehicle over very long distances.

The mobile 20 channel receiver was placed on board an RAF flight from RAF Brize Norton in England to the North Pole via Thule in Greenland. The reference 20 channel receiver was at Leeds throughout the whole flight. L1 carrier phase and C/A code data was taken at a 1Hz rate from all GPS and GLONASS satellites in view. Data was taken for the whole trip from England to Thule, then on a return trip from Thule which passed over the North Pole, and finally from Thule back to England. The flight path above 89° latitude and over the North Pole is shown in latitude and longitude in Figure 13.

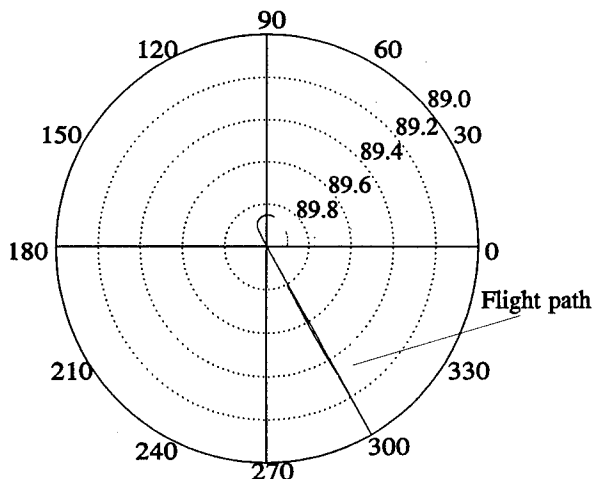


Figure 13 Plot of aircraft path over North Pole

Differential data was successfully recorded over the pole. There are a number of outages after the polar crossing which were caused by technical failures due to the high temperatures experienced at the receivers position on the plane. This version of the receiver has not been designed to work over a very large temperature range. After this part of the flight the receiver was moved and no further problems were experienced.

The number of satellites visible for GPS/GLONASS, GPS, and GLONASS differential solutions is shown in Figure 14. It should be noted that the number is the number of jointly visible satellites from both Leeds and the North Pole. The plane passed over the pole at 15:48:28 hours when 8 GPS satellites were visible and 5 GLONASS. A maximum of 13 satellites were observed with a maximum of 8 GPS satellites and 6 GLONASS satellites. The outages were for the reasons described above. An elevation mask of 0° was used.

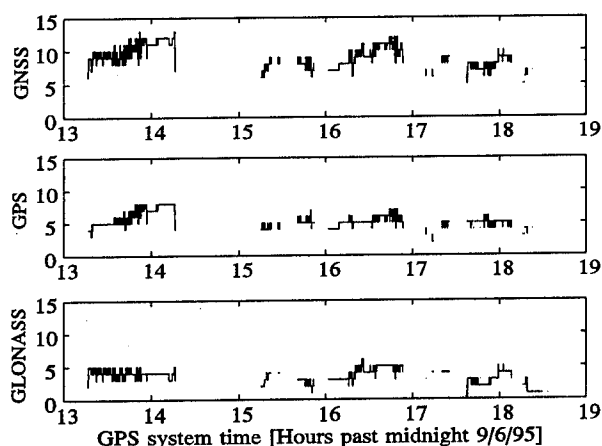


Figure 14 Number of GPS/GLONASS, GPS and GLONASS satellites visible during flight over North Pole (co-visible with Leeds)

The increase in number of satellites available would be significant for performing integrity analysis, eg RAIM tests.

An analysis of the GPS/GLONASS position accuracy has been carried out. Trimble Navigation (UK) have kindly supplied Leeds with position information obtained from an ionospherically free carrier phase solution using their own receivers. The Trimble reference station was at Thule so a comparison with the Leeds solution with a reference station in England can only be approximate! A plot of the height difference between the Leeds differential GNSS solution and the TRIMBLE solution during and after a take off from Thule is shown in the lower plot in Figure 15. The top plot is of the actual height of the aircraft.

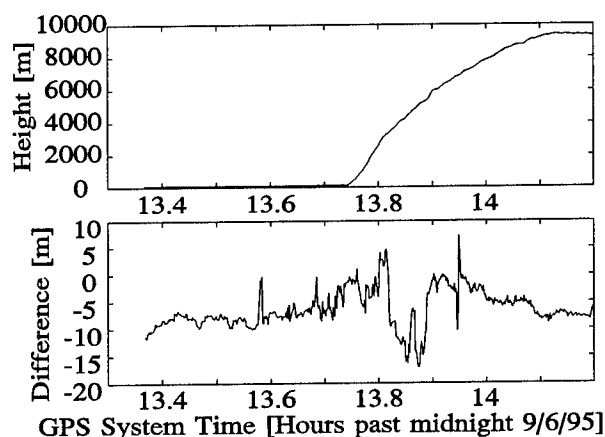


Figure 15 Height of aircraft and difference in height between GPS/GLONASS solution and carrier phase solution

An accurate comparison of the heights is not possible because the antennas on the plane were not coincident and the vector between the reference stations (one in Thule and one in Leeds) is not accurately known. But the results indicate that the two solutions do not widely differ, especially considering that the Leeds reference

station was over 3600 km away at Leeds!

CONCLUSION

This paper has described the performance of differential smoothed and unsmoothed GPS/GLONASS positioning using the Leeds 20 channel receiver. The increased GPS/GLONASS satellite availability and the differential positioning accuracy has been described. Comparisons with GPS and GLONASS alone have been given. Examples have also been given of the performance of GPS/GLONASS positioning for two applications, vehicle positioning in urban areas and flight tests.

ACKNOWLEDGEMENTS

The authors would like to acknowledge the contribution from Trimble Navigation (UK) for the tests described in this paper. The authors would also like to thank the RAF for providing the flight.

REFERENCES

- [1] S.Riley, "An Integrated Multichannel GPS/GLONASS Receiver", Proc. ION-GPS 92, ION Satellite Division, 5th International Technical Meeting, Albuquerque, New Mexico, September 16-18, 1992.
- [2] S.Riley & P.Daly, "Architecture and results from the Leeds University 20 Channel GNSS receiver", Proceedings of the ION National Technical meeting, Anaheim, CA, January 1995.
- [3] S.Riley, D.Walsh & P.Daly "Navigation Results from a 20 Channel GPS/GLONASS Receiver", DSNS 95, Bergen, April 1995.
- [4] R.Hatch, "The Synergism of GPS Code and Carrier Measurements", Proc. 4th International Geodetic Symposium on Satellite Positioning, Las Cruces, New Mexico, 1982.

Differential GLONASS, Differential GPS and Integrated Differential GLONASS/GPS – Initial Results

Dr. Jacques Beser, Anushia Balendra, Eric Erpelding, and Sonia Kim
3S Navigation

BIOGRAPHIES

Dr. Jacques Beser has worked on satellite navigation-related projects for over 17 years. He is currently V.P. and Director of 3S Navigation, responsible for satellite navigation products. Dr. Beser pioneered the differential use of GPS and led the design of the Range Applications Program Reference Receiver Pseudorange Corrections Generator. He holds degrees from CALTECH and Stanford University. He is a member of ION and IEEE.

Mrs. Anushia Balendra received an M.S. degree in Electrical Engineering from the Tennessee Technological University in 1992. She is currently a systems analyst at 3S Navigation involved in software development and analysis for integrated GPS/GLONASS applications.

Mr Eric Erpelding received an M.S. degree in Mathematics from the University of California, Irvine, in 1986. He is currently developing software for integrated GPS/GLONASS receivers at 3S Navigation.

Ms Sonia Kim received a B.S. degree in Information & Computer Science from the University of California, Irvine, in 1990. She is currently a senior programmer at 3S Navigation involved in software development for integrated GPS/GLONASS receivers.

ABSTRACT

Differential techniques have been used with GPS with great success to provide meter and even submeter accuracy. The same techniques can be applied to the GLONASS satellites, which will be fully deployed by the end of 1995. Both code and carrier differential corrections can be generated for each constellation and individual as well integrated navigation solutions can be calculated.

The RTCM-SC-104 has formed a workgroup with the objective of defining differential GLONASS messages similar to their GPS counterparts. In close coordination with Russian GLONASS representatives, tentative messages have been defined and will be briefly addressed in the paper.

3S Navigation receivers providing single frequency GPS C/A code and dual frequency GLONASS C/A and P code were used to generate differential corrections. Issues specific to GLONASS and integrated GLONASS/GPS are discussed and initial results are presented.

1.0 INTRODUCTION

3S Navigation has been involved in the development of integrated GPS/GLONASS receivers for several years and has published several papers discussing the advantages of using both constellations (Refs 1,2,3,4). With the GPS constellation fully deployed and the GLONASS constellation expected to be completed by the end of 1995, interest in the combined use of both systems is growing. Differential GPS has been used successfully for several years with most receivers supporting the RTCM-SC-104 standard (Ref 5). Over the last few years, differential messages suitable for differential GLONASS and combined GLONASS/GPS applications were developed and will be included in the next version of the standard (version 2.2). A brief overview is provided herein. The paper also presents differential results for both code and carrier phase measurements. Two types of receivers were used to obtain the necessary data. Both are PC-based receivers, providing extensive outputs and user interface capabilities. The 10-channel L1, C/A code, R-100/20 was used for integrated GPS/GLONASS code differential tests, while the 10-channel version of the dual frequency, C/A and P code GLONASS R-100/40 was used for GLONASS carrier phase differential tests.

2.0 DIFFERENTIAL OPERATIONS

2.1 GPS

The RTCM-SC-104 Standard (Ref 5) describes specific differential correction messages for both code and carrier phase GPS measurements. The primary code and carrier messages are listed in Table 2.1.

2.2 GLONASS

The RTCM-SC-104 standard document is currently being revised to address the needs of the entire GNSS community, to

include GPS, GLONASS as well as other potential navigation aids. Messages defined for GLONASS code and carrier corrections are listed in Table 2.2. Note that in the case of the carrier phase corrections, the same message type is used for both GPS and GLONASS. This is because a provision was made in the definition of these messages for up to 64 satellites, thereby allowing to differentiate the GPS and GLONASS constellations.

TABLE 2.1 PRIMARY GPS DIFFERENTIAL MESSAGES

| TYPE No | TYPE |
|---------|-------------------------------|
| 1 | Differential GPS Corrections |
| 3 | GPS Reference Station Param. |
| 5 | GPS Constellation Health |
| 6 | GPS Null Frame |
| 7 | DGPS Radiobeacon Almanac |
| 9 | GPS Partial Correction Set |
| 16 | GPS Special Message |
| 18 | RTK Uncorrected Carr. Phases |
| 19 | RTK Uncorrected Pseudoranges |
| 20 | RTK Carrier Phase Corrections |
| 21 | RTK Pseudorange Corrections |

TABLE 2.2 PRIMARY GLONASS DIFFERENTIAL MESSAGES

| TYPE No | TYPE |
|---------|-------------------------------|
| 31 | Differential GLONASS Correct. |
| 32 | GLONASS Ref. Station Param. |
| 33 | GLONASS Constellation Health |
| 34 | GLONASS Partial Correct. Set |
| | GLONASS Null Frame |
| 35 | DGLONASS Radiobeacon Almanac |
| 36 | GLONASS Special Message |
| 18 | RTK Uncorrected Carr. Phases |
| 19 | RTK Uncorrected Pseudoranges |
| 20 | RTK Carrier Phase Corrections |
| 21 | RTK Pseudorange Corrections |

2.3 Integrated GPS/GLONASS

Differential operations using both GPS and GLONASS satellites are possible. There are two issues to keep in mind while combining measurements from both constellations. The first one relates to the use of different datums by both systems, specifically WGS-84 for GPS vs SGS-90 for GLONASS. The second issue relates to the different time references. GPS time "follows" UTC(USNO) but without leap seconds adjustments, and GLONASS time "follows" UTC(SU) with leap seconds adjustments. Excluding the leap seconds, a typical GPS to GLONASS system time difference is on the order of 17 microsecond, with GLONASS time ahead of GPS time. UTC(SU) is typically ahead of UTC(USNO) by 5.4 microsecond.

The different datums issue is best handled by maintaining two separate reference receiver position solutions, one in each datum and processing each constellation corrections in its respective datum. This offers the additional advantage that the corrections are usable by both single constellation receivers and dual constellation receivers. The dual constellation user receiver will have to take care of the dual datum problem, as it must already do in the stand-alone mode anyway.

The reference receiver clock bias contribution to the differential corrections is usually not a problem in differential GPS operations, as this bias is simply added to the user receiver clock bias and does not affect navigation accuracy. For integrated GPS/GLONASS operations, since a different bias is contributed to the GPS and GLONASS corrections, the corrections have to be handled carefully by the user receiver. The preferred way is for the receiver to maintain separate GPS and GLONASS estimates of the clock errors. Another possibility is to include a GPS-to-GLONASS time bias in the differential data. However, any error in this bias

will degrade the accuracies of the corrections and therefore of the ultimate navigation solution. Since the number of satellites in view should not be an issue, solving for two independent biases is a safer approach avoiding contaminating GLONASS with SA effects.

3.0 DIFFERENTIAL TESTS

3.1 Receivers

The receivers used for the differential tests are manufactured by 3S Navigation.

The R-100/20 is a single frequency, 10-channel C/A code, GPS/GLONASS navigation receiver. The R-100/40 is a dual frequency, 4 channel, GLONASS C/A and P code navigation receiver. For these tests the R-100/40 was expanded to 10 channels. Two R-100/20 and two R-100/40 were used.

Combined processing of GPS and GLONASS signals is tightly integrated in the R-100 family architecture. When applicable, individual satellite tracking channels can be arbitrarily assigned to any GPS or GLONASS satellite. As shown schematically on figure 3-1, the R-100 receiver includes a broadband antenna, an RF/IF subsystem, and a GPS/GLONASS Digital Signal Processor, which is implemented on an IBM PC XT/AT-compatible expansion board. The user operates the receiver through the PC host computer utilizing either NMEA 0183-formatted commands or an interactive menu-style user interface. In the R-100/20, hardware channels are allocated for processing up to 6 GLONASS or 6 GPS C/A-code signals in the L1 frequency band, or 6 GLONASS and 4 GPS, 5 GLONASS and 5 GPS, or 3 GLONASS and 6 GPS. The Antenna/Preamp assembly includes a circularly polarized L1, or L1/L2, as appropriate, broadband marine-grade antenna, preselection filter, and low noise preamplifier. The assembly is bolt mountable and constructed for all-weather use. A single coaxial cable

connects the assembly to the RF/IF Unit. Sufficient gain is provided to permit cable lengths of up to 100 feet using RG-223 coaxial cable. The RF/IF unit amplifies and filters the RF signal from the antenna, down converts to various intermediate frequencies (IF), selectively amplifies the desired spectra, down converts to near baseband, and digitizes in-phase and quadrature-phase samples at 17.5 MHz. The L1 and L1/L2 RF/IF Units synthesize their own 10 MHz reference frequency or optionally accept an external 5 or 10 MHz input. A coupling unit at the input provides DC power to the Antenna/PreAmp Assembly. A cable connects the RF/IF Unit to the GPS/GLONASS Digital Signal Processor. The R-100/20 GPS/GLONASS Digital Signal Processor (DSP) receives digital samples from the RF/IF Unit and continuously tracks multiple GPS and/or GLONASS satellites. It tracks phase and frequency errors due to clock drifts, satellite Doppler, receiving platform motion and thermal noise. It also provides fast-sequencing tracking. It extracts ephemeris and almanac data from satellite data messages and transfers separate channels of satellite data to the PC host. It occupies two standard PC expansion cards which plug into PC 8-bit bus

expansion slots. The R-100/40 consists of one standard PC expansion card per channel, providing dedicated parallel tracking. Interchannel delay calibration is performed at the start of the tracking session. The PC Host Computer provides an easy-to-operate user interface. It controls receiver operation and selects healthy satellites that provide best solution geometry. It calculates and displays filtered two- or three-dimensional position and velocity as well as time and status information. Solutions as well as error estimates and satellite status are displayed to the user, logged to the PC hard disk, and transferred to an RS-232C output port. NMEA 0183 and RTCM SC-104 formats are supported. The tracker software is downloaded from the PC to the Digital Signal Processor boards, along with the Doppler frequency and search strategy to be used by the tracker. An IEEE-488 interface between the host computer and a customer-supplied computer is also available as an option. For accurate time transfer applications, a 1 PPS output as well as synchronization with a 1 PPS input are available.

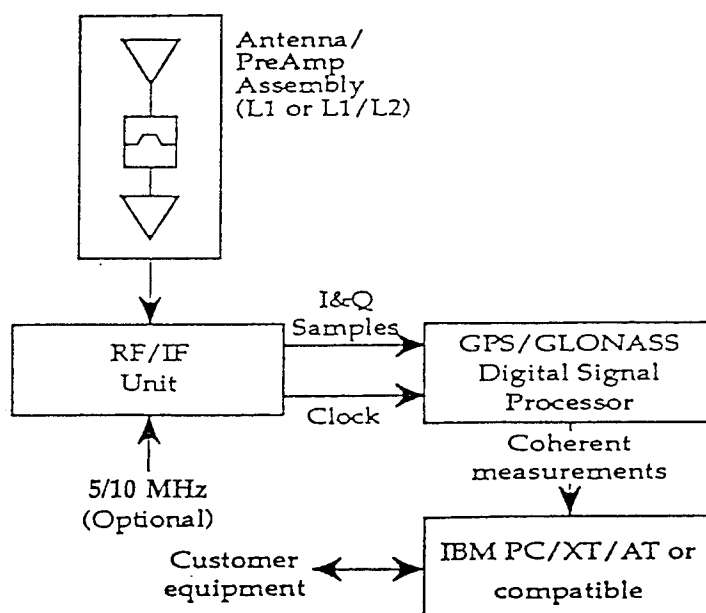


FIGURE 3-1. R-100 INTEGRATED GPS/GLONASS RECEIVER ARCHITECTURE.

3.2 Code Differential Tests

Zero baseline tests were conducted at 3S navigation offices in Laguna Hills, California utilizing two separate R-100/20 receivers connected to the same antenna. Data were collected on 9 September 1994 from 21:32 to 21:55 UTC. Four GLONASS satellites (slots 5, 6, 16, and 21) and five GPS satellites (PRN 1, 17, 21, and 28) were tracked. During post-processing, pseudorange measurements from one of the receivers were processed to generate GPS and GLONASS differential corrections at a one Hz rate. These corrections were applied to the measurements of the other receiver, after proper extrapolation. The corrections for the GLONASS and GPS measurements are shown in figures 3-2 and 3-3, respectively. For GPS, the SA effects are clearly visible except for satellite PRN 28 which is not SA-capable. Integrated GLONASS/GPS navigation solutions were generated for the second receiver using first the uncorrected measurements, then the differentially corrected measurements. Figures 3-4 and 3-5 present the East-North position and velocity errors, respectively, for both the baseline and differentially corrected solutions. HDOP ranged from 1.2 to 1.5 during the test.

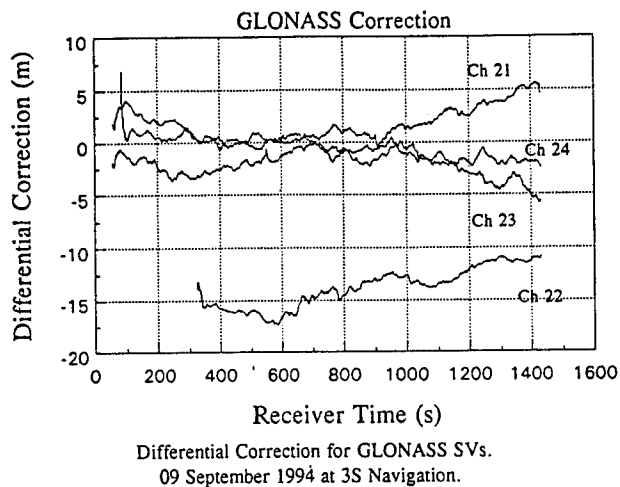


FIGURE 3-2.

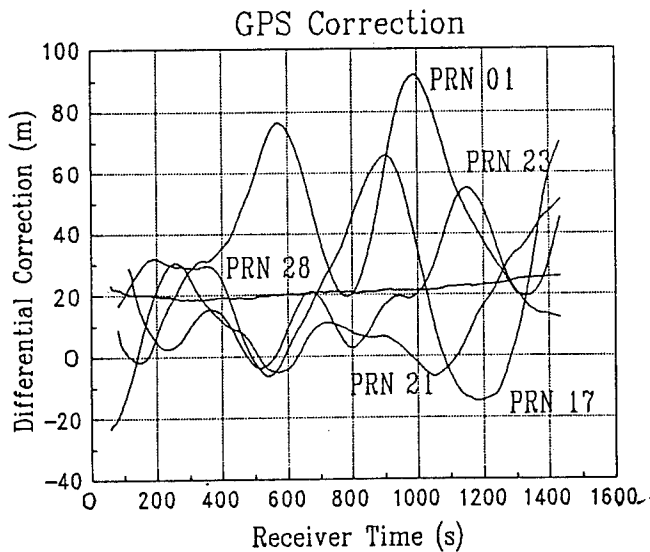
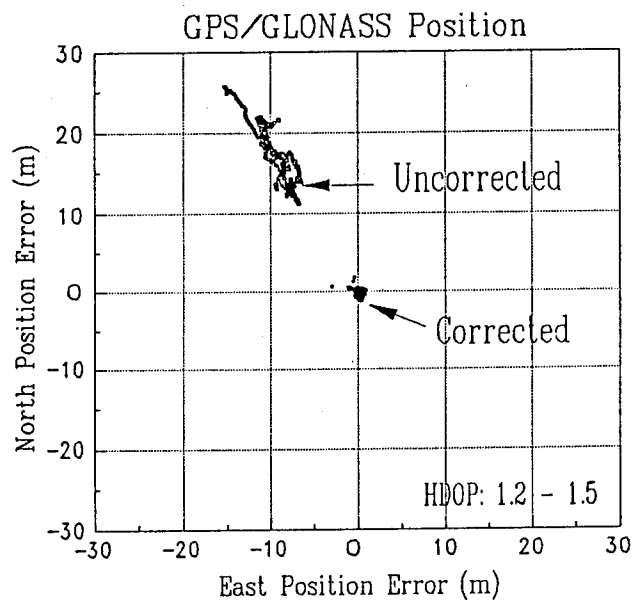
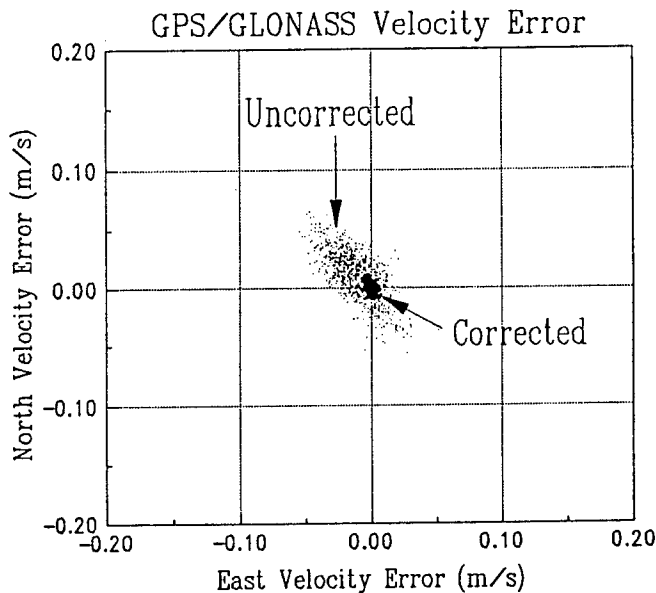


FIGURE 3-3.



Horizontal Position Error using Uncorrected
& Differentially Corrected Measurements. 09 Sept. 1994.

FIGURE 3-4.



Horizontal Velocity Error using Uncorrected
& Differentially Corrected Measurements. 09 Sept. 1994.

FIGURE 3-5.

3.3 Carrier Phase Differential Tests

Two ten-channel, dual frequency, P code GLONASS R-100/40 receivers were used over a known baseline at 3S Navigation in Laguna Hills, California. The baseline was as follows:

1. East : 0.838 meter
2. North: 23.395 meter
3. Up : 0.051 meter

Five GLONASS satellites were continuously and simultaneously tracked by both receivers on L1 and L2 and code and accumulated carrier phase measurements were generated for both. One satellite switch was commanded at both receivers during the tracking session.

Data were collected on 4 May 1995 from 5:00 UTC to 6:00 UTC. The satellites tracked were (slot/frequency) 03/21, 04/12, 12/22, 14/09, 18/10, 19/03.

The following processing was performed:

The carrier phase measurement can be represented as:

$$\phi = R + c(\delta t_{ue} - \delta t_{sv}) - \text{iono} + \text{tropo} + N\lambda$$

where:

R is the range to the satellite in meters
 c is the speed of light
 δt_{ue} is the receiver clock bias
 δt_{sv} is the satellite clock bias
 iono is the ionospheric delay
 tropo is the tropospheric delay
 N is the integer carrier cycle ambiguity

A residual can be formed by subtracting from ϕ , estimates for R and $c\delta t_{sv}$, or

$$\phi_{res} = \phi - R_{est} + c\delta t_{sv_{est}}$$

$$=R_{err}+c(\delta t_{ue}-\delta t_{sv_{err}})-iono+tropo+N\Gamma$$

where the err subscript is the remaining error.

If N_0 is the integer number of cycles in the initial carrier phase residual ϕ_{res0} , we have, after reducing the residual by $N_0\Gamma$:

$$\phi_{res}=\phi-N_0\Gamma-R_{est}+c\delta t_{sv_{est}}$$

$$=R_{err}+c(\delta t_{ue}-\delta t_{sv_{err}})$$

$$-iono+tropo+(N-N_0)\Gamma$$

By applying ϕ_{res} to the carrier phase measurements of another receiver, we obtain,

$$\phi_{res2}=\phi_2-R_{est2}+c\delta t_{sv_{est}}$$

$$=R_{err2}-R_{err1}+c(\delta t_{ue2}-\delta t_{ue1})$$

$$-iono_2+iono_1+tropo_2-tropo_1+(N_2-N_1+N_0)\Gamma$$

Since the baseline is short, we assume common values for both the ionospheric and tropospheric delays at both receivers, and,

$$\phi_{res2}=$$

$$R_{err2}-R_{err1}+c(\delta t_{ue2}-\delta t_{ue1})+(N_2-N_1+N_0)\Gamma$$

The receiver clock errors are common to all satellites and will therefore appear in all residuals.

Clearly, then, ϕ_{res2} will be a measure of the error in the receiver baseline along the satellite line of sight. If the baseline is correct, the residuals will remain constant (or drift at the same rate for all satellites due to receiver clock drifts) for all

satellites as a function of time. Any error in the baseline will show as unequal drifts in the satellites residuals.

These differentially corrected carrier phase residuals are plotted in figure 3-6, using the known surveyed baseline. All residuals are pretty much constant, thereby verifying the accuracy of the baseline. In figure 3-7, a one meter error is introduced in each axis of the baseline. The unequal drifts clearly point to an erroneous baseline. In figure 3-8, a 5 cm error is introduced in one axis only. Even here, the residual curves are not constant, thereby again pointing to an erroneous baseline.

The above results indicate the sensitivity of the single difference carrier phase residuals to baseline errors. Obviously, in differential operations, one does not know the baseline, but is instead trying to determine it. The results presented herein do show that this baseline can be determined from single difference measurements using a search technique whose goal is to identify the baseline for which the double difference residuals are constant.

For the correct baseline, all residuals should be and remain at zero (to within an integer number of cycles). This is not the case in the data presented here. One reason might be different hardware biases for different frequencies, another would be multipath effects. More work is needed in this area. But, as long as they are constant, these biases will not affect our ability to precisely measure the baseline. Also note that there is no need to measure the carrier cycle ambiguities in order to determine the baseline.

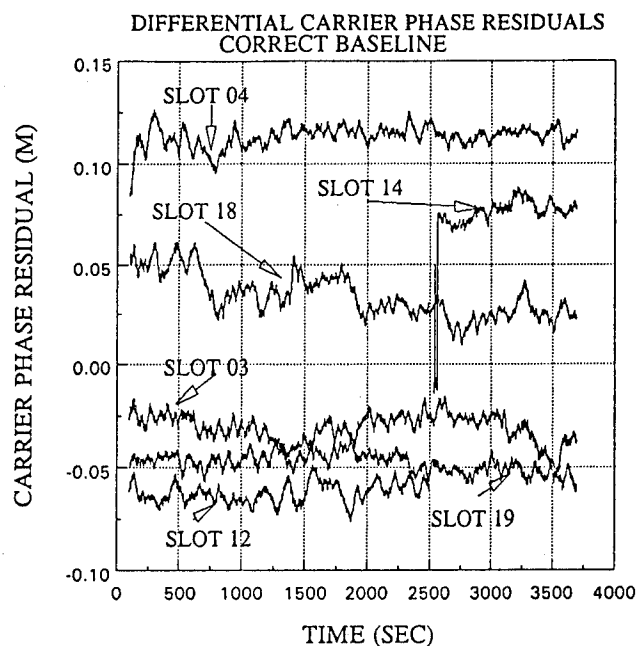


FIGURE 3-6. DIFFERENTIAL CARRIER PHASE RESIDUALS WITH CORRECT BASELINE. 5 MAY 1995.

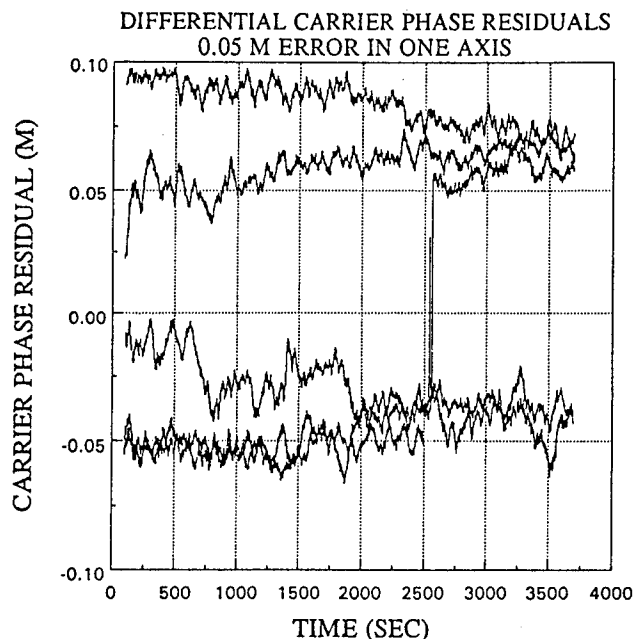


FIGURE 3-8. DIFFERENTIAL CARRIER PHASE RESIDUALS WITH 0.05 METER ERROR IN ONE AXIS. 5 MAY 1995.

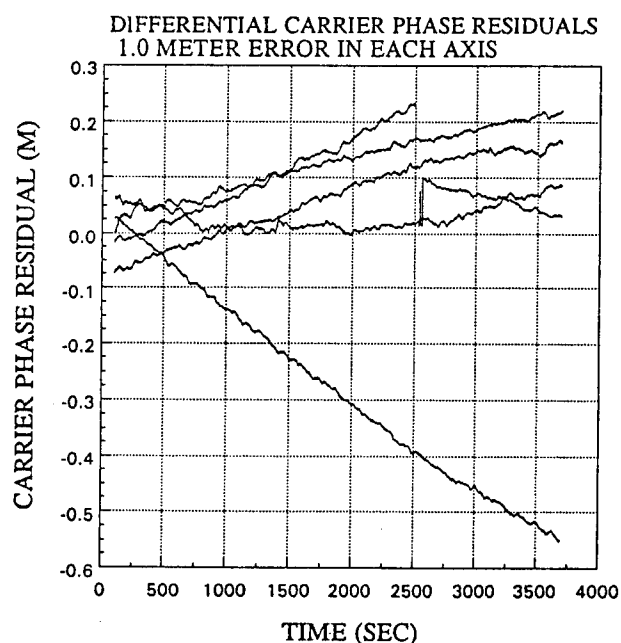


FIGURE 3-7. DIFFERENTIAL CARRIER PHASE RESIDUALS WITH 1.0 METER ERROR IN EACH AXIS. 5 MAY 1995.

4.0 CONCLUSIONS

Differential code and carrier techniques developed for GPS can be used for integrated GPS/GLONASS operations. The next version of the RTCM-SC-104 Standard will include messages for GLONASS measurements. The sensitivity of GLONASS differential carrier phase residuals to baseline errors was shown to detect an error of 0.05 meter in one axis without the need to resolve the carrier cycle ambiguities or the hardware channel biases.

5.0 ACKNOWLEDGMENTS

The authors acknowledge the entire 3S Navigation staff whose tireless and dedicated efforts produced the receivers without which this paper could not have been written.

6.0 REFERENCES

1. Beser, J., GPS and GLONASS Visibility Characteristics and Performance Data of the 3S Navigation R-100 Integrated GPS/GLONASS Receiver, Proceedings ION-GPS-92, September 1992.
2. Beser, J. and Danaher, J., The 3S Navigation R-100 Family of Integrated GPS/GLONASS Receivers: Description and Performance Results, Proceedings, ION 1993 National Technical Meeting, San Francisco, CA January 1993.
3. Beser, J. and Balendra, A., Integrated GPS/GLONASS Navigation Results, Proceedings, ION GPS 93, Salt Lake City, UT, September 1993.
4. Balendra, A., Kim, S. and Beser, J., Fully Integrated GLONASS Dual Frequency P Code and GPS/GLONASS Single Frequency C/A Code Receiver. Features and Performance, ION GPS 94, Salt Lake City, UT, September 1994.
5. Anon., RTCM Recommended Standards for Differential NAVSTAR GPS Service, Version 2.1, January 3, 1994

Performance Evaluation of a Global IGS-Based Differential GPS System

Don English, Gene Howell, and Wang Tang
ARINC

BIOGRAPHY

Don W. English is the Manager of the System Integration and Test Engineering (SITE) Laboratory at the ARINC San Diego Office. He has worked with the Global Positioning System for 10 years. Mr. English holds a B.S. degree in electrical engineering from University of Idaho.

Gene Howell is a Senior Principal Engineer at ARINC. He has worked in the field of aided navigation systems for 15 years. He holds B.S. and M.S. degrees in mathematics from Southern Illinois University in Carbondale.

Wang Tang is Technical Director of the Systems Integration Department at ARINC. He has 16 years experience in the field of navigation and guidance systems. He is the recipient of the 1994 ARINC Technical Excellence Award. He received a B.S. degree from National Cheng Kung University, Taiwan, an M.S. degree from University of Texas at El Paso, and a Ph.D. degree from Iowa State University, all in electrical engineering. He is a registered Professional Engineer in the Commonwealth of Massachusetts.

ABSTRACT

Differential GPS (DGPS) has long been recognized as a very cost-effective testing tool to evaluate the position and velocity accuracy of other navigation systems. Typical Differential GPS operation involves a reference station, installed at a precisely surveyed location, which provides pseudorange corrections to all users in the vicinity. With several advances in correlation technology and multipath reduction, it is believed that the achievable positioning accuracy of DGPS is on the order of a meter.

A major problem associated with the single station DGPS operation is that the accuracy degrades as the separation between the reference station and user increases due to spatial decorrelation. One method

to overcome this problem is to install many reference stations so that users spread over a large area will always be in close proximity to a reference station. Obviously, this is not a desirable nor feasible solution for areas such as the North Atlantic Ocean.

The objective of this paper is to describe ARINC's IGS-based Differential GPS (AIDGPS) system. AIDGPS is a post-processed Wide Area DGPS system which derives its corrections from data from the International GPS Service (IGS) for Geodynamics. The IGS routinely provides pseudorange and carrier phase measurements from more than 80 globally distributed stations. By relying on the IGS, the AIDGPS user does not need to establish a unique reference station network. Since the IGS network is comprised of dual-frequency receivers, AIDGPS is able to measure and compensate for delays due to the ionosphere.

This paper will introduce the AIDGPS system and describe its utilization of the IGS. Detailed algorithms and accuracy performance of the AIDGPS system also will be discussed.

INTRODUCTION

Differential GPS, as described by numerous other papers, is a cost effective means of determining accurate position information. At the heart of any DGPS system is its reference station(s). Local Area DGPS (LADGPS) systems rely on a single reference station to provide DGPS correction data to the users. The potential for position errors increases as the distance between the user and the reference station increases. Wide Area DGPS (WADGPS) systems are more robust. The WADGPS corrections are based on the output of several reference stations distributed about a region. Thus WADGPS errors are minimized throughout the area of interest.

This paper describes the ARINC IGS-Based Differential GPS (AIDGPS) system. AIDGPS creates its WADGPS correction data based on data which is

obtained from the International GPS Service for Geodynamics (IGS). The IGS provides carrier phase and pseudorange measurements from more than 80 globally distributed reference stations. IGS data is available on the INTERNET.

AIDGPS is a post-processed WADGPS system with a significant cost benefit over other DGPS systems. That cost benefit is realized through the elimination of the need to either establish or subscribe to a DGPS service. Also, AIDGPS takes advantage of the IGS's L1 and L2 measurements, thus insuring a high degree of accuracy over the user defined region.

This paper will briefly describe the IGS and AIDGPS's exploitation of the IGS. The remainder of the paper will describe the results of field testing of the AIDGPS system under various conditions.

IGS BACKGROUND

The International Association of Geodesy (IAG) officially established the International GPS Service for Geodynamics on January 1, 1994 [1]. The primary objective of the IGS is to provide precise GPS data products for geodetic and geophysical research activities. The data disseminated by the IGS consists of:

- High quality orbits for all GPS Satellites (20 cm accuracy)
- Earth rotation parameters
- L1 and L2 phase and pseudorange observations for each IGS station
- IGS site information

Each IGS station consists of a high-precision dual-frequency P-code GPS receiver which records satellite pseudorange and carrier phase measurements at 30 second intervals. Five IGS Operational Data Centers are responsible for retrieving each station's raw data, formatting the data into the RINEX [2] standard, and forwarding the data to the Regional or Global Data Centers. The Data Centers provide the on-line interface for the user community to retrieve the IGS data. Data for most IGS stations are usually available at the Data centers within hours of GMT midnight each day.

IMPLEMENTATION

AIDGPS determines the position of a remote GPS receiver based on pseudorange measurements from

the remote receiver, corrected by AIDGPS generated corrections. The remote receiver may be any GPS receiver capable of outputting pseudorange measurements. AIDGPS determines the pseudorange correction data by processing IGS stations' pseudorange observations, ephemerides, along with the precisely surveyed IGS stations' positions. The remote GPS receiver's recorded pseudoranges are compensated by the AIDGPS correction data. AIDGPS then computes the DGPS position solution.

Since the major source of position error for differential GPS is due to ionospheric decorrelation [3], the ionospheric delay is estimated and compensated for by AIDGPS. The IGS L1 and L2 carrier phases and pseudoranges are filtered to produce estimates of the delay. The measured pseudoranges are then corrected with the calculated delays. Although not necessary, the satellite clock errors are derived from the recorded ephemerides and then used to compensate the pseudoranges. This is performed as a reasonableness check on the computed corrections since variations among the resulting corrections should be approximately at the level of Selective Availability (SA).

The positions of the IGS stations' antennas are used in conjunction with satellite ephemerides to obtain the geometric range from the antennas to the satellites. By differencing the geometric ranges with the compensated (for ionospheric delay and satellite clock error) pseudorange measurements, the pseudorange corrections are obtained.

The pseudorange corrections are found for all satellites tracked by the IGS stations in the network during the time interval of the recorded remote GPS receiver data. The network is defined to consist of whichever IGS stations' data files the operator has chosen to download from the INTERNET. However, AIDGPS will limit the network to only those IGS stations which track at least one satellite in common with the remote GPS receiver.

The IGS observation data is recorded in RINEX files at 30 second intervals. Once the corrections are determined, a cubic spline is performed to yield 1 Hz corrections. After compensation for satellite clock error and ionospheric delay, the dominating error source is SA. To validate the cubic spline generated 1 Hz corrections, a second order Markov process was used to model SA [4] with a pseudorange error of 17 meters RMS. It was found that the error contributed by the cubic spline was less than 3.5% of the

total random error in the correction term. From this it is concluded that there is negligible performance degradation in using the low frequency IGS data to estimate higher frequency pseudorange corrections. As a result of this process, 1 Hz pseudorange corrections, compensated for ionospheric delay and satellite clock error, are generated for every satellite tracked by each IGS station in the network.

The next step is to formulate the WADGPS corrections based on the network's stations' corrections. The 1 Hz pseudorange corrections include the receiver biases from each of the respective stations. Inter-station biases are estimated in order to reference all corrections to one time base. One station is selected to be primary. The other stations are checked to find any satellite tracked in common with the primary. When found, the average of the differences in the corrections for common satellites is used as an estimate of the inter-station clock bias, which is then subtracted from all the corrections of the station under consideration. This process is repeated until all possible connections to the primary station are exhausted. For example, if stations A and B track no satellites in common, but stations A and C have common satellites as do stations B and C, then the receiver biases for stations A and B can be related through C.

After the receiver bias correlation, the network of stations is partitioned into sets with no satellites in common. Because no station is used that does not track at least one of the remote GPS receiver's satellites, all stations will be used in correcting the recorded pseudoranges. Consequently, there will be as many receiver biases to estimate as there are sets in the partition. This imposes the condition that the number of sets in the partition plus three (three position errors) must be less than or equal to the number of satellites tracked by the remote GPS receiver. For example, with a 5 channel remote receiver, the maximum number of sets in the partition would be two.

Once the corrections are referenced to a common time frame, a weighted average of corrections to each satellite are computed. The weighting factor is the sine of the elevation angle from the IGS station to the satellite. The implicit assumption is that lower elevation satellites will have noisier pseudorange measurements. A function of the carrier-to-noise ratios would be a preferable weighting factor but the ratios are not available in the IGS observation files.

Once the pseudorange corrections have been found, the remaining task is to apply the corrections to the remote receiver's pseudoranges. However, those pseudoranges include ionospheric delay error. Therefore, the delay must be estimated and compensated before application of the network corrections. The ionospheric delay is estimated using the WAAS algorithms [5][6] with the exception that the grid resolution is 5 degrees. Since a predictive model is required for the algorithm, the ionospheric delay model defined in ICD-GPS-200 [7] is implemented with the parameters broadcast in the navigation message. The stations in the network provide all measurements that are used by the WAAS algorithm in forming the grid of ionospheric delays. The grid is recomputed every two minutes.

The remote receiver measured pseudoranges are compensated for ionospheric delay, derived from the WAAS grid. Since it not known a priori how many sets will be in the network partition, an iterative least squares is employed to estimate the position errors and remote/network receiver clock bias from the corrected pseudoranges and satellite positions. With n satellites tracked partitioned into sets $\{1, 2, \dots, k\}$ and $\{k+1, k+2, \dots, n\}$, the measurement matrix is given by:

$$H = \begin{pmatrix} -u_x^1 & -u_y^1 & -u_z^1 & 1 & 0 \\ \vdots & \vdots & \vdots & \vdots & \vdots \\ -u_x^k & -u_y^k & -u_z^k & 1 & 0 \\ -u_x^{k+1} & -u_y^{k+1} & -u_z^{k+1} & 0 & 1 \\ \vdots & \vdots & \vdots & \vdots & \vdots \\ -u_x^n & -u_y^n & -u_z^n & 0 & 1 \end{pmatrix}$$

where u^m is the user-to-satellite line-of-sight vector. With the initial estimate of position given by the uncorrected navigation solution from the remote receiver, and a clock bias of zero, the estimated errors are found iteratively via

$$\delta x_j = (H^T H)^{-1} H^T z_j$$

with

$$\begin{aligned} z_j &= \|x_j\| - \rho \\ x_j &= x_{j-1} + \delta x_{j-1} \end{aligned}$$

where by abuse of notation, $\|x_j\|$ represents the magnitude of the position vector plus the appropriate estimate of clock bias. The variable x_j is the 4-tuple on iteration j with the first three components being the ECEF position vector of the airborne receiver and fourth component the clock bias (or 5-tuple with two clock bias terms if there are two partitions of the network).

TEST RESULTS

Stationary Tests

To validate the pseudorange correction and position determination calculations, static tests were used. The initial tests of AIDGPS were conducted on data collected from a remote GPS receiver with its antenna at a surveyed position on the ARINC laboratory roof. IGS data from the INTERNET was collected to correct the GPS data.

Numerous static trials under varying satellite conditions were executed. Statistical results of a few of these tests are given in Table I.

These results were obtained by AIDGPS's processing of data from a five channel OEM remote GPS receiver. The AIDGPS position data was compared to the surveyed position of the remote receiver's antenna. No data smoothing was employed, thus every calculated position sample was independent.

The combined three dimensional position error standard deviation was 4.9 meters. This is typical of what is normally seen with a DGPS system and certainly better than the uncorrected three dimensional position error standard deviation of nearly 60 meters.

Low Dynamic Tests

To prove AIDGPS in a dynamic environment, ARINC's 1988 Buick station wagon was drafted as a test bed. A laptop computer was connected to a GPS receiver for the purpose of collecting pseudorange and ephemeris data. The GPS receiver's antenna was mounted, via magnet, on the roof of the test bed.

ARINC's Sub-Centimeter Offset Recording Equipment (SCORE) was employed as the 'truth' source. SCORE is a kinematic carrier phase tracking system for high precision trajectory determination [8]. The SCORE GPS receiver's antenna was also mounted on the roof of the test bed via magnet.

The test bed was driven around Fiesta Island in Mission Bay in San Diego ten times at a relatively constant speed. The island has a paved roadway around its perimeter of about four miles in length. Fiesta Island was chosen as a 'test range' because of its proximity to the ARINC office and the fact that there is no terrain masking. The ten circuits of the island were executed to verify the repeatability of the AIDGPS results.

Figure I was generated by plotting the uncorrected horizontal GPS position data on a horizontal plane. Note the random effects of Selective Availability caused the circuits of the island to be non-overlapping.

Figure II was generated by plotting the horizontal AIDGPS position data on a horizontal plane. At this scale the individual circuits of the island are indistinguishable.

Table I Static Test Results

| Date | No. of Samples | East Bias/Sigma | North Bias/Sigma | Vertical Bias/Sigma |
|----------|----------------|-----------------|------------------|---------------------|
| March 16 | 2203 | 0.2/2.0 M | 0.0/1.9 M | -1.5/3.6 M |
| March 27 | 1033 | 0.6/2.0 M | -0.6/2.1 M | -2.2/3.8 M |
| March 28 | 909 | 0.0/3.6 M | -1.4/2.7 M | -0.8/3.1 M |
| March 29 | 1053 | 0.0/1.7 M | -1.6/2.1 M | 1.6/4.5 M |
| March 30 | 1170 | 0.8/1.9 M | -0.4/2.3 M | -1.4/3.8 M |

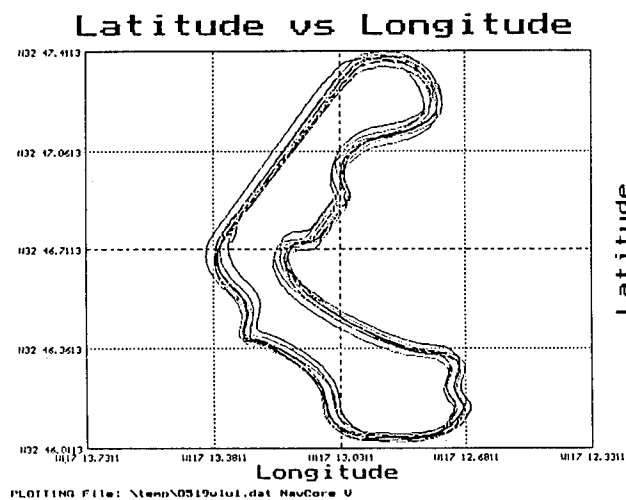


Figure I. Low Dynamics, Uncorrected Horizontal Trajectory

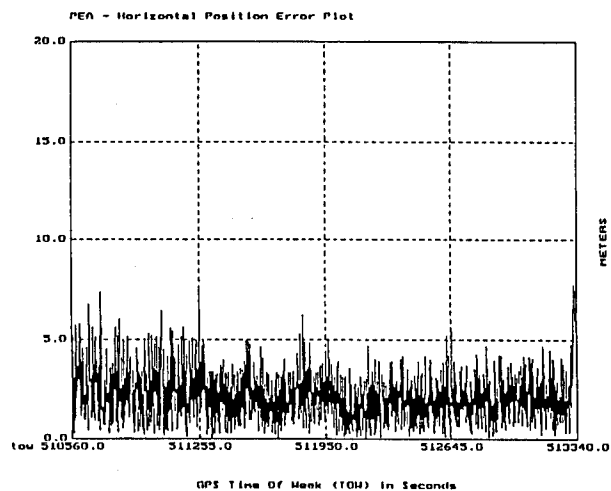


Figure III. Low Dynamics, AIDGPS Horizontal Position Error

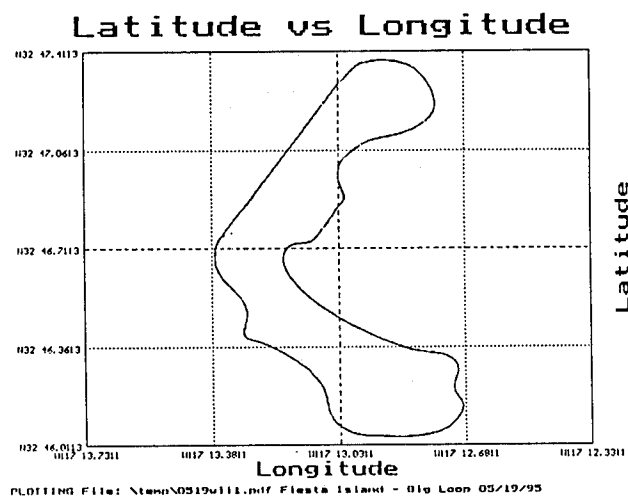


Figure II. Low Dynamics, AIDGPS Horizontal Trajectory

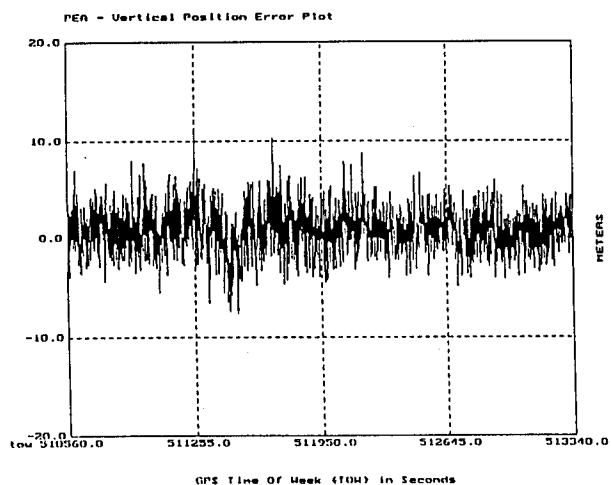


Figure IV. Low Dynamics, AIDGPS Vertical Position Error

Comparisons of the AIDGPS position data to the SCORE truth position data are shown in the following figures. Figure III is a plot of the horizontal position error during ten circuits of the island. Figure IV is a plot of the vertical position error during the same time period.

The standard deviations of the horizontal and vertical position errors were 2.4 and 2.3 meters, respectively.

Medium Dynamic Tests

To prove AIDGPS at higher dynamics, data was collected from a remote GPS receiver installed in the cockpit of a Grumman Tiger aircraft. SCORE was again used as the truth source. Figure V is a plot of

the height of the aircraft during the test. As shown in the plot, the pilot took off, climbed to 1,400 feet, circled the airport, descended, executed a 'touch and go', circled the airport again, descended again, executed another 'touch and go', circled the airport a final time, and landed.

Comparisons of the AIDGPS position data to the SCORE truth position data are shown in the following figures. Figure VI is a plot of the horizontal position error during the course of the flight. Figure VII is a plot of the vertical position error during the same time period.

The standard deviation of the horizontal and vertical errors were 3.7 and 4.4 meters, respectively. In com-

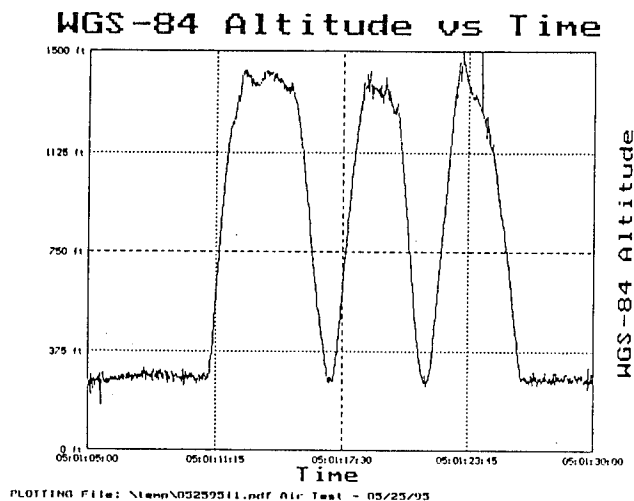


Figure V. Medium Dynamics, Vertical Trajectory

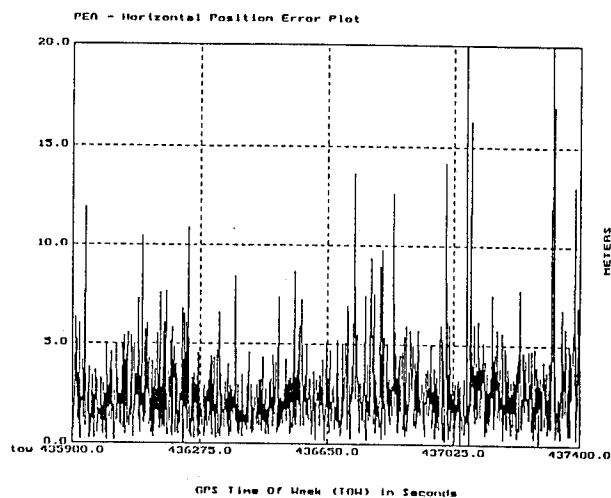


Figure VII. Medium Dynamics, Vertical Position Error

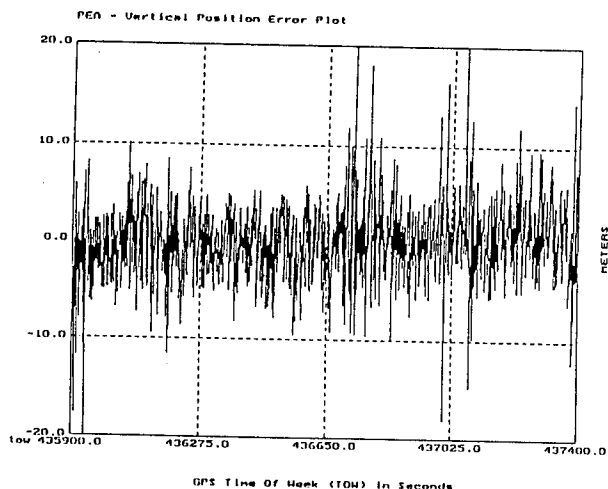


Figure VI Medium Dynamics, Horizontal Position Error

paring these plots to the low dynamics test results, it is apparent that this data is more noisy. This is because this set of data had a PDOP of about four as compared to a PDOP of about three experienced during the low dynamics testing. The poorer PDOP was due to the restricted satellite visibility experienced by the remote receiver mounted in the aircraft's cockpit.

APPLICATIONS

AIDGPS will be utilized to assess the feasibility of reducing the Vertical Separation Minimum (VSM) of aircraft over the North Atlantic above flight level (FL) 290 [9]. The FAA and ICAO are in the process of

implementing guidelines for reducing the vertical separation of aircraft over North Atlantic (NAT) airspace. This effort, called the Reduced Vertical Separation Minimum (RVSM), will reduce the vertical separation of aircraft from the current 2000 foot minimum to a 1000 foot minimum between FL 290 and FL 410, inclusive. Prior to implementation of the RVSM, the FAA and ICAO wish to monitor the height keeping performance of a large sample of commercial and general aviation flights.

To gather the necessary GPS observables, GPS Monitoring Units (GMUs) are non-intrusively installed on the aircraft. The GMUs have two antennas which are attached to windows on opposing sides of the cockpit. The GMU's GPS receiver is connected to a notebook personal computer which records pseudorange and ephemeris data. The GMU data files are processed by AIDGPS to determine the absolute height of the aircraft during flight. Atmospheric data will be used to allow the comparison of the absolute height information to the reported pressure altitude of the aircraft.

CONCLUSION

The results presented here were obtained from the processing of data from a five channel OEM GPS receiver. Better results would be expected when using an all-in-view receiver. AIDGPS, also has the ability to smooth the pseudorange data, however that feature was turned 'off' during the processing of this data. Even without data smoothing, the standard

deviation of AIDGPS's output position error is generally less than 5 meters.

AIDGPS is a cost effect post-processed differential GPS tool. This unique, reconfigurable tool may be adapted to provide WADGPS coverage virtually anywhere on the globe. The utilization of data from the IGS makes the tool geographically portable. Also, AIDGPS is able to process GPS pseudorange observables from a variety of GPS receivers, thus AIDGPS is not dependent on a particular manufacturer's product.

Obviously, AIDGPS is a post-processed system, therefore it is not effective for real-time applications. However, for applications not requiring immediate position reporting, the flexibility of AIDGPS makes it an attractive alternative for many DGPS applications.

ACKNOWLEDGEMENTS

The authors would like to express their appreciation of Diane Davis, Hana Maquet, and Gerald Schmit in the development and testing of the AIDGPS software.

REFERENCES

- [1] Zumberge, J. F., et al, The International GPS Service for Geodynamics - Benefits to Users, Proceedings of Institute of Navigation 7th International Technical Meeting (ION GPS-94), Salt Lake City, UT, September 1994, pp 1660-1663.
- [2] Gurtner, Werener, RINEX-The Receiver Independent Exchange Format, in GPS World, July 1994, v.5, no. 7, pp 48-52.
- [3] Brown, A., Extended Differential GPS, Navigation, Journal of the Institute of Navigation, Vol-36, No. 3, Fall 1989, pp 265-285.
- [4] Chuo, H. An Anti-SA Filter for Non-Differential GPS Users, Proceedings of The International Technical Meeting (ION-GPS-90), Colorado Springs, Colorado, September 1990, pp 535-542.
- [5] SatNav, Satellite Navigation, Specification for the Wide Area Augmentation System, Draft, no date.
- [6] El-Arini, M., et al, Comparison of Real-Time Ionospheric Algorithms for a GPS Wide Area Augmentation System (WAAS), Navigation, Journal of the Institute of Navigation, Vol. 41, No. 4, Winter 1994-1995, pp 393-413.
- [7] NAVSTAR GPS Space Segment/Navigation User Interfaces, ICD-GPS-200C, Code Identification Number 6Z691, 10 October, 1993.
- [8] Tang, Dr. W., et al, A Kinematic Carrier Phase Tracking System for High Precision Trajectory Determination, Proceedings of Institute of Navigation 7th International Technical Meeting (ION GPS-94), Salt Lake City, UT, September 1994, pp 783-789.
- [9] Colamosca, B., K. Joyce, R. Rigolizzo, A. Schust, and W. Smoot, Summary Report of United States Studies on 1,000-foot Vertical Separation Above Flight Level 290. DOT/FAA/DS-88/10. Washington, D.C.; Advanced System Design Services, Federal Aviation Administration, July 1988.

Satisfying Airport Operational Requirements Using Seamless GNSS Techniques, Procedures and Processing

Lois Pilley and H. Robert Pilley
DSDC

BIOGRAPHY

Ms. Lois Pilley is the CEO and co-founder of DSDC. DSDC specializes in hardware, software and systems engineering for GPS applications with a concentration in navigation and Air Traffic Control technologies. DSDC's research has led to the development of a low cost, GPS-based airport navigation and management system for use in aircraft, surface vehicles and the airport control tower. Ms. Pilley has over eleven years experience in the software design and development of air traffic control systems for the U.S. Air Force and the FAA.

Mr. Robert Pilley is the president of DSDC. Mr. Pilley has over twelve years experience in FAA programs and is the co-chair for RTCA SC-159, working group 4B, Airport Surface Navigation and Surveillance. In 1993, Mr. Pilley was awarded a U.S. patent for a GPS-based Airport Control & Management System.

Both Mr. and Ms. Pilley have contributed to RTCA SC-166, SC-159, SC-186, the RTCA GNSS Task Force, the Transportation Research Board, and the Airport Surface Traffic Automation (ASTA) Technical Interchange Group (ATIG). Mr. and Ms. Pilley are the co-authors of a technical engineering source book entitled, GPS-BASED AIRPORT OPERATIONS - Requirements, Analysis & Algorithms.

ABSTRACT

The successful implementation of a seamless, DGPS-based airport navigation, control and management system is dependent on the successful integration of avionics and Air Traffic Management (ATM) technologies. Differential GPS (DGPS) position, velocity and time (PVT) data can provide pilots with world-wide, all-weather navigation capabilities, including forms of precision approach, taxi and departure guidance. An integrated datalink can give all participants a dynamic view of the airspace (or airport surface) and provide the ATM system with the inputs it needs to manage air and ground traffic safely and efficiently. Using common, safety-enhancing algorithms, GPS and datalink can provide improved benefits to the vast majority of aviation system users and operators.

To maximize the strength and versatility of an integrated GPS-based airport system, international standards are required for navigation, geodesy, avionics, and datalink(s). The first step in developing these standards is the definition of high-level operational requirements for seamless airport operations.

This paper describes a set of key, high-level

operational requirements for a DGPS-based airport navigation, control and management system. The requirements are translated into a specific technology implementation utilizing GPS and datalink. The concepts presented here are based on the real time test activities conducted by DSDC at the Manchester, NH airport.

OPERATIONAL PERSPECTIVES

There is a clear consensus throughout the aviation industry that terminal area operations must be enhanced in order to meet the rising demands for air service. To achieve the FAA's stated goals of a 15 percent reduction in average taxi-in and taxi-out delays and an 80 percent reduction in runway incursions, automation aids are being sought which will improve airport-wide operations.

It is critical that the airport automation system be architected to provide seamless, 4-D terminal operations which can provide a smooth transition to and from en route airspace. Surface automation should form the baseline for an airport-independent processing system, improving operating efficiencies and enhancing safety.

Onboard equipment should satisfy multiple mission needs, accommodating all classes of aircraft. The equipment installed in aircraft for use in the terminal area should be the same as that used in en route airspace [3]. Traffic on the airport surface should merge seamlessly with arriving and departing aircraft. Ground vehicles, maneuvering within the airport movement area, should be managed and monitored with aircraft to ensure safe and efficient operations.

In addition to supporting diverse user needs, the system should also allow for cost effective installation at large and small airports, allowing full flexibility for the application of appropriate levels of services in all terminal areas [3]. Finally, benefits should be realizable in all types of weather and not be limited to low visibility conditions.

This paper describes two operational perspectives - one for airport functions, the other for aircraft. When integrated together, the combined functions have the potential to improve airport capacity through the sharing of information between air traffic controllers, airport operators and airport users. The operational requirements supporting these perspectives have been derived from a series of FAA, ICAO, NASA and

RTCA documents. Brackets are used to denote specific sources. Where possible, the actual requirement is re-stated for consistency with the referenced document.

Airport Operational Perspective

Surveillance

For enhanced terminal area automation, surveillance will be provided through Automatic Dependent Surveillance Broadcast (ADS-B). With ADS-B, each properly equipped aircraft derives its position, speed, heading and other information using its onboard avionics. The information is periodically broadcast and is received by other, similarly equipped users or ground-based management facilities. In addition, various classes of surface vehicles may be configured with GPS/ADS-B equipment to broaden the surveillance coverage to include all authorized vehicles movements.

Within the terminal area, ADS-B will provide all control authorities with surveillance for the airport's airspace and maneuvering area (i.e., surface areas used for takeoff, landing and taxiing of aircraft). Where feasible, surveillance coverage will begin from at least 10 nmi from touch-down and extend to the airport boundary including those parts of the ramps and maintenance areas used for the movement of aircraft. [2] Coverage will be provided for moving and static aircraft and vehicles, providing positive identification on authorized movements. [2]

The vast majority of airports have no low altitude surveillance for aircraft on final approach. Even fewer have any form of ground surveillance. For those airports that currently have radar coverage, there is no simple means by which to merge air and ground traffic. ADS-B will provide improved monitoring capabilities for all airports which will, through improved position reporting, lead to reduced aircraft separation on final approach. On the airport surface, ADS-B will provide improved management of ground movements, merging surface vehicles with aircraft to provide a comprehensive view of the airport's operations. The integrated management of air and surface movements will increase the airport's capacity through the more efficient utilization of existing airspace and runways.

As ADS-B messages are received by the Airport Traffic Management (ATM) system, they are used as inputs into the conflict detection and resolution, conformance monitoring, and automated lighting functions. Shared databases will allow for the mirrored processing of these functions onboard the aircraft and required surface vehicles as well. The following subsections describe each of these functions and the planning function in greater detail.

Conflict Detection and Resolution

For each ADS-B equipped aircraft and surface vehicle operating within the airport maneuvering area, the ATM system will extract the position and velocity information from the ADS-B message and use the data to project the aircraft/vehicle's position ahead in time.

The ATM will continuously monitor the aircraft/vehicle's current and projected positions with respect to all possible conflicts. Detectable conflicts include:

- Collision with a moving aircraft/vehicle
- Collision with a static aircraft/vehicle
- Collision with a known, static obstacle (towers, buildings, mountains)
- Incursion into a restricted area (weight/wingspan limited areas, closed areas, construction areas)
- Incursion into a controlled area (runways, taxiways, special use airspace, ILS critical areas, approach/departure envelopes)
- Incursion into a hazardous weather area

The terminal ATM system will provide, via its datalink, automated advanced warning messages about potential traffic conflicts. [3] Alerts and instructions to resolve the conflict will be brought to the attention of the controlling authority and the affected aircraft/vehicle. Other aircraft/vehicle(s) in the vicinity, but not directly involved in the conflict, may also be provided with an alert notification by the ATM system through voice or digital means.

Aircraft/vehicle type classification, status and clearance information will play an important role in conflict detection processing. Individual areas may be restricted to certain vehicles and not others. For example, a taxiway may be off limits to vehicles over a specified weight. In this case, a conflict or taxiway incursion alert will be generated if a heavy vehicle approaches or enters the taxiway while a lighter vehicle would have unrestricted access. In addition, aircraft/vehicle's may be 'cleared' to enter selected areas at specific times. For example, if an aircraft/vehicle is cleared for a runway, it may enter it without restriction. If an uncleared aircraft/vehicle enters the runway, however, a runway incursion alert will be generated.

To detect potential conflicts between aircraft or between an aircraft and a surface vehicle, a conflict-protected volume will be projected around each aircraft/vehicle in question. The conflict-protected volume around each aircraft in managed air/ground space should accommodate safety requirements and the need to minimize the airspace reserved by each instant by each aircraft. [3] The volumes may be moved forward in time, based on the aircraft's velocity and travel path information. If the aircraft's conflict-protected volume intersects with another vehicle's volume within a predetermined minimum time, a potential collision condition will be triggered. Other data, including trend, intent and aircraft capabilities may be factored into the collision detection processing to minimize false alarms.

Conformance Monitoring

In addition to conflict detection and resolution, the ATM system shall provide automated monitoring of all aircraft and selected ground vehicles to ensure adherence to authorized taxi instructions. [5] After a

travel path has been issued to an aircraft or vehicle, the ATM system can perform a series of navigation functions, mirroring those performed on board the aircraft/vehicle using its ADS-B position reports. A set of waypoints will be maintained for each cleared vehicle. The vehicle's 3-D range to waypoint and cross track error may be computed for each subsequent ADS-B report and used to determine whether the aircraft/vehicle is on or off course. If an off course condition is detected, a warning message will be displayed to the controller at the ATM workstation.

Short term warnings will be provided when the computed deviation for an aircraft/vehicle falls outside of its preset/predefined maximum route deviation. [2] Alerts will also be generated if an aircraft/vehicle enters or is about to enter an occupied taxiway which is not on his assigned route. [2]

Planning

The surveillance information provided by ADS-B will be utilized by the airport planning function to improve the efficiency of the airport. ADS-B will provide the planning function with accurate and frequent knowledge of aircraft position, speed, and heading such that clearances can be coordinated and performed in the appropriate time and location on the runways. [4] This information will enable the planning function to provide sequencing of aircraft after landing or when departing from the parking positions to ensure minimum delay and minimum utilization of the available capacity of the airport. [2]

For arriving and departing aircraft, ADS-B will provide the tower controllers with the information they need to sequence and optimize the traffic flow. The local controller is responsible for the sequencing, spacing and issuance of clearances and instructions to arriving and departing aircraft. In sequencing aircraft, the controller considers the position, type, speed, and direction of movement of aircraft desiring to land; estimates future positions; the number and capabilities of aircraft wishing to depart from the airport; the pattern, length, direction, and condition of runways available for use; wind speed and direction; noise abatement requirements; wake turbulence; and traffic information. The local controller also determines:

The order, time and direction of takeoff and necessary turns.

Where inbound aircraft are to enter the traffic pattern and whether distances between aircraft are shortened or lengthened to control the spacing and to assure a safe, orderly flow of aircraft on the final approach to the landing runway.

Runway use including possible simultaneous use of other runways and designated areas.

The times and methods by which arrivals and departures can be interspersed with the least delay to traffic.

When to issue clearances to landing and departing aircraft to assure standard separation.

When VFR flights through the airport traffic area can be authorized.

Provides timely coordination with other controllers on movements of arrivals / departures / overflight aircraft.

When the aircraft clears the runway, control is passed to the ground controller. The ground controller is responsible for controlling the movement of aircraft and other vehicles on all parts of the airport except the runways in use. Specific duties include:

Determining when aircraft and other vehicles may safely cross runways and movement areas.

Issuing control instructions to aircraft and surface vehicles.

Formulating and issuing taxi clearances and instructions to aircraft and vehicles.

Maintaining separation among taxiing aircraft and vehicles.

Operating designated field lighting systems.

Collecting, analyzing and distributing reports regarding hazards, potential hazards and operational status of facilities/equipments.

The planner will utilize ADS-B data to facilitate the automation of these functions, using predictive software to accurately determine arrival and departure times. Similar information will also be provided to ramp controllers, enabling them to sequence and merge their needs and expectations with those of the airport tower.

Lighting Control

Automated intersection lights may be provided to indicate activity on a given runway. [7] As in the conflict detection processing, the aircraft/vehicle's current and projected positions will be compared to a defined 'airport lighting area'. If the aircraft/vehicle is inside the area, or is within a predetermined minimum distance from the area, the lights will be enabled to indicate the runway is active. When the aircraft/vehicle exits the area, the lights will be disabled. A runway incursion will force the lights to switch to a alert state, signalling that the runway has been compromised.

The automated control of airport lights will serve as an airfield safety alert, providing a clear indication to the users of current status and alert conditions. The use of ADS-B for automated lighting control eliminates the need for costly, single-purpose, ground-based sensors.

Aircraft Operational Perspective

Navigation

With differential GPS data provided onboard the aircraft, highly accurate navigation is available for

departure guidance, precision approach and ground taxi operations. Standards for avionics equipment which will support GPS-based precision approaches down to Category III are currently being developed by RTCA. To facilitate this capability, The system design for airports and heliports should allow for full zero-zero taxi and take-off guidance and for some airports, as needed, to be equipped for full zero-zero landing on some runways. [3]

For seamless navigation, the pilot must be provided with continuous guidance and control during the landing roll-out, while taxiing to the parking position and from the parking position up to the runway holding point and to line up for an appointed take-off position. [2] When assigned a travel path, the aircraft/surface vehicle will perform conformance monitoring to ensure adherence to the designated route. The navigation function will provide the capability to determine the current/predicted lateral deviation from the cleared path. [4] The aircraft shall be provided with guidance cues to return to true path if the maximum deviation has been exceeded. [4]

As part of the navigation system, the pilot and vehicle driver shall be provided with warnings of incursions into unauthorized areas, particularly runways and taxiways. [2] The guidance system will also be capable of indicating routes and areas either restricted or not available for use. [2] Incursion warnings will be generated if the aircraft/vehicle enters a restricted area.

Navigation may also be augmented through the use of a cockpit map display. With an onboard map presentation, the aircraft/vehicle's GPS position may be used to provide the pilot/operator with a graphical representation as to his current position with respect to the airport layout. Route description and conformance monitoring may also be provided graphically, alerting the pilot/operator to any deviations from the desired course.

The use of cockpit map displays with visualization of taxi paths and hold short instructions will serve to reduce pilot/operator confusion and the occurrence of 'blunders' on the airport surface.

CDTI/Situational Awareness

Through the integration of ADS-B information, cockpit moving map displays may be augmented through the presentation of other traffic in the immediate vicinity. Cockpit Display of Traffic Information (CDTI) may be provided for airborne and surface operations, integrating the two seamlessly during takeoff and approach operations.

With CDTI, the current position, ID, and intent of proximate aircraft and vehicles will be shown with respect to self. [4] It will provide true 'traffic awareness', providing the pilot/operator with 3-D situational awareness, regardless of the current visibility conditions.

CDTI can also aid the pilot in navigation, providing a clear view of the aircraft to follow during taxi operations, including an indication of his spacing from the preceding aircraft. [2]

The implementation of CDTI has the potential to reduce separation standards, provide improved utilization of area.

Collision Avoidance

ADS-B will provide enhanced aircraft-to-aircraft and aircraft-to-vehicle collision detection and avoidance capabilities. As ADS-B messages are received from other aircraft/vehicles, the pilot (and vehicle driver) will be provided with information to prevent collision with other aircraft, vehicles or temporary (known) obstacles. [2] For airborne applications, true 3-D collision detection will be achievable for vertical and horizontal maneuvers. The collision detection processing performed on board the aircraft should mirror that performed on the ground at the ATM system.

Station Keeping/Self Separation

ADS-B will allow for appropriately equipped aircraft to share in the responsibility for separation, sequencing and spacing by means of an on-board traffic display. [3] CDTI will provide pilots with more latitude in determining how they maintain separation with proximate aircraft.

With 'free flight', properly equipped aircraft will be permitted to proceed with 'due regard' for other traffic. In trail-descent, in trail-climb and aircraft-to-aircraft station keeping will reduce controller workload, increase efficiency by better utilizing airspace, and reduce separation standards, thereby increasing airspace capacity.

PERFORMANCE REQUIREMENTS AND ACCURACY

To support the airport and aircraft operational perspectives described above, the ADS-B message must include the following parameters at a minimum:

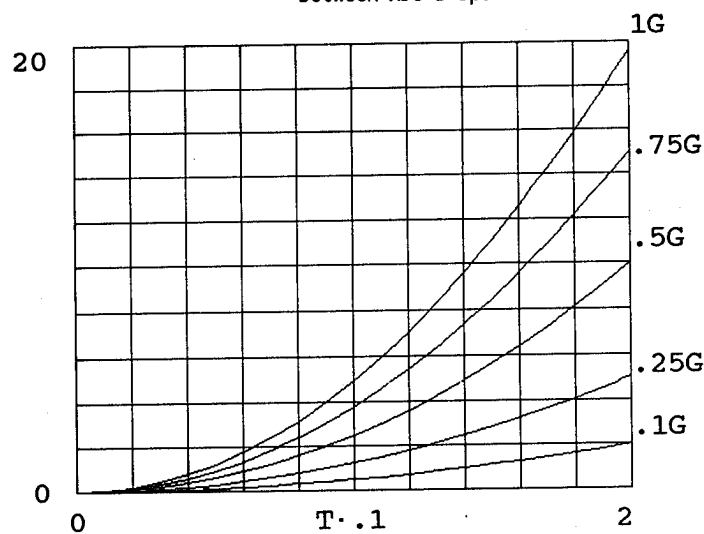
ID
Type Classification
3-D Position
Velocity
Direction

The following performance parameters have been derived from the referenced documents for airport surface operations:

| | |
|---------------------|-----------------------------------|
| ADS-B update rate | <= 1/second |
| Positional accuracy | < 3 m, with a resolution of 1.5 m |
| Direction | < 2 degrees |
| Velocity | < 5 knots |

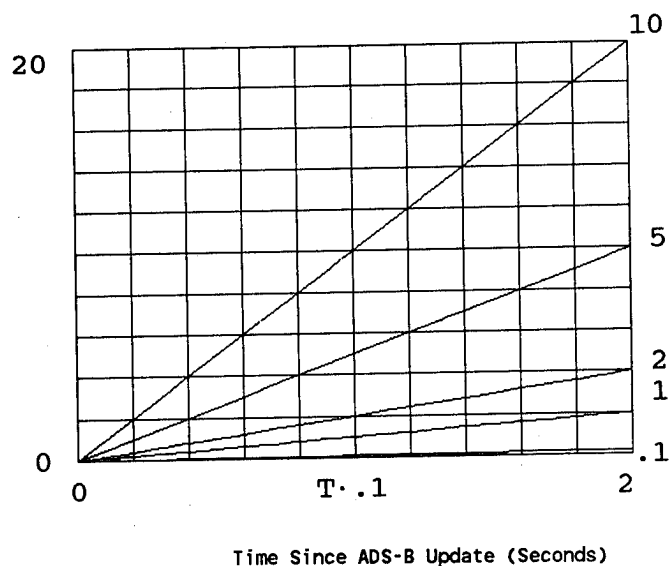
The charts below show potential positional errors which may be introduced through inaccuracies in acceleration, velocity and heading data. In the first chart which follows, the vertical axis represents the positional offset in meters. The horizontal axis represents the time since last update in seconds. Each line represents a different acceleration value beginning with 0.1 G at the bottom and continuing with 0.25 G, 0.5 G, 0.75 G, and 1.0 G.

Positional Error Due to Acceleration
Between ADS-B Updates



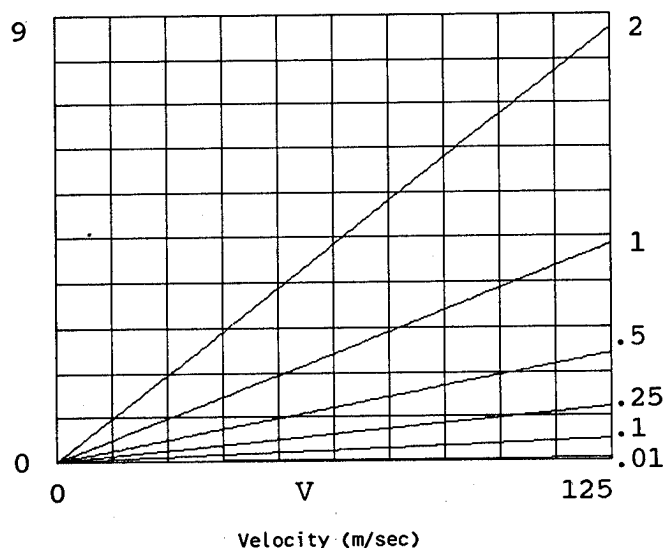
As shown above, the positional error introduced for acceleration is relatively low, particularly at the lower acceleration (0.1 G) typical of most airport operations.

Positional Error Due to Reported ADS-B Velocity Error



Here, the positional error due to velocity inaccuracies of 0.1 m/sec, 1.0 m/sec, 2.0 m/sec, 5.0 m/sec, and 10.0 m/sec are provided. Assuming the velocity is accurate to better than 5 knots (~ 2.5 m/sec), the positional error introduced each second is on the order of approximately 3.0 meters.

Cross Track Error Due to 2 Degree Heading Error
Reported in ADS-B Message



In this chart, the vertical axis represents the cross track error, in meters, introduced by a 2 degree heading error. The horizontal axis represents the velocity from 0 to 125 m/sec (~ 250 knots). Each line represents time, in seconds, starting with 0.01 and continuing with 0.1, 0.25, 0.5, 1.0 and 2.0. The cross track error introduced at the maximum velocity at the end of one second is relatively small (less than six (6.0) meters).

The overheads imposed by the position determination, radio and local processing functions translate into a finite system delay. Latency compensation is required to accurately represent the positions of the aircraft/vehicles on the 3-D airport map and to accurately perform the time-synchronized processing functions.

To compensate for this type of system delay factor, the precise DGPS derived velocity components may be used to project the position ahead. The amount of required latency compensation time (t) may be determined through the use of precise GPS time. The compensation factor is determined by multiplying the velocity by the compensation time (t). The compensation factor is applied to the current position to determine a new, compensated position. The compensated position may then be considered the current position and may be used throughout the navigation and processing algorithms. This technique works well in low dynamic environments where the course is relatively steady as in final approach, landing and takeoff for commercial and GA airport operations. High dynamic conditions may require hybrid solutions involving the integration of additional sensors and the inclusion of acceleration information in the ADS-B message. Given the stated frequency of the ADS-B broadcasts (≤ 1 /second) and the relatively small velocity errors (< 5 knots) at the receiving station, the acceleration factor has little impact for normal airport operations. This may be observed again in the following example which defines a compensation technique to reduce the processing and display

uncertainties between ADS-B updates.

$$\text{ADS-B RATE} = 1 \text{ HZ } (T = 1)$$

The ADS message is broadcast at a once per second rate. The position and velocity information are correct (3 m +/- 1.5 m and < 5 knots, respectively) at the time of broadcast.

$$1 \text{ G MAXIMUM GROUND SIDE ACCELERATION} = 9.8 \text{ M/S}^2$$

The maximum acceleration is assumed to be 1 G in the commercial airport ground environment. This acceleration is assumed to change linearly over a one second period (Jerk = 9.8 M/S^3). The distance travelled due to the constant jerk of 9.8 M/S^3 over the one second period is found by integrating the jerk three times.

$$250 \text{ KNOT MAXIMUM GROUND VELOCITY} = 128.6 \text{ M/S}$$

The maximum speed for airport surface movement is 250 knots. Assuming the maximum speed and acceleration, the positional change between ADS-B updates is determined below:

$$128.6 * 1 + \frac{|9.8T^3|}{(2*3)} = 130.2 \text{ METERS}$$

Latency compensation can be performed at the ATM to smooth the perceived jump in position reports. In the example below, the processor clock at the ATM station internally updates all positions 100 times per second.

$$\text{REAL TIME CLOCK RESOLUTION} = .01 \text{ SECONDS}$$

$$128.6 * .01 + \frac{|9.8T^3|}{(2*3)} = 2.8 \text{ METERS}$$

By using the time clock interrupt to project the reported ADS-B position ahead, the position error is less than three (3.0) meters under maximum dynamic conditions.

The above example may be repeated for a thirty (30.0) knot taxi speed.

$$30 \text{ KNOT TAXI SPEED} = 15.4 \text{ M/S}$$

$$\text{ADS-B UPDATE RATE} = 1 \text{ HZ}$$

$$15.4 * 1 + \frac{|9.8T^3|}{(2*3)} = 17.1 \text{ METERS}$$

$$\text{REAL TIME CLOCK RESOLUTION} = .01 \text{ SECONDS}$$

$$15.4 * .01 + \frac{|9.8T^3|}{(2*3)} = 1.8 \text{ METERS}$$

Here, the position offset between ADS-B updates is 17.1 meters. Latency compensation techniques, employed every .01 seconds can reduce this offset to less than two (2.0) meters.

For conflict detection processing, the current position may be projected ahead ten (10.0) or more

seconds depending on phase of flight and vehicle type. Under a constant jerk of 9.8 M/S^3 , the worst case positional offset is determined below. By multiplying the change in velocity due to the constant jerk over the 1 second update period by the projection time, the offset can be determined.

$$\frac{\text{Velocity} * \text{Projection}}{\text{change} \quad \text{time}} = \text{Position offset}$$

$$\frac{|9.8 * 1^2|}{2} * 10 = 49.0 \text{ METERS}$$

A general purpose latency compensation scheme utilizing the Earth Centered Earth Fixed (ECEF) velocity and position data is provided below. This processing is performed for latency compensation and projection processing in the zone incursion and collision algorithms.

PROJECT ECEF POSITION

$$X_t, Y_t, Z_t = \text{ECEF position}$$

$$NX_t, NY_t, NZ_t = \text{ECEF Projected position}$$

$$VX_t, VY_t, VZ_t = \text{Velocity components along ECEF axes}$$

$$T = \text{Latency time (in seconds)}$$

$$NX_t = X_t + VX_t * T$$

$$NY_t = Y_t + VY_t * T$$

$$NZ_t = Z_t + VZ_t * T$$

PROJECT ECEF POSITION USING TIME, VELOCITY AND ACCELERATION DATA

$$X_t, Y_t, Z_t = \text{ECEF Position}$$

$$NX_t, NY_t, NZ_t = \text{ECEF Projected Position}$$

$$VX_t, VY_t, VZ_t = \text{Velocity components along ECEF axes}$$

$$AX_t, AY_t, AZ_t = \text{ECEF Acceleration}$$

$$T = \text{Latency time (in seconds)}$$

$$NX_t = X_t + VX_t * T + \frac{AX_t}{2} * T^2$$

$$NY_t = Y_t + VY_t * T + \frac{AY_t}{2} * T^2$$

$$NZ_t = Z_t + VZ_t * T + \frac{AZ_t}{2} * T^2$$

COORDINATE REFERENCE SYSTEM CONSIDERATIONS FOR ADS-B

The use of a common coordinate reference system is an important factor for efficient and seamless operations

within the airport environment. Each aircraft and vehicle must be capable of determining its current position with respect to a common origin. The precise location of key physical or geographic areas of interest must be known with respect to the same coordinate reference. The table below compares ECEF to the more traditional Latitude/Longitude/Altitude reference systems.

| POSITION FORMAT | LINEAR | CONTINUOUS | CONSTANT SCALE | SINGLE POINT ORIGIN |
|-------------------------|--------|------------|-------------------|------------------------|
| ECEF X,Y,Z | Yes | Yes | Yes | Yes |
| LAT, LON | No | No | No | No |
| Ellipsoidal Altitude | Yes | Yes | Yes | No |
| Baro Alt | Yes | Variable | No | No |
| MSL Alt | Yes | Variable | No | No |

Varying, discontinuous scales and mixed variable position formats complicate processing and introduce processing errors making seamless, airport-independent processing unattainable.

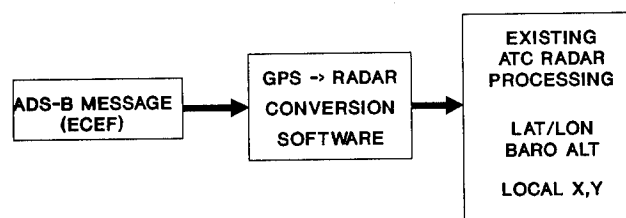
Seamless airport operations are further simplified when implementing ECEF X,Y,Z velocity as well. As with the ECEF 3-D position data, the velocity components are linear, continuous, have a single point origin and a constant scale. Many receivers output the three velocity components in a North/East/Up format. Though this represents a linear velocity, it does not have a single point origin and, when combined with Latitude/Longitude position, can introduce additional processing overheads. It is, however, preferred over the more traditional combination of compass heading, airspeed and baro vertical rate which suffers from several limitations. Compass heading varies with location and is susceptible to corruption by stray magnetic fields and may suffer from local geographic anomalies. The second element, air speed, is not useful for ground movement and varies with time and place. Baro rate also varies and requires calibration. Though these parameters are required by the pilot, they are not necessarily required, nor are they the optimal choices for use in the primary processing algorithms for airport automation.

Precise, seamless airport control, navigation and management is greatly simplified using ECEF-based position and velocity formats. This framework provides simplified mathematical processing for navigation, conflict detection and resolution, collision avoidance and airport management processing. Because the ECEF coordinate reference system is world-wide, the developed processing algorithms are airport independent, eliminating the need for specialized airport processing and local, site-dependent scaling adjustments.

TRANSITION

During the transition from local navigation and surveillance to a world-wide, seamless system, the

full capabilities of a GPS or GNSS-based solution should not be compromised. Compatibility with present systems should not limit the overall accuracies and effectiveness of GNSS. Though multi-sensor data fusion may be required during this phase, the operating environment should be based on GNSS operations while gracefully phasing out outdated systems. The figure below provides a high level overview for combining GNSS data with radar processing. Rather than constraining all GNSS operations to fit in a radar-based world, a converter is shown which translates the GNSS coordinates for compatibility with the radar processing. This approach is preferable as it maximizes the future operational benefits of a GNSS-based system while still providing compatibility with today's terrestrial based systems.



GPS-RADAR CONVERSION

CONCLUSIONS

Since approach, departure and surface operations represent the most difficult phases of flight due to traffic congestion, complexity of the airport and ATC operations, and since these operations demand the highest levels of accuracy and performance, the requirements for these functions should act as the foundation, driving the requirements that form the baseline for improved terminal area operations.

If the high level operational requirements are not addressed, the true benefits and cost effectiveness of GPS and digital communications will not be realized in the airport environment. Care must be taken to avoid the pitfalls of the past - new systems must be architected to support a fully integrated, system-wide concept. Standards for avionics, ADS-B, and ATM must be developed in parallel with new Air Traffic Control (ATC) procedures and pilot operations.

REFERENCES

1. Pilley, H. Robert & Lois V., GPS-BASED AIRPORT OPERATIONS - Requirements, Analysis & Algorithms, Volume I, Deering System Design Consultants, Inc. (DSDC), September 1994. (Available through the Navtech Book and Software Store.)
2. ICAO AWOPS, Proposed Operational Requirements for Advanced Surface Movement Guidance & Control Systems, Draft 9, May 1995.
3. RTCA SC 166, User Requirements for Future Airport and Terminal Area Communications, Navigation and

Surveillance, Document No. RTCA/DO-211, October 1992.

4. NASA, Airport Surface Operational Requirements Analysis, NASA CR-191508, Contract NAS1-18027, Boeing Commercial Airplane Group, NASA Langley Research Center.

5. Harrison, Michael. Aerodrome Surface Movement Planner for Advanced Surface Movement Guidance and Control Systems (A-SMGCS). 1995.

6. FAA, The Future Airport Surface Movement Safety, Guidance, and Control System: A Vision for Transition into the 21st Century. 1993

7. FAA, Airport Surface Traffic Automation, Draft Statement of Work. 1994.

8. Pilley, H. R. Airport Control/Management System. U.S. Patent No. 5,200,902, April 6, 1993.

Selective Availability via the Levinson Predictor

Timothy Barnes
Zeta Associates, Inc.

BIOGRAPHY

Timothy Barnes is employed by Zeta Associates Incorporated and works primarily in the areas of estimation and signal processing. Previously, he was employed by The Analytic Sciences Corporation (TASC) and the National Oceanic and Atmospheric Administration (NOAA) working primarily in orbital dynamics and satellite navigation. He received a B.S. in Aerospace Engineering and a Master of Engineering in Systems Engineering from the University of Virginia.

ABSTRACT

The use of a generalized Levinson Predictor to provide estimates of future values of Selective Availability (SA) is explored. The prediction of SA provides the DGPS user a means for overcoming the latency of the corrections. The predicted estimates are derived from a linear combination of prior measurements of SA. An iterative method for deriving the weights, choosing the interval between data samples against which the weights are applied, and generating an estimate of the mean square error of the predictor. The accuracy of the estimate is presented as a function of prediction interval.

The RMS of the errors in predicting future values of SA using a Levinson predictor are approximately 0.2, 2.0, and 4.0 meters for predictions of 8, 30 and 60 seconds using code ranging data smoothed with carrier phase. The weights are determined from an estimate of the SA autocorrelation made at the beginning of each collection pass.

The SA process tends to be wide-sense stationary in that the weights determined from one pass can be applied to future passes without significant degradation of prediction accuracy. Additionally, a set of weights determined from one PRN can be applied to other PRN's without significant degradation in predictor accuracy.

Finally, the user, with a modest amount of computation, can select the prediction interval desired given past SA values and an autocorrelation function.

INTRODUCTION

The current performance of the Global Positioning System is degraded due to the implementation of Selective Availability. Selective Availability (SA) appears to the user as slowly time varying sinusoidal error to the pseudo range measurements with an RMS of 25 meters.

Differential GPS (DGPS) is a technique that is frequently used to correct for SA induced ranging errors. However, the time delay (latency) between the generation of corrections and their application by the user can result in large residual errors. These errors can be reduced if the SA-induced error can be predicted for relatively short periods of time.

This paper presents the Levinson Predictor as a robust and flexible technique for predicting SA.

LEVINSON PREDICTOR

The Levinson predictor forms an estimate of the future (output) based on a moving average of past data. The predicted output is given by:

$$\hat{y}(t) = - \sum_{j=1}^n a_j y(t-j) \quad (1)$$

where present time corresponds to $j=1$. The Levinson predictor is guaranteed stable and the coefficients (a_1, \dots, a_n) are chosen to minimize the mean square error. This yields a cost function:

$$J_n = E \{ [y(t) - \hat{y}(t)]^2 \} \quad (2)$$

The predictor can be augmented to allow for variable prediction intervals by restating equation 1 as:

$$\hat{y}(t) = - \sum_{j=m}^{n-1} a_{j-m+1} y(t-j) \quad (3)$$

where the prediction interval is equal to m samples and $n-m$ samples is the length of the data span used in the prediction. Substituting equation 3 into equation 2 yields:

$$J_n = E \{ [y(t) + a_1 y(t-m) + a_2 y(t-m-1) + \dots + a_{n-m} y(t-n+1)]^2 \} \quad (4)$$

The coefficients of the predictor are determined by taking the partial of J_n with respect to a_j and setting the result equal to 0 which yields:

$$\frac{\partial J_n}{\partial a_j} = E \{ (y(t) - \hat{y}(t)) y(t-j) \} = 0 \quad (5)$$

for $j=m, \dots, n-1$. Expanding and separating equation 5 yields:

$$E \{ y(t) y(t-j) \} = E \{ \hat{y}(t) y(t-j) \} \quad (6)$$

Substituting equation 3 into equation 6 yields:

$$E \{ y(t) y(t-j) \} = \quad (7)$$

$$E \left\{ \left(\sum_{k=m}^{n-1} -a_{k-m+1} y(t-k) \right) y(t-j) \right\}$$

for $j=m, \dots, n-1$. Expanding the right hand side of 7 gives:

$$E \{ y(t) y(t-j) \} = E \{ -a_1 y(t-m) y(t-j) - a_2 y(t-m-1) y(t-j) - \dots - a_{n-m} y(t-n+1) y(t-j) \} \quad (8)$$

This yields $n-m$ equations for a predictor of length of $n-m$. Note that the left hand side of equation 8 is just the autocorrelation of the SA process beginning at the time delay corresponding to the index m . Letting $C_j = E \{ y(t) y(t+j) \}$ we can restate the cost function as:

$$J_n = E \{ y(t) [y(t) - \hat{y}(t)] \} \quad (9)$$

$$= C_0 + \sum_{j=m}^{n-1} a_{j-m+1}^{n-m} C_j$$

The superscript on the weights used in equation 9 denotes the interval length of the past data used in the predictor. This notation is used throughout the remainder of this paper. Writing equation 8 in matrix form:

$$\begin{bmatrix} C_0 & C_1 & C_2 \dots & C_{n-m-1} \\ C_1 & C_0 & C_1 \dots & C_{n-m-2} \\ C_2 & C_1 & C_0 \dots & C_{n-2} \\ C_{n-m-1} & C_{n-m-2} & C_{n-m-3} \dots & C_0 \end{bmatrix} \begin{bmatrix} a_1^{n-m} \\ a_2^{n-m} \\ a_3^{n-m} \\ a_{n-m}^{n-m} \end{bmatrix} = \begin{bmatrix} -C_m \\ -C_{m+1} \\ -C_{m+2} \\ -C_{n-1} \end{bmatrix} \quad (10)$$

Recall that the C 's come from computing the autocorrelation of the Selective Availability time series. The autocorrelation matrix in equation 10 is a Toeplitz matrix and can be solved for iteratively as shown by Levinson. That is, increasing the length of the predictor to an $(n+1-m)$ predictor uses the coefficients from the $n-m$ length predictor. Let the autocorrelation matrix in equation 10 equal A_k and the right hand side equal $-c_k$. Additionally, let $n-m=k$, and the $k+1$ system can be written as

$$\begin{bmatrix} A_k & E_k r \\ r^T E_k & C_0 \end{bmatrix} \begin{bmatrix} a_i^{k+1} \\ a_{k+1}^{k+1} \end{bmatrix} = \begin{bmatrix} -c_k \\ -c_{k+1} \end{bmatrix} \quad (11)$$

where ' r ' is a vector of autocorrelation C_1 through C_n and E_k is an operator that reverses the indices of the vector it operates on. Solving equation 11 for a_i^{k+1} yields the following equation:

$$a_i^{k+1} = A_k^{-1} (-c_k - a_{k+1}^{k+1} E_k r) = a_i^k + a_{k+1}^{k+1} E_k z_i^k \quad (12)$$

where

$$z_i^k = A_k^{-1} r \quad (13)$$

which is the Levinson-Durbin algorithm solution of equation 10 when the right side equals $-r$. The iterative solution for the z 's due to Durbin is:

$$z_{k+1}^{k+1} = \frac{-\left(C_{k+1} + \sum_{j=1}^k z_j^k C_{k+1-j}\right)}{\left(C_0 + \sum_{j=1}^k z_j^k C_j\right)} \quad (14)$$

$$z_i^{k+1} = z_i^k + z_{k+1}^{k+1} z_{k+1-i}^k \quad (15)$$

with equations 14 & 15 initialized by

$$z_1^1 = \frac{-C_1}{C_0} \quad (16)$$

The last coefficient of equation 11 is similar to equation 14, that is:

$$a_{k+1}^{k+1} = \frac{-\left(C_{k+1} + \sum_{j=1}^k a_j^k C_{k+1-j}\right)}{\left(C_0 + \sum_{j=1}^k z_j^k C_j C_0\right)} \quad (17)$$

An estimate of the mean square error can be computed for each predictor of increased window length directly from the cost function using equation 9.

DATA COLLECTION

The GPS ranging data was collected using a 16 channel integrated GPS/GLONASS receiver manufactured by 3S Navigation. Both code and carrier phase data are collected and can be processed at variable rates. Nominally, data are output at a 1 Hz rate. The carrier phase measurements were used to smooth the code data using a "Hatch filter" technique. The smoothed pseudo-range data were used in all analyses. The collection suite also includes an FTS (Frequency and Time Systems, Inc.) model 4065 cesium clock.

The smoothed pseudo-range data were corrected for tropospheric delay and then differenced with expected range. These differences were subsequently corrected for clock offset and drift using a second order clock model for the cesium reference yielding a time series of the magnitude of SA. Figure 1 is an example of the results of this process.

The data used in this paper were collected while tracking PRN's 1, 4 and 5 from May 18-20, 1995.

SA PREDICTION

The Levinson predictor was used to estimate future values of SA given a time series of past values and the autocorrelation

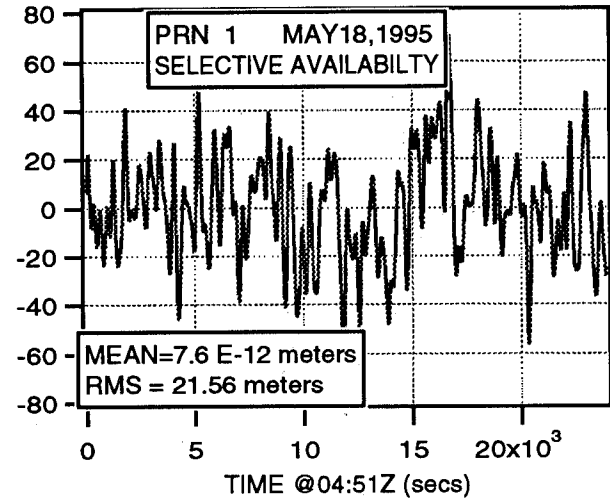


FIGURE 1. Selective Availability

lation of SA. The autocorrelation function was determined from 90 minutes of SA data at the beginning of the pass and is not updated throughout the remainder of the pass. The present realization of the predictor allows the user to specify several input parameter selections. The parameters are:

1. sampling rate of the data
2. length of the past data interval
3. amount of data used to determine the autocorrelation function
4. prediction time

The cost function has been used to optimize the selection for the first two parameters. Using shorter intervals to determine the autocorrelation function has been explored but is not presented here. The prediction times presented here are 8, 30, and 60 seconds.

Figure 2 shows a plot of the predicted and actual SA for a prediction interval of 8 seconds for portions of the PRN 1 pass on May 18, 1995. The two plots are virtually identical for the 8 second predictions. A data interval of 12 seconds is used with a coefficient computed every second and the autocorrelation matrix is determined from 90 minutes of data. The second plot in Figure 2 is the difference between the predicted and actual SA values. The RMS of this difference 0.20 meters and is based on data from the entire pass of approximately 6.5 hours in duration and computes more than 23,000 SA predictions and differences.

Figure 3 shows the same plots for a prediction interval of 30 seconds for approximately the same portion of the pass shown in figure 2. The data interval or window has been increased to 60 seconds with a coefficient computed every 5 seconds and the autocorrelation matrix determined from 90 minutes of data. The second plot is the difference plot

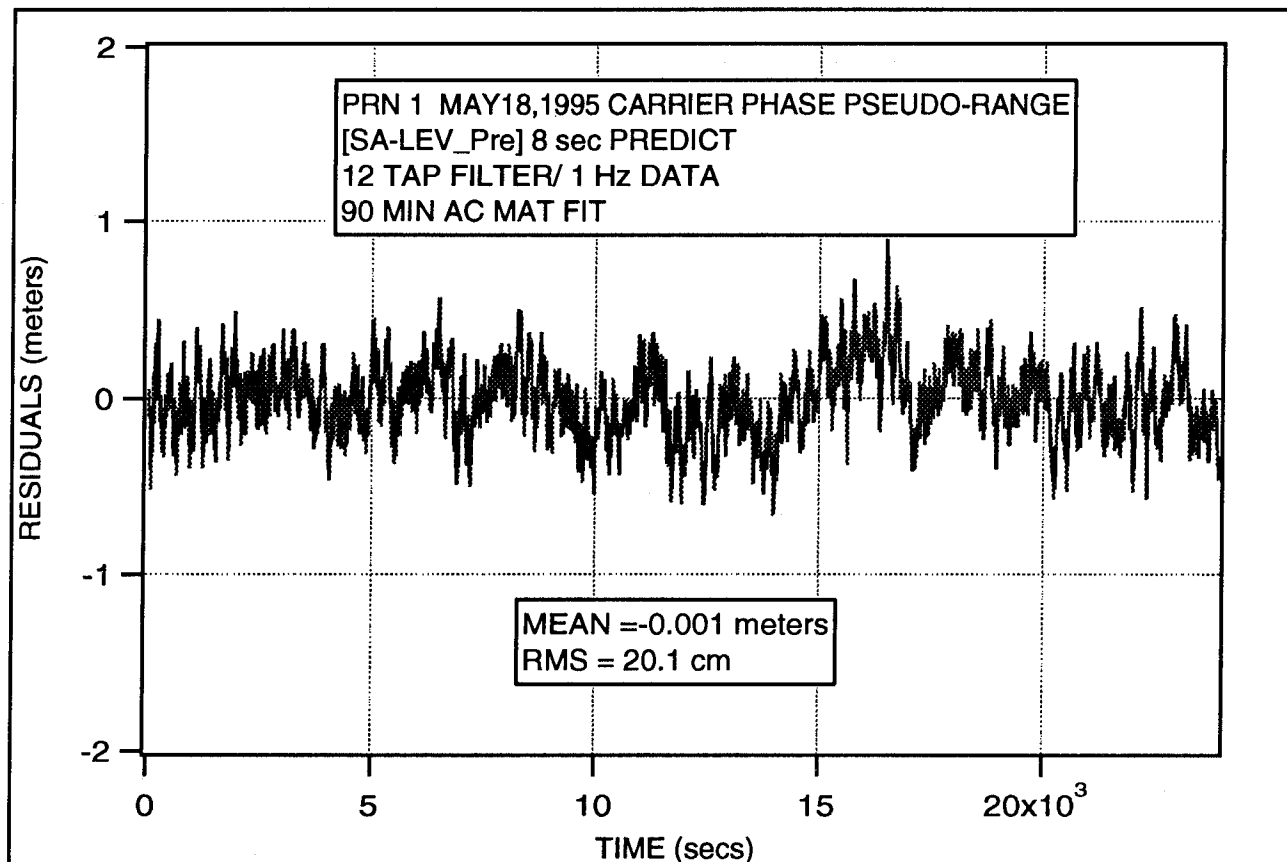
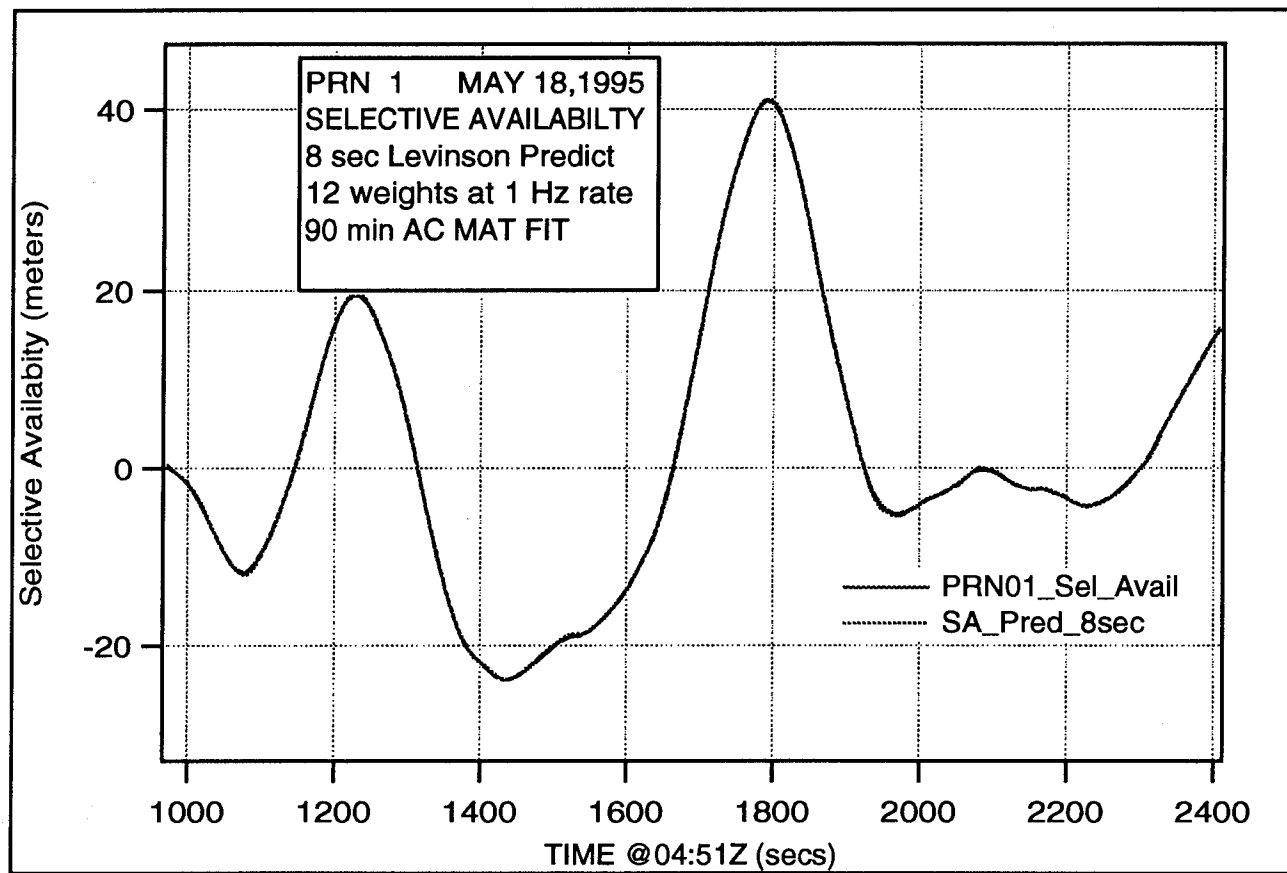


FIGURE 2. PRN 1 Predicting 8 seconds MAY 18, 1995

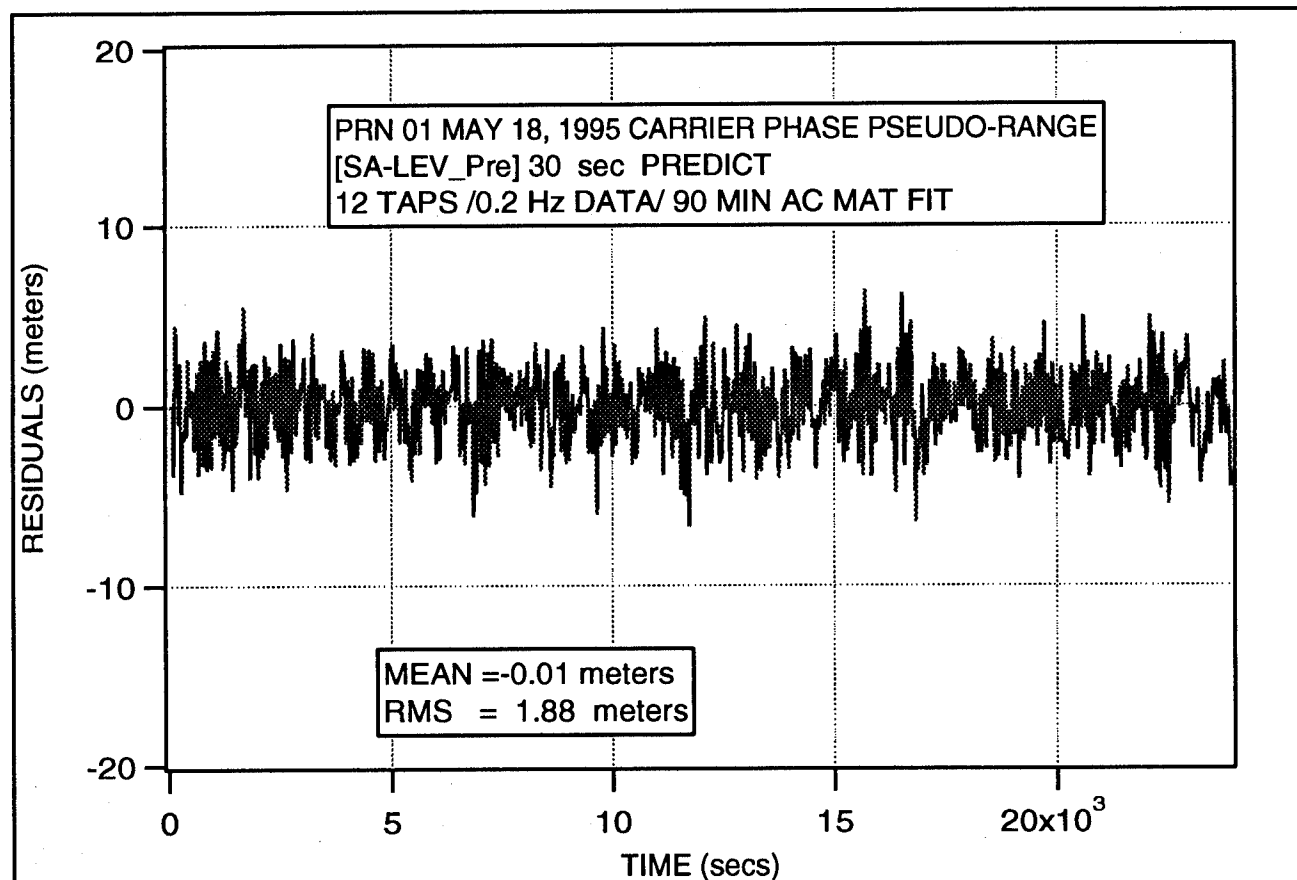
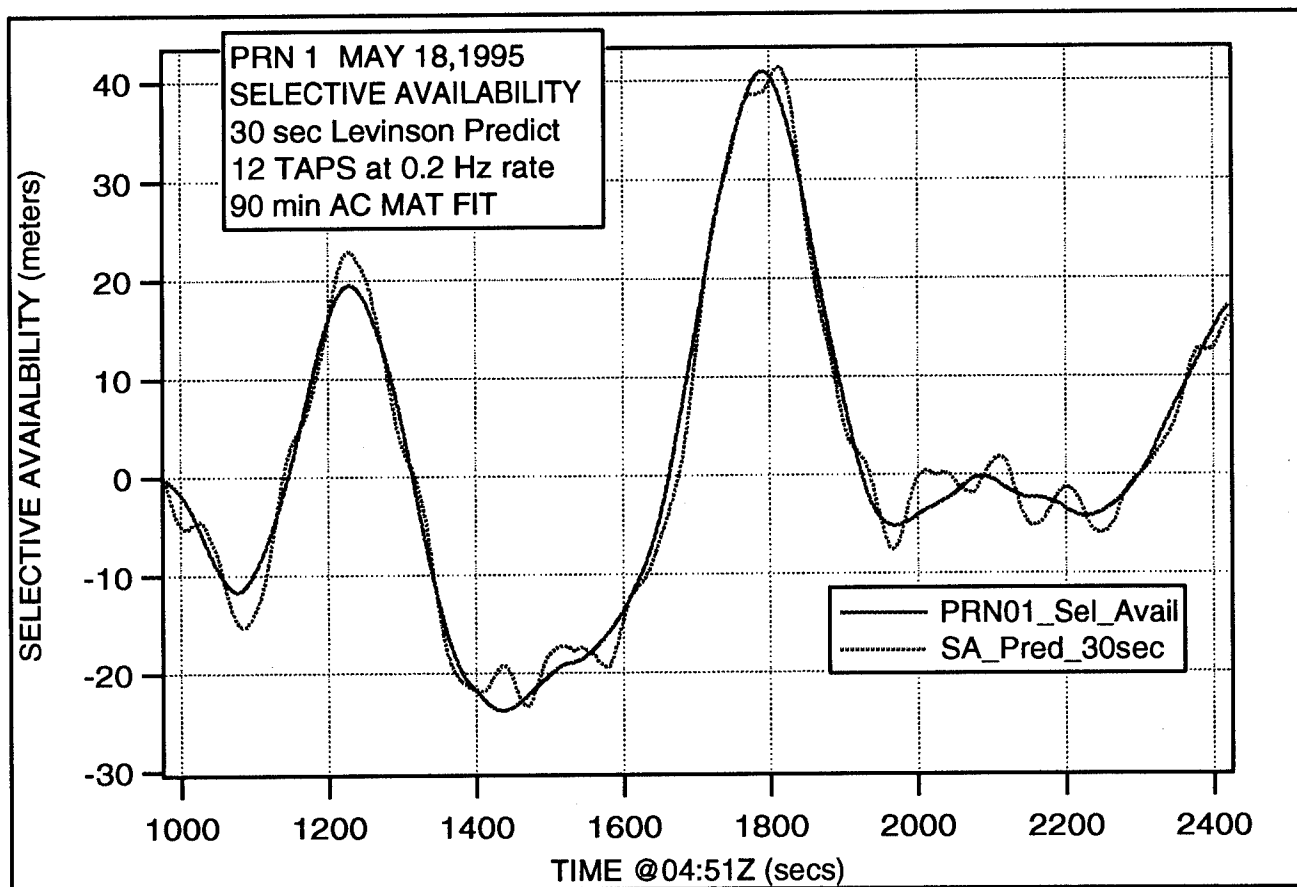


FIGURE 3. PRN 1 PREDICTING 30 SECONDS

again for a 30 second prediction. The RMS of this difference is 1.88 meters.

Figure 4 is similar to figures 2 and 3 with the prediction interval increased to 60 seconds. The data length is 60 seconds and weights are applied to data samples separated by five seconds. The RMS for 60 second prediction is 3.59 meters. Note that the prediction error in both figures 3 and 4 is largest when the second derivative of SA is at its maximum.

Predicting SA on Future Passes

Data were collected for three consecutive passes of PRN 1 on three consecutive days. The data from the first pass were used to determine the predictor weights which were used to predict SA on the 20 May pass. Once again, prediction intervals of 8, 30 and 60 seconds were chosen. The results are shown in figure 5. The RMS errors in prediction are 0.21, 1.98, and 3.76 meters respectively. These results are equivalent to those shown earlier where the weights were applied on the same pass as they were determined. This result implies that for PRN1 in this two day interval SA tends to be a wide-sense stationary process.

Predicting SA Across PRNs

The filter weights determined from the 18 May 1995 pass of PRN 1 were applied to SA data collected from PRN 4. As before, prediction intervals of 8, 30, and 60 seconds were chosen. The errors in the predicted data are shown in figure 6. The RMS of the differences between SA and the Levinson predictor are 0.22, 1.94 and 3.85 meters respectively. These results yield essentially the same performance as when applied to the PRN 1 data and demonstrate that the autocorrelation of SA is nearly identical across PRN's.

CONCLUSIONS

A summary of the results is shown in table 1. The RMS of

TABLE 1. Levinson Predictor Results Summary

| RMS Predicted SA error | | | |
|------------------------|---|--------------|--------------|
| Prediction time, sec | Predictor weights from PRN 1 on 18 May applied to | | |
| | PRN 1 18 May | PRN 1 20 May | PRN 4 18 May |
| 8 | 0.20 | 0.21 | 0.22 |
| 30 | 1.88 | 1.98 | 1.94 |
| 60 | 3.59 | 3.76 | 3.85 |

the errors in predicting future values of SA using a

Levinson predictor are bounded by 0.2, 2.0, and 4.0 meters for predictions of 8, 30 and 60 seconds. Additionally the weights determined from one PRN and one pass can be applied across passes and PRN's without significant degradation of prediction accuracy.

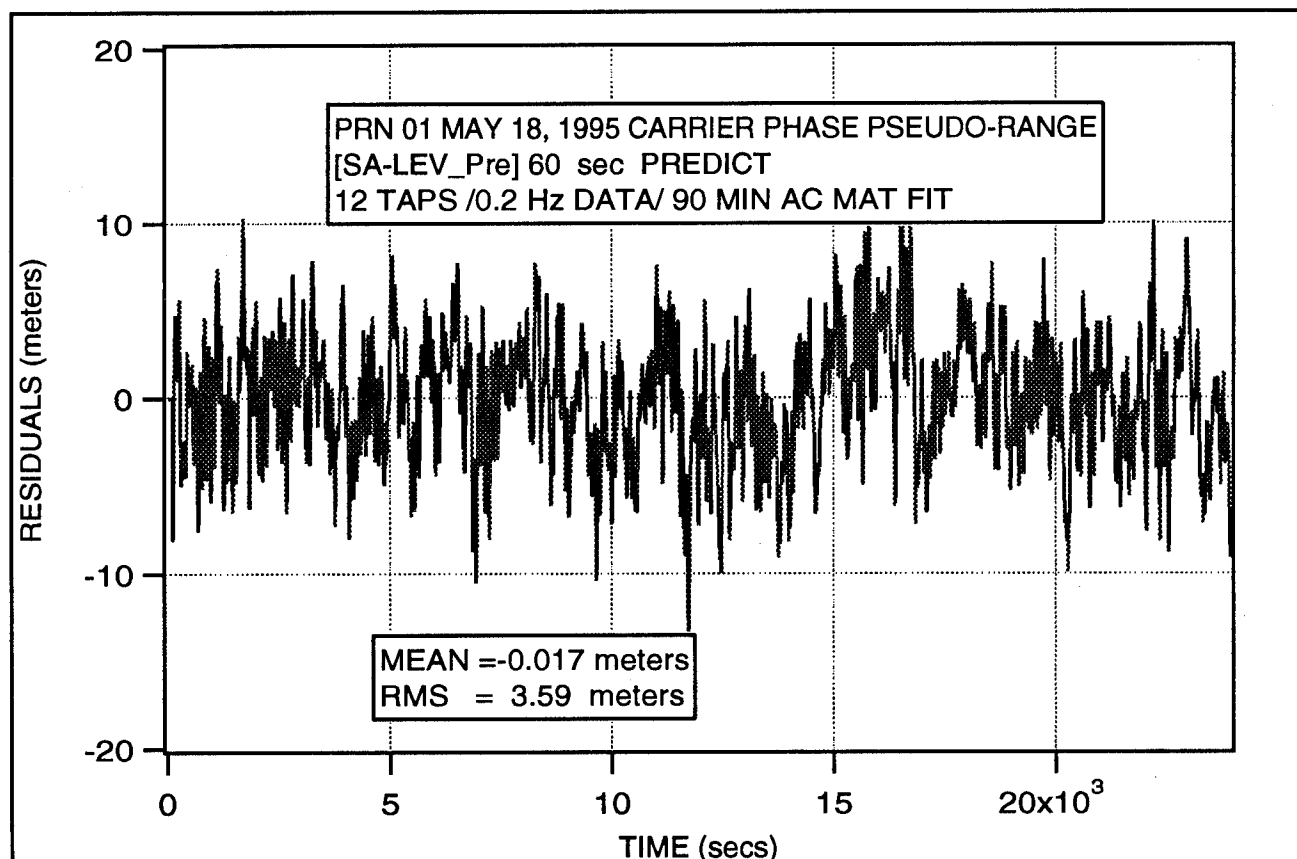
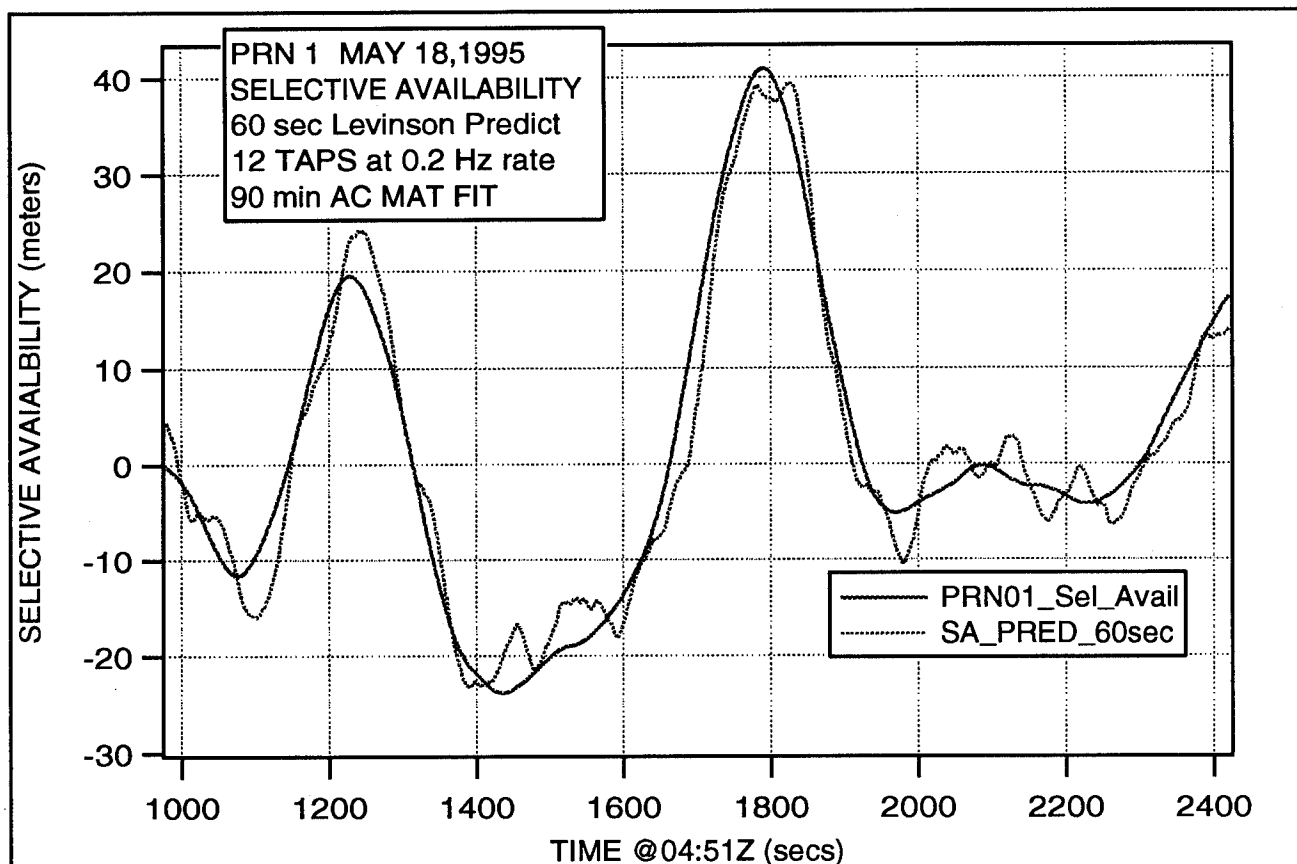


FIGURE 4. PRN 1 PREDICTING 60 SECONDS

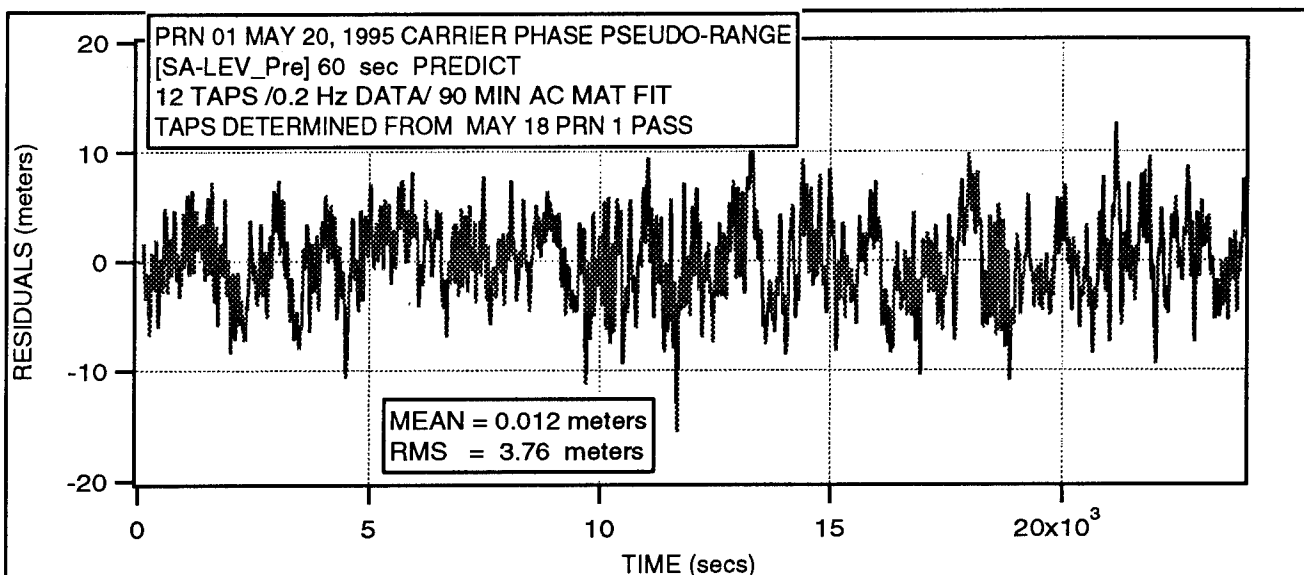
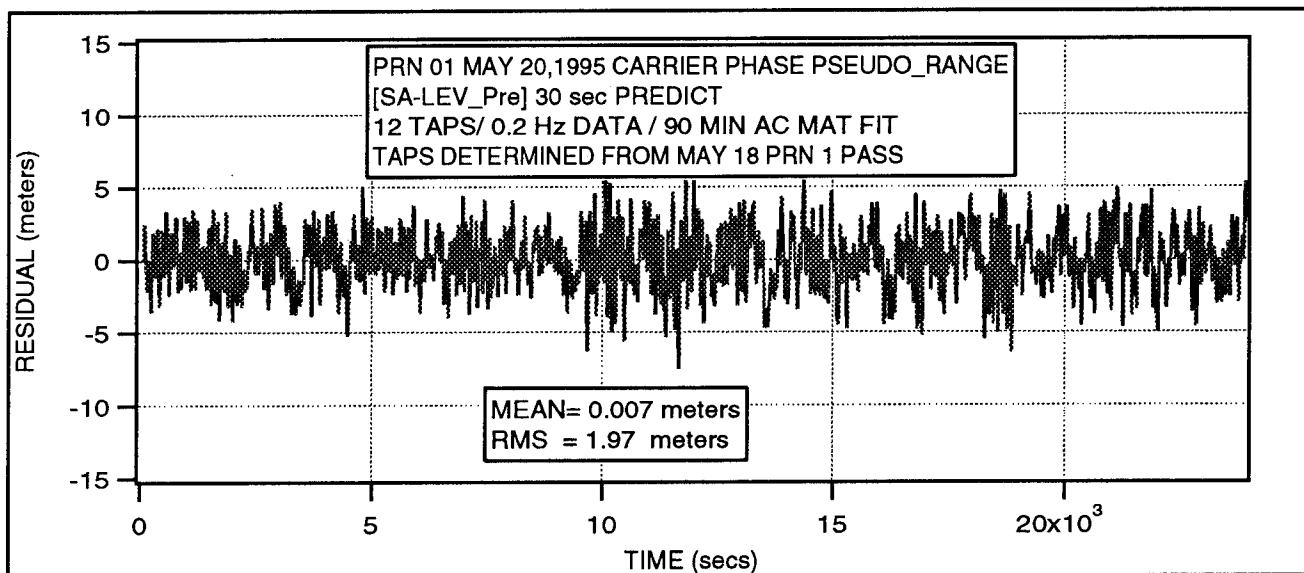
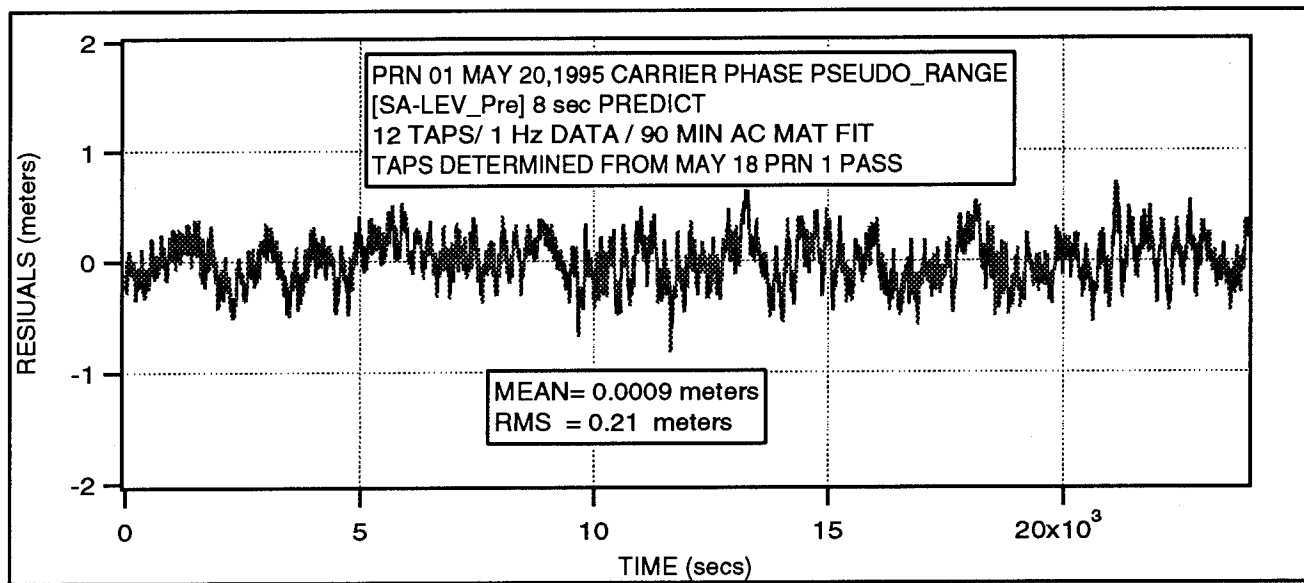


FIGURE 5. PRN1 WEIGHTS DETERMINED FROM MAY 18 APPLIED TO MAY 20 SA

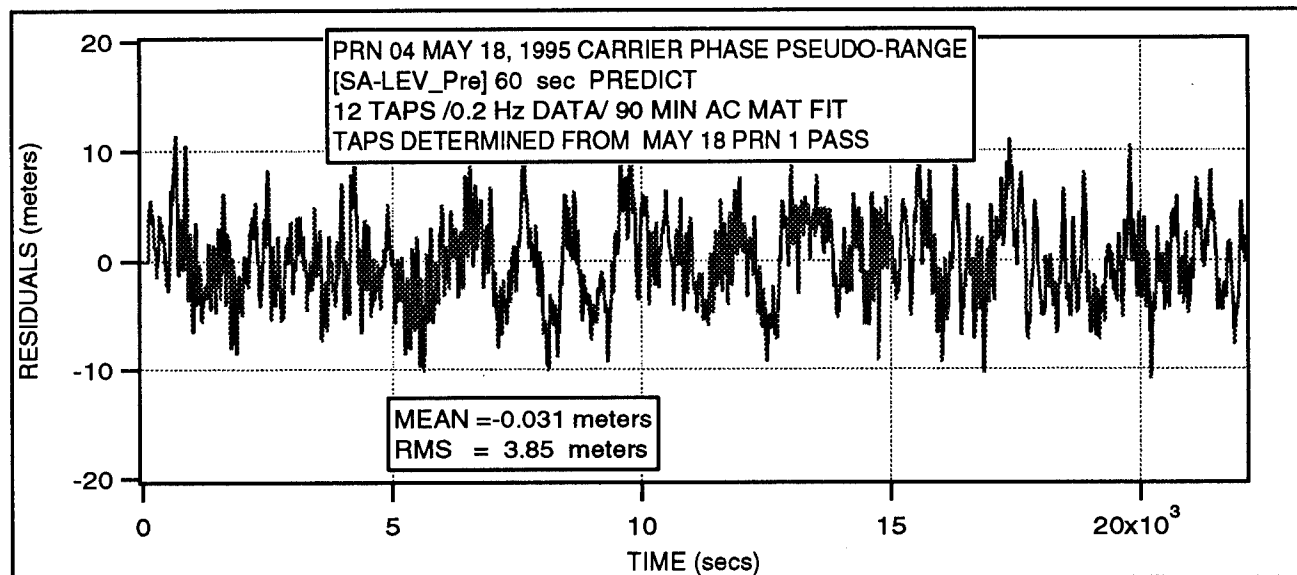
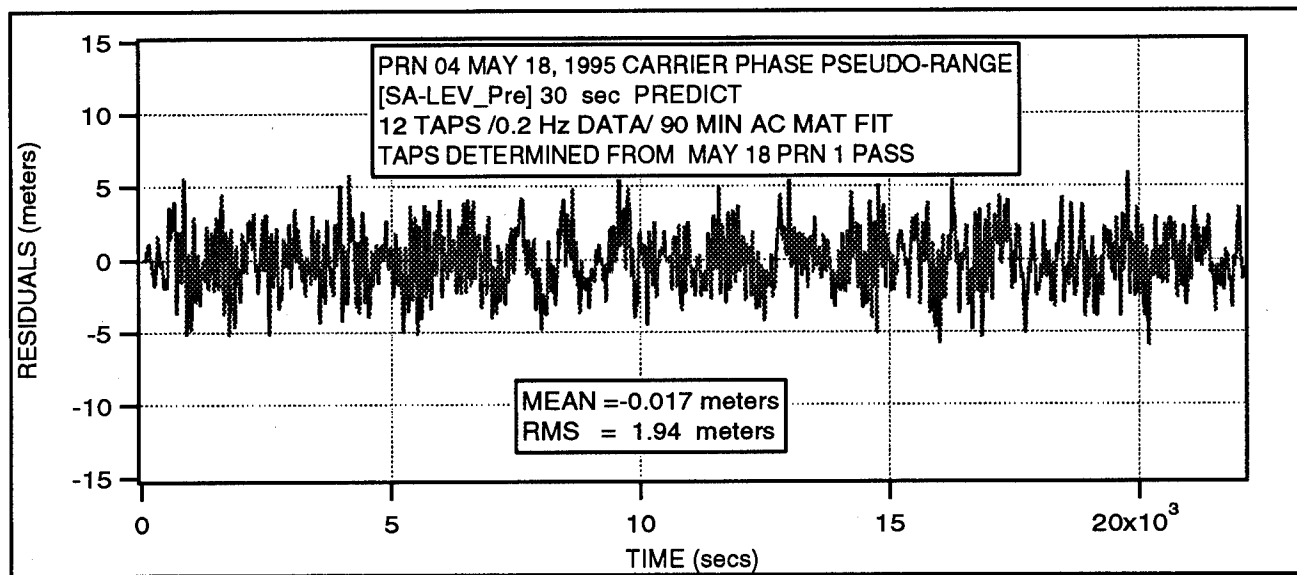
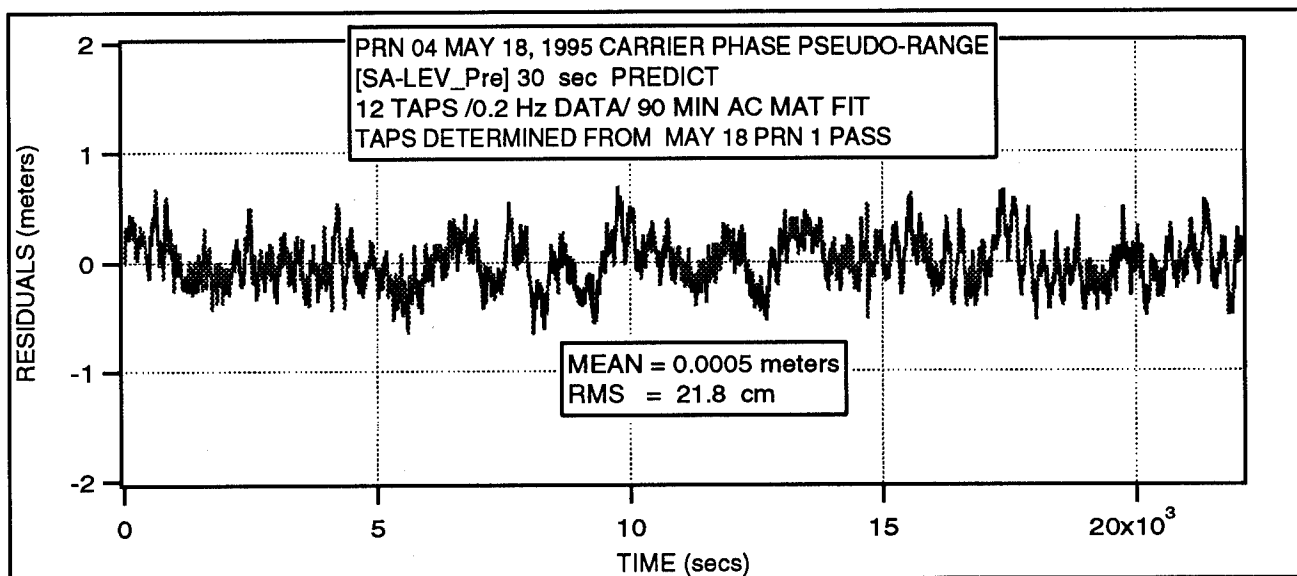


FIGURE 6. PRN 04 PREDICTED FROM PRN 1 WEIGHTS MAY 18,1995

ACKNOWLEDGEMENTS

The author would like to thank Dr. Jerry Fields for his contributions and reviews and Dr. J. Monty Schumpert for his reviews. Both are with Zeta Associates Inc. Additionally, the author would like to thank Dr. Terry McGurn of the U.S. Government for his support of this work.

REFERENCES

1. Golub and Van Loan(1983). *Matrix Computations*, Johns Hopkins Press, Baltimore, Md. pp.125-130.
2. Goodwin and Sin (1984). *Adaptive Filtering Prediction and Control*, Prentice Hall, Englewood Cliffs, NJ. pp. 280-283.
3. Strobach (1991). "New Forms of Levinson and Schur Algorithms", IEEE Signal Processing Magazine. January 1991. pp. 12-36.



Session C2

Space: Orbit and Attitude

Chair:

Dr. Bob Schutz

University of Texas at Austin

Co-Chair:

Mr. Kenn Gold

University of Colorado

GPS Attitude Determination and Navigation Flight Experiment

J. Kurt Brock, Rich Fuller, Brian Kemper, Dave Mleczo, J. Rodden, and Alfred Tadros
Space Systems/LORAL

BIOGRAPHY

Kurt Brock received his M.S. from Stanford University in Aeronautics and Astronautics and his B.S. from the University of California at Berkeley in Mechanical Engineering. In 1992/1993 he served as Chief Systems Engineer on the Globalstar Program and then as the GPS Tensor Program Manager. His current position is Executive Director of Satellite Navigation and Air Traffic Control at Space Systems/LORAL in Palo Alto, California.

Rich Fuller received his B.S. from Boston University in Aerospace Engineering and an M.S. from Stanford University in Aeronautical and Astronautical Engineering. Mr. Fuller has worked primarily on the GPS Tensor attitude determination and systems engineering activities. Mr. Fuller has worked on the attitude determination and control system design for Space Systems/LORAL on various programs.

Brian Kemper received his B.S. from the University of Illinois in Aeronautical Engineering and M.S. from Stanford University in Aeronautics and Astronautics. He is working in the area of software testing and systems analysis for the GPS Tensor development at Space Systems/LORAL.

Dave Mleczo received his B.S. from University of California at Santa Barbara in Electrical Engineering. Mr. Mleczo is leading the software development for the GPS Tensor Program at Space Systems/LORAL.

J. Rodden is a member of the Systems Analysis Department of Space Systems/LORAL. He has B.S., M.S. from the University of California at Berkeley in Mechanical Engineering, Ph.D. in Engineering Mechanics from Stanford. He is leading the systems engineering for the GPS Tensor development for application on the Globalstar Program. His experience is in the development of spacecraft Guidance and Control Systems.

Alfred Tadros received his B.S. in Aerospace Engineering and M.S. in Mechanical Engineering from Massachusetts Institute of Technology. Mr. Tadros is working in the area of software testing and systems analysis for the GPS Tensor development at Space Systems/LORAL.

ABSTRACT

A GPS attitude and navigation receiver operated successfully in space as a flight experiment on the Daimler-Benz Aerospace (DASA) CRISTA-SPAS free flying satellite. This flight resulted in the first space operation of GPS derived attitude determination. The satellite was launched from, separated and subsequently recovered by Space Shuttle Atlantis, STS 66, November 3-14, 1994. The vehicle operated at a distance of several kilometers from the Shuttle during the 11 day mission. The spacecraft attitude was maintained with a stellar-inertial attitude determination system using mass expulsion actuators for control to point the Crista telescope at a pre designated point on the Earth's limb. The GPS TANS Vector receiver navigated and determined three axes attitude with respect to an antenna reference frame fixed to the CRISTA-SPAS vehicle but not aligned to it. An alignment transformation between the GPS antenna system and the spacecraft was derived post flight. The GPS receiver operated satisfactorily during the flight.

INTRODUCTION

A GPS attitude and navigation receiver operated successfully in space as a flight experiment on the Daimler-Benz Aerospace CRISTA-SPAS free flying satellite. This flight resulted in the first space operation of GPS derived attitude determination. The satellite was launched from, separated and subsequently recovered by Space Shuttle Atlantis, STS 66, November 3-14, 1994. The vehicle operated at a distance of several kilometers from the Shuttle during the 11 day mission. The spacecraft attitude was maintained with a stellar-inertial attitude determination

system using mass expulsion actuators for control to point the CRISTA telescope at a pre designated point on the earth's limb. Except for brief calibration maneuvers the vehicle was controlled within arc seconds at an attitude fixed to keep the telescope line of sight at a tangent altitude over the oblate Earth.

The GPS TANS Vector receiver navigated and determined three axes attitude with respect to an antenna reference frame fixed to the ASTRO-SPAS vehicle but not aligned to it. An alignment transformation between the GPS antenna system and the spacecraft was derived post flight. The GPS receiver operated satisfactorily during the flight. Flight results and analysis of the receiver acquisition, navigation, and attitude determination are shown in the paper. The paper discusses the integration of the GPS receiver with the CRISTA-SPAS system. The flight operation of the receiver generating navigation and attitude determination on the separable spacecraft is described along with a presentation and discussion of the flight results.

ASTRO-SPAS

SPAS is the acronym for "Shuttle Pallet Satellite" which is launched into Earth orbit by the U.S. Shuttle, deployed for a free flight period of a few days at a distance up to 120 km from the Shuttle, then retrieved and returned to Earth. In continuation of past successful US-German cooperation in Space Science, NASA and the German Space Agency, DARA GmbH, have agreed to perform at least 4 joint missions with the ASTRO-SPAS system striving to exercise different scientific payload components provided by both the USA and Germany.

The first mission in the ASTRO-SPAS series was conducted in 1993 under the name ORFEUS-SPAS-I. That system was dedicated to astronomical observations at very short wavelengths, specifically the two spectral ranges Far Ultraviolet and Extreme Ultraviolet. The second mission, CRISTA-SPAS was an exploratory mission to analyze dynamical processes in the middle atmosphere. The name CRISTA is from Cryogenic Infrared Spectrometers and Telescopes for the Atmosphere. The CRISTA experiment was conducted by the University of Wuppertal, Germany. The scientific payload is complemented by MAHRSI for Middle Atmosphere High Resolution Spectrograph Investigation ultraviolet experiment supplied by the US Naval Research Laboratory, Washington, DC. An experiment Surface Effects Sample Monitor, SESAM, was conducted by the German Aerospace Research Establishment, DLR, Braunschweig, Germany.

The scientific objective of the flight experiments was to learn more about the Earth's atmosphere.

USE OF GPS ON ASTRO-SPAS

The spacecraft builder, Daimler Benz Aerospace formally Deutsche Aerospace or DASA required GPS for Navigation. In addition the position data was used directly to modify the spacecraft pointing commands to account for variations of tangent altitude direction on an oblate Earth. This correction was adjusted in flight. The nominal attitude reference was provided by a stellar-gyro attitude determination system. Attitude control was from a set of 0.01 Newton mass expulsion thrusters.

The spacecraft GPS unit was supplied by Standard Elektrik Lorenz Co. now part of Alcatel Company. An additional GPS receiver was supplied by SS/L for operation on the CRISTA-SPAS as an experiment. A precursor GPS receiver to the GPS Tensor was a modified commercial TANS Vector from Trimble Navigation Co. TANS is an acronym for Trimble Advanced Navigation System. The Space Systems/LORAL supplied TANS Vector unit had attitude determination capability. The four antennas for the TANS Vector GPS receiver can be seen on the photo of the spacecraft being released by the Shuttle arm in Figure 1.

GPS OPERATION

The most significant feature of the GPS Tensor is its ability to determine not only the normal GPS outputs of position, velocity and time, but the attitude of the spacecraft as well. The attitude determination algorithm is the one developed by Dr. Clark Cohen of Stanford University(ref. 1). Dr. Cohen developed a scheme of multiplexing RF outputs from 4 antennas, measuring the carrier phase between them and determining attitude from those measurements. The scheme leads to an economization of size, weight, power and parts count. The TANS Vector has incorporated the attitude technology developed by Dr. Cohen. A development of a space qualified GPS receiver for attitude and orbit determination has been in progress at Space Systems/LORAL since early 1994. Space Systems/LORAL licensed the technology of the commercial TANS Vector from Trimble and Stanford University to use as a starting point for a receiver called the GPS Tensor (ref. 2).

SYSTEM ARCHITECTURE

The four antennas with hemispherical sensitivity patterns are to be located on a spacecraft facing upward away from the earth with their relative distances from

each other maximized. The GPS Functional Block Diagram is shown in Figure 2. The four antennas connect to preamps each with split outputs to accommodate the dual receivers. The signals are multiplexed, and down-converted in frequency, then correlated to attain carrier and code lock. The block diagram in Figure 3 shows the digital correlators of one channel of the GPS receiver which is comprised of the Phase Lock Loop (PLL) and the Delay Lock Loop (DLL) coupled by the Code Generator. The incoming GPS signal from the microwave front end goes to both the carrier and code correlators. The Carrier Correlator provides the carrier tracking error. The error of one of the antennas designated the "master" through compensation generates the Doppler Range Rate in a closed loop which is applied to the Phase Pumped Oscillator (PPO). The PPO is a numerically controlled oscillator (NCO). The PLL acting on the non-master or "slave" antennas outputs the carrier phase measurements that are used in determining the satellite attitude. The Code Correlator is in a closed loop, DLL, that aligns in time the received C/A code with the code clock generating the code Epoch and code phase correction time which gives the pseudo range measurement.

THE NAVIGATION ALGORITHM

The basic receiver computes the position and the velocity of the spacecraft from pseudorange and pseudorange rate measurements from at least four GPS satellites. Typically, four satellites with the minimum Position Dilution of Precision (PDOP) are selected. The pseudoranges are derived from time measurements obtained by aligning the receiver generated code with the time-tagged C/A code from the GPS satellites. The correlation of the two signals is done in a code-tracking loop. The pseudorange rates are computed from the frequency shift of the carrier signal. At least four measurements are required to get a position and velocity fix because the receiver clock bias and drift need to be resolved as well. The position is computed from iterating on a set of nonlinear equations for position and clock offset bias.

THE ATTITUDE ALGORITHM

The attitude algorithm uses carrier phase measurements at the different antennas from identified GPS SV positions in the sky. The basic navigation receiver was augmented to add a capability for determining attitude. The changes included the addition of three more antennas with attendant preamplifiers, a multiplexer for time sequencing the different antenna signals under software control, and separate filtering of the phase measurements. The sampled "master" antenna derived phase is controlled to null through closed loop control of the NCO. Additional processing

and memory has been added to perform the calculations for attitude determination.

Carrier signals are continuously received at all the spacecraft GPS antennas. These GPS SV sources are identified by the code matching process. Each receiver channel processes a single code carrier. The differential range, Δr , is the distance from a wave front plane normal to the line of sight from a GPS SV to one of the antenna locations on the spacecraft. For a unit vector line of sight direction, S_i , from the i th GPS SV and a baseline distance, x_j , from the "master" antenna to the j th antenna, the differential range as shown in Figure 4 is the dot product:

$$\Delta r_{ij} = S_i \cdot x_j = S_i^T A^T x_j$$

The second expression in vector-matrix format involves the matrix, A , which is the angular transformation from the GPS reference coordinate system to the spacecraft body coordinates. The transform, A^T , is the transpose of A . The carrier phase at an antenna location is the differential range less the integer number, k , of wave length, λ , these distances are established for each antenna and specific GPS SV. Measured in units of wave length and including antenna line bias, b , the phase is:

$$\Delta \phi_{ij} = S_i^T A^T x_j - k_{ij} \lambda + b_j$$

Attitude determination is achieved by iteratively improving estimates of the transformation matrix, A , from successive measurements of carrier phase, $\Delta \phi$.

Essential to the master equation solution above is the predetermination of the base line vectors, x_j , in body coordinates and the individual antenna line bias values. This determination is done in a process called Self Survey prior to attitude operation. The Integer Ambiguity Resolution is also required before attitude operation, but once done, the integer values are updated through monitoring of the phase data.

A block diagram of the GPS Attitude Determination Software Flow is shown in Figure 5. The initialization process of Self Survey determines the vector distances between the master antenna and the others. The line biases are also determined in this process. This process is performed on the ground on a stationary platform with known orientation with respect to the local earth centered reference coordinates. This data is not expected to change during operation. The integer determination is conducted just before attitude operation. It is relatively straight forward to keep track of changes in differential range, Δr , simply by counting the number of times a differential phase wraps around a full 360° . Several integer resolution techniques are implemented. One relies on GPS SV

motion, one relies on receiver attitude changes and another relies on the logical elimination of incongruous integer/attitude combinations. Changes in the relative carrier phase measured over time reveal the spacecraft attitude and correspondingly, the integer ambiguities. As attitude calculations are generated, the integer values are continuously updated and separate integrity checks made. See reference 2.

FLIGHT OPERATION

A pictorial of the CRISTA-SPAS vehicle showing the location of the GPS TANS Vector antennas is shown in Figure 6 along with the coordinate systems used. The vehicle z axis is aligned with the line of sight of the CRISTA telescope. The mission had the line of sight trailing the velocity direction with an azimuth offset $\lambda = 18.6086^\circ$. The telescope axis is pitched down on the average by 15.2035° with a variation up to a degree to maintain the line of sight at a tangent altitude nominally of 62.9 km above the World Geodetic System 1984 oblate Earth model.

Data taken from the TANS Vector during the flight was stored on the ASTRO-SPAS tape recorders. These consisted of packets of 31 words at 0.5 second intervals or 3 seconds for the complete set of 6 packets. These data included navigation, attitude and a variety of internal software parameters. These include time tags, Satellite Vehicle identifications, signal to noise levels, code phases, carrier beat phases, Doppler shifts, and differential phase between antennas. "Quick look" data was taken during the flight during twice daily periods when the Shuttle communication antenna was directed at the ASTRO-SPAS for uplinking commands and collecting real time data.

SELF SURVEY

The self survey process is required to determine the antenna baseline lengths and the RF line bias associated with each antenna/cable path. Baseline and line bias parameters are required for the solution of the attitude determination algorithm. The self survey is usually performed after the receiver system is configured on the spacecraft but could be done on a separate platform. A final step in the process includes determination of data for derivation of direction cosine transformation between the laboratory coordinates of East-North-Up, (ENU), and those of the spacecraft. This transformation is needed since the processing establishes the baselines in a computer defined reference frame that must be related to the specific spacecraft for subsequent use in attitude determination.

The object of the self survey alignment procedure is to determine the transformation between the local East-North-Up reference frame at the time of self survey

data taking and the spacecraft reference frame. The transformation is then calculated in terms of the Euler angle sequence Azimuth(about UP) - Pitch(about the displaced East) - Roll(about the displaced North). The Up axis is the local vertical as determined by nominal leveling methods. If this is significantly different from WGS84 an additional correction is required. The North axis is in the local horizontal (orthogonal to UP) in the plane of UP and "true" North of the earth's axis of rotation. The spacecraft axes are those associated with the mechanical layout of the vehicle and are commonly measured from the mirror surfaces of an alignment cube.

The self survey starts with GPS equipment configured in a flight configuration i.e. receiver, preamps, cables and 4 antennas in an area that has RF access to the GPS Constellation. The spacecraft is not to be moved during the Self Survey data collection. Antenna/cables etc. not to be moved within spacecraft henceforth from initiation of Self Survey process.

The antenna axes nominally established by the self survey data processing is an orthogonal frame defined as a single azimuth rotation about the local UP direction. The rotation angle nominally is the angle in the local horizontal between the horizontal projection of the baseline 2 vector (master-#2 antenna) with respect to the E-N-U frame. Subsequent attitude angles are referenced to this antenna frame unless it is over written for an externally defined spacecraft reference.

The Self Survey data acquisition starts with GPS equipment on the spacecraft instrumented with alignment devices. Data is accumulated for about 9 hours (about 120 data bytes every 5 minutes). Post processing the data provides the estimate of antenna baselines and line biases.

Optical alignment techniques are normally used on the vehicle to establish offsets of the spacecraft with respect to the E-N-U reference frame calibrated in the self survey area. The attitude roll, pitch, and yaw angles are generated with respect to this spacecraft coordinate system or default antenna axes. The self survey alignment data in terms of Euler angles is input to the GPS software to overwrite the default settings. Comparison of baseline vectors in spacecraft coordinates with mechanical dimensions of antenna locations can be used for approximate verification. When no externally measured transformation from spacecraft to local ENU reference is provided, the GPS software maintains a default transformation. The default transformation is one that relates the coordinate frame of the antennas with the local ENU. The horizontal projection of the no. 2 or y antenna axis passing through the designated Master antenna to the

no. 2 antenna is taken as the starting reference. This axis is transformed to be in alignment with the local horizontal North direction with a single axis rotation about the local Up axis. This transformation, unless modified, is used to coordinatize the baseline distance vectors with respect to the spacecraft reference axes. The antenna coordinate frame is used subsequently for all attitude calculations. The no. 1 or antenna x axis is in that same rotation plane and orthogonal to the no.2 axis between the Master and # 2 antenna. That is the pitch, roll and azimuth calculated are the rotations of the antenna reference axes that were related to ENU coordinates as they existed at the time of the self survey. To reference the attitude calculations to a specific spacecraft coordinate frame the Euler angles between that spacecraft frame and the antenna coordinates must be over written by those calculated by the self survey data processing.

Optical measurements are used to derive a transformation between a spacecraft and the local ENU frame at the time of the self survey process. This transformation is required to re-reference the self survey baselines to the spacecraft coordinates. The transformation of spacecraft axes to ENU is first found from external measurements. The transformation between ENU and the antenna frame is mathematically generated in the self survey data processing. The offset azimuth, pitch, and roll is calculated from that measured transformation and input to the GPS software overwriting the self survey calculated angles between the antenna frame and the local ENU.

SELF SURVEY AND COORDINATES FOR CRISTA-SPAS

The self survey for CRISTA-SPAS was not taken on the spacecraft. Instead a plywood mockup of the antenna configuration was made replicating the mechanical positions planned for the spacecraft as shown on Figure 7. The self survey data collection for 9.3 hours took place in Palo Alto on that mockup. This survey determined the GPS baselines and line biases by a long term averaging process using antenna phase measurements from live satellites. These baseline vectors are in local East-North-Up coordinates at the survey location as calculated by the TANS Vector software.

Self Survey Antenna Data for 3 Baselines Vectors(cycles)

| East | North | Up |
|---------|---------|---------|
| -3.2410 | -4.1092 | 0.1679 |
| -6.4092 | -2.0818 | -0.0508 |
| -3.6007 | 2.0368 | 0.1733 |

Orientation of Antenna Frame

From ENU in degrees

| Azimuth | Pitch | Roll |
|---------|-------|-------|
| 252.005 | 0.000 | 0.000 |

Line Bias Estimates (cycles)

| Baseline 1 | Baseline 2 | Baseline 3 |
|------------|------------|------------|
| 0.099 | 0.977 | 0.262 |

No over-write of the calculated rotation of the Master-no. 2 antenna was input so the local ENU coordinates are the computational reference. That is the antenna coordinates are defined as being aligned with the #2 axis along the Master-no. 2 antenna which in this case is rotated some 252.005° away and with no pitch or roll offsets. The #1 axis is orthogonal to #2 and in the plane of #2 and the local North direction. The #3 axis is defined to complete the orthogonal set.

The transformation must be defined between this antenna frame and the ASTRO-SPAS spacecraft coordinates. This transformation could have been unity if the coordinates of the spacecraft reference frame had been measured with respect to the local ENU and the offset pitch, roll, and azimuth angles been over-written into the GPS self survey data.

The method used to find the transformation between the antenna frame and the spacecraft started by determining the North direction vector, transpose (0 1 0), as a linear combination of the baseline antennas vectors in ENU. The coefficients thus determined are used to mathematically construct the North vector in spacecraft coordinates using the baseline distances in spacecraft coordinates assumed to be aligned to the mechanical centers of the GPS patch antennas. The antennas 1-2-3 axes can now be generated in spacecraft coordinates. With the antenna coordinate frame defined in both ENU(at the self survey data taking) and the spacecraft, the transformation between them can be generated. Figure 8 shows the antenna positions and the ASTRO-SPAS coordinates in the Self survey ENU coordinates. The #2 antenna axis is about 14.7° away from the CRISTA-SPAS z or telescope axis and in the plane of the CRISTA-SPAS z and y axes.

NAVIGATION FLIGHT DATA

Figure 9 shows the radial distance from the earth center of the ASTRO-SPAS as determined by the GPS TANS Vector Receiver. The orbital period radial variation of about 6 km indicates a near zero eccentricity about 0.0003. The distortions of the wave shape is primarily attributed to the J2 gravitational effect. This waveshape has been seen in simulations of this Shuttle orbit. The velocity magnitude from the

GPS measurements show a gradual increase over about 2 and half revs of some 220 m/s which is attributed to the effect of atmospheric drag of the Shuttle altitude about 500 km. A difference in position and velocity as determined by the TANS Vector and the SEL receivers is shown in Figure 10. Except for noise in the data these differences are mostly within a few hundred meters and a few meters/second.

ATTITUDE DETERMINATION FLIGHT DATA

The inclination angle during the mission was exactly 57° as predicted, but the precise value differed a little during every orbit, $<0.1^\circ$. The CRISTA-SPAS yaw angle of 18.6086° stayed constant during the nominal measurement times of the mission, but the pitch angle nominally 15.2035° was adjusted to maintain the telescope line of sight at the tangent altitude height over the oblate Earth nominally at 62.9 km. The on board attitude determination system controls the vehicle to an axis frame determined by a quaternion based attitude command. Those quaternions refer to J2000. The processing accounts for precession, nutation, and earth rotation Polar motion is ignored. Figure 11 shows the attitude of the CRISTA-SPAS as determined by this truncated quaternion data. The roll and yaw angles were determined within about 0.05° of the nominal values. The pitch angles show the variation due to the earth oblateness.

Figure 12 shows a comparison of the attitude as determined by the Tans Vector and that derived from the ASTRO-SPAS quaternions and the derived spacecraft to antenna transformation. The attitude difference between measured and derived attitude for a representative four hour data file is shown in Figure 13. The attitude and attitude deviation from a fitted polynomial curve over a 20 minute time segment shows the structure of the attitude measurements in Figure 14 and 15.

ATTITUDE PERFORMANCE ACCURACY

Over a set of samples covering a span of close to 24 hours of operation the Root Mean Square (RMS) attitude variations around mean motion was about 0.19° in roll, 0.15° in pitch, and 0.26° in azimuth. To eliminate uncertainties in the true attitude, the mean motion was taken with respect to a polynomial fit of the data over each sample interval.

GPS RECEIVER OPERATION

The TANS Vector operated satisfactorily for both navigation and attitude determination within several hours of turn on in space. The software established

GPS SV acquisition from virtually cold star conditions. The power to the TANS Vector was cycled at least four times during the mission with acquisition being achieved from cold start conditions each time. After about four days the attitude solution stopped. This anomaly was not unexpected. The attitude determination circuitry and processor is separate and was integrated with the navigation elements in the TANS Vector design with some shared memory connection. Both navigation and attitude processors operate independently. An interference in the common interface circuitry is a statistical event that causes lock-up in the attitude determination software. Reloading attitude software and restarting the processing is the nominal solution. This solution was not possible in the flight system on ASTRO-SPAS due to the limited command capability allowed to the TANS Vector. The only command available during flight was power on or off. The GPS Tensor under development has only one processor and has no segmented processing and memory elements therefore this lock-up can not occur in the GPS Tensor.

SUMMARY

A successful GPS operation of navigation and attitude determination occurred in space with the Tans Vector operating on the ASTRO-SPAS on STS 66, November 3-14, 1994. The operation met performance expectations.

ACKNOWLEDGMENTS

We recognize and appreciate the helpfulness and support of Dr. Konrad Moritz, ASTRO-SPAS Program Manager, and Matthias Vogel, ASTRO-SPAS Electrical Systems Manager of Daimler Benz Aerospace, Ottobrun, Germany. In addition we appreciate the help of the entire ASTRO-SPAS group. We also recognize the support of members of the GPS Tensor team at Space Systems/LORAL including Rod Fan, and Jim Conley.

REFERENCES

- C. Cohen, Attitude Determination Using GPS, PhD Dissertation, December 1992, Stanford University
- J.K. Brock et al, GPS Attitude and Orbit Determination for Space, Presented at the ION GPS-94 Conference Salt Lake City, UT, Sept. 20-23, 1994
- J. K. Brock, J.J. Rodden, GPS Tensor Development, GPS Solutions, Vol. 1, No. 2, Fall 1995, Official Publication of GPS International Association

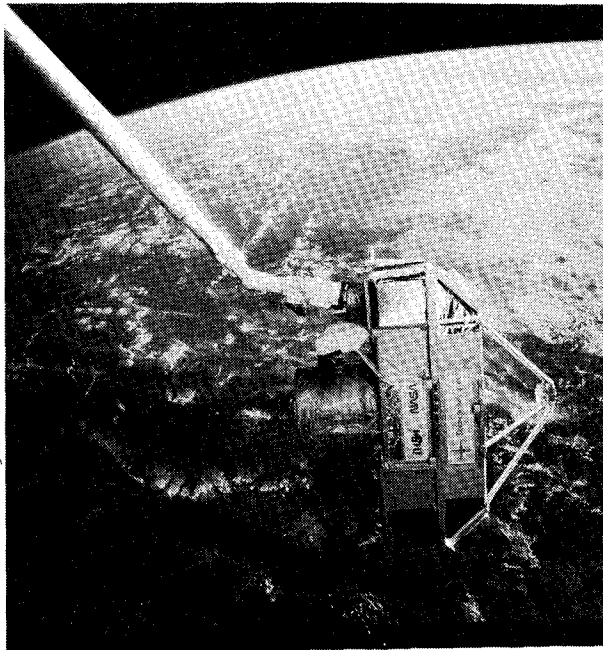


Figure 1, CRISTA -SPAS in Orbit

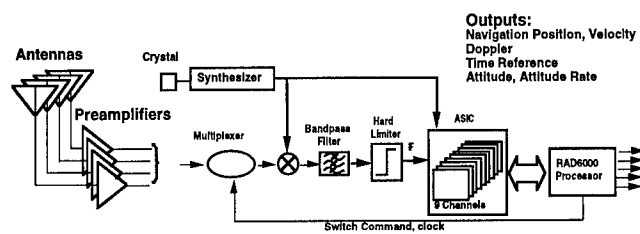


Figure 2, GPS Receiver Functional Block Diagram

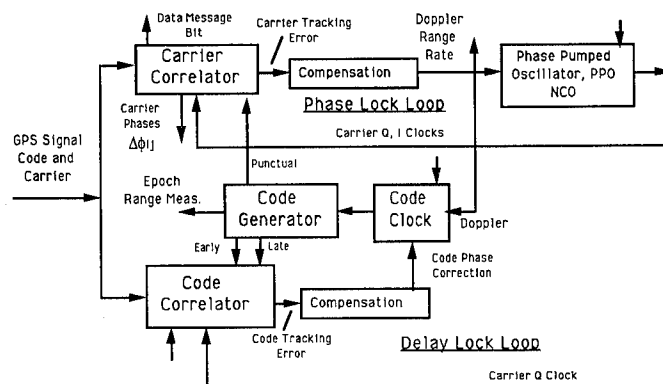
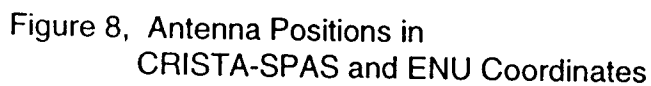


Figure 3, GPS Receiver Channel



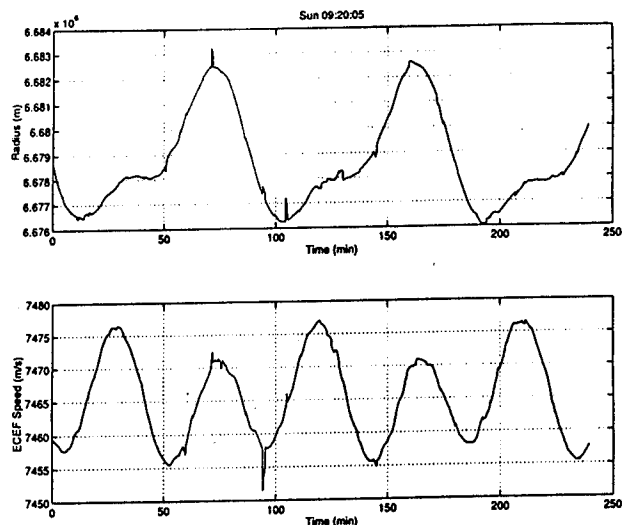


Figure 9, GPS Measured Radius Distance and ECEF Velocity

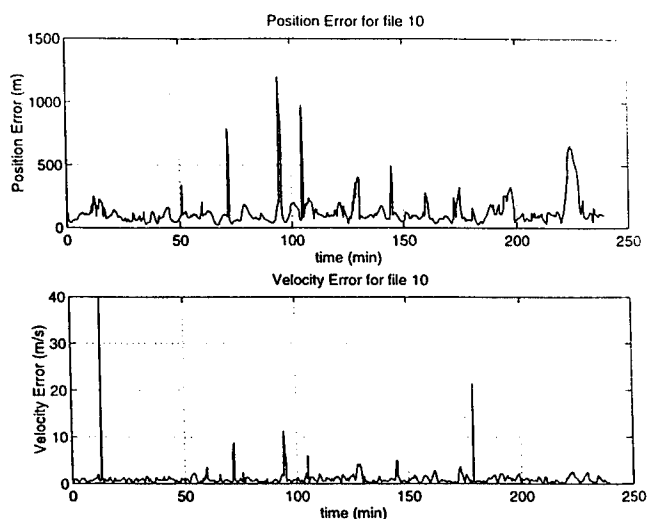


Figure 10, Difference in Position and Velocity Between TANS Vector and SEL Receivers

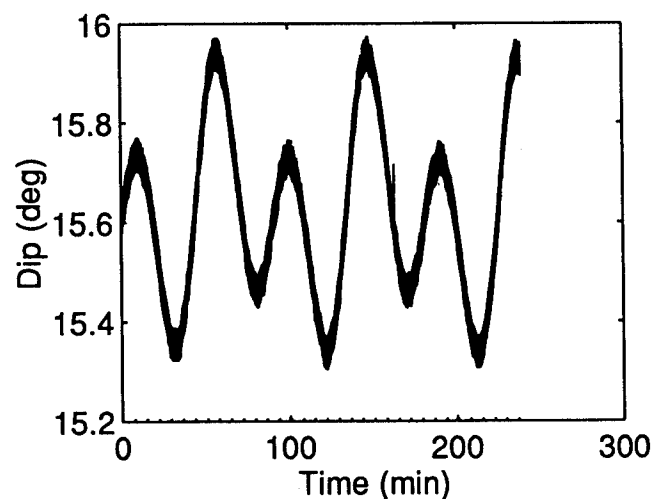


Figure 11, Dip angle of CRISTA-SPAS Telescope Axis With Respect to Local Horizontal

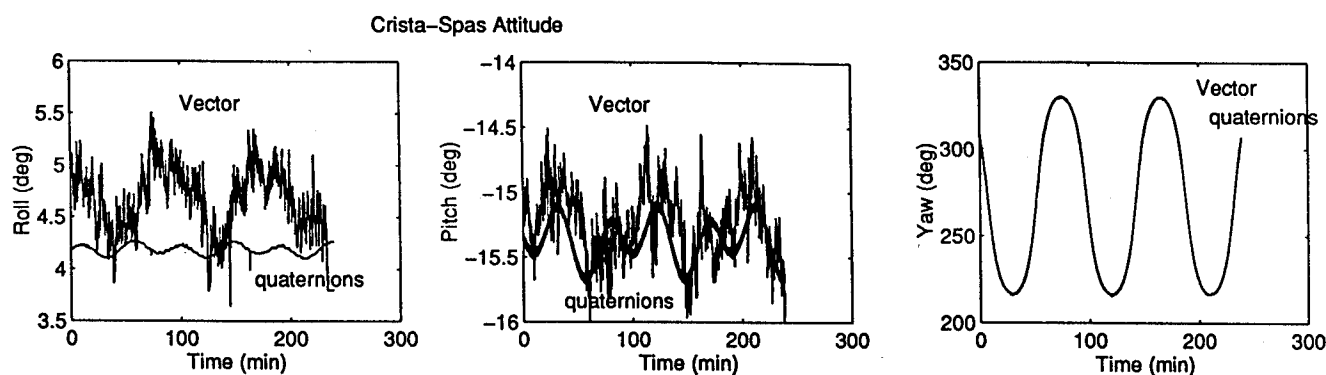
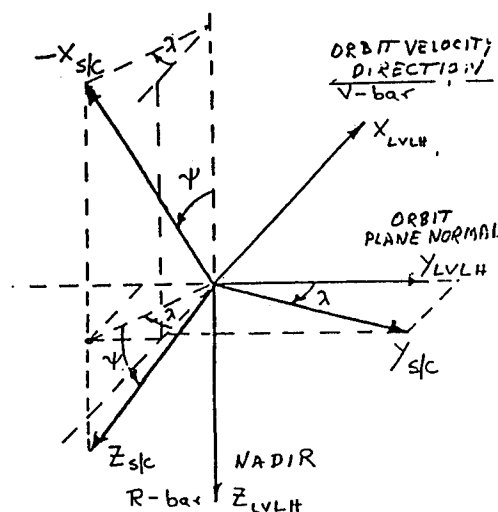


Figure 12, Attitude From GPS Compared to CRISTA-SPAS Quaternion Derived Data

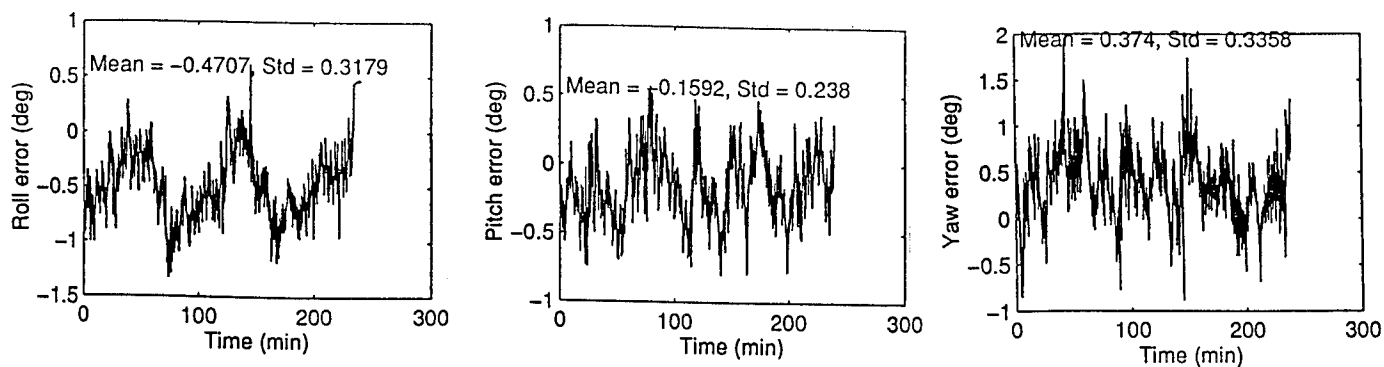


Figure 13, Attitude Difference Between GPS Measured and Derived Data

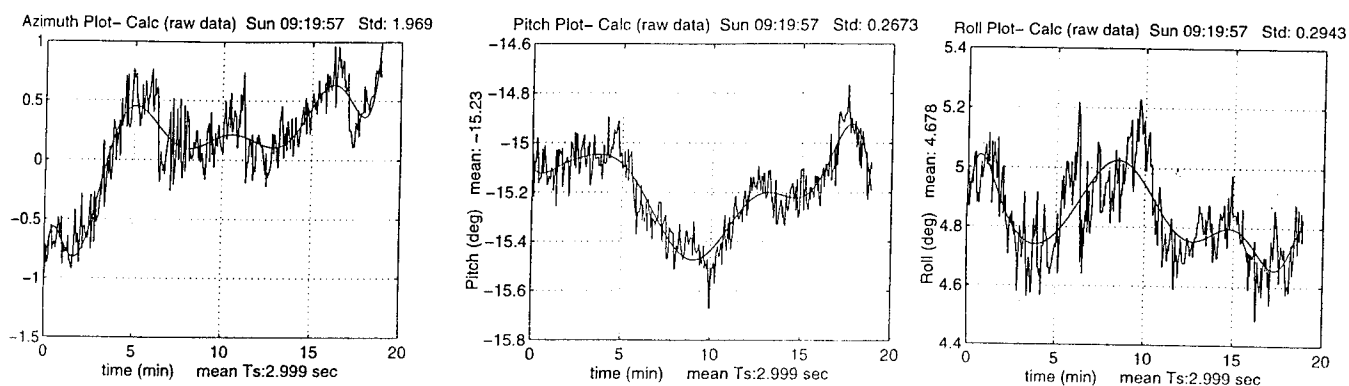


Figure 14, GPS Attitude For 20 Minute Interval

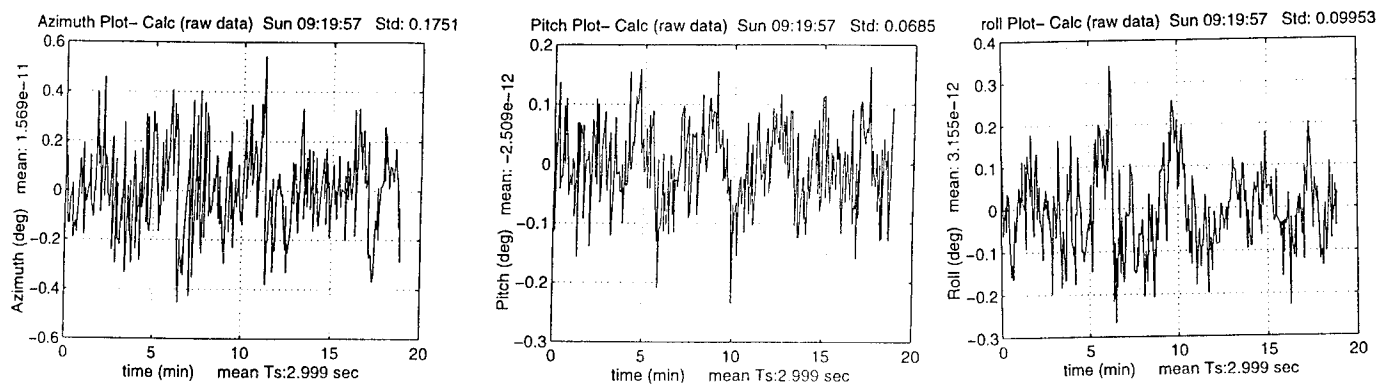


Figure 15, Attitude Difference Between GPS Data and Fitted Polynomial

The GPS Attitude Determination Flyer (GADFLY): A Space-Qualified GPS Attitude Receiver on the SSTI-Lewis Spacecraft

Frank Bauer, E. Glenn Lightsey, Stephen Leake, Jon McCullough,
James O'Donnell, Jr., Kate Hartman, and Roger Hart
NASA Goddard Space Flight Center

ABSTRACT

The Global Positioning System (GPS) Attitude Determination Flyer (GADFLY) experiment is slated to fly on the Small Satellite Technology Initiative (SSTI) Lewis spacecraft in July, 1996. The primary objective of the GADFLY experiment is to demonstrate and validate the cost-saving, systems engineering features that can be exploited by using GPS receivers in space vehicles. The experiment's physical hardware includes four GPS antennas and preamplifiers, cross-strapped to two Space Systems/Loral GPS Tensor receivers. This will be the first flight of a fully space-qualified GPS receiver capable of simultaneously sensing space vehicle attitude, orbit and providing a precise time reference.

INTRODUCTION

The SSTI program was established by the NASA Administrator as a demonstration platform for new science and engineering technologies. Two SSTI spacecraft are currently being developed for NASA Headquarters; "Lewis", by TRW, and "Clark" by CTA. Both are technology demonstration spacecraft with Earth Science objectives that are meant to illustrate the NASA philosophy of "smaller, faster, better, cheaper" by being developed in two years. SSTI-Lewis will be flying six other science and engineering experiments in addition to GADFLY, and has a five year design life.

The Space Systems/Loral GPS Tensors are being flown on GADFLY primarily as an attitude determination experiment, providing the first long-term, on-orbit flight of a space-qualified GPS receiver capable of deriving spacecraft attitude. This experiment will also demonstrate precise time distribution and provide autonomous real-time navigation solutions to the spacecraft subsystems and other experiments. The spacecraft clock will use a timing signal and a "time at the tone" message from the GPS Tensor to maintain a timing accuracy to better than two milliseconds. A GPS timing testbed is being

developed at the Goddard Space Flight Center to develop and test the techniques of getting this timing information from the GPS Tensor onto a MIL-STD-1553 spacecraft bus. In addition to the timing information, navigation solutions provided by the GPS Tensor will be used by the spacecraft to support its science experiments. To improve on the real-time navigation accuracy delivered by the GPS Standard Positioning Service, the GPS Enhanced Orbit Determination Experiment (GEODE) is being developed for GADFLY. GEODE, an enhanced navigation filter developed at the Goddard Space Flight Center, is expected to be embedded in the Tensor to provide navigation accuracy on the order of 20 meters 1σ . The GADFLY performance goals are shown in table 1.

| | Spacecraft Requirement | GADFLY Goals |
|--------------------------|--|---|
| Attitude Determination | None (using GPS) | $0.45^\circ 3\sigma$ |
| Orbit Determination | 150 m 3σ in-track 150 m 3σ cross-track 230 m 3σ radial Time Tags: 2 msec, 1 Hz update | 450 m 3σ unfiltered 150 m 3σ Tensor filtered 60 m 3σ GEODE Time Tags: < 1 msec 1 Hz update |
| Precise Timing Reference | 1 msec, 1 Hz update | Time Tags < 1 msec Discrete Pulse < 1 μ sec |

Table 1: GADFLY Performance Goals

Because SSTI-Lewis has primarily Earth Science objectives, it is an Earth pointing spacecraft. See figure 1. Four GPS antennas with one foot diameter aluminum ground planes are located on the spacecraft's zenith-pointing side as shown in the figure. The two GPS Tensors will be cross-strapped to these four antennas for redundancy. Figure 2 represents the location of the Tensor and preamplifier/splitter module within the Lewis spacecraft and figure 3 represents the GADFLY hardware block diagram. Each Tensor receiver will provide attitude and attitude rate (calculated from GPS signal doppler measurements) information at a minimum update rate of 4 Hz. While the GPS-derived attitude information will not be used for closed-loop control, information from the

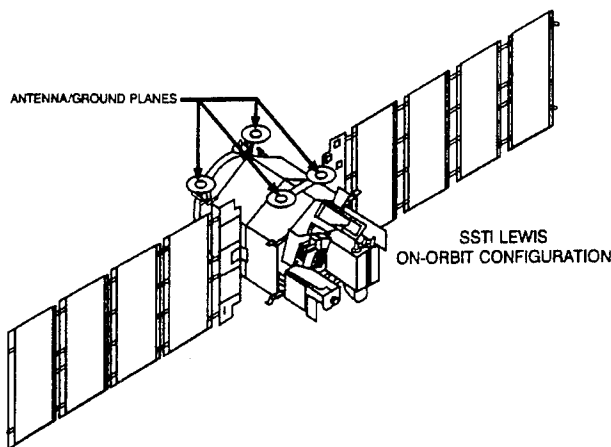


Figure 1: SSTI-Lewis On-Orbit Configuration

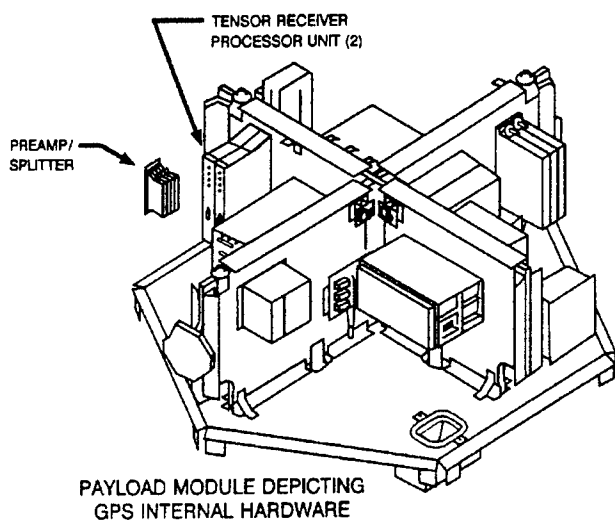


Figure 2: Payload Module with GPS Hardware

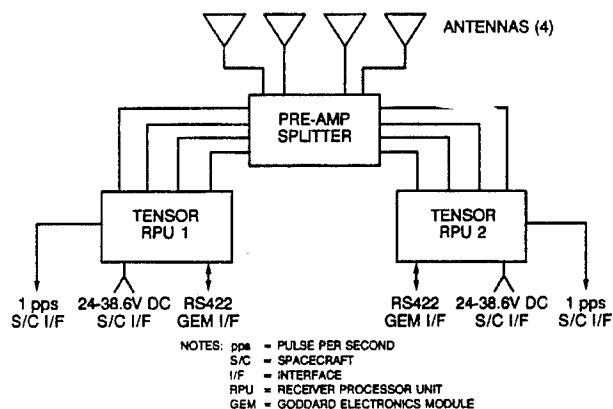


Figure 3: GADFLY Hardware Block Diagram

other attitude sensors onboard, including a CCD Star Tracker and an Earth Sensor, will be used to calibrate and verify the output of the GPS receivers.

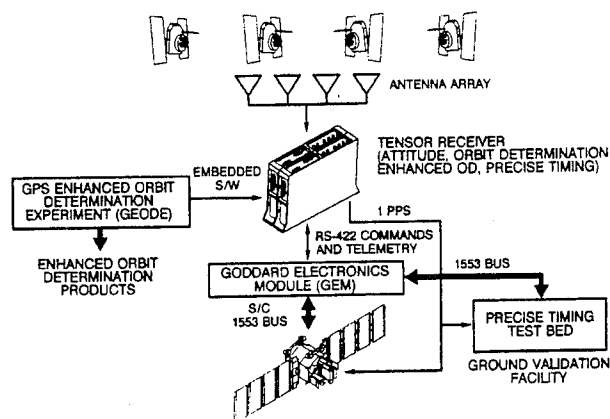


Figure 4: GADFLY System Configuration

Figure 4 shows an end-to-end diagram of the configuration of the GADFLY experiment, from the GPS constellation shown at top, through the GPS antennas and receiver, and into the other hardware and software systems that will be used to fulfill the various aspects of its mission. The GADFLY experiment will be the first space mission to use a fully space-qualified GPS receiver capable of calculating spacecraft attitude, orbit and time. In addition, because of the long duration of the mission, and the fact that other sensors and capabilities will be available to verify and calibrate the GPS attitude, orbit and time, the experiment will provide invaluable, long term information on the use of GPS in space.

TENSOR DESCRIPTION

The SS/Loral Tensor receiver is being developed as a flight-qualified attitude determination, orbit determination and precise timing sensor which uses the radio frequency signals received by the constellation of 24 GPS satellites.

The Tensor uses the GPS Standard Positioning Service (SPS) Course Acquisition (C/A) code, which operates at the GPS L1 (1575.25 MHz) frequency. The receiver offers 13 real-time output states; time, and three-axis attitude, attitude rate, position, and velocity. The Tensor to be flown on SSTI-Lewis is a redundant unit comprised of three major assemblies: two Receiver Processor Units (RPUs), a four channel preamplifier/splitter and four L1 frequency GPS patch antennas. A mechanical drawing of a redundant Tensor receiver processing unit, with pertinent physical characteristics is shown in figure 5. Similarly, the preamplifier/splitter and the antennas are illustrated in figure 6.

The Tensor has nine physical channels and uses multiplexing to enable the four antennas to each track up to nine satellites simultaneously, effectively making it a 36 channel receiver. The Tensor uses a RAD6000 RISC

- SPACE SYSTEMS/LORAL (SS/L) PART NUMBER: E034580
- EXTERNAL FINISH:
 - MOUNTING SURFACE CONTACT AREA: CHEM FILM PER MIL-C-5541, CLASS 3
 - EXTERIOR SURFACES: BLACK CHEMGLAZE Z306 PAINT
 - THERMAL CONTROL EMISSIVITY: 0.9
- THERMAL DISSIPATION: 14.0 WATTS, AVERAGE
- UNIT WEIGHT: 8.9 LBS
- DIMENSIONS: 3.15 x 10.83 x 7.05 IN
- MOUNTING SURFACE CONTACT AREA: 34 SQ. IN.

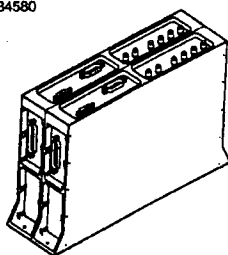
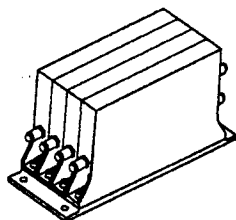


Figure 5: Tensor Receiver Processing Unit

- FOUR CHANNEL PREAMPLIFIER/SPLITTER
- THERMAL DISSIPATION: 1.0 WATT, ORBIT AVERAGE
- UNIT WEIGHT: 0.9 LBS.
- DIMENSIONS: 2.00 x 5.43 x 3.01 IN.
- MOUNTING SURFACE CONTACT AREA: 4.6 SQ. IN.



- GPS ANTENNA (1 OF 4)
- BALL GPS ANTENNA PART NUMBER 301700-500
- ELECTRICAL SPECIFICATIONS:
 - FREQUENCY: 1573.4 - 1577.4 MHz
 - VSWR: 2.0:1.0
 - GAIN (AS MEASURED ON 16 INCH GROUND PLANE): 4.5 dBi
 - AZIMUTH COVERAGE: OMNI-DIRECTIONAL
 - ELEVATION COVERAGE: HEMISPHERICAL
 - POLARIZATION: RIGHT HAND CIRCULAR
- THERMAL DISSIPATION: 0 WATTS
- UNIT WEIGHT: 0.20 LBS
- DIMENSIONS: 2.87 x 2.87 x 0.34 IN.

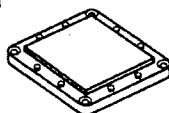


Figure 6: Tensor Preamp/Splitter and Antennas

microprocessor operating at 20 MHz. Attitude data from the Tensor can be provided to the spacecraft at update rates of up to 10 Hz. For the GADFLY application, a 4 Hz update rate is provided. Tensor data is fed to a specially designed Goddard Electronics Module (GEM) through an RS-422 serial data interface operating at 9600 baud. The GEM then converts the RS-422 serial data from the Tensor to MIL-STD-1553 data interface format which is accepted by the Lewis spacecraft data system.

Redundancy is accomplished by cross strapping the four preamplifiers/splitters and antennas to the two identical RPUs. If one of the antennas or preamplifiers/splitters fail on-orbit, the remaining three can still perform the time and orbit functions at full accuracy and the attitude function at reduced accuracy.

Schedule Risk Mitigation

The SSTI-Lewis development and launch schedule is very ambitious. Moreover, the Tensor receiver is a new product still under development. Thus, there is a quantifiable risk that the flight Tensor delivery would arrive late in the spacecraft integration and testing activities. To mitigate the potential risk associated with a late delivery to the spacecraft, several plans were put in place. First, a Tensor emulator was developed at the Goddard Space Flight Center to emulate the timing

interface and the data packet format. This emulator is intended to expedite the interface testing of the GEM. In addition, a Brass Board Engineering model of the Tensor was delivered to the GSFC in mid-July, 1995. From a mechanical and electrical interface standpoint, this unit can be used as a form, fit and function replacement to the Tensor. It possesses the same chassis and mounting interfaces. It will allow the SSTI-Lewis team to perform about 90% of the interface verification checks. Its primary differences reside in the fact that it is a six (versus nine) channel receiver, it uses several Field Programmable Gate Arrays on a daughter board, instead of a single ASIC, and it possesses a lower voltage DC/DC Converter to supply input power.

GPS TIME CODE TEST BED

Precise timing, using GPS, promises to significantly reduce spacecraft development and systems operations costs. Expensive, onboard precision oscillators, such as the \$400,000 oscillators flown on the X-Ray Timing Explorer, can be replaced with less precise, inexpensive (\$10,000 or less) oscillators that are updated frequently using GPS. In addition, the current state of the practice in time distribution requires a significant time distribution harnessing infrastructure to synchronize all the spacecraft subsystem clocks. By using GPS through a spacecraft bus architecture, a significant harness weight savings and integration and testing time savings can be realized. The GPS time distribution approach, planned for future spacecraft, will significantly enhance spacecraft autonomy by eliminating the ground-based manual labor and multiple ground stations that are required to correlate the spacecraft clock to UTC. Currently, many spacecraft require daily clock updates from the ground to maintain the clock precision required to meet the spacecraft mission objectives. This ground intervention activity will be totally eliminated with the GPS time distribution approach planned for Lewis and future spacecraft. Also, the existence of an onboard precise time reference will allow science data to be time-tagged upon downlink to the ground, and will facilitate the performance of concurrent science by multiple spacecraft and/or sites. The future direction of spacecraft time management is illustrated in Table 2.

To adequately validate the Lewis spacecraft time distribution concept, a GPS Timing Test Bed is being developed at the GSFC. This test bed will evaluate and characterize GPS time distribution through a series of time monitoring measurements. The test bed intends to validate the GPS/spacecraft time distribution interface, to measure the accuracy and stability provided by the GPS time distribution design and to determine the complexity of the user clock to meet various mission objectives. This

| | Time Correlation | Time Distribution |
|-------------------|---|--|
| What we have... | Range delay method using manual operations (accurate to $\approx 100 \mu\text{sec}$) | Distribution of multiple clocks with discrete interfaces + time code via 1553/1773 |
| What we'd like... | Autonomous onboard time maintenance (accurate to $\approx 10 \mu\text{sec}$) | Distribution of time sync and time code solely via 1553/1773 |
| Why? | Reduce mission operations costs and improve accuracy | Reduce spacecraft complexity and development cost |

Table 2: Time Management Direction

facility is being developed to characterize not only the SS/L Tensor receiver, but any receiver that provides time code information. A block diagram of the timing test bed is shown in figure 7. As shown, all major components in this test bed can be linked through a MIL-STD-1553 or 1773 data interface. For the SSTI-Lewis application, a 1553 interface is used. Using the time monitor, connected to the bus as a remote terminal, the data latency and clock stability of the GPS time distribution can be monitored. As shown, various components can be added to the bus to determine how data bus sharing and loading will impact the timing distribution.

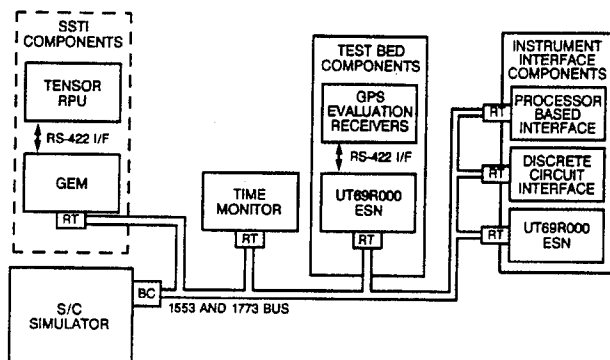


Figure 7: GPS Time Code Test Bed

Design details of the GPS time distribution technique envisioned for future NASA spacecraft are shown in figures 8–10. Currently, spacecraft time distribution is performed through hardware discretes. Future spacecraft will distribute timing data through the spacecraft 1553/1773 bus, as shown in figure 8. A special interface is in development to capture the 1 Hz timing pulse from the GPS receiver and the “time at the tone” information from the GPS data interface (in this example an RS-422 interface) and broadcast the timing data over the bus. Thus, all subsystems, components and the spacecraft master computer would receive this timing data simultaneously. Figure 9 illustrates how the various components in the spacecraft would update their timing

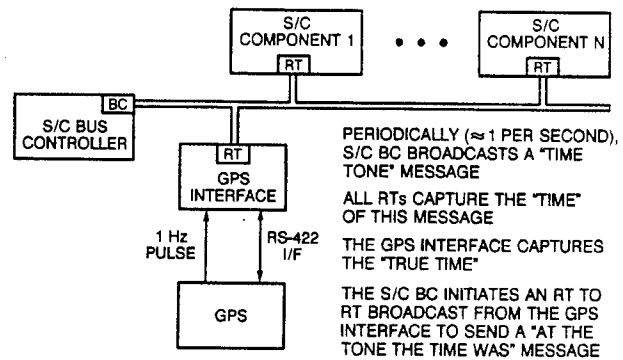


Figure 8: GPS Time Distribution via S/C Data Bus

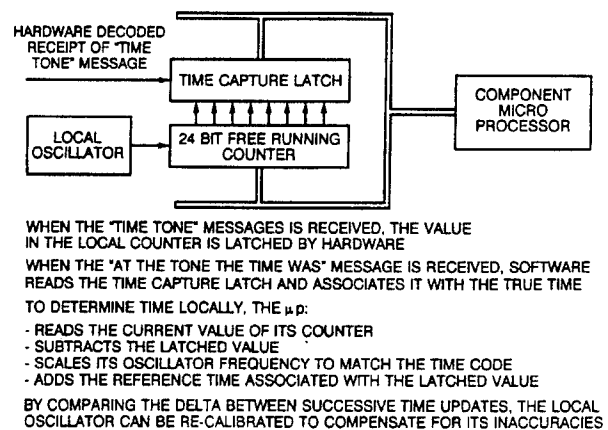


Figure 9: Spacecraft Component Clock Calibration

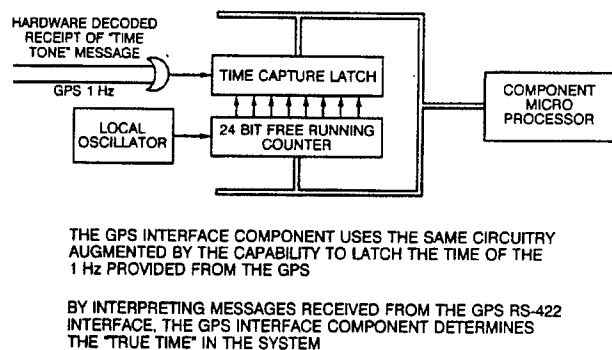
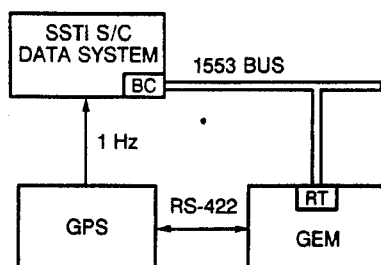


Figure 10: GPS Interface to Spacecraft Bus

signal with this broadcast data. Figure 10 illustrates, from a top level, the design of the GPS interface circuitry which accepts the 1 Hz timing discrete from the GPS receiver and the “time at the tone” data and produces the spacecraft time reference. The eventual goal of the time distribution activity is to reduce the size of the GPS interface block, shown in figure 8, to a multichip module for 1553 and 1773 data systems. This can then be

embedded into the various GPS receivers to save weight, size and power.

The GPS time distribution techniques described above could not be totally implemented on the SSTI-Lewis spacecraft due to the ambitious development and launch schedule. In particular, the 1 Hz discrete pulse is delivered directly to the spacecraft data system instead of being processed by the GPS interface card (the GEM) and sent through the bus. See figure 11. The "time at the tone" information is, however, sent through the bus. The methods to be flown on SSTI-Lewis represent an important incremental step in the development of a precise, autonomous, onboard system for maintaining and distributing time information derived from GPS.



GEM RECEIVES MESSAGES VIA THE RS422 INTERFACE
 GEM INTERPRETS THE "AT THE NEXT 1 Hz, THE TIME WILL BE" MESSAGE
 GEM MAKES THIS TIME AVAILABLE FOR THE S/C BUS CONTROLLER
 IN SSTI, THE S/C WILL READ THE GEM \approx 512 MILLISECONDS TO OBTAIN THIS TIME

Figure 11: SSTI-Lewis Time Distribution Concept

GADFLY ENHANCED ORBIT DETERMINATION EXPERIMENT

The current state of the practice for space vehicle orbit determination is to provide a periodic uplink of the vehicle ephemeris data based on ground station ranging techniques. This scenario is very labor and ground operations intensive. By flying a GPS receiver on a spacecraft, it becomes possible to determine the spacecraft's position onboard, autonomously. However, the accuracy of this position with a C/A code GPS receiver is on the order of 100–200 meters, and the GPS-derived velocity is not accurate enough to derive good orbit predictions for the spacecraft. The purpose of the GADFLY Enhanced Orbit Determination Experiment (GEODE) is to develop and implement a filter for the GPS position and velocity in order to increase the accuracy of the position to the order of 20–50 meters, and improve the accuracy of the velocity to allow a

completely autonomous onboard orbit determination scheme. The combination of these two functions will satisfy the majority (>95%) of NASA's upcoming Earth orbiting space missions.

Table 1 depicts the GADFLY performance goals, including the orbit determination requirements. As shown, filtered point solutions generated by a C/A code receiver under selective availability are expected to meet the requirements of the most stringent instrument on the SSTI-Lewis spacecraft—the Hyperspectral Imager (HSI) Earth Observer. However, additional orbit determination filtering can yield better orbit determination accuracy. While the HSI requirements are met using the standard C/A code receiver with point filtering, enhanced science can be obtained with more accurate orbit determination. In particular, the HSI instrument has a 70 meter orbit determination goal to meet its enhanced science objectives. Since there is excess CPU and memory capacity on the Tensor, the opportunity arose to incorporate filtering software in the receiver that will produce vectors accurate enough to exceed the HSI navigation goal. The objective of the GEODE team is to develop filtering algorithms for enhanced orbit determination to be integrated into the Tensor. A block diagram of the GEODE hardware and data throughput configuration is shown in figure 12.

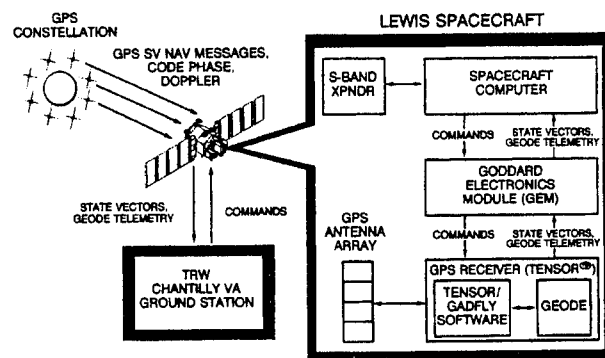


Figure 12: GEODE Configuration

Expected Benefits

In addition to providing improved positions for the HSI instrument, the GEODE filter provides a strong dynamic coupling between the position and velocity that is lacking in point solutions. This is particularly important when the state vectors are to be used for ephemeris prediction. The improved dynamics allow the receiver to continue to generate accurate states during signal outages or degraded coverage while the filter propagates the state without measurements. Enhanced GPS states that are downlinked can now be propagated accurately for science planning

and scheduling, eliminating the added cost of ground processing which was previously performed to enhance the real-time onboard solutions. The GEODE software is being developed to be portable, and modular, allowing it to be reused on other missions and incorporated in other GPS receivers.

GEODE Heritage

To meet more accurate onboard orbit requirements and to reduce operations costs for spacecraft that use NASA's TDRSS communications satellites, Goddard's Flight Dynamics Division developed an autonomous navigation system that derives onboard tracking data from the nominally scheduled communications uplink signal. The TDRSS Onboard Navigation System (TONS) coordinates the transponder and flight computer to acquire tracking data and compute orbit solutions, creating a navigation system from existing spacecraft systems that imposes few or no hardware or power requirements in addition to the communications needs. TONS implements an extended Kalman filter with high fidelity force and statistical models to sequentially process Doppler observations output by the transponder carrier tracking loop and is capable of producing solutions on the level of the GPS precise positioning service. In a demonstration with the EUVE spacecraft the filter operated without divergence for 320 days, comparing to high-accuracy definitive solutions to 25 meters 1σ . The filter also propagated over data gaps of up to 24 hours with only 150 meters of error growth and with immediate recovery at the next contact. GEODE will use applicable experience and software from TONS to substantially shorten the development schedule and meet the Lewis milestones.

Software Development

While TONS uses integrated Doppler observations as inputs to the filter, the Tensor provides pseudorange, carrier phase, and Doppler. However, the filter structure and spacecraft dynamics are not dependent on data type, and the intent is to modify the TONS filter to accept the GPS observations and reuse much of the flight software developed for the TONS application on EOS-AM1.

Key algorithms to be developed for GEODE include measurement models for the GPS observables and a routine for satellite selection. Extraction of the GPS broadcast data message is done by the Tensor, and the basic GPS constellation position and timing information will be available to the GEODE software in memory. See figure 13.

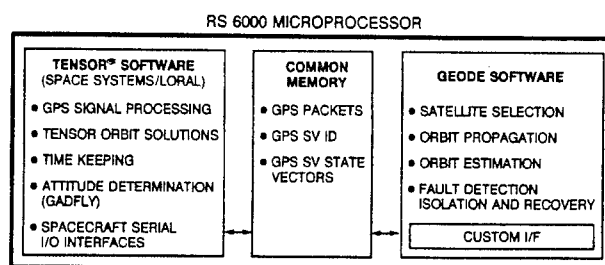


Figure 13: Software Architecture

Code development will take place on a Sun workstation and an RS/6000 workstation. Another RS/6000 workstation will be used to emulate the Tensor to gain experience in downloading code and to evaluate timing and code size before the Tensor delivery.

Flight software is being developed in two builds. The first is to be ready by delivery of the Tensor. It will include new functions, not reused from TONS, such as interfaces to the Tensor software, basic observation models, and one-second state generator. The second build, to be completed prior to spacecraft integration and test, will implement the full orbit determination capability.

Flight Testing

The spacecraft state, as well as covariances and other parameters sufficient for full performance evaluation will be downlinked in telemetry. Raw observations from the Tensor will be post-processed in combination with data from a network of GPS receivers on the ground to produce high-accuracy solutions that can be used as a baseline of comparison. Orbits derived from S-band tracking will be used to provide an independent check of the GEODE solutions.

GADFLY PRE-FLIGHT TEST PLANS

Prior to the delivery of the Tensor receiver to GSFC, several environmental tests are to be performed to validate flight worthiness. In particular, a 14.14 Grms one minute vibration of the RPUs, preamplifiers and antennas will be performed. This will be followed up with a 8 cycle thermal vacuum test which will be completed over a -34°C to +77°C temperature range. Electromagnetic Interference (EMI) testing will be completed on the qualification Tensor unit. Upon completion of these tests as well as a full performance evaluation and software validation of the Tensor, the receiver will be delivered to NASA GSFC. GADFLY integration and testing includes the timing validation in the timing test bed, GEM interface testing and GEODE software build development, load and testing. See figure 14. Final GEODE software validation is expected to be performed

using the GSFC 40 channel attitude and orbit GPS constellation simulator. Spacecraft level integration and test activities includes integration and aliveness testing, environmental testing and a self survey. During the self survey, the antenna baselines will be measured relative to an optical cube on one of the antenna ground planes. See figure 15. These measurements are similar to those performed on the Spartan GPS Attitude Determination and Control System (GADACS) experiment [ref 2].

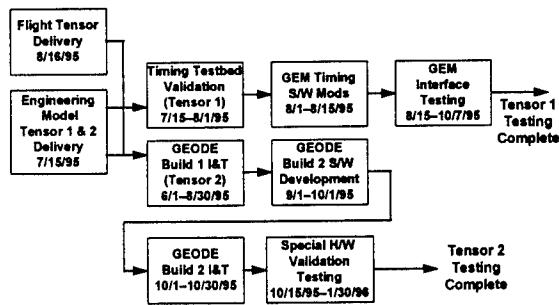


Figure 14: GADFLY Integration and Test Plan

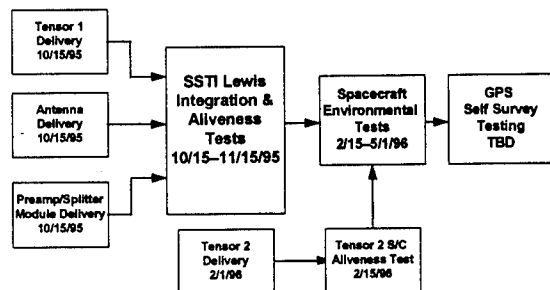


Figure 15: GADFLY S/C Level I&T Plan

POST LAUNCH TESTING

There are four primary on-orbit data evaluation activities that will be accomplished with GADFLY. These include Tensor receiver robustness quantification, attitude performance evaluation, GEODE performance assessment and GPS timing evaluation.

Throughout the SSTI-Lewis mission, key parameters will be checked and archived to quantify the robustness of the Tensor receiver and GPS, in general. A database is being planned to record and track key parameters such as time to first fix after a cold start, time to first fix after a warm start, and GPS data dropouts, for example. Information such as vehicle attitude and orbit position shall be noted, stored, and evaluated in an attempt to improve the robustness of future receiver builds.

The attitude performance of GADFLY will be evaluated by acquiring the SSTI-Lewis sensor data from the star

tracker, earth sensor, and gyro and comparing these to the GPS receiver data. Through this activity, a long-term understanding of the attitude capabilities of GPS can be gleaned. Moreover, the effects of multipath can be better studied and quantified in an orbital velocity environment. The Tensor receiver, to be flown on GADFLY will include an option to use the double difference technique to remove line bias effects. The advantages and disadvantages of this technique will also be quantified as part of the testing.

During the Lewis mission, the spacecraft time distribution scheme will be monitored. System performance will be compared to the ground-based test bed and timing accuracy will be quantified using standard ranging techniques.

As stated previously, orbit determination data from the Tensor receiver GEODE software will be compared to high accuracy ground-based solutions and S-band tracking data.

CONCLUSIONS

The GADFLY experiment on the SSTI-Lewis spacecraft is expected to be a pathfinder to demonstrate several GPS technologies for use in future spacecraft. This will be the first flight of a fully space-qualified GPS receiver capable of simultaneously sensing space vehicle attitude, orbit and providing a precise time reference. The GPS attitude determination experiment will provide a long-term high accuracy quantification of system performance, including the degradation effects of vehicle multipath and attitude rates derived from GPS signal doppler measurements. The long-term aspects of this flight will provide an outstanding platform to quantify the effects of receiver robustness. Of particular importance is receiver data dropouts, radiation degradations (if any), and single event effects, including latchups and bit upsets. The new techniques to be demonstrated on Lewis to distribute GPS time over the spacecraft data bus will provide much lower cost, less weight, and autonomous alternatives to the current practice. The GEODE software, being developed at GSFC and embedded in the Tensor receiver will provide an autonomous onboard orbit determination scheme which is expected to serve over 95% of all Earth orbiting spacecraft. Significant system cost, power and weight reductions are expected from exploiting GPS in space vehicles. If it is fully successful, the GADFLY experiment promises to help rewrite the books on how to design future spacecraft.

ACKNOWLEDGMENTS

The authors wish to gratefully acknowledge the multi-organizational team who have made the GADFLY experiment possible. In particular, we wish to acknowledge the support from NASA Headquarters Code XS for their financial and payload sponsorship, and Codes OT, OI and OS for financial support and their vision to reduce mission costs through strategic investments, Dom Conte, our SSTI-Lewis interface engineer and the SSTI-Lewis team at TRW who had the insight to manifest GADFLY, the government and industry team at NASA Goddard, particularly the members of the Guidance and Control Branch (Code 712), the Flight Dynamics Division (Code 550), and the Flight Data Systems Branch (Code 735) especially Phil Luers, John Allen, and Evan Webb, the rest of the government and industry support team including our team at the Johnson Space Center, particularly Penny Saunders, the support and guidance provided by Clark Cohen and Brad Parkinson at Stanford University, and Kurt Brock and Bill Slingland at Space Systems/Loral. All have been crucial to the success of this program.

REFERENCES

1. Cohen, C. E. (1992). Attitude determination using GPS. Ph.D. dissertation. Stanford University, Stanford, California.
2. Bauer, F. H., Lightsey, E. G., et. al. (1994), Pre-Flight Testing of the Spartan GADACS Experiment, *ION-GPS-94*. Salt Lake City, Utah.
3. Lightsey, E. G., C. E. Cohen and B. W. Parkinson. (1993). Application of GPS attitude determination to gravity gradient stabilized spacecraft. *AIAA Guidance, Navigation, and Control Conference*. Monterey, California.
4. Cohen, C. E., E. G. Lightsey, B. W. Parkinson and W. A. Feess. (1993). Space flight tests of attitude determination using GPS: preliminary results. *ION GPS-93*. Salt Lake City, Utah.
5. Lightsey, E. G., C. E. Cohen, and B. W. Parkinson (1994). Attitude determination and control for spacecraft using differential GPS. *ESA International Conference on Spacecraft Guidance, Navigation, and Control*. Noordwijk, The Netherlands.

Argos Navigation and Attitude Determination System

Dr. Jon Petway
Rockwell

BIOGRAPHY

Dr. Jon W. Petway received his B.S.E.E. degree from the University of Kentucky (Lexington) in 1962 and his M.S.E.E. and Ph.D. from the Georgia Institute of Technology in 1963 and 1966, respectively. He then returned to the University of Kentucky as a faculty member for 3 years. Experience gained from summer employment during Apollo led him to seek a full time position in the aerospace industry. Since May 1969 he has been employed by Rockwell working in the area of design and error analysis of multi-sensor navigation systems (including attitude determination).

ABSTRACT

The ARGOS (Advanced Research Global Observation Satellite) vehicle carries eight DOD related experiments and is scheduled for launch into a nominally circular sun synchronous orbit in March 1997. A major objective of the navigation/attitude determination subsystem design has been to reduce cost by utilizing the GPS sensor in such a way that on-board hardware, software, and ground tracking requirements are simplified.

In order to meet the attitude determination accuracy requirement, our primary concern, an approach comprising two mechanizations was used. The first of these utilizes GPS information (position and velocity) to determine the transformation matrix between the J2000 Earth Centered Inertial (ECI) frame and a set of axes referred to as Local Vertical Orbit Plane (LVOP). This latter set of axes would be a locally level set of axes for a spherical (non-oblate) earth. The second mechanization of the ARGOS attitude determination system is designed to hold the spacecraft to an earth geocenter pointing attitude such that vehicle BODY axes track the LVOP axes. This is accomplished by using orbital gyrocompassing and horizon sensor measurements to detect and control attitude deviations from LVOP alignment.

Attitude errors result from imperfections in both of the mechanizations. In order to demonstrate compliance with

accuracy requirements, a comprehensive error analysis was conducted. For the transformation matrix component, a covariance simulation was developed. This includes both the eight state Kalman filter embedded in the GPS receiver and a high fidelity simulation of the GPS constellation. Outputs of this simulation were used to derive the errors in the ECI to LVOP transformation matrix. For the orbital gyrocompassing/horizon sensor component, horizon sensor noise and gyro drift as specified by the vendors were used to compute RMS errors in controlling the spacecraft to alignment with LVOP axes.

A backup navigation capability was implemented based upon using GPS outputs to compute a set of orbital elements while GPS is active and reliable.

INTRODUCTION

The P91-1, or ARGOS (Advanced Research Global Observation Satellite), mission is to carry eight DOD experiments into orbit. There have been other such satellites. The author is familiar with one of those, referred to as P80-1. The on-board software supporting maintenance of the P80-1 navigation solution was very substantial. Ground tracking would have been (P80-1 was never launched) a big expense. Attitude determination was driven by the Teal Ruby Experiment and the performance requirement was at the 0.015° (1σ) level using gyros and a star sensor. Currently the P91-1 vehicle is being assembled and tested. Navigation and attitude determination are supported by a horizon sensor, gyros and a GPS sensor with no star sensor. The on-board computer effort is greatly lessened, as is ground tracking, while analysis predicts attitude determination accuracy to be approximately 0.018° (1σ).

This paper will describe how navigation and attitude determination are mechanized around a GPS sensor. The coordinate system considerations which must be dealt with will be discussed first to lay the groundwork. A section is included wherein a detailed error analysis of the GPS based attitude determination function is described

and results are presented. Another section describes the backup navigation capability that has been designed into the system wherein a set of orbital elements are maintained by processing GPS position and velocity, and then used for navigation purposes in the event of a GPS non-availability.

COORDINATE SYSTEM

Standard GPS outputs of position and velocity are referred to the WGS84 Earth Centered Earth Fixed (ECEF) coordinate frame (Reference 1) which rotates with the earth. However, all P91-1 requirements which GPS supports are based in the ECI coordinate frame. Therefore, it was requested that the GPS supplier modify the outputs to be referenced to the ECI frame. This modification amounts to constructing a coordinate transformation between the ECEF and ECI frames. Four component matrices would be necessary for the maximum accuracy transformation. However, sub-maximum but adequate accuracy might be obtainable using only a subset of the four component matrices. The following discussion develops some background information and then shows how the decision on implementation of the ECEF to ECI transformation was made.

Since the parameters which are used to define an inertial frame are actually continually changing, it has been customary to define an inertial frame in terms of the parameters as they were or will be at some particular time. Thus there was the M50 frame which was useful for many years, but now has been largely supplanted by the J2000, or ECI, frame. This is the new standard inertial frame geared to star positions on the celestial sphere at the start of the new Julian century. Question is: If we know the position of a vehicle in ECEF coordinates at some particular time on some particular date in a year remote from the year 2000, what are the necessary steps for re-expressing these position coordinates in the ECI frame?

Recent developments in Astronomy have led to a model which concisely relates the ECEF of date (at the particular time on the particular date in the remote year) components of a vector to the ECI components of the same vector. Since the earth's orientation with respect to ECI varies in four basic ways, it is not surprising that the re-expressing of vector components involves four matrices. These four matrices comprise an A matrix which accounts for the phenomenon of polar motion, a B matrix which accounts for the diurnal rotation about the Z axis, and the C and D matrices which account for nutation and precession, respectively. It is these latter two which are to be dealt with here; the A matrix involves very small unpredictable effects and is updated on a near real-time basis via measurement data, and the B matrix is very straightforward, requiring nothing more than accurate time for its generation. On the other hand, the effects accounted for by the C and D matrices, while not large over periods of a few years, still need to be evaluated so that a decision can be made as to how often these matrices

should be updated in order to keep ECI position and velocity errors at acceptable levels. These corrections are not so straightforward as the A and B matrices. The necessary algorithms will be set forth and discussed in the remainder of this section.

The overall algorithm for accounting for precession consists of nine lower level algorithms for computing the elements of the 3x3 D matrix. This is based on theory developed in the late nineteenth century by an astronomer named Simon Newcomb (for details see Reference 2 and Reference 3). The idea is based on the fact that the ascending node of the sun's apparent orbit around the earth is defined by the intersection of the ecliptic and equatorial planes. Both of these planes move, so the ascending node (this is the vernal equinox) moves. What makes the ecliptic move is gravitational pull of the planets and this motion is called planetary precession. The equatorial plane moves partly because of the gravitational effect of the sun and moon on the earth's equatorial bulge (called lunisolar precession) and partly due to other short term effects (called nutation). Newcomb developed a scheme for determining how the precession effects cause the vernal equinox to move between two known epochs (reference times) in terms of three Euler rotations (a 3-2-3 sequence) and he also provided a polynomial method for calculating the value of the rotations if the two epochs are known. The polynomials in current use are based on models adopted by the International Astronomical Union (IAU) circa 1980.

We now state the transformation matrix, which is the product of the three Euler rotations.

$$D(\epsilon_F, \epsilon_D) = R_3(-Z_A) R_2(\theta_A) R_3(-\zeta_A)$$

where ϵ_F and ϵ_D are epochs and $R_k(\theta)$ is a matrix modeling a rotation through angle θ about the k th coordinate axis. Multiplication of the three matrices on the right produces the following:

$$D = \begin{bmatrix} \cos Z_A \cos \theta_A \cos \zeta_A & -\cos Z_A \cos \theta_A \sin \zeta_A & -\cos Z_A \sin \theta_A \\ -\sin Z_A \sin \zeta_A & -\sin Z_A \cos \zeta_A & 0 \\ \sin Z_A \cos \theta_A \cos \zeta_A & -\sin Z_A \cos \theta_A \sin \zeta_A & -\sin Z_A \sin \theta_A \\ +\cos Z_A \sin \zeta_A & +\cos Z_A \cos \zeta_A & 0 \\ \sin \theta_A \cos \zeta_A & -\sin \theta_A \sin \zeta_A & \cos \theta_A \end{bmatrix}$$

The polynomials given in Reference 1 have been adapted to the P91-1 scenario and evaluated to determine the following numerical values for the three Euler rotations based on ϵ_F being 1 January 2000 (the J2000 ECI frame) and ϵ_D being 30 September 1995, the original planned launch date. The argument t is to be the Julian date of ϵ_D minus the Julian date of ϵ_F divided by 36525 so that it works out to be how far past 1 January 2000 ϵ_D is in units of Julian centuries. In the current case $t = -0.0425$.

Thus,

$$\zeta_A(t) = 2306.2181t + 0.30188t^2 + 0.017998t^3 \text{ arcsecond}$$

$$\zeta_A(-0.0425) = -98.01 \text{ arcsecond (or } -0.0272^\circ)$$

$$Z_A(t) = 2306.2181t + 1.09468t^2 + 0.018203t^3 \text{ arcsecond}$$

$$Z_A(-0.0425) = -98.01 \text{ arcsecond (or } -0.0272^\circ)$$

$$\theta_A(t) = 2004.3109t + (-0.42665)t^2 - 0.041883t^3 \text{ arcsecond}$$

$$\theta_A(t)(-0.0425) = -85.18 \text{ arcsecond (or } -0.0236^\circ)$$

When these values are used to calculate the elements of the D matrix, the result is

$$D = \begin{bmatrix} 0.9999994644 & -0.0009494589 & 0.0004118976 \\ 0.0009494589 & 0.9999995493 & 0.0000001955 \\ -0.0004118976 & -0.0000001955 & 0.9999999152 \end{bmatrix}$$

Since the off diagonal terms are rotations in units of radians about the X, Y, Z axes, we can identify the following small angular misalignments between properly precessed and unprecessed coordinate frames.

$$\begin{aligned} -0.0403 & \text{ arcsecond about X (or } 0.00001119^\circ) \\ 84.95 & \text{ arcsecond about Y (or } 0.0235^\circ) \\ 195.84 & \text{ arcsecond about Z (or } 0.0544^\circ) \end{aligned}$$

These show the effect of precession in 4 years and 3 months. Obviously, the D matrix must be included in the calculation of ECI outputs within the GPS receiver or else the errors due to omitting the D matrix will overwhelm the attitude error budget of 0.05 degrees. It was decided that the D matrix must be implemented and a frequency of updating the D matrix of once per day was chosen. The reason attitude errors are affected is that the ECI position and velocity, which are directly affected, are used to compute the transformation matrix which relates ECI axes to LVOP axes as will be shown in detail in the next section.

The precession phenomenon discussed above is concerned with long term (or long period) changes in the earth's rotation axis. There are other short term changes which are grouped under the heading of "nutations". These are numerous (there are 106) and have periods ranging from 18.6 years down to 5 days. The current accepted model is the "1980 IAU Theory of Nutation" which provides a method for evaluating two parameters, $\Delta\epsilon$ and $\Delta\psi$, quantifying the deviation of the true coordinate frame from the mean (accounts for precession only) coordinate frame at a particular time within the range of validity of the model. Since the approximate amplitude of nutation motions is 9 arcseconds or 0.0025 degrees, it is a small effect and the decision was not to implement the C matrix containing the nutation correction.

Of course, the B matrix, which accounts for the 15°/hr earth rate rotation about the Z axis must be implemented.

The final component of the ECEF to ECI transformation is the A matrix which accounts for the phenomenon of polar motion. One way of looking at this phenomenon is to picture the earth as having a very thin surface layer which has limited freedom to move around. The result is that latitudes and longitudes of various landmarks are observed to change very slightly. These effects are exceedingly small and are not believed to impact P91-1 sufficiently to call for implementation of the A matrix. The transformation which must be implemented in the GPS receiver to convert its ECEF position components to ECI is as follows:

$$\begin{bmatrix} \text{X position component} \\ \text{Y position component} \\ \text{Z position component} \end{bmatrix} = A * B * C * D \begin{bmatrix} \text{X position component} \\ \text{Y position component} \\ \text{Z position component} \end{bmatrix}$$

(in ECEF Frame) (in ECI Frame)

where the unimplemented A and C matrices would become identity matrices and be omitted. The transformation for the velocity vector would be similar except that the $\omega \otimes R$ term due to earth's rotation would have to be accounted for.

VEHICLE ATTITUDE

Attitude will be maintained by determining at a 1 Hz rate, two rotational transformation matrices such that multiplication of these matrices in the proper order produces the transformation between ECI axes and BODY axes. The two matrices are:

1. $C_{LVOP/ECI}$ When a vector expressed in ECI axes is pre-multiplied by this matrix the result is the components of the same vector expressed in LVOP axes.
Note: Local Vertical Orbit Plane (LVOP) coordinates are defined as having z toward the geocenter, y opposite the angular momentum vector and x completing a right handed coordinate system with origin at the P91-1 center of mass.
2. $C_{BODY/LVOP}$ In correspondence with the above, this matrix re-expresses the LVOP components of a vector in BODY axes.

The product of these two matrices re-expresses ECI components as components in the BODY axis frame.

$$C_{BODY/ECI} = C_{BODY/LVOP} * C_{LVOP/ECI}$$

The LVOP coordinate frame is defined by three orthogonal unit vectors; u_z directed toward the geocenter, u_y perpendicular to the orbit plane in the direction opposite to the angular momentum vector, and u_x in such a direction as to complete a right handed coordinate system. These unit vectors will be constructed from the

ECI outputs of GPS position and velocity, and therefore will be expressed in the ECI frame. Thus if the dot product of any vector in the ECI frame with one of these unit vectors is formed, the result is the corresponding component of the ECI vector in the LVOP frame. This, by definition, is what the transformation does. Therefore, the ECI to LVOP transformation matrix can be constructed as a matrix whose rows are the transposed unit vectors u_x , u_y , and u_z .

The computation of u_x , u_y , and u_z is as follows. The symbol \otimes denotes the vector cross product operation and $|\underline{R}|$ denotes the magnitude of the vector \underline{R} . A superscript T indicates the transpose of a vector or a matrix.

Given GPS position and velocity outputs expressed in ECI coordinates:

\underline{R} --- position
 \underline{V} --- velocity

Compute the following:

$$\begin{aligned} u_z &= \frac{-\underline{R}}{|\underline{R}|} \\ \underline{H} &= \underline{R} \otimes \underline{V} \\ u_y &= \frac{-\underline{H}}{|\underline{H}|} \\ u_x &= u_y \otimes u_z \end{aligned}$$

Form the required transformation matrix:

$$C_{LVOP/ECI} = \begin{bmatrix} u_x^T \\ u_y^T \\ u_z^T \end{bmatrix}$$

LVOP axes can be considered to be in nominal alignment with BODY axes so that the transformation between these two frames is modeled in terms of three small rotations as either a vector or a skew-symmetric matrix. The form is as follows:

$$C_{Body/LVOP} = \begin{bmatrix} 1 & \psi & -\theta \\ -\psi & 1 & \phi \\ \theta & -\phi & 1 \end{bmatrix}$$

where ϕ , θ , and ψ are the misalignments in radians about the x, y, and z BODY axes, respectively. Because all of the transformations considered here are pure rotations of orthogonal frames the transpose is equal to the inverse and either operation reverses the direction of the transformation. The ϕ , θ , and ψ are produced by an orbital gyrocompassing mechanization. The concept of orbital gyrocompassing is discussed in the following paragraphs.

The "classical" gyrocompassing system has been in use as an attitude reference in ocean-going vessels since the development of the gyroscope. This system relies on the ability of the gyros to sense the earth's angular velocity.

Damping in the devices causes settling in a position having zero sensed earth angular velocity - north.

Spacecraft applications of the gyrocompass technique use the same approach, but measure orbit rate rather than the earth's rotation rate. A prime example of this application is that of the Agena spacecraft, which used roll horizon sensor data to augment roll - yaw decoupling logic driving a gimbaled platform reference system. Many spacecraft gyrocompass systems have operated in a similar manner; by torquing gimbaled gyros to provide rate integration. A slightly different approach, using strapdown gyros with the integration performed in the logic, has been known since at least 1961. It is the strapdown gyro version of gyrocompass control that was implemented on the P80-1 spacecraft and is also used for P91-1 (Reference 4).

In its simplest form, the P91-1 gyrocompassing method is a means to obtain yaw control using horizon sensor and rate gyro measurements to generate spacecraft attitude commands. The theory is pictorially described in Figure 1. The roll gyro normally measures only roll rate; however, it will also detect a component of the orbit rate if there is a yaw angle present. Roll attitude is nominally about the velocity vector (x-axis); hence, if an attitude rate error is measured by the roll gyro and no attitude rate error is seen in the roll channel of the horizon sensor, the system assumes the error to be in yaw attitude. Part of the information measured by the roll sensors may therefore be used to control the yaw attitude.

This simple mechanization, providing very loose roll and yaw control, can be improved by the use of a yaw gyro and additional logic. The equations of angular velocity, reduced to small angle approximations, show the complete set of gyro signals:

$$\underline{\omega}_0 = \begin{bmatrix} \dot{\phi} - \omega_0 \psi \\ \dot{\theta} - \omega_0 \phi \\ \dot{\psi} - \omega_0 \theta \end{bmatrix}$$

The first component will be recognized as the roll gyro measurement discussed above. Roll and yaw are seen to be coupled due to orbital motion. It is apparent that high quality roll and yaw information will result when the coupling terms are removed - and the logic has been designed to accomplish this. Figure 2 presents the complete gyrocompassing logic as it is currently used.

The outputs of the orbital gyrocompassing mechanization are used as the elements of the BODY to LVOP transformation matrix. When this matrix is post-multiplied by the previously computed ECI to LVOP transformation matrix the total attitude matrix is determined.

$$C_{BODY/ECI} = C_{BODY/LVOP} * C_{LVOP/ECI}$$

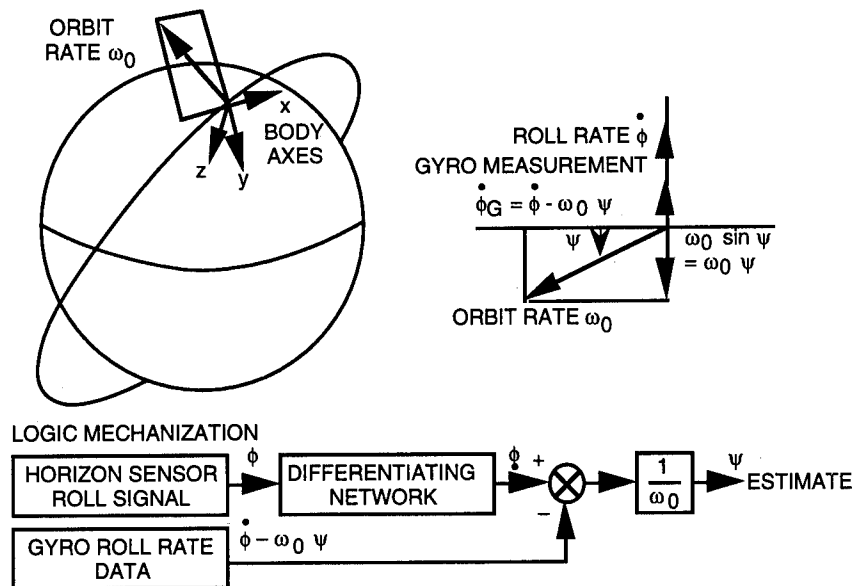


Figure 1. Basic Theory of Gyrocompassing

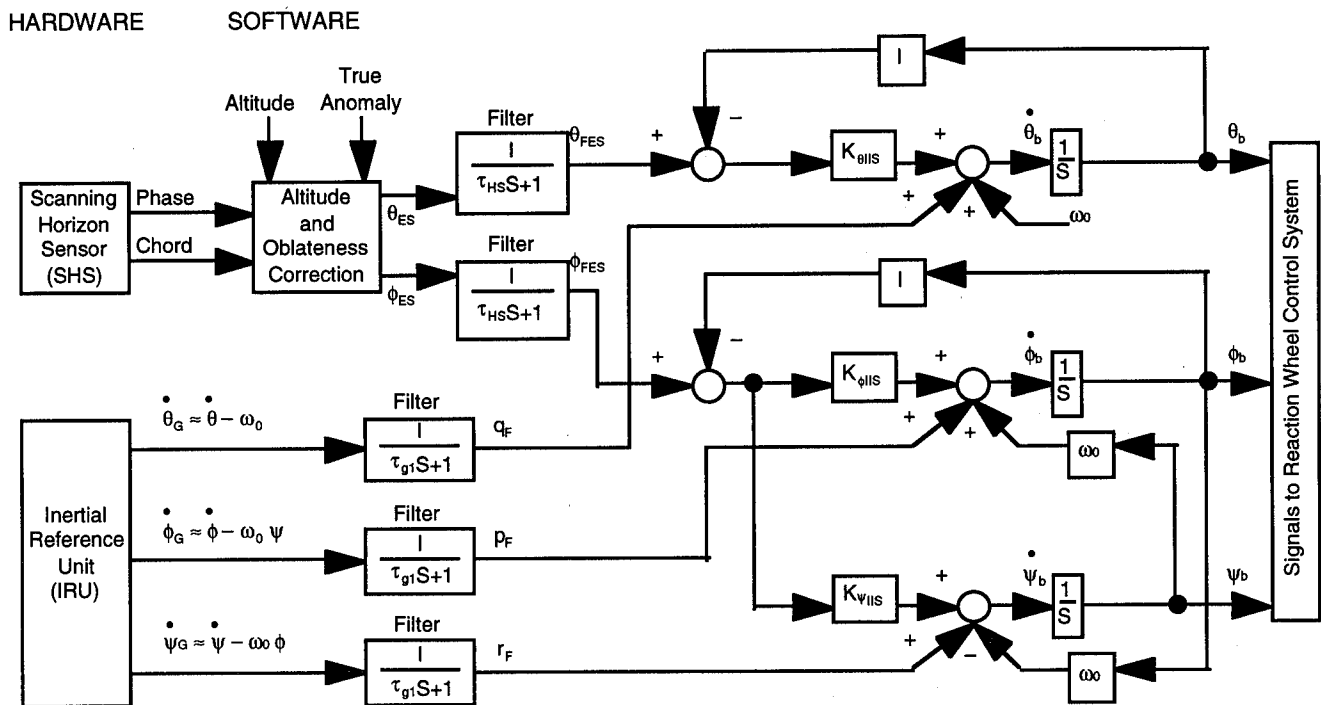


Figure 2. Gyrocompass Attitude Determination for P91-1

The next section will show how this attitude matrix is used to determine vehicle attitude.

ATTITUDE VIA EULER ANGLES

The attitude of P91-1 BODY axes with respect to ECI axes can be specified by a set of three Euler rotations and the sequence of axes about which the rotations are performed. There are twelve choices for this set of rotations (Reference 5). There is one set which seems to

appeal to intuition, and this is the set of Euler rotations which was chosen for the specification of P91-1 attitude. The selected set bears a strong relationship to the three orbit elements which determine the location of the orbit plane. It is strongly emphasized that the rotations discussed here are based upon the BODY axes being in an arbitrary orientation and subsequently rotated into alignment with ECI axes.

Diagram illustrating the geometry of orbital elements and coordinate frames:

- ECI Frame:** Earth-Centered Inertial frame with axes X_{ECI} , Y_{ECI} , and Z_{ECI} .
- Body Frame:** Frame attached to the body with axes X_{BODY} , Y_{BODY} , and Z_{BODY} .
- Orbit Trace:** The path of the body in the orbital plane.
- ECI XY Plane:** The plane defined by the X_{ECI} and Y_{ECI} axes.
- Line of Nodes:** The intersection of the ECI XY plane and the orbital plane.
- Angles:**
 - θ_0 : Angle between Z_{ECI} and Z_{BODY} .
 - Ω : Angle between X_{ECI} and the line of nodes.
 - i : Angle between Z_{ECI} and the normal to the orbit plane.
 - γ : Angle between X_{ECI} and X_{BODY} .
 - γ' : Angle between X_{ECI} and X'' .
 - γ'' : Angle between X_{ECI} and Y'' .
 - γ''' : Angle between X_{ECI} and Y' .
 - γ'''' : Angle between X_{ECI} and Y' perpendicular to orbit plane.
- Other Labels:**
 - Y' PERPENDICULAR TO ORBIT PLANE
 - LINE OF NODES IN ECI XY PLANE
 - (VERNAL EQUINOX)

The first Euler rotation is about the y-BODY axis and its magnitude is equal to the orbit angle plus 90 degrees. This rotation places the x-prime axis in the ECI xy plane and the z-prime axis tangent to the orbit pointing in the direction of vehicle travel. The second Euler rotation is about the x-prime axis with magnitude equal to 90 degrees minus the inclination angle i . This leaves the newz-double prime axis parallel to the z-ECI axis and the y-double prime axis in the ECI xy plane. The third and final Euler rotation is about the z-double prime or z-ECI axis with a magnitude equal to 360 degrees minus the Right Ascension of the ascending node. This latter rotation was chosen particularly so that all three Euler rotations would be in a positive sense. The transformation matrix between the ECI and LVOP coordinate frames is as follows.

$$C_{\text{ECI/Body}} = \begin{bmatrix} CR_3CR_1 + SR_3SR_2SR_1 & SR_3CR_2 & -CR_3SR_1 + SR_3SR_2CR_1 \\ -SR_3CR_1 + CR_3SR_2SR_1 & CR_3CR_2 & +SR_3SR_1 + CR_3SR_2CR_1 \\ CR_2SR_1 & -SR_2 & CR_2CR_1 \end{bmatrix}$$

ascending node has the standard symbol Ω . The angle from the ascending node around the orbit to the vehicle

$$R_7 = 90 - i$$

$$R_3 = 360 - \Omega$$

$$CR_K = \cos (R_K)$$

$$SR_K = \sin (R_K)$$

By forming appropriate quotients of elements of the above matrix and evaluating the appropriate inverse trigonometric functions of these quotients, the three Euler rotations are readily determined.

The attitude determination accuracy requirement for P91-1 is 0.05 degrees 1 sigma. In order to verify analytically that the system described in the previous sections will meet this requirement, a comprehensive error analysis was performed. Each component subsystem, the GPS based transformation matrix determination and the orbital gyrocompassing mechanization, was considered separately, and their errors subsequently combined to determine the overall attitude error.

The GPS portion of the error analysis presented a peculiar problem--the bugaboo of S.A. (Selective Availability). The P91-1 GPS function will not operate in the classified PPS (Precise Positioning Service) mode, and therefore will be subject to S.A. Since the ground rules of S.A. are that a certain level of accuracy will be guaranteed for position information but that there is no guarantee of accuracy with regard to velocity information, the problem of error analysis is frustrated. The error analysis presented here is based upon GPS operation in the PPS mode because that mode of operation leads to a tractable error analysis. Recently a model which may support sophisticated error analysis of GPS operation in the S.A. mode has been obtained. However, this came too late for results to be included in this current presentation.

568

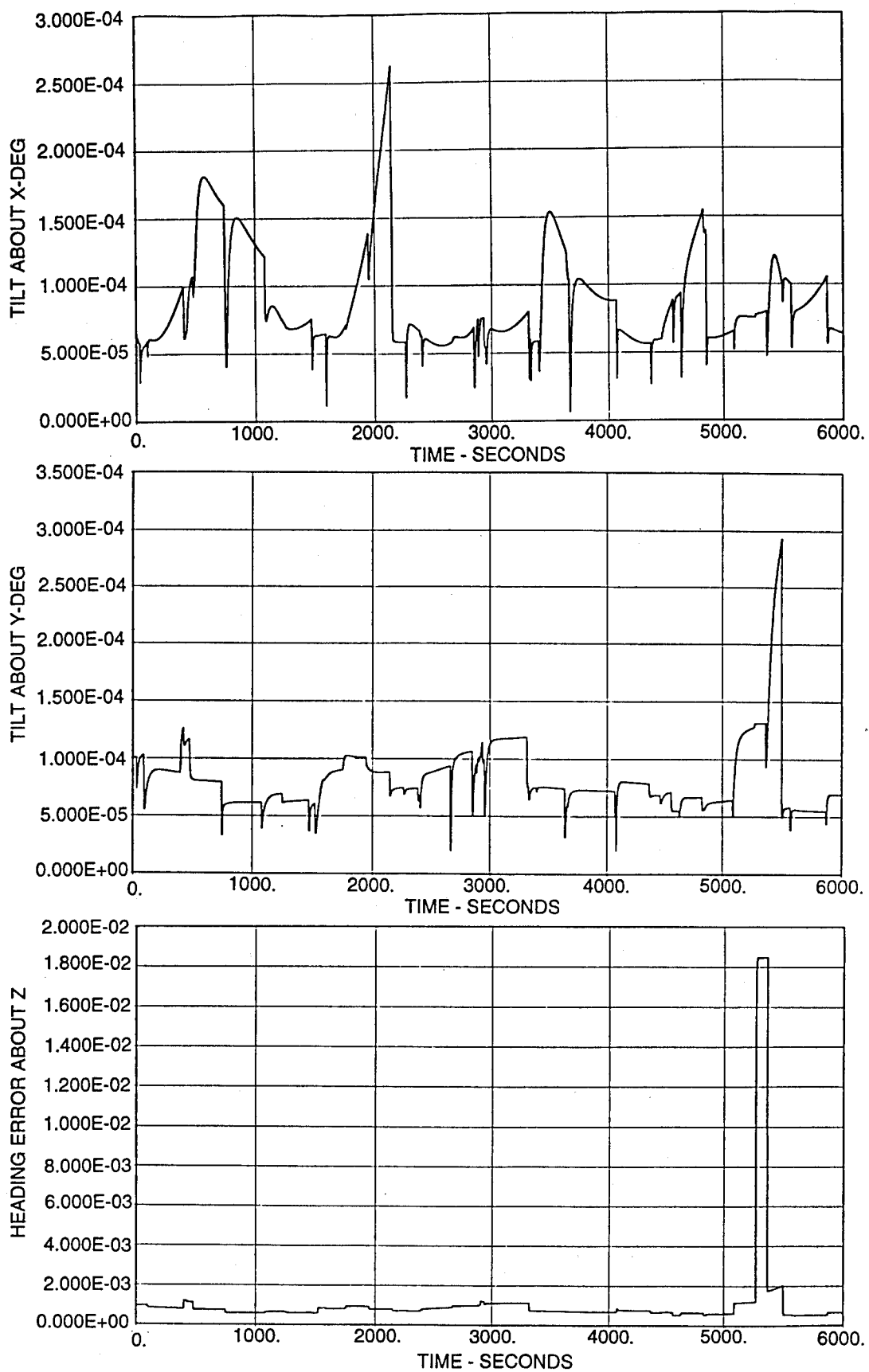


Figure 4. Tilt and Heading Errors Due to GPS Errors (1σ)

Errors in the determination of misalignment of BODY axes from LVOP axes (i.e. orbital gyrocompassing errors) were evaluated in terms of spectral information and the gyrocompassing mechanization transfer function. The error sources are horizon sensor white noise in both roll and pitch, and gyro bias and random walk for the roll, pitch, and yaw gyros. Their resulting rms values are listed under "gyrocompassing contribution" in Table I. They are rms values which are independent of time. These errors and the GPS based LVOP tilt and heading errors are deemed to be independent, so the total attitude error can be evaluated by simple rss methods. However, the tilt and heading errors are square roots of covariances which vary with time. In order to have a representative overall value, each tilt plot and the heading error plot were reviewed and an estimated representative value was determined. Since these plots were generated using parameters of the high accuracy PPS mode, a multiplying factor of 10 was applied to account for the lower S.A. accuracy level. The resulting representative values (including the factor of 10) are listed in Table I under "GPS contribution." Table I also contains a third column where gyrocompassing and GPS contributions are combined (rss) for each axis, and a final entry combining (rss) the total error about the three axes to give a total overall attitude error. The value, 0.018° , shows that attitude determination accuracy is within spec.

Table I. Attitude Determination Error

| | GPS Contribution* | Gyro- compassing Contribution | rss of Contributions | Total Attitude Determin- ation Error |
|--------------------|----------------------|-------------------------------------|-------------------------|---|
| Roll (about x) | 0.0012 | 0.00076 | 0.0014 | } 0.018° |
| Pitch (about y) | 0.0010 | 0.00050 | 0.0011 | |
| Yaw (about z) | 0.0150 | 0.00913 | 0.0176 | |

* Contains adjustment for S.A. - see text.

BACKUP NAVIGATION MODE

The GPS receiver (in actual fact there are two - a primary and a secondary receiver) on-board P91-1 is a tremendous asset. Very significant performance enhancements and lowered ground support requirements are obtained. However, there is a downside. There is always the possibility that GPS supplied information will cease being available. This could happen because of a malfunction of the receiver itself, because of radiation induced problems, because of antenna blockage, or for other as yet unknown reasons. It was realized early-on that prudence required that some sort of a backup navigation capability be implemented. The original purpose was to provide the necessary information to get the secondary receiver up, initialized and running in the event of failure of the primary receiver. But there are other reasons for having a backup navigation capability. The GPS receiver has the capability to maintain a navigation solution by integrating gravity which will carry the P91-1 vehicle through short

periods of mild radiation exposure causing loss of signals. However, in a protracted period of loss of GPS two functions must be maintained or the satellite will die. These are keeping the solar arrays pointed well enough to charge the batteries and maintaining sufficient knowledge of the earth's magnetic field to support momentum dumping which is required if the attitude control system is to continue functioning. Backup navigation supports these two functions very well.

The scheme for backup navigation is based upon using GPS position and velocity to periodically (once per hour so as to avoid senescence) compute and store a set of orbit elements. Then when there is a time of GPS non-availability the orbit elements can be used to provide temporary degraded navigation data. Such a source of information could be used to initialize the secondary GPS receiver if position and velocity were transformed to the ECEF coordinate frame.

The implementation of the orbit element computation is very straightforward (Reference 6) and requires no elaboration here. The other aspect, that of using the orbit elements to compute vehicle position and velocity, was implemented using a scheme found in many GPS receivers (Reference 3). It will not be discussed in any detail here, but the performance seems to be more than adequate. The precession of the ascending node is modeled so that earth's oblateness is accounted for. This mechanization was run for over three orbits along with a high fidelity orbit propagator - both starting from the same initial condition. The maximum difference between the respective position outputs occurred in the y position component and had a value of approximately 0.10 meters. For velocity, the maximum difference occurred in the z component and had a value of 10-4 meters per second. These two plots are shown in Figure 5. The growing oscillation nature of the error is believed to be due to numerical precision. The high fidelity propagator was a FORTRAN based program, while the flight software simulation was compiled from C code. The accuracy of the backup navigation information appears to be very good.

ACKNOWLEDGMENTS

The author would like to gratefully thank Tom Witham, Ken Ryan, and Cliff Kelly for applying their expertise to getting the error analysis results out of the computer, Sherry Whetzel for her magic in producing the finished paper, Hari Hablani for his valuable suggestions, and P91-1 management, namely Jim Jansz, Wil Swan, Dave Triplett, Frank Rotter and Cliff Rogers, for their encouragement and help.

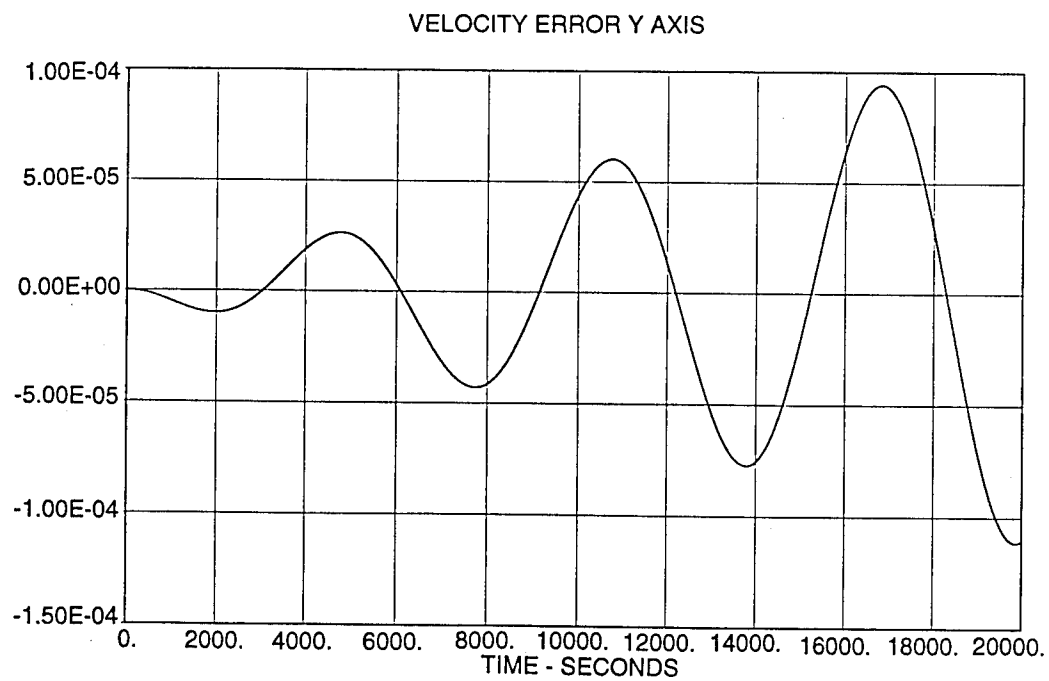
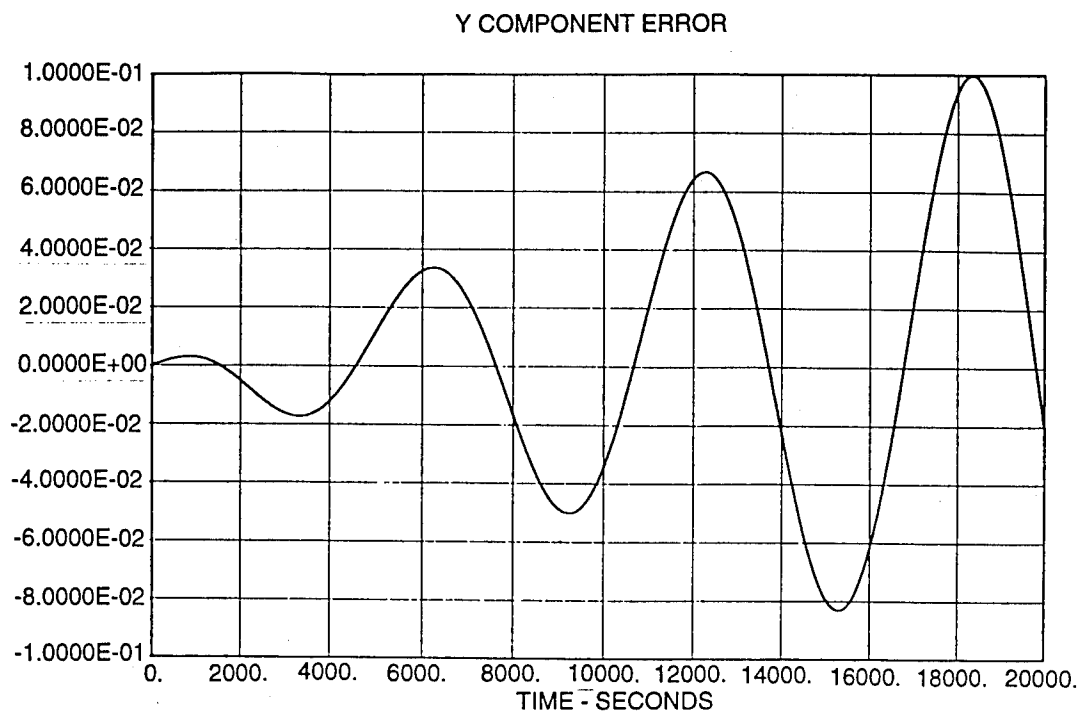


Figure 5. Maximum Position and Velocity Errors of Backup Navigation Mode

CONCLUSIONS

It has been shown that a GPS sensor in combination with orbital gyrocompassing can be an effective means of attitude determination for an earth pointing satellite in a circular orbit. The quality of attitude knowledge produced is comparable to that produced by a system utilizing a star sensor. Ground tracking cost is greatly reduced, as in on-board navigation software cost. However, a simple backup navigation capability is retained which shows quite good performance.

REFERENCES

1. Defense Mapping Agency Technical Report (DMA TR8350.2, 30 Sept. 1987), "Department of Defense World Geodetic System, 1984."
2. Seidelmann, P. K. (Ed.), "Explanatory Supplement to the Astronomical Almanac," University Science Books, Mill Valley, CA, 1992.
3. Leick, Alfred, GPS Satellite Surveying, Wiley-Interscience, 1990.
4. Lyons, M.G., and D. B. DeBra, "A Reduced State Estimator for Orbital Heading Reference," Journal of Spacecraft, Vol. II, No. 2, February 1974.
5. Wertz, J. R. (editor), "Spacecraft Attitude Determination and Control," D. Reidel Co., Boston, 1978.
6. Bate, R., D. Mueller and J. White, "Fundamentals of Astrodynamics," Dover Publications, 1971.

Experimental Results of Using the GPS for SFU Onboard Navigation

Tsutomu Ichikawa and Keiken Ninomiya
The Institute of Space and Astronautical Science

Susumu Kumagai and Masaki Mistutake
Hitachi, Ltd.

ABSTRACT

SFU (Space Flyer Unit) satellite has been launched by H-II booster on the 18th March 1995. This satellite will rendezvous dock on a space shuttle and return to earth after cruising circular orbit during about nine or ten months. In the point of navigation , it is one of characteristic to carried GPS receiver which we has been developed several years ago.

This paper describe the outline of onboard GPS receiver configuration and functions, and the first experimental results of it's behavior and performance. This GPS receiver is having function of two modes. The one is geometric position determination using four Navstars signal directly, which does not consider the dynamics of the satellite. The other is orbit estimation with using onboard Extended Kalman filter algorithm.

1. OUTLINE OF SFU GPS

Block diagram of SFU with onboard GPS Receiver (GPSR) and antennas (GPSA-1, GPSA-2) is shown in figure-1. GPSR is five channels parallel receiver and single frequency (L1-C/A code) receiver. Resources of GPSR are as below
 mass: about 11 (kg)

Dimensions: about 200x300x180 (mm)

Power consumption: about 34 (watt)

GPSR is connected to two antennas installed the body. And FOV of each antenna is about 160 degrees as shown figure-2. The signals from two antennas are down converted into intermediate frequency at RF (Radio Frequency) section and distributed to five channels of synchronization of spread spectrum signals and acquisition, tracking, measurement of pseudo range/pseudo range-rate and demodulating GPS

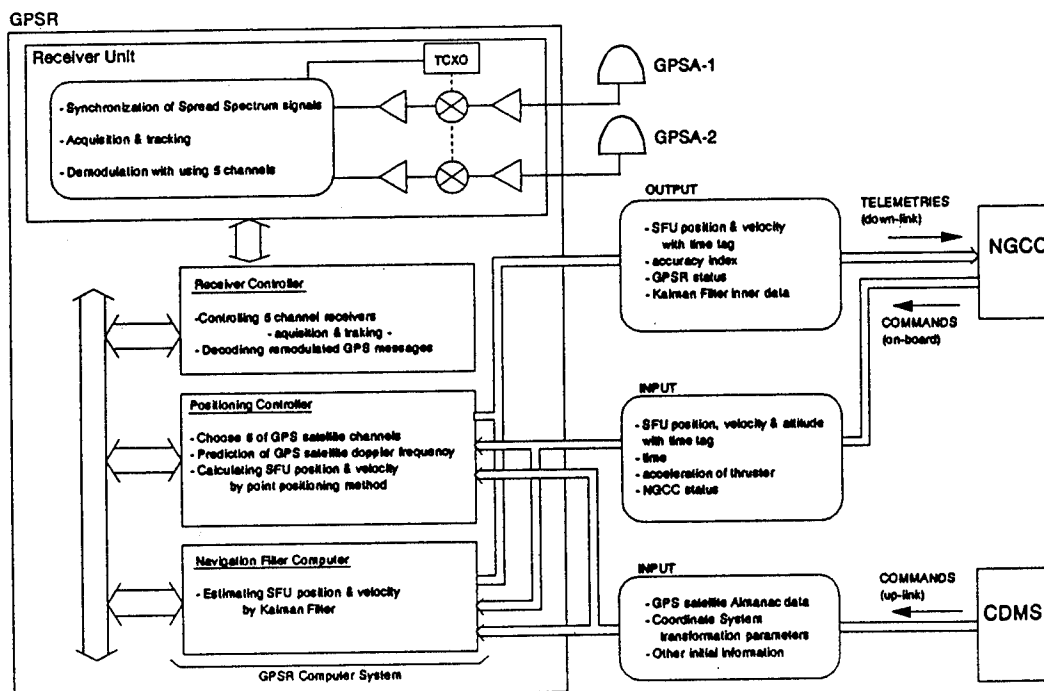


Figure-1 SFU GPS block diagram

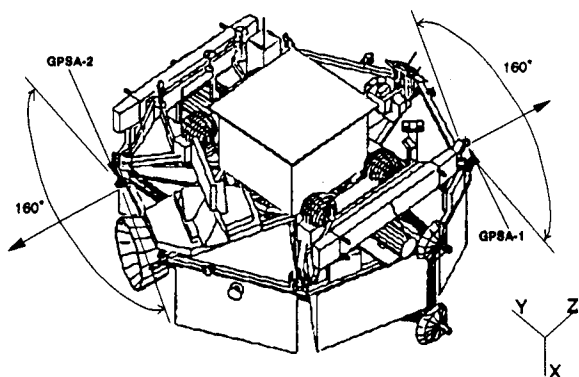


Figure-2 GPSA FOV

messages are performed.

Three microcomputers are installed in GPSR to form a multiprocessor sharing the function. There are Positioning controller, Receiver controller, and Navigation filter computer.

Positioning controller is main computer system of GPSR. This controller perform two main tasks which are the acquisition/tracking control and the point positioning navigation.

(1) Acquisition/tracking control : Positioning controller chooses five GPS satellites (Navstars) and select antenna which set up the body for each channel And it predicts Doppler frequency of each channel by processing the signal of GPS satellites while utilizing the orbit elements and attitude data simultaneously. The update results is controlled this system.

(2) Point positioning navigation : Point positioning navigation is simply geometric navigation using four GPS satellites ranging data. The results of point positioning navigation includes SFU orbital elements and clock bias/drift of GPSR system clock (TCXO). Then Positioning Controller uses them for acquisition and tracking control and achieve the short time acquisition by the precise prediction of Doppler frequency.

Receiver controller controls each channel hardware following the commands from Positioning controller. And then Receiver controller readout GPS messages and ranging data which is measured each channel. Positioning controller and Navigation filter computer use the GPS messages and ranging data for each navigation process.

Navigation filter computer estimates orbit elements of SFU with Extended Kalman filter (EKF). The EKF has SFU dynamics model and GPSR clock model. And it performs time update and observation update using a observation

model.

Positioning controller and Navigation filter computer operates independently. Namely, GPSR always keeps two navigation results which are point positioning data and the estimation data. But GPSR telemetry has the area for only one navigation result. Therefore GPSR has two telemetry modes (point positioning mode and filter mode). The telemetry mode is changed by up-link commands.

2. ACQUISITION AND TRACKING ON ORBIT

When GPSR acquire GPS satellite signals during cruising the orbit, the range of Doppler frequency signals is about 100 kHz. It is about ten times as wide as one on the ground receiver. If GPSR does not predict the precise Doppler frequency, it is impossible to acquire the signal from the GPS satellite. In such this case, it is guessed that the frequency prediction error which causes from clock bias/drift of GPSR is occurred. There are orbit elements errors of SFU and the GPS satellites too as other source.

We classify the accuracy of frequency prediction into two levels. The first level is start up condition in which the clock bias/drift errors of GPSR are unknown and SFU orbit elements errors are coarse. The second level is tracking condition in which the clock bias/drift errors of GPSR and SFU orbital elements error are reduced. Then the precise orbit can be determined. Namely, navigation status is successful.

It is explained the method of GPSR receiving process in Start-up mode and Tracking mode in this section.

2-1 START-UP MODE PROCESS

After GPSR is turned on, GPSR does not have sufficient data for start-up. At GPSR start-up operation, GPSR receives up-link commands containing data for start-up (almanac data elements for the GPS Satellites and parameters for transformation of time/coordinate systems).

Almanac data elements in the commands give the orbit elements in WGS84 coordinate system of the first acquisition GPS satellites. And parameters for transformation of time/coordinate systems in the commands make the coordinate systems transformation between WGS84 and EME50. EME50 is the inertial coordinate system which is NGCS (Navigation and Guidance Control Subsystem) interface coordinate system and is used to describe SFU dynamics.

At first, GPSR calculates the visibility and Doppler Frequency of two GPS satellites using almanac, coarse SFU

orbital elements and its attitude elements.

The coarse SFU orbit and attitude elements are given by NGCC (Navigation and Guidance Control Computer) which is the main computer of NGCS. The attitude data is used to derive the view of each GPSA.

And then GPSR tries the first acquisition using all (five) channels. At the start-up mode, the Doppler frequency prediction is inaccurate data in usually. We estimate the error is 10kHz at maximum. Then using five channels, GPSR has five times wide pull in range. The range is enough to acquire the signal under the start-up condition. After first acquisition, GPSR measure the real Doppler frequency and compensate the Doppler frequency prediction. Then GPSR can acquire the second GPS satellite signal using less than five channels (tracking channels can not use for signal acquisition).

Tracking the signals of the first two GPS satellites, GPSR takes the almanac elements of other GPS satellites. And GPSR predict the third and the fourth GPS satellite data. Four GPS satellites signals can be received sequentially.

At start-up mode, Navigation filter computer is driven by using initial state vector of EKF which is provided the coarse orbital elements from NGCC with onboard.

2-2 TRACKING MODE PROCESS

When receiving four GPS satellites signals, GPSR start point positioning task. Then GPSR shift to tracking mode. At tracking mode, the prediction data is accurate because GPSR uses navigation results (orbit elements, clock bias/drift of GPSR) in order to predict the Doppler frequency. GPSR can acquire the GPS satellite signals easily. So, GPSR tries to keep GDOP lower controlling the five channels.

At tracking mode, Navigation filter computer can be driven by using EKF which given initial states from the point positioning result .

2-3 RESULT OF ACQUISITION AND TRACKING

The result of acquisition and tracking is shown in figure 3 and figure-4. GPSR shifted to start-up mode at 16:40 (UTC) on 19th, March, 1995. About eight minutes later, GPSR shifted to tracking mode and started to control GDOP. Then we confirmed that GDOP was almost kept less than four after 17:00 (UTC). When GDOP exceed four in some points, one channel lock loss occurred and GPSR calculated using the combination of remained four channels, in which the GDOP was greater than four. We confirmed that GPSR acquisition and tracking operation was under good condition.

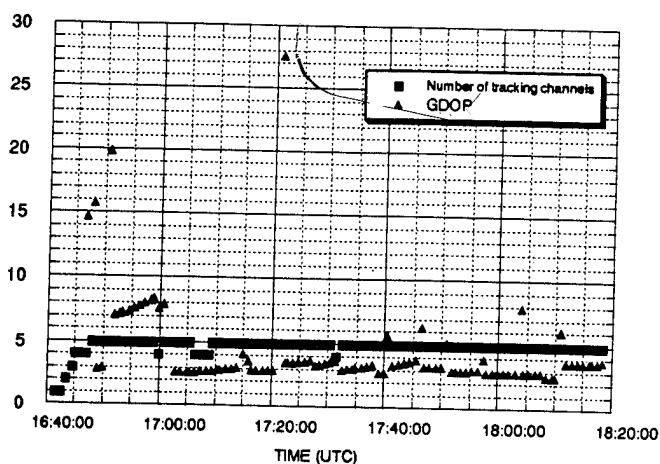


Figure-3 START-UP and TRACKING Results

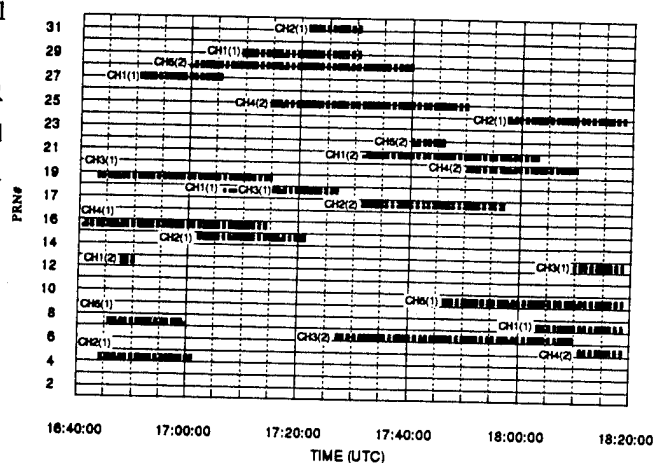


Figure-4 GPS satellites selection results

3. NAVIGATION RESULTS

GPSR was operated during the initial operation phase of SFU, in which the main functions of SFU (communication, attitude control, power management, etc.) was checked out and SFU was transferred into nominal circular orbit (Altitude : about 500 km). Finishing the initial operation phase, SFU operation was shifted to the mission phase and GPSR was turned off at the same time because of preserving electric power and controlling thermal condition.

At the initial operation phase, we checked the function of GPSR mainly. But we did not evaluate the navigation performance enough, because the amount of GPSR telemetries was controlled lower to keep main mission data of SFU and the Earth-based orbit determination (OD) data were not sufficient for the evaluation yet.

Therefore we describe the rough evaluation results (First experiment result) in this paper. They are the comparison between the orbit elements of GPSR navigation and the

Earth-based orbit determination results by using radiometric data. But the Earth-based orbit determination did not use enough radiometric data. So, the comparison results include the unknown error of Earth-based OD. And the comparison results has unknown bias. We confirm only the dispersion of navigation results.

The quantitative analysis of GPS navigation performance will start from this September after finished the mission phase of SFU.

3-1 POINT POSITIONING RESULTS

The results of point positioning navigation of GPSR are shown in figure-5. Figure-5 plots point position navigation errors against the Earth-based OD and GDOP as a function of time. In figure-5, the relations between the navigation error and GDOP are clear, and GPSR almost kept GDOP less than four.

The variance of the position error is less than about 200 meters and the bias error is about 400 meters. The tracking direction errors account for the majority part of the bias errors and the radial direction errors and outer plane direction errors scarcely include bias components. Therefore, it is estimated that the bias error mainly occurred from the propagation error of the Earth-based OD or time estimation error of point positioning.

Point positioning navigation has no countermeasure for Selective Availability (SA). We consider the navigation results of point positioning which include the effect of SA are reasonable.

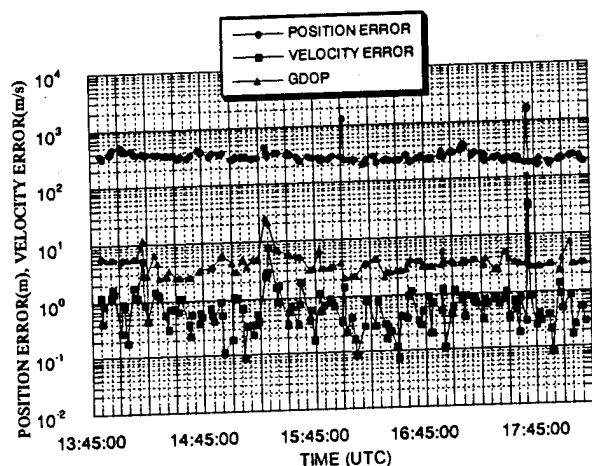


Figure-5 Comparison between Point Positioning and Earth- based OD

3-2 EXTENDED KALMAN FILTER ESTIMATION RESULTS

The results of EKF with onboard navigation of GPSR are shown in figure-6. Figure-6 plots point position navigation errors against the Earth-based OD and accuracy index as a function of time. Accuracy index indicates the mode of EKF algorithm. When the accuracy index is less than two, the EKF estimates the orbit elements under the no limitation condition (no overflow, no over thresholds). Therefore, EKF calculate estimation parameter in the stable condition.

Checking the telemetries of GPSR, we confirmed the EKF software operate normally on orbit.

In figure-6, accuracy index became less than two after 4:50 (UTC). Before 4:50, accuracy index almost greater than two, and the estimation error was discontinuous at 4:40. At 4:40, the self-reset of the EKF was occurred which was caused by limitation over of covariance in the EKF. After the self-reset, the EKF took in the point positioning result for initial states and restarted the estimation.

The covariance of the position error is less than about 200 meters. It is the same level as point positioning error. But the errors were varied smoothly as a function of time.

In figure-6, it is difficult to consider about the bias error, because the amount of the estimation data is poor. The period of SFU orbit is about one hour and half, then we need more than three hours data in which accuracy index is less than two. But we have not gotten enough data.

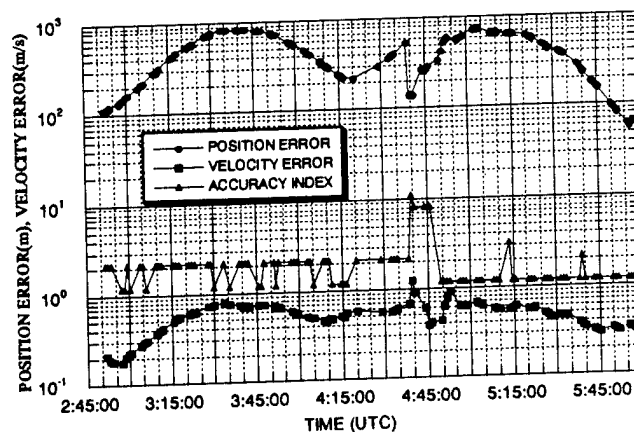


Figure-6 Comparison between EKF navigation and Earth-based OD

CONCLUDING AND REMARKS

In this paper we describe consists of GPSR with onboard microcomputer and the first experimental results in orbit.

Navigation results by using point position mode or the filter mode which approach Extended Kalman Filter are reasonable at first experimental situation. In terms of the accuracy, it is evaluated by comparison with Earth-based orbit solution based on radiometric data. These results are relativity because each other result with covariance include several disturbances (measurement noise, system noise, geometrical observation condition, and so on). We plan the detail experiment for autonomous navigation with onboard GPSR in this month. The outline of experiment is shown as following.

(1) The Extended Kalman Filter parameter set up optimization.

(2) Navigation, guidance and control: This experiment carried out to connect NGC system. After small orbitmaneuver execution, the filter is provided a measurement value from NGC which utilized the accelerometer and estimate a posteriori orbit elements and maneuver parameter.

(3) Differential GPS experiment: We experiment on between ground GPS receiver and onboard GPS receiver. There is reason to expect that the effect of SA and the troposphere is evaluated.

We would like to update the evaluation and analysis to onboad GPS at the result of experiment in this month. This research contribute to the autonomous navigation in future satellite.

ACKNOWLEDGMENTS

The author acknowledges the tracking support and orbit determination task to SFU of JPL Navigation team and NASDA (Japan) tracking support team.

REFERENCES

- (1) Joan B.Dunham, "Mathematical Specifications of the Onboard Navigation Package (ONPAC) Simulator (REVISION.1)", NASA-TM-84797, Feb.1981.
- (2) Howard Heuberger, "Performance of the GPS Package on LANDSAT-5", IEEE Position Location and Navigation Symp. , 1984
- (3) R. Steven Nerem, "Expected Orbit Determination Performance for the TOPEX/Poseidon Mission", IEEE Trans. on Geoscience and Remote sensing, 1993
- (4) G. J. Bierman, "Factorization Method for Discrete

Sequential Estimation", Academic Press, 1977

- (5) T. Nishimura, "Error Bonus of Continuous Kalman Filters and the Application to Orbit Determination Problems", IEEE Trans. AC, 1967

A Practical Demonstration of Low Cost Autonomous Orbit Determination Using GPS

Martin Unwin and Martin Sweeting
University of Surrey

BIOGRAPHIES

Martin Unwin is completing his Ph.D. in the University of Surrey, UK on the subject of GPS applications for microsatellites. As part of his studies, he has implemented and is managing the GPS experiment on both the PoSAT-1 and the FASat-Alfa microsatellites. He received his B.Sc. in Physical Electronic Engineering from Lancaster University in 1989 and worked for two years at Thorn EMI Electronics on microwave design. Martin Unwin has won student prizes at the ION GPS-93, DSNS 94 and IAF 94 conferences.

Martin Sweeting is the deputy Director of the Centre for Satellite Engineering Research at the University of Surrey. He has been responsible for all of the eleven UoSAT missions since UoSAT-1 in 1980, and is the Managing Director and CEO of Surrey Satellite Technology Limited, also based at the University of Surrey. Professor Sweeting was recently awarded an OBE and a Royal Academy of Engineering medal for his pioneering work in satellite engineering.

ABSTRACT

The GPS Navigation Unit experiment on the PoSAT-1 microsatellite has been operating successfully since the satellite's launch in September 1993. The primary aims of the experiment are to develop a low-cost and precise means of tracking a satellite as an alternative to the use of published NORAD orbital elements. PoSAT-1 is the first microsatellite to make use of a GPS receiver and the first satellite of any kind to generate autonomously its own orbital elements using GPS.

Orbital elements are required both on the ground and in space. Ground-stations require elements for mission operations planning. The spacecraft's attitude determination and control system (ADCS) also requires knowledge of position. The performance of magnetometer and star-sensor-based ADCS is greatly enhanced when on-board position estimates are improved to the level of 1 km accuracy or better. In all

cases, this can be obtained most simply by having an autonomous orbit determination capability on-board the satellite itself. The payloads that satellites carry, from communications to space science, have widely varying position accuracy requirements, but elements generated from GPS data are able to meet most of these needs directly.

There are many cases when a small satellite cannot spare the power to operate a GPS receiver continuously. Fortunately, to maintain a reasonable estimate of the orbit, this is actually not necessary. The experiment on PoSAT-1 demonstrates the ability of a small satellite to determine its own orbit autonomously through an intermittently-operated GPS receiver.

This paper discusses the system design of an autonomous Navigation Unit suitable for a small satellite based on a GPS receiver. The performance of the Trimble TANS GPS receiver on board PoSAT-1 is discussed, and also the on-board control of the receiver and the processing of the GPS data. The accuracy of the raw GPS data is evaluated, along with the accuracy of the final determined orbit. Comparisons are made to NORAD elements, and to alternative tracking methods. Finally an experimental demonstration of autonomous operation through the implementation of the GPS Navigation Unit is described.

INTRODUCTION

Satellites have found many applications in science, communications and remote sensing. The traditional large satellite is now being challenged by a smaller variety, which is sometimes just as capable, but quicker and cheaper to develop. Such small satellites can make use of the latest terrestrial technologies and advances in microprocessors to give more flexibility and enhance capabilities.

One of the major costs associated with the space industry is the operation and control of satellites. The cost of some ground stations may be as much as \$1000 per satellite pass for tracking and telemetry functions.¹

Therefore there is a desire to give satellites as much autonomy as possible, with reduced requirements on the ground station. This would also benefit future planned communications constellations that are likely to suffer from complexity of operations due to the number of satellites under control from one ground station.

The use of GPS on a satellite to provide autonomous navigation (or self-tracking) was foreseen in the 1970s² but it is only recently that the GPS constellation has been completed and the receiver technology has become suitable for such a practical application.³ On-board GPS offers many advantages over ground-based ranging and other tracking techniques. The small size and low cost of the hardware, the global coverage and the high performance of the tracking and the operational convenience make GPS an ideal self-tracking sub-system for small satellites. GPS offers the potential for orbit determination, time transfer and experimental scheduling by position, and ultimately the potential for attitude determination and control, and even autonomous orbit maintenance.

Autonomous tracking systems do not have to be implemented on-board the satellite, and the automated ground-based processing of downloaded logged GPS data may be suitable, and potentially provides far more accuracy.⁴ However, commercial missions usually have a limited down-link bandwidth, and an on-board method of reducing the tracking information may be vital.

AUTONOMY IN THE UOSAT MISSIONS

The University of Surrey in the UK has pioneered the construction and use of microsatellites. A commercial company, Surrey Satellite Technology Ltd, has grown to develop and market these satellites and to date, eleven satellites have been launched, recently at a rate of two per year. The satellites may carry communications or remote sensing payloads or may be part of a technology transfer programme. The UoSAT microsatellites are a good example of the smaller, faster, cheaper ethos and they also demonstrate relative autonomy of the satellite.

As the programs typically take only 12 months from contract to launch, new technologies can be flown promptly. The short time scales, amongst other factors, lead to a lower cost: a satellite may cost only \$3m including launch. While the satellites are typically only 50 kg, they carry plenty of advanced technologies, such as GaAs solar cells, CCD cameras and star sensors. The layering of new technologies over tried and tested architecture improves the reliability, while not compromising the research. FASat-Alfa, the latest

microsatellite, carries 20 microprocessors giving great flexibility and processing power.

The ground station requirements for a UoSAT microsatellite are minimal, being based on three PCs, a transceiver, a modem and a steerable mast antenna. At the ground station in Surrey, there are two antenna channels. Six satellites are actively under control, while another three satellites are being monitored. Most of the operations are autonomous, with ADCS (attitude determination control system) software, power load optimisation software and other housekeeping tasks continually active on the main OBC (On-board computer). Most information on the satellite is handled in terms of files, and these are stored in the satellite RAM-Disk. The store and forward communications messages, the experimental data and the telemetry log-files are all downloaded automatically through a no-data-loss packet protocol. Within the ground station, this data is unpacked, processed and archived without the need for any supervision. If a problem should occur, for example a telemetry value out of range, then a pager will alert the duty officer.

As part of an Air Force contract, JPL developed a scale of 0-11 to describe the level of autonomy of a satellite.⁵ Many satellites cannot store software and timed command sequences, and so are classified as Level 1 or 2. The latest UoSAT spacecraft fall into the category of Level 4, even though this does not take into account the ground station autonomy.

At present, there are still some operations that need user input. Every day or so, the clocks on all of the satellite OBCs are synchronised from the ground using the station's GPS receiver. Every week, new orbital elements originating from NORAD are uploaded to the satellites to broadcast to all users and to maintain the ADCS magnetometer IGRF model accuracy. About once every ten days, new *sched-files* which schedule commands and events according to time must be uploaded to specify the telemetry logging regime. Sched-files are also used to operate payloads and experiments.

This level of operational autonomy has been developed over a number years, and has helped to reduce the work-load of the ground-station operator. The satellite OBC operating system and software has been developed to give a high level of integrity: the OBC ran on UoSAT-3 for over three years before needing a software re-load. If the OBC program does crash then the spacecraft is in little danger. The hardware telemetry and telecommand system continues to operate, and the operating system and OBC software can usually be re-loaded from the ground within a couple of satellite passes.

GPS offers the means to increase the autonomy by eliminating the two remaining regular interactions with the ground: setting the OBC clocks and providing mean orbital elements. The use of GPS may further assist in the scheduling of payloads through triggering by position.

The GPS experiment on PoSAT-1 has been used to prove some of these capabilities, and future UoSAT-class microsattellites will also carry GPS receivers, moving the sub-system from experimental to operational status.

THE GPS NAVIGATION UNIT

A GPS receiver on a satellite has special requirements, not only in terms of internal algorithms, but also the external operation and control. A small satellite has demanding power constraints, and so the GPS receiver should be operated intermittently. Mean orbital elements must be generated from the GPS data, and the position propagated as required during the time that the receiver is off. If the clocks are to be synchronised to GPS time, then the regularity must be established and controllable. If on-board autonomy is to be achieved, then the capability for scheduling these events and facilities must be included.

To provide a structured framework for the implementation of these facilities, the concept of the GPS Navigation Unit was defined.⁶ This is a satellite sub-system based on a low-cost commercial GPS receiver (modified for orbital operation) supported by a computer system for receiver control and processing of the data. The fundamental purpose of the Navigation Unit is to provide a set of services to the satellite. A number of example small satellite missions were considered that could make use of such a sub-system. These missions included store and forward messaging satellites, real-time communication satellites, and low and high resolution remote sensing satellites. The requirements from these missions were compiled into a list of services as follows:

- Position, velocity, time.
- GPS Measurement data logging.
- Clock Synchronisation.
- Mean Orbital Element Generation.
- Data Logging.
- Payload Triggering by position.
- Status Monitoring.

The characteristics of each of these services were analysed in terms of accuracy, operational mode and format options. A system design was then developed that took into account the practicalities of the operation

of a GPS receiver and the environment of a typical small satellite.

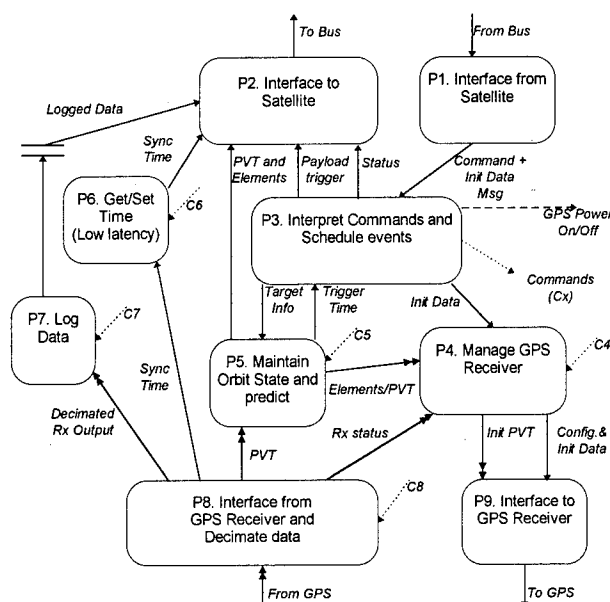


Figure 1: Data Flow Diagram Level 1 for the GPS Navigation Unit

The method for the system design was largely based on the commonly used structured design and analysis technique.⁷ This method orients the development in the information domain and models data flow through a series of processes. Figure 1 shows the Data Flow Diagram for the GPS Navigation Unit. The rounded boxes represent processes, and the solid lines are data items.

The processes can fairly directly be translated into software modules, and the real-time nature of the problem dictates that modules will be either interrupt driven or parallel tasks, depending on the specific implementation environment. The main module of the GPS Navigation Unit is P3, which is responsible for interpreting commands and scheduling events. The events include the periodic operation of the GPS receiver through telecommand, the periodic generation of mean orbital elements and the issuing of payload trigger commands. Subordinate modules are commanded by P3 to fulfil these functions, and these command lines are represented by the dotted lines labelled Cx.

The data items are expanded in a requirements dictionary to specify exactly what information is required in which module. Further partitioning of the modules is necessary, and, and each of the processes is broken down into lower level Data Flow Diagrams. To translate this into practical software, development in terms of State Transition Diagrams and flow charts was necessary. The interfaces of the GPS Navigation Unit were defined to provide the services to the satellite and also to program the Unit.

POSAT-1 GPS RECEIVER PERFORMANCE

The GPS experiment on PoSAT-1 provides an opportunity for implementation of the GPS Navigation Unit concept as well as more general research into the use of GPS in orbit.⁸ PoSAT-1 was launched in September 1993 on the Ariane V59 flight into an 800 km circular orbit with an inclination of 98°.

The GPS receiver is a 6 channel C/A code Trimble TANS Sensor, and it is operated through software running on the Transputer Data Processing Unit. The receiver is a version of a commercial model with orbital firmware, and is made from industrial-rated parts. The transputer T800 is a 32-bit RISC architecture microprocessor that operates at 20 MHz and contains a built in floating point unit. The GPS antenna is a Trimble-supplied active Teflon patch which is mounted on the +Z-facet of the satellite. There are a number of protrusions on the satellite that will tend to block the GPS signals, including the boom and the horizon sensors, but static ground-based tests indicated that GPS position fixes could be made for 99% of the time.

The performance of the GPS receiver was characterised in terms of number of GPS satellites tracked, percentage time of position fixes and Time To First Fix (TTFF). These figures depend on a large number of factors, including GPS receiver hardware, firmware, initialisation, antenna visibility and satellite orbit. However, they give a good indication of the operation of the GPS receiver and can be compared with ground-based tests.

Table 1: Tracking performance for typical run

| | |
|--------------------------|-----------------|
| 4 or more GPS satellites | 86% of the time |
| 5 or more GPS satellites | 54% |
| 6 or more GPS satellites | 13% |

Table 1 summarises the orbital tracking performance from a continuous 3 hour GPS operation. Ground tests on a model of the PoSAT-1 +Z-facet gave figures of 97-99% for 4 or more satellites. However, in ground-based mode, the receiver is able to track 8 satellites through multiplexing of some of the 6 channels, whereas in space, only 6 satellites are tracked. Therefore a degradation is expected.

The position fix performance has been monitored separately over a period of many operations, and gives the results shown in Table 2.

Table 2: Position Fix Performance

| | |
|--------------------------|-----------------|
| 3-D Position Fix (LEO) | 84% of the time |
| 3-D Position Fix (Bench) | 99% |

In some operations, it has been noted that the position fix performance does fall below 70%, especially if the position initialisation is not optimal. The gaps that occur between position fixes rarely seem to be longer than 30 seconds, and so the data is well spread over the orbit. For most medium accuracy applications, even a fix rate of only once every 30 seconds would be adequate. It therefore appears that there is plenty of margin in the antenna visibility pattern, and future similar missions should have a good margin for useful operation.

The Time to First Fix is a common measure of a GPS receiver initialisation performance, and is of particular interest for orbital applications, where the initialisation is complicated by the user velocity. The TANS is initialised by supplying time and GPS Almanac and a set of orbital elements that enable the prediction of the position by the receiver. The propagator in the receiver tends to drift with time, and so the elements had to be supplied with an up-to-date epoch to the GPS receiver. This means that the GPS receiver cannot sustain operation for more than a few days without re-initialisation, however, it is understood that the latest firmware for the orbital TANS now automatically updates the internal osculating elements for initialisation from its position fixes.

Once the mechanism for initialisation had been established in the controlling software, the TTFF performance has been consistent and fast. In Figure 2, some example TTFFs are shown as the GPS Almanac ages. Operations with even older Almanacs, in one case five months old, indicates that the TTFF is not very sensitive with Almanac age. However, the old Almanac would be likely to become unreliable if the GPS satellites perform orbital manoeuvres as might be expected every six months or so.

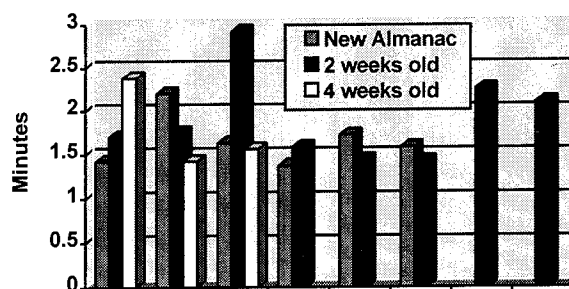


Figure 2: Time to First Fix

POSITION FIX ACCURACY

The Trimble TANS receiver is able to produce both position fixes and the raw measurement data, but for on-board medium accuracy applications, the position

fixes are the most straight-forward data to use. No phase data is available from the single antenna version of the receiver.

The position and velocity fixes were analysed through conversion to orbital elements. The Selective Availability characteristic wandering was visible, as was the lower level noise floor of the measurements themselves. However, a more serious source of error was that from time to time, a single data point was to be observed to be several kilometres different from the rest of the data. These outlying points appear to be caused by bad measurement time-tag handling when satellites are changed over, and typically there is a 0.2 second timing error. When a 3-sigma outlier removal algorithm was tried out an orbit of the data, about 1% of data was removed. Another anomaly that has been observed only on a couple of occasions is a gross error of perhaps 100s of kilometres which may continue for a number of readings before the satellite selection is changed. An obvious symptom for this is when the clock drift term jumps to another value quite different from its normal bias rate. Further investigation is required to find the cause of this error.

Apart from these receiver-specific anomalies the GPS data does appear to be as accurate as theory states that it should be. To verify the accuracy, a request was made with a UK-based satellite tracking facility to track PoSAT while the GPS experiment was operating. Figure 3 illustrates some of the radar data points made available for analysis.



Figure 3: Radar Tracking of PoSAT-1

The GPS solutions were propagated to the radar points, and GPS/radar residuals derived and rotated into an axis aligned with the radar range. This is because the accuracy of the radar measurements is considerably

better in the range axis than in its other axes, and it is only the range that has comparable accuracy to stand-alone GPS measurements. For the purpose of these comparisons, the outlying GPS points were removed from the data.

Figure 4 shows the results from one pass expressed in range, satellite-velocity and cross-track components (1σ RMS). It can be seen that the range residual is by far the smallest, and typically varies from 20-70 metres. The other axes show increasing errors at the beginning and the end of the pass, characteristic of radar angular uncertainties. The range measurement of the radar is almost certainly more accurate than the GPS measurement, so this residual then is a measure of the GPS positioning accuracy.

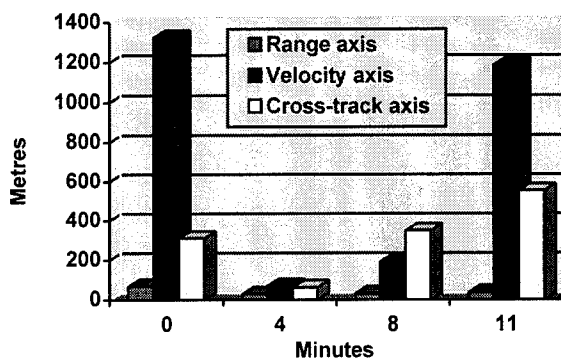


Figure 4: Radar and GPS residuals

Three passes of concurrent GPS and radar data were used for the tracking cross-comparison. Converting the resultant residuals to 3-D 2σ RMS gives 150 metres from the three passes of data used. This compares with 174 metres expected with the ground-based use of GPS.

This is not a rigorous proof of the accuracy of GPS in orbit, as only about 1/2 hour of data has been considered. To obtain stable statistics with GPS, several hours or even days of data are required. Secondly an assumption has been made that GPS has the same characteristics in the two axes other than radar range. This is not strictly true, but is unlikely to be far wrong as the radar range axis rotates significantly with respect to WGS-84 during the course of a satellite pass.

Even so, the comparison has been useful to verify that a low-cost commercial GPS receiver is capable of tracking a satellite to the level of 100 metres.

DEVELOPMENT OF ORBIT DETERMINATION ROUTINE

The system study for the GPS Navigation Unit revealed that for most small satellite applications, the high accuracy of GPS is not necessary on-board, and

an accuracy of 1-5 kilometres is more than adequate to support operations, communications and experiments. What is required from the Navigation Unit is the ability to propagate the orbit to give a medium accuracy while the GPS receiver is off. Another requirement is the generation of orbital elements for the ground based user, preferably compatible with the NORAD elements that have been used until now.

The method that was adopted for implementation made use of the SGP4 analytical propagator (the recommended propagator when using NORAD elements).⁹ The individual position and velocity fixes from the GPS receiver are converted to osculating elements, and transformed into mean elements through the use of the SGP4 propagator. Successive element sets can then be combined over time through a least-squares fit to obtain a single mean orbital element set.

The accuracy of the NORAD element sets for PoSAT were characterised so that valid comparisons could be made between the two sources of elements. It was found that the self-consistency from one set to a set a week later was about 2 kilometres for PoSAT's orbit. Naturally, lower altitude orbits gave worse agreements.

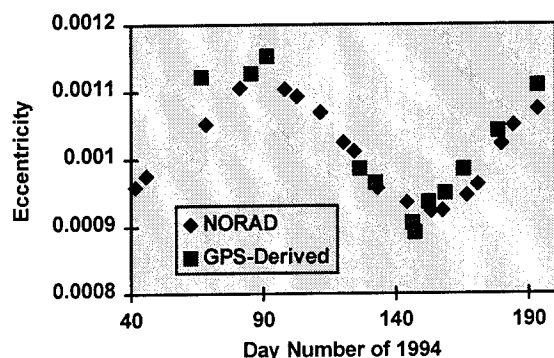


Figure 5 Eccentricity Comparison

Typical experimental operations have seen the GPS receiver being operated for one orbit at a time, and it is from this period of data that the element sets have been generated. The current implementation of the algorithm does not filter the outlying points from the data to reduce the complexity in the autonomous system but still achieves reasonable accuracy. Figure 5 shows the GPS-derived values of eccentricity as compared to the NORAD values. The agreement is generally within 5%, although it appears that the GPS-derived results are more noisy than the NORAD values.

A similar reasonably close agreement was found with all the elements. The GPS-derived elements were then used to predict the position at epoch with SGP4, and this was compared with the prediction based on NORAD elements, Figure 6, and the combined RMS residual over a number of weeks was 1.5 km.

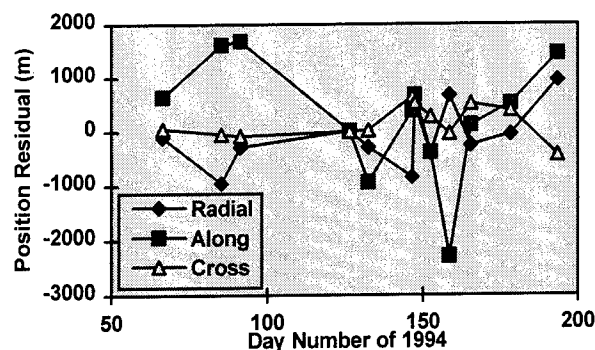


Figure 6 GPS / NORAD Element Set Residuals at Epoch

The only element where the agreement was not entirely satisfactory was the mean motion. This element determines the long term stability of the orbit prediction, and so a greater precision is required than with the other elements. The problem lies in the short sample period of one orbit. The SGP4 propagator does not account for the Earth's sectoral harmonics (slight variation in the shape of the Earth with longitude), and also GPS is less accurate in the radial axis ($159 \text{ metres } 2\sigma$). Longer periods of data would help average out these effects but the autonomous operation of the GPS receiver may be limited to one orbit by power and operational constraints.

The solution to this problem was to use the previous set of elements which would be already stored by the GPS Navigation Unit. This prior element set can be used to lever the data collected and determine a far more accurate mean motion through a least-squares technique. Figure 7 shows the determination of the mean motion with and without the prior weighting compared to the NORAD values.

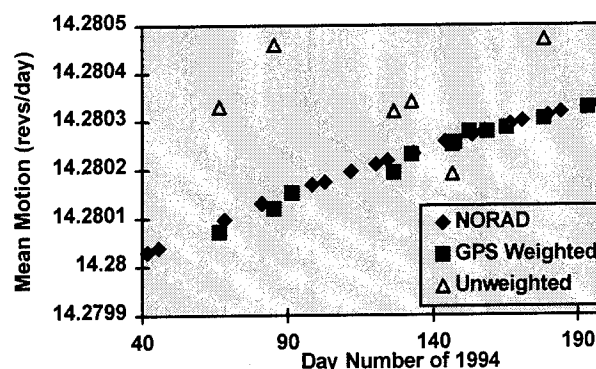


Figure 7 Mean Motion Comparison

The results are good: the comparison between the GPS and the NORAD mean motions gives a mean semi-major axis agreement of 5.3 metres RMS. The discrepancy in the position prediction after 2 weeks is less than 10 kilometres.

Currently the drag term is not being determined in the on-board algorithm as it is found to have a small effect: at PoSAT's altitude, the resultant secular drag causes less than one second delay every two weeks. If the drag is set to an average value, and new elements are generated every week, then the resultant drag error is too small to be noticed. However, when the Navigation Unit is implemented in a lower orbit on a future satellite, or even if the atmospheric density increases at PoSAT's altitude as a result of solar activity, then the drag will have a more significant effect. Therefore, a drag modelling capability will be added in the near future.

IMPLEMENTATION OF NAVIGATION UNIT

As a proof of concept, the GPS Navigation Unit was implemented on the Transputer Data Processing Unit on-board PoSAT-1. The code was written mostly in parallel modules in the Occam programming language with some imported 'C' functions. The use of parallel modules in Occam permits the simple implementation of multitasking on one or more processors without the need for a full-fledged multitasking operating system.

The orbit determination and propagation routine was implemented as described in the previous section. The accuracy of the determination algorithm has been characterised for operation on PoSAT-1 in a flexible manner, either to be operated once a day, or once a week. The numerical algorithms are stable, and a simulation operated successfully on five months of real GPS data. If the Unit tries to use bad prior elements, they are rejected, and the orbit determination algorithm is reset to use only new GPS data. The elements are generated together with a report on the fit quality.

A real-time analysis was performed during the implementation to ensure that the transputer could handle the processing load. The most computationally intensive process is the iterative conversion from position to mean elements, which is performed for every data point, i.e. every second. Through modifying bench test results to account for hardware differences, it was estimated that this process only takes 40 or 80 milliseconds on the transputer hardware, depending on whether the EDAC circuitry is present or not. Therefore, there is a considerable processing margin, and in fact the same code could just about be supported by a transputer with no floating point unit.

While not all of the functions defined for the GPS Navigation Unit have been fully implemented at this stage, the concept has been largely proven in orbit. Specifically, the following services have now been demonstrated on PoSAT-1 from the GPS experiment:

- Position: The position can be requested at any time together with velocity and time.
- Time: A clock synchronisation message can be generated by the GPS clock, or the Transputer clock when the GPS receiver is off. The message can be used in conjunction with the GPS Pulse per second.
- Orbital Elements can be generated automatically to get an prediction accuracy of 1-10 km for two weeks.
- Orbital GPS Data can be logged at specified repetitive intervals and durations.
- Status Request: At any time.
- Autonomous mode: The Navigation Unit sends a GPS power cycling command, initialises the GPS receiver, sends a GPS-derived synchronising message to the satellite, generates and broadcasts orbital elements, and shuts down the GPS receiver again on a specified periodic basis.

In fact only a demonstration, rather than full autonomy of the Navigation Unit can be achieved on PoSAT due to two limitations. The memory used by the transputer is not protected against SEUs, so the program would only be expected to run for one or two months before needing a re-load. Secondly, the OBC program memory limit has been reached, and so there are restrictions on the number of payloads in concurrent operation. Both of these issues are addressed in the latest design for the FASat-Alfa mission.

In the autonomous operation mode, the average power consumption of the GPS receiver is low. For medium accuracy purposes, the GPS receiver would be operated once a day for an orbit duration, giving a daily clock synchronisation and orbital element generation. The resultant mean power consumption of the GPS receiver is less than 0.15 watts, which is an appropriately low level for a microsatellite. Using the receiver only once a week would lower the average power to 0.02 watts. In the case of the PoSAT-1 experiment, this figure is offset by the power consumption of the transputer supporting the GPS and Star Imaging experiments. This consumes a steady 0.75 watts, although through the software control of the clock speed, it can be reduced to half of that figure.

There are new technology microprocessors emerging of an equal or better performance with a lower power consumption than the T800 transputer. Some are based on a static architecture, and so the clock can be stopped until an interrupt from a timer or a communications peripheral starts the clock again. Alternatively, the GPS Navigation Unit software, as specified, could be implemented in the GPS receiver itself, so eliminating the power consumption of the separate computer altogether.

CONTINUING THE USE OF GPS IN ORBIT

The FASat-Alfa microsatellite mission is the first Chilean satellite (Figure 8), and has been constructed under a Technology Transfer Programme between the Chilean Air Force and Surrey Satellite Technology Ltd. FASat-Alfa uses the 50 kg modular UoSAT bus, similar to PoSAT-1, but carries new technology and experiments. As well as the GPS experiment, FASat carries an Ozone layer monitoring experiment, a 100 metre resolution imaging system, and a DSP data transfer experiment.

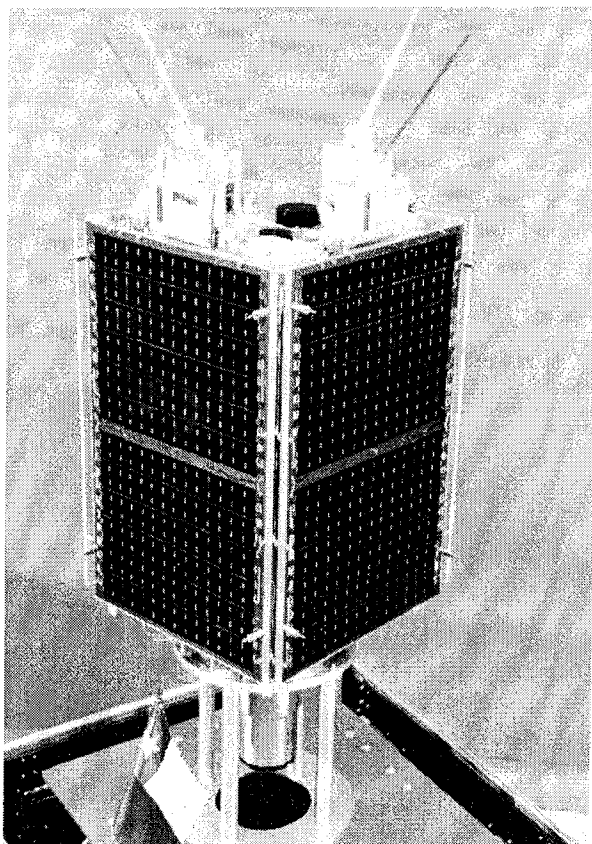


Figure 8 The FASat-Alfa microsatellite in launch configuration

FASat-Alfa was launched on a Ukrainian Tsiklon launcher on 31st August 1995. FASat-Alfa was carried as a passenger satellite attached to the primary Ukrainian SICH-1 remote sensing satellite. Unfortunately at the time of writing the two satellites had failed to separate, so although SICH-1 is functioning, it has not yet been possible to command and commission FASat-Alfa.

The GPS experiment on FASat is very similar to the system on PoSAT, with a few minor improvements. The transputer memory has been increased to 2 Mbytes, and is now EDAC protected. The OBC has been enhanced, an i386-based second OBC has been added to the satellite platform, and a new high speed data-bus has been introduced, so the GPS experiment is

better supported. Pulse per second signals now go from the GPS receiver to four of the microprocessors on-board for the purposes of accurate clock synchronisation.

Should it prove not possible to activate FASat-Alfa, there is a strong possibility that a replacement microsatellite with the latest system design and carrying the same GPS experiment will be built within the next 12 months. The GPS Navigation Unit will therefore continue to be developed to gain full autonomy, new orbit determination methods will be implemented, and payloads triggered autonomously by position.

In the third quarter of 1996, the UoSAT-12 minisatellite is scheduled for launch. This is a new design of satellite which is larger than the UoSAT microsatellite bus (300 kg instead of 50 kg). It will carry advanced imaging systems and a small bi-propellant propulsion system to experiment with orbital manoeuvring. The current plan is to include on UoSAT-12 a GPS receiver which is capable of determining attitude through phase difference measurements between GPS antennas. Together with the propulsion system, this offers the opportunity for autonomous attitude and orbit control.

SUMMARY

The commercially-rated Trimble TANS GPS receiver on PoSAT-1 is still functioning nominally after nearly 2 years in orbit. The GPS receiver can be initialised typically within 2 minutes, but the receiver must be re-initialised occasionally if being operated continuously. Position fixes will on average be available for 80% of the time, although in some cases falling to 60%. There are outliers in the data, and occasional gross errors, but for most of the time the position fixes are accurate to the expected levels of about 100 metres, as verified by external radar tracking.

A system design for a GPS Navigation Unit has been described that is suitable for various small satellite applications. The Navigation Unit is capable of operating autonomously and provides a number of services to the satellite. This concept has been proven in orbit: PoSAT-1 has become the first satellite to autonomously generate mean orbital elements in orbit. The orbit determination method used only requires the GPS receiver to consume an average power of 0.15 watts or less, and yet can determine the mean semi-major axis to 5 metres.

The full potential of GPS for small satellites has not yet been reached: GPS can be used on the satellite to simplify or eliminate day-to-day operational scheduling, and eventually to perform autonomous attitude

and orbit maintenance for a satellite, enhancing the platform's capabilities significantly while maintaining the low cost of the satellite and the operations.

ACKNOWLEDGEMENTS

This research has been supported by EPSRC and SSTL. The PoSAT microsatellite mission is funded by a consortium of Portuguese organisations led by INETI. The FASat-Alfa mission is funded FACH, Chile.

¹ Anastasiou I, "Satellite Autonomous Navigation: World-wide Survey of Projects, Operators' Attitudes and Perspectives", AAS/GSFC Int. Symp. on Space Flight Dynamics, NASA GSFC, April 1993.

² Van Leewen A. et al., "The Global Positioning System and its Application in Spacecraft Navigation", Proc. ION NAS 1979, Institute of Navigation.

³ Treder A.J., "Autonomous Navigation - When Will We Have It?", Navigation, Journal of the Institute of Navigation, Vol 34, No.2, Summer 1987.

⁴ Lichten S. et al., "An Automated Low-Earth Orbit Determination System with High Accuracy Real-Time Capability", Proc. ION NTM, Institute of Navigation, Anaheim, Jan 1995.

⁵ Marshall M.M., (principal author) "Goals for Air Force Autonomous Spacecraft", JPL Report 7030-1 (USAF Report SD-TR-81-72); March 1981.

⁶ Unwin M.J., "The Design and Implementation of a Small Satellite Navigation Unit Based on a Global Positioning System Receiver", PhD Thesis, Sept 1995.

⁷ Pressman R.S., "Software Engineering: A Practitioner's Approach", McGraw Hill, 1992.

⁸ Unwin M.J., "The PoSAT Microsatellite GPS Experiment", Proc. ION GPS-93, Institute of Navigation, Salt Lake City, Sept 1993.

⁹ Space Track Report No.3, Aerospace Defense Command, USAF, December 1980.

Applicability of GPS-based Orbit Determination Systems to a Wide Range of HEO Missions

Jorge Potti and Pelayo Bernedo
GMV S.A.

Alessandro Pasetti
ESA/ESTEC

BIOGRAPHIES:

Jorge Potti (e-mail: jpotti@gmv.es) is Project Manager at GMV (Spain). He received his M.S. degree in Aeronautical Engineering in 1986 from the Polytechnic University of Madrid (Spain) where he gained the third national award of university studies. Since that time he is working at GMV (Grupo de Mecánica del Vuelo) in the research and development group of the Flight Dynamics and Avionics Division. At present his major areas of research are satellite guidance, navigation and control, including GPS applicability and operational issues.

Pelayo Bernedo received his M.S. degree in Aeronautical Engineering from the Polytechnical University of Madrid, Spain in 1988. He worked for McDonnell Douglas in the MD-80 twinjet series within the structures group. Since 1991 he works in the Simulation Division in GMV, where he specializes in GPS based navigation for airborne applications and tracking systems for fleets of ground vehicles.

Alessandro Pasetti is Control System Engineer with ESA-ESTEC in The Netherlands. He has a first degree in Electrical Engineering at the University of Trieste in Italy and holds a MSc in Control Systems from Imperial College of London. He has been working in the Attitude and Orbit Control Section of ESTEC, the main research establishment of the European Space Agency, since 1989. His areas of interest include satellite navigation and the application of GPS to satellite attitude determination.

ABSTRACT:

This paper presents the most significant objectives, results and conclusions of the "*Study on Orbit Determination for Satellites at HEO*". This study was promoted by the European Space Research and Technology Centre (ESTEC) and was developed by GMV S.A. One of its major objectives is the investigation of different real-time orbit determination techniques for application on-board satellites operating in highly elliptical orbits (HEO).

The study addresses those technical areas of particular concern towards the applicability of GPS to the orbit determination of satellites at HEO. Among others, we must mention techniques for attenuating the disturbing effect of the ionosphere and of selective availability, the problem of the link budget at high altitudes, investigations of GPS antenna(s) configuration optimality, the need for an on-board propagation model, techniques for attenuating the disturbing effect of orbit control manoeuvres and the importance of the GPS-receiver clock stability.

Four HEO scenarios were considered during the study (M-HEO(8), Molniya, Tundra and ISO-type orbit). For each scenario, computer simulations were performed to ascertain the achievable orbit determination accuracy. The results show that for typical HEO telecommunication missions (on M-HEO or Molniya orbits) a single GPS antenna connected to a low-cost GPS receiver and implementing a relatively simple Kalman filter with a low-cost orbit dynamics model, is able to provide an orbit positioning accuracy in the order of 100 m. Such orbit determination accuracy is sufficient for many HEO applications. Some HEO scientific missions in ISO-type of orbit, however, require higher accuracies. Our study demonstrates that for such missions the maximum achievable accuracy implementing state-of-the-art GPS technology lies in the order of 10 m. For HEO missions in Tundra orbit the achievable orbit determination accuracy lies in an approximate range of 50-100 m depending on the quality of GPS technology implemented. Extrapolations to GEO from the Tundra case becomes also possible from the results of the study.

1. PROBLEM DEFINITION: ANALYSIS OF HEO MISSIONS

The entry point of the study is the definition of four representative HEO scenarios on which various orbit determination algorithms will be tested. For each scenario, an analysis of orbit disturbances is performed followed by an analysis of on-board/on-ground orbit determination models (GPS, conventional tracking,

etc.) and identification of suitable orbit determination techniques.

1.1. Identification of mission scenarios

A very wide range of HEO orbits with very different characteristics exist. Only a few could be studied in detail within the scope of the study. Accordingly, the first part of the study briefly surveyed past, present and future HEO's and selected four representative orbits from which four mission scenarios were defined and used as test cases to assess the orbit determination techniques. The selected mission scenarios are the following (table 1 illustrates the orbital elements of the four selected HEO mission scenarios):

- Scenario 1: telecommunication mission at multi-regional HEO 8-hour orbit with low perigee (hereinafter referred to as M-HEO(8)).
- Scenario 2: navigation mission at Tundra-24 hour orbit. Such an orbit is very similar to a GEO orbit and therefore this study can be used to confirm the results of similar orbit determination studies for GEO (see, e.g. ref. [2]).
- Scenario 3: scientific mission at HEO with high accuracy positioning requirements. A geosynchronous 24-hour orbit has been selected for this scenario. This orbit is characterised by a perigee

of 1,000 Km and an apogee of 70,572 Km. This will be referred to as ISO-type orbit in the remainder of the document.

- Scenario 4: telecommunication mission at Molniya-type orbit.

1.2. Orbit Determination requirements for HEO missions

The orbit determination requirements depend on the selected orbit scenario and on the type of mission. Scientific HEO missions often require a very accurate spacecraft positioning. The selected orbit determination requirement for the scientific mission scenario (ISO-type orbit) would correspond to a very stringent VLBI mission. The following values have been selected: 1 m accuracy in position and 1 cm/s accuracy in velocity (1σ). For a navigation mission, the position of each spacecraft of the constellation must be known with a high precision. In our study, the Tundra type orbit is assumed to be used for very high precision navigation purposes. A position error of 30 m (1σ) is selected as orbit determination requirement. Communication missions are not very demanding on orbit determination requirements. Therefore a position error of 1 Km (1σ) is considered for the communications MHEO 8 hour and Molniya orbit scenarios.

| | M-HEO(8) | Tundra | ISO-type | Molniya |
|-----------------|------------|------------|-----------|------------|
| Orbital period | 8 hour | 24 hour | 24 hour | 12 hour |
| Semi-major axis | 20,278 Km | 42,164 Km | 42,164 Km | 26,578 Km |
| Eccentricity | 0.636 | 0.266 | 0.825 | 0.722 |
| Perigee height | 1,000 Km | 24,000 Km | 1,000 Km | 1,000 Km |
| Apogee height | 26,800 Km | 47,000 Km | 70,572 Km | 39,400 Km |
| Inclination | 63.435 deg | 63.435 deg | 5.25 deg | 63.435 deg |

Table 1: Selected HEO mission scenarios

2. GPS-BASED ORBIT DETERMINATION

2.1. General

The approach followed in our analyses is to find the minimal hardware configuration which allows on-board GPS-based orbit determination at the prescribed accuracy for each of the selected HEO mission scenarios. For the cases of M-HEO(8) and Molniya, the low demanding orbit determination accuracy allows to design an on-board GPS-based orbit determination system based on the use of a low-cost C/A code GPS receiver. The more demanding orbit determination (OD) accuracy requirements for the Tundra and ISO-type scenarios implies a need for state-of-the-art dual-frequency GPS receiver and maybe the support of differential GPS. In all the cases, being an on-board application, it is particularly important to minimise the hardware demands on-board the spacecraft. This means that the resulting algorithms should be simple enough to fit

within the GPS receiver processor and, therefore, the on-board dynamics model shall be simple enough.

C/A-code GPS receivers (M-HEO(8) and Molniya scenarios) are assumed to provide pseudo-range, integrated Doppler (continuous carrier phase) and carrier phase only at the L1 frequency. State-of-the-art dual-frequency GPS receivers (Tundra and ISO-type scenarios) are assumed to provide differential (L1-L2) continuous carrier phase measurements in addition to the C/A-code pseudo-range, integrated Doppler (continuous carrier phase) and carrier phase measurements at the L1 frequency. The errors affecting the GPS observations are assumed as follows: 0.5 m and 0.25 m for pseudoranges provided by C/A code and dual-frequency GPS receivers, respectively, and 1 mm carrier phase noise.

C/A-code GPS receivers (M-HEO(8) and Molniya scenarios) provide measurements at L1 frequency only

which means that ionosphere effects cannot be compensated on-board unless provisions are made for estimating the ionosphere refraction correction. On this respect it must be noted that:

- For the cases where the satellite at M-HEO(8) or Molniya orbit has a GPS antenna pointing in the zenith direction, then the ionosphere refraction correction error can be neglected for practical purposes.
- For the cases where the satellite at M-HEO(8) or Molniya orbit has a GPS antenna pointing in the nadir direction, then the ionosphere range error can attain values of 100 m which require implementation of some mechanism to overcome it. Several compensation methods have been discussed and it is proposed to use a method to reject ionosphere affected signals. This can be easily done by enlarging by 1,000 Km the size of the Earth; using this 1,000 Km constraint the ionosphere effects are almost null. Obviously this mechanism implies worse visibility conditions as will be shown later.

Dual-frequency GPS receivers (Tundra and ISO-type scenarios) provide continuous carrier phase measurements at both frequencies L1 and L2, which means that ionosphere effects can be compensated on-board (since ionosphere errors are a function of the frequency of the signal being transmitted). It is therefore assumed that ionosphere refraction error can almost entirely be compensated on-board. Finally, differential GPS (needed for the ISO-type scenario) allows removing entirely the effects of GPS clocks and vastly compensates the effects of GPS ephemeris. With this technique the measurements are differenced with those simultaneously made at ground tracking sites observing the same set of GPS satellites.

2.2. Observability analysis

Due to the nature of the orbits under consideration (see figure 1), and assuming that the nominal S/C attitude is Earth pointing, there appear the following possibilities for locating the GPS receiver antenna:

- M-HEO(8) and Molniya scenarios: both nadir-view and zenith-view location would bring GPS satellite signals within the GPS receiver antenna field of view. The advantage of the zenith-view antenna is that the ionosphere disturbing effect does not appear and that the GPS signals travel is shorter. On the other hand, a zenith-view antenna gives a worse GPS satellite visibility as will be shown later.
- Tundra scenario: the only sensible orientation of the GPS receiver antenna is in nadir-view. As discussed earlier, due to the demanding OD accuracy requirements, it is assumed that the ionosphere

disturbance is removed by the availability on-board of a dual frequency GPS receiver.

- ISO-type scenario: due to very demanding OD accuracy requirements, both zenith-view and nadir-view antennas are assumed.

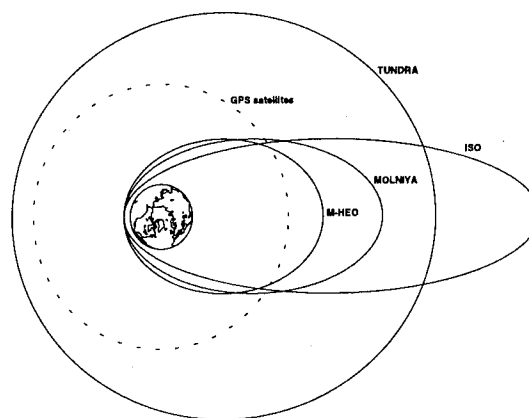


Figure 1: Geometry of the HEO mission scenarios and GPS constellation

Figures 2 and 3 show the visibility charts¹ for the HEO mission scenarios under consideration.

Analysis of these figures reveals that for the M-HEO(8) and Molniya orbit scenarios the zenith-view antenna case implies a large proportion of time with no visible satellites. In addition, the nadir-view antenna provides a mean number of visible GPS satellites significantly higher than that provided by the zenith-view case. It is therefore concluded that further investigations will concentrate in the nadir-view case; the zenith-view case is discarded.

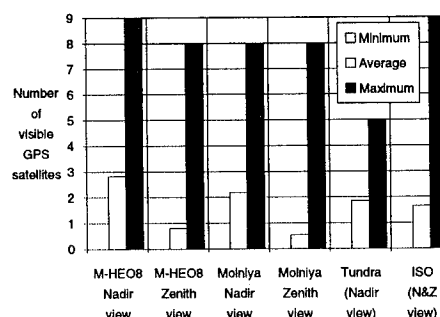


Figure 2: Number of visible GPSS¹ for each candidate target mission and GPS receiver antenna pointing.

¹ The results presented correspond to geometric visibility conditions, i.e. it has been assumed that the power level and signal-to-noise ratio of the GPS signals arriving at the GPS receiver are unconstrained (i.e. infinite GPS receiver sensitivity). This particular problem will be discussed later. However, for the M-HEO(8) and Molniya nadir-view antennas, as discussed earlier, an on-board technique has been put in place to reject those signals which are suspected of crossing the ionosphere. Therefore, ionosphere crossing signals are not considered as visible.

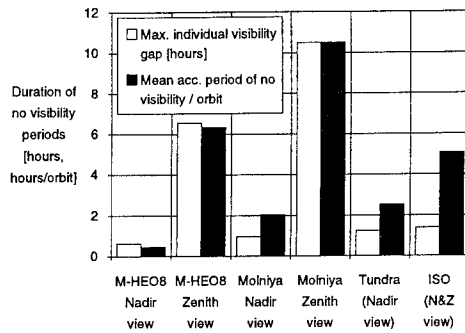


Figure 3: Analysis of loss of visible GPSS¹ for each candidate mission and GPS receiver antenna pointing.

2.3. Link budget

GPS satellite signals power reception levels at Earth surface is -160 dBW as minimum (although current power levels are typically of about -154 dBW). Taking into account that in the case of a satellite at HEO the GPS-HEO signal travel can be significantly longer, geometric visibility does not imply signal availability at the required power levels. Two parameters play an important role:

- The power level of the received GPS signals: commercial receivers are designed taking into account the minimum signal power level guaranteed by the USA DoD (-160 dBW). Due to the relatively large distance in this application (for the cases of the GPS antenna pointing in the Nadir direction and the satellite being close to its orbit apogee) it is likely that the received power level is less than that value.
- More important yet is the received C/N_0 ratio of the GPS signals. While a weak signal can be amplified to reach the desired power level, nothing can be done if the contribution of the different noise sources is such that the overall C/N_0 ratio is less than the receiver sensitivity. From ref. [7], the nominal C/N_0 at the input of the LNA unit shall be of 46 dBHz at L1 frequency and the minimum carrier-to-noise power density ratio for signal acquisition shall be of 38 dBHz (both measured at the LNA input).

The antenna gain pattern of the GPS satellites deserves special attention. Based on actual GPS signal levels, which are around 5 dB higher than specifications, it has been considered that the GPS satellites EIRP (in the maximum gain direction) is 30 dBW.

From ref.'s. [2] and [4] it is possible to derive the following formulation for the power level and C/N_0 ratio of the GPS signal received:

$$P_r = EIRP + L_t + L_s + L_b + G_r + L_a$$

$$C/N_0 = EIRP + L_t + L_s + L_b + G_r + L_a - 10 \log_{10} T_s + 228.6$$

where:

P_r is the power level at the GPS receiver

$EIRP$ is the effective isotropic radiated power by the emitting GPS satellites in the maximum gain direction. Based on actual GPS signal levels, which are around 5 dB higher than specifications, it has been considered that the GPS satellites EIRP (in the maximum gain direction) is 30 dBW.

L_t is the transmitter antenna gain loss with respect to the maximum gain direction. This term accounts for the antenna gain pattern of the GPS satellites.

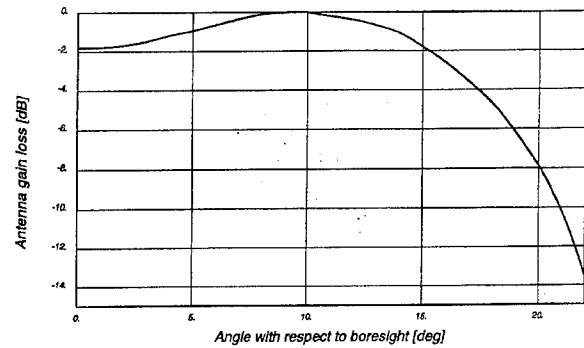


Figure 4: GPS emitting antenna gain loss vs reception direction

G_r is the receiver GPS antenna gain in the maximum gain direction. From ref. [6], typical low-cost GPS antennas provide a gain of 6 dB

L_a is the attenuation of the GPS signal when received from a direction different from the GPS antenna maximum gain. It is a function of the deviation of the incoming signal from the maximum gain direction.

L_s is the free-space loss, given by

$$L_s = 20 \log_{10} \left(\frac{\lambda_0}{4\pi d} \right)$$

where λ_0 is the wavelength (corresponding to L1 frequency) and d is the distance between the GPS-satellite and the GPS receiver

L_b encompasses other system losses like polarisation mismatch, etc., assumed as being -2 dBW

T_s is the system noise temperature, assuming that the antenna is pointing at the Earth, this is 290 K, otherwise this is 180 K.

The above formulation and related assumptions (adopted from ref.'s [2], [4] and [6]) allow us to calculate the resulting power level and associated C/N_0 ratio of every signal arriving at the GPS receiver. Computer

simulations were performed to compute the effective observability charts when power level and signal-to-noise ratio constraints are put in place. Figures 6 and 7 correspond to the visibility charts of the previous section but now any GPS signal arriving at the GPS receiver with a signal-to-noise ratio below 38 dB is considered as not visible. The assumptions which have been made as concerns the GPS receiver antenna are summarised in table 3. Inspection of these plots reveals the following conclusions:

- M-HEO(8) and Molniya scenarios: there is a significant loss in the number of GPS satellites observed at the required C/N_0 level: the mean number of GPS satellites observed falls to 1.480 (M-HEO(8)) / 1.165 (Molniya) from 2.792 (M-HEO(8)) / 2.192 (Molniya) described in previous section. However, the resulting visibility charts appear still promising to reach the specified OD accuracy requirement. It must be noted that the power level becomes as low as -165.980 (M-HEO(8)) / -165.970 (Molniya) dB and, thus, there is a need to raise the power level by some 6 dBw by means of a low noise amplifier. An alternative to this would be to mount on-board the M-HEO(8) or Molniya orbiting S/C, a high gain antenna which would raise both the C/N_0 and power level. But in this case the price to pay is a reduced antenna field of view which would result in still reduced visibility conditions (mean number of visible GPS satellites is reduced by about 25%) and, thus, worse OD accuracy (simulations reveal that OD accuracy loss is of approximately 50-60%).
- Tundra scenario: analysis reveal that at Tundra altitudes the GPS signals arrive at the GPS receiver antenna within a narrow cone of approximately 20 degrees (half-cone angle). This allows to utilise a high gain antenna and the reduced field of view does not affect the visibility conditions. Even with a high gain antenna (12 dB in the maximum gain direction) there is a significant loss of visible GPS satellites at the required C/N_0 levels: it falls to 1.168 from 1.862. It must be noted that the power level becomes as low as -165.970 and, thus, there is also a need to raise it by the aid of a low noise amplifier between the GPS receiver antenna and the GPS receiver LNA input.
- ISO scenario: the zenith-view antenna does not pose any problem. On the other hand, even with a high gain nadir-view antenna (12 dB in the maximum gain direction) there is a loss of visible GPS satellites at the required C/N_0 levels (it falls to 1.108 from 1.659) and the power level becomes as low as -167.940 and, thus, there is a need to raise it by some 8 dBw with the aid of a low noise amplifier.

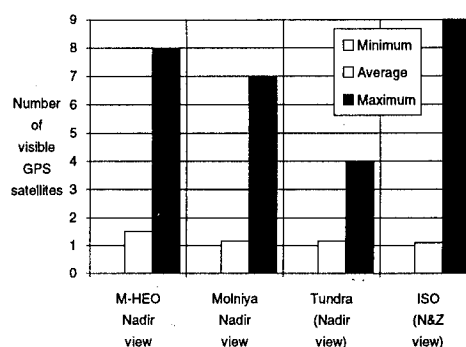


Figure 6: Number of visible GPSS for each mission and GPS receiver antenna pointing at the required power level.

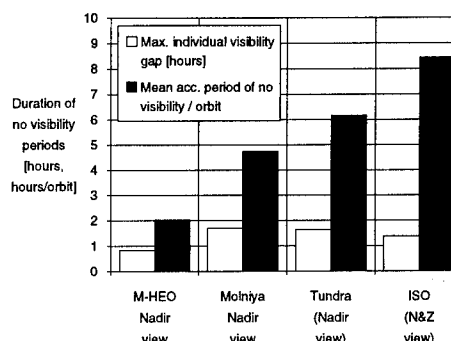


Figure 7: Analysis of loss of visible GPSS for each mission and GPS receiver antenna pointing at the required power level.

2.4. On-board orbit dynamic models

Due to the fact that the GPS-based orbit determination algorithms are targeted to run on-board the spacecraft, there is a need for implementing a low-cost² dynamics model. Since the on-board estimation filter relies on both the measurements model and the on-board dynamics model to derive an optimum estimate of the spacecraft location, then the quality of the on-board dynamics model is one of the driving factors of the orbit determination algorithm performances. This is particularly important in orbital arcs where there is no available measurement as was discussed before. Analyses have been conducted to identify an optimum on-board orbit dynamics model for each of the HEO scenarios under consideration with the following conclusions:

- M-HEO(8) and Molniya orbits: due to low demanding OD accuracy requirements, an extremely simplified orbit dynamics model has been selected, implementing only the Earth's gravity field model to the order and degree 2, i.e. the central gravity plus the J_2 and J_3 terms.

² Low-cost here refers to the requirements imposed by the selected dynamics model on the on-board processor in terms of memory requirements and CPU demands.

- Tundra and ISO orbits: due to high demanding OD accuracy requirements, a more sophisticated orbit dynamics model has been selected, implementing an Earth's gravity field model to the order and degree 4, third body perturbations due to Sun and Moon following an analytical ephemeris model and solar radiation pressure perturbations following a rough analytical model.

2.5. Preliminary analysis of OD accuracy

A GPS-based estimation filter implementing the algorithms described in section 3 has been built to assess the performances of such a system in the selected HEO scenarios. The estimation technique employed is based on an extended Kalman filter is used to perform estimation of the following state vector:

$$\bar{x}_{state} = \{\bar{x} \quad \bar{v} \quad E_{clock} \quad \Delta T_B \quad \bar{b} \quad \bar{I}\}^T$$

where \bar{x} is the spacecraft position vector, \bar{v} is the spacecraft velocity vector, E_{clock} is the normalised frequency of the GPS receiver clock, ΔT_B is the time bias of the GPS receiver clock, \bar{b} are the range biases at each of the GPS receiver channels (these are modelled as a 1st order Gauss-Markov processes, attempting to attenuate the disturbing effect of selective availability) and \bar{I} are the Doppler integration constants at each of the GPS receiver channels.

The orbit dynamics models discussed in paragraph 2.4 are used for the propagation of the position and velocity state vector components. Both pseudo-range and integrated Doppler measurements are processed in a sequential fashion to perform state vector update. For the dual-frequency GPS receiver concept (Tundra and ISO-type orbit scenarios) it is assumed that the on-board algorithm precisely know the disturbing effect of ionosphere at 95% confidence level. For the differential GPS concept (ISO-type orbit scenario) it is assumed that the on-board algorithms are able to entirely remove the disturbing effect of selective availability.

Table 3 summarises the most significant input data which have been used to perform the simulations as well as the resulting HW/SW requirements for each mission scenario. The results are here summarised:

RMS Position estimation errors (m)

| | Along-track | Across-track | Radial | TOTAL |
|-----------------|-------------|--------------|---------|---------|
| Molniya | 138.135 | 237.857 | 129.347 | 303.347 |
| M-HEO(8) | 61.270 | 61.270 | 104.011 | 153.362 |
| Tundra | 45.512 | 23.090 | 22.628 | 55.826 |
| ISO-type | 5.230 | 2.299 | 12.543 | 13.782 |

Table 2: Resulting OD accuracy for each mission.

| | | | M-HEO(8) | Molniya | Tundra | ISO-type |
|-----------------------|-------------------------------|-------------------------|------------------|------------------|--------------------------|----------------|
| Hardware requirements | GPS receiver | Type | C/A | C/A | Dual-frequency | Dual-frequency |
| | | Number of channels | ≥ 9 | ≥ 9 | ≥ 4 | ≥ 9 |
| | | Pseudo-range noise | 0.5 - 5 m | 0.5 - 5 m | 0.25 m | 0.25 m |
| | | Carrier phase noise | 1 - 10 mm | 1 - 10 mm | 1 mm | 1 mm |
| | | Clock | Low-cost crystal | Low-cost crystal | State-of-the-art crystal | Atomic |
| | | Sensitivity (C/N_0) | ≥ 38 dBHz | ≥ 38 dBHz | ≥ 38 dBHz | ≥ 38 dBHz |
| | | Sensitivity (PWR) | ≥ -160 dBw | ≥ -160 dBw | ≥ -160 dBw | ≥ -160 dBw |
| | GPS receiver antenna 1 | Orientation | Nadir-view | Nadir-view | Nadir-view | Nadir-view |
| | | Beam-width | 160 deg | 160 deg | 60 deg | 60 deg |
| | | Max. antenna gain | 6 dB | 6 dB | 12 dB | 12 dB |
| | | Max. antenna gain loss | 6.6 dB | 6.6 dB | 1.1 dB | 1.1 dB |
| | | LNA gain | 6 dB | 6 dB | 6 dB | 6 dB |
| | GPS receiver antenna 2 | Orientation | - | - | - | Zenith-view |
| | | Beam-width | - | - | - | 160 deg |
| | | Max. antenna gain | - | - | - | 6 dB |
| | | Max. antenna gain loss | - | - | - | 6.6 dB |
| LNA gain | | - | - | - | - | |
| Software requirements | OD filtering technique | | Kalman | Kalman | Kalman | Kalman |
| | Ionosphere effects mitigation | | Reject | Reject | Dual-frequ. | Dual-frequ. |
| | On-board orbit dynamics model | | 2×2 | 2×2 | 4×4+ | 4×4+ |
| | Measurements processed | | PRN, NDOP | PRN, NDOP | PRN, NDOP | PRN, NDOP |
| Differential GPS | | | No | No | No | Yes |

Table 3: Overview of HW/SW requirements for the proposed GPS-based OD system of each mission scenario

2.6. Conclusions

Table 3 summarises the HW/SW demands on each selected mission scenario to achieve the prescribed OD accuracy targets. It must be noted that they are largely met in both the M-HEO(8) and Molniya orbit scenarios. For the Tundra case no dual-frequency GPS-based OD method allows orbit determination at the prescribed accuracy (30 m, 1σ). However, the proposed hardware/software configuration allows orbit determination at an accuracy of 60 m (1σ) not far from the specified target. Finally, for the ISO-type orbit scenario there is no way for an on-board GPS-based orbit determination method to reach the prescribed OD accuracy (1 m, 1σ). The best we can do implementing a state-of-the-art dual-frequency GPS receiver with two GPS receiver antennas and having the support of differential GPS to remove the disturbing effect of selective availability, is an orbit determination accuracy of approximately 10 m (1σ).

3. GPS-BASED ORBIT DETERMINATION ALGORITHMS

The on-board software required for performing the autonomous GPS based OD is summarised in figure 8 which represents a particular application case of an extended Kalman filter. Such an algorithm is able to provide real-time estimation, i.e. the time at which the estimate is output coincides with the last measurement point.

In figure 8 it has been omitted the selection of the GPS satellites to be tracked since it is assumed to be performed by the receiver itself. In our case we are assuming having 9 channels which is already a conservative assumption, since most of the GPS receivers currently under development foresee an "all-in-view" approach, which means, in practice, that they are being designed with 12 or even more receiver channels.

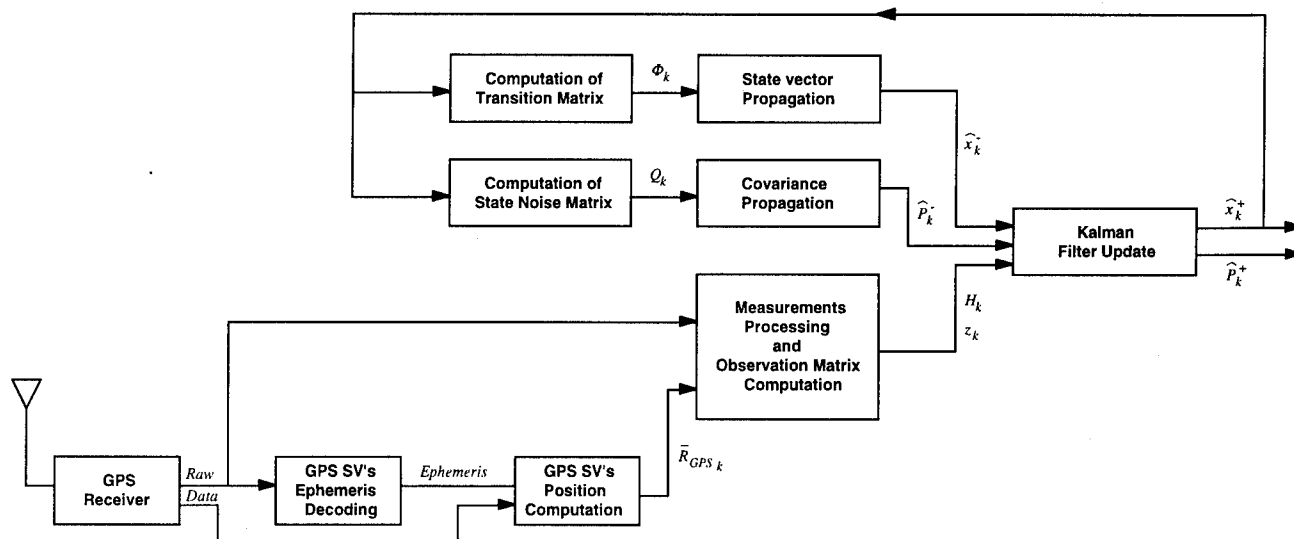


Figure 8: Orbit determination function architecture.

The functionalities required are here briefly summarised:

- *Acquisition of GPS receiver data:* the GPS receiver will output the following data which drive our estimation filter: identification of the GPS satellites tracked, the raw GPS measurements (pseudo-range and integrated Doppler) in all the receiver channels and antennas, time of measurement in the receiver clock, and, GPS satellite navigation message data, including the ephemeris of the GPS satellites being tracked.
- *Prediction of the GPS satellites state vector:* some GPS satellite data are required for the measurement processing (i.e., GPS satellite position, velocity and acceleration vectors for the observables

on-board prediction and for the observation matrix computation, see below). Hence, a GPS satellites state vector prediction is required. Such prediction will be performed from the GPS satellites ephemeris contained in the GPS Navigation Message Data using Keplerian propagation modified with second order harmonic perturbations.

The on-board GPS based OD function will consist of the following modules:

- *Initialisation of the state vector and covariance matrix for orbit determination:* as discussed in paragraph 2.5, the augmented state vector used will consist of $(8+2n_c)$ components as follows (n_c stands for the number of GPS receiver channels).

The initialisation of this vector (mean and covariance) is performed from input parameters.

- *Propagation of the mean augmented state vector:* the augmented state vector is propagated as follows: if there is a change of the GPS satellite tracked in a receiver channel, the elements of the estimated augmented state vector corresponding to the associated range bias and integrated Doppler constant should be initialised, the propagation of the spacecraft position and velocity is performed by integrating numerically the equations of motion in the inertial frame, and, the propagation of the estimated parameters (i.e., other elements of the augmented state vector apart from the spacecraft position and velocity) is performed analytically from the corresponding dynamic error model selected (e.g., bias, ECRV, etc.).
- *Propagation of the augmented state vector error covariance matrix:* the augmented state vector error covariance matrix is propagated as follows: if there is a change of the GPS satellite tracked in a receiver channel, the elements of the estimated covariance matrix corresponding to the associated range bias and integrated Doppler constant should be initialised, the transition matrix of the spacecraft position and velocity vectors is computed analytically by using the formulation of a second order Runge Kutta numerical integrator. The required dynamic matrix is computed analytically from the linearised formulation and using the estimated state vector. The transition matrix of the estimated parameters is constructed analytically from their modelled dynamics, and, the error covariance matrix associated to the augmented state vector is propagated using discrete formulation. The above mentioned transition matrix, the covariance matrix at previous time and the system noise covariance matrix are used. The system noise associated to the spacecraft state vector is computed analytically from the uncertainties in the on-board orbit dynamics model, whereas the system noise covariance matrix associated to the estimated parameters is directly constructed from their on-board modelled dynamics. The covariance matrix propagation will be done by using its U-D factorisation in order to reduce the on-board computer workload as well as to improve the numerical stability.
- *Processing of measurements:* the raw measurements provided by the receiver will be processed as follows: the observables selected for the orbit determination (namely, pseudo-range and integrated Doppler) will be predicted on-board by using non-linear formulation (an extended Kalman filter is used) and by using the a-priori estimate of the augmented state vector, spacecraft data (namely measurement time) and selected

GPS satellite data (namely, position, velocity and acceleration vectors) provided by a GPSS state vector prediction algorithm, the on-board predicted values of the observables are used to compute the corresponding innovations (or measurement residuals): difference between the raw measurement (pseudo-range or integrated Doppler) through the channel under consideration and the predicted values, the observation matrix to be used for the filtering process is computed analytically using an appropriate formulation obtained after linearising (with respect to the mean estimate of the augmented state vector), and, a constant and GPS receiver dependent value of the pseudo-range and integrated Doppler measurements noise is assumed.

- *Update of the augmented state vector and covariance matrix:* an extended Kalman filter is used to update the augmented state vector and associated error covariance matrix. The measurements are processed sequentially (i.e. one-by-one) by the filtering algorithm for reducing the number of operation required, and the covariance matrix update is made using the U-D factorisation. The Kalman gain matrix is computed by weighting the a-priori estimate of the error covariance matrix in order to improve the convergence characteristics of the filtering process.

4. PERFORMANCE ANALYSIS OF GPS-BASED ORBIT DETERMINATION FOR ARCHIMEDES

A detailed sensitivity analysis has been performed only for the M-HEO(8) scenario. The main results are presented below.

4.1. Sensitivity analysis w.r.t. different selective availability models

Tests have been performed to investigate the robustness of the orbit determination techniques to changes in the selective availability models. This was done by running several simulations which differed only in the type of selective availability model implemented.

A summary of the results is shown in table 4 from which one can conclude that the proposed algorithms exhibit a remarkable robustness with respect to changes of selective availability models.

Even for the case of the time series selective availability models (i.e. Lear Arima 2x1, Zyla Arima 3x2 and RTCA Gauss Markov SA model, which are regarded as too pessimistic since they provide an output which is too noisy compared to actual SA measurements), the proposed algorithms are able to maintain the positioning estimation accuracy very close to the nominal case:

maximum OD error differences with respect to the nominal case are always below 10%.

| SA MODEL | RMS position estimation error (m) | | | |
|---------------------|-----------------------------------|-------------|--------|-------|
| | Along-track | Cross-track | Radial | Total |
| None | 62.5 | 42.3 | 100.9 | 126.0 |
| Lear deterministic | 75.7 | 80.6 | 112.0 | 157.4 |
| Lear random | 76.1 | 61.5 | 106.9 | 145.0 |
| Martínez-Molina | 83.2 | 52.0 | 107.6 | 145.7 |
| Rater Jerk analytic | 95.0 | 61.3 | 104.0 | 153.4 |
| Lear Arima 2x1 | 90.3 | 82.2 | 115.5 | 168.1 |
| Zyla Arima 3x2 | 83.1 | 74.7 | 115.3 | 160.6 |
| RTCA Gauss Markov | 81.9 | 88.3 | 111.1 | 163.9 |

Table 4: Orbit Determination RMS errors summary results for different SA models

4.2. Sensitivity analysis w.r.t. GPS receiver clock stability

In the frame of this study it has been assumed for the M-HEO(8) orbit scenario that a low-cost crystal clock would be sufficient for achieving the proposed target orbit positioning accuracy. The GPS receiver clock is modelled as follows:

$$E_{clock}(t + \Delta t) = E_{clock}(t) + \dot{E}_{clock}\Delta t + w$$

$$\Delta T_B(t) = \int_0^t E_{clock}(\tau) d\tau$$

where E_{clock} is the normalised clock frequency error which is driven by a constant drift (\dot{E}_{clock}) and a noisy term (w) representing the clock stability; ΔT_B is the time bias of the GPS receiver clock which is obtained through integration of the normalised clock frequency error. The term \dot{E}_{clock} has been assumed as being 10^{-13} (s/s)/s as discussed in ref. [8] for a low cost crystal clock and this value is regarded as conservative. Therefore, no sensitivity analysis will be performed with respect to the GPS receiver clock drift/ageing. Another subject is the clock stability (driven by the term w above). Ref. [8] suggests a value of 10^{-11} (this is regarded as a quite pessimistic value) for low-cost crystal clocks and for a sampling rate of 1 sec. A sensitivity analysis will be conducted with respect to various values of this parameter ranging from 10^{-9} to 10^{-11} .

It should be noted that the changes in receiver clock stability were matched by corresponding changes in the estimation filter tuning (the clock error is one of the terms estimated by the on-board filter). In practice, this means that we assume that the user has a relatively good knowledge of the clock characteristics.

A summary of the simulation results is presented in table 5. It will be seen that the proposed estimation technique is very robust to variation in clock characteristics with the total error remaining within $\pm 15\%$ of its

nominal value even for a hundredfold deterioration in clock stability.

| Clock stability term w | RMS position estimation error (m) | | | |
|-----------------------------|-----------------------------------|--------------|--------|-------|
| | Along-track | Across-track | Radial | TOTAL |
| 0 | 95.3 | 61.3 | 104.0 | 153.6 |
| 10^{-11} | 100.3 | 61.5 | 102.5 | 156.0 |
| 10^{-10} | 114.8 | 57.3 | 109.9 | 168.9 |
| 10^{-9} | 116.8 | 55.3 | 124.1 | 179.1 |

Table 5: OD RMS errors summary results for different values of the GPS receiver clock stability

One can, therefore conclude that the clock stability is not a crucial issue for our application case. The reason why clock stability does not affect the accuracy of the orbit estimation method is due to the fact that the proposed GPS-based Orbit Determination algorithm is based on dynamic filtering where two sources of information (the measurements provided by the GPS receiver and the orbital dynamics knowledge) are merged together. To this one must add that the observation matrix (the matrix with the partial derivatives of the measurements with respect to the state vector elements) of our system is such that the clock related state elements (both the normalised clock frequency error and the time bias of the GPS receiver clock) are highly observable. This makes that after periods of non-visibility of the GPS satellites, during which the receiver clock is drifting (and, thus, the corresponding state estimate is becoming worse and worse), the filter uses its orbit dynamics model to propagate the orbital estimates (S/C position and velocity vectors). Since periods of non visibility last at the most one hour, the error accumulated by the on-board orbit propagator is comparatively small. When the GPS satellites come into view again, the receiver clock has accumulated a certain error. This error will, however, be quickly corrected by the filter thanks to the still quite accurate estimate of the orbital position and high observability of clock related state components.

4.3. Sensitivity analysis w.r.t. GPS receiver antenna / amplifier gain

Previously the link budget for the GPS signals at M-HEO(8) altitudes was discussed. It was shown that in order to raise the power level above -160 dBw it is necessary to add an amplifier to increase the power level by some 6 dBw. This result is based on a number of assumptions including the assumed GPS receiver antenna gain pattern. Since there is some technological margin related to this requirement we are interested in knowing what is the sensitivity of our proposed GPS-based OD algorithms to this parameter (the GPS receiver antenna amplifier gain). It must be noted that this parameter is functionally equivalent to the GPS receiver antenna gain in the maximum gain direction. Several simulations were performed for different values

of the GPS receiver antenna amplifier gain (2, 3, 4, 5, 6, 7, 8, 9 and 10 dBw), the rest of the input data being identical in all the cases. A summary of the simulation results is shown in table 6 which yields the following conclusions:

- Values of the GPS receiver antenna amplifier gain above 6 dBw is of no interest. The number of measurements processed by the OD filter stays constant and therefore, the OD accuracy keeps constant to the very last digit.
- Decreasing the value of the GPS receiver antenna amplifier gain below 6 dBw implies that the number of measurements processed by the OD filter decreases and, therefore, the OD accuracy degrades. The amount of performance degradation is of less than 1% in the case where the gain loss is of 1 dBw. However, for the cases where the gain loss is of 4 dBw, then the performance degradation becomes as high as 27.6%.

| GPS receiver antenna amplifier gain (dBw) | RMS position estimation error (m) | | | |
|---|-----------------------------------|-------------|--------|-------|
| | Along-track | Cross-track | Radial | Total |
| 10 | 95.0 | 61.3 | 104.0 | 153.4 |
| 9 | 95.0 | 61.3 | 104.0 | 153.4 |
| 8 | 95.0 | 61.3 | 104.0 | 153.4 |
| 7 | 95.0 | 61.3 | 104.0 | 153.4 |
| 6 | 95.0 | 61.3 | 104.0 | 153.4 |
| 5 | 95.3 | 59.9 | 105.2 | 154.0 |
| 4 | 94.7 | 68.0 | 144.4 | 185.6 |
| 3 | 105.5 | 68.2 | 126.9 | 178.5 |
| 2 | 120.0 | 90.6 | 125.2 | 195.7 |

Table 6: OD RMS errors results for different values of the GPS receiver antenna amplifier gain

4.4. Sensitivity analysis w.r.t. GPS satellite outages

As indicated previously, the nominal performances of our GPS-based OD filter have been obtained under the assumption of the GPS constellation being composed of 24 satellites, all of them operating continuously. It becomes interesting to analyse the effect on the filter performance of the absence of one or more GPS satellites. For such purpose identical simulations have been performed and one, two and three GPS satellites were considered unavailable.

Extensive simulations have been performed for the 1 GPS satellite failure, i.e. 24 simulations have been performed corresponding to a single failure of any of the GPS satellites. The results reveal how there is a big sensitivity of the achieved orbit determination accuracy depending on which is the GPS satellite failed. Under worst case conditions, failure of a single GPS satellite can degrade the OD accuracy by a factor of 1.44. The results of the single GPS satellite failure simulations allows to select the worst case for 2 and 3 GPS satellites failures as those which disturb more seriously the OD

performances (note that the number of possible combinations of 2 or 3 GPS satellite failures is huge and therefore we have not explored all possible combinations). These are the following:

- 2 GPS satellites failed: worst case is failure of GPS satellites numbers 2 and 9, in which case the OD performances are degraded by a factor of 1.5
- 3 GPS satellites failed: worst case is failure of GPS satellites numbers 2, 9 and 16, in which case the OD performances are degraded by a factor of 1.7

5. REFERENCES

- [1] Lear, W.M., "GPS Navigation for Low Earth Orbiting Vehicles", NASA, Mission Support Directorate - Mission Planning and Analysis Division, 1989.
- [2] Legido, J.M., Martínez-Olague, M.A., "Tracking of Geostationary Satellites with GPS, GPS-GEOTRACK, Phases 1 & 2 Final Report", Doc. No. GMVSA 2070/94, issue 1, July 1994.
- [3] CNES, "Measurement of the RGIC Signal Code/Carrier Coherency with a GPS Receiver", Proceedings of the ION GPS-92, Albuquerque, New Mexico, USA, September 1992.
- [4] Wertz, J.R., Larson, W.J. (ed.), "Space Mission Analysis and Design", Kluwer Academic Publishers, 1991.
- [5] Potti, J., Peláez, A., "SOAP S/W User's Requirements Document", Doc. No. GMV/ODISHEO/SW/URD (GMVSA 2079/94), issue 01, August 1994. Study on Orbit Determination for Satellites at HEO (ODISHEO).
- [6] Micro Pulse GPS antennas specification (commercial information).
- [7] Howard, N., "Support to Receiver Characteristics", Study of Autonomous Orbit and Attitude Determination Techniques for Low-Earth Observation Systems (ATLEOS), The CAA Institute of Satellite Navigation, Department of Electronic and Electrical Engineering, The University of Leeds.
- [8] Busca, G., Rochart, P. and Schlueter, B., "Study of Potential Applications for Atomic Clocks in Space", Final Report of ESTEC Contract No. 9099/90/NL/US(SC), Work Order No. 9, Observatoire Cantonal de Neuchâtel, November 1994.

Performance Evaluation of the GPS Yaw Bias Implementation

Yoaz Bar-Sever
Jet Propulsion Laboratory

BIOGRAPHY

Yoaz Bar-Sever has a Ph.D. in Applied Mathematics from the Technion - Israel Institute of Technology and a M.S. in Electrical Engineering from the University of Southern California. Since 1989 he has been a member of the Earth Orbiter System Group at JPL where his current focus is on high precision orbit determination with GPS and its applications in Earth sciences.

ABSTRACT

On June 6, 1994, the US Air force implemented a yaw bias on most GPS satellites. By January 1995 the implementation was extended to all Block II satellites. The yaw bias was introduced as a way to make the yaw attitude of the GPS satellites modelable during shadow crossings. A yaw attitude model was written to simulate the new satellite attitude during eclipse seasons. This model was made freely available to the GPS community. Proper utilization of the yaw attitude model significantly improves the overall accuracy of precise positioning with GPS. Failure to account for the new attitude model could result in large positioning errors due to the mismodeling of the antenna phase center of the GPS satellite and of the carrier phase wind-up. After 6 months experience with the biased constellation a new yaw attitude model was written that is more efficient and accurate than the first model.

In this paper we discuss the implementation of the new attitude model in JPL's IGS process which produces daily GPS orbits of the highest quality. The design of the new model will be outlined, as well as guidelines for its implementation in POD schemes. The experience gained after a year of operations with the yaw-biased GPS constellation will be analyzed to evaluate the performance of the attitude models and assess optimal estimation

strategies based on the observed variability of the relevant parameters. Finally, we will discuss operational aspects of implementing the new model.

INTRODUCTION

On June 6, 1994, the US Air Force implemented a yaw bias on most GPS satellites. By January 1995 the implementation was extended to all the satellites except SVN10. The yaw bias was introduced as a way to make the yaw attitude of the GPS satellites modelable during shadow crossings (Bar-Sever et al., 1995). The yaw attitude of a biased GPS satellite during eclipse seasons is markedly different from the yaw attitude of a non-eclipsing satellite, or from that of an unbiased satellite. The yaw attitude of the GPS satellite has a profound effect on precise geodetic and space applications. This required the development of a special attitude model for biased GPS satellites. In addition to the yaw bias effects, that model also corrected other mismodeling that existed in the old model, namely, that of the "noon turn".

The first attitude model written for the biased constellation, named GYM94 (for "GPS Yaw attitude Model - 94"), was made freely available to the GPS community in the form of a collection of FORTRAN routines (Bar-Sever, 1994). GYM94 was implemented in JPL's GIPSY software and, in various forms, in other high-precision geodetic packages. A second generation model, GYM95, replaced GYM94 in GIPSY in early 1995. The design of the new model is outlined below.

More than a year after the implementation of the yaw bias, it is time to evaluate the success of this endeavor and to review its operational aspects. This is not an easy task since the biased and the unbiased constellations do not exist side by side and cannot be compared directly. Some

preliminary results have already indicated significant improvement in precise geodetic and space applications (Bar-Sever et al., 1995) but only now we possess enough data to have meaningful statistical comparisons between the performance of the biased and the unbiased constellations. Some of these statistical comparisons are reported in this paper. Also demonstrated here is the critical dependence of the yaw attitude model on the yaw rate parameter and the need either to estimate this parameter or to use a good a-priori value. This will lead us to a discussion of the operational aspects of the biased constellation and to propose a simplification of these operations.

THE NEW YAW ATTITUDE MODEL (GYM95)

The analysis that led to the implementation of the yaw bias on GPS satellites is described in Bar-Sever et al. (1995). A general description of the first yaw attitude model (GYM94) can also be found there. GYM94 computed the satellite yaw angle through numerical integration of a control law. Its output was a large file containing the yaw attitude history and, optionally, partial derivatives of the yaw attitude with respect to the yaw rate parameter. This file could later be interpolated to retrieve a yaw angle at the requested time. This process required relatively large amounts of computer memory and CPU time. In addition, the model's complex control law - a simulation of the on-board attitude determination algorithm did not allow much physical insight into the problem and was hard to tune. To overcome all these deficiencies the GYM95 model was created. GYM95 is simple enough to be described by a small set of formulas, allowing easy implementation in different computing environments. Its analytic nature, as opposed to the numerical nature of GYM94, allows queries at arbitrary time points with great savings in computer resources. Finally, it allows more flexibility in tuning and adapting it to the changing conditions of the GPS constellation.

The yaw attitude of a GPS satellite can be divided into four regimes: nominal attitude, shadow crossing, post-shadow maneuver and noon turn. Shadow crossing, together with the post-shadow maneuver comprise the "midnight turn". Most of the time (and for non-eclipsing satellites all the time) the satellite is in the nominal attitude regime. The post-shadow maneuver begins immediately after emerging from the Earth's shadow and lasts until the satellite has regained its nominal attitude.

This phase can last from zero to 40 minutes. The noon turn maneuver does not occur until the beta angle goes below about 5° and can last between zero and 40 minutes. During each regime the satellite yaw attitude is given by a simple formula with the main parameters being the time of entry to the regime and the yaw rate. For example, during shadow crossing the yaw attitude, Ψ , is given by:

$$\Psi = \Psi_i + \dot{\Psi}_i * (t - t_i) + 0.5 * |RR| * \text{SIGN}(b) * (t - t_i)^2 \text{ for } t < t_i + t_1$$

and

$$\Psi = \Psi_i + \dot{\Psi}_i * t_1 + 0.5 * |RR| * \text{SIGN}(b) * t_1^2 + |R| * \text{SIGN}(b) * (t - t_i - t_1) \text{ otherwise.}$$

b is the yaw bias, R is the maximal yaw rate, RR is the yaw rate rate, Ψ_i is the yaw angle upon shadow entry, $\dot{\Psi}_i$ is the yaw rate upon shadow entry and t_i is the time of shadow entry. t_1 is the spin-up/down time and is given by:

$$t_1 = (|R| * \text{SIGN}(b) - \dot{\Psi}_i) / (|RR| * \text{SIGN}(b)).$$

This formula expresses the simple fact that during shadow crossing the satellite is yawing at the maximum rate, R . It also takes into account the transition period, t_1 , from nominal yaw just before shadow entry to maximal yaw. This transition depends on the sign of the yaw bias and on the maximal yaw rate rate, RR . As discussed below, the Air Force is maintaining the yaw bias such that the sign of the bias is opposite to that of the orbit's beta angle. This requires changing the sign of the bias twice a year when the orbit's beta angle crosses zero. The effect of having the beta angle and the bias of opposite sign is to reverse the yaw direction of the satellite as soon as it crosses into shadow. The satellite, then, spins down and then spins up again in the other direction until it reaches its maximum yaw rate. It keeps yawing at that rate until it crosses into clear again and reacquires the Sun in its sensors. It then performs the quickest maneuver needed to resume nominal attitude. This may result in another yaw rate reversal. The satellite usually resumes nominal attitude within 30 minutes after shadow exit. Figures 1 and 2 illustrate the two types of yaw maneuvers of a conventionally biased satellite during shadow crossing. A satellite having a bias with the same sign as that of the beta angle will spin up as it enters into shadow instead of reversing its sense of rotation.

THE YAW RATE PARAMETER

The central parameter in the GPS yaw attitude model is the satellite maximal yaw rate (Bar-Sever et al., 1995). 10% Error in the yaw rate value will lead to a significant 35° error in yaw attitude during long shadow events. In order to minimize yaw rate errors they are being routinely estimated at JPL for each satellite and for each shadow event. The estimated yaw rate is treated as a piece-wise constant parameter for each satellite. The parameter value is allowed to change twice per revolution, mid-way between noon and midnight. Since a small error in the yaw rate can cause a large yaw error over time and since our a-priori knowledge of the yaw rate is not sufficiently accurate, we found it necessary to iterate on the yaw rate value. JPL routinely publish the final estimates for the yaw rates. They are available as daily text file via anonymous ftp to 128.149.70.41, directory "pub/jpligsac". Due to a software bug, yaw rates prior to February 16, 1995, are not available. The yaw rates were observed to be, indeed, both satellite-dependent and time-dependent. Most users of the new yaw attitude model are currently not estimating the yaw rates and, instead, treat them as constants with three possible values that were supplied early on by JPL. These values are: $0.113^\circ/\text{sec}$ for Block II satellites, $0.103^\circ/\text{sec}$ for Block IIA satellites and $0.087^\circ/\text{sec}$ for those Block II satellites with a reaction wheel failure (SVNs 14, 16, 18, 19 and 20). A review of the estimated midnight yaw rate values over the last six months (Figure 3) reveals that the three a-priori values need to be corrected, but the current behavior displayed by the estimated yaw rates preclude any constant value from being a good approximation over the whole eclipse season.

The most striking feature in Figure 3 is the discontinuity of the estimated yaw rates in the middle of eclipse season. This, as yet unexplained behavior, is exactly correlated with the time of the upload of a new yaw bias to the satellite attitude control system. This upload occurs twice per year at the middle of eclipse season for each satellite. Only SVNs 22, 25 and 29 do not seem to suffer from a yaw rate jump, but only SVNs 22 and 25 should be considered an exception, though, because SVN 29 does not undergo a bias switch.

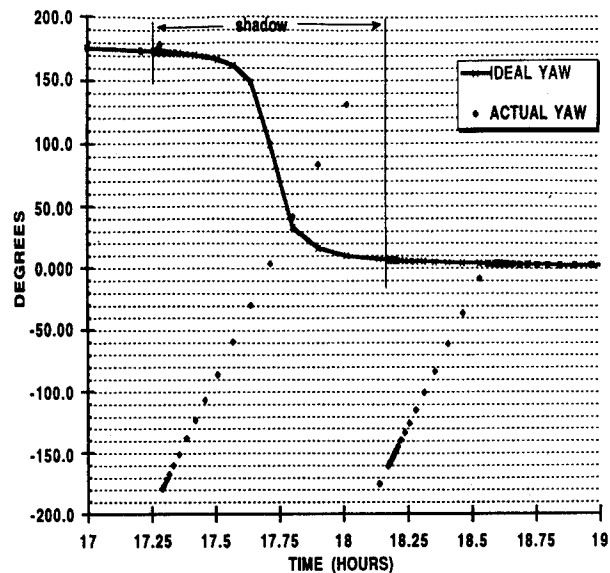


Figure 1. An illustration of a typical yaw maneuver during shadow crossing when no yaw rate reversal is needed upon shadow exit. The "ideal" yaw is what the satellite would have done if it could see the Sun and it is the way the old yaw attitude was modeled.

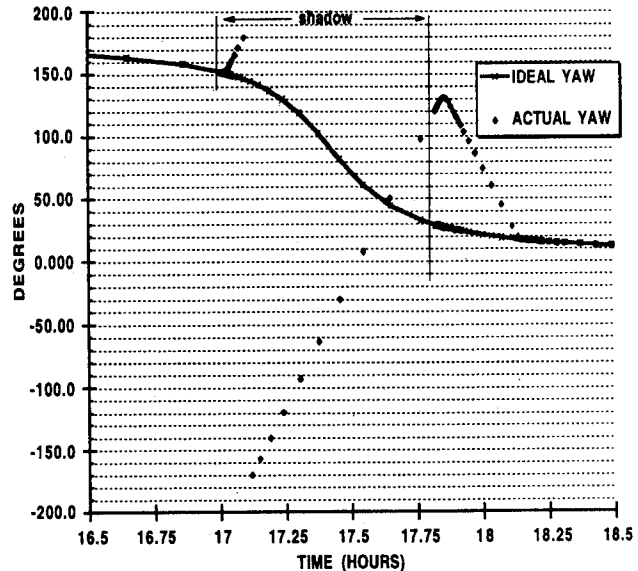


Figure 2. Same as Figure 1 but with yaw rate reversal upon shadow exit.

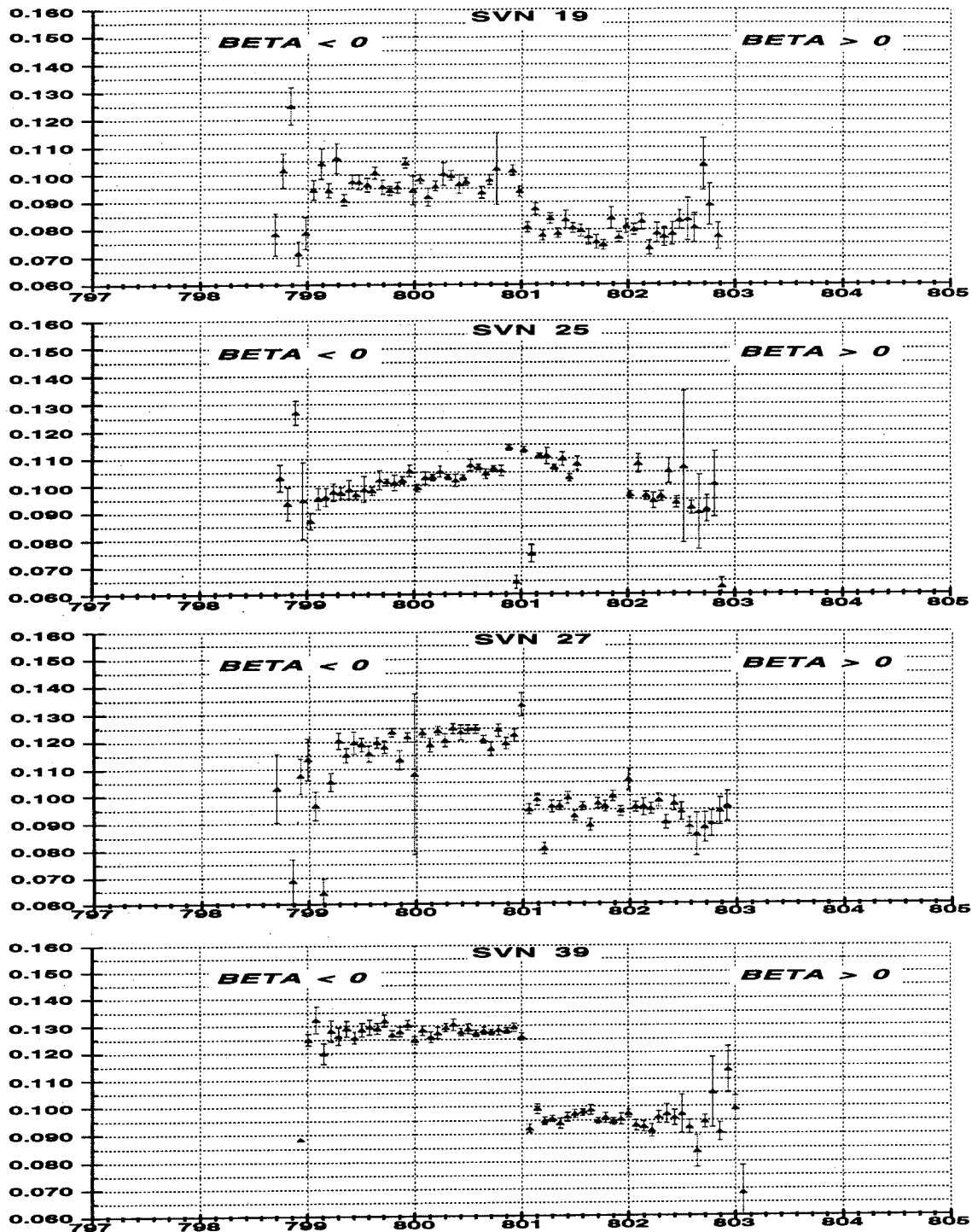


Figure 3a. Estimated midnight turn yaw rates for plane A satellites between March and August, 1995, along with their formal errors. The abscissa scale is in GPS week and the ordinate scale is in degrees/seconds.

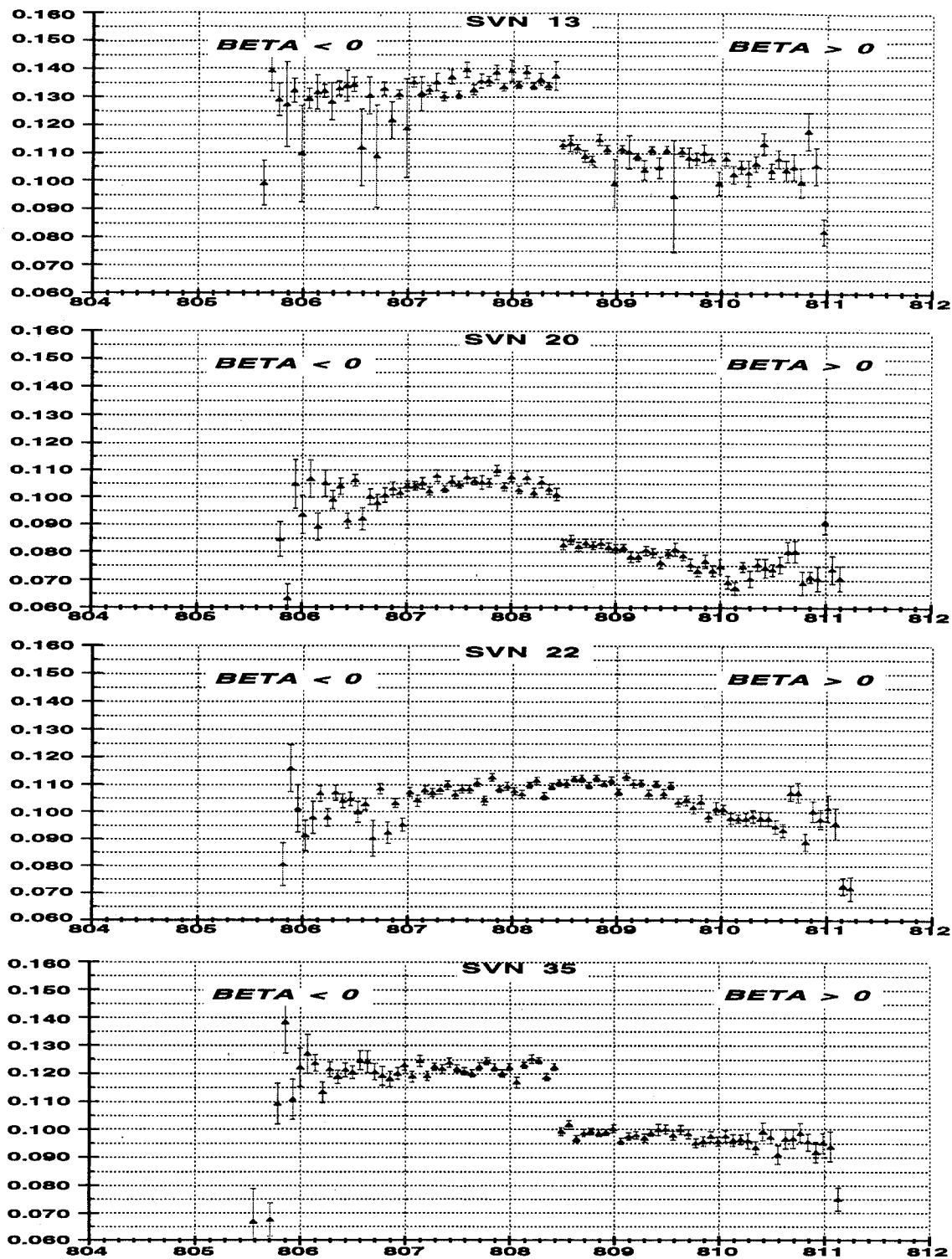


Figure 3b. Same as Figure 3a but for plane C satellites.

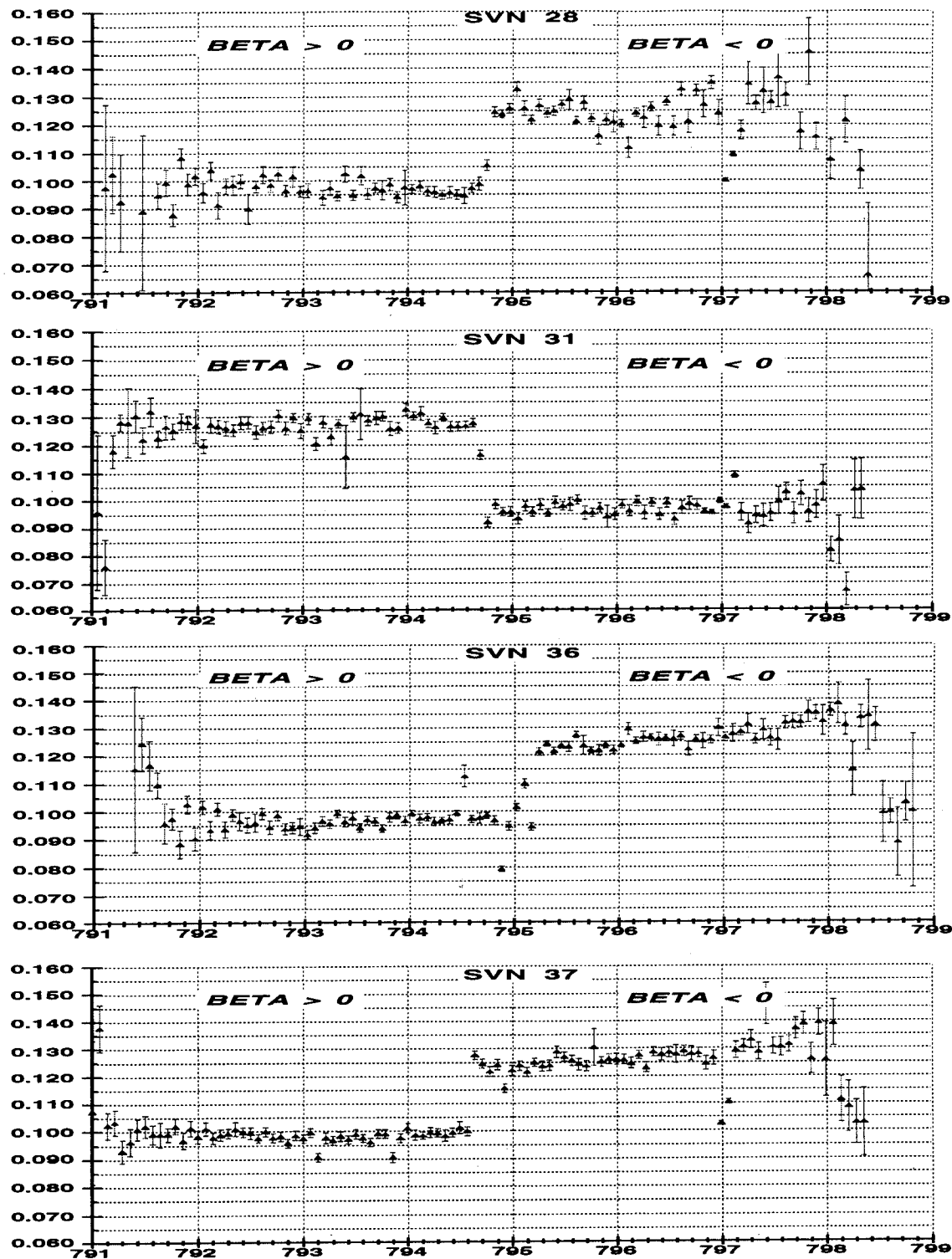


Figure 3c. Same as Figure 3a but for plane D satellites.

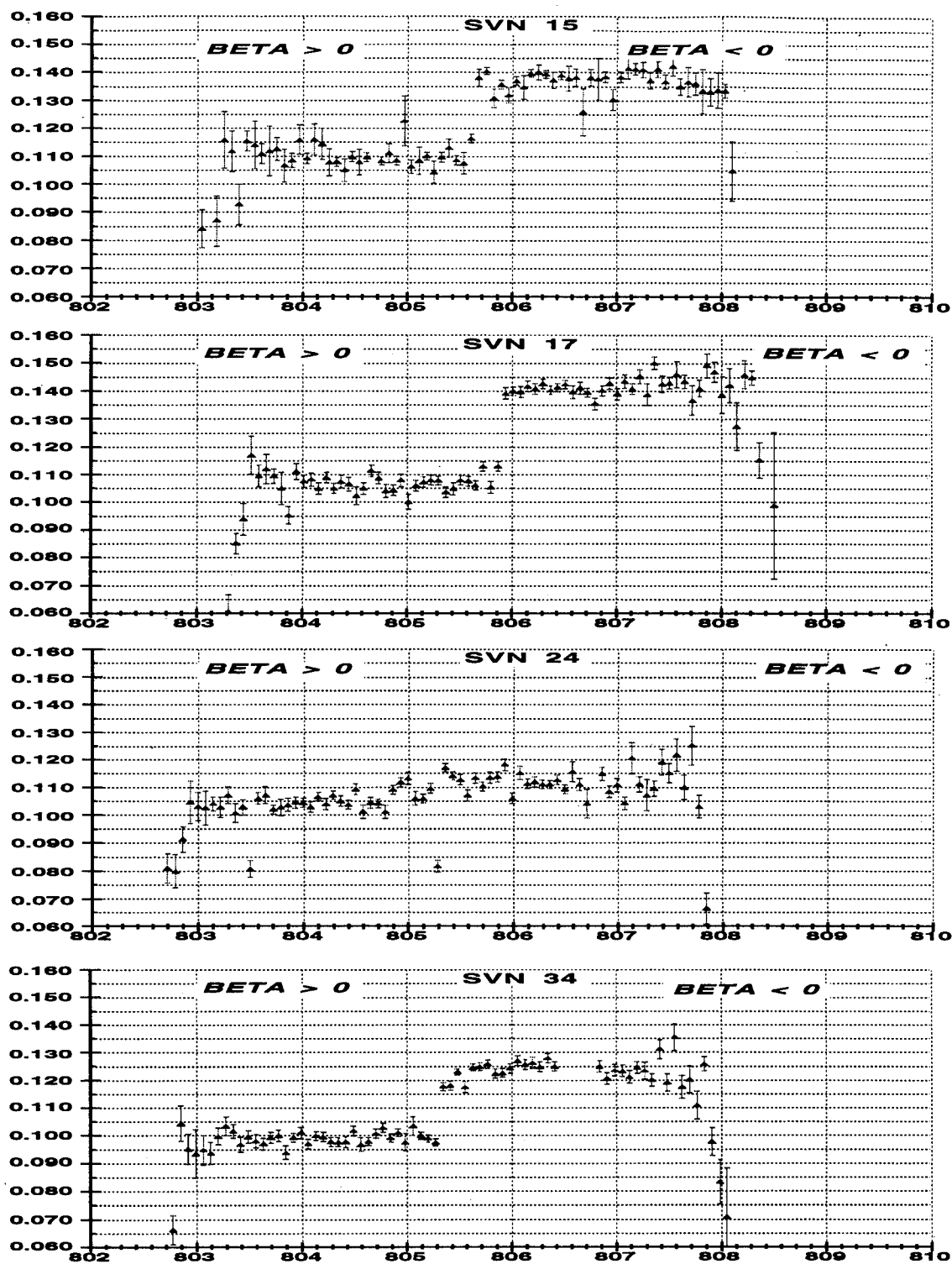


Figure 3d. Same as Figure 3a but for plane E satellites.

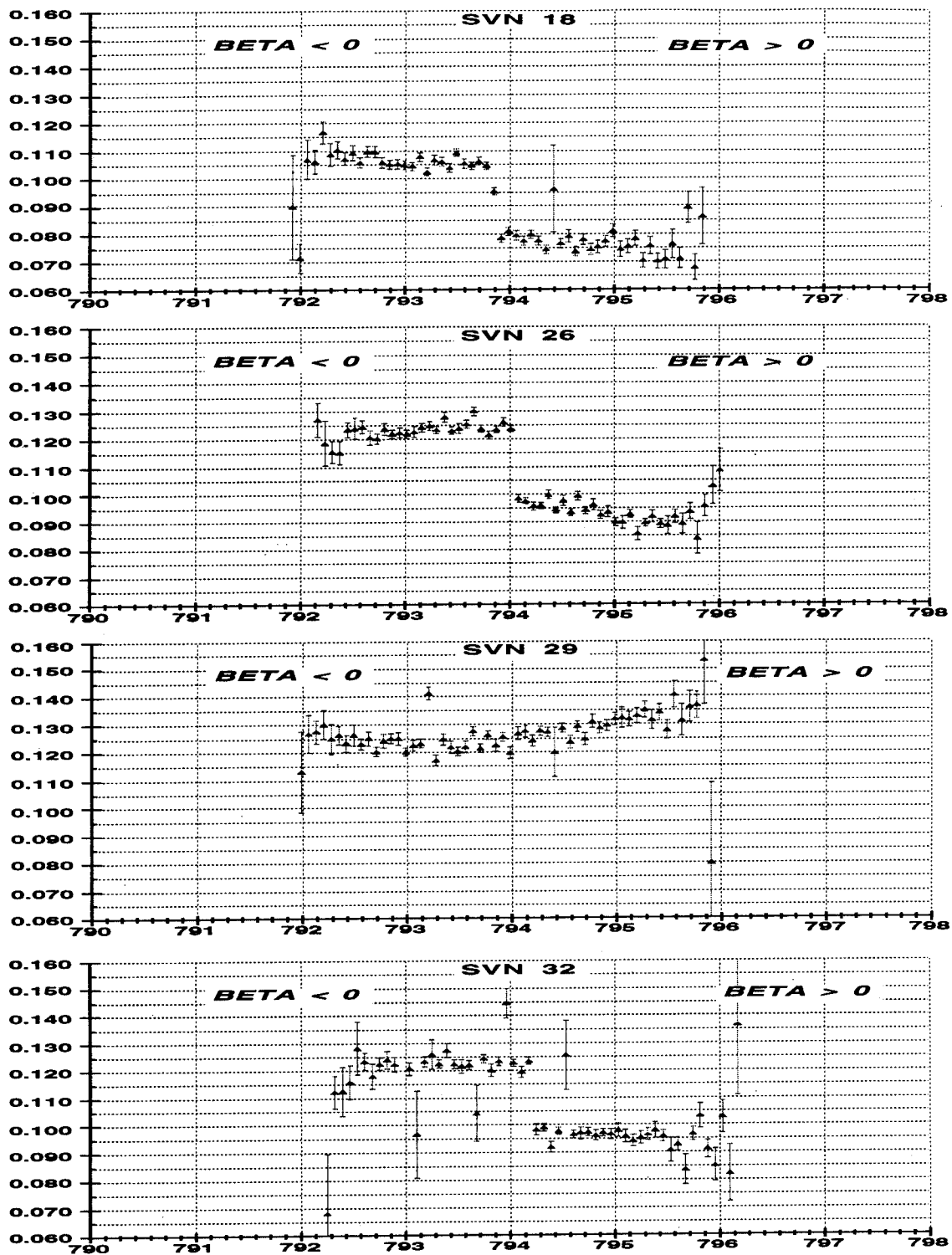


Figure 3e. Same as Figure 3a but for plane F satellites.

PERFORMANCE EVALUATION OF THE BIASED CONSTELLATION

Great care needs to be exercised when comparing the performance of the GPS prior to June 6, 1994 - the unbiased constellation, to that of the current, biased, constellation. This is because there are constant improvements in GPS data processing and it is hard to isolate the effects of the yaw bias on observed improvements in the quality of GPS-based products. Nevertheless, some judgment can be made as to the success of yaw-biasing the constellation by comparing carefully-selected statistics from before and after the yaw bias implementation.

One useful comparison is that of the post-fit residuals. This measure of solution quality is most sensitive to the quality of the modeling and to the number of degrees of freedom in the estimation scheme. The most important improvement in the IGS processing at JPL in the past year has been in the global distribution of the ground network. Assuming everything else is kept constant, this should have little effect on the post-fit residuals. To further isolate the yaw bias effects we will only compare post-fit residuals of eclipsing satellites to that of non-eclipsing satellites. Theoretically, the only difference between eclipsing and non-eclipsing satellites is in the modeling of their navigation signal.

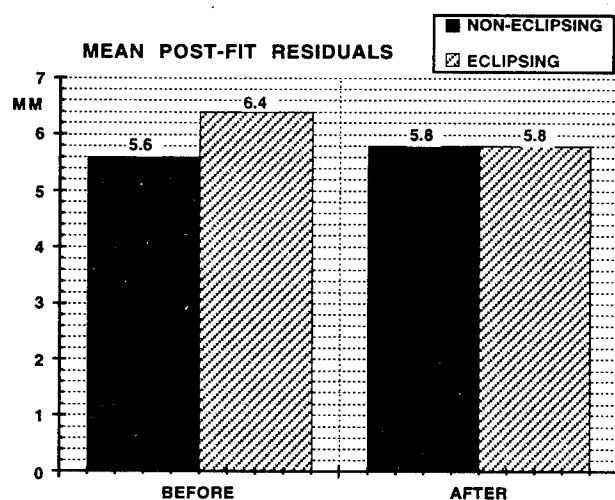


Figure 4. Comparison of post-fit residuals of eclipsing and non-eclipsing satellites. The "after" results are based on the JPL IGS products from June 18 to July 27, 1995 (Zumerge & Bertiger, 1995). The "before" results are based on reprocessing data from January 8 to February 27, 1994 with the current estimation technique. Roughly the same satellites are eclipsing in both periods.

Figure 4 demonstrates that we are now doing a much better job in modeling eclipsing satellites than before the yaw bias was implemented. In fact, there is now no evidence for any mismodeling of eclipsing satellites.

It is not clear, though, how much of the additional data strength suggested by the improved level of post-fit residuals is going toward improving the actual products. The GPS orbits themselves are one such product. In fact, observations about GPS orbits were the motivation that led to the study of the yaw attitude problem and to the implementation of the yaw bias. A good measure for the quality of orbit solutions is overlap repeatabilities. JPL's daily solutions span 30 hours, centered on noon of each day, resulting in a six-hour overlap between consecutive days. The RMS difference between the two daily solutions during this overlap period is indicative of the quality of the orbit. Figure 5, from 1993, shows the mean of the orbit overlap of all GPS satellites as the constellation was in transition to a period when there are no eclipsing satellites. A consistent improvement in overlap repeatabilities during such a transition was typical before the bias was implemented, suggesting the existence of a problem in modeling eclipsing satellites.

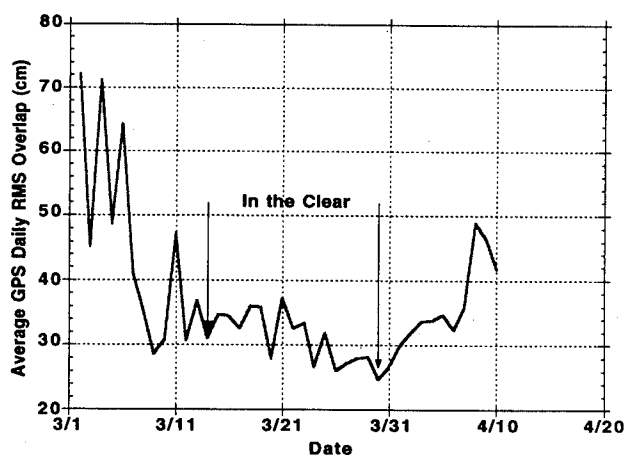


Figure 5 Mean daily overlap repeatability of all GPS satellites during March and April, 1993, when the GPS constellation transitioned in and out of a period when no satellites were eclipsing.

A long-term comparison of overlap repeatabilities clearly demonstrates that this pattern ceased to exist immediately after the implementation of the yaw bias. Figure 6 depicts weekly averages of overlap repeatabilities of all GPS

satellites from January, 1994, to August, 1995. The GYM94 model was implemented in JPL's GIPSY software in September 1994 as the GPS constellation was emerging out of a period when all satellites were in the clear. It is evident from Figure 6 that from then on, periods when all satellites were in the clear are no longer local minima for the mean orbit repeatabilities, suggesting that the mismodeling of satellites during eclipse seasons no longer exist.

A more direct measure of the improvement to orbits of eclipsing satellites can be seen from Figure 7 which shows that after the yaw bias was implemented the quality of the orbits of eclipsing satellites is essentially the same as that of non-eclipsing satellites, in marked contrast to the situation before the implementation, where eclipsing orbit were 18% worse off than non-eclipsing satellites.

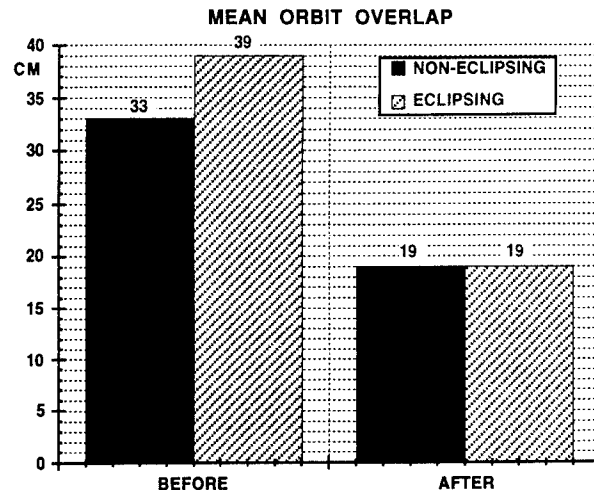


Figure 7. Same as Figure 4 but for orbit overlaps

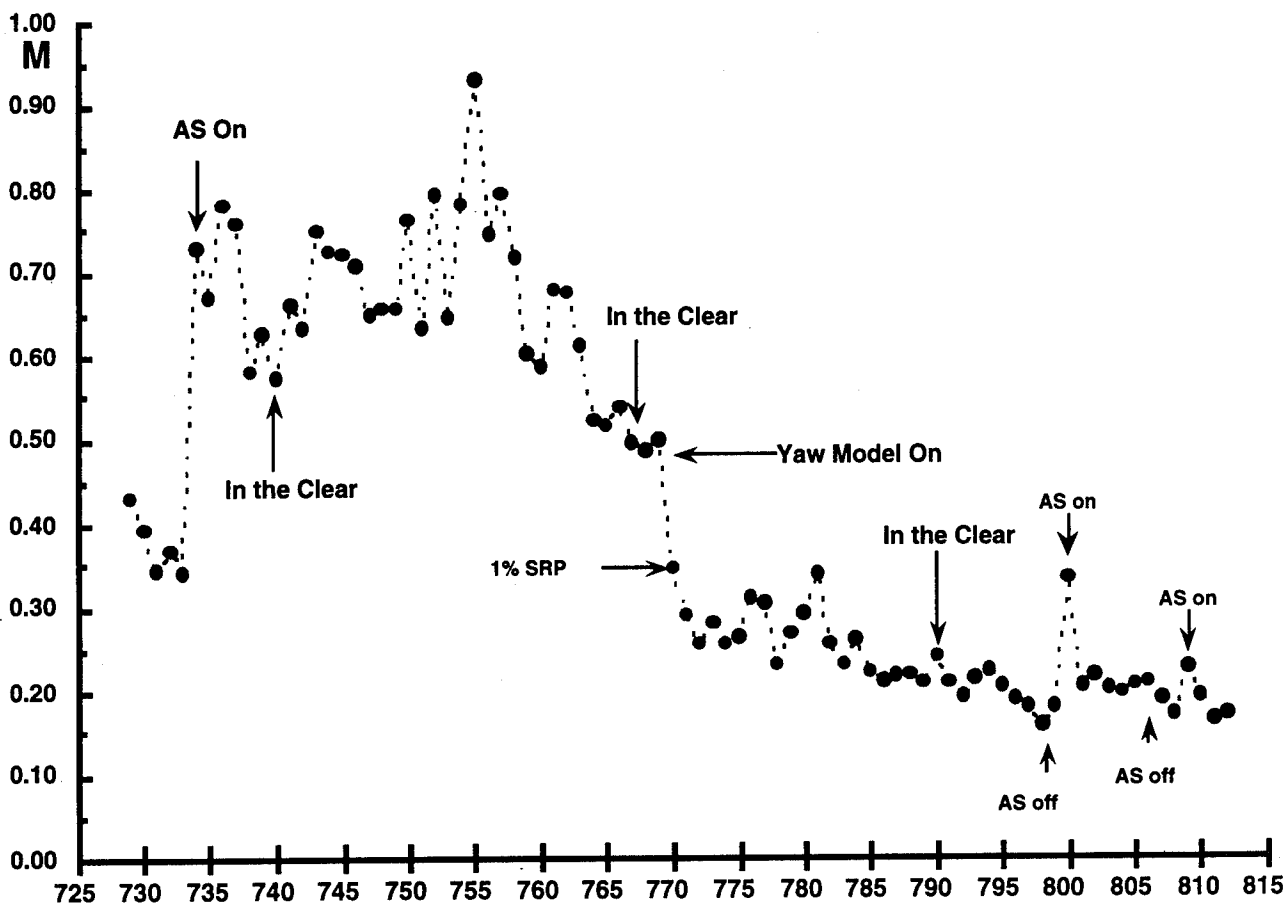


Figure 6. Weekly mean GPS orbit repeatabilities of the JPL solutions for the IGS. The mean is taken over all satellites and over a full week. The yaw model was implemented at JPL on September 20, 1994 (GPS week 767). The abscissa scale is in GPS week. The ordinate scale is in meters. (From David Jefferson, JPLIGSAC)

OPERATIONAL ASPECTS OF THE BIASED CONSTELLATION

Except for SVN 29, which suffers from a problem that precludes its yaw bias from being changed, The Air Force is maintaining the yaw bias on all satellites such that the sign of the bias is opposite the sign of the orbit's beta angle. This requires the upload of a new yaw bias twice a year for every satellite. This upload is done roughly when the orbit's beta angle crosses zero. As was described earlier, knowledge of the sign of the yaw bias is critical for proper modeling of the satellite attitude. Because of operational constraints, the exact upload time is not known sufficiently in advance. This, and the lack of formal communications channel between the GPS operators and the GPS-user community causes delay in the dissemination of the bias switch timing information. As a result, the radiometric signal from the eclipsing satellites is often mismodeled during a few-day period around the time beta angle crosses zero (when the eclipse period is maximal).

The reason behind the yaw bias switching is to minimize the time it takes for the spacecraft to recover nominal attitude after shadow exit. As is shown bellow, keeping the sign of the yaw bias opposite to that of the beta angle does imply faster recovery of the nominal attitude on average - but only by a very small margin. Furthermore, it will be argued here that there are no clear benefits to be gained from a quicker recovery of the nominal attitude.

A simulation was performed to asses the time needed to recover the nominal attitude after shadow exit. The recovery time is equal to the yaw error upon shadow exit, time the maximal yaw rate, after adjustment is made to account for possible reversing of the yaw rate direction and the resulting spin down and spin up time. The yaw error upon shadow exit was computed as a function of the shadow length, where account has been taken of the spin down and spin up time after shadow entry if the sign of the bias is opposite that of the beta angle. The recovery time was computed for a variety of realistic yaw rates and for all possible shadow duration. Two cases where

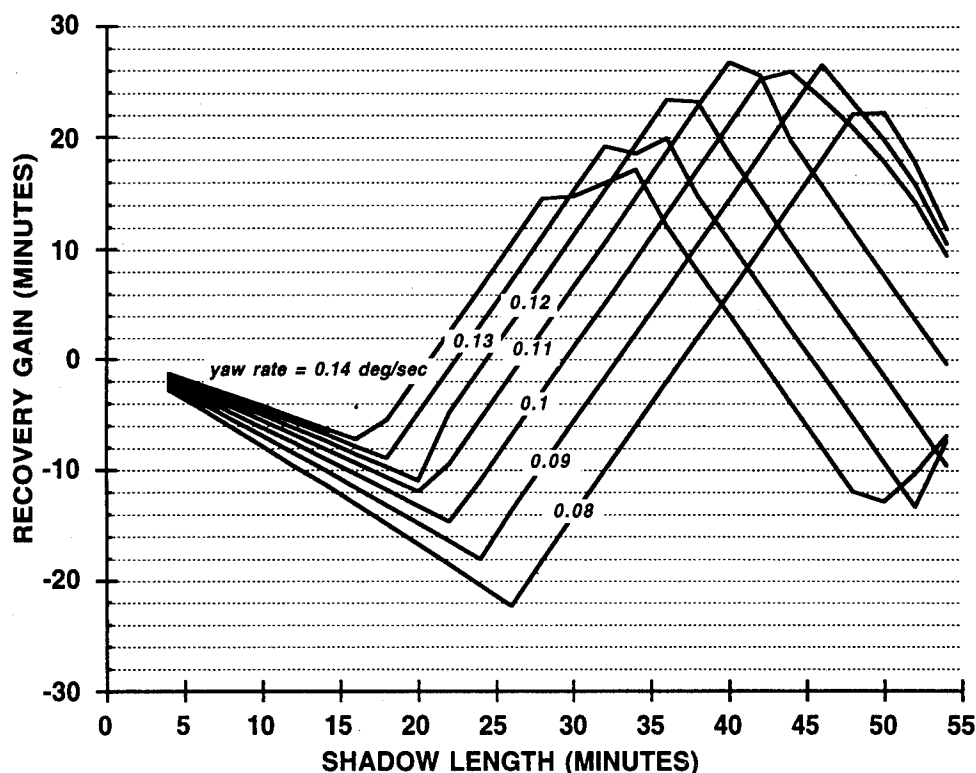


Figure 8. Given a positive beta angle, the recovery gain is the difference between the recovery time with yaw bias equal to -0.5° and the recovery time with yaw bias equal to $+0.5^\circ$. The recovery time is defined as the time from shadow exit until the nominal yaw attitude is recovered.

Table 1. Seasonal and yearly mean values of the recovery gains for seven realistic yaw rate values.

| yaw rate (deg/sec) | 0.8 | 0.9 | 1.0 | 1.1 | 1.2 | 1.3 | 1.4 |
|-------------------------------------|------|-----|-----|-----|-----|-----|-----|
| Average gain over half a year (min) | -2.7 | 1.1 | 3.8 | 4.1 | 2.9 | 1.7 | 0.5 |
| Average gain over a year (min) | -1.4 | 0.5 | 1.9 | 2.0 | 1.4 | 0.9 | 0.3 |

compared: one with the yaw bias and beta angle having opposite signs (the current situation), and the second one is with the yaw bias and beta angle having the same sign. The difference in recovery time between these two cases is termed here "the recovery gain". The results of this comparison are presented in Figure 8. The recovery gain is seen to change during eclipse season and it attains both positive and negative values for every choice of the yaw rate. This suggests that the figure of merit should be the seasonal average of the recovery gains. These averages are presented in Table 1, below. It can be seen that under the most favorable conditions, that is, satellites with yaw rate of about 1.1 deg/sec, the gain in recovery time is just 4.1 minutes. For the more commonly observed yaw rate values of 0.95 deg/sec and 1.3 deg/sec the gain is about 3

and 2 minutes, respectively. For the five slowly-spinning reaction-wheel "cripples" there is actually a negative gain of about two minutes. Note that if the yaw bias remains unchanged during the whole year then half the time it will have a sign opposite to that of the beta angle and, consequently, half the time the recovery rate will be optimal and averaging over a full year will yield recovery gains that are smaller than 2 minutes in the most extreme case.

But recovering nominal attitude a bit sooner or later has really no effect on the functionality of the spacecraft. The only concern might be to avoid delay in the resumption of power supply from the solar panels, but this has no relation to the duration of the attitude recovery time. The

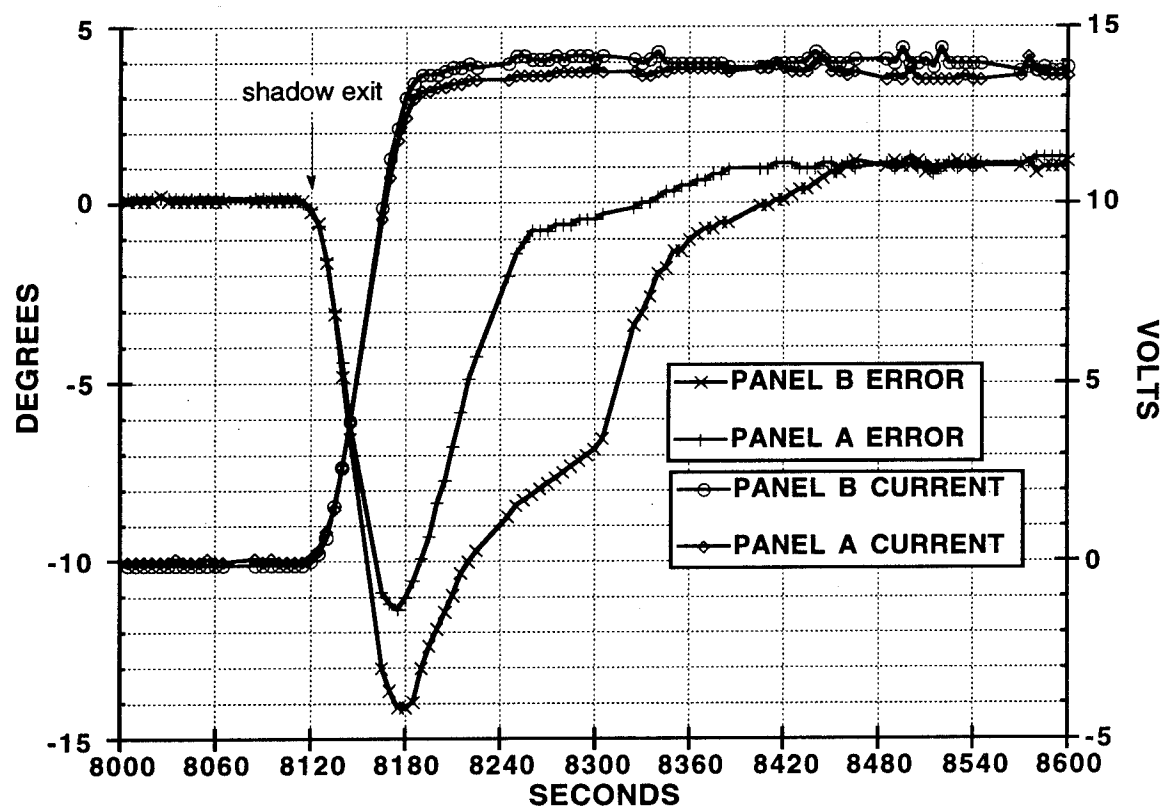


Figure 9. Solar panel pitch error (left ordinate) and current supply (right ordinate) immediately after shadow exit, during eclipse season in 1993. The origin of the abscissa scale is arbitrary. This satellite was yaw biased.

reason is that the solar panels are never more than 28 degrees in error upon shadow exit and the average error is probably much smaller. This guarantees sufficient power supply immediately upon shadow exit. Since the array pitch rate is about 0.1 deg/sec, optimal power supply will resume in less than 5 minutes, regardless of any yaw maneuver the satellite is undergoing. These facts are evident in Figure 9 which was constructed from SVN 24 telemetry during maximum eclipse - a worst case scenario. The pitch error is corrected within 5 minutes after shadow exit and full power supply is available 1 minute after shadow exit.

In conclusion, it is recommended that the yaw bias on all GPS satellites will be permanently set to +0.5 (the unchangeable value on SVN 29). JPL will continue to estimate and monitor the yaw rates of all GPS satellite in an effort to publish a set of values that will always be accurate enough to be used as a-priori for precise GPS applications.

ACKNOWLEDGMENTS

The author wishes to thank the GPS operations team at 2SOPS, Falcon Air Force Base, for an outstanding level of cooperation and openness. Thanks also to David Jefferson and the JPL IGS Analysis Center team for providing their daily GPS solutions. The work described in this paper was carried out in part by the Jet Propulsion Laboratory, California Institute of Technology, under contract with the National Aeronautics and Space Administration.

REFERENCES

- Bar-Sever, Y., 1994. Improvement to the GPS Attitude Control Subsystem Enables Predictable Attitude During Eclipse Seasons. IGS Mail #0591, May, 1994.
- Bar-Sever, Y., Anselmi, J., Bertiger, W., Davis, E., 1995. Fixing the GPS Bad Attitude: Modeling GPS Satellite Yaw During Eclipse Seasons. Proceedings of the ION National Technical Meeting, Anaheim, CA, January 1995.
- Zumberge J.F., Bertiger, W.I., 1995. The Global Positioning System - Theory and Application. Vol. I, Chapter 16, "Ephemeris and Clock Navigation

Message Accuracy", Senior Editors: B.W. Parkinson, J.J. Spilker Jr.; Editors: P. Axelrad, P. Enge. In press.

Effect of GPS Orbit Accuracy on GPS-determined Topex/Poseidon Orbit

H. J. Rim, B. E. Schutz, P. A. M. Abusali, and B. D. Tapley
Center For Space Research, University of Texas at Austin

BIOGRAPHIES

H. J. Rim received his B.S. and M.S. from Seoul National University, Department of Aeronautical Engineering. He received his Ph.D. from the University of Texas at Austin, Department of Aerospace Engineering and Engineering Mechanics, in 1992. He is currently Research Associate at the Center for Space Research, where his efforts include GPS-based precise orbit determination for Topex/Poseidon, EOS ALT/GLAS, and geodetic applications of GPS.

B. E. Schutz is Professor of Aerospace Engineering and Engineering Mechanics at the University of Texas at Austin and holds the Gulf Oil Foundation Centennial Fellowship in Engineering. He is also Associate Director of the Center for Space Research and a member of the Applied Research Laboratory staff. He is Science Team Leader for the EOS Geoscience Laser Altimeter System.

P. A. M. Abusali is Research Scientist with the Center for Space Research at the University of Texas at Austin.

B. D. Tapley is Professor of Aerospace Engineering and Engineering Mechanics at the University of Texas at Austin and holds the Clare Cockrell Williams Centennial Chair in Engineering. He established the orbit mechanics program in the ASE-EM department in 1961 and the Center for Space Research in 1981, developing both into international centers for study and research. He also serves as the Director of the Texas Space Grant Consortium.

ABSTRACT

From the very successful TOPEX/POSEIDON (T/P) oceanographic satellite mission, it has been demonstrated that the GPS tracking system could provide better than 3 cm radial orbit accuracy using the GPS dual-frequency carrier phase observable. To achieve this 3 cm T/P orbit accuracy, analysis requires precise GPS ephemerides, which become one of the major sources of error for the precise T/P positioning using this data type. There are two approaches to obtain the precise GPS ephemeris: 1) solve the GPS orbit simultaneously with the T/P orbit, and 2) fix the GPS ephemeris to an independent determination,

such as the International GPS Service for Geodynamics (IGS). For the simultaneous solution of T/P and the GPS constellation, two strategies were compared in terms of forming the double-differenced GPS phase measurement. If the explicit double differences were formed between T/P and each ground station, the data provides continuous tracking of the T/P orbit, while the coverage for a GPS satellite is only about 25-30% of the orbit. Adding the double differences between the ground stations, even though these data do not contain T/P orbit information, allows higher coverage for GPS orbit. Also, the effect of empirical GPS parameters on the GPS orbits and the T/P orbit was investigated. For each case, the resulting GPS orbit was compared to the IGS GPS ephemerides. For the case where the GPS orbits were fixed, several GPS orbit related parameters were adjusted to minimize the effect of GPS orbit error on the T/P orbit.

INTRODUCTION

Since the successful launch of T/P in August 1992, this mission has presented a unique opportunity to evaluate different satellite tracking systems. The satellite laser ranging (SLR) system provides very accurate slant range information during short intervals (10-15 min). However, there exists large coverage gaps because of their incomplete tracking. The DORIS system provides more coverage from 40-50 station ground network using a Doppler measurement. The GPS tracking system provides continuous and globally dense data set with high precision phase measurement. However, the GPS orbits are a potential error source for the T/P orbit.

Several different POD approaches were proposed for the T/P POD using GPS measurement. Those include 1) fully dynamic approach which requires precise models of the forces acting on T/P and GPS satellites. 2) the reduced dynamic approach (Wu et al., 1991) which uses both geometric and dynamic information and weighs their relative strength by solving for process noise accelerations in the T/P force model to absorb dynamic model errors. For both approaches, the GPS satellite's positions are computed using a fully dynamic approach. In this paper, the T/P orbit was computed using a fully dynamic approach.

There are two approaches to obtain the precise GPS ephemeris in the T/P orbit determination using GPS tracking data. One is to solve the GPS orbit simultaneously with the T/P orbit. The other is to fix the GPS ephemeris to an independent determination.

For the simultaneous solution of T/P and the GPS constellation, two strategies were compared in terms of forming the double-differences. If the explicit double differences were formed between T/P and each ground station, this data provides continuous tracking of the T/P orbit, while the coverage for a GPS satellite is only about 25-30% of the orbit. Adding the double differences between the ground stations, even though these data do not contain T/P orbit information, allows higher coverage for the GPS orbit. The GPS orbit accuracy depends not only on the coverage of the GPS orbit, but also on the parameterizations for GPS. The effect of empirical parameters, such as constant along-track parameters (C_t) and once per orbital revolution (1-cpr) parameters, on the GPS orbit accuracy was investigated for the different combinations of double-differences.

Since the precise orbit determination (POD) of GPS satellites is a key requirement for GPS-based precise geodetic applications, much effort has been devoted to improve the GPS orbit accuracy for geodetic applications. After establishing globally distributed permanent GPS tracking sites by the IGS, the GPS orbits are routinely computed with the estimated accuracy of better than 20 cm (Zumberge et al., 1994). Several different center's IGS orbits were used for T/P orbit computation when the GPS orbits were fixed to independently determined ephemerides. For this case, GPS orbit related measurement parameters were introduced to minimize the effect of GPS orbit error on the T/P orbit.

DATA SETS

Two types of double-differenced GPS phase observations were processed. One is the double-differenced data between ground stations, referred to as IGS data. The other is the double-differenced data between a ground station and the T/P satellite, referred to as Topex data. Five days of data for both data type were processed from April 23, 1995, which corresponds to the GPS week 798, and the T/P Cycle 96. Twenty four GPS satellites from 32 ground stations were used for the IGS data, while from 24 stations were used for the Topex data. The data were sampled at 2 min interval for both data sets, and a 15° elevation cut-off applied to the ground GPS receivers, while the data above the T/P local horizon were used for the Topex data.

SOLUTION STRATEGIES

The T/P standard models were used (Tapley et al., 1994a; McCarthy, 1992) as the reference models. The JGM-3 gravitational model (Tapley et al., 1994b) was used as the reference geopotential field (70x70 for T/P; 12x12 for GPS). The T/P tuned ocean tide model (Eanes, 1994) was used as the reference ocean tide model. The GPS non-gravitational model included the ROCK4T radiation pressure and y-axis force (Fliegel et al., 1992). The GPS station coordinates are given in the IERS Terrestrial Reference Frame (ITRF93). The SLR-derived series for Earth polar motion and UT1 were used as the Earth orientation model. (Eanes and Watkins, 1993). More in-depth description of dynamic and measurement models could be found in Schutz et al., 1994.

Two approaches of obtaining the precise GPS ephemeris in the Topex data processing were investigated. One resulted from adjusting the GPS orbit simultaneously with the T/P orbit—denoted as “adjusted GPS case”. The other resulted from fixing the GPS orbit to an independent determination, such as IGS—denoted as “fixed GPS case”.

For the IGS data and adjusted GPS case for Topex data, 30 hour arcs were used to get the middle 24 hour orbits. The epoch state, a scale factor of ROCK4 (C_r), and 15 hour y-bias parameters were adjusted for each GPS. And these estimated C_r and y-bias parameters were fixed for the case when empirical parameters—30 hour C_t and 1-cpr parameters in transverse (T) and normal (N) directions—were adjusted for GPS. The double-differenced ambiguity parameters, 2.5 hour zenith delay parameters, and coordinates of selected ground stations were estimated for every cases. The epoch state, 6 hour C_t , and 30 hour 1-cpr in T and N directions were adjusted for T/P. For the fixed GPS case, 1-day arcs were used instead of 30 hour arcs.

For the adjusted GPS case, two strategies were compared in terms of forming the double-differenced GPS phase measurement. One is to process only the double-differences between T/P and a ground station—denoted as Case A. The other is to add the double-differences between the ground stations to Case A—denoted as Case B. Also, for each case, empirical parameters for GPS, such as C_t and 1-cpr parameters—denoted as (II), were investigated in addition to the y-bias and C_r parameters—denoted as (I)—to evaluate the effect of these parameters on GPS orbit accuracy.

For the fixed GPS case, the orbit element correction parameters were introduced as the measurement parameters to reduce the effect of GPS orbit errors on the T/P orbit. Those errors were modeled as,

$$\rho_{\text{new}} = \rho + \sum_{i=1}^6 \frac{\partial \rho}{\partial \text{oe}_i} \cdot \delta \text{oe}_i$$

where

ρ_{new} = corrected station-GPS or GPS-T/P range
 ρ = uncorrected station-GPS or GPS-T/P range
 oe_i = i -th orbit element
 δoe_i = i -th orbit element correction parameter

Four orbit element correction parameters were estimated with a tight constraint for each GPS orbit pass, while the semi-major axis and the mean anomaly were fixed.

GPS ORBIT COMPARISON

To evaluate the GPS orbit solutions for the adjusted GPS cases, the GPS orbit solutions were compared with the JPL-IGS orbits (Zumberge et al., 1993). The mean orbit repeatability—mean of 6 hour orbit overlap differences—for the JPL's orbit solution for GPS week 798 was 15.7 cm.

Table 1 summarizes GPS orbit comparisons with the JPL-IGS ephemeris. Case A (I), where only station-T/P double-differenced data were processed using nominal GPS parameters, showed the largest orbit difference of 33 cm in 3D RSS. CSR (I) case, where only station-station double-differenced data were processed, had better agreement of 29 cm. This was expected because of the reduced coverage of the GPS orbit for the station-T/P double-differenced data. Case B (I), where the station-T/P and station-station double-differenced data were combined, demonstrated the least difference of 23 cm for the nominal GPS parameterization of y -bias and C_r . This suggests that by adding station-T/P double-differenced data to the station-station double-differenced data, the GPS orbit accuracy could be improved, especially in T and N components.

It was demonstrated that the empirical parameters for GPS contributed in reducing the orbit difference with JPL-IGS ephemeris. CSR (II) case, where the empirical parameters were estimated for GPS, reduced the transverse difference by 4 cm, and 3 cm in 3D RSS, comparing with CSR (I) case, where the nominal GPS parameters were adjusted. 7 cm and 4 cm improvements in the 3D RSS orbit difference were achieved by employing the empirical parameters for Case A and Case B, respectively. It is interesting to note that the GPS orbit solutions for CSR (II) and Case A (II) had the similar level of orbit differences against JPL-IGS orbits. Now, the GPS orbit difference became less than 20 cm for Case B (II), where the station-station and station-T/P double-differenced data were combined, and the empirical GPS parameters were adjusted.

TOPEX ORBIT COMPARISON

The T/P orbit solutions were compared with the JPL's reduced dynamic solution (Bertiger et al., 1994). Since the reduced dynamic solution is less sensitive to dynamic

model errors, this orbit is considered to be a useful comparison orbit.

Adjusted GPS Case

Table 2 summarizes T/P orbit comparisons with the JPL's reduced dynamic solution for adjusted GPS cases. The orbit difference in 3D RSS marginally reduced by mixing the station-station double-differenced data with the station-T/P double-differenced data when the nominal GPS parameters were estimated. The difference in the radial (R) component, however, increased by 2 mm, while the difference in N component decreased about 7 mm. When the empirical GPS parameters were adjusted, the 3D RSS difference decreased by 6 mm by combining the station-station and the station-T/P double-differenced data. Note that the difference in R component was not affected, while 3 mm and 7 mm improvement occurred in the orbit agreement in T and N components.

It is evident that estimating empirical GPS parameters helps in reducing the T/P orbit difference against the JPL's reduced dynamic solution. For the station-T/P double-differenced data, 2 mm, 6 mm, and 2 mm reduction in RTN orbit difference, respectively, was demonstrated. For the mixed double-differenced data, there were 4 mm, 8 mm, and 2 mm decreases in RTN orbit difference. Now, the T/P orbit difference became 5.2 cm in 3D RSS for Case B (II), where the mixed double-differenced data were processed with empirical GPS parameters.

Fixed GPS Case

For the fixed GPS case, the GPS ephemeris from four different IGS centers were tested, along with the CSR (I) and CSR (II) solutions. Those IGS centers were: 1) JPL, 2) Astronomical Institute, University of Berne (CODE), 3) GeoForschungsZentrum (GFZ), and 4) Scripps Institution of Oceanography, University of California, San Diego (SIO).

Table 3a summarizes T/P orbit comparisons with JPL's reduced-dynamic orbit, when the GPS orbit was fixed to solutions from different centers. Since the only difference in these cases is the GPS ephemeris, it serves as an indirect way of evaluating the quality of GPS orbit solutions. JPL's ephemeris generated T/P orbit, which agreed the best with JPL's reduced-dynamic orbit—1.7 cm, 4.7 cm, and 2.4 cm in RTN components, respectively, and 5.5 cm in 3D RSS. This agreement is better than most of the adjusted GPS cases, except Case B (II). SIO's orbit resulted T/P orbit, which differed the most with JPL's reduced-dynamic orbit—4.1 cm, 9.3 cm, and 3.5 cm in RTN components, respectively, and 10.7 cm in 3D RSS. The other center's IGS orbits performed nicely to generate T/P orbits, which agreed with the JPL's reduced-dynamic orbit at 2–2.4 cm level in R component, 5.2–6.6 cm in T

component, 2.7–3.2 cm in N component, and 6.2–7.7 cm in 3D RSS. Comparison of CSR (I) and CSR (II) cases shows the effect of the empirical GPS parameters on the T/P orbit for the fixed GPS case—4 mm, 7 mm, and 2 mm in RTN components, respectively, and 8 mm in 3D RSS.

In Table 3b, T/P orbit comparisons with the JPL's reduced-dynamic orbit were summarized when the orbit element correction parameters were adjusted for the fixed GPS cases. It is evident from this table that the T/P orbit accuracy approached to a certain level no matter which center's GPS orbit was used. The orbit difference ranged 1.7–1.8 cm, 4.3–5.3 cm, and 2.2–2.7 cm in RTN components, respectively, and 5.1–6.2 cm in 3D RSS. Even SIO's ephemeris generated T/P orbit which had commensurate radial accuracy with those generated by fixing to other center's GPS ephemeris. Note also that these agreements with the JPL's reduced-dynamic orbit were better for most cases than those for the adjusted GPS cases.

CONCLUSIONS

When the T/P orbit is determined by processing the GPS phase observable, the GPS orbit should be determined either by adjusting the GPS orbit with the T/P orbit, or by fixing it to independently determined precise orbit. For the adjusted GPS case, the empirical GPS parameters, such as C_1 and 1-cpr parameters, played an important role in improving the GPS orbit accuracy, which, in turn, reduced the effect of GPS orbit error on the resulting T/P orbit. For the double-differenced GPS measurement, mixing the station-T/P double-differences with the station-station double-differences provided better GPS orbit coverage, which resulted in improved GPS orbit solutions. However, the improvement in the T/P orbit was marginal. For the fixed GPS case, the T/P orbit accuracy varied depending on the quality of GPS orbits. By employing the orbit element correction parameters for fixed GPS case, T/P orbit accuracy improved, and these parameters somewhat desensitize the effect of GPS orbit error on the T/P orbit.

ACKNOWLEDGMENTS

This research was sponsored by NASA Contract NAS 5-33021. The data preprocessing efforts by Y. Nam is deeply appreciated.

REFERENCES

- Bertiger, W. I., Y. E. Bar-Sever, E. J. Christensen, E. S. Davis, J. R. Guinn, B. J. Haines, R. W. Ibanez-Meier, J. R. Jee, S. M. Lichten, W. G. Melbourne, R. J. Muellerschoen, T. N. Munson, Y. Vigue, S. C. Wu, T. P. Yunck, B. E. Schutz, P. A. M. Abusali, H. J. Rim, M. M. Watkins, and P. Willis, GPS precise tracking of TOPEX/POSEIDON: Results and implications, *J. Geophys. Res.*, 99(C12), 24449-24464, December 15, 1994.
- Eanes, R. J. and M. M. Watkins, Earth orientation and site coordinates from the Center for Space Research, *International Earth Rotation Service Tech. Note 14*, ed. P. Charlot, Observatoire de Paris, pp. L-7 to L-11, September 1993.
- Eanes, R. J., Diurnal and semidiurnal tides from TOPEX/POSEIDON altimetry, *EOS Transactions, AGU*, 75(16), April 19, 1994.
- Fliegel, H., T. Gallini, and E. Swift, Global Positioning System radiation force model for geodetic applications, *J. Geophys. Res.*, 97(B1), 559-568, January 10, 1992.
- McCarthy, D. D. (ed), IERS Standards, *International Earth Rotation Service Tech. Note 13*, Observatoire de Paris, July 1992.
- Schutz, B. E., B. D. Tapley, P. A. M. Abusali, and H. J. Rim, Dynamic orbit determination using GPS measurements from TOPEX/Poseidon, *Geophys. Res. Lett.*, 21(19), 2179-2182, September 15, 1994.
- Tapley B. D., J. C. Ries, G. W. Davis, R. J. Eanes, B. E. Schutz, C. K. Shum, M. M. Watkins, J. A. Marshall, R. S. Nerem, B. H. Putney, S. M. Klosko, S. B. Luthcke, D. Pavlis, R. G. Williamson, and N. P. Zelensky, Precision orbit determination for TOPEX/POSEIDON, *J. Geophys. Res.*, 99(C12), 24383-24404, December 15, 1994a.
- Tapley B. D., M. M. Watkins, J. C. Ries, G. W. Davis, R. J. Eanes, S. R. Poole, H. J. Rim, B. E. Schutz, and C. K. Shum, R. S. Nerem, F. J. Lerch, E. C. Pavlis, S. M. Klosko, N. K. Pavlis, R. G. Williamson, The JGM-3 gravity model, European Geophysical Society XIX General Assembly, Grenoble, France, 1994b.
- Wu, S. C., T. P. Yunck, and C. L. Thornton, Reduced-dynamic technique for precise orbit determination of low Earth satellites, *J. Guid., Control Dyn.*, 14(1), 24-30, 1991.
- Zumberge, J. F., G. Blewitt, D. Jefferson, M. B. Heflin, and F. H. Webb, Earth orientation parameters from the Jet Propulsion Laboratory using GPS, *International Earth Rotation Service Tech. Note 14*, ed. P. Charlot, Observatoire de Paris, pp. P-33 to P-37, September 1993.
- Zumberge, J. F., R. E. Neilan, G. Beutler, and W. Gurtner, The International GPS Service for Geodynamics - Benefits to users, *Proc. ION GPS-94*, Salt Lake City, Utah, September 20-23, 1994.

Table 1. GPS Orbit Comparison with JPL's IGS Orbit (cm)

| Cases | Radial | | Transverse | | Normal | | RSS |
|-------------|--------|-------|------------|-------|--------|-------|-------|
| | mean | RMS | mean | RMS | mean | RMS | |
| CSR (I) | 1.89 | 8.59 | 6.65 | 23.40 | 1.90 | 14.37 | 28.77 |
| CSR (II) | 1.31 | 7.15 | 5.50 | 19.33 | 1.85 | 14.97 | 25.47 |
| Case A (I) | 1.89 | 10.53 | 6.26 | 25.32 | 2.65 | 17.53 | 32.54 |
| Case A (II) | 0.96 | 7.72 | 5.56 | 18.72 | 2.89 | 16.04 | 25.83 |
| Case B (I) | 3.41 | 9.01 | 5.84 | 18.15 | 2.19 | 10.87 | 22.99 |
| Case B (II) | 2.93 | 8.24 | 5.67 | 13.88 | 2.40 | 10.14 | 19.06 |

**Table 2. Topex Orbit Comparison with JPL's reduced-dynamic Orbit
Adjusted GPS case (cm)**

| Cases | DD rms | Radial | | Transverse | | Normal | | RSS |
|-------------|--------|--------|------|------------|------|--------|------|------|
| | | mean | RMS | mean | RMS | mean | RMS | |
| Case A (I) | 1.28 | 0.21 | 1.92 | 1.46 | 5.01 | -0.14 | 3.47 | 6.39 |
| Case A (II) | 1.13 | 0.19 | 1.73 | 0.65 | 4.45 | -0.19 | 3.26 | 5.78 |
| Case B (I) | 1.50 | 0.18 | 2.11 | 0.85 | 4.96 | -0.20 | 2.79 | 6.07 |
| Case B (II) | 1.38 | 0.20 | 1.73 | 0.77 | 4.18 | -0.23 | 2.57 | 5.20 |

**Table 3a. Topex Orbit Comparison with JPL's reduced-dynamic Orbit
Fixed GPS case—no orbit element correction parameters (cm)**

| Orbits | DD rms | Radial | | Transverse | | Normal | | RSS |
|----------|--------|--------|------|------------|------|--------|------|-------|
| | | mean | RMS | mean | RMS | mean | RMS | |
| JPL | 1.47 | -0.22 | 1.69 | 1.53 | 4.66 | -0.23 | 2.36 | 5.49 |
| CODE | 1.94 | 0.16 | 2.31 | 1.83 | 5.92 | -0.26 | 2.42 | 6.80 |
| GFZ | 2.16 | 0.30 | 2.24 | 1.50 | 6.63 | -0.31 | 3.23 | 7.71 |
| SIO | 2.80 | 0.11 | 4.05 | 0.42 | 9.31 | -0.15 | 3.46 | 10.73 |
| CSR (I) | 2.29 | 0.09 | 2.42 | 0.81 | 5.87 | -0.19 | 2.93 | 6.99 |
| CSR (II) | 2.11 | 0.14 | 2.03 | 0.83 | 5.17 | -0.21 | 2.71 | 6.18 |

**Table 3b. Topex Orbit Comparison with JPL's reduced-dynamic Orbit
Fixed GPS case—with orbit element correction parameters (cm)**

| Orbits | DD rms | Radial | | Transverse | | Normal | | RSS |
|----------|--------|--------|------|------------|------|--------|------|------|
| | | mean | RMS | mean | RMS | mean | RMS | |
| JPL | 1.03 | 0.17 | 1.78 | 0.42 | 4.37 | -0.20 | 2.31 | 5.25 |
| CODE | 1.05 | 0.17 | 1.71 | 0.34 | 4.29 | -0.22 | 2.54 | 5.27 |
| GFZ | 1.06 | 0.17 | 1.69 | 0.02 | 4.16 | -0.22 | 2.42 | 5.10 |
| SIO | 1.08 | 0.17 | 1.76 | 0.86 | 5.27 | -0.19 | 2.67 | 6.16 |
| CSR (I) | 1.05 | 0.18 | 1.78 | 0.62 | 4.54 | -0.19 | 2.43 | 5.45 |
| CSR (II) | 1.05 | 0.18 | 1.79 | 0.53 | 4.35 | -0.20 | 2.21 | 5.20 |

Use of GPS for Precise and Operational Orbit Determination at ESOC

Tomás Martín Mur, Dr. John Dow, and Nicolas Bondarenco
European Space Operations Centre, European Space Agency

Dr. Stefano Casotto
Dipartimento di Astronomia of the Università Padova

Dr. Joachim Feltens
mbp Informationstechnologie GmbH

Carlos García Martínez
GMV S.A.

BIOGRAPHIES

Tomás Martín Mur is a Mathematical Analyst at the Near Earth Navigation and Geodesy Section of ESOC, the European Space Operations Centre of the European Space Agency, ESA.

Dr. John Dow is the head of the Near Earth Navigation and Geodesy Section of ESA/ESOC.

Dr. Stefano Casotto has been working for Logica at the Near Earth Navigation and Geodesy Section of ESA/ESOC and now is working in the Dipartimento di Astronomia of the Università di Padova.

Nicolas Bondarenco is a Young Graduate at the Near Earth Navigation and Geodesy Section of ESA/ESOC.

Dr. Joachim Feltens works for EDS-mbp at the Near Earth Navigation and Geodesy Section of ESA/ESOC.

Carlos García Martínez works for GMV S.A. at the Near Earth Navigation and Geodesy Section of ESA/ESOC.

ABSTRACT

A GPS Tracking and Data Analysis Facility (GPS-TDAF) has been operating now for three years at the European Space Operations Centre (ESOC). This facility was developed in order to support future ESA projects that involve GPS.

The GPS-TDAF has been used for our participation in the International GPS Service for Geodynamics, as both Operational Data Centre and Analysis Centre, from the start of the IGS. ESOC is currently providing GPS tracking data from 5 ESA ground stations, precise orbits, precise clocks, earth orientation parameters (eop's) and station coordinate solutions.

ESOC is especially interested in the use of GPS for satellite orbit determination. In this context we have analyzed GPS data from two very different satellites,

Topex/Poseidon and Astropas. With the Topex/Poseidon data we have obtained orbits that could be used to support applications that require a very precise orbit (e.g. altimeter). The Astropas data do not have the same quality, but is of high interest because it is closer to the kind of data that will have to be processed in some missions that will use GPS for automated navigation and rendezvous.

The ESOC approach to GPS data analysis is presented, together with the last results obtained for the different applications.

INTRODUCTION

The Near Earth Navigation and Geodesy Section of ESOC was established to perform the orbit determination and other navigation tasks needed for a series of Near Earth satellites of the European Space Agency. It was foreseen that some of these satellites would have very demanding orbit determination accuracy requirements. Navigation software was developed to include all the measurement types needed for precise and operational orbit determination. The software has been used to its full capabilities with the ERS-1 and ERS-2 satellites, that had stringent orbit determination accuracy requirements to allow for the full utilization of the altimetry data (Ref. 1).

When the software was first developed it was required that it be able to process the most important tracking measurements at that time: microwave ranging, laser ranging, and altimetry. As time passed new tracking methods for Near Earth satellites have been developed: GPS, DORIS and PRARE. These tracking types have also been incorporated into the software. PRARE data from Meteor-3 was successfully processed at our section (Ref. 2) and we are now ready to process ERS-2 data as soon as it is available. DORIS will be used by Envisat and we have already processed data from the Topex/Poseidon satellite (Ref. 3). GPS is foreseen for In Orbit Infrastructure applications like ARP and ATV and for use in small Earth Observation satellites.

We started our GPS activities with the processing of GIG-91 data (Ref. 4). The orbit and geometric parameter estimation software had to be adapted to accommodate the measurement types and processing techniques needed for GPS. This started the development of the ESA GPS Tracking and Data Analysis Facility (GPS-TDAF), that includes not only the data analysis system but also a number of GPS receivers at ESA ground stations and the associated communications and control software and hardware. This paper describes the ESA GPS TDAF and the orbit determination activities that have been performed using the facility.

The ESA GPS-TDAF

The ESA GPS Tracking and Data Analysis Facility started as an extension of our Precise Orbit Determination Facility (Ref. 5) to incorporate GPS measurement types. The first opportunity to analyze GPS data came with the GIG-91 campaign and it was clear that an extensive effort was needed in order to preprocess the data before it could be fed into our existing orbit determination software.

Our orbit determination software is optimized for its most important use, that is operational orbit determination and prediction. A typical case of this is the routine orbit determination for the ERS-1 and ERS-2 satellites. These satellites are routinely tracked by only one ground station, Kiruna, with about 10 passes per day of some minutes. The need to obtain a precise orbit with sparse tracking data and the need to be able to accurately propagate it so that it can be used for the scheduling of instruments and ground station operations were important for the selection of the estimation algorithm and force modelling. A batch least-squares was selected, with acceleration modelling based on state of the art dynamic models.

When GPS observables had to be incorporated in the software, those suited for batch estimators were used. Our best results have been obtained using double differences of ionospheric free carrier phase and we have also implemented double difference pseudo-ranges. These measurement types have been implemented for pairs of ground stations, in order to improve the GPS satellite orbits or for geodesy, and for orbiting receiver/ground station pairs, in order to obtain precise orbits of the satellite carrying the GPS receiver.

GPS preprocessing software was needed to convert the basic GPS observables to double difference observables. A cycle slip algorithm based on integer almost ionospheric free combinations was implemented and also an algorithm to select a set of independent double difference combinations. Antenna phase center and center of mass corrections were also

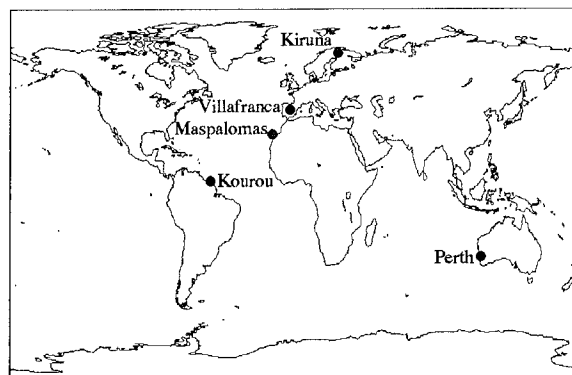


Figure 1. ESA Ground Stations equipped with high precision GPS receivers

included in the preprocessing software.

Post-processing software had also to be adapted for the GPS measurements. The most important part is the multi-arc orbit and geodetic parameter estimation software that has been used to obtain station coordinates solutions (Ref. 6). A completely new development was needed in order to obtain precise clock bias values (Ref. 7). These were estimated in post-processing using the estimated orbits and correction parameters obtained processing double differences.

A simultaneous development to that of the analysis software was the deployment of high precision geodetic GPS receivers at the ESA ground stations. Receivers have been installed and are operating in Maspalomas (Canary Islands, Spain), Kourou (French Guyana), Kiruna (Sweden), Perth (Australia) and Villafranca (Spain) (Fig. 1). The reasons for installing this GPS network were:

- To be able to obtain near-real-time GPS data to support operational and precise orbit determination of satellites equipped with GPS receivers.
- To be able to compute local ionospheric models using dual frequency GPS data to correct one frequency microwave ranging data.
- To be able to accurately determine the positions of the stations in a global reference frame.

These GPS receivers are remotely controlled from ESOC. Highly automated controlling and communications software had to be developed to minimize both on-site support and operator intervention.

Participation in the International GPS Service for Geodynamics

Having participated in some of the early discussions concerning the establishment of an operational service for generation of high precision GPS orbit parameters, a proposal was submitted by ESOC in May 1991 in response to the call for participation issued by the

International Association of Geodesy/International Union of Geodesy and Geodynamics (IAG/TUGG). Our proposal was based on two starting points which could provide a significant contribution to the development of such a service:

- the existence of a network of globally distributed ESA ground stations, already equipped with communications, atomic standard timing systems and other relevant infrastructure.
- a state-of-the-art orbit and geodetic determination software that allowed for consistent processing of different types of geodetic satellite data (in particular SLR and GPS).

Our first solutions for orbital and polar motion parameters were transmitted to the IGS about one month after the start of the IGS-92 campaign. ESOC continued to process IGS data after the decision to continue the IGS activity in the form of an "IGS Pilot Service" and from 1 January 1994 as an operational service (Ref. 8).

We are now operating our five GPS receivers as IGS stations. ESOC acts as the Operational Data Centre for these receivers, retrieving the data and delivering them to the designated IGS Data Centres. We are also contributing as Analysis Centre, processing data from about 50 IGS stations to obtain high accuracy GPS daily products, with a delay of less than 10 days.

The data and products that we provide are the following:

- RINEX observation files, containing dual frequency phase and pseudo-range data at 30 seconds intervals from our five ground stations.
- Improved GPS satellite orbits, with an accuracy estimated to be of about 15 cm per axis.
- Improved earth orientation parameters (eop), with accuracy at the level of 0.3-0.4 milliarcsec.
- Precise GPS satellite clock biases, with accuracies in the nanosecond range.
- Station coordinate solutions with accuracies in the cm range, with the last submission in the form of a full covariance matrix for position and velocity estimates.

The orbit and clock solutions provided by the different IGS Analysis Centers are used to compute a combined IGS solution (Ref. 9) that is being widely used for applications (geodetic and other) for which accurate GPS orbits are needed.

Our clock bias estimates have also been used for time transfer experiments such as the one described by Tor Melgaard in these proceedings.

Topex/Poseidon GPS data analysis

Topex/Poseidon has been a satellite of unique

importance for the evaluation of on-board GPS. It carries a high precision dual-frequency receiver producing long cycle-slip free carrier phase passes as well as P-code pseudo-range measurements. It was launched when the GPS constellation was almost complete and when the IGS network of high precision receivers had started to provide globally distributed tracking data.

As a high precision altimetry mission, very accurate orbit determination was vital to its success. The satellite was equipped with several tracking systems: laser ranging retroreflectors (SLR), a doppler receiver (DORIS), and an experimental GPS receiver. This has made Topex/Poseidon a veritable precise orbit determination laboratory that allows the inter-comparison of the three tracking techniques.

As the ESOC precise orbit determination system adopts a fully dynamic approach, the high accuracy expected for Topex/Poseidon required the best possible force models and an accurate reconstitution of the attitude of the satellite, in order to compute surface forces and to correct measurements for centre of mass offset.

The force models used in the processing of the data were (Ref. 3):

- The JGM-2 (70x70) gravity model, that was specially developed to support this mission (Ref. 10).
- MSIS air density model combined with a variable area model based on a geometric description of the spacecraft as a composite of simple geometric bodies (Fig. 2), with surface properties provided by the Topex/Poseidon Macro-Model (Ref. 11).
- Lunisolar perturbations.
- Solid Earth tides (Wahr's model).
- Extended Schwiderski ocean tides.
- Solar radiation pressure using the spacecraft model already described.
- One cycle per revolution empirical forces (transverse

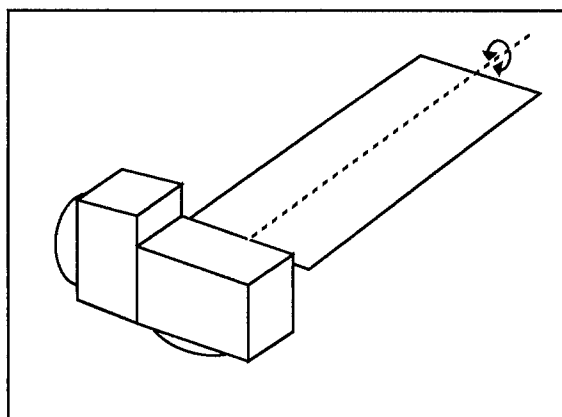


Figure 2. Topex/Poseidon spacecraft model used to compute surface forces

| | | DORIS | SLR+ DORIS | GPS (1) (2) | |
|----------------|---|-------|---------------|----------------|-----|
| SLR | R | 1.8 | 1.0 | 3.1 | 1.9 |
| | T | 6.2 | 2.6 | 16.1 | 9.4 |
| | N | 12.6 | 1.0 | 7.5 | 2.1 |
| DORIS | R | | 1.2 | 1.7 | 1.1 |
| | T | | 4.7 | 13.5 | 5.8 |
| | N | | 12.4 | 12.3 | 3.0 |
| SLR + DORIS | R | | | 2.0 | 1.3 |
| | T | | | 14.2 | 6.9 |
| | N | | | 7.5 | 2.2 |

Table 1: Average comparison statistics for ESOC orbits. Shown is difference rms in cm for the radial, transverse and normal components (R,T,N). For GPS orbits (1) before and (2) after Helmert transformations

and normal).

The reconstitution of the attitude of the satellite was needed in order to calculate surface forces and centre of mass corrections. Topex/Poseidon is a three axis stabilized satellite with the radar altimeter constantly pointing downwards normal to a reference ellipsoid. In order to maintain the solar panel facing the sun, a sophisticated attitude law consisting of a combination of yaw steering about the local vertical and solar array pitching about its axis has been devised (Ref. 11). The different regimes of the attitude law and the transition modes were implemented in the software.

Other orbit determination modelling, including the definition of the reference frames, was done in consistency with the IERS Standards of 1992 (Ref. 12).

A 10-day period (repeat cycle 21) was selected for the analysis of the orbit restitution capability of the three techniques: SLR, DORIS, and GPS, although longer intervals were processed for SLR and DORIS data.

The SLR tracking for the period was about 20 passes per day, with a total of 22 stations performing some tracking in the 10-day period. The geographical distribution of the data shows that 76% of the tracking was performed from Europe and the US. The orbits were computed using three-day arcs and the average value of the residuals for all stations was at the level of 5 cm.

The DORIS tracking scenario is very different from that of SLR, as 43 DORIS beacons were active during the period. An almost complete geographical coverage without significant data gaps was achieved. The number of passes per day was about 130 with very

| | | JPL Reduced Dynamics (1) (2) | | DUT Reduced Dynamics (1) (2) | | DUT Full Dynamics (1) (2) | |
|----------|---|---------------------------------------|-----|---------------------------------------|-----|------------------------------------|-----|
| ESOC | R | 3.2 | 2.8 | 3.2 | 2.9 | 2.1 | 1.5 |
| Full | T | 16.4 | 8.2 | 10.6 | 8.1 | 8.7 | 5.3 |
| Dynamics | N | 24.8 | 4.5 | 10.8 | 4.1 | 10.3 | 2.7 |

Table 2: Average comparison statistics for GPS orbits. Shown is difference rms in cm for the radial, transverse and normal components (R,T,N) (1) before and (2) after Helmert transformations

marginal day to day variations. Range-rate and tropospheric (zenith delay) biases were estimated for each pass. Average DORIS residuals so obtained were of 0.50 mm/s.

An improved station coordinate solution had been calculated for the processing of DORIS and SLR data. This solution was based in the processing of 3.5 months of Lageos SLR together with 18 days of Topex/Poseidon DORIS and SLR data. With this solution we could achieve a reduction from 0.54 mm/s to 0.50 mm/s in our DORIS residuals.

Topex/Poseidon orbits computed using a combination of SLR and DORIS were also generated with the combined station coordinate solution. The level of residuals obtained was about the same as that obtained in the individual solutions.

For the GPS processing (Ref. 13), Topex/Poseidon observations were used together with data from 17 to 20 ground receivers from the IGS network. The four eclipsing satellites during the period were not used, due to the erratic attitude behavior during and shortly after eclipse. From the rest, a total of 15 GPS SV's were used. Ionospheric free carrier phase double differences involving Topex and a ground receiver were the data type chosen for analysis. Additionally, and in order to solve for the orbits of the GPS SV's, ground based double differences were used. Measurements were generated every 2 minutes when involving the orbiting receiver and every 4 minutes when involving only ground stations. A Kalman filter was used to estimate receiver clock biases and drifts, but no appreciable drift was ever detected in the Topex/Poseidon clock.

The coordinates used for GPS were those from the IGS (ITRF), following a similar approach to that of the IGS Analysis by fixing the coordinates of a core set of stations and estimating the others. Drag scaling factors for Topex/Poseidon were estimated every 12 hours. The double difference phase measurements were fit to a level of 17 mm for those involving Topex/Poseidon.

In order to assess the performance of the different tracking data types, the ephemerides generated by each method were compared with each other and with ephemerides obtained by JPL (for GPS only) and by the Delft University of Technology (DUT) (Ref. 14). The results of these comparisons are shown on Table 1 for internal comparisons and in Table 2 for inter-centre comparisons.

Internal comparison with respect to our GPS orbits display relatively high values in the transverse and normal directions which are associated with large mean components and very small standard deviations. This occurrence can be interpreted as due to reference frame incompatibilities, mainly the inclusion or not of small empirical celestial pole corrections. In order to get rid of reference frame differences a Helmert transformation was applied individually to each arc to get the GPS orbit in the reference of the other orbit. The agreement between the different orbits is very good, even without Helmert transformations.

The Table 2 shows the comparisons between the ESOC GPS orbit and external GPS orbits. Our GPS orbit agrees best with the DUT dynamical solution, but the agreement between our solution and the reduced dynamics solutions is also very good, especially in the radial component.

These results indicate that GPS can be used for precise orbit determination and that the orbits so obtained are very close to the orbits obtained using other precise tracking methods. They also validate our software with respect to the use of GPS observables for precise orbit determination.

Astrospace GPS data analysis

A second aspect of GPS orbit determination is its use for operational navigation of satellites. There have been a number of satellites that use a GPS receiver to calculate on-board the position and even the orbit of the spacecraft. It is foreseen that some elements of support to the International Space Station will be equipped with GPS receivers for this purpose. These receivers used for operational navigation may not be dual-frequency P code receivers. The receiver that is being planned for ARP (ATV Rendezvous Pre-development and Verification) is a C/A code one-frequency receiver. The GPS SPS Signal Specification (Ref. 15) only specifies the characteristics of the L1 C/A code. The use of other kinds of measurements (P code, L2) has to be based on empirical and unguaranteed sources.

One of our goals is to obtain absolute positioning of user spacecraft. These absolute positions can then be used as a yardstick for absolute on-board navigation

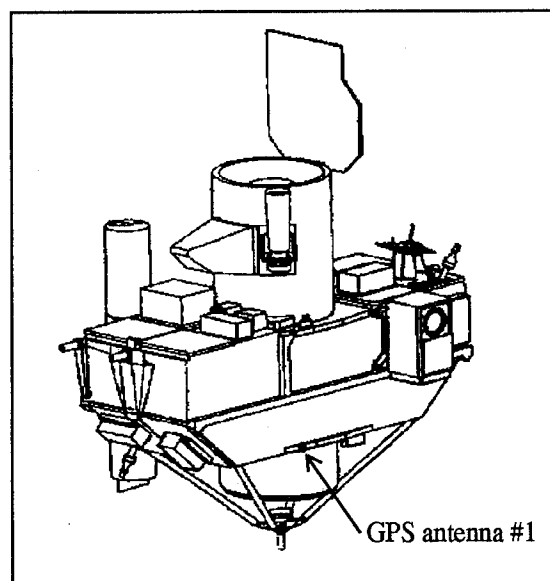


Figure 3. The Orfeus-Spas in flight configuration

and relative rendezvous experiments.

In operational orbit determination, an important role of on-ground orbit determination with GPS is to obtain predicted orbits to be used in operations scheduling.

ESOC had the opportunity to obtain GPS data from the September 1993 flight of the Astrospace spacecraft (Orfeus-Spas mission). Astrospace is a reusable Shuttle dedicated satellite that carries a telescope as prime payload instrument (Fig. 3). The spacecraft is deployed from the Shuttle by the Orbiter RMS, it operates for some days in Shuttle's vicinity and is then retrieved and brought back to ground by the Shuttle. It has a one-frequency receiver recording C/A pseudo-range and L1 carrier phase from up to 6 GPS SV's at any time. The operating environment and GPS receiver of this spacecraft are similar to those of future Space Station missions.

The most important differences between the GPS data analysis performed for Topex/Poseidon and that needed for Astrospace are:

- Data quality: Topex/Poseidon carries a high precision GPS receiver that is optimized to obtain long cycle slip free carrier phase passes. The receiver in Astrospace is optimized for best GDOP, even if this means changing the set of tracked satellites.
- The Topex/Poseidon clock is steered to minimize its clock bias, while the Astrospace clock is in free drift, of about 0.04 ms/s, with clock resets every 8 minutes
- Topex/Poseidon has a GPS antenna on top of a mast with a choke-ring to minimize multipath, while Astrospace has two antennas to maximize visibility of the GPS constellation.
- Topex/Poseidon is kept in a very well known attitude, controlled by reaction wheels. Astrospace is oriented to

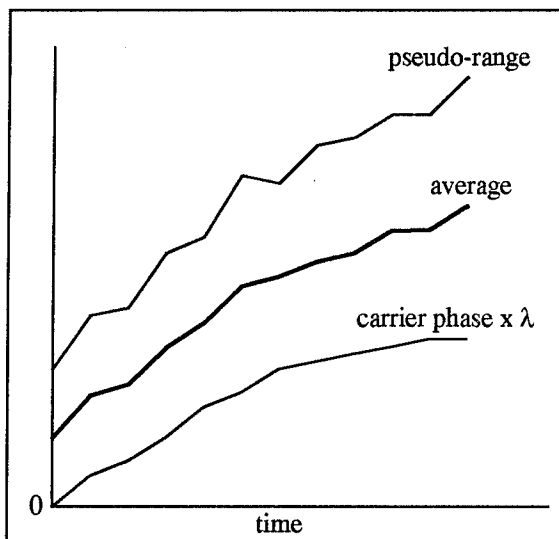


Figure 4. Average measurement

different astronomical sources with periods of observation of 20-40 minutes and it changes its attitude using cold gas thrusters. This may cause dynamic modelling problems.

- The ionospheric correction for Topex/Poseidon can be obtained using the dual-frequency data, but for Astropas this is not possible. Ground based ionospheric corrections may not be applicable for an orbiting receiver, because the spacecraft is inside the ionosphere and not below it.

There are two possible ways of obtaining ionospheric free measurements for a single frequency receiver. One is to obtain an average of the carrier phase and the pseudo-range measurement. This new measurement will be free of ionospheric effect, but it will have a noise at the level of that of the pseudo-range and an ambiguity as the carrier phase. Figure 4 shows an example of this technique.

The second way is to obtain a smoothed approximation of the half difference between pseudo-range and carrier phase for a pass and to use this smoothed function to correct the phase measurements. Figure 5 shows an example of this technique and Figure 6 shows the smoothing of the half difference using real Astropas data. The value of the smooth function at the measurement time is added to the carrier phase value to correct it for the ionospheric effect. The post-fit residuals of the smoothing are an indicator of the pseudo-range noise and for Astropas they are typically in the 2 meter rms range.

Both ionospheric correction techniques rely on the use of long cycle-slip free carrier phase passes. Short carrier phase passes are useless for orbit determination, because of the need to estimate the ambiguity. Undetected cycle slips will introduce errors in our

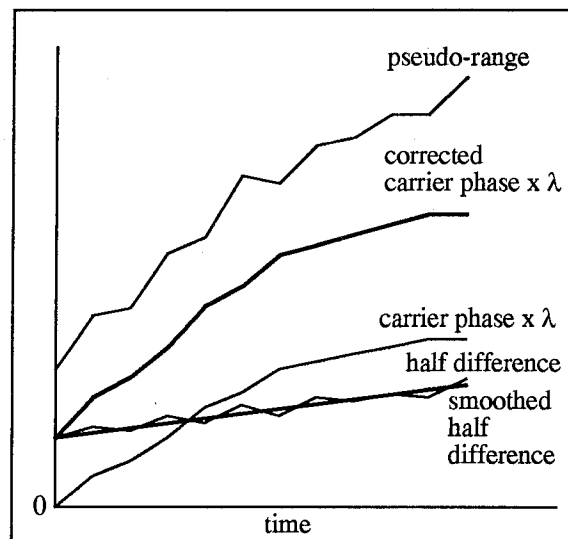


Figure 5. Ionospheric corrected phase measurement

derived measurements.

The first step in the preprocessing is then to obtain carrier phase and pseudo-range measurements at the same epochs as our ground based measurements, so they can be combined to obtain double differences. This process is very difficult because it has to be performed simultaneously with the cycle slip detection. We are currently investigating possible interpolating algorithms to obtain long cycle slip free carrier phases. The first data that should be checked with on-board GPS data is the on-board reconstitution of the position of the satellite. The earth-fixed positions obtained on-board can be fitted to an orbit. An example of this fit is shown in Figure 7. This is a one-orbit period in the middle of a 3-day arc of position measurements that were fitted using our orbit determination program. The residual fit was about 56 m per component, with higher

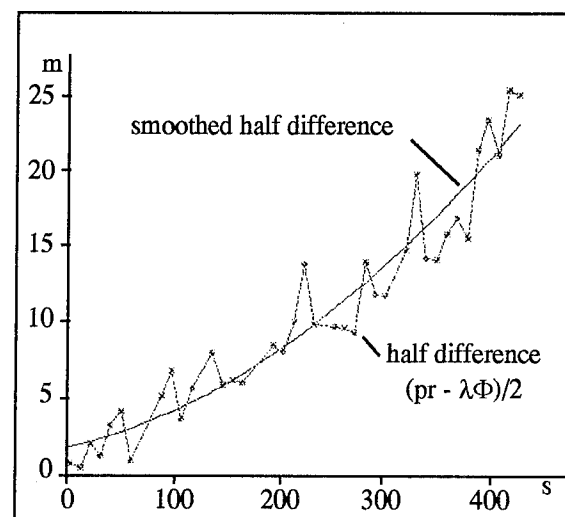


Figure 6. Real data example of smoothed ionospheric correction

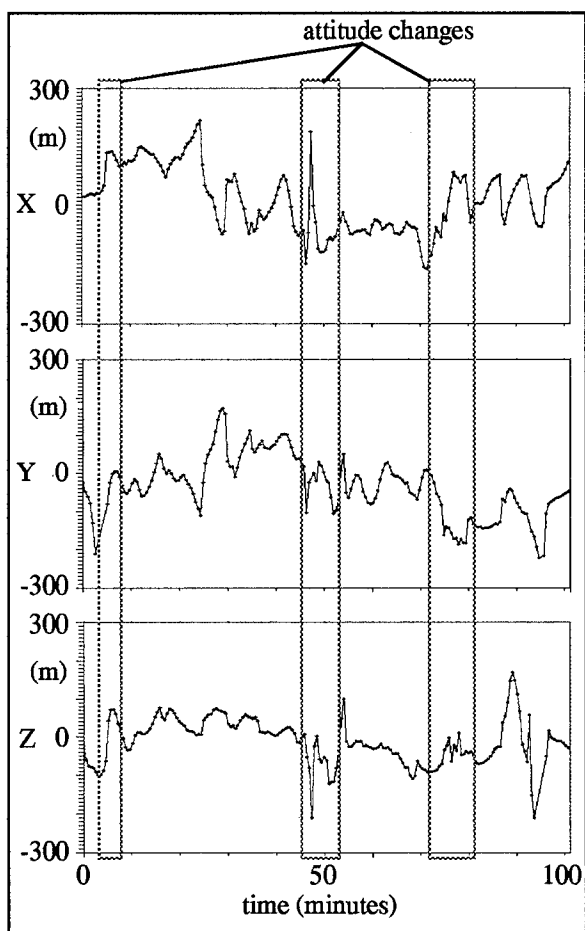


Figure 7. Difference between on-board derived position and fitted orbit

residuals in x and y components than in z. The orbit was modelled using JGM-2 (70x70) gravity model and linear Cd's in 6 hour intervals. The Cd's so obtained were between 1.5 and 2.8 for a typical area of 9 m². The orbit so computed can then be used to preprocess the basic GPS measurements.

In order to study the effect of the ionospheric delay another test run was performed using three hours of double difference pseudo-range measurements, combining ionospheric free pseudo-ranges from the ground stations with C/A pseudo-ranges from Astrospas. The orbits of the GPS satellites were those obtained by our routine IGS processing. In this test the pseudo-range residuals, due mainly to the uncorrected ionospheric delay, were of 11 meters.

Another possible test is to compute clock bias corrections and use precise GPS SV's orbits to perform precise pseudo-range point positioning. The ionospheric correction will be again the limiting factor for the accuracy of the reconstituted positions. We plan to obtain precise clock values for the period of the flight in order to compare these positions with those obtained on-board.

CONCLUSION

ESOC has developed a GPS Tracking and Data Analysis Facility that has demonstrated the feasibility of using GPS for precise orbit determination, with results of similar quality to those obtainable with other precise tracking methods, like SLR and DORIS. This facility can also be used to support missions for which an on-board GPS receiver is used for autonomous navigation. The Facility can analyze the results of the on-board navigation and it can obtain more precise off-line orbits that can be used to validate autonomous navigation using GPS. Work is on-going in order to provide higher precision orbits even for spacecraft that are not equipped with high precision GPS receivers.

ACKNOWLEDGMENTS

Miguel Romay-Merino is gratefully acknowledged for helping us to describe the details of his work on SLR and DORIS orbit determination for Topex/Poseidon. The Astrospas data were kindly supplied to ESA by DARA (Deutsche Agentur fuer Raumfahrt-Angelegenheiten).

REFERENCES

1. Zandbergen, R., Dow, J.M., Romay Merino, M.M., Piriz, R., "ERS-1 and ERS-2 Operational and Precise Orbit Determination", *Adv. Space Res.* 16, (12)105-108, 1995.
2. Romay Merino, M., Dow, J.M., "Meteor-3 PRARE Data Analysis at ESOC", presented at the ERS-2 PRARE User Workshop, Potsdam, Nov. 8-9, 1994.
3. Casotto, S., Romay Merino, M.M., Martin Mur, T.J., Dow, J.M., "Sub-decimetres Determination of the Topex/Poseidon Orbit", OAD Working Paper No. 544, Darmstadt, Aug. 1994.
4. Dow, J.M., Feltens, J., Duque, P., Sarti, F., "A GPS Orbit Determination and Analysis Facility", in *Proceedings of the 6th International Symposium on Satellite Positioning*, Columbus (Ohio), Mar. 17-20, 1992.
5. Dow, J.M., Martin Mur, T.J., Romay Merino, M.M., "ESA's Precise Orbit Determination Facility", *ESA Bulletin* No. 78, May 1994.
6. Martin Mur, T.J., Dow, J.M., Feltens, J., Garcia Martinez, C., "Annual Report from the ESOC/IGS Analysis Centre to the IERS for 1993", in *IERS Technical Note 13*, Observatoire de Paris, Sep. 1994.
7. Martin Mur, T.J., "Estimation of Precise GPS Clock Bias Values by the ESOC IGS Analysis Centre", in *Proceedings of the 1995 IGS Workshop*, Potsdam, May

15-17, 1995.

8. Dow, J.M., Martin Mur, T.J., Garcia Martinez, C., Feltens, J., "High Precision Orbits for the International GPS Service for Geodynamics (IGS)", *Adv. Space Res.* 16, (12)51-54, 1995.

9. Beutler G., Kouba, J., Springer, T., "Combining Orbits of the IGS Processing Centres", in *Proceedings of the IGS Analysis Centre Workshop*, Ottawa, Canada, Oct. 12-14, 1993.

10. Nerem, R.S., Lerch, F.J., Marshall, J.A., Pavlis, E.C., Putney, B.H., Tapley, B.D., Eanes, R.J., Ries, J.C., Schutz, B.E., Shum, C.K., Watkins, M.M., Klosko, S.M., Chan, J.C., Luthcke, S.B., Patel, G.B., Pavlis, N.K., Williamson, R.G., Rapp, R.H., Biancale, R., Nouel, F., "Gravity Model Development for Topex/Poseidon: Joint Gravity Models 1 and 2", *J. Geophys. Res.*, 99, 24,421-24,447, 1994.

11. Marshall, J.A., Luthcke, S.B., Antreasian, P.G., Rosborough, G.W., "Modelling Radiation Forces Acting on Topex/Poseidon for Precise Orbit Determination", NASA TM 104564, 1992.

12. McCarthy, D.D. (ed), "IERS Standards (1992)", *Observatoire de Paris, International Earth Rotation Service, Technical Note 13*, Paris, 1992.

13. Casotto, S., Romay Merino, M.M., Martin Mur, T.J., Dow, J.M., "Topex/Poseidon Precise Orbit Determination Using GPS Double Difference Phase Observables", *Adv. Space Res.* 16, (12), 1995.

14. Smith, A.J.E., Hesper, E.T., Kuijper, D.C., Mets, G.J., Visser, P.N.A.M., Ambrosius, B.A.C., Wakker, K.F., "Topex/Poseidon Data Analysis Study", ESOC Contract Report, ESA CR(P) 3849, 1994.

15. "Global Positioning System Standard Positioning Service Signal Specification", U.S. DoD, Nov. 5 1993.



Session D2

Wide Area Augmentation Systems

Chair:

Dr. Sally Basker
Racal Research

Co-Chair:

Mr. Bruce DeCleene
FAA

A Wide Area Augmentation System (WAAS) Service Volume Model and Its Use in Evaluating WAAS Architectures and Design Sensitivities*

Dr. Walter Poor, Thomas Albertson, and Pauline Yen
The MITRE Corporation

Biographies

Dr. Poor is a Member of the Technical Staff in the MITRE Corporation's Center for Advanced Aviation System Development (CAASD). His current work is on the availability of GPS for use in the National Airspace System. Other work at MITRE included an algorithm for the data analysis of TCAS. He has a Ph.D. in Mathematics from SUNY at Stony Brook.

Mr. Albertson is a Technical Aide in the MITRE Corporation's CAASD. His major concentration is software engineering with a focus on GUI (graphical user interface) development and Client/Server issues. He is working toward a Master's degree in Computer Science and Information Systems at American University.

Ms. Yen is a senior software engineer with the Planning System Incorporated (PSI), a subcontractor for the MITRE Corporation on FAA projects. She has over 18 years of experience in software engineering. She programs mostly using the object-oriented approach in C++, with X/Windows and MOTIF for the GUI. She graduated from George Mason University with a degree in mathematics.

Abstract

The Federal Aviation Administration Satellite Program Office, AND-510, is developing a Wide Area Augmentation System (WAAS) based on the Global Positioning System (GPS) to support a precision approach capability down to a Category I (CAT I) decision height (DH) of 200 feet. This paper reports on the development of a stochastic service volume model (SVM) to estimate the coverage for initial and end-state GPS/WAAS based on combinations of various system design elements. The SVM will be used to help validate the performance of proposed WAAS designs and to determine the sensitivities to design changes. Using statistical as well as deterministic input parameters, the model graphically identifies regions of WAAS coverage (system availability of accuracy, integrity, and continuity of service) for varying levels of navigation service down to Category I precision approach. This paper describes

the model and shows how it can be used to analyze the availability of GPS/WAAS.

Introduction

The Federal Aviation Administration (FAA) Satellite Program Office, AND-510, is developing a Wide Area Augmentation System (WAAS) [1] to enhance the usefulness of the Global Positioning System (GPS). Wide-area Reference Stations (WRS) are to record the pseudorange and carrier-phase data from the GPS satellites as seen from different geographic locations, and pass the data to Wide-area Master Stations (WMS). The WMSs will analyze the data, develop differential corrections, and send the corrections to ground earth stations (GES). The GESs will broadcast the corrections, along with GPS-like navigation signals, to users via dedicated equipment aboard geostationary satellites (GEOS). Experiments indicate that given a sufficient number of WRSs and GEOS in the proper locations, the corrected navigation signals from the GPS and GEOS should support Category I (CAT I) precision approach (PA), as well as enroute and non-precision approach (ER/NPA) operations.

The initial version of WAAS (IWAAS) is expected to use three Inmarsat3 GEOS and 24 WRSs to meet a specified set of requirements for the availability of navigation accuracy, integrity, and continuity of service [1]. It is anticipated that more WRSs and GEOS will be needed to meet the more stringent requirements for end-state WAAS (EWAAS). For example, the specified "precision-approach service volume" for IWAAS is the airspace over the conterminous United States (CONUS), and PA supported by IWAAS must be 95% available over at least half of this specified volume. For EWAAS, however, the PA service volume is defined to be the airspace over CONUS, Alaska, Hawaii, and Puerto Rico; PA supported by EWAAS must be 99.9% available over this entire volume. A still larger service volume is specified for ER/NPA operations.

This paper describes the current version of a WAAS SVM built for FAA's AND-510 organization to assist in the analysis of various coverage availability issues for

* This paper is based on system analysis studies performed by MITRE's Center for Advanced Aviation System Development (CAASD). This paper reflects the views of the authors, who are solely responsible for the accuracy of the facts, analyses and suggestions presented herein; it does not reflect the official views or policies of the FAA.

WAAS. The analysis presented in the paper is an example of how the SVM can be used to assess alternative WAAS designs. The results show some of the effects of extra GEOS and WRSs on the availability of PA operations supported by GPS/WAAS; results are shown for CONUS only.

Description of the SVM and Analysis Examples

The SVM was developed from the Global Navigation Satellite System (GNSS) Air Traffic Operations Model (GATOM) developed previously for the FAA [2]. GATOM is a detailed, Markov-process availability model that estimates the unavailability¹ of navigation accuracy, integrity, and continuity of service for GPS augmented with various combinations of GEOS, pseudolites, and altimeter data; GATOM also analyzes "critical sets" of satellites to aid in the understanding of the operational impact of availability shortfalls [3, 4]. Since the basic computations in the SVM are the same as in GATOM, the reader is referred to [2, 3, 4] for details on the computations.

The initial requirements for the SVM were very different from those of GATOM, and features such as receiver autonomous integrity monitoring (RAIM) and critical-satellite analysis [3, 4] were temporarily removed to allow the rapid development of a flexible, near real-time model. A user-interface (written in C++) allows one to change system parameters during an analysis run for rapid, easy assessment of the sensitivity of availability and coverage to changes in these parameters. Parameters of interest include the following:

- The number and locations of GEOS providing navigation signals.
- The number of GEOS (including required redundancy) that must be visible to the user for receipt of the WAAS message.
- GPS and GEOS failure and restoration statistics.
- The number and locations of WMSs, WRSs, and GESs in operation.
- WMS, WRS, and GES failure and restoration statistics.
- Ground network connectivity, availability, and reliability.
- Various service volumes of interest (for IWAAS PA, EWAAS PA, or ER/NPA).

Restoration of service after multiple satellite failures is assumed to be carried out in series rather than in parallel. The mean-time between failures (MTBF) and mean-time to restore (MTTR) statistics for each GPS satellite are as follows:

- Short-term MTBF = 5,309 hours, short-term MTTR = 12.2 hours.

- Long-term MTBF = 120 months, long-term MTTR = 2 months.

The failure and restoration statistics for each GEOS are as follows:

- Short-term MTBF = 7,300 hours, short-term MTTR = 36 hours.
- Long-term MTBF = 130 months, long-term MTTR = 1 month.

Different failure and restoration statistics are also included in the SVM, and have been used for other analyses, but do not significantly affect the sample results in this paper.

Accuracy

Although the WAAS navigation requirements are stated directly in terms of navigation position-error rather than dilution of precision (DOP), the unavailability of user-specified DOPs is computed and may be displayed along with the unavailability of the specified position-error accuracy bounds. The accuracy model is based on the following equation from Appendix E of the WAAS MOPS [5] for the variance of the pseudorange error for satellite i as a function of its elevation angle El_i :

$$\sigma_i^2 = \sigma_{UDRE_i}^2 + F^2(El_i) \sigma_{UIVE_i}^2 + \sigma_{SNR_i}^2 + \frac{\sigma_{m45}^2}{\tan^2 El_i} + \frac{\sigma_{trv}^2}{\sin^2 El_i} + \sigma_{latency}^2$$

where

- $\sigma_{UDRE_i}^2$ is the variance of the pseudorange correction (except for ionosphere and troposphere).
- $\sigma_{UIVE_i}^2$ is the variance of the vertical ionospheric correction and $F(El_i)$ is the obliquity factor for elevation angle El_i .
- $\sigma_{SNR_i}^2$ is the receiver noise variance.
- σ_{m45}^2 is the variance of the multipath error at 45° elevation.
- σ_{trv}^2 is the variance of the tropospheric error.
- $\sigma_{latency}$ is the latency error bound (to be applied if no fast corrections have been received for satellite i within six seconds).

These parameters are set to constant values in the current build of the SVM; in particular, the accuracy model in the current build of the SVM is not tied to the number or locations of WRSs. These constants will be replaced by appropriate models in follow-on builds of the SVM.

Continuity of Function

The model for the continuity of accurate navigation in the SVM is at present based on the work in [3, 4]. With this approach, the user can specify the minimum number of satellites that can be used for navigation. For example,

¹ Unavailability equals one minus availability, that is, unavailability is the probability that the service criteria are not met.

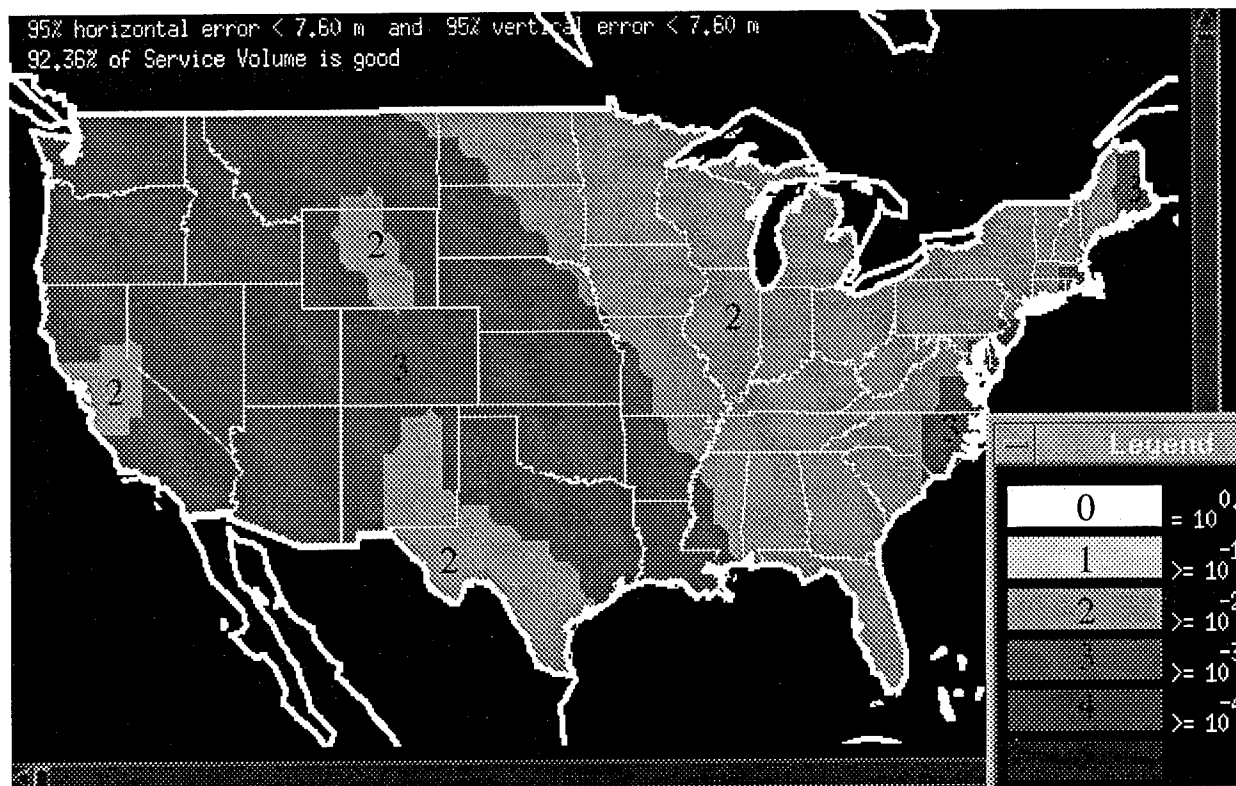


Figure 1. The Unavailability of Navigation Accuracy and Continuity for Precision Approach with IWAAS at One Sample Time.

suppose that a minimum of five satellites are required in the navigation solution. In many cases, navigation could continue after the failure of any one of the five; on a probabilistic level, the effect is roughly equivalent to requiring one redundant satellite for the sake of continuous service, and we refer to this as "level-one redundancy". Similarly, "level-two redundancy" (a requirement for two redundant satellites) would be approximated in the SVM by requiring a minimum of six satellites in the navigation solution. The calculations in [3, 4] show that these are acceptable approximations for WAAS continuity analysis. Other models for continuity are also under study for follow-on builds of the SVM.

The Unavailability of Navigation Accuracy and Continuity for Precision Approach with IWAAS

As a sample of the output from the SVM, Figure 1 shows an unavailability contour plot for PA accuracy and continuity with IWAAS (that is, with 24 GPS, 3 Inmarsat3 GEOS, and 24 WRSSs). At each location, the quantity of interest is the unavailability of the IWAAS PA requirements "95% vertical error ≤ 7.6 m and 95% horizontal error ≤ 7.6 m, with continuity" at the time chosen by the user. Level-one continuity was required, that is, a minimum of five satellites were required as an approximation to a requirement for a redundant satellite. Since the unavailability is calculated at a specific time

rather than a time average, this is referred to as an *instantaneous* unavailability plot.

The analysis included postulated failure and restoration statistics for GPS and Inmarsat3, but did not assume any WRS or ground network failures (with subsequent degradation of the accuracy of the WAAS corrections). The worst unavailabilities in this case are between 0.001 and 0.01 (indicated by the light gray²). According to Shively [3, 4], unavailability > 0.01 usually corresponds to the existence of a critical satellite.

Previous work with GATOM indicates that *instantaneous* unavailability at any location varies dramatically with time; this has been confirmed with the SVM, but examples of this variation are not included due to the lack of space.

Figure 2 shows the *daily average* of unavailability of navigation accuracy and continuity across CONUS for PA with IWAAS. The worst average unavailability of accuracy in this case is less than $10^{-1.5}$, that is, the worst

² The gray-scale resolution in the figures is limited by the copy machine used to reproduce this paper, not by the SVM; the SVM provides much greater precision than is shown in the figures, and all unavailabilities quoted are based on digital output from the SVM, rather than from the gray scale in the figures.

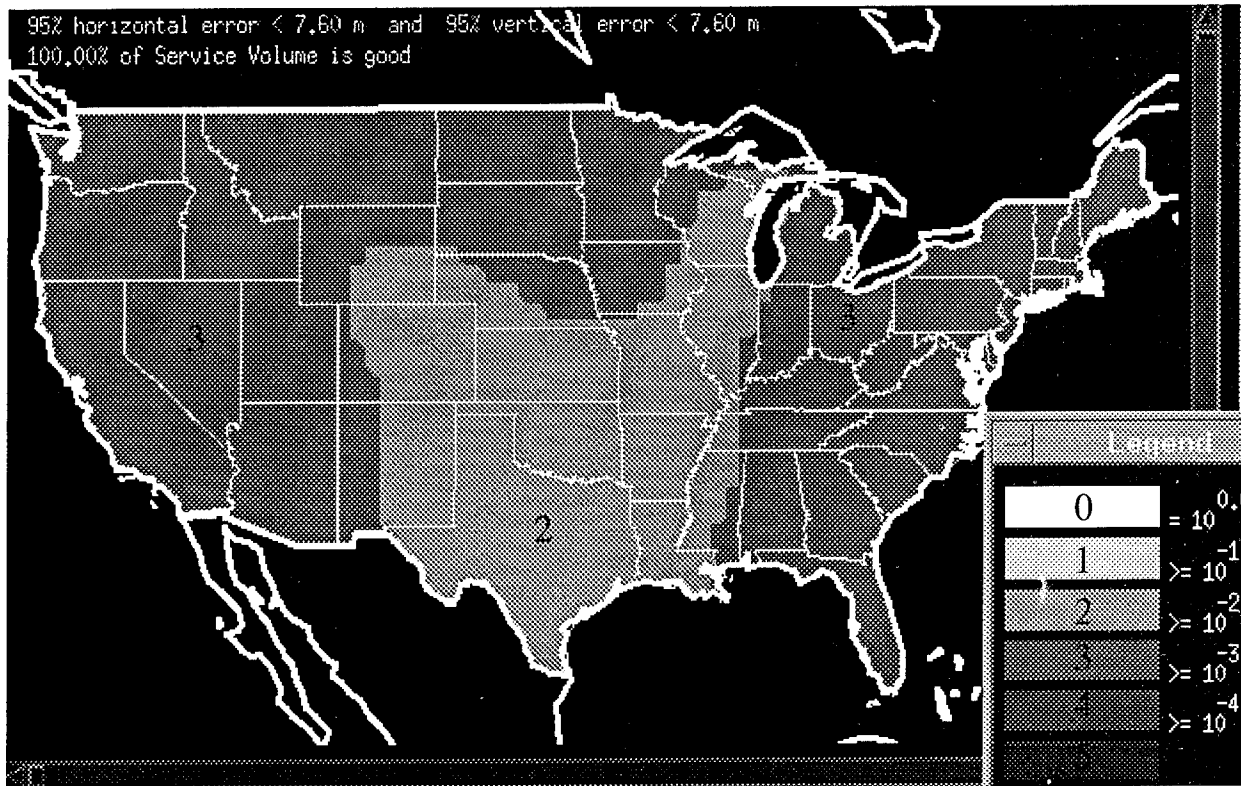


Figure 2. The Daily Average of Unavailability of Navigation Accuracy and Continuity for Precision Approach with IWAAS.

daily average availability is approximately 0.97 or better. Although the results of most availability analyses are phrased in terms of the daily averages, it is crucial to understand the operational impact of instantaneous unavailability and coverage, since air operations are taking place at a specific instant in time, rather than at some abstract, average time. Nevertheless, the majority of the results in this paper will be phrased in terms of averages so the reader can compare them with previously published results.

Figure 2 ignores the fact that, by definition, WAAS service is not available to any user unable to see at least one GEOS. Figure 3 therefore shows the effect if the additional requirement is imposed that at least one GEOS be visible to each user. The effect is shown mainly by the light-gray region in the central part of CONUS: only one Inmarsat3 is visible there, so the unavailability of this Inmarsat3 dominates the WAAS unavailability in that region. As in Figure 1, unavailability this large corresponds to the existence of a critical satellite: failure of the single GEOS visible in the central part of CONUS would deny WAAS service. The availability problem caused by this critical satellite is being addressed in the WAAS design.

If the visibility requirement were strengthened so that each user must see at least two GEOS for a redundant WAAS message (for a backup in case one GEOS fails), then the

central part of CONUS (the light-gray region in Figure 3) would have an outage because only one of the three Inmarsat3 GEOS is visible there; in this case the color would change from light-gray to white.

In all subsequent figures, at least one GEOS must be visible for reception of the WAAS broadcast.

The Unavailability of Navigation Accuracy and Continuity for Precision Approach with IWAAS and GEOS Augmentation

One way to increase system performance is to add ranging and broadcast resources. If we add a new GEOS, for example, then the redundancy of the WAAS broadcast, as well as the availability of accuracy and continuity, increases in those areas from which the satellite is visible. One suggestion is to add a GEOS at longitude 120° West. Since a GEOS at this location can be seen everywhere in CONUS, it would solve the critical-satellite problem shown in Figure 3. This is demonstrated by Figure 4, where part of the light gray region in Figure 3 has changed to the next darker shade of gray; the remaining light gray is due to the combination of the continuity and broadcast requirements. The overall increase in availability can be seen by comparing the total content of Figures 3 and 4.

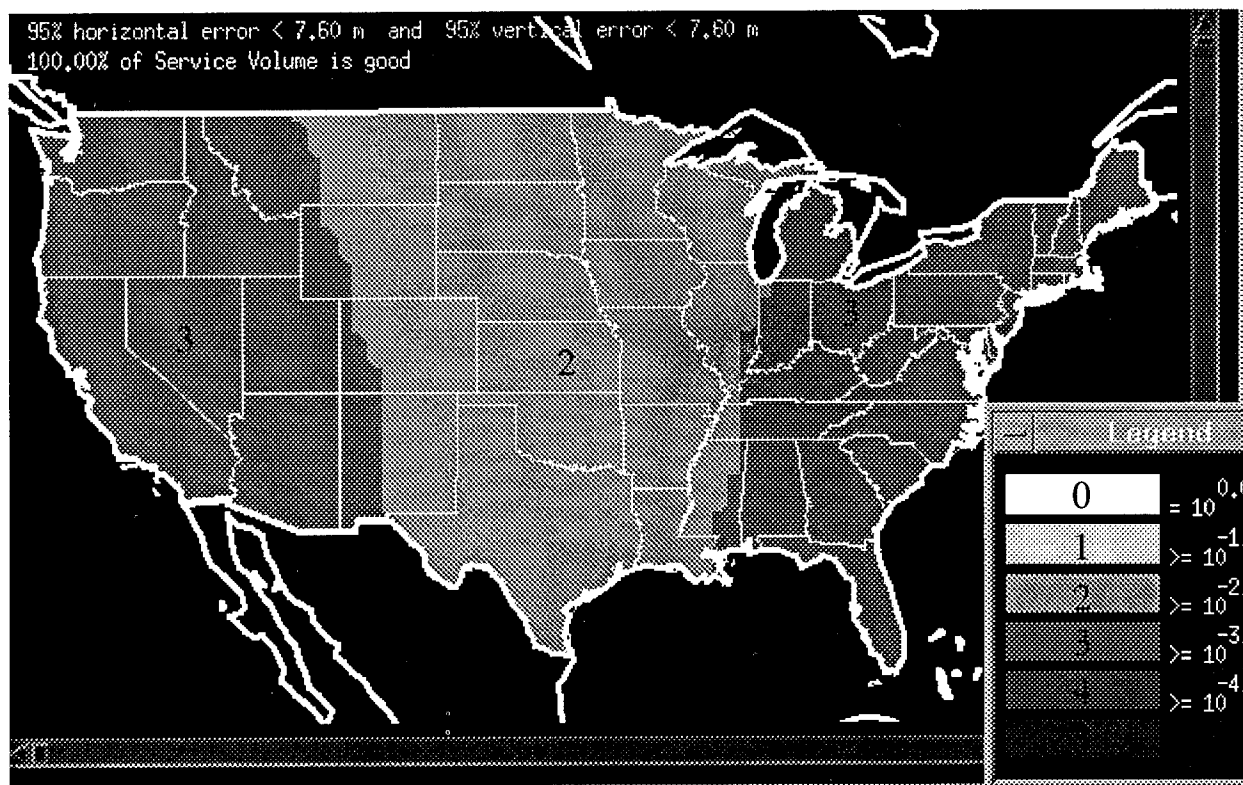


Figure 3. The Daily Average of Unavailability of Navigation Accuracy, Continuity and the WAAS Broadcast for Precision Approach with IWAAS.

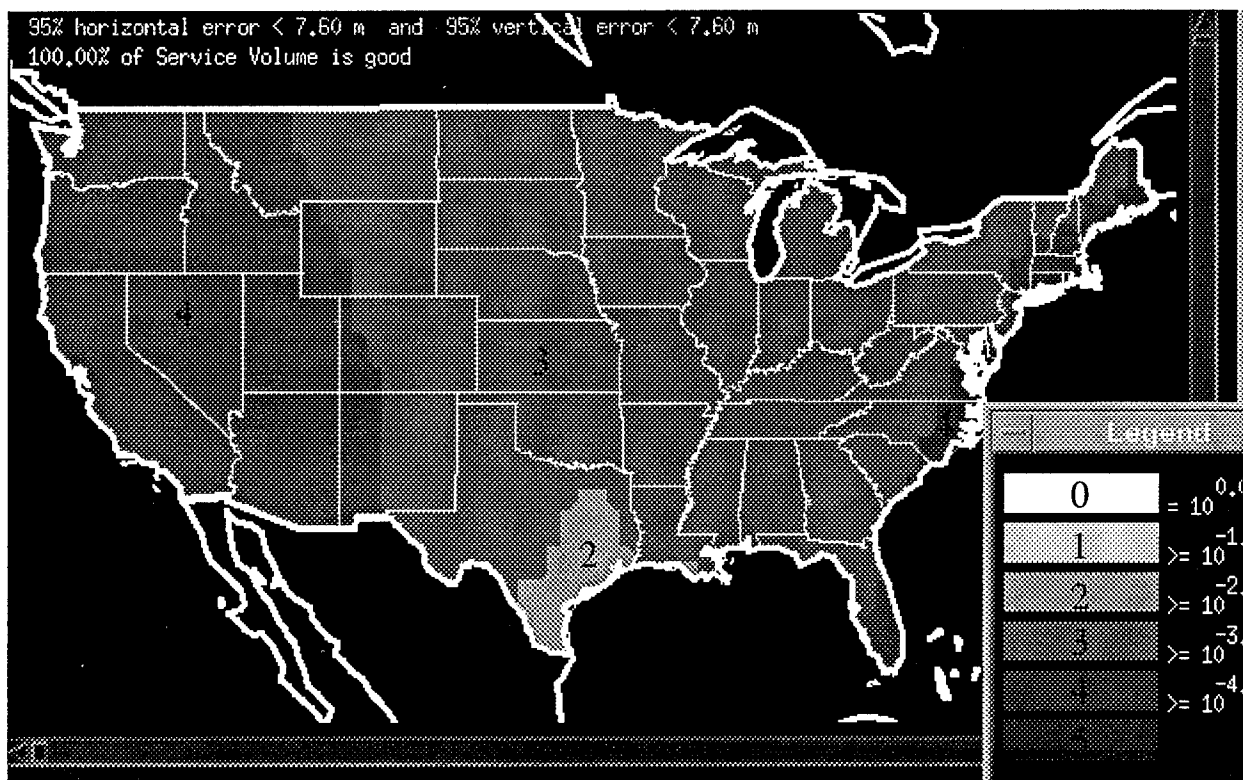


Figure 4. The Daily Average of Unavailability of Navigation Accuracy, Continuity and the WAAS Broadcast for Precision Approach with IWAAS, Augmented by a GEOS at Longitude 120° West.

Integrity

As various differential-correction and integrity algorithms are developed and tested for possible incorporation into WAAS, their effects on availability will be assessed by including relevant calculations in the SVM. For example, one of the ingredients in any WAAS integrity algorithm is a 99.9% bound on the ionospheric error (or something equivalent). Reference [6] presents research on the conditions under which a 99.9% ionospheric error bound is available for integrity calculations. These conditions depend on the number and locations of the WRSs as well as the orbital data for the GPS and GEOS.

The criterion in [6] for the availability of the 99.9% ionospheric error bound has been incorporated into the SVM to show the coarse sensitivity of coverage availability to different WRS configurations. This is obviously only one element of a comprehensive integrity criterion for WAAS. Since the overall integrity assurance scheme for WAAS is still under study, a completely different approach with a different availability criterion may ultimately be selected. This proposed integrity criterion may in fact be unnecessarily strict since it is based on test data from a small number of test-bed sites; if this is so, then the resulting unavailability estimates in this paper may perhaps be too pessimistic. Thus no decision on the required number of WRSs can be made based on this analysis, but nevertheless the trend is informative.

The analysis of the 99.9% ionospheric error bound presented in [6] uses a measure of the geographic distribution of the ionospheric pierce points at the time of interest (a pierce point is defined as the point where the line-of-sight vector from the WRS to a satellite intersects the layer in the ionosphere 350 km above the surface of the earth). The distribution of pierce points has been used in a number of other analyses, for example [7], which modelled the accuracy contours for WAAS in terms of the pierce points. In general, increasing the density of pierce points improves both service accuracy and integrity. Requiring higher densities, however, imposes an availability penalty, given no additional WAAS resources. A greater number of pierce points can be gained by adding WRSs or ranging satellites.

For the analysis here and in [6], the fundamental concept is the distribution of pierce points with respect to a rectangular grid with ionospheric grid points spaced 5° apart in latitude and longitude (see Figure 5).

- An ionospheric grid point will be called "available" if at least three of the four grid rectangles that meet at the grid point each contain at least one pierce point. Otherwise it is "unavailable".
- A grid rectangle will be called "available" if at least three of its four corner grid points are available. Otherwise it is "unavailable".

According to the analysis in [6], WAAS should be able to provide a 99.9% ionospheric error bound to any user located inside an available grid rectangle, but integrity *may* not be guaranteed (or achieved with sufficient certainty) in unavailable rectangles. This is the criterion for the availability of integrity (with respect to ionospheric corrections) currently implemented in the SVM: WAAS is considered unavailable inside any unavailable grid rectangle (unavailability = 1), regardless of the availability of navigation accuracy and continuity at points in the rectangle.

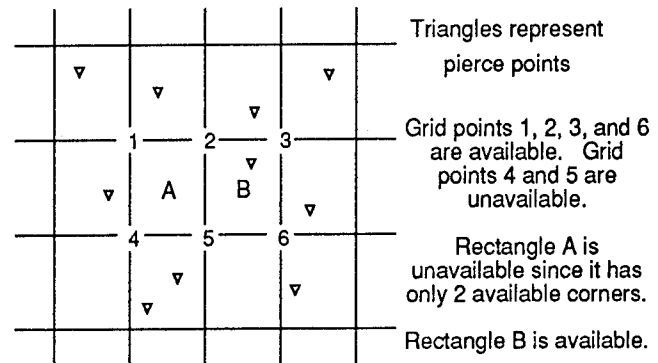


Figure 5. Examples of available and unavailable ionospheric grid points and rectangles.

Two points must be emphasized:

- This methodology does not address the integrity of WAAS with respect to error sources other than the ionosphere, nor does it include the constraint that the vertical protection error (VPE) should be ≤ 19.2 m [1].
- The exact form of an ionospheric integrity algorithm for WAAS has not been determined, as mentioned previously; this methodology is just a candidate.

With these caveats, hereafter the word integrity will refer to this proposed criterion for the availability of the 99.9% ionospheric error bound. The effect of the constraint "VPE ≤ 19.2 m" will be discussed in a future paper.

The Unavailability of Navigation Accuracy, Continuity, and Integrity for Precision Approach with IWAAS

Figure 6 shows two instantaneous unavailability plots of IWAAS for the northwestern part of the U.S. The service requirements are accuracy, continuity, WAAS broadcast, and integrity for PA. The white triangles are the pierce points. With all WRSs active, all grid rectangles in this part of the country are available for integrity, as shown in Figure 6a (several critical pierce points over Canada are off the edge of the Figure).

Figure 6b shows the result if the WRS at Billings (Montana) fails at this time. The loss of pierce points generated by this WRS produces an integrity outage,

which extends from the Pacific Coast east to Wisconsin along the U.S./Canadian border, and south into Utah, Colorado and Nebraska.

It should be noted that the new outage area need not occur in the immediate vicinity of the failed WRS; the reason is that pierce points produced by a WRS may be some distance away, and the outage reflects the location of the pierce points more than the location of the WRS. For example, the failure at Billings removes the pierce point north of Minnesota in Figure 6a; without this pierce point, the ionospheric grid points with coordinates (50°N, 90°W), (50°N, 95°W), and (50°N, 100°W) are unavailable

for integrity, and therefore the rectangles between latitudes 45° and 50° North, and longitudes 90° and 100° West are unavailable. Similar problems cause the other rectangles in Figure 6b with outages for the 99.9% ionospheric error bound.

As the satellites move during the day, the pierce points move with them, changing the locations of any integrity outages. Figure 7 shows the daily average of the unavailability of accuracy, continuity, the WAAS broadcast, and integrity for IWAAS plus a fourth GEOS (at longitude 120° W).

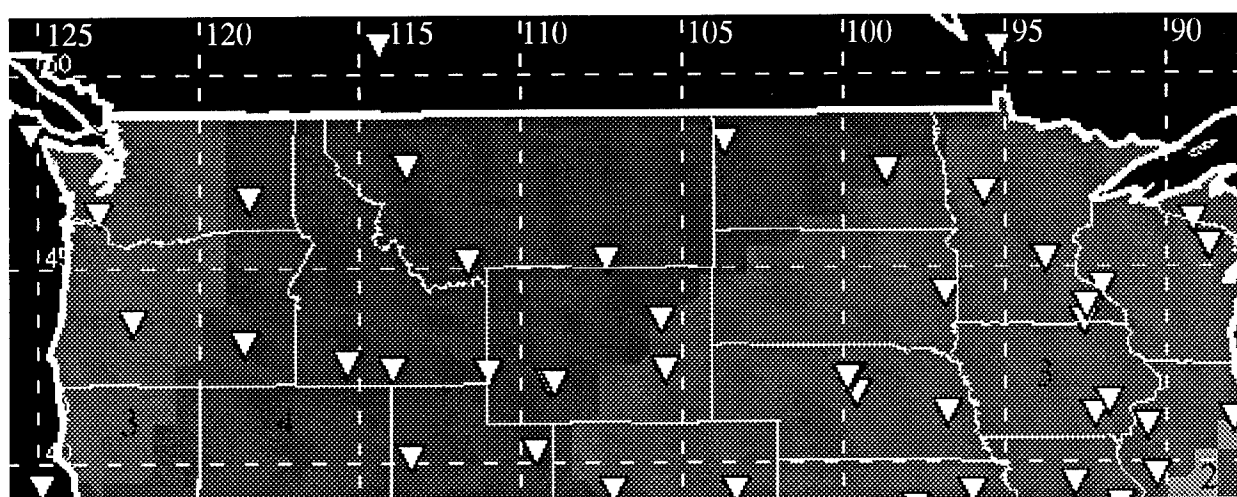


Figure 6a. All WRSs are operational.

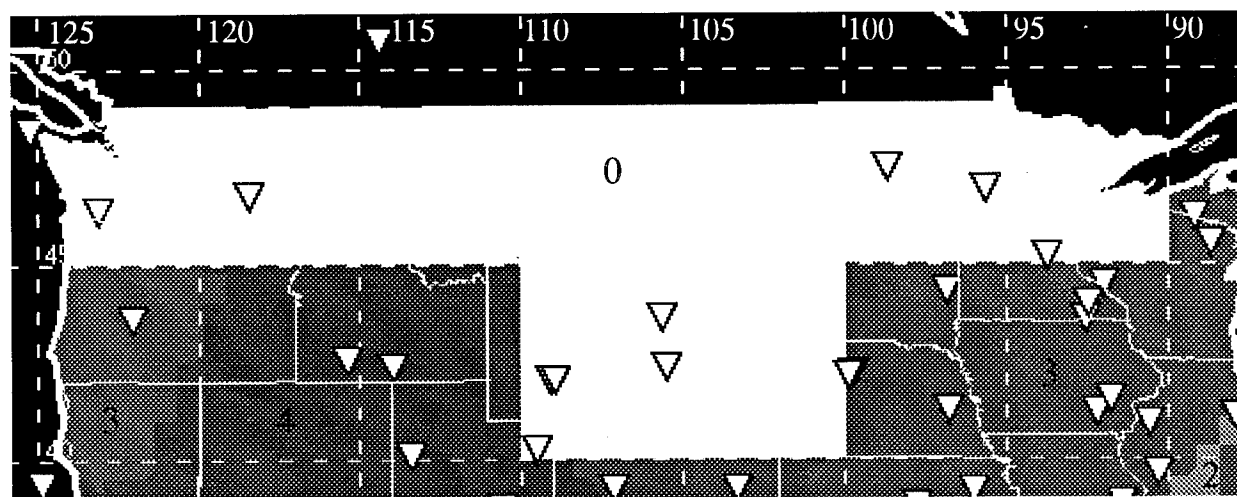


Figure 6b. The Billings WRS has failed.

Figure 6 . The Effect of a WRS Failure on the Instantaneous Unavailability of Precision Approach at One Sample Time.

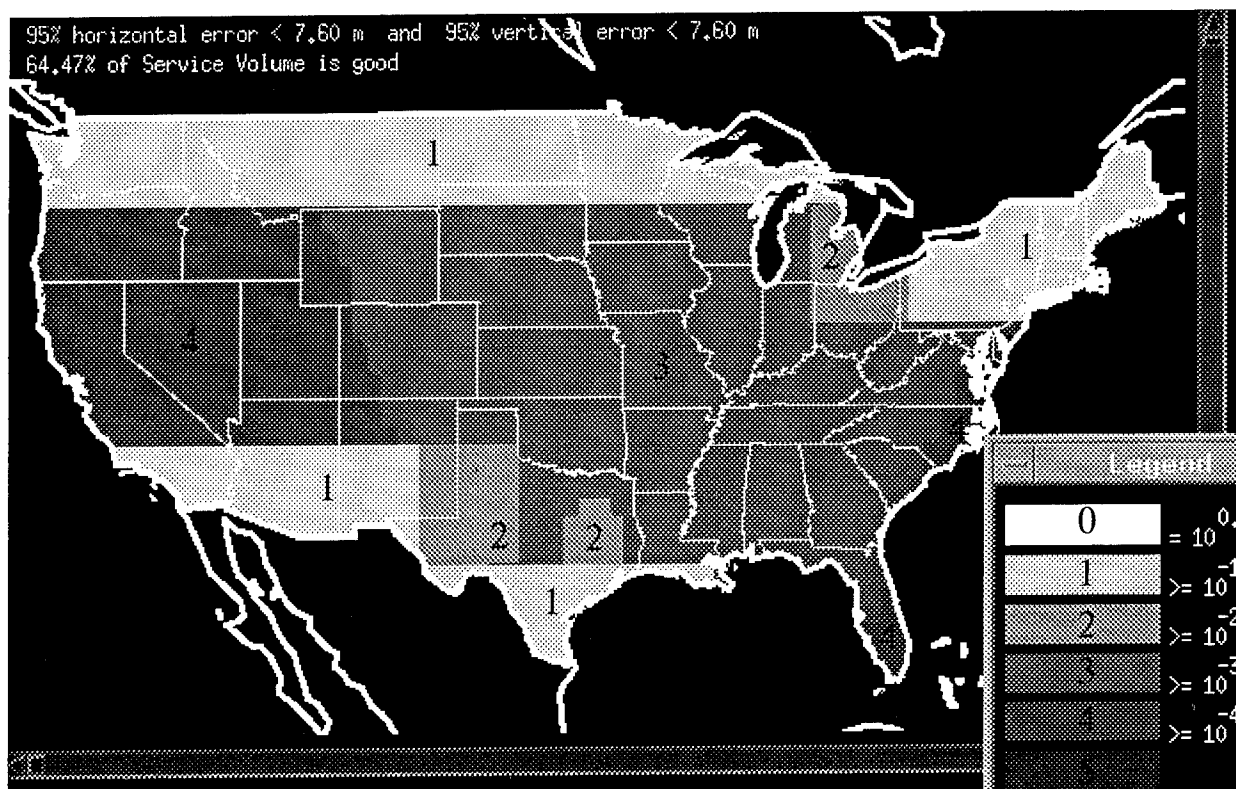


Figure 7. The Daily Average of Unavailability of Navigation Accuracy, Continuity, the WAAS Broadcast, and Integrity for Precision Approach with IWAAS, Augmented by a GEOS at Longitude 120° West.

The Unavailability of Navigation Accuracy, Continuity and Integrity for PA with IWAAS Augmented by Extra GEOS and WRSs

The option exists for up to 49 CONUS sites and 20 international sites for the WRSs, and analysis has been conducted with the SVM for more than 20 WAAS configurations containing more than 24 WRSs. This analysis helped to understand the interaction between extra WRSs and the proposed criterion for the availability of integrity cited above.

Figure 8 is an instantaneous unavailability chart for one of these larger configurations. It shows the pierce points for a time of day with an integrity outage in the southwestern part of CONUS and the northwestern part of Mexico. Three of the grid rectangles in the figure have no pierce points. As a result, the ionospheric grid points with coordinates (35° N, 115° W) and (30° N, 115° W) are unavailable for integrity. This is the reason for the integrity outage in the two grid rectangles covering southern California and southwestern Arizona (and which also affects northwestern Mexico).

This integrity outage could be eliminated either by adding satellites to the constellation (presumably by GEOS rather than GPS), or by adding WRSs to the WAAS network. However, the particular distribution of the pierce points in this example suggests that a modification of the proposed integrity method might be preferable.

In this case, the grid rectangle on the left (containing the integrity outage over southern California) contains 7 pierce points. Further research on GPS/WAAS integrity may show that these 7 pierce points are sufficient for integrity in this rectangle, especially considering the fact that the 9 grid rectangles centered on this one contain more than 20 pierce points in all. Similarly, the 9 grid rectangles centered on the rectangle on the right (containing the integrity outage over southwestern Arizona) contain more than 30 pierce points in all. Even with no pierce points in the rectangle itself, the pierce points in the surrounding rectangles may be sufficient for integrity. This feeling is bolstered by the observation that moving two pierce points less than a degree in the right directions (in Figure 8) would remove the outage without significantly changing any of the information available to WAAS for integrity calculations. The bottom line is that Figures 6-8 will look significantly better if this proposed integrity criterion can safely be relaxed or otherwise adjusted appropriately.

Summary

The SVM was built to provide analytical support to AND-510 on questions about the WAAS. The examples presented in this paper demonstrate how the SVM can be used to check the sensitivity of WAAS availability to things such as:

- The WAAS architecture, for example, the number and locations of GEOS and WRSs.
- Design parameters, for example, the failure and restoration rates for GPS and GEOS.
- Proposed geometry constraints and integrity algorithms.

Detailed analysis will be required to determine the WRS configuration for EWAAS; this analysis must also consider other facets of the availability problem, such as the connectivity and failure/restoration statistics of the ground segment now being incorporated into the SVM.

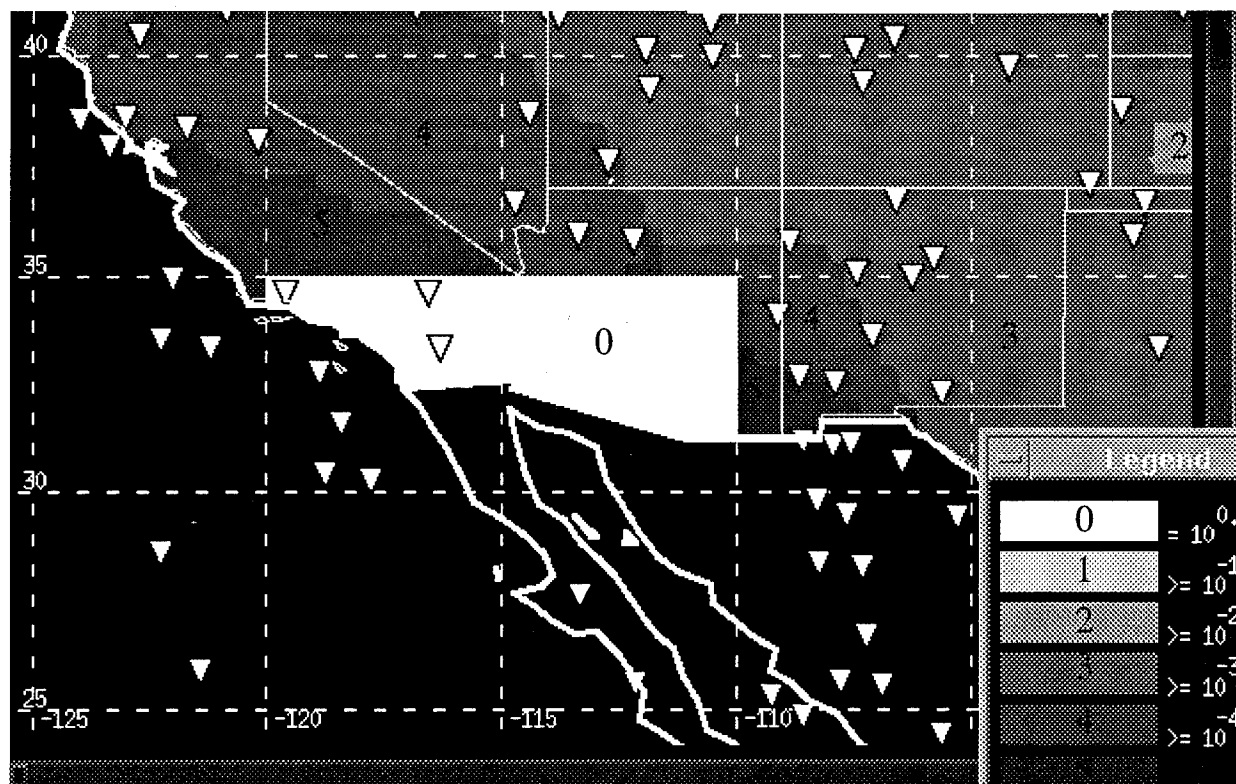


Figure 8. An Instantaneous Unavailability Chart Showing the Sensitivity of the Integrity Outages to the Criterion for Availability of Grid Rectangles.

Acknowledgements

The authors would like to acknowledge Robert S. Conker, M. Bakry El-Arini, Kelly R. Markin, James K. Reagan, and Curtis A. Shively from MITRE/CAASD for many helpful discussions during the development of the SVM, and for reviewing this paper. The authors would also like to acknowledge Joseph Dorfner, the manager of the FAA Satellite Program Office (AND-510), who is the sponsor of this work.

References

1. *Specification for the Wide Area Augmentation System (WAAS)*, FAA-E-2892A, 2 August 1995.
2. Poor, W.: *Availability Estimates for GNSS*, Institute of Navigation Technical Meeting, January 1993.
3. Shively, C.: *Satellite Criticality Concepts for Unavailability and Unreliability of GNSS Satellite Navigation*, MITRE MP 93W0000051, October 1993.
4. Shively, C.: *Availability Analysis of GPS Wide Area Augmentation System (WAAS) Space Segment Considering Continuity Requirements*, Institute of Navigation Technical Meeting, January 1995.
5. *Minimum Operational Performance Standards for Sensors Using Global Positioning System / Wide Area Augmentation System, Draft 6*, RTCA, 24 July 1995.
6. Conker, S., El-Arini, B., Albertson, T., Klobuchar, J., Doherty, P.: *Development of Real-Time Algorithms to Estimate the Ionospheric Error Bounds for WAAS*, Institute of Navigation Satellite Division Meeting, September 1995.
7. Pullen, S. P., Enge, P. K., and Parkinson, B. W.: *A New Method for Coverage Prediction for the Wide Area Augmentation System (WAAS)*, Institute of Navigation Meeting, June 1995.

An Algorithm for Inter-frequency Bias Calibration and Application to WAAS Ionosphere Modeling

Yi-chung Chao, Yeou-Jyh Tsai, Todd Walter, Changdon Kee, Per Enge, and Brad Parkinson
Stanford University

BIOGRAPHY

The authors are part of the WAAS development team at Stanford University. The team has been focusing on developing and verifying different WAAS algorithms and concepts for both accuracy and integrity improvement. Their WAAS innovations are all validated by real time flight trials. The WAAS development team at Stanford is also working on various navigation applications.

ABSTRACT

The Wide Area Augmentation System (WAAS) was invented to improve both the differential GPS accuracy as well as the integrity monitoring over a large geographical region. [Kee et al, 1990, Walter et al, 1994] The ionosphere model parameters are one of the most important messages for the single frequency WAAS users. However, the embedded inter-frequency biases in both GPS satellites and dual-frequency Wide Area Reference Station (WRS) receivers make the WAAS generate biased ionospheric delay measurements. As the airborne single frequency avionics retrieve this WAAS ionospheric corrections, a systematic error will be transformed into user's navigation solution. These biases must be reduced to obtain the best possible performance of WAAS. Furthermore, the biased ionospheric delay measurement will also offset the ionosphere-free pseudorange estimates. Thus these biases not only offset the ionosphere model but will also corrupt the WAAS corrections for satellite clocks and ephemerides.

Without appropriate modeling, the bias can be as large as several meters. An alternative software calibration methodology has been developed at Stanford University for estimating these inter-frequency biases. This method allows a constant monitoring and a preliminary report has been presented earlier [Chao, et al, 1995]. Since then the algorithm has been enhanced in several aspects: 1) The data from several stations are processed together rather than the previous single station processing. 2) The spherical harmonics model order is increased from 1 to 2.

3) The process is more efficient and more automatic. The new results show a better than half meter consistency.

When the new biases are incorporated into Stanford's Master Station algorithm, the ionospheric model shows greater agreement with the corrected dual-frequency measurements. Most importantly, as will be shown later, new corrections significantly improve the positioning accuracy for a single frequency user. These lower and more zero-centered navigation fixes will allow us to further analyze the system in more detail as well as monitor with better integrity.

1 INTRODUCTION

The purpose of Wide Area Augmentation System (WAAS) is not only to improve the differential GPS accuracy but also to provide integrity monitoring. The accuracy improvement is achieved by reducing the spatial decorrelation effects in GPS satellite orbit error and ionospheric delay in differential corrections. With geostationary satellite broadcasting correction message on L1 frequency, WAAS facilitates the application of differential GPS to civilian users since signals can be easily accessed while no local broadcasting equipment needs to be setup. Furthermore, via the real time network monitoring, WAAS will be able to provide an integrity warning within the time to alarm. The Stanford lab has been a part of the FAA cross country WAAS network since 1992 and is responsible for three WRS's in the west coast. This small size experimental network has been used to develop and validate WAAS algorithms with real time flight tests. The Stanford flight test results [Walter, et al 1994, Kee et al, 1995, Tsai, et al, 1995] demonstrate that CAT I precision approach accuracy can be achieved with this system.

Figure 1.1 is the overview of the Stanford WAAS experimental network. This figure shows the three WRS's (Elko, Nevada, Arcada, California and San Diego, California), and Stanford's static and dynamic users with the western coastline of North America. A snap shot of the ionosphere pierce points (IPP's) seen by

the entire network are also shown in the same figure. These ionospheric delay measurements from the three WRS's are used to generate the ionosphere model parameters for a geographical region coverage of approximately 40 degree by 40 degree.

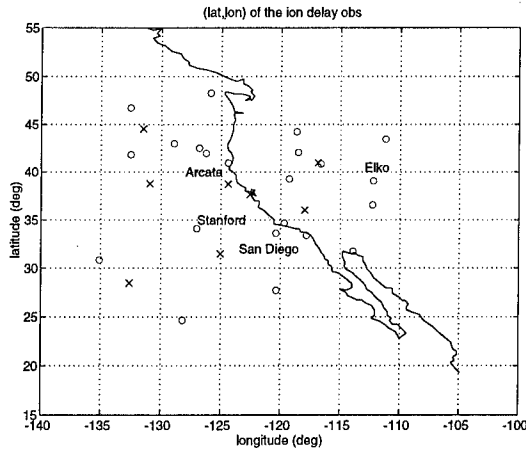


Figure 1.1. Stanford WAAS network and ionosphere pierce point locations. Circles are the IPPs from WRS's and crosses are IPPs from the Stanford user.

As technology improves and new applications develop, the accuracy requirement of Differential GPS becomes higher and higher. Therefore, smaller error starts to reveal themselves, become more important and need better modeling and treatment. One such source is the inter-frequency biases embedded in the GPS transmitters and receivers. The inter-frequency biases make the WAAS generate the biased ionospheric delay measurements. As the airborne single frequency avionics retrieve the WAAS ionospheric corrections, a systematic error will be transformed into user's navigation solution. Without appropriate modeling the combination of the transmitter-receiver inter-frequency biases can be as large as several meters. Because the WAAS user is single frequency and need and ionosphere correction, these several-meter interfrequency biases will offset navigation solutions.

One common practice to this problem is to pre-calibrate receivers and rely on either broadcast information or other separate estimates of the satellite biases. The current information of satellites' inter-frequency biases, also known as T_{gd}^j , are from pre-launched calibration data and are in GPS navigation messages. Due to the lack of monitoring and updating, this information is usually regarded as only marginally accurate. On the other hand, the receivers can also be hardware-calibrated and a calibration value can be obtained for each individual receiver. However, these approaches are both time

consuming and difficult to acquire. Moreover, even if the inter-frequency biases are pre-calibrated, they must be constantly monitored for either bias drifting or hardware switching. Therefore, to provide WAAS adequate accuracy and improved integrity monitoring, a more convenient calibration method is needed. In addition, this method must be repeated periodically on the receivers installed in the field.

The purpose of this research is to develop a calibration methodology which can be easily applied and useful to reduce the offset and jumpiness caused by the inter-frequency bias while providing better accuracy constraint for integrity monitoring. A preliminary report [Chao et al, 1995] demonstrated a half-meter consistency of the estimation results. Since then the algorithm has been enhanced in several aspects: 1) The data from several stations are processed together rather than the previous single station processing. 2) The spherical harmonics model order is increased from 1 to 2. 3) The process is more efficient and more automatic.

2 INTERFREQUENCY BIAS ESTIMATION

2.1 GPS Signal Models and Definition of the Inter-frequency Biases

To clearly understand the role that the inter-frequency bias plays in the ionospheric delay measurements, it is best to start with the basic GPS observables, code and carrier phases on L1 and L2 frequencies. The models for the GPS measurements used are:

$$PR_{L1} = \tilde{\rho} + I_{L1} + T_{gd}^j + M_{PR1} + E_{PR1} \quad (2.1)$$

$$PR_{L2} = \tilde{\rho} + \gamma \cdot I_{L1} + \gamma \cdot T_{gd}^j + R_i + M_{PR2} + E_{PR2}$$

$$\phi_{L1} = \tilde{\rho} - I_{L1} + T_{gd,\phi}^j + N_1 \lambda_1 + m_{\phi_1} + \varepsilon_{\phi_1}$$

$$\phi_{L2} = \tilde{\rho} - \gamma \cdot I_{L1} + \gamma \cdot T_{gd,\phi}^j + R_{i\phi} + N_2 \lambda_2 + m_{\phi_2} + \varepsilon_{\phi_2}$$

where

$$\gamma \equiv (L_1 / L_2)^2 = (77 / 60)^2$$

$\tilde{\rho}$ is the pseudorange, including the tropospheric delay, receiver and satellite clock biases and all elements common to all the four observables in equation (2.1).

I_{L1} is the ionospheric delay at L1 frequency.

T_{gd}^j is the actual (as opposed to the broadcast) transmitter inter-frequency bias in code-phase on L1 for the j-th satellite. $T_{gd,\phi}^j$ is the respective bias on the carrier-phase.

R_i is the receiver differential inter-frequency bias on L2 for the i -th receiver. Because of the timing of the GPS receivers is dependent on L1 C/A code, the inter-frequency bias on L1 is zero by definition.

M_{PR} and m_ϕ are the non-white noises contributed from multipath effect. The large case (M) represents larger error in pseudorange and the lower case (m) represents at least a order or more smaller multipath on carrier phase.

E_{PR} and ϵ_ϕ are the measurement noises. They also represent larger noise on pseudorange and smaller noise on carrier phase. These measurement noises are also assumed to be white noise as opposed to the colored multipath effect.

Note that different transmitter and receiver inter-frequency biases have been assumed for the code phase and the carrier phase measurements to take into account the different tracking loop and to be more realistic. However, from the following analysis, these inter-frequency biases on carrier phase measurements can be lumped with the constant cycle ambiguities and do not need to be treated separately.

2.2 Dual Frequency Ionospheric Delay Measurements

In the usual sense of dual frequency GPS measurement, the ionospheric free pseudorange will not be affected by the satellite inter-frequency biases [GPS-ICD-200]. However, since the WAAS user equipment is single frequency and uses ionospheric corrections, the following analysis will show that both the satellite and the receiver inter-frequency biases, T_{gd}^j and R_i , introduce errors to the ionospheric measurements as well as to the smoothed pseudorange through carrier-smoothing. These biased measurements will then corrupt the WAAS ionospheric, satellite clock and ephemeris corrections. From each WRS, the ionospheric dual frequency measurements can be calculated from both code phase and carrier phase as:

$$\begin{aligned} I_{L1,PR} &\equiv \frac{PR_{L2} - PR_{L1}}{\gamma - 1} \\ &= I_{L1} + (T_{gd}^j + \frac{R_i}{\gamma - 1}) + v_{PR} \end{aligned} \quad (2.2)$$

$$\begin{aligned} I_{L1,\phi} &\equiv \frac{\phi_{L1} - \phi_{L2}}{\gamma - 1} \\ &= I_{L1} - (T_{gd}^j + \frac{R_{i,\phi}}{\gamma - 1}) + \frac{N_1\lambda_1 - N_2\lambda_2}{\gamma - 1} + v_\phi \\ &= I_{L1} + Amb + v_\phi \end{aligned} \quad (2.3)$$

where we assumed the inter-frequency biases are very slowly time varying and thus can be lumped into the ambiguity term for a data collection session. The ionospheric delay derived from carrier phase, equation (2.3), will be used to smooth the code phase equation (2.2), as part of the algorithm for Stanford real-time experimental WAAS. Clearly, the quantity $T_{gd}^j + \frac{R_i}{\gamma - 1}$ in

$I_{L1,PR}$, which will be used to generate the WAAS ionospheric corrections, prevent us from obtaining the correct ionospheric delay. This $T_{gd}^j + \frac{R_i}{\gamma - 1}$ is satellite as

well as receiver dependent and can have values of several meters. We call this quantity the *inter-frequency bias*, i.e. we define

$$\text{Inter-frequency Bias} \equiv T_{gd}^j + \frac{R_i}{\gamma - 1}$$

For the above reason, a calibration method is needed to improve the accuracy of WAAS. The current methods for obtaining the GPS satellite and receiver inter-frequency biases are through either global data estimation [Wilson, et al, 1994] or direct hardware calibration. Since the Stanford experimental WAAS network has only limited geographical coverage, and also because the hardware calibration is time consuming and the biases may subject to drift, the following estimation algorithm provides an easier way to estimate and monitor these biases.

2.3 Estimation Algorithm

This section details the post-processing algorithm for estimating the inter-frequency biases. A basic assumption of the inter-frequency biases is that they are quite constant over a long period of time. This assumption will be verified later.

The idea of estimating the interfrequency bias is the following: if we can separate the ionospheric delay from the ambiguity term in the almost noiseless equation (2.3), then we can plug in and cancel this ionospheric delay in equation (2.2). After an averaging to reduce the code phase noise and multipath, the estimate of the inter-frequency bias can be obtained.

In essence, this estimation scheme exploit the obliquity factor used with a spherical harmonics model to separate the ionospheric delay from the inter-frequency biases [Cohen et al, 1992]. Another assumption for using this scheme is that the ionosphere will be constant for a course of 2 to 3 hours when expressed in the Solar-Magnetic frame [Knecht et al, 1985].

Figure 2.1 depicts the concept of ionosphere pierce point and the obliquity factor. The ionosphere is a layer above the surface of Earth and the ionosphere pierce point (IPP) is the intersection of user's line of sight to the satellite and the center of the ionosphere slab. The obliquity factor is the ratio of ionospheric delay along the user's line of sight to the delay in the vertical direction through the same IPP. The user is actually the static WRS in this figure. The obliquity factor is assumed to be a pure geometric function of satellite elevation angle.

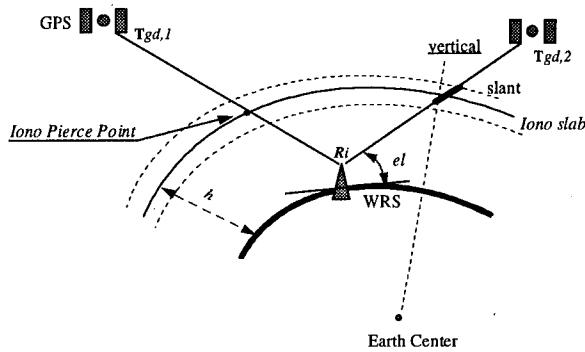


Figure 2.1. Ionospheric Pierce Point (IPP) Concept.

Even if the ionospheric delay measurements from both code phase and the carrier phase have the same measurements of ionosphere with different offsets, the carrier phase measurement is more preferable to use for the ionosphere modeling because of its much smaller multipath and measurement noise. Explicitly, the noiseless equation (2.3) can be re-written with the obliquity factor (Ob) as

$$I_{L,\phi} = Ob \cdot I_{L,vert} + N \quad (2.4)$$

where N is a constant offset.

With the assumption that the ionosphere is constant for a 3-hour period in the Solar-Magnetic frame, all the IPPs' geographical latitudes and longitude are transformed to the Solar-Magnetic frame and a spherical harmonic model is the ideal candidate for modeling the constant ionosphere in this spherical coordinate system.

After a Least Squares fit of the model coefficients, the ionosphere can be separated from the constant offsets in equation (2.4). Again advantages has been taken of the change of satellite elevation angle and thus obliquity factor, Ob . Usually a half-an-hour satellite observation period is necessary to provide sufficient elevation angle change and therefore sufficient separation.

Once we separate the constant offset from the ionospheric delay in (2.4), we can back substitute the ionospheric delay into equation (2.2) and what is left from the code phase measurement will be

$$T_{gd}^j + \frac{R_i}{\gamma - 1} = \hat{I}_{L,PR} - Ob \cdot \hat{I}_{vert} - v_{PR} \quad (2.5)$$

By further assuming the colored noise, which dominated by multipath effect, can be averaged out, an estimate value for the inter-frequency biases can be obtained as:

$$\text{inter-frequency bias} \equiv \left\langle T_{gd}^j + \frac{R_i}{\gamma - 1} \right\rangle \quad (2.6)$$

where operator $\langle \rangle$ represents time averaging

Cycle slips in the ionospheric delay measurement can easily be fixed with 1 Hz data both because the limited physical variation speed in the ionosphere as well as because the satellite clock biases (mainly due to Selective Availability) been canceled out. Therefore a linear extrapolation can be used for a cycle slip to centimeter level.

3. Data Processing

The database used in this study is real data collected from each of the Stanford WRS's and also the Stanford user for performance validation. All three WRS's and Stanford user are equipped with Trimble 4000 SSE receivers. Data is mostly collected around midnight and at noon to avoid the larger ionosphere gradient in the sunrise and sunset periods. This practice allows the obliquity factor be calculated more accurately.

The ionosphere is assumed to be constant in the Solar-magnetic coordinate frame for at least 2 to 3 hours. As a result of this assumption, the noon time estimation results have larger variation than those from midnight processing. However, this is the only way to obtain the complete estimates for all satellites in the GPS constellation.

The processing of multi-station data has several advantages over the single WRS. First of all, multi-station data provides more consistency when modeling the ionosphere simultaneously than separately. Second, the multi-station data set provide far more complete coverage of the sky and therefore a higher order spherical harmonics can be used for the ionospheric delay

modeling reliably . Hence more detailed variations can be correctly modeled. Figure 3.1 shows a set of IPP ground tracks in one data processing session, a total of 43 satellite-receiver pairs have been included in this run.

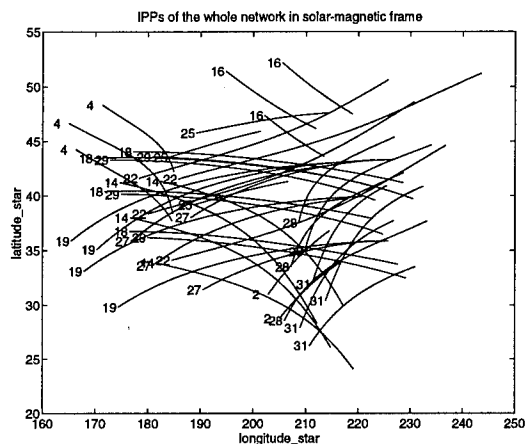


Figure 3.1, ground track of ionospheric pierce points in a multi-station processing session. total of 43 satellite-receiver pairs been included in this run.

To obtain the final estimates, the following strategy was employed: A set of seven-day data was collected. Then for each midnight and noon time 5-hour data period, one multi-station estimation result was obtained for each 3-hour data subset. These 3-hour subsets usually overlap for an hour. Therefore, for each 5-hour period, three to four multi-station estimates as well as the confidence number will be calculated for all possible satellite-in-view as well as the confidence number for each estimates. These estimate will be combined in a weighted-average to get one estimate for that 5-hour period. After repeating the process for all the data, the final estimate will be another weighted average over all midnight and noon time sessions.

Currently, the program handles all processing automatically, including choosing satellites according to the time period specified, cycle slip fixing and performing the estimation. Since the greater multipath effect is at lower elevation, a exponential weighting function is used for computing the time averaging in equation (2.6).

Figure 3.2 shows one example for the time-averaged result presented in equation (2.6).

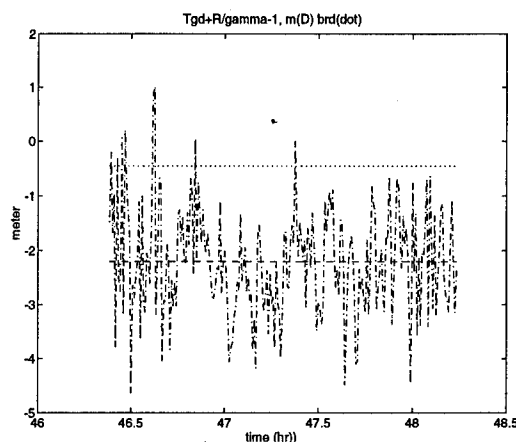


Figure 3.2. The noisy line is the mix of the *inter-frequency bias* and the colored noise in equation (2.5). After time averaging, the *interfrequency bias* is given by the dotted line. Also presented is the same bias based on the broadcast Tgd and pre-calibrated receiver bias (old value).

4 RESULTS AND VERIFICATION

Results and several verification schemes will be provided to prove the usefulness of this estimation algorithm. Since it is hard to find any independent and direct means to verify the validity of our estimates , several verification methods [Chao, et al, 1995] i.e. single-difference between receivers/satellites, the rms error in both WAAS ionospheric modeling and navigation fixes will be used in this paper to assess the estimates.

4.1 Verification by Single Differences

The single difference between two receivers viewing the same satellite is used to check the consistency of the estimation. This process cancels the satellite bias and forms the relative receiver bias ΔR_i . This quantity should agree to within the error limit regardless which satellite is used for forming the single difference. Table 4.1 presents the statistics for different $\frac{\Delta R_i}{\gamma - 1}$ using all 25

GPS satellites in the current status. The last column i.e., the standard deviation, indicates the estimation results agree to better than 0.5 meters. These estimated bias also agreed with the earlier estimation results to within the error bound [Chao et al, 1995]. As these results compared to the two-year-old hardware calibrated values, one of the single-difference is off by one meter or so. This shows the needs for constant monitoring of the inter-frequency biases.

| all 25 Svs | mean (m) | std (m) |
|----------------------|----------|---------|
| Arcata - Stanford | 1.86 | 0.44 |
| Elko - Stanford | 5.68 | 0.49 |
| San Diego - Stanford | 3.09 | 0.33 |

Table 4.1. Statistics of relative receiver biases from single differences between receivers of estimated inter-frequency biases using common satellites. For comparison, the two-year-old hardware calibration single-differences are also listed: between Arcata and Stanford was 1.40 meter, between Elko and Stanford was 4.54 meters, between San Diego and Stanford was 3.19 meters.

4.2 RMS Error in WAAS Ionospheric Modeling

The WAAS broadcasts the ionosphere model parameters for single frequency users to correct ionospheric error. Not considering the inter-frequency biases will cause the Wide Area Master Station (WMS) to generate a biased and even skewed ionosphere map. The error could be as large as several meters as shown in Table 4.1. The rms error of the user ionospheric should be reduced after taking the biases into account.

For the Stanford WAAS network, carrier smoothed measurements along with a confidence indicator are used to obtain the ionospheric delay at each WRS. The data is then transmitted back to the WMS at Stanford campus. The tasks of WMS are to generate the ephemeris correction, the satellite clock correction and ionospheric delay model [Walter et al, 1994, Kee et al, 1995, Tsai et al, 1995].

The current implementation of the ionospheric delay model in Stanford WAAS conforms to the RTCA-SC-159 Working Group 2 (WG2) Grid algorithm [RTCA-WG2]. The formula to generate each grid is

$$\hat{I}_{grid,V} = \hat{I}_{Klob,V} \cdot \left\{ \frac{\sum_{k=1}^K \left(\frac{I_{meas,V,k}}{I_{Klob,V,k}} \right) \cdot w_k}{\sum_{k=1}^K w_k} \right\} \quad (4.1)$$

where $\hat{I}_{grid,V}$ is the estimated vertical ionosphereic delay at the grid, $\hat{I}_{Klob,V}$ is the ionospheric delay calculated from broadcast Klobuchar model, $I_{meas,V,k}$ is the measured ionospheric delay at the IPP and $I_{Klob,V,k}$ is the ionospheric delay from Klobuchar model at the IPP. K is the total number of IPP's. Finally, $w_k = 1/d_k$ is used as a

weighting function, where d_k is the distance from the k -th IPP to the grid.

For the Stanford WAAS, 76 grid points are used to cover an approximately 40 degree by 40 degree geographical region with 5 degree grid spacing. Because the Klobuchar model is used [Klobuchar, 1986], the above algorithm automatically accounts for the time and seasonal effects between the IPP and grid. For our implementation, the weighting function has been modified to include the confidence from the smoothing function as [Kee et al, 1995]:

$$w'_k = \sqrt{1/\sigma_{smth}^2 + 1/d_k^2} \quad (4.2)$$

The mean and rms error of the ionospheric delay at Stanford dual frequency static user is presented in Table 4.2. for comparison. Note that Stanford has a dual frequency static user for this statistical comparison.

| user ionospheric RMS error | Modified Grid user ionospheric RMS | | | |
|----------------------------------|------------------------------------|--------|---------------------|--------|
| | w/o ifb correction | | with ifb correction | |
| | mean | stdev | mean | stdev |
| | -0.31 m | 0.82 m | -0.05 | 0.37 m |

Table 4.2 Comparison of user ionospheric delay RMS error through WAAS modified grid algorithm, with and without inter-frequency biases (ifb) correction. The statistics is based on August 26, 1995, 14-hour data.

4.3 WAAS Navigation Solutions

The last and the most important test of the estimated interfrequency bias is the improvement of WAAS navigation fixes. Both the ionospheric delay correction and the satellite clock and ephemeris correction will be affected by the biases through frequency smoothing for both pseudorange and ionosphere measurements. Figure 4.1 shows a 14-hour Stanford WAAS real-time flight test vertical error without adjusting the interfrequency biases. An about one-meter offset was in the vertical direction and similar half meter offset in the east and north direction.. After adjusting the interfrequency biases, Figure 4.2 shows the offset in the vertical direction has been greatly reduced to be more zero-centered for the same data.

Table 4.2 presents the 95% and 99.9% percentile of the WAAS navigation fix error over this 14-hour session. Table 4.3 shows the means as well as the sample worst cases for the same set of data. It is apparent that with the inter-frequency bias correction, not only the mean of the

navigation errors been reduced, but also the distribution of the errors been greatly reduced.

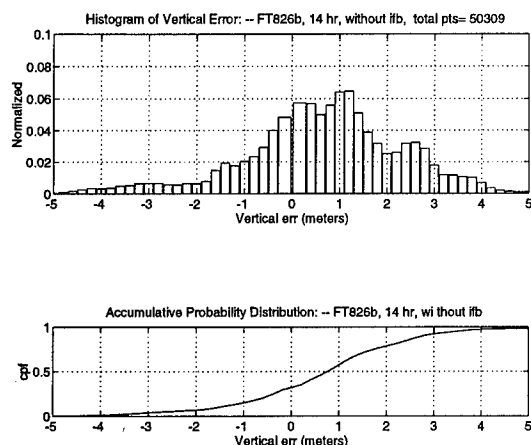


Figure 4.1 Histogram of WAAS navigation solution flight errors before adjusting the estimated inter-frequency biases.

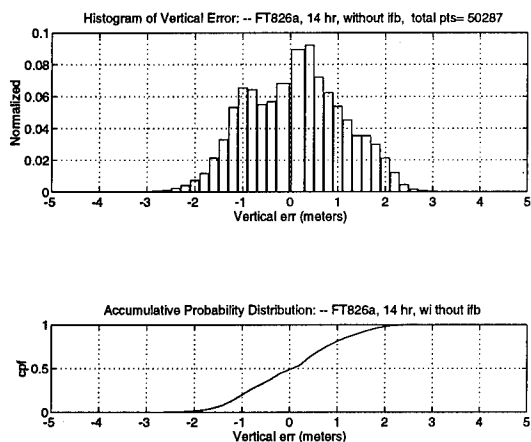


Figure 4.2 Histogram of WAAS navigation solution flight errors after adjusting the estimated inter-frequency biases.

| Percentile | without ifb correction | | with ifb correction | |
|------------|------------------------|-----|---------------------|-----|
| | between (meters) | | between (meters) | |
| 95% | -4.7 | 6.7 | -1.85 | 2.4 |
| 99.9% | -5.0 | 7.2 | -2.8 | 2.8 |

Table 4.2 95% and 99.9% of the WAAS vertical navigation error. Comparison for with and without applying inter-frequency biases (ifb). The statistics is based on a 14-hour data from August 26, 1995, 54000 epochs.

| | w/o ifb correction | | | with ifb correction | | |
|----------|--------------------|-------|-------|---------------------|-------|-------|
| | worst cases | | | worst cases | | |
| | mean | lower | upper | mean | lower | upper |
| Vertical | +0.79 | -5.4 | +7.6 | +0.11 | -4.4 | +4.6 |
| East | 0.41 | -3.8 | +2.8 | +0.06 | -1.6 | +3.4 |
| North | 0.20 | -3.0 | +4.2 | -0.12 | -2.6 | +1.6 |

Table 4.3 Comparisons of WAAS navigation error statistics with and without inter-frequency bias (ifb) correction: mean and worst cases in meters. Data is from August 26, 1995, 54000 epochs.

This result shows the necessity of correctly adjusting the inter-frequency biases. The fact that the distributions are more closely centered about zero shows that the biases have largely been removed from the corrections. Thus despite the fact that there is no independent mean to absolutely validate bias estimates obtained by this method, all consistency checks that have been performed indicate that they are correct.

5 FUTURE WORK AND CONCLUSIONS

A working estimation algorithm has been developed for estimating the interfrequency biases between L1 and L2 frequencies embedded in both the GPS satellites and the WAAS reference receiver. With this calibration scheme, the ionospheric correction accuracy has been improved to only 5 cm in the mean of the errors. The WAAS navigation fix errors have also been reduced greatly. Most importantly, the navigation errors are more zero-centered and a 2-meter 95% accuracy has been demonstrated after adjusting the interfrequency. This will enable more effective integrity monitoring.

It is worthwhile to mention that multi-station data processing improves the estimation by more consistent ionosphere modeling as well as by being able to use a higher order spherical harmonics model.

For the future, work will focus on

- Development of sequential algorithm and preparation for the coming high solar activity period.
- Continuously monitor the interfrequency bias and creating a larger data base.
- Searching for better obliquity model for better ionospheric modeling.

6 ACKNOWLEDGEMENTS

The authors would like to gratefully thank the support and assistance of the FAA AGS-100, the Satellite Program Office, FAA Technical Center and the FAA

personnel at the WRS's. We would also want to thank all our colleagues in the Stanford GPS group.

REFERENCES

- Cohen C., B. Pervan, B. Parkinson, *Estimation of Absolute Ionospheric Delay Exclusively through Single-Frequency GPS measurements*, Proceeding of Institute of Navigation 1992 Annual Meeting of the Satellite Division (ION-GPS-92), Albuquerque, NM, Sept, 1992.
- El-Arini M.B., P.A. O'Donnel, P.M. Kellam, J.A. Klobuchar, T.C. Wisser and P.J. Doherty *The FAA Wide Area Differential GPS (WADGPS) Static Ionospheric Experiment*, Proceeding of the Institute of Navigation 1993 National Technical Meeting, January 1993
- ICD-GPS-200 Revision B-PR, Rockwell International, July 1991
- Klobuchar, J.A *Design and Characteristics of the GPS ionospheric Time Delay Algorithm for Single Frequency Users* IEEE Position Location and Navigation Symposium, Las Vegas, NV, Nov. 1986.
- Kee C., B. Parkinson, P. Axlerad, *Wide Area Differential GPS Navigation*, Journal of the US Institute of Navigation, vol.38, no.2, Summer, 1991.
- Kee, C., T. Walter, Y.C. Chao, Y.J.Tsai, J.Evans, A.K.Barrows,E. Abbott, D. Powell, P. Enge, B. Parkinson, *Comparison of Full Vector and Common View WAAS Algorithm*, ION 51th Annual Conference, Colorado Spring, Colorado, June 7, 1995.
- Knecht, D.J. Shuman, B.M. *Handbook of Geophysics and the Space Environment, chapter of the geomagnetic field.*, 1985
- RTCA Special Committee 159 Working Group 2 *Wide Area Augmentation System Signal Specification*, March 1994
- Tsai Y.J., Y.C. Chao, T. Walter, C. Kee, D. Powell, P. Enge, B. Parkinson *Evaluation of Orbit and Clock Models for Real Time WAAS*. Proceeding of the Institute of Navigation 1993 National Technical Meeting, CA, January 1995
- Tsai, Y.J., P.Enge, Y.C. Chao, T. Walter, C.Kee, J.Evans, A.Barrows, D.Powell, B.Parkinson, *Validation of the RTCA Message Format for WAAS*, ION-GPS-95
- Walter T., C. Kee, Y.C. Chao, Y.J. Tsai, U. Peled, J. Ceva, A. Barrows, E. Abbott, D. Powell, P. Enge and B. Parkinson *Flight Trials of the Wide Area Augmentation System (WAAS)*, Proceeding of Institute of Navigation 1994 Annual Meeting of the Satellite Division (ION-GPS-94), Salt Lake City, Salt Lake City, Sept, 1994
- Wilson B., A. Mannucci *Extracting Ionospheric Measurements from GPS in the Presence of Anti-Spoofing* Proceeding of Institute of Navigation 1994 Annual Meeting of the Satellite Division (ION-GPS-93), Salt Lake City, Sept, 1994.

Incorporation of Orbital Dynamics to Improve Wide-Area Differential GPS

Juan Ceva and Bradford Parkinson
Stanford University

Willy Bertiger, Ronald Muellerschoen, and Thomas Yunck
Jet Propulsion Laboratory

Biographies

Juan Ceva obtained a B.S. degree in Aerospace Engineering at St. Louis University and a M.S. and Eng. degree in Aeronautics and Astronautics at Stanford University. As a graduate student of Professor Parkinson and as a summer intern at the Jet Propulsion Laboratory (JPL), he has worked on a variety of topics involving GPS, in particular WAAS (the topic of his Engineer thesis).

Willy Bertiger received his Ph.D. in Mathematics from the University of California, Berkeley, in 1976. In 1985, he began work at JPL as a Member of the Technical Staff in the Earth Orbiter Systems Group. His work at JPL has been focused on the use of GPS for high precision orbit determination and positioning.

Ronald Muellerschoen received a B.S. degree in physics at Rensselaer Polytechnic Institute and a M.S. degree in Applied Mathematics at the University of Southern California. He is currently a Member of the Technical Staff in the Earth Orbiter Systems Group at the Jet Propulsion Laboratory (JPL). His work at JPL has concentrated on the development of efficient filtering/smoothing software for processing GPS data and the processing of Topex/Poseidon-GPS data.

Tom Yunck received his B.S.E.E. from Princeton University, and his Ph.D. in Systems and Information Science from Yale University. He is currently Deputy Manager of the Tracking Systems and Applications Section at JPL, where he is involved in the application of GPS to precise orbit determination and geodesy.

Bradford Parkinson is Professor at Stanford University and is Program Manager of the Relativity Gyro Gravity Probe B Experiment, which utilizes GPS extensively. He served as the first Program Director of the GPS joint Program Office, and was instrumental in the system's development. He is a past chairman of the ION Satellite Division, and the 1991 winner of the Kepler award.

Abstract

A powerful dynamical technique to compute precise GPS satellite orbits for the FAA real-time Wide-Area Augmentation System (WAAS) has been evaluated. The dynamical technique estimates GPS satellite states from a long history of measurements, which are related to the current states through precise models of satellite dynamics. This contrasts with non-dynamical techniques, in which an inverted form of the navigation fix solution yields the instantaneous position of the satellite, without introducing dynamical information. The dynamical orbit determination method not only yields much more accurate and robust orbit solutions, it enables complete separation of orbit and satellite clock errors. Results with real data show that a network of 12 monitor stations distributed over North America, producing dual frequency pseudorange data, yields 3-dimensional orbit accuracies of better than three meters within the service volume, as compared with the JPL precise ephemerides. This is about a factor of three improvement over the broadcast ephemerides.

In a WAAS simulation the dynamical orbit estimation technique produced the most accurate user results. Over the 30 simulated users, the mean of the eastern, northern and vertical components of the users' standard deviations were 20.5 cm east; 25.0 cm north; and 28.4 cm vertical. This represents the orbit and satellite clock components of the user position error. No latency, tropospheric, or user measurement noise are included in the simulated user ranges (although measurement errors were of course present in the data used to compute the orbits). A comparison with the results obtained with the broadcast and non-dynamical orbits is presented.

The dynamical orbit estimation process and the slow correction generation can be done in about 2.5 seconds well in advance of its use. Thus the dynamical slow correction generation adds no latency to the process

of the message generation. Real-time performance of the dynamical orbit estimation is easily achievable in a WAAS scenario.

1 Introduction

The Federal Aviation Administration (FAA) is currently developing a GPS-based navigation system that is intended to become the primary navigation aid for commercial aviation during all phases of flight—including Category I precision approach. This revolutionary navigation system will be based on the concept of WADGPS (Kee 1993). Called by the FAA the Wide-Area Augmentation System (WAAS), it will make use of a network of 20 to 30 Wide-area Reference Stations (WRSs) distributed throughout the National Airspace System. These reference stations will collect pseudorange and atmospheric measurements, and will send them to one, or perhaps more, Wide-area Master Stations (WMSs). The WMS will process the data to provide a *vector correction* for each GPS satellite. The vector correction will include as separate components the GPS ephemeris errors, satellite clock bias and ionospheric delay estimate. The FAA distinguishes two kinds of corrections: a *slow correction* and a *fast correction*. The slow correction contains, as its name indicates, the slowly varying errors—the ephemeris error and long-term clock errors. Due to its slowly varying nature, this error need be transmitted only every 5 minutes. On the other hand, the satellite clock error is quickly varying—due to SA—and demands a faster correction rate, on the order of one correction message every six seconds. The corrections will be sent to the users by means of a Geosynchronous Earth Orbit (GEO) satellite using a signal and data format designed by RTCA¹ Special Committee 159. The WAAS is expected to provide supplemental radio navigation by the year 1997, and eventually to become the primary system of navigation. The system will add to the current GPS system the following features: a ranging function that will improve *availability* and *reliability*; differential GPS corrections that will improve *accuracy*; and *integrity* monitoring that will enhance safety. To meet the requirements associated with a primary navigation system, WAAS should be able to provide fault-free position fix with a time *availability* of 0.999 for Category I approaches, and 0.99999 for domestic *en route*, terminal and non-precision approach phases of flight.

¹Radio Technical Commission for Aeronautics.

Section 2 describes dynamical orbit determination and assesses the accuracy of the GPS ephemeris obtained using this technique. Section 2.3 presents the user positioning accuracy obtained in a WAAS scenario simulation. Section 3 discusses the advantages that a dynamical orbit determination introduces over non-dynamical techniques. The real-time aspects of a dynamical orbit determination technique are mentioned in Section 4. The conclusions are drawn in Section 5.1.

2 Dynamical Orbit Determination

By dynamical orbit determination we refer to a technique that computes precise satellite orbits from a collection of measurements that are related to the satellite states by precise dynamical models that accurately describe the orbital motion of the satellite. The relationship between satellite states and observables is inherently non-linear. The commonly implemented statistical estimation technique requires linear relationships between states and observables; therefore, the equations describing the motion of the satellite are linearized with respect to a nominal trajectory.

2.1 State vector, numerical propagation models and orbit estimator

Our solutions for the GPS ephemeris are implemented in a software set known as GIPSY/OASIS II (GOA II). The filter implementation is a Square Root Information Filter (SRIF) which yields increased numerical stability compared to non-square root implementations (cf. Bierman (1977), Wu et al. (1990)). Assuming no numerical problems, the SRIF is equivalent to other Kalman implementations.

When solving for GPS ephemeris errors, our state vector consists of a GPS epoch state, GPS clock, station troposphere, station clocks, as well as Y bias and solar pressure scaling factor for each GPS satellite. One station clock is held as a reference. Station tropospheres are treated as random walks. We use 30-hour data arcs in the solutions presented in this paper. The epoch state for GPS refers to the position and velocity at the beginning of the 30-hour arc for GPS.

In the dynamical ephemeris solution no process noise is added to the GPS epoch state (position and velocity), since the dynamical model used represents accurately

enough the orbit during the 30-hour data arcs. An operational system will run continuously rather than in 30-hour discrete steps. This can be achieved by adding a small amount of process noise to cause earlier data to fade from the solution.

For the nondynamical ephemeris adjustments, an acceleration vector is added to the filter state for each GPS with an independent update at each measurement time. The constraint at each measurement time is so loose that the position solutions for GPS are essentially uncorrelated.

The following models are recommended to be used to obtain a satisfactory nominal trajectory:

- A 12×12 expansion of the JGM-3 gravity model (Watkins et al. 1994).
- Third-body effect for the Sun and the Moon only (Newhall, Standish & Williams 1983).
- Solid Earth tide (Wahr 1981) and ocean tide (Nerem 1994) models.
- Direct solar radiation pressure model (Fliegel & Gallini 1992).

No models for relativistic gravitational effects, Earth albedo and atmospheric drag perturbations are required for the GPS constellation.

2.2 WAAS dynamical orbit determination results

To evaluate WAAS orbit determination strategies, we selected a network of existing GPS tracking stations was selected across the continental U.S. and Canada, plus Bermuda (see Fig. 1 and Table 1). These tracking stations, which represent the Wide-Area Remote Stations or WRSs in a WAAS network, belong to the IGS global network of GPS receivers and are equipped with TurboRogue receivers built by Allen Osborne Associates. From these stations real carrier-smoothed pseudorange measurements² were collected thirty seconds apart during a period of thirty hours on January 10-11, 1995. The estimation method selected was the one that implements numerical propagation of the dynamical models together with a position-velocity state vector as described in Sec. 2.1. The tropospheric delay

²The TurboRogue receivers already output carrier-smooth pseudorange, saving one step in the data processing.

error was not estimated; in its place, the estimated values obtained from the JPL precise ephemerides were used³. The initial spacecraft state was taken from the results of the JPL precise orbits⁴.

2.2.1 Comparison with the JPL precise orbit

We can assess the accuracy of the estimated orbits by comparing them with other estimated orbits known to be more precise. In this case the results of the GPS orbits for January 10, 1995, obtained with the WAAS network, were compared with the JPL precise GPS orbits, which have a 3-D $1\text{-}\sigma$ accuracy of 20 cm (Zumberge et al. 1995). Table 2 shows the RMS differences between the orbits over the service area of the simulated WAAS network in the radial, along-track, and out-of-plane orbital components. Carrier phase

| The WAAS Dynamical Orbit Accuracy | |
|-----------------------------------|--------------------------|
| Orbit component | Accuracy (m, 1σ) |
| Radial | 0.65 |
| Cross-track | 1.37 |
| Long-track | 1.96 |

Table 2: The WAAS dynamical orbit accuracy. The accuracy is established as the difference between the orbit estimated using the WAAS stations and dynamical information and the JPL precise orbit over the service area of the WAAS network.

measurements would substantially improve the solution (Yunck et al. 1995), but they are not to be used, according to the WAAS specifications (FAA 1994). Post-process smoothing of the resulting orbit is not suitable for a real-time application.

³This was done in anticipation of the user positioning simulation presented in Sec. 2.3. In this simulation, the measurements are generated using the precise JPL ephemeris. The use of the same tropospheric estimates in both the orbit estimation process and the user positioning simulation assures a perfect cancellation of the tropospheric delay bias, which, although of great importance, is not the main object of this research.

⁴Of course, this cannot be done in the real-time application; however, in the worst case, one could always start the orbit estimation process with an initial state based on the broadcast ephemerides that are always available. Also, the use of accurate dynamical models permits the propagation of the orbits when new measurements are not available; in the case of the JPL precise ephemerides, the orbital errors can remain under one meter even when propagated three days ahead without incorporating new observations. Note that once the nominal orbit is good enough to linearize the problem, the solution is essentially insensitive to that nominal orbit. In other words, any two reasonable nominal trajectories will yield the same estimate.

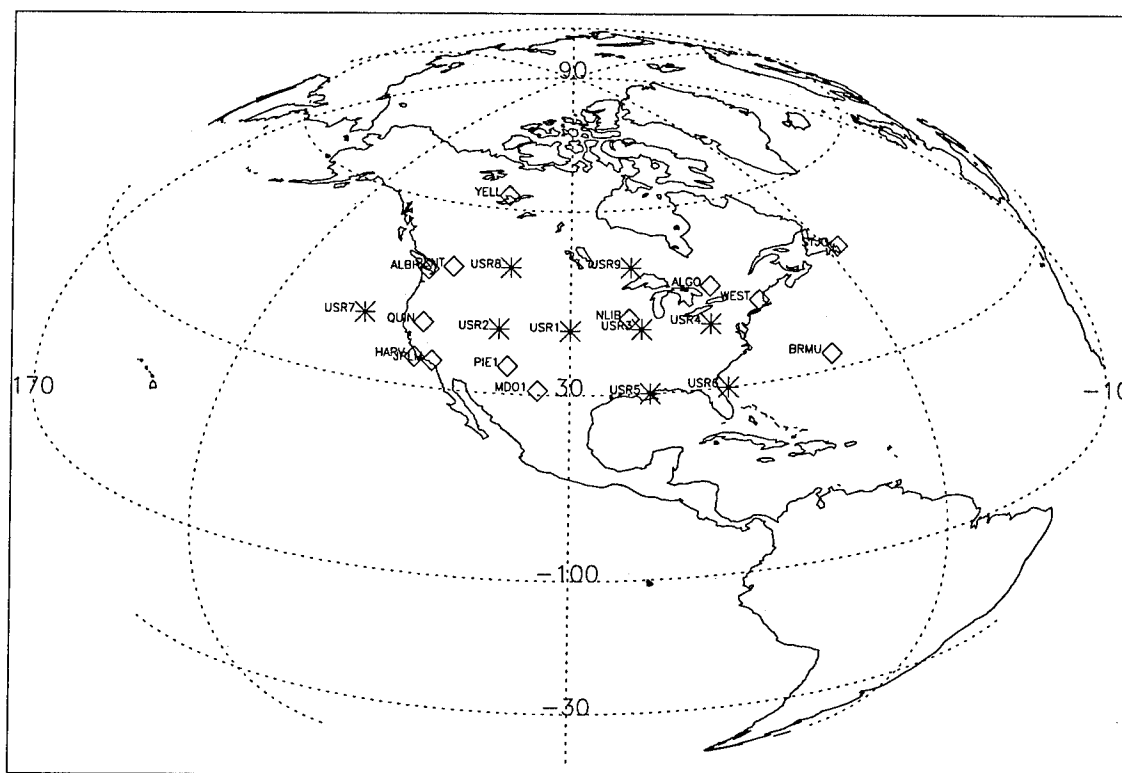


Figure 1: The WAAS simulated network. The WRSs are symbolized with diamonds. Users were placed in the locations represented by asterisks as well as in the vicinity of the WMSs with the exception of Bermuda.

2.2.2 Comparison with the broadcast orbit

The dynamical orbit generated with the WAAS network shows a threefold improvement over the broadcast orbit. The broadcast orbit for December 10, 1995, was differenced with respect to the JPL precise orbit in the same manner as before. Table 3 shows the RMS differences between the orbits over the service area of the WAAS network in the radial, along-track, and out-of-plane orbital components.

Given the high quality of the broadcast orbit, we believe that there are no SA effects imposed on them (Zumberge & Bertiger 1996). However, if SA were to degrade the broadcast orbits, an independent ephemeris source such as the one presented here would be imperative to maintain the accuracy required by WAAS.

| The Broadcast Orbit Accuracy | |
|------------------------------|--------------------------|
| Orbit component | Accuracy (m, 1σ) |
| Radial | 1.6 |
| Cross-track | 2.6 |
| Long-track | 7.5 |

Table 3: The broadcast orbit accuracy. The accuracy is established as the difference between the broadcast orbit and the JPL precise orbit over the service area of the WAAS network.

2.3 The WAAS user positioning simulation

A simulation was conducted to assess the improvement that the dynamical orbit estimation technique offers to the WAAS users. In it, nine static users were distributed (see Table 1) within the simulated WAAS net-

| The WAAS Simulated Network Station and User Locations | | | | | |
|---|------------|------------------|---------|----------------|-----------------|
| Type | 4 char. ID | City | Country | Latitude (deg) | Longitude (deg) |
| WRS & USR | ALBH | Albert Head | Canada | 48.39 | -123.49 |
| WRS & USR | ALGO | Algonquin | Canada | 45.96 | -78.07 |
| WRS | BRMU | Bermuda | U. K. | 32.37 | -64.70 |
| WRS & USR | HARV | Harvest Platform | USA | 34.47 | -120.68 |
| WRS & USR | JPLM | Pasadena | USA | 34.20 | -118.17 |
| WRS & USR | MDO1 | McDonald | USA | 30.68 | -104.01 |
| WRS & USR | NLIB | North Liberty | USA | 41.77 | -91.57 |
| WRS & USR | PENT | Penticton | Canada | 49.32 | -119.62 |
| WRS & USR | PIE1 | Pie Town | USA | 34.30 | -108.12 |
| WRS & USR | QUIN | Quincy | USA | 39.97 | -120.94 |
| WRS & USR | STJO | Saint John's | Canada | 47.60 | -52.68 |
| WRS & USR | WEST | Westford | USA | 42.61 | -71.49 |
| WRS & USR | YELL | Yellowknife | Canada | 62.48 | -114.48 |
| USR | USR1 | | USA | 40.00 | -100.00 |
| USR | USR2 | | USA | 40.00 | -110.00 |
| USR | USR3 | | USA | 40.00 | -90.00 |
| USR | USR4 | | USA | 40.00 | -80.00 |
| USR | USR5 | | USA | 30.00 | -90.00 |
| USR | USR6 | | USA | 30.00 | -80.00 |
| USR | USR7 | | USA | 40.00 | -130.00 |
| USR | USR8 | | Canada | 50.00 | -110.00 |
| USR | USR9 | | Canada | 50.00 | -90.00 |

Table 1: The WAAS simulated network station and user locations.

work depicted in Fig. 1, and another eleven users were placed over twelve of the thirteen (all but Bermuda) WRSs in the network.

The range observables were created by computing geometric ranges from the users to the GPS satellite positions as prescribed by the JPL precise ephemeris for the period of January 9, 1995, 23:59:50 GMT to January 10, 1995, 23:58:50 GMT. The actual SA clock dithering to each GPS was sampled using precise GPS satellite clock solution obtained with the precise orbits. The purpose of the simulation was to assess only the contribution of the orbit accuracy, in the presence of SA clock dithering, to the user positioning error after performing the slow and fast corrections. No measurement noise was added to the generated measurements; no ionospheric delays were included, and, furthermore, the tropospheric delay biases were largely removed by using the JPL precise orbit tropospheric bias estimates for that day. These atmospheric biases (especially the ionospheric) are the dominant error sources, but are not the topic of interest in this study.

To simulate the slow and fast corrections, the following steps were taken:

1. Using the previously estimated dynamical orbit from the WAAS network, the satellite position component of the simulated pseudorange was subtracted. This is the so-called slow correction. Note that since the orbit generated by the WAAS network and the JPL precise orbit differ, some ephemeris error remains. It is precisely how this ephemeris error combines with the satellite clock error in the final user positioning error that is of interest in this simulation. (Recall that the orbit and clock corrections are performed with real data.)
2. The tropospheric delay values that the JPL precise orbit provided for that day were subtracted from the measurements. Since these are the same values that went into the WAAS orbit estimation, a perfect cancellation took place. This helps to isolate the ephemeris and clock errors.

3. The GPS fast corrections (dominated by the SA imposed on the clocks) were estimated from the measurements once the slow corrections (and the tropospheric delay biases) were removed from the WRS data ⁵.
4. Using the slow orbit corrections and the fast corrections from step 3, an estimator was run to estimate the user location. The coordinates of the location were estimated as white noise stochastic parameters, essentially solving for a point position independently at every epoch, as would be more characteristic of a moving user, e.g., an airplane. The standard deviation of the point positioning history was computed for every station along eastern, northern and vertical components. The mean of the standard deviation of all stations was also computed in the eastern, northern and vertical components. The typical VDOP value was in the order of 1.2.

The vertical component is the one of interest, for it is the hardest to determine and has the most stringent requirement in the FAA landing category specifications. Figure 2 and Table 4 show the mean standard deviation of all the user positioning error when using the WAAS network dynamical orbit, and, for comparison, the results when using the broadcast orbit. Figure 2 reflects user error due to ephemeris error only, whereas Table 4 reflects the error due to ephemeris error and satellite clock error in the presence of SA. It can be seen in the figure that the WAAS dynamical orbit results in a mean standard deviation of the vertical error of 9.15 cm 1σ (orbit error only). It must be emphasized that these results do not include the dominant source of error for single frequency users, namely, the ionospheric delay. However, using ionospheric delay estimation algorithms such as the one presented in Mannucci, Wilson & Edwards (1993), the ionospheric delay can be estimated with an accuracy of half a meter (Mannucci, Wilson & Yuan 1994). In any event, the WAAS dynamical orbit considerably improves the user positioning when compared with the broadcast orbit that has a vertical error of 38.6 cm 1σ (orbit error only). As Table 5 shows, the introduction of dy-

namical information prevents the degradation of the user positioning on the periphery of the network.

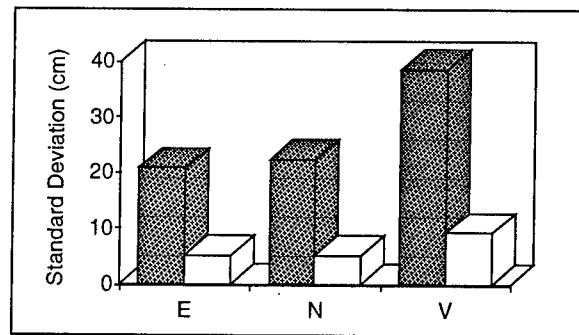


Figure 2: Results of the WAAS user positioning simulation. The numbers show the mean standard deviation in the eastern, northern and vertical components of the point positioning history of the simulated WAAS users. The results obtained with the WAAS network-generated dynamical orbit (white bars) are contrasted with the results achieved using the broadcast orbit (dark bars). These values represent only the contribution of the orbital error to the user error.

2.4 Conclusion

The dynamical orbit generated with the simulated WAAS network results in user positioning accuracies that not only exceed the requirements of the FAA category I approach, but that are also closer in accuracy to the more demanding category II approach. The introduction of dynamical information prevents the degradation of the user solution in the periphery of the network as is the case with nondynamical techniques. Finally, the ability to properly separate clock and ephemeris errors permits the use of the slow/fast scheme that is demanded in the FAA WAAS specifications.

3 Improvement Over Nondynamical Techniques

The dynamical orbit determination contrasts with the nondynamical technique, in which an inverted form of the navigation fix solution yields the instantaneous position of the satellite, without introducing dynamical information. It also contrasts with a kinematic

⁵A previous study of the latency effect is reported in Yunck et al. (1995). In this study the effect of the user extrapolation of the last fast correction under the effect of SA is addressed. The study concludes that (after using different extrapolation techniques, involving the use of pseudorange and combinations of pseudorange and phase as well as linear and quadratic models) a linear extrapolation with pseudorange data alone will not suffice and suggest the introduction of phase data that improves the accuracy by an order of magnitude.

| The WAAS User Positioning Summary Results | | | |
|---|-----------------------|------------------------|---------------------------|
| Orbit Type | East (cm, 1σ) | North (cm, 1σ) | Vertical (cm, 1σ) |
| WAAS Dynamical | 20.5 | 25.0 | 28.4 |
| Broadcast | 33.1 | 38.5 | 54.9 |

Table 4: Results of the WAAS user positioning simulation. The numbers show the mean standard deviation in the east, north and vertical components of the point positioning history of the simulated WAAS users. The dynamical orbit results are contrasted with the ones obtained using the broadcast orbit. These values represent the contribution of orbit error and satellite clock error to the user positioning error.

technique (Tsai et al. 1995) in which the first time-derivative of the satellite position error is also estimated, again without the use of dynamics.

Some fundamentals of satellite range tracking must be understood to appreciate the superiority of the dynamical techniques. Orbit estimation sensitivity with differential techniques as well as clock and ephemeris range bias separation are among these fundamental aspects.

3.1 Nondifferential and differential satellite tracking

Figure 3 shows that when a single station tracks a satellite, the tracking station is less sensitive to along- and cross-track motion and mostly senses radial motion. In the example illustrated in Fig. 4, two stations difference their range measurements to a commonly viewed satellite. In this case the sensitivity reverses; now the differenced measurements are not sensitive to radial displacements (along the bisecting line of the angle subtended by the satellite and the stations) but only to motion parallel to the baseline. This is proven mathematically (for the 2-D case) in Section 3.2.

It is also important to note that when several stations observing a commonly viewed satellite try to solve for the unknowns of the system, namely, the position of the satellite, its clock bias, and the station clock biases, two options exist: the first one calls for the elimination of the satellite and station clocks by differencing the measurements; the second calls for solving for all system clocks but one, de facto referencing all the satellite and station clocks to the one omitted ⁶. The first of

⁶These approaches are mathematically equivalent under some conditions (Wells, Doucet & Lindlohr 1986, Grafarend & Schaffrin 1986). Kuang, Schutz & Watkins (1995) show that estimating the receiver clock error and eliminating the bias by differencing the measurements at each measurement epoch are

these approaches has performed an obvious differentiation of the measurements, and the second one has performed an implicit differentiation by referencing all adjusted clocks to one held fixed ⁷. In both cases the relative station solutions are virtually insensitive to satellite radial displacements.

3.2 The UDRE concept

The User Differential Range Error (UDRE) is defined (FAA 1994) as "the 99.9% accuracy of the corrections for the designated satellite, indicating the accuracy of combined fast and slow corrections, not including the accuracy of the ionospheric corrections. The ephemeris accuracy component is an 'equivalent' range accuracy for the worst location in the coverage region." The combined error due to slow and fast corrections will be smaller than the absolute range error from just the slow ephemeris error (Yunck et al. 1995). The ephemeris component of the UDRE can be calculated by computing the sensitivity of the range measurement to the satellite position. According to Fig. 5, it can be shown (Yunck et al. 1995) that the sensitivities of the range r_u^k with respect to satellite height H and lateral

mathematically equivalent, provided that no a priori clock information is used in the undifferenced case and all receivers see the same satellites.

⁷Consider the example in which two tracking stations of known positions obtain range measurements to a commonly visible satellite. The system contains five unknowns, namely, the three components of the satellite position, its clock bias and the two station clock biases. In the second case, the two measurements from stations to satellite are not differenced, one reference station is selected and its clock bias is eliminated from the list of unknowns. This leaves two measurements and five unknowns or a $5 - 2 = 3$ deficiency. In the first case mentioned, the two measurements are differenced, reducing the number of measurements to one, eliminating the satellite clock and leaving the difference between station clocks as an unknown together with the satellite position. Again, an identical $4 - 1 = 3$ deficiency exists.

| The WAAS User Simulation Results | | | |
|----------------------------------|------------------------|-------------------------|----------------------------|
| 4 char. ID | East (cm, 1 σ) | North (cm, 1 σ) | Vertical (cm, 1 σ) |
| ALGO | 17.7 | 22.1 | 27.0 |
| NLIB | 13.8 | 20.6 | 26.0 |
| PENT | 16.5 | 22.2 | 25.6 |
| PIE1 | 14.9 | 20.2 | 27.2 |
| USR1 | 13.7 | 20.0 | 26.1 |
| USR2 | 14.8 | 19.5 | 25.8 |
| USR3 | 14.9 | 21.2 | 26.1 |
| USR4 | 13.7 | 20.0 | 26.1 |
| USR8 | 14.6 | 19.9 | 25.2 |
| USR9 | 15.8 | 20.1 | 25.6 |
| ALBH | 18.5 | 22.6 | 25.8 |
| JPLM | 16.3 | 23.2 | 28.0 |
| MDO1 | 15.3 | 23.1 | 28.8 |
| QUIN | 17.3 | 21.7 | 26.1 |
| STJO | 26.8 | 36.2 | 33.6 |
| USR5 | 17.1 | 25.4 | 28.4 |
| USR6 | 15.5 | 23.0 | 28.8 |
| USR7 | 21.8 | 25.1 | 27.8 |
| WEST | 19.4 | 25.9 | 27.6 |
| YELL | 19.5 | 36.2 | 32.0 |

Table 5: Results of the WAAS user positioning simulation. The numbers show the standard deviation in the eastern, northern and vertical components of the point positioning history of the simulated WAAS users. The first block shows the users inside the network whereas the second block show the peripheral users.

position L are given by

$$\frac{\partial r_u^k}{\partial H} = \frac{h}{r_u^k} = \cos \theta, \quad (1)$$

$$\frac{\partial r_u^k}{\partial L} = \frac{d}{r_u^k} = \sin \theta, \quad (2)$$

where θ is the angle between the line of sight of user u to satellite k and the direction of line h .

Since the GPS satellites orbit at a high altitude, the angle θ is small (less than 14 degrees); hence, the non-differential User Range Error (URE) is more sensitive to changes in radial position of the satellite than to along- and cross-track changes. However, in the differential case the opposite is true. That is to say, the range difference between the users u and monitor station m (see Fig. 6) is more sensitive to along-track satellite motion than to radial motion. Mathematically the sensitivities of the differential range are given (for the 2-D case) by the difference of the partials of r_u^k and r_m^k as given by Eqs. (1) and (2). The maximal

sensitivity of the differential range Δr ,

$$\Delta r \triangleq |r_m^k - r_u^k|,$$

to a radial error occurs in the configuration depicted in Fig. 6, where the monitor receiver m is directly below the satellite and the user u is located at the maximal distance possible (≈ 7430 km). This results in the angle $\theta \approx 13.8^\circ$. Therefore, the sensitivities of the differential range for this worst case are given by

$$\begin{aligned} \frac{\partial \Delta r}{\partial H} &= \left| \frac{\partial r_m}{\partial H} - \frac{\partial r_u}{\partial H} \right|_{(1)} = |\cos(0) - \cos(13.8)| \\ &= 0.03, \end{aligned} \quad (3)$$

$$\begin{aligned} \frac{\partial \Delta r}{\partial L} &= \left| \frac{\partial r_m}{\partial L} - \frac{\partial r_u}{\partial L} \right|_{(2)} = |\sin(0) - \sin(13.8)| \\ &= 0.24. \end{aligned} \quad (4)$$

It can be seen in this “worst radial sensitivity” case that the sensitivity to the lateral component of the ephemeris error is eight times greater than the radial component; a 1-m error in the radial ephemeris component causes a 3-cm error in the differential range,

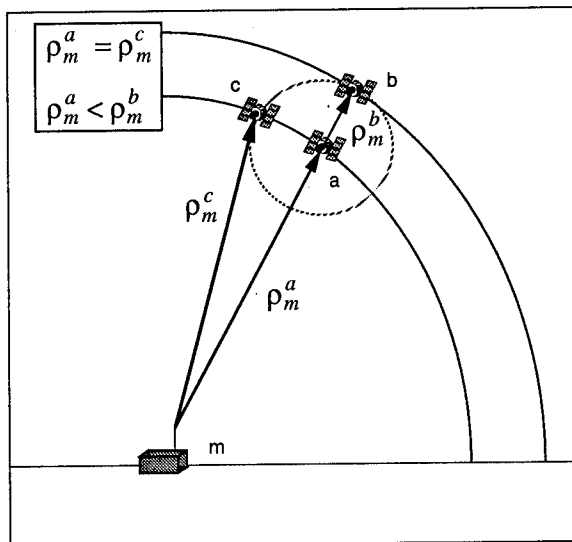


Figure 3: Nondifferential GPS tracking sensitivity. A single satellite is being tracked by a monitor station m . The station cannot distinguish between positions a and c (lateral motion), and can only sense vertical motion such as changes from position a to position b .

whereas a 1-m error in the lateral ephemeris component (along-track) causes a 24-cm error in the differential range. On the other hand, the worst case for the lateral sensitivity occurs when the satellite is located in the mid-point distance between the monitor station and the user, and the monitor station and the user are located at both sides of the Earth's limb as viewed by the satellite. In this case a 1-m ephemeris lateral (along-track) error with a 7420-km baseline between stations results in 34-cm differential range error. The radial and cross-track (in 3-D) sensitivities would be zero in this case.

With dynamical orbit estimation, the radial orbit error is generally smaller than the horizontal error. That, combined with the overall reduced sensitivity of UDRE to the radial component, makes the absolute radial orbit error a relatively unimportant contributor to the UDRE.

3.3 Separation of ephemeris and clock biases

Another important aspect of the orbit estimation problem is the separation of satellite position errors and clock errors. A station tracking an orbiting satel-

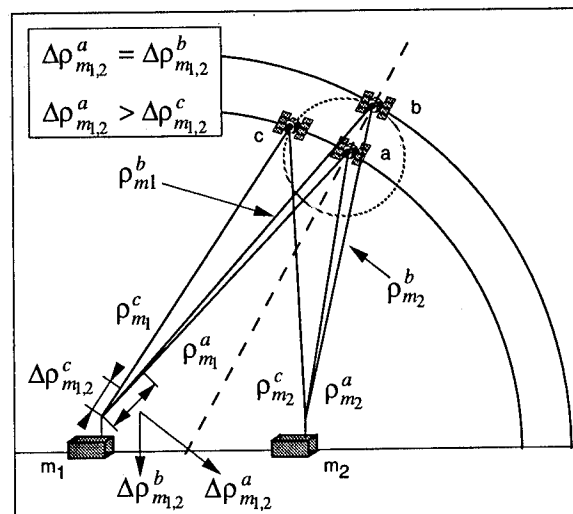


Figure 4: Differential GPS tracking sensitivity. A single satellite is being tracked by a couple of stations m_1, m_2 that combine their individual range measurements to form a differential range measurement $\Delta \rho_{m1,2}$. The differential range is insensitive to radial satellite motion (position change from a to b), and can only sense transverse motion (position change from a to c).

lite with range measurements over a period of time can use the fact that the satellite moves in a dynamically prescribed orbit to measure the orbital period. This period is related (directly in the case of a circular orbit) to the orbiting altitude of the satellite. This extra information can be used to determine what portions of the range bias are due to ephemeris errors versus clock errors. If the satellite dynamics is ignored, distinguishing the biases becomes difficult, and only the sum of the two contributions can be accurately estimated. This concept is illustrated in Fig. 7.

If one solves nondynamically for orbit and clock parameters, the error ellipsoid of the orbit solution is prolate in the differential mode; that is, there is more error in the radial direction (the direction that cannot be observed) than in the cross- or along-track directions. When dynamical information is incorporated into the problem, the uncertainty of the radial component of the orbit is readily constrained by Newtonian motion. Although the radial component is poorly observed, it is related to the two other observed components by dynamical relationships. In this (dynamical) case, the ellipsoid error assumes an oblate shape as the results shown in Tables 2 and 3 confirm.

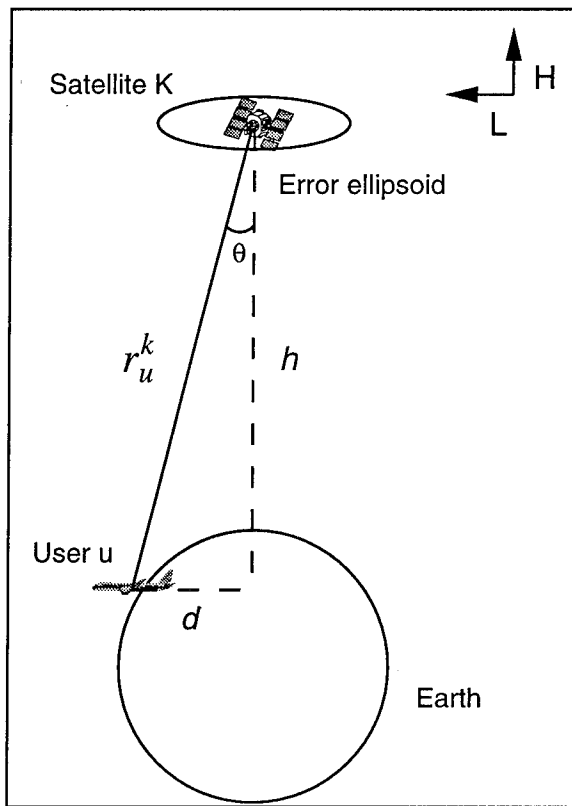


Figure 5: Sensitivities of the URE and UDRE due to radial L and lateral H ephemeris errors.

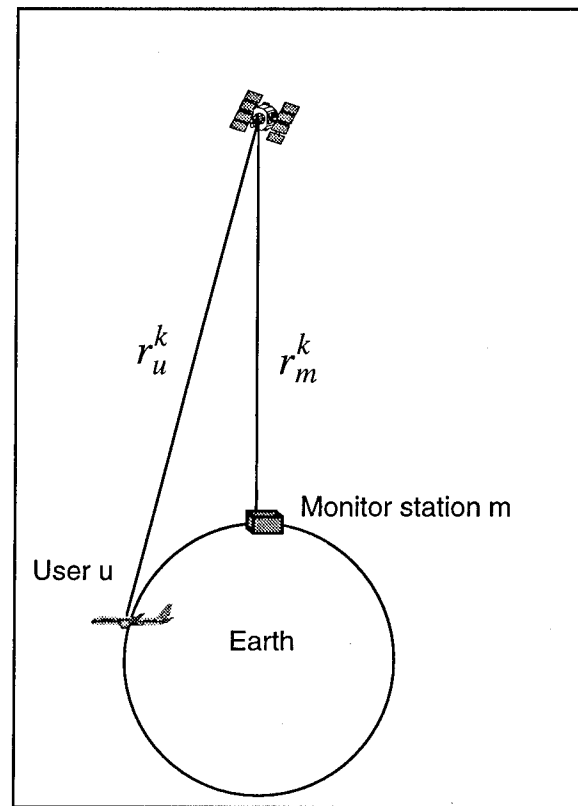


Figure 6: The worse case of UDRE due to radial error occurs when the monitor station is below the tracking satellite and the user is located at the Earth's limb.

When no dynamical information is used, it is better to follow the strategy that the Stanford University uses, in which ephemeris errors and clock biases are solved simultaneously in the fast correction. Although the individual estimates of these parameters are not accurate, because of compensating correlations, the overall pseudorange correction is very satisfactory, as the Stanford flight trials show (Walter et al. 1994). In fact, a simulation shows that when no dynamical information is used, and a separated slow/fast correction scheme is exercised, the vertical error (just due to orbit error) is on the order of 500 cm (1σ) with a noticeable degradation on the periphery of the network⁸. This result is contrasted in Table 6 with the much better results obtained in the Stanford University simulation and flight trials (Walter et al. 1994).

The algorithm implemented by Stanford University in its flight trials makes use of a minimum-norm so-

lution without a priori constraints on the ephemeris and clock errors (Ceva 1995, Tsai et al. 1995). On the other hand, the Stanford simulation presented in Pullen, Enge & Parkinson (1995), which considers a network that spans the continental U.S., makes use of a priori orbit constraints and uses a Kalman filter implementation. The fact that a priori orbit constraints are needed with a wide-area network in the absence of satellite dynamics is consistent with the results obtained here. Suffice to say that when a priori constraints of a few meters are added to the non-dynamical orbit estimation, the 3-D RSS of the orbit error (as compared with the JPL precise ephemerides) is on the order of 9 meters. (That contrasts with a 3-D RSS orbital error of 200 meters when no a priori constraint is applied.)

⁸Note that the fast correction will always absorb part of the ephemeris error that is left after the slow correction is applied.

| User Positioning Accuracy with a Nondynamical Orbit Estimation | | |
|--|--|--|
| Stanford University Simulation (cm, 2σ) | Stanford University Flight Trials (cm, 2σ) | Slow/Fast Correction Simulation (cm, 1σ) |
| 340 | 300 | 571 |

Table 6: User positioning accuracy with a nondynamical orbit estimation. The Stanford University simulation and flight trials, in which ephemeris and clock parameters are solved simultaneously, are contrasted with the results of a simulation in which the ephemeris and clock errors are solved using a slow/fast correction scheme. The Stanford University approach proves much superior when a nondynamical orbit estimation is implemented.

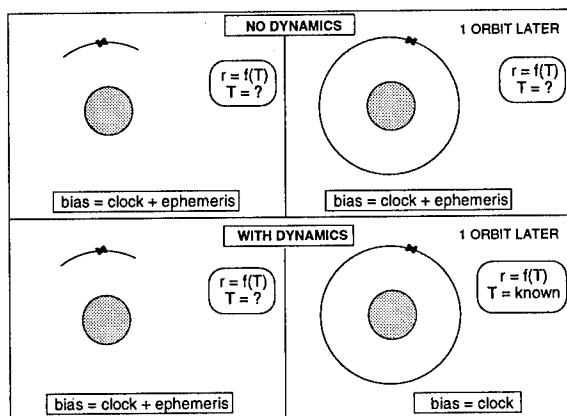


Figure 7: Dynamical vs. nondynamical orbit estimation. The dynamical information can be used to determine what portions of the range bias are due to ephemeris errors versus clock errors.

3.4 Conclusion

Differential techniques lose sensitivity to radial orbital errors and can benefit from dynamical information to help recover the information missing from the observed transverse components. The ephemeris contribution to UDRE is dominated by the lateral (along-track) ephemeris errors and not radial ephemeris error. As mentioned in Sec. 2.3, the ability to separate clocks and ephemeris errors permits the use of the slow/fast scheme that is required in the FAA WAAS specifications. The ability to separate these two error sources adds integrity to the system by enabling the detection and identification of errors in the estimates of either ephemeris or clock biases.

4 The Real-Time Aspect

The WAAS must operate in real-time. In the case of the slow corrections, they must be broadcast every five minutes⁹. That means that the corrections must be computed, verified, packaged and broadcast in less than five minutes. (The orbits, however, could be computed much less often.)

Table 7 shows the computational times of the complete algorithm implemented on an HP 9000/755 workstation with a 26-Megaflops (Megaflop per second) performance. The computational times presented do not include estimates of the time that the system will require for data validation, verification, and input/output protocols.

The assumptions in the calculations presented are:

1. Orbit integration.
 - (a) Integration of 24 GPS satellites with the full model described in Section 2.1.
2. Slow correction generation.
 - (a) 9 state parameters for each of the 27 satellites (24 GPS satellites and 3 GEO satellites) i.e., position, velocity, clock, Y bias and solar scale factor.
 - (b) 2 state parameters for each of the 24 WRSs i.e., clock and tropospheric bias.
3. The fast (pseudorange) correction.
 - (a) 24 GPS satellites.
 - (b) 24 WRSs with 12-channel receivers.

⁹The only reason they have to be updated so often is that they are in the form of x, y, z (position) corrections, which are valid for only a short time. If they were in the form of corrections to broadcast orbital parameters, they could be updated much less frequently.

| Computational Times | |
|--|----------------|
| Task | Execution Time |
| Integrate 24 orbits for 5 min; Compute predicted pseudoranges | < 0.5 sec |
| Slow (5 min) orbit corrections (pseudorange only) | < 1.9 sec |
| Slow (5 min) orbit corrections (pseudorange and phase) | < 20 sec |
| 1 sec fast pseudorange correction | < 50 msec |

Table 7: Computational times on HP 9000/755 workstation.

It can be seen that the ephemeris prediction and slow correction calculation take (not including data validation, verification, and input/output protocols) less than 2.5 seconds with pseudorange processing only. Since the dynamical solution can be propagated into the future for hours with little loss of accuracy, the estimate from the previous (rather than the current) five-minute interval would be broadcast. The 2.5-second orbit computation would thus add no latency to the message generation.

The packing (on a 486-60 PC) and transmission times of the correction message can be based on the Stanford experience (Walter et al. 1994), where the whole RTCA SC 159 WAAS message is sent in 27 milliseconds.

Finally it is important to note that although the state-of-the-art models used in the dynamical orbit estimation are very sophisticated, they are well understood and the computational time that they demand easily meets the WAAS specification.

5 Summary of Conclusions

5.1 Summary of conclusions

- A nine-state vector, i.e., position, velocity, clock bias, Y bias and solar pressure scaling factor can accurately characterize the GPS satellites orbits over many hours.
- A continental U.S. WAAS network can estimate GPS orbits that are a factor of three better than the current uncorrupted broadcast orbits.
- The orbit accuracy improvements lead to a user

positioning improvement of a factor of four over the broadcast orbits (excluding nonephemeridal errors). When SA-dithered clock errors are added the improvement is twofold.

- With the use of dynamics in the orbit estimation process, the ephemeris and clock biases can be properly separated, thus accommodating the FAA WAAS scheme of slow and fast corrections.
- The orbital dynamical models implemented permit the propagation of the last orbital estimate, to allow future predictions without new measurements, hours ahead with little or no loss of accuracy. This indicates that less sophisticated models, whose predictions would be good for tens of minutes, could be used in a WAAS scenario.
- The ability to separate ephemeris biases from clock biases adds integrity to the system by introducing the capability to detect and identify errors in the estimate of either parameter.
- The dynamical orbit estimation process, the slow correction generation, and its broadcast can be done in 2.5 seconds on an HP 9000/755 workstation with a 26-Megaflops performance. This estimate does not include the time that the system will require for data validation, verification, and input/output protocols. Since the orbits can be accurately propagated ahead, the dynamical orbit estimation process adds no latency to the slow message generation.

Acknowledgements

The work described in this paper was carried out in part by the Jet Propulsion Laboratory, California Institute of Technology, under contract with the National Aeronautics and Space Administration (NASA) and by the Stanford University under NASA grant # NAS8-36125 and under Federal Aviation Administration (FAA) grant # 93-G-004/FAA.

References

- Bierman, G. (1977), *Factorization Methods for Discrete Sequential Estimation*, Academic Press.
- Ceva, J. (1995), Real-time dynamical GPS ephemeris prediction for WAAS applications, Engineer's

- thesis, Stanford University, Department of Aeronautics and Astronautics, Stanford, CA 94305.
- FAA (1994), Wide Area Augmentation Systems (WAAS) specifications, Technical report, Department of Transportation.
- Fliegel, H. & Gallini, T. (1992), 'Global Positioning System radiation force model for geodetic applications', *Journal of Geophysical Research* **97**(B1), 559–568.
- Grafarend, E. & Schaffrin, B. (1986), General classes of equivalent linear models by nuisance parameter elimination—applications to GPS observations, in 'Proceedings of the Fourth International Geodetic Symposium on Satellite Positioning', Vol. I, Austin, Texas, pp. 721–733.
- Kee, C. (1993), Wide Area Differential GPS (WADGPS), PhD thesis, Stanford University, Department of Aeronautics and Astronautics, Stanford, CA 94305.
- Kuang, D., Schutz, B. & Watkins, M. (1995), 'On the structure of geometric positioning in GPS measurements', *Manuscripta Geodaetica*. In revision.
- Mannucci, A., Wilson, B. & Edwards, C. (1993), A new method for monitoring the Earth's ionospheric total electron content using the GPS Global Network, in 'Proceedings of the ION GPS 93', The Institute of Navigation, Salt Lake City, Utah.
- Mannucci, A., Wilson, B. & Yuan, D. (1994), An improved ionospheric correction method for Wide-Area Augmentation Systems, in 'Proceedings of the ION GPS 94', The Institute of Navigation, Palm Springs, California.
- Nerem, R. (1994), 'Gravity model development for TOPEX/POSEIDON: Joint gravity models 1 and 2', *Journal of Geophysical Research* **99**(C12), 24383–24404.
- Newhall, X., Standish, E. & Williams, J. (1983), 'DE 102: a numerically integrated ephemeris of the moon and planets spanning forty-four centuries', *Journal of Astronomy and Astrophysics* pp. 150–167.
- Pullen, S., Enge, P. & Parkinson, B. (1995), A new method for coverage prediction for the Wide Area Augmentation System (WAAS), in 'Proceedings of the 51st ION Annual Meeting', Colorado Springs, Colorado, pp. 501–513.
- Tsai, Y. et al. (1995), Evaluation of orbit and clock models for real-time WAAS, in 'Proceedings of the National technical meeting', The Institute of Navigation, Anaheim, California, pp. 539–547.
- Wahr, J. (1981), 'Body tides on an elliptical, rotating, elastic and oceanless Earth', *Journal of Royal Astronomical Society* **64**, 677–703.
- Walter, T. et al. (1994), Flight trials of the Wide-Area Augmentation System, in 'Proceedings of the 1994 ION GPS Meeting', Salt Lake City, Utah, pp. 1537–1546.
- Watkins, M. et al. (1994), The JGM-3 gravity model, In preparation.
- Wells, D., Doucet, K. & Lindlohr, W. (1986), First order geodetic GPS network design: some consideration, in 'Proceedings of the Fourth International Geodetic Symposium on Satellite Positioning', Vol. I, Austin, Texas, pp. 801–819.
- Wu, S. et al. (1990), Global positioning system (GPS) precision orbit determination (POD) software design, Technical report, Jet Propulsion Laboratory. JPL internal report JPL D-7275.
- Yunck, T. et al. (1995), A robust and efficient new approach to real time Wide Area Differential GPS navigation for civil aviation, Technical report, Jet Propulsion Laboratory. JPL internal report JPL D-12584.
- Zumberge, J. & Bertiger, W. (1996), *GPS—Theory and Applications*, Vol. I of *AIAA Educational Series*, American Institute of Aeronautics and Astronautics, chapter 2.
- Zumberge, J. et al. (1995), IGS analysis center 1994 annual report, Technical report, International GPS Service for Geodynamics. In press.

Validation of the RTCA Message Format for WAAS

Yeou-Jyh Tsai, Per Enge, Yi-Chung Chao, Todd Walter, Changdon Kee, Jennifer Evans,
Andrew Barrows, David Powell, and Bradford Parkinson
Stanford University

BIOGRAPHIES

The authors are presently at Stanford University where their research concentrates on all aspects of the Wide-Area Augmentation System.

ABSTRACT

The Wide Area Augmentation System (WAAS) will augment GPS by broadcasting:

- additional ranging signals from geostationary satellites.
- integrity data for each satellite
- multiple-component differential corrections for each satellite

The ranging function will improve the availability and reliability of the position fix; the integrity data will improve the safety of the fix; and the differential GPS corrections will provide non-precision and Category I precision approach capability.

The WAAS data format was designed by Working Group 2 of RTCA Special Committee 159, and is gaining wide acceptance as the standard for WAAS transmissions. This remarkable format allows for the broadcast of differential corrections and integrity data on the GPS-like ranging signal. As such, it must pack this data into 250 bits/second, because higher data rates would require higher signal powers which might interfere with GPS.

This paper is the first to report on a nearly full implementation of the RTCA data format. It is based on the experimental WAAS flight system maintained by Stanford University for the FAA. The paper describes the

separation of the error components, message scheduling and packing, and flight results.

1 Introduction

The Wide Area Augmentation System (WAAS) consists of a signal-in-space and a ground network [1][2][8]. The signal-in-space carries GPS integrity and correction data to users and also provides a ranging signal that augments the primary GPS constellation. Initially, the WAAS signal will be broadcast to users from geostationary satellites.

The Wide Area Augmentation System will augment GPS so that it can be used as the primary navigation sensor for enroute through precision approach air navigation. The WAAS augments GPS with: additional ranging signals from the geostationary satellites, as well as differential corrections and *don't use* messages contained in the WAAS data stream. Taken together, the differential corrections and the improved geometry will improve nominal user accuracy to better than 8 meters (2drms) in the vertical, which is adequate for aircraft Category I precision approach. The integrity data will improve user safety by flagging GPS satellites whose incorrect behavior cannot be ameliorated. In fact, the WAAS can deliver health warnings to the pilot within 6 seconds of a GPS satellite malfunction.

The WAAS data format was designed by Working Group 2 of RTCA Special Committee 159, and is gaining wide acceptance as the standard for WAAS transmissions. This remarkable format allows for the broadcast of vector differential corrections and integrity data on the GPS-like ranging signal. As such, it must pack this data into 250 bits/second, because higher data rates would require higher signal powers which might interfere with GPS signals.

To date, studies on vector corrections of GPS signals for prototypes of WAAS have demonstrated the potential to achieve vertical positioning accuracy of 2-3 meters or better [2]. Simulation results on coverage prediction show WAAS meets the accuracy requirements over a large area [5]. Experimental data, which include static and dynamic test environments, collected using wide-area reference stations several hundred miles away from the user site further confirm Category I accuracy is achievable[3] [4].

The WAAS takes advantages of the characteristics of the error components of the pseudorange errors. Satellite clock errors, mostly from Selective Availability (SA), are varying much faster than satellite ephemeris errors. It is crucial to be able to separate these two components because the WAAS data capacity is limited to 250 bps. Therefore, efficient scheduling of message based on successful fast/slow separation enables the maximal usage of GEO navigation payloads.

This paper presents the Stanford WMS algorithm for separating satellite *location/clock* error. To date, our approach to estimate the satellite location/clock errors takes no advantage of well-understood models of GPS satellite dynamics. As such, it does not provide an accurate estimate of the satellite ephemeris. However, it does provide an estimate of the satellite location which is helpful for users located inside the network coverage area. Current research [13] strives to improve the overall performance of WAAS by incorporating satellite dynamic information.

To our knowledge, this paper is the first one to report on a nearly full implementation of the RTCA data format. It is based on the experimental WAAS flight system maintained by Stanford University for the FAA. Section 2 describes the RTCA message format, including integrity, fast/slow corrections, masks and geostationary satellite's navigation message. Section 3 discusses Stanford's WMS algorithm in estimating satellite's location/clock errors. Section 4 gives a brief description of message packing and scheduling. In Section 5, we will present both the static test results, using the receiver at Stanford campus as a passive user. Also, we will show the flight test results at Palo Alto and Livermore airport. Finally, we will summarize and give conclusions in Section 6.

2 RTCA Message Format

For each GPS satellite, the WAAS message contains separate corrections for the quickly varying component

of the pseudorange error (mostly satellite clock) and the slowly varying component of the pseudorange error (mostly satellite location). The WAAS message also carries estimates of the vertical ionospheric delay for a grid of locations.

The basic WAAS message is 250 bits in length. At the data rate of 250 bps, the duration of a WAAS message is one second, and the start of the message block is synchronous with a six second GNSS time epoch. Each block consists of: an 8 bit (distributed) preamble, a 6 bit message type, a 212 bit data field, and a 24 bit CRC parity.

The preamble is a 24-bit unique word, distributed over 3 successive blocks. An 8-bit preamble is adequate because the WAAS message is one second in duration and remains in synchronism with the GPS time epoch of six seconds. The message type field is 6 bits long, which allows for 64 different messages. The currently defined message types are summarized in Table 1.

| Type | Contents | Used |
|-------|--|------|
| 0 | Don't use GEO for anything (for testing) | no |
| 1 | PRN mask assignments | yes |
| 2 | Fast pseudorange error estimates | yes |
| 3-8 | Reserved for future messages | no |
| 9 | GEO navigation message | no |
| 10-11 | Reserved for future messages | no |
| 12 | WAAS Network/UTC offset parameters | no |
| 13-16 | Reserved for future messages | no |
| 17 | GEO satellite almanacs | no |
| 18 | Ionospheric pierce point mask 1 | yes |
| 19 | Ionospheric pierce point mask 2 | yes |
| 20 | Ionospheric pierce point mask 3 | no |
| 21 | Ionospheric pierce point mask 4 | no |
| 22 | Ionospheric pierce point mask 5 | no |
| 23 | UDRE zone radii and weights | no |
| 24 | Mixed fast/long-term satellite errors | no |
| 25 | Long-term satellite error estimate | yes |
| 26 | Ionospheric delay error estimate | yes |
| 27-63 | Reserved for future messages | no |

Table 1: WAAS Message Types

The WAAS message format serves an extremely ambitious goal: provide Category I precision approach accuracy over a continental area using only a data rate of 250 bits per second. Indeed, greater bit rates would require the received signal power from the geostationary WAAS satellites to be greater than the received power from the GPS satellites - an undesirable outcome. Yet the WAAS message stream must carry corrections for

all 24 GPS satellites and any GNSS satellites in orbit. In contrast, local area DGPS data links typically use 100 bits per second or more to provide a similar capability to ranges of two or three hundred kilometers. Moreover, local links need only carry corrections for the 6 to 12 satellites which are in view of a single reference station.

The details of the WAAS message format are given in [8]. However, the WAAS message format basically achieves highly efficient use of very limited capacity as follows.

Fast and Slow Corrections Fast correction messages carry the quickly varying component of the pseudorange errors for each satellite (mostly clock error). They will also carry the *use/don't use* integrity data for each GPS satellite. As such, they must be sent much more frequently than any other message (every 6 to 10 seconds), but they do not decorrelate spatially. Consequently, a single fast correction per satellite suffices for the entire footprint of the WAAS satellite. The GPS error components which vary more slowly are separated and sent much less frequently.

No Rate Corrections Unlike most local area DGPS data formats, the WAAS carries no rate corrections for the quickly varying component of the satellite error. As shown in [10], it is more efficient for the user receiver to estimate the rate by differencing the most recent fast corrections.

Masks A *mask* is used to designate which satellite belongs to which slot in the fast correction messages. A mask is used to assign slots so that satellite identifications need not be sent with every fast correction. A similar ionospheric mask is used to associate each slot in the ionospheric correction message with a geographic location.

Geostationary Navigation Message In contrast to the GPS satellites, the WAAS satellites are geostationary; so their location need only be updated every 2 minutes or so.

Parity The WAAS uses a much stronger parity algorithm than the extended Hamming code used in the GPS navigation message (and typically used for the transmission of differential corrections). To reduce the probability of failing to detect a bit error, the parity scheme uses 24 bits and thus reduces the

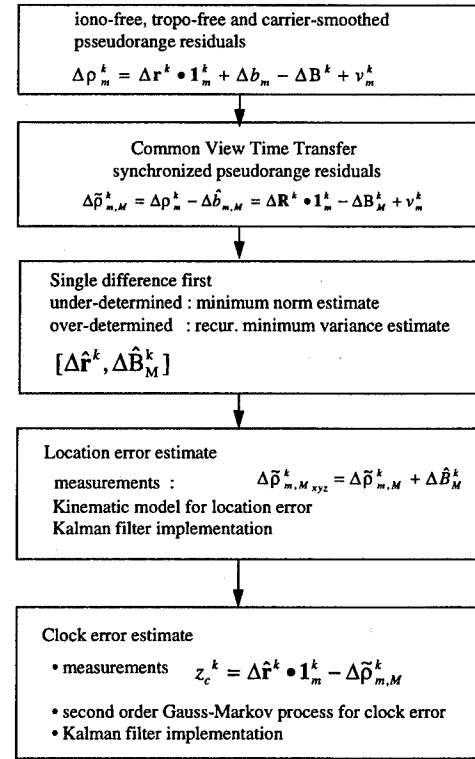


Figure 1: Block Diagram of Stanford Satellite Location/Clock Estimator

probability of failing to detect an interference burst to $2^{-24} = 5.96 \times 10^{-8}$. In contrast, GPS adds 6 parity bits to every 24 data bits for an overhead of $6/30 = 0.20$. The WAAS overhead is $24/250 \approx 0.096$.

3 Satellite Location/Clock Estimator

The Wide Area Reference Station (WRS) uses dual frequency receiver to estimate the ionospheric delay and weather station to estimate the tropospheric delay [3]. Processing of these ionospheric delay data to generate a "grid" of ionospheric estimates is described in [11][12]. This paper will focus on the estimation of satellite location and clock errors.

The Wide Area Master Station (WMS) receives the following *iono and tropo-free, carrier-smoothed* pseudorange residuals from the reference stations

$$\{\{\Delta \rho_m^k = \Delta r^k \cdot \mathbf{1}_m^k + \Delta b_m - \Delta B^k + v_m^k\}_{k=1}^{K_m}\}_{m=1}^M \quad (1)$$

In this equation, the $\Delta \mathbf{r}^k$ and the ΔB^k are the estimanda of interest. Estimates of these parameters will be broadcast to the users. In contrast, the user has no interest in the reference station clock offsets (Δb_m). However, these *nuisance* parameters must still be estimated by the master station to yield an accurate estimate of the data of interest. Finally, the ν_m^k is the measurement noise.

For the time being, the Stanford WMS uses the simpler strategy, as shown in Figure 1, which estimates the satellite *location/clock* errors directly as described in the following paragraphs.

Common view time transfer [6] is used to remove the WRS clock offsets from the measurements as follows

$$\begin{aligned}\Delta \tilde{\rho}_{m,M}^k &= \Delta \rho_m^k - \hat{\Delta b}_{m,M} \\ &= \Delta \mathbf{r}^k \cdot \mathbf{1}_m^k - \Delta B_M^k + v_m^k\end{aligned}\quad (2)$$

After the WRS clock offsets are removed, the observation equations are uncoupled and synchronized to master clock. In other words, the observations which depend on the clock and location errors of the k^{th} satellite do not depend on the clock or location errors of any other satellite.

A single difference

$$\begin{aligned}\tilde{\Delta}_{m,M}^k &= \Delta \tilde{\rho}_m^k - \Delta \tilde{\rho}_M^k \\ &= \Delta \mathbf{r}^k \cdot (\mathbf{1}_m^k - \mathbf{1}_M^k) + v_{m,M}^k\end{aligned}\quad (3)$$

is then used to remove the satellite clock offsets from the measurements. At this point, the reduced observations only depend on the location errors ($\Delta \mathbf{r}^k$) for the given satellite. The linear system of Eqn.(3) can be rewritten in a more compact formula. Define \mathbf{z} , \mathbf{G} and \mathbf{v} such that

$$\mathbf{z} = \mathbf{G} \cdot \Delta \mathbf{r}^k + \mathbf{v}\quad (4)$$

A simple linear estimator is used to estimate the three components of satellite location error. If the satellite of interest is only in view of three or fewer WRSs, then a minimum norm solution is used. If the satellite is in view of four or more WRSs, then an *a priori* covariance $\mathbf{\Lambda} = E[\Delta \mathbf{r}^k (\Delta \mathbf{r}^k)^T]$ for the satellite location error is included in the estimator's cost function and recursive minimum variance estimator [15] [16] which minimizes the error covariance is used. This is described in the following equation

$$\Delta \hat{\mathbf{r}}^k = \begin{cases} \mathbf{G}^T (\mathbf{G} \mathbf{G}^T)^{-1} \cdot \mathbf{z} & \text{if } M < 4 \\ \mathbf{\Lambda} \mathbf{G}^T (\mathbf{R} + \mathbf{G} \mathbf{\Lambda} \mathbf{G}^T)^{-1} \cdot \mathbf{z} & \text{if } M \geq 4 \end{cases}\quad (5)$$

The location error estimates are subtracted from the original observations, which are then used to estimate

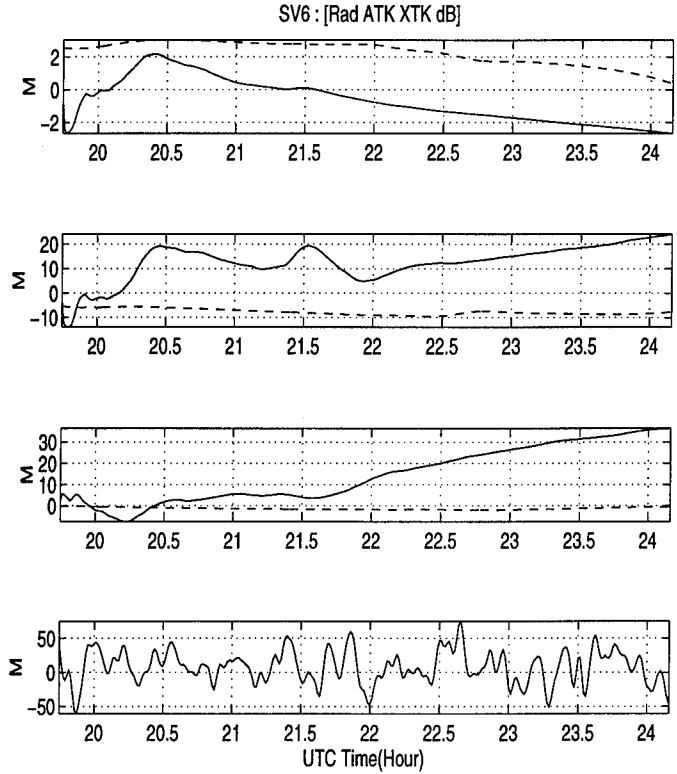


Figure 2: Satellite Location/Clock Error Estimates for PRN 6. Shown here are the radial, along track and cross track errors and clock errors. Post-processed precise ephemeris are plotted as dashed lines.

the satellite clock offsets as follows

$$\Delta \hat{B}^k = \frac{1}{M} \sum_{m=1}^M (\Delta \hat{\mathbf{r}}^k \cdot \mathbf{1}_m^k - \Delta \tilde{\rho}_{m,M}^k)\quad (6)$$

A simple kinematic orbit model is used for satellite location error. We use the satellite clock error from previous *snapshot* estimator to derive the measurement

$$z_{om}^k = \tilde{\Delta}_{m,M}^k + \hat{B}^k\quad (7)$$

The process and measurement models are described by the following equations

$$\mathbf{x}_o(k+1) = \Phi_o(k) \mathbf{x}_o(k) + \mathbf{B}_o(k) \mathbf{w}_o(k)\quad (8)$$

$$\mathbf{z}_o(k) = \mathbf{H}_o(k) \mathbf{x}_o(k) + \mathbf{v}_o(k)\quad (9)$$

We then use a Kalman filter implementation to estimate $\hat{\mathbf{x}}_o(k)$, which includes satellite location and velocity errors. The estimates $\hat{\mathbf{x}}_o(k)$ are subtracted from the original observations, which are then used to form the measurements for satellite clock error as follows

$$z_{cm}^k = \hat{\mathbf{r}}^k \cdot \mathbf{1}_m^k - \Delta \tilde{\rho}_{m,M}^k\quad (10)$$

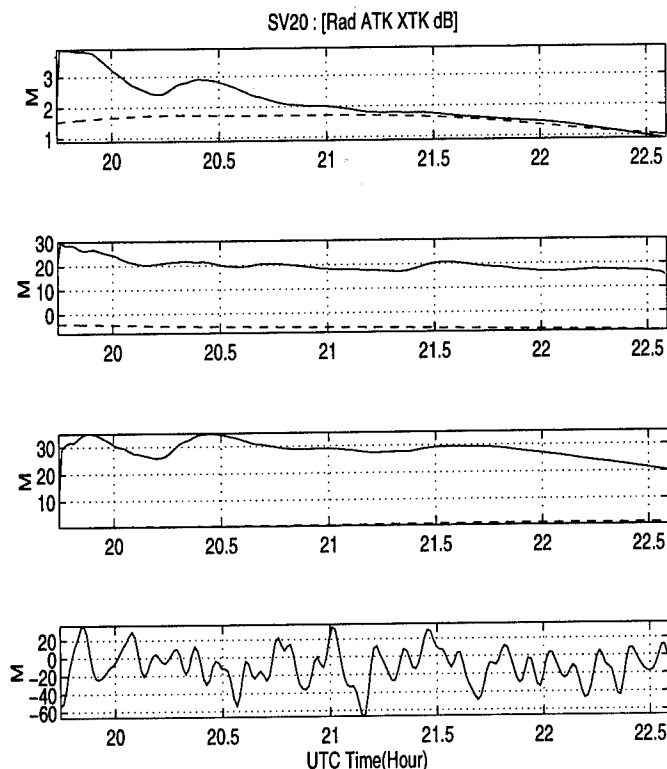


Figure 3: Satellite Location/Clock Error Estimates for PRN 20. Shown here are the radial, along track and cross track errors and clock errors. Post-processed precise ephemeris are plotted as dashed lines.

A second order Gauss Markov process model [14]

$$\mathbf{x}_c(k+1) = \Phi_c(k)\mathbf{x}_c(k) + \mathbf{B}_c(k)\mathbf{w}_c(k) \quad (11)$$

$$\mathbf{z}_c(k) = \mathbf{H}_c(k)\mathbf{x}_c(k) + \mathbf{v}_c(k) \quad (12)$$

is used. Vector estimates $\hat{\mathbf{x}}_c(k)$ which includes clock error and clock error velocity are then generated using another Kalman filter.

Estimated corrections are shown in Figures 2 and 3. As shown, these corrections are smoother, as compared to the "snapshot" corrections. In addition, changes of observation geometry do not cause an abrupt jump of the estimates, as is in the snapshot approach [6]. Figure 2 shows the filtered estimate of PRN 6 for about 5 hours and Figure 3 shows the filtered estimate of PRN 20 for about 3 hours. Clearly satellite location errors are slowly varying, as compared to satellite clock error.

This approach takes no advantage of well-understood models of GPS satellite dynamics. As such, it does not provide an accurate estimate of the satellite ephemeris. As shown in Figures 2 and 3, our location estimates

are different from post-processed precise ephemeris. However, these location estimates do provide an estimate of the satellite location which is helpful for users located inside the reference stations. Current research [13] strives to improve the overall performance of WAAS by incorporating satellite dynamic information.

4 WAAS Message Scheduling and Packing

WAAS message broadcast is limited at 250 bps and there are only 212 bits data field for corrections to be put in. Therefore, it is important to schedule the message broadcast efficiently, while at the same time users just acquiring WAAS must have a short *time to first fix* (TTFF).

Our message scheduler is based on the receiver in our laboratory which is used as a passive user to receive and decode WAAS messages. This passive user generates predictions for the satellite clock and location error predictions using decoded messages. As such, correction latency because of message broadcast and precision loss because of fixed data bits are included. The WMS compares the differences between generated corrections with the user predicted corrections to decide which type of message is to be sent.

WAAS messages are scheduled as follows.

- Mask (satellite PRN and iono. grid) message is sent every 2 to 5 minutes, or if for some reasons the mask changes. For example, a new satellite is launched or taken out of service. This will ensure prompt service for users entering WAAS.
- Satellite clock errors are the fast varying components of corrections and have to be sent every 6 to 10 seconds. If the difference between WMS generated corrections and user predicted corrections exceeds a threshold, a fast correction will be broadcast.
- Satellite location corrections are sent every 2 to 5 minutes normally. However, if the projection to user-satellite line of sight of the difference between WMS generated and user predicted satellite location error exceeds a threshold, a slow correction will be broadcast.
- Vertical ionospheric delays at grid points are sent every 2 to 5 minutes.

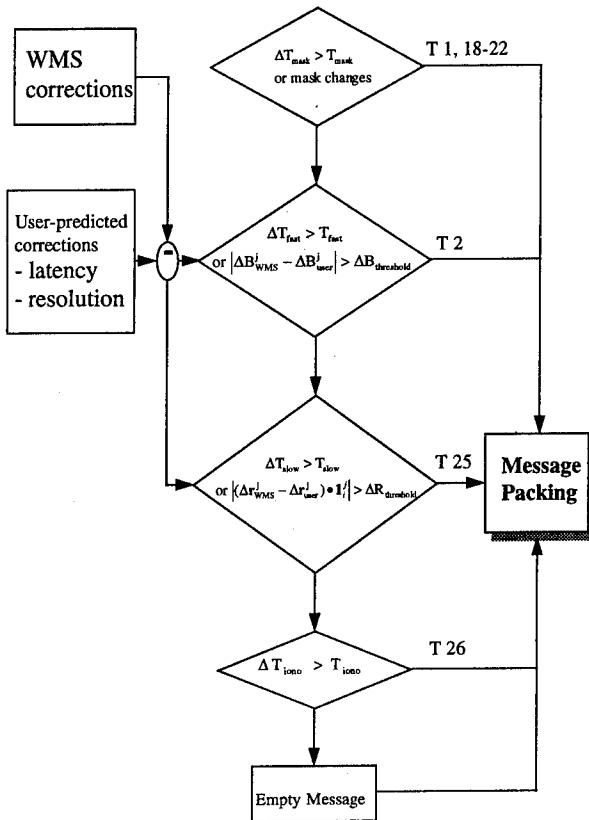


Figure 4: Stanford WAAS Message Scheduling Algorithm

- If none of the above message has been sent, an empty message will be broadcast.

Figure 4 summarizes our current message scheduling algorithm. Because our network does not have full GPS constellation in view at the same time, we only have to send corrections for satellites which are observed by our network. It is not surprising that most of the time an empty message is sent (about 50 %). It is important to keep in mind that Stanford experimental WAAS network is not using geostationary satellite to broadcast WAAS message, therefore no GEO navigation messages are scheduled. However, there will be no difficulty at all to accommodate the GEO messages and other reserved messages in the future. Column 3 of Table 1 shows the currently implemented message types.

After deciding which message is to be sent, WMS packs the correction according to data format described in Section 2. We use UHF data link to broadcast WAAS messages to our airborne user. The UHF transmitter is operated at 464.475 MHz and transmits data at 9600

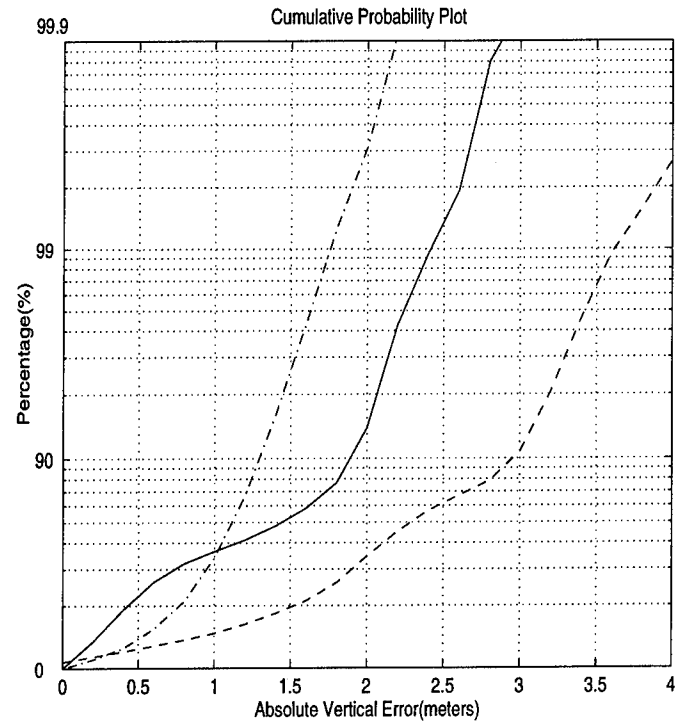


Figure 5: Cumulative Probability Plot of Absolute Vertical Errors. The dashed line shows result before inter-frequency biases are removed. The solid line shows result after inter-frequency biases are removed. The dashdot line shows result for a dual frequency user.

bits per second. As such, our WAAS data, which is 250 bits in length, uses only a small portion of UHF receiver's capacity.

The exceptions from RTCA data format include

1. No geostationary satellite navigation message is scheduled. To broadcast the correction messages, we use UHF data link.
2. Time tag is added in both fast (type 2) and slow (type 25) correction messages. This is because we are not using geostationary satellite for broadcasting that we cannot use message preamble to synchronize with the GPS time.
3. Empty message is scheduled, because mostly of the time our network sees only 8 or 9 satellites. For operational WAAS, a fast correction should be scheduled in this case.

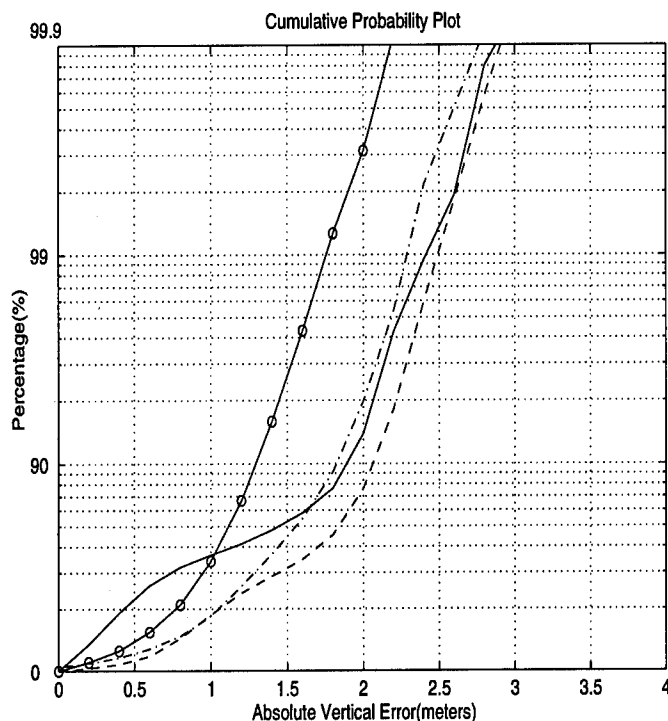


Figure 6: Cumulative Probability Plot of Absolute Vertical Errors. The inter-frequency bias has been calibrated. Results shown here include our regular WMS operation (solid), using broadcast ephemeris (dashed), using dual frequency receiver (solid line with "o") to estimate ionospheric delays and results applying post-processed precise ephemeris (dashdot).

5 Results

All the data presented here were collected in real time using Stanford experimental WAAS network. Our reference stations are located at Arcata, Elko and San Diego [3]. These reference stations send the GPS observations over phone lines to the WMS on campus. The vector differential corrections are derived from these observables. These corrections are then put into RTCA data format and then broadcast using a UHF transmitter. The results of static and dynamic tests are described below.

5.1 Static Tests

Data presented in this section were collected with the passive reference station colocated at Stanford with the WMS. Stanford data, though, is not used in the formation of the corrections. The received WAAS mes-

sage is "unpacked" and applied to the Stanford station.

Figure 5 shows the 4-hour data which we compare the results before and after the inter-frequency biases at the reference stations and satellites were calibrated. These inter-frequency biases, if not calibrated, will affect our satellite *location/clock* estimator. In addition, it also influences the ionospheric delay estimation using current grid algorithm. The dashed line shows the result before the biases were calibrated, while the solid line is after applying the bias calibration [11][12]. With the bias calibration, we are able to separate errors caused by ionospheric delay from those caused by satellite ephemeris and clock errors. The improvement over the vertical errors at 95 % changes from greater than 3 meters to less than 2 meters. Also shown in this figure is the performance for a dual frequency user. This user would have the best result because he can use measurements on both frequencies to estimate delay from the ionosphere.

Figure 6 shows the same 4-hour data which we compare several situations. Inter-frequency biases have been calibrated for all cases.

1. **Broadcast** Using broadcast ephemeris only. In this case, our fast corrections are composed of weighted pseudorange residuals from our WRSs, while satellite location errors are set to be zero. The result is shown in dashed line.
2. **Regular** Using corrections generated by our satellite location and clock estimator. The result is shown in solid line.
3. **Post-Processed Precise Ephemeris** Using post-processed precise ephemeris from International Geodynamics Service (IGS) for slow corrections (satellite ephemeris errors) and satellite clock error is derived from the pseudorange residuals using the post-processed precise ephemeris. The result is shown in dashdot line.
4. **Dual Frequency User** Using corrections generated by our satellite location and clock estimator, but using measurements on both frequency to estimate the ionospheric delay. The result is shown in solid line with "o".

Our **Regular** case shows the improvements over using **Broadcast** ephemeris, and is quite close to the result from using **Post-Processed Precise Ephemeris**. However, given the limited amount of data points, the first three cases have close results. In addition, the user is located almost at the center of our network which should have better results than the boundary users.

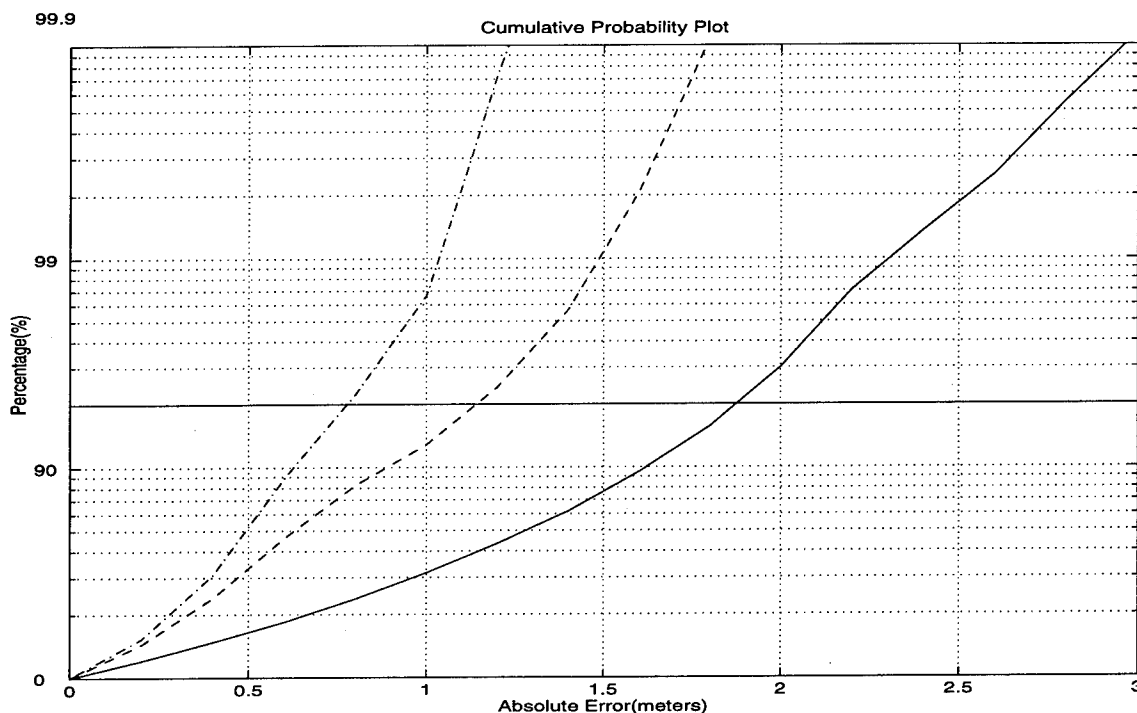


Figure 7: Statistics of the Absolute Errors in east-west (dashdot), south-north (dashed) and vertical (solid) directions. The solid horizontal line indicates the cumulative probability at 95 %.

The best result is achieved for a dual frequency user. Longer data will have to be collected in the future to make better comparisons and conclusions.

To present the statistics of static test results, Figure 7 shows the distributions of the absolute errors in the east-west (dashdot), south-north (dashed) and vertical (solid) directions for our regular case, with the inter-frequency biases calibrated. These data were collected over several days and includes both daytime and nighttime period. The length of the data are more than 32 hours, at 1 Hz epoch rate. Positioning performance is better in the horizontal directions. The 95 % value for the absolute vertical error is better than 2 meters.

5.2 Dynamic Tests

The flight trials were conducted at Palo Alto airport. As a truth source, we have surveyed ends of the runway of the airports. We have applied a flat runway model from surveyed results and it should be accurate to better than one meter.

The RTCA messages were broadcast to Professor David Powell's Piper Dakota using a UHF data link.

The airborne user has a 10 channel single frequency receiver to receive the GPS signals and a UHF radio modem to receive our WAAS messages. In the future, the WAAS messages will be broadcast from geostationary satellites. The data presented here were collected **before** the inter-frequency bias calibration.

Figure 8 shows 20 *touch-and-gos* we did on the same day at the Palo Alto airport. This flight test lasted about one and a half hour. These points include flight technical error in addition to the navigation sensor error. Zero altitude is the surface of the runway. The vertical errors when the airplane was on the runway (roughly from 50 meters to 450 meters in the along-track direction), are always within the ± 4.1 meters 95 % navigation sensor error limits (shown as dashed line) required for a Category I ILS landing system. In addition, the vertical errors are very consistent for all approaches and have the mean at about -2 meters.

It is important to note that this flight trial was conducted before the bias calibration. Interestingly, results from our static passive user show a mean vertical error of about -1.5 meters. After we post-processed the data with the bias calibration, the mean is about 0 meters. We believe the vertical errors on this flight

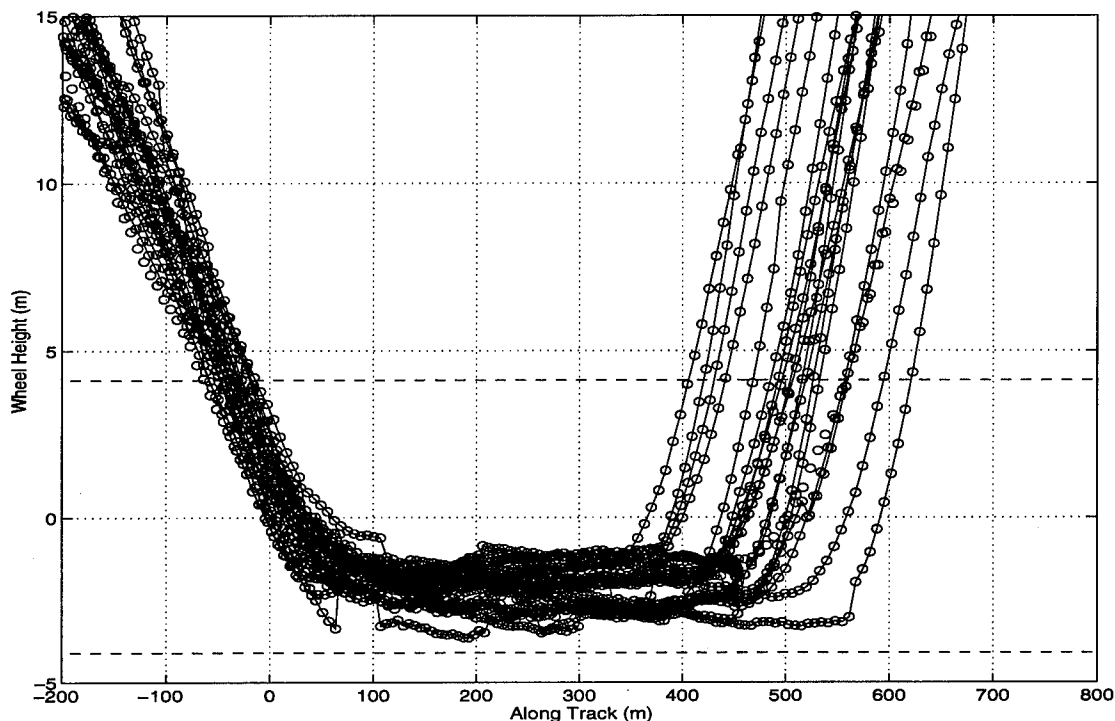


Figure 8: Flight Trials at Palo Alto Airport, without bias calibration

trial are majorly caused by the inter-frequency biases and the errors should be centered around the 0 meters if we have the inter-frequency biases calibrated. There are a few jumps in Figure 8. We think they come from the signal multipath effect when the airplane was on the ground.

6 Summary and Conclusions

This paper reports a nearly full implementation of the RTCA data format. We have demonstrated that our satellite *location/clock* error estimator is capable of separating the slowly and quickly varying error components. As such, the error estimates can be packaged and broadcast in the *fast/slow* messages according to RTCA data format. This will make the most use of WAAS messages, which have the limits of 250 bits per second.

We also described our current message scheduling and packing algorithm. Slight modifications were made because we are using a UHF data link and our network only sees limited number of satellites at a time. However, there will be no difficulty for operating a real time WAAS network which covers a larger area.

Improved performance has been achieved with the bias calibration. Static test results obtained from Stanford receiver yield vertical errors better than 2 meters 95 percent of the time. Flight trial conducted at Palo Alto airport shows our WAAS accuracy can achieve Category I ILS precision approach accuracy requirements, even before inter-frequency biases were calibrated.

ACKNOWLEDGMENTS

Help on the flight trials from Eric Abbott, Awele Ndili and students at Stanford University are highly appreciated. The authors gratefully acknowledge support from the FAA Satellite Program Office (AGS-100) and the FAA Technical Center. In particular, Joseph Dorfler, J.C. Johns, David Peterson, Leo Eldredge, Barbara Fuller and Fred Snyder have been particularly helpful. In addition, we would like to thank Bruce DeCleene of FAA Certification (AIR-100), and the FAA personnel at the San Diego, Elko, and Arcata Flight Service Stations.

REFERENCES

1. C. Kee, B.W. Parkinson, and P. Axelrad, "Wide Area Differential GPS," *Navigation, Journal of the U.S. Institute of Navigation*, vol. 38, no. 2, Summer 1991.
2. C. Kee, "Wide Area Differential GPS," PhD. Dissertation, Stanford University, December 1993.
3. T. Walter, C. Kee, Y.C. Chao, Y.J. Tsai, et.al., "Flight Trials of the Wide Area Augmentation System (WAAS)," *Proceedings of ION-GPS 94*, Salt Lake City, UT., Sept. 22-24, 1994, pp.1245-1254.
4. C. Kee, T. Walter, Y.C. Chao, Y.J. Tsai, et.al., "Comparison of Full Vector and Common View WAAS Algorithms," *Proceedings of the Annual Meeting of the Institute of Navigation*, Colorado Springs, June 1995.
5. S. Pullen, P.K. Enge and B.W. Parkinson, "A New Method for Coverage Prediction for the Wide Area Augmentation System (WAAS)," *Proceedings of the Annual Meeting of the Institute of Navigation*, Colorado Springs, June 1995.
6. Y. Tsai, Y. Chao, T. Walter, C. Kee, D. Powell, P. Enge and B. Parkinson, "Evaluation of Orbit and Clock Models for Real Time WAAS," *Proceedings of the National Technical Meeting of the Institute of Navigation*, Anaheim, CA, pp. 539-547, January 1995.
7. S. M. Lichten and J. S. Border, "Strategies for High Precision Global Positioning System Orbit Determination," *Journal of Geophysical Research*, Vol.92, No.B12, pp.12,751-12,762, Nov. 1987.
8. P.K. Enge and A.J. Van Dierendonck, "The Wide Area Augmentation System," *Proceedings of the Eighth International Flight Inspection Symposium*, Denver, June 1994.
9. RTCA Special Committee 159 Working Group 2, "Wide-Area Augmentation System Signal Specification," March 1994.
10. C.J. Hegarty, "Optimal Differential GPS for a Data Rate Constrained Broadcast Channel," *Proceedings of the Sixth International Technical Meeting of the Satellite Division of the Institute of Navigation*, Salt Lake City, pp. 1527-1535, September 1993.
11. Y.C. Chao, Y.J. Tsai, T. Walter, C. Kee, et.al., "The Ionospheric Delay Model Improvement for the Stanford WAAS Network," *Proceedings of ION National Technical Meeting 95*, Anaheim, CA., Jan. 18-20, 1995.
12. Y.C. Chao, Y.J. Tsai, T. Walter, C. Kee, et.al., "An Algorithm for Inter-frequency Bias Calibration and Application to WAAS Ionosphere Modeling," *Proceedings of ION-GPS 95*, Palm Springs, CA., Sept. 12-15, 1995.
13. J. Ceva, W. Bertiger, R. Mullerschoen, T. Yunk and B. Parkinson, "Incorporation of Orbital Dynamics to Improve Wide-Area Differential GPS," *Proceedings of ION-GPS 95*, Palm Springs, CA., Sept. 12-15, 1995.
14. J. Studenny, "Simulation of a Second-Order Gauss-Markov Process," *RTCA Paper No.148-93/SC159-424*, March 17, 1993.
15. D. G. Luenberger, "Optimization by Vector Space Methods," John Wiley & Sons, Inc., 1969.
16. G. J. Bierman, "Factorization Methods for Discrete Sequential Estimation," Academic Press, 1977.

The Ability of a RADGPS to Provide the Accuracy and Integrity Required for En-route Navigation

Dr. Richard Farnworth
UK National Air Traffic Service

Stuart Jolley
Roke Manor Research

Andrew Lovett
Racal Avionics

BIOGRAPHIES

Dr. Richard Farnworth is a research engineer employed by the United Kingdom's National Air Traffic Services which is part of the Civil Aviation Authority (CAA). His responsibilities include the management of R&D projects relating to the application of satellite navigation systems in civil aviation.

Stuart Jolley is Group Leader of the Air Traffic Management Group within Roke Manor Research who provide support for the ATM division of Siemens Plessey Systems.

Andrew Lovett is Satellite Programme Manager for Racal Avionics where he is responsible for satellite communications and navigation systems. After leaving the Royal Air Force in 1989 he joined STC Navigation Systems, later to become Cosser Electronics Ltd. where he was involved in the development of P(Y) code GPS receivers. He joined Racal Avionics in 1989 as GPS Applications Manager.

ABSTRACT

A satellite navigation system providing a primary means of en-route navigation will have to meet exacting accuracy, availability, integrity and continuity of service requirements. The UK National Air Traffic Services in collaboration with the Racal Group, Roke Manor Research and Siemens Plessey Systems have set up a trial to investigate the use of a satellite navigation system for providing en-route navigation in the future.

The GPS system and a network of regional monitor stations have been used to investigate the provision of differential corrections and timely integrity warnings to aircraft and air traffic control facilities. Integrity

data and pseudorange corrections are derived from a number of Racal Skyfix reference stations located in and around the UK. The data is uplinked to a suitably equipped British Airways Boeing 767 using the high integrity C-Band datalink provided by the Siemens Plessey MLS at Heathrow Airport. The data is also transferred to a NATS facility to allow system monitoring to be performed so that Air Traffic Controllers can be made aware of navigation system outages.

Integrity and availability cannot be demonstrated by the use of flight trials so a Hazard Analysis has been performed to identify the levels achievable with currently available technology. The levels of augmentation and redundancy needed to meet the integrity and availability requirements can then be determined.

INTRODUCTION

The introduction of Global Navigation Satellite Systems provides an alternative to the ground based navigation aids such as DME and VOR which have served the aviation community well for many years. Before such systems can be used operationally it must be demonstrated that they can meet the exacting required navigation performance (RNP) parameters specified by the International Civil Aviation Organisation (ICAO). When satellite navigation systems are introduced into civil aircraft operations new procedures will also be necessary to advise Air Traffic Control staff of the navigation system status in their airspace.

This paper describes a study undertaken to investigate the potential use of a regional area differential GPS system for en-route air navigation. The study involves theoretical analysis and a practical demonstration

which will enable the performance of the system to be measured against the ICAO RNP.

A discussion is also included on how controllers and airspace planners might manage the ongoing changes in the GPS constellation.

OBJECTIVES

The RNP requirements for various phases of flight as they are currently defined by ICAO are summarised in

Table 1. Much work has been presented to demonstrate the high levels of accuracy achievable using satellite positioning systems but further work is necessary to demonstrate that the remaining RNP requirements can be met. All the requirements defined by the RNP must be met simultaneously before national authorities will certify any system for aviation use.

| Phase of Flight | Accuracy | | Integrity | Availability | Continuity |
|------------------------|-------------------------|------------------------|---------------------------------------|------------------------|--|
| | Lateral | Vertical | | | |
| B-RNAV | ±5 NM | | | $1-1 \times 10^{-4}$ | |
| P-RNAV | ±1 NM | | | $1-1 \times 10^{-5}$ | |
| En-route | ±330' | - | 10s warning | $1-1 \times 10^{-5}$ | |
| Non Precision Approach | ±330' | - | 10s warning | $1-1 \times 10^{-5}$ | |
| CAT I | ±132' at height 200' | ±40' at height 200' | 3.3×10^{-7} 6 sec warning | $1-2.5 \times 10^{-3}$ | 1×10^{-5} 15 sec operation |
| CAT II | ±70' at height 100' | ±15' at height 100' | 3.3×10^{-8} 2 sec warning | $1-1.5 \times 10^{-3}$ | 4×10^{-6} 15 sec operation |
| CAT III | ±50' at height 50' | ±5' at height 50' | 3.3×10^{-9} 1 sec warning | $1-1 \times 10^{-3}$ | 4×10^{-6} 30 sec operation |

Note: Integrity and continuity are per hour for en-route applications and per approach for precision approach applications

Table 1. Provisional Values for Required Navigation Performance (RNP)

The current GPS constellation does not meet the RNP parameters for any phase of flight without some kind of augmentation. One reason for this is the lack of system integrity monitoring. There are, of course, methods designed to improve the integrity such as RAIM and the integration of other sensors like inertial reference systems and barometric altimeters but these have limitations. Differential systems provide a level of integrity monitoring and the US and Europe with WAAS and EGNOS intend to provide monitor systems covering vast areas. These systems will be very costly and it will be at least five years to become operationally usable. The objective of this study is to gain some experience with GNSS monitoring systems using system components already available today. The Regional Area Differential GPS is similar to WAAS and EGNOS but less complex and on a smaller scale. Another objective of the work

is to evaluate the necessary augmentation required for the GPS system to meet the RNP for the en-route phase of flight.

The study is broken down into three separate activities. Firstly a practical demonstration of the use of a regional area monitoring system is being undertaken at Heathrow airport involving the transmission of integrity data and differential corrections to an operational aircraft. Secondly a fault tree analysis is being undertaken to identify the levels of integrity and continuity achievable using the proposed regional or wide area augmentation systems. Finally an investigation is being carried out into the potential for presentation of navigation system status information to air-traffic control (ATC) authorities so that airspace can be managed in an efficient and safe manner.

PRACTICAL DEMONSTRATION

The practical trials and data collection make use of elements of the local area differential GPS system currently undergoing evaluation at London's Heathrow Airport. Racal's SKYFIX network provides the ground monitoring stations located around the UK and Europe. A British Airways 767 equipped with ILS, MLS and DGPS systems receives the integrity and correction data each time it approaches Heathrow and stores the information for off line analysis.

The system configuration is illustrated in Figure 1. Data from five of the skyfix reference stations is fed to the Racal control centre at Aberdeen where it is processed to generate differential corrections which

are valid for a virtual reference station at the centroid of the original stations. The integrity monitoring software makes use of 8 of the skyfix reference stations and the virtual pseudorange corrections to apply consistency checks to the corrections enabling the detection and isolation of satellite or monitor station anomalies. An integrity bit is generated for each satellite which acts as a use/don't use indication for the airborne receiver. The quality of the pseudorange corrections is also indicated in the UDRE parameter in the differential message. The data is then converted into the format required for uplinking to the aircraft and sent via X25 data link to Heathrow airport. The locations of the ground monitor stations is illustrated in figure 2.

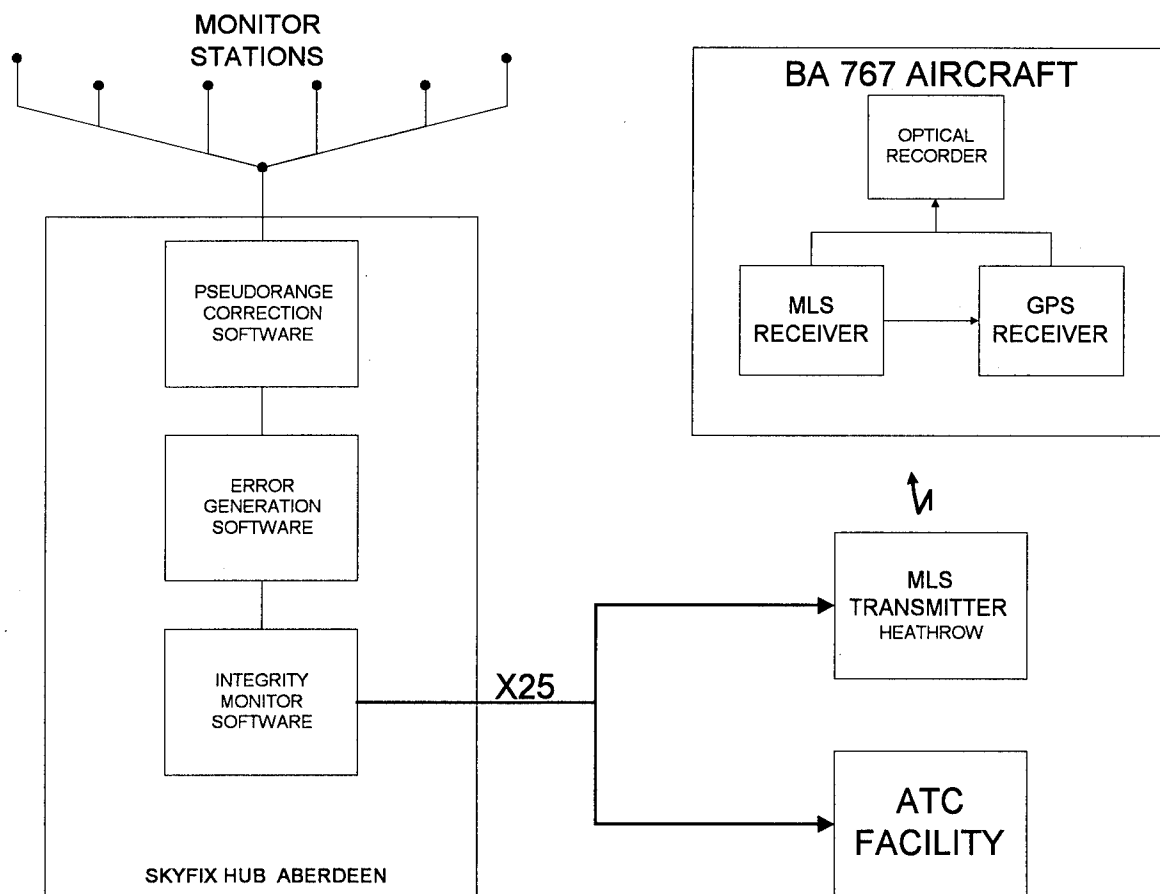


Figure 1. RADGPS System Configuration

The uplink makes use of the MLS C-Band communications channel available at Heathrow. This is not the ideal method for communicating corrections over a wide area but it is a ground to air datalink already in place and is ideal for the purpose of system evaluation. An extension to the trial will investigate other methods of communicating the differential and integrity data to the aircraft such as terrestrial VHF transmitters or geostationary satellites. The MLS Azimuth transmitter broadcasts the data via the auxiliary C-words on the MLS data channel.

On the aircraft the MLS receiver decodes the C-words to extract the corrections and feeds them over the ARINC 429 bus to the GPS receiver. Here the corrections are applied in order to determine the

position of the aircraft. Data from the onboard GPS, MLS and ILS receivers are stored using an optical quick access recorder for off-line analysis and processing. The data is automatically recorded each time the aircraft approaches Heathrow airport.

In parallel the data is routed to a NATS facility where the status of the GPS and the reference stations can be monitored.

For evaluation purposes an error generation system has been included in the system at Aberdeen to introduce artificial pseudorange errors on individual satellites. The application of these errors allows the latency of the system to be calculated which will help in computing the estimated time to alarm.



Figure 2 Location of SKYFIX Ground Monitor Stations

The data acquired during these approaches will be used to investigate the accuracy, integrity and latency of the Regional Area Differential GPS system. The accuracy will be investigated by the comparison of DGPS position with MLS, ILS and an optical ground truth system. The accuracy of the regional system will be compared with the local area differential system.

FAULT TREE ANALYSIS

The high levels of integrity and continuity required for the certification of aviation navigation aids cannot be demonstrated by the use of flight trials. For example the experimental confirmation of an integrity of 5×10^{-8} per flight hour as required for continental en-route navigation would require in excess of 20 million hours of flight trials.

An alternative approach to certification is top use safety case analysis. This involves the identification and analysis of conditions and events which result in a loss of performance or system failure. Integrity and continuity of a system can then be determined using fault trees and failure modes and effects analysis. The resulting fault trees will have top level events representing the continuity and integrity risks and will branch down to lower level events that contribute to the overall risk.

Fault Trees have been developed for a differential GPS system representative of a RADGPS or WADGPS. A top level fault tree is illustrated in figure 3 which identifies the major components of the system that will contribute to the integrity and continuity risks.

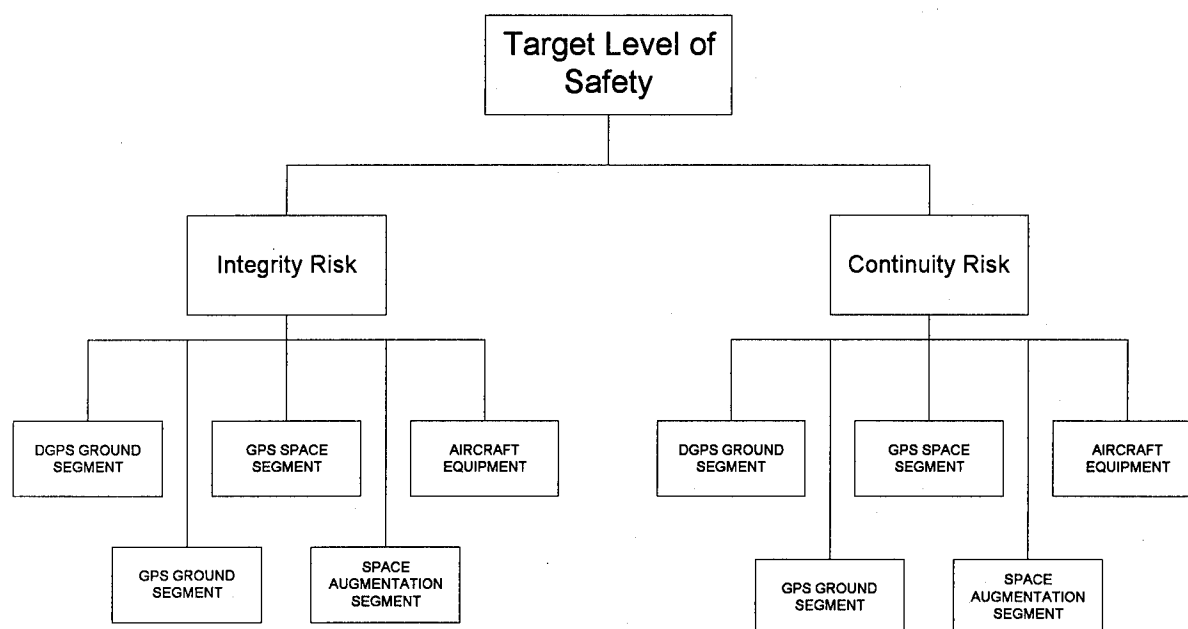


Figure 3 Top Level Fault Tree

After developing the fault trees they were used to undertake a top-down analysis of risk apportionment for each of the lower level events base on the RNP requirements. This allows performance requirements to be imposed on each element of the system.

It was originally proposed to carry out a similar bottom up analysis making use of knowledge of the reliability of existing system components to illustrate the levels of integrity and continuity achievable. This

analysis has not been feasible at this time due to the lack of representative performance

PRESENTATION TO ATC

In addition to the transmission of data to aircraft it is also necessary to provide system information to Air Traffic Control Staff. Airspace planning must take into account the ongoing changes in the satellite constellation. On a relatively long timescale such

changes come about as old satellites are taken out of service and replaced by new ones. In the shorter term changes come about when satellites are taken out of service for maintenance or when a satellite develops a malfunction. For planned maintenance considerable warning times may be available such that Air Traffic Control (ATC) could adjust some of its operations in order to minimise the impact of an outage. This is only a realistic possibility if a reliable notification system is in place. An assessment of the current sources of information provided on the constellation changes indicates that these cannot be relied upon to form the basis of a warning system for ATC.

In the case of a malfunction there may be no significant warning but it could still assist ATC if the monitoring system identifies the malfunction and warns the control centre of the potential impact of such a failure. The response of ATC may be to increase separations, re-route aircraft or simply advise pilots of the situation.

The presentation of information to active controllers may need to be different to that for the airspace planner who has more time to assess the implications. Initial discussions on this subject have raised a number of questions, the answers to which may help to identify the optimum presentation method.

An important consideration is the proportion of outages that are planned versus unplanned. If the majority of outages are planned then it becomes important to have an effective system of notification. The planned outages must be controlled so that suitable warning time is given and the predicted outages will occur at the times specified. The consequences of an outage for any region can then be investigated using a simulator. A problem arises when considering different airborne architectures. The effect on a system with barometric or inertial aiding will be different than that on a stand alone receiver. It will be necessary to group effects into a small number of architectures or assume a worst case equipment fit. It will not please airlines who have spent money equipping with sophisticated equipment if they find themselves restricted because of worst case assumptions on the part of the controlling authorities. These questions are currently being addressed by the UK CAA and results will be published in the near future.

CONCLUSIONS

This paper has described a three part study currently being undertaken to investigate GPS monitoring and display systems and their ability to fulfil the RNP for en-route navigation. The data collection at Heathrow

is still underway and analysis will be carried out shortly. The fault tree analysis has resulted in the preparation of a number of Fault Trees whose complexity make it impossible to present at this forum. Initial assessment appears to suggest that the continuity of service requirements are likely to be more stringent than the integrity requirements. The investigation into methods of presenting information to ATC has opened up a significant area of work that is currently under consideration and this information will be published when completed.

ACKNOWLEDGEMENTS

The authors would like to express their gratitude for all the assistance received on this project. British Airways allowed us to make use of their operational aircraft to carry evaluation equipment and provide flight data. Rolf Johansson of Lambourne Navigation has provided constructive support in discussions about GPS outages and how to illustrate them to ATC.

Integrating WAAS with LAAS to Avoid Signal Spoofing

Dr. Vis Sankaran and Donald Benson
Dynamics Research Corporation

BIOGRAPHIES

Vis Sankaran and Donald Benson are Systems Analysis Engineers at Dynamics Research Corporation where they are involved in marine applications of GPS. Dr. Sankaran and Mr. Benson identified several potential problems with real-time tactical GPS computer algorithms and provided the necessary information for their resolution prior to becoming costly problems in the fleet. Dr. Sankaran received a dual B.S. degree in Physics and Electrical Engineering from India, M.S. in Electrical Engineering from the University of Waterloo, Canada, and Ph.D. in Information and Control Sciences from Southern Methodist University. Mr. Benson received B.S. degree in Physics and M.S. in Aerospace Engineering, both from Massachusetts Institute of Technology.

ABSTRACT

The purpose of this paper is to show how a system satisfying strictest aviation requirements can be made immune to terrorist spoofing. The system combines Wide Area Augmentation System (WAAS) and Local Area Augmentation System (LAAS). It also uses secured independent signals for WAAS accuracy corrections that was recommended by Joint Program Office (JPO).

WAAS is on the verge of becoming a full-scale development program for the Federal Aviation Administration (FAA) and was planned to be operational by 1997. However, national security concerns regarding the broadcast of GPS accuracy corrections on a global scale for WAAS was the subject of considerable discussions during early 1995. JPO has recommended "GPS dual use opportunities," with secured independent WAAS uplink. In addition, WAAS can meet aviation requirements for all phases of flight down to CAT I precision approaches. But to get

the requirements for CAT II/III precision approaches and landing (PAL), local area differentials are needed for augmenting with GPS. The concept, referred to as LAAS within the FAA, has been recommended as an additional augmentation. Here the differential technique is to locate a GPS monitor receiver at a surveyed reference site in the vicinity of an airport. The data is processed on the ground to determine pseudo-range corrections of GPS signals which are sent to the airborne receiver over a data link. By combining both WAAS and LAAS concepts, advantages of both systems could be merged for avoiding signal spoofing.

This paper describes a conceptual development and integration of WAAS with LAAS to avoid signal spoofing for aviation requirements. Recommended configurations and generic specifications for interfacing WAAS, recently presented by JPO, with LAAS concept currently in study will be presented. In addition, how terrorist spoofing of the unsecured signals from the local area could be avoided by using the secured wide area signals will be discussed. A difference monitoring with a threshold will be provided. Finally, benefits of the integration concepts to provide uniformity in products regardless of manufacturer will be discussed.

INTRODUCTION

In order to meet both civil and military radionavigation needs, the Federal Government has established a series of radionavigation systems over a period of years [1 - 3]. Each system utilized the latest technology available at the time it was introduced. The new high-technology radionavigation system, the Global Positioning System (GPS), has wide civil as well as military application on a global basis. Developed by the Department of Defense, Full Operational Capability (FOC) of the GPS for radionavigation purposes was declared in April 1995.

For aviation, GPS FOC represents the most significant development in 50 years. However, GPS alone cannot meet all the requirements of worldwide civil aviation. It needs augmentation services offering unprecedented accuracies for positioning and stand-alone navigation for aviation users [4-5]. The need to augment GPS and the desire to provide GPS user services as quickly as possible has resulted in FAA's Wide Area Augmentation System (WAAS) [6]. WAAS provides three aviation requirements critical to safety of flight (integrity, accuracy, and availability) that are lacking in GPS. However, WAAS can not meet the requirements for all phases of flight. It can meet flight down to category I precision approaches only. The requirements for the different phases of flight are being evaluated by FAA specifically for the WAAS. Analyses, computer simulations, and testing have already started. WAAS Initial Operational Capability (IOC) is expected in 1997.

To satisfy the requirements for Category II and III precision approaches and landing, local area differential GPS (LADGPS) corrections are needed for augmenting with GPS. The concept referred to as Local Area Augmentation System (LAAS) within the FAA has been recommended as an additional augmentation [7]. Here the differential technique is to locate a GPS monitor receiver at a surveyed reference site in the vicinity of an airport. This concept is being developed and flight tests are being performed to verify the feasibility. LAAS development phase is expected in 1996.

During early 1995, some security concerns raised by DOD to broadcast wide-area differential corrections in an unprotected form was the subject of debate between DOD and DOT. Several rounds of meetings between DOD and DOT officials produced a tentative agreement that will allow FAA to move forward with its WAAS design and procurement. The agreement is classified. DOD will not interpose itself further in the WAAS process, pending the outcome of tests of techniques that would allow DOD to selectively jam the WAAS signal in military theaters or other regions of security concerns [8].

In this paper, we describe the civil aviation requirements, following which we describe a conceptual development and operational plan for both WAAS and LAAS. Then, jamming and signal spoofing, which are a subject of considerable debate, are discussed. We show that the LAAS spoofing is the most critical spoofing issue. JPO recommendation, "GPS Dual Use Opportunities," [9] with secured independent WAAS uplink is provided as an example to avoid LAAS signal spoofing. A conceptual design architecture that

integrates WAAS and LAAS systems to avoid LAAS signal spoofing for aviation requirements is discussed. Finally, benefits of the integration concepts to provide uniformity in products by selecting Non Developmental Items (NDI) and Commercially available Off The Shelf (COTS) products will be discussed.

AVIATION REQUIREMENTS

GPS, a satellite-based radionavigation system operated by the DOD and jointly managed by the DOD and DOT, provides two levels of service: a Standard Positioning Service (SPS) and a Precise Positioning Service (PPS). While SPS accuracy can be better than 30 meters (2 drms), with the activation of Selective Availability (SA) that accuracy is degraded to 100 meters (2 drms) for civil users. Nevertheless, GPS provides all-weather global coverage, 24 hours a day at unprecedented accuracies. PPS provides 22 meters (2 drms) accuracy to U.S. and allied military and U.S. Federal Government users. Yet even GPS, with its remarkable accuracies, still does not meet aviation requirements. By Augmenting GPS with other services, called Augmented GPS (AGPS), to satisfy integrity, accuracy, and availability, GPS will meet the aviation requirements. Table 1 outlines the accuracies of GPS services verses aviation requirements.

TABLE 1. Accuracy of GPS Services Vs Aviation Requirements

| | | Aviation Requirements | | |
|------------|-------------------|--|---------------------------|----------------------------------|
| | | En Route through Non-Precision Landing | Precision Landing CAT I | Precision Landing CAT II/III |
| Services | Accuracy (meters) | > 100 m | Hor: 17.1 m Ver: 4.1 m | Hor: 4.1-5.2 m Ver: 0.6-1.7 m |
| SPS | 100 | YES | NO | NO |
| SPS w/o SA | 30 | YES | NO | NO |
| PPS | 22 | YES | NO | NO |
| AGPS | < 10 | YES | YES | YES |

Aviation requirements are described in two basic phases: en route/terminal and approach/landing. The en route/terminal phase includes all portions of flight to within 18,500 meters (10 nm) of the runway. It includes oceanic, domestic, and terminal subphases. The approach/landing phase includes that portion of flight conducted prior to touchdown. The navigation and positioning requirements for aviation are summarized in Table 2.

Table 2. Aviation Navigation and Positioning Requirements

| Aviation Category | Accuracy (2 drms) | Time to Alarm | Availability | Coverage Altitude |
|------------------------------------|---------------------------|---------------|--------------|-------------------|
| En Route Oceanic | 23 km (12.6 nm) | 30 seconds | 99.977% | 8400-12,200 m |
| En Route Domestic | 1000 m | 10 seconds | 99.977% | 150-18,300 m |
| Terminal | 500 m | 10 seconds | 99.977% | 150-5500 m |
| Approach/Landing Non-Precision | 100 m | 10 seconds | 99.977% | 75-900 m |
| Approach/Landing Precision CAT I | Hor: 17.1 m Ver: 4.1 m | 6 seconds | 99.999% | 30-900 m |
| Approach/Landing Precision CAT II | Hor: 5.2 m Ver: 1.7 m | 2 seconds | 99.999% | 15-900 m |
| Approach/Landing Precision CAT III | Hor: 4.1 m Ver: 0.6 m | 2 seconds | 99.999% | 0-900 m |

Since Aviation requirements are only met by augmentations, it is no wonder that aviation users are clamoring for immediate augmentation implementation. Therefore, Federal Aviation Administration (FAA), in cooperation with other DOT organizations and DOD, is planning to augment the GPS SPS with both a wide area and a local area system, called WAAS and LAAS, respectively.

WAAS AND LAAS CONCEPTS

The current 24 GPS operational satellites alone cannot satisfy the aviation stringent requirements. It fails to meet three requirements critical to safety of flight:

1. Integrity: The ability of a system either to provide timely warnings to users or to shut itself down when it should not be used for navigation.
2. Accuracy: The difference between the measured position at any given time to the actual or true position.
3. Availability: The ability of a system to be used for navigation whenever it is needed by the users, and its ability to provide that service throughout a flight operation.

The need to augment GPS and the desire to approve or provide user services as quickly as possible has resulted in FAA's augmentation strategy, WAAS and LAAS.

Initial analyses and testing by FAA determined that a wide area broadcast system would require about 24 Wide-area Reference Stations (WRS) and transponders on several Geostationary (GEO) satellites. Figure 1 shows a conceptual WAAS architecture in developmental stage. The WAAS will be a safety-critical system consisting of the equipment and software

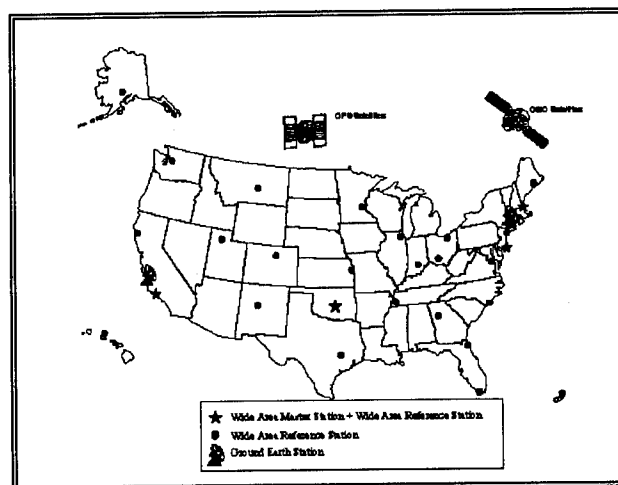


Figure 1. WAAS Architecture

which augments the GPS SPS. It will provide a signal in space to WAAS users with the specific goal of supporting aviation navigation for en route through Category I precision approach phases of flight. The signal in space will provide three services: (1) integrity

data on GPS and GEO satellites, (2) wide area differential corrections for GPS satellites, and (3) an additional ranging capability.

The GPS satellites' data is to be received and processed at widely dispersed sites, referred to as WRS. These data are forwarded to data processing sites, referred to as Wide-area Master Stations (WMS), which process the data to determine the integrity, differential corrections, residual errors, and ionospheric information for each monitored satellite and generate GEO satellite navigation parameters. This information is to be sent to a Ground Earth Station (GES) and uplinked along with the GEO satellites. These GEO satellite will then downlink this data on the GPS Link I (LI) frequency with a modulation similar to that used by GPS.

In addition to providing GPS integrity, the WAAS will verify its own integrity and take any necessary action to ensure that the system meets the WAAS performance requirements. The WAAS also has a system operations and maintenance function that provides information to FAA's National Airspace System (NAS) personnel.

The WAAS user receiver will process: (1) the integrity data to ensure that the satellites being used are providing in-tolerance navigation data, (2) the differential correction and ionospheric information data to improve the accuracy of the user's position solution, and (3) the ranging data from one or more of the GEO satellites for position determination. The WAAS user receivers are not considered part of the WAAS.

FAA has been testing the use of WAAS and initial operational capability (IOC) is expected in 1997. Once these WAAS services are available, some of the benefits to the aviation community will include increased fuel savings as a result of more direct user preferred routing, and improved safety for non-precision approaches, and approach course guidance at airports. As users equip and implement WAAS, the FAA's ground based infrastructure will be reduced thus avoiding expenditures for replacement systems and maintenance costs for those systems. Currently many aviation navigation aids are used. Among them Instrument Landing System (ILS) and Microwave Landing System (MLS) are primarily used for instrument precision landing and approaches. As shown in Figure 2, they will remain to be the only precision landing system in the near future. Other benefits of WAAS include Automatic Dependent Surveillance (ADS) and traffic alert and collision avoidance. Using ADS, aircraft will report position, identification, and speed every second, thus reducing the chance of surface conflicts and runway

incursions. Finally, FAA will develop standards for cockpit moving maps, called as Electronic Chart Display Information System (ECDIS).

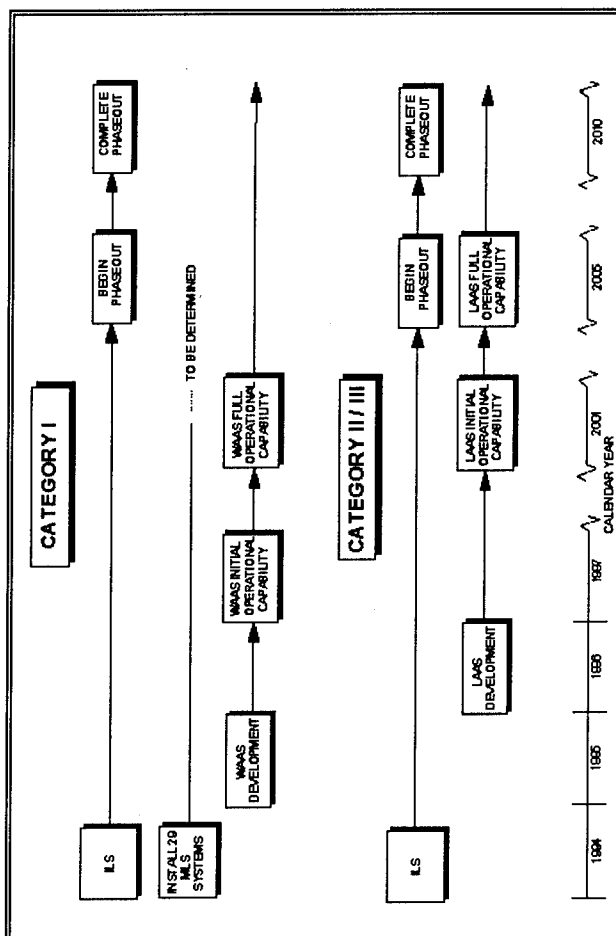


Figure 2. Operating Plan for Precision Landing Systems

Presently, the ILS ground-based system is the only system used to support CAT II/III operations. GPS without proper LADGPS augmentation cannot support CAT II/III operations. GPS can be augmented by a Local Area Augmentation System (LAAS) that will improve the integrity, accuracy, and availability of GPS-based satellite navigation for all categories of precision approaches. The most commonly used differential technique is to locate a GPS monitor receiver at a surveyed reference site in the vicinity of an airport. The data is processed on the ground to determine pseudo-range corrections of GPS signals which are sent to the airborne receiver over a data link. These corrections enable the GPS avionics to calculate a more precise position than is possible using GPS signals alone. The

ground monitor can also provide integrity information to notify the user of a system fault and the same data link could also provide ranging information to increase availability.

LAAS concept is being developed and flight test are being performed to verify the feasibility. LAAS development phase is expected in 1996. Again, Figure 2 shows the operating plan for precision landing systems, CAT I and CAT II/III.

Tables 3-5 show the current status of WAAS and LAAS comparisons for aviation requirements based on results of the tests [10-12] for the three critical areas. Table 3 is for the en route through non-precision landing phase, Table 4 is for precision landing CAT I phase, and Table 5 is for the precision landing CAT II/III phase.

Table 3. WAAS Vs LAAS Comparison for En Route Through Non-Precision Landing Phase of Aviation

| | Critical Areas | | |
|-------------|----------------|----------|--------------|
| | Integrity | Accuracy | Availability |
| WAAS | YES | YES | YES |
| LAAS | N/A | N/A | N/A |

Table 4. WAAS Vs LAAS Comparison for Precision Landing CAT I Phase of Aviation

| | Critical Areas | | |
|-------------|----------------|----------|--------------|
| | Integrity | Accuracy | Availability |
| WAAS | YES | YES | YES |
| LAAS | YES ? | YES ? | YES ? |

? Technically achievable; Feasibility to be verified

Table 5. WAAS Vs LAAS Comparison for Precision Landing CAT II/III Phase of Aviation

| | Critical Areas | | |
|-------------|----------------|----------|--------------|
| | Integrity | Accuracy | Availability |
| WAAS | YES | NO | YES |
| LAAS | YES ? | YES ? | YES ? |

? Technically achievable; Feasibility to be verified

JAMMING AND SPOOFING

WAAS and LAAS, will provide accuracies of 1-5 meters verses GPS SPS accuracies of 100 meters. Therefore, aviation application employing augmentations will be much more sensitive than those applications using basic GPS SPS. As stated earlier this accuracy is critical to safety of flight. The controversy between DOD and FAA in the early part of 1995 was primarily due to the fact that DOD was concerned with potential for misuse of widely broadcast differential corrections without any protection. Specifically, proper countermeasures should be developed to jamming and spoofing.

The term "jamming" refers to intentional and unintentional radio frequency (RF) interference of transmitted signals received by a user. The term "spoofing" refers to the transmission of counterfeit signals to provide undetectable falsification of service.

Unintentional jamming includes known RF sources that coincidentally interfere with the GPS or AGPS signal. Typical sources that can unintentionally interfere with GPS or AGPS systems include mobile communication systems and television station transmitters.

Intentional jamming and spoofing sources include signals deliberately transmitted to interfere with the GPS or AGPS signal. The objective of an intentional jammer or spoofer is to cause havoc in system applications resulting in total denial or mistrust of the system. Jamming and spoofing can be accomplished using information from open literature which defines signal format and data structure and off-the-shelf hardware and software. Persons or groups who might

want to intentionally jam or spoof GPS or AGPS systems would include hackers, extortionists, and terrorists.

The GPS uses a spread spectrum signal design which provides some inherent resistance to jamming. Spread spectrum signals provide a means for a receiver to enhance the power of a GPS signal spread over a given frequency band, while conversely dispersing a high power jamming signal transmitted at a given frequency. Therefore, intentional jamming is a complicated process. However spoofing is somewhat simplified process. There are two kinds of spoofing: GPS SPS spoofing and AGPS spoofing.

To spoof GPS SPS, a spoofer must emulate a GPS signal and capture users within a specific target area. Spoofer power must be high enough to ensure this capability. Additionally, capturing a GPS receiver requires that the spoofer's code phase coincide with the time of arrival of the code phase of the real GPS satellite at the user location. Due to this time-of-arrival constraint, normal expectation are that a spoofer would only spoof one satellite at a time. Also GPS SPS spoofing is somewhat complicated.

However, GPS augmentations rely on some type of differential GPS link. Therefore, spoofing AGPS may be more effective than spoofing GPS SPS. This is particularly true for local area DGPS (LADGPS) systems. The spoofer would replicate and transmit a LADGPS signal with falsified data to users in the surrounding area. Further, unlike GPS SPS, no time-of-arrival complexities are involved since the LADGPS signal does not require code phase synchronization. Also, WAAS has ranging capability, and therefore, the same time-of-arrival constraints as those identified for GPS SPS would apply for WAAS spoofing. Thus the primary jamming and spoofing issue is to avoid the LAAS spoofing.

DOT's January 1994 Strategic Plan has established the goal to promote safe and secure transportation. To meet this objective, the plan specifies that DOT will identify and implement new measures to enhance security on all modes of transportation to achieve personal security and national security goals.

DUAL USE OPPORTUNITIES

JPO director, COL. Mike Wiedemer, in his ION GPS-94 presentation sketched out several additional no-cost opportunities for dialogue about dual-use system: joint policy on management and control of precise navigation

signals, joint definition of WADGPS signal architecture, and joint exploration of advanced over-the-air integrity systems. This was a strawman proposal designed to stimulate conversation within the DOD and the DOT about joint investment. It looks like this would save hundreds of millions of dollars if this investment is undertaken. The WAAS joint program is called the extended WAAS system. This has wider support, since it is a joint investment program, involving both civil and military users. [13,14]

It describes a common geostationary communication link and architecture, a "bus," that would be shared by civil and DOD users, with a separate operational control facilities. A couple of new design twists include the capability for encryption of the wide-area differential GPS corrections and an offset of 10.3 MHz from the main GPS L1 frequency on which the WAAS messages are sent. Once the word encryption is mentioned, it is often associated with some war-fighting mode designed for meeting the security concerns. In this particular case, that is not it at all. On the contrary, it is to avoid "spoofing," and for aviation it is for safety of flight.

CONCEPTUAL DESIGN ARCHITECTURE FOR INTEGRATING WAAS AND LAAS

As discussed earlier, the FAA has developed and is testing both WAAS and LAAS programs to provide real-time aviation positioning and navigation accuracy shown in Table 2. WAAS provides accuracy to all phases down to precision landing category I and LAAS provides precision landing category II/III. Both are needed, but at any time only one is needed. So both can be integrated in one unit or box to provide the aviation requirements. Also security is one issue which has not been explored in detail. Some of the questions one should consider are:

1. Should both WAAS and LAAS be encrypted?
2. Will there be operator error during precision landing if LAAS is encrypted?
3. Can both WAAS and LAAS be integrated?

The answer to all these questions is yes.

On the first question, FAA wants to identify and implement security on all modes of transportation to achieve security and safety of flight. Therefore, both WAAS and LAAS should be encrypted.

On the second question, there could be operator error decoding the LAAS encryption during precision landing

category II/III due to lack of time. Also using the wrong encryption key could contribute to the error.

On the third question, since at any time only one system is needed, they could both be integrated in one unit to take advantage of both.

As discussed earlier, the first two questions limit the aviation requirements and causes additional burden during precision landing phase. A mitigating factor to these two questions is the fact that both WAAS and LAAS could be integrated in one unit or box. Some benefits by integration are LAAS could primarily be used to meet the accuracy requirement of the flight and WAAS still could be used for integrity and availability enhancements. Also only WAAS has to be encrypted and by differencing the WAAS and LAAS data, the LAAS could be monitored to avoid spoofing. Since WAAS covers a wider area, encryption on WAAS is a better choice. Further, JPO has a strawman proposal for dual use opportunities where the WAAS signals are encrypted separately for both DOD and DOT. Again, LAAS spoofing is the more vulnerable spoofing of the AGPS spoofing. Though it is early to provide the difference threshold level, based on test results, a threshold of 1 - 3 meters should be considered.

At this writing, AGPS hardware and software are not available in a single unit or box that can integrate both configurations. As indicated before, WAAS primarily used to find the flight location and LAAS primarily used for flight landing. Therefore, we refer to this unit as a Flight Locator and Lander (FLL) hereinafter. Recommendations for FLL are the following:

FLL should use NDI and COTS technology. GPS receivers and differential corrections are easy and economical to build in one box. Also all of the differential corrections are in standard RTCM SC-104 or RTCA formats so that a wide variety of GPS receivers can be integrated. Therefore, it is suggested that integrating WAAS and LAAS in one unit with differences between each used to counteract LAAS spoofing.

FLL should be able to operate with one internal or one external battery power, or combination of both. Additional external backup power supply system should also be developed.

FLL should be capable of interfacing with any personal computer, printer, and display terminal.

FLL should have a large mass storage device so that all data can be stored for future processing and analysis.

Finally, test and evaluate the hardware and software developed so that a comprehensive and appropriate decision could be made for all aviation implementation. This should include extensive data collection at various places so that the results could be analyzed scientifically. Evaluation should include current compatibility and future enhancement easy and simple to implement. In short, the conceptual design architecture is practical, with extensive applications and future charters for the aviation.

SUMMARY AND CONCLUSIONS

Fitting GPS and Augmentation services (WAAS and LAAS) into current and future worldwide aviation efforts will require considerable skill and coordination. A joint investment effort is needed among DOD and DOT in order to simultaneously satisfy both parties requirements at a minimum expense. When you attempt to optimize one solution set, you are probably not going to satisfy every user completely.

This paper has discussed some issues associated with GPS and augmentation services. Specifically, we started with the civil aviation requirements, which can only be satisfied by augmentation technique. Two augmentations, WAAS and LAAS, were discussed and current status provided. Some of the security concerns on jamming and spoofing were addressed. We showed that LAAS spoofing is the most critical spoofing issue. Finally, how spoofing can be avoided by integrating both WAAS and LAAS for aviation requirement was discussed. This integration provides the benefit of providing uniformity in using COTS products and NDI items, regardless of manufacturer. Further DOD/DOT study, design, and testing is required.

ACKNOWLEDGMENTS

The authors would like to thank Dr. George Koehler, Mr. Herbert Sandberg, and Mr. Alan Zorn for comments provided to clarify and focus the paper. The authors would also like to thank Mr. John Enright for advice and support.

REFERENCES

1. 1994 Federal Radionavigation Plan, DOD/DOT, US Government Publication, May 1995.

2. Kruh P., et al, A Strategy for Buildup to the Operational NAVSTAR/GPS Constellation, Proceeding of the Institute of Navigation/National Aerospace Conference, March 1983.
3. Nelson A., Civil Standardization of the Global Positioning System for the Aviation Community, Presented at IEEE PLANS 92 Conference, April 1992.
4. A Technical Report to the Secretary of Transportation on a National Approach to Augmented GPS Services, Institute for Telecommunication Sciences (ITS) Report, December 1994.
5. Loh Robert, Seamless Aviation: FAA's Wide Area Augmentation System, GPS World, April 1995.
6. Till Robert, Wanner William, and Loh Robert, "FAA's Wide Area Augmentation System (WAAS) Test Concepts for Early Implementation," Proceeding of ION-GPS-94, September 1994.
7. "Local Area Augmentation System (LAAS Quarterly Review," FAA SATNAV Program Office, RTOA Paper No. 422-94, 1994.
8. "Washington View," GPS World, January - July 1995.
9. COL. Wiedemer Mike, "GPS Dual Use Opportunities," Proceedings of ION GPS-94, September 1994.
10. Wulschleger Victor, et. Al., "FAA's Wide Area Augmentation System (WAAS) Summary of Ground & Flight Test Data," Proceeding of ION-GPS-94, September 1994.
11. Walter Todd, et. al., "Flight Trials of the Wide Area Augmentation System (WAAS)," Proceeding of ION-GPS-94, September 1994.
12. Casewell Ian, et. al., "A European Wide Area DGPS Experiment: Final Results," Proceeding of ION-GPS-94, September 1994.
13. "Face to Face: COL. Mile Wiedemer, Director, GPS Joint Program Office," GPS World, April 1995.
14. "The Global Positioning System: Charting the Future Summary Report," NAPA and NRC Report, May 1995.

Exact Formula For User Range Error in Wide Area Differential GPS

Henry Beisner
Consultant, Paradeigma, Inc.

Arthur Dorsey
Loral Federal Systems

BIOGRAPHIES

Dr. Henry M. Beisner is a consultant to Loral Corporation developing differential GPS navigation systems. He is president of Paradeigma, Inc., consulting in applied physics, signal processing and analysis. He has had nine years of experience with IBM developing the GPS Control Segment. He characterized satellite clock error and demonstrated system estimation of orbits and clock biases from measurements. He proved the validity of the Control Segment coordinate system, developed the orbit integrator standard, monitored GPS system user navigation error and demonstrated that the GPS system met the user navigation error specification. He received a Ph.D., in physics from the Ohio State University and is author of a number of papers in the field of navigation.

Dr. Arthur J. Dorsey is an advisory engineer in the Loral Air Traffic Control division involved in radar surveillance algorithms. His direct responsibility is the design and development of multiple-sensor tracking and radar registration algorithms. From 1981 to 1985, Dr. Dorsey was with the IBM Federal System division and involved in the design, development and field deployment of the Global Positioning System Control Segment. His direct responsibility was the design and development of a real-time Kalman filter to estimate the satellite position and clock. For his work, Dr. Dorsey was awarded the IBM Outstanding Technical Achievement Award in 1984. Dr. Dorsey received a BS (1974), an MS (1978) and a PhD (1983) degree in Electrical Engineering from the University of Maryland.

ABSTRACT

A wide area differential GPS system is defined with GPS satellite orbits and a network of reference station locations. For routinely attained GPS ephemeris accuracies, a Service Volume Model shows that the

ephemeris component of user range error is negligible. Given such GPS ephemeris accuracies and a subset of satellites observed by all reference stations, an exact expression is derived for the covariance matrix of the reference station and satellite clock biases. The clock covariance matrix is used to derive an exact expression for user range error:

$$\sigma_{URE} = \frac{\sigma_{Meas.}}{\sqrt{M}}$$

where $\sigma_{Meas.}$ is the pseudorange measurement error and M is the number of reference stations. This establishes a lower bound on user range error. Expressions are derived for: reference station and satellite clock bias estimation errors, time transfer error to a user, and time transfer error to a surveyed user.

INTRODUCTION

The Global Positioning System (GPS) [Logsdon,1992; Hofmann-Wellenhof,1993; DOD,1993], having become fully operational (including Selective Availability (SA) [Braasch,1990]), provides the civil community with the basis for developing differential GPS systems. Such differential GPS systems can provide increased navigational accuracy by nullifying the effects of SA. One such system, developed by the Jet Propulsion Laboratory, provides geodetic survey position accuracies to centimeter levels [Yunk,1993].

Two distinctly different differential GPS systems are being developed: Local Differential GPS (LDGPS) and Wide Area Differential GPS (WADGPS). The LDGPS employs a Reference Station (RS), at a known location, to measure the GPS signal and obtain a position fix. The resulting differences between the RS known and calculated positions is a measure of the error in the received GPS signal. The LDGPS system transmits this error to a local user (within 100 miles or so from the RS) who can, then, correct his GPS location to meter accuracy.

Alternately, the WADGPS [FAA,1994; Kee,1991; Kee,1994; Loh,1994; Phlong,1993; Mueller,1994] employs numerous reference stations placed within a Service Volume spaced several hundred miles from one another. To attain accuracies approaching those of LDGPS over a wide area, the GPS data received from all the RS's must be condensed to a single signal. This signal must, then, be transmitted within required time constraints to all users within the Service Volume, along with indicators of signal quality.

To attain the desired accuracies in WADGPS, various models have been developed to interpolate and extrapolate the corrections at the RS's throughout the Service Volume. WADGPS performance depends to a large degree on the validity of these models.

As a WADGPS system is designed and developed, one desires "rules of thumb" of navigational accuracy to aid the various system trade-offs. The objective of this paper is to develop such "rule of thumb" formulas for User Range Error (URE). The results are based on a rigorous derivation of system clock errors and serve as an absolute lower bound on navigation error. The formulas were validated using a sophisticated Service Volume Model, employing covariance analysis.

URE depends on three error sources: Satellite (SV) ephemeris error, SV clock estimation error and SV clock dither prediction error, i.e., Selective Availability (SA) [Braasch,1990; Kee,1991; Kee,1994]. The SV ephemeris and SV clock errors are separable in WADGPS, given their widely distinct time constants. The SV ephemeris error is on the order of 15 minutes, while SV clock error is on the order of a second. The SV clock dither prediction error, although a challenging problem in itself, can be easily separated from SV ephemeris and SV clock estimation errors.

Although complex, the estimation of GPS SV ephemerides is a well understood science, once the SV clocks [Beisner,1980] have been removed from the problem. The contribution of the network of SV and RS clocks to the WADGPS navigation error is not so clear, however. The derivation presented below reveals the workings of the network of clocks and provides an exact measure of the effect of the clock errors on URE performance. This also gives a lower bound on user range error.

PROBLEM FORMULATION

Given a set of Reference Stations (RS's), satellites (SV's) and the pseudorange measurements between them,

one can estimate the SV ephemeris and SV and RS clock biases [Kee,1994; Johnson,1995]. The instantaneous pseudorange measurement from the n -th SV to the m -th reference station can be written as:

$$\rho_{mn} = \sqrt{(\vec{r}_n - \vec{R}_m)^2} + c\tau_m - ct_n + \eta_{mn}$$

where \vec{r}_n is the earth centered inertial (ECI) position of SV n , \vec{R}_m is the ECI location of reference station m , c is the velocity of light, τ_m is the bias of the reference station clock, t_n is the bias of the SV clock and η_{mn} is the measurement error.

Linearize the SV ephemeris about a reference trajectory \vec{r}_{nREF} by defining

$$\Delta\vec{r}_n = \vec{r}_n - \vec{r}_{nREF}$$

and

$$r_{mnREF} = \sqrt{(\vec{r}_{nREF} - \vec{R}_m)^2}$$

Assume that N GPS SV's can be observed by M reference stations. For the pseudorange measurement vector, ρ , of the form:

$$\rho = (\rho_{11}, \rho_{12}, \dots, \rho_{1N}, \rho_{21}, \rho_{22}, \dots, \rho_{2N}, \dots, \rho_{M1}, \rho_{M2}, \dots, \rho_{MN})^T$$

and the SV ephemeris and clock bias vector, x , of the form:

$$x = c(\tau_1, \tau_2, \dots, \tau_M, t_1, t_2, \dots, t_N, \Delta\vec{r}_1, \Delta\vec{r}_2, \dots, \Delta\vec{r}_N)^T$$

where T denotes transpose, we define the measurement partial derivative matrix, H as follows:

$$H = \frac{\partial \rho}{\partial x}$$

One may now write, in vector form,

$$\rho = r_{REF} + Hx + \eta$$

Following classical least squares [Bierman,1977; Kee,1994; Johnson,1995; Gelb,1974], one can estimate the SV ephemeris and clock biases, \hat{x} , by minimizing

$(\hat{\rho} - \rho)^2$ over \hat{x} , where (\dots) means expected value. and

$$\hat{\rho} = r_{REF} + H\hat{x}$$

The resulting SV ephemeris and clock bias estimator has the form:

$$\hat{x} = [H^T H]^{-1} H^T (\rho - r_{REF})$$

The associated SV ephemeris and clock covariance matrix, Ξ , has the form:

$$(\hat{x} - x)(\hat{x} - x)^T = \Xi = \sigma_{Meas.}^2 [H^T H]^{-1} \quad (1)$$

where $\sigma_{Meas.}$ is the root-mean-square of the measurement errors:

$$\sigma_{Meas.}^2 = \frac{1}{MN} \sum_{m=1}^M \sum_{n=1}^N \eta_{mn}^2$$

The User Range Error (URE) has the form [DOD, 1993]:

$$\sigma_{URE}^2 = \frac{Tr\{K_p \tilde{H} \Xi \tilde{H}^T K_p^T\}}{Tr\{K_p K_p^T\}} \quad (2)$$

where \tilde{H} is the partial derivative matrix of the user's pseudorange measurements and the position estimator K_p matrix (as defined in [DOD, 1993]) maps the user's pseudorange measurements onto his location estimate.

The expression for URE is complex, involving the estimation accuracy of the SV ephemeris and SV clocks and the projection of those components onto each user location in the Service Volume. We used the Loral Service Volume model to evaluate URE and found that the influence of the ephemeris error on URE was small. This observation lead to the result of this paper, i.e., that a simple lower bound for URE can be derived, based only on the SV and RS clock errors.

CLOCK COVARIANCE MATRIX

Assuming that SV ephemeris, \tilde{r}_n , errors are sufficiently small to have a negligible effect on user range error, the SV clock bias vector has the form:

$$x = c(\tau_1, \tau_2, \dots, \tau_M, t_1, t_2, \dots, t_N)^T$$

and the measurement partial derivative matrix, H has the form:

$$H = \frac{\partial \rho}{\partial x} =$$

| | τ_1 | τ_2 | \dots | τ_M | t_1 | t_2 | \dots | t_N |
|-------------|----------|----------|---------|----------|-------|-------|----------|-------|
| ρ_{11} | 1 | | | | -1 | | | |
| ρ_{12} | 1 | | | | | -1 | | |
| \vdots | \vdots | | | | | | \ddots | |
| | 1 | | | | | | | -1 |
| ρ_{1N} | 1 | | | | | | | -1 |
| ρ_{21} | | 1 | | | -1 | | | |
| ρ_{22} | | 1 | | | | -1 | | |
| \vdots | \vdots | | | | | | \ddots | |
| | | 1 | | | | | | -1 |
| ρ_{2N} | | 1 | | | | | | -1 |
| \vdots | | | \dots | | | | \dots | |
| ρ_{M1} | | | | 1 | -1 | | | |
| ρ_{M2} | | | | 1 | | -1 | | |
| \vdots | | | | \vdots | | | \ddots | |
| | | | | 1 | | | | -1 |
| ρ_{MN} | | | | 1 | | | | -1 |

Define the clock portion of the pseudorange to be

$$\rho'_{mn} = \rho_{mn} - \sqrt{(\tilde{r}_n - \tilde{R}_m)^2}$$

Then, in vector form,

$$\rho' = Hx + \eta$$

Define \hat{x} to be an estimate of x giving an estimate of ρ' :

$$\hat{\rho}' = H\hat{x}$$

Then the clock bias estimate has the form:

$$\hat{x} = [H^T H]^{-1} H^T \rho'$$

and the associated clock covariance matrix, Ξ , has the form:

$$(\hat{x} - x)(\hat{x} - x)^T = \Xi = \sigma_{Meas.}^2 [H^T H]^{-1} \quad (3)$$

where

$$H^T H =$$

| | τ_1 | τ_2 | \cdots | τ_M | t_1 | t_2 | \cdots | t_N |
|----------|----------|----------|----------|----------|----------|----------|----------|----------|
| τ_1 | N | | | | -1 | -1 | \cdots | -1 |
| τ_2 | | N | | | -1 | -1 | \cdots | -1 |
| \vdots | | | \ddots | | \vdots | \vdots | \cdots | \vdots |
| τ_M | | | | N | -1 | -1 | \cdots | -1 |
| t_1 | -1 | -1 | \cdots | -1 | M | | | |
| t_2 | -1 | -1 | \cdots | -1 | | M | | |
| \vdots | \vdots | \vdots | \vdots | \vdots | | | \ddots | |
| | -1 | -1 | \cdots | -1 | | | | M |
| t_N | -1 | -1 | \cdots | -1 | | | | M |

This matrix can be expressed in a spectral [Gantmacher,1960], i.e., eigenvector-eigenvalue, representation:

$$H^T H = 0\chi_0\chi_0^T + NP_{RS} + MP_{SV} + (M+N)\chi_{M+N}\chi_{M+N}^T \quad (4)$$

where

$$\begin{aligned} \chi_0 &= \frac{1}{\sqrt{M+N}} \begin{pmatrix} \mathbf{1}_M \\ \mathbf{1}_N \end{pmatrix} \\ \chi_{M+N} &= \frac{1}{\sqrt{MN(M+N)}} \begin{pmatrix} N\mathbf{1}_M \\ -M\mathbf{1}_N \end{pmatrix} \\ \mathbf{1}_M &= (1,1,\dots,1)^T, \text{ } M \text{ dimensional} \\ \mathbf{1}_N &= (1,1,\dots,1)^T, \text{ } N \text{ dimensional} \end{aligned}$$

P_{RS} is a projection operator, in τ_m space, which projects a vector onto a subspace orthogonal to $\mathbf{1}_M$ and P_{SV} is a projection operator, in t_n space, which projects a vector onto a subspace orthogonal to $\mathbf{1}_N$. Note, the matrix, $\chi_0^T \chi_0$, has zero weight in (4), the spectral decomposition of $H^T H$.

These two representations for $H^T H$ are equivalent in that they both have the same eigenvectors and eigenvalues. By direct calculation, it can be shown that χ_0 and χ_{M+N} are eigenvectors of $H^T H$, specifically:

$$\begin{aligned} H^T H \chi_0 &= 0\chi_0 \\ H^T H \chi_{M+N} &= (M+N)\chi_{M+N} \end{aligned}$$

Let χ_N be a vector in τ_m space, orthogonal to $\mathbf{1}_M$. Then,

$$(\mathbf{1}_M^T, 0_N^T) \chi_N = 0$$

and

$$P_{RS} \chi_N = \chi_N$$

where

$$0_N = (0,0,\dots,0)^T, \text{ } N \text{ dimensional}$$

Also,

$$(0_M^T, \mathbf{1}_N^T) \chi_N = 0$$

and

$$P_{SV} \chi_N = 0$$

where

$$0_M = (0,0,\dots,0)^T, \text{ } M \text{ dimensional}$$

Then,

$$\chi_0^T \chi_N = 0$$

$$\chi_{M+N}^T \chi_N = 0$$

$$H^T H \chi_N = N\chi_N$$

and χ_N is an eigenvector of $H^T H$. There are $M-1$ of these eigenvectors and they form the subspace of the range of the projection operator P_{RS} .

Following a similar development, one can show that

$$H^T H \chi_M = M\chi_M$$

where χ_M is a vector in t_n space, orthogonal to $\mathbf{1}_N$. These $N-1$ eigenvectors form the projection operator P_{SV} .

The zero eigenvalue in (4) expresses the fact that absolute time cannot be obtained from time difference measurements. The eigenvector χ_0 is an unobservable one dimensional subspace in the estimation problem and has been analyzed using the concepts of transparent variations and the composite clock [Brown, 1991]. A way to overcome the difficulty of the zero eigenvalue is to require the mean clock bias estimation error to be zero:

$$\chi_0^T (\hat{x} - x) = 0 \quad (5)$$

From (3), one obtains the clock covariance matrix Ξ by applying (4) and (5) and using the spectral form of the matrix inversion theorem [Gantmacher,1960; Campbell,1979]:

$$\Xi = \sigma_{Meas}^2 \left[\frac{1}{N} P_{RS} + \frac{1}{M} P_{SV} + \frac{1}{M+N} \chi_{M+N} \chi_{M+N}^T \right] \quad (6)$$

To obtain the URE in (2) using (6), one ignores the ephemeris and RS clock states. One can, then, set \tilde{H}

equal to the identity matrix by redefining K_p , the user's position estimator matrix [DOD,1993] as follows:

$$K_p = \begin{bmatrix} 0_M^T, k_E^T \\ 0_M^T, k_N^T \\ 0_M^T, k_V^T \end{bmatrix}$$

where k_E , k_N and k_V are estimator vectors for the user's east, north and vertical location error components:

$$\begin{pmatrix} \hat{x}_E \\ \hat{x}_N \\ \hat{x}_V \end{pmatrix} = K_p \hat{x}$$

Note that

$$(1_M^T, 0_N^T) K_p^T = 0$$

$$(0_M^T, 1_N^T) K_p^T = 0$$

and

$$Tr\{K_p K_p^T\} = PDOP^2$$

Therefore

$$\chi_{M+N}^T K_p^T = 0$$

$$P_{RS} K_p^T = 0$$

$$P_{SV} K_p^T = K_p^T$$

By substituting the above into (2), we obtain the User Range Error:

$$\sigma_{URE}^2 = \frac{Tr\{K_p \Xi K_p^T\}}{Tr\{K_p K_p^T\}} = \frac{\sigma_{Meas.}^2}{M} \quad (7)$$

This is the principal result of the paper.

In other words, the URE clock component depends only on the measurement accuracy, $\sigma_{Meas.}$ (assumed to be the same across all RS and users) and the number of RS's. In case that the N SV's and M RS's are not all seen by one another, N and M can be replaced by their average or effective values. The exact form of the clock covariance matrix in (6) is the basis for understanding and computing time transfer and user location accuracies. The validity of (7) has been confirmed with a covariance model developed in the APL language and by the Service Volume Model.

TIME INDETERMINACY

In developing the clock covariance matrix, Ξ in (6), the space of the eigenvector

$$\chi_0 = \frac{1}{\sqrt{M+N}} (1_M^T, 1_N^T)^T$$

was removed [Gantmacher,1960; Campbell,1979]. This is necessary due to a fundamental indeterminacy in estimating clocks using only time measurement differences. Absolute time cannot be measured.

When this singularity is removed in (5), the clock covariance matrix Ξ represents the variance of the clock bias estimates from the true biases, if the mean of the true biases were known, i.e., the implied probability density is a conditional density.

This time indeterminacy provides a natural "lever", i.e., a means of steering, system time to follow an external standard. One uses the single degree of freedom provided by the indeterminacy to define system time by constraining the clock bias estimates to a weighted average:

$$t_{WAve.} = \sum_{m=1}^M w_{RSm} \tau_m + \sum_{n=1}^N w_{SVn} t_n$$

for which

$$\sum_{m=1}^M w_{RSm} + \sum_{n=1}^N w_{SVn} = 1$$

The variance of a clock bias estimate with respect to the external standard is, therefore, the sum of the variance with respect to system time and the variance of system time from the external standard.

In the early days of GPS, this clock singularity was removed by defining one clock as the Master Clock. This precluded the use of all GPS clocks as an ensemble and limited the GPS system time accuracy to the accuracy of the Master Clock. When the GPS clock ensemble capability was developed, GPS system time keeping was significantly improved [Brown,1991]. Note that the Master Clock is a special case of the weighted average.

RS CLOCK BIAS ESTIMATION ERROR

As will be justified in the Service Volume Model section, assume SV ephemeris errors are negligible (< 1 m). For RS number m , the variance of τ_m is the diagonal element of Ξ

$$\sigma_{RST}^2 = \Xi_{mm} = \sigma_{Meas.}^2 \left[\frac{1}{N} - \frac{1}{MN} + \frac{N}{M(M+N)^2} \right] \approx \frac{\sigma_{Meas.}^2}{N}$$

Take typical values

$$\begin{aligned} \sigma_{Meas.} &= 1.1 \text{ m} \\ M &= 15 \\ N &= 12 \end{aligned}$$

Then,

$$\sigma_{RST} = 1.03 \text{ ns}$$

$$\sigma_{RST} \approx 1.06 \text{ ns}$$

A good approximate expression, in this case, for RS clock bias estimation error is, therefore,

$$\sigma_{RST} \approx \frac{\sigma_{Meas.}}{\sqrt{N}}$$

where N is the effective number of SV's seen by the RS.

CURRENT SV CLOCK BIAS ESTIMATION ERROR

Assume SV ephemeris error is negligible. For SV number n , the variance of t_n is the diagonal element of Ξ

$$\sigma_{SVT}^2 = \Xi_{nn} = \sigma_{Meas.}^2 \left[\frac{1}{M} - \frac{1}{MN} + \frac{M}{N(M+N)^2} \right] \approx \frac{\sigma_{Meas.}^2}{M}$$

For typical values

$$\sigma_{SVT} = 0.919 \text{ ns (0.276 m)}$$

$$\sigma_{SVT} \approx 0.947 \text{ ns}$$

A fair approximation to the current SV clock bias estimation error is, therefore,

$$\sigma_{SVT} \approx \frac{\sigma_{Meas.}}{\sqrt{M}}$$

USER TIME AND LOCATION ERROR

As a result of the clock analysis giving the Clock Covariance Matrix Ξ , one can directly calculate user time and, as well, location estimation error. The User Time-Location Covariance Matrix is

$$C_U = K \Xi K^T + K K^T (\sigma_{SVH}^2 A^2 + \sigma_{Dither}^2 + \sigma_{UMeas.}^2)$$

where

$$K = \begin{bmatrix} 0_M^T, k_E^T \\ 0_M^T, k_N^T \\ 0_M^T, k_V^T \\ 0_M^T, k_T^T \end{bmatrix}$$

is the standard user location-time estimation matrix [DOD,1993]. Note that:

$$K(0_M^T, \mathbf{1}_N^T)^T = (0,0,0,1)^T$$

$$HDOP^2 = k_E^2 + k_N^2$$

$$VDOP^2 = k_V^2$$

$$PDOP^2 = k_E^2 + k_N^2 + k_V^2$$

$$TDOP^2 = k_T^2$$

$$\sigma_{Dither} = \text{SV clock dither prediction error}$$

$$\sigma_{UMeas.} = \text{user measurement error}$$

$$\sigma_{SVH} = \text{a priori horizontal SV ephemeris error}$$

$$A = \text{effective angle from user to SV to centroid of RS's}$$

TIME TRANSFER, USER LOCATION ERROR AND URE

Time transfer error for the normal user is given by

$$\sigma_{UT}^2 = C_{U44} = k_T^2 \left[\sigma_{URE}^2 + \sigma_{UMeas.}^2 \right] - \left[\frac{1}{MN} - \frac{M}{N(M+N)^2} \right] \sigma_{Meas.}^2$$

(Note that the variance cannot be negative for k_T^2 is greater than or equal to $1/N$.) User location error is given by

$$(\sigma_{UE}^2, \sigma_{UN}^2, \sigma_{UV}^2) = (C_{U11}, C_{U22}, C_{U33}) = (k_E^2, k_N^2, k_V^2)(\sigma_{URE}^2 + \sigma_{UMeas.}^2)$$

The horizontal error is given by

$$\sigma_{UH}^2 = \sigma_{UE}^2 + \sigma_{UN}^2$$

In the above

$$\sigma_{URE}^2 = \frac{1}{M} \sigma_{Meas.}^2 + \sigma_{SVH}^2 A^2 + \sigma_{Dither}^2$$

is exact for the coefficient of $\sigma_{Meas.}^2$. A typical value (with $M = 15$) is

$$\sigma_{URE} = 0.415 \text{ m}$$

and, ignoring ephemeris,

$$\sigma_{URE} \approx 0.413 \text{ m}$$

The contribution of the ephemeris (0.6m<1m) can be ignored in the approximation. This was confirmed with the Service Volume Model and with a covariance model written in the APL language. Note that URE depends mainly on three quantities (again, ignoring ephemeris errors) : the RS measurement error, the effective number of RS's and the dither prediction error

$$\sigma_{URE} \approx \sqrt{\frac{\sigma_{Meas.}^2}{M} + \sigma_{Dither}^2}$$

INSTANTANEOUS TIME TRANSFER TO A SURVEYED USER

A surveyed user puts equal weight on all SV's

$$k_T = \frac{1}{N} \mathbf{1}_N$$

Calculating user time transfer error, one obtains

$$\sigma_{UT}^2 = \frac{1}{N} (\sigma_{SVH}^2 A^2 + \sigma_{Dither}^2 + \sigma_{UMeas.}^2) + \frac{M}{N(M+N)^2} \sigma_{Meas.}^2$$

with

$$\sigma_{UMeas.} = 1.1 \text{ m}$$

$$\sigma_{Dither} = 0.3 \text{ m}$$

$$N = 12$$

$$M = 15$$

$$\sigma_{Meas.} = 1.1 \text{ m}$$

$$\sigma_{SVH} = 0.6 \text{ m}$$

$$A = 4^\circ$$

gives

$$\sigma_{UT} = 1.11 \text{ ns}$$

To good approximation

$$\sigma_{UT} \approx \frac{\sigma_{UMeas.}}{\sqrt{N}} = 1.06 \text{ ns}$$

Therefore, time transfer to a surveyed user is limited by user measurement error.

SERVICE VOLUME MODEL

The purpose of the Loral Service Volume Model is to demonstrate that the accuracy portion of the system availability [FAA,1994] is met for a wide area differential GPS system throughout the Service Volume or to measure the fraction of the Service Volume which meets these requirements.

The model serves not only as a system design tool, but, ultimately, to support on-line monitoring and control of a WADGPS system. In particular, this would include the capability to detect loss of the advertised service levels and daily certification of the system level navigational performance. Examples of such real time performance metrics are in use by the operational GPS Control Segment today: observed range deviation (ORD), estimated range deviation (ERD) and monitor station nav solutions. Each provides a real time detection mechanism to ensure that the GPS advertised services are achieved.

The Service Volume Model, operating efficiently on an IBM RISC 6000 model 590, simulates 24 GPS satellites using actual almanac data. These satellite (SV) locations along with those of 8 geostationary (GEO) satellites are calculated as a function of time and transformed to Earth Centered Earth Fixed (ECEF) coordinates. Reference station (RS) and user locations are calculated using the WGS-84 Geoid. The model can handle as many as 44 reference stations.

To cover the service volume, the Model simulates several thousand user locations. The user is allowed to employ 4, 5 or 6 visible SV's, each of which must see 5 or more RS's. These are picked to minimize PDOP.

The fast (on the order of 1 second) processing is modeled with one clock state for each RS and one clock state and three position states for each GPS and GEO satellite. The slow (on the order of 15 minutes) processing is modeled with an approximate a priori covariance matrix which represents the resulting accuracy of the long term processing.

The partial derivatives of the pseudorange measurements are calculated from the satellite and RS positions, given visibility. An information matrix is calculated from the a priori covariance matrix, the RS receiver measurement accuracy and the partial derivatives of the measurements. This matrix is inverted to obtain the System State Covariance Matrix (1) which is augmented by the GPS satellite clock dither prediction process noise to form the Predicted State Covariance Matrix.

The advantage of representing errors with covariance matrices, as compared to monte carlo methods, is that, statistically, much greater ground can be covered with the same computing resource. The dimensionality of a WADGPS system can be quite large, e.g., 32 satellites and 44 reference stations, with a minimum of four states per satellite. To obtain reliable variances in this space, one must calculate a very large number of monte carlo points.

The Predicted State Covariance Matrix is projected along the pseudorange measurements to the user. The location estimation error of the user is calculated from this pseudorange covariance matrix, the user's estimator (K) matrix and the user's measurement error.

The user estimator (K) matrix is calculated by inverting a 4 by 4 matrix obtained from the partial derivatives of the pseudoranges with respect to the user location [DOD,1993]. This K matrix implies the Dilution of Precision measures (PDOP, HDOP, VDOP). Visibility of at least 4 satellites is required.

The inputs to the model allow one to specify a set of user grids, GPS satellite and GEO orbits and RS locations. Input parameters may be set for a priori covariances, system and user receiver measurement errors, ionosphere error and GPS satellite clock dither prediction error. Various performance test thresholds may be set. User ionosphere error is also input.

The outputs consist of a variety of user location error measures including all measures of Accuracy Availability.

These consist of five measures: Total Accuracy Availability, Vertical Position Error, Vertical Position Accuracy, Horizontal Position Accuracy and URE. Vertical Position Error includes user ionospheric error as defined in the Specification [FAA, 1994; Loh, 1994].

Sensitivities of various performance parameters were studied with respect to system definition parameters. Dependence was determined of URE on orbit accuracy, long term satellite and RS clock estimation accuracy, and GPS satellite clock dither prediction error. We found that long term clock accuracy could be ignored, that orbit accuracy of better than a meter caused little improvement, and that GPS satellite clock dither prediction had a significant effect on URE.

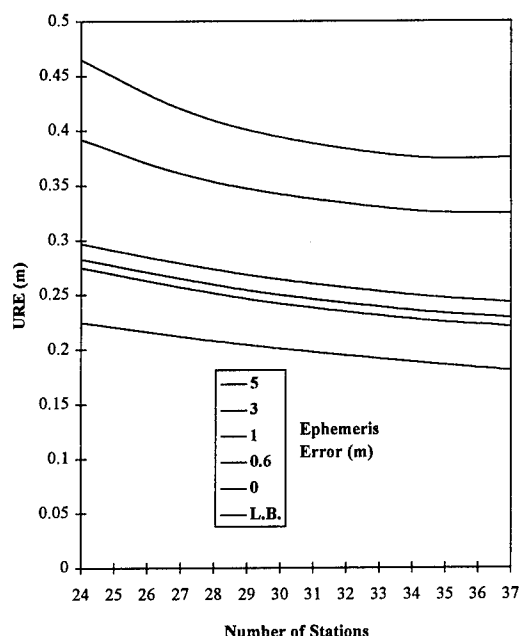


Figure 1. Dependence of URE on the Number of Stations and A Priori Ephemeris Error, Zero SV Clock Dither Prediction Error

Figure 1 shows user range error as a function of the number of reference stations, parametric in a priori ephemeris error. The absolute lower bound, of equation (7), is also shown. Note that the zero ephemeris error curve can be obtained by replacing the total number of stations by an effective, or average, number of stations seen per SV. These data were produced by the Service Volume Model with parameter values set for precision approach. A 24 hour (simulated) run was made with 24 to 37 RS's, 24 GPS SV's and 6 GEO's.

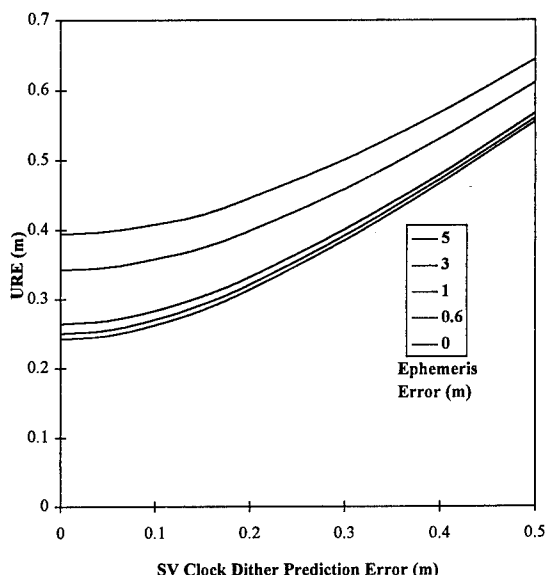


Figure 2. Sensitivity of URE to Ephemeris and SV Clock Dither Prediction Errors, 30 Stations

Figure 2 shows the sensitivity of URE to ephemeris error and GPS satellite clock dither prediction error. URE is plotted for a range of values of ephemeris estimation error and SV clock dither prediction error for 30 stations. Note that, when the ephemeris error is reduced below 1 meter, the effect on URE is significantly diminished. Clock dither prediction error begins to dominate at 0.2 meters.

CONCLUSIONS

An exact expression was derived for the effect of the network of SV and RS clocks on User Range Error (URE) in Wide Area Differential GPS. The expression serves as a lower bound on URE.

This was accomplished by means of an exact solution of the Clock Covariance Matrix. Corresponding expressions were derived for station and satellite clock bias error, time transfer error to a user and time transfer error to a surveyed user.

An approximate expression was derived for User Range Error, including SV ephemeris and SA prediction error. This was confirmed by a sophisticated Service Volume Model employing covariance analysis.

ACKNOWLEDGMENTS

The authors wish to thank the Loral Corporation for supporting this work. Thanks are due to Russell Y. Nakamura, Sherman G. Francisco, Peter Hoch, Dwight Divine III, Arthur G. Gower IV and Timothy C. Parker for their support, encouragement and helpful suggestions.

REFERENCES

- Beisner, H. M.; "Clock Error with a Wiener Predictor and by Numerical Calculation," IEEE Transactions on Instrumentation and Measurement, Vol. IM-29, No. 2, June 1980, pp. 105-113
- Bierman, G. J.; Factorization Methods for Discrete Sequential Estimation, Academic Press, New York, 1977
- Braasch, M. S.; "A Signal Model for GPS," Navigation, Vol. 37, No. 4, Winter 1990-91, pp. 363-377
- Brown, K. R.; "The Theory of the GPS Composite Clock," ION GPS 91, Sept. 11, 1991
- Campbell, S. L.; Meyer, C. D.; Generalized Inverses of Linear Transformations, Dover, New York, 1979
- Department of Defense, U. S.; "Global Positioning System Standard Positioning Service, Signal Specification," Nov. 5, 1993
- Federal Aviation Administration, U. S. Department of Transportation; "Specification, Wide Area Augmentation System (WAAS)," June 8, 1994
- Gantmacher, F. R.; The Theory of Matrices, Vol. I, Chelsea, New York, 1960
- Gelb, A. (ed.); Applied Optimal Estimation, MIT Press, Cambridge, 1974
- Hofmann-Wellenhof, B.; Lichtenegger, H.; Collins, J.; Global Positioning System, Theory and Practice, 2nd. ed., Springer-Verlag, New York, 1993
- Johnson, A.; Mueller, T.; Christofferson, E.; "Space-Based Navigation System Accuracy Performance Model," Institute of Navigation National Technical Meeting, Anaheim, CA, Jan 18-20, 1995
- Kee, C.; Parkinson, B. W.; Axelrad, P.; "Wide Area Differential GPS," Navigation, Vol. 38, No. 2, Summer 1991, pp. 123-144
- Kee, C.; Parkinson, B. W.; "Wide Area Differential GPS," PLANS '94 Conference, April 13, 1994
- Logsdon, T.; The Navstar Global Positioning System, Van Nostrand Reinhold, New York, 1992
- Loh, R.; Fernow, J. P.; "Integrity Concepts for a GPS Wide-Area Augmentation System (WAAS)," Institute of Navigation National Technical Meeting, San Diego, CA, Jan 24-26, 1994
- Mueller, T.; "Wide Area Differential GPS," GPS World, June, 1994, pp. 36-44
- Phlong, W. S.; Elrod, B. D.; "Availability Characteristics of GPS and Augmentation Alternatives," Navigation, Vol. 40, No. 4, Winter 1993-94
- Yunk, T. P.; "Coping with the Atmosphere and Ionosphere in Precise Satellite and Ground Positioning," Environmental Effects on Spacecraft Positioning and Trajectories, Geophysical Monograph 73, IUGG Volume 13, International Union of Geodesy and Geophysics and the American Geophysical Union, 1993

WAAS Sensor Interference Testing

Dr. Trent Skidmore
Ohio University

Mark Johnson
Rockwell International

BIOGRAPHIES

Trent A. Skidmore, Ph.D.

As a Research Scientist and Adjunct Assistant Professor at the Ohio University Avionics Engineering Center, Dr. Skidmore is involved in a variety of GPS-related projects. These currently include the study of GPS interference, the development of the Satellite Coverage Research Analysis Model (SCRAM) for studying the availability and integrity of satellite-based navigation systems, and spectrum engineering issues associated with differential GPS and the SCAT-I ground-to-aircraft data link. Dr. Skidmore is the secretary of Working Group-4 of RTCA Special Committee-159 and also participates in the FAA/NASA Joint University Program for Air Transportation Research. He is a graduate of Ohio University and Michigan Technological University.

Mark W. Johnson

Mr. Johnson is a senior systems design engineer in GPS receiver development at Rockwell International Corporation in Cedar Rapids, Iowa. He holds a BS in Computer Engineering from Iowa State University and a MSE in Electrical Engineering from Arizona State University. He has experience doing GPS hardware, software, and systems engineering at Rockwell and Motorola. He is involved in industry/government specification development for civil aviation GNSS in the RTCA committees.

ABSTRACT

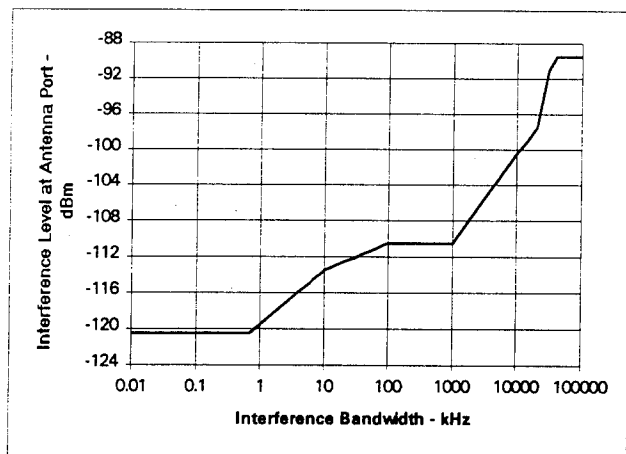
The concern over potential radio frequency interference to the planned FAA Wide Area Augmentation System (WAAS) can be greatly reduced with the careful development of testing procedures designed to ensure proper operation of a WAAS sensor in the presence of various types of interference. This paper provides the

justification and theoretical background for the interference tests that a WAAS sensor/receiver must be subjected to before certification. These tests follow the information contained in the RTCA Minimum Operational Performance Standard (MOPS) for Global Positioning System/Wide Area Augmentation System Airborne Equipment. The interference types to be tested fall into three primary categories: narrow-band (continuous wave) interference, broad-band interference, and pulsed interference, each of which has a unique requirement and test procedure. The requirements and tests are further categorized depending upon the particular phase of flight (en route, non precision approach, and precision approach) for which the sensor is designed. Described are the specific parameters to be quantified, including navigation-mode position accuracy, channel specific pseudorange accuracy, or data demodulation (bit error rate). Also included is a discussion of the test procedure for validating that the receiver produces no harmful misleading information (HMI), under any level of interference, that could constitute an integrity threat. This paper is of particular interest to two groups: 1) GPS/WAAS manufacturers whose sensors must show compliance, and 2) Civil aviation authorities who must certify the sensors and also determine appropriate regulatory measures given the limitations of the WAAS receivers.

INTRODUCTION

This paper contains a summary of the interference test procedures required for GPS/WAAS equipment that is to be certified for en route, terminal, and non precision approach operations (Class 1 and 2 Equipment). The interference tests for Category I precision approach avionics will be addressed in the future as the precision approach MOPS are developed. The tests discussed herein were designed in order to allow a manufacturer to show compliance, in a sound statistical fashion, with the

standard interference environment specified in Appendix C of the Draft MOPS [1] and shown in Figures 1 and 2 below. It should be noted that these test procedures are subject to change based on the Plenary review of the MOPS by RTCA Special Committee 159.



Note: Interference power density will not exceed -110.5 dBm in the frequency band of $L1 \pm 10$ MHz

Figure 1. WAAS MOPS In-Band Interference Level Requirements

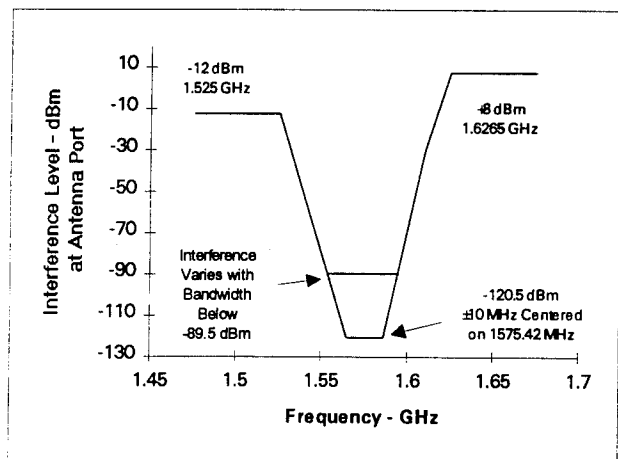


Figure 2. WAAS MOPS Out-of-Band Interference Level Requirements

The focus of this paper will be to look in detail at the tests and associated pass/fail criteria intended to show compliance with the following three requirements:

1. Initial Acquisition Time
2. No Hazardously Misleading Information (HMI) Test, also known as the Interference Integrity Test.
3. Steady-State Accuracy

While interference affects other requirements such as satellite acquisition time, satellite reacquisition time, and message loss rate, significant insight into the testing philosophy can be gained by considering the cases listed above. For all of these tests, it is assumed that the power of the GPS satellites is -134.5 dBm and that the power of the WAAS satellites is -135.5 dBm, at the antenna port of the receiver under test. This accounts for the maximum 4.5 dB antenna attenuation at 5° and assumes that the satellite power does not change as a function of elevation angle.

INITIAL ACQUISITION TIME TEST

The key requirement for initial acquisition time can be summarized as follows:

“the time from application of power to the first valid position fix shall be less than 5 minutes”

This requirement assumes that the receiver has been initialized in position and time and the receiver has valid almanac. Furthermore, this requirement must be met under the standard interference environment of the MOPS Appendix C. Therefore, the tests to verify initial acquisition performance must be run for each of the GPS/WAAS signal generator (simulator) scenarios described below. The two scenarios account for both inside and outside of WAAS coverage.

Scenario #1: Initial Acquisition (GPS Only)

- Exactly 6 GPS satellites.
- Selective Availability disabled.
- Platform dynamics: Constant velocity of 800 kt beginning at 5,000 ft (MSL) and performing a 3° climb.

Scenario #2: Initial Acquisition (GPS & WAAS)

- Exactly 5 GPS satellites and 1 WAAS satellite.
- Selective Availability disabled.
- Platform dynamics: Constant velocity of 800 kt beginning at 5,000 ft (MSL) and performing a 3° climb.

The interference conditions to be tested are shown in Table 1. These are all broadband noise values whose center is at 1575.42 MHz. In each test, the interference is to be applied to the receiver before it is powered on or the simulator is engaged.

Table 1. Initial Acquisition Time Test Interference Conditions

| Noise Bandwidth | Total Power (dBm) |
|-----------------|-------------------|
| 100 kHz | -116.5 |
| 20 MHz | -103.5 |

Combining Simulator Scenarios 1 and 2 with [Table 1](#) shows that the entire initial acquisition time test consists of a total of four (4) situations to be tested: Simulator Scenario 1 with the two interference conditions listed in [Table 1](#) and Simulator Scenario 2 again with the same two noise conditions.

The following steps are performed for the initial acquisition test:

1. The interference to be applied is turned on and connected to the sensor.
2. The airborne equipment (sensor) is powered and initialized to a position with total radial error equal to 60 nautical miles, and one minute (60 seconds) of error in time with respect to the starting position and time reference in the simulator. It is assumed that the receiver has obtained a valid almanac for the simulator scenario to be tested prior to conducting these tests.
3. The simulator scenario is engaged and the satellites' RF shall be turned on.
4. The time to first valid position fix (TTFF), defined as the time from when the simulated satellites' RF is engaged until the first valid position (with integrity) is output, must be observed. For simulator Scenario #1 (6 GPS satellites), integrity must be provided by the sensor's Fault Detection and Exclusion (FDE) algorithm. For simulator Scenario #2 (5 GPS satellites and 1 WAAS satellite), integrity must be provided by WAAS. Along with the TTFF, at least the next 60 seconds of continuous position fixes (a minimum of 60 data points) after the initial fix must also be recorded in order to verify the accuracy requirement.
5. Precise ephemeris must be purged or rendered invalid at the end of each acquisition attempt.
6. Go to Step 2 and repeat as required.

In order to determine the pass/fail criteria, not only must the TTFF be met, but the position fix must also be valid.

Turning Selective Availability (SA) off translates the 100 meter (95%) horizontal accuracy into a new derived requirement of 15 meters (95%). For the purpose of the interference tests, the accuracy statistic is computed using the 2drms formula shown below.

$$2drms = 2 \sqrt{\frac{\sum_{i=1}^N \left(\frac{1.5(d_i)}{HDOP_i} \right)^2}{N}}$$

where

- 2drms: Twice the distance, root-mean-square
 d_i : Instantaneous 2-D horizontal position error (meters)
 N : Number of points considered
 $HDOP_i$: Instantaneous Horizontal Dilution of Precision

The use of the 2drms formula provides a conservative estimate of the 95% error and effectively weights large position errors which may be caused by unwanted interference. A failure by the sensor to produce a position output after 5 minutes indicates a failure mode, and results in declaring the test a failure.

Scaling the instantaneous 2-dimensional position error (d_i) by $1.5/HDOP_i$ provides a means of normalizing the tests to a constant $HDOP = 1.5$ and accounts for fluctuations in the satellite coverage due to changing geometries. $HDOP_i$ may be obtained from the receiver under test or calculated separately. Only those satellites used in the position solution are included in the $HDOP_i$ calculation. The manufacturer must demonstrate the validity of the values chosen for $HDOP_i$.

To determine the initial acquisition pass/fail criteria, consider a single trial where the sensor under test provides a valid position fix within the required time (5 minutes) and maintains the required accuracy (15 m, 95%) for at least the next 60 seconds. This sensor is considered to have passed one (1) trial. [Table 2](#) shows the total test disposition and represents a "quit-while-ahead" testing approach designed to keep testing times at a reasonable length. This testing philosophy is a subset of the testing required by the Department of Defense (DoD) [2].

Table 2. Graduated Sampling Pass/Fail Criteria

| Trials | Cumulative Failures within Specified Time | Test Disposition |
|------------------|---|-----------------------------|
| First 10 Trials | Zero (0) One (1) Two (2) or More | Pass Run 10 More Fail |
| Second 10 Trials | Zero (0) One (1) or Two (2) Three (3) or More | Pass Run 10 More Fail |
| Third 10 Trials | Zero (0) One (1) or More | Pass Fail |

For example, if no failures occur in the first ten trials, success for that simulator and interference case would be declared and the current test terminated. A single failure in the first set of ten trials necessitates running the next set of ten trials. Two or more failures during the first ten trials indicates that the sensor has failed that particular test, and so on. Justification for the above-stated criteria is shown in Appendix M of the MOPS [1] and summarized below.

ACQUISITION TESTING JUSTIFICATION

Tests for initial acquisition and satellite (re)acquisition time can be considered to follow a binomial distribution based on the following assumptions:

1. Each acquisition attempt is an independent trial, i.e. the results of any single trial do not depend on the results of any previous trial, and
2. Only two test states are possible - acquire (within the specified time and accuracy) or not acquire.

The binomial distribution is represented by the following:

$$\sum_{y=0}^n P(y) = \sum_{y=0}^n \binom{n}{y} p^y q^{n-y}$$

where:

$$\binom{n}{y} = \frac{n!}{n!(n-y)!}$$

and

| | | |
|--------|---|---------------------------------------|
| $P(y)$ | = | Probability of failing a test |
| y | = | Number of failures (0, 1, or 2) |
| n | = | Number of trials |
| p | = | Probability of failing a single trial |
| q | = | Probability of passing a single trial |

A graduated sampling approach is employed in order to keep test times within reason. The number of failures per 10 trials (y) is allowed to vary between zero and two, according to the approach shown in [Table 2](#). The acquisition test is broken out into a series of three segments each composed of ten trials. The "quit-while-ahead" concept is used. For example, if no failure occurs in the first 10 trials, success is declared and the current test terminated. If one failure occurred in the first 10 trials, at least 10 more trials (after the first 10) are required prior to declaring the test successful. Therefore let:

| | | |
|----------|---|--|
| α | = | Probability of rejecting a good receiver |
| β | = | Probability of accepting a bad receiver |

Rational for this method of testing is based on achieving an acceptably low β risk with a small number of samples and deferring rejection of a good receiver (low α) until a larger sample is obtained. Such a test concept will, on the average, shorten the duration of the testing. The overall probability of passing the three-segment, 30 trial test is related to the probability of success per individual trial. Receivers that are nominally designed to have a

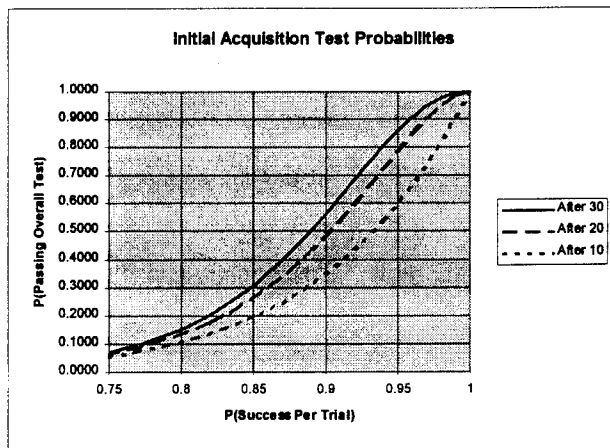


Figure 3. Acquisition Test Probability Statistics

0.95 probability of passing a single test will have 0.86 probability of passing the overall test. Conversely, the probability of a “bad” receiver, one that has a 0.80 chance of passing a single trial, will only pass the overall test with a probability of 0.16. Thus, this graduated test procedure has a high probability of rejecting a bad receiver. [Figure 3](#) shows the probability of passing the overall test after each 10-segment trial for receivers of varying quality.

INTERFERENCE INTEGRITY TEST FOR CLASS 1 & 2 SENSORS

The key interference integrity requirement for equipment that is to be certified for en route, terminal, and non-precision approach operations (Class 1 and 2 equipment) can be summarized by stating that the GPS/WAAS equipment shall maintain integrity even under interference conditions greater than those specified in the MOPS Appendix C. These tests must incorporate Selective Availability as specified in the MOPS Appendix B [1].

Tests are run for each of the GPS/WAAS signal generator (simulator) scenarios described below:

Scenario #1: Interference Integrity Test (GPS Only)

- Exactly 6 GPS satellites.
- Selective Availability enabled.
- Case 1: Stationary sensor.
- Case 2: Dynamics as specified in [Table 3](#), referencing [Figures 4 and 5](#).

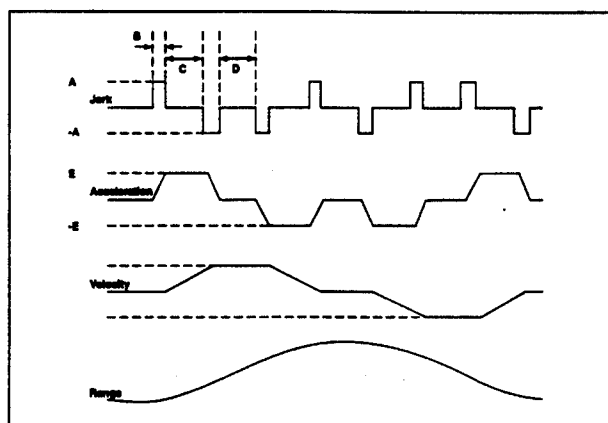
Scenario #2: Interference Integrity Test (GPS and WAAS)

- Exactly 3 GPS satellites and 1 WAAS satellites.
- Selective Availability enabled.
- Case 1: Stationary sensor.
- Case 2: Dynamics as specified in [Table 3](#), referencing [Figures 4 and 5](#).

The dynamic profile values in [Table 3](#) are derived from the maximum abnormal non-precision/precision approach maneuver dynamics as specified in the MOPS. [Figure 4](#) shows one cycle of motion. The simulated motion shall alternate between horizontal and vertical motion as indicated in [Figure 5](#).

Table 3. Dynamic Profile Values For The Interference Integrity Tests

| Description/Label | Horizontal | Vertical |
|----------------------------------|-----------------------|-----------------------|
| Maximum Jerk (A) | 7.3 m/s ³ | 7.3 m/s ³ |
| Jerk Period (B) | 2.7 s | 2.0 s |
| Constant Acceleration Period (C) | 3.9 s | 6.7 s |
| Constant Velocity Period (D) | 3.9 s | 6.7 s |
| Maximum Acceleration (E) | 19.6 m/s ² | 14.7 m/s ² |
| Cycle Duration | 52.4 s | 69.9 s |



(Conceptual Picture Only: Not Drawn to Scale)

Figure 4. Generic Dynamic Profile

It should be noted that the velocity profile has been drawn showing either constant or linearly changing values. The simulator realization of this profile is required to produce accurate nonlinear velocity and range profiles as needed.

Note: Manufacturers using simulator equipment unable to generate the specified dynamic profiles must create tests that generate equivalent information.

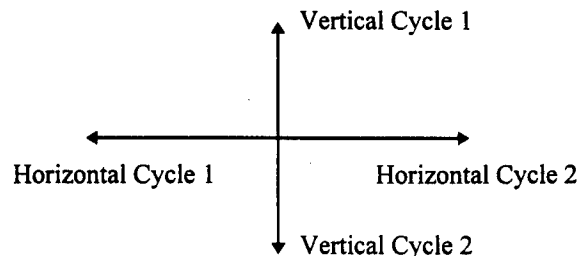


Figure 5. Dynamic Profile Horizontal And Vertical Motion

The continuous wave interference frequencies to be tested are shown in [Table 4](#). The beginning steady-state power values are shown in the table. During the initial acquisition phase, the applied interference power at 1575.42 MHz is 6 dB less than that shown in the table. The I/S ratio is varied according to the test procedures.

Table 4. Initial Interference Integrity Test CW Interference Values

| Frequency (MHz) | Power (dBm) | I/S (dB) |
|-----------------|-------------|----------|
| 1525.0 | -12.0 | 122.5 |
| 1555.42 | -89.5 | 45.0 |
| 1575.42 | -120.5 | 14.0 |
| 1595.42 | -89.5 | 45.0 |
| 1610.0 | -30.0 | 104.5 |
| 1618.0 | -12.0 | 122.5 |
| 1626.0* | +8.0 | 142.5 |

* Only Required for Aircraft with SATCOM

The following steps are to be performed for the interference integrity test:

1. The interference to be applied is turned on and connected to the sensor. Note that the power of the interference during initial acquisition is lower than that for steady-state operation.
2. The airborne equipment is powered and initialized to a position with a total radial error of 60 nautical miles, and one minute (60 seconds) of error in time with respect to the starting position and time reference in the simulator. It is assumed that the receiver has obtained a valid almanac for the simulator scenario to be tested prior to conducting these tests.
3. The simulator scenario is engaged and the satellites' RF turned on.
4. The sensor is allowed to reach steady state. When the sensor has reached steady state, the power of the interference is adjusted (adjustment necessary only at 1575.42 MHz) to the values shown in [Table 4](#) and maintained for 200 seconds.
5. The position and integrity status indicator must be recorded during this interval. Note that for Simulator Scenario 1 (Cases 1 & 2) integrity must be provided by FDE, and for Scenario 2 (Cases 1 & 2), the integrity must be provided by WAAS.

6. The power of the interfering signal is increased by 10 dB and maintained for 200 seconds. The position and integrity status indicator must be recorded during this interval.
7. Go to Step 6 and repeat until the interference power equals +30 dBm (I/S = +164.5 dB) or until no status change has occurred over the last two 10 dB power increases; i.e., the sensor indicates loss of integrity and no position/navigation information is being output.
8. Decrease the interference power in 10 dB steps, remaining at each level for 200 seconds. Integrity and position information must be recorded when the sensor resumes operation as the interference power is decreased.
9. Go to Step 8 and repeat until the interference has returned to the values specified in [Table 4](#).
10. Go to Step 2 and repeat as required. Precise ephemeris must be purged or rendered invalid at the start of each new interference frequency being applied.

To determine the interference integrity pass/fail criteria, the instantaneous horizontal position error (computed using the 2drms accuracy statistic) and integrity indicator flag is observed. The equipment fails the interference integrity test if the 2-D position error exceeds the Horizontal Protection Level (HPL) or Horizontal Alert Limit (HAL) without indicating a loss of integrity monitoring, and a loss of navigation is not indicated.

STEADY-STATE ACCURACY TEST

The key steady-state accuracy requirement states that the GPS/WAAS equipment must maintain an accuracy of 100 m (95%). However, with SA off, the accuracy threshold is given as 15 m (95%).

The tests to verify steady-state accuracy performance are run for each of the GPS/WAAS signal generator (simulator) scenarios described below:

Scenario #1: Steady-State Accuracy Test (GPS Only)

- Selective Availability disabled.
- Dynamics as specified in [Table 5](#), referencing [Figures 4 and 5](#).
- Exactly 6 GPS Satellites for 300 seconds.
- Then, exactly 4 GPS Satellites for the remainder of test.

Scenario #2: Steady-State Accuracy Test (GPS & WAAS)

- Selective Availability disabled.
- Dynamics as specified in Table 5, referencing Figures 4 and 5.
- Exactly 4 GPS satellites and 2 WAAS satellites for 300 seconds.
- Then, exactly 2 GPS satellites and 2 WAAS satellites for the remainder of the test.

Note: Removal of the GPS satellites for the steady-state portion of the test must be accomplished by disabling the RF of those satellites in the simulator and not by de-selection in the receiver.

The dynamic profile values in Table 5 are derived from the maximum normal non-precision/precision approach maneuver values specified in the MOPS. The simulated motion must alternate between horizontal and vertical motion as indicated in Figure 5. The total duration of the test must be at least 105 minutes. This includes the time required by the sensor to reach steady-state.

Table 5. Dynamic Profile Values For The Steady-State Tests (See Figures 4 and 5)

| Description/Label | Horizontal | Vertical |
|----------------------------------|----------------------|----------------------|
| Maximum Jerk (A) | 2.5 m/s ³ | 2.5 m/s ³ |
| Jerk Period (B) | 2.3 s | 2.0 s |
| Constant Acceleration Period (C) | 20.3 s | 24.2 s |
| Constant Velocity Period (D) | 20.3 s | 24.2 s |
| Maximum Acceleration (E) | 5.7 m/s ² | 4.9 m/s ² |
| Cycle Duration | 180.8 s | 209.8 s |

For these tests, a maximum of four satellites will be used to verify that the receiver, once in steady state, can continue to compute a position when a specific set of satellites is required. Note that using only four GPS satellites in the GPS only case will cause an integrity warning, which is to be ignored for these tests as long as a position output is continually generated.

The interference conditions to be evaluated are shown in Tables 6, 7, and 8. Table 6 contains the broadband noise values (whose center is at 1575.42 MHz). Table 7 contains the continuous wave (CW) cases to be tested. Shown in Table 8 are the pulsed interference conditions

to be tested. In all cases, the interference is to be applied to the WAAS sensor before the simulator is engaged.

The power levels indicated in Tables 6 and 7 are for the steady-state portion of the tests and correspond to Classes 3 and 4 equipment and installations with SATCOM. The power during the first 300 seconds (initial acquisition) of each broadband test is 6 dB lower than those listed in Tables 6. Power levels for Class 1 & 2 equipment steady-state operations are 6 and 3 dB lower than those listed in the Table 6 and the 1575.42 MHz CW value in Table 7, respectively.

Table 6. Steady-State Accuracy Test Broadband Interference Values

| Noise Bandwidth | Total Power (dBm) |
|-----------------|-------------------|
| 100 kHz | -110.5 |
| 2 MHz | -97.5 |

Table 7. Steady State Accuracy Test CW Interference Values

| Frequency (MHz) | Power (dBm) | I/S (dB) |
|-----------------|-------------|----------|
| 1525.0 | -12.0 | 122.5 |
| 1555.42 | -89.5 | 45.0 |
| 1575.42* | -120.5 | 14.0 |
| 1595.42 | -89.5 | 45.0 |
| 1610.0 | -30.0 | 104.5 |
| 1618.0 | -12.0 | 122.5 |
| 1626.0** | +8.0 | 142.5 |

* Interference power is decreased 6.0 dB during initial acquisition

** Only Required for Aircraft with SATCOM

Table 8. Steady-State Accuracy Test Pulsed Interference Values

| Frequency (MHz) | GPS Only Scenario Pulsewidth (milliseconds) | GPS & WAAS Scenario Pulsewidth (microseconds) |
|-----------------|---|---|
| 1525.0 | - | 125.0 |
| 1555.42 | 1.0 | 125.0 |
| 1575.42 | 1.0 | 125.0 |
| 1595.42 | 1.0 | 125.0 |
| 1610.0 | - | 125.0 |

For the pulsed interference tests, a pulse modulated carrier (CW) with peak carrier level of +30 dBm (1.0 Watt) and duty factor of 10% shall be used. This applies to both the 1.0 msec pulses for the GPS only case and the

125.0 μ sec pulses for the GPS & WAAS case. This corresponds to an I/S ratio of +164.5 dB.

Therefore, the entire steady-state accuracy test will include a total of sixteen (16) cases to be tested: Simulator Scenario 1 (GPS Only) with the three (3) conditions of Table 8 and Simulator Scenario 2 (GPS & WAAS) with the thirteen (13) interference conditions listed in Tables 6, 7, and 8. Equipment for use in Satcom equipped aircraft requires an additional CW case to be tested.

The following steps are to be performed for the steady-state accuracy test:

1. The interference to be applied is turned on and connected to the sensor. The power is set to the appropriate initial acquisition level.
2. The airborne equipment is powered and initialized to a position with total radial error equal to 60 nautical miles, and one minute (60 seconds) of error in time with respect to the starting position and time reference in the simulator. It is assumed that the receiver has obtained a valid almanac for the simulator scenario to be tested prior to conducting these tests.
3. The simulator scenario is engaged and the satellites' RF is turned on.
4. Position fixes are to be observed (recorded) beginning no later than 5 minutes after application of the simulator output to the sensor. After the initial 5 minutes, the power of the is adjusted to the required steady-state level. The steady-state data must be recorded once per minute for no less than 100 minutes. The sampling interval is set to one minute in order to obtain independent samples.
5. Go to Step 2 and repeat as required. Precise ephemeris must be purged or rendered invalid after each trial.

The accuracy statistic must be computed using the 2drms formula as shown above. The pass/fail criteria for the steady-state accuracy interference tests is a comparison between the 2drms accuracy computed over the steady-state portion of the test and a scaled version of the accuracy requirement. With selective availability disabled and no multipath, it can be assumed that the 5 m pseudorange noise component, including interference effects, translates into a maximum of position error of 15

m (95% 2-dimensional accuracy), where $15 \text{ m} = (2) * (5 \text{ m}) * (\text{HDOP} = 1.5)$.

The actual pass/fail threshold value depends on the duration of the test and follows a chi-square distribution (see MOPS Appendix M). The evaluation process consists of determining the variance of 100 steady-state data points (sampled at once per minute) with a desired confidence of 0.99. Using the chi-squared distribution with 99% confidence it can be shown that the maximum allowable 2drms error is equal to 12.5 m. Therefore, in order to determine the test disposition, the 2drms error is computed beginning 300 seconds after test initiation until the total 105-minute test is complete. This 2drms error value is compared with 12.5 m. If the 2drms error is less than or equal to 12.5 meters, the sensor has passed that interference condition test. If the 2drms error is greater than 12.5 m, the sensor has failed the test.

If it is necessary to run the test longer in order to move the decision threshold closer to the limit of 15.0 meters, Appendix M of the WAAS MOPS [1] should provide the necessary framework for accomplishing this.

STATISTICAL JUSTIFICATION FOR ACCURACY TEST REQUIREMENTS

It can be shown that the percent confidence (α) of the variance (σ^2) for a normally distributed random variable can be upper bounded by using the computed sample variance (s^2) according to the following:

$$\sigma^2 \leq \frac{(n-1)s^2}{\chi_{\alpha, n-1}^2}$$

where

| | |
|--------------------------|--------------------------|
| n: | Number of data points |
| $\chi_{\alpha, n-1}^2$: | Chi-squared distribution |
| α : | Percent confidence |

For example, in the steady-state accuracy test of section 2.5.8, it is required that the 2drms (95% 2σ) accuracy be 15 m (with SA off). Given a required confidence of $\alpha = 0.99$ and 100 data points ($n = 100$), the chi-squared distribution dictates that $s^2 = 39.3 \text{ meters} = ((12.5 \text{ meters})/2)^2$;

$$\sigma^2 \leq \frac{(99)(39.3)}{69.2} = 56.25$$

which yields $\sigma \leq 7.5$ m, thus meeting the $2\sigma \leq 15$ m requirement.

Therefore, when the sampled 2drms value is less than or equal to 12.5 meters, it is known with 99.0% confidence that the 15 m (95%) error component due to pseudorange noise requirement is not exceeded.

SUMMARY

Following extensive study, the RTCA and FAA are taking a new approach to specifying and testing interference effects on GNSS receivers. The intent is to provide test methods with statistically based assurances of receiver performance. These tests can be categorized as Acquisition, Interference Integrity, and Steady-State Accuracy tests. With the approval of the new WAAS MOPS these requirements and tests will be the standard by which the interference performance of FAA-certified GNSS receivers is judged.

REFERENCES

- [1] "Minimum Operational Performance Standard For Global Positioning System/Wide Area Augmentation System Airborne Equipment," Final Draft (Draft 6), RTCA Paper No. 369-95/SC-159-661, July 24, 1995.
- [2] "Interface Control Document ICD-GPS-204A NAVSTAR GPS Instrumentation and Connector Standards," NAVSTAR GPS Joint Program Office Space Division, March 1992.

ACKNOWLEDGMENTS

The authors wish to thank the members of RTCA SC-159 and their colleagues on the WAAS MOPS Authors Committee for their invaluable comments during the development of these test procedures. Special thanks go to A.J. Van Dierendonck, Per Enge, Bruce DeCleene, Bob Erlandson, Daryl McCall, John Studenny, and Frank van Graas. Dr. Skidmore's contribution to this project was supported by the FAA under a University Research Grant with the FAA Satellite Program Office. Mr. Johnson's contribution to this project was primarily supported by Rockwell Collins Commercial Avionics Division, SATNAV program.

A Study for Performance Enhancements of the Asian-Australian GPS Augmentation System (AAAS)*

Dr. Yanming Feng, Prof. Kurt Kubik, and Jizhang Sang
Queensland University of Technology

Prof. Jingnan Liu
Wuhan Technical University of Surveying and Mapping

BIOGRAPHY

Dr. Yanming Feng received his PhD degree in Satellite Geodesy from Wuhan Technical University of Surveying and Mapping, P. R. China in 1990. He is currently working as Senior Technologist at the Space Centre for Satellite Navigation, Queensland University of Technology, Brisbane, Australia. He has been active in GPS field for 10 years, particularly in the areas of satellite orbital determination, high accuracy positioning, DGPS kinematic positioning, WADGPS, GPS Integrity Monitoring and Wide Area Augmentation Systems (WAAS).

Professor Kurt Kubik completed his PhD studies in Geodetic Engineering at the Technical University of Vienna, Austria in 1967. He has held Chairs in Surveying and Numerical Mathematics at Universities in Germany, Denmark, USA and Australia. In 1992, he was awarded the position of Honorary Professor at the Wuhan Technical University of Surveying and Mapping (WTUSM). Prof. Kubik is the founding Director of the Space Centre for Satellite Navigation, the federally supported Australian Centre of Excellence in GPS studies. He has published three books and more than 150 scientific papers in the fields of Mathematics, Surveying and Mapping, and Computer Sciences.

Professor Jingnan Liu is the Dean of Faculty of Earth Science and Surveying Engineering at Wuhan Technical University of Surveying and Mapping (WTUSM), P. R. China. He has 20 years experience in Satellite Navigation and Space Geodesy. He is the leader of a number of national-level GPS related programs in China,

including GPS Satellite Tracking Network of China and China Wide Area Differential GPS (WADGPS) system. He is one of the leading scientists in the field of Satellite Navigation and Space Geodesy in China. Professor Liu is also author or co-author of several books and more than 60 journal and conference papers.

ABSTRACT

Three separate Wide Area Augmentation Programs have been proposed independently by Australia, P. R. China and Japan within the same geographical region. This paper discusses the opportunity to combine or integrate these three systems into one unified WAAS system for the whole Asian-Australian area. This resulting system, which we may call "Asian-Australian Augmentation System" (AAAS) would provide full integrity, accuracy and an additional ranging capability for all phases of flight such as oceanic, domestic, non-precision- and precision approach for most of the countries in East-Asia and Australia.

The paper first addresses the configuration and operational strategy for the AAAS system. The performance enhancements provided by the AAAS are then examined, in particular the geometric precision of GEOs orbit determination. Then, Navigation Availability and Receiver Autonomous Integrity Monitoring (RAIM) Availability are studied over the areas of Australia, China, Japan and South-East Asia for the non-precision approach phase of flight. Different combinations and configurations of GPS and GEOs are evaluated. The results demonstrate that the accuracy of GEO orbit determination from the AAAS ground network is vastly superior to country-wide operation. AAAS achieves RAIM availability of 100 percent, using the integrated constellation of the 6 GEO satellites from the individual networks, and their ranging functions.

* The paper reflects the views of the authors, who are responsible for the technical details, computation results and suggestions presented herein. It does not reflect official views of the authorities of Australia, P. R. China and Japan.

1. INTRODUCTION

The Wide-Area Augmentation System (WAAS) concept has been widely accepted as one of the most important means to improve GPS integrity, accuracy and availability for sole means of civil aviation [1]. It provides GPS-like ranging signals from the geostationary relay satellites to increase navigation availability and RAIM capability for all phases of flight. It also broadcasts GPS failure messages and differential GPS corrections (determined by a ground integrity monitoring and reference network) modulated onto the L1 carrier phase to GPS/WAAS user receivers, in order to provide full integrity and accuracy for precision approach down to Category I.

Recognising its potential, similar WAAS programs have been proposed independently for Australia, Japan and P. R. China. In Australia, the Civil Aviation Authority (CAA, now Air Services Australia, ASA) proposed in 1993 to implement an Australian Wide Area Augmentation Systems (Australian WAAS) in order to improve the integrity and availability of the GPS system, to meet the criteria for sole means of navigation in civil aviation. Current planning envisages the use of this system for all phases of flight down to Non-Precision Approach (NPA) within the Australia Area of Interest (AAOI) [2]. In Japan, the Japanese Civil Aviation Bureau (JCAB) and Ministry of Transport (MOT) are jointly developing a GPS Integrity Channel (GIC) network to broadcast GPS integrity and differential information for Civil Air Navigation. The first phase of the system will be implemented in 1998. JCAB and MOT are also considering the augmentation of the Global Navigation Satellite System (GNSS) by GEO's navigation overlay service in order to improve availability and positioning accuracy for Civil Air Navigation in Japan [3]. In P. R. China, the Civil Aviation Administration of China (CAAC) has determined to gradually set up a WAAS in order to fulfil the integrity, availability and continuity requirements for all phases of flight down to non-precision approach [4]. The ultimate objective of the Chinese WAAS is to provide a sole means of navigation facility for all phases of flight down to CAT I precision approach and landing.

Initial proposals to coordinate these three independently developing WAAS systems into an enhanced WAAS system for the Asian-Australian region are contained in [5,6]. Bilateral agreements on technical corporation and coordination have already been signed between some of the interested parties (CAAC, JCAB and ASA) and with the US FAA [5]. The combined and unified system, which we may call Asian-Australian Augmentation System (AAAS), would provide superior integrity,

accuracy and additional ranging capability for most of the Austral-Asian countries and for all phases of flight such as oceanic, domestic, non-precision and precision approaches.

This paper aims to study the technical improvements possible through such an AAAS system: The AAAS system could use the monitoring data from all three countries to improve upon the accuracy of GEOs orbit determinations, and it provides more geostationary satellites to enhance the availability of the system service. In the following, we will first give an overall description of the AAAS configuration and a proposed operational strategy. The performance enhancements provided by the AAAS are examined in terms of accuracy of GEO's orbit determination, and Navigation and RAIM availability over the areas of Australia, P.R. China, Japan and South-East Asia for the non-precision approach phase of flight, as this is the most stringent navigation requirement.

2. DESCRIPTION OF THE ASIAN-AUSTRALIAN-AUGMENTATION SYSTEM (AAAS)

The WAAS as currently planned by FAA sets a conceptual example for GPS-based navigation augmentation systems. Regardless of particular ground control regions, the architecture and operational principle of different WAAS systems are basically the same. A WAAS system consists of Geostationary satellites (GEOs), Wide Area Reference Stations (WRSS) and Wide area Master Stations (WMSs) and Ground Earth Stations (GESs). Earlier availability studies have shown that a NPA navigation availability of 100% can be achieved with at least two GEO satellites, which provide ranging signals or navigation overlay service for their footprint users. RAIM availability will also improve with the number of GEO satellites in view. The number of WRSS may vary and depends on the size of the covered region or service volumes. One WMS station and one GES station are required to run at all time, and one or more extra stations serve as hot-stand-by facility. The data link amongst these ground stations is typically over terrestrial lines, but may involve GEOs standard communication channels where appropriate.

Table 1 compares the configuration parameters of different GPS wide area augmentations, as developed or proposed by US FAA, JCAB, ASA, CAAC and AAAS. These parameters are approximate and have not been finalised. The proposed AAAS system is a straightforward combination of the Japanese WAAS, Australian WAAS and Chinese WAAS systems.

Table 1 Configuration parameters of the individual WAAS and of the AAAS systems

| Augmentation | # of WRSs | # of WMSs | # of GESs | # of GEOs | Service area |
|-----------------|-----------|----------------|----------------|-----------|----------------|
| US FAA WAAS | 15 - 30 | 2- 4 | 2-4 | 2 - 6 | CONUS |
| Japanese WAAS | 4 | 1 active | 2 (one active) | 2 | Japan |
| Australian WAAS | 10 - 12 | 2 (one active) | 2 (1 active) | 2 -3 | AAOI |
| Chinese WAAS | 8- 15 | 2 (one active) | 2 (1 active) | 2-3 | China |
| AAAS | 22 - 31 | 3 (3 active) | 4 (2 active) | 4 -6 | Asia-Australia |

In the early stage of the AAAS development, the AAAS would consist of all the ground stations and geostationary satellites of the individual systems. The system service area covers China, Japan, South-East Asia and Australia. The locations of various ground stations can be seen in Figure 1.

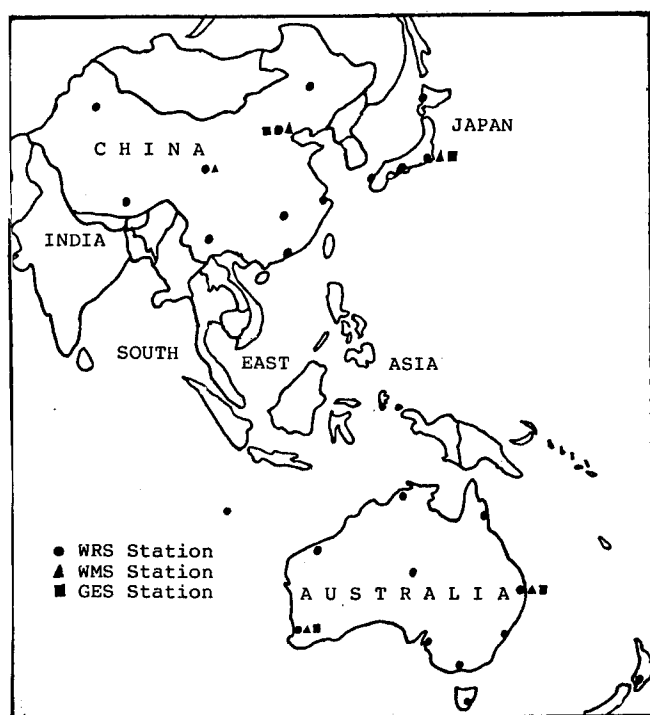


Figure 2 Possible AAAS Ground Stations

The unified AAAS allows to make full use of the resources and observation data to provide an enhanced navigation service. On the other hand, it also increases the degree of difficulty in system operation and coordination. In a simple solution, the three systems function relatively independently, but exchange the pre-processed monitoring data for post-processing of GPS and GEO orbit determination. In particular, the proposed operational strategy for the AAAS is as follows:

- Each Wide Area Reference Station (WRS) station collects measurements from all the GPS- and GEO satellites in view, processes and aggregates the data according to an unified algorithm and sends this data to its own country Wide Area Master Station (WMS);

- Each country WMS is responsible for preparing and formatting the user data messages including satellite integrity messages, differential corrections and ionospheric delay information. These country-dependent messages are then transmitted to the one currently active Ground-Earth Station (GES) within the AAAS (the other two country GESs are in stand-by mode). The three country WMSs also compress and mutually exchange their observation data. For cross-check purposes, each WMS centre creates GEO- and GPS orbits by using all the data collected from all the three countries according to unified orbit determination software.
- At the active GES, the results from the three country WMS are cross-checked, integrated and then uplinked to all the GEO satellites, together with the navigation signals generated in the GES.

This strategy requires a minimum of coordination between the systems and authorities. It allows distributed authority and thus flexibility in the implementation and operation of the AAAS. Even though, efficient collaboration amongst the countries involved is still a necessity.

3. PERFORMANCE IMPROVEMENTS THROUGH AAAS

We now examine the performance improvements which can be attained through the integration of the individual systems into the unified AAAS. Here, RAIM is of particular importance as it is an essential component in system integrity and flight safety enhancement. RAIM availability criteria for non-precision approaches are most stringent, and most sensitive to the constellations of GEO satellites. Also, the accuracy of GEOs orbit determination will directly impact on user positioning capability. Thus, we focus on these two parameters in our study of AAAS's performance characteristics.

3.1 Precision of GEOs Orbit Solutions

GEOs broadcast ephemerides have to be created at the WMS from the tracking data of the WRSs.. Assuming that the locations of the ground stations are precisely

known, the accuracy of GEOs orbit solutions depends mainly on the GEOs ranging errors and on the geometry of ground tracking network in their footprint. The errors of the GEOs position solutions are a primary error contribution to the UERE in the GPS/WAAS positioning solution. Thus, the improvement of the GEOs orbit solutions is an important objective in the performance enhancement of the navigation system.

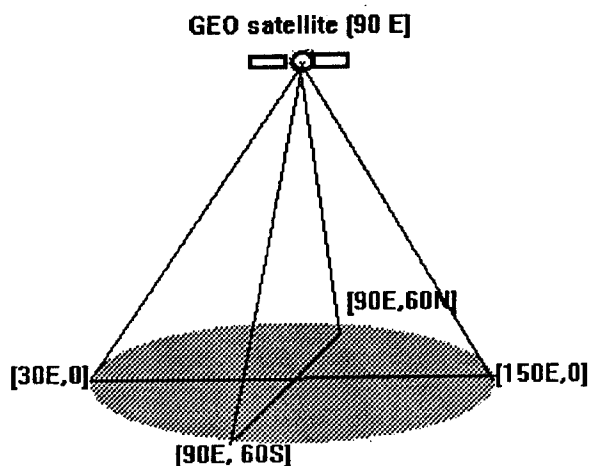


Figure 2 An ideal tracking network for a GEO at [90E,0]

An ideal tracking network for a GEO satellite consists of 4 or more ground stations, uniformly-distributed along the perimeter of its (circular) footprint. Figure 2 gives an example of such a network and of the footprint, which extends for 120 degrees in latitude and longitude. Any country network can only cover a fraction (less than one sixth) of this footprint area. The AAAS concept however allows the use of appropriately widely dispersed ground stations on both sides of the equator, covering a half to two third of the footprint area. This allows a significant strengthening of the geometry of GEOs orbit solutions. We may use the concept of Geometric Dilution Of Precision (DOP) to evaluate the relative suitability of a given ground network configuration for GEO orbit determination.

Table 2 lists the DOP values of GEO orbit determinations, when tracked from the individual ground networks in Japan, China and Australia, and when combining the networks into one AAAS network. The ranging RMS errors for all the GEO measurements are assumed to be identical. The symbols NDOP, EDOP and UDOP denote the DOP values of the Northing (cross track), Easting (along track) and Upward (radial) components of the GEO position errors. The results show that the DOP values of GEOs orbit determination for the AAAS network are 5 times as favourable as for the three individual country networks: If, for instance, we achieve

from the Australian country network a GEO orbit accuracy of 50 metres in the Upward component, the accuracy of the corresponding AAAS orbit determination would be about 10 metres. This reduces the GEO orbit error component in UERE from tens of metres to the level of a few metres, making it into a minor factor in the UERE budget. As a result, this gives a simple explanation for the assumption of $\sigma_{\text{GEO}} = 15$ metres in the following availability evaluations. The 1σ error of 15 metres is also the level of GPS UERE without Selective Availability on.

3.2 Navigation Availability and RAIM Detection Availability

The Navigation availability and RAIM availability for each individual country WAAS system and for the unified AAAS system were studied. Availability is defined as the percentage of time the system provides the required performance for a given phase of flight. For non-precision approach, we define availability as the average over a 24 hour period. The evaluation approaches for navigation and RAIM availabilities follow ref [7]. In this context, the Navigation function is deemed available if $2 \text{ HDOP } \sigma_{\text{GPS}} < 0.3 \text{ nmi}$, where $\sigma_{\text{GPS}} = 33.0$. The RAIM Detection function is automatically determined to be unavailable if fewer than 5 satellites are visible to the user. If 5 or more satellites are visible, the Approximate Radial-error Protection (ARP) value for a given time-space point is computed. If the computed ARP values exceed the ARP ceiling values, which vary with the number of visible satellites, RAIM is declared unavailable. The computational assumptions are summarised in Table 3, which also lists the scenarios to be evaluated. We study the individual WAASs as independently proposed by the three countries (cases 2,3 and 4), the independent country use of all visible GEOs (case 5), and the proposed unified AAAS with improved GEO ranging (case 6). In addition, we study the scenario of unified (improved) orbit determination, but limiting the user ranging to the countries' own GEOs (cases 2a, 3a and 4a). Table 4 shows the Navigation and RAIM detection availabilities, listing country/region averages and worst location availability. The main findings are:

- 1) For all GEO augmentations, NPA Navigation availability (Containment within tunnel without integrity check) is 100% over the areas of interest. Unaided GPS availability is on average, 99.8%, which falls short of the required navigation performance of 99.999 %.
- 2) GPS Augmentation through the individual country systems significantly improves RAIM Detection Availability but fails by far to meet the required integrity performance levels for civil aviation. For all countries,

Table 2 DOP values of GEO orbital determinations from different ground tracking networks

| GEO location | | 60 E | 80 E | 105 E | 110 E | 120 E | 135 E | 140 E | 150E | 165E |
|-----------------------------------|------|------|-------|-------|-------|-------|-------|-------|-------|-------|
| Japan 4 WRS stations | NDOP | | | | | 37.94 | | | 39.02 | |
| | EDOP | | | | | 20.07 | | | 22.15 | |
| | UDOP | | | | | 44.24 | | | 43.71 | |
| China 5 WRS stations | NDOP | | 18.17 | | 16.37 | | | 14.41 | | |
| | EDOP | | 13.42 | | 1.92 | | | 12.85 | | |
| | UDOP | | 14.20 | | 14.58 | | | 11.55 | | |
| Australia 5 WRS stations | NDOP | | | 11.14 | | | 10.96 | | | 10.34 |
| | EDOP | | | 12.32 | | | 2.06 | | | 12.67 |
| | UDOP | | | 16.36 | | | 16.79 | | | 14.65 |
| 3 countries 14 WRS stations | NDOP | 1.80 | 0.87 | 0.60 | 0.57 | 0.54 | 0.52 | 0.52 | 0.54 | 0.62 |
| | EDOP | 5.57 | 2.23 | 1.13 | 1.03 | 0.94 | 1.07 | 1.18 | 1.50 | 2.38 |
| | UDOP | 4.51 | 2.40 | 2.20 | 2.17 | 2.12 | 2.10 | 2.11 | 2.15 | 2.89 |

RAIM availability values are in the order of 60% for unaided GPS, improving to 88-96% for the individual augmentation schemes of the country WAASs, and to about 98%, if each individual country independently utilises all available GEO satellites.

3) The AAAS concept, with its utilisation of common orbit determination (section 3.1) results in 100% RAIM detection availability for all countries involved. The performance of the GEO augmentation system could thus be significantly enhanced by improving the GEOs ranging accuracy. Note that the level of 99.999% RAIM availability might also be achieved with 3 GEO satellites only, but it assumes availability of 24 GPS satellites and barometric aiding [9].

4. SUMMARY AND CONCLUSIONS

Compared with the individual WAAS systems of China, Australia and Japan, the proposed AAAS system provides two significant technical advantages. Firstly, by utilising the monitoring data collected in both northern and southern hemispheres and the resulting better geometry in GEO orbit determination, the accuracy of GEOs orbit determination can be significantly improved. The results show a reduction of the GEO DOPs by an average factor of 5 or more. This enables to reduce the effect of GEO's orbit error in the UERE from tens of

metres to a few metres. Secondly, the AAAS system allows ranging to more GEO satellites thus improving upon RAIM-Detection availability. A RAIM detection availability of 100 percent can be achieved for most of the Areas of Interest, such as Australia, China, Japan and South-East Asia. The same level of RAIM Availability can not be achieved by individual country-wide WAAS systems based on a 21 GPS satellite configuration.

The AAAS concept is analogue to the WAAS system currently implemented in USA. Only a low level of coordination is required between the countries: They must exchange observation data for improved GEO orbit determination and integrity warnings. This ensures a large degree of autonomy for each individual country system, requiring low levels of coordination.

The AAAS program, if implemented, would provide enhanced satellite-based navigation service for most of the Asian countries, Australian and the West-Pacific areas. It would create a golden opportunity for a broad collaboration among the involved countries in the areas of space technology and economic development. The authors believe that all the countries in these areas could make good contributions to the program and would greatly benefit from the AAAS long into the next century.

Table 3: Assumptions for the Availability Computations

| GPS constellation | Optimal 21 satellites (defined in [8]) |
|---|---|
| GEO satellite Constellations: (these locations are assumed for availability studies only) | 3 over AAOI: 105 E, 135 E, 165 E; 2 over Japan FIR: 120 E, 140 E 3 over China: 80 E, 110 E, 140 E; 6 over all the areas: 60 E, 85 E, 110 E, 130 E, 150 E, 1650E |
| Mask elevation angle | 7.5 degrees |
| DOP algorithms | all-in-view(3d position + time bias) |
| Sample points : (The Locations of the biggest airports) | 4 in Japan; 10 in Australia (1 in NZ) 9 in China; 9 in South-East Asia, 1 min step over a 24 hr period |
| 1 σ GPS pseudorange error (σ_{GPS}) and 1 σ GEO range error (σ_{GEO}) | $\sigma_{GPS} = 33.0$ m, $\sigma_{GEO} = 33.0$ $\sigma_{GPS} = 33.0$ m, $\sigma_{GEO} = 15.0$ |
| Evaluation cases: Case 1: 21 GPS SVs over all the areas Case 2, 2a : 21 GPS SVs + 3 GEOs over China ($\sigma_{GPS} / \sigma_{GEO} = 1$, $\sigma_{GPS} / \sigma_{GEO} = 2.2$) Case 3, 3a : 21 GPS SVs + 2 GEOs over Japan ($\sigma_{GPS} / \sigma_{GEO} = 1$, $\sigma_{GPS} / \sigma_{GEO} = 2.2$) Case 4, 4a: 21 GPS SVs + 3 GEOs over AAOI ($\sigma_{GPS} / \sigma_{GEO} = 1$, $\sigma_{GPS} / \sigma_{GEO} = 2.2$) Case 5: 21 GPS SVs + 6 GEOs over all the areas ($\sigma_{GPS} / \sigma_{GEO} = 1$ Case 6: 21 GPS SVs + 6 GEOs over all the areas ($\sigma_{GPS} / \sigma_{GEO} = 2.2$) | |

Table 4. Navigation and RAIM Detection Availabilities for Non-Precision Approach Navigation

| Area | Case | Navigation Availability(%) | | RAIM Detection Availability(%) | |
|-----------------|---------|----------------------------|---------|--------------------------------|---------|
| | | Average | Worst | Average | Worst |
| Japan | Case 1 | 99.688 | 99.097 | 65.382 | 57.986 |
| | Case 3 | 100.000 | 100.000 | 93.090 | 88.611 |
| | Case 3a | 100.000 | 100.000 | 97.205 | 94.236 |
| | Case 5 | 100.000 | 100.000 | 99.548 | 98.819 |
| | Case 6 | 100.000 | 100.000 | 100.000 | 100.000 |
| China | Case 1 | 100.000 | 100.000 | 70.154 | 60.486 |
| | Case 2 | 100.000 | 100.000 | 97.917 | 94.861 |
| | Case 2a | 100.000 | 100.000 | 99.599 | 99.028 |
| | Case 5 | 100.000 | 100.000 | 99.722 | 98.472 |
| | Case 6 | 100.000 | 100.000 | 100.00 | 100.000 |
| Australia | Case 1 | 99.772 | 98.472 | 76.212 | 64.931 |
| | Case 4 | 100.000 | 100.000 | 98.782 | 96.319 |
| | Case 4a | 100.000 | 100.000 | 99.861 | 99.167 |
| | Case 5 | 100.000 | 100.000 | 99.596 | 97.637 |
| | Case 6 | 100.000 | 100.000 | 100.000 | 100.000 |
| South-East Asia | Case 1 | 99.931 | 99.375 | 88.495 | 64.931 |
| | Case 5 | 100.000 | 100.000 | 99.923 | 99.306 |
| | Case 6 | 100.000 | 100.000 | 100.000 | 100.000 |

REFERENCES

- [1] A Technical Report to the Secretary of Transportation on a National Approach to Augmented GPS Service, NTIA Special Publication 94-30, 1994.
- [2] Australian Civil Aviation Authorities, Description of the Australian Wide Area Augmentation System (WAAS), in Response to the INMARSAT call for Allocations for Implementation of Navigation Payload Operational Service, October, 1994.
- [3] Civil Aviation Bureau, MOT of Japan, Development and Implementation Plan for GNSS in Japan, June 1994.
- [4] Civil Aviation Administration of China, The Implementation Strategic Policy of CAAC CNS/ATM System, Civil Aviation Economy and Technology, Vol. May 1995.
- [5] Wei, X, A Proposal of Wide Area Augmentation System (WAAS) for China and A tentative Consideration for Asia and Oceania Regional System, The proceedings of Satellite Navigation Technology: 1995 and beyond, Brisbane, June 1995.
- [6] Feng, Y.,K, Kubik, J. Sang, and F. Faruqi, A Feasibility Study for Asian-Australian GPS Augmentation System (AAAS), Proceedings of the First Conference on Space Technology and Developing Countries, Tehran, May 1995.
- [7] Chin, G.Y., J.H. Kraemer and R. G. Brown, GPS RAIM: Screening Out Bad Geometries Under Worst-Case Bias Conditions, Navigation, Journal of The Institute of Navigation, Vol. 39 No. 4 1992-93.
- [8] Greens, G. et al. The GPS 21 Primary Satellite Constellation, NAVIGATION, Journal of The Institute of Navigation, Vol 36, No. 1989.
- [9] Nicholson, W., RAIM Availability for Augmented GPS-based Navigation System, Proceeding of 7th International Technical Meeting, Salt Lake City, 1994.



Session A3

Precision Landing

Chair:

Dr. Per Enge
Stanford University

Co-Chair:

Ms. Cecelia Feit
Sierra Technologies

FAA – Wilcox Electric Category IIIB Feasibility Demonstration Program Flight Test Results

W. Hundley, S. Rowson, and G. Courtney
Wilcox Electric

V. Wullschlegler and R. Velez
FAA Technical Center

R. Benoist
Litton Aero Products

P. O'Donnell
MITRE/CAASD

ABSTRACT

Wilcox Electric has been working since June 1994 on a contract from the General Services Administration under the technical cognizance of the FAA's Satellite Program Office to demonstrate the feasibility of a local area DGPS to provide Category III B autoland capability. Accuracy and integrity features supported by actual technical demonstrations are the principal focus of the program although the contractor must also show how the proposed system design would satisfy continuity of service and availability requirements if developed for production and operational use. Wilcox has been assisted in this effort by Litton Aero Products, NovAtel Communications and Federal Express.

The focus in this paper is on the Category III B accuracy requirements, the system approach directed toward meeting these requirements, and the flight test results which demonstrate the actual in-flight capability of the system to conduct Category III B autolands.

The basic system approach is described. It utilizes high accuracy C/A code tracking with emphasis on design features which enhance accuracy and integrity. One noteworthy enhancement is the use of the new MEDLL (Multipath Estimating Delay Lock Loop) technology in the ground station.

This is followed by a description of the flight test program at the FAA Technical Center, Atlantic City, NJ, including a discussion of the ground station installation, the avionics installation in the FEDEX Boeing B727 and the data acquisition systems.

Test results based on in-depth statistical analysis (provided by the FAA Technical Center and

MITRE/CAASD) of 102 successful autolands are presented.

INTRODUCTION

There is an ongoing multi-faceted drive within the aviation community to apply GPS technology in a safe and cost beneficial manner to that most critical phase of flight - precision approach and landing under instrument meteorological conditions (IMC). Participation in this effort is widespread including but not limited to the FAA (Satellite Program Office, SOIT, Technical Center), ICAO, RTCA, MITRE, various universities and industrial organizations.

A key program in this effort is the FAA's Category IIIB Differential GPS Feasibility Demonstration Program in which Wilcox Electric is a participant. Category IIIB is defined in Advisory Circular 120-28C as "a precision instrument approach and landing with no decision height (DH), or with a DH below 50 feet and controlling runway visual range less than 700 feet but not less than 150 feet." DGPS as defined for the program can include such techniques as code corrections or carrier phase tracking on a real time kinematic basis but is limited to the information provided by the Standard Positioning Service (SPS). This latter restriction did not preclude the use of dual receiver, codeless techniques but did preclude the use of information from satellite systems other than GPS such as GLONASS or INMARSAT or hybrid systems utilizing ILS or MLS with GPS.

Emphasis in the program was placed on demonstrating the ability of the contractor's system design to provide automatic landing capability to the specified accuracy and on the performance of the contractor's integrity monitor. The contractor also had to analyze the proposed system design capability in the areas of integrity risk, continuity of function risk and availability if developed for production and operational use.

The demonstrations included two phases: 1. Flight tests at a Government facility in a contractor provided

transport type aircraft with autoland capability. 2. Simulator tests at a Government simulator facility. The flight test phase has been concluded and its results are the principal topic of this paper. The simulator demonstration is just under way at the NRAD facility at Warminster, PA.

The contracting authority for the program was the General Services Administration (GSA) Federal Systems Integration and Management Center (FEDSIM). Technical oversight resided in the FAA Satellite Program Office. The Wilcox team for the program included three key team members in addition to Wilcox. These were Litton Aero Products, NovAtel Communications and Federal Express.

Litton's responsibilities included the design, build and test of the avionics and the airborne data acquisition and recording equipment and support throughout the system integration and test.

NovAtel provided the GPS engines for the ground station and the avionics plus support during the design reviews.

Federal Express provided and operated the autoland equipped Boeing B727-200 certified for CAT III ILS autolands. Their responsibilities also included the integration and installation of the avionics and the airborne data acquisition system into the aircraft.

Wilcox Electric provided overall program management as well as system design and analysis; ground station design, build and test; data link transmitter and receiver design, build and test; and systems integration and test, including ground tests, flight readiness, flight trials and simulator test.

REQUIREMENTS FOR PRECISION APPROACH

In order to provide the basic precision approach function with the required degree of hazard-free operation, all precision approach systems must satisfy demanding standards of accuracy, integrity, and continuity of function. Taken together, these parameters define the RNP (Required Navigation Performance) necessary to execute precision approaches safely. A fourth RNP parameter is system availability. High availability of service, while not a direct safety consideration, is extremely desirable from an operations point of view. These are the four key requirements that must be satisfied by any precision approach system.

As an initial step toward determining whether any DGPS system architecture satisfies these RNP requirements, the

parameters themselves must first be quantified. Risk analysis based on a target level of safety (TLS) combined with a tunnel (or TERPS surfaces) concept are methodologies that are useful in assigning quantitative values to accuracy, integrity, and continuity of function parameters for precision approach and landing. The TLS for precision approach and landing is generally agreed to be no more than one accident in 10^8 landings.

Current accuracy, integrity and continuity of function requirements for Category III ILS also provide a valuable baseline in quantifying these requirements. In the case of availability, we start with what we are achieving today with ILS and translate it to a satellite-based system. The translation is not straightforward. For example an ILS unavailability normally impacts a single runway end whereas DGPS unavailability could involve an entire airport or region of airports.

The FAA Category IIIB DGPS Feasibility Program required that the accuracy and integrity monitoring logic of the proposed system design be verified by flight trials and taxi tests. Satellite simulator tests will further characterize these performance parameters, particularly the integrity monitoring logic under conditions not readily achieved during flight testing. The principal quantitative output of the flight trials is a measure of the accuracy of the proposed DGPS system approach and its capability to provide autolands to Category IIIB standards with an actual in-service aircraft and is the principal focus of this paper.

Two types of accuracy requirements were specified for the Program:

- 1) DGPS Navigation Sensor Error (NSE).
- 2) Total System Error (TSE).

The contractor was permitted to choose which type of requirement the system design must satisfy. If a contractor elected the total system error requirement, which Wilcox did, then its system must also meet aircraft touchdown and roll-out accuracy requirements which are critical to Category IIIB autolands. Both types of accuracy requirements are important and both were measured during the program and their performance evaluated.

In determining the navigation sensor error (NSE) requirement the principal guidelines are the current ILS specifications promulgated in ICAO Annex 10 for error components that make up the NSE. These components include ground equipment bias, airborne receiver bias and ground equipment course structure (beam bends).

The 95% NSE is taken as the root sum square of the 95% value of these three error components. Table 1 lists these values of NSE for Category III ILS for the final critical part of the approach path. The table also lists similar NSE requirements defined for the FAA CAT III Feasibility Program plus a set of requirements contained in the RTCA Paper No 252-95/SC-159-652 -FAA SOIT

Consensus on Requirements for the Local Area Augmentation System (LAAS) ORD, James Fernow, 19 April, 1995. This latter set of requirements was employed in the recent FAA/GSA LAAS RFP. In this case the numbers in parenthesis in Table 1 represent the objective and the nonparenthetical numbers are the minimum acceptable.

Table 1 - Requirements for Category III 95% Navigation Sensor Error (NSE) -meters

| Height above Threshold (feet) | Distance from Threshold (feet) | Lateral Requirement (meters) | | | Vertical Requirement (meters) | | |
|-------------------------------|--------------------------------|--------------------------------------|--|-----------------------|--------------------------------------|--|---------------------|
| | | ILS ¹ ICAO Annex 10 | FAA CAT III Feasibility Program | FAA / GSA LAAS RFP | ILS ² ICAO Annex 10 | FAA CAT III Feasibility Program | FAA/GSA LAAS RFP |
| 50 | 0 | 5.3 | 4.4 | 5.5 (4.4) | 0.6 | 1.2 | 1.8 (1.3) |
| 100 | 954 | 5.8 | 4.4 | 5.5 (4.4) | 1.3 | 1.2 | 1.8 (1.3) |
| 200 | 2862 | 6.9 | 5.1 | 5.5 (4.4) | 2.7 | 2.4 | 1.8 (1.3) |
| 500 | 8586 | 16.5 | | 5.5 (4.4) | 7.0 | 6.1 | 1.8 (1.3) |

Notes ¹ Assumes 10000 feet localizer to threshold distance

Notes ² Assumes 3° glide path, 50 feet threshold crossing height

The data in Table 1 indicates a much more difficult requirement in the vertical axis than the lateral axis. The disparity in the lateral and vertical linear accuracy requirements derives both from the fact that ILS is an angular system and that the localizer and glide slope guidance sources are separated by distances that are typically 7000 to 10,000 feet. A Category III ILS is basically a 0.1 degree angular system. This fact plus the typical physical separation of the lateral and vertical guidance elements leads directly to the current ± 18 foot (± 5.3 m) localizer, ± 2 foot (± 0.6 m) glide slope requirement at the threshold. The lateral requirement 95% ± 18 feet) is actually a larger lateral sensor error than one would like in order to assure touching down in the desired touchdown zone and the ± 2 feet vertical error is better than required. This trend can be discerned in the

more current DGPS requirements set forth in the Table. The substantially superior linear accuracy characteristic of DGPS compared to ILS at distances a half mile and greater from the threshold has the potential to enable the autopilot to provide improved flight stability on the approach path and also offers the potential for improving the efficiency of air space utilization, obstacle clearance and noise abatement.

For the second accuracy measurement criterion - total system error - the requirements were based on the tunnel-in-space concept. Since this concept is relatively new the actual tunnel dimensions can be expected to undergo further refinement with time. The TSE requirements as they were specified for the Program are listed in Table 2.

Table 2 - Requirements for 95% Total System Error (TSE) for FAA Category IIIB DGPS Feasibility Program

| Height above Threshold (feet) | Distance from Threshold (feet) | Requirements | |
|-------------------------------|--------------------------------|------------------------|-------------------------|
| | | Lateral Error (meters) | Vertical Error (meters) |
| 50 | 0 | 15.5 | - |
| 100 | 954 | 22.9 | 4.6 |
| 200 | 2,862 | 33.5 | 9.8 |
| 750 | 13,357 | 83.8 | 27.1 |

The TSE methodology also requires that for Category III the equipment demonstrates that the 95th percentile accuracy of the autoland touchdowns will not exceed a ± 27 foot lateral dispersion about runway centerline and that the total 95% longitudinal dispersion is no greater than 1500 feet.

It is important to note that the ± 18 foot lateral NSE allowed at the threshold for current Category III ILS (Refer to Table 1) represents a major part (67%) of the ± 27 foot TSE while the ± 2 foot vertical displacement from a 3 degree glide path translates into a 38 foot longitudinal error, which is less than 3% of the 1500 foot longitudinal TSE requirement.

In addition Advisory Circulars AC 20-57A and AC120-28C specify that Category III systems must demonstrate by a combination of flight test, simulation and/or analysis that the probability that an aircraft touchdown will be outside a prescribed runway area is less than 10^{-7} . Further the probability that during roll out the outboard landing gear comes within 5 feet of the lateral limits of a 150 foot wide runway must be less than 10^{-6} .

SYSTEM DESIGN APPROACH

The fundamental GPS technique used in the system is C/A code tracking for determination of pseudorange and range rate. This serves as the underpinning of a basically simple, robust and reliable design. At one point in time it was believed that code tracking would not provide sufficient accuracy for automatic landing and that more complex carrier phase tracking approaches would be required. This was true of what was then conventional code tracking. However, code tracking with narrow width correlators as exemplified by the NovAtel GPS card has already been demonstrated by Wilcox[1] to be at least two to three times more accurate than standard width correlators and capable of meeting autoland accuracy requirements.[2] The narrow width correlation technique greatly [3] minimizes the effects of receiver noise and multipath which are the two major residual GPS error sources when operating in the local differential mode. For the ground station used in the FAA feasibility program the multipath rejection capability of the narrow correlator has been further enhanced by the use of the MEDLL (Multipath Estimating Delay Lock Loop) technology developed by NovAtel. [4] The MEDLL separately estimates the parameters of both the direct line-of-sight and the reflected signals and removes the multipath component at the signal level. A standard NovAtel narrow correlator card is used in the avionics.

For the total system error (TSE) concept which includes flight technical error (FTE), an important element of the integrity monitoring, of necessity, resides in the aircraft. This is the implementation of a TSE warning whenever the aircraft is in danger of penetrating an outer tunnel safety boundary. The warning algorithm implemented in the avionics was

$$\text{WARN if } |FTE| + K\sigma_{NSE} > T$$

where: FTE = measured flight technical error
 σ_{NSE} = estimated standard deviation of the system navigation sensor error
 K = constant
 T = outer tunnel limit

Separate values are computed for the lateral and vertical errors. A large value of K will improve the probability of missed detection but at the expense of increasing the false alarm rate. A value of K = 3 was implemented for the demonstration equipment.

FLIGHT EVALUATION EQUIPMENT

The ground station used in the demonstration program was a single thread system (see Figure 1), that is, a single reference unit, single data link and single integrity monitor. For actual operational use this configuration would be expanded to include the redundancy necessary to provide continuity/integrity performance required by Category IIIB requirements. The reference unit and the integrity monitor each contained its own MEDLL receiver. Their GPS antennas were separated by 300 feet in order to place them in environments with uncorrelated multipath, were mounted on 8 ft poles to be compatible with eventual operational requirements (clearance for snow, mowers, etc.), and were fitted with choke rings to reduce multipath effects not already eliminated by the MEDLL technology. Multipath effects were further mitigated through use of long time constant carrier phase smoothing in the receivers.

The monitor unit looked at pseudorange corrections (PRC) and range rate corrections computed by the reference unit both before and during transmission to the aircraft. A software algorithm was used to remove the effects of any clock bias between the two receivers so that reference and monitor pseudorange corrections could be meaningfully compared. Any of a number of conditions could cause the monitor to remove corrections from the signal in space for a particular satellite (e.g. large PRC differences, satellite not tracked by the monitor). Using the removal of a satellite's corrections, as opposed to sending an explicit "don't use" message is more fail-safe.

PRC differences between the reference and monitor units were used to compute a UDRE (user differential range error) for each satellite. UDREs were transmitted to the aircraft, along with PRC corrections and rate corrections at 5 Hz. Each UDRE was recomputed every 200 msec.

The ground station also transmitted approach pathpoints (checked by the monitor) to the aircraft for comparison with the pathpoints stored in the avionics. This is a key integrity feature.

The data link transmitter operated in the VOR navigation band and used GMSK modulation. The data link antenna was horizontally polarized and omnidirectional.

Figure 2 is a high level block diagram of the avionics system. The principal unit, the GPS Landing System Unit (GLSU), was a modified Litton LTN-2001 MK2 which consisted of a NovAtel narrow correlator GPS receiver, a processor and I/O to handle the interfaces with the aircraft autopilot and the PC based airborne data acquisition system. The VHF data link receiver for obtaining the ground station corrections was connected to an existing VOR antenna on the aircraft. The GLSU processor converted DGPS navigation sensor position information into ILS "look alike" lateral and vertical deviation signals that drove the B727-200 flight control system. The deviations were actually transmitted to the autopilot at a 20 Hz rate. This was accomplished using the differentially corrected GPS velocities to "project ahead" the 5 Hz position data at 50 msec intervals. It is important to note that the B727 does not utilize an inertial system and the DGPS navigation solution was not augmented in any way.

As previously indicated an important component of the integrity monitoring scheme was implemented in the avionics. The ground station UDREs for all satellites used in the position solution were averaged, multiplied by HDOP or VDOP, and combined with an avionics position uncertainty obtained from the GLSU Kalman filter covariance matrix to obtain an estimate of the 3σ NSE vertical and lateral error bounds. The 3σ NSE bounds were then added to the indicated flight technical error (FTE) to determine whether the aircraft was potentially outside the total system error (TSE) outer integrity tunnel. Excursions outside this tunnel (vertically or laterally) would cause a "tunnel alarm" indication to be latched, warning that a missed approach should be executed.

Although operational avionics would be duplicated or triplicated, the system tested was single thread with

parallel outputs to the multiple flight control system inputs normally provided by the ILS.

The FEDEX B727-200 flight control system is driven by the Sperry/Honeywell SP-150 Automatic Flight Control System (AFCS). This is an analog system and is approved for fail-passive autolands, Category IIIA, 50 ft DH in the B727-200 of which FEDEX has about 90 such aircraft in operation. The SP-150 is divided into a yaw damper subsystem and an autopilot subsystem. The yaw damper system controls the rudders to dampen out oscillations about the vertical (yaw) axis without affecting normal aircraft turns.

The autopilot system consists of two control channels.

- A. The roll channel controls aileron position, thereby controlling roll attitude and heading changes.
- B. The pitch control channels control the aircraft about the lateral axis. The elevators are used to maneuver the aircraft and the stabilizer is used to trim the aircraft for a stable flight condition. There are two pitch channels. Each can be selected individually to control one elevator with the other elevator acting as a slave. During an autoland approach both pitch channels are used to drive the two elevators independently and simultaneously.

The SP-150 does not have an autothrottle subsystem thereby requiring the pilot to manually control the throttles during autolands. One of the more interesting aspects of the program was to see how DGPS would fare with an older flight control system in an autoland environment.

Ground truth during the flight trials was primarily provided by the FAA Technical Center laser tracker. The laser radiation illuminates a retroreflector mounted on the bottom of the fuselage near the nose of the aircraft. The reflected laser energy is tracked and provides azimuth, elevation and range to the retroreflector with respect to the laser tracker origin. Laser tracker azimuth and elevation are reported to be accurate to 20 arc seconds (1σ) and the range accuracy is ± 1 ft 1σ out to 5 nmi. The laser tracker was backed up by modified NIKE - Hercules tracking radar. Co-mounted with the tracking radar was a video camera which recorded an image of the aircraft landing gear tagged with GPS time and was used to determine the actual time of aircraft touchdown.

DESCRIPTION OF TESTS

The flight trials were conducted at the Atlantic City, NJ International Airport in conjunction with the FAA Technical Center. There are two intersecting runways at the airport-RW 13/31 and RW 4/22. Runway 13 is the preferred approach direction (traffic and wind conditions permitting) because it has the best geometry with respect to the laser tracker and because of its length.

After completion of a Flight Readiness Review on Friday, April 14, autoland flight tests began Monday morning, April 17. A total 102 successful autolands out of 106 approaches were achieved by Friday afternoon, April 21. 76 of the 102 autolands were made to Runway 13, 4 were to Runway 31, 8 to Runway 04 and 14 to Runway 22. Runway approach selection was accomplished through a pilot-operated RUNWAY SELECT switch. No other actions were required in the avionics or ground station in order to change runways.

Of the 102 successful autolands 92 were touch and go and 10 of them were continued through roll-out.

All 102 were routine autolands with no indication of any problems.

Concerning the 4 unsuccessful approaches, 3 of them resulted in missed approaches and were caused by the autopilot failing to capture in the lateral channel. FEDEX produced documentation of a history of occasional localizer capture failures with this model autopilot during ILS approaches. Replacing the roll channel computer in the autopilot cleared the problem. The fourth unsuccessful approach resulted when the avionics equipment indicated loss of differential corrections, displayed the localizer and glide slope flags, illuminated the tunnel warning light and stopped recording data. This loss of guidance occurred near the runway threshold and the pilot completed the landing manually rather than execute a missed approach. At the time of this anomaly it was thought the data link receiver had failed. It was replaced and all remaining 26 autolands were completed successfully. The replaced data link receiver was later tested and found to be operating normally. Inspection of the recorded ground station data showed that it was transmitted normally during this period. It is now hypothesized that the failure was due to a glitch in the avionics single channel power system.

The normal approach procedure was to execute a 30 degree intercept with the autopilot engaged at about 7 n mi from the runway threshold and an altitude of 1800 feet and remain in the autoland mode until touchdown. Airborne data recording started with the aircraft on the approach path about 5 nmi from the threshold. The Laser Tracker normally acquired the aircraft 6 to 7 miles out on the approach. Ground station data was recorded continuously. All data is GPS time tagged for post processing synchronization. Four (4) taxi tests were also conducted in which the aircraft was taxied in and out of the lateral and vertical outer tunnel integrity alarm boundaries in order to check the functioning of the integrity alarm logic.

TEST RESULTS

The raw data measured by both the avionics and ground station data acquisition systems for each approach were converted to the format specified for the program, then merged with the ground truth data from the laser tracker. This data was then processed by both the FAA Technical Center and MITRE/CAASD to produce the final official test results. Wilcox Electric and Litton Aero Products also processed parts of the data. As would be expected the test results as processed by the different organizations are in very close agreement with only negligible differences in the numbers.

Two classes of statistical analysis were applied to the test data.

- 1) Hypothesis Testing
- 2) Estimation Statistics.

The hypothesis testing process which is a standard manufacturing quality control technique was used to determine whether or not the system satisfied the requirements of a specific measure of success (MOS) specified in the contract. For example, it was specified that for the 100 approaches analyzed for TSE the level of significance is 5% and the allowed percentage of out of tolerance errors was 5%. Based on these parameters 91 approaches must be successful for the MOS to be satisfied. For an approach to be considered successful the measured TSE must always be within the inner tunnel over the evaluation region. All MOS's were easily satisfied since there were no out of tolerance conditions on any one of the 102 approaches analyzed.

The estimation statistics are of much greater interest since they quantitatively characterize the system performance actually achieved during the flight test. A number of statistical parameters were computed from the data ensemble obtained from the 102 approaches, the

most significant of which is $|\mu| + 2\sigma$ or the sum of the absolute value of the mean plus twice the standard deviation. This is considered to be a conservative representation of the 95% error and is employed throughout this paper unless otherwise noted.

The test results which characterize the accuracy performance in terms of navigation sensor error, flight technical error and total system error are enumerated below:

Navigation Sensor Error (NSE): The Navigation Sensor Error (NSE) is the difference between the aircraft position as indicated by the DGPS system and the "true" aircraft position as indicated by the laser tracker. It includes the effects of errors in the DGPS ground equipment and the DGPS avionics. The indicated NSE also includes a small error due to imperfections in the laser tracker. The NSE is expressed in runway coordinates in terms of along track error, cross track error and vertical error with only the latter two errors being significant for the precision approach function.

Table 3 summarizes the NSE performance based on test data from 102 approaches. From 200 ft HAT to touchdown - the final critical part of the approach - the values of lateral NSE as computed by the three different organizations vary from 0.76 meters to 0.96 meters. This is far better performance than any current requirement.

For vertical NSE from 200 ft HAT to 50 ft HAT (runway threshold) the values of NSE vary from 1.20 meters to 1.37 meters. At altitudes lower than 50 ft HAT vertical guidance in an autoland is provided by the on-board radar altimeters. These figures are compatible with the objective values delineated in the recent LAAS RFP (Refer to Table 1) and well within the listed threshold values.

The last line of Table 3 represents the 95% error statistics for an ensemble of data taken every 0.1 nmi from threshold out to 2 nmi from threshold for all approaches (about 2,000 data points). These statistics are slightly larger than the values shown for the specific near-in HAT in the Table. This is not unexpected since the laser tracker is less accurate for points further out on the approach path. Figure 3 is a plot of the vertical NSE trajectories and estimation statistics along the trajectories for the 100 autolands. As can be seen from the data for the majority of the time the vertical NSE is less than 1 meter.

The values reported in Table 3 are unfiltered NSE. Another method for characterizing navigation sensor performance is in terms of path following error (PFE) and control motion noise (CMN). The PFE is a low frequency component of the NSE which will cause the aircraft to deviate from the desired path. The CMN is a higher frequency component which will not cause any aircraft deviation but can cause disturbing control surface motions, attitude oscillations and control column motion in an autopilot driven aircraft. The PFE and CMN values are obtained by passing the unfiltered NSE for an approach through PFE and CMN filters the parameters of which have been defined by ICAO for MLS and which represent typical transport aircraft response characteristics. Both MITRE and Wilcox independently performed the necessary data processing and got the same results which can be summarized as follows;

- 1) There is little or no difference between the 95% values of the unfiltered NSE and the PFE. This has been a consistent result with previous Wilcox tests.

- 2) CMN performance was excellent and well within current MLS specifications (Refer to Figures 4 and 5). This has also been a consistent result with previous Wilcox tests and is a positive factor for pilot acceptance.

Flight Technical Error (FTE): Flight Technical Error which is the difference between the aircraft position as defined by the DGPS navigation equipment and the aircraft position defined by the desired flight path is a measure of how well the aircraft flight control system can respond to its guidance inputs. Table 4 tabulates both mean and the 95% statistics for the FTE as measured for the 102 autolands executed by the B727-200. The Table shows a significant bias for the lateral FTE. It is noted that there were persistent - approaching 10 knots at times - cross winds present throughout the flight test.

As a point of comparison in the recent autoland flight tests with the UPS Boeing 757 aircraft [5] the lateral FTE over the final 4 nmi was less than 13 m (95%) for 43 approaches and at threshold was 2.4 m (95%) with a mean of 0.0m. For the same 43 approaches the vertical FTE was 1.6 m (95%) over the final 4 nmi and 1.6 m (95%) at threshold. In the case of autoland tests with the NASA Langley Boeing 737-100 aircraft [2] which has been modified for flight research the measured FTE at 150 ft. HAT was 2.2 m (95%) lateral and 2.3 m (95%) vertical. The improvement in these latter two cases over the B727-200 can be attributed to the more advanced digital autopilots installed in these aircraft.

TABLE 3 - 95% Navigation Sensor Error
102 Autolands
FAA/WILCOX CAT IIIB Demonstration

| Height Above Threshold (feet) | Lateral NSE (Meters) | | | Vertical NSE (Meters) | | |
|-------------------------------|-------------------------------|---------------------------|--------------------------------|-------------------------------|---------------------------|--------------------------------|
| | FAA Tech Center Data Analysis | MITRE CAASD Data Analysis | Wilcox Electric* Data Analysis | FAA Tech Center Data Analysis | MITRE CAASD Data Analysis | Wilcox Electric* Data Analysis |
| 0 | | .96 | | | | |
| 50 | .90 | .86 | | 1.30 | 1.25 | |
| 100 | .87 | .74 | | 1.37 | 1.35 | |
| 200 | .86 | .86 | .76 | 1.27 | 1.31 | 1.20 |
| 700 to 50 | .99 | | .90 | 1.41 | | 1.35 |

*92 Autolands

TABLE 4 - 95% Flight Technical Error
102 Autolands
FAA/WILCOX CAT IIIB Demonstration

| Height above Threshold (feet) | Distance from Threshold (feet) | Lateral FTE (Meters) | | Vertical FTE (Meters) | |
|-------------------------------|--------------------------------|----------------------|-------------------|-----------------------|-------------------|
| | | Mean (μ) | $ \mu + 2\sigma$ | Mean (μ) | $ \mu + 2\sigma$ |
| 50 | 0 | -2.43 | 6.43 | 0.36 | 3.16 |
| 100 | 954 | -2.43 | 6.56 | 0.38 | 3.19 |
| 200 | 2862 | -2.81 | 9.18 | -0.16 | 2.75 |
| 700 to 50 | 12,403 to 0 | -2.84 | 13.73 | 0.19 | 3.28 |

Total System Error (TSE): The TSE which is the displacement of the true aircraft position from the desired aircraft position is the final answer as to the accuracy of the overall precision approach system. It includes all the effects of errors in both the navigation system performance (including ground and airborne equipment) and in the performance of the aircraft flight control system be it automatic or manual. The TSE is expressed in terms of the instantaneous lateral and vertical displacements of the actual position of the aircraft from the desired flight path.

Table 5 indicates the 95% values of TSE. In all cases the TSE requirements were met with margin. The test results clearly demonstrate that with the current high precision NSE provided by the Wilcox DGPS system the total system error is completely dominated by the B727-200 flight technical error (Refer to Figure 6). Any further improvements in NSE would have no impact on TSE. Figure 7 shows the touchdown dispersions for 93 autolands as plotted by the FAA Tech. Center. 93 are

plotted instead of 102 because the ground truth system could not track the aircraft beyond the threshold on one of the runways. As can be seen all 93 autolands were well within the 95% touchdown zone specified in AC20-57A. The lateral dispersion ($|\mu| + 2\sigma$) was 5.71 meters (18.7 ft). The 2σ longitudinal dispersion was 113.2 meters (371.4 ft). In no case was the outboard landing gear anywhere near 5 feet from the runway edge. This performance certainly equals and is probably better than would be obtained with ILS inputs to the B727 flight control system.

TABLE 5 - 95% Total System Error
102 Autolands
FAA/WILCOX CAT IIIB Demonstration

| Height above Threshold (feet) | Lateral TSE - (Meters) | | | Vertical TSE - (Meters) | | |
|--|--------------------------------------|---------------------------------|--|--------------------------------------|---------------------------------|--|
| | FAA Tech. Center Data Analyses | MITRE CAASD Data Analysis | FAA CAT III Program Requirement See Table 2 | FAA Tech. Center Data Analysis | MITRE CAASD Data Analysis | FAA CAT III Program Requirement See Table 2 |
| 0 | 5.71 | 5.51 | 8.23 | - | - | - |
| 50 | 6.41 | 6.20 | 15.50 | 3.73 | 3.25 | - |
| 100 | 6.41 | 6.71 | 22.90 | 3.89 | 3.27 | 4.6 |
| 200 | 9.16 | 9.80 | 33.50 | 3.29 | 3.13 | 9.8 |

As previously indicated taxi tests were conducted to test the integrity monitor TSE alarm logic. In all cases the alarm activated shortly before the outer tunnel TSE alarm boundary was penetrated by the taxiing aircraft and returned to normal when the aircraft was taxied back inside the tunnel. This was the expected result. The integrity test data is still being analyzed for quantitative performance in the areas of time to alarm and the precision of the NSE estimated by the system compared with the true NSE. The results of this analysis together with the results from the simulator test program will be reported in the future.

CONCLUSIONS

- The additional multipath rejection capability provided by the MEDLL technology resulted in a significant improvement in DGPS accuracy.
- The 95% navigation sensor error of ± 0.9 meters lateral and ± 1.3 meters vertical continues a trend of improving accuracy attainable with C/A code tracking DGPS and is the best performance achieved to date.
- The tests demonstrated that code tracking local area DGPS can provide Category III autoland capability to older in-service aircraft equipped with less than state of the art flight control systems.

ACKNOWLEDGMENTS

The authors wish to express their appreciation to avionics engineers Ray Cole and Steve Fink of FEDEX and Bill Pagel of Litton for their valuable contributions to the program. We would also like to thank the FEDEX flight crew - Capt. Dave Pace, First Officer Gary McCracken,

Second Officer Bill Shidler, Second Officer Todd Menning - for their dedication and hard work. Finally thanks are in order to Ray Swider of the FAA Satellite Program Office for his enthusiasm and support.

REFERENCES

1. Hundley W, Rowson S, Courtney G, Wullschleger V, Velez R, and O'Donnell P; **Flight Evaluation of a Basic C/A Code Differential GPS Landing System for Category I Precision Approach;** NAVIGATION, Journal of the Institute of Navigation, Vol. 40, No. 2 Summer 1993
2. Rowson S, Courtney G, and Hueschen R; **Performance of Category IIIB Automatic Landings Using C/A - Code Tracking Differential GPS;** NAVIGATION, Journal of the Institute of Navigation, Vol 41, No 2 Summer 1994
3. VanDierendonck A.J., Fenton P, and Ford T; **Theory and Performance of Narrow Correlator Spacing in a GPS Receiver;** NAVIGATION, Journal of the Institute of Navigation, Vol 39, No. 3, Fall 1992
4. Townsend B, VanNee R, Fenton P, and VanDierendonck K; **Performance Evaluation of the Multipath Estimating Delay Lock Loop;** Proceedings ION National Technical Meeting; Jan. 18-20, 1995
5. VanGraas F, Diggle D, Wullschleger V, Velez R, Kuehl G, Hilb R, and Dimeo M; **FAA/Ohio University/UPS Autoland Flight test Results;** Proceedings ION National Technical Meeting; Jan. 18-20, 1995

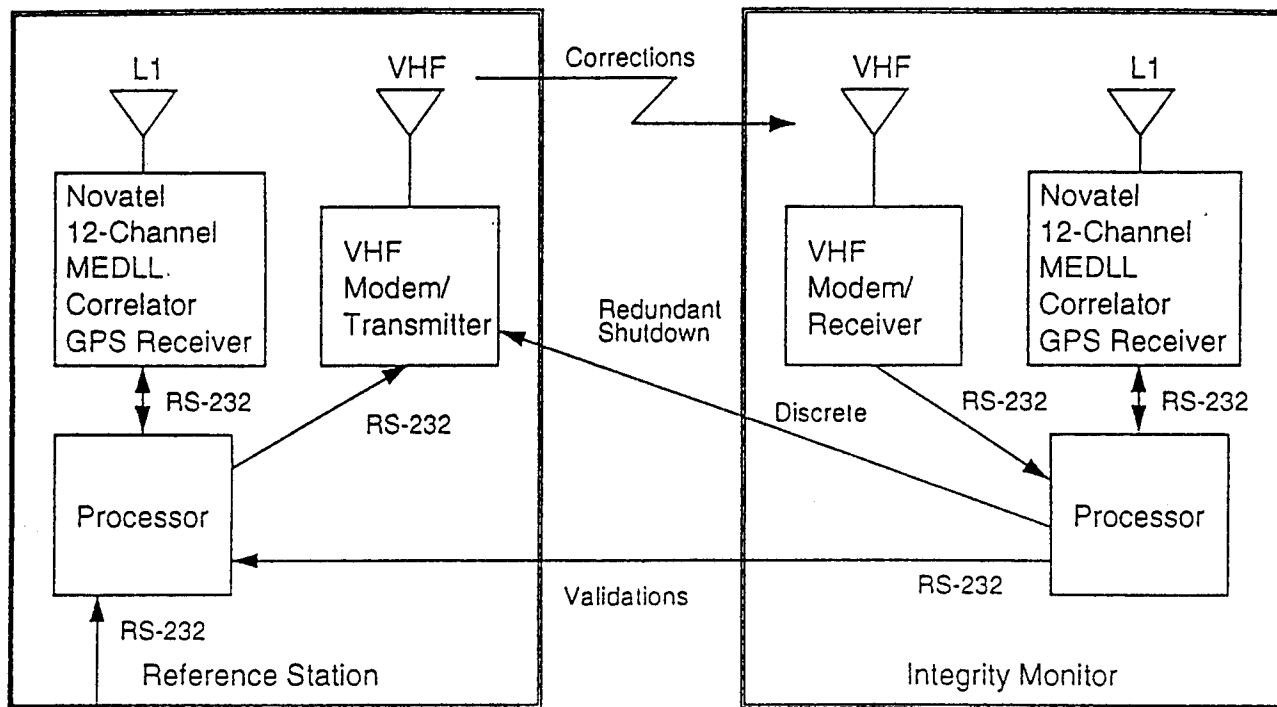


Figure 1: DGPS Ground Station, Block Diagram

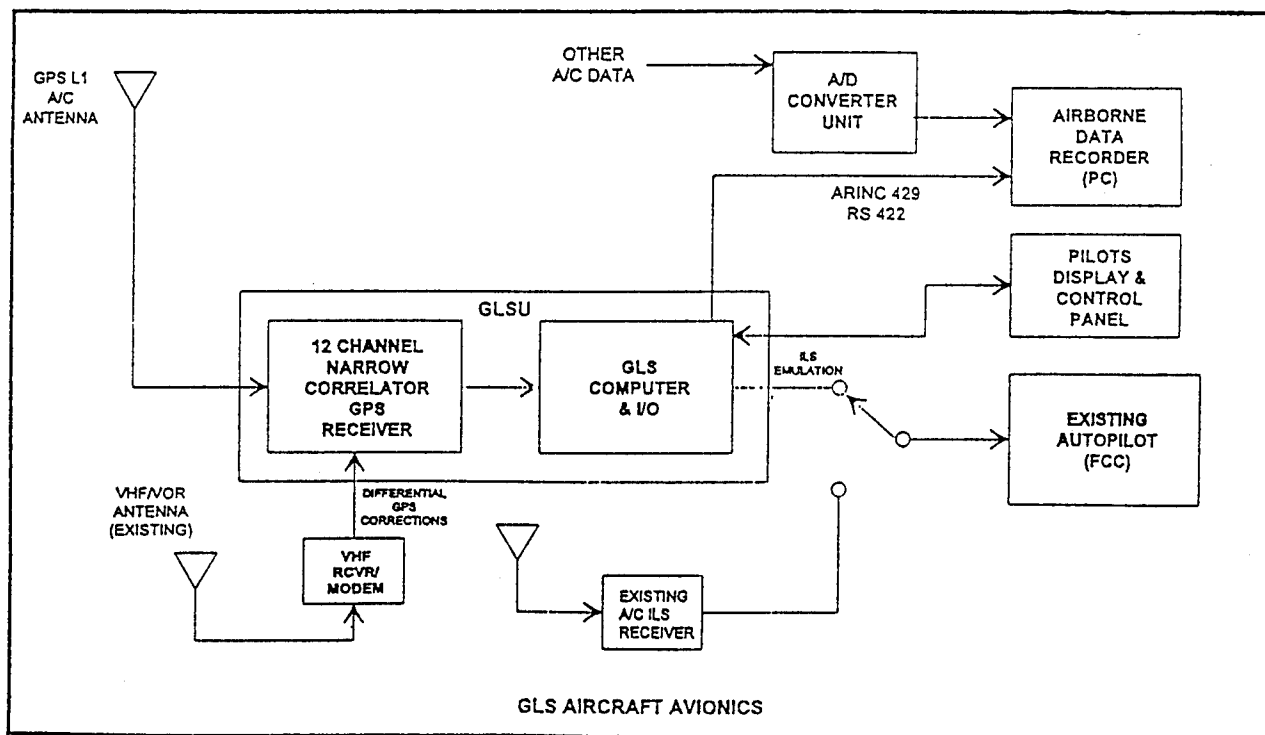


Figure 2: DGPS Airborne Station, Block Diagram

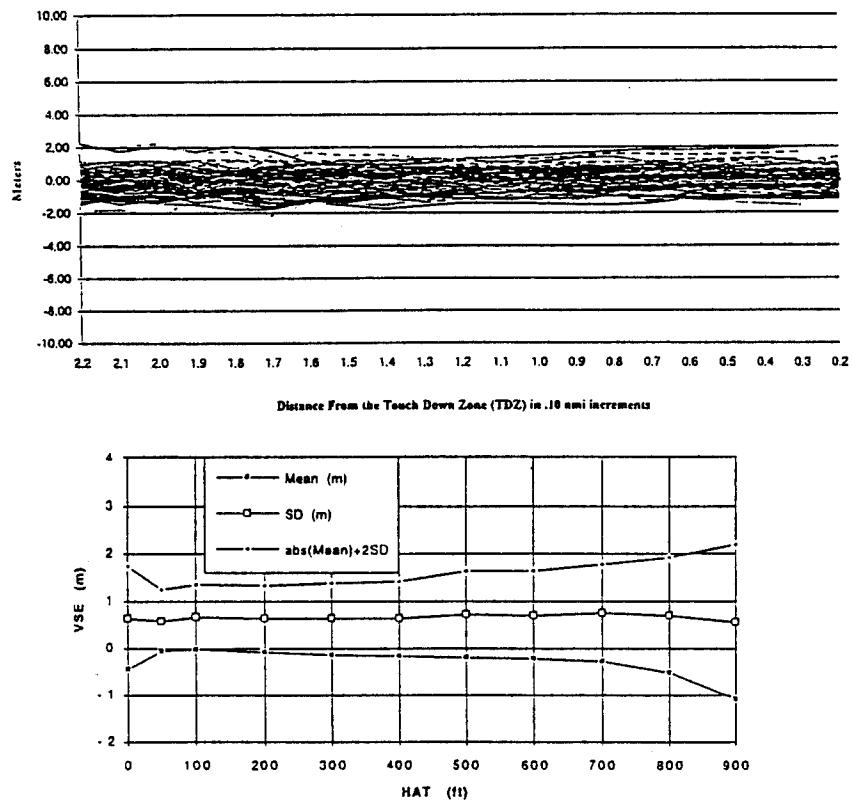
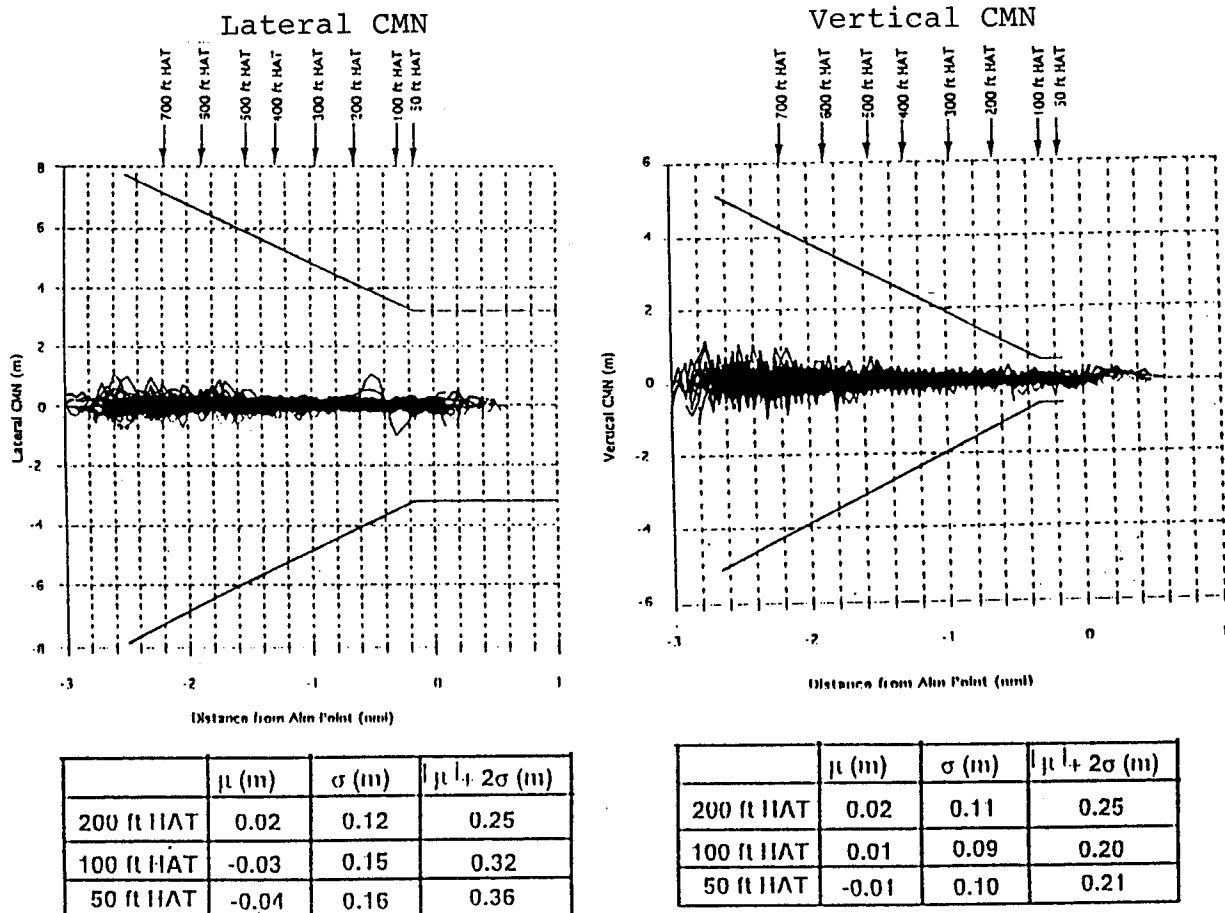


Figure 3: Vertical NSE Trajectories and Estimation Statistics



Figures 4,5: Lateral and Vertical CMN Trajectories and Estimation Statistics

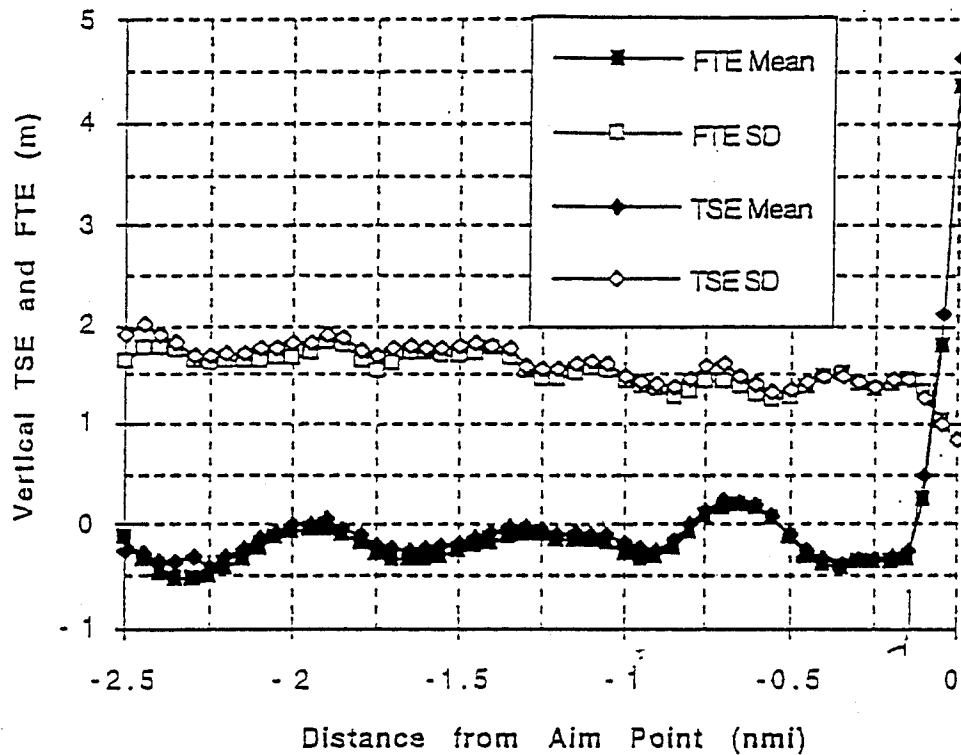


Figure 6: Comparison of Vertical TSE and FTE.

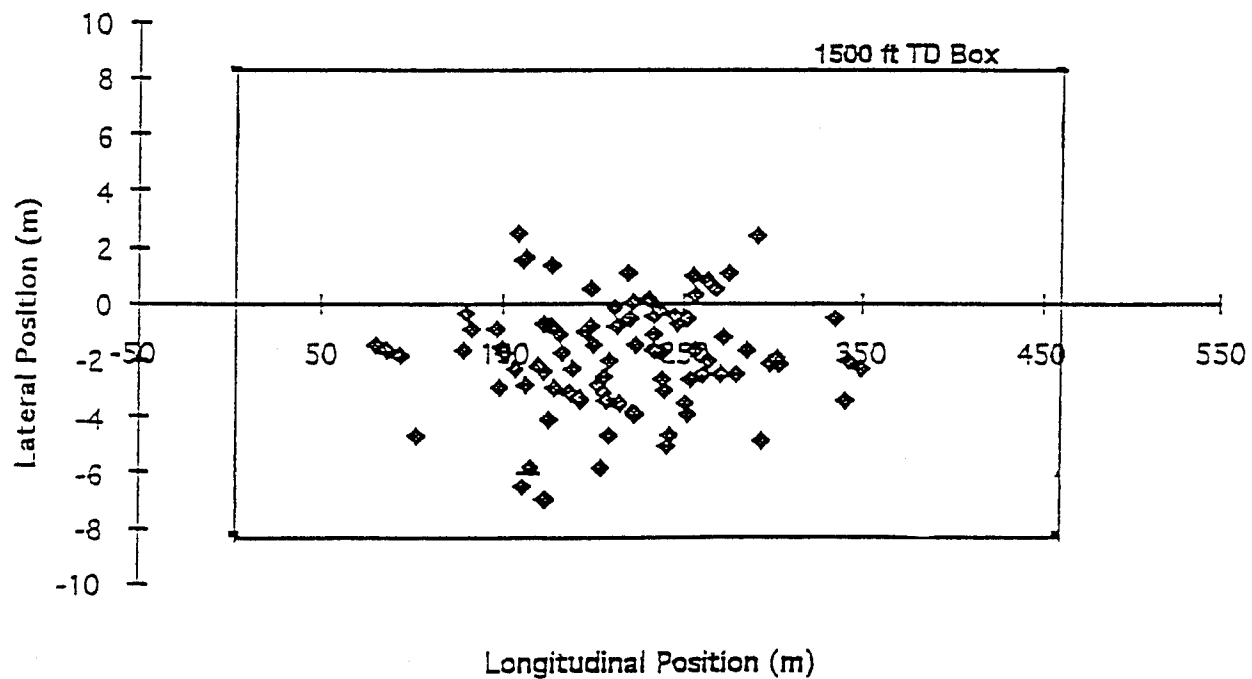


Figure 7: Touch down Dispersion - 93 Autolandings

FAA/Ohio University/United Parcel Service

DGPS Autoland Flight Test Demonstration

Frank van Graas, David Diggle, and Maarten Uijt
Avionics Engineering Center, Ohio University

Victor Wullschlegler and Ruben Velez
FAA Technical Center

Dave Lamb and Mark Dimeo
System Resources Corporation

Greg Kuehl and Robert Hilb
United Parcel Service

BIOGRAPHIES

Frank van Graas is Associate Professor of Electrical Engineering and Computer Science at Ohio University, Athens, OH and a Principal Investigator with the Ohio University Avionics Engineering Center. His research interests center on all facets of GPS including aircraft flight reference and precision approach and landing.

David W. Diggle is a Research Scientist with the Ohio University Avionics Engineering Center. He has recent experience with GPS kinematic flight reference systems and aircraft flight test.

Maarten Uijt de Haag is a Research Engineer with the Ohio University Avionics Engineering Center. He supports the GPS software development and flight test operations.

Victor Wullschlegler is an Electronics Engineer with the FAA Technical Center (FAATC), Atlantic City, NJ. He is assigned to the Satellite Navigation Group and is project manager in charge of cooperative industry and university GPS-based flight testing for precision approach applications.

Ruben Velez is a Software Engineer at the FAATC. He supports GPS-based flight testing and data analysis for the Satellite Navigation Program.

Mark F. Dimeo is a Computer Programmer for System Resources Corporation. His work for the FAATC supports a variety of programs including GPS.

Dave Lamb is an Electronics Engineer at System Resources Corporation. He is involved in the test and evaluation of GPS-based landing systems in support of the FAA's Local Area Augmentation (LAAS) program.

Greg Kuehl is an Avionics Engineer with United Parcel Service (UPS), Louisville, KY. His experience includes familiarity with the avionics suites of most commercial

aircraft flown by UPS including the Boeing 757. He is currently responsible for evaluating new technology for applicability to the UPS aircraft fleet.

Robert C. Hilb directs the Advanced Flight Projects Department at UPS. He is an airline Captain and is type rated in a variety of commercial aircraft. He currently flies the Boeing 727 and 757 in both line and flight test operations for UPS.

ABSTRACT

Test results are presented from a feasibility determination of Differential Global Positioning System (DGPS) Category (CAT) IIIb precision approach and landings. A code-based DGPS architecture with integrity monitoring was used. In addition, the feasibility of a combined DGPS/Instrument Landing System (ILS) architecture was evaluated.

A total of 50 approaches were flown: thirty-two approaches used DGPS for both lateral and vertical guidance, 14 used DGPS for lateral and ILS for vertical guidance, and 4 approaches used ILS only. A United Parcel Service Boeing 757 was the test aircraft for all flight tests.

The results of the tests show that code-based DGPS as well as combined DGPS/ILS, when used as the input to an autopilot, can attain vertical and lateral accuracies consistent with Required Navigation Performance for CAT IIIb.

INTRODUCTION

The Federal Aviation Administration (FAA) Satellite Program Office, has a research program in place to determine the feasibility of augmenting the Global Positioning System (GPS) for aircraft Category IIIb precision approach and landing operations. Candidate differential GPS (DGPS) architectures are evaluated in accordance with the FAA Category IIIb Feasibility Flight

Test Plans [1-3].

Under this FAA program, Ohio University has developed a code-based DGPS navigation/landing system which was tested during two flight test periods at the FAA Technical Center in Atlantic City, NJ. The first flight test period occurred in October 1994, during which a total of 50 automatic DGPS landings were performed [4]. The second series of flight tests were conducted from 17 through 20 February 1995. The latter flight tests included DGPS, Instrument Landing System (ILS), as well as combined DGPS/ILS landings. Furthermore, the DGPS system was upgraded with an integrity monitor station.

This paper provides a brief overview of the code-phase DGPS architecture, followed by a detailed description of the integrity monitoring function. Aircraft integration and test procedures are briefly addressed and flight test results are summarized for both series of automatic landing experiments. Detailed information on the flight tests can be found in references [4] and [5].

SYSTEM ARCHITECTURE

Figure 1 is a block diagram of the ground and airborne elements which comprise the DGPS system.

On the ground, a single-frequency (L1 at 1575.42 MHz) GPS antenna with an integrated low-noise amplifier (LNA) provides the GPS signal to a 10-channel, narrow-correlator GPS receiver. The antenna is sited at a presurveyed location. Raw measurement data from the receiver are provided to the reference-station processor at a rate of once per second. The processor then formats two data link messages: the first contains only raw data (code and carrier) while the second consists of derived Selective Availability (SA) range-rate corrections. The two ground messages are handed-off to a 2400 bps modem/transmitter operating in the Instrument Landing System (ILS) glideslope band. Each message is broadcast at a rate of once per second.

In addition, a second identical receiver and a GPS single-satellite simulator are incorporated for integrity purposes. A detailed discussion of this aspect of the ground system is presented in the next section. Not shown is a dual-frequency GPS receiver used to provide post-processed kinematic reference data.

Aboard the B-757 aircraft, a dual-frequency antenna provides GPS signals to two airborne receivers. As in the ground system, one of the units is a 10-channel, narrow-correlator, single-frequency (L1) GPS receiver. The other (not shown) is a dual-frequency GPS receiver, operating as an independent source to provide post-

processed aircraft kinematic reference data. Information from the data-link receiver/modem and the single-frequency GPS receiver are combined in the airborne processor. Data-link messages arrive once every second, while GPS measurement data is taken from the airborne receiver at a rate of four times per second. Data rates of up to 10 times per second can be accommodated if required. Ephemeris data, as it becomes available, is also taken from the airborne GPS receiver. Differentially-corrected GPS aircraft position and velocity data are then calculated and converted to ILS deviations and deviation rates. The ILS deviation data, presented in terms of the *difference of depth of modulation* or ddm, are then sent to the I/O processor which provides ILS look-a-like signals through an ARINC-429 interface to the autoland system. This guidance data has a very low noise level since it is derived from differentially-corrected GPS velocity. The DGPS velocity is of low noise level (below 0.01 m/s rms), since it is calculated from successive receiver integrated-Doppler measurements. Reference [4] presents further details about the B-757 autoland system and DGPS-aircraft integration.

Additional flexibility was incorporated into the airborne system to provide three distinct operating modes for the autoland system. In Mode 1, DGPS derived localizer and glideslope information was provided to the ARINC-429 interface unit. In Mode 2, DGPS derived localizer information along with the glideslope output from the B-757 right-channel ILS receiver was fed to the interface. For Mode 3, the source of both localizer and glideslope signals was the right-channel ILS receiver.

INTEGRITY DESIGN

A novel DGPS integrity architecture was used during the flight tests. The system uses integrated Doppler frequency shift measurements (also referred to as carrier phase measurements) in addition to code phase measurements to achieve a high level of availability of the DGPS integrity function. It is noted, however, that the system does not try to resolve the integer carrier-cycle ambiguities.

Another key element of the design is the use of a single-channel GPS simulator, which eliminates the need for a common clock between the reference and the monitor GPS receivers. Some of the integrity principles used in this design were previously documented in reference [6].

The integrity philosophy that resulted in this design is based on the following:

- 1) Minimize the complexity of the integrity logic (small fault tree, few "what ifs," and avoid

misinterpretation of the requirements);

2) Allocate the integrity requirements clearly to ground and airborne components for interoperability;

3) Robust behavior under anomalous conditions (including anticipated and unanticipated phenomena, such as monitor clock malfunctions, high ionospheric phase rates, and hardware failures);

4) Design for the use of hardware redundancy.

Robust Carrier-Phase Smoothing

Instantaneous DGPS code-phase noise is too large to meet CAT III accuracy and integrity requirements. Therefore, all code-based DGPS architectures use some level of carrier smoothing of the code phase to reduce the level of noise. Usually, the smoothing period is on the order of a few seconds up to several minutes. Carrier-phase smoothing (CPS) can be very effective, as long as no undetected cycle slips are incurred and the ionospheric divergence between code and carrier phase is accounted for. The proposed system architecture uses CPS over several minutes to increase the DGPS accuracy, which in turn also increases the availability of the integrity monitoring function.

Cycle slips are detected and corrected by evaluating the difference between two successive phase differences which are corrected for receiver clock offset [6]. The smoothing itself, however, is performed in the aircraft position solution after the ground station data has been incorporated into the airborne processing. The aircraft calculates both an unsmoothed differential code-phase solution as well as a differential delta-carrier-phase update. The delta-carrier-phase update is corrected for SA range-rate as determined by the reference station. The corrected delta-carrier-phase update is used to bring the previous position estimate to the current time with centimeter accuracy. In addition, integrity monitoring (RAIM) is performed on this update to detect measurement inconsistencies. Next, the unsmoothed differential code-phase solution is used to update the position estimate. The gain on this update is fairly small, such that the position estimate is strongly smoothed (the time constant is on the order of 100 seconds). This technique mitigates ionospheric divergence errors, because the smoothing occurs after the differential corrections have been applied. Furthermore, by bringing the position solution forward in time with the delta-carrier-phase updates, discontinuities in the position solution do not occur when satellites are switched in and out of the solution.

Ground Integrity Monitor

Figure 2 shows the block diagram of the ground station. The ground station is configured around two GPS antennas, two GPS receivers, a single-channel GPS satellite simulator, and a ground processor. The two GPS antennas are separated such that the multipath errors between the two antennas are decorrelated. The remainder of the equipment is co-located. A single-channel GPS satellite simulator is used as a calibration input into both GPS receivers.

Single differences (SD) are calculated for each of the satellites in view and for the satellite simulated by the GPS simulator. Since the separation distance between the two GPS antennas is small, the errors that are dominant in the SDs are:

- 1) Clock offset between the two GPS receivers;
- 2) Multipath and receiver noise differences between the two GPS receivers.

Next, a double difference (DD) test statistic is calculated for each of the GPS satellites in view by differencing their SDs against the SD derived from the simulated satellite, corrected for the known DD geometry.

In summary, the SD equations are given by:

$$SD^i = \underline{b} \underline{e}^i + \Delta t_{R-M} + e_{R-M}^i$$

$$SD^s = \underline{b} \underline{e}^s + \Delta t_{R-M} + e_{R-M}^s$$

where: superscript i denotes GPS satellites; superscript s denotes the simulated GPS satellite; \underline{b} is the baseline vector connecting the two antennas; \underline{e} are the unit vectors to the satellites; Δt_{R-M} is the clock offset between the reference and monitor GPS receivers; e_{R-M} represents the multipath and receiver noise differences between the reference and monitor GPS receivers. After differencing the SDs with respect to the simulated SD, the DD equation is given by:

$$DD^i = (\underline{e}^i - \underline{e}^s) \underline{b} + e_{R-M}^i - e_{R-M}^s$$

The resulting test statistic is

$$p^i = e_{R-M}^i - e_{R-M}^s$$

Because the satellite simulator does not have any errors except for noise, the second term of the test statistic is small. Therefore, the test statistic can be used to detect differences between the two GPS receivers for each GPS satellite separately.

Figure 3 shows a plot of the unsmoothed DD residuals for an actual data collection session. The residuals are shown for a period of time of approximately one hour, during

which the satellite elevation angle changes from 61 to 33 degrees. The standard deviation of the residuals is 0.24 m.

Key to the overall system integrity design is the combination of two fault detection techniques:

- 1) Detection of slowly changing anomalies is performed on the ground by examining the DD residuals. Because of the aircraft smoothing technique, the time to alarm for slowly changing anomalies does not need to satisfy the desired 1 second time-to-alarm for CAT III operations. The reason is that the error will not be able to have a rapid effect on the position solution.
- 2) Detection of rapid changing anomalies is performed both on the ground using thresholds on the unsmoothed DD residuals; and in the aircraft using fault detection techniques on a redundant velocity update.

Detection of slowly changing anomalies

The reference/monitor DD residuals for each satellite are averaged over 100 uncorrelated updates (50 seconds of data at an update rate of two per second). The noise component of the averaged residuals is thus reduced from 0.24 m to $0.24/10 = 0.024$ m. To allow for a slowly changing residual bias of 0.3 m (to account for temperature changes and multipath) and to achieve a false detection rate of less than 10^{-7} (5.2 standard deviations), the detection threshold is set at

$$T_D = 0.3 + 5.2(0.024) = 0.42 \text{ m}$$

Next, the minimum detectable bias is calculated from the desired probability of missed detection of 10^{-9} :

$$\mu_M = T_D + \sigma \sqrt{2} \operatorname{erfc}^{-1}(2 \times 10^{-9}) \text{ or}$$

$$\mu_M = 0.42 + 0.024(5.9) = 0.56 \text{ m}$$

In other words, the probability of a missed detection for a bias error of greater than 0.56 m is less than 10^{-9} . The reference station removes a satellite from the uplink if the detection threshold is exceeded. Upon detection, the satellite will remain excluded for at least 50 seconds.

The worst case failure for the above processing technique would be a step error which is exactly the value of the minimum detectable bias. Because of the airborne smoothing time constant of 100 seconds, this bias will only reach 50% of its maximum impact on the position solution before it is detected by the reference station. Therefore, the airborne position solution would calculate its protection limits using only half the minimum

detectable bias. The impact of each potential satellite malfunction on the position solution is calculated and the worst case malfunctions determine the horizontal and vertical protection limits: HPL and VPL, respectively. The above technique has good availability, because potential satellite malfunctions are detected before the ranging error exceeds 0.28 m. This allows for the protection of vertical and horizontal position errors that are consistent with CAT III operations.

Detection of rapid changing anomalies

Rapid changing anomalies are detected using the unsmoothed DD residuals which have a standard deviation of 0.24 m. The detection threshold is set at

$$T_D = 0.3 + 5.2(0.24) = 1.55 \text{ m}$$

The minimum detectable bias for a missed detection probability of 10^{-9} is given by

$$\mu_M = 1.55 + 0.24(5.9) = 2.97 \text{ m}$$

This type of detection is included to avoid large sudden errors which can easily be detected and removed from the position solution. Furthermore, it provides a reduced level of integrity for users who have not yet smoothed their position solution for 100 seconds.

The second rapid detection method is performed by the aircraft integrity processing. It consists of a standard RAIM-type technique operated on the delta-carrier-phase updates [6, 8]. For a typical delta-carrier-phase noise of 0.5 cm, this provides a VPL of better than 0.15 m with high availability.

GROUND TRACKING

Figure 4 shows the locations of the GPS ground station and truth sources with respect to the runways at the Atlantic City International Airport (ACY).

Truth data was collected via the FAA's laser tracker and a separate DGPS-based Time Space Position Information (TSPI) system. The laser tracker azimuth and elevation measurements were accurate to within 20 arc seconds, 1 sigma. The range measurements were accurate to within one foot (for measurements out to 5.0 nmi). This translates into approximately a 30-cm vertical accuracy ($|\mu| + 2\sigma$ or 95%) at the runway 13 threshold. The laser tracker uses a six-inch-diameter retroreflector, mounted on the B-757 nose landing gear, to track the aircraft. A laser calibration check of a known target was performed prior to each run. The TSPI is comprised of two Ashtech Z-12 GPS receivers. One of the receivers was located at a surveyed location and the other receiver was located in the aircraft. The TSPI accuracy was approximately 0.1

m. The laser tracker provided the primary truth source while the TSPI system served as a source for quality control.

In addition to the laser tracker and the TSPI system, the FAA technical Center's NIKE tracking radar/video camera system was used to collect data for precise touchdown determination. A GPS derived time tag is associated with the collected video information. This data yields the precise time of touchdown and the corresponding laser derived position of the aircraft is then determined for each approach. This information also supplements the weight-on-wheels data collected on the aircraft and additionally allows the lateral and longitudinal touchdown dispersion for each approach to be determined.

TEST PROCEDURE

A total of 50 approaches were flown: 45 were touch-and-go approaches with the remaining five consisting of touchdown and rollout to a full stop. Modes 1, 2 and 3 were exercised to varying degrees (see Flight Test Results). The approaches were flown to Runway 13 at the ACY on February 18th and 19th, 1995. Runway 13 was selected due to its 10,000 ft length and, more importantly, the presence of a commissioned ILS required for Modes 2 and 3 operations.

Each approach began at the Initial Approach Fix (IAF) located a distance of 5.0 nmi on runway heading from threshold. The pilot initiated capture of the 3°-glideslope at the IAF and data collection commenced at the Final Approach Fix (FAF). The FAF was a distance of 3.25 nmi on runway heading from threshold. This flight profile was flown for all 50 of the system accuracy flights and for in-flight integrity tests which occurred on February 20th.

The latter consisted of three approaches where satellite pseudorange errors were deliberately introduced into the DGPS system. During each approach, a pseudorange error of 0.1 m/s was introduced at the ground station into one of the GPS satellites being actively used for the aircraft position solution. During these tests, the detection thresholds were enlarged to allow for a significant error build-up during the approach. Timing was such that the induced pseudorange error exceeded the integrity limit of 2.0 m just as the aircraft reached the runway threshold. To accomplish this, the introduction of the error occurred as the aircraft passed the FAF at about 3.0 nmi distance from threshold. Upon exceeding the 2.0 m pseudorange integrity limit, the transmission of data from the ground system concerning the offending satellite ceased forcing the airborne system to remove the satellite from the all-in-view solution computed onboard the

aircraft. During these tests, the aircraft was tracked by both the TSPI and the laser tracker. Prior to the in-flight integrity tests, the concept was subjected to stationary tests with the ground system and the aircraft located on the FAA Technical Center ramp.

DATA ANALYSIS

The data analysis was performed as set forth in the FAA Category IIb Feasibility Study Level 2 and Level 3 flight test plans [2, 3]. These test plans are based on Required Navigation Performance (RNP) requirements [7].

Based on the laser tracker position, navigation sensor error (NSE) and total system error (TSE) were calculated in terms of vertical and lateral (cross-track) performance. NSE is the difference between the aircraft position as computed by DGPS and that measured by the laser tracker. TSE is the difference between the tracked-aircraft position and the desired (3-degree nominal) approach path. TSE includes all components of error which are predominantly FTE and NSE. Path following error (PFE) and control motion noise (CMN) analyses were not performed since the system was evaluated on a total system performance basis.

The system integrity testing consisted of two phases: ramp tests followed by in-flight testing. For the former, of interest was the system reaction to a physically induced pseudorange error in a given satellite and detection of excessive satellite multipath. The ramp tests were qualitative in nature intended more to demonstrate the system's integrity logic. The in-flight testing was based not only on the ability of the system to remove an out-of-tolerance satellite from the solution; but, the time to alarm as well, i.e. the time elapsed between detection of the out-of-tolerance satellite and the removal of the satellite from the solution.

FLIGHT TEST RESULTS

In Table 1 are given flight test results from both the October '94 flight test and the February '95 flight test. During the October '94 flight test, a total of 50 approaches were flown using DGPS guidance. During the February '95 flight test, a total of 50 approaches were also flown; but, there were three different configurations:

- 1) 32 Mode 1 approaches were flown with DGPS as the only source of guidance;
- 2) 14 Mode 2 approaches were flown with DGPS providing lateral guidance and ILS providing vertical guidance; and,
- 3) 4 Mode 3 approaches were flown with ILS as the sole source of guidance.

Table 1 represents only the Mode 1 (DGPS) approaches.

In contrast, the navigation sensor error (NSE) from the October '94 flight test is somewhat larger than that from the February '95 test data for two reasons:

- 1) the lack of precise aircraft attitude data, which is used to compute a lever arm correction between the aircraft retroreflector (used for laser tracking) and the guidance point on the aircraft; and,
- 2) the configuration of the October '94 system did not employ all of the signal processing techniques, in particular the carrier-phase-based velocity determination, which was implemented for the February '95 flight test.

The vertical TSE for the February '95 flight test was 1.9 m, $(|\mu| + 2\sigma)$. This result demonstrates the exceptional performance of the autopilot when coupled to the OU DGPS system. Vertical FTE is seen to be 1.2 m and vertical NSE is 1.1 m. The root-sum-square of vertical FTE and NSE equals 1.6 m. This serves as a check to validate the vertical TSE which, by definition, is the difference between the desired path in space and the laser tracker position.

Figure 5 is a composite plot of 28 approaches flown in the Mode 1 (DGPS) configuration (four approaches were not available for detailed analysis due to a data recording error). The 95 percent, Required Navigation Performance (RNP) tunnel requirements are overlaid onto this figure. All of the approaches easily fall within the RNP tunnel, which is ± 15 ft at the point marked "50' HAT". The overall performance is smooth and consistent with the exception of one approach which was marred by a late capture of the glidepath. The mean and standard deviation shown on the figure result from statistics calculated on all data points from 700 ft height above threshold (HAT) to 50 ft HAT.

Figure 6 demonstrates the excellent total system lateral performance. It can be seen that all approaches are well within the RNP tunnel requirements.

Figure 7 shows the vertical TSE when the ILS was providing the vertical guidance to the autopilot (and DGPS was providing the lateral guidance). The performance, although the ILS at Atlantic City is only certified to Category I, demonstrated comparable total system performance to that of the completely coupled DGPS system. Note the scalloping due to a beam bend in the ILS signal.

All touchdowns for both flight test periods occurred within the 95% touchdown zone (an area 1500 ft long by 54 ft wide). Furthermore, there was no discernable difference between the statistics of the DGPS and the ILS

touchdowns.

CONCLUSIONS

The results of the flight tests show that code-based DGPS as well as combined DGPS/ILS, when used as the input to an autopilot, can attain vertical and lateral accuracies consistent with Required Navigation Performance for CAT IIb. The vertical Total System Error (TSE) at 50 ft height above threshold (HAT) was 1.9 m $(|\mu| + 2\sigma)$, while the vertical Navigation Sensor Error (NSE) was 1.1 m $(|\mu| + 2\sigma)$.

Integrity monitoring was implemented at both the ground reference station and the aircraft. Initial integrity tests support the feasibility of providing integrity for DGPS-based CAT IIb operations.

ACKNOWLEDGEMENTS

The work presented in this paper was supported and funded through several funding agencies. Prime among them was the FAA Satellite Program Office under University Research Grant 92-G-023. Additional funding came through the Joint University Program for Air Transportation Research sponsored by the NASA Langley Research Center and the FAA Technical Center under Grant NGR 36-009-017.

Aircraft tracking support at the FAATC was provided by Diane Bansback and Ron Morganweck who operated the laser tracker, and Brad West and David Moore, the operators of the Nike radar tracker.

REFERENCES

1. O'Donnell, P.A., Braff, R., Shively, C., "CAT IIb Level 1 Test Plan for Global Positioning System (GPS)", DOT/FAA/RD-93/21, The MITRE Corporation, August 1993, McLean, VA.
2. O'Donnell, P.A., Braff, R., "CAT IIb Level 2 Flight Test Plan for the Global Positioning System (GPS)", DOT/FAA/NG-95/01, The MITRE Corporation, October 1994, McLean, VA.
3. Wulschleger, V., "DGPS CAT IIb Feasibility Demonstration Program Level 3 Flight Test Plan: Ohio University/United Parcel Service Code-Based Differential GPS", The FAA Technical Center, 10 February 1995, Atlantic City, NJ.
4. Van Graas, F., D. W. Diggle, V. Wulschleger, R. Velez, G. Kuehl, R. C. Hilb, and M. Dimeo, "FAA/Ohio University/UPS Autoland Flight Test Results",

Proceedings of the 1995 National Technical Meeting of The Institute of Navigation, 18-20 January 1995, Anaheim, CA.

5. Wullschleger, V., R. Velez, D. Lamb, and M. Dimeo, "FAA/Ohio University/UPS DGPS CAT IIIb Flight Test", Aviation Technology Directorate Report, Preliminary Report, The FAA Technical Center, 23 March 1995, Atlantic City, NJ.

6. Van Graas, F. and Shane-Woei Lee, "High-Accuracy Differential Positioning For Satellite-Based Systems Without Using Code-Phase Measurements", Proceedings of the 1995 National Technical Meeting of The Institute of Navigation, 18-20 January 1995, Anaheim, CA.

7. Kelly, R.J. and J.M. Davis, "Required Navigation Performance (RNP) for Precision Approach and Landing with GNSS Application", NAVIGATION: Journal of The Institute of Navigation, Vol. 41, No. 1, Spring, 1994.

8. Joyner, G., "RAIM Experiences", All Weather Operations Panel (AWOP), Fifteenth Meeting, 26 September to 12 October, 1994, Montreal, Canada.

Table 1. Summary of DGPS Flight Test Results at 50 feet Height Above Threshold (HAT)

| UPS B-757 | OU Oct. '94 Flight Test | | OU Feb. '95 Flight Test | |
|-------------------|-------------------------|---------|-------------------------|---------|
| $ \mu + 2\sigma$ | Vertical | Lateral | Vertical | Lateral |
| NSE | 1.9 | 1.7 | 1.1 | 1.4 |
| FTE | 1.4 | 2.4 | 1.2 | 2.5 |
| TSE | 2.3 | 3.1 | 1.9 | 3.7 |

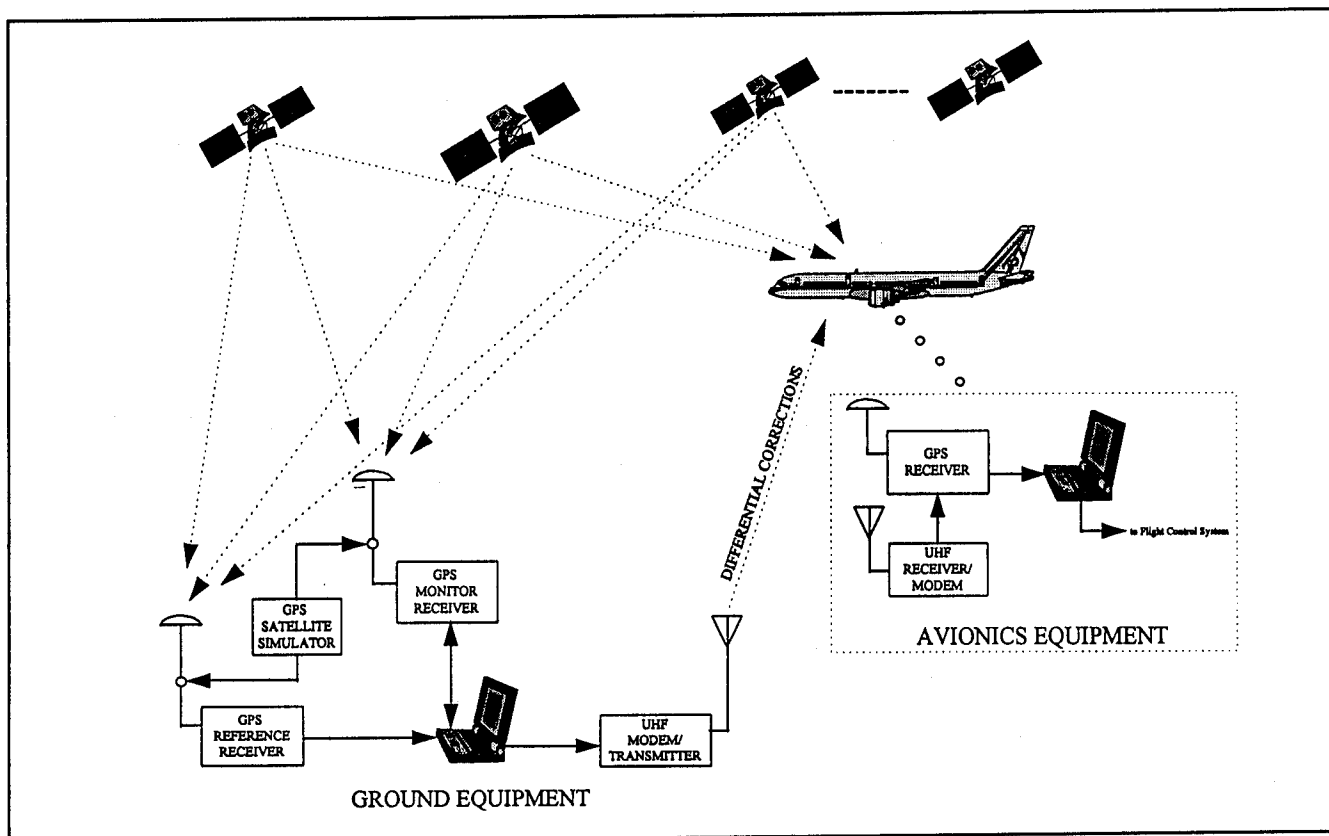


Figure 1. Ohio University DGPS System Block Diagram

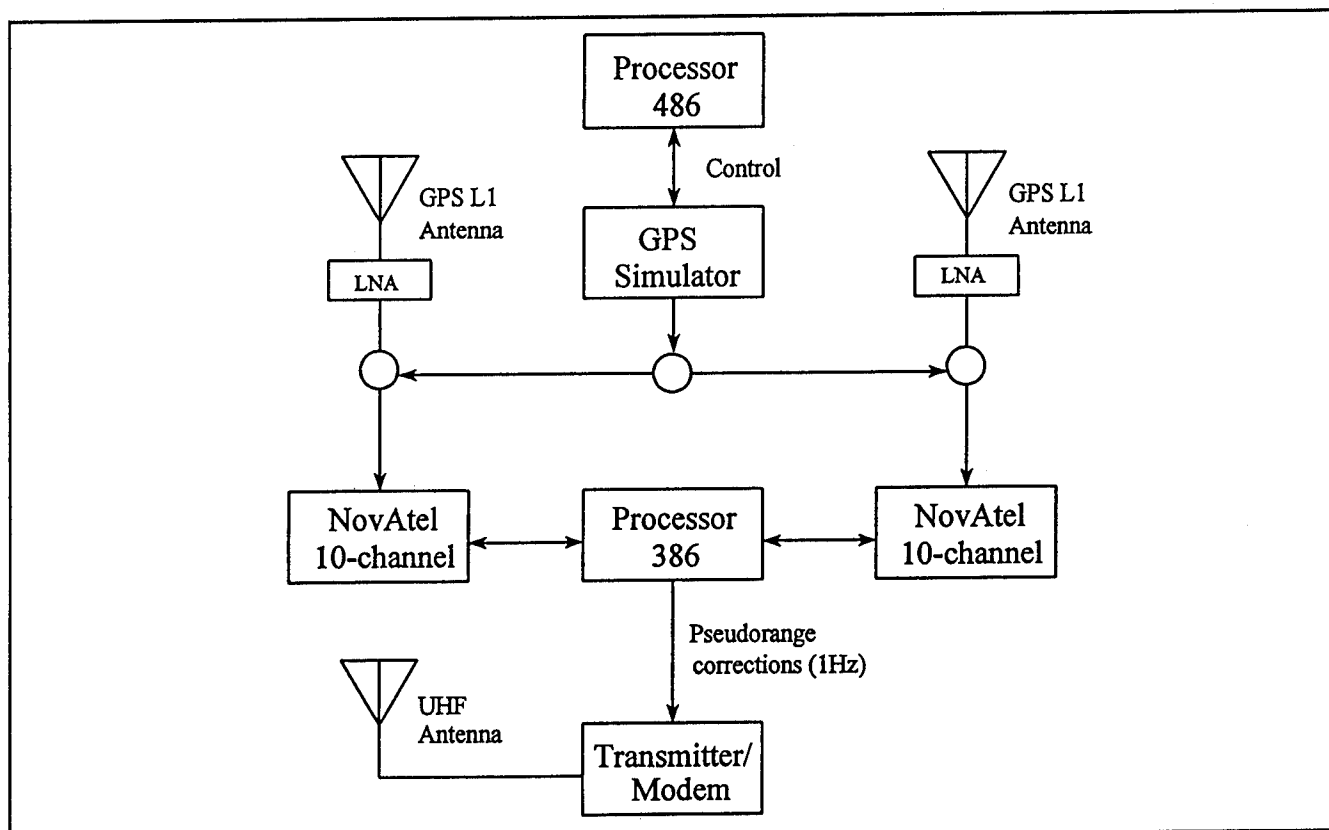


Figure 2. Ohio University Ground Station Block Diagram

INTEGRITY MONITOR DOUBLE DIFFERENCE RESIDUALS

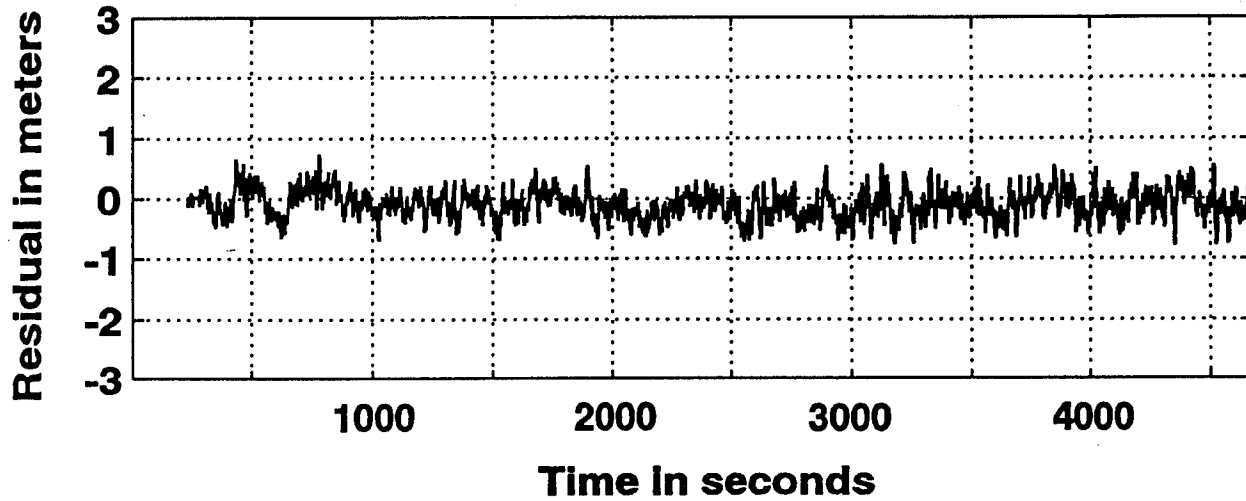


Figure 3. Ground Integrity-Monitor Residuals

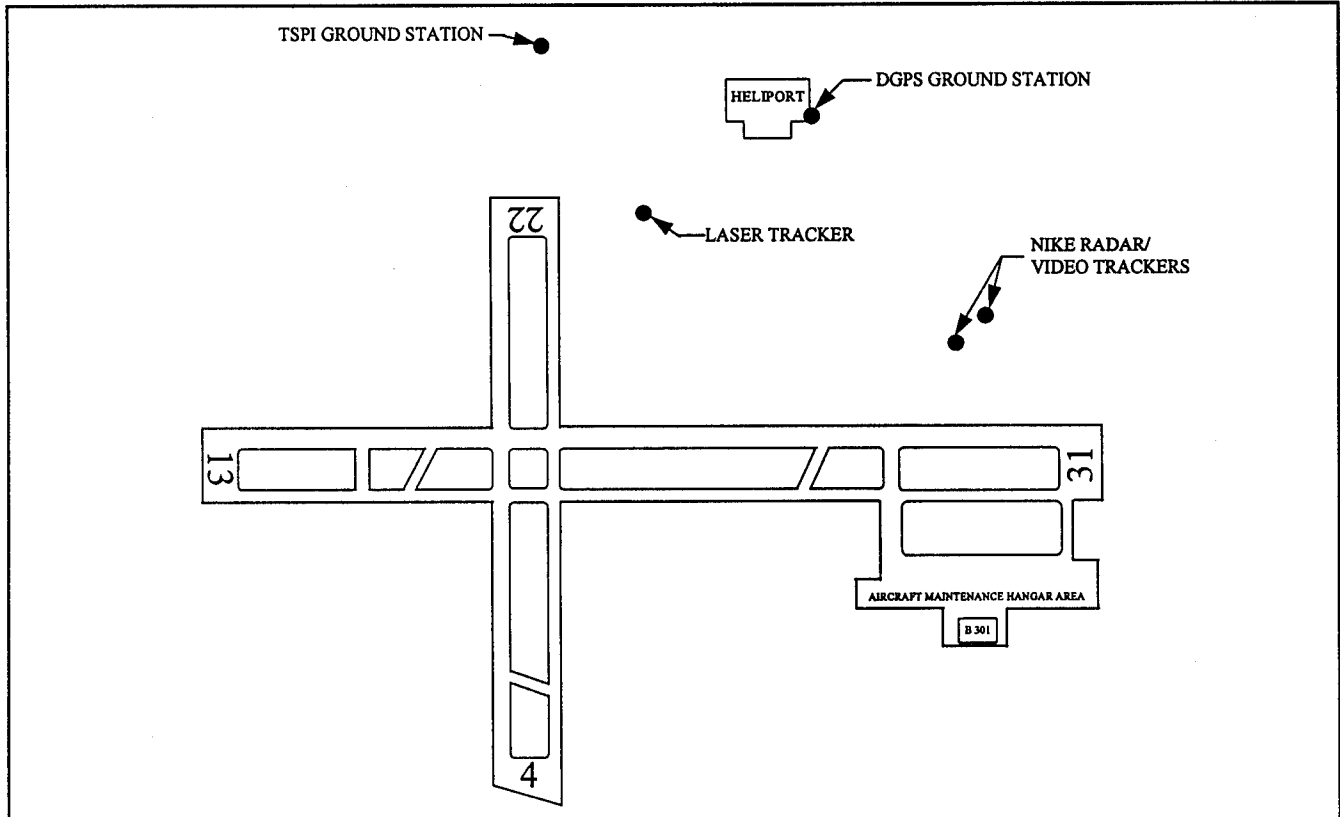


Figure 4. Ohio University DGPS Ground Test Setup Locations

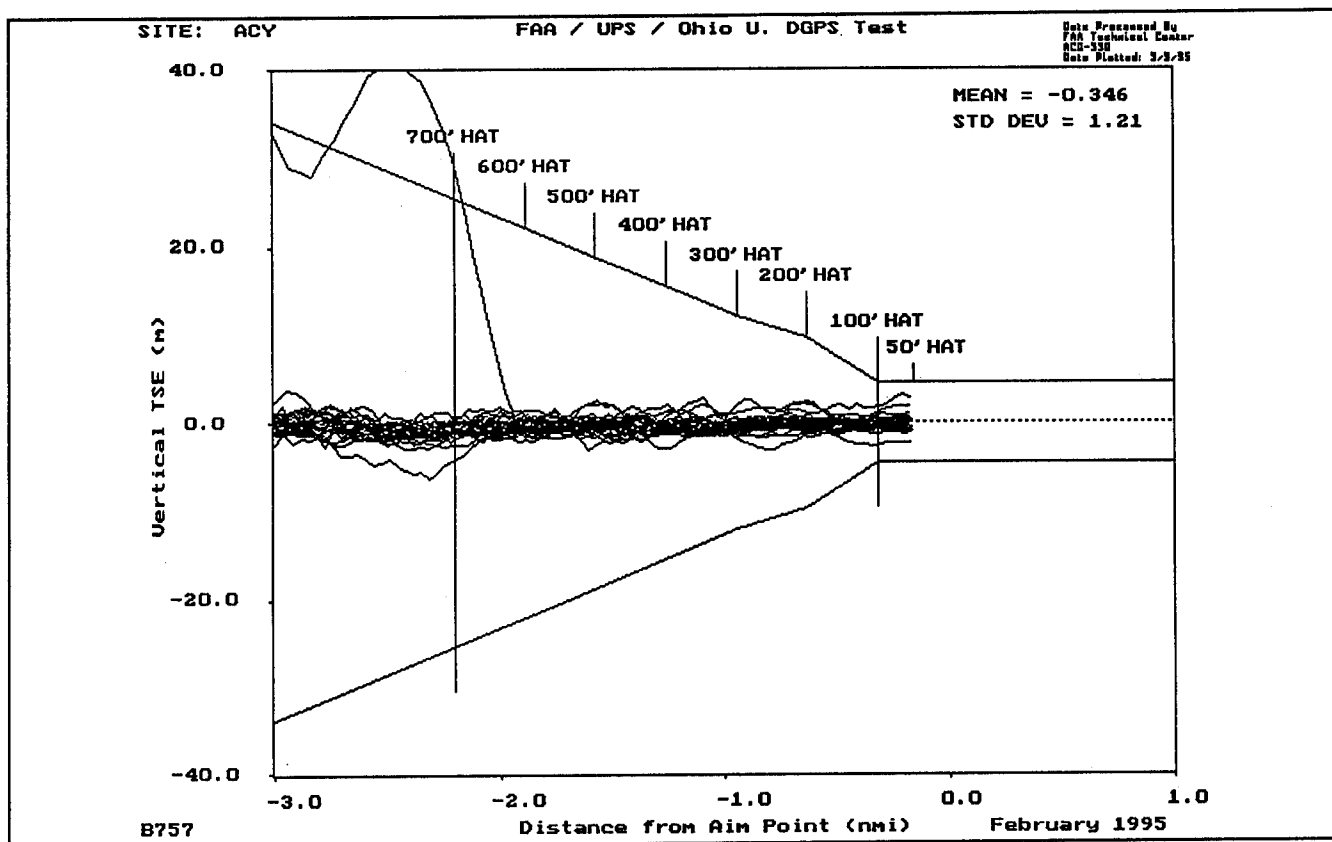


Figure 5. Vertical Total System Error for All DGPS Approaches (m)

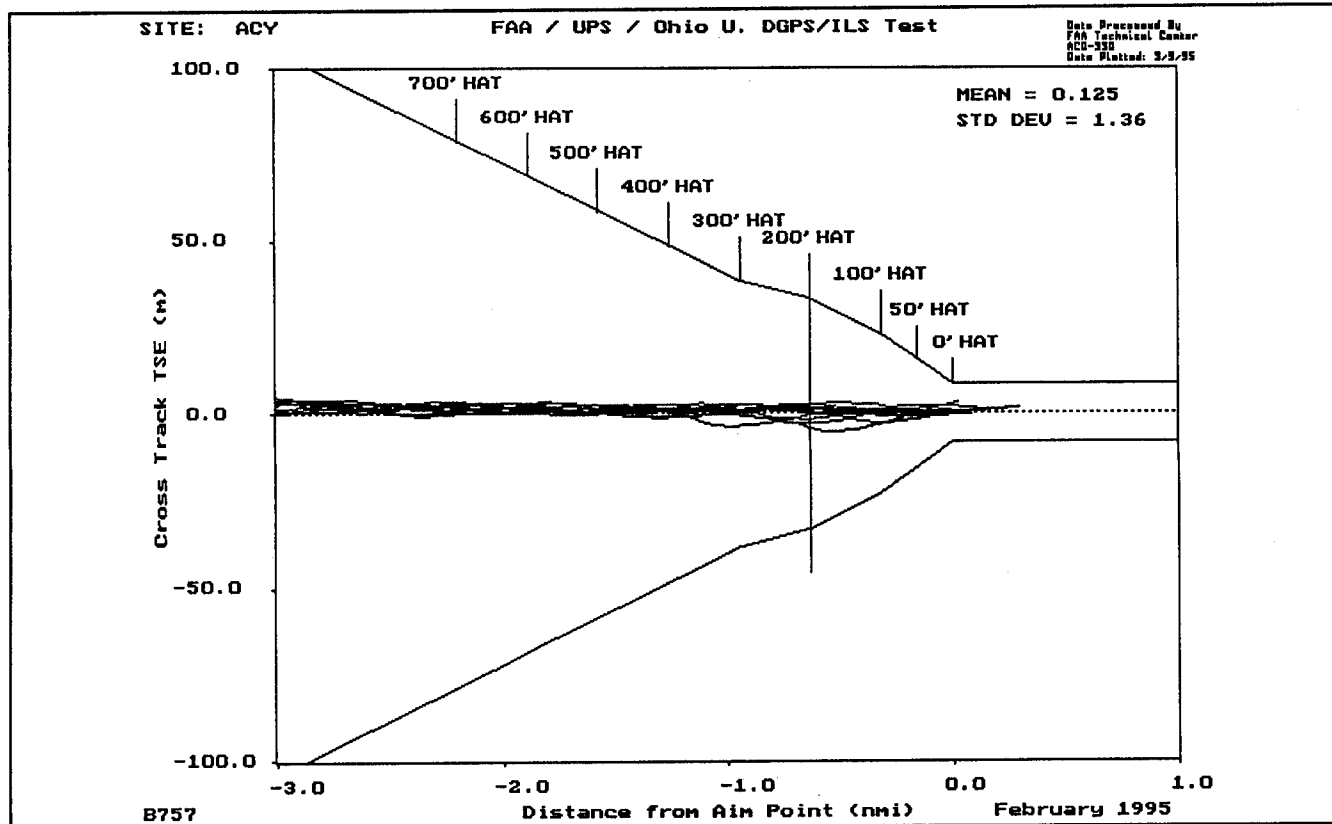


Figure 6. Lateral Total System Error for All DGPS Approaches (m)

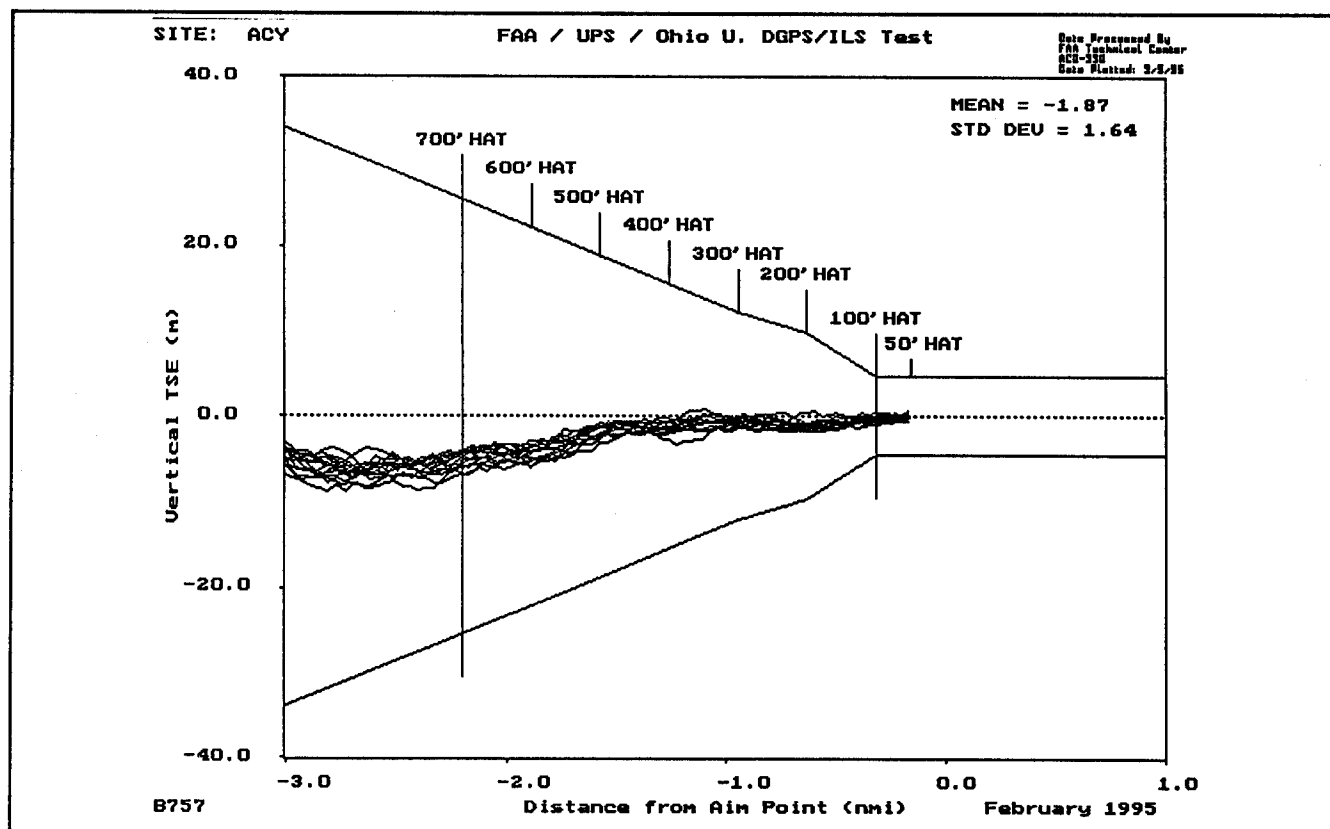


Figure 7. Vertical Total System Error for All ILS Approaches (m)

FAA/FEDSIM – E-Systems Cat IIIB Feasibility Demonstration Flight Test Preliminary Results

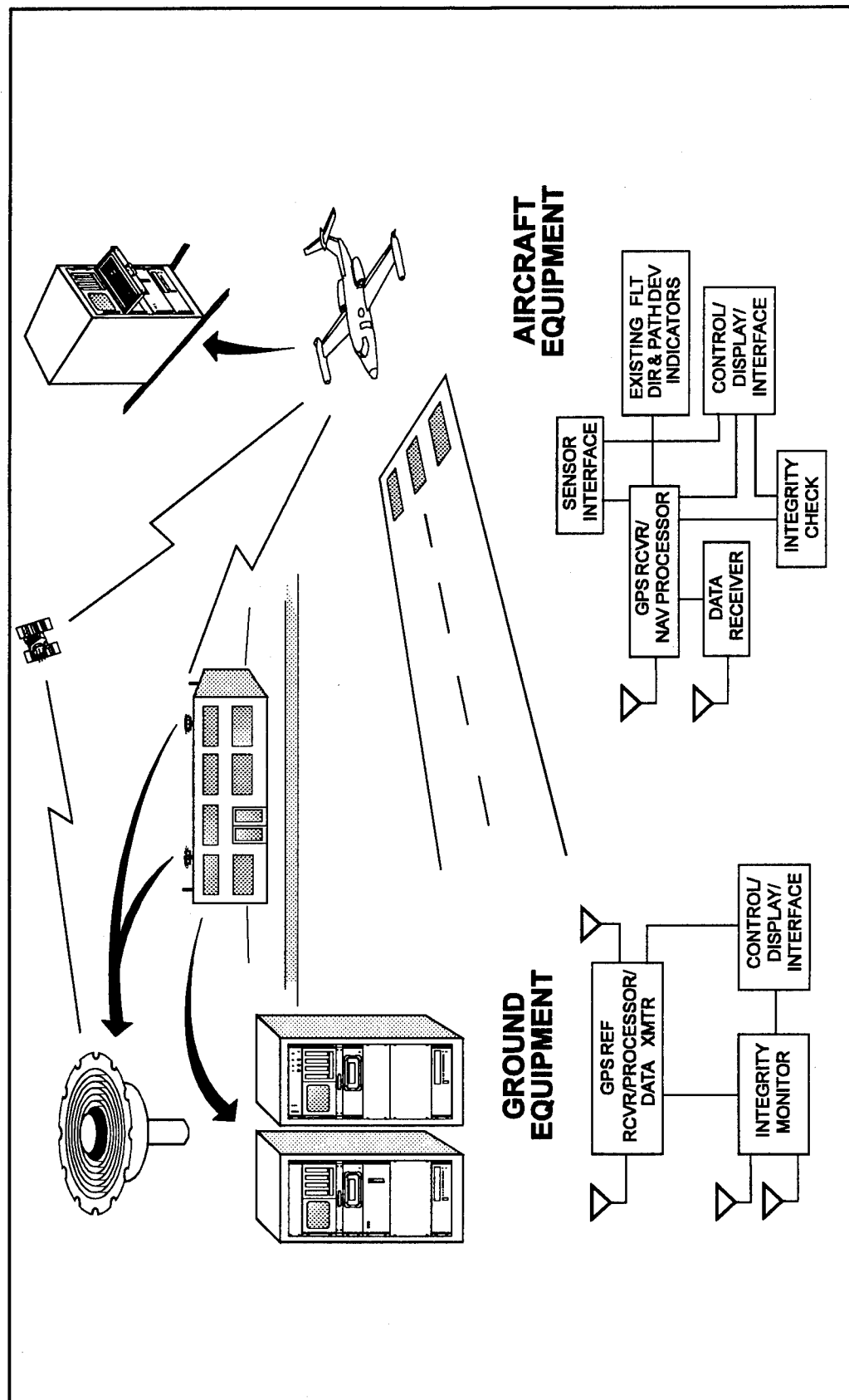
Glyn Romrell, Ron Brown, and Greg Johnson
E-Systems

Dave Kaufmann
NASA Ames

DGPS Cat IIIb Feasibility Demo

- **FAA Client, FEDSIM contract awarded June 1994**
- **Demonstrate feasibility of Cat IIIb DGPS Landings**
 - Accuracy and Integrity
- **Measures of Success (MOS)**
 - Navigation Sensor Error (Selected)
 - Total System Error
- **E-Systems advanced GPS Technology**
 - “On-the-fly” Integer Phase Ambiguity Resolution
 - Kinematic Carrier Phase Tracking
 - Ground Integrity Monitoring and Airborne RAIM

Cat IIIB Demo System Configuration



System Overview

- **Ground Equipment**
 - Measures & Verifies All GPS Observables
 - Verifies Integrity of GPS & Uplink Signals
 - Uplinks Measurements & Site Data, VHF D8PSK
 - Provides Data Recording
- **Airborne Equipment**
 - Receives GPS Signals-In-Space
 - Verifies Uplink Message Integrity
 - Generates Position/Velocity/Time (PVT) Solution
 - Unique RAIM Protects Position Alarm Limits
 - ILS Like Deviations to Aircraft Flt Dir & Indicators
 - Provides Data Recording

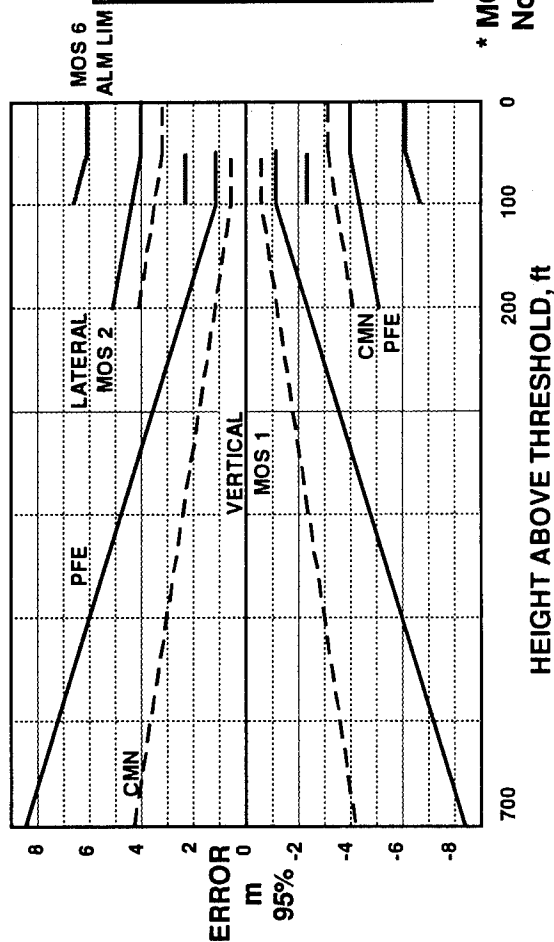
Nav Sensor Accuracy & Alarm Limits

VERTICAL ERROR, 95% - MOS 1

| HAT, ft | PFE, m | CMN, m |
|---------|--------|--------|
| 700 | 8.4 | 4.2 |
| 200 | 2.4 | 1.2 |
| 100 | 1.2 | 0.6 |
| 50 | 1.2 | 0.6 |

LATERAL SENSOR ERROR, 95% - MOS 2

| HAT, ft | PFE, m | CMN, m |
|------------|--------|--------|
| 200 | 5.1 | 4.1 |
| 100 | 4.4 | 3.5 |
| 50 | 4.0 | 3.2 |
| TD/ROLLOUT | 4.0 | 3.2 |



MONITOR ALARM LIMITS
FOR POSITION ERRORS -

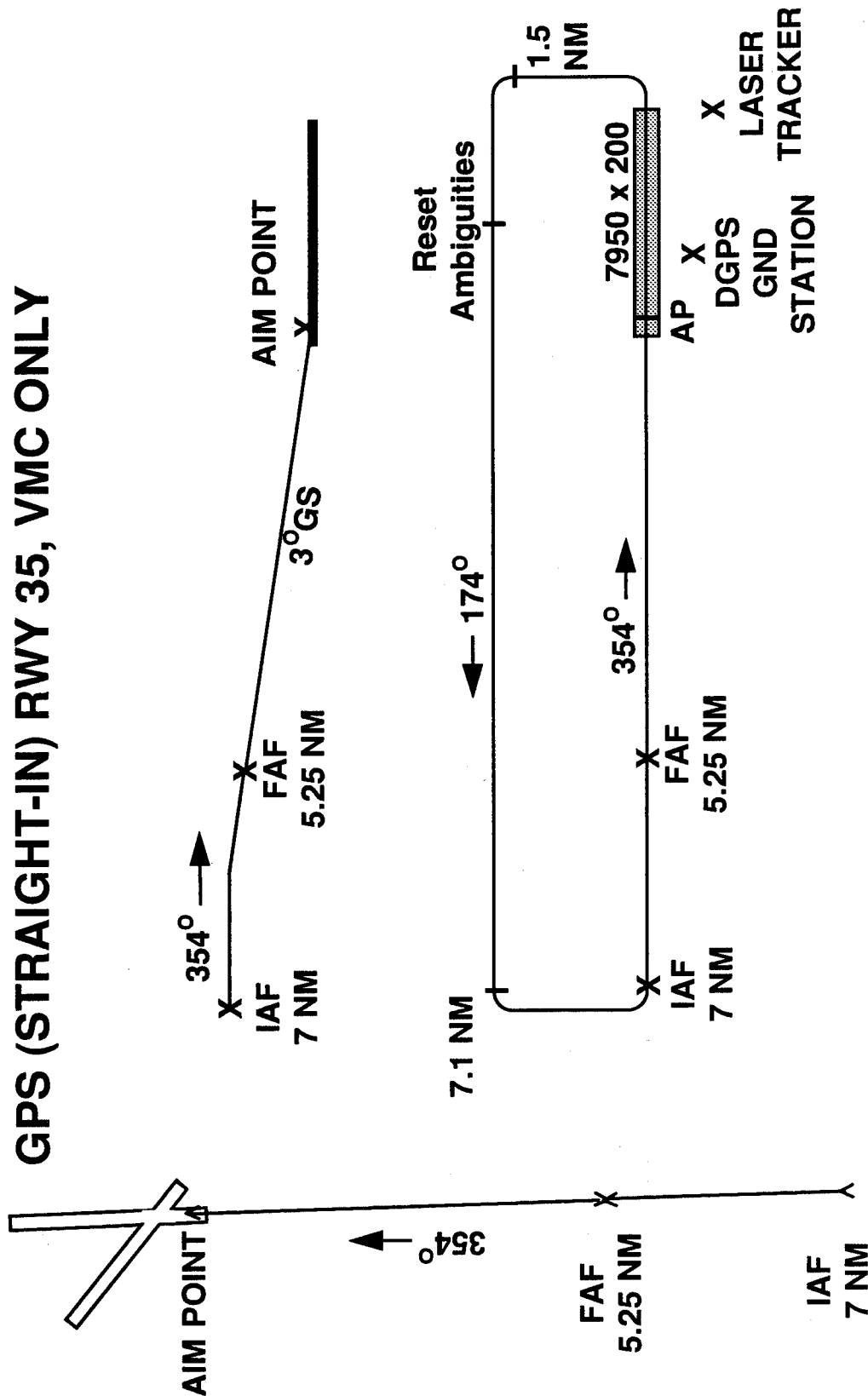
| HAT, ft | VERT. LIMIT Half Width, m | LAT. LIMIT Half Width, m |
|---------|------------------------------|-----------------------------|
| 700 | 16.0 | - |
| 200 | 4.6 | 7.8 |
| 100 | 2.3 | 6.7 |
| 50 | 2.3 | 6.1 |

* MOS 6 - Must Alarm Within 2 Seconds When Limit Exceeded,
No Missed Alarms, No More Than One False Alarm

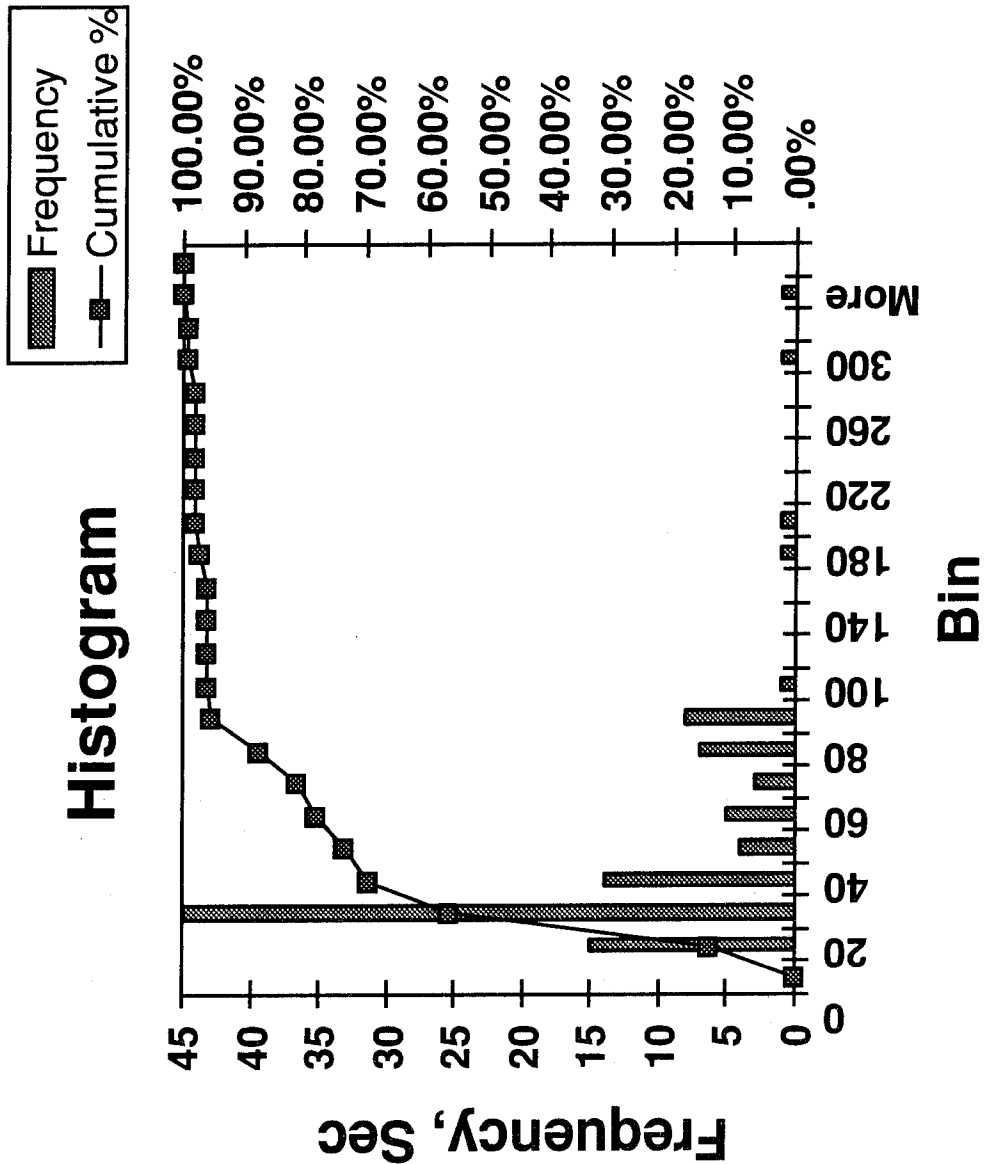
E-Systems Flight Test at NASA Ames Crows Landing June 1995 Preliminary Results

Flight Test Profile - Crows Landing

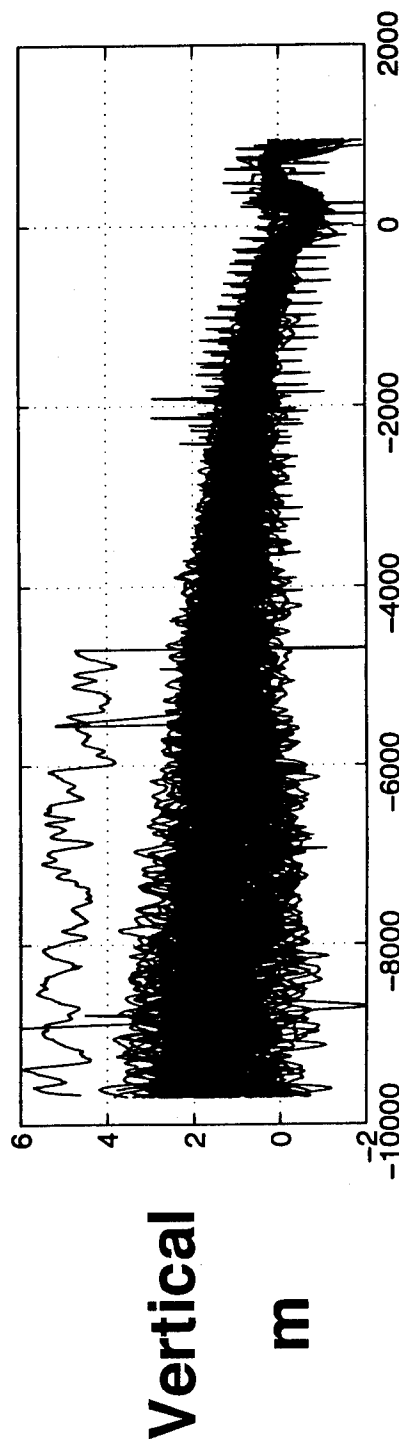
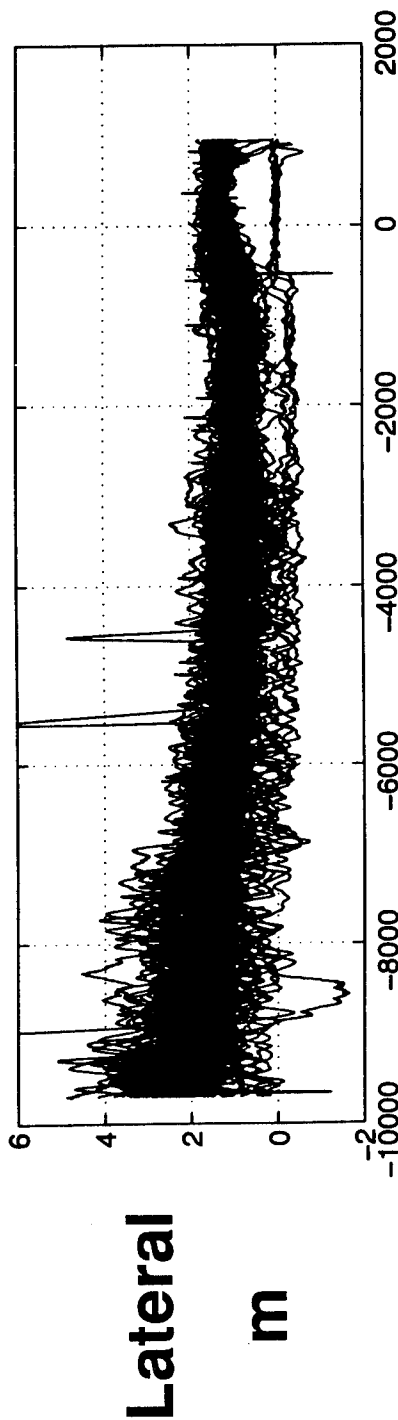
GPS (STRAIGHT-IN) RWY 35, VMC ONLY



Time to Resolve Ambiguities

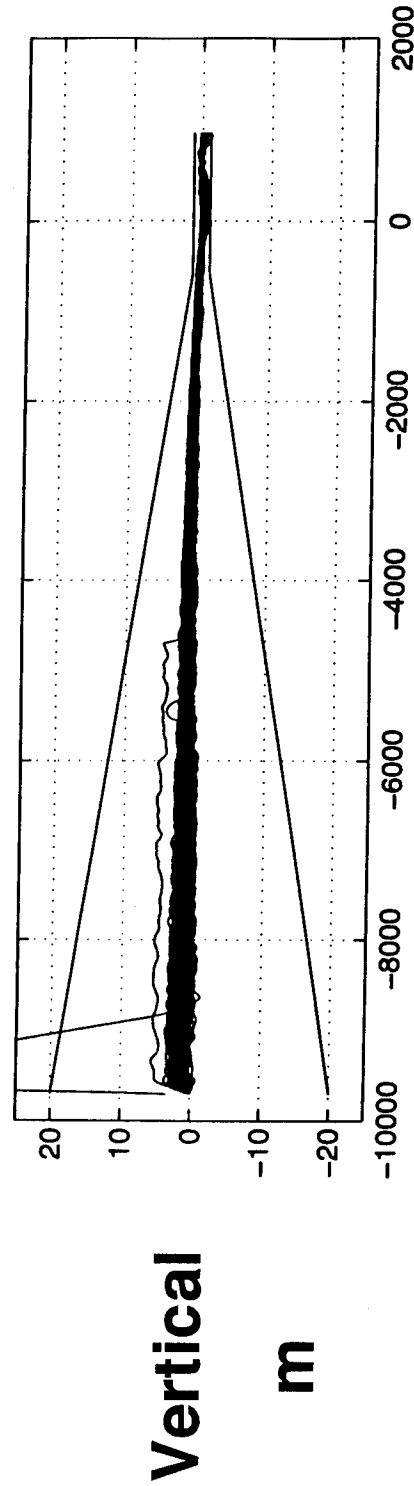
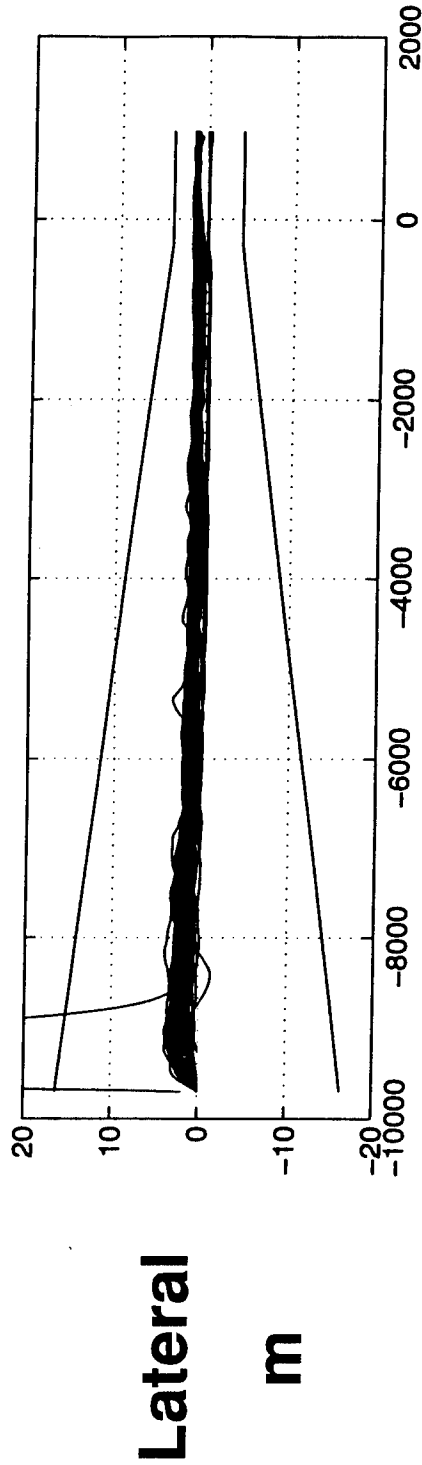


Unfiltered Error 100 Approaches



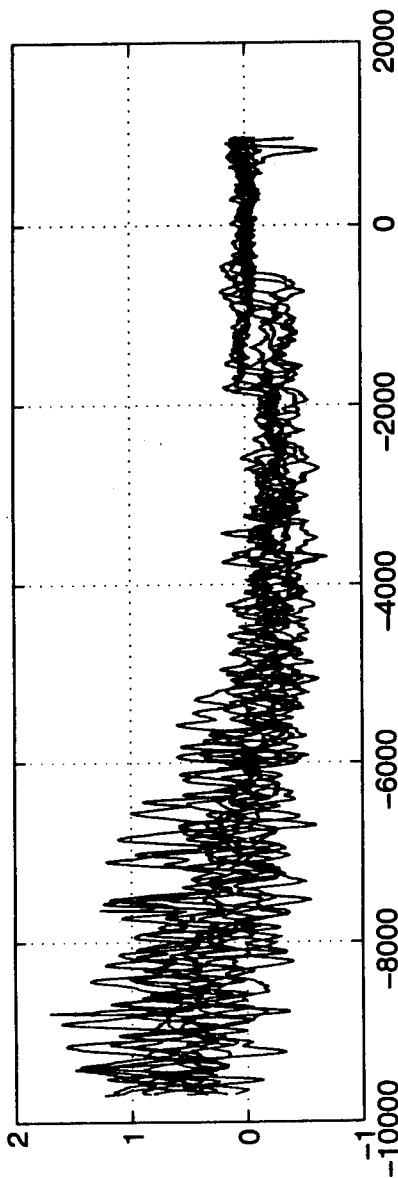
Distance to Aim Point

PFE Output 100 Approaches



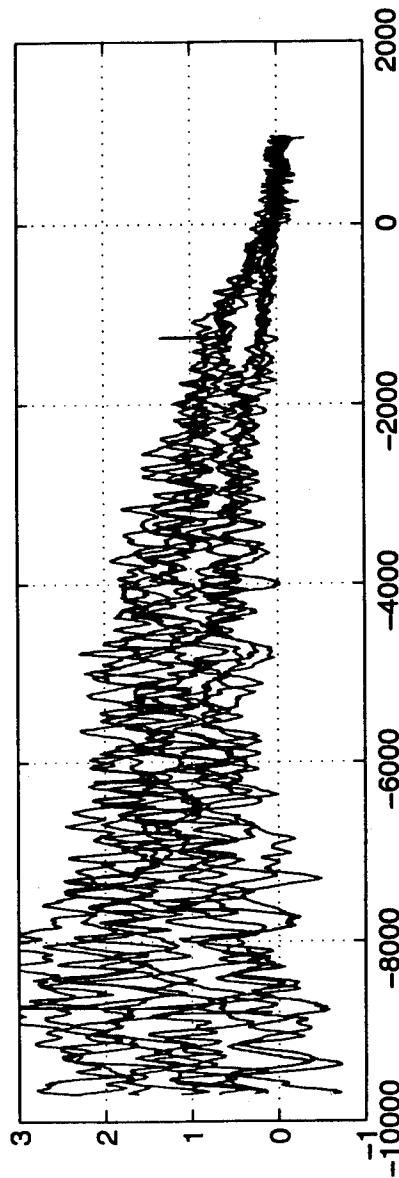
Distance to Aim Point

Unfiltered Error - 9 With Attitude



Lateral

m

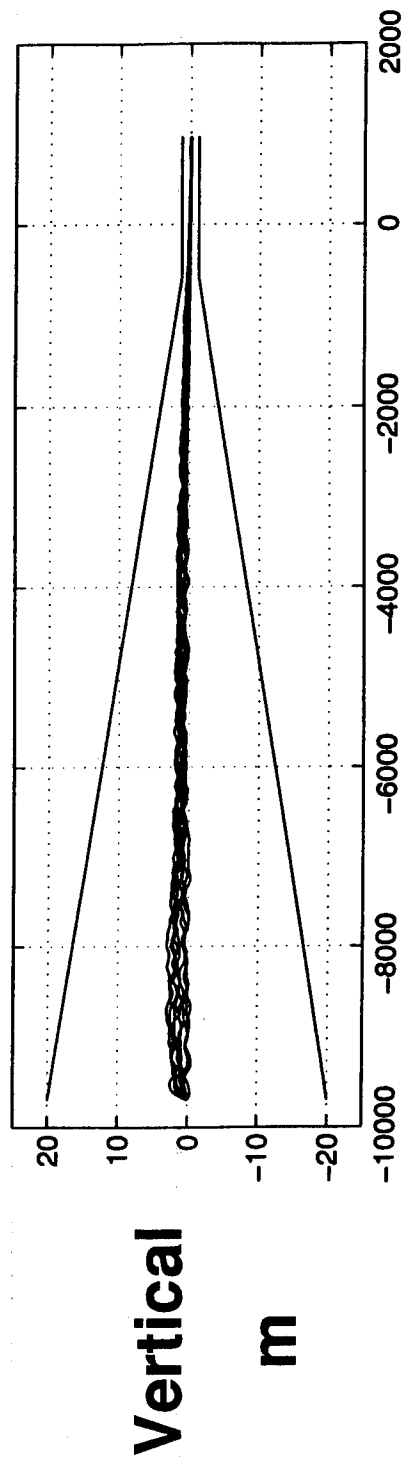
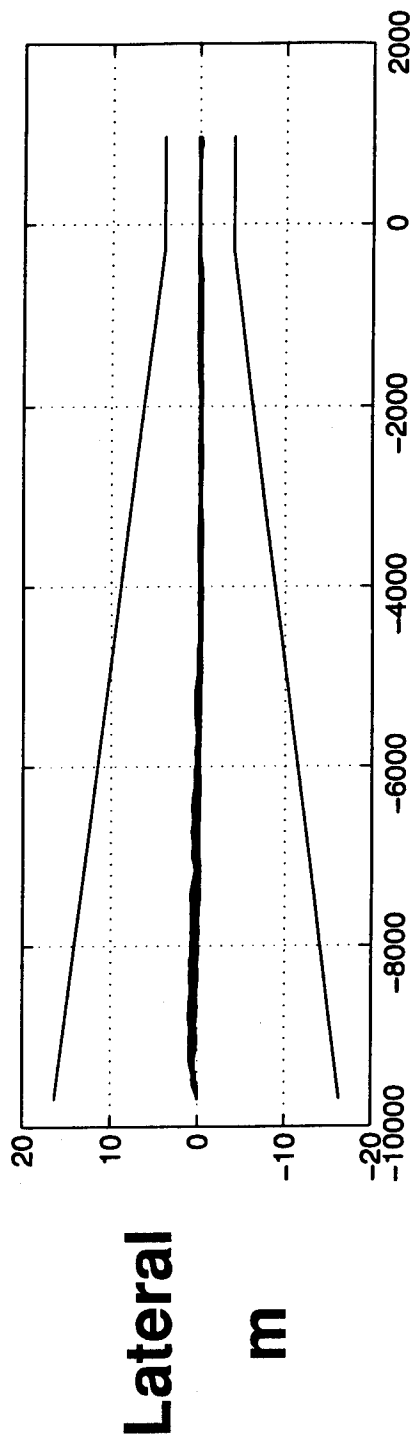


Vertical

m

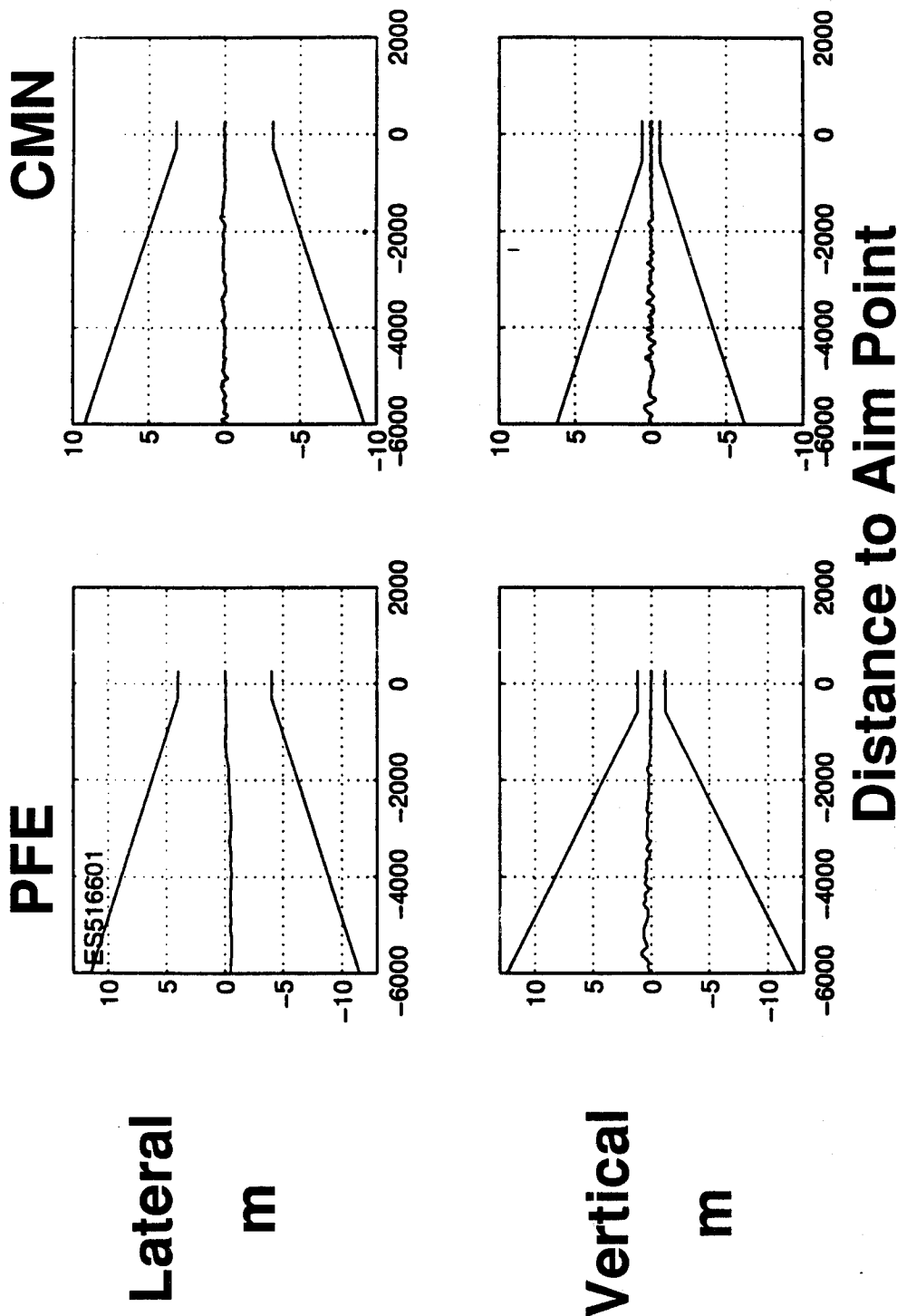
Distance to Aim Point

PFE Output - 9 With Attitude

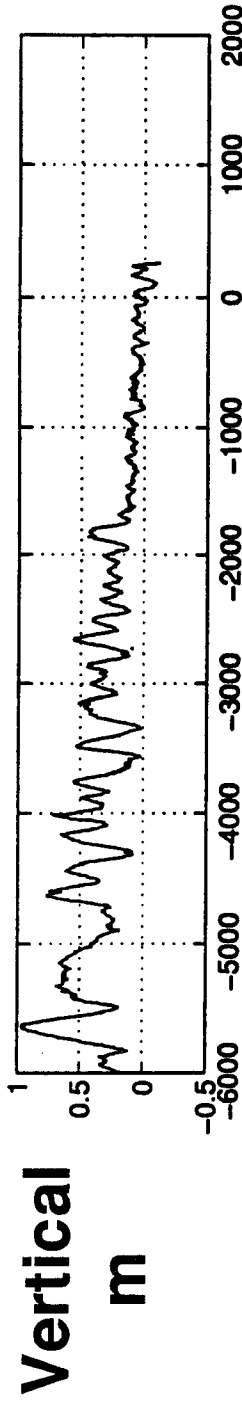
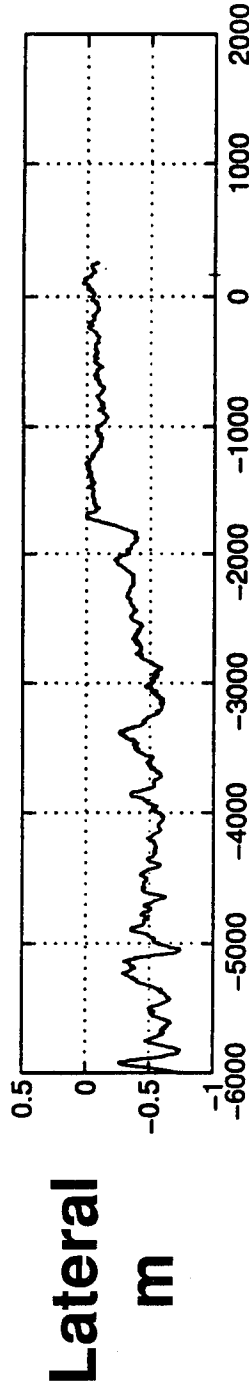
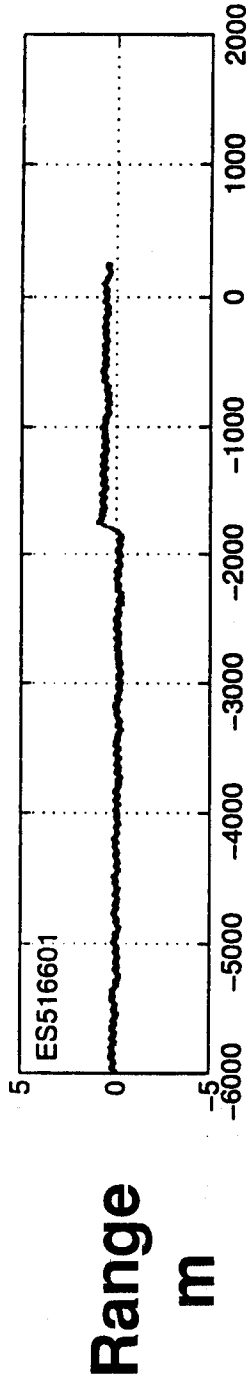


Distance to Aim Point

PFE/CMN Typical - 1 Approach



Unfiltered Error - 1 Approach



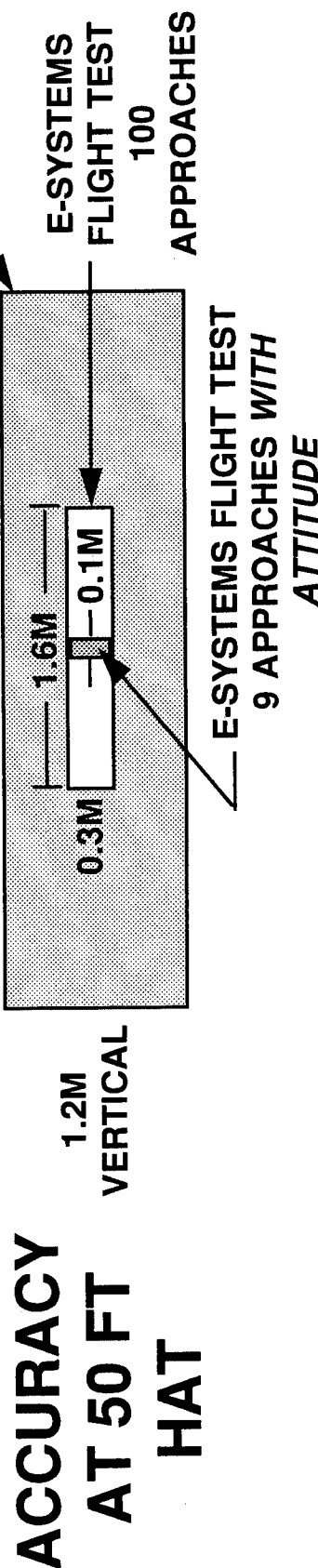
Distance to Aim Point

© 1995 E-Systems, Inc.

Summary - Flight Test Prelim Result

- Completed 100 Approaches & 10 Integrity Static Tests that Passed FAA Measures of Success
- Demonstrated Integrity Alarms Within 2.3 m Limit
- Demonstrated Nav Sensor Accuracies Meeting ILS Requirements From Final Approach Fix

95% Error of 0.3 m Vert. & 1.6 m Lat. at 50 ft. HAT
(Improved to 0.1m Lateral with Attitude Data)



Application of INS/GPS Systems Integration to Increase Performance of Automatic Landing Systems

Dr.-Ing. Jochen Meyer-Hilberg and Dr. rer. nat. Harald Harder
Daimler-Benz Aerospace AG, Navigation and Flight Guidance Systems

Biography

Dr.-Ing. Jochen Meyer-Hilberg was born on February 19, 1960 in Berlin. He received his Diploma in Communications Engineering in 1984 and his Ph. D. in Digital Processing in 1989 from the Technical University of Darmstadt, Germany.

Since 1990 he has been a Systems Engineer at Daimler-Benz Aerospace (Dasa) in Ulm, Germany, and is responsible for the software development of Dasa's Integrated Navigation and Landing System.

Dr.-Ing. Meyer-Hilberg is a Prize Winner of the VDE/ITG (Verband Deutscher Elektrotechniker/Informationstechnische Gesellschaft) Literature Award 1991 for his publications.

Abstract

Ever since Global Positioning System (GPS) became operational, it has been used in numerous applications. A field of very interesting application is the use of GPS in the area of air traffic control. Enroute navigation, automatic take-off and landing, taxi guidance and collision avoidance are some tasks that can be aided by using GPS. The highest challenge is the use of GPS for automatic landing systems because of the stringent requirements. Accuracy requirements can be met using GPS in differential mode (DGPS). However, it is hard to meet the requirements for availability, continuity of function and integrity with DGPS alone. This problem can be solved by integrating GPS with an Inertial Navigation System (INS).

In this paper, the Integrated Navigation & Landing System (INLS) developed by Daimler-Benz Aerospace (Dasa/Ulm, Germany) is discussed:* the

* This project has been partly sponsored by the German Space Agency (DARA). The responsibility for the content of this publication lies with the authors.

emphasis is to show how an INS can help to increase availability, continuity of function and integrity. After explanation of INLS system concept, flight test results are presented. The behaviour of the INLS, especially during phases of flight with satellite maskings and satellite outages, is illustrated using real flight test data.

After discussion of some exemplary flight tests, final results of flight test series with a total number of approaches in the order of 150 are presented. These flight tests were performed in 1993 and 1994, feeding INLS output data directly to an autopilot and using a laser tracker as an absolute reference of aircraft position. Our results show that system integration of INS and GPS leads to an operational landing system that satisfies accuracy, availability, continuity of function and (in principle) integrity requirements. Compared with conventional Instrument Landing Systems (ILS), INS/GPS landing systems are less expensive and need less ground equipment.

1 Introduction

Conventional systems used in air traffic control are old-fashioned and have reached their capacity limits long ago. The main problem of such systems like radar or Instrument Landing System (ILS) is to determine positions and velocities of aircraft. Modern technology can be used (see Fig. 1) to fix positions and velocities on board of the aircraft (with satellite navigation, e.g. GPS), to transmit these data to central air traffic control stations (e.g. with VHF data link or satellite communication) and to check aircraft data if there are any conflict situations between aircraft (e.g. with expert systems) [1].

To use GPS for automatic landing systems, its accuracy must be improved e.g. with differential techniques (DGPS). Accuracies in the order of one meter can be achieved using DGPS with carrier smoothed code [2], but system safety cannot be guaranteed

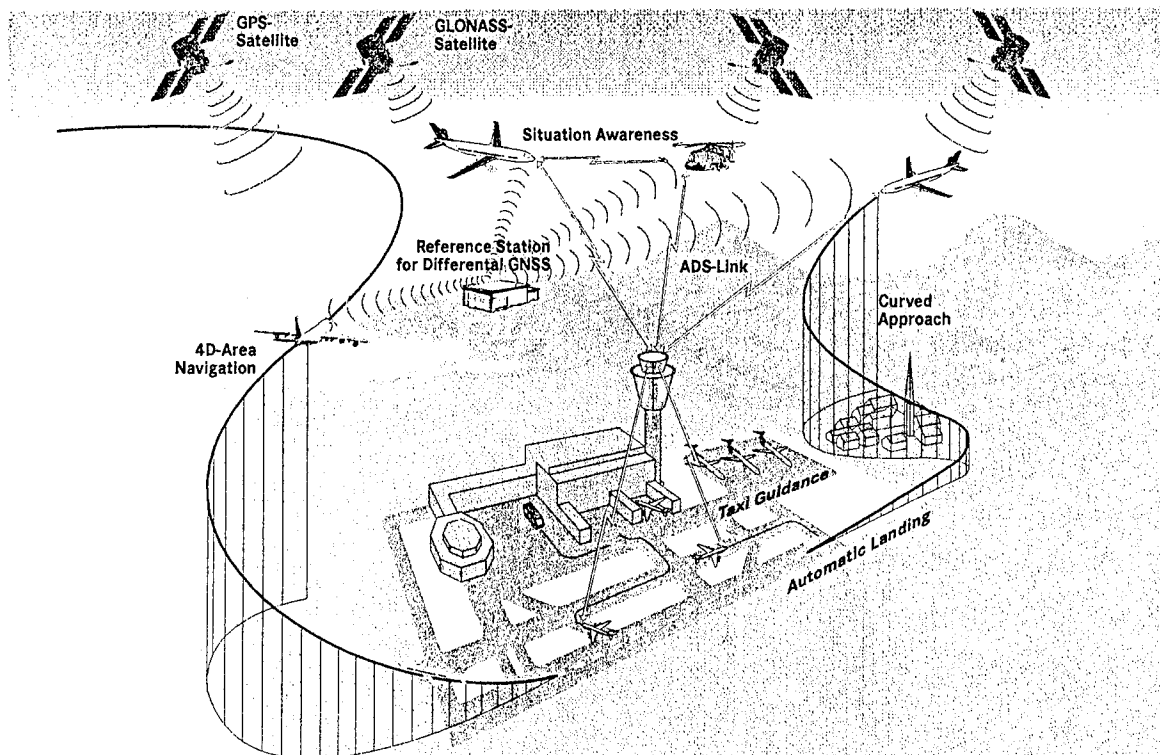


Fig. 1: Application of GPS in the Area of Air Traffic Control.

due to possible undetected satellite errors. Using a second, independent navigation system with complementary characteristics (Inertial Navigation System, INS [3,4]), availability, continuity of function and integrity of the *total* navigation system can be increased. Therefore Daimler-Benz Aerospace (Dasa/Ulm, Germany) has developed an Integrated Navigation & Landing System (INLS) which consists of a DGPS/low-cost INS combination and software completely written in Ada. Ada is *the* adequate language for safety critical applications due to its strict type checking and readability.

2 System Concept of the INLS

The main advantage of GPS is its excellent long-term position accuracy, the main disadvantages are its poor short-term accuracy (e.g. due to noise and multipath) and possible loss of position data due to satellite maskings. An INS is a good counterpart of GPS because of its good short-term accuracy and the absence of position drop-outs. However, long-term accuracy of INS is bad due to accumulating sensor errors.

Dasa's system concept of the integrated system can be described as a complementary filter: GPS positions are low-pass filtered to gain the good long-term accuracy and to suppress short-term position errors. INS positions are high-pass filtered to eliminate the long-term position drift and to obtain the good short-term accuracy.

In Fig. 2, system concept of the INLS is shown in principle. Aircraft motion is measured by DGPS and by inertial sensors (low-cost sensors). Inertial measurements including sensor errors are accelerations $\vec{a} + \Delta\vec{a}$ and angular rates $\vec{\Omega} + \Delta\vec{\Omega}$. These data are processed in a navigation computation algorithm resulting in the INS position $\vec{X} + \Delta\vec{X}$. The difference between INS and DGPS positions (i.e. the difference of INS position error $\Delta\vec{X}$ and DGPS position error $\delta\vec{X}$) is fed into a Kalman filter. The Kalman filter estimates main errors of the INS, e.g. acceleration sensor offset $\Delta\vec{a}$, gyro drift $\Delta\vec{\Omega}$ and position error $\Delta\vec{X}$. These estimates are used to calibrate the INS continuously in-flight. During phases of flight with satellite maskings, the INS within the INLS is operating alone. Due to continuous calibration, performance of the low-cost sensors has been improved to laser gyro quality provided that maximum duration of maskings is in the range of several minutes [4].

The INLS has been tested during numerous flight tests. The results of these tests will be presented in the following sections. On the basis of an exemplary flight test, the quality of INS calibration is demonstrated in section 3. Using artificial satellite maskings with a duration of 60 seconds each, the INS drift is estimated. Continuity of function is ensured in spite of complete DGPS position drop-outs.

During another approach, satellite constellation changed 40 s before touch down leading to an DGPS

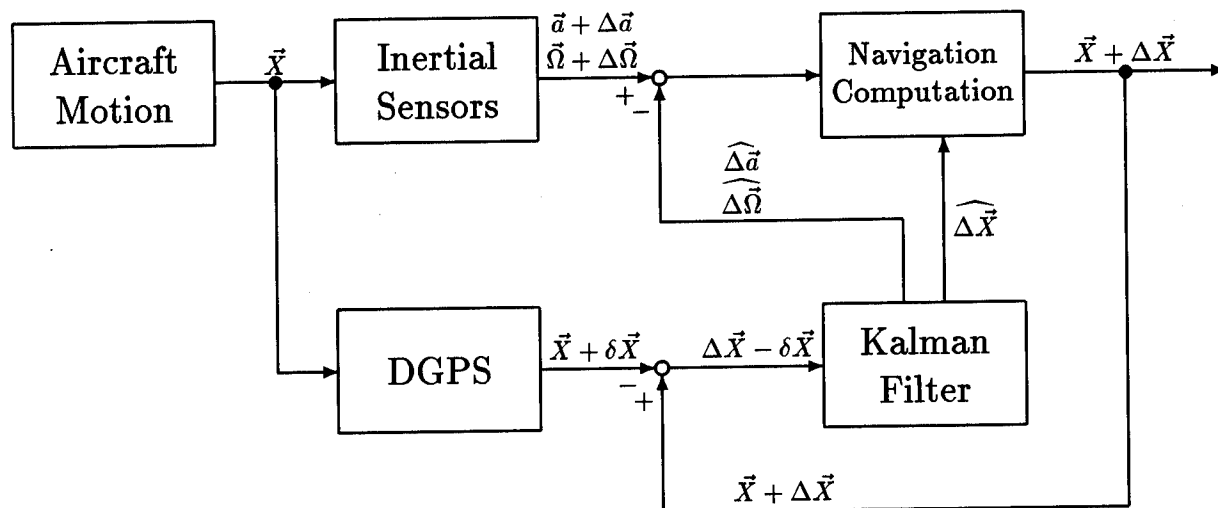


Fig. 2: System Concept of the INLS.

altitude error of some meters. Using an INS, this DGPS error can be detected and eliminated. However, only short-term DGPS errors can be corrected, it is not possible to identify offset-type errors with an INS. It is illustrated in section 4 how an INS can help to increase integrity and availability.

Section 5 contains summarized results of Dasa's flight test series with the INLS in 1993 and 1994.

3 Performance of the INS within the INLS

Data of a flight test on 5. October 1994 (mission 2) are used to demonstrate the calibration quality of the INS within the INLS. During this flight test, seven approaches are flown with INLS coupled to an autopilot. In Fig. 3, the flight track is shown. It is considerable how accurate the aircraft follows its glidepath for the last 150 meters of altitude before touch down!

To check INS quality, artificial GPS maskings which lead to total loss of DGPS position data are used. Each time period of GPS masking has a duration of 60 seconds and its end exactly coincides with the moment of touch down. Therefore, no DGPS positions are available during the last 4 km of these approaches and INS is operating alone.

Fig. 4 shows the errors of INS positions. A laser tracker is used as an absolute position reference and Path Following Errors (PFE) are calculated according to ICAO Annex 10 [5]. Position error $\Delta \vec{X}$ at the end of a satellite masking period with a duration Δt_{mask} can be estimated [4]:

$$\Delta \vec{X}(\Delta t_{\text{mask}}) \approx \frac{1}{2} \cdot \Delta \vec{a} \cdot \Delta t_{\text{mask}}^2$$

Acceleration sensor offset $\Delta \vec{a}$ can be divided into horizontal and vertical components Δa_{hor} and Δa_{vert} . Horizontal errors are larger than vertical because misalignment ε_{hor} of the vertical axis leads to a faulty compensation of gravity g which couples in as a horizontal acceleration error:

$$|\Delta a_{\text{hor}}| = g \cdot \sin |\varepsilon_{\text{hor}}|$$

With values of Fig. 4, maximum misalignment $|\varepsilon_{\text{hor}}|$ of the vertical is estimated to a value in the order of some hundredth of a degree!

Average position drift $\dot{\Delta \vec{X}}$ of the INS can be calculated [4]:

$$\dot{\Delta \vec{X}}(\Delta t_{\text{mask}}) \approx \frac{1}{2} \cdot \Delta \vec{a} \cdot \Delta t_{\text{mask}}$$

With the values above, mean horizontal and vertical drifts $|\dot{\Delta X}_{\text{hor}}|$ and $|\dot{\Delta X}_{\text{vert}}|$ can be estimated to some centimeters per second. These values are comparable to typical drift rates of laser gyro INS. Satellite maskings in the range of minutes can be bridged, continuity of function of the INLS is guaranteed. Moreover, the Kalman filter estimates position accuracies, therefore accuracy degradations due to satellite maskings are known and can be monitored.

4 Behaviour of the INLS after GPS Errors

In Fig. 5, aircraft positions of a test flight on 11. October 1994 (mission 2, 4th approach) are shown versus time. During this approach, satellite constellation changed leading to a bad VDOP and to large DGPS altitude errors. At time $t = 233\,100$ s, a satellite that was needed for good vertical accuracy disappeared. Low-dynamic flight condition

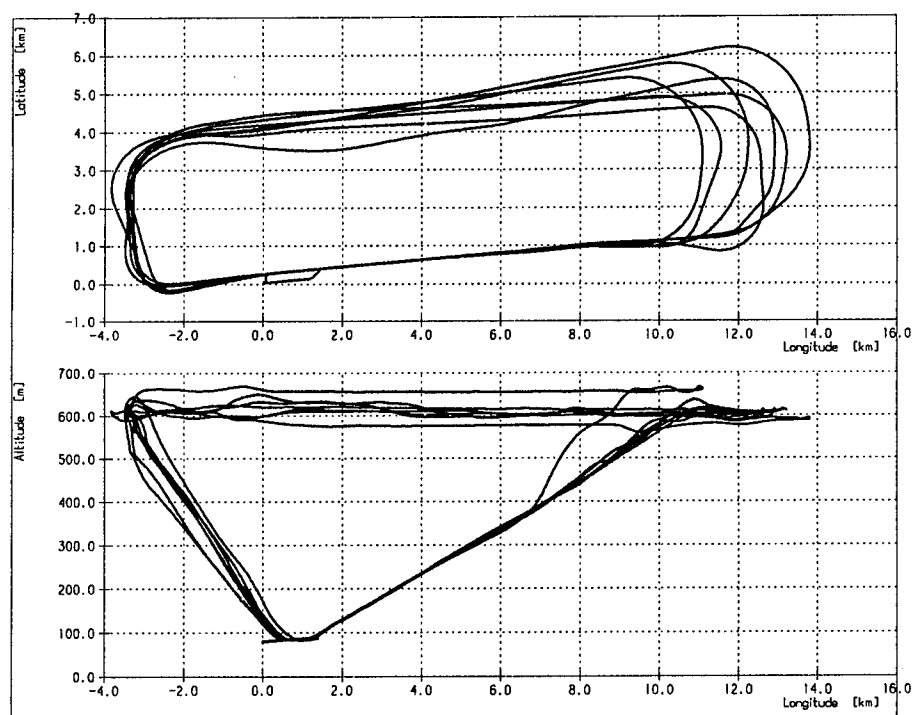


Fig. 3: Flight Track of Test Flight on 5. October 1994, Mission 2 (Latitude versus Longitude and Altitude versus Longitude).

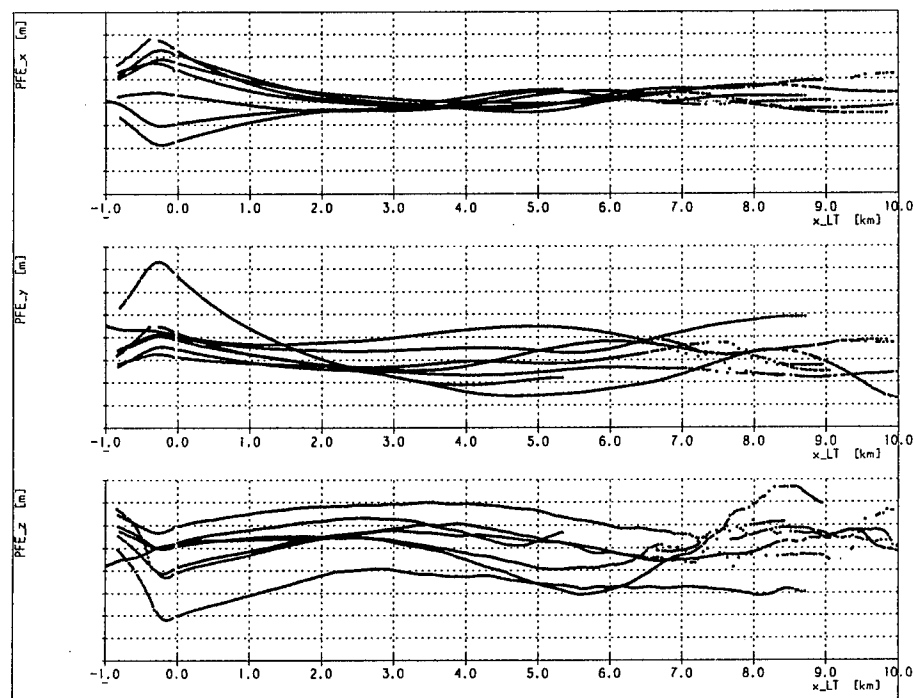


Fig. 4: Typical Path Following Errors (PFE) versus Distance $x.LT$ to Touch Down Zone (TDZ) with $x \hat{=}$ In-Track, $y \hat{=}$ Cross-Track and $z \hat{=}$ Vertical Direction. The Last 60 Seconds before Touch Down ($4 \text{ km} \geq x.LT \geq 0 \text{ km}$), GPS is Masked and INLS is Operating with INS Alone.

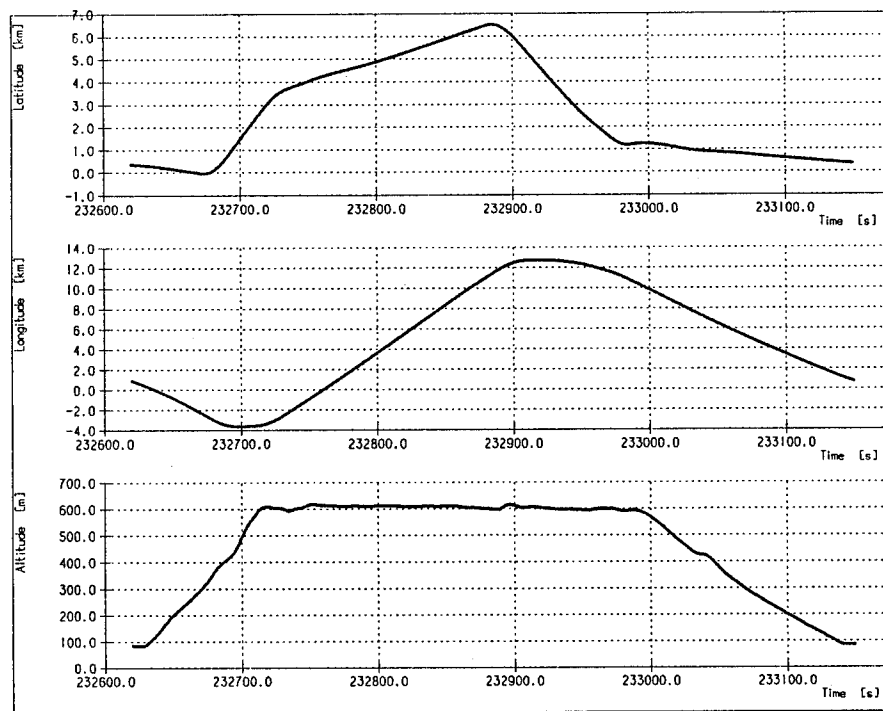


Fig. 5: Aircraft Positions (Latitude, Longitude and Altitude) versus Time (Test Flight on 11. October 1994, Mission 2, Approach 4).

has been reached at this time (look at positions in Fig. 5). The aircraft flew at an altitude of about 120 meters above Touch Down Zone and 40 seconds are left to touch down.

The following figures illustrate the typical behaviour of the INS within the INLS after sudden degradations of GPS position accuracy. Due to the low-pass characteristic of the DGPS branch in Fig. 2, short-term DGPS position errors are eliminated. In Fig. 6, "internal" position errors, i.e. differences of INLS and DGPS positions, are plotted versus time. These differences are input values of the Kalman filter (see Fig. 2) and no external references (e.g. laser tracker) are needed. Discontinuities of the curves in Fig. 6 are DGPS position errors due to satellite constellation changes, while INLS position errors rise slowly. For time $t < 233\,000$ s, changes are caused by satellite maskings due to large roll angles. At time $t = 233\,100$ s, DGPS altitude error jumps about some meters!

Fig. 6 shows a mixture of DGPS and INLS errors. To separate DGPS and INLS errors, a laser tracker is used providing a position reference. Path Following Errors (PFE) have been calculated according to ICAO Annex 10 [5]. In Fig. 7, Path Following Errors of DGPS and INLS are plotted versus height above Touch Down Zone (TDZ). At a height of 120 meters, DGPS altitude error jumps from zero to some meters (see Fig. 6 also!). DGPS Path Following Errors are basically low-pass filtered DGPS posi-

tion errors. That is the reason why Fig. 7 shows an exponentially increasing function without any discontinuities (see upper curve in lower plot).

The integrated navigation system is able to eliminate short-term DGPS errors, but it cannot compensate long-term errors (offset errors). This behaviour can be seen in Fig. 7: INLS vertical Path Following Error (lower curve in lower plot) does not show a jump at a height of 120 meters above TDZ, but gets closer to DGPS PFE gradually. At the moment of touch down, INLS PFE nearly equals DGPS PFE.

Cross-track and vertical PFEs shown in Fig. 7 as separate components are visualized in a common picture in Fig. 8 using autostereogram technique [6]. Cross-track PFE_y is plotted in vertical direction, height z_{LT} above TDZ in horizontal direction and vertical PFE_z in the direction perpendicular to paper plane. Background is plane with PFE_z = 0. See reference [6] on how to view this picture. The lower curve corresponds to DGPS PFE which does not meet CAT III accuracy. DGPS accuracy during this approach is suitable only for a CAT I landing. On the other hand, INLS Path Following Error meets CAT III accuracy requirements!

With an integrated navigation system, integrity and availability can be increased in comparison to GPS alone. Short-term GPS errors can be detected and lack of availability due to bad satellite geometry can be compensated. For a maximum duration of about

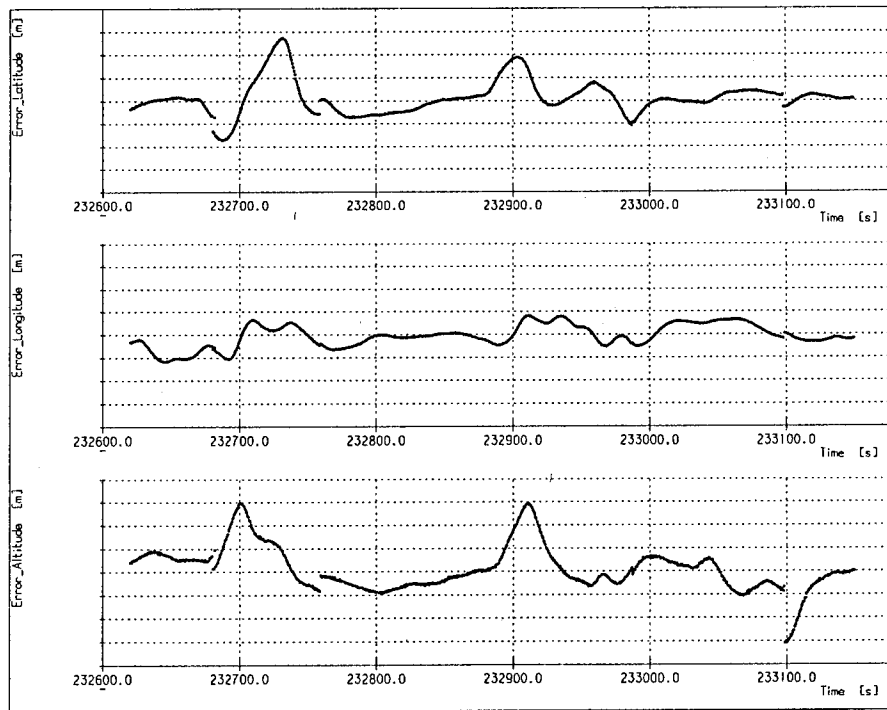


Fig. 6: Typical “Internal” Position Errors (INLS ↔ DGPS) versus Time (Test Flight on 11. October 1994, Mission 2, Approach 4). The Discontinuity of Altitude Error at Time = 233 100 s is Due to a Constellation Change of GPS Satellites.

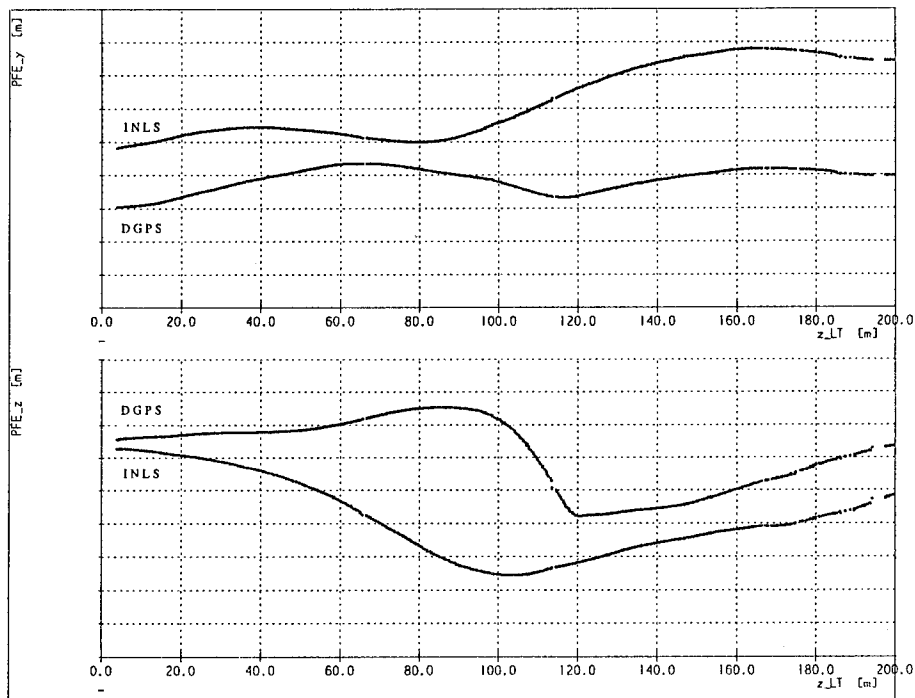


Fig. 7: Typical Path Following Errors (PFE) of DGPS and INLS versus Height z_{LT} above Touch Down Zone (TDZ) with $y \hat{=}$ Cross-Track and $z \hat{=}$ Vertical Direction (Test Flight on 11. October 1994, Mission 2, Approach 4).



Fig. 8: Autostereogram (3-Dimensional Picture) of Path Following Errors (PFE) from Fig. 7 (Lower Curve: DGPS, Upper Curve: INLS).

Vertical Direction: Cross-Track PFE_y (Same Scale as in Fig. 7),

Horizontal Direction: Height z_{LT} above TDZ (Same Scale as in Fig. 7),

Depth: Vertical PFE_z (Background is Plane with PFE_z = 0).

30 seconds, CAT III requirements can be met even if there are GPS accuracy degradations!

5 Final Results of INLS Flight Tests

Several flight test series have been performed in 1993 and 1994 in Braunschweig, Germany. A total number of 149 landings was flown, most of them with autopilot driven by INLS output data. A laser tracker was used as an independent position reference. The summarized results of these flight tests are shown in Table 1. Table entries show how many approaches met CAT I/II/IIIb accuracy requirements [7] having good or bad satellite geometry ($\text{GDOP} < 4$ or $\text{GDOP} \geq 4$). Due to the sharp vertical accuracy requirements of ± 1.2 m, a total of 30 approaches (20 %) did not meet CAT IIIb requirements (automatic landing). Most of these failures are due to exceptional flight conditions before or during these approaches. 8 failures are due to bad satellite constellations and 22 failures are due to GPS receiver errors (NovAtel receiver). However,

all 149 approaches met CAT IIIb horizontal accuracy requirements and maximum altitude error is about 2.88 meters ($\text{GDOP} = 4$)! Our results correspond to results of other examinations [8,9,10].

6 Summary

GPS can be used for automatic landing systems. Accuracy requirements can be met quite easily using differential GPS. Meeting availability, continuity of function and integrity requirements is possible with INS/GPS system integration. Results of flight tests showed that Dasa's integrated navigation system INLS is a precision navigation system without the disadvantages of GPS (position drop-outs) and INS (drift). CAT IIIb automatic landing requirements can be met even if GPS fails for a duration not exceeding 30 seconds. The INLS estimates position accuracies to maintain accuracy monitoring. In case of accuracy degradations, warnings are issued to the pilot.

| | GDOP < 4 | | GDOP ≥ 4 | | Σ | |
|-------------------------|----------|---------|----------|--------|--------|---------|
| Number of Flights | 129 | | 20 | | 149 | |
| Accuracy within CAT I | 128 OK | 1 Fail | 19 OK | 1 Fail | 147 OK | 2 Fail |
| Accuracy within CAT II | 108 OK | 21 Fail | 13 OK | 7 Fail | 121 OK | 28 Fail |
| Accuracy within CAT IIb | 107 OK | 22 Fail | 12 OK | 8 Fail | 119 OK | 30 Fail |

Table 1: Summary of INLS Flight Tests in 1993 and 1994. The Large Number of Failures is Due to Exceptional Flight Conditions (High Accelerations!).

References

- [1] Th. Jacob, H.-G. Wippich, H. Schmidt, J. Meyer-Hilberg, G. Bantle, W. Rösch: GPS/GNSS for ATM. In: AGARD Conference Proceedings 538: Machine Intelligence in Air Traffic Management. Neuilly-Sur-Seine, France: Advisory Group for Aerospace Research & Development, October 1993, ISBN 92-835-0724-X, pp. 8/1-8/10.
- [2] X. Gu, A. Lipp: DGPS Positioning Using Carrier Phase for Precision Navigation. Proceedings of the 1994 IEEE Position Location and Navigation Symposium (PLANS '94), Las Vegas, NV, April 1994, ISBN 0-7803-1435-2, pp. 410-417.
- [3] P. G. Savage: Strapdown Inertial Navigation Lecture Notes. Plymouth, MN 55441, USA: Strapdown Associates, February 1990.
- [4] J. Meyer-Hilberg, Th. Jacob: Accuracy Performance of Dasa's Integrated Navigation & Landing System. Proceedings of the 1995 National Technical Meeting of the Institute of Navigation, Anaheim, CA, January 1995, pp. 549-556.
- [5] International Civil Aviation Organization (ICAO): International Standards, Recommended Practices and Procedures for Air Navigation Services, Aeronautical Telecommunications, Annex 10 to the Convention on International Civil Aviation, Volume I. Fourth Edition of Volume I, April 1985.
- [6] Stereogram. San Francisco, CA: Cadence Books, 1994, ISBN 0-929279-85-9.
- [7] R. Braff, P. O'Donnell, C. Shively, R. Swider: FAA's DGPS CAT III Feasibility Program: Update and Test Methodology. Proceedings of the 1994 IEEE Position Location and Navigation Symposium (PLANS '94), Las Vegas, NV, April 1994, ISBN 0-7803-1435-2, pp. 239-245.
- [8] F. van Graas, D. Diggie, V. Wulschleger, R. Velez, G. Kuehl, R. Hilb, M. Dimeo: FAA/Ohio University/UPS Autoland Flight Test Results. Proceedings of the 1995 National Technical Meeting of the Institute of Navigation, Anaheim, CA, January 1995, pp. 145-156.
- [9] R. Paielli, R. Bach, B. McNally, R. Simmons, D. Warner, T. Forsyth, G. Kanning, C. Ahtye, D. Kaufmann, J. Walton: Carrier Phase Differential GPS Integrated with an Inertial Navigation System: Flight Test Evaluation with Auto-Coupled Precision Landing Guidance. Proceedings of the 1995 National Technical Meeting of the Institute of Navigation, Anaheim, CA, January 1995, pp. 711-724.
- [10] C. Cohen, D. Lawrence, H. S. Cobb, B. Pervan, J. D. Powell, B. Parkinson, G. Aubrey, W. Loewe, D. Ormiston, B. D. McNally, D. Kaufmann, V. Wulschleger, R. Swider: Preliminary Results of Category III Precision Landing With 110 Automatic Landings of a United Boeing 737 Using GNSS Integrity Beacons. Proceedings of the 1995 National Technical Meeting of the Institute of Navigation, Anaheim, CA, January 1995, pp. 157-166.

A340 – DGPS Landing Experiment

Julie de Cevins
Airbus Industrie

Pascal Ponsot
Aerospatiale

BIOGRAPHY

Julie de Cevins joined Airbus Industrie in 1993. She is responsible for coordinating the design of navigation sensors for all in-production and in-service aircraft.

Previously, she worked on the design and testing of avionics systems for A330 and A340 with Aerospatiale, and also with Intertechnique and SFENA (now part of Sextant Avionique).

Mrs de Cevins holds a Diplôme d'Ingénieur from Ecole Polytechnique Féminine (1987) and a Masters qualification in Aerospace Electronics from Ecole Nationale Supérieure de l'Aéronautique et de l'Espace (1988).

Pascal Ponsot works at AEROSPATIALE Design Office since 1982 as an Avionics engineer. From 1982 to 1992, he was responsible for airborne, Navigation radars development and Qualification for military Aerospace. He joined AEROSPATIALE/AIRBUS DIVISION Avionics department in 1992 for radio Navigation development on Airbus aircraft. After working for first SATCOM certification on Airbus, he is responsible since 1994 for the DGPS precision approach experimentation on Airbus A340, and for Radar, TCAS and ATC development on all Airbus aircraft.

ABSTRACT

Since October 95, Airbus Industrie has been performing Differential GPS approaches and landings on A340 test aircraft on Toulouse and other airports. The main goal was to prove DGPS Cat 1 accuracy feasibility on a big airplane such as A340 and, if possible, Cat 2.

The DGPS airborne equipment is linked to the auto-pilot and to the displays, in order to provide "ILS-like" information to the auto-pilot and to the

crew.

The objectives of this experiment are of different types :

- . test the chosen airborne architecture, and especially the flight management system interface and the auto-pilot interface with DGPS.
- . test different vendor equipment (Litton and Sextant) and evaluate accuracy,
- . test interoperability between the different ground and airborne equipment,
- . evaluate the environmental contribution on airborne and ground stations.

180 approaches have been performed with Sextant and Litton, using a SCATI Wilcox/Thomson ground station equipment. They show very good results, and at least Cat 1 and Cat 2 accuracy. First approach was good enough to be autoland and rollout.

These approaches have been performed on different airports in France (Montpellier and Toulouse), in China (Beijing, Shanghai and Canton), in South Africa (Mmabatho) and in Mauritius (Plaisance).

Results show that there is :

- . better than 2 meters lateral and 3 meters vertical accuracy,
- . simplicity and ease of installation of the ground station
- . importance of the ground station antenna location to avoid multipath and masking of the satellites,
- . importance of ground station integrity

and availability.

- excellent results to "envisage" Cat 3 autoland with improvement of Ground Station Integrity, Availability and Monitoring.

This experiment is part of a more global project which is to certify DGPS initially for Category 1 landing minima by mid 1997.

Next steps of this program will be to confirm the aircraft architecture, to check the availability and the integrity of the system by simulation, to study and define the Human Machine Interface, and last but not least to go through the certification process itself. This phase will be the most critical one, as the standards are still being written and as the ground station and airborne receiver will probably in a first approach have to be certified all together.

1. INTRODUCTION

Until now, many Differential GPS experiments have been performed on different types of aircraft, but Airbus and Aerospatiale considered that it was necessary to perform their own DGPS trial in order to test the ability of Airbus aircraft to interface with this new system.

The main objectives were :

- 1 - to demonstrate, for the first time in the world, that it was feasible to land a civil widebody aircraft using a differential GPS technique, with auto-flight systems as designed today.
- 2 - to verify that DGPS performances were compatible with Category 1, and, if possible, with Category 2 (low visibility landing requirements).
- 3 - to test the interoperability between different ground stations and airborne receivers.

As a consequence, it was necessary to observe the aircraft systems behaviour and to study some technical aspects : architecture, data link, data to upload, trajectory calculation, update rate, interface, displays, tunnel concept, mask angle, time to alarm

This experimentation was launched at the end of 1993 with the support of French Civil Aviation

Authority (STNA : Service Technique de la Navigation Aérienne) for the use of the ground station, and of two avionic manufacturers : Sextant and Litton.

2. ARCHITECTURE

2.1 Ground based equipment

In order to test the interoperability of the system , two types of ground station have been used during Airbus experiment.

A fixed one was provided by the STNA and was built by Thomson/Wilcox.

A second one was an experimental portable station provided by Sextant.

2.1.1 STNA Ground station

This station is a Thomson/Wilcox GLS 2000 equipment designed according to the SCAT I MASPS dated 1994. It is located in a shelter close to the overrun area of runway 33 L on Toulouse airport. The antennas are located on top of the shelter.

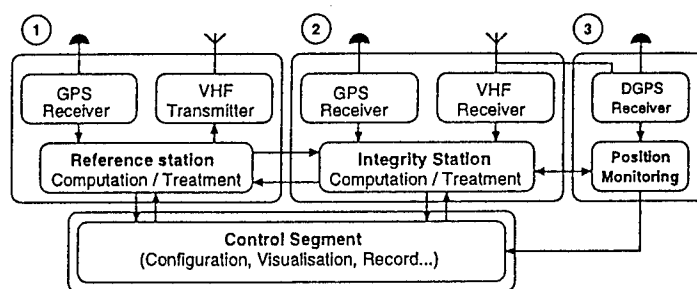


Figure N° 1 : STNA ground station

This station is composed of three parts :

Reference station : Receives the GPS signals, calculates the GPS position, compares to the WGS 84 reference position, elaborates the corrections for each satellite, sends the corrections to the airplane via VHF data link.

Integrity monitoring station : Receives the GPS signals, receives the differential corrections via the VHF data link, subtract the differential corrections to the ground station reference position, compares the result to the GPS position.

Position monitoring : This monitoring is ensured by a DGPS receiver which calculates a GPS corrected

position using corrections transmitted via VHF and compares it to the reference position.

If the position monitoring or the integrity monitoring detects any anomaly, integrity is set to false and the data link transmits a non availability information.

Remark :

Multipath signals are minimized by the shock-ring type GPS antennas, and with specific software.

2.1.2 Sextant portable ground station prototype

This ground station, which is a prototype, was the first one available, and was used during the first part of the tests. It was designed by Sextant according to SCAT I recommendations for the data link (same definition as STNA). It is a portable equipment powered by a 12 VDC battery. The GPS antenna is located on the ground at a distance of about 20 meters from the equipment.

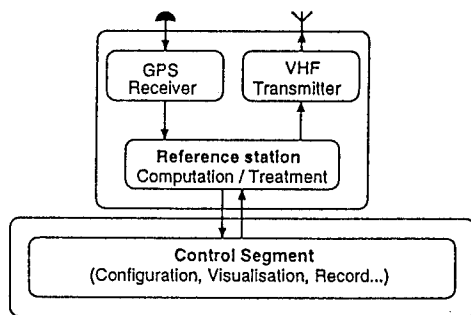


Figure N° 2 : Sextant portable ground station

This station consists only of a reference station which calculates the differential corrections and sends them via the VHF data link. This station does not provide any integrity monitoring.

This portable system is designed to obtain the reference coordinates and related data of the flight paths in less than 3 hours. It offers the possibility to perform trials on different environments with a very short preparation time. This capability was used several times for demonstration purpose.

2.2 Data link

The data link used for this experiment was the same for all ground stations. It is described in RTCA SCAT I document appendix F. It is in the VHF communication band (experiment frequency is 122.475 MHz), with an hybrid Modulation Shift Keying (MSK), a transmission rate of 2400 bits per second, and a refresh rate of 1 Hz.

Information sent are :

Pseudo range corrections,
User Difference Range Error,
Acceleration Bound Error,
Range Rate Correction,
Reference time.

A 4th VHF antenna has been installed on board the aircraft for the DGPS data link purpose. This antenna is linked to a specific VHF receiver designed for the datalink purpose, located on the DGPS pallet.

2.3 Airborne equipment

As already mentioned, the objective was to implement the DGPS on board the aircraft with no modification of the connected systems : all the DGPS interfaces were strictly identical to the ILS interfaces.

The experimental architecture is based on a single DGPS installation.

Both vendors provided the same type of DGPS pallet consisting of :

- . A GPS receiver based on ARINC 743A definition providing Position/ Velocity/Time
- . A VHF data link receiver, in accordance with SCAT I protocol
- . DGPS system computing : (refer to Fig. N° 3)
 - the corrected GPS position of the aircraft,
 - the approach path according to the runway selected by the pilot through the MCDU (the ideal path is calculated using the WGS 84 reference points (The 2 runway thresholds) and the glide slope stored in the DGPS data base),
 - the deviations between the aircraft DGPS position and the approach path, using the proper lever arm corrections (static and dynamic) between GPS antenna and ILS G/S antenna position on the aircraft, which is the reference position for the automatic guidance.

Sextant and Litton equipment were experimented during this trial.

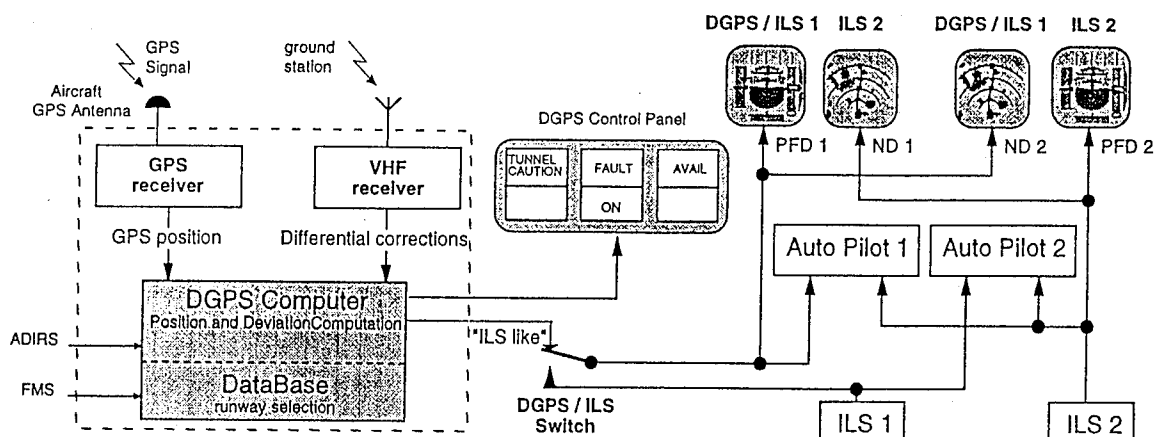


Figure N° 3 : Airborne receiver

2.3.1 Sextant airborne equipment specificities

The airborne GPS landing equipment is based on an ARINC 743 GNSS sensor (TOPSTAR equipment from Sextant Avionique), which has been modified to contain the differential GPS Landing functions. The basic navigation functions are :

- 10 parallel channel GPS signal processing (code/phase) all-in-view (0° mask angle), L1, C/A
- RAIM algorithm
- Position, Velocity, Time (P.V.T.) calculations at 10 Hz

2.3.2 Litton airborne equipment specificities

This equipment is composed of a 12 channel Novatel card, using a narrow correlator technique.

It receives IRS velocity information to perform a Kalman filtering between differential GPS position and IRS information. This function named by Litton "Coasting mode", allows to propagate DGPS position information calculation up to several tens of seconds after differential corrections loss.

2.3.3 Airborne equipment interfaces

Inputs :

- "DGPS/ILS" Switch : this switch is located on the center pedestal and allows the crew to choose to select an ILS approach or a DGPS approach.
- Flight Management System (FMS) : The DGPS receives from the FMS the ILS frequency and the ident of the runway selected by the crew through the MCDU or the RMP.

Remark : For the trial purpose, when an approach must be performed on a non ILS equipped runway, a dummy ILS frequency is introduced in the FMS in order to be able to access the runway reference points.

- Air Data Inertial Reference System (ADIRS) : The DGPS receives the aircraft position for initialization of the GPS receiver, and the attitude information for the dynamic lever arm correction calculation, and the velocity for Litton coasting.

Outputs :

- ILS-like position information : When the DGPS/ILS switch is set to "DGPS", the lateral and vertical deviations are sent to the Auto pilot for guidance control law computation, and to the Display Management Computers for display on the Primary Flight Display and the Navigation Display. A look-alike glide deviation and a look-alike localizer deviation are transmitted with an angular format.
- DGPS Control Panel :

This control panel is located on top of the glareshield. It is composed of four lights :

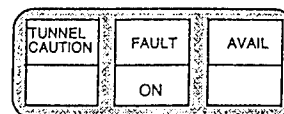


Figure N° 4 : DGPS control panel

- . DGPS "ON" : The aircraft systems receive the DGPS ILS like information instead of the ILS information
- . DGPS "AVAIL" : DGPS system is operational and data link is correct - When an integrity anomaly has been detected by the ground station or the on-board equipment or when a performance degradation has been detected by the DGPS on-board equipment, this light flashes.
- . TUNNEL "CAUT" : Linked to the RNP tunnel principle - Flashes when aircraft is outside the Inner tunnel but in the outer tunnel, and lights when aircraft is outside the outer tunnel.
Reminder : the inner tunnel defines the typical 95th percentile aircraft flight deviations, and the outer tunnel defines the 10^{-7} rare event aircraft containment surface.
- . DGPS "FAULT" : Lighted when a DGPS receiver failure is detected.

2.3.4 Displays

The DGPS ILS-like deviations are displayed on Primary Flight Display 1 (Captain side) and on Navigation Display 2 (First officer side) while ILS 2 information is still displayed on PFD 2 and ND1 for crosscheck.

Remark : This is the same architecture as today ILS definition where ILS 1 is displayed on PFD 1 and ND 2, ILS 2 is displayed on PFD 2 and ND 1.

Runway heading computed using DGPS data base waypoints are displayed on PFD 1 and ND 2.

ILS frequency and runway ident used for the DGPS approach selection are displayed on PFD/ND as with ILS classical information today.

Note : the human machine interface has been defined for the test purpose only. It is being improved for production implementation.

3. RESULTS

3.1 Trial conditions

After the system design and aircraft modifications during early 1994, the ground station prototypes were installed on Toulouse airport on September 1994.

The DGPS flight trial campaign begun on October 1994. Three steps can be distinguished :

- Debug flights

- Performance flights for fine analysis.
- Demonstration flights for airlines on different airports.

During the first flight on 13 October 1994, in view of the good behavior during the first manual approach, the test pilots performed successfully 9 automatic DGPS captures, approaches, including autolands and roll-out with success on two Toulouse runways.

At the end of 1994, DGPS autolands were performed for system adjustment, and then, in 1995, the two different LITTON and SEXTANT pallets were tested and demonstrations were performed on several airports in France, China, Mauritius, and South Africa.

The DGPS system has been tested in different environmental conditions :

- different constellation geometries,
- different weather conditions,
- different locations for the ground station.

During the 7 months of the Airbus DGPS experimentation, the A340 n°1 performed a total of 180 DGPS approaches and landings (113 autolands), on 7 airports and 15 different runways.

Using the Sextant airborne receiver : 70 landings in Toulouse + 60 for airlines demonstration in China, Mauritius and South Africa.

Using the Litton airborne receiver : 50 landings at Toulouse airport.

3.2 Analysis means

A340 n° 1 is the Airbus Industrie flight test vehicle, fully equipped for development flights with :

- recorders (all aircraft parameters recorded)
- real time telemetry
- microwave trajectography (accuracy 0.5 m in the three axes).

The DGPS parameters are recorded onboard and simultaneously sent by telemetry for real time analysis on the ground. Telemetry also allows real time discussions between ground engineers and the flight test crew on board the aircraft.

Microwave trajectography was used to measure around 60 approaches.

Litton also used their "FLYKIN" process which is a post processing DGPS, based on a phase tracking technique for quick analysis.

3.3 Results

3.3.1 Accuracy

The analysis of aircraft system behavior and DGPS performance, show that the DGPS system provides at least the accuracy needed for Cat 2 precision approach down to autoland.

The accuracy of the DGPS system for precision approach can be separated into two different categories :

- NSE : Navigation System Error represents the intrinsic error of the DGPS system.
- FTE : Flight Technical Error, is the guidance system error including guidance loop, weather, wind, aircraft characteristics,...

The Total System Error $TSE = FTE + NSE$ is the accuracy of the complete aircraft guidance : navigation + autopilot.

Navigation system error :

The dispersion for the STNA ground station was measured when installed on the airport on static point :

lateral : +/- 1.2 m and vertical : +/- 2.5 m.

The accuracy of the complete DGPS system, measured using trajectography during the approach, is :

lateral : +/- 1.8 m and vertical : +/- 2.8 m.

These values are the 95 % deviations on around 50 approaches.

The extreme conditions encountered for the whole DGPS approaches and landings are displayed on Table 1.

The accuracy observed during the trial is indicated on Table 2.

For comparison, on Table 3, are indicated the required ILS accuracy (ICAO Annex 10).

Comments

The lateral accuracy, as expected, is better than the vertical accuracy. Furthermore, accuracy is continuous all along the approach.

The average values included the dispersion of the

ground station, the accuracy of the trajectography and the error of the DGPS system.

The 95 % error results are in accordance with expected performances.

Figures show that DGPS accuracy complies with ILS Cat 1 and ILS Cat 2 requirements, but not with ILS vertical Cat 3 requirements. However, below 100 ft, the autoflight system uses aircraft vertical position calculated using not only ILS-like vertical position. Below 50 ft, DGPS vertical position is not used, anymore by autoflight. As a consequence, DGPS vertical accuracy should not be an issue to perform autoland.

Total System Error

The aircraft touch-down point on the runway for DGPS landing are shown on the following figure, for 44 autolands :

| | MIN | AVERAGE | MAX |
|------------------------|-----|---------|-----|
| Nbr Tracked Satellites | 4 | 6 | 7 |
| H DOP | 0.9 | - | 3.9 |
| V DOP | 1.2 | - | 4.1 |

TABLE 1 : GPS Constellation on Toulouse Airport during DGPS approaches

| HEIGHT | 200 FT | | 100 FT | | 50 FT | | Touchdown | |
|-------------------|-----------|-----------|-----------|-----------|-----------|-----------|-----------|-----------|
| | \bar{x} | 2σ | \bar{x} | 2σ | \bar{x} | 2σ | \bar{x} | 2σ |
| Lateral (metres) | - 0.1 | 1.8 | - 0.1 | 1.8 | - 0.1 | 1.6 | - 0.2 | 1.8 |
| Vertical (metres) | - 0.1 | 3.2 | 0.1 | 2.8 | 0.4 | 2.4 | 0.4 | 2.4 |

\bar{x} : Average Value

TABLE 2 : Accuracy (DGPS vs trajectography)

| | Cat 1 (200 ft) | Cat 2 (100 ft) | Cat 3 (< 100 ft) |
|----------|----------------|----------------|------------------|
| Lateral | +/- 18.7 m | +/- 6.3 m | +/- 4.6 m |
| Vertical | +/- 5.4 m | +/- 2.5 m | +/- 0.8 m |

TABLE 3 : ICAO Annex 10 - ILS Performance Requirements

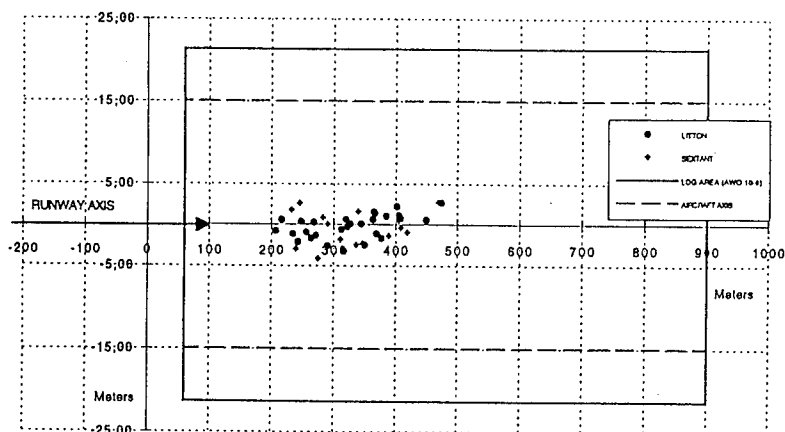


Figure N° 5 : Touch Down Position

The Total System Error estimated for the lateral touch down accuracy is :
Average: - 0.35 m

σ : 1.70 m

Max Lateral value < 4 m.

Those figures are inside the performance landing area (AWO 10-6).

The dotted line correspond to the performance landing area for the A340 centerline according to the A340 landing gear width.

The touching points (as displayed on Figure N° 5) are very close to the centerline (always better than 3 meters), but spread over 200 meters on the X axis due to weather and guidance conditions.

Influence of the satellite constellation :

It was difficult to find a direct simple link between the satellite geometry (dilution of precision HDOP, VDOP), and the accuracy of the DGPS position. It

depends on geometry and other factors as satellite elevation, number of satellites with low elevation, signal/noise ratio, multipath, etc...

In fact, the accuracy is degraded when several satellites are at low elevation despite a good HDOP/VDOP.

On the contrary, with a less good HDOP/VDOP, but with no satellite at low elevation, the performance is better.

This trial confirms that the LADGPS accuracy is good enough to perform Cat 1 and Cat 2 approaches. Thanks to the very good performances of the A340 autopilot, the DGPS could also be used to perform autolands.

3.3.2 Integrity

The integrity monitoring is performed by the ground station. Sextant airborne DGPS equipment also uses RAIM. Figures can only be obtained with calculation because of the very high requirements (10^{-7} in certain cases), which would require a huge number of flight hours.

However, for Sextant equipment (it is the only one which contains a DGPS RAIM algorithm), when RAIM algorithm detects a satellite failure and deselects the failed satellite, a DGPS position variation can be observed. To counteract this issue, a specific filtering has been introduced in the algorithm.

3.3.3 Continuity of service

Two cases have been identified causing an interruption of the continuity of service. Consequences are the followings :

- The ground station antenna must be located on a clear area with no metallic structure around it, as well as in a place above which aircraft do not fly. For instance, the ILS LOC shelter location must be avoided because the aircraft may mask the satellites tracked by the ground station and cause multipath when landing, causing a loss of GPS signals from the satellites.
- During aircraft turns with bank angles over 20° (capture situation), some satellites can be lost by the airborne GPS receivers because the aircraft masks some satellites. This may last several seconds. However, there is no operational consequence because high rate turns occur far from the runway threshold, and because the DGPS re-acquires the GPS satellites very quickly.

Data link failures were simulated during the approach, and after the 15 seconds delay (SCAT I recommendations), the Sextant DGPS provided a position with no accuracy degradation.

Using the Litton "Coasting mode", landings were tested with datalink failure simulated under 700 ft (around 1 minute before touch). A vertical error leading to an earlier touch-down was observed, as well as a lateral error of a maximum of 3 meters. These are very good results regarding the data link loss delay.

3.2.4 Interoperability

Each ground station has been tested with each airborne equipment. Each configuration worked properly. No anomaly was detected.

3.3.4 Qualitative results

ILS look-alike observations

- The ILS look-alike principle is compatible with current ILS precision approach operations on a modern aircraft such as A340. The DGPS receiver emulates correctly all the aircraft equipment up to autoland. It has been observed that ILS like deviations were very clean and smooth compared to ILS deviations.
- The 10 Hz refresh rate of the DGPS output deviations are lower than the refresh rate of the ILS information (20 Hz). However, they are compatible with the autopilot and displays system performances
- Experiment shows that dynamic lever arm corrections of the antenna positions are not really necessary. If this is not used, it does not have any impact on guidance performance provided GPS antenna position, which is on top of the aircraft, has been projected on to the ILS Glide antenna axis. However, in case of landing with cross wind, as the GPS antenna is located far behind the ILS LOC antenna, the main gear of the aircraft will be closer to the runway centre line and the nose of the aircraft will be beside it.

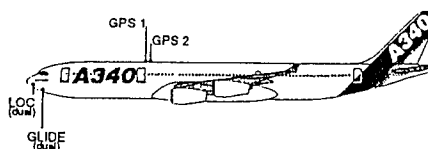


Figure N° 6 : Antennas position

- The runway selection means have not been modified compared to the classical ILS selection. However, it will have to be modified in the future.
- DGPS system should allow to display the distance between aircraft and runway threshold, information which today is obtained with markers and DMEs.
- For this experiment purpose and in order to keep the operational aspects (HMI) as much as possible compatible with today's ILS procedures, the Loc-like and Glidelike deviations have been displayed under angular indications. In order to take full advantage of the DGPS capabilities, linear deviations have to be considered.

3.3.5 Miscellaneous

- According to SCAT I definition, Sextant system performances are not degraded while a 15 seconds data link loss occurs.
- The Litton "coasting mode" which propagates corrections when the data link is interrupted was tested between 700 ft and 400 ft altitude. It showed a propagation of the corrections which was good enough to perform autoland.
- This trial showed that the measurement and the input of the descent path had to be performed very accurately.
- The quality of the data link is also very important and very specific work will have to be performed on the integrity of the data link.
- The tunnel alarms, as defined in the RTCA SCAT I document, have been tested. Preliminary feelings are that these alarms don't fulfill operational needs. This concept has to be improved with an HMI study.

4. DEMONSTRATION

In view of the excellent results obtained during the trials performed in Toulouse, the Airbus A340 N°1 realized demonstrations, with no specific preparation, in different places over the world :

- On another French airport : Montpellier
- On 3 Chinese airports : Beijing, Shanghai, Guangzhou
- On Plaisance airport in Mauritius
- On Mmabatho airport in South Africa.

These demonstrations were performed using the Sextant portable ground station which is designed for rapid installation, measurement, and usage, and Sextant airborne equipment.

More than 60 approaches including 35 autolands were performed by different airline pilots, which were very positively impressed by the accuracy, and the user-friendliness of the system.

These approaches were made in manual mode, flight director mode, and autopilot mode. In most cases, the approaches were extended down to touch down and roll-out.

The DGPS system even allowed to perform autolands (Cat 3 conditions) from the first trial day.

5. CONCLUSION AND PERSPECTIVE

The analysis of the DGPS test flights is not totally completed yet, but the results already obtained demonstrate that the accuracy of the DGPS, coupled to autopilot, already fulfills the Cat 1 and Cat 2 accuracy requirements in principle for the aircraft system interface.

More than 110 autolands were performed with Airbus A340, with this experimental installation without modification on the main aircraft system.

The integrity, availability, and continuity of service parameters remain to be analysed with simulations, and other GPS augmentations may be necessary to obtain the safety required for autoland.

The interoperability was tested with different airborne and ground stations.

The main lessons are the following :

- Good understanding of the DGPS by the pilots, who find the same presentation, behavior, ergonomics as ILS information.
- Good behavior of aircraft systems, such as the display system and the autopilot (same behavior as with the standard ILS).
- Proper filtering and extrapolation for the deviation computations are needed.
- Lateral precision < 1.8 m (95 %) - Vertical Precision < 2.8 m (95 %) obtained complies with Cat 1 and Cat 2 accuracy requirements.
- Ground station must be improved (multipath, availability, integrity monitoring,...)

In view of the very good results obtained during the experiment as well as its excellent portability, Airbus has decided to launch a Differential GPS development and certification program. The development will be realized in the frame of a Multi-Mode Receiver including an ILS receiver and a DGPS receiver on the base of a dual installation.

The Airbus objective is to certify this new equipment for category 1 landing using DGPS by mid 1997.

Excellent performances already obtained associated with improved integrity monitoring and availability of the ground station should allow to certify Category 3 approaches.

FAA's CAT III Feasibility Program: Status and Accomplishments

R. Braff and P. O'Donnell
The MITRE Corporation

V. Wulschleger, C. Mackin, and R. Velez
FAA Technical Center

R. Swider and Per Enge
Stanford University

F. van Graas
Ohio University

D. Kaufmann
NASA Ames Research Center

ABSTRACT

The FAA has been conducting a Category III (CAT III) feasibility program. This paper reviews both planning and technical aspects of the program. The background and schedule for the CAT III program is summarized, including the relationship to the FAA's Local Area Augmentation System (LAAS) and Wide Area Augmentation System (WAAS) programs. Results and insights gained from four of the CAT III flight test campaigns are summarized, and several major remaining work areas for CAT III feasibility are discussed.

INTRODUCTION

Background

The FAA early on recognized the tremendous potential of the GPS Standard Positioning Service (SPS) for civil aviation. Consequently, the FAA established a program for satellite navigation that sought to incrementally introduce GPS service into use within the National Airspace System (NAS). This program has been extremely successful and has prompted the FAA to embark upon a development program for augmentation of the SPS in order to meet aviation requirements that exceed the capabilities of SPS. This development program has capitalized upon advances in differential GPS (DGPS) technology. Besides improving the accuracy provided by SPS, DGPS provides a check of system/signal-in-space integrity, and may enhance navigation continuity of service and availability. These four parameters--accuracy, integrity, continuity, and availability--constitute the required navigation performance (RNP) that GPS-SPS, an SPS augmentation scheme, or any other navigation system must meet in order to qualify as a "primary" means of navigation for a particular phase of navigation. Phases of navigation are defined generally as oceanic-en route, domestic-enroute,

terminal area, approach and landing, and surface navigation.

The most effective and efficient use of DGPS technology that the FAA is developing is the Wide Area Augmentation System (WAAS). WAAS makes use of a network of DGPS ground-reference stations distributed throughout the NAS that monitor SPS performance, correct for SPS errors, and broadcast correction and integrity messages throughout the NAS via transponders on geostationary satellites. The extensive coverage area provided by the geostationary-satellite broadcasts gives WAAS its wide-area coverage. WAAS will augment SPS by providing aviation users a primary means of navigation for every phase of navigation. Precision approach will be supported by WAAS to Category I (CAT I) minima--down to 200 ft above the runway surface. This service will be sufficient for the vast majority of aviation user needs and, most likely, for many non-aviation users.

The FAA is also pursuing DGPS in a local area configuration--the Local Area Augmentation System (LAAS). An individual LAAS will have much less coverage, probably out to the range of a one-way local-area DGPS (LADGPS) broadcast sufficient to cover terminal airport operations. This limited coverage, however, is necessary in order to realize the benefits of LAAS. Although the LAAS will overlap with WAAS coverage in providing terminal area and CAT I precision approach, it will also support operations that WAAS cannot support, due to limitations in accuracy, integrity, continuity, and availability. Specifically, LAAS will support CAT II precision approaches (instrument descent to within 100 feet of the runway surface), CAT III automatic landings (instrument descent below 50 ft of the runway surface), and airport surface navigation. LAAS will also be useful to extend the availability of precision approach service at high traffic airports and where there is no WAAS coverage, i.e., at high latitudes or remote/island destinations or in areas with terrain masking of the geostationary satellites.

The design of both the WAAS and LAAS will be complementary. The goal is to provide for seamless, satellite-based navigation service as the primary means of navigation within the NAS and perhaps, on a global basis. The advantages of such a system are enormous: the FAA, and other service providers, could dispense with an extensive and expensive inventory of terrestrial systems now required for aviation; the aviation community would have a single navigation system for all possible needs, thereby reducing the cost of aircraft equipage, maintenance, and pilot training; other, non-aviation users would have access to these services.

CAT III Feasibility Program

The FAA's CAT III feasibility research program is part of the LAAS program. The FAA embarked upon an ambitious program to establish the feasibility of supporting CAT III automatic landings based upon LADGPS in 1992. This program concentrated on demonstrating that LADGPS techniques could provide the required accuracy and signal integrity for CAT III automatic landings, the most stringent of the requirements that the LAAS is expected to meet. The centerpiece of the program was a request for proposals (RFP) to industry that was released in September of 1993. The program was to conclude flight testing--the basis for feasibility determination--in mid-1995. That milestone has been met. In parallel, the feasibility study included research work (including flight tests) with Ohio University, Stanford University, and NASA Ames to mitigate any contractual risks incurred with release of the RFP. An overall program schedule is shown in Figure 1. A more detailed summary of the CAT III feasibility program may be found in [1].

The RFP anticipated multiple contracts, and, in fact, contracts were let with Wilcox Electric of Kansas City, Missouri and E-Systems Montek Division of Salt Lake City, Utah in June of 1994. Both contracts called for a phased approach. Phases 1 and 2 involved system design and culminated in design reviews for both contractors. These activities were completed in October 1994. Phase 3 included system development, culminating in a flight readiness review. Originally this phase was to be completed in early 1995 but the flight readiness review was shifted to immediately precede flight testing. Both contractors successfully concluded this phase in April (Wilcox) and June 1995 (E-Systems). Phase 4 was the flight test phase upon which this paper's results are drawn. Wilcox successfully concluded flight tests in April and E-Systems did so in June of 1995. Phase V calls for extensive simulator and laboratory experimentation, and will begin September 1995.

The Ohio University, Stanford University, and NASA Ames programs proceeded along parallel lines, although some of the contract phase requirements were not included. Nonetheless, the flight test plans used for the

two contractors were closely adhered to, where possible, when testing the systems developed by the universities. Additionally, Ohio University developed two different LADGPS configurations for flight testing and for simulation; neither the Stanford nor NASA Ames systems were tested in the simulator. Stanford University completed flight testing in October 1994, Ohio University flight tested in October 1994 and February 1995, and NASA Ames completed flight tests in June of 1995. The Ohio simulation test was run in December of 1994.

All experimentation with DGPS systems from developers in the feasibility study has been successful, and has prompted the FAA to declare that its accuracy feasibility determination has been met by mid-1995 (as planned). The integrity feasibility based on testing was extremely encouraging, but requires more study and detailed analysis of the various integrity algorithms. This analysis is part of the charter of the FAA's LAAS Integrity Panel (LIP). The LIP is an independent panel consisting of both government and private members.

RESULTS AND INSIGHTS

The CAT III feasibility program allowed some insights to be gained on accuracy, integrity, continuity, and availability as well as concrete test results. The Level 1 and Level 2 Test Plans [2,3] describe the experiment design in detail.

Accuracy

The CAT III feasibility program allowed a DGPS system developer two choices for evaluation of accuracy.

Navigation Sensor accuracy. Navigation sensor accuracy (NSE) was one of the choices for accuracy evaluation. To meet the NSE requirements, a system had to meet the CAT III vertical and lateral accuracy requirements for the Instrument Landing System (ILS) at 100 ft height above threshold (HAT) as derived from ICAO, Annex 10 [4]. NSE is measured in runway coordinates and is defined as the difference between the aircraft position as derived by the navigation system and the laser tracker truth system. Since real-time carrier phase methods have position accuracies on the order of a decimeter, those developers who used carrier phase elected to be evaluated with respect to NSE.

Total system error. The other choice for accuracy was total system error (TSE). TSE is defined as the lateral and vertical offset errors from the desired flight path. TSE is measured in runway coordinates as the offset of the aircraft position from the desired flight path as determined by the laser tracker ($TSE = \text{Tracker} - \text{Desired}$) or by $TSE = NSE + FTE$, where FTE is the flight technical error. FTE is the flight control system's error, when used in the operating environment, in correcting the offset from the desired flight path as indicated by the navigation system.

The equivalence of the two methods of measuring TSE was verified by the flight tests as shown in Figure 2. Note in Figure 2 that the ensemble standard deviations are essentially equal along the approach, and the ensemble means vary only slightly. The code developers elected to be evaluated with respect to preliminary TSE requirements that were available at the time of RFP release [5]. These requirements are with respect to navigation performance boundaries about the desired flight path (sometimes called the "tunnel") within which the aircraft must remain during the approach.

Summary of accuracy results. The details of the accuracy results are available in other papers presented by the developers of the DGPS systems and the test organizations [6-11]. This discussion presents an integrated look at the results from four flight test campaigns that were conducted as part of the CAT III feasibility program. Table 1 summarizes these flight tests.

Figure 3 contains a graphical representation of the accuracy results in terms of NSE and TSE; FTE results can be inferred from the figure as being approximately equal to $TSE - NSE$. Results are given at approximately 50 ft HAT in terms of the absolute value of the mean + twice the standard deviation ($|\mu| + 2\sigma$). Note that data for all these parameters were collected during all of the flight tests except for E-Systems (E-Systems did not have an autoland capability). Comparing the two code systems (Wilcox and Ohio University) indicates that their NSEs are comparable, but the Ohio University TSE is significantly smaller than that of Wilcox. This is due to the superior autopilot performance of the newer B-757 as compared to the B-727.

The two carrier phase systems had comparable NSEs. The carrier-phase NSEs are certainly more accurate than indicated since the main error component is the laser tracker error (≈ 0.3 m [95 percent]). All 300 tallied approaches for autoland aircraft (Wilcox, Ohio University, and Stanford University) landed within the FAA's 95 percent touchdown box thus indicating that either form of DGPS can consistently provide sufficient accuracy for successful CAT III autoland approaches.

Integrity

The function of a DGPS integrity algorithm is to ensure that a defined navigation error is always less than a known error bound. Depending upon whether DGPS is based on code phase or carrier phase this function was carried out by two basic methods.

Code phase integrity. Since state-of-the-art code phase DGPS has not yet produced vertical accuracy less than ~ 1 m (95 percent), the ILS CAT III NSE protection levels (e.g., 1.2 m vertical at 50 ft HAT) for the signal-in-space can not be used because they would cause an unacceptable high alarm rate. Therefore, a protection level based upon TSE was used. The general algorithm is

given by $|FTE| + NSE_{bnd}(g' \oplus a') > T - M$, where FTE is indicated flight technical error, $NSE_{bnd}(\bullet)$ is an estimated navigation sensor error bound, g' accounts for the DGPS correction errors as determined on the ground, a' accounts for the airborne portion of NSE, \oplus is a general symbol for addition (e.g., root-sum-square [RSS] or linear), T is outer performance boundary half-dimension (tunnel) that can only be penetrated with less than $1 \cdot 10^{-7}$ probability per approach, and M is half-dimension of aircraft, including wheels. The purpose of this algorithm is to estimate and monitor the magnitude of the total system error ($TSE = FTE + NSE$) to prevent the aircraft from penetrating the outer performance boundary. Since FTE is measured directly, the fundamental problem of the integrity algorithm is determining $NSE_{bnd}(\bullet)$.

Knowledge of the integrity algorithms of a number of developers indicates that each has a different way of determining $NSE_{bnd}(\bullet)$. Therefore, a general method for evaluating the performance of $NSE_{bnd}(\bullet)$ for a flight test is to compare its real-time calculated value at time t to the actual NSE as determined by the laser-tracker truth source. Unfortunately, the original CAT III flight test plan did not specify that $NSE_{bnd}(\bullet)$ be recorded, but $NSE_{bnd}(\bullet)$ may be recovered through postprocessing. The Wilcox flight test did not produce any undesired integrity alarms (no missed or false alarms) since the aircraft was always well within the performance boundaries by a comfortable margin. To explicitly exercise the integrity algorithm, a zig-zag taxi maneuver was conducted along the runway to cause the aircraft to intentionally penetrate the lateral outer performance boundary. However, it was discovered that each integrity alarm occurred a few feet prior to the penetration of the outer performance boundary. This early alarming appears to be inevitable due to $NSE_{bnd}(\bullet)$ bounding the actual NSE.

Carrier phase integrity. Since carrier phase provides positioning accuracy on the order of a decimeter, the integrity position protection level can be that of ILS. Since accuracy is so high, receiver autonomous integrity monitoring (RAIM) is employed for carrier phase [12,13]. In other words, carrier phase allows the detection of avionics and multipath errors at the aircraft, as well as any errors in the DGPS corrections. For E-Systems, a series of special tests were conducted. While the aircraft was parked, the DGPS data of one of the tracked satellites was subjected to an induced ramp error. The results of this test indicated that when the RAIM performance parameters are set (e.g., missed detection and alarm rate), alarms frequently occur at NSE values that are less than 0.5 m even though the protection level is > 1 m. In other words, with carrier phase a 0.5 m NSE indicates something is wrong. This situation is acceptable as long as the alarm rate is within specification. During 100 approaches each for E-Systems and Stanford University there were no false alarms.

Availability and Continuity

The concepts of availability and continuity may be expressed as follows. Availability is the probability the system will provide service when needed. Continuity is the probability that while the system is being used it will continue to provide service.

Code phase availability. The traditional method of estimating availability for code phase systems has been to calculate the availability of achieving a vertical-dilution-of-precision (VDOP) less than some maximum permissible value. Since $\text{accuracy} = 2\sigma_{\text{range}} \cdot \text{VDOP}$ (95 percent), decreasing $2\sigma_{\text{range}}$ would allow a greater allowable VDOP, and hence a higher availability. However, from the Wilcox flight tests it was discovered that up to about a maximum VDOP = 5, the NSE appears to be independent of VDOP as shown in Figure 4. Therefore, the use of a VDOP criterion for availability may be too conservative. An analysis of why NSE appears to be independent of VDOP will be conducted.

Code phase continuity. No continuity problems were experienced with code phase systems during the CAT III flight tests. However, code phase could be susceptible to continuity interruptions due to nuisance integrity alarms if a ground-monitor alarm limit is set too low. In the Wilcox CAT III DGPS system, an alarm limit for a pseudorange-correction comparison between a reference and a monitor receiver was arbitrarily set to about 5 m to avoid a high alarm rate that could lead to declaration of a satellite(s) as unusable. The 5 m value is much too large to screen out significant errors if they should occur. Thus, the Wilcox integrity algorithm was essentially based on the *user differential range error (UDRE)* for each pseudorange correction that was broadcast as part of the DGPS message from the ground. However, in the Ohio University system, the pseudorange alarm limit was 0.8 m and no false alarms were recorded. To meet signal-in-space continuity requirements, an analysis described in [13] showed that code phase may require 2 monitor receivers on the ground and both need to show the alarm to provide a low enough alarm rate for a reference-monitor comparison test.

Carrier phase availability. During the E-Systems flight test of a kinematic on-the-fly ambiguity resolution system, the lowest-elevation satellite sometimes was dropped from the integer ambiguity resolution process. Unless this satellite was dropped, the integer ambiguity resolution would not converge. In effect, dropping a satellite lowers system availability in that it is somewhat equivalent to raising the mask angle. This could cause carrier phase to lose some of its advantage with respect to code phase in accommodating higher DOPS.

Carrier phase continuity. Based on the Stanford University flight test, the integrity beacon (pseudolite bubble) provides excellent continuity. Except for a GPS satellite failure detected by the system, over 100

approaches were executed without any interruptions. The apparent susceptibility of the conventional on-the-fly system with respect to low elevation satellites may have an impact on continuity since if a satellite can not be used for ambiguity resolution there may not be enough remaining satellites to provide for ambiguity resolution.

Pseudolites. Pseudolites have the potential to increase availability by providing a source of additional ranging signals. Although the CAT III feasibility program had encouraged the use of pseudolites as extra ranging and DGPS data sources, only the Stanford University system used them as the basis of their system. A short flight test campaign employing the Stanford Telecommunications (STel) pseudolite in a data link capacity only was conducted. This pseudolite used pulsed transmissions and was offset from L1 by the first null in the power spectrum [15]. Preliminary results indicated that the pseudolite transmissions, when properly functioning, did not interfere with the utilization of the GPS constellation signals either at the reference station or the aircraft. Preliminary results also indicated that satisfactory reception of the pseudolite transmissions could be obtained through the use of a top-mounted aircraft antenna. A follow-on flight test is scheduled for later this year which will utilize the pseudolite as both a data link and ranging source.

REMAINING CAT III WORK AREAS

This section discusses several of the remaining areas of work that need to be completed before a proper configuration for LADGPS CAT III can be chosen.

Code versus carrier. It can be assumed that code phase will be used for CAT I approaches. With respect to CAT II, the continual advance in code accuracy seems to indicate that code accuracy will be suitable for CAT II (1.7 m [95 percent]). A system based on code phase also is preferable for CAT III because it is simpler—one unit covers all runway ends at an airport, and the aircraft knows that it has CAT III capability at the initial approach fix rather than having to wait until integer ambiguities have been determined. However, although testing indicates that an aircraft can be landed with sufficient accuracy, it is still not certain that code accuracy allows enough margin for CAT III integrity. Also, the integrity requirements for the user solution are very stringent. This would not be a problem for a carrier phase implementation because it has more than enough accuracy to be able to use RAIM (e.g., the Stanford University integrity beacon). To solve the code phase integrity problem, Ohio University is developing a method that allows for both precision integrity monitoring on the ground and in the avionics. The method uses carrier phase data transmitted as part of the DGPS message to establish a reference trajectory to check the code solution. In addition, ground monitoring is facilitated through the use of a GPS signal generator to precisely synchronize the

reference and monitor receiver clocks and remove inherent biases due to temperature, etc.

Optimize integrity algorithms. Although the integrity algorithms examined in the CAT III feasibility program have so far appeared to function properly, they still need to be improved and subjected to more concentrated testing and analysis. Further testing is being carried out by NRad (Warminster, PA) in their signal-simulation laboratory. In the laboratory, user equipment will be subjected to a variety of signal failure modes. Detailed analysis of the premises and logic of integrity algorithms will be conducted by the FAA's GPS LIP, which will evaluate integrity concepts with respect to a fixed set of evaluation criteria.

Evaluate pseudolites. More work needs to be done in the evaluation of high-powered pseudolites with respect to providing additional ranging signals to enhance continuity and availability. The role of a pseudolite data link will also be explored further.

Benefit/cost analysis. A benefit/cost (B/C) analysis needs to be performed to compare DGPS to a ground-based CAT III landing system. This is necessary in order to obtain funding for implementation.

SUMMARY

The FAA's Local Area Augmentation System (LAAS) provides operational capabilities that can not be provided by the Wide Area Augmentation System (WAAS). The Category III feasibility program is part of the LAAS. The CAT III program has concentrated on demonstrating that local area differential GPS (LADGPS) techniques provide the required accuracy and signal integrity for CAT III automatic landings. Over 400 successful approaches from four different developers were demonstrated. For the first time, real-time integrity monitoring systems have been used and evaluated in landing operations.

Figure 3 summarizes the accuracy capabilities of the four systems. The two carrier phase systems (E-Systems and Stanford University) demonstrated comparable positioning accuracies with errors that were only a few tenths of a meter. Most likely, the largest component of the error was contributed by the laser tracker position-truth source. The demonstrated accuracies shown in Figure 3 for real-time carrier phase systems are better than the accuracy provided by a CAT III ILS.

The vertical accuracy of the two code phase systems (Wilcox and Ohio University) is not as good as the vertical-accuracy requirement for CAT III ILS, but lateral accuracy is 3 to 4 times better than the ILS requirement. Both systems demonstrated that they provide sufficient accuracy for consistent automatic landings within the required "touchdown box" dimensions and keep an aircraft inside the navigation performance boundaries.

With respect to integrity, no false alarms were generated during the flight tests. Special tests of one of the code phase (Wilcox) and one of the carrier phase (E-Systems) systems indicated that integrity alarms were properly generated when a significant intentional error was introduced. However, the integrity testing was limited, as were the integrity methods. Further efforts will be devoted to perfecting and testing integrity methods.

Since both code phase and carrier phase appear as viable alternatives for CAT III, follow-on work will concentrate on selecting the best technique. This effort will be part of the LAAS architecture selection process.

REFERENCES

1. Braff, R., P. O'Donnell, C. Shively, and R. Swider, *FAA's DGPS CAT III Feasibility Program: Update and Test Methodology*, Proceedings of the IEEE Position, Location And Navigation Symposium, Las Vegas, Nevada, April 1994.
2. O'Donnell, P., R. Braff, C. Shively, *Category (CAT) IIIb Level 1 Test Plan for Global Positioning System (GPS)*, Final Report, Federal Aviation Administration, DOT/FAA/RD-93/21, September 1993.
3. O'Donnell, P. and R. Braff, *Category (CAT) IIIb Level 2 Flight Test Plan for the Global Positioning System (GPS)*, Federal Aviation Administration, DOT/FAA/NG-95/01, February 1995.
4. Anonymous, *International Standards, Recommended Practices, and Procedures for Air Navigation Services, Aeronautical Telecommunications*, Annex 10 to the Convention on International Civil Aviation, Volume 1, International Civil Aviation Organization, April 1985.
5. Kelly, R. and J. Davis, *Required Navigation Performance (RNP) for Precision Approach and Landing with GNSS Application*, NAVIGATION, The Journal of the Institute of Navigation, Vol. 41, No. 1, Spring 1994.
6. van Graas, F. and S-W Lee, *High-Accuracy Differential Positioning for Satellite-Based Systems Without Using Code-Phase Measurements*, Proceedings of the 1995 National Technical Meeting, Anaheim, California, January 1995.
7. van Graas, F., D. Diggle, V. Wulschleger, R. Velez, G. Kuehl, R. Hilb, and M. DiMeo, *FAA/Ohio University/UPS Autoland Flight Test Results*, Proceedings of the 1995 National Technical Meeting, Anaheim, California, January 1995.
8. Kaufmann, D., *Flight Test Evaluation of the E-Systems Differential GPS Category III Automatic Landing System*, NASA Ames Research Center, Moffett Field, CA.

9. Hundley, W., S. Rowson, G. Courtney, V. Wullschleger, P. O'Donnell, *FAA-Wilcox Electric Category IIIB Feasibility Demonstration Program - Flight Test Results*, Proceedings of ION-GPS 95' Meeting, Palm Springs, California, September 1995.

10. van Graas, F., D. Diggle, V. Wullschleger, R. Velez, G. Kuehl, R. Hilb, D. Lamb, M. DiMeo, E. Breeuwer, *FAA/Ohio University/United Parcel Service DGPS Autoland Flight Test Demonstration*, Proceedings of the ION-GPS 95' Meeting, Palm Springs, California, September 1995.

11. Cohen, C., et al, *Autoland a 737 Using GPS Integrity Beacons*, NAVIGATION, The Journal of the Institute of Navigation, Vol. 42, No. 3, Fall, 1995.

12. Pervan, B., C. Cohen, and B. Parkinson, *Integrity Monitoring for Precision Approach Using Kinematic GPS*

and a Ground-Based Pseudolite, NAVIGATION, The Journal of the Institute of Navigation, Vol. 41, No. 2, Summer 1994.

13. Brown, R., R. Hall, G. Romrell, and J. Waid, *RAIM Availability for CAT IIIB Operation*, Proceedings of the 51st Annual Meeting of the Institute of Navigation, Colorado Springs, Colorado, June 1995.

14. Braff, R. *Alarm Limits and Avionics Algorithm for Local-DGPS Integrity Monitoring*, Differential Satellite Navigation Symposium (DSNS) '95, Bergen, Norway, April 1995.

15. Elrod, B. and A. Van Dierendonck, *Testing of GPS Augmented With Pseudolites for Precision Approach Applications*, Proceedings of ION GPS-94, 7th Annual International Technical Meeting, The Institute of Navigation, Salt Lake City, Utah, September 1994.

Table 1 CAT III Feasibility Flight Tests

| Developer | Location of Test/ Host Aircraft | Date of Test | No. of Approaches | Evaluation Criteria |
|---------------------|---|--------------|-------------------|---------------------|
| Wilcox | FAA Technical Center/ Boeing 727-200 FEDEX | 4/95 | 100 | TSE (Code) |
| E-Systems | NASA Crows Landing/ Westwind II | 6/95 | 100 | NSE (Carrier) |
| Ohio University | FAA Technical Center/ Boeing 757-200 UPS | 10/94,2/95 | 100 | TSE (Code) |
| Stanford University | NASA Crows Landing/ Boeing 737-300 UA | 10/94 | 100 | NSE (Carrier) |

| | 1993 | 1994 | 1995 | 1996 |
|-------------------------------------|------|------|------|------|
| ACTIVITY | | | | |
| Proposal Request & Prep | □△ | | | |
| Proposal Evaluation & Award | →△ | | | |
| System Design (Phases I & II) | | △→△ | | |
| Develop/Flight Ready (Phase III) | | | →△ | |
| Flight Test (Phase IV) | | | →△ | |
| Simulator Test (Phase V - optional) | | | →△ | △ |

Figure 1. CAT III Feasibility Program Schedule

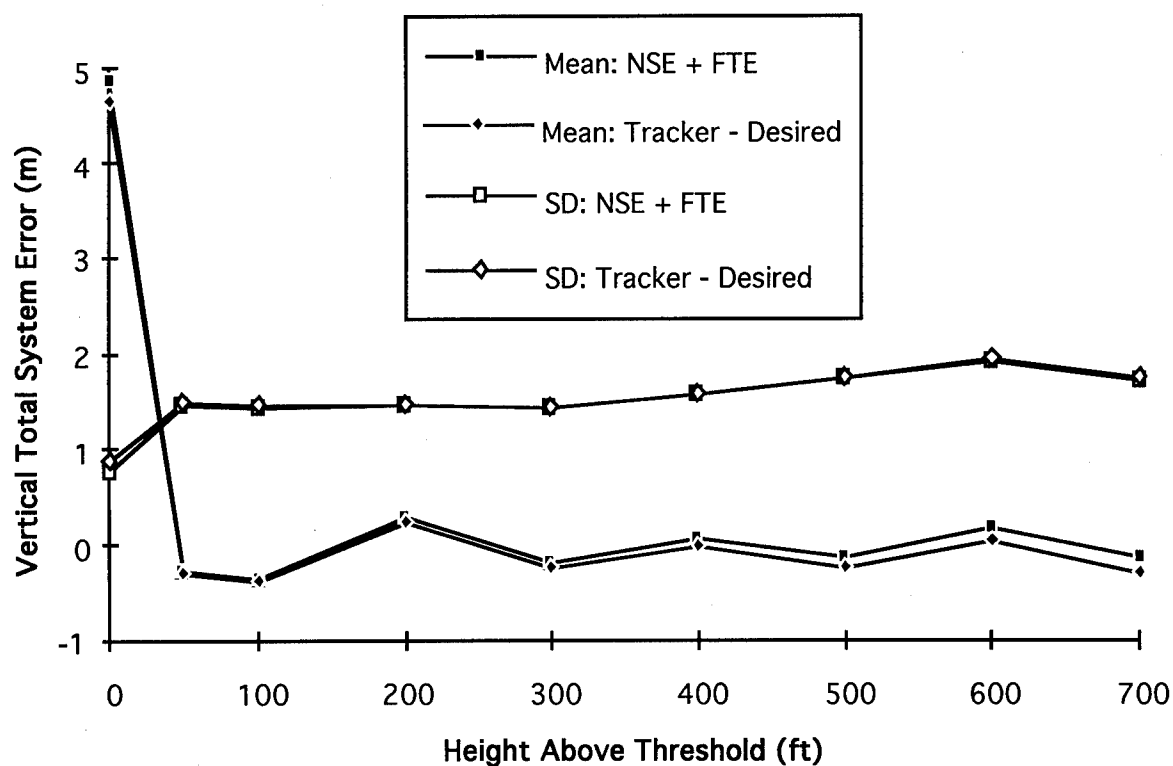


Figure 2 Equivalence of Two Methods of Measuring Total System Error

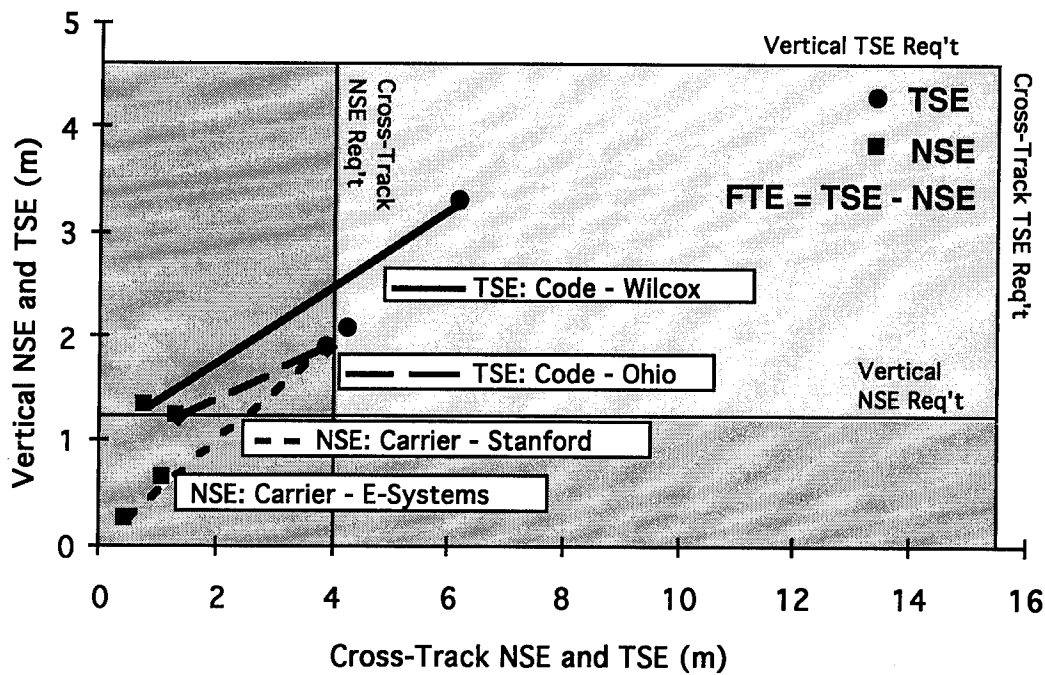


Figure 3 Summary of CAT III Feasibility Flight Test Results (In Terms of $|\mu| + 2\sigma$)

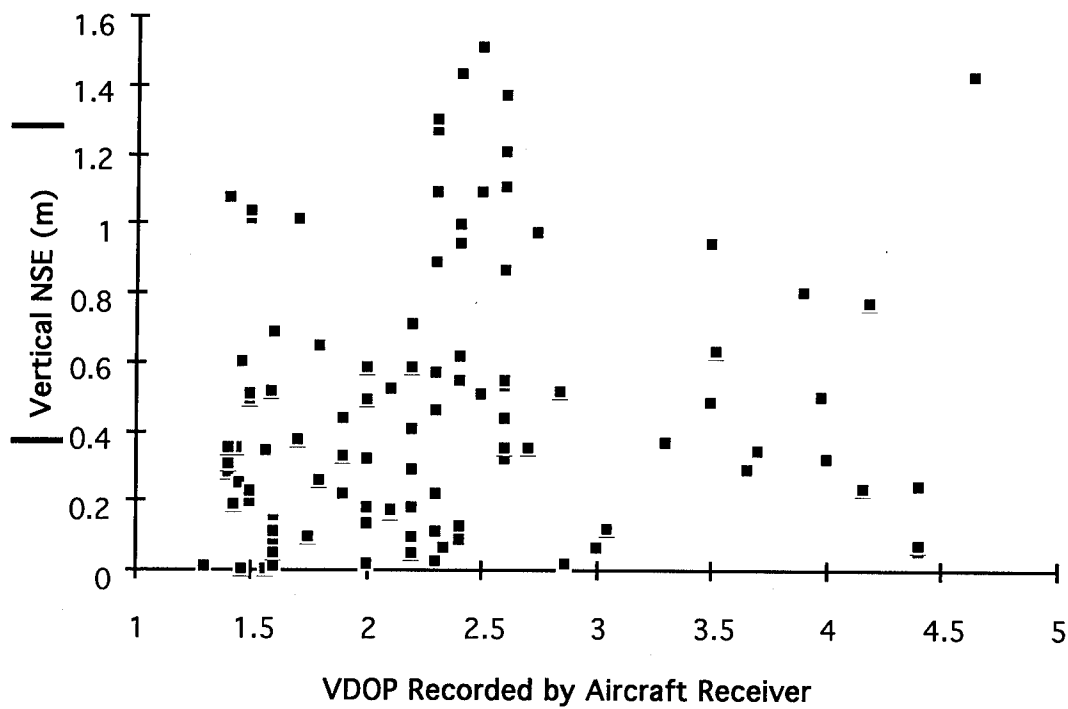


Figure 4 Relationship Between Navigation Sensor Error and VDOP

GNSS Receiver Interference: Susceptibility and Civil Aviation Impact

Mark Johnson and Robert Erlandson
Rockwell

BIOGRAPHIES

Mark Johnson is a senior systems design engineer in GPS receiver development at Rockwell International Corporation in Cedar Rapids, Iowa. He holds a BS in Computer Engineering from Iowa State University and a MSE in Electrical Engineering from Arizona State University. He has experience doing GPS hardware, software, and systems engineering at Rockwell and Motorola. He is involved in industry/government specification development for civil aviation GNSS in the RTCA committees.

Robert Erlandson is a Principal Engineer at Collins Commercial Avionics, Rockwell International Corporation, Cedar Rapids, Iowa. He holds BEE and MS(EE) degrees from the University of Minnesota and has extensive experience in GPS and other microwave avionics hardware design and system analysis at Collins since 1975. In 1993 he was a Rockwell representative to the FCC Mobile Satellite Service Above 1 GHz Negotiated Rulemaking Committee and is currently an active member of RTCA SC-159.

ABSTRACT

There are several potential sources of interference to a GNSS (Global Navigation Satellite System) receiver in a civil aviation application. These sources are on-board the same aircraft, on nearby aircraft, or are non-aircraft sources, and include in-band RFI, out-of-band RFI, and physical interference.

The paper presents an introduction to the interference problem, discusses GPS and GLONASS receiver interference susceptibility including an analysis of interference bandwidth versus receiver susceptibility, and provides an overview of the potential sources of interference to GNSS receivers. It presents a derivation of the minimum receiver to interference source separation

distance during enroute and precision approach and a detailed GNSS interference link analysis.

INTRODUCTION

Table 1 lists the sources of interference that have been identified as potential concerns for GNSS receivers in the civil aviation environment.

In-band RFI includes harmonics, spurious, and intermodulation products falling in the nominal GPS (1565-1586 MHz) or GLONASS (1595-1610 MHz) band segments. Out-of-band RFI includes powerful signals near the nominal GPS and GLONASS bands strong enough to overcome the receiver's passive RF filtering. Physical interference (not listed) includes multipath, shadowing, terrain masking, and other interference caused by the physical environment.

As shown in the table, the potential interference sources are numerous. Many of the interference sources can be shown to be of negligible concern after more scrutiny. SATCOM, VHF Harmonics, and MSS remain as serious interference concerns, however dedicated efforts have resolved most of the concerns for SATCOM and VHF.

L-Band Aeronautical SATCOM is a multi-channel data and voice system in which the aircraft unit transmits up to +25 dBW EIRP per channel in the 1626.5-1660.5 MHz band. Its active intermodulation products are controlled by frequency management and transmitter filtering to provide adequate protection for GPS receivers [1]. GPS receivers have been specified to provide adequate out-of-band passive RF filtering to accommodate interference from SATCOM band emissions. The SATCOM-to-GLONASS interference problem is being actively worked and potential solutions look promising as well, although stringent out-of-band filtering may be required in the GLONASS receiver.

Table 1: Potential Sources of Interference to GNSS Receivers

| RFI Source | Type | Location |
|--|------------------------|-------------------------------------|
| Mobile Satellite Services (MSS) | In-Band Out-of-Band | Non-A/C |
| VHF Comm Harmonics & Passive Intermod Products | In-Band | Same A/C Nearby A/C |
| SATCOM (AMSS) | In-Band Out-of-Band | Same A/C Nearby A/C |
| ACARS Harmonics | In-Band | Same A/C, Nearby A/C, Non-A/C |
| Flight Telephone Services | Out-of-Band | Same A/C Nearby A/C |
| DME | Out-of-Band | Same A/C Nearby A/C Non-A/C |
| HF Harmonics | In-Band | Same A/C |
| Mode S | In-Band Out-of-Band | Same A/C Nearby A/C Non-A/C |
| Amateur Radio | In-Band | Non-A/C |
| FM Harmonics and Passive IM | In-Band | Non-A/C |
| TV Harmonics | In-Band | Non-A/C |
| VHF/UHF Land Mobile Harmonics | In-Band | Non-A/C |
| VOR Harmonics | In-Band | Non-A/C |
| Personal Electronic Devices (PED) | In-Band | Same A/C |

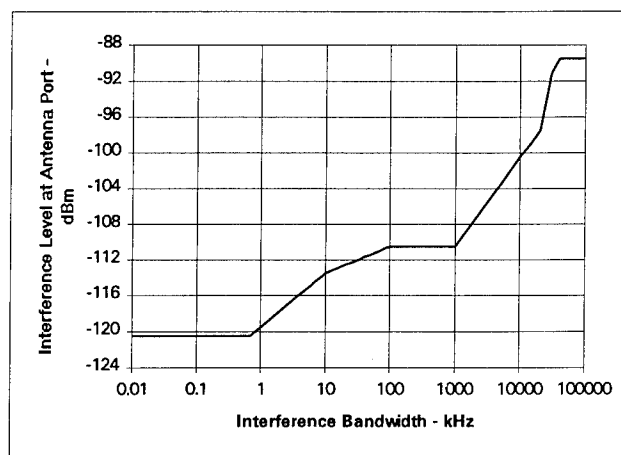
VHF is a civil aviation voice and data air to ground radio link in the 118 to 136 MHz band. The 12th and 13th harmonics of several 25 kHz VHF channels fall in-band to GPS and/or GLONASS. VHF antenna to GNSS antenna interference can adequately be controlled by means of in-line filtering of the VHF transmitted signal. Shielding and proper installation provides GNSS receivers with adequate protection from VHF box to box and box to antenna emissions. [1]

Mobile Satellite Service (MSS) is a new communications link intended to provide the equivalent of global cellular telephone service. Handsets transmit voice or data signals in the 1610-1626.5 MHz band at about 0.5 W to a network of low earth orbiting (LEO) satellites. They, in turn, route the signal down to other receiving handsets or, via ground stations, to the standard telephone network. Handset emission spill-over into the adjacent GNSS band is a primary concern to civil aviation GPS and

GLONASS. Details of the MSS interference problem are presented in the "LINK ANALYSIS FOR MSS INTERFERENCE TO GNSS" section later in this paper.

GPS RECEIVER INTERFERENCE SUSCEPTIBILITY

Because the minimum GPS signal is specified to be only -130 dBm (-160 dBW) [2], even very small interfering signals can cause tracking failure of a GPS receiver trying to receive that signal. The in-band interference specification level proposed by RTCA/SC-159 for the Wide Area Augmentation System (WAAS) Minimum Operational Performance Standards (MOPS) varies versus the bandwidth of the interfering signal, lowest for CW, highest for wideband (>40 MHz). See figure 2 below.



Note: Interference power density will not exceed -110.5 dBm/MHz in the frequency band of L1 ±10 MHz

Figure 2: GPS In-Band Interference Level Requirements

This varying level of interference rejection capability is due to the length (and therefore repetition period) of the GPS C/A codes. The gold code sequences are 1 ms long, resulting in a line spectrum with lines spaced at 1 kHz instead of a continuous spectrum. Since each discrete spectral line contains the energy that would be spread over a kilo-Hertz of continuous spectrum, the average level of the discrete lines is increased by $10 \log_{10}(1000) = 30$ dB. Thus, instead of the theoretical spectral peak value of $10 \log_{10}(1.023 \times 10^6) = -60$ dB, the average peak is only about -30 dB. Additionally, the level of many of the individual lines is higher than the envelope of the theoretical continuous spectrum. The exact level of the worst case spectral line varies from code to code (SV number), with the worst case lines for the worst case codes providing an effective processing gain of less than 20 dB against CW interference signals.

IN-BAND SUSCEPTIBILITY VS INTERFERENCE BANDWIDTH

As stated above, the susceptibility of a GPS receiver to interference varies depending on the bandwidth of the interference. The correlation function of the receiver spreads the incoming interference signal according to the spectrum of the C/A code for that particular SV number while de-spreading the desired GPS signal.

An analysis of interference susceptibility vs. bandwidth for SV #6 C/A tracking was performed. The power spectral density (PSD) function for the SV #6 C/A code sequence is shown in figure 3. As stated above it is a discrete spectrum with 1 kHz spaced spectral lines. SV #6 was picked since it has the worst case (highest) spectral lines of the C/A codes.

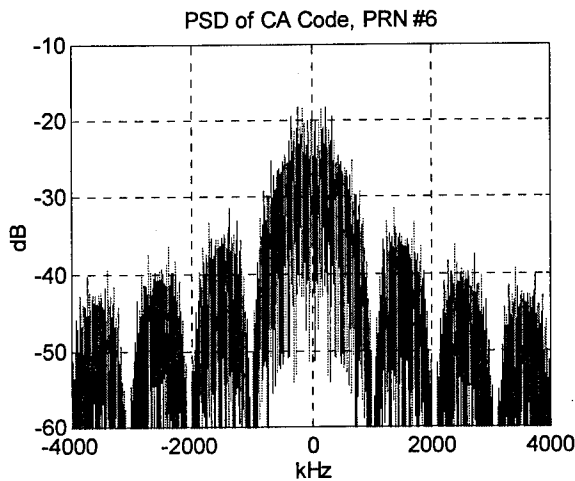


Figure 3: GPS C/A Code PSD, PRN #6

The simulation model is shown in figure 4. The incoming interference signal is multiplied by the internal C/A code to obtain the post-correlation Power Spectral Density (PSD) (Point A in figure 4) as shown in figures 5 through 11.

The simulation model was actually implemented in the frequency domain (in units Hz) as a convolution of two PSD's followed by a 50 Hz filter. The justification of this approach is as follows:

let $f(t)$ be the interference signal and $g(t)$ be the C/A code sequence, then,

$$y(t) = f(t) \cdot g(t)$$

and ,

$$S_{yy}(f) = \mathcal{F}\{R_{yy}(\tau)\}$$

where $\mathcal{F}\{\}$ represents the Fourier Transform, so,

$$R_{yy}(\tau) = E\{y(t)y(t-\tau)\} = E\{f(t)g(t)f(t-\tau)g(t-\tau)\}$$

which, for independent f & g ,

$$= E\{f(t)f(t-\tau)\} E\{g(t)g(t-\tau)\}$$

$$R_{yy}(\tau) = R_{ff}(\tau) \cdot R_{gg}(\tau)$$

so,

$$S_{yy}(f) = \mathcal{F}\{R_{ff}(\tau) \cdot R_{gg}(\tau)\}$$

$$S_{yy}(f) = S_{ff}(f) * S_{gg}(f)$$

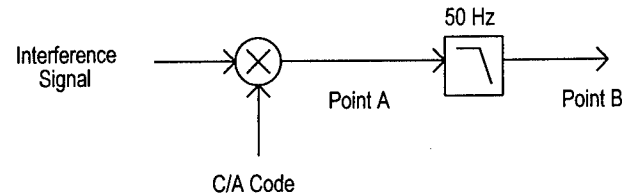


Figure 4: Interference Susceptibility vs. Interference Bandwidth Simulation Model

As can be seen in the figures the peak spectral line out of the multiplier is at a maximum for CW interference and continues to drop for wider interference bandwidths. The total interference power is held constant throughout these figures (resulting, of course, in a reduced power density level as bandwidth increases).

For a CW interferer the resulting power spectral density function out of the correlation multiplier is shown in

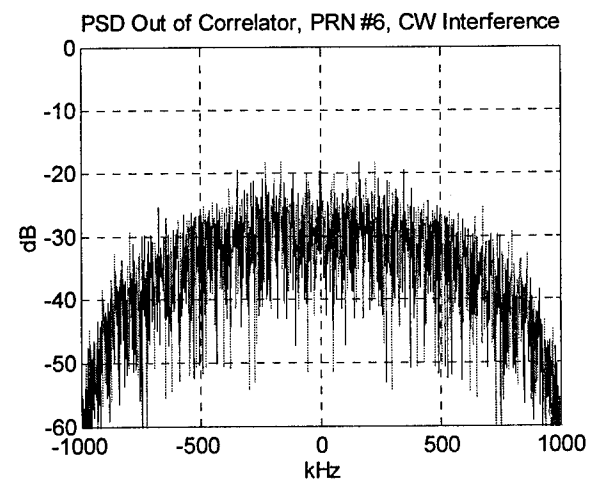


Figure 5: PSD Out of Correlation Multiplier, PRN #6, CW Interference

figure 5. Its peak correlator spectral output of -18.3 dB occurs at offsets of 163 kHz and 227 kHz. Thus a CW interference signal striking the GPS antenna at a frequency of $L1 \pm 163$ kHz or ± 227 kHz would be translated by means of the correlator to land directly on

the L1 frequency (assuming zero doppler and no frequency standard offset).

As the bandwidth of the interference signal widens, the correlation function spreads the interference energy across more and more C/A code spectral lines and the spectrum out of the correlator begins to smooth out. Eventually enough lines are included inside the interference bandwidth to yield correlation processing gain equivalent to that predicted by the continuous sinc² function. As can be seen in figures 7 and 8 this has not yet occurred at an interference bandwidth of 100 kHz, but has occurred at an interference bandwidth of 1 MHz.

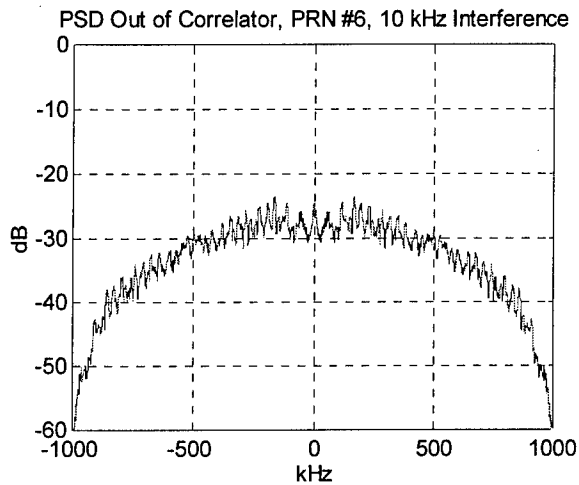


Figure 6: PSD Out of Correlation Multiplier, PRN #6, 10 kHz Interference

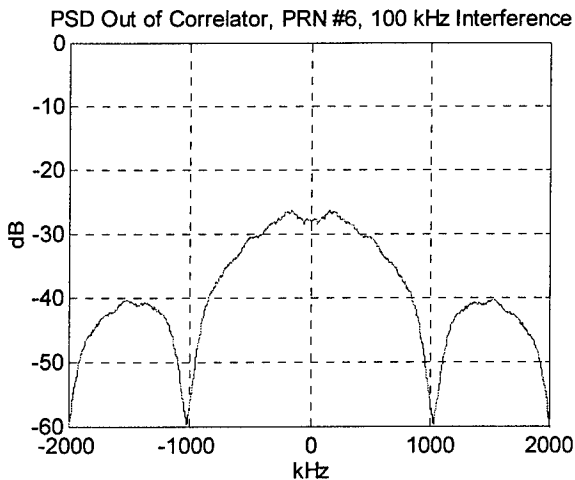


Figure 7: PSD Out of Correlation Multiplier, PRN #6, 100 kHz Interference

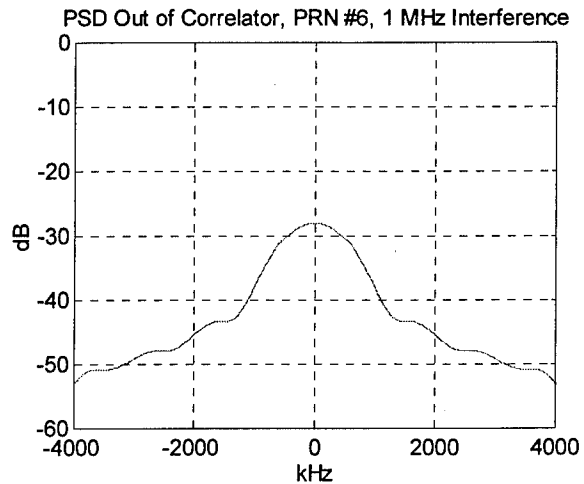


Figure 8: PSD Out of Correlation Multiplier, PRN #6, 1 MHz Interference

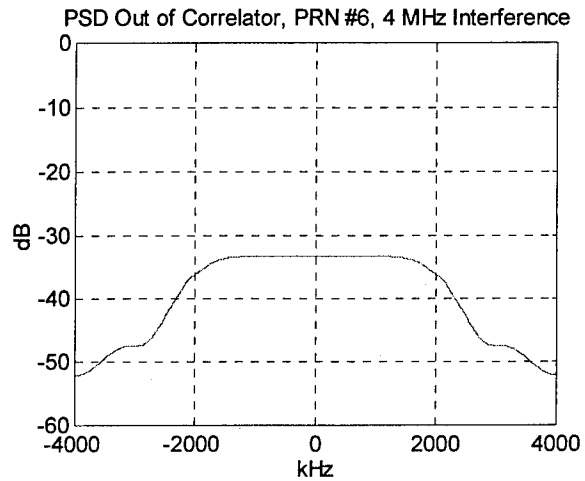


Figure 9: PSD Out of Correlation Multiplier, PRN #6, 4 MHz Interference

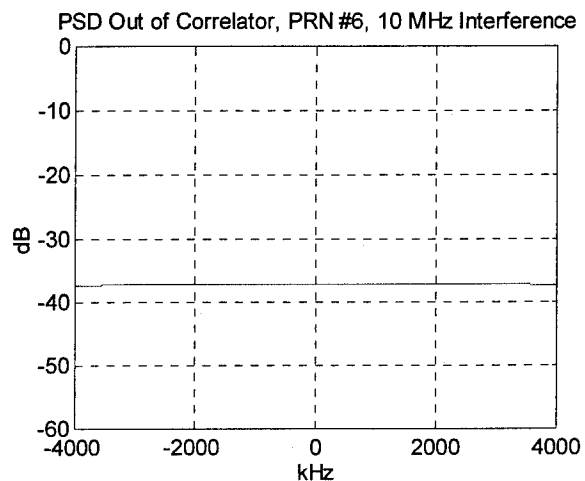


Figure 10: PSD Out of Correlation Multiplier, PRN #6, 10 MHz Interference

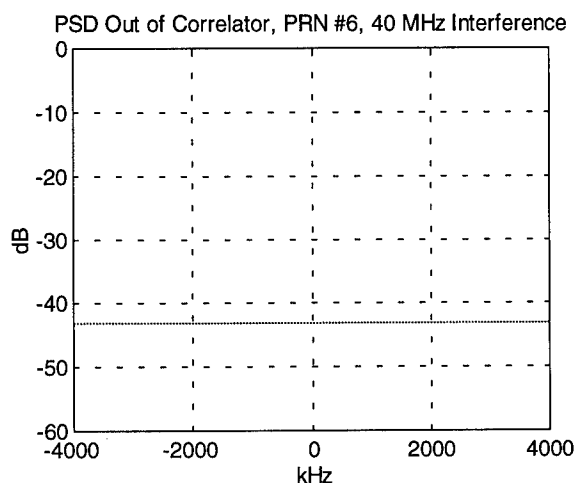


Figure 11: PSD Out of Correlation Multiplier, PRN #6, 40 MHz Interference

The second stage of the correlation function is the integrate and dump filter (IDF) which is a digital realization of a low pass filter whose cutoff frequency is at the GPS data rate of 50 Hz. Since the frequency response of this filter is a sinc function its noise equivalent bandwidth is exactly 1/2 its first null bandwidth or 25 Hz, one sided. Thus an approximation of a 50 Hz, two-sided, "square" filter was used in the model. The effect of this filter is to remove all but the middle 50 Hz of frequency components in the PSD at point A, to obtain the expected processing gain.

Figure 12 below shows a summation of the processing gain for SV #6. As can be seen, the minimum processing gain (corresponding to the maximum spectral point out of the correlator) varies from 18 dB for a CW interferer to 56 dB for a 40 MHz wideband interference source for a spread of 38 dB in interference handling capability. Note that the processing gain increase up through 1 MHz is due to increasing correlation processing gain as interference bandwidth increases, peaking at 43 dB ($=10\log(1,023,000/50)$). Above 1 MHz, however, additional *apparent* processing gain is actually just due to the reduction in I_o as the bandwidth of the interferer increases (constant P_{in} , where $P_{in} = I_o \times \text{Bandwidth}$). Processing gain here is defined as {total interference power in} divided by {total interference power out}, of the correlation function.

Note the general agreement in curve shape between the WAAS MOPS requirements in figure 2 and the available processing gain shown in figure 12. As shown in figure 13, with the exception of CW interference, the minimum post-correlation signal to interference ratio for SV #6 is

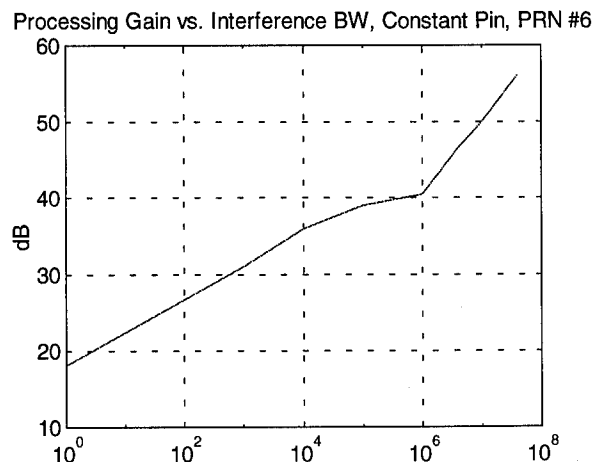


Figure 12: GPS C/A Code Minimum Processing Gain vs. Interference Bandwidth, PRN #6

nearly constant vs. interference bandwidth, ranging only from 15 to 16.5 dB. For CW interference to SV #6, however, the WAAS MOPS requirement leaves a minimum post-correlation signal to interference ratio of only 4 dB. It should be noted, however, that this low S/I ratio is for the worst case line of the worst case C/A code spectrum. Since the probability of CW interference coinciding in frequency with a large C/A code spectral line is small, and such coincidence is unique in frequency to each SV, the problem for CW interference appears worse in figure 13 than it nominally is. Additionally, the worst case spectral line for a typical SV is 5-10 dB lower (resulting in a 5-10 dB higher worst case post-correlation S/I ratio). Further analysis is warranted on the appropriate selection of the CW interference requirement.

It should also be pointed out that all the interference spectrums used in the analysis above are flat across their entire spectrum. The proposed interference requirements for the WAAS MOPS only allow an interference level of -110.5 dBm/MHz (-140.5 dBW/MHz) in the "notch" bandwidth of $L1 \pm 10$ MHz for interference bandwidths greater than 20 MHz. Even though the total interference power for the notched cases remain at the levels shown in figure 2, a noticeable change in post-correlation S/I results. This is because the majority of interference power into the correlator for greater than 20 MHz interference is outside $L1 \pm 10$ MHz, while the majority of the power out of the correlator is passed through the middle few MHz of the C/A spectrum. Thus the high interference levels outside of $L1 \pm 10$ MHz have negligible effect on post-correlation S/I. Further analysis shows that using the flat 40 MHz interference spectrum increases the post-correlation S/I ratio by 4.9 dB vs. the notched 40 MHz interference. The flat spectrum 40 MHz interference case is shown by the square marker in figure 13.

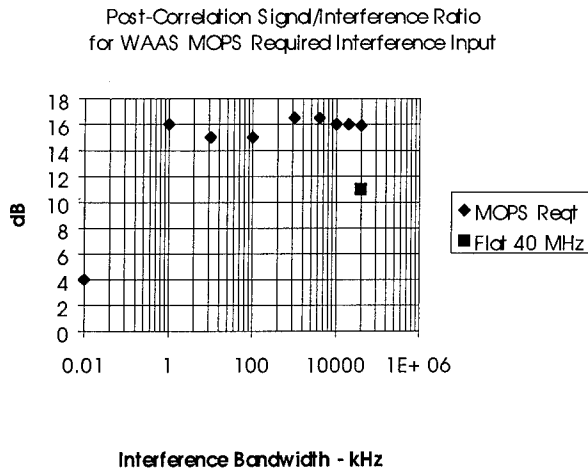


Figure 13: Worst Case Post-Correlation S/I Ratio for WAAS MOPS Required Interference Input, PRN #6

OUT-OF-BAND INTERFERENCE SUSCEPTIBILITY

The out-of-band interference specification level proposed by RTCA/SC-159 for the Wide Area Augmentation System (WAAS) Minimum Operational Performance Standards (MOPS) varies versus the frequency of the interference signal as shown in Figure 14. For ease of test and analysis the interference is considered to be CW, which is the worst case interferer. The corresponding diagram for GLONASS receivers is still under development and will likely be much more difficult for the receiver to meet.

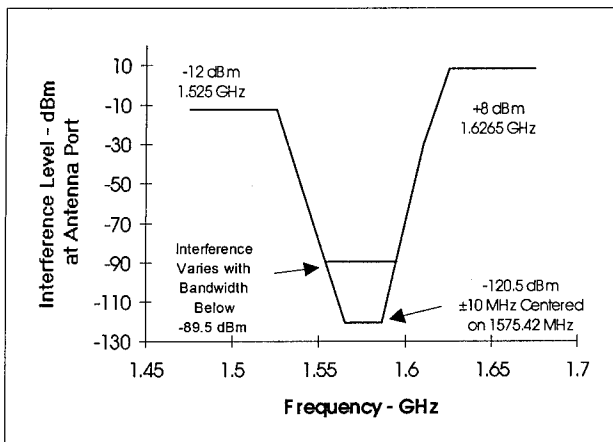


Figure 14: GPS Out-of-Band Interference Level Requirements

An SPS GPS receiver rejects out-of-band interference two ways. First, it heavily RF filters the received signal using a filtering section with a combined frequency response similar to an inverted and normalized version of Figure

14. Second, the correlation process yields a processing gain against the interference signal that grows as the frequency of the interferer is removed from L1. The level of processing gain follows the envelope of the worst case C/A code sinc-squared function, whose minimum processing gain is less than 20 dB in the main signal lobe (see in-band discussion above).

The out-of-band interference affects a GPS receiver by overcoming the rejection capability of the receiver's RF filtering and correlator processing gain. When strong enough, the interference saturates the RF front end of the receiver causing GPS signal suppression and receiver tracking failure. The current specification requires the GPS receiver to include passive filtering that yields approximately 90 dB rejection at 1525 MHz and 1626.5 MHz (see Figure 14). (90 dB = 128.5 dB - inherent interference rejection capability of an SPS GPS receiver 50 MHz away from L1)

INTERFERENCE SOURCE SEPARATION

Source Location for Precision Approach

During final approach the minimum separation from an interference source is governed by several factors in addition to decision height. Consider the approach geometry views in Figure 15. The top view (Fig. 15a) shows the Required Navigation Performance (RNP) outer tunnel lateral limits [3] overlaid on the final approach and approach light surfaces [4]. The ideal approach path is the centerline. The vertical cross-section view (Fig. 15b) through the ideal glidepath shows the approach light and final approach surface slopes in relation to the RNP outer tunnel vertical limits. Recall that the outer tunnel is defined as that volume which contains the extremities of the aircraft on all but one in 10^7 approaches. Its semi-dimensions are $5.73 \sigma_i$ + aircraft semi-dimension; where σ_i is the vertical or lateral total system error (TSE) standard deviation. The inner tunnel (not shown) is a volume of space around the ideal glidepath which encloses the aircraft navigation reference point with 95% probability (semi-dimension = $2\sigma_i$). The approach light and final approach surfaces define the upper limit of ground obstacles in the vicinity of the approach path. FAA layout guidelines prescribe that above-ground objects (other than essential navaids) are to be outside the runway object-free area [5] which extends at least 1000' beyond the runway threshold and 400' either side of the runway centerline.

An inspection of Figure 15 suggests the closest an uncontrolled ground based interference source could get to an aircraft on Category II/III approach is at a point directly under the approach path just beyond the edge of the runway object-free area and just below the 50:1

approach light surface. Thus the source is 1000' from the runway threshold, 2000' from the ideal touchdown point and 16' ($\{2000-1200\}/50$) above the extended runway surface. At that distance from touchdown, the ideal 3° glidepath is 104.8' ($2000 \cdot \tan 3^\circ$) above the runway surface or just above the 100' Cat II decision height.

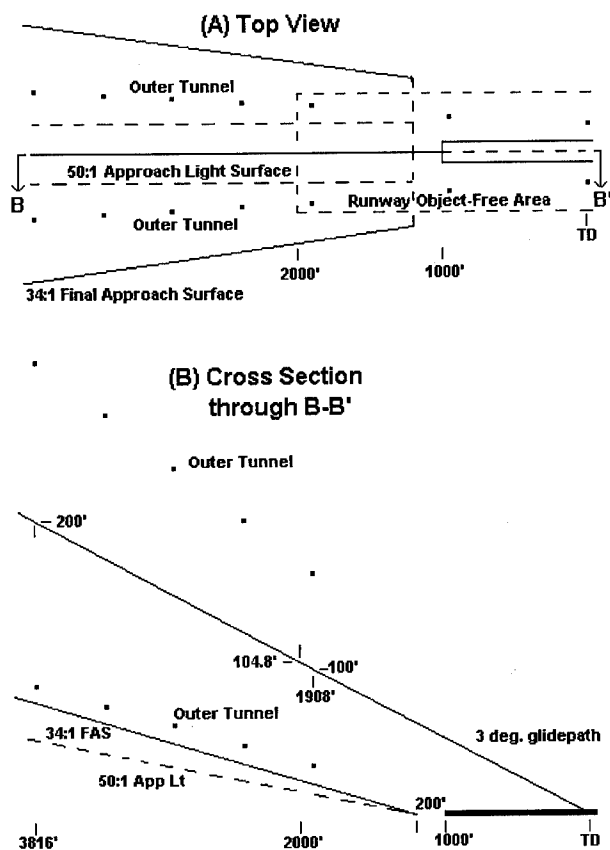


Figure 15: Views of a Precision GNSS Approach

Mobile interference sources can commonly have easy access on a regular roadway to a point about 1000' from a runway threshold underneath the approach path. A familiar example is Aviation Boulevard near Los Angeles International Airport. It crosses under the Runway 25L Cat II approach path at 1200' from the runway threshold and level with the extended runway surface.

The equivalent situation for a Category I precision approach would put the interference source directly under the 200' decision height point on the glide path and just beneath the 50:1 approach light surface. That point is 3816' from the ideal touchdown point and 52' ($\{3816-1200\}/50$) above the extended runway surface. Though mobile interference sources could get closer to the aircraft inside of the 200' decision height point, the aircraft will no longer be on instrument approach and thus less sensitive to upset by interference.

Antenna Separation for Cat II/III Precision Approach

An estimate of the height of the aircraft above the interferer assumes that the aircraft deviation below the ideal glidepath is 1.5 times the Cat II inner tunnel semi-dimension (3σ TSE). It is also assumed that the ideal glidepath actually represents the trajectory of the GNSS antenna. This is the case now for ILS/MLS approaches and it is reasonable to extend the assumption to Cat II and III GNSS approaches. The RNP inner tunnel lower surface is 15' below the glidepath at the 100' Cat II decision height [3]. By linear interpolation the (2σ) inner tunnel dimension is 15.8' at the nearby approach point directly above the interferer (104.8' above the runway extended surface). The estimated aircraft height, H_a , is given by

$$\text{EQ 1} \quad H_a = H_{\text{ideal}} - 3\sigma \text{TSE}$$

Since H_{ideal} , the ideal glidepath height, is 104.8' and $3\sigma \text{TSE}$ is 23.7', EQ 1 yields an H_a value of 81.1'.

From the previous section the maximum interference source height, H_i , at this point is 16'. Therefore the Cat II minimum GNSS antenna-to-interference separation, h , is the difference in heights,

$$\text{EQ 2} \quad h = H_a - H_i \text{ or } h = 65' \text{ (rounded to integer)}$$

An estimate of minimum antenna separation distance for Cat III comes from the High Intensity RF fields study [2] by subcommittee AE4R of the Society of Automotive Engineers. They concluded in the "severe" environment that a 50' slant range should be used between an aircraft on the ground and other mobile emitters within the airport perimeter. The HIRF study also suggests a maximum enroute spacing of 500'

Antenna Separation for Cat I Precision Approach

A similar aircraft height estimate with the 3σ TSE method can be made using Category I parameters. In that case at 200' decision height the outer and inner tunnel vertical semi-dimensions are 110' and 32', respectively. The value for $3\sigma \text{TSE}$ is then 48' and EQ 1 yields 152' for H_a (200-48). From the source location analysis the maximum Cat I source height is 52'. Therefore for Cat I parameters EQ 2 yields an antenna separation, h , of 100' (152-52). The same method for the non-precision approach case also yields about 100'.

LINK ANALYSIS FOR MSS INTERFERENCE TO GNSS

GNSS Signal and Interference Propagation Parameters

A determination of the interference effects on an airborne GNSS receiver requires values for the emitter power and antenna directivity, the separation range, the navigation

antenna directional performance, and the receiver sensitivity and susceptibility factors. Minimum satellite signals are -161 dBW for GLONASS and WAAS and 160 dBW for GPS at the output of a lossless isotropic circular polarized antenna. These values are modified by the gain factor for the actual GNSS antenna. The analysis reference point is the GNSS antenna terminals.

The simplest and most straightforward method to describe the interference source emission is with the maximum spurious effective isotropic radiated power (EIRP) value in the GNSS frequency band. EIRP is the product of transmitter power and transmit antenna gain. The MSS mobile earth terminal (MET) spurious EIRP requirement near the GPS L1 frequency is -70 dBW/MHz broadband and -80 dBW narrowband emission [7]. The GLONASS band spurious broadband EIRP requirement is currently under discussion in RTCA SC-159 Working Group 6. Values range from -70 to -50 dBW/MHz (-130 to -110 dBW/Hz). For the purpose of this analysis it is assumed that the MSS MET maximum EIRP is in the direction to the GNSS antenna. The assumption is reasonable because, in general, the MSS MET emission is likely to be directed upward in a broad, low gain, cardioid-like antenna pattern and the GNSS-equipped aircraft will be above the MET.

Free space line-of-sight propagation between the MSS MET and the GNSS antenna is a good representation of the actual interference encounter. Runway approach paths are relatively free of tall obstacles in the vicinity of the final approach area so foliage attenuation or diffraction should be negligible. Multipath fading of the interference signal, if it takes place, should not affect the average received interference power. Excess path attenuation from rain or other absorption mechanisms are negligible at L-Band. Thus the sole factor controlling propagation loss in the analysis is the line-of-sight distance (slant range) between the MET and GNSS antenna. Slant range minimum values have been determined from aircraft navigation requirements and airport approach layout constraints. They are 500 feet (enroute), 100 feet (non-precision approach and Cat I), and 50 feet (Cat II / III). See "Interference Source Separation" section above.

Navigation Antenna Parameters

The GNSS receive antenna pattern controls both signal and interference levels. The ARINC 743A and GPS / WAAS antenna MOPS specifications require a minimum signal gain of -4.5 dBic at +5 degrees elevation. This value represents a reasonable limit based on actual antenna measurements. The gain for interference signals arriving from below the horizon (negative elevation angles) is unspecified, however, and subject to significant influence from the aircraft fuselage and wing structures.

Very little measured antenna pattern data for aircraft installations is available in the open literature. One published report by Owens [8], however, gives relative pattern data on a BAC1-11 (about the size of a Boeing 737-200 with rear fuselage-mounted engines like a DC-9). The pattern has good upper hemisphere coverage, but high gain sidelobes centered at -60 degrees elevation ahead and either side of the fuselage. These sidelobes have approximately the same gain as that for the minimum elevation satellite (0 dB rel. gain) and substantial angular extent. Comparison to the peak upward gain shows that aircraft structure diffraction has limited the installed GNSS antenna to about a 10 dB minimum front-to-back gain ratio. This result is representative of at least mid-sized air transport aircraft.

The angular direction for the strongest sidelobe will, in general, be different on different aircraft depending on structure diffraction details. However, it can be generally assumed that the sidelobe will be in a sufficiently downward direction to offer a relatively short path length to ground-based interference. In the BAC1-11 example, the path length to the ground in the maximum sidelobe direction is 15% (1.2 dB) longer than to a ground point directly below the aircraft, but the antenna gain in the sidelobe is higher by about 10 dB. Given the pattern complexities of actual aircraft and the need to establish a reasonable bound on side- and backlobe gain, a conservative assumption for the GNSS interference analysis is that minimum elevation satellite and interference gains are equal (-4.5 dB) for Cat I with minimal allowance for Cat II/III. Cat II/III may need improved antenna installation for link margin considerations. By the same reasoning no polarization mismatch loss is assumed.

GNSS Receiver Parameters

The receiver factors affecting GNSS system performance are the system noise temperature, the pre-correlator implementation loss and the receiver carrier-to-total noise density ratio required for proper output quality. The noise power spectral density at the antenna terminals is

$$EQ\ 3 \quad N_0 = k \cdot T_s$$

where T_s is the total system noise temperature (sum of sky noise and receiver system noise) and k is Boltzmann's constant (1.38×10^{-23} W/Hz/K). For this analysis N_0 has been set at -201.5 dBW/Hz, which corresponds to a T_s value of 512.8 K. A sky noise allocation of 100 K is reasonable given that the antenna pattern coverage for low elevation satellites necessary for good navigation performance also allows in some warm earth blackbody radiation. A 412.8 K receiver requires a good noise figure (3.8 dB) and a low loss installation.

The pre-correlator implementation loss, L_{imp} , takes into account such effects as imperfections in the RF/IF transfer function, the non-ideal A/D converter factor, and non-ideal satellite signal loss. RF/IF hardware transfer function loss is typically around 0.5 dB and includes such things as filter dispersion, local oscillator phase noise, and AGC setpoint inaccuracies. Quantization loss in the A/D converter ranges from 2 dB for a 1-bit converter to less than the 0.5 dB for multi-bit converters. Non-ideal satellite signal loss is 0.6 dB maximum for GPS and GLONASS and 1 dB for WAAS. Implementation loss values range from about 1 to 3 dB. Values below about 2 dB are considerably more expensive to achieve with manufacturing margins; this analysis will use 2.5 dB.

Several post-correlator implementation parameters are factored into the relation between the receiver carrier-to-total noise density ratio, C/N_{tot} , and the appropriate navigation system performance probability. Details of the relation will not be discussed here. The system performance parameter driving WAAS reception is a word error rate of 10^{-4} per second. A carrier-smoothed code-tracking receiver can achieve the 10^{-4} rate with a C/N_{tot} value of 30 dB-Hz. The driving requirement for Cat I GPS or GLONASS reception is a pseudo-range measurement standard deviation of 0.7 meters. A carrier-smoothed code-tracking receiver can achieve 0.7 m standard deviation at a C/N_{tot} value of 30 dB-Hz. A GLONASS receiver tracking loop parameters can be adjusted to compensate for its longer chip length and achieve equal pseudo-range performance to GPS.

Cat I Link Analysis with MSS Interference

In the link analysis the derived value of C/N_{tot} (CNIR) is compared with the computed value of its defining equation, $C/(N_0 + I_0)$; where C is the signal carrier power, and N_0 and I_0 are the thermal noise and interference densities, respectively, at the antenna terminals. The interference density is calculated with the free-space propagation equation given the specified interference source emission and the other propagation parameters.

The carrier power, C (in dBW), at the antenna terminals is given by

$$EQ 4 \quad C = 10 \cdot \log(S \cdot G_s / L_{imp});$$

where S is the minimum satellite signal level (in Watts) for either GPS, WAAS, or GLONASS referenced to an isotropic circular antenna. The other parameters, G_s and L_{imp} (previously defined) are in power ratio terms.

The free-space path loss (in dB) from the interference source is given by

$$EQ 5 \quad PathLoss = 20 \cdot \log\{299.8 / Freq / (4 \cdot \pi \cdot Range)\};$$

where "Freq" is the signal frequency (in MHz) and "Range" is the antenna separation (in meters). The broadband interference density at the antenna terminals (in dBW/Hz) is given by

$$EQ 6 \quad I_{obb} = EIRP_{bb} - PathLoss + InterfcAntGain;$$

where "EIRP_{bb}" is the maximum broadband spurious emission at the MSS MET (in dBW/Hz). Similarly the equivalent narrowband interference density at the antenna terminals (in dBW/Hz) is given by

$$EQ 7 \quad I_{onb} = EIRP_{nb} - PathLoss + InterfcAntGain - InterfcGBnb;$$

where "EIRP_{nb}" is the maximum narrowband spurious emission at the MSS MET (in dBW) and "InterfcGBnb" is the narrowband spreading factor. This factor quantifies the correlator spreading of the CW interference signal into an equivalent power density value. For the GPS and GLONASS pseudo-random codes it is typically less than the ideal $10 \cdot \log(\text{chip rate})$ value due to finite code lengths and other code imperfections (cf. "In-Band Susceptibility" sect.). Because of the maximal length nature of the GLONASS code compared to the GPS Gold codes, the GLONASS code has a higher spreading factor than GPS even though its chip rate is half the GPS rate.

The $C/(N_0 + I_0)$ values for broad- and narrowband interference in logarithmic terms are

$$EQ 8 \quad CNIR_{bb} = -10 \cdot \log\{10(N_0 - C)/10 + 10(I_{obb} - C)/10\},$$

$$EQ 9 \quad CNIR_{nb} = -10 \cdot \log\{10(N_0 - C)/10 + 10(I_{onb} - C)/10\}$$

These values are compared with the derived C/N_{tot} requirements (Req CNIR) for a measure of link margin.

The Cat I link summary (Table 2) shows the WAAS link has essentially 0 dB margin for the specified broad- and narrowband MSS MET emission levels at the $100'$ (30.48 m) separation distance. The GLONASS link results show large negative margin for the -110 dBW/Hz broadband interference level at $100'$. Though not shown the

GLONASS link does not close even at 500' en-route separation. If the -130 dBW/Hz proposed limit were used, the GLONASS Cat I link would also close with 0 dB margin. Because of a 1 dB larger minimum satellite signal the Cat I GPS link (Table 3) has 1 dB margin at 100'. The calculations assume that the EIRP levels are maintained to a sufficiently large frequency separation from the receive center frequency (approx. ± 10 MHz for GPS, WAAS, ± 5 MHz for GLONASS) to avoid excess noise in the correlator sidelobes.

Table 2: Category I Link Budget Summary

| Parameter | Units | WAAS | GLON |
|---------------------|--------|---------|---------|
| Freq | MHz | 1575.42 | 1604.25 |
| Sat Sig Pwr | dBW | -161.00 | -161.00 |
| Sat Ant Gain | dB | -4.50 | -4.50 |
| Impl. Loss | dB | 2.50 | 2.50 |
| C (ant term) Eq5 | dBW | -168.00 | -168.00 |
| No (ant term) | dBW/Hz | -201.50 | -201.50 |
| Interfc EIRP bb | dBW/Hz | -130.00 | -110.00 |
| Interfc EIRP nb | dBW | -80.00 | -80.00 |
| Range | meters | 30.48 | 30.48 |
| Path Loss Eq6 | dB | 66.08 | 66.23 |
| Interfc Ant Gain | dB | -4.50 | -4.50 |
| Interfc G*B nb | dB-Hz | 50.10 | 52.10 |
| Io(ant term) bb Eq7 | dBW/Hz | -200.58 | -180.73 |
| Io(ant term) nb Eq8 | dBW/Hz | -200.68 | -202.83 |
| CNIR bb Eq9 | dB-Hz | 30.00 | 12.70 |
| CNIR nb Eq10 | dB-Hz | 30.06 | 31.11 |
| Req CNIR | dB-Hz | 30.00# | 30.00 * |

requirement derived from $WER = 10^{-4}$

In an actual interference encounter C/N_{tot} is time-varying due to GNSS platform relative motion. It dips briefly (approx. 0.5 sec) to the tabulated value at the minimum path loss point from a higher baseline (large path loss to interference) and then returns to the baseline. This transient C/N_{tot} dip is long enough to impact the receiver tracking loops and is therefore treated as a quasi-steady state phenomenon in this analysis.

Cat II/III Link Analysis

A comparison of the GPS link performance (Table 3) for the Cat I vs. Cat II/III cases shows that about 5 dB of improvement in the receiver system-related parameters is needed. This is to overcome the reduced source separation of 50' (15.2 m) for Cat II/III with the same spurious EIRP limits. The set of modified Cat II/III system parameters in the calculation (1dB less Impl. Loss, 3 dB less Interfc. Ant. Gain, 1 dB less CNIR) is only one of many workable combinations. Though no C/N_{tot}

requirement is listed for the Cat II/III link, Cat III flight test data and analysis suggest that a carrier smoothed narrow-correlator receiver with suitable processing can meet the $0.1 \text{ m } 1\sigma$ pseudo-range jitter needed for overall accuracy at the 30 dB C/N_{tot} . Further study of appropriate interference link budget allocations for Cat II/III approach is needed.

Table 3: GPS Link Budget Comparison

| Parameter | Units | Cat I | Cat II/III |
|---------------------|--------|---------|------------|
| Freq | MHz | 1575.42 | 1575.42 |
| Sat Sig Pwr | dBW | -160.00 | -160.00 |
| Sat Ant Gain | dB | -4.50 | -4.50 |
| Impl. Loss | dB | 2.50 | 1.50 |
| C (ant term) Eq5 | dBW | -167.00 | -166.00 |
| No (ant term) | dBW/Hz | -201.50 | -201.50 |
| Interfc EIRP bb | dBW/Hz | -130.00 | -130.00 |
| Interfc EIRP nb | dBW | -80.00 | -80.00 |
| Range | meters | 30.48 | 15.24 |
| Path Loss Eq6 | dB | 66.08 | 60.06 |
| Interfc Ant Gain | dB | -4.50 | -7.50 |
| Interfc G*B nb | dB-Hz | 50.10 | 50.10 |
| Io(ant term) bb Eq7 | dBW/Hz | -200.58 | -197.56 |
| Io(ant term) nb Eq8 | dBW/Hz | -200.68 | -197.66 |
| CNIR bb Eq9 | dB-Hz | 31.00 | 30.08 |
| CNIR nb Eq10 | dB-Hz | 31.06 | 30.16 |
| Req CNIR | dB-Hz | 30.00 * | |

*requirement derived from pseudo-range $\sigma = 0.7 \text{ m}$

CONCLUSIONS

The primary in-band interference sources of concern to a GNSS receiver are VHF communications radio harmonics, Mobile Satellite Services (MSS) transmissions, and SATCOM (AMSS) intermodulation products. SATCOM is also a potential out-of-band interference source for GNSS. MSS remains as the single biggest interference concern to GNSS.

GNSS receiver interference susceptibility varies as much as 25 dB versus the bandwidth of the interference from CW up through 1 MHz broadband interference due to the discrete nature of the C/A code spectrum.

Precision approach geometries allow the GNSS antenna to be very close to a potential interference source: as close as 50 feet for Cat II/III and 100 feet for Cat I.

The GNSS receiver susceptibility, combined with conservatively estimated approach geometries yield a GPS/WAAS receiver link budget with MSS interference

having minimal margin during Cat I approach. The GLONASS Cat. I receiver link budget has -20 dB margin for MSS interference at maximum proposed levels. The GPS Cat. III receiver link budget can reasonably be expected to close with an additional 5 dB improvement in system parameters.

ACKNOWLEDGMENTS

The authors would like to acknowledge the helpful comments of Bob Kelly, Chris Hegarty, and Bruce DeCleene, fellow members of the RTCA/SC-159 GNSS Interference Working Group. Much of the analysis and data in this paper was developed in support of this committee's efforts. We would also like to thank our Rockwell colleagues Gary McGraw and George Cobley for their many insights. This project was primarily supported by Rockwell Collins Commercial Avionics Division, SATNAV program.

REFERENCES

- [1] Johnson, M. W., "Interference to GNSS Receivers in the Civil Aviation Environment", Proceedings of ION GPS-94 Conference, Part 1, 9/20/94-9/23/94, pg 1127.
- [2] RTCA, RTCA Paper No. 396-95/SC-159-661, Final Draft of Minimum Operational Performance Standard Global Positioning System/Wide Area Augmentation System Airborne Equipment, July 24, 1995, Prepared by SC-159.
- [3] RTCA / DO-217, "Minimum Aviation System Performance Standards, DGNSS Instrument Approach System: Special Category I," 27 August 1993 (Rev 1).
- [4] FAA Advisory Circular 120-29 (Change 3).
- [5] FAA Advisory Circular 150/5300-13 (Change 4).
- [2] SAE, HIRF Users Manual, Sec. 4, RTCA Paper No. 489-94/SC159-582A.
- [7] Federal Communications Commission, Report and Order on CC Docket No. 92-166, Amendment of the Commission's Rules to Establish Rules and Policies Pertaining to a Mobile Satellite Service in the 1610-1626.5/2483.5-2500 MHz Frequency Bands, FCC 94-261, Oct. 14, 1994.
- [8] Owen, J. I. R., "A Review of the Interference Resistance of SPS GPS Receivers for Aviation," Navigation: Journal of the Institute of Navigation, Vol. 40, No. 3, Fall 1993, pp 249-259.

Observed GPS Signal Continuity Interruptions

H. Stewart Cobb, David Lawrence, Jock Christie, Todd Walter,
Y.C. Chao, J. David Powell, and Bradford Parkinson
Stanford University

ABSTRACT

During an autoland flight test of Stanford's Integrity Beacon Landing System in October 1994, one approach was aborted before landing due to a temporary satellite outage. Analysis showed that both the aircraft and ground reference GPS receivers lost lock on one satellite for six seconds. In subsequent weeks, we observed similar outages on most of the Block II satellites. Analysis of this data did not indicate a cause for these outages.

According to the satellite operators, this is a generic spacecraft problem. Command uplinks to Block II (but not IIA) satellites occasionally cause a conflict in the spacecraft computer. A conflict causes the spacecraft to emit a non-standard PRN code during one navigation data subframe (six seconds). These conflicts occur roughly 0.3 times per satellite per day. A simple Monte Carlo analysis shows that, in the worst case, this phenomenon could reduce availability of GPS precision landing systems by a factor of ten.

This type of outage is not described in the standard literature on GPS spacecraft reliability, nor is it monitored by the FAA's Performance Analysis Network (PAN). The FAA has recently contracted to upgrade PAN to continuously monitor spacecraft signals. As a result, accurate data on spacecraft signal continuity will soon be available to researchers.

THE QUESTION

During October 1994, Stanford University conducted a flight test of its Integrity Beacon Landing System (IBLS). Conducted in cooperation with United Airlines and the Federal Aviation Administration (FAA), the test involved navigating a Boeing 737 airliner down a precision approach to a fully automatic landing. The object of the test was to confirm that GPS-based systems are capable of providing the navigation accuracy and integrity needed to land aircraft even in the worst weather conditions.

The test was a complete success, resulting in 110 successful automatic landings [1]. One landing approach was aborted due to a brief loss of signal from one GPS satellite, as described below. That one abort attracted our

interest because it spoiled an otherwise perfect record. We carried out an extensive postflight analysis to trace the cause of this signal loss.

At the time, the IBLS system used a six-channel GPS receiver. Two channels are required to track the Integrity Beacon pseudolites on the ground, leaving only the necessary minimum of four channels to track GPS satellites. If the receiver lost lock on even one satellite, the system would be required to abort the approach. (The current version of IBLS uses a nine-channel GPS receiver and would not cause an abort in this situation.) To avoid this possibility, we carefully selected a set of healthy high-elevation satellites before each approach.

Our postflight analysis showed that both our airborne and ground reference receivers had simultaneously lost lock on spacecraft (PRN) 17. Six seconds later, both receivers simultaneously regained lock on the signal from that spacecraft. No other satellite signals were affected on either receiver. We performed tests for several days at the same sidereal time (constellation configuration) and this phenomenon did not recur. This made us suspect a one-time satellite signal failure, as our alternative explanations (a common receiver failure mode or a precise burst of interference) seemed highly improbable.

The Navigation Information Service (NIS) operated by the US Coast Guard is the designated point of contact for civilian questions about the GPS system. We called the NIS, explained the situation to the watchstander, and asked whether anything had happened to PRN 17 at the instant we lost its signal.

The Coast Guard watchstander called the 2nd Space Operations Squadron (2SOS) at Falcon Air Force Base, Colorado. 2SOS controls the satellite constellation, but only military users can contact them directly. The watchstander reported back to us that 2SOS had been sending commands to that spacecraft at the time the glitch occurred and that 2SOS had also seen the glitch. The watchstander added that 2SOS had given him the impression that such glitches were not uncommon, although he himself had never heard of them before.

Unable to get a better explanation, we fell back on our own resources. We set up a GPS receiver in our lab to monitor the constellation continuously and report any glitches. We duplicated the experiment in another lab using a different receiver with a different internal architecture, to eliminate the possibility that we were seeing some kind of internal receiver error. After two weeks of taking data, we had observed a total of eleven glitches similar to the one which caused our landing abort. Each glitch occurred simultaneously on both receivers. The only common thread we could detect was that we observed glitches on Block II spacecraft only, not on Block I or on Block IIA.

As we collected and analyzed the data, it became clear that we had discovered some sort of generic spacecraft problem which was not reflected in the literature on spacecraft failure modes and failure rates. This presented us with a dilemma. Members of our group were analyzing the ability of various air navigation system designs to meet specified Required Navigation Performance (RNP) parameters, including system availability and continuity. The analysis was based on the published failure models, but we now had data showing that those models were incomplete.

To resolve this dilemma, we decided to contact 2SOS directly. We outlined our observations, our concerns, and our need for accurate failure models in a letter requesting a better description of this phenomenon. To their credit, 2SOS responded very quickly with a full explanation.

THE ANSWER

Each GPS spacecraft continually broadcasts its own ephemeris and other data to user receivers. Current spacecraft are not capable of generating this data on their own. Instead, the data is read in realtime from a buffer memory on board the spacecraft, which the satellite operators must periodically refill with new data. This refilling process is called a "navigation data upload." Each satellite is refilled about once a day, on the average. Due to the amount of data involved, each upload takes about ten minutes to complete.

During the upload, one part of the spacecraft computer program is writing to the buffer memory, while another part of the program is reading broadcast information from that same memory. On the Block II spacecraft, it seems that these two processes occasionally conflict, and the broadcast data for one navigation data subframe does not reach the navigation signal transmitter in time. The transmitter shifts to a *non-standard C/A code* for the duration of that subframe, as it is designed to do

whenever its broadcast data is invalid. This non-standard C/A code is intended to be "invisible" to user receivers; the receiver sees this event as a loss of signal from that satellite. The loss of signal lasts for one subframe, or six seconds.

The characteristics of the glitch we saw match this explanation perfectly. Unfortunately, the precise cause of this conflict is unknown, and there appears to be no feasible workaround to prevent it. It does not happen during every upload. Statistics collected by 2SOS show that the frequency of occurrence is roughly 0.3 glitches per spacecraft per day. Because the current constellation contains nine Block II spacecraft, we would expect to see about three glitches per day in the constellation. (According to 2SOS, a similar glitch was seen one time on one Block IIA satellite. Future satellites are not expected to exhibit this problem.)

The glitches are not uniformly distributed. According to 2SOS, most uploads are performed during the second shift (2200 to 0600 UTC) to satellites in view of the control station in Colorado. This is done for reasons of operational convenience rather than necessity, however, and the procedure may change at any time.

THE IMPACT

Of all GPS applications, precision landing is perhaps the one which can least easily tolerate short signal outages. Most applications can "ride out" a six-second navigation outage. However, precision landing systems are required to announce a navigation failure within one or two seconds, and automatic landing systems must abort the approach after a navigation failure.

To gauge the impact of this satellite signal failure mode on our ongoing analyses, we performed a simple Monte Carlo study of landing system availability with and without this glitch. For 20,000 random trials, the study considered whether at least four satellites (the minimum required for navigation) were visible above a 7.5 degree elevation mask angle at one of nine Category III airports worldwide. Because a precision landing system could not tolerate the Block II uplink glitch with only four satellites available, we flagged those cases for separate treatment. The study introduced spacecraft failures at appropriate rates using the satellite availability model published by Phlong and Elrod [2].

The study showed that the availability of GPS for precision landing, without considering the Block II uplink glitch, was 99.965 percent. Removing the cases where only four satellites were available, and at least one of

them was a Block II satellite, the availability of GPS navigation fell to 99.34 percent, over ten times worse. This difference illustrates the impact that incomplete spacecraft failure models can have on system analyses.

This study shows a *relative* difference between two sets of assumptions, but it should not be considered as a guide to *absolute* levels of GPS availability. The study considered a relatively small number of cases, and it did not address augmentation methods such as pseudolites or geostationary satellites. Nevertheless, it does show the need for more accurate models.

THE IMPLICATIONS

The discovery of these glitches was a surprise to us and to most of our fellow researchers. The second surprise was that the glitches were *no* surprise to the satellites' builders and operators. Every time a spacecraft shifts to non-standard code, it sends a message to the control center. This uplink glitch was even seen in prelaunch testing of the Block II spacecraft. Nevertheless, we have not seen it mentioned in the literature. No one tried to cover up the problem; rather, those who knew about it seemed to believe no one else would be interested.

We have illustrated above the importance to researchers of accurate models of spacecraft behavior. The fact that this glitch was unknown to the research community for so long begs an important question: Are there other spacecraft anomalies with similar impact which remain unknown today? If so, tomorrow's systems may not perform as well in the real world as today's analyses predict.

Fortunately, the Federal Aviation Administration (FAA) has just begun a program which will help answer that question. This is the Performance Analysis Network (PAN), which is operated under contract by Overlook Technologies. The PAN monitors the signals of the GPS constellation from three locations within the United States, and logs any deviations from the Standard Positioning Service specification. The PAN has actually been in operation since 1993, but the data collected to date has generally been too sparse to provide accurate signal continuity models [3].

Last spring, the FAA modified the PAN contract to support development of the Wide Area Augmentation System (WAAS). One of the new provisions requires the PAN to collect availability, continuity, and accuracy data

at a once-per-second rate on all spacecraft in view of each monitor station. The PAN will not begin operating in this mode until late 1995, and it will take some time after that to collect enough data to develop accurate statistics. However, it will not be too long before models of spacecraft performance based on actual data, rather than predictions, become available to the research community. This should help quell the fear that our spacecraft models may not reflect reality.

THE MESSAGE

The purpose of this paper is to document this particular satellite signal failure mode in the literature. Analysis of highly demanding navigation applications, such as precision landing, must incorporate all known failure modes and rates, else they may lead to inaccurate conclusions. The PAN is about to start collecting signal continuity data from actual experience. We expect that PAN data will serve as an accurate baseline for future analyses.

ACKNOWLEDGMENTS

We gratefully acknowledge the help of the Air Force's 2nd Space Operations Squadron, especially Captain Chris Shank, for explaining the cause of this glitch and collecting system-wide statistics on its frequency. Mark Fryt of Overlook Technologies explained their past and future PAN data collection efforts. Sam Pullen, Boris Pervan, and Per Enge helped us understand the impact of this glitch. Finally, this work would not have been possible without the moral and financial support of the Federal Aviation Administration.

REFERENCES

1. C.E. Cohen et al. "Preliminary Results of Category III Precision Landing with 110 Automatic Landings of a United Boeing 737 Using GNSS Integrity Beacons." *Proceedings of ION-NTM-95*, Anaheim, California, January 1995.
2. W.S. Phlong and B.D. Elrod. "Availability Characteristics of GPS and Augmentation Alternatives." *Navigation*, Vol. 40, No. 4, Winter 1993-94.
3. J.C. Johns and R. Conley. "A Summary of GPS SPS Performance as Observed by the FAA's GPS Performance Analysis Network." *Proceedings of ION-GPS-94*, Salt Lake City, Utah, September 1994.

Integrity and Continuity of Service Analysis of LADGPS and WADGPS Architectures with SNAPSYS Simulator

Dr. D. Flament and N. Marchal
Thomson - CSF

B. Christophe
Onera

J. L. Jonquiere
DGAC/STNA

BIOGRAPHY

Name : D. Flament

Nationality : French

Experience : D. Flament graduated from ECL (Ecole Centrale de Lille) in 1984. He obtained his doctorate degree in Automatic Science from ECL in 1986.

In 1987 he joined the systems department of ONERA where he has in charge of satellite navigation system studies for CNES in the context of the European Complement to GPS and then for the French Civil Aviation DGAC where he developed the simulator SNAPSYS for DGNSS performance analysis.

Since January 1995, he is at THOMSON-CSF where he is in charge of the system activities for the development of the french EURIDIS step 1 Ranging system for CNES and DGAC/STNA and technical responsible for ESA GNSS2 study.

Name : B. Christophe

Nationality : French

Experience : B. Christophe graduated from ENSAE Toulouse in 1990. In 1989, he made at ONERA a training period and was in charge of study for CNES about CE-GPS availability. In 1990, he joined definitely the ONERA. Up to 1994, he was in charge of studies for CNES about airbreathing and rocket launcher trajectory and flexible launcher trajectory simulation. Since 1994, he is involved in satellite navigation system studies and responsible of GNSS software support and development.

Name : J.L. Jonquiere

Nationality : French

Experience : Jean Louis Jonquiere is graduated from the Civil Aviation National School (1969). For last years, he has been in charge of teaching in the Electronics Department. His areas of interest are Radionavigation and Signal Processing.

Now, in the french Civil Aviation Department, he is working in the Division of new Systems Communications, Navigation and Surveillance of the Air Navigation Technical Service. He is GNSS project manager. He is responsible of the technical part of the

local Area Differential Experimentation at Toulouse Airport. he participates to the European regional Augmentation project EGNOS. He is adviser of the France member of the OACI GNSS Panel.

Name : N. Marchal

Nationality : French

Experience : Nicole Marchal graduated as an engineer from the Ecole Centrale de Lyon (France) in 1990 and from the Technische Hochschule of Darmstadt (Germany). In 1991, she joined THOMSON-CSF. Since 1993, she has been working as a project engineer for navigation systems and has more particularly studied the requirements and performances aspects.

ABSTRACT

Since few years, the so-called WADGPS (Wide Area DGPS) and LADGPS (Local Area DGPS) systems are extensively studied and now considered as possible means for Civil Aircraft landing for phases of flight until Precision Approach CAT 1 (WADGPS) and even further (until CAT 3) for LADGPS.

Operational requirements have been defined for each given phase of flight independantly of the navigation sensor. They have been expressed in the so called Required Navigation Performances (RNP) and Tunnel concept. The RNP are translated in Accuracy, Availability, Integrity and Continuity of Service. Under French Civil Aviation (DGAC/STNA) contract, Thomson-CSF has conducted theoretical analyses on the RNP requirements and then proposed both LADGPS and WADGPS architectures compliant with Precision Approach RNP requirements. More particularly, Thomson-CSF proposed an Integrity Monitoring System working at different levels in the navigation system. The more recent analyses were dealing with the difficult Integrity and Continuity Of Service performance assessments offered by the proposed system in various scenarii. These analyses have been carried on with the ONERA simulator.

ONERA has developed, under CNES contract then under STNA contract, a simulation tool called SNAPSIS 'Satellite NAVigation systems Performance analysIS simulation Software'. This simulator has been designed to modelise different types of differential system architectures and to analyse their performance in term of RNP. At a previous congress, preliminary results with LADGPS and WADGPS architectures have been presented. Since, new modelisations, both for the spatial segment and for the user segment, have been developed and their influence on the performances has been studied. Moreover, new methodologies have been used for the statistical evaluations of performances.

At first, this paper will present the main Thomson-CSF conclusions about the RNP analysis and the resulting LADGPS and WADGPS solutions mainly from the Integrity and COS points of view. More particularly, we will expose the different elements of the Integrity Monitoring System.

Then the different modules which compose SNAPSIS and which have allowed to simulate finely and accurately the different architectures with a great choice of possible components will be presented (ground segments, integrity monitoring algorithms, pseudolites, etc.).

Some illustrative results showing the great sensitivity of the RNP performances to some system parameter (SA dither characteristics, for instance) will be given. Finally, we will insist on the methodology applied to perform extensive Integrity and COS analyses based on a preliminary theoretical approach of these RNP parameters and the use of probability scaling in the simulations in order to achieve high confidence (99%).

1. INTRODUCTION

The WADGPS is now known as a possible means to offer a landing navigation service for Civil Aviation, even for the CAT1 precision approach phase of flight. The WAAS system is currently developed by the FAA and a similar project is now under progress in Europe.

Preliminary studies about the now well known RNP 'Required Navigation Performances' assessment expressed in terms of Accuracy, Availability, Integrity and Continuity Of Service have been conducted, especially for some results on LADGPS and WADGPS performances (ref.1).

The present article gives the THOMSON-CSF results on proposed solutions to provide Accuracy, Availability, Integrity and COS. The analyses presented here are mainly concerned by Integrity and Continuity of Service. Therefore some Integrity Monitoring System solutions with their associated performances in probability of alarm and probability of missed detection will be described. They are based on a study and system simulation supported by the French Civil Aviation Administration (STNA) and

the French Space Agency (CNES). The THOMSON-CSF architectures and scenarii are tested with the always upgraded model SNAPSIS, developed by the French Aerospace Research Laboratory, ONERA (ref.2 and 3).

2. RNP REQUIREMENTS

The Required Navigation Performances (RNP) to be satisfied by the navigation system are translated in accuracy, availability, integrity and Continuity of Service (COS) which are applicable in the airspace where precision approaches are occurring.

The tunnel concept (ref.4) introduces a solid operational reference to link up these four RNP requirements. The Total System Error (TSE) which is the difference between the aircraft true position and the ideal landing path shall meet the tunnel requirement. The TSE is defined as the quadratic sum of the Flight Technical Error FTE (aircraft command and pilot error) and of the Navigation System Error NSE. The NSE is directly allocated to the navigation system. From a tradeoff analysis, THOMSON-CSF already proposed (ref 1) a choice of Navigation System Requirements which is presented in table 1 for CAT 1 precision approach.

The system accuracy is usually expressed in terms of the smallest radius of horizontal or vertical circle that encompasses 95% of the position error measurements (STANAG ref 5). These figures have been adopted here in the case of the NSE (95%) (H: horizontal, V: vertical).

| | CAT1 |
|---|---------------------|
| Accuracy | |
| H NSE 95% | 18,7 m |
| V NSE 95% | 5,4 m |
| Integrity | |
| Prob. of undetected failure (per 150 s) | $1,3 \cdot 10^{-7}$ |
| H alarm limit | 33,5 m on NSE |
| V alarm limit | 9,8 m on NSE |
| time to alarm | 6 s |
| COS | |
| Prob of alarm per 15 s | $1 \cdot 10^{-5}$ |
| Availability | not determined |

Table 1 : Proposed Navigation System Requirements for CAT1

These four service characteristics are strongly correlated what makes their analysis difficult.

For instance, the Availability requirement expresses the probability that the positioning service meet the accuracy requirement **and** that the Integrity monitoring declares the service safe at a given instant. The Availability analysis leads then the System designer to firstly perform both the positioning service availability analysis and the Integrity monitoring service availability analysis. This double aspect makes the Availability requirement assessment a difficult task that remain currently under discussion and that will need a further detailed study.

The probability of undetected failure requirement is strongly limited ($<1.3 \cdot 10^{-7}$). This is the probability that the NSE exceeds the alarm limit **and** that the integrity monitoring system doesn't detect it and warn the user within the time to alarm.

It is obvious that the best way to solve the Integrity Issue is to provide both a better geometry (PDOP figure) and more accurate measurements, i.e. to reduce the sigma(URE) in order to ensure a low level of NSE. But anyway, for Precision Approach, the level of the undetected failure probability requirements implies that sophisticated Integrity monitoring methods must be implemented in order to guarantee the robustness of the service to any unplanned system failure (space component sudden failure, straightforward HW/SW in the ground segment, etc.).

The time to alarm (requirement of 6 s) is not detailed in this paper, even if it is a critical part of the system. Indeed, the processing times in the different components have not been studied nor simulated during the study. Qualitative budgets have shown the relative feasibility of this constraint for CAT1. It is then assumed that the problem of the time to alarm can be decorrelated from the other integrity or accuracy requirements.

The Continuity of Service 'COS' is the probability that the performance of the Navigation System is within tolerance throughout the phase of flight period (150s divided in ten segments of 15s) given that it was within tolerance at the start of the period. Planned losses of service do not affect continuity. The Continuity losses are then mainly due to unplanned sudden unavailability caused by the integrity monitoring system alarms and outages.

The RNP are all correlated through the NSE distribution, what makes their analyses such a critical problem. In fact, the NSE distribution bounds the RNPs through the following conditions:

We have $NSE\ 95\% < \text{Accuracy threshold}$, which expresses the accuracy requirement and which can also be written as: $\text{Prob.}(NSE > \text{Accuracy Threshold}) \leq 5\%$. This performance will then impact on the Availability one.

We also have this complex condition: $\text{Prob.}(NSE > \text{Alarm limit}) \leq \text{Probability of Alarm}$ which bounds together the NSE distribution to the Integrity performance (Alarm limit) and to the COS performance (max probability of alarm allowed).

3. WADGPS AND LADGPS ARCHITECTURES FOR CAT1 PRECISION APPROACH

3.1 WADGPS components description:

The space segment includes the 24 GPS constellation plus 1 to 3 INMARSAT3 geostationary satellites (AORE; AORW; IOR).

The ground segment is composed by 7 tracking and monitoring stations MS located around the world:

Toulouse (south of France) where is also located the control station CS and six low latitudes stations (Ascension, Nairobi, Guam, Kourou, Papeete and Singapour). The level of relative synchronization of each MS / CS is 15 ns (1 sigma).

The CS performs the satellite orbit determination with a Kalman filter processing of MS smoothed pseudoranges and distributes to the MS the predicted ephemeris for the monitoring function. The instantaneous monitoring measurement of each MS is affected by noise and multipath (1.8m, 1 sigma). The CS computes then the final message from the different corrections sent by each MS at each instant for each satellite in view. The WADGPS final message is composed mainly by fast and slow corrections and by the UDRE (defining the global correction accuracy). This message format has been proposed at RTCA (ref.6).

As the service is not perfectly real time, there is a latency delay which represents the 'age' of the corrections. This delay is here supposed to be bounded by 4 and 6 seconds.

The user grid covers Europe. The minimum elevation angle for using a satellite is 5°. The user receiver is able to track all the satellites in view (at least 13 channels). Finally, the user pseudorange is affected by noise and multipath (1.2m, 1 sigma).

3.2 LADGPS architecture description

The ground segment is mainly composed by the reference station located at Toulouse tracking all the satellites in view above 5 degrees of elevation angle. The instantaneous pseudorange correction of the reference station is affected by noise and multipath (1.2m, 1 sigma) and by the effects of latency delays (less than two seconds).

The use of additional pseudolites (up to two) can be considered also. Their signal is supposed to be affected by noise whose level remains very low near the pseudolite and increases linearly with the distance to the pseudolite as it is proposed in the literature.

3.3 WADGPS and LADGPS Integrity Monitoring System

The WADGPS Integrity Monitoring System proposed by Thomson-CSF is based on three successive monitoring levels :

- a consistency check of the whole ground segment monitoring output data (fast, slow corrections and UDRE) in order to detect a possible unplanned failure in one ground component; this first level can already be efficient as soon as there is enough redundancy in the ground segment (enough monitoring stations, cf FAA system 'WAAS' architecture) ;

- a user on board real time Integrity Monitoring level relying whether on a sophisticated Differential RAIM algorithm or on the use of the UDRE broadcast in the WADGPS message ;

- an additional near real time end to end Integrity Monitoring level relying on the instantaneous positioning error monitored in a nearby station (named IMSt: Integrity Monitoring Station).

The user is of course supposed to get these two last different levels information. A priority order will have to be defined previously.

The LADGPS Integrity Monitoring System proposed by Thomson-CSF is limited to the two last previous monitoring levels.

3.3.1 User on board integrity monitoring methods

The last RAIM algorithm implemented in SNAPSIS and that has been extensively analysed is the sophisticated algorithm proposed by F. Van Graas at the RTCA (ref.7). In fact this algorithm is used in a differential mode (DRAIM).

This last method is based on a FDE (Fault Detection and Exclusion) algorithm working in the parity space. This algorithm determines automatically the threshold from the inputs (expected PA, Pmd and pseudorange accuracy (σ_{URE})).

The Van Graas RAIM algorithm includes an availability test comparing a function of the pseudorange residuals to the alarm limits (horizontal and vertical). When one of the two alarm limits is exceeded, the algorithm can not conclude and the integrity monitoring is declared unavailable. Then there are the detection process followed by the exclusion process in case of failure detection. Then an alarm can be transient, i.e. can occur at the detection level and disappear after the exclusion process. There are finally three possible status concluded by this FDE algorithm:

- service is safe (green status: G)
- service is not safe (red status or alarm : R)
- no conclusion (orange status : O), the integrity monitoring is declared unavailable.

The second on board integrity monitoring method is based on the use of the UDRE message component. The principle is to project the UDRE vector supposed to give the pseudorange accuracy achieved instantaneously with each satellite in the user time-position space. The user could then be able to estimate his NSE (horizontal and vertical) and to compare them directly to the alarm limits. As the UDRE definition has not been precisely specified until now, it is difficult and not really useful to perform fine analyses of this integrity monitoring method.

3.3.2 End to end integrity monitoring in the IMSt (for both WADGPS and LADGPS)

The last level proposed by Thomson-CSF is an end to end monitoring realized in a station IMSt which is precisely located and which processes the satellite signals exactly as a user. This station is then able to estimate directly its positioning error whose main part is due to the Navigation System: NSE(IMSt)

(horizontal and vertical) and to trigger an alarm when the alarm limit (horizontal or vertical) is exceeded. The efficiency of this method mainly to reduce the user missed detection and false alarm rates depends only on the correlation of the NSE estimated by the IMSt with the true NSE of the user.

We have analysed the correlation between NSE(IMSt) and NSE(user) achieved with our WADGPS for different local sets of IMSt covering Europe and for a user grid covering a region of 2200 km around Strasbourg (France). The results showed that even with only 7 IMSt, a good correlation was achieved, degraded only by the short term errors (noise+multipaths) of the user and IMSt receivers.

This detection level can be completed. In fact, the integrity monitoring function performed by this station can be developed to exclude or isolate the wrong pseudorange(s) among the instantaneous navigation solution. This second level information would be sent to the ground segment control center for its general system integrity monitoring.

4. SNAPSIS PRESENTATION

The current version of SNAPSIS stems from different studies for CNES then DGAC (ref 9). Its main purpose is to allow complex Satellite Navigation System studies. It complements another tool developed at ONERA, ANACON (ref 10), which is limited to availability studies. The SNAPSIS software can simulate systems with architecture based on GPS or DGPS (LADGPS and WADGPS) principles. The simulation is the most precise to allow fine analysis of the performance (integrity, continuity of service, accuracy, ...). The architecture modelisation is defined by different parameters the user can easily modify.

4.1 Overall design

There are mainly five successive steps (or segments) in the simulation process. Each one is realized by a specific module (see figure 1). These five main tasks are:

- Orbit generation and determination module (for GPS and geostationary satellites);
- Broadcast ephemeris module;
- WADGPS correction message determination;
- WADGPS message selection and communication module;
- LADGPS correction generation and User processings module.

Each module uses data input files (typically one only or one per satellite) resulting from the execution of the prior modules and generate data output files (typically one only or one per satellite) which will be read by the next modules.

4.2 Orbit generation and determination module

This is the first and very important simulation segment of the process. It consists in two successive

tasks, each one is realized by one submodule.

The first submodule performs a realistic simulation of the whole constellation satellite orbit and clock offset. Prior studies on the problems of, first the CE-GPS and then the GPS satellite orbit determination have led us to establish sophisticated models of:

- geostationary (GS) complement as the CE-GPS and GPS satellite dynamics;
- GPS satellite natural clock offset;
- Satellite clock offset high frequency alteration due to SA (SA dither);
- GS (geostationary) and GPS satellite observations (pseudorange, simple or double difference) and observation errors (atmospheric effects, synchronisation errors between tracking stations, etc.).

These models are used to produce the true satellite (geostationary and GPS) orbit and clock offset files and also the true observations files that a tracking ground stations network realizes for every satellite.

The second submodule performs the orbit determination computed at the master control center from the observations done by the tracking network with an Extended Kalman Filtering method. We have shown in past studies that even in case of SA, a quite good GPS orbit accuracy can be achieved. The possibility to track several satellites simultaneously in order to improve the observability of some ground station errors (synchronisation bias) and consequently the orbit determination accuracy has also been recently tested.

So this second processing will provide the Monitoring Stations with accurate orbit prediction with the associated covariance matrix for typically the next 12 hours. The data resulting from this second calculus are concatenated to the true orbit and clock offset data. The output files of this first module (one file per satellite) contain then:

- satellite true orbit, clock offset and SA dither;
- satellite predicted orbit and predicted covariance matrix.

4.3 Broadcast Ephemeris module

The second simulation step consists in creating an ephemeris degradation in order to take into account the effect of possible Selective Availability on the GPS satellite navigation data. The modelling of this degradation has been exposed in the previous communication and has not changed. It will then not be reproduced here (ref. 3).

4.4 WADGPS message determination

The third simulation step is the cornerstone of a WADGPS system. It must produce eventually the extended differential correction data about every satellite. These data are computed by each station of the ground network and will be then sent to the master control station. As in the CE-GPS context, this

differential data determination function is ensured simultaneously with the tracking function by the same stations.

To compute these messages, the station is provided with the following data :

- broadcast satellite position (degraded by SA);
- raw pseudorange (between satellite and station true positions and mainly degraded by SA satellite clock dither);
- predicted satellite position with its covariance matrix (outcome of orbit determination processing);
- predicted pseudorange between predicted satellite and estimated station positions corrected with estimated pseudorange errors (atmospheric effects, synchronisation offsets, etc.).

The RTCA WADGNSS message format (ref 6) has been used as reference. Among the different data included in this format, only the major components which have a direct effect on the performances have been computed in the software. They are:

- the fast correction;
- the long term satellite error corrections;
- the User Differential Range Error (UDRE) which must qualify the global correction accuracy;
- the "Use" / "Don't Use" flag.

Until now, neither ionospheric correction data nor range rate correction data are present in the message. The UDRE proposed here is computed by the ground segment and is representative of the uncertainty (1 sigma) on the global (fast+slow) correction before coding and transmission.

The transmissions involved (between the monitor station and the user) introduce delays. This delay is a function of the transmission conditions and can then be represented by a variable drawn at random at each instant in each station for each satellite. Then the differential corrections calculus is delayed of this value.

A linear regression algorithm has been implemented to estimate the instantaneous satellite clock error rate and to predict the value of the fast correction a few seconds later (the mean expected value of the transmission delays).

It is also possible at this level to trigger a typical clock failure on a satellite or on a monitoring station in order to be able to analyse its effect on the final performances.

4.5 WADGPS message selection and coding module

The control station has to elaborate for each satellite only one set of corrections smoothed over the different simultaneous sets transmitted by the network of monitoring stations. Some additional processings to increase the integrity of the whole process are possible at this level (to detect a station or satellite sudden clock failure as important ramp or bias for instance).

4.6 LADGPS message generation and User processings module

This is the last simulation segment of the process. It gathers the local differential corrections generation modelling (ground segment composed by a reference station and some secondary stations) the various user processings (positioning, non integrity detection), and an another process of non integrity detection, independant of users, with some station named IMSt (Integrity Monitoring Station).

4.6.1 LADGPS message generation and diffusion

Stations modelisation :

Each station is considered as a specific user with an error budget :

- exact knowledge of its position;
- exact synchronisation with the GPS time;
- tropospheric and ionospheric delay model (mono- or bi-frequency receiver).

Pseudo range correction (PRC):

The correction is the difference, at the reference station level, of the predicted pseudorange (with its position knowledge) and the measured pseudorange. This correction is code as specified in the RTCA SCAT I DGPS message format (ref.11).

Transmission delay :

The transmission delays between the reference station and the users have been taken into account like in WADGPS (see paragraph IV.4). The coding respects the RTCA SCAT I DGPS format (ref.11).

At this level, like in WADGPS context, it is possible to trigger typical clock failures in the reference station to study their effect at the final level (user).

4.6.2 Pseudolites signals

A pseudolite can be compared to a ground GPS satellite with no-degraded messages, as described in paragraph 3.2.

4.6.3 User processings

Until now, the users are considered to be static and composed a user network. This user set is easily selected in the control file, it can be a grid covering the INMARSAT satellite visibility area (typical WADGPS performance analysis) or a local area surrounding an airport location (typical LADGPS performance analysis).

A lot of control parameters must be defined in the global data input file to characterize the constellation declared available (with/without geostationary or pseudolite ranging), the user equipment and its basic satellite selection mode (all in view, best PDOP, etc..). The user can select either the use of the UDRE based technic or the DRAIM to perform his own integrity monitoring. The DRAIM technic used in SNAPSYS is the FDE (ref.7).

4.6.4 End to end integrity monitoring by

additional Stations IMSt

End to end integrity monitoring has been proposed by THOMSON and described in paragraph 3.3.2. This additional integrity monitoring is simulated.

4.7 Performances analysed

The new developments of this last module of SNAPSYS are rather numerous and important and allow to take into account in a faithful manner a lot of different elements of a WADGPS or LADGPS system (constellation, monitoring station, reference station, secondary station, pseudolite, receiver algorithm, etc..). Every one of these system components is mainly defined and characterized in a specific file (ex: pseudosat.d is the pseudolite catalogue file containing an exhaustive parameter list for each pseudolite).

The performances analyzed are mainly:

- DOP statistics;
- the URE achieved (1 sigma);
- the raw positioning error between the true position and the GPS fix (raw GPS data);
- the corrected positioning error between the true position and the GPS corrected fix (GPS pseudoranges corrected with differential data);
- user's on board alarm counting and length;
- service outage, false alarm and missed detection counting.
- IMSt own alarm and missed detection counting;
- IMSt confirmation of user integrity diagnostics.

4.7.1 SA model influence for WADGPS architecture

The WADGPS architecture is described in paragraph 3.1 (+ 2 Geostationary satellites) with users in Europe (error budget of 4ns). We simulate the system during one day, with a positioning every 300 seconds.

The following table presents the results with a first order markov process SA model ($\sigma_{SA}=21m$, $\tau=180s$) and a second order markov process SA model ($\sigma_{SA}=23m$, $\sigma_{dSA/dT}=0.28m/s$, $\tau=118s$).

| | SA model | |
|-----------------------|-----------|-----------|
| | 1st order | 2nd order |
| $\sigma(URE)$ (m) | 7.1 | 5.1 |
| NSE(95%) Vertical (m) | 21.0 | 14.8 |
| NSE(95%) Hor. (m) | 10.6 | 6.9 |

The performances are ameliorated of 25 to 30% with a second order SA model.

4.7.2 Transmission delay influence for LADGPS architecture

The LADGPS architecture is described in paragraph 3.2 (with 2nd order model SA). We simulate the system during one day, with a positioning every second.

The following table presents the results with a transmission delay of 0 to 2s and of 2 to 4s.

| | Transmission delay | |
|--------------------------|--------------------|----------|
| | 0 to 2 s | 2 to 4 s |
| $\sigma(\text{URE})$ (m) | 1.56 | 2.11 |
| NSE(95%) Vertical (m) | 4.43 | 5.09 |
| NSE(95%) Hor. (m) | 2.68 | 3.06 |

The degradation appears directly on the measure quality. We can note this effect is dependent of SA model.

5. INTEGRITY AND COS PERFORMANCE ANALYSES

Basically, the performance analysis that can be made by simulation is based on the following principle, for each instantaneous user position fix:

1. the on board user integrity monitoring can produce 2 main conclusions:
 - the service is declared safe;
 - the service is declared unsafe (alarm);
2. at the same time the end to end IMSt can produce 2 main conclusions:
 - the NSE estimated at the IMSt does't exceed the alarm limit ;
 - the NSE estimated at the IMSt exceeds the alarm limit ==> IMSt alarm ;
3. while the true position error is:
 - smaller than the alarm limit;
 - larger than the alarm limit.

When a complementary IMSt information is available to the user, there are then 8 possible events to count. At the end of the simulation run, the eight counters give the false/true alarm rates and the missed detection rate allowing to compute the COS losses and the Non Integrity cases.

5.1 WADGPS Continuity of Service performance analysis

As presented before (§ 2), the Continuity losses are determined by the unplanned user integrity monitoring alarms and outages. More precisely, we have the following formula:

$$1-\text{COS} = \text{Ds} \cdot \text{Pf} \cdot \text{Pdet} + \text{Ds} \cdot (1-\text{Pf}) \cdot \text{PA} + (1-\text{Ds}) \quad (1)$$

where we have:

Ds: availability of the integrity monitoring

Pf: probability of failure (probability of having NSE > alarm limit)

Pdet: probability of detection of the failure by the integrity monitoring

PA: probability of alarm

In the previous development Pf must be considered as the sum of:

Pf/current system = probability of having NSE > alarm limit with the current system (no failing component); previous analyses done by Thomson-CSF with ONERA SNAPSIS tool for the French Civil Aviation Authority (ref.1) have shown that for our current WADGPS architecture (involving a $\sigma(\text{URE})$ of 5m), this figure was close to 10^{-4} for Horizontal positioning;

and

Pf/failing system = probability of having NSE > alarm limit with a failing component in the system;

So the previous formula (1) can be computed twice with each one of the two Pf presented before.

The simulation runs involved here allow to estimate the most important and difficult part of these two components of the COS performance involving the current system. The second component could be assessed in a similar way from the precise definitions of system component failure modes with their associated conditional probabilities.

As the COS requirement is a very low probability figure (10^{-5} per 15s), the amount of test runs necessary to enable realization of high confidence (> 50%) can be very large (involving 10^{+7} to 10^{+8} snapshots) for a system designed to meet the requirement. This kind of analysis could then be very time consuming.

The feature adopted here to circumvent this difficulty is probability scaling. We adapted the method proposed within RTCA by J.L.Farrell and F.V.Graas (ref 8) for GNSS sole means integrity testing to our Differential GNSS architecture.

The method consists in amplifying input noise level to increase the expected number of events (alarms for COS analysis, missed detections for Integrity analysis).

The statistical hypothesis is that the combined effect of error sources affecting the user corrected pseudorange is normally distributed with zero mean. On this basis, the amount of noise amplification is calculated to produce an average rate of alarm of around 0.01 (generating 100 alarms for 10000 alarm snapshots). The complete procedure will not be presented here. It is very close to what J.L.Farrell proposed for its 'NPA simulations with no SV failure' (ref.9). The tests have been performed in a similar manner in order to produce high confidence (99%) conclusions instead of the usual 50% confidence attached to the classical experimental average.

The main difference is that we are here testing the performances of a Differential system. So the noise amplification will not be applied on the satellite clock SA (as in ref.8), what would be useless because the system would correct it, but at the user receiver level. Moreover, among the total of alarms triggered at one user level during the complete set of simulations, the only alarms counted are those supposed to create a loss of COS and then are those following a state when service was declared available.

The results presented in the table 2 illustrate the performances achieved with DRAIM (Van Graas ref.7) as on board integrity monitoring in case of no forced system failure. The following table shows the relatively high number of orange cases.

| expec. PA $\sigma(\text{psd})$ | Direct unav. :O | trans. al R=>O | trans. al R=>G | def. al. R=>R |
|-----------------------------------|--------------------|-------------------|-------------------|------------------|
| 10^{-5} ; 4,9m | 47 | 0 | 0 | 0 |
| 0,01 ; 7,6m | 235 | 161 | 8 | 0 |

table 2: Unavailabilities of DRAIM induced by the internal test (total of 52000 snapshots)

The Van Graas DRAIM algorithm includes a preliminary availability test (see § 3.3.1). When one of the alarm limit is exceeded (the vertical alarm limit is low (9,8m) compared to the pseudorange accuracy (4,9m or 7,6m)), the algorithm can not conclude and the integrity monitoring is declared unavailable. We can see in the table 1 that these cases are quite numerous. These cases could reduce the COS performance to a large extent. The efficiency of this test for the Integrity performance will have to be proven by a detailed analysis in the future.

In order to decorellate the problems, in the following simulations we remove this internal test from the integrity monitoring algorithm.

| expected PA; $\sigma(\text{psd})$ | trans. al. R=>G | def. al. R=>R | exp. PA | unscaled PA (99%) |
|--------------------------------------|--------------------|------------------|---------|----------------------|
| 10^{-5} ; 4,9m | 0 | 0 | 0 | |
| 0,001 ; 6,3m | 8 | 0 | 0,00015 | $0,08 \cdot 10^{-6}$ |
| 0,005 ; 7,1m | 54 | 0 | 0,00103 | $0,1 \cdot 10^{-5}$ |
| 0,01 ; 7,62m | 362 | 0 | 0,0069 | $0,54 \cdot 10^{-5}$ |
| 0,1 ; 10,3m | 2621 | 107 | 0,052 | $0,5 \cdot 10^{-5}$ |

table 3: DRAIM Alarm Probability performances for WADGPS (around 52000 snapshots)

The final PA determination takes into account all the alarms (transients and definitives) what could be considered as a pessimistic attitude from an operational point of view. The reason is that probability scaling is associated to the first level of the FDE algorithm only and can not take into account any exclusion step.

If we stay at the DRAIM detection level, we can conclude that we achieve consistent results leading to an alarm probability figure (99%) of $0,5 \cdot 10^{-5}$ as soon as the event sample size is large enough (two last cases), what proves a rather good behaviour of the probability scaling process.

Another conclusion is that in this context (no system component failure), the DRAIM exclusion process is quite efficient to find a navigation solution which does not violate the algorithm internal threshold and then which will not create a loss of COS.

So, we can already conclude that in the routine case (with no system component failure), the contribution of the on board DRAIM integrity monitoring described before to the Continuity losses is very small in comparison with the CAT 1 requirement.

5.2 LADGPS Continuity of Service performance analysis

The same kind of analysis has been performed for our LADGPS system. The same procedure (ref.7) has been applied. The nominal pseudorange correction accuracy is around 1.6m . As for WADGPS analysis, the amount of noise amplification is calculated to produce an average rate of alarm of around 0.01 (what implies a global $\sigma(\text{psd})$ growing from 1.6m to around 2.5m).

The analysis is more difficult here because at this level of range accuracy, the Alarm rate PA is theoretically very sensitive to any slight increase of $\sigma(\text{psd})$.

The conclusions draught from the results obtained are similar to the previous one.

| expect. PA; $\sigma(\text{psd})$ | experim. PA | unscaled PA 99% |
|----------------------------------|-------------|----------------------|
| 0,001 ; 2,06m | 0,00032 | $0,27 \cdot 10^{-5}$ |
| 0,01 ; 2,5m | 0,00646 | $0,42 \cdot 10^{-5}$ |
| 0,04 ; 2,9m | 0,0274 | $0,44 \cdot 10^{-5}$ |

table 4: DRAIM Alarm Probability performances for LADGPS

5.3 WADGPS Integrity performance analysis

The Integrity performance is measured by the probability of non-integrity PNI which is expressed as follows:

$$\text{PNI} = D_s \cdot P_f \cdot P_{md} + D_s \cdot P_f \cdot (1 - P_{md}) \cdot P(\text{warning delay} > \text{time to alarm}) \quad (2)$$

with: P_{md} : probability of missed detection

$P(\text{warning delay} > \text{time to alarm})$ supposed to be = 0 (ensured by the system design)

The simulation runs involved here allow to estimate the P_{md} parameter in case of a WADGPS failure supposed to create an exit of the outer tunnel (NSE H > 33,5m or NSE V > 9,8m) in order to test the integrity monitoring. Two different levels of system failures have been simulated :

- a bias 'type 1' occurring at the user level on one user receiver channel which then doesn't affect the IMSt positioning ;

- a bias 'type 2' occurring at the ground segment Control Center level on one of the PRC broadcast to the users and of course also to the IMSt ;

The simulations operate around 10^{+6} user position fixes. The missed detection results are expressed at the algorithm level (the DRAIM missed the bias detection) and at the User NSE level (after having taking into account the algorithm conclusion, the NSE alarm limit is finally exceeded).

First of all, the table 5 shows clearly the detection and exclusion performances of the DRAIM algorithm. They become obvious from a certain bias level (around 50m). This experimental result is in good

accordance with the theoretical value of the minimum detectable bias predicted by the algorithm itself.

We can also verify that the system is basically not accurate enough for vertical positioning. There is a big amount ($> 27\%$) of missed detection proving it and that can not be reduced by the FDE method alone. The efficiency of the IMSt additional monitoring to reduce this md rate is particularly noticeable ($> 50\%$).

For the horizontal positioning service, we can resume our integrity analysis by the table 6.

5.4 LADGPS Integrity performance analysis

The simulation runs involved here allow to estimate the Pmd parameter in case of a LADGPS failure supposed to produce a systematic error (50m bias) on one satellite pseudorange correction (the satellite tracked by the first channel of the receiver for instance, supposed to be failing). According to the previous definitions this is a bias 'type 2' occurring at the ground segment level on one of the PRC broadcast to the users and of course also to the IMSt. The IMSt is supposed to be located near the reference station.

The simulations operate around 10^{+5} user position fixes. The missed detection results are expressed at the algorithm level (the DRAIM missed the bias detection) and at the User NSE level (after having taking into account the algorithm conclusion, the NSE alarm limit is finally exceeded).

The results appear in the table 7. It shows clearly the detection and exclusion performances of the DRAIM algorithm. This excellent results are mainly due to the fact that the bias level is greatly higher than the pseudorange accuracy ($\sigma(\text{psd}) = 1.6\text{m}$).

We can also verify the efficiency of the IMSt monitoring to reduce the md rate for vertical positioning.

6. CONCLUSION

The general concern of this communication was to present the last important results on the local and wide area solutions to provide the RNP for CAT 1 precision approach studied by THOMSON-CSF and ONERA with the support of the French Civil Aviation Authority (DGAC/STNA) and of the French Space Agency (CNES). The WADGPS and LADGPS preliminary architectures have already been presented in past papers (ref 2 and 1). The recent developments focused on the Integrity and COS issues that are surely very delicate to analyse and to solve. An efficient and robust integrity monitoring system acting at three successive levels in the system has been proposed by THOMSON-CSF which two main components are:

- an on board integrity monitoring based on either the performant DRAIM algorithm proposed by F.V. Graas at RTCA, or on the projection of the UDRES provided by the ground segment;

- and an interesting complementary monitoring means realized in a nearby station IMSt.

The overall design and the successive steps realized in each module have been briefly exposed. The software structure and its detailed possibilities allow to focus the analysis on a specific aspect (orbit determination accuracy, differential correction accuracy, transmissions delays influence, etc.). This quite exhaustive parametric approach should help to the system designer to tune the system specifications in order to satisfy operational requirements.

SNAPSIS can already been considered as a powerful simulation tool allowing exhaustive and reliable analysis of the different integrity monitoring concepts that have been appearing since several years.

An extensive and original approach has been adopted using the SNAPSIS simulator (ref.2 and 3) developed at ONERA to perform Integrity and COS performance analysis for WADGPS and LADGPS architectures. This approach is based firstly on a preliminary fine analysis of the different independant probability figures involved in the definition of the COS and PNI requirements, secondly on probability scaling allowing high 99% confidence.

The results show that CAT 1 H RNP requirements are already met with the proposed architecture in the context of the various scenarii tested and that CAT 1 V could interestingly be achieved locally through a combined improvement of the PRC accuracy and a complementary integrity monitoring performed by IMSt in the service area.

The authors wish to thank the CNES navigation team, and S. LODDO (Thomson-CSF) for their constructive participation.

REFERENCES

1. Gouni P.; Marchal N.(THOMSON); Jonquière J.L.(STNA); Carlier T.(CNES)
Description and Assessment of Integrity Performances for LADGPS and WADGPS architectures
DSNS, April 94, London (UK)
2. Flament D.(ONERA); Jonquière J.L.(STNA) ; Carlier.T.(CNES)
SNAPSIS: Software for GNSS and DGNSS performance analysis - Application to Civil Aviation for Precision Approach - DSNS 94, London (UK)
- 3.Flament D.(ONERA); Durand J.M.(CNES)
European Complement to GPS - RGIC systems simulation software - ION-GPS 92, Alb. NM (USA)
4. Davis J.; Kelly B.
RNP tunnel Concept for Precision Approach and Landing, - Satellite Operational Implementation Team Meeting, January 1993

5. Standardization Agreement 4294 Draft issue L. 1
August 1990 - Navstar GPS System characteristics

6. Wide Area Augmentation System Signal
Specification - RTCA paper n° 114-94/SC159-508
prepared by SC-159 WG2, April 1994

7. Van Graas F. (Ohio Univ. - USA)
Baseline Fault Detection and Exclusion Algorithm -
4th draft - RTCA paper n° 474-93/SC159-482

8 Farrell J.L. (NaVIGIL); Van Graas F. (Ohio Univ.)
Integrity testing for GNSS sole means
ION Nat. meeting - San Diego Ca USA - Jan. 94

9. Flament D., Christophe B.
Architecture GPS Différentiels pour l'approche de
précision (compléments)
ONERA Report - Jan. 1995 - DGAC Contract

10. Michal T., Christophe B.
Etude de la disponibilité du système GPS
ONERA - May 1990 - CNES Contract

11. Minimum Aviation System Performance
Standards DGNSS Instrument Approach System
Special Category I - Proposed Final Draft - Document
RTCA No 272-93/SC159-443 June 25 1993

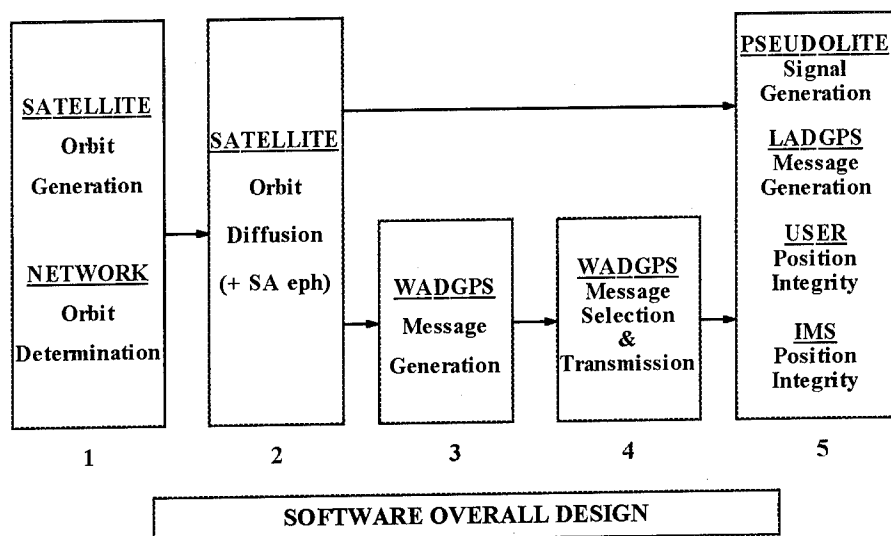


Figure 1

| | DRAIM level | | | User NSE level | | | |
|---------------|---------------------|-----------------------|----------------------|--------------------------------|-------------------|---------------------------------|------|
| System bias | def. al R=>R | trans. al R=>G | DRAIM md | User md -HOR alone ; + IMSt | | User md - VER alone ; + IMSt | |
| no | 0 | 0 | - | 0 | | 0,27 | |
| type 1 - 50m | $3,3 \cdot 10^{-2}$ | $93,8 \cdot 10^{-2}$ | $2,9 \cdot 10^{-2}$ | $3 \cdot 10^{-4}$ | $3 \cdot 10^{-4}$ | 0,41 | 0,24 |
| type 2 - 50m | $3,8 \cdot 10^{-2}$ | $93,7 \cdot 10^{-2}$ | $2,5 \cdot 10^{-2}$ | $4 \cdot 10^{-4}$ | $3 \cdot 10^{-4}$ | 0,44 | 0,11 |
| type 1 - 100m | 0 | $99,99 \cdot 10^{-2}$ | $0,01 \cdot 10^{-2}$ | $7,5 \cdot 10^{-5}$ | 0 | 0,31 | 0,03 |

table 5: Prob. results at DRAIM and User levels (with/without IMSt) in case of WADGPS system failures

| failure | effect | prob. Pf | User int. monit. | User Pmd | PNI |
|--------------------------|---------------|----------------|------------------|---------------------|--|
| bias > 50m on one PRC | NSE H > 33,5m | $Pf < 10^{-4}$ | DRAIM (V.Graas) | $< 4 \cdot 10^{-4}$ | $< 4 \cdot 10^{-8}$ (req. $< 1,3 \cdot 10^{-7}$) |

table 6: PNI analysis for horizontal CAT 1 with WADGPS

| Failure : 50 m bias on one PRC | DRAIM level | | | User NSE level | | | |
|-----------------------------------|-----------------------|------------------------|-------------|--------------------------------|---------------------|---------------------------------|---------------------|
| Space seg. | def. al R=R | trans. al R=>G | DRAIM md | User md -HOR alone ; + IMSt | | User md - VER alone ; + IMSt | |
| 24 GPS | $0,37 \cdot 10^{-2}$ | $99,63 \cdot 10^{-2}$ | 0 | $13 \cdot 10^{-4}$ | $< 1 \cdot 10^{-5}$ | $33 \cdot 10^{-4}$ | $5 \cdot 10^{-5}$ |
| 24 GPS + AORE | $0,042 \cdot 10^{-2}$ | $99,958 \cdot 10^{-2}$ | 0 | $< 1 \cdot 10^{-5}$ | $< 1 \cdot 10^{-5}$ | $15 \cdot 10^{-4}$ | $< 1 \cdot 10^{-5}$ |

table 7: Prob. results at DRAIM and User levels (with/without IMSt) in case of LADGPS system failure

Interoperability and Traditional Nav-aid Considerations for DGPS Standards

Lori Hill and Ken Ganther
Wilcox Electric

BIOGRAPHY

Lori M. Hill is the software lead for conventional navigation aids and research and development projects at Wilcox Electric including local area GPS development. Ms. Hill holds a BSEE, MSEE, and MBA from the University of Missouri. Ken Ganther is the manager of electronic design engineering at Wilcox Electric and has more than 15 years experience with traditional navigation design. Mr. Ganther holds a BSEE from the University of Kansas.

ABSTRACT

In the coming year the subject of Category I/II/III Local Area Differential GPS (DGPS) requirements will be more closely examined for aircraft private and public use. This paper is the result of a study by Wilcox to evaluate Category I/II/III DGPS current standards with respect to possible interoperability between the ground station and airborne equipment, as well as conflicts with the traditional navigation standards and experiences. This paper presents possible resolutions and standards definitions to provide interoperability and to guarantee integrity and reliability that exist today in our traditional navigation devices.

Considered are the following interoperability issues: unusable satellite definition, Acceleration Error Bound (AEB) definition, normalized Pseudorange Corrections (PRCs), working ground station definition. These interoperability issues primarily have an effect on ground equipment availability but also address some possible accuracy issues.

Also considered in this paper is a study of traditional nav-aid principles that should be incorporated into DGPS standards. These principles have evolved over the long and successful history of traditional nav-aids in providing common everyday navigation around the world. These

principles include the integrity of the total navigation solution, system architecture, Signal in Space (SIS) shadowing, approach guidance path and identification, guidance signal response time, monitor architecture, SIS integrity and failure warning time, monitor failure (monitor fail-safe), general comments on redundancy, and resistance to interference.

INTEROPERABILITY

Standards are developed to prevent interoperability issues from arising. In the development stage of these standards, consideration is needed in establishing requirements that will clarify interfaces and requirements between sub-systems. In the case of DGPS, requirements and standards need to be established that allow all aircraft avionics and ground stations to work together. In initial implementation of the current Minimum Aviation System Performance Standards DGNSS Instrument Approach System: Special Category I (SCAT - I) RTCA/DO-217 (MASPS RTCA/DO-217)¹ several areas were discovered that may cause confusion or misinterpretation that would prevent the full capability intended by the SCAT - I specifications. These interoperability issues, described in the following paragraphs, are: antenna siting, unusable satellite definition, AEB definition, normalized PRCs, and working ground station definition.

Unusable Satellite Definition

The ground station definition of a bad satellite must first consider that the reference and integrity monitor(s) must both have a satellite visible before declaring the satellite unusable by the aircraft. Differing antenna sitings of the reference and integrity antennas could cause a reduction of satellite availability. Once the reference and the integrity monitor have established a subset of available satellites, the ground subsystem then must compute

similar PRCs and Range Rate Corrections (RRCs) for the individual satellite.

When comparing the reference and the integrity PRCs and RRCs, a limit must be established on the allowable deviation. This deviation must take into consideration differences in clock offsets and clock drifts between the reference and integrity monitor GPS receivers. The precision of the clocks in each of the reference and integrity monitor GPS receivers will determine the allowable limits on the PRCs and RRCs deltas. This limit must also consider satellite availability. Restrictive limits will reduce the set of satellites available and possibly affect the continuity of service for the ground station.

One way to accommodate the lack of a precise clock is to remove the clock bias before making a comparison. Otherwise, the difference limits would have to include the largest clock difference into the allowable limit difference. The clock bias can be computed by averaging PRC differences over all satellites tracked by both receivers, with compensation for elevation angle affects. Satellites with the highest elevation should have more weight since these satellites are less affected by noise and multipath.

If a satellite is not available to both reference and integrity monitor or does not pass the difference limits on PRCs or RRCs, the satellite should be marked as unusable or removed from the transmitted message by the ground station. This is unclear in the MASPS RTCA/DO-217 when pertaining to the coast mode. In section 2.2.3.1.3 it is stated "For Class B, C, or D2 equipment the navigation solution may "coast" with three or fewer satellites for a period of time and still maintain required system accuracy." To be properly implemented an unusable satellite should be marked 'don't use' if integrity was not met, and not simply removed from the type 1 message. This prevents the airborne subsystem from utilizing a known 'bad' satellite during a coast mode.

Lowest elevation satellites have the greatest multipath errors, yet give position calculations the best geometrical solutions. Our experimentation shows that 5-7 degrees was determined to be the best mask angle for the ground station to provide satellite corrections that had the cleanest signals without ground interference. An aircraft in flight will typically have more satellites in view than the ground station due to increased viewable range, although the ground station may well represent the satellites viewable at decision height or runway threshold.

In establishing the ground stations observable satellites, either a standard mask angle needs to be determined or a minimum signal strength needs to be defined before the ground station is permitted to report a satellite as available.

AEB Definition

The MASPS RTCA/DO-217 states for AEB definition "The estimate should be the maximum acceleration measured on any visible and operating satellite, determined to be valid by the ground subsystem, during any 15 second observation for at least the previous 30 minutes, or the period of visibility whichever is less". First, it is unclear if "acceleration" is average acceleration or instantaneous acceleration. If averaged, it is unclear if a satellite should be considered usable during the first 15 seconds of visibility. A satellite should not be reported as usable for the first 15 seconds of visibility without being reported in the AEB calculation.

Since some airborne subsystems use AEB as a predictive measure, the AEB definition should be exact so implementation for all ground station and avionics manufacturers are the same. If the airborne subsystems use AEB as a predictive measure, AEB should not have rapid shifts. It is suggested that AEB be averaged over 15 seconds. The accuracy of the ground station clock will determine the smoothness of the AEB calculations. Therefore, the ground station clock should be of equal or greater accuracy than the avionics clock. Anytime a parameter affects the overall performance of the system, like the possible AEB shifts, these parameters need to have limits determined and specified to avoid subsystem conflicts.

Normalized PRCs

The ground station clock precision is again an issue in PRC and RRC calculations. Without a very precise ground station clock, the clock will drift. It is possible for the clock to drift so far as to put the PRC and RRC values outside of the transmittable ranges (respectively +/- 655.34 m, +/-4.094 m/s). Therefore, to keep the PRC and RRC values in range, the clock must be adjusted periodically. During the clock adjust, PRC and RRC, and the resultant AEB values will jump. The MASPS RTCA/DO-217 does not specify if clock adjustments are allowed, and if so, to what extent are the PRCs and RRCs allowed to spike during adjustment. The MASPS RTCA/DO-217 does state under section 2.2.3.2.2 "If the receiver filters code or Doppler measurements in developing a pseudorange estimate, the differential

corrections shall be applied immediately before computing a position. (This ensures that ground station clock drift does not affect position measurement accuracy)." This implies that clock drift is expected at the ground subsystem. But, without proper definition, the airborne subsystems and ground subsystems suppliers can implement different solutions that would be compatible.

Working Ground Station Definition

The MASPS RTCA/DO-217 does not make it clear if the ground station should consider sending differential corrections if less than four GPS satellites are usable or should the type 1 message be marked with "Station not working". With less than four GPS satellites in view, differential corrections are invalid because clock drift cannot be calculated. It is stated, though, in section 2.3.3.1.1 that "Use of any other Global Navigational Satellite System (GNSS) constellation is permissible but not required". The ground station should alert that the GPS constellation is not available, if GNSS satellites are not a consideration. The area of cross utilization of GPS and GNSS needs further consideration in establishing requirements, particularly with respect to monitoring. This would allow the avionics to apply both GPS and GNSS satellites to maintain differential mode even without the required number of GPS satellites available. For instance, under sections 2.2.3.1.5 it is stated "For Class A or D1 equipment, navigation for final approach requires a minimum of 4 satellites to be tracked for which differential corrections are being received." It is unclear if GNSS satellites are permissible in this definition.

TRADITIONAL NAV-AID CONSIDERATIONS

As discussed in the article "Terrestrial Radionavigation Technologies"² in the 50th anniversary issue of the ION Journal, what are now called "traditional nav-aids" have established a benchmark of excellent performance against which GPS based precision landing aids can be compared. The Instrument Landing System (ILS), which is in widespread use worldwide, is the default reference standard for new precision landing systems. The Microwave Landing System (MLS) has added the important new concepts of Path Following Error (PFE) and Control Motion Noise (CMN) that are not included in MASPS RTCA/DO-217.

This section discusses significant differences between Category I ILS performance, as specified in ICAO Annex 10³, and Special Category I DGNSS (SCAT-I) performance, as specified in MASPS RTCA/DO-217¹. Accuracy and coverage issues are not discussed in this

section. The focus is on a comparison of signal-in-space and monitoring characteristics which mainly affect system integrity.

ILS Block Diagram

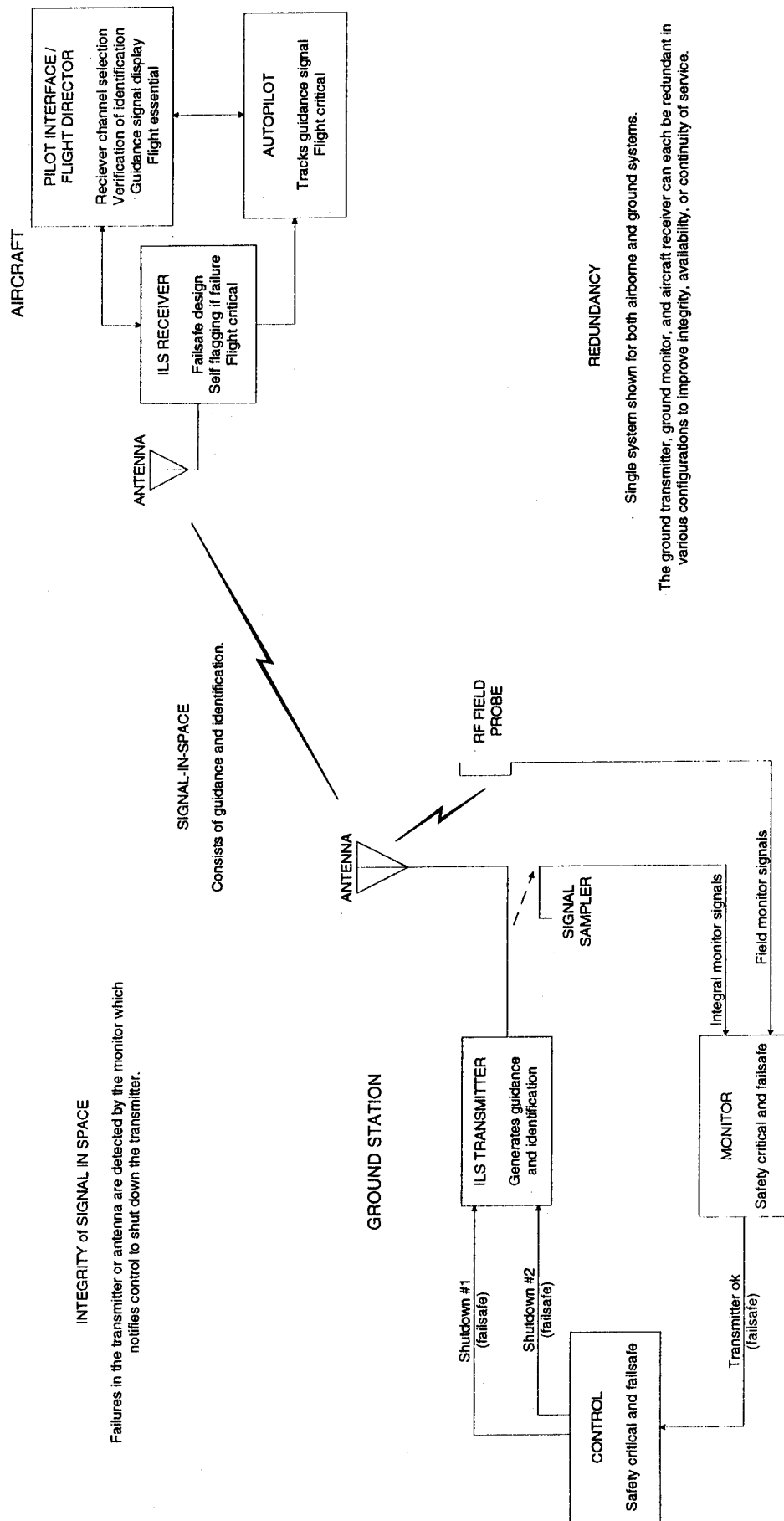
ICAO Annex 10 Standards and Recommended Practices for ILS describes the system block diagram shown in Figure 1. The ground system is responsible for all characteristics of the signal in space (SIS). The airborne system is reduced in concept to the simplest possible form to minimize the cost to aircraft owners and minimize the pilot/autopilot workload without compromising integrity. Cost and workload burdens are shifted to the ground system to the fullest practical extent, where regulatory agencies that are charged with maintaining flight safety can exercise direct control over the integrity of the guidance signal.

The airborne ILS receiver and autopilot are flight critical, which places on them the highest airborne standards of reliability and failsafe operation. This presumes, however, that a SIS is present with a correct guidance signal and correct runway identification code. Minimizing the amount of functionality within the flight critical category provides the lowest failure rate and cost. In operation the pilot simply selects the channel for the desired runway end, and listens for the correct Morse code identification embedded in the SIS. If no ILS signal is received, or if the Morse code is incorrect or missing, then the pilot knows that the ILS for the selected runway end is not usable. The redundancy consisting of selection followed by verification is simple, low cost, reliable, and failsafe provided that the ground system does not radiate an out-of-tolerance guidance signal with a proper Morse code identification, and provided that the airborne equipment is of a failsafe design.

The SIS, consisting of guidance and identification, is created by the ground transmitter and antenna, which provide most of the SIS accuracy. The rest of the SIS accuracy is determined by signal propagation errors, such as multipath, which are characterized by a commissioning flight test, and verified through periodic flight inspections. Undetected propagation errors are the weak link in ILS integrity. The main characteristic of the transmitter that affects the integrity of the SIS is that it contains two shutdown control inputs such that either control input can remove the entire SIS. Therefore, except for the redundant shutdowns, it is not necessary for the transmitter to be of failsafe design.

SIS integrity is provided mainly by the Monitor and Control functions. These functions are safety critical and failsafe. In effect, a failure anywhere within these

ICAO ILS ARCHITECTURE



functions will either have no effect on their ability to shutdown a defective transmitter, or will shutdown the transmitter regardless of whether it is defective or not. These false shutdowns result in a degradation in availability and continuity of function, but do not compromise integrity. Certification of the ground station then mainly consists of the commissioning flight check and verification that the monitor and control functions work properly.

The ILS SIS is usable to full performance specifications for Category I, II, and III by any aircraft type with a minimum investment in airborne equipment. Airborne technology consists of simple VHF/UHF receivers and audio frequency processing circuits.

The following is a more detailed comparison of ICAO Annex 10 with MASPS RTCA/DO-217. The format for each topic is to describe the ILS first, describe SCAT-I second, and add a general comment.

SIS Shadowing

ILS - Full continuity of function is provided for aircraft attitudes of up to +/- 20 degrees bank, +/- 10 degrees yaw, and +/- 10 degrees pitch, in any combination.

SCAT-I - Paragraph 2.2.3.1.3 recognizes that SIS outages will occur with aircraft attitude changes, and allows for reacquisition times of 5, 10, or 30 seconds depending on the length of the outage. The airborne equipment is allowed to "coast" during the reacquisition time using three or fewer satellites and some means of prediction of the next true "fix". Inertial guidance during an outage is also possible, but it typically will be used only by aircraft that normally carry inertial platforms.

Comment - The best way to eliminate the need for coasting goes well beyond the scope of SCAT-I by adding more ranging sources, such as the launch of more GPS satellites, inclusion of GLONASS satellites, Wide Area Augmentation System (WAAS) GEO ranging sources, or local pseudolites. Any of these would help keep shadowing, due to aircraft maneuvers, from reducing the number of visible ranging sources below four. Any approach that requires expensive airborne equipment would preclude the use of the precision landing service by the operators of small aircraft. Alternatively, coasting during SIS outages may be acceptable for Category I operations since ICAO states that responsibility for meeting the global integrity risk factor "is vested more or less completely in the pilot".

Approach Guidance Path and Identification

ILS - The ILS transmits all guidance signals relative to the desired runway threshold. The approach path definition and runway identification are high integrity ground system functions that are verified by a commissioning flight check, and are subsequently controlled by the commissioning body. The localizer part of the ILS transmits unique Morse Code identification specific to each runway and approach direction on the same radio frequency carrier as the guidance signal without interfering with the guidance signal. The identification signal is transmitted at least six times per minute, and is suppressed whenever the guidance signals are not usable. The Morse code provides positive confirmation that the correct runway end is selected. The Morse code is the letter I followed by a unique combination of three letters and numerals.

SCAT-I - Runway threshold identification and approach path definition (waypoint data) are contained only in Message Type 4, which is optional. Moving these functions to the airborne receiver also moves the data integrity risk with them, which conflicts with the ICAO principle of simplifying the airborne equipment for low cost and complexity. Guidance information is created by the airborne receiver comparing GPS position updates (corrected by the broadcast differential corrections) with the approach path definition waypoints.

Comment - The ILS precedent suggests that the high integrity functions of approach path (waypoint) definition and runway identification be kept in the ground station. This can be done by making Message Type 4 mandatory, and remove the responsibility for correct waypoint definition from the airborne equipment. Reliable transmission of this data from the ground to the air is well covered in MASPS RTCA/DO-217. Tailoring of the approach path to fit specific aircraft types (if desired) could still be accomplished in the aircraft equipment by generating different paths that are referenced to the high integrity path contained in Message Type 4.

Guidance Signal Response Time

ILS - The SIS is a continuous amplitude modulated radio signal. The system response time is governed by the aircraft receiver operating in accordance with a particular airborne receiver specification, since ICAO Annex 10 does not specify a requirement. A typical specification is ARINC 710 which states that the Course Deviation Indicator (CDI) needle deflection must reach 63% of it's final position within 0.1 second of a half-scale step change in the signal-in-space. ARINC 429 and ARINC 710 also provide for ILS receiver deviation updates of at least 15 per second (20 preferred) on the ARINC-429 bus.

SCAT-I - GPS receiver updates occur at discrete times. Paragraph 2.2.1.9 of MASPS RTCA/DO-217 specifies a display update rate of 5 per second with no more than 0.2 seconds difference between the time tag of the position estimate and the time at which the guidance signal is presented to the display. Prediction of future (or intermediate) display indications based on Differential Global Satellite System (DGNSS) velocity (extrapolation or interpolation) is allowed provided that no instability occurs due to the presence of wind gusts or reasonable pilot control commands. More stringent requirements may be necessary when driving an autopilot.

Comment - Verification of the MASPS RTCA/DO-217 stability condition is yet to be determined.

Monitor Architecture

ILS - As seen in Figure 1 the ILS monitor primarily samples the output of the transmitter with special RF sampling devices, and secondarily, samples intermediate signals from the transmitter and the radio field. The designs of the monitor and control functions are fundamentally different from the transmitter thus minimizing possible common mode errors. The monitor views the transmitter signals as though it were a precision aircraft receiver at a fixed location. ILS monitored parameters are then defined in terms that correlate to position relative to the runway threshold. This type of "position monitoring" derives naturally and intuitively from the type of signals generated by the ILS ground transmitter. The system effect upon detection of failure is that the ILS must cease radiation of guidance signals.

SCAT-I - There are, by necessity, three different monitors in a DGNSS. By providing differential corrections, the basic function of the DGNSS is a GPS constellation integrity monitor. The constellation monitor and differential corrections must then be monitored for correctness. Lastly, the signals broadcast by the DGNSS ground station must be monitored. The SCAT-I ground station requirements do not clearly define the partitioning between the three monitor types. The specified integrity monitor monitors the DGNSS broadcast, and uses a voting scheme in which two very similar (or identical) constellation monitors are compared with each other such that, if they do not agree, a fault is declared. This type of monitoring may be susceptible to common mode errors, i.e., if both paths make a common mistake it may not be detected since they both agree.

Comment - MASPS RTCA/DO-217 should be revised to clearly differentiate between the three monitors and

adopt appropriate requirements for each. MASPS RTCA/DO-217 should also be revised to account for the possibility of common mode error contributions to loss of integrity. Note that common mode errors tend to be very difficult to predict.

SIS Integrity and Failure Warning Time

ILS - SIS integrity resides primarily in the monitor and control functions. This is a simple, conservative, and widely accepted philosophy. The ILS monitor and control functions have shutdown control over the ILS SIS. The transmitter may have single or multiple failures and, if an out-of-tolerance SIS is created, the monitor will detect the out-of-tolerance condition (to some level of integrity risk) and the control function will remove the SIS. The glideslope SIS is removed (or changed-over to the standby equipment for a dual transmitter station) within six seconds of the onset of an out-of-tolerance condition. Upon removal of the SIS the problem becomes one of missed approach procedures. If this happens too often then availability and continuity of function are degraded (but not integrity). The time duration of six seconds is reduced to one second for Category III stations.

SCAT-I - The GPS constellation radiates continuously and is not subject to control by the DGNSS. The GPS constellation itself does not provide timely warnings (less than six seconds) of satellite errors. The DGNSS provides indirect monitoring of individual GPS satellites by broadcasting pseudorange corrections.

Comment - In keeping with the conservative ICAO philosophy, the unaugmented GPS constellation should be considered to have an integrity value of zero within a six second window of failure warning. MASPS RTCA/DO-217 should be revised to provide individual satellite integrity warnings, and aircraft on precision approach should not be allowed to use the GPS signals unless the DGNSS provides a positive indication that each satellite in use for that approach is healthy.

Also, the conservative monitoring philosophy of ILS should be adopted. This philosophy is that guidance signal sources are not to be trusted. Integrity should be vested in the monitoring and control functions to the fullest practical extent. This philosophy applies equally to both GPS and other GNSS satellites that may be added to the total navigation solution.

Monitor Failure (Monitor Fail-Safe)

ILS - The essence of the text of ICAO Annex 10 is as follows: "Design and operation of the monitor system

shall be consistent with the requirement that ... radiation shall cease ... in the event of failure of the monitor system itself”.

SCAT-I - No requirement.

Comment - Wording similar to the ILS requirement should be adopted for each monitor type.

General Comments on Redundancy

Dual ground transmitters improve availability and continuity of service of the SIS by quickly providing (less than 6 seconds) replacement equipment to continue transmitting a within-tolerance SIS.

Dual ground station monitoring, such that either monitor can keep the transmitter on the air, improves continuity of service and availability by preventing a failure in one monitor from removing an in-tolerance SIS.

Multiple aircraft receivers improve the probability of mission success. Airborne equipment is of a failsafe design such that a component failure in the equipment causes either no effect on the guidance display or a complete loss of the guidance display (flag in view). The pilot, or autopilot, then has the option of immediately switching to the standby equipment for guidance.

Interference Resistance

ILS - ILS operates completely within bands that are protected by international treaty for ILS and VOR use only. Resistance to in-band adjacent channel interference and out-of-band spurious signals is normally specified in documents such as ARINC 710, RTCA/DO-195, and RTCA/DO-192. ICAO, however, has recently added a requirement that new localizer airborne receivers be resistant to FM broadcast interference, which is the most troublesome out-of-band unintentional interference source. ICAO now requires that a localizer receiver operating with a desired signal at -86 dBm and receiving two interfering signals in the FM broadcast band at -10 to +15 dBm (two-tone intermodulation test) not produce more than a 10% change in CDI deflection.

Resistance to intentional jamming or spoofing is not an explicit part of the system design, but the ILS contains some built-in rejection characteristics. Since the system uses narrowband AM modulation the interfering signal would need to be nearly the same strength as the ILS signal and be on-channel to have an effect. Also, as the aircraft approaches closer to the airport the necessary interference power increases as the inverse square of the distance of the aircraft from the ILS transmitting

antennas. At the decision height the aircraft is very close to the glideslope transmitter, which is typically located very near the runway threshold.

SCAT-I - Resistance of the GPS receiver to out-of-band continuous wave interference is specified.

Comment - MASPS RTCA/DO-217 should add requirements for resistance to in-band CW interference, and in- or out-of-band pulse type interference (since GPS operates in a frequency region where pulse modulation is extensively used). Requirements for resistance to intentional interference should also be adopted, since GPS transmitters are much farther away from the user receivers, thus making it much easier to produce interference. In effect, many GPS users could be affected at one time by a single interference source of relatively low power.

Another reason for adding interference requirements is the publication of the relatively recent (January 1994) U.S. Department of Transportation (DOT) Strategic Plan⁴, in which the DOT establishes the goal to “Promote Safe and Secure Transportation”. This plan further specifies that the DOT will “Identify and implement new measures to enhance security on all modes of transportation to achieve personal security and national security goals.”

SUMMARY

In establishing the standards for interoperability between the ground station and the airborne equipment, the standards should be defined to prevent conflict or misinterpretations by differing manufacturers. Also in establishing standards, knowledge gained from years of traditional navigation experience should be brought into consideration.

ACKNOWLEDGMENTS

The authors would like to thank Steve Rowson, Chris Hammond, Lowell Snapp, and Warren Hundley for their inputs.

REFERENCES

1. RTCA, *Minimum Aviation System Performance Standards DGNSS Instrument Approach System: Special Category I (SCAT I)*, Document No. RTCA/DO-217, August 27, 1993.
2. Enge, P., Swanson, E., Mullin, R., Ganther, K., Bommarito, A., and Kelly, R., *Terrestrial Radionavigation Technologies*, NAVIGATION: Journal

of the Institute of Navigation, Vol. 42, No. 1, Special Issue, September, 1995.

3. ICAO, *International Standards, Recommended Practices and Procedures for Air Navigation Services, Aeronautical Telecommunications, Annex 10 to the Convention of International Civil Aviation, 4th Edition of Vol. 1*, April 1985.

4. DeBolt, R.O., et. al., *A Technical Report to the Secretary of Transportation on a National Approach to Augmented GPS Services*, Appendix E, Institute for Telecommunication Sciences, National Telecommunications and Information Administration, U.S. Dept. of Commerce, Boulder, Colorado, 1995.



Session B3

Specialized User Equipment Technology

Chair:

Capt. Ben Peterson
U.S. Coast Guard Academy

Co-Chair:

Dr. Triveni Upadhyay
Mayflower Communications

Development and Testing of a Mobile Pseudolite Concept for Precise Positioning

Tom Holden, *Stanford Telecom*

John Raquet¹, Gerard Lachapelle, Weigen Qiu, and C. Pelletier, *The University of Calgary*

Anthony Nash, *746th Test Squadron, Holloman AFB*

Patrick Fenton, *NovAtel*

ABSTRACT

The concept of using a pseudolite (PL) in the reverse mode where the PL is positioned with respect to receivers deployed at known points is presented. In order to eliminate clock and other code and carrier phase biases, two types of double differencing approaches are described and analyzed, namely double differencing between two receivers (RX), one space vehicle (SV) and one fixed or mobile PL, and double differencing between two RX, one fixed PL and one mobile PL. The PL and GPS receiver modifications required to implement this concept are described. The results of an initial test conducted in a land vehicle at Holloman AFB, N.M., under the direction of the 746th Test Squadron are described. The test range consisted of a 600m course surrounded by six receivers deployed in a non-coplanar configuration at distances ranging from 100m to 1,500m from the vehicle. The PL code and carrier phase data was used to assess its quality in terms of equipment noise, multipath, cycle slips, etc. The data was also analyzed in the position domain to assess the differential positioning performance of this augmented GPS system. Further development and testing plans are outlined, with emphasis on enhancing GPS-based testing capabilities at the 746th Test Squadron.

INTRODUCTION

A novel flight reference system concept has been developed by the 746th Test Squadron in anticipation of future testing requirements. The purpose of this system is to provide a reference (true) trajectory for aircraft against which other navigation systems can be tested and analyzed. At the top level, there are three driving requirements for this system, including i) very high position and velocity accuracy (on the order of 0.1m and 0.005m/s), ii) ability to easily install on all aircraft in the

Air Force inventory, and iii) ability to operate in the presence of jamming at GPS frequencies.

The reference system concept which is expected to meet these requirements is shown in Figure 1. This system represents an inverse of the procedure normally used to perform precise carrier-phase positioning. Normally, relative positioning is performed between two GPS receivers tracking many common GPS satellites, and optionally from one or more ground-based fixed pseudolites. In the new reference system concept, relative positioning is performed between two pseudolites transmitting GPS-like signals which are collected by many common GPS receivers at precise three-dimensional coordinates on the ground. If one of the pseudolites is at a fixed, known point on the ground, then the position of the mobile pseudolite (which is on the aircraft) can be determined.

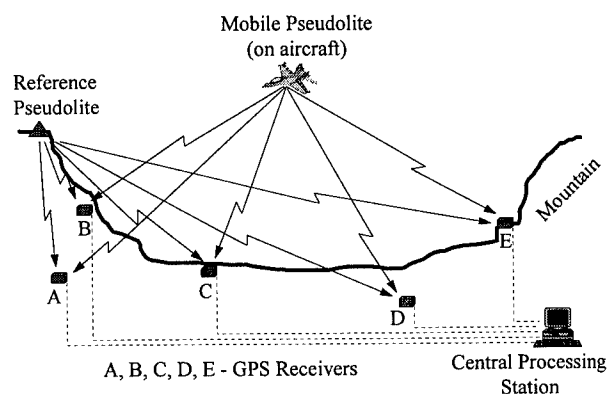


Figure 1: Inverted Pseudolite Reference System Concept

This configuration boasts two distinct advantages over the traditional concept of placing the GPS receiver in the aircraft. First, immunity to intentional GPS jamming is gained by placing the receivers on the ground, away from

¹ Capt Raquet is a graduate student at The University of Calgary under sponsorship from The Air Force Institute of Technology

the focus of the jamming beam on the aircraft. Any residual jamming signals on the receivers can be shielded locally at each receiver as shown in Figure 2. This concept is currently being tested by the 746th Test Squadron.

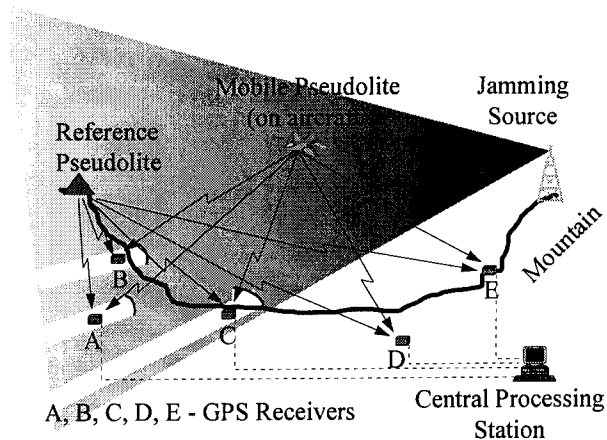


Figure 2: Receiver Shielding During Jamming

Secondly, flexibility is gained and cost is reduced by placing most of the hardware and software infrastructure on the ground, where power, size, and computational load constraints can be more easily accommodated. The only equipment required on-board the aircraft is a GPS pseudolite and antenna, which are relatively small and could be easily placed on most aircraft, using several placement options (empty missile pod, empty fuel tank, wing/fuselage mount, etc.).

This paper presents test results from a proof-of-concept test which took place at the 746th Test Squadron in April, 1995. The results demonstrate the feasibility of generating an accurate trajectory of a transmitting pseudolite on a mobile platform.

In the past, pseudolites have been shown to improve GPS signal geometry for mobile receivers.¹ Pseudolites have also been used to help with ambiguity resolution and autonomous integrity monitoring during aircraft precision approach and landing.^{2,3,4} This is the first time that the pseudolite itself has been positioned using carrier-phase data in a double-difference mode.

TEST DESCRIPTION

The 746th Test Squadron mobile test van was selected as the mobile platform for this proof-of-concept test. The van is a modified touring bus with on-board power supplies, antenna mounts, and equipment racks which make it ideally suited for this type of mission.

Finding an adequate test site for this test was a challenge. In order to obtain a reasonable three-dimensional solution, it was important for the ground receivers to be placed in a configuration that was as non-coplanar as possible to avoid a critical configuration singularity.⁵ This meant that the receivers needed to be placed at varying altitudes. Another constraint was that each receiver had to maintain signal lock with the pseudolite for the entire test route. This meant that, at a minimum, line-of-sight was to be maintained between the ground receivers and the moving vehicle. Additionally, the range between each receiver and the pseudolites (~100-1000m). After two days of initial system checkouts and testing, the test route shown in Figure 3 was selected. This route covered a segment of straight, level road. A large hill was located to the northeast of the road, which permitted placement of the receivers at varying altitudes while maintaining line-of-sight to the vehicle. The total length of the test route was 600m.

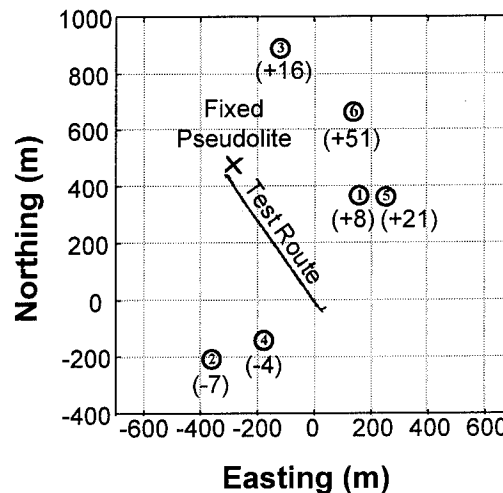


Figure 3: Receiver Geometry of Test (6 Receivers)
(Nominal Altitude (m) Above Trajectory in Parenthesis)

A total of six fixed receivers were used for the test. The positions of the receivers relative to the test route are shown in Figure 3. The nominal height difference between the test route (which was nearly level) and each receiver is given in parenthesis. A vehicle (car or pickup) was placed at each receiver location to provide power. Receivers 1 through 5 were 12-channel NovAtel model 3151R receivers in Powerpack™ enclosures. Data was transferred real-time through the RS-232 port for storage on separate laptop computers. Receiver 6 was a NovAtel PC card model 3951R that was mounted directly in a

laptop computer. All of the receivers used NovAtel's Narrow Correlator™ technology.⁶ NovAtel model 501 dome antennas were used with each receiver. The antennas for receivers 2-6 were mounted directly on the roof of the vehicles with a magnetic mount. In order to improve reception along the test trajectory, the antennas were placed on the edge of the vehicle roofs at a 10°-20° inclination towards the trajectory. The antennas for receiver 1 and the fixed pseudolite were mounted on surveying tripods in pickup truck beds. All receivers and the fixed pseudolite remained stationary during the entire test.

The coordinates of the fixed GPS receivers were determined from GPS measurement data collected by the receivers themselves. First, a floating ambiguity survey was performed between receiver 4 and the 746th Test Squadron reference receiver, located 16km away from the test site. From that point on, the position of receiver 4 was considered the true reference point against which all other positioning was performed. Next, each fixed GPS receiver was positioned using an integer ambiguity solution relative to each of the other GPS receivers, using about two hours of data and the SEMIKIN™ software.⁷ A network adjustment algorithm was then used to combine this redundant set of relative surveys to generate the final positions of each of the fixed receiver antennas. Using this method, the estimated relative positioning accuracy of the fixed receivers is 1-2 cm.

The pseudolite transmitters were Stanford Telecom Model 7201 Wideband Signal Generators. The data rate for the broadcast was set at 50 bps, and a prerecorded GPS message was transmitted. Two Mini-Circuits broadband amplifiers were used to amplify the RF output from its standard level of -50 dBm to an output of between -15 dBm and -10 dBm in order to obtain the desired transmission range. Each unit was controlled by a laptop computer running an in-house Stanford Telecom software product called Synchronicity™, which was designed to simulate GPS, WAAS, and other pseudolite environments.

The fixed and mobile pseudolites transmitted on L_1 using the PRN 10 and PRN 8 gold codes, respectively. Each of the receivers had the first two channels manually locked onto PRN 10 and PRN 8, and the remaining 10 channels remained free to receive as many GPS satellites as possible. No other modifications were made to the pseudolites or the receivers. Single frequency (L_1) pseudorange, carrier phase, and Doppler measurements were collected at a 2 Hz rate from the pseudolites and each tracked satellite.

The fixed pseudolite's antenna was mounted on a tripod in the back of a pickup truck in a position visible to all of the fixed receivers. The position of the pseudolite antenna was determined by attaching one of the NovAtel GPS receivers to the antenna for a GPS survey (relative to the fixed GPS receivers) after the pseudolite testing was complete.

Three phases of testing were performed on April 7, 1995. Each phase consisted of several passes along the test route at speeds between 5 and 20 m/s. During one of the phases, pseudolite 8 was mounted on the roof of the test van, and pseudolite 10 was placed at the fixed location shown in Figure 3. The majority of this paper describes the analysis of this data. During another phase, both pseudolites were mounted on the test van—one towards the front and one towards the rear. The data from this phase has not yet been analyzed, and no results are presented in this paper. During the last phase, receiver 1 was mounted on the bus, using the same antenna that had been used earlier by the mobile pseudolite. During this phase, the receiver collected measurements from the fixed pseudolite and all visible GPS satellites. As described later in the paper, this mobile receiver data has proven helpful in characterizing the performance of the mobile pseudolite positioning algorithms.

MEASUREMENT DOMAIN ANALYSIS

Before attempting to generate a position solution, the raw measurements were analyzed to determine basic measurement quality. Of primary interest was the effect of multipath on the code and carrier measurements. High levels of multipath were expected because both the receivers and pseudolites were ground-based, and the GPS signal would have many potential reflected paths in addition to the straight-line path.

The placement of the pseudolite antenna on the test van was also conducive to multipath. In order to increase reception at low elevations and to maximize visibility to the fixed receivers, the pseudolite antenna was mounted on a wood post 25 cm above a flat 1m x 1m metal plate, which was itself mounted 21 cm above the rounded metal roof of the test van. While this configuration was necessary to accommodate the necessary constraints in a ground-based test, it did create ideal conditions for multipath (a worst case scenario).

Additionally, significant multipath was anticipated because the signal to noise ratio (C/N_0) on each of the receivers tended to noticeably drop whenever there was relative motion between the pseudolite and receiver antennas. This effect may have been caused by

uncharacteristically high, rapidly changing levels of multipath. due to the large potential for reflected signals described above.

Analysis was performed on the data collected during all phases of the test, but all results in this paper are shown for a 1673 sec time period when one pseudolite was mounted on the van and the other pseudolite was at a fixed site on the ground. This time period was the only large segment in which all six receivers maintained continuous carrier lock on both of the pseudolites with no cycle slips (cycle slip detection and correction were not of primary importance in this proof of concept demonstration). The measurement data from this time period are representative of the entire test.

Code/carrier difference plots are shown in Figure 4. The motion of the mobile pseudolite can be inferred from the bottom plot, which shows latitude as a function of time. Because carrier phase multipath is very small relative to code multipath, the code minus carrier difference is a good measure of code multipath (plus measurement noise). As expected, there is a relatively high level of multipath variation in the signal from the mobile platform. This multipath correlates strongly with vehicle motion. In contrast, the signal from the stationary pseudolite is relatively flat (note the difference in scale). This does not mean that there is no multipath, but that the multipath (if any) is nearly constant. The apparent multipath from the satellite is relatively small in magnitude from the moving pseudolite, and is uncorrelated with vehicle motion (since the receiver is on the ground). Note that the receivers used in this test feature NovAtel's Narrow Correlator SpacingTM technology, which reduces code multipath effects.⁸

POSITION DOMAIN ANALYSIS

The primary goal for this test was to demonstrate the ability to position a mobile pseudolite using carrier phase processing techniques. This case is analogous to the more typical case of positioning a GPS receiver (differentially) using GPS satellites. The two pseudolites in this test correspond to the two receivers in the typical case, and similarly the fixed receivers on the ground correspond to the satellites. By considering the problem this way, standard methods for ambiguity resolution and positioning were utilized to generate the desired trajectory. Two types of double differencing were used in the position domain analysis.

Type 1 double differencing (SV as base): This type of double differencing is between two receivers (RX), a mobile pseudolite (PL) on the test van, and a space

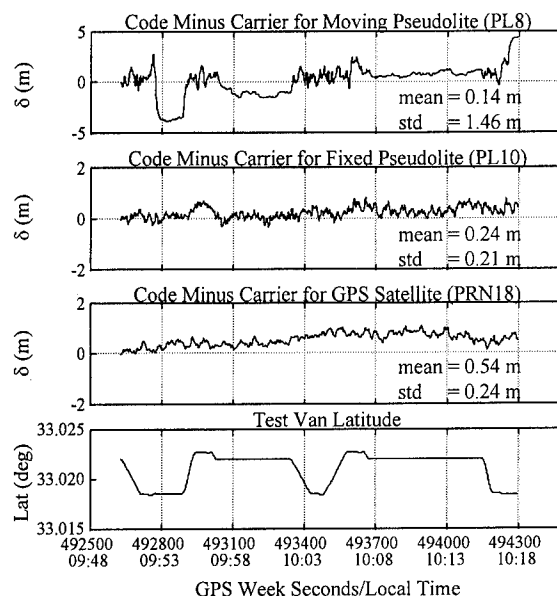


Figure 4: Code Minus Carrier for Receiver 1
(All plots on identical time scale,
bottom plot shows movement of mobile pseudolite)

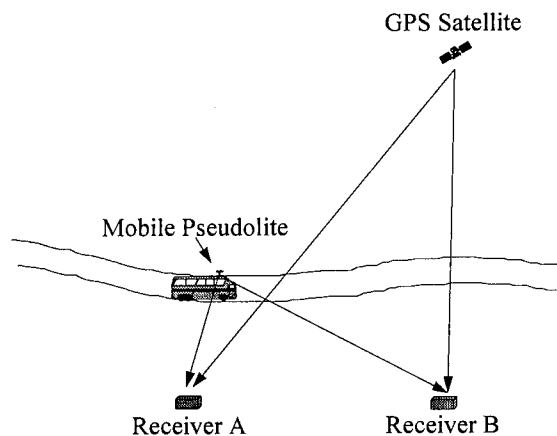


Figure 5: Type 1 Double Differencing (SV as Base)

vehicle (SV) as the base transmitter (analogous to the base receiver in a typical case). See Figure 5.

With type 1 double differencing, all clock errors are eliminated, and differential atmospheric errors are insignificant (for the short baseline of this test case). The positioning geometry (DOP) is a function of the relative location of the mobile pseudolite and the receivers on the ground. The GPS SV is used only in the double difference process to remove some of the errors, and it has no bearing on the DOP values. A plot of the VDOP (vertical) and HDOP (horizontal) values is shown in Figure 6 as a function of time. The latitude is also given to demonstrate that the DOP values are a function of the

position of the mobile pseudolite. Note the relatively high values for VDOP (between 10 and 13), caused by having all of the receivers and the moving pseudolite in nearly the same plane.

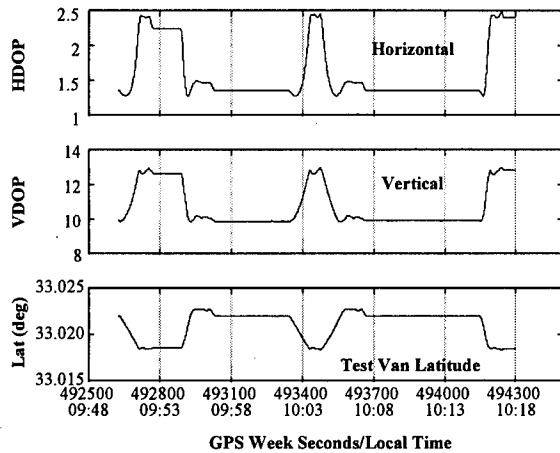


Figure 6: Dilution of Precision (DOP) Plots

For a fixed set of double difference integer ambiguities $\nabla\Delta\mathbf{N}$ and carrier phase measurements $\nabla\Delta\Phi$, the measurement residual is defined as

$$\mathbf{v} = \underbrace{\nabla\Delta\Phi + \nabla\Delta\mathbf{N}}_{\text{"measured value"}} - \underbrace{\nabla\Delta\mathbf{R}_{calc}(\mathbf{p}_{mobile}, \mathbf{p}_{base}, \mathbf{p}_{rec1}, \mathbf{p}_{rec2}, \dots, \mathbf{p}_{rec6})}_{\text{"expected value"}} \quad (1)$$

where $\nabla\Delta\mathbf{R}_{calc}$ is the calculated double difference of the ranges, based upon the position of the mobile PL (\mathbf{p}_{mobile}), the base SV (\mathbf{p}_{base}), and the positions of each of the six receivers ($\mathbf{p}_{rec1}, \mathbf{p}_{rec2}, \dots, \mathbf{p}_{rec6}$). The error in this residual as a function of errors in the assumed positions of the PL, SV, and receivers is expressed by

$$\delta\mathbf{v} = \mathbf{H}_{mobile}\delta\mathbf{p}_{mobile} + \mathbf{H}_{base}\delta\mathbf{p}_{base} + \mathbf{H}_{rec_6}\delta\mathbf{p}_{rec_6} + \sum_{j=1}^5 \mathbf{H}_{rec_j}\delta\mathbf{p}_{rec_j} \quad (2a)$$

$$\mathbf{H}_{mobile} = \begin{bmatrix} \mathbf{e}_m^1 - \mathbf{e}_m^6 \\ \mathbf{e}_m^2 - \mathbf{e}_m^6 \\ \vdots \\ \mathbf{e}_m^5 - \mathbf{e}_m^6 \end{bmatrix}, \quad \mathbf{H}_{base} = \begin{bmatrix} \mathbf{e}_b^6 - \mathbf{e}_b^1 \\ \mathbf{e}_b^6 - \mathbf{e}_b^2 \\ \vdots \\ \mathbf{e}_b^6 - \mathbf{e}_b^5 \end{bmatrix}, \quad \mathbf{H}_{rec_6} = \begin{bmatrix} \mathbf{e}_b^6 - \mathbf{e}_m^6 \\ \mathbf{e}_b^6 - \mathbf{e}_m^6 \\ \vdots \\ \mathbf{e}_b^6 - \mathbf{e}_m^6 \end{bmatrix} \quad (2b)$$

where \mathbf{e}_m^k is the unit line-of-sight vector from the mobile PL to receiver k , \mathbf{e}_b^k is the unit line-of-sight vector from the base SV to receiver k , and \mathbf{H}_{rec_j} is a 5x3 design matrix in which the j^{th} row is $\mathbf{e}_b^j - \mathbf{e}_r^j$ and all other rows

are 0. In this case, receiver 6 was chosen as the common receiver in order to minimize the vertical dilution of precision (VDOP) term. Because the receivers and the roving PL are very close to each other relative to their distance from the SV, $\mathbf{e}_b^x \approx \mathbf{e}_b^y$ for all combinations x and y . This means that $\mathbf{H}_{base} \approx \mathbf{0}$, and the residual error equation becomes

$$\delta\mathbf{v} = \mathbf{H}_{mobile}\delta\mathbf{p}_{mobile} + \mathbf{H}_{rec_6}\delta\mathbf{p}_{rec_6} + \sum_{j=1}^5 \mathbf{H}_{rec_j}\delta\mathbf{p}_{rec_j} \quad (3)$$

To determine the position of the roving PL (\mathbf{p}_{mobile}), a nominal position is chosen. The error in this position is calculated using the least squares method under the assumption that the errors in receiver positions are zero:

$$\delta\mathbf{p}_{mobile} = (\mathbf{H}_{mobile}^T \mathbf{H}_{mobile})^{-1} \mathbf{H}_{mobile}^T \delta\mathbf{v} \quad (4)$$

The roving pseudolite position is then corrected by $\delta\mathbf{p}_{mobile}$, a new set of residuals are calculated, and the process is repeated until the solution has sufficiently converged.

Type 2 double differencing (PL as base): This type of double differencing is the same as type 1, except that the space vehicle used as the base transmitter has been replaced by a fixed pseudolite (see Figure 7).

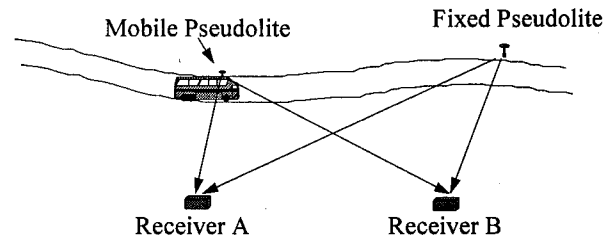


Figure 7: Type 2 Double Differencing (PL as Base)

With type 2 double differencing, all of the sensitivity (\mathbf{H}) matrices in equation 2 are non-zero and cannot be eliminated. The roving pseudolite position is calculated in the same manner as type 1 double differencing (using equation 4), only in this the errors in the base pseudolite position are also assumed to be zero. The VDOP and HDOP values for this case are the same as those shown in Figure 6. Measurements from the GPS SV's were used to provide a common time base for each of the receivers, but they are not used in the double differencing process.

Double difference ambiguity resolution. To generate the most accurate solution, the correct set of integer ambiguities $\nabla\Delta N$ must be determined. Standard ambiguity resolution techniques were employed which included generating an initial estimate of the ambiguities (using code minus carrier double differences), generating an integer search space about the initial estimate, calculating the sum of squares of the residuals for each of the candidate ambiguity sets, and selecting the correct ambiguity set based upon a statistical criterion.⁹ For the cases at hand, the residuals over the entire trajectory were calculated for each candidate integer ambiguity set.

For type 2 double differencing (PL as base), the above procedure seemed to work very well, generating a trajectory which closely matched the known trajectory (as described below), and which had low measurement residuals throughout. However, in the type 1 case, the correct set of integer ambiguities was not definitely identified. The ambiguity set with the minimum residuals did not generate a valid solution (the altitude was several meters below the known altitude). This apparent inconsistency is due to the faulty assumption that the errors in receiver positions (δp_{rec}) were zero. The relative positioning accuracy of the receivers is actually 1 cm, which is about the same magnitude as the residuals themselves (for the correct set of ambiguities). The residuals are therefore highly dependent not only upon the position of the roving receiver, but also the position errors in the fixed receivers. Equation 4, however, attempts to minimize the residuals by only varying the roving receiver's position. In effect, the receiver positioning errors are adding "noise" to the residuals, because they have not been properly accounted for from an estimation point of view. Efforts are currently underway to explicitly model some or all of the receiver position errors in an effort to handle this problem appropriately.

It's interesting to note that the error in residuals with type 2 double differencing is a function of positioning errors of the base PL as well as the fixed receivers (see equation 2), but the minimum residual in this case did yield a good set of integer ambiguities. What most likely occurred is that the errors in pseudolite positioning canceled some of the receiver positioning errors, resulting in a good solution. A Monte-Carlo analysis showed that when the receiver and pseudolite positions were artificially and randomly moved 1cm (1σ) in each axis, the residual could increase as much as 300% or decrease as much as 54%. The average change was an increase of 42%. This demonstrated the high sensitivity of the residuals to small positioning errors of the fixed PL and receivers.

In order to arrive at a good set of integer ambiguities for type 1 double differencing, an altitude criterion was also added based upon *a priori* knowledge of the true altitude. The ambiguity set chosen for the type 1 double differencing represents the minimum residual case of those that generate a solution near to the correct altitude. While this is not an acceptable long term approach to the ambiguity resolution problems unique to this particular configuration, it does allow the generation of an accurate position of the roving pseudolite, which was the primary goal of this demonstration.

DEMONSTRATION RESULTS

Comparison between type 1 and type 2 double differencing. The difference between the trajectories generated by type 1 and type 2 double differencing is shown in Figure 8. Both the absolute difference (dashed traces) and the DOP-normalized plots (black traces) are presented. DOP-normalization is important due to the poor receiver geometry that is unique to this ground-based test.

All of the errors in Figure 8 include receiver and fixed pseudolite survey error (as described above), multipath, measurement noise, and possibly a small error in the integer ambiguities for one or both of the solutions. (Recall that the integer ambiguities were uncertain in the type 1 case because of the propagation of survey errors into the residuals--see "Position Domain Analysis" above). The errors appear to be primarily a function of geometry, which is evident by comparing the shapes of the plots in Figure 8 with the trajectory from Figure 6.

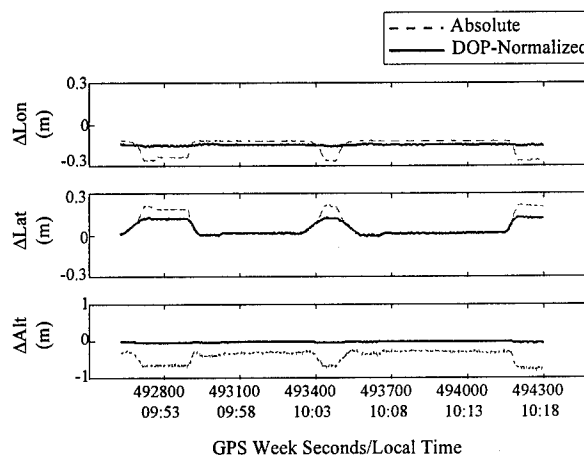


Figure 8: Position Difference Between Type 1 and Type 2 Double Differencing

Residuals for the two types of double differencing are shown in Figure 9. The residuals for type 2 double differencing look reasonable, with magnitudes on the order of 1-2 cm. The type 1 residuals are larger, with two traces at about ± 3 cm. These two traces correspond to receivers 1 and 5, and they are nearly mirror images of each other. This indicates that there may be a survey error in either (or both) of the receivers which the least squares fit absorbs and splits evenly between the two receivers.

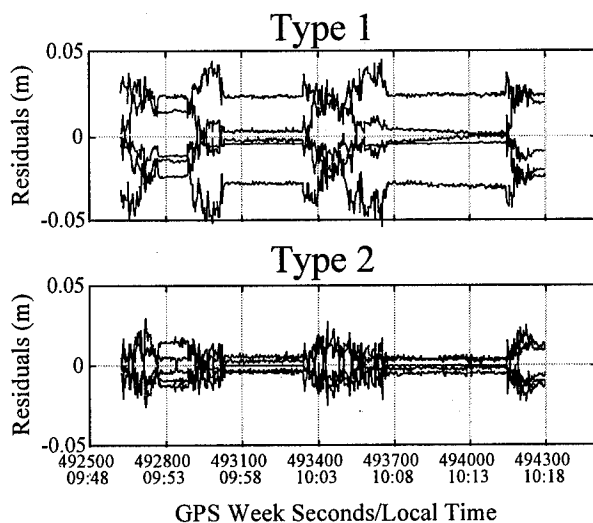


Figure 9: Residuals from Type 1 and Type 2 Double Differencing

To test out this theory, receiver 1 was moved by 5.3 cm to the northeast (2 cm north, 5 cm east), a distance that was chosen by hand after looking at the receiver geometry. After receiver 1 was moved, the trajectory and residuals were recalculated. The trajectory did not exhibit any significant change (< 1 cm in each axis), but the residuals were greatly improved as shown in Figure 10. This example provides a clear demonstration of the sensitivity of the residuals to receiver survey errors.

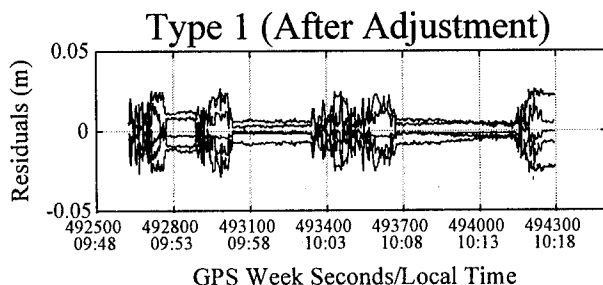
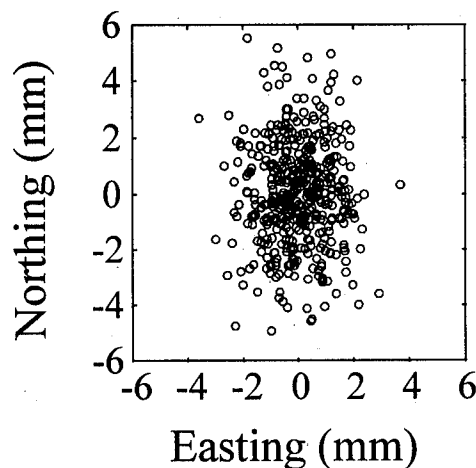


Figure 10: Type 1 Double Difference Residuals After Adjusting Position of Receiver 5

Stationary positioning stability. As shown in the bottom plot of Figure 6, there were several time periods when the van was stationary. The van also stopped during the final phase of the testing, when the NovAtel receiver was attached to the antenna previously used by the pseudolite.

Figure 11 shows the pseudolite position during one of these stops (note that the scale is in millimeters). A comparison of the standard deviations of the positions during all stop periods is given in Table 1. In order to provide a fair comparison independent of geometry, the values are also normalized by the appropriate dilution of precision (DOP) term. Based upon these results, the stability of the pseudolite position looks very good in comparison to the GPS receiver position.



**Figure 11: Stability of Type 2 Pseudolite Double Difference Solution
(GPS Time 493083-493333 Seconds)**

Comparison with GPS receiver trajectory. Because it is not possible to correlate the pseudolite and GPS receiver trajectories by time, an alternative means of comparison has been developed. Each data point has been transformed into a new coordinate frame with its origin near the southeast end of the test trajectory, the x-axis pointing northwest directly along the trajectory, the y-axis pointing horizontally southwest normal to the test trajectory, and the z-axis pointing upward. If put in terms of the path or "track" of the vehicle, the x-axis corresponds to down-track position (with the origin near the southeast end of the trajectory and increasing to the northwest), the y-axis to cross-track position, and the z-axis to above-track position. After performing this coordinate transformation, the trajectory can be correlated by down-track (x) position. This is especially useful for

Table 1: Position Solution Stability Comparison

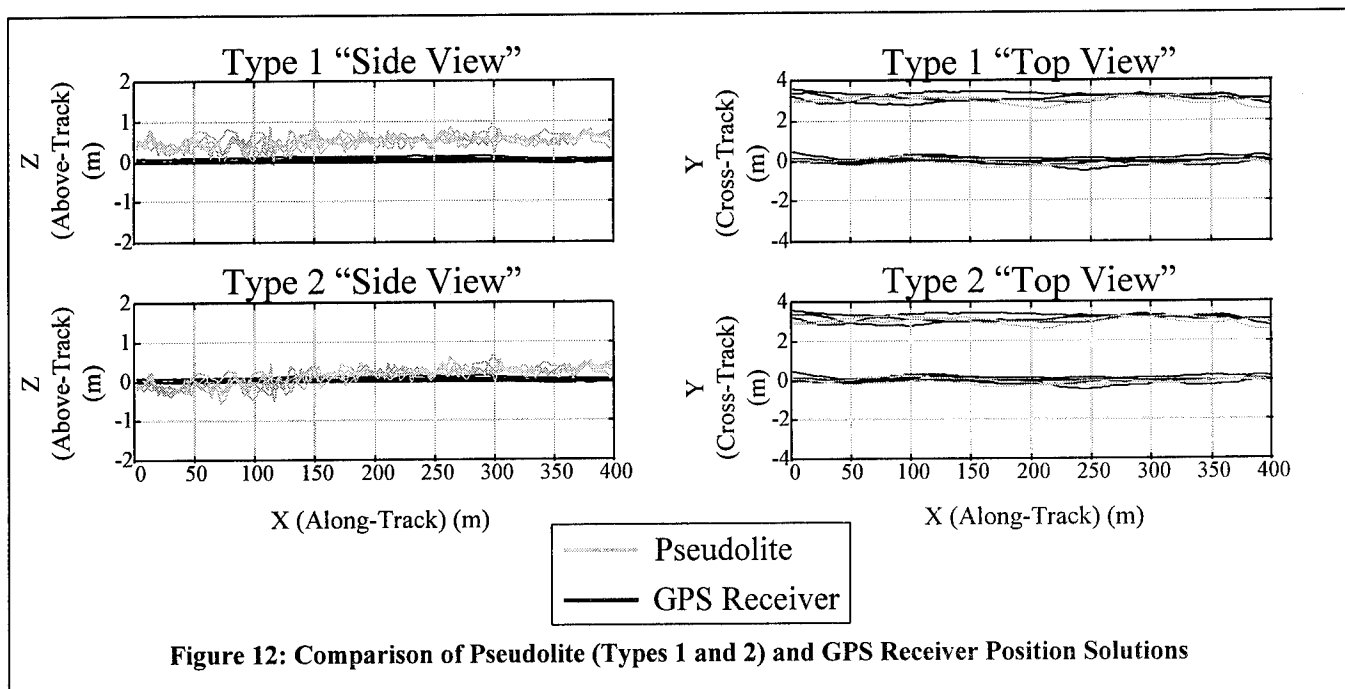
| Positioning Method | GPS Time (sec) | Std Deviation of Position (mm) | | | DOP-Normalized Std Deviation of Position (mm) | | |
|---------------------------|----------------|--------------------------------|-------|----------|--|-------|----------|
| | | East | North | Vertical | East | North | Vertical |
| Pseudolite (Type 1 DD) | 493083-493333 | 0.9 | 1.3 | 16.7 | 1.2 | 1.2 | 1.7 |
| | 493739-494089 | 1.9 | 2.7 | 17.2 | 2.4 | 2.4 | 1.7 |
| Pseudolite (Type 2 DD) | 493083-493333 | 1.1 | 1.9 | 18.4 | 1.4 | 1.8 | 1.9 |
| | 493739-494089 | 1.8 | 2.5 | 17.5 | 2.3 | 2.2 | 1.8 |
| NovAtel GPS Receiver | 497812-498013 | 2.3 | 3.0 | 4.2 | 6.0 | 9.9 | 3.7 |
| | 498389-498539 | 2.7 | 6.7 | 6.5 | 15.2 | 34.3 | 8.7 |

the vertical axis, since the road is relatively flat, and the altitude of the antenna is sufficiently determined by the down-track position on the road. The cross-track component is also a function of down-track position, but is less repeatable because it depends upon the van driver's ability to follow the same path each time.

The data collected by the mobile GPS receiver during the final phase of testing was processed using The University of Calgary's SEMIKIN™ software, which determined the correct set of integer ambiguities and generated a time history of position.⁷ Residuals and other quality measurements were monitored to make certain that the trajectory was correct. As a result, the GPS receiver trajectory is considered a "truth" reference against which the pseudolite positioning can be compared. The

estimated accuracy of the GPS trajectory is 1-3 cm, depending primarily upon carrier-phase multipath.

The trajectories generated by type 1 double differencing, type 2 double differencing, and the GPS receiver alone were transformed into the new x-y-z coordinate system, and the results are shown in Figure 12. The plots on the left show the altitude generated from the type 1 and type 2 double differencing methods as a function of down-track position. These plots depict a "side view" of each of the trajectories. Both the GPS receiver and the pseudolite traversed the same section of road several times (5 for the receiver and 4 for the PL), and the plots give a measure of repeatability of the solution. The pseudolite-generated altitudes exhibit about 0.5m of noise, which is good considering the high VDOP values during this test.



The plots on the right show the cross-track component of the trajectory as a function of down-track position. The X-Y plots represent the view "looking down" onto the road. The two distinct paths are the two opposite sides of the road. The bottom traces show the southeast to northwest runs, and the top traces show the return. The trajectories generated by the GPS receiver and the pseudolite (using either type of double differencing) are indistinguishable, and they agree to within ~0.5 m. This is as good as could be expected, since each line was a separate trip for the van, and the driver could not be expected to repeat the same trajectory to an accuracy better than 0.5 m under normal conditions.

Comparison with tape measure positioning. One final analysis technique was used in an effort to provide an independent measure of the van's antenna position against which the pseudolite and GPS solutions can be compared. On each southward pass of the trajectory, the van stopped for a period of time near a fixed survey point on the middle of the road. (These are the same points that were used to analyze position stability above). Three measurements were made with a tape measure at each stop point to determine the position of the edge of the van tires with respect to the centerline of the road and the survey marker. These measurements were later converted into measures of the horizontal position and heading of the van at each stop point. After making an assumption about the roll and pitch angles, the exact position of the antenna was calculated. An error analysis determined that approximate 1σ error values for this method are 6 cm for down-track (x) axis, 19 cm for cross-track (y) axis, and 7 cm for vertical (z) axis. The high y-axis uncertainty is due to the uncertainty in the roll angle.

The comparison between the tape-measure and the PL/GPS receiver positioning methods are given in Table 2. While not sub-decimeter in all cases, these results do show agreement between the independent measurements to a level of 10-20 cm horizontal and 30-60 cm vertical, which is reasonable considering the accuracy of the tape

measure method and the poor vertical geometry in the pseudolite case.

CONCLUSION

The results from this demonstration clearly show that it is possible to generate an accurate position of a transmitting mobile pseudolite using an array of GPS receivers fixed on the ground. Accuracies on the order of 10-30 cm were demonstrated. Given the somewhat severe conditions which existed in this demonstration relative to an operational system (e.g. very poor vertical geometry, high multipath potential, inadequate knowledge of receiver positions), these results are encouraging that such a system may be a feasible means to meet the reference system requirements for high accuracy (better than 10 cm).

The analysis of the data also pointed out areas that require attention in order to develop a system which is reliable. In particular, it is important to determine the position of the fixed receivers and fixed pseudolite to a very high degree of accuracy (through better surveys and/or error modeling techniques), due to the close proximity of the pseudolites and receivers.

REFERENCES

- ¹ D. Klein, B.W. Parkinson, "The Use of Pseudo-Satellites for Improved GPS Performance," *Global Positioning System*, Vol. III, The Institute of Navigation 1986.
- ² C. Cohen, D. Lawrence, B. Pervan, S. Cobb, A. Barrows, D. Powell, B. Parkinson, V. Wullschleger, and S. Kalinowski, "Flight Test Results of Autocoupled Approaches Using GPS Integrity Beacons," proceedings of ION GPS-94, Salt Lake City, Sep 20-23 1994, pp. 1145-1153.

Table 2: Difference Between Tape-Measure and PL/GPS Receiver Positions at Survey Stop Points.

| Positioning Method | GPS Time (sec) | Position Error vs. Tape Measure Method | | |
|-------------------------------------|----------------|--|-----------------|-----------------|
| | | Along-Track (X) | Cross-Track (Y) | Above-Track (Z) |
| Pseudolite (Phase II, Type 1 DD) | 493083-493333 | 18.7 cm | 13.1 cm | 60.7 cm |
| | 493739-494089 | 18.8 cm | 14.1 cm | 63.6 cm |
| Pseudolite (Phase II, Type 2 DD) | 493083-493333 | 8.5 cm | 7.16 cm | 30.1 cm |
| | 493739-494089 | 8.6 cm | 7.86 cm | 36.0 cm |
| NovAtel GPS Receiver (Phase III) | 497812-498013 | 17.6 cm | 0.56 cm | 2.8 cm |
| | 498389-498539 | 25.6 cm | 4.46 cm | 1.1 cm |

³ H.S. Cobb, C.E. Cohen, and B.W. Parkinson, "Theory and Design of Pseudolites," proceedings of the ION National Technical Meeting, San Diego, Jan 24-26 1994, pp. 69-75.

⁴ B.S. Pervan, C.E. Cohen, and B.W. Parkinson, "Autonomous Integrity Monitoring for Precision Approach Using DGPS and a Ground-Based Pseudolite," proceedings of ION GPS-93, Salt Lake City, Sep 22-24 1993, pp. 475-485.

⁵ G. Blaha, *Investigations of Critical Configurations for Fundamental Range Networks*, Reports of the Department of Geodetic Science number 150, Ohio State University, 1951.

⁶ A.J. Van Diredonck, P. Fenton, T. Ford, "Theory and Performance of Narrow Correlator Spacing in a GPS Receiver," *NAVIGATION*, Journal of the Institute of Navigation, Vol. 39 No. 3 (1992), pp. 265-283.

⁷ M.E. Cannon, "High-Accuracy GPS Semikinematic Positioning: Modeling and Results," *NAVIGATION*, Journal of the Institute of Navigation, Vol. 37 No. 1 (1990), pp. 53-64.

⁸ B. Townsend, P. Fenton, "A Practical Approach to the Reduction of Pseudorange Multipath Errors in a L1 GPS Receiver," proceedings of ION GPS-94, Salt Lake City, Sep 21-23 1994, pp. 143-148.

⁹ G. Lachapelle, M.E. Cannon, G. Lu, "High Precision GPS Navigation with Emphasis on Carrier Phase Ambiguity Resolution," *Marine Geodesy*, Vol. 15 No. 4 (1992), pp. 253-269.

Precision Landing Tests with Improved Integrity Beacon Pseudolites

H. Stewart Cobb, David Lawrence, Boris Pervan, Clark Cohen,
J. David Powell, and Bradford Parkinson
Stanford University

ABSTRACT

Stanford's Integrity Beacon Landing System uses ground-based pseudo-satellite transmitters known as Integrity Beacons to resolve carrier phase ambiguities on final approach, giving IBLs both high integrity and centimeter-level accuracy. This paper discusses two improved Integrity Beacon designs and the results of flight tests with these new beacons.

The original Integrity Beacons were not synchronized to GPS time. The IBLs reference station was required to measure the beacon carrier phase reference information using a direct cable connection to each Integrity Beacon, which proved inconvenient in practice. We therefore constructed a pair of *Autonomous Integrity Beacons*, pseudolites whose transmitted signals are synchronized to GPS satellite signals using the *Omni-Marker* principle invented at Stanford. Flight tests using these beacons showed that IBLs performance was maintained with the reference station in a convenient location some six kilometers from the beacons.

The original Integrity Beacons produced a short-range "bubble" of usable signals. While this was sufficient to demonstrate the IBLs concept, a longer-range beacon would have additional applications. To this end, we constructed an Autonomous Integrity Beacon with a

range of greater than four kilometers, using a pulsing scheme similar to that recommended by RTCM-104 to alleviate the near/far problem. Flight tests showed that this long-range beacon provided useful information to IBLs everywhere within its expanded bubble, without blocking satellite reception by IBLs or conventional GPS receivers.

INTRODUCTION

The *Integrity Beacon Landing System* (IBLS) developed at Stanford University exceeds the navigation requirements for Category III "blind" landings [6-8]. The capabilities of this system have been demonstrated in several flight test campaigns [1-4] culminating in 110 successful automatic landings of a Boeing 737 [5].

IBLS uses differential carrier-phase GPS navigation to achieve the high levels of accuracy and integrity required for Category III landings. The IBLs receiver on board the landing aircraft forms differential GPS measurements by comparing the code and carrier signals it receives against an equivalent set of signals received by the IBLs reference station on the ground.

The carrier phase integer ambiguities are resolved as the landing aircraft flies over a set of *Integrity Beacons* placed underneath the approach path. These beacons are

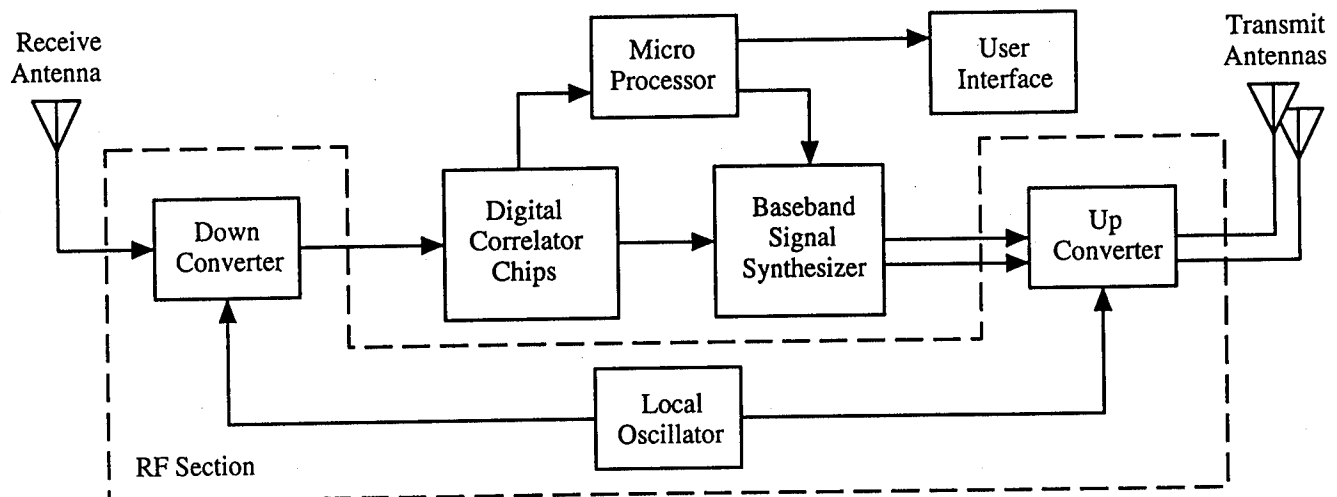


Figure 1: Block Diagram of Autonomous Integrity Beacon

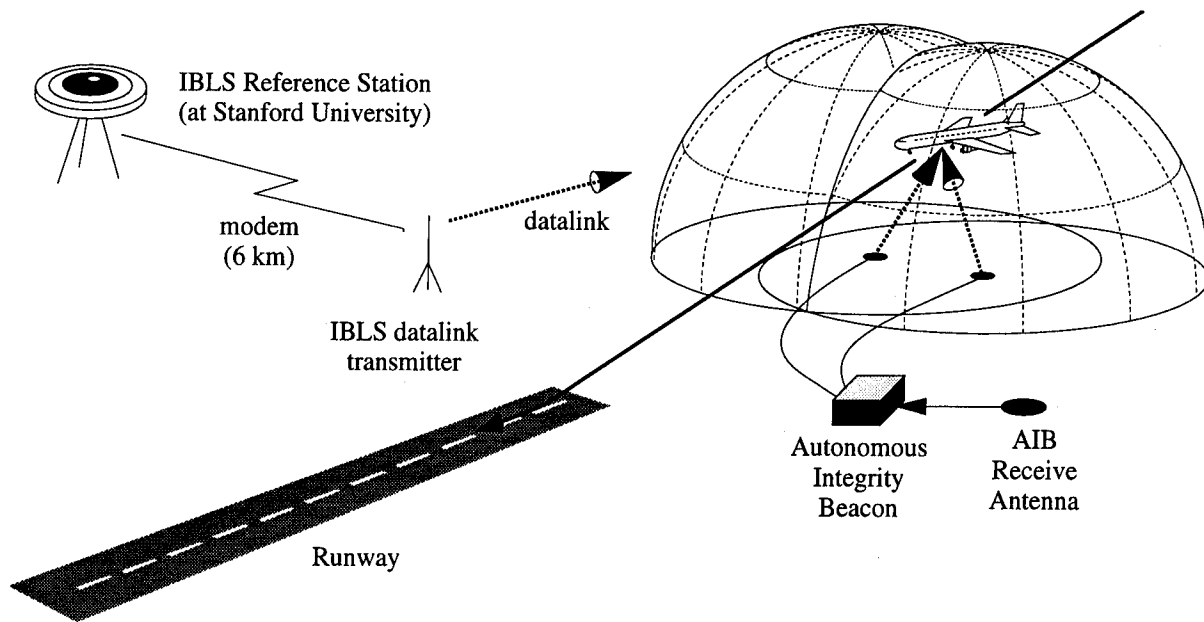


Figure 2: Integrity Beacon Landing System with Autonomous Integrity Beacon

ground-based pseudo-satellite or *pseudolite* transmitters which emit signals very similar to GPS satellite signals. As the aircraft flies over the beacons, its IBL receiver collects carrier phase data from the satellites and the beacons. The IBL system assembles this data into a matrix and performs a nonlinear least-squares batch algorithm to determine the integer ambiguities [3, 7].

GPS is a timing-based system which inherently requires precise clocks at each transmitter. However, the Integrity Beacons used in all previous flight tests contained comparatively poor clocks which were available and affordable. The original IBL system calibrated these clocks by directly connecting the beacon signals to the IBL reference receiver. The reference receiver measured the beacon signals and the satellite signals simultaneously, which effectively synchronized the beacon transmitters to precise GPS time.

While this approach worked in theory and in initial flight tests, it proved inconvenient as the test program expanded. The requirement for a direct connection forced us to locate the reference station near the beacons under the approach path, a kilometer or more from the runway. This distant location reduced the reliability of the datalink between the reference station and the aircraft. As a result, the datalink absorbed the largest fraction of our installation efforts at each new site.

To solve our datalink problems and move the reference station back near the runway, we needed another way to synchronize the Integrity Beacons to the GPS satellite

signals. As necessity is the mother of invention, this necessity gave birth to the *Omni-Marker* concept [2, 9].

The Omni-Marker was invented by Dr. Clark Cohen at Stanford University. It can be thought of as an "electronic mirror" which reflects signals from selected GPS satellites. By comparing the direct and "reflected" satellite signals, a user receiver can compute an extremely precise differential range measurement.

In practice, the Omni-Marker consists of a GPS receiver closely linked to a pseudolite transmitter. The receiver controls the transmitter so that the transmitted signal has the same code phase and carrier phase as the signal received from a satellite. The PRN code of the transmitted signal differs from the satellite signal, so that the user receiver can tell the two signals apart.

AUTONOMOUS INTEGRITY BEACON

The Autonomous Integrity Beacon (AIB) uses the Omni-Marker Principle to synthesize two or more Integrity Beacon signals synchronized to a single GPS satellite. It consists of one receive antenna, two or more transmit antennas, an electronics package, and cables connecting these units (see Figure 1). With an AIB installed, the IBL reference station can be relocated from the approach path to a more convenient site, chosen to optimize datalink coverage or satellite visibility.

To demonstrate the feasibility of this concept, we designed and constructed an AIB based on a six-channel Trimble TANS receiver. The baseband code and carrier

signals we needed to synthesize the beacon signals were available as test outputs on the receiver's digital correlator chips, and the local oscillator signals we needed to drive the transmitter's upconverter were available on the RF circuit board. (This was pure serendipity; in more highly integrated receivers, these signals are generally unavailable.) The baseband carrier signal was taken from the output of a numerically controlled oscillator, which was not designed for this application and contained a great deal of jitter. Unfortunately, this jitter could not be eliminated from the transmitted signal.

We developed a custom circuit board to amplify, upconvert, and filter the transmitted signals. A set of fast RF switches were added to support the pulse tests described later. Bench tests of the breadboard AIB showed that it did indeed generate signals which our IBLS receivers could track. The breadboard AIB consumes approximately 5 watts from a 12-volt supply.

The carrier-phase noise level on the signals transmitted by our breadboard AIB appears to be 3 to 4 times higher than the equivalent noise level on the GPS satellites themselves. This result is undoubtedly due to the carrier jitter present in this breadboard AIB. A purpose-built AIB chipset would generate a much cleaner carrier signal. Nevertheless, this noise level is low enough to support IBLS testing.

AIB FLIGHT TESTS

Our goal for this series of tests was to confirm that IBLS could use signals from a standalone AIB to resolve the carrier phase integer ambiguities correctly, while the IBLS ground station was located some distance away. We installed the breadboard AIB under the approach path at Palo Alto airport, where many of our previous IBLS flight tests were conducted. The AIB reflected a high-elevation satellite (chosen according to the time of each flight test) to form two Integrity Beacon signal "bubbles" which overlapped the approach path. The AIB's transmit power was adjusted so that the signal bubbles were approximately the same size as in earlier IBLS tests.

For all the tests described in this paper, the IBLS reference station remained in our lab at Stanford, over six kilometers away. An IBLS datalink transmitter, placed near the runway, received data from the reference station through a telephone modem (see Figure 2). The IBLS user receiver on board the aircraft was essentially the same as in previous tests, with only small software changes required to accommodate the AIB.

We tested the breadboard AIB during a total of eleven landing approaches over two days. Each day of tests began with a static survey which determined the carrier-phase integers in the IBLS receiver for later comparison. During each approach, the aircraft flew through the AIB signal "bubbles" and then performed a touch-and-go landing. After each pass through the bubbles, the IBLS software processed the bubble data in a batch algorithm to resolve the carrier phase integer ambiguities.

AIB FLIGHT TEST RESULTS

Each bubble pass was successful in that the IBLS realtime integrity checks declared that the batch algorithm had successfully estimated the cycle ambiguity integers. The batch algorithm actually estimates each integer ambiguity as a floating point number. One measure of the quality of the Integrity Beacon data is the difference between each computed number and the known integers determined from the preflight static survey.

A histogram of these differences, for all the integers estimated during this test, is shown in Figure 3. Note that all differences are safely below the threshold of 0.5 which could cause an erroneous cycle ambiguity resolution. We believe that these differences would be even lower were it not for the carrier jitter present in our breadboard AIB. Although a purpose-built AIB would probably give even better results, the success of these tests does show that the Autonomous Integrity Beacon concept is feasible.

PULSED INTEGRITY BEACON

Every pseudolite transmits a "bubble" of usable signals. Outside the radius of that bubble (the *far* radius), the pseudolite's signal is too weak for a GPS receiver to detect. The Integrity Beacons used in IBLS tests until now generated a continuous signal, which meant they had a *near* radius as well. The near radius is the distance at which the pseudolite signal is so strong that it jams the receiver, preventing the receiver from detecting the signals from the GPS satellites. For such a pseudolite, the far radius is roughly ten times the near radius, regardless of the absolute size of either. This ratio is determined by the cross-correlation properties of the PRN codes used for the GPS C/A signals [9].

Increasing the pseudolite's transmitted power increases the far distance at which its signals can be heard, at the cost of increasing the near distance within which all signals are jammed. This *near/far problem* is well-known to GPS researchers.

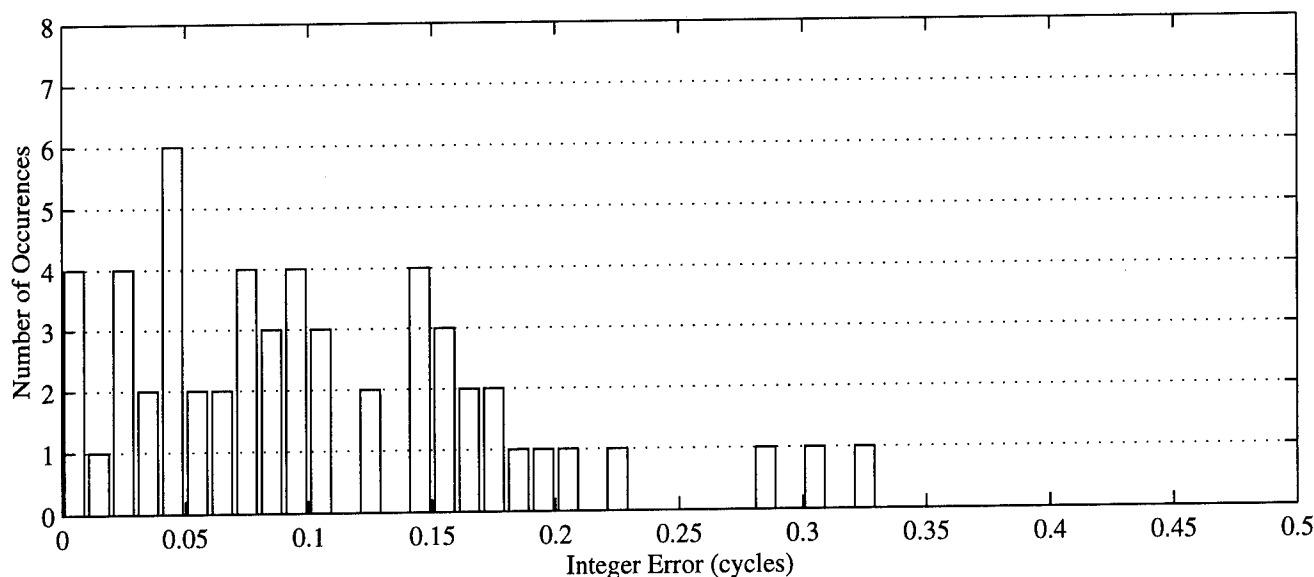


Figure 3: Histogram of Integer Differences during AIB Flight Tests

IBLS avoids the near/far problem by locating the Integrity Beacons below the aircraft's approach path. The beacons' power levels are set so that aircraft flies across the signal bubble, between the near and far radii. The near radius is close enough to the ground that the aircraft will not stray inside it by mistake.

Although the IBLS system design does not require it, there would be advantages to including longer-range pseudolites. An incoming aircraft could check that the Integrity Beacons and its own receivers were working before committing to a bad-weather approach. A long-range beacon could also be used as an additional ranging source to improve the geometry of a navigation solution or the availability of Receiver Autonomous Integrity Monitoring (RAIM).

Before increasing the power of the Integrity Beacons, one must find a way to mitigate the near/far problem. One way to do this is to transmit the beacon signal in short pulses, as suggested by the RTCM-104 committee a decade ago [10]. The user receiver will see only the pseudolite signal for the duration of the pulse; the rest of the time, it will see only the satellite signals. If the pulses are short, perhaps 100 microseconds out of every millisecond epoch, then the GPS satellite signals will be detected with only a slight decrease in signal-to-noise ratio. A sufficiently strong pseudolite signal can be received even if it only transmits ten percent of the time.

To experimentally verify this concept, we built a pulsing device into our Autonomous Integrity Beacon. We discovered in earlier experiments that the transmit pulses

must be synchronized to the C/A code epochs; the AIB provided a convenient way to do this, as the epoch pulses were readily available.

The RTCM-104 standard recommends a complex pulse pattern which is comparatively difficult to generate. For our experiments, we chose instead to generate a simple pulse at a fixed time delay from the epoch pulse. To ensure that the unmodified IBLS receiver could track the pulsed signal accurately without cycle slips, we increased the transmit pulse length to 125 microseconds. (A receiver designed to track pulsed signals would function well with pulses 100 microseconds or shorter.)

The pulses were produced by a set of fast PIN-diode switches in the path of the transmitted signal. RTCM-104 recommends that the pulse generator provide at least 100 dB of isolation when the pulse turns off. We used two 60 dB switches in series to provide a theoretical isolation of 120 dB when off.

The AIB output signal level is roughly -30 dBm, and the cables to the transmit antennas attenuate these signals by about 20 dB. We used a 45 dB low-noise amplifier at each transmit antenna to boost the output signals to roughly -5 dBm for the short-range pulsed bubble tests. For the long-range tests, however, we needed +15 dBm or more. However, we did not have enough amplifiers to drive both transmitted signals at this level, so the long-range tests used only a single bubble. (The power levels cited are approximate, as we could not measure them accurately in the field.)

PULSED FLIGHT TESTS

We performed three sets of tests with the pulsed AIB. The first test was intended simply to demonstrate that the concept worked. We placed the pulsed AIB atop a parking structure near our lab on the Stanford campus, with the IBLS reference station and datalink transmitter nearby. Our flight test aircraft maneuvered over the AIB at about 500 meters altitude to measure the characteristics of the pulsed bubble. We plotted in Figure 4 a top view of the points where a valid AIB signal was received. The plot shows that the AIB signal was usable out to about three kilometers.

During these maneuvers, the IBLS software attempted to resolve the carrier phase ambiguities using the AIB, even though the geometry of each solution attempt was quite poor. These solution attempts each converged to an answer, but the answers generally were not precise enough to uniquely identify the integers because of the poor geometry. Each attempt did correctly update the position covariances, however, and after several attempts the solution converged on the correct integers. This process was repeated several times, and post-processing confirmed that the integers were always identified correctly. This result shows the robustness of the IBLS technique.

The second test placed the AIB in the usual IBLS approach and landing configuration with both bubbles pulsed at the highest available power level, about -5 dBm. We performed seven approaches in this configuration. IBLS successfully identified the integers

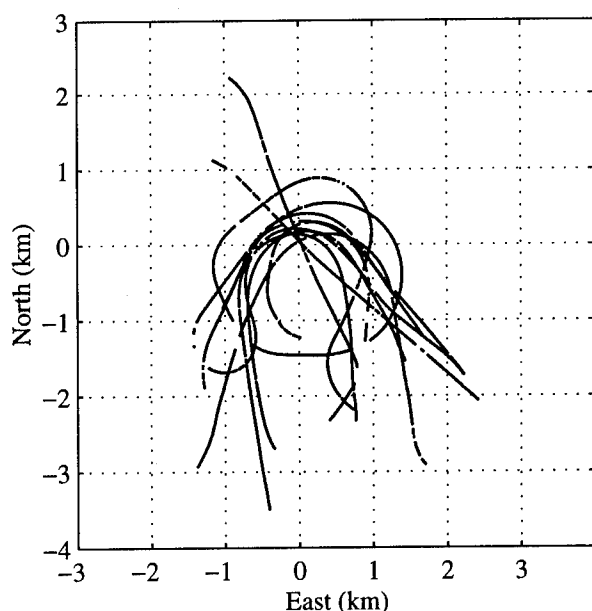


Figure 4: First Pulsed AIB Range Test

each time, as confirmed by post-processing comparison with a preflight static survey. This result demonstrates that IBLS accuracy was not degraded by the pulsed beacon signals.

For the final test, we left the AIB in the same location but reconfigured the amplifiers to provide the maximum possible output power (about $+22$ dBm) to a single transmit antenna. Our flight test aircraft flew around the airport traffic pattern to measure the coverage area of the pulsed AIB signal. Figure 5 is a top view of the airport area showing the points where a valid AIB signal was received. Also shown, for reference, are the runway and a circle representing the size of the original, non-pulsed AIB signal bubbles.

The figure shows that the AIB signal was lost in the crosswind turns and, to a lesser extent, in the base turns. During these turns, the beacon receive antenna on the bottom of the aircraft was pointed away from the AIB transmit antenna. We believe the signal was lost in these turns because the fuselage blocked the beacon signal.

The maximum range achieved in this test was approximately 4.5 kilometers. At that point, the aircraft was low on the horizon as seen from the AIB. Both the transmit and receive antennas are patch antennas whose gain patterns fall off sharply at low elevation angles. We believe signals were lost at this point because the antenna patterns provided insufficient gain. We are exploring ways to improve the AIB and aircraft antenna patterns and to mitigate the blockage effect.

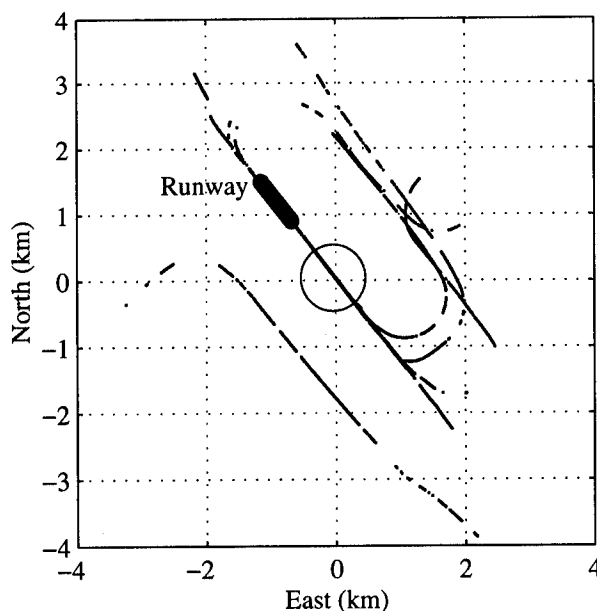


Figure 5: Pulsed AIB Range Test at Airport

INTERFERENCE TESTS

During both flight tests with the high-power pulsed signals, we attempted to measure the "near" radius within which the AIB transmissions jammed the satellite signals in non-cooperating receivers. On the theory that the least expensive receivers would be the least tolerant of interference, we acquired two low-cost handheld receivers from different manufacturers. We set each receiver to display the relative signal strengths for the satellites it was tracking and examined the trends in those displays under different conditions. The results for the two receivers were virtually identical.

As expected, each receiver showed a noticeable but negligible drop in signal strength on each satellite when we turned on the pulsed AIB transmitters. No additional signal degradation was noted until the receivers were brought within about ten meters of one transmit antenna. From a radius of ten meters down to about one meter, the signal strengths slowly declined. At a distance of one meter from the antenna, both receivers were still doing position fixes, although the displayed signal strengths were very low. When the receivers were brought still closer to the antenna, the satellite signals disappeared entirely and both receivers complained of poor satellite visibility.

Theoretically, a pulsed pseudolite transmitter should not jam the satellite constellation at any distance. We believe that the close-in jamming we saw can be attributed to signal leakage through the pulse switches or to thermal noise being amplified when the switches were off. Careful system design could probably reduce the size of this "near" radius, if necessary. If not, locating the beacon transmitters within a ten-meter clear zone should not present operational difficulties.

While a single pulsed pseudolite can be installed so as not to interfere with the GPS satellite signals, it may be more difficult to install multiple pulsed pseudolites in the same vicinity without mutual interference. Two pseudolites which share the same pulse time slot will be subject to the near/far problem with each other. Unless the distances and signal strengths are carefully controlled, as in the placement of IBLIS Integrity Beacons, one will be heard and the other will be jammed. One possible solution is to use separate pulse time slots, but the combined duty cycle of all the pulses together cannot exceed 20 or 25 percent without unacceptably degrading the signals from the GPS constellation. Clearly, more research is needed in this area before multiple pulsed pseudolites see widespread use.

CONCLUSION

Our flight test results with a breadboard Autonomous Integrity Beacon show that the AIB concept is feasible. It is no longer necessary to locate the IBLIS ground reference station within a cable's length of the Integrity Beacons themselves.

Our flight test results with a pulsed AIB show that a long-range pseudolite is also feasible. Signals from a long-range pseudolite can improve the availability of GPS navigation and Receiver Autonomous Integrity Monitoring, help resolve carrier-phase ambiguities, and carry digital data as well.

Both of these developments remove previous constraints on designs for GPS precision landing systems. However, more research is necessary before multiple long-range pseudolites can be used at the same airport.

ACKNOWLEDGMENTS

We gratefully acknowledge the help of our fellow graduate students Jock Christie, Gabe Elkaim, Mike O'Connor, Andy Barrows, and Jennifer Evans in performing these tests. Trimble Navigation provided all the GPS receivers we used for the flight experiments. Finally, this research would not have been possible without the moral and financial support of the Federal Aviation Administration.

REFERENCES

1. C.E. Cohen, B.S. Pervan, H.S. Cobb, D.G. Lawrence, J.D. Powell, and B.W. Parkinson. *Real-Time Cycle Ambiguity Resolution using a Pseudolite for Precision Landing of Aircraft with GPS*, DSNS-93, Amsterdam, The Netherlands, March-April 1993.
2. C.E. Cohen, B.S. Pervan, D.G. Lawrence, H.S. Cobb, J.D. Powell, and B.W. Parkinson. *Real-Time Flight Testing Using Integrity Beacons for GPS Category III Precision Landing*, NAVIGATION, Vol. 41, No. 2, Summer 1994.
3. C.E. Cohen, B.S. Pervan, D.G. Lawrence, H.S. Cobb, J.D. Powell, and B.W. Parkinson. *Achieving Required Navigation Performance using GNSS for Category III Precision Landing*, DSNS-94, London, UK, April 1994.
4. C.E. Cohen et al. *Flight Test Results of Auto-coupled Approaches using GPS and Integrity*

Beacons, ION GPS-94, Salt Lake City, Utah, September 1994.

5. C.E. Cohen et al. *Preliminary Results of Category III Precision Landing With 110 Automatic Landings of a United Boeing 737 Using GNSS Integrity Beacons*. ION National Technical Meeting, Anaheim, California, January 1995.
6. B.S. Pervan, C.E. Cohen, and B.W. Parkinson. *Integrity Monitoring for Precision Approach using Kinematic GPS and a Ground-Based Pseudolite*, NAVIGATION, Vol. 41, No. 2, Summer 1994.
7. B.S. Pervan, C.E. Cohen, and B.W. Parkinson. *Integrity in Cycle Ambiguity Resolution for GPS-Based Precision Landing*, DSNS-94, London, UK, April 1994.
8. B.S. Pervan, C.E. Cohen, and B.W. Parkinson. *Autonomous Integrity Monitoring for GPS-Based Precision Landing Using Integrity Beacon Pseudolites*, ION GPS-94, Salt Lake City, Utah, September 1994.
9. H.S. Cobb, C.E. Cohen, and B.W. Parkinson. *Theory and Design of Pseudolites*, ION National Technical Meeting, San Diego, California, January 1994.
10. T.A. Stansell. *RTCM SC-104 Recommended Pseudolite Signal Specification*, NAVIGATION, Vol. 33, No. 1, Spring 1986.

A Combined GPS/GLONASS High Precision Receiver for Space Applications

Dr. Stuart Riley, Dr. Neil Howard, Eric Aardoom, and Prof. Peter Daly
ISN, University of Leeds

Pierluigi Silvestrin
ESA, ESTEC

Biography

Dr. Stuart Riley graduated from the University of Leeds in 1990 with a BEng and in 1994 with a PhD in Electronic and Electrical Engineering. Since 1990 he has been active in integrated GPS/GLONASS receiver design and observable processing. He is the Leeds project manager for the GNSS receiver development, and has specific responsibilities for the system architecture, tracking software and observable processing.

Dr. Neil Howard graduated from the University of York in 1990 with a BEng and in 1994 with a DPhil in Electronics. Since then he has been at the University of Leeds developing the channel hardware for the ESA GPS/GLONASS receiver.

Eric Aardoom received the M.Sc.EE degree from Delft University of Technology, the Netherlands, in 1989. Subsequently, he worked at the same university on the design of an integrated navigation system using GPS, Loran-C, Omega and MLS. In 1994 he joined the ISN to work on the development of the GNSS receiver.

Prof. Peter Daly is Director of the CAA Institute of Satellite Navigation in the University of Leeds and has been involved with GPS/GLONASS satellite navigation issues since 1982.

Pierluigi Silvestrin is a Senior Systems Engineer in the Earth Observation Preparatory Programme Division of the European Space Research and Technology Centre (ESTEC) in Noordwijk (The Netherlands). He graduated in Electronic Engineering at the University of Padova (Italy) in 1985, specialising in control systems design. After working for one year at the Joint European Torus (JET) in Abingdon (UK), he joined in 1987 the Attitude and Orbit Control Systems Section of ESTEC. In 1989 he joined the Earth Observation Preparatory

Programme Division, where he is presently responsible for studies of space systems and supporting technologies for future Earth observation missions of the European Space Agency.

Abstract

The University of Leeds are developing a prototype multichannel combined GPS/GLONASS receiver capable of simultaneously tracking the C/A and P codes, and when anti-spoofing (A-S) is present operating in a codeless mode. The primary application is for earth observation radio occultation measurements on board a low earth orbiting (LEO) satellite. However, the architecture allows for a variety of applications such as earth-based reference stations or spacecraft attitude determination.

The channel digital signal processing is presented. Each channel is capable of simultaneous L1 and L2 P code, and L1 C/A code tracking. Details of the firmware are given, including the tracking strategy and filter bandwidths. Finally, initial results showing the code and carrier phase precision are provided.

Introduction

Space applications of GPS or, more generally, GNSS receivers can be divided into two main classes: applications in support of spacecraft operation, such as navigation and attitude determination, and scientific applications. The latter class can be related to three main areas of the Earth sciences: geodesy, atmospheric monitoring, and ionospheric science.

In geodesy, precise tracking data from an orbiting receiver can help in several different ways. Very precise orbit determination (POD) by post-processing of the tracking data from the orbiting receiver as well as from a ground reference network is now a well demonstrated application of spaceborne GNSS. Impressive results have been achieved in the

Topex-Poseidon mission in terms of accuracy of the reconstituted orbits, better than 3cm rms for the radial component [1]. Future space missions for ocean altimetry and land topography are expected to build upon such experience. Gravity field determination [2] is another geodetic application of spaceborne GNSS which has much in common with POD. In this case, the POD is geared towards the continuous refinement of existing gravity field models, which are at the moment strongly limited in both accuracy and spatial resolution. Depending on the altitude of the spacecraft, which needs to be as low as possible to detect gravity anomalies at medium as well as long wavelengths, an improvement of the geoid determination up to 2.5cm for gravity models with degree and order $n,l = 40$ has been predicted by various studies. GNSS tracking in combination with gravity gradiometry for high resolution geoid determination is baselined for the Gravity and Ocean Circulation Explorer satellite, an Earth science mission presently studied by the European Space Agency (ESA).

In the atmospheric sciences, the main interest lies with the application of radio occultation techniques which have been developed over a period of 30 years in relation to studies of planetary atmospheres and ionospheres. These limb sounding techniques provide a new approach for monitoring atmospheric temperatures, pressures and humidities on a global scale and with high accuracy and spatial resolution [3]. When the receiver on board a low Earth orbiting satellite tracks GPS or GLONASS satellites that are observed to rise or set through the atmosphere, the arrival time of the received signal is retarded because of the refractive bending and slowing of the signal as it crosses the atmosphere. By measuring with high accuracy and sampling rate the change in carrier phase, one can determine the atmospheric refractive index as a function of altitude. Pressure and temperature profiles can then be derived using the gas law, the known relationship between refractivity and dry air density, and the assumption of hydrostatic equilibrium. Accuracies in the temperature retrieval better than 1K at altitudes between 10 and 30km have already been demonstrated in the frame of the GPS-MET proof-of-concept experiment [4], with vertical resolutions better than 1km. The possibility to extend these measurements well into the troposphere (below 10km) and in the upper stratosphere (up to about 45km) is the subject of intense research worldwide. As a single orbiting GNSS receiver can observe about 1000 setting GPS and GLONASS satellites, each providing a high accuracy temperature sounding, it is clear that this all-weather technique will greatly contribute to the global atmospheric monitoring, with large impacts expected in operational meteorology and

climatology. Operational meteorology suffers from the scarcity of observations over the oceans and the less developed countries, which will be entirely eliminated when the data from a few orbiting receivers is available. Climatology needs long term observations free from calibration problems, which strongly affect current space-based atmospheric remote sensing. The GNSS radio occultation technique relies on precise time delay measurements, and can therefore provide the needed long term reference monitoring of the atmosphere. Global mapping of the ionosphere is yet another important application of precise spaceborne GNSS receivers. In concert with ground networks of GNSS receivers, the tracking data from space receivers can help probing the ionosphere along many paths. The derived measurements of Total Electron Content (TEC) can be used to develop maps of electron distributions in two or three dimensions. Ionospheric tomography techniques are in particular going to benefit from the vastly improved observation geometry including near-horizontal scanning of the ionosphere. Ionospheric structures, such as the mid-latitude trough, and their dynamics will be studied and monitored far better than today by means of ionospheric tomography. The flight of GNSS receivers capable of radio occultation observations has been proposed for all future ESA Earthscience missions.

Observation Requirements

The scientific applications impose a common set of requirements on (space qualified) GNSS receivers. The basic observables for these applications are carrier phase measurements at both L1 and L2 frequencies, which must be output with millimetric precision and, for atmospheric and ionospheric remote sensing, also at a relatively high data rate (10Hz at least). Code phase observations are of lesser importance, but still valuable for POD. Although the signal dynamics resulting from the orbital motion is rather modest (always less than 2g), the Doppler shifts and Doppler rates on the signals in the occultation geometry can be quite strong, especially when the signals cross the tropopause or particular structures of the ionosphere. Simulations performed with atmospheric and ionospheric models show that the receiver should keep reliable tracking even with TEC variations of the order of $1 \times 10^{16} \text{ e/m}^2/\text{s}^2$. When crossing the troposphere, signals can also be attenuated by several dB's, which calls for low receiver noise figure and tracking threshold. Dual-frequency operation produces negligible ionospheric errors for the most demanding observations of the neutral atmosphere[5].

The use of GLONASS in addition to GPS provides

very significant advantages for scientific applications. It obviously results in about twice as many observations of the atmosphere and ionosphere as with GPS only, which strongly increase the spatial distribution of measurements. The availability of dual frequencies signals unaffected by A-S is another important advantage, as it eliminates the need for the performance degrading codeless tracking of the L2 frequency signals. The receiver design should however be flexible enough to cope with a possible change in the GLONASS signal policy and implement codeless tracking techniques to be used in the event of a signal encryption similar to GPS. As GLONASS is an FDMA system, care has to be taken that the consequent satellite-dependent receiver biases and their variations be limited by design or by internal calibration means, as first mentioned by Raby [6]. This is critical for geodetic applications, but less so for atmospheric monitoring because of the short duration (about 1 minute) of occultation events.

Spaceborne GNSS Receiver Development

Whereas space qualified receivers for real-time navigation and attitude determination are commercially available, no civilian GNSS space receiver is available today. This fact led ESA to initiate a development activity, starting with the design and breadboarding of a precision receiver, largely based on the digital GNSS receiver studies carried out at the CAA Institute of Satellite Navigation of the University of Leeds, which is now approaching completion. In parallel the preparation of the implementation of the receiver with space qualified VLSI components has also been started. The receiver design has also taken into account the need to be compatible with ground applications in reference stations for geodesy and atmospheric/ionospheric monitoring.

Receiver Specification

The initial ESA specification calls for a twelve-channel receiver capable of operating on either an earth based or LEO platform (200km to 1000km orbital height). The maximum TEC velocity as seen from the LEO is $3.8 \times 10^{17} \text{ e/m}^2/\text{s}$ with a maximum TEC acceleration of $3.3 \times 10^{16} \text{ e/m}^2/\text{s}^2$. The platform jerk, rotation rate and rotation acceleration are specified as negligible. For a nominal input CNR of 46dBHz (L1) and 43dBHz (L2), the one-sigma precision of 1Hz measurements should be 50cm (GPS) and 1m (GLONASS) for the C/A code, and 25cm (GPS) and 50cm (GLONASS) for the P-code. The carrier observable should have a maximum measurement rate of 10Hz and precision of 1mm for L1 and L2 at the specified input level.

Down-Conversion

The L-band signals are received by a passive helical antenna developed by Saab-Ericsson for ESA. The antenna has been designed to accommodate dual frequency GPS and GLONASS signals and minimize multipath. Following the antenna the signal enters a low-loss pre-selection filter to attenuate interference sources. Separate L1 and L2 outputs are provided from the filter unit and are amplified by Miteq LNAs each with a guaranteed maximum noise figure of 0.8dB. L1 and L2 signals are fed to the receiver where all further processing occurs. The RF/IF processing has been developed to minimize the group delay in the GLONASS band with the final L1 and L2 GNSS signals all at a similar IF to allow common sampling hardware to be used for all signals.

Sampling

In the current receiver the sampling unit has been designed to simultaneously process GPS L1 and L2, and GLONASS L1 and L2 from one antenna. However, the receiver has been developed with additional flexibility to allow multiple antenna feeds. The basic block diagram of a single sampling unit is shown in Figure 1. The input signal S, which has a centre frequency near 14.25 MHz, is 4-bit sampled in I at 57 MHz. A FIR filter in an FPGA produces 2-bit I and Q samples at 28.5MHz having down-converted the IF frequency by 14.25MHz. The output carrier frequency is close to baseband and allows removal of the GLONASS channelization with the channel's carrier NCO. Sampling only in-phase while producing lower rate I and Q samples has the advantage of reduced IF analogue components which are susceptible to group delay variations with temperature. Four input bits are used to prevent rounding errors in the FIR filters affecting the quality of the two output bits. To account for variations of the input signal level an AGC is implemented.

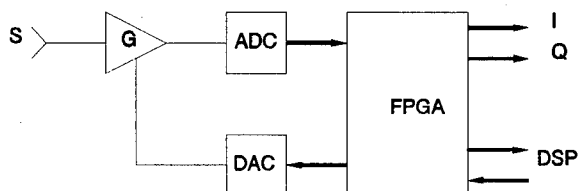


Figure 1 Simplified block diagram of the sampler.

Histogram counters in the FIR filter FPGA, linked to the tracking DSP, control an analogue variable gain amplifier and a digital gain block attempting to maintain a Gaussian sample distribution. Although not implemented in the current firmware release, the AGC architecture would allow interference detection and enhanced mitigation.

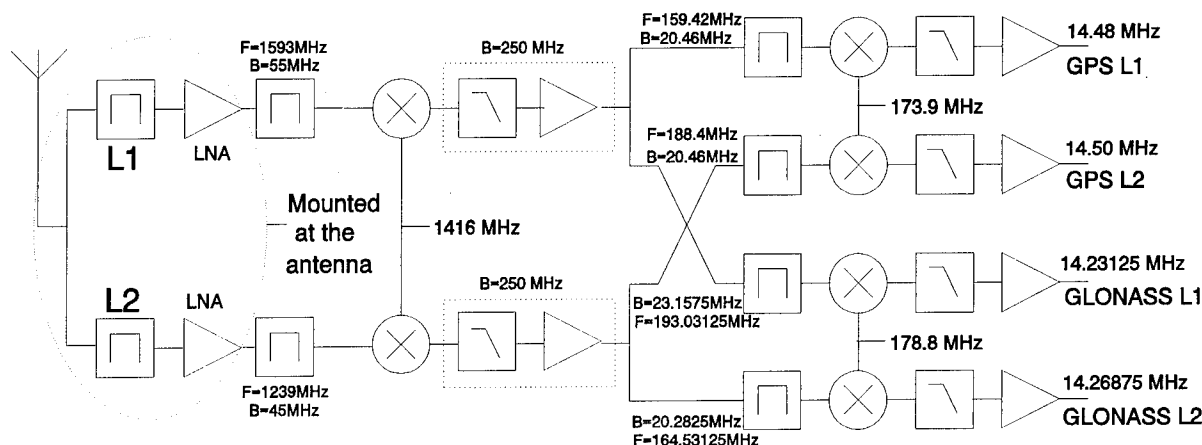


Figure 2 GNSS receiver front-end configuration.

Channel Hardware

Each channel can simultaneously track the C/A-code, and P-code at L1 and L2 of either a GLONASS or GPS satellite. Two-bit, dual frequency samples from both systems enter each channel. A multiplexer is used to select the relevant system's samples. To reduce the number of gates the orthogonal relationship between the C/A and P(L1) is used, consequently only a single L1 carrier NCO is implemented. From the I and Q correlation summations this assumption has been shown to be true for GPS. However, for GLONASS the mean deviation from orthogonal between C/A and P(L1) has been measured up to 5° . The carrier loop is driven by the C/A code, the code discriminators are non-coherent and so this error does not affect the P(L1) code observable. The digital image reject mix is used to maximize the CNR. The carrier NCO produces four phase control bits and counts modulo-twelve so that the mixer rotates the input samples in steps of 30° which fits conveniently with the input and output two bit amplitude quantization.

Each sub-channel (C/A, P(L1) and P(L2)) has four correlators during steady-state tracking - punctual and 'early minus late' in both I and Q. During acquisition, all twelve correlators (six I and Q) can be configured to operate with the C/A code and search over a six-chip window to reduce the acquisition time. A second C/A code generator is also implemented to allow the channel to track the L1 C/A code of two different satellites if P-code tracking is not required. This also has the advantage that, if GPS or the new GLONASS-M satellites start transmitting C/A code at L2, this can be tracked with the CNR gain and the consequent increase in observable precision over encrypted P-code (A-S). Alternatively, the receiver can be used for all-in-view GPS and GLONASS single frequency navigation or monitoring.

High precision C/A code tracking is achieved by using narrow correlation [7], a variety of spacings are available with a minimum early/late delay of 70ns (two cycles of the 28.5MHz sample clock). The hardware accumulation period has various software controllable settings between 0.25ms and 20ms. This allows the possibility of very rapid acquisition of high CNR satellites as a search of all C/A code phases can be performed quickly. Long integration during steady state tracking increases the SNR in the tracking loops. The integration time flexibility allows the receiver to be used with high data rate pseudolites and Inmarsat-III transmissions. At the end of the accumulation period the summations are latched and the processor interrupted. The NCO frequency control words are double buffered with the new word applied at the start of the accumulation period. This provides a constant delay between the end of the correlation period and the application of the new NCO frequencies. Consequently the tracking performance is invariant to changes in the DSP processing load as the delay is accounted for in the tracking loops. Figure 3 provides a simplified schematic of the channel.

To reduce the hardware complexity of the channel, only a single P-code generator is used (Figure 4). Separate L1 and L2 P code NCOs clocked at the sample speed provide up/down signals to a cycle difference counter. The output of the cycle difference counter is used to control a multiplexer which has an input N states of a shift register clocked on the P(L1) code clock. The single P-code generator is driven by the P(L1) code NCO. The output of the code generator is fed to the shift register. The P(L1) code used in the correlation process is delayed by M samples to allow for an effective negative L1-L2 delay. This can occur because of GNSS satellite relative L1/L2 and group delay differences in the L1 and L2 signal paths in the RF/IF processing of the receiver. The P(L2) code is taken from the output of

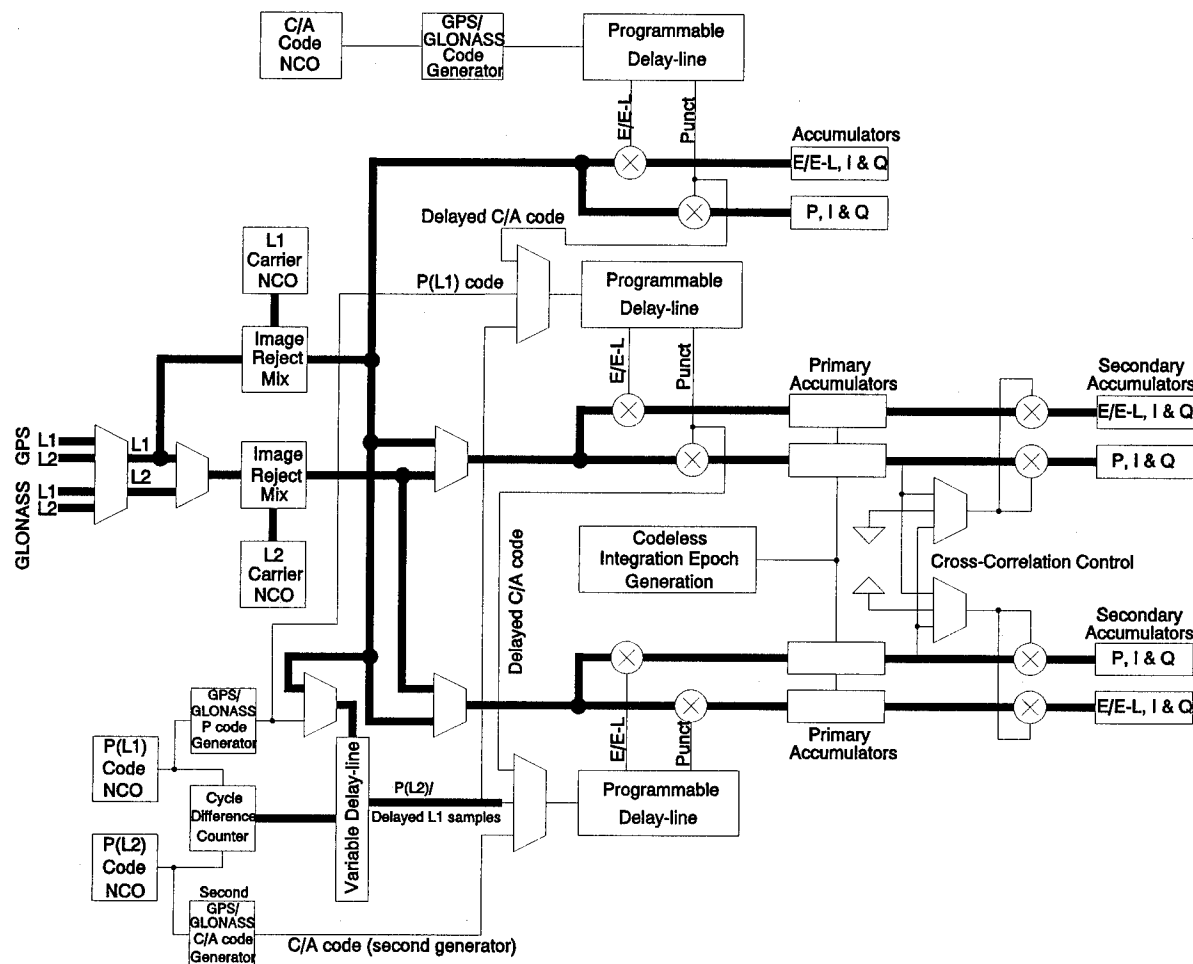


Figure 3 Channel processing hardware.

the multiplexer, and is identical to the signal produced if a separate code generator were used.

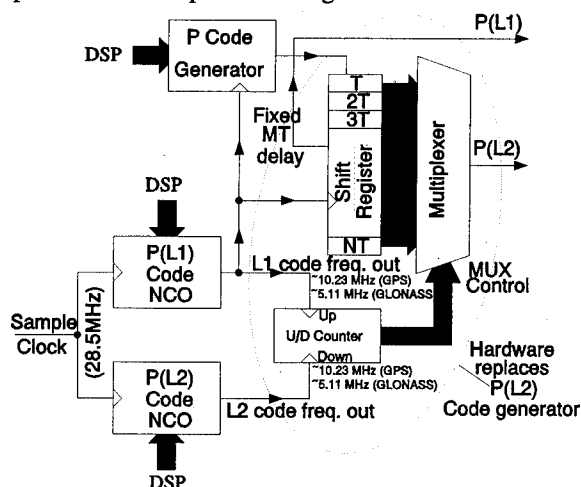


Figure 4 P code generation hardware.

The hardware allows for a variety of codeless techniques to be implemented. These include enhanced CNR techniques such as pre-correlation with the P-code followed by a type of L1/L2 cross-correlation or L2 squaring as well as standard cross-correlation. The preferred method is to take advantage of the Y code (encrypted P-code) being a

modulo-two addition of the P-code and a lower rate W-code [8]. The L1 and L2 samples are correlated with the P-code in primary accumulators. The L1 and L2 accumulation sums are cross-correlated approximately every 20 P-code chips, the result is summed in the secondary accumulators. This reduces the bandwidth of the noise and so increases the CNR which produces higher precision observables.

All observables are generated in hardware by counting integer cycles and latching the phase outputs of the NCOs on a common receiver measurement epoch. The current maximum sample rate of the code observable is 1Hz and 10Hz for the carrier. More rapid rates could be achieved by changing the frequency of the observable strobe, although the filter bandwidths would need to be widened in order to provide contiguous independent observables.

Figure 5 provides an overview of the carrier observable hardware. An 18-bit counter is clocked by the most-significant-bit (MSB) of the carrier NCO and counts the number of integer carrier cycles over the measurement period. The counter will wrap over several times as the digital IF frequencies are a up to several megahertz for some of the GLONASS

channels. However, by removing the integer number which would occur on the counter over the measurement period with no Doppler, the number of Doppler cycles can be unambiguously measured for velocities in excess of $\pm 10\text{km/s}$. By adding the partial phase latched from the phase register of the NCO the sub-cycle component of the carrier measurement can be made. Twelve bits of partial phase are latched however, due to the NCO counting modulo-twelve the resolution of the carrier measurement is $1/3072$ (approximately 0.06mm for L1 GPS).

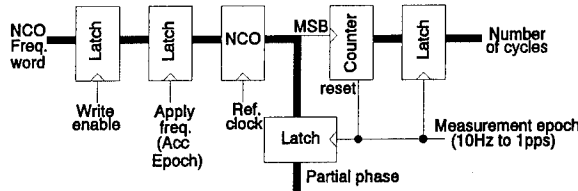


Figure 5 Carrier phase measurement hardware.

An overview of the C/A code phase measurement is given in Figure 6. Sixteen bits of the partial phase of the code NCO are latched on the 1pps measurement epoch giving a GPS C/A code resolution of approximately 4.6mm . A counter reset on the code epoch provides the number of integer chips modulo 1ms. To produce a pseudorange without the 1ms ambiguity a counter is reset during acquisition when the received system epoch in the data message is detected. The counter is incremented on the code epoch and counts modulo-1000.

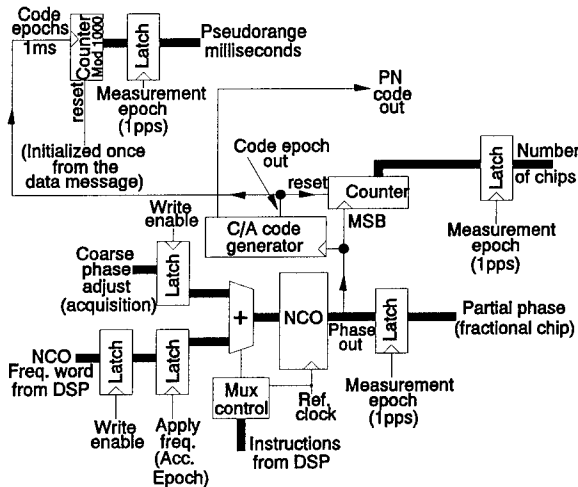


Figure 6 C/A code phase measurement hardware.

Receiver Firmware

The normal method for warm acquisition in the receiver is to set the code and carrier Doppler frequencies to the *a priori* estimate using satellite almanac information and a receiver position estimate. The C/A code is generated, I and Q correlation values are produced every millisecond synchronous with the C/A code epoch. All correlators used in the

channel are configured to search for C/A code energy with a spacing between them of one chip. If energy is not detected the code is shifted. In order for the receiver to have locked a detection threshold must be exceeded. Consider the case when there is no signal, I and Q correlation sums are independent with zero expectation, a standard deviation σ and are assumed Gaussian. The detection function is $I^2 + Q^2$. For the noise only case it can be shown using standard expressions [9] that:

$$E(I^2 + Q^2)_{\text{noise}} = 2\sigma^2 \quad (1)$$

$$\text{variance}(I^2 + Q^2)_{\text{noise}} = 4\sigma^4 \quad (2)$$

Because two independent Gaussian distributions have been squared and summed, the resulting distribution is Chi-squared (χ^2) with two degrees of freedom. The signal plus noise case must now be considered. Using the relationship [10]:

$$\frac{A^2}{\sigma^2} = 2 \frac{C}{N_0} T \quad (3)$$

where T is the correlation period, σ the receiver noise, A signal and C/N_0 is the CNR. It can then be shown that:

$$E(I^2 + Q^2)_{\text{signal} + \text{noise}} = 2\sigma^2 \left[1 + \frac{C}{N_0} T \right] \quad (4)$$

$$\text{variance}(I^2 + Q^2)_{\text{signal} + \text{noise}} = 4\sigma^4 \left[1 + 2 \frac{C}{N_0} T \right] \quad (5)$$

the resulting distribution is non-centralised χ^2 , due to the correlator totals having non-zero expectation. From this it is possible to analyze the probability of missed detection and false alarm for a given CNR and hence calculate the mean time to acquisition. A threshold was set to allow acquisition of satellites within the receiver specification and the acquisition performance was analyzed.

Once the threshold is passed the tracking progresses to the next state where a 200Hz bandwidth frequency lock loop (FLL) operates for 20ms . During this time the twenty independent values of $I^2 + Q^2$ are accumulated and compared against a threshold with a very low probability of false alarm in order to confirm lock. During all stages of the tracking progressively more stringent checks are made on the correlation values to confirm lock, without incorrectly flagging a low CNR satellite as having unlocked. A 10Hz non-coherent one-chip delay lock loop is also initiated aided by the FLL. Provided the threshold is exceeded the carrier tracking hands over to a third order 100Hz PLL. The early correlator is switched over to generate early minus late, this leaves the late correlator free (it is later used for P-code tracking) and the discriminator is changed to a non-coherent dot-product. The bandwidths of the PLL and DLL

are reduced until they are 10Hz and 1Hz respectively. The correlation chip spacing is also reduced. The data bit edges are determined and then the hardware correlation period is increased from 1ms to 10ms. This has the advantage of reducing the processor load by a factor of 10 while increasing the signal-to-noise ratio in the tracking loops. Apart from differences in the code/carrier ratio constants used in the tracking loop aiding, the source for the above algorithms is common to GPS and GLONASS operation.

At this stage the C/A code is fully locked and ready to produce observables once any transients have ceased. A search for the pre-amble is initiated. Once it is found a parity check is performed and, if successful, the time from the message is extracted for measurement time-tagging. With this time information, the GPS or GLONASS P-code generator can be initiated such that the L1 code is exactly in phase with the incoming signal, except for Gaussian C/A tracking noise and multipath. P(L2) will be in error by the ionosphere and relative L1/L2 receiver group delay. Typically this will be less than a few chips and so, once time information is available, dual-frequency P-code acquisition is very rapid. GPS provides the time at the beginning of each six-second line. Included in the HOW word is a flag to indicate whether A-S is enabled. If encrypted, the receiver automatically acquires and tracks the satellite's P-code in a codeless mode. GLONASS only transmits the time once every thirty seconds. Fortunately, as the GLONASS P code repeats every second, it is not necessary to know the time only the position within the data message; the GLONASS P-code starts synchronous with the beginning of each two-second line. A GLONASS codeless tracking mode is available however, as GLONASS has never been observed to have any encryption invoked it is not possible to analyze how successful the tracking would be, for example if a future encryption modulated a different PN code onto the L1 and L2 carriers the present tracking would fail. The L2 carrier loop is aided by the L1 loop which is driven by the C/A code (for GPS the transmitted L1 C/A code power is 3dB greater than P(L1) and 6dB greater than P(L2) [11]). Both the L1 and L2 P code tracking is also aided by the C/A carrier loop. The nominal bandwidth for the code loops is 1Hz with 10Hz for the carrier.

When the codeless tracking is invoked the data message is removed. Consequently much longer integration periods are possible in order to increase the tracking loop SNR. This is implemented in the current firmware. Also, as the BPSK data has been removed, a $\pm 180^\circ$ arctangent look-up-table can be used to increase the operating region of the carrier discriminator.

Receiver Processing Unit

The processing is split between an Analog Devices ADSP21020 DSP which is currently undergoing an ESA sponsored spatialisation program and the host PC. The PC software provides the user interface, navigation solution, observable storage, satellite selection, acquisition *a priori* Doppler calculation and extraction of the navigation parameters from the received binary data. These functions will be ported to the DSP or a new processor, depending on processor load, during the next phase of the receiver development. The PC communicates with the DSP via dual-port RAM (DPRAM) accessed from the PC ISA bus. The DSP performs signal acquisition, receiver control, satellite tracking, sampling board control (AGC functions), and observable generation. The DSP board consists of the processor with boot EPROMs, 32K words of program SRAM, 32K words of data SRAM, 4Kx16 bits of DPRAM, a DUART and an FPGA. The FPGA is used for receiver time base generation and processor glue logic. Flexibility has been built into the processor board to allow development. The processor can be booted from the EPROMs, a serial port, the DPRAM or a JTAG port, and can address up to 4 antennae and 64 channels (this may be useful for attitude determination applications). All core components on the DSP board (RAM, DSP and DPRAM) can be obtained in package and electrically compatible ESA approved space grades allowing easy migration to a space-qualified receiver. All code has been written in 'C' which provides easy maintenance and portability.

Calibration Issues

GLONASS uses FDMA therefore, unlike GPS, the receiver has a different group delay at each channel frequency. Any bandpass element will introduce these delays, i.e. the antenna, filters and amplifiers. In a survey mode these errors cancel for GPS when two pseudoranges or carrier phase-ranges are differenced on the same receiver - the single difference. For GLONASS this is not the case [6,12]. In order to minimize these delays all the filter elements in the receiver have been designed to provide flat group delay characteristics and a low variation with temperature. Although not implemented in the current prototype, a real-time calibration scheme has been investigated. In the next model of the receiver a dedicated channel will be used to track a locally generated L1/L2 signal which will switch between the GLONASS channels. This will allow accurate GLONASS inter-channel bias calibration and also provide a means of measuring and removing the relative L1/L2 receiver delay variation.

Results

This section illustrates the tracking performance of the receiver. The final RF/IF and sampling sections of the prototype are not yet complete, and so all results shown use one-bit samples from a RF/IF section modified from a previous Leeds receiver design [13]. Consequently, there is some L2 degradation. Delivery of the antenna pre-selection filter is expected in October. At present, an active Trimble dual frequency antenna is used (circa 1990) which is not ideal for GLONASS, especially at L2. The residual when the accumulated delta range is subtracted from the pseudorange is given to highlight the tracking performance and is defined as follows:

Pseudorange observable:

$$\rho = R + T + \frac{I}{f_{1,2}^2} + \eta_{code} \quad (6)$$

Accumulated delta range (ADR) observable:

$$\phi = R + T - \frac{I}{f_{1,2}^2} + \eta_{carrier} + N\lambda \quad (7)$$

R - geometric satellite to receiver range

T - clock offset

η_{code} and $\eta_{carrier}$ are the tracking noise

N - carrier observable integer ambiguity

λ - carrier wavelength

$I/f_{1,2}^2$ - frequency dependent ionospheric delay

The residual is given by:

$$\rho - \phi = \eta_{code} - \eta_{carrier} - N\lambda + \frac{2I}{f_{1,2}^2} \quad (8)$$

provided carrier lock is maintained N is constant. Consequently the noise on the code observable is given (since $\eta_{code} \gg \eta_{carrier}$). By manipulating the L1 and L2 ADR it is possible to remove the ionospheric profile. In any practical situation the code phase noise will include a significant contribution from multipath.

GPS Data

Figure 7 provides dual frequency observables from a GPS satellite, taken when A-S was not active. The data shown in this graph was taken at 1Hz with L1 and L2 code bandwidths of 1Hz, carrier bandwidths of 10Hz and an integration time of 10ms. No carrier smoothing or filtering has been applied to the data. A linear combination of L1 and L2 ADR has been subtracted to remove the ionospheric affect, all three curves are flat and therefore the receiver is correctly tracking the L1/L2 ionospheric divergence.

The C/A and P(L1) have a correlation coefficient of approximately 0.7 with a zero time shift, this is due to multipath reflections with a differential path length

of less than approximately 15m. In this region the P and C/A code discriminators produce the same error for a multipath signal. The P(L1) and P(L2) data is uncorrelated due to the different carrier wavelength.

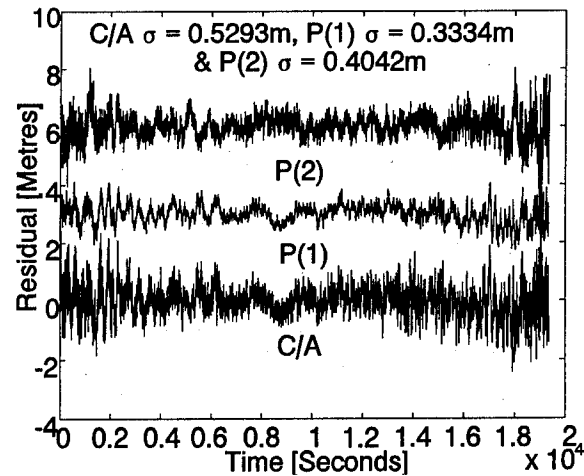


Figure 7 Ionospherically corrected pseudorange minus ADR for C/A, P(1) & P(2). Average values offset for presentation.

Although the multipath signal will have the same additional path length for L1 and L2, the number of carrier cycles (and in particular the partial phase) will be different for L1 and L2 due to the different wavelengths. Therefore, the degree of constructive/destructive interference to the direct signal is different for the two frequencies. This affects the error in the code loop. The measurement correlation can be seen in Figure 8.

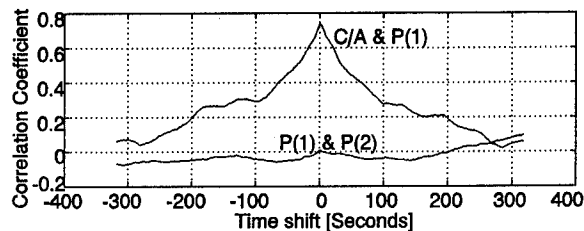


Figure 8 Cross-correlation between C/A & P(1), and P(1) & P(2).

To show the performance comparison against a commercial receiver the antenna feed was also connected to a Trimble 4000SSE and both receivers instructed to track the same satellite. Figure 9 shows the resulting C/A code data for a one hour segment when the satellite was close to zenith. The Trimble had a standard deviation of 24.5cm, the Leeds receiver was slightly noisier at 29.5cm. The Leeds bandwidths were as stated above, no data for the Trimble tracking loops was available. The low frequency noise, on the order of a few minutes, are caused by multipath and are correlated between the receiver - see Figure 10.

Codeless GPS Data

Figure 12 shows a five hour segment of data tracking

GPS P-code in a codeless mode. The current algorithm is still under development however, as can be seen, the receiver is successfully tracking the P-code when A-S is enabled. The P-code tracking loops used during the tracking session presented in Figure 12 had a bandwidth of 0.1Hz, integration period of 100ms, and are aided by the C/A code. To confirm that the tracking is not correlating the P(L1) and P(L2) measurements, the cross-correlation was produced - Figure 11. The expected correlation between C/A and P(L1) is due to multipath, whereas P(L1) and P(L2) are uncorrelated. Any further processing of the data would use the C/A code as the L1 code observable.

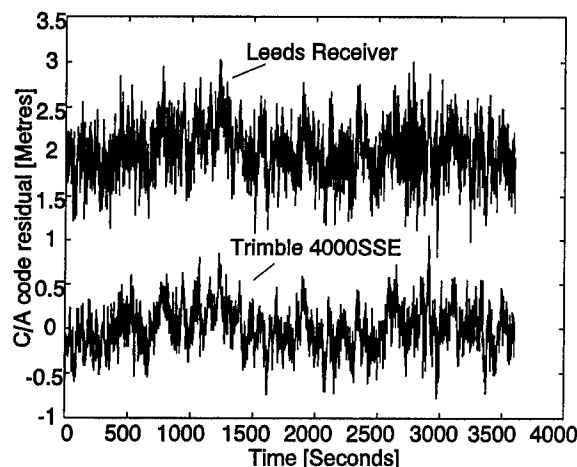


Figure 9 C/A code pseudorange minus accumulated delta range for PRN15 on 7th August 1995 from a Trimble 4000SSE and the University of Leeds GNSS receiver on a zero baseline.

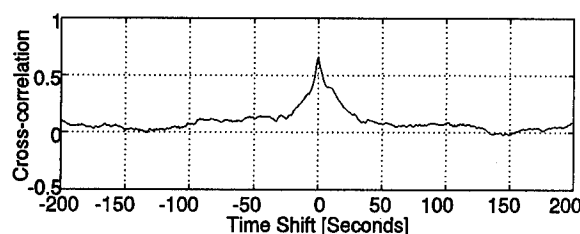


Figure 10 Cross-correlation of the Trimble and Leeds data given in Figure 9.

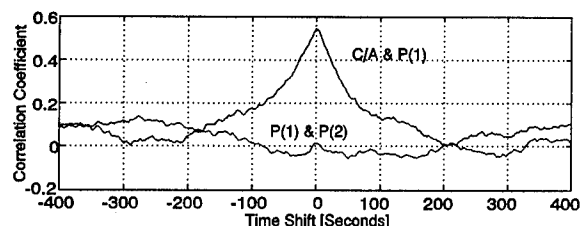


Figure 11 Cross-correlation between C/A & P(1), and P(1) & P(2) for the data in Figure 12.

Figure 13 gives data from PRN 14 taken on 5/9/95, during this session the codeless P-code loops were increased to 1Hz. To show the carrier tracking precision of the data, the L2 carrier phase was subtracted from the L1. This produces a profile

which changes according to ionospheric activity.

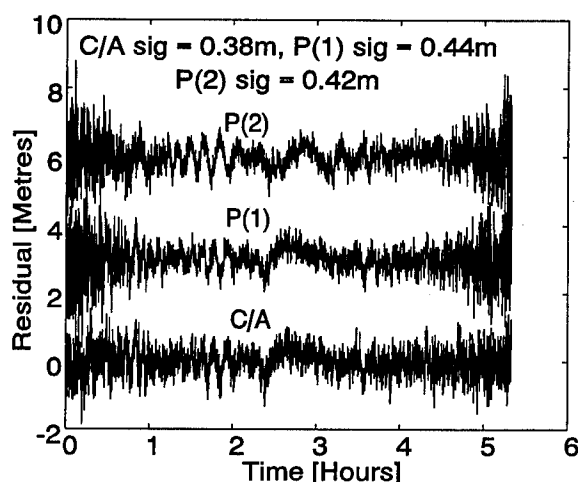


Figure 12 Ionospherically corrected pseudorange minus ADR for C/A, P(1) & P(2) of PRN 9 on 26th August 1995 (A/S on). Code tracking bandwidths of C/A 1Hz, codeless P(1) & P(2) 0.1Hz.

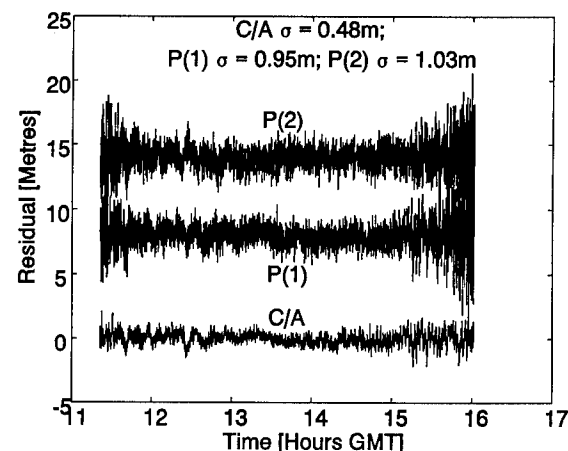


Figure 13 PRN 14 on 5/9/95 (A/S on). Codeless bandwidths 1Hz.

To produce an estimate of the carrier phase measurement noise the data was split into overlapping 30 minutes segments. A quadratic fit was removed from each section to remove the ionosphere divergence. The standard deviation of the 30 minutes of de-trended data was then calculated and plotted, this is given in Figure 14. The elevation angle is also given in the plot. It can be seen that at high elevations the standard deviation of the difference in L1 and L2 carrier phase observables is as low as 2mm, the L1 carrier phase is obtained from tracking the C/A code (10Hz bandwidth), L2 is from codeless tracking of P(L2) (1Hz bandwidth). Remaining errors are multipath and residual ionospheric effects.

GLONASS Data

Figure 15 shows ionospherically-corrected residual data from GLONASS almanac 15 (channel number 4) taken on 30/8/95. The L2 data is degraded due to the commercial GPS Trimble antenna unit used during

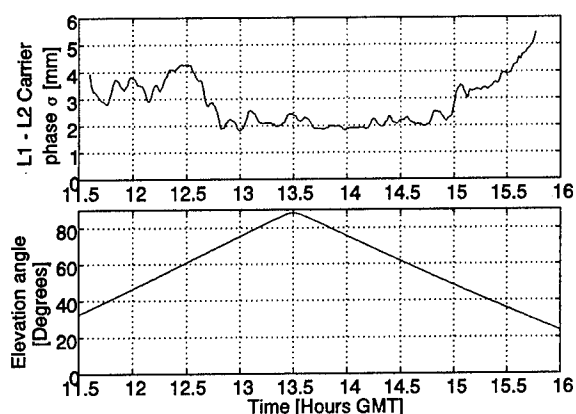


Figure 14 Thirty minute standard deviations of L1 minus L2 (minus quadratic fit) carrier phase and satellite elevation from the same data set as given in Figure 13.

the test. The measured L2 return loss at the GLONASS frequency is -5dB and at GPS it is -25dB. No data was available for the antenna gain at GLONASS frequencies. The measurements generally have approximately twice the standard deviation of that for GPS for similar CNR due to the chip length of GLONASS being twice that of GPS. Because of the difference in chip lengths, GLONASS is affected by multipath with differential path lengths twice that of GPS; this also adds to the standard deviation of the code phase measurements.

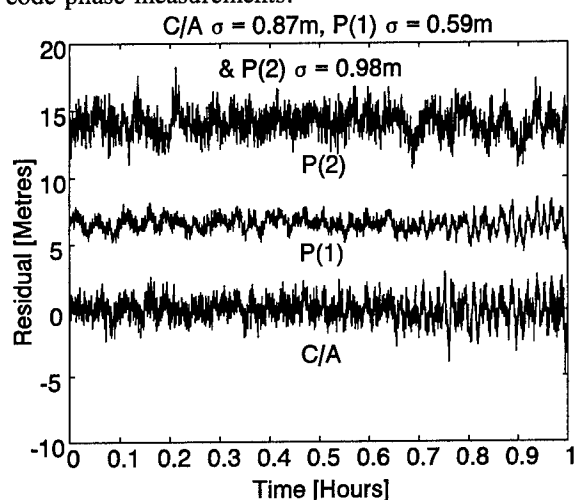


Figure 15 Ionospherically corrected pseudorange minus ADR for C/A, P(1) & P(2). Average values offset for presentation.

Future Developments

The results shown above are from provisional tests at Leeds. The current receiver is a 19" rack-mount unit with considerable power consumption due to the large number of FPGAs. The channel processing hardware resides entirely within FPGAs and the development of a space-qualified multichannel ASIC is a major part of the next phase of the program. IMEC in Belgium and Alcatel Espace in Spain with the help

of the Leeds team are currently producing VHDL code from the FPGA schematics. Also during the next phase, the RF/IF circuitry will be miniaturized and code resident on the PC ported to the DSP.

Acknowledgements

This work has been funded by ESA. The authors would like to thank Trimble Navigation UK for the loan of the Trimble 4000SSE. Alcatel Espace, Toulouse are acknowledged for the RF/IF filters.

References

- [1] W.Bertiger W, et al., "The First Low Earth Orbiter with precise GPS Positioning: Topex/Poseidon", *Proc of the ION GPS-93*, Salt-lake City, Utah, USA, 22-24 Sept. 1993.
- [2] O.L.Colombo, "Mapping the Earth's Gravity Field with Orbiting GPS Receivers", *Proc of the IAG Symposium 102: GPS and Other Radio Tracking Systems*, Edinburgh, Scotland, 3-12 August 1989.
- [3] W.G.Melbourne et al., "The Application of Spaceborne GPS to Atmospheric Limb Sounding and Global Change Monitoring", JPL Publication 94-18, Pasadena, CA, USA, April 1994.
- [4] B.M.Herman, D.Feng, W.Schreiner and M.Exner, "Early Results of the GPS/MET Program", presented at the URSI Working Group AFG1 Conference on Atmospheric Research and Applications using Observations based on the GPS/GLONASS Systems, Danish Meteo Institute, Copenhagen, 8-9 June 1995.
- [5] H.P.Ladreitner and G. Kirchengast, "GPS/GLONASS-Sensing of the Neutral Atmosphere: Model Independent Correction of Ionospheric Influences", submitted to *Radio Science*, June 1995.
- [6] P.Raby and P.Daly, "Using the GLONASS System for Geodetic Survey", *Proc. of ION GPS-93*, ION Satellite Division, 6th International Technical Meeting, Salt-Lake City, Utah, USA, 22-24 September, 1993.
- [7] A.J.Van Dierendonck, P.Fenton and T.Ford, "Theory and Performance of narrow correlator spacing in a GPS receiver", *Proc. ION National Technical Meeting*, San Diego, CA, 27 January 1992.
- [8] R.G.Keegan, "P-Code Aided Global Positioning System Receiver", United States Patent 4972431, 20th November 1990.
- [9] A.Papoulis, *Probability, Random Variable, and Stochastic Processes*, 3rd Edition, McGraw-Hill, Inc., 1991.
- [10] S.Hinedi and J.I.Statman, "Digital Accumulators in Phase and Frequency Tracking Loops", *IEEE Transactions on Aerospace and Electronic Systems*, Vol 26, No. 1, January 1990.
- [11] NATO MAS Standardisation Agreement - NAVSTAR GPS System Characteristics. STANAG 4294 Draft Issue N, May 1991.
- [12] P.Raby and P.Daly, "Surveying with GLONASS: Calibration, Error Sources and Results", *Proc. of the 3rd International conference on Differential systems*, London, April, 1994.
- [13] S.Riley, "An Integrated Multichannel GPS/GLONASS Receiver", *Proc. of ION-GPS 92*, ION Satellite Division, 5th International Technical Meeting, Albuquerque, New Mexico, September 16-18, 1992.

Integrated GPS/GLONASS Antenna for High Performance Applications

Taymoor Hekmat and Norbert Niklasch
ViCon Engineering GmbH

Martin Maurer
MAN Technologie AG

BIOGRAPHIES

Taymoor Hekmat received his M.S. in Electrical Engineering in 1992 from the Technical University of Munich. He worked as a research assistant in the area of polarimetric remote sensing and antenna systems at the Technical University of Munich. He joined the ViCon Engineering company, as a scientific coworker, in 1994, where he is currently responsible for antenna research and development.

Norbert Niklasch, received a M.S. in Electrical Engineering in 1983 from the University of the Federal Armed Forces, Munich. He worked in the area of electronic reconnaissance, on system design and software development for differential reference, integrity monitoring stations, and satellite navigation systems. Since 1993 he is owner of the ViCon Engineering company.

Martin Maurer, received a M.S. in physics in 1974 and a Ph.D. in 1984 from the University of Munich. He is a specialist for system design and software development for advanced differential reference and integrity monitoring stations. He is responsible for the MAN Technologie AG study project team for future satellite navigation systems GNSS 1 and 2 in the framework of the studies issued by the European Space Agency.

ABSTRACT

The combined utilization of both the GPS and GLONASS systems is of particular interest for improving the availability, accuracy and reliability of satellite positioning data, especially in certain civil applications that require high levels of precision and integrity. On the other hand, high-precision applications such as integrity monitoring or differential reference systems require antennas with a high level of multipath rejection and a high degree of phase uniformity, while covering the upper hemisphere with a smooth gain pattern and with minimum axial ratio.

In this paper, we shall present an antenna system which has been developed to satisfy the above stated requirements in the frequency band of both the GPS L1/L2 and GLONASS L1/L2 systems. The antenna element is built up as a superstrate loaded stacked microstrip configuration flushmounted on a corrugated ground-plane. Performance optimization with emphasis on multipath rejection has been carried out and will be presented here. Some special techniques for improving the radiation pattern and AR level have been incorporated and are described. Design considerations covering broadbanding the AR, input reflection coefficient, and antenna gain properties are also discussed.

INTRODUCTION

The multipath phenomenon is one of the most dominant error sources in high-precision satellite positioning and navigation. Particularly in phase tracking systems it can lead to significant relative errors [1]. In differential GPS (DGPS) it has been well-established as the dominant error source [2]. In order to achieve an efficient multipath rejection, one needs an antenna with sharp pattern roll-off at low elevation angles. The multipath error investigation of Braash [2] shows that not only for low elevation angle satellites but even for the high elevation angle ones multipath error occurs. Hence for an optimum antenna design very low levels of side- and backlobes are also required. We have improved the multipath rejection property in a powerful manner through the proper combination of substrate and superstrate and through the use of a corrugated ground-plane.

Using two stacked flat resonators, which are driven separately, exhibits many advantages for a dual-band GPS/GLONASS reception. Due to the enhanced isolation between the patcher, there is an inherent band separation and thus preventing undesired signals outside of the frequency bands. The phase center locations of the two stacked microstrip antennas are relatively stable. With some improvement techniques we can achieve an acceptable multipath property. And the overall AR level is also good.

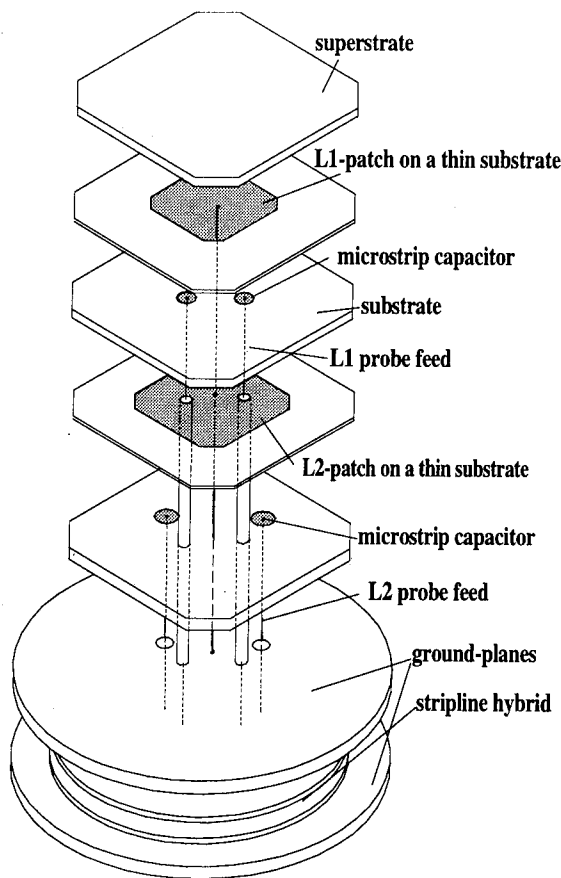


Fig. 1

Furthermore is a bandwidth of more than 3.4% for each frequency band L1/L2 necessary for the reception of both GPS and GLONASS signals. Since microstrip antennas exhibit an inherent narrow bandwidth, broadbanding techniques are necessary to maintain the desired VSWR, AR and gain level within each frequency band. Desired bandwidth is achieved by means of the decreased quality factor of the antenna. This technique has nevertheless some disadvantages which should be minimized.

Another effort is adapting the radiation pattern to the hemispherical coverage. Some investigations are done to find the suited configuration. Lowering the AR level is another concern in an optimum antenna design. It is found that higher order modes and unequal E- and H-plane radiation patterns of the linear patches at low elevation angles are the main sources of circular polarized crosspolarisation. These effects should also be minimized.

Antenna requirements:

Frequency bands: L1 1.565-1.620 GHz

L2 1.217-1.262 GHz

Radiation pattern: Hemispherical up to 5 degrees elevation;

Sharp pattern roll-off at the elevation angles below 5 degrees;
Very low side- and backlobes.

Polarization: Right-hand circular polarized;
AR- level over the entire coverage area. lower than 3 dB.

Phase response: Uniform over the entire coverage area.

Computation method

The analysis and determination of the antenna structure is carried out by means of the full-wave analysis method [16]. It applies the mixed potential integral equation formulation based on Green's function treatment and the method of moments. This method provides the most accurate results among the other computing models and enables the consideration of the mutual coupling effects between the patches and the capacitors, the effect of the superstrate and also the effect of the short circuiting of the lower patch as well as the consideration of the surface waves. A full-wave analysis program has been used to perform the antenna simulations. For all simulations infinite extension of the substrate and the ground-plane is assumed. Close agreement between simulated and measured results has been observed.

Antenna configuration

It is well known that single-fed microstrip antennas have a narrow AR bandwidth. Thus a dual-fed configuration is chosen for the excitation of circular polarization. Two probe feeds are excited with equal amplitude and with 90° difference phase by means of an hybrid coupler. Fig 1 illustrates the configuration of the antenna. The antenna is built up as a superstrate loaded, piggyback microstrip configuration. A phase shifting circuit is designed in stripline technique and placed on the backside of the antenna ground-plane to avoid spurious radiation. It consists of two separate hybrid couplers, respectively for L1 and L2 bands. This separation provides an inherent band isolation and optimum hybrid properties for each frequency band.

The piggyback configuration has the advantage of inherent band separation of each radiating patch. Furthermore, the simulations have shown that the radiation pattern of each patch is not affected and thus not degraded by the other patch (Fig. 2). In contrast to the piggyback configuration, an alternative arrangement such as the electromagnetically coupled stacked patches exhibits large patterns of imbalance [3].

The antenna consists of two stacked four-corner truncated patches. The patches are fed by means of two microstrip capacitors which are connected through the probe feeds with the corresponding hybrid. The probe feed of the upper patch is a small diameter coaxial probe extending through the substrate of the lower patch. Thus the lower patch is short circuited at

two points by the outer conductor of the probes and acts as the ground-plane of the upper patch. The upper patch is loaded with a superstrate. The substrate and the superstrate of the upper patch acts as the superstrate of the lower patch.

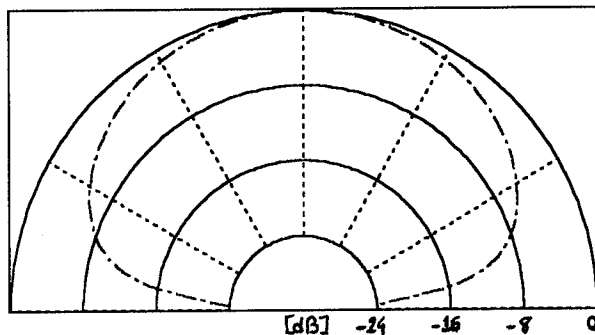


Fig. 2 : Radiation pattern of a lower patch in a piggyback antenna configuration.

Broadbanding and AR-level

Various techniques of broadbanding have already been investigated by several authors. It is well known that arranging parasitic elements either above [4] or beside [5] the radiating patch improves the bandwidth. However plane parasitic elements have the disadvantage of some pattern asymmetry and pattern change at different frequencies. Stacked parasitic configurations have also reduced efficiency and it is complicated to incorporate them in a dual frequency stacked patch design. Another wideband technique is the use of impedance matching networks [6]. The proper matching network for four feeds requires a too big area and can not be placed in the central cavity of a corrugated ground-plane.

The bandwidth of microstrip antennas can also be increased by means of a patch element with a low quality factor Q_r , i.e. by increasing the thickness of the substrate and decreasing its dielectric constant. This method yields the most structural simplicity and exhibits good radiation properties. On the other hand it has the disadvantages of increased surfacewave radiation, increased higher-order mode excitation, and increased input reactance by probe feeds. These disadvantages have to be minimized.

Several antenna configurations have been simulated to investigate the effects which give rise to cross-polarization and increased AR-level. Some results are shown in the figures 3 and 4. Fig.3-a and -b show that with lowering of the Q_r , the level of cross-polarization increases. Feeding with four probes respectively with 0° , 90° , 180° and 270° phase differentials provides a significant improvement in the boreside region (Fig 3-c). Four-probe feeding is a well known method for suppression of the higher-order modes [7], thus the higher-order modes may be the dominant source of cross-polarization at least in the boreside region. The

increased cross-polar level at low elevation angles is due to the unequal radiation of linear polarized components in H- and E-planes for infinite extension of ground-plane and substrate. The effect of applied superstrate on the cross-polarization and AR-level is negligible (Fig. 3-d).

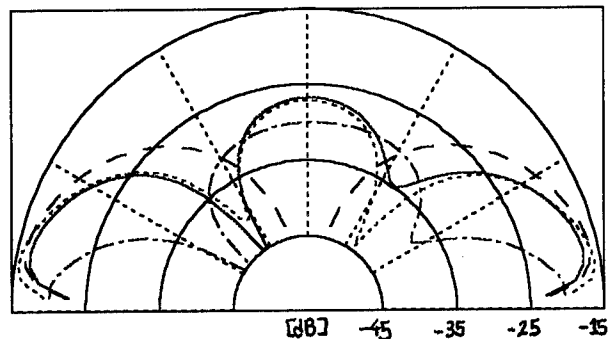


Fig.3 : Crosspolar radiation pattern. a) (---) Antenna with Q_r equal to 42, b) (-.-.-) Antenna with Q_r equal to 33, c) (—) Antenna with Q_r equal to 33 and four feed points, d) (—) Antenna with Q_r equal to 33 and with superstrate.

Since the four-feed method requires a big area for its phase shifting, a novel configuration was developed to reduce the generation of higher-order modes, and thus the AR-level of the antenna : a four corner truncated rectangular patch. Teshirogi and Goto [8] have already used the circular polarizer notches in microstrip disc antennas to suppress the higher-order modes. Generating circular polarization by means of two truncated corners is also a well known method [9]. Depending on the orientation of the truncated corners and the feed, the antenna will be right- or left-hand polarized. Therefore a dual-feed antenna with only two truncated corners generates both right- and left-hand polarizations and the higher-order mode suppression will be not efficient enough. Using four truncated corners results in a remarkable improvement of crosspolarization, particularly in the boreside region. Fig. 4 shows this effect. At first the truncation geometry has been determined with the simple closed equation presented by Haneishi et. al. [9]. With these a priori values the accurate geometry is then determined by means of the fullwave simulations.

Low quality factor has also the disadvantage of increasing the reactance of the probe feed and thus a mismatch, even at resonance. This mismatch decreases the VSWR-bandwidth and worsens the AR properties of the antenna. By means of a microstrip capacitor which is placed below the radiating patch (Fig. 1), the probe reactance is canceled out within the radiating structure. The bandwidth is increased from 2.2 percent to 3.4 percent and low AR level is maintained due to the coincidence of resonant frequency of the antenna and the middle frequency of the operation band. The microstrip capacitors cause a slight increase of cross-coupling of the feeds and thus a small

increase of AR level. However, the measured AR-levels show that this effect has not greatly influenced the AR-properties of the antenna.

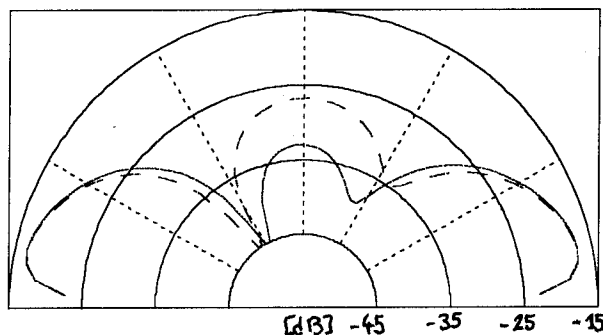


Fig 4 : Crosspolar radiation pattern. (---) Rectangular patch with low quality factor. (—) Four corner truncated rectangular patch with low quality factor.

Radiation pattern

The ideal antenna would have uniform gain from zenith to 5 degrees elevation angle, then an immediate roll-off for all other angles below 5 degrees. Some techniques to approximate the ideal radiation pattern have been investigated. The primary idea was to combine two different radiation patterns of two radiating elements to achieve the desired pattern. In order to have a relative simple stacked configuration, the radiating elements had to be in the same plane and be coupled electromagnetically. An annular-ring-loaded circular-disc radiator, in which the TM_{21} -mode in annular-ring and TM_{11} -mode in circular-disc are excited, appeared to be the most proper candidate. The simulations and the measurements showed only a poor coupling between the probe feed excited circular-disc and the annular-ring. The radiation pattern of the circular-disc was not affected by the ring and thus the desired pattern could not be achieved.

The next possibility, the effects of the substrate properties on the radiation patterns, have also been investigated. It has been observed that by increasing the relative permittivity, the gain at the middle and lower elevation angles also increases and the radiation pattern tends to be an hemispherical one. On the other hand, by increasing the relative permittivity, the gain at 5 degrees and lower elevation angles also increases and the multipath rejection will fail.

However, the simulation of several superstrates has shown that one can overcome this problem with a proper combination of the superstrate and the substrate. The effect which could be applied is that the proper superstrate gives rise to a strong elevation angle dependent decrease of the gain. It means that the decrease of the elevation angle first becomes remarkable and significant at 15 degrees and 10 degrees elevation angle respectively. Thus with a

proper combination of substrate and superstrate it is possible to achieve both an approximated hemispherical pattern and an acceptable rejection. Fig. 5 illustrates this effect.

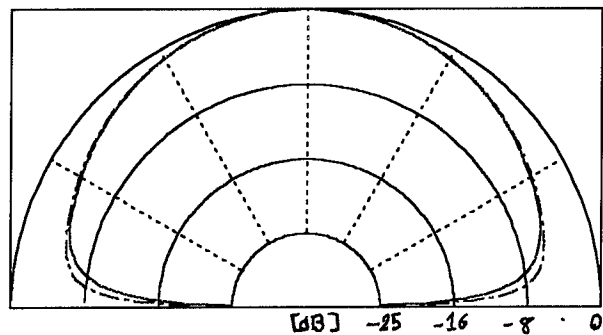


Fig 5 : (---) Antenna without superstrate. (—) Antenna with superstrate.

Corrugated ground-plane

Generating hybrid modes through the corrugated surfaces is a well-known method for achieving radiation pattern symmetry and very low crosspolarisation in corrugated horns. As a simple approximation one can consider the corrugated wall as a reactive surface with a vanishing admittance $Y=0$ at a proper corrugation depth. The field under this condition has then zero azimuthal dependence and the cutoff corrugated surface will prevent the propagation of surface waves. Considering the corrugated ground-plane as a wide flare angle corrugated horn with a semi flare angle equal to 90° , one can use the same theory and design considerations as for corrugated horns to determine the structure of a corrugated ground plane.

Several models have been proposed to predict the properties of corrugated horns. The space harmonic model, proposed by Cloaricoats and Olver [10] yields under considering of the full slot geometry accurate results for corrugated horns with a semi flare angle up to 15° . Cloaricoats and Saha [11] presented also the spherical-mode model for predicting the properties of conical horns with semi flare angles greater than 15° . Tranquilla et al. [12] applied this model to predict the farfield characteristics of several GPS antenna types flushmounted to a corrugated ground-plane. Their computed results are in close agreement with measured data.

The corrugation depth is approximately $\lambda/4$ or more and dependent on aperture size and flare angle. However for accurate determination of its value, the full geometry of the slots should be considered. By the proper choice of corrugation geometry, the number of slots per wavelength is not critical but a minimum number of slots per wavelength are needed to prevent the effect of the non-resonating slot. On the other hand

the corrugation becomes less frequency dependent as the slot width to ridge width ratio increases [13]

For L1/L2 dual band operation one can choose either a unique corrugation depth corresponding to the lower edge of the L2 frequency-band or one can choose two corrugation depths, each corresponding with one frequency band. Both techniques are already successfully used in wideband corrugated horns.[14][15].

Based on the spherical-mode model, the corrugation depths have been determined various diameters and several corrugated ground-planes with corrugation depths equal and higher to these values have been produced and will be measured.

Fig. 9a and b shows the measured radiation pattern of the microstrip antenna flushmounted to a corrugated ground-plane. The corrugations are 0.26λ depth at the band middle frequency and have a ridge width to slot width ratio of 0.1. The ground-plane diameter is equal to 1.86λ . Sharp pattern roll-off at low elevation angles is achieved. The side-lobes have vanished and the back-lobe level has decreased to -38 dB. Furthermore, the AR-properties have improved, particularly in boreside direction. The pattern symmetry has also improved.

Experimental results

Applying the techniques presented in this paper, an antenna element flushmounted to a corrugated ground-plane for the L1 band has been produced and measured. Some measurement results have been shown in Fig. 7-9. The desired performances are achieved. The antenna flushmounted to the ground-plane has excellent AR-properties over the entire coverage area. The multipath rejection due to sharp pattern roll-off and very low side- and backlobes is performed and the 3.4% bandwidth is also maintained. The antenna gain is equal to 7 dBic.

CONCLUSIONS

High-precision applications of GPS and GLONASS systems require antennas with a high level of multipath rejection and a high degree of phase uniformity. They should also cover the upper hemisphere with a smooth gain pattern and minimum axial ratio. An antenna system has been presented which has been developed to satisfy the above requirements for both systems. It has been shown that powerful multipath rejection is possible by means of a proper substrate-superstrate combination and by the use of a corrugated ground-plane. Some techniques for maintaining 3.5% bandwidth have also been presented. Proposed techniques performed excellent AR properties over the entire frequency band and over the entire coverage area. An antenna element

flushmounted to a corrugated ground-plane has been produced and measured. The measurements have confirmed the presented design techniques.

REFERENCES

- [1] Tranquilla, J.M., "Multipath and imaging problems on GPS receiver antennas", Proc. 4th Int. Symp. Satellite Positioning, Austin, TX, Apr.28 - ay 2, 1986, pp. 557-561.
- [2] Braasch, M., "Optimum Antenna Design for DGPS Ground Reference Stations", Proc. of the ION - GPS 94, pp 1291-1297.
- [3] Sensiper, S., Williams, D., and Mc Kone, J.P., "An integrated global positioning satellite antenna-low noise amplifier system", IEEE Int. Conf. Antenna & Propg. 1987, Part 1, pp 51-54.
- [4] Chen, C.H., Tulintseff, A., and Sorbello, R.M., "Broadband two-layer microstrip antenna", IEEE AP-S Sym. Digest, 1984, Boston, MA, pp. 251-254.
- [5] Kumar, G., and Gupta, K.C., "Nonradiating edges and four edges gap-coupled multiple resonator broad-band microstrip antennas", Microstrip Antenna Design (Artech House Inc., Norwood, 1988),p 276.
- [6] Sakaguchi, K., Hasebe, N., "A feeding technique for broadbanding and dual-banding microstrip antenna", Electr.&Comm.in Japan, Part 1, Vol.76, No 4, 1993, pp 102-111.
- [7] Chiba, T., Suzuki, Y., and Miyano, N., "Suppression of higher modes and cross polarised component for microstrip antennas", IEEE AP-S Int. Symposium Antennas and Propagat. Digest, 1982, pp.285-288.
- [8] Teshirogi, T., and Goto, N., "Recent phased array work in Japan", ESA/COST 204 Phased-Array Antenna Workshop, 1983, pp. 37-44.
- [9] Haneishi, M., and Yoshida, S., "A design method of circularly polarized rectangular microstrip antenna by one-point feed", Microstrip Antenna Design (Artech House Inc., Norwood, 1988), p 313.
- [10] Clarricoats, P.J.B., and Olver, A.D., "Corrugated horns for microwave antennas", (Peter Peregrinus Ltd., London, 1984).
- [11] Clarricoats, P.J.B., and Saha, P.K., "Propagation and radiation behaviour of corrugated feeds, Part 2 - Corrugated-conical-horn feed", Proc. IEE, vol. 118, No. 9, pp 1177-1186, Sept. 1971.

- [12] Tranquilla, J.M., Carr, J.P., and Al-Rizzo, H.M., "Analysis of a choke ring groundplane for multipath control in global positioning system (GPS) Applications", IEE Trans. 1994 - AP 42, pp 905-911.
- [13] Thomas, B.Mac A., James, G.L., and Greene, K.J., "Design of wide-band corrugated conical horns for cassegrain antennas.", IEEE Trans. AP-34, 186, pp 750-757.
- [14] Rao, K.S., "A simple dual-band corrugated horn with low cross polarization", IEEE Trans. 1990, AP-38, no. 6, pp. 946-950.
- [15] Olver, A.D., Yang, K.K., and Clarricoats, P.J.B., "Propagation and radiation behaviour of dual-depth corrugated horns microstrip antenna design", IEE Proc. H, 1984, 131, Ppp. 179-185.
- [16] Mosig, J.R., and Gardiol, F.E., "General integral equation formulation for microstrip antennas and scatterers" Microstrip Antenna Design (Artech House Inc., Norwood, 1988), p179.

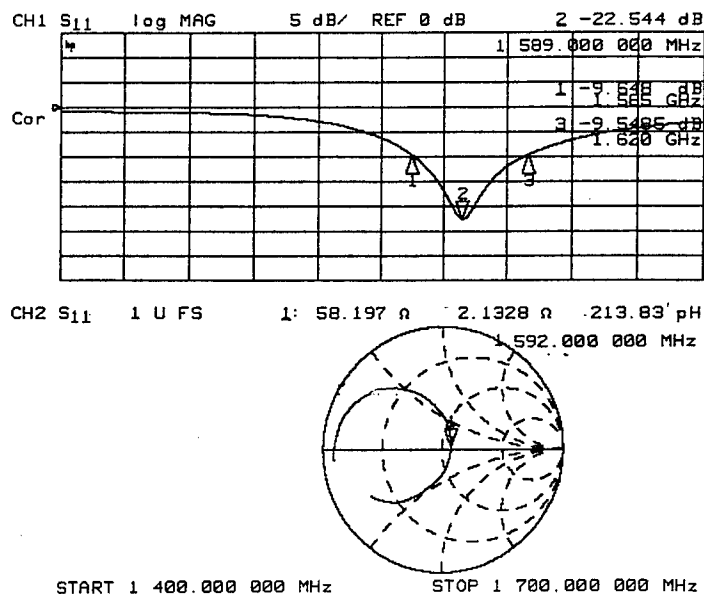


Fig.7 : Return loss and input impedance of the L1-antenna.

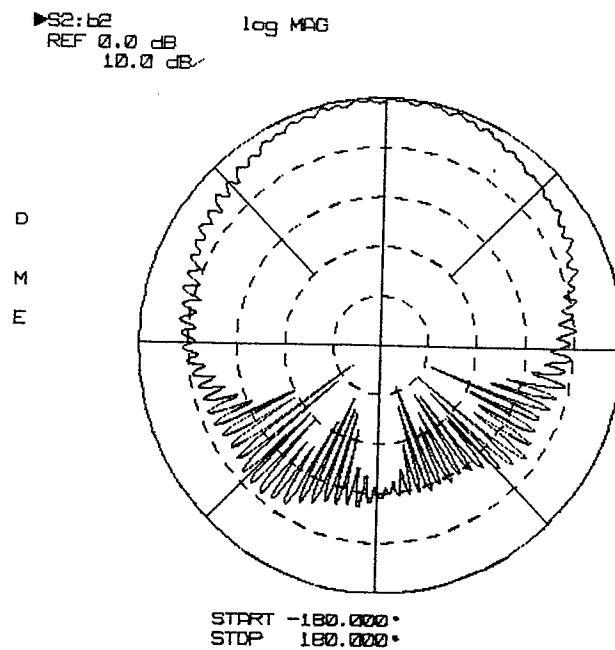


Fig. 8a: Measured radiation pattern of the antenna without corrugated ground-plane. Frequency 1,565 GHz.

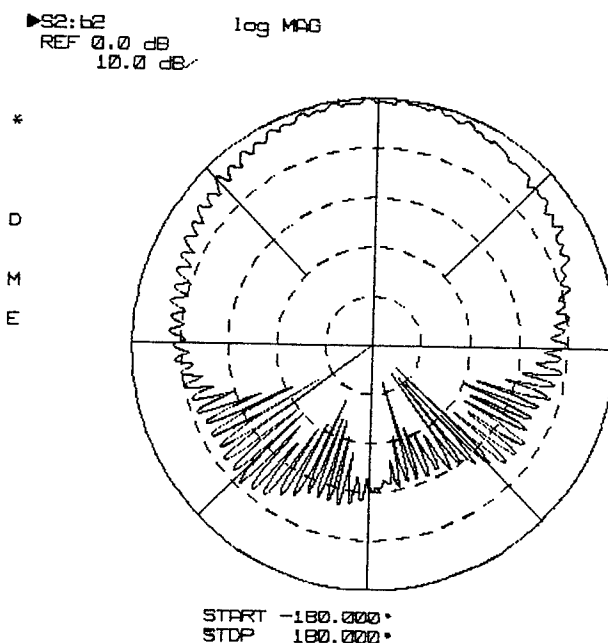


Fig. 8b: Measured radiation pattern of the antenna without corrugated ground-plane. Frequency 1,620 GHz.

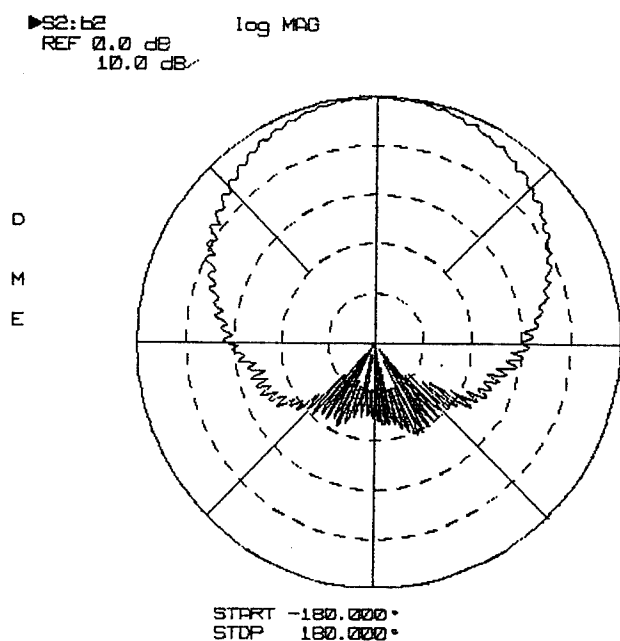


Fig. 9a: Measured radiation pattern of the antenna flushmounted to the corrugated ground-plane. Frequency 1,565 GHz.

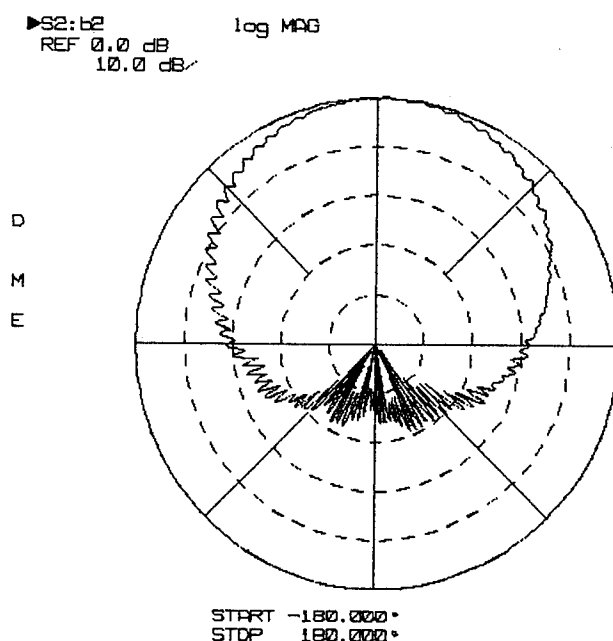


Fig. 9b: Measured radiation pattern of the antenna flushmounted to the corrugated ground-plane. Frequency 1,620 GHz.

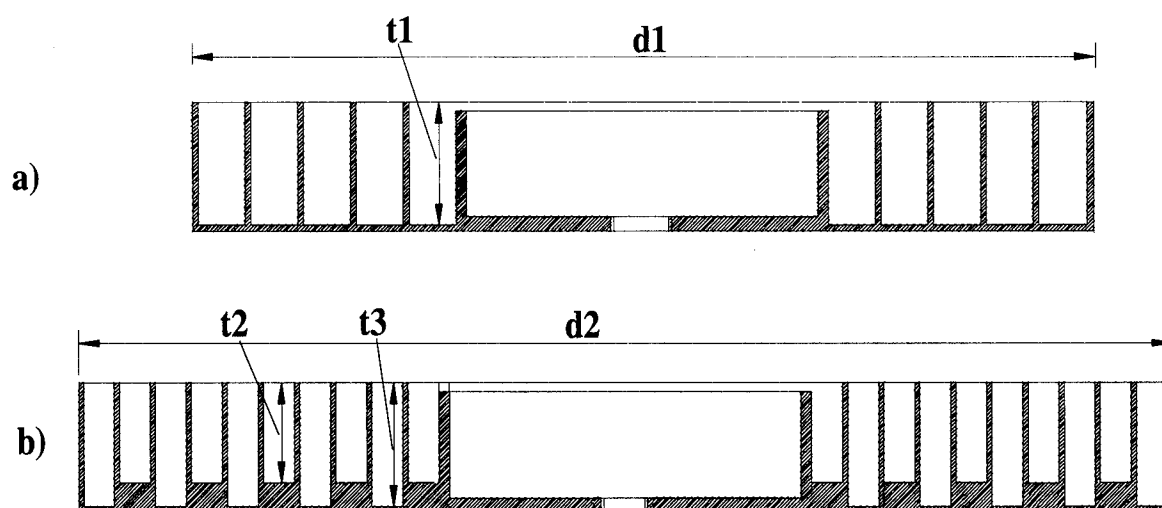


Fig. 10: Corrugated ground-planes.

a) L1-version, $b_1 = 1.86\lambda$, $t_1 = 0.26\lambda$ at the L1 center frequency.

b) L1/L2-version, $b_2 = 1.85\lambda$, $t_2 = 0.2\lambda$, $t_3 = 0.26\lambda$ at the L2 center frequency.

Tracking Measurements From a Miniature GLONASS Receiver

Dr. Oliver Leisten, Dr. Geraint Ffoulkes-Jones, Gerald Whitworth, and David Belton
Navstar Systems Ltd.

BIOGRAPHIES

Oliver P. Leisten is the R.F. Group Leader of Navstar Systems Limited of Northampton, England. Dr Leisten received a PhD in microwave electronics in conjunction with Philips Research Labs. He has also worked for Plessey Avionics and Communications, Plessey Military Communications and GEC Plessey Avionics. Dr Leisten has specialist knowledge in the fields of microwave and I.F. high integration receiver design.

Gerald Whitworth BSc is Software Group Leader of Navstar Systems Ltd. He joined Navstar Systems Ltd (formerly known as Polytechnic Electronic Plc) in 1983 and has been involved in the design and development of the company's range of GPS products from the XR1, launched in 1984, to the latest 6/12 Channel receiver product the XR5.

David Belton Bsc is Hardware Engineering Group Leader at Navstar Systems Limited in Northampton, England. He joined Navstar Systems Limited (formerly known as Polytechnic Electronics plc) in 1989 as part of the design team for the company's Decca based vehicle navigation system. He has also been involved in the design and development of a number of subsequent GPS receivers including the latest 12 channel receiver product, the XR5.

Geraint Ffoulkes-Jones is a Software Engineer with Navstar Systems Ltd, and specialises in navigation, position fixing and surveying techniques. Dr Ffoulkes-Jones obtained his PhD at the IESSG at the University of Nottingham for research into Fiducial GPS surveying. Before joining Navstar he was a senior research assistant at the IESSG where he was the co-author of the GAS (GPS Analysis Software) fiducial network package.

ABSTRACT

The structure of a GLONASS LI receiver, that is related to and derived from Navstar Systems integrated GPS chipset has previously been presented ⁽¹⁾. This chipset was designed to primarily work within the GPS system but with the capability to convert to GLONASS operation as the use of the dual standard receiver architectures was anticipated. A relatively compact and capable GLONASS LI receiver has been implemented and from this some tracking measurements which demonstrate promising performance are presented.

The receiver utilises the 20 MHz master oscillator of the XR5 GPS instrument in a receiver synthesiser system that achieves phase noise advantage by means of a dual stage $\Delta f_{L01} = 0.5$ MHz and derived $\Delta f_{L02} = 0.0625$ MHz local oscillator systems. The GLONASS receiver shares the device structure of its XR5 GPS parent except for the addition of a single synthesiser chip. The code tracking, carrier frequency tracking and hopefully ultimately carrier code tracking, together with data recovery is carried out in the standard NAVSTAR SYSTEMS designed multi-channel D.S.P. device. A fast sequencing GLONASS receiver is housed in a box 6.75 inch x 3 inch x 2.5 inch in size. The D.S.P device is capable of simultaneously processing GPS and GLONASS inputs.

Recent tracking measurements have demonstrated approximately 5 metres peak to peak pseudorange rate noise. This implies that our prototype instrument should be capable of unaided position fixing accuracy that is significantly better than the 100m CEP level that is provided by S/A degraded GPS.

INTRODUCTION

In recent years an increasing number of reports have been published on the design of GLONASS instruments and the integration of GLONASS with GPS (references 2,3,4,5,6,7,8,9). Generally these contributions have been concerned with the demonstration of the performance of the GLONASS or integrated GPS/GLONASS systems. The focus of this contribution is to demonstrate the tracking capability of a fast sequencing GLONASS instrument that has high integration and low cost. The object is to reduce the complexity of the GLONASS engine to be comparable to GPS so that marketable integrated GPS/GLONASS or GLONASS aided products are possible.

The designer of a low cost integrated GPS/GLONASS instrument faces the challenge of how to embody the significantly different system frequency plans into the instrument chipset. This thorny problem has been described as "a problem in numerology and factorising" ⁽²⁾. By constraining the XR5 based instrument to the GPS and GLONASS L1 services a receiver frequency plan has been captured which may be considered elegant for either service. This has enabled the design of devices which are GLONASS adaptable but technologically competitive in the mainstream GPS application.

The XR5 ASIC device-set comprises a GPS/GLONASS receiver chip ⁽¹⁰⁾, a three level adaptive quantiser chip and a 6 channel digital processor chip which can operate with the L1 GPS and L1 GLONASS services. The digital processor device embodies digital synthesis processes which capture the otherwise complex frequency planning arithmetic in a way which minimises the build complexity of the receiver. However in addition to this a principal simplifying feature is that of the receiving strip frequency plan which is described in the foregoing:-

NAVSTAR'S XR5 GPS RECEIVER STRUCTURE AND ITS ADAPTATION TO GLONASS

The XR5 GPS receiver's device structure is shown in figure 1. The structure was organised to be adaptable to implement a GLONASS receiver with the minimum of change as will be described.

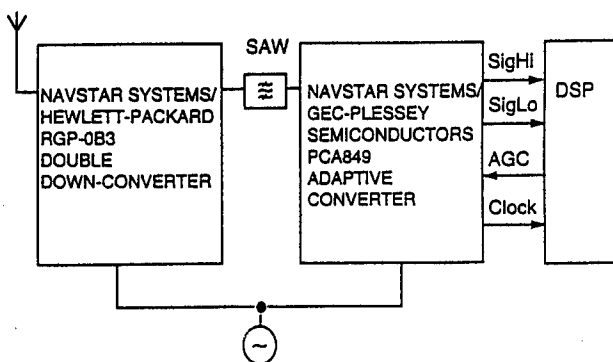


Figure 1: Device structure of the XR5 GPS Receiver.

The configuration of the RGP-03B receiver on Chip (ROC) device was designed to be usable in conjunction with a synthesiser chip to permit the receiver to tune selected GLONASS channels into the SAW filter pass-band. It can be shown that the use of a divide by eight divider to derive the second local oscillator input to the second down-converter stage is in many respects an optimum frequency plan. Basically it supports the use of a 20 MHz master reference oscillator in both GPS and GLONASS receivers in a way which takes advantage of common factors. The derivation of the second local oscillator input from the first local oscillator using a divide by eight process provides a convenient scheme for synthesising the $\frac{9}{16}$ MHz channel steps in two $\frac{1}{2}$ MHz and $\frac{1}{16}$ MHz components as shown in figure 2:-

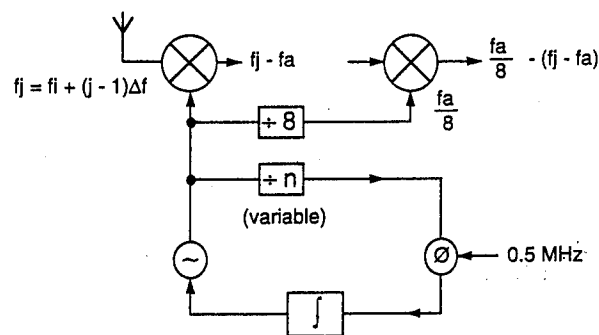


Figure 2: Optimum GLONASS synthesiser/receiver structure with derived second local oscillator.

A phase locked loop noise benefit of approximately 18 dB has been gained ⁽¹⁾ using the stepping frequency of 0.5 MHz of the first local oscillator rather than the $\frac{1}{16}$ MHz common demonstrator between 20 MHz and $\frac{9}{16}$ MHz that

would otherwise be necessary without the derived second local oscillator strategy.

GLONASS RECEIVER IMPLEMENTATION

The synthesiser/down-conversion part of the XR5 based GLONASS receiver is shown in figure 3:-

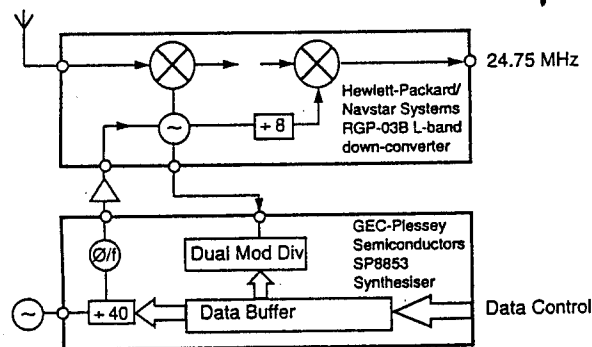


Figure 3: Use of SP8853 synthesiser to control local oscillator frequencies.

It was found to be convenient to use the SP8853 synthesiser to control the local oscillator frequencies. This GEC-Plessey Semiconductors part has fast tuning arrangements, low phase noise and the ability to tune between two set frequencies in response to a logic transition rather than in response to a relatively slow code-change sequencing.

The complete GLONASS test instrument includes a quadrifilar helix antenna pre-amplifier assembly of NAVSTAR SYSTEMS design. This antenna module incorporates two specially designed R.F. filters and sufficient gain to permit remote mounting from the receiver to the extent of 15 metres of RG-58 cable.

The GLONASS receiver strip is housed on a card measuring $6\frac{1}{2}$ inches by $2\frac{3}{4}$ inches and is implemented with three application specific filter designs. The front-end section includes two microstrip band-pass filters and a capacitor loaded interdigital filter operating at a centre frequency of 156.75 MHz selects out the first I.F. frequencies. At both of these stages GLONASS channels occupy different centre-frequencies and it is important not to introduce significant delay dispersion. Care has been taken to situate the GLONASS channel frequencies and first I.F. channel frequencies at the group delay saddle-point of the front end and first I.F. filters respectively.

The GLONASS receiver shares a common surface acoustic wave (SAW) channelising filter with the GPS receiver. The filter was designed for optimum phase linearity and with a 3dB bandwidth of approximately 1.35 MHz.

The conversion to digits in the GPS and GLONASS forms of the XR5 instruments is accomplished using a 2-level automatic gain controlled process which is implemented with the PCA849 adaptive converter device together with the digital signal processor. This system affords the XR5 receiver the high receiver dynamic range that characterises the multi-level conversion class of spread-spectrum receivers. It is important to draw an architectural distinction here between the channel dedicated receiver architecture employed in the XR5 based GLONASS instrument and the digitally channelised GLONASS receiver structures that have elsewhere been proposed (in some references). One of the primary advantages that the GLONASS system may be considered to possess over GPS is that of anti-jam robustness. This is because in addition to the spreading advantage that it has in common with GPS, the GLONASS system has channel selectivity to the extent that has been implemented in the channelising filters. It can be expected therefore that these specifying the use of GLONASS instruments in life dependant systems will require a high level of rejection adjacent channel interference together with proper spreading advantage. It seems that the digital channelising schemes that have been proposed can not achieve high rejection of adjacent channel interference because no individual channel adaptation is possible if the same digitised input is provided to all channels.

TRACKING GLONASS WITH GPS DIGITAL HARDWARE

The current developments in GLONASS at Navstar Systems Ltd are performed using a standard XR5 GPS digital board. The XR5 GPS digital board consists of a 68EC020 microprocessor, RAM, EPROM, a real-time clock chip, and an ASIC. The ASIC is a Navstar Systems Ltd, in house design, and was initiated in 1990. The ASIC contains 6 GPS parallel tracking channels and all the "glue" logic normally associated with the 68K family of microprocessors. Each GPS tracking channel has its own carrier NCO, CODER, a set of four correlators, and all of the control and mixing logic. Common to all channels is a code NCO, each channel selecting the required phase of the code

frequency. GLONASS signals are tracked with the ASIC by reorganising the internal channel structure. Two GPS channels are configured to be a single GLONASS channel. One of the channel NCO's being used to generate the 511 kHz GLONASS code frequency for the other channel, which generates the carrier frequency using its "own" NCO. The design of the CODER incorporates variable taps in the shift registers. This allows not just the GPS codes to be generated, but also GLONASS and other non-GPS gold codes. Basically, each stage of the shift registers are ANDed with an enable signal and combined into an exclusive OR gate. This results in the microprocessor having to initialise the CODER taps once each time the receiver is powered on or reset. A relatively minor overhead. For GLONASS the second (G2) shift register is set to all zeros and effectively not used. The ASIC was also designed to allow each of its channels to track several satellites by fast sequencing. A principle first used by Navstar Systems Ltd in its XR3 product launched in 1986. Navstar's XR5M6 product contains one ASIC and tracks up to eight satellites by multiplexing two of the parallel channels each with two satellites. A single ASIC combined GPS/GLONASS receiver could then potentially track 8 GPS satellites, two in each of its GPS parallel channels, and four GLONASS satellites, multiplexed in the other channel. A dual ASIC configuration, such as the XR5M12, could then be used to track 8 parallel GPS satellites, each non-multiplexed, and up to eight GLONASS satellites. The digital logic is modular and potentially there is no reason why up to 4 ASICs could be employed in a single receiver, which would then contain 16 parallel GPS channels and 4 parallel GLONASS channels, with each channel still retaining the ability to multiplex up to four satellites.

GLONASS RECEIVER TRACKING PERFORMANCE

The receiver was commissioned using a home-made simulator and made it's first satellite acquisition on Tuesday 22nd August. Within three working days of experimentation the hardware was developed to its present performance and no doubt considerable scope for continued refinement exists. The GLONASS L1 signals proved to be strong and easy to track, with correlation levels that would be usually good for GPS.

The XR5 digital signal processor supports facilities for independently measuring code and carrier phase so that code/carrier aiding is possible. For

reasons which are not clear the Costas carrier phase locked loop was not successfully closed but carrier frequency lock was obtained using the automatic frequency control (AFC) loop that is normally used in acquisition. However the tracking arrangements were reliable and sustained tracking observations were made to yield the foregoing measurements.

In order to support a navigational process the GLONASS receiver needs to measure sufficient satellite pseudorange measurements. These measurements are the raw uncalibrated range measurements containing the errors which the navigational computation seeks to quantify so that correct position can be determined. Pseudorange measurements from GLONASS satellite 7 (channel 21) are shown in figure 4:-

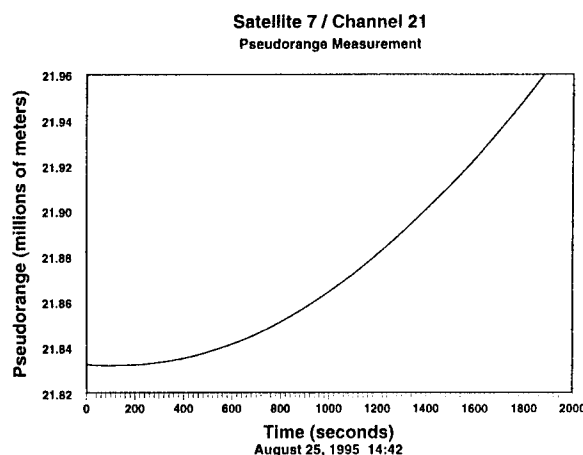


Figure 4: Pseudorange measurement of GLONASS satellite 7.

In the course of observation of satellite 7 it passed over it's zenith position with aspect to our Northampton, England position.

At the enormous scale associated with the range in metres to the GLONASS satellites the shape of the pseudorange curve is very smooth. To analyse the quality of the tracking function it is more instructive to measure the pseudorange rate in metres per second, a measurement of this is shown in figure 5:-

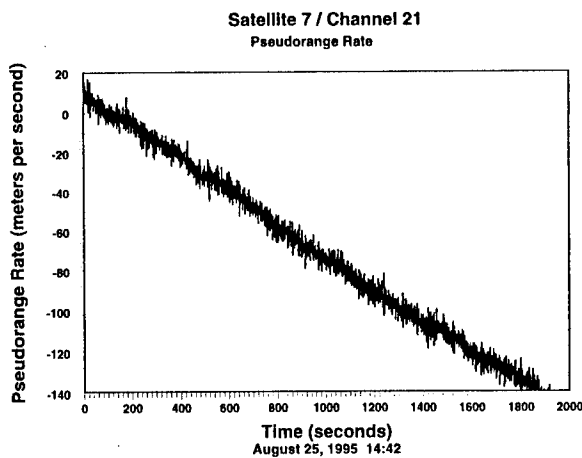


Figure 5: Pseudorange rate observations taken from satellite 7

The pseudorange observations shown in figure 7 show a steady slope which is due to a combination of receiver clock error and satellite frequency doppler shift. However the noise superimposed on this segment of data indicates that the tracking ambiguity to this satellite is approximately 5 metres peak to peak. At this stage of the development of the GLONASS receiver this result is considered to be most promising.

In order to direct the tracking process it is necessary to track the satellite's doppler shift to accommodate this source of frequency error in the correlation process. A short segment of observation of satellite 8 which was radiating on channel 2 is shown in figure 6:-

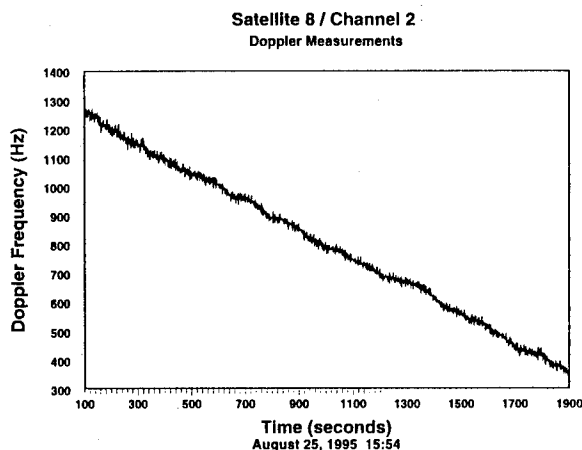


Figure 6: Doppler frequency shift measurements on satellite 8.

Underlying the process of tracking the satellite doppler shift is the ability to measure carrier phase. Using the automatic frequency control loop it was possible to log the angular change between milli-second observation intervals. This

type of measurement typically produced the outcome shown in figure 7:-

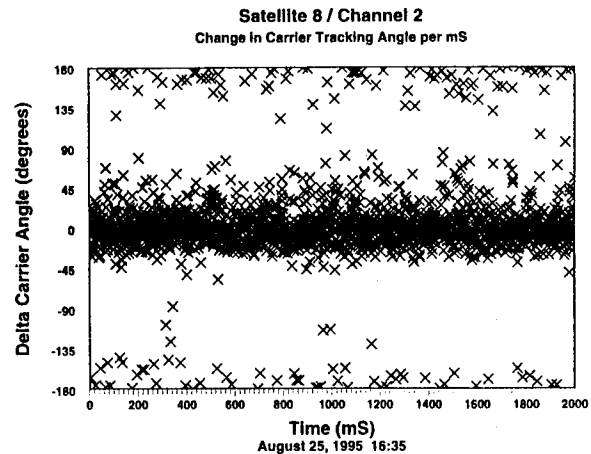


Figure 7: Carrier phase-angular change between milli-second intervals.

The graph shown in figure 6 was interesting because it shows a dense band of measurements in the centre and less frequent outliers distributed about ± 180 degrees. The width of the centre band of observation is attributable to locally generated instrument phase noise. However the cause of the outlier measurements was investigated further. Figure 8 shows a segment of the carrier phase angular change graph plotted to a higher resolution.

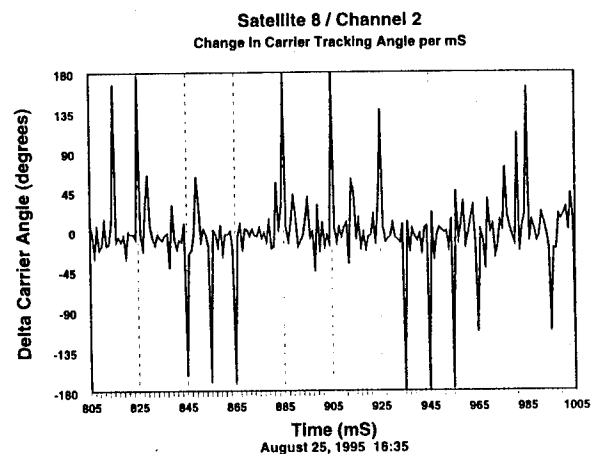


Figure 8: Short segment of phase-angular change data between milli-second intervals.

Examinations of the carrier phase angular change data presented in figure 8 leads to conclusion that the outlier transitions take place at exactly 10ms opportunities in line with the GLONASS data rate of 100 bps. It was therefore a relatively trivial task to process the data to toggle the data logic level on receipt of 180 degree carrier phase transitions.

The data can be interpreted by comparing the data and inverted data against certain pre-amble sequences to determine the sense of the correct toggle transitions. Figure 9 shows a sequence of data processed this way and aligned to consistent 10 ms edge boundaries.

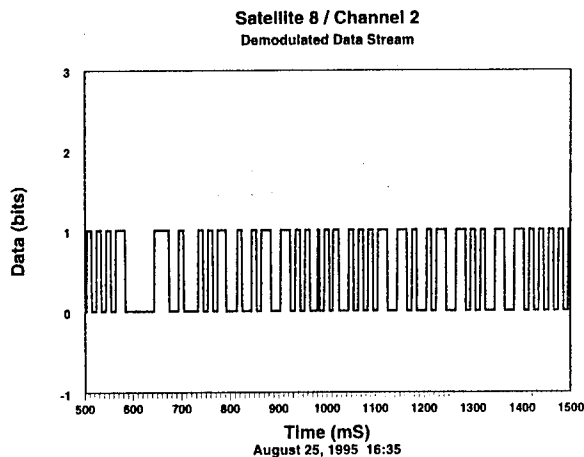


Figure 9: GLONASS demodulated data stream.

GLONASS FUTURE DEVELOPMENTS

This paper demonstrates the ability to track, measure pseudoranges and decode navigation data from GLONASS satellites within the basic structure of Navstar XR5 GPS ASIC. At present the future GLONASS developments planned include the following:

- Utilising the GLONASS multiplexing capability to track at least 4 satellites on the same XR5 ASIC.
- To decode the navigation data and successfully perform computations with these values.
- To perform a stand alone navigation solution in a separate GLONASS Kalman within the XR5.
- Investigate the datum and clock differences between the GPS and GLONASS systems.
- Develop a combined GPS/GLONASS navigation solution operating within the same Kalman. It is possible that this will lead to a GPS aided GLONASS navigator (i.e. use GPS aid the initial acquisition of GLONASS satellites and then use the higher precision of the GLONASS system to give higher accuracies than are possible with S/A corrupted GPS).

- Develop an integrity monitoring system within the XR5 which constantly compares the data and solutions from both GPS and GLONASS systems.
- Obtain carrier lock on the GLONASS signal and produce precise carrier phase measurements.
- Develop a technique to calibrate the small GLONASS inter-channel biases that remain in the measured data, so that the precision of the carrier phase measurements can be fully utilised.
- Utilise the GLONASS carrier phase measurements to help the ambiguity resolution process in precise kinematic applications. It is anticipated that they would only be used to improve the time to resolution and provide better quality control, and not actually be used in the position solution.

CONCLUSIONS

A highly integrated GLONASS receiver has been demonstrated to be able to track satellites sufficiently well to support good quality GLONASS stand-alone fixes. Used in combination with GPS an interesting range of powerful instrument combinations are possible. These should be manufacturable at reasonable cost using NAVSTAR SYSTEMS' existing technology. Instruments offering fast acquisition, 25m CEP stand-alone accuracy and the robustness of a combined 48 satellite constellation are possible.

ACKNOWLEDGEMENTS

The authors wish to thank Navstar Systems and in particular its General Manager, Tony Haddrell for supporting this work.

The GLONASS tracking receivers were built and commissioned by Hussein Khawaja. We acknowledge the generous provision of sample synthesiser chips from GEC-Plessey Semiconductors and wish to thank David O'Neill for these.

Martin Hall wrote the Windows based channel control software. Special thanks are due to Andrea Collins, Donna Blackwell and Sarah Payne who produced this paper in a very short time.

REFERENCES

1. O.P. Leisten
Compact Circuitry for GLONASS Reception.
Institute of Navigation Conference
Salt Lake City
September 20-23, 1994
2. R.A. Eastwood
An Integrated GPS/GLONASS Receiver
Institute of Navigation Conference
San Diego
Jan 23/25, 1990
3. P.Raby, K.Harris, P.Gibson, P.Mans and G.Morrison
A Dual Navstar GPS/GLONASS Satellite Receiver
Institute of Navigation Conference
Colorado Springs
September 19-21, 1990
4. R.G.Hartman, M.A.Bremner and N.M.Kant
GPS/GLONASS Flight Test, Lab Test and Coverage Analysis Tests
Institute of Navigation Conference
New Mexico
September 11-13, 1991
5. S.Riley
An Integrated Multi-channel GPS/GLONASS Receiver
Institute of Navigation Conference
Albuquerque, New Mexico
September 16-18, 1992
6. H.Hojo, S.Kawashima, M.Nakamura, K.Yui, A.Okuyama and K.Washizu
An Integrated GPS/ GLONASS Receiver
Institute of Navigation Conference
Salt Lake City
September 22-24, 1993
7. J.Beser and A.Balendra
Integrated GPS/GLONASS Navigation Results
Institute of Navigation Conference
Salt Lake City
September 22-24, 1993
8. A.Balendra, S.Kim and J.Beser
Fully Integrated GLONASS Dual Frequency, P-Code and GPS/GLONASS Single Frequency, C/A Code Receiver: Features and Performance
Institution of Navigation Conference
Salt Lake City
September 20-23, 1994
9. B.Peterson, E.Chamberlin, T.Vogler, P.Daley, S.Riley
GPS/GLONASS Time Difference Measurements and Test Bed Development
Institution of Navigation Conference
Salt Lake City
September 20-23, 1994
10. K.J.Negus, R.A.Koupal, D.Millicker, C.P.Snapp
FA 14.6: Silicon Bipolar Mixed-Signal Parameterised - Cell Array for Wireless Applications to 4 GHz
IEEE International Solid -State Circuits Conference 1992

Power Minimization Techniques for GPS Null Steering Antenna

Anton Gecan
E-Systems

Michael Zoltowski
Purdue University

Biographies

Anton S. Gecan received his BSEE from Purdue University in 1971, his MSEE and Ph.D. from the University of South Florida in 1984 and 1992, respectively. He is a Staff Engineer in the GPS products group at E-Systems, St. Petersburg, Fl. Dr. Gecan was the principal architect of the AE-1A algorithm and is presently conducting IR&D efforts on advanced null steering algorithms for GPS applications. Dr. Gecan served as a Navy officer and is a Vietnam veteran.

Michael D. Zoltowski completed his BSEE and MSEE at Drexel University in 1983. He received his Ph.D. from the University of Pennsylvania in 1986. Dr. Zoltowski is an associate professor of Electrical Engineering at Purdue University. He is the author of over 20 journal and 40 conference papers on the subject of adaptive array processing. Dr. Zoltowski is presently funded by E-Systems to assist in IR&D efforts addressing GPS null steering applications.

Abstract

This paper explores the performance that can be achieved from a null steering array antenna using both a subgradient-search power minimization technique as well as an LMS-related power minimization method. Consideration is given to expected performance of the algorithms in both static and dynamic environments.

A simple, subgradient-based nulling algorithm is presented with simulation results indicating the ability of the algorithm to achieve a known optimal solution under static conditions. Subsequently, the LMS-related approach to nulling via power minimization is formulated. Simulation results employing the LMS-related technique in a static geometry are presented and compared with the subgradient search method and the optimal solutions.

The paper then explores the performance of both algorithms in a dynamic situation where the array rapidly changes its orientation with respect to the interference.

Introduction

Protection of the GPS receiver from both deliberate and inadvertent interference has become an important issue within the GPS community. Recent investigation by the Defense Science Board (DSB) of the vulnerability of the GPS signal to interference has highlighted the disturbing ease with which GPS signals can be jammed. The DSB went on to cite null steering antennas as one technology that can be used to protect the GPS receiver from jammers and inadvertent interference.

This paper, tutorial in nature, explores the interference protection that can be achieved using an adaptive array with a simple power minimization algorithm directing the action of the array. Power minimization as a technique to combat interference was first suggested by Zahm [1] and Compton [2]. While Zahm originally discussed nulling a strong interference signal to enhance reception of a weak desired signal, for GPS the situation is somewhat simplified. Since the GPS signal itself is 30+ dB below the thermal noise floor - any signal above the noise floor can be considered interference. Consequently, the nulling action of the array can be set to attack any incoming signal with a power level above noise. An additional, attractive feature of power minimization is that the method can be implemented in hardware relatively inexpensively.

Power Minimization via Subgradient Search

The geometry of a four element circular array is shown in Figure 1A. The reference element is located in the center of the array. The three auxiliary elements are positioned 120° apart surrounding the reference at a radius R.

Figure 1B presents a block diagram of a power minimization implementation employing a four element adaptive array. As shown in the figure, each signal from

an antenna element is multiplied by a complex valued weighting factor before being routed to a summer. The complex weight can increase or attenuate the magnitude of an element's signal while rotating the phase of the signal some angular amount. After summing the individual array element signals, the composite signal at RF can be routed to a receiver or translated to a convenient IF frequency and then passed to the receiver.

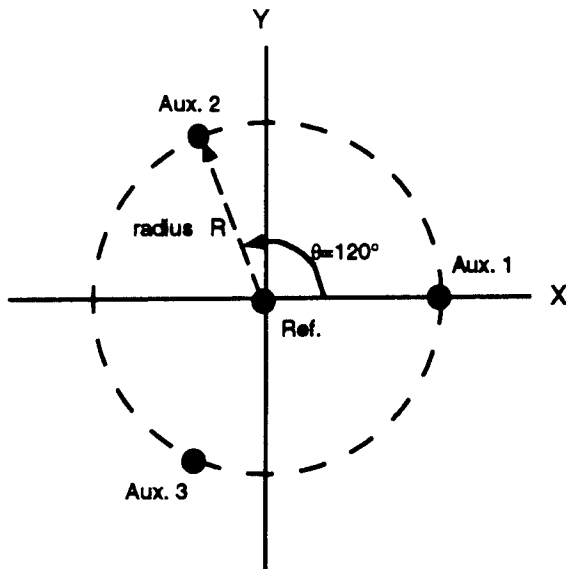


Figure 1A Four Element Circular Array

To drive the algorithm, a portion of the translated IF signal is provided to the power estimation function. The power function uses a simple time average to estimate the power on the array. The null steering algorithm embedded in the processor systematically manipulates the weights on the antenna elements to continually lower the array power.

In the absence of any interference, the array power level should be within a few dB of the thermal noise floor. However, when interference sources are present in the bandpass of the GPS signal, the power on the array will rise to the level of the incident (non-GPS) signals. By manipulating the weights to minimize power, the algorithm seeks to return the overall array power to near noise floor levels. The residual power on the array will again approach the noise floor when the minimization algorithm has successfully placed nulls in the directions of the interfering sources.

Array power is a quadratic function of the weighted element signals. Consequently, the overall power can be considered, mathematically, as a convex, parabolic surface, as depicted in Figure 2A (for a two element array). As shown in the figure, there is a weight setting, W_{opt} , that results in minimum power on the array. The task of the minimization algorithm is to find this point.

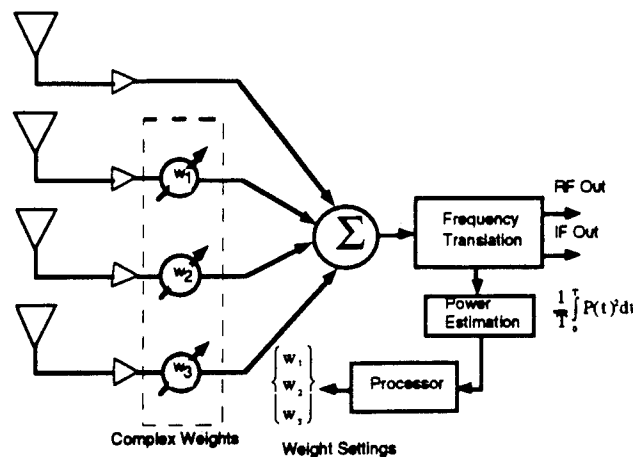


Figure 1B. Adaptive Four-Element Array

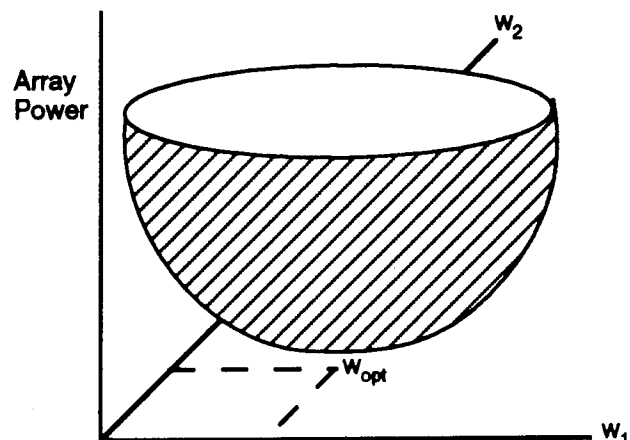


Figure 2A. Convex Power Surface for Two Element Array

Curves of equal array power levels can be projected onto the W_1 - W_2 plane of the graph as shown in Figure 2B. The projected curves form concentric ellipses-shaped contours centered at the minimum power point. At the onset of jamming, the minimization algorithm begins at, say, point A in Figure 2B. The actual start point is determined by the power of the interfering sources and their angular relationship (or "geometry") with respect to the array.

Given a start point, we seek to move toward the center of the contours where power will be minimal. To do this we must determine two things: (1) a direction of movement and (2) a distance to move in the chosen direction. We will call these choices the direction and step size.

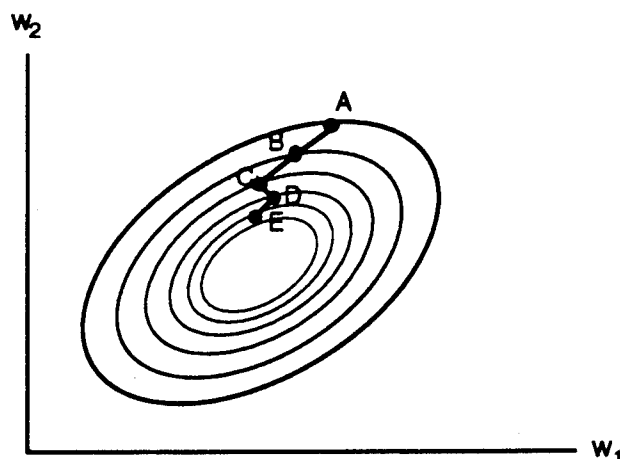


Figure 2B. Contours of Power Surface for Two Element Array

We might consider attempting a steepest descent technique. We could manipulate the array to estimate the gradient, e.g., using a method described by Hudson[3]. Such an approach requires three separate, sequential power estimates for a four element array. Each of the power estimates is formed by time averaging the power on the array over some period, e.g. 20 usecs. We could then move along the gradient direction in small steps (each requiring a separate power estimate) until power ceases to decrease.

At this new point we could again re-compute the gradient and repeat the procedure. While we would eventually approach the point of minimum power, the convergence time of the method is excessive in that three power estimates are needed before any actual movement to decrease power is attempted. Moreover, additional power estimates are needed as one progresses along the defined descent direction.

To speed convergence we choose to implement a subgradient search method[4]. That is, we seek a search direction that when followed, moves us closer (in a Euclidean sense) to the optimum point. The search direction is not usually the line of fastest descent (i.e., the gradient) but rather, an easily found direction that leads to reduced power. With a suitable search direction defined, we then move along that direction some predetermined, fixed step size (large when overall power is large, and small when near the noise floor). This action is indicated in Figure 2B by the trajectory from A to B to C, etc.

To find a search direction at a given point (i.e., at a given level curve of Figure 2B), the individual element weights are manipulated one at a time. Each complex valued weight is sequentially set to one of four possible settings: $[Ae^{j0}, Ae^{j180}, Ae^{j90}, Ae^{j270}]$, where A is a function of the predetermine step size and the $e^{j\phi}$'s effect angular rotations of 0, 180, 90, and 270 degrees. These

settings first increase or decrease the real part of the weight, followed by an increase/decrease in the imaginary part of the weight.

If a given setting results in a reduction of power on the array, the setting is retained and one moves to the next element of the array. After a complete pass has been made through all the elements, the order of the element search and the ordering of the search directions are reversed. This is done to help each antenna element of the array to contribute equally to the nulling action. After a number of passes through all the antenna elements, the algorithm will have converged the weights to values that result in the power on the array being near the noise floor level. An antenna pattern taken with the converged weight settings will show nulls in the direction of the jamming sources.

Evaluating Optimal Solutions

In order to evaluate the performance of nulling algorithms, it is useful to have analytically derived the optimal weights. It is well known [3,5,6] that the optimal weights for the auxiliary elements of the array are:

$$W_{a_opt} = R_{aa}^{-1} r_{oa} \quad (1)$$

W_{a_opt} is the 3×1 vector of optimal weights for the auxiliary elements; R_{aa} is the 3×3 covariance matrix of the auxiliary elements. the 3×1 vector r_{oa} is the correlation vector of the auxiliary elements with the reference element (denoted element 0).

If there are three jammers incident on the array, then R_{aa} is full rank and one can solve for W_{opt} straightway. However, when a single jammer is incident on the array R_{aa} can have widely disparate eigen values (one at jammer power level and two at noise power level) leading to ill conditioning of R_{aa} . While there are methods to solve (1) even with ill conditioning, it is useful to develop the optimal solution for a single interferer intuitively to gain a better understanding of nulling. Consider a simple *three* element array problem with a single jammer as shown in Figure 3.

Figure 3 depicts a phasor plot of a single jammer incident on a *three* element array. The jammer is in the in-phase position as seen by the reference element. At the first auxiliary element, the jammer is seen as the same signal as at the reference but with a phase rotation of ϕ_1 . Similarly, the jammer signal at second auxiliary element has the same magnitude as the reference (in-phase) signal and a phase offset of ϕ_2 . We wish to manipulate the two jammer signals captured on the auxiliaries to null out the in-phase, reference element jammer.

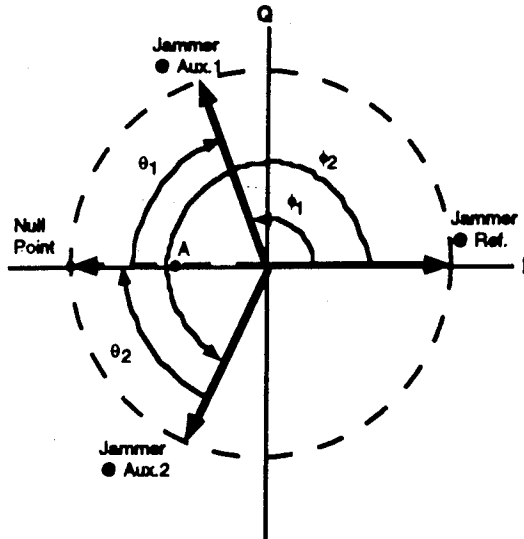


Figure 3. Single Jammer Geometry

Recall that multiplication by a complex weight can cause a signal to attenuate magnitude and rotate phase. If we multiply the signal on the first auxiliary by a complex weight that rotates the signal through an angle θ_1 while attenuating the signal to half its value, the resultant phasor will be from the origin to point A. Similarly, if we rotate the second auxiliary element's signal through θ_2 degrees while attenuating by half we obtain another phasor from the origin to point A.

As shown in Figure 3, the resultant sum of the two weighted phasors is the vector from the origin to the null point. When this sum phasor is added to the jammer signal on the reference, the resulting sum or array output signal is zero. Thus, by appropriately attenuating and rotating the auxiliary signals prior to adding them to the reference signal, we have nulled out the incident jammer. Note that in this formulation each auxiliary element contributes an equal magnitude component to the nulling vector. This equal contribution of each element is the optimal solution against a single jammer since it provides the narrowest null - preserving as much of the field of view as possible. More generally, in the *single* jammer case the optimal solution will be:

$$W_{a_opt}[i] = \frac{1}{M} e^{j(180 - \phi[i])} \quad i = 1, \dots, M \quad (2)$$

where the index runs across the M auxiliary elements (e.g., $M=3$ for a four element array). The weight on the reference element itself is always

$$W[ref] = 1.0 \quad (3)$$

LMS-Related Power Minimization

A power minimization algorithm can be formulated from an LMS perspective. Let T_s be the sample interval and $1/T_s$ be the rate at which all the auxiliary element weights are updated. Let

$$x_{ref}(n) = x_{ref}(t) \Big|_{t=nT_s} \quad (4)$$

be the output of the reference element at $t=nT_s$. Denote the output vector of the auxiliary elements (i.e., 3×1 for a four element array) as

$$\bar{x}_a(n) = \bar{x}_a(nT_s) \quad (5)$$

Then define an "error" signal:

$$e(n) = x_{ref}(n) - \sum_{i=1}^M w_i^* x_i(n) = x_{ref}(n) - \bar{w}_a^H \bar{x}_a(n) \quad (6)$$

where both w_a and x_a are 3×1 vectors and the superscript H denotes conjugate transpose and superscript $*$ signifies conjugate. We wish to find the weight vector w_a that minimizes the expected value (denoted by $E\{\cdot\}$) error, that is

$$\bar{w}_{a_opt} = \underset{\bar{w}_a}{\text{Min}} E\{|e(n)|^2\} \quad (7)$$

We can expand $E\{|e(n)|^2\}$ as follows:

$$\begin{aligned} E\{|e(n)|^2\} &= E\{(x_{ref}(n) - \bar{w}_a^H \bar{x}_a(n)) \\ &\quad \times (x_{ref}^*(n) - \bar{x}_a^H(n) \bar{w}_a)\} \\ &= E\{x_{ref}^2(n)\} - \bar{w}_a^H E\{x_{ref}^*(n) \bar{x}_a(n)\} \\ &\quad - E\{x_{ref}(n) \bar{x}_a^H(n)\} \bar{w}_a + \bar{w}_a^H E\{\bar{x}_a(n) \bar{x}_a^H(n)\} \bar{w}_a \end{aligned} \quad (8)$$

Define

$$\bar{r}_{oa} \equiv E\{x_{ref}^*(n) \bar{x}_a(n)\} \quad (9)$$

and

$$\bar{R}_{aa} \equiv E\{\bar{x}_a(n) \bar{x}_a^H(n)\} \quad (10)$$

then

$$E\{|e(n)|^2\} = E\{x_{ref}^2(n)\} - \bar{w}_a^H \bar{r}_{oa} - \bar{r}_{oa}^H \bar{w}_a + \bar{w}_a^H \bar{R}_{aa} \bar{w}_a \quad (11)$$

Taking the complex gradient with respect to w_a , one obtains

$$\nabla_{\bar{w}_a} (E\{|e(n)|^2\}) = -2\bar{r}_{oa} + 2\bar{R}_{aa}\bar{w}_a \quad (12)$$

As an aside, if (12) is set equal to zero and solved for w_a , one immediately obtains the Weiner solution cited in (1). Using (12), a gradient search can be constructed as

$$\bar{w}_a(n+1) = \bar{w}_a(n) - \mu(n) \{\bar{r}_{oa} - \bar{R}_{aa}\bar{w}_a(n)\} \quad (13)$$

where $\mu(n)$ is the step size at $t=nT_s$. We do not have asymptotic values for r_{oa} nor R_{aa} ; however, we can estimate these quantities via their instantaneous values to achieve an LMS formulation

$$\begin{aligned} \bar{r}_{oa} &\approx x_{ref}^*(n)\bar{x}_a(n) \\ \bar{R}_{aa} &\approx \bar{x}_a(n)\bar{x}_a^H(n) \end{aligned} \quad (14)$$

If we substitute (14) in (13), fix the step size, and do some algebraic manipulation, we obtain the weight update equation

$$\bar{w}_a(n+1) = \bar{w}_a(n) + \mu \{x_{ref}(n) - \bar{w}_a^H \bar{x}_a(n)\} \bar{x}_a(n) \quad (15)$$

This is an LMS-based scheme that updates all the weights simultaneously.

Performance Comparison - Static Case

For a performance comparison of the two nulling algorithms, consider two cases

Case 1: Single CW Jammer
Elevation: 10° above array plane
Azimuth: 60° , mid-way between array elements 1 and 2 (see Figure 1B)
Jammer Power: +50 dB over noise level

Case 2: Three CW Jammers
Elevation: all 10° above array plane
Azimuth: 60° , 180° , and 300° , mid-way between the auxiliary elements
Jammer Power: +30, +40 and +50 dB over noise floor

Using the methods described in a previous section, the optimal solutions for the two cases can be found. A metric can then be generated that compares the "distance" (norm squared value) of the achieved nulling weight set from the theoretical optimal values:

$$Metric = \|\bar{w}_{opt} - \bar{w}_{actual}\|^2 \quad (16)$$

The following metrics were computed for the static cases:

| | Subgradient | LMS |
|---------------|-------------|--------|
| Single Jammer | 0.1164 | 0.0043 |
| Three Jammers | 0.1539 | 0.1207 |

Figures 4 and 5 shown the results of applying the two methods to the cases.

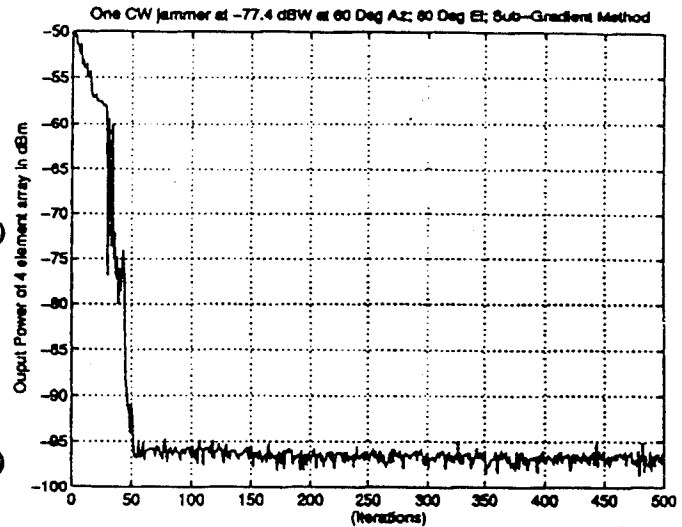


Figure 4A. Subgradient Single CW Jammer Nulling

As shown in Figure 4A, the subgradient power minimization nulls a single CW jammer into the noise floor (~ -98 dBm) in approximately 50 iterations of the algorithm. The 50 iterations occur over roughly five passes through the three auxiliary elements. It should be noted that each iteration requires an integrate and dump interval (say, 20 μ secs) to estimate the power plus time to set/reset weight values and have the changed values settle. Consequently, the time for the 50 iterations will be a function of the hardware implementation.

Figure 4B shows the simulation results of the subgradient method employed against three CW jammers. The three jammers exercise the full degrees of freedom of the array. After 500 iterations the method is still approximately 20 dB above the noise floor, but the algorithm appears to be continuing to make very slow progress toward the noise floor. Generally, the method is slowed by multiple jammers with differing power levels. At first, the search attacks the strongest jammer and in the process of countering that jammer unmasks lower power interference.

3 CW jammers at -77.4, -87.4 & -97.4 dBW at 60, 180 & 300 Deg Az; 60 Deg El; Sub-Gradient Method

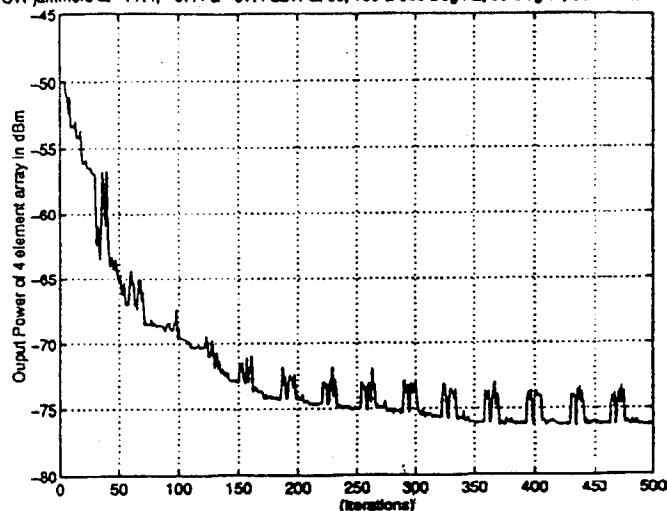


Figure 4B. Subgradient Nulling of Three CW Jammers

Upon unmasking other sources, the algorithm must "walk" the weights from the position dictated by the dominant jammer to positions that counter the lower power jammers as well as the strong source. The gradual descent observed after, say, the 200th iteration indicates that the algorithm is using a small step size as it tries to migrate to the optimal weights versus the three jammers. Speed and depth of convergence in multi-jammer cases will be affected greatly by how the step size at a given null depth is chosen within the algorithm.

In Figure 5A, the LMS based power minimization algorithm attacks a single CW jammer. The jammer is nulled into the noise floor in roughly 20 iterations. Again, the speed of convergence will be a function of the hardware implementation. However, the LMS method is working with the instantaneous values of sampled signals where the sample rate is quite high, i.e. megahertz. Consequently, the convergence time of the LMS will be vastly superior to that of the subgradient technique - on the order of microseconds versus milliseconds.

In Figure 5B, the LMS technique nulls out three CW sources quite effectively. A close look at the figure shows the null is on average approximately 5 dB above the noise floor by the 20th iterations. The method appears to average to the noise floor by about the 120th iteration. Clearly, the performance of the LMS method is superior to subgradient power minimization.

One CW Jammer at -77.4 dBW at 60 Deg Az; 60 Deg El; LMS

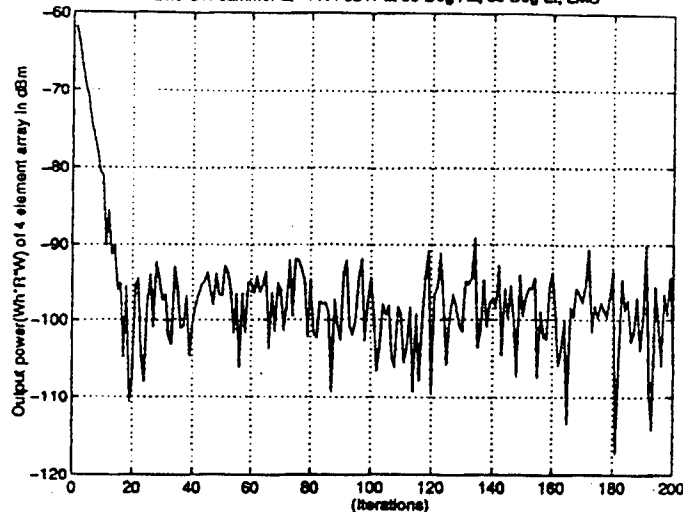


Figure 5A. LMS Nulling of Single CW Jammer

Three CW Jammers at -77.4, -87.4 & -97.4 dBW at 60, 180 & 300 Deg Az; 60 Deg El; LMS

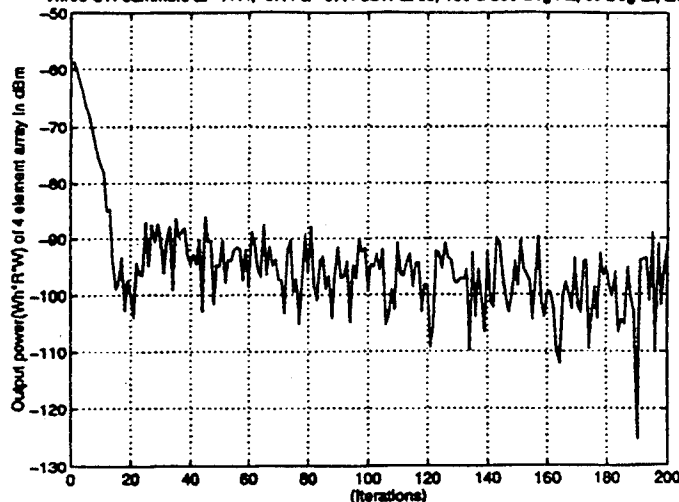


Figure 5B. LMS Nulling of Three CW Jammers

Performance Comparison - Dynamic Case

We begin with the static alignment of the two cases cited above, then rotate the array at a rate of 300+°/sec about an axis through auxiliary element #1 and the reference element.

The following metrics were computed for the dynamic cases:

| | Subgradient | LMS |
|---------------|-------------|--------|
| Single Jammer | increasing | 0.0201 |
| Three Jammers | 0.1448 | 0.1348 |

Figure 6A and 6B shows the nulling results when the subgradient methods is employed. As the array rotates, the phase relationships of the jammers at the antenna elements change with time. This causes the null point (or optimal weights) to migrate away from the values set by the algorithm. The search method must then chase the null point to maintain the null.

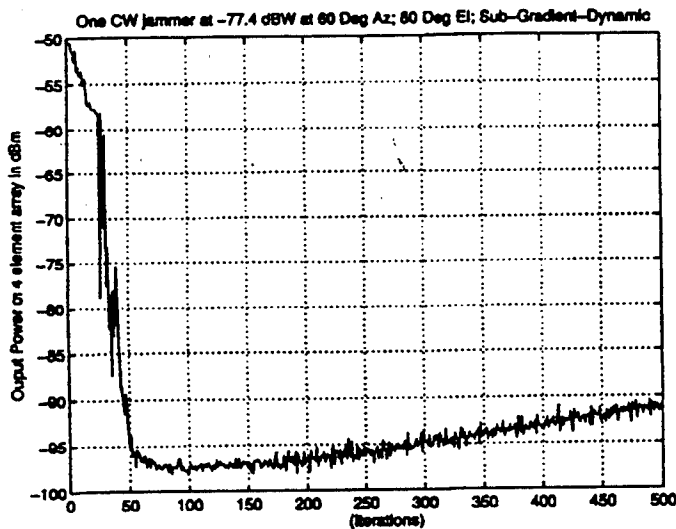


Figure 6A. Subgradient Nulling of Single CW Jammers

When the null moves away at a rate faster than the stepping mechanism of the search, the null degrades as shown in the Figure 6A for the single jammer case. For the subgradient search to have an chance of success in high dynamics the algorithm must include features that sense movement of the null point and open search step size selection as appropriate so that the search has the "legs" to chase the null point.

When this is done, the algorithm can maintain nulling action in dynamics but with some degradation. This capability is shown in Figure 6B where the step sizing mechanism is allowed to open to chase the null point. The algorithm is holding the null to about 28-30 dB above the noise floor during the rotation. At the 500th iteration the null is about 5 dB worse than the it was in the static case (compare 4B and 6B).

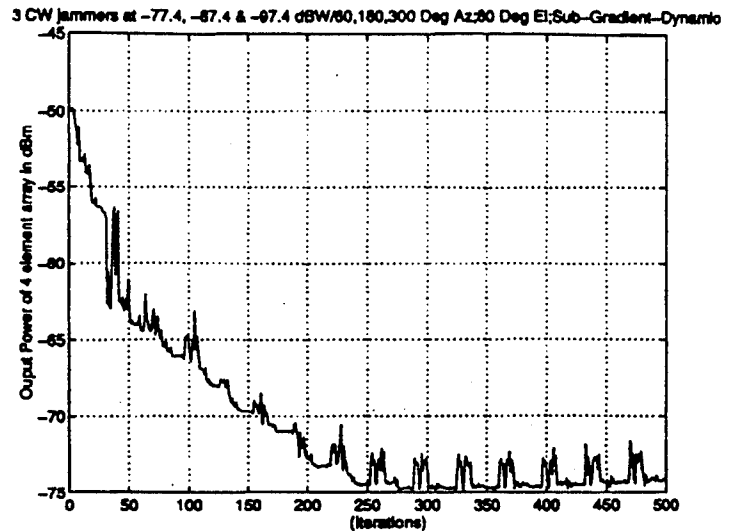


Figure 6B. Subgradient Nulling of Three CW Jammers

Figures 7A and 7B depict the nulling performance of the LMS based power minimization. The method benefits greatly from its high speed implementation and the use of instantaneous values. Even though the antenna element phase relationships are time varying, this algorithm is fast enough to track the change and maintain its nulls.

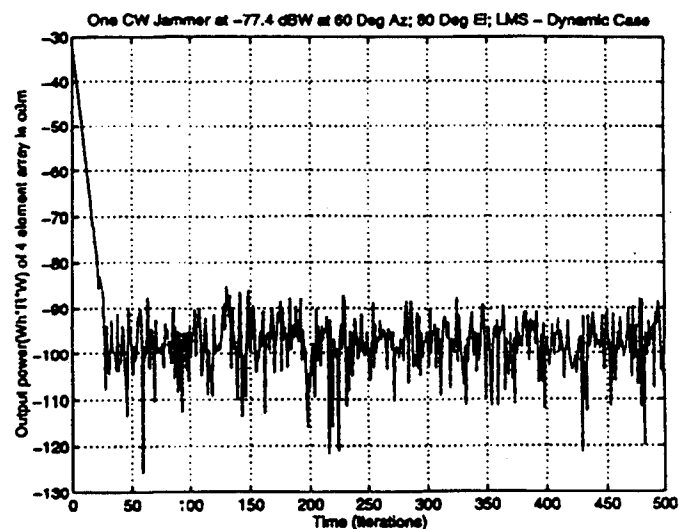


Figure 7A. LMS Nulling of Single CW Jammer

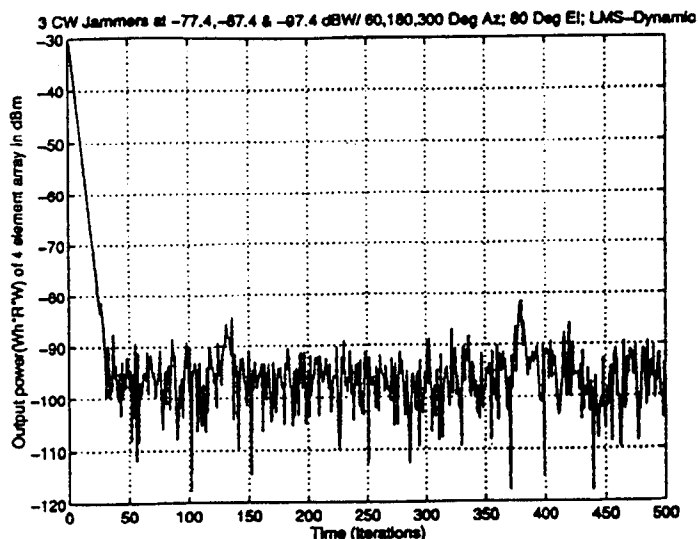


Figure 7B. LMS Nulling of Three CW Jammers
Final Comment

The above results indicate a significant performance benefit from using the LMS approach over a simple search method. One is immediately tempted to opt for an LMS-like technique. However, the hardware implementation of LMS requires significantly more complex and expensive equipment. For null steering applications, the real driving issue is - what level of protection does my GPS receiver need to perform in its anticipated environment? While the performance of the LMS technique is attractive, the fact remains that the simple and inexpensive search method can be entirely adequate in many applications.

Acknowledgments

The authors wish to express their appreciation to Dr. D. Stephens of E-Systems and Dr. S. Ananthaiyer of Purdue University who assisted in the preparation of this paper.

References

1. C. L. Zahm, "Application of Adaptive Array to Suppress Strong Jammers in the Presence of Weak Signals", *IEEE Transactions on Aerospace and Electronic Systems*, AES-9, no. 2; March, 1973
2. R. T. Compton Jr., "The Power Inversion Adaptive Array: Concept and Performance," *IEEE Transactions on Aerospace and Electronic Systems*, AES-15, no. 6; November, 1979
3. J. E. Hudson, *Adaptive Array Principles*, Peter Pererinus Ltd. on behalf of IEE; London, 1981

4. M. Bazaraa, C. Shetty, *Nonlinear Programming*, John Wiley & Sons, 1979

5. R. T. Compton Jr., *Adaptive Antennas*, Prentice-Hall, Inc., 1988

6. R. A. Monzingo, T. W. Miller, *Introduction to Adaptive Arrays*, John Wiley & Sons, 1980

Performance of a Miniature Dielectrically Loaded Volute Antenna

Dr. Oliver Leisten and Dr. Geraint Ffoulkes-Jones
Navstar Systems Ltd.

BIOGRAPHY

Oliver P Leisten is the RF Group Leader of Navstar Systems Ltd of Northampton, England. Dr Leisten received a PhD in Microwave Electronics in conjunction with Philips Research Labs. He has also worked for Plessey Avionics and Communications, Plessey Military Communications and GEC Plessey Avionics. Dr Leisten has specialist knowledge in the fields of microwave component characterisation and simulation.

ABSTRACT

This paper describes the design and predicted characteristics of a miniature dielectrically loaded quadrifilar helix antenna which is 5mm in diameter and approximately 20mm long. The antenna is considerably foreshortened with respect to its equivalent dimensions in air by the use of a Zirconium Tintinate ceramic dielectric core. The Zirconium Tintinate material used is produced by Morgan Matroc Ltd as a high stability microwave ceramic dielectric material and possesses a relative dielectric constant (ϵ_r) of 36. The intention is to provide a quadrifilar antenna of small physical size which should possess excellent phase centre stability and also low angle discrimination that is superior to that of the conventional microstrip patch antennas.

The antenna element is realised on a rod section of ceramic material with a co-axial feed passing axially, through the centre of the rod to the feed connection point at the top surface. the base portion of the antenna is formed into a metallised

sleeved balun which creates the conditions for the required balanced feed at the top feed point. This base section also serves as a convenient metal surface to solder to a circuit board or alternatively as a clamping surface for incorporation into a mechanical assembly.

The radiating section consists of two loop pairs which are respectively fed from the individual inputs comprising the balanced pair of feeds. Each loop pair consists, in clockwise order, of a helix element that is 45 degrees short, followed by a helix element that is 45 degrees longer than half a wavelength at the operating frequency. This feed scheme creates the necessary orthogonality (at the radiation resistive normalisation impedance).

The antenna element is small and light enough to be incorporated as tips into communication whip aerials.

INTRODUCTION

The combination of helical and loop structure antennas into resonant mode antiphase feed circularly polarised antennas was proposed by C.C.Kilgus ⁽¹⁾. Numerous forms of this original 'volute' antenna structure have been used to receive GPS signals. An air-dielectric volute antenna has been manufactured at Navstar Systems for some years. It sports an azimuthal pattern that is typical of this class of antennas (Figure 1).

NAVSTAR XR4 GPS ANTENNA

The polar plots shown below were produced by an independent antenna test facility, as part of an investigation into GPS antennas. Reproductions of the plots are "as received".

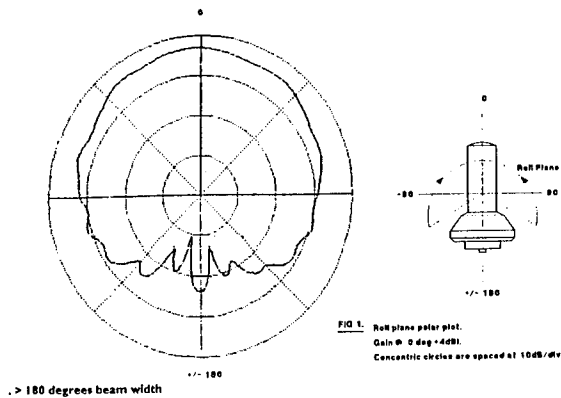


Figure 1 - Azimuthal Roll-plane Pattern of the NAVSTAR SYSTEMS Air Dielectric Volute Antenna

The Navstar Systems air-dielectric antenna has many of the electrical characteristics which approach those of the ideal GPS antenna. Axial ratio is better than 3dB over the full degree beamwidth with the outcome that good multipath rejection is provided. The beamwidth is broader than is possible with patch antennas so that the antenna can accommodate some pitch and roll motions whilst maintaining usable reception for GPS navigation.

The main disadvantage of volute antennas with respect to conventional patch antennas concerns their focal point. Modern survey antennas must have well behaved and precisely known phase centres to be able to perform their survey function at the high resolution that has become possible. This and the obvious miniaturisation benefits of dielectrically foreshortened antennas have together motivated the research into the small volute antennas.

The use of Zirconium Tintinate ceramic dielectric of relative dielectric constant $\epsilon_r = 36$ promotes a significant size reduction with respect to the original Navstar air dielectric element (Figure 2). This approach, though very bold in terms of the degree foreshortening sought, has the merit that it realises antennas which can be packaged in a number of novel ways, such as within car-phone antennas.

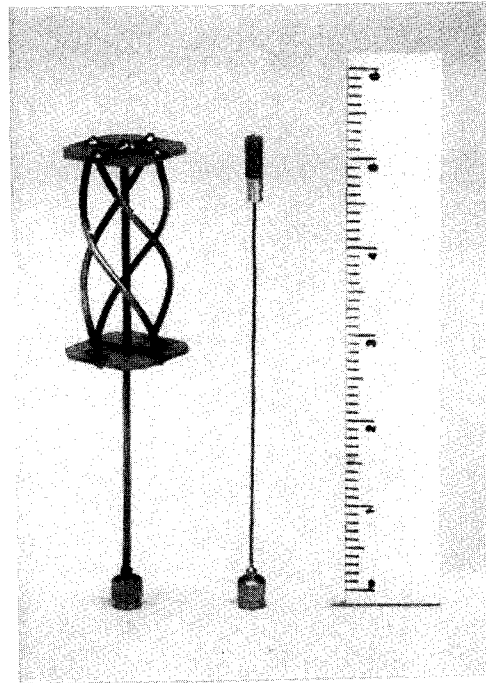


Figure 2 - Size Reduction due to Dielectric Loading

ANTENNA STRUCTURE

Innovation into dielectric foreshortening of quadrifilar helix antennas requires fundamental research into two areas:

- Structures of foreshortened antenna feed networks giving balanced anti-phase feed at the top feed-point.
- Wave propagation along helical transmission lines (and meandered helical transmission lines) on a cylindrical surface of high relative dielectric constant material with an axial ground column.

The chosen structure, schematically shown in Figure 3, is designed to be top fed using a semi-rigid co-axial cable passing axially through the centre of the element from the base. Obviously this is a single-ended transmission media since the outer of the co-axial cable is grounded. The base part of the antennas is a 90° resonant sleeve balun element whose purpose is to choke the outer of the co-axial cable and to impose a close to infinite impedance to ground on that line. From this point of imposed input impedance balance, balance degenerates with

increasing radiating section length and due to the imbalance between the line inductances in the outer and inner conductors of the co-axial cable. This line inductance imbalance can be minimised if the co-axial line characteristic impedance is kept low since the external inductance of inner and outer is dependant on their respective diameters (which converge as impedance is reduced).

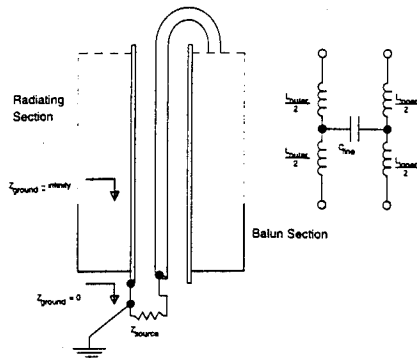


Figure 3 - Schematic Diagram showing Operation of Sleeve Balun Feed

The radiating section of the dielectric loaded antenna is a close adaptation of an approach that was proposed by Kilgus ⁽¹⁾, Kilgus showed that if balanced feed is available at the feed-point of the radiating section then orthogonality, between the four helix elements comprising two loop pairs, can be achieved by each loop pair to be composed of a short helix with electrical length 45° shorter than $\lambda/2$ resonance and of a long helix with electrical length 45° longer than resonance. In order to select right hand circular polarisation the short and long helix elements have to be organised in clockwise progression about the face of the cylindrical surface of the dielectric. In fact to organise this phasing correctly it is necessary to set the respective short and long helix reactances to as seen at the top feed point to be conjugate and equal to the average radiation resistance of the two helix elements. To select the nominally 180° beamwidth desired from the antenna the helices are wound to half a turn round the cylindrical surface. The process for creating the incremental delay in the long helices with respect to the delay of the

short helices was to meander the long helices sinusoidally to slow the wave velocity resolved into the helical direction. The artwork shown in Figure 4 is a developed view of the conductor pattern on a dielectric loaded antenna of the topology.

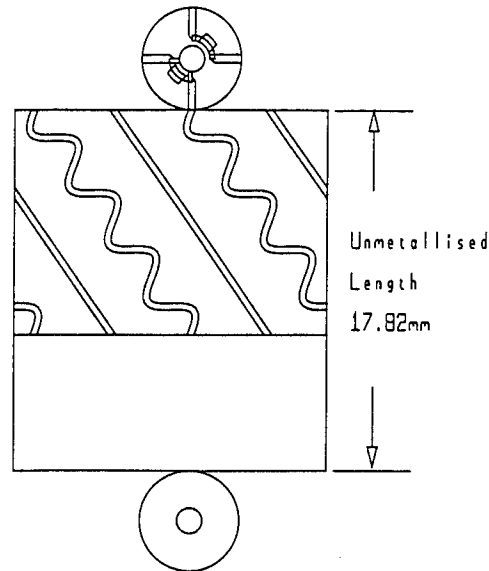


Figure 4 - Developed Artwork for Dielectric Loaded Volute

An iterative rough-cut design of the dielectric loaded volute, working at the GPS L1 frequency, with planar (microstrip) wave propagation modelling was initially carried out. This analysis led to the adoption of the 5mm dielectric diameter for the antenna. The feed cable hole diameter was set at 50 thousands of an inch (mils) to accommodate standard UT-47 semi-rigid cable. The rough dimensions provided from this analysis were used to set the proportions of a set of 20 different calibration standards that were used to empirically characterise the wave propagation characteristics of the helix and meandered helix lines.

HELICAL LINE CHARACTERISATION

A set of 20 standard transmission line elements were built using the Zirconium Tintinate material as the dielectric. Each standard was devised to be used in combination with others to characterise the wave propagation properties of lines of various helical pitch angles and various

meander amplitudes. Also a special calibration jig-set was constructed to be able to reproducibly apply spring-loaded wedge launch contacts onto the surface line for connection into an automatic vector network analyser. The jig-set was designed to permit free and independent rotation of the launchers about the ground centre-axis of the guide medium so that waves could be launched and received at any point on the periphery of the standard at an angle offset due to the helical rotation of the test line. Calibration software was also written to permit automatic measurement of transmission line delay eigen-values that characterise the various standard transmission line media.

The measurement of the standard set was repeated until accurate data was assured and a body of knowledge concerning relative dielectric constant was extracted. This data underpinned the analytical design of the dielectric volute antenna which served as the entry into electromagnetic simulation.

ELECTROMAGNETIC MODELLING OF DIELECTRIC LOADED VOLUTE ANTENNA™

A time domain Transmission Line Modelling (TLM) approach to electromagnetic simulation was adopted using the Micro-Stripes™ package that is produced by Kimberley Communications Consultants Limited of Nottingham, England. At initial time (t_0) a large voltage transition is created between the inner and outer conductors of the feed cable. The working area of the antenna and surrounding space is discretised into a fine orthogonal mesh. The philosophy of the TLM modelling algorithm is that the pulse travels along notional transmission lines connecting each cell to its neighbours. The pulse scatters from each cell in accordance with the geometrical features contained within that cell. For instance metal surfaces promote total or partial reflection at the interface between cells. In each cell linear combinations of pulses at the cell are used to calculate the E and H field components at the centre of the cell. In a similar way to SPICE™ simulation of oscillators, Fourier transformation provides the frequency response E and H fields at given points. Thus it is possible to elicit

resonance mode information. The software computes surface currents and voltages, electric, magnetic, power density and energy density fields and provides far-field transformation to obtain simulated antenna patterns.

A Visual Basic™ program was written to capture the geometric description of the simulation target antenna in terms of the Micro-Stripes™ geometric language. A unified unit system encompassing the meander dimensions and dielectric cylinder dimensions is possible by scaling the antenna into radii and radians and mathematical description of the antenna is relatively easy. This process yields a geometrical description of the antenna that is approximately 4000 lines long! An example geometry, captured into Micro-Stripes'™ geometrical language is shown in Figure 5.

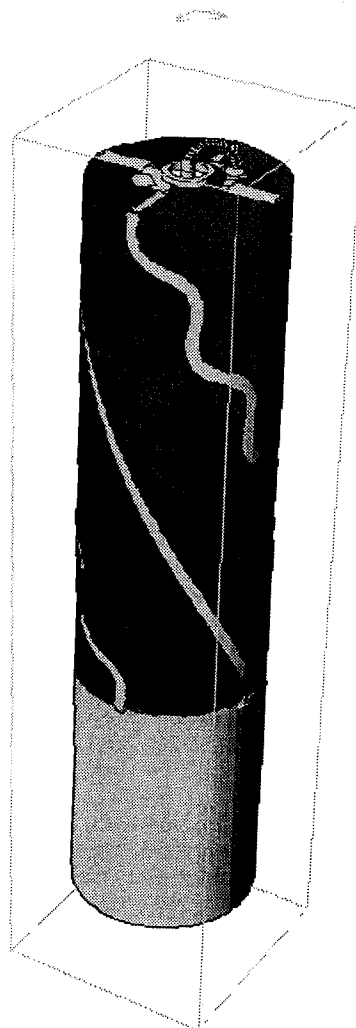


Figure 5 - Micro-Stripes Geometrical Representation of a Captured Dielectric Loaded Volute Antenna Geometry

- The geometrical description of the antenna is formulated in regular Cartesian co-ordinates which renders discretisation into cells relatively simple. The goal here is to optimise computational efficiency by discretising into a fine mesh only in areas where high resolution is absolutely vital. The model is bounded by absorptive walls to simulate free space and also a rectangular space-domain surface is defined to enclose the entire antenna apart from its feed entrance point. The space-domain surface is caused to support currents that are equivalent to those flowing in the antenna structure by a field manipulation. This is a necessary part of the process of creating a far-field transformation to the simulated antenna patterns.

ELECTROMAGNETIC SIMULATION RESULTS

The basic electromagnetic model of the GPS L1 dielectric loaded volute takes 17 hours to run on a Sun Sparc model 20. Finer resolution and hence longer run-time may be necessary once convergent criteria towards fully working antennas have been identified. At present the analytical synthesis of antenna geometry is not accurate enough to accurately predict the resonance frequency. To reveal the working operation of the antenna it is generally necessary to determine resonant modes of the structure using Fourier transformation of fields at indicative points close to resonant members. This process indicates a frequency which can be used for full electromagnetic field evaluation. This process has been used to reset the analysis frequency in the example that will be presented to 1.8 GHz.

Analysis of a complex resonating field structure is a demanding task. Fortunately the operation is aided by the electromagnetic simulator's ability to compute line integral voltages and currents integrated through surfaces. Generally what is required is a proper ordering of fields in accordance with the required function of the elements of the structure. For example the operation of the balun structure seems to be correctly ordering the outer and inner voltages into

balance as shown in a field section in Figure 6.

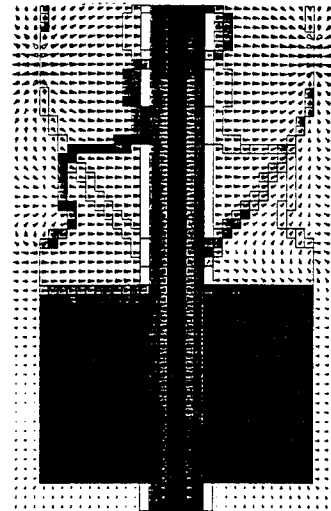


Figure 6 - Helical Antenna Simulation: X-Y plane Surface Currents and Electric Field Distribution showing Electric Fields within Balun Sleeve

Although the direction of the electric field within the co-axial feed cable is ambiguous due to the presence of a mismatch standing wave in that structure it is clear that a balancing action is developing between the sleeve and the transmission line outer. Electric fields have been ordered to develop a potential between the sleeve ground and the co-axial cable outer. This conclusion is further confirmed by the plot of electric fields at the plane of the balance rim as shown in Figure 7.

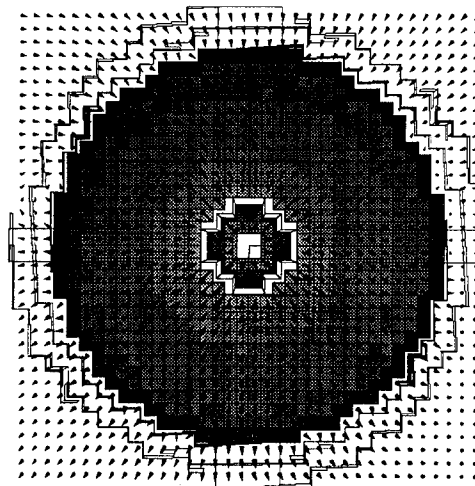


Figure 7 - Helical Antenna Simulation : Base Surface Currents and Electric Field at Plane of Balun rim

Plotted through the entire centre section of the antenna at a different scale (Figure 8) it is clear that the electric fields are most

intense at the resonant voltage mode of the helices at the half height of the radiating section.

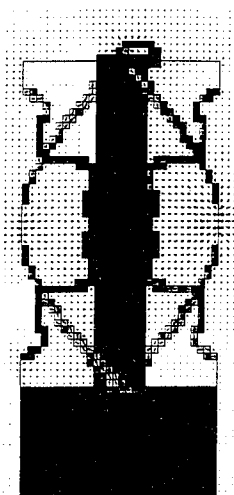


Figure 8 - Helical Antenna Simulation - Surface Currents and Electric Field through the X-Y Plane

The magnetic field, again plotted in the same plane as the electric field (Figure 9) is ordered to peak at the positions of maximum surface current in the helices. Since the antenna is resonating in the helix mode this condition occurs at the top and base of the helices.

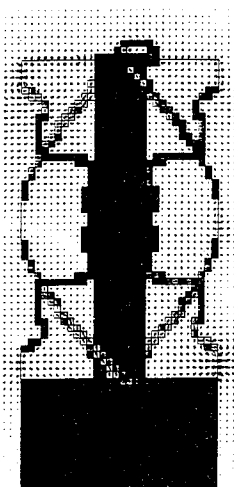


Figure 9 - Helical Antenna Simulation - Surface Currents and Magnetic Field through the X-Y Plane

The electromagnetic simulator computes the power density field from the cross product at E and H fields. From Figure 10 it can be seen that the power flows are generally in opposition in the left and right hand side respectively. This ordering

occurs in accordance with the balanced nature of the antenna feed.

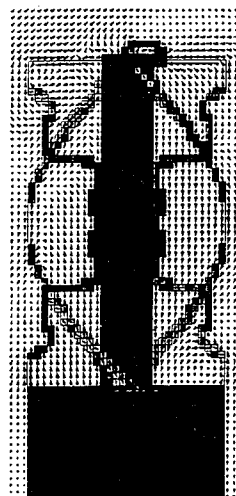


Figure 10 - Helical Antenna Simulation, Surface Currents and Field Power Density Through X-Y Plane

The conditions for preferential selection of right hand circularly polarised radiation require current balance in all helix elements and phase orthogonality between them. The resonance mode developed in this simulation example does not quite meet these criteria as shown from the top surface feed in Figure 11. Clearly some current magnitude difference exists and the example antenna may not possess particularly good selectivity of right hand circular polarisation.

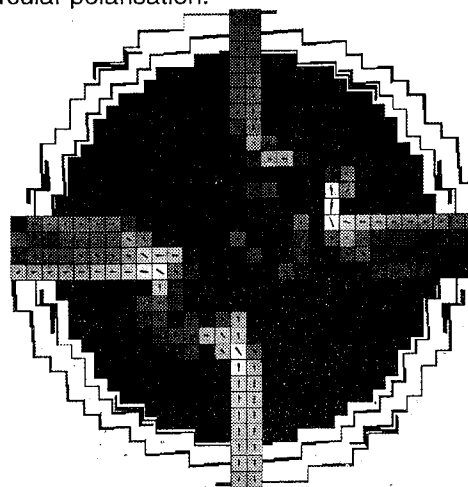


Figure 11 - Helical Antenna Simulation - Surface Currents at Top Feed Point

FAR FIELD SIMULATION RESULTS

So far simulation trials have failed to isolate the true quadrifilar helix resonant mode in the dielectric loaded volute antenna. In other words it has been difficult to set conditions that promote proper orthogonality in the helix members of the antenna. For this reason no volute cardioid type responses have so far been obtained and it has not yet been possible to demonstrate selectivity in favour of right hand circular polarisation. Therefore mixed polarisation far-field simulated patterns should be evaluated against the standpoint of indicated radiation efficiency, particularly in the light of the apparent poor match indicated by the standing wave in the diagram of Figure 6. The simulated predictions for azimuthal pattern are shown in the x-y plane and z-y planes in Figures 12 and 13 respectively and the prediction for horizontal plane in Figure 14. In all three figures the radial scale is set at -30dB to 0dB with respect to isotropic.

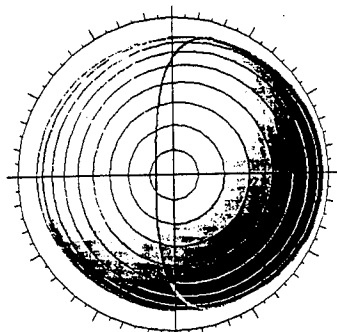


Figure 12 - X-Y Plane Azimuthal Simulated Far-Field Pattern for the 1.8GHz Antenna

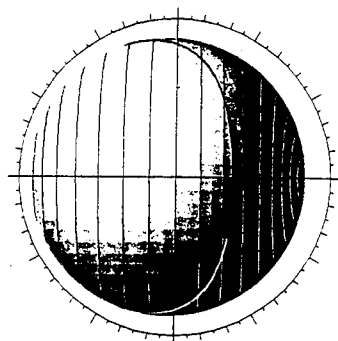


Figure 13 - Z-Y Plane Azimuthal Simulated Far-Field Pattern for the 1.8GHz Antenna

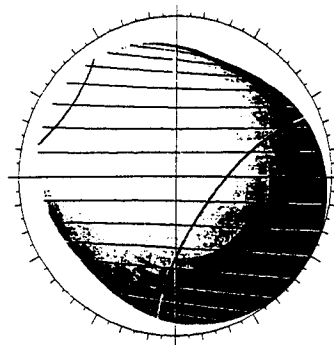


Figure 14 - X-Y Horizontal Plane Simulated Far-Field Pattern for the 1.8GHz Antenna

MEASURED RESULTS

At present two artwork versions of dielectric loaded quadrifilar helix antennas have been constructed. The design of these antennas was conducted early in the project and their purpose was primarily to test the accuracy of the electromagnetic simulation model. It was found that the simulator could predict resonance frequency to within a few MHz accuracy. As might have been expected for an antenna that has been miniaturised to this extent the operating bandwidth is low (Figure 15):

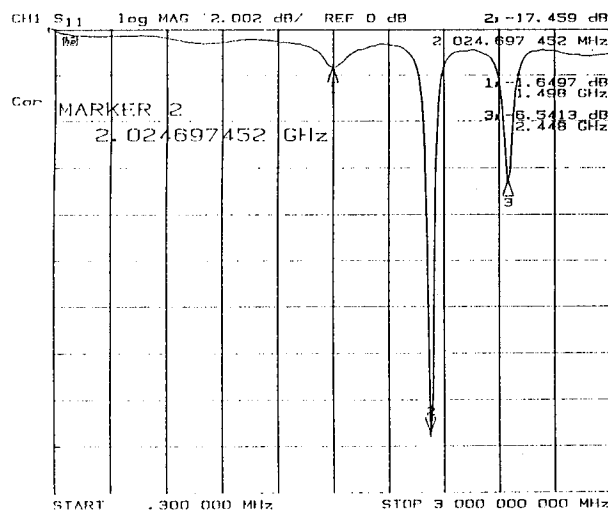


Figure 15 - Input Reflection Coefficient of the Version 1 Dielectric Loaded Antenna

It has been found that there are generally three resonance modes with the present topology of antenna. These are associated with long-loop resonance, parallel long and short loop resonance, and short loop resonance modes in turn. The measured radiation patterns were not particularly well ordered but occasionally patterns were measured which correlated well with the simulation theory. For example a pattern associated with the short loop modes of Figure 15 is shown in Figure 16. It correlates well with the theory for the radiation pattern for which a single loop is dominant.

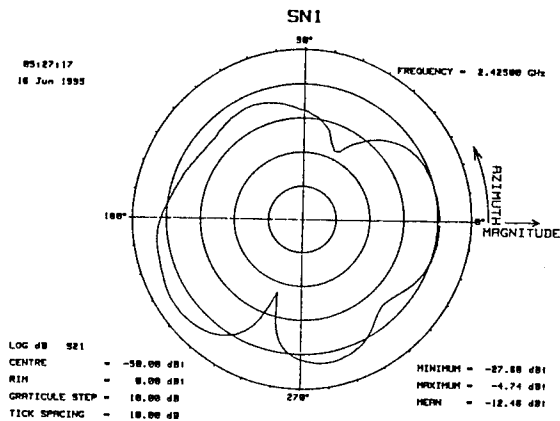


Figure 16 - Measured Right Hand Circular Azimuthal Radiation Pattern for a Dielectric Loaded Quadrifilar Helix Antenna

TARGET SPECIFICATION FOR THE DIELECTRICALLY LOADED VOLUTE ANTENNA

Since the radiation efficiency of the antenna is apparently reasonably good it is supposed that the dielectrically loaded volute antenna can exhibit patterns that are similar to those of an equivalent air-covered volute, but over a narrower bandwidth. This was the starting assumption at the inception of this research and though such performance has yet to be demonstrated the research results are promising. The development goals are:

- To develop a viable GPS antenna which is approximately 5mm in diameter and 20 mm in length.
- The antenna should exhibit approximately 0dBic gain over a 180° beamwidth.
- The antenna should possess discrimination in favour of right hand polarisation, particularly with respect to left hand polarisation. It should therefore possess good multi-path rejection characteristics.

The antenna should be configurable for PCB mounting onto a circuit board (Figure 17) or alternatively for connection to a long co-axial cable feed perhaps as the top part of a whip-mount stack of antennas. (Figure 18).

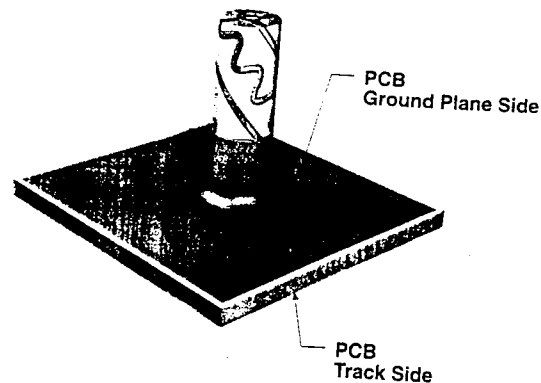


Figure 17 - Circuit Board Mounting of Dielectric Loaded Volute

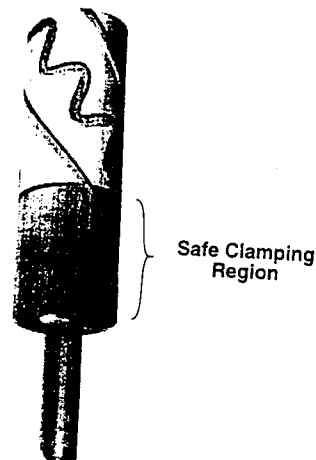


Figure 18 - Whip-mounting of Dielectric Loaded Volute

FURTHER WORK AND CONCLUSION

The choice of topology that has been adopted is complex but elegant in terms of mounting flexibility. NAVSTAR SYSTEMS have mounted a determined effort to realise the potential performance of this structure. A design route towards this miniature dielectric loaded volute antenna has been established, but the approach needs further refinement if the correctly phased resonance mode is to be found. A particularly important step in this regard is to build the model so that it characterises the helical radiation resistance per helix so that proper phasing can be designed.

ACKNOWLEDGEMENTS

Thanks are due to many Navstar Systems colleagues who worked hard to realise the characterisation hardware for this research. In particular Rob Gee designed the jig-set, administered its manufacture and assisted with measurements. Thanks are due to General Manager Tony Haddrell and Commercial manager Mike Duckham for their material and moral support.

The team at Morgan Matroc Unilator division at Ruabon, North Wales have worked hard to produce calibration standards and test elements. Thanks are due to David Hutchinson who ported designs into their system. Keith Linaker and Kay Griffiths lent the project valuable effort. The project enjoyed the support of Managing Director Bob Jackson and Technical Director David Cannell who no doubt diverted valuable resources to support it.

Special thanks are due to Paul Risinger (Vice Chairman of our holding company - Symmetricom) who has given particular support to this venture. It has been our pleasure to serve a company that is so committed to the development of new technology.

REFERENCES

C.C. Kilgus
Resonant Quadrifilar Helix Design
The Microwave Journal
December 1970

An Effective GPS Application for Helicopter Operations

William O'Keefe
Newcomb Communication, Inc.

BIOGRAPHY

Fairleigh Dickinson University, MBA degree, Cum Laude in Business Management, concentration in operations research and information technologies.

United States Naval Academy, BS degree in Naval Science, concentration in electrical engineering.

Law Enforcement Manager. Leader in the product development for law enforcement applications of the Newcomb Satellite Tracking System. Designed system modifications leading to more effective covert installations and operations of tracking and communications including message encryption, miniaturization, and automatic surveillance configurations.

A senior member in Advanced Concepts Development at a US Government Research and Development Laboratory. Designed and developed an international information tracking and data fusion facility. Managed several projects involving covert tracking, information flow and decision support technologies. Participated as a principal in the conceptualization and design of a global satellite tracking system. Effectively coalesced talents, abilities and resources culminating in operationally successful counterdrug target tracking and information gathering.

Adjunct Professor, at Boston College. Created a course and authored the textbook entitled *Information Science: Applications and Overview*. Taught five courses over the years in such areas as Database design, Programming Logic, Networking and Open Systems, and Business Applications.

Formerly served in the National Aeronautics and Space Administration, Electronics Research Center; Bell Telephone Laboratories; and as an officer in the U.S. Navy.

ABSTRACT

The primary technical innovation involves the effective use of a unique satellite transmitter and receiver message

configuration and protocols and the antenna system for use on board helicopters. A combined L-band transmit, C-band receive, and GPS antenna system allows automatic dispatch/flight following operations and safety communications from helicopters operating in the Gulf of Mexico. A helicopter presents a very inhospitable environment for satellite, or upward looking, antennas. A carefully selected group of antennas have been designed that makes such an L-band transmitter, C-band receiver, and GPS receiver work to full advantage in such an environment.

The objectives are to allow helicopter pilots performing frequent low altitude ferrying between wellhead oil platforms in the Gulf of Mexico to report their position and intentions to the company while also actually decreasing their workload. One organization operates about 240 of the total of 600 such aircraft serving in the Gulf area. Dispatcher flight following for this organization now requires 22 people at several bases. The personnel requirement could be reduced to 10 people with SATCOM. One flight following system under consideration uses a Mode-S transponder technology, rather than SATCOM. The Mode-S system does not work below 300 feet altitude, rendering it of little value for such helicopter operations. Some of these aircraft perform up to 70 individual flight operations per day.

The results from an extensive SATCOM demonstration on board a Bell 206 aircraft have been encouraging. The value lies primarily in that these helicopters no longer need to climb up to approximately 1000 feet to report positions or alter flight plans as was necessary using the standard UHF radio for this purpose. The operations generally take place from 50 to 200 miles out over water and are effectively over-the-horizon from the UHF radio system. Such communications tasks are now operating so as to relieve all of the position reporting communications workload from the pilot. It also eliminated the extra fuel that was consumed in the climb outs required to reach the UHF radio horizon.

It is concluded that such a satellite based GPS position reporting and communication system has been demonstrated to be completely effective largely due to the efficient message protocols and configuration design.

This new technology application now allows seamless organizational asset tracking and emergency situation notification for possible extraction and rescue.

INTRODUCTION

The central philosophy here is to provide an opportunity for a practical and automatic flight following and dispatching capability. The main thrust being the technology involving message transmission configuration and protocols. A chronic situational dilemma is that of getting the critical position information back to the control and dispatching center in a rapid and secure manner. This paper explains the unique application of advanced technology in the areas of position information transmission via new configuration of available antenna systems and the idea of Spread Spectrum Code Division Multiple Access (CDMA) digital message transmission.

The ability to remotely conduct flight following by using satellite transmitting devices over continent-wide areas is now commercially available. This system uses commercial satellites without risk of signal detection or losing position reports. Advances in microchip development along with Chip-On-Board (COB) manufacture, and the best developments in micro GPS engines support this so called automatic dependent surveillance. Newcomb Communications, Inc. of New Hampshire is applying digital Direct Sequence Spread Spectrum (DSSS) techniques to the position reporting and tracking system. Based on the pioneering work by Dr. Gerry O'Neill, DSSS by Newcomb transmits reliable identity and position reporting signals to Geostationary satellites over 22,000 miles from the surface using bursts of only a few watts of energy lasting less than a tenth of a second. Such advanced technology has enabled the manufacture of small, low power position reporting and communication systems. Proprietary designs leverage a form of DSSS signal transmission called Code Division Multiple Access (CDMA), ensuring every position report sent will be received. A unique feature is that the transmissions appear up to 1000 times below the naturally occurring background noise at the receiver. Accurate position information is determined using embedded, miniature Global Positioning System (GPS) receivers.

The main issue is how best to get the position (navigational) information back to the organizational element that needs to conduct the flight operations. These are the dispatchers or controllers. All of the GPS systems provide such information to the entity carrying the receiver, but relies on various radio links, often

depending on extensive surface assets to complete the communication task. The task often adds considerable to the pilot's workload. This task should be as fully automated as possible, and yet allow emergency traffic and routine optional traffic as needed.

The main technical innovations of interest involve the effective use of a unique satellite transmitter and receiver antennas for use on board aircraft, particularly helicopters. L-band transmit, GPS and C-band receive antennas allow automatic real-time dispatch/flight following operations. Safety communications from the aircraft include timely reporting of selected telemetry of any information considered critical to the individual operation.

Helicopter pilots performing frequent low altitude ferrying between wellhead oil platforms in the Gulf of Mexico are required to report their position and intentions to the company dispatcher while also considerably decreasing their workload. One organization operates about 300 of the total of 600 such aircraft serving in the Gulf area. In one particular case the dispatcher flight following for this organization now requires 22 people at several bases. The personnel requirement could be reduced to about 10 people with this advanced technology SATCOM and tracking capability. The FAA secondary surveillance radar tracking does not perform well when the aircraft are operating below 300 feet, rendering it of little value for such off-shore helicopter operations. The pilot workload is high as some of these aircraft perform up to 70 individual flight operations per day.

The GPS Subsystem

The GPS Subsystem determines precise geographic position, altitude, velocity, and time from L1 GPS, 1575.42 MHz Standard Positioning Service signals generated by at least four GPS satellites. Positional accuracy is 25 meters CEP using Full Accuracy C/A Code and 10 meters CEP using optional Differential GPS. The GPS subsystem provides this derived information to the transmitter and KDU subsystems periodically, typically once per second.

The GPS subsystem consists of OEM units such as the Trimble SVeeSix or Rockwell MicroTracker units.

The Antenna Subsystem

The antennas are omnidirectional. They consist of flat plate, approximately 0.5" high by 6" diameter and a "cell phone" type whip. The flat plate antenna generally consists of a patch or quadrifiler device with left-hand

spin and axillary rates of 4 dB. There are several antenna configurations available for this system. They are:

- L/C band patch 3dBi gain antenna and a separate active GPS antenna.
- L/C band TX/RX Aircraft left hand circular polarized L-band and Vertical polarized C-band receive antenna and a separate active GPS antenna.
- GPS 20mA active aircraft antenna.
- GPS 20mA active ground antenna.
- L/C band and GPS combined patch antenna.

The Workstation

The Newcomb Supervisory Control and Tracking (NSCAT) workstation is the basic unit that provides graphical tracking of assets equipped with Newcomb Communications, Inc. mobile satellite transmitters. Both real-time and historical displays are available.

The normal platform for this package is a 90 megahertz Pentium with 24 meg of ram, a 500 meg IDE disk plus a 1 gig SCSI disk. A tape back up system is also included. The video subsystem is a PCI graphics adapter with 2 meg of RAM. A CD ROM drive is included for loading of programs and data to disk and is not intended for live access. This selection of hardware was chosen to provide good performance and proper storage space.

This program provides the link to the Newcomb Communications, Inc. ground station. Connection can be made either through a direct dial up or through a local Internet provider. (Automating local Internet connections is a custom option). Data collected is added to the NSCAT data base for future retrieval and display.

MESSAGE CONFIGURATION AND PROTOCOLS

Spread Spectrum Background

Spread spectrum communication was borne of the need for secure communications during World War II. "Spectrum spreading was a natural result of the Second World War battle for electronic supremacy, a war waged with jamming and anti jamming [AJ] tactics. On the Allied side by the end of the war, every heavy bomber was equipped with at least two jammers developed by the Radio Research Laboratory (RRL) at Harvard." In a postwar RRL report, the following comment on AJ design is notable: "In the end, it can be stated that the

best anti-jamming is simply good engineering design and the spreading of the operating frequencies."¹

Transmitting position information using spread spectrum is now a well established technique for highly reliable communication. Today such successful military programs as the Joint Tactical Information Distribution System (JTIDS) and Global Positioning System (GPS) use spread spectrum techniques.

Spread Spectrum, CDMA

The Newcomb systems use direct sequence spread spectrum techniques. This is accomplished by Binary Phase Shift Keyed (BPSK) modulation of the fundamental carrier, along with carrier suppression, producing a double side band signal occupying a spectrum twice as wide as the modulation rate. The signal elements used to determine phase shifts are the "ones" and "zeros", called "chips", of "pseudo-noise" (PN) generated by any one of many millions of binary polynomials. Chips are taken in groups and assigned to represent the data bits of a digital message. Each group of chips is either inverted (binary ones-complemented) or not, depending on the value of the bit being encoded. This results in signal which, in addition to being at a low power level, has all the characteristics of thermal noise to any receiver not sharing the exact PN pattern.

Thousands of position report messages may share a single radio channel, providing they are staggering the timing of a given PN code. This sharing is known as CDMA. Each CDMA signal is automatically encoded with the identification of its individual transmitter, and contains patterns enabling recognition, detection and position report recovery by a properly synchronized earth station which knows the particular PN code used. This facilitates a decentralized satellite communication network.² Several receivers, each sharing a private PN code with its population of transmitters, may concurrently use a single channel. To any receiver not privy to a PN code, the channel appears to have nothing but naturally occurring noise, as the signals are camouflaged, to have all the properties of an empty frequency.

Certain salient characteristics of this form of communication, making it ideal for reliable delivery of position information to remote controllers and dispatchers, are:

- **Low Power**, Small flat "patch" antennas can reach the satellite.

- **Security, Low Probability of Detection, (LPD)** An extremely low average power density (less than thermal noise at reasonable distance from the transmitting antenna) combined with noise-like encoding makes signal difficult to detect.
- **Security, Low Probability of Interception (LPI),** In the unlikely event that signals are detected, they cannot be decoded, or even demodulated, without knowing the particular PN code in use. In addition, the actual position report data may easily be encrypted.
- **Multiple Access CDMA,** This allows unscheduled transmissions by multiple users, even when messages may overlap. It provides reliable message reception with an overall system capacity of more than 2 million messages per hour.
- **Near / Far Performance,** The combination of spread spectrum coding and satellites creates a synergy particularly suited for wide area covert communications, tracking and surveillance. Targets outside the normal operating areas may be monitored from any distance, while dispatchers remain in communication without effective loss of communication.

To demonstrate the effectiveness of making real-time automatic information available to the operators that need it, a 30 day position reporting demonstration was recently completed. The Newcomb satellite tracking system was installed on board a Bell 206 aircraft that was very active in serving wellhead platforms. The results were encouraging. The value was primarily in that the helicopters no longer had to climb up to approximately 1000 feet to report their positions. This often forced them to alter flight plans made necessary because the standard UHF radio was below the horizon.

These operations generally take place from 50 to 200 miles out over water and are effectively over-the-horizon from the UHF radio system. On board the equipped aircraft, communications tasks are operating so as to relieve all of the position reporting communications workload from the pilot. The operation also eliminated the extra fuel that was consumed in the climb outs required to reach the UHF radio horizon. This system is being considered by the FAA to fulfill the requirements for Automatic Dependent Surveillance (ADS) techniques.

Transparent Data Transfer Mode

Unlike the other modes of operation, the transparent data transfer mode presumes that the other side of its interface is governed by a program or process running on a microprocessor connected to this serial interface. We'll use the term, mobile process, to refer to this process attached to the aircraft beacon. We presume that the mobile process wants to use this mode of the interface to exchange reliable, ordered streams of 8-bit data with a compatible process at the customer's base station. We'll use the term, base process, to refer to this base station process that's exchanging data streams with the mobile process. Since the base process must log into the satellite gateway to get its data, and since the satellite gateway's protocols cannot avoid adding protocol data to the data being exchanged, some portion of the base process must adapt the 8-bit data stream to the protocols in use. We'll use the term, protocol adapter, to refer to that part of the base process. Specifically, inbound packets from the aircraft beacon to the gateway cannot be acknowledged without help from the base process. Therefore, the aircraft beacon transparent data transfer mode requires cooperation from the customer's protocol adapter to insure reliable, ordered delivery of the 8-bit data streams. This works in the following way.

When transferring inbound data in this mode, the aircraft beacon will accumulate every 8-bit byte from the mobile process into a packet conforming to the Simple Transport Protocol (STP), (closely related to the CCITT X.25 network layer protocol). The aircraft beacon, recognizing that it's in transparent data transfer mode, will provide STP acknowledgments back to the protocol adapter, and then disassemble the STP packets into an ordered 8-bit stream of data, which is presented to mobile process across this interface.

Once in this mode, data bytes do not exert any influence on the operation of the interface; to wit, there are no bytes that are considered control characters. In general, RTS/CTS is used to control the inbound flow of data, from the mobile process to aircraft beacon (toward the base process); and DTR/DSR is used to control the outbound flow of data, from the aircraft beacon to the mobile process. The specific control signal usage in this mode is as follows:

- CD:** The aircraft beacon asserts Carrier Detect only when it has established an STP connection with the protocol adapter. It removes CD whenever this connection is lost.

RTS: The mobile process asserts Request To Send to indicate that it wants to transmit data to the base process. It removes RTS in order to force the inbound data stream to stop, and thereby forces completion of any partially constructed packets.

CTS: The aircraft beacon asserts Clear To Send whenever it's ready to accept inbound data for transmission toward to the protocol adapter. This is true whenever there's a connection, and thus only if CD is true. It drops CTS to halt the flow of data from the mobile process.

DSR: The aircraft beacon asserts Data Set Ready whenever it may have outbound data to present to the mobile process. This is true whenever there's a connection, and therefore whenever CD is true.

DTR: The mobile process asserts Data Terminal Ready whenever it's ready to receive outbound data from the aircraft beacon. It removes DTR in order to halt the data it's receiving from the aircraft beacon.

After the mode entry sequence, the aircraft beacon will attempt to make an STP connection to the protocol adapter. After the connection is made, it will assert the CD, CTS, and DSR signals.

The aircraft beacon will continue assembling and sending packets as long as they are acknowledged by the customer's protocol adapter. Whenever the protocol adapter indicates that it's not ready to receive more packets, it will stop the flow of bytes from the mobile process by removing the CTS signal.

A similar process operates on the outbound channel. As packets arrive from the protocol adapter via the satellite gateway, the aircraft beacon sends back acknowledgments to the satellite gateway and STP sliding window acknowledgments to the protocol adapter.

The service is characterized as unreliable because -- although messages are never delivered out of order or in mangled condition -- the messages are sometimes lost and not delivered at all. This happens for a number of reasons: the attitude of the aircraft or boat may move the antenna out of sight of the relevant satellite; or the mobile unit may pass underneath a physical obstruction like an overpass; or the information may be lost after it's been passed into the internet, etc. -- none of which can be

prevented. To compensate for this, we must add a transport-level protocol that guarantees end-to-end delivery of every packet's worth of data that's sent. The Simple Transport Protocol (STP), has been customized designed to do this.

Why is a customized transport protocol necessary? There are several widely accepted, standard transport protocols that have already proven themselves -- e.g. TCP/IP and the many classes of ISO transport protocols. Unfortunately, none of these standard protocols is practical under these circumstances, for several reasons:

- They have to pay a proportionately high price in overhead -- both processing overhead, and data space overhead.
- The protocols restrict the data-carrying capacity of their packets to about 90 bytes.
- TCP/IP headers would add up to 48 bytes, or more than half of the available packet size.
- Standard protocols make significant assumptions about the presence of, properties of, and services offered by standard protocol layers lower down in the communications stack.

Therefore, it's impossible to take an existing, proven implementation and adapt it with only minor modifications. The whole thing -- or at least most of it -- would have to be rewritten from scratch, yielding a grossly overweight implementation, with a great many unused but irremovable features, that therefore becomes extraordinarily difficult to test. The only proven part that would survive would be the rules of the protocol and their effect on communication.

The X.25 fixed-size sliding window used for acknowledgments can provide sequencing and flow control, but cannot simultaneously detect missing packets. Therefore, we simply add the proven technique of accredit allocation to the X.25 protocol and add a corresponding credit field to the header. Then we eliminated certain header fields and their associated facilities. We eliminated X.25's Q-, D-, and M-bits from the header, since their associated functions serve no useful purpose here. As a result, we end up with the minimal transport protocol described below, for which there is prima facie evidence that it will retain the proven benefits of the X.25 protocol.

Timing and Time-outs

When an aircraft beacon transmits a packet, it takes about 70 milliseconds to send a maximal length packet. The packet will take approximately 0.25 seconds to travel up to the satellite and back down to the satellite gateway. Once inside the satellite gateway, there will be an apparently negligible delay before the information is translated to the record format. If the data travels to the customer's site via internet, this adds delays of about 2 seconds (normal delay) to 10 seconds (typical long delays). So the total inbound delay is expected to be somewhere in the vicinity of 4 to 12 seconds.

We'll assume that the time spent in the customer's system is negligible and try to estimate the outbound travel time. The size of the SHIS DATA command for a maximal packet is approximately 197 bytes, which takes 0.8 seconds at 2400 baud. Once the DATA command has been entered, the delay until it's transmitted will be less than a minute. Let's say it's delayed 30 to 60 seconds in the satellite gateway. The transmission of approximately 100 bytes at 1200 baud will take about 0.8 seconds. And the satellite transit delay will be 0.25 seconds once again. So the outbound delay is expected to be somewhere around 35 to 65 seconds.

The total round-trip time for a packet and its acknowledgment, or confirmation, is thus expected to be around 40 to 80 seconds, with considerable variability. Therefore, we specify that all STP time-out periods should be set to a minimum of 90 seconds. When an attempted connection times out, this interval will increase arithmetically until it reaches the two way aircraft beacon's automatic transmission interval.

One further note on throughput. The two way aircraft beacon, for internal physical reasons, will limit its transmissions to no more frequently than one every 10 seconds. Therefore its average data throughput can be no greater than 9 bytes per second, or 90 baud. The outbound throughput is limited to 1200 baud for all outbound 100-byte packets to all connected mobile units. Therefore, the outbound connections are limited to 1200 baud divided by the number of two way aircraft beacons that are currently connected.

CURRENT APPLICATIONS

Newcomb Communications, Inc. is now building both transmit-only (model CP-1) and transmit/receive (model AV-2) long range mobile satellite communication systems for continent wide tracking and covert surveillance. Extensive demonstration and test programs with such agencies as the U.S. Army, U.S. Coast Guard,

U.S. Customs Service, and the Drug Enforcement Administration, have been conducted with success. The system configurations demonstrated are a full digital aircraft radio. These are packages in a 1/4 ATR Short Chassis and are manufactured using surface mount technology. Power requirements are between 6 and 8 watts. Future models will use MMIC and ASIC devices to further reduce size, weight, and power.

Military Command and Control

The Army is using this system as a secure long range vehicle communications for virtual situation control, helicopter flight following, and communications operations. Anticipated applications include secure communications and control links in the Army Special Forces and US Special Operations Command. The salient LPI/LPD features and the ability of the entire system to handle millions of messages per hour can provide communications support for tactical commanders. Commanders can now have surveillance coverage, positive control, and covert communications with all equipped forces independent of distance and ground obstructions.

Coast Guard VTS and SAR Operations

The Coast Guard has demonstrated this form of communication because of the total system capacity afforded by CDMA DSSS and the real time nature of the communications. These applications include Vessel Traffic Systems (VTS) and Search and Rescue (SAR) operations on the high seas. The vessel traffic control system application was demonstrated in the Narragansett Bay and New Orleans areas by placing a CP-1 type transmitter on work boats, ferry boats, and even a Mississippi River Boat. The search and rescue operations have demonstrated the possibility of eliminating the "Search" portion of the scenario owing to the track following behavior of the system when any interruption may indicate a problem calling for help.

Counterdrug Tracking

The U.S. Customs and DEA have ongoing test operations involving tracking of both overt and covert target vehicles, including cars, boats, and aircraft. The nature of the tracking workstation to include customized mapping allows operational control with a strong decision support aspect. The inclusion of an "emergency switch" feature, enabling the vehicle operator to change the nature of the automatically transmitted signal without any other person noticing this action, is a strong inducement to use such a position reporting system in this type of work. Counterdrug work has caused the beacons to be mounted on containers, allowing suspect

shipments to be tracked without placing any agents in danger.

FUTURE ENHANCEMENTS

Message Encryption

The Newcomb DES system is a complete system whose data is controlled and encrypted at the point of origin and decrypted at the end point. This type of system has the greatest chance for integrity.

The Newcomb DES system consists of an Encryption Device for encryption at the beacon and a decryption device for decryption at the user workstation. Both shall have the ability to encrypt and decrypt messages, but must be unique for the CP-1 beacon. The decryption device at the tracking workstation shall not be identical to those used at beacon sites due to processing limitations.

In the DES CP-1 system, there is only one unique key per tracking workstation. Therefore, a tracking workstation may only decrypt those units supplied with the same one key. It may receive other transmissions from units supplied with a different key, but it cannot extract any information from the coded message.

The encoded portion of the message throughout the DES CP-1 system shall consist of GPS location information followed by an optional message from the beacon keyboard or a PC.

The encryption device at the beacon shall be permanently mounted, preferably internal to the beacon. The host PC is optional in a remote site with the beacon.

Emergency Situation Indicator

An emergency situation on board the vehicle, plane, or boat being tracked, such as a call for extraction, can be sent in a covert manner. This is accomplished through a remote switch, button or an radio frequency key that can be used to change the message header content at any time while the beacon is transmitting during a mission. This is in preference to using the standard laptop keyboard to effect such a change in situation call. The appearance of the keyboard would make the existence of the tracking system obvious to the "bad guys" that may be in the vicinity of the operator.

Video Capture

A miniature monochrome video camera may be included with the CP-1 unit allowing an automatically controlled

or directed video frame to be captured, compressed and transmitted to the workstation

A 50 to 1 compression software module is added to the CP-1 mobile earth station so that a video frame can be captured (such as in the use of a "frame Grabber" or video switch sequence), compressed, packetized, and sent to the tracking workstation as message content in a small number of messages from the transmitter. These image content type messages are then decompressed at the receiving workstation, assembled and displayed. The image frames are time stamped and archived without operator intervention. Such a capability enables an effective remote automated operation to be rapidly deployed without regard to any existing terrestrial communications infrastructure.

Personal tracking

Looking at the next generations of this system, several derivations are being designed. One is for the individual, such personally carried miniature transmitters can be built using advanced integrated chip and manufacturing technology to compact the designs bringing the total system weight down from the current seven (7) pounds to less than two (2). This will provide two way communications, location tracking, and identification in almost any location.

Downed Pilot Locator

Remembering the recent Capt. Scott O'Grady rescue operation in Bosnia, we are anticipating that the Air Force would have a future interest in a miniturized personal communication and tracking system. Basically, a small two-way satcom unit talking to a synchronous satellites, renders the signal almost impossible to detect or jam and does not require a local rescue search operation to make the pilot's location and situation known. A smaller transmitter would provide a secure, difficult to detect or intercept, and unlimited range "get me the hell out of here" type message. The built in GPS receiver provides an accurate position along with that message. This answers several needs in such a situation.

Command and Control

Comprehensive operational control of assets both on the surface, at sea, and in the air can now create a real-time satellite view of any rapidly changing situation. The technique of Intransit Visibility is now possible.

It is recognized that the ability to communicate using satellites without large antenna dishes, power supplies, power amplifiers and other support equipment is an indispensable feature in an efficient wide area operation.

This type of communication is secure, dependable, and efficient.

Remotely Piloted Vehicles

This area shows promise in that more accurate and real-time control adds the concept of mission variation and emergency response to the operating envelope of Remotely Piloted Vehicle (RPV) operations. Opening up multiple CDMA channels on a single aircraft beacon will enable high data rates that encompass real-time video, extensive telemetry, and precise control.

Data Collection

The placement of small, low power beacons that transmit a pre-selected data stream or burst will make remote automated weather or environmental reporting an efficient option for the advanced warning of natural disasters, storm warnings, or the control of smoothly operating "just on time" inventory deliveries.

CONCLUSION

Such a satellite based GPS position reporting and communication system has been demonstrated to be completely effective largely due to the efficient antenna coupling, transmission protocols, and message configuration design. This new technology application now allows seamless organizational asset tracking and emergency situation notification for such situations as extraction and rescue.

The significance of the message engineering is that the position information is effectively available at a remote workstation when required. This now promotes greater reliability and security of signal transmission. The cost savings are considerable for such tracking and flight following operations, and the increased safety resulting from real-time position reporting are considerable.

This integration of a variety of technologies in electronics and software provides the capability for flexible, long range, and secure tracking of all assets.

ACKNOWLEDGMENTS

The support and encouragement of the scientists and engineers of the Newcomb Communications organization are gratefully acknowledged. Particularly the technical and engineering information provided by Carlton Williams, John Hopkins, Wayne Eddy, Jim Lenahan, John Wall, and Scott Normandeau.

REFERENCES

Satellite Based Covert Communications and Tracking, Scott W. Normandeau, Carleton Williams, and John Hopkins, Newcomb Communications, Inc. 1993.

System Descriptions of CP-1 and AV-2 SatCom units, Newcomb Communications, Inc. 1994

¹ Spread Spectrum Communications, Vol 1, Simon, Omura Scholtz and Levitt, Computer Science Press 1989

² Satellite Communications, Prett, Boston, John Wiley & Sons, New York 1986



Session C3

Maritime Applications

Chair:

Mr. Jim Morgan

Chevron Petroleum Technology Co.

Co-Chair:

Mr. Fred Forbes

Canadian Coast Guard

Verification of USCG DGPS Broadcast Parameters

Lt. Mark Lunday, Joseph Spalding, and Marylouise Dowd
USCG R&D Center

BIOGRAPHY

LT Mark Lunday, USCG, is an electronics engineer assigned to the Advanced GPS Research project at the United States Coast Guard Research and Development Center in Groton, CT. He received a B.S.E.E. from the Coast Guard Academy in 1986, and an M.S.E.E. from the Georgia Institute of Technology in 1992. He has served as student engineer and assistant Chief Engineer aboard the Coast Guard Cutter *DEPENDABLE*, and as Executive Officer aboard the Coast Guard Cutter *MONHEGAN*.

Mr. Joseph W. Spalding is project manager of the Advanced GPS project at the United States Coast Guard Research and Development Center in Groton, CT. Mr. Spalding has been conducting research in GPS and DGPS for ten years. Current projects include GPS and DGPS integrity monitors, receiver autonomous integrity monitoring, and GPS attitude determination. He holds a Bachelors in Electrical Engineering from the State University of New York Maritime College, and an M.S. in Computer Science from the University of New Haven.

Ms. Marylouise Dowd is a Ph.D. student at RPI, and has been working as a Co-op at the Coast Guard Research and Development Center for three years. She has a B.S. in Computer Science from Duquesne University, an M.S. in Computer Science from St. Joseph's University, and an M.S. in Industrial Management Engineering from RPI. She has been working in expert system and navigation support system research for the Department of Transportation for six years.

Ed Note: *Views expressed in this paper are those of the authors, and should not be construed as official or reflecting the views of the Commandant or of the U.S. Coast Guard.*

ABSTRACT

This report presents the results of performance tests conducted on several state-of-the-art Differential Global Positioning System (DGPS) Minimum-Shift-Keyed (MSK) receivers under varying conditions. Previous papers have theorized that specific data rates and RTCM SC-104 message types will produce greater data throughput and thus better navigational solution accuracies, particularly in the presence of atmospheric noise. The purpose of this effort was to determine the capability of commercially available receivers with regard to proposed USCG DGPS broadcast parameters; additionally, the tests attempted to validate theorized optimal broadcast parameters (message type and speed) with regard to static noise and carriers/jammer interference. The performance testing, conducted at the U.S. Coast Guard (USCG) Research and Development Center (RDC) in Groton, CT, was done in three phases. In the first phase, the MSK receivers were tested under real-time atmospheric noise conditions. In the second phase of testing, DGPS corrections of various ages were received to determine throughput as a function of correction latency. In the third phase, the receivers were tested in the presence of a controlled CW carrier functioning as an interference/jamming source. Performance was quantized for each of the phases, which resulted in a collection of performance data that was correlated to atmospheric noise and interfering CW signal strength and frequency.

INTRODUCTION

The Coast Guard is charged under 14 U.S. Code 81 with the establishment, maintenance, and operation of electronic aids to navigation in order to prevent disasters, collisions, and wrecks of vessels and aircraft[1]. The Coast Guard's role as a primary provider and user of radionavigation prompted the Coast Guard Research and Development Center (RDC) to begin GPS-related research in 1983. The research program concluded that real-time DGPS corrections could significantly improve the accuracy, provide a high level of

integrity, increase the usable coverage, and provide local control of the civilian portion of GPS without interfering with the military operation of the system. The research program also recommended that these improvements be incorporated in future navigational services utilizing GPS as a standard[2].

In 1988, the Coast Guard's Office of Navigation and Waterways Safety selected DGPS as the tool to fill requirements for harbor and harbor approach navigation contained in the Federal Radionavigation Plan (FRP). The Coast Guard developed an implementation plan that would establish a network of DGPS broadcast stations. Under the plan, the network would be operational in 1996, and would cover both coasts of the U.S., Hawaii, Alaska, and Puerto Rico. The format of the corrections would be based on message and data standards developed by a multi-disciplinary committee under the sponsorship of the Radio Technical Commission For Maritime Services Special Committee 104 (RTCM SC-104)[3]. Currently, the Coast Guard operates numerous DGPS broadcasts in the Marine Beacon Band (MBB) in prototype form, from New Hampshire to Texas and California, with other transmitters operating along the Mississippi in a joint venture with the Army Corps of Engineers.

Due to the rapid development and relatively recent emergence of DGPS as a navigational technology, there have been few detailed studies that measured receiver characteristics in the presence of noise and signal interference. Performing such tests is not a trivial task, since a signal testing facility is required. While several DGPS beacons are transmitting corrections as part of the prototype system, control of the signal required for testing purposes is difficult to obtain. Many of the transmitter sites are remotely located; additionally, a method of generating signals whose content is known in advance precludes the use of these prototype transmissions, since they are transmitting real-time correction data.

Due to the difficulties with performing such tests, and the need to validate USCG DGPS broadcast parameters, the Coast Guard R&D Center was directed to utilize existing equipment and facilities, suited to these types of tests, to determine MSK receiver performance characteristics. There were three main areas of interest.

The first area was the ability of a receiver to detect signals at significant distances from the transmitter site in the presence of atmospheric noise. The second area, closely related to the first, was the susceptibility of MSK receivers in general to atmospheric noise, even in the presence of a strong MSK transmitter. The third area of interest was the vulnerability of MSK receivers to man-made signal interference, either from

unintentional carrier interference or intentional DGPS broadcast signal jamming efforts.

The R&D Center purchased four types of commercial off-the-shelf (COTS) DGPS MSK receiver models. These receivers represented a range of features, capabilities, and demodulation techniques. Since the receivers were already being manufactured in large numbers, the Coast Guard had some concerns about the existing designs of COTS units. When the final DGPS implementation plan underwent modifications in 1991 and 1993, the R&D Center was directed to look at the capabilities of all of the receivers under the modified broadcast parameters, in addition to the original request of determining susceptibility to atmospheric noise and man-made signal interference. This final plan eliminated receiver to receiver comparison in favor of absolute performance determination against an ideal receiver that was impervious to all interference and noise.

EQUIPMENT

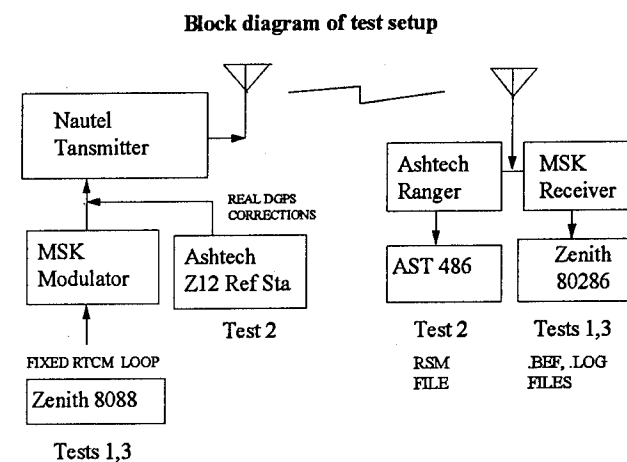


Figure 1

For this testing, control of signal frequency, bit rate, and data content was required. The first two tests, Bit Error Rate (BER) and Interference/Jamming (INTJAM), required the creation of a repetitive loop of MSK data; this enabled actual bit error rates (BER) to be determined from the data output by the receiver. A loop size of one message containing four RTCM 30 bit words was selected as an optimum pattern. This equated to a loop size of 120 bits. The program that created the RS-232 data for this was written in Borland C, and was run on a Zenith 8088 laptop computer. The third test, Message Throughput/Navigation Accuracy (MTNA), required the generation of real-time DGPS corrections. Ashtech Z-12 reference stations were used at the main RDC building to generate this information.

MSK modulators that converted the RS-232 data to MSK signals at the desired frequencies were used in all three tests. The modulator was based upon a design originally created by the R&D Center in 1989, and used direct digital synthesis to create the MSK signal. For the third test, modulators within the Ashtech reference stations were used to generate the MSK signals.

The MSK signal was transmitted by using a Nautel Marine Beacon Band (MBB) radio beacon amplifier. This amplifier is the standard used at Coast Guard radio beacon sites. It is a wide-band class A amplifier, with a maximum forward power of 100 watts. This amplifier was the same used by Enge in field testing in New Orleans[4].

Antenna design for this testing presented a number of unique challenges. The final antenna design for the BER and MTNA tests was a ten-turn rectangular loop, with dimensions of 4' x 16' mounted on the R&D Center roof, orientated in the y-z plane, with the antenna plane orthogonal to the receiving site. Due to the high SWR of this design, input power was kept to a minimum; in spite of this, there was sufficient signal strength at the receiving hut to replicate the desired MSK beacon signal strength.

For the INTJAM tests, antenna modification was required. A much stronger signal was needed at the receiving hut; a traveling wave antenna, approximately 250 feet in length, served as a much more efficient radiator; typical SWR values were 3:1, and for a forward power of 5 watts, the reflected power was only 2 watts.

Due to the electromagnetic noise at the R&D Center (from computers and other electrical equipment), a remote location was selected for MSK receiver placement. At this location, an enclosed housing made of fiberglass and measuring 20'x10'x10' was utilized to store the receivers. The building had 120VAC power, and air-conditioning/heating for climate control. To further reduce non-atmospheric noise at the receiver location, laptop computers with LCD screens were selected to record data and control the receivers; linear DC power supplies for the equipment were incorporated; and incandescent lighting was used instead of fluorescent lighting. The result was a receiving location that had a noise floor 30 dBm lower than the main R&D Center building.

The MSK radio beacon receiver whip antennas and their respective couplers were mounted on the top of the fiberglass enclosure. Each antenna was attached to the top of a vertically mounted piece of four foot long 1" ODE pipe. Each antenna was kept at least three feet apart from the others. Whip antennas were selected for use during the testing in order to permit equitable comparisons among the units.

For the MTNA tests, real-time calculation of radial error (RE) was required. This necessitated a GPS receiver at the receiving site, along with a surveyed antenna that would allow navigation error calculations to be performed. A location was chosen on the roof of the receiving site building, and its position was surveyed using Ashtech surveying algorithms.

The MSK signal used in the tests was adjusted to simulate reception at the fringe of beacon coverage. Coast Guard MBB radio beacons have adjustable power output levels; each beacon is set up to provide a specific coverage range over sea water. The beacon coverage is defined by the signal's field strength, in microvolts per meter, at a specified distance, in nautical miles (NM). The Montauk Point radio beacon, for example, has a specified transmitted field strength of 75 microvolts per meter at a distance of 150 NM. This range is typically referred to as the "edge of coverage."

A Field Intensity Meter (FIM) was used to take field strength measurements of Montauk Point at the receiving location. These values were averaged and compared to the spectrum analyzer signal measurement of the Montauk Point beacon, in dbm at the output of the antenna coupler of the model D100 receiver. A mathematical relationship between the spectrum analyzer and the FIM measurements at the receiving site was thus established. With this information, the output power of the local signal was adjusted until the appropriate signal level on the spectrum analyzer corresponded to a FIM measurement of 75 microvolts per meter.

Data recording equipment at the receiving location included laptop 286 series CPUs, in conjunction with software developed by the R&D Center, to control the MSK receivers and to correlate the known fixed RTCM data pattern to the data stream received by the receivers. Correlation was performed by shifting the known data pattern loop and performing bit comparisons (exclusive OR) with the received data bits. Statistics on the receiver data output were collected in a log file, and included the total number of bits received and incorrect bits. In addition, the log file contained totals for received RTCM words and RTCM messages, along with receiver performance statistics (SS and SNR). Bit error event data was stored in a bit error file. This file contained the date, time, and location in the message of every bit error occurrence. These two data files provided sufficient information to allow post-processing and analysis of receiver performance.

For the MTNA testing, real-time radial error measurements were required; after setting up the Ashtech reference stations at the main R&D Center building, Ashtech Ranger receivers with a single surveyed antenna at the receiving hut were established. Using specialized software developed by the

R&D Center for integrity monitoring, termed Reference Station Monitor (RSM), DGPS correction age and radial error were recorded in real time to a log file. This correction age information was later used during data throughput tests to determine the obtainable navigation accuracy in the presence of atmospheric noise data collected during the BER tests. Tables of radial error versus message age for RTCM message types 1 and 9-3 were created from the RSM data; these tables were formed by using MATLAB and a least-mean-squares matrix algorithm to interpolate and curve-fit the RSM data.

For the INTJAM tests, additional specialty equipment was required. A Hewlett-Packard HP-8904 frequency synthesizer was used to generate the CW interference signal; specialized QuickBasic code was developed to control the HP-8904A and record signal levels in a log file.

TEST DESIGN

Bit Error Rate

The purpose of the Bit Error Rate (BER) test was to determine receiver susceptibility to atmospheric noise. This test examined the effect of high atmospheric noise on data throughput at the bit level, using bit error rates detected at the receivers. Data throughput was examined as differences between the four different receivers, and differences for any given receiver between receiving data at 100 BPS vs. 200 BPS. This test of the bit error rates set the stage for the next set of tests which examined which message types (Type 1 or Type 9-3) might do better in times of high atmospheric noise.

Due to the real-world setting and the inability to control atmospheric noise, a "shotgun approach" to data collection was taken; testing was conducted on approximately 40 days during the summer and fall of 1993 and 1994, representing more than 500 hours worth of data collection in order to achieve a broad spectrum of samples. From this large collection, six days were selected as a representative of atmospheric conditions from relatively quiet to extremely noisy. Receiver signal-to-noise ratio (SNR) values factored into the selection of the six days. Samples which had significant atmospheric noise were chosen for analysis.

Message type - navigation accuracy

The purpose of this test was to examine the effect of high atmospheric noise on the throughput of two message types (Type 1, Type 9.3) being broadcast at different speeds (100 BPS, 200 BPS) to gain insight into the relationship between these variables and navigational accuracy/performance. Previous calculations and field trials conducted by Enge have shown that RTCM Type 9 messages, in spite of reduced data transmission efficiency and increased clock complexities,

have distinct advantages over Type 1 messages in the presence of atmospheric noise[4]. The current USCG DGPS implementation plan calls for all transmissions to be done using RTCM Type 9-3 message formats.

With the data files collected in the BER test, some additional analysis was made regarding the ability of specific message types at certain speeds to "pass through" the noise during static impulse lulls, and thus reach the receiver. By post-processing the data and examining the time periods between bit losses, a calculation was made in terms of message throughput. With this information, a determination of navigation position radial error was performed. Over a given period of time, comparisons between RTCM message types and MSK bit rates were made, and conclusions were drawn about signal parameters under varying atmospheric noise conditions.

Interference/Jamming

The purpose of the Interference-Jamming (INTJAM) test was to look at COTS receiver technology in terms of susceptibility to man-made signal interference. This was done by broadcasting two MSK signals with the same data on different frequencies; one signal would be the control, and the other would suffer from intentional interference attempts, conducted by a controlled CW carrier. By collecting bit hit statistics in real time and comparing the data to information about the CW interference carrier, conclusions were made regarding the susceptibility of MSK receivers to man-made interference.

For this test, two MSK signals were used; the first on 316.5 kHz, served as the "victim" of interference by the jammer. The second MSK signal, at 313.5 kHz, functioned as the control of the experiment.

ANALYSIS AND DISCUSSION BY TEST

Bit Error Rate

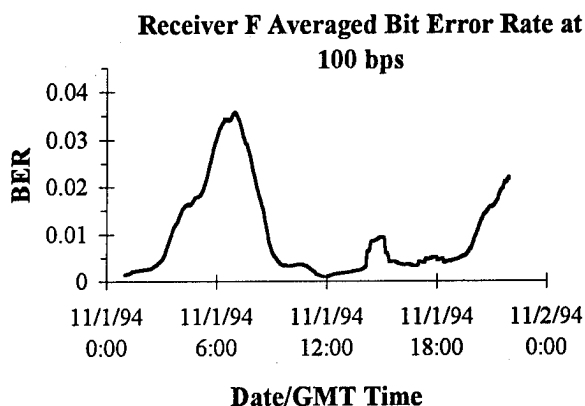


Figure 2

The first step in the analysis was to graph the average bit error rates for the 24 hour period of the test (an example of the graphs used for comparison are shown in Figures 2 and 3). Graphs were produced at 100 and 200 BPS for each receiver type for each day. The graphs show a discernible difference in performance between receivers, as well as between transmission rates.

With this anecdotal evidence, a set of Analyses of Variance (ANOVA) was performed on the data. ANOVA is a form of hypothesis testing which allows testing for several means, and was used here to determine if there were statistically significant differences in the bit error rates detected between the four different receivers. ANOVAs were performed for the four receivers at both the 100 BPS and 200 BPS levels for each day of the sample. The results concurred with the anecdotal graph evidence, showing a significant difference between the receivers for detected bit error rates.

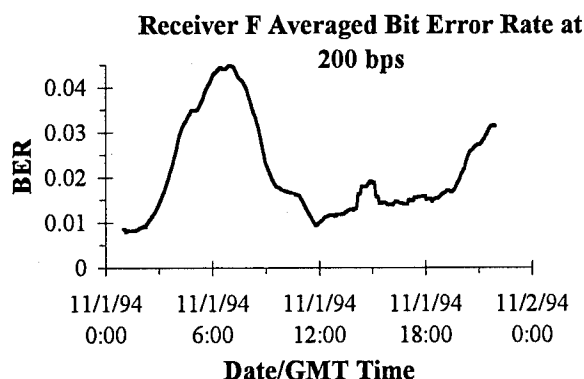


Figure 3

The next step was to perform a set of T-test to determine if there was a significant difference between the bit error rates detected by each receiver at 100 BPS vs. 200 BPS for each day of the sample. T-tests are a form of hypothesis testing, and were used here to determine if the differences between data collected from the same receiver type at different transmission rates were statistically significant. Once again, the T-test confirmed the anecdotal evidence, in general showing the difference to be statistically significant.

On most of the days tested, the majority of receivers performed better at 100 BPS than at 200 BPS. On one of the days, where there was a sustained period of low atmospheric noise followed by a period of high atmospheric noise, half of the receivers showed no significant difference in performance between the 100 BPS and 200 BPS. It was hypothesized that the sustained period of low noise "swamped" the effects of transmission rate during the higher noise. A second set of T-tests were performed for that day, splitting out the time of high atmospheric noise, and once

again, all receivers performed better at 100 BPS than at 200 BPS.

This provided some insight into how the receivers tested are impacted by high atmospheric noise when receiving data at either 100 BPS or 200 BPS. Additionally, it suggests how these same variables may affect navigational accuracy. The next set of test were designed to examine this question.

Message type

Once again, the initial step was to graph the message types at 100 BPS and 200 BPS for each receiver type for each day. The graphs indicated a discernible difference in performance between message types, as well as between transmission rates.

Next, sets of T-tests were run to determine if the differences detected between samples of different broadcast speed (100 vs. 200 BPS) and message type (Type 1 vs. Type 9-3) were statistically significant. The T-test concurred with the anecdotal graphical evidence, showing the differences to be statistically significant.

Finally, graphs were constructed that compared radial error over time for specific message types and bit rates. One sample of data is shown here. This period of time was characterized by significant BER values due to relatively high atmospheric noise. Figure 4 shows a comparison of radial error over time for message types 1 and 9-3 at 100 BPS. From this information, we can state that for signals at 100 BPS, the optimum messaging algorithm is type 9-3.

Radial Error vs. Time, Day 292 Rcvr C

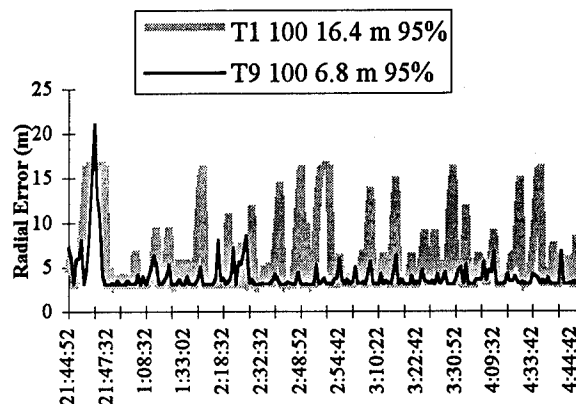


Figure 4

Figure 5 shows a comparison of radial error over time for message types 1 and 9-3 at 200 BPS. From this information

we can state that for signals at 200 BPS, the optimum messaging algorithm is also type 9-3.

Radial Error vs. Time, Day 292 Rcvr C

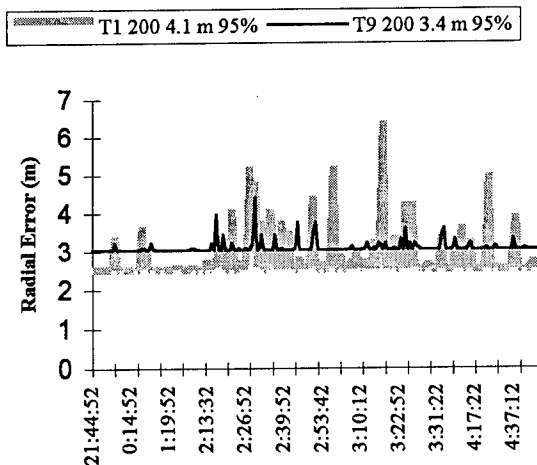


Figure 5

Figure 6 compares the radial error over the same time period for 100 BPS and 200 BPS for message type 9-3. This data indicates that 200 BPS is a better data rate for type 9-3. This is interesting, and suggests that perhaps all transmissions should be done at 200 BPS for type 9-3. However, there are mitigating circumstances such as location and nominal range of the beacon, as well as the beacon's intended users. One example is whether the beacon is designed to provide service to a nearby high-traffic shipping lane like New York Harbor (which has a beacon at Sandy Hook, NJ transmitting at 200 BPS), or for harbor and harbor approach navigation other than high-traffic areas over a larger geographic area, such as Long Island Sound (which has a beacon at Montauk Point, NY transmitting at 100 BPS).

These tests do confirm the earlier research finding that the optimum message type for DGPS corrections is type 9-3 at a transmission rate of 200 BPS.

Radial Error vs. Time, Day 292 Rcvr C

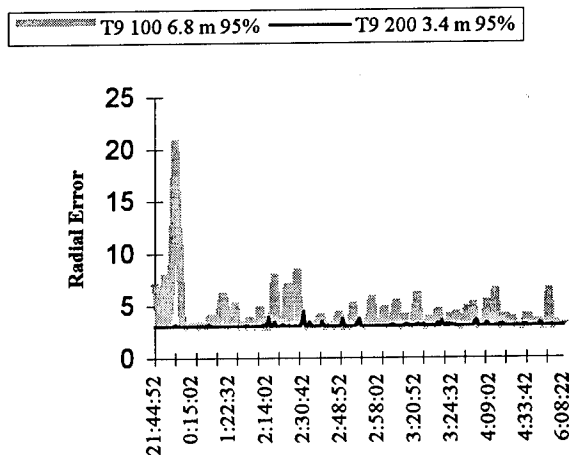


Figure 6

Interference/jamming

Five tests were conducted to ascertain susceptibility to signal interference. The specifics of each test are shown in Table 1. All tests used 313.5 kHz as the control (labeled Ctl), and 316.5 kHz as the variable (labeled Int). The control and variable signal strengths varied within a few points of -56 dBm due to varying humidity and rainfall at the testing site. The starting and ending voltages (V) were selected in an attempt ensure a weak signal to begin with, and a sufficiently strong signal to produce interference.

The graphs presented here are for two representations of the data. The first graph shows message count as a function of various jammer parameters; total messages and bad messages at each jammer frequency and jammer signal level are indicated as time progressed in the test. The second graph shows SNR as a function of time during the test, with jammer signal levels at progressing frequencies also plotted.

Test 1 was used to confirm proper operation of the apparatus, and to do an early detection of possible "jamming weaknesses" by the MSK receivers. At no point did the jammer signal level equal or exceed the MSK signal in Test 1. The frequency range covered the upper half of the 316.5 kHz signal, but at widely spaced sampling points. The results showed no apparent effects upon MSK signal reception by the jammer.

Table 1

| Test # | Int freq | dBm | Clf freq | dBm | Start V(dBm) | End V(dBm) | Step (dBm) | Start f (kHz) | End f(kHz) | Step (kHz) |
|--------|----------|-------|----------|-------|--------------|------------|------------|---------------|------------|------------|
| 1 | 316.5 | -58 | 313.5 | -57.5 | -80 | -60 | 2.5 | 318 | 316.5 | 0.1 |
| 2 | 316.5 | -58 | 313.5 | -57.5 | -80 | -60 | 2.5 | 316.53 | 316.52 | 0.001 |
| 3 | 316.5 | -54.5 | 313.5 | -54 | -80 | -60 | 2.5 | 316.53 | 316.52 | 0.001 |
| 4 | 316.5 | -56.8 | 313.5 | -57.1 | -72 | -51.6 | 2 | 316.527 | 316.523 | 0.001 |
| 5 | 316.5 | -56.8 | 313.5 | -57.1 | -72 | -51.6 | 2 | 316.527 | 316.523 | 0.0005 |

Test 2, with Test 3 as a revalidation, was guided by a hypothesis that the MSK signal is most vulnerable to interference at its upper and lower shift frequencies (316525 Hz and 316475 Hz for a 100 BPS signal). For this test, the jammer frequency was run from 316530 to 316520 Hz. Figure 6 shows the performance of receiver A in comparison to its control

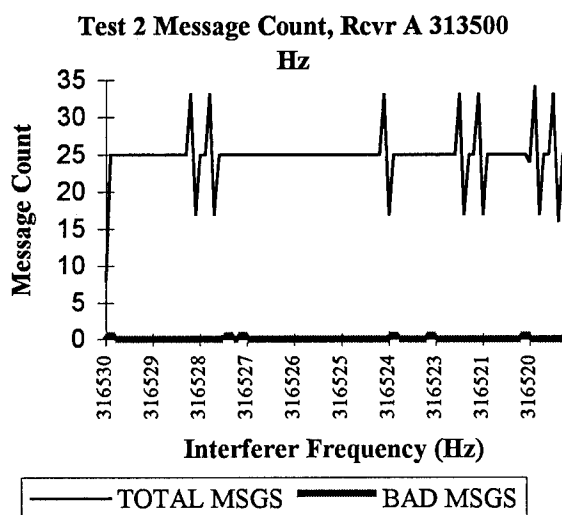


Figure 7

While there are some messages that are bad (did not make it through to the receiver), there is no apparent correlation between jammer signal strength, jammer frequency proximity to 316525 Hz, and bad bit counts. This behavior was repeated by the other receiver types. Figure 7 shows the performance for receiver A at 313500 Hz. Figure 8 is for receiver A at 316500 Hz. Again, a couple of the messages did not make it through, but there is no apparent correlation to jammer frequency or signal strength.

Test 4, with Test 5 as a validation, was conducted using jammer signal levels ranging from relatively weak to noticeably stronger than the MSK signal. These tests produced some very interesting results.

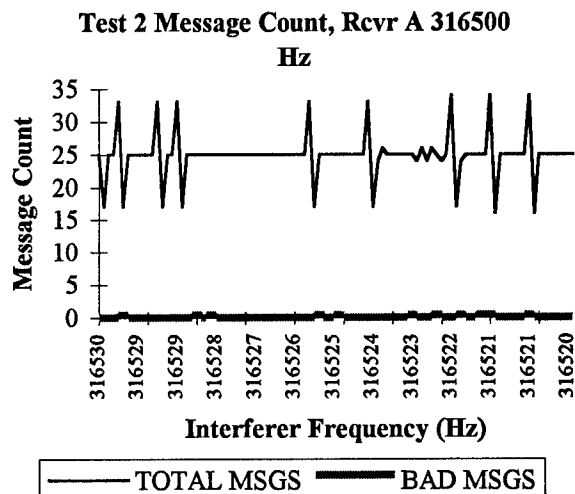


Figure 8

The control at 313.5 kHz did not lose any messages during the test. The 316.5 kHz signal, however, did suffer catastrophic message losses whenever the jammer reached its peak; in this test, the jammer went from 15 dBm below to 5 dBm above the MSK signal

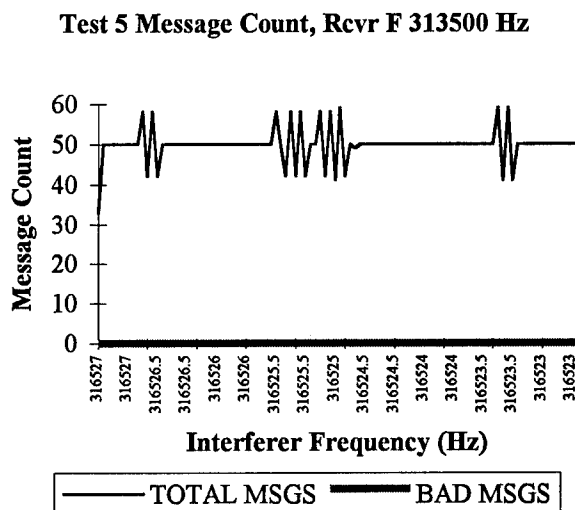


Figure 9

This evidence is shown quite vividly in Figures 9 and 10. Clearly, what messages did get through (and the count was reduced) were almost all lost. This behavior of message loss was repeated almost exactly the same for all four receivers, with greatest vulnerability shown at jammer frequencies of 316.5260 kHz and 316.5255 kHz. This data indicates that the receivers are susceptible to jamming in the presence of strong signals, even when those signals may be up to 5 Hz away from the "critical shift frequency." These results tend to contradict those of Test 2 and Test 3; however, the atmospheric noise in Tests 2 and 3 was more significant than the interference from the jamming signal, due to strong summer storms. Therefore, Tests 2 and 3 neither contradict nor support the "vulnerable frequency" hypothesis.

Test 5 Message Count, Rcvr F 316500 Hz

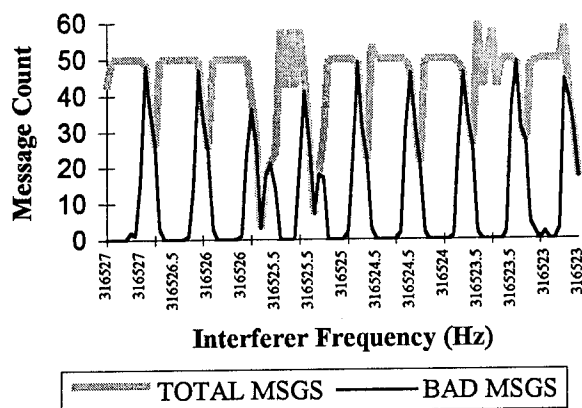


Figure 10

There is an interesting phenomenon that was observed during the testing, shown in Figures 11 and 12. These Figures compare SNR over time for 316500 Hz and 313500 Hz as the jammer steps through quantized signal levels, then progresses through frequency samples.

Test 5 SNR, Rcvr C 313500 Hz

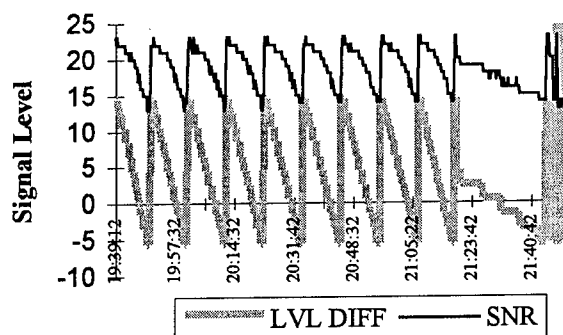


Figure 11

Test 5 SNR, Rcvr C 316500 Hz

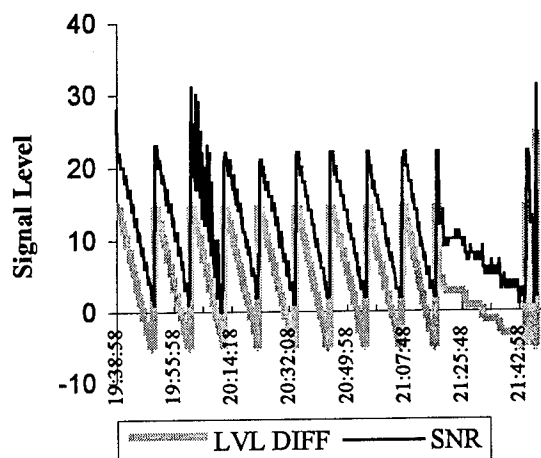


Figure 12

These Figures compare SNR over time between 316500 Hz and 313500 Hz as the jammer steps through quantized signal levels, then progresses through frequency samples. In the 316500 Hz receiver, the SNR was significantly degraded, particularly in the vicinity of 316525 Hz.

In the 316500 Hz receiver, the SNR was significantly degraded, particularly when the jammer was in the vicinity of 316525 Hz. However, even though the control receiver did not lose any messages, its SNR was also degraded. While the degradation for the control was not as much, it is substantial and would make a difference if the MSK signal at 313.5 kHz was weaker. This behavior was replicated by all receivers, and may be attributable to one of two factors. First, there is the possibility of receiver front-end overload due to the test setup. This is unlikely, given that SNR plots for Tests 1 through 3 showed no decrease in SNR for the receiver at 313.5 kHz, but the receiver at 316.5 kHz did have a degraded SNR as expected. The more plausible explanation is that this is due to a tendency by the receivers to suffer from adjacent channel interference or intermodulation effects, even when the jammer signal is several kHz away.

CONCLUSIONS

The data shows that all the tested units can receive MSK signals under the proposed USCG broadcast parameters. In the presence of atmospheric noise, message type 9-3 had an advantage over type 1 in the presence of atmospheric noise; this agrees with predicted results.

With regard to interference from other CW signals, all receivers demonstrated similar vulnerability; in particular, very strong jammers had an effect upon MSK signal reception, even when the jammer frequency was several kHz away from the MSK frequency.

This research examined a broad topic of issues regarding MSK receiver performance. We recommend that additional research should be conducted into the area of jamming. This topic is worthy of further investigation, and holds major implications as the USCG DGPS broadcast network nears completion.

REFERENCES

1. Alsip, D., Bulter, J., Radice, J., "Implementation of the U.S.Coast Guard's Differential GPS Navigation Service", June 1993
2. Coast Guard Research and Development Center Project Implementation Plan Document for FY94, November 1993.
3. Coast Guard Commandant's Instruction COMDTINST M16577.1, "Broadcast Standard for the USCG DGPS Navigation Service", Coast Guard Office of Navigation and Waterways Safety, Coast Guard Headquarters, Washington, D.C., April, 1993.
4. Enge, P. et al, "DGPS/Radiobeacon Field Trials, Which Compare Type 1 & Type 9 Messaging", Proceedings of the 49th Insititute of Navigation (ION) Annual Meeting, June 1993, Cambridge, MA.

DGPS Positioning Accuracy Performance Analysis with RTCM Message Types 1/9 and 18-21 Using Various Receiver Technologies

G. Lachapelle, M. E. Cannon, H. Lan, and C. Tang
The University of Calgary

S. Wee and S. Ryan
Canadian Coast Guard, Ottawa

ABSTRACT

The synchronous and asynchronous RTCM message Types 1 and 9, respectively, which can be generated using either code or carrier phase smoothed code, are used in single differencing mode to obtain DGPS positions. Types 18-21 messages contain carrier phase and range measurements and corrections thereof which can be used in double differencing mode. In the latter case, two options are possible, namely integer ambiguity resolution on the fly if dual-frequency data is available, or/and ambiguity float solution if only L1 data is available. The results of an investigation performed to analyse the accuracy performance achievable using both Type 1/9 and Types 18-21 with the ambiguity float option are described. In order to assess the impact of the receiver technology used, three all-in-view receiver Types were tested, namely standard wide correlator C/A code, Narrow Correlator™ C/A code and Super C/A code/Y1/Y2 semicodeless. Extensive land tests with reference station-remote separations of over 400 km and airborne and shipborne trials were used to generate and intercompare DGPS positions using the approaches and equipment described above. The data was post-processed and time latencies of 5 to 25 seconds were successively introduced to analyse corresponding effects on accuracy performance. While a horizontal accuracy of 5 m (95th percentile) required by the Canadian Coast Guard was met by all receivers and all methods, it was found the ambiguity float method implemented using Types 18-21 messages produced better positioning results in most cases, namely 1 m (horizontal - 95th percentile) for distances between the reference station and remote in excess of 100 km and 50 cm for distances less than 100 km, assuming latencies of up to 15 seconds.

INTRODUCTION

Two classes of protocols have been defined by the Radio Technical Commission for Maritime Services (RTCM) Special Committee (SC) No. 104 for the real-time transmission of GPS data from a reference station to a remote station to generate differentially corrected positions at the remote [RTCM 1994].

The first class, which encompasses message Types 1 and 9, generates differential range and range rate corrections. These are generated using either code or carrier phase smoothed code measurements. If Type 1 is used, the reference generation time is the same z-count (synchronous). Due to unavoidable time delays caused by firmware and data transmission limitations, the corrections are received at the remote with a latency of typically a few to several seconds and the range rate correction is used to predict the range correction for the current epoch. In order to minimize delays, the corrections can also be generated and transmitted for each satellite as fast as the firmware permits. In this case, however, the reference z-count is not the same (asynchronous) for all satellites and message Type 9 is used to transmit this Type of data. A major advantage of message Types 1 and 9 is a relatively low transmission rate requirement of 50 to 100 bps (bits per second). The message Type is also tolerant to correction reception outages at the remote because the latest range rate received can be used to predict the differential range correction for the current epoch. The resulting accuracy degradation is significant however and compounds the nominal latency effect. The between-receiver single difference method is used in conjunction with Types 1 and 9.

The second class of messages, namely Types 18-21, transmits either raw code and carrier phase measurements (Types 18-19) or related code and carrier phase corrections (Types 20-21) which enable the remote to reconstruct raw code and carrier phase observations. The detailed message formulation and related advantages and limitations are described in [RTCM 1994]. The interval at which the measurements are transmitted is user-selectable but is constrained by the data link and firmware used; the transmission rate requirement is typically above 1,000 bps if the code and carrier phase measurements are transmitted every second. With the availability of the raw reference code and carrier phase measurements at the remote, the double difference method can be used to process the measurements. If dual-frequency observables are available, the integer ambiguities can be resolved, resulting in a so-called class of RTK (Real Time Kinematic) systems. Successful integer ambiguity resolution is however

sensitive to many parameters, with the distance from the reference station and uninterrupted reception of reference data being two critical ones, as demonstrated by a variety of investigators [e.g., Lachapelle et al 1992, Chen & Lachapelle 1995]. The alternative is to use the ambiguity float solution, which is described in the next Section. In this case, L1 measurements are sufficient, and the distance from the reference station is no longer critical. The method is also somewhat tolerant to data reception interruptions. These advantages however come at the cost of a significant accuracy degradation. The actual accuracy achievable will be a function of receiver characteristics, processing method and other operational factors such as the distance from the reference station which will still affect the magnitude of differential atmospheric corrections.

The two major objectives of this investigation are to intercompare the accuracy performance of both classes of message Types and to quantify the effect of receiver selection on accuracy.

The WGS84 coordinates of the reference station are required to generate the differential corrections and to calculate the DGPS position of the remote. Reference coordinate errors will result in remote DGPS coordinate distortions due to non-linearity effects. Another objective is to quantify the magnitude of these distortions.

METHODOLOGY

Processing Approaches

Message Types 1 and 9 were tested using a between-receiver single difference approach which can be written as

$$\Delta p = \Delta p + \epsilon(\Delta p) \quad (1)$$

if one neglects the effects of differential orbital and atmospheric errors. Δp is the differential pseudorange or carrier phase smoothed pseudorange formed at the remote, Δp is the correct but unknown differential range which contains the unknown coordinates of the remote and $\epsilon(\Delta p)$ is the error term which includes receiver noise and multipath. The use of both raw and carrier phase smoothed pseudoranges was tested. The recursive algorithm employed to smooth pseudoranges consists of two parallel filters operating simultaneously on each satellite. The DGPS positions were derived using the C³NAVTM software which employs a least-squares algorithm [e.g., Cannon & Lachapelle 1992].

Each data set was first post-processed with no (0 second) latency to assess the accuracy performance achievable in post-mission and to obtain a reference solution against which to assess solutions obtained with various latency effects. Latencies of 5 to 25 seconds were tested by delaying the data generated at the reference station by such an offset. For each latency tested, the same time offset was

equally applied to each satellite pseudorange. This implies the use of message Type 1 and the worst case of Type 9. The latency tests are therefore valid for both message Types if a conservative approach is used. For the purpose, the two message Types will be referred to as Type 1/9.

Message Types 18-20 were tested using a double difference approach which can be written as follows for pseudorange and carrier phase observables:

$$\nabla \Delta p = \nabla \Delta p + \epsilon(\nabla \Delta p) \quad (2a)$$

$$\nabla \Delta \Phi = \nabla \Delta \Phi + \lambda \Delta \nabla N + \epsilon(\Delta \nabla \Phi) \quad (2b)$$

if, again, one neglects the effects of differential orbital and atmospheric errors. $\nabla \Delta p$ is the correct but unknown double difference range which contains the unknown coordinates of the remote, $\Delta \nabla N$ is the double difference integer ambiguity term, and $\epsilon(\nabla \Delta p)$ and $\epsilon(\Delta \nabla \Phi)$, the pseudorange and carrier phase errors, respectively. Since $\epsilon(\Delta \nabla \Phi) \ll \epsilon(\nabla \Delta p)$, it is advantageous to use carrier phase measurements despite the presence of the ambiguity term. If n satellites are observed simultaneously at both receivers, there are $n-1$ ambiguities. When the integer ambiguities can be determined, they become deterministic and only the three coordinate components are left in the estimation process. This is why fixed integer ambiguity solutions are accurate to the cm-level. In the ambiguity float approach used here, the $(n-1)$ $\Delta \nabla N$'s remain stochastic quantities and their estimated values are updated at each epoch. The DGPS kinematic positions of the remote were derived with the FLYKINTM software [e.g., Lachapelle et al 1993] in ambiguity float mode. A Kalman filter is used and the dynamics of the receiver are modelled using a constant velocity model. The state vector for the ambiguity float mode is

$$\delta x = \{\delta x, \delta y, \delta z, \delta v_x, \delta v_y, \delta v_z, \delta \Delta \nabla N_1, \delta \Delta \nabla N_2, \dots, \delta \Delta \nabla N_{n-1}\}$$

The measurement and system noise was selected based on a combination of receiver specifications, estimated ambient multipath and experience. The software was modified to test user selectable latencies; message Types 20-21 were selected for this purpose. As for the case of message Type 1/9, each data set was first post-processed with no (0 second) latency to assess the accuracy performance achievable in post-mission. Solutions with latencies of 5 to 25 seconds were then obtained.

Field Measurements

Three data sets were observed to test the two message Types, namely land, airborne and shipborne sets. The land test was conducted over a two day period in October 1994 between Calgary and Havre, Montana. Three receiver Types were used simultaneously, namely

- Wide correlator spacing 12-channel Magnavox MX9212

- Narrow Correlator™ spacing NovAtel GPSCard™ 951 [Van Dierendonck et al 1992]
- Super C/A code/semicodeless Y1/Y2 Ashtech Z12 [e.g., Van Dierendonck 1994]

All receivers were in static mode and data was collected at every second to simulate kinematic mode. The distance between the two groups of receivers was 424 km. The configuration is shown in Figure 1.

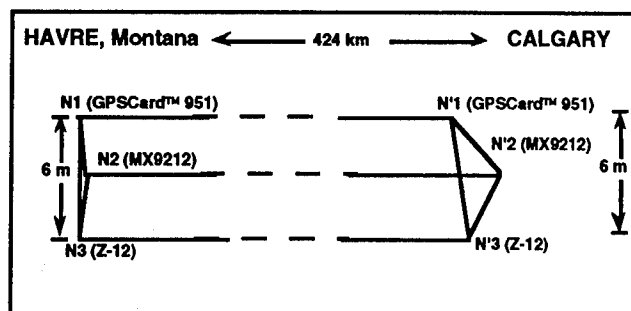


Figure 1: Receiver Configuration, Land Test, Calgary - Havre, October 94

The airborne trial was conducted by the Naval Air Warfare Center (NAWC), Warminster, in July 1994 off Florida's east coast as shown in Figure 2. A P3 Orion aircraft was used. The availability of two reference stations at distances of up to 1,200 km from the aircraft was used to test the effect of the reference station distance from the remote on accuracy. NovAtel GPSCard™ 951 receivers was used to collect data every second. More details on the flight trial are available in [Lachapelle et al 1995a].

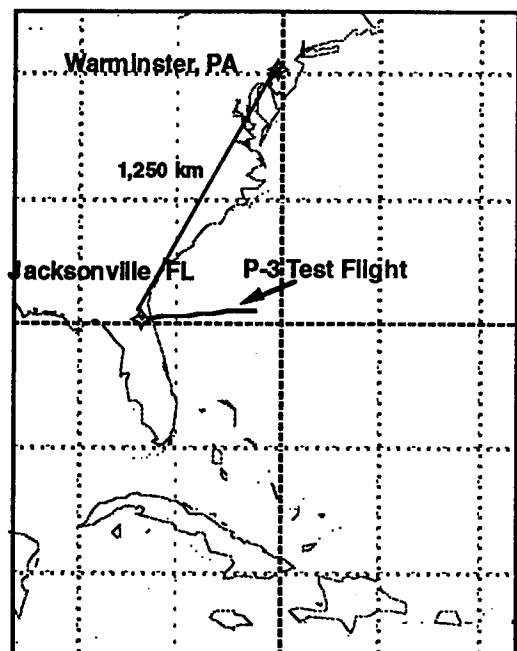


Figure 2: NAWC P3 Aircraft Trajectory and Reference Stations, July 94

The shipborne trial was conducted by the Canadian Department of National Defence/Defence Research Establishment Ottawa off Vancouver Island's west coast in November 1994, as shown in Figure 3. The distance from the shore-based reference station to the remote reached 100 km. Two Ashtech Z-12 receivers were used to collect data every second. More details on the ship trial are available in [Lachapelle et al 1995b].

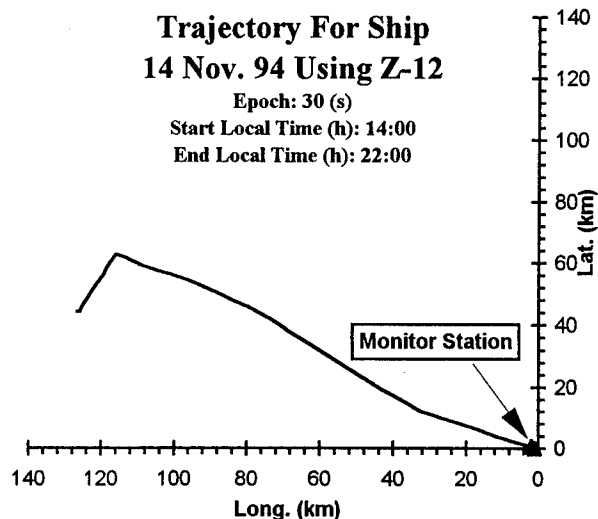


Figure 3: Ship Trajectory, Offshore Vancouver Island, November 94

RESULTS AND ANALYSIS

The land test analysis, which includes a comparison of receiver performance, is first presented. The airborne and shipborne trial results, which were obtained using specific receiver pairs, are then described. Finally, the distortion effects of reference station coordinate errors on remote coordinates are discussed.

Land Test

The measurements collected simultaneously with the three receiver pairs described in the previous section over a two day period were processed successively using Type 1/9 and 20-21 approaches, with latencies of up to 25 seconds. The no or 0 second latency case, which is that corresponding to post-mission processing, was also used for comparison purpose.

In order to illustrate the effect of latency on Type 1/9 range corrections, mean and RMS differences between range corrections calculated for the 0 latency case and for latencies of 5, 10, 15 and 25 seconds are shown in Figure 4 for a 50-minute data segment observed in Calgary with the GPSCard™ receiver. For all satellites, the RMS difference is below 1 m except for a latency of 25 seconds. This is within anticipated limits with Selective Availability on.

PRN12 is a Block I satellite which is not affected by Selective Availability; this is why the mean and RMS differences are smaller than the other satellites, especially for a latency of 25 seconds.

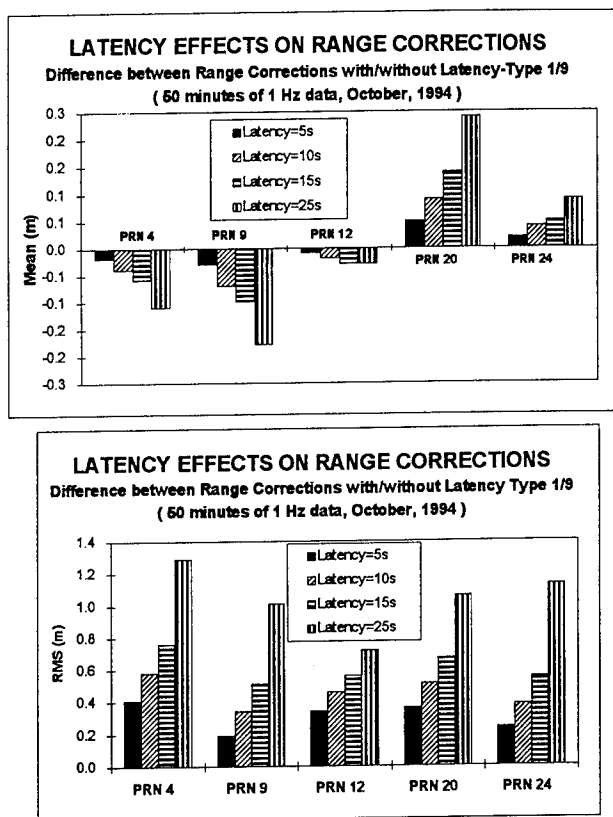


Figure 4: Land Test - Mean and RMS Effect of Latency on Type 1/9 Range Corrections

The various accuracy statistics presented below in the position domain are based on a comparison between the particular solution tested and an average of several batch static solutions to determine the coordinate differences between Calgary and Havre based on several hours of data with all receiver pairs. An ionospherically corrected solution with the Z-12 receiver pair was also performed to estimate the differential effect of the ionosphere on the 424-km baseline. This effect was found to be of the order of 10 cm. The accuracy of the average solution is estimated to be equal to or better than 1 ppm or 40 cm.

The accuracy of the Type 1/9 carrier phase smoothed code solutions obtained with all three receiver pairs for latencies of 0, 5, 10, 15 and 25 seconds are shown in Figure 5. In this case, the Ashtech Z-12 data used is the Super C/A code L1 data. The horizontal 95th percentile accuracy is better than 4 m in all cases. This is well within the 5-m threshold required by the Canadian Coast Guard. The height standard deviation (\approx 68th percentile) is < 3 m. The best accuracy performance are achieved by the GPSCard™ 951 pair, followed closely by the Z-12 C/A code data. The MX9212 accuracy performance are slightly lower due to the use of a

wide correlator technique, as anticipated. The effect of a latency of up to 15 seconds on the horizontal 95th percentile and height standard deviation is less than 0.5 m. For a latency of 25 seconds, the effect reaches about 2 m.

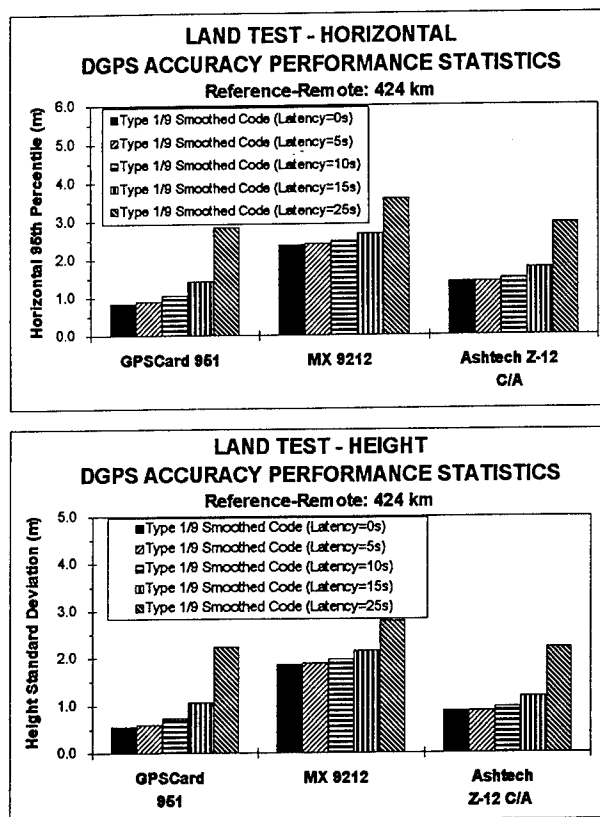


Figure 5: Land Test - Effect of Latency on Type 1/9 Solutions

Type 1/9 code versus carrier phase smoothed code versus Type 20-21 solutions (ambiguity float) are shown in Figure 6 for the 0 latency case. The statistics for each of the two days are shown separately to illustrate the high level of repeatability between the two days. The Type 1/9 Z-12 Y1 code and carrier phase smoothed code solutions are similar to the Z-12 Super C/A code solution, which indicates that the use of a semicodeless technology to obtain Y1 does not substantially reduce accuracy in this case. The Type 20-21 solutions are significantly better, than the Type 1/9 carrier phase smoothed code solutions i.e., 0.5 m to 1.5 m, for the case of the MX9212 and Z-12 receivers. No relative improvement occurs in the case of the GPSCard™ 951 receivers due to the high accuracy already achieved by the Type 1/9 solutions in view of the low noise and high multipath rejection capability of the Narrow Correlator™ spacing technique. The MX9212 results show the greater relative accuracy improvement between the Type 1/9 code and Type 20-21 solutions, illustrating the greater weight on carrier phase data in the Type 20-21 solution.

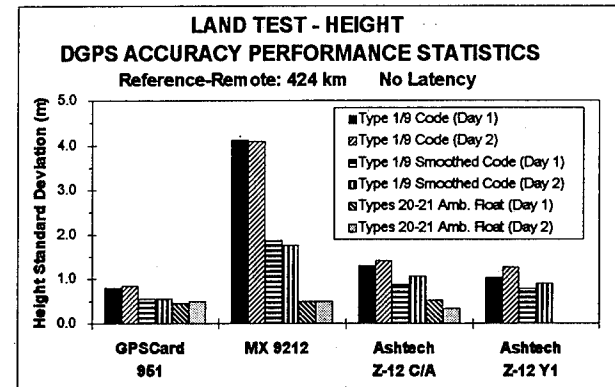
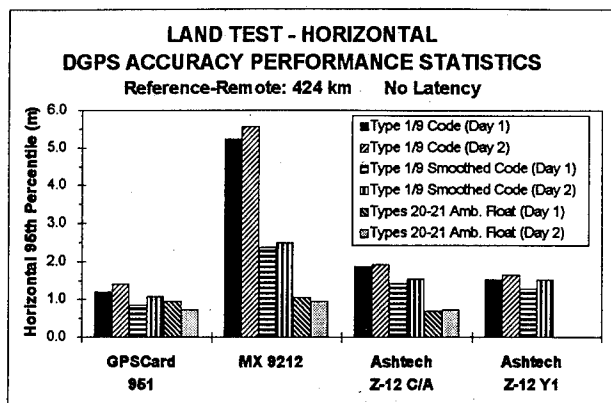


Figure 6: Land Test - Comparison of Type 1/9 and 20-21 Solutions

The effect of latency on Type 20-21 solutions are shown in Figure 7 for the GPSCard™ 951 receivers and in Figure 8 for the MX9212 receivers. The latency effect on Type 1/9 carrier phase smoothed solutions is repeated in the figures for direct comparison purposes. The position error growth due to latencies of up to 15 seconds is relatively small for both solution Types. For the case of a 15-second latency, the Type 20-21 solution yields a 95th horizontal and height accuracy better than 2 m for both receiver Types.

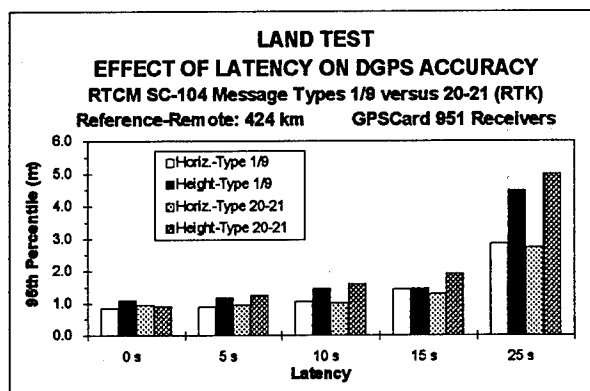


Figure 7: Land Test - Effect of Latency on Type 1/9 and 20-21 Solutions (GPSCard™ Receivers)

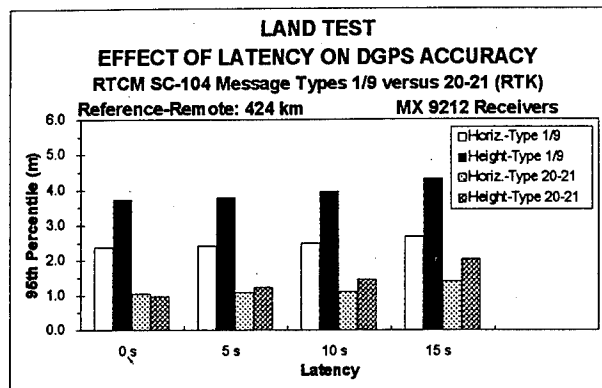


Figure 8: Land Test - Effect of Latency on Type 1/9 and 20-21 Solutions (MX9212 Receivers)

The accuracy performance achieved using different receivers at the reference station and remote using Type 1/9 solutions was analysed for selected combinations. The results are summarized in Figure 9 for the horizontal case. The accuracies shown for each mixed pair are approximately half way between the accuracies reported earlier with each identical pair, as anticipated.

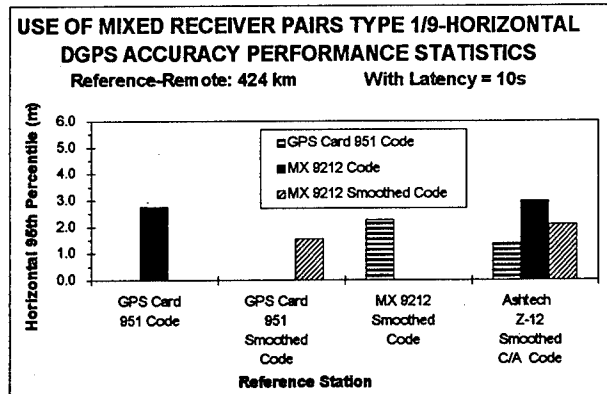


Figure 9: Land Test - Accuracy of Mixed Receiver Pairs for a Latency of 10 Seconds

Aircraft Trial

The aircraft, whose trajectory is shown in Figure 2, reached a speed of several hundred km per hour and a height of 2000 m above sea level. An accurate reference trajectory could be determined separately for the aircraft because, during takeoff in Jacksonville, the reference station was less than one km away and the L1 integer ambiguities were resolved to their correct integer values which were maintained for a period of 40 minutes. By that time, the aircraft was over 450 km away from the Jacksonville reference station. An inspection of the double difference carrier residuals obtained from the fixed integer ambiguity solution showed that the correct ambiguities were used during that period, resulting in a reference trajectory accurate to a few decimeters. The only error source which would prevent a sub-decimeter accuracy

from being reached is the differential ionospheric effect when the aircraft is a few hundred km from the reference station. This reference trajectory was used to assess the message Types 1/9 and 20-21 solutions derived subsequently and to derive the statistics presented in Figures 11 and 12.

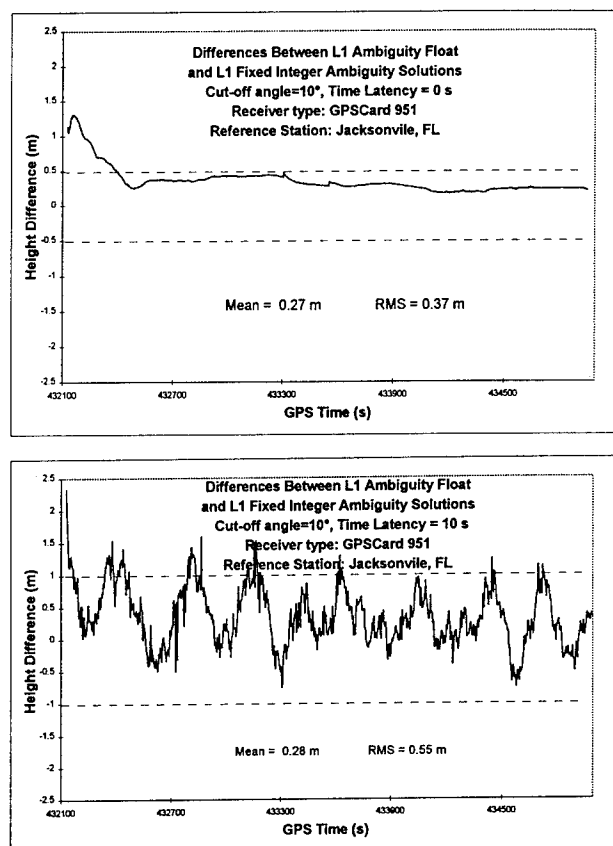


Figure 10: Difference Between Aircraft Height Profiles Obtained from Fixed Integer Amb. and Type 20-21 Solutions (Jacksonville Ref. St.)

The data was then processed successively using message Types 1/9 and 20-21. In the case of Type 1/9, a carrier phase smoothed code solution was used, while in the case of Types 20-21, an ambiguity float solution approach was used. Latencies of 10 and 25 seconds were tested. The difference between the aircraft height profiles obtained from the fixed integer ambiguity and Types 20-21 solutions using the Jacksonville reference station are shown in Figure 10 for latencies of 0 and 10 s, respectively. The latency effect is clearly visible. The accuracy performance statistics obtained when using the Jacksonville reference station are summarized in Figure 11. The message Type 20-21 solutions are significantly better than the message Type 1/9 solutions, the 95th percentile horizontal and height accuracies remaining better than 1 m even when a latency of 10 seconds is introduced. For the 0 second latency case, the 95th percentile accuracy is of the order of 50 cm, which is similar to the results obtained by Ford and Neumann [1994] using a similar technique. The reason for the lower accuracy

of the Type 1/9 solutions is that these solutions rely more heavily on the code measurements which are significantly affected by relatively high multipath caused by the fuselage, as shown previously [Lachapelle et al 1994]. When the latency reaches 25 seconds however, the performance of both Types 1/9 and 20-21 are similar because latency effects become dominant and mask the other error sources.

Types 20-21 solutions were also derived using the Warminster reference station to assess the effect of a longer distance reference-remote on accuracy. During the trial, the distance to Warminster varied between 1126 and 1255 km. The accuracy performance statistics are summarized in Figure 12. For the no latency case, the 95th percentile horizontal and height errors are around 2 m, as compared to less than 0.5 m when the Jacksonville reference station is used. The difference is caused by a combination of differential orbital and atmospheric errors. Over such a distance, the differential effect of a quiet ionosphere in a North-South direction can easily be over 1 ppm or 1.2 m over 1,200 km. The error growth when a latency of 10 s is introduced is very small but it becomes significant when the latency is increased to 25 s.

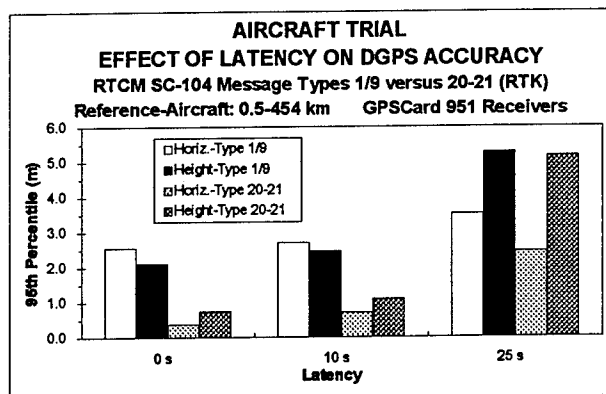


Figure 11: Aircraft Trial - Type 1/9 and 20-21 Accuracy Performance (Jacksonville Ref. St.)

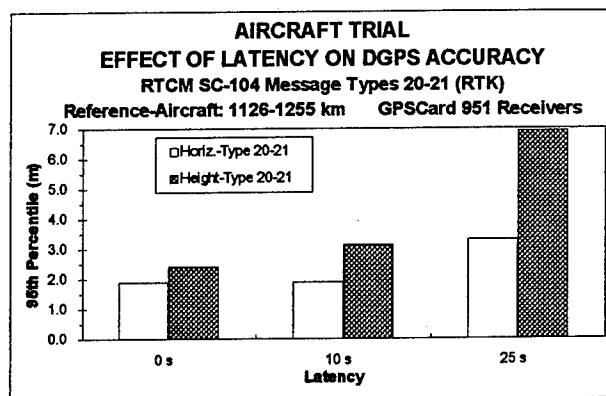


Figure 12: Aircraft Trial - Type 20-21 Accuracy Performance (Warminster Ref. Station)

Ship Trial

Since dual-frequency measurements were available, the fixed integer ambiguities were recovered and a 10-cm reference trajectory was therefore obtained for the purpose of assessing the accuracy of the Types 1/9 and 20-21 solutions which were obtained using the Y1 range and carrier phase measurements. The accuracy statistics are summarized in Figure 13 for the 0, 10 and 25 seconds latency cases. For the 0 second latency case, the 95th percentile accuracies are of the order of a few decimeters when using the message Types 20-21 solution. This compares to 0.8 m (horizontal) and 1.6 m (height) for the message Type 1/9 solution. When latencies of 10 and 25 seconds are introduced, the accuracy of the Types 20-21 solutions remain better than the corresponding Type 1/9 solutions but the accuracy performance ratio decreases due to the masking effect of latency errors.

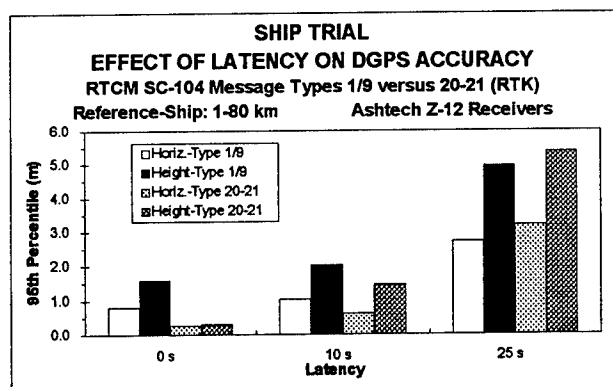


Figure 13: Ship Trial - Message Type 1/9 and 20-21 Accuracy Performance

Effect of Reference Station Coordinate Errors

The coordinates of a reference station should be in WGS84 to avoid distortion errors in the estimated coordinates of the remote due to non-linearity effects. The reference station coordinates enter in the formation of the least-squares or Kalman filter design matrix and, if incorrect values are used, the DGPS coordinates of the remote will be distorted by an effect which cannot be recovered through coordinate transformations. The magnitude of the effect depends on the distance between the reference and remote, the coordinate errors of the reference, satellite geometry, and the duration of observations in the case of a static remote station.

The effect can be estimated for specified cases by inserting errors in the reference station coordinates and calculating the resulting distortions on the DGPS coordinates of the remote. Several cases were studied here using data collected on the 424-km land static and shorter baselines. In Figure 14, the effect caused by shifts of 1, 10, 100 and 1,000 m in each of the three coordinate components are shown for a static case where observations of the 424-km baseline are

made over periods of 1, 2 and 3 hours, respectively. The effect is calculated as the difference between the DGPS coordinates of the remote obtained using correct reference station coordinates and the corresponding coordinates obtained using incorrect reference station coordinates but corrected for the nominal errors induced in the reference station coordinates. The effect, which reaches a few decimeters when an error of 10 m is inserted, was found to be a function of satellite geometry and repeats itself if a data segment observed during the same sidereal time period another day is used. For a different data segment, the effect would be different but its magnitude about the same.

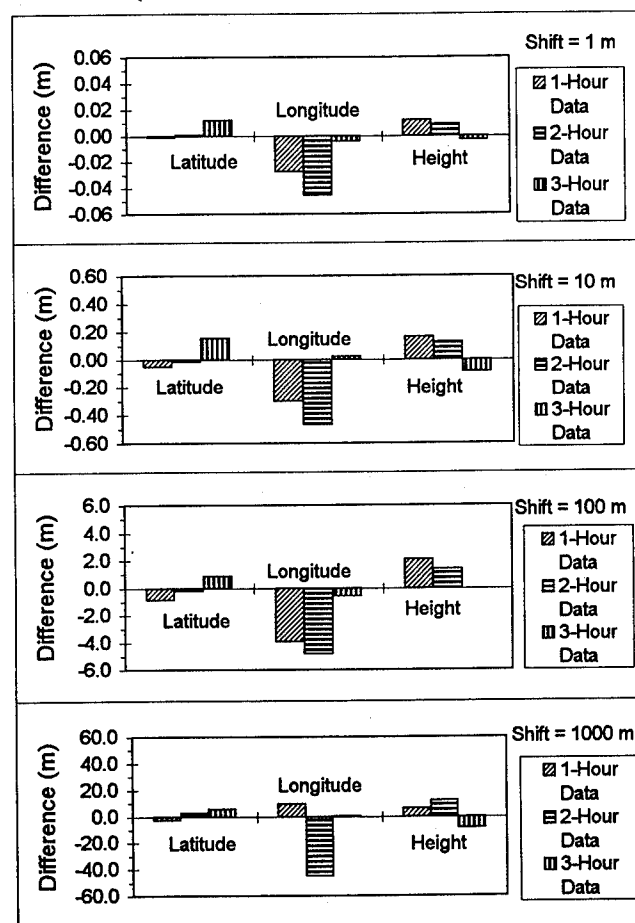


Figure 14: Effect of Reference Station Coordinate Errors on DGPS Coordinates of Remote Station - Static Case, 424 km Inter-Station Distance

In Figure 15, corresponding results for a 6-hour data segment observed on the same baseline and processed in kinematic mode are shown. The effect occasionally exceeds 10 cm when an error of 10 m is input in each coordinate component of the reference station, i.e., about 1 % of the reference station coordinate errors. Other tests revealed that the effect is approximately proportional to the distance between the two stations. If the effect is to be kept below 50 cm for a distance of 400 km to the reference station, the reference station WGS84 coordinates should be known with an accuracy of about 25 to 50 m.

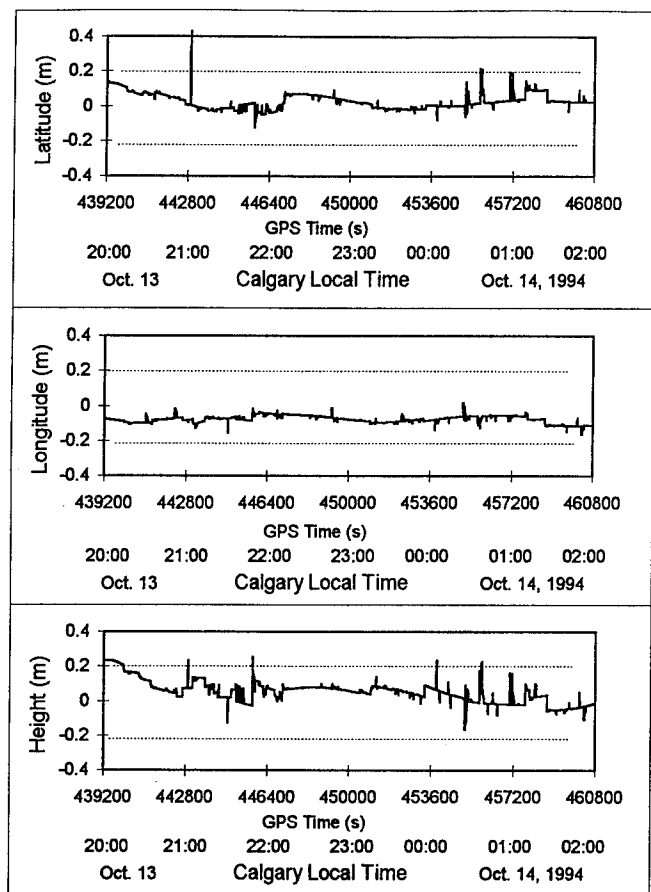


Figure 15: Effect of 10-m Reference Station Coordinate Errors on DGPS Coordinates of Remote - Kinematic Case, 424 km Inter-Station Distance

CONCLUSIONS

The results reported herein demonstrates that carrier phase smoothed RTCM SC-104 messages Type 1/9 can easily meet the DGPS 95th percentile horizontal accuracy requirement set by the Canadian Coast Guard for all three receiver Types tested and for latencies in excess of 15 seconds, which is well beyond the 5 to 8 seconds latency expected for most firmware systems operating in conjunction with marine radiobeacons. The use of Types 18-21 solutions with L1 data in ambiguity float mode yields a yet better accuracy. For distances of up to several hundred km from the reference station, a 95th percentile accuracy of ≤ 1 m was obtained for all land, airborne and shipborne cases tested. Some accuracy degradation occurs over long distances however due to the decorrelation of orbital and atmospheric effects. The effect of WGS84 reference station coordinate errors on DGPS remote coordinates was estimated to be 1 - 2% of the reference coordinate error for distances of 400 km to the reference station.

ACKNOWLEDGMENTS

The analysis of the P3 aircraft data by The University of Calgary was sponsored by the Naval Air Warfare Center, U.S. Department of the Navy, Warminster, PA.

REFERENCES

- CANNON, M.E., and G. LACHAPELLE [1992] Analysis of a High Performance C/A Code GPS Receiver in Kinematic Mode. *Navigation*, 39, 3, The Inst. of Navigation, Alexandria, VA, 285-299.
- CHEN, D., and G. LACHAPELLE (1995) A Comparison of the FASF and Least-Squares Search Algorithms for Ambiguity Resolution On The Fly. *Navigation*, 42, 2, Alexandria, VA.
- FORD, T., and J. NEUMANN [1994] NovAtel's RT20 - A Real-Time Floating Ambiguity Positioning System. Proc. of GPS-94, The Inst. of Navigation, Alexandria, VA, 1067-1076.
- LACHAPELLE, G., M.E. CANNON, and G. LU (1992) Ambiguity Resolution On The Fly - A Comparison of P Code and High Performance C/A Code Receiver Technologies. Proc. ION of GPS-92, 1025-1032.
- LACHAPELLE, G., H. SUN, M.E. CANNON, and G. LU [1994] Precise Aircraft-to-Aircraft Positioning Using a Multiple Receiver Configuration. Proc. of ION National Technical Meeting, 793-799.
- LACHAPELLE, G., M.E. CANNON, W. QIU, and C. VARNER [1995a] An Analysis of Differential and Absolute GPS Aircraft Positioning. Proc. of ION National Technical Meeting, 701-710.
- LACHAPELLE, G., H. SUN, M.E. CANNON, and C. McMILLAN [1995b] Precise GPS Shipborne Positioning Experiments with Semicodeless Receivers. Proc. of ION 51st Annual Meeting, 613-620.
- RTCM [1994] RTCM Recommended Standards for Differential Navstar GPS Service, Version 2.1, RTCM SC-104, Washington, D.C.
- VAN DIERENDONCK, A.J. [1994] Understanding GPS Receiver Terminology: A Tutorial on What those Words Mean. Proc. of Intern. Symp. on Kinematic Systems in Geodesy, Geomatics and Navigation - KIS94, Dept of Geomatics Eng., The University of Calgary, 15-24.
- VAN DIERENDONCK, A.J., FENTON, P., and FORD, T. [1992] Theory and Performance of Narrow Correlator Spacing in a GPS Receiver, *NAVIGATION*, The Inst. of Navigation, Alexandria, VA, 39, 3, 265-283.

Boosting Shipboard RAIM Availability

James LaMance and Alison Brown
NAVSYS Corporation

Joseph Spalding
US Coast Guard R&D Center

BIOGRAPHIES

JAMES LaMANCE

Dr. LaMance is a GPS Design Engineer at NAVSYS Corporation. He received his PhD in Aerospace Engineering from the University of Colorado and Boulder in 1994. Previous areas of research have included precise orbit determination and satellite oceanography. Dr. LaMance currently conducts research in the areas of real-time kinematic processing and integrity monitoring in GPS.

JOSEPH SPALDING

Mr. Spalding is an Electronics Engineer at the US Coast Guard Research and Development Center. He has been working in GPS and DGPS for ten years. He currently serves as Advanced GPS Research project manager. Current research includes DGPS integrity monitors, RAIM for DGPS users, GPS azimuth determination, and development of standards for maritime use of GPS and DGPS. He has an MS in computer science from the University of New Haven and a BE in Electrical Engineering from the State University of New York Maritime College. Mr. Spalding is a licensed Third Mate of Oceans, Steam, or Motor Vessels of any Gross Tons.

ALISON BROWN

Dr. Brown is the President of NAVSYS Corporation, which specializes in developing GPS technology. She has fifteen years experience in GPS receiver design and has seven GPS related patents. She has published numerous technical papers on GPS application and is on the editorial board for GPS World and GIS World magazines. Dr. Brown currently conducts research in various areas of GPS, including advanced GPS receiver design, high accuracy GPS, differential GPS techniques, GPS integrity monitoring, and low cost GPS sensors. Dr. Brown completed her graduate studies at MIT and UCLA. In 1987 she served as chairman for the RTCA SC-159 GPS Integrity working group. In 1987 and 1988 she was Technical and General Chairman, respectively, for the Institute of Navigation Satellite Division National Technical Meeting.

Presented at ION Fall Meeting, Palm Springs,
CA, September 16-19, 1995

ABSTRACT

Differential GPS (DGPS) is becoming widely used for a variety of precise positioning applications. Test results have demonstrated the capability to provide real-time navigation data to an accuracy of 2 meters. This exceeds the accuracy requirement of 10 meters (2 dRMS) established for the majority of radionavigation applications. However, on occasion, transient errors are observed in the DGPS solution where, for a short period of time, the navigation error exceeds 10 meters. These errors can be caused by transients in the satellite signals (e.g. selective availability), errors in the reference station (e.g. multipath), or errors in the DGPS receiver itself.

Many of the applications for DGPS require a highly reliable solution. One such application is navigation buoy positioning. Currently, buoys are located by the USCG using DGPS. DGPS can provide the capability for locating buoys in all weather conditions with a high level of reliability. However, current methods do not always include an integrity measure on the DGPS solution. In addition to the real time integrity monitoring, the Coast Guard desires that data be archived and the integrity status be regenerated if the need arises (e.g. post-mission validation for litigation considerations).

This paper describes an autonomous DGPS Fault Detection and Isolation (FDI) algorithm which can be implemented in the user's DGPS receiver. The algorithm makes use of redundant measurements to test the validity of the DGPS solution. An additional redundant measurement can be obtained through the use of a tide model and altitude aiding the FDI algorithm. With altitude aiding, the algorithm can be implemented in any DGPS receiver with 6 or more channels.

The DGPS FDI algorithm was tested on board the US Coast Guard Cutter RED WOOD and at the Research and Development Center in Groton, CT to demonstrate the ability of the algorithm to detect navigation accuracy failures and the contribution of the altitude aiding to reduce false alarms. The tests were conducted underway from December 11-14, 1994 and on land from February 24 through March 1, 1995. During the tests the tide models

December 11-14, 1994 and on land from February 24 through March 1, 1995. During the tests the tide models were shown to reliably add information to the FDI process and reduce the percentage of yellow warning alarms. During the land tests the contribution of high accuracy differential corrections was analyzed. The FDI algorithm has previously been demonstrated to reliably detect failures through simulation and field testing. With the improvements of the altitude aiding and high accuracy differential corrections, false alarms and warnings have been virtually eliminated.

INTRODUCTION

Government-provided DGPS service is currently planned for all coastal waters of the US to provide harbor approach navigation. Positioning aids-to-navigation (AToN) was a major impetus to the DGPS implementation. The US Coast Guard currently maintains tens of thousands of navigational buoys using several methods of positioning. Through four years of field experience, DGPS has consistently proven to be the most reliable and accurate method of placing a buoy at its assigned latitude and longitude.

Over the past two decades, the Coast Guard has significantly improved its method of positioning buoys with horizontal sextant angles. This method has been refined to yield accurate positioning and create enough information to properly defend the Coast Guard from potential legal actions regarding AToN not being on their proper station. Extra observables are used to create an over-determined solution, and all the measurements are recorded so that the solution can be calculated at any point in the future.

DGPS has presented technical challenges to meet the same legal requirements as those specified for horizontal sextant angle positioning. Most DGPS receivers do not provide the reporting and analytical features to resolve legal issues. To satisfy this requirement, the USCG R&D Center funded and directed the development of NavSafe, a RAIM system for DGPS. NavSafe measures the integrity of the DGPS position solution and indicates the quality of the solution, and can also record enough data to return the integrity equations for fault detection at a later date.

The specific challenge to be met by the NavSafe RAIM software was to provide integrity guarantees for the task of buoy positioning by the US Coast Guard. This task requires a navigation accuracy of 10 m (R95).

The NavSafe integrity software uses a Fault Detection and Isolation (FDI) algorithm that continually checks for biases on the GPS receiver's pseudo-range measurements and sets alarms whenever the required integrity is not achieved. One of the major problems with previous RAIM algorithms was the inability of the algorithms to determine within a certain probability if there was in fact a failure or if the solution was valid. This situation occurs often in cases of low signal-to-noise (SNR) ratios, poor tracking geometry, and insufficient number of redundant satellites. In this situation the RAIM

algorithm has failed to provide the required integrity information. To augment the RAIM process for this application, additional information is provided to the RAIM software by means of a tide model.

THE NAVSAFE RAIM ALGORITHM

The NavSafe RAIM algorithm uses pseudo-range residuals as its inputs. This makes the algorithm generic so it can be used with any GPS receiver that outputs the residuals (for example, using the \$GPGRS NMEA message). The algorithm continually looks for biases on the pseudo-range measurements. Using the pseudo-range residuals, the algorithm calculates the most likely bias. This is standard in Fault Detection and Isolation [3, 4, 5, 7]. NMEA adopted the \$GPGBS message in version 2.01 published last year for reporting the most likely bias.

All RAIM calculations are a function of the noise on the measurements. The NavSafe RAIM algorithm uses a technique to compute the variance of the noise from the residuals. Tests done on NavSafe show that this variance calculation is accurate to within 5% of variance measurements calculated independently using the known receiver position.

Having computed the most likely bias, the algorithm uses a proprietary technique to compute the relative probabilities of any other biases on other channels. This allows the algorithm to consider all possible biases, not just the most likely, although when a significant bias is present the set of possibilities rapidly reduces to the single true bias.

The algorithm computes the worst case radial position error (RPE) that could result from any of the set of possible biases. The RPE is a function of the bias and of the noise on all the measurements. The standard mathematical model for the distribution of the RPE is the non-central chi-squared probability distribution function (PDF) [1, 2, 5, 6]. NavSafe uses a novel approach to solve the non-central chi-squared probability function in real-time. This allows the algorithm to calculate the expected error to any required accuracy (in the case tested here the accuracy is 10 m, R95).

The NavSafe package produces three alarm states, green, yellow, and red, to report on the current accuracy of the measurements. If the expected error is within the accuracy requirement, then a green light is shown and the user is assured that the required accuracy has been achieved. All the relevant data can be logged so that the calculations can be reproduced to verify the accuracy and satisfy the legal requirements surrounding aids-to-navigation. If the expected error is outside the accuracy requirement, then the NavSafe algorithm computes the probability of false alarm. If this is low, then a red alarm is raised, indicating a probable error. Otherwise, a yellow alarm is raised, warning the user that the test cannot be performed reliably.

The probability of false alarm can be shown to be a function of the change in HDOP that occurs after the suspected

biased satellite has been removed from the computation. This change in HDOP is called the *integrity geometry* and is as important to RAIM as ordinary HDOP is to navigation. If the integrity geometry is bad (large), then even a small suspected bias will lead to a large distribution of possible error, and the algorithm must raise an alarm. So one can see that bad integrity geometry will lead to a high alarm rate. The worst case integrity geometry is, of course, predictable by using the almanac data to compute future positions of satellites. The NavSafe package provides a look-ahead feature that produces an on-screen plot of the expected alarm rate for any time period. Using this feature, users can plan critical navigation tasks to coincide with periods of good integrity geometry.

TIDE MODELS

There are two different tide models which can be used with the altitude aided version of NavSafe. The NavSafe default mode uses a global model based on satellite altimeter cross-over data [8]. This model will predict the tides in areas of open ocean, but will not resolve the tidal signatures of some estuaries, sounds, or coastal areas. The model does not attempt to resolve the tides in river areas. In these areas, the user can enter data from the tide tables which will be used for a local tide model computation instead of the global model. As data is collected, the tide model in use will be calibrated to account for changes in location of the antenna relative to the sea surface and coordinate system differences inherent in the measurement. If the global model is valid in a particular area, data will be collected and logged even if the global model is not currently in use. This way, if the tide model is switched from either no model or the user input local model to the global model, the global model will already be calibrated. Proper calibration of the global model should take between 12 and 24 hours.

The global tide model is based on a least squares fit of the first 40 cycles of TOPEX/POSEIDON [9] to the Laplace Tidal Equations as determined by Egbert et al [8]. The tides are provided as complex amplitudes of the earth-relative sea-surface elevation for eight primary harmonic constituents (M2, S2, N2, K2, K1, O1, P1, Q1) (Lambeck, 1980) on a 512x256 grid between 79.71° South and 69.71° North. This gridded data is bilinearly interpolated to the desired location. A tidal synthesis program uses the interpolation of the tidal admittances in the diurnal and semi-diurnal bands to include 9 additional constituents (2N2, MU2, NU2, L2, T2, J1, NO1, OO1, RHO1). The synthesis program also adds the long period constituents of MF, MM, SSA using the equilibrium equations.

The user supplied local tide information will be used to fit a model of the tide using the M2 tidal frequency. Over short periods of time, the M2 signal will dominate the tidal signature. The function used to represent this tide model is

$$h_{user tide} = \alpha \cos \omega t + \beta \sin \omega t + b \quad (1)$$

where ω is the M2 tidal frequency.

TIDE MODEL CALIBRATION AND COMPARISON

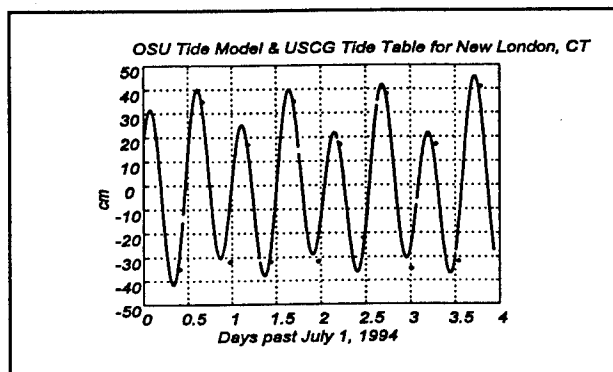


Figure 1 Global Model and Tide Tables: New London

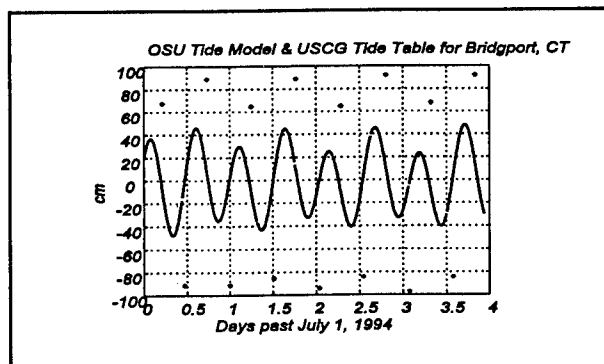


Figure 2 Global Model and Tide Tables: Bridgeport

Each of the tide models used for altitude aiding will need to be calibrated. This calibration will account for the offset between the antenna and the sea surface height and any differences in the coordinate systems used. For example, when the high and low tides are given from a user entry, they will be relative to a local low water mean, whereas the navigation solution will be in the WGS-84 coordinate system. The estimation of a bias to account for this type of local difference provides a more intuitive approach over keeping track of all the local coordinate transformations.

For the global tide model, a bias will be used to calibrate the model. The global model performance provides fits to the tide gauge data below the 50 cm level once the bias is removed. Comparisons of the global model and the high and low tides from four tide tables, with the bias removed, are shown in Figure 1 through Figure 4.

The comparison at Bridgeport, CT is the worst case with an offset in gain and phase. However, even for this case, the errors are less than 50 cm. With this type of global model calibration, there will be no need for user input and the model should yield sigmas on the height information in the altitude aiding equations of less than 1 meter. The bias will be adjusted as measurements are collected and can be allowed to adjust over short periods of time to account for actions such as taking on fuel, unloading cargo, and burning fuel.

For the local model shown in equation (1), the parameters α and β will be estimated from the two days of tide table information provided by the user. As data is collected, the bias, b , will be estimated. This bias, like the bias in the global model, will be adjusted as measurements are taken to account for taking on fuel, unloading cargo, and burning fuel. This tide model will be accurate to the 20-30 cm level over the period of time given from the tide tables.

TEST RESULTS

The NavSafe RAIM package was tested at the USCG R&D facility at Groton, CT, during December 1994 and February 1995. Differential corrections were generated by a Coast Guard reference station.

SEA TESTS

The altitude aiding addition to NavSafe was tested during December 11-14, 1994 aboard the USCG Cutter Red Wood. These tests document the decrease in yellow alarms through the use of altitude aiding and the accuracy of the global tide model. The GPS data input into NavSafe was taken from a single antenna and split into two different receivers and PCs, both running NavSafe. One version of NavSafe was running with the altitude aiding disabled and the other with the altitude aiding in the auto mode. In auto mode, the altitude aiding is used when there is a yellow alarm. If there is a green or red alarm, altitude aiding is not used. Both versions had the parameters RPE max set to 10 meters, PFA max=5%, and PMD max=5%.

Data for these tests were collected continuously over about 4 days. Table 1 shows the percentage of green, yellow, and red alarms for the four days. The altitude aiding is used to reduce the number of yellow alarms by adding information into the FDI algorithm about the height component of the navigation solution. This table clearly shows the improvement when altitude aiding is used in reducing the number of yellow alarms from 27.4% down to 8.8%. However, some additional explanation of the high percentage of red and yellow is needed. The high number of non-green alarms is due to two factors in this test scenario. First, by splitting the antenna, there is a 3 dB loss in the GPS signal which will translate directly into noise on the pseudo-range measurement. Second, the differential corrections were lost for brief periods of time. Both of the factors will generate yellow and red alarms.

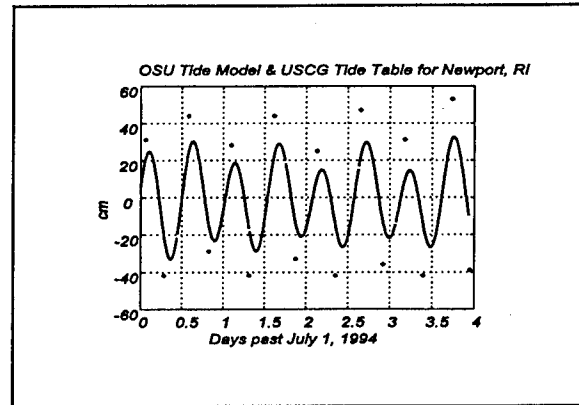


Figure 3 Global Model and Tide Tables: Newport

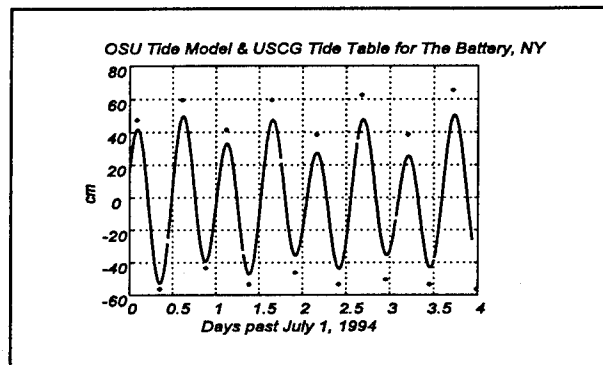


Figure 4 Global Model and Tide Tables: The Battery

The global tide model was also verified during these sea tests. The tide height, tide residuals (used in the FDI), and the tide sigmas (also used in the FDI) are shown for both the altitude aided and the non-altitude aided versions of NavSafe in Figure 5 through Figure 10. The tide signature for both cases is very similar. For both cases the tide height varies by about 5 meters and the twice diurnal M2 tide signal is apparent. The choppy, non-tidal signature is caused by having the time constant on the tide bias set too low, therefore allowing the bias to adjust too quickly. This

Table 1 Altitude Aiding Sea Test Results

| | No Altitude Aiding | Altitude Aiding (used 26.3% of the time) |
|--------|--------------------|--|
| Green | 68.78% | 85.56% |
| Yellow | 27.40% | 8.84% |
| Red | 3.82% | 5.59% |

was done to verify that the tide bias and time constant were operating properly. This is validated through the tide sigma shown in Figure 9 and Figure 10. The large outages on the

residuals and sigmas are due to restarts of the specific PC or recalibration of the tide. These instances were necessary during the 4 days of testing. These results show that the tide sigmas vary from about 1 to 2 meters. This accuracy of data provides a solid reference to help the FDI algorithm.

TESTING WITH HIGH ACCURACY DIFFERENTIAL CORRECTIONS

To further test the altitude aiding contribution to the decrease in yellow alarms and the contribution of very accurate differential corrections, another set of test data was collected. The alarm statistic settings used were the same as for the sea test. During this test, however, only one receiver was used. Data were collected from February 24 to March 1, 1995, two days using an altitude aided FDI and the other two days with the altitude aiding disabled. The results from 1 day of altitude aiding on and 1 day with altitude aiding off of this test are shown in Table 2.

An operational differential station, located at Montauk Point and occupied by an Ashtech Z-XIIR was used for this testing. A Novatel running in a PC was used for the remote receiver. This hardware was chosen to demonstrate the capability of the system without the addition of expensive GPS hardware.

These results show a tremendous reduction of yellow alarms over the use of the prototype differential reference receivers where the yellow alarm rate was about 21% [10]. In addition, with altitude aiding, the yellow alarm rate goes from about 5% to 0.00%.

Table 2 Sea Testing with Highly Accurate Differential Corrections

| | Green | Yellow | Red |
|----------------------------------|--------|--------|------|
| 2/24/95 1.3 days Aiding On | 99.93% | 0.00% | .07% |
| 3/1/95 1.1 days Aiding Off | 94.7 | 5.36 | .53 |

CONCLUSION

NavSafe and the FDI algorithms described in this report have been tested for over two years and proven to be a reliable method of determining the integrity of a GPS navigation solution without affecting the navigation solution. The use of tide models to help constrain the FDI process combined with accurate differential receivers virtually eliminates the yellow alarms. The use of these

algorithms and software will provide the user with an accurate and reliable method of monitoring a GPS navigation solution.

The test results showed that the NavSafe RAIM package accurately computes the variance of the noise on the pseudo-range measurements, and reliably detects biases whenever they occur. The calculation of the expected error is achieved in real-time so that alarms occur as soon as the actual error approaches the limits set by the user. The system performance with operational differential reference stations was found to be good at distances of 23 miles, showing similar results to those achieved in zero-baseline tests.

REFERENCES

- [1] M. Abramowitz, I.A. Stegun, eds, *Handbook of Mathematical Functions*, New York, Dover, 1970.
- [2] A. Brown, M. Sturza, "The Effect of Geometry on Integrity Monitoring Performance," ION National Technical Meeting, June 1990.
- [3] K.C. Daly, E. Gai, J.V. Harrison, "Generalized Likelihood Test for FDI in Redundant Sensor Configurations," *Journal of Guidance and Control*, Vol 2, Jan-Feb 1979.
- [4] S.R. Hall et al, "In-Flight Parity Vector Compensation for FDI," *IEEE Transactions on Aerospace and Electronic Systems*, Vol AES-19, No 5, Sept 1983.
- [5] M.A. Sturza, "Fault Detection and Isolation (FDI) Techniques for Guidance & Control Systems," *NATO AGARD Graph GCP/AG.314: Analysis, Design & Synthesis Methods for Guidance and Control Systems*, 1988.
- [6] M.A. Sturza, "Navigation System Integrity Monitoring Using Redundant Measurements," *Navigation: Journal of the Institute of Navigation*, Vol 35, No 4, Winter 1988-89.
- [7] A.S. Willsky, "A Survey of Design Methods for Failure Detection in Dynamic Systems," *Automatica*, Vol 12, 1976.
- [8] G.D. Egbert, A.F. Bennett, M.G.G. Foreman, "TOPEX/POSEIDON Tides Estimated Using a Global Inverse Model," *J. Geophys Res*, in press.
- [9] P.S. Callahan, "Topex/Poseidon NASA GDR Users Handbook," *JPL Technical Report D-8590, Rev C*, JPL, Pasadena, CA, 1993.
- [10] NAVSYS Corporation, "Autonomous Failure Detection for Differential GPS," *SBIR Phase II Final Report*, NAVSYS, Colorado Springs, CO, 1995.

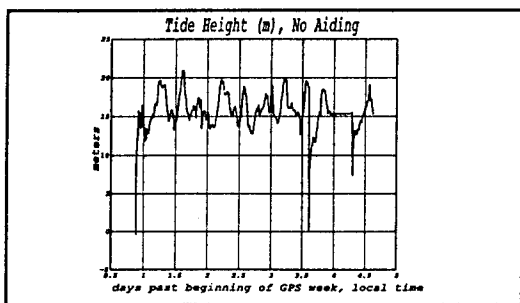


Figure 5 Tide Model Verification: Tide Height, No Aiding

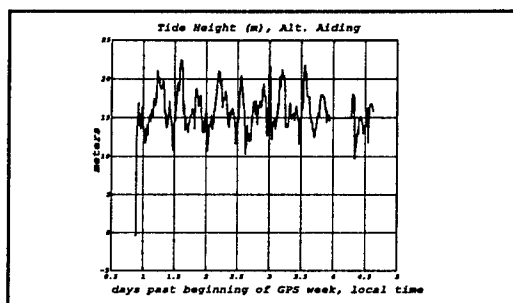


Figure 6 Tide Model Verification: Tide Height, Altitude Aiding

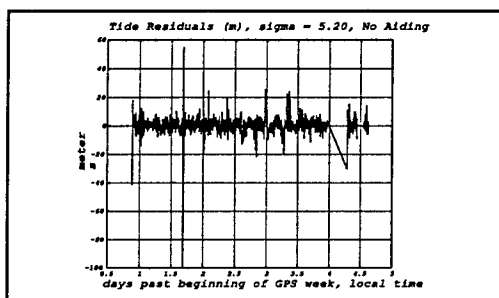


Figure 7 Tide Model Verification: Tide Residuals, No Aiding

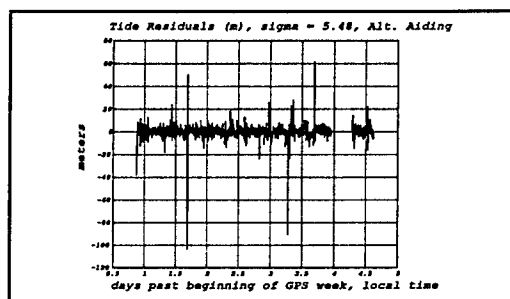


Figure 8 Tide Model Verification: Tide Residuals, Altitude Aiding

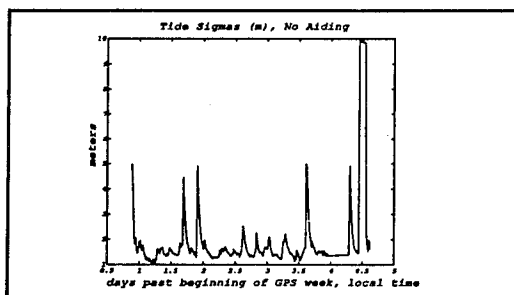


Figure 9 Tide Model Verification: Tide Sigmas, No Aiding

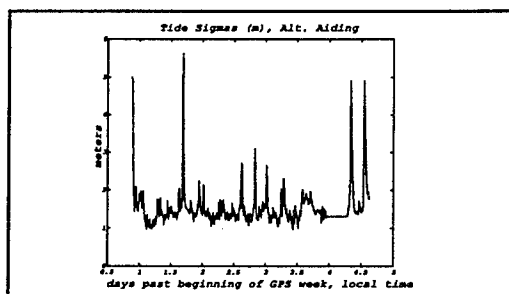


Figure 10 Tide Model Verification: Tide Sigmas, Altitude Aiding

The Virtual Anchor

Glen Robertson
Rhodan Marine Equipment

John Webster
Holst-Webster Enterprises

BIOGRAPHIES

Glen E. Robertson is CEO of Mini-Systems, Inc., which he founded in 1968 and he is President of Rhodan Marine Equipment, Inc. Mini-Systems specializes in hybrid thick and thin film products and hermetic packages for Military, Aerospace and Medical Electronic applications. Rhodan Marine concentrates on specialized products for maritime applications. An enthusiastic advocate and user of GPS, Mr. Robertson studied electrical engineering at the University of Illinois at Champaign-Urbana.

John L. Webster is V.P. of Engineering for Holst-Webster Enterprises specializing in software for Differential GPS applications, prior to this he was Chief Engineer for the Chrysler Corporation's Electronics Division in Huntsville, Alabama, where one of his projects was the development of an experimental GPS navigation system for automobiles. Mr. Webster is a licensed professional engineer in Alabama and attended the University of Alabama's Huntsville Campus.

ABSTRACT

In the Commercial Fishing Industry there exists the need for a Virtual Anchor for small and medium sized boats. This system was initially intended to replace a physical anchor for short duration parking of a boat during the harvesting of Lobsters or Crabs by commercial fishermen. Scuba Divers can also utilize the system to maintain their Dive Boat's location over environmentally sensitive coral reefs, where physical anchors, which damage the reef, are prohibited. Day Party Fishing Boat Captains can also use the system to park their boat directly over known good fishing spots in deep water.

A novel virtual anchor has been developed, installed and demonstrated aboard a 34 foot boat at sea. In calm seas, with disturbing wind forces of less than 10 knots, using a USCG Differential Beacon for corrections, the system maintained the boat's bow position within a four meter radius. The one sigma standard deviation was approximately two meters during one hour anchoring trials. A production version of the system could be marketed for under \$10,000.

The DGPS based Virtual Anchoring system is both technically and economically feasible for commercial vessel operators. The bow positioning accuracy of the system is far superior to that obtained from a single physical anchor because it continuously corrects. The long "scope" of a conventional physical anchor line or "Rode" allows a boat to swing about a large radius unless multiple anchors are deployed.

In the lucrative lobster harvesting application, the system price can be paid back within one annual harvesting season due to time savings from not deploying and recovering a physical anchor at each lobster habitat harvested.

INTRODUCTION

There are several maritime operational scenarios in which a vessel is required to anchor for relatively short durations. This involves dropping an anchor upwind or upcurrent from the position that the boat will be in. When operations at this location are completed the anchor must be retrieved and stowed. Occasionally the anchor does not set well and the boat drags the anchor off site, or the anchor becomes fouled on the bottom and additional time is lost while freeing and retrieving the anchor.

The need for a Virtual Anchor was specifically motivated by a Commercial Lobster harvesting operation. In this scenario, a number of lobster habitats are situated on the sea floor at pre-recorded DGPS latitude and longitude positions and at depths of less than 45 feet. No marker buoys are used to reduce the risk of pirate harvesting. The harvesting boat and crew will work several dozen habitats a day. Harvesting is accomplished by two free divers working from the boat. The time spent anchoring and un-anchoring the boat at each habitat is unproductive time.

CONCEPT DESCRIPTION

Conceptually, the Virtual Anchoring System consists of an accurate Differential GPS Receiver, A Steerable Thruster and a Control Computer. The GPS Receiving Antenna is mounted at the bow of the boat and the desired anchoring point is like a waypoint which, the Thruster Control System continually seeks.

When the vessel operator presses the "Set Anchor" command button, the desired Anchoring coordinates are instantly stored in the Control Computer's memory. Once an Anchoring Site has been selected, the control computer continually utilizes the DGPS Receiver fixes to calculate a Range and Bearing to the Anchoring Site. These Range magnitudes are generally much less than five meters.

In the Control Computer, the current Thruster Heading is compared to the Bearing to the Anchoring Site and a Steering Correction signal is derived. The DGPS Receiver Latitude and Longitude Fixes are communicated to the Control Computer via a standard 4800 baud NMEA serial data interface. The Thruster's Heading information is also communicated to the Control Computer via a similar serial data interface. Since the DGPS Fixes are only updated once per second and the Thruster Heading is only updated at a few samples per second, we are dealing with a Sampled Data Control algorithm. The maximum steering rate of our present thruster steering servo is limited to about sixty degrees per second. To minimize hunting, the steering algorithm issues corrections sized accordingly.

The Range information is used to determine the amount of Thruster Power needed. The current Electric Thruster uses a Pulse-Width modulation scheme to control Thruster power. The Control Computer has a four bit parallel port Digital to Analog interface to the Pulse Width Modulator which gives the system sixteen levels of Thrust. The system was initially tested with a thruster capable of 45 pounds thrust, but is currently utilizing a 65 pound thruster to provide more authority in higher wind and sea current conditions.

Range/Rate information is also calculated to provide a second order control. This rate or velocity information is used to provide control system damping to minimize overshooting and hunting. Control algorithm coefficients are adjustable to suit the vessel's weight inertia and hull drag. When the thruster has achieved sufficient velocity toward the desired anchoring site, the thruster power is reduced accordingly to avoid overshoot. Velocity away from the desired anchoring site quickly results in maximum corrective thrust to prevent loss of position.

DGPS CORRECTION SOURCES

Differential Corrections are available from a variety of sources. This Virtual Anchoring System has been experimentally implemented with three different Differential Correction schemes. Initially the system was implemented using a private VHF Narrow Band FM Packet Data Radio link. The base station DGPS reference receiver was initially a Navstar XR4 with its antenna located at a surveyed position. The XR4 base station was later updated to an XR-5M with some improvement of performance. A VHF

receiver and packet radio modem aboard the vessel received the pseudorange and range rate corrections for the on-board DGPS receiver. Initially an XR4 DGPS receiver was used on-board. It was later upgraded to an XR5, but was quickly replaced by an Ashtech Sensor II, which provided superior accuracy at less cost.

The second method of obtaining differential corrections involved subscribing to the DCI RDS service which was broadcast on a subcarrier from a nearby FM Radio Broadcast Station. The DCI Model RDS-3000 receiver receives the differential GPS corrections and provides them via a serial data output to the on-board Ashtech DGPS receiver.

The third method of obtaining differential corrections involved the use of the U.S. Coast Guard's Low Frequency beacon broadcasts of differential corrections. A low frequency beacon receiver aboard the vessel receives and demodulates the MSK modulated differential correction data and transmits it to the on-board DGPS receiver via a 4800 baud serial data link.

The XR4 and XR5 implementations used RTCM 104 Type 1 and Type 2 messages. The DCI subscription service is available with either Type 1 or Type 9 messages. During our tests, we used the signal from an FM station near Tampa, Florida. The USCG Low Frequency beacon broadcasts were initially Type 1, but are currently being changed over to Type 9. We used the Type 9 signals broadcast from the Egmont Key beacon during our tests at Sarasota, Florida.

Using the Ashtech Sensor II DGPS receiver on-board the test boat, we observed comparable accuracy from all three sources of differential correction information. Base line distances were on the order of 60 km for the DCI service, 30 km for the USCG beacon and 5 km for the private reference station VHF radio data link.

SYSTEM ARCHITECTURE

The Differential Corrections Receiver receives the RTCM-104 Type 9 correction messages and sends them over a 4800 baud serial data link to the on-board DGPS receiver.

Latitude and Longitude fix data from the on-board DGPS receiver is sent to the Virtual Anchor Control Computer via another 4800 baud serial data link.

Thruster heading information is obtained serially via a third 4800 NMEA data link from a KVH flux-gate digital compass mounted on the thruster steering mechanism. Slip Rings are required for these connections. High current slip rings are used to connect the Pulse-Width Power Controller to the Thruster Motor.

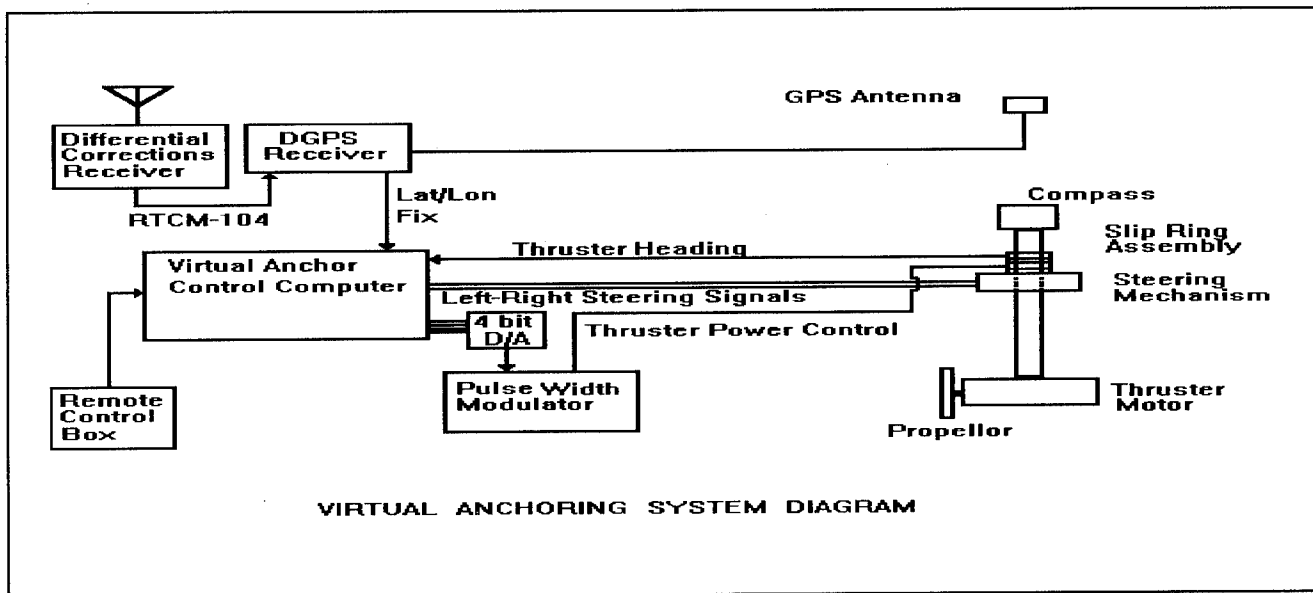


Figure 1

This block diagram indicates all of the functional elements of the Virtual Anchoring System.

The Remote Control Box provides the human boat operator interface. From this conceptual control panel, the operator can "Set Anchor" and "Release Anchor".

An "Audible Alarm Annunciator" is contained in the remote control box to alert the boat operator in case of large range errors or loss of differential mode.

PERFORMANCE EVALUATIONS

DIFFERENTIAL FIX ACCURACY

To evaluate the accuracy of the Differential GPS fixes, several hours of operation were conducted while at dockside. Using the earlier Navstar XR4 DGPS receiver, the differential fix errors were in the five to ten meter range which was deemed unacceptable.

After replacing the XR4 units with Navstar's newer XR5 model, the errors dropped into the three to five meter range. This usually provided anchoring accuracies better than those obtained with a single physical anchor. The Ashtech Sensor II DGPS receiver provided an even better differential fix. With this present configuration, the fix errors are generally in the one to two meter range.

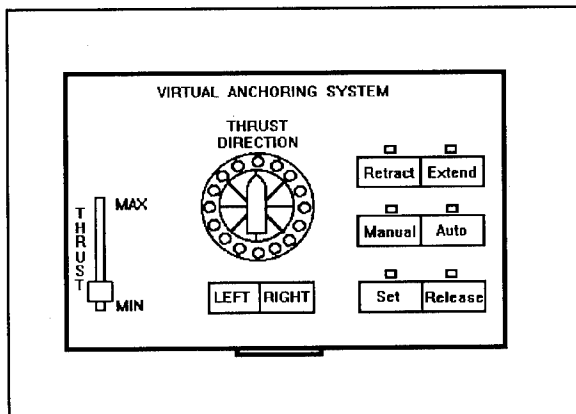


Figure 2

Red LED indicates power is on and system is not anchored. A Green LED indicates that the Virtual Anchor has been activated.

The Remote Control Box also allows the thruster to be used manually; for this usage, the controls include the "Retract/Extend" selector, the "Manual/Auto" selector, "Left/Right" steering buttons, and "Thrust" rheostat. This manual control capability provides additional maneuvering capability and can be used to assist docking. To facilitate this usage, a sixteen point "Thruster Relative Heading" display is provided.

THE SEA TRIALS

A 34-foot Scarab boat was available for the initial system testing. A temporary bow-thruster mounting platform, without a retract mechanism, was installed on the Scarab.

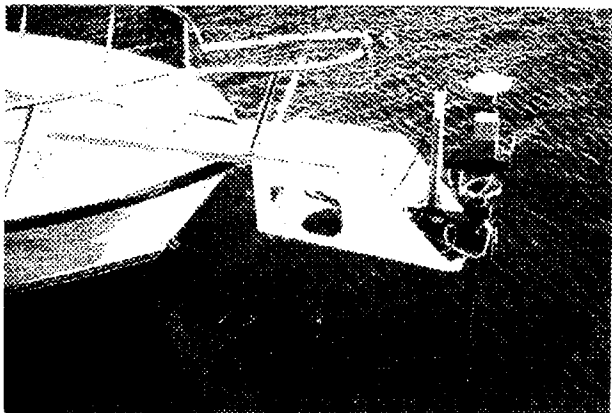


Figure 3

Note that the GPS receiving antenna is located directly over the bow thruster.

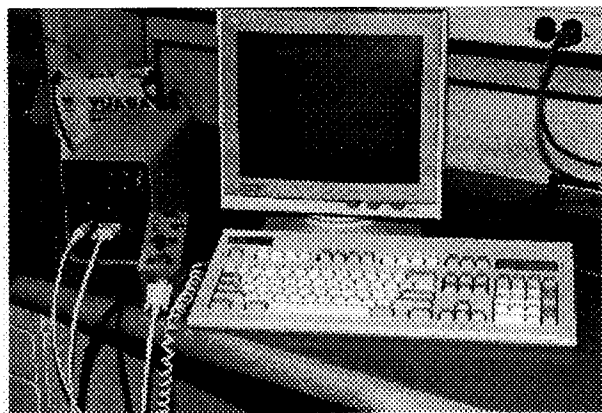


Figure 4

This photo shows the Virtual Anchoring System Control Computer.

The prototype system utilizes a single board IBM 486-33 PC/AT compatible computer. For test data collection, a virtual drive RAM card was included on the prototype. A conventional computer keyboard interface was added during R&D tests to facilitate parameter changes. A VGA monitor interface was also added during these R&D tests to facilitate performance data monitoring.

BOAT DYNAMIC FACTORS

The 34-foot Scarab's twin 250 HP Outboard Engines concentrate the mass at the stern of the boat and its long stiletto shape places the center of wind pressure well forward of the center of mass. This gives the wind a good bit of leverage and causes the bow to want to swing toward the downwind direction. The Scarab weighs about 5 tons which gives it a significant amount of momentum, once any velocity is achieved. Its wind surface area is small when

heading into the wind but becomes quite large when broadside to the wind.

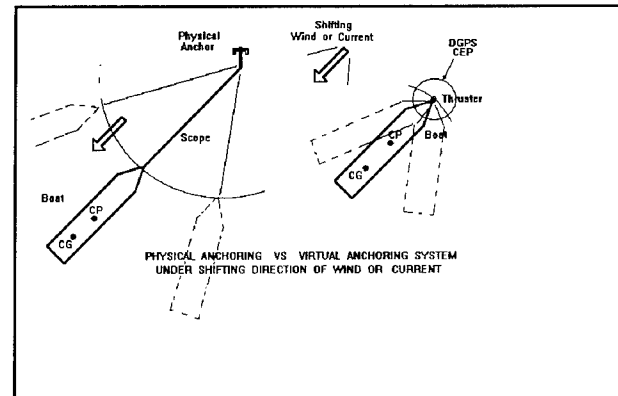


Figure 5

The dynamics of this boat represent a severe challenge to the Virtual Anchor Control System. The lobster harvesting boats are 25 foot Robalos, are lighter weight and have a lower length to beam width ratio. The lobster storage compartments are located forward, so, as the work day progresses, the center of mass moves slightly forward. This will tend to compensate for the decreasing fuel mass.

ANCHORING TESTS

Three types of tests were conducted to determine proper selection of the Coefficients that determine the Dynamic performance of the Sampled Data Ship Positioning System. Initial testing was performed in a protected basin with calm water and light winds. Trial and error selections of the Range and Range Rate thrust coefficients provided an empirical feel for the test boat's dynamics. A Lap-Top PC was used to log fix data during the on-board tests.

An offshore test was conducted in three to five foot seas near the Sarasota Sea Buoy. Problems were encountered here. Due to the test boat's configuration, the bow thruster was being lifted completely out of the water as the boat rode over the larger waves.

A third type of test was conducted in a narrow channel during a tidal flow which increased to two knots of current.

From these early tests, it was determined that the 45 pound thruster limitation allowed us to anchor the Scarab in calm water at winds up to 15 knots, in calm winds at tidal currents up to 2 knots and at sea in a moderate situation of combined wind and wave motion. To provide increased control system authority, a 65 pound bow thruster has been procured for the Scarab installation.

ACCURACY DATA

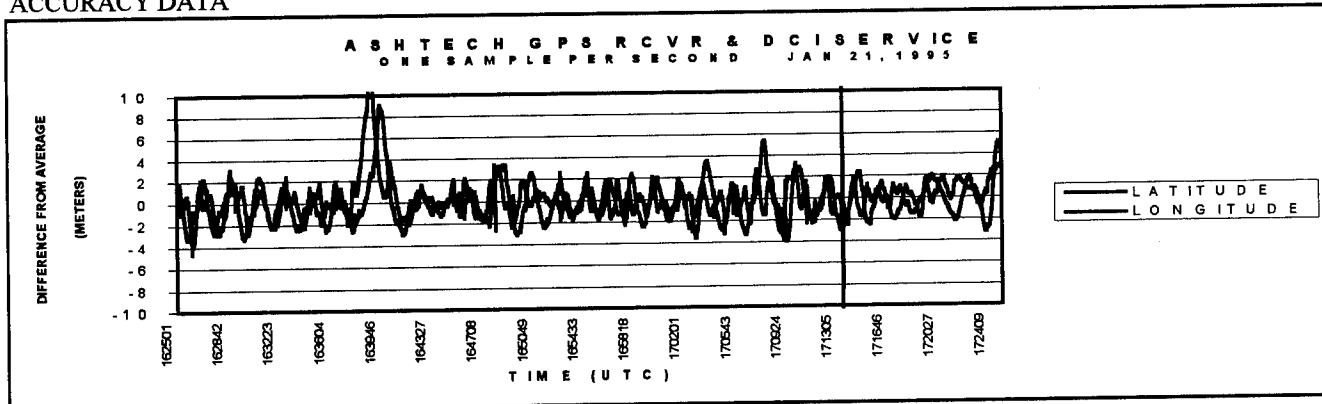


Figure 6

This plot shows a one hour anchoring test in a protected basin with winds of about 10 knots. Note that the one sigma standard deviation for this hour of anchoring is less than two meters.

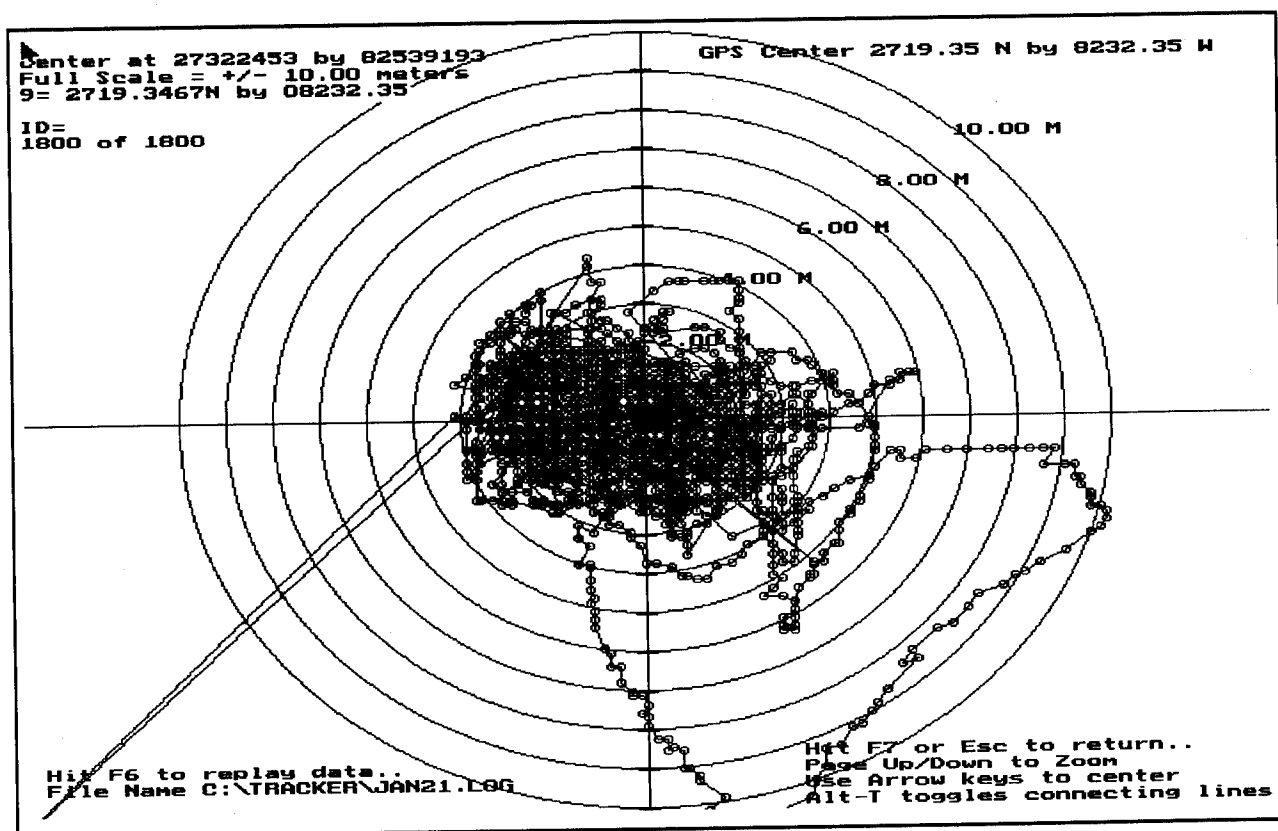


Figure 7

This XY plot of the same data from Figure 6 shows how well the boat's position was being held during the virtual anchoring test. The plot includes a bad data point in the lower left corner and the excursion in the lower right occurred while the anchoring system was disabled to make some experimental coefficient changes.

This figure is a screen capture from a tracking program supplied by Holst-Webster Enterprises.

POTENTIAL IMPROVEMENTS

Although the system has already demonstrated superior anchoring accuracy when compared to a single physical anchor, several improvement possibilities arose during the on-board tests.

An anemometer to measure windspeed and direction could be added, at a moderate cost, as an additional sensor input to a multi-state Kalman filter added to the software. At substantial cost, On-The-Fly kinematic DGPS computations could be performed to provide centimeter accuracy for the anchoring site control system input.

ALTERNATE CONFIGURATIONS

It is obvious that several alternate system configurations could be implemented.

For example, two fixed (non-steerable) reversible thrusters could be utilized in place of a steerable thruster. Differential thrust would replace the steering mechanism. In this implementation, the ship's compass could be utilized if it has a suitable NMEA data output. At the cost of a second thruster, the steering mechanism and slip-ring assemblies would be eliminated.

Putting duplicate systems on a vessel to maintain both the bow and stern position could keep a vessel in a fixed heading as well as in a precise location.

CONCLUSIONS

It has been demonstrated that the Virtual Anchoring System is both technically and economically feasible for installation aboard commercial fishing and lobster harvesting boats or pleasure crafts. With the proper Thruster, the system can virtually snub a small boat's bow to an imaginary piling using a six foot line.

In the lobster harvesting application, the increased productivity due to anchoring time saving alone shows an installation investment payback well within one harvesting season.

ACKNOWLEDGEMENTS

The authors of this paper would like to gratefully acknowledge the pleasant experience of working with brothers, Heath and Timothy Higgs of Marsh Harbor in the Bahamas whose fishing methods showed the need for a "Virtual Anchor"; Walter Jchu, a Circuit Design Engineer for Mini-Systems, Inc. for computer/controller interface, designing/packaging; Walter K. McCall, E.E. for valuable

suggestions and sketches; John Scott, who skillfully innovated and fabricated the fixtures to implement the system on various boats; Elaine Panos, Secretary for proofing and organizing text.

Use of DGPS For an In Water Acoustic Survey For the PTS SWIMSS

Robert Reid
Naval Undersea Warfare Center

BIOGRAPHY

Robert Reid has been an electronics engineer at the Naval Undersea Warfare Center (NUWC) Division, Newport, RI, since 1981. He earned his bachelor of science degree in electrical engineering from the University of Massachusetts (Dartmouth). He was project engineer for the Portable Tracking System (PTS) during the execution of the experiment. He is currently working as the program manager on the Hawaiian Shallow Water Range Program. He holds one patent and several patents pending, as well as a number of papers published in the area of underwater acoustic tracking and radiated noise measurements.

ABSTRACT

The Portable Tracking System (PTS) is being designed to support the U.S. Navy's requirement to perform open-ocean testing in diverse environmental conditions, including shallow water. The Shallow Water In-line Multiplexed Sensor System (SWIMSS) is a prototype system used to track the position of in-water vehicles that are performing naval operations. SWIMSS is designed to be deployed in water depths up to 2000 feet. It consists of 10 in-line sensor hydrophones that time-division multiplex (TDM) acoustic data over a single-mode fiber-optic cable. An installation and testing of SWIMSS was conducted 10-18 September 1994, 120 miles off the coast of Newport, RI, at 39° 53.5'N and -72° 07.2'W in approximately 300 feet of water.

In order to perform this kind of in-water tracking operation, each hydrophone sensor must be acoustically surveyed in a geodetic coordinate system. The survey of the sensor nodes requires a mobile survey ship to "ping" at various key range points. Aboard the survey vessel is a Differential Global Positioning System (DGPS) receiver and UHF RF telemetry equipment, as well as an underwater acoustic projector. The survey vessel received differential corrections from the Montauk Point, Long

Island, New York Coast Guard Station. The SWIMSS cable is terminated to a moored surface ship where the acoustic pings are detected. The receive vessel is logging the DGPS position of the survey vessel via the RF link on a SUN Workstation. Personnel on the receive vessel vector the survey vessel to the various survey waypoints for data collection. The underwater projector, hull-mounted to the survey vessel, transmits a "ping" that is synchronized with DGPS time. The ping is received by the SWIMSS sensor, multiplexed on the fiber, and demultiplexed by shipboard electronics aboard the receive vessel. The time delay caused by the transition of the ping through the water is measured by an acoustic digital signal processor interfaced to the shipboard demultiplexer and DGPS. The signal processor in turn is interfaced to the SUN, and the transit times through the water are displayed and stored. A "4" course is run over the SWIMSS sensor by the survey vessel. Based on the known time of the transmission, the position of the survey vessel acquired via DGPS, and the RF link, the transit time of the ping through the water and the velocity of sound in the water, the latitude, longitude, and depth of the SWIMSS hydrophone sensor can be calculated.

The new innovation here regards the fact that shallow water is a harsh environment for the transmission of acoustic pings. In the past, with deep-water acoustic tracking range surveys, several hydrophones would be making detections on a direct-path transmission from pinger to hydrophone. This technique ties the hydrophones together as they relate to each other. This is not possible in shallow water because the direct-path acoustic transmission is shorter, necessitating the requirement of a single hydrophone survey. This is the case because hydrophones may not be receiving the same acoustic paths. DGPS was the tool that makes possible hydrophone position in shallow water.

INTRODUCTION

The Navy has shifted the emphasis of testing from deep ocean water to the shallow, near-shore environment because of the shift of threat conditions. However, shallow water proves to be a very harsh environment for the task of underwater communications between undersea vehicles and a series of hydrophones positioned on the ocean floor. This problem is currently being investigated by the PTS program to support the U.S. Navy's requirement to conduct shallow-water testing in the littoral environment.

The accomplishment of this requirement will be satisfied by the PTS final production shallow-water system, which is a 100-hydrophone sensor node assemblage designed to cover 100 square nautical miles of open ocean.

The Naval Undersea Warfare Center Division, Newport is responsible for the execution of the PTS. It was decided early in the program to develop a prototype shallow-water system for testing, increasing the knowledge, and developing in-house experience for this type of system. This prototype was the Shallow Water In-line Multiplex Sensor System (SWIMSS), which provided the hardware. Special techniques were required during and after installation to acoustically position the SWIMSS sensor nodes. Figure 1 is a graphic depiction of SWIMSS as installed.

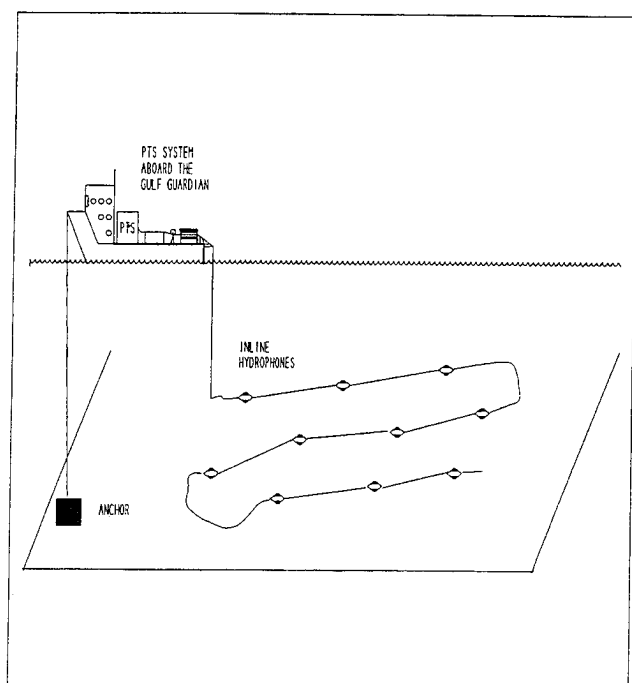


Figure 1. SWIMSS Conceptual Installation

BACKGROUND

Acoustic underwater tracking ranges consist of a series of hydrophones that are typically laid out in a geometric pattern of equilateral triangles. In order to perform the acoustic tracking function, the exact position and the inter-relationship between these hydrophones must be established. Acoustic tracking is performed on an undersea vehicle with the use of a cooperatively installed device called a "pinger." The pinger transmits a sonic signal that is detected by the bottom-mounted hydrophones. If enough hydrophones make detections on a given ping, the position of the vehicle can be calculated using 3-D triangulation algorithms.

On deep-water acoustic tracking ranges, the positions of the hydrophones are achieved through an acoustic survey using the Vanderkulk technique (1). After the hydrophones have been installed, a surface vessel, equipped with a synchronous pinger is used for the acoustic survey. This pinger is configured to transmit on the 1 second mark of GPS. The hydrophones are interfaced to a digital signal processor (DSP) where the in-water signals are detected. The DSP is also synchronized with GPS time. When the survey vessel pings, the signal travels through the water, is acquired by the bottom-mounted hydrophones, and detected with the DSP. Since the exact time of the transmission is known, the transit time of the ping signal through the water is also known. The speed of sound in the water is also known via the Sound Velocity Profile (SVP) which can be measured with various devices. Knowing the transit time from the pinger to the hydrophone and the speed of sound of water, the distance of this slant range can also be calculated.

Acoustic underwater tracking ranges are typically laid out in a hexagon with a hydrophone at the center as graphically depicted in Figure 2. The Vanderkulk process requires the survey vessel to ping at key geometric points over the hydrophone field. These points are located at the bisectors of baselines, over hydrophones, and at the geometric centroid of the equilateral triangles. Transit times from 3 to 7 hydrophones are required to calculate the relationship between the hydrophone on a relative coordinate system. The hydrophones are surveyed as triad groups. For the 7-hydrophone array shown in Figure 2, 25 survey points with multiple hydrophone replies per ping are required for the Vanderkulk process to function. In shallow water, the multiple replies required to perform this type of survey are rare; therefore, a technique to provide a single hydrophone survey was needed to solve this problem.

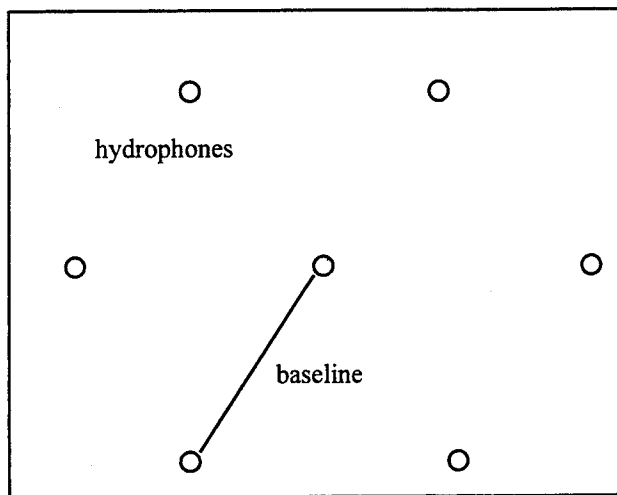


Figure 2. Acoustic Range Hydrophone Layout

TEST DESIGN

The SWIMSS was installed 10-18 September, 1994, 120 miles off the coast of Newport, RI, at 39° 53.5' north latitude and -72° 07.2' west longitude in approximately 300 feet of water. Figure 3 depicts the actual deployment location. The 10 nautical mile SWIMSS was laid out in a horseshoe configuration off the Motor Vessel GULF GUARDIAN, referred to as the receive vessel.

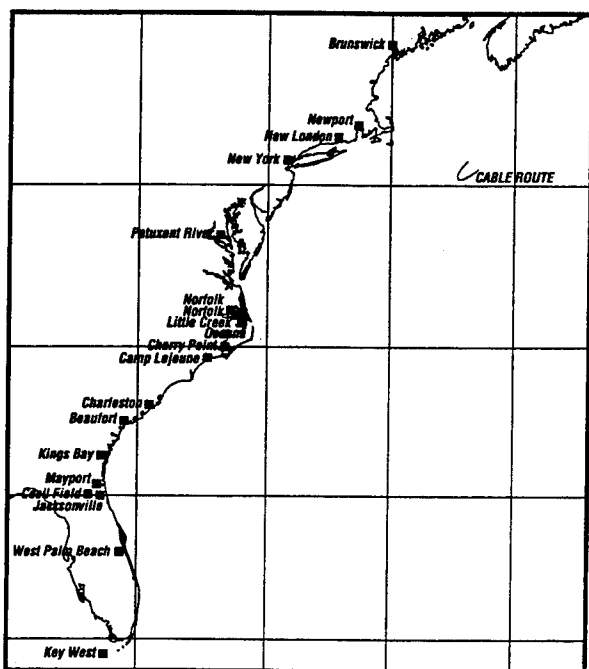


Figure 3. The Deployment Location for SWIMSS

Figure 4 is a plot of the GPS track of the cable lay. The end of the SWIMSS Electrical Mechanical Optical (EMO) cable was connected to an electronics enclosure aboard the GULF GUARDIAN. When the cable lay was complete, the GULF GUARDIAN dropped anchor and remained at moor for the remainder of the trip until recovery of the system.

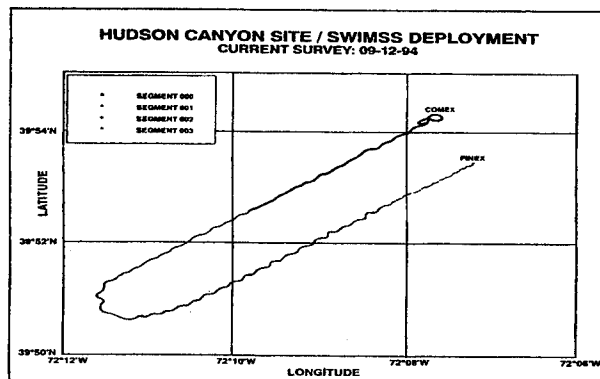


Figure 4. SWIMSS Cable Lay Track

Figure 5 shows the GULF GUARDIAN fully loaded out with the PTS and the SWIMSS system.

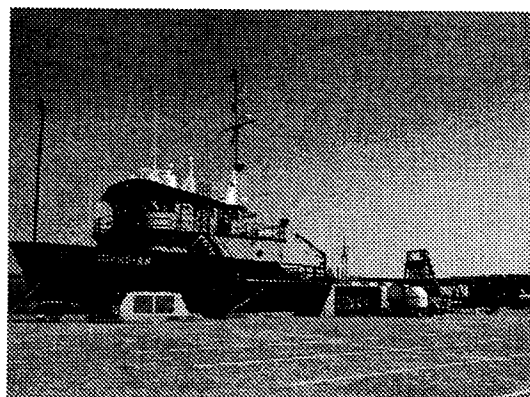


Figure 5. Installation Vessel GULF GUARDIAN

The acoustic tracking array was laid out in a configuration of 2 x 5 hydrophones. This layout provides a rectangular tracking area of approximately 1.5 x 4 nautical miles.

A second vessel was required to assist as the survey vessel. This vessel was the TORPEDO RETRIEVER 841. The RETRIEVER is referred to as the survey vessel.

TEST INSTRUMENTATION

The two vessels were outfitted with various equipment to conduct the single phone survey. The instrumentation setup is graphically depicted in Figure 6. Both the survey vessel and the receive vessel were equipped with 12-channel DGPS satellite receivers that provide 24-hour 3-D tracking. This receiver accepts differential corrections in an RTCM SC-104 format and interfaces to a control computer via a control and data RS-232 port.

The differential correction was supplied via the U.S. Coast Guard Mid-Frequency transmitter located at Montauk Point, Long Island, New York. This differential reference station is one of a Coast Guard Network that will cover the entire U.S. coast line by the year 1996. Both the receive and the survey vessels were equipped with DGPS capability.

The DGPS position of the survey vessel was transited to the receive vessel via a radio modem. The survey vessel was configured as the transmitter and the receiver vessel as the receiver. The DGPS position of the survey vessel was interfaced to a SUN Microsystems 670 workstation computer. The position from both the receive and the survey vessels was logged continuously.

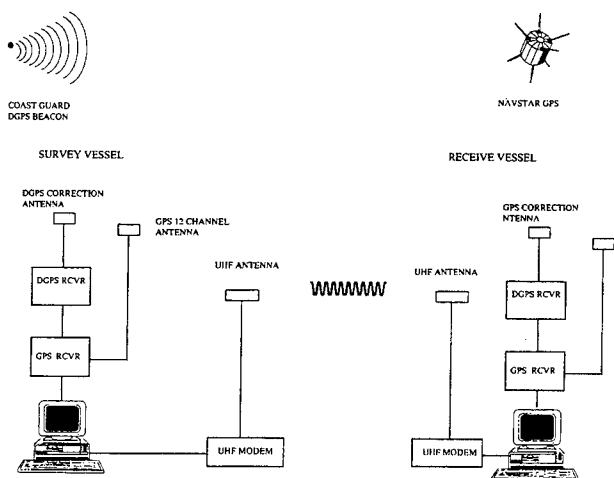


Figure 6. SWIMSS Vessel Instrumentation

X-SURVEY

The X-Survey algorithm was designed to locate the PTS shallow-water tracking sensors. Each sensor is located one at a time and independently. A synchronized pinger at a known depth on a survey vessel is used to generate acoustic data. All delays must be taken into account. Acoustic data on transit times are collected within the radius of direct path signals from the pinger to the sensor.

In addition to the acoustic data, time-correlated DGPS tracking data, including X, Y coordinates and the course of the survey vessel are also collected. If the DGPS antenna and pinger do not align, then the parallax is used to track the pinger. The DGPS course is used in this computation.

A simple run geometry is used by the survey vessel while collecting data. Two passes forming an x or + pattern are made for each sensor, as shown in Figure 7.

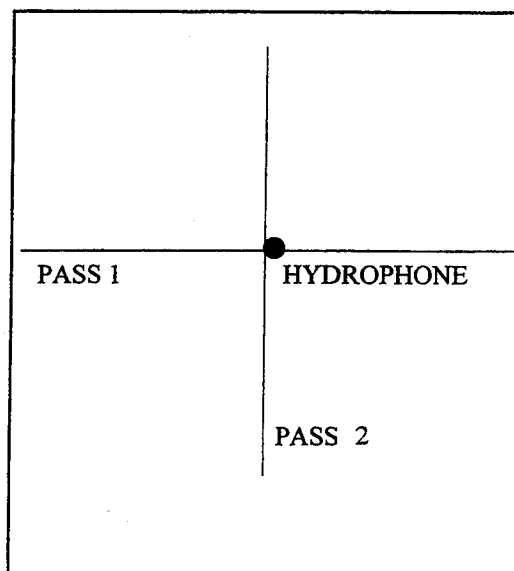


Figure 7. Simple Run Geometry

During each pass, an attempt is made to go over or close to the deployed position of each hydrophone. The straight lines in Figure 7 are the representation of the survey vessel track.

Figure 8 graphically depicts an actual DPGS plot of the survey vessel around two of the hydrophone sensors.

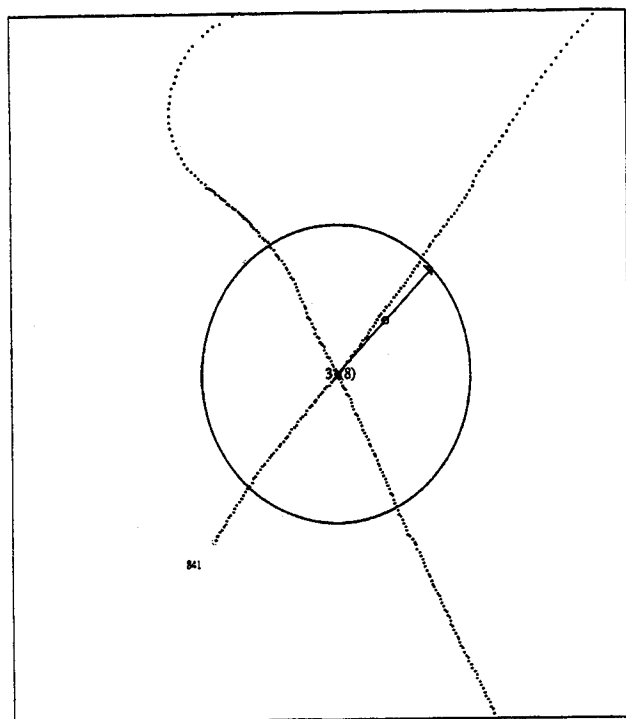


Figure 8a. DPGS X Survey Run

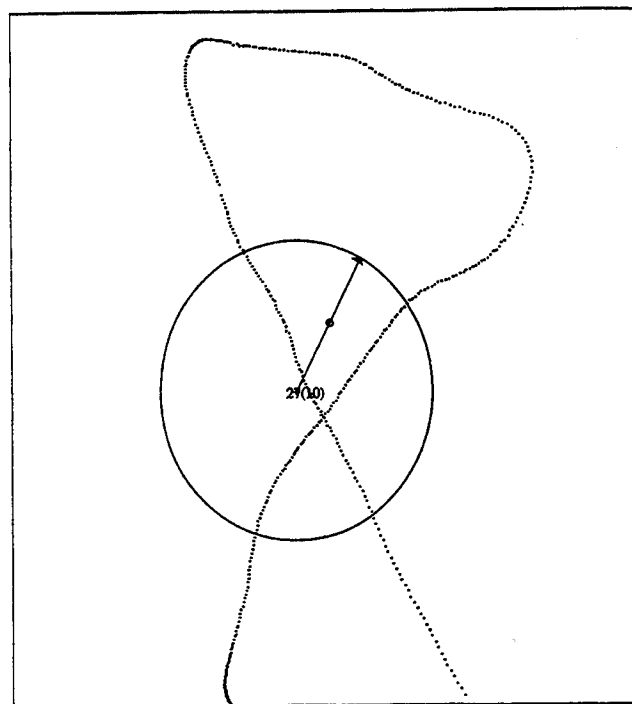


Figure 8b. DPGS X Survey Run

CONCLUSION

The use of DGPS for the navigation positioning of the survey vessel permitted the use of these mathematics to solve the problem of locating underwater acoustic tracking sensors. Figure 9 displays the planned, deployed, and surveyed location for this test. This technology saved much time and equipment needed to support shore stations that historical surveys would have required.

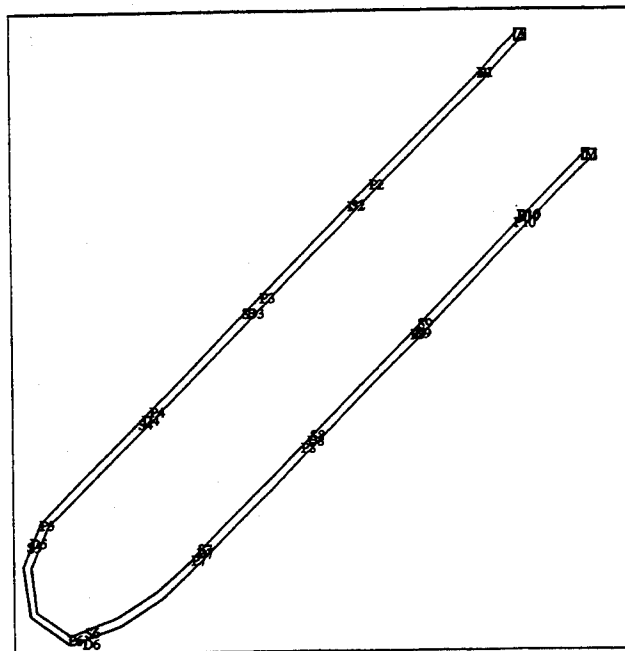


Figure 9. Salmon Hydrophone Locations

ACKNOWLEDGMENTS

The author would like to acknowledge Richard C. Pacheco of the Measurements and Analysis Branch of Naval Undersea Warfare Center Division, Newport for his development and execution of the algorithm to accomplish the positioning of the signal sensor node for the PTS.

REFERENCES

1. W. Vanderkulk, "Remarks on a Hydrophone Location Method," IBM No. 60-914-21, Navy Systems Engineering, 9 December 1960.

Autonomous Underwater Vehicle Navigation

Stewart Cannon, *Pelagos Corporation*

Jeff Smith, *Applied Remote Technology*

BIOGRAPHY

Mr. Cannon graduated from the University of New Brunswick (B.Sc. Survey Engineering) in 1980. He has over 14 years experience designing and developing integrated navigation systems for commercial and military applications. Mr. Cannon has been involved in offshore operations worldwide his entire career, and is the lead software architect for Pelagos Corporation's object-oriented integrated navigation and data management system. He has built up Pelagos' offshore surveying group which specializes in systems development, acoustic positioning and field operations.

Mr. Smith graduated from the University of Washington (M. S., Electrical Engineering) in 1984. At Applied Remote Technology, Mr. Smith was a principal Electrical Engineer working on the MK-30 Target Undersea Vehicle program. Mr. Smith has over 14 years experience in the areas of Electro-optic Laser systems and undersea vehicle development. His experience includes system requirements analysis, software design and development, and hardware/software system integration. Mr. Smith also holds patents in the field of Inertial Reference Systems. His recent design efforts at ART have included Fiber Optic Telemetry systems and the electrical design of ART's latest LLSS-4096 Laser Line Scan Sensor electronics.

ABSTRACT

The development of autonomous underwater vehicles (AUVs) has finally reached the point that their use on commercial projects is now being seriously considered. Much of the research and development efforts to date have been funded primarily by military organizations to meet defense objectives. In this paper the authors examine the navigation problems and their potential

solutions that will permit the reliable use of AUVs on commercial survey and inspection operations. These techniques include the global positioning system, inertial navigation systems, Doppler speed logs, bathymetry-aided navigation, acoustic measurements from chase ships, acoustic measurements from transponders (breadcrumb technique), and multiple cooperative AUVs.

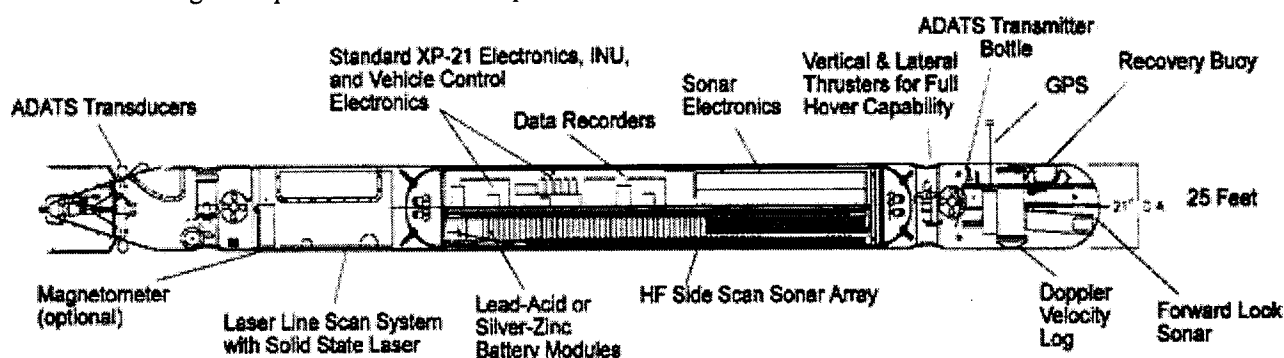
The current level of development for each of the approaches will be discussed and its future potential assessed. Finally, the authors' development efforts and current level of implementation relating to the XP-21 AUV will be presented.

INTRODUCTION

Autonomous Underwater Vehicles (AUV's) represent the next logical step in offshore operational capability and hold the promise of significantly reducing costs. Before this becomes a reality, however, many obstacles must be overcome with navigation being one of the most significant. An object-oriented system architecture is proposed as being highly suited to the integrated navigation of autonomous vehicles. This paper presents insights gained on AUV navigation system design obtained while fielding an AUV system equipped with a state-of-the-art suite of sensors.

Autonomous Underwater Vehicles

AUV's are a subset of Unmanned Undersea Vehicle's (UUV's). The type and construction of these vehicles is dependent on the mission requirements. A vehicle may have only a forward propulsion system (i.e.: single propeller) or have hovering and station-keeping capability in six degrees of freedom provided by multiple thrusters. The size of a system depends on the application or mission of the UUV.



A UUV is always tethered to a support ship and uses this tether for both power and control. Therefore, very high power levels are available and a high communication bandwidth is possible, particularly if a fiber-optic telemetry system is used. The key feature of a UUV is extended work time on site and it is most capable for large projects at specific locations. On the downside, a host platform with an expensive crew and facilities is required, maneuvering range is limited, tether handling systems are expensive, operations are limited by sea state, and tether drag limits vehicle capabilities.

An AUV may communicate with the support ship with a standard cable, a fiber-optic cable, an acoustic telemetry link or via an RF link. The distinguishing feature of an AUV is that it is self-powered. Therefore, longer ranges from the support ship are possible since there is no large tether to manage. This also minimizes tether effects on vehicle performance. In some applications fiber-optic payout packs are used to extend high bandwidth communication range from the support ship. A minimal crew is required, and potentially, operations may be conducted at a much lower cost than with tether-powered systems. On the downside, limited battery capacity may reduce vehicle range significantly. Lead-acid batteries provide a low tech, low cost solution, but only give a 4 to 8 hour vehicle life. Silver-zinc batteries provide a medium tech, high cost solution and give 15 to 40 hours of operational life. Aluminum-oxygen fuel cells provide a medium tech, high cost solution and give 80 plus hours of operational life.

A typical mission for an AUV would be medium- to long range (1 to 20 km) and cover a medium- to large survey area. A host platform would be required for launch and recovery operations, to provide mission planning updates, and for sensor information processing. The AUV's navigation capability may include an inertial navigation unit with doppler velocity and magnetic heading aids. Acoustic beacons may also be available for positioning. An AUV would typically be equipped with a side scan sonar, a laser-line-scan imaging system, a video imaging system, a laser ranging system and magnetic sensors.

The closest relatives of the AUV from a navigation perspective are the cruise missile and the torpedo, and even this analogy breaks down quickly. The requirements to navigate autonomously over long distances are similar; however, a weapons goal is to intercept its target while moving, whereas an AUV may have to hover, sample data at a specific point and move on to the next target.

Navigation System Requirements For AUVs

The exact context experienced by the navigation system on an AUV is difficult to define. Traditionally, navigation systems have been called upon to determine the position and velocity of a vehicle and to provide guidance information to reach a desired goal. In more recent times, interaction with control systems has become commonplace. The ultimate AUV navigation, guidance and control (NGC) system would be capable of computing position, velocity, acceleration and attitude of a vehicle from all available sensors, interacting in an optimal manner with the vehicle's control system and interpreting sensor data to generate guidance information pertinent to the vehicle's safety and the mission's objectives. Rather than try to design a system capable of performing all of these objectives immediately, a staged approach based on an extensible architecture is proposed. This meshes well with the current level of development of AUV's and allows the architecture to be applied to non-AUV applications in order to reduce costs.

The varying degrees of autonomous operation currently implemented in AUV's allow NGC problems to be solved in stages. Having a high-bandwidth tether allows all of the sensor data to be uploaded to computers on a support ship and allows control data to be downloaded to the vehicle's control system. Operators on the support ship may then perform many of the more advanced functions which the NGC system would have to perform for true autonomous operation. For example, the designer of the navigation system in a tethered AUV may first concentrate on decoding and organizing the sensor data so that during operations the system can be manually configured to suit different operational modes. The next stage would be to automate the configuration to match the modes. Having an operator manipulate the control system of the AUV removes the requirement for direct subsystem coupling in the early design stages. As each subsystem becomes more robust, it can be coupled and then tested, with an operator ready to take over control in the event of any irregularities.

The guidance functionality assigned to the navigation system provides the most challenging portion of the system design. The fundamental requirements are to travel to waypoints and to follow pre-programmed survey lines, and these are easily solved. If sensors which can observe the surrounding physical environment are installed on the vehicle, their output may be interpreted to produce guidance information in order to avoid local obstacles and to identify features important to the mission's objectives. Having an observer available to interpret the sensor output allows automated guidance

decisions to be removed from the system's functionality in early design stages.

Implementation of the of the extensible architecture requires the functionality of the system to be examined in general terms. The system must be capable of decoding data from many sensors, and organizing these data into logical structures. These structures must be optimally combined to compute the vehicle's position, velocity and attitude. The current operational mode of the vehicle must be determined and any guidance calculations, such as the range and bearing to a waypoint, must be made. The results must be presented to the control system for thruster and control surface activation.

The data provided by the sensors may be classified into the following functional groups: position data; velocity/acceleration data; attitude data; and, remote sensing data. Each of these data groups has its own characteristics. Position data provide enough information to establish the coordinates of a vehicle. GPS is an example of a positioning system. Velocity/acceleration data measure the dynamics of the vehicle. A doppler speed log is an example of a velocity/acceleration system. Velocity and acceleration data are particularly useful as input to control systems. Attitude data provide information on the orientation of a vehicle in three dimensions. Magnetic heading is an example of attitude data. Attitude data are also useful to the vehicle's control system. Remote sensing data provide the vehicle with information on the outside world. Side scan sonar is an example of remote sensing data. Although remotely sensed data are not considered position information, one must know the position and attitude of the vehicle in order to interpret the data.

The interactions among these sensors is complex and dynamic. In order for one system to contribute to the knowledge of the vehicle's state or its surroundings, data from other sensors may have to be considered. The sensors produce large volumes of data which must be processed and recorded. Fortunately, advances in computer hardware and software are making this problem tractable. Object-oriented software design has been successfully applied to AUV navigation and offers the flexibility to provide a system which is capable of combining many types of data in many modes.

Object-Oriented Navigation System Design

Object-oriented programming is a recently developed programming paradigm which allows systems to be configured in a much more dynamic fashion than was formerly possible. Pelagos' WinFrog system was

designed using object-oriented technology to allow maximum configuration flexibility. The primary challenge for the AUV navigation is to allow switching among the sources of position data from various sensors and to feed different data to various devices during different operational modes. In addition, using the C++ programming language and object-oriented design techniques permits implementation details of the objects used in the software to be hidden from each other and thus to prevent undesirable interactions. This technique lends itself to team programming and allows individual programmers to concentrate on the object they are assigned to develop. C++ also provides an inheritance mechanism which may be used during the design stage to define fundamental *Base Classes* which may be then used to derive *Classes* which implement the details of the application. *Base Classes* act as templates for *Derived Classes*, thus forcing consistency of functionality during development. A *Base Class* is used as a template for functions which control the general operation of all the *Derived Classes*. The *Derived Classes* are given a group of data variables appropriate to the purpose of the *Class*, and the functions from the *Base Class* are overridden to act on these variables. In addition to holding data, some of these classes are used to hold configuration information.

Modern navigation systems must be capable of dealing with multiple vehicle situations efficiently. Consequently, a *Vehicle Class* has been developed to encapsulate the functionality of all of the vehicles with which the system must deal. This class provides waypoint and line tracking, graphical presentation, and position calculations. The position is part of a *State Class* which also contains the heading, elevation, attitude and the dynamics of the vehicle. The *State Class* can propagate itself and its covariance matrix through time, and may be updated by measurements as they become available.

These measurements are represented by derivations of the *Data Records Base Class*. *Data Records* have an *updateState* function which is used to make a measurement contribution to a *Vehicle's State*; it also has a *configuration* function which is used to define how the contribution is made. For example, a *Position* is an example of a *Data Record*. A *Position* contains latitude, longitude, accuracy and offset data members. The *updateState* function uses the heading contained in the *State Class* to move the latitude and longitude by the offset amount where they can be combined with the *State Class* position. The *configuration* function produces a dialog box in order to edit the offsets and accuracy.

The *Data Records Base Class* has been used to derive the following set of Classes used for the AUV's navigation system:

Position Class: This Class encapsulates the concept of a position measurement. It has configurable x, y and z offsets and accuracy. The dialog box displayed when the configuration function is selected is shown below:

Heading Class: This Class encapsulates the concept of a heading measurement. It has a configurable offset and accuracy.

Velocity Class: This class encapsulates the concept of dual-axis velocity measurements relative to the water or to the bottom. These velocities may be vehicle- or north referenced. This class has configurable offsets and accuracy.

Attitude Class: This class encapsulates the concept of pitch, roll and yaw measurements which have an accuracy associated with them. It has configurable x, y and z offsets.

Elevation Class: This Class encapsulates the concept of an elevation measurement. The *Elevation Class* has a configurable z offset and accuracy.

USBL Hydrophone Class: This class encapsulates the concept of a ship-mounted hydrophone. It gathers the position and orientation of the vehicle with which it is associated and no measurements are produced. It has configurable x, y and z offsets.

USBL Beacon Class: This class encapsulates the concept of relative range, bearing, and elevation angle

measurements made from a ship-mounted hydrophone to a beacon. The measurements may be converted to an absolute position using the position and orientation of a *USBL Hydrophone Class*. The *Beacon Class* has configurable x, y and z offsets and accuracy.

Each *Vehicle* contains an array of *Data Records* which are used to update its *State*. A *Communication Device Base Class* is used to encapsulate the functionality of the devices connected to the computer. Derived Classes contain an array of *Data Records* corresponding to the types of measurements supplied by the device being modeled. A *read* function parses input into the *Data Records* array. An *update* function is provided to copy *Data Records* from the *Communication Device's Data Records* array to the *Vehicle's Data Records* array where they can be used to update its *State*. A *configure* function is provided to remotely control the settings of the device. In addition to providing actual *Data Records*, the *Communication Device Classes* provide a list of names of the *Data Records* they are capable of providing. *Vehicles* have a function to display the names and let an operator select which *Data Records* are to be used. This mechanism provides an extremely dynamic calculation environment.

The *Main Program* is used to hold all of the *Vehicles* and *Communication Devices*, provide the menu and toolbar functionality, provide a parent window for displaying the child windows and drive real-time operation of the system. This is where data from *Communication Devices* are gathered and passed to *Vehicles*, as required.

XP-21 AUV SUMMER 1995 SEA TRIALS

In July 1995, ART's XP-21 AUV was demonstrated in Scotland. The XP-21 is capable of maneuvering in six degrees of freedom and was equipped with a fiber-optic tether for the trials. During the demonstration, operators were used to run the navigation system, vehicle control system, and to interpret the data from the sensors. The control system was interfaced directly to a compass, attitude sensor, pressure sensor and a doppler speed log. The mission objectives were to demonstrate an AUV's applicability for mine-hunting and pipeline inspection. For the mine-hunting phase, several mine shaped-objects were placed on the bottom for inspection by the AUV. For the pipeline inspection phase, an actual pipeline in the area was used.

Data fusion was accomplished using Pelagos' WinFrog Integrated Navigation and Data Management system. A host computer located on the support vessel was interfaced to the INU with a serial interface multiplexed

over the fiber-optic cable, and to the Vehicle Operating System (VOS), which was, in turn, interfaced to the rest of the sensors on the vehicle. The INU and VOS were both modeled as *Communication Devices Class* derivations. The *INU Communication Device Class* was given a *configure* function to allow the operator to remotely control operation of the set. The dialog box produced when the configure function is executed is shown below:

This dialog box allows various initialization data to be entered and various modes of operation to be set.

The following sensors were installed on the vehicle and interfaced to the host computer on the support ship:

Sensor Name: RDI Doppler Current Profiler
System Type: Doppler Velocity Sensor
Input Required: None
Data Produced: Vehicle relative *Velocity Data Records*. This system is interfaced via the *VOS Communication Device Class*.

Sensor Name: Litton LN-100
System Type: Inertial Navigation Unit (INU)
Input Required: *Position, Velocity, Elevation and Heading Data Records* are required to initialize the INU on a moving platform. *Velocity, Heading and Elevation Data Records* are used to control errors during operation. *Position Data Records* may be sent to the INU if they are available.

Data Produced: *Position, Velocity, Heading, Attitude, and Elevation Data Records*. This system is interfaced via the *INU Communication Device Class*.

Sensor Name: KVH Flux Gate
System Type: Magnetic Heading Sensor
Input Required: None
Data Produced: *Heading Data Records*. This system is interfaced via the *VOS Communication Device Class*.

Sensor Name: Trackpoint Beacon
System Type: Ultra Short Baseline
Input Required: *USBL Hydrophone Data Records*
Data Produced: *USBL Beacon Data Records*. This system is interfaced via the *Trackpoint Communication Device Class*.

Sensor Name: Paroscientific Pressure Sensor
System Type: Pressure-Derived Depth
Input Required: None
Data Produced: *Elevation Data Records*. This system is interfaced via the *VOS Communication Device Class*.

In addition to the sensors on the vehicle, several sensors were mounted on the support ship and interfaced to the host computer. Each of these sensors was modeled as a *Communication Devices Class* derivation.

The following sensors were installed on the support ship and interfaced to the host computer:

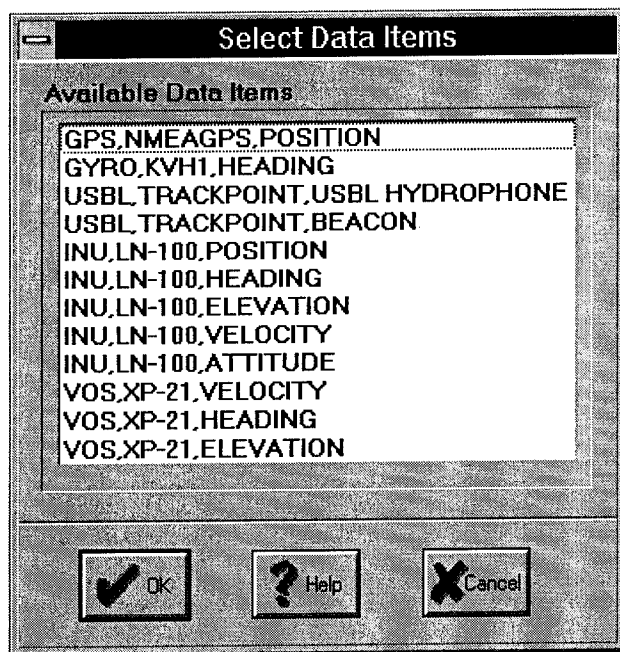
Sensor Name: Trimble DGPS
System Type: Differential GPS
Input Required: RTCM Data
Data Produced: *Position, Velocity, and Elevation Data Records*. This system is interfaced via the *NMEA GPS Communication Device Class*.

Sensor Name: KVH Flux Gate
System Type: Magnetic Heading
Input Required: None
Data Produced: *Heading Data Records*. This system is interfaced via the *KVH Communication Device Class*.

Sensor Name: Trackpoint Hydrophone
System Type: Ultra Short Baseline
Input Required: *Position and Heading Data Records*
Data Produced: None. This system is interfaced via the *Trackpoint Communication Device Class*.

Once all of the *Communication Devices* were interfaced to the host computer, the operator could associate *Data Records* with a vehicle using a dialog box which provides a list of all the *Data Records* supplied by all of the

Communication Devices. An example of the dialog box is shown below:



For the sea trials the support ship had the following *Data Records* associated with it:

| System | Name | Data Record |
|--------|------------|-----------------|
| GPS | NmeaGps | Position |
| Gyro | KVH1 | Heading |
| USBL | Trackpoint | USBL Hydrophone |

For the sea trials the vehicle had the following *Data Records* associated with it:

| System | Name | Data Record |
|--------|------------|-------------|
| USBL | Trackpoint | Beacon |
| INU | LN-100 | Position |
| INU | LN-100 | Heading |
| INU | LN-100 | Elevation |
| INU | LN-100 | Velocity |
| INU | LN-100 | Attitude |
| VOS | ART | Velocity |
| VOS | ART | Heading |
| VOS | ART | Elevation |
| VOS | ART | Attitude |

Once the *Data Records* had been associated with the support ship and the vehicle, it was possible to configure each *Data Record* independently. The operator could then dynamically configure the data flow and state calculation as the vehicle changed modes.

Various operational modes were identified and had to be performed during the demonstration. The operator would set up the navigation system by designating the appropriate *Data Records* as a Primary system to be used to update the state and setting the rest to Secondary so they would only be monitored. The *Communication Devices Classes* were then used to set up the sensors to accept any necessary data. The following outlines the operational modes along with their system requirements:

Operational Mode: Transiting to site

Guidance Requirements: The support ship uses its *Data Records* to compute its *State*. The range and bearing to the launch point are computed, and pre-programmed charts are used to avoid obstacles.

Navigation System Requirements: The INU on the vehicle requires *Position*, *Velocity*, *Heading* and *Altitude Data Records* to initialize. To accomplish this *Position* and *Velocity Data Records* from the DGPS system and the *Heading Data Record* from the compass on the ship were associated with the vehicle and set to Primary. The USBL's *Beacon Data Record* was set to Secondary. The INU's *Position*, *Heading*, *Elevation*, *Velocity* and *Attitude Data Records* were set to be secondary. The VOS's *Velocity*, *Heading*, and *Elevation Data Records* were also set to Secondary. The INU *Communication Devices Class's* configuration dialog box was used to set the system to Sea Align Mode with PVT (Position Velocity and Time) messages on. The position and velocity of the *State* were then fed into the INU to let the system initialize at sea.

Operational Mode: Vehicle Deployment

Guidance Requirements: Autonomous navigation begins as the vehicle is launched from the support ship and transits to the sea bottom. The navigation system's graphics displays are used to track the support ship and vehicle's locations and to avoid obstacles using pre-programmed charts.

Navigation Requirements: The INU *Communication Devices Class's* configuration dialog box was used to set the system to Sea Navigation Mode and turn PVT messages off. The INU's *Position*, and *Velocity Data Records* and the VOS's *Elevation*, *Heading* and *Attitude Data Records* were set to be Primary. Once the vehicle was underwater, the graphic output for the USBL's *Beacon Data Record* was turned on to allow visual position comparison.

Operational Mode: Finding initial point

Guidance Requirements: The vehicle travels to the initial point using the navigation data to generate range and bearing and the sensor data to avoid local obstacles and stay close to the bottom. The navigation system's

graphics displays are used to track the support ship and vehicle's locations and to avoid obstacles using pre-programmed charts.

Navigation Requirements: Once the Doppler Sonar acquired bottom lock, it could be used to contribute to the vehicle's *State*. The INU's *Velocity Data Record* was set to Secondary and the VOS's *Velocity Data Record* was set to Primary. The INU *Communication Devices Class's* configuration dialog box was used to turn on HVEL messages which fed velocity, heading and elevation from the vehicle's *State* to the INU.

Operational Mode: Surveying

Guidance Requirements: The vehicle uses the navigation data to follow the lines and the sensor data to avoid local obstacles and stay close to the bottom. As targets of interest are identified, they may be logged by the navigation system and investigated more closely.

Navigation Requirements: The requirements for the navigation system are essentially the same as when finding the initial point. Velocity, elevation and heading are derived from the sensors interfaced via the VOS and are fed to the INU. Position is derived from the INU and the USBL system is used to graphically keep track of the drift in the INU. Occasionally, the INU was updated by sending it the position of the *USBL Beacon Data Record* via the INU *Communication Devices Class's* configuration dialog box.

Operational Mode: Recovering vehicle

Guidance Requirements: The vehicle uses the navigation data to travel directly to the surface while the support ship positions itself for recovery. The navigation system's graphics displays are used to track the support ship and vehicle's locations and to avoid obstacles using pre-programmed charts. The support ship locates the vehicle, attaches a tether and recovers it.

Navigation Requirements: The Doppler Sonar loses bottom lock and can't be used to contribute to the vehicle's *State*. The VOS's *Velocity Data Record* was set to Secondary and the INU's *Velocity Data Record* was set to Primary. The INU *Communication Devices Class's* configuration dialog box was used to turn off HVEL messages. The USBL's *Beacon Data Record* was used for visual position comparison.

FUTURE DEVELOPMENTS WITH XP-21 SENSOR SUITE

The navigation system implemented for the 1995 sea trials was used to support operation of the vehicle in a tethered mode with an operator in the loop. The first set of improvements should be to automate the configuration changes required to implement the operational modes

identified in the last section. This would allow the system to be initialized and operate without the need for an operator. The next step would be to improve the absolute positioning capabilities of the system. The current system requires a support ship with a USBL system to monitor the drift of the INU, a requirement which would not be practical for autonomous operations. The following operational modes have differing requirements for absolute positioning:

Operational Mode: Point sampling

Guidance Requirements: The vehicle must identify the point of interest and then hold a stable position relative to the point to be sampled.

Navigation Requirements: The control system requires high-frequency data to hold a stable position. This is normally accomplished by using the doppler speed log. The problem with this is that there are no bounds on the position error, and the hover point may drift with time. The navigation system must control this position error relative to the point of interest with a high degree of precision. Identifying the point of interest is considered outside the context of the navigation system; however, the image may be required to assist with station-keeping.

Operational Mode: Autonomous linear surveying

Guidance Requirements: The vehicle must traverse a pre-defined route while taking data samples.

Navigation Requirements: The absolute position of the vehicle must be determined to a level necessary to stay on the track and to allow the data being collected to be interpreted properly.

Operational Mode: Docking

Guidance Requirements: Vehicle must identify the docking point and then close slowly in on it.

Navigation Requirements: The position of the vehicle relative to the docking point must be determined with a high degree of accuracy.

These requirements may be met by using imaging sensors which are not thought of as traditional navigation system inputs. The data produced by an imaging sensor may be combined with navigation data to produce digital representations of the area over which the vehicle travels. These representations may then be correlated with previously captured representations in memory to provide absolute positioning capabilities to the system. The most concrete example of this type of navigation is terrain contour matching. From a software perspective the imaging data must then be fused with navigation data and passed on to the specialized processes for correlation with stored data. When correlations are made, the results are passed back to the navigation system as *Position Data*

Records which allows them to be logged and presented to the vehicle's control system. The specialized processes are considered to be outside the context of the navigation system and may even reside on other computers and be accessible over a network.

The following imaging sensors were mounted on the vehicle, but were not used in the navigation solution:

Sensor: EG&G DF-1000

System Type: Sidescan sonar

Input Required: *Position, Elevation and Attitude Data Records*

Data Produced: Geo-referenced sonar backscatter scans are produced by combining sonar scans with position data. These scans may be combined to produce a mosaic image of the area over which the vehicle travels. Features identified on this mosaic may be compared to features stored from a previous survey and correlations may be converted into a position with an accuracy estimate. These may contribute to the vehicle's *State* by using the *Position Data Record* model. The vehicle must be moving to produce a mosaic, so these data are not useful during hovering maneuvers.

Sensor: ART LLSS-4096

System Type: Laser imaging system

Input Required: *Position, Elevation and Attitude Data Records*

Data Produced: Geo-referenced laser scans are produced by combining laser scans with position data. These scans may be combined to produce a mosaic image of the area over which the vehicle travels. Features identified on this mosaic may be compared to features stored from a previous survey and correlations may be converted into a position with an accuracy estimate. These may contribute to the vehicle's *State* by using the *Position Data Record* model. The vehicle must be moving to produce a mosaic, so these data are not useful during hovering maneuvers.

Sensor: Video Camera

System Type: Video imaging system

Input Required: *Position, Elevation and Attitude Data Records*

Data Produced: Stabilized video images are produced by combining video images with position and attitude data. Rather than use the images to produce a mosaic, these may be used most effectively to provide a precise position relative to an object in view, as is required during point sampling mode. Once a feature has been identified on one frame, the vehicle's position is noted and any deviations of the image from its original location are converted to distances and combined with the initial position to derive a position with an accuracy estimate.

These may contribute to the vehicle's *State* by using the *Position Data Record* model. For precise positioning requirements, image matching may be used to remove low-frequency drift from the Doppler velocity sensor.

Sensor: Reson Sea-Bat

System Type: Multibeam look-ahead sonar

Input Required: *Position, Elevation and Attitude Data Records*

Data Produced: Geo-referenced bathymetry swaths are produced by combining this system's scans with position data. These scans may be combined to produce a bathymetric map of the area over which the vehicle travels. Profiles derived from this map may be compared with a map stored from a previous survey, and correlations may be converted into a position with an accuracy estimate. These may contribute to the vehicle's *State* by using the *Position Data Record* model. The vehicle must be moving to produce a profile, so these data are not useful during hovering maneuvers. Terrain contour matching is the most viable of the image-matching techniques due to its proven performance on missile systems and the large database of bathymetry currently available.

ADDITIONAL POSITIONING SENSORS

In addition to the sensors considered so far, other sensors may be used to derive the position of an AUV. Chief among these is Long Baseline Acoustic Navigation (LBL). This technique involves placing and precisely coordinating transponders on the sea floor and measuring ranges to them from a transceiver on the AUV. Sets of these ranges may then be used to compute the position of the transceiver. LBL systems have been used for AUV positioning in local areas and is probably the most practical method for computing the absolute position of a non-tethered vehicle.

The primary restriction on using LBL techniques for wider area navigation is the cost and limited range of the transponders. By using the relative navigation capabilities provided by the dead-reckoning sensors, LBL techniques may be extended for use in linear surveys. Transponders may be placed along the route and spaced such that only one can be received by the AUV at any time. As the AUV passes a given transponder, the change in geometry provides an effective update to the vehicle's position. This is sometimes referred to as the "bread-crumbs" technique.

One of the major limitations of this technique is the requirement for deploying and coordinating the transponders along the route. After the AUV has been

deployed at the start of the survey area, the support ship must deploy and coordinate the transponders along the entire route and then return to the AUV to download the coordinates of the transponders. Using a support ship to perform this function is expensive and time-consuming

COMPLEMENTARY AUTONOMOUS VEHICLES

The final step in AUV navigation considered in this paper is the use of complementary vehicles. Some of the navigation problems discussed in previous sections may be overcome by using more than one vehicle during an operation. In addition to solving navigation problems, using several vehicles allows simultaneous spatial sampling, which is generally not possible by any other method. The following sensors may be used in multiple vehicle operations:

Sensor: Data telemetry and local USBL

System Type: Acoustic digital telemetry

Input Required : None

Data Produced: This type of system may form part of an integrated communication and positioning system. Several transducers may be placed on an AUV to measure the direction of an incoming communication signal by correlating a coded start of message sequence. If these directions are to be used for positioning, the location of the transmitter must be known. The communication link may be used to download the location of the transmitter. The position of the vehicle cannot be determined with only a single direction measurement, so the relative navigation capabilities provided by the dead-reckoning sensors must be used to gather data as the geometry between the two vehicles changes.

Sensor: AUV mounted GPS

System Type: Global Positioning System

Input Required: none

Data Produced: *Position and Velocity Data Records.*

Combining the data telemetry, local USBL and AUV mounted GPS systems provides a potential solution to absolute positioning over long areas. One vehicle can travel close to the surface to get GPS fixes and use the data telemetry system to transmit its position to another vehicle on the bottom. The local USBL capabilities of the vehicle on the bottom may then be used to determine the direction of the transmission for use in its state calculation. The vehicle near the surface would maneuver to positions suggested by the vehicle near the bottom to provide geometrical strength to its position, as required.

ACKNOWLEDGMENTS

The authors would like to thank the following people for their support and assistance over the course of the project.

Ken Collins, Bill Aucoin and Mark Iwanoski of Applied Remote Technology; and Tony Ellis, Dave Caswell and Donna Mount of Pelagos Corp.

REFERENCES

Hutchinson, B.L. and Skov, B.E., "A System Approach to Navigating and Piloting Small UUV's", Proceedings of the Symposium on Autonomous Underwater Vehicle Technology, June 1990.

Stambaugh, J.S. and Thibault, R.B. "Navigation Requirements for Autonomous Underwater Vehicles"

Lin, C.F., "Modern Navigation, Guidance and Control Processing", Prentice-Hall, Inc., Englewood Cliffs, NJ, 1991.

G. L. Mealy and Tang, W. "Application of Multiple Model Estimation to a Recursive Terrain Height Correlation System" (IEEE Transactions on Automatic Control, March 1983), Kalman Filtering: Theory and Application, IEEE Press, New York, 1985.

I. Bar Shalom, Yaakov, ed., "Multitarget-Multisensor Tracking: Applications and Advances Volume II", Artech House, MA 1992.

Stewart, W. Kenneth, Jr., "Multisensor Modeling Underwater with Uncertain Information", Technical Report 1143, MIT Artificial Intelligence Laboratory, 1988.

Performance Analysis of the Interrupted Data Acquisition Receiver Obtained From Operational Missions

Gerald Whitworth
Navstar Systems Ltd.

David Meldrum
Dunstaffnage Marine Laboratory

BIOGRAPHIES

Gerald Whitworth BSc is Software Group Leader at Navstar Systems Ltd. in Northampton, England.

He joined Navstar Systems Ltd. (formerly known as Polytechnic Electronics Plc) in 1983 as part of the design team for the company's first GPS product, the XR1. He has been involved in the design and development of all subsequent GPS and Loran receivers since then including the latest 12 channel receiver product, the XR5, and specialised GPS timing instruments.

David Meldrum BSc leads the Marine Technology Group at the Dunstaffnage Marine Laboratory in Oban, Scotland.

He has been involved in instrumentation development for 20 years, firstly as a research associate at the Scott Polar Research Institute, University of Cambridge, working on radar studies of the Antarctic ice-cap, and latterly as a marine physicist at Dunstaffnage, with a specialised interest in oceanographic applications for satellites.

ABSTRACT

Navstar Systems Ltd is closely involved with Dunstaffnage Marine Laboratory (DML) to design and develop a GPS navigation system for an Autonomous Underwater Vehicle (AUV), called Autosub, currently under development. The GPS receiver is required to generate a position solution while the AUV is surfaced, under a range of sea states that interrupt the GPS signal due to vessel roll and periodic wave washover of the GPS antenna.

This paper is the third in a series detailing the development process. The first paper described the physical requirements of the receiver, including the antenna system, and the simulation of wave washover effects, and the modelling of ephemeris collection algorithms. The second paper described in detail the various techniques that were developed in the receivers firmware to overcome the problems of frequent intermittent loss of the GPS signal, including initial acquisition and ephemeris collection by reconstituting the small contiguous samples of data collected.

INTRODUCTION

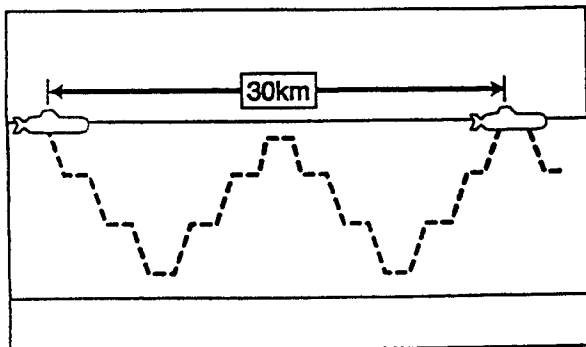
The UK Natural Environment Research Council (NERC) took the initiative to establish the Autosub Community Research Project in the late 1980's, following international concerns about the Earth's climatic changes. The oceans are a major contributing factor to global climate regulation, although the actual mechanisms are currently inadequately understood. To further understand the process, and ultimately generate a predictive model, represents a formidable challenge. Much of the raw data about the oceans is today gathered from a combination of earth observation satellites and surface vessels. Satellites are now capable of remotely sampling the ocean surface whilst ships provide the deep ocean measurements. Both of these methods remain limited in their capabilities and are obviously costly to set-up, operate and maintain. This substantial constraint led to the proposal of using autonomous underwater vehicles (AUV's) to perform the routine data-gathering tasks. Such vehicles would work well in the open oceans and also in the scientifically important but generally inaccessible polar regions.

HISTORY

Although several maritime countries are currently developing such underwater vehicles, none at present exist that have all the required capacity of payload, depth and range and the ability to perform extended submerged missions. The Autosub Community Research Project was established with the aim of using current advances in technologies to establish an AUV capability for routine, cost effective data collection from the deep oceans.

The AUV is being designed to undertake extended data gathering missions. Part of the mission requirement is for the vessel to surface periodically to upload and download data from its control base. During the brief period on the surface the AUV will use GPS to determine its position and to correct any errors that have accumulated during the submerged phase of the mission.

AUV Mission Profile

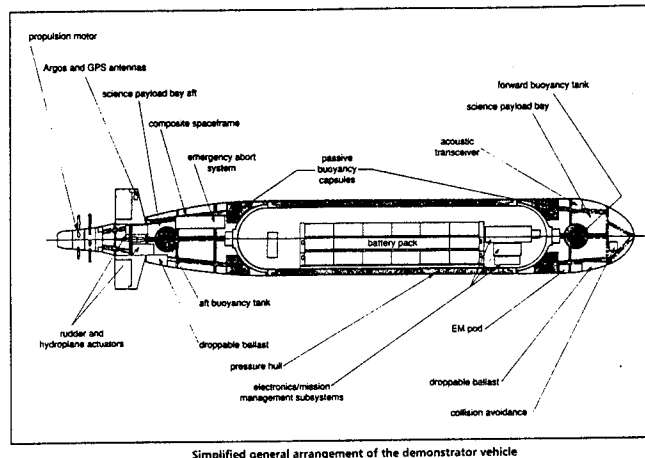


Dunstaffnage Marine Laboratory, based at Oban, Scotland, are managing the satellite communications features of the project. Navstar Systems Ltd are involved as the prime GPS contractor supplying the GPS equipment for the harsh environment anticipated for the AUV.

THE DEMONSTRATOR VEHICLE

A $\frac{3}{4}$ size scale model of the AUV demonstrator vehicle has already been prepared for hydrographic tests at the Defence Research Agency. The full size demonstrator will be 7 meters in length with a mass of 2.8 tonnes. Of particular interest is the location of the GPS antenna. Early design stages envisaged that the vehicle would surface in a nose-up attitude, with a nose mounted antenna. It now seems certain that the demonstrator vehicle at least will surface horizontally, and use a tail-fin mounted antenna.

Both scenarios have been examined with regard to their GPS performance.



SOFTWARE CONSIDERATIONS

A conventional GPS receiver utilises the continuous data stream of the GPS satellites to perform synchronisation and demodulation of the satellite data. The GPS signal structure consists of a basic frame of data, repeated every 30 seconds. Each frame is comprised of 5 subframes, three of which contain the satellite ephemeris. Each subframe consists of 10 thirty-bit words with the first two words in each subframe containing synchronisation and timing data. Traditionally, GPS receivers collect subframes by continuous signal reception. If the GPS signal is interrupted during a subframe transmission the subframe is generally collected 30 seconds later when repeated. One of the major features of the AUV installation is that there is likely to be continual wave washover of the GPS antenna, resulting in a signal that is never available to the receiver for the duration of a complete subframe (6 seconds).

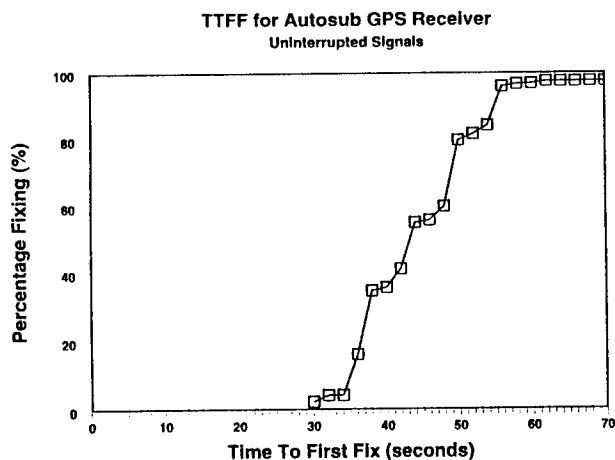
Navstar Systems Ltd undertook to modify the receiver software from its standard six-channel parallel receiver, the XR5M6, to operate in this environment. Known as the Interrupted Data Acquisition Receiver (IDAR), this project generated some challenging problems to be solved by enhancing the receiver's software. The three main areas of adaptation included:

- 1) Initial synchronisation from a non-continuous GPS signal.
- 2) Reducing the reacquisition time to a minimum in order to collect data bits rapidly.
- 3) Reconstruction of the ephemeris subframes from the small non-contiguous

The software aspects and the features for the Interrupted Data Acquisition Receiver were presented in a paper at ION-94.

UNINTERRUPTED SIGNAL PERFORMANCE

In order to provide a baseline for test analysis, a pair of modified XR5M6 GPS receivers were subjected to a long term Time To First Fix (TTFF) characterisation. The object of the exercise was to measure the elapsed time from powering on the receiver to the time the receiver first generated a position solution. The receiver software had been specially modified such that satellite ephemerides could be cleared by command and the receiver reset. Normally, the XR5M series retains satellite ephemerides in non-volatile memory to achieve TTFF's of less than 30 seconds. By clearing the ephemerides the increased TTFF when subjected to an interrupted signal could be measured and quantified. With an uninterrupted signal the receivers had a TTFF of less than 60 seconds, of which 30 seconds can be attributed to ephemeris collection. The histogram below summarises the TTFF scatter when the receiver had its ephemeris cleared, and was reset by command, in excess of 1200 times. Over 96.5% of the measurements generated a TTFF of less than 60 seconds, with the average TTFF being 44 seconds.



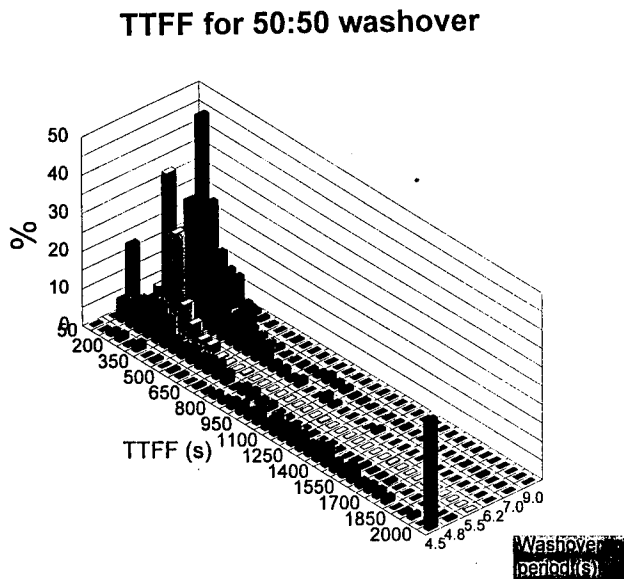
SIMULATED 50:50 WASHOVER

In order to simulate an interrupted signal, a PC program was written to generate a control signal output. The control signal was used to operate a relay switching the co-axial signals from the

antenna off and on. The program was designed to produce a 50:50 mark/space ratio control signal at a user selectable period.

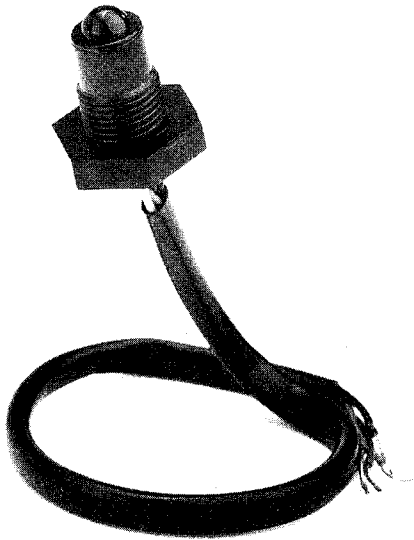
Various simulated washover periods were performed from $4\frac{1}{2}$ seconds to 9 seconds. For periods of less than $4\frac{1}{2}$ seconds the receiver began to take significantly longer to generate a first solution. This is partly due to the small amount of time that the signal is available ($2\frac{1}{4}$ seconds) and partly due to the period beating with the satellite data. At a period of exactly $4\frac{1}{2}$ seconds there are exactly four such simulated washover cycles every three complete subframes.

The graph below illustrates how the TTFF histograms shift significantly to the right once the period drops below 4.8 seconds. Above this figure the TTFF is affected only to a minimal extent.

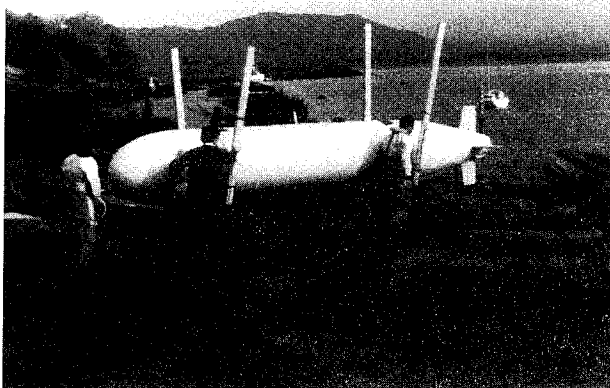


MODEL HULL RESULTS

The next testing stage consisted of recording the actual washover motion of a full scale model of the Autosub. Affixed to the rear of the model was an instrumented wave staff containing six optical immersion switches.

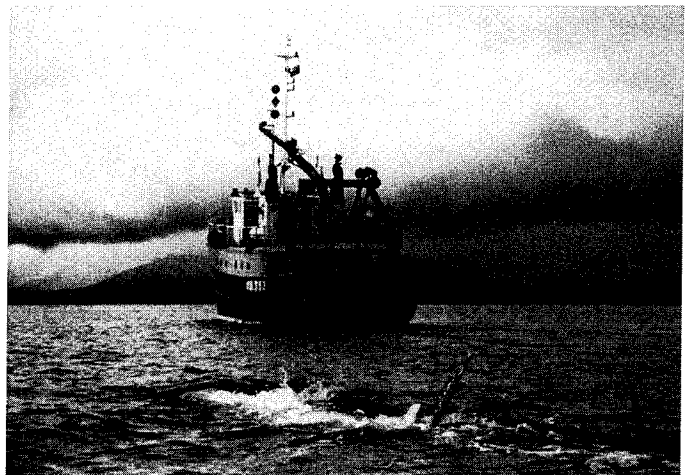


The switches are small, reasonably inexpensive, housed in a polysulphone body and contain no moving parts. This makes them ideal for this purpose. The switch operates using the principal of total internal reflection. An integral LED and photosensor are arranged so that when a liquid does not cover the sensor, a light path is established between them.



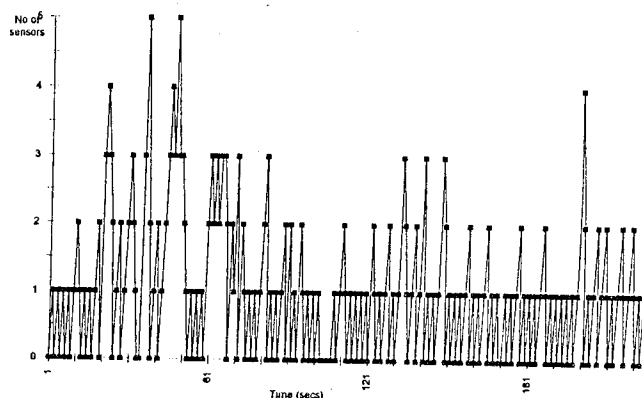
The sensors were fitted at 10 cm intervals with the lowest sensor located at a level corresponding to the calm water level. The sensor array can be

seen located just aft of the model hull's top fin. The lower two sensors can be seen to be below the top of the fin. As the GPS antenna is anticipated to be located on the top of the fin this test provided valuable washover masking data, both representative, from the second lowest sensor, and worst case from the lowest sensor. Should both of these two locations have proven to be unacceptable, data from the remaining sensors would have provided a means of determining the optimum height for some sort of antenna mounting mechanism.

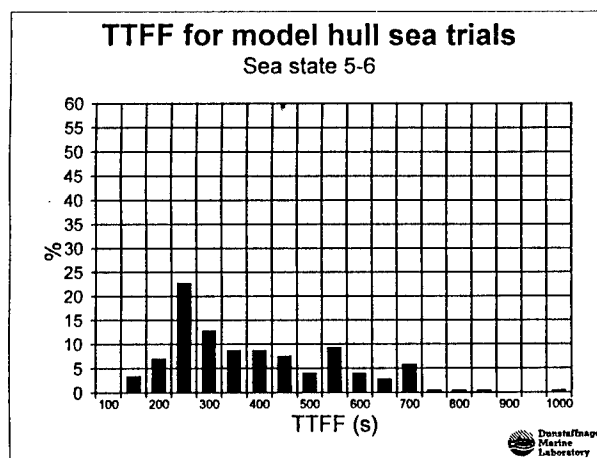
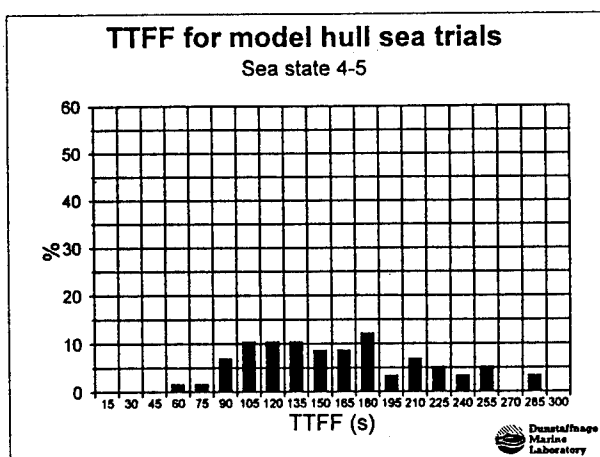
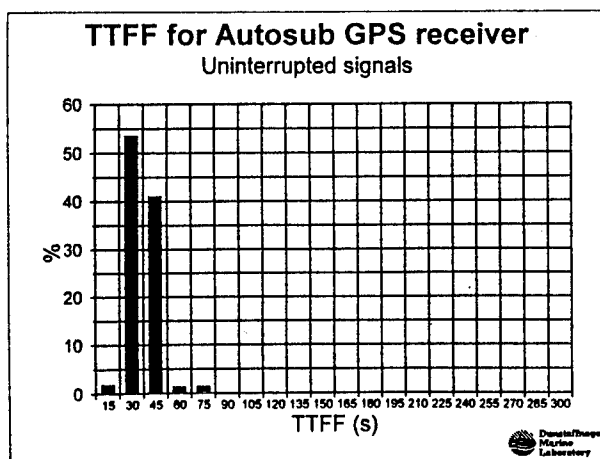


The model Autosub was deployed in the Firth of Lorne, which is off the west coast of Scotland. At the time of the mission the sea state was estimated to be between 4 and 5. Throughout the mission, an on-board computer monitored the state of the sensors and recorded which ones were obscured by wave washover.

AUTOSUB WASHOVER 02-03-95 1200-1205Z



The above graph illustrates a small sample of the data collected. It can be seen that, as expected, the lowest two sensors are obscured for a significant proportion of the time. Back at the laboratory, the washover data was stitched into a continuous loop. This was used to generate an interrupted GPS signal which replicated that which would have been seen by a vessel mounted receiver. Feeding this signal into the receivers then allowed TTFF measurements to be made as though the receivers were actually located on the Autosub. This method allowed testing to be performed for extensive periods and significant statistics gathered.

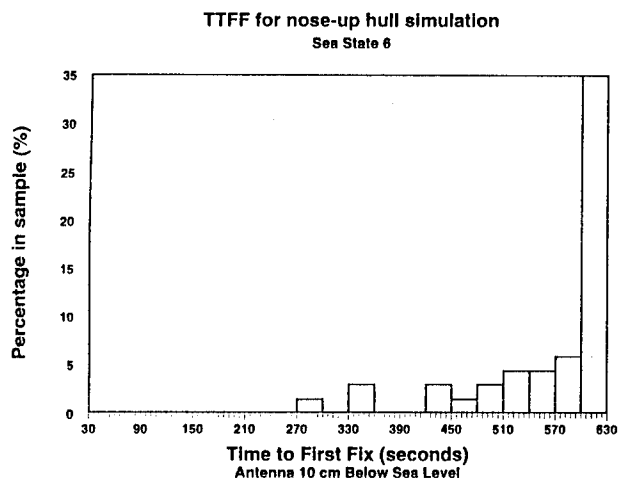
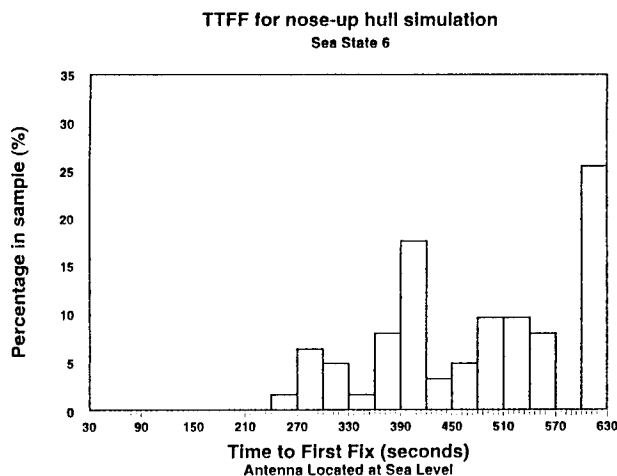
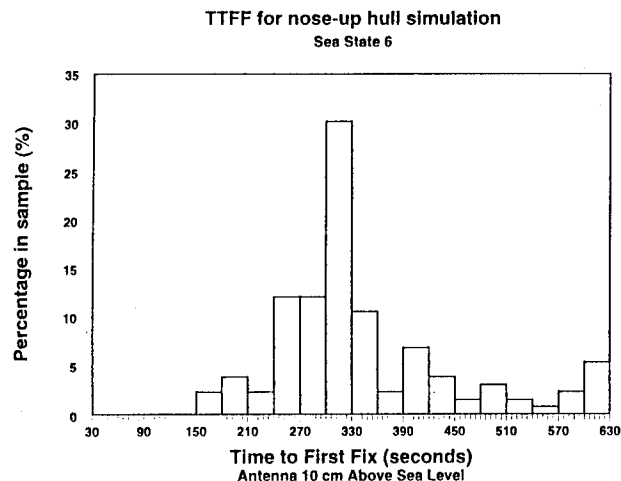


The above graphs show how the TTFF figure of the receiver is increased when subjected to an interrupted signal. In the uninterrupted case, the average TTFF is around 45 seconds. With the signal interrupted by a sea-state of 4-5 the TTFF is increased to several minutes with the majority of tests first fixing between 1 and 4 minutes. The TTFF is degraded further to between 3 and 12 minutes with a sea-state of 5-6. While the spread of these figures is in some part due to the randomness of the sea, the TTFF is also dependant on the receivers initial switch on state and the search strategy in the presence of interrupted signals, the optimisation of which is an area targeted for further study. The figures were produced using data from the lowest sensor. A fix in less than four minutes is acceptable under these conditions. As the lowest sensor is below the top of the fin which is where the GPS antenna is anticipated to be fitted, the eventual performance is expected to better this result.

SIMULATED SEA-STATE 6 RESULTS: NOSE-UP ATTITUDE

The third testing method consisted of generating simulated waveforms of washover obstruction for a sea-state of 6. The washover data being derived from a detailed dynamic simulation of the behaviour of a nose-up vehicle. Various antenna heights were simulated, with 10 cm above the static water line being closest point to the anticipated eventual antenna mounting location. The graphs below show the majority of TTFF's as being between 3 and 10 minutes under these conditions, with less than 10% of the tests taking longer than 10 minutes to fix. For comparison, results were also obtained for antenna locations located at the static water line and also 10 cm below the static water line. The last example is particularly interesting as this location is actually below the calm water level. At this point a calm sea is actually worse than a rough sea as the GPS

signals are never unobscured. Even at this antenna location, the receiver managed to generate a position solution in under 10 minutes in over 25 % of the tests.



RECEIVER ENHANCEMENTS

During the testing phase at Dunstaffnage Marine Laboratory, several suggestions were made whereby the performance of the Interrupted Data Acquisition Receiver could be enhanced. These were discussed between DML and Navstar Systems Ltd and will be incorporated into the next stage of the receiver development.

- 1) Should predicted satellites not immediately be found the search algorithm should not increase search windows or allocate alternate satellites until a reasonable time has elapsed.
- 2) Navigation from satellite almanac should be allowed if the ephemeris cannot be demodulated in severe conditions.
- 3) Inconsistency tests should be refined, e.g. by implementing a cross-checking between satellite almanac and ephemeris to prevent occasional incorrect data being processed and resulting in large positional errors.

COMMERCIAL EXPLOITATION

Several of the features of the Interrupted Data Acquisition Receiver, although specifically developed for the harsh Autosub environment, have already been used in other Navstar products.

The fast signal reacquisition routines were incorporated into a receiver specially developed for use in built-up areas where satellite signals may only be available for a few seconds at road intersections.

The optimised bit and data synchronisation routines were incorporated into all XR5M family members resulting in a reduction of the TTFF by six seconds.

FUTURE DEVELOPMENT

The receiver has been extensively bench-tested using real and simulated washover data, the real data having been gathered using an instrumented wave staff attached to a full size model hull deployed in open waters close to Dunstaffnage. Nonetheless, the receiver itself has still to go to sea.

The next trials phase, therefore, consists of integrating the receiver, a data logger and an immersion resistant antenna within the model hull.

Results of Testing on a GPS-Based Compass

Joseph Spalding and Lt. Mark Lunday
USCG R&D Center

BIOGRAPHY

Mr. Joseph W. Spalding is project manager of the Advanced GPS project at the United States Coast Guard Research & Development Center in Groton, CT. Mr. Spalding has been conducting research in GPS and Differential GPS (DGPS) for ten years. While at the R&D Center, he developed several systems that apply GPS and DGPS to marine applications. Current projects include DGPS integrity monitors, receiver autonomous integrity monitoring and GPS attitude determination. He holds a bachelors degree in electrical engineering from the State University of New York Maritime College and an MS in computer science from the University of New Haven. Mr. Spalding is a licensed Merchant Marine officer holding a rating of Third Mate of Oceans, steam or motor, any gross tons.

LT Mark Lunday, USCG, is an electronics engineer assigned to the Advanced GPS Research project at the United States Coast Guard Research and Development Center in Groton, CT. He received a B.S.E.E. from the Coast Guard Academy in 1986 and an M.S.E.E. from Georgia Institute of Technology in 1992. He served as student engineer and assistant Chief Engineer aboard the Coast Guard Cutter *DEPENDABLE* and as Executive officer aboard the Coast Guard Cutter *MONHEGAN*.

[Ed. Note: Views expressed in this paper are those of the authors and should not be construed as official or reflecting the views of Commandant or of the U.S. Coast Guard.]

ABSTRACT

The use of GPS to determine vessel heading and azimuths as applied to marine navigation was investigated. By observing the GPS constellation using a multi-antenna array, the orientation of the array can be calculated relative to the GPS coordinate system. A device of this type is not subject to: variations in the earth's magnetic field, deviations due to ship specific magnetic field effects, inertial effects caused by changes in vessel motion, inaccuracies in polar regions (above 70° latitude). A GPS based heading device also has advantages in areas of reliability (no moving parts) and the ability to get on line and settled out in minutes rather than hours. To investigate this technology and promote its development the Coast Guard R&D Center contracted through the DOT Small Business Innovative Research Program to have a device built for testing marine navigation applications. In 1994 Adroit Systems Incorporated delivered the *TriADS™* prototype attitude determination unit.

Tests conducted at land based and shipboard installations demonstrated the ability of the system to reliably calculate heading. However, the short baselines in the antenna arrays exhibited unacceptable amounts of process noise for instantaneous heading solutions. Filtering of the GPS heading output was tried, but this induced unacceptable lag into the heading result.

The potential for GPS devices to perform this task was clearly demonstrated. Several recommendations are given that could aid manufacturers in developing future units with acceptable performance.

INTRODUCTION

Determination of vessel heading and azimuth of objects has always been a crucial part of marine navigation. Magnetic and gyroscopic compasses have been the tools for this task. With the development of the Global Positioning System, the potential for a new heading determination tool exists. By observing the GPS constellation using a multi-antenna array, the orientation of the array can be calculated relative to the GPS coordinate system. A device of this type would not be subject to: variations in the earth's magnetic field, deviations due to ship specific magnetic field effects, inertial effects caused by changes in vessel motion or inaccuracies in Polar regions (above 70° latitude). A GPS-based heading device would also have advantages in areas of reliability (no moving parts) and the ability to get on-line and settled out in minutes rather than hours. To investigate this technology the Coast Guard R&D Center contracted to have a practical device built for use in marine navigation. Tests were conducted on an antenna test facility and on board an ocean going ship. The system was integrated with the ship's heading displays for navigational purposes. The results of these USCG conducted tests are presented here. Finally, conclusions regarding the performance and potential for GPS based compasses are discussed.

BACKGROUND

In the late 1980's several researchers [1,2,3,4] developed and demonstrated the ability to measure the attitude (heading, roll, and pitch) of dynamic platforms by using an array of GPS antennae. In order to explore the practical marine applications of this technology, the Coast Guard R&D Center participated in the 1991 DOT Small Business Innovative Research program with the following topic:

DYNAMIC MARINE PLATFORM ATTITUDE DETERMINATION USING GPS CARRIER PHASE

"It is possible to receive the signals of the NAVSTAR Global Positioning System (GPS) using several antennae and calculate the orientation of the antennae relative to the NAVSTAR GPS earth-centered, earth-fixed coordinate system. The objective of this research is to develop economical equipment capable of performing this calculation continuously aboard a maneuvering marine platform such as a U.S. Coast Guard cutter in all weather conditions and sea states. The equipment should convert the calculated orientation and present the ship's heading in a manner

similar to a gyrocompass. Suitable pitch and roll indicators should also be developed. The accuracy should be equal to or better than current attitude determination devices. Successful completion of this research should result in an attitude determining device that would have uniform accuracy at all latitudes."

Several proposals were received, and Adroit Systems Incorporated (ASI) was chosen the winner of the Phase I contract. ASI proposed a solution that represented an innovative antenna design combined with off-the-shelf GPS and computer components. The phase I study concluded that the unit could be economically produced because of the availability of off-the-shelf components, and proved preliminary algorithm design and methods using an existing, though limited capability, demonstration unit.

For Phase II, ASI proposed producing this design. GPS circuit boards, single board PC computer, patch type GPS antennae and various minor components were procured. A custom antenna base plane and custom serial interface board were built. A real-time operating system was selected. The embedded software to control the GPS boards and calculate attitude was developed. The system was tested by the contractor in-house at ASI, on board a tug in Baltimore, Maryland, on a 41' Coast Guard utility boat, and on board the M/V Kings Pointer at the US Merchant Marine Academy.

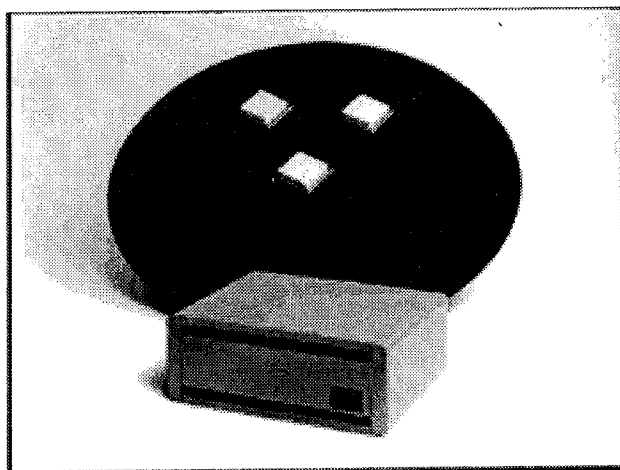
MEASURING HEADING WITH GPS

The technical details of measuring heading with GPS are well documented in the literature [5,6,7] and in the Phase I final report from this effort. A brief description follows:

The orientation of GPS antennae with respect to each other can be made with great accuracy through the use of phase interferometry of the 1575.42 MHZ GPS carrier signal. The 19 cm wavelength of GPS allows measurement of phase down to the millimeter level. These principles are the basis of all precision GPS techniques, the most common being baseline geodetic surveying to the centimeter level. In GPS surveying, one antenna is designated the base at a known location and the other is at an unknown location. For attitude determination both antenna locations are unknown but the length of the vector between the two is precisely known. The calculation of the orientation of this vector yields the antenna array's attitude in three dimensions and therefore the heading, roll, and pitch of the vessel. For marine surface navigation,

heading and the ability to measure the azimuth of objects of interest is the primary concern.

ADROIT *TriADS™*



Adroit *TriADS™*

TriADS™ was developed from 1992-1994 by Adroit Systems Incorporated. the fundamental approach was to create a relatively low-cost easily produced system. Wherever possible, off the shelf components were used. The system consists of a processing unit and an antenna assembly. The processing unit consists of 3 GPS circuit boards, a single board computer, and a custom interface card in a water resistant enclosure. The antenna assembly consists of 3 Ball™ GPS antennae with integrated low noise amplifiers, and an electronic inclinometer unit, all mounted to a custom fabricated antenna base plane designed to minimize multipath signals.

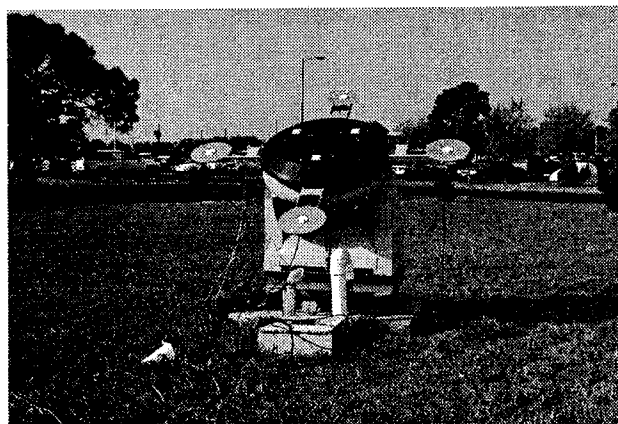
Two different antenna systems were available for this test, a 17 cm and a 50 cm baseline design. The two antenna are similar in appearance (see figure above), the difference being the length of the legs of the triangular antenna arrangement. The advantages of the 17 cm design are that it is easier to handle, mount, and simplifies the processing of the carrier phase information. Since all of the phase measurements are within one wavelength (19 cm) there is no carrier cycle ambiguity to be resolved. The 50 cm baseline antenna advantage is accuracy. Given the same amount of process noise at each of the three individual antennae, the 50 cm baseline will yield better accuracy because the noise will be a smaller percentage of overall baseline length. For example; given 0.5 cm of noise at each antenna, the 17 cm baseline would yield angular noise on the order of 1.7 degrees while the 50 cm antenna would be 0.6 degrees.

PRELIMINARY TESTS OF *TriADS™*

During the development cycle Adroit Systems Incorporated conducted testing under static conditions, on a land vehicle, and underway on a tug in Baltimore harbor. The results of these tests are presented in [6,7,8]. In these technical papers Adroit concluded that "GPS ADS (attitude determination system) is a viable navigation sensor for maritime use." "The test results demonstrated the performance of the system in a marine environment. The results indicated good system performance in the presence of obstacles such as bridges and RADAR, and demonstrated repeatable accuracies in repetitive dynamic maneuvers."⁸

E-SYSTEMS TESTS

In March 1995, engineers from the R&D Center and Navy Research and Development (NRaD) in Warminster, PA conducted testing at E-Systems, E.C.I. Division facility in ST. Petersburg, Florida. Through a cooperative effort arranged by NRaD we were able to utilize E.C.I.'s outdoor antenna test facility. The capability of most interest was a test pedestal with 360 degrees of horizontal rotation and plus or minus 45 degrees in one vertical axis. Using this tool we



E-Systems Test Pedestal (Photo courtesy ECI Photo Lab)

were able to evaluate the *TriADS™* capability in a controlled situation. Different tests were performed to stress the system in areas such as multi-path and dynamics. Data was collected over a three day period using the Adroit *TriADS™*. Different tests were conducted using various pitch, roll and azimuth angles. Although the test platform had only one vertical axis, that axis could be aligned at any azimuth allowing roll and pitch to both be tested. The antenna pedestal was located near the E-systems parking lot which was used in testing the susceptibility to multipath.

GPS Static Stability test (90 deg) Mean = 90.39 Std dev = 0.39

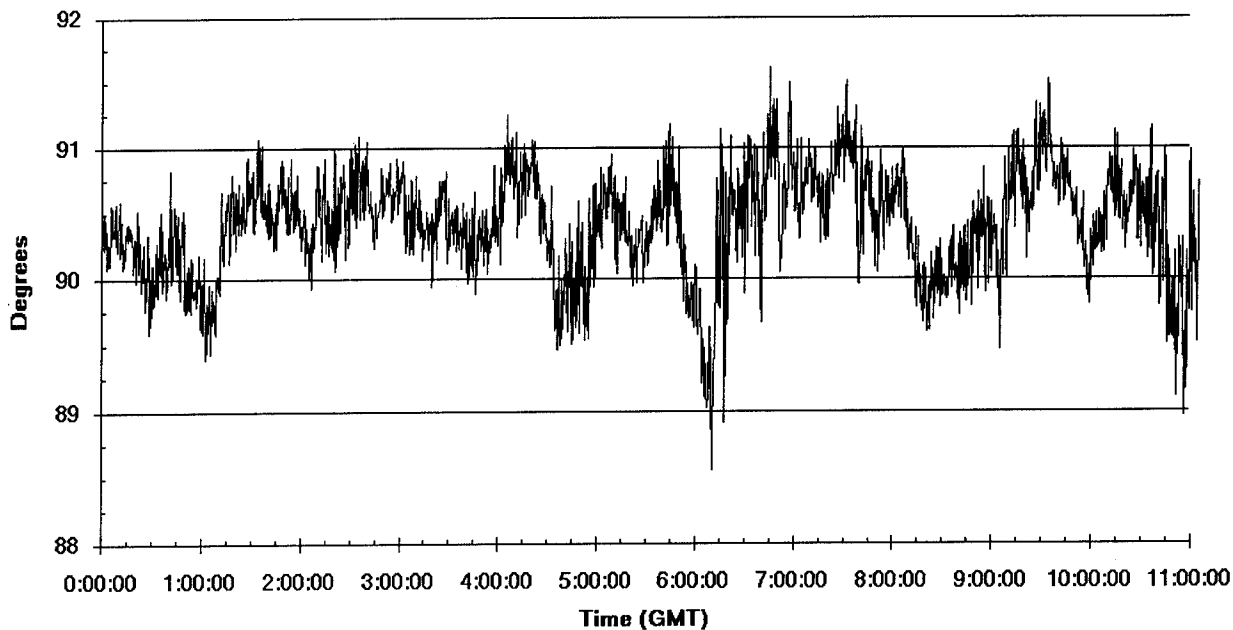


Figure 3

Collection of data for several hours at a fixed azimuth and vertical angle were done to examine the stability of the system. Several tests were also done to test the system under dynamic conditions. These dynamic tests were limited by the speed of motion of the test pedestal. We considered the rotation rate sufficient to simulate real world heading changes but the vertical angle rate was slower than the rate a vessel could roll.

It was our intention to test the TriADS with both the standard 17 cm baseline antenna and the newer 50 cm baseline antenna Adroit had developed for another application. However, the 17 cm baseline antenna was lost in shipment to Florida and was not recovered. All test results from this test at E-Systems presented here are with the TriADS™ 100 using the 50 cm antenna. Due to the integer cycle ambiguity resolution required when using the 50 cm baseline the TriADS™ 100 could only achieve an update rate of about one point every five seconds. The TriADS™ 100 also has a Kalman filter to smooth the heading response. Earlier shipboard tests had shown that the unfiltered solutions were excessively noisy for practical use. However, during the majority of testing at E-Systems the system was run with the filter off in order to observe the instantaneous measurement capability of the system.

To test the stability of the system we set the pedestal

at known azimuths for an extended period of time. For the data presented here the system was set at 90 degrees for 11 hours. Figure 3 shows the system performance over the first 11 hours. The standard deviation was calculated to be 0.39 degrees. There was a mean bias of 0.39 degrees. We attribute this bias to difficulty in aligning the Adroit antenna with the test pedestal.

To evaluate the response of the system we executed rapid heading changes on the pedestal and observed the result (figure 4). In this test we swung

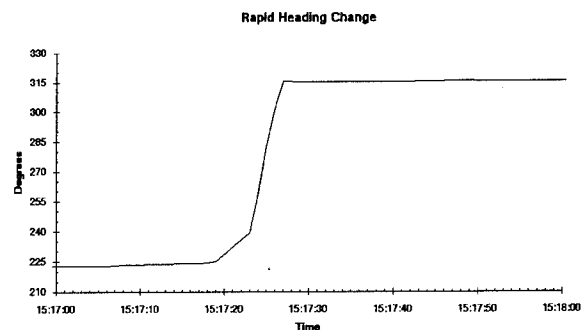


Figure 4

the pedestal from a steady state of 225 degrees to 315 degrees at about 20 degrees per second. The Kalman filter was off.

Our final series of tests for heading was to evaluate the performance of the Kalman filtered solution. We performed rapid changes of heading and observed a significant performance problem in the heading

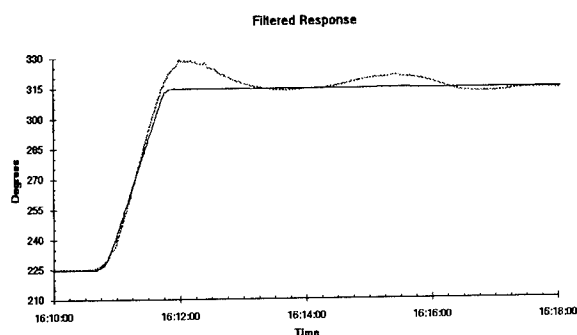
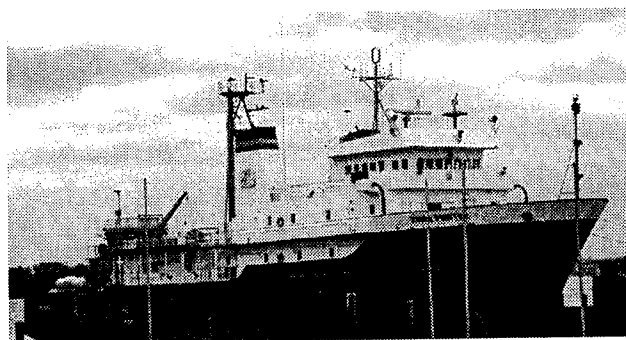


Figure 5

response. The filter response lagged and then overshoot the final pedestal position. The slow update rate of the system with the 50 cm baseline antenna contributed to this problem.

KINGS POINTER COMPARISON TESTS

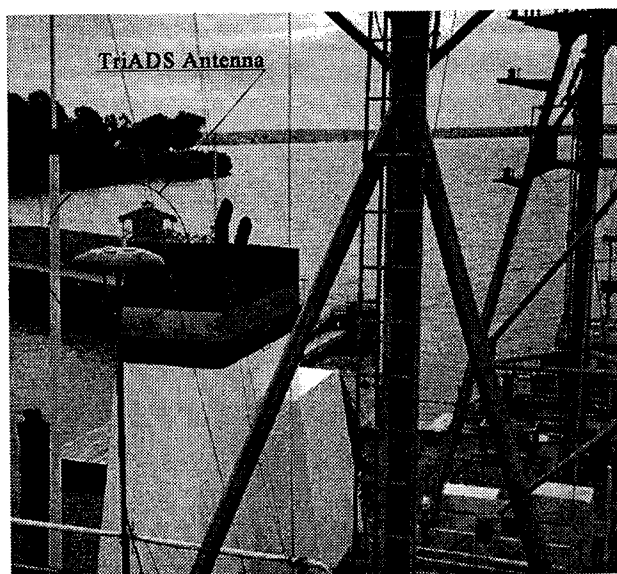
In May 1995 we conducted detailed final performance testing of the TriADS™ on board the M/V Kings Pointer. The Kings Pointer is the U.S.



M/V Kings Pointer

Merchant Marine Academy training vessel. USMMA Midshipman are familiarized with ships systems, learn ship handling and take short cruises on board the 224' vessel. The ship is the former USNS Contender, a T-AGOS 2 class vessel built by the Navy for ocean surveillance. The antenna was mounted above the bridge on a 10' (3 m) long pole. We felt the antenna location was less than optimal due to blockage from the RADAR mast, but felt that this would be representative of a real world installation.

A 17 cm base line antenna was used on the Kings Pointer. It exhibited the expected amount of increased process noise. Standard deviation when differenced



Antenna Location

with the gyro compass during straight runs was 1.8 degrees. More importantly, for this dynamic trial, the unit was able to maintain a 1 Hz output rate due to the 17 cm baseline being less than the 19 cm GPS carrier wavelength. Another advantage of the short baseline is the ease of mounting of the antenna array. An inexpensive 2" (5 cm) pole and common U-bolts made the mounting relatively simple compared to larger baseline systems.

The performance of the TriADS™ was compared to the gyrocompass on board the Kings Pointer. Data was collected over several hours with the vessel performing harbor piloting in the East River. Data was collected dockside in order to calibrate any bias in the alignment of the GPS and the gyro compass. We found a consistent bias of 2.5 degrees between the GPS and the gyro. We attribute this bias primarily to misalignment of the GPS antenna array. Figure 8 shows the heading with both the GPS and gyro over a two hour period dockside.

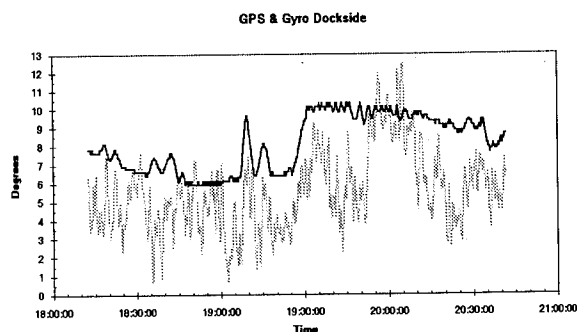
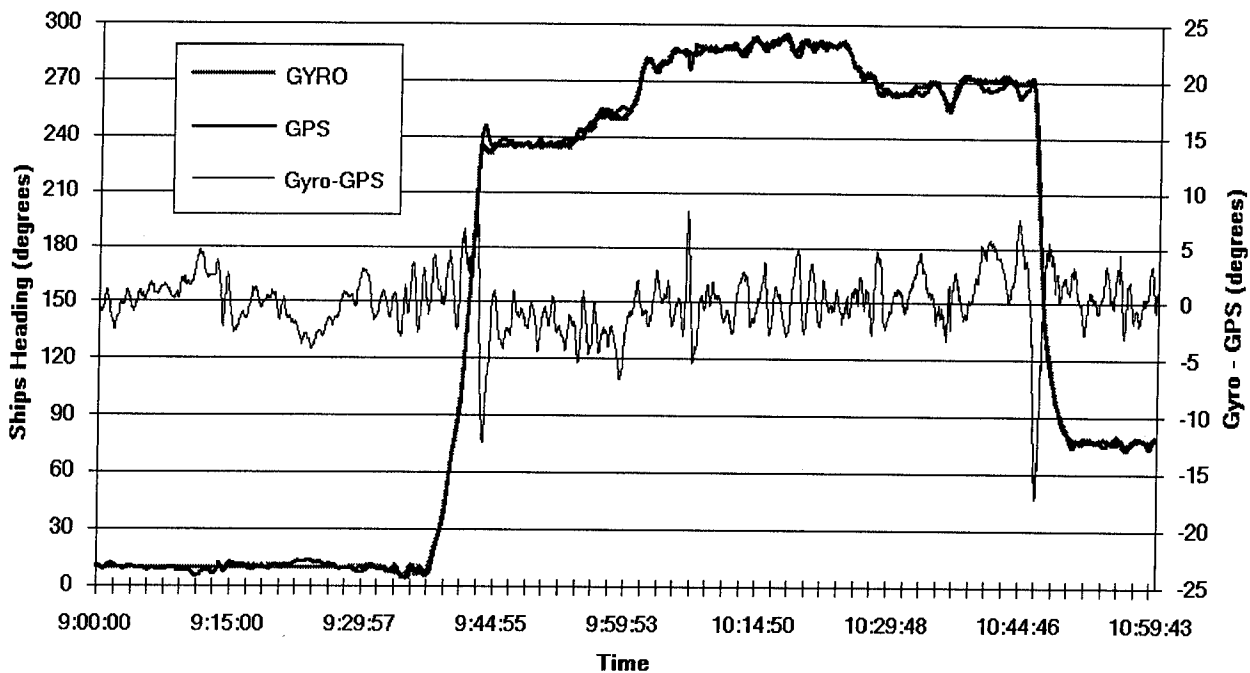


Figure 8

Underway Performance Comparison



Once the bias was characterized we compared the performance of the GPS to the gyrocompass underway. Figure 9 shows the gyro measurements with the GPS measurements (corrected for the bias) plotted on top. The third line is referenced to the right hand scale and represents the difference between the gyro and GPS. It became immediately apparent that we still had problems with the filter performance despite the higher output rate from the unit due to use of the smaller 17 cm antenna. Figure 10 shows the area in the beginning of the turn showing the GPS lagging the gyro by about 20 seconds. At the completion of the turn the filtering

showing a classic over-damped filter response.

KINGS POINTER OPERATIONAL TESTS

As a final test of GPS based heading, an operational test involving piloting of the Kings Pointer strictly with GPS derived heading was tried. The TriADS™ was used to provide heading information for the vessel in place of the master gyrocompass. In order to accomplish this the R&D Center built a custom interface to make the TriADS™ output simulate the gyrocompass output.

GYRO SYSTEM INTERFACE

On board the M/V Kings Pointer the Sperry MK 227 gyro compass drives an extensive electromechanical gyro repeater system that provides the helm, RADAR, bridge wings, and various stations throughout the ship with heading information. The gyro compass itself outputs stepper sequences using 20 volts on three lines. This method yields six states to indicate heading to 1/6 of a degree. Each complete sequence through the six states is one degree. There is no absolute heading distributed, each gyro repeater must be manually aligned to the gyrocompass current heading. Once aligned, the gyro repeaters maintain the heading quite reliably.

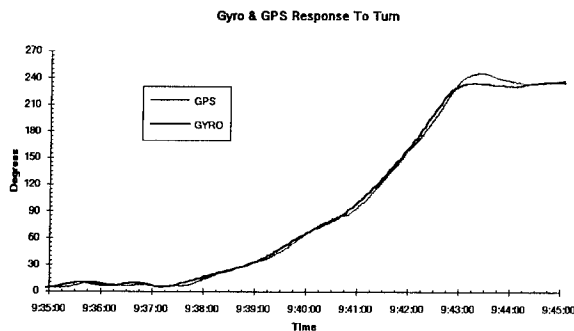


Figure 10

causes the GPS to over shoot the gyrocompass response. At this point the heading filter in the GPS is

| Heading increment | Line 1 | Line 2 | Line 3 |
|-------------------|--------|--------|--------|
| 1/6 | 0 | 1 | 0 |
| 2/6 | 0 | 1 | 1 |
| 3/6 | 0 | 0 | 1 |
| 4/6 | 1 | 0 | 1 |
| 5/6 | 1 | 0 | 0 |
| 6/6 | 1 | 1 | 0 |

Table 1

In order to provide useful heading information to the ship, we had to find a way to drive the gyro repeater system with the TriADS™. The TriADS™ was built to provide output via RS232 using NMEA-0183 messages. In order to drive the gyro repeaters, we created a system to take the NMEA-0183 VHW message and convert it into incremental stepper heading changes (Table 1). The program is hosted on a 80286 laptop, reads the NMEA-0183 \$GPVHW message, extracts the true heading, and changes the output states of three lines of the parallel port to give the proper stepper position output. The 5 volt signals from the parallel port drive electronic relays that provide the required 20 volt level for the ship's system. The Sperry MK 227 gyro binnacle is wired to accept an external input from a backup gyro. We utilized this connection yielding easy integration and a built in switch to toggle between gyro and GPS generated input signals.

OPERATIONAL TEST RESULTS

On August 21, 1995 at 1650 EDT we got underway on the Kings Pointer, with the TriADS™ providing the ship's heading for a cadet piloting training run. The three hour cruise traversed the area between Execution Rocks in Long Island sound and the Whitstone bridge in the East River. In steering the vessel, it soon became apparent that the lag in the GPS solution made course changes difficult. The helmsmen were instructed to use physical landmarks to guide their steering as they were not getting sufficient real time feedback from the TriADS™. After a few maneuvers, the helmsman was able to adapt his steering to the lag in the gyro update.

The accuracy of the unit seemed to be generally sufficient for position fixing using optical and RADAR bearings to objects. These bearings and fixes are generally taken while the vessel is on a steady course.

During any maneuvers, the lag in the heading output would have caused significant navigational positioning fixing errors.

An additional feature of the shipboard gyro repeater system is its ability to indicate the rate of turn. This is done through audible clicks, one click per each change of state of the stepper function or 1/6 of a degree. This audible feedback gives the conning officer valuable feedback on the performance of the helmsman and the progress of the vessel through a particular maneuver.

With the GPS driving the gyro repeaters the clicks for each 1/6 of a degree would come in bursts. As the TriADS would give one \$GPVHW output each second, when there was a heading change the gyro interface program would proceed through the required stepper increments quite quickly in order to avoid any delay. The test subjects were not comfortable with the bursts of heading changes.

CONCLUSIONS

GPS has the potential to provide a practical alternative to a gyrocompass or magnetic compass for navigation. The benefits of low cost and high reliability make this technology particularly attractive. Our goal of achieving equivalent performance to the gyrocompass was not realized. The short baseline GPS antenna arrays tested in this effort exhibit unacceptable amounts of process noise. Filtering of the output is required to achieve a low noise level. Alignment of the GPS antenna array must be performed with a high degree of precision. This alignment was difficult with the TriADS™ antenna. Substituting the gyro compass signal for the master compass on commercial vessels equipped with gyrocompasses is relatively simple and allows the use of GPS versus gyrocompass to be transparent to the users.

RECOMMENDATIONS

Alignment aids are required on the GPS antenna array, and an alignment procedure must be developed to achieve acceptable alignment of the antenna array relative to the vessel.

Manufacturers should consider the use of inexpensive solid state, fiber optic or quartz rate gyros to aid in filtering the heading output.

Industry should create GPS heading devices with update rates on the order of 5 Hz.

When simulating gyrocompass stepper output a GPS device will have to maintain a high output rate to

indicate smooth rate of turn indications through the gyro repeaters audible indication.

ACKNOWLEDGMENTS

The authors would like to acknowledge the assistance of Ed Zantek and Steven Kravets of Navy Research & Development in Warminster, Pennsylvania; E-systems, E.C.I. Division, especially Geri Lodato and Richard Hall; and ENS Kevin Quilliam, USCG for their assistance in the land based testing.

The authors would also like to acknowledge the participating midshipman of the USMMA and especially Commander Gary Gehring, Master of the M/V Kings Pointer, whose willingness to test the next generation of navigation equipment, both provides us with a valuable test platform and enhances the midshipman's training.

REFERENCES

1. Brown A. K., W. M. Bowles and T. P. Thorvaldsen (1982). "Interferometric Attitude Determination Using The Global Positioning System: A New Gyrotheodolite", Proceedings of the Third International Geodetic Symposium on Satellite Doppler Positioning, Las Cruces N. Mex. 8-12 February, Vol. II pp.1289-1304.
2. Kruczynski L. R., P. C. Li, A. G. Evans and B. R. Hermann (1988). "Using GPS To Determine Vehicle Attitude", ION GPS-88 Proceedings of the Satellite Division's International Technical Meeting, Colorado Springs Colo., 21-23 September, pp.139-145
3. Lucas, R., R. Okkes, and W. Kriedte (1988). "Attitude Determination With GPS", ION GPS-88, Proceedings of the Satellite Division's International Technical Meeting, Colorado Springs, Colo., 21-23 September, pp 85-88
4. Nesb, I. (1988). "Applications Of GPS Determined Attitude For Navigation", ION GPS-88, Proceedings of the Satellite Division's International Technical Meeting, Colorado Springs, Colo., 21-23 September, pp 95-100.
5. Jurgens, Richard D., Rodgers, Charles E., and Fan, Leopold C., "GPS Azimuth Determining System (ADS) Cycle Resolution, System Design, and Army Test Results", Proceedings of the National Technical Meeting, Institute of Navigation, Phoenix, Arizona, January 22-24, 1991.
6. Diefes, D., Fan, L., Rodgers, C., "Dynamic GPS Attitude Determining System for Marine Applications, Concept Design and Developmental Test Results", Proceedings of the 1993 National Technical Meeting, Institute of Navigation, San Francisco, California, January 20-22, 1993.
7. Diefes, D., Hazel, G., Greenlee, D., "GPS Based attitude Determining System for Marine Navigation", Proceedings of ION GPS-93, Sixth International Technical Meeting of the Satellite Division, Institute of Navigation, Salt Lake City, Utah, September 22-24, 1993.
8. Diefes, D., Hazel, G., Greenlee, D., "Test results of GPS Based attitude determining System for Marine Navigation", Proceedings of the 1994 National Technical Meeting, Institute of Navigation, San Diego, California, January 24-26, 1994.
9. Diefes, D., "GPS Based Attitude Determining Systems for Integrated Navigation Systems", Proceedings of ECDIS '94, March 1-2, 1994.
10. Hazel, G., Smith, S., "Instantaneous GPS Attitude tests: cycle Ambiguity resolved", Proceedings of ION GPS-94, Seventh International Technical Meeting of the Satellite Division, Institute of Navigation, Salt Lake City, Utah, September 20-23, 1994.

The Use of GPS for Underwater Navigation, Sea Trial Results

M. H. G. Thomas
ACSA

BIOGRAPHY

ACSA, Advanced Concepts and Systems Architecture, is a company based in the south of France involved in the development of new techniques for the application of GPS to underwater navigation and mobile robotics (UUVs).

The author, M. H. THOMAS has been involved in underwater navigation equipment development since 1975. Initially with INTERSUB, as survey engineer, then as technical manager.

In 1980, he founded a company SBS specialized in integrated navigation software and mapping.

In September 1994, the author presented a paper [2] at OCEAN-94-OSATES describing " New Advanced Underwater Navigation Techniques Based On Surface Relay Buoys" . Today, he presents the sea trial results of a new set of equipment called Surface Long Base Line (SLBL).

ABSTRACT

Solutions have been proposed for the use of GPS for underwater navigation since 1992 [1]. This paper relates new techniques using upward flows of acoustic data being transmitted by a mobile to a set of GPS buoys. A radio network allows data exchange between the buoys, a D-GPS station and a PC based control station.

Sea trials were performed during the 1995 summer. They are presented and analyzed herein. They demonstrate that the acoustic propagation does not degrade the accuracy of the GPS system. The third dimension, depth, is measured using a pressure sensor and coded in the upward acoustic flow of data.

Those techniques which apply to remote control over long distances of UUVs (Unmanned Underwater Vehicles) are covered by international patents .

1/ INTRODUCTION

GPS receivers are now widely used for aircraft, ships and land vehicles . In 1992, the US-AF announced the use of GPS for underwater navigation [1] . Very few publications have presented equipment or experimental results since then. As a matter of fact, GPS can be of great use to assist locating underwater objects (wrecks) or mobiles. It requires buoys to convert radar waves into acoustic signals.

Very often, the mobile does not require to know its position; but it is the external world that requires to know the position of the underwater object. That is the case of a ROV's pilot, that is the case of a survey ship towing seismic flutes, that is the case for salvage operations, ...

For that reason, but also for size of equipments, cost and power consumption, we have decided to use upward flow of acoustic data for localization purposes and downwards flow for Control and Command of the underwater vehicle .

The picture below gives a view of the scene .

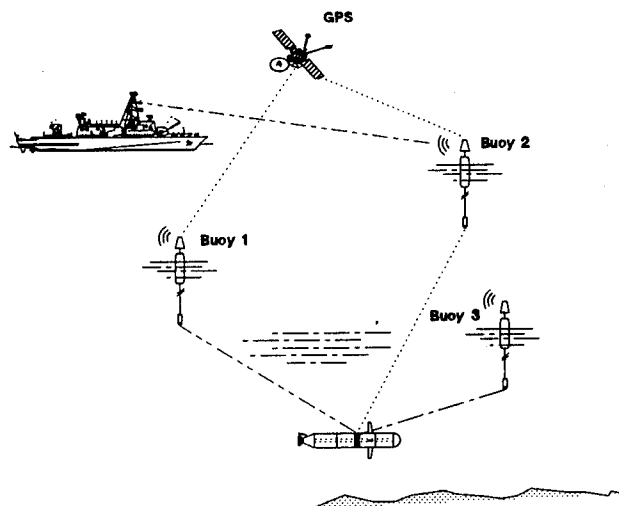


Figure 1 : General View

2/ THE USE OF GPS FOR UNDERWATER NAVIGATION

The basic principle for localizing an underwater vehicle consists of having a pinger on board the vehicle itself. The signal, transmitted at regular intervals, is received by a set of buoys located in the vicinity of the vehicle.

Each time, a buoy receives an acoustic pulse, the time of arrival is very accurately dated within the GPS Time Base. The buoy then transmits by radio its position and the time of arrival.

That allows a central station to calculate the pseudo-ranges from the buoys to the vehicle for each acoustic signal transmitted. Coordinates of the mobile can then be calculated (intersection of spheres or circles if the vehicle's depth is known).

3/ EQUIPMENTS USED

The equipment used to demonstrate the feasibility of GPS for tracking underwater mobiles consisted of :

- 1 Control station,
- 1 D-GPS station,
- 4 Buoys,
- 1 Local radio network,
- 1 Acoustic transmitter.

Their main characteristics are :

Control Station

The control station allows to remotely control the surface relay buoys and D-GPS station through the radio network and to acquire navigation data.

The control station is composed of :

- 1 Color Portable PC 486-50 Mhz,
- 1 GPS 8 channels, OEM Card,
- 1 Microprocessor control unit MCU,
- 1 200 Mhz Radio-Modem - 100 mw.

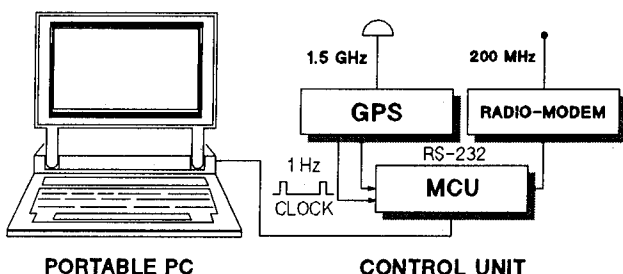


Figure 2 : Control Station Block Diagram

The control station can be either, a network controller, or, a passive data receiver.

In the first mode, the control station transmits commands or requests to the buoys and D-GPS station in order to configure them, for self-tests or for quality control of data. For example, the radio network can be set to one particular frequency in the band 200-230 Mhz after a spectrum analysis over the full frequency band.

In the second mode, "Real-Time Navigation", the control station remains passive and receives data streams coming, either from the D-GPS station or, from the buoys. All radio transmissions are synchronized within a time window (150 msec. wide) allocated to each piece of equipment.

The main features of the control station are :

- Configuration and test of equipments via radio network,
- Activation, de-activation of radio broadcasts,
- Real-time data acquisition and processing,
- Raw data storage for off-line data analysis,
- Graphic display of mobile's route and depth,
- Quality control of data,
- Off-line processing.

Programs on the Portable-PC use interactive multiple graphic windows facilities.

D-GPS Station

The aim of the D-GPS station is to transmit RTCM-104 messages to the GPS receivers installed on board the buoys.

As we use only one frequency for the radio network, the frames of data must be transmitted within the time windows allocated to the D-GPS station. For this reason, a microprocessor control unit MCU is integrated in the D-GPS station.

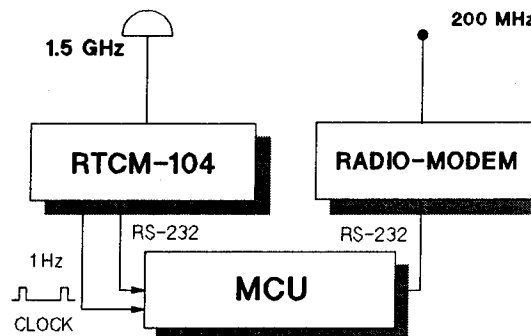


Figure 3 : D-GPS station Block Diagram

GPS-Buoys

Each buoy includes 4 modules:

- 1 GPS 8 channels OEM card,
- 1 Acoustic module,
- 1 200 Mhz radio transmitter,
- 1 Microprocessor based central processing unit, MCU.

The main functionality of the buoys are :

- Acquire RTCM-104 corrections,
- Detect acoustic signals and date them,
- Transmit to control station data frames.

The size of the buoy is 90 cm long and 14 Cm in diameter. Its weight is 12 Kg.

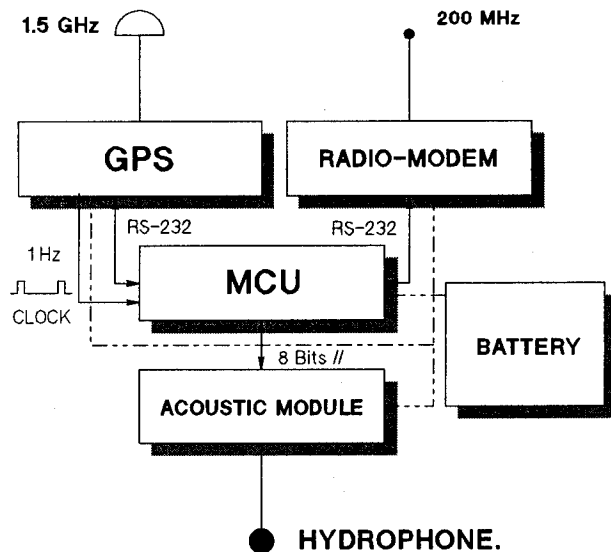


Figure 4 : GPS-Buoys block diagram.

The hardware developed can date the acoustic signal interrupts with a resolution of 10^{-5} sec., giving a pseudo-range resolution for underwater distances measurements of 1.5 Centimeters .

The frame of data transmitted by each buoy to the control station consists of :

- Buoy's ID number,
- Transmission sequence number,
- Buoy's coordinates,
- Acoustics' signals arrival times,
- Quality control data,
- Checksum caracters.

In order to avoid loss of data in case of radiotransmission errors, the frame of data

contains redundant informations. Data are transmitted at 1 hertz.

Radio Network

The radio network consist of a set of VHF radio transmitter working at 9.600 BPS. All radios are synchronised using GPS time signals in order to avoid data frames overlaps.

The main radio characteristics are :

- Frequency band : 200-230 Mhz,
- RF Power output : 100 mw,
- Size : 12 x 8 x 6 Cm .

Acoustic transmitter

Whereas, an ordinary pinger can be used, we manufactured a special acoustic transmitter for the purpose of our trials. This transmitter has a very stable clock which can be synchronised prior to the dive using a GPS 1 PPS clock signal output, through an IR link.

The main characteristics of our transmitter are :

- Frequency : 30 Khz,
- Repetition rate : 1 Sec.,
- Long term clock stability : 10^{-8} / month,
- Clock consumption : 2 mamps,
- Pressure sensor : 0-30 bars, 1°/oo.

The quartz was calibrated using GPS receiver's PPS signals. The repetition rate measured of the quartz was : 0,99999799 sec.

4/ SITE AND EXPERIMENTS

The first evaluations of the system took place on august, the 24th, 1995 in the Mediterranean sea, near Toulon's harbor, in very shallow water depths (15 m).

The D-GPS station was installed near the green lighthouse marking the southern entrance of "La Grande Jetée ". GPS positions have been averaged during 3 minutes, giving the following coordinates for the D-GPS station :

⇒ N 43° 05' .404
⇒ E 005° 55' .500

Continuous radio-transmission of RTCM-104 correction messages was then set at 1 sec. intervals.

The aim of the first experiment was to evaluate the position stability of a set of 4 buoys aligned on the quay.

Further, the 4 buoys were moored in Toulon's Grand Rade, in the direct vicinity of the D-GPS station. A pinger was then towed, within the buoys pattern, at a water depth of 5 to 10 meters.

5/ TRIALS RESULTS

Pinger's clock stability

The pinger's clock stability was confirmed, allowing to easily calculate acoustic ranges from acoustic pseudo-ranges (distances pinger to buoys).

Static performances of buoy's GPS receivers

The last digits giving the coordinates of the buoys aligned on the quay during the static test are given below:

| | |
|-------------|--------------------|
| Buoy N° :10 | X= 753.5, Y= 814.5 |
| Buoy N° :11 | X= 735.1, Y= 802.1 |
| Buoy N° :10 | X= 756.1, Y= 834.1 |
| Buoy N° :10 | X= 749.5, Y= 800.3 |

They can be correlated with the measured distances between the buoys on the quay.

| Buoy's Number | 10 | 11 | 12 | 13 |
|---------------|------|------|------|------|
| 10 | - | 22.2 | 19.8 | 14.8 |
| 11 | 22.8 | - | 38.3 | 14.5 |
| 12 | 20.5 | 43.3 | - | 34.4 |
| 13 | 14.5 | 8.3 | 35.0 | - |

Table giving distances between buoys on the quay.

(Above the diagonal, figures represent distances between buoys as calculated; below ,as measured.)

Dynamic performanc. of buoy's GPS receivers

The first plot on the next page shows the dispersion obtained in locating the buoy N°: 11 as moored at sea. Typically, the dispersion was +/- 10 meters.

Dynamic performance of acoustic detectors

The second plot given on following page shows the acoustic ranges between the pinger and the four buoys. The repetability of the measurements is close to 30 cm.

A plot of the track of the underwater pinger towed below the ship, within the buoys' pattern, is given next page.

6/ CONCLUSIONS

The first sea trials have allowed to fully test the complete underwater localization system.

The results demonstrate that GPS buoys can be a very powerful tool to accurately locate underwater vehicles in real time.

By using GPS real-time submetric kinematics techniques, metric accuracies should be achieved in positioning underwater vehicles at depths over 1000 meters.

Those techniques which apply to remote control at long distances of UUVs (Unmanned Underwater Vehicles) are covered by international patents .

* * *

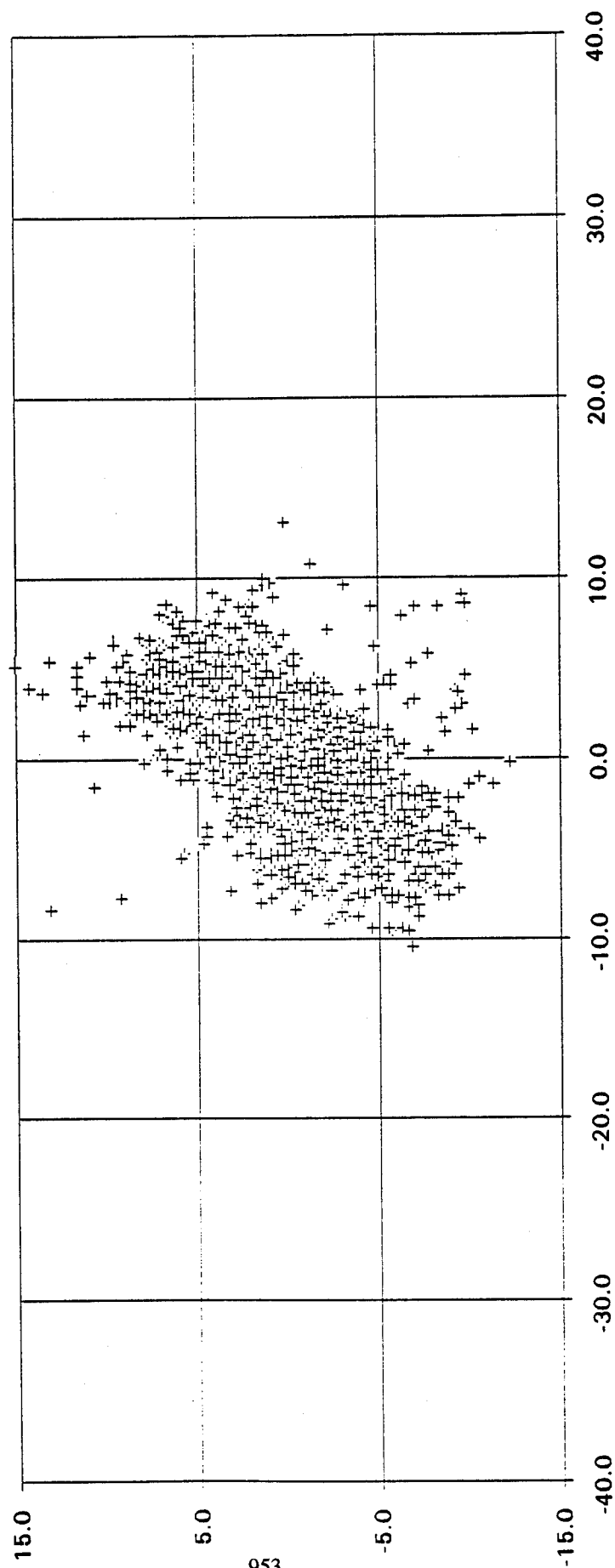
REFERENCES

[1] July 1992, " *Nouveau procédé pour l'utilisation sous-marine du GPS* ", Revue NAVIGATION N°: 159, J.W. YOUNGBERG US-AF.

[2] September 1994 : " *New Advanced Underwater Navigation Techniques Based On Surface Relay Buoys* " OCEANS-94-OSATES - M. H. THOMAS.

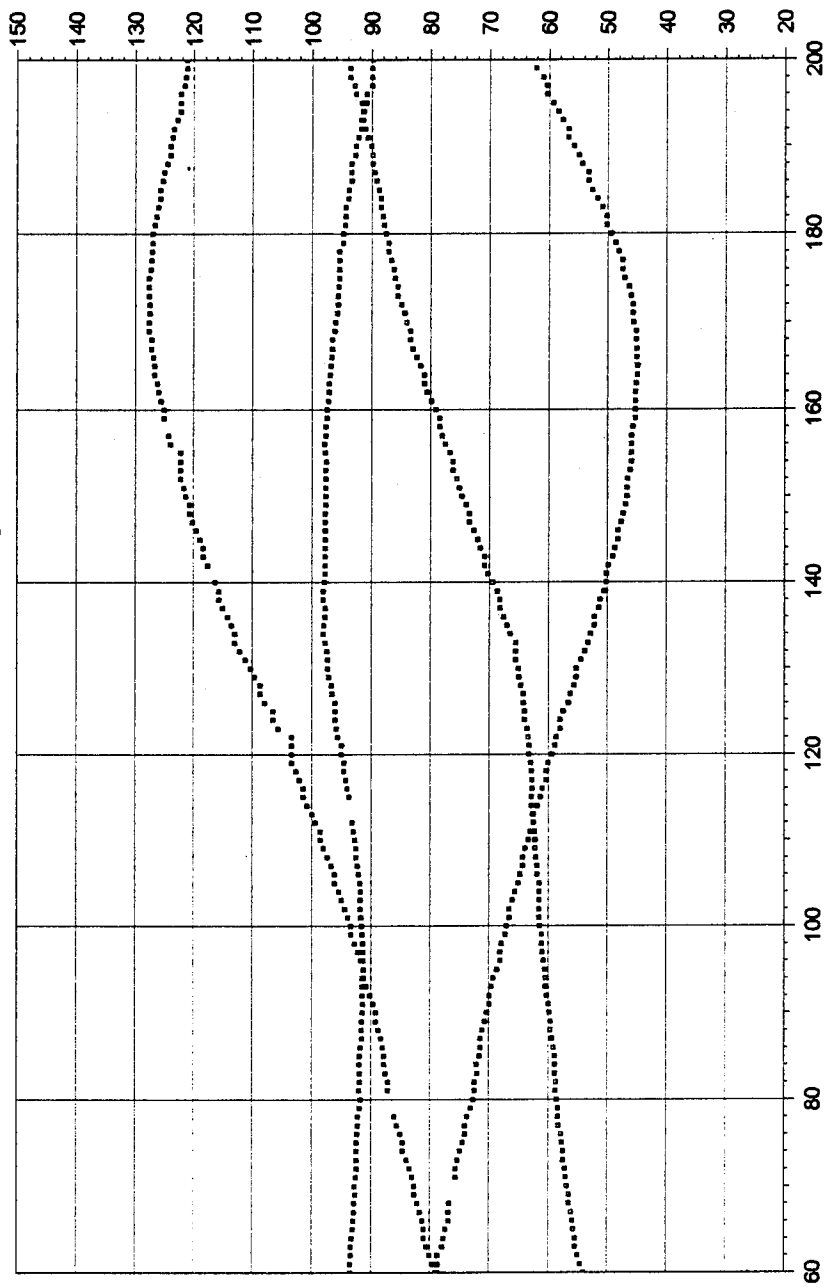
* * *

Buoy N°: 12 - X-Y DISPERSION PLOT



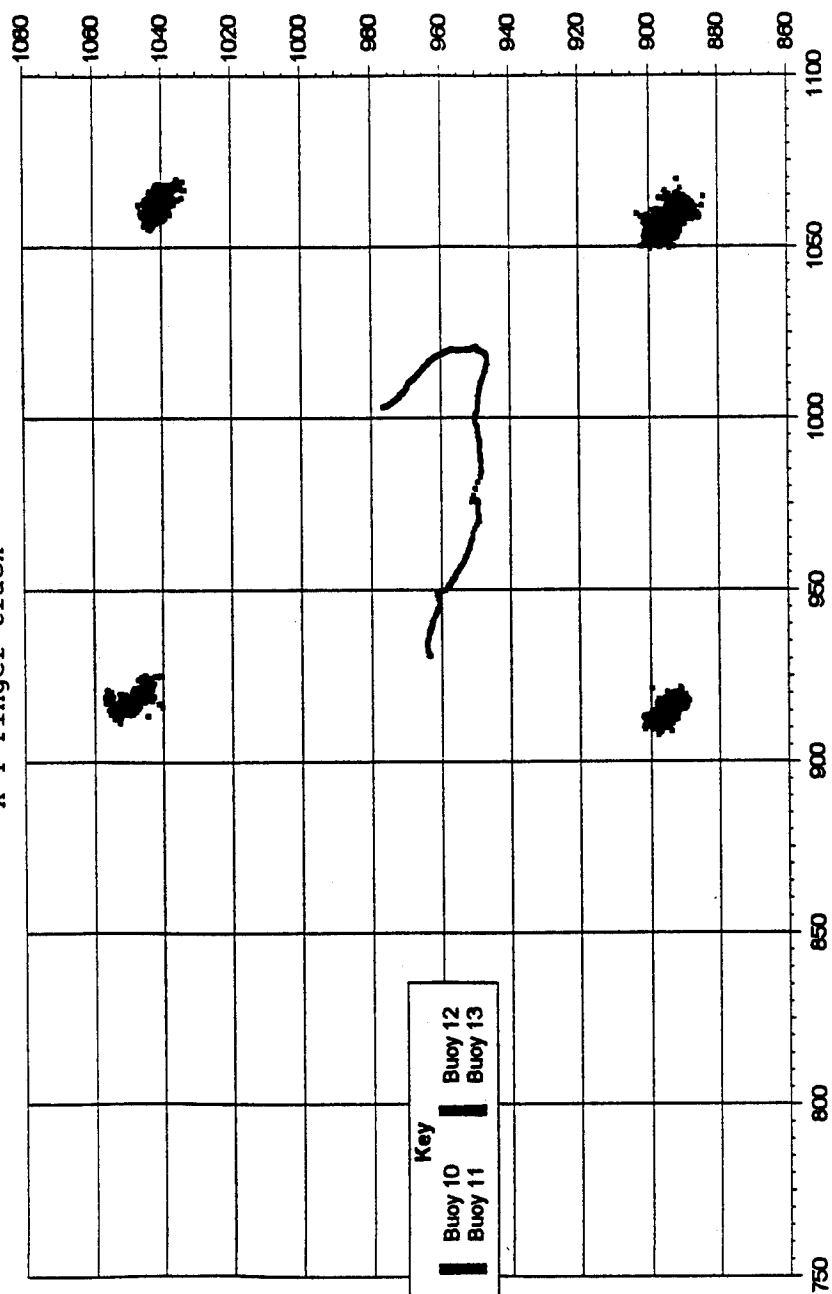
24/8/95

Acoustic Pseudo-Ranges



24/08/95

X-Y Finger track





Session D3

GLONASS

Chair:

Mr. Scott Fearheller
U.S. Air Force

Co-Chair:

Dr. Jacques Beser
3S Navigation

The GLONASS System Status and Prospects for Development

Michael Lebedev and Victor Gorev
CSIC

Alexander Ganin and Victor Kulnev
Central Research Institute of the Russian Space Forces

BIOGRAPHY

Michael M. Lebedev was born in 1950; Russian; in 1974 graduated at Moscow Aviation Institute and in 1984 from Dzerzhinsky Military Academy, Moscow. Specialist in the sphere of development and utilization of space systems of different application, including GLONASS system.

Victor V. Gorev was born in 1947; Russian; In 1971 graduated at Military Command and Engineering College, Kharkov. Specialist in the sphere of development and utilization of space systems of different application, including GLONASS system.

Alexander A. Ganin was born in 1959; Russian; in 1981 graduated at Mozhaysky Institute of Military Engineering, Leningrad; Doctor of technical sciences since 1988; more than 15 years he specializes in space radionavigation.

Victor V. Kulnev was born in 1953, Russian; in 1976 graduated at Dzerzhinsky Military Academy, Moscow; Doctor of technical sciences since 1985, more than 20 years he specializes in space radionavigation.

INTRODUCTION

Carrying out the Decree of the President of the Russian Federation dated September 24, 1993 and the Decree of the Government of the Russian Federation №237 dated March 7, 1995, the Russian Space Forces in the current year continue to conduct the planned activity on deployment the orbital constellation of GLONASS system and to control the system as a whole, and the organizing and coordinating activity in user's navigation equipment creation and further development of GLONASS program.

Three satellites of the 25-th block were successfully launched in March, the next 26-th block was put into the orbit in July, and up to the end of the year it is planned to make 2-3 launches and that will provide the fulfilling of obligations to deploy the full constellation in 1995.

However even now 22 operational satellites of GLONASS system provide continuous navigational field, which enable users in standard mode using standard precision channel to determine position with 50-70 m accuracy and velocity measuring with 15 cm/sec accuracy. Such accuracy

characteristics are available for mass domestic and foreign users and they can be improved significantly by using special technical and mathematical methods of conducting and processing the measurements.

The fact that the characteristics of GLONASS system are not worse as compared with similar American GPS system and, because of high inclinations of orbits, GLONASS possesses even more favorable characteristics of satellites observation in north latitudes, many times was confirmed by Russian and foreign experts and practices. Besides, as using of selective access mode is absent in GLONASS system it is more preferable for civilian users in accuracy.

However, we are sure, the fact of existence of two global satellite navigation systems belonging to two different countries must not assume their indispensable opposition, but on the contrary, allows to work out a wide range of tasks in the interests of world society.

For the first time the proposal on international civilian use of GLONASS system's navigation field and free access of standard precision channel was made to ICAO by Russian party on May 9, 1988 and from that day our course to the integration and cooperation with foreign navigation means remain stable.

The joint use of navigation fields of GLONASS and GPS allows to increase the reliability of navigation determinations, and to increase the integrity index of combined navigation system as well, including realization in receivers autonomous integrity monitoring mode.

The advantage of joint GLONASS-GPS use during these years became undeniable fact and confident realization of GLONASS program will promote the fastest implementation of both systems in many spheres of world economy and science.

MAIN DIRECTIONS OF SYSTEM DEVELOPMENT

1. If we are talking about the main directions of GLONASS system's development, first of all it is necessary to note that in the first quarter of 1996 Russian Space Forces plan to start flight tests of new GLONASS-M program. The new modernized GLONASS-M satellite will have higher guarantee period of service (5 years instead of 3 at the moment) and better technical characteristics. This enable to increase the reliability and accuracy of the system as a whole.

2. The second direction to which Russian Space Forces give much attention is a work on introduction the space navigation technologies in Russian economy and science, and creation the new generation of user's navigation equipment, stations of differential corrections and integrity control.

At the current moment according to the order of Russian Space Forces our designers and scientists create a whole range of very interesting and prospective models, which have no analogues in the world.

By the end of 1995 it is planned to produce 3-4 types of test samples of user's navigation equipment and differential corrections and integrity control stations as well. The nomenclature of user's navigation equipment and differential stations, offered for creation and serial manufacturing, according to their composition and characteristics allow to use them directly (or after some technical changes) practically in all areas of civilian applications.

It is necessary to note separately that all prospective samples of equipment, which are currently created in Russia are combined and can work using GLONASS, GPS or GLONASS-GPS signals.

3. The third direction of development is working out and realization the conception of Russian wide area differential subsystem on the base of Russian space vehicles control complex infrastructure and it's interaction with departmental local differential subsystems, situated both on Russian territory and abroad.

4. The next direction of Russian Space Forces' activity within the frameworks of GLONASS integration with foreign means is work on progress the cooperation with different international and foreign organizations and firms in the sphere of expansion the possibilities of using GLONASS satellite navigation system for broad sections of users.

One part of this activity is an active participation of Russian Space Forces' representatives in the work to prepare the formal proposals of Russia on GLONASS system' using in ICAO and IMO international organizations, and working out and concordance the Standards and Recommended practice for international GNSS system.

Besides, the very active work is in the process on signing bilateral agreements with different organizations and firms on using GLONASS potential and joint development and manufacturing user's equipment and drawing-up a common approaches for creation differential subsystems and integrity control systems.

A widening interest to GLONASS system was shown At 41-st International Aerospace Exhibition in Le-Bourget. During the Show we have reached an understanding with some firms to prepare corresponding agreements and contracts on different aspects of using GLONASS advantages in the regions of Europe, South-East Asia, South America and south of Africa.

And today we once again confirm our readiness for collaboration on all questions of using GLONASS system's possibilities, it's development and integration with foreign navigation means.

5. Besides, Russian Space Forces continue activity on solving the problems, connected with use of joint navigation fields of GLONASS and GPS systems in the interests of broad sections of world society users. Here we can highlight the following directions:

- search of common approaches for granting space navigation systems to world society;
- concordance of base coordinate systems;
- concordance of system time scales;
- drawing up a measures on non-admission the using of space navigation systems to the detriment of national security.

The work in this direction is doing together with representatives of GPS system' administration.

Within the frameworks of highlighted problem I would like to express my opinion according to the prospects of creation so-called independent civilian systems as an alternative to GLONASS and GPS systems. Not taking in consideration the economic valuation of huge expenses on development and creation a new civilian systems when we have two ready operational satellite systems, I will only stop on the aspect, which one forget, I do not know why, criticizing GLONASS and GPS.

The main argument, putting forward to motivate the necessity of alternative system's creation, is affirmation of some specialists and organizations that as GLONASS and GPS are under the control of military structures so if there is aggravation of the international situation, the military departments of states-owners of navigation systems can undertake the special measures, making difficult or even excluding the possibility for civilian use of the systems. To our opinion this argument is not durable enough, because proposed for creation new civilian navigation system will not be absolutely independent from international situation as well.

This conclusion is brought by our opinion that in a hard periods of world's political situations the so-called civil navigation systems will be indirectly subordinated under a policy of governments and States which took part in the systems creation. Under the circumstances these systems will not independents. Besides, in these periods the basic elements of the system control complexes the most probably will be under control and protection of power structures are close to army, and it will doing in the interest of security.

That is why we think the only GLONASS and GPS with appropriate augmentation are real systems which may be effectively used by both military and civil users.

GLONASS and GPS have the exceptional characteristics of accuracy and coverage. They are operated by the ones of most stable state structures - the ministries of defense, and in addition they are the state navigation systems.

The Coordinational Scientific Information Center (CSIC) is responsible within the Russian Space Forces for purposive and consistent policy in the field of GLONASS development and operation, and of its implementation and integration with foreign navigation systems. CSIC determine the main directions of development, render to users an consulting, informing and scientific-methodical services with the aims of more effective GLONASS use. CSIC is the official representative of the Ministry of Defense on a talks, meetings and conferences.

In conformity with the Russian Federation Government's Decree number 237 from March 7, 1995 "On executing works in use of the GLONASS global satellite system for the sake of civil users" CSIC is responsible for providing the civil users with formal information on GLONASS status. CSIC distribute also a technologic information on GLONASS, including:

- notice on GLONASS status;
- notice-advisory to GLONASS users on any changes in GLONASS status;
- notice-advisory to GLONASS users on others important events in GLONASS (e.g. GLONASS launch, etc.);
- GLONASS almanac.

Besides, in case of special inquiry CSIC provides an additional information on GLONASS.

An availability of GLONASS in any point of Earth and at any time predetermine a principles of information interaction between CSIC and domestic and foreign users as follows:

- an access to technologic information on GLONASS 24 hours a day, with a minimal delay;
- distribution of information by various ways including electronic and printed formats;
- distribution of information both on Russian and English;
- using of up-to-date information technologies: Usenet, Internet, BBS etc.

We have no doubts that our efforts on a fastest introduction of satellite navigation systems in everyday life will be successful and will promote development of science, economy and international cooperation of all interested partners.



RUSSIAN SPACE FORCES

**COORDINATION SCIENTIFIC INFORMATION CENTER
M. LEBEDEV AND V. GOREV**

**CENTRAL RESEARCH INSTITUTE
A. GANIN and V. KULNEV**

THE GLONASS SYSTEM STATUS AND PROSPECTS OF DEVELOPMENT

ION 95



THE CORE ISSUES

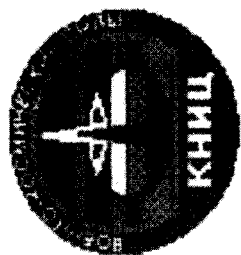
- THE GLONASS SYSTEM OF TODAY
- MAIN DIRECTIONS OF THE GLONASS DEVELOPMENT
- TASKS AND DIRECTIONS OF ACTIVITIES OF THE COORDINATIONAL SCIENTIFIC INFORMATION CENTER

ION '95

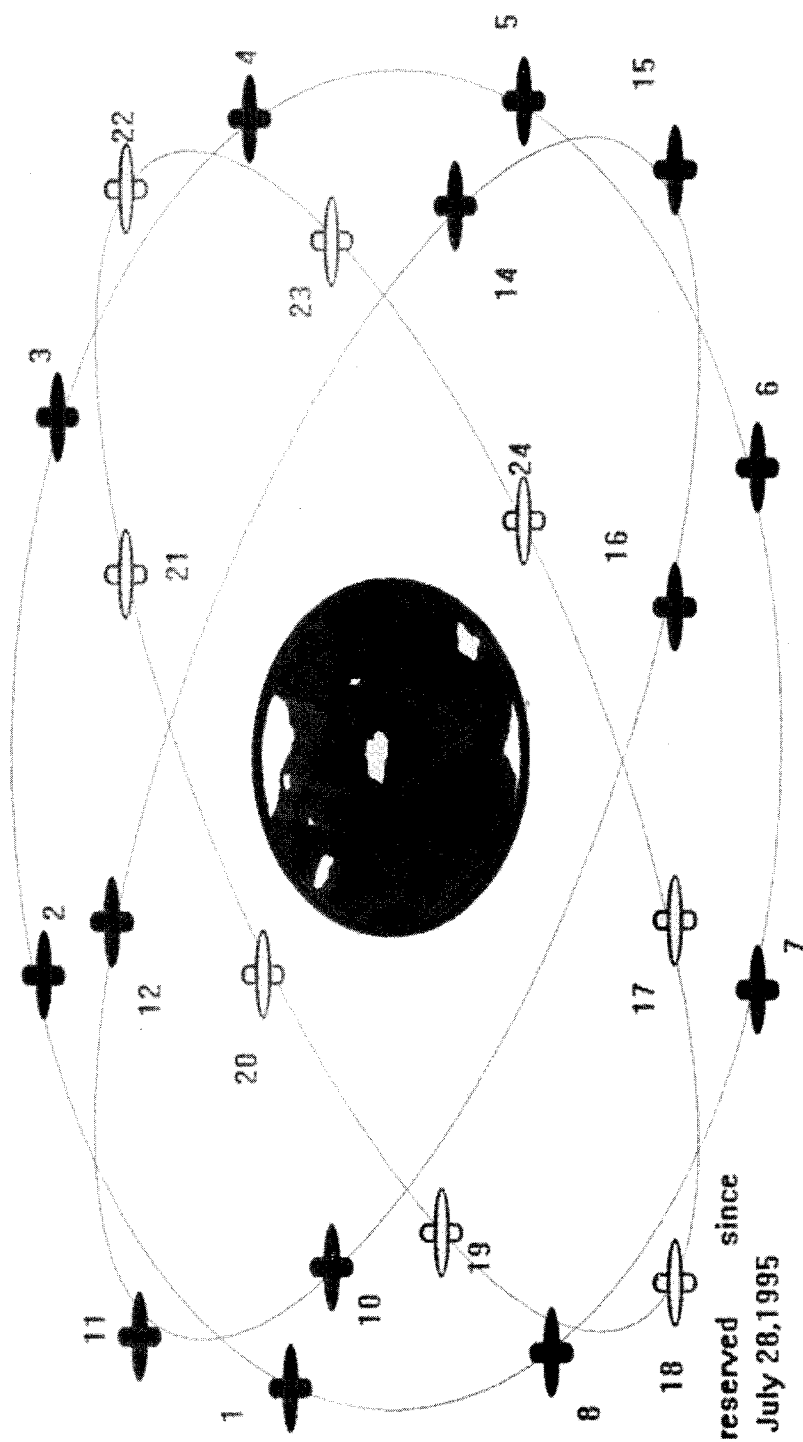


THE CORE DOCUMENTS CONCERNING GLONASS USE

- **DECREE OF THE PRESIDENT OF THE
RUSSIAN FEDERATION dated September 24, 1993
on putting into operation the GLONASS system**
- **DECREE OF THE GOVERNMENT OF THE
RUSSIAN FEDERATION N.237 dated March 7, 1995
“On executing works in use of the GLONASS global
navigation system for the sake of civil users”**
- **REGULATIONS ON INTERACTION BETWEEN
MINISTRIES AND DEPARTMENTS**
- **THE GLONASS INTERFACE CONTROL
DOCUMENT**



GLONASS CONSTELLATION



ORBIT Parameters:

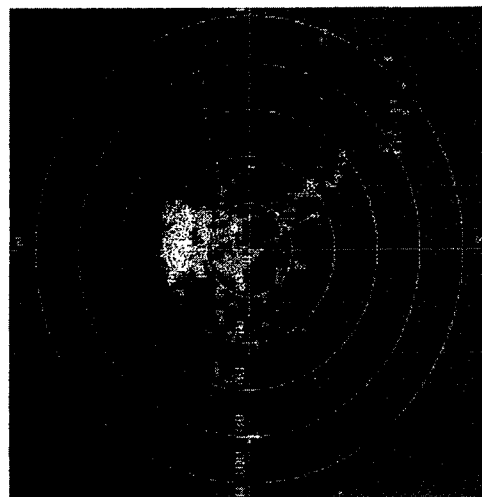
- Height:
about 19100 km
- Period:
about 11 h 15 min
- Inclination:
64.8 deg

reserved since
July 28, 1995

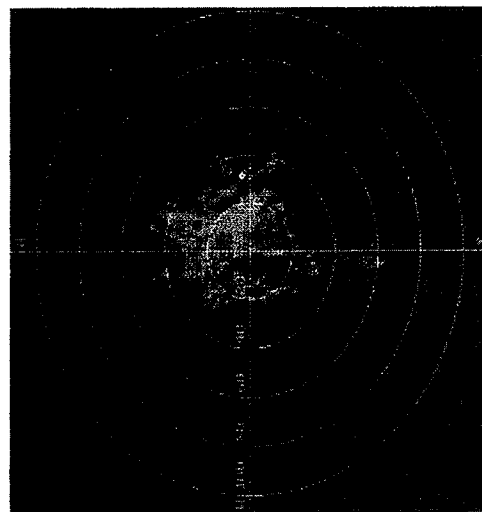


ESTIMATION OF 2D-POSITIONING ACCURACY

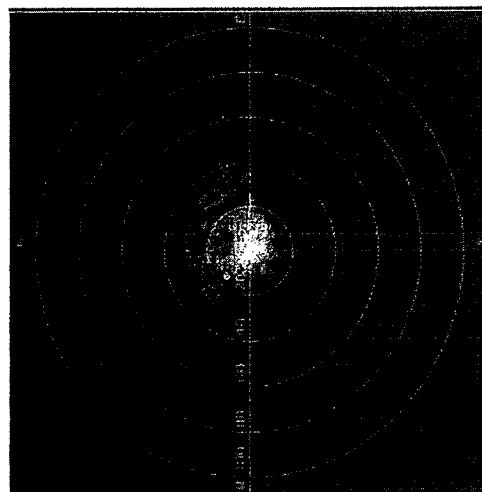
Moscow 6000 observations



GPS



GPS+GLONASS



GLONASS



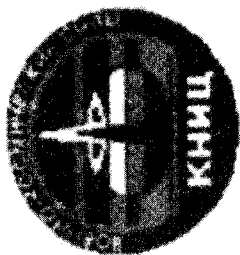
MAIN DIRECTIONS OF GLONASS DEVELOPMENT

- Starting the GLONASS-M flight in 1996.
- Creation the new generation of GLONASS/GPS user's equipment and its implementation in Russia.
- Realization the conception of united differential system creation in Russia.
- Development of international cooperation in the sphere of expansion the possibilities of GLONASS use.
- Works in the field of joint GLONASS/GPS use.

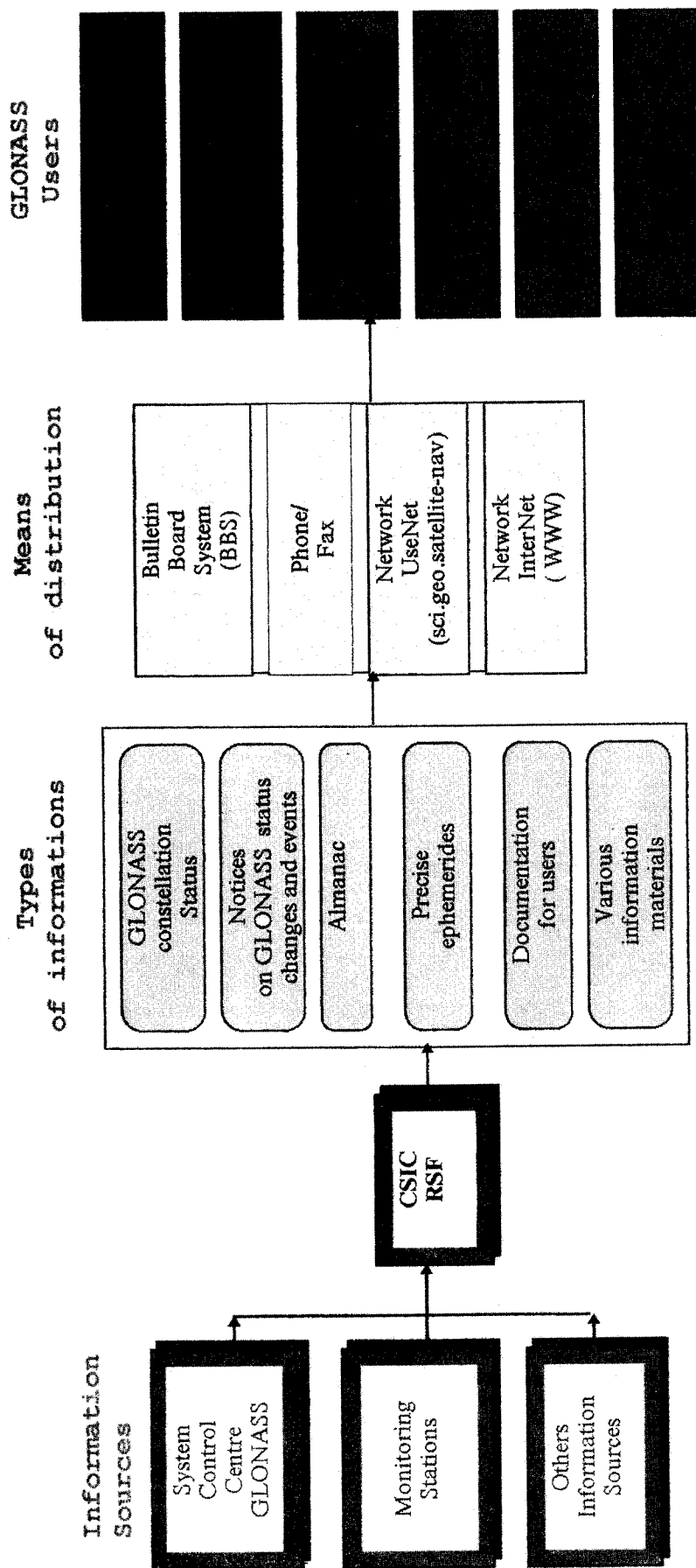


ADVANTAGES OF GLONASS AND GPS JOINT USE

- Increasing reliability of positioning caused of augmented constellation use during:
 - vessels traffic control in coastal area;
 - air traffic control in airport area;
 - surface traffic control in city area;
 - positioning in area with broken relief (wooded, mountainous, etc);
 - trajectory determination of high dynamic objects;
 - positioning in complicated conditions of interference or when there are restrictions on wide-directional receiving antenna use.
 - Increasing the integrity characteristics.
-



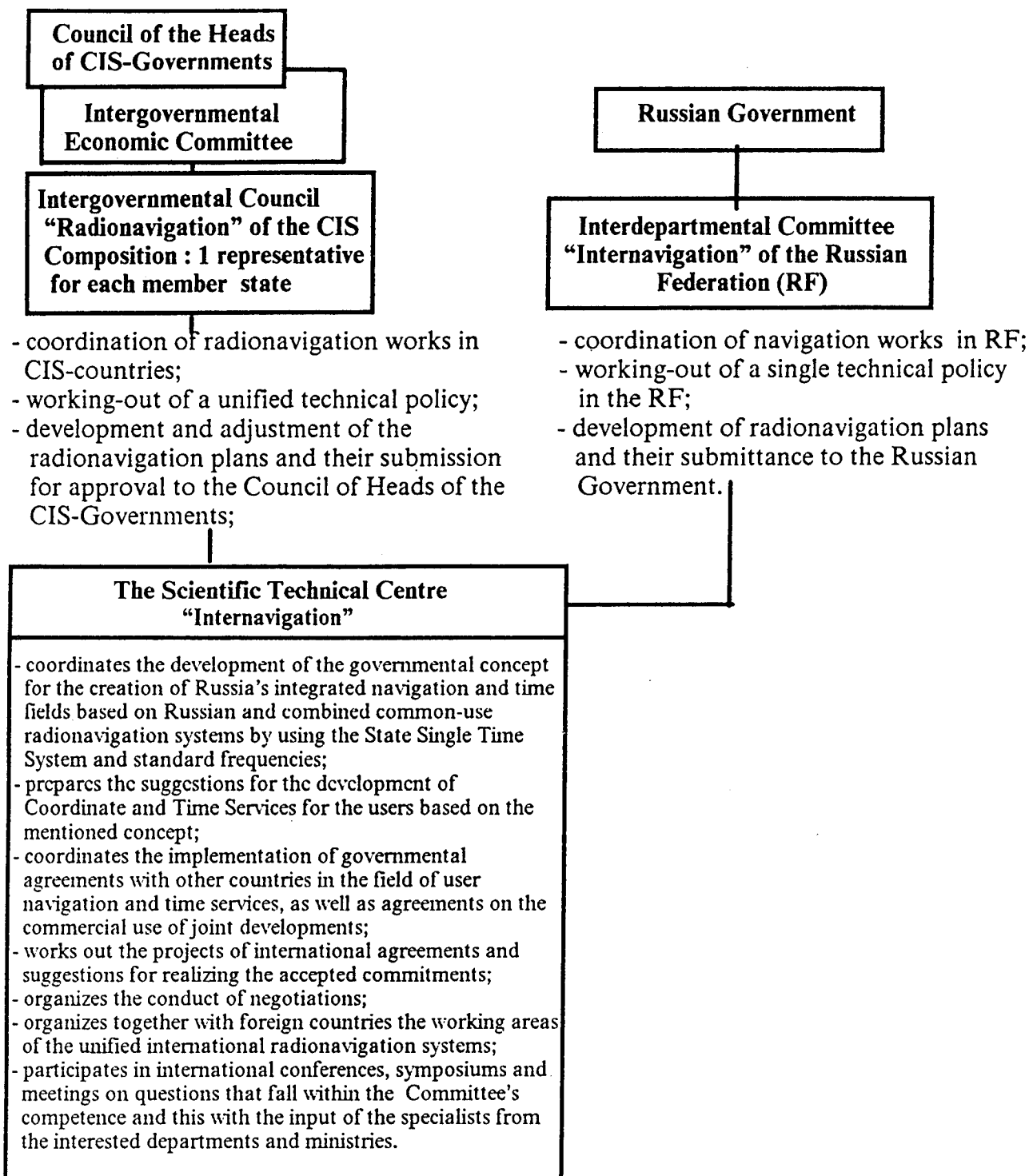
INFORMATION INTERACTION BETWEEN CSIC RSF AND GLONASS USERS



The Place of GLONASS in the Radionavigation Plan of the CIS

Vladimir Denisov

*Radionavigation Intergovernmental Council
Internavigation Research and Technical Center*



The role and position of the GLONASS radionavigation system within the CIS radionavigation plan

The navigation policy of the member states of the Commonwealth of Independent States (CIS) is determined by the :

- general and economic policy of the CIS-states;
- character of the economic problems and the requirements of the navigation services to solve them
- condition of the navigation services.

Considering the current state and taking into account the current economic difficulties the realization of the navigation services programme of the CIS-users is planned in two stages (Fig.1) :

Stage 1 : (till 1997) carrying out the works needed to increase the effectiveness of the use of radionavigation systems for general use, which are currently being used :

- the completion of the GLONASS SNS configuration;
- carrying out conjugation works of the Russian and foreign navigation systems for common use, the creation of unified systems and systems for combined use;
- the creation of differential subsystems of the GLONASS, ALFA, CHAYKA navigation systems and their introduction;
- the development of different types of integrated receiver indicator equipment for air, naval and ground users;
- the development of automatized control systems for all kinds of transport based on radionavigation fields;
- the creation of a single structure for CIS navigation services.

Stage 2 : (till 2000) the integration of Russian and foreign navigation systems for general use, the introduction of a single structure for the CIS navigation services into the navigation systems of Europe and the rest of the world :

- the organization of the serial production of different types of integrated receiver indicator equipment in a way that satisfies the needs of aviation, naval and ground users;

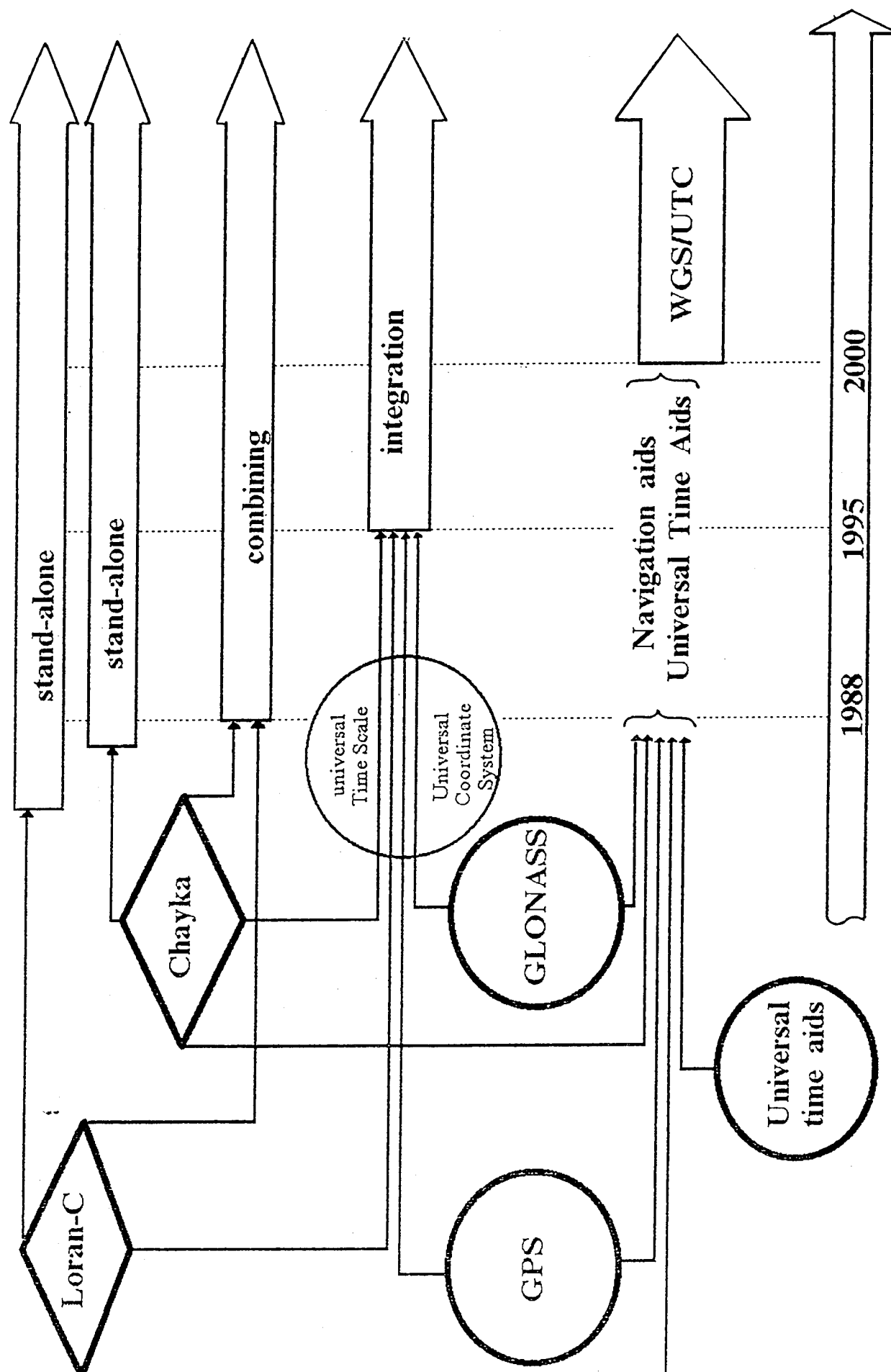


Fig.1. PNS application phases

- the introduction in practice of ways of applying integrated navigation systems for air and naval navigation;
- the creation and introduction of automated control systems of all types of transport based on radionavigation fields;
- the development of a network of ground stations of the CHAYKA/LORAN-C systems based on new generation equipment;
- working out perspective trends for the realization of technical navigation means;
- the functioning of a single structure for CIS navigation services within the navigation structures in Europe and the rest of the world.

In the radionavigation plan of the Russian Federation and CIS the development of the RNSS GLONASS has the highest priority. The RNSS which are based on the coordinated use of movement and radiation of the signals from a satellite network, are global systems which function continuously and almost instantaneously provide navigation applications.

The level of technical solutions which in time has grown, has allowed the RNSS to substantially enhance the accuracy of the determination coordinates and user movement parameters. This is why the RNSS represent a qualitative new phase in the development of radionavigation technical science.

The basic advantages of RNSS are : the unlimited scope of operation in near space; the high accuracy of coordinate and speed component determination in space; the simple navigation determinations transmitted in one coordinate system for all users; the accuracy does not depend on the time of day, seasons or hydrometeorological conditions; the high reliability; the endless number of objects that can be served; the possibility in one and the same radionavigation field to use receiver indicator equipment with different levels of accuracy and operation capabilities with a different composition of the determined parameters. Up to now none of the existing varieties of radiotechnical means for close and distant navigation has been able to fulfil the needs for accuracy and range of operation needed for the navigation services for several objects. The RNSS are the first RNS which provide a strictly accurate navigation on a global scale. This is why they are

the first systems with a worldwide application which are able to solve navigation problems for any moving object. The improvement of navigation services for moving objects during the 90ies and at the beginning of the 21th century will depend first of all on the development and introduction in practice of exactly these systems, although for economic and reliability reasons they will be used in combination with RNS with a ground network of support points.

Future ways for developing and improving radionavigation systems.

The analysis results (tests performed by radionavigation services) of the degree of satisfaction concerning the demands of different groups of users suggest that the following steps should be undertaken :

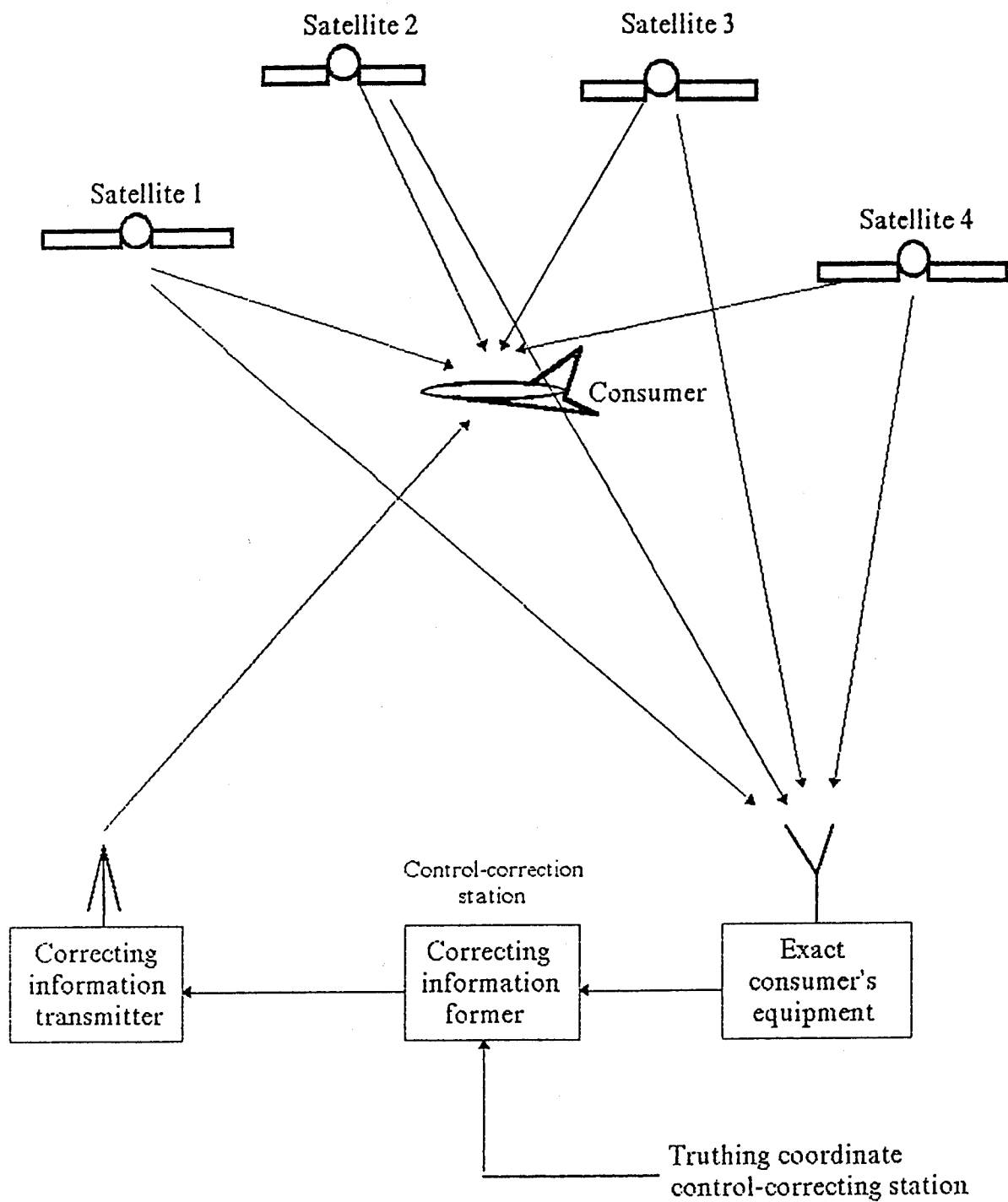
- enhancement of the accuracy to determine an object's position;
- improvement of the system's availability;
- increase of RNS integrity;

These problems can be solved by :

- using differential subsystems (modes) and relative navigation means;
- integrating the different radionavigation systems and creating a single radionavigation field;
- improving the technical characteristics of the radionavigation systems and user receiver indicator equipment.

Differential subsystems of space radionavigation systems

One of the possible versions of a differential subsystem can be the implementation of a reference station as a pseudo-satellite which transmits differential corrections simultaneously with the navigation signal similar to the signal transmitted by a navigation system satellite (Fig.2).



Subsystem Differential Structure

The implementation of the GLONASS SNS differential subsystem will provide an absolute position determination accuracy of 2 to 5 metres and a relative position determination accuracy of about 1 metre. A higher accuracy of the relative position determination of several centimetres ($\pm 10^{-6}$ of the baseline length) will be provided by geodetic measurements using carrier phase and special processing techniques.

Integration of radionavigation systems

The land RNS systems (primary and supplementary) are the radionavigation systems most widely used up to now. Their further application will not permit to satisfy the ever-increasing requirements of primary user groups concerning accuracy, availability and navigation support integrity.

With the introduction of the new-generation GLONASS (Russia) and GPS (US) space radionavigation systems it will become possible to satisfy the basic user needs for navigation support accuracy. However, also in this case availability and integrity user requirements (for air and marine users, in particular) may remain unsatisfied.

To improve such navigation support characteristics as availability and integrity it is expedient to establish integrated RNS systems (Fig.3). Improved availability and integrity of the integrated RNS is achieved through multiple radionavigation coverage.

The simultaneous operation of several Russian and foreign space and land radionavigation systems enables a combined and integrated usage in order to achieve higher accuracy, availability and integrity.

The following integrity versions are possible:

1. Space RNS - space RNS;
2. Space RNS - land RNS;
3. Land RNS - land RNS.

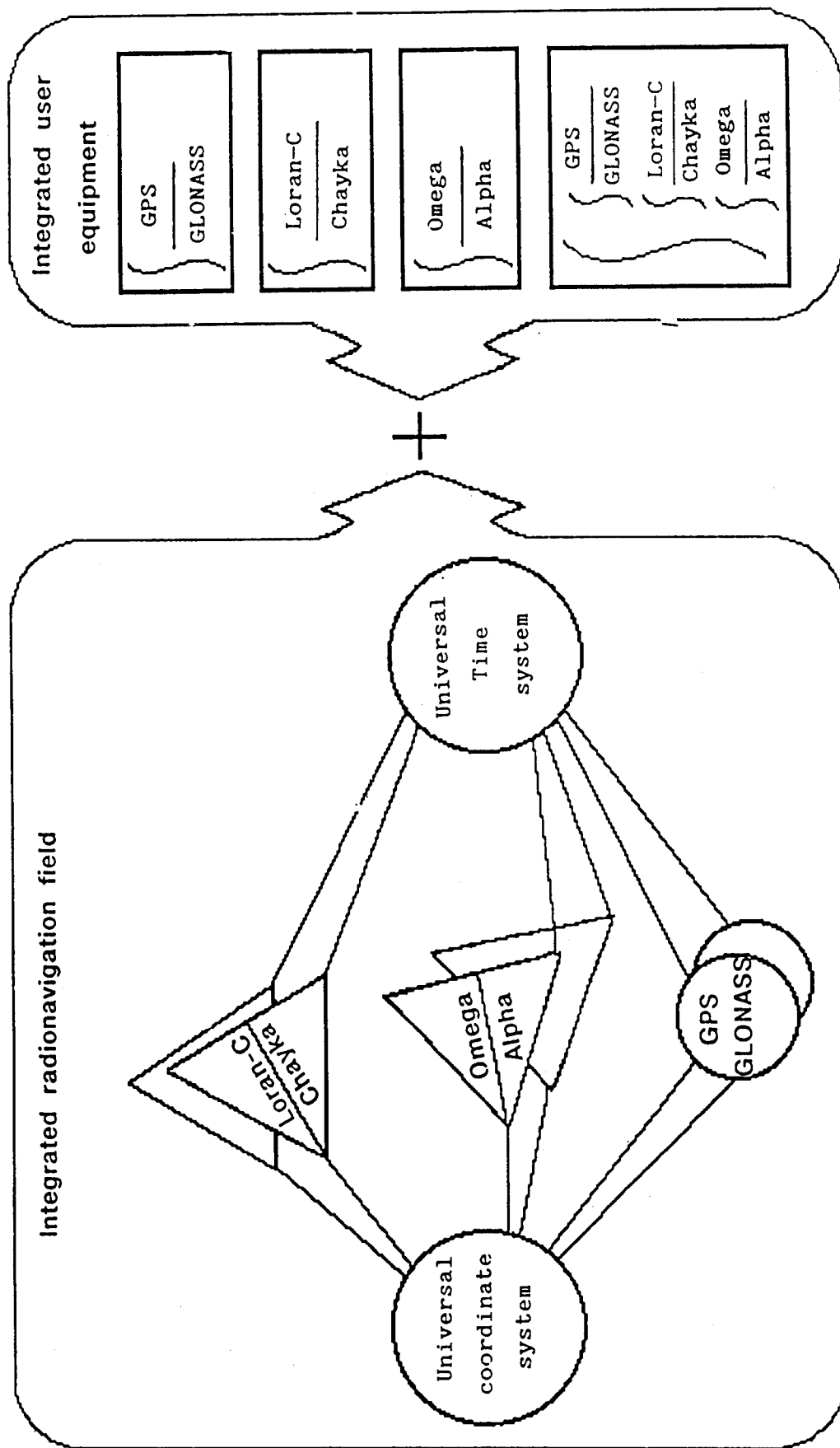


Fig.3. Concept of RNS integration

Integration of space radionavigation systems

The purpose of integrating space radionavigation systems is establishing a versatile RNS which will function as the primary radionavigation system for air, marine, land and space users.

The integration of the GLONASS (RF) and GPS (US) SNS systems is one of the most promising ways to integrate two SNS.

Integrating the GLONASS and GPS systems means:

integrating their radionavigation fields, i.e. the possibility of the combined use of navigation parameters by each of the integrated systems when solving navigation problems;

integrating user receiver equipment operating in the GLONASS/GPS systems. The combined utilization of navigation parameters (pseudo-ranges and pseudo-speeds) requires the elimination of discrepancies in the GLONASS and GPS coordinate systems and time scales.

Ephemeris data received from the satellites of each system is calculated in its own coordinate system: i.e. PZ-90 for GLONASS and WGS-84 for GPS. To convert from one coordinate system to the other, transition matrix elements should be specified by way of experiment with the GLONASS and GPS user equipment.

Frequency and time corrections must be regularly determined and inserted into the coordinate and time data onboard each satellite of the GLONASS system in order to remove the discrepancies between their time scales.

The realization of the GLONASS/GPS SNS integration depends on how fast the issues on radionavigation field integration can be settled and user receiver equipment designed and standardized.

The integration of the GLONASS/GPS space systems will permit to establish the basic global radionavigation system, which meets present-day and future air, marine, land and space user requirements.

Integration of land and space radionavigation systems

The integration of land and space radionavigation systems will allow the establishment of an integrated radionavigation system outperforming each of its component systems. The implementation of integrated land and space systems requires the integration of their radionavigation fields and user receiver equipment which necessitates removing the discrepancies in the coordinate systems and time scales.

The combination of both the Chayka/GLONASS systems is one of the ways in which the Russian land and space radionavigation systems may be integrated.

The integration of the above mentioned systems will help improve their availability and integrity in geographic regions limited by the coverage of the land RNS chains. The availability and integrity of the land and space systems lies between 0.997 to 0.998, whereas in the integrated RNS these factors will reach 1.0.

The integrated Chayka/GLONASS radionavigation system can be further employed as the primary system for all phases of navigation, except categorized approach and landings and manoeuvring in port areas.

The concept of establishing a single radionavigation field

The concept of establishing a radionavigation field presupposes the integration of radionavigation systems.

A single radionavigation field is a totality of integrated space- and land-based RNS radionavigation fields which possess a unified (or congruent) coordinate-time basis and coordinated structure of navigation signals.

The efficiency of operations in a single radionavigation field will depend on the degree of concordance of the coordinate systems and time scales in the integrated systems.

The single coordinate-time basis and coordinated signal structure will provide the development of unified receiver modules. Such a modular structure should give the possibility that the necessary receiver types may be chosen by any user depending on the composition of the employed integrated radionavigation systems.

The combined processing of the navigation parameters through measurements taken from any three radionavigation signals (one satellite and two ground-based stations, two satellites and one ground-based station, etc) will improve the probability (reliability) of the navigation determinations. The redundancy of navigation measurements in the unified radionavigation field will also permit to monitor the system's quality almost in real time.

The accuracy improvement of the characteristics to a few metres (centimetres for carrier phase measurements) with simultaneous enhancement of availability and integrity of the navigation support in the regions equipped with ground RNS stations can be achieved through combining the functions of ground RNS with those of the pseudo-satellites and through the realization of the GLONASS differential mode.

The united radionavigation field can be based on the GLONASS SNS radionavigation field which will supply the unified time scale (UTS SU) and coordinate system (PZ-90) for all ground RNS systems.

The use of a single radionavigation field will make it possible to satisfy the navigation support needs of the primary user groups, and it will also increase the probability of a continuous navigation support and the possibility of mutual control by the space- and land-based RNS.

In the first phase this united radionavigation field will cover separate regions in the CIS-countries, covered by the ground RNS, and it will further be expanded as the ground network is being extended.

Future development of the RNS user equipment

The development of receiver equipment must be directed towards:

improving the accuracy through utilizing correction reception differential modes and reducing measurement channel instrumental errors;

improving functional capabilities and services, including application of electronic maps;

improving reliability, interference resistance and electromagnetic compatibility;

providing autonomous integrity monitoring means;

reducing dimensions and weight;

reducing equipment costs and providing its availability to the mass user;

providing the opportunity of complex utilization with other autonomous and navigation means;

unifying units and elements used in the navigation equipment for various applications;

constructing integrated modular user equipment.

A unified family of equipment is the most promising direction for further development of air, marine, land and space user equipment.

The development of integrated user equipment is one of the conditions for establishing a single radionavigation field. The optimum construction of integrated user equipment presupposes a joint utilization of navigation parameter measurements from various RNS systems for solving navigation problems.

The following integrated equipment types are possible depending on the type of the integrated RNS systems:

- the integrated equipment for the GLONASS/GPS space radio-navigation systems;

- the integrated equipment for the ground and space RNS systems: Chayka/GLONASS, Alfa/GLONASS;

The development of integrated user equipment of the Chayka/GLONASS, Alfa/GLONASS, Chayka/Loran-C types must be a constituent part of the general programme for establishing integrated RNS.

Conclusion

Today, the information about user coordinates and time is provided by systems and means which are being developed separately.

The basic goal of the Radionavigation Plan is the creation of a single time and coordinate system which will function continuously via a single information algorithm and as the sum of the means and systems for the ground and space navigation as well as time-study, metrology, astronomy, geodynamics and fundamental and applied geodesy. This will allow the users to determine their coordinates with the required accuracy, reliability and operation capabilities as well as establish the time correlation in which the users are interested.

The GLONASS and GLONASS-M Programs

V. Kazantsev
NPOPM

BIOGRAPHY

M.F.Reshetnev -General Designer and General Director of NPO PM, Academician, graduated from Moscow Aviation Institute.

A.G.Kozlov First Deputy of General Designer of NPO PM, graduated from Tomsk Polytechnical Institute.

V.F.Chеремisin - Deputy Head of Division, NPO PM, graduated from Bauman Higher Technical School, Moscow.

V.N.Kazantzev - The leading designer of NPO PM, graduated from Kazan Aviation Institute.

INTRODUCTION

On September 24, 1993, the President of Russian Federation gave orders to put into operation the global navigation satellite system GLONASS consisted of 12 satellites. Simultaneously the decision was made to extend the system up to 24 satellites in 1995. At the present moment 22 satellites of the system are injected. In IV quarter of 1995 the launch of 3 satellites block is planned to be performed. Thus, the GLONASS system will be completed.

Previously the documentation was presented to the international organizations (ICAO and IMO) with guarantees to provide the use of GLONASS system in the interests of the world community during 15 years, not less. The completion of the system in 1995 was confirmed

by Decree of Russian Government N 237 of 07.03.95. Due to this Decree the Ministry of Defence, the Russian Space Agency and the Ministry of Transportation were ordered to develop a program of civil use of GLONASS system including design and production of navigation equipment, development of differential subsystem as well as to continue the use of this system as the international one.

CONSTALLATION STRUCTURE

Figure 1 shows the structure of system constellation on July, 1995. On launching on 25.07.95, the satellites were injected in the 10th, 11th and 15th orbital slots, and as the result now we have 22 functional satellites in orbits.

Table 1

| I surface | | II surface | | III surface | |
|-----------|-------|------------|-------|-------------|-------|
| Sat. | Life | Sat. | Life | Sat. | Life |
| 1 | 2,504 | 9 | - | 17 | 0,723 |
| 2 | 2,452 | 10 | 0,001 | 17 | 0,723 |
| 3 | 0,696 | 11 | 0,001 | 19 | 0,819 |
| 4 | 0,696 | 12 | 1,000 | 20 | 0,819 |
| 5 | 4,647 | 13 | 1 | 21 | 3,005 |
| 6 | 0,696 | 14 | 1,000 | 22 | 0,819 |
| 7 | 2,452 | 15 | 0,001 | 23 | 0,723 |
| 8 | 2,504 | 16 | 1,000 | 24 | 3,005 |

Orbit constellation July, 1995

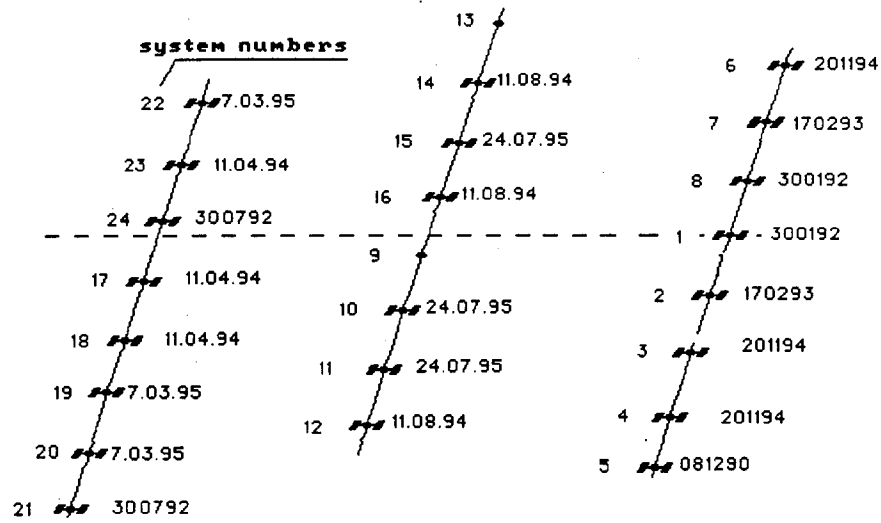


Fig 1.

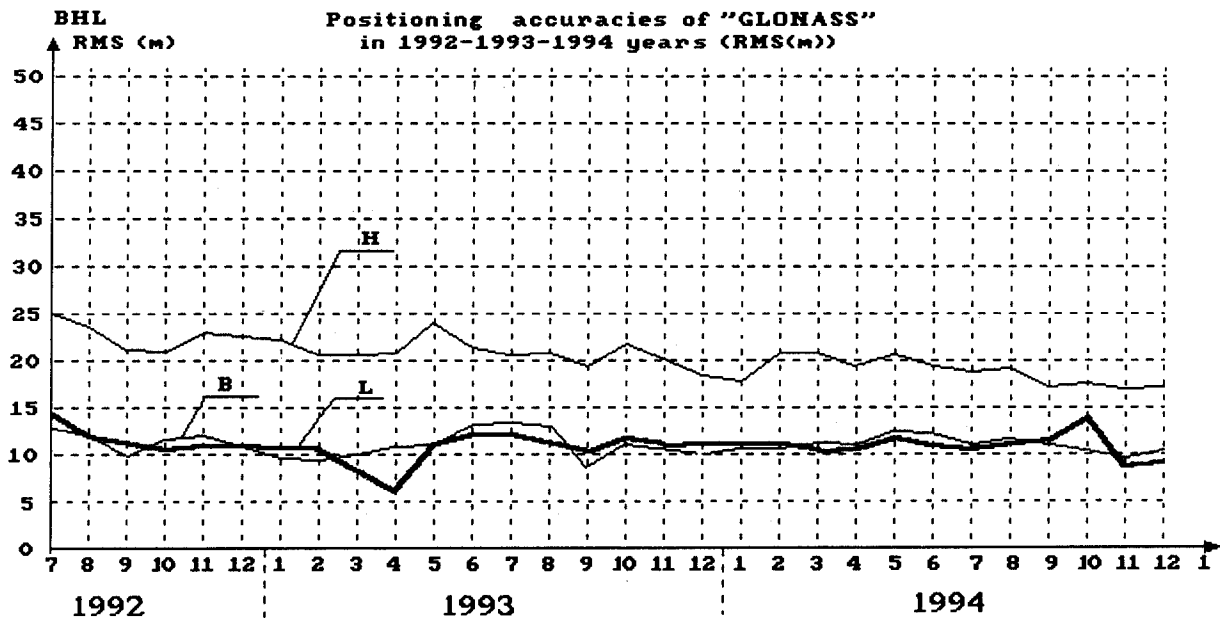


Fig.2

According to the data on July 1995 (the assessment of 23 selected satellites beginning with "Kosmos 1948"), the lifetime was equal to 3,43 years (the calculated value was equal to 3,14 years).

The spent life time period data expressed in terms of years on July, 1995, is shown in the Table 1.

The analysis of spent life period data in Table 1 shows that after the successful launch of the next block of satellites till the end of 1995 the total number of satellites is planned to be up to 24.

In GLONASS system the characteristics are provided with the accuracy of 0,95 in the case of 21 satellites in orbit. Thus, August of 1995 is considered to be the formal date of full-scale use of GLONASS.

GLONASS system is based on the principle of satellite replacement by injecting 3 satellites block in the event of one satellite fails in orbital plane. In this case two remained satellites will represent the orbital redundancy. In these terms the orbital constellation may consist of up to 6 redundant satellites. It allows to reduce the time required to replace the failed satellites.

SYSTEM ACCURATE CHARACTERISTICS

Table 2 shows the experimental data on positioning accuracy from January till July, 1995, which were obtained with the control-testing equipment of navigation field on the posts of Moscow and Komsomolsk-on-Amur. Data are presented as the point estimations (M) and RMS values of coordinate errors determined under the selection of measurements at the month's interval.

Table 2.

| | JAN | FEB | MART | JUN | JUL |
|-------|------|------|------|------|------|
| RMS | | | | | |
| B | 7.8 | 11.3 | 9.1 | 7.2 | 8.3 |
| H (m) | 12.8 | 15.9 | 14.2 | 14.0 | 14.2 |
| L | 8.4 | 11.7 | 9.2 | 9.6 | 8.6 |
| M | | | | | |
| B | 2.8 | 1.4 | 1.2 | 1.3 | 1.5 |
| H (m) | 15.0 | 13.6 | 14.3 | 17.2 | 16.2 |
| L | 2.0 | 3.0 | 1.0 | -0.4 | 1.2 |

The analysis of the analogue data in 1992, 1993 and 1994 given in Fig. 2 shows the stability of these data. The scatter in the data on the

month's base does not exceed 10%. The ionosphere plays the main role in the values of expectation of vertical component as the control-testing equipment of navigation field conducts the measurements on one frequency.

Program of GLONASS system modification

In order to improve the efficiency of system and accuracy of its characteristics, the GLONASS modification program was begun in 1989.

The program provides:

- satellite modification;
- modification of on-ground control segment;
- improvement of accuracy of system's characteristics.

In this program the satellite modification is the key element for the major characteristic of the system. The satellite modification includes the following:

- extension of guaranteed lifetime of satellite up to 5 years;
- transition to frequency band (1598,0625 - 1605,3750) ± 0.511 MHz; reduction of out-of-band interference level to satisfy the ITU (International Telecommunication Union) standards;
- improvement of stability of on-board synchronizing device up to 1×10^{-13} relative units;
- improvement of satellite dynamic in order to improve the accuracy of ephemeris forecast;
- navigational signal transmission on F2 frequency for civil users in order to eliminate the ionospheric component;
- transmission of warning signal of satellite unsuitability as a component of navigational information within 10 seconds after the fault occurs.

Modification of on-ground control segment includes the modification of the control centre, the development of up-to-date measuring devices for radio monitoring of orbit and control devices, modification of contact between control stations and control centre.

The implementation of these items allows to increase the ephemeris accuracy by $30 \div 40\%$, to increase the accuracy of navigational signal phase synchronization twice or thrice (15ns), to eliminate the ionospheric component of pseudorange error.

At the present moment the progress of modern technology allows to produce the user navigational equipment with the accuracy of pseudorange measurement within limits of $0,1 \div 0,2$ to $1 \div 5$ meters.

Table 3 shows the planned assessment of accurate characteristics for standard orbital constellation when the user works with 4 satellites with the pseudorange measurement accuracy of 5 m, radial pseudospeed of 0,01 m/sec for fixed user and with ideal ballistic structure.

Table 3

| Coordination error [M;SM/s] | Probability level | | |
|--------------------------------|-------------------|------|------|
| | 0,997 | 0,95 | 0,68 |
| B, m | 16,0 | 10,4 | 4,0 |
| H, m | 36,8 | 24,0 | 10,0 |
| L, m | 16,8 | 10,4 | 5,0 |
| V _B , sm/s | 1,6 | 0,9 | 0,5 |
| V _H , sm/s | 3,6 | 2,2 | 1,6 |
| V _L , sm/s | 1,7 | 1,0 | 0,5 |

Table 4 represents the accuracy characteristics of GLONASS/GPS combined navigational field; these characteristics are averaged within 24 hours interval on Earth surface. The data are obtained for undisturbant orbital structures, and include the following items:

- user operation with all visible satellites;
- error of intersynchronization of GLONASS and GPS systems is equal to 15 ns;
- angle of user radiovisibility is equal to 5 degree;
- error of system coordinate correlation is equal 1,5m;
- error of pseudorange measurement for GLONASS system is equal to 3m and for GPS system is equal to 4m.

In this case the GPS system operation was simulated using the coarse ephemeris mechanism and time correction (these error components

were applied according to standard law of distribution).

Table 4

| Coordination error [M] | Probability level | | |
|---------------------------|-------------------|------|------|
| | 0,997 | 0,95 | 0,68 |
| B | 41,6 | 27,2 | 12,8 |
| H | 99,2 | 64,0 | 32,0 |
| L | 46,4 | 28,0 | 14,4 |

The analysis of data of Tables 3 and 4 shows that the deterioration of GLONASS-M system accuracy level is resulted from coarsing the information of GPS system under the standard mode of positioning. To our mind, the usage of more complicated methods of processing the navigational information with the priority of GLONASS-M system being more precise, will allow the accuracy of combined navigational field to approach the level of GLONASS-M accuracy.

With the completed GLONASS/GPS constellation the users can get the advantages of combined navigational field right now.

Table 5 represents the estimating meanings of accuracy characteristics of combined navigational field for various probability levels and constellations of (21+21) and (24+24) satellites.

The results are obtained using the same initial data as the ones represented in Table 4 plus ionospheric component of error which then is converted into vertical component for very probability level and increases it by 27 m.

Table 5

| | Coordination error [M] | Probability level | | |
|-------|---------------------------|-------------------|-------|------|
| | | 0,997 | 0,95 | 0,68 |
| 21+24 | B max | 48,0 | 32,0 | 16,0 |
| | H max | 154,0 | 101,0 | 63,0 |
| | L max | 58,0 | 36,0 | 18,0 |
| 24+24 | B max | 42,0 | 26,0 | 14,0 |
| | H max | 133,0 | 91,0 | 59,5 |
| | L max | 46,0 | 30,0 | 14,0 |

Table 5 shows that the use of GLONASS/GPS constellation of 42-48 satellites allows to improve accuracy of positioning.

SYSTEM RADIONAVIGATIONAL PLAN

The following schedule of step-by-step changes of frequency band was approved to provide electromagnetic compatibility of GLONASS system and radio position service systems, mobile satellite service and radioastronomers.

At the first stage (up to 1998) GLONASS system will use the navigational signals with characters from 1 to 14 and from 21 to 24. Antipodal satellites will use the same characters. At this stage the modified GLONASS satellite is planned to be developed in order to transmit the signals within frequency range of L1 $1601,4375 \pm 1598,0625$ Mhz, L2 $1242,9375 \pm 1245,5625$ Mhz with the negative characters from -7 to -1. The satellite is proposed to be equipped with the filters to reduce the wide-band radiation in the frequency range of $1630 \div 1670$ MHz to the radiation level recommended by CCIR. At the second stage (up to the 2004) the satellites with the characters from 0 to 12 will be under operation continuously, and the satellite with the character 13 will be used as technological one on case by case base. Simultaneously the modified satellites newly commissioned can also have the characters from -7 to -1. At the third stage (beginning from 2005) all the satellites being under operation will use the navigational signal with characters from -7 to +6, and characters from +5 and +6 will be used only as technological ones within limited periods of time.

PROPOSALS OF GLONASS/GPS COMBINED USAGE

Since GLONASS and GPS systems being offered for international purposes as well as concepts for combined use of these systems being developed, the Russian and American sides (FAA, DOD, ARINC, Honeywell, North West Airline, etc.) have been cooperating profitably in developing standards for aircraft equipment. The approached technical solutions allowed to refuse the deeper integration of systems with specified level of accuracy when the combined navigational field is used. Simultaneously the limitation of each system in terms of availability and integrity for aviation users were established.

It should be noticed that aviation user requirements are more strict ($0,999 \div 0,99999$) and require the special development. To our opinion these requirement would be met using two navigational systems and additional communication subsystem. This subsystem must

consist of communication satellites in geosynchronous orbits (in geostationary orbits or in orbits of "TUNDRA" type) and on-ground control equipment of navigational field performing the functions of differential station network and control. Communication satellite can settle the following problems:

- to transit the information for automatic dependent surveillance (ADS) in the interests of ATM;
- to transit differential corrections for ADS zone and worldwide, if necessary;
- to transit the information of GLONASS and GPS integrity. The studying of the different solutions of the above problems were held in [4, 5, 6]. We also have at least two problems to be solved in the future.

They are:

- the connection of coordinate systems used - ПЗ-90 and WGS-84
- synchronization of UTC (SU) and UTC (USNO) time scales.

At the present moment GLONASS and GPS use two equal accurate coordinate systems with the following main characteristics (see Table 5).

Russian geodesists received by the indirect means the variables to assess the connection of these two systems:

$$\begin{aligned}x &= y = 0, \quad z = 1,5, \quad m = 0, \\W_x &= W_y = 0, \quad W_z = -0,076''\end{aligned}$$

These assessments are preliminary [8]. Neglect of these connections variables of two systems may lead to errors in positioning in limits within $10 \div 15$ m. Taking into account the specified level of system accuracy characteristics (in limits within $100 \div 150$ m approximately) and the given accurate redundancy of GLONASS, the value of $10 \div 15$ m practically does not impact the specified level of positioning accuracy if the user works with the satellites of two positioning systems at a moment. But in the case of improvement of systems accuracy characteristics within the limits of $10-20$ m one should take this value into account.

Table 6

| Characteristics | RMS error | |
|--|-----------|-----------|
| | ИЗ-90 | WGS-84 |
| Post locations relative to Earth's centre of mass, m | 2 | 2 |
| Relative locations of posts, m | 0,2 | 0,1 ÷ 0,5 |
| Geoid altitude above terrestrial ellipsoid, m | 1,5 | 1,5 |

Table 6 shows that the range of coordinate systems accuracy possibilities by a factor of 100 differs the same characteristics of GLONASS and GPS. The analysis of radionavigational plan shows the largely extension of system possibilities depending on the given accuracy [2, 3]. In this connection the trend to provide the higher accuracy to the civil users will exist in the future as well. The second problem is to provide the synchronization of systems time scales with the correction accuracy transmitted in navigational frame (message). Modified satellites of GLONASS-M are designed to transmit the corrections to GLONASS time scale relative to GPS time scale. The calculation of these corrections with the accuracy adopted for each system would allow to solve the problem on any four satellites from the constellation of 48 satellites with the standard mode of positioning. To solve these problems one should have the set of highly accurate equipment to fix the time scale of GPS connected with the central synchronizer of GLONASS system. Conceptually the more precise decision of this problem is possible. For this purpose one should use the analogue set mounted at the place of GPS time reference. The set provides the subsequent exchange of measuring information and calculations of corrections throughout the whole number of measurements.

CONCLUSIONS

1995 is the date of completion of GLONASS system consisting of 24 satellites and the date of the beginning of its full-scale operation. As it was mentioned previously the Russian Ministry of Defence and the Russian Space Agency guarantee that the system will be under operation during 15 years period. Simultaneously we continue to modify the system in order to have the accurate characteristics of 30-40 m (limiting values) in the future. The usage of GLONASS/GLONASS-M navigational field combined with GPS allows to improve the positioning reliability

and to reduce the effect of geometrical factors of positioning. Under this conditions the presence of coarsing mode in GPS system combined with the usage of combined navigational field in standard mode of positioning results in the deterioration of level of GLONASS-M accuracy. To our mind, the usage of more complicated methods of processing the navigational information with the priority of GLONASS-M system being more precise, will allow the accuracy of combined navigational field to approach the level of GLONASS-M accuracy.

REFERENCE

- 1) GLONASS system technical characteristics and performance, ICAO DOC. FANS/4-WP 75, 1988
- 2) Radionavigational plan of Russia, Internavigatsia, 1994
- 3) Federal Radionavigation Plan 1990, DOD and DOT US, DOT-VNTSC-RSPA-90-3.
- 4) Navigation 1987-1988, v34, N4, p297-306.
- 5) Navigation 1985-1986, v32, N4, p334-350.
- 6) Kinal G.V. and Singh J.P. "An International Geostationary Overlay for GPS and Glonass, Navigation, N37, N 1, 1990
- 7) MISRA P. and other, Receiver Autonomous Integrity Monitoring of GPS and Glonass, Navigation, v40, N1, 1993
- 8) Boikov V.V. and others "The use of geodetic satellites to solve the fundamental problems". Geodesya and Kartographya, N11, 1993 Moscow ISSN 0016-7126

Ways of GLONASS System Advancing

Nicolay Ivanov, Vadim Salischev, and Alexander Vinogradov
RISDE

BIOGRAPHY

Dr. Nicolay E. Ivanov is the Director of Research and Development field at Russian Institute of Space Device Engineering (RISDE). The main focus of his activity involves development of radio engineering complexes for satellite navigation and geodetic systems. These complexes consist of vehicle-born radio engineering equipment for satellites, earth-located control complexes, and user equipment for these systems. Dr. Ivanov is a technical manager for the geodetic system Geo Ik and the navigation systems Tsikada and GLONASS. Dr. Ivanov is also responsible for the development of command systems for automatic spacecraft. Dr. Ivanov has the academic degree of doctor of technical sciences.

Dr. Vadim A. Salischev is a Chief of Department in the RISDE. The sphere of his activity relates to research and development of satellite-based navigation and geodetic systems and equipment for users of these systems. He took an active part in development of systems principles, signal's structure and designing equipment for Tsikada, Geo-IK and GLONASS systems. Dr. Salishev graduated from the Moscow Aviation Institute and has been working in the space technology area since 1959. He has the academic degree of doctor of technical sciences.

Mr. Alexander A. Vinogradov is a chief of the sector of the RISDE. The sphere of his activity relates to research and development of satellite-based navigation and geodetic systems and equipment for users of these systems. He took an active part in development of systems principles, signal's

structure and designing software for user equipment of the GLONASS system. Mr. Vinogradov graduated from Moscow Aviation Institute and has been working in the space technology area since 1975. At present, his research interests are connected with development of software for GLONASS user's equipment of different types.

ABSTRACT

Currently, the GLONASS system is in its final phase of full deployment. As it was declared earlier, full deployment of the system consisting of 24 satellites would be finished by the end of 1995.

It is known, that frequency band of the GLONASS navigation signals overlaps with the band used by the Radio Astronomy. In order to avoid interferences in the Radio Astronomy band, the plan have been developed and is implemented now for gradual changing of the GLONASS navigation frequency bandwidths.

In order to improve navigation accuracy for civil users, the modernization of the navigation L2-signal is undertaken. Modernized GLONASS-M satellites will broadcast L2-signals destined as for military as for civil use. This will allow civil users to exclude automatically that portion of measurement error caused by the ionospheric refraction.

One of the most important tasks linked with the full system's deployment is a task of integrity maintenance. For the sake of this task, creation of additional GLONASS integrity monitoring stations will be started on the territory of Russia in 1995. These stations will be linked into a single network with an internal information exchange, allowing fast detection and uploading aboard the satellites information on possible degradation of navigation signal's quality. These monitoring station will at the same time serve as differential stations and will form the wide area differential network. The monitoring station will be based upon the 16-channel combined GLONASS/GPS receivers, allowing

to monitor integrity and form differential corrections for satellites of both GLONASS and GPS systems.

Combined usage of the GLONASS and GPS systems in near terms should become the real factor improving reliability and availability of navigation for civil users.

Analysis made on similar and different features of both systems confirms existence of two aspects requiring mutual discussions and further cooperation between the Russian and the US specialists. These aspects are differences in time scales and coordinate systems adopted in the GLONASS and GPS.

Russian specialists are ready for cooperation in this area and intended to broadcast the time scale difference within the GLONASS navigation message. However, the divergence between the GLONASS and GPS coordinate systems can be determined most accurately and reliably by means of mutual efforts of the Russian and US specialists.

1. INTRODUCTION

The GLONASS system currently is in its final phase of full deployment. As it was declared earlier, full deployment of the system consisting of 24 satellites would be finished by the end of 1995.

The process of transformation of the GLONASS into continuously operating system attracts advanced requirements to reliability of space and ground segments and to compatibility of GLONASS navigation signals with signals of other radio systems. Also, there is a constant growth of user's requirements in terms of navigation accuracy and integrity, where the term integrity means the ability of a system to provide timely warnings to users when the system shouldn't be used for navigation.

2. GLONASS ADVANCING

Due to the above mentioned reasons, the GLONASS system is being modernized currently, following directions listed below:

- improving compatibility of the GLONASS with other radio systems;
- improving navigation accuracy and improving services represented by the system to users;
- increasing reliability and lifetime of on-board satellite equipment and improving system integrity;
- deployment of differential subsystem.

Currently, nominal values of carrier frequencies for navigation radiosignals transmitted within L1 and L2 bandwidths are defined as follows [1]:

$$f_{L1} = f_{01} + K\Delta f_1 \quad (1)$$

$$f_{L2} = f_{02} + K\Delta f_2 \quad (2)$$

where: $K = 0, 1, 2, \dots, 24$;

$$f_{01} = 1602 \text{ MHz}; f_{02} = 1246 \text{ MHz}$$

$$\Delta f_1 = 562.5 \text{ KHz}; \Delta f_2 = 437.5 \text{ KHz}$$

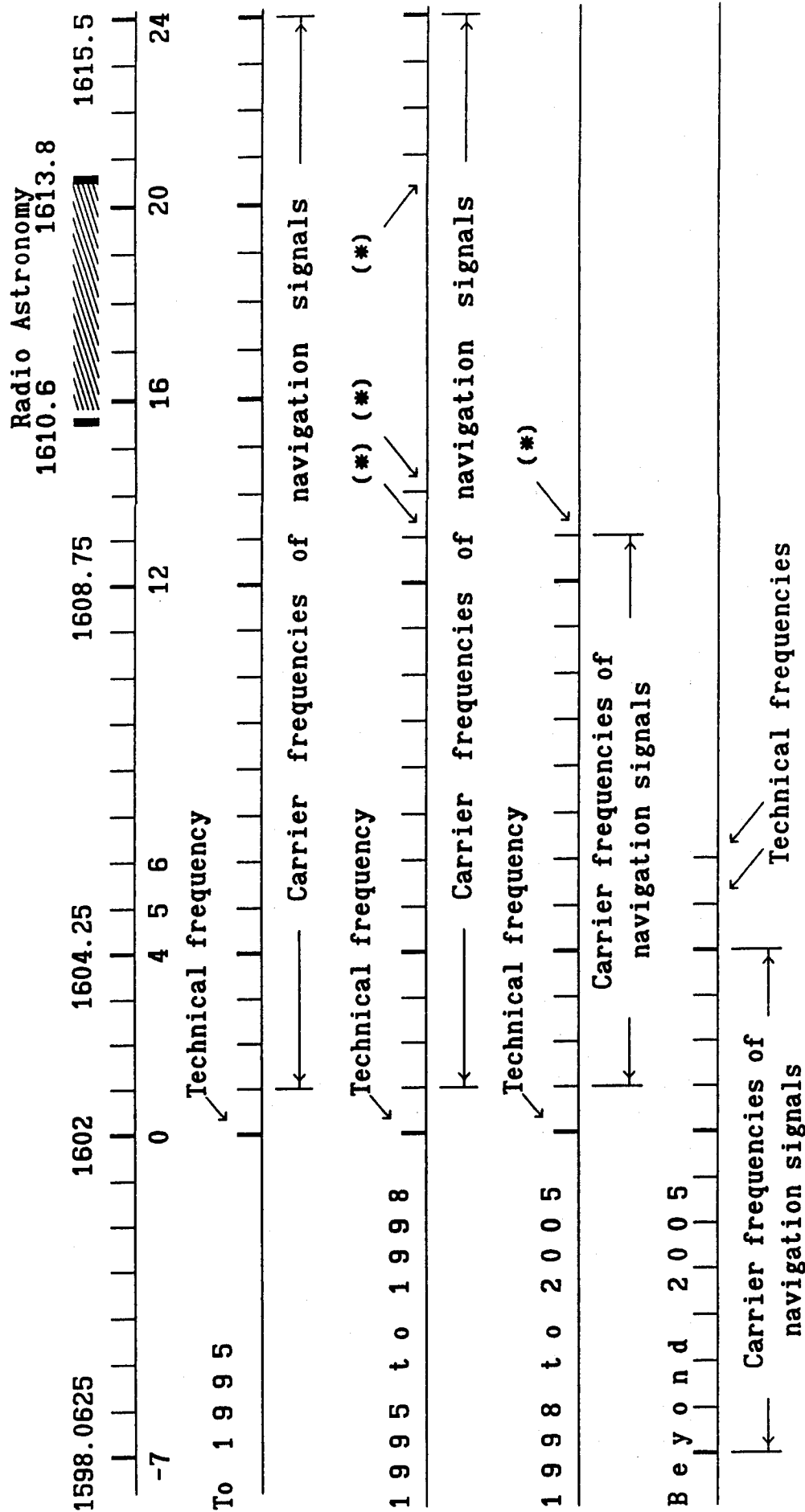
$$f_{L2}/f_{L1} = 7/9 \quad (3)$$

The carrier frequency with $K=0$ doesn't used for navigation. It is necessary for testing spare navigation spacecraft in orbit.

Thus, the GLONASS navigation signals for civil use occupy in L1 bandwidth the frequencies (fig.1):

$$\Delta f = (1602.5625 \div 1615.5) \pm 0.511 \text{ MHz}$$

The use of frequencies specified above by the GLONASS satellites, creates interferences to Radio Astronomy within the bandwidth $1610.6 \div 1613.8 \text{ MHz}$.



***) - Carrier frequencies, which may be used under exceptional circumstances**

Fig. 1: GLONASS Frequency Plan.

Moreover, according to resolutions of WARC-87 and WARC-92, the bandwidth 1610.0÷1626.5 MHz is allocated on primary base to Radiodetermination-Satellite Service ("Earth-to-space") and Mobile-Satellite Service ("Earth-to-space"). The bandwidth 1613.8÷1626.5 MHz is allocated to Mobile-Satellite "space-to-Earth" service on secondary base.

Considering for these factors, modernization of the GLONASS system includes gradual shifting and shrinkage of the bandwidth occupied by the system signals. The principle of frequency division between navigation signals will be maintained, but total number of frequencies will be reduced to 12. To avoid internal interferences between the satellites of modernized GLONASS system, the satellites broadcasting on the same frequency will occupy opposite orbital points.

The process of changing GLONASS frequencies will include several stages [2].

Stage 1: present to 1998.

During this stage satellites stop transmission of signals on frequencies with $K = 16, 17, 18, 19, 20$, i.e. within the bandwidth 1610.6÷1613.8 MHz, used in Radio Astronomy. Operating at that time satellites broadcast their signals on frequencies with $K = 0 \div 12$ and $K = 22, 23, 24$. Carrier frequencies with $K = 13, 14, 21$ will have limited use: during setting up the satellite into operation mode after its launch, and during the satellite's prophylactics.

Stage 2: 1998-2005.

The GLONASS-M satellites will broadcast their signals on carriers with $K = 0 \div 12$. As an exception, sometimes the carrier with $K = 13$ may be used.

The on-board equipment of modernized GLONASS-M satellites will contain filters rejecting out-of-band emissions in the 1660÷1670 MHz, as recommended by the ITU-R RA.769 ($-238 \text{ dBW}/(\text{m}^2\text{Hz})$).

Stage 3: beyond 2005.

During this period the GLONASS-M satellites will broadcast navigation signals on carriers with $K = -7 \div +4$.

Carriers with $K = 5, 6$ will be used as technical frequencies for interaction with ground control segment.

The on-board equipment of GLONASS-M satellites operating at that time will contain filters rejecting out-of-band emissions in the $1610.6 \div 1613.8$ MHz and $1660 \div 1670$ MHz, as recommended by the ITU-R RA.769 (-238 dBW/(m^2 Hz)).

In order to increase the navigation accuracy, the new cesium frequency reference will be used on the board of the GLONASS-M satellites, whose instability will account 10^{-13} per day [3], compared with 5×10^{-13} per day for GLONASS satellites.

Currently, the signal for civil use only is broadcasted in the L1 bandwidth. Meanwhile, the ionospheric error component can be as high as 30 m and more during the periods of maximum solar activity.

That is why the GLONASS-M satellites will broadcast signals for civil use on two bandwidths (L1 and L2). This will allow users equipped with two-frequency receivers to reduce significantly measurement error component due to the ionosphere.

The power of the signal transmitted on L2 for civil users will be equal to 10 W. The gain of transmitting antenna is 8.8 dB along the central axis directed to Earth, and 11 dB and 9 dB for angles $\pm 15^\circ$ and $\pm 19^\circ$ off the central axis, respectively.

The ranging code of civil L2 signal will be formed as pseudorandom sequence of maximal length with repetition period of 1 ms and bit rate 511 Kbit/s. The forming polynomial is as follows:

$$G(x) = 1 + x^5 + x^9$$

Due to the transmission of ranging code for civil users in L2-bandwidth, the additional parameter $\Delta\tau_n$ is introduced in the GLONASS-M navigation message. This parameter characterizes a difference between delays of ranging codes in L1 and L2 equipment of the satellite. If $\Delta\tau_n > 0$, then L2-delay is larger than L1-delay. If $\Delta\tau_n < 0$, then

L1-delay is larger than L2-delay. An error of transmitted $\Delta\tau_n$ -value is less than 2×10^{-9} s.

Besides the $\Delta\tau_n$ - parameter, some more parameters are introduced in navigation messages, increasing reliability of navigation determinations of users.

The GLONASS satellites transmit in their navigation messages a τ_c - parameter, which characterizes the difference between the time scale of Central Synchronizer (to which phases of satellite ranging codes are referenced) and the UTC(SU) time scale, to which the satellite's ephemerides are calculated. The UTC(SU) scale can be corrected by 1 sec once, or twice per year, depending on astronomic time. The correction can be implemented at midnights December,31-January,1, March,31-April,1, June,30-July,1, September,30-October,1.

The GLONASS-M navigation messages will contain the sign of expectation of 1-sec correction to UTC(SU). This sign can have four states:

- 10 - solution on implementing the time correction is not adopted yet;
- 00 - there will be no corrections;
- 01 - the correction is expected by +1 sec;
- 11 - the correction is expected by -1 sec.

In the case, when the solution on implementing the UTC SU correction is adopted, the information on that will be introduced into the navigation message not later than two months before implementation.

Combined usage of GLONASS and GPS systems give users additional advantages, the basic of which are increasing the availability, reliability of navigation and reduction of GDOP, due to increased number of satellites in view. But currently, application of two systems simultaneously for 3-D positioning requires availability of 5 satellites in view, minimum. This is caused by the introduction of the new unknown - difference of ranging code phases between the GLONASS and GPS satellites.

It is expected to transmit the difference between the GLONASS and GPS time scales ($\tau_{\text{GPS-GLN}}$) within the GLONASS-M

navigation message. This parameter will have the range $\pm 1.9 \times 10^{-3}$ s and the value of order bit as 1×10^{-9} s.

Also, the navigation message will contain the satellite identity as follows:

00 - GLONASS;

01 - GLONASS-M.

The onboard equipment of the GLONASS-M satellites will include additional devices and additional cross-links between devices, in order to increase reliability of onboard electronic equipment during satellite's lifetime.

The system integrity monitoring in the GLONASS system is implemented in two ways [1].

First, each navigation satellite autonomously monitors operation of its onboard systems. When a malfunction occurs which may degrade the quality of navigation signal, the satellite begins to transmit within its navigation message the sign, signaling on bad "health status". This method of autonomous monitoring of status of onboard systems is quite quick, but it doesn't capable of discovering all possible malfunctions in operation of the on-board systems.

Second, a quality of navigation signals of all satellites of the system is constantly monitored by the Navigation Integrity Control and Monitoring Equipment, included in the GLONASS Subsystem of Control and Monitoring (ground segment). When a malfunction occurs which degrades the quality of broadcasted navigation signal, the sign Cn is introduced into satellite's navigation message indicating the bad "health status" of a satellite.

Improvement of the GLONASS system integrity is planned to carry out acting in two directions: expanding the range of circuits of onboard subsystems monitored autonomously by the on-board means, and deployment the network of ground-based stations providing continuous system integrity monitoring.

At the Russian Institute of Space Device Engineering the monitoring station have been developed based on 16-channel GLONASS/GPS receiver. This multichannel receiver

is capable of receiving with each its channel signals of both GLONASS or GPS.

Figure 2 shows the probability density for numbers of GLONASS and GPS satellites of fully deployed systems, observed simultaneously.

The receiver was designed considering for cost-to-effectivity ratio and has 16 channels (fig.3).

The purposes of monitoring station are the following:

- continious tracking of up to 16 GLONASS and GPS satellites, storing in computer memory all received measurement and digital information;

- continuous real-time navigation using constellations consisting of:

 - GLONASS satellites only;

 - GPS satellites only;

 - both GLONASS and GPS satellites.

- analysis of error components of navigation determinations and measurements of pseudo ranges and pseudo range rates;

- monitoring of GLONASS and GPS navigation signal's and message's quality;

- generation of differential corrections to measured navigation parameters and "health" statuses of observed satellites.

Monitoring and differential station can operate autonomously, or being controlled manually by operator.

Operation of the receiver and its reliability are constantly controlled by central computer of the monitoring station. This control is provided by means of telemetry information exchange between the computer and receiver in real time, without interrupting signal reception and measurement processing.

The following functions and parameters are monitored constantly:

- operation of delay-locked loop of the ranging code, phase-locked and frequency-locked loops of received signal;

- noise and signal levels in each receiver channel;

- content of received digital information (using

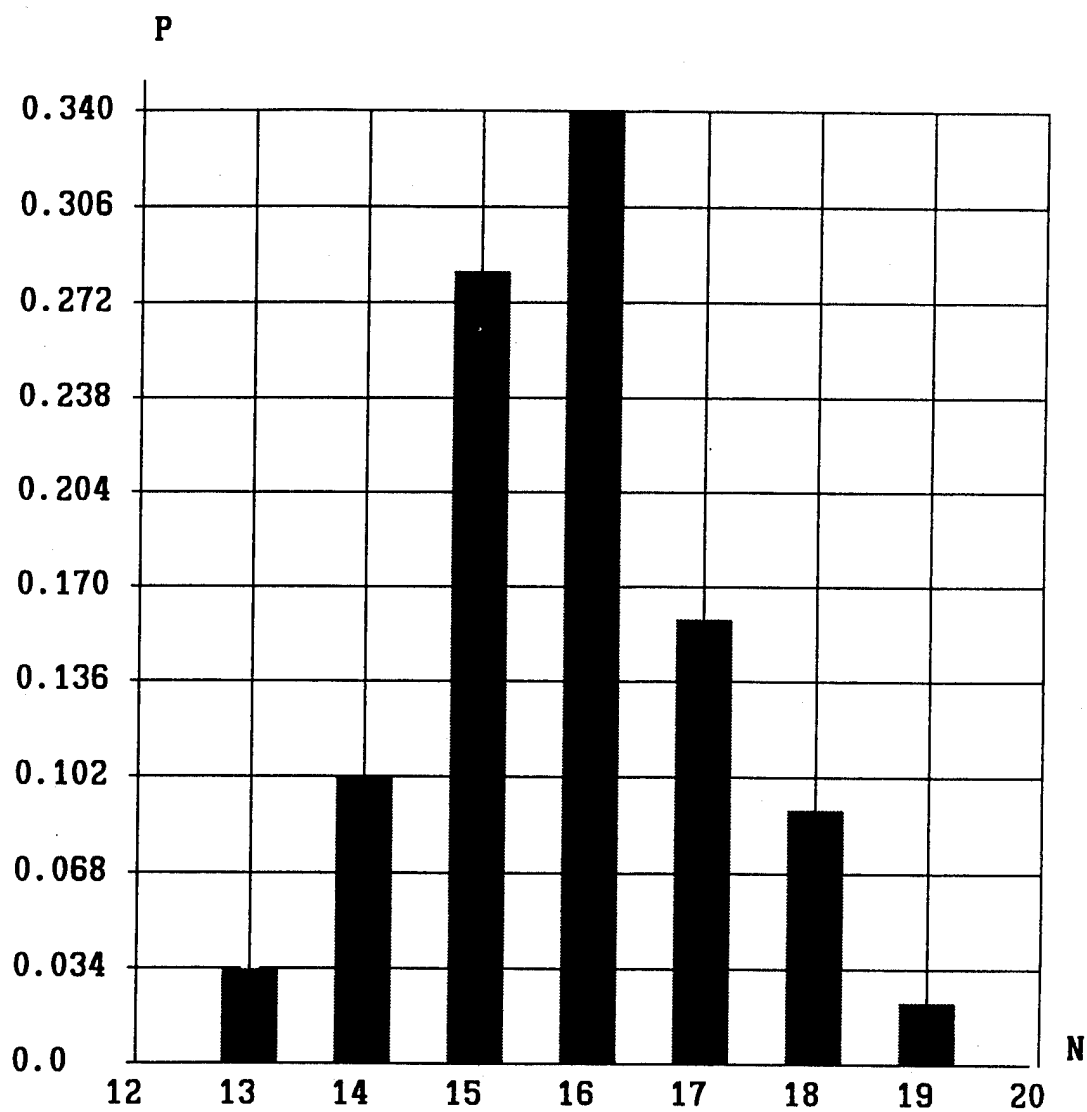


Fig. 2: Density Probability of GLONASS and GPS Visible Satellite Numbers of Fully Deployed Systems.

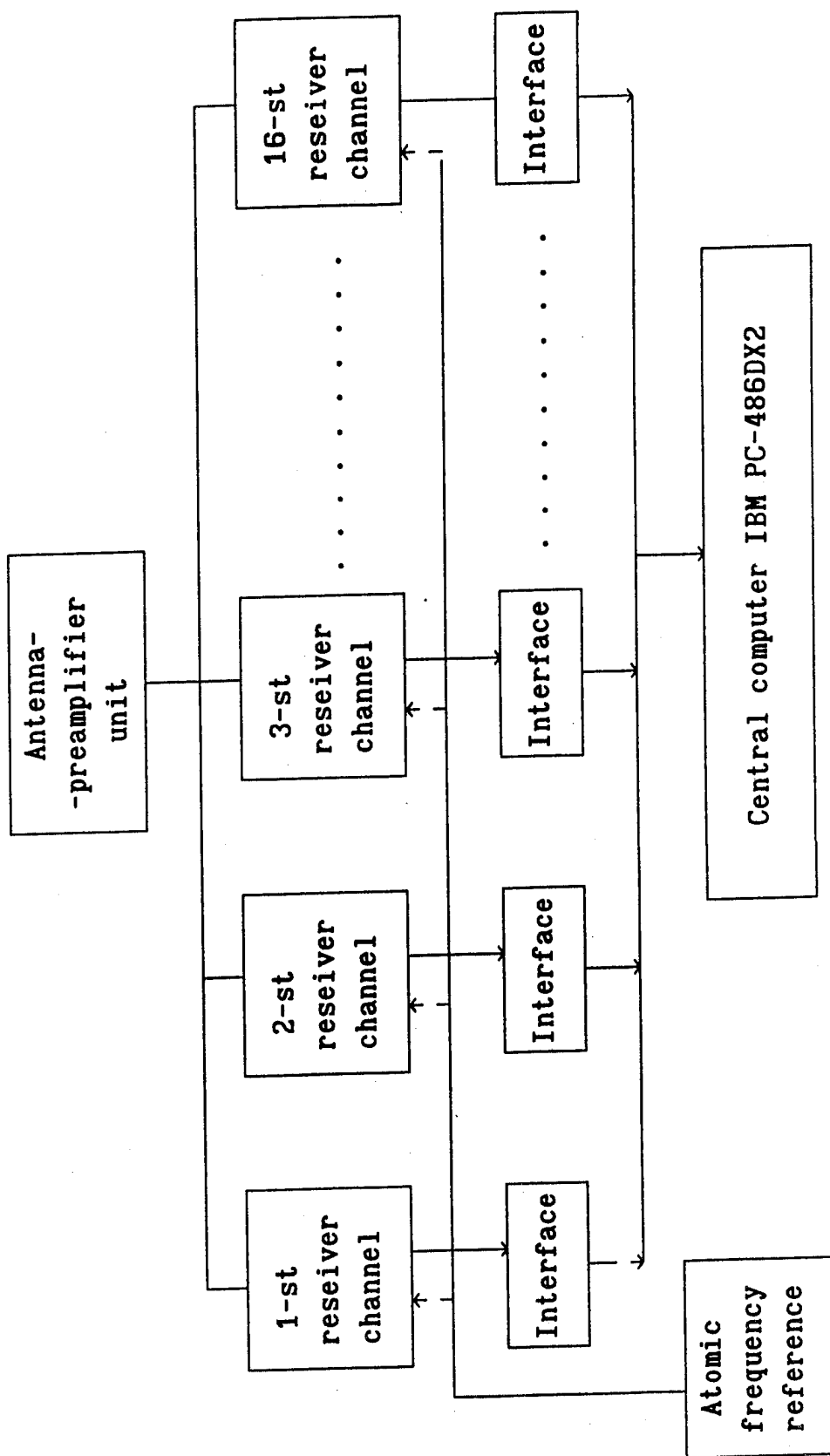


Fig. 3: GLONASS/GPS Monitoring Station.

Hamming Code, and comparison of subsequent information frames).

If any anomalous measurement of pseudo range and pseudo range rate are discovered, then all, or several receiver channels start reception of signal from that satellite, which yields anomalous measurements. If all signals received by these dedicated channels would yield anomalous measurements, then the solution can be adopted on bad "health" status of this particular satellite.

For example, figure 4 shows delta ranges $\delta S(t)$, obtained on GPS satellite measurements:

$$\delta S(t) = S(t) - S(t - \Delta t);$$

and calculated delta ranges δR for the same time interval:

$$\delta R(t) = R(t) - R(t - \Delta t).$$

$$\Delta t = 1 \text{ s}$$

Figure 5 shows delta range rates $\delta \dot{S}(t)$, obtained based on real measurements using the same GPS satellite and the same as above time interval:

$$\delta \dot{S}(t) = \dot{S}(t) - \dot{S}(t - \Delta t);$$

Figure 6 shows differences of calculated and measured parameters, obtained using different GPS satellites NS4 and NS1.

$$\Delta R_{4-1}(t) = [S_4(t) - R_4(t)] - [S_1(t) - R_1(t)];$$

$$\Delta \dot{R}_{4-1}(t) = [\dot{S}_4(t) - \dot{R}_4(t)] - [\dot{S}_1(t) - \dot{R}_1(t)];$$

Figure 7 shows the same differences for GLONASS satellites.

General estimation of navigation signal's quality is performed using continuously obtained positioning results.

For instance, figures 8 and 9 show positioning

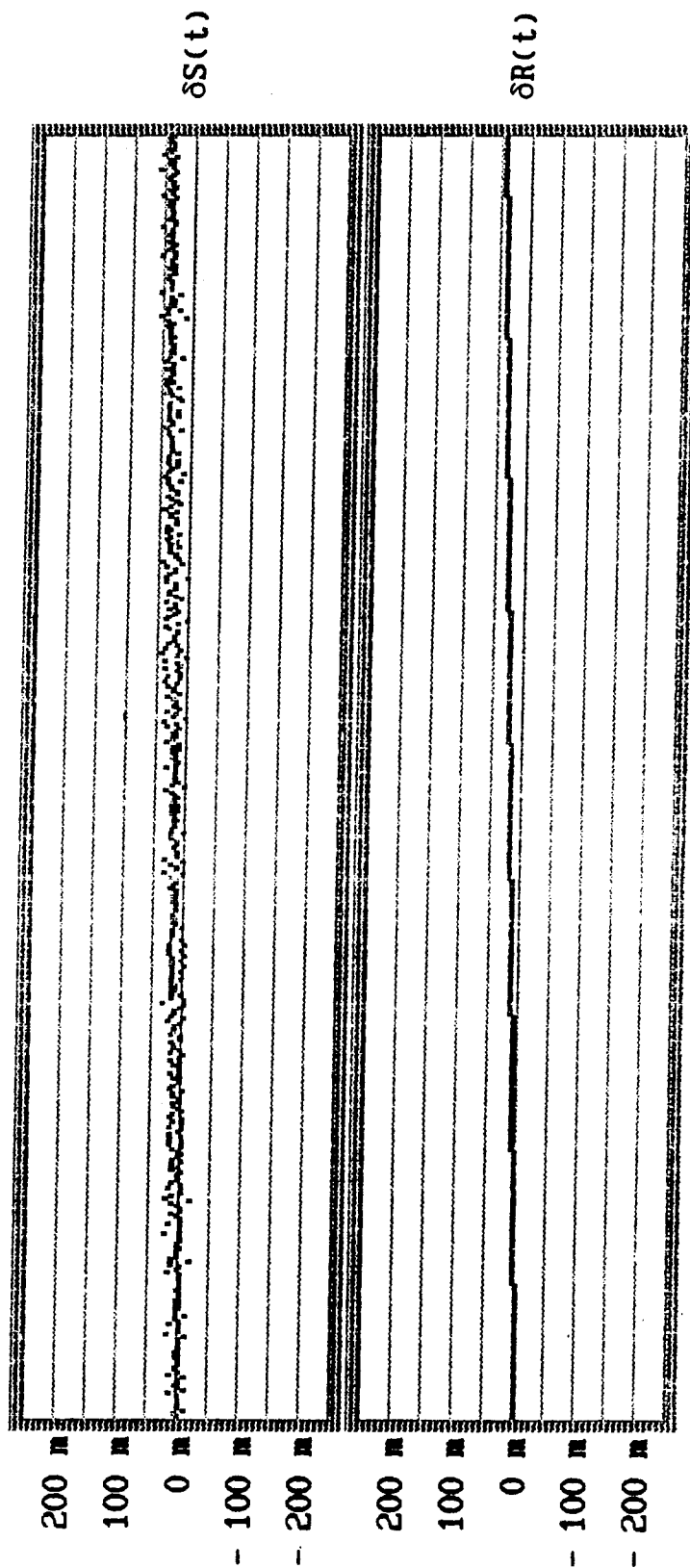


Fig. 4: Measured and Calculated Delta Ranges for GPS Satellites.

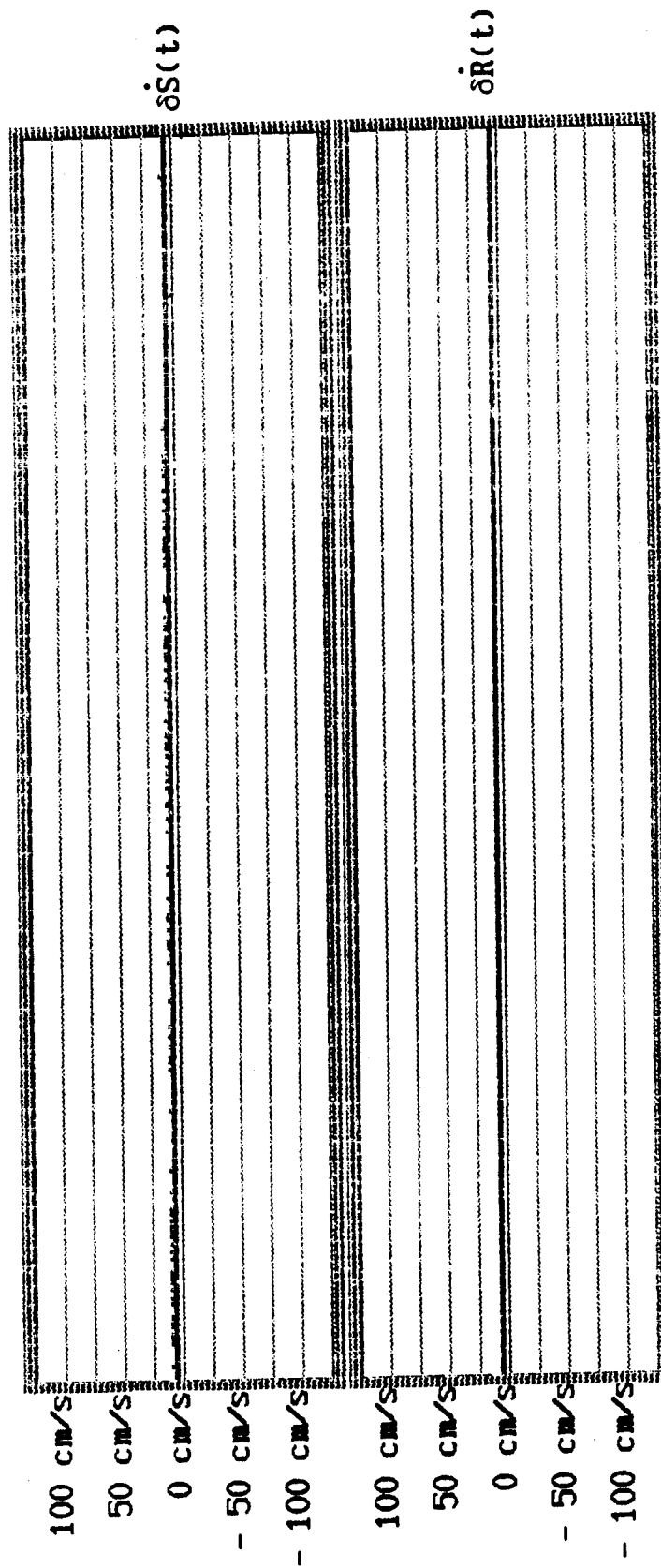


Fig.5: Measured and Calculated Delta Range Rates for GPS Satellites.

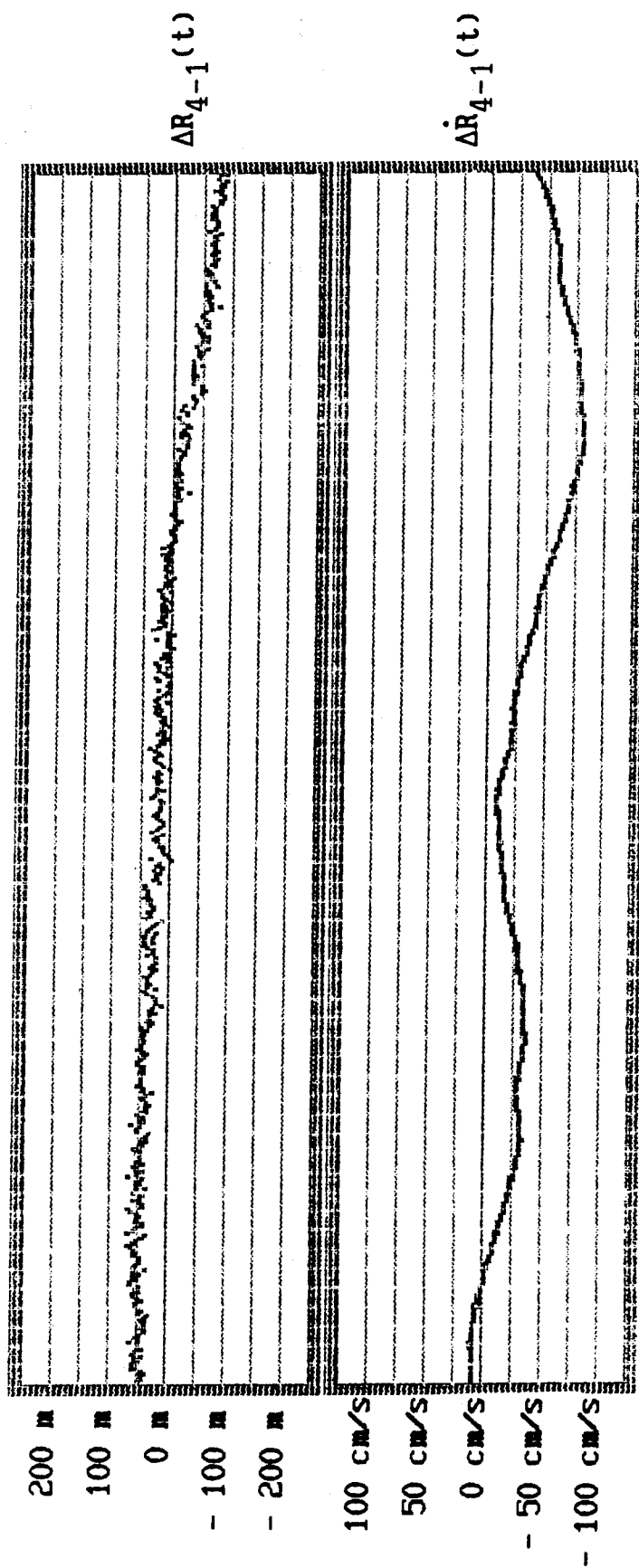


Fig.6: Differences between the Calculated and Measured Parameters
for Different GPS Satellites.

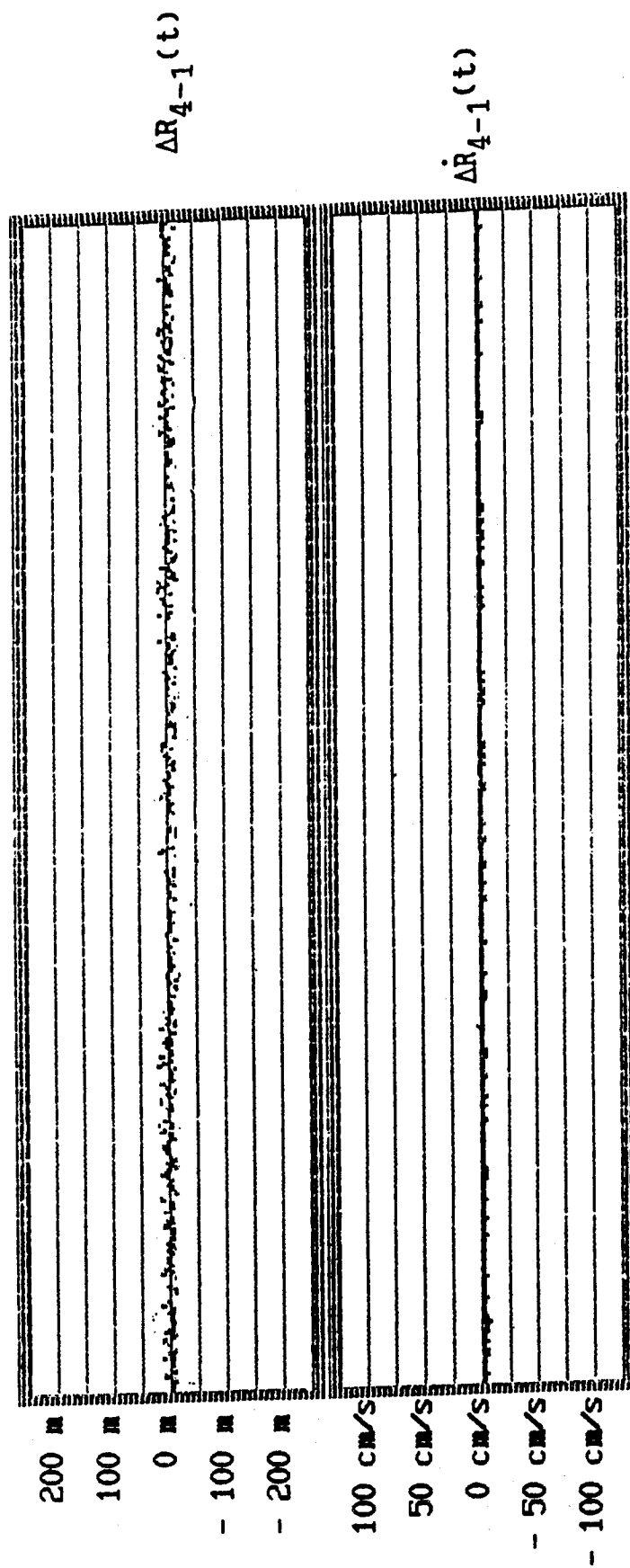
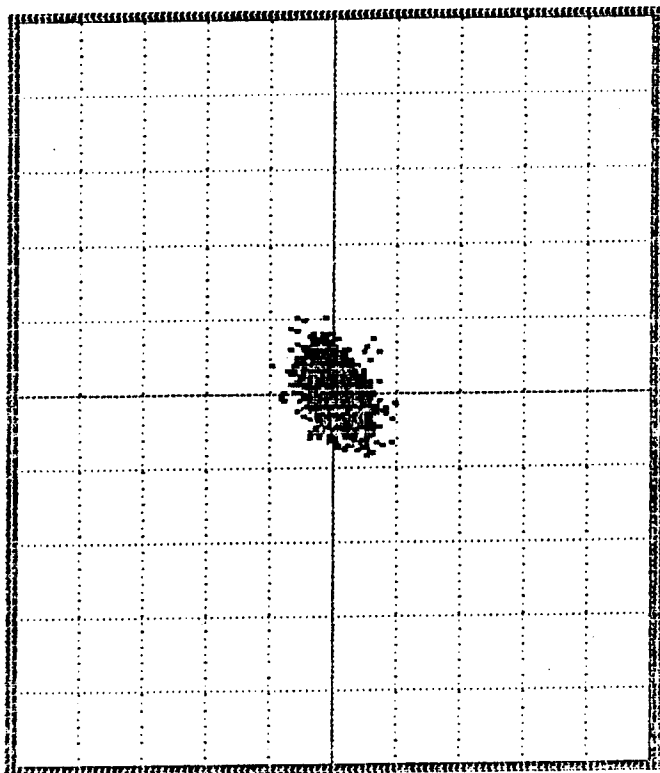
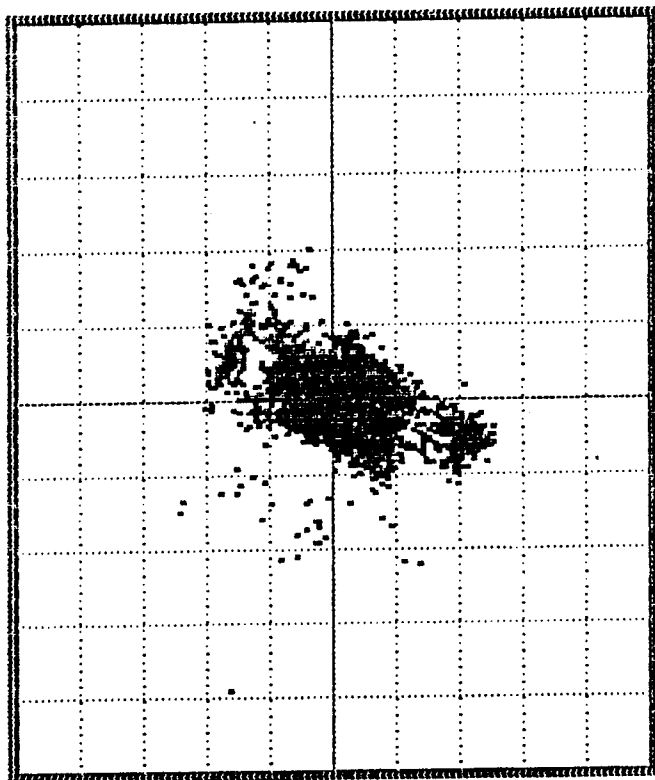


Fig.7: Differences between the Calculated and Measured Parameters
for Different GLONASS Satellites.



Latitude - Longitude Deviation
(small square - 30 x 30 m)

Fig.8: Positioning Results for GLONASS. Averaging Time - 1 s.



Latitude - Longitude Deviation
(small square - 30 x 30 m)

Fig.9: Positioning Results for GPS. Averaging Time - 1 s.

results, averaged during $T_o = 1$ sec and obtained using GLONASS and GPS satellites respectively.

Monitoring station's hard- and software are capable of continuous estimating clock offset between the GLONASS and GPS systems, and divergence between the SGS and WGS reference frames at station's location. Station is capable of generating differential corrections to measurements made with all satellites observed.

Standard interface of the station corresponds to interface of IBM PC486DX2. This interface makes possible transmission of differential corrections and any other information generated by the monitoring station to external consumers via link channel.

It is planned to connect all monitoring stations located on the territory of Russia into wide area network, providing users with integrity information and GLONASS/GPS clock offset. This network will also provide users with differential corrections, whose accuracy practically will not depend on distance to station, given that user is on the territory covered by the network.

Combined application of the GLONASS and GPS systems in near terms should become the real factor improving reliability and availability of navigation for civil users in the world.

Analysis made on similar and different features of both systems [4,5] shows that the largest portion of differences will insignificantly impact the complexity and cost of combined GLONASS/GPS receivers, due to high speed of operation and high integration level of modern electronic components. The GLONASS/GPS clock difference will be transmitted within the GLONASS-M navigation messages. The only factor still capable to degrade the navigation accuracy of combined GLONASS/GPS receiver is the divergence between the WGS and SGS reference frames, which is not yet defined accurately enough. However, having in mind growing tendency to mutual cooperation, the divergence between the GLONASS and GPS coordinate systems can be determined most accurately and reliably by means of mutual efforts of the Russian and

US specialists and other interested states.

It worth noting, that discussing technical and institutional problems of connection of differential networks being created in Russia, Europe, USA and other countries into common network could become a real step toward creating a world-wide differential and integrity monitoring network.

3. ACKNOWLEDGEMENTS

Authors would like to appreciate the active participation of Mr. M.G.Lebedev, Mr V.V. Gorev, Mr. A.A.Ganin, the leaders of the Coordination Scientific Information Center of Russian Space Forces and Mr. J.V. Medvedkov, the Chief Advisor of the Russian Space Agency in discussing the main aspects GLONASS system advancing described in this paper.

Authors are also grateful to Mr. Jungstand from the DLR firm (Germany), for testing the monitoring station and making valuable comments and proposals.

4. REFERENCES

1. Global Navigation Satellite System. Interface Control Document.
2. Summary Record of the Meeting between the Administrations of the United States of America and Russian Federation (Working Group I), 26-30 September, 1994.
3. J.Gouzhva, A. Guevorkyan, A. Bassevich, P. Bogdanov: "High- Precision Time and Frequency Dissemination with GLONASS". GPS World, July, 1994.
4. N. Ivanov, V. Salischev: "GLONASS and GPS: Prospects for a Partnership", GPS World, April, 1991.
5. N. Ivanov, V. Salischev: "GLONASS System - An Overview". Paper presented at the 1991 Conference of Royal Institute of Navigation, London, 1991.

Marine Radiobeacon DGPS/DGLONASS Service and Regional Centers for Differential GLONASS/Alpha/Chayka Services

Pyotr Bogdanov, Valery Chistyakov, Sergey Filatchenkov, Arvid Gevorkyan, and Vladlen Khimulin
Russian Institute of Radionavigation and Time

BIOGRAPHY

Pyotr P. Bogdanov is chief of laboratory at RIRT. He received a candidate of science degree in general engineering in 1984.

Valery V. Chistyakov is RIRT dipl. engineer.

Sergey V. Filatchenkov is chief of laboratory at RIRT. He received a candidate of science degree in general engineering in 1989.

Arvid G. Gevorkyan heads research branch at RIRT. He received a doctor of science degree in general engineering in 1991, and academic status of professor in radiophysics in 1994.

Vladlen I. Khimulin is chief of research department at RIRT.

ABSTRACT

In this paper a concept and performances of the Russian Differential GNSS (DGNSS) marine radiobeacon service as well as a description of a Regional Center for monitor/differential services are presented.

Use of both GPS and GLONASS has been proposed by the International Maritime Organization as a solution for future navigation needs. So, there is expediency to distribute differential data for both GPS and GLONASS users because of the tenfold improvement in accuracy over conventional positioning in areas where differential data are available.

Such a possibility will be realized in the Russian radiobeacon DGNSS service. Thanks to functional redundancy as compared to the widely used DGPS service, the marine public will

benefit by having a larger positioning opportunities. In some cases, such as degradation of GPS or GLONASS or specific local operational requirements, the generation of corrections for one GNSS is only possible.

Each correction distribution mode's specific features are caused by differences in main operational performances. Along with evaluation of these performances for different modes, the overview of DGNSS service and principles of differential data distributions are presented. Besides, some noise immunity coding implementation problems are described.

The purpose of a Regional Center development is supporting GLONASS, very low-frequency (VLF) navigation system ALPHA, low-frequency (LF) navigation system CHAYKA and State System of Common Time and Reference Frequencies by monitoring of navigation /timing fields of these systems over the Russian territory.

INTRODUCTION

Radiobeacon DGNSS Service

Since 1990 the Russian Institute of Radionavigation and Time (RIRT) has been conducting researches in Differential GNSS, both DGPS and DGLONASS. One direction of these works is dealt with development of DGNSS Radiobeacon Service.

Presently, the radiobeacons of many countries are being used to broadcast differential corrections for GPS users only, while Russian DGNSS Service being under development will produce both DGLONASS and DGPS corrections in joint DGNSS mode as well as in separate DGLONASS only or DGPS only ones. The Head Department of

Navigation and Oceanography of the Ministry of Defence, a leading Russia's marine navigation agency, has announced plans to provide a DGNSS radiobeacon service to cover coastal areas of Russia [1].

All three possible modes are supporting all positioning functions with varying levels of functional performances. The choice of operational mode depends on conditions of every GNSS and local positioning requirements. In this paper emphasis will be made on DGLONASS mode's specific features, joint DGNSS mode implementation, features of service design, comparison of some performances of different modes.

The improvement of critical DGNSS operational performances can be connected with the noise immunity coding implementation. Some coding issues are also discussed.

Regional Center

GLONASS, VLF navigation system ALPHA, LF navigation system CHAYKA and State System of Common Time and Reference Frequencies are main means for positioning/ timing support of various users within the Russian territory. But monitoring of navigation and time fields generated by these system don't cover all over the country. Besides, information which is being transmitted to the users about the state and quality of fields is not operative and effective.

Specialists of RIRT have developed a project to increase positioning and timing support of above systems by using Regional Centers of navigation and time information. These centers should be additional points for monitoring over the Russian territory. They can as well provide differential corrections and operative broadcast about the state of navigation and time fields to users.

The views expressed herein are those of the authors and are not to be construed as official.

DGNSS SERVICE OVERVIEW

The following main principles were taking into account for the Russian DGNSS Radiobeacon Service design process:

- Simultaneous broadcast both direction finding signals and differential corrections for GLONASS and/or GPS by joint DGNSS or DGLONASS

alone or DGPS alone operational modes. GNSS integrity check and DGNSS monitoring.

- Joint correction distribution via united data link met to the International Telecommunication Union Recommendations (ITU) [7].

- Agreement of DGPS message generation and distribution, including message scheduling, with the SC-104 RTCM Recommendations [9] and USCG Broadcast Standard [2] for the compability with existing variety of DGPS equipment. Use of SC-104 RTCM general message format for DGLONASS data distribution for the DGNSS software simplifying and a single beacon receiver using for all modes.

- Opportunity of positioning of either DGNSS user (i.e. user without transformation abilities for frame and time) during the joint DGNSS mode. Retaining of positioning performances of either DGNSS and message frame synchronization performances of DGPS during the joint DGNSS mode.

- Opportunity of baud rate and message schedule variations depending on operational mode.

- Opportunity of noise immunity coding implementation.

- Separate notifications on healths and conditions of DGLONASS and DGPS.

- Broadcast of Special Messages on both Russian and English with use of extended ASCII codes.

The necessity of implementation of these principles is dictated by an appearance of integrated GNSS equipment as well as by wide using of equipment of a single GNSS. Then, the SC-104 RTCM Recommendations and ITU maritime radiobeacon data link parameters have already been accepted by many National Services of Navigation and introduced into serial equipment by many manufacturers; the SC-104 RTCM has prospect to fix the DGLONASS messages also [9].

The possibility of above concept fulfilling is based on similarity of both GNSS performances and DGNSS differential data, such as pseudorange and pseudorange rate ranges, signal/noise ratios (SNR), number of satellites, etc. Since GLONASS is non-selective availability (SA) - degraded and there is no plan to introduce such a degradation deliberately, the DGLONASS error growth due to

correction latency is less than that of DGPS, as shown in Figure 1.

Therefore, the DGLONASS correction update interval about 90s is quite acceptable, while the DGPS update interval will not exceed 15s. The last fact, along with limitation of a number of DGPS messages (see [2]; one high update rate message only), allows to introduce infrequent DGLONASS messages into a stream of DGPS messages without accuracy degradation, as shown in earlier paper [3].

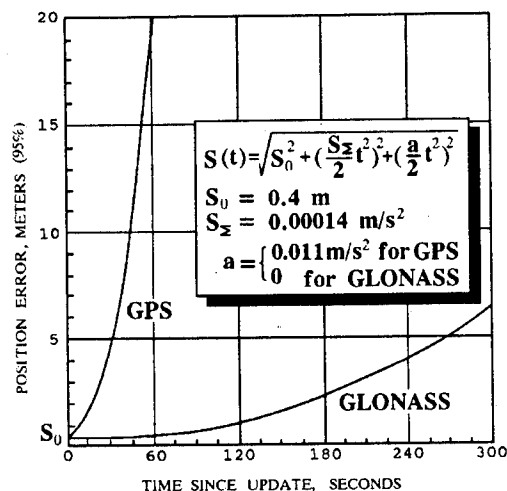


FIGURE 1. DIFFERENTIAL ERROR GROWTH

Details of DGLONASS messages and specific features of DGLONASS and DGNSS correction distributions was described in [3]. The list of messages is presented in Table 1.

Briefly, the main specific features of DGLONASS messages are dealt with following GLONASS specific parameters:

- Datum, Age of Navigation Data and Satellite Identities, that taken account of Correction, Constellation Health and Reference Station Parameter Messages;

- Time reflected in Headers of all Messages;

- Satellite health indications reflected in Constellation Health Message.

The purposes of other DGLONASS messages are:

- notice about beacon type (Type 33 Message);

- notice about GLONASS/DGLONASS

healths and conditions (Headers of all DGLONASS messages);

- Special Message broadcasts in Russian and/or English for navigation safety and/or on GLONASS/DGLONASS state (Type 36 Message).

Table 1. Messages of Russian Maritime DGNSS Service

| Title | Message Type N | |
|---|----------------|---------|
| | GPS | GLONASS |
| Differential GNSS Corrections | 1 | 31 |
| Reference Station Parameters | 3 | 32 |
| Constellation Health | 5 | 33 |
| Null Frame | 6 | 34# |
| Beacon Almanac | 7 | 35 |
| Partial Satellite Set Differential GNSS Corrections | 9 | 34 |
| Special Message | 16 | 36 |

number of words after the Header is 0 or 1.

There is currently a draft describing the Russian DGNSS Radiobeacon Service entitled "Broadcast Standard For Russian DGPS/DGLONASS Lighthouse Service" that defines the key radiobeacon broadcast characteristics [1]. The use of Service corrections will give a possibility to determine the coordinates with accuracy better than 10 meters. The service also provides accuracy check and user warning within less than 10 s. The planned availability is 99.8% for a 30 day period and reliability is 99.97% for 1 year measurement interval. The transmission rates are 100 bps for DGNSS and DGPS modes and 25 or 50 bps for DGLONASS mode. The "Type 9-3" and "Type 34-1" methods will be used for correction distributions during DGNSS mode. The broadcast of Type 1 and Type 31 messages is reserved.

The planned architecture of DGNSS Service as a whole is similar to that of DGPS [2]. It will comprise a set of Reference Stations (RS) with

associated Integrity Monitors (IM) and the Control Station. Currently, only the experimental RS and IM are manufacturing and all control and monitor functions are incorporated in the united software executing with the RS computer. The service architecture specific feature is the co-location of the IM at the RS site. This approach ensures a similarity of satellite's multipaths for RS and IM antennas as well as avoids the IM function being dependent on a communication link, which improves the Service availability. At the same time, the possibility of off-site monitor and display exists.

The RS monitoring is realized by two ways. Firstly, the IM receives RS and GNSS data and verifies that they are within a tolerance. The second check level is intended for separation of RS receiver and transmitter faults for the benefit of fast fault detection and reducing of outages. This task is solved in RS modulator by decoding of data arrived by a feedback from transmitter.

Due to a low DGLONASS baud rate and a Partial Satellite Set Correction distributions the RS utilizes a highly stable frequency source.

DGNSS PERFORMANCE EVALUATION

Each DGNSS mode has unique performances dealt with the number of available GNSS, correction transmission rate and, somewhat, quantity of equipment required for the correction producing. All above causes affect a service availability; the first factor is influencing on accuracy and reliability also; the second one is influencing on coverage and time to alarm; the third cause in the some cases changes reliability performances.

A software tools were developed and utilized to compute all following estimations. Simulation results dealt with environmental signal effects presented herein were calculated for signal propagation over sea at the Baltic Sea East and the atmospheric level which is exceeded 0.1% of the time annually. The data of [4] and [11] was used.

Accuracy

The standard GLONASS positioning has an accuracy advantage over the standard GPS positioning because of S/A error lack, however the

differential mode cancels the GPS S/A errors. Hence, the accuracies of DGPS and DGLONASS modes are approximately equal, but DGNSS mode provides better accuracy due to the lower Dilution of Precision (DOP). As shown in [8], the joint GNSS constellation provides Position DOP (PDOP) of 1.9 and Horizontal DOP (HDOP) of 0.99 ($P \geq 0.95$), while, for example, GPS provides PDOP=4.5 and HDOP=2 ($P \geq 0.95$). The significant sacrifice of accuracy for marine users can occur during the storms, when the desperate extremity of positioning is exist. Moreover, a very large heels can evoke an disability of positioning by one GNSS use or receiver autonomous integrity monitoring disability. Such positioning losses are caused by opportunity of occasional satellite's signal losses and, hence, a DOP variances. A heel exerts influence on a little ships mainly. The predicted accuracy aggravation factor due to up to 20 degrees heel and satellite mask angle of 10 degrees for joint DGNSS will not exceed of 1.5 - 1.6. The use of signals of one GNSS only evokes up to 5 - 7 times accuracy degradation. These results are based on simulations of GNSS constellations for casual points of Earth and casual times [6].

Coverage

A simulation was designed to determine the coverages associated with baud rate, bit error rate and radiated power.

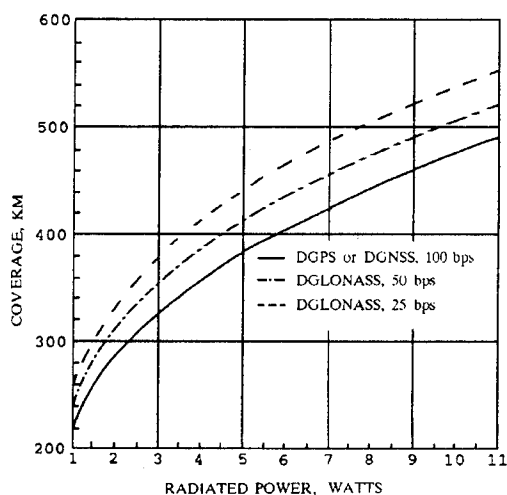


FIGURE 2. COVERAGE VIA RADIATED POWER

A low DGLONASS mode's update rate evokes the increase of SNR and, hence, the DGLONASS coverage is greater than that of DGNSS or DGPS. The DGLONASS coverage gain depends on radiated

power and can achieve dozens of kilometers; it is illustrated by Figure 2 for 10^{-3} bit error rate requirement of 10^{-3} (see [7]), above locality and noise parameters.

The beacon percentage coverage growth due to the twofold baud rate reduction can be approximately evaluated as $300E_s^{-1}$, where E_s is a signal strength for required bit error rate in dBuV/m.

Availability and Integrity

A low DGLONASS correction update rate gives some preferences in availability and integrity fields also, as compared to DGNSS and DGPS modes. We follow some approaches to our estimations of these performances.

Assuming that outages of a DGNSS Service equipment are "constant" for all modes and corrections are broadcasting continuously, we supposed that positioning availability is in proportion to the ratio of received and broadcasted messages for the all visible satellites on condition that local atmospheric noise level within a required period is unexceeded. Taking into account the mode's specific features described above, a simulation was performed to determine how often all the corrections for all visible satellites would be successfully received.

The simulation results for nine satellites and radiated power of 1 Watt are shown in Figure 3.

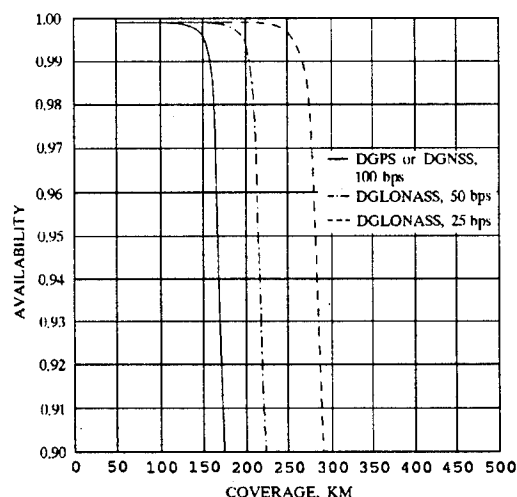


FIGURE 3. ALARM MESSAGE AVAILABILITY

The coverages of annual availability of 0.997, which requires about of $1 \cdot 10^{-6}$ - $2 \cdot 10^{-6}$ bit error rates for different modes, are about of 145 km

for both DGNSS and DGPS mode, 190 km for 50 bps DGLONASS mode and 250 km for 25 bps one.

At the distances less than 100 km the correction signal availabilities are approximately identical for all the modes, and positioning availability of DGNSS mode will be 1.02 times that of other modes.

Since the DGNSS service not only enhances the positioning accuracy but also provides a real time integrity check, it can augment user's integrity capabilities in areas where radiobeacon data are available. The augmentation factor depends on probability of integrity message reception for time to alarm. For this time in the fault cases the alarm messages have a broadcast preference though the allowable correction update rate for health satellites have to be kept. Moreover, the distribution of alarm messages must begin without fail after completing of a running message to support the frame synchronization.

In the DGNSS mode the unhealthy conditions include as full GNSS malfunction as that of some satellite. It is planned to indicate the first condition by the Null Frame message's Station Health field and the second condition by the pseudorange alarm values of Correction Message field (see [1]).

In the DGLONASS mode the full GLONASS unhealthy conditions will be indicated the same as in DGNSS mode. The unfitness GLONASS satellite can be indicated by both pseudorange alarm in Correction Message and by Constellation Health Message. The last method shortens the duration of alarm notice due to the shorter message length which is importantly during the low data rate of DGLONASS mode. It will be noted that about of 15 bps data rate that usable for accuracy features can't augments integrity capabilities for unfitness satellite within time to alarm of 10s.

Table 2 presents the predicted coverages of annual 0.99999 probability of alarm information receiving within 10s for 1 Watt radiated power and above alarm mechanisms. These results are calculated on the assumption that there is only one satellite malfunction within time to alarm and the correction latency positioning error growth due to the additional alarm message broadcasts is less than

0.1 m.

The bit error rate required for above probability achieves $5 \cdot 10^{-8}$ for the 25 bps DGLONASS mode. For the other modes such requirements are weaker.

Table 2. Coverage of alarm information receiving

| Malfunction kind | Number of alarm messages | Coverage, km |
|--------------------------|--------------------------|--------------|
| <u>DGNSS mode</u> | | |
| Both GNSS | 6 | 220 |
| GPS only | 14 | 250 |
| GLONASS only | 5 | 210 |
| GPS or GLONASS satellite | 5 | 200 |
| <u>DGLONASS mode</u> | | |
| GLONASS, 50 bps | 8 | 300 |
| 25 bps | 4 | 330 |
| GLONASS satellite | | |
| 50 bps | 3/4# | 240/260 |
| 25 bps | 1/1# | 230/230 |

notice by Type 34-1/33 Messages.

Reliability

The service reliability evaluation was based on considerations that, firstly, the unforecast DGNSS service outage can arise due to failure of both reference station equipment and GNSS and, secondly, performing of specified DGNSS function can be fulfilled by use of one GNSS only. The DGNSS interconnection model developed for each mode was used to establish the mode's relative reliability scores. Assuming that GNSS failures are equally likely to occur at either GNSS and taking into account the current architecture of Russian DGNSS Reference Station (it is very essential circumstance) we reckon that total DGNSS service reliability is 1.36 times than DGPS and 1.66 times than DGLONASS ones.

CODING OF DGNSS DATA

It is known that a practicable radiobeacon coverage is usually less than coverage where the very corrections are valid, due to the atmospheric noises. That is why the attractivity of error correction coding is exist.

Coding provides greater noise immunity gain over uncoded operations especially on condition of a little error rates. Besides, the error rate gain of DGLONASS mode during the coding operation is greater than that of other modes (with identical coding schemes for all modes). It is illustrated by Figure 4 for the Reed-Solomon (31,15) code recommended for radiobeacon data link in [5].

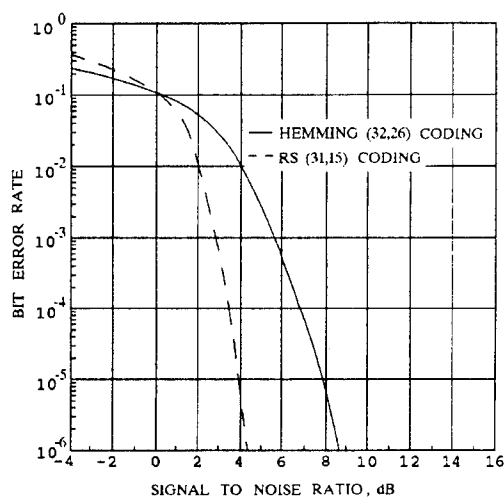


FIGURE 4. UPPER BOUND OF BIT ERROR RATE

But coding incorporating has two restrictions: limitation of radiobeacon data link bandwidth and lack of international recommendations on the coding schemes.

The first restriction during the 100 bps DGPS and DGNSS modes prevents from the use of higher than 1/2-rate codes. Thus, there is impossibility of qualitative positioning performance improvements by coding. For the DGLONASS mode a more powerful, up to 1/8-rate codes are permitted owing to the greater allowable correction latency. This mode has lesser sensitivity to the additional time for the coding and decoding also.

However even 1/2-rate code can improve practically all service performances anyhow. Thus, according to simulations, a (31,15) Reed-Solomon coding for radiated power of 1 Watt,

bit error rate of 10^{-6} and 100 bps data rate, provides of 17% coverage growth over uncoded operation. Such coding provides 20% - 60% growth of the coverage of 0.99999 alarm reception probability (this value depends on error rate requirements for different malfunction kinds) also, etc.

The second coding implementation restriction is more significant. The worldwide service compatibility requires international agreement on type of code. Moreover, the DGPS receivers without coding capabilities has currently manufactured in quantity. So there are essential problems in DGPS and, consequently, in DGNSS code implementations. But in the DGLONASS mode the coding may be used with lesser problems due to the current lack of DGLONASS equipment. The coding schemes of 25 bps and 50 bps DGLONASS modes and possibilities of coding implementations are scrutinizing now. The coding solution may be location dependent.

REGIONAL CENTER FOR MONITOR AND DIFFERENTIAL SERVICES

The main purpose of Regional Center development is supporting GLONASS, ALPHA and CHAYKA navigation systems as well as State System of Common Time and Reference Frequencies by monitoring of navigation and timing fields of these systems over the specified regions. The GPS, LORAN-C and OMEGA can be supported also.

The Regional Center is intended for improving system's efficiencies by

- monitoring navigation and time data distributed by GNSS, VLF and LF navigation and time services;
- integrity monitoring GNSS, VLF and LF navigation systems;
- time signal transfers;
- correction distributions for navigation/synchronization augmentations;
- international cooperation to provide joint use possibility of Russia's and US navigation systems.

The functional elements of the Regional Center include:

Time/Frequency Reference Standard. Provides monitoring time signals distributed by GNSS as well as VLF/LF Time Services and TV-channels based on comparison and joint processing of timing data of above sources. Also, the differential synchronization corrections are calculated here on the

basis of simultaneous measurements of VLF/LF stations' and TV-channels' signals, on one side, and GNSS signals on the other side. This element as well provides timing data transmitting for synchronization of regional users.

GNSS, VLF and LF navigation system Monitor Units. The systems' health determination, performance data archiving and processing are accomplished here. The calculated positions would be compared to the precisely known Regional Center position to determine if the systems' operational performances were within tolerances.

Reference Stations of GNSS, VLF and LF navigation systems. This element includes equipment to calculate local differential corrections for above systems.

Communication Network. Provides links between Regional Center and Control Centers of GLONASS, ALPHA and CHAYKA as well as the State System of Common Time and Reference Frequencies.

Integrity/Correction Data Links. Communication terminals providing integrity and/or correction messages distribution for the regional users.

The equipment for this project implementation as well as formats and contents of information messages are discussed now. The messages dealt with GNSS will take into account the ARINC 743A, SC-159 RTCA and SC-104 RTCM recommendations.

SUMMARY

This paper has reviewed the architecture and performance evaluations of the Russian DGNSS radiobeacon service. The signals distributed by the DGNSS service can be utilized by the users of one GNSS without sacrificing of its own positioning characteristics. The joint correction broadcast improves positioning accuracy, especially in a heavy sea's time, and reliability as well as positioning availability at a relatively short distances, as compared to other modes. The DGLONASS mode, thanks to a lower correction update, rate has a maximum coverage, integrity availability as well as positioning availability at long ranges. Due to the operational flexibility the DGNSS Service can operatively support different requirements to meet needs of different localities and conditions.

The full deployment of DGNSS Service requires the development of special Standard for RS, IM, Control Station and data interfaces and protocols. The Standard must take account of as DGLONASS as joint DGNSS modes' specific features and, also, RTCM Recommendations for DGPS Service [10]. This work is underway in RIRT.

Besides, the paper has described the main functions of Regional Center of navigation and time information as well as its operational principles. In some cases the regional centers can additionally provide differential modes of navigation and time synchronization.

REFERENCES

- [1]. Broadcast Standard For Russian DGPS/DGLONASS Lighthouse Service of HDONO MD, 1995.
- [2]. Broadcast Standard For the USCG DGPS Navigation Service. COMDTINST M16577.1. April, 1993.
- [3]. V. Chistyakov, S. Filatchenkov, V. Khimulin "Parameters of Differential GLONASS/GPS Service on the Base of Russian Marine Radiobeacons". The 4th International Conference on Differential Satellite Navigation Systems., Vol.1., Bergen, April 1995.
- [4]. P.K. Enge, et al., "Coverage of DGPS Radiobeacons". Proceedings of ION GPS-92.
- [5]. P.K. Enge "Forward Error Correction for Radiobeacon Broadcast of Differential GPS Data", IEEE Transactions on Aerospace and Electronic Systems, January 1993
- [6]. N.V. Ivantsevich, I.G. Murashkina "Investigation of Geometric Characteristics of a Joint Constellation of GLONASS/GPS Navigational Satellites". Radionavigation and Time (Russia), N 1,2, 1993
- [7]. ITU, Doc.8c/TEMP/22 (Rev.1)-E.1 Nov., 1993
- [8]. R. Mirza et al., "Integrated use of GPS and GLONASS in Civil Aviation Navigation I: Coverage & Data Models". Proceedings of ION GPS-90.
- [9]. RTCM Recommended Standards for Differential GNSS Service. First Draft. December 22, 1994.
- [10]. RTCM Recommended Standard for Differential Navstar/GPS Maritime Reference Station and Integrity Monitors. Draft, November 5 1994
- [11]. World Distribution and Characteristics of Atmospheric Radio Noise. International Radio Consultative Committee Report 322, 1964

GLONASS Approaches Full Operational Capability (FOC)

Peter Daly
The University of Leeds

Biography

Peter Daly is Professor of Electronic Engineering and Director of the CAA Institute of Satellite Navigation at the University of Leeds, UK. His research interests include GPS, GLONASS and integrated GPS/GLONASS navigation systems for space, aviation & maritime applications.

Abstract

There are two Global Navigation Satellite Systems (GNSS) available for world-wide civil use. The two systems are Navstar GPS which reached full operational capability (FOC) early in 1995 and GLONASS which is just one successful launch away from FOC. In the near future, augmentation of these two systems will be provided initially by geostationary satellites such as Inmarsat-3. Particularly in view of the interest in joint GPS/GLONASS initiatives, the progress of GLONASS towards a full operational complement deserves constant attention. Observations on the GLONASS signal structure and satellite space segment provided useful insights into the question of GPS/GLONASS interoperability.

Brief review of GLONASS launch history

GLONASS launches take place from Tyuratam (Baikonur Cosmodrome) in the CIS republic of Kazakhstan. The satellites are launched three at a time into inclined orbits with period 11.25 hrs. The full complement of satellites will occupy three orbital planes 120° apart with 8 equally-spaced satellites in each plane. By September 1995, there had been a total of 26 launches since the very first in 1982. In the early stages of the programme, only one or two of the satellites launched were active satellites, the others acting as make-weights. In 1986 the first launch took place with all three satellites forming part of the GLONASS navigation programme. Prior to August 1994, all satellites were launched into either plane 1 or plane 3. Since

that date there have been 2 launches into plane 2.

As individual satellites were lost they were gradually replaced over the years since 1982 with a very slow & gradual increase in the total number of satellites available for general use. The overall gain-loss situation is summarised in Figures 1 - 4 which cover 3 year intervals since 1986 - details prior to 1986 are not available to the author. Launches are indicated by upward-pointing arrows; launch sequence numbers are given together with GLONASS numbers devised at the University of Leeds. As is apparent from Figure 4, there are currently 22 active GLONASS satellites and after one further launch FOC can be anticipated.

Almanacs for all valid satellites are transmitted in sequence in the data message according to the rubric:- plane 1 (almanacs numbers 1-8), plane 2 (almanac numbers 9-16) and plane 3 (almanac numbers 17-24). In what follows active satellites are referred to by both GLONASS and channel numbers.

Plane 1

| | | | | | | | | |
|---------|----|----|----|----|----|----|----|----|
| Channel | 23 | 05 | 21 | 12 | 23 | 13 | 21 | 02 |
| Almanac | 01 | 02 | 03 | 04 | 05 | 06 | 07 | 08 |
| GLONASS | 55 | 60 | 68 | 70 | 49 | 69 | 61 | 54 |

Plane 2

| | | | | | | | | |
|---------|----|----|----|----|----|----|----|----|
| Channel | / | 09 | 04 | 22 | / | 09 | 04 | 22 |
| Almanac | 09 | 10 | 11 | 12 | 13 | 14 | 15 | 16 |
| GLONASS | / | 75 | 76 | 65 | / | 67 | 74 | 66 |

Plane 3

| | | | | | | | | |
|---------|----|-----|----|----|----|----|----|----|
| Channel | 24 | 10* | 03 | 01 | 24 | 10 | 03 | 01 |
| Almanac | 17 | 18 | 19 | 20 | 21 | 22 | 23 | 24 |
| GLONASS | 62 | 64 | 72 | 73 | 57 | 71 | 63 | 56 |

* satellite due to return to service 13 Sept 1995.

Table 1

At the start of September 1995, there were 22

GLONASS Space Vehicles (SV's) in orbit, 8 SV's in plane 1, 6 in plane 2 and 8 in plane 3. Satellites are listed by plane in order of almanac number in Table 1.

As is clear from the Table, both planes 1 and 3 are complete and one further triple launch into plane 2 would leave that plane complete and with an in-orbit spare. For reference purposes a list of the current satellites with satellite international identifiers, Cosmos & GLONASS numbers, transmit channels, almanac slots and planes is presented in Figure 5. It should be noted that the oldest of the current satellites which is in plane 1 at almanac slot 5 is due to complete 5 years of service in December 1995.

Amongst user communities of GNSS, in particular civil aviation, there is a requirement for continuous availability and integrity of navigation satellites for precise approach and landing procedures. In order to meet these requirements it is necessary to have a sufficient number of satellites to allow on-board integrity checking (RAIM) on a continuous basis. The availability of (i) GPS and (ii) GPS + GLONASS at a typical European location is shown in Figure 6, from which the advantage of combined use of GPS/GLONASS is immediately apparent.

Further launches planned during 1995

It is understood that there is to be one further GLONASS triple launch in 1995. It seems probable that this launch will take place into plane 2 as both planes 1 and 3 are complete already. Should this launch be successful and should there be no further satellite failures, the GLONASS space segment will then consist of 25 active satellites.

GLONASS-M

A new improved GLONASS satellite has been under development in the CIS for some time - GLONASS-M - which promises a number of new attractive features. The new satellites are designed to have an active lifetime of 5 years, improved on-board atomic clocks and the facility for transmitting a C/A code on both L1 and L2 frequencies - see next section. Use of a C/A code on two frequencies allows a precise estimate of the ionospheric ray bending effect with obvious implications for improved accuracy.

Testing of GLONASS-M has been conducted all during 1995 with the first launch planned in the first quarter of 1996. This launch will carry 2 GLONASS satellites and 1 GLONASS-M although the Proton launcher is capable of launching 3

GLONASS-M SVs simultaneously.

GLONASS frequency plan

The GLONASS transmission plan calls for a scheme of Frequency Division Multiple Access (FDMA), each satellite sending the same code but a different carrier frequency. Two carriers are transmitted in L-band, one around 1.6 GHz (L1) and the other around 1.2 GHz (L2). Satellites are distinguished by channel number with channel 0 (used for test purposes only) at centre frequency (L1) 1602 MHz and the 24-satellite system using channels 1-24 with channel 24 at 1615.5 MHz (spacing 0.5625 MHz). Transmit frequencies and channel spacings at L2 are in the ratio of 7/9 as compared with L1 frequencies. Satellites transmit both a low-precision (C/A) and a high-precision (P) code at L1 and a high-precision (P) code only at L2. Since the high-precision code operates at 5.11 Mb/s and uses a bandwidth of approximately 10 MHz, the signal spectrum occupied by GLONASS is defined at the upper limit by the highest transmit frequency plus 5 MHz and at the lower limit by the lowest transmit frequency minus the 5 MHz. The resulting spectrum requirement spans the range 1597-1620.5 MHz, a total bandwidth of 23.5 MHz, actually larger than the bandwidth requirements of GPS (20 MHz) in spite of the fact that GPS operates at twice the chipping rate of GLONASS.

Interference and WARC'92 allocations

During the ITU (World Administrative Radio Conference) WARC'92 meeting held during March in Torremolinos, two frequency allocations were made in L-band which had important ramifications for GLONASS. The first allocation was of the band 1610 - 1626.5 MHz (bandwidth 16.5 MHz) to Low Earth Orbiting (LEO) satellites on a world-wide primary basis. Satellites of this type (such as the Iridium and Globalstar system) are planned to provide voice communication services globally. Although these LEO satellites are constrained in terms of the interference permitted to other systems, there is clearly a potential problem related to interference caused to GLONASS at the upper part of the L1 band as a result of the new allocation.

The second allocation which impacted GLONASS operations was that of the band 1610.6 - 1613.8 MHz which corresponds roughly to GLONASS channels 15-21, allocated to radio-astronomy again on a primary basis. Whereas the first allocation had the potential to cause interference to GLONASS reception, the second allocation impacted both GLONASS transmit levels and operating frequency

band in that GLONASS was now constrained not to cause interference to radio-astronomy.

In addition to the difficulties raised by the new allocations, there is an additional problem to be considered involving the use of GLONASS on aircraft as is recommended in the ICAO Future Air Navigation Systems (FANS) plans for Global Navigation Satellite Systems (GNSS). Because aircraft already use a satellite-earth link via a geostationary link which operates at (relatively) high power and in the frequency range 1646.5-1656.5 MHz, potential interference from the aircraft satellite communication links makes the design of the airborne GLONASS receiver much more difficult than would be the case if the upper range of the GLONASS band were reduced.

Since the WARC'92 agreements, changes have been made to the GLONASS signal structure to respond to the problem of interference to radio-astronomy. Already in October 1991 an undertaking had been given by the GLONASS administration to the IUCAF (Inter-Union Commission on Frequency Allocations for Radio Astronomy and Space Science, set up in 1960 by URSI, IAU and COSPAR), to reduce emissions from GLONASS satellites in the neighbouring radio-astronomy band of 1660 - 1670 MHz by using improved output filtering techniques on all GLONASS satellites launched from 1994 onwards.

In late 1992, a series of tests was conducted [1] in conjunction with the Large Telescope facility at Jodrell Bank, UK to estimate the effect of altering channel allocations on GLONASS satellites. Tests were conducted in four phases:-

- (a) normal GLONASS operation
- (b) no use of channels 15-21
- (c) only channels 1-12 and
- (d) only channels 1-6

Following these tests a Russian proposal was made to re-use frequencies within the GLONASS band and also to lower the effective range of frequencies employed.

Frequency re-use & re-location.

Frequency re-use involves allocating to antipodal satellites in the GLONASS system the same transmit frequency. In this way satellites on opposite sides of the earth do not interfere with each other, allowing the entire space segment to be

implemented with only 12 channels. One exception to this rule would be high-flying receivers on-board satellites attempting to use GLONASS for navigation purposes. However even in cases such as these, modern receiver techniques are sophisticated enough to distinguish between the two mutually-interfering signals. The removal of the top 12 channels of GLONASS would reduce the required bandwidth by 6.75 MHz, saving spectrum where it is most needed - at the top of the band.

The phasing-in of this new strategy is already nearly complete. During September 1993, the first pairs of antipodal satellites were allocated channels 23 and 24. Since then the re-use of frequency has increased to the point in September 1995 where 9 pairs of the 22 available satellites employ a common transmit frequency with no use of any channel in the range 15-20.

In the longer term, it is intended to lower the entire frequency range employed by GLONASS satellites. The timescale of the proposed plan is summarised in Table 2.

GLONASS frequency & RF interference issues

● 1994 → 1998

- channels 0 to 12, 22, 23 & 24 with no carriers in the 1610.6 - 1613.8 MHz band (channels 15 - 21). Channels 13, 14 & 21 under exceptional circumstances, only.

● 1998 → 2005

- channels 0 to 12 with 13 to be used only in extreme circumstances
Use filters to protect Radio Astronomy (RA) band from 1660 to 1670 MHz.

● 2005 →

- channels -7 to 4 for navigation and 5 & 6 as technical frequencies
Use filters to protect RA in both 1660-1670 and 1610.6-1613.8 MHz bands.

Table 2

The "half-way" solution to be implemented by the year 2005 improves the resistance of GLONASS to external interference and also helps to resolve the problems faced by radio-astronomy. The "new" spectrum would then extend from 1594 - 1610.5 MHz (bandwidth 16.5 MHz).

Another solution to the problems of interference caused to/by GLONASS would be for GLONASS to use a single transmit frequency, as close as possible to the GPS frequency, possibly even the

GPS frequency itself, and code division multiple access (CDMA) as GPS does. In this way GPS and GLONASS compatibility would be vastly improved and some interference problems minimised.

GPS/GLONASS signal architecture

Ever since the start of the GPS & GLONASS space programmes, there has been a remarkable similarity in the signal architecture in space. GPS & GLONASS both employ a coarse code (C/A) at the upper of the two L-band frequencies (L1) but not at the lower (L2) frequency and the two systems employ a fine code (P) at both L1 and L2 frequencies. As is well known satellites are distinguished in GPS by a characteristic code known as Code Division Multiple Access (CDMA) whereas GLONASS uses the method of Frequency Division Multiple Access (FDMA). A distinguishing feature of GPS not observed in GLONASS is the use of Selective Availability (SA) to reduce accuracy to non-authorised users and anti-spoofing (AS) to prevent access to the fine (P) code. The situation is summarised in Table 3.

GNSS SIGNAL STRUCTURE

| | |
|------------------|------------------|
| ○ GPS | ○ GLONASS |
| ● C/A CODE L1 | ● C/A CODE L1 |
| ● P CODE L1 | ● P CODE L1 |
| ● NO C/A CODE L2 | ● NO C/A CODE L2 |
| ● P CODE L2 | ● P CODE L2 |
| ● CDMA | ● FDMA |
| ● SA/AS | ● NO SA/AS |

Table 3

It should be noted that steps are being taken [2] by the National Academy of Public Administration (NAPU) within the US to alter the strategy with regard to GPS so as to improve matters for the civil user. Firstly there is a proposal to turn SA to zero immediately and to deactivate it after 3 years. This would bring GPS into line with GLONASS which does not employ SA although there can be no doubt that the capability to do so is present. Secondly NAPU proposes the use of the coarse C/A code so as to allow the user to estimate ionospheric delay and so to improve accuracy. In parallel but independent of these moves, the GLONASS administration has planned for some time now transmit the C/A code at both L1 and L2

frequencies on the new GLONASS-M satellites, the first of which is to appear early in 1996. If both these steps are taken (i) not remove SA on GPS and (ii) to implement an added C/A code at L2, it would bring GPS & GLONASS very much into line with each other with regard to capability and improve the available accuracy of both to the civil user significantly.

GLONASS time references

Individual GLONASS satellite transmit data relating to two time references (i) SV time to GLONASS system time and (ii) GLONASS system time to UTC(SU). The navigator is not normally directly interested in the latter of these two references as it is sufficient to relate all events to system time. However, the behaviour of the national Universal Coordinated Time (UTC) reference is extremely important in defining UTC itself. The performance and stability of UTC (which represents essentially World Time) allows the satellite systems themselves to function more accurately and precisely in terms of both position and time. So in an indirect, long-term sense, the quality of the UTC references supporting both GPS & GLONASS impinges strongly on the ultimate performance capability. For some time now the US national reference, UTC(USNO) has been steered towards UTC itself. Over the past 5 years there has been no steering with UTC(SU) but at 00h, 23rd March 1995, a frequency change was implemented - see Figure 7 - leading to very much lower rates of change of phase with time (about 2ns/day). The change which came about [3] as a result of analysis of data from updated primary Cesium atomic clocks at the National Time & Frequency Standard of Russia consisted simply of a step in time scale of -10 E -14 s/s.

The parameter (A0) in the GLONASS data message which relates GLONASS system time to UTC(SU) has a resolution (LSB) of 7 ns and is normally only updated to satellites once a day (and often less frequently) by the control segment. As a result, a plot of A0 against time shows a step-like behaviour as may be observed in Figure 8 which presents data received from one of the GLONASS satellites (GLONASS 64) over a period of 200 days. Some of the steps in the data amount to 100 - 200 ns. Clearly the parameter as transmitted provides only a very crude description of the (actual) smooth relation between system time and UTC(SU) and is unsatisfactory for the purposes of precise time transfer. It would lead to much improved capability for time transfer purposes were the parameter A0 to be allocated a much higher resolution (say 1 ns) and be uplinked much more frequently.

Alternatively an additional frequency offset could be transmitted to the user.

GLONASS information sources

Within the last year, a Coordinated Scientific Information Center (CSIC) of the Russian Space Forces has been introduced [4] to provide information relating to the GLONASS system. The CSIC may be contacted by mail, fax, phone, e-mail and now has a home page on the Internet.

Typically the CSIC provides details on:-

- (i) constellation status
- (ii) forthcoming launches
- (iii) notice advisories

The constellation status lists all operational satellites by GLONASS and Cosmos number. Until fairly recently, GLONASS launches were not announced in advance. However the most recent launch (#26 of 24 July 1995) was declared by the CSIC on 19 July with full details of intended launch plane, final position and transmit channel of the three satellites. For many years now, GPS users have had access to Notice Advisories to Navstar Users (NANUs). Now GLONASS users can access NAGUs issued by CSIC giving current information about individual GLONASS satellites.

A second Russian source [5] has recently become available which also provides information relating to the GLONASS system.

Summary

GPS has already reached Full Operational Capability (FOC); there can be little remaining doubt that GLONASS will reach the same milestone by the end of 1995 or early in 1996. There are a number of important aviation, maritime and surveying applications of global satellite navigation which demand the use of more than one system from the viewpoint of independence, redundancy, availability and system integrity.

There are of course a number of problems associated with dual use of GPS/GLONASS not least in the area of satellite control. The lifetime of GLONASS satellites is still less than their GPS counterparts. However, the new GLONASS-M satellites will appear on the scene during the first part of 1996 offering improved lifetimes of 5 years and more stable on-board atomic clocks.

The planned changes to existing use of frequencies in and around the GLONASS band are necessary to avoid problems with interference from mobile satcomms to and from GLONASS to radio astronomy. Any of the measures that have been outlined are likely to cause some disruption to receiver manufacturers and users of the system, although a reduction in the bandwidth used by the system would be an advantage in the long term. The current level of C/A code performance of the GLONASS system is better than that of GPS with Selective Availability, despite the lower code chipping rate of GLONASS and as there are no known plans by the CIS to introduce any SA type degradation of the signals, this is likely to remain so.

References

- [1] R J Cohen: "The GLONASS-Radio Astronomy joint experiment" 12th International Wroclaw Symposium on Electromagnetic Compatibility, EMC 1994, pp.530-534, ISBN 83-901999-0-4.
- [2] "Charting the future of GPS", Office of Communications of the US National Academy of Public Administration (NAPU), 31 May 1992, Washington DC.
- [3] N B Koshelyaevski, VNIIFTRI, Russian State Time & Frequency Service, private communication.
- [4] Coordinated Scientific Information Center (CSIC), Russian Space Forces, Kazakova St 23, Moscow, Russia 103064.
- [5] Intergovernment Navigation & Information Center (INIC), 2 B. Vusovsky Lane, Moscow, Russia 109028.

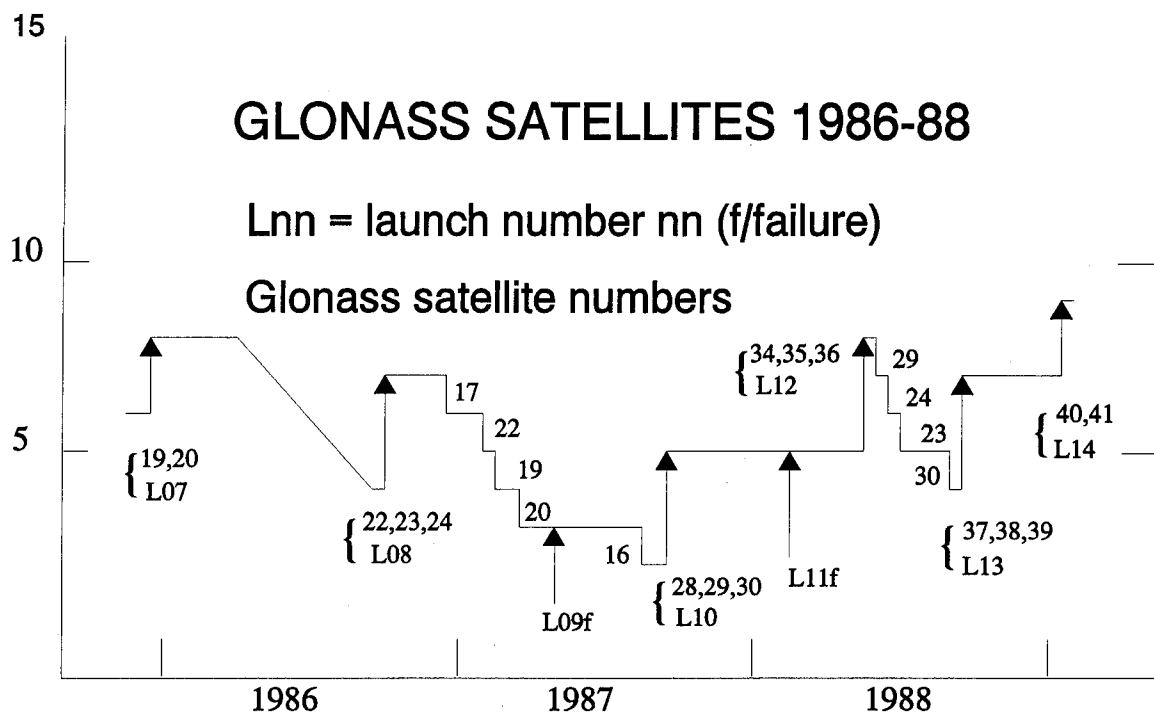


Figure 1. GLONASS launches during 1986-88

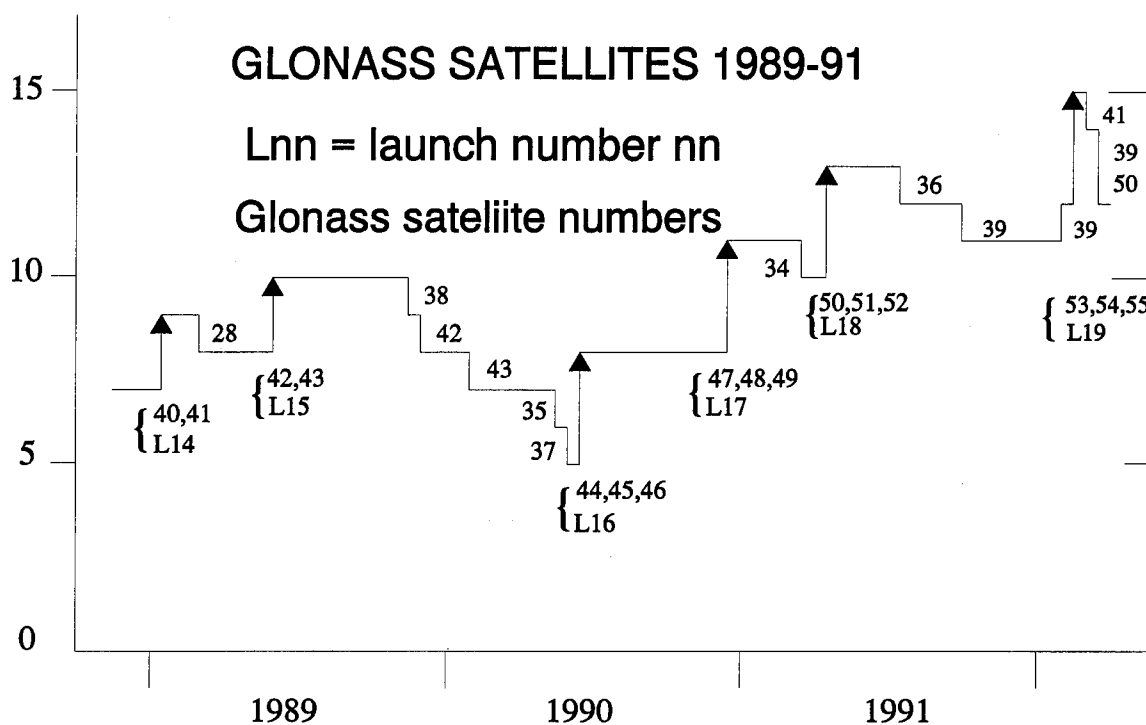


Figure 2. GLONASS launches during 1989-91

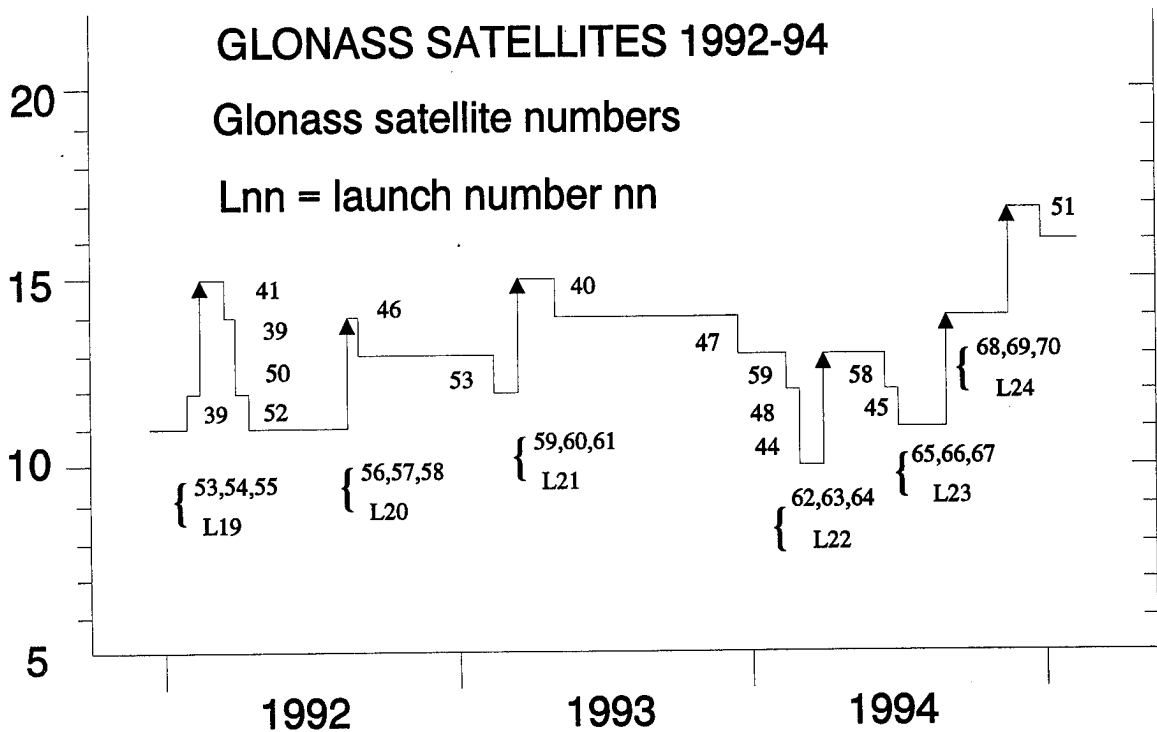


Figure 3. GLONASS launches during 1992-94

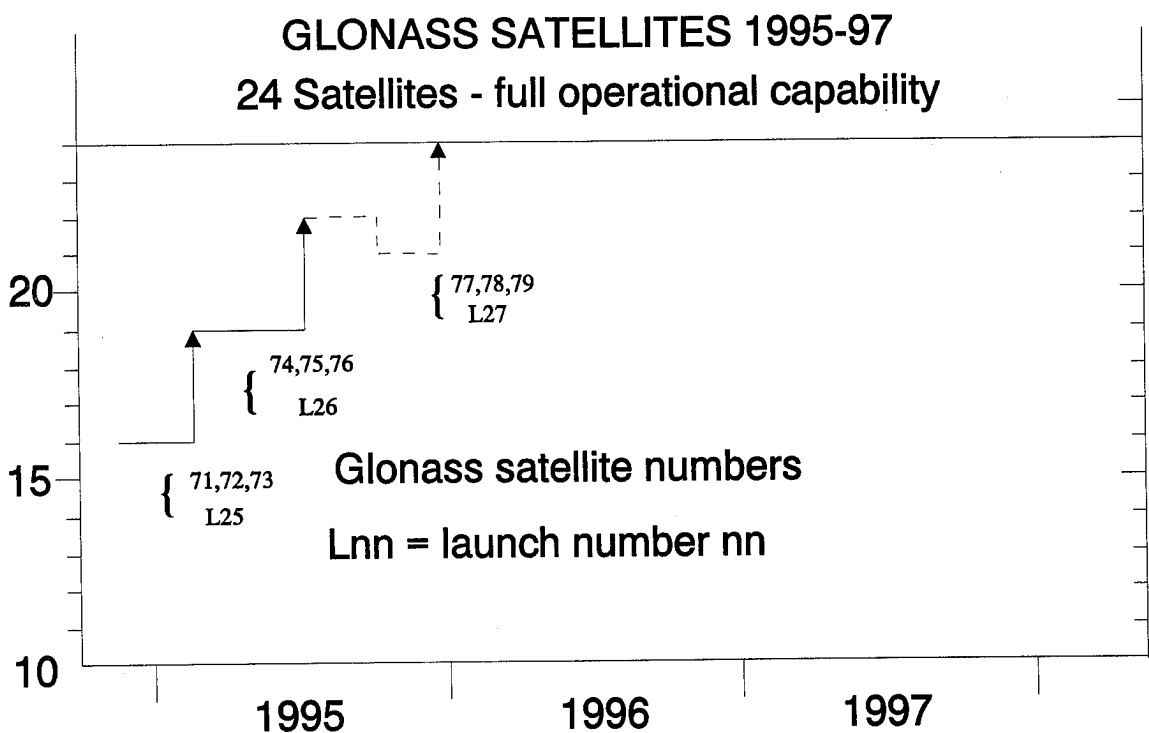


Figure 4. GLONASS launches during 1995-97

GLONASS - SEPT 95 → 22 SV's

| SAT ID | Cosmos | GLN | CHN | ALM | Plane |
|-----------|--------|-----|-----|-----|-------|
| 1992- 5C | 2179 | 55 | 23 | 1 | 1 |
| 1993- 10B | 2236 | 60 | 5 | 2 | 1 |
| 1994- 76A | 2295 | 68 | 21 | 3 | 1 |
| 1994- 76C | 2294 | 70 | 12 | 4 | 1 |
| 1990-110C | 2111 | 49 | 23 | 5 | 1 |
| 1994- 76B | 2296 | 69 | 13 | 6 | 1 |
| 1993- 10C | 2235 | 61 | 21 | 7 | 1 |
| 1992- 5B | 2178 | 54 | 2 | 8 | 1 |
| \ | \ | \ | \ | 9 | 2 |
| 1995- 37A | 2317 | 74 | 9 | 10 | 2 |
| 1995- 37B | 2318 | 75 | 4 | 11 | 2 |
| 1994- 50A | 2287 | 65 | 22 | 12 | 2 |
| \ | \ | \ | \ | 13 | 2 |
| 1994- 50C | 2289 | 67 | 9 | 14 | 2 |
| 1995- 37C | 2316 | 76 | 4 | 15 | 2 |
| 1994- 50B | 2288 | 66 | 22 | 16 | 2 |
| 1994- 21A | 2276 | 62 | 24 | 17 | 3 |
| 1994- 21C | 2275 | 64 | 10 | 18 | 3 |
| 1995- 9B | 2309 | 72 | 3 | 19 | 3 |
| 1995- 9C | 2307 | 73 | 1 | 20 | 3 |
| 1992- 47C | 2204 | 57 | 24 | 21 | 3 |
| 1995- 9A | 2308 | 71 | 10 | 22 | 3 |
| 1994- 21B | 2277 | 63 | 3 | 23 | 3 |
| 1992- 47A | 2206 | 56 | 1 | 24 | 3 |

Figure 5. Status of GLONASS in-orbit - September 1995

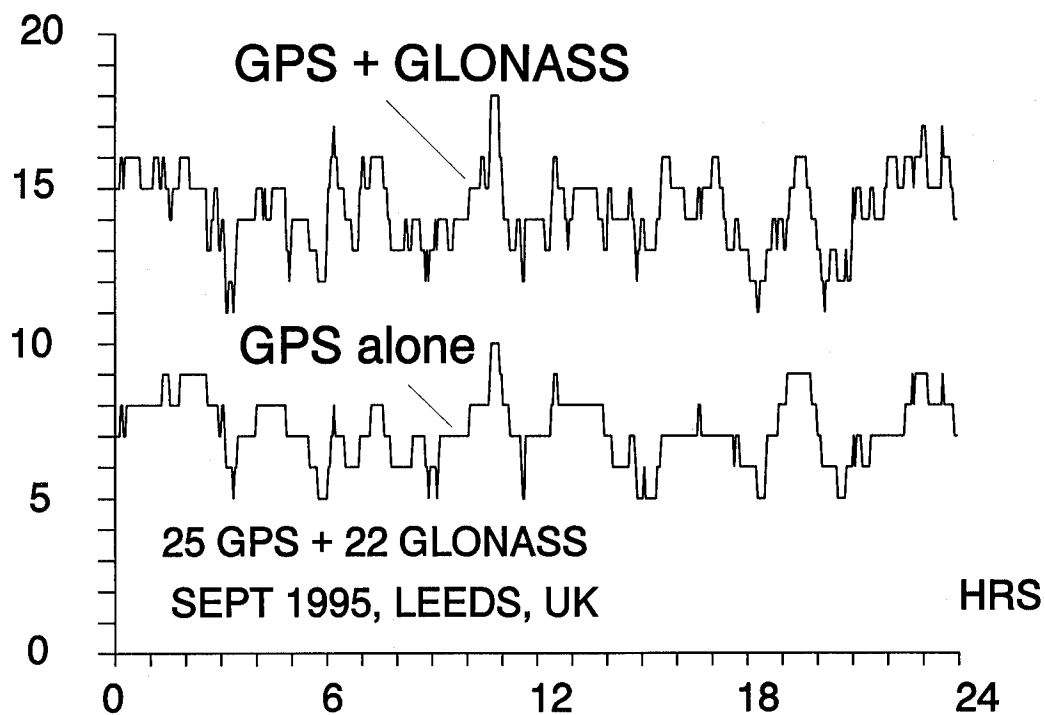


Figure 6. GPS & GLONASS availability

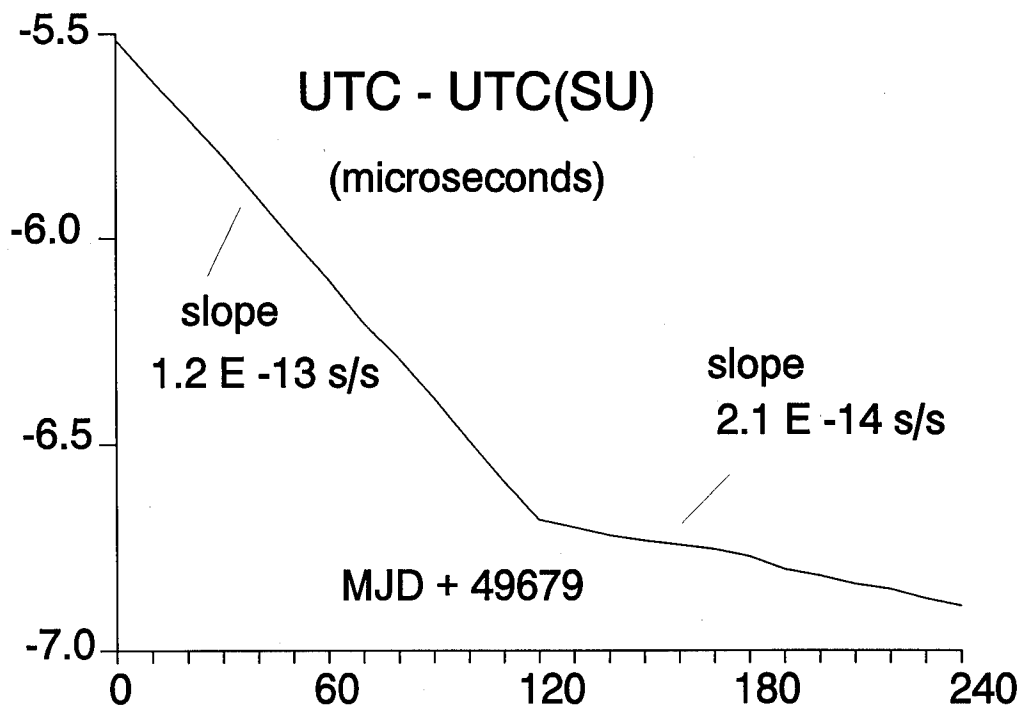


Figure 7. UTC - UTC(SU) versus Modified Julian Day (MJD)
Change of slope at MJD 49799 - 23 March 1995

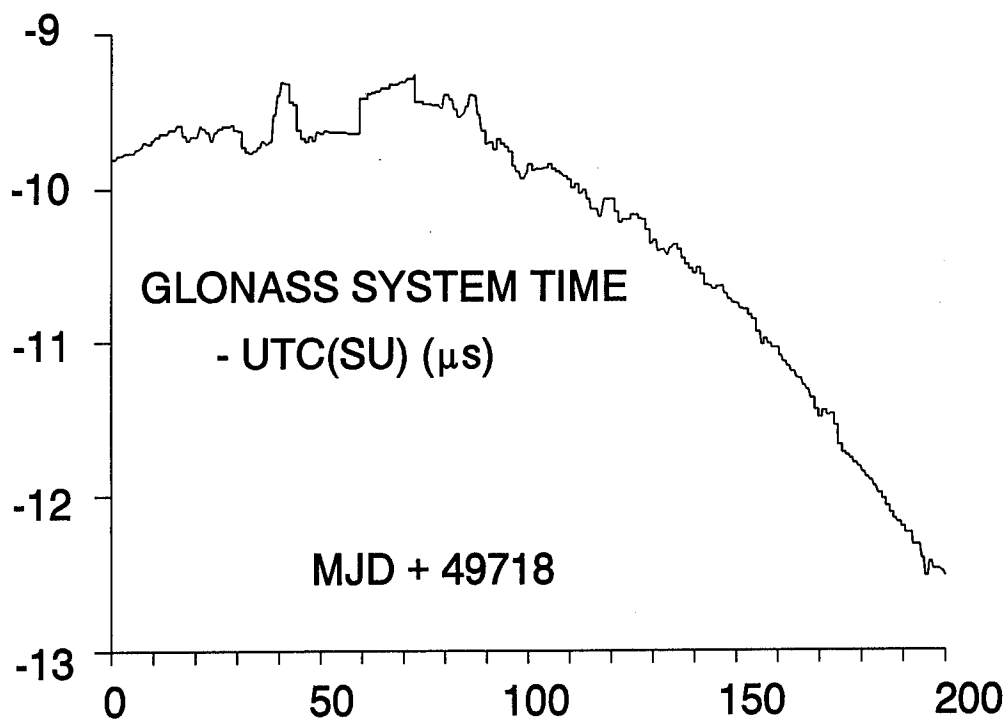


Figure 8. Data transmitted by GLONASS satellites
Modified Julian Day (MJD) 49718 corresponds to 1/1/95

Evaluation of GLONASS Performance in Practical Applications: Comparison with GPS-Based Ionospheric TEC Values

Dr. Nestor Zarraoa, Dr. Esther Sardon, Dr. Dietmar Klähn, and Arne Jungstand
DLR-DFD Neustrelitz

BIOGRAPHY

The authors work at the Remote Sensing Ground Station Neustrelitz, part of the German Aerospace Research Establishment. Both N. Zarraoa and E. Sardon hold Ph.D. degrees in mathematics from the Universidad Complutense de Madrid (Spain), and have worked in several areas of Space Geodesy, including VLBI, GPS and GLONASS. D. Klähn holds a Ph.D. degree in physics from the University of Rostock and has a long experience with satellite receiving systems, including GPS and DGPS applications. A. Jungstand holds a B.S. degree in physics from the University of Rostock, and has worked in ionospheric physics and satellite navigation.

ABSTRACT

After GPS has reached the operational status, the Russian Navigation Satellite System GLONASS, is also approaching the stage of constellation completion. However, the knowledge about the capacities of GLONASS, as compared with those of GPS, is rather scarce, because of the reduced number of receivers available, and the little literature published so far.

The DLR Remote Sensing Station Neustrelitz has started several activities around GLONASS. Some of the purposes we have are the proper evaluation of the quality and integrity of the Russian system, the distribution of updated information about the system to other users, and the extensive testing of the capabilities of GLONASS, as compared with the current GPS performance, in areas like positioning, navigation and ionospheric monitoring. In this paper we will present part of our work in the evaluation of the GLONASS system and a first detailed comparison of the applicability of GLONASS for ionospheric monitoring, as stand alone or combined with GPS.

Ionospheric monitoring based on GPS is one important line of research in DLR Neustrelitz, and we are providing a regular distribution of ionospheric TEC values for other users, using our permanent GPS reference station and also other stations from the IGS network. The inclusion of GLONASS data into the

scheme of this monitoring is a rather natural application of the system, and an excellent test base to evaluate the data quality and the possible complications of the GLONASS structure for this purpose. Moreover, the use of the new observables from GLONASS, increases the spatial coverage of the data when monitoring with a single station by more than 50%.

We have used for our comparisons a combination of two receivers, one GLONASS (3S_R101) and one GPS (Turbo-Rogue) in the same site. We have studied the performance of the GLONASS receiver in terms of reliability and integrity, and we have adapted the existing algorithms for TEC monitoring from GPS to the combination of both techniques. In this paper we will present the results of these tests and the comparison of the results that are obtained using each technique independently or both together, in terms of ionospheric corrections monitoring.

INTRODUCTION

The Russian counterpart to GPS, GLONASS (Global Navigation Satellite System) is approaching the constellation completion. Currently there are 19 satellites operational (22 after the launch in July), and it is scheduled to have the complete set up during 1995.

GLONASS specifications (i.e. Bartenev et al., 1994) are rather similar to GPS. The main difference is that each satellite transmits in its own frequencies, while in GPS all transmit in the same frequency, being distinguished by the code transmitted. Otherwise, both systems use L-band in two frequencies to correct ionospheric delays, the altitude of the satellites and their orbits are comparable, and also the quality of the signals are nominally similar for both.

The main drawback of GLONASS nowadays is the user's segment. There are very few receiver manufacturers, most of them in Russia, and many of the receivers available have been designed for very specific purposes, and are not well suited for civil uses like precise geodetic measurements or light-weighted surveying or navigation.

In DLR-Neustrelitz, we have a long experience as a monitor station for GPS signals with purposes like differential navigation, ionospheric monitoring or system integrity checking. Among other activities related to GPS, we are operating one permanent Turbo Rogue GPS receiver for real time ionospheric monitoring and system integrity checks. We are also providing regular post-processed ionospheric TEC information from GPS data, via anonymous FTP, to the scientific community.

Since 1993, GLONASS has become one of the priorities in DLR-Neustrelitz. Through several agreements with Russian Institutes, we acquired three C/A-code GLONASS receivers and we have also purchased a 3S Navigation R101 GLONASS receiver, currently used as permanent monitoring station, much the same as our reference Turbo Rogue for GPS.

In the first part of this paper we will present some of the comparisons performed between the different GLONASS receivers available in our Institute, both in the integrity of the receivers and on the actual precision of the real-time positioning output.

In the second part we will discuss more in detail the performance of the 3S_R101 receiver, and the application of the GLONASS data into our activities as ionospheric monitoring station, both as an stand-alone system and also with the combination of both GPS and GLONASS data.

GLONASS SET UP AT NEUSTRELITZ

At Neustrelitz we have four different GLONASS receivers, the R101 from the US manufacturer 3S Navigation, plus three receivers manufactured in Russia by the Institute of Radionavigation and Time (ASN-16) and the Institute of Space Device Engineering (ISDE-16 and Skipper). In figure 1 we show a simple diagram of our set up.

The four receivers have different characteristics, and they also belong to different technological generations. The ISDE-16 is a receiver specially designed and produced to be used as GLONASS monitoring station in Neustrelitz and Moscow, based upon the architecture of the Skipper receivers. It offers interesting improvements over its predecessor, like the use of 16

physical channels instead on one, the ability of track either GPS or GLONASS in C/A code, and the capability of producing RTCM differential corrections. Currently both hardware and software are being thoroughly tested in Neustrelitz.

The 3S_R101 receivers can track P1 and P2 codes for GLONASS, and it can also track simultaneously GPS satellites, but these only in C/A. The standard output of the receiver includes the carrier phase on either C/A, P1 or P2 channels (Beser, 1994).

The 3S_R101 has in principle the capability of being used for ionospheric monitoring (it tracks both frequencies) and precise geodesy or navigation (tracks P1 and P2, which, unlike GPS today, are not affected by anti-spoofing or selective availability), so it was a good candidate for a permanent monitoring GLONASS station.

EVALUATION OF OUR GLONASS RECEIVERS

Considering that most of our receivers only use C/A codes, one of the most straight forward tests is to compare directly their real-time positioning outputs in order to check, not only their agreement but also their internal precision.

The four receivers have been operating in parallel for a limited time span. The ISDE-16 was installed in Neustrelitz during March 1995, and since June we have had problems with both the ASN-16 and the Skipper. We selected one day within this period (April 26, 1995) in which all receivers were operating with no apparent problems, and we compared the position outputs given by each of them. The results were presented in a previous report, where we found that the performance of the ISDE-16 receiver was rather weak. After testing the hardware, we found some problems with the power output of our frequency standard, which was substituted by a new oscillator. This change improved significantly the results of the ISDE-16.

Figure 2 shows the density distribution of the estimates in the local horizontal plane for each receiver. Figure 3 shows their vertical components estimated as a function of time. While for the ASN-16, Skipper and 3S_R101 we have used April 26th, for the ISDE-16 we have used data from August 8th.

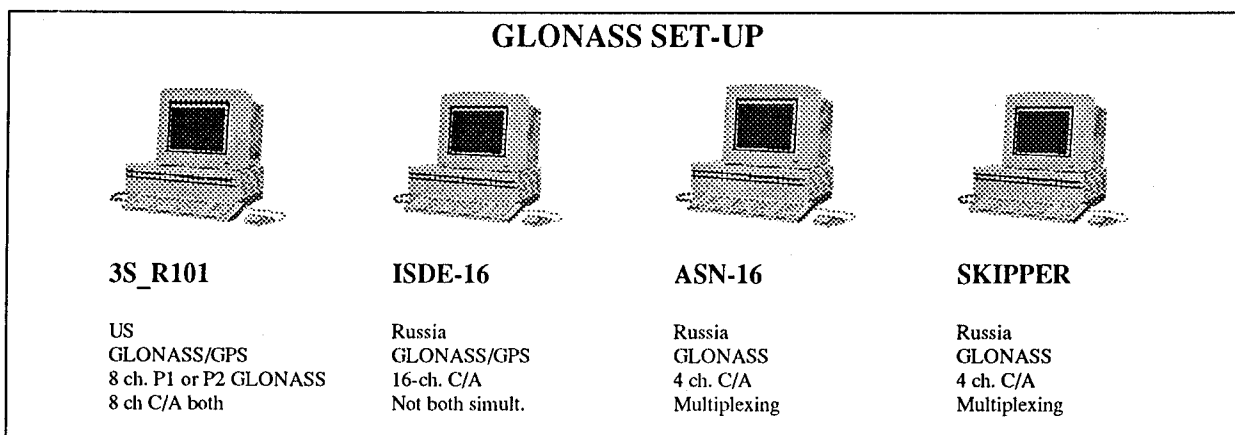


Figure 1. Main characteristics of the GLONASS receivers at DLR-Neustrelitz

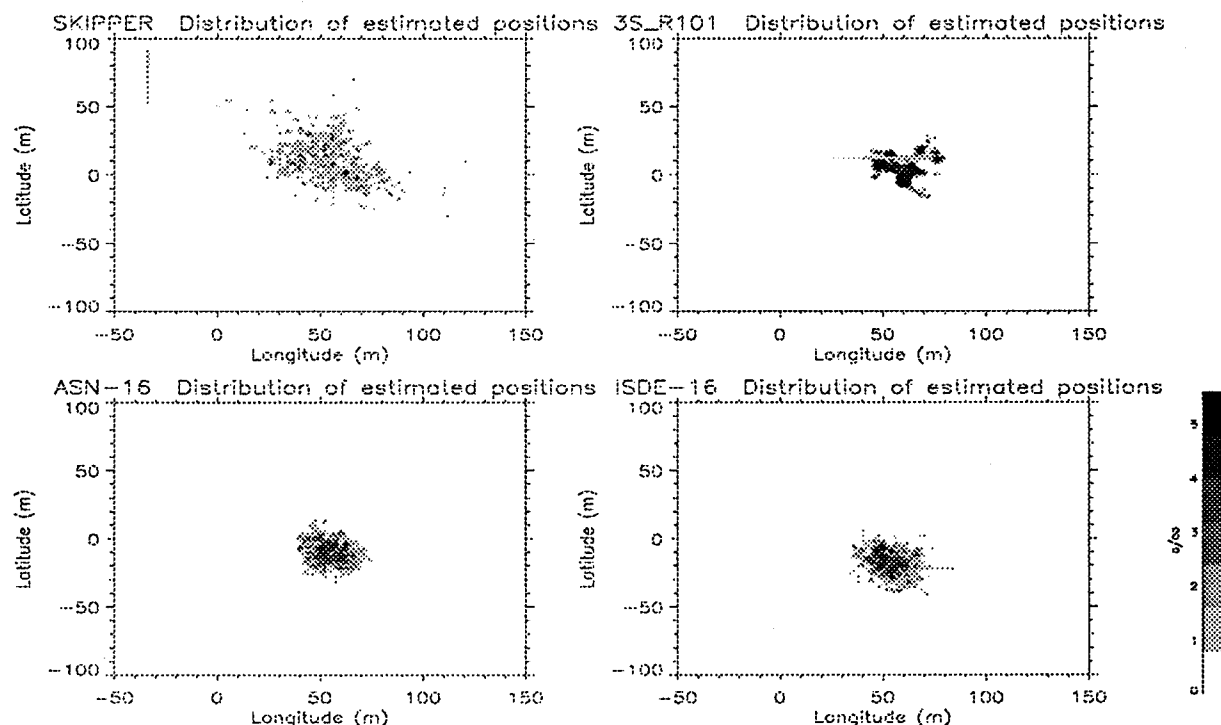


Figure 2. Density of the horizontal distribution of the estimates from the 4 GLONASS receivers

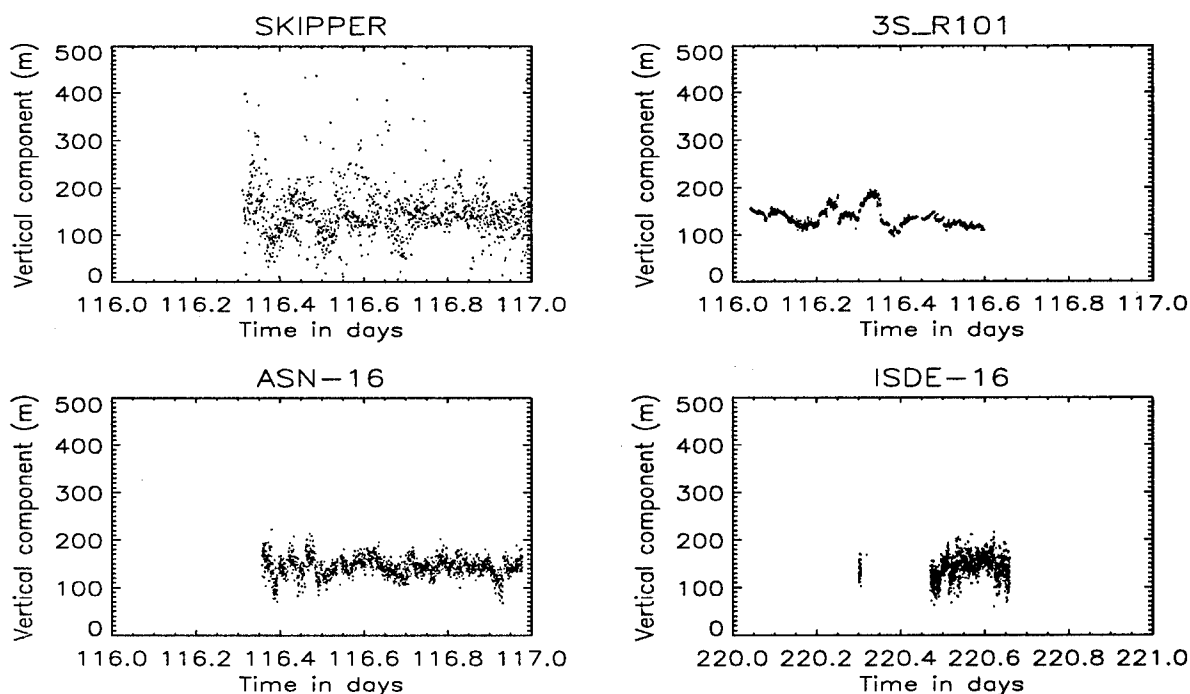


Figure 3. Vertical estimates from the 4 GLONASS receivers

The results are summarised on table 1 for the local components, corrected by the eccentricity between antennas. In terms of precision, they show the superior performance of the 3S_R101 receiver. This makes also use of the P-code pseudoranges, not only C/A as the others. Its density peaks up in a small section of the horizontal plane (8 m. rms in both coordinates).

From the other three receivers, operating with C/A code, the results show that the ASN-16 and ISDE-16 receivers give rather good performance, slightly better for the ASN-16. This receiver operates on multiplexing mode (only one physical channel) and only tracks four satellites simultaneously.

Nevertheless, the results are very good, with standard deviations of 10 to 12 meters. The ISDE-16 produces standard deviations on the same level. Note that the ISDE-16 is designed for integrity monitoring, not for positioning, so the results are not filtered or optimized in any way. The Skipper receiver is much weaker than the others. Both the Skipper and the ISDE-16 present a considerable number of outliers in the estimation.

In the vertical component, we see the same rating of quality. The 3S_R101 shows a very narrow noise level, although with changes from time to time that degrade the standard deviation, probably caused by differences in the visible scenario or by the changes of the satellite broadcast ephemerides. The ASN-16 performs also very good with more noise, but without the systematic changes present in the 3S_R101. The ISDE-16 shows some more noise than the ASN-16. For these three, the standard deviation of the vertical component is about 20 meters. The Skipper is clearly poorer, again with a considerable number of outliers.

All antennas were located at the roof of our main building, with a maximum difference of 3.5 meters. The mean positions given by each receiver, referred to the same reference point are given in table 1.

Table 1. Estimates of the position and standard deviations (all referred to the same reference point) given by all four receivers with their rms values. All numbers in meters.

| | North | East | Up |
|---------|------------------|------------------|-------------------|
| 3S_R101 | +63.29 8.15 | +5.48 8.39 | +137.00 19.00 |
| ASN-16 | +55.37 10.59 | -9.43 12.40 | +144.07 18.00 |
| ISDE-16 | +55.02 10.773 | -16.07 11.575 | +145.87 22.255 |
| SKIPPER | +56.27 23.23 | +14.15 22.14 | +140.49 38.43 |

The agreement between receivers is not very good with differences in the range of tens of meters. Not all receivers observed the same amount of time or during the same period (The ISDE-16 data comes from August), so some of the difference could be accounted to different satellite configurations. Other possible causes are under study.

Quality of GLONASS observables versus GPS

In order to be used in high precision applications, we must check the quality of the observables produced by our reference GLONASS receiver, particularly compared with the current status of GPS.

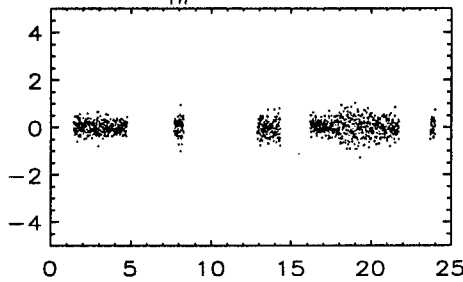
We have computed the noise level for the P-code at both frequencies in GLONASS using the R101 receiver. The expression used for this comparison takes the two observables (carrier phase and pseudorange) over two consecutive times in the following way:

$$N_i(t_n) = P_i(t_n) - P_i(t_{n-1}) - [L_i(t_n) - L_i(t_{n-1})] \cdot \lambda_i$$

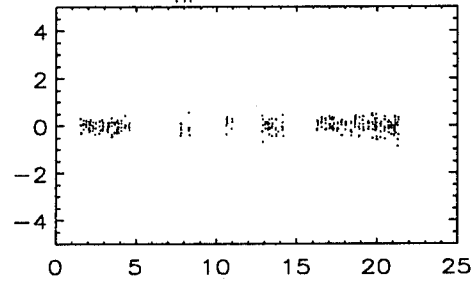
$P_i(t)$ and $L_i(t)$ are the observed pseudorange and carrier phase at frequency i at the time t , and λ_i is the wavelength at frequency i . The resulting quantity is thus free from the geometry, troposphere and clock effects, as well as from the initial phase ambiguities.

The only terms that contribute to N are the change in ionospheric delays between the two consecutive times (not larger than 1-2 cm for 30 seconds data rate under normal ionospheric conditions), the contribution from multipath and the random noise from the four observables. As the carrier phases are one or two orders of magnitude more precise than the pseudoranges, this term reflects, in practice, the noise level of the P-code pseudorange. This expression has been applied to GPS and GLONASS data from the Turbo-

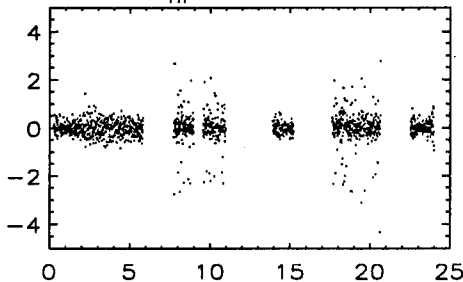
GLONASS frq# 21 P1 rms = 0.29



GLONASS frq# 21 P2 rms = 0.22



GLONASS frq# 22 P1 rms = 0.45



GLONASS frq# 22 P2 rms = 0.52

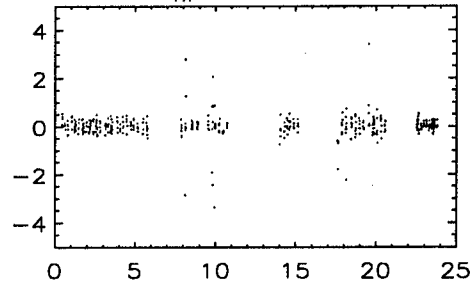


Figure 4. Noise level for GLONASS satellites (frequencies 21 and 22) at both P1 and P2

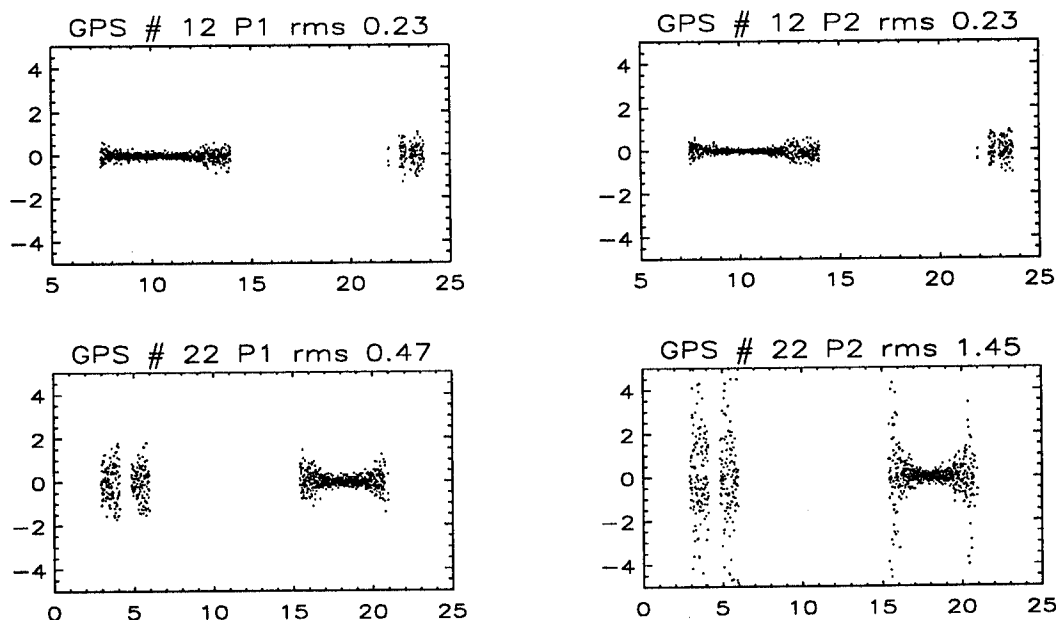


Figure 5. Noise level for GPS satellites (PRN 12 and 22) at both P1 and P2

Rogue and 3S_R101 receivers at Neustrelitz, for all satellites and in both frequencies. We have also been able to compare the noise level to GPS satellites with and without anti-spoofing (A/S).

In figures 4 and 5 we compare the results for P1 and P2 using two GLONASS satellites, one normal, and one with some problems (reported also by the Coordinational Scientific Information Center, Russian Space Forces, private communication), and the same for two GPS satellites, one with A/S on and one without.

From the GLONASS data (fig. 4) the rms of the noise is of about 20-30 cm, consistently in both frequencies, which is in agreement with the nominal expected precision and better than other published results presented at an earlier stage of the system (e.g. Riley and Daly, 1993). It is important to note that the GLONASS frequency number is assigned to two different satellites, located in the same orbit plane, but in antipodal locations. Then, each of the plots is representing two spacecrafts.

For the frequency number 22, the satellites located at slot 16 is the one with the problems mentioned above, and it shows in a worse rms value of about 0.5 m. due to several large outliers.

For the GPS data (fig. 5) of satellite 12, with A/S off, we see an excellent performance, with rms level of 20 cm, even considering the lower elevation cut-off of the Rogue receiver, so the low-elevation data present contributes to an increase of the total rms. For satellite 22, however, with A/S on, we can appreciate a degradation in the quality of the signal both in P1 (which in fact is the C/A GPS code) with an rms of 0.5 m and even worse at P2, 1.45 m, which is computed by a cross-correlation of the incoming phases plus the C/A code.

The conclusion is that GLONASS code data has a precision comparable to the GPS without Anti-Spoofing, although the latter is slightly better. However, GLONASS is superior to GPS with A/S on.

IONOSPHERE MONITORING WITH GLONASS

The dual frequency used in satellite systems like GPS or GLONASS permits the elimination of ionospheric effects for navigation or positioning activities. However, it can also be used to determine the absolute value of the ionospheric delays, which in turn, can be applied to a number of other activities, like correction of single frequency receivers by differential correction dissemination.

So far, GPS has been extensively tested in its capacity of ionospheric modelling (e.g. Lanyi, 1988; Coco, 1991 or Zarraoa & Sardón, 1995). In principle GLONASS could also be used for the same purpose, either as stand alone system or in combination with GPS, and some initial efforts have been presented by several groups (Danaher et al., 1993; Riley and Daly, 1993; Bishop et al, 1994).

In DLR Neustrelitz, there are several activities towards the accurate estimation of ionospheric delays from GPS signals. A real-time monitoring system has been developed, which can be used to rapidly disseminate corrections and/or information about the ionospheric conditions, which are applicable to a large region within Germany. Moreover, a regular analysis of a global network (based on IGS) over Europe, is being used to produce ionospheric TEC maps and instrumental bias time series, which are available via FTP to the scientific community.

In this environment, it is specially interesting to test the capability of GLONASS data from the 3S_R101

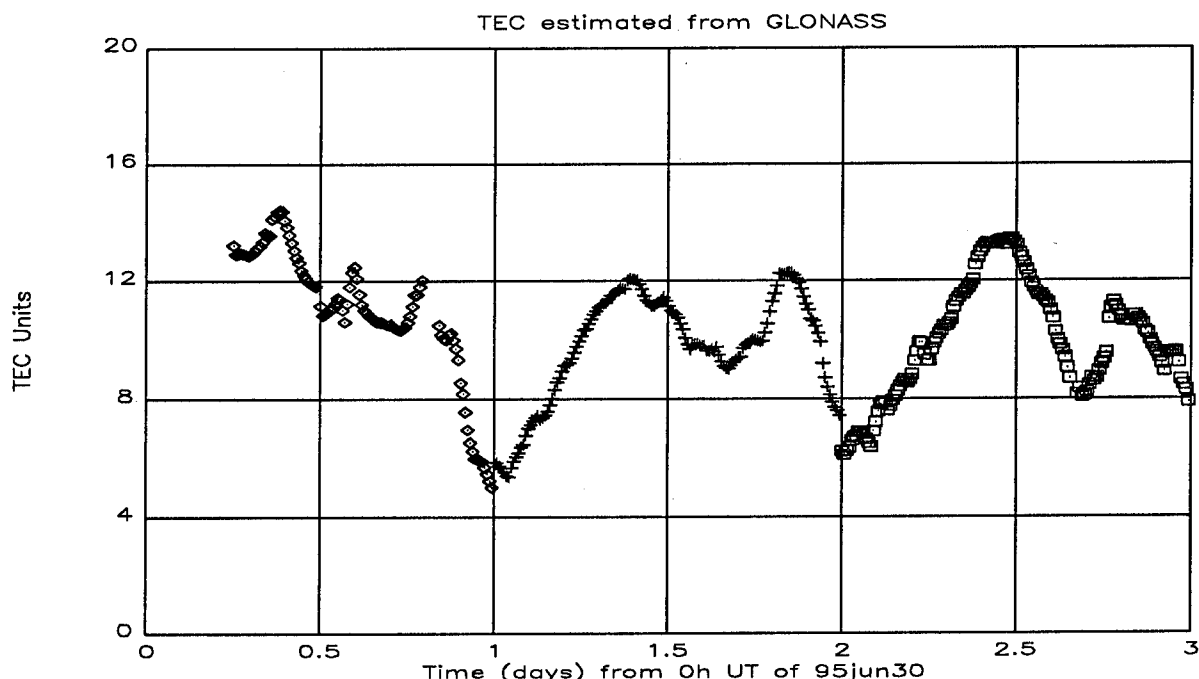


Figure 6. Vertical TEC at Neustrelitz estimated from GLONASS data (3S_R101 receiver) from June 30th to July 2nd, 1995

receiver to monitor also the ionosphere, alone or in combination with GPS.

Our 3S_R101 receiver has 8 channels able to receive GLONASS P-Code data, in either L1 or L2 frequencies, but not both in the same channel. Thus the output per channel is the pseudorange and the carrier phase observable in either P1 or P2 for the selected satellite.

In order to investigate the use of GLONASS data for the determination of ionospheric delays we have used the receiver in several special epochs in a manual "IONO" mode, where an scenario of 4 satellites was selected for each instant, and observed each satellite in P1 and P2 in consecutive channels.

Our software for post processing GPS data for TEC determination (Sardón et al, 1994) has been successfully adapted to GLONASS data and we have selected a test epoch (30th of June to 2nd of July 1995) with data from both GLONASS and GPS.

The GLONASS data was analysed independently and absolute TEC values and satellite instrumental biases obtained for the first time.

Our main concerns about the GLONASS use for ionosphere were the calibration of these instrumental biases. Due to the multifrequency character of GLONASS, the existence of inter channel bias into the receiver had to be verified, so a series of tests have been also carried out in this direction.

INSTRUMENTAL BIASES IN 3S_R101

In the case of one of the Turbo Rogue receivers at Neustrelitz, we have performed some tests in the past,

confirming that the inter-channel delays were negligible. We have also studied the long term stability of several receivers of the International GPS Service for Geodynamics (IGS) network, with the conclusion that the rms variation of these biases from one day to the next is below 0.5 nanoseconds for the differential delay between P1 and P2 measurements.

For GLONASS, and the 3S_R101 receiver, we have also investigated the stability of the instrumental delays over channels, by performing a series of calibration tests, where all channels observed the same satellite, alternating P1 and P2 in the 8 channels of the 3S_R101. This tests can be used to determine the possible inter channel bias, its stability in time, and its dependence of the satellite frequency observed.

The results of the inter channel bias calibration show some interesting features. The comparison of the four P1 channels with respect to the mean P1 at each time, show a step-like decreasing bias from 2.8 cm to -2.7 cm, with rms values of slightly over 1 cm and a similar trend is also in the P2 channels. See table 2.

Table 2. Inter channel biases with respect to the mean of P1 and of P2 and differential bias for each channel pair. (All numbers in centimetres)

| chn | 0 | 1 | 2 | 3 | 4 | 5 | 6 | 7 |
|-------|------|-----|------|-----|-------|------|------|------|
| P1 | 2.8 | | 0.9 | | -1.0 | | -2.7 | |
| P2 | | 2.5 | | 0.8 | | -0.6 | | -2.7 |
| P1-P2 | 0.24 | | 0.10 | | -0.41 | | 0.06 | |

In general, the channels are sampled in consecutive order, although all observables are referred to the same time in the output. An explanation for these decrease

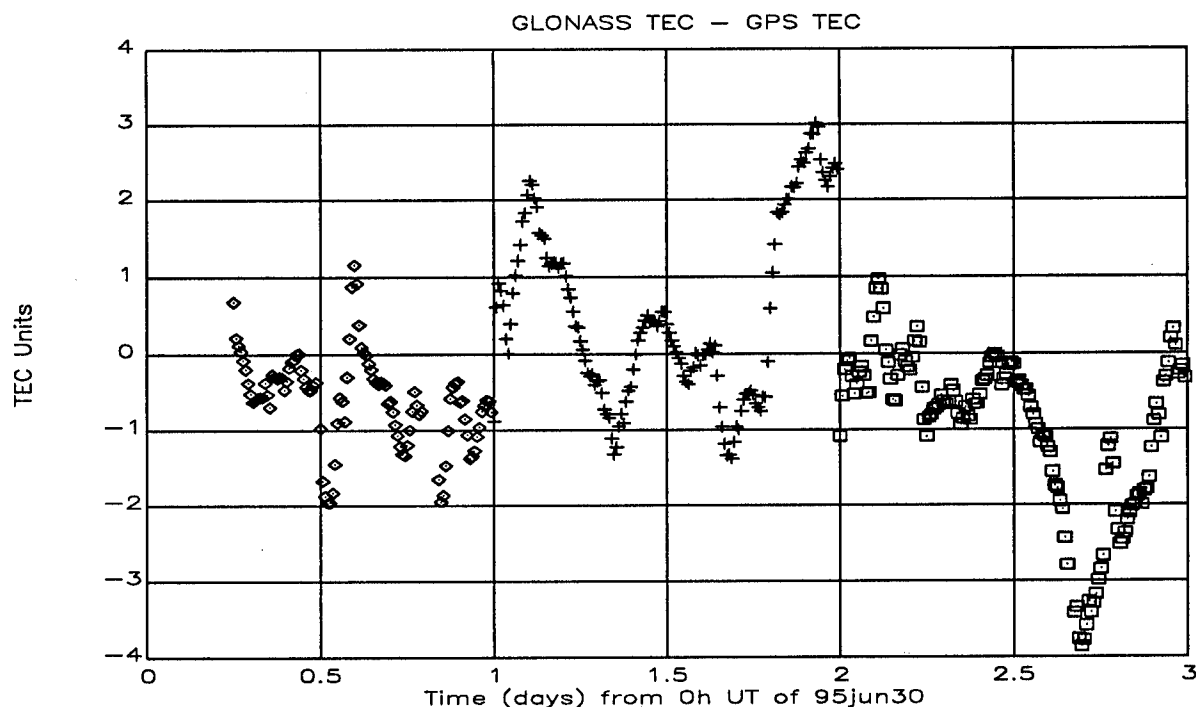


Figure 7. Differences between independent GLONASS and GPS TEC measurements at Neustrelitz from June 30th to July 2nd, 1995

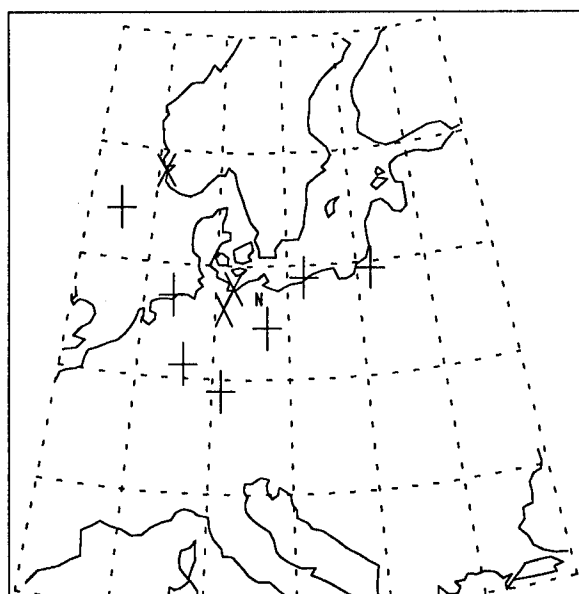


Figure 8. GPS (+) and GLONASS (x) scenario over Neustrelitz (N) at one particular moment

could be a small time delay in the actual sampling time with respect to the time given as nominal, which, acting in a sequential mode, might be (in average) the same between any two consecutive channels.

Under this assumption, by using two consecutive channels for P1 and P2 of each satellite, we can reduce the differential delay between pairs, which is the term affecting the ionospheric estimation. In our case the difference between any two pairs reach a maximum level of 6 mm. This is not negligible, but its influence is moderate. All the data presented in this paper was acquired using this channel distribution.

RESULTS OF IONOSPHERIC TEC ESTIMATION FROM GLONASS

In figure 6 we present the TEC estimated using only the 3S_R101 receiver for the test period.

Our algorithms applied to GPS data have been checked against independent ionospheric techniques in the past (Sardón et al, 1993; Solé et al, 1994), so the direct comparison with TEC models derived from GPS should be a straight forward validation method for the GLONASS results. In figure 7 we show the differences between the GLONASS and GPS estimates of the TEC for the same period as in figure 5. The rms differences is of 1.58 TEC units which is in agreement with the expected accuracy of our estimation method, from one to two TECU (Zarraoa & Sardón, 1995).

The same TEC is reproduced by both systems, although some differences remain, which in general correspond to periods where the number of available GLONASS satellites is small.

Once we have proven that GLONASS can operate as an stand along ionospheric monitoring system, which is consistent with similar GPS analysis, we can try to combine the two sets of data in a single analysis.

The advantages of this combination are several. First, the number of observables can be increased by more than 50% with our current receiver and GLONASS constellation, and the observed geometry improves. This is illustrated in figure 8 where the two sets of observables at Neustrelitz are plotted for a certain time, showing how GLONASS adds points in empty zones of the GPS scenario. For the test period, the increase in data when GLONASS was added to GPS

was over 55%. Second, instrumental effects can be better evaluated with the combination of data from different receivers.

We have merged both data sets for an unique estimation of the ionospheric TEC. With this combination we have also been able to produce an improved set of instrumental biases for the GLONASS system. In figure 9 we show the TEC estimated by GPS and GLONASS alone, and also the combined data set when the biases have been fixed to those estimated in the combined solution. Table 3 presents the instrumental biases estimated for the GLONASS satellites for that day, relative to the receiver bias, which can not be estimated without an external calibration. We must note that the stability in time of these values has not been confirmed yet, and we are currently processing a longer data set to verify it.

Table 3. Instrumental biases of the GLONASS satellites referred to our 3S_R101 receiver, estimated for July 2nd, 1995. (nanoseconds)

| Slot | | Slot | | Slot | |
|------|------|------|------|------|-------|
| 1 | - | 9 | - | 17 | 2.53 |
| 2 | 1.54 | 10 | - | 18 | -0.05 |
| 3 | 1.05 | 11 | - | 19 | 0.26 |
| 4 | 3.92 | 12 | 3.37 | 20 | 0.49 |
| 5 | 4.80 | 13 | - | 21 | 0.61 |
| 6 | 1.92 | 14 | 5.07 | 22 | 0.32 |
| 7 | 2.48 | 15 | - | 23 | 7.05 |
| 8 | - | 16 | 5.45 | 24 | 1.67 |

With the exception of the period between 14:00 and 18:00 where GLONASS could only observe one satellite, we can see that the three systems produce very much the same results. The rms differences between GLONASS and the combined solution are of only 0.3 TECU, and between GPS and the combined solution are of 0.15 TECU.

CONCLUSIONS

The results showed here are part of an extensive effort in testing the reliability and integrity of the GLONASS system for positioning, navigation and ionospheric monitoring.

Our first conclusion is that the GLONASS concept is perfectly alive and walking rapidly towards system completion, in spite of the economic and logistic problems in Russia. The constellation is almost complete and the performance of the system is according to the expected specifications.

The data quality is comparable with the GPS P-code standards, with the advantage of the lack of Anti-Spoofing systems, which makes the GLONASS P-code to be significantly more precise than the current GPS performance under Anti-Spoofing.

Some receivers are nowadays able to use the full accuracy of the GLONASS signal, like the 3S Navigation R101 series, with access to P-code and phases of both frequencies. However, the receiver side is still the weakest point in GLONASS. Few receiver types are available, and most of them are not suitable for high accuracy requirements and are not designed for light-portable navigation uses either.

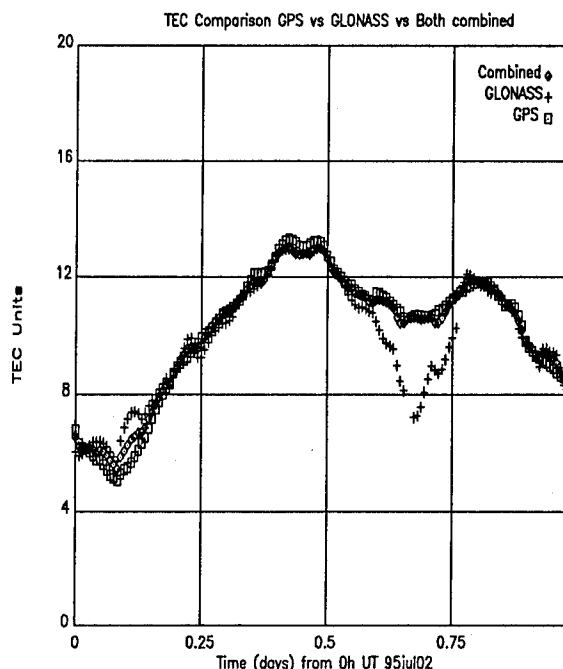


Figure 9. TEC estimations for July 2nd, 1995, obtained by GPS, GLONASS and the combination of both, when the instrumental biases are estimated from the combination.

The quality of the high precision (P-code and carrier frequency) GLONASS data has been demonstrated in its application to ionospheric monitoring. GPS and GLONASS have been successfully combined in a regular analysis procedure to obtain both TEC values and instrumental systematic errors, improving by 55% the amount of data available from GPS only, and thus improving the results and coverage of our ionospheric corrections for external users.

ACKNOWLEDGEMENTS. This work has been financed by the German Space Agency (DARA) through several projects in the last few years.

REFERENCES

- Bartenev, V.A. and 16 authors more (1994). Russia's Global Navigation Satellite System. Ed. ANSER.
- Danaher, J., A. Balendra, M. Danaher, E. Erpelding, J. Beser, R. Gerlach (1993). GLONASS dual frequency ionospheric sounder. Proceedings of the ION GPS-93. Ed. The Institute of Navigation.

Beser, J. (1994). A new line of GPS/GLONASS receivers and simulators. Proceedings of the ION GPS-94. Ed. The Institute of Navigation.

Bishop, G., S. Riley, P. Daly, A. Mazzella, E. Holland (1994). Analysis of temporal stability of GPS and GLONASS group delay correction terms seen in various sets of ionospheric delay data. Proceedings of the ION GPS-94. Ed. The Institute of Navigation.

Coco, D. (1991). GPS - Satellites of opportunity for ionospheric monitoring. GPS World. October 91.

Lanyi, G. (1986) Total ionospheric electron content calibration using SERIES GPS satellite data. TDA Progress Report 42-85. JPL.

Riley, S. & P. Daly (1993). Performance of the GLONASS P-Code at L1 and L2 frequencies. Proceedings of ION GPS-93 Technical Meeting. Ed. The Institute of Navigation.

Sardón, E., N. Jakowski, A. Rius (1993). Comparison of ionospheric TEC obtained from Faraday rotation of geostationary satellite signals and from GPS data. Proc. GPS/Ionosphere Workshop Neustrelitz. Ed. DLR/DFD Neustrelitz.

Sardón, E., A. Rius, N. Zarraoa (1994). Estimation of the transmitter and receiver differential biases and the ionospheric total electron content from GPS observations. Radio Science V. 29, No. 3, 577-586.

Sole, G., E. Sardón, S.M. Radicella (1994). Comparison of TEC data obtained from GPS data and from models using V.I. ionogram data. Proceedings of the International Beacon Satellite Symposium, Aberyswyth. Ed. L. Kersley, Univ. of Wales.

Zarraoa, N. & E. Sardón (1995). Test of GPS as a tool for ionospheric monitoring in high latitudes. Annales Geophysicae (in press).

Processing GLONASS Carrier Phase Observations – Theory and First Experience

Dr. Alfred Leick and Dr. Jinye Li
University of Maine

Dr. Jacques Beser
3S Navigation

Dr. Gerald Mader
National Geodetic Survey

BIOGRAPHY

Dr. Jacques Beser is Vice President of 3S Navigation in Laguna Hills, California, a company that has developed several GLONASS receivers. Dr. Alfred Leick is Associate Professor at the University of Maine. He is author of the book *GPS Satellite Surveying*. Dr. Jinye Li completed his graduate studies at the University of Maine in August 1995 and is now employed at Trimble, Sunnyvale, California. Dr. Gerald Mader is a research scientist at the National Geodetic Survey having extensive experience with GPS.

ABSTRACT

The GLONASS (ICD-92) double difference carrier observables must be transformed to either a common frequency or to linear distances in order for the relative receiver clock errors to cancel. Such a scaling causes the double difference equations to contain single difference ambiguities whose coefficients depend on the GLONASS frequencies. Pseudoranges are used to compute an approximate single difference ambiguity value for the base satellite. This additional step, which is not required for GPS, allows the double difference ambiguity formulation. However, this initial approximation of the single difference ambiguity must meet certain accuracy limitations. Dual-frequency pseudoranges and carrier phase observations to 5 GLONASS satellites are used to verify software implementation and to draw conclusions such as the need for frequency-dependent hardware delay calibrations and the need for accurate pseudoranges.

INTRODUCTION

GLONASS is becoming increasingly important in forming, together with GPS, an important element in the GNSS (Global Navigation Satellite System). GLONASS's attractiveness is largely attributed to the lack of selective availability (SA) and antispooing, making two P-code observables available to Civilian users in addition to both carrier phases. Modern positioning techniques, such as on-the-fly (OTF) ambiguity resolution, which blur the distinction between surveying and navigation, perform better the more satellites are observable. The fact that the satellites of both systems transmit at different frequencies will further enhance the combination solution.

In order to begin exploring GLONASS for precise positioning either as a stand-alone satellite system or in combination with GPS, it is necessary to study the peculiarities of GLONASS carrier phases and to modify existing GPS software. We modified the program KARS which was developed at the National Geodetic Survey for kinematic and rapid static surveys by G. Mader. This modification and the respective verification is the major objective of the initial phase of this study.

Test data were collected with two 10-channel, 3S Navigation R100/40 GLONASS receivers. The R100/40 is nominally a four-channel, dual frequency C/A and P-code GLONASS receiver. It can be expanded to ten channels by the addition of Digital Signal Processing (DSP) boards. The R100/40 is a PC-based receiver providing extensive outputs and user interface capabilities. The receiver consists of a broadband antenna, an RF/IF sub-system and digital signal processor boards installed in IBM PC/AT-compatible expansion slots. The user operates the receiver through the host PC. The RF/IF unit synthesizes its own 10 MHz reference frequency or accepts an external 5 or 10 MHz input. The ten parallel channels allow for continuous tracking of five GLONASS satellites on both L1 and L2. Code and carrier phase measurements were

generated at each receiver within 1 msec of GLONASS 1-second epochs.

The baseline was located on the roof of the 3S Navigation building. As with so many other roof-top test baselines, it suffers from a strong multipath environment. The baseline was also measured with Ashtech Z-12 GPS receivers in order to generate a standard for comparison. The R100/40 receivers were connected to the same Cesium clock. However, no attempt was made to assure that the differential clock error for both receivers is zero. It was further learned that the R100/40 receivers occasionally generated half-cycle slips at the time of data collection. This deficiency has since been corrected.

GLONASS DOUBLE DIFFERENCES

The GLONASS carrier frequencies at L1 band, denoted by a subscript 1, follow from the expression

$$f_1^p = 9(178 + C \times 0.0625) \text{ MHz} \quad (1)$$

where the C denotes the frequency number. GLONASS satellites are identified by either the frequency number or the PRN number (p). Table 1 lists the satellites used in this experiment. The L2-band frequencies, denoted by the subscript 2, are related to those of L1 as

$$f_2^p = \frac{7}{9} f_1^p \quad (2)$$

For the purpose of this study we introduce the mean GLONASS frequencies

$$f_{1,GLO} \equiv f_1^p (C = 12.5) \quad (3)$$

$$f_{2,GLO} = \frac{7}{9} f_{1,GLO} \quad (4)$$

for which the inequality

$$0.995 \leq \frac{f_{1,GLO}}{f_1^p} = \frac{f_{2,GLO}}{f_2^p} \leq 1.005 \quad (5)$$

holds.

Table 1: GLONASS Satellites Used

| PRN(p, q, \dots) | Frequency (C) | Elevation (deg) |
|----------------------|---------------|-----------------|
| 3 | 21 | 48 |
| 4 | 12 | 30 |
| 12 | 22 | 21 |
| 18 | 10 | 42 |
| 19 | 3 | 33 |

In order to eliminate receiver clock errors, the GLONASS carrier phase observations are scaled to the mean frequencies. For example, the scaled undifferenced GLONASS carrier phase observation at station k to satellite p at L1 band is

$$\begin{aligned} \phi_{k,1,GLO}^p &\equiv \frac{f_{1,GLO}}{f_1^p} \phi_{k,1}^p \\ &= \frac{f_{1,GLO}}{c} \rho_k^p + \frac{f_{1,GLO}}{f_1^p} N_{k,1}^p + \frac{f_{1,GLO}}{c} \dot{\rho}_k^p dt_k - f_{1,GLO} dt_k \\ &\quad + f_{1,GLO} dt^p + \frac{f_{1,GLO}}{f_1^p} I_{k,1,\phi}^p(f_1^p) + \frac{f_{1,GLO}}{c} T_k^p + \\ &\quad \frac{f_{1,GLO}}{f_1^p} \left[d_{k,1,p,\phi} + d_{k,1,p,\phi}^p + d_{1,p,\phi}^p + \epsilon_{k,1,\phi} \right] \end{aligned} \quad (6)$$

The terms on the right hand side of this equation refer to the topocentric distance, the integer ambiguity, the topocentric range rate, the receiver clock error, the satellite clock error, the ionosphere, the troposphere, receiver hardware delay, multipath, satellite hardware delay, and observation noise respectively. The subscript p in the hardware delay terms and the multipath term indicates the possibility of a frequency dependency.

As with GPS, the satellite clock error and the satellite hardware delay cancel in single differences. The ionospheric effects cancel for short baseline. The observations can be corrected for the topocentric range rate term using a receiver clock error derived from the pseudoranges. The double difference between stations k and m , and satellites p and q becomes

$$\begin{aligned} \phi_{km,1,GLO}^{pq} &\equiv \left[\phi_{k,1,GLO}^p - \phi_{m,1,GLO}^p \right] - \left[\phi_{k,1,GLO}^q - \phi_{m,1,GLO}^q \right] \\ &= \frac{f_{1,GLO}}{c} \rho_{km}^{pq} + \frac{f_{1,GLO}}{f_1^p} N_{km,1}^p - \frac{f_{1,GLO}}{f_1^q} N_{km,1}^q \\ &\quad + \frac{f_{1,GLO}}{c} T_{km}^{pq} + d_{km,1,\phi}^{pq} + \epsilon_{km,1,\phi}^{pq} \end{aligned} \quad (7)$$

The d -term in (7) represents hardware delays and multipath. Equation (7) differs from the respective GPS double difference expression primarily by the coefficients

of the single-difference ambiguities. These coefficients depend on the satellite frequencies. The single difference ambiguities are linearly dependent and cannot be separately determined from (7) without additional information.

In order to obtain an explicit double difference ambiguity formulation, we introduce an approximate value for the single difference ambiguity to satellite p such that

$$N_{km,1}^p = N_{km,1,0}^p + dN_{km,1}^p \quad (8)$$

Substituting (8) into (7) gives

$$\begin{aligned} \Phi_{km,1,GLO}^{pq} - \frac{f_{1,GLO}}{f_1^p} N_{km,1,0}^p &= \frac{f_{1,GLO}}{c} \rho_{km}^{pq} \\ &+ \frac{f_{1,GLO}}{f_1^q} \Delta N_{km,1}^{pq} + \frac{f_{1,GLO}}{c} T_{km}^{pq} + \psi_{km,\Phi}^p + d_{km,1,\Phi}^{pq} \end{aligned} \quad (9)$$

where

$$\psi_{km,\Phi}^p = -\frac{f_{1,GLO}}{f_1^q} \left[\frac{f_1^p - f_1^q}{f_1^q} - \left(\frac{f_1^p - f_1^q}{f_1^q} \right)^2 + \dots \right] dN_{km,1}^p \quad (10)$$

$$|\psi_{km,\Phi}^p| \leq \frac{1}{125} dN_{km,1}^p \quad (11)$$

is the model error caused by the error in approximation of the single difference ambiguity to satellite p . The newly created double difference ambiguity is

$$\Delta N_{km,1}^{pq} = dN_{km,1}^p - N_{km,1}^q \quad (12)$$

Equation (9) can be modified further by introducing approximate values for the single difference ambiguity to satellite q . However, such an additional expansion of the ambiguity does not gain anything; it merely results in a coefficient of 1 for the reformulated double difference ambiguity parameter. Replacing the subscript 1 by 2 in equations (9-12) yields the respective expressions for L2-band observations.

The satellite p denotes the base satellite. This is usually the satellite with the highest elevation angle. The single difference ambiguity approximation can be derived from the carrier phases and pseudoranges using the wide-lane expressions

$$\begin{aligned} N_{k,w}^p &= (\varphi_{k,1}^p - \varphi_{k,2}^p) - (f_1^p P_{k,1}^p + f_2^p P_{k,2}^p) / 8c \\ &+ (d_{k,1,p,\Phi}^p + d_{k,1,p,\Phi}^p + d_{1,p,\Phi}^p) - (d_{k,2,p,\Phi}^p + d_{2,p,\Phi}^p + d_{2,p,\Phi}^p) \\ &- 0.65(d_{k,1,p}^p + d_{k,1,p}^p + d_{1,p}^p) - 0.50(d_{k,2,p}^p + d_{k,2,p}^p + d_{2,p}^p) \end{aligned} \quad (13)$$

$$N_{km,1,0}^p = \varphi_{km,1}^p + \frac{9}{2} [N_{km,w}^p - (\varphi_k^p - \varphi_m^p)] \quad (14)$$

$$N_{km,2,0}^p(1) = \varphi_{km,1}^p + \frac{7}{2} N_{km,w}^p - \frac{9}{2} (\varphi_k^p - \varphi_m^p) \quad (15)$$

The symbol c denotes the velocity of light. The numerical values in equations (13-15) apply to GLONASS frequencies. The subscript 2 in (15) indicates the single difference ambiguity of L2. In both (14) and (15) the single-difference ionospheric term has been neglected. The determination of the wide-lane ambiguity from (13) depends on the hardware delays and the multipath, i.e. the d -terms. Since the base satellite p is at a high elevation angle, the multipath should be at a minimum.

Instead of scaling the GLONASS observations to the mean frequency according to equation (9), the receiver clock errors also cancel in double differences if the undifferenced carrier phases are first converted to linear distances. In that case we obtain

$$\begin{aligned} \Phi_{km,1}^{pq} - \frac{c}{f_1^p} N_{km,1,0}^p &= \rho_{km}^{pq} + \frac{c}{f_1^q} \Delta N_{km,1}^{pq} \\ &+ T_{km}^{pq} + \psi_{km,\Phi}^p + d_{km,1,\Phi}^{pq} \end{aligned} \quad (16)$$

with

$$\psi_{km,\Phi}^{pq} = -\frac{c}{f_1^q} \left(\frac{f_1^p - f_1^q}{f_1^q} - \dots \right) dN_{km,1}^p \quad (17)$$

In our modification of KARS we implemented (9).

DIFFERENTIAL PSEUDORANGE SOLUTION

Because pseudoranges determine the approximate single difference ambiguity value to the base satellite via equation (13), there is a need to ascertain the quality of the pseudoranges. The misclosure

$$\begin{aligned}
M_{k,1}^p &\equiv P_{k,1}^p + \left(\frac{2}{1-\alpha} - 1\right) \frac{c}{f_1^p} \phi_{k,1}^p - \left(\frac{2}{1-\alpha} - 1\right) \frac{c}{f_2^p} \phi_{k,2}^p \\
&= \left(\frac{2}{1-\alpha} - 1\right) \frac{c}{f_1^p} N_{k,1}^p - \left(\frac{2}{1-\alpha} - 1\right) \frac{c}{f_2^p} N_{k,2}^p \\
&\quad + (d_{k,1,p} + d_{k,1,p}^p + d_{1,p}^p) \\
&\quad + \left(\frac{2}{1-\alpha} - 1\right) \frac{c}{f_1^p} (d_{k,1,p,\phi} + d_{k,1,p,\phi}^p + d_{1,p,\phi}^p) \\
&\quad - \left(\frac{2}{1-\alpha} - 1\right) \frac{c}{f_2^p} (d_{k,2,p,\phi} + d_{2,p,\phi}^p + d_{2,p,\phi}^p)
\end{aligned} \tag{18}$$

where

$$\alpha \equiv \left(\frac{f_1^p}{f_2^p}\right)^2 \tag{19}$$

The variation of the misclosure (18) with time is shown in Figure 1 for 900 epochs at 1-second spacing (Station m). Since there was no cycle slip during this interval the variation seen in Figure 1 is primarily due to the multipath on the P1-pseudoranges.

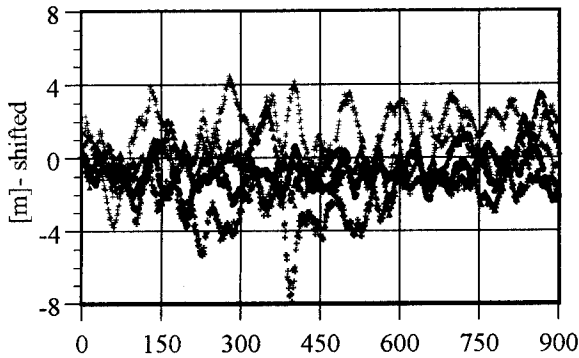


Figure 1: Misclosure (m,L1)

The differential P1-code solutions for stations k and m are shown in Figure 2. The GPS derived carrier phase solution is shown for comparison. The differential receiver clock correction, seen in Figure 3, reflects the stability of the Cesium clock; the variations are due to multipath. The differential receiver clock error is about $26.44\mu\text{sec}$. The residuals in Figure 4 show a large variation for satellite 12. The cause for this variation is unknown.

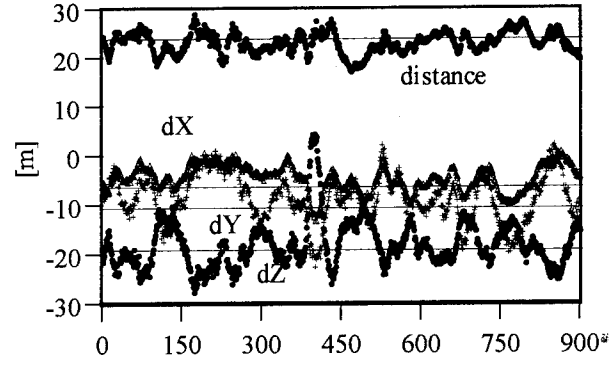


Figure 2: Diff. Pseudorange Solution (k,m,L1)

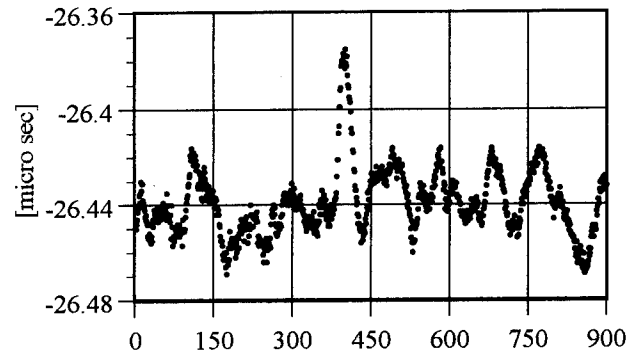


Figure 3: Differential Station Clock (k,m,L1)

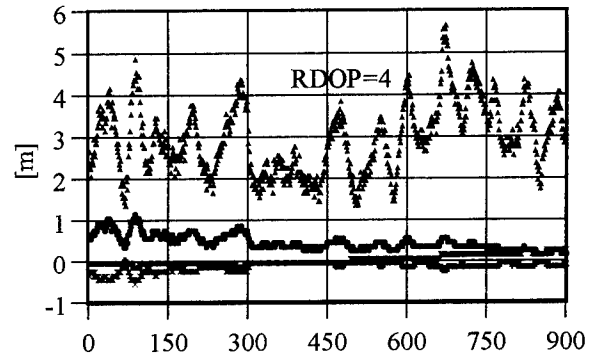


Figure 4: Pseudorange Residuals (k,m,L1)

CARRIER PHASE MISCLOSURES

The epochs between 300 and 400 are used in the carrier phase processing. An initial assessment of the quality of the dual-frequency carrier phases follows from Figure 5 which shows the ionospheric change from one epoch to the next using all satellites observed at both stations. The observations at Station m appear to be noisier than those of Station k . The cause is probably due to the use of an inline amplifier for the Station m antenna connection due to the longer distance. The amplifier was tuned for L1 frequencies and a specific cable length. Since a different

cable length was used, the overall gain at both L1 and L2 could have been affected, resulting in reduced carrier-to-noise ratios and therefore noisier measurements.

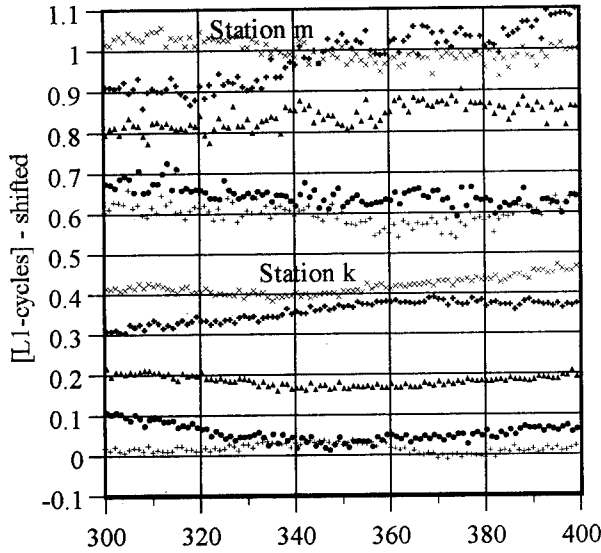


Figure 5: Ionospheric Change

The double difference carrier phase misclosures were computed from

$$dN_{km,1}^p + d_{km,1,\varphi}^{pq} = \frac{f_1^q}{f_{1,GLO}} \left[\varphi_{km,1,GLO,b}^{pq} - \frac{f_{1,GLO}}{f_1^p} N_{km,1,0}^p - \frac{f_{1,GLO}}{c} \rho_{km,a}^{pq} \right] \quad (20)$$

where the subscript b denotes the observation, and subscript a refers to the GPS-derived station coordinates. The fractional parts are shown in Figures 6 and 7. The integer parts were (21,-3,12,-1) and (17,-4,12,-1) for the double differences (3-4,3-12,3-18,3-19) indicating the suitability of equation (13) to approximate single difference ambiguities. The ambiguities to the non-base satellites were also expanded (otherwise the left-hand side of (20) would be arbitrarily large).

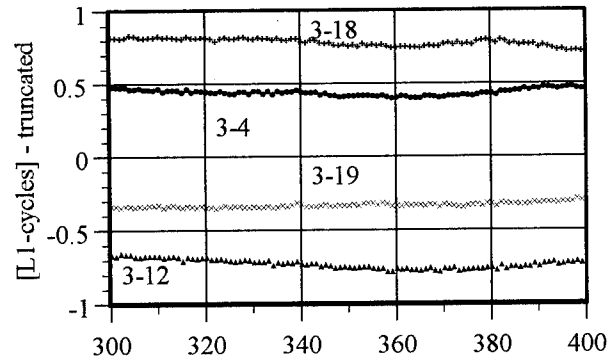


Figure 6: Double Difference Misclosures (k,m,L1)

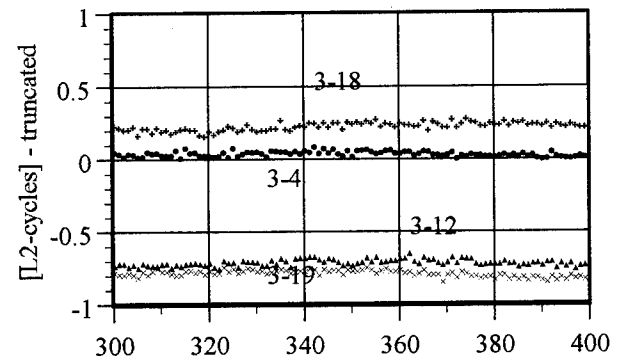


Figure 7: Double Difference Misclosure (k,m,L2)

Figures 6 and 7 require a cautious interpretation. Because of the model errors (10), caused by errors in the approximation of the ambiguities to the base satellite, the misclosures should not exactly coincide with integers even if the hardware and multipath terms are zero. Rather, these values should be shifted by the amount

$$\psi_{km,1}^{pq} = \left(\frac{f_1^p - f_1^q}{f_1^q} \right) dN_{km,1}^p \quad (21)$$

before coincidence with integers can be expected. Note that the same approximate single difference ambiguity value was used for all epochs. Figure 8 shows the variation of ε with dN . The initial values at $dN = 0$ are those of epoch 300 in Figure 6. It is seen that only the double differences (3-18) and (3-19) transit integers at the same place, i.e. $dN \approx 50$. The fact that not all double differences transit integers for the same dN indicates that hardware delays and the multipath effects are not negligible. In fact, a frequency dependency of the hardware delays cannot be excluded. Prior to data collection no attempts were made to calibrate the hardware phase delays (Raby and Daly, 1993). Some of the lines in Figure 8 could also shift due to half cycle slips in the observations.

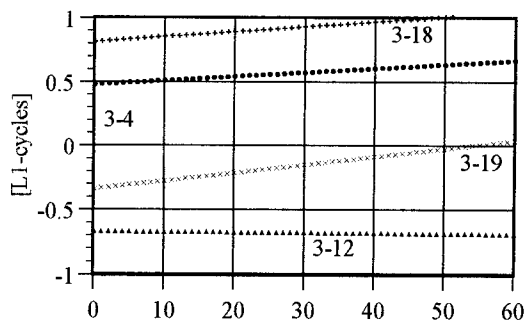


Figure 8: Error in Wide-Lane Ambiguity for Base Satellite (L1)

OTF CARRIER PHASE SOLUTIONS

In order to study the GLONASS phase observations for OTF positioning, the offsets in Figures 6 and 7 were averaged and the double difference observation corrected respectively. In order to make the OTF computations more realistic, the approximation of the single difference ambiguity was allowed to change from epoch to epoch according to the variation of the wide lane computed from (13). Figures 9 and 10 show the variation of the multipath according to

$$M_{k,w}^p = -0.65M_{k,1}^p - 0.50M_{k,2}^p \quad (22)$$

and the resulting variation in the wide lanes. Note that a wide-lane variation of 1 causes a change of 4 or 5 in the ambiguity according to equation (14), which in turn causes a model error of about 0.04 cycles according to equation (11).

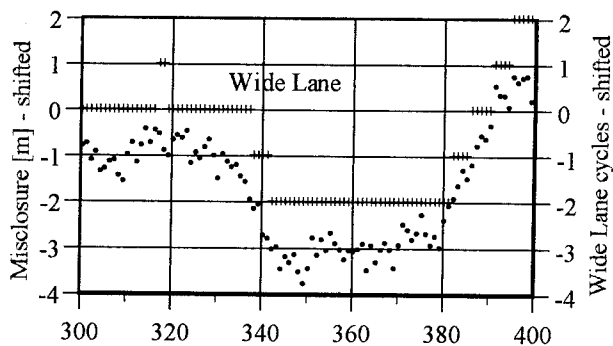


Figure 9: Misclosure and Wide Lane to Base Satellite (k,L1)

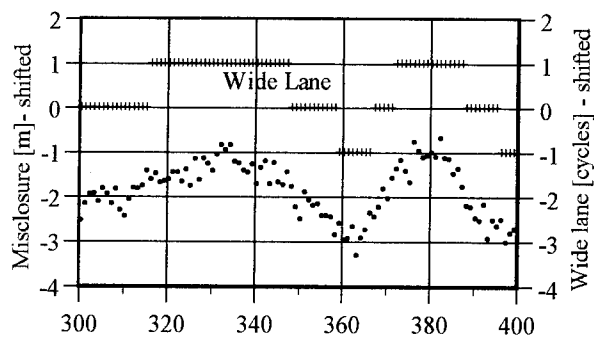


Figure 10: Misclosure and Wide Lane to Base Satellite (m,L1)

Using an ambiguity threshold value of 0.9, all 100 OTF solutions qualified and fell into 7 clusters as depicted in Figure 11. A total of 72 solutions fell into Cluster 1 which contains the correct solution. See the first column of Figure 11. The fact that the other clusters received solutions is attributed to the variation of the approximate single difference ambiguity to the base satellite and the noise of the observations. Unfortunately the contrast never exceeded 0.07 which is, again, a reflection of the observational noise, but also the fact that only 5 satellites were available. Usually a contrast of 0.1 is necessary to assure that false maxima are identified and eliminated.

The impact of the wide lane, and consequently the approximation of the single difference ambiguities of the base satellite were investigated by adding the same constant to the wide lane at each epoch. Four tests were made adding 1, 3, 5, and 10 wide-lane cycles respectively. The result is documented in Figures 11 to 14.

Figure 11 shows a clear decline in the number of solutions falling into (the correct) Cluster 1 and a corresponding increase for the other clusters. All clusters remain surprisingly dense. Figure 12 shows that the average distance with respect to the cluster mean barely changes. The rms phase residuals increase only slightly according to Figure 13. Figure 15 shows the change in the maximum ambiguity value if a wide-lane constant of 20 is added.

It appears that a small error in the wide lane of 2 or 3 cycles, as expected from the multipath variation, could be tolerated in OTF application. However, additional studies are necessary in order to understand better the impact of additional satellites.

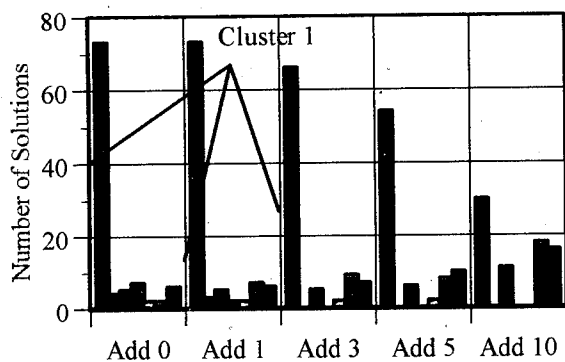


Figure 11: Cluster Population

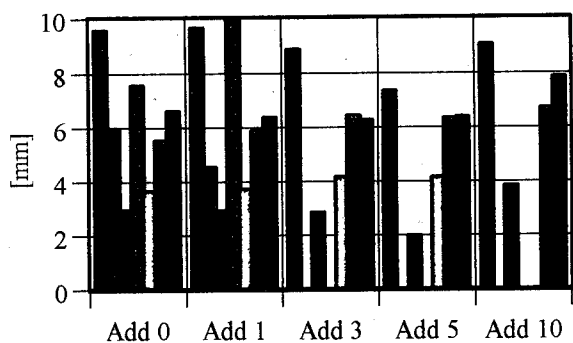


Figure 12: Average Distance from Cluster Mean

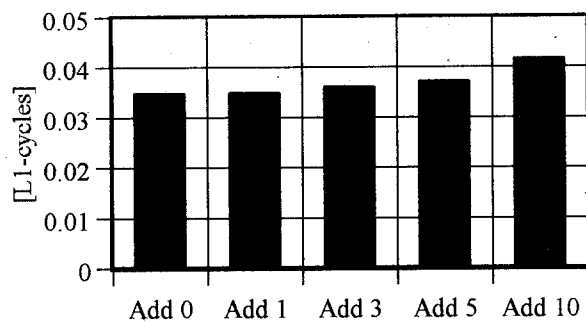


Figure 13: RMS Residuals

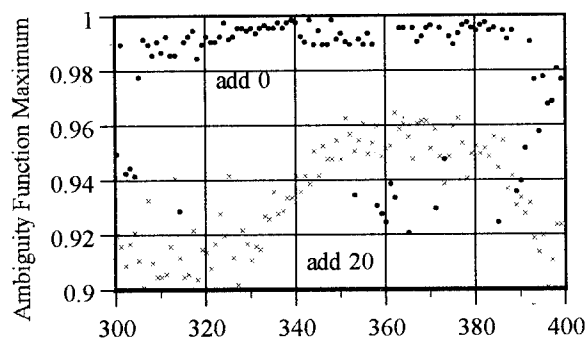


Figure 14: Ambiguity Function vs Error in Wide Lane

CONCLUSIONS

The KARS program has been successfully modified to process GPS and GLONASS carrier phase and pseudorange observations. The modified KARS program will be used for additional research on GLONASS carrier phase positioning.

The initial GLONASS data set, containing dual-frequency pseudoranges and carrier phases to 5 satellites, served primarily to test software modifications. However, the analysis demonstrated the need to focus future tests on the determination and calibration of hardware delays which might, in addition, be frequency-dependent.

The dual-frequency pseudoranges are used to determine an initial estimate to the single difference ambiguity of the base satellite. These estimates must be sufficiently accurate in order to reduce the mathematical model error. Our analysis seems to indicate that the variation of these initial estimates, caused by multipath, might be tolerable in OTF application. Clearly the role of the pseudoranges and the wide-lane ambiguity must be further investigated. However, it seems clear that the successful uses of GLONASS carrier phase observation in kinematic applications depends much more on accurate pseudoranges, and as such on high-quality antennas, than is the case for GPS.

REFERENCES

ICD-92. *Global Satellite Navigation System GLONASS - Interface Control Document* (second wording). RTCM Paper No. 518-91/SCI59-317.

Raby, P. and Daly, P. (1993). "Using the GLONASS System for Geodetic Survey." *Proceedings of the ION GPS-93*, pp. 1129-1138. The Institute of navigation.

Differential GLONASS in Russia: The Ways of Development

Alexander Ganin

GLONASS Coordination Research and Information Center

BIOGRAPHY

Alexander A. Ganin was born in 1959; Russian; in 1981 graduated at Mozhaysky Institute of Military Engineering, Leningrad; Doctor of technical sciences since 1988; more than 15 years he specializes in space radionavigation.

Victor V. Kulnev was born in 1953, Russian; in 1976 graduated at Dzerzhynsky Military Academia, Moscow; Doctor of technical sciences since 1985, more than 20 years he specializes in space radionavigation.

INTRODUCTION

The GLONASS space navigation system performance meets the accuracy requirements of most mass users. However, there are the series of important applications which require a more high accuracy (about few or only one meter) in real time, and the usual autonomous mode of GLONASS use cannot provide this accuracy level.

Particularly, this is very relevant to air traffic control during an approach and landing phases of flight, vessels traffic services for harbour approaches and restricted waters, trajectory monitoring of space vehicle launchers, etc. But the differential GLONASS and GPS systems allow to provide the required level of accuracy for these applications.

HISTORY AND THE STATUS OF THE PROBLEM

In Russia, an active research in the field of differential GLONASS system was begun in the end of the seventies, that is practically at the same time when GLONASS itself had been developed. The scientists of Central Research Institute of the Russian Space Forces (TsNII VKS), Russian Research Institute of Space Device Engineering (RNII KP), Scientific Producing Corporation of Applied Mechanics (NPO PM) took active part in these research works.

A developed by them theoretical aspects of differential GLONASS special features allowed to substantiate a ways of DGLONASS implementation and move on to an experimental phase of research.

As a result, an analytical and numerical descriptions of a differential stations operating zones was obtained, and a boundaries of zone, within of which a main errors of GLONASS differential mode are decorrelated, was developed. A methods of

differential mode residual errors reduction was also developed.

However, owing to various objective causes an implementation of differential GLONASS in Russia was dragged on. A lack of the Selective Availability mode in GLONASS system played a not unimportant role in the process. The standard accuracy of GLONASS on the few ten meters level met the requirements of common users in Russia.

But the works in this field had been speeded up in 1990-1991.

It should be noted that the operating zones of some foreign DGPS networks are partly spreading over the Russian territories and aquatories. Besides, a some foreign companies are displaying the great interest in penetration to the Russian market of users equipment, and in deployment of its own differential systems in Russia.

Under these circumstances, an interest of Russian users and users equipment manufacturers in differential mode of navigation are increasing. Therefore, the works on creation of differential stations for various applications had been speeded up.

For instance, Russian Institute of Radio Navigation and Time (RIRV) developed a differential station integrated with maritime radiobeacon. The station provides a maritime GLONASS/GPS users with the differential corrections data.

RNII KP developed a ground-based differential station providing GLONASS/GPS users with the differential corrections in RTCM SC-104 format. Besides, the station have the capabilities to provide a ground-based navigation system with the signals of synchronization, and to perform an integrity monitoring. The Russian Space Forces demonstrated this station, and the others prospective models of users equipment completely providing as the differential mode as the combined GLONASS/GPS positioning, at the 2nd International Air Show "MAKS-95" in Zhukovsky (August 22-27, 1995).

At present, there are the plans of creation of local-area and regional-area differential system for air traffic control and vessels traffic services. Taking into account its departmental specialization caused, on the whole, by channels selected for differential corrections transmission, the use of these systems by common users is problematical. Therefore, it should be expected on the appearance of intentions to create others differential systems in the future, e.g. for the sake of surface transportation control.

Thus, it can be noted there is the tendency to create the Russian network of departmental differential systems oriented towards specified users. These systems are a local-area differential systems (LADS), and its operating zones do not cover all the Russian territory. The way of differential systems deployment realized by the simple increasing of LADS number is too hard justified from the standpoint of economics. That is why the other way of differential system deployment was proposed.

In 1994, Central Research Institute of the Russian Space Forces jointly with Coordinational Scientific Information Center of the Russian Space Forces (KNITs VKS) developed a project of the future Russian differential system with the use of ground-based infrastructure of the Russian space vehicles control complex. This differential system will be able to serve practically all the GLONASS users in Russia.

Principles of operation of this system and algorithms of differential corrections calculation and formation were formerly developed and examined using as measuring data from GLONASS ground-based control complex, as results of TsNII VKS/KNITs VKS/Russian Maritime Geodetic Company joint works in Far-East and South-East Asia regions.

The analysis of domestic and foreign situation concerning differential systems development performed by TsNII in 1994 clearly indicated that an isolated development of WADS and LADS do not meet up-to-date requirements. In order to coordinate the development of detached differential systems in Russia and its subsequent integration within United (State) differential system (UDS), the Concept of differential GLONASS system design had been assigned to develop. Interdepartmental resolution "On executing works in different-level differential systems and integrity monitoring system development" from 1994, contains this assignment. The Concept was developed by the Russian Space Forces (VKS) jointly with the Russian Space Agency (RKA) and the Ministry of Transport. At present, the first version of the document is on the approval at concerned ministries and departments.

The following principles of UDS design was proposed:

1) the differential system performance will meet all the requirements of main group of users;

2) the high-precise navigation field of UDS will cover the most important, from point of view of economics and defense, territories and aquatories of the Russian Federation and a neighboring States. A potential capabilities of extending the UDS operating zone, reconfiguration of high-precise navigation field (or UDS ground-based facilities density redistribution over the Russian Federation and neighboring States) will be foreseen;

3) the basic differential system features is the formation and distribution of correcting and additional data. The UDS differential corrections will be formed and transmitted for the sake as GLONASS as GPS users in any combinations. The combined transmission of GLONASS/GPS differential corrections will not

decrease any positioning capability of only one navigation system users;

4) the UDS will be created with the minimal costs through the rational integration of wide-area, regional-area and local-area differential systems. The existing Russian infrastructure containing GLONASS ground-based control complex, ground-based radionavigation systems and data communication facilities will be used;

5) standardization and unification of differential stations equipment, transmissions channels, and data formats will be executed taking into account domestic and international standards and international experience. The UDS structure will allow to rationally combine an ability to meet the users requirements with a maximal unification of the UDS basic elements;

6) the capability of interaction between UDS and differential GPS systems will be foreseen and the interaction between UDS, GPS, GNSS and its subsystems will be based on appropriately approved international agreements;

7) in the process of UDS creation it will take into account the specified requirements of aviation and maritime users;

8) transition from LADS to regional-area differential system (RADS) and WADS will be staged. An extension of the UDS operating zone will be performed simultaneously with UDS integration for the sake of various users;

9) the UDS operation will be checked by the Government of the Russian Federation taking into account the Russian defense and economics interests, and the existing commitments to international users community. The machinery of State checking and coordination of UDS creation will realized on a interdepartmental basis with a participation of the concerned departments, developers and users.

The following issues will be coordinated during the process:

- determination and checking of adherence to the State policy in the field of the UDS creation and development, taking into account the Russian national interests;

- determination of rules, standards and recommendations concerning the UDS creation, implementation and operation, as well a checking of adherence to these documents too;

- an allocation of State share of funds distribution;

- certification of system components and the whole system;

- integration into an international system taking into account a corresponding requirements.

The Concept determine that the Russian differential system will have the three-level hierarchic structure including WADS, RADS and LADS. Each level of UDS is the autonomous system performing its own tasks. In the aggregate, the system are united system providing the users with the precise navigation service.

The wide-area differential system (WADS) will contain the Center of collecting and processing of data, the monitoring stations, the differential stations and data transmissions facilities.

The regional-area differential system (RADS) will contain the differential stations and data transmission facilities united into network for the regional users service (on land and coasts regions).

The local-area differential system (LADS) will contain the static or mobile differential station and the data transmission facility operating for the sake of specified users.

The basic elements of the united differential system are the centers of collecting and processing of data, differential stations, monitoring stations, satellite-based and ground-based data links, data interchange systems and users equipment.

The first level of the UDS is the WADS which provides:

- collecting and processing of data received from monitoring stations, 2nd- and 3rd-level differential stations in order to promptly correct the parameters of regional ionosphere model, and GLONASS ephemerides, clock corrections and integrity data;
- transmissions of needed WADS data to 2nd- and 3rd-level differential stations or directly to users;
- interaction between the WADS and the GLONASS Control Center (navigation field monitoring division).

The required number of the 1st-level differential stations is from three to five. Each of the stations is the WADS Center. The accuracy of positioning provided within the 1500-2000 km area is from 5 to 10 meters.

By our opinion, the arrangement of 1st-level differential stations network is possible on a basis of existing infrastructure of Russian space vehicles control complex which contain the ground-based control complex sites, data interchange systems and a powerful computation facilities.

The following circumstances are propitious for this idea:

- the ground-based elements of the Russian space vehicles control complex are placed over a wide area of all the Russia, allowing to create the full coverage by differential service of main Russian regions;
- the infrastructure of the Russian space vehicles control complex have the excellent capabilities to collect and process navigation data from many sites;
- the most simple way to arrange an interaction between GLONASS Control Complex and differential system facilities is to do it within the WADS. And the WADS will use the data from RADS and LADS.

The second level of UDS is RADS (specialized differential system), which will be created in order to cover the highly developed regions having a powerful

economics and a great many users. The RADS can be deployed in areas of an intensive traffic (air, maritime, surface, railway), complicated meteo conditions, and where the surveying is performing, etc.

The accuracy of positioning provided by 2nd-level differential station within the 500 km area is from 3 to 10 m.

The third level of the UDS is the LADS which will be deployed in detached regions in order to provide a particular economic, scientific or defense applications. The LADS will be able also provide the performing of special (episodic) departmental works, including the post-processing of data. The precise LADS will be able to provide within the few tens of kilometers area the decimeter level of positioning accuracy.

The LADS can be also created in a mobile version. 3rd-level differential systems may contain the pseudolites.

The key problem of the differential system creation is to arrange a data transmission channel providing the users with differential corrections and additional information. In order to arrange an information interaction between the elements of the differential system the data channels will be provide a continuous transmission of differential corrections and the additional data to users, and the required probability of the correct data reception by them within operating zone.

The use of GLONASS navigation channel to transmit the differential corrections to users is the one of prospective methods of resolving the problem.

The terms and stages of the Russian differential system creation depend on many factors. However, it may be expected the Russian RADS and LADS will be actively deployed in 1996-1997, then they will be integrated into the UDS in 1998-2000. The UDS will use the capabilities of infrastructure of the Russian space vehicles control complex.

THE WAYS OF INTEGRATION WITH FOREIGN DIFFERENTIAL SYSTEMS

At first, an integration between Russian differential system and foreign LADS and WADS should be directed to maximal unification of correcting data formats and the transmission channels. This requirement caused by economic expediency and by increasing Russian cooperation with others countries. The cooperation in the field of differential navigation will have a beneficial effect on air and vessels traffic control in area of responsibility of corresponding Russian services.

During the process of developing economic cooperation between Russia and international community, the positing of problem, concerning the integration of Russian differential system with international differential systems (e.g. in European, Baltic regions, etc.) may be legitimate.

By our opinion, on the first stage of such integration a joint scientific-theoretical and experimental works in the field of perfecting the principles of unification for national differential systems to be integrated, methods and algorithms of calculation and formation of correcting data, algorithms of global and local monitoring will be the one of form of mutually beneficial and fruitful cooperation. Besides, it will be expediency to consider the possibility of differential station joint development with concerned foreign partners.

CONCLUSION

1. At present there is an objective need in Russian differential GLONASS system.
2. The most expediency from standpoint of economics is to create the future Russian differential system as the three-level hierarchic structure including wide-area, regional-area and local-area differential systems.
3. The use of capabilities of infrastructure of the Russian space vehicles control complex is the most rational way of the domestic wide-area differential system creation.
4. During the process of the Russian differential system deployment in 1998-2000 it is expediency to execute the works aimed at perfecting of interaction between differential GLONASS and GPS jointly with concerned foreign partners.



RUSSIAN SPACE FORCES

CENTRAL RESEARCH INSTITUTE
Dr. A.GANIN and Dr. V. KULNEV

DIFFERENTIAL GLONASS IN RUSSIA. THE WAYS OF DEVELOPMENT.

ION '95



THE CORE ISSUES

- HISTORY AND STATUS OF THE PROBLEM
- PRINCIPLES OF THE GLONASS UNITED DIFFERENTIAL SYSTEM DESIGN
- THE WAYS OF INTEGRATION WITH FOREIGN DIFFERENTIAL SYSTEMS



THE PRINCIPLES OF THE UNITED DIFFERENTIAL SYSTEM DESIGN

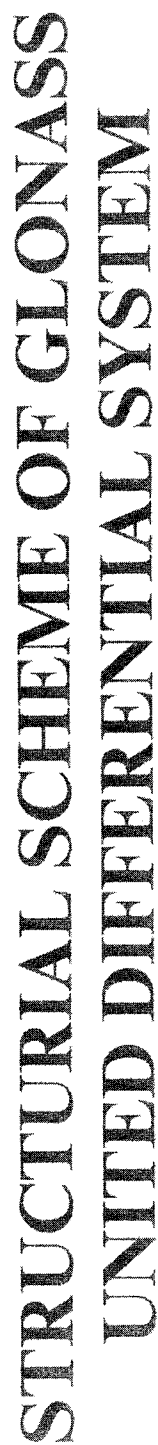
- Meet the requirements of the main groups of users;
- Providing the high-precise navigation over the most important regions of Russia;
- Formation of differential corrections for GLONASS and GPS users;
- Minimizing of coast for differential system creation;
- Standardization and unification of system components;
- Capabilities of integration with GPS differential networks;
- Formation of differential corrections for GLONASS and GPS users;
- Meet the requirements of international organizations;
- Staged development of the system;
- State checking of system creation and use with consideration of national safety interests.



THE MAIN CHARACTERISTICS OF DIFFERENTIAL SYSTEMS

| type of system | accuracy, m | operating zone, km | differential corrections | data links |
|----------------|-------------|---|---|--|
| wide-area | 5-15 | 2000-3000 | ephemerides, clock correction, ionospheric corrections | channels of ground-based radionavigation systems |
| regional-area | 3-10 | < 500 for only one differential station | corrections to pseudoranges | satellite channels, channels of ground-based navigation system, VHF/SW communications links, radio beacon channels |
| local-area | 3-10 | < 500 | corrections to pseudoranges | channels of ground-based navigation system, VHF/SW communications links, radio beacon channels |
| | 0.1-1.0 | 10-40 | corrections to pseudoranges during carrier phase measurement mode | VHF communications links |

100000





THE WAY OF INTEGRATION WITH FOREIGN DIFFERENTIAL SYSTEM

- Joint the teoretical and experimental works in the field of perfecting of GLONASS/GPS differential corrections formation methods, and local and global monitoring of navigational fields;
 - Coordination of differential corrections transmission standards, and unification of data links;
 - Joint development and creation of GLONASS/GPS differential stations and users equipment;
 - Joint works in integration of GLONASS and GPS differential networks.
-



CONCLUSION

- At present there is objective need in Russian differential GLONASS system.
 - The most expediency from standpoint of economic is to create the future Russian differential system as three-level hierarchic structure including wide-area, regional-area and local area differential systems.
 - The use of capabilities of infrastructure of the Russian space vehicles control complex is the most rational way of the domestic wide-area differential system creation.
 - During the process of the Russian differential system deployment in 1998-2000 it is expediency to execute the works aimed at perfecting of integration between GLONASS and GPS jointly with concerned foreign partners.
-

Kalman Filter Procedures for GPS/GLONASS-Signals

Norbert Niklasch
ViCon Engineering

Martin Maurer and Martin Haunschild
MAN Technologie AG

Walter Richert
LMU

BIOGRAPHIES

Norbert Niklasch received a diploma in Electrical Engineering in 1983 from the University of Federal Armed Forces, Munich. His main areas of work are design and development of RF-systems and components for satellite communications and navigation, software engineering and consultancy in the area of communication and navigation. Since 1993 he is owner of the company ViCon Engineering GmbH.

Martin Maurer received diploma in physics in 1974 and Ph.D. in 1984 from the University of Munich. He is specialist for the development of numerical codes, the performance of simulations, and software engineering for the solution of nonlinear systems related to space borne applications. Currently he is performing system design and software development for advanced differential reference and integrity monitoring stations. He is responsible for the MAN Technologie AG study project team for future satellite navigation systems GNSS1 and GNSS2 in the framework of the studies issued by the European Space Agency.

Martin Haunschild received diploma in Aerospace Engineering in 1985 and Ph.D. in 1989 from the Technical University of Munich. He is Head of the Satellite Navigation Project Group of MAN Technologie AG. Since 1990 he was project leader of various ESA-projects as NAVSAT Phase B1 Study, Monitoring of the GPS/GLONASS navigation satellites and the GNSS2 Mission Analysis Study. Currently he is project coordinator for the combined GPS/GLONASS/GNSS receiver product line as well as for the GLOGINAV-project (GLONASS-GPS-Inertial System-Navigation) of the German Luftfahrtforschungsprogramm (Aerospace Research Progr.).

Walter Richert received Ph.D. in 1972 in numerical mathematics from the University of Munich. Since 1980 he is professor of numerical mathematics at the Mathematical Institute of the University of Munich. His research interests are optimization, modeling and simulation for applications ranging from partial differential equations to eigenvalue problems. Currently he is working in design of filters and algorithms for satellite navigation systems.

ABSTRACT

Satellite navigation signals underlie several perturbations. These include effects such as atmospheric perturbations, noise, measurement and clock errors as well as multipath in the surroundings of a receiver. In addition artificial errors like jamming or selective availability (SA) can make worse the availability of the signal or the accuracy of position determination. At present only GPS is affected with SA which is the dominant error for stand alone users. Since GLONASS is available now this system can be used in combination with GPS. The model presented here uses these systems applying a filter algorithm derived from Kalman filter techniques for filtering SA contributions to enhance the accuracy and the predictability of the position even if GLONASS is unavailable for certain times. After SA-filtering, the signal containing noise contributions is then treated by Kalman filter techniques.

1. INTRODUCTION

Since several years the influence of perturbations of GPS-signals is under consideration. There are well known effects such as atmospheric perturbations including ionospheric delay and atmospheric attenuation, and influences on the kinematics of the space vehicles caused by gravitational and non-gravitational forces. These influences are of physical nature which do not depend on the specific system and are the major reason of errors in the determination of the user position. These errors can partially reduced by application of correction models for systematic errors which can be found for a short review e.g. in ref.1.

Another category of errors are due to equipment characteristics like code generation signal processing, clock errors and receiver measurement noise (clock noise and diffuse multipath). Concerning suppression of noise the importance of linear and non-linear forms of Kalman-filter procedures was shown in many publications.

A third source of potential errors can be found in the surroundings of a receiver antenna where shadowing and specular multipath of the signal caused by obstacles can occur. These effects are problematic e.g. for users on the ground or in the landing phase of airplanes. For these user groups modern antenna technology can be a help for multipath rejection. An example for this technology is presented in another paper (ref.2).

Besides the 'natural' sources of errors which in general can occur in every satellite navigation system like GPS, GLONASS or future GNSS, in addition artificial errors can be added to the signal itself which can make worse the availability of the signal or the accuracy of the position determination by varying the clock or ephemeris data. To the first item jamming can be added while the second effect is represented by the selective availability (SA), described in ref 1, ref 3 and ref 4 or in many other publications not mentioned here. This selective availability is implemented in GPS satellites but not in GLONASS.

The elimination of SA is discussed in many publications which make investigations for SA corrections in the GPS system only. An overview can be found in ref. 4. A treatment of SA using Kalman filter estimations was made in ref.5 where a real-time restitution of GPS time was performed.

Since it is intended that GLONASS will be installed completely in 1996, it seems now to be suitable to use the combination of both systems. In this combination a larger number of satellites is available leading to higher accuracy and availability. Thus it will be possible to reduce SA using GLONASS for a database to determinate an optimal filter for the treatment of GPS data with SA.

The model presented here applies a combined filter algorithm derived from Kalman filter techniques for the suppression of SA and additional noise filtering. In this way it is possible to enhance the accuracy and the predictability of the position even if GLONASS is unavailable for certain times. Also this method may make it easier to track GLONASS satellites.

To make this procedure treatable for the stand-alone user an accurate treatment of signal input by the receiver hard- and software becomes pertinent for the present GPS or GLONASS and especially for future satellite navigation systems. Thus suitable receivers for simultaneous use of these systems must be available. A description of new receiver development for this purpose can be found in refs. 6 and 7.

2. GPS AND SELECTIVE AVAILABILITY

NAVSTAR GPS is has reached already the fully operational phase with 24 [block 2] satellites in operation. As it is well known satellites have an orbital altitude of 20200 km and a orbital period of 12 h. For the carrier frequencies the two bands L1 in the range 1565.2 - 1585.7 Mhz and L2 in the range 1217.4 - 1237.8 were used. Besides the P-code used for mainly military purposes the C/A code is available for civil applications. For this code the US Department of Defense implemented an artificial error, the Selective Availability (SA) to degrade the GPS signal derived security. This is accomplished by manipulations of broadcast ephemeris data and dithering of the satellite clock (ref 4). For non-differential applications of GPS the SA is the largest error source. While the UERE (User Equivalent Range Error) of GPS without SA is in the range of 10 m, SA increases the UERE to the range of 25-100 m. A detailed discussion of SA effects can be found in ref.4 and the literature cited there.

Even for the application of differential GPS the SA influences accuracy as shown in fig. 1 where the range error in dependence on the time since update of correction data is plotted. It can be seen that due to SA a rapid increase of this error occurs. Thus transmission speed and data rate are determined to a large extent by SA. Without this perturbations requirements on these parameters would be considerably less strict.

Therefore it is of great interest to find procedures to suppress or minimize SA influence. Models of SA based on observations was developed by Braasch (ref. 1) and others (see e.g. refs. 5, 8). However, for all investigations open questions remain whether SA is equal for all satellites, whether SA is a stationary random process, and what is the orbital SA.

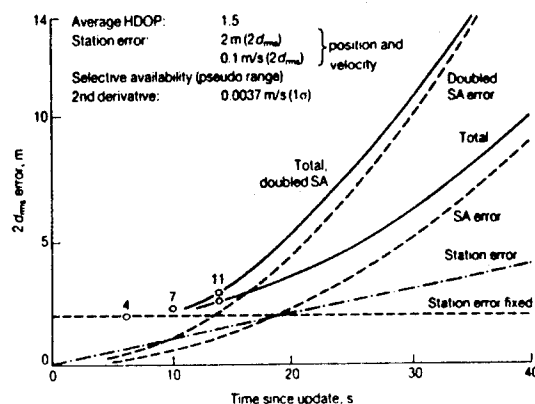


Fig.1: Errors versus time in DGPS due to SA (ref.3)

3. GLONASS AND COMBINATION WITH GPS

For the treatment of the problems described above until now only GPS data were used. Since it is intended to operate GLONASS fully during 1996 it should be considerable to use also this system for SA suppression.

The complete system will consist of 24 satellites in nearly circular orbits with an altitude of 19130 km and an orbital period of 11.25 h (refs. 6, 7, 9, 10). The inclination of 64.8° leads to a higher visibility of these satellites in northern regions where the coverage by GPS satellites is reduced.

In contrast to GPS, whose satellites transmit on the same frequency using different codes to distinguish between satellites, GLONASS satellites use the same code sequence, but transmit on different frequencies. These frequencies are

$$f_k = 1602 + k \cdot 0.5625 \text{ Mhz for the L1 frequency band}$$

$$f_k = 1246 + k \cdot 0.4375 \text{ Mhz for the L2 frequency band}$$

where k is the satellite frequency number. Also the orbital information is different from that of GPS (ref. 9). A further difference to GPS, which is advantageous for the use of GLONASS satellites, is the absence of techniques like SA. Thus the GLONASS positioning solution is more coherent than a GPS solution. The UERE due to GLONASS is in the range of 9 m which is slightly larger than the UERE of GPS without SA. This is caused by the fact that the ionospheric delay is not corrected.

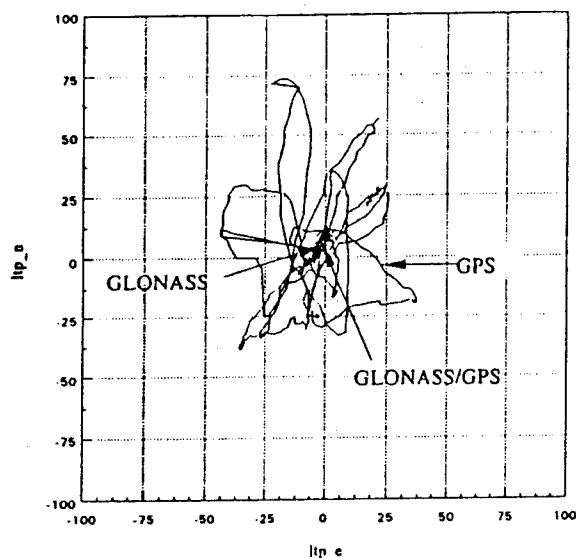


Fig.2: Position Errors for GPS, GLONASS, and GLONASS/GPS (ref.6)

With respect to coordinate transformation, ephemeris transformation, and time transformation between GPS and GLONASS differences can be tolerated or can be handled by special algorithms (e.g. Kalman filter techniques for time transformations). Thus the combined use of GPS and GLONASS in an integrated system is considerable. Since now receivers are available which are suitable for parallel tracking of satellites in both systems measurements can be performed easily. An example of such measurements is shown in fig.2 where position measurements were made with the R100 receiver of the company 3S Navigation (ref.6). The graphs show the different paths of position errors for GPS, GLONASS alone, and for the combination of GPS/GLONASS varying with time. It can be seen that position errors of GPS are mostly within a circle of 50 m while GLONASS and the combination are within a circle of 5 m which is 1/10 of GPS error. This figure shows impressively the advantage of the combined system. Altogether the advantages of the combined use of GPS/GLONASS are

- simultaneous visibility of more satellites (> 5)
- improvement of GDOP (< 3)
- enhanced accuracy without application of differential techniques
- Applicability of fast algorithms for the resolution of phase ambiguity for geodetic applications and reduction of measurement time
- reduction of SA effect of GPS
- enhancement of integrity
- enhancement of reliability

Thus the use of a combined system will be suitable for future applications.

Nevertheless there remains a problem in time ranges where the total number of satellites is sufficient for an accurate positioning measurement but the number of available GLONASS satellites is too small. In this case accuracy will be dominated by the data of the GPS satellites such that an instantaneous change in the accuracy will occur until the GLONASS constellation is usable again.

4. MODEL AND FILTER PROCEDURE

To bridge this gap a model is considered which uses the GLONASS data for the filtering of SA in GPS data. Based on this filtered data it is possible to continue the determination of position using GPS data including SA with the accuracy which is obtained from the entire system. When the GLONASS constellation is favorable again the filter will be calibrated anew. Fig. 3 shows the processing schedule of the model. For a first time interval and a fixed user position both GLONASS and

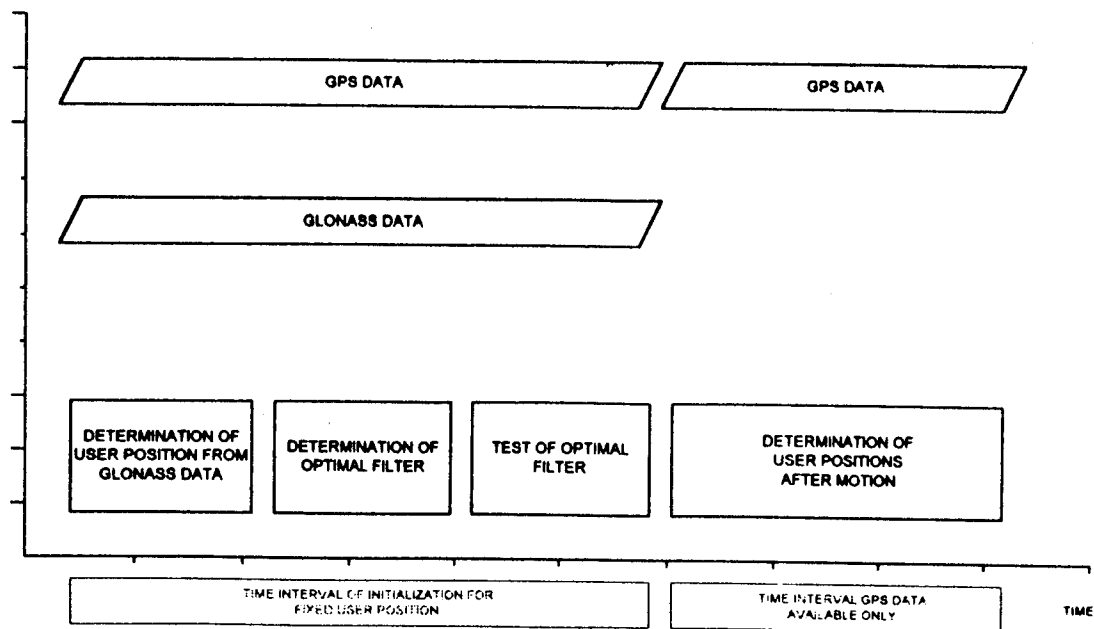


Fig. 3 : Schedule for the development of the filter model

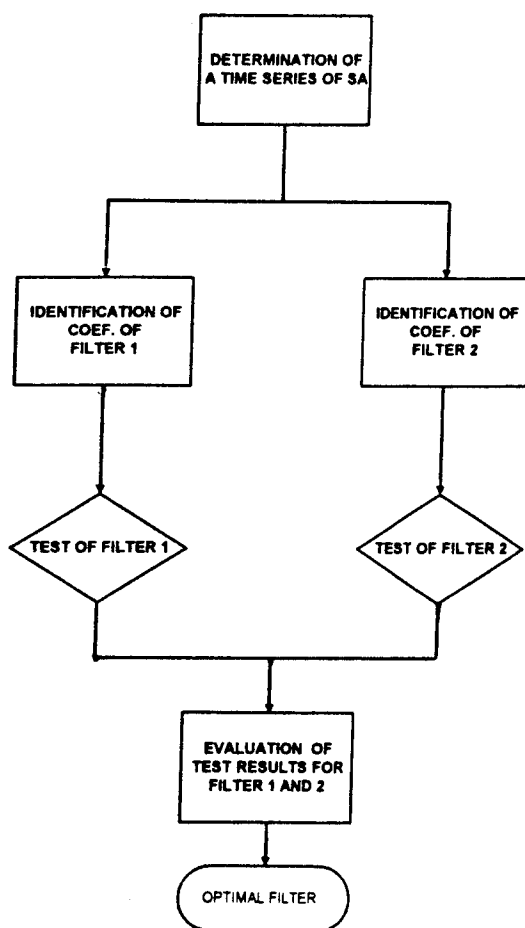


Fig. 4 : Schedule for evaluation of an optimal filter

GPS data are collected and the user position will be determined from GLONASS data. This is the data base for the determination of an optimal filter. The filter procedure chosen is an algorithm derived from a Kalman filter algorithm which was developed by Richert (ref.11). To determinate an optimal filter for the problem in a first step the SA for *one* measurement has to be determined. To do this a procedure is implemented in the algorithm which performs the following minimization problem:

As an assumption the following data set is given:

$[T_1, T_2]$ time interval between two updates of GPS ephemerids

$\tilde{t}_0 \in [T_1, T_2]$ time of signal transmission by GPS satellites $j=1, \dots, 4$ including SA

$d^{(j)}(\tilde{t}_0)$ pseudorange determined by a signal transmitted by satellite j at time \tilde{t}_0

$$d(\tilde{t}_0) := \begin{pmatrix} d^{(1)}(\tilde{t}_0) \\ d^{(2)}(\tilde{t}_0) \\ d^{(3)}(\tilde{t}_0) \end{pmatrix}$$

array of transmitted pseudoranges of a set of instantaneous measurements of three satellites

$s^{(j)}(\tilde{t}_0)$ position of a GPS satellite j at time \tilde{t}_0
in WGS 84

$$s(\tilde{t}_0) = \begin{pmatrix} s^{(1)}(\tilde{t}_0) \\ s^{(2)}(\tilde{t}_0) \\ s^{(3)}(\tilde{t}_0) \end{pmatrix};$$

array of a set of three GPS satellites

$u(s, d)$ position of the user determined by the
vector s (which consists of the *positions*
of 3 satellites) and the vector d (which
consists of the *pseudoranges* of the
3 satellites) in GPS

$u_{GLONASS}$ user position determined by GLONASS
satellites in WGS 84;

With the knowledge of this data set we can determine the
time \hat{t}_0 to be a minimal point of the following minimi-
zation problem:

$$\min_{\Delta t \in [\tilde{t}_0 - \varepsilon, \tilde{t}_0 + \varepsilon]} \|u_{GLONASS} - u(s(\tilde{t}_0 + \Delta t), d(\tilde{t}_0 + \Delta t))\|$$

Computing this minimization problem the time \hat{t}_0
obtained then represents an approximation to the time
 t_0 which is the true point of time of signal transmission
for the GPS signal. For the transformation of GLONASS
data from SGS-85 to the GPS reference system a first
version of a transformation procedure is used which is
under development by the authors. Since the func-
tionality of the filter algorithm was the more important
aim of our investigations at present, some inaccuracy of
the transformation was neglected for the moment.

Repeating these computations for subsequent time steps a
data set is obtained which defines a time series of SA and
can be used as an input for the filter procedure. The basic
idea of this procedure is that the data to be identified can
be considered as the output of a linear filter whose input
is white noise. This means that the stochastic models
employed here are based on the idea that the time series
in which successive values are highly dependent on the
preceding values can be regarded as generated from a
series of an independent white noise process with fixed
normal distribution having zero mean. So this white
noise process is supposed to be transformed to the
stochastic process by a linear filter. Thus the processes
for SA filtering can be described by an auto-regressive,
moving average (ARMA) filter model (see refs.1,11) of a

given order. For the filter model described here two sets
of parameters are chosen for evaluation. This evaluation
leads to the optimization of the entire filter procedure for
the specific SA data set under consideration (see fig.4).

Following fig.3 after optimization and test a filter
mechanism is defined which also can be applied in the
case where position determination by GLONASS data is
not possible. Errors due to SA will be reduced and the
accuracy of position determination will increase. Thus it
is possible to bridge the time gap where GLONASS is
not available.

To the filter for SA reduction a post-processed Kalman
filter procedure can be added which was also evaluated
by the authors. In this combination the remaining noise
parts of the signals can be treated and a further reduction
of position errors is possible.

This algorithm implemented in receivers with
GPS/GLONASS capability should help the users to
obtain an enhanced accuracy for a lot of applications
without the need of differential services. Applications are
considerable in all areas of users interests, from
aeronautics to marine application and also for ground
mobile applications where additional difficulties may
occur by e.g. topographical constraints. In this case the
simultaneous lack of a sufficient number of satellites of
GPS and GLONASS can be mitigated if the total number
of GPS and GLONASS satellites is sufficient for position
determination and SA will be reduced by the filter
procedure described here. Even if differential methods
are used in addition the procedure described above may
be useful for the reduction of the requirements on the
transmission speed and the data rate for differential
corrections.

5. FIRST RESULTS

In a first step this filter procedure was tested with respect
to its functionality and efficiency. To perform these tests
a data set was generated which is representative for the
behavior of SA. This was done by the use of data
collected in ref.1. To test the filter optimization a model
was chosen which was a mixture of two models used in
ref.1. In this approach additional errors like ionospheric
delay could be excluded. These errors have to be treated
separately. For the timesteps arbitrary units were chosen.

Fig. 5 demonstrates the application of the filter proce-
dure to SA. The SA in this figure is a composition of two
types of SA, which are well identified. The type changes
in point 400. The optimal filter is determined based on
the time steps from 0 to 200. For the rest of this time
series this optimal filter is applied.

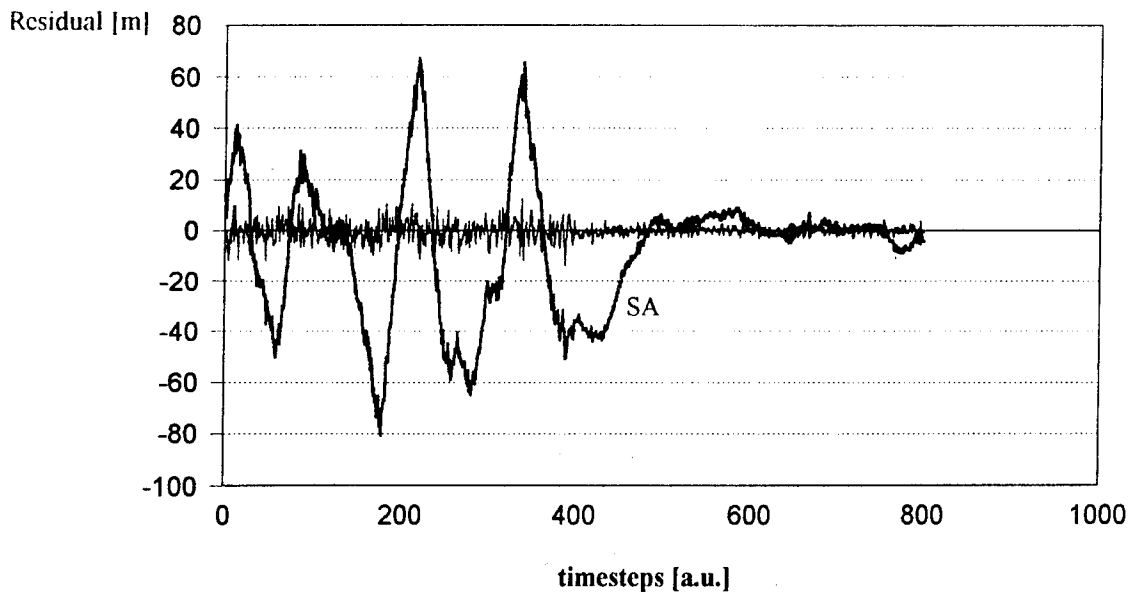


Fig. 5: Pseudorange Residuals with SA turned on and pseudorange residual after application of an optimal filter to SA

While the residuals due to SA comprise a large range with deviations up to 80 m, the application of the optimal filter leads to a reduction of the residual caused by SA to a range of 7-10 m which will result in a reduction of about a factor of ten. The remaining residual is containing only the noise parts of the signal.

The second step leads to a reduction of the influence of the noise. As described above Kalman filtering is applied to the remaining part of the residual in fig. 5 which is plotted in a smaller scale in fig. 6. The application of Kalman filtering can be seen in fig. 7. The residual is smoothed noticeably and a reduction of about a factor of

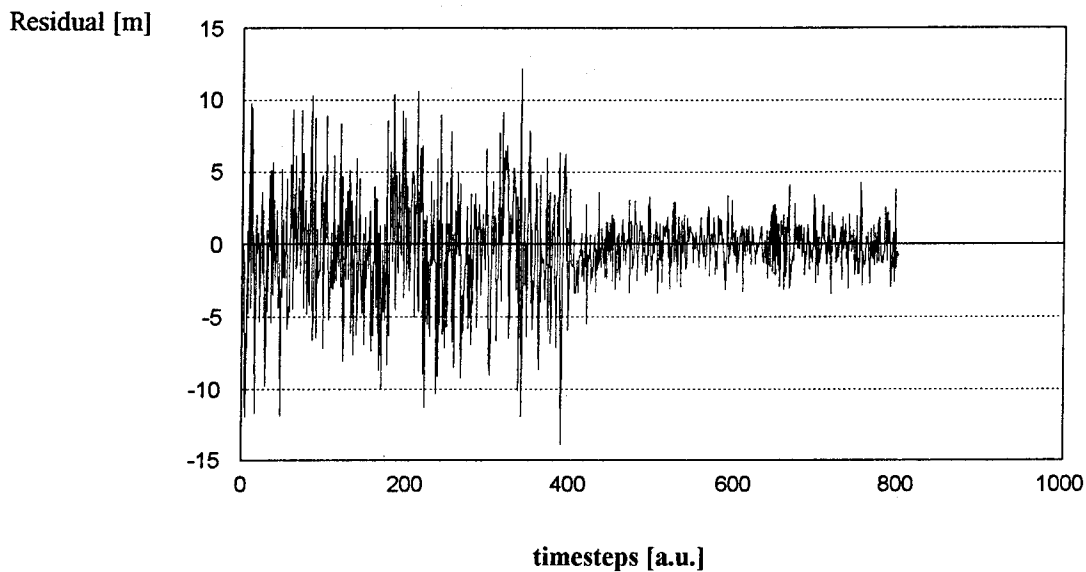


Fig. 6: Pseudorange residual after application of an optimal filter to SA (Noise contribution)

$s^{(j)}(\tilde{t}_0)$ position of a GPS satellite j at time \tilde{t}_0
in WGS 84

$$s(\tilde{t}_0) = \begin{pmatrix} s^{(1)}(\tilde{t}_0) \\ s^{(2)}(\tilde{t}_0) \\ s^{(3)}(\tilde{t}_0) \end{pmatrix};$$

array of a set of three GPS satellites

$u(s, d)$ position of the user determined by the
vector s (which consists of the *positions*
of 3 satellites) and the vector d (which
consists of the *pseudoranges* of the
3 satellites) in GPS

$u_{GLONASS}$ user position determined by GLONASS
satellites in WGS 84;

With the knowledge of this data set we can determine the
time \hat{t}_0 to be a minimal point of the following minimi-
zation problem:

$$\min_{\Delta t \in [\tilde{t}_0 - \varepsilon, \tilde{t}_0 + \varepsilon]} \|u_{GLONASS} - u(s(\tilde{t}_0 + \Delta t), d(\tilde{t}_0 + \Delta t))\|$$

Computing this minimization problem the time \hat{t}_0
obtained then represents an approximation to the time
 t_0 which is the true point of time of signal transmission
for the GPS signal. For the transformation of GLONASS
data from SGS-85 to the GPS reference system a first
version of a transformation procedure is used which is
under development by the authors. Since the func-
tionality of the filter algorithm was the more important
aim of our investigations at present, some inaccuracy of
the transformation was neglected for the moment.

Repeating these computations for subsequent time steps a
data set is obtained which defines a time series of SA and
can be used as an input for the filter procedure. The basic
idea of this procedure is that the data to be identified can
be considered as the output of a linear filter whose input
is white noise. This means that the stochastic models
employed here are based on the idea that the time series
in which successive values are highly dependent on the
preceding values can be regarded as generated from a
series of an independent white noise process with fixed
normal distribution having zero mean. So this white
noise process is supposed to be transformed to the
stochastic process by a linear filter. Thus the processes
for SA filtering can be described by an auto-regressive,
moving average (ARMA) filter model (see refs. 1, 11) of a

given order. For the filter model described here two sets
of parameters are chosen for evaluation. This evaluation
leads to the optimization of the entire filter procedure for
the specific SA data set under consideration (see fig. 4).

Following fig. 3 after optimization and test a filter
mechanism is defined which also can be applied in the
case where position determination by GLONASS data is
not possible. Errors due to SA will be reduced and the
accuracy of position determination will increase. Thus it
is possible to bridge the time gap where GLONASS is
not available.

To the filter for SA reduction a post-processed Kalman
filter procedure can be added which was also evaluated
by the authors. In this combination the remaining noise
parts of the signals can be treated and a further reduction
of position errors is possible.

This algorithm implemented in receivers with
GPS/GLONASS capability should help the users to
obtain an enhanced accuracy for a lot of applications
without the need of differential services. Applications are
considerable in all areas of users interests, from
aeronautics to marine application and also for ground
mobile applications where additional difficulties may
occur by e.g. topographical constraints. In this case the
simultaneous lack of a sufficient number of satellites of
GPS and GLONASS can be mitigated if the total number
of GPS and GLONASS satellites is sufficient for position
determination and SA will be reduced by the filter
procedure described here. Even if differential methods
are used in addition the procedure described above may
be useful for the reduction of the requirements on the
transmission speed and the data rate for differential
corrections.

5. FIRST RESULTS

In a first step this filter procedure was tested with respect
to its functionality and efficiency. To perform these tests
a data set was generated which is representative for the
behavior of SA. This was done by the use of data
collected in ref. 1. To test the filter optimization a model
was chosen which was a mixture of two models used in
ref. 1. In this approach additional errors like ionospheric
delay could be excluded. These errors have to be treated
separately. For the timesteps arbitrary units were chosen.

Fig. 5 demonstrates the application of the filter proce-
dure to SA. The SA in this figure is a composition of two
types of SA, which are well identified. The type changes
in point 400. The optimal filter is determined based on
the time steps from 0 to 200. For the rest of this time
series this optimal filter is applied.

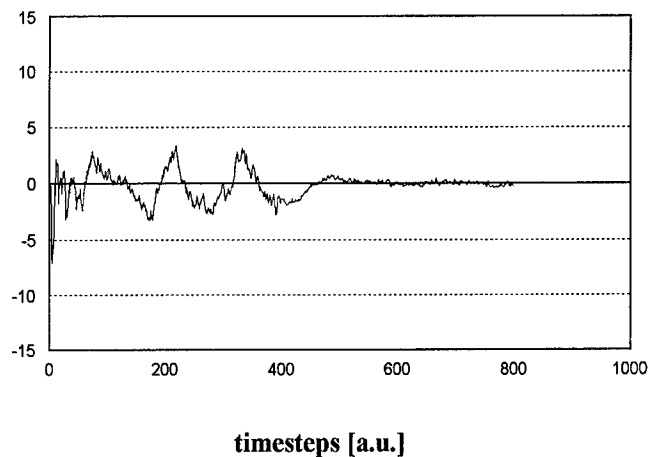


Fig. 7: Filtering of noise contributions

two can be achieved additionally. Altogether a reduction of SA error in the range of a factor of 20 could be reached in this tests.

Of course further work has to be performed using data from direct measurements to prove the algorithm in practical use. To do this, however, models of other error sources have to be implemented in the procedures in order to eliminate these errors before the application of the filter procedures. This work is done at present and will be published in the near future.

6. CONCLUSIONS

A suitable numerical procedure for single frequency users was presented which is able to reduce SA errors. The factor of reduction can be estimated to be in the magnitude of ten. Together with noise filtering a factor of 20 can be achieved for the entire reduction.

One of the most important features of this procedure is the use of combined GPS/GLONASS data which is suitable for the calibration of the filter.

Besides many applications in the area of single frequency users the procedure may also be usable for differential services in order to reduce the requirements on the transmission speed and the data rate.

To achieve a good performance of this procedure additional work like e.g. treatment of other errors for GLONASS satellites has to be done. Further problems must be treated with respect to the transformation of the different geodetic systems of GPS and GLONASS which will be important for the determination of SA values.

These problems are handled at present and new results can be expected in the near future.

7. REFERENCES

- [1] M.S. Braasch : A Signal Model for GPS. Navigation, vol.37, No. 4 1991
- [2] T. Hekmat, N. Niklasch, M.Maurer: Integrated GPS/GLONASS Antenna for High Performance Application, Presentation B3, No.4 on the ION GPS 95
- [3] B. Forsell: Radionavigations Systems, ed. Prentice Hall London, 1991
- [4] M.S. Braasch et.al.: Improved Modelling of GPS Selective Availability. Proc. ION-GPS p325, Albuquerque, NM, USA 1992
- [5] C. Thomas: Real Time Restitution of GPS Time Through a Kalman Estimation. Metrologia **29**, p397, 1992
- [6] A. Balendra, S. Kim, J. Beser: Fully Integrated GLONASS Dual Frequency P Code and GPS/GLONASS Single Frequency C/A Code Receiver, Features and Performance. Proc. ION GPS 94, Salt Lake City, 1994
- [7] B. Eisfeller, G.W. Hein, U. Roßbach: Experiences in DGPS/DGLONASS Combination. Proc. ISPA 95, Braunschweig 1995
- [8] H. Chou: An Anti-SA Filter for Non-differential GPS Users. ION GPS-90, Colorado Springs, CO, USA 1990
- [9] ISDE: Main Aspects of GLONASS System Development, Some Questions of System Use for Navigation Determinations. Technical Report Prepared for MAN Technologie AG, Moscow, CIS 1992
- [10] J. Beser, M. Haunschild: Advantages of GLONASS and Integrated GPS/GLONASS Operations over GPS-Only Operations. Submitted to publication, 1995.
- [11] W. Richert: Zur Algorithmischen Darstellung von Kalman-Filtern. MAN Technologie Report SRD 001, 1991